

# 付 録



# Macrophage Migration Inhibitory Factor and Stearoyl-CoA Desaturase 1: Potential Prognostic Markers for Soft Tissue Sarcomas Based on Bioinformatics Analyses

Hiro Takahashi<sup>1,2,3,4\*</sup>, Robert Nakayama<sup>4,5,6</sup>, Shuhei Hayashi<sup>7</sup>, Takeshi Nemoto<sup>4,8</sup>, Yasuyuki Murase<sup>9</sup>, Koji Nomura<sup>9</sup>, Teruyoshi Takahashi<sup>2</sup>, Kenji Kubo<sup>2</sup>, Shigetaka Marui<sup>2</sup>, Koji Yasuhara<sup>2</sup>, Tetsuro Nakamura<sup>2</sup>, Takuya Sueo<sup>3</sup>, Anna Takahashi<sup>3</sup>, Kaname Tsutsumiuchi<sup>2</sup>, Tsutomu Ohta<sup>4</sup>, Akira Kawai<sup>10</sup>, Shintaro Sugita<sup>11</sup>, Shinjiro Yamamoto<sup>7</sup>, Takeshi Kobayashi<sup>2,3</sup>, Hiroyuki Honda<sup>9</sup>, Teruhiko Yoshida<sup>4</sup>, Tadashi Hasegawa<sup>11,12</sup>

**1** Graduate School of Horticulture, Chiba University, Matsudo, Chiba, Japan, **2** Graduate School of Bioscience and Biotechnology, Chubu University, Kasugai, Aichi, Japan, **3** Plant Biology Research Center, Chubu University, Kasugai, Aichi, Japan, **4** Division of Genetics, National Cancer Center Research Institute, Tokyo, Japan, **5** Cancer Transcriptome Project, National Cancer Center Research Institute, Tokyo, Japan, **6** Department of Orthopaedic Surgery, Keio University School of Medicine, Tokyo, Japan, **7** Department of Applied Life Science, Faculty of Biotechnology and Life Science, Sojo University, Kumamoto, Japan, **8** Department of Dermatology, Tokyo Medical and Dental University, Tokyo, Japan, **9** Department of Biotechnology, School of Engineering, Nagoya University, Nagoya, Aichi, Japan, **10** Orthopedics Division, National Cancer Center Hospital, Tokyo, Japan, **11** Department of Surgical Pathology, Sapporo Medical University School of Medicine, Sapporo, Hokkaido, Japan, **12** Pathology Division, National Cancer Center Hospital, Tokyo, Japan,

## Abstract

The diagnosis and treatment of soft tissue sarcomas (STSs) has been particularly difficult, because STSs are a group of highly heterogeneous tumors in terms of histopathology, histological grade, and primary site. Recent advances in genome technologies have provided an excellent opportunity to determine the complete biological characteristics of neoplastic tissues, resulting in improved diagnosis, treatment selection, and investigation of therapeutic targets. We had previously developed a novel bioinformatics method for marker gene selection and applied this method to gene expression data from STS patients. This previous analysis revealed that the extracted gene combination of *macrophage* migration inhibitory factor (MIF) and stearoyl-CoA desaturase 1 (SCD1) is an effective diagnostic marker to discriminate between subtypes of STSs with highly different outcomes. In the present study, we hypothesize that the combination of *MIF* and *SCD1* is also a prognostic marker for the overall outcome of STSs. To prove this hypothesis, we first analyzed microarray data from 88 STS patients and their outcomes. Our results show that the survival rates for *MIF*- and *SCD1*-positive groups were lower than those for negative groups, and the *p* values of the log-rank test are 0.0146 and 0.00606, respectively. In addition, survival rates are more significantly different ( $p = 0.000116$ ) between groups that are double-positive and double-negative for *MIF* and *SCD1*. Furthermore, *in vitro* cell growth inhibition experiments by MIF and SCD1 inhibitors support the hypothesis. These results suggest that the gene set is useful as a prognostic marker associated with tumor progression.

**Citation:** Takahashi H, Nakayama R, Hayashi S, Nemoto T, Murase Y, et al. (2013) Macrophage Migration Inhibitory Factor and Stearoyl-CoA Desaturase 1: Potential Prognostic Markers for Soft Tissue Sarcomas Based on Bioinformatics Analyses. PLoS ONE 8(10): e78250. doi:10.1371/journal.pone.0078250

**Editor:** Dennis J. Templeton, University of Virginia, United States of America

**Received:** May 26, 2013; **Accepted:** September 10, 2013; **Published:** October 22, 2013

**Copyright:** © 2013 Takahashi et al. This is an open-access article distributed under the terms of the Creative Commons Attribution License, which permits unrestricted use, distribution, and reproduction in any medium, provided the original author and source are credited.

**Funding:** This work was supported by the Ministry of Education, Culture and Sports, Science and Technology of Japan [Grants-in-Aid for Scientific Research to Young Scientists (B) (No. 21710211 and 24710222 to HT) and by Futaba Electronics Memorial Foundation. The funders had no role in study design, data collection and analysis, decision to publish, or preparation of the manuscript.

**Competing interests:** The authors have declared that no competing interests exist.

\* E-mail: hiro.takahashi@chiba-u.jp

## Introduction

Soft tissue sarcomas (STSs) are a group of highly heterogeneous tumors that exhibit a diverse spectrum of mesenchymal differentiations. In addition, the molecular diagnosis of tumor heterogeneity has been hampered by the relatively low incidence of these tumors; an annual incidence of

soft tissue sarcoma is around 50 per million population[1,2], i.e. <1% of all malignant tumors. Significant differences were observed in 5-year survival rates among STS subtypes, e.g., 100% for well-differentiated liposarcoma (WLS), 71% for synovial sarcoma (SS), 46% for pleomorphic malignant fibrous histiocytoma (MFH), and 92% for myxofibrosarcoma (MFS). Recently, MFH is frequently called “undifferentiated

pleomorphic sarcoma (UPS)", because it was renamed as such in 2002 by the World Health Organization (WHO) [3]. The primary objective of molecular diagnosis is to identify a set of marker genes that facilitates accurate differential diagnosis of sarcoma subtypes. Discrimination between MFH and MFS, for example, is particularly difficult because there is a histological overlap between the two and because of the high heterogeneity of MFH [4]. Information on such subtype-specific genes may also help in understanding the molecular pathways that are activated in each subtype of the different biological malignancies. To this end, we had previously developed the projective adaptive resonance theory (PART) filtering method [5] for gene filtering and the boosted fuzzy classifier with SWEEP operator (BFCS) method [6,7] for model construction. Further, we developed a combination of these method, termed PART-BFCS [8-12], and applied this method to analyze gene expression data from STSs [12]. Our previous analysis showed that the 28 extracted genes are useful markers and that the most frequently selected combination of genes, *macrophage migration inhibitory factor* (MIF) and *stearoyl-CoA desaturase 1* (SCD1), represents an effective diagnostic marker combination to discriminate between MFH and MFS.

In general, the objective of a statistical or informatical analysis is the enrichment of important information [13-18]. The use of statistical or informatical analysis is both practical and useful [19-28]. In the present study, we hypothesized that the combination of *MIF* and *SCD1* can serve not only a diagnostic marker for discrimination between MFH and MFS, but also act as a prognostic marker for the overall outcome of STS, since an elevated expression of *MIF* and *SCD1* is observed in various highly malignant tumors [29-32]. Accordingly, using clinical and microarray data from STS patients, we conducted a simulation based on the permutation test, to extract genes that have both the functions of "a diagnostic marker to discriminate between MFH and MFS" and "a prognostic marker for the outcome of overall STS", which yielded four statistically significant genes, including *MIF* and *SCD1*. Furthermore, we investigated the potential of the combination of *MIF* and *SCD1* as a prognostic marker using clinical and microarray data from STS patients. We also investigated the *in vitro* cell growth inhibition induced by MIF and SCD1 inhibitors in a mouse MFH cell line. These experiments suggest that the combination of *MIF* and *SCD1* is useful as a prognostic marker for tumor progression.

## Materials and Methods

### Ethics statement

The study was conducted according to the principles expressed in the Declaration of Helsinki, and the ethics committee of the National Cancer Center approved the study protocol and all patients provided written informed consent to participate.

### Patients and tumor samples

Characteristics of the 88 soft tissue tumors used in this study are shown in Table S1. All patients had received a histological diagnosis of primary soft tissue tumor at National Cancer

Center Hospital, Tokyo, between 1996 and 2002. Tumor samples were obtained at the time of excision and cryopreserved in liquid nitrogen until use.

### Microarray analysis

For RNA extraction, trained pathologists carefully excised the tissue samples from the main tumor, leaving a margin clear from the surrounding non-tumorous tissue. Microscopically, the samples may still contain several non-tumor cells. Elimination of non-tumor stromal cells is important for gene expression analyses in carcinomas since tumor tissues contain a significant number of non-tumor stromal cells, including fibroblasts, endothelial cells, and inflammatory cells. Otherwise, tumor tissues contain very few non-tumor stromal cells for soft tissue sarcomas. Furthermore, soft tissue sarcomas contain non-tumor stromal cells, which are difficult to eliminate since soft tissue sarcoma originates from mesenchymal cells. Therefore, laser microdissection was not performed in this study. Total RNAs extracted from the bulk tissue samples were biotin-labeled and hybridized to high-density oligonucleotide microarrays (Human Genome U133A 2.0 Array, Affymetrix, Santa Clara, CA, USA) comprising 22,283 probe sets representing 18,400 transcripts, according to the manufacturer's instructions. The scanned array data were processed by Affymetrix Microarray Suite v.5.1 (MAS5), which scaled the average intensity of all the genes on each array to the target signal of 1,000. The microarray data in the present paper are available from the Genome Medicine Database of Japan (GeMDBJ) (<https://gemdbj.nibio.go.jp/dgdb/>) under the accession number EXPR058P.

### Data processing

We excluded 68 controls and 2,343 genes that were subject to cross-hybridization according to NetAffx Annotation ([www.affymetrix.com](http://www.affymetrix.com)). Furthermore, we excluded those genes for which more than 10 percent (8/88) of the samples showed an absent call (i.e., the detection call determined by MAS5 based on the  $p$  value of the one-sided Wilcoxon signed-rank test; absent call corresponds to  $p \geq 0.065$ , which is the default threshold in MAS5), since this indicates that the expression signal was undetectable. We also excluded those genes that showed an interquartile range value of less than 2,000. In total, 1,376 genes were selected, to which we applied log-transformation or binarization using the median values as the threshold for each gene. The two types of datasets, binarized and log-transformed, were used for Welch's  $t$ -test and the log-rank test, respectively.

### Simulation on the basis of permutation test

We calculated  $p$  values by applying Welch's  $t$ -test for discrimination between MFH and MFS, and by applying the log-rank test in the survival analysis of all STS patients for the 1,376 filtered genes. We defined the integrated statistic  $p'$  as  $p_1 \times p_2$ , where  $p_1$  indicates the  $p$  value calculated by Welch's  $t$ -test and  $p_2$  indicates the  $p$  value calculated by the log-rank test. STS patients ( $n = 35$ ; 20 MFH patients and 15 MFS patients) were used in both these tests, and the outcomes between MFH and MFS were significantly different. We therefore conducted a

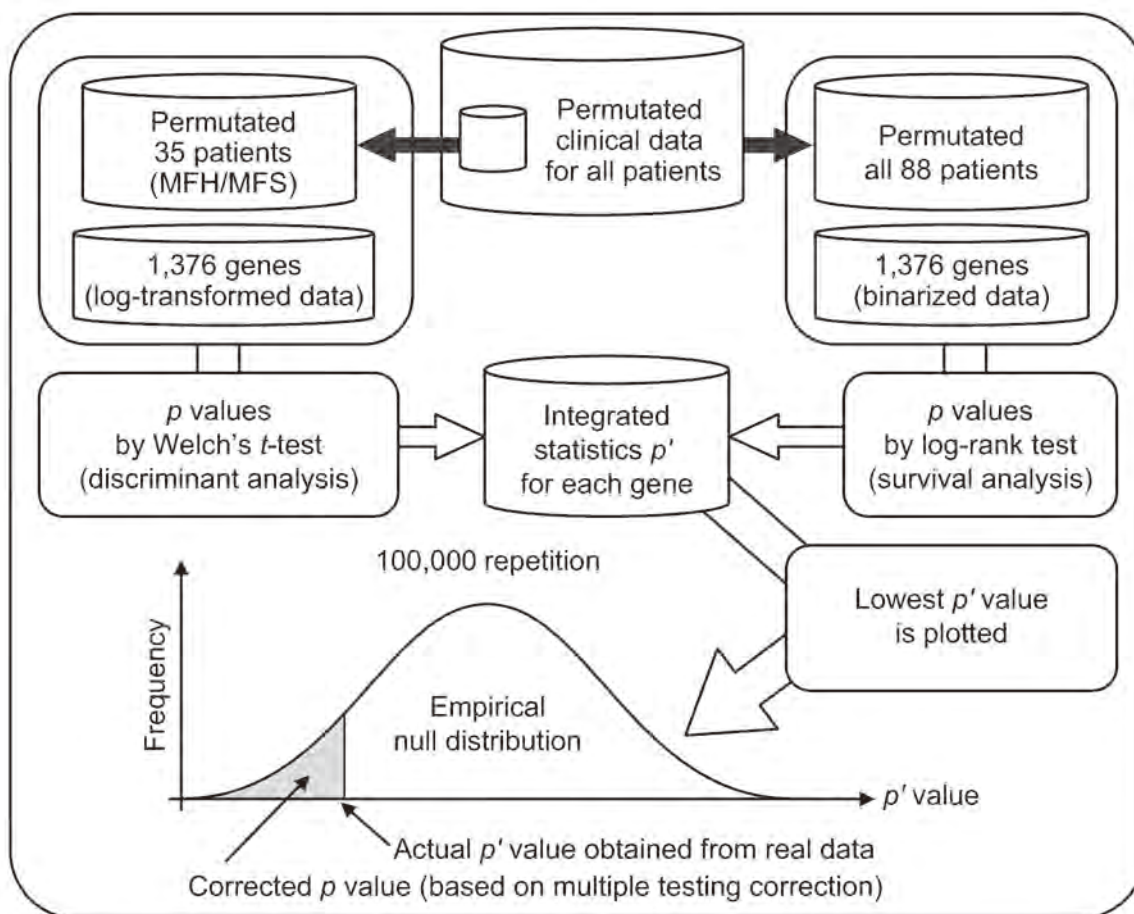


**Figure 1. A schematic of the simulation conducted based on the permutation test.** Clinical data for all patients were permuted. Permuted data for 35 STS patients (20 MFH patients and 15 MFS patients) were extracted from permuted data for all patients. For these data,  $p$  values ( $p_1$ ) were calculated by applying Welch's  $t$ -test to the log-transformed gene expression data to discriminate between MFH and MFS. Otherwise, permuted data for 88 patients were used for survival analysis. For these data,  $p$  values ( $p_2$ ) were calculated by applying log-rank test to the binarized gene expression data to analyze the outcome in the STS patient group. The integrated statistic  $p'$  was defined as  $p_1 \times p_2$ . The lowest  $p'$  value was selected for each repetition. This procedure was repeated 100,000 times, and an empirical null distribution was constructed. Using the distribution, the actual  $p'$  value obtained from real data was converted to the corrected  $p$  value (based on the correction for multiple testing).

doi: 10.1371/journal.pone.0078250.g001

simulation based on the permutation test as shown in Figure 1 to estimate the corrected  $p$  values to address this problem, as well as the multiple testing problems.

### Statistical analysis

Median values of gene expression signals for each gene were calculated and patients were divided into 2 groups using the median values as the threshold for each gene. Log-rank tests [33] were conducted for the outcome of STS patients for each gene, and Spearman's rank correlation coefficients for relationships between histological grades (or tumor metastases) and gene expression signals were also calculated. In the present study, we analyzed over 50 months of follow-up information as censored data. Kaplan-Meier curves [34] were

drawn for all STS patients, and those positive for *MIF*, *SCD1*, and the combination of *MIF* and *SCD1*.

### Cell lines and culture conditions

Murine sarcoma Sendai (MuSS) [35], a malignant fibrous histiocytoma cell line, was provided by the Cell Resource Center for Biomedical Research Institute of Development, Aging and Cancer, Tohoku University. Cells were maintained in RPMI 1640 medium containing 2% fetal bovine serum (FBS) and 1% penicillin-streptomycin solution. Cell cultures were incubated at 37°C, 5% CO<sub>2</sub>, and 100% humidity. 4-Iodo-6-phenylpyrimidine (4-IPP) (purchased from TOCRIS Bioscience, Bristol, UK) and A939572 (purchased from Biofine International, Vancouver, BC, Canada) were dissolved in dimethyl sulfoxide (DMSO).

**Table 1.** Genes extracted by simulation based on the permutation test.

Affymetrix probe ID	Accession no.	Gene symbol	<i>P</i> value <i>t</i> -test	Log-rank test	Integrated statistics <i>p</i> '	Corrected <i>p</i> value
207543_s_at	NM_000917	<i>P4HA1</i>	1.22E-04	5.73E-04	7.01E-08	0.00487
217871_s_at	NM_002415	<i>MIF</i>	5.31E-06	1.46E-02	7.75E-08	0.00523
201231_s_at	NM_001428	<i>ENO1</i>	1.06E-04	1.06E-03	1.12E-07	0.00693
200832_s_at	AB032261	<i>SCD1</i>	7.36E-05	6.06E-03	4.46E-07	0.01976

doi: 10.1371/journal.pone.0078250.t001

**Cell growth assays**

For the determination of concentrations for the combination of 4-IPP (MIF inhibitor) and A939572 (SCD1 inhibitor), cells were plated in 96-well plates (10,000 cells per well). After 24 h of incubation, cells were treated with 4-IPP at concentrations ranging from 5µM to 50 µM, A939572 at concentrations ranging from 1 nM to 1000 nM, a combination of both, or DMSO only (control). After 24 h of incubation of cells with these compounds, cell viability was measured using the 3-(4,5-dimethylthiazol-2-yl)-2,5-diphenyl-tetrazolium bromide (MTT) assay [36]. Metabolically active cells can convert the yellow tetrazolium salt MTT to indigo blue formazan. For the assay, the medium were removed gently and the cells were washed with PBS. Subsequently, medium containing 0.5 g/L MTT was added to each well. After 2 h of incubation of the cells with MTT, the medium was removed gently and the cells were washed with PBS. To dissolve the indigo blue formazan crystals, 100µL DMSO was added. The optical density was measured on a microplate reader at 540 nm. All *in vitro* studies were repeated 3 times.

**Results**

**Discrimination between MFH and MFS by using gene expression levels of *MIF* and *SCD1***

Our previous analysis revealed that *MIF* and *SCD1* is an effective diagnostic marker to discriminate between MFH and MFS [12]. In the present study, we first analyzed microarray data from 35 STS patients (20 MFH patients and 15 MFS patients) by using expressions of *MIF* and *SCD1*, as shown in Figure 2. Figure 2 shows that STS patients are clearly classified into two groups (MFS and MFH).

**Extraction of genes with both diagnostic and prognostic marker functions by simulation on the basis of the permutation test**

In the present study, we hypothesized that the combination of *MIF* and *SCD1* is useful not only a diagnostic marker for discrimination between MFH and MFS, but also represents a prognostic marker for the overall outcome of STS. Therefore, we first conducted a simulation based on a permutation test for the outcome of overall STS, from which four genes, including *MIF* and *SCD1*, were extracted (Table 1). From this analysis, it can be seen that the corrected *p* values are 0.00523 and 0.0198 for *MIF* and *SCD1*, respectively. This result suggests that *MIF* and *SCD1* have functions of both a diagnostic marker

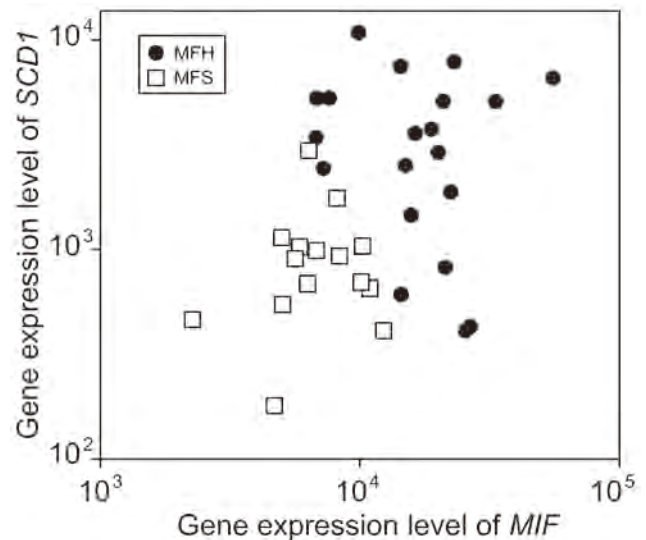


**Figure 2.** Discrimination between MFH and MFS by using expressions of *MIF* and *SCD1*. Open square indicates MFS patient. Filled circle indicates MFH patient.

doi: 10.1371/journal.pone.0078250.g002

to discriminate between MFH and MFS and prognostic marker for the overall outcome of STS.

**Association analysis of clinical and gene expression data**

We next conducted a log-rank tests of STS patient outcomes and a correlation analysis between tumor metastasis and each clinical parameter, as shown in Tables 2 and 3, respectively. Table 2 shows that only the histological grade is significantly associated with patient outcomes (*p* = 0.00102 as calculated by the log-rank test). Table 3 shows that histological grade is strongly correlated with incidence of tumor metastasis in STS patients (*p* = 0.486, *p* = 1.56 × 10<sup>-6</sup> as calculated by the Spearman's rank correlation coefficient). The histological grade is a useful conventional index, and pathologists trained in the detection of specific tumors can diagnose these indices in patients. Therefore, it is important to identify factors that correlate with histological grade and patient outcomes for the diagnosis of STS patients. We conducted log-rank tests of STS patient outcomes and a correlation analysis of the histological grade or incidence of tumor metastasis with the expression of

**Table 2.** Relationships between clinical parameters and outcome of STS patients.

Clinical parameters		Number of patients	$p$ value of log-rank test
Gender	Male	46	0.652
	Female	42	
Age	< 55	45	0.173
	≥55	43	
Tissue-type	MLS	20	0.0670
	MFH	20	
	MFS	15	
	SS	17	
	LMS	6	
	FS	5	
Histological grade	MPNST	5	0.00102
	1	14	
	2	23	
	3	51	

MLS: Myxoid liposarcoma, MFH: Pleomorphic malignant fibrous histiocytoma, MFS: Myxofibrosarcoma, SS: Synovial sarcoma, LMS: Leiomyosarcoma, FS: Fibrosarcoma, MPNST: Malignant peripheral nerve sheath tumor.

doi: 10.1371/journal.pone.0078250.t002

**Table 3.** Correlation between clinical parameters and tumor metastasis of STS patients.

Clinical parameters		Number of patients	Spearman's rank correlation coefficient	
			$\rho$	$p$ value
Gender	Male	46	-0.206	0.0543
	Female	42		
Age		88	0.0327	0.762
Histological grade	1	14	0.486	1.56E-06
	2	23		
	3	51		

doi: 10.1371/journal.pone.0078250.t003

four genes selected by the permutation test, as shown in Table 4. Table 4 shows that *MIF* has a high correlation with histological grade ( $\rho = 0.421$ ,  $p = 4.41 \times 10^{-5}$ ) and tumor metastasis ( $\rho = 0.308$ ,  $p = 3.47 \times 10^{-3}$ ), whereas *SCD1* has no correlation with histological grade ( $\rho = -0.0191$ ,  $p = 0.860$ ) and tumor metastasis ( $\rho = 0.0237$ ,  $p = 0.826$ ). This result suggests that *MIF* expression is strongly related with tumor metastasis, whereas *SCD1* expression can be used in combination with the histological grade to diagnose the STS outcome.

#### Analysis of the outcomes of STS patients using gene expression data

Patients were divided into 2 groups using the median values as the threshold for each gene for binarization of independent variable. For example, the median values were 10,171 and 1,879 for *MIF* and *SCD1*, respectively. The interquartile range values (difference in median values between positive and

**Table 4.** Correlation analysis using Spearman's rank correlation coefficient.

Affymetrix probe ID	Accession no.	Gene symbol	Spearman's rank correlation coefficient			
			with histological grade		with tumor metastasis	
			$\rho$	$p$ value	$\rho$	$p$ value
207543_s_at	NM_000917	<i>P4HA1</i>	0.449	1.12E-05	0.424	3.89E-05
217871_s_at	NM_002415	<i>MIF</i>	0.421	4.41E-05	0.308	3.47E-03
201231_s_at	NM_001428	<i>ENO1</i>	0.356	6.66E-04	0.247	2.01E-02
200832_s_at	AB032261	<i>SCD1</i>	-0.0191	0.860	0.0237	0.826

doi: 10.1371/journal.pone.0078250.t004

negative groups) were 10,142 and 2,681 for *MIF* and *SCD1*, respectively. We conducted log-rank tests of STS patient outcomes by using binarized data. In the present study, we focused on *MIF* and *SCD1* to test the hypothesis that the combination of *MIF* and *SCD1* could be a prognostic marker for the overall outcome of STSs. Thus, Kaplan-Meier curves were drawn for all STS patients, and those positive for *MIF*, *SCD1*, and the combination of *MIF* and *SCD1*, as shown in Figure 3. Figure 3B shows that the survival rate of the *MIF*-positive group ( $n = 44$ ) was significantly lower than that of the *MIF*-negative group ( $n = 44$ ) ( $p = 0.0146$  as calculated by the log-rank test). Similarly, Figure 3C shows that the survival rate of the *SCD1* positive group ( $n = 44$ ) was significantly lower than that of the *SCD1*-negative group ( $n = 44$ ) ( $p = 0.00606$  as calculated by the log-rank test). Furthermore, Figure 3D shows that the survival rates among groups that are double-positive ( $n = 20$ ), single-positive ( $n = 48$ ), and double-negative ( $n = 20$ ) for *MIF* and *SCD1* are significantly different ( $p = 0.000327$  as calculated by the log-rank test), and that the survival rate of the double-positive group ( $n = 20$ ) was much lower than that of the double-negative group ( $n = 20$ ) with greater significance ( $p = 0.000116$  as calculated by the log-rank test). These results indicate that *MIF*, *SCD1*, and the combination of *MIF* and *SCD1* are not only diagnostic markers to discriminate between MFH and MFS, but also potential prognostic markers for the overall outcome of STS. Furthermore, the combination of *MIF* and *SCD1* is superior to the single markers, *MIF* or *SCD1*, as a prognostic marker.

#### Survival analysis for each tissue type using a combination of *MIF* and *SCD1*

The differential diagnosis of soft tissue sarcomas is not difficult, with the exception of discrimination between MFH and MFS. We conducted a survival analysis by classifying patients into one of three groups based on a combination of *MIF* and *SCD1* expression for each tissue type, as shown in Table 5. The survival rates among groups that are double-positive ( $n = 2$ ), single-positive ( $n = 13$ ), and double-negative ( $n = 5$ ) for *MIF* and *SCD1* are significantly different ( $p = 0.0150$  as calculated by the log-rank test) for MLS patients, as shown in Figure 4 and Table 5. This result suggests that a combination of *MIF* and *SCD1* is a potential prognostic maker for MLS. The

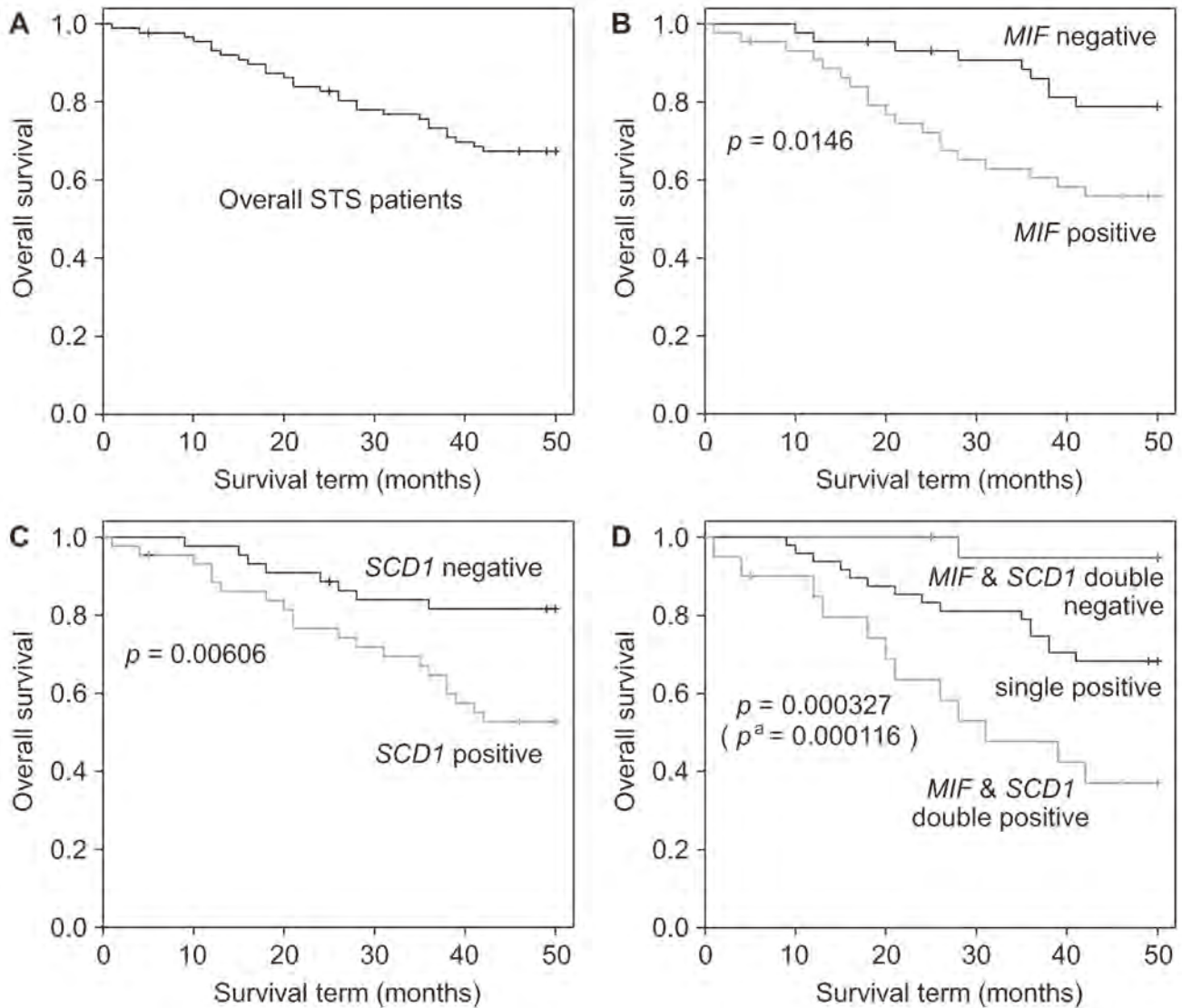


**Figure 3. Kaplan-Meier curves and log-rank test for all STS patients.** (A) All STS patients (B) The *MIF*-positive group (*MIF* > 10171, median of *MIF* signals for 88 patients) consisted of 44 patients (red line) and the *MIF*-negative group consisted of 44 patients (black line). (C) The *SCD1*-positive group (*SCD1* > 1879, median of *SCD1* signals for 88 patients) consisted of 44 patients (red line) and of *SCD1*-negative group consisted of 44 patients (black line). (D) The *MIF* and *SCD1* double-positive group (*MIF* > 10171 and *SCD1* > 1879) consisted of 20 patients (red line), the *MIF* or *SCD1* single-positive group consisted of 48 patients (black line), and the *MIF* and *SCD1* double-negative group consisted of 20 patients (blue line). The *p* values were calculated by the log-rank test. <sup>a</sup> indicates the *p* value for the comparison of the double-positive vs. the double-negative groups.

doi: 10.1371/journal.pone.0078250.g003

number of patients in each category is relatively small however, and these results should be validated in future studies.

**Cell growth inhibition assay using MIF inhibitor and SCD1 inhibitor**

We conducted cell growth inhibitory experiments using the MuSS cell line with a MIF inhibitor and a SCD1 inhibitor to investigate the role of MIF, SCD1, and the combination of MIF and SCD1 for tumor progression. In the present study, 4-IPP

and A939572 were used as MIF and SCD1 inhibitors, respectively. The effects of 4-IPP, A939572, and the combination of 4-IPP and A939572 on cell proliferation were evaluated in a 24-hour growth inhibition assay, as shown in Figure 5. Figure 5A and 5B show concentration response curves for cells treated with 4-IPP and A939572, respectively. This is clearly dose-dependent. Furthermore, we selected 15 μM 4-IPP and 50 nM A939572 as concentrations that showed weak cell growth inhibition (approximately 10%) to evaluate the inhibitory effect of the combination of inhibitors on MuSS cells.

**Table 5.** Survival analysis for each tissue type using a combination of *MIF* and *SCD1*.

Tissue-type	Number of patients	P value of log-rank test
MLS	20	0.0150
MFH	20	0.868
MFS	15	0.638
SS	17	0.231
LMS	6	0.638
FS	5	0.0634
MPNST	5	0.886

MLS: Myxoid liposarcoma, MFH: Pleomorphic malignant fibrous histiocytoma, MFS: Myxofibrosarcoma, SS: Synovial sarcoma, LMS: Leiomyosarcoma, FS: Fibrosarcoma, MPNST: Malignant peripheral nerve sheath tumor.

doi: 10.1371/journal.pone.0078250.t005

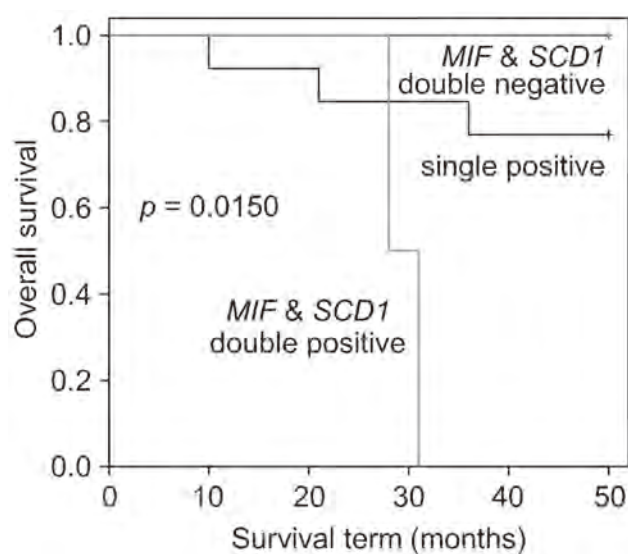


**Figure 4.** The Kaplan-Meier curve and log-rank test for MLS patients. The *MIF* and *SCD1* double-positive group ( $MIF > 10171$  and  $SCD1 > 1879$ ) consisted of 2 patients (red line), the *MIF* or *SCD1* single-positive group consisted of 13 patients (black line), and the *MIF* and *SCD1* double-negative group consisted of 5 patients (blue line). The  $p$  value was calculated by the log-rank test.

doi: 10.1371/journal.pone.0078250.g004

Figure 5C shows that cell growth was significantly inhibited to a greater extent by the combination of inhibitors than by the single inhibitors. This result was statistically significant ( $p < 0.05$  as calculated by the Welch's  $t$ -test and corrected by the Bonferroni correction). These results indicate that *MIF* and *SCD1* are potential essential factors of cell growth for STSs.

## Discussion

In the present study, we conducted the simulation based on the permutation test for the extraction of genes that have both

functions of the diagnostic marker to discriminate between MFH and MFS and the prognostic marker for the outcome of overall STS. Consequently, only four genes, including *MIF* and *SCD1*, were extracted and their corrected  $p$  values were statistically significant ( $p < 0.05$ ). We focused on the combination of *MIF* and *SCD1*.

*MIF* was first reported in the 1960s as a factor capable of inhibiting the random migration of macrophages during delayed-type hypersensitivity responses [37-39]. Recently, studies have been conducted on the roles of *MIF* in various inflammatory diseases, such as rheumatoid arthritis [40] and atherosclerosis [41]. (S,R)-3-(4-hydroxyphenyl)-4,5-dihydro-5-isoxazole acetic acid methyl ester (ISO-1), which has been used for the treatment of various inflammatory diseases, was reported to be an inhibitor of the biological activity of *MIF* [42]. Subsequent to our report[12], *in vitro* *MIF* inhibition experiments have been conducted using small molecules for various cancers, such as colon cancer inhibited by ISO-1 [43], prostate cancer inhibited by ISO-1 [44], lung cancer inhibited by ISO-1 [45], and 4-Iodo-6-phenylpyrimidine (4-IPP) [45], glioblastoma inhibited by ISO-1[46-48], and adenoid cystic carcinoma inhibited by ISO-1[49]. In addition, several experiments have been conducted on animal models (*in vivo*) such as those for colorectal cancer inhibited by ISO-1 [50], and prostate cancer inhibited by ISO-1 [44]. As mentioned, *MIF* inhibition is an effective treatment method for various tumors. Although *MIF* inhibition suppresses both cell growth and metastasis in many tumors, its inhibition of cell growth is not universal. For example, *MIF* depletion or pharmacologic inhibition in breast tumor cells changed tumor growth only slightly, but blocked metastasis, as reported by Simpson et al [51].

*SCD* catalyzes the conversion of saturated fatty acids (SFAs) to  $\Delta 9$  monounsaturated fatty acids (MUFAs). These enzymes preferentially convert stearic acid (C18:0) to oleic acid (C18:1) and palmitic acid (C16:0) to palmitoleic acid (C16:1)[52]. In humans, 2 genes have been characterized (*SCD1* and *SCD5*), *SCD1* being co-orthologous to the 4 mice genes [53]. SFAs and MUFAs, the most abundant fatty acid species, have many divergent biological effects including the regulation of cell proliferation, programmed cell death, and lipid-mediated cytotoxicity [54]. Recently, a number of reports have implicated *SCD1* expression and activity in the pathogenesis of cancer [55]. Overexpression of human *SCD1* was observed in a variety of human cancers, including colon, esophageal, and hepatocellular carcinomas relative to the corresponding normal tissues [30]. Subsequent to our report[12], *in vitro* *SCD1* inhibition experiments were conducted using small molecules for several cancers, such as lung cancer and breast cancer inhibited by N-(2-(6-(3,4-dichlorobenzylamino)-2-(4-methoxyphenyl)-3-oxopyrido[2,3-b]pyrazin-4(3H-yl)ethyl)acetamide (CVT-11127) [56-58], pharyngeal cancer and lung cancer inhibited by 4-(2-chlorophenoxy)-N-(3-(3-methylcarbamoyl)phenyl)piperidine-1-carboxamide (A939572) [59], and colon cancer inhibited by 5-tetradecyloxy-2-furoic acid (TOFA) [60]. In addition, a single *in vivo* study has been conducted using a human gastric cancer xenograft model that

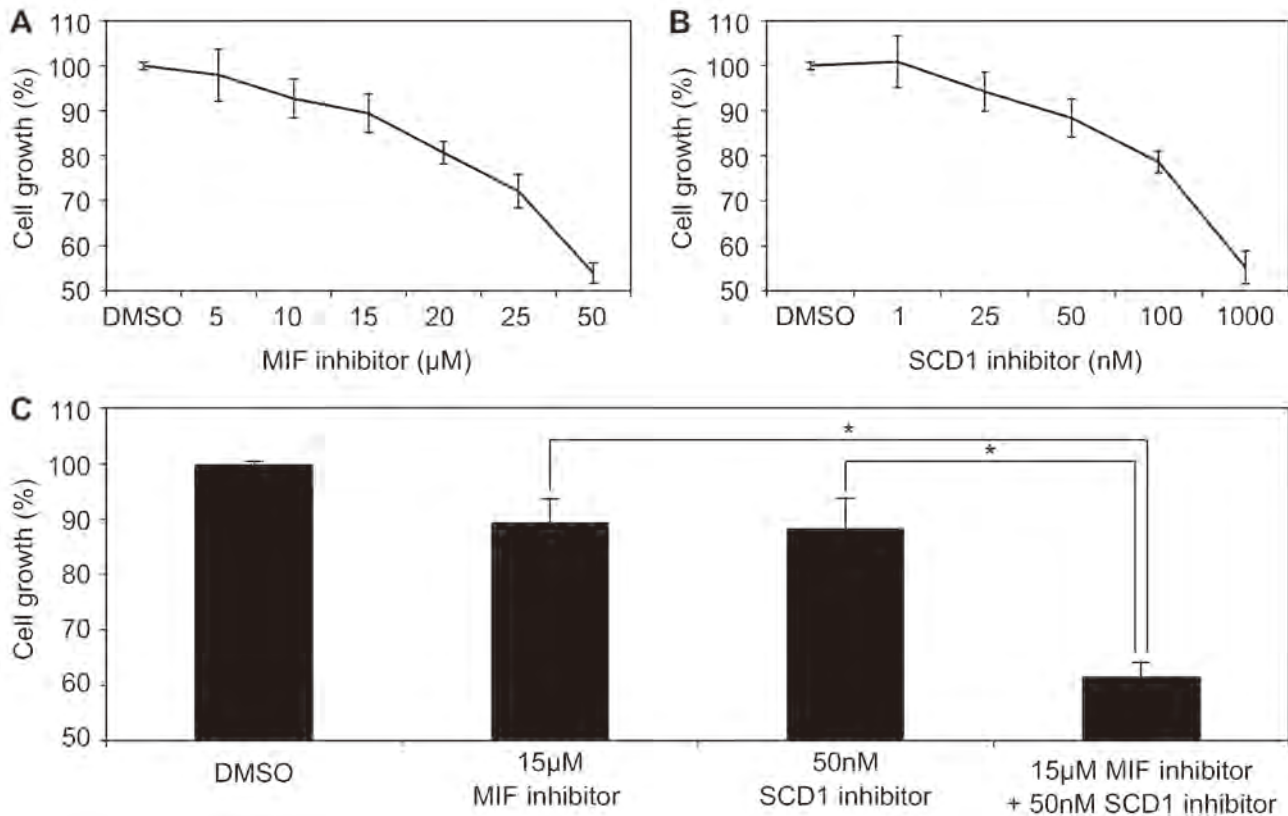


**Figure 5. Cell growth inhibitory effects of 4-IPP and A939572 for MuSS cell line.** (A) Inhibition of cell viability at varying concentrations of 4-IPP (MIF inhibitor) in MuSS cells relative to DMSO-treated control cells. (B) Inhibition of cell viability at varying concentrations of A939572 (SCD1 inhibitor) in MuSS cells relative to DMSO-treated control cells. (C) Inhibition of cell viability by DMSO only (control), 15 μM MIF inhibitor, 50 nM SCD1 inhibitor, and the combination of 15 μM MIF inhibitor and 50 nM SCD1 inhibitor in MuSS cells relative to DMSO-treated control cells. Data are shown for cells treated for 24 h in media containing 2% FBS. Cell viability was determined using the MTT assay in 3 independent replicates at each dose level. Error bars represent the SD from the mean. \* indicates  $p < 0.05$  ( $p$  value was calculated by Welch's  $t$ -test and corrected by Bonferroni correction for multiple testing).

doi: 10.1371/journal.pone.0078250.g005

was inhibited by A939572 [59]. As mentioned, SCD1 inhibition is an effective treatment method for several tumors.

In the present study, cell growth arrest for STS cells was observed by experiments using MIF and SCD1 inhibitors, as shown in Figure 5. However, the cancer cell growth assay is not the first report of the use of MIF or SCD1 inhibitors to retard cancer cell growth. MIF or SCD1 inhibitors have been used to restrict the growth or metastasis of many types of cancers [43-48,56-60], although not STS. Moreover, gene silencing of MIF or SCD1 has been carried out for many kinds of cancers [44,48,54,59-67], again with the exception of STS. Although MIF- or SCD1 inhibition has not been reported in the case of STS, and our assay is insufficient to show the effects of MIF- or SCD1-inhibition for STS, many previous studies have suggested that MIF and SCD1 are potential therapeutic targets in the treatment of STS patients. Our association analysis, which examines overall outcome and metastasis in STS patients, also supports this hypothesis.

Although we did not conduct experiments to identify the molecular mechanism of action of MIF- and SCD1 inhibitors,

several studies examining MIF and SCD1 pathways have been reported to date, as shown in Figure 6. Secreted MIF interacts with cell surface CD74 [68]. CD74 lacks a signal-transducing intracellular domain but interacts with the proteoglycan CD44 and mediates signaling via CD44 to induce the activation of a Src-family kinase and mitogen-activated protein kinase (MAPK)/extracellular signal-regulated kinase (ERK), to activate the phosphatidylinositol 3-kinase (PI3K)/Akt pathway, or to initiate p53-dependent inhibition of apoptosis [69]. MIF also can induce invasion and metastasis via G-protein-coupled chemokine receptors (CXCR2 and CXCR4) [43,70]. While the SCD1 enzyme activates the Akt pathway by regulation of the MUFA/SFA balance in mammalian cell lipids [55,71]. As mentioned above, both MIF and SCD1 regulate cell viability through various pathways and there is a common signaling pathway downstream of MIF and SCD1. Furthermore, MIF is related with incidence of tumor metastasis in patients. They are therefore reasonable potential therapeutic targets. Combination chemotherapy may prevent drug resistance in cancer patients. However, further studies, such as analysis of the molecular

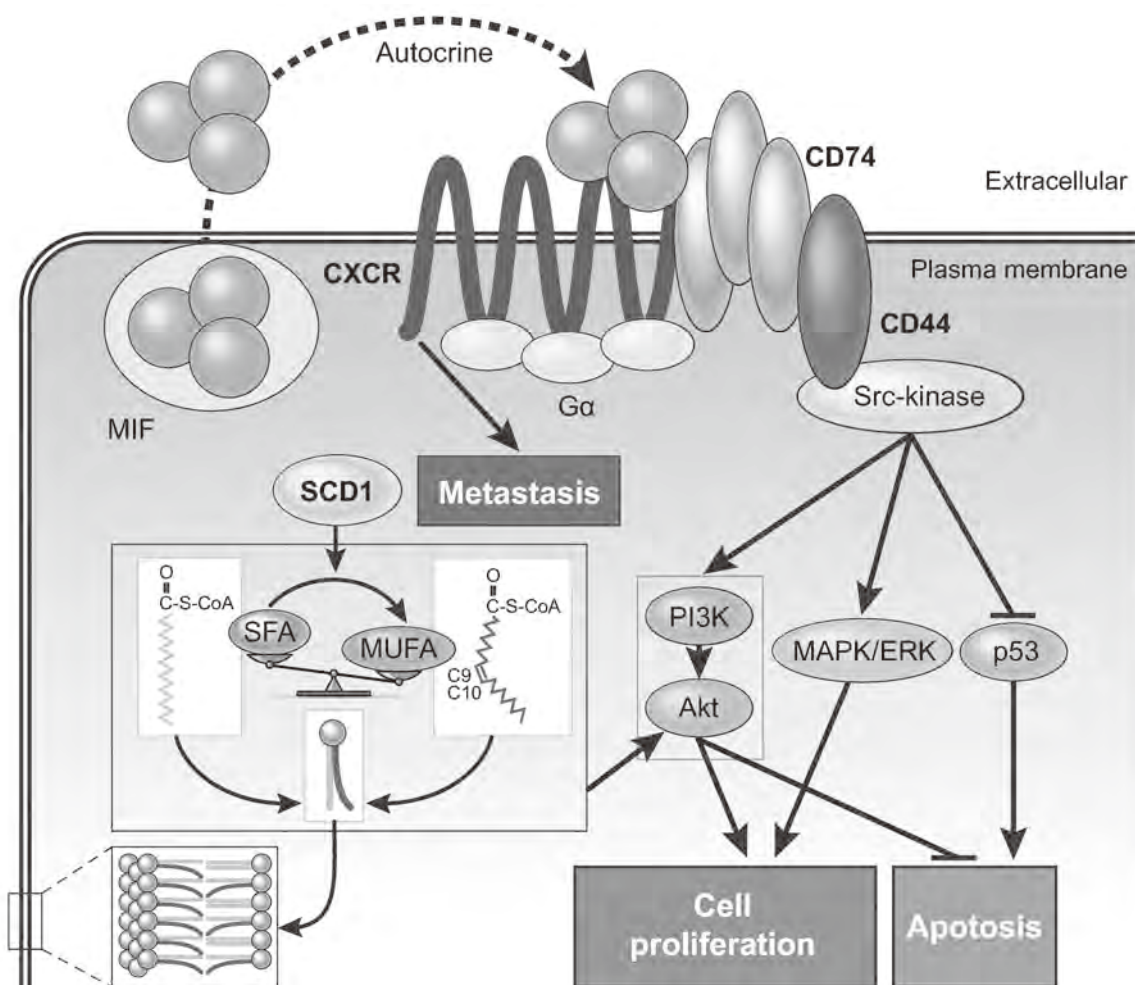


**Figure 6. Hypothetical regulation model for metabolic and signaling control by MIF and SCD1.** MUFA, monounsaturated fatty acids; SFA, saturated fatty acids; SCD1, stearoyl-CoA desaturase 1; MIF, macrophage migration inhibitory factor; CXCR, CXC chemokine receptor; PI3K, phosphoinositide 3-kinase; MAPK, extracellular signal-regulated kinase; ERK, mitogen-activated protein kinase.

doi: 10.1371/journal.pone.0078250.g006

mechanism, invasion, apoptosis assays, and other experiments should be conducted for STS cells in the future.

MIF inhibitors have been developed as anti-inflammatory drugs and some anti-inflammatory drugs have a MIF inhibitory effect. For example, Ibudilast (current development codes: AV-411 or MN-166) is an anti-inflammatory drug that was initially developed for the treatment of bronchial asthma and inhibits MIF activity [72]. Safety evaluation for Ibudilast has been conducted by a clinical trial [73]. Furthermore, the occurrence of MIF inhibitors in cruciferous vegetables as a natural product [74] suggests that MIF will be more a promising therapeutic target in the future. On the other hand, SCD1 inhibitors have been developed as drugs for diabetes and dyslipidemia [75]. Studies have been conducted to establish the therapeutic window for the SCD1 inhibitor MK-8245 using various animals, such as mouse, rat, dog, and monkey [75]. Therefore, MIF and SCD1 inhibitors have high potential as

drugs, because the safety of these inhibitors has been validated for various diseases other than cancer, as mentioned above. Although a differential diagnosis between MFH and MFS is difficult even for trained pathologists. Our bioinformatics analysis has shown the combination of *MIF* and *SCD1* is a useful diagnostic marker, and can hence be useful in this context. Furthermore, our analysis has demonstrated that the utility of *MIF* and *SCD1* is not limited to discrimination between MFH and MFS. Specifically, *MIF* expression correlates to the incidence of metastasis and histological grade in all STS patients, and *SCD1* expression provides novel information in addition to histological grade, which would help in determining the prognosis of STS.

In conclusion, we conducted exhaustive gene expression analysis of STS patients and *in vitro* growth inhibition assays using an MFH cell line to test the hypothesis that the gene combination of *MIF* and *SCD1* (identified by a bioinformatics

approach) is not only a diagnostic marker for discrimination between MFH and MFS, but also a prognostic marker for the overall outcome of STS. Our results from these experiments suggest that the combination of *MIF* and *SCD1* is potentially useful as a prognostic marker associated with tumor progression or metastasis in patients.

## Supporting Information

**Table S1. Clinical data of 88 STS patients.**

## References

- Gatta G, van der Zwan JM, Casali PG, Siesling S, Dei Tos AP et al. (2011) Rare cancers are not so rare: the rare cancer burden in Europe. *Eur J Cancer* 47: 2493-2511. doi:10.1016/j.ejca.2011.08.008. PubMed: 22033323.
- Gustafson P (1994) Soft tissue sarcoma. *Epidemiology and prognosis in 508 patients*. *Acta Orthop Scand Suppl* 259: 1-31. PubMed: 8042499.
- Fletcher CDM, Unni KK, Mertens F, editors (2002) *Pathology and Genetics of Tumors of Soft Tissue and Bone*. Lyon: IARC Press.
- Nakayama R, Nemoto T, Takahashi H, Ohta T, Kawai A et al. (2007) Gene expression analysis of soft tissue sarcomas: characterization and reclassification of malignant fibrous histiocytoma. *Mod Pathol* 20: 749-759. doi:10.1038/modpathol.3800794. PubMed: 17464315.
- Takahashi H, Kobayashi T, Honda H (2005) Construction of robust prognostic predictors by using projective adaptive resonance theory as a gene filtering method. *Bioinformatics* 21: 179-186. doi:10.1093/bioinformatics/bth473. PubMed: 15308545.
- Takahashi H, Honda H (2005) A new reliable cancer diagnosis method using boosted fuzzy classifier with a SWEEP operator method. *J Chem Eng Jpn* 38: 763-773. doi:10.1252/jcej.38.763.
- Takahashi H, Honda H (2006) Prediction of peptide binding to major histocompatibility complex class II molecules through use of boosted fuzzy classifier with SWEEP operator method. *J Biosci Bioeng* 101: 137-141. doi:10.1263/jbb.101.137. PubMed: 16569609.
- Kawamura T, Takahashi H, Honda H (2008) Proposal of new gene filtering method, BagPART, for gene expression analysis with small sample. *J Biosci Bioeng* 105: 81-84. doi:10.1263/jbb.105.81. PubMed: 18295727.
- Takahashi H, Aoyagi K, Nakanishi Y, Sasaki H, Yoshida T et al. (2006) Classification of intramural metastases and lymph node metastases of esophageal cancer from gene expression based on boosting and projective adaptive resonance theory. *J Biosci Bioeng* 102: 46-52. doi:10.1263/jbb.102.46. PubMed: 16952836.
- Takahashi H, Honda H (2006) Lymphoma prognostication from expression profiling using a combination method of boosting and projective adaptive resonance theory. *J Chem Eng Jpn* 39: 767-771. doi:10.1252/jcej.39.767.
- Takahashi H, Murase Y, Kobayashi T, Honda H (2007) New cancer diagnosis modeling using boosting and projective adaptive resonance theory with improved reliable index. *Biochem Eng J* 33: 100-109. doi:10.1016/j.bej.2006.08.004.
- Takahashi H, Nemoto T, Yoshida T, Honda H, Hasegawa T (2006) Cancer diagnosis marker extraction for soft tissue sarcomas based on gene expression profiling data by using projective adaptive resonance theory (PART) filtering method. *BMC Bioinformatics* 7: 399. doi:10.1186/1471-2105-7-399. PubMed: 16948864.
- Takahashi H, Takahashi A, Naito S, Onouchi H (2012) BAIUCAS: a novel BLAST-based algorithm for the identification of upstream open reading frames with conserved amino acid sequences and its application to the *Arabidopsis thaliana* genome. *Bioinformatics* 28: 2231-2241. doi:10.1093/bioinformatics/bts303. PubMed: 22618534.
- Kojima S, Iwasaki M, Takahashi H, Imai T, Matsumura Y et al. (2011) Asymmetric leaves2 and Elongator, a histone acetyltransferase complex, mediate the establishment of polarity in leaves of *Arabidopsis thaliana*. *Plant Cell Physiol* 52: 1259-1273. doi:10.1093/pcp/pcr083. PubMed: 21700721.
- Takahashi H, Honda H (2006) Modified signal-to-noise: a new simple and practical gene filtering approach based on the concept of projective adaptive resonance theory (PART) filtering method. *Bioinformatics* 22: 1662-1664. doi:10.1093/bioinformatics/btl156. PubMed: 16632489.
- Takahashi H, Iwakawa H, Nakao S, Ojio T, Morishita R et al. (2008) Knowledge-based fuzzy adaptive resonance theory and its application to the analysis of gene expression in plants. *J Biosci Bioeng* 106: 587-593. doi:10.1263/jbb.106.587. PubMed: 19134556.
- Takahashi H, Nakagawa A, Kojima S, Takahashi A, Cha BY et al. (2012) Discovery of novel rules for G-quadruplex-forming sequences in plants by using bioinformatics methods. *J Biosci Bioeng* 114: 570-575. doi:10.1016/j.jbiosc.2012.05.017. PubMed: 22721688.
- Takahashi H, Iwakawa H, Ishibashi N, Kojima S, Matsumura Y et al. (2013) Meta-analyses of microarrays of *Arabidopsis* asymmetric leaves1 (as1), as2 and their modifying mutants reveal a critical role for the ETT pathway in stabilization of adaxial-abaxial patterning and cell division during leaf development. *Plant Cell Physiol* 54: 418-431. doi:10.1093/pcp/pct027. PubMed: 23396601.
- Iwasaki M, Takahashi H, Iwakawa H, Nakagawa A, Ishikawa T et al. (2013) Dual regulation of ETTIN (ARF3) gene expression by AS1-AS2, which maintains the DNA methylation level, is involved in stabilization of leaf adaxial-abaxial partitioning in *Arabidopsis*. *Development* 140: 1958-1969. doi:10.1242/dev.085365. PubMed: 23571218.
- Nakagawa A, Takahashi H, Kojima S, Sato N, Ohga K et al. (2012) Berberine enhances defects in the establishment of leaf polarity in asymmetric leaves1 and asymmetric leaves2 of *Arabidopsis thaliana*. *Plant Mol Biol* 79: 569-581. doi:10.1007/s11103-012-9929-7. PubMed: 22684430.
- Sano M, Aoyagi K, Takahashi H, Kawamura T, Mabuchi T et al. (2010) Forkhead box A1 transcriptional pathway in KRT7-expressing esophageal squamous cell carcinomas with extensive lymph node metastasis. *Int J Oncol* 36: 321-330. PubMed: 20043065.
- Chiba Y, Mineta K, Hirai MY, Suzuki Y, Kanaya S et al. (2013) Changes in mRNA stability associated with cold stress in *Arabidopsis* cells. *Plant Cell Physiol* 54: 180-194. doi:10.1093/pcp/pcs164. PubMed: 23220693.
- Matsuo N, Mase H, Makino M, Takahashi H, Banno H (2009) Identification of ENHANCER OF SHOOT REGENERATION 1-upregulated genes during in vitro shoot regeneration. *Plant Biotechnol* 26: 385-393. doi:10.5511/plantbiotechnology.26.385.
- Takahashi H, Kaniwa N, Saito Y, Sai K, Hamaguchi T et al. (2013) Identification of a candidate single-nucleotide polymorphism related to chemotherapeutic response through a combination of knowledge-based algorithm and hypothesis-free genomic data. *J Biosci Bioeng* (. (2013) doi:10.1016/j.jbiosc.2013.05.021. PubMed: 23816762.
- Takahashi H, Tomida S, Kobayashi T, Honda H (2003) Inference of common genetic network using fuzzy adaptive resonance theory associated matrix method. *J Biosci Bioeng* 96: 154-160. doi:10.1016/S1389-1723(03)90118-6. PubMed: 16233501.
- Yoshimura K, Mori T, Yokoyama K, Koike Y, Tanabe N et al. (2011) Identification of alternative splicing events regulated by an *Arabidopsis* serine/arginine-like protein, atSR45a, in response to high-light stress using a tiling array. *Plant Cell Physiol* 52: 1786-1805. doi:10.1093/pcp/pcr115. PubMed: 21862516.
- Kotooka N, Komatsu A, Takahashi H, Nonaka M, Kawaguchi C et al. (2013) Predictive value of high-molecular weight adiponectin in subjects with a higher risk of the development of metabolic syndrome: From a population based 5-year follow-up data. *Int J Cardiol* 167: 1068-1070. doi:10.1016/j.ijcard.2012.10.066. PubMed: 23194783.
- Yajima I, Kumasaka MY, Naito Y, Yoshikawa T, Takahashi H et al. (2012) Reduced GNG2 expression levels in mouse malignant melanomas and human melanoma cell lines. *Am J Cancer Res* 2: 322-329. PubMed: 22679562.
- Krockenberger M, Kranke P, Häusler S, Engel JB, Horn E et al. (2012) Macrophage migration-inhibitory factor levels in serum of patients with

(XLS)

## Author Contributions

Conceived and designed the experiments: HT SY TK HH TY TH. Performed the experiments: SH TT KK KY T. Nakamua TS AT. Analyzed the data: HT YM KN SM. Contributed reagents/materials/analysis tools: RN T. Nemoto KT TO AK SS. Wrote the manuscript: HT RN SH.

- ovarian cancer correlates with poor prognosis. *Anticancer Res* 32: 5233-5238. PubMed: 23225421.
30. Li J, Ding SF, Habib NA, Farmor BF, Wood CB et al. (1994) Partial characterization of a cDNA for human stearyl-CoA desaturase and changes in its mRNA expression in some normal and malignant tissues. *Int J Cancer* 57: 348-352. doi:10.1002/ijc.2910570310. PubMed: 7909540.
  31. Liao B, Zhong BL, Li Z, Tian XY, Li Y et al. (2010) Macrophage migration inhibitory factor contributes angiogenesis by up-regulating IL-8 and correlates with poor prognosis of patients with primary nasopharyngeal carcinoma. *J Surg Oncol* 102: 844-851. doi:10.1002/jso.21728. PubMed: 20872800.
  32. Wang XB, Tian XY, Li Y, Li B, Li Z (2012) Elevated expression of macrophage migration inhibitory factor correlates with tumor recurrence and poor prognosis of patients with gliomas. *J Neuro Oncol* 106: 43-51. doi:10.1007/s11060-011-0640-3. PubMed: 21725855.
  33. Mantel N (1966) Evaluation of survival data and two new rank order statistics arising in its consideration. *Cancer Chemother Rep* 50: 163-170. PubMed: 5910392.
  34. Kaplan EL, Meier P (1958) Nonparametric estimation from incomplete observations. *J Am Stat Assoc* 53: 457-481. doi:10.1080/01621459.1958.10501452.
  35. Watanabe I, Kurosawa N, Nishihira T (1998) Establishment and characterization of a murine cell-line derived from malignant fibrous histiocytoma of A/Jackson mouse. *Tohoku J Exp Med* 184: 173-187. doi:10.1620/tjem.184.173. PubMed: 9591335.
  36. Mosmann T (1983) Rapid colorimetric assay for cellular growth and survival: application to proliferation and cytotoxicity assays. *J Immunol Methods* 65: 55-63. doi:10.1016/0022-1759(83)90303-4. PubMed: 6606682.
  37. Bloom BR, Bennett B (1966) Mechanism of a reaction in vitro associated with delayed-type hypersensitivity. *Science* 153: 80-82. doi:10.1126/science.153.3731.80. PubMed: 5938421.
  38. David JR (1966) Delayed hypersensitivity in vitro: its mediation by cell-free substances formed by lymphoid cell-antigen interaction. *Proc Natl Acad Sci U S A* 56: 72-77. doi:10.1073/pnas.56.1.72. PubMed: 5229858.
  39. George M, Vaughan JH (1962) In vitro cell migration as a model for delayed hypersensitivity. *Proc Soc Exp Biol Med* 111: 514-521. doi:10.3181/00379727-111-27841. PubMed: 13947220.
  40. Leech M, Metz C, Hall P, Hutchinson P, Gianis K et al. (1999) Macrophage migration inhibitory factor in rheumatoid arthritis: evidence of proinflammatory function and regulation by glucocorticoids. *Arthritis Rheum* 42: 1601-1608. doi:10.1002/1529-0131(199908)42:8. PubMed: 10446857.
  41. Lin SG, Yu XY, Chen YX, Huang XR, Metz C et al. (2000) De novo expression of macrophage migration inhibitory factor in atherosclerosis in rabbits. *Circ Res* 87: 1202-1208. doi:10.1161/01.RES.87.12.1202. PubMed: 11110779.
  42. Lubetsky JB, Dios A, Han J, Aljabari B, Ruzsicska B et al. (2002) The tautomerase active site of macrophage migration inhibitory factor is a potential target for discovery of novel anti-inflammatory agents. *J Biol Chem* 277: 24976-24982. doi:10.1074/jbc.M203220200. PubMed: 11997397.
  43. Dessen AF, Stechly L, Jonckheere N, Dumont P, Monté D et al. (2010) Autocrine induction of invasive and metastatic phenotypes by the MIF-CXCR4 axis in drug-resistant human colon cancer cells. *Cancer Res* 70: 4644-4654. doi:10.1158/1538-7445.AM10-4644. PubMed: 20460542.
  44. Meyer-Siegler KL, Iczkowski KA, Leng L, Bucala R, Vera PL (2006) Inhibition of macrophage migration inhibitory factor or its receptor (CD74) attenuates growth and invasion of DU-145 prostate cancer cells. *J Immunol* 177: 8730-8739. PubMed: 17142775.
  45. Winner M, Meier J, Zierow S, Rendon BE, Crichlow GV et al. (2008) A novel, macrophage migration inhibitory factor suicide substrate inhibits motility and growth of lung cancer cells. *Cancer Res* 68: 7253-7257. doi:10.1158/0008-5472.CAN-07-6227. PubMed: 18794110.
  46. Baron N, Deuster O, Noelker C, Stürer C, Strik H et al. (2011) Role of macrophage migration inhibitory factor in primary glioblastoma multiforme cells. *J Neurosci Res* 89: 711-717. doi:10.1002/jnr.22595. PubMed: 21360573.
  47. Piette C, Deprez M, Roger T, Noël A, Foidart JM et al. (2009) The dexamethasone-induced inhibition of proliferation, migration, and invasion in glioma cell lines is antagonized by macrophage migration inhibitory factor (MIF) and can be enhanced by specific MIF inhibitors. *J Biol Chem* 284: 32483-32492. doi:10.1074/jbc.M109.014589. PubMed: 19759012.
  48. Schrader J, Deuster O, Rinn B, Schulz M, Kautz A et al. (2009) Restoration of contact inhibition in human glioblastoma cell lines after MIF knockdown. *BMC Cancer* 9: 464. doi:10.1186/1471-2407-9-464. PubMed: 20038293.
  49. Liu H, Chen G, Zhang W, Zhu JY, Lin ZQ et al. (2013) Overexpression of macrophage migration inhibitory factor in adenoid cystic carcinoma: correlation with enhanced metastatic potential. *J Cancer Res Clin Oncol* 139: 287-295. doi:10.1007/s00432-012-1330-z. PubMed: 23064787.
  50. He XX, Chen K, Yang J, Li XY, Gan HY et al. (2009) Macrophage migration inhibitory factor promotes colorectal cancer. *Mol Med* 15: 1-10. doi:10.2119/molmed.2008.00116. PubMed: 19009023.
  51. Simpson KD, Templeton DJ, Cross JV (2012) Macrophage migration inhibitory factor promotes tumor growth and metastasis by inducing myeloid-derived suppressor cells in the tumor microenvironment. *J Immunol* 189: 5533-5540. doi:10.4049/jimmunol.1201161. PubMed: 23125418.
  52. Enoch HG, Catalá A, Strittmatter P (1976) Mechanism of rat liver microsomal stearyl-CoA desaturase. Studies of the substrate specificity, enzyme-substrate interactions, and the function of lipid. *J Biol Chem* 251: 5095-5103. PubMed: 8453.
  53. Castro LF, Wilson JM, Gonçalves O, Galante-Oliveira S, Rocha E et al. (2011) The evolutionary history of the stearyl-CoA desaturase gene family in vertebrates. *BMC Evol Biol* 11: 132. doi:10.1186/1471-2148-11-132. PubMed: 21595943.
  54. Scaglia N, Igal RA (2008) Inhibition of Stearyl-CoA Desaturase 1 expression in human lung adenocarcinoma cells impairs tumorigenesis. *Int J Oncol* 33: 839-850. PubMed: 18813799.
  55. Igal RA (2010) Stearyl-CoA desaturase-1: a novel key player in the mechanisms of cell proliferation, programmed cell death and transformation to cancer. *Carcinogenesis* 31: 1509-1515. doi:10.1093/carcin/bgq131. PubMed: 20595235.
  56. Hess D, Chisholm JW, Igal RA (2010) Inhibition of stearylCoA desaturase activity blocks cell cycle progression and induces programmed cell death in lung cancer cells. *PLOS ONE* 5: e11394. doi:10.1371/journal.pone.0011394. PubMed: 20613975.
  57. Nashed M, Chisholm JW, Igal RA (2012) Stearyl-CoA desaturase activity modulates the activation of epidermal growth factor receptor in human lung cancer cells. *Exp Biol Med* 237: 1007-1017. doi:10.1258/ebm.2012.012126. PubMed: 22946088.
  58. Scaglia N, Chisholm JW, Igal RA (2009) Inhibition of stearylCoA desaturase-1 inactivates acetyl-CoA carboxylase and impairs proliferation in cancer cells: role of AMPK. *PLOS ONE* 4: e6812. doi:10.1371/journal.pone.0006812. PubMed: 19710915.
  59. Roongta UV, Pabalan JG, Wang X, Ryseck RP, Fargnoli J et al. (2011) Cancer cell dependence on unsaturated fatty acids implicates stearyl-CoA desaturase as a target for cancer therapy. *Mol Cancer Res* 9: 1551-1561. doi:10.1158/1541-7786.MCR-11-0126. PubMed: 21954435.
  60. Mason P, Liang B, Li L, Fremgen T, Murphy E et al. (2012) SCD1 inhibition causes cancer cell death by depleting mono-unsaturated fatty acids. *PLOS ONE* 7: e33823. doi:10.1371/journal.pone.0033823. PubMed: 22457791.
  61. Armstrong ME, Gantier M, Li L, Chung WY, McCann A et al. (2008) Small interfering RNAs induce macrophage migration inhibitory factor production and proliferation in breast cancer cells via a double-stranded RNA-dependent protein kinase-dependent mechanism. *J Immunol* 180: 7125-7133. PubMed: 18490711.
  62. Du X, Wang QR, Chan E, Merchant M, Liu J et al. (2012) FGFR3 stimulates stearyl CoA desaturase 1 activity to promote bladder tumor growth. *Cancer Res* 72: 5843-5855. doi:10.1158/0008-5472.CAN-12-1329. PubMed: 23019225.
  63. Hagemann T, Wilson J, Kulbe H, Li NF, Leinster DA et al. (2005) Macrophages induce invasiveness of epithelial cancer cells via NF-kappa B and JNK. *J Immunol* 175: 1197-1205. PubMed: 16002723.
  64. Han I, Lee MR, Nam KW, Oh JH, Moon KC et al. (2008) Expression of macrophage migration inhibitory factor relates to survival in high-grade osteosarcoma. *Clin Orthop Relat Res* 466: 2107-2113. doi:10.1007/s11999-008-0333-1. PubMed: 18563508.
  65. Rendon BE, Roger T, Teneng I, Zhao M, Al-Abed Y et al. (2007) Regulation of human lung adenocarcinoma cell migration and invasion by macrophage migration inhibitory factor. *J Biol Chem* 282: 29910-29918. doi:10.1074/jbc.M704898200. PubMed: 17709373.
  66. Sun B, Nishihira J, Suzuki M, Fukushima N, Ishibashi T et al. (2003) Induction of macrophage migration inhibitory factor by lysophosphatidic acid: relevance to tumor growth and angiogenesis. *Int J Mol Med* 12: 633-641. PubMed: 12964047.
  67. Sun B, Nishihira J, Yoshiki T, Kondo M, Sato Y et al. (2005) Macrophage migration inhibitory factor promotes tumor invasion and metastasis via the Rho-dependent pathway. *Clin Cancer Res* 11: 1050-1058. PubMed: 15709171.

68. Morand EF, Leech M, Bernhagen J (2006) MIF: a new cytokine link between rheumatoid arthritis and atherosclerosis. *Nat Rev Drug Discov* 5: 399-410. doi:10.1038/nrd2029. PubMed: 16628200.
69. Zernecke A, Bernhagen J, Weber C (2008) Macrophage migration inhibitory factor in cardiovascular disease. *Circulation* 117: 1594-1602. doi:10.1161/CIRCULATIONAHA.107.729125. PubMed: 18362243.
70. Bernhagen J, Krohn R, Lue H, Gregory JL, Zernecke A et al. (2007) MIF is a noncognate ligand of CXC chemokine receptors in inflammatory and atherogenic cell recruitment. *Nat Med* 13: 587-596. doi:10.1038/nm1567. PubMed: 17435771.
71. Igal RA (2011) Roles of StearoylCoA Desaturase-1 in the Regulation of Cancer Cell Growth, Survival and Tumorigenesis. *Cancers* 3: 2462-2477. doi:10.3390/cancers3022462.
72. Cho Y, Crichlow GV, Vermeire JJ, Leng L, Du X et al. (2010) Allosteric inhibition of macrophage migration inhibitory factor revealed by ibudilast. *Proc Natl Acad Sci U\_S\_A* 107: 11313-11318. doi:10.1073/pnas.1002716107. PubMed: 20534506.
73. Rolan P, Gibbons JA, He L, Chang E, Jones D et al. (2008) Ibudilast in healthy volunteers: safety, tolerability and pharmacokinetics with single and multiple doses. *Br J Clin Pharmacol* 66: 792-801. doi:10.1111/j.1365-2125.2008.03270.x. PubMed: 19032723.
74. Cross JV, Rady JM, Foss FW, Lyons CE, Macdonald TL et al. (2009) Nutrient isothiocyanates covalently modify and inhibit the inflammatory cytokine macrophage migration inhibitory factor (MIF). *Biochem J* 423: 315-321. doi:10.1042/BJ20091170. PubMed: 19723024.
75. Oballa RM, Belair L, Black WC, Bleasby K, Chan CC et al. (2011) Development of a liver-targeted stearoyl-CoA desaturase (SCD) inhibitor (MK-8245) to establish a therapeutic window for the treatment of diabetes and dyslipidemia. *J Med Chem* 54: 5082-5096. doi:10.1021/jm200319u. PubMed: 21661758.

# Simultaneous Determination of Post-Translational Racemization and Isomerization of *N*-Terminal Amyloid- $\beta$ in Alzheimer's Brain Tissues by Covalent Chiral Derivatized Ultraperformance Liquid Chromatography Tandem Mass Spectrometry

Koichi Inoue,<sup>†</sup> Daiju Hosaka,<sup>†</sup> Nana Mochizuki,<sup>†</sup> Hiroyasu Akatsu,<sup>‡,§</sup> Kaname Tsutsumiuchi,<sup>||</sup> Yoshio Hashizume,<sup>‡</sup> Noriyuki Matsukawa,<sup>§</sup> Takayuki Yamamoto,<sup>‡</sup> and Toshimasa Toyooka<sup>\*,†</sup>

<sup>†</sup>Laboratory of Analytical and Bio-Analytical Chemistry, School of Pharmaceutical Sciences, University of Shizuoka, Shizuoka, Japan

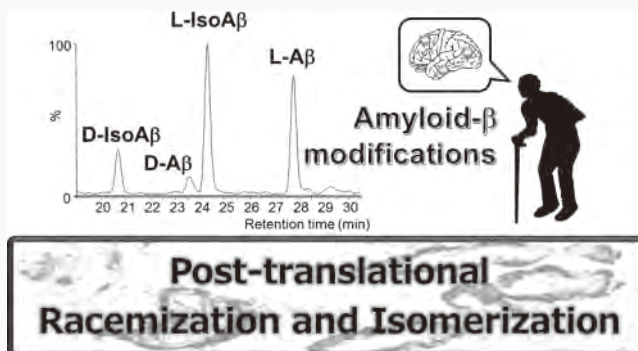
<sup>‡</sup>Department of Neuropathology, Choju Medical Institute, Fukushima Hospital, Toyohashi, Japan

<sup>§</sup>Department of Neurology, Nagoya City University, Graduate School of Medical Sciences, Nagoya, Japan

<sup>||</sup>College of Bioscience and Biotechnology, Chubu University, Kasugai, Japan

## Supporting Information

**ABSTRACT:** Typical markers of protein aging are spontaneous post-translational modifications such as amino acid racemization (AAR) and amino acid isomerization (AAI) during the degradation of peptides. The post-translational AAR and AAI could significantly induce the density and localization of plaque deposition in brain tissues. Alzheimer's disease (AD) is reliably related to the formation and aggregation of amyloid- $\beta$  peptide ( $A\beta$ ) plaques in the human brain. No current analytical methods can simultaneously determine AAR and AAI during the degradation of  $A\beta$  from AD patients. We now report a covalent chiral derivatized ultraperformance liquid chromatography tandem mass spectrometry (CCD-UPLC-MS/MS) method for the determination of post-translational AAR and AAI of *N*-terminal  $A\beta$  ( $N$ - $A\beta_{1-5}$ ) in human brain tissues. When subjected to tryptic  $N$ - $A\beta_{1-5}$  from post-translationally modified natural  $A\beta$  in focal brain tissues by the CCD procedure, it was monitored at  $m/z$  989.6  $\rightarrow$  637.0/678.9 during electrospray collision-induced dissociation. These  $N$ - $A\beta_{1-5}$  fragments with L-aspartic acid (L-Asp), D-Asp, L-isoAsp, and D-isoAsp could be separated using the UPLC system with a conventional reversed-phase column and mobile phase. The quantification of these peptides was determined using a stable isotope [<sup>15</sup>N]-labeled  $A\beta_{1-40}$  internal standard. The CCD-UPLC-MS/MS assay of potential  $N$ - $A\beta_{1-5}$  allowed for the discovery of the present and ratio levels of these  $N$ - $A\beta_{1-5}$  sequences with L-Asp, D-Asp, L-isoAsp, and D-isoAsp.



The spontaneous accumulation of the post-translational modifications within biological proteins can be regarded as an aging process. The accumulation of modified proteins may disrupt biochemical functions by affecting protein expression, clearance, turnover, cell signaling, and induction of apoptosis, suggesting that protein aging could have both physiological and pathological markers. Nearly all age-related neurodegenerative diseases involve the misfolding and accumulation of specific proteins in the brain regions. More than 50 diseases of abnormal protein deposition have been identified in the brain and systemic tissues of humans.<sup>1</sup> Under pathogenic conditions such as amino acid substitutions, the post-translational modifications such as cleavage, phosphorylation, oxidation, protein density, and/or misfolding of structured proteins, some proteins are liable to be dysfunctional, self-aggregate, and accumulate inside or outside of neuron cells in specific brain regions.

Amyloidosis, the most widely known appearance of frequent pathology, may still dramatically impact the outcome from therapy and prevention with aging degeneration. The pathogenic aggregation of the amyloid- $\beta$  ( $A\beta$ ) peptides is considered a hallmark of the progression of Alzheimer's disease (AD), the leading cause of senile dementia in the elderly and one impact of dementia as an increasing threat to global health. Efforts to extract and analyze the composition of  $A\beta$  plaques from human brains of AD patients started in the 1970s.<sup>2,3</sup> The first successful protocol to purify and analyze the  $A\beta$  sequence of amino acids was developed using amino acid analyzer liquid chromatography (LC) techniques.<sup>4</sup> They reported the sequence of the *N*-terminal 24 amino acids in  $A\beta$ , showing

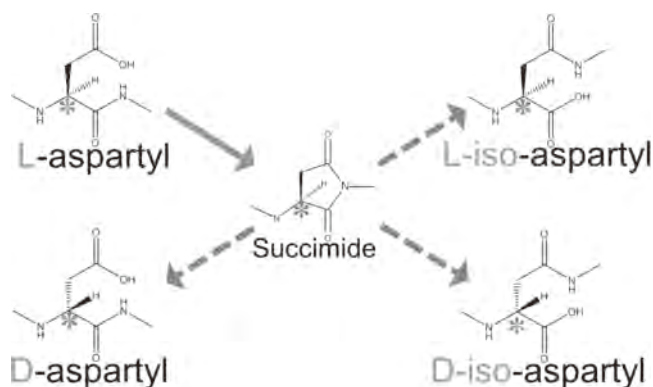
Received: October 14, 2013

Accepted: November 27, 2013

Published: November 27, 2013

similarity between AD and Down's syndrome. In the 1990s, various reports strongly suggested that  $A\beta$  sequences isolated from AD and Down's syndrome brains were post-translationally modified by racemization and isomerization of the amino acids in protein.<sup>5–9</sup> The *N*-terminal structure of  $A\beta$ , extracted from senile plaques such as neuritic deposits, showed cleaved *N*-terminal aspartic acid (<sup>1</sup>Asp) of about 8%, the formation of isoaspartate forms (iso<sup>1</sup>Asp) of about 20%, pyroglutamate-3 (p3Glu), the cyclization of the *N*-terminal glutamyl residue of about 51%, and the native form of only about 20% by amino acid analysis and mass spectrometric (MS) analysis with the tryptic digestion and Edman degradation.<sup>10</sup> These pathways of the post-translational *N*-terminal modification of  $A\beta$  are characterized to represent the most frequent type of aging protein damage. These reactions proceed through the formation of a cyclic succinimide intermediate, which rapidly processed to spontaneous chemical modifications such as amino acid racemization (AAR) and amino acid isomerization (AAI) during the degradation of Asp-included peptides (Scheme 1).<sup>11</sup> During the spontaneous chemical modification

**Scheme 1. Formation of a Cyclic Succinimide Intermediate That Occurred by Spontaneous Chemical Modifications Such As Amino Acid Racemization (AAR) and Amino Acid Isomerization (AAI) during Degradation of Asp-Included Peptides**



Isomerization and racemization of *L*-aspartate occur spontaneously in proteins and proceed through a common transient cyclic succinimidyl intermediate. Succinimide is hydrolyzed immediately to form two more stable compounds: *L*-isoaspartate and *L*-aspartate. Alternatively, *L*-succinimide racemizes to *D*-succinimide, which is rapidly hydrolyzed to *D*-isoaspartate and *D*-aspartate.

of  $A\beta$ , the AAR and AAI of Asp for protein functionality is the existence of a specific repair system based on protein *L*-isoaspartyl *O*-methyltransferase (PIMT).<sup>12</sup> However, the PIMT repair system is not completely efficient in that the *D*-Asp residue is not recognized and equally functional in all tissues.<sup>13</sup> It has been reported that the modified Asp sequence dramatically increased with aging in the brain.<sup>14</sup> The AAR and AAI represent the major nonenzymatic and chemical modifications affecting the  $A\beta$  folding and degradation in the pathology of aging dementia. Recently, an interesting study was reported that when isoAsp is present at position 672 in the amyloid precursor protein (APP), cathepsin B can catalyze the cleavage between methionine (Met) at 671 and isoAsp at 672 with a high efficiency.<sup>15</sup> Since spontaneous AAI cannot readily take place in the post-translational *N*-terminal modification, iso<sup>1</sup>Asp formation in the native  $A\beta$  can only occur as an early

event in the  $A\beta$  production before the  $\beta$ -secretase cleavage (BACE1). This means that the detection of AAR and AAI in the *N*-terminal sequence has two aspects used to evaluate the production and aggregation of  $A\beta$ . In any case, the consequences of these chemical modifications are site-specific and can affect the age-related accumulation according to the structural alterations produced by the site-specific incorporation of modified *N*-terminal residues. There have been many studies of AAR and AAI events of  $A\beta$  in vivo and/or in vitro, but its role in the natural  $A\beta$  pathogenesis in the focal brain tissues is still unclear.

In the case of AAR in the  $A\beta$  sequence, Edman degradation with LC amino acid analysis was used for the determination of the chiral free-amino acids from extracted natural or artifact  $A\beta$ s.<sup>9,16</sup> The *O*-acyl isopeptide method was developed for evaluation of the solubility and stability of  $A\beta$  related to AAR.<sup>17</sup> In the case of AAI in the  $A\beta$  sequence, the frequently employed methods for AAI in the  $A\beta$  sequence are MS techniques.<sup>18,19</sup> Sargaeva et al. used electron capture dissociation (ECD) Fourier-transform ion cyclotron resonance (FTICR) MS for the identification of Asp and isoAsp in the  $A\beta$  sequence based on signature backbone cleavage ions ( $m/z$   $c + 57$  and  $z - 57$ ) produced upon radical-mediated fragmentation.<sup>18</sup> Ni et al. applied electron transfer dissociation (ETD) MS based on the same cleavage ions.<sup>19</sup> However, an MS assay may be not utilized to discover signature ions of both Asp residues in the  $A\beta$  sequences from the spurious background noise of biological samples. To chromatographically separate the AAI peptides using LC techniques, sufficient results could not be acquired with model peptide sequences.<sup>19–21</sup> On the other hand, LC separation would be needed to analyze nondifferences in the Asp-isomers with identical mass in biological samples. In this study, covalent chiral derivatized ultraperformance liquid chromatography tandem mass spectrometry (CCD-UPLC-MS/MS) was used to simultaneously analyze the post-translational AAR and AAI of *N*-terminal  $A\beta$  ( $N$ - $A\beta_{1-5}$ ) in the human brain. When subjected to tryptic  $N$ - $A\beta_{1-5}$  from post-translationally modified natural  $A\beta$  in brain tissues monitored by CCD-electrospray ionization (ESI) with collision-induced dissociation (CID), these  $N$ - $A\beta_{1-5}$  sequences with *L*-Asp, *D*-Asp, *L*-isoAsp, and *D*-isoAsp could be separated using the UPLC system with a conventional reversed-phase column and mobile phase. Our approach overcomes the limitations of simultaneous AAR and AAI monitoring of the modified  $A\beta$  peptides in AD brain.

## ■ EXPERIMENTAL SECTION

**Materials.** Synthetic  $N$ - $A\beta_{1-5}$  peptides with *L*-Asp, *D*-Asp, *L*-isoAsp, and *D*-isoAsp (peptide purity: >95%, molecular weight: 636.65) were obtained from Eurofins Operon (Wien, Austria).  $A\beta_{1-40}$ ,  $1-42$ ,  $1-43$  and stable isotope [<sup>15</sup>N]-labeled  $A\beta_{1-40}$  were obtained from the rPeptide Co. (Athens, GA). The covalent chiral derivatized reagent of (R)-(-)-4-(*N*, *N*-dimethylaminosulfonyl)-7-(3-isothiocyanatopyrrolidin-1-yl)-2,1,3-benzoxadiazole (R-DBD-Py-NCS) for HPLC labeling was obtained from the Tokyo Chemical Industry (Tokyo, Japan). All other chemicals were of analytical grade and were used without further purification.

**UPLC-MS/MS Equipment and Conditions.** The UPLC-MS/MS was performed using a Waters ACQUITY UPLC/Xevo TQ-S system (Waters, Milford, MA) that was coupled to a triple quadrupole mass spectrometer fitted with an electrospray ionization (ESI) source. LC separation was performed

using an Acquity UPLC BEH C18 (2.1 × 100 mm, 1.7 μm; Waters, Milford, MA). The mobile phase consisted of 50 mM aqueous ammonium formate with 0.01% formic acid (Solvent A) and 0.01% formic acid in methanol (Solvent B). Other conditions are shown in the Supporting Information.

**Preparation and Covalent Chiral Derivatization of Aβ Peptides.** The Aβ peptides were dissolved in their original vial with water and acetonitrile (50/50, v/v) by sonication for 30 s to produce 1 mM solutions. This water/acetonitrile solution was already applied to prepare the Aβ<sub>1-16</sub> and Aβ<sub>1-40</sub> peptides for the LC/MS experiment.<sup>22,23</sup> For the optimal derivatized conditions, this protocol was used for measuring the AAR and AAI of N-Aβ<sub>1-5</sub> as derivatives in the brain tissues (Supporting Information).

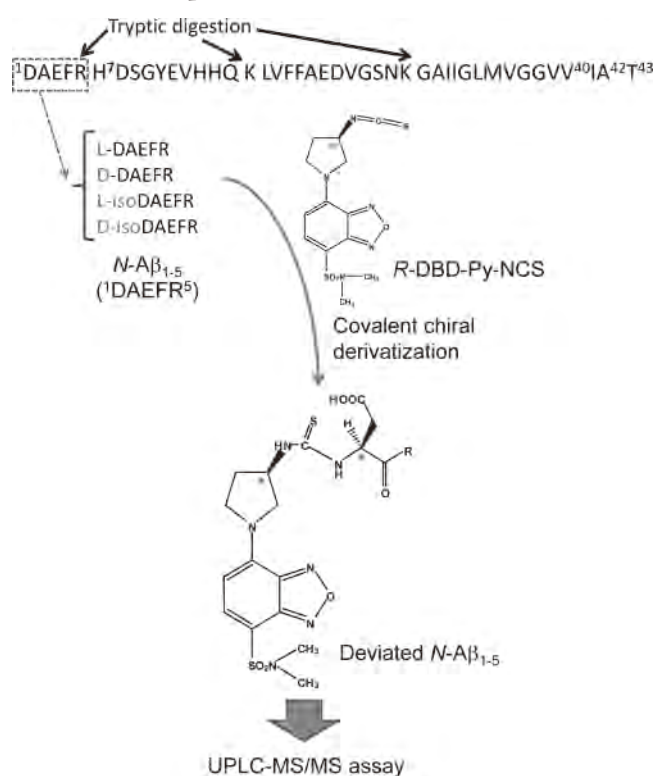
**Extraction, SPE, and Tryptic Procedure.** In the first step, the brain tissues and zirconia beads (5.0 mm) in the tubes were placed in the holes of an aluminum block and immediately homogenized for 3 min by a Shake Master (Bio Medical Sciences, Tokyo, Japan). These supernatant solutions were applied to the solid phase extraction (SPE) using InterSep MC-1 (30 mg/1 mL, GL Science Co., Tokyo, Japan). These eluants were dried under a stream of nitrogen at 30 °C. These samples were dissolved in 90 μL of 50 mM ammonium hydrogen carbonate in water, 10 μL of trypsin, and were then incubated at 37 °C for 6 h. These solutions were then subjected to derivatization. For the optimal extraction and tryptic procedures of Aβ, we utilized the UPLC-MS/MS analysis of the stable tryptic part of LVFFAEDVGSNK (*m/z* 663.6 → *m/z* 185.2) from the AD brain tissues.

**Sample Information.** The utilized tissues from the Fukushima Brain Bank were used for the accurate, reliable, and detailed pathological evaluation of AD.<sup>24</sup> All of our cases were reviewed and discussed with several doctors at a clinicopathological conference regarding neuropathological staining.<sup>25</sup>

## RESULTS AND DISCUSSION

**CCD-UPLC-MS/MS Analysis of N-Terminal Aβ Sequence.** The Aβ sequences in the plaque, aggregation, fibrils, insoluble polymers, and soluble oligomers were built from the N-terminal position starting with Asp to the C-terminal position at 40, 42, 43, or others in the AD brain. After tryptic digestion, four main parts of the fragments were dissected, as shown in Scheme 2. In this study, the N-terminal part of Asparagine (Asp)-glutamic acid (Glu)-phenylalanine (Phe)-arginine (Arg) (<sup>1</sup>DAEFR<sup>5</sup>; N-Aβ<sub>1-5</sub>) was the focus based on three reasons from previous reports. First, cathepsin B is more effective than BACE1 in processing the <sup>672</sup>Asp-containing peptide derivatives and can cleave the <sup>672</sup>isoAsp-containing peptides such as APP, which occurs with a high catalytic efficiency.<sup>15</sup> BACE1 is a type I transmembrane aspartyl protease that is involved in the generation of the Aβ component in brain tissue. This enzyme has been found to be especially efficacious to hydrolyze the variant of APP and was in fact discovered using this APP sequence as molecular bait. BACE1 was able to cleave readily only the sample peptide representing the APP Swedish mutated sequence at the prior position <sup>1</sup>Asp, while cathepsin B hydrolyzed the structures of the isoAsp residue at position-1 in APP.<sup>15</sup> BACE1 and cathepsin B could jointly participate in cleaving the N-terminal part, including <sup>672</sup>Asp or <sup>672</sup>isoAsp. The majority of AD dementia patients may be altered in the extent of cleavage and clearance of APP, and therefore, specific inhibitors of cathepsin

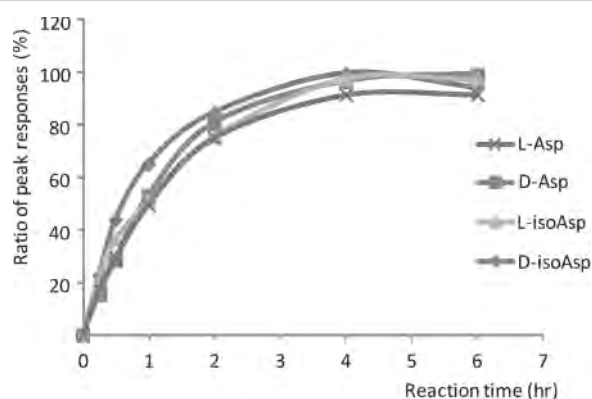
**Scheme 2. Tryptic Digestion and Experimental Approach for the Post-Translational AAR and AAI Formation of N-Terminal Aβ Sequences**



Natural Aβ sequences are termed from the N-terminal Asp to the C-terminal <sup>38</sup>Gly, <sup>40</sup>Val, <sup>42</sup>Ala, <sup>42</sup>Ala, or other types. Moreover, <sup>13,14</sup>His and/or <sup>35</sup>Met are oxidized. These Aβ sequences were cleavage by trypsin and produced to four fragments such as DAEFR, HD SGYEVVHQ, and others. The N-terminal fragment (DAEFR) is focused for determining AAR and AAI formation of N-terminal <sup>1</sup>Asp in the natural Aβ sequence. This N-terminal fragment is deviated by R-DBD-Py-NCS for the UPLC separation of AAR and AAI formation of N-terminal <sup>1</sup>Asp in natural Aβ sequences.

B represent candidate drugs for AD dementia.<sup>26,27</sup> Second, the formation of pyroglutamate-modified Aβ is a multistep process requiring the removal of the two N-terminal amino acids, such as <sup>1</sup>Asp and <sup>2</sup>Ala, by elimination to expose the <sup>3</sup>Glu site at the third position of the Aβ peptides.<sup>28</sup> Third, the AAR of the N-terminal <sup>1</sup>Asp residue could suppress the Aβ fibril formation regarding Asp at position 7 or 23.<sup>29</sup> Thus, a valuable idea was conceived that the AAR of the N-terminal <sup>1</sup>Asp is accelerated for the inhibition of the Aβ fibril and aggregation. Accordingly, the analysis of the N-terminal Aβ sequence in the AD brain would be needed for discussing these queries related to the N-terminal <sup>1</sup>Asp. In this study, based on a novel CCD-UPLC-MS/MS assay of N-Aβ<sub>1-5</sub>, an initial experiment was performed to determine the CCD reaction and MS ionizations of the Aβ model peptides. The full scan and daughter mass spectra were evaluated to determine the relative intensities of ions in a given mass range in the positive ESI mode. These N-Aβ<sub>1-5</sub> sequences with the L-Asp, D-Asp, L-isoAsp, and D-isoAsp structures could be reacted with R-DBD-Py-NCS in a solution of triethylamine. It was clear that the CCD reaction of the N-Aβ<sub>1-5</sub> model peptides occurs at higher temperatures from 20 to 70 °C. In this study, the reaction condition was the highest at 70 °C and achieved a plateau after 4 h in the solution of 2% triethylamine

(Figure 1). The mass spectrum of the typical  $A\beta_{1-5}$  peptide ( $N$ - $A\beta_{1-5}$  sequence with  $L$ -Asp) showed a signal at  $m/z$  989.6 [M]

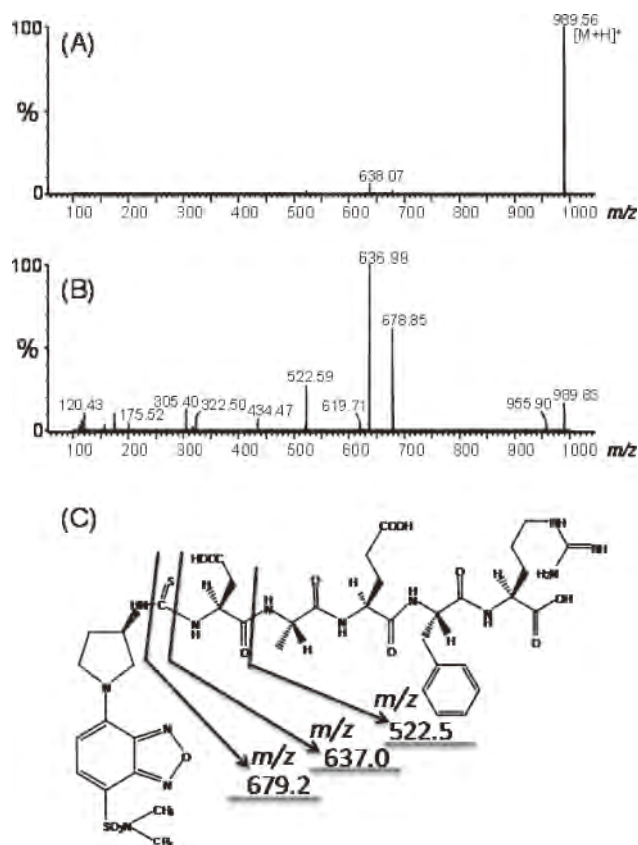


The derivatized condition was used for measuring the AAR and AAI of  $N$ - $A\beta_{1-5}$  by UPLC-MS/MS assay. A 100  $\mu$ L solution of the standard was added to 50  $\mu$ L of 5 mM R-DBD-Py-NCS in acetonitrile and 50  $\mu$ L of 2% triethylamine at 70  $^{\circ}$ C for 0–6 h. The mixed solution was dried and added to 50  $\mu$ L of the mobile phase solution.

<sup>1</sup>Investigation of optimal reaction time at 70  $^{\circ}$ C for the covalent chiral derivatized  $N$ - $A\beta_{1-5}$  model peptides.

+H]<sup>+</sup> by the CCD reaction (Figure 2A). The results of the daughter scan from the precursor ions of  $m/z$  678.9, 637.0, and 522.6 are shown in Figure 2B. These fragment patterns of  $m/z$  678.9, 637.0, and 522.6 from the typical  $A\beta_{1-5}$  peptide are shown in Figure 2C. When the collision energy (40 V) was used in the product ions of [M + H]<sup>+</sup>, the major fragment ions at  $m/z$  989.6  $\rightarrow$   $m/z$  637.0/678.9 were observed using a collision energy of 20 eV. Moreover, other  $A\beta$  model peptides showed comparable MS spectral patterns in the ESI positive mode. Based on this result, these ions in the SRM mode were used for the analysis of  $N$ -terminal  $A\beta$  sequences with AAR and AAI in biological samples.

To utilize an MS assay of nondifferences of peptide sequences with an identical mass in biological samples, the chromatographic techniques should be needed for the development of an accurate, reliable, and sensitive method for biological samples. In the effort of chromatographically separating the AAR and AAI peptides, we think that this sufficient result could not be acquired using traditional separation techniques. In our laboratory, an indirect derivatization-based assay could be used to identify potential low molecules such as drug, pesticide, and biomarkers in various complicated samples for the analysis of chiral compounds based on the reversed-phase LC system.<sup>30–32</sup> The CCD-UPLC-MS/MS assay to simultaneously screen the AAR and AAI of peptides as an effective method in biological samples, however, has not been reported. In this study, several reversed-phase columns and mobile phases (added formic acid, acetic acid, and TFA: concentration of 0.1% in water/acetonitrile or methanol) were evaluated for the separation of these  $N$ - $A\beta_{1-5}$  sequences with  $L$ -Asp,  $D$ -Asp,  $L$ -isoAsp, and  $D$ -isoAsp (Figure 3B). On the basis of this result, a separation of  $L$ -Asp (retention time (RT): 28.5 min),  $D$ -Asp (RT: 24.3 min),  $L$ -isoAsp (RT: 25.0 min), and  $D$ -isoAsp (RT: 21.3 min) could be achieved using the UPLC BEH C<sub>18</sub> column with a mobile phase consisting of 0.1% formic acid in water/methanol. The RT of [<sup>15</sup>N]-labeled  $N$ -terminal Asp residue internal standard from a stable isotope  $A\beta_{1-40}$  was

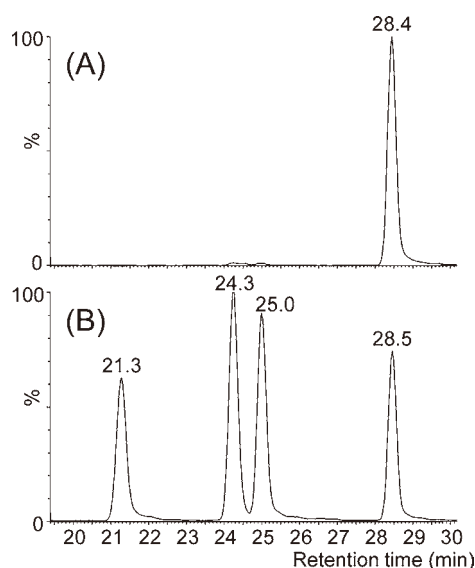


(A) MS spectrum of  $N$ - $A\beta_{1-5}$  in ESI-positive mode. (B) MS/MS spectrum ( $m/z$  989.56  $\rightarrow$ ) of  $N$ - $A\beta_{1-5}$  in ESI-positive mode. (C) MS/MS fragment pattern of covalent chiral derivatized  $N$ - $A\beta_{1-5}$ . The UPLC-MS/MS was performed using a Waters ACQUITY UPLC/Xevo TQ-S system that was coupled to a Quadrupole mass spectrometer fitted with an ESI source in the positive ionization mode. The mobile phase consisted of 50 mM aqueous ammonium formate with 0.01% formic acid and 0.01% formic acid in methanol with the flow rate of 0.4 mL/min.

<sup>2</sup>Mass spectra and fragment pattern of the typical  $A\beta_{1-5}$  peptide ( $N$ - $A\beta_{1-5}$  sequence with  $L$ -Asp).

28.4 min in the SRM mode ( $m/z$  989.6  $\rightarrow$   $m/z$  637.0/678.9) (Figure 3A).

**Sample Preparation and Tryptic Digestion of Full-Length  $A\beta$  Peptides in Human Brain Tissues.** For the analysis of the natural  $A\beta$  peptides from brain tissues using our developed method, extraction, cleanup and tryptic digestion would be needed. Thus, we investigated each condition and operation of the full-length natural  $A\beta$  peptides. For the extractive process of natural  $A\beta$  peptides, we investigated various kinds of solutions using the tryptic part of LVFFAEDVGSNK ( $m/z$  663.6  $\rightarrow$   $m/z$  185.2) from AD brain tissues. This result is shown in Figure 4A. In addition, previous studies showed that the compact of natural  $A\beta$  plaques in the human brain often used the FA solution.<sup>33–36</sup> In this study, we used 50% FA in water for the extraction of the natural  $A\beta$  peptides in the brain tissues. For the cleanup procedure of the full-length natural  $A\beta$  peptides, we then employed the SPE method as a reference.<sup>37</sup> It suggested that recovery was approximately 90% for these  $A\beta$  species, and the key to obtaining a high recovery was in meticulously altering the elutropic composition and ion pair strength of the SPE solvents with the acetonitrile and ammonium combination as the best

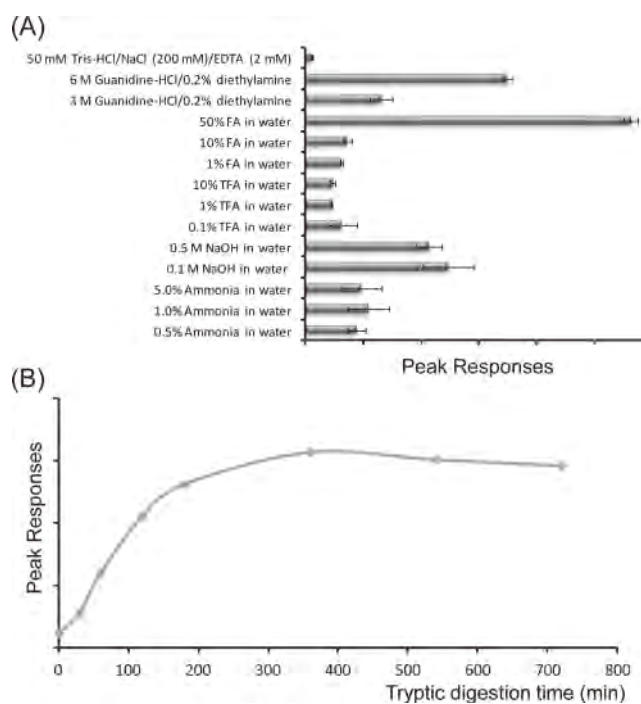


(A) SRM chromatogram ( $m/z$  989.6  $\rightarrow$   $m/z$  637.0/678.9) for the isotope stable [ $^{15}\text{N}$ ]-labeled  $N$ -terminal peptide from  $A\beta_{1-40}$  (retention time (RT): 28.4 min). (B) SRM chromatogram ( $m/z$  989.6  $\rightarrow$   $m/z$  637.0/678.9) for the  $N$ - $A\beta_{1-5}$  with L-Asp (RT: 28.5 min), D-Asp (RT: 24.3 min), L-isoAsp (RT: 25.0 min), and D-isoAsp (RT: 21.3 min). This separation of the derivatized  $N$ - $A\beta_{1-5}$  fragment included with L-Asp, D-Asp, L-isoAsp, and D-isoAsp was achieved using the UPLC BEH C18 column with a mobile phase consisting of 0.1% formic acid in water/methanol.

<sup>3</sup>SRM chromatograms of  $N$ - $A\beta_{1-5}$  standard solution.

recovery solvent.<sup>37</sup> We then targeted the  $N$ -terminal  $A\beta$  sequence in the brain tissues regarding the tryptic digestion procedure. In previous reports, we investigated the tryptic digestion of the full-length  $A\beta_{1-40}$  and  $A\beta_{1-42}$  peptides under the buffer's condition.<sup>22,23</sup> The reaction time was investigated using the tryptic part of LVFFAEDVGSNK from the full-length  $A\beta_{1-40}$ ,  $A\beta_{1-42}$  and  $A\beta_{1-43}$  standards, as shown in Figure 4B. The reaction time of about 6 h was used in this study. Ultimately, in this study, we used the stable isotope full-length  $A\beta_{1-40}$  for evaluating the recovery of the natural  $A\beta$  peptides using the extraction, SPE, and tryptic procedures. The recovery of the full-length  $A\beta_{1-40}$  in the control brain tissues was analyzed using the dilution stable isotope tryptic [ $^{15}\text{N}$ ]-labeled  $N$ - $A\beta_{1-5}$ , which ranged from 96.1 to 102.3% (Average 99.2%, RSD: 2.2%,  $n = 5$ ).

**Examination of AAR and AAI of  $N$ -Terminal  $A\beta$  Sequence in AD Brain Tissues.** Shimizu et al. reviewed the AAR and AAI formation; although seizure is not a common symptom of AD patients, rapid accumulation of isomerized proteins may cause an epileptic seizure, while chronic accumulation may cause neurodegeneration.<sup>11</sup> Alternatively, it is speculated that most proteins isomerized in matured or aged brains are associated with the progression of neurodegeneration. Moreover, the  $N$ -terminal  $A\beta$  sequence in senile plaque from AD patients indicated that DL-Asp is only 10%, and the predicted L-Asp is about 2% based on the D/L-iso7Asp ratio (55.7/19.2%) in this review.<sup>11</sup> Successively, most of them wonder about this influence of the AAR and AAI formations on the AD brain. Thus, we examined the AAR and AAI formations of the  $N$ -terminal  $A\beta$  sequence in AD and control brain tissues (frontal lobe region) using our developed CCD-UPLC-MS/MS assay. Table 1 shows that the  $N$ -terminal  $A\beta$  sequence in the AD and control brain tissues was calculated using the unit of



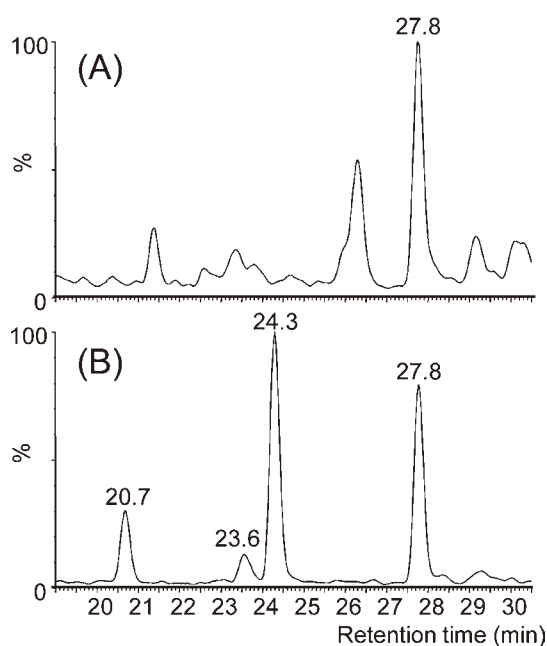
(A) Investigation of extraction solution for the natural  $A\beta$  peptides in AD brain tissue. (B) Investigation of tryptic digestion time for the natural  $A\beta$  peptides in AD brain tissue. In the extractive process and tryptic digestion time of natural  $A\beta$  peptides, various kinds of solutions and tryptic digestion time were investigated using the stable tryptic part of LVFFAEDVGSNK ( $m/z$  663.6  $\rightarrow$   $m/z$  185.2) from AD brain tissues.

<sup>4</sup>Investigation of extraction and tryptic procedures for the natural  $A\beta$  peptides using the stable tryptic part of LVFFAEDVGSNK from AD brain tissues.

picomoles per milligram of tissue. In addition, the typical SRM chromatograms of  $N$ - $A\beta_{1-5}$  and the internal standard in AD brain tissues are shown in Figure 5. The concentration levels of the post-translational AAR and AAI formation of the  $N$ -terminal  $A\beta$  sequence were detected in the AD brain tissues. Thus, the specificity is very important, and it is defined as the noninterference at the retention times of  $N$ - $A\beta_{1-5}$  and internal standard from the endogenous brain components in the SRM chromatograms. From this result for analysis of the control, no significant peaks from the  $A\beta$  presence (sample nos. 11–13, 15, 16, and 18–20 in Table 1) were found at the retention time corresponding to  $N$ - $A\beta_{1-5}$  in almost all cases. Moreover, the relationship between the Braak stage and  $A\beta$  levels is not a possibility definitive correlation and will be discussed using large scale samples. On the other hand, based on this result for the AD brain, the post-translational AAR and AAI formation of the  $N$ -terminal  $A\beta$  sequence was detected in all patients. These patterns for the aging and gender difference in AD patients are shown in Figure 6. The detection levels of the  $N$ -terminal  $A\beta$  sequence from AD patients of the predictable L-Asp of about  $59.0 \pm 26.0\%$  based on the D/L-iso/D-isoAsp ratio ( $4.8 \pm 5.7/25.4 \pm 15.0/10.8 \pm 11.2\%$ , AD patients,  $n = 10$ ) were observed. This pattern of aging and gender difference allowed for the discovery of significantly interesting results in the AD patients (Figure 6). Thus, the possible AAR and AAI and the effects of the post-translational modification in AD patients would be investigated using a greater number of subjects. On the basis of the antibody's study of the  $A\beta$  in AAI, Szendrei et al. reported

Table 1. Post-Translational AAR and AAI Formation of N-Terminal A $\beta$  Sequence for AD and Control Brain Tissues ( $n = 20$ )<sup>a</sup>

no.	state	age	Braak	sex	N-terminal AP sequence (pmol/mg)				total
					L-Asp	D-Asp	L-isoAsp	D-isoAsp	
1	AD	86	6	male	3.2	ND	0.6	ND	3.8
2	AD	87	4	female	0.3	ND	0.4	0.2	0.9
3	AD	96	4	female	0.2	0.1	0.2	0.1	0.6
4	AD	86	4	male	1.8	0.1	0.3	0.1	2.3
5	AD	85	6	male	1.8	0.1	0.2	ND	2.1
6	AD	77	4	male	2.3	0.1	0.4	ND	2.8
7	AD	83	6	female	7.1	ND	0.6	0.2	7.9
8	AD	92	5	female	1.7	0.2	2.2	0.7	4.8
9	AD	76	4	male	0.3	0.1	0.3	0.1	0.8
10	AD	88	4	female	0.1	ND	0.1	0.1	0.3
11	control	82	1	male	ND	ND	ND	ND	ND
12	control	87	1	female	ND	ND	ND	ND	ND
13	control	95	1	female	ND	ND	ND	ND	ND
14	control	89	2	male	0.7	0.1	0.7	0.3	1.8
15	control	85	2	male	ND	ND	ND	ND	ND
16	control	76	1	male	ND	ND	ND	ND	ND
17	control	87	2	female	0.2	ND	ND	ND	0.2
18	control	96	2	female	ND	ND	ND	ND	ND
19	control	73	1	male	ND	ND	ND	ND	ND
20	control	89	2	female	ND	ND	ND	ND	ND

<sup>a</sup>ND < 0.1 pmol/mg.

(A) SRM chromatogram ( $m/z$  989.6  $\rightarrow$   $m/z$  637.0/678.9) for the isotope stable [<sup>15</sup>N]-labeled N-terminal peptide from A $\beta$ <sub>1-40</sub> (retention time (RT): 27.8 min). (B) SRM chromatogram ( $m/z$  989.6  $\rightarrow$   $m/z$  637.0/678.9) for the N-A $\beta$ <sub>1-5</sub> with L-Asp (RT: 27.8 min), D-Asp (RT: 23.6 min), L-isoAsp (RT: 24.3 min), and D-isoAsp (RT: 20.7 min). Concentration levels showed (Table 1) that the N-terminal A $\beta$  sequence in the AD and control brain tissues was calculated using the unit of picomoles per milligram of tissue.

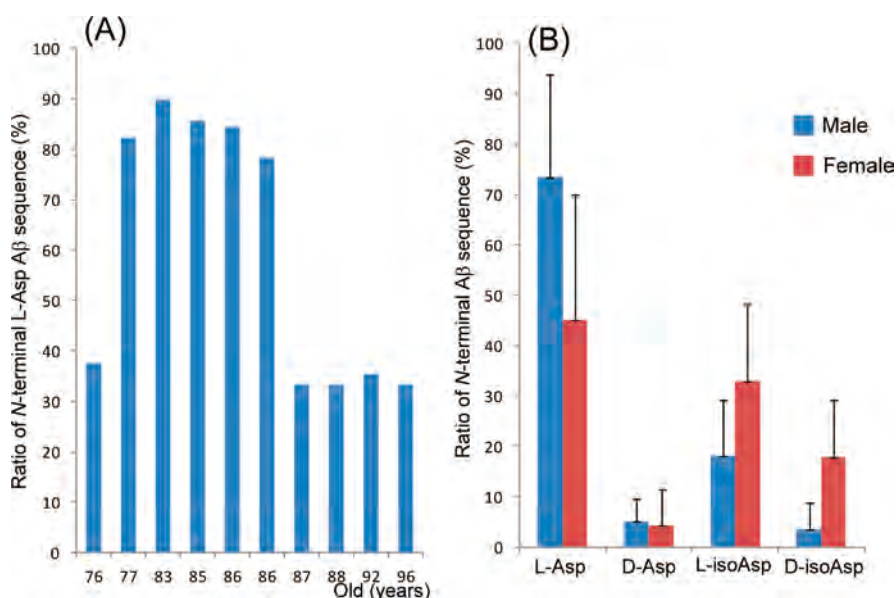
<sup>5</sup>SRM chromatograms of N-A $\beta$ <sub>1-5</sub> in brain tissue from AD patients.

that the diisomerized decapeptide (Asp at position 1 and 7) was used as an immunogen to generate polyclonal antibody 14 943 that recognizes the isomerized peptides preferentially when the peptide antigen structures are conserved during the enzyme-

linked immunoassay procedure.<sup>38</sup> They suggested a possible mechanism of the retention of the isomerized A $\beta$  peptide in the affected brains.<sup>38</sup> In addition, Iwatubo et al. used the six different antibodies that specifically recognize distinct N-terminal structures of A $\beta$  for suggesting that initial deposits in diffuse plaques begin with N-terminal A $\beta$  with or without structural modifications such as isomerization and racemization.<sup>8</sup> Future researchers would investigate the questions by examining the influence of different antibody epitopes and isotypes on plaque clearance and neuronal protection. In addition, the isotype of an antibody is important for either Fc- or complement-mediated phagocytosis of N-terminal A $\beta$  by microglial cells because antibody isotype defines its affinity for Fc receptors as well as its ability to activate complement for the design of antibodies with therapeutic potential.<sup>39</sup> Thus, the accurate analytical method should be used for the evaluation of antibody and binding effects of N-terminal A $\beta$  modifications in brain tissues. At the present stage, we cannot determine what is behind the emergence, pathological effects, elimination, and useful biomarkers of the post-translational AAR and AAI formation of the N-terminal A $\beta$  sequence for AD. On the basis of these data, we show for the first time that the N-A $\beta$ <sub>1-5</sub> levels in AD brain tissues were compared by a reliable CCD-UPLC-MS/MS method.

## CONCLUSIONS

In this study, the analytical assay to simultaneously analyze the AAR and AAI of N-terminal A $\beta$  sequence was developed and applied to monitoring the post-translational modified A $\beta$  in brain tissues from AD patients. Our CCD-UPLC-MS/MS assay of potential N-A $\beta$ <sub>1-5</sub> allowed for the discovery of the presence and ratio levels of these N-A $\beta$ <sub>1-5</sub> sequences with L-Asp, D-Asp, L-isoAsp, and D-isoAsp. Future work is needed so that the cause-and-effect sequence of the A $\beta$  aggregated events with AAR and AAI will be investigated using this assay.



(A) Pattern of aging difference for each AD patient ( $n = 10$ ). (B) Pattern of gender difference of average AD patient (male,  $n = 5$ , and female,  $n = 5$ ) for the decreased L-Asp. The detection levels of the N-terminal A $\beta$  sequence from AD patients of the predictable L-Asp of about  $59.0 \pm 26.0\%$  based on the D/L-iso/D-isoAsp ratio ( $4.8 \pm 5.7/25.4 \pm 15.0/10.8 \pm 11.2\%$ , AD patients,  $n = 10$ ) were observed.

<sup>c</sup>Pattern of the post-translational AAR and AAI formation of N-terminal A $\beta$  sequence for AD brain ( $n = 10$ ).

## ■ ASSOCIATED CONTENT

### Supporting Information

Additional information as noted in the text. This material is available free of charge via the Internet at <http://pubs.acs.org>.

## ■ AUTHOR INFORMATION

### Corresponding Author

\*E-mail: [toyooka@u-shizuoka-ken.ac.jp](mailto:toyooka@u-shizuoka-ken.ac.jp). Fax: +81 54 264 5593. Tel: +81 54 264 5656.

### Author Contributions

K.I., D.H., and N.M. carried out most of the analytical experiments. H.A. and Y.H. performed the pathological examination, and H.A. designed and supervised the clinical work for the AD patients. N.M. conducted biological discussion. K.T. prepared and suggested the peptide's synthesis. K.I., H.A., N.M., T.Y., and T.T. contributed to preparation of materials and provided advice on project planning and data interpretation. K.I. designed and supervised the project and wrote the manuscript.

### Notes

The authors declare no competing financial interests.

## ■ ACKNOWLEDGMENTS

This study was supported by grants from the Japanese Brain Bank Network for Neuroscience Research and the Ministry of Education, Culture, Sports, Science, and Technology of Japan. We thank Norihiro Ogawa, Takeshi Kanesaka, and Chie Taniguchi for technical assistance in the clinical and pathological study, and we thank all patients and relatives of patients for organ donation.

## ■ REFERENCES

- Walker, L. C.; LeVine, H., III *J. Biol. Chem.* **2012**, *287*, 33109–33115.
- Nikaido, T.; Austin, J.; Rinehart, R.; Trueb, L.; Hutchinson, J.; Stukenbrok, H.; Miles, B. *Arch. Neurol.* **1971**, *25*, 198–211.
- Allsop, D.; Landon, M.; Kidd, M. *Brain Res.* **1983**, *259*, 348–352.
- Glenner, G. G.; Wong, C. W. *Biochem. Biophys. Res. Commun.* **1984**, *120*, 885–890.
- Shapira, R.; Austin, G. E.; Mirra, S. S. *J. Neurochem.* **1988**, *50*, 69–74.
- Mori, H.; Ishii, K.; Tomiyama, T.; Furiya, Y.; Sahara, N.; Asano, S.; Endo, N.; Shirasawa, T.; Takio, K. *Tohoku J. Exp. Med.* **1994**, *174*, 251–262.
- Saido, T. C.; Yamao-Harigaya, W.; Iwatsubo, T.; Kawashima, S. *Neurosci. Lett.* **1996**, *215*, 173–176.
- Iwatsubo, T.; Saido, T. C.; Mann, D. M.; Lee, V. M.; Trojanowski, J. Q. *Am. J. Pathol.* **1996**, *149*, 1823–1830.
- Roher, A. E.; Lowenson, J. D.; Clarke, S.; Wolkow, C.; Wang, R.; Cotter, R. J.; Reardon, I. M.; Zürcher-Neely, H. A.; Heinrikson, R. L.; Ball, M. J.; Greenberg, B. D. *J. Biol. Chem.* **1993**, *268*, 3072–3083.
- Kuo, Y. M.; Emmerling, M. R.; Woods, A. S.; Cotter, R. J.; Roher, A. E. *Biochem. Biophys. Res. Commun.* **1997**, *237*, 188–191.
- Shimizu, T.; Watanabe, A.; Ogawara, M.; Mori, H.; Shirasawa, T. *Arch. Biochem. Biophys.* **2000**, *381*, 225–234.
- Shimizu, T.; Matsuoka, Y.; Shirasawa, T. *Biol. Pharm. Bull.* **2005**, *28*, 1590–1596.
- Lowenson, J. D.; Clarke, S. *J. Biol. Chem.* **1992**, *267*, 5985–5995.
- David, C. L.; Orpizewski, J.; Zhu, X. C.; Reissner, K. J.; Aswad, D. W. *J. Biol. Chem.* **1998**, *273*, 32063–32070.
- Böhme, L.; Hoffmann, T.; Manhart, S.; Wolf, R.; Demuth, H. U. *Biol. Chem.* **2008**, *389*, 1055–1066.
- Iida, T.; Matsunaga, H.; Santa, T.; Fukushima, T.; Homma, H.; Imai, K. *J. Chromatogr., A* **1998**, *813*, 267–275.
- Sohma, Y.; Yoshiya, T.; Taniguchi, A.; Kimura, T.; Hayashi, Y.; Kiso, Y. *Biopolymers* **2007**, *88*, 253–262.
- Sargaeva, N. P.; Lin, C.; O'Connor, P. B. *Anal. Chem.* **2009**, *81*, 9778–9786.
- Ni, W.; Dai, S.; Karger, B. L.; Zhou, Z. S. *Anal. Chem.* **2010**, *82*, 7485–7491.
- Krokhin, O. V.; Antonovici, M.; Ens, W.; Wilkins, J. A.; Standing, K. G. *Anal. Chem.* **2006**, *78*, 6645–6650.
- Güttler, B. H.; Cynis, H.; Seifert, F.; Ludwig, H. H.; Porzel, A.; Schilling, S. *Amino Acids* **2013**, *44*, 1205–1214.
- Inoue, K.; Garner, C.; Ackermann, B. L.; Oe, T.; Blair, I. A. *Rapid Commun. Mass Spectrom.* **2006**, *20*, 911–918.
- Inoue, K.; Kaneko, M.; Hino, T.; Oka, H. *J. Agric. Food Chem.* **2010**, *58*, 9413–9417.

- (24) Akatsu, H. *Brain Nerve* **2010**, *62*, 1043–1052.
- (25) Inoue, K.; Tsutsui, H.; Akatsu, H.; Hashizume, Y.; Matsukawa, N.; Yamamoto, T.; Toyo'oka, T. *Sci. Rep.* **2013**, *3*, 2364.
- (26) Haque, A.; Banik, N. L.; Ray, S. K. *Drug Targets* **2008**, *7*, 270–277.
- (27) Hook, V.; Hook, G.; Kindy, M. *Biol. Chem.* **2010**, *391*, 861–872.
- (28) Jawhar, S.; Wirths, O.; Bayer, T. A. *J. Biol. Chem.* **2011**, *286*, 38825–38832.
- (29) Sakai-Kato, K.; Naito, M.; Utsunomiya-Tate, N. *Biochem. Biophys. Res. Commun.* **2007**, *364*, 464–469.
- (30) Tsutsui, H.; Mochizuki, T.; Maeda, T.; Noge, I.; Kitagawa, Y.; Min, J. Z.; Todoroki, K.; Inoue, K.; Toyo'oka, T. *Anal. Bioanal. Chem.* **2012**, *404*, 1925–1934.
- (31) Tsutsui, H.; Fujii, S.; Sakamoto, T.; Min, J. Z.; Todoroki, K.; Toyo'oka, T. *J. Sep. Sci.* **2012**, *35*, 1551–1559.
- (32) Inoue, K.; Prayoonhan, N.; Tsutsui, H.; Sakamoto, T.; Nishimura, M.; Toyo'oka, T. *J. Sep. Sci.* **2013**, *36*, 1356–1361.
- (33) van Helmond, Z.; Heesom, K.; Love, S. J. *Neurosci. Methods* **2009**, *176*, 206–212.
- (34) Youmans, K. L.; Leung, S.; Zhang, J.; Maus, E.; Baysac, K.; Bu, G.; Vassar, R.; Yu, C.; LaDu, M. J. *J. Neurosci. Methods* **2011**, *196*, 51–59.
- (35) Delacourte, A.; Sergeant, N.; Champain, D.; Wattez, A.; Maurage, C. A.; Lebert, F.; Pasquier, F.; David, J. P. *Neurology* **2002**, *59*, 398–407.
- (36) Izco, M.; Pesini, P.; Pérez-Grijalba, V.; Fandos, N.; Sarasa, M. J. *Alzheimer's Dis.* **2013**, *34*, 835–839.
- (37) Lame, M. E.; Chambers, E. E.; Blatnik, M. *Anal. Biochem.* **2011**, *419*, 133–139.
- (38) Szendrei, G. I.; Prammer, K. V.; Vasko, M.; Lee, V. M.; Otvos, L., Jr. *Int. J. Pept. Protein Res.* **1996**, *47*, 289–296.
- (39) Bard, F.; Barbour, R.; Cannon, C.; Carretto, R.; Fox, M.; Games, D.; Guido, T.; Hoenow, K.; Hu, K.; Johnson-Wood, K.; Khan, K.; Kholodenko, D.; Lee, C.; Lee, M.; Motter, R.; Nguyen, M.; Reed, A.; Schenk, D.; Tang, P.; Vasquez, N.; Seubert, P.; Yednock, T. *Proc. Natl. Acad. Sci. U.S.A.* **2003**, *100*, 2023–2028.

# Simultaneous Determination of Trigonelline, Caffeine, Chlorogenic Acid and Their Related Compounds in Instant Coffee Samples by HPLC Using an Acidic Mobile Phase Containing Octanesulfonate

Kana ARAI,\*<sup>1</sup> Hiroyuki TERASHIMA,\*<sup>2</sup> Sen-ichi AIZAWA,\*<sup>3</sup> Atsushi TAGA,\*<sup>4</sup> Atsushi YAMAMOTO,\*<sup>5</sup> Kaname TSUTSUMIUCHI,\*<sup>5</sup> and Shuji KODAMA\*<sup>1†</sup>

\*<sup>1</sup> School of Science, Tokai University, 4-1-1 Kitakaname, Hiratsuka, Kanagawa 259-1292, Japan

\*<sup>2</sup> GL Sciences Inc., 6-22-1 Nishishinjuku, Shinjuku, Tokyo 163-1130, Japan

\*<sup>3</sup> Graduate School of Science and Engineering, University of Toyama, 3190 Gofuku, Toyama 930-8555, Japan

\*<sup>4</sup> Faculty of Pharmacy, Kinki University, 3-4-1 Kowakae, Higashi-Osaka 577-8502, Japan

\*<sup>5</sup> Department of Biological Chemistry, College of Bioscience and Biotechnology, Chubu University, 1200 Matsumoto-cho, Kasugai, Aichi 487-8501, Japan

In order to analyze trigonelline, caffeine, chlorogenic acid, and their related compounds simultaneously, an HPLC method using an InertSustain C18 column and a mobile phase containing octanesulfonate as an ion-pairing reagent under an acidic condition was developed. The optimum mobile phase conditions were determined to be 0.1% phosphoric acid, 4 mM octanesulfonate, and 15% methanol at 35°C. Using the proposed method, trigonelline, nicotinic acid, caffeine, theophylline, chlorogenic acid, and caffeic acid in ten instant coffee samples were analyzed. These analytes except for theophylline were detected in all samples. An increase in the caffeine content in instant coffee samples tended to decrease in both trigonelline and chlorogenic acid contents, and the trigonelline content was found to be correlated well with the chlorogenic acid content ( $R^2 = 0.887$ ).

**Keywords** Instant coffee, trigonelline, caffeine, chlorogenic acid, HPLC

(Received April 23, 2015; Accepted May 13, 2015; Published August 10, 2015)

## Introduction

Coffee, a popular beverage all over the world, has characteristic taste and aroma. Typical compounds in coffee, such as caffeine, trigonelline and chlorogenic acid, are known to influence coffee flavor, contributing to the acidity and conferring astringency and bitterness.<sup>1,2</sup> These compounds are known to be biologically active as reviewed.<sup>3-7</sup> Caffeine, an alkaloid, stimulates the central nervous system, heart rate and respiration. Chlorogenic acid exhibits various biological properties including anti-bacterial, anti-oxidant and anti-carcinogenic activities, particularly hypoglycemic and hypolipidemic effects. Chlorogenic acids are a family of esters formed between caffeic acid and (–)-quinic acid. According to Clifford,<sup>8</sup> using the preferred IUPAC numbering,<sup>9</sup> chlorogenic acid is generally referred to as 5-caffeoylquinic acid, while it is still often called chlorogenic acid or 3-caffeoylquinic acid (pre-IUPAC numbering). Trigonelline, which is derived from the methylation of the nitrogen atom of nicotinic acid, has hypoglycemic, hypolipidemic, sedative, anti-migraine, anti-bacterial, anti-viral and anti-tumor effects, and potency to improve memory

retention and inhibit platelet aggregation.

Two coffee tree species are distributed worldwide. *Coffea arabica* (Arabica) and *Coffea canephora* (commonly known as Robusta) are adapted to very different ecological environments, which may cause different taste and aroma. Arabica, with its lower bitterness and better flavor, is more appreciated by consumers, and its cost is higher than that of Robusta. Some chemicals in coffee such as sucrose and trigonelline, give appreciated flavor, while other chemicals such as chlorogenic acid and caffeine increase bitterness.<sup>10,11</sup> To evaluate the quality of coffee commodities from chemical constituents and their contents, sensitive, precise, and accurate analytical means are required for determining these chemicals.<sup>12</sup>

A number of investigations for the determination of components in coffee, including caffeine, chlorogenic acids, and/or trigonelline, have been conducted by high-performance liquid chromatography (HPLC) as reviewed.<sup>12-14</sup> Casal *et al.* reported that two coffee species, Arabica and Robusta, could be clearly distinguished by their trigonelline and caffeine contents,<sup>15</sup> but that neither trigonelline nor caffeine could be used to identify the geographical origin of the roasted coffee. Ky *et al.* reported higher trigonelline and sucrose contents in Arabica and higher chlorogenic acid and caffeine contents in Robusta.<sup>10</sup> The roasting process is also one of the important factors concerning the characteristic flavor and the final quality of coffee. The key

† To whom correspondence should be addressed.

E-mail: kodama@tokai-u.jp

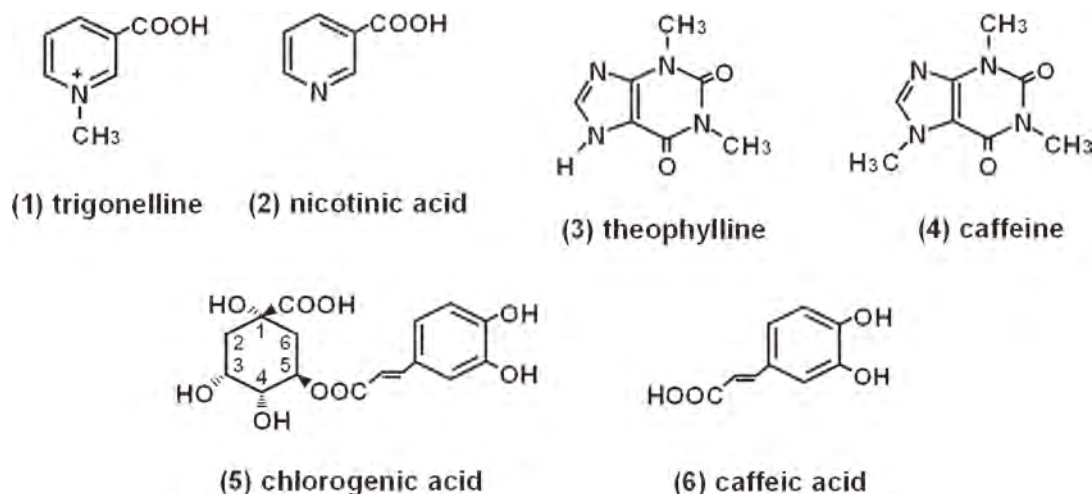


Fig. 1 Structural formulas of trigonelline, caffeine, chlorogenic acid, and their related compounds.

substances are subjected to chemical changes in this process.<sup>16</sup> For example, green coffee beans contain high levels of chlorogenic acids in their composition, while these levels were drastically reduced during roasting.<sup>17</sup> The loss of trigonelline was strongly dependent upon the degree of roasting and was associated with the formation of nicotinic acid, but caffeine levels were decreased only slightly.<sup>18</sup> Considerable stability of caffeine during roasting was also shown for both Arabica and Robusta samples by Bicho *et al.*<sup>19</sup>

The simultaneous determination of these compounds can be useful for the quality control of raw coffee beans and monitoring of coffee roasting conditions.<sup>20</sup> However, the three typical compounds (trigonelline, caffeine, and chlorogenic acid) in coffee have not been determined at the same time by one HPLC method. For example, trigonelline and caffeine were simultaneously analyzed, while chlorogenic acid was separately analyzed by another HPLC method.<sup>10,19,21</sup> Rodrigues and Bragagnolo used an HPLC method for the determination of caffeine and chlorogenic acids, and another HPLC method for determining trigonelline, nicotinic acid, 5-hydroxymethylfurfural, theobromine and theophylline.<sup>22</sup> De Maria *et al.* reported a simultaneous determination of trigonelline, caffeine, and total chlorogenic acid, in green coffee samples by high-performance gel filtration chromatography<sup>23</sup> other than reversed phase HPLC. The aim of the present study was to develop a method for the simultaneous analysis of trigonelline, caffeine, chlorogenic acid, and their related compounds (nicotinic acid, theophylline, and caffeic acid, as shown in Fig. 1) in instant coffee samples by a reversed phase HPLC using a mobile phase containing octanesulfonate as an ion-pairing agent under an acidic condition.

## Experimental

### Reagents and chemicals

Trigonelline hydrochloride, theophylline, chlorogenic acid hydrate, and sodium 1-octanesulfonate were obtained from Tokyo Kasei (Tokyo, Japan). Methanol was from Kanto (Tokyo, Japan). Nicotinic acid, caffeic acid, caffeine, and other chemicals (analytical grade) were obtained from Wako Pure Chemicals (Osaka, Japan).

### HPLC apparatus and chromatographic conditions

The HPLC system consisted of a Jasco (Tokyo, Japan) Model PU-2080 pump, a Jasco Model UV-2075 detector, a Rheodyne (Cotati, CA) manual injector, a Shimadzu (Kyoto, Japan) Model CTO-10A column oven, and a Shimadzu Model DGU-14A degasser. An InertSustain C18 column (4.6 mm i.d. × 150 mm, GL Sciences, Tokyo, Japan) was used. A mobile phase consisted of 0.1% phosphoric acid, 4 mM octanesulfonate, and 15% methanol. Elution was carried out at a flow rate of 1.0 mL/min at 35°C. Analytes were detected at 220 nm. Data acquisition and processing were conducted with a Chromato-PRO (Runtime Instruments Co., Kanagawa, Japan).

### Standard solution and sample preparation

Stock solutions (10 mM) of trigonelline, nicotinic acid, caffeine, theophylline, chlorogenic acid, and caffeic acid were separately prepared with purified water or 20% acetonitrile. Nine brands of instant coffee, one brand of decaffeinated instant coffee and one brand of regular coffee were purchased from a local market. Analytes in these instant coffee samples (0.0500 g) were extracted with ultrasonication in 10 mL of 15% methanol at 43 kHz for 5 min at room temperature. Then, the mixture was centrifuged at approximately 1200g for 5 min and the supernatant was filtered with 0.45 μm filter and was analyzed by the HPLC method.

### Preparation of 3-, 4-, and 5-caffeoylquinic acids

Commercial regular coffee (10 g) was added to 100 mL of hot purified water at 80°C. After stirring for one minute, the mixture was centrifuged at approximately 1200g for 5 min. The supernatant was filtered with 0.45 μm filter and was applied to HPLC described by Tfouni *et al.*<sup>16</sup> with minor corrections, using an InertSustain C18 column thermostated at 40°C. A mobile phase consisted of 0.1% phosphoric acid and 20% acetonitrile. Elution was carried out at a flow rate of 1.0 mL/min and analytes were detected at 320 nm. Three fractions, corresponding to the 3-, 4-, and 5-caffeoylquinic acids, were separately collected.

## Results and Discussion

### Factors affecting separation

Among the six analytes in Fig. 1, the purine related compounds, caffeine and theophylline, were retained by the ODS column and could be analyzed by reversed phase HPLC using neutral mobile phases. When the acidic mobile phase was used, chlorogenic and caffeic acids were easily analyzed by reversed phase HPLC,<sup>16,22,24-26</sup> because their protonated forms are neutral. However, trigonelline and nicotinic acid, which are cationic in an acidic medium and zwitterionic and anionic, respectively, in neutral or alkaline media, are difficult to be analyzed under any pH conditions. We examined the retention behaviours of trigonelline and nicotinic acid using HPLC with an InertSustain C18 column and a mobile phase containing 0.1% phosphoric acid and 15% methanol. As a result, trigonelline and nicotinic acid were detected at 1.6 and 2.1 min, respectively. This result were almost the same compared to previous reports,<sup>10,19,21</sup> showing that these zwitterionic compounds were difficult to be retained by an ODS column with an acidic mobile phase. The ionic nature of the analyte is suppressed by association with an ion-pair reagent of the opposite charge. The resulting uncharged ion-pair interacts with a non-polar stationary phase. HPLC with a mobile phase containing the ion-pair reagent (known as ion-pair chromatography) can be used for the simultaneous determination of both ionic and neutral compounds. Ion-pair chromatography is versatile and offers more possibilities for changing the stationary and/or mobile phase parameters.<sup>27</sup> Waksmundzka-Hajons<sup>28</sup> and Cecchi<sup>29</sup> have discussed the retention mechanism of ion-pair chromatography in detail. It was shown that the addition of C7-C9 alkylsulfonates to a mobile phase at concentrations over the range of ~1-10 mM can provide the separation of compounds having amino groups.<sup>30</sup> Octanesulfonate, a C8 alkylsulfonate, as an ion-pair reagent has been widely used for the analysis of basic and zwitterionic compounds in foods and other real samples.<sup>31-35</sup>

In order to analyze all analytes by using a reversed HPLC method, we added octanesulfonate to the acidic mobile phase as an ion-pairing reagent for the cationic analytes. The effect of the octanesulfonate concentration (2-8 mM) on the retention times of analytes was evaluated (Fig. 2). An increase in the octanesulfonate concentration brought about increases in the retention times of both trigonelline and nicotinic acid. However, the retention times of the other four analytes were gradually decreased with increasing the octanesulfonate concentration. These facts suggest that the hydrophobic interaction between neutral analytes and the C18 group on the column were weakened by adding octanesulfonate having a hydrophobic alkyl group, while ion-pairing between the cationic analytes and the sulfonate group could promote the interaction between the analytes and the hydrophobic ODS column. The 4 mM octanesulfonate concentration was adopted for the simultaneous separation of all analytes considering the separation of the positional isomers of coffeoylquinic acid and other contaminants contained in the instant coffee samples (*vide infra*).

By increasing the methanol concentration (10-25%), the retention times of all the analytes in the acidic mobile phases decreased, where the degree of the effect of methanol pronouncedly depends on the analytes. The methanol concentration was fixed at 15% for the simultaneous separation of all the analyte considering a moderately short retention time and the separation of the positional isomers of coffeoylquinic acid and other contaminants contained in the instant coffee

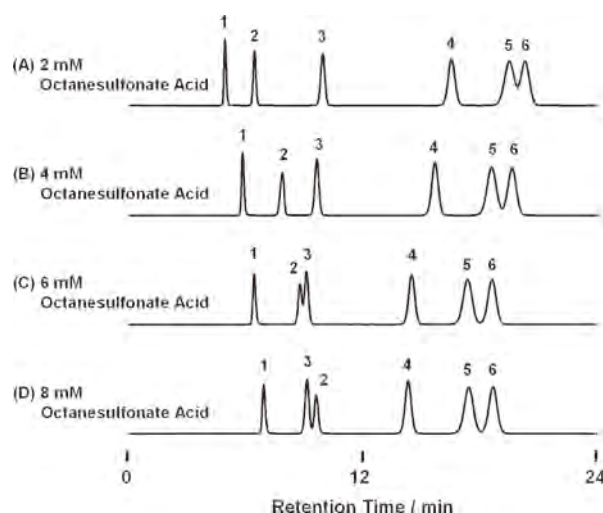


Fig. 2 Effect of the octanesulfonate concentration on the separation of six analytes. HPLC was done by using an InertSustain C18 column and mobile phases consisting of 0.1% phosphoric acid, 2-8 mM octanesulfonate, and 15% methanol. 1, trigonelline; 2, nicotinic acid; 3, theophylline; 4, caffeine; 5, chlorogenic acid; 6, caffeic acid.

samples (*vide infra*). Therefore, the optimum mobile phase conditions were determined to be 0.1% phosphoric acid, 4 mM octanesulfonate, 15% methanol at 35°C.

### Analysis of instant coffee samples

Six analytes were subjected to the HPLC method using the above optimum conditions. The detection limit, defined as a signal-to-noise ratio of 3, was 0.3  $\mu\text{M}$  for all analytes. Linearity ( $R^2 > 0.992$ ) was demonstrated in the range of 1  $\mu\text{M}$  - 3 mM for the standard curves of all the analytes. Good reproducibilities of the peak areas (RSD < 0.6%) and the migration times (RSD < 0.13%) were obtained by five consecutive determinations at 1 mM for all six analytes. Recoveries were between 96.5 and 100.1%.

Roasting is a time-dependent process, whereby chemical changes are induced in the coffee beans.<sup>17</sup> Bicho *et al.* reported that the caffeine contents did not vary significantly with the roasting degree for the Arabica and Robusta samples, revealing a considerable stability during roasting.<sup>19</sup> However, the trigonelline contents in both coffees decreased significantly with the roasting intensity and the levels of chlorogenic acids remained higher in Robusta coffee beans, but decreased sharply with the roasting intensity. Rodrigues *et al.* reported that regular roasted ground coffee brews showed higher contents of chlorogenic acids, chlorogenic acid lactones, trigonelline, nicotinic acid, caffeine, and theobromine than regular soluble coffee brews.<sup>22</sup> In this work, trigonelline, nicotinic acid, theophylline, caffeine, chlorogenic acid, and caffeic acid in ten instant coffee samples were analyzed by using the proposed HPLC method (Table 1) and a representative chromatogram is shown in Fig. 3B. The amounts of trigonelline, caffeine, and chlorogenic acid in sample A\* extracted with hot water were almost the same as those in sample A extracted with 15% methanol using ultrasonication at 43 kHz for 5 min. The amounts of nicotinic acid and caffeic acid in sample A were higher than those in sample A\*. Thus, analytes in samples A - J were extracted with 15% methanol. The caffeine levels in samples A - I ranged from 28.8 to 35.0 mg/g, while caffeine level in decaffeinated sample J was understandably only

Table 1 The amounts of coffee components in instant coffee samples (mg g<sup>-1</sup>)

Instant coffee	Trigonelline	Nicotinic acid	Theophylline	Caffeine	Chlorogenic acid	Caffeic acid
A*	4.78 ± 0.01	0.0474 ± 0.0041	ND	33.8 ± 0.1	4.24 ± 0.03	0.0567 ± 0.00376
A	4.68 ± 0.04	0.294 ± 0.001	ND	32.5 ± 0.1	4.39 ± 0.04	0.102 ± 0.001
B	4.72 ± 0.04	0.292 ± 0.001	ND	35.0 ± 0.1	4.52 ± 0.04	0.0879 ± 0.0001
C	3.02 ± 0.02	0.364 ± 0.001	ND	34.7 ± 0.2	2.65 ± 0.01	0.107 ± 0.003
D	6.71 ± 0.06	0.315 ± 0.005	ND	34.6 ± 0.2	10.6 ± 0.1	0.168 ± 0.003
E	6.94 ± 0.07	0.339 ± 0.007	ND	34.1 ± 0.2	8.14 ± 0.16	0.0489 ± 0.0017
F	7.06 ± 0.08	0.300 ± 0.001	ND	31.7 ± 0.6	9.45 ± 0.07	0.0734 ± 0.0013
G	7.59 ± 0.09	0.233 ± 0.004	ND	32.8 ± 0.3	9.10 ± 0.009	0.0644 ± 0.0039
H	7.73 ± 0.08	0.391 ± 0.001	ND	32.2 ± 0.3	9.81 ± 0.22	0.316 ± 0.011
I	9.76 ± 0.13	0.531 ± 0.022	ND	28.8 ± 0.3	11.6 ± 0.3	0.161 ± 0.006
J	6.67 ± 0.05	0.327 ± 0.005	ND	0.947 ± 0.010	9.43 ± 0.08	0.232 ± 0.013

Analytes in instant coffee samples were extracted with 15% methanol (A - J) or hot water (A\*).

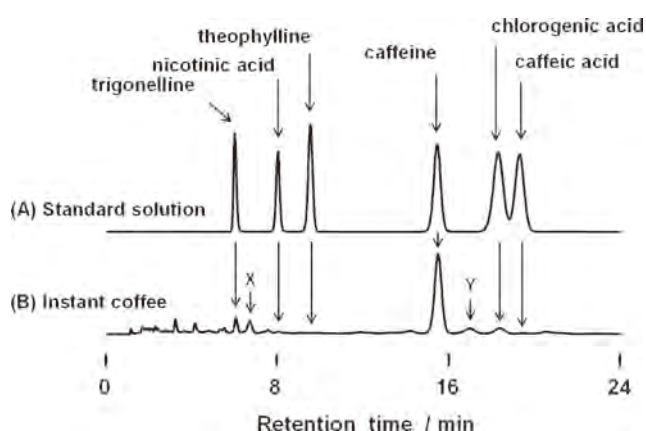


Fig. 3 Chromatograms of standard solution (A) and instant coffee sample (B). An instant coffee (0.0500 g) was dissolved by 15% methanol (10 mL). HPLC was done by using an InertSustain C18 column and mobile phases consisting of 0.1% phosphoric acid, 4 mM octanesulfonate, and 15% methanol. Analytes were detected at 220 nm.

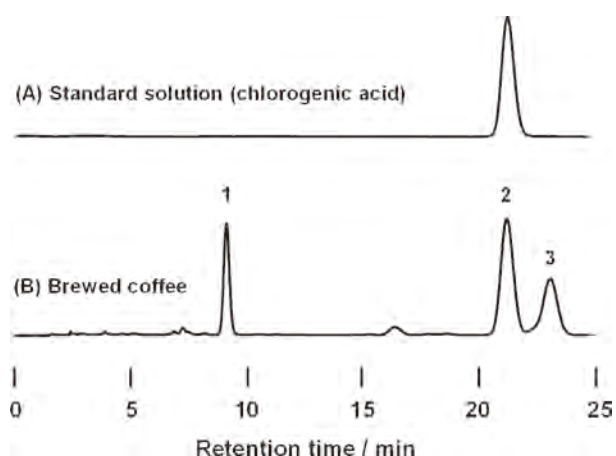


Fig. 4 Chromatograms of standard solution of chlorogenic acid (A) and brewed regular coffee (B). A regular coffee (10 g) was added to 100 mL of hot purified water (80°C). HPLC was done by using an InertSustain C18 column and mobile phases consisting of 0.1% phosphoric acid, 4 mM octanesulfonate, and 15% methanol. Analytes were detected at 320 nm. 1, 3-caffeoylquinic acid; 2, 5-caffeoylquinic acid; 3, 4-caffeoylquinic acid.

0.947 mg/g. It seems that those samples with higher concentrations of caffeine tend to have lower concentrations of trigonelline and chlorogenic acid. However, the trigonelline levels in samples A - I were found to be correlated well with the concentration of chlorogenic acid. The regression equation for the relationship between the amounts of trigonelline ( $x$ ) and chlorogenic acid ( $y$ ) was expressed as  $y = 1.48x - 1.74$  with a correlation coefficient ( $R^2$ ) of 0.887. Further studies are needed to clarify whether this correspondence resulted in coffee varieties, roasting processes and/or manufacturing process of instant coffee.

When instant coffee samples were analyzed by the proposed method with UV detection at 320 nm instead of at 220 nm, two peaks X and Y as well as a peak of chlorogenic acid, which were detected at 220 nm in Fig. 3B, were also detected at 320 nm. Chlorogenic acids are a family of esters formed between caffeic acid and (-)-quinic acid, which is referred to 5-caffeoylquinic acid. The three positional isomers of *mono*-caffeoylquinic acids, 3-, 4-, and 5-caffeoylquinic acid, were contained in regular coffee, where the isomer contents were increased in this order.<sup>19,25</sup> In order to assign the peaks X and Y in Fig. 3B, the three isomers of *mono*-caffeoylquinic acids were prepared by a similar method reported by Tfouni *et al.*,<sup>16</sup> as stated above. The chromatographic pattern in Fig. 4B was almost the same as that by Tfouni *et al.*,<sup>16</sup> and the three major peaks 1, 2, and 3 corresponded to 3-, 5-, and 4-caffeoylquinic acids, respectively. These three fractions were separately collected and each of those was applied to the proposed HPLC method. As a result, peaks X and Y were found to be peaks for 3- and 4-caffeoylquinic acids, respectively.

In conclusion, trigonelline, caffeine, chlorogenic acid, and their related compounds were simultaneously analyzed by the HPLC method using octanesulfonate as the ion-pairing reagent under an acidic condition. These analytes in instant coffee samples could be analyzed using the proposed HPLC method. As a result, the amounts of trigonelline and chlorogenic acid in instant coffee samples were found to be correlated well to each other.

## References

1. K. L. Johnston, M. N. Clifford, and L. M. Morgan, *Am. J. Clin. Nutr.*, **2003**, *78*, 728.
2. H. Liu, J. Shao, Q. Li, Y. Li, H. M. Yan, and L. He, *J. AOAC Int.*, **2012**, *95*, 1138.
3. S. Meng, J. Cao, Q. Feng, J. Peng, and Y. Hu, *Evidence-Based Complementary Altern. Med.*, **2013**, 801457.

4. E. Fuentes and I. Palomo, *Vasc. Pharmacol.*, **2014**, *63*, 155.
5. R. Upadhyay and L. J. M. Rao, *Crit. Rev. Food Sci. Nutr.*, **2013**, *53*, 968.
6. J. Zhou, L. Chan, and S. Zhou, *Curr. Med. Chem.*, **2012**, *19*, 3523.
7. I. A. Ludwig, M. N. Clifford, M. E. J. Lean, H. Ashihara, and A. Crozier, *Food Funct.*, **2014**, *5*, 1695.
8. M. N. Clifford, *J. Sci. Food Agric.*, **2000**, *80*, 1033.
9. IUPAC, Nomenclature of cyclitols, *Biochem. J.*, **1976**, *153*, 23.
10. C.-L. Ky, J. Louarn, S. Dussert, B. Guyot, S. Hamon, and M. Noirot, *Food Chem.*, **2001**, *75*, 223.
11. C. A. B. De Maria, L. C. Trugo, F. R. Aquino Neto, R. F. A. Moreira, and C. S. Alviano, *Food Chem.*, **1996**, *55*, 203.
12. A. A. Nuhu, *ISRN Nutr.*, **2014**, 384230.
13. A. Belay, *Int. J. Phys. Sci.*, **2011**, *6*, 6373.
14. P. N. Patil, *Int. J. Pharm. Sci. Rev. Res.*, **2012**, *12*, 76.
15. S. Casal, M. B. P. P. Oliveira, M. R. Alves, and M. A. Ferreira, *J. Agric. Food Chem.*, **2000**, *48*, 3420.
16. S. A. V. Tfouni, L. B. Carreiro, C. R. A. Teles, R. P. Z. Furlani, K. M. V. A. B. Cipolli, and M. C. R. Camargo, *Int. J. Food Sci. Technol.*, **2014**, *49*, 747.
17. A. Farah, T. Paulis, L. C. Trugo, and P. R. Martin, *J. Agric. Food Chem.*, **2005**, *53*, 1505.
18. S. Casal, M. B. Oliveira, and M. A. Ferreira, *Food Chem.*, **2000**, *68*, 481.
19. N. C. Bicho, A. E. Leitao, J. C. Ramalho, and F. C. Lidon, *Eur. Food Res. Technol.*, **2011**, *233*, 303.
20. D. Perrone, C. M. Donangelo, and A. Farah, *Food Chem.*, **2008**, *110*, 1030.
21. L. Maeztu, S. Andueza, C. Ibanez, Paz de Pena, J. Bello, and C. Cid, *J. Agric. Food Chem.*, **2001**, *49*, 4743.
22. N. P. Rodrigues and N. Bragagnolo, *J. Food Composit. Anal.*, **2013**, *32*, 105.
23. C. A. B. De Maria, L. C. Trugo, R. F. A. Moreira, and M. Petracco, *Food Chem.*, **1995**, *52*, 447.
24. N. Manchon, L. Mateo-Vivaracho, M. Darrigo, G. Lafuente, E. Guillamon, A. Villares, and M. A. Rostagno, *Czech. J. Food Sci.*, **2013**, *31*, 483.
25. K. Fujioka and T. Shibamoto, *Food Chem.*, **2008**, *106*, 217.
26. G. Budryn, E. Nebesny, A. Podsedek, D. Zyzelewicz, M. Materska, S. Jankowski, and B. Janda, *Eur. Food Res. Technol.*, **2009**, *228*, 913.
27. A. D. Smolenkov and O. A. Shpigun, *Talanta*, **2012**, *102*, 93.
28. M. Waksmundzka-Hajnos, *J. Chromatogr. B*, **1998**, *717*, 93.
29. T. Cecchi, *J. Liq. Chromatogr. Relat. Technol.*, **2015**, *38*, 404.
30. A. D. Amolenkov, S. A. Ponomarenko, and O. A. Shpigun, *Russ. J. Chem. A*, **2009**, *83*, 478.
31. M. Yasuda, T. Ota, A. Morikawa, K. Mawatari, T. Fukuuchi, N. Yamaoka, K. Kaneko, and K. Nakagomi, *J. Chromatogr. B*, **2013**, *934*, 41.
32. N. Kumar and D. Sangeetha, *J. Liq. Chromatogr. Relat. Technol.*, **2013**, *36*, 1835.
33. R. Ando, Y. Makino, T. Tamura, N. Yamamoto, R. Nishigaki, T. Kimura, N. Yokote, and H. Yamamoto, *Biomed. Chromatogr.*, **2010**, *24*, 301.
34. P. Garcia del Morala, M. J. Arina, J. A. Resinesb, and M. T. Diez, *J. Chromatogr. B*, **2007**, *855*, 276.
35. T. Lavizzari, M. T. Veciana-Nogues, S. Bover-Cid, A. Marine-Font, and M. C. Vidal-Carou, *J. Chromatogr. A*, **2006**, *1129*, 67.

Phase I clinical study of a new hyperthermia therapy using a capacitive heating device and magnetic nanoparticles in castration-resistant prostate cancer

Noriyasu Kawai<sup>1</sup>, Takeshi Kobayashi<sup>2</sup>, Daichi Kobayashi<sup>1</sup>, Kaname Tsutsumiuchi<sup>3</sup>, Keitaro Iida<sup>1</sup>, Toshiaki Etani<sup>1</sup>, Taku Naiki<sup>1</sup>, Ryosuke Ando<sup>1</sup>, Kentaro Mizuno<sup>1</sup>, Aisushi Okada<sup>1</sup>, Keiichi Tozawa<sup>1</sup>, Takahiro yasui<sup>1</sup>

1. Department of Nephro-urology, Nagoya City University Graduate School of Medical Sciences
2. Research Institute for Biological Function, College of Bioscience and Biotechnology, Chubu University
3. Department of Biological Chemistry, College of Bioscience and Biotechnology, Chubu University

Corresponding author

Noriyasu Kawai, MD, Ph.D.

Department of Nephro-urology, Nagoya-City University Graduate School of Medical Sciences.

1 Kawasumi, Mizuho-cho, Mizuho-ku, Nagoya, 467-8601, Japan

Tel: +81 528538266; Fax: +81 528523179; E-mail: n-kawai@med.nagoya-cu.ac.jp

**Abstract**

**Purpose:** Magnetites (iron oxide nanoparticles in Fe<sub>3</sub>O<sub>4</sub>) coated with positively charged liposomes are called as magnetic cationic liposomes (MCL). MCLs used in an 8-MHz radiofrequency (RF) capacitive heating device can increase the temperature of a specific site to up to 45°C. The aim of this study was to evaluate the safety of regional 8-MHz RF capacitive hyperthermia combined with MCL in castration-resistant prostate cancer (CRPC) patients.

**Materials and methods:** Three CRPC patients resistant to standard cancer therapy were enrolled in this study. The patients were injected with 0.5 ml MCL containing Fe (30 mg/ml) into the prostate, followed by the application of heat using an 8 MHz RF capacitive heating device. The primary end point was the presence or absence, as well as the degree of adverse events. The secondary end point was to obtain preliminary efficacy data.

**Results:** The temperature of the tumor was increased by more than 2°C following MCL injection when compared with the RF-8 treatment alone. No severe adverse events were noted in the prostate, rectum, or the bladder. IL-6 levels were increased in the tissues.

**Conclusion:** The present study confirms the safety of regional 8-MHz RF capacitive hyperthermia combined with MCL.

**Keywords:** prostate cancer, hyperthermia, magnetic cationic liposome, alternating magnetic field

**Introduction**

The incidence of prostate cancer, the most frequently diagnosed malignancy in

Western males, is increasing rapidly in Japan [1-4]. It has the highest morbidity and second-highest mortality rates among most male malignancies, and the rate of detection of this cancer has increased remarkably, especially during the early phase, due to the discovery and spread of the prostate-specific antigen (PSA), specific for the prostate gland [5]. Hormone therapy is the first choice of treatment in cases presenting with distant metastasis at the time of diagnosis. However, although extremely effective at first, most prostate cancer patients eventually develop resistance to the treatment. The taxane-based anticancer drug docetaxel was proven to be effective for the treatment of castration-resistant prostate cancer (CRPC), and was expected to have a prolonged prognosis. But, resistance to the drug led to its ineffectiveness against castration-resistant prostate cancer.

Therapeutic treatments for relapsed prostate cancer following the ineffectiveness of docetaxel include anti-androgenic drugs, (abiraterone, enzalutamid), anticancer drugs (cabazitaxel), bone metastases therapeutic drugs, immunotherapy, and radiotherapy. However, these medications extend the progression-free survival of the patients up to a period of three months only. Besides, it is important to consider the quality of life of the cancer patient during treatment planning.

The common treatments of prostate cancer include surgery, radiation and medication (anticancer drugs). Nonetheless, the tumors become resistant to these treatments resulting in their recurrence. On the other hand, hyperthermia, a less popular form of cancer treatment, is based on the principle that mammalian cells perish at a temperature of 42.5°C or more. The efficacy of hyperthermia has been seen in several cancer patients during the clinical phase. The capacitive heating method is the most common type of hyperthermia therapy provided in Japan. This method involves the picking up of the tumor between two electrodes and running a radiofrequency (RF) wave

(approximately 10 MHz) through it. Based on this principle of hyperthermia, excellent therapeutic effects of the combination of chemotherapy and hyperthermia, for malignant tumors (e.g. osteosarcoma and liver cancer), have been reported by our university [6,7]. Whereas microwave warming is mainly limited to the warming of the superficial areas of the tumor, the RF wave is useful for the treatment of deep seated tumors. In capacitive hyperthermia, normal tissue surrounding the tumor is also warmed by the electrodes. The specific adsorption rate of electric energy is dependent on the electrical properties of the tissue such as, permittivity and electric resistance. Since there are no significant differences in the electrical properties between the tumor and the surrounding normal tissues, it is difficult to heat only the tumor tissues during this treatment. Therefore, in order to prevent excessive heating of normal tissues, "mild" heating conditions (< 40°C) are often applied leading to insufficient heating of the tumor, thereby resulting in incomplete tumor suppression. Hence, for these reasons hyperthermia is less popular when compared to the other methods used for the treatment of cancer.

Iron oxide nanoparticles expressed in  $Fe_3O_4$  are called magnetite. Magnetite generates heat with irradiation of the alternating magnetic field (AMF). The hyperthermia using magnetite and AMF is called as magnetic nanoparticle (MNP) mediated hyperthermia (MNHT). MNHT treatment consists of two major technical approaches: the first is to accumulate MNPs into the tumor tissue, and the second is to apply an AMF in order to generate local heat through the nanoparticles. The application of MNHT uniformly increases the temperature of the tumor tissue to above 43°C, and is different from the capacitive heating method commonly used in Japan.

We developed the magnetic cationic liposome (MCL), wherein the magnetite nanoparticle is coated with positively charged liposomes to improve its biocompatibility.

We repeated the basic MNHT method for the treatment of prostate cancer as MHNT ideally warms the prostate gland up to a temperature of 43°C.

However, AMF generating devices have not been used for cancer treatment during the clinical phase in Japan. In a previous study, we have demonstrated that the magnetic nanoparticles serve as a medium that induces efficient heat generation during RF-capacitive heating [8]. In an in vivo experiment, it has been noted that heat generation using magnetic nanoparticles is similar to that obtained with inductive heating involving an AMF [9]. Thus, in cases where mild hyperthermia is applied, it is possible to generate heat to temperatures greater than 43°C using MCL injections, thereby raising the critical temperature of only the tumor tissue to that required for cancer cell death. In contrast, tissues that have not been injected with MCL do not experience an increase in temperature beyond 43°C even if picked up between the electrodes. Therefore, magnetic nanoparticles are considered to be a promising heat-generating medium not only for inductive heating but also for capacitive hyperthermia.

Herein, we have aimed at developing a new hyperthermia method for cancer treatment using the regional 8-MHz RF capacitive hyperthermia combined with MCL. The aim of this phase I study was to evaluate the safety of this method in treating prostate cancer patients resistant to standard therapy.

## Patients and methods

### Eligibility Criteria

*The inclusion criteria were:*

- patients with a histologically confirmed diagnosis of prostate cancer.

- treatment by medication or radiation only without radical prostatectomy,
- evidence of castration-refractory prostate cancer which did not respond to standard hormonal or anti-cancer agents.

Other inclusion criteria included the following: age 20–80 years, and an Eastern Cooperative Oncology Group (ECOG) performance status of 0 to 2.

*Exclusion criteria included the following:*

- patients with radical prostatectomy,
- presence of metals (pacemaker, implant denture, iron clip bolt) in the body which may react with the magnetic field,
- patients with pleural effusion, ascitis, and pericardial effusion requiring urgent treatment,
- presence of active infections,
- patients with the multiple primary cancers with less than five years disease-free interval,
- patients who were unable to communicate,
- cases where local anesthesia was contraindicated,
- patients with circulatory conditions and inadequately controlled diabetes mellitus,
- anticoagulation,
- cases deemed unsuitable for this study by a chief physician.

This study protocol conforms to the ethical guidelines of the 1975 Declaration of Helsinki and has been approved by the institutional review board of the Nagoya City University Hospital, Japan. Written informed consent was obtained from all patients before enrollment.

The patients were screened by the principal investigator (AO) to ensure that the eligibility requirements were met. Weight, vital signs, and EOCG performance status were evaluated. Adequate hematopoietic (absolute neutrophil count  $\geq 1,500/\mu\text{l}$ ; hemoglobin  $\geq 8.0\text{g/dl}$ ; platelet count  $\geq 100 \times 10^9/\text{L}$ ) and hepatic (serum total bilirubin within normal institutional range, and serum AST and ALT levels  $\leq 2.5 \times$  the institutional upper limit of normal) were required.

#### **Study Drug and Preparation**

##### *Information*

##### *Magnetic cationic liposome (MCL)*

MCL consists of two units, magnetite and liposome. Magnetite is composed of fine ( $\leq 50$  nanometers) particles of iron. The hydrophilic colloidal solution of the superparamagnetic iron oxide coated with carboxydextran is approved as a pharmaceutical formulation in Japan, where it is used as a liver contrast media for MRI by the generic names of feructrotan and ferumoxide. On the other hand, liposome is applied in clinical practice as a lipid membrane that wraps and coats an anticancer, antifungal or gene therapeutic drug. Some of the drugs coated with liposome such as doxorubicin HCl liposome and liposomal amphotericin B, have already been approved for use in Europe and America, because drugs coated with liposome are absorbed only by target cells and not the normal cells. In Japan, a liposomal drug has been used in the phase I clinical trial of  $\beta$  interferon gene therapy for glioma [10] and melanoma [11]. In October, 2007, clinical trials of hyperthermia immunotherapy were conducted using the anti-melanoma antibody immobilization magneto liposome for the treatment of advanced melanoma. MCLs contain magnetite particles that are coated with liposome and possess a positive electric charge, thus enabling them to adhere to the negatively

changed tumor cell surfaces by electrostatic forces. The MCLs are subsequently engulfed into the cells by phagocytosis indicating that positive charges on magnetite promote the entry of these particles into the target cell [12]. The injection of magnetite into regional tumors generates heat by irradiation of the AMF[13]; hence, regional interstitial hyperthermia can be performed only in cancer cells.

##### *Thermotron RF-8*

The body was placed between the two plates of electrode (2.5 and 30 cm in diameter), followed by the release of high frequency electromagnetic waves (8-MHz) into the tissue. This resulted in the selective warming (up to  $43^\circ\text{C}$ ) of the deep part of the human body. The output power ranged from 800–1500W. This treatment is applicable to all sites except the brain and the eyeball. As it is a local treatment, it does not affect the whole body and can be used to treat outpatients, if required. If used in combination with chemotherapy and radiotherapy, the synergistic effect would reinforce the effect of the treatment with very few side effects.

#### **Drug administration**

##### *Injection of MCL*

The patients were moved to a fluoroscopy room, and sacral epidural anesthesia was provided with 10 ml of 2% Xylocaine. Additional anesthesia was provided by administering pentazocine (25 mg) and hydroxyzine hydrochloride (15 mg), intravenously. Next, 0.5ml MCL along with 30mg/ml Fe was injected slowly in the peripheral zone (PZ), transition zone (TZ), and central zone (CZ) of the prostate; the injections were identified by ultrasonography and fluoroscopy (Figure 1). Then, 18 -gauge catheters were inserted into the prostate gland next to the points of MCL.

injection with the aid of a four-point microthermocouple sensor for measuring the tumor temperature. The patients were regularly monitored for any adverse reactions over a period of 30 minutes. CT scans of the pelvis were performed to confirm the presence of MCL at the initial points of injection.

#### *Hyperthermia*

The patient was moved from the CT room to the hyperthermia therapy room and made to lie down on the treatment table. A four-point microthermocouple sensor was placed in the previously inserted catheter. The output was controlled at 43°C with a treatment duration of 30 minutes. Blood pressure and pulse measurements were taken during the treatment procedure and an electrocardiogram monitor was set up. The 18-gauge catheter was removed after the treatment, and patients were returned to their room where the vital signs were checked after 1, 3, 6, 12 and 24 hours. Hemostatic drugs and antibiotics were administered as required.

#### *Evaluation of objective response and toxicity*

After a single treatment, CT scans were performed to evaluate local injuries to the prostate and urethra, including pelvic abscess. Physical examinations and blood studies were performed; prostate specific antigen levels were evaluated. All toxicities were graded according to the Common Terminology Criteria for Adverse Events (CTCAE; ver. 4.0)

#### *Dose Escalation*

The primary end point was to evaluate the presence, or absence, as well as the degree of adverse events. The secondary end point was to obtain preliminary efficacy data. In the present study, MCL was used as a medium to increase the temperature of the tumor

tissue, and not as a drug. It is necessary to inject the least required amount of MCL in order to raise the temperature to 43°C. The injection of higher doses to increase the temperature above 43°C is not advisable. Generally, the weight of the prostate gland is measured by imaging studies (ultrasound or CT scan) using phantom or large animals following which, the appropriate amount of MCL required is then estimated. In the present study, a dose escalation system was not adopted, and the amount of MCL to be used was estimated decided on each of the three patients.

The injection of 0.5 ml MCL (with an iron concentration of 30 mg/ml) resulted in the elevation of the temperature to 43°C within a spherical area (radius, 1 cm). The bulbar volume of a sphere with a 1 cm radius is approximately 4.2 cm<sup>3</sup>. In the case of a prostate weighing 25 ml, the injection of 0.5 ml MCL each at six points will heat the whole gland to a temperature of 43°C.

Adverse events were evaluated by CTC/AE. Preliminary efficacy was based on the level of the tumor marker, PSA, in each patient four weeks posttreatment.

## **Results**

### *Patients' characteristics*

The characteristics of the three patients (median age, 74 years; age range, 69–79 years), who participated in this study are shown in Table 1. In cases 1 and 2, the tumor had invaded into the surrounding tissues with multiple bone and lymph node metastases during the initial diagnosis phase. In case 3, the cancer had invaded into the bladder, with signs of lung metastasis. Gleason's score of prostate cancer during initial diagnoses of cases 1, 2 and 3 were 4 + 5 = 9, 4 + 5 = 9, and 5 + 5 = 10, respectively. The PSA levels in cases 1, 2 and 3 during initial diagnosis were 1180, 3360, and 20 ng/ml,

respectively.

Prior treatment of the patients in this phase clinical study is described briefly. None of the three patients had any indications for surgery, and androgen deprivation therapy:ADT was performed in all three cases. In cases 1 and 2, bisphosphonate preparations were provided for multiple bone metastases after ADT, following which docetaxel was induced. Case 1 underwent 25 courses of docetaxel, whereas in case 2, a maximum of two courses were provided owing to the strong side effects of the drug. Patient number 3 presented with locally invasive localized prostate cancer, but underwent ADT and not surgery. Docetaxel was introduced due to progression of the cancer. Irradiation of the whole pelvis was performed after five courses of docetaxel. Subsequently, another two courses of the drug were added. EOCG performance scores at the start of the clinical trials was one in all three patients. The PSA levels just before the Phase I clinical trial in cases 1, 2 and 3 were 123, 85, and 1.2 ng/ml, respectively, whereas IL-6 levels were 1.8, 1.9, 1.7 pg/ml, respectively.

***Injection and distribution of MCL***

MCL was injected bilaterally into the PZ and TZ (four places in total) of the prostate. A catheter was inserted on each side of the paired MCLs for thermometry (Figure 1a, b). CT images in Figure 2 show the distribution of MCL after infusion. The right and left TZ and PZ were injected with 0.5 ml MCL containing 30 mg/ml of iron in all three patients and numbered as follows: right TZ, No.1; right PZ, No.2; left TZ, No.3; and left PZ, No.4. The power output of RF-8 and the temperatures of the four catheters (Nos. 1–4) in the three cases are shown in Table 2.

In case 1, the No. 4 catheter was inserted with closest proximity to the paired No. 4 MCLs when compared with the other catheters. On the other hand, the No. 3 catheter

was inserted at the farthest point from the site of the paired No. 3 MCLs. The temperature of the No. 3 catheter depicted the temperature of the prostate, which was unaffected by the MCL. The power output of RF-8 was gradually raised from 350W to 500W from the start of this hyperthermia until seven minutes later. The output had to be reduced due to heating of the abdominal skin close to the electrode; it was reduced to zero at one point of time for ten minutes after which, it was turned back on and warming was resumed at approximately 370W for 20 minutes. The maximum temperature of the No. 4 catheter was 38.5°C, which differed from that of the No. 3 thermometer (36.5°C) by 2.0°C. The No. 4 catheter for thermometry was inserted closest to the paired No. 4 MCL, whereas the No. 3 catheter was placed at the furthest point from the paired No. 3 MCL (Figure 2). As a result, the temperature at the site of MCL infusion was increased by at least 2°C when compared with the site without MCL (Figure 3a).

In case 2, the power output of RF-8 was lowered to zero seven minutes from the start, for a period of five minutes; yet, it was possible to raise the final power output to 700W. In retrospect, the maximum temperature of the No.1 catheter for thermometry was 41.5°C, and was 2.3°C higher than that of the No. 3 catheter at 39.2°C, which was the lowest recorded temperature of the four catheters. The No. 1 catheter was inserted closest to the paired No. 1 MCL, whereas the No. 3 catheter was placed further most from the paired No. 3 MCL (Figure 3b).

In case 3, the power output of RF-8 was lowered to zero for three minutes at the ninth minute of treatment and then turned on at 550W for five minutes. The power output was stopped again for three minutes, and subsequently turned on for another five minutes. This step was repeated three times. The maximum temperature in this case was 40.8°C with the No. 1 catheter for thermometry, and the rise in temperature was approximately

equal to that of the No. 2 catheter at 39.5°C with a differences of 1.3°C. The catheters for thermometry were located at equal distances from the paired MCLs in cases 1 and 2 (Figure 3c).

#### **Toxicity and adverse events**

Grade 1 burn injuries of the skin were detected by CTCAE in all three cases. This adverse event is usually observed in patients treated with RF-8 alone, and is therefore not specific to this phase I clinical trial. No adverse events were noted in the prostate, rectum and bladder. Similarly, adverse events were absent at the implant site of the perineum. No abnormalities in blood biochemical findings were observed. Consciousness disorders and anaphylactic shock were absent.

#### **Discussion**

The present study confirms the safety of the regional 8-MHz RF capacitive hyperthermia combined with MCL. Several factors were taken into consideration for this new therapy.

#### ***Hyperthermia for prostate cancer***

There are some reports about the effect of hyperthermia therapy on prostate cancer [14-16]. The combination therapy of radiation to the pelvis and hyperthermia for localized prostate cancer has been shown to suppress the biological recurrence of PSA [14] when compared with radiation therapy alone. Furthermore, the biological recurrence of PSA was found to be suppressed by interstitial hyperthermia, when compared with regional hyperthermia, in patients who underwent the combination

therapy of both radiation and hyperthermia for localized prostate cancer treatment [15]. The combination therapy of radiation and transrectal hyperthermia without hormonal therapy has been reported to inhibit the recurrence of PSA for a period of five years [16]. However, hyperthermia therapy on its own is not sufficient for the treatment of prostate cancer; the anticancer agents have several side effects with dose-limiting toxicity. Similarly, in the case of radiation therapy, the optimal dosage is predetermined, and the treatment cannot be carried out repeatedly above this optimal dosage.

#### ***Magnetic nanoparticle-mediated hyperthermia (MNHT)***

We developed MNHT, which can optionally control the temperature of the lesion injected with MCL by AMF irradiation. Studies have shown that antibody-conjugated MCLs can be accumulated within the specific lesion containing the specific antigen [17,18]. The efficacy of MNHT has been demonstrated in animal models of melanoma [19], glioma [20], breast cancer [21,22], renal cancer [18] and osteosarcoma [23]. Previously, we have reported the in vivo findings of the application of hyperthermia using MCLs on recurrent prostate cancer and bone metastases [24-27].

Interestingly, MNHT is thought to induce hyperthermic immunoreactivity; Yanase et al. observed antitumor immune responses induced by hyperthermia using MCLs in an experimental T-9 rat glioma model where the tumor was transplanted into both femurs<sup>18</sup>. The heating of one tumor above 43°C using MCL injection via MNHT resulted in the complete disappearance of the other tumor as well; no increase in temperature was noted in the tumor that did not receive the MCL injection [20]. This is explained by the fact that large quantities of heat shock protein (HSP) released from the necrotic tumor tissue can induce strong tumor immunoreactivity [28].

**The regional 8-MHz RF capacitive hyperthermia combined with MCL**

At present, there is no magnetic field generator that can be used in clinical practice for the treatment of prostate cancer. Therefore, we have developed a new hyperthermic therapy using an 8-MHz RF capacitive hyperthermic heating device (Thermotron RF-8), which is available in Japan and used in our university hospital. Results of several experiments using phantoms and animal models have revealed that inductive hyperthermia by RF-8 with MCL injected into the target lesion could elevate the temperature 46°C and more. It is thought that hyperthermia using RF-8 alone cannot elevate the temperatures of lymph node metastatic lesions and tumors exhibiting local recurrence. In such cases, the lesions can be heated to over 43°C by injecting MCL. In small animal models, hyperthermia therapy using RF-8 with MCL injection into the tumor lesion has suppressed the growth of gliomas [8].

In conventional hyperthermia therapy with RF-8, the power output could not be raised in order to increase the temperature of the deep lesion to 43°C or more because the patients could not tolerate the heat generated by the electrodes in contact with their abdominal skin. Therefore, due to insufficient power output RF-8 thermotherapy by itself was not effective in controlling the cancer.

The inclusion of MCL injection to the RF-8 therapy raised the temperature of the lesion by 2 to 3°C when compared with lesions that did not receive MCL injections. Thus, a mild power output to raise the temperature to 40–41°C, which can be tolerated by the patients, along with the injection of MCL, which raises the temperature to 43°C is ideal to kill the cancer cells.

**Injection methods of MCL and catheter for thermometry**

In this phase I study, the injection of MCL and the catheter for thermometry were

performed under sacral epidural anesthesia in the lithotomy position, without the use of a template. MCL (0.5 ml) was injected into the PZ and TZ, followed by the insertion of the catheter for thermometry in close proximity to the insertion points of the MCLs. It is critical that the catheter is accurately inserted next to the insertion points of MCL in order to conduct accurate temperature measurements. We intend to promote the original template and also establish the setting of the catheter for thermometry at appropriate positions beside the MCLs.

**CT findings of the distribution of MCL**

The spread area was at a distance of 2 mm in diameter from the injection point. In case 1, CT demonstrated the existence of MCL four months after the injection, whereas in case 2, the existence of MCL was curtailed by the CT findings after a period of nine months. In the case 3, the patient was had a follow-up period of one year after the treatment. In all cases, CT demonstrated the existence of almost all MCLs one month after treatment, and 90% of the MCLs remained even after nine months posttreatment (Figure 4). These findings suggest that *the regional 8-MHz RF capacitive hyperthermia combined with MCL* can be performed repeatedly for the treatment of prostate cancer.

**Speculation about thermometry**

Thermometry was performed by using a thermocouple. However, the thermometer was not set at the ideal position beside the four MCL insertion points; therefore, it is important to use a template during the insertion of the catheter. Due to the invasive nature of the process further studies addressing this issue regarding catheter insertion are warranted.

reject the possibility of using this therapy in future.

**IL-6**

In recent years, the association between hyperthermia and interleukin-6 (IL-6) has been studied. IL-6 is produced by T cells, B cells, macrophages, fibroblasts, vascular endothelial cells, and kidney mesangial cells. IL-6 is thought to promote the antibody production of B cells and also the differentiation and activation of T cells. It has recently been demonstrated that IL-6 induces the migration of T cells into the tumor microenvironment, thereby suppressing cancer growth [289]. This therapy appears to activate cancer immunity because local hyperthermia treatment elevated IL-6 levels in localized prostate cancer.

**Conclusion**

Thus, RF-8 hyperthermia with injected MCL has been performed safely in this Phase I clinical study. However, because one of the eligibility criteria in this study was progressive prostate cancer in patients with multiple metastasis, the effect of the treatment on decreased PSA levels has not been demonstrated. The maximum temperature did not reach 43°C in the patients, as accurate temperature measurements were not performed. RF-8 hyperthermia with injected MCL is known to activate tumor immunity. Nevertheless, it is important to ascertain the quantity and point of injection in the case of MCL. Besides, the injection of MCL as well as the catheter for thermometry must be performed using a template.

Tumor-specific hyperthermia using MCLs with RF-capacitive heating appears to be the treatment of choice for lymph node metastases and local recurrence of urinary

**Adverse events**

Adverse events over grade 2 with regard to the injection of MCL or temperature elevation were not noted during this phase I study. Furthermore, no rectal fistula, bladder injury, or prostatic infections were observed. In addition, no liver dysfunction nor renal dysfunction were observed. No reactions to MCL injection (such as anaphylactic shock) were noted in any of the patients. Patient 1 died four months after this phase I study due to the progression of prostate cancer. This study was not related to the death of the patient. The case 3 patient is alive without cancer progression for more than one year due to the effect of enzalamide. Ninety percent of the initially injected MCL was present in the body of the patient during the one year follow-up period; no adverse events owing to MCL were noted. These findings indicate that MCL injection has no toxicity effects in the human body.

**PSA**

PSA levels were not decreased in any of the three patients. In fact, PSA levels had gradually increased in the three patients during the observation period. The main eligibility criteria of this phase I study was castration refractory prostate cancer and evidence of no effect of standard therapy for the treatment of this cancer. All three patients in this study presented with bone and lung metastasis. However, the target of hyperthermia in this study was limited to the prostate. Even if localized therapy had been performed in patients with progressive prostate cancer presenting with multiple metastasis, the general condition of these patients would deteriorate because of the progression of multiple metastatic lesions. We think that the rise in PSA level does not

system cancers that are located deep within the trunk. However, such lesions are typically located adjacent to the abdominal aorta, inferior vena cava, or the common internal, or external iliac artery/vein. We have already confirmed that this therapy does not cause injury to the great vessels near the tumor tissue [30].

In the next phase, we aim to design a study wherein the effect of the therapy can be evaluated. To that end, one of the eligibility criteria should include patients with localized recurrent prostate cancer.

#### **Acknowledgement**

The authors thank Mr. Tetsuya Sekiguchi and Mr. Tetsushi Nomura for medical advice about RF-8 running.

#### **Declaration of interest**

This work was supported by Grant-in-Aid for Scientific Research of Japan, number 24592403 and 15K10602. The authors alone are responsible for the content and writing of the paper.

#### **Reference**

1. Sim HG, Cheng CW. Changing demography of prostate cancer in Asia. *Eur J Cancer*, 2005, 41:834-45.
2. Chia SE, Tan CS, Lim GH, et al. Incidence, mortality and five-year relative survival ratio of prostate cancer among Chinese residents in Singapore from 1968 to 2002 by metastatic staging. *Ann Acad Med Singapore*, 2010, 39 :466-71.
3. Crocetti E, De Angelis R, Buzzoni C, et al. Cancer prevalence in United States, Nordic Countries, Italy, Australia, and France: an analysis of geographic variability. *Br J Cancer*, 2013, 9:109:219-28.
4. Znaor A, van den Hurk C, Primm-Zakej M, et al. Cancer incidence and mortality patterns in South Eastern Europe in the last decade: gaps persist compared with the rest of Europe. *Eur J Cancer*, 2013, 49: 1683-91.
5. Etzioni R, Legler JM, Feuer EJ, et al. Cancer surveillance series: interpreting trends in prostate cancer--part III: Quantifying the link between population prostate-specific antigen testing and recent declines in prostate cancer mortality. *J Natl Cancer Inst*, 1999, 91: 1033-39.
6. Otsuka T, Yonezawa M, Kamiyama F, et al. Results of surgery and

- radio-hyperthermo-chemotherapy for patients with soft-tissue sarcoma. *Int J Clin Oncol*, 2001, 6: 253-258.
7. Nojiri S, Kusakabe A, Shinkai N, et al. Factors influencing distant recurrence of hepatocellular carcinoma following combined radiofrequency ablation and transarterial chemoembolization therapy in patients with hepatitis C. *Cancer Manag Res*, 2011, 3:267-272.
8. Shinkai M, Ueda K, Ohtsu S, et al. Effect of functional magnetic particles on radiofrequency capacitive heating. *Jpn J Cancer Res*, 1999, 90: 699-704.
9. Shinkai M, Ueda K, Ohtsu S, et al. Effect of functional magnetic particles on radiofrequency capacitive heating: an in vivo study. *Jpn J Cancer Res*, 2002, 93:103-8.
10. Yoshida J, Mizuno M. Clinical gene therapy for brain tumors. Liposomal delivery of anticancer molecule to glioma. *J Neurooncol*, 2003, 65:261-267.
11. Kubo H, Ashida A, Matsumoto K, et al. Interferon beta therapy for malignant melanoma: the dose is crucial for inhibition of proliferation and induction of apoptosis of melanoma cells. *Arch Dermatol Res*, 2008, 300:297-301.
12. Shinkai M, Yanase M, Honda H, et al. Intracellular hyperthermia for cancer using magnetite cationic liposomes: in vitro study. *Jpn J Cancer Res*, 1996, 87:1179-83.
13. Yanase M, Shinkai M, Honda H, et al. Intracellular hyperthermia for cancer using magnetite cationic liposomes: An in vivo study. *Jpn J Cancer Res*, 1998, 89:463-469.
14. Zelefsky MJ, Reuter VE, Fuks Z, et al. Influence of local tumor control on distant metastases and cancer related mortality after external beam radiotherapy for prostate cancer. *The Journal of urology*, 2008, 179:1368-73.
15. Van Vulpen M, De Leeuw AA, Raaymakers BW, et al. Radiotherapy and hyperthermia in the treatment of patients with locally advanced prostate cancer: preliminary results. *BJU international*, 2004, 93:36-41.
16. Fosmire H, Hynynen K, Drach GW, et al. Feasibility and toxicity of transrectal ultrasound hyperthermia in the treatment of locally advanced adenocarcinoma of the prostate. *Int J Radiat Oncol Biol Phys*, 1993, 26:253-259.
17. Ito A, Shinkai M, Honda H, Kobayashi T. Medical application of functionalized magnetic nanoparticles. *J Biosci Bioeng*, 2005, 100:1-11.
18. Shinkai M, Le B, Honda H, et al. Targeting hyperthermia for renal cell carcinoma using human MN antigen-specific magnetoliposomes. *Jpn J Cancer Res*, 2001;92:1138-45.
19. Suzuki M, Shinkai M, Honda H, et al. Anticancer effect and immune induction by hyperthermia of malignant melanoma using magnetite cationic liposomes. *Melanoma Res*, 2003,13:129-35.
20. Ohno T, Wakabayashi T, Takemura A, et al. Effective solitary hyperthermia treatment of malignant glioma using stick type CMC-magnetite. In vivo study. *J Neurooncol*, 2002, 56:233-39.
21. Ito A, Kuga Y, Honda H, et al. Magnetite nanoparticle-loaded anti-HER2 immunoliposomes for combination of antibody therapy with hyperthermia. *Cancer Lett*, 2004,212:167-75.
22. Kikumori T, Kobayashi T, Sawaki M, et al. Anti-cancer effect of hyperthermia on breast cancer by magnetite nanoparticle-loaded anti-HER2 immunoliposomes. *Cancer Res Treat*, 2009,113:435-41.
23. Matsuoka F, Shinkai M, Honda H, et al. Hyperthermia using magnetite cationic

- liposomes for hamster osteosarcoma. *Biomagn Res Technol*, 2004,2:3.
24. Kawai N, Ito A, Nakahara Y, et al. Anticancer effect of hyperthermia on prostate cancer mediated by magnetite cationic liposomes and immune-response induction in transplanted syngeneic rats. *Prostate*, 2005, 64:373-81.
25. Kawai N, Ito A, Nakahara Y, et al. Complete regression of experimental prostate cancer in nude mice by repeated hyperthermia using magnetite cationic liposomes and  
 and  
 a newly developed solenoid containing a ferrite core. *Prostate*, 2006, 66:718-27.
26. Kawai N, Futakuchi M, Yoshida T, et al. Effect of heat therapy using magnetic nanoparticles conjugated with cationic liposomes on prostate tumor in bone. *Prostate*, 2008, 68:784-92.
27. Kobayashi D, Kawai N, Sato S, et al. Thermotherapy using magnetic cationic liposomes powerfully suppresses prostate cancer bone metastasis in a novel rat model. *Prostate*, 2013, 73:913-22.
28. Ito A, Shinkai M, Honda H, Augmentation of MHC class I antigen presentation via heat shock protein expression by hyperthermia. *Cancer Immunol Immunother*, 2001, 50:515-22.
29. Mikucki ME, Fisher DT, Ku AW, et al. Preconditioning thermal therapy: flipping the switch on IL-6 for anti-tumour immunity. *Int J Hyperthermia*, 2013, 29:464-473.
30. Kawai N, Kobayashi D, Yasui T, et al. Evaluation of side effects of radiofrequency capacitive hyperthermia with magnetite on the blood vessel walls of tumor metastatic lesion surrounding the abdominal large vessels: an agar phantom study. *Vasc Cell*, 2014, 15:6:15.

### Figure legends

**Figure 1** Schematic diagrams of the cross-sectional view of the prostate gland (a). horizontal section of the prostate. The dotted area represents the peripheral zone (PZ), whereas the central white area represents the transitional zone (TZ). X demonstrates the point where MCL was injected. No. 1, right TZ; No. 2, right PZ; No. 3, left TZ; and No. 4, left TZ. Central gray area is the central zone (CZ). (b). Sagittal section of the prostate. Black long bars indicate the catheters for thermometry, inserted beside the points of MCL injection.

**Figure 2** CT image of the horizontal section of the prostate (Case 1) after injection of MCL and catheter insertion. White arrows indicate the points of insertion of the

catheters, whereas the solid black triangles indicate the points of MCL injection. The No. 4 catheter was at closest to the paired MCLs, whereas the No. 3 catheters were located farthest away from the paired MCL.

**Figure 3** Graphs indicating the temperature (line), RF-8 power output (bar) and treatment time in the three (Cases 1–3) patients. Circle dot line is No. 1, bar plus dot line is No. 2, square dot line is No. 3 and black line is No. 4. (a). Case 1. The maximum temperature of the No. 4 catheter for thermometry was 38.5°C, but the difference in temperature when compared with the No. 3 thermometer (36.5°C) was 2.0°C. (b). Case 2. The maximum temperature of the No. 1 catheter for thermometry was 41.5°C, and was 2.3°C was higher than that of the No. 3 catheter for thermometry, which at 39.2°C was lowest temperature measured. (c). Case 3. The maximum temperature was 40.8°C for the No. 1 catheter. The rise in temperature was approximately equal to that of the No. 2 (39.5°C).

**Figure 4** CT images of horizontal sections of the prostate from Case 3 demonstrating the three points. Several white spots were seen on the prostate indicating the presence of MCL in the tissue. CT image of the prostate of just after MCL injection (a) demonstrated sharpen several white spots. CT image of the prostate one month after MCL injection (b) still showing the white spots. One year later, there is a slight reduction in the number of white spots compared with the image taken one month after MCL injection (c).

Table 1

Patient's characteristics			
	Case 1	Case 2	Case 3
Age (Years)	69	74	79
Clinical stage at initial diagnosis	cT4N1M1	cT4N1M1	cT4N0M1
Metastatic lesion	Lymph node Bone	Lymph node bone	lung
Treatment summary until phase 1 clinical trials	1. MAB 2. bisphosphonate 3. docetaxel (25)	1. MAB 2. bisphosphonate 3. docetaxel (1)	1. MAB 2.docetaxel (5) 3.radiation for pelvis 4. docetaxel (2)
ECOG Performance status	1	1	1
Gleason's score	4+5=9	4+5=9	5+5=10
PSA at initial examination (ng/ml)	1,180	3,360	20
PSA before phase 1 clinical study (ng/ml)	123	85	1.2
IL-6 before phase 1 clinical study (pg/ml)	1.8	1.9	1.7

MAB: maximal androgen blockade

Docetaxel ( ): docetaxel cycle

Table 2

Results of "The regional 8-MHz RF capacitive hyperthermia combined with MCL"

	Case 1	Case 2	Case 3
Max power of RF-8	500	700	550
Treatment time (min)	40	41	42
Max. temperature (°C)	38.5	41.5	40.8
PSA (pre/post) (ng/ml)	123/205	85/105	1.2/1.3
IL-6 (pre/post) (ng/ml)	1.8/3.2	1.9/2.0	1.7/4.1
Adverse events (CTCAE v4.0)			
MCL injection			
Prostate	0	0	0
Bladder	0	0	0
Rectum	0	0	0
Metabolism	0	0	0
Infusion reaction	0	0	0
Allergy	0	0	0
Hyperthermia			
Skin burn	1	1	1

PSA: prostate specific antigen

IL-6: interleukin 6

CTCAE: Common Terminology Criteria for Adverse Events

MCL: magnetic cationic liposome

Figure 1

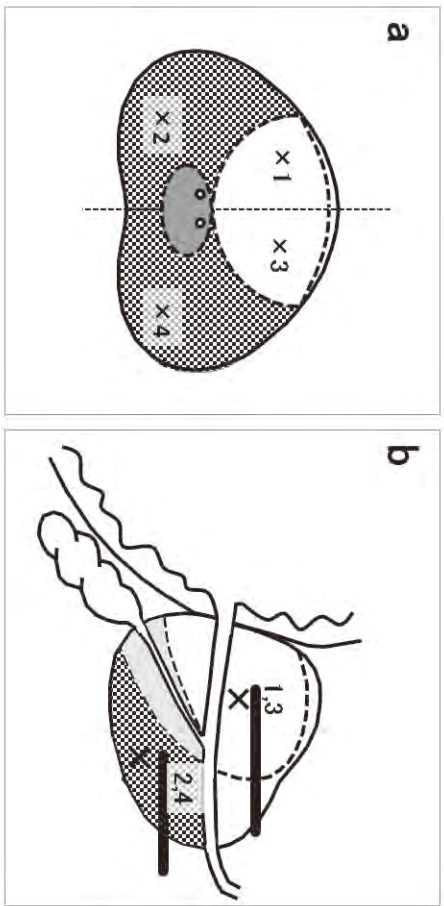
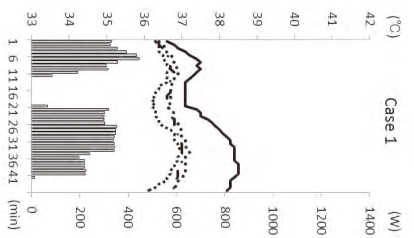
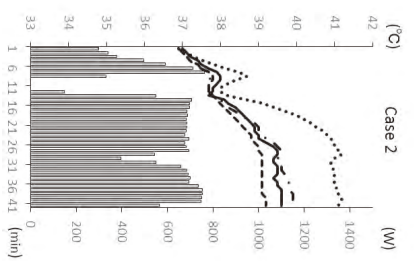


Figure 3 a



b



c

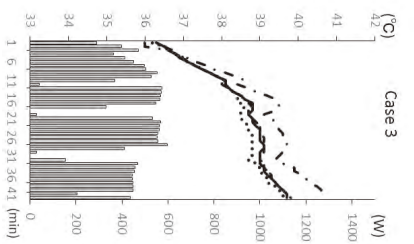


Figure 2

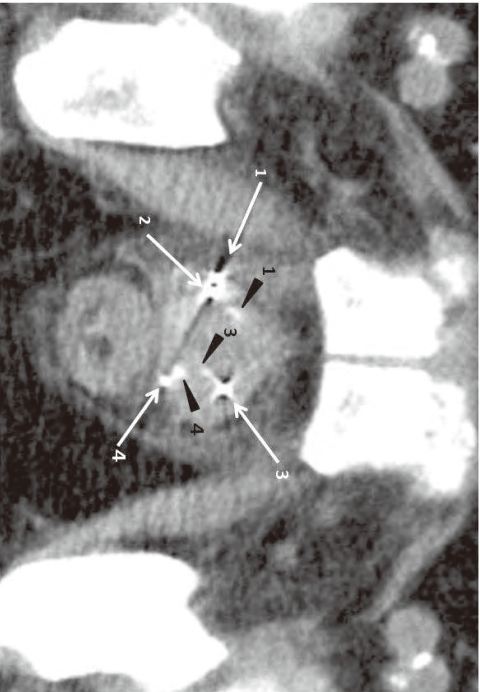


Figure 4





## Fargesin, a component of *Flos Magnoliae*, stimulates glucose uptake in L6 myotubes

Sun-Sil Choi · Byung-Yoon Cha · Bong-Keun Choi ·  
 Young-Sil Lee · Takayuki Yonezawa ·  
 Toshiaki Teruya · Kazuo Nagai · Je-Tae Woo

Received: 15 March 2012 / Accepted: 20 June 2012 / Published online: 12 July 2012  
 © The Japanese Society of Pharmacognosy and Springer 2012

**Abstract** *Flos Magnoliae* (FM) is a commonly used Chinese medicinal herb for symptomatic relief of allergic rhinitis, sinusitis and headache. Although several FM species have been used as substitutes or adulterants for clinical use, possible differences in their pharmacological actions have not been reported. To confirm the effects of FM on skeletal muscle glucose metabolism, we tested the effects of several compounds isolated from FM on glucose uptake by L6 myotubes. We found that fargesin, a component of FM, dose-dependently stimulated glucose consumption in L6 myotubes, which was accompanied by enhanced glucose transporter (GLUT)-4 translocation to the cell surface. Fargesin-stimulated glucose uptake was blocked by wortmannin, a phosphatidylinositol-3 kinase (PI3 K) inhibitor. Fargesin stimulated Akt phosphorylation, a key component in the insulin signaling pathway, which was completely inhibited by wortmannin. Here, we demonstrated that fargesin, a bioactive component of *Flos Magnoliae*, increases basal glucose uptake and GLUT4

translocation in L6 myotubes by activating the PI3 K–Akt pathway.

**Keywords** *Flos Magnoliae* · Fargesin · L6 cells · Glucose uptake · Insulin signaling

### Introduction

Insulin plays a key regulatory role in stimulating glucose transport from the blood into peripheral tissues via glucose transporter (GLUT)-4, which is predominantly expressed in skeletal muscle and adipose tissue [1]. Skeletal muscle constitutes the major mass of the peripheral tissue, representing about 40 % of the total body mass and accounting for >30 % of the total energy expenditure. Notably, skeletal muscle accounts for >80 % of insulin-stimulated glucose transport in the postprandial state and hence plays a major role in glucose homeostasis [2]. Thus, impaired skeletal muscle glucose uptake is largely responsible for the development of type 2 diabetes mellitus (T2DM) [3]. Accordingly, identification of novel compounds that can enhance skeletal muscle glucose uptake is important to facilitate the development of new treatments for insulin resistance and T2DM.

The two main regulators of glucose transport are phosphatidylinositol-3 kinase (PI3 K) and AMP-activated protein kinase (AMPK), which control glucose uptake into the cytoplasm by stimulating the translocation of intracellular GLUT4 to the cell membrane [4, 5]. PI3 K is activated by insulin and, in turn, phosphorylates a central regulator of glucose uptake, the serine/threonine kinase protein kinase B (PKB/Akt) [6]. In insulin-resistant skeletal muscle, activation of PI3 K has a weaker effect on glucose uptake than in normal skeletal muscle [7, 8]. AMPK is composed

S.-S. Choi · B.-Y. Cha (✉) · B.-K. Choi · Y.-S. Lee ·  
 T. Yonezawa · K. Nagai · J.-T. Woo  
 Research Institute for Biological Functions,  
 Chubu University, 1200 Matsumoto, Kasugai, Aichi, Japan  
 e-mail: bycha@isc.chubu.ac.jp

T. Teruya  
 Faculty of Education, University of the Ryukyus,  
 1 Senbaru, Nishihara, Okinawa 903-0213, Japan

T. Teruya  
 Department of Biological Chemistry, Chubu University,  
 1200 Matsumoto, Kasugai, Aichi, Japan

K. Nagai · J.-T. Woo  
 Department of Research and Development, Erina Co., Inc.,  
 1-9-2 Hagashi-Shinbash, Minato-ku, Tokyo 105-0021, Japan

of three subunits,  $\alpha$ ,  $\beta$  and  $\gamma$  [9]. In mammalian cells, AMPK acts as an energy sensor and is activated by exercise/contraction and compounds such as metformin, thiazolidinediones and polyphenols [10–12].

*Flos Magnoliae* (FM; Chinese name: Xin-yi; *Magnolia biondii*) is one of the most commonly used Chinese medicinal herbs. It has a long history of clinical use for managing rhinitis, sinusitis and headache. Pharmacologic studies have revealed that FM has anti-allergic, anti-inflammatory, antimicrobial and anti-angiogenic effects [13, 14]. FM was also reported to protect against streptozotocin-induced type 1 diabetes by suppressing streptozotocin-mediated  $\beta$ -cell damage [15]. Although several pharmacologic studies of FM have been done, more than 20 different FM species are now in clinical use, which makes species identification and evaluation of the pharmacological effects of individual components of FM difficult.

In this study, we examined the effects of several compounds isolated from FM on glucose uptake and investigated the underlying mechanisms using skeletal muscle cells. We found that fargesin stimulated glucose uptake in L6 myotubes by inducing GLUT4 translocation to the cell membrane, in a process involving activation of the insulin signaling component Akt.

## Materials and methods

### Chemical reagents

Insulin and anti- $\beta$ -actin were purchased from Sigma-Aldrich (St. Louis, MO, USA). Polyclonal antibodies against GLUT4, phospho-Akt (Ser473), Akt, phospho-AMPK (Thr702) and AMPK were purchased from Cell Signaling Technology Inc. (Beverly, MA, USA). Horseradish peroxidase-conjugated anti-rabbit IgG and anti-mouse antibodies, and polyvinylidene difluoride (PVDF) membranes were purchased from Amersham (Buckinghamshire, UK).

### Plant material

Commercially available air-dried FM was authenticated and provided by Daikoshoyaku Co. Ltd. (Nagoya, Japan, lot 028209004).

### Isolation and identification of fargesin, epimagnolin and kobusin

FM (1.5 kg) was extracted in methanol (12 L) for 7 days. The extract was then filtered, concentrated (185.6 g) and partitioned between ethyl acetate and water. The ethyl acetate-soluble fraction (131.2 g) was further partitioned

between aqueous methanol and *n*-hexane. The material obtained from the aqueous methanol portion (110.7 g) was chromatographically resolved on a silica gel using stepwise gradient elution in *n*-hexane and ethyl acetate (9:1, 8:2, 7:3, 5:5, 4:6 and 0:1, v/v, 10 fractions; FM-1 to FM-10). Fargesin (4.76 g, Fig. 1a) was obtained from FM-4 (9.7 g) and FM-5 (4.5 g) on fractional crystallization. FM-6 (6.7 g) and FM-8 (38.3 g) were fractionated by reverse-phase preparative HPLC with OSD column [mobile phase, water and acetonitrile at 50:50 (v/v); size, 20 mm  $\times$  250 mm, COSMOSIL Cholesterol Waters; flow rate of the mobile phase, 5 ml/min, UV = 215 nm]. The eluted fractions were subsequently identified as kobusin (3.9 g) and epimagnolin (21.8 g), respectively (Fig. 1a). The analysis of purified fargesin, epimagnolin and kobusin were determined by NMR. The  $^1\text{H-NMR}$  (400 MHz,  $\text{CD}_3\text{Cl}$ ) and  $^{13}\text{C-NMR}$  (100 MHz,  $\text{CD}_3\text{Cl}$ ) spectra were obtained on a FT NMR (JEOL, Japan) and compared with the data reported in the literature [16–18].

### Cell culture

L6 rat myoblasts were grown in Dulbecco's modified Eagle's medium (DMEM) (Gibco BRL, NY, USA) supplemented with 10 % fetal bovine serum (FBS; Biosource, Inc., NY, USA) and antibiotics (100 U/ml penicillin and 100  $\mu\text{g/ml}$  streptomycin; Gibco BRL) at 37 °C under a humidified 5 %  $\text{CO}_2$  atmosphere. At 2–3 days after reaching confluence, the L6 myoblasts were transferred to DMEM supplemented with 2 % horse serum (Gibco BRL) for differentiation, and were incubated for 7 days. The extent of differentiation was established by observing multinucleation of cells. Approximately 90 % of the myoblasts fused into myotubes.

### Glucose consumption assay

Glucose consumption was determined in L6 myoblast or L6 myotubes cells grown in 96-well plates. L6 myoblasts or myotubes were incubated for 1 h with the specified compounds. Cells were washed twice and incubated with serum-free DMEM. After 3 h, the cells were incubated with or without 100 nM insulin in Krebs–Henseleit–HEPES (KHH) buffer (118 mM NaCl, 4.7 mM KCl, 2.5 mM  $\text{CaCl}_2$ , 1.2 mM  $\text{MgSO}_4$ , 25 mM  $\text{Na}_2\text{HPO}_4$ , 1.2 mM  $\text{KH}_2\text{PO}_4$ , 0.1 % BSA, 1 mM glucose, 10 mM HEPES and 2 mM sodium pyruvate, pH 7.4) followed by incubation with the indicated concentration of fargesin for 3 h. The glucose concentration in the buffer was determined by the glucose oxidase method (Wako, Osaka, Japan). Intracellular glucose was calculated by subtracting the glucose concentration of the medium from the total glucose concentration in the blank wells.

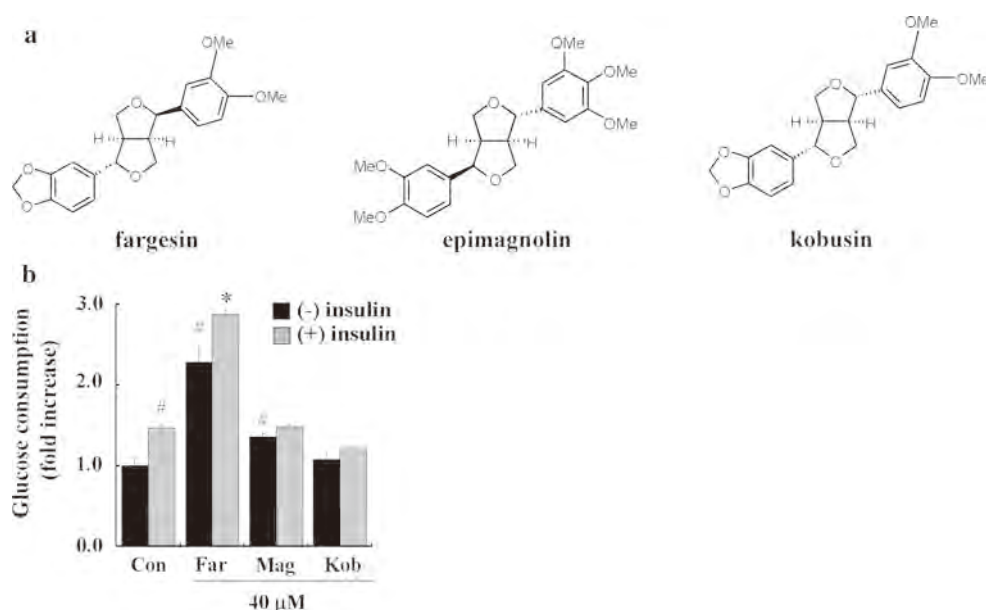


**Fig. 1** Chemical structures of the compounds isolated from *Flos Magnoliae* (**a**, **b**) and their effects on glucose consumption (**c**). **a**  $^1\text{H-NMR}$  (400 MHz,  $\text{CD}_3\text{Cl}$ ),  $^{13}\text{C-NMR}$  (100 MHz,  $\text{CD}_3\text{Cl}$ ) spectrum and chemical structure of fargesin, epimagnolin and kobusin. **b** Differentiated L6 myotubes were treated with 40  $\mu\text{M}$  of the compounds isolated from *Flos Magnoliae* (40  $\mu\text{M}$ ) for 1 h, and

glucose concentrations were measured as described in “Materials and methods”. Values are mean  $\pm$  standard deviation ( $n = 3$ ) of three independent experiments. # $P < 0.05$  versus control cells (basal state) and \* $P < 0.05$  versus insulin-treated control cells. *Far* fargesin, *Mag* epimagnolin, *Kob* kobusin

#### Protein extraction and immunoblotting

Cells were washed with ice-cold PBS and the subcellular fraction and whole-cell lysates were collected as follows. To prepare the subcellular fraction, cells were harvested in buffer A (0.25 M sucrose, 10 mM Tris-HCl pH 7.4, 2 mM EDTA, 1 mM PMSF). The lysates were centrifuged at 760 g for 10 min to remove nuclei and unbroken cells. The supernatant was centrifuged at 12,000 g for 20 min to pellet the crude plasma membrane. The supernatant was collected as the cytosolic fraction and the crude plasma membrane pellets were re-suspended in buffer A. All samples were frozen at  $-80^\circ\text{C}$  until use.

To prepare the whole-cell lysate, cells were washed with ice-cold PBS and harvested in lysis buffer (50 mM Tris-HCl pH 7.4, 150 mM NaCl, 1 mM EDTA, 1 % Triton X-100, 1 % sodium deoxycholate, 0.1 % SDS, 1 mM PMSF). The lysates were centrifuged at 12,000 g for 20 min and the supernatants were collected.

Proteins in the whole-cell and subcellular extracts were separated by 10 % SDS-PAGE and electrotransferred to PVDF membranes. The membranes were blocked in Tris-buffered saline containing 0.1 % Tween-20 and 5 % nonfat dried milk, and then incubated with the primary antibodies and appropriate secondary antibodies according to the manufacturers’ instructions. Antigen-antibody complexes were detected by enhanced chemiluminescence (Amersham, UK).

#### Cytotoxicity

The cytotoxicity of fargesin was determined using MTT assays. Briefly, L6 myoblasts on 96-well plates were treated with the indicated concentrations of fargesin. After 24 h, the cells were incubated with 10 mg/ml MTT solution (final concentration 0.1 mg/ml) at  $37^\circ\text{C}$  for 3 h. Cells were lysed with DMSO and the absorbance of purple formazan was measured at 570 nm. Cell viability is expressed as the percent reduction of MTT absorbance in treated cells compared with untreated cells.

#### Statistical analysis

All the data are presented as mean  $\pm$  standard deviation. One-way analysis of variance (ANOVA) followed by Dunnett’s test was used to determine the statistical significance of the differences between the experimental groups. A  $P$  value  $< 0.05$  was considered significant.

#### Results

##### Effects of components of FM on glucose consumption in rat L6 myotubes

We first examined the effects of fargesin, epimagnolin and kobusin, isolated from FM, on glucose consumption in L6

myotubes. At a concentration of 40  $\mu\text{M}$ , fargesin (2.6-fold) and epimagnolin (1.3-fold), but not kobusin, significantly stimulated glucose consumption without any cytotoxicity in L6 myotubes (Fig. 1b).

Cytotoxicity of fargesin in L6 myoblasts

Next, we examined the cytotoxicity of fargesin in L6 myoblasts using the MTT assay. As shown in Figure 2a, fargesin did not show cytotoxicity at concentrations of up to 80  $\mu\text{M}$ .

Fargesin increases glucose consumption in L6 myotubes and myoblasts

To determine the role of fargesin in glucose metabolism, we first examined the effects of fargesin on glucose consumption in L6 myotubes. We found that fargesin dose-dependently increased basal glucose consumption, with a maximum response at 40  $\mu\text{M}$  in L6 myotubes (Fig. 2b). This activity was associated with enhanced glucose uptake in the myotubes. However, there was no difference in glucose consumption between myotubes pre-incubated with fargesin for 1 h and those pre-incubated for 24 h (data not shown). We also determined whether fargesin increased glucose consumption in L6 myoblasts, which respond poorly to insulin because of low GLUT4 expression [19]. As shown in Figure 2c, fargesin did not significantly increase glucose consumption in L6 myoblasts.

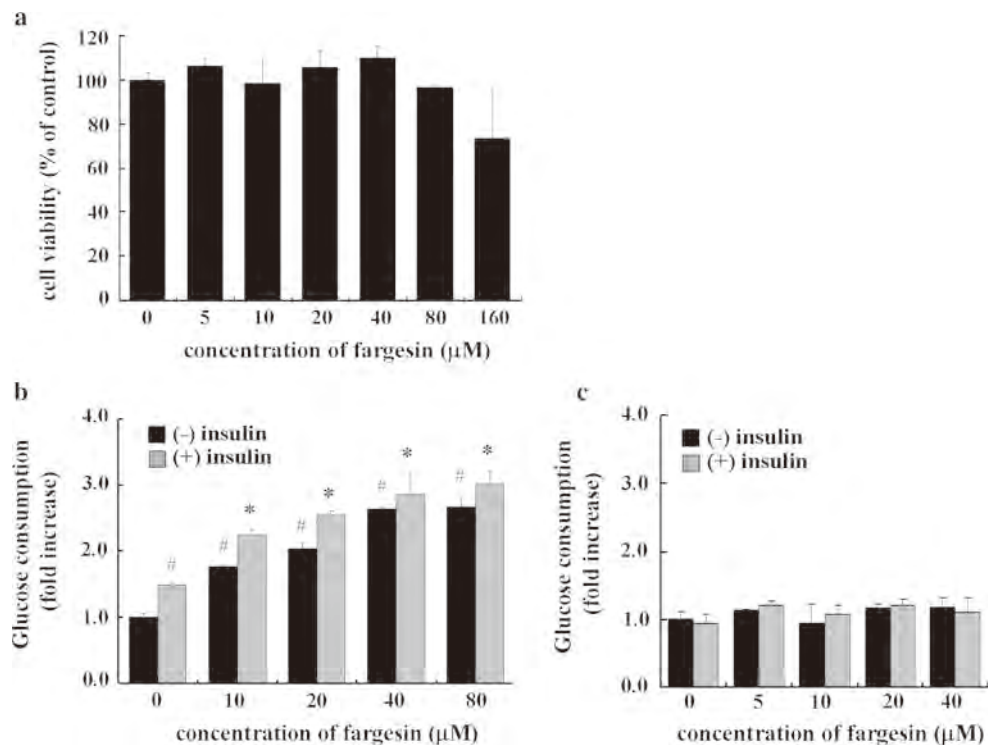
Fargesin promotes GLUT4 translocation in L6 myotubes

Glucose transport is the rate-limiting step in glucose utilization. One of the major factors regulating glucose transport in skeletal muscle is the quantity of GLUT4 at the cell surface [20]. To understand the mechanisms by which fargesin influences glucose metabolism, we measured GLUT4 expression in the plasma membrane. In fargesin-treated cells, plasma membrane GLUT4 expression was increased compared with that in control cells (Fig. 3a) without differences in total GLUT4 expression between these two groups (Fig. 3b).

Fargesin-mediated glucose uptake does not involve the AMPK pathway

Glucose transport is activated in peripheral tissues by two distinct pathways. In the first pathway, glucose transport is stimulated by insulin through IRS-1/PI3 K signaling. In the second pathway, muscle contraction and exercise activate AMPK, a conserved intracellular energy sensor that plays a central role in the regulation of glucose and lipid metabolism, and also induces the expression and translocation of GLUT4 in muscle [5, 21]. Therefore, we investigated whether AMPK activation is involved in the effect of fargesin on glucose uptake in L6 myotubes. Fargesin stimulated glucose uptake, even in the presence of compound C, an AMPK inhibitor (Fig. 4a). As shown in Figure 4b,

**Fig. 2** Effects of fargesin on cell viability (a) and glucose consumption in L6 myotubes (b) and L6 myoblasts (c). **a** The percent viability of cells treated with the indicated concentrations of fargesin for 24 h was determined by an MTT assay. Data are representative of three independent experiments. \* $P < 0.05$  versus the basal value in control cells. **b, c** Differentiated L6 myotubes (b) and undifferentiated L6 myoblasts (c) were treated with the indicated concentrations of fargesin for 1 h, and glucose concentrations were measured as described in “Materials and methods”. Values are mean  $\pm$  standard deviation ( $n = 3$ ) of three independent experiments. # $P < 0.05$  versus control cells (basal state) and \* $P < 0.05$  versus insulin-treated control cells



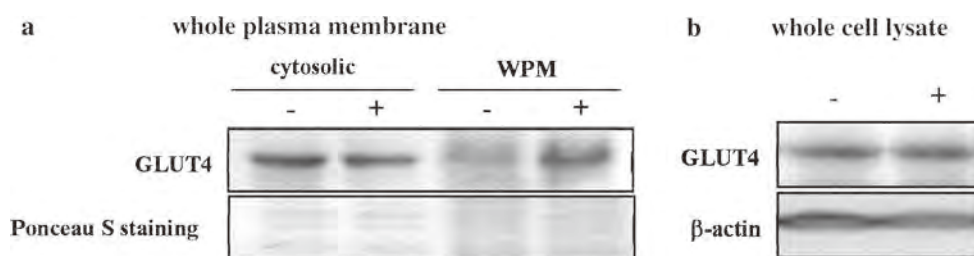


**Fig. 3** Effects of fargesin on GLUT4 translocation in L6 myotubes. Cells were treated with 40  $\mu$ M fargesin for 1 h. The whole plasma membrane fraction (*WPM*) (a) and whole-cell lysates (b) were extracted after further incubation with 40  $\mu$ M fargesin for 30 min.

The membrane fraction and total protein were subjected to Western blotting to determine membrane and total GLUT4 expression, respectively. The data shown are representative of three independent experiments

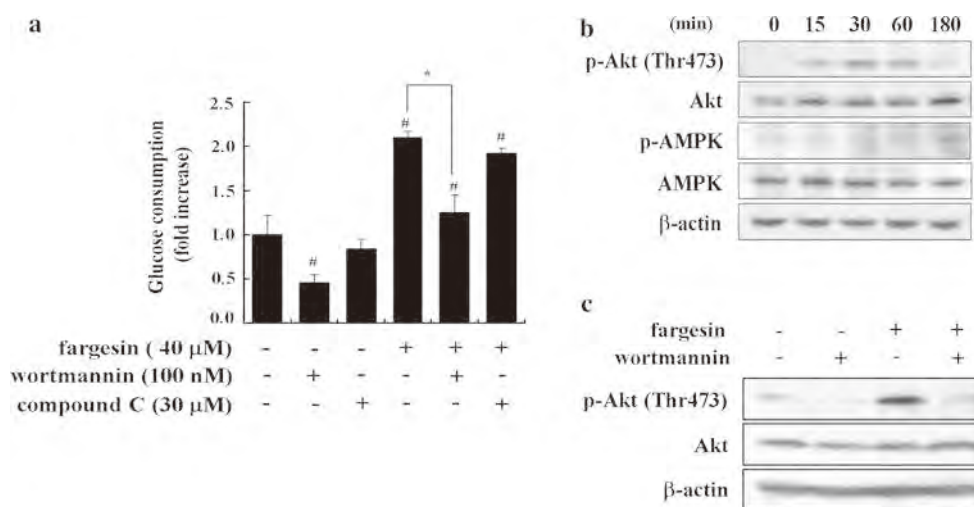


**Fig. 4** Effect of fargesin on activation of the AMPK- and PI3 K-dependent pathways in L6 myotubes. **a** Cells were incubated with 40  $\mu$ M fargesin for 1 h in the absence or presence of 100 nM wortmannin or 30  $\mu$ M compound C. Glucose concentrations were measured as described in “Materials and methods”. Values are mean  $\pm$  standard deviation ( $n = 3$ ).  $\#P < 0.05$  versus control cells (basal state) and  $*P < 0.05$  versus fargesin-treated cells. **b** Time-dependent phosphorylation of AMPK and Akt by fargesin. Cells were

stimulated for the indicated times with 40  $\mu$ M fargesin and cell lysates were subjected to Western blotting, as described in “Materials and methods”. **c** PI3 K-dependent phosphorylation of Akt. Cells were pretreated with 100 nM wortmannin and then stimulated with 40  $\mu$ M fargesin. The cell lysates were subjected to Western blotting, as described in “Materials and methods”. The data shown are representative of three independent experiments

phosphorylation of AMPK seemed to be increased but it did not show a significant difference in densitometry analysis (data not shown). Therefore, the AMPK pathway does not appear to contribute to the effects of fargesin on glucose uptake.

Fargesin activates the Akt pathway in a PI3 K-dependent manner

Next, we treated cells with wortmannin, a selective PI3 K inhibitor, to examine the contribution of PI3 K to fargesin-induced glucose uptake. As shown in Figure 4a, the stimulatory effects of fargesin were completely inhibited by 100 nM wortmannin, indicating that PI3 K plays an important role in fargesin-stimulated glucose uptake. Akt, an important downstream target of PI3 K, is a serine/

threonine protein kinase that promotes translocation of GLUT4 to the plasma membrane [22]. Therefore, we next examined the effects of fargesin on Akt activation. As shown in Figure 4b, treatment with 40  $\mu$ M fargesin significantly enhanced Akt phosphorylation at 30 min. Interestingly, fargesin-induced phosphorylation of Akt was inhibited in cells treated with 100 nM wortmannin (Fig. 4c). Taken together, these results indicate that fargesin stimulates glucose uptake by activating Akt in a PI3 K-dependent manner.

Discussion

Metabolic syndrome is a complex and chronic disease associated with adverse functioning of many organs.

Among the metabolic syndrome components, hyperglycemia caused by insulin resistance is the main contributor to the associated disorders [1]. Thus, regulating glucose uptake is important for the treatment of diabetes and metabolic syndrome. FM is one of the most commonly used Chinese and Korean medicinal herbs and has reported to have several pharmacological effects [13–15]. However, the pharmacological effects of individual components are largely unknown. Most of the recent studies of fargesin, kobusin and epimagnolin have focused on their anti-inflammatory effects [23–26]. Hence, in the present study, we isolated these three components from FM and examined their effects on glucose uptake in L6 myotubes. We found that, of the three compounds, fargesin showed the most potent stimulatory effects on glucose uptake. Fargesin significantly increased glucose uptake in a dose-dependent manner in differentiated myotubes, but not in undifferentiated myoblasts. Thus, the effects of fargesin-stimulated glucose consumption might be associated with GLUT4 expression, translocation and/or activity.

To understand the mechanism by which fargesin stimulates glucose transport, we assessed GLUT4 distribution and the relative signal in this process in L6 myotubes. GLUT4 is the predominant glucose transporter in skeletal muscle and adipose tissues, and is primarily responsible for insulin-stimulated glucose transport, following its translocation to the plasma membrane [27]. Insulin resistance is believed to result from defects in insulin's downstream signals that induce translocation of GLUT4 to the cell surface [3]. Therefore, screening for agents that can increase glucose uptake by increasing the expression and/or stimulation of GLUT4 translocation is one of the main strategies for identifying new therapeutic agents for T2DM. In the present study, we showed that fargesin stimulated basal glucose uptake in L6 myotubes, which was accompanied by enhanced translocation of GLUT4 to the cell membrane without affecting total GLUT4 protein expression. Thus, fargesin-stimulated glucose consumption might be accompanied by increased GLUT4 translocation.

Glucose uptake via GLUT4 translocation is achieved by two distinct pathways mediated by insulin and muscle contraction [27]. AMPK regulates GLUT4-dependent glucose transport in response to a diverse range of cellular stressors, including contraction, hypoxia and agents that disrupt the intracellular ATP:AMP ratio [10–12]. Activation of PI3 K is a major event in the insulin signaling cascade and promotes GLUT4 translocation [19]. Binding of insulin to its receptor activates PI3 K and hence phosphorylation of the downstream target Akt [22]. In our study, fargesin did not affect AMPK activation, but did increase Akt phosphorylation. We also found that inhibition of PI3 K with a PI3 K-specific inhibitor blocked fargesin-induced glucose uptake. Therefore, we think that

fargesin promotes glucose uptake by modulating GLUT4 translocation, which is achieved by activating Akt in a PI3 K-dependent manner. These results point towards insulin-like properties of fargesin in terms of its mechanism of action. Considering this concept, we now need to determine whether fargesin initiates the insulin signaling pathway at the level of the insulin receptor substrate, which is ultimately responsible for insulin-induced GLUT4 translocation.

In conclusion, we have demonstrated that fargesin, a bioactive compound isolated from FM, increases basal glucose uptake and GLUT4 translocation in muscle cells by activating the PI3 K–Akt pathway. These results help to clarify the glucose-lowering effects and anti-diabetic properties of fargesin and FM, and further support their potential use in the treatment of diabetes.

**Acknowledgments** This study was performed at a laboratory supported by an endowment from Erina Co., Inc.

## References

- Zaid H, Antonescu CN, Randhawa VK, Klip A (2008) Insulin action on glucose transporters through molecular switches, tracks and tethers. *Biochem J* 413:201–215
- Smith AG, Muscat GE (2005) Skeletal muscle and nuclear hormone receptors: implications for cardiovascular and metabolic disease. *Int J Biochem Cell Biol* 37:2047–2063
- DeFronzo RA, Gunnarsson R, Bjorkman O, Olsson M, Wahren J (1985) Effects of insulin on peripheral and splanchnic glucose metabolism in noninsulin-dependent (type II) diabetes mellitus. *J Clin Invest* 76:149–155
- Musi N, Hayashi T, Fujii N, Hirshman MF, Witters LA, Good-year LJ (2001) AMP-activated protein kinase activity and glucose uptake in rat skeletal muscle. *Am J Physiol Endocrinol Metab* 280:E677–E684
- Zheng D, MacLean PS, Pohnert SC, Knight JB, Olson AL, Winder WW, Dohm GL (2001) Regulation of muscle GLUT-4 transcription by AMP-activated protein kinase. *J Appl Physiol* 91:1073–1083
- Saltiel AR, Kahn CR (2001) Insulin signalling and the regulation of glucose and lipid metabolism. *Nature* 414:799–806
- Björnholm M, Kawano Y, Lehtihet M, Zierath JR (1997) Insulin receptor substrate-1 phosphorylation and phosphatidylinositol 3-kinase activity in skeletal muscle from NIDDM subjects after in vivo insulin stimulation. *Diabetes* 46:524–527
- Dohm GL, Tapscott EB, Pories WJ, Dabbs DJ, Flickinger EG, Meelheim D, Fushiki T, Atkinson SM, Elton CW, Caro JF (1998) An in vitro human muscle preparation suitable for metabolic studies. Decreased insulin stimulation of glucose transport in muscle from morbidly obese and diabetic subjects. *J Clin Invest* 82:486–494
- Towler MC, Hardie DG (2007) AMP-activated protein kinase in metabolic control and insulin signaling. *Circ Res* 100:328–341
- Zhou G, Myers R, Li Y, Chen Y, Shen X, Fenyk-Melody J, Wu M, Ventre J, Doebber T (2001) Role of AMP-activated protein kinase in mechanism of metformin action. *J Clin Invest* 108:1167–1174
- Konrad D, Rudich A, Bilan PJ, Patel N, Richardson C, Witters LA, Klip A (2005) Troglitazone causes acute mitochondrial

- membrane depolarisation and an AMPK-mediated increase in glucose phosphorylation in muscle cells. *Diabetologia* 48:954–966
12. Hwang JT, Kwon DY, Yoon SH (2009) AMP-activated protein kinase: a potential target for the diseases prevention by natural occurring polyphenols. *N Biotechnol* 26:17–22
  13. Shen Y, Li CG, Zhou SF, Pang EC, Story DF, Xue CC (2008) Chemistry and bioactivity of *Flos Magnoliae*, a Chinese herb for rhinitis and sinusitis. *Curr Med Chem* 15:1616–1627
  14. Kobayashi S, Kimura I, Kimura M (1996) Inhibitory effect of magnosalin derived from *Flos magnoliae* on tube formation of rat vascular endothelial cells during the angiogenic process. *Biol Pharm Bull* 19:1304–1306
  15. Kim EK, Song MY, Kim IS, Moon WS, Ryu DG, So HS, Park R, Park JW, Kwon KB, Park BH (2008) Beneficial effect of *Flos magnoliae* extract on multiple low dose streptozotocin-induced type 1 diabetes development and cytokine-induced beta-cell damage. *Int J Mol Med* 22:481–488
  16. Ahmed AA, Mahmoud AA, Ali ET, Tzakou O, Couladis M, Mabry TJ, Gáti T, Tóth G (2002) Two highly oxygenated eudesmanes and 10 lignans from *Achillea holosericea*. *Phytochemistry* 59:851–856
  17. Mitsuo M, Hiroyuki K, Hiromu K (1994) Microbial oxidation of (+)-epimagnolin a by *Aspergillus niger*. *Phytochemistry* 35:1191–1193
  18. Biavatti MW, Vieira PC, da Silva MF, Fernandes JB, Degani AL, Cass QB, Schefer AB, Ferreira AG (2001) Separation and NMR studies on lignans of *Raulinoa echinata*. *Phytochem Anal* 12:64–68
  19. Mitsumoto Y, Burdett E, Grant A, Klip A (1991) Differential expression of the GLUT1 and GLUT4 glucose transporters during differentiation of L6 muscle cells. *Biochem Biophys Res Commun* 175:652–659
  20. Ziel FH, Venkatesan N, Davidson NB (1998) Glucose transport is rate limiting for skeletal muscle glucose metabolism in normal and STZ-induced diabetic rats. *Diabetes* 37:885–890
  21. Holmes BF, Kurth-Kraczek EJ, Winder WW (1999) Chronic activation of 5'-AMP-activated protein kinase increases GLUT-4, hexokinase, and glycogen in muscle. *J Appl Physiol* 87:1990–1995
  22. Farese RV, Sajan MP, Standaert ML (2005) Insulin-sensitive protein kinases (atypical protein kinase C and protein kinase B/Akt): actions and defects in obesity and type II diabetes. *Exp Biol Med (Maywood)* 230:593–605
  23. Guo T, Deng YX, Xie H, Yao CY, Cai CC, Pan SL, Wang YL (2011) Antinociceptive and anti-inflammatory activities of ethyl acetate fraction from *Zanthoxylum armatum* in mice. *Fitoterapia* 82:347–351
  24. Lim H, Son KH, Bae KH, Hung TM, Kim YS, Kim HP (2009) 5-Lipoxygenase-inhibitory constituents from *Schizandra fructus* and *Magnolia flos*. *Phytother Res* 23:1489–1492
  25. Kim JS, Kim JY, Lee HJ, Lim HJ, Lee DY, Kim DH, Ryu JH (2010) Suppression of inducible nitric oxide synthase expression by furfuran lignans from flower buds of *Magnolia fargesii* in BV-2 microglial cells. *Phytother Res* 24:748–753
  26. Chae SH, Kim PS, Cho JY, Park JS, Lee JH, Yoo ES, Baik KU, Lee JS, Park MH (1998) Isolation and identification of inhibitory compounds on TNF-alpha production from *Magnolia fargesii*. *Arch Pharm Res* 21:67–69
  27. Watson RT, Pessin JE (2007) GLUT4 translocation: the last 200 nanometers. *Cell Signal* 19:2209–2217

## RESEARCH ARTICLE

# Long-term supplementation of honokiol and magnolol ameliorates body fat accumulation, insulin resistance, and adipose inflammation in high-fat fed mice

Young-Je Kim<sup>1\*</sup>, Myung-Sook Choi<sup>1,2\*</sup>, Byung Yoon Cha<sup>3\*</sup>, Je Tae Woo<sup>4</sup>, Yong Bok Park<sup>5</sup>, Sang Ryong Kim<sup>5,6</sup> and Un Ju Jung<sup>2</sup>

<sup>1</sup> Department of Food Science and Nutrition, Kyungpook National University, Daegu, Republic of Korea

<sup>2</sup> Center for Food and Nutritional Genomics Research, Kyungpook National University, Daegu, Republic of Korea

<sup>3</sup> Research Institute for Biological Functions, Chubu University, Kasugai, Japan

<sup>4</sup> Yuto Teruya, Oknawa Research Center Co. Ltd., Suzaki, Uruma, Okinawa, Japan

<sup>5</sup> School of Life Sciences and Biotechnology, Kyungpook National University, Daegu, Republic of Korea

<sup>6</sup> Brain Science and Engineering Institute, Kyungpook National University, Daegu, Republic of Korea

**Scope:** This study investigated the effect of honokiol (HON) and magnolol (MAG), phenolic compounds in *Magnolia* plants, on adiposity and adiposity-related metabolic disturbances in mice fed high-fat diet (HFD), and the potential underlying mechanisms focusing on the lipid metabolism and inflammatory response.

**Method and results:** C57BL/6J mice were fed HFD (45 kcal% fat) with or without HON (0.02%, w/w) or MAG (0.02%, w/w) for 16 wk. Despite no changes in body weight, food intake, and hepatic fat accumulation, HON and MAG significantly lowered the weight of white adipose tissue (WAT) as well as adipocyte size and protected against insulin resistance induced by HFD. These effects were associated with increases in energy expenditure and adipose fatty acid oxidation and decreases in fatty acid synthase activity and expression of genes related to fatty acid synthesis, desaturation, and uptake, as well as adipocyte differentiation in WAT. Moreover, HON and MAG significantly lowered the expression of proinflammatory genes in WAT and elevated the plasma IL-10 level. Particularly, HON significantly decreased the plasma resistin level and increased the plasma adiponectin level compared to the control group.

**Conclusion:** HON and MAG have potential as novel agents for amelioration of adiposity and associated insulin resistance and inflammation.

Received: February 8, 2013

Revised: May 6, 2013

Accepted: May 7, 2013

## Keywords:

Adipogenesis / Antiobesity / Honokiol / Inflammation / Magnolol



Additional supporting information may be found in the online version of this article at the publisher's web-site

**Correspondence:** Dr. Un Ju Jung, Center for Food and Nutritional Genomics Research, Kyungpook National University, 1370 San-Kyuk Dong, Puk-Ku, Daegu 702-701, Republic of Korea

**E-mail:** jungunju@naver.com

**Fax:** +82-53-958-1230

**Abbreviations:** **FAS**, fatty acid synthase; **FAT/CD36**, fatty acid translocase/cluster of differentiation 36; **HFD**, high-fat diet; **HOMA-IR**, homeostatic index of insulin resistance; **HON**, honokiol; **IPGTT**, intraperitoneal glucose tolerance test; **IRS2**, insulin receptor substrate 2; **MAG**, magnolol; **MCP-1**, monocyte chemoattractant protein-1; **NF-κB**, nuclear factor kappa-light-chain-enhancer of activated B cells; **PPAR-γ**, peroxisome pro-

## 1 Introduction

Obesity is defined as excessive fat accumulation that may have adverse effects on health [1]. It is well known as a potent risk factor for metabolic diseases including type 2 diabetes, dyslipidemia, atherosclerosis, hepatic steatosis, and cancer, and insulin resistance in obesity is the underlying cause for metabolic syndrome [2]. Obesity-induced inflammation, a key

liferator activated receptor- $\gamma$ ; **SCD1**, stearoyl-CoA desaturase; **SREBP1c**, sterol-regulatory-element-binding protein 1c; **TLR2**, toll-like receptor 2; **TNF- $\alpha$** , tumor necrosis factor- $\alpha$ ; **WAT**, white adipose tissue

\*These authors contributed equally to this work.

feature of adipose tissue dysfunction, has been proposed to be an important link between obesity and insulin resistance [3]. Adipose tissue can respond rapidly and dynamically to excess energy intake through adipocyte hypertrophy and hyperplasia [4], and enlarged adipose tissue results in altered production of various adipokines (e.g. adiponectin, resistin, and leptin) and inflammatory chemokines and cytokines (e.g. monocyte chemoattractant protein-1 (MCP-1), tumor necrosis factor- $\alpha$  (TNF- $\alpha$ ), IL-6, and IL-10), which impacts insulin sensitivity [5]. The level of circulating resistin and mRNA expression of proinflammatory chemokines and cytokines, including MCP-1 and TNF- $\alpha$ , in adipose tissue were increased in mice on a high-fat diet (HFD) that developed obesity and insulin resistance [6, 7]. In contrast, plasma adiponectin and anti-inflammatory IL-10 levels were low in subjects with obesity and type 2 diabetes, and they are positively correlated with insulin sensitivity [8, 9].

Consumption of a diet high in fat is considered a major factor in promoting obesity, insulin resistance, and other metabolic diseases in humans as well as in various animal models [4, 10, 11]. Conversely, high-level consumption of vegetables, fruits, and whole grains is associated with lower inflammation [10] and reduced risk for obesity and metabolic disease [11]. *Magnolia* plants have been used as Korean and Brazilian complementary and alternative medicines for the treatment of diabetes and diabetic complications [12] and as Japanese and Chinese traditional herb medicine for the treatment of various ailments, including fever, headache, anxiety, stroke, diarrhea, and anemia, due to their antithrombotic, antidepressant, and antibacterial properties [13]. Honokiol (HON) and magnolol (MAG) (Supporting Information Fig. 1), biphenolic structural isomers isolated from the stem bark of *Magnolia* plants, are considered as their major bioactive constituents [14]. It is reported that HON and MAG exert anti-inflammatory effects by inhibiting the downstream pathway of MEKK-1 in nuclear factor kappa-light-chain-enhancer of activated B cells (NF- $\kappa$ B) activation signaling [15]. MAG reduced fasting blood glucose and plasma insulin levels in type 2 diabetic rats without altering body weight [16], and induced glucose uptake in 3T3-L1 adipocytes [17]. HON also enhanced insulin signaling pathways such as the Ras/ERK1/2 and phosphoinositide-3-kinase/Akt signaling pathways [18], and ameliorated alcoholic steatosis by blocking fatty acid synthesis regulated by sterol-regulatory-element-binding protein 1c (SREBP1c) [19]. Moreover, a recent study showed that HON and MAG possessed antioxidant and anti-inflammatory activities, along with low cytotoxicity [20]. However, the effects of HON and MAG on diet-induced obesity have not been explored.

In the present study, we investigated whether HON and MAG attenuate adiposity, insulin resistance, hepatic steatosis, and inflammation in C57BL/6J mice fed HFD, a widely used animal model for obesity [21]. To elucidate their potential underlying mechanisms, we evaluated not only plasma adipokines and cytokines levels, but also the activity of lipid-regulating enzymes and/or the expression of genes involved

in lipid metabolism and inflammation in visceral adipose tissue and liver.

## 2 Materials and methods

### 2.1 Isolation and identification of HON and MAG

Commercially available air-dried bark of *Magnolia obovata* was purchased from Daikoshoyaku Co. Ltd. (Nagoya, Japan, lot 7G25M). *M. obovata* bark (dry weight, 3 kg) was extracted in methanol (8 L) for 2 wk. The evaporated methanol extract (362.5 g) was dissolved in distilled water, and successively fractionated with ethyl acetate (220.2 g), hexane (90.17 g), and 90% methanol (125 g). The 90% methanol-eluted fraction was fractionated using a silica gel open column (BW silica gel; BW-820M, Fuji Silysia Chemical Ltd., Japan; methanol and chloroform (0:1, 1:20, 1:10, 1:5, 1:1, and 1:0, v/v). Part of the eluted fractions was further fractionated using an octadecylsilyl silica gel (Cosmosil 75C18-OPN, 60% aqueous methanol to methanol). The eluted fractions were subsequently established as HON and MAG by the  $^1\text{H}$  NMR (400 MHz,  $\text{CDCl}_3$ ) and  $^{13}\text{C}$  NMR (100 MHz,  $\text{CDCl}_3$ ) spectra obtained on an FT NMR system (JEOL, Japan) (Supporting Information Figs. 2 and 3) [22].

### 2.2 Animals and diets

Obesity-prone C57BL/6J mice (4 wk old, male) were purchased from Jackson Laboratories (Bar Harbor, ME, USA). All mice were individually housed under a constant temperature (24°C) with a 12-h light/dark cycle, and fed a normal chow diet for acclimation for 1 wk after delivery. At 5 wk of age, they were randomly divided into three groups of ten mice each and fed an HFD (D12451, Research Diets, New Brunswick, NJ, USA) with or without HON (0.02%, w/w, approximately 17 mg/kg body weight per day) or MAG (0.02%, w/w, approximately 17 mg/kg body weight per day) for 16 wk. The HFD contains 45 kcal% fat, 20 kcal% protein, and 35 kcal% carbohydrate. In the HFD, 87.7% w/w of total fat was from lard, which contains high amounts of saturated fat, and 12.3% w/w of total fat was from soybean oil, an unsaturated fat source. They were given free access to food and distilled water, and food consumption and body weight were measured daily and weekly, respectively. At the end of the experimental period, all the mice were anesthetized with isoflurane (5 mg/kg body weight, Baxter, USA) after a 12-h fast, and blood samples were collected from the inferior vena cava into heparin-coated tube for determination of their plasma lipids, adipokines, and cytokines levels. The blood was centrifuged at  $1000 \times g$  for 15 min at 4°C, and the plasma was separated. After blood collection, epididymal white adipose tissue (WAT), perirenal WAT, retroperitoneal WAT, mesentery WAT, subcutaneous WAT, and liver were promptly removed, rinsed with physiological saline, and weighed. Among them, epididymal WAT

and liver were immediately frozen in liquid nitrogen and stored at  $-70^{\circ}\text{C}$  until enzyme activity and/or RNA analyses. Studies were performed under protocols for animal studies approved by the Kyungpook National University Ethics Committee (Approval No. KNU-2011–49).

### 2.3 Energy expenditure

Energy expenditure was measured using an indirect calorimeter (Oxylet; Panlab, Cornella, Spain). The mice were placed into individual metabolic chambers at  $25^{\circ}\text{C}$ , with free access to food and water.  $\text{O}_2$  and  $\text{CO}_2$  analyzers were calibrated with highly purified gas. Oxygen consumption and carbon dioxide production were recorded at 3-min intervals using a computer-assisted data acquisition program (Chart 5.2; AD Instrument, Sydney, Australia) over a 24-h period, and the data were averaged for each mouse. Energy expenditure was calculated according to the following formula:

$$\text{EE}(\text{kcal}/\text{day}/\text{bodyweight}^{0.75}) = \text{V}_{\text{O}_2} \times 1.44 \times [3.815 + (1.232 \times \text{V}_{\text{O}_2}/\text{V}_{\text{CO}_2})]$$

### 2.4 Fasting blood glucose, intraperitoneal glucose tolerance test (IPGTT), and homeostatic index of insulin resistance (HOMA-IR)

The blood glucose concentration was measured with whole blood obtained from the tail veins after withholding food for 12 h using a glucose analyzer (Glucocard, Arkray, Japan) based on the glucose oxidase method. The IPGTT was performed on the 15th wk. After a 12-h fast, the mice were injected intraperitoneally with glucose (0.5 g/kg body weight). The blood glucose level was determined from the tail vein at 0, 30, 60, and 120 min after the glucose injection. The cumulative changes in blood glucose responses were quantified by the incremental area under the curve. Homeostatic index of insulin resistance (HOMA-IR) was calculated according to the homeostasis of the assessment as follows:

$$\text{HOMA-IR} = [\text{fasting glucose}(\text{mmol}/\text{L}) \times \text{fasting insulin}(\mu\text{LU}/\text{mL})]/22.51$$

### 2.5 Plasma biomarkers

Plasma insulin, adipokines (adiponectin, resistin, and leptin), and cytokines (IL-10, IL-6, TNF- $\alpha$ , and MCP-1) were determined with a multiplex detection kit from Bio-Rad (Hercules, CA, USA). All samples were assayed in duplicate and analyzed with a Luminex 200 Labmap system (Luminex, Austin, TX, USA). Data analyses were done with Bio-Plex Manager software version 4.1.1 (Bio-Rad).

Plasma lipid concentrations were determined with commercially available kits: Plasma free fatty acid and phospholipid levels were measured using the Wako enzymatic kit (Wako Chemicals, Richmond, VA, USA), and triglyceride, total cholesterol, and HDL-cholesterol levels were determined using the Asan enzymatic kits (Asan, Seoul, Republic of Korea).

### 2.6 Hepatic lipids contents

Hepatic lipids were extracted [23], and then the dried lipid residues were dissolved in 1 mL of ethanol for triglyceride and cholesterol assays. Triton X-100 and a sodium cholate solution in distilled water were added to 200  $\mu\text{L}$  of the dissolved lipid solution for emulsification. The hepatic triglyceride and cholesterol contents were analyzed with the same enzymatic kit used for the plasma analysis.

### 2.7 Lipid-regulating enzyme activity

To measure the lipid-regulating enzymes activities in the epididymal WAT, samples were prepared and analyzed as previously described [24]. Briefly, fatty acid synthase (FAS) activity was determined with a spectrophotometric assay according to the method by Carl et al. [25]; one unit of FAS activity represented the oxidation of 1 nmol of NADPH per minute at  $30^{\circ}\text{C}$ . Carnitine palmitoyltransferase activity was determined according to the method by Markwell et al. [26] and the results were expressed as nmol/min/mg protein. Fatty acid  $\beta$ -oxidation was measured spectrophotometrically by monitoring the reduction of NAD to NADH in the presence of palmitoyl-CoA as described by Lazarow [27], with slight modification. Protein concentration was measured by the Bradford method using BSA as the standard [28].

### 2.8 Analysis of gene expression

Epididymal WAT and liver were homogenized in TRIzol reagent (Invitrogen Life Technologies, Grand Island, NY, USA) and total RNA was isolated according to the manufacturer's instructions. The total RNA was converted to cDNA using the QuantiTect Reverse Transcription Kit (Qiagen GmbH, Hilden, Germany). The RNA expression was quantified by quantitative real-time PCR using the QuantiTect SYBR green PCR kit (Qiagen GmbH) and the SDS7000 sequence-detection system (Applied Biosystems, CA, USA). Each cDNA sample was amplified using primers labeled with SYBR Green dye for glyceraldehyde-3-phosphate dehydrogenase. The amplification was performed as follows: 10 min at  $90^{\circ}\text{C}$ , 15 s at  $95^{\circ}\text{C}$ , and 60 s at  $60^{\circ}\text{C}$  for a total of 40 cycles. The cycle threshold values obtained were those cycles at which a statistically significant increase in the SYBR green emission intensity occurred. Ct data were normalized using glyceraldehyde-3-phosphate

**Table 1.** Effects of dietary HON and MAG supplementation on body weight, food intake, food efficiency ratio, and plasma adipokine, cytokine, and lipid levels in mice fed HFD for 16 wk

	CON	HON	MAG
Initial body weight (g)	18.60 ± 0.39	18.48 ± 0.48	18.27 ± 0.44
Final body weight (g)	44.76 ± 1.04	46.38 ± 0.82	45.13 ± 0.80
Body weight gain (g/day)	0.23 ± 0.009	0.25 ± 0.001	0.24 ± 0.005
Food intake (g/day)	3.96 ± 0.14	4.04 ± 0.09	4.01 ± 0.09
Food efficiency ratio	0.06 ± 0.003	0.06 ± 0.002	0.06 ± 0.002
Plasma			
Resistin (ng/mL)	575.91 ± 23.79 <sup>a)</sup>	403.33 ± 41.52 <sup>b)</sup>	517.91 ± 51.49 <sup>ab)</sup>
Adiponectin (μg/mL)	13.43 ± 0.41 <sup>a)</sup>	15.13 ± 0.40 <sup>b)</sup>	14.00 ± 0.37 <sup>ab)</sup>
IL-10 (ng/mL)	1049.12 ± 77.09 <sup>a)</sup>	1304.57 ± 59.76 <sup>b)</sup>	1258.58 ± 51.46 <sup>b)</sup>
Free fatty acid (mmol/L)	0.91 ± 0.07	0.89 ± 0.07	1.01 ± 0.06
Triglyceride (mmol/L)	1.10 ± 0.08	1.22 ± 0.21	1.38 ± 0.11
Phospholipid (mmol/L)	2.53 ± 0.14 <sup>a)</sup>	2.06 ± 0.14 <sup>b)</sup>	1.82 ± 0.16 <sup>b)</sup>
Total cholesterol (mmol/L)	4.64 ± 0.38	4.57 ± 0.29	4.26 ± 0.26
HDL cholesterol (mmol/L)	1.94 ± 0.26	1.77 ± 0.19	1.72 ± 0.17

Mean ± SEM ( $n = 10$ ).

<sup>ab)</sup> Means in the same row not sharing a common superscript are significantly different among groups at  $p < 0.05$ .

CON = mice fed a high-fat diet (HFD) alone; HON = honokiol (0.02%, w/w) supplemented mice fed an HFD; MAG = magnolol (0.02%, w/w) supplemented mice fed an HFD.

dehydrogenase, which was stably expressed in mice. Relative gene expression was calculated with the  $2^{-\Delta\Delta C_t}$  method [29]. Primer sequences are shown in the Supporting Information Table 1.

### 2.9 Histological analysis

Epididymal WAT and liver were fixed in a buffer solution of 10% formalin. Fixed tissues were processed routinely for paraffin embedding, and 4-μm sections were prepared and stained with hematoxylin eosin and/or Masson's trichrome. Stained areas were viewed using an optical microscope (Nikon, Tokyo, Japan) with a magnifying power of  $\times 200$ , and epididymal adipocyte size was measured with the Leica Application Suite software version 2.8.1 (Leica, Bensheim, Germany).

### 2.10 Statistical analysis

Data were expressed as the mean ± SEM. Significant differences among the groups were determined using one-way analysis of variance in SPSS (version 11.0, SPSS Inc., Chicago, IL, USA). Duncan's multiple-range test was performed if differences were identified between the groups at  $p < 0.05$ .

## 3 Results

### 3.1 Effect on food intake, body weight, body fat mass, and adipocyte morphology

There were no significant differences in daily food intake and body weight among the three groups during the 16-wk

feeding period (Table 1). However, the supplementation of dietary HON or MAG significantly reduced the weight of visceral WAT, including the epididymal and retroperitoneal WAT as well as the subcutaneous WAT compared to the HFD control group (Fig. 1A). Furthermore, histological analysis revealed that HON- and MAG-supplemented mice had a smaller epididymal adipocyte size relative to the control mice (Fig. 1B and C).

### 3.2 Effects on insulin sensitivity

We next examined whether HON and MAG influenced HFD-induced insulin resistance. The supplementation of dietary HON and MAG resulted in a significant decrease in HOMA-IR in HFD-fed mice, although the fasting blood glucose and plasma insulin levels were not significantly altered by HON and MAG supplementation (Fig. 2A–C). Furthermore, in the IPGTT, the blood glucose level was significantly lowered in the HON and MAG groups compared to the control group at 120 min after glucose loading (Fig. 2D). The level of area under the curve was also markedly decreased in the HON- and MAG-supplemented mice compared to the control obese mice (Fig. 2E).

### 3.3 Effect on plasma adipokines, cytokines, and lipids levels

The supplementation of dietary HON significantly reduced the plasma resistin level in HFD-fed mice compared to the control group, whereas plasma adiponectin and IL-10 levels were significantly higher in the HON group compared to the control group (Table 1). MAG also significantly increased

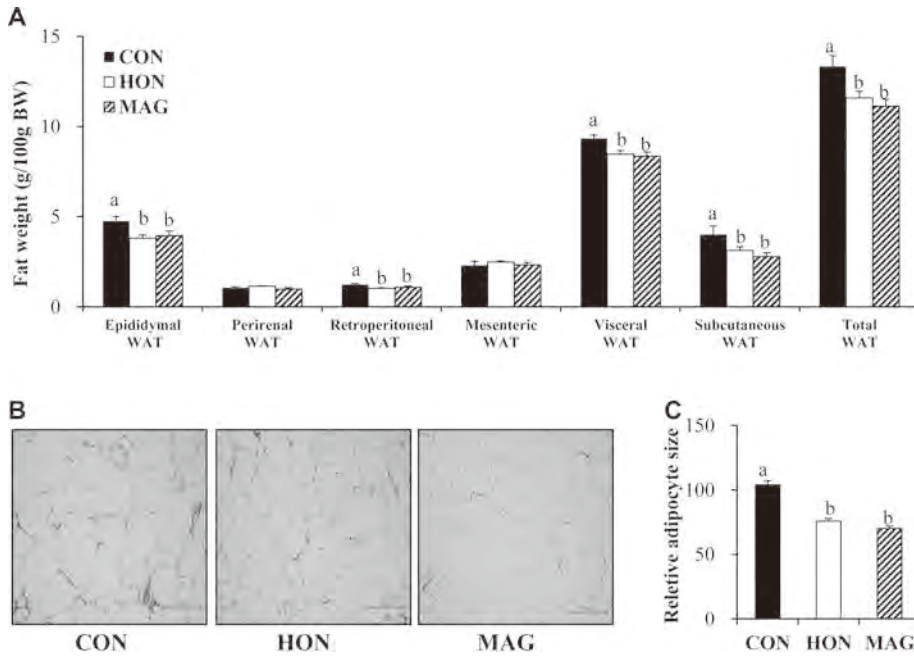


**Figure 1.** Effects of dietary HON and MAG on body fat mass (A) and adipocyte size (B and C) in mice fed HFD for 16 wk. (A and C) Data shown as the mean ± SEM ( $n = 10$ ). <sup>ab</sup>Means not sharing common letters are significantly different among the groups at  $p < 0.05$ . (B) Representative photographs of adipocytes in the epididymal WAT of mice, ×200 magnification. CON, mice fed a high-fat diet (HFD) alone; HON, honokiol (0.02%, w/w) supplemented mice fed an HFD; MAG, magnolol (0.02%, w/w) supplemented mice fed an HFD; WAT, white adipose tissue.

the plasma IL-10 level compared to the control group, and it showed a tendency to increase the adiponectin level and decrease the resistin level in plasma although they were not statistically significant. However, there were no significant differences in the plasma leptin, TNF- $\alpha$ , IL-6, and MCP-1 levels among the groups (data not shown). We also found that HON and MAG supplementation did not significantly affect the plasma free fatty acid, triglyceride, total cholesterol, and HDL-cholesterol levels in HFD-fed mice, while

plasma phospholipid level was lowered in the HON- and MAG-supplemented mice (Table 1).

### 3.4 Effect on energy expenditure and adipose lipid regulating enzyme activity

To determine how HON and MAG ameliorate adiposity induced by HFD, we measured energy expenditure and the activities of enzymes that can regulate lipid accumulation in

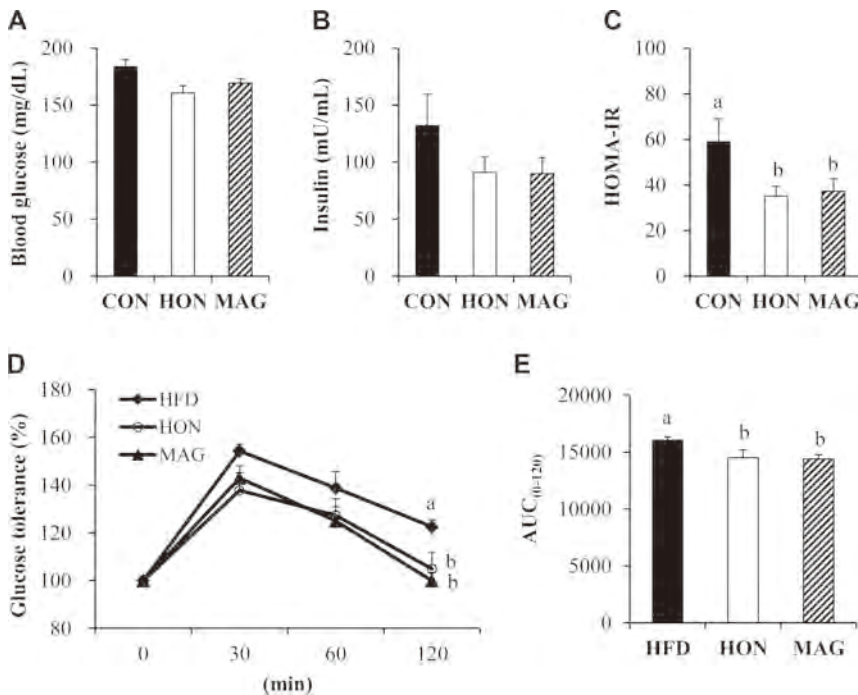


**Figure 2.** Effects of dietary HON and MAG on blood glucose (A), plasma insulin (B), HOMA-IR (C), and glucose tolerance (D and E) in mice fed HFD for 16 wk. Data shown as the mean ± SEM ( $n = 10$ ). <sup>ab</sup>Means not sharing common letters are significantly different among the groups at  $p < 0.05$ . CON, mice fed a high-fat diet (HFD) alone; HON, honokiol (0.02%, w/w) supplemented mice fed an HFD; MAG, magnolol (0.02%, w/w) supplemented mice fed an HFD; AUC, area under the curve; HOMA-IR, homeostatic index of insulin resistance.

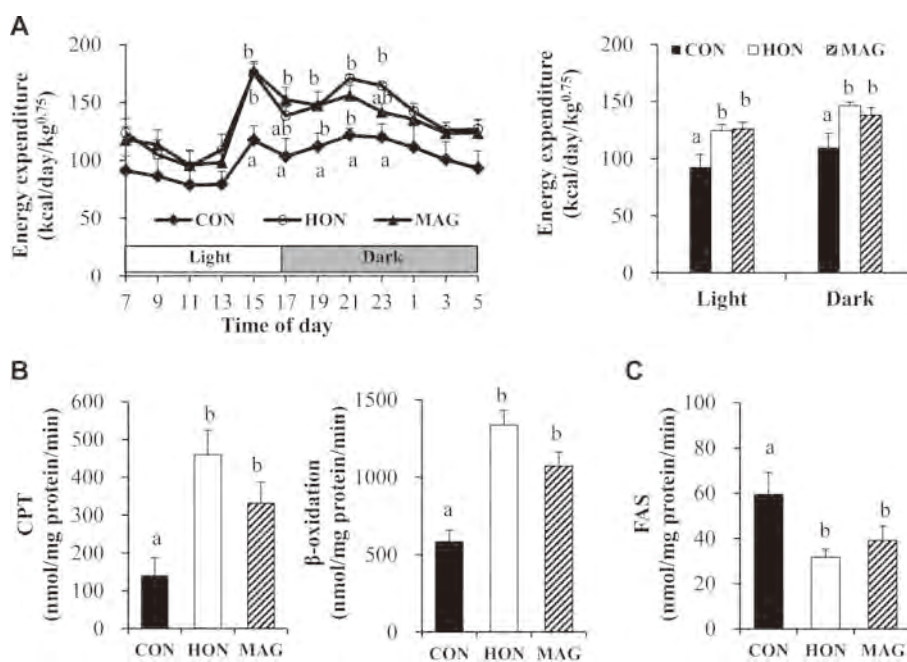


**Figure 3.** Effects of dietary HON and MAG on energy expenditure (A) and epididymal WAT lipid-regulating enzymes activities (B and C) in mice fed HFD for 16 wk. Data shown as the mean  $\pm$  SEM ( $n = 10$ ). <sup>ab</sup>Means not sharing common letters are significantly different among the groups at  $p < 0.05$ . CON, mice fed a high-fat diet (HFD) alone; HON, honokiol (0.02%, w/w) supplemented mice fed an HFD; MAG, magnolol (0.02%, w/w) supplemented mice fed an HFD; CPT, carnitine palmitoyltransferase; FAS, fatty acid synthase.

adipose tissue. HON- and MAG-supplemented mice showed a significant increase in energy expenditure during both the light and dark phases (Fig. 3A). Furthermore, dietary HON and MAG supplementation resulted in a significant increase in the activities of carnitine palmitoyltransferase and  $\beta$ -oxidation in the epididymal WAT (Fig. 3B). In contrast, the activity of FAS was significantly decreased in the epididymal WAT of HON- and MAG-supplemented mice compared to the control mice (Fig. 3C).

### 3.5 Effect on adipose gene expression involved in adipogenesis and inflammation

To understand the molecular mechanisms underlying the antiadipogenic role of HON and MAG, we assessed changes in the expression of genes controlling lipogenesis and adipocyte differentiation in epididymal WAT (Fig. 4A). The supplementation of HON as well as MAG significantly downregulated the mRNA expression of FAS, stearoyl-CoA desaturase 1 (SCD1), fatty acid translocase/cluster of differentiation 36 (FAT/CD36), and insulin receptor substrate (IRS2) in the epididymal WAT of HFD-fed mice. Furthermore, HON- and MAG-supplemented mice showed a significant decrease in the mRNA expression of their transcription factors, SREBP1c, and peroxisome proliferator activated receptor- $\gamma$  (PPAR- $\gamma$ ), in the epididymal WAT compared to the control mice.

Next, we explored whether HON and MAG influenced the expression of adipose inflammatory genes in HFD-fed mice (Fig. 4B). The mRNA levels of toll-like receptor 2 (TLR2) in HON and MAG groups were significantly lower than those in the control group. Moreover, the mRNA levels of proinflammatory cytokine, TNF- $\alpha$ , and its transcription factor NF- $\kappa$ B

were significantly downregulated in the epididymal WAT of HON- and MAG-supplemented mice compared to the control mice. However, there were no significant changes in the mRNA levels for TLR4, MCP-1, and IL-10 between the groups.

### 3.6 Effect on hepatic fat accumulation and hepatic gene expression involved in lipid metabolism and inflammation

We next examined the effects of HON and MAG on hepatic steatosis in HFD-fed mice. There were no significant changes in hepatic lipid droplet accumulation and hepatic triglyceride and cholesterol content (Fig. 5A and B). Also, the supplementation of HON and MAG did not significantly alter mRNA expression of genes and transcription factors involved in fatty acid and cholesterol synthesis, fatty acid  $\beta$ -oxidation, and inflammation in the liver of HFD-fed mice (Fig. 5C).

## 4 Discussion

Adipocyte hypertrophy (increase of cell size) and hyperplasia (increase of cell number) were observed in various rodent models, including HFD-fed mice, and adipocyte hypertrophy is the main contributor to the increase in body fat mass [4]. In particular, WAT is the primary site of fuel storage, mainly in the form of triglycerides, via the uptake of lipogenic substrate from the diet and de novo lipogenesis, and abnormal regulation of adipocyte differentiation as well as lipogenesis is linked to obesity [30]. We found that the

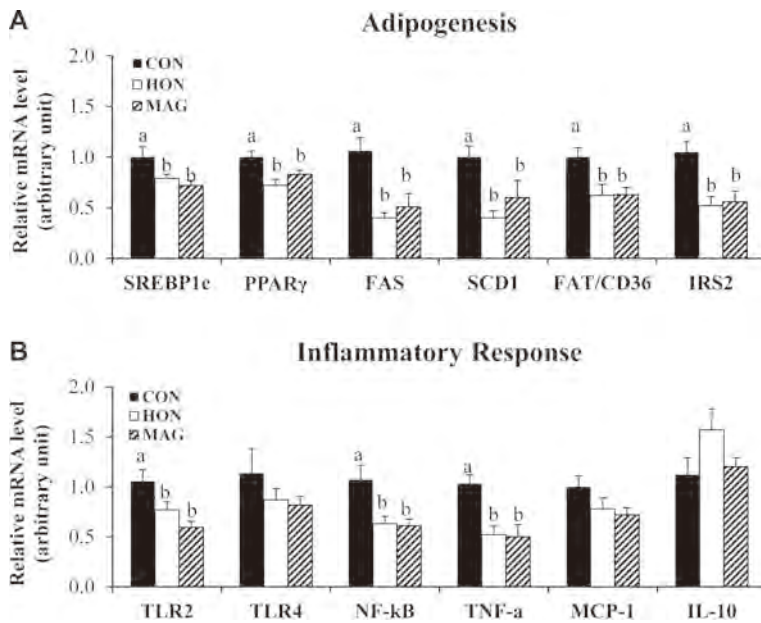


**Figure 4.** Effects of dietary HON and MAG on mRNA expression of genes related to adipogenesis (A) and inflammatory response (B) in epididymal WAT of mice fed HFD for 16 wk. Data shown as the mean  $\pm$  SEM ( $n = 10$ ). <sup>ab</sup>Means not sharing common letters are significantly different among the groups at  $p < 0.05$ . CON, mice fed a high-fat diet (HFD) alone; HON, honokiol (0.02%, w/w) supplemented mice fed an HFD; MAG, magnolol (0.02%, w/w) supplemented mice fed an HFD; FAS, fatty acid synthase; FAT/CD36, fatty acid translocase/cluster of differentiation 36; IRS2, insulin receptor substrate 2; MCP-1, monocyte chemoattractant protein-1; NF- $\kappa$ B, nuclear factor kappa-light-chain-enhancer of activated B cells; SCD1, stearoyl-CoA desaturase; PPAR- $\gamma$ , peroxisome proliferator activated receptor  $\gamma$ ; SREBP1c, sterol-regulatory-element-binding protein 1c; TLR2, toll-like receptor 2; TNF- $\alpha$ , tumor necrosis factor- $\alpha$ .

decrease of adipocyte size and body fat mass in HON- and MAG-supplemented mice was associated with a significant decrease in activity of FAS and in the mRNA expression of key genes involved in fatty acid synthesis (FAS, SCD1) and uptake (FAT/CD36) as well as adipocyte differentiation (IRS2) in epididymal WAT. Interestingly, HON and MAG did not alter body weight, which may be due to an increase in lean body mass or bone mass by these phytonutrients [31, 32], although we did not determine it.

The SREBP1c is highly expressed in adipose tissue and plays a central role in the induction of lipogenic genes such as FAS and SCD1 that catalyze the de novo synthesis of saturated and monounsaturated fatty acids, respectively [33, 34]. The expression of FAS was increased in the adipose tissue of both genetic and nutritional obese mice as well as patients with obesity and type 2 diabetes, whereas mice lacking FAS or SCD1 prevented obesity induced by HFD [35, 36]. PPAR- $\gamma$  is another important adipocyte transcription factor that can regulate the expression of a number of genes involved in lipid metabolism and adipocyte differentiation. The fatty acid transporter FAT/CD36, one of the target genes of PPAR- $\gamma$ , controls circulating fatty acids uptake into adipose tissue [37]. The mRNA level of FAT/CD36 was increased in the adipose tissue of animals with obesity and insulin resistance [38], whereas FAT/CD36 deficiency protected against adiposity and body weight gain in HFD-fed mice [37]. IRS2 gene expression was also increased in 3T3-L1 adipocytes and human primary adipocytes in response to the PPAR- $\gamma$  activator [39]. Miki et al. [40] have suggested that IRS2 plays a critical role in adipocyte differentiation through PPAR- $\gamma$  activation. PPAR- $\gamma$  activation was also related to the expression of FAS and SCD1 in adipose tissue [35, 41]. Taken together, our observation suggests that the downregulation of SREBP1c and PPAR- $\gamma$  gene expression by HON and MAG

supplementation may have numerous effects on various adipogenic pathways regulated by these transcription factors, including those that support lipogenesis and adipose differentiation. Furthermore, the protection from adiposity observed in HON- and MAG-supplemented mice may also be explained by the increased energy expenditure and fatty acid oxidation. In contrast to our in vivo findings, in vitro proadipogenic effects of HON and MAG have been reported [42–44], which may be due to the fact that the physiological conditions and complex interactions are absent in the in vitro system.

Excess adiposity, especially in visceral WAT, is considered to cause insulin resistance [4]. Although PPAR- $\gamma$  agonists such as thiazolidinedione acted as insulin sensitizer by potentiating insulin signaling in adipocytes [45], decreasing PPAR- $\gamma$  activity, either by PPAR- $\gamma$  antagonist treatment or by heterozygous PPAR- $\gamma$  deficiency, protected against HFD-induced adipocyte insulin resistance as well as hypertrophy in mice [46] as observed in the HON- and MAG-supplemented mice. Similarly, mice lacking FAS or SCD-1 either in all cells or specifically in adipocytes were protected from the deterioration of glucose homeostasis induced by HFD [34, 36, 47]. In addition, enhanced  $\beta$ -oxidation increased insulin sensitivity [48]. Thus, these results indicate that the antiadipogenic effects of HON and MAG partially account for overall improvement in insulin resistance.

In particular, the increase in insulin sensitivity by HON supplementation may also be related to the increased level of adiponectin and decreased level of resistin in plasma, since adiponectin and resistin have been considered as a potential link between obesity and insulin resistance [6, 8, 49–51]. Serum resistin was elevated in obesity and insulin resistance [6], and resistin deficiency in mice led to improved glucose homeostasis [49]. Conversely, circulating adiponectin

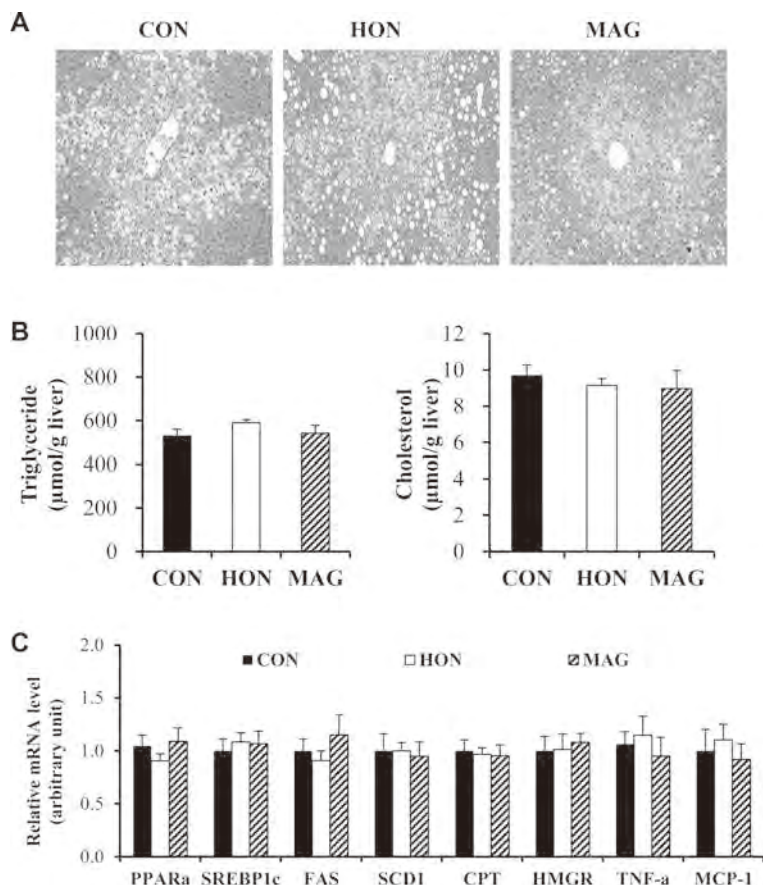


**Figure 5.** Effects of dietary HON and MAG on hepatic morphology (A), lipid content (B), and mRNA expression of genes related to lipid metabolism and inflammation (C) in mice fed HFD for 16 wk. (A) Hepatic lipid droplet accumulation in fixed transverse liver sections stained with hematoxylin and eosin. Original magnification  $\times 200$ . (B and C) Data shown as the mean  $\pm$  SEM ( $n = 10$ ). CON, mice fed a high-fat diet (HFD) alone; HON, honokiol (0.02%, w/w) supplemented mice fed an HFD; MAG, magnolol (0.02%, w/w) supplemented mice fed an HFD; CPT, carnitine palmitoyltransferase; FAS, fatty acid synthase; HMGR, 3-hydroxy-3-methylglutaryl-CoA reductase; MCP-1, monocyte chemoattractant protein-1; SCD1, stearoyl-CoA desaturase; PPAR- $\alpha$ , peroxisome proliferator activated receptor  $\alpha$ ; SREBP1c, sterol-regulatory-element-binding protein 1c; TNF- $\alpha$ , tumor necrosis factor- $\alpha$ .

level was negatively correlated with adiposity and insulin resistance [8]. Adiponectin-deficient mice showed glucose intolerance and insulin resistance [50], whereas overexpression of adiponectin ameliorated insulin resistance in mice [51]. Recently, the adiponectin–resistin ratio was suggested to be useful as integrated diagnostic biomarkers for insulin resistance [52].

In obesity, increased accumulation of adipose tissue is accompanied by chronic adipose inflammation, which has been proposed to have an important role in the pathogenesis of obesity-related insulin resistance [3]. Among several inflammatory pathways, HFD feeding activated the NF- $\kappa$ B proinflammatory signaling cascade in adipose tissues, which led to increased expression of several proinflammatory cytokines, including TNF- $\alpha$  and IL-6, in the adipose tissue of obese animals [53]. Furthermore, the innate immune receptors, TLR2 and TLR4, initiated signals that activate the NF- $\kappa$ B pathway [54]. The expression of TLR2 and TLR4 in adipose tissue was activated by HFD feeding, and mice lacking TLR2 or TLR4 were protected against HFD-induced insulin resistance by downregulating the expression of proinflammatory genes in adipose tissue [55, 56]. Interestingly, TLR2 deficiency did not alter circulating proinflammatory markers but reduced transcript abundance of proinflammatory mediators, including MCP-1 and TNF- $\alpha$ , in the adipose tis-

sue of HFD-fed mice [56]. In the current study, we observed that the mRNA expression of TLR2, NF- $\kappa$ B, and TNF- $\alpha$  was markedly decreased in the epididymal WAT of the HON- and MAG-supplemented mice. However, similar to a previous study [56], the supplementation of HON and MAG did not change the plasma TNF- $\alpha$  level, indicating that circulating TNF- $\alpha$  was not reflected within the epididymal WAT. Recently, Pamir et al. [57] also reported that transcript levels of several adipokines (e.g. TNF- $\alpha$ , MCP-1) did not reflect the overall plasma protein levels and suggested the possibility of dissociation between their transcript and protein levels and differences in cytokine clearance and/or utilization, which can occur between adipose and blood compartments.

Unlike proinflammatory TNF- $\alpha$  and MCP-1, IL-10 is an anti-inflammatory cytokine with a lower plasma level in animals and subjects with obesity and insulin resistance [9, 58]. IL-10 increased glucose uptake and protected adipocytes from TNF- $\alpha$ -induced insulin resistance [58]. It is reported to be a potent inhibitor of proinflammatory responses [59]. Thus, the beneficial effects of MAG and HON on diet-induced insulin resistance may be also partly due to the increased level of circulating IL-10 as well as the decreased expression of proinflammatory genes in adipose tissue.

In conclusion, this study first demonstrated that long-term supplementation of dietary HON and MAG ameliorates

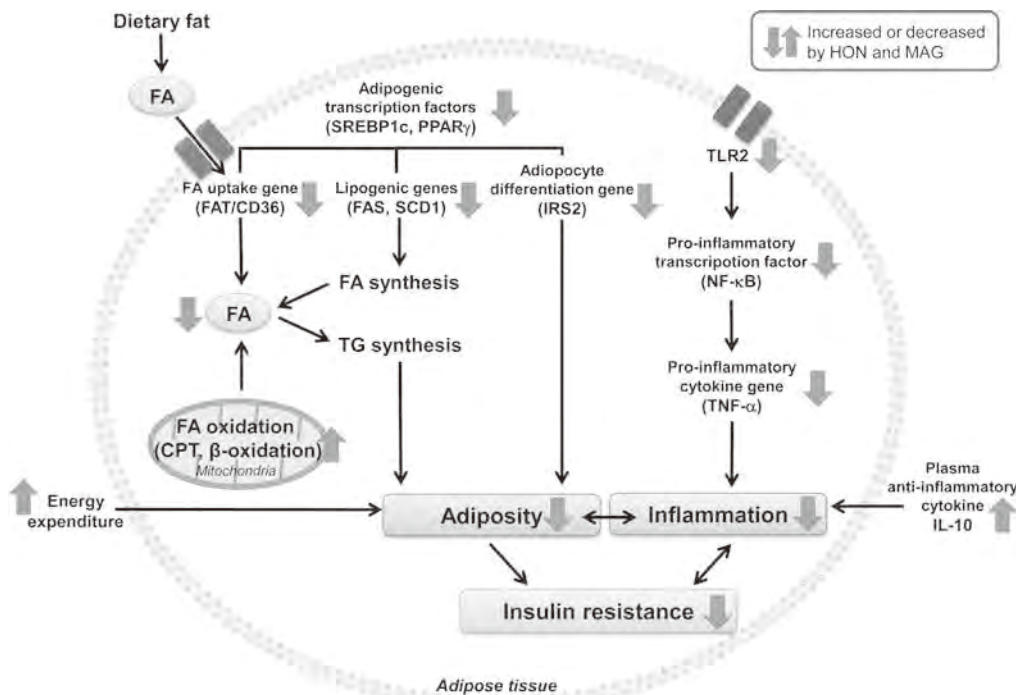


**Figure 6.** Proposed mechanisms of HON and MAG for antiobesity. The supplementation of HON and MAG downregulates mRNA expression of key adipogenic transcription factors, SREBP1c and PPAR- $\gamma$ , which in turn decreases mRNA expression of their target genes involved in fatty acid synthesis, fatty acid uptake, and adipocyte differentiation, as well as FAS activity in the epididymal WAT, and simultaneously increases energy expenditure along with the activities of CPT and  $\beta$ -oxidation in the epididymal WAT, indicating that these changes may be potential mechanisms for improving body fat accumulation and insulin resistance induced by HFD. Furthermore, the antiadiposity and insulin-sensitizing action of HON and MAG may be associated with the increased anti-inflammatory IL-10 level in plasma and downregulated mRNA expression of proinflammatory transcription factor NF- $\kappa$ B and its target gene TNF- $\alpha$  as well as TLR2 in epididymal WAT. CPT, carnitine palmitoyltransferase; FAS, fatty acid synthase; FAT/CD36, fatty acid translocase/cluster of differentiation 36; IRS2, insulin receptor substrate 2; NF- $\kappa$ B, nuclear factor kappa-light-chain-enhancer of activated B cells; PPAR- $\gamma$ , peroxisome proliferator activated receptor  $\gamma$ ; SCD1, stearoyl-CoA desaturase; SREBP1c, sterol-regulatory-element-binding protein 1c; TLR2, toll-like receptor 2; TNF- $\alpha$ , tumor necrosis factor- $\alpha$ .

adipogenesis in mice fed HFD by increasing energy expenditure and visceral WAT fatty acid oxidation and a simultaneous decrease in the expression of key genes involved in adipogenesis as well as enzyme activity for fatty acid synthesis in visceral WAT. Furthermore, HON and MAG exhibited a protective role against insulin resistance induced by HFD. These changes were partly associated with the downregulation of proinflammatory gene expression in visceral WAT and the increase of the anti-inflammatory IL-10 level in plasma. Figure 6 illustrates the possible mechanisms of the HON and MAG effects for antiobesity. Thus, our findings suggest that HON and MAG may be useful novel agents for the control of obesity and obesity-related insulin resistance.

*This research was supported by the Basic Science Research Program (number 2011-0022387) and the SRC program (Center for Food & Nutritional Genomics: number 2012-0000644) through the National Research Foundation of Korea (NRF) funded by the Ministry of Education, Science and Technology.*

*The authors have declared no conflict of interest.*

## 5 References

- [1] Rossner, S., Obesity: the disease of the twenty-first century. *Int. J. Obes.* 2002, 26, S2–S4.
- [2] Gallagher, E.-J., Leroith, D., Karnieli, E., Insulin resistance in obesity as the underlying cause for the metabolic syndrome. *Mt. Sinai. J. Med.* 2010, 77, 511–523.
- [3] Wellen, K.-E., Hotamisligil, G.-S., Inflammation, stress, and diabetes. *J. Clin. Invest.* 2005, 5, 1111–1119.
- [4] Jo, J., Gavrilova, O., Pack, S., Jou, W. et al., Hypertrophy and/or hyperplasia: dynamics of adipose tissue growth. *PLoS Comput. Biol.* 2009, 5, e1000324.
- [5] Antuna-Puente, B., Feve, B., Fellahi, S., Bastard, J.-P., Adipokines: the missing link between insulin resistance and obesity. *Diabetes Metab.* 2008, 34, 2–11.
- [6] Stepan, C.-M., Bailey, S.-T., Bhat, S., Brown, E.-J. et al., The hormone resistin links obesity to diabetes. *Nature* 2001, 409, 307–312.
- [7] Chiang, S.-H., Bazuine, M., Lumeng, C.-N., Geletka, L.-M. et al., The protein kinase IKKepsilon regulates energy balance in obese mice. *Cell* 2009, 138, 961–975.

- [8] Weyer, C., Hypoadiponectinemia in obesity and type 2 diabetes: close association with insulin resistance and hyperinsulinemia. *J. Clin. Endocrinol. Metab.* 2001, *86*, 1930–1935.
- [9] van Exel, E., Gussekloo, J., de Craen, A.-J., Frölich, M. et al., Low production capacity of interleukin-10 associates with the metabolic syndrome and type 2 diabetes: the Leiden 85-Plus Study. *Diabetes* 2002, *51*, 1088–1092.
- [10] Calder, P.-C., Ahluwalia, N., Brouns, F., Buetler, T., Dietary factors and low-grade inflammation in relation to overweight and obesity. *Br. J. Nutr.* 2011, *106*, S5–S78.
- [11] Heidemann, C., Scheidt-Nave, C., Richter, A., Mensink, G.-B., Dietary patterns are associated with cardiometabolic risk factors in a representative study population of German adults. *Br. J. Nutr.* 2011, *106*, 1253–1262.
- [12] Mors, W.-B., Rizzini, C.-T., Pereira, N.-A. (Eds.), *Medicinal Plants of Brazil*. Reference Publication, Inc., Michigan, 2002.
- [13] Tomas, S. C.-Li. (Ed.), *Chinese and Related North American Herbs: Phytopharmacology and Therapeutic Values*. CRC Press, Boca Raton, FL 2002.
- [14] Maruyama, Y., Kuribara, H., Overview of the pharmacological features of honokiol. *CNS Drug. Rev.* 2000, *6*, 35–44.
- [15] Lee, J., Jung, E., Park, J., Jung, K., Anti-inflammatory effects of magnolol and honokiol are mediated through inhibition of the downstream pathway of MEKK-1 in NF-kappaB activation signaling. *Planta. Med.* 2005, *71*, 338–343.
- [16] Sohn, E.-J., Kim, C.-S., Kim, Y.-S., Jung, D.-H., Effects of magnolol (5,5\_-diallyl-2,2\_-dihydroxybiphenyl) on diabetic nephropathy in type 2 diabetic Goto-Kakizaki rats. *Life Sci.* 2007, *80*, 468–475.
- [17] Choi, S.-S., Cha, B.-Y., Lee, Y.-S., Yonezawa, T. et al., Magnolol enhances adipocyte differentiation and glucose uptake in 3T3-L1 cells. *Life Sci.* 2009, *84*, 908–914.
- [18] Choi, S.-S., Cha, B.-Y., Iida, K., Sato, M. et al., Honokiol enhances adipocyte differentiation by potentiating insulin signaling in 3T3-L1 preadipocytes. *J. Nat. Med.* 2011, *65*, 424–430.
- [19] Yin, H.-Q., Kim, Y.-C., Chung, Y.-S., Kim, Y.-C. et al., Honokiol reverses alcoholic fatty liver by inhibiting the maturation of sterol regulatory element binding protein-1c and the expression of its downstream lipogenesis genes. *Toxicol. Appl. Pharmacol.* 2009, *236*, 124–130.
- [20] Murakami, Y., Kawata, A., Seki, Y., Koh, T. et al., Comparative inhibitory effects of magnolol, honokiol, eugenol and bis-eugenol on cyclooxygenase-2 expression and nuclear factor-kappa b activation in RAW264.7 macrophage-like cells stimulated with fimbriae of *Porphyromonas gingivalis*. *In Vivo* 2012, *26*, 941–950.
- [21] Collins, S., Martin, T.-L., Surwit, R.-S., Robidoux, J., Genetic vulnerability to diet-induced obesity in the C57BL/6J mouse: physiological and molecular characteristics. *Physiol. Behav.* 2004, *81*, 243–248.
- [22] Choi, S.-S., Cha, B.-Y., Iida, K., Sato, M. et al., Honokiol enhances adipocyte differentiation by potentiating insulin signaling in 3T3-L1 preadipocytes. *J. Nat. Med.* 2011, *65*, 424–430.
- [23] Folch, J., Lees, M., Sloan-Stanley, G. H., A simple method for isolation and purification of total lipids from animal tissues. *J. Biol. Chem.* 1957, *226*, 497–509.
- [24] Kim, H.-J., Lee, K.-T., Park, Y.-B., Jeon, S.-M. et al., Dietary docosahexaenoic acid-rich diacylglycerols ameliorate hepatic steatosis and alter hepatic gene expressions in C57BL/6J-Lep(ob/ob) mice. *Mol. Nutr. Food Res.* 2008, *52*, 965–973.
- [25] Carl, M.-N., Lakshmanan, M.-R., Porter, J.-W., Fatty acid synthase from rat liver. *Meth. Enzymol.* 1975, *35*, 37–44.
- [26] Markwell M, A.-K., McGroarty, E.-J., Bieber, L.-L., Tolbert, N.-E., The subcellular distribution of carnitine acyltransferases in mammalian liver and kidney. *J. Biol. Chem.* 1973, *248*, 3426–3432.
- [27] Lazarow, P.-B., Assay of peroxisomal  $\beta$ -oxidation of fatty acids. *Meth. Enzymol.* 1981, *72*, 315–319.
- [28] Bradford, M.-M., A rapid and sensitive method for the quantitation of microgram quantities of protein utilizing the principle of protein-dye binding. *Anal. Biochem.* 1976, *72*, 248–254.
- [29] Schmittgen, T.-D., Livak, K.-J., Analyzing real-time PCR data by the comparative C(T) method. *Nat. Protoc.* 2008, *3*, 1101–1108.
- [30] Moller, D.-E., Flier, J., Insulin resistance-mechanism, syndromes, and implications. *N. Engl. J. Med.* 1991, *325*, 938–948.
- [31] Anderson, R. A., Chromium and polyphenols from cinnamon improve insulin sensitivity. *Proc. Nutr. Soc.* 2008, *67*, 48–53.
- [32] Sacco, S. M., Horcajada, M. N., Offord, E., Phytonutrients for bone health during ageing. *Br. J. Clin. Pharmacol.* 2013, *75*, 697–707.
- [33] Kim, J.-B., Spiegelman, B.-M., ADD1/SREBP1 promotes adipocyte differentiation and gene expression linked to fatty acid metabolism. *Genes Dev.* 1996, *10*, 1096–1107.
- [34] Sampath, H., Miyazaki, M., Dobrzyn, A., Ntambi, J.-M., Stearoyl-CoA desaturase-1 mediates the pro-lipogenic effects of dietary saturated fat. *J. Biol. Chem.* 2007, *282*, 2483–2493.
- [35] Lodhi, I.-J., Yin, L., Jensen-Urstad, A.-P., Funai, K. et al., Inhibiting adipose tissue lipogenesis reprograms thermogenesis and PPAR- $\gamma$  activation to decrease diet-induced obesity. *Cell Metab.* 2012, *16*, 189–201.
- [36] Ntambi, J.-M., Miyazaki, M., Stoehr, J.-P., Lan, H. et al., Loss of stearoyl-CoA desaturase-1 function protects mice against adiposity. *Proc. Natl. Acad. Sci. USA* 2002, *99*, 11482–11486.
- [37] Hajri, T., Hall, A.-M., Jensen, D.-R., Pietka, T.-A. et al., CD36-facilitated fatty acid uptake inhibits leptin production and signaling in adipose tissue. *Diabetes* 2007, *56*, 1872–1880.
- [38] Priego, T., Sánchez, J., Palou, A., Picó, C., Leptin intake during the suckling period improves the metabolic response of adipose tissue to a high-fat diet. *Int. J. Obes.* 2010, *34*, 809–819.
- [39] Smith, U., Gogg, S., Johansson, A., Olausson, T. et al., Thiazolidinediones (PPARgamma agonists) but not PPARalpha agonists increase IRS-2 gene expression in 3T3-L1 and human adipocytes. *Faseb. J.* 2001, *15*, 215–220.

- [40] Miki, H., Yamauchi, T., Suzuki, R., Komeda, K. et al., Essential role of insulin receptor substrate 1 (IRS-1) and IRS-2 in adipocyte differentiation. *Mol. Cell. Biol.* 2001, 21, 2521–2532.
- [41] Yao-Borengasser, A., Rassouli, N., Varma, V., Bodles, A.-M. et al., Stearoyl-coenzyme A desaturase 1 gene expression increases after pioglitazone treatment and is associated with peroxisomal proliferator-activated receptor-gamma responsiveness. *J. Clin. Endocrinol. Metab.* 2008, 93, 4431–4439.
- [42] Choi, S.-S., Cha, B.-Y., Lee, Y.-S., Yonezawa, T. et al., Magnolol enhances adipocyte differentiation and glucose uptake in 3T3-L1 cells. *Life Sci.* 2009, 84, 908–914.
- [43] Alonso-Castro, A. J., Zapata-Bustos, R., Domínguez, F., García-Carrancá, A. et al., Magnolia dealbata Zucc and its active principles honokiol and magnolol stimulate glucose uptake in murine and human adipocytes using the insulin-signaling pathway. *Phytomedicine* 2011, 18, 926–933.
- [44] Choi, S.-S., Cha, B.-Y., Iida, K., Sato, M. et al., Honokiol enhances adipocyte differentiation by potentiating insulin signaling in 3T3-L1 preadipocytes. *J. Nat. Med.* 2011, 65, 424–430.
- [45] Jiang, G., Dallas-Yang, Q., Li, Z., Szalkowski, D. et al., Potentiation of insulin signaling in tissues of Zucker obese rats after acute and long-term treatment with PPARgamma agonists. *Diabetes* 2002, 51, 2412–2419.
- [46] Rieusset, J., Touri, F., Michalik, L., Escher, P. et al., A new selective peroxisome proliferator-activated receptor gamma antagonist with antiobesity and antidiabetic activity. *Mol. Endocrinol.* 2002, 16, 2628–2644.
- [47] Wueest, S., Rapold, R.-A., Schumann, D.-M., Rytka, J.-M. et al., Deletion of Fas in adipocytes relieves adipose tissue inflammation and hepatic manifestations of obesity in mice. *J. Clin. Invest.* 2010, 120, 191–202.
- [48] Perdomo, G., Commerford, S.-R., Richard, A.-M., Adams, S.-H. et al., Increased beta-oxidation in muscle cells enhances insulin-stimulated glucose metabolism and protects against fatty acid-induced insulin resistance despite intramyocellular lipid accumulation. *J. Biol. Chem.* 2004, 279, 27177–27186.
- [49] Banerjee, R.-R., Rangwala, S.-M., Shapiro, J.-S., Rich, A.-S. et al., Regulation of fasted blood glucose by resistin. *Science* 2004, 303, 1195–1198.
- [50] Maeda, N., Diet-induced insulin resistance in mice lacking adiponectin/ACRP30. *Nat. Med.* 2002, 8, 731–737.
- [51] Yamauchi, T., Kamon, J., Minokoshi, Y., Ito, Y. et al., Adiponectin stimulates glucose utilization and fatty-acid oxidation by activating AMP-activated protein kinase. *Nat. Med.* 2002, 8, 1288–1295.
- [52] Lau, C.-H., Muniandy, S., Novel adiponectin-resistin (AR) and insulin resistance (IRAR) indexes are useful integrated diagnostic biomarkers for insulin resistance, type 2 diabetes and metabolic syndrome: a case control study. *Cardiovasc. Diabetol.* 2011, 10, 1–8.
- [53] Cho, S., Choi, Y., Park, S., Park, T., Carvacrol prevents diet-induced obesity by modulating gene expressions involved in adipogenesis and inflammation in mice fed with high-fat diet. *J. Nutri. Biochem.* 2011, 23, 192–201.
- [54] Medzhitov, R., Toll-like receptors and innate immunity. *Nat. Rev. Immunol.* 2001, 1, 135–145.
- [55] Shi, H., Kokoeva, M.-V., Inouye, K., Tzameli, I. et al., TLR4 links innate immunity and fatty acid-induced insulin resistance. *J. Clin. Invest.* 2006, 116, 3015–3025.
- [56] Davis, J.-E., Braucher, D.-R., Walker-Daniels, J., Spurlock, M.-E., Absence of TLR2 protects against high-fat diet-induced inflammation and results in greater insulin-stimulated glucose transport in cultured adipocytes. *J. Nutri. Biochem.* 2011, 22, 136–141.
- [57] Pamir, N., McMillen, T.-S., Edgel, K.-A., Kim, F. et al., Deficiency of lymphotoxin- $\alpha$  does not exacerbate high-fat diet-induced obesity but does enhance inflammation in mice. *Am. J. Physiol. Endocrinol. Metab.* 2012, 302, E961–E971.
- [58] Lumeng, C.-N., Bodzin, J.-L., Saltiel, A.-R., Obesity induces a phenotypic switch in adipose tissue macrophage polarization. *J. Clin. Invest.* 2007, 117, 175–184.
- [59] Ouyang, W., Rutz, S., Crellin, N.-K., Valdez, P.-A. et al., Regulation and functions of the IL-10 family of cytokines in inflammation and disease. *Annu. Rev. Immunol.* 2011, 29, 71–109.

## Dehydroglyasperin C, a component of liquorice, attenuates proliferation and migration induced by platelet-derived growth factor in human arterial smooth muscle cells

Hyo Jung Kim<sup>1</sup>†, Byung-Yoon Cha<sup>2</sup>†, In Sil Park<sup>1</sup>, Ji Sun Lim<sup>1</sup>, Je-Tae Woo<sup>2</sup> and Jong-Sang Kim<sup>1</sup>\*

<sup>1</sup>*School of Applied Biosciences, Food Science and Biotechnology, BK21 Research Team for Developing Functional Health Food Materials, Kyungpook National University, Daegu 702-701, Republic of Korea*

<sup>2</sup>*Research Institute for Biological Functions, Chubu University, 1200 Matsumoto, Kasugai, Aichi, Japan*

(Submitted 10 August 2012 – Final revision received 2 November 2012 – Accepted 5 November 2012 – First published online 9 January 2013)

### Abstract

Liquorice is one of the botanicals used frequently as a traditional medicine in the West and in the East. Platelet-derived growth factor (PDGF)-BB is involved in the development of CVD by inducing abnormal proliferation and migration of vascular smooth muscle cells. In our preliminary study, dehydroglyasperin C (DGC), an active compound of liquorice, showed strong antioxidant activity. Since phytochemicals with antioxidant activities showed beneficial effects on chronic inflammatory diseases, the present study aimed to investigate the effects of DGC on PDGF-induced proliferation and migration of human aortic smooth muscle cells (HASMC). Treatment of HASMC with DGC for 24 h significantly decreased PDGF-induced cell number and DNA synthesis in a dose-dependent manner without any cytotoxicity, as demonstrated by the 3-(4,5-dimethyl-thiazol-2-yl)-2,5-diphenyltetrazolium bromide test and thymidine incorporation. Upon cell cycle analysis, DGC blocked the PDGF-induced progression through the G<sub>0</sub>/G<sub>1</sub> to S phase of the cell cycle, and down-regulated the expression of cyclin-dependent kinase (CDK); 2, cyclin E, CDK4 and cyclin D1. Furthermore, DGC significantly attenuated PDGF-stimulated phosphorylation of PDGF receptor-β, phospholipase C-γ1, AKT and extracellular-regulated kinase 1/2, and DGC inhibited cell migration and the dissociation of actin filaments by PDGF. In a rat vascular balloon injury model, DGC suppressed an excessive reduction in luminal diameters and neointimal formation compared with the control group. These results demonstrate the mechanistic basis for the prevention of CVD and the potential therapeutic properties of DGC.

**Key words:** Dehydroglyasperin C: Vascular smooth muscle cells: Platelet-derived growth factor-BB: Platelet-derived growth factor signalling pathway: Proliferation: Migration

Accumulation of vascular smooth muscle cells (VSMC) is a key event in the formation and development of lesions in atherosclerosis. The excessive accumulation of VSMC is due to a combination of directed migration from the media into the intima of the artery accompanied by proliferation and possibly decreased apoptosis. The proliferation and migration of VSMC are associated with vascular change through intimal lesion formation, and these can be induced by growth factors, such as PDGF. PDGF is expressed in various vascular cells such as VSMC, endothelial cells, platelets and macrophages, and platelet-derived growth factor-BB (PDGF-BB) is a more potent inducer of VSMC proliferation and migration than PDGF-AA and -AB<sup>(1–4)</sup>.

However, the mechanisms related to the PDGF-stimulated proliferation and migration of smooth muscle cells have not yet been fully elucidated. Several studies have shown that PDGF disrupts actin filament assembly and increases the expression of the PDGF-β receptor (PDGFR-β) in injured carotid arteries<sup>(5)</sup>. PDGF-BB developed intimal thickening and VSMC migration from the media to the intima in a rat model of angioplasty<sup>(6)</sup>. Consistent with the results, it has been shown that a selective PDGF-receptor tyrosine kinase blocker attenuated activation, migration, proliferation and neointimal formation after balloon injury in a swine model<sup>(7)</sup>. Some studies have also reported that phosphorylations of mitogen-activated protein kinases are related to PDGF-mediated cytoplasmic signalling such as DNA synthesis and the

**Abbreviations:** CDK, Cyclin-dependent kinase; DGC, dehydroglyasperin C; ERK, extracellular-regulated kinase; HASMC, human aortic smooth muscle cells; PDGF, platelet-derived growth factor; PDGFR-β, platelet-derived growth factor-β receptor; PLCγ1, phospholipase C-γ1; VSMC, vascular smooth muscle cells.

\* **Corresponding author:** J.-S. Kim, fax +82 53 950 6750, email vision@knu.ac.kr

† Both authors contributed equally to this work.

mitogenic process<sup>(8)</sup>, and the PDGF-induced activation of phospholipase C- $\gamma$ 1 (PLC $\gamma$ 1) and phosphatidylinositol-3 kinase/AKT is implicated in the induction of smooth muscle cell migration<sup>(9)</sup>. Furthermore, PDGF generates reactive oxygen species as a mediator of signal transduction to elicit its mitogenic effect. Thus, PDGF-BB and PDGFR signal transduction are essential for the development and pathogenesis of proliferative vascular disease.

Recently, several compounds from plants have exhibited beneficial effects in the regulation of atherosclerosis, heart diseases and autoimmune disorders. The antioxidant properties of these kinds of compounds have been suggested to explain their beneficial effects. Phytochemicals present in the Leguminosae family of plants have an inhibitory mechanism for PDGF-induced mitogenic signalling in mesangial cells<sup>(10)</sup>. Treatment with phytochemicals derived from soyabean by a biotic elicitor in human aortic VSMC resulted in a significant inhibition of PDGF-mediated cellular proliferation and migration<sup>(11)</sup>.

Liquorice, the *Glycyrrhiza* species (*Glycyrrhiza uralensis* Fisher), is one of the most frequently utilised plants as a traditional medicine and a natural sweetener since Egyptian, Greek and Roman times, and ancient China<sup>(12)</sup>. Besides antioxidant activity, liquorice root possesses potential beneficial effects against inflammation, viral infection, tumorigenesis, malaria and CVD<sup>(13–20)</sup>, as well as peptic ulcers, hepatitis C, and pulmonary and skin diseases<sup>(21,22)</sup>.

Glycoumarin (*G. uralensis*), glabridin (*Glycyrrhiza glabra*) and licochalcone A (*Glycyrrhiza inflata*) have the potential to function as indicators of liquorice<sup>(23)</sup>. As the other bioactive constituents present in liquorice, dehydroglyasperin C (DGC) and dehydroglyasperin D have shown increased PPAR- $\gamma$  ligand-binding activity and anti-inflammatory activity<sup>(12,24)</sup>, and isoangustone A has also shown antibacterial effects against methicillin-resistant *Staphylococcus aureus* (MRSA) strains<sup>(25)</sup>, suppression of inflammation in renal mesangial cells<sup>(26)</sup>, and induction of G<sub>1</sub> arrest and apoptosis in prostate cancer cells<sup>(27,28)</sup>.

Although the beneficial effect of liquorice has been postulated in several studies, the protective effect of DGC, a bioactive constituent of liquorice root, on atherosclerosis is not yet known. In the present study, the anti-atherosclerotic effects of DGC were evaluated, and it was found that this compound could inhibit PDGF-stimulated proliferation and migration of human aortic smooth muscle cells (HASMC).

## Experimental methods

### Preparation of dehydroglyasperin C

Purification of DGC from liquorice root was performed according to the method described previously<sup>(29)</sup>. Briefly, the *n*-hexane–ethanol extract of *G. uralensis* (90 g, 0.9% yield) was produced by dip extraction with *n*-hexane–ethanol at a ratio of 9:1 (v/v) of dried and ground roots of *G. uralensis* (1 kg). A portion of the extract (5.2 g) was subjected to flash column chromatography with silica gel (Macherey-Nagel Kieselgel), eluted by gradient systems of *n*-hexane–ethyl acetate

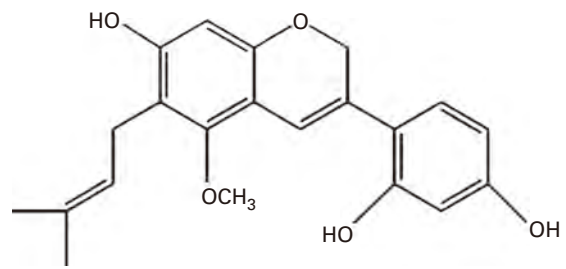


Fig. 1. Molecular structure of dehydroglyasperin C.

(5:5, v/v) to obtain twenty fractions. The fractions (0.7 g) showing NAD (P)H:quinone oxidoreductase 1 (NQO1) induction activity were combined and further purified by recrystallisation to recover compound 1 (35 mg). The structure of the compound was elucidated as DGC (Fig. 1) by comparison of the spectral data with an authentic sample.

### Cell culture

HASMC were obtained from Cascade Biologics, Inc. For routine maintenance, cells were grown in Dulbecco's modified Eagle's medium (Gibco) supplemented with 10% heat-inactivated fetal bovine serum at 37°C in an atmosphere of 5% CO<sub>2</sub>–95% air under saturating humidity and passaged every week (1:4 split ratio) by trypsinisation with 0.25% trypsin/0.02% EDTA sodium salt solution (Thermo Fisher Scientific, Inc.).

### Cell proliferation assay

The experimental procedures were performed according to previously described methods with some modifications. Briefly, HASMC were trypsinised and plated into ninety-well plates with DMEM at an initial concentration of  $1 \times 10^4$  cells per well, and incubated in an atmosphere consisting of 5% CO<sub>2</sub> in air at 37°C for 24 h. Then, the medium was removed and replaced by a medium containing various concentrations of the test compounds in serum-free DMEM. The bioassay was terminated on day 1 by removing the medium from the wells, and adding 3-(4,5-dimethyl-thiazol-2-yl)-2,5-diphenyltetrazolium bromide solution (0.5 mg/ml in phenol red-free culture medium). After 2 h, the solution was removed and 200  $\mu$ l dimethyl sulphoxide was added. After 10 min, absorbance was determined at 540 nm by a microplate reader (Tecan). Cell proliferation of each group was calculated as the relative absorbance of the treatment group to the control.

### DNA synthesis assay

Thymidine incorporation experiments were carried out according to a previously described method<sup>(30)</sup>. HASMC were cultured until they reached about 40% confluency. The culture medium was replaced with serum-free medium and incubated for 24 h. The serum-deprived cells were then pre-incubated with DGC for 24 h and stimulated with/without PDGF or with/without DGC for 20 h. After the incubation period, 1  $\mu$ Ci, (37 kBq) of [<sup>3</sup>H]thymidine was added to the

cultures and incubated for 4 h at 37°C. The cells were harvested using a Universal Harvester (Perkin Elmer), and transferred to a GF/C filter (Perkin Elmer). The filter was dried and the level of radioactivity was determined using a microplate scintillation and luminescence counter (TopCount NXT; Perkin Elmer). The values were calculated from absolute counts to a percentage of the control to allow comparison between the experimental groups.

#### Cell cycle analysis

Cell-cycle progression analysis was measured as described previously<sup>(31)</sup>. HASMC were seeded in six-well plates at  $2 \times 10^5$  cells/well and incubated until the cell density reached to 80% confluency; thereafter, the medium was replaced with serum-free medium and incubated for 24 h. The cells were then pre-incubated with DGC for 24 h and stimulated with/without PDGF or with/without DGC for 24 h. HASMC were harvested, resuspended in 70% ethanol and incubated at  $-20^\circ\text{C}$  for 4 h. The fixed cells were washed twice with PBS, and incubated at 37°C for 60 min using a solution containing DNase-free RNase (200 µg/ml). After incubation, the cells were stained with propidium iodide (50 µg/ml) at 4°C for 30 min and subjected to a flow cytometric analysis (Becton Dickinson).

#### Migration assay

Cell migration was measured with a modified Boyden transwell chamber (twenty-four-well plate) assay as described in our previous study<sup>(30)</sup>. Starved cells were trypsinised and cell suspension in a basal medium (500 µl,  $5 \times 10^4$  cells/well) was seeded in the upper chamber. Then, 760 µl of serum-free medium with or without experimental compounds were added to the lower chamber. After incubation for 24 h, the cells were labelled by the fluorescence dye calcein acetoxy-methyl ester (4 µg/ml). The cells that migrated to the lower chamber were measured with a fluorescence microplate reader at an excitation wavelength of 485 nm and an emission wavelength of 530 nm. Each treatment was repeated in three independent transwells.

#### Western blotting

HASMC were homogenised in pre-cooled radioimmunoprecipitation assay buffer (pH 7.4) containing 50 mM-Tris-Cl, 150 mM-NaCl, 1 mM-EDTA, 1% Triton-X, 0.5% sodium deoxycholate and 0.1% SDS. The homogenates were cleared by centrifugation at 7600 g for 5 min at 4°C, and the supernatants were denatured in sample buffer for 5 min at 95°C. Proteins were separated by electrophoresis on a 10% SDS-polyacrylamide gel for 1.5 h at 70–150 V and transferred onto nitrocellulose membranes (Amersham Biosciences) for 2 h at 250 mA. The membranes were incubated with antibodies to p-PDGFR-β, PDGFR-β, p-PLCγ1, PLCγ1, p-AKT, AKT, p-extracellular-regulated kinase, extracellular-regulated kinase (ERK), cyclin-dependent kinase (CDK)2, CDK4, cyclin D1, cyclin E and β-actin at dilutions of 1:1000 overnight at

4°C. The bands were detected using a chemiluminescence kit (Pierce). Densitometry analysis was performed with Lab Image software (Scion Corporation).

#### Angioplasty balloon surgery

Balloon injury in rats was performed as described previously<sup>(32)</sup>. All surgical procedures were performed according to the principles of the Kyungpook National University Animal Care and the Guild for the Care and Use of Laboratory Animals. The animals were divided into four groups: negative control (vehicle alone,  $n$  3); balloon injured only ( $n$  3); balloon injured plus DGC (0.5 mg,  $n$  3); balloon injured plus DGC (1 mg,  $n$  3); balloon injured plus DGC (2 mg,  $n$  3). Male Sprague–Dawley rats, 8 weeks old (Daehan Biolink), were anaesthetised using an intraperitoneal injection of Zoletil (1 ml/kg body weight) and Rompun (0.25 ml/kg body weight). The right carotid artery was surgically exposed and injured using a balloon catheter (Edwards Lifescience). After balloon injury, 100 µl of Pluronic gel with or without DGC were applied to the adventitial surface of the injured carotid rat artery.

#### Tissue preparation and morphological analysis

Carotid arteries were dissected, rinsed with physiological saline and weighed. The tissues were fixed in 10% buffered formalin (pH 7.6). The fixed tissues were serially sliced at a thickness of 5.0 µm using a microtome (Model RM 2125RT; Leica Microsystems). The sections were stained with Harry's haematoxylin–eosin, and the luminal, neointimal and medial areas of the different sections were quantified with light microscopy and an image analysis program (NIS-Elements F3.00; Nikon Corporation).

#### Statistical analysis

Data were tested by ANOVA, followed by Duncan's multiple range test, using SPSS software (SPSS, Inc.). The level of significance was set at  $P < 0.05$ .

## Results

### *Effects of dehydroglyasperin C on human aortic smooth muscle cell proliferation and platelet-derived growth factor-stimulated cycle progression*

When HASMC were stimulated by PDGF-BB (20 ng/ml), the number of cells was increased by about 35% compared with the control group. Treatment of PDGF-stimulated HASMC with DGC (0.1–1 µM) resulted in a significant decrease in cell number, which was not a result of cell death. The ratio of inhibition was 17.3 (SD 3.0), 15.7 (SD 7.8) and 31.0 (SD 6.7)% at 0.1, 0.5 and 1 µM, respectively (Fig. 2(A)). There was no significant change in cell morphology in the cultures treated with PDGF plus DGC (data not shown).

To confirm the effect of DGC on VSMCC proliferation, we performed DNA synthesis analysis. The effect of DGC on DNA synthesis was assayed by [<sup>3</sup>H]thymidine incorporation.

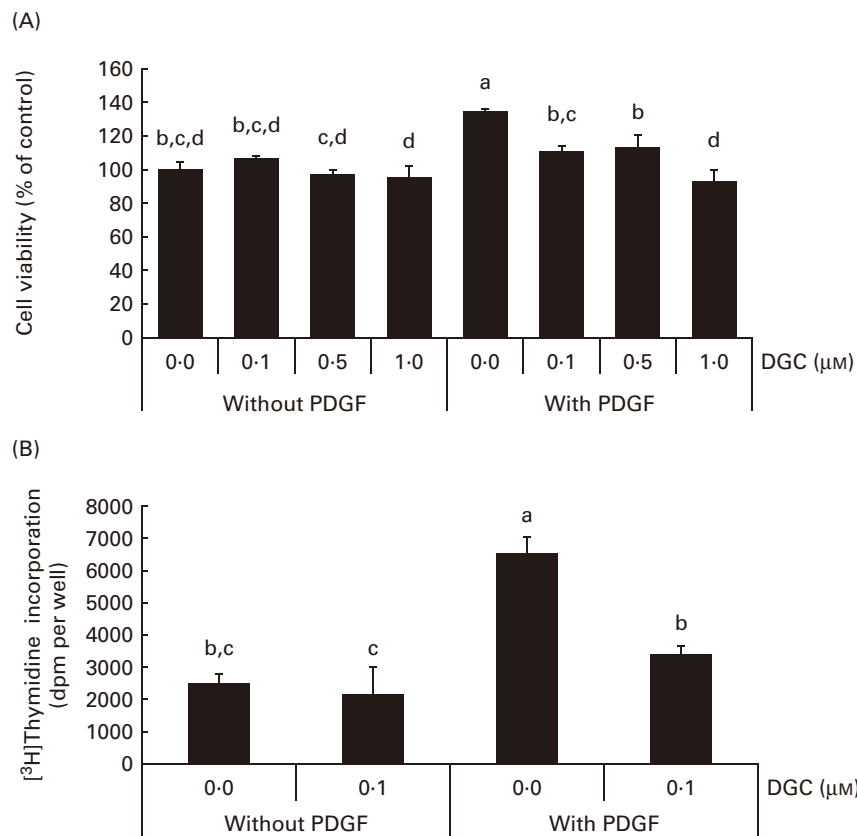


**Fig. 2.** Effects of dehydroglyasperin C (DGC) on platelet-derived growth factor (PDGF)-induced proliferation of human aortic smooth muscle cells (HASMC). HASMC were treated with or without 1 μM-DGC in the presence or absence of 20 ng/ml PDGF after pre-incubation with or without DGC for 24 h. After incubation for 20–24 h, the cells were processed for the 3-(4,5-dimethyl-thiazol-2-yl)-2,5-diphenyltetrazolium bromide assay (A) or [<sup>3</sup>H]thymidine incorporation (B) as described in the Experimental methods section. Values are means of three separate independent experiments, with standard deviations represented by vertical bars. <sup>a,b,c,d</sup>Mean values with unlike letters were significantly different (*P* < 0.05).

As shown in Fig. 2(B), incubation of the cells with 20 ng/ml of PDGF led to a significant increase in [<sup>3</sup>H]thymidine incorporation, which corresponded to approximately a 2.6-fold increase in vehicle-stimulated cells. DGC effectively inhibited the PDGF-induced [<sup>3</sup>H]thymidine incorporation into DNA. The inhibition percentage of DGC was about 47.9 (SD 4.1)% at 1 μM. These data demonstrate that DGC blocks DNA synthesis in VSMC, resulting in the attenuation of proliferation.

The DNA content was also analysed by propidium iodide staining to investigate the effect of DGC on cell cycle progression in HASMC. PDGF-BB induced an increase in the S phase from 3.4 to 30.5% compared with the non-stimulated cells. DGC decreased the accumulation at the S phase to 4.6% with 0.1 μM, 5.9% with 0.5 μM and 5.7% with 1 μM in PDGF-treated cells. These results indicate that DGC was effective in arresting PDGF-stimulated cell cycle progression in HASMC (Fig. 3(A) and (B)).

*Effects of dehydroglyasperin C on the expression of cell cycle-related proteins*

Growth factors increase the expression of cyclin D1 in the G<sub>1</sub> phase of the cell cycle to allow entry of the cells into the S phase. Cell cycle progression is tightly regulated through a complex network of positive and negative cell-cycle

regulatory molecules such as CDK and cyclins. Along with CDK4, the expression of cyclin E-dependent kinase CDK2 is also essential for the progression of the cells from the G<sub>1</sub> to the S phase<sup>(33)</sup>. To investigate whether the inhibition of proliferation by DGC is involved in the regulation of cell cycle-related proteins, we assessed the expression of G<sub>1</sub>-checkpoint proteins in DGC-treated cycle-arrested cells. As shown in Fig. 3(C), we observed slightly decreased levels of CDK4, cyclin D1, CDK2 and cyclin E in cells incubated with DGC (1 μM). Therefore, these findings suggest that DGC affects the transition of HASMC from the G<sub>1</sub> to the S phase, together with its inhibitory effects on HASMC proliferation.

*Effects of dehydroglyasperin C on the platelet-derived growth factor-induced signalling pathway*

Several phospho-specific antibodies were used to quantify the PDGF-regulated downstream molecules. PDGF-induced activated proteins such as PDGFR-β, PLCγ1 and AKT were detected to determine the inhibitory mechanism of DGC on the signal transduction pathway of PDGF for HASMC proliferation and migration. HASMC were stimulated with PDGF-BB (20 ng/ml) for 15 min, which caused the obvious phosphorylation of PDGFR-β, PLCγ1 and AKT, and the increased phosphorylation

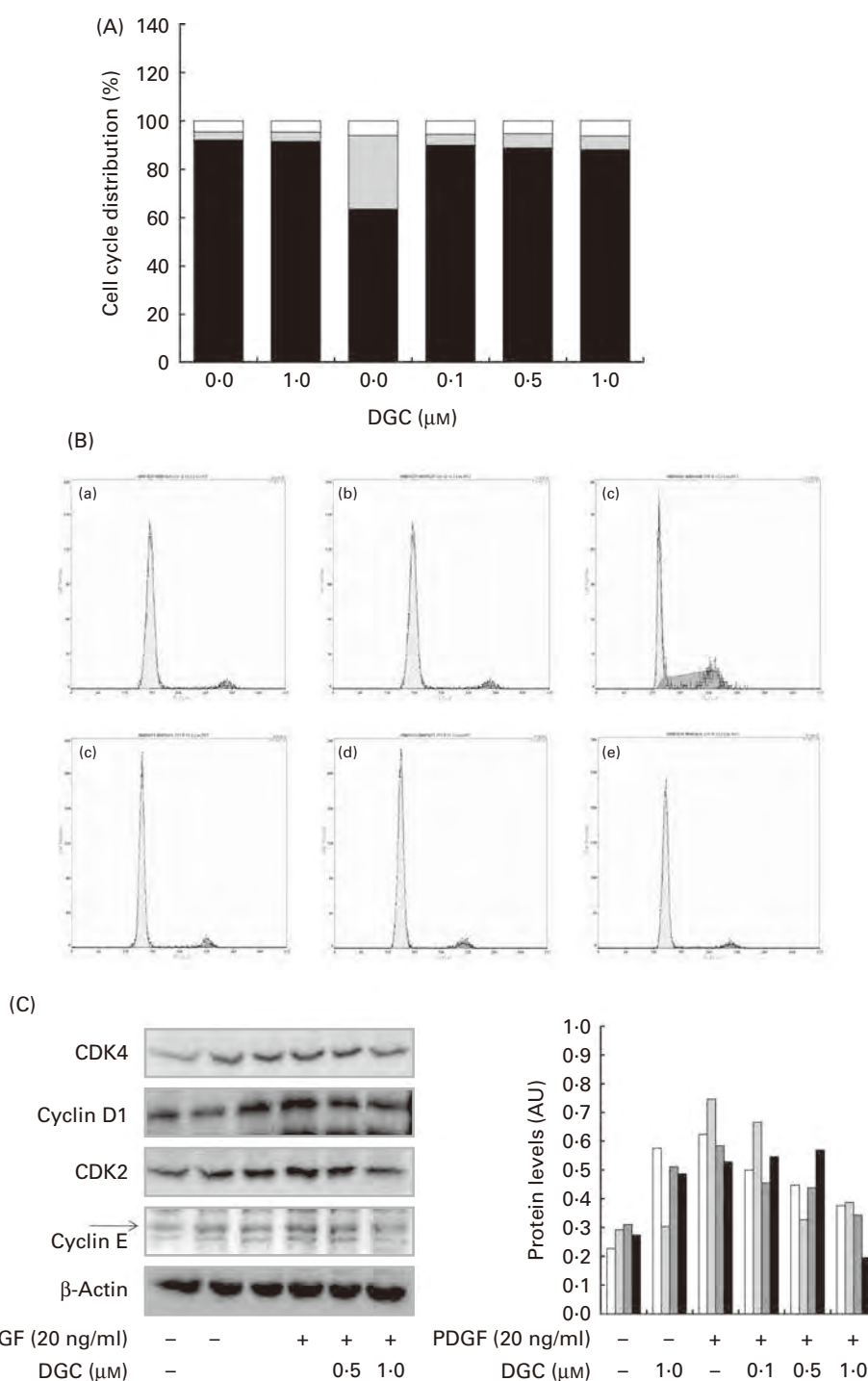


**Fig. 3.** Effects of dehydroglyasperin C (DGC) on cell cycle progression in human aortic smooth muscle cells (HASMC) stimulated by platelet-derived growth factor (PDGF). HASMC were treated as described in Fig. 2. (A) Representative DNA histograms of propidium iodide fluorescence in cells assessed by flow cytometry are shown. □, G<sub>2</sub>/M; ▤, S; ■, G<sub>0</sub>/G<sub>1</sub>. (B) For evaluation of the expression of proteins related to cell cycle progression, whole-cell extracts (20 μg) were subjected to (C) Western blot analysis for CDK4 (□), cyclin D1 (▤), CDK2 (▥) or cyclin E (■). AU, arbitrary units. (A colour version of this figure can be found online at <http://www.journals.cambridge.org/bjn>).

was suppressed with various concentrations of DGC (0.1, 0.5 and 1 μM), suggesting that the anti-proliferative effect of DGC was implicated in the early signal transduction by PDGF (Fig. 4(A)–(C)). Since PDGF is capable of inducing the activation of mitogen-activated protein kinases for VSMC proliferation<sup>(9)</sup>, we investigated the effects of DGC on the PDGF

signalling pathway by measuring the phosphorylation levels of ERK1/2 with Western blotting (Fig. 4(D)) in HASMC. The results showed that PDGF substantially increased ERK1/2 phosphorylation, whereas cells incubated with DGC at various concentrations (0.1, 0.5 and 1 μM) diminished ERK1/2 phosphorylation in a dose-dependent manner.

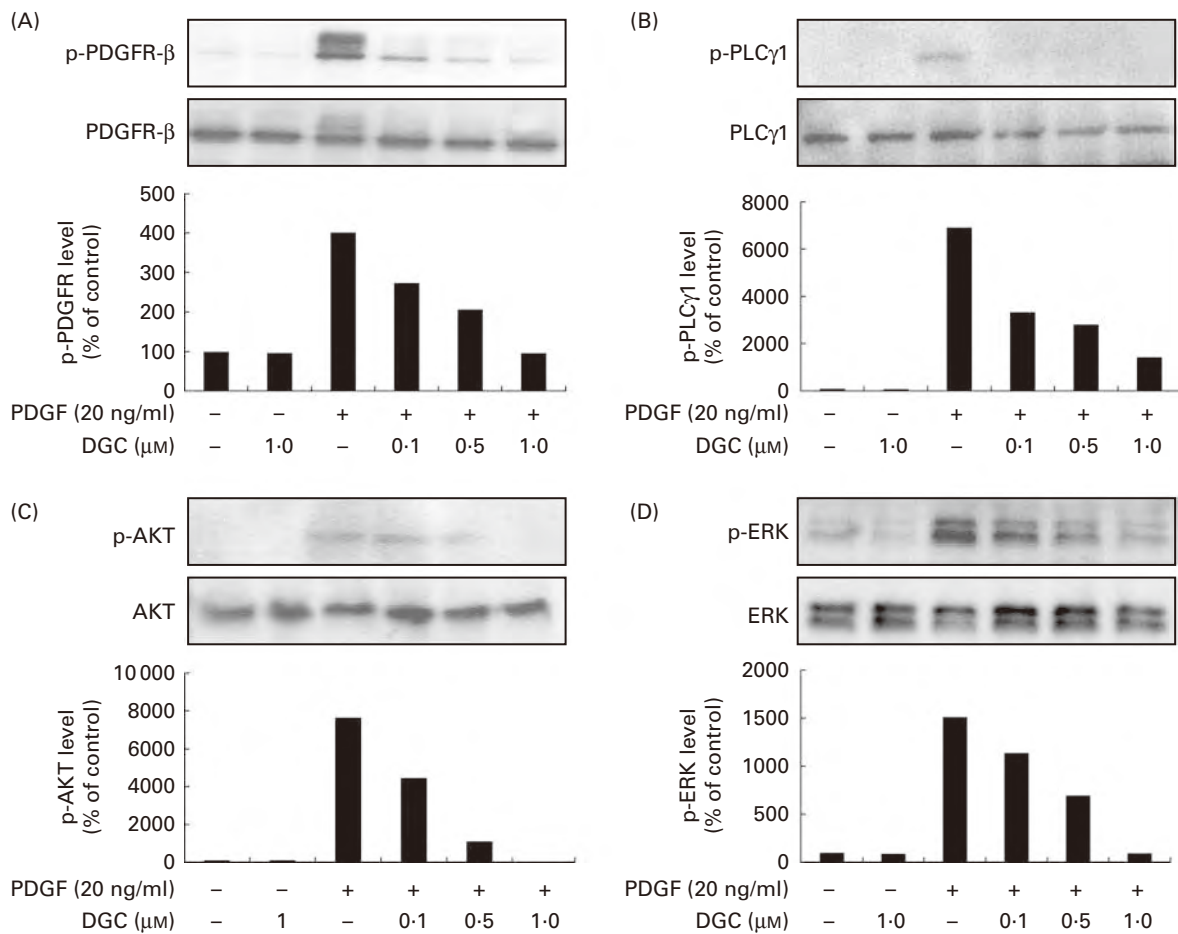


**Fig. 4.** Effects of dehydroglyasperin C (DGC) on the platelet-derived growth factor (PDGF) signalling pathway. Western blot of the phosphorylation of (A) PDGF receptor-β (PDGFR-β), (B) phospholipase C-γ1 (PLC-γ1) and (C) AKT, and (D) the activation of mitogen-activated protein kinases was performed for human aortic smooth muscle cells treated with or without 20 ng/ml of PDGF-BB for 15 min after pre-incubation with DGC for 24 h.

*Effects of dehydroglyasperin C on platelet-derived growth factor-stimulated migration of human aortic smooth muscle cells*

VSMC migration is affected by the stimulation of PDGFR-β by PDGF<sup>(32)</sup>. In order to investigate the effects of DGC on HASMC migration, the cells were treated for 24 h with different concentrations of DGC in the presence or absence of PDGF in a Boyden chamber. The cells migrated to the lower chamber were stained with calcein acetoxyethyl ester, and were photographed with a fluorescence microscope. As shown in Fig. 5, treatment with DGC alone had no significant effect on HASMC migration compared with the vehicle-treated cells. However, PDGF significantly increased the migration up to about 304.4 (SD 29.1)%, while DGC effectively inhibited the PDGF-stimulated cell migration at 1 μM.

*Effects of dehydroglyasperin C on the rearrangement of actin filaments induced by platelet-derived growth factor*

Regardless of the cell type, since effective reorganisation of the actin cytoskeleton is absolutely important for migration<sup>(34)</sup>, we attempted to determine the effects of DGC on the PDGF-induced rearrangement of actin filaments (Fig. 6).

Indeed, we observed that HASMC underwent a reorganisation of actin after the addition of PDGF, and DGC alone did not show any change in the actin microfilaments of HASMC. On the contrary, incubation with DGC (1 μM) in the presence of PDGF blocked the loss of microfilaments, and the appearance of the actin filaments looked similar in the cells treated with either the vehicle or DGC alone.

*Dehydroglyasperin C inhibits neointimal formation in an animal model of angioplasty restenosis*

DGC induced a dose-dependent reduction in intimal hyperplasia compared with the untreated group (Fig. 7(A) and (B)). Treatment with DGC inhibited the balloon injury-induced decrease in the luminal area (balloon injured only, 0.146 (SD 0.001); balloon injured plus DGC (0.5 mg), 0.219 (SD 0.005); balloon injured plus DGC (1 mg), 0.261 (SD 0.006); balloon injured plus DGC (2 mg), 0.285 (SD 0.024)). As shown in Fig. 7(B), a significant reduction in the luminal area by DGC was related to the intima:media area ratio. In addition to the reduction in the medial area (about 18%), the DGC-treated group also showed a reduced neointima:media area ratio than the vehicle-loaded Pluronic

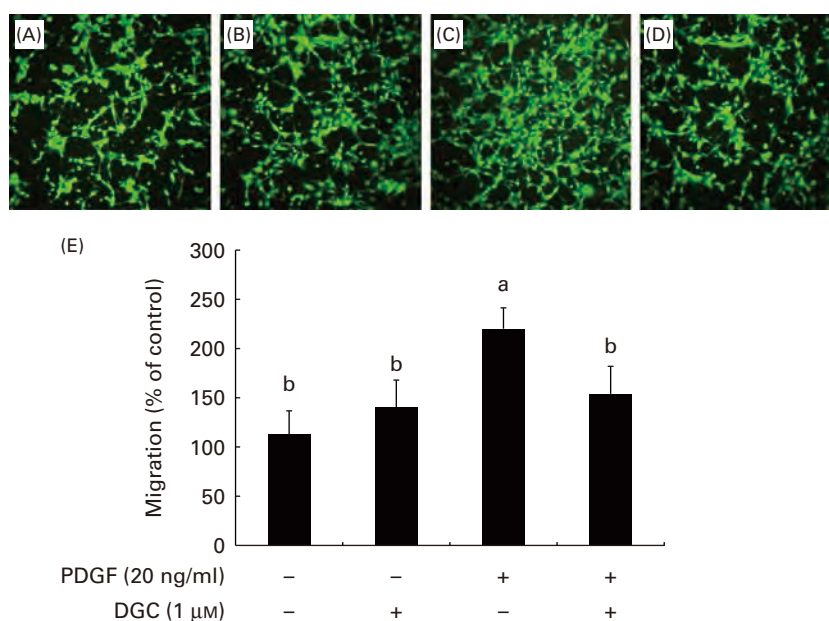


**Fig. 5.** Effects of dehydroglyasperin C (DGC) on platelet-derived growth factor (PDGF)-induced migration of human aortic smooth muscle cells (HASMC). HASMC were seeded onto the transwell plate with or without 1  $\mu$ M-DGC in the presence or absence of 20 ng/ml of PDGF-BB for 24 h. The migrated HASMC were analysed with fluorescence calcein acetoxyethyl ester staining. The representative photomicrographs of the migrated cells to the lower chambers after calcein acetoxyethyl ester staining are shown as follows: (A) control; (B) DGC (1  $\mu$ M); (C) PDGF; (D) PDGF + DGC (1  $\mu$ M). The percentage of migrated cells relative to the control is shown in the bar graph (E). Values are means of three separate independent experiments, with standard deviations represented by vertical bars. <sup>a,b</sup> Mean values with unlike letters were significantly different ( $P < 0.05$ ). (A colour version of this figure can be found online at <http://www.journals.cambridge.org/bjn>).

gel group in a dose-dependent manner (balloon injured plus DGC (0.5 mg), approximately 38%; balloon injured plus DGC (1 mg), approximately 68%; balloon injured plus DGC (2 mg), approximately 84%).

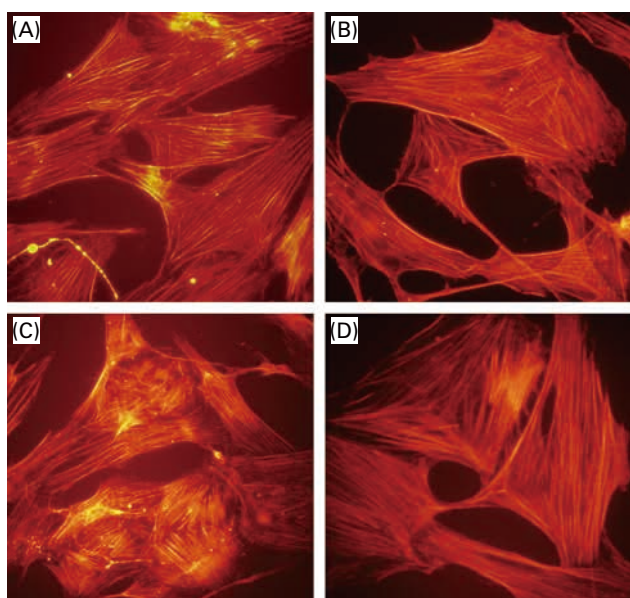


**Fig. 6.** Effects of dehydroglyasperin C (DGC) on platelet-derived growth factor (PDGF)-stimulated cytoskeletal reorganisation. The cells grown on a coverslip were treated with or without 1  $\mu$ M-DGC in the presence or absence of 20 ng/ml of PDGF-BB for 24 h. The cells were fixed, and the actin filaments were stained with rhodamine phalloidine and photographed using a fluorescent microscope. (A) Control; (B) DGC (1  $\mu$ M); (C) PDGF; (D) PDGF + DGC (1  $\mu$ M). Magnification 200 $\times$ . (A colour version of this figure can be found online at <http://www.journals.cambridge.org/bjn>).

## Discussion

VSMC are major cells present in arterial structures, and play a very important role in the maintenance of normal vascular structures and functions. VSMC are normally quiescent, at low proliferative indices, and remain in the  $G_0/G_1$  phase of the cell cycle<sup>(35)</sup>. The growth of VSMC is an indicator for the formation and development of atherosclerosis through proliferative responses and promoting the expression of other growth factors in VSMC<sup>(36,37)</sup>.

Several studies have shown that liquorice-derived compounds have beneficial effects on atherosclerotic processes including the adhesion and migration of leucocytes<sup>(19)</sup>, development of visceral obesity, regulation of HDL levels<sup>(18)</sup> and lipidaemia<sup>(20)</sup>, and vascular growth factor-induced proliferation of VSMC<sup>(38)</sup>. In addition to vascular protective effects, liquorice is also known to possess antioxidant activity<sup>(16)</sup>.

Although the constituents of liquorice are desirable candidates acting as anti-atherosclerotic agents, little is known regarding their effects on PDGF-induced proliferation and migration of VSMC. In the present study, we tested the inhibitory effects of DGC on PDGF-induced proliferation and migration of HASMC, and attempted to explain its associated mechanisms. PDGF was used as a positive control to evaluate the effect of DGC on the proliferation of VSMC. We provide the first evidence that DGC inhibits PDGF-stimulated proliferation and DNA synthesis without induced apoptosis.

pRb, CDK, cyclins, CDK inhibitor proteins, p21<sup>cip1</sup> and p27<sup>kip1</sup>, and tumour-suppressor proteins including p53<sup>(33,39,40)</sup> are implicated in controlling the cell cycle for the  $G_1$ , S,  $G_2$  and M phases. While normal VSMC maintain the  $G_0$  phase for a quiescent state, an increase in the accumulation of VSMC in the intima and media

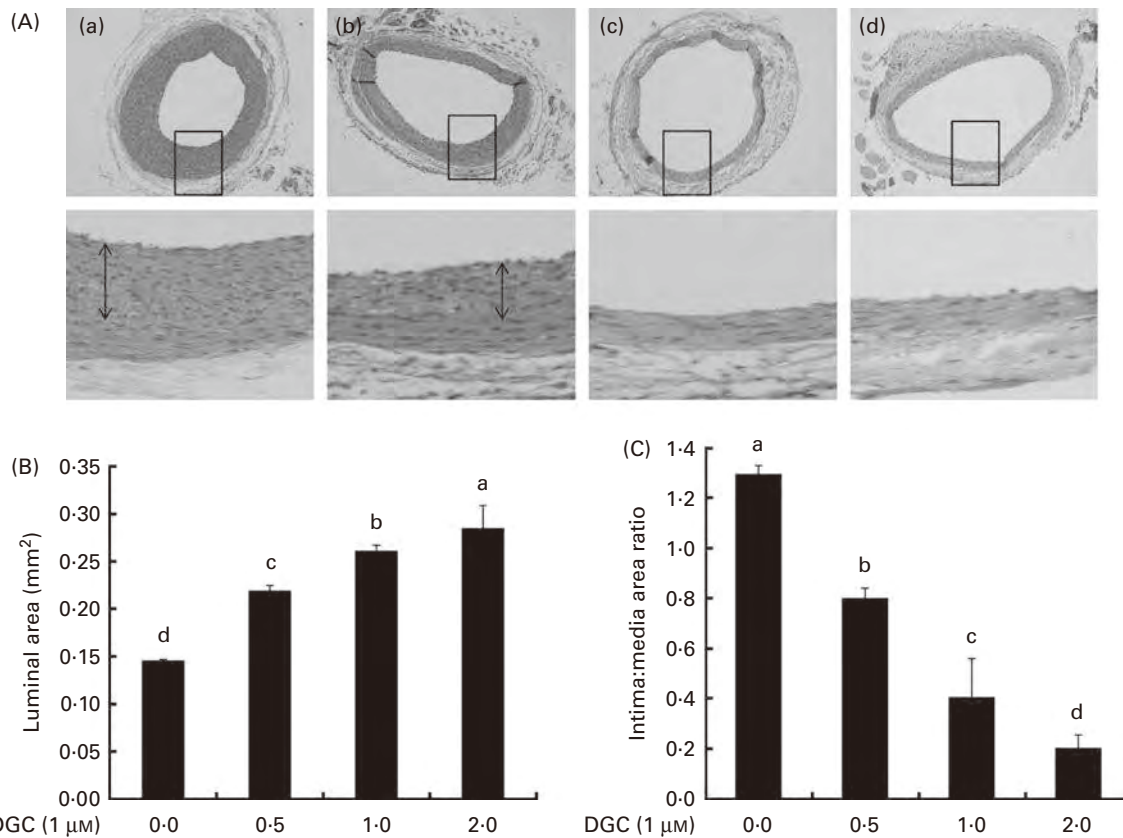


**Fig. 7.** Effects of dehydroglyasperin C (DGC) on rat carotid artery morphology after balloon injury. DGC (0.5 and 1 mg) diminished the formation of intimal smooth muscle cells on the 16th day after balloon catheter injury. (A) Control (a), 0.5 mg DGC (b), 1 mg DGC (c) and 2 mg DGC (d). Magnification 100 × and 400 ×. (B) Luminal area and (C) intima:media area ratios of the four groups (*n* 4 per group). <sup>a,b,c,d</sup>Mean values with unlike letters were significantly different (*P* < 0.05). (A colour version of this figure can be found online at <http://www.journals.cambridge.org/bjn>).

is related to excessive proliferation and diminished VSMC death. CDK2 and CDK4, important mediators in modulating the G<sub>0</sub>/G<sub>1</sub>-to-S-phase progression of the cell cycle and function by building complexes with cyclin E and cyclin D1, respectively, increase the activation of pRb and release transcription factors, resulting in the promotion of DNA synthesis<sup>(33,40–42)</sup>. On that account, the methods controlling proliferation and reducing apoptosis in abnormal VSMC have been developed as a new therapy<sup>(43)</sup>. In the present study, DGC restrained the PDGF-induced proliferation at a concentration of 1 μM, which may be attributable to the arrest of the G<sub>0</sub>/G<sub>1</sub>-S phase by reducing the expression of cyclin E/CDK2 and cyclin D1/CDK4. This reduced expression suggests that PDGF-stimulated expression of cell-cycle regulatory proteins is necessary for this inhibitory activity of DGC to alleviate the abnormal proliferation of VSMC.

PDGFR-β was expressed in the VSMC of atherosclerotic lesions<sup>(44)</sup>. It has been reported that the activated PDGFR in PDGF-BB-stimulated VSMC produces H<sub>2</sub>O<sub>2</sub>, resulting in the phosphorylation of the mitogen-activated protein kinases ERK1/2<sup>(45)</sup> and PLCγ1<sup>(45–47)</sup>. In addition to reactive oxygen species, PDGFR-β phosphorylated by PDGF interacts with PLCγ, Ras guanine 5'-triphosphatase-activating protein, phosphatidylinositol-3 kinase, tyrosine phosphatase SH2 domain-containing tyrosine phosphatase 2 (SHP-2) and members of the signal transducers and activators of the transcription family that are present in the cytoplasm<sup>(48)</sup>.

Recently, DGC among the bioactive compounds from liquorice root has been shown to induce the expression of detoxifying enzymes through the transcription factor Nrf2 in hepatoma cells<sup>(29)</sup>, and exhibited antioxidant activity against 2,2'-azino-bis(3-ethylbenzothiazoline-6-sulfonic acid) (ABTS<sup>+</sup>) radicals<sup>(49)</sup>. In our preliminary study, DGC showed an antioxidant property in rat tissues (data not shown), which has been proved by a significant inhibition of lipid peroxidation, increased proliferation of oestrogen receptor (ER)-positive MCF-7 cells, elevated oestrogenic activity on yeast-based ER activity and higher affinity to ER-β than to ER-α. The animal study performed by Hsieh *et al.*<sup>(50)</sup> also demonstrated that an α-tocopherol derivative inhibited PDGF-stimulated neointimal formation after angioplasty through the inhibition of reactive oxygen species-mediated PLCγ1-PKCδ and Janus kinase 2 (JAK2)-signal transducers and activators of transcription 3 activation, which cause the cell cycle arrest of the G<sub>2</sub>/M phase. Furthermore, the constituents derived from the plant containing antioxidant activities were elucidated to have anti-proliferative properties in vascular cells induced by PDGF<sup>(11)</sup>. Considering the correlation among atherosclerosis, the oxidation process and the influence of natural oestrogen derived from plants<sup>(51–53)</sup>, there is a possibility that DGC may control vascular growth factor-mediated morphological changes in the blood vessels. As expected, the present results showed that DGC regulated the

proliferation of vascular cells by reducing Akt and PLC $\gamma$ 1 in PDGF-treated HASMC.

ERK1/2 controls the PDGF-induced proliferation of VSMC through the regulation of the cell cycle modulators cyclin D1 and p27kip1<sup>(42,54–56)</sup>. Mitogenic stimulation activates the kinase MEK1/2 and induces the subsequent phosphorylation of ERK1/2 that activates downstream transcription factors such as Elk-1<sup>(57)</sup>, which is involved in DNA synthesis in VSMC<sup>(58)</sup>. Consistent with previous studies, the present data showed that DGC significantly decreased the PDGF-induced phosphorylation of ERK1/2.

VSMC migration from the media to the intima in the blood vessels leads to intimal thickening. In this process, PDGF is an important migratory factor for VSMC during neointimal formation<sup>(59)</sup>. Although the mechanisms of PDGF-stimulated migration have not been fully understood so far, there are several interesting studies. For instance, PDGF-BB facilitated intimal hyperplasia through the media-to-intima migration of VSMC in an animal model<sup>(6)</sup>, and the blocking of PDGF receptor signalling markedly retarded VSMC growth and neointimal formation by injury<sup>(7)</sup>. In addition, it is known that PDGF disturbs actin filament assembly and gives rise to an excessive increase in PDGFR expression after angioplasty<sup>(5)</sup>.

Taken together, the present study demonstrates that DGC has the ability to inhibit not only PDGF-stimulated proliferation of VSMC, which is attributable to interference with the cell cycle, but also VSMC migration. The possible mechanisms of DGC responsible for inhibiting the proliferation of VSMC are related to the inactivation of PDGFR- $\beta$ , PLC $\gamma$ 1, AKT and ERK. The results of the present study will be helpful in better understanding the mechanism of the pharmacological activity of DGC in the treatment of atherosclerosis.

### Acknowledgements

This study was supported by the Basic Science Research Program through the National Research Foundation of Korea (NRF) funded by the Ministry of Education, Science and Technology (2010-0027204). J.-S. K. and J.-T. W. planned the study. H. J. K. and B.-Y. C. performed the proliferation, Western blotting, migration and cytoskeletal reorganisation assay. H. J. K., I. S. P. and J. S. L. carried out the angioplasty balloon surgery. H. J. K., B.-Y. C. and J.-S. K. wrote the paper. The authors declared no conflict of interest.

### References

- Ross R (1993) The pathogenesis of atherosclerosis: a perspective for the 1990s. *Nature* **362**, 801–809.
- Raines EW (2004) PDGF and cardiovascular disease. *Cytokine Growth Factor Rev* **15**, 237–254.
- Jiang B, Yamamura S, Nelson PR, *et al.* (1996) Differential effects of platelet-derived growth factor isoforms on human smooth muscle cell proliferation and migration are mediated by distinct signaling pathways. *Surgery* **120**, 427–431.
- Koyama N, Hart CE & Clowes AW (1994) Different functions of the platelet-derived growth factor- $\alpha$  and - $\beta$  receptors for the migration and proliferation of cultured baboon smooth muscle cells. *Circ Res* **75**, 682–691.
- Sirois MG, Simons M & Edelman ER (1997) Antisense oligonucleotide inhibition of PDGFR- $\beta$  receptor subunit expression directs suppression of intimal thickening. *Circulation* **95**, 669–676.
- Jawien A, Bowen-Pope DF, Lindner V, *et al.* (1992) Platelet-derived growth factor promotes smooth muscle migration and intimal thickening in a rat model of balloon angioplasty. *J Clin Invest* **89**, 507–511.
- Banai S, Wolf Y, Golomb G, *et al.* (1998) PDGF-receptor tyrosine kinase blocker AG1295 selectively attenuates smooth muscle cell growth *in vitro* and reduces neointimal formation after balloon angioplasty in swine. *Circulation* **97**, 1960–1969.
- Bornfeldt KE, Raines EW, Nakano T, *et al.* (1994) Insulin-like growth factor-I and platelet-derived growth factor-BB induce directed migration of human arterial smooth muscle cells via signaling pathways that are distinct from those of proliferation. *J Clin Invest* **93**, 1266–1274.
- Bornfeldt KE, Raines EW, Graves LM, *et al.* (1995) Platelet-derived growth factor. Distinct signal transduction pathways associated with migration versus proliferation. *Ann NY Acad Sci* **766**, 416–430.
- Venkatesan B, Ghosh-Choudhury N, Das F, *et al.* (2008) Resveratrol inhibits PDGF receptor mitogenic signaling in mesangial cells: role of PTP1B. *FASEB J* **22**, 3469–3482.
- Kim HJ, Cha BY, Choi B, *et al.* (2012) Glyceollins inhibit platelet-derived growth factor-mediated human arterial smooth muscle cell proliferation and migration. *Br J Nutr* **107**, 24–35.
- Mae T, Kishida H, Nishiyama T, *et al.* (2003) A licorice ethanolic extract with peroxisome proliferator-activated receptor- $\gamma$  ligand-binding activity affects diabetes in KK-Ay mice, abdominal obesity in diet-induced obese C57BL mice and hypertension in spontaneously hypertensive rats. *J Nutr* **133**, 3369–3677.
- Fukai T, Marumo A, Kaitou K, *et al.* (2002) Anti-*Helicobacter pylori* flavonoids from licorice extract. *Life Sci* **71**, 1449–1463.
- Shin YW, Bae EA, Lee B, *et al.* (2007) *In vitro* and *in vivo* antiallergic effects of *Glycyrrhiza glabra* and its components. *Planta Med* **73**, 257–261.
- Gupta VK, Fatima A, Faridi U, *et al.* (2008) Antimicrobial potential of *Glycyrrhiza glabra* roots. *J Ethnopharmacol* **116**, 377–380.
- Chin YW, Jung HA, Liu Y, *et al.* (2007) Anti-oxidant constituents of the roots and stolons of licorice (*Glycyrrhiza glabra*). *J Agric Food Chem* **55**, 4691–4697.
- Zhang L, Yang Y, Yu L, *et al.* (2011) Cardioprotective effects of *Glycyrrhiza uralensis* extract against doxorubicin-induced toxicity. *Int J Toxicol* **30**, 181–189.
- Eu CH, Lim WY, Ton SH, *et al.* (2010) Glycyrrhizic acid improved lipoprotein lipase expression, insulin sensitivity, serum lipid and lipid deposition in high-fat diet-induced obese rats. *Lipids Health Dis* **9**, 81.
- Chang YL, Chen CL, Kuo CL, *et al.* (2010) Glycyrrhetic acid inhibits ICAM-1 expression via blocking JNK and NF- $\kappa$ B pathways in TNF- $\alpha$ -activated endothelial cells. *Acta Pharmacol Sin* **31**, 546–553.
- Lim WY, Chia YY, Liong SY, *et al.* (2009) Lipoprotein lipase expression, serum lipid and tissue lipid deposition in orally-administered glycyrrhizic acid-treated rats. *Lipids Health Dis* **8**, 31.
- Haraguchi H, Ishikawa H, Mizutani K, *et al.* (1998) Antioxidative and superoxide scavenging activities of retrochalcones in *Glycyrrhiza inflata*. *Bioorg Med Chem* **6**, 339–347.
- Shibata S (2000) A drug over the millennia: pharmacognosy, chemistry, and pharmacology of licorice. *Yakugaku Zasshi* **120**, 849–862.

23. Kondo K, Shiba M, Yamaji H, *et al.* (2007) Species identification of licorice using nrDNA and cpDNA genetic markers. *Biol Pharm Bull* **30**, 1497–1502.
24. Kuroda M, Mimaki Y, Sashida Y, *et al.* (2003) Phenolics with PPAR-gamma ligand-binding activity obtained from licorice (*Glycyrrhiza uralensis* roots) and ameliorative effects of glycyrrin on genetically diabetic KK-A(y) mice. *Bioorg Med Chem Lett* **13**, 4267–4272.
25. Hatano T, Shintani Y, Aga Y, *et al.* (2000) Phenolic constituents of licorice. VIII. Structures of glicophenone and glicoisoflavanone, and effects of licorice phenolics on methicillin-resistant *Staphylococcus aureus*. *Chem Pharm Bull (Tokyo)* **48**, 1286–1292.
26. Li J, Lim SS, Lee ES, *et al.* (2011) Isoangustone A suppresses mesangial fibrosis and inflammation in human renal mesangial cells. *Exp Biol Med (Maywood)* **236**, 435–444.
27. Seon MR, Park SY, Kwon SJ, *et al.* (2012) Hexane/ethanol extract of *Glycyrrhiza uralensis* and its active compound isoangustone A induce G<sub>1</sub> cycle arrest in DU145 human prostate and 4T1 murine mammary cancer cells. *J Nutr Biochem* **23**, 85–92.
28. Seon MR, Lim SS, Choi HJ, *et al.* (2010) Isoangustone A present in hexane/ethanol extract of *Glycyrrhiza uralensis* induces apoptosis in DU145 human prostate cancer cells via the activation of DR4 and intrinsic apoptosis pathway. *Mol Nutr Food Res* **54**, 1329–1339.
29. Seo JY, Park J, Kim HJ, *et al.* (2009) Isoalantolactone from *Inula helenium* caused Nrf2-mediated induction of detoxifying enzymes. *J Med Food* **12**, 1038–1045.
30. Cha BY, Shi WL, Yonezawa T, *et al.* (2009) An inhibitory effect of chrysoeriol on platelet-derived growth factor (PDGF)-induced proliferation and PDGF receptor signaling in human aortic smooth muscle cells. *J Pharmacol Sci* **110**, 105–110.
31. Erl W, Weber C & Hansson GK (2000) Pyrrolidine dithiocarbamate-induced apoptosis depends on cell type, density, and the presence of Cu(2+) and Zn(2+). *Am J Physiol Cell Physiol* **278**, 1116–1125.
32. Clowes AW, Reidy MA & Clowes MM (1983) Kinetics of cellular proliferation after arterial injury. I. Smooth muscle growth in the absence of endothelium. *Lab Invest* **49**, 327–333.
33. Sherr CJ & Roberts JM (1999) CDK inhibitors: positive and negative regulators of G<sub>1</sub>-phase progression. *Genes Dev* **13**, 1501–1512.
34. dos Remedios CG, Chhabra D, Kekic M, *et al.* (2003) Actin binding proteins: regulation of cytoskeletal microfilaments. *Physiol Rev* **83**, 433–473.
35. Xiong Y, Hannon GJ, Zhang H, *et al.* (1993) p21 is a universal inhibitor of cyclin kinases. *Nature* **366**, 701–704.
36. Ferns GA, Raines EW, Sprugel KH, *et al.* (1991) Inhibition of neointimal smooth muscle accumulation after angioplasty by an antibody to PDGF. *Science* **253**, 1129–1132.
37. Newby AC & Zaltsman AB (2000) Molecular mechanisms in intimal hyperplasia. *J Pathol* **190**, 300–309.
38. Park JH, Lim HJ, Lee KS, *et al.* (2008) Anti-proliferative effect of licochalcone A on vascular smooth muscle cells. *Biol Pharm Bull* **31**, 1996–2000.
39. Braun-Dullaeus RC, Mann MJ, Sedding DG, *et al.* (2004) Cell cycle-dependent regulation of smooth muscle cell activation. *Arterioscler Thromb Vasc Biol* **24**, 845–850.
40. Sherr CJ (1996) Cancer cell cycles. *Science* **274**, 1672–1677.
41. Jirawatnotai S, Aziyu A, Osmundson EC, *et al.* (2004) Cdk4 is indispensable for postnatal proliferation of the anterior pituitary. *J Biol Chem* **279**, 51100–51106.
42. Martin A, Odajima J, Hunt SL, *et al.* (2005) Cdk2 is dispensable for cell cycle inhibition and tumor suppression mediated by p27(Kip1) and p21(Cip1). *Cancer Cell* **7**, 591–598.
43. Guevara NV, Chen KH & Chan L (2001) Apoptosis in atherosclerosis: pathological and pharmacological implications. *Pharmacol Res* **44**, 59–71.
44. Wilcox JN, Smith KM, Williams LT, *et al.* (1998) Platelet-derived growth factor mRNA detection in human atherosclerotic plaques by *in situ* hybridization. *J Clin Invest* **82**, 1134–1143.
45. Sundaresan M, Yu ZX, Ferrans VJ, *et al.* (1995) Requirement for generation of H<sub>2</sub>O<sub>2</sub> for platelet-derived growth factor signal transduction. *Science* **270**, 296–299.
46. Brown DI & Griendling KK (2009) Nox proteins in signal transduction. *Free Radic Biol Med* **47**, 1239–1253.
47. Choi MH, Lee IK, Kim GW, *et al.* (2005) Regulation of PDGF signalling and vascular remodelling by peroxiredoxin II. *Nature* **435**, 347–353.
48. Heldin CH & Westermark B (1999) Mechanism of action and *in vivo* role of platelet-derived growth factor. *Physiol Rev* **79**, 1283–1316.
49. Lee YS, Kim SH, Kim JK, *et al.* (2010) Rapid identification and preparative isolation of antioxidant components in licorice. *J Sep Sci* **33**, 664–671.
50. Hsieh CY, Liu CL, Hsu MJ, *et al.* (2010) Inhibition of vascular smooth muscle cell proliferation by the vitamin E derivative pentamethylhydroxychromane in an *in vitro* and *in vivo* study: pivotal role of hydroxyl radical-mediated PLCgamma1 and JAK2 phosphorylation. *Free Radic Biol Med* **49**, 881–893.
51. Sosroseno W, Bird PS & Seymour GJ (2003) Intracellular proteins involved in *Porphyromonas gingivalis*-induced opsonophagocytic activities of a murine macrophage cell line (RAW 264.7 cells). *J Microbiol Immunol Infect* **36**, 229–235.
52. Pan W, Ikeda K, Takebe M, *et al.* (2001) Genistein, daidzein and glycitein inhibit growth and DNA synthesis of aortic smooth muscle cells from stroke-prone spontaneously hypertensive rats. *J Nutr* **131**, 1154–1158.
53. Kim HJ, Suh HJ, Kim JH, *et al.* (2010) Estrogenic activity of glycoellins isolated from soybean elicited with *Aspergillus sojae*. *J Med Food* **13**, 382–390.
54. Wei GL, Krasinski K, Kearney M, *et al.* (1997) Temporally and spatially coordinated expression of cell cycle regulatory factors after angioplasty. *Circ Res* **80**, 418–426.
55. Lavoie JN, L'Allemain G, Brunet A, *et al.* (1996) Cyclin D1 expression is regulated positively by the p42/p44MAPK and negatively by the p38/HOGMAPK pathway. *J Biol Chem* **271**, 20608–20616.
56. Castro C, Diez-Juan A, Cortes MJ, *et al.* (2003) Distinct regulation of mitogen-activated protein kinases and p27Kip1 in smooth muscle cells from different vascular beds. A potential role in establishing regional phenotypic variance. *J Biol Chem* **278**, 4482–4490.
57. Yang Z, Madinova A, Kozai T, *et al.* (2002) Felodipine inhibits nuclear translocation of p42/44 mitogen-activated protein kinase and human smooth muscle cell growth. *Cardiovasc Res* **53**, 227–231.
58. Adam RM, Borer JG, Williams J, *et al.* (1999) Amphiregulin is coordinately expressed with heparin-binding epidermal growth factor-like growth factor in the interstitial smooth muscle of the human prostate. *Endocrinology* **140**, 5866–5875.
59. Jalvy S, Renault MA, Leen LL, *et al.* (2007) Autocrine expression of osteopontin contributes to PDGF-mediated arterial smooth muscle cell migration. *Cardiovasc Res* **75**, 738–747.

# Nobiletin Prevents Body Weight Gain and Bone Loss in Ovariectomized C57BL/6J Mice

Young-Sil Lee<sup>1</sup>, Midori Asai<sup>1</sup>, Sun-Sil Choi<sup>1</sup>, Takayuki Yonezawa<sup>1</sup>, Toshiaki Teruya<sup>2</sup>, Kazuo Nagai<sup>1</sup>, Je-Tae Woo<sup>3,4</sup>, Byung-Yoon Cha<sup>1\*</sup>

<sup>1</sup>Research Institute for Biological Functions, Chubu University, Kasugai, Japan

<sup>2</sup>Faculty of Education, University of the Ryukyus, Nishihara, Japan

<sup>3</sup>Department of Biological Chemistry, Chubu University, Kasugai, Japan

<sup>4</sup>Department of Research and Development, Erina Co., Inc., Tokyo, Japan

Email: \*[bycha@isc.chubu.ac.jp](mailto:bycha@isc.chubu.ac.jp)

Received 10 August 2014; revised 8 September 2014; accepted 19 September 2014

Copyright © 2014 by authors and Scientific Research Publishing Inc.

This work is licensed under the Creative Commons Attribution International License (CC BY).

<http://creativecommons.org/licenses/by/4.0/>



Open Access

---

## Abstract

Obesity and osteoporosis are associated with estrogen deficiency following menopause. Therefore, it is important to prevent and treat both disorders to maintain a healthy life in postmenopausal women. Nobiletin, a polymethoxylated flavone, exhibits various pharmacologic effects, including anti-tumor and anti-inflammatory activities. Therefore, in this study, we examined the effects of nobiletin on obesity, obesity-related metabolic disorders, and bone mass in ovariectomized (OVX) mice. Mice were divided into four groups and underwent sham operation or OVX. OVX mice were treated with 50 or 100 mg/kg nobiletin, or received vehicle alone (0.3% carboxyl methyl cellulose/0.5% dimethyl sulfoxide). Nobiletin decreased body weight gain and white adipose tissue weight in OVX mice. Nobiletin also decreased triglyceride levels, and tended to reduce plasma total cholesterol and glucose levels. Additionally, nobiletin prevented the reduction in bone mineral density of the trabecular region of the femur in OVX mice. Taken together, our results suggest that nobiletin improves adiposity, dyslipidemia, hyperglycemia, and prevents bone loss in OVX mice. Therefore, nobiletin is expected to have beneficial effects for the prevention and improvement of metabolic disorders and osteoporosis in postmenopausal women.

## Keywords

Nobiletin, Ovariectomy, Obesity, Lipid and Glucose Metabolism, Bone Mineral Density

---

\*Corresponding author.

## 1. Introduction

Estrogen is an important factor for protection against obesity in females. Estrogen deficiency leads to osteoporosis, as well as body weight gain [1] [2]. Recent studies have shown that postmenopausal women have greater body fat and visceral fat compared with premenopausal women [1]-[4]. Obesity is associated with several metabolic disorders including dyslipidemia, insulin resistance, and cardiovascular disease [1] [2]. Because osteoporosis and obesity are major health problems in postmenopausal women, it is important to identify strategies to prevent or treat these disorders and maintain a healthy life in postmenopausal women.

Natural phytoestrogens are increasingly being used to prevent or improve metabolic disorders, and are thought to reduce the risk of osteoporosis in postmenopausal women [5] [6]. Additionally, phytoestrogens seem to lack the undesirable side effects associated with estrogen. Therefore, there is growing interest in using natural compounds to prevent and improve metabolic disorders and osteoporosis in postmenopausal women.

Nobiletin is a polymethoxylated flavone present in some citrus fruits such as *Citrus depressa* (shikuwasa) and *Citrus sinensis* (oranges) [7] [8]. Nobiletin was reported to exhibit biological effects via its anti-inflammatory, anti-tumor, and neuroprotective properties [9]-[11]. It was also recently reported that nobiletin can regulate bone metabolism by inhibiting osteoclast formation and bone resorption induced by interleukin (IL)-1 in osteoblasts, and preventing bone loss in OVX mice [12]. Recent reports have also revealed that nobiletin may be able to regulate lipid metabolism. Nobiletin enhances lipolysis and suppresses adipogenesis, although it is also reported that nobiletin induces adipocyte differentiation [13]-[15]. Our previous studies revealed that nobiletin reduces adiposity, plasma triglyceride (TG) levels, and insulin resistance in high-fat diet (HFD)-induced obese mice [16]. In the present study, we investigated the effects of nobiletin on obesity and bone mass in OVX mice.

## 2. Materials and Methods

### 2.1. Isolation of Nobiletin

Nobiletin was isolated and identified as described in our previous report [16].

### 2.2. Animals and Experimental Design

Female C57BL/6J mice were purchased from Japan SLC (Shizuoka, Japan) at 6 weeks of age. The mice were housed under temperature—( $23^{\circ}\text{C} \pm 3^{\circ}\text{C}$ ) and humidity-controlled conditions with a 12-h light/dark cycle, and were given free access to food and water throughout the experiment. After acclimatization for 1 week with a standard rodent normal-fat diet (CRF-1; Charles River, Japan), the mice underwent either sham-operation (sham,  $n = 8$ ) or ovariectomy (OVX,  $n = 24$ ). After surgery, mice were allowed to recover under normal conditions. Two days later, the OVX mice were randomly divided into three groups ( $n = 8$  mice/group) and treated with 50 (OVX + 50NOB) or 100 (OVX + 100NOB) mg/kg nobiletin, or vehicle (OVX control group). The vehicle was 0.3% carboxyl methyl cellulose/0.5% dimethyl sulfoxide. Nobiletin and vehicle were administered by oral gavage once daily for 12 weeks. Mice in the sham control group were administered with vehicle alone. Body weight and food intake for each mouse was measured two times per week during the study. The study was approved by The Animal Experimental Committee of Chubu University, and the mice were maintained in accordance with their guidelines.

### 2.3. Plasma, Tissue, and Bone Sampling

At the end of the 12-week study, the mice were anesthetized with a high dose of ether. Plasma samples were obtained by centrifuging blood samples at  $5000 \times g$  for 15 min at  $4^{\circ}\text{C}$ . The resulting plasma samples were stored at  $-80^{\circ}\text{C}$  until analysis. Liver, white adipose tissues (WAT; reproductive, perirenal, and mesenteric WAT), and the uterus were immediately excised, rinsed, and weighed. The femurs were also excised, soft tissue was carefully removed from the bone without damaging trabecular tissue, and the femoral bones were fixed in 70% ethanol.

### 2.4. Plasma Biochemistry

Plasma total cholesterol (T-CHO), TG, and glucose levels were determined using commercially available enzyme assay kits (Cholesterol E-Test, Triglyceride E-Test, and Glucose C II-Test, respectively; Wako Pure Chemical Industries, Osaka, Japan) according to the manufacturer's protocols.

## 2.5. Peripheral Quantitative Computed Tomography (pQCT) Analysis

Isolated bones were measured by pQCT (XCT Research, SA<sup>+</sup>, Stratec Medizintechnik GmbH, Pforzheim, Germany) with a tube voltage of 50.5 kV and a tube current of 0.281 mA. The scan speed was 5 mm/s with a voxel resolution of 0.07 mm. The analytical parameters for cortical bone mineral density (BMD) were set as a threshold of 690 mg/cm<sup>3</sup> and a peel mode of 20. Trabecular BMD was <395 mg/cm<sup>3</sup> with a peel mode of 20. A femur slice located 0.6 mm from the distal end of the growth plate was used to measure trabecular and cortical BMD. Trabecular bone was defined by setting an internal area of 35% of the total cross-sectional area. Total BMD, trabecular BMD, and cortical BMD were calculated using pQCT software (Makejob; StratecMedizintechnik GmbH).

## 2.6. Statistical Analysis

Data are expressed as means  $\pm$  standard error of the mean. Differences in mean values between each group were analyzed by one-way analysis of variance, followed by Dunnett's test. Values of  $p < 0.05$  were considered to indicate statistical significance. All analyses were conducted using IBM-SPSS version 20 (IBM, New York, NY, USA).

## 3. Results

### 3.1. Effects of Nobiletin on Body Weight Gain and Food Intake

Body weight gain and food intake are shown in **Figure 1**. Body weight gain was significantly greater in the OVX group than in the sham group ( $p < 0.005$ ). Body weight gain was significantly lower in the OVX + 100NOB group than in the OVX group ( $p < 0.05$ ) but was not significantly different between the OVX + 50NOB and OVX groups. Food intake was comparable among all four groups.

### 3.2. Effects of Nobiletin on Organ Weight

Organ weight is shown in **Figure 2**. Uterus weight was significantly lower in the OVX group than in the sham group ( $p < 0.005$ ), indicating that the mice were estrogen deficient. Uterus weight tended to be higher in the OVX + 100NOB group than in the OVX group, although did not significantly. Liver weight did not differ among the four groups. WAT weight was significantly higher in the OVX group compared with the sham group ( $p < 0.005$ ). The reproductive, perirenal, and total WAT weights were significantly lower in the OVX + 100NOB group than in the OVX group (all,  $p < 0.05$ ). However, there was no difference in WAT weights between the OVX + 50NOB group and the OVX group.

### 3.3. Effects of Nobiletin on Plasma Biochemistry

**Figure 3** shows the effects of nobiletin on plasma biochemistry. Plasma T-CHO levels were significantly higher in the OVX group than in the sham group ( $p < 0.05$ ). Plasma T-CHO levels were decreased in the OVX + 100NOB group compared with the OVX group, although not significantly. Plasma TG levels were significantly

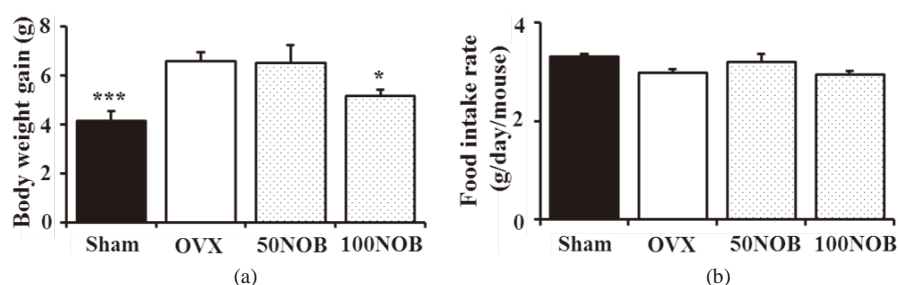


**Figure 1.** Effects of nobiletin on body weight gain (a) and food intake (b). Sham: sham-operated mice; OVX: ovariectomized mice; 50NOB: OVX + 50 mg/kg nobiletin; 100NOB: OVX + 100 mg/kg nobiletin. Values are means  $\pm$  standard error of the mean ( $n = 8$  mice/group). \*  $p < 0.05$  and \*\*\*  $p < 0.005$  vs the OVX group.

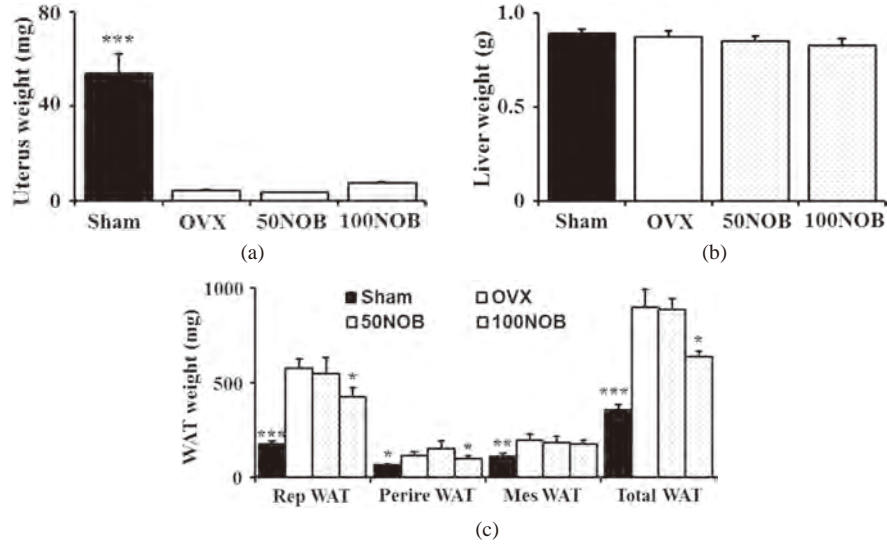


**Figure 2.** Effects of nobiletin on uterus weight (a), liver weight (b) and white adipose tissue (WAT) weight (c). RepW: reproductive WAT; PeriW: perirenal WAT; MesW: mesenteric WAT; TotalW: total WAT weight; Sham: sham-operated mice; OVX: ovariectomized mice; 50NOB: OVX + 50 mg/kg nobiletin; 100NOB: OVX + 100 mg/kg nobiletin. Values are means  $\pm$  standard error of the mean ( $n = 8$  mice/group). \*  $p < 0.05$ , \*  $p < 0.01$ , and \*\*\*  $p < 0.005$  vs the OVX group.

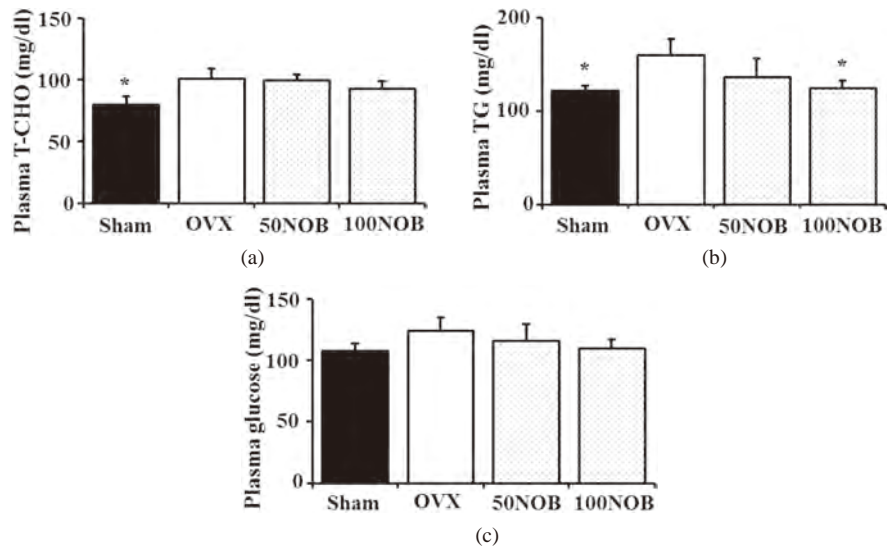


**Figure 3.** Effects of nobiletin on plasma total cholesterol (T-CHO; (a)), triglyceride (TG; (b)), and glucose (c) levels. Sham: sham-operated mice; OVX: ovariectomized mice; 50NOB: OVX+50 mg/kg nobiletin; 100NOB: OVX + 100 mg/kg nobiletin. Values are means  $\pm$  standard error of the mean ( $n = 8$  mice/group). \*  $p < 0.05$  vs the OVX group.

higher in the OVX group than in the sham group ( $p < 0.05$ ). Plasma TG levels were lower in the OVX + 100NOB group, but not in the OVX + 50NOB group, compared with the OVX group. Plasma glucose levels did not differ between the sham and OVX groups, although they tended to be lower in the OVX + 100NOB group than in the OVX group.

### 3.4. Effects of Nobiletin on BMD

Figure 4 shows the effects of nobiletin on BMD in OVX rats. Total femoral BMD and trabecular BMD were

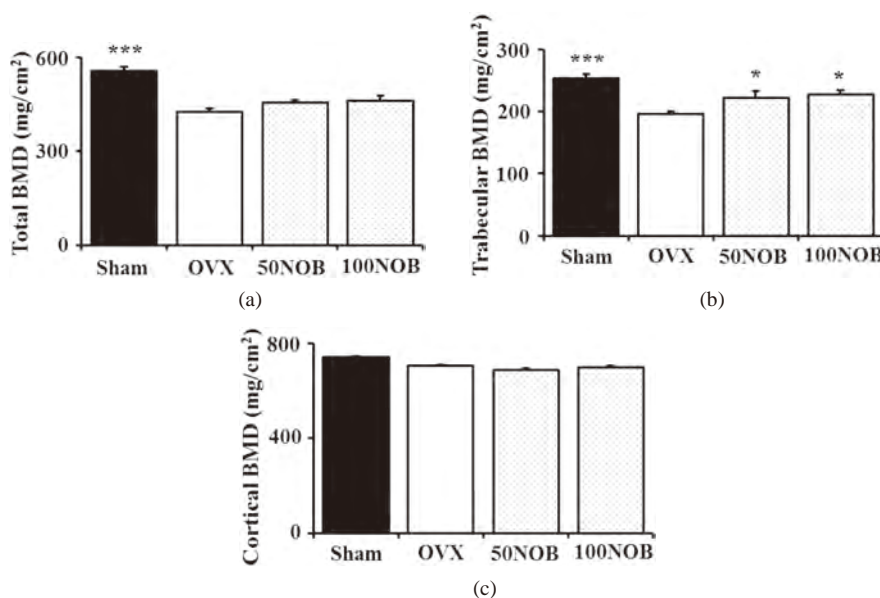


**Figure 4.** Effects of nobiletin on total femoral bone mineral density (BMD; (a)), trabecular BMD (b), and cortical BMD (c). Sham: sham-operated mice; OVX: ovariectomized mice; 50NOB: OVX + 50 mg/kg nobiletin; 100NOB: OVX + 100 mg/kg nobiletin. NFD: normal-fat diet; HFD: high-fat diet. Values are means  $\pm$  standard error of the mean ( $n = 8$ ). \* $p < 0.05$  and \*\*\* $p < 0.005$  vs the OVX group.

significantly lower in the OVX group than in the sham group (both,  $p < 0.005$ ). The decrease in total femoral BMD caused by OVX was attenuated by both doses of nobiletin, although this not significantly. Trabecular BMD was significantly greater in both OVX + NOB groups than in the OVX group (both,  $p < 0.05$ ). Cortical BMD did not differ among the four groups.

#### 4. Discussion

In the present study, we examined whether nobiletin could reduce obesity, obesity-related metabolic disorders, and osteoporosis in OVX mice. To our knowledge, the present study is the first to show that nobiletin prevents the increases in body weight, WAT weight, and plasma TG, as well as bone loss, in OVX mice.

In the present study, nobiletin reduced increases in body weight gain and WAT weight in OVX mice. It has been reported that estrogen is capable of preventing obesity in females. OVX mice are characterized by increased food intake and decreased energy expenditure, which lead to obesity [17]. It was reported that treating OVX mice with estradiol prevented the development of obesity [18].

In the present study, food intake was similar in the sham and OVX groups, and was not affected by nobiletin. Therefore, the reduction in body weight gain and WAT weight in this study were not caused by changes in food intake. Recent studies and our own *in vivo* data indicate that nobiletin regulates adipogenesis and lipolysis. For example, nobiletin enhances lipolysis in differentiated adipocytes by activating the cAMP-response element-binding pathway and suppresses lipid accumulation by downregulating peroxisome proliferator-activated receptor (PPAR) $\gamma$ , and activating AMP-activated protein kinase. However, it was reported that nobiletin can induce adipocyte differentiation [13]-[15]. Furthermore, we previously reported that nobiletin increased the expression of energy expenditure-related genes, such as PPAR $\alpha$  and carnitine palmitoyltransferase I, in HFD-induced obese mice [16]. Based on these earlier findings, it is likely that increased lipolysis and energy expenditure may be involved in the reduced body weight gain and WAT weight in nobiletin-treated mice. Further studies are needed to examine the effects of nobiletin on the expression of lipid metabolism-related genes.

Obesity-related metabolic disorders, such as hyperlipidemia, hyperglycemia, and glucose intolerance, are significant problems in postmenopausal women. In the present study, nobiletin reduced plasma TG levels and tended to reduce plasma T-CHO and glucose levels in OVX mice. In our previous study, we showed that nobiletin improved hypertriglyceridemia [16]. These results suggest that nobiletin may improve obesity-related meta-

bolic disorders, such as hyperlipidemia, in postmenopausal women.

Osteoporosis is a skeletal disease characterized by a reduction in bone strength, increasing the risk of fracture. Osteoporosis in postmenopausal women is caused by a decrease in estrogen levels and an increase in bone resorption [19]. In our present study, we showed that nobiletin inhibited the decrease in trabecular BMD of OVX mice and showed tendency to increase total femoral BMD in OVX mice. Previous studies have shown that nobiletin suppresses osteoclast formation and bone resorption by inhibiting nuclear factor- $\kappa$ B-dependent transcription and prostaglandin E production in osteoblasts via the activity of IL-1. This report also showed that nobiletin prevents bone loss in OVX mice [12] (Harada *et al.* 2011). Based on our results and this earlier report, nobiletin is expected to prevent osteoporosis in postmenopausal women.

## 5. Conclusion

In conclusion, treatment with nobiletin decreased body weight gain, WAT weight, and plasma TG levels in OVX mice. Nobiletin tended to decrease plasma T-CHO levels and glucose levels in OVX mice, and prevented the decrease in BMD following OVX. These results suggest that nobiletin may improve adiposity, hypertriglyceridemia, and bone metabolism in OVX mice, as a model of the postmenopausal state. Therefore, nobiletin may have beneficial effects for the prevention and treatment of metabolic disorders and osteoporosis in postmenopausal women.

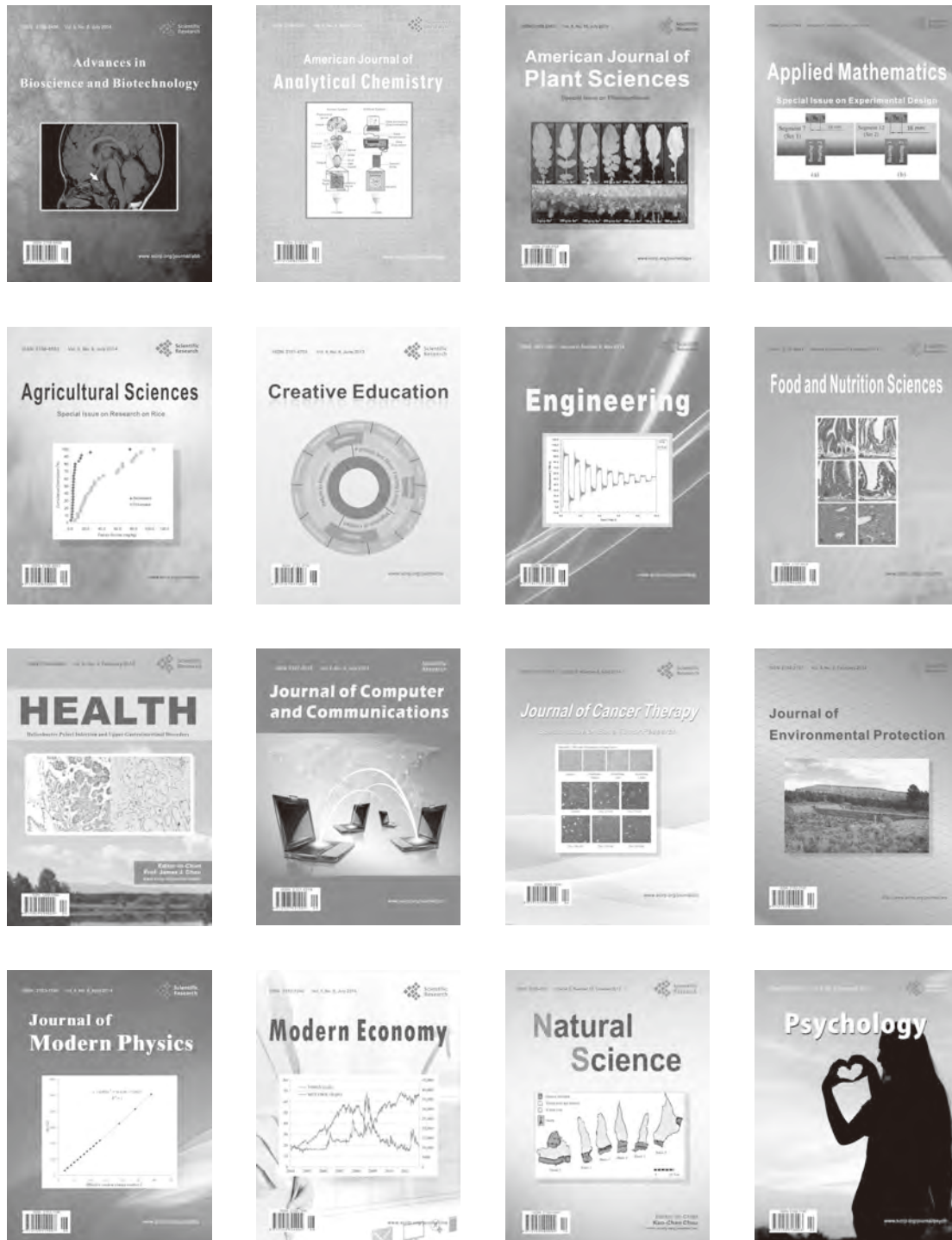
## References

- [1] You, T., Ryan, A.S. and Nicklas, B.J. (2004) The Metabolic Syndrome in Obese Postmenopausal Women: Relationship to Body Composition, Visceral Fat, and Inflammation. *The Journal of Clinical Endocrinology Metabolism*, **89**, 5517-5522.  
[http://press.endocrine.org/doi/abs/10.1210/jc.2004-0480?url\\_ver=Z39.88-2003&rfr\\_id=ori:rid:crossref.org&rfr\\_dat=cr\\_pub=pubmed&http://dx.doi.org/10.1210/jc.2004-0480](http://press.endocrine.org/doi/abs/10.1210/jc.2004-0480?url_ver=Z39.88-2003&rfr_id=ori:rid:crossref.org&rfr_dat=cr_pub=pubmed&http://dx.doi.org/10.1210/jc.2004-0480)
- [2] Kaaja, R.J. (2008) Metabolic Syndrome and the Menopause. *Menopause International*, **14**, 21-25.  
<http://min.sagepub.com/content/14/1/21.abstract>  
<http://dx.doi.org/10.1258/mi.2007.007032>
- [3] Cooke, P.S. and Naaz, A. (2004) Role of Estrogens in Adipocyte Development and Function. *Experimental Biology and Medicine* (Maywood), **229**, 1127-1235. <http://ebm.sagepub.com/content/229/11/1127.abstract>
- [4] Lobe, R.A. (2008) Metabolic Syndrome after Menopause and the Role of Hormones. *Maturitas*, **60**, 10-18.  
[http://www.maturitas.org/article/S0378-5122\(08\)00039-X/abstract](http://www.maturitas.org/article/S0378-5122(08)00039-X/abstract)  
<http://dx.doi.org/10.1016/j.maturitas.2008.02.008>
- [5] Anderson, J.W., Johnstone, B.M. and Cook-Newell, M.E. (1995) Meta-Analysis of the Effects of Soy Protein Intake on Serum Lipids. *The New England Journal of Medicine*, **333**, 276-282.  
<http://www.nejm.org/doi/full/10.1056/NEJM199508033330502>  
<http://dx.doi.org/10.1056/NEJM199508033330502>
- [6] Messina, M.J. (2002) Soy Foods and Soybean Isoflavones and Menopausal Health. *Nutrition in Clinical Care*, **5**, 272-282. <http://onlinelibrary.wiley.com/doi/10.1046/j.1523-5408.2002.05602.x/abstract>  
<http://dx.doi.org/10.1046/j.1523-5408.2002.05602.x>
- [7] Mercader, J., Wanecq, E., Chen, J. and Carpené, C. (2011) Isopropyl-norsynephrine Is a Stronger Lipolytic Agent in Human Adipocytes than Synephrine and Other Amines Present in Citrus Aurantium. *Journal of Physiology and Biochemistry*, **67**, 443-452. <http://link.springer.com/article/10.1007%2F978-94-007-0078-2>
- [8] Nagata, U., Sakamoto, K., Shiratsuchi, H., Ishi, T., Yano, M. and Ohta, H. (2006) Flavonoid Composition of Fruit Tissues of Citrus Species. *Bioscience, Biotechnology, and Biochemistry*, **70**, 178-192.  
[https://www.jstage.jst.go.jp/article/bbb/70/1/70\\_1\\_178/article](https://www.jstage.jst.go.jp/article/bbb/70/1/70_1_178/article)
- [9] Murakami, A., Nakamura, Y., Torikai, K., *et al.* (2000) Inhibitory Effect of Citrus Nobiletin on Phorbol Ester-Induced Skin Inflammation Oxidative Stress, and Tumor Promotion in Mice. *Cancer Research*, **60**, 5059-5066.  
<http://cancerres.aacrjournals.org/content/60/18/5059.long>
- [10] Silalahi, J. (2002) Anticancer and Health Protective Properties of Citrus Fruit Components. *Asia Pacific Journal of Clinical Nutrition*, **11**, 79-84. <http://onlinelibrary.wiley.com/doi/10.1046/j.1440-6047.2002.00271.x/abstract>  
<http://dx.doi.org/10.1046/j.1440-6047.2002.00271.x>
- [11] Nakajima, A., Yamakuni, T., Haraguchi, M., Omae, N., Song, S.Y., Kato, C., *et al.* (2007) Nobiletin, a Citrus Flavonoid

- that Improves Memory Impairment, Rescues Bulbectomy-Induced Cholinergic Neurodegeneration in Mice. *Journal of Pharmacological Sciences*, **105**, 122-126. [https://www.jstage.jst.go.jp/article/jphs/105/1/105\\_1\\_122/article](https://www.jstage.jst.go.jp/article/jphs/105/1/105_1_122/article)
- [12] Harada, S., Tominari, T., Matsumoto, C., Hirata, M., Takita, M., Inada, M. and Miyaura, C. (2011) Nobiletin, a Polymethoxy Flavonoid, Suppresses Bone Resorption by Inhibiting NF $\kappa$ B-Dependent Prostaglandin E Synthesis in Osteoblasts and Prevents Bone Loss Due to Estrogen Deficiency. *Journal of Pharmacological Sciences*, **115**, 89-93. [https://www.jstage.jst.go.jp/article/jphs/115/1/115\\_10193SC/article](https://www.jstage.jst.go.jp/article/jphs/115/1/115_10193SC/article)  
<http://dx.doi.org/10.1254/jphs.10193SC>
- [13] Saito, T., Abe, D. and Sekiya, K. (2007) Nobiletin Enhances Differentiation and Lipolysis of 3T3-L1 Adipocytes. *Biochemical and Biophysical Research Communications*, **357**, 371-376. <http://www.sciencedirect.com/science/article/pii/S0006291X07006109>
- [14] Kanda, K., Nishi, K., Kadota, A., Nishimoto, S., Liu, M.C. and Sugahara, T. (2011) Nobiletin Suppresses Adipocyte Differentiation of 3T3-L1 Cells by an Insulin and IBMX Mixture Induction. *Biochimica et Biophysica Acta*, **1820**, 461-468. <http://www.sciencedirect.com/science/article/pii/S0304416511002923>
- [15] Choi, Y., Kim, Y., Ham, H., Park, Y., Jeong, H.S. and Lee, J. (2011) Nobiletin Suppresses Adipogenesis by Regulating the Expression of Adipogenic Transcription Factors and the Activation of AMP-Activated Protein Kinase (AMPK). *Journal of Agricultural and Food Chemistry*, **59**, 12843-12849. <http://pubs.acs.org/doi/abs/10.1021/jf2033208>  
<http://dx.doi.org/10.1021/jf2033208>
- [16] Lee, Y.S., Cha, B.Y., Saito, K., Yamakawa, H., Choi, S.S., Yamaguchi, K., *et al.* (2010) Nobiletin Improves Hyperglycemia and Insulin Resistance in Obese Diabetic *ob/ob* Mice. *Biochemical Pharmacology*, **79**, 1674-1683. <http://www.sciencedirect.com/science/article/pii/S0006295210000936>  
<http://dx.doi.org/10.1016/j.bcp.2010.01.034>
- [17] Roger, N.H., Perfield II, J.W., Strissel, K.J., Obin, M.S. and Greenberg, A.S. (2009) Reduced Energy Expenditure and Increased Inflammation Are Early Events in the Development of Ovariectomy-Induced Obesity. *Endocrinology*, **150**, 2161-2168. [http://press.endocrine.org/doi/abs/10.1210/en.2008-1405?url\\_ver=Z39.88-2003&rft\\_id=ori:rid:crossref.org&rft\\_dat=c\\_rft\\_pub=pubmed](http://press.endocrine.org/doi/abs/10.1210/en.2008-1405?url_ver=Z39.88-2003&rft_id=ori:rid:crossref.org&rft_dat=c_rft_pub=pubmed)  
<http://dx.doi.org/10.1210/en.2008-1405>
- [18] Kolta, S., De Vernejoul, M.C., Meneton, P., Fectenbaum, J. and Roux, C. (2003) Bone Mineral Measurements in Mice: Comparison of Two Devices. *Journal of Clinical Densitometry*, **6**, 251-258. <http://www.sciencedirect.com/science/article/pii/S109469500660276X>  
<http://dx.doi.org/10.1385/JCD:6:3:251>
- [19] Riggs, B.L. (1992) Osteoporosis. In: Wyngaarden, J.B., Ed., *Textbook of Medicine*, 19th Edition, Saunders, Philadelphia, 1426-1430.

Scientific Research Publishing (SCIRP) is one of the largest Open Access journal publishers. It is currently publishing more than 200 open access, online, peer-reviewed journals covering a wide range of academic disciplines. SCIRP serves the worldwide academic communities and contributes to the progress and application of science with its publication.

Other selected journals from SCIRP are listed as below. Submit your manuscript to us via either [submit@scirp.org](mailto:submit@scirp.org) or Online Submission Portal.



## Research Communication

# Antidiabetic effect of nepodin, a component of *Rumex* roots, and its modes of action *in vitro* and *in vivo*

Byung Geun Ha<sup>1</sup>  
Takayuki Yonezawa<sup>1,2</sup>  
Myoung Jin Son<sup>3</sup>  
Je Tae Woo<sup>1,4</sup>  
Shinsuke Ohba<sup>2,5</sup>  
Ung-Il Chung<sup>2,5</sup>  
Kazumi Yagasaki<sup>1,3\*</sup>

<sup>1</sup>Department of Nutriproteomics, Graduate School of Medicine, The University of Tokyo, Bunkyo-Ku, Tokyo, Japan

<sup>2</sup>Department of Bioengineering, Graduate School of Engineering, The University of Tokyo, Bunkyo-Ku, Tokyo, Japan

<sup>3</sup>Department of Applied Biological Chemistry, Tokyo University of Agriculture and Technology, Fuchu, Tokyo, Japan

<sup>4</sup>Department of Research and Development, Erina Co., Inc., Minato-Ku, Tokyo, Japan

<sup>5</sup>Center for Disease Biology and Integrative Medicine, The University of Tokyo, Bunkyo-Ku, Tokyo, Japan

## Abstract

Many active components derived from edible natural resources such as plant extracts have recently attracted attention for their potential use as functional foods or drugs for preventing and treating metabolic diseases such as diabetes. To obtain a novel modulator of glucose metabolism, we conducted screening of a small compound library in cultured L6 myotubes. We identified nepodin that stimulated glucose uptake dose-dependently in differentiated L6 myotubes. The stimulatory effect of nepodin on glucose uptake was abrogated by a 5'-adenosine monophosphate-activated protein kinase (AMPK) inhibitor. In addition, nepodin stimulated the phosphorylation of AMPK. Nepodin also stimulated the transloca-

tion of GLUT4 to the plasma membrane in L6 myoblasts transfected with a Glut4 cDNA-coding vector and in differentiated L6 myotubes. In *in vivo* study, nepodin suppressed the increases in fasting blood glucose levels and improved the glucose intolerance of C57BL/KsJ-*db/db* mice, a type 2 diabetic animal model. Nepodin rescued the impaired phosphorylation of AMPK in the skeletal muscle of *db/db* mice. These results suggest that nepodin has an anti-diabetic effect, which is at least partly mediated by stimulation of GLUT4 translocation via AMPK activation by nepodin. © 2014 BioFactors, 40(4):436–447, 2014

**Keywords:** nepodin; diabetes; AMPK; GLUT4; db/db mouse

Additional Supporting Information may be found in the online version of this article.

**Abbreviations:** ACC1, acetyl-CoA carboxylase 1; AMPK, 5'-adenosine monophosphate-activated protein kinase; FAS, fatty acid synthase; GLUT, glucose transporter; G6Pase, glucose-6-phosphatase; GS, glycogen synthase; LGP, liver glycogen phosphorylase; PEPCK, phosphoenolpyruvate carboxykinase; SCD1, stearoyl-coenzyme A desaturase 1.

© 2014 International Union of Biochemistry and Molecular Biology

Volume 40, Number 4, July/August 2014, Pages 436–447

\*Address for correspondence: Kazumi Yagasaki, PhD, Department of Applied Biological Chemistry, Tokyo University of Agriculture and Technology, Fuchu, Tokyo 183–8509, Japan. Tel./Fax: +81-42-367–5714; E-mail: yagasaki@cc.tuat.ac.jp.

Received 13 February 2014; accepted 4 April 2014

DOI 10.1002/biof.1165

Published online 23 April 2014 in Wiley Online Library

(wileyonlinelibrary.com)

## 1. Introduction

Type 2 diabetes is characterized by insulin resistance and hyperglycemia, which leads to multiple diabetic complications like nephropathy, neuropathy, retinopathy, ketoacidosis, cardiovascular disease, and hypertension. Currently, the global prevalence of type 2 diabetes is rapidly increasing, resulting in a significant financial and social burden worldwide [1]. Numerous studies for the treatment of the type 2 diabetes have focused on maintaining normal levels of blood glucose by increasing glucose clearance in peripheral tissues such as skeletal muscle and adipose tissue [2].

Natural products such as plant extracts have recently attracted attention for their potential uses as functional foods or drugs for preventing and treating metabolic diseases such as diabetes [3]. A number of active components derived from natural resources have been determined to exhibit antidiabetic activity by functioning in the regulation of the diabetic pathophysiological signaling pathway including 5'-adenosine monophosphate-activated protein kinase (AMPK) pathway [3–5]. AMPK is a major cellular and whole-body energy sensor and a master regulator of metabolic homeostasis, and this kinase is activated by decreases in an energy state as reflected by an increased AMP/ATP ratio [6]. AMPK has also been known as an attractive therapeutic target for metabolic disease including obesity and diabetes [4,6,7]. Several studies have reported that antidiabetic natural compounds such as resveratrol and berberine can activate AMPK and that the AMPK activation is important for their antidiabetic action [4,5]. We have also demonstrated that activation of AMPK is involved in the stimulation of glucose uptake induced by natural polyphenols, such as genistein, piceatannol, aspalathin, daidzein, and equol, which improve hyperglycemia in type 2 diabetic model mice [8–12].

We have carried out screening of various food components and phytochemicals for small molecule activators of glucose uptake in cultured L6 myotubes. Among several candidates screened, we identified nepodin as a hit compound. Nepodin, acetyl-1,8-dihydroxy-3-methylnaphthalene, is a component found from the root of *Rumex japonicus* [13]. *Rumex japonicus* are very common perennial herbs growing mainly in East Asia, including China, Japan, and Korea. Young leaves of *Rumex japonicus* have been eaten as an edible wild plant and its infusion has been drunk as a tea. It has traditionally been used for the treatment of acute and chronic cutaneous diseases, constipation, jaundice, uterine hemorrhage, and hematemesis [14,15]. Antioxidant activity and antibacterial activity of *Rumex japonicus* have also been reported [16]. However, antidiabetic action of nepodin is poorly understood.

In this study, we investigated the effect of nepodin on glucose uptake and the mechanisms of glucose uptake enhancement using cultured L6 myotubes. To determine the effect of nepodin on type 2 diabetes *in vivo*, we also examined the fasting blood glucose level and glucose tolerance using male C57BL/KsJ-*db/db* mice, which were genetically engineered to carry obese and diabetic phenotypes.

## 2. Materials and Methods

### 2.1. Materials

L6 myoblasts were purchased from American Type Culture Collection (Rockville, MD, USA; ATCC® numbers: CRL-1458). Nepodin was purchased from Fluorochem (Glossop, UK). The following items were purchased from the cited commercial sources: glucose CII test kit, triglyceride assay kit, cholesterol E assay kit, compound C, and carboxymethyl cellulose (CMC) from Wako Pure Chemical Industries (Osaka, Japan); high-range insulin ELISA kit from Mercodia AB (Uppsala, Sweden); thiobarbituric acid-reactive substances (TBARS) assay kit from ZeptoMetrix Corporation (Buffalo, NY, USA); 5-aminoimidazole-4-carboxamide 1- $\beta$ -D-ribofuranoside from Toronto Research Chemicals (Toronto, ON, Canada); Pefabloc SC from Roche Applied Science (Indianapolis, IN, USA); Dulbecco's modified Eagle's medium (DMEM) and fetal bovine serum (FBS) from Sigma (St. Louis, MO, USA); phospho-AMPK and anti-AMPK antibodies from Cell Signaling Technology (Beverly, MA, USA); anti-Na<sup>+</sup>/K<sup>+</sup>-ATPase  $\alpha$ -1 antibody from Millipore (Billerica, MA, USA); anti-glucose transporter 4 (GLUT4) antibody from AbD Serotec (Oxford, UK); horseradish peroxidase-conjugated anti-mouse and anti-rabbit IgG antibodies from Invitrogen (Carlsbad, CA, USA); and ECL Plus Western blotting detection reagents and Hybond ECL nitrocellulose membrane from GE Healthcare (Buckinghamshire, UK).

### 2.2. Culture of L6 Myoblasts

L6 myoblasts were cultured in DMEM containing 10% (v/v) FBS, penicillin G (100 U/mL), and streptomycin (100  $\mu$ g/mL) in a humidified 5% CO<sub>2</sub> incubator at 37°C. To differentiate myotubes, L6 myoblasts ( $5 \times 10^3$ ,  $5 \times 10^4$ , or  $7 \times 10^5$ ) were seeded in Falcon 96-well plates, 24-well plates, or 60-mm culture dishes and cultured to 90% confluency for 3 days. Then the cells were cultured to form myotubes in DMEM containing 2% FBS for 1 week. The medium was renewed every 2 days. Cell viability was determined by the 3-(4,5-dimethylthiazol-2-yl)2,5-diphenyl tetrazolium bromide (MTT) assay described previously [17].

### 2.3. Determination of Glucose Uptake by Cultured L6 Myotubes

L6 myotubes were incubated in filter-sterilized Krebs-Henseleit-HEPES buffer (1.2 mM MgSO<sub>4</sub>, 7.3 mM KH<sub>2</sub>PO<sub>4</sub>, 47.6 mM KCl, 118 mM NaCl, 3.3 mM CaCl<sub>2</sub>, 25 mM NaHCO<sub>3</sub>, pH 7.4) containing 0.1% bovine serum albumin, 10 mM HEPES, and 2 mM sodium pyruvate (KHH buffer) for 2 h. The myotubes were then cultured for 4 h in KHH buffer containing 11 mM glucose without or with nepodin (10–100  $\mu$ M) and without or with compound C (5  $\mu$ M), an AMPK inhibitor. The differences in the glucose concentrations in the KHH buffer before and after culture were determined by the absorbance at 505 nm using a microplate reader (Model AD200; Beckman Coulter, Brea, CA, USA) and the glucose CII test kit. The amounts of glucose consumed were calculated [18].



## 2.4. Subcellular Fractionation and GLUT4 Translocation Analysis

To prepare plasma membrane and postplasma membrane fractions, we carried out a rapid plasma membrane preparation as described previously [19]. Briefly, L6 myotubes were harvested with buffer A (50 mM Tris-HCl, pH 8.0, 0.5 mM DTT) containing 0.1% Nonidet P-40 (NP-40), protease inhibitors (1 mM PMSF and 0.2 mg/mL Pefabloc SC), and a phosphatase inhibitor (1 mM  $\text{Na}_3\text{VO}_4$ ) and homogenized by 10 passages through a 30-gauge syringe needle. Each homogenate was centrifuged at 1,000g for 10 min at 4°C, and the pellet was resuspended in NP-40-free buffer A. After incubation on ice for 10 min with occasional mixing, the samples were centrifuged at 1,000g for 10 min at 4°C. The pellet was resuspended in buffer A containing 1% (v/v) NP-40, incubated on ice for 1 h with occasional mixing, and centrifuged at 16,000g for 20 min at 4°C. The supernatant was collected as the plasma membrane fraction. The supernatants from the first and second centrifugations at 1,000g were pooled and centrifuged at 16,000g for 20 min at 4°C. This supernatant was collected as the postplasma membrane fraction.

## 2.5. Western Blotting Analysis

L6 myotubes were solubilized in a lysis buffer (10 mM Tris-HCl, pH 7.4, 150 mM NaCl, 1% NP-40, 0.5% sodium deoxycholate, 0.1% SDS, 0.5 mM DTT, 0.2 mg/mL Pefabloc SC, 1 mM  $\text{Na}_3\text{VO}_4$ ) for 30 min at 4°C. The lysates were then sonicated for 10 sec and centrifuged at 12,000g for 15 min at 4°C. The protein concentrations of the supernatants were evaluated using a protein assay reagent (Bio-Rad Laboratories, Hercules, CA). Equal amounts of protein (20  $\mu\text{g}$  per lane) were loaded onto precasted 10% polyacrylamide gels (Wako Pure Chemical Industries), separated by electrophoresis, and transferred to nitrocellulose membranes. The membranes were incubated in a blocking solution containing 3% BSA in Tris-buffered saline (TBS; 25 mM Tris, 150 mM NaCl, 2 mM KCl, pH 7.4) for 1 h. After the incubation, the membranes were washed in TBS and incubated with antiphospho-AMPK and anti-AMPK, anti- $\text{Na}^+/\text{K}^+$ -ATPase  $\alpha$ -1, or anti-GLUT4 antibodies overnight at 4°C. The membranes were then washed in TBS containing 0.1% (v/v) Tween-20 for 30 min and incubated with horseradish peroxidase-conjugated anti-mouse or anti-rabbit IgG antibodies at a dilution of 1:5,000 for 1 h at room temperature. Immunoreactive bands were detected using ECL Plus Western blotting detection reagents. The intensity of each band was analyzed with a lumino image analyzer (Model LAS-4000 Mini; Fujifilm, Tokyo, Japan) coupled with image analysis software (Multi Gauge Ver. 3.0; Fujifilm).

## 2.6. Transfection and Immunocytochemistry of pFN21A (HaloTag®7)-Glut4 in L6 Myoblasts

pFN21A (HaloTag®7)-Glut4 was constructed by inserting the rat Glut4 cDNA into the pFN21A (HaloTag®7) CMV Flexi® vector (Promega KK, Tokyo, Japan) as described previously [9,10]. L6 myoblasts were used for the transfection and detec-

tion of pFN21A (HaloTag®7)-Glut4, because the transfection efficiency into L6 myotube was very low and we could hardly detect the HaloTag® expression as described previously [9]. Briefly, to support cell attachment and growth, an eight-well chamber slide was coated with collagen (Cellmatrix Type I-C, Nitta Gelatin, Osaka, Japan). L6 myoblasts were seeded at a density of  $5 \times 10^3$  cells per well on collagen-coated eight-well chamber slides (NUNC, Roskilde, Denmark). After culture for 24 h, pFN21A (HaloTag®7)-mock control vector and pFN21A (HaloTag®7)-Glut4 expression vector (0.3  $\mu\text{g}$  per well) were transfected using FuGENE®6 (Roche Diagnostics, Indianapolis, IN, USA) and then cultured for 36 h. After 36 h, the transfected cells were incubated in KHH buffer for 2 h and for another 30 min in KHH buffer containing 11 mM glucose without or with 30  $\mu\text{M}$  nepodin. The cells were immediately fixed in ice-cold 3.7% formaldehyde in PBS for 10 min, followed by permeabilization by 30-min treatment with 0.1% Triton X-100 and blocking for 1 h with 3% skim milk. Cells were incubated overnight with anti-HaloTag® rabbit polyclonal antibody (Promega KK, Tokyo, Japan) and anti-caveolin-3 goat polyclonal antibody (Santa Cruz Biotechnology, Santa Cruz, CA, USA), followed by anti-rabbit IgG Alexa Fluor 555 (Invitrogen, Carlsbad, CA, USA) and anti-goat IgG fluorescein isothiocyanate conjugate secondary antibodies (Santa Cruz Biotechnology) for 1 h. Image acquisition was performed using a laser scanning confocal microscope (Axiovert 200M; Carl Zeiss, Oberkochen, Germany).

## 2.7. Animals Experiment

C57BL/KsJ-*m/m* and C57BL/KsJ-*db/db* mice (5 weeks old) were obtained from Charles River Japan (Kanagawa, Japan). All animal experiments were conducted in accordance with the guidelines established by the Animal Care and Use Committee of the University of Tokyo, and the protocols were approved by this committee (M-P09-063). The mice were housed in an air-conditioned room with a temperature of  $22^\circ\text{C} \pm 2^\circ\text{C}$ , a relative humidity of  $60\% \pm 5\%$ , and an 8:00–20:00 light cycle. All the mice were maintained on a stock CE-2 pellet diet (Oriental Yeast, Tokyo, Japan). To determine the effect of nepodin, C57BL/KsJ-*db/db* mice were used as an animal model of type 2 diabetes and C57BL/KsJ-*m/m* as the nondiabetic normal group. The *db/db* mice (6 weeks old) were divided into three groups: control, nepodin 2 mg/kg/day, and nepodin 10 mg/kg/day, with similar fasting blood glucose levels and body weights (0 week). Nepodin was dissolved in 0.2% CMC solution and orally administered for 5 weeks. Likewise, the nondiabetic and diabetic control groups were given 0.2% CMC only for 5 weeks. Water and food were always available. After oral nepodin administration and concomitant fasting for 3 h, blood was collected from the tail vein every week, and the concentration of blood glucose was determined using the glucose CII test kit. After final nepodin administration and blood collection from tail vein for the final determination of fasting blood glucose levels at the 5th week of feeding, whole blood was collected from all mice (11 weeks old) via postcaval vein under pentobarbital

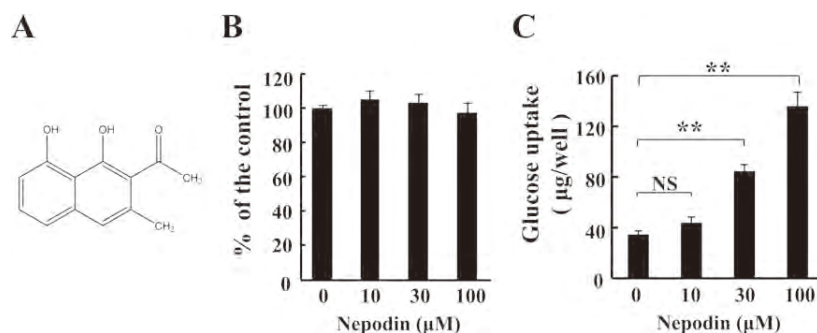


FIG 1

Effect of nepodin treatment on cell viability and glucose uptake in L6 myotubes. Chemical structure of nepodin (A). Effects of nepodin on the viability of L6 myotubes. Cell viability was measured by the MTT assay (B). Effects of nepodin on glucose uptake in L6 myotubes. For glucose uptake assay, L6 myotubes were preincubated in Krebs-Henseleit-HEPES buffer (KHH buffer) without glucose for 2 h. The cells were then incubated in KHH buffer containing 11 mM glucose without or with nepodin for 4 h, and the glucose uptake was measured using a glucose CII test kit (C). Each value represents the mean  $\pm$  SEM for 6 wells. \*\* $P < 0.01$ , significant difference versus the control (nepodin 0  $\mu$ M) group by Dunnett's multiple comparisons test; NS, not significant.

anesthesia. Blood was left to clot at room temperature to obtain serum. Concentrations of serum triglyceride, cholesterol, TBARS, glucose, and insulin were measured with commercial kits. The liver was quickly removed, washed with cold 0.9% NaCl, blotted on filter paper, and weighed. Total lipids from the liver were extracted according to the procedure proposed by Folch et al. [20]. After aliquots of the chloroform phase had been dried, liver triglyceride and cholesterol contents were determined as previously described [21].

### 2.8. Intraperitoneal Glucose Tolerance Test

Intraperitoneal glucose tolerance test (IPGTT) was performed at 4 weeks after oral administration of nepodin as described previously [10,18] with slight modifications. Briefly, mice were fasted overnight, and an intraperitoneal injection of glucose (0.2 g/mL/100 g body weight) was performed 3 h after oral administration of nepodin (2 mg/kg and 10 mg/kg body weight). Blood glucose levels at 0, 30, 60, 90, 120, and 180 min were determined.

### 2.9. Quantitative RT-PCR Analysis

Total RNA was isolated from the liver using ISOGEN (Nippon Gene, Toyama, Japan), and cDNA was synthesized using a ReverTra Ace qPCR RT Kit (Toyobo, Osaka, Japan) according to the manufacturer's instructions. Real-time PCR was performed with FastStart SYBR green Master Mix (Roche Diagnostics, Mannheim, Germany) in an ABI Prism 7500 Sequence Detection System (Applied Biosystems, Foster City, CA, USA). The PCR reaction was performed in triplicate. The relative expression levels of the target genes to the expression level of the endogenous reference gene actin were calculated using the delta cycle threshold method. The primer sequences are listed in Supporting Information Table S1.

### 2.10. Statistical Analysis

All data are presented as the mean  $\pm$  SEM. The data were evaluated by a one-way analysis of variance. Differences between the mean values were assessed using Dunnett's multi-

ple comparisons test. Statistical significance was considered for values of  $P < 0.05$ .

## 3. Results

### 3.1. Effect of Nepodin on Glucose Uptake in Cultured L6 Myotubes

We performed screening of a small compound library containing about 2,400 compounds for small molecule activators of glucose uptake in cultured L6 myotubes and identified nepodin having naphthalene skeleton (Fig. 1A) as a candidate compound. To investigate the effect of nepodin on cell cytotoxicity and glucose uptake, we performed an MTT assay and glucose uptake assay in cultured L6 myotubes. Nepodin at 10–100  $\mu$ M had no cytotoxicity in cultured L6 myotubes (Fig. 1B). Nepodin significantly stimulated glucose uptake in dose-dependent and insulin-independent manners (Fig. 1C).

### 3.2. Effect of Nepodin on AMPK Phosphorylation in L6 Myotubes

To clarify the involvement of AMPK in the action of nepodin, we examined the effect of compound C, an ATP-competitive inhibitor of AMPK, on nepodin-promoted glucose uptake. The result showed significant inhibition of glucose uptake by the treatment with compound C (Fig. 2A). This result suggested that the stimulatory effect of nepodin on glucose uptake was dependent on the AMPK pathway. To confirm the activity of AMPK on nepodin-induced glucose uptake, we performed Western blotting with anti-AMPK and antiphospho-AMPK antibodies. In differentiated L6 myotubes, nepodin stimulated the phosphorylation of AMPK in dose-dependent manner (Fig. 2B) and time-dependent manner (Fig. 2C). These results suggest that glucose uptake by nepodin is, at least partly, mediated by the AMPK pathway.

### 3.3. Effect of Nepodin on GLUT4 Translocation to the Plasma Membrane in L6 Myocytes

To explore regulatory mechanisms for promotion of glucose uptake by nepodin, we determined the translocation of GLUT4,

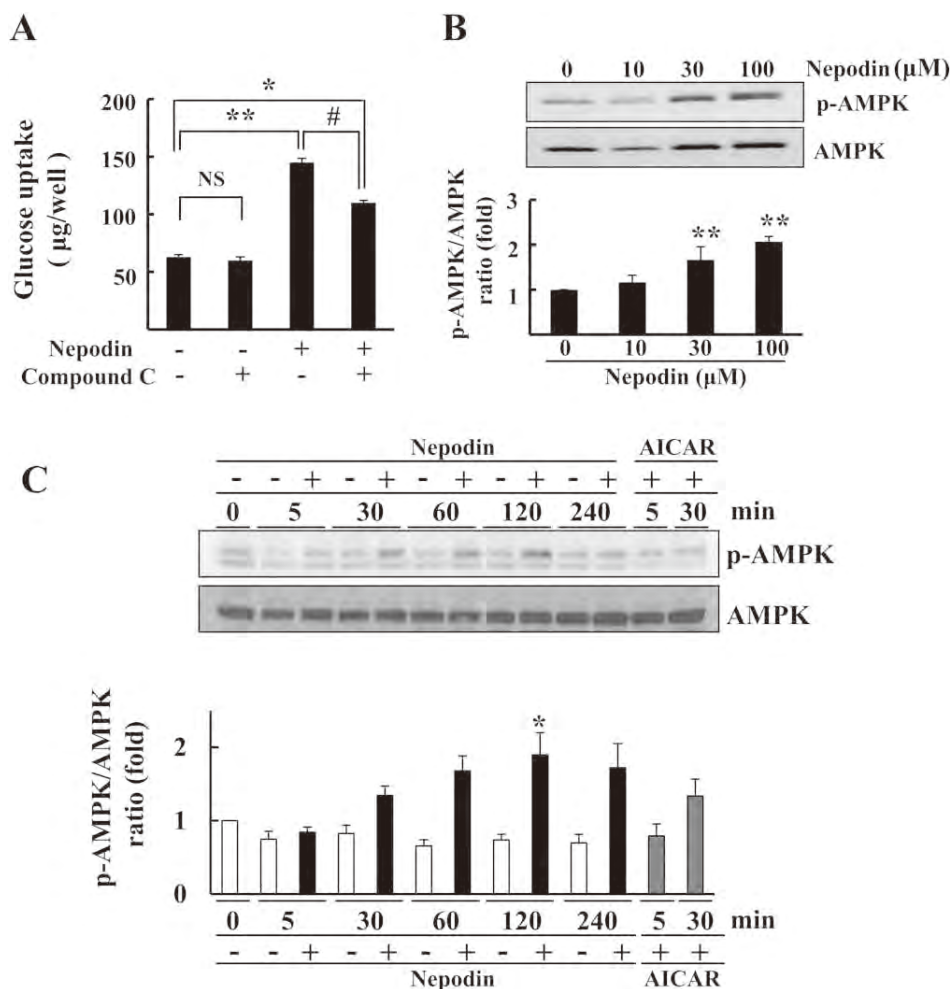


FIG 2

Effect of nepodin treatment on AMPK pathway in cultured L6 myotubes. L6 myotubes were preincubated in Krebs-Henseleit-HEPES buffer (KHH buffer) without glucose for 2 h. The cells were then cultured for 4 h in KHH buffer containing 11 mM glucose without or with 30 µM nepodin and without or with 5 µM compound C (A) and for 30 min at the indicated nepodin concentrations (B). For the time course measurement, 30 µM nepodin and 1 mM 5-aminoimidazole-4-carboxamide 1-β-D-ribofuranoside (AICAR) were used (C). Total lysates were analyzed by immunoblotting with antiphospho-AMPK and anti-AMPK antibodies. Each immunoblot is a representative of three independent experiments. Each value represents the mean ± SEM for 6 (A) and 3 (B, C). \*P < 0.05 and \*\*P < 0.01, significant difference versus the control (0 µM nepodin) group, #P < 0.05, nepodin only versus nepodin + inhibitor group by Dunnett's multiple comparisons test. p-AMPK, phospho-AMPK; NS, not significant.

known as a main glucose transporter in the skeletal muscle system, by Western blotting. Nepodin stimulated the translocation of GLUT4 to the plasma membrane time-dependently in cultured L6 myotubes (Fig. 3A). Next, the effect of nepodin on GLUT4 translocation was also confirmed by immunocytochemistry. We expressed Halo epitope-tagged GLUT4 in L6 myoblasts. Caveolin-3 was used as a membrane marker, as it is a muscle-specific structural protein of membrane caveolae. Halo-GLUT4 was evenly observed in the whole area of the cell in the absence of nepodin (Fig. 3B, center-red). However, robust immunofluorescent signal for Halo-GLUT4 was expressed on the cell surface membrane compartment after nepodin treatment for 30 min (Fig. 3B, bottom-red). Furthermore, Halo-GLUT4 was colocalized with caveolin-3 (Fig. 3B,

bottom-green, yellow). These results suggest that nepodin stimulates the increase in glucose uptake by promoting the translocation of GLUT4 to the plasma membrane.

### 3.4. Effect of Nepodin on Fasting Blood Glucose Level, Glucose Intolerance, and Serum Insulin Level and Homeostasis Model Assessment for Insulin Resistance in db/db Mice

To test our initial findings that nepodin treatment significantly stimulated glucose uptake in L6 myotubes *in vivo*, we investigated the effect of nepodin on a type 2 diabetic animal model, using male C57BL/KsJ-*db/db* mice, a genetic mouse model for obesity and diabetes, and C57BL/KsJ-*m/m* mice as the nondiabetic lean group. Significant increase in the fasting blood

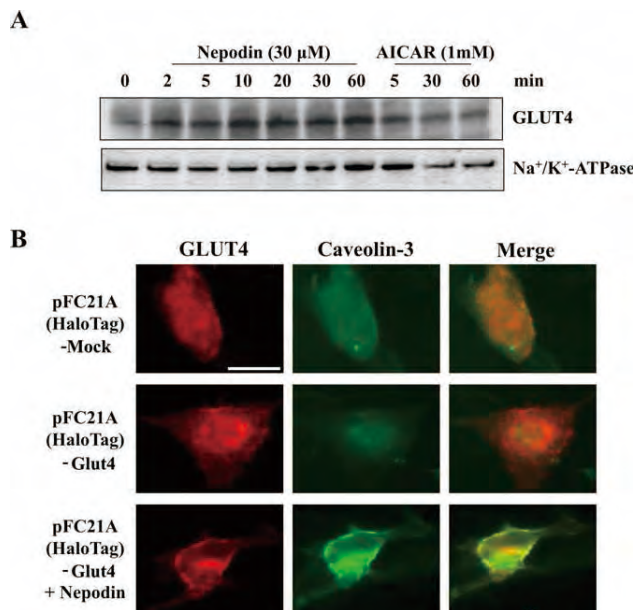


**FIG 3**

Effect of nepodin treatment on the translocation of GLUT4 to the plasma membrane in cultured L6 myocytes. L6 myotubes were preincubated in Krebs-Henseleit-HEPES buffer (KHH buffer) without glucose for 2 h and were then incubated with 11 mM glucose in KHH buffer containing 30 μM nepodin or 1 mM 5-aminoimidazole-4-carboxamide 1-β-D-ribofuranoside (AICAR) for the indicated times. Subcellular membrane fractions of the L6 myotubes were prepared by a rapid plasma membrane preparation method. The plasma membrane fractions (20 μg) were subjected to SDS-PAGE and Western blotting analyses using anti-GLUT4 and anti-Na<sup>+</sup>/K<sup>+</sup>-ATPase antibodies (A). L6 myoblasts were transfected with pFN21A (HaloTag®7)-Mock control vector and pFN21A (HaloTag®7)-Glut4 expression vector. After culture for 36 h, L6 myoblasts were incubated in KHH buffer without glucose for 2 h and for another 30 min in KHH buffer containing 11 mM glucose without or with 30 μM nepodin. Scale bars, 20 μm (B).

glucose was observed in *db/db* mice when compared with lean mice after a week (7 weeks old), and the increase was dose-dependently suppressed by oral administration of nepodin (Fig. 4A). Nepodin administration itself did not affect the food intake or body weight in either the *db/db*-control group or the two nepodin-administered groups (Supporting Information Fig. S1). To further examine the effect of nepodin on type 2 diabetes, we conducted an IPGTT. The zero time fasting glucose levels did not differ among *db/db* groups. However, 60–180 min after glucose injection, the administration of high-dose (10 mg/kg) nepodin constantly improved the impaired glucose tolerance of *db/db* mice (Fig. 4B). Nepodin administration also decreased an increase in plasma insulin concentration of *db/db* mice in a dose-dependent manner (Fig. 4C). Homeostasis model assessment for insulin resistance, a method used to quantify insulin resistance, showed that nepodin administration ameliorated insulin resistance of *db/db* mice (Fig. 4D).

Therefore, these results suggest that nepodin has antihyperglycemic potential and improves insulin resistance.

### 3.5. Effect of Nepodin on Phosphorylation of AMPK in Skeletal Muscle of *db/db* Mice

On the basis of our *in vitro* findings, to determine whether or not nepodin would stimulate AMPK activity *in vivo*, we investigated the phosphorylation of AMPK in the skeletal muscle of nondiabetic mice, control *db/db* mice, and nepodin-administrated *db/db* mice. The phosphorylation of AMPK in control *db/db* mice was decreased considerably when compared with nondiabetic mice. Nepodin administration in *db/db* mice for 5 weeks increased the phosphorylation of AMPK about two times in comparison with control *db/db* mice (Fig. 5).

### 3.6. Effect of Nepodin on Liver and Serum Lipid Levels of *db/db* Mice

To investigate whether nepodin also influences lipid metabolism, we investigated the levels of total triglyceride and cholesterol in the liver and serum. Total triglyceride and cholesterol in both the liver and serum were significantly higher in the *db/db* control group than in the nondiabetic lean group. However, the hepatic triglyceride and cholesterol were significantly decreased in the nepodin-administrated groups (Fig. 6A). The serum triglyceride and cholesterol were also decreased dose-dependently in the nepodin-administrated groups (Fig. 6B). In addition, nepodin suppressed the rise in serum concentrations of TBARS, an index of lipid peroxidation and oxidative stress in *db/db* mice (Fig. 6B).

### 3.7. Effect of Nepodin on mRNA Expression Levels of Enzymes Related to Glucose and Lipid Metabolism in the Liver of *db/db* Mice

We next investigated gluconeogenic and lipogenic gene expression in the liver of *db/db* mice. Nepodin administration did not affect gluconeogenic genes such as phosphoenolpyruvate carboxykinase (PEPCK) and glucose 6-phosphatase (G6Pase) expression (Fig. 7A), but slightly increased the expression of glycogen synthase (GS). However, the expression of liver glycogen phosphorylase was not changed by nepodin administration (Fig. 7B). These results suggest that nepodin does not affect gluconeogenesis and glycogenolysis but can stimulate glycogenesis. Moreover, nepodin did not affect the expression of acetyl-coenzyme A carboxylase 1 (ACC1) but significantly reduced the expression levels of lipogenic genes such as fatty acid synthase (FAS) and stearoyl-coenzyme A desaturase 1 (SCD1; Fig. 7C). These results suggest that nepodin not only stimulates the expression of hepatic genes related to glycogenesis but also suppresses hepatic lipogenic gene expression.

## 4. Discussion

Five major findings of this study are recognized. Nepodin significantly stimulated glucose uptake dose-dependently in

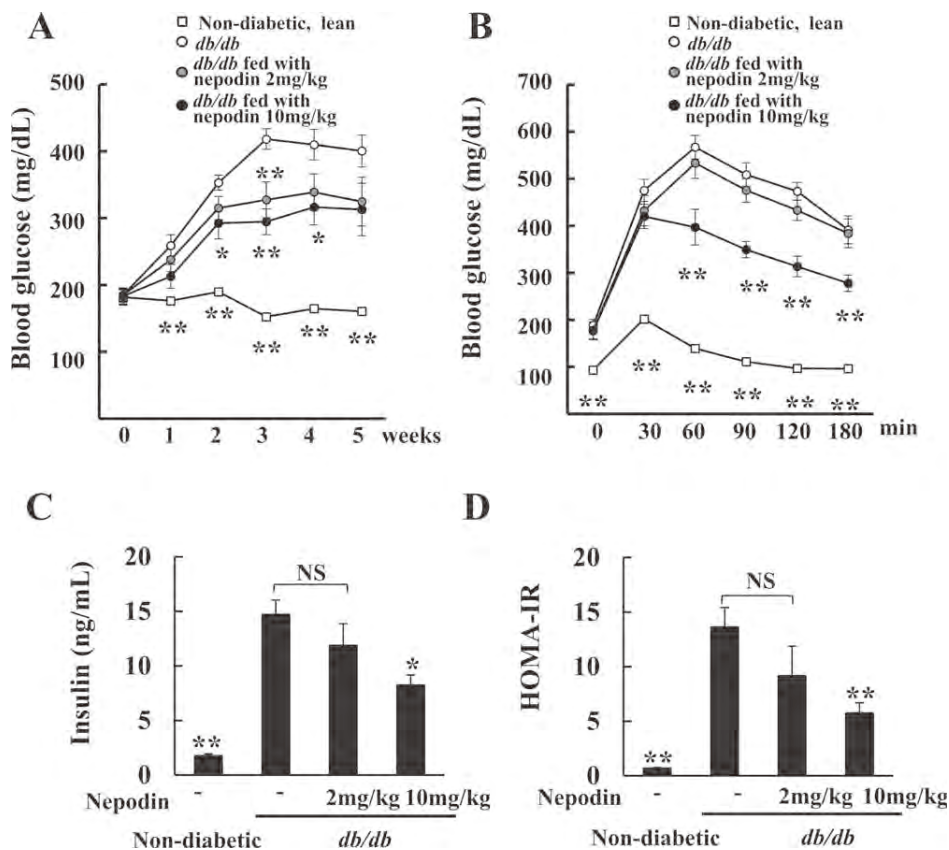


FIG 4

Effect of nepodin administration on fasting blood glucose level and glucose intolerance in db/db mice. During 5 weeks of oral nepodin administration (open square: nondiabetic lean; open circle: db/db control; gray circle: 2 mg/kg/day; closed circle: 10 mg/kg/day), fasting blood glucose level was measured once a week (A). For IPGTT, after 4 weeks of nepodin administration, nondiabetic lean mice or db/db mice were fasted for 18 h. Then mice received intraperitoneal injection of glucose (2 g/kg body weight), and blood glucose concentrations were measured at the indicated times (B). Serum insulin concentration was measured using an ELISA insulin kit at 5 weeks of nepodin administration (C). Homeostasis model assessment for insulin resistance was calculated according to the following equation: glucose  $\times$  insulin/405. Glucose and insulin concentrations are given in mg/dL and ng/mL, respectively (D). Each value represents the mean  $\pm$  SEM (db/db control, n = 10; others, n = 6). \*P < 0.05, \*\*P < 0.01, significant difference versus the db/db control group by Dunnett's multiple comparisons test; NS, not significant.

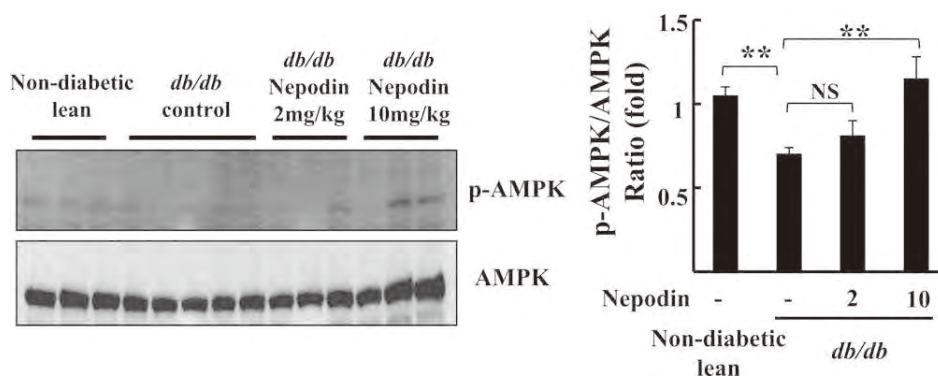
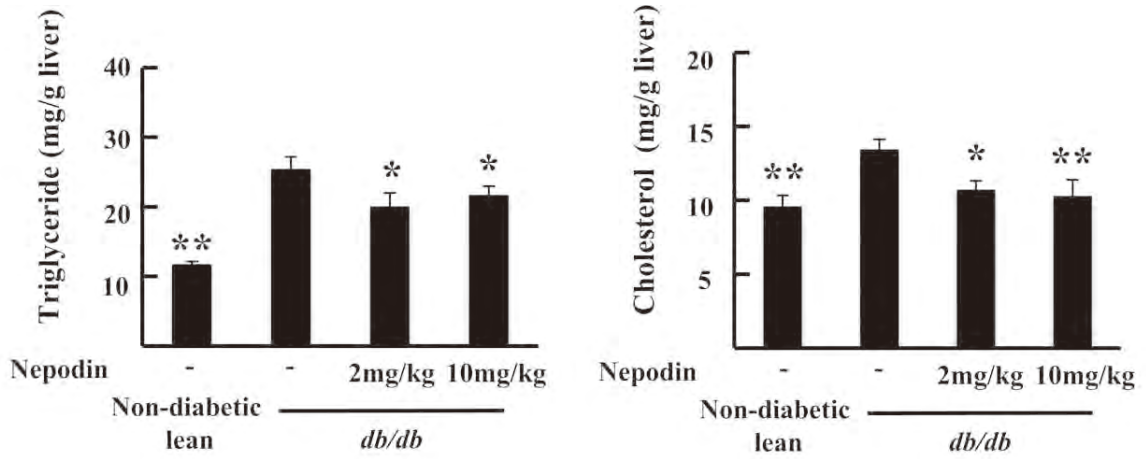


FIG 5

Effect of nepodin administration on the phosphorylation of AMPK in gastrocnemius muscle of db/db mice. After 5 weeks of oral nepodin administration, homogenates (20  $\mu$ g) of gastrocnemius muscle were subjected to SDS-PAGE and Western blotting analyses using antiphospho-AMPK and anti-AMPK antibodies. Right panel shows quantification of blotting data shown in left panel. Each value represents the mean  $\pm$  SEM (db/db control, n = 10; others, n = 6). \*\*P < 0.01, significant difference versus the db/db control group by Dunnett's multiple comparisons test; NS, not significant.

A



B

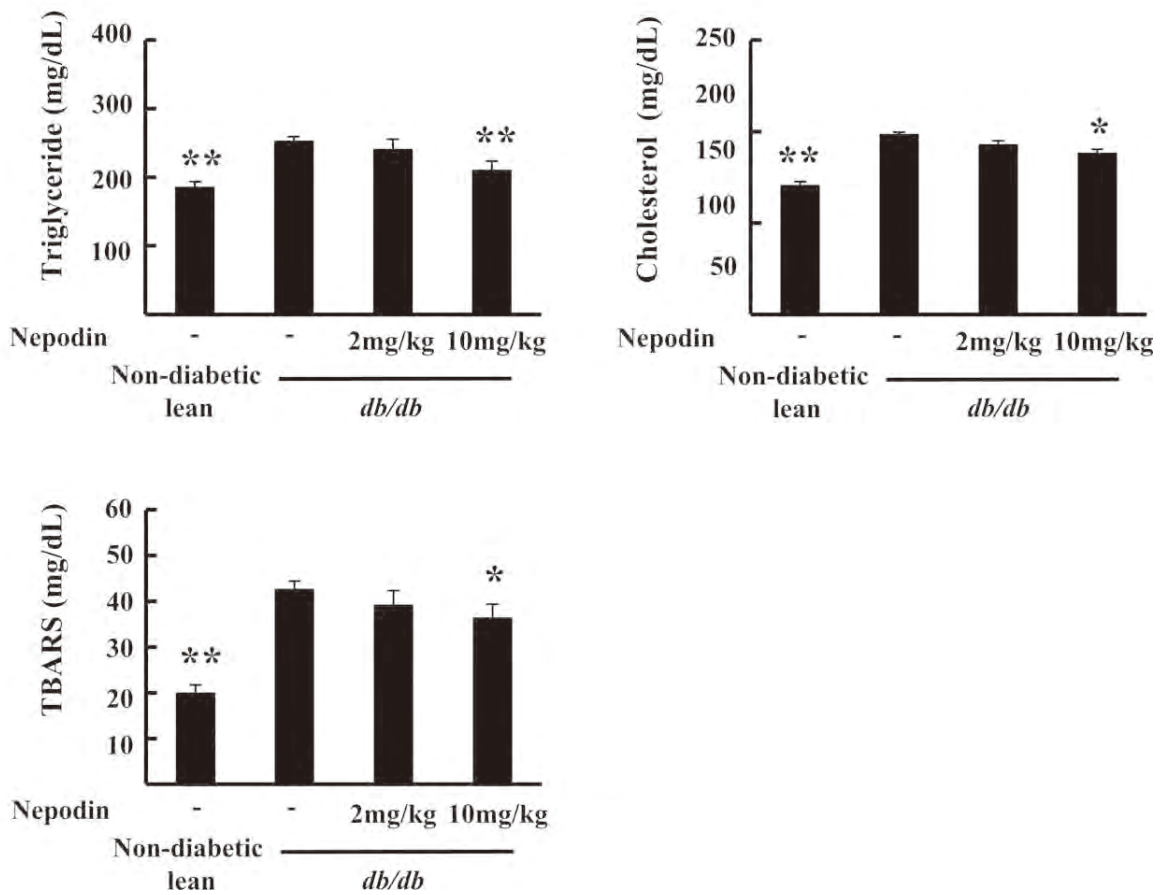


FIG 6

Effect of nepodin treatment on liver (A) and serum (B) lipid levels in db/db mice. The levels of triglyceride and cholesterol were measured at 5 weeks of oral nepodin administration. Mice were deprived of food for 4 h before the measurements. TBARS are substances formed as a byproduct of lipid peroxidation. Each value represents the mean  $\pm$  SEM (db/db control, n = 10; others, n = 6). \*P < 0.05 and \*\*P < 0.01, significant difference versus the db/db control group by Dunnett's multiple comparisons test.

cultured L6 myotubes in the absence of insulin. Nepodin stimulated the phosphorylation of AMPK in dose- and time-dependent manners in L6 myotubes. Nepodin increased the

translocation of GLUT4 to the cell surface in skeletal muscle cells. Oral administration of nepodin greatly attenuated the hyperglycemic condition without changes of food intake and

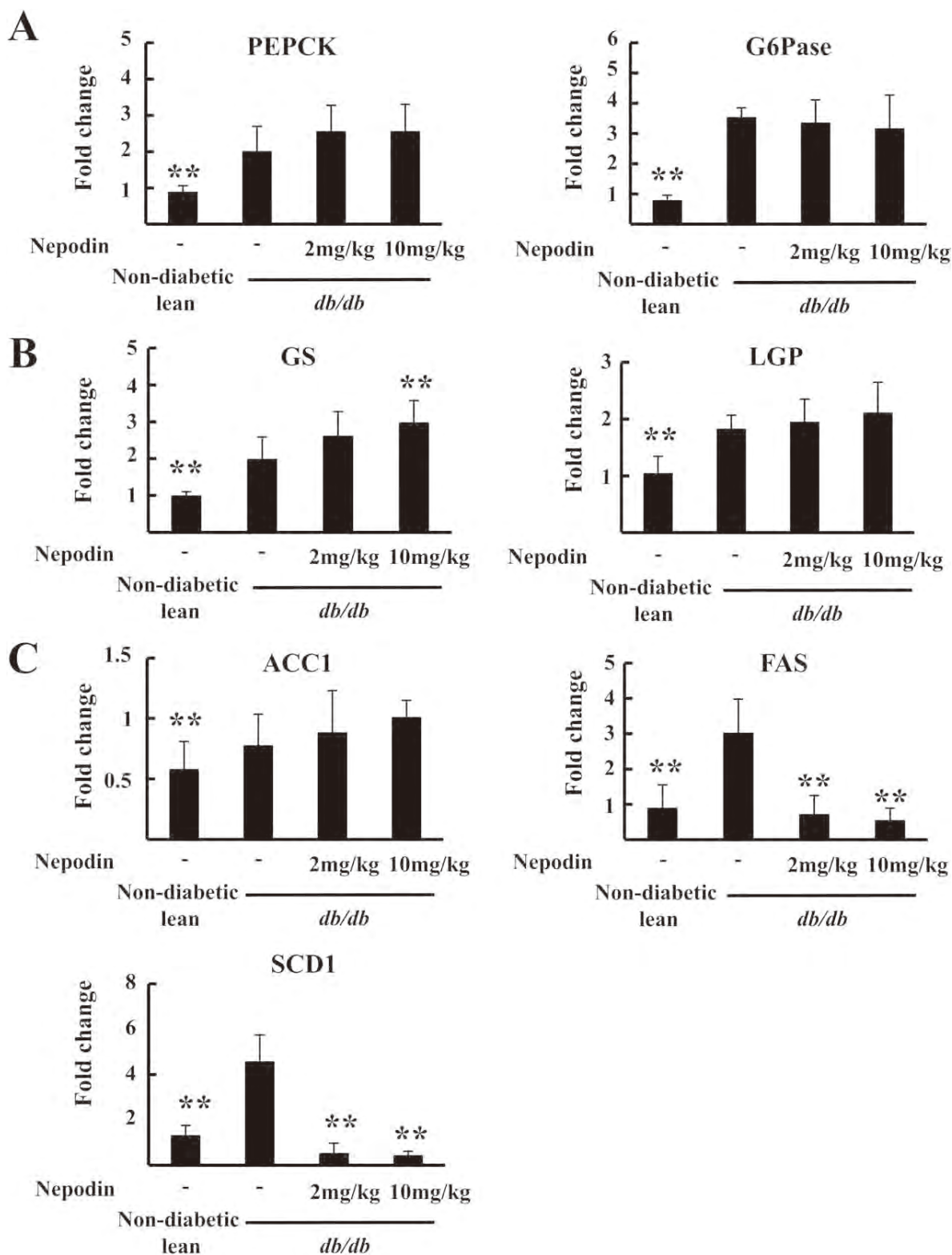


FIG 7

Effect of nepodin on mRNA expression levels of enzymes related to glucose and lipid metabolism in the liver of db/db mice. After oral nepodin administration for 5 weeks, livers (0.2 g/mouse) from mice were collected. Real-time PCR was used to measure relative mRNA levels of PEPCK, G6Pase in gluconeogenesis (A), GS and LGP in glycogen synthesis and degradation (B), and ACC1, FAS, and SCD1 in fatty acid synthesis (C). Each value represents mean  $\pm$  SEM (db/db control, n = 10; others, n = 6). \*\*P < 0.01, significant difference versus the db/db control group by Dunnett's multiple comparisons test. PEPCK, phosphoenolpyruvate carboxykinase; G6Pase, glucose 6-phosphatase; GS, glycogen synthase; LGP, liver glycogen phosphorylase; ACC1, acetyl-CoA carboxylase 1; FAS, fatty acid synthase; SCD1, stearoyl-coenzyme A desaturase 1.

weight and improved the impaired glucose tolerance of C57BL/KsJ-*db/db* mice. Finally, nepodin rescued the impaired phosphorylation of AMPK in the skeletal muscle of C57BL/KsJ-*db/db* mice. These findings suggest that nepodin has an antihyperglycemic effect able to prevent the increase in fasting blood glucose levels and improvement of impaired glucose tolerance, at least partly, by stimulating the translocation of GLUT4 *via* activating AMPK.

Among recent studies about antidiabetic components derived from foods and natural resources, resveratrol and berberine are notable as they have been tested and used successfully in human diabetes mellitus as well as in animal models [22–24]. A common feature of these antidiabetic components is that they exert hypoglycemic effects through AMPK activation and GLUT4 translocation. Moreover, these components have been reported to have antiobesity potential as well as antidiabetic potential [25,26]. Unlike these compounds, nepodin seems to be the unique one which has a specific hypoglycemic property because it greatly attenuates the hyperglycemia condition and improves the impaired glucose tolerance without affecting body weight and food intake in C57BL/KsJ-*db/db* mice.

Previous reports showed that sustained high glucose and insulin exposure decreases insulin-stimulated GLUT4 translocation in L6 myotubes [27], 3T3-L1 adipocytes [28], and primary cultured rat adipocytes [29]. The 24- to 48-h pretreatment with high glucose and insulin resulted in decreases in insulin-stimulated glucose uptake and GLUT4 translocation to the cell surface [28,29]. Hence, we postulated that sustained normal and high glucose culture conditions may induce glucose uptake by a different mechanism in L6 myotubes. However, we could not find differences in nepodin-induced glucose uptake or its mode of action in differentiated cultured L6 myotubes under normal and high glucose conditions (Ha et al., unpublished observations). These results suggest that nepodin is a strong stimulator of glucose uptake regardless of the glucose concentration in L6 myotubes.

Adiponectin has been proposed to be a major insulin-sensitizing adipokine that modulates a number of metabolic processes including glucose and fatty acid metabolism [30]. Antidiabetic thiazolidinediones, such as troglitazone and pioglitazone, and resveratrol have been known to improve insulin resistance through adiponectin-dependent pathways [31–33]. Natural products such as metformin improve insulin resistance through adiponectin-independent pathways [34]. Oral nepodin administration did not affect the level of serum adipokines such as adiponectin, MCP-1, and TNF- $\alpha$  in *db/db* mice (data not shown), which suggests that nepodin exerted its antidiabetic effect in an adiponectin-independent manner.

Oral nepodin administration resulted not only in a decrease of triglyceride levels in serum and liver, as reported in previous studies on resveratrol [25] and berberine [35], but also resulted in an inhibitory effect of cholesterol levels in both liver and serum. Moreover, as expected, nepodin, as a component of *Rumex japonicus* known for having antioxidant activity

[17], inhibited serum concentrations of TBARS, an index of lipid peroxidation and oxidative stress. In terms of hepatic glucose and lipid metabolism, nepodin increased the gene expression of GS and specifically inhibited the expressions of genes related to fatty acid synthesis such as FAS and SCD1, although it did not affect the expression of gluconeogenic genes such as PEPCK and G6Pase. In another type 2 diabetic model *ob/ob* mice, we observed a decreased expression of hepatic GS and an increased expression of PEPCK in untreated *ob/ob* mice when compared with normal lean mice. These changes in GS and PEPCK are considered to increase glucose supply to blood stream and hence induce rises in the blood glucose levels. Some phytochemicals such as aspalathin [10] and equol [12] reversed these changes in hepatic gene expression of GS and PEPCK; the decreased expression of hepatic GS and the increased expression of PEPCK in untreated *ob/ob* mice were normalized by the treatment of such phytochemicals, leading to reduction of glucose production in the liver of *ob/ob* mice. In contrast, the hepatic gene expression of GS in *db/db* mice was significantly increased like that of PEPCK in the current study, and nepodin further increased the expression of GS without affecting that of PEPCK (Figs. 7A and 7B). Mechanisms underlying hyperglycemia induction may be slightly different between *ob/ob* and *db/db* mice. Thus, the further increase in hepatic gene expression of GS by nepodin in *db/db* mice seems to contribute toward its antihyperglycemic action through a reduction of glucose supply into blood stream from the liver. These results suggest that nepodin ameliorates hyperglycemia and hypertriglyceridemia of *db/db* mice through the enhancement of hepatic glycogenesis and the inhibition of hepatic lipogenesis without affecting gluconeogenesis.

GLUT4 is a principal glucose transporter protein that plays a key role in regulating whole-body glucose homeostasis. The number of GLUT4 molecules at the surface of skeletal muscle cells increases rapidly in response to insulin, contraction, depolarization, or energy deprivation [36]. Several studies showed that antidiabetic components derived from natural resources induced glucose uptake through the translocation of GLUT4 in skeletal muscle cells [37]. We also confirmed that nepodin stimulates the translocation of GLUT4 to the plasma membrane, suggesting that nepodin increased insulin-independent glucose uptake through promotion of GLUT4 translocation to the cell surface in skeletal muscle. It has been well established that activation of AMPK stimulates glucose uptake by increasing GLUT4 translocation to the cell surface [38]. Several studies suggest that activation of AMPK enhances insulin sensitivity and increases glucose cellular uptake *in vitro* and *in vivo* [39–41]. Abnormal AMPK activity has been implicated in the progression of obesity and diabetes [42].

To determine how nepodin stimulates glucose uptake, we investigated mechanisms explaining glucose uptake in skeletal muscle. A glucose-uptake assay using several kinase inhibitors showed that the stimulatory effect of nepodin on glucose uptake was associated with AMPK pathway. In this study, we confirmed that nepodin specifically stimulated the



phosphorylation of AMPK dose- and time-dependently, although it did not affect the phosphorylation of phosphatidylinositol 3-kinase and Akt that are related to insulin-signaling pathways (data not shown). Moreover, in the skeletal muscle of *db/db* mice, we have found that nepodin rescues the impaired phosphorylation of AMPK. Therefore, these findings suggest that nepodin may stimulate glucose uptake through activation of AMPK and subsequent translocation of GLUT4 to the cell surface in skeletal muscles.

In conclusion, we have identified for the first time nepodin as a novel AMPK activator having antidiabetic potential. We propose nepodin as a new functional food or drug candidate for modifying imbalanced lipid and glucose homeostasis thereby reducing the risk of metabolic syndrome and type 2 diabetes complications.

## Acknowledgements

The authors thank Ms. Rima Tanabe-Masamura and Ms. Akino Wada for their excellent technical assistance.

## References

- [1] Marx, J. (2002) Unraveling the causes of diabetes. *Science* 296, 686–689.
- [2] Moller, D. E. (2001) New drug targets for type 2 diabetes and the metabolic syndrome. *Nature* 414, 821–827.
- [3] Liu, Q., Chen, L., Hu, L., Guo, Y., and Shen, X. (2010) Small molecules from natural sources, targeting signaling pathways in diabetes. *Biochim. Biophys. Acta* 1799, 854–865.
- [4] Hwang, J., Kwon, D. Y., and Yoon, S. H. (2009) AMP-activated protein kinase: a potential target for the diseases prevention by natural occurring polyphenols. *New Biotechnol.* 26, 17–22.
- [5] Hardie, D. G. (2011) Sensing of energy and nutrients by AMP-activated protein kinase. *Am. J. Clin. Nutr.* 93, 891S–896S.
- [6] Hardie, D. G. (2008) AMPK: a key regulator of energy balance in the single cell and the whole organism. *Int. J. Obes. (Lond.)* 32 (Suppl. 4), S7–S12.
- [7] Fogarty, S., and Hardie, D. G. (2010) Development of protein kinase activators: AMPK as a target in metabolic disorders and cancer. *Biochim. Biophys. Acta* 1804, 581–591.
- [8] Ha, B. G., Nagaoka, M., Yonezawa, T., Tanabe, R., Woo, J. T., et al. (2012) Regulatory mechanism for the stimulatory action of genistein on glucose uptake *in vitro* and *in vivo*. *J. Nutr. Biochem.* 23, 501–509.
- [9] Minakawa, M., Miura, Y., and Yagasaki, K. (2012) Piceatannol, a resveratrol derivative, promotes glucose uptake through glucose transporter 4 translocation to plasma membrane in L6 myocytes and suppresses blood glucose levels in type 2 diabetic model *db/db* mice. *Biochem. Biophys. Res. Commun.* 422, 469–475.
- [10] Son, M. J., Minakawa, M., Miura, Y., and Yagasaki, K. (2013) Aspalathin improves hyperglycemia and glucose intolerance in obese diabetic *ob/ob* mice. *Eur. J. Nutr.* 52, 1607–1619.
- [11] Cheong, S. H., Furuhashi, K., Ito, K., Nagaoka, M., Yonezawa, T., et al. (2014) Daidzein promotes glucose uptake through glucose transporter 4 translocation to plasma membrane in L6 myocytes and improves glucose homeostasis in Type 2 diabetic model mice. *J. Nutr. Biochem.* 25, 136–143.
- [12] Cheong, S. H., Furuhashi, K., Ito, K., Nagaoka, M., Yonezawa, T., et al. (2014) Antihyperglycemic effect of equol, a daidzein derivative, in cultured L6 myocytes and *ob/ob* mice. *Mol. Nutr. Food. Res.* 58, 267–277.
- [13] Nishina, A., Kubota, K., Kameoka, H., and Osawa, T. (1991) Antioxidizing component, Musizin, in *Rumex japonicus* Houtt. *J. Am. Oil Chem. Soc.* 68, 735–739.
- [14] Li, Y. P., Takamiyagi, A., Ramzi, S. T., and Nonaka, S. (2000) Inhibitory effect of *Rumex japonicus* Houtt on the porphyrin photooxidative reaction. *J. Dermatol.* 27, 761–768.
- [15] Zee, O. P., Kim, D. K., Kwon, H. C., and Lee, K. R. (1998) A new epoxynaphthoquinol from *Rumex japonicus*. *Arch. Pharm. Res.* 21, 485–486.
- [16] Elzaawely, A. A., Xuan, T. D., and Tawata, S. (2005) Antioxidant and antibacterial activities of *Rumex japonicus* Houtt. Aerial parts. *Biol. Pharm. Bull.* 28, 2225–2230.
- [17] Mosmann, T. (1983) Rapid colorimetric assay for cellular growth and survival: application to proliferation and cytotoxicity assays. *J. Immunol. Methods* 65, 55–63.
- [18] Kawano, A., Nakamura, H., Hata, S., Minakawa, M., Miura, Y., et al. (2009) Hypoglycemic effect of aspalathin, a rooibos tea component from *Aspalathus linearis*, in type 2 diabetic model *db/db* mice. *Phytomedicine* 16, 437–443.
- [19] Nishiumi, S., and Ashida, H. (2007) Rapid preparation of a plasma membrane fraction from adipocytes and muscle cells: application to detection of translocated glucose transporter 4 on the plasma membrane. *Biosci. Biotechnol. Biochem.* 71, 2343–2346.
- [20] Folch, J., Lees, M., and Sloane Stanley, G. H. (1957) A simple method for the isolation and purification of total lipides from animal tissues. *J. Biol. Chem.* 226, 497–509.
- [21] Kojima, T., Uesugi, T., Toda, T., Miura, Y., and Yagasaki, K. (2002) Hypolipidemic action of the soybean isoflavones genistein and genistin in glomerulonephritic rats. *Lipids* 37, 261–265.
- [22] Bhatt, J. K., Thomas, S., and Nanjan, M. J. (2012) Resveratrol supplementation improves glycemic control in type 2 diabetes mellitus. *Nutr. Res.* 32, 537–541.
- [23] Yin, J., Xing, H., and Ye, J. (2008) Efficacy of berberine in patients with type 2 diabetes mellitus. *Metabolism* 57, 712–717.
- [24] Zhang, Y., Li, X., Zou, D., Liu, W., Yang, J., et al. (2008) Treatment of type 2 diabetes and dyslipidemia with the natural plant alkaloid berberine. *J. Clin. Endocrinol. Metab.* 93, 2559–2565.
- [25] Kim, S., Jin, Y., Choi, Y., and Park, T. (2011) Resveratrol exerts anti-obesity effects via mechanisms involving down-regulation of adipogenic and inflammatory processes in mice. *Biochem. Pharmacol.* 81, 1343–1351.
- [26] Lee, Y. S., Kim, W. S., Kim, K. H., Yoon, M. J., Cho, H. J., et al. (2006) Berberine, a natural plant product, activates AMP-activated protein kinase with beneficial metabolic effects in diabetic and insulin-resistant states. *Diabetes* 55, 2256–2264.
- [27] Huang, C., Somwar, R., Patel, N., Niu, W., Török, D., et al. (2002) Sustained exposure of L6 myotubes to high glucose and insulin decreases insulin-stimulated GLUT4 translocation but upregulates GLUT4 activity. *Diabetes* 51, 2090–2098.
- [28] Kozka, I. J., Clark, A. E., and Holman, G. D. (1991) Chronic treatment with insulin selectively down-regulates cell-surface GLUT4 glucose transporters in 3T3-L1 adipocytes. *J. Biol. Chem.* 266, 11726–11731.
- [29] Garvey, W. T., Olefsky, J. M., Matthaiei, S., and Marshall, S. (1987) Glucose and insulin co-regulate the glucose transport system in primary cultured adipocytes. A new mechanism of insulin resistance. *J. Biol. Chem.* 262, 189–197.
- [30] Kadowaki, T., Yamauchi, T., Kubota, N., Hara, K., Ueki, K., et al. (2006) Adiponectin and adiponectin receptors in insulin resistance, diabetes, and the metabolic syndrome. *J. Clin. Invest.* 116, 1784–1792.
- [31] Maeda, N., Takahashi, M., Funahashi, T., Kihara, S., Nishizawa, H., et al. (2001) PPAR $\gamma$  ligands increase expression and plasma concentrations of adiponectin, an adipose-derived protein. *Diabetes* 50, 2094–2099.
- [32] Phillips, S. A., Ciaraldi, T. P., Kong, A. S., Bandukwala, R., Aroda, V., et al. (2003) Modulation of circulating and adipose tissue adiponectin levels by antidiabetic therapy. *Diabetes* 52, 667–674.
- [33] Kang, L., Heng, W., Yuan, A., Baolin, L., and Fang, H. (2010) Resveratrol modulates adipokine expression and improves insulin sensitivity in adipocytes: relative to inhibition of inflammatory responses. *Biochimie* 92, 789–796.
- [34] Huybens, P., Quartier, E., Pipeleers, D., and Van de Castele, M. (2005) Metformin reduces adiponectin protein expression and release in 3T3-L1 adipocytes involving activation of AMP activated protein kinase. *Eur. J. Pharmacol.* 518, 90–95.

- [35] Chen, C., Zhang, Y., and Huang, C. (2010) Berberine inhibits PTP1B activity and mimics insulin action. *Biochem. Biophys. Res. Commun.* 397, 543–547.
- [36] Huang, S., and Czech, M. P. (2007) The GLUT4 glucose transporter. *Cell. Metab.* 5, 237–252.
- [37] Yagasaki, K. (2014) Anti-diabetic phytochemicals that promote GLUT4 translocation via AMPK signaling in muscle cells. *Nutr. Aging* 2, 35–44.
- [38] Kurth-Kraczek, E. J., Hirshman, M. F., Goodyear, L. J., and Winder, W. W. (1999) 5' AMP-activated protein kinase activation causes GLUT4 translocation in skeletal muscle. *Diabetes* 48, 1667–1671.
- [39] Musi, N., and Goodyear, L. J. (2003) AMP-activated protein kinase and muscle glucose uptake. *Acta Physiol. Scand.* 178, 337–345.
- [40] Shaw, R. J., Lamia, K. A., Vasquez, D., Koo, S., Bardeesy, N., et al. (2005) The kinase LKB1 mediates glucose homeostasis in liver and therapeutic effects of metformin. *Science* 310, 1642–1646.
- [41] McConell, G. K., Manimmanakorn, A., Lee-Young, R. S., Kemp, B. E., Linden, K. C., et al. (2008) Differential attenuation of AMPK activation during acute exercise following exercise training or AICAR treatment. *J. Appl. Physiol.* 105, 1422–1427.
- [42] Hardie, D. G. (2007) AMP-activated protein kinase as a drug target. *Annu. Rev. Pharmacol. Toxicol.* 47, 185–210.

## Original Article

# Hyperpigmentation mechanism of methyl 3,5-di-caffeoylquininate through activation of p38 and MITF induction of tyrosinase

Hyo Jung Kim<sup>1,†</sup>, Jin Sook Kim<sup>2,†</sup>, Je-Tae Woo<sup>1,3</sup>, Ik-Soo Lee<sup>2</sup>, and Byung-Yoon Cha<sup>1,\*</sup>

<sup>1</sup>Research Institute for Biological Functions, Chubu University, Kasugai, Aichi 487-8501, Japan, <sup>2</sup>KM Convergence Research Division, Korea Institute of Oriental Medicine, Daejeon 305-811, Republic of Korea, and <sup>3</sup>Department of Research and Development, Erina Co., Inc., Minato-ku, Tokyo 105-0021, Japan

<sup>†</sup>These authors contributed equally to this work.

\*Correspondence address. Tel/Fax: +81-568-51-6189; E-mail: bycha@isc.chubu.ac.jp

Received 7 January 2015; Accepted 20 March 2015

## Abstract

Methyl 3,5-di-caffeoylquininate (3,5-diCQM) has been used for the treatment of various diseases in oriental medicine, but its effect on melanogenesis has not been reported yet. In this study, the molecular mechanism of 3,5-diCQM-induced melanogenesis was investigated. It was found that 3,5-diCQM induced synthesis of melanin pigments in murine B16F10 melanoma cells in a concentration-dependent manner. Treatment of cells with 3,5-diCQM for 48 h increased extracellular and intracellular melanin production and tyrosinase activity. The expressions of tyrosinase, tyrosinase-related protein 1 (TRP1), and TRP2 were up-regulated in a dose-dependent manner 48 h after 3,5-diCQM treatment. Western blot analysis showed that 3,5-diCQM increased the phosphorylation of p38 mitogen-activated protein kinase and cAMP responsive element binding as well as the expression of microphthalmia-associated transcription factor. In addition, 3,5-diCQM-stimulated cAMP production, and 3,5-diCQM-induced tyrosinase activity and melanin synthesis were attenuated by H89, a protein kinase A inhibitor. These results suggested that 3,5-diCQM-mediated activation of the p38 pathway may represent a novel approach for an effective therapy for vitiligo and hair graying.

**Key words:** methyl 3,5-di-caffeoylquininate (3,5-diCQM), melanogenesis, tyrosinase, microphthalmia-associated transcription factor (MITF), p38 mitogen-activated protein kinase (p38 MAPK)

## Introduction

Melanin is a biological pigment found in the skin, hair, eyes, ear, brain, and other parts of the human body. Dermal pigmentation is dependent on either the number, size, composition, and distribution of melanocytes or the activity of melanogenic enzymes [1]. Production of melanin is needed for scavenging free radicals [2,3] and protecting metabolically active keratinocytes from extensive environmental stimuli. A lack of epidermal melanin gives rise to susceptibility to skin cancers [1,4] and skin aging [5]. Furthermore, skin pigment loss can lead to decrease in immunity, resulting in conditions such as vitiligo [6,7].

Melanins are synthesized in melanosomes of melanocytes containing specific enzymes for proper melanin production, including tyrosinase, tyrosinase-related protein 1 (TRP1), and TRP2. Tyrosinase catalyzes the hydroxylation of tyrosine to produce 3,4-dihydroxyphenylalanine (DOPA) and the oxidation of DOPA to DOPA quinone. TRP1 oxidizes 5,6-dihydroxyindole-2-carboxylic acid (DHICA) to indole-5,6-quinone-2-carboxylic acid in mice, but not in humans, and TRP2 isomerizes DOPA chrome to DHICA.

Several important signaling pathways have been reported to be involved in melanin synthesis, such as the cyclic adenosine monophosphate (cAMP)-mediated pathway. An elevated level of intracellular

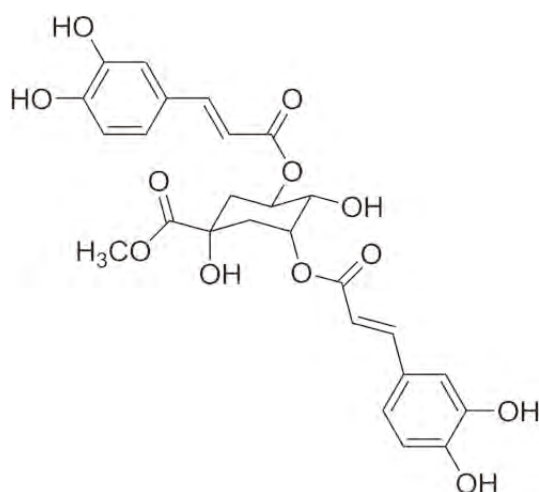


Figure 1. Chemical structure of 3,5-diCQM

cAMP allows the activation of protein kinase A (PKA), which can phosphorylate cAMP responsive element binding (CREB) protein and CREB binding protein (CBP), leading to the increase in the expression of microphthalmia-associated transcription factor (MITF). MITF activates the promoters of melanogenic genes, thereby increasing melanogenesis [8,9]. A study on the dominant negative mutant of MITF lacking the transactivation domain demonstrated that MITF is required for cAMP-induced stimulation of tyrosinase expression. The second critical pathway is the PKC-mediated pathway, which remains controversial. In addition, p38 mitogen-activated protein kinase (MAPK) and PI3K/AKT signaling pathways are also related to the regulation of melanogenesis. The phosphorylation of p38 MAPK increases the expressions of MITF and tyrosinase, resulting in the stimulation of melanin synthesis [10]. Furthermore, the activation of PI3K/AKT reduces melanin synthesis through down-regulation of MITF, tyrosinase, and TRPs, whereas inhibition of the PI3K/AKT pathway increases the production of melanin by MITF activation and tyrosinase expression induction [11,12].

Derivatives of caffeoylquinic acid have been used to cure various diseases in traditional oriental medicine and exhibit wide ranges of biological activities, such as anti-tumor [13], hepatoprotective [14,15], anti-inflammatory [16], anti-microbial [17], and antimutagenicity activities [18], indicating that these derivatives may exert beneficial effects against various human diseases. In addition to inhibition of human immunodeficiency virus-1 integrase and its replication [19–21], the antioxidant activities of caffeoylquinic acid derivatives [15,22] were also reported. However, no previous study has examined the activity of methyl 3,5-di-caffeoylquinic acid (3,5-diCQM) (Fig. 1), a caffeoylquinic acid derivative, on melanogenesis. In the present study, we explored the effect of 3,5-diCQM on the induction of pigmentation through activation of the melanin synthesis-related pathway.

## Materials and Methods

### Isolation of 3,5-diCQM

3,5-diCQM was isolated from the stems and leaves of *Erigeron annuus* [23] and its chemical structure was identified by comparing its physicochemical and spectral data with those in the literature [17]. In brief, air-dried stems and leaves of *E. annuus* (3.3 kg) were

extracted with a total of 60 l MeOH (three times, 20 l each) at room temperature for 7 days, filtered, and concentrated to give a MeOH extract (330 g). The extract was suspended in 2 l H<sub>2</sub>O and successively partitioned with *n*-hexane (3 × 2 l), EtOAc (3 × 2 l), and *n*-BuOH (3 × 2 l) to give *n*-hexane- (51 g), EtOAc- (29 g), and *n*-BuOH-soluble fractions (56 g), respectively. The EtOAc-soluble fraction (29 g) was chromatographed over silica gel (6.5 × 47 cm; 70–230 mesh) as the stationary phase using a CHCl<sub>3</sub>–MeOH gradient (20:1 → 0:1) to afford 12 fractions (F01–F12). Of these, fraction F08 (1.7 g) was further purified by a Sephadex LH-20 column (5.0 × 65 cm) and eluted with a MeOH–H<sub>2</sub>O gradient (1:1 → 1:0) to obtain 3,5-diCQM (80 mg).

### Cell culture

B16F10 murine melanoma cells were purchased from American Type Culture Collection (Manassas, USA) and plated in 6-well plates (2 × 10<sup>5</sup> cells/well) with Eagle's minimal essential medium (Wako Pure Chemical Industries Ltd., Osaka, Japan) containing 10% fetal bovine serum (Life Technologies, Carlsbad, USA), 100 U/ml penicillin, and 0.1 mg/ml streptomycin (Life Technologies). The cells were grown in an atmosphere of 5% CO<sub>2</sub> at 37°C for 24 h and treated with different doses of 3,5-diCQM for 24 or 48 h for tyrosinase activity or melanin content assay, respectively. Human epidermal melanocytes (moderately pigmented donor, HEMn-MP) were obtained from Life Technologies. The cells were seeded in 6-well plates at a density of 2 × 10<sup>5</sup> cells/well with 254 medium (Life Technologies) containing 1% human melanocyte growth supplements, 100 U/ml penicillin, and 0.1 mg/ml streptomycin and incubated in atmosphere of 5% CO<sub>2</sub> at 37°C for 24 h and then, the normal melanocyte growth medium was removed and replaced with 254 medium containing transferrin (5 µg/ml), insulin (5 µg/ml), heparin (3 µg/ml), and hydrocortisone (0.18 µg/ml) for treatment with sample. The treated cells were further incubated in atmosphere of 5% CO<sub>2</sub> at 37°C for 48 h. Human melanoma MMAC cells were purchased from RIKEN BioResource Center (Ibaraki, Japan) and cultured with Dulbecco's modified Eagle's medium (Wako Pure Chemical Industries Ltd.) containing 10% fetal bovine serum, 100 U/ml penicillin, and 0.1 mg/ml streptomycin. The cells were treated with sample for 48 h and melanin content was measured.

### Cell morphology and cell viability measurement

Cell morphology was examined under a CKX41 microscope (Olympus, Tokyo, Japan). Cell viability was assayed by adding 3-(4,5-dimethylthiazol-2-yl)-2,5-diphenyltetrazolium bromide (MTT; Dojin-do Laboratories, Kumamoto, Japan) solution (0.5 mg/ml in phenol red-free culture medium). After discarding the culture medium of the cells, MTT solution was added to cells and incubated for 2 h. The medium was removed, and dimethyl sulfoxide (DMSO) was added. The absorbance was determined at 570 nm (ref. 630 nm) using a microplate spectrophotometer (Dainippon, Osaka, Japan). The cell proliferation of each group was calculated as the absorbance of the treatment group relative to the control.

### Cellular tyrosinase activity assay

Tyrosinase activity assay in B16F10 cells was carried out according to the method previously described [24]. Cells were lysed with 0.5% Triton X-100 solution containing 1% sodium deoxycholate for 2 h. A reaction mixture containing Solutions A, B, and C (2:1:1) (Solution A, 2% *N,N*-dimethylformamide in 100 mM sodium phosphate, pH 7.1; Solution B, 5 mM L-DOPA in 100 mM sodium phosphate, pH 7.1; Solution C, 20 mM MBTH in H<sub>2</sub>O) was added and then, the cells were incubated at 37°C for 10 min. The product dopachrome was

detected at 505 nm (ref. 490 nm) by a multi-plate reader (Dainippon) and normalized with protein content.

### Melanin measurement

Extracellular melanin content in the cell culture media (phenol red free) was measured by using a multi-plate reader. After the medium was collected, the cells were washed twice with ice-cold phosphate-buffered saline, followed by lysis with RIPA buffer for 40 min on ice, and the lysates were centrifuged at 10,000 g for 20 min. Supernatants containing protein were subject to the protein assay and the pellets with intracellular melanin were solubilized in 200  $\mu$ l of 1 M NaOH for 2 h at 60°C. Melanin amount was determined spectrophotometrically at 405 nm (ref. 570 nm) by a multi-plate reader. The melanin amount was calculated by normalizing the total melanin values with protein content (abs melanin/ $\mu$ g protein).

### Measurement of cAMP concentration

The cAMP level was measured using a cAMP kit (R&D Systems Inc., Minneapolis, USA). In brief, cells were lysed in 0.1 M HCl and centrifuged, and the supernatants were collected, neutralized, and diluted. Alkaline phosphate-labeled cAMP was added to compete with cAMP in the cell lysates for sites on a rabbit antibody immobilized on a 96-well plate. After washing, a substrate solution was added into each well to determine the bound enzyme activity. Color development was stopped, and the absorbance was measured (405 nm). The intensity of the color was expressed to be inversely proportional to the concentration of cAMP in the cell lysates.

### Western blot analysis

The treated cells were lysed in RIPA lysis buffer consisting of 50 mM Tris-HCl, 150 mM NaCl, 1 mM EDTA, 1% Triton X-100, 1% sodium deoxycholate, 0.1% SDS, pH 7.4, 1 mM PMSF, and protease inhibitors, incubated for 40 min on ice, and centrifuged (10,000 g, 20 min). After protein assays, the lysates were denatured in sample buffer, separated on 10% SDS polyacrylamide gels at 200 V, and transferred onto membranes for 60 min at 100 V. Membrane blocking was performed with 5% skim milk solution for 1 h and the membrane was incubated with anti-tyrosinase (anti-goat), TRP1 (anti-rabbit), TRP2 (anti-rabbit), p-CREB (anti-rabbit)/CERB (anti-mouse), MITF (anti-mouse), p-AKT (anti-rabbit)/AKT (anti-rabbit), p-p38 (anti-rabbit)/p38 (anti-rabbit), p-ERK (anti-rabbit)/ERK (anti-rabbit), p-JNK (anti-rabbit)/JNK (anti-rabbit), and  $\beta$ -actin (anti-mouse) antibodies at dilutions of 1:1000 at 4°C overnight. Anti-tyrosinase, TRP1, and TRP2 antibodies were from Santa Cruz Technology (Finnell Street, Dallas, USA), anti-p-CREB/CERB, p-AKT/AKT, p-p38/p38, p-ERK/ERK, p-JNK/JNK, and  $\beta$ -actin antibodies were from Cell Signaling Technology (Danvers, USA), and anti-MITF antibody was from Millipore (Billerica, USA). And then, they were further incubated with the corresponding secondary antibody for 2 h. The targeted proteins were detected by using a chemiluminescence kit (Amersham, Buckinghamshire, UK) according to the manufacturer's instructions and visualized after exposure to chemiluminescence film (Fujifilm, Tokyo, Japan).

### Statistical analysis

Data were expressed as the mean  $\pm$  SD and unpaired Student's *t*-test was used for statistical analysis. A *P*-value of <0.05 was considered of significant difference.

## Results

### Morphological changes of melanoma cells induced by 3,5-diCQM

While normal melanoma cells show short dendrites, differentiating melanocytes show increased dendrite production [25]. Our results showed that murine melanoma B16F10 cells treated with 3,5-diCQM for 24 h did not show any increase in cell number or cytotoxicity (Fig. 2A), and did not induce any change in cell morphology when compared with the control cells (Fig. 2B).

### 3,5-diCQM stimulates tyrosinase activity and melanin content

Since tyrosinase is known to play an important role in melanin production, the effect of 3,5-diCQM on tyrosinase activity in melanoma cells was measured. Our results showed that 3,5-diCQM treatment increased tyrosinase activity in a dose-dependent manner (control, 100%  $\pm$  6.2%; 12.5  $\mu$ M, 136%  $\pm$  13.9%; 25  $\mu$ M, 175.2%  $\pm$  5.8%; 50  $\mu$ M, 242.9%  $\pm$  19.8%) (Fig. 3A). As shown in Fig. 3B, extracellular and intracellular melanin amount showed the same increasing trend in response to 3,5-diCQM treatment (extracellular melanin: control, 100%  $\pm$  4.4%; 12.5  $\mu$ M, 320.9%  $\pm$  10.2%; 25  $\mu$ M, 504.2%  $\pm$  20.3%; 50  $\mu$ M, 764.6%  $\pm$  0.0%; intracellular melanin: control, 100%  $\pm$  7.3%; 12.5  $\mu$ M, 197.2%  $\pm$  12.6%; 25  $\mu$ M, 222.4%  $\pm$  12.5%; 50  $\mu$ M, 285.4%  $\pm$  32.2%).

### Effect of 3,5-diCQM on the expressions of TRPs

Since 3,5-diCQM increased tyrosinase activity and melanin production, we next aimed to elucidate the melanogenic signaling pathway related to the stimulatory activity of 3,5-diCQM. After treatment with 3,5-diCQM, western blotting was performed to examine the expressions of melanogenesis-related proteins (MRPs) such as tyrosinase, TRP1, and TRP2. Tyrosinase and TRP1 protein expressions were clearly augmented after treatment with 3,5-diCQM at different concentrations (12.5, 25, and 50  $\mu$ M) for 48 h (Fig. 4), and 3,5-diCQM treatment distinctly induced the expression of tyrosinase and TRP1 in a dose-dependent manner. However, the treatment of with 3,5-diCQM had little effect on the expression of TRP2.

### 3,5-diCQM enhances CREB activation and induces the expressions of MITF and p-MITF

Studies [8,9] have shown that CREB and MITF act as mediators of melanocyte differentiation through increased phosphorylation and expression, respectively. According to the previous reports, MITF expression is enhanced in skin by UV irradiation and it acts as a master regulator of melanin production, and the phosphorylation of MITF regulates the transcription of genes encoding MRPs through interactions with M- and E-boxes present in the promoter regions of tyrosinase, TRP1, and TRP2 [26]. Therefore, we hypothesized that both of CREB and MITF may be involved in 3,5-diCQM-induced melanogenesis. As expected, our results showed that phosphorylation of CREB (Fig. 5A) was clearly enhanced to  $\sim$ 2 folds at the highest concentration of 3,5-diCQM for 15 min compared with cells treated with 0.1% DMSO only.

A significant increase was also shown in the expression of total and phosphorylated MITF by 3,5-diCQM treatment for 24 h (Fig. 5B), suggesting that 3,5-diCQM-mediated elevation of the MITF and activation of the MITF might be cAMP-dependent.

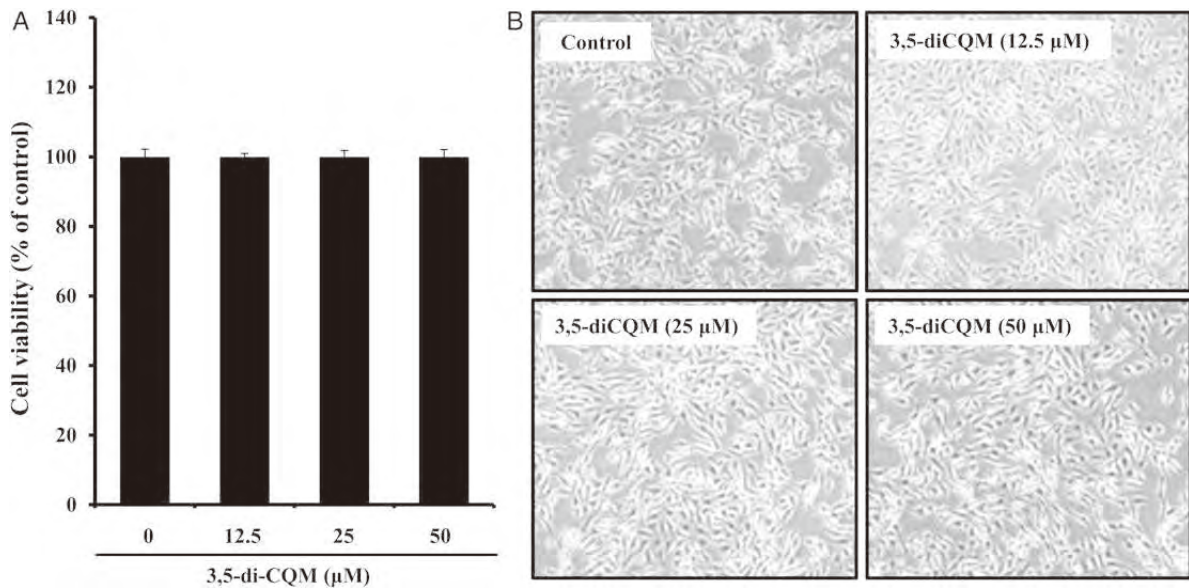


**Figure 2. Effects of 3,5-diCQM on cell viability and morphology** B16F10 cells were treated with 0.1% DMSO as vehicle or with 3,5-diCQM at 12.5, 25, and 50 μM for 24 h. (A) Cell viability was measured by MTT assay. (B) Cell morphology was observed under a microscope. Magnification, ×200. Values are expressed as the mean ± SD of three separate independent experiments.

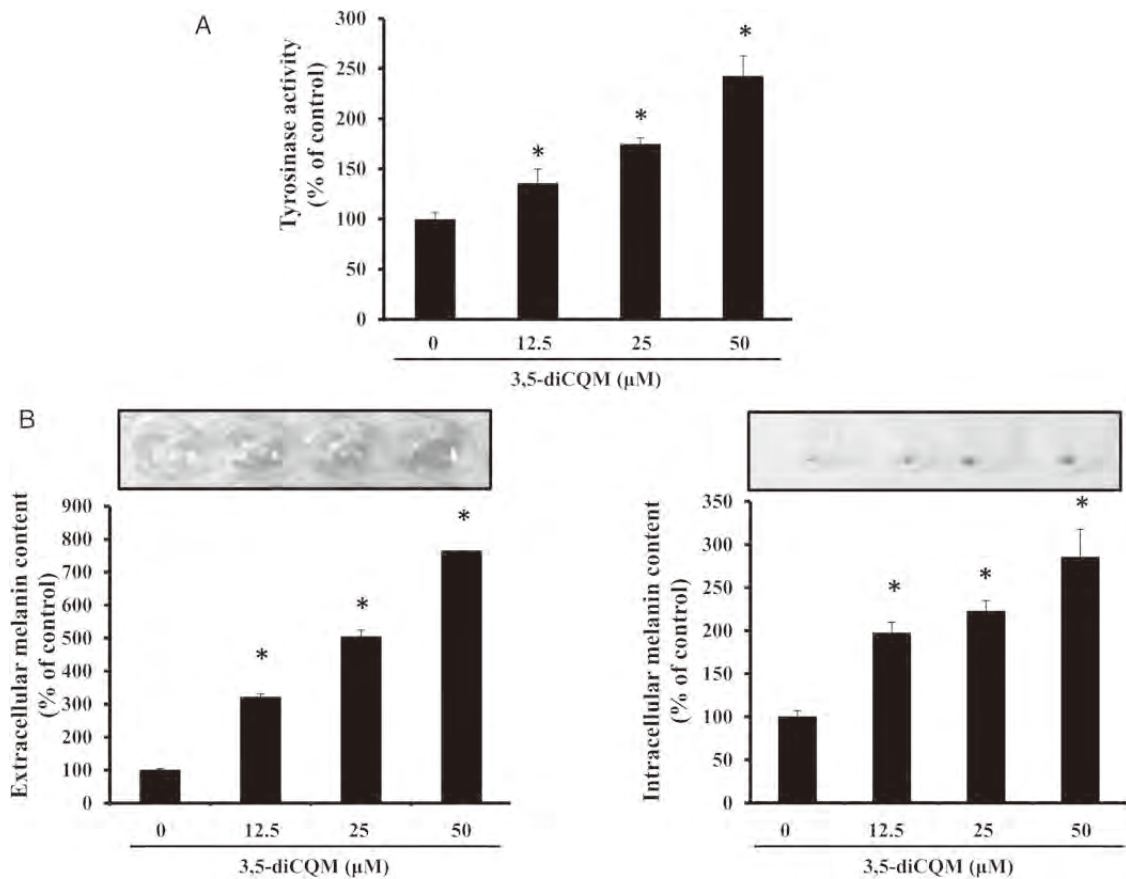


**Figure 3. Effects of 3,5-diCQM on tyrosinase activity and melanin content** B16F10 cells were treated with 3,5-diCQM at 12.5, 25, and 50 μM for 24 h. (A) Tyrosinase activity was determined by L-DOPA oxidation assay. B16F10 cells were treated with 3,5-diCQM at 12.5, 25, and 50 μM for 48 h. (B) Melanin content was assayed. Each percentage value in the treated cells was calculated with respect to that in the control cells. Values are expressed as the mean ± SD of three separate independent experiments. \**P* < 0.05 compared with control.

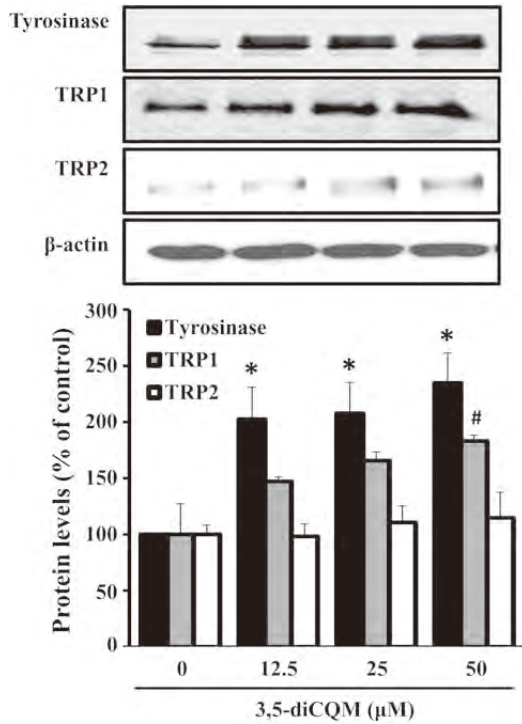


**Figure 4. Effects of 3,5-diCQM on expression of TRPs** B16F10 cells were treated with 3,5-diCQM at 12.5, 25, and 50 μM for 48 h. Tyrosinase, TRP1, and TRP2 protein expression were detected by western blotting, and β-actin was used as a loading control. Values are expressed as the mean ± SD of three separate independent experiments. \*,#P<0.05 compared with control.

**3,5-diCQM increases cAMP level**

Since cAMP requires the activation of CREB for its responsiveness to the MITF promoter [25], we explored whether 3,5-diCQM affects the induction of cAMP, which is a crucial step in melanogenesis. To evaluate this hypothesis, we assessed intracellular cAMP level after 3,5-diCQM treatment. As seen in Fig. 6A, the level of cAMP was increased 12 h after 3,5-diCQM addition. cAMP accumulation has been shown to cause the activation of PKA, leading to melanin synthesis. Thus, we evaluated the effect of H89, an inhibitor of cAMP-dependent PKA, on the 3,5-diCQM-mediated induction of tyrosinase activity and melanin content. As shown in Fig. 6B, H89 (1 μM) abrogated 3,5-diCQM (30 μM)-induced enhancement of tyrosinase activity on incubation for 24 h. In addition, H89 (1 μM) also reduced the melanin content up-regulated by 3,5-diCQM (30 μM) treatment for 48 h compared with controls (Fig. 6C). These results imply that cAMP/PKA signaling is directly involved in 3,5-diCQM-mediated melanogenesis.

**3,5-diCQM induces activation of p38 MAPK**

Phosphorylation of MAPK or inhibition of PI3K/AKT activation has also been reported as one of the signaling processes in hyperpigmentation. Thus, we performed western blot analysis on cells after 3,5-diCQM treatment at 12.5, 25, and 50 μM for 15 min to evaluate MAPK and PI3K/AKT in 3,5-diCQM-regulated melanogenesis. Phosphorylation of p38 MAPK, but not JNK or ERK, was significantly increased after 1 h at different concentrations of 3,5-diCQM treatment compared with controls (Fig. 7). In particular, the addition of 25 and 50 μM 3,5-diCQM increased the activation of p38 MAPK. In contrast, 3,5-diCQM did not induce any significant up-regulation of AKT phosphorylation. Even co-treatment with ERK inhibitor (PD98059), AKT inhibitor or JNK inhibitor (SP600125) either increased 3,5-diCQM-induced tyrosinase activity or did not influence

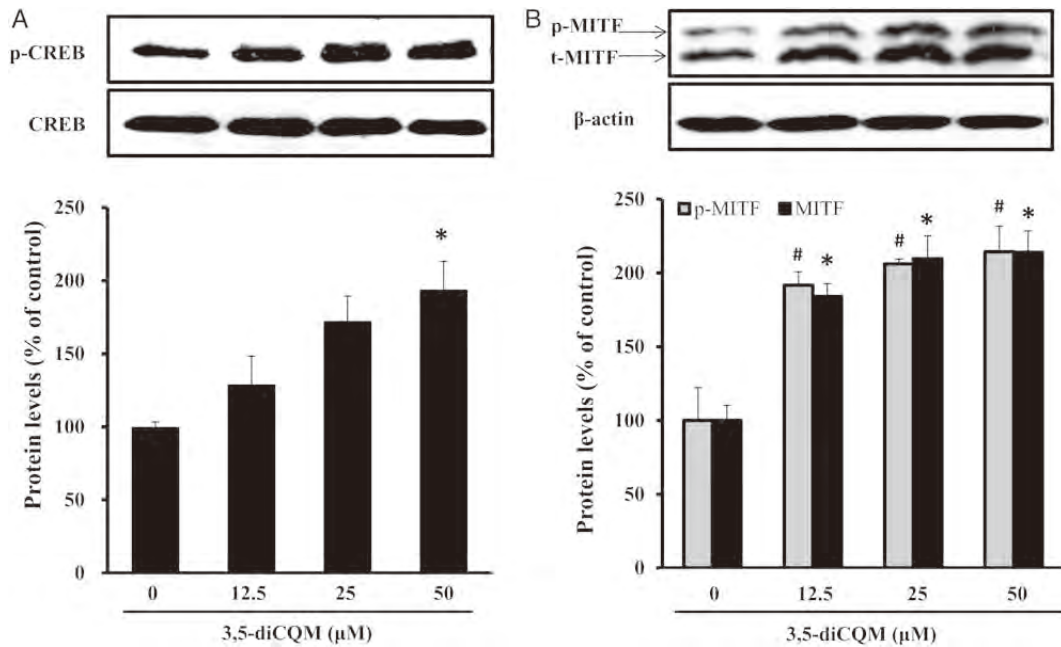


**Figure 5. Induction of CREB activation and MITF up-regulation by 3,5-diCQM** After incubation of B16F10 cells with 3,5-diCQM at 12.5, 25, and 50 μM for 15 min (CREB activation) or 24 h (MITF expression), western blotting was carried out using specific antibodies against phospho-CREB (p-CREB) (A), total (t-MITF) and phosphorylated MITF (p-MITF) (B), and β-actin. Values are expressed as the mean ± SD of three separate independent experiments. \*,#P<0.05 compared with control.

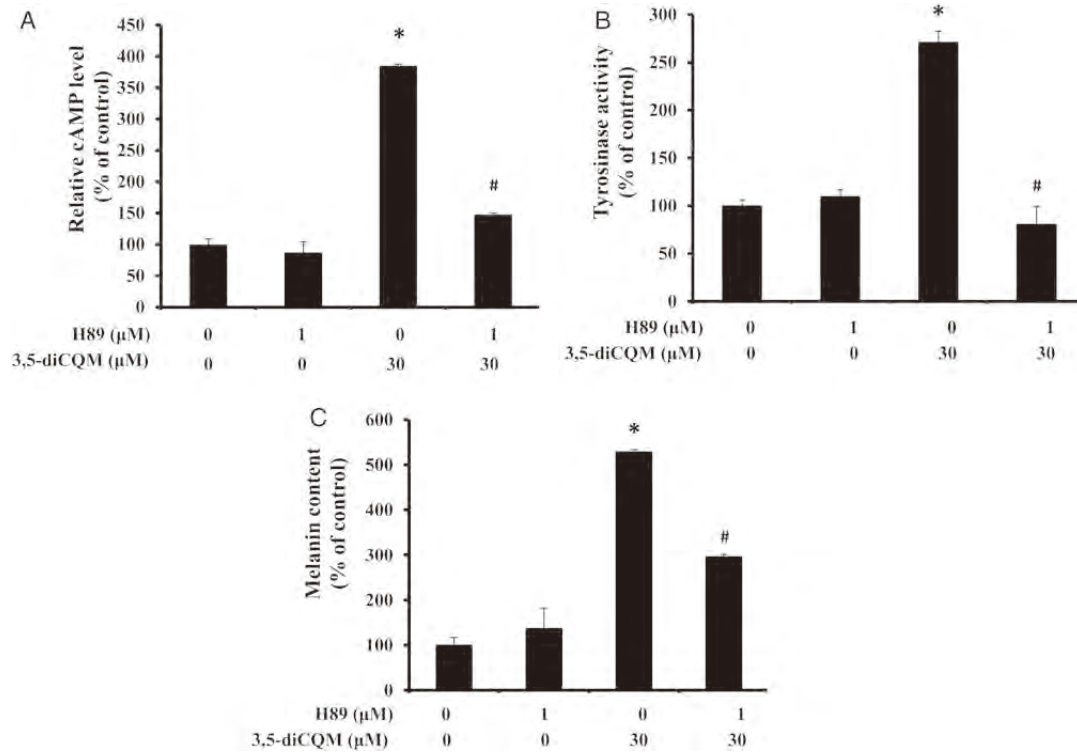


**Figure 6. Induction of cAMP level by 3,5-diCQM** B16F10 cells were pre-incubated with H89 (1 μM) for 2 h before 3,5-diCQM (30 μM) was added, and then incubated for 12 h for the measurement of cAMP level (A). For the tyrosinase activity (B) and melanin content (C), cells were co-treated with H89 (1 μM) and 3,5-diCQM (30 μM) for 24 and 48 h, respectively. Values are expressed as the mean ± SD of three separate experiments. \* $P < 0.05$  compared with control; # $P < 0.05$  compared with 3,5-diCQM stimulation.

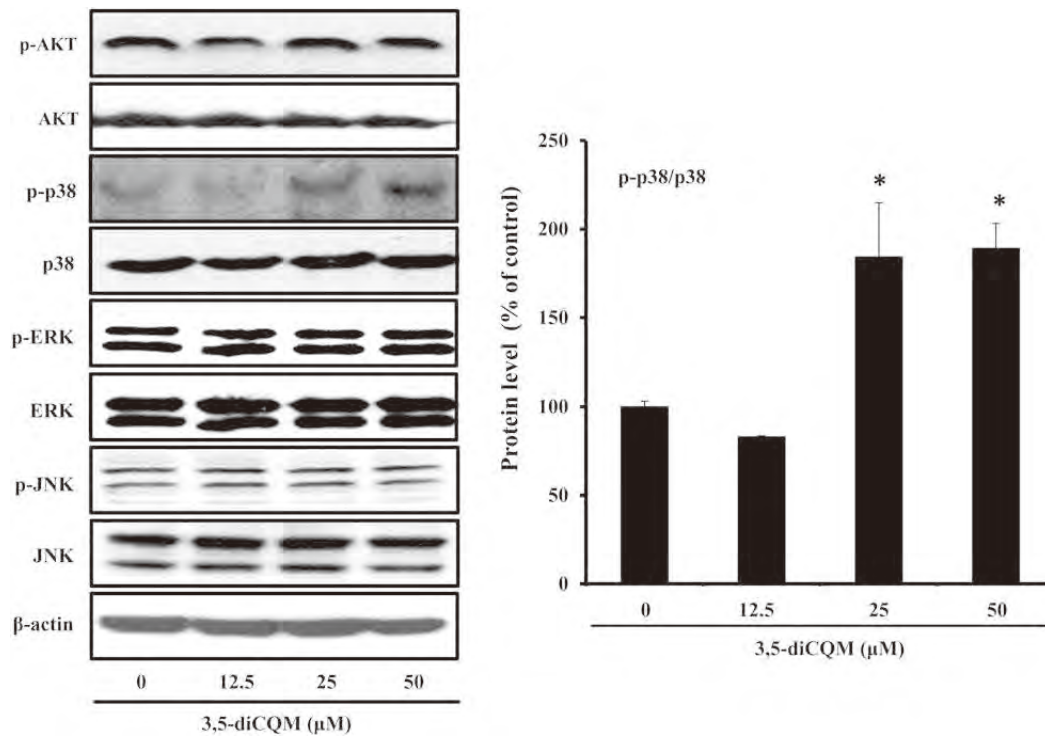


**Figure 7. Effects of 3,5-diCQM on the activation of MAPKs and AKT signaling pathway** B16F10 cells were treated with 3,5-diCQM at the 12.5, 25, and 50 μM for 15 min, and the phosphorylation of ERK, p38, JNK, and AKT was measured by western blotting. Values are expressed as the mean ± SD of three separate independent experiments. \* $P < 0.05$  compared with control.

tyrosinase activity, revealing that ERK, AKT, and JNK are not directly involved in the upstream pathway of melanogenesis mediated by 3,5-diCQM (Fig. 8A–C). However, the p38 MAPK inhibitor SB203580 significantly reduced 3,5-diCQM-triggered tyrosinase activity by 40.6% compared with control (Fig. 8D).

### 3,5-diCQM induces the hyperpigmentation in normal human epidermal melanocytes

To ascertain the inducing effects of 3,5-diCQM on hyperpigmentation, we assessed the melanin content in the cells treated with 3,5-diCQM in normal human epidermal melanocytes. After 48 h treatment, 3,5-diCQM induced an increase in melanin content when compared with the untreated control cells (control, 100%  $\pm$  3.0%; 3,5-diCQM, 131.1%  $\pm$  1.0%) (Fig. 9A). In accordance with its effect in normal human epidermal melanocytes, 3,5-diCQM enhanced the production of melanin in MMac human melanoma cells as well (control, 100%  $\pm$  0.0%; 3,5-diCQM, 161.6%  $\pm$  4.6%) (Fig. 9B).

### Discussion

Melanogenesis plays a pivotal role in solar UV irradiation-induced skin injury and the decline in hair pigmentation, namely hair graying, which is attributed to the lack of melanization signals, low level of GSH, loss of melanocytes, and an indicator of hair aging [27–30]. Currently, many researchers have focused on the specific mechanisms

involved in melanogenesis with the aim of developing new therapeutic agents for hair graying and depigmented skin disease, such as vitiligo on pigmentation. In hypopigmentation therapy [31,32], the induction of melanin production and functional melanocytes was the focus of study to develop effective treatments. Natural resources have been screened for the development of pigmentation agents, and several previous studies using murine melanoma and human melanocytes have shown the pigmentation inducing effects of natural compounds, including quercetin [33], naringenin [34], cubebin [10], lotus flower [35], and glycyrrhizin [36].

Here, we investigated the effects of 3,5-diCQM on skin pigmentation induction and the mechanism by which 3,5-diCQM elicits activating effects on melanogenesis in murine B16F10 cells. Our results showed that 3,5-diCQM increased melanin production via the induction of the melanogenic enzyme tyrosinase and pigmentation-related transcription factor MITF. These data suggest that one of the mechanisms for 3,5-diCQM-induced melanogenesis in B16F10 cells is associated with the increase of the expression of the melanogenic enzyme tyrosinase through a master regulator of melanocyte activity, MITF.

cAMP enhances the expression of MITF through the activation of PKA and CREB, which binds to the CRE consensus motif in the MITF promoter [37] and subsequently results in the indirect activation of the tyrosinase promoter by MITF [38]. In accordance with previous studies, we observed that 3,5-diCQM induces the phosphorylation of CREB and enhances the production of cAMP compared with

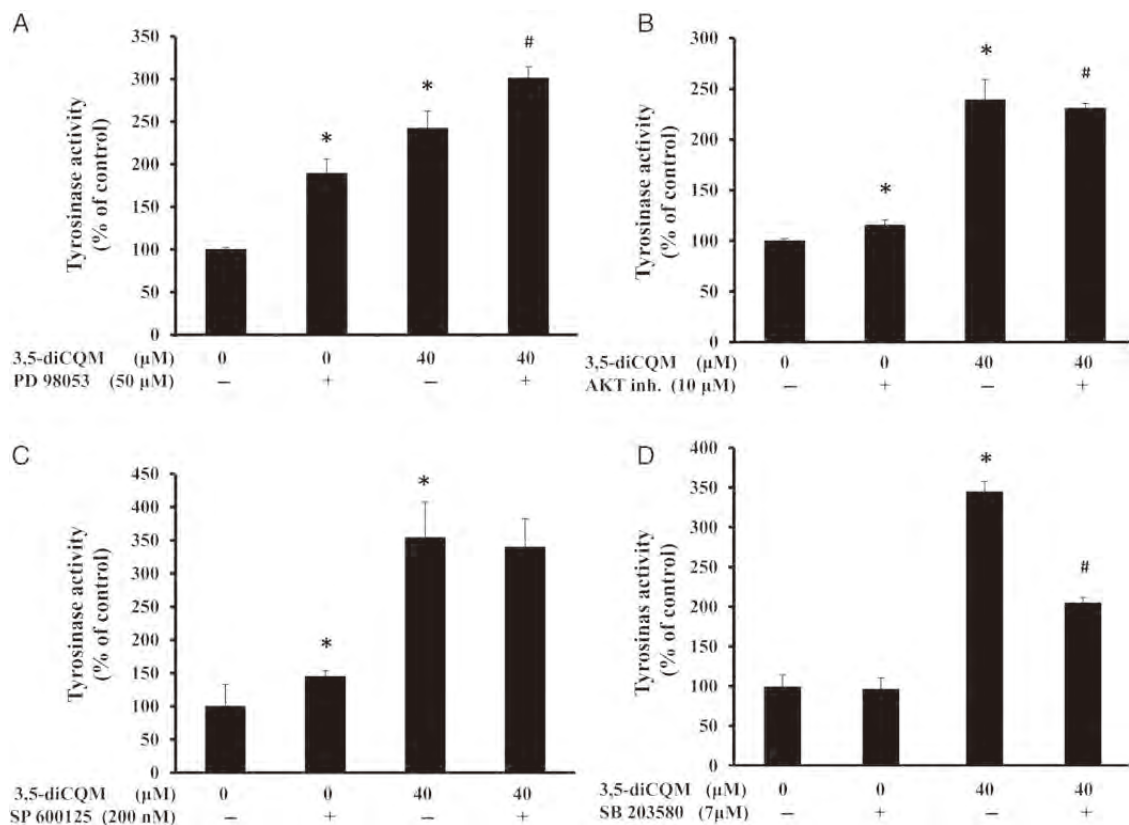


**Figure 8. Effects of inhibitors of MAPKs and AKT on 3,5-diCQM-induced tyrosinase activity** (A–D) Inhibitors were pre-incubated with B16F10 cells for 2 h before addition of 3,5-diCQM at 40 μM, followed by an additional incubation for 24 h. Each percentage value in the treated cells was calculated with respect to that in the control cells. Values are expressed as the mean  $\pm$  SD of three separate experiments. \* $P$  < 0.05 compared with control; # $P$  < 0.05 compared with 3,5-diCQM stimulation.

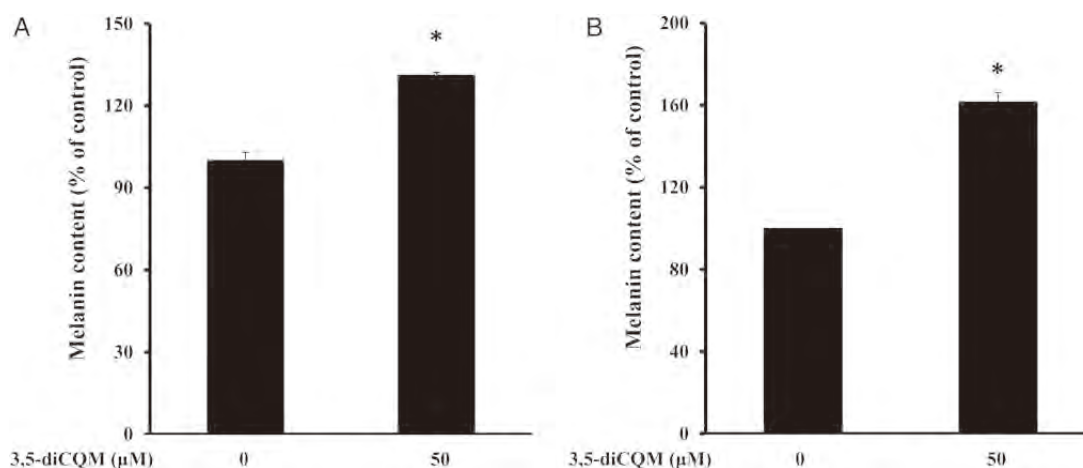


**Figure 9. Effects of 3,5-diCQM on melanin content in human melanocytes and melanoma cells** Normal human epidermal melanocytes (A) and human melanoma cells (MMAc) (B) were treated with 3,5-diCQM at 50  $\mu$ M for 48 h and then melanin contents were measured as described in 'Materials and Methods' section. Values are expressed as the mean  $\pm$  SD of three separate independent experiments. \* $P < 0.05$  compared with control.

untreated cells, indicating that 3,5-diCQM-mediated MITF activation relies on cAMP/PKA signaling.

Recently, it was demonstrated that the p38 MAPK was involved in melanogenesis by treatment with UV light, Lupeo or  $\alpha$ -MSH in melanoma cells [39–41]. Co-treatment with the p38 inhibitor, SB203580, abolished the  $\alpha$ -MSH-induced increase in melanin synthesis, indicating that p38 is closely related to the  $\alpha$ -MSH-induced melanogenic pathway. Mallick *et al.* [42] reported that a lipid fraction has activities to stimulate pigmentation and that activation of the p38-stress-activated signaling pathway is related to the melanogenesis process in murine melanoma cells. Furthermore, the activation of ERK and JNK/SAPK suppresses melanin synthesis [43–45] or the phosphorylation of ERK was induced by cAMP elevating agents [46]. In addition, inhibition of PI3K/AKT induces hyperpigmentation by stimulating activation of MITF and expression of its downstream pathway-related proteins such as tyrosinase and TRPs [11,12], whereas the phosphorylation of PI3K/AKT decreases melanin production by reducing MITF, tyrosinase, and TRPs in MSH-treated cells [47]. Our result on p38 MAPK phosphorylation is consistent with previous studies. That is, treatment with 3,5-diCQM markedly enhanced the phosphorylation of p38 MAPK, and co-incubation with p38 MAPK inhibitor SB203580 clearly abrogated 3,5-diCQM-stimulated tyrosinase activity. Unlike its effect on p38 MAPK, 3,5-diCQM did not cause the phosphorylation of ERK, JNK, or AKT, and their inhibitors did not reduce the 3,5-diCQM-stimulated melanogenic process either. These results suggested that among the upstream pathways involved in melanogenesis, p38 MAPK is responsible for the pigmentation process mediated by 3,5-diCQM in melanoma cells. These results suggested that 3,5-diCQM-caused p38 MAPK phosphorylation which then stimulated phosphorylation of MITF. This led to increased tyrosinase activity as well as expression of tyrosinase, TRP1, and TRP2, and finally enhanced the melanin production.

Additionally, the melanogenic effect of 3,5-diCQM was confirmed by assessing enhanced level of melanin production in normal human epidermal melanocytes and human melanoma cells.

Regarding the increasing demand to treat hypopigmentation in skin and hair, it is tempting to speculate that natural compounds with antioxidant activity such as 3,5-diCQM might induce pigmentation in the hair graying model caused by loss of antioxidant enzymes

and dysfunction of melanization. However, additional potential mechanisms of action should be considered and explored in future studies.

Taken together, our results show that 3,5-diCQM is capable of inducing pigmentation, and the molecular mechanism underlying 3,5-diCQM-induced pigmentation is through the activation of the p38 signaling pathway which, via phosphorylation and activation of the CREB, leads to induction of the transcription factor MITF and subsequent activation of tyrosinase and melanin production.

## Funding

This work was supported by an endowment from Erina Co., Inc. (Tokyo, Japan) (No. 20140070).

## References

1. Sturm RA. Skin colour and skin cancer-MC1R, the genetic link. *Melanoma Res* 2002, 12: 405–516.
2. Mason HS, Ingram DJE, Allen B. The free radical property of melanin. *Arch Biochem Biophys* 1960, 86: 225–230.
3. Sarn T. Properties and function of the ocular melanin—a photobiophysical view. *J Photochem Photobiol B* 1992, 12: 215–258.
4. Yoshida M, Fuchigami M, Nagao T, Okabe H, Matsunaga K, Takata J, Karube Y, *et al.* Antiproliferative constituents from Umbelliferae plants VII active triterpenes and rosmarinic acid from *Centella asiatica*. *Biol Pharm Bull* 2005, 28: 173–175.
5. Gilchrist BA, Blog FB, Szabo G. Effects of aging and chronic sun exposure on melanocytes in human skin. *J Invest Dermatol* 1979, 73: 141–143.
6. Uehara M, Miyauchi H, Tanaka S. Diminished contact sensitivity response in vitiliginous skin. *Arch Dermatol* 1984, 120: 195–198.
7. Hatchome N, Aiba S, Kato T, Torinuki W, Tagami H. Possible functional impairment of Langerhans' cells in vitiliginous skin. Reduced ability to elicit dinitrochlorobenzene contact sensitivity reaction decreased stimulatory effect in the allogeneic mixed skin cell lymphocyte culture reaction. *Arch Dermatol* 1987, 123: 51–54.
8. Hearing VJ. Biochemical control of melanogenesis and melanosomal organization. *J Invest Dermatol* 1999, 4: 24–28.
9. Scream RA, Conkright MD, Katoh Y, Best JL, Canetti G, Jeffries S, Guzman E, *et al.* The CREB coactivator TORC2 functions as a calcium- and cAMP-sensitive coincidence detector. *Cell* 2014, 119: 61–74.

10. Hirata N, Naruto S, Ohguchi K, Akao Y, Nozawa Y, Inuma M, Matsuda H. Mechanism of the melanogenesis stimulation activity of (-)-cubebin in murine B16 melanoma cells. *Bioorg Med Chem* 2007, 15: 4897–4902.
11. Khaled M, Larrriere L, Bille K, Ortonne JP, Ballotti R, Bertolotto C. Microphthalmia associated transcription factor is a target of the phosphatidylinositol-3-kinase pathway. *J Invest Dermatol* 2003, 121: 831–836.
12. Lee J, Jung K, Kim YS, Park D. Diosgenin inhibits melanogenesis through the activation of phosphatidylinositol-3-kinase pathway (PI3K) signaling. *Life Sci* 2007, 81: 249–254.
13. Mishima S, Inoh Y, Narita Y, Ohta S, Sakamoto T, Araki Y, Suzuki KM, et al. Identification of caffeoylquinic acid derivatives from *Brazilian propolis* as constituents involved in induction of granulocytic differentiation of HL-60 cells. *Bioorg Med Chem* 2005, 13: 5814–5818.
14. Basnet P, Matsushige K, Hase K, Kadota S, Namba T. Four di-O-caffeoylquinic acid derivatives from propolis. Potent hepatoprotective activity in experimental liver injury models. *Biol Pharm Bull* 1996, 19: 1479–1484.
15. Lin YL, Lu CK, Huang YJ, Chen HJ. Antioxidative caffeoylquinic acids and flavonoids from *Hemerocallis fulva* flowers. *J Agric Food Chem* 2011, 24: 8789–8795.
16. Góngora L, Gíner RM, Máñez S, Recio M, Del C, Schinella G, Ríos J. Effects of caffeoyl conjugates of isoprenyl-hydroquinone glucoside and quinic acid on leukocyte function. *Life Sci* 2002, 71: 2995–3004.
17. Zhu X, Zhang H, Lo R. Phenolic compounds from the leaf extract of artichoke (*Cynara scolymus* L.) and their antimicrobial activities. *J Agric Food Chem* 2004, 52: 7272–7278.
18. Yoshimoto M, Yahara S, Okuno S, Islam MS, Ishiguro K, Yamakawa O. *Biosci Biotechnol Biochem* 2002, 66: 2336–2341.
19. Robinson WE Jr, Cordeiro M, Abdel-Malek S, Jia Q, Chow SA, Reinecke MG, Mitchell WM. Dicafeoylquinic acid inhibitors of human immunodeficiency virus integrase: inhibition of the core catalytic domain of human immunodeficiency virus integrase. *Mol Pharmacol* 1996, 50: 846–855.
20. Zhu K, Cordeiro ML, Atienza J, Robinson WE Jr, Chow SA. Irreversible inhibition of human immunodeficiency virus type 1 integrase by dicafeoylquinic acids. *J Virol* 1999, 73: 3309–3316.
21. Yang B, Meng Z, Dong JX, Yan LP, Zou LB, Tang ZM, Dou GF. Metabolic profile of 1,5-dicafeoylquinic acid in rats, an *in vivo* and *in vitro* study. *Drug Metab Dispos* 2005, 33: 930–936.
22. Hung TM, Na M, Thuong PT, Su ND, Sok DE, Song KS, Seong YH, et al. Antioxidant activity of caffeoyl quinic acid derivatives from the roots of *Dipsacus asper* Wall. *J Ethnopharmacol* 2006, 108: 188–192.
23. Jang DS, Yoo NH, Kim NH, Lee YM, Kim CS, Kim J, Kim JH, et al. 3,5-Di-O-caffeoyl-epi-quinic acid from the leaves and stems of *Erigeron annuus* inhibits protein glycation, aldose reductase, and cataractogenesis. *Biol Pharm Bull* 2010, 33: 329–333.
24. Winder AJ, Harris H. New assays for the tyrosine hydroxylase and dopa oxidase activities of tyrosinase. *Eur J Biochem* 1991, 1: 317–326.
25. Buscà R, Ballotti R. Cyclic AMP a key messenger in the regulation of skin pigmentation. *Pigment Cell Res* 2000, 13: 60–69.
26. Bertolotto C, Bille K, Ortonne JP, Ballotti R. In B16 melanoma cells, the inhibition of melanogenesis by TPA results from PKC activation and diminution of microphthalmia binding to the M-box of the tyrosinase promoter. *Oncogene* 1998, 2: 1665–1670.
27. Kaidbey KH, Agin PP, Sayre RM, Kligman AM. Photoprotection by melanin—a comparison of black and Caucasian skin. *J Am Acad Dermatol* 1979, 1: 249–260.
28. Kollias N, Sayer RM, Zeise L, Chedekel MR. Photoprotection by melanin. *J Photochem Photobiol B Biol* 1999, 9: 135–160.
29. Trüeb RM. Oxidative stress in ageing of hair. *Int J Trichol* 2009, 1: 6–14.
30. Galván I, Alonso-Alvarez C, Negro JJ. Relationships between hair melanization, glutathione levels, and senescence in wild boars. *Physiol Biochem Zool* 2012, 85: 332–347.
31. Westerhof W, D'Ischia M. Vitiligo puzzle: the pieces fall in place. *Pigment Cell Res* 2007, 20: 345–359.
32. Spritz RA. The genetics of generalized vitiligo and associated autoimmune diseases. *Pigment Cell Res* 2007, 20: 271–278.
33. Nagata H, Takekoshi S, Takeyama R, Homma T, Osamura R. Quercetin enhances melanogenesis by increasing the activity and synthesis of tyrosinase in human melanoma cells and normal human melanocytes. *Pigment Cell Res* 2004, 17: 66–73.
34. Connor M, Christie MJ. Opioid receptor signalling mechanisms. *Clin Exp Pharmacol Physiol* 1999, 26: 493–499.
35. Jun S, Kim NH, Koo BS, Kim JY, Lee AY. Lotus (*Nelumbo nucifera*) flower essential oil increased melanogenesis in normal human melanocytes. *Exp Mol Med* 2009, 41: 517–524.
36. Jung GD, Yang JY, Song ES, Par JW. Stimulation of melanogenesis by glycyrrhizin in B16F1 melanoma cells. *Exp Mol Med* 2001, 33: 131–135.
37. Lin JY, Fisher DE. Melanocyte biology and skin pigmentation. *Nature* 2007, 22, 445: 843–850.
38. Park HY, Gilchrist BA. Signaling pathways mediating melanogenesis. *Cell Mol Biol (Noisy-le-grand)* 1999, 45: 919–930.
39. Galibert MD, Carreira S, Goding CR. The Usf-1 transcription factor is a novel target for the stress-responsive p38 kinase and mediates UV-induced tyrosinase expression. *EMBO J* 2001, 20: 5022–5031.
40. Hata K, Hori K, Takahashi S. Role of p38 MAPK in lupeol-induced B16 2F2 mouse melanoma cell differentiation. *J Biochem* 2003, 134: 441–445.
41. Bellei B, Maresca V, Flori E, Pitisci A, Larue L, Picardo M. p38 regulates pigmentation via proteasomal degradation of tyrosinase. *J Biol Chem* 2010, 5: 7288–7299.
42. Mallick S, Mandal SK, Bhadra R. Human placental lipid induces mitogenesis and melanogenesis in B16F10 melanoma cells. *J Biosci* 2002, 27: 243–249.
43. Kim DS, Kim SY, Lee JE, Kwon SB, Joo YH, Youn SW, Park KC. Sphingosine-1-phosphate-induced ERK activation protects human melanocytes from UVB-induced apoptosis. *Arch Pharm Res* 2003, 26: 739–746.
44. Park SH, Kim DS, Kim WG, Ryou IJ, Lee DH, Huh CH, Youn SW, et al. Terrein: a new melanogenesis inhibitor and its mechanism. *Cell Mol Life Sci* 2004, 61: 2878–2885.
45. Bu J, Ma PC, Chen ZQ, Zhou WQ, Fu YJ, Li LJ, Li CR. Inhibition of MITF and tyrosinase by paeonol-stimulated JNK/SAPK to reduction of phosphorylated CREB. *Am J Chin Med* 2008, 36: 245–263.
46. Englaro W, Rezzonico R, Durand-Clement M, Lallemand D, Ortonne JP, Ballotti R. Mitogen-activated protein kinase pathway and AP-1 are activated during cAMP induced melanogenesis in B-16 melanoma cells. *J Biol Chem* 1995, 270: 24315–24320.
47. Jang JY, Lee JH, Jeong SY, Chung KT, Choi YH, Choi BT. Partially purified *Curcuma longa* inhibits alpha melanocyte stimulating hormone stimulated melanogenesis through extracellular signal regulated kinase or Akt activation mediated signalling in B16F10 cells. *Exp Dermatol* 2009, 18: 689–694.

## Nobiletin, a Polymethoxy Flavonoid, Reduced Endothelin-1 Plus SCF-Induced Pigmentation in Human Melanocytes

Hyo Jung Kim<sup>1</sup>, Takayuki Yonezawa<sup>1</sup>, Toshiaki Teruya<sup>2</sup>, Je-Tae Woo<sup>1,3</sup> and Byung-Yoon Cha<sup>1</sup>

<sup>1</sup>Research Institute for Biological Functions, Chubu University, Kasugai, Aichi, Japan

<sup>2</sup>Faculty of Education, University of the Ryukyus, Nishihara, Okinawa, Japan

<sup>3</sup>Department of Research and Development, Erina Co., Inc., Minato-ku, Tokyo, Japan

Received 31 October 2014, accepted 2 December 2014, DOI: 10.1111/php.12400

### ABSTRACT

**Nobiletin is a unique flavonoid having polymethoxy groups and has exhibited anti-inflammatory and antiobesity effects. Here, we examined the inhibition of nobiletin on melanogenesis induced by endothelin-1 (ET) and stem cell factor (SCF) in normal human melanocytes. Nobiletin dose dependently reduced ET plus SCF-stimulated tyrosinase activity without causing cytotoxicity. Nobiletin reduced cAMP-response element-binding protein (CREB) phosphorylation and microphthalmia-associated transcription factor (MITF) expression, which is a key transcription factor for tyrosinase expression in pigmentation induced by ET plus SCF stimulation. Nobiletin treatment effectively decreased ET plus SCF-induced Raf-1, MEK and ERK1/2 phosphorylation and also downregulated the forskolin-induced phosphorylation of CREB. Furthermore, nobiletin inhibited ET plus SCF-triggered production of melanin and expression of MITF/tyrosinase in a three-dimensional human epidermal model. In accordance with protein expression, the expression of genes related to the pigmentation was also increased in the cells stimulated with ET plus SCF and the cotreatment with nobiletin decreased obviously the ET plus SCF-triggered gene expressions of tyrosinase, PMEL, TRP1 and MITF. Nobiletin contributes to hypopigmentation by downregulating MITF and tyrosinase expression through reduced Raf-1 phosphorylation. Our findings implicate nobiletin as a potential new whitening agent.**

### INTRODUCTION

Melanocytes are present in the basal layer of the epidermis and produce melanin, a pigmented polymer, which provides skin, hair bulb and eyes their pigments. Excessive synthesis of melanin gives rise to hyperpigmentary diseases such as solar lentigo, freckles and chloasma (1). Environmental stimuli, such as UV irradiation, play a pivotal role in the mechanism underlying melanin synthesis. On exposure to UV radiation, activated keratinocytes produce paracrine cytokines including endothelin-1 (ET) (2,3),  $\alpha$ -melanocyte stimulating hormone ( $\alpha$ -MSH) (4,5) and stem cell factor (SCF) (6,7). These cytokines stimulate the proliferation of melanocytes, followed by the expression and activation of tyrosinase. As a result, melanin is synthesized in melanosomes

and the melanosomes are transported to the surrounding epidermal keratinocytes by phagocytosis (8).

A great deal of attention has focused on the application of natural products in the cosmetics industry (9,10), and extracts from natural sources are being employed as new agents in functional cosmetics (11,12). In particular, a large number of flavonoids from natural sources have been targeted for drug development both in pharmacological and in cosmetic research (11,13). Several natural inhibitors of melanin production have been used as cosmetic additives for skin whitening. Many studies have aimed to identify compounds effective in the inhibition of tyrosinase expression in the control of melanogenesis, due to its role as the catalyst in the rate-limiting reaction of the melanogenic pathway. However, these compounds that inhibit melanin production actually caused risks leading to hypopigmentation even in normal skin color conditions, carcinogenic potential, or weak whitening effects. Therefore, these clinical results suggest that downregulation of environmental stimuli-induced melanogenesis without affecting constitutive pigmentation could be an improved method for the measurement of antimelanogenic effects.

Among the melanogenic cytokines, ET and SCF act as potent mitogens and melanogens in UV-exposed human epidermis and several human hyperpigmentary disorders (14–16). ET-1 and SCF regulate the expression of microphthalmia-associated transcription factor (MITF) through the mitogen-activated protein kinase pathway, and subsequently stimulate the transcription and translation of tyrosinase. Tyrosinase catalyzes the rate-limiting reaction of the pigmentation process and functions as the main regulator of melanin synthesis (17,18).

Nobiletin (5,6,7,8,3',4'-hexamethoxy flavone, Fig. 1) is a polymethoxy flavonoid abundantly present in *Citrus* fruits, including *shikuwasa*. Recent studies have shown that nobiletin exhibits anti-inflammatory (19–21), antiallergenic (22,23), anti-atherosclerotic (24) and antitumor activities (25). In addition, nobiletin has been demonstrated to improve obesity (26–28), attenuate neuroinflammation (29,30) and prevent pigmentation (31). However, the antipigmentation properties and its inhibitory mechanism of nobiletin are not yet known.

This study evaluated for the first time the inhibitory effects of polymethoxy flavonoid nobiletin on the melanogenesis signaling pathway stimulated by ET together with SCF. Here, we show the inhibitory effects of nobiletin on ET and SCF-induced melanogenesis and the possible mechanism underlying these

\*Corresponding author email: bycha@isc.chubu.ac.jp (Byung-Yoon Cha)  
© 2014 The American Society of Photobiology

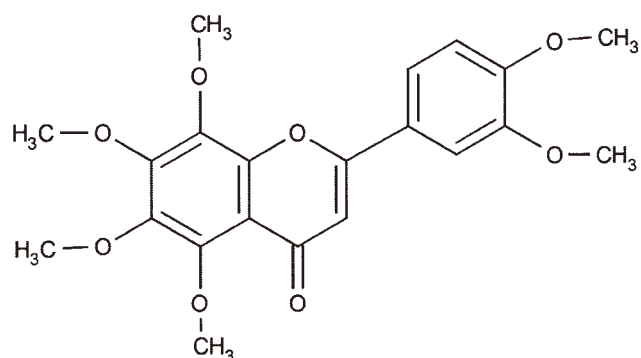


**Figure 1.** Chemical structure of nobiletin.

physiological effects in human melanocytes and a three-dimensional human epidermal model.

## MATERIALS AND METHODS

**Preparation of nobiletin.** Shiikuwasa (*C. depressa*) was purchased from Teruyanusan (Ohigimison, Okinawa, Japan). The dried peels of *shiikuwasa* (dry weight, 6 kg) were extracted in methanol (35 L) for 1 week. The evaporated methanol extract (503.8 g) was partitioned between ethyl acetate and water. The separated organic phase was then partitioned between hexane and 90% methanol. The concentrated 90% methanol phase was chromatographed on a silica gel column (BW-820MH; Fuji Silysia Chemical, Nagoya, Japan) using a stepwise gradient with a solvent consisting of hexane and ethyl acetate (90:10, 80:20, 60:40, 20:80 and 0:100, v/v). The fractions obtained with 20:80 and 0:100 (v/v; 16 g) hexane and ethyl acetate generated crystals that were identified as nobiletin by high-performance liquid chromatography and nuclear magnetic resonance (NMR). The  $^1\text{H}$  and  $^{13}\text{C}$  NMR data of purified nobiletin were consistent with those reported elsewhere (27).

**Cell culture.** Human normal melanocytes were obtained from Life Technologies (Carlsbad, CA). The cells were seeded in 35 mm dishes at a density of  $2 \times 10^5$  cells with 254 medium containing 1% human melanocyte growth supplement (HMGS), 100 U/mL penicillin, 0.1 mg/mL streptomycin and incubated in an atmosphere consisting of 5%  $\text{CO}_2$  at 37°C for 24 h. For experimental conditions, the melanocyte growth medium was removed and replaced with 254 medium containing transferrin (5  $\mu\text{g}/\text{mL}$ ), insulin (5  $\mu\text{g}/\text{mL}$ ), heparin (3  $\mu\text{g}/\text{mL}$ ) and hydrocortisone (0.18  $\mu\text{g}/\text{mL}$ ) and incubated at 37°C in 5%  $\text{CO}_2$ . Each experiment was performed with cells at 80% confluence. Changes in cell viability were not observed in any of the experiments.

**Cell morphology and cell viability measurement.** The morphology of human normal melanocytes was examined under a microscope (CKX41; Olympus Optical, Tokyo, Japan). The medium was removed from cells, and cell viability was assayed by adding 3-[4,5-dimethylthiazol-2-yl]-2,5-diphenyltetrazolium bromide (MTT) solution (0.5 mg/mL in culture medium). After 2 h, the medium was removed, and 200  $\mu\text{L}$  of DMSO was added. The absorbance was determined at 570 nm (reference at 630 nm) by a microplate spectrophotometer (Dainippon, Osaka, Japan). Cell proliferation was calculated as the absorbance of the treatment group relative to the control.

**Assay of cellular tyrosinase activity.** Tyrosinase activity was assayed as previously described with modifications (32). Cells were washed using cold PBS and lysed with 1% sodium deoxycholate and 0.5% Triton X-100 for 2 h. A total of 150  $\mu\text{L}$  of reaction mixture containing solution A, B and C (2:1:1) (Solution A, 2% N,N-dimethyl formamide in 100 mM sodium phosphate (pH 7.1); Solution B, 5 mM L-DOPA in 100 mM sodium phosphate (pH 7.1); Solution C, 20 mM MBTH in  $\text{H}_2\text{O}$ ) were added and the cells were incubated at 37°C for 10 min. The oxidation of L-DOPA to dopachrome was measured at 505 nm (reference at 490 nm) by a multiplate reader and normalized with protein content. Experiments were performed at least three times. For indirect inhibition of tyrosinase activity, the cell lysates were transferred into 96-well plates, incubated with sample at 37°C for 2 h, mixed with solution containing L-DOPA and measured using a plate reader.

**Western blotting.** Human melanocytes were lysed with RIPA lysis buffer (50 mM Tris-HCl, 150 mM NaCl, 1 mM EDTA, 1% Triton X-100, 1% sodium deoxycholate, 0.1% SDS, pH 7.4, 1 mM PMSF and protease inhibitors). The cells were then placed on ice and vortexed for 15 s every 10 min for a total of 40 min, followed by centrifugation (10 000  $\times g$ , 20 min). After boiling with sample buffer, 10  $\mu\text{g}$  of proteins was separated on 10% SDS polyacrylamide gels at 80–150 V and transferred onto membranes for 60 min at 100 V. The membrane was blocked for 30 min with 5% skim milk solution and incubated with primary antibody at dilutions of 1:1000 at 4°C overnight. The bands were detected using a chemiluminescence kit (Amersham, Buckinghamshire, UK) according to the manufacturer's instructions and visualized after exposure to chemiluminescence film (Fujifilm, Tokyo, Japan).

**Melanoderm assay.** The Labcyte Melano-Model (Japan Tissue Engineering Co., Ltd. Gamagori, AICHI, Japan) is a reconstituted human three-dimensional tissue model. Foreskin-derived human keratinocytes and melanocytes were seeded on the nylon mesh basement membrane. Melanoderm tissue was transferred into a 24-well plate with a cell culture insert on top of a culture stand. Nobiletin was dissolved in DMSO, medium containing different concentrations of compounds was placed on top of the cell inserts, and the medium with ET and SCF was added below the cell insert. Medium was changed three times per week. After 2 weeks of treatments, images were obtained from the top view with a phase contrast microscope at 100 $\times$  magnification. MTT assay, melanin content measurement and western blotting were performed according to the instructions of the Labcyte Melano-Model.

**RNA extraction and GeneChip microarray.** Total RNA was prepared using Isogen reagent (Wako Pure Chemical Industries, Ltd., Osaka, Japan) according to the manufacturer's instructions. RNA was further purified using RNeasy columns (Qiagen, Valencia, CA) and treatment with ribonuclease-free deoxyribonuclease I (Qiagen). Total RNA was used to generate cRNA, which was labeled with biotin according to the techniques recommended by Affymetrix (Santa Clara, CA). cRNA was then hybridized to Affymetrix GeneChips (Human gene 2.0 ST Array). After washing, the chips were scanned and analyzed using GeneChip scanner 3000 7G (Affymetrix). Average intensities for each GeneChip were globally scaled to a target intensity of 150. Further analysis was performed using GeneSpring software version 5.0.1 (Silicon Genetics, Redwood City, CA) to obtain fold change relative to the control treated with 0.1% DMSO (v/v).

**Statistical analysis.** All values are expressed as mean  $\pm$  SD and for statistical significance, unpaired Student's *t*-tests were used. A significant difference was taken for  $P < 0.05$ .

## RESULTS

### Effect of nobiletin on normal human melanocyte viability

We first evaluated the effects of nobiletin on cellular morphology and cytotoxicity of normal human melanocytes. The cells were treated with nobiletin at concentrations of 5, 10 and 20  $\mu\text{M}$  for 24 h, and cells were evaluated by microscopy and MTT assay. Nobiletin treatment alone did not induce any cytotoxicity, morphological changes or changes in cell number. To determine whether nobiletin could inhibit melanogenesis, cells were treated with nobiletin in the absence and presence of ET plus SCF. Both the morphological analysis and MTT results showed that this treatment did not lead to any cytotoxicity (Fig. 2).

### Effect of nobiletin on tyrosinase activity in normal human melanocytes

Since the inhibition of tyrosinase activity is involved in the anti-melanogenic process, we examined the effects of nobiletin on ET plus SCF-induced tyrosinase activities. Human melanocytes were pretreated with various doses of nobiletin for 2 h before ET (10 nM) and SCF (5 nM) stimulation. As shown in Fig. 3a,

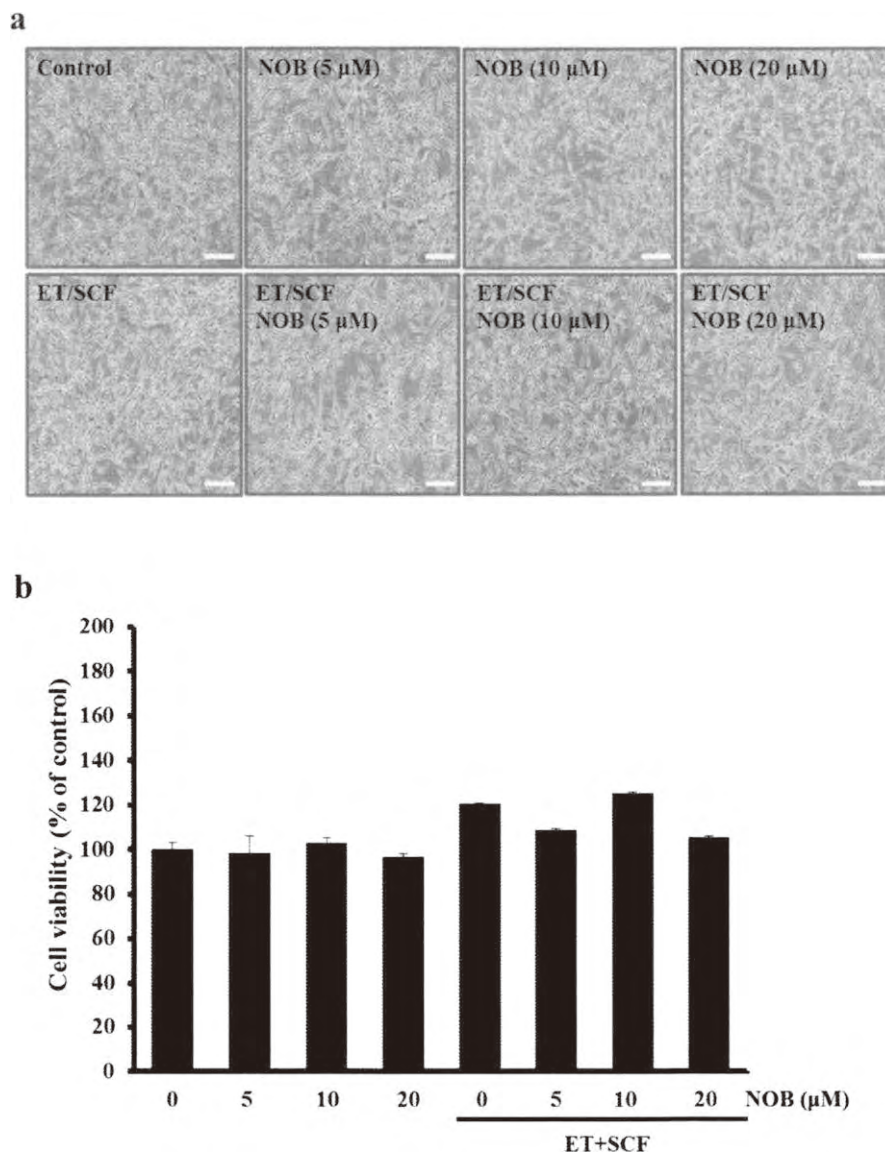


**Figure 2.** Effects of nobiletin on cell viability. Normal human melanocytes were pretreated with nobiletin for 2 h, and then cultured in the presence of ET (10 nM) plus SCF (5 nM) for 24 h. The photographs were taken under a microscope to observe morphological changes. Scale bar, 100  $\mu$ m (a). The influence of nobiletin on ET plus SCF stimulation on viability of human melanocytes was evaluated by the 3-(4,5-dimethyl-thiazol-2-yl)-2,5-diphenyltetrazolium bromide assay (b). Values are the means  $\pm$  SD of three measurements.

ET plus SCF stimulation increased the level of tyrosinase activity compared to the incubation with 0.1% DMSO (v/v). Nobiletin reduced the ET plus SCF-stimulated level of tyrosinase activity in a dose-dependent manner.

Tyrosinase activity was next examined using cell lysate obtained from cells treated with ET plus SCF for 24 h. Figure 3b shows that nobiletin did not influence the tyrosinase activity increased by ET plus SCF treatment. This result implies that nobiletin might induce antimelanogenic effects through the indirect inhibition of tyrosinase activity, but it does not directly inhibit tyrosinase activity.

**Effect of nobiletin on the expression of MITF and phosphorylation of CREB in normal human melanocytes**

MITF is the key transcription factor that regulates the expression of the tyrosinase gene. To investigate if the inhibitory

activity of nobiletin is related to changes in tyrosinase expression, melanocyte lysates were examined by western blot analysis. Figure 4a shows that the expression level of MITF was markedly increased in the ET plus SCF-stimulated melanocytes (ET + SCF,  $404 \pm 24.9$ ) and then nobiletin showed similar inhibitory effects in all concentrations tested (ET + SCF + 5  $\mu$ M nobiletin,  $353 \pm 17.0$ ; ET + SCF + 10  $\mu$ M nobiletin,  $359.0 \pm 25.0$ ; ET + SCF + 20  $\mu$ M nobiletin,  $360.0 \pm 6.6$ ).

Phosphorylation of CREB is associated with the activation and expression of tyrosinase through upregulation of MITF gene expression. Nobiletin attenuated the CREB activation triggered by ET plus SCF and inhibited CREB phosphorylation to similar levels in all concentrations tested (ET + SCF,  $656.0 \pm 26.6$ ; ET + SCF + 5  $\mu$ M nobiletin,  $478.0 \pm 75.6$ ; ET + SCF + 10  $\mu$ M nobiletin,  $413.0 \pm 66.5$ ; ET + SCF + 20  $\mu$ M nobiletin,  $415.0 \pm 90.3$ ) (Fig. 4a).

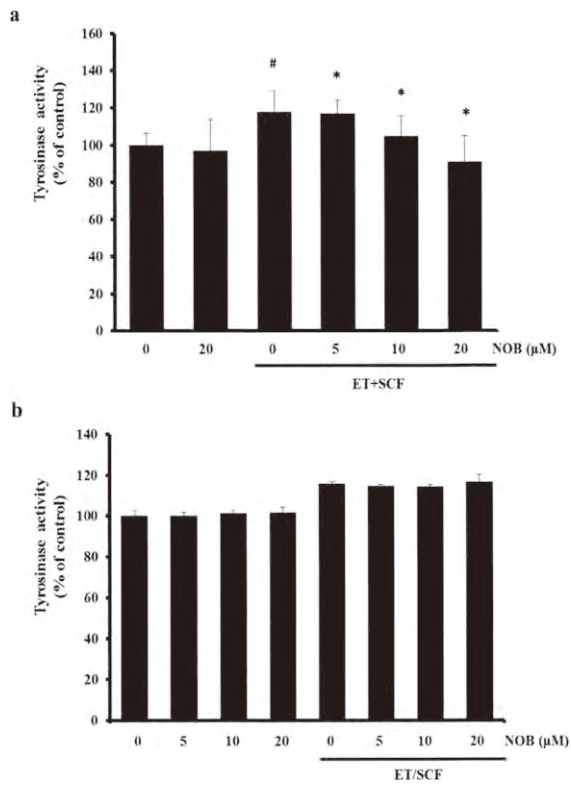


**Figure 3.** Effects of nobiletin on ET plus SCF-induced tyrosinase activity in normal human melanocytes. (a) Melanocytes were preincubated with nobiletin (NOB) for 2 h and cotreated with ET (10 nM) plus SCF (5 nM) for 24 h, and then tyrosinase activity was examined. (b) Melanocytes lysates which were stimulated with ET (10 nM) plus SCF (5 nM) for 24 h were incubated with nobiletin (NOB) for 1 h, and tyrosinase activity was examined. The results are expressed as mean ± SD of three separate experiments. <sup>#</sup>*P* < 0.05 compared to control; <sup>\*</sup>*P* < 0.05 compared to ET plus SCF stimulation.

**Effect of nobiletin on inhibitory signaling pathways of melanogenesis in normal human melanocytes**

Dephosphorylation of Raf-1, MEK and ERK has been reported to induce the degradation of MITF, which subsequently reduces the level of tyrosinase expression (33). Therefore, we evaluated whether nobiletin affects these intracellular signaling pathway factors. Phosphorylation of Raf-1, MEK and ERK1/2 in the cells was induced at 15 min after ET plus SCF treatment, whereas the treatment of cells with nobiletin alone had no effect on phosphorylation of these factors. As expected, nobiletin inhibited the effects of ET plus SCF on inducing Raf-1, MEK and ERK1/2 phosphorylation (Fig. 4b). Regarding ET signaling in melanocytes, it has been reported that both activated RSK and PKA could phosphorylate CREB. Therefore, we evaluated whether nobiletin inhibits the tyrosinase activity and CREB phosphorylation induced by cAMP/PKA activation. The incubation with nobiletin in presence of forskolin diminished the forskolin-triggered phosphorylation of CREB as well as tyrosinase activity (Fig. 5a,b). Together this indicates that nobiletin regulates all two upstream signaling pathways for tyrosinase expression.

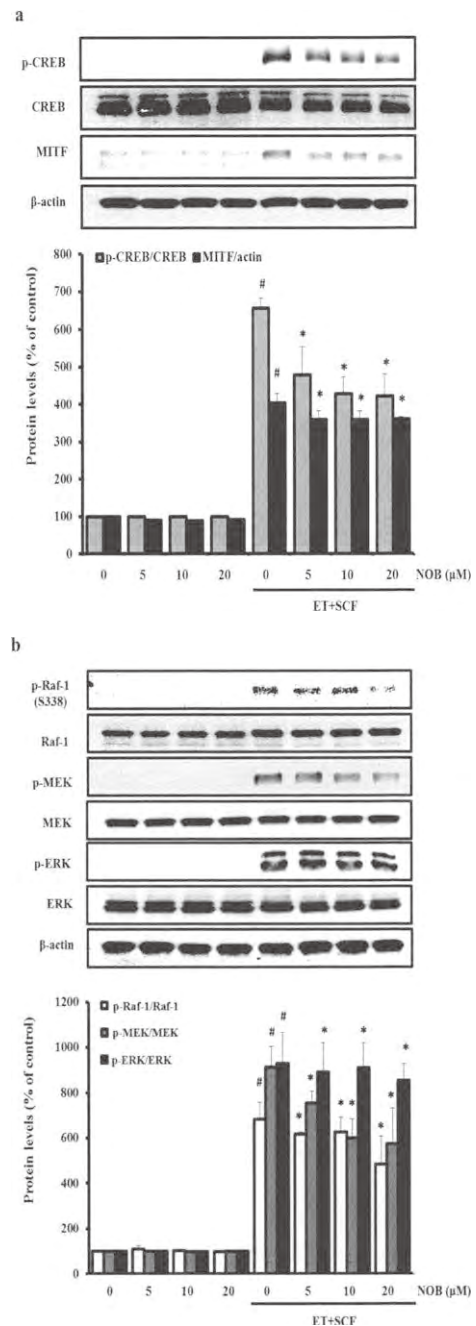


**Figure 4.** Effects of nobiletin on ET plus SCF-induced signaling pathway in normal human melanocytes. Western blot analysis of melanocytes preincubated with nobiletin and treated with or without ET plus SCF (a) for CREB, p-CREB and MITF and (b) for p-c-Raf-1, p-MEK and p-ERK. The results are expressed as mean ± SD of three separate experiments. <sup>#</sup>*P* < 0.05 compared to control; <sup>\*</sup>*P* < 0.05 compared to ET plus SCF stimulation.

**Effects of nobiletin on ET plus SCF-stimulated hyperpigmentation in a cultured human epidermis model**

To confirm the inhibitory effects of nobiletin observed in normal human melanocytes, we used cultured human epidermis consisting of multilayered epidermal melanocytes and keratinocytes. After 2 weeks of treatment, all experimental groups tested showed no decrease in cell viability by MTT assay or changes in cellular

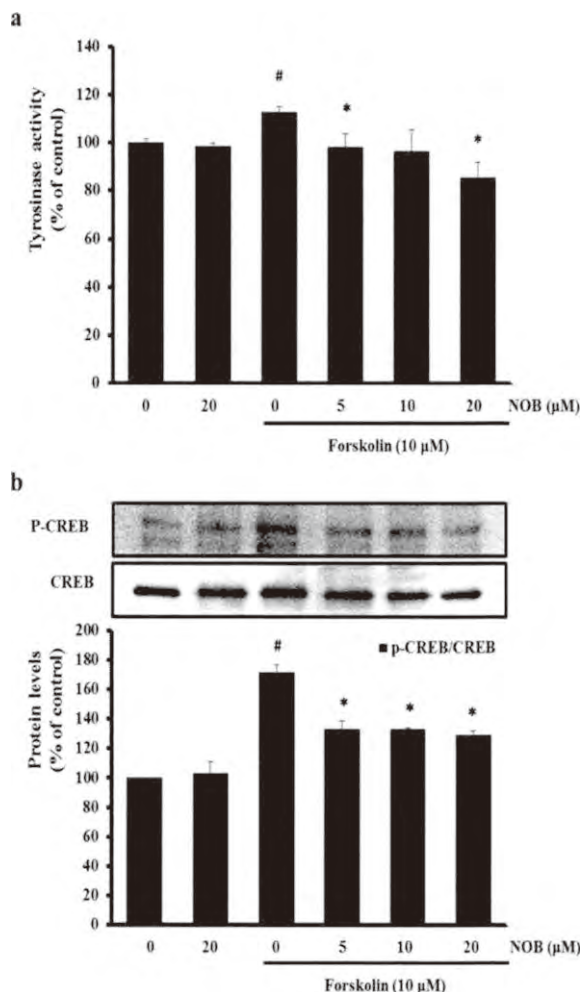


**Figure 5.** Effects of nobiletin on forskolin-induced pathway in normal human melanocytes. Tyrosinase activity assay (a) and Western blot analysis (b) of melanocytes preincubated with nobiletin and treated with or without forskolin for CREB and p-CREB. The results are expressed as mean  $\pm$  SD of three separate experiments. # $P < 0.05$  compared to control; \* $P < 0.05$  compared to ET plus SCF stimulation.

morphology (Fig. 6a). We observed an increase in visible hyperpigmentation in the human epidermal model following the addition of ET plus SCF (10 and 5 nM, respectively) compared with the cells treated with 0.1% DMSO (v/v) as vehicle and the hyperpigmentation was declined upon increasing amounts of nobiletin treatment (Fig. 6b). In accordance with this result, melanin content assay also revealed that the ET plus SCF stimulation significantly accelerated melanin production, and nobiletin interrupted the ET plus SCF-induced melanin content at doses of 5, 10 and 20  $\mu$ M (Fig. 6c). Western blot analysis further showed that the expression levels of tyrosinase and MITF were upregulated at 14 days of treatment with ET plus SCF, and the addition of nobiletin markedly abolished the ET plus SCF-induced expression of melanogenic proteins at all concentrations tested (Fig. 6d).

**Effects of nobiletin on ET plus SCF-stimulated melanogenic gene expression in a cultured human epidermis model**

To analyze the gene expression profiles in three-dimensional model, we performed cDNA microarray analysis (Table 1). The

gene expression levels were compared between two groups: control vs ET plus SCF, control vs nobiletin and ET plus SCF vs ET plus SCF plus nobiletin. Tyrosinase, tyrosinase-related protein1 (TRP1), tyrosinase-related protein2 (TRP2), oculocutaneous albinism II and melan-A are well known as melanogenesis-related genes and as expected, they were highly expressed in the group treated with ET plus SCF in this study. Besides, the incubation with nobiletin only reduced those melanocyte-specific gene expressions, its addition to ET plus SCF treatment obviously downregulated the ET plus SCF-increased levels of melanogenic genes, and the nobiletin distinctly downregulated the MITF gene expression in both absence and presence of ET plus SCF.

**DISCUSSION**

In this study, we investigated the antipigmentary effects of nobiletin and its molecular mechanisms in ET plus SCF-induced melanogenesis. Our findings showed that nobiletin interrupted melanogenesis via inhibition of an upstream pathway involved in ET plus SCF-induced CREB activation and MITF upregulation both in human melanocytes and in a human epidermal tissue model.

From the industrial point of view, natural cosmetics are becoming more prevalent and important in the global market. Recently, the development of natural products from herbs or plants has become a new approach for the inhibition of melanogenesis and the prevention of abnormal pigmentation (34–37). Development of skin-whitening cosmetics has focused on identifying depigmenting compounds on the basis of inhibition of tyrosinase activity, tyrosinase expression, and transfer of melanosomes from melanocytes to keratinocytes. Among these activities, the downregulation of tyrosinase activity has been proposed to be mainly responsible for reduced melanin production. In recent years, however, since safety issues to formulate plant extracts or phytochemicals as cosmetic agents have been prioritized, a change in the research and development of whitening cosmetics has been required. Active compounds that are commercially used as skin-whitening agents for treating and preventing hyperpigmentation disorders have caused many side effects including depigmentation in normal skin color as well as skin irritation, contact dermatitis and exogenous ochronosis in dark skin. Because of these problems, their use in cosmetics has been strictly limited, not only in Europe and USA but also in Asia (38,39). In light of these concerns, we have carefully evaluated the effects of nobiletin alone in normal human melanocytes. Fortunately, nobiletin did not induce any direct changes on basal cell activities as shown in the results of the cell viability and tyrosinase activity assays using cell lysate. Nobiletin exhibited inhibitory functions on ET plus SCF-accumulated melanin production, suggesting that nobiletin might show antipigmentary effects in abnormally hyperpigmented conditions, but not in normal skin conditions, thus emphasizing its *in vitro/in vivo* safety.

Exposure to sunlight promotes the overexpression of growth factors like ET and SCF in keratinocytes and melanocytes, which could lead to paracrine activation and proliferation that in turn renders cells more susceptible to transformation, subsequently resulting in the synthesis and activation of tyrosinase for melanin induction (40–42).

Previous studies have demonstrated that the production of melanin could be enhanced by ET, SCF or ET plus SCF

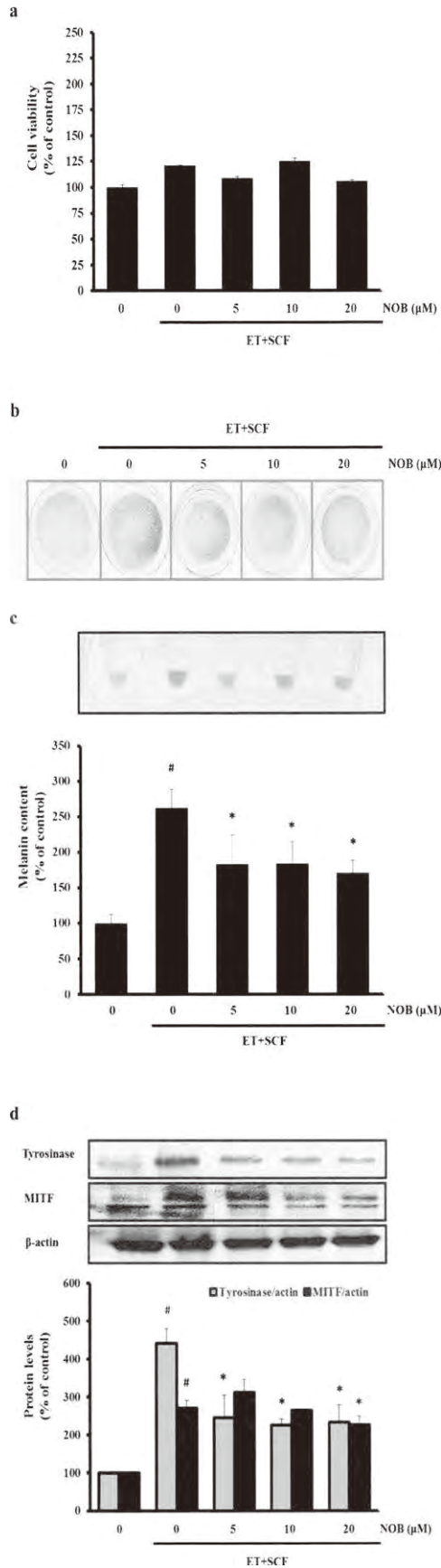


**Figure 6.** Effects of nobiletin in a cultured human epidermis model. After preincubation with nobiletin for 1 day, the cells were stimulated with ET plus SCF for 14 days. The epidermis model was examined by MTT assay (a), microscopic observation (b,  $\times 100$  magnification), melanin content measurement (c), and western blotting (d). Data are expressed as mean  $\pm$  SD of three independent experiments. <sup>#</sup> $P < 0.05$  compared to control; <sup>\*</sup> $P < 0.05$  compared to ET plus SCF stimulation.

(33,43,44). The stimulation of ET or SCF in melanocytes have induced the increased levels of tyrosinase activity, tyrosinase expression, and its upstream pathway with regard to melanin synthesis, as shown in other reports and in our study as well. Interestingly, treatment with nobiletin of human melanocytes inhibited the ET plus SCF-induced tyrosinase activity and tyrosinase expression.

ET initiates its action by binding EDNB receptor, followed by the activation of PKC, which induces phosphorylation of Raf-1 to phosphorylate MEK, ERK1/2, RSK and CREB. At the same time, ET-activated PKC increases the intracellular cAMP levels and then activates PKA, subsequently causing the phosphorylation of CREB. The ET-elicited MAPK-RSK and cAMP-PKA signaling pathways are implicated in induction of MITF gene expression by CREB phosphorylation (45). SCF also stimulates CREB phosphorylation as a result of activation of c-kit and MAPKs, whereas SCF signaling does not increase intracellular cAMP levels unlike the signaling cascade of ET (9,10). Based on the intracellular transduction signaling pathways of ET and SCF, we examined the effects of nobiletin on the ET plus SCF-induced phosphorylation of Raf-1, MEK, ERK1/2, CREB and MITF. Similar to previous findings, our result showed upregulated levels of MAPKs, CREB and MITF in cells stimulated with ET plus SCF. In addition, the treatment of melanocytes with nobiletin decreased the ET plus SCF-triggered phosphorylation of Raf-1, MEK, ERK1/2 and CREB, as well as expression of MITF. Since ET-activated PKC and cAMP could induce CREB phosphorylation (45), we tested whether the inhibitory effect of nobiletin on CREB phosphorylation is also related to abrogation of the cAMP/PKA pathway. Our result revealed that the CREB phosphorylation induced by forskolin, a cAMP-dependent PKA activator was decreased by preincubation with nobiletin prior to forskolin addition. This result indicates that nobiletin also decreases the ET-induced activation of CREB and MITF by interrupting both PKC/MAPK and cAMP/PKA cascade.

Raf-1 is phosphorylated at various sites, including serine 259 and 338, by the activation of PKC and Ras, respectively (46–48). Interestingly, nobiletin diminished the ET plus SCF-induced Raf-1 phosphorylation at serine 338, but not at serine 259 (data not shown), suggesting that inhibition of Raf-1 phosphorylation at serine 338 by nobiletin is its major signaling mechanism to inhibit the ET plus SCF-intracellular linkage.

In accordance with previous report (43), we have also found that gene expressions of tyrosinase, TRP1, TRP2 and PMEL are enhanced on ET plus SCF treatment over 7 days, the increased melanocyte-specific genes are accompanied by upregulation of MITF gene expression level which plays important role to lead the melanogenesis-specific genes and proteins. In addition, we confirmed that the incubation with nobiletin attenuates ET and SCF-induced melanogenic gene expressions including TYR, TRP1, PMEL, oculocutaneous albinism II and melan-A, but not TRP2. Interestingly, the MITF gene level increased by the stimulation with ET plus SCF was markedly abrogated by cotreatment

**Table 1.** Effects of nobiletin on the melanogenic genes associated with endothelin-1 and SCF in a cultured human epidermis model.

Gene	Probe Set ID	Expression value			
		Control	NOB	ET + SCF	ET + SCF + NOB
Tyrosinase	16729865	233.3	152.7	634.9	383.2
Tyrosinase-related protein1	17083595	1393.2	1207.5	3220.4	2727.6
Tyrosinase-related protein2	16780208	111.4	247.1	159.0	353.7
Microphthalmia-associated transcription factor	16942576	73.7	79.5	202.9	151.1
Premelanosome protein	16765848	357.1	281.5	936.7	769.2
Oculocutaneous albinism II	16806249	144.1	125.3	341.9	290.5
Melan-A	17083417	173.6	176.2	492.9	428.3

with nobiletin, suggesting that nobiletin attenuates the ET plus SCF-triggered melanogenesis by interrupting the MITF gene expression. Among the melanin synthesis-related enzymes including tyrosinase, TRP1 and TRP2, TRP1 and TRP2 also function in the biosynthesis of melanin downstream of tyrosinase and modulate tyrosinase activity. Namely, TRP1 influences tyrosinase activity by forming a complex with it and/or stabilizing it and TRP2 regulates the quantity and quality of the melanin produced during melanin biosynthesis. In other word, tyrosinase plays the main role in melanogenesis as rate-limiting enzyme, catalyzing the hydroxylation of tyrosine to form 3, 4-DOPA, followed by oxidation of DOPA to produce DOPA-quinone. Therefore, its inhibition has been targeted for the development of skin-whitening agents in cosmetics. In this study, even though nobiletin shows the increased gene expression of TRP2 both in the absence and presence of melanogenic cytokines, its remarkable inhibition on ET plus SCF-triggered gene expression of tyrosinase is worthy of note. Therefore, it is suggested that the antipigmentary effects of nobiletin are closely implicated in the decrease of tyrosinase expression.

Recently published data demonstrated that nonflavonoid compounds could attenuate the melanin synthesis of melanocytes through inhibition of mechanisms involving ET and/or SCF (33,43,44). The blocking of melanin synthesis by arenarol is involved a reduction in ET-stimulated MEK activation in human melanocytes (33) and administration of N-linked carbohydrate modifiers abrogated the pigmentation response by blocking ET/SCF-induced MITF mRNA levels in a human epidermal equivalent model (43), and astaxanthin treatment decreased SCF-induced stimulation of MITF expression (44). Unlike these compounds, nobiletin is one of the polymethoxy flavonoid and in recent study it has been shown that nobiletin protects the brain from ischemic damage through activating the Akt/CREB signaling pathway and improving blood-brain barrier permeability (49).

Taken together, we attribute the depigmentary effects of nobiletin on ET plus SCF stimulation to inhibition of Raf-1 phosphorylation. Furthermore, the antipigmentary effects of nobiletin were also confirmed in a human epidermal equivalent model. This is the first research emphasizing the antimelanogenesis potential of nobiletin and suggesting the possibility of beneficial applications in the cosmetic industry on the basis of its advantages such as flavonoid of unique structure, high intestinal permeability, and no direct action on tyrosinase activity of normal skin. Clinical studies focused on dose, bioavailability, efficacy and safety are required to further develop the use of these promising therapeutic agents.

**Acknowledgements**—This research was supported by an endowment from Erina Co., Inc. (Tokyo, Japan) and Cooperative Research Program for Agriculture Science & Technology Development (Project No. PJ009583) of Rural Development Administration (Republic of Korea).

## REFERENCES

- Briganti, S., E. Camera and M. Picardo (2003) Chemical and instrumental approaches to treat hyperpigmentation. *Pigment Cell Melanoma Res.* **16**, 101–110.
- Imokawa, G., Y. Yada and M. Miyagishi (1992) Endothelins secreted from human keratinocytes are intrinsic mitogens for human melanocyte. *J. Biol. Chem.* **267**, 24675–24680.
- Imokawa, G., M. Miyagishi and Y. Yada (1995) Endothelin-1 as a new melanogen: coordinated expression of its gene and the tyrosinase gene in UVB-exposed human epidermis. *J. Invest. Dermatol.* **105**, 32–37.
- Abdel-Malek, Z., V. B. Swope, I. Suzuki, C. Akcali, M. D. Harriger, S. T. Boyce, K. Urabe and V. J. Hearing (1995) Mitogenic melanogenic stimulation of normal human melanocytes by melanotropic peptides. *Proc. Natl Acad. Sci. USA* **92**, 1789–1793.
- Suzuki, R. D., S. Cone, J. Im, Z. A. Nordlund and Z. A. Abdel-Malek (1996) Binding of melanotropic hormones to the melanocortin receptor MC1R on human melanocytes stimulates proliferation and melanogenesis. *Endocrinology* **137**, 1627–1633.
- Hachiyu, A., A. Kobayashi, A. Ohuchi, Y. Takema and G. Imokawa (2001) The paracrine role of stem cell factor/c-kit signaling in the activation of human melanocyte in ultraviolet B-induced pigmentation. *J. Invest. Dermatol.* **116**, 578–586.
- Hachiyu, A., A. Kobayashi, Y. Yoshida, T. Kitahara, Y. Takema and G. Imokawa (2004) Biphasic expression of two paracrine melanogenic cytokines, stem cell factor and endothelin-1, in ultraviolet B-induced human melanogenesis. *Am. J. Pathol.* **65**, 2099–2109.
- Tsatmali, M., J. Ancans and A. J. Thody (2002) Melanocyte function and its control by melanocortin peptides. *J. Histochem. Cytochem.* **50**, 125–133.
- Shimizu, K., S. Yasutake and R. Kondo (2003) A new stilbene with tyrosinase inhibitory activity from *Chlorophora excelsa*. *Chem. Pharm. Bull.* **51**, 318–319.
- Park, S. H., D. S. Kim, W. G. Kim, I. J. Ryoo, D. H. Lee, C. H. Huh, S. W. Youn, I. D. Yoo and K. C. Park (2004) Terrein: a new melanogenesis inhibitor and its mechanism. *Cell. Mol. Life Sci.* **61**, 2878–2885.
- Aburjai, T. and F. M. Natsheh (2003) Plants used in cosmetics. *Phytother. Res.* **17**, 987–1000.
- Wang, K. H., R. D. Lin, F. L. Hsu, Y. H. Huang, H. C. Chang, C. Y. Huang and M. H. Lee (2006) Cosmetic applications of selected traditional Chinese herbal medicines. *J. Ethnopharmacol.* **19**, 353–259.
- Ohizumi, Y. (1997) Application of physiologically active substances isolated from natural resources to pharmacological studies. *Jpn. J. Pharmacol.* **73**, 263–289.
- Imokawa, G., Y. Yada and M. Kimura (1996) Signalling mechanisms of endothelin-induced mitogenesis and melanogenesis in human melanocytes. *Biochem. J.* **15**(314), 305–312.

15. Imokawa, G., T. Kobayashi and M. Miyagishi (2000) Intracellular signaling mechanisms leading to synergistic effects of endothelin-1 and stem cell factor on proliferation of cultured human melanocytes. Cross-talk via trans-activation of the tyrosine kinase c-kit receptor. *J. Biol. Chem.* **27**(275), 33321–33328.
16. Kadono, S., I. Manaka, M. Kawashima, T. Kobayashi and G. Imokawa (2001) The role of the epidermal endothelin cascade in the hyperpigmentation mechanism of lentiginosus. *J. Invest. Dermatol.* **116**, 571–577.
17. Bertolotto, C., R. Buscà, P. Abbe, K. Bille, E. Aberdam, J. P. Ortonne and R. Ballotti (1998) Different cis-acting elements are involved in the regulation of TRP1 and TRP2 promoter activities by cyclic AMP: pivotal role of M boxes (GTCATGTGCT) and of microphthalmia. *Mol. Cell. Biol.* **18**, 694–702.
18. Hemesath, T. J., E. R. Price, C. Takemoto, T. Badalian and D. E. Fisher (1998) MAP kinase links the transcription factor Microphthalmia to c-Kit signalling in melanocytes. *Nature* **15**, 298–301.
19. Wu, Y. Q., C. H. Zhou, J. Tao and S. N. Li (2006) Antagonistic effects of nobiletin, a polymethoxyflavonoid, on eosinophilic airway inflammation of asthmatic rats and relevant mechanisms. *Life Sci.* **78**, 2689–2696.
20. Imada, K., N. Lin, C. Liu, A. Lu, W. Chen, M. Yano, T. Sato and A. Ito (2008) Nobiletin, a citrus polymethoxy flavonoid, suppresses gene expression and production of aggrecanases-1 and -2 in collagen-induced arthritic mice. *Biochem. Biophys. Res. Commun.* **373**, 181–185.
21. Choi, S. Y., J. H. Hwang, H. C. Ko, J. G. Park and S. J. Kim (2007) Nobiletin from citrus fruit peel inhibits the DNA-binding activity of NF- $\kappa$ B and ROS production in LPS-activated RAW 264.7 cells. *J. Ethnopharmacol.* **113**, 149–155.
22. Kobayashi, S. and S. Tanabe (2006) Evaluation of the anti-allergic activity of Citrus unshiu using rat basophilic leukemia RBL-2H3 cells as well as basophils of patients with seasonal allergic rhinitis to pollen. *Int. J. Mol. Med.* **17**, 511–515.
23. Jang, S. E., K. R. Ryu, S. H. Park, S. Chung, Y. Teruya, M. J. Han, J. T. Woo and D. H. Kim (2013) Nobiletin and tangeretin ameliorate scratching behavior in mice by inhibiting the action of histamine and the activation of NF- $\kappa$ B, AP-1 and p38. *Int. Immunopharmacol.* **17**, 502–507.
24. Whitman, S. C., E. M. Kurowska, J. A. Manthey and A. Daugherty (2005) Nobiletin, a citrus flavonoid isolated from tangerines, selectively inhibits class A scavenger receptor-mediated metabolism of acetylated LDL by mouse macrophages. *Atherosclerosis* **178**, 25–32.
25. Miyata, Y., T. Sato, M. Yano and A. Ito (2004) Activation of protein kinase C  $\beta$ II/epsilon-c-Jun NH2-terminal kinase pathway and inhibition of mitogen-activated protein/extracellular signal-regulated kinase 1/2 phosphorylation in antitumor invasive activity induced by the polymethoxy flavonoid, nobiletin. *Mol. Cancer Ther.* **3**, 839–847.
26. Lee, Y. S., B. Y. Cha, K. Saito, H. Yamakawa, S. S. Choi, K. Yamaguchi, K. Nagai and J. T. Woo (2010) Nobiletin improves hyperglycemia and insulin resistance in obese diabetic ob/ob mice. *Biochem. Pharmacol.* **79**, 1674–1683.
27. Lee, Y. S., B. Y. Cha, S. S. Choi, B. K. Choi, T. Yonezawa, T. Teruya, K. Nagai and J. T. Woo (2013) Nobiletin improves obesity and insulin resistance in high-fat diet-induced obese mice. *J. Nutr. Biochem.* **24**, 156–162.
28. Nichols, L. A., D. E. Jackson, J. A. Manthey, S. D. Shukla and L. J. Holland (2011) Citrus flavonoids repress the mRNA for stearoyl-CoA desaturase, a key enzyme in lipid synthesis and obesity control, in rat primary hepatocytes. *Lipids Health Dis.* **10**, 36.
29. Ihara, H., H. Yamamoto, T. Ida, H. Tsutsuki, T. Sakamoto, T. Fujita, T. Okada and S. Kozaki (2012) Inhibition of nitric oxide production and inducible nitric oxide synthase expression by a polymethoxyflavone from young fruits of Citrus unshiu in rat primary astrocytes. *Bio-sci. Biotechnol. Biochem.* **76**, 1843–1848.
30. Cui, Y., J. Wu, S. C. Jung, D. B. Park, Y. H. Maeng, J. Y. Hong, S. J. Kim, S. R. Lee, S. J. Kim, S. J. Kim and S. Y. Eun (2010) Anti-neuroinflammatory activity of nobiletin on suppression of microglial activation. *Biol. Pharm. Bull.* **33**, 1814–1821.
31. Sasaki, K. and F. Yoshizaki (2002) Nobiletin as a tyrosinase inhibitor from the peel of Citrus fruit. *Biol. Pharm. Bull.* **25**, 806–808.
32. Winder, A. J. and H. Harris (1991) New assays for the tyrosine hydroxylase and dopa oxidase activities of tyrosinase. *Eur. J. Biochem.* **1**, 317–326.
33. Choi, B. K., B. Y. Cha, T. Fujiwara, A. Kanamoto, J. T. Woo, M. Ojika and G. Imokawa (2013) Arenarol isolated from a marine sponge abrogates endothelin-1-stimulated melanogenesis by interrupting MEK phosphorylation in normal human melanocytes. *Cytotechnology* **65**, 915–926.
34. Oh, M. J., M. A. Hamid, S. Ngadiran, Y. K. Seo, M. R. Sarmidi and C. S. Park (2011) Ficusdeltoidea (Mas cotek) extract exerted anti-melanogenic activity by preventing tyrosinase activity in vitro and by suppressing tyrosinase gene expression in B16F1 melanoma cells. *Arch. Dermatol. Res.* **303**, 161–170.
35. Lee, N. H., W. J. Lee, H. B. Koh, M. J. Kim, W. J. Yoon and C. G. Hyun (2010) Effect of Korean red sea cucumber (*Stichopus japonicus*) on melanogenic protein expression in murine B16 melanoma. *Int. J. Pharmacol.* **6**, 37–42.
36. Yoon, W. S., M. J. Kim, J. Y. Moon, H. J. Kang, G. O. Kim, N. H. Lee and C. G. Hyun (2010) Effect of palmitoleic acid on melanogenic protein expression in murine B16 melanoma. *J. Oleo Sci.* **59**, 315–319.
37. Kim, S. S., C. G. Hyun, Y. H. Choi and N. H. Lee (2012) Tyrosinase inhibitory activities of the compounds isolated from *Neolitsea aciculata* (Blume) Koidz. *J. Enzyme Inhib. Med. Chem.* **28**, 685–689.
38. Lima, L. L., R. M. Lima, A. F. da Silva, A. M. do Carmo, A. D. da Silva and N. R. Raposo (2013) Azastilbene analogs as tyrosinase inhibitors: new molecules with depigmenting potential. *Sci. World J.* **2013**, 274643. doi: 10.1155/2013/274643.
39. Sheth, V. M. and A. G. Pandya (2011) Melasma: a comprehensive update: part II. *J. Am. Acad. Dermatol.* **65**, 699–714.
40. Moretti, S., C. Pinzi, A. Spallanzani, E. Berti, A. Chiarugi, S. Mazzioli, M. Fabiani, C. Vallecchi and M. Herlyn (1999) Immunohistochemical evidence of cytokine networks during progression of human melanocytic lesions. *Int. J. Cancer.* **84**, 160–168.
41. Sriwiriyant, P., A. Ohuchi, A. Hachiya, M. O. Visscher and R. E. Boissy (2006) Interaction between stem cell factor and endothelin-1: effects on melanogenesis in human skin xenografts. *Lab. Invest.* **86**, 1115–1125.
42. Imokawa, G. (2004) Autocrine and paracrine regulation of melanocytes in human skin and in pigmentary disorders. *Pigment Cell Res.* **17**, 96–110.
43. Wakabayashi, Y., H. Nakajima and G. Imokawa (2013) Abrogating effect of N-linked carbohydrate modifiers on the stem cell factor and endothelin-1-stimulated epidermal pigmentation in human epidermal equivalents. *J. Dermatol. Sci.* **69**, 215–228.
44. Nakajima, H., K. Fukazawa, Y. Wakabayashi, K. Wakamatsu, K. Senda and G. Imokawa (2012) Abrogating effect of a xanthophyll carotenoid astaxanthin on the stem cell factor-induced stimulation of human epidermal pigmentation. *Arch. Dermatol. Res.* **304**, 803–816.
45. Sato-Jin, K., E. K. Nishimura, E. Akasaka, W. Huber, H. Nakano, A. Miller, J. Du, M. Wu, K. Hanada, D. Sawamura, D. E. Fisher and G. Imokawa (2008) Epistatic connections between microphthalmia-associated transcription factor and endothelin signaling in Waardenburg syndrome and other pigmentary disorders. *FASEB J.* **22**, 1155–1168.
46. Marais, R., Y. Light, C. Mason, H. Paterson, M. F. Olson and C. J. Marshall (1998) Requirement of Ras-GTP-Raf complexes for activation of Raf-1 by protein kinase C. *Science* **280**, 109–112.
47. Abraham, D., K. Podar, M. Pacher, M. Kubicek, N. Welzel, B. A. Hemmings, S. M. Dilworth, H. Mischak, W. Kolch and M. Baccarini (2000) Raf-1-associated protein phosphatase 2A as a positive regulator of kinase activation. *J. Biol. Chem.* **275**, 22300–22304.
48. Chong, H., H. G. Vikis and K. L. Guan (2003) Mechanisms of regulating the Raf kinase family. *Cell. Signal.* **15**, 463–469.
49. Zhang, L., H. Zhao, X. Zhang, L. Chen, X. Zhao, X. Bai and J. Zhang (2013) Nobiletin protects against cerebral ischemia via activating the p-Akt, p-CREB, BDNF and Bcl-2 pathway and ameliorating BBB permeability in rat. *Brain Res. Bull.* **96**, 45–53.

# Antiproliferative Activity of Acerogenin C, a Macrocyclicdiarylheptanoid, on PDGF-Induced Human Aortic Smooth Muscle Cells Proliferation

Byung-Yoon Cha<sup>1</sup>, Wen Lei Shi<sup>2</sup>, Kotaro Watanabe<sup>3</sup>, Takayuki Yonezawa<sup>1</sup>, Toshiaki Teruya<sup>1</sup>, Kiyotake Suenaga<sup>3</sup>, Yuichi Ishikawa<sup>3</sup>, Shigeru Nishiyama<sup>3</sup>, Kazuo Nagai<sup>1,2</sup>, Je-Tae Woo<sup>1,2</sup>

<sup>1</sup>Research Institute for Biological Functions, Chubu University, Matsumoto, Japan

<sup>2</sup>Department of Biological Chemistry, Chubu University, Matsumoto, Japan

<sup>3</sup>Department of Chemistry, Faculty of Science and Technology, Keio University, Yokohama, Japan

Email: [bycha@isc.chubu.ac.jp](mailto:bycha@isc.chubu.ac.jp)

Received 22 September 2014; accepted 6 February 2015; published 10 February 2015

Copyright © 2015 by authors and Scientific Research Publishing Inc.

This work is licensed under the Creative Commons Attribution International License (CC BY).

<http://creativecommons.org/licenses/by/4.0/>



Open Access

## Abstract

Platelet-derived growth factor (PDGF)-BB is one of the most potent factors in the development and progression of various vascular disorders, such as atherosclerosis and restenosis. PDGF is a major stimulant for vascular smooth muscle cells (VSMCs) proliferation via the mitogenesis signaling pathway. In the present study, we investigated the effect of acerogenin C, a macrocyclicdiarylheptanoid, on PDGF-BB-stimulated human aortic smooth muscle cells (HASMCs) proliferation. Acerogenin C significantly inhibited PDGF (20 ng/mL)-BB-induced [<sup>3</sup>H]-thymidine incorporation into DNA at concentrations of 0.1, 1 and 10  $\mu$ M without any cytotoxicity. Acerogenin C also blocked PDGF-BB-stimulated phosphorylation of PLC $\gamma$ 1 and Akt but had no effect on extracellular signal-regulated kinase 1/2 (ERK1/2) and PDGF beta-receptor (R $\beta$ ) activation. In addition, acerogenin C (0.1 - 10  $\mu$ M) induced cell-cycle arrest in the G<sub>1</sub> phase, which was associated with the down-regulation of cyclins and the up-regulation of p27<sup>kip1</sup>. These results suggest that acerogenin C blocks PDGF-BB-stimulated HASMCs proliferation via G<sub>0</sub>/G<sub>1</sub> arrest in association with the induction of p27<sup>kip1</sup> and the suppression of PLC $\gamma$ 1 and phosphatidylinositol 3-kinase (PI3-K)/Akt signaling pathways. Furthermore, acerogenin C may be used for prevention and treatment of atherosclerosis during restenosis after coronary angioplasty.

## Keywords

HASMCs, Acerogenin C, PDGF-BB, p27<sup>kip1</sup>, Cell Cycle

**How to cite this paper:** Cha, B.-Y., Shi, W.L., Watanabe, K., Yonezawa, T., Teruya, T., Suenaga, K., Ishikawa, Y., Nishiyama, S., Nagai, K. and Woo, J.-T. (2015) Antiproliferative Activity of Acerogenin C, a Macrocyclicdiarylheptanoid, on PDGF-Induced Human Aortic Smooth Muscle Cells Proliferation. *Pharmacology & Pharmacy*, 6, 47-55.

<http://dx.doi.org/10.4236/pp.2015.62007>

## 1. Introduction

Whereas PDGF is expressed at low levels in arteries in healthy adults, its expression is increased in conjunction with the inflammatory-fibroproliferative response that characterizes atherosclerosis [1]. Thus, studies of balloon catheter-injured arterial tissue [2]-[4], naturally occurring atherosclerosis [5]-[8], coronary arteries after percutaneous transluminal coronary angioplasty [9], and experimentally induced atherosclerosis [10] [11] revealed increased expression of PDGF and PDGF receptors in these lesions.

It is well-known that binding of signal transduction molecules to different phosphorylated tyrosine residues in PDGF-R $\beta$  and PDGF-BB triggers the PI3-K/PKB (Akt) and PLC $\gamma$ 1 pathways in addition to the ERK pathway [12]. PI3-K mediates many different cellular responses, including actin reorganization, chemotaxis, cell growth and the serine/threonine kinase Akt/PKB for the antiapoptotic effect [13]-[15]. Interestingly, full activation of PLC $\gamma$  is dependent on PI3-K; the PI(3,4,5)P<sub>3</sub> formed by PI3-K binds the PH domain of PLC $\gamma$  and may anchor the enzyme at the membrane [16]. Mitogenic growth factors such as PDGF-BB share a final common signaling pathway in the cell cycle. Quiescent (G<sub>0</sub>) cells enter a gap period (G<sub>1</sub>), during which the factors necessary for DNA replication in the subsequent synthetic (S) phase are assembled. After DNA replication is completed, the cells enter another gap phase (G<sub>2</sub>) in preparation for mitosis (M). Restriction points at the G<sub>1</sub>-S and G<sub>2</sub>-M interphases ensure orderly cell cycle progression [17].

In the arterial media, VSMCs are normally quiescent, proliferate at low indices (<0.05%), and remain in the G<sub>0</sub>/G<sub>1</sub> phases of the cell cycle [18]. After vessel injury, vascular smooth muscle cells migrate into the intimal layer of the arterial wall, where they leave their quiescent state and reenter the cell cycle [1]. In many cells, transit through G<sub>1</sub> of the cell cycle and entry into the S phase require the binding and activation of cyclin/CDK complexes, predominantly cyclin D1/CDK4 and cyclin E/CDK2 [19] [20]. The kinase activities of the cyclin/CDK complexes are negatively regulated by CDK inhibitors, such as p27<sup>kip1</sup> [21] [22].

Acerogenin is a diarylheptanoid whose characteristic structural feature is the presence of two hydroxylated aromatic rings tethered by a linear seven-carbon chain. Acerogenin C (**Figure 1**) was isolated from stems of *Boswellia ovalifoliolata* BAL. & HENRY (Bursaceae) [23], while acerogenin C has been synthesized by Gonzalez G. I. *et al.* [24]. This diarylheptanoid exhibits a broad range of potent biological activities that include anti-inflammatory, antihepatotoxic, antifungal, antibacterial and related effects [23] [25].

However, the mechanism by which acerogenin C affects VSMCs function is still largely unknown. The present study aimed to investigate, for the first time, the inhibitory effects of acerogenin C on PDGF-induced proliferation and signaling transduction pathways in HASMCs.

## 2. Materials and Methods

### 2.1. Materials and Reagents

PDGF-R $\beta$ , Akt, PLC $\gamma$ 1, ERK1/2, cyclin D1, CDK4, cyclin E, CDK2, p27<sup>kip1</sup> and  $\alpha$ -actin antibodies were purchased from Cell Signaling Technology Inc. (Beverly, MA, USA). Acerogenin C was a gift of Dr. Nishiyama (Department of Chemistry, Faculty of Science and Technology, Keio University; 3-14-1 Hiyoshi, Kohoku-ku, Yokohama 223-8522, Japan).

### 2.2. Cell Cultures

HASMCs were purchased from Cascade Biologics, Inc. (Portland, OR, USA). HASMCs were grown in Dulbecco's Modified Eagle Medium (DMEM) supplemented with 10% FBS, 100 IU/mL penicillin and 100  $\mu$ g/mL

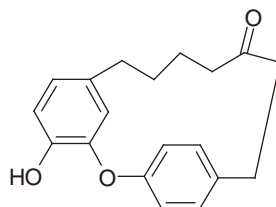


**Figure 1.** Chemical structures of acerogenin C.

streptomycin at 37°C in a humidified 95% air/5% CO<sub>2</sub> atmosphere. Cells were used at passages three through eight. For all experiments, HASMCs were grown to 80% - 90% confluence and quiescence was induced by starvation for at least 24 h.

### 2.3. [<sup>3</sup>H]-Thymidine Incorporation Assay

HASMCs proliferation was determined by [<sup>3</sup>H]-thymidine incorporation. HASMCs were incubated for 20 h with or without PDGF-BB (20 ng/mL) and various concentrations of acerogenins and then pulse-labeled with 1 μCi/mL of [<sup>3</sup>H]-thymidine for 4 h. Cells were harvested using a Universal Harvester (Perkin Elmer, Waltham, MA, USA) and then transferred to a GF/C filter (Perkin Elmer). The filter was dried and counted in scintillation fluid using a Microplate Scintillation and Luminescence Counter (Topcount NXT, Perkin Elmer).

### 2.4. Cell Viability

Cell viability was determined using the trypan blue dye exclusion method. Cells were incubated for 24 h with or without PDGF-BB (20 ng/mL) and various concentrations of acerogenin C and were then harvested from the dishes using a 0.1% w/v trypsin solution. Cell viability was examined by the trypan blue dye exclusion test. The number of viable cells was estimated by microscopic cell counting using a hemocytometer.

### 2.5. SDS-PAGE and Immunoblotting

Western blotting for protein analysis was performed as described previously [26]. Cells were harvested in lysis buffer containing 1 μM sodium vanadate, 1 μM phenylmethylsulfonyl fluoride, 5 μg/mL aprotinin and 5 μg/mL leupeptin. The protein concentration was determined by the Bradford assay (Bio-Rad, Hercules, CA, USA). Lysates corresponding to equal amounts of proteins were boiled in Laemmli sample buffer and the supernatants were loaded onto gels for SDS-PAGE. Proteins were transferred onto PVDF membranes and probed with the following primary antibodies: anti-phospho-PDGF-Rβ, anti-PDGF-Rβ, anti-phospho-PLCγ1 (Tyr783), anti-PLCγ1 anti-phospho-ERK1/2, anti-ERK, anti-phospho-Akt (Thr308) and anti-Akt. Appropriate horseradish peroxidase-coupled secondary antibodies were used at 1:10,000. Immunoreactive bands were visualized using enhanced chemiluminescence (ECL; Amersham Pharmacia Biotech, UK). The detected proteins were normalized to α-actin or the respective total protein, as appropriate. The intensities of bands were quantified using Sicon-Image for Windows (Scion Corporation, Frederick, MA, USA).

### 2.6. Cell Cycle Analysis

HASMCs were seeded in 6-well culture plates and grown in DMEM medium with growth supplement at 37°C in a humidified 95% air/5% CO<sub>2</sub> atmosphere. Cells were grown to 80% confluence and made quiescent by starvation for at least 24 h. Cells were incubated for 24 h with or without PDGF-BB (20 ng/mL) and various concentrations of acerogenin C. Cells were harvested, fixed in 70% ethanol for 12 h, and stored at -20°C. Cells were then washed twice with ice-cold PBS and incubated with 100 μg/mL RNase and 50 μg/mL propidium iodide and cell-cycle phase analysis was performed by flow cytometry using a Cytomics FC500 and CXP Software Ver. 2 software (Beckman Coulter, JAPAN).

### 2.7. Statistical Analysis

Experimental results are expressed as means ± S.E.M. One-way analysis of variance (ANOVA), followed by Dunnett's test, was used for multiple comparisons. P values of <0.05 and <0.01 were considered statistically significant.

## 3. Results

### 3.1. Effect of Acerogenins on PDGF-Induced HASMCs Proliferation and DNA Synthesis

In the [<sup>3</sup>H]-thymidine incorporation assay (**Figure 2(a)**), stimulation with PDGF-BB (20 ng/mL) increased cell proliferation by about 10-fold. Acerogenin C (0.1 to 10 μM) inhibited PDGF-induced cell proliferation in a concentration-dependent manner with about 90% inhibition observed at 10 μM. When quiescent cells were

treated with acerogenin C (0.1 to 10  $\mu\text{M}$ ) for 24 h in the absence of PDGF-BB, no significant difference was observed in the extent of [ $^3\text{H}$ ]-thymidine incorporation, suggesting that acerogenins are not cytotoxic at the concentrations tested. In particular, the lack of cytotoxicity of acerogenin C at the concentrations used in these experiments was confirmed by the trypan blue exclusion assay (Figure 2(b)). The number of cells was significantly increased after 20 ng/mL PDGF-BB stimulation ( $28.3 \pm 0.3 \times 10^4$  cells/well) compared with the non-stimulated group ( $13.1 \pm 0.1 \times 10^4$  cells/well) and the increased cells were significantly reduced to  $21.2 \pm 0.2$ ,  $15.3 \pm 0.3$  and  $14.2 \pm 0.2 \times 10^4$  cells/well at concentrations of 0.1, 1 and 10  $\mu\text{M}$ , respectively (Figure 2(b)).

### 3.2. Effect of Acerogenin C on PDGF-Induced PDGF-R $\beta$ , PCL $\gamma$ 1, Akt and ERK 1/2 Activation

The HASMCs were pre-incubated in the presence or absence of various concentrations of acerogenin C in a serum-free medium for 24 h and then stimulated for 10 min with 20 ng/mL PDGF-BB. As shown in Figure 3, PDGF-BB markedly increased phosphorylation levels on the PDGF-R $\beta$  but acerogenin C treatment had no significant effect. To determine the effects of acerogenin C on the downstream intracellular signal transduction pathway of PDGF-BB, we determined the phosphorylation of PLC $\gamma$ 1, Akt and ERK1/2. PDGF-BB treatment clearly increased phosphorylation levels on the PLC $\gamma$ 1, Akt and ERK1/2. Acerogenin C blocked the phosphorylation of PLC $\gamma$ 1 and Akt in a concentration-dependent manner but had no effect on ERK 1/2 phosphorylation.

### 3.3. Effect of Acerogenin C on Cell Cycle Progression in HASMCs

Flow cytometric analysis was performed to determine whether acerogenin C-induced cell growth inhibition was due to an arrest in a specific point of the cell cycle. As shown in Figure 4, pre-incubation of HASMCs in a serum-free medium for 24 h resulted in approximately  $91.8 \pm 2.5\%$  synchronization of the cell cycle in the G0/G1 phase. During cell cycle analysis, stimulation with PDGF-BB (20 ng/mL) increased the percentage of cells in the S phase from  $5.6 \pm 1.3\%$  to  $27.5 \pm 2.1\%$ . Acerogenin C (0.1 to 10  $\mu\text{M}$ ) significantly blocked cell cycle progression in a concentration-dependent manner. The percentage of cells in the S phase was significantly reduced to  $12.6 \pm 1.2\%$  ( $P < 0.05$ ,  $n = 3$ ),  $7.4 \pm 1.4\%$  ( $P < 0.05$ ,  $n = 3$ ) and  $5.4 \pm 1.4\%$  ( $P < 0.05$ ,  $n = 3$ ) at concentrations of 0.1, 1 and 10  $\mu\text{M}$  acerogenin C, respectively (Figure 4). These results suggest that acerogenin C may act against DNA synthesis in the early events of the cell cycle.

### 3.4. Effect of Acerogenin C on Cell Cycle Regulatory Protein Expression

Using immunoblot analysis, we analyzed the protein expressions of the cyclins and CDKs, which are known to

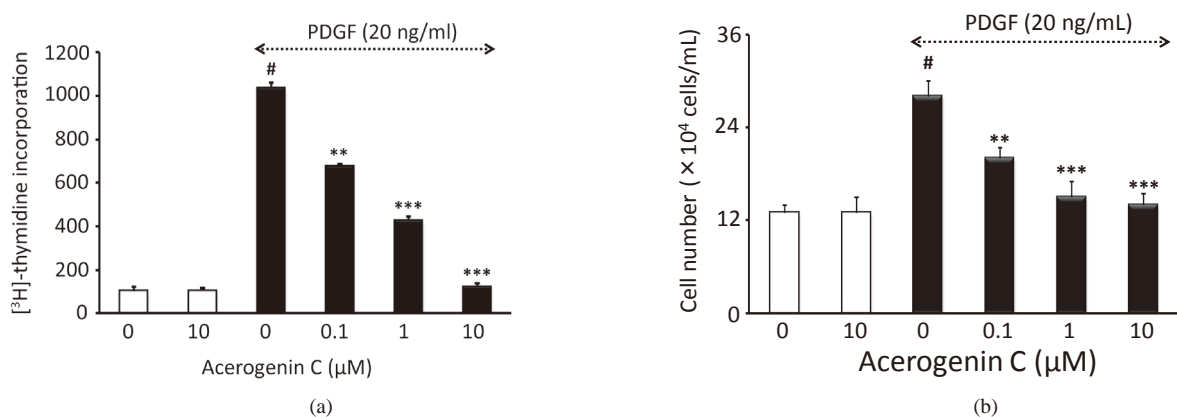


**Figure 2.** The effect of acerogenin on PDGF-BB-stimulated HASMCs proliferation. Cells were incubated for 20 h with or without PDGF-BB (20 ng/mL) and various concentrations of acerogenin C, and then pulse-labeled with [ $^3\text{H}$ ]-thymidine for 4 h (a). The cells were pre-incubated for 24 h with or without PDGF-BB and indicated concentrations of acerogenin C. The cells were trypsinized and then counted using a hemocytometer (b). Results are means  $\pm$  S.E.M. from three independent experiments. # $P < 0.005$  compared with control; \*\* $P < 0.01$  and \*\*\* $P < 0.001$  compared with PDGF-stimulation.

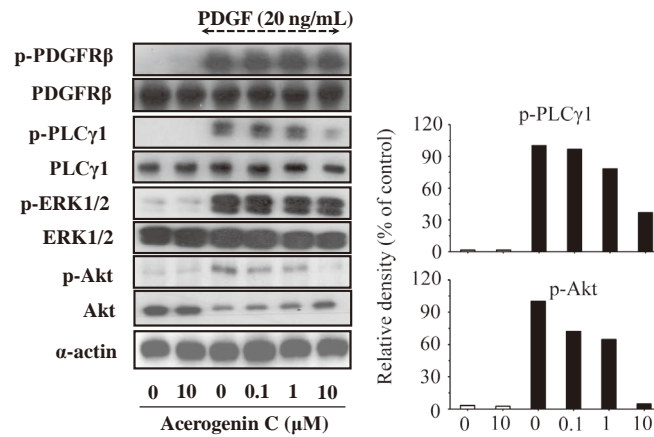


**Figure 3.** The effect of acerogenin C on PDGF-stimulated PDGF-R $\beta$ , ERK 1/2, PLC $\gamma$ 1, and Akt phosphorylation in HASMCs. The cells were incubated for 10 min with or without PDGF-BB and various concentrations of acerogenin C in 6-well culture plates. Cells were lysed and lysates were immunoblotted with antibodies. Total protein was used for respective normalization. After densitometric quantification, data are representative of at least three independent experiments with similar results.

be regulated by p27<sup>kip1</sup>, following treatment with acerogenin C. As shown in **Figure 5**, acerogenin C decreased the protein expression of cyclin E and CDK2, as well as cyclin D1 and CDK4, in a concentration-dependent manner. In addition, the expression of p27<sup>kip1</sup>, one of the cyclin-dependent kinase inhibitors, was down regulated by PDGF-BB treatment. In contrast, the p27<sup>kip1</sup> protein level was significantly increased by acerogenin C treatment in a concentration-dependent manner.

#### 4. Discussion

In the present study, we found that acerogenin C inhibited DNA synthesis in response to PDGF-BB (**Figure 2(a)**). As a result, acerogeninC showed a concentration-dependent inhibition of the incorporation of [<sup>3</sup>H]-thymidine into HASMCs. Furthermore, the antiproliferative effect of acerogenin C on HASMCs was not due to cellular cytotoxicity, as demonstrated by the cell counting (**Figure 2(b)**) and MTT assays (data not shown).

To understand the mechanism of down-regulation of PDGF-BB-stimulated HASMCs proliferation, we examined whether the effect of acerogenin C is mediated by down-regulation of the intracellular signaling pathways.

The PDGF-BB-stimulated mitogenesis signaling pathway has been well characterized. Binding of PDGF-BB to PDGF-R $\beta$  can activate three major signal transduction pathways, PI3-K/Akt, PLC $\gamma$ 1 and ERK1/2, by activating Raf-1 [12]. As shown **Figure 3**, acerogenin C had no effect on the PDGF-BB-induced phosphorylation of PDGF-R $\beta$  at various concentrations. This result suggests that the inhibition of acerogenin C on HASMCs proliferation does not occur at the receptor level. Thus, we did Western blotting to understand the effect of acerogenin C on the downstream signal transduction, such as the PI3-K/Akt, PLC $\gamma$ 1 and ERK1/2 signaling pathways. As shown in **Figure 3**, we observed that acerogenin C specifically inhibited PDGF-stimulated PLC $\gamma$ 1 and Akt activation but not PDGFR and ERK1/2 MAP kinase activation in HASMCs. These results are similar to a previous study, in which JM91 inhibited PDGF-induced PI3-K/Akt and ERK1/2 MAP kinase activation but not PDGF R $\beta$  in HASMCs [12]. In the present study, PDGFR $\beta$ , PLC $\gamma$ 1, ERK1/2 and Akt were used as a control for protein loading. However, the total amount of Akt rapidly decreased upon its activation. PDGF causes a rapid decrease in the Akt protein levels, concomitant with Akt activation. PDGF causes the regulated proteolytic down-regulation of Akt, which is dependent on PI3-K and proteasome activities. The proteasome-dependent down-regulation of Akt might be a fundamental mechanism that regulates the activity and function of Akt in VSMCs [27]. Interestingly, full activation of PLC $\gamma$  is dependent on PI3-K; the PI(3,4,5)P3 formed by PI3-K binds the PH domain of PLC $\gamma$  and may anchor the enzyme at the membrane [16]. PLC $\gamma$  appears not to be of primary impor-

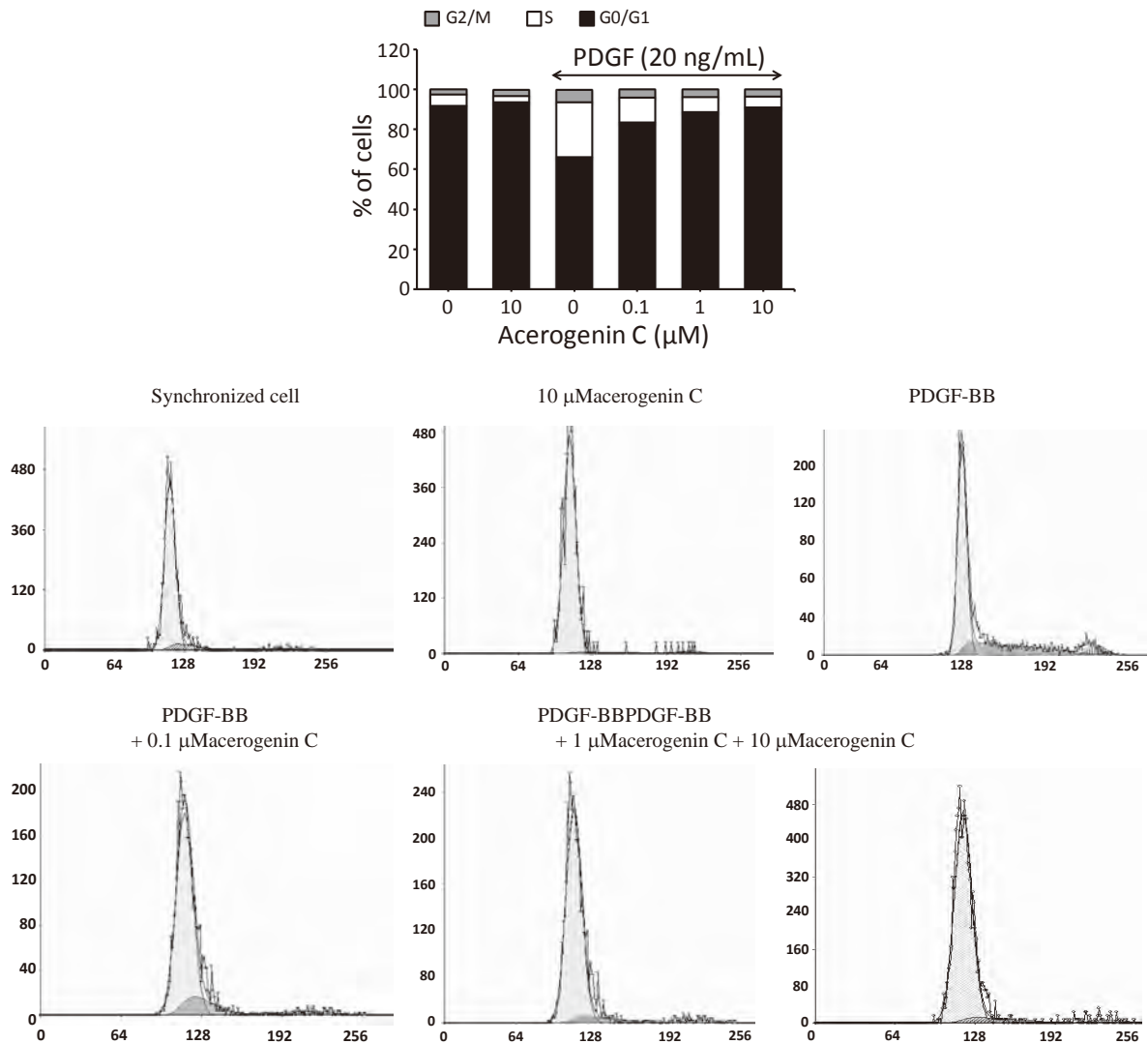


**Figure 4.** The effect of acerogenin C on PDGF-BB-stimulated cell cycle progression in HASMCs. The cells were incubated for 24 h with or without PDGF-BB and various concentrations of acerogenin C in 6-well culture plates. The cells were trypsinized and then analyzed by flow cytometry. Each item is derived from a representative experiment where data from at least 10,000 events were obtained. Data are representative of at least three independent experiments with similar results.

tance for the stimulation of cell growth and motility in most cell types. However, in certain cell types, PLC $\gamma$  affects these responses [28]. Members of the PI3-K family that bind to and are activated by tyrosine kinase receptors consist of a regulatory subunit, p85, and a catalytic subunit, p110. Their preferred substrate is phosphatidylinositol 4,5-bisphosphate [PI(4,5)P2], which is phosphorylated to phosphatidylinositol 3,4,5-trisphosphate [PI(3,4,5)P3]. Phosphatidylinositol 3-kinase plays a central role in intracellular signal transduction; it can be activated by several different signals, it has a number of downstream effector molecules, and it mediates many different cellular responses, including actin reorganization, chemotaxis, cell growth and antiapoptosis [15].

In addition, cell cycle analysis was performed to investigate the antiproliferative effect of acerogenin C. As shown in **Figure 4**, acerogenin C inhibits PDGF-BB-stimulated HASMCs proliferation via G<sub>0</sub>/G<sub>1</sub> arrest. Several reports suggest that the G<sub>1</sub> phase is a major point of control for cell proliferation in mammalian cells [29]. Many studies have attributed the regulation of G<sub>1</sub> cell-cycle arrest to a number of cellular proteins, including the CDK inhibitor, p27<sup>kip1</sup> [22]. Our data demonstrates a significant up-regulation of p27<sup>kip1</sup>. However, under similar experimental conditions, the expression levels of another cyclin-dependent kinase inhibitor, p21<sup>waf1</sup> protein, was not changed (data not shown), suggesting that p21<sup>waf1</sup> is unlikely to be involved in the cell-cycle arrest induced

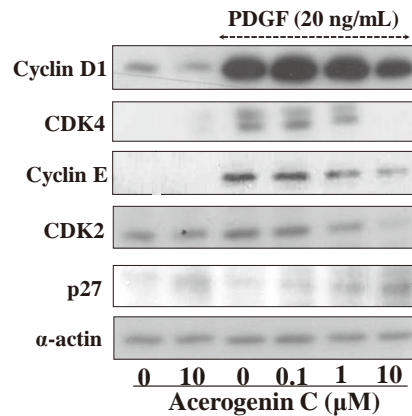


**Figure 5.** The effect of acerogenin C on PDGF-stimulated expression of cell cycle regulatory proteins in HASMCs. The cells were incubated for 24 h with or without PDGF-BB and various concentrations of acerogenin C in 6-well culture plates. The cells were lysed and proteins were analyzed by SDS-PAGE and immunoblotting.  $\alpha$ -actin was used for normalization. Data are representative of at least three independent experiments with similar results.

by acerogenin C. We assessed the effect of acerogenin C treatment on the cyclins and CDKs operative in the  $G_1$ -phase of the cell cycle, such as cyclin D1, CDK4, cyclin E and CDK2. Acerogenin C inhibited the expression of cyclin D1, CDK4, cyclin E and CDK2 in a concentration-dependent manner. Our results indicate that cell cycle arrest in the  $G_1$ -phase might be due to the down-regulation of CDKs/cyclins complex expression.

## 5. Conclusion

We showed that acerogenin C inhibited PDGF-BB-induced HASMCs proliferation via  $G_0/G_1$  arrest, in association with the down-regulation of the expression of cyclin D1, CDK4, cyclin E and CDK2 and the up-regulation of p27<sup>kip1</sup>. Therefore, acerogenin C may be useful for prevention and treatment of vascular diseases, such as restenosis after coronary angioplasty.

## Acknowledgements

This study was performed at a laboratory supported by an endowment from Erina Co., Inc.

## References

- [1] Ross, R. (1993) The Pathogenesis of Atherosclerosis: A Perspective for the 1990s. *Nature*, **362**, 801-809. <http://dx.doi.org/10.1038/362801a0>
- [2] Kanzaki, T., Shinomiya, M., Ueda, S., Morisaki, N., Saito, Y. and Yoshida, S. (1994) Enhanced Arterial Intimal Thickening after Balloon Catheter Injury in Diabetic Animals Accompanied by PDGF Beta-Receptor Overexpression of Aortic Media. *European Journal of Clinical Investigation*, **24**, 377-381. <http://dx.doi.org/10.1111/j.1365-2362.1994.tb02179.x>
- [3] Majesky, M.W., Reidy, M.A., Bowen-Pope, D.F., Hart, C.E., Wilcox, J.N. and Schwartz, S.M. (1990) PDGF Ligand and Receptor Gene Expression during Repair of Arterial Injury. *Journal of Cell Biology*, **111**, 2149-2158. <http://dx.doi.org/10.1083/jcb.111.5.2149>
- [4] Uchida, K., Sasahara, M., Morigami, N., Hazama, F. and Kinoshita, M. (1996) Expression of Platelet-Derived Growth Factor B-Chain in Neointimal Smooth Muscle Cells of Balloon Injured Rabbit Femoral Arteries. *Atherosclerosis*, **124**, 9-23. [http://dx.doi.org/10.1016/0021-9150\(95\)05742-0](http://dx.doi.org/10.1016/0021-9150(95)05742-0)
- [5] Libby, P., Salomon, R.N., Payne, D.D., Schoen, F.J. and Pober, J.S. (1989) Functions of Vascular Wall Cells Related to Development of Transplantation-Associated Coronary Arteriosclerosis. *Transplantation Proceedings*, **21**, 3677-3684.
- [6] Libby, P., Warner, S.J., Salomon, R.N. and Birinyi, L.K. (1988) Production of Platelet-Derived Growth Factor-Like Mitogen by Smooth-Muscle Cells from Human Atheroma. *New England Journal of Medicine*, **318**, 1493-1498.

- <http://dx.doi.org/10.1056/NEJM198806093182303>
- [7] Rubin, K., Tingström, A., Hansson, G.K., Larsson, E., Rönstrand, L., Klareskog, L., *et al.* (1988) Induction of B-Type Receptors for Platelet-Derived Growth Factor in Vascular Inflammation: Possible Implications for Development of Vascular Proliferative Lesions. *Lancet*, **1**, 1353-1356. [http://dx.doi.org/10.1016/S0140-6736\(88\)92177-0](http://dx.doi.org/10.1016/S0140-6736(88)92177-0)
- [8] Wilcox, J.N., Smith, K.M., Williams, L.T., Schwartz, S.M. and Gordon, D. (1988) Platelet-Derived Growth Factor mRNA Detection in Human Atherosclerotic Plaques by *in Situ* Hybridization. *Journal of Clinical Investigation*, **82**, 1134-1143. <http://dx.doi.org/10.1172/JCI113671>
- [9] Ueda, M., Becker, A.E., Kasayuki, N., Kojima, A., Morita, Y. and Tanaka, S. (1996) *In Situ* Detection of Platelet-Derived Growth Factor-A and -B Chain mRNA in Human Coronary Arteries after Percutaneous Transluminal Coronary Angioplasty. *American Journal of Pathology*, **149**, 831-843.
- [10] Golden, M.A., Au, Y.P., Kirkman, T.R., Wilcox, J.N., Raines, E.W., Ross, R., *et al.* (1991) Platelet-Derived Growth Factor Activity and mRNA Expression in Healing Vascular Grafts in Baboons. Association *in Vivo* of Platelet-Derived Growth Factor mRNA and Protein with Cellular Proliferation. *Journal of Clinical Investigation*, **87**, 406-414. <http://dx.doi.org/10.1172/JCI115011>
- [11] Ross, R., Masuda, J., Raines, E.W., Gown, A.M., Katsuda, S., Sasahara, M., *et al.* (1990) Localization of PDGF-B Protein in Macrophages in All Phases of Atherogenesis. *Science*, **248**, 1009-1012. <http://dx.doi.org/10.1126/science.2343305>
- [12] Seo, J.M., Jin, Y.R., Ryu, C.K., Kim, T.J., Han, X.H., Hong, J.T., *et al.* (2008) JM91, a Newly Synthesized Indole-dione Derivative, Inhibits Rat Aortic Vascular Smooth Muscle Cells Proliferation and Cell Cycle Progression through Inhibition of ERK1/2 and Akt Activations. *Biochemical Pharmacology*, **75**, 1331-1340. <http://dx.doi.org/10.1016/j.bcp.2007.11.013>
- [13] Dudek, H., Datta, S.R., Franke, T.F., Birnbaum, M.J., Yao, R., Cooper, G.M., *et al.* (1997) Regulation of Neuronal Survival by the Serine-Threonine Protein Kinase Akt. *Science*, **275**, 661-665. <http://dx.doi.org/10.1126/science.275.5300.661>
- [14] Kauffmann-Zeh, A., Rodriguez-Viciana, P., Ulrich, E., Gilbert, C., Coffey, P., Downward, J., *et al.* (1997) Suppression of c-Myc-Induced Apoptosis by Ras Signalling through PI(3)K and PKB. *Nature*, **385**, 544-548. <http://dx.doi.org/10.1038/385544a0>
- [15] Vanhaesebroeck, B., Leever, S.J., Panayotou, G. and Waterfield, M.D. (1997) Phosphoinositide 3-Kinases: A Conserved Family of Signal Transducers. *Trends in Biochemical Sciences*, **22**, 267-272. [http://dx.doi.org/10.1016/S0968-0004\(97\)01061-X](http://dx.doi.org/10.1016/S0968-0004(97)01061-X)
- [16] Falasca, M., Logan, S.K., Lehto, V.P., Baccante, G., Lemmon, M.A. and Schlessinger, J. (1998) Activation of Phospholipase C $\gamma$  by PI 3-Kinase-Induced PH Domain-Mediated Membrane Targeting. *EMBO Journal*, **17**, 414-422. <http://dx.doi.org/10.1093/emboj/17.2.414>
- [17] Elledge, S.J. (1996) Cell Cycle Checkpoints: Preventing an Identity Crisis. *Science*, **274**, 1664-1672. <http://dx.doi.org/10.1126/science.274.5293.1664>
- [18] Gordon, D., Reidy, M.A., Benditt, E.P. and Schwartz, S.M. (1990) Cell Proliferation in Human Coronary Arteries. *Proceedings of the National Academy of Sciences of the United States of America*, **87**, 4600-4604. <http://dx.doi.org/10.1073/pnas.87.12.4600>
- [19] Sherr, C.J. (1994) G1 Phase Progression: Cycling on Cue. *Cell*, **79**, 551-555. [http://dx.doi.org/10.1016/0092-8674\(94\)90540-1](http://dx.doi.org/10.1016/0092-8674(94)90540-1)
- [20] Sherr, C.J. (1996) Cancer Cell Cycles. *Science*, **274**, 1672-1677. <http://dx.doi.org/10.1126/science.274.5293.1672>
- [21] Xiong, Y., Hannon, G.J., Zhang, H., Casso, D., Kobayashi, R. and Beach, D. (1993) p21 Is a Universal Inhibitor of Cyclin Kinases. *Nature*, **366**, 701-704. <http://dx.doi.org/10.1038/366701a0>
- [22] Toyoshima, H. and Hunter, T. (1994) p27, a Novel Inhibitor of G1 Cyclin-Cdk Protein Kinase Activity, Is Related to p21. *Cell*, **78**, 67-74. [http://dx.doi.org/10.1016/0092-8674\(94\)90573-8](http://dx.doi.org/10.1016/0092-8674(94)90573-8)
- [23] Akihisa, T., Taguchi, Y., Yasukawa, K., Tokuda, H., Akazawa, H., Suzuki, T., *et al.* (2006) Acerogenin M, a Cyclic Diarylheptanoid, and Other Phenolic Compounds from *Acer nikoense* and Their Anti-Inflammatory and Anti-Tumor-Promoting Effects. *Chemical and Pharmaceutical Bulletin*, **54**, 735-739. <http://dx.doi.org/10.1248/cpb.54.735>
- [24] Gonzalez, G.I. and Zhu, J. (1997) First Total Synthesis of Acerogenin C and Aceroside IV. *Journal of Organic Chemistry*, **62**, 7544-7545. <http://dx.doi.org/10.1021/jo9714324>
- [25] Keseru, G.M. and Nogradi, M. (1995) The Chemistry of Natural Diarylheptanoids. In: Rahman, A.U., Ed., *Studies in Natural Products Chemistry*, Vol. 17, Elsevier, Amsterdam, 357-394.
- [26] Cha, B.Y., Shi, W.L., Yonezawa, T., Teruya, T., Nagai, K. and Woo, J.T. (2009) An Inhibitory Effect of Chrysoeriol on Platelet-Derived Growth Factor (PDGF)-Induced Proliferation and PDGF Receptor Signaling in Human Aortic Smooth Muscle Cells. *Journal of Pharmacological Sciences*, **110**, 105-110. <http://dx.doi.org/10.1254/jphs.08282FP>

- 
- [27] Adachi, M., Katsumura, K.R., Fujii, K., Kobayashi, S., Aoki, H. and Matsuzaki, M. (2003) Proteasome-Dependent Decrease in Akt by Growth Factors in Vascular Smooth Muscle Cells. *FEBS Letters*, **554**, 77-80. [http://dx.doi.org/10.1016/S0014-5793\(03\)01109-8](http://dx.doi.org/10.1016/S0014-5793(03)01109-8)
- [28] Heldin, C.H. and Westermark, B. (1999) Mechanism of Action and *in Vivo* Role of Platelet-Derived Growth Factor. *Physiological Reviews*, **79**, 1283-1316.
- [29] Fang, F. and Newport, J.W. (1991) Evidence That the G1-S and G2-M Transitions Are Controlled by Different cdc2 Proteins in Higher Eukaryotes. *Cell*, **66**, 731-742. [http://dx.doi.org/10.1016/0092-8674\(91\)90117-H](http://dx.doi.org/10.1016/0092-8674(91)90117-H)

## RESEARCH ARTICLE

# Rosmarinic acid exerts an antiosteoporotic effect in the RANKL-induced mouse model of bone loss by promotion of osteoblastic differentiation and inhibition of osteoclastic differentiation

Ji-Won Lee<sup>1,2,3</sup>, Midori Asai<sup>3</sup>, Sang-Kyung Jeon<sup>4</sup>, Tadahiro Iimura<sup>1,5</sup>, Takayuki Yonezawa<sup>3</sup>, Byung-Yoon Cha<sup>3</sup>, Je-Tae Woo<sup>3</sup> and Akira Yamaguchi<sup>2</sup>

<sup>1</sup> Division of Bio-Imaging, Proteo-Science Center (PROS), Ehime University, Ehime, Japan

<sup>2</sup> Section of Oral Pathology, Graduate School of Medicine and Dental Sciences, Tokyo Medical and Dental University, Tokyo, Japan

<sup>3</sup> Research Institute for Biological Functions, Chubu University, Aichi, Japan

<sup>4</sup> Food Science and Technology, Keimyung University, Daegu, Korea

<sup>5</sup> Translational Research Center, Ehime University Hospital, Ehime, Japan

**Scope:** Bone homeostasis is ensured by the balance between bone formation and resorption. Thus, control of the recruitment, proliferation, and differentiation of bone cells is essential to maintain bone mass. The aim of this study was to elucidate the effects of rosmarinic acid as a potential therapeutic agent on bone metabolism using bone cells and a mouse model.

**Methods and results:** Rosmarinic acid increased alkaline phosphatase activity and induced mineralization in osteoblasts. Addition of rosmarinic acid to cultures of calvarial osteoblastic cells prepared from T-cell factor/ $\beta$ -catenin TOP-GAL mutant mice strongly induced the expression of LacZ and promoted stabilization of  $\beta$ -catenin in the cytoplasm of ST2 cells, suggesting that rosmarinic acid affects the canonical Wnt signaling pathway. Moreover, rosmarinic acid inhibited not only osteoclast formation in cocultures of mouse bone marrow cells and osteoblasts, but also receptor activator of nuclear factor kappa-B ligand (RANKL)-induced osteoclastic differentiation in bone marrow-derived macrophages. RANKL-induced p38 mitogen-activated protein kinase and the expression of nuclear factor of activated T cell, c-Jun, and c-Fos were inhibited by rosmarinic acid in bone marrow macrophages. Finally, we confirmed that rosmarinic acid improved bone mass in a soluble RANKL-induced bone loss mouse model.

**Conclusion:** Rosmarinic acid has dual regulatory effects on bone metabolism and may control the bone functions by controlling osteoblastic and osteoclastic differentiation.

Received: March 6, 2014  
Revised: October 17, 2014  
Accepted: October 20, 2014

## Keywords:

$\beta$ -Catenin / Osteoblast / Osteoclast / Rosmarinic acid / Wnt



Additional supporting information may be found in the online version of this article at the publisher's web-site

**Correspondence:** Professor Je-Tae Woo, Research Institute for Biological Functions, Chubu University, 1200 Matsumoto, Kasugai-shi, Aichi 487-8501, Japan

**E-mail:** jwoo@isc.chubu.ac.jp

**Fax:** +81-568-51-6189

**Abbreviations:** **3D**, three-dimensional; **ALP**, alkaline phosphatase; **BMNC**, bone mineral content; **BMD**, bone mineral density; **BMCs**, bone marrow cells; **BMMs**, bone marrow macrophages; **BMP**, bone morphogenetic protein; **IkB**, inhibitory

kappa B; **JNK**, anti-c-Jun N-terminal kinase; **LiCl**, lithium chloride; **MAPK**, mitogen-activated protein kinase; **M-CSF**, macrophage colony-stimulating factor; **NFATc1**, nuclear factor of activated T cell; **OCN**, osteocalcin; **OPG**, osteoprotegerin; **PTH**, parathyroid hormone; **p.o.**, per os (oral administration); **RANKL**, receptor activator of nuclear factor kappa-B ligand; **sRANKL**, soluble RANKL; **Tb. BMD**, trabecular BMD; **TCF/LEF**, T-cell factor/lymphoid enhancer-binding factor; **TNF- $\alpha$** , tumor necrosis factor-alpha; **TRAP**, tartrate-resistant acid phosphatase

## 1 Introduction

Bone provides mechanical support, protects the various organs of the body, and serves as a depository for minerals. As microscopic units, bone is continuously remodeled by the balance between the activities of osteoblasts and osteoclasts both of which are present on the bone surface. Osteoblasts are mononucleated bone-forming cells that are derived from mesenchymal cells. They produce an organic mixture known as osteoid that mineralizes to form new bone, while osteoclasts, which are multinucleated cells derived from multipotent hematopoietic stem cells, resorb the bone [1, 2]. Upon completion of resorption, a reversal period follows during which osteoblasts fill the resulting cavity with osteoid that becomes mineralized, a process termed as remodeling [3]. Signals that determine the replication, differentiation, function, and death of cells in both of these lineages dictate the degree of bone remodeling, a process necessary to maintain calcium homeostasis and to remove and prevent the accumulation of aged or weakened bone [4].

Osteoporosis is a progressive bone disease that is characterized by a decrease in bone mass and density, which leads to bone fractures. In particular, the most common cause of age-related bone loss occurs in women who are associated with estrogen deficiency after menopause [5]. Estrogen replacement therapy is only recommended for women who have menopausal symptoms and no contraindications, which appears to be an effective osteoporosis treatment, although some side effects may occur [6]. Numerous medications have been developed for the treatment of osteoporosis, such as antiresorptive agents (e.g. estrogen) and bone formation-stimulating agents (e.g. growth hormone) [7]. However, the currently available bone-forming agents may either have serious side effects (e.g. breast cancer and cardiovascular disease) or fail to sufficiently improve bone quality to reduce the fracture susceptibility [8]. Thus, the discovery of natural products that minimize bone loss in postmenopausal women would be beneficial.

Traditional plants and their active natural products are major sources for novel drug discovery and development [9]. Rosemary (*Rosmarinus officinalis* L.) is a perennial herb used for food flavoring, which is widely distributed in the Mediterranean region. According to the National Nutrient Database of the United States Department of Agriculture, fresh rosemary has an energy content of 131 kcal consisting of 16% carbohydrates, 6% protein, 20% total fat, 37% dietary fiber, and various vitamins and minerals. In folk medicine, rosemary is known as a digestive, tonic, astringent, diuretic, and diaphoretic, and is useful for treating urinary ailments [10]. Furthermore, numerous studies demonstrate that extracts, essential oils, and chemical constituents isolated from rosemary have biological activities such as antioxidant, anti-HIV-I, antiulcerogenic, anticarcinogenic, and antimicrobial effects. Rosmarinic acid ( $\alpha$ -*o*-caffeoyl-3,4-dihydroxyphenyl-lactic acid) is one of the chemical constituents of rosemary,

which has a therapeutic potential including anticyclooxygenase, antioxidant, and anti-inflammatory effects. Therefore, rosmarinic acid might have pharmaceutical effects for the treatment or prevention of several inflammatory diseases, cancer, and ageing [10–14]. Rosmarinic acid has been recently reported to increase alkaline phosphatase (ALP) activity and mineralized bone nodule formation in ST2 murine bone marrow stromal cells [15]. However, the functional activities and mechanisms of action remain to be elucidated. Here, we demonstrate the therapeutic potential of rosmarinic acid in bone metabolism by regulating osteoblastic and osteoclastic differentiation.

## 2 Materials and methods

### 2.1 Reagents

An osteocalcin (OCN) sandwich ELISA kit was obtained from Biomedical Technologies Inc. (Stoughton, MA). Recombinant soluble RANKL (sRANKL, where is RANKL receptor activator of nuclear factor kappa-B ligand) was purchased from PeptoTech EC Ltd. (London, UK). Recombinant sRANKL for in vivo experiments was kindly supplied by Oriental Yeast Co. Ltd. (Tokyo, Japan).  $1\alpha,25$ -Dihydroxyvitamin D<sub>3</sub> [ $1\alpha,25$ -(OH)<sub>2</sub>D<sub>3</sub>] and prostaglandin E<sub>2</sub> were purchased from Wako Pure Chemical Industries Ltd. (Osaka, Japan). Specific PCR primers for mouse ALP, OCN, RANKL, osteoprotegerin (OPG), macrophage colony-stimulating factor (M-CSF), Wnt3a, Tcf4, and glyceraldehyde-3-phosphate dehydrogenase (GAPDH) were synthesized by Life Technologies Inc. (Tokyo, Japan). A type I collagen gel solution (Cell matrix type IA) was obtained from Nitta Gelatin Co. (Osaka, Japan). Anti- $\beta$ -catenin, anti-c-Jun N-terminal kinase (JNK), antiphospho-JNK, anti-p38 mitogen-activated protein kinase (MAPK), antiphospho-p38 MAPK, antiinhibitory kappa B ( $I\kappa$ B), anti-c-Jun, anti-c-Fos, and anti-nuclear factor of activated T cell (NFATc1) mouse polyclonal antibodies were purchased from Cell Signaling Technology Inc. (Beverly, MA). An anti- $\beta$ -actin mouse polyclonal antibody was purchased from Sigma Chemical Co. (St. Louis, MO). Rosmarinic acid was purchased from Tokyo Chemical Industry (Tokyo, Japan). All other chemicals and reagents were analytical grade.

### 2.2 Animals

Male Std ddY mice (6–9 weeks of age) were purchased from Japan SLC Co. (Hamamatsu, Japan). Wnt reporter TOP-GAL mice were obtained from Prof. Ota Masato (Tokyo Medical and Dental University). The experimental animal study was approved and maintained in accordance with the guidelines of the Animal Experiment Committee of Chubu University.

## 2.3 Osteoblast experiments

### 2.3.1 Cell culture

MC3T3-E1 and ST2 cells were grown in  $\alpha$ -MEM (Gibco BRL, New York, NY) supplemented with 10% fetal bovine serum (Gibco BRL) at 37°C in a humidified atmosphere containing 5% CO<sub>2</sub>. The medium was changed every 3 days. At confluency, the medium was replaced with osteogenic medium ( $\alpha$ -MEM containing 50  $\mu$ g/mL phosphate ester of ascorbic acid (Sigma, St. Louis, MO) and 10 mM  $\beta$ -glycerophosphate (Sigma) in the absence or presence of rosmarinic acid dissolved in DMSO. Primary calvarial osteoblasts were obtained from neonatal ddY mice and TOP-GAL mutant mice by tissue digestion with collagenase (Wako Pure Chemical Industries Ltd.) and dispase (Godo Shusei Co., Tokyo, Japan) as described previously [16].

### 2.3.2 Determination of osteoblastic cell proliferation and differentiation

Osteoblast proliferation was measured by an 3-(4,5-dimethylthiazol-2-yl)-2,5-diphenyltetrazolium bromide (MTT) assay. MC3T3-E1 and ST2 cells were cultured under the same conditions used for osteogenic experiments. MTT reagent was added at 3 h before the end of the culture. Culture supernatants were removed carefully and the remaining formazan crystals were dissolved in DMSO. Absorbance at 570 nm was then measured using a microplate reader. To measure ALP activity, MC3T3-E1 and ST2 cells were grown in 96-well plates and then treated with rosmarinic acid for 4 days. After treatment, the cells were rinsed twice with PBS and fixed with 10% formalin for 10 min. ALP activity was then measured using an ALP kit (Wako Pure Chemical Industries Ltd.) according to the manufacturer's protocol. The absorbance was measured at 405 nm. The ALP activity was standardized to the relative control as a percentage. After determination of ALP activity, the cells were stained using an ALP kit (Sigma).

### 2.3.3 Measurement of OCN and alizarin red staining

After MC3T3-E1 cells were cultured to confluency in culture dishes, the cells were treated with rosmarinic acid in osteogenic medium for 14 days. OCN content in the culture medium was then measured using the sandwich ELISA assay kit according to the manufacturer's protocol. Total protein was determined using a BCA protein assay kit (Bio-Rad, Hercules, CA). To confirm calcium deposition, we performed alizarin red staining.

### 2.3.4 Detection of TOP-GAL activity by X-gal staining

Primary calvarial cells isolated from TOP-GAL transgenic mice were seeded at  $1 \times 10^4$  cells/well in 96-well plates and cultured until confluency. The cells were then cultured

in osteogenic medium for 7 days with or without rosmarinic acid. To detect  $\beta$ -galactosidase activity, the cells were fixed in 10% formalin for 10 min, washed twice in PBS, and immersed in an X-gal (5-bromo-4-chloro-3-indolyl- $\beta$ -D-galactopyranoside) substrate solution (1 mg/mL X-gal in 5 mM K<sub>4</sub>Fe(CN)<sub>6</sub>, 5 mM K<sub>3</sub>Fe(CN)<sub>6</sub>, and 5 mM MgCl<sub>2</sub>) for 12–24 h.

### 2.3.5 Immunohistochemical staining for $\beta$ -catenin

ST2 cells grown on eight-chamber culture slides were fixed with 4% paraformaldehyde in PBS for 20 min, permeabilized with 0.05% Triton-X 100 (Sigma) in PBS for 20 min, and then blocked with 10% BSA in Tris-buffered saline (20 mM Tris-HCl, pH 7.5, and 137 mM NaCl) plus 0.1% Tween-20 (TBS-T) for 1 h. The cells were then sequentially incubated with a mouse anti- $\beta$ -catenin monoclonal primary antibody (1:500) and Alexa Fluor-conjugated anti-mouse secondary antibody (1:1000). After three washes with PBS, the cells were counterstained with 4,6-diamidino-2-phenylindole for 5 min and washed three times with PBS. The slides were removed from the chambers, rinsed in PBS, and mounted with antifade-mounting medium. Fluorescent signals were examined with a fluorescence microscope (Carl Zeiss, Oberkochen, Germany).

## 2.4 Osteoclast experiments

### 2.4.1 Mouse bone marrow cells (BMCs) and cocultures

BMCs were obtained from the tibiae of 4- to 6-week-old ddY male mice. In the coculture system, BMCs were cocultured with calvarial osteoblasts in 24-well plates in the presence of  $1 \times 10^{-8}$  M  $1\alpha,25\text{-(OH)}_2\text{D}_3$  for 5 days. The cells were then fixed and stained for tartrate-resistant acid phosphatase (TRAP), a marker of osteoclasts.

### 2.4.2 Osteoclast differentiation from mouse bone marrow macrophages (BMMs)

To obtain BMMs, BMCs were cultured for 1 day in  $\alpha$ -MEM containing 10% fetal bovine serum and M-CSF (50 ng/mL) in 60-mm dishes. After 18 h of culture, unattached cells were collected and considered as BMMs. In the BMM culture system, BMMs were cultured in 96-well plates in the presence of M-CSF (50 ng/mL) for 3 days and then treated with RANKL (100 ng/mL), for a further 3 days. The cells were sequentially fixed with 10% formalin for 10 min and ethanol for 1 min, and then dried. Subsequently, the cells were incubated in 0.1 mL phosphatase substrate (5 mM *p*-nitrophenyl phosphate in 50 mM citrate buffer, pH 4.6) in the presence of 10 mM sodium tartrate at 37°C for 30 min. The reaction was stopped

by addition of 0.1 N NaOH and the absorbance was measured at 405 nm. After determination of TRAP activity, the cells were stained with a TRAP-staining solution (0.1 mg/mL naphthol AS-MX phosphate and 0.6 mg/mL fast red violet LB salt in 0.1 M sodium acetate buffer, pH 5.0, containing 50 mM sodium tartrate). TRAP-positive multinucleated cells with five or more nuclei were counted. Osteoclast proliferation was determined by an Alamar blue assay (Biosource International, Camarillo, CA) according to the manufacturer's instructions. Mouse BMCs ( $5 \times 10^4$  cells/well) were cultured in 96-well plates with M-CSF for 3 days and then treated with various concentrations of rosmarinic acid for 24 h. After addition of the Alamar blue reagent and incubation for 3 h, the fluorescence was measured at an excitation wavelength of 560 nm and emission wavelength of 590 nm.

### 2.4.3 RT-PCR and real-time PCR

Total RNA was extracted using TRIzol (Life Technologies Inc.). First-strand cDNA was synthesized from the total RNA with an oligo (dT)<sub>12–18</sub> primer and ReverTra Ace reverse transcriptase (ToYoBo, Tokyo, Japan) and then subjected to PCR amplification with Ex Taq polymerase (Takara Biochemicals, Tokyo, Japan). PCR products were separated by electrophoresis in 2% agarose gels and visualized by ethidium bromide staining under UV light. Real-time RT-PCR to quantitate gene expression was performed using Fast SYBR Green (Roche Diagnostics Ltd., Lewes, UK). The primers were as follows: *Wnt3a* (5'-TAC CCG ATC TGG TGG TCC TTG GC-3' and 5'-GCA TGA TCT CCA CGT AGT TCC TG-3'); *Rankl* (5'-CGC TCT GTT CCT GTA CTT TCG AGC G-3' and 5'-TCG TGC TCC CTC CTT TCA TCA GGT T-3'); *Tcf4* (5'-GCC TCT CAT CAC GTA CAG CA-3' and 5'-GGA TGG GGG ATT TGT CCT AC-3'). The SYBR green signals were detected using a LightCycler Nano System (Roche). Glyceraldehyde-3-phosphate dehydrogenase was used as an internal control for normalization. The PCR products were analyzed by gel electrophoresis, and the specificity of amplification was confirmed by melting curves.

### 2.4.4 Western blot analysis

To obtain total proteins, cells were lysed with RIPA buffer (20 mM Tris-HCl, pH 7.5, 150 mM NaCl, 1 mM EDTA, 50 mM  $\beta$ -glycerophosphate, 1% NP-40, 1 mM  $\text{Na}_3\text{VO}_4$ , 1 $\times$  phosphatase inhibitor, and 1 $\times$  protease inhibitor cocktail). Cytoplasmic fractions were prepared using NE-PER nuclear and cytoplasmic extraction reagents (Sigma) according to the manufacturer's protocol. Protein concentrations were determined by the BCA protein assay kit with BSA as the standard. Protein samples (20  $\mu$ g) were denatured in SDS sample buffer and resolved in a 10% SDS-polyacrylamide gel. The separated proteins were transferred to polyvinylidene difluoride membranes in 25 mM Tris, 192 mM glycine, and 20% methanol.

The membranes were blocked with TBS-T containing 3% dried milk powder. Subsequently, the membranes were reacted with specific antibodies. Loading differences were normalized using an anti- $\beta$ -actin antibody. Peroxidase activity on the polyvinylidene difluoride membranes was visualized on X-ray film using an ECL Western blotting detection system (Amersham Pharmacia Biotech, Ltd.).

## 2.5 Animal experiments

### 2.5.1 Mouse preparation and in vivo experiments using the RANKL-induced bone loss model

The sRANKL-induced mouse model of bone loss was established using 6-week-old female C57BL/6NcrJ mice (Charles River Laboratories Japan Inc., Shizuoka, Japan). The mice were housed in a temperature-controlled room ( $23 \pm 3^\circ\text{C}$ ) with  $55 \pm 5\%$  humidity in a 12-h/12-h light/dark cycle and provided free access to food (CRF-1; Oriental Yeast Co. Ltd.) and distilled water. The mice were allowed to acclimatize for 7 days. To establish the bone loss model, sRANKL was administered to mice [17]. Briefly, the mice were injected intraperitoneally with sRANKL (1 mg/kg) or PBS (vehicle) at 24-h intervals for 4 days. On the fourth day, the sRANKL-administered mice were randomly assigned to five groups ( $n = 5$  mice/group) and treated for 26 days as follows: PBS (sRANKL control, oral administration; (p.o.)); parathyroid hormone (PTH, intraperitoneally), 100  $\mu$ g/kg/day; low-dose rosmarinic acid (1 mg/kg/day, p.o.); mid-dose rosmarinic acid (10 mg/kg/day, p.o.), and high-dose rosmarinic acid (100 mg/kg/day, p.o.). The highest dose of rosmarinic acid (100 mg/kg) administered to the animal model was equivalent to approximately 30 mM. According to bioavailability [18], genotoxicity [19], and doses applied in previous in vivo experiments (10–100 mg/kg) [20–22], we administered rosmarinic acid at doses of 1, 10, and 100 mg/kg. After the treatments, the mice were euthanized and blood samples were collected for serum isolation. Femora were also removed and fixed with 70% ethanol for bone mass measurement.

### 2.5.2 Histomorphometric and histological analyses of bone

Tomographic measurements of bone mineral density (BMD), bone mineral content (BMNC), and bone strength were performed by peripheral quantitative computed tomography using an XCT Research SA+ (Stratec Medizintechnik, Pforzheim, Germany) with a voxel size of 0.7 mm. Image analysis was carried out using integrated XCT 2000 software. Two sections of the distal femoral metaphysis starting at 1 mm from the growth plate were scanned at 0.2 mm intervals to measure the trabecular bone density. Three-dimensional (3D) images of the distal femoral metaphysis were reconstructed by  $\mu$ CT analysis of the growth plate of the right

femur distal metaphysis using a CT R<sub>m</sub>CT2 (Rigaku Corp., Tokyo, Japan). X-ray irradiation was performed at a tube voltage of 90 kV and current of 160  $\mu$ A for 3 min. Image analysis was carried out using integrated TRI/3D-BON (Ratoc System Engineering Co. Ltd., Tokyo, Japan). For histological staining, femurs were fixed with 4% paraformaldehyde in 0.1 M phosphate buffer (pH 7.4) for 24 h at 4°C. The specimens were prepared as described previously [16]. TRAP and ALP staining were performed according to the manufacturer's protocols for histology. Serum levels of TRAP5b (IDS Ltd., Tyne and Wear, UK) and OCN (Takara, Japan) were measured according to the manufacturer's protocols.

## 2.6 Statistical analysis

Data are expressed as the means  $\pm$  SD. Statistical analysis was performed using the unpaired two-tailed Student's *t*-test assuming unequal variances. Values of  $p < 0.05$  were considered to indicate statistical significance.

## 3 Results

### 3.1 Effects of rosmarinic acid on the proliferation and differentiation of osteoblasts

In our previous study, we found that a rosemary extract (methanol extract) increased ALP activity (an early differentiation marker of osteoblasts) in MC3T3-E1 cells using our screening system. Furthermore, we compared the induction of ALP activity by two major compounds in the extract, carnosic acid, and rosmarinic acid. In this study, compared with control cells, we found that rosmarinic acid treatment caused significant induction of ALP activity (Fig. 1B–D) without affecting the proliferation of MC3T3-E1 cells. In contrast, carnosic acid had no ability to increase ALP activity (data not shown). To confirm OCN expression as a late-stage differentiation marker of osteoblasts, we determined the secreted level of OCN protein in the culture medium by ELISA, and found that it was significantly increased by rosmarinic acid treatment (Fig. 1F). To investigate the effect of rosmarinic acid on mineralization, cells were cultured for 14 days in osteogenic medium and then stained with alizarin red that specifically binds to calcium (Fig. 1E). Addition of rosmarinic acid to the cell cultures significantly enhanced bone nodule formation by osteoblasts. These results prompted us to investigate rosmarinic acid and its mechanism of action more precisely in osteoblasts.

### 3.2 Effects of rosmarinic acid on Wnt/ $\beta$ -catenin signaling in osteoblasts

Because Smad proteins play important roles downstream of bone morphogenetic protein (BMP) signaling in osteoblastic differentiation, we first examined the effects of rosmarinic acid on the Smad signaling pathway by Western blotting

(Fig. 2A). Smad1 and Smad5 are major signaling molecules that induce differentiation of C2C12 cells into osteoblasts [23, 24]. Recombinant bone morphogenetic protein 2 dramatically increased the levels of phospho-Smad1/5/8 in MC3T3-E1 cells, whereas rosmarinic acid did not show any induction of Smad protein phosphorylation. Next, to investigate the possibility of Wnt/ $\beta$ -catenin involvement in rosmarinic acid-induced osteoblastic differentiation, we examined the effects of rosmarinic acid on Wnt signaling. Wnt/ $\beta$ -catenin signaling plays an important role in the induction of bone formation [25]. Therefore, we examined the effects of rosmarinic acid on ALP expression and activity in lithium chloride (LiCl)-treated ST2 cells. LiCl is known to act as a GSK3 $\beta$  inhibitor by inducing its phosphorylation, which increases osteoblastic differentiation by enhancing  $\beta$ -catenin stability [26]. As shown in Fig. 2B, LiCl significantly increased ALP activity compared with that in control cells. Compared with the LiCl treatment control, ALP activity was increased further by rosmarinic acid synergistically and dose dependently. These findings imply that the action of rosmarinic acid may involve costimulation of the Wnt pathway induced by LiCl rather than a single effect. The stability of  $\beta$ -catenin in the cytosol is critical for controlling Wnt/ $\beta$ -catenin signaling. In the cytosol,  $\beta$ -catenin acts as a coactivator of the T-cell factor/lymphoid enhancer-binding factor (TCF/LEF) family of DNA-binding proteins to regulate Wnt-mediated target genes for osteogenesis [27, 28]. Therefore, we examined the amounts of cytoplasmic  $\beta$ -catenin (Fig. 2C). ST2 cells were treated with LiCl and rosmarinic acid for 1, 3, 6, or 9 days, followed by isolation of cytosolic protein fractions. In rosmarinic acid-treated cells, the level of  $\beta$ -catenin in the cytoplasm was increased compared with that in control cells. Moreover, the cytoplasmic  $\beta$ -catenin level was increased not only synergistically, but also by treatment with rosmarinic acid alone. To confirm the effects of rosmarinic acid on TCF/LEF-dependent gene transcription, we performed X-gal staining of primary calvarial osteoblasts from TOP-GAL transgenic mice, a reporter strain that expresses  $\beta$ -galactosidase in the presence of TCF/LEF-mediated signaling and activated  $\beta$ -catenin. The addition of rosmarinic acid increased X-gal activity in a dose-dependent manner (Fig. 2D). We also examined the effects of rosmarinic acid on  $\beta$ -catenin accumulation by immunocytochemical staining of  $\beta$ -catenin in ST2 cells.  $\beta$ -Catenin levels were increased in the cytosol and nucleus by treatment with rosmarinic acid alone for 3 days (Fig. 2E). Finally, the gene expression levels of *Wnt3a*, *Tcf4*, and *Rankl*, which are Wnt-related markers, were determined by real-time PCR. Activation of Wnt signaling downregulates RANKL expression, whereas overexpression of full-length  $\beta$ -catenin inhibits RANKL promoter activity [29]. Compared with control cells, the gene expression levels of *Wnt3a* and *Tcf4* were significantly increased while *Rankl* gene expression was significantly inhibited by treatment with rosmarinic acid (Fig. 2F). These findings suggest that the action of rosmarinic acid may involve Wnt/ $\beta$ -catenin signaling in osteogenesis through a synergistic effect as an agonist of Wnt signaling.

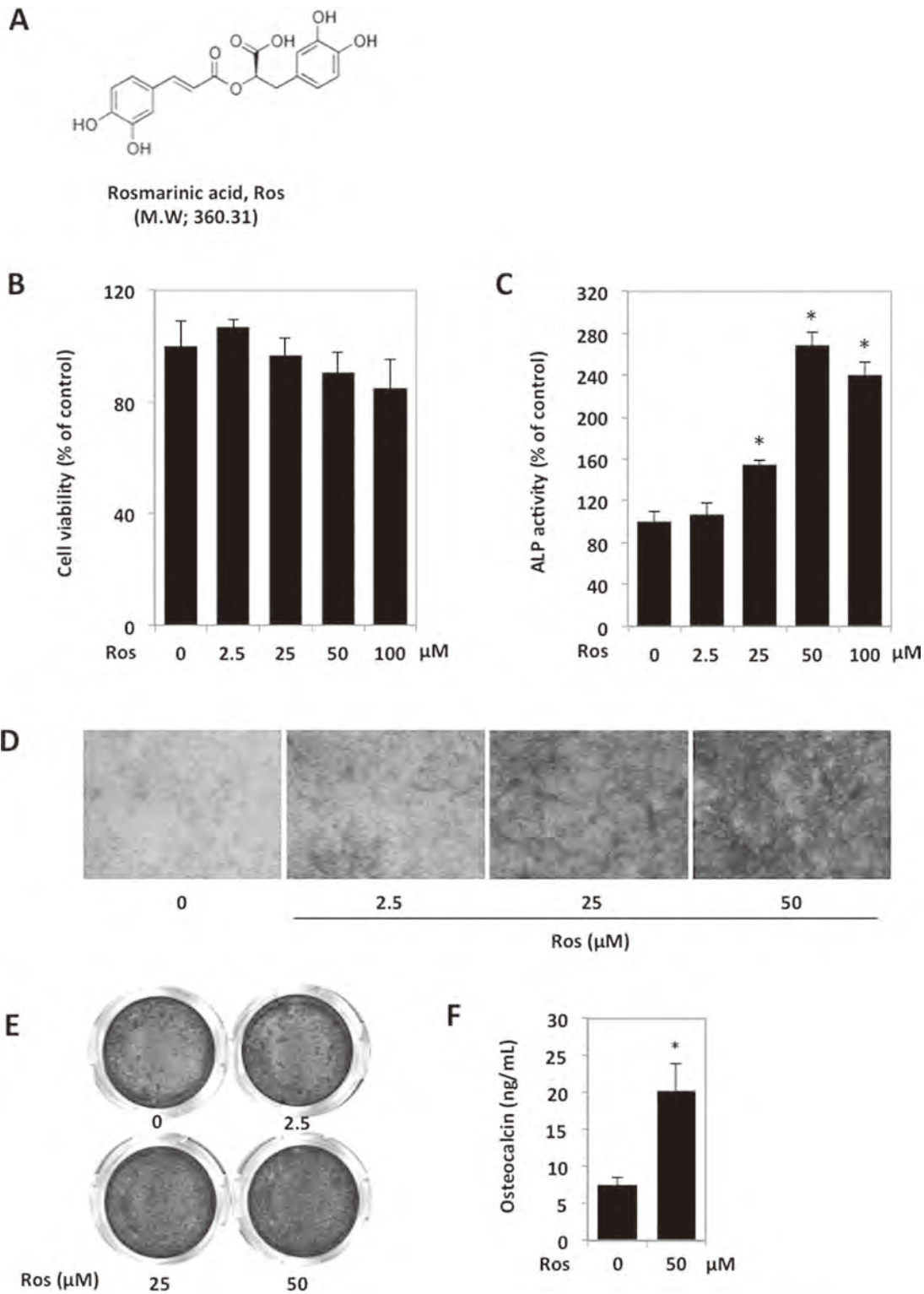


**Figure 1.** Effects of rosmarinic acid on osteoblastic differentiation. (A) Structure of rosmarinic acid. (B, C) Effects of rosmarinic acid on the proliferation and ALP activity of MC3T3-E1 cells. MC3T3-E1 cells were cultured for 4 days in osteogenic medium with various concentrations of rosmarinic acid. (D, E) Culture plates containing osteoblastic cells were subjected to ALP and alizarin red staining after 7 and 14 days of rosmarinic acid treatment, respectively. (F) OCN secreted into the culture medium was measured by ELISA before alizarin red staining. Results are expressed as the means  $\pm$  SD of three cultures. \* $p < 0.05$ .

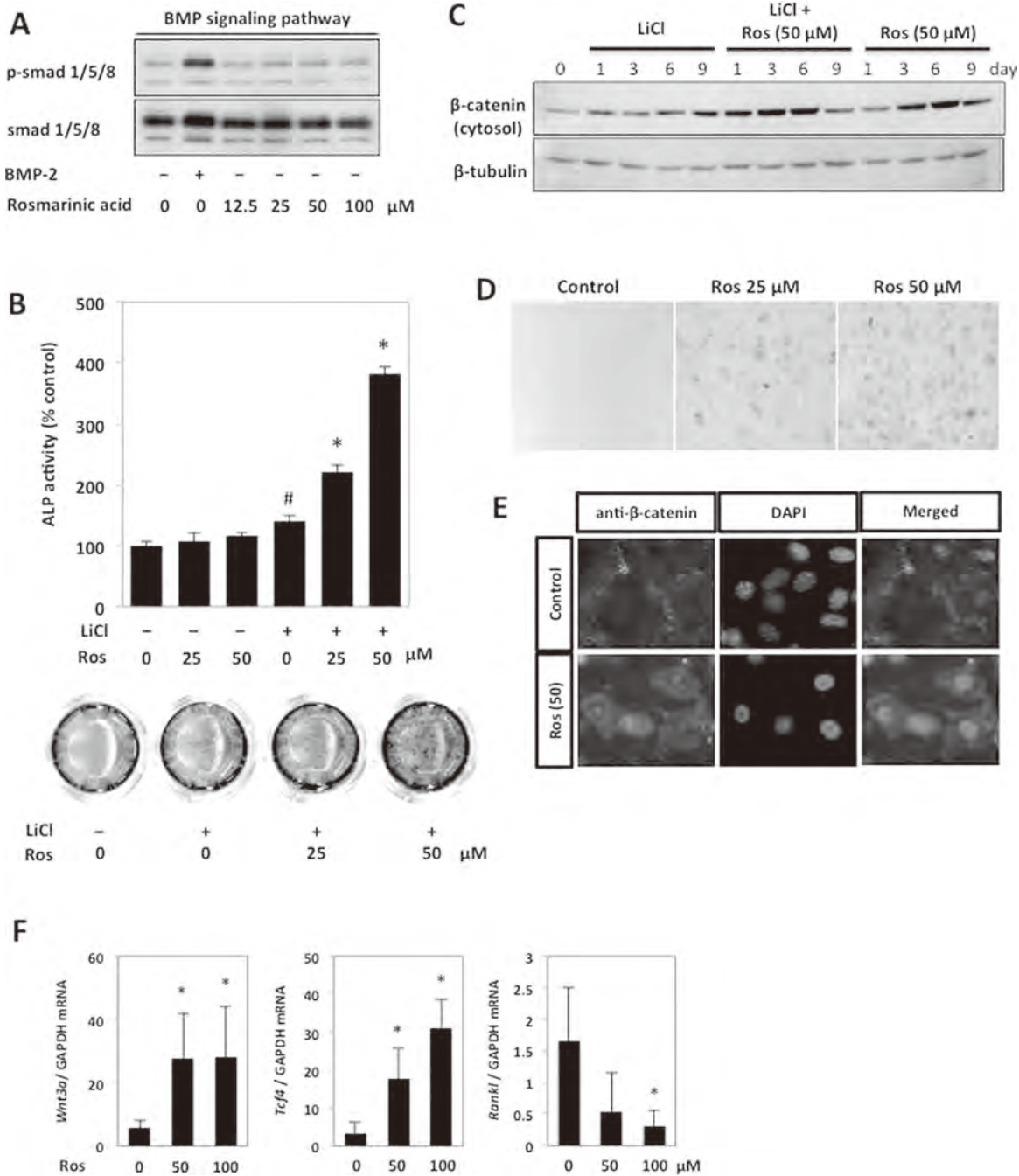


**Figure 2.** Effects of rosmarinic acid on differentiation via Wnt/β-catenin signaling. (A) The levels of phospho-Smad1/5/8 and Smad1/5/8 were determined in MC3T3-E1 cells. (B) Rosmarinic acid treatment increases ALP activity in ST2 cells treated with LiCl. ST2 cells were cultured in 48-well plates for 4 days. The results are expressed as the means ± SD of three cultures. #*p* < 0.05 for control versus LiCl. \**p* < 0.05 for LiCl versus addition of rosmarinic acid. The cells were fixed with 10% formalin and ALP activity in the presence of rosmarinic acid was determined before ALP staining. (C) Rosmarinic acid induces accumulation of cytosolic β-catenin in a dose-dependent manner. ST2 cells were treated with the vehicle or rosmarinic acid at 0, 25, and 50 μM for 1, 3, and 6 days with or without LiCl. Cytoplasmic protein fractions were isolated and subjected to Western blotting for β-catenin. (D) X-gal staining of TOP-GAL activity in calvarial osteoblast-like cells from TOP-GAL mutant mice. To detect β-galactosidase in mouse calvarial osteoblast-like cells from TOP-GAL mice, the cells were cultured in 96-well plates with rosmarinic acid for 7 days. After fixation with 10% formalin, the cells were washed twice with PBS and stained overnight in an X-gal solution at 37°C. β-Gal-positive cells were stained blue. (E) Immunocytochemical staining for β-catenin in MC3T3-E1 cells. The cells were treated with 50 μM rosmarinic acid for 24 h. (F) Real-time PCR analyses of *Wnt3a*, *Tcf4*, and *Rankl* mRNA expression levels in ST2 cells treated with rosmarinic acid for 2 days. Results are expressed as the means ± SD of three cultures. \**p* < 0.05.

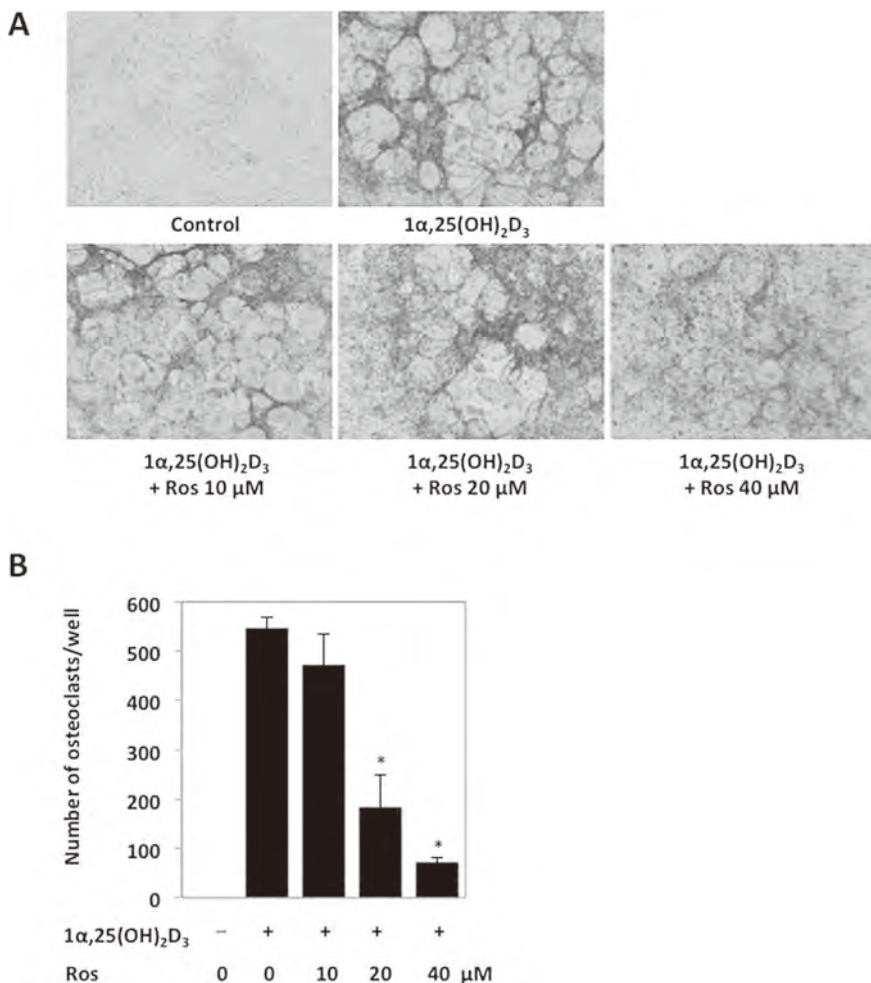


**Figure 3.** Effects of rosmarinic acid on  $1\alpha,25\text{-(OH)}_2\text{D}_3$ -induced osteoclastogenesis in cocultures. (A) Primary calvarial osteoblasts and BMCs were cocultured in 24-well plates for 5 days in the presence of  $1\alpha,25\text{-(OH)}_2\text{D}_3$  ( $1 \times 10^{-8}$  M). Subsequently, the cells were fixed with 10% formalin and stained for TRAP. (B) TRAP-positive multinucleated cells containing five or more nuclei were counted as osteoclasts. Results are expressed as the means  $\pm$  SD of three cultures. \* $p < 0.05$ .

### 3.3 Effects of rosmarinic acid on osteoclastic differentiation in the coculture system

To clarify the effects of rosmarinic acid on osteoclastogenesis, we first examined the effects of rosmarinic acid on cocultures of osteoblasts and BMCs. BMCs were cocultured with calvarial osteoblast cells in the presence of  $1\alpha,25\text{-(OH)}_2\text{D}_3$ . Many TRAP-positive osteoclasts appeared in the cocultures within 5 days in response to  $1\alpha,25\text{-(OH)}_2\text{D}_3$ . We found that rosmarinic acid dose-dependently decreased the number of osteoclasts remaining in the cultures without affecting the number of osteoblasts (Fig. 3A and B). Complete inhibition of osteoclast formation was observed in cocultures treated with rosmarinic acid at 40  $\mu\text{M}$ .

### 3.4 Effects of rosmarinic acid on RANKL-induced osteoclastic differentiation and its signaling pathway

To determine the effects of rosmarinic acid on osteoclastic differentiation of osteoclast progenitor cells in the absence

of osteoblasts, we used mouse BMMs. BMMs were cultured with rosmarinic acid in the presence of RANKL and M-CSF to differentiate into osteoclasts. The proliferation of BMMs was not significantly affected by treatment with rosmarinic acid for 24 h (Fig. 4A). As shown in Fig. 4B and C, RANKL dramatically induced osteoclastic differentiation of BMMs, whereas rosmarinic acid significantly inhibited the osteoclastic differentiation induced by RANKL in a dose-dependent manner. To elucidate the inhibitory pathway influenced by rosmarinic acid, osteoclast precursors were cotreated with rosmarinic acid and RANKL for 0–60 min. A key signaling event induced by RANKL binding to RANK is activation of MAPKs and  $\text{I}\kappa\text{B}$  signaling. The phosphorylation levels of MAPKs and  $\text{I}\kappa\text{B}$  reached maximal levels within 10 min and then returned to basal levels in response to RANKL (Fig. 4D). Phosphorylation of  $\text{I}\kappa\text{B}$  and JNK was not impaired but phosphorylation of p38 MAPK was markedly reduced by treatment with rosmarinic acid. Furthermore, we examined the effects of rosmarinic acid on c-Jun, c-Fos, and NFATc1 signaling pathways, as essential transcription factors that play critical roles in osteoclast development. Rosmarinic acid strongly impaired RANKL-stimulated expression of these transcription factors

Fig.4. Lee et al.

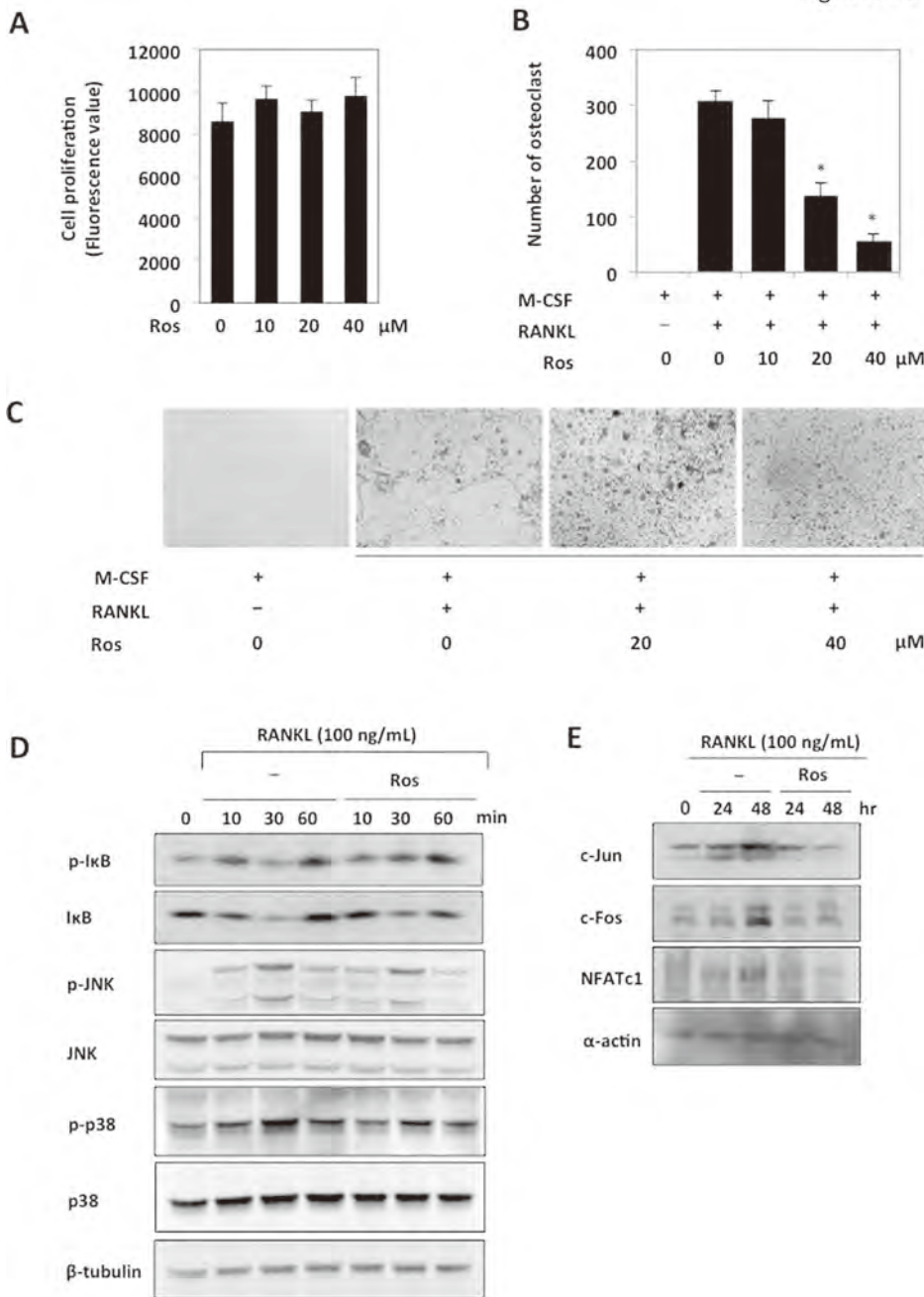


**Figure 4.** Effects of rosmarinic acid on RANKL-induced osteoclastic differentiation of mouse BMMs. (A) BMCs were cultured with rosmarinic acid for 24 h in 96-well plates. Cell proliferation was determined by the Alamar blue assay. (B, C) Mouse BMMs were cultured with 100 ng/mL RANKL and 50 ng/mL M-CSF. After culture for a further 3 days, the cells were fixed and stained for TRAP. TRAP-positive multinucleated cells containing five or more nuclei were counted as osteoclasts. Results are expressed as the means ± SD of three cultures. \**p* < 0.05. (D) BMMs were treated with rosmarinic acid and RANKL for the indicated time periods, and then phosphorylation levels of I-κB, JNK, and p38 MAPK were assessed. (E) BMMs were treated with or without rosmarinic acid and stimulated with 100 ng/mL RANKL for 24 and 48 h. The effects of rosmarinic acid on the expression levels of c-Jun, c-Fos, and NFATc1 during osteoclastogenesis were determined by Western blot analysis.

(Fig. 4E). Collectively, these findings suggest that rosmarinic acid directly acts on osteoclast precursors and subsequently inhibits osteoclastic differentiation.

### 3.5 Effects of rosmarinic acid on the function of mature osteoclasts

To investigate the function of osteoclasts, we examined the effects of rosmarinic acid on bone resorption by mature osteo-

clasts differentiated in the mouse coculture system by  $1\alpha,25\text{-(OH)}_2\text{D}_3$  and prostaglandin  $\text{E}_2$ . Mature osteoclasts formed in cocultures with BMCs, and calvarial osteoblasts readily created resorption pits on dentin sections (Fig. 5A). Risedronate is a bisphosphonate [30] that is known to disrupt osteoclast activation. Although mature osteoclasts treated with  $1\ \mu\text{M}$  risedronate were found on dentin sections, which positively stained for TRAP activity, their typical round shape was shrunken and they concomitantly failed to resorb bone because of a disturbed sealing zone. Rosmarinic acid failed

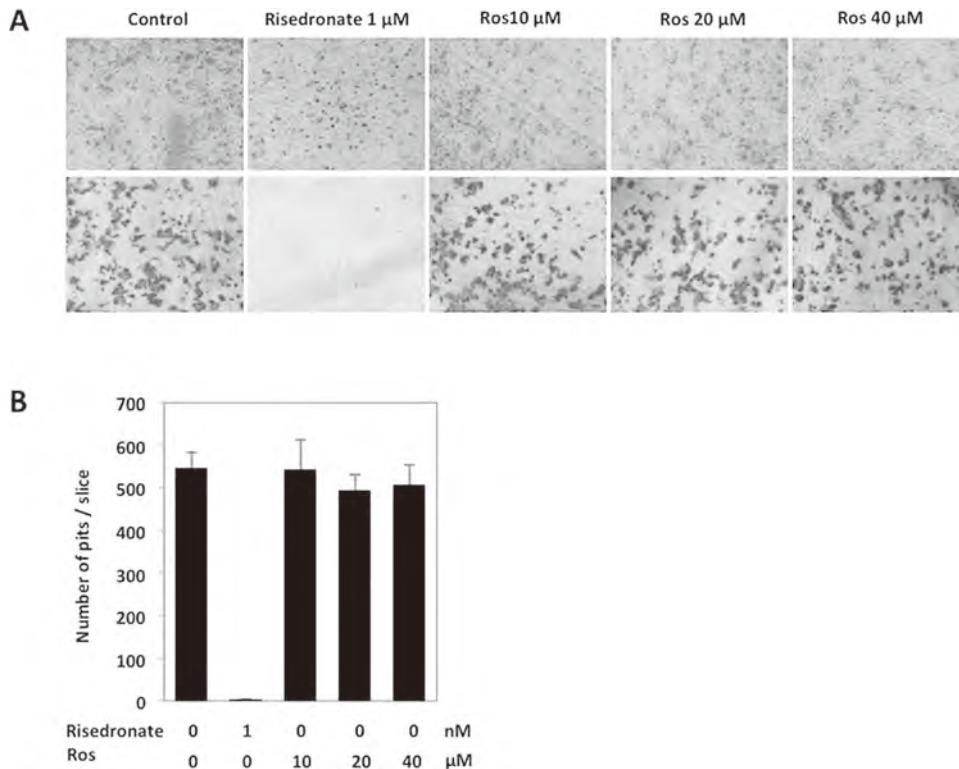


**Figure 5.** Effects of rosmarinic acid on bone resorption. Mature osteoclasts on dentin sections were treated with various concentrations of rosmarinic acid. (A) After 48 h, the cells were left on the dentin sections and stained for TRAP (upper panels). Subsequently, the cells were removed and the dentin sections were stained with Mayer's hematoxylin to identify resorption pits (lower panels). (B) The numbers of resorption pits were counted. Results are expressed as the means ± SD of three cultures.

to inhibit the pit formation on the dentin sections at all examined doses without affecting mature osteoclasts on the dentin (Fig. 5B). Taken together, these findings indicate that rosmarinic acid impairs osteoclastic differentiation of osteoclast precursors through the p38 MAPK pathway, but has no effect on the function of mature osteoclasts, suggesting a different pathway from that of bisphosphonates.

### 3.6 Effects of rosmarinic acid on the sRANKL-induced mouse model of bone loss

To ascertain the biological potency *in vivo*, we examined the effects of rosmarinic acid using an sRANKL-induced bone loss mouse model (Supporting Information Fig. 2). Overall, the groups showed no significant differences in their body weights (data not shown). Marked increases in femoral trabecular 3D images obtained by  $\mu$ CT in the rosmarinic acid-injected group were distinguishable from those observed in the control group (Fig. 6A). In terms of osteoclast activity, PTH-injected mice exhibited significant increases in serum TRAP5b levels and the number of osteoclasts (Fig. 6B). However, rosmarinic acid-treated mice showed no significant differences compared with control mice. Furthermore, serum levels of OCN, a marker of bone mineralization, were significantly increased in rosmarinic acid-treated mice as well as PTH-treated mice. These results were consistent with the histological results of staining for TRAP and ALP activity (Supporting Information Fig. 3). Injection of sRANKL significantly decreased the total BMD and trabecular BMD (Tb.

BMD; Fig. 6C), and administration of PTH significantly increased the total and Tb. BMDs. Administration of high-dose rosmarinic acid also significantly increased the Tb. BMD in RANKL-induced bone loss, but had a lower effect than PTH. On the other hand, no differences were observed in the cortical BMD, even in RANKL- and PTH-injected groups. Although the cortical BMNC was not significantly changed, the total BMNC, trabecular BMNC, and cortical bone inner length were improved by administration of high-dose rosmarinic acid. In addition, the Y-axis strength-strain index was significantly increased by high-dose rosmarinic acid administration. These findings suggest that, similar to PTH, rosmarinic acid has the potential to affect bone-remodeling activity by stimulation of bone turnover via upregulation of osteoblast activity while sustaining osteoclast activity *in vivo*.

## 4 Discussion

To identify natural compounds with anabolic effects that regulate bone metabolism, we first investigated effects on induction of osteoblastic differentiation. We found that a treatment with a crude extract of rosemary resulted in significant induction of ALP activity in MC3T3-E1 cells compared with that in control cells as well as dose-dependent increases in cell proliferation (Supporting Information Fig. 1). It is known that rosemary powder and essential oil inhibit bone resorption in the aged ovariectomized rat model [31]. To identify the responsible compounds as possible therapeutic targets, we investigated the major compounds in rosemary extracts, rosmarinic

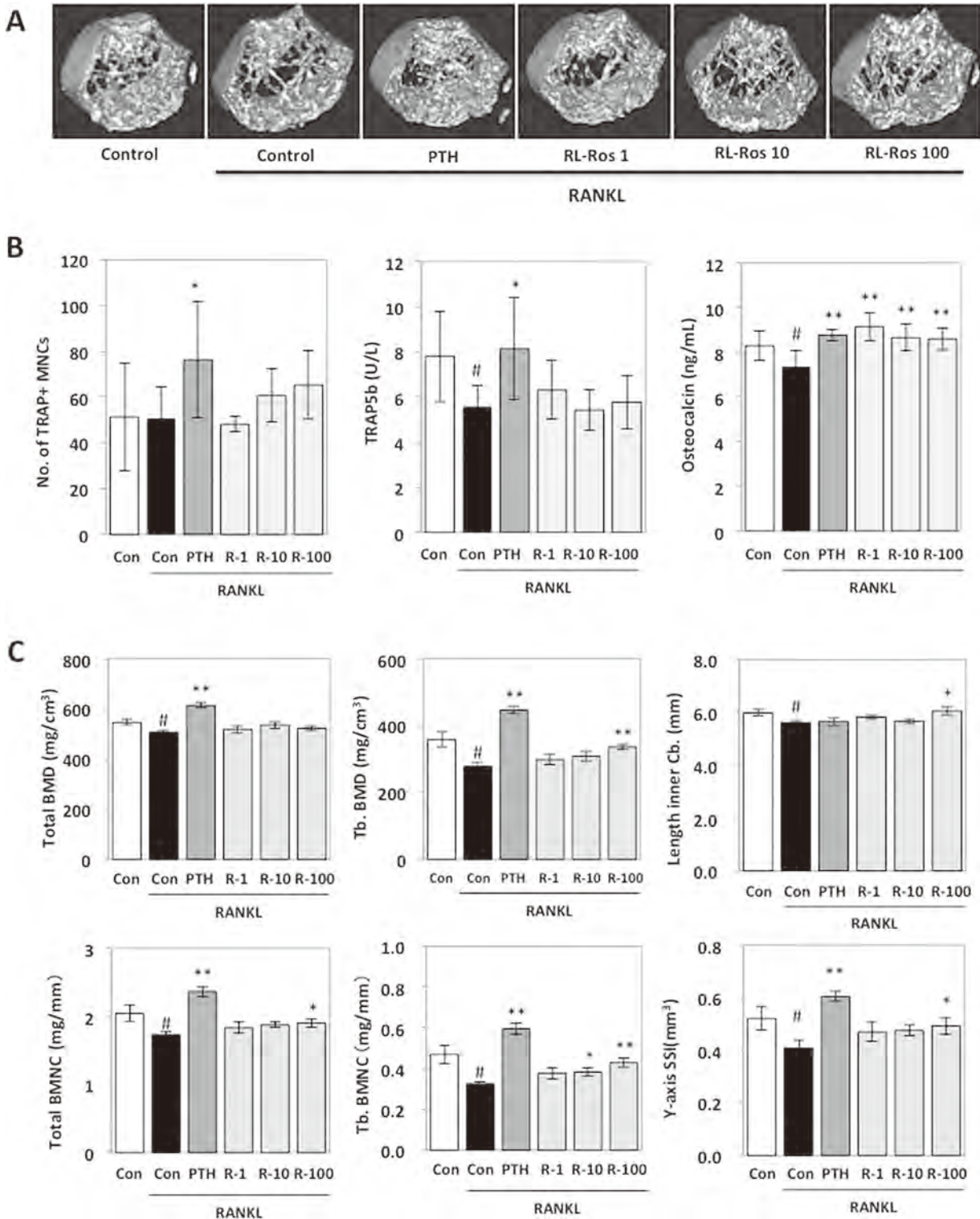


**Figure 6.** Effects of rosmarinic acid evaluated in a mouse model of RANKL-induced bone loss. (A) Morphometric analysis of 3D  $\mu$ CT data. Three-dimensional images of the distal femoral metaphysis were reconstructed by  $\mu$ CT analysis of the growth plate from the right femur distal metaphysis. (B) Number of osteoclasts and serum biochemical analyses. Serum levels of TRAP5b and osteocalcin (OCN) are shown. (C) Tomographic measurements of BMD, BMNC, and bone strength were performed by peripheral quantitative computed tomography. Image analysis was carried out using integrated XCT 2000 software. Data are expressed as the means  $\pm$  SD of three cultures. # $p < 0.05$  for vehicle versus RANKL group; \* $p < 0.05$  and \*\* $p < 0.001$  for RANKL control versus rosmarinic acid administration.

acid and carnosic acid, as a phenolic acid and diterpene, respectively. We found that rosmarinic acid caused significant induction of ALP activity, whereas carnosic acid had no such effect. Therefore, we focused on rosmarinic acid as a potential therapeutic compound to clarify its mechanism of action based on osteoblastic differentiation and mineralization.

To verify the effects of rosmarinic acid on osteogenesis, we first investigated the possible involvement of the BMP signaling pathway. This pathway is important for osteoblastic differentiation and has been studied extensively. BMPs promote commitment of multipotent mesenchymal stem cells to the osteoblast lineage by regulating signals that stimulate specific transcriptional programs required for bone formation during embryonic skeletal development and postnatal bone remodeling [32, 33]. Signal transduction studies have revealed that Smad1, 5, and 8 are the immediate downstream molecules of BMP receptors and play central roles in BMP signal transduction [32]. However, in our study, addition of rosmarinic acid did not affect the levels of Smad protein phosphorylation, as the main pathway of the BMP cascade, whereas bone morphogenetic protein 2 significantly increased the levels of Smad1/5/8 phosphorylation. These results suggest that rosmarinic acid is not involved in BMP-induced osteoblastic differentiation.

The Wnt/ $\beta$ -catenin signaling pathway plays critical roles in osteoblastic cell differentiation and bone formation. Mutations in Wnt receptors that cause alterations in Wnt signaling result in profound changes in bone mass. In bone cells, Wnt signals through the canonical Wnt/ $\beta$ -catenin signaling pathway [34]. This pathway is initiated upon binding of Wnt ligands to seven transmembrane receptors of the Frizzled family and representatives of the single-pass LDL receptor-related protein family (LRP5/6). Wnt, Frizzled, and LRP5/6 form a ternary complex that initiates a cascade of molecular interactions leading to stabilization of  $\beta$ -catenin. Subsequently,  $\beta$ -catenin enters the nucleus where it associates with TCF/LEF to regulate gene transcription [35, 36].

Many small compounds have been suggested to have regulatory effects through the Wnt pathway [37–41], such as controlling cell proliferation via the modulatory effects of Wnt signaling at transcriptional levels. In particular, baicalin induces an osteogenic effect in rat primary osteoblasts by activation of the Wnt pathway, resulting in phosphorylation of GSK3 $\beta$  and induction of nuclear accumulation of  $\beta$ -catenin. Furthermore, Lee et al. [42] reported that baicalin and isorhamnetin act on human adipose tissue-derived stem cells. These effects are also mediated through activation of the Wnt pathway that inhibits the differentiation of adipose stem cells into adipocytes. It is intriguing that individual effects of small compounds have been found in specific cell lines rather than all cell types.

In the case of rosmarinic acid, Yang et al. [43, 44] reported a relationship between Wnt signaling and rosmarinic acid. They demonstrated that rosmarinic acid acts on liver fibrosis by *Ppar $\gamma$*  derepression mediated by suppression of canonical Wnt signaling in hepatic stellate cells. Bone marrow-derived

mesenchymal stem cells can differentiate into various cell types of mesenchymal origin. Osteoblasts and adipocytes differentiate from common pleiotropic mesenchymal stem cells under the transcriptional control by numerous factors and multiple intracellular signaling pathways. Consistent with this process, cell fate determinations are regulated by various signaling pathways. Our results indicated that rosmarinic acid might affect the Wnt-mediated pathway depending on the cell type. Thus, we first considered the possibility that rosmarinic acid induces osteogenesis depending on Wnt/ $\beta$ -catenin signaling in a LiCl-dependent manner. This notion was supported by rosmarinic acid treatment resulting in: (i) induction of LiCl-mediated ALP activity in ST2 cells, (ii) increased stabilization of  $\beta$ -catenin and nuclear translocation, (iii) increased LacZ expression in calvarial osteoblasts from TOP-GAL transgenic mice, and (iv) responses of specific target genes of Wnt/ $\beta$ -catenin signaling. Taken together, these results suggest that rosmarinic acid activates the Wnt/ $\beta$ -catenin signaling cascade to promote osteoblastic differentiation.

Osteoclasts originate from hematopoietic precursor cells of the phagocyte lineage and differentiate into multinucleated cells by fusion of mononuclear progenitors [45]. Mature osteoclasts resorb bone and mediate excessive bone loss in several bone disorders, including osteoporosis, arthritis, periodontitis, bone metastasis, and corticosteroid-induced bone loss [46, 47]. Osteoclasts can be induced to differentiate by three osteoblast-derived cytokines essential for osteoclastic differentiation, namely RANKL, M-CSF, and OPG, which is currently recognized as a decoy receptor for RANKL-RANK interactions. We found that osteoclasts were formed in response to these factors. Although RT-PCR analyses showed that rosmarinic acid did not affect  $1\alpha,25\text{-(OH)}_2\text{D}_3$ -induced mRNA expression levels of RANKL, OPG, and M-CSF in osteoblasts (data not shown), addition of rosmarinic acid to cocultures of mouse BMCs and primary osteoblasts with  $1 \times 10^{-8}$  M  $1\alpha,25\text{-(OH)}_2\text{D}_3$  caused significant inhibition of osteoclastogenesis. In addition, rosmarinic acid inhibited the osteoclastic differentiation of BMMs induced by RANKL. These results support the validity of our coculture data indicating that rosmarinic acid directly acts on osteoclast precursors.

MAPK family members are divided into three groups: ERK, JNK, and p38 MAPK groups. Phosphorylation of p38 MAPK by MAPK kinase (MKK) 3/6 results in its activation. A previous study has shown that the expression of dominant-negative forms of p38 MAPK and MKK6 in RAW264 cells inhibits RANKL-induced differentiation of these cells into osteoclasts [48]. Furthermore, p38 MAPK-mediated signals are required for osteoclastic differentiation but not osteoclast functions [49]. Similar to RANKL, tumor necrosis factor- $\alpha$  (TNF- $\alpha$ ) has been shown to stimulate osteoclastic differentiation of monocyte/macrophage lineage cells including BMMs. TNF- $\alpha$ -induced osteoclastic differentiation of BMMs is strongly inhibited by SB203580, a specific inhibitor of p38 MAPK [50, 51]. Thus, the p38 MAPK pathway plays crucial roles not only in RANKL-mediated osteoclast differentiation,

but also in TNF- $\alpha$ -mediated osteoclastic differentiation. Some reports show that rosmarinic acid reduces the phosphorylation of p38 MAPK in normal endothelial cells and neuronal cells [52, 53]. Hsu et al. [54] reported that rosmarinic acid strongly inhibits phosphorylation of RANKL-induced p38 MAPK as well as ERK and JNK signals in BMMs. Moreover, DC-STAMP and  $\beta$ 3 integrin mRNA expression is significantly inhibited by rosmarinic acid, implying disturbance of osteoclast fusion for maturation and attachment to the bone surface, respectively. Concomitantly, RANKL-induced osteoclastic differentiation and functions are inhibited in response to rosmarinic acid. Consistently, our results showed that rosmarinic acid suppressed RANKL-induced phosphorylation of p38 MAPK, although it did not affect I- $\kappa$ B or JNK activity in the present study. However, compared with other reports, we did not exclude effects of the treatment concentration of rosmarinic acid. Although 10–40  $\mu$ M rosmarinic acid had no effect on either dentin-resorption activity or the pit number in dentin sections with mature osteoclasts, another study [54] reported that 60–120  $\mu$ M rosmarinic acid has an inhibitory effect on the bone-resorbing activity of mature osteoclasts in a pit formation assay. This finding indicates that a high concentration of rosmarinic acid might have potent effects to inhibit mature osteoclasts. It has been shown that c-Fos induces NFATc1 expression and that c-Fos and NFATc1 cooperatively regulate osteoclastogenesis in response to RANKL treatment. As a master transcription factor, NFATc1 has been shown to play a critical role in the differentiation of osteoclasts induced by RANKL [55, 56]. Furthermore, our data demonstrated that rosmarinic acid significantly suppressed not only RANKL-induced c-Fos, but also NFATc1. Thus, we suggest that inhibition of RANKL-induced c-Fos expression by rosmarinic acid treatment is a relevant factor in the suppression of downstream NFATc1 signaling pathways. Moreover, osteoclastic differentiation induced by TNF- $\alpha$  and M-CSF was inhibited by addition of a p38 MAPK inhibitor. p38 MAPK is phosphorylated in BMMs in response to RANKL, but not in mature osteoclasts [57]. These results indicated that the p38 MAPK inhibitor acted directly on osteoclast precursors to inhibit osteoclastic differentiation. Taken together, these findings raise the possibility that rosmarinic acid inhibits osteoclastic differentiation through inhibition of RANKL-induced NFATc1 expression via regulation of p38 MAPK phosphorylation.

Low-calcium diet, denervation, tail suspension, and ovariectomized rats have been recognized as standard models for osteoporosis [58–61]. In this study, we performed *in vivo* experiments using an sRANKL-induced bone loss model. This model undergoes rapid bone loss by injections of sRANKL in a procedure that is completed within 50 h [17]. The rapid decrease in the BMD of this model appears to be caused not only by stimulation of the terminal differentiation of osteoclast progenitors, but also by activation of the preexisting pool of osteoclasts. In this model, the increased ALP level was accompanied by an increased TRACP5b level, suggesting that the elevated osteoclastic differentiation and activation initiated stimulation of bone formation. From 50 h to 4 weeks

after sRANKL injection, mild bone formation proceeds. In our study, treatment with sRANKL markedly decreased all examined markers including total BMD, BMNC, and 3D  $\mu$ CT images, indicating that the model was established successfully. We tested this model by evaluation with PTH, a potent anabolic agent for bone remodeling. PTH treatment dramatically increased the total BMD and BMC compared with those in the control group. Orally administered rosmarinic acid at its highest dose (100 mg/kg) also increased all markers, and the 3D  $\mu$ CT images confirmed the results of peripheral quantitative computed tomography analyses. Although rosmarinic acid treatment did not lead to any significant difference in the total BMD, it increased the tb. BMD, trabecular BMC, and cortical bone inner length, revealing anabolic effects that would be useful for pharmaceutical application. We also found inhibitory effects of rosmarinic acid on the differentiation, but not function, of osteoclasts as well as effects on osteoblastic differentiation by *in vitro* assays. In comparison with these *in vitro* activities, the *in vivo* results (serum levels of TRAP5b and OCN) support the notion that the induction of bone formation by rosmarinic acid occurs as a direct anabolic effect on osteoblastic differentiation. Furthermore, rosmarinic acid had direct inhibitory effects on osteoclastogenesis affected by osteoclast precursors, but no effects on bone resorption by mature osteoclasts. However, the precise mechanisms of rosmarinic acid in the prevention of bone loss or induction of bone formation *in vitro* and *in vivo* remain under investigation.

Pharmacological treatments for osteoporosis can be divided into two categories: anabolic agents that stimulate osteoblastic differentiation and antiresorptive agents that inhibit osteoclastic differentiation and bone resorption. In our screening experiments to identify an agent with these dual functions in bone metabolism, we found that rosmarinic acid had at least two functions: osteogenic properties via promotion of Wnt/ $\beta$ -catenin signaling and antiosteoclastogenic properties via suppression of p38 MAPK-mediated differentiation signaling. These dual functions of rosmarinic acid may serve a milestone in the development of multitargeted drugs for osteoporosis. Because rosmarinic acid only constitutes 19.3–58.5 mg/g of dried rosemary [62], habitual consumption of rosemary may not exert an antiosteoporotic effect. However, if rosmarinic acid is taken as a dietary supplement, it may be worthy of consideration as a new pharmacological agent, which may contribute to justification of its clinical application to prevent bone metabolic diseases.

*We thank Dr. Hisataka Yasuda (Oriental Yeast) for generously providing the sRANKL. The authors also thank Dr. Ota Masato (Tokyo Medical and Dental University) for kindly supplying the transgenic TOP-GAL mice. This work was performed at a laboratory supported by an endowment from Erina Co. Inc. and the MEXT-supported Program for the Strategic Research Foundation at Private Universities (Japan). This work was carried out with the support of the Japan Society for the Promotion of Science Post-Doc fellowship received by Dr. J.-W Lee for carrying out*

research activities at Prof. Yamaguchi's Laboratory at the Tokyo Medical and Dental University, Tokyo, Japan.

Potential conflict of interest statement: The work was performed in a laboratory partially supported by Erina Co. Inc.

## 5 References

- [1] Ryoo, H. M., Lee, M. H., Kim, Y. J., Critical molecular switches involved in BMP-2-induced osteogenic differentiation of mesenchymal cells. *Gene* 2006, *366*, 51–57.
- [2] Kwan Tat, S., Padrines, M., Theoleyre, S., Heymann, D. et al., IL-6, RANKL, TNF-alpha/IL-1: interrelations in bone resorption pathophysiology. *Cytokine Growth Factor Rev.* 2004, *15*, 49–60.
- [3] Canalis, E., The fate of circulating osteoblasts. *N. Engl. J. Med.* 2005, *352*, 2014–2016.
- [4] Canalis, E., Update in new anabolic therapies for osteoporosis. *J. Clin. Endocrinol. Metab.* 2010, *95*, 1496–1504.
- [5] Gruber, H. E., Ivey, J. L., Baylink, D. J., Matthews, M. et al., Long-term calcitonin therapy in postmenopausal osteoporosis. *Metabolism* 1984, *33*, 295–303.
- [6] Genant, H. K., Baylink, D. J., Gallagher, J. C., Estrogens in the prevention of osteoporosis in postmenopausal women. *Am. J. Obstet. Gynecol.* 1989, *161*, 1842–1846.
- [7] Turner, C. H., Toward a cure for osteoporosis: reversal of excessive bone fragility. *Osteoporos. Int.* 1991, *2*, 12–19.
- [8] Rodan, G. A., Martin, T. J., Therapeutic approaches to bone diseases. *Science* 2000, *289*, 1508–1514.
- [9] Phillipson, J. D., Anderson, L. A., Ethnopharmacology and Western medicine. *J. Ethnopharmacol.* 1989, *25*, 61–72.
- [10] al-Sereiti, M. R., Abu-Amer, K. M., Sen, P., Pharmacology of rosemary (*Rosmarinus officinalis* Linn.) and its therapeutic potentials. *Indian J. Exp. Biol.* 1999, *37*, 124–130.
- [11] Kelm, M. A., Nair, M. G., Strasburg, G. M., DeWitt, D. L., Antioxidant and cyclooxygenase inhibitory phenolic compounds from *Ocimum sanctum* Linn. *Phytomedicine* 2000, *7*, 7–13.
- [12] Petersen, M., Simmonds, M. S., Rosmarinic acid. *Phytochemistry* 2003, *62*, 121–125.
- [13] Yang, E. J., Ku, S. K., Lee, W., Lee, S. et al., Barrier protective effects of rosmarinic acid on HMGB1-induced inflammatory responses in vitro and in vivo. *J. Cell. Physiol.* 2012, *228*, 975–982.
- [14] Yun, S. Y., Hur, Y. G., Kang, M. A., Lee, J. et al., Synergistic immunosuppressive effects of rosmarinic acid and rapamycin in vitro and in vivo. *Transplantation* 2003, *75*, 1758–1760.
- [15] Xu, Y., Jiang, Z., Ji, G., Liu, J., Inhibition of bone metastasis from breast carcinoma by rosmarinic acid. *Planta Med.* 2010, *76*, 956–962.
- [16] Lee, J. W., Kobayashi, Y., Nakamichi, Y., Udagawa, N. et al., Alisol-B, a novel phyto-steroid, suppresses the RANKL-induced osteoclast formation and prevents bone loss in mice. *Biochem. Pharmacol.* 2010, *80*, 352–361.
- [17] Tomimori, Y., Mori, K., Koide, M., Nakamichi, Y. et al., Evaluation of pharmaceuticals with a novel 50-hour animal model of bone loss. *J. Bone Miner. Res.* 2009, *24*, 1194–1205.
- [18] Baba, S., Osakabe, N., Natsume, M., Terao, J., Orally administered rosmarinic acid is present as the conjugated and/or methylated forms in plasma, and is degraded and metabolized to conjugated forms of caffeic acid, ferulic acid and m-coumaric acid. *Life Sci.* 2004, *75*, 165–178.
- [19] De Oliveira, N. C., Sarmiento, M. S., Nunes, E. A., Porto, C. M. et al., Rosmarinic acid as a protective agent against genotoxicity of ethanol in mice. *Food Chem. Toxicol.* 2012, *50*, 1208–1214.
- [20] Chu, X., Ci, X., He, J., Jiang, L. et al., Effects of a natural prolyl oligopeptidase inhibitor, rosmarinic acid, on lipopolysaccharide-induced acute lung injury in mice. *Molecules* 2012, *17*, 3586–3598.
- [21] Jang, A. H., Kim, T. H., Kim, G. D., Kim, J. E. et al., Rosmarinic acid attenuates 2,4-dinitrofluorobenzene-induced atopic dermatitis in NC/Nga mice. *Int. Immunopharmacol.* 2011, *11*, 1271–1277.
- [22] Lucarini, R., Bernardes, W. A., Ferreira, D. S., Tozatti, M. G. et al., In vivo analgesic and anti-inflammatory activities of *Rosmarinus officinalis* aqueous extracts, rosmarinic acid and its acetyl ester derivative. *Pharm. Biol.* 2013, *51*, 1087–1090.
- [23] Fujii, M., Takeda, K., Imamura, T., Aoki, H. et al., Roles of bone morphogenetic protein type I receptors and Smad proteins in osteoblast and chondroblast differentiation. *Mol. Biol. Cell* 1999, *10*, 3801–3813.
- [24] ten Dijke, P., Korchynskyi, O., Valdimarsdottir, G., Goumans, M. J., Controlling cell fate by bone morphogenetic protein receptors. *Mol. Cell. Endocrinol.* 2003, *211*, 105–113.
- [25] Day, T. F., Guo, X., Garrett-Beal, L., Yang, Y., Wnt/beta-catenin signaling in mesenchymal progenitors controls osteoblast and chondrocyte differentiation during vertebrate skeletogenesis. *Dev. Cell* 2005, *8*, 739–750.
- [26] Li, J., Khavandgar, Z., Lin, S. H., Murshed, M., Lithium chloride attenuates BMP-2 signaling and inhibits osteogenic differentiation through a novel WNT/GSK3- independent mechanism. *Bone* 2011, *48*, 321–331.
- [27] Logan, C. Y., Nusse, R., The Wnt signaling pathway in development and disease. *Annu. Rev. Cell Dev. Biol.* 2004, *20*, 781–810.
- [28] Miller, L. D., Park, K. S., Guo, Q. M., Alkharouf, N. W. et al., Silencing of Wnt signaling and activation of multiple metabolic pathways in response to thyroid hormone-stimulated cell proliferation. *Mol. Cell. Biol.* 2001, *21*, 6626–6639.
- [29] Spencer, G. J., Utting, J. C., Etheridge, S. L., Arnett, T. R. et al., Wnt signalling in osteoblasts regulates expression of the receptor activator of NFkappa B ligand and inhibits osteoclastogenesis in vitro. *J. Cell Sci.* 2006, *119*, 1283–1296.
- [30] Russell, R. G., Bisphosphonates: the first 40 years. *Bone* 2011, *49*, 2–19.
- [31] Muhlbauer, R. C., Lozano, A., Palacio, S., Reinli, A. et al., Common herbs, essential oils, and monoterpenes potentially modulate bone metabolism. *Bone* 2003, *32*, 372–380.
- [32] Chen, D., Zhao, M., Mundy, G. R., Bone morphogenetic proteins. *Growth Factors* 2004, *22*, 233–241.

- [33] Wozney, J. M., Rosen, V., Celeste, A. J., Mitscock, L. M. et al., Novel regulators of bone formation: molecular clones and activities. *Science* 1988, 242, 1528–1534.
- [34] Westendorf, J. J., Kahler, R. A., Schroeder, T. M., Wnt signaling in osteoblasts and bone diseases. *Gene* 2004, 341, 19–39.
- [35] Almeida, M., Han, L., Bellido, T., Manolagas, S. C. et al., Wnt proteins prevent apoptosis of both uncommitted osteoblast progenitors and differentiated osteoblasts by beta-catenin-dependent and -independent signaling cascades involving Src/ERK and phosphatidylinositol 3-kinase/AKT. *J. Biol. Chem.* 2005, 280, 41342–41351.
- [36] Tu, X., Joeng, K. S., Nakayama, K. I., Nakayama, K. et al., Noncanonical Wnt signaling through G protein-linked PKCdelta activation promotes bone formation. *Dev. Cell* 2007, 12, 113–127.
- [37] Syed, D. N., Afaq, F., Maddodi, N., Johnson, J. J. et al., Inhibition of human melanoma cell growth by the dietary flavonoid fisetin is associated with disruption of Wnt/beta-catenin signaling and decreased Mitf levels. *J. Invest. Dermatol.* 2011, 131, 1291–1299.
- [38] Song, D. H., Sussman, D. J., Seldin, D. C., Endogenous protein kinase CK2 participates in Wnt signaling in mammary epithelial cells. *J. Biol. Chem.* 2000, 275, 23790–23797.
- [39] Kim, J., Zhang, X., Rieger-Christ, K. M., Summerhayes, I. C. et al., Suppression of Wnt signaling by the green tea compound (-)-epigallocatechin 3-gallate (EGCG) in invasive breast cancer cells. Requirement of the transcriptional repressor HBP1. *J. Biol. Chem.* 2006, 281, 10865–10875.
- [40] Dashwood, W. M., Orner, G. A., Dashwood, R. H., Inhibition of beta-catenin/Tcf activity by white tea, green tea, and epigallocatechin-3-gallate (EGCG): minor contribution of H(2)O(2) at physiologically relevant EGCG concentrations. *Biochem. Biophys. Res. Commun.* 2002, 296, 584–588.
- [41] Amado, N. G., Cerqueira, D. M., Menezes, F. S., da Silva, J. F. et al., Isoquercitrin isolated from *Hyptis fasciculata* reduces glioblastoma cell proliferation and changes beta-catenin cellular localization. *Anticancer Drugs* 2009, 20, 543–552.
- [42] Lee, H., Bae, S., Kim, K., Kim, W. et al., Beta-Catenin mediates the anti-adipogenic effect of baicalin. *Biochem. Biophys. Res. Commun.* 2010, 398, 741–746.
- [43] Yang, M. D., Chiang, Y. M., Higashiyama, R., Asahina, K. et al., Rosmarinic acid and baicalin epigenetically derepress peroxisomal proliferator-activated receptor gamma in hepatic stellate cells for their antifibrotic effect. *Hepatology* 2012, 55, 1271–1281.
- [44] Miyahara, T., Schrum, L., Rippe, R., Xiong, S. et al., Peroxisome proliferator-activated receptors and hepatic stellate cell activation. *J. Biol. Chem.* 2000, 275, 35715–35722.
- [45] Suda, T., Nakamura, I., Jimi, E., Takahashi, N., Regulation of osteoclast function. *J. Bone Miner. Res.* 1997, 12, 869–879.
- [46] Boyle, W. J., Simonet, W. S., Lacey, D. L., Osteoclast differentiation and activation. *Nature* 2003, 423, 337–342.
- [47] Chambers, T. J., Regulation of the differentiation and function of osteoclasts. *J. Pathol.* 2000, 192, 4–13.
- [48] Matsumoto, M., Sudo, T., Saito, T., Osada, H. et al., Involvement of p38 mitogen-activated protein kinase signaling pathway in osteoclastogenesis mediated by receptor activator of NF-kappa B ligand (RANKL). *J. Biol. Chem.* 2000, 275, 31155–31161.
- [49] Li, X., Udagawa, N., Takami, M., Sato, N. et al., p38 Mitogen-activated protein kinase is crucially involved in osteoclast differentiation but not in cytokine production, phagocytosis, or dendritic cell differentiation of bone marrow macrophages. *Endocrinology* 2003, 144, 4999–5005.
- [50] Azuma, Y., Kaji, K., Katogi, R., Takeshita, S. et al., Tumor necrosis factor-alpha induces differentiation of and bone resorption by osteoclasts. *J. Biol. Chem.* 2000, 275, 4858–4864.
- [51] Kobayashi, K., Takahashi, N., Jimi, E., Udagawa, N. et al., Tumor necrosis factor alpha stimulates osteoclast differentiation by a mechanism independent of the ODF/RANKL-RANK interaction. *J. Exp. Med.* 2000, 191, 275–286.
- [52] Iuvone, T., De Filippis, D., Esposito, G., D'Amico, A. et al., The spice sage and its active ingredient rosmarinic acid protect PC12 cells from amyloid-beta peptide-induced neurotoxicity. *J. Pharmacol. Exp. Ther.* 2006, 317, 1143–1149.
- [53] Ku, S. K., Yang, E. J., Song, K. S., Bae, J. S., Rosmarinic acid down-regulates endothelial protein C receptor shedding in vitro and in vivo. *Food Chem. Toxicol.* 2013, 59, 311–315.
- [54] Hsu, Y. C., Cheng, C. P., Chang, D. M., *Plectranthus amboinicus* attenuates inflammatory bone erosion in mice with collagen-induced arthritis by downregulation of RANKL-induced NFATc1 expression. *J. Rheumatol.* 2011, 38, 1844–1857.
- [55] Ishida, N., Hayashi, K., Hoshijima, M., Ogawa, T. et al., Large scale gene expression analysis of osteoclastogenesis in vitro and elucidation of NFAT2 as a key regulator. *J. Biol. Chem.* 2002, 277, 41147–41156.
- [56] Takayanagi, H., Kim, S., Koga, T., Nishina, H. et al., Induction and activation of the transcription factor NFATc1 (NFAT2) integrate RANKL signaling in terminal differentiation of osteoclasts. *Dev. Cell* 2002, 3, 889–901.
- [57] Li, X., Udagawa, N., Itoh, K., Suda, K. et al., p38 MAPK-mediated signals are required for inducing osteoclast differentiation but not for osteoclast function. *Endocrinology* 2002, 143, 3105–3113.
- [58] Anderson, J. J., Garner, S. C., Mar, M. H., Boass, A. et al., The ovariectomized, lactating rat as an experimental model for osteopenia: calcium metabolism and bone changes. *Bone Miner.* 1990, 11, 43–53.
- [59] Dehority, W., Halloran, B. P., Bikle, D. D., Curren, T. et al., Bone and hormonal changes induced by skeletal unloading in the mature male rat. *Am. J. Physiol.* 1999, 276, E62–E69.
- [60] Kalu, D. N., Liu, C. C., Hardin, R. R., Hollis, B. W., The aged rat model of ovarian hormone deficiency bone loss. *Endocrinology* 1989, 124, 7–16.
- [61] Sessions, N. D., Halloran, B. P., Bikle, D. D., Wronski, T. J. et al., Bone response to normal weight bearing after a period of skeletal unloading. *Am. J. Physiol.* 1989, 257, E606–E610.
- [62] Shekarchi, M., Hajimehdipoor, H., Saeidnia, S., Gohari, A. R. et al., Comparative study of rosmarinic acid content in some plants of Labiatae family. *Pharmacogn. Mag.* 2012, 8, 37–41.

## RESEARCH ARTICLE

## Honokiol, Magnolol, and a Combination of Both Compounds Improve Glucose Metabolism in High-fat Diet-induced Obese Mice

Young-Sil Lee, Sun-Sil Choi, Takayuki Yonezawa, Toshiaki Teruya, Je-Tae Woo, Hyo Jung Kim, and Byung-Yoon Cha

Received May 26, 2014; revised October 24, 2014; accepted October 27, 2014; published online August 31, 2015  
© KoSFoST and Springer 2015

**Abstract** Honokiol and magnolol are neolignans contained in the Chinese medicinal herb *Magnolia officinalis* that exert anti-tumor and anti-inflammatory effects. Both compounds have been reported to enhance glucose uptake. Little is known about effects when used in combination. The effects of honokiol, magnolol, and a combination of both compounds on lipid and glucose metabolism in high-fat diet-induced obese mice were investigated, and underlying mechanisms were examined. All 3 treatments significantly ( $p < 0.05$ ) reduced plasma total cholesterol and glucose levels, and improved glucose tolerance, compared with controls. In addition, treatments increased mRNA expression of the peroxisome proliferator-activated receptor (PPAR)- $\gamma$ , glucose transporter (GLUT)-4, and adiponectin genes in white adipose tissue (WAT). Both compounds individually and in combination significantly ( $p < 0.05$ ) increased Akt phosphorylation and GLUT4 protein expression in WAT compared to the control group. Honokiol and magnolol improve dyslipidemia and hyperglycemia and act synergistically when used in combination.

**Keywords:** honokiol, magnolol, combination, high-fat

Young-Sil Lee, Sun-Sil Choi, Takayuki Yonezawa, Je-Tae Woo, Hyo Jung Kim, Byung-Yoon Cha (✉)  
Research Institute for Biological Functions, Chubu University, 1200 Matsumoto, Kasugai, Aichi, Japan  
Tel: +81-568-51-6189; Fax: +81-568-52-6189  
E-mail: bycha@isc.chubu.ac.jp

Toshiaki Teruya  
Faculty of Education, University of the Ryukyus, 1 Senbaru, Nishihara, Okinawa 903-0213, Japan

Young-Sil Lee  
Division of Bioscience and Bioinformatics, College of Natural Science, Myongji University, Yongin, Gyeonggi 449-728, Korea

Je-Tae Woo  
Department of Research and Development, Erina Co. Inc., 1-9-2 Hagashi-Shinbash, Minato-ku, Tokyo 105-0021, Japan

diet-induced obese mouse, glucose metabolism

### Introduction

Type 2 diabetes mellitus (T2DM) is a disease characterized by hyperglycemia caused by defects in secretion and action of insulin. T2DM is associated with abdominal obesity, dyslipidemia, and insulin resistance. Because of a progressive increase in the incidence of T2DM, there is a clear need for new treatments and/or therapeutic targets and strategies to prevent or treat this disease (1). Well established targets for treatment of T2DM already exist. The peroxisome proliferator-activated receptor (PPAR)- $\gamma$  is a ligand-activated nuclear receptor that forms heterodimers with the retinoid X receptor (RXR). These PPAR $\gamma$ -RXR heterodimers play an important role in both lipid and glucose homeostasis by regulation of gene expression associated with both the lipid and glucose metabolisms (2). Thiazolidinedione (TZD), a PPAR $\gamma$  agonist, decreases plasma low-density lipoprotein-cholesterol, triglyceride, and glucose levels, and enhances insulin sensitivity by an increase in insulin-stimulated glucose uptake and suppression of hepatic glucose production in diabetic animal models, and in patients with T2DM (3). PPAR $\gamma$ /RXR heterodimer complexes can be activated by RXR ligands alone. Binding of a ligand to RXR was reported to enhance recruitment of co-activators to the PPAR $\gamma$ /RXR heterodimer, and some RXR ligands can increase expression of genes targeted by PPAR $\gamma$  ligands (4). Similar to TZD, RXR ligands lowered plasma glucose levels in obese diabetic mice (5). Therefore, ligands for nuclear receptors, particularly PPAR $\gamma$  and RXR, have been used for prevention and treatment of the metabolic syndrome. Natural bioactive compounds are less toxic than existing agents and could reduce the risk of T2DM development and the metabolic syndrome (6). Honokiol and magnolol

are low molecular weight (Mw) neolignans present in the Chinese medicinal herb *Magnolia officinalis*, which is widely used in traditional Chinese medicine (7). These 2 compounds are structural isomers and have a number of pharmacological effects, including pro-apoptotic, anti-oxidative, antitumor, and anti-inflammation (8,9). Honokiol and magnolol improve both the glucose and lipid metabolisms (10-12) and inhibit acyl-CoA cholesterol acyltransferase (ACAT), which catalyzes formation of cholesteryl esters from cholesterol and long-chain fatty acyl-CoA (12). Furthermore, Honokiol, an RXR ligand, regulates the cholesterol metabolism via upregulation of ATP-binding cassette transporter (ABCA) expression, and enhancement of insulin-stimulated glucose uptake in adipocytes (13,14). Magnolol can activate PPAR $\gamma$  as a ligand, induce adipocyte differentiation, and enhance insulin-stimulated glucose uptake in animal models (10,15). In this study, the effects of honokiol, magnolol, and a combination of both compounds on the lipid and glucose metabolisms and the underlying mechanisms in high-fat diet (HFD)-induced obese mice were investigated.

## Materials and Methods

**Compounds** Honokiol and magnolol were purchased from Wako Pure Chemical Industries (Osaka, Japan).

**Animal study** Four week old male C57BL/6J mice were purchased from Japan SLC (Shizuoka, Japan). Mice were housed under temperature (23 $\pm$ 3°C) and humidity controlled conditions with a 12 h light/dark cycle and given free access to water and food throughout the experimental period. After acclimatization to a standard rodent normal-fat diet (NFD) (CRF-1; Charles River, Tokyo, Japan) for 1 week, mice were fed either the NFD (Charles River) (NFD control,  $n=8$ , protein (casein/L-Cystine); 25%, carbohydrate (maltodextrin/sucrose); 61%, fat (lard/soybean oil); 14% and other, 3.59 kcal/g), or the HFD ( $n=32$ ; Rodent diet D12492; Research Diets, New Brunswick, NJ, USA; protein (casein/L-Cystine); 20%, carbohydrate (maltodextrin/sucrose); 20%, fat (lard/soybean oil); 60%, and other, 5.24 kcal/g) for 8 weeks to induce obesity. Based on body weights and plasma glucose levels, mice fed the HFD were divided into 4 experimental groups ( $n=8$ /group) and treated without (HFD control) and with 100 mg/kg of honokiol (HFD+100H), 100 mg/kg of magnolol (HFD+100M), or honokiol plus magnolol (50 mg/kg (HFD+50H+50M). Chemicals were mixed with 0.3% carboxymethylcellulose and administered using oral gavage once daily for 8 weeks with continuation of the HFD. The control NFD and HFD groups were administered vehicle alone. Body weight and food intake were measured twice per week throughout the

study period. The experimental design was approved by the Animal Experiment Committee of Chubu University (Kasugai, Japan) and mice were maintained in accordance with committee guidelines (CHUBU 2110024).

**Collection of plasma, liver, and white adipose tissues (WAT)** Mice were sacrificed at the end of the 8 week treatment period using cervical dislocation after collection of blood samples from the tail vein. Plasma was prepared using centrifugation (himac CF16RX; Hitach Koji Co., Ltd., Tokyo, Japan) of blood samples at 5,000 $\times$ g for 15 min at 4°C. Plasma samples were stored at -80°C (MDF-382; Sanyo, Osaka, Japan) until analysis. Liver, muscle, and WAT (epididymal, perirenal, and mesenteric WAT) were immediately excised, rinsed, weighed, frozen in liquid nitrogen, and stored at -80°C (MDF-382; Sanyo) until analysis.

**Plasma biochemical analysis** Plasma total cholesterol (T-CHO), triglyceride (TG), and glucose levels were determined using enzymatic methods with commercial assay kits (Cholesterol E-Test, Triglyceride E-Test, NEFA C Test, and Glucose C II-Test; Wako Pure Chemical Industries).

**Oral glucose tolerance testing (OGTT)** After 52 days of treatment, mice were fasted overnight and a basal blood sample (0 min) was collected from the tail vein. Mice were then orally administered glucose (2 g/kg of body weight) and additional blood samples were collected at 30, 60, and 120 min. Blood samples were centrifuged (himac CF16RX; Hitach Koji Co., Ltd.) at 5,000 $\times$ g for 15 min at 4°C and plasma samples were stored at -80°C (MDF-382; Sanyo) until analysis. Plasma glucose levels were measured using a Glucose C II-Test kit (Wako Pure Chemical Industries).

**Total RNA isolation and gene expression analysis** Total RNA was isolated from WAT of mice from each group ( $n=8$ ) using the Isogen reagent (Nippon Gene, Tokyo, Japan) according to the manufacturer's protocol. Total RNA (1.5  $\mu$ g) was reverse-transcribed to cDNA using a reverse transcription system (a3500; Promega, Madison, WI, USA) with the oligo (dT) primer. mRNA expression levels of adipokines and glucose metabolism related genes were determined using gene-specific primers with real-time PCR and a FastStart universal SYBR Green Master PCR kit (Roche, Mannheim, Germany) on an ABI Prism 7700 system (Applied Biosystems, Foster City, CA, USA). Forward and reverse primers for PPAR $\gamma$ 2 were 5'-GAG CTG ACC CAA TGG TTG CTG-3', and 5'-GCT TCA ATC GGA TGG TTC TTC 3'; GLUT4, 5'-CAA CGT GGC TGG GTA GGC A-3' and 5'-ACA ACA TCAG CCC AGC CGG T-3', and for adiponectin were 5'-GTT GCA

AGC TCT CCT GTT CC-3' and 5'-CTT GCC AGT GCT GTT GTC AT-3'. All samples were normalized for expression of GAPDH. The expression level of the gene of interest in each treatment group relative to the expression level of the gene in HFD control group mice was calculated using the  $2^{-\Delta\Delta C_t}$  formula where  $C_t$  is the cycle number at which the fluorescence became higher than the background level. Specifically,  $\Delta C_t = \Delta C_{t \text{ interest}} - \Delta C_{t \text{ GAPDH}}$  and  $\Delta\Delta C_t = \Delta C_{t \text{ treated group}} - \Delta C_{t \text{ HFD control group}}$ , which was normalized to 1.

**Protein extraction and Western blotting** For preparation of whole cell lysates, WAT samples were homogenized in RIPA buffer (50 mmol/L of Tris-HCl, pH 7.4, 1% NP-40, 0.2% sodium deoxycholate, 0.2% sodium dodecylsulfate (SDS), 1 mM PMSF) for Western blotting. Homogenates were centrifuged Equipment (Centrifuge 5417R; Eppendorf, Hamburg, Germany) at  $760\times g$  for 5 min at  $4^\circ\text{C}$  to remove nuclei and intact cells. Resulting supernatants were further centrifuged (Centrifuge 5417R; Eppendorf) at  $12,000\times g$  for 20 min at  $4^\circ\text{C}$  and final supernatants were collected. Subcellular fractionation of WAT was carried out using the methods of Rampal *et al.* (16) with slight modification. WAT samples were homogenized in a buffer (0.25 M sucrose, 10 mM Tris-HCl pH 4.2, 2 mM EDTA, 1 mM protease inhibitor, and 1 mM phosphatase inhibitor (Sigma-Aldrich, St. Louis, MO, USA). The homogenate was centrifuged (himac CF16RX; Hitach Koji Co., Ltd.) at  $760\times g$  for 5 min at  $4^\circ\text{C}$ , then the resulting supernatant was centrifuged (Centrifuge 5417R; Eppendorf) at  $12,000\times g$  for 20 min at  $4^\circ\text{C}$  to pellet the whole plasma membrane, pellets of which were suspended in RIPA lysis buffer and frozen at  $-80^\circ\text{C}$  (MDF-382; Sanyo). Protein concentrations were determined based on assays (Bradford; Bio-Rad, Hercules, CA, USA), using bovine serum albumin (Wako Pure Chemical Industries) as a standard.

Protein samples (50  $\mu\text{g}$  of whole lysate, 20  $\mu\text{g}$  of the whole plasma membrane fraction) were separated using SDS-polyacrylamide gel electrophoresis (Bio-Rad) and transferred to polyvinylidene difluoride membranes (Amersham, Cleveland, OH, USA). Membranes were blocked with 5% (w/v) non-fat dry milk in Tris-buffered saline (Wako Pure Chemical Industries) containing 0.1% Tween 20 (Sigma-Aldrich) (TBS-T) and incubated with anti-mouse GLUT4 (AbD SeroTec, Oxford, UK, 1:1,000) or anti-rabbit phospho-Akt (ser473), Akt, and GAPDH (Cell Signaling Technology, Beverly, MA, USA, 1:1,000) antibodies in 5% BSA (Wako Pure Chemical Industries). After incubation, membranes were washed with TBS-T (Wako Pure Chemical Industries), then incubated with a horseradish peroxidase-conjugated anti-rabbit or anti-mouse IgG secondary antibody (Santa Cruz Biotechnology, Santa Cruz, CA, USA) in TBS-T (Wako Pure Chemical Industries) containing 5% non-fat dry milk (Wako Pure Chemical Industries). After washing,

immunocomplexes were visualized using enhanced chemiluminescence (Amersham). Exposed X-ray films were scanned and obtained images were subjected to densitometric analysis using Scion Image Release Beta 4.02 software (Scion Corporation, Frederick, MD, USA). The expression levels of GLUT4 and phospho-Akt/Akt levels were calculated relative to their expression levels in HFD control group mice and expressed as fold induction.

**Statistical analysis** Data were expressed as a mean  $\pm$  SEM. Differences in mean values between 2 groups were analyzed using Student's *t*-test and a one-way analysis of variance (ANOVA) using Origin 7 Software (MicroCal Software, Northampton, MA, USA). Values of  $p < 0.05$  were considered statistically significant.

## Results and Discussion

**Effects of honokiol, magnolol, and a combination on body weight gain, food intake, and organ weight** Body weight gain, food intake, and organ weights are shown in Fig. 1. Body weight gain in HFD control group mice was significantly ( $p < 0.005$ ) higher than in NFD group mice. Body weight gain was lower in HFD+100H and HFD+100M group mice than in HFD control group mice, although differences were not significant ( $p > 0.05$ ). Notably, body weight gain in HFD+50H+50M group mice was significantly ( $p < 0.05$ ) less than in HFD control group mice (Fig. 1A). Whereas food intake was not significantly ( $p > 0.005$ ) different among HFD control and treated group mice, the food intake of HFD was significantly ( $p < 0.05$ ) lower compared to the NFD group mice (Fig. 1B). Liver weight was significantly ( $p < 0.05$ ) lower in both HFD+100H and HFD+50H+50M group mice, compared with HFD group mice, but there was no significant change ( $p > 0.05$ ) in HFD+100M group mice compared with HFD group mice (Fig. 1C). WAT weight (epididymal, perirenal, mesenteric, and total) was significantly ( $p < 0.005$ ) greater in HFD group mice than in NFD group mice. Similar to body weight gain, WAT weight also did not significantly ( $p > 0.05$ ) reduce among HFD+100H, HFD+100M, and HFD group mice. WAT weight was significantly ( $p < 0.05$ ) lower in HFD+50H+50M group mice than in HFD group mice (Fig. 1D). A combination of honokiol plus magnolol inhibited visceral fat accumulation better than both honokiol and magnolol alone, without affecting food intake.

It was recently reported that honokiol and magnolol from the Chinese medicinal herb *Magnolia officinalis* regulated lipid and glucose metabolism *in vitro* (10,14). In this study, honokiol, magnolol and a combination were investigated for use in prevention or treatment of disordered

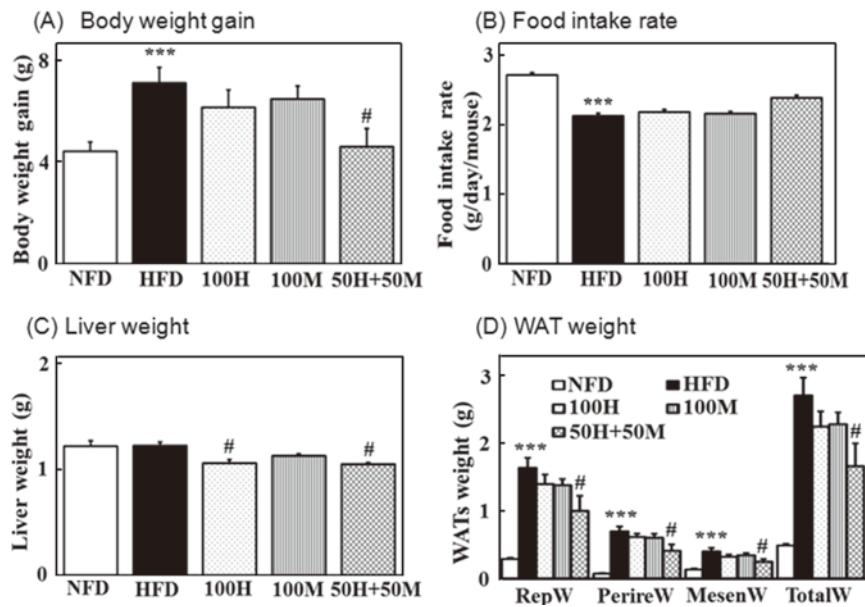


**Fig. 1. Effects of honokiol, magnolol, and a combination on body weight gain, food intake, and organ weight.** (A) Body weight gain, (B) Food intake rate, (C) Liver weight, (D) WAT weight. RepW, reproductive WAT; PeriW, perirenal WAT; MesenW, Mesenteric WAT; TotalW, RepW+PeriW+MesenW. NFD, Normal-fat diet; HFD, High-fat diet; 100H, HFD plus 100 mg/kg of honokiol; 100M, HFD plus 100 mg/kg of magnolol. 50H+50M, HFD plus honokiol and magnolol at a dose of 50 mg/kg each. Values are expressed as a mean±SEM ( $n=8$ ). \*\*\* $p<0.05$  vs, the NFD group; # $p<0.05$  vs. the HFD group.

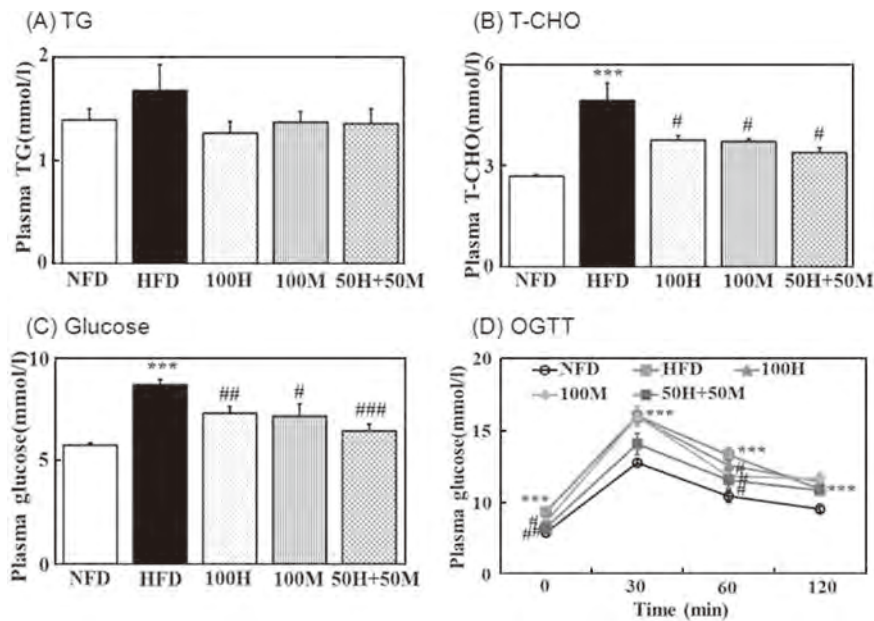


**Fig. 2. Effects of honokiol, magnolol, and a combination on biochemical plasma parameters.** (A) Plasma TG levels, (B) Plasma T-CHO levels, (C) Plasma glucose levels, (D) OGTT. NFD, Normal-fat diet; HFD, High-fat diet; 100H, HFD plus 100 mg/kg of honokiol; 100M, HFD plus 100 mg/kg of magnolol. 50H+50M, HFD plus honokiol and magnolol at a dose of 50 mg/kg each. Values are expressed as a mean±SEM ( $n=8$ ). \*\*\* $p<0.05$  vs. the NFD group; # $p<0.05$ , ## $p<0.01$ , and ### $p<0.005$  vs. the HFD group.

lipid and glucose metabolisms in HFD-induced obese mice. The reduction of body weight in the group administered with honokiol and magnolol individually was not significant ( $p>0.05$ ). A combination of these compounds significantly ( $p<0.05$ ) reduced body weight gain and WAT weight compared to the controls.

**Effects of honokiol, magnolol, and a combination on plasma biochemistry and glucose tolerance** Plasma biochemical parameters are shown in Fig. 2. The plasma TG level did not differ among mice of any group (Fig. 2A). The plasma T-CHO and glucose levels were significantly ( $p<0.005$ ) greater in HFD group mice than in NFD group

mice. On the other hand, both T-CHO ( $p < 0.05$ ) and glucose levels ( $p < 0.01$ ) were significantly lower in HFD+100H mice, significantly ( $p < 0.05$  for both) lower in HFD+100M mice, and significantly lower in HFD+50H+50M mice (T-CHO at  $p < 0.05$  and glucose at  $p < 0.005$ ) group mice than in HFD group mice (Fig. 2B and C). For evaluation of glucose tolerance, OGTT was performed after 53 days of treatment with both T-CHO and glucose. Plasma glucose levels were significantly ( $p < 0.005$ ) higher in HFD control group mice for all treatment times after glucose administration, compared with NFD group mice. Honokiol, magnolol, and a combination significantly ( $p < 0.05$  for all) reversed this effect at 60 min after glucose administration (Fig. 2D). Thus, honokiol, magnolol, and a combination suppressed glucose and lipid disorders in HFD-induced obese mice.

**Effects of honokiol, magnolol, and a combination on PPAR $\gamma$  and target gene expressions** The effects of honokiol, magnolol, and a combination on the mRNA levels of PPAR $\gamma$  and target genes in WAT were investigated. PPAR $\gamma$  mRNA expression levels were significantly ( $p < 0.05$ ) increased in NFD group mice, compared with HFD group mice. PPAR $\gamma$  mRNA expression levels were also significantly ( $p < 0.01$  for all) increased in HFD+100H, HFD+100M, and HFD+50H+50M group mice, compared with HFD group mice (Fig. 3A). GLUT4 and adiponectin expression levels of PPAR $\gamma$  target genes were significantly ( $p < 0.05$  for both) increased in NFD group mice, and in HFD+100H ( $p < 0.01$  for both), HFD+100M ( $p < 0.01$  and  $p < 0.005$ , respectively), and HFD+50H+50M group mice ( $p < 0.05$  and  $p < 0.01$ , respectively), compared with HFD control group mice (Fig. 3B and C). Thus, honokiol, magnolol and a combination upregulated mRNA expression of PPAR $\gamma$  and target genes in WAT.

Both compounds and a combination also significantly ( $p < 0.05$ ) decreased the plasma cholesterol levels, but not in plasma TG levels ( $p > 0.05$ ). It has been reported that honokiol and magnolol are ligands for RXR and PPAR $\gamma$ , respectively (10,13). Treatment with an RXR ligand alone and co-treatment with RXR and PPAR $\gamma$  ligands inhibited body weight gain and fat accumulation in Zucker fatty rats (17,18), and led to an increase in anti-diabetic activity without the increase in TG levels that is associated with RXR agonist treatment and the increase in lipid accumulation that is associated with TZD treatment (5,18). RXR can also heterodimerize with the liver X receptor (LXR) to promote efflux of excess cholesterol from macrophages due to regulation of ABCA1 expression (14).

PPAR $\gamma$  ligands regulate ABCA1 expression based on induction of LXR-RXR dimerization (19). It was also reported that honokiol and magnolol inhibited ACAT, which catalyzes formation of cholesteryl esters from cholesterol and long-chain fatty acyl-CoA (12). This process represses

accumulation of total cholesterol by inhibition of very low-density lipoprotein production in the liver and facilitation of cholesterol efflux from macrophages (20). Therefore, the mechanism by which honokiol and magnolol improve adipose and lipid disorders could be attributed, at least for regulation of genes involved in lipid metabolism, to activation of nuclear receptors as ligands and to inhibition of ACAT activity. Furthermore, the synergistic effects of a combination that were reported herein may be related to the activities of these 2 ligands for honokiol and magnolol. In addition to effects on the lipid metabolism, honokiol and magnolol reduced plasma glucose levels and improved glucose intolerance. To examine the mechanisms by which honokiol and magnolol improved glucose metabolism, the effects of both compounds on cellular signaling pathways involved in reduction of plasma glucose levels and improvement of glucose intolerance were investigated. One possible mechanism was an increase in expression of PPAR $\gamma$  and target genes. PPAR $\gamma$  regulates glucose metabolism by modulation of numerous gene expressions, including GLUT4 and adiponectin (21,22). GLUT4, a member of the GLUT family, plays an important role in glucose uptake in tissues. Activation of PPAR $\gamma$  by TZD increased GLUT4 expression and insulin-dependent glucose uptake in adipose tissue in an animal model, and also in type 2 diabetes patients (23).

Adiponectin, an adipocyte-derived hormone, is a target gene of PPAR $\gamma$ . Adiponectin stimulates glucose uptake by enhancement of GLUT4 gene expression in adipocytes and by an increase in fatty acid oxidation in muscles, resulting in enhanced insulin sensitivity (24). Expression and plasma levels of GLUT4 are down-regulated in obese and insulin resistance individuals, but are induced in animals and humans by thiazolidinediones (25-27). mRNA expression levels of PPAR $\gamma$ , GLUT4, and adiponectin in WAT of HFD-induced obese mice were increased by honokiol and magnolol when treated both individually and in combination (Fig. 3). Although honokiol and magnolol both individually increased gene expression levels of PPAR $\gamma$  and the target genes GLUT4 and adiponectin compared to the HFD group, honokiol showed weaker induction of these genes than magnolol, probably due to differences in ligand activities.

A previous study reported that some genes are regulated by both RXR agonists and by the RXR permissive partner nuclear receptor (28). These results are consistent with a report that honokiol and magnolol increased expression of PPAR $\gamma$  genes during adipocyte differentiation (10,11). Honokiol and magnolol may, at least in part, enhance glucose metabolism by activation of PPAR $\gamma$  and expression of target genes. The anti-diabetic effects and increases in PPAR $\gamma$  and target expressions also occurred in a synergistic manner when honokiol and magnolol were administered in combination.

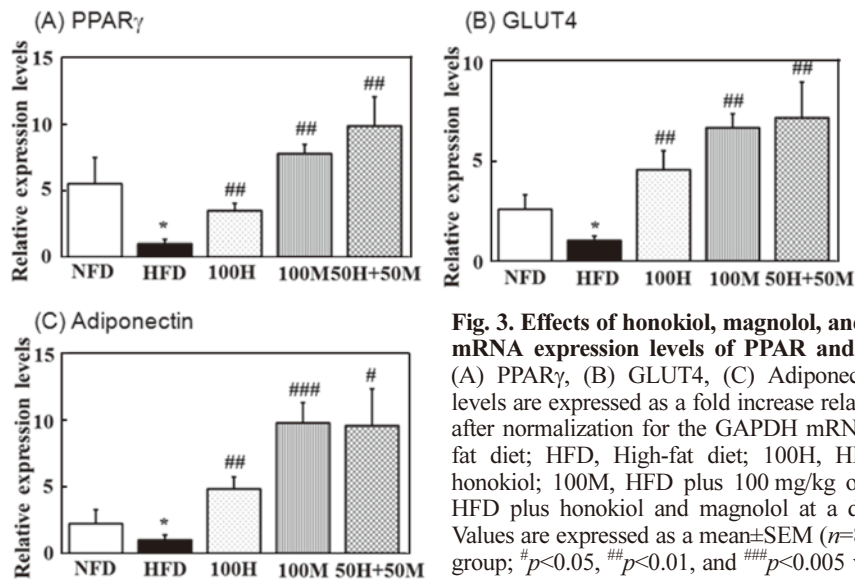


**Fig. 3. Effects of honokiol, magnolol, and a combination on the mRNA expression levels of PPAR and target genes in WAT.** (A) PPAR $\gamma$ , (B) GLUT4, (C) Adiponectin. mRNA expression levels are expressed as a fold increase relative to HFD group mice after normalization for the GAPDH mRNA level. NFD, Normal-fat diet; HFD, High-fat diet; 100H, HFD plus 100 mg/kg of honokiol; 100M, HFD plus 100 mg/kg of magnolol. 50H+50M, HFD plus honokiol and magnolol at a dose of 50 mg/kg each. Values are expressed as a mean $\pm$ SEM ( $n=8$ ). \* $p<0.05$  vs. the NFD group; # $p<0.05$ , ## $p<0.01$ , and ### $p<0.005$  vs. the HFD group.

**Effects of honokiol, magnolol, and a combination on the insulin signaling pathway in WAT** The effects of honokiol and magnolol on activation of the insulin signaling pathway were investigated. p-Akt levels were significantly ( $p<0.05$ ) increased in both NFD and HFD+100H group mice, compared with HFD group mice, but not in HFD+100M and HFD+50H+50M groups compared to HFD group ( $p>0.05$ ). GLUT4 protein levels was significantly ( $p<0.05$ ) higher in NFD, HFD+100H, HFD+100M, and HFD+50H+50M group mice, compared with HFD group mice (Fig. 4A and B). Whole plasma GLUT4 levels look like increasing in HFD+100H, HFD+100M, and HFD+50H+50M group mice, compared with HFD group mice (Fig. 4C), but the results was not significant ( $p>0.05$ ). Thus, honokiol, magnolol, and a combination apparently activate Akt and, hence, up-regulate GLUT4 expression resulting in increased glucose uptake.

Another possible mechanism whereby honokiol and magnolol can influence the glucose metabolism in WAT is insulin-dependent PI3K-Akt signaling. In general, the PI3K-Akt pathway is responsible for glucose uptake. Binding of insulin to a receptor causes phosphorylation of the receptor which, subsequently, phosphorylates the insulin receptor substrate (IRS), PI3K, and Akt. In this pathway, Akt stimulates GLUT4 expression and translocation of GLUT4 to the plasma membrane, thus enhancing glucose uptake (29). It has also been reported that PPAR $\gamma$  and RXR activation can influence the insulin signaling pathway by modulation of expression and/or phosphorylation of signaling cascade molecules (21,30). On GLUT4 protein expression levels, the cells treated with honokiol, magnolol, and combination of honokiol and magnolol did not induce

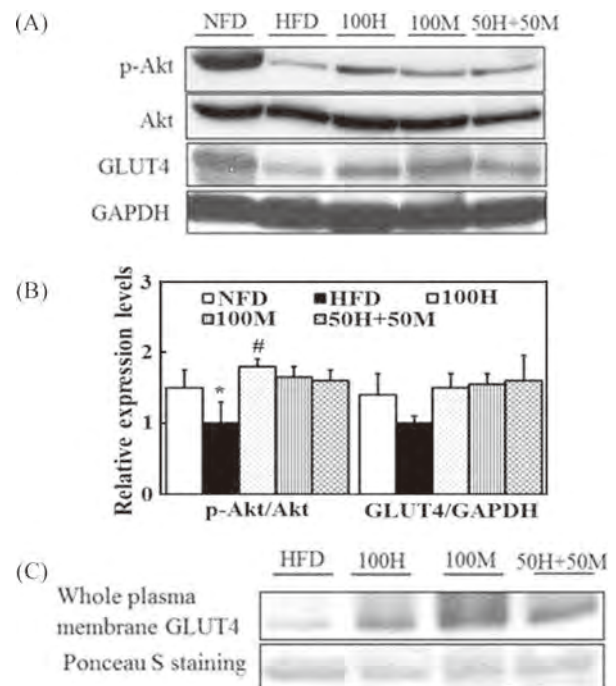


**Fig. 4. Effects of honokiol, magnolol, and a combination on the insulin signaling pathway in WAT.** (A) Whole lysates p-Akt, Akt and GLUT4 protein expression levels. Representative immunoblots are shown. (B) Densitometric analysis of p-Akt and GLUT4 expressions. The relative p-Akt and GLUT4 expression levels were normalized for total protein (Akt) or GAPDH, respectively, and compared with corresponding expression levels in HFD group mice, which were assigned a value of 1.0. (C) Whole plasma membrane GLUT4 protein expression levels. NFD, Normal-fat diet; HFD, High-fat diet; 100H, HFD plus 100 mg/kg of honokiol; 100M, HFD plus 100 mg/kg of magnolol. 50H+50M, HFD plus honokiol and magnolol at a dose of 50 mg/kg each. Values are expressed as a mean $\pm$ SEM ( $n=8$ ). \* $p<0.05$  vs. the NFD group; # $p<0.05$  vs. the HFD group.

any significant increase compared to the control (Fig. 4). In contrast, earlier reports showed honokiol and magnolol increased insulin-stimulated glucose uptake via the insulin signaling pathway (10-14). The beneficial effects of honokiol and magnolol on glucose metabolisms were probably driven by increased glucose uptake following activation of the Akt-GLUT4 pathway.

In conclusion, honokiol and magnolol improved lipid and glucose metabolisms in HFD-induced obese mice. These effects, particularly the hypoglycemic one, were accompanied by increased GLUT4 and adiponectin expression following activation of PPAR $\gamma$ , and by increased glucose use/uptake via enhanced activity of the insulin signaling pathway in WAT. Furthermore, honokiol and magnolol, when used in combination, exerted synergistic pharmacological effects, including improvements in the lipid and glucose metabolisms. Thus, honokiol, magnolol and a combination may be useful for prevention of hyperlipidemia and hyperglycemia.

**Disclosure** The authors declare no conflict of interest.

## References

- Hu FB, van Dam RM, Liu S. Diet and risk of type II diabetes: The role of types of fat and carbohydrate. *Diabetologia* 44: 805-817 (2001)
- Lee CH, Olson P, Evans RM. Mini review: Lipid metabolism, metabolic disease, and peroxisome proliferators-activated receptors. *Endocrinology* 144: 2201-2207 (2003)
- Nolan JJ, Ludvik B, Beerdson P, Joyce M, Olefsky J. Improvement in glucose tolerance and insulin resistance in obese subjects treated with troglitazone. *New Engl. J. Med.* 331: 1188-1193 (1994)
- Schulman IG, Shao G, Heyman RA. Transactivation by retinoid X receptor-peroxisome proliferator-activated receptor  $\gamma$  (PPAR $\gamma$ ) heterodimers: Intermolecular synergy requires only the PPAR $\gamma$  hormone-dependent activation function. *Mol. Cell. Biol.* 18: 3483-3494 (1998)
- Mukherjee R, Davies PJ, Crombie DL, Bischoff ED, Cesario RM, Jow L, Hamann LG, Boehm MF, Mondon CE, Nadzan AM, Paterniti JR Jr, Heyman RA. Sensitization of diabetic and obese mice to insulin by retinoid X receptor agonists. *Nature* 386: 407-410 (1997)
- Sharpe PA, Blanck HM, Williams JE, Ainsworth BE, Conway JM. Use of complementary and alternative medicine for weight control in the United States. *J. Altern. Complem. Med.* 13: 217-222 (2007)
- Yin HQ, Je YT, Kim YC, Shin YK, Sung S, Lee K, Jeong GS, Kim YC, Lee BH. *Magnolia officinalis* reverse alcoholic fatty liver by inhibiting the maturation of sterol regulation element-binding protein-1c. *J. Pharmacol. Sci.* 109: 486-495 (2009)
- Ogata M, Hoshi M, Shimotohno K, Urano S, Endo T. Anti-oxidant activity of magnolol, honokiol and related phenolic compounds. *J. Am. Oil Chem. Soc.* 74: 557-562 (1997)
- Lee J, Jung E, Park J, Jung K, Lee S, Hong S, Park J, Park E, Kim J, Park S, Park D. Anti-inflammatory effects of magnolol and honokiol are mediated through inhibition of the downstream pathway of MEKK-1 in NF- $\kappa$ B activation signaling. *Planta Med.* 71: 338-343 (2005)
- Choi SS, Cha BY, Lee YS, Yonezawa T, Teruya T, Nagai K, Woo JT. Magnolol enhances adipocytes differentiation and glucose uptake in 3T3-L1 cell. *Life Sci.* 84: 908-914 (2009)
- Choi SS, Cha BY, Iida K, Sato M, Lee YS, Teruya T, Yonezawa T, Nagai K, Woo JT. Honokiol enhances adipocyte differentiation by potentiating insulin signaling in 3T3-L1 preadipocytes. *J. Nat. Med.* 65: 424-430 (2011)
- Kwon BM, Kim MK, Lee SH, Kim JA, Lee IR, Kim YK, Bok SH. Acyl-CoA: Cholesterol acyltransferase inhibitors from *Magnolia obovata*. *Planta Med.* 63: 550-551 (1997)
- Jung CG, Horike H, Cha BY, Uhm KO, Yamauchi R, Yamauchi T, Hosono T, Iida K, Woo JT, Michikawa M. Honokiol increases ABCA1 expression level by activating retinoid X receptor beta. *Biol. Pharm. Bull.* 33: 1105-1111 (2010)
- Kotani H, Tanabe H, Mizukami H, Makishima M, Inoue M. Identification of a naturally occurring rexinoid, honokiol, that activates the retinoid X receptors. *J. Nat. Prod.* 73: 1332-1336 (2010)
- Sohn EJ, Kim CS, Kim YS, Jung DH, Jang DS, Lee YM, Kim JS. Effects of magnolol (5,5'-diallyl-2,2'-dihydroxybiphenyl) on diabetic nephropathy in type 2 diabetic Goto-Kakizaki rats. *Life Sci.* 80: 468-475 (2007)
- Rampal AL, Jhun BH, Kim S, Liu H, Manka M, Lachal M, Spangler RA, Jung CY. Okadaic acid stimulates glucose transport in rat adipocytes by increasing the externalization rate constant of GLUT4 recycling. *J. Biol. Chem.* 270: 3938-3943 (1995)
- Emilsson V, O'Dowd J, Wang S, Liu YL, Sennitt M, Heyman R, Cawthorne MA. The effects of rexinoids and rosiglitazone on body weight and uncoupling protein isoform expression in the Zucker *fa/fa* rat. *Metabolism* 49: 1610-1615 (2000)
- Leibowitz MD, Ardecky RJ, Boehm MF, Broderick CL, Carfagna MA, Crombie DL, D'Arrigo J, Etgen GJ, Faul MM, Grese TA, Havel H, Hein NI, Heyman RA, Jolley D, Klausung K, Liu S, Mais DE, Mapes CM, Marschke KB, Michellys PY, Montrose-Rafizadeh C, Ogilvie KM, Pascual B, Rungta D, Tyhonas JS, Urcan MS, Wardlow M, Yumibe N, Reifel-Miller A. Biological characterization of a heterodimers-selective retinoid X receptor modulator: Potential benefits for the treatment of type 2 diabetes. *Endocrinology* 147: 1044-1053 (2006)
- Chawla A, Boisvert WA, Lee CH, Laffitte BA, Barak Y, Joseph SB, Liao D, Nagy L, Peter A, Edwards PA, Curtiss LK, Evans RM, Tontonoz P. A PPAR $\gamma$ -LXR-ABCA1 pathway in macrophages is involved in cholesterol efflux and atherogenesis. *Mol. Cell* 7: 161-171 (2001)
- An S, Jang YS, Park JS, Kwon BM, Paik YK, Jeong TS. Inhibition of acyl-coenzyme A: Cholesterol acyltransferase stimulates cholesterol efflux from macrophages and stimulates farnesoid X receptor in hepatocytes. *Exp. Mol. Med.* 40: 407-417 (2008)
- Spiegelman BM. PPAR-gamma: Adipogenic regulator and thiazolidinedione receptor. *Diabetes* 47: 507-514 (1998)
- Wu Z, Xie Y, Morrison RF, Bucher NL, Farmer SR. PPAR $\gamma$  induces the insulin-dependent glucose transporter GLUT4 in the absence of C/EBP $\alpha$  during the conversion of 3T3 fibroblasts into adipocytes. *J. Clin. Invest.* 101: 22-32 (1998)
- Furuta M, Yano Y, Gabazza EC, Araki-Sasaki R, Tanaka T, Katsuki A, Hori Y, Nakatani K, Sumida Y, Adachi Y. Troglitazone improves GLUT4 expression in adipose tissue in an animal model of obese type 2 diabetes mellitus. *Diabetes Res. Clin. Pr.* 56: 159-171 (2002)
- Fu Y, Luo N, Klein RL, Garvey WT. Adiponectin promotes adipocytes differentiation, insulin sensitivity and lipid accumulation. *J. Lipid Res.* 46: 1369-1379 (2005)
- Hu E, Liang P, Spiegelman BM. Adipo Q is novel adipose-specific gene dysregulated in obesity. *J. Biol. Chem.* 271: 10697-10703 (1996)
- Yu JG, Javorschi S, Hevener AL, Kruszynska YT, Norman RA, Sinha M, Olefsky JM. The effect of thiazolidinediones on plasma adiponectin levels in normal, obese, and type 2 diabetic subject. *Diabetes* 51: 2968-2974 (2002)
- Pajvani UB, Hawkins M, Combs TP, Rajala MW, Doebber T, Berger JP, Wagner JA, Wu M, Knopps A, Xiang AH, Utzschneider KM, Kahn SE, Olefsky JM, Buchanan TA, Scherer PE. Complex distribution, not absolute amount of adiponectin, correlated with thiazolidinedione-mediated improvement in insulin sensitivity. *J.*

- 
- Biol. Chem. 279: 12152-12162 (2004)
28. Széles L, Póliska S, Nagy G, Szatmari I, Szanto A, Pap A, Lindstedt M, Santegoets SJ, Rühl R, Dezsö B, Nagy L. Research resource: Transcriptome profiling of genes regulated by RXR and its permissive and nonpermissive partners in differentiating monocyte-derived dendritic cells. *Mol. Endocrinol.* 24: 2218-2231 (2010)
29. Pessin JE, Saltiel AR. Signaling pathway in insulin action: Molecular targets of insulin resistance. *J. Clin. Invest.* 106: 165-169 (2000)
30. Shen Q, Cline GW, Shulman GI, Leibowitz MD, Davies PJ. Effects of rexinoids on glucose transport and insulin-mediated signaling in skeletal muscles of diabetic (*db/db*) mice. *J. Biol. Chem.* 279: 19721-19731 (2000)

# Identification and Structure Determination of Novel Anti-inflammatory Mediator Resolvin E3, 17,18-Dihydroxyeicosapentaenoic Acid\*<sup>§</sup>

Received for publication, January 7, 2012, and in revised form, January 23, 2012. Published, JBC Papers in Press, January 24, 2012, DOI 10.1074/jbc.M112.340612

Yosuke Isobe<sup>‡§</sup>, Makoto Arita<sup>†¶1</sup>, Shinnosuke Matsueda<sup>‡</sup>, Ryo Iwamoto<sup>§</sup>, Takuji Fujihara<sup>§||</sup>, Hiroki Nakanishi<sup>\*\*</sup>, Ryo Taguchi<sup>\*\*</sup>, Koji Masuda<sup>§||</sup>, Kenji Sasaki<sup>††</sup>, Daisuke Urabe<sup>††</sup>, Masayuki Inoue<sup>††</sup>, and Hiroyuki Arai<sup>‡</sup>

From the Departments of <sup>‡</sup>Health Chemistry and <sup>††</sup>Integral Analytical Chemistry, <sup>§</sup>Business-Academia-Collaborative Laboratory, Graduate School of Pharmaceutical Sciences, and <sup>\*\*</sup>Department of Metabolome, Graduate School of Medicine, University of Tokyo, 7-3-1 Hongo, Bunkyo-ku, Tokyo 113-0033, the <sup>||</sup>Shionogi Research Laboratories, 3-1-1 Futaba-cho, Toyonaka, Osaka 561-0825, and <sup>¶</sup>PRESTO, Japan Science and Technology Agency, 4-1-8 Honcho, Kawaguchi, Saitama, Japan

**Background:** Endogenous mediators that control aberrant inflammation are of interest as potential targets of new therapeutics.

**Results:** Here, we identified a novel omega-3 fatty acid-derived anti-inflammatory mediator 17,18-diHEPE, denoted as resolvin E3.

**Conclusion:** Resolvin E3 has a potent inhibitory action on neutrophil chemotaxis both *in vitro* and *in vivo*.

**Significance:** The significance of this study is the identification of a novel endogenous lipid mediator with a potent anti-inflammatory property.

Bioactive mediators derived from omega-3 eicosapentaenoic acid (EPA) elicit potent anti-inflammatory actions. Here, we identified novel EPA metabolites, including 8,18-dihydroxyeicosapentaenoic acid (8,18-diHEPE), 11,18-diHEPE, 12,18-diHEPE, and 17,18-diHEPE from 18-HEPE. Unlike resolvins E1 and E2, both of which are biosynthesized by neutrophils via the 5-lipoxygenase pathway, these metabolites are biosynthesized by eosinophils via the 12/15-lipoxygenase pathway. Among them, two stereoisomers of 17,18-diHEPE, collectively termed resolvin E3 (RvE3), displayed a potent anti-inflammatory action by limiting neutrophil infiltration in zymosan-induced peritonitis. The planar structure of RvE3 was unambiguously determined to be 17,18-dihydroxy-5Z,8Z,11Z,13E,15E-EPE by high resolution NMR, and the two stereoisomers were assigned to have 17,18R- and 17,18S-dihydroxy groups, respectively, using chemically synthesized 18R- and 18S-HEPE as precursors. Both 18R- and 18S-RvE3 inhibited neutrophil chemotaxis *in vitro* at low nanomolar concentrations. These findings suggest that RvE3 contributes to the beneficial actions of EPA in controlling inflammation and related diseases.

In many human diseases, uncontrolled inflammation is suspected as a key component of pathogenesis (1). Acute inflam-

\* This work was supported by Japan Science and Technology Agency Precursor Research for Embryonic Science and Technology (to M. A.), Core Research for Evolutional Science and Technology (to H. A. and R. T.), grant-in-aid for scientific research from the Ministry of Education, Culture, Sports, Science, and Technology of Japan (to M. A.), Ono Medical Research Foundation (to M. A.), and the Program for Promotion of Basic and Applied Research for Innovations in Bio-Oriented industry (to H. A.).

✂ Author's Choice—Final version full access.

<sup>§</sup> This article contains supplemental Figs. S1–S4, Tables S1 and S2, and "Methods".

<sup>1</sup> To whom correspondence should be addressed: 7-3-1 Hongo, Bunkyo-ku, Tokyo 113-0033, Japan. Tel.: 81-3-5841-4723; Fax: 81-3-3818-3173; E-mail: marita@mof.u-tokyo.ac.jp.

mation is an indispensable host response to foreign challenges or tissue injury that, if unopposed, could lead to loss of tissue structure and function. In healthy conditions, inflammatory processes are self-limiting and self-resolving, suggesting the existence of endogenous control mechanisms in the course of acute inflammation and resolution (for reviews see Ref. 2, 3). Therefore, the identification of such endogenous anti-inflammatory and/or pro-resolution mechanisms is of wide interest.

Omega-3 polyunsaturated fatty acids, such as eicosapentaenoic acid (EPA)<sup>2</sup> and docosahexaenoic acid (DHA), both of which are enriched in fish oils, have beneficial effects in many inflammatory disorders, including cardiovascular disease, arthritis, colitis, and asthma (4, 5). Omega-3 polyunsaturated fatty acids are widely held to act via several possible mechanisms, serving as an alternative substrate producing less potent products (6) or being converted to potent anti-inflammatory and protective mediators, namely resolvins, protectins, and maresins (7–11). Resolvin (Rv) E1 (5S,12R,18R-trihydroxy-6Z,8E,10E,14Z,16E-EPE) and RvE2 (5S,18R-dihydroxy-6E,8Z,11Z,14Z,16E-EPE) are biosynthesized by human polymorphonuclear leukocytes (PMNs) via the 5-lipoxygenase (5-LOX) pathway from a common precursor 18-hydroxyeicosapentaenoic acid (18-HEPE) (8–10). 18-HEPE formation *in vivo* is related to dietary intake of EPA (9), and a recent study demonstrated two parallel stereospecific pathways, 18R- and 18S-, in the biosynthesis of E series resolvins both in human sera and murine exudates (12). Resolvins were first isolated from the self-limited inflammation and were found to serve as stop signals for PMN infiltrations in murine peritonitis (13). These lipid mediators are not only anti-inflammatory but also

<sup>2</sup> The abbreviations used are: EPA, eicosapentaenoic acid; HEPE, hydroxyeicosapentaenoic acid; EPE, eicosapentaenoic acid; LOX, lipoxygenase; MRM, multiple reaction monitoring; PMN, polymorphonuclear leukocyte; PG, prostaglandin; LTB<sub>4</sub>, leukotriene B<sub>4</sub>.

## Novel Anti-inflammatory Mediator 17,18-diHEPE

promote resolution back to the noninflamed state to maintain tissue homeostasis (14).

Here, we report the identification of a novel EPA-derived anti-inflammatory mediator formed via the leukocyte 12/15-LOX pathway. The basic structure of this bioactive EPA metabolite was identified as 17,18*R/S*-dihydroxy-5*Z*,8*Z*,11*Z*,13*E*,15*E*-EPE, denoted 18*R*-RvE3 and 18*S*-RvE3, respectively.

### EXPERIMENTAL PROCEDURES

**Materials**—Racemic 18-HEPE and 15-HETE-d8, LTB<sub>4</sub>-d4, and PGE<sub>2</sub>-d4 were purchased from Cayman Chemical. Zymosan A was purchased from Wako Chemicals. Synthetic RvE2 was prepared as in Ref. 15. Dexamethasone, A23187, and soybean 15-LOX (type I-B) were purchased from Sigma. Male C57BL/6 mice (7–8 weeks) were purchased from CLEA Japan, Inc. 12/15-LOX-deficient mice on C57BL/6 background were purchased from The Jackson Laboratory. Animal studies were approved by the University of Tokyo Animal Committee.

**Isolation of Peripheral Blood Leukocytes**—Peripheral blood neutrophils and eosinophils were isolated from nonatopic healthy subjects as described previously (16). Briefly, red blood cells (RBC) were removed from 40 ml of heparinized peripheral blood using Dextran T-500 (GE Healthcare) and mononuclear cells by centrifugation over 1.083 g/ml Histopaque (Sigma). After hypotonic cell lysis to remove any remaining RBC, neutrophils and eosinophils were separated by a CD16-negative selection using CD16-labeled magnetic microbeads and autoMACS (Miltenyi Biotec). Ethical approval was obtained from the University of Tokyo Research Ethics Committee.

**Neutrophil and Eosinophil Incubations**—Neutrophils or eosinophils were divided into  $5 \times 10^5$  cells in 0.5 ml of Hanks' balanced salt solution and stimulated with calcium ionophore (A23187, 2  $\mu$ M) at 37 °C in the presence of 18-HEPE (1.6  $\mu$ g). After 30 min, 1 ml of ice-cold methanol was added to stop the reaction.

**Mediator Lipidomics, Product Isolation and Extractions**—Samples were extracted by solid-phase extraction using Sep-Pak C18 cartridges (Waters) with a deuterium-labeled internal standard (LTB<sub>4</sub>-d4). LC-MS/MS-based lipidomic analyses were performed using an HPLC system (Waters UPLC) with a linear ion trap quadrupole mass spectrometer (4000 QTRAP; Applied Biosystems) equipped with Acquity UPLC BEH C<sub>18</sub> column (1.0 mm  $\times$  150 mm  $\times$  1.7  $\mu$ m; Waters). Samples were eluted with mobile phase composed of water/acetate (100:0.1, v/v) and acetonitrile/methanol (4:1, v/v) (73:27) for 5 min and ramped to 30:70 after 15 min to 20:80 after 25 min and held for 8 min, ramped to 0:100 after 35 min, and held for 10 min with flow rates of 70  $\mu$ l/min (0–30 min), 80  $\mu$ l/min (30–33 min), and 100  $\mu$ l/min (33–45 min). MS/MS analyses were conducted in negative ion mode, and fatty acid metabolites were identified and quantified by multiple reaction monitoring (MRM). Quantitation was performed using calibration curves constructed for each compound, and recoveries were monitored using added deuterated internal standards (15-HETE-d8, LTB<sub>4</sub>-d4, PGE<sub>2</sub>-d4). Compounds were monitored with MRM transitions of 18-HEPE (317 > 259 *m/z*), RvE3 (333 > 213 *m/z*), and PGE<sub>2</sub> (351 > 271 *m/z*).

**Transfection Studies**—HEK293 cells ( $3.0 \times 10^5$  cells) were transiently transfected with 1.0  $\mu$ g of pCAGGS (17) or pCAGGS containing mouse 12/15-LOX or human 15-LOX cDNA using Lipofectamine 2000 transfection reagent (Invitrogen). After 24 h, cells were incubated with 18-HEPE (10  $\mu$ M) or arachidonic acid (10  $\mu$ M) and calcium ionophore (A23187, 10  $\mu$ M). After 30 min, ice-cold methanol was added to stop the reaction.

**Enzymatic Conversion of 18-HEPE with Soybean 15-LOX**—Soybean 15-LOX (type I-B) was incubated with racemic 18-HEPE, 18*R*-HEPE, or 18*S*-HEPE in borate buffer (10 ml, pH 9.0) at 4 °C. The reaction was terminated at 90 min, and hydroperoxide intermediates were reduced with excess NaBH<sub>4</sub>. Incubations were extracted by using Sep-Pak C18 cartridges (Waters). To separate and isolate conversion products, reverse-phase HPLC was carried out by using a Waters XBridge C<sub>18</sub> column (100 mm  $\times$  4.6 mm  $\times$  5  $\mu$ m) with mobile phase methanol/water/acetate (65:35:0.0035, v/v/v) at 0.7 ml/min of flow rate.

**Murine Zymosan-induced Peritonitis**—Peritonitis was performed as in Ref. 13. Compounds were administered intravenously through a tail vein and followed by 1 ml of zymosan A (1 mg/ml) into peritoneum. Peritoneal lavages were collected at 2 h, and cells were enumerated. Differential leukocyte counts were performed by Wright-Giemsa stain and light microscopy. For LC-MS/MS analysis, mice were sacrificed at 48 h after zymosan challenge, and peritoneal exudates were collected.

**Neutrophil Chemotaxis Assay**—Chemotaxis experiments were conducted using EZ-TAXIScan chamber (Effector Cell Institute, Tokyo, Japan). The EZ-TAXIScan is a visually accessible chemotactic chamber, in which one compartment containing chemoattractant and another compartment containing cells are connected by a microchannel (18, 19). PMNs were isolated from mouse bone marrow. Bone marrow cells were obtained by flushing femurs of C57BL/6 male mice (8–10 weeks) with Hanks' balanced salt solution supplemented with 20 mM HEPES, pH 7.4, and 0.5% FCS. RBC were lysed with 0.2% NaCl, and the PMNs were isolated over a 62% Percoll gradient by centrifugation for 30 min at  $1,000 \times g$ .

The EZ-TAXIScan chamber was assembled with a 260  $\mu$ m wide  $\times$  4  $\mu$ m thick silicon chip on an untreated slide glass and filled with RPMI 1640 medium, 0.1% BSA. One microliter of test compounds was then added directly to the lower and upper reservoir. PMNs ( $6 \times 10^3$  cells) were preincubated with test compounds for 5 min and were added to the lower reservoir of each of the six channels and allowed to line up by removing 10  $\mu$ l of buffer from the upper reservoir. One microliter of chemoattractant (LTB<sub>4</sub>, 10 nM) was then added to the upper reservoir, and PMN migration at room temperature was recorded every 30 s for 40 min and was analyzed with TAXIScan Analyzer 2 software.

**NMR Experiments of RvE3**—<sup>1</sup>H and two-dimensional NMR spectra of RvE3 (10  $\mu$ g, 30 nmol of compound V, and 20  $\mu$ g, 60 nmol of compound VI, respectively) in CD<sub>3</sub>OD (0.25 ml) were recorded at 298.1 K on a Varian Unity Inova 800 instruments (800 MHz for <sup>1</sup>H NMR) equipped with a cold probe. Chemical shifts are denoted in  $\delta$  (ppm) relative to residual solvent peaks as internal standard (CD<sub>3</sub>OD, <sup>1</sup>H  $\delta$  3.31).

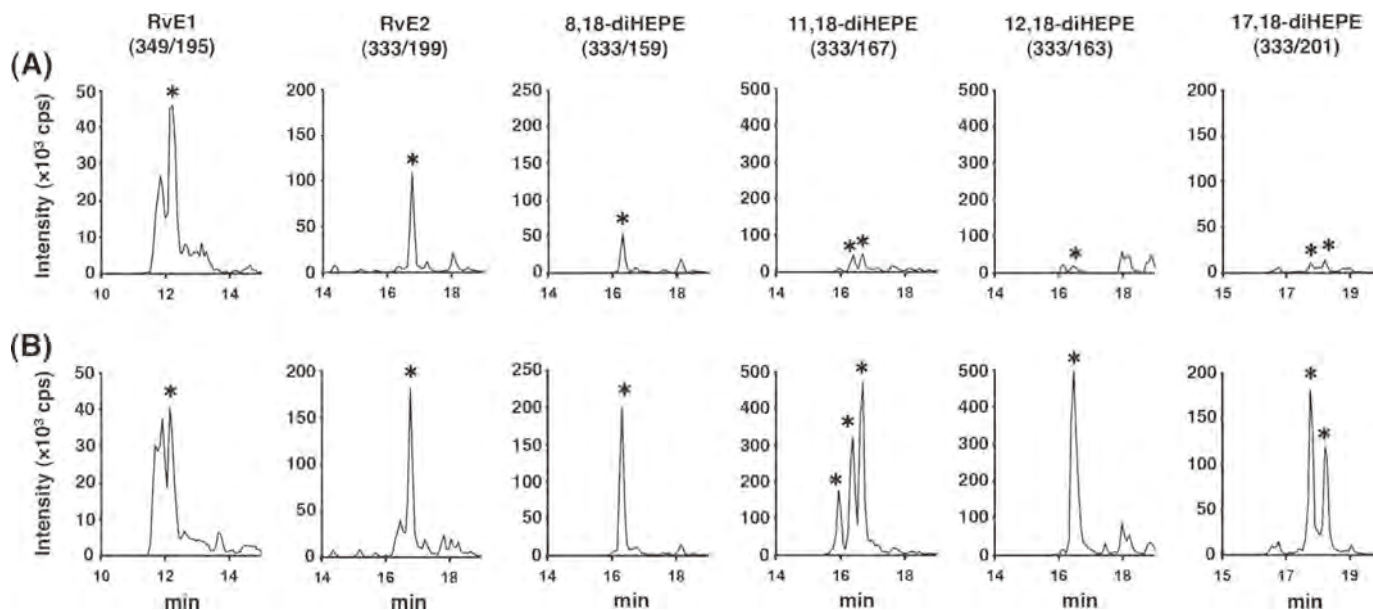


FIGURE 1. **Formation of 18-HEPE metabolites from human leukocyte incubations.** MRM chromatograms of the 18-HEPE incubation products with human PMN (A) and eosinophils (B) were separated by reverse-phase HPLC. 18-HEPE metabolites were monitored by MRM mode using established transitions for RvE1 (349/195  $m/z$ ) and RvE2 (333/199  $m/z$ ) as well as predicted transitions for 8,18-diHEPE (333/159  $m/z$ ), 11,18-diHEPE (333/167  $m/z$ ), 12,18-diHEPE (333/163  $m/z$ ), and 17,18-diHEPE (333/201  $m/z$ ). Peaks of each metabolite are marked by asterisks.

**Statistical Analysis**—Results are expressed as mean  $\pm$  S.E. Statistical significance was determined by Student's *t* test;  $p < 0.05$  was considered significant.

## RESULTS

**Formation of Novel Metabolites by Eosinophils**—Because human PMNs incubated with 18-HEPE in the presence of a calcium ionophore produced E series resolvins (*i.e.* RvE1 and RvE2) via 5-LOX pathway (7), we questioned whether other EPA metabolite(s) with potent anti-inflammatory property could be formed by other cell types. Because our previous study demonstrated that eosinophils are recruited to the inflamed loci during the resolution phase of acute peritonitis and promote resolution by producing pro-resolving mediators (20), we focused on eosinophils. Human eosinophils were isolated from peripheral blood and were incubated with racemic 18-HEPE in the presence of a calcium ionophore. Unbiased target lipidomics using liquid chromatography-tandem mass spectrometry (LC-MS/MS)-based analyses were performed, and several hydroxylated products were identified using MRM with established or predicted precursor-product ion pairs. Side-by-side MRM chromatograms of products from human PMN and eosinophil incubations with 18-HEPE (Fig. 1, A and B, respectively) clearly demonstrate that human PMN converted 18-HEPE into RvE1 and RvE2, as reported previously (10, 12). However, isolated human eosinophils converted 18-HEPE into novel 8,18-dihydroxy-EPE (8,18-diHEPE), 11,18-diHEPE, 12,18-diHEPE, and 17,18-diHEPE in addition to RvE1 and RvE2. Because human eosinophils express higher levels of leukocyte-type 15-LOX than PMNs (21), we reasoned that 8,18-diHEPE, 11,18-diHEPE, 12,18-diHEPE, and 17,18-diHEPE might be formed via the 15-LOX pathway. To this end, we isolated eosinophils from wild type or mice deficient in leukocyte-type 12/15-LOX, a murine orthologue of human 15-LOX (22),

and incubated them with 18-HEPE. As expected, much less of the novel products was detected from the incubation of 12/15-LOX-deficient murine eosinophils (Fig. 2).

To further confirm the 12/15-LOX-dependent formation of novel products, HEK293 cells were transiently transfected with expression plasmid encoding 12/15-LOX and were incubated with 18-HEPE in the presence of calcium ionophore. Cells expressing mouse leukocyte-type 12/15-LOX or human 15-LOX efficiently converted 18-HEPE into 8,18-diHEPE, 11,18-diHEPE, 12,18-diHEPE, and 17,18-diHEPE (Fig. 3A). As reported previously (22), when arachidonic acid was used as a substrate, murine 12/15-LOX exhibited a major arachidonic acid 12-LOX activity (C10-hydrogen abstraction), whereas the human orthologue acts predominantly as 15-LOX (C13-hydrogen abstraction) (Fig. 3B). Similarly, murine 12/15-LOX formed predominantly 8,18-diHEPE and 12,18-diHEPE from 18-HEPE possibly through C10-hydrogen abstraction, whereas human 15-LOX preferentially converted 18-HEPE into 11,18-diHEPE and 17,18-diHEPE, possibly through C13-hydrogen abstraction (Fig. 3A). Side-by-side comparison of arachidonic acid- or 18-HEPE-derived products from eosinophil incubations also demonstrated the species difference between mouse and human (Fig. 3, C and D). These results indicate the different enzyme species convert 18-HEPE to a same series of oxidized products with different ratios both *in vitro* and in cells.

To synthesize 18-HEPE conversion products *in vitro*, racemic 18-HEPE was incubated with soybean 15-LOX. A total of six products (compounds I–VI) carrying chromophore of conjugated triene were generated (Fig. 4A). Based on the MS/MS spectra, compounds I–IV were assigned as 11,18-diHEPE, and compounds V and VI were assigned as 17,18-diHEPE (Fig. 4B). 11,18-diHEPEs and 17,18-diHEPEs had UV absorbance peaks at 268 and 273 nm, respectively, demonstrating the presence of

## Novel Anti-inflammatory Mediator 17,18-diHEPE

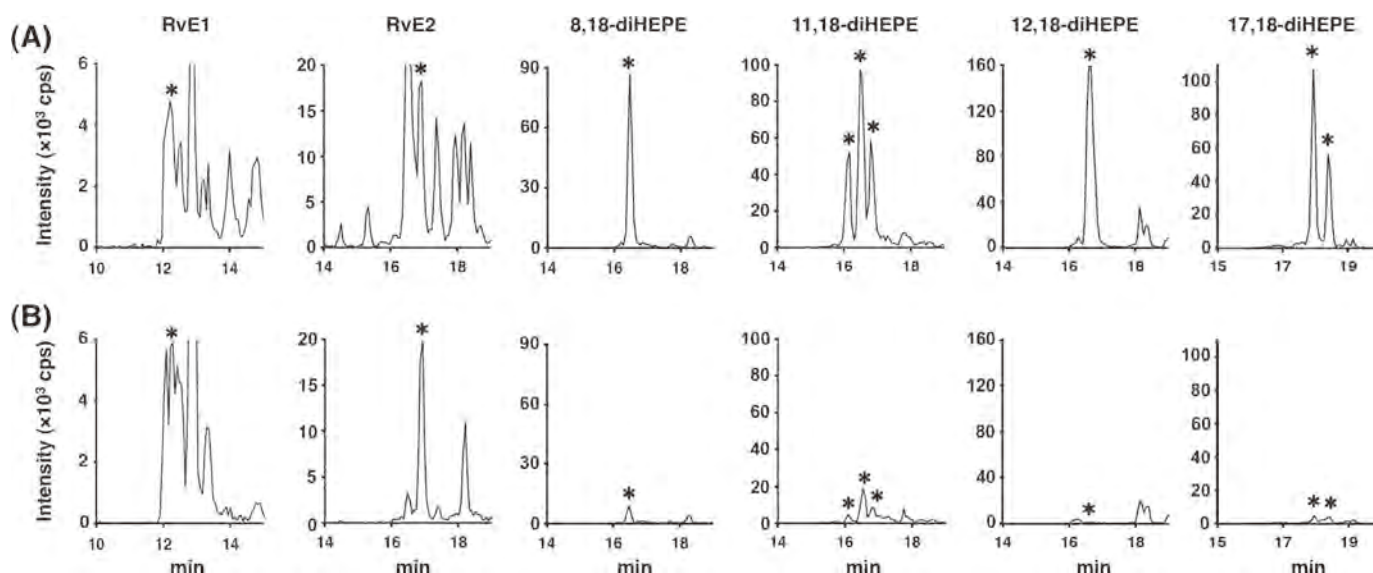


FIGURE 2. 12/15-LOX-dependent formation of 18-HEPE metabolites from mouse eosinophils. Lipidomic profiles of 18-HEPE incubation products of mouse eosinophils (A) and 12/15-LOX-deficient mouse eosinophils (B) were compared.

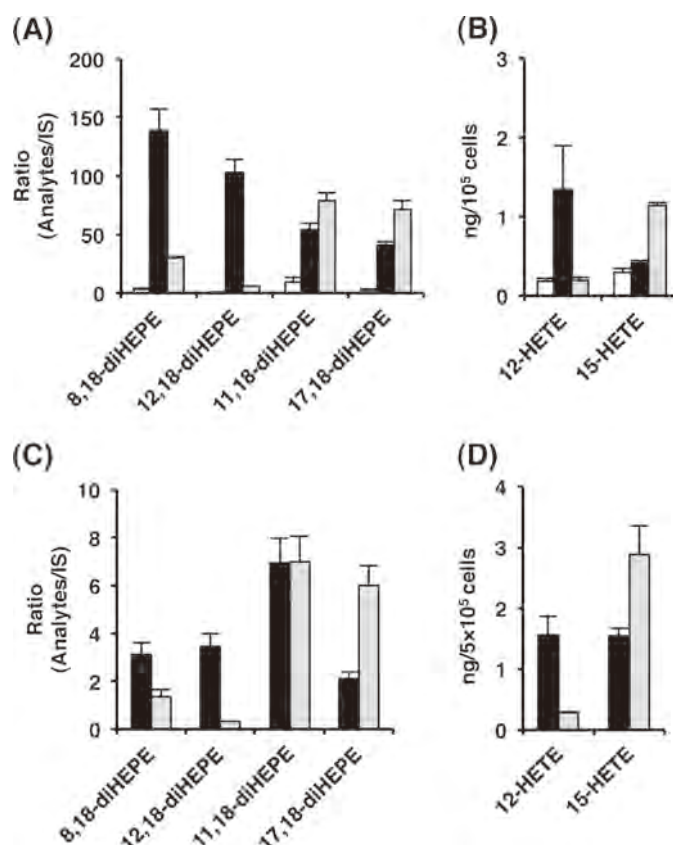


FIGURE 3. Formation of 18-HEPE metabolites by cells expressing mouse 12/15-LOX or human 15-LOX. Lipidomic profiles of 18-HEPE (A) or arachidonic acid (B) incubation products of HEK293 cells transiently transfected with mock (white bars), mouse 12/15-LOX (black bars), or human 15-LOX (gray bars) cDNA plasmids are shown. Lipidomic profiles of 18-HEPE (C) or arachidonic acid (D) incubation products of mouse (black bars) or human (gray bars) eosinophils are shown. Relative production was determined by calculating peak area ratio of each analyte to deuterium-labeled internal standard (LTB<sub>4</sub>-d<sub>4</sub>). Values represent mean  $\pm$  S.E.,  $n = 3-5$ .

conjugated triene structures (Fig. 4B). These enzymatically generated compounds co-eluted with eosinophil-derived products at 16.2 min (compound I), 16.6 min (compounds II and III), 16.9 min (compound IV), 18.1 min (compound V), and 18.5 min (compound VI), respectively (Fig. 5). Therefore, we used these

enzymatically generated compounds to further assess their biological activities *in vivo*.

**Inhibition of PMN Infiltration in Murine Peritonitis**—Earlier studies demonstrated that nanogram doses of E series resolvins (RvE1 and RvE2) significantly reduced PMN infiltration *in vivo*

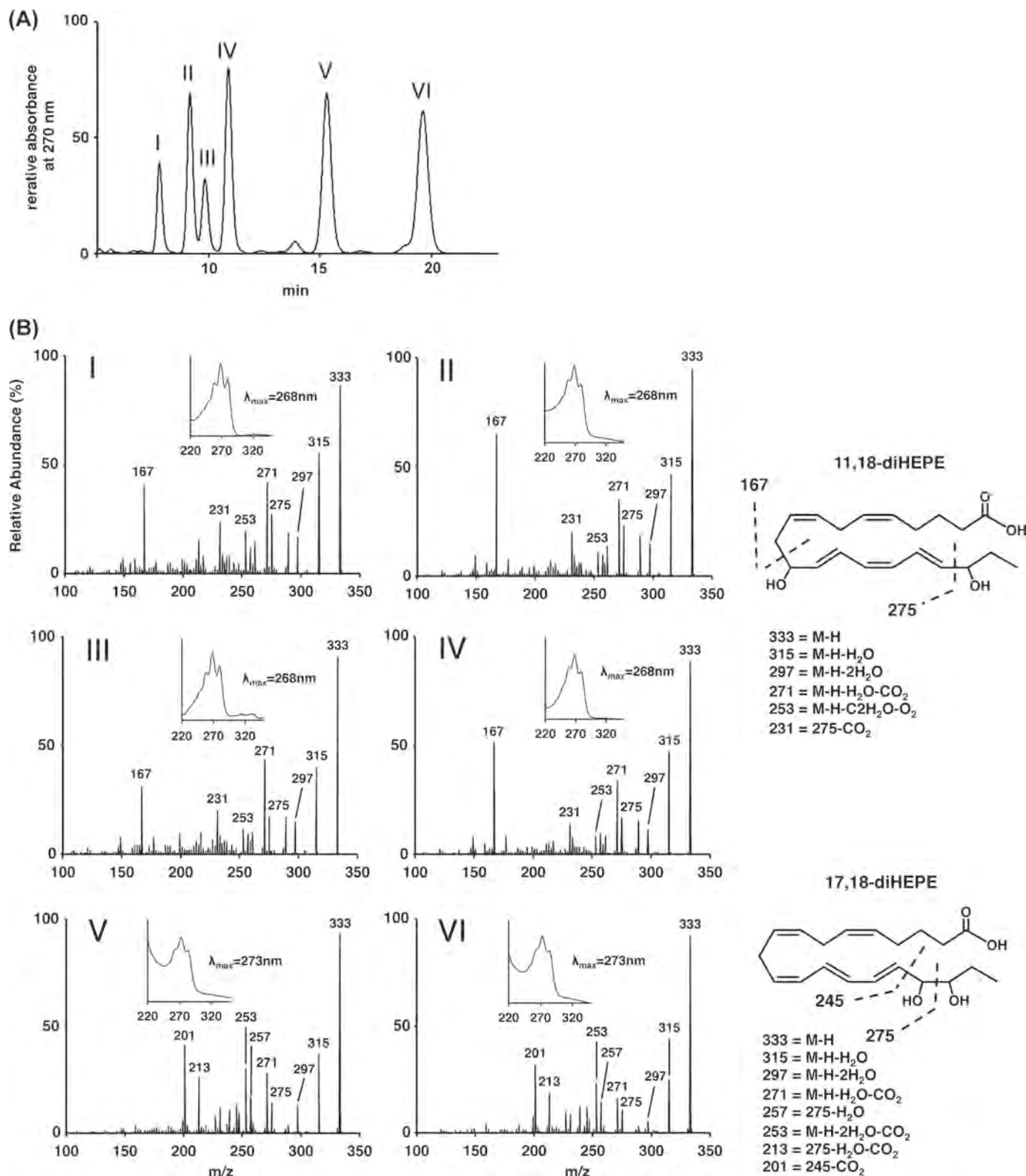


FIGURE 4. Enzymatic formation of 18-HEPE metabolites and their anti-inflammatory properties *in vivo*. A, reverse-phase HPLC chromatogram of the 18-HEPE incubation products with soybean 15-LOX monitored with UV absorbance at 270 nm. B, UV and tandem mass spectra of major products isolated from soybean 15-LOX incubation. Based on the MS/MS spectra, compounds I to IV were assigned as 11,18-diHEPE with corresponding fragments at *m/z* 333(M-H), 315(M-H-H<sub>2</sub>O), 297(M-H-2H<sub>2</sub>O), 271(M-H-H<sub>2</sub>O-CO<sub>2</sub>), 253(M-H-2H<sub>2</sub>O-CO<sub>2</sub>), and diagnostic fragments at *m/z* 275, 231(275-CO<sub>2</sub>), and 167. Compounds V and VI were assigned as 17,18-diHEPE with corresponding fragments at *m/z* 333(M-H), 315(M-H-H<sub>2</sub>O), 297(M-H-2H<sub>2</sub>O), 271(M-H-H<sub>2</sub>O-CO<sub>2</sub>), 253(M-H-2H<sub>2</sub>O-CO<sub>2</sub>), and diagnostic ions at *m/z* 275, 257(275-H<sub>2</sub>O), 245, 213(275-H<sub>2</sub>O-CO<sub>2</sub>), and 201(245-CO<sub>2</sub>).

Downloaded from www.jbc.org at CHUBU DAIGAKU TOSHOKAN, on January 7, 2013

## Novel Anti-inflammatory Mediator 17,18-diHEPE

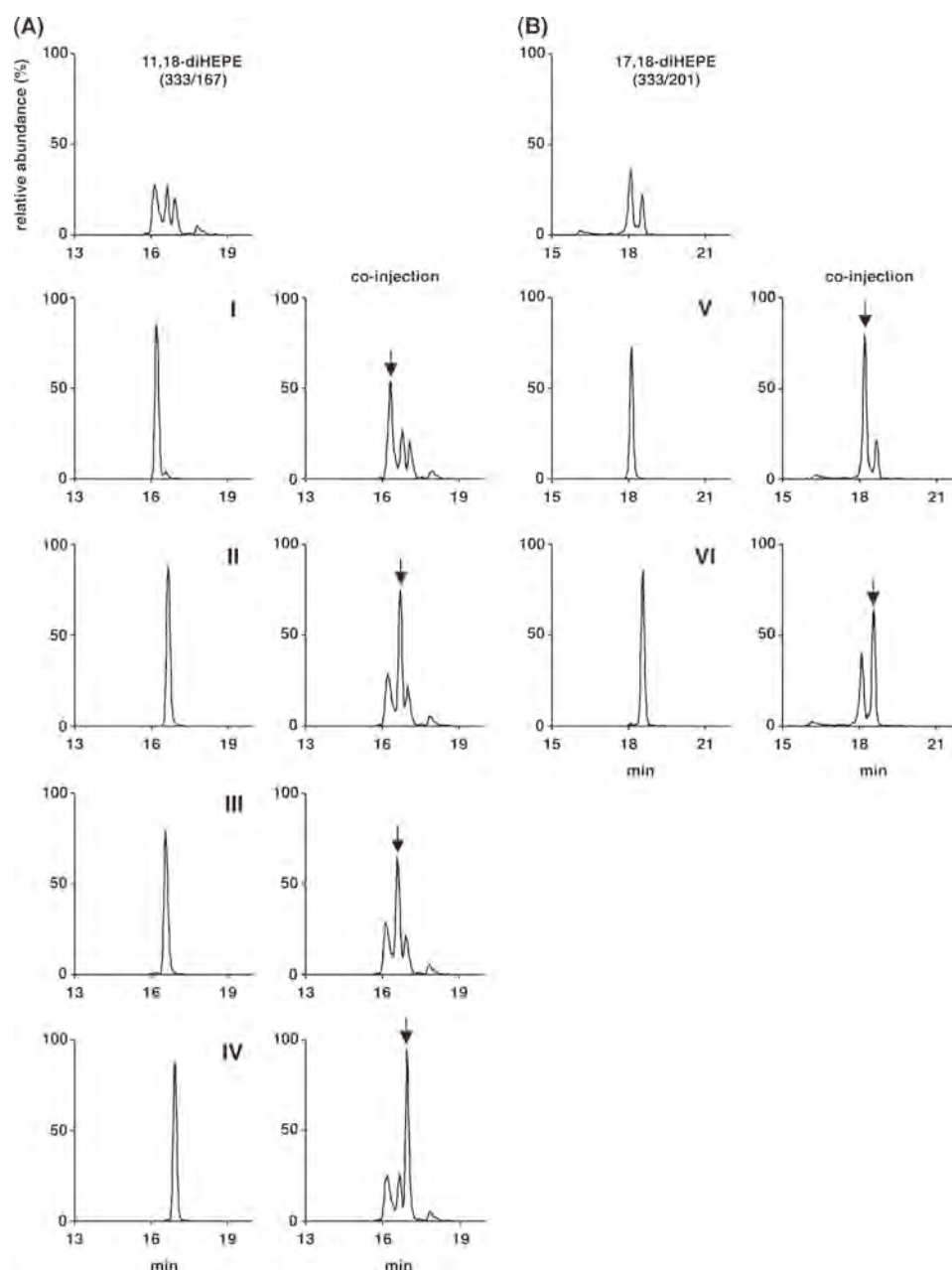
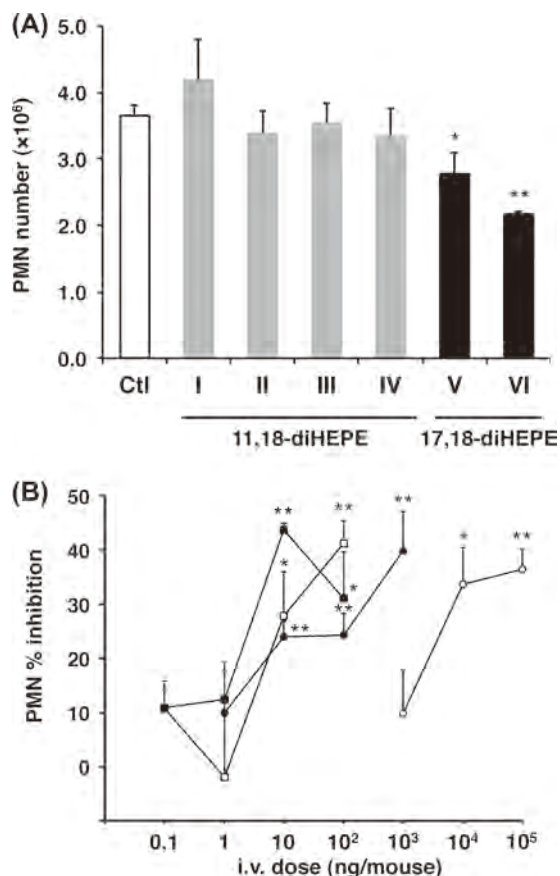


FIGURE 5. **Comparison of eosinophil-derived 18-HEPE metabolites with enzymatically generated products.** Top panel, MRM chromatograms of 11,18-diHEPE (A) and 17,18-diHEPE (B) obtained from eosinophil incubation with 18-HEPE. Lower panels, MRM chromatograms of compounds I–VI obtained from soybean 15-LOX-catalyzed synthesis and co-injection of these enzymatically generated products with eosinophil derived products. Note that compounds II and III co-eluted in this liquid chromatographic condition.

(8–10). We determined whether enzymatically generated compounds displayed anti-inflammatory actions *in vivo*. Zymosan A, a glucan from a yeast cell wall, was used to induce sterile peritonitis characterized by acute PMN infiltration. Administration of 10 ng/mouse of the 17,18-diHEPE isomers (compounds V and VI) significantly blocked PMN infiltration by  $27.9 \pm 8.2$  and  $43.7\% \pm 1.3\%$ , respectively (Fig. 6A). In contrast, little effect was observed by the administration of 11,18-diHEPEs (compounds I–IV), which show the structure-specific activity of 17,18-diHEPEs. Compound V at 100 ng/mouse and compound VI at 10 ng/mouse dramatically inhibited PMN infiltration and were almost as potent as higher doses of RvE2 (1  $\mu\text{g}/\text{mouse}$ ) or dexamethasone (10  $\mu\text{g}/\text{mouse}$ ) (Fig. 6B). For

comparison in this model, EPA administration at 100 ng/mouse gave no effect on PMN numbers ( $(3.36 \pm 0.7) \times 10^6$  versus  $(3.31 \pm 0.3) \times 10^6$  cells,  $n = 4$ ), suggesting that EPA requires metabolic conversion to exert its actions on leukocyte infiltrations *in vivo*. Given their biosynthetic route and their potent anti-inflammatory actions, the two isomers of 17,18-diHEPE (compounds V and VI) were collectively denoted RvE3.

**Structure Determination of RvE3 Isomers by NMR**—Minute amounts of the two enzymatically prepared RvE3 isomers (30–60 nmol) were analyzed by high field NMR. The planar structures of the two RvE3 isomers (compounds V and VI), including the positions of the hydroxy groups and the geometries of the olefins, were unambiguously established using  $^1\text{H}$



**FIGURE 6. Inhibition of PMN infiltration in zymosan-induced peritonitis.** A, compounds I–VI were injected intravenously (10 ng/mouse) via tail vein followed by peritoneal injection of zymosan A (1 mg/ml). After 2 h, peritoneal lavages were collected, and PMN leukocyte numbers were counted. Values represent mean  $\pm$  S.E.,  $n = 3$ –12, \*,  $p < 0.05$ ; \*\*,  $p < 0.01$  as compared with vehicle control. B, dose-dependent comparison of the actions of compound V (□), compound VI (■), RvE2 (●) and dexamethasone (○) on PMN infiltration. Values represent mean  $\pm$  S.E.,  $n = 4$ –12, \*,  $p < 0.05$ ; \*\*,  $p < 0.01$  as compared with vehicle control.

NMR and  $^1\text{H}$ - $^1\text{H}$  COSY spectra ( $\text{CD}_3\text{OD}$ , 800 MHz) (supplemental Figs. S1 and S2 and supplemental Table S1). The coupling constants of the olefinic protons from C11 to C16 clearly indicated that both RvE3 isomer possessed 11Z,13E,15E-conjugated trienes (Fig. 7A). Therefore, we concluded that RvE3 is 17,18-dihydroxy-5Z,8Z,11Z,13E,15E-EPE and that compounds V and VI are stereoisomers of 17,18-hydroxy groups.

**Stereoselective Synthesis of 18R- and 18S-RvE3**—The 18R- and 18S-HEPE enantiomers were chemically synthesized (supplemental Fig. S3) and were submitted to the 15-LOX reaction to better understand stereochemical structures of RvE3 isomers. Separate treatment of the synthesized 18R- and 18S-HEPE by soybean 15-LOX delivered the different diastereomers of 17,18-diHEPEs. The  $^1\text{H}$  NMR spectra and the HPLC retention time of 17,18S-diHEPE and 17,18R-diHEPE were found to be identical to those of compounds V and VI, respectively (Fig. 7, B and C). Importantly, these enzymatically generated products co-eluted with 17,18-diHEPEs formed *in vivo* within inflammatory exudates of murine peritonitis (Fig. 8). By combining these results, the structures of endogenously formed RvE3 isomers were determined to be 17,18S-dihydroxy-5Z,8Z,11Z,13E,15E-EPE (compound V, 18S-RvE3) and

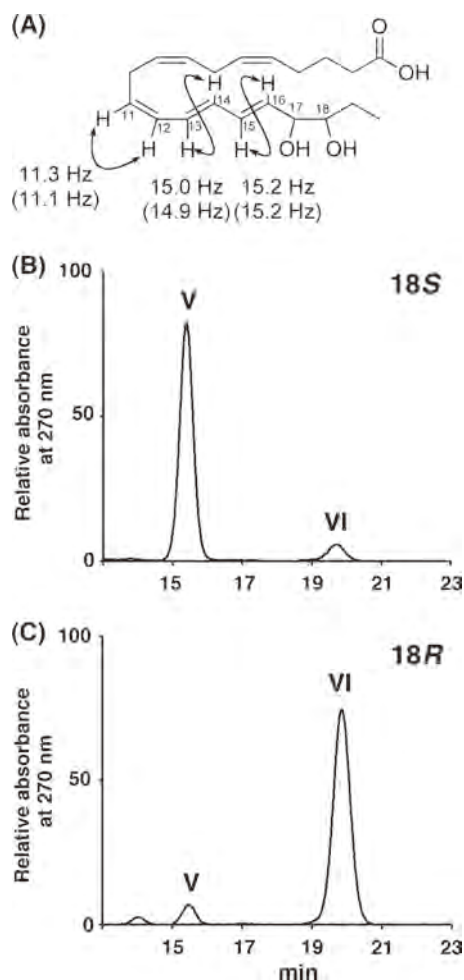


**FIGURE 7. Physical and spectroscopic properties of RvE3.** A,  $^1\text{H}$ - $^1\text{H}$  coupling constants of conjugated triene and full structure of RvE3 (compound V and VI). B and C, reverse-phase HPLC chromatogram of synthetic 18S-HEPE or 18R-HEPE incubation products with soybean 15-LOX monitored with UV absorbance at 270 nm.

17,18R-dihydroxy-5Z,8Z,11Z,13E,15E-EPE (compound VI, 18R-RvE3), respectively. Endogenous levels of 18R-RvE3, 18S-RvE3, and their precursor 18-HEPE in inflammatory exudates of murine peritonitis were  $\sim 14$ , 32, and 222 pg/mouse, respectively. These levels were comparable with that of  $\text{PGE}_2$  (100 pg/mouse) in this model. Moreover, when EPA was supplemented, we could detect much higher levels of 18R-RvE3, 18S-RvE3, and 18-HEPE in the peritoneal fluid (supplemental Table S2).

**Inhibition of PMN Chemotactic Migration**—Next, we examined whether these RvE3 isomers affect PMN chemotaxis *in vitro*. Murine PMNs isolated from bone marrow were applied to an EZ-TAXIScan chemotaxis chamber (18) in which a stable chemoattractant gradient was formed (Fig. 9A). Cell movements were time-lapse recorded such that the path and migration speed of an individual PMN could be determined. Both 18S- and 18R-RvE3 at nanomolar concentrations significantly reduced PMN migration speeds toward  $\text{LTB}_4$  (Fig. 9, B and C). Thus, both RvE3 isomers directly act on PMNs to control chemotaxis as did 15-epi-lipoxin  $\text{A}_4$  tested in parallel for direct comparison. These PMN responses were not observed by EPA,

## Novel Anti-inflammatory Mediator 17,18-diHEPE

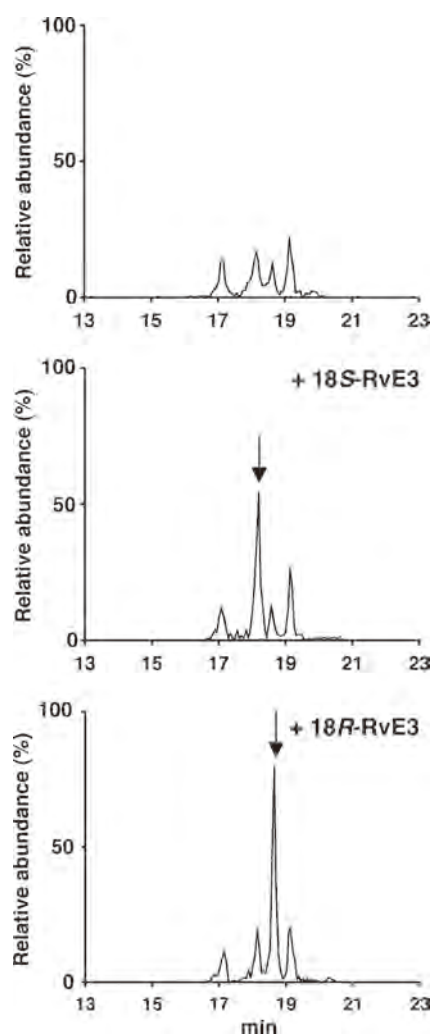


FIGURE 8. **RvE3 formation *in vivo*.** Comparison of endogenously formed 17,18-diHEPEs in mouse inflammatory exudates with enzymatically generated RvE3 isomers. *Top panel*, MRM chromatogram with established transition of 333/201 *m/z* to monitor 17,18-diHEPEs present in murine peritoneal exudates 48 h after zymosan challenge. *Middle and lower panel*, MRM chromatogram obtained from co-injection of enzymatically generated 18S-RvE3 (*middle panel*) or 18R-RvE3 (*lower panel*) with 17,18-diHEPEs present in murine peritoneal exudates 48 h after zymosan challenge.

a metabolic precursor of RvE3, when introduced at equal concentrations in the chambers (Fig. 9B).

RvE3 had little effect on cyclic AMP, intracellular calcium level, and morphology of mouse bone marrow PMNs (supplemental Fig. S4). Also, RvE3 treatment had little effect on the LTB<sub>4</sub>-induced calcium influx. This result suggests that the inhibitory effect of RvE3 on PMN chemotaxis is not simply due to LTB<sub>4</sub> receptor antagonism or cytotoxic action.

## DISCUSSION

The results of this study uncover the structure and anti-inflammatory property of a new EPA-derived mediator RvE3. Human and mouse eosinophils generated RvE3 from 18-HEPE via leukocyte-type 12/15-LOX pathway. Enzymatically generated RvE3 had the same physical properties as endogenously biosynthesized products and displayed a potent anti-inflammatory action by stopping PMN infiltration in zymosan-induced peritonitis. The structures of the two diastereomeric RvE3

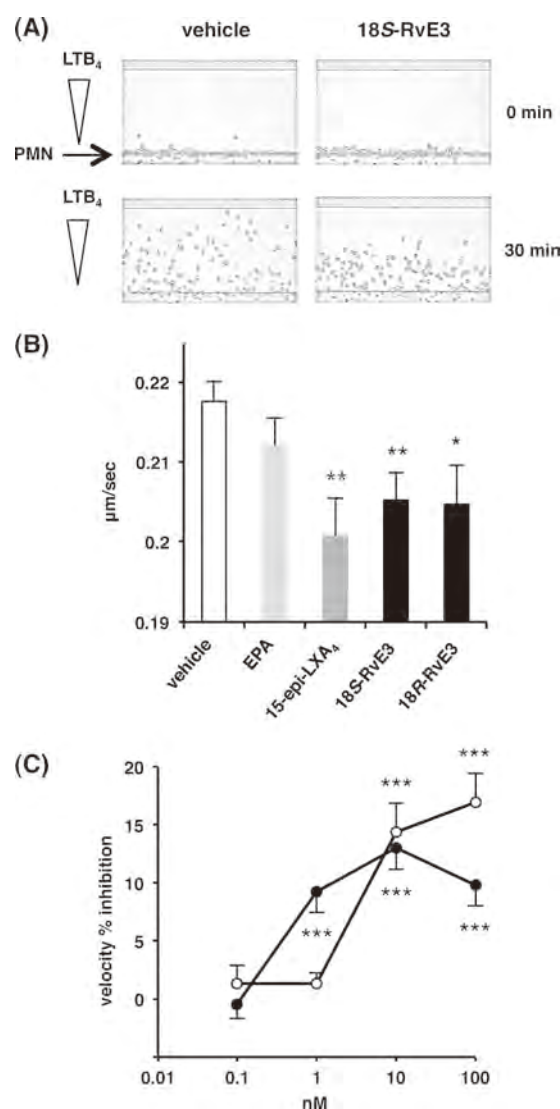


FIGURE 9. **RvE3 reduces mouse PMN chemotaxis efficiency.** Effect of RvE3 on chemotaxis of mouse bone marrow PMNs toward LTB<sub>4</sub>. *A*, bone marrow PMNs were incubated with 10 nM 18S-RvE3 during the assay. Images of PMNs are shown at 0 and 30 min after addition of LTB<sub>4</sub> (10 nM) as a chemoattractant. *B*, velocity of the motile cells were determined from digital time lapse movies. *C*, concentration dependence of 18S-RvE3 (○) and 18R-RvE3 (●) on reduced velocity of PMN chemotaxis. Values represent mean ± S.E., *n* ≥ 20 cells, \*, *p* < 0.05; \*\*, *p* < 0.01; \*\*\*, *p* < 0.001 as compared with vehicle control.

were determined to be 17,18S-dihydroxy-5*Z*,8*Z*,11*Z*,13*E*,15*E*-EPE (compound V, 18S-RvE3) and 17,18*R*-dihydroxy-5*Z*,8*Z*,11*Z*,13*E*,15*E*-EPE (compound VI, 18*R*-RvE3), respectively. Both 18*S*- and 18*R*-RvE3 inhibited PMN chemotaxis *in vitro* at low nanomolar concentrations as evidenced by decreased velocity. Reduced chemotaxis of PMN is relevant in many diseases where uncontrolled inflammation is the underlying pathophysiology (1, 2, 7). Hence reduced PMN chemotaxis by RvE3 would be relevant in all conditions where PMN-mediated tissue injury is important.

Although the E series resolvins (*i.e.* RvE1 and RvE2) are formed via the 5-LOX pathway, this study uncovered a novel route of anti-inflammatory cascade via the 12/15-LOX pathway (Fig. 10). EPA is converted to 18-HEPE by aspirin-acetylated COX-2 (8) or cytochrome P450 monooxygenase (23). 18-HEPE is further converted via sequential actions of lipoxygenases,

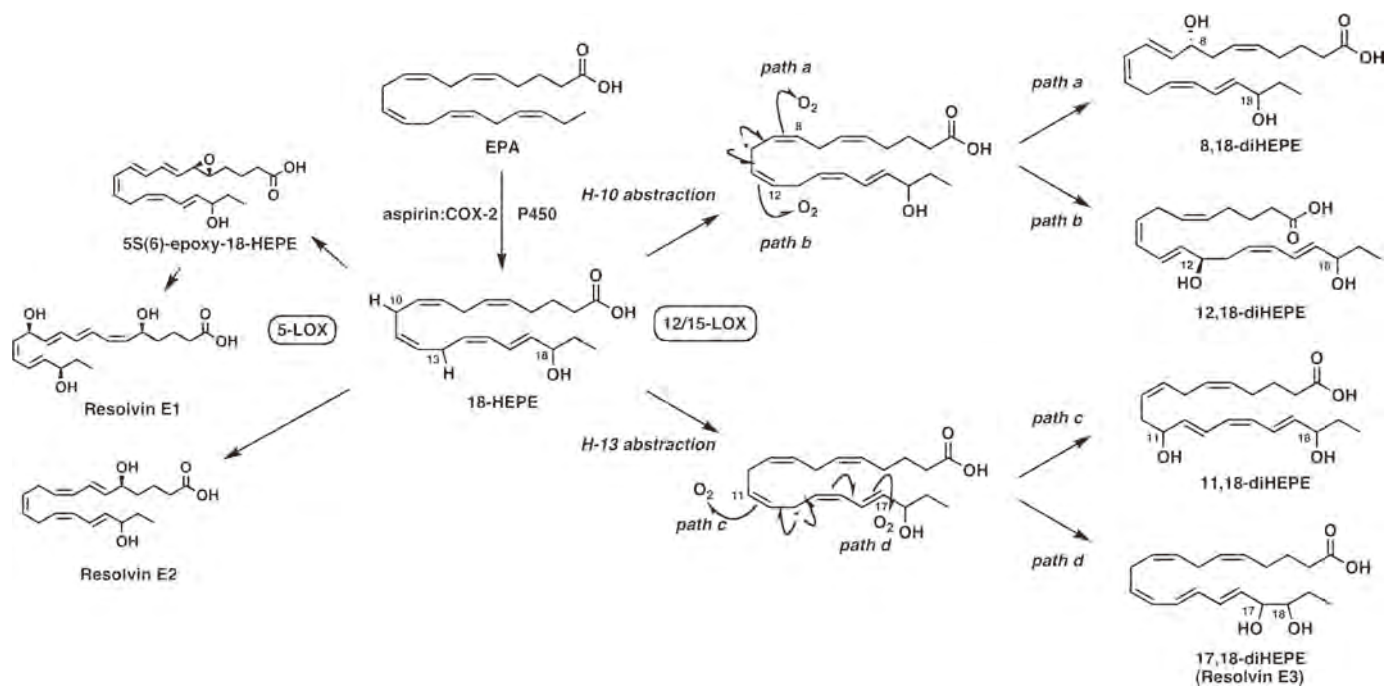


FIGURE 10. **Proposed scheme for biosynthesis of E series resolvins and related products.** E series resolvins are generated from a common precursor 18-HEPE. EPA is converted to 18-HEPE by aspirin-acetylated COX-2 or cytochrome P450 monooxygenase. 18-HEPE is further converted via the sequential actions of lipoxygenases, which leads to formation of E series resolvins. 5-LOX expressed in PMNs converts 18-HEPE into RvE1 and RvE2. The stereochemistry of RvE1 and RvE2 was established (9, 12). In addition, 18-HEPE is converted by 12/15-LOX present in eosinophils or resident macrophages into 8,18-diHEPE, 11,18-diHEPE, 12,18-diHEPE, and 17,18-diHEPE (RvE3). The stereochemistry of the alcohols in 8,18-diHEPE and 12,18-diHEPE is depicted as tentative.

which leads to the formation of E series resolvins. It is likely that hydrogen abstraction from C13 by 12/15-LOX induced a stereospecific oxygen insertion at C11 or C17, leading to the formation of 11,18-diHEPE and RvE3. After 12/15-LOX abstracts pro-S-hydrogen from the C13 position of 18-HEPE, molecular oxygen is generally inserted at C17 in an antarafacial fashion (24), resulting in formation of the 17*R*-hydroxylated compounds. Therefore, both RvE3 isomers are likely to have 17*R*-hydroxy groups. Also, hydrogen abstraction from C10 induced the insertion of oxygen at C8 or C12 to form 8,18-diHEPE and 12,18-diHEPE, respectively (Fig. 10). It is important to note that leukocyte-type 12/15-LOX is an enzyme present in murine cells, and in humans there are at least two different enzymes (15-LOX and 15-LOX2) (22). Murine 12/15-LOX exhibits a major arachidonic acid 12-LOX activity (C10-hydrogen abstraction), whereas the human orthologue acts predominantly as 15-LOX (C13-hydrogen abstraction) when arachidonic acid is used as a substrate. We showed the difference in enzymatic property between mouse 12/15-LOX and human 15-LOX when 18-HEPE was used as a substrate. Murine 12/15-LOX formed predominantly 8,18-diHEPE and 12,18-diHEPE possibly through C10-hydrogen abstraction, whereas human 15-LOX preferentially converted 18-HEPE into 11,18-diHEPE and RvE3, possibly through C13-hydrogen abstraction (Fig. 3).

The contribution of eosinophils to the biosynthesis of RvE3 and other 12/15-LOX-derived mediators such as lipoxins and protectins (25–27) is of interest in controlling acute inflammation and resolution. A recent study has demonstrated that eosinophils are recruited to the inflamed loci during the resolution phase of acute peritonitis and promote resolution by producing pro-resolving mediators in mice (20). Besides eosino-

phils, 12/15-LOX is expressed in tissue resident macrophages, dendritic cells, mast cells, and airway epithelial cells (22). Also, the expression level of 12/15-LOX is up-regulated in various cell types by Th2 cytokines, including interleukin(IL)-4 and IL-13 (22). Cells expressing 12/15-LOX might be involved in regulating inflammatory responses by locally producing anti-inflammatory lipid mediators such as RvE3. This is consistent with reports that document exacerbated inflammatory responses in 12/15-LOX-deficient mice in several disease models (25–27).

PMNs constitute the first line of defense against foreign pathogens. In response to stimuli, PMNs migrate into inflamed tissues, where they protect their host by engulfing, killing, and digesting pathogens. Conversely, excessive and sustained PMN activation can cause tissue damage and uncontrolled inflammation. Therefore, PMN function needs to be well controlled, and endogenous mediators that control these PMN responses are of interest. In this study, RvE3 proved to be a potent inhibitor of PMN chemotaxis *in vitro* and also significantly reduced PMN numbers in zymosan-induced peritonitis model *in vivo*. Intravenous administration of 18*R*- and 18*S*-RvE3 in a dose as small as 10 ng/mouse gave 30–45% inhibition of PMN infiltration that was maintained at the 100-ng doses. The characteristics of partial inhibition of PMN infiltration may benefit potential anti-inflammatory roles of these mediators without compromising host defense via immune suppression. Hence, it might be useful to consider RvE3 as a new endogenous anti-inflammatory compound to protect against an aberrant or uncontrolled innate inflammatory response and as a potential new therapeutic.

## Novel Anti-inflammatory Mediator 17,18-diHEPE

*Acknowledgments*—We are grateful to Michiko Kamio for skillful technical assistance, and Dr. Shigeru Matsuoka (University of Tokyo) for performing NMR experiments.

### REFERENCES

- Nathan, C., and Ding, A. (2010) Nonresolving inflammation. *Cell* **140**, 871–882
- Gilroy, D. W., Lawrence, T., Perretti, M., and Rossi, A. G. (2004) Inflammatory resolution. New opportunities for drug discovery. *Nat. Rev. Drug Discov.* **3**, 401–416
- Serhan, C. N., Chiang, N., and Van Dyke, T. E. (2008) Resolving inflammation. Dual anti-inflammatory and pro-resolution lipid mediators. *Nat. Rev. Immunol.* **8**, 349–361
- GISSI-Prevenzione Investigators (1999) Dietary supplementation with *n*-3 polyunsaturated fatty acids and vitamin E after myocardial infarction. Results of the GISSI-Prevenzione trial. Gruppo Italiano per lo Studio della Sopravvivenza nell'Infarto miocardico. *Lancet* **354**, 447–455
- Simopoulos, A. P. (2002) Omega-3 fatty acids in inflammation and autoimmune diseases. *J. Am. Coll. Nutr.* **21**, 495–505
- Schmitz, G., and Ecker, J. (2008) The opposing effects of *n*-3 and *n*-6 fatty acids. *Prog. Lipid Res.* **47**, 147–155
- Serhan, C. N. (2007) Resolution phase of inflammation. Novel endogenous anti-inflammatory and proresolving lipid mediators and pathways. *Annu. Rev. Immunol.* **25**, 101–137
- Serhan, C. N., Clish, C. B., Brannon, J., Colgan, S. P., Chiang, N., and Gronert, K. (2000) Novel functional sets of lipid-derived mediators with anti-inflammatory actions generated from omega-3 fatty acids via cyclooxygenase 2-nonsteroidal anti-inflammatory drugs and transcellular processing. *J. Exp. Med.* **192**, 1197–1204
- Arita, M., Bianchini, F., Aliberti, J., Sher, A., Chiang, N., Hong, S., Yang, R., Petasis, N. A., and Serhan, C. N. (2005) Stereochemical assignment, anti-inflammatory properties, and receptor for the omega-3 lipid mediator resolvin E1. *J. Exp. Med.* **201**, 713–722
- Tjonahen, E., Oh, S. F., Siegelman, J., Elangovan, S., Percarpio, K. B., Hong, S., Arita, M., and Serhan, C. N. (2006) Resolvin E2. Identification and anti-inflammatory actions. Pivotal role of human 5-lipoxygenase in resolvin E series biosynthesis. *Chem. Biol.* **13**, 1193–1202
- Serhan, C. N., Yang, R., Martinod, K., Kasuga, K., Pillai, P. S., Porter, T. F., Oh, S. F., and Spite, M. (2009) Maresins. Novel macrophage mediators with potent anti-inflammatory and pro-resolving actions. *J. Exp. Med.* **206**, 15–23
- Oh, S. F., Pillai, P. S., Recchiuti, A., Yang, R., and Serhan, C. N. (2011) Pro-resolving actions and stereoselective biosynthesis of 18 S E-series resolvins in human leukocytes and murine inflammation. *J. Clin. Invest.* **121**, 569–581
- Serhan, C. N., Hong, S., Gronert, K., Colgan, S. P., Devchand, P. R., Mirick, G., and Moussignac, R. L. (2002) Resolvins. A family of bioactive products of omega-3 fatty acid transformation circuits initiated by aspirin treatment that counter proinflammation signals. *J. Exp. Med.* **196**, 1025–1037
- Schwab, J. M., Chiang, N., Arita, M., and Serhan, C. N. (2007) Resolvin E1 and protectin D1 activate inflammation-resolution programs. *Nature* **447**, 869–874
- Ogawa, S., Urabe, D., Yokokura, Y., Arai, H., Arita, M., and Inoue, M. (2009) Total synthesis and bioactivity of resolvin E2. *Org. Lett.* **11**, 3602–3605
- Powell, W. S., Chung, D., and Gravel, S. (1995) 5-Oxo-6,8,11,14-eicosatetraenoic acid is a potent stimulator of human eosinophil migration. *J. Immunol.* **154**, 4123–4132
- Sakagami, H., Aoki, J., Natori, Y., Nishikawa, K., Takehi, Y., Natori, Y., and Arai, H. (2005) Biochemical and molecular characterization of a novel choline-specific glycerophosphodiester phosphodiesterase belonging to the nucleotide pyrophosphatase/phosphodiesterase family. *J. Biol. Chem.* **280**, 23084–23093
- Kanegasaki, S., Nomura, Y., Nitta, N., Akiyama, S., Tamatani, T., Goshoh, Y., Yoshida, T., Sato, T., and Kikuchi, Y. (2003) A novel optical assay system for the quantitative measurement of chemotaxis. *J. Immunol. Methods* **282**, 1–11
- Nishio, M., Watanabe, K., Sasaki, J., Taya, C., Takasuga, S., Iizuka, R., Balla, T., Yamazaki, M., Watanabe, H., Itoh, R., Kuroda, S., Horie, Y., Förster, I., Mak, T. W., Yonekawa, H., Penninger, J. M., Kanaho, Y., Suzuki, A., and Sasaki, T. (2007) Control of cell polarity and motility by the PtdIns(3,4,5)P3 phosphatase SHIP1. *Nat. Cell Biol.* **9**, 36–44
- Yamada, T., Tani, Y., Nakanishi, H., Taguchi, R., Arita, M., and Arai, H. (2011) Eosinophils promote resolution of acute peritonitis by producing proresolving mediators in mice. *FASEB J.* **25**, 561–568
- MacMillan, D. K., Hill, E., Sala, A., Sigal, E., Shuman, T., Henson, P. M., and Murphy, R. C. (1994) Eosinophil 15-lipoxygenase is a leukotriene A4 synthase. *J. Biol. Chem.* **269**, 26663–26668
- Kühn, H., and O'Donnell, V. B. (2006) Inflammation and immune regulation by 12/15-lipoxygenases. *Prog. Lipid Res.* **45**, 334–356
- Arita, M., Clish, C. B., and Serhan, C. N. (2005) The contributions of aspirin and microbial oxygenase to the biosynthesis of anti-inflammatory resolvins. Novel oxygenase products from omega-3 polyunsaturated fatty acids. *Biochem. Biophys. Res. Commun.* **338**, 149–157
- Schneider, C., Pratt, D. A., Porter, N. A., and Brash, A. R. (2007) Control of oxygenation in lipoxygenase and cyclooxygenase catalysis. *Chem. Biol.* **14**, 473–488
- Gronert, K., Maheshwari, N., Khan, N., Hassan, I. R., Dunn, M., and Laniado Schwartzman, M. (2005) A role for the mouse 12/15-lipoxygenase pathway in promoting epithelial wound healing and host defense. *J. Biol. Chem.* **280**, 15267–15278
- Merched, A. J., Ko, K., Gotlinger, K. H., Serhan, C. N., and Chan, L. (2008) Atherosclerosis. Evidence for impairment of resolution of vascular inflammation governed by specific lipid mediators. *FASEB J.* **22**, 3595–3606
- Krönke, G., Katzenbeisser, J., Uderhardt, S., Zaiss, M. M., Scholtyssek, C., Schabbauer, G., Zarbock, A., Koenders, M. I., Axmann, R., Zwerina, J., Baenckler, H. W., van den Berg, W., Voll, R. E., Kühn, H., Joosten, L. A., and Schett, G. (2009) 12/15-Lipoxygenase counteracts inflammation and tissue damage in arthritis. *J. Immunol.* **183**, 3383–3389

# LPIAT1 regulates arachidonic acid content in phosphatidylinositol and is required for cortical lamination in mice

Hyeon-Cheol Lee<sup>a</sup>, Takao Inoue<sup>a,\*</sup>, Junko Sasaki<sup>b</sup>, Takuya Kubo<sup>a</sup>, Shinji Matsuda<sup>a</sup>, Yasuko Nakasaki<sup>a</sup>, Mitsuharu Hattori<sup>c</sup>, Fumiharu Tanaka<sup>a</sup>, Osamu Udagawa<sup>a</sup>, Nozomu Kono<sup>a</sup>, Toshiki Itoh<sup>d</sup>, Hideo Ogiso<sup>e</sup>, Ryo Taguchi<sup>e</sup>, Makoto Arita<sup>a</sup>, Takehiko Sasaki<sup>b</sup>, and Hiroyuki Arai<sup>a,f</sup>

<sup>a</sup>Graduate School of Pharmaceutical Sciences and <sup>e</sup>Department of Metabolome, Graduate School of Medicine, University of Tokyo, Tokyo 113-0033, Japan; <sup>b</sup>Department of Medical Biology, Akita University School of Medicine, Akita 010-8543, Japan; <sup>c</sup>Department of Biomedical Science, Graduate School of Pharmaceutical Sciences, Nagoya City University, Aichi 467-8603, Japan; <sup>d</sup>Department of Biochemistry and Molecular Biology, Kobe University Graduate School of Medicine, Hyogo 650-0017, Japan; <sup>f</sup>Core Research for Evolutional Science and Technology, Japan Science and Technology Agency, Tokyo 102-0075, Japan

**ABSTRACT** Dietary arachidonic acid (AA) has roles in growth, neuronal development, and cognitive function in infants. AA is remarkably enriched in phosphatidylinositol (PI), an important constituent of biological membranes in mammals; however, the physiological significance of AA-containing PI remains unknown. In an RNA interference–based genetic screen using *Caenorhabditis elegans*, we recently cloned *mboa-7* as an acyltransferase that selectively incorporates AA into PI. Here we show that lysophosphatidylinositol acyltransferase 1 (LPIAT1, also known as MBOAT7), the closest mammalian homologue, plays a crucial role in brain development in mice. *Lpiat1*<sup>−/−</sup> mice show almost no LPIAT activity with arachidonoyl-CoA as an acyl donor and show reduced AA contents in PI and PI phosphates. *Lpiat1*<sup>−/−</sup> mice die within a month and show atrophy of the cerebral cortex and hippocampus. Immunohistochemical analysis reveals disordered cortical lamination and delayed neuronal migration in the cortex of E18.5 *Lpiat1*<sup>−/−</sup> mice. LPIAT1 deficiency also causes disordered neuronal processes in the cortex and reduced neurite outgrowth in vitro. Taken together, these results demonstrate that AA-containing PI/PI phosphates play an important role in normal cortical lamination during brain development in mice.

**Monitoring Editor**  
John York  
Vanderbilt University

Received: Sep 18, 2012  
Revised: Oct 18, 2012  
Accepted: Oct 18, 2012

This article was published online ahead of print in MBoC in Press (<http://www.molbiolcell.org/cgi/doi/10.1091/mbc.E12-09-0673>) on October 24, 2012.

\*Present address: Division of Cellular and Gene Therapy Products, National Institute of Health Sciences, Tokyo 158-8501, Japan.

Requests for the LPIAT1-knockout mice should be addressed to H.A. (harai@mol.f.u-tokyo.ac.jp) or T.S. (tsasaki@med.akita-u.ac.jp).

Address correspondence to: Hiroyuki Arai (harai@mol.f.u-tokyo.ac.jp).

Abbreviations used: AA, arachidonic acid; AA-CoA, arachidonoyl-CoA; FADS1,  $\Delta^5$ -fatty acid desaturase; FADS2,  $\Delta^6$ -fatty acid desaturase; LPIAT1, lysophosphatidylinositol acyltransferase 1; PC, phosphatidylcholine; PE, phosphatidylethanolamine; PI, phosphatidylinositol; PIP, PI monophosphate; PI3P, PI 3-phosphate; PIP<sub>2</sub>, PI bisphosphate; PUFA, polyunsaturated fatty acid.

© 2012 Lee et al. This article is distributed by The American Society for Cell Biology under license from the author(s). Two months after publication it is available to the public under an Attribution–Noncommercial–Share Alike 3.0 Unported Creative Commons License (<http://creativecommons.org/licenses/by-nc-sa/3.0>). "ASCB®" "The American Society for Cell Biology®," and "Molecular Biology of the Cell®" are registered trademarks of The American Society of Cell Biology.

## INTRODUCTION

Polyunsaturated fatty acids (PUFAs) in membrane phospholipids play critical roles in regulating the structure, dynamics, and permeability of membranes. In mammals, the PUFA composition affects many cellular processes, including modulation of ion channels (Chyb et al., 1999; Xiao et al., 2001) and activities of membrane-associated enzymes that are sensitive to the biophysical properties of lipid membrane (Goldberg and Zidovetzki, 1997). Postnatal PUFA depletion causes various abnormalities, including sterility, ulceration, and dermatitis, and PUFA supplementation can alleviate most of those symptoms (Stoffel et al., 2008; Stroud et al., 2009; Roqueta-Rivera et al., 2010; Williard et al., 2001). Arachidonic acid (AA; 20:4n-6) is the most enriched n-6 PUFA in the brain and is involved in multiple aspects of neuronal development and function, including neurite outgrowth, signal transduction, and membrane fluidity. The prenatal

and postnatal status of AA is associated with early postnatal neurological function (Dijck-Brouwer *et al.*, 2005; Zhao *et al.*, 2009). There are several lines of evidence suggesting that AA has more beneficial effects than other n-6 fatty acids for perinatal infants. Human infants, as well as neonatal animals, have a reduced ability to elongate/desaturate fatty acids to an appropriate degree, and supplementation with linoleic acid and linolenic acid is not sufficient to overcome a PUFA-deficiency state (Abad-Jorge, 2008). AA is preferentially transferred across the placenta compared with other n-6 fatty acids (Davis-Bruno and Tassinari, 2011). Moreover, a neurological optimality score that quantifies the quality of neonatal neurological functioning is positively related with AA but not with other n-6 fatty acids (Dijck-Brouwer *et al.*, 2005). Nutritional studies also suggest that AA supplementation ameliorates cognitive function in aged animals (Kotani *et al.*, 2003; Okaichi *et al.*, 2005) and helps to protect against a variety of mental disorders (Maekawa *et al.*, 2009).

Among membrane phospholipids, phosphatidylinositol (PI) is unique in its fatty acid composition, that is, most of the fatty acid attached to the sn-2 position of PI is AA (20:4n-6), whereas other major membrane phospholipids such as phosphatidylcholine (PC) and phosphatidylethanolamine (PE) contain various PUFAs, including docosahexaenoic acid (DHA; 22:6n-3; Jungalwala *et al.*, 1984; Patton *et al.*, 1982; Nakagawa *et al.*, 1985; Tanaka *et al.*, 2003). However, the physiological significance of the enrichment of AA in PI is unclear. AA-containing PI is formed by fatty acid remodeling after the de novo synthesis of PI through sequential deacylation and reacylation reactions (Holub and Kuksis, 1971; Baker and Thompson, 1973; Luthra and Sheltawy, 1976). Although high levels of lysophosphatidylinositol acyltransferase (LPIAT) activities were detected from various mammalian tissues by *in vitro* assays (Baker and Thompson, 1973; Inoue *et al.*, 1984; Sanjanwala *et al.*, 1989; Yashiro *et al.*, 1995), the gene responsible for the activity was not identified until recently. In an RNA interference-based genetic screen using *Caenorhabditis elegans*, we identified a gene encoding an acyltransferase that selectively incorporates AA into PI and named it *mboa-7* (Lee *et al.*, 2008). We also showed that a human orthologue of *mboa-7* exhibited arachidonoyl-CoA (AA-CoA):LPIAT activity and that small interfering RNA-mediated knockdown selectively reduced the AA-CoA:LPIAT activity and [<sup>14</sup>C]AA incorporation into the PI fraction in HeLa cells. Voelker's group named a mammalian orthologue of *mboa-7* "MBOAT7" and showed that MBOAT7 is an LPIAT with remarkable specificity for AA-CoA by using mass spectrometry-based enzyme assays (Gijón *et al.*, 2008). *Drosophila* orthologue also prefers AA-CoA as an acyl donor (Steinhauer *et al.*, 2009). Shindou and Shimizu (2009) renamed MBOAT7 as LPIAT1 based on its substrate specificity and by the order of its publication in their review. In the present study, we generated LPIAT1-knockout mice to elucidate the physiological significance of AA in PI.

## RESULTS

### Targeted deletion of the *Lpiat1* gene in the mouse

To determine the physiological role of LPIAT1 in mammals, we generated LPIAT1-deficient mice (*Lpiat1*<sup>-/-</sup> mice) by gene targeting (Figure 1, A and B). A targeting vector substituted a neomycin-resistant gene for exons 2–4 of the *Lpiat1* gene, deleting the initiation codon. Western blot analysis of wild-type mice revealed high expression of LPIAT1 in the brain among the tissues tested (Figure 1C). In the fetal brain, expression of LPIAT1 was observed in the cerebral cortex (Figure 1D), the CA regions and the dentate gyrus of the hippocampus (Figure 1E), the external plexiform layer and the mitral cell layer of the olfactory bulb (Figure 1F), and the granular cell layer of the cerebellum (Figure 1G). In contrast, LPIAT1 protein was not

detected in tissues from *Lpiat1*<sup>-/-</sup> mice (Figure 1, C–G). LPIAT activity with AA-CoA as an acyl donor was almost absent in the membranes of the brain (Figure 1H), but acyltransferase activities toward other lysophospholipids were not changed (Figure 1I). AA-CoA:LPIAT activity was also undetectable in the membranes of the liver, kidney, and testis from *Lpiat1*<sup>-/-</sup> mice (Figure 1H). These data indicate that LPIAT1 is the predominant enzyme that catalyzes the incorporation of AA into lysoPI in mice.

### *Lpiat1*<sup>-/-</sup> mice show reduced AA content in PI and PI phosphates

PI participates in various types of signal transduction through distinct phosphorylated derivatives of the inositol head group (Di Paolo and De Camilli, 2006; Sasaki *et al.*, 2009). Therefore we analyzed the fatty acyl species of PI and PI phosphates in the *Lpiat1*<sup>-/-</sup> brain. The amount of AA in total PI fatty acids in the *Lpiat1*<sup>-/-</sup> brain (28%) was significantly less than that in the *Lpiat1*<sup>+/+</sup> brain (43%; Figure 2A). Conversely, other fatty acids, such as palmitic acid (16:0) and DHA in PI, were increased in the *Lpiat1*<sup>-/-</sup> brain. Consistent with this observation, liquid chromatography–electrospray ionization mass spectrometry (LC/ESI-MS) analysis revealed that the amount of 18:0/20:4 PI (38:4 PI) was significantly reduced in the *Lpiat1*<sup>-/-</sup> brain (Figure 2, B and C). The molecular species compositions of PC and PE were not significantly affected (Figure 2, D and E). PI content was slightly decreased in the *Lpiat1*<sup>-/-</sup> brain (Figure 2F). In addition to the reduced content of AA in PI, the fatty acyl species of PI mono-phosphate (PIP; primarily phosphatidylinositol 4-phosphate [PI4P]) and PI bisphosphate (PIP<sub>2</sub>; primarily phosphatidylinositol 4,5-bisphosphate [PI(4,5)P<sub>2</sub>]) were affected in a manner similar to that of PI (Figure 2, G and H). The contents of PI phosphates in the *Lpiat1*<sup>+/+</sup> and *Lpiat1*<sup>-/-</sup> brains could not be measured because the values fluctuated from experiment to experiment.

As shown previously (Palmer, 1986), acyltransferase activity with AA-CoA as an acyl donor toward lysoPI4P or lysoPI(4,5)P<sub>2</sub> was almost undetectable in the membranes of the brain from wild-type mice compared with the activity toward lysoPI (Figure 3A). Overexpression of LPIAT1 did not increase the acyltransferase activity toward lysoPI4P or lysoPI(4,5)P<sub>2</sub> (Figure 3B). These data indicate that AA-containing PI phosphates are not formed by incorporation of AA into lysoPI phosphates.

### AA metabolites in *Lpiat1*<sup>-/-</sup> mice

AA cleaved from phospholipids is converted to bioactive mediators such as prostaglandins and leukotrienes. An LC-MS/MS analysis showed that the amounts of free AA and its metabolites such as prostaglandin D<sub>2</sub> (PGD<sub>2</sub>) and 5-hydroxyeicosatetraenoic acid (5-HETE) were slightly but not significantly reduced in the *Lpiat1*<sup>-/-</sup> mouse brain compared with the *Lpiat1*<sup>+/+</sup> mouse brain (Table 1). Leukotrienes were not detectable under the present conditions.

### *Lpiat1*<sup>-/-</sup> mice show abnormal brain morphology

Matings between *Lpiat1* heterozygous mice yielded significantly fewer P0 *Lpiat1*<sup>-/-</sup> progeny than expected according to Mendelian inheritance (18.0%; *p* = 0.0027, chi-square test), whereas the genotypes of embryonic day 16.5 (E16.5) and E18.5 progeny followed the expected Mendelian frequencies (Table 2). The number of surviving *Lpiat1*<sup>-/-</sup> mice diminished markedly in the 4 wk after birth (Figure 4A). *Lpiat1*<sup>-/-</sup> mice were significantly smaller than *Lpiat1*<sup>+/+</sup> and *Lpiat1*<sup>+/+</sup> littermates (Figure 4, B and C).

At E18.5, the forebrain of *Lpiat1*<sup>-/-</sup> mice was smaller in size, whereas the midbrain appeared to be normal in size (Figure 4D). Histological analysis revealed that the sizes of the cerebral cortex

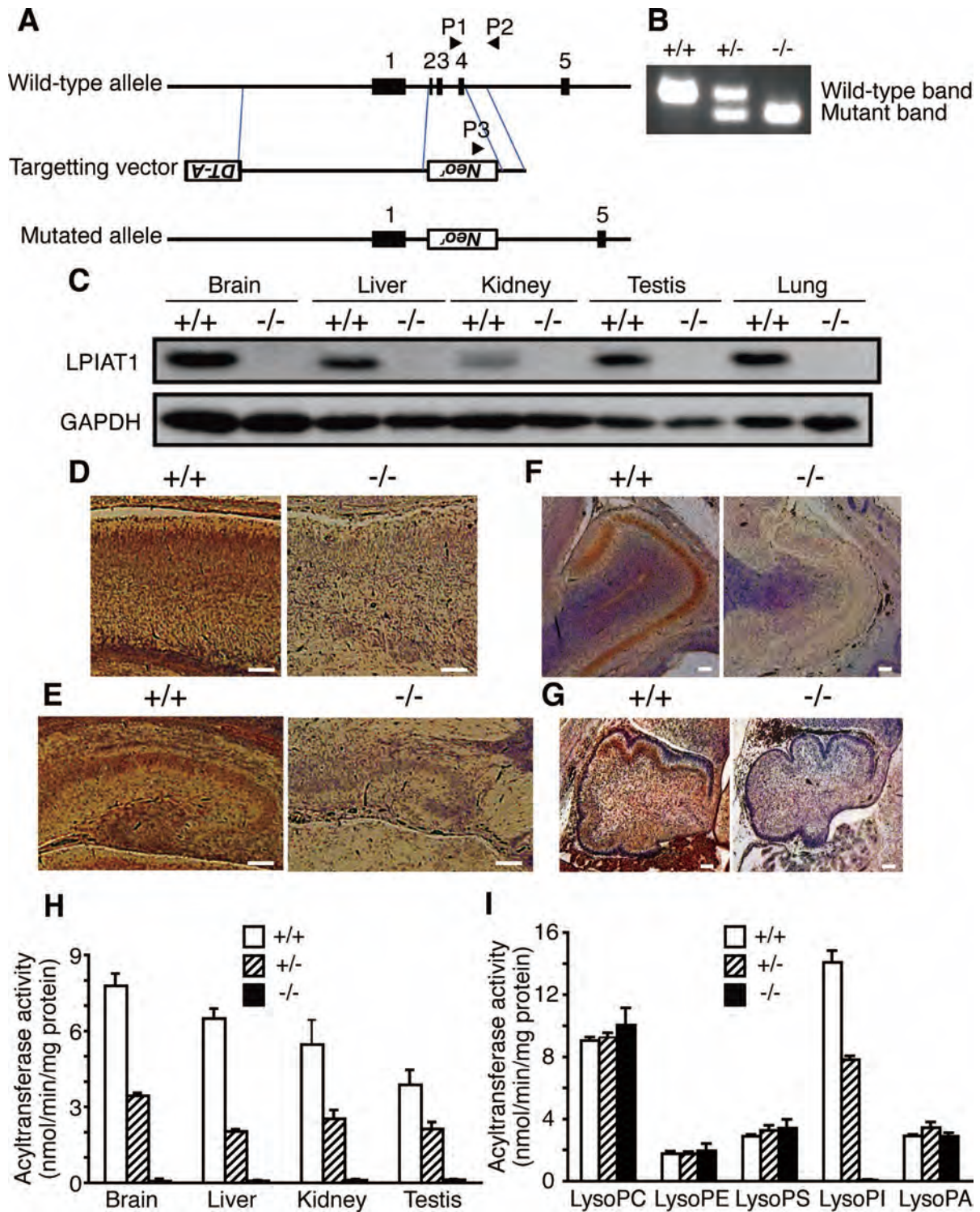


**FIGURE 1:** *Lpiat1*<sup>-/-</sup> mice lack AA-CoA:LPIAT activity. (A) Diagram of the *Lpiat1* genomic locus and the targeting vector. The positions of the PCR primers (P1, P2, and P3) are indicated. All three primers were used in the same PCR. (B) PCR analysis of genomic DNAs from *Lpiat1*<sup>+/+</sup>, *Lpiat1*<sup>+/-</sup>, and *Lpiat1*<sup>-/-</sup> mice. (C) Immunoblot analysis of LPIAT1. Each tissue was prepared from 2-wk-old *Lpiat1*<sup>+/+</sup> and *Lpiat1*<sup>-/-</sup> mice. Control GAPDH was run simultaneously in a different gel. The same amount of protein was loaded in each lane. (D–G) LPIAT1 expression in the brain. Sagittal sections of the brains from E18.5 *Lpiat1*<sup>+/+</sup> and *Lpiat1*<sup>-/-</sup> littermates were stained with antibodies against mouse LPIAT1. Neocortex (D), hippocampus (E), olfactory bulb (F), and cerebellum (G) are shown. LPIAT1 was also detected in granule cells in accessory olfactory bulb. Scale bar, 100  $\mu$ m. (H) AA-CoA:LPIAT activity in the membrane fractions of each tissue from *Lpiat1*<sup>+/+</sup>, *Lpiat1*<sup>+/-</sup>, and *Lpiat1*<sup>-/-</sup> mice at 2 wk of age. [<sup>14</sup>C]AA-CoA, lysoPI, and 5  $\mu$ g of protein were used. Data are means  $\pm$  SD (n = 3). (I) AA-CoA:lysophospholipid acyltransferase activity of the *Lpiat1*<sup>+/+</sup>, *Lpiat1*<sup>+/-</sup>, and *Lpiat1*<sup>-/-</sup> brains using the indicated lysophospholipids as the indicated lysophospholipids as indicated. PS, phosphatidylserine; PA, phosphatidic acid. Protein at 20  $\mu$ g was used. Data are means  $\pm$  SD (n = 3).

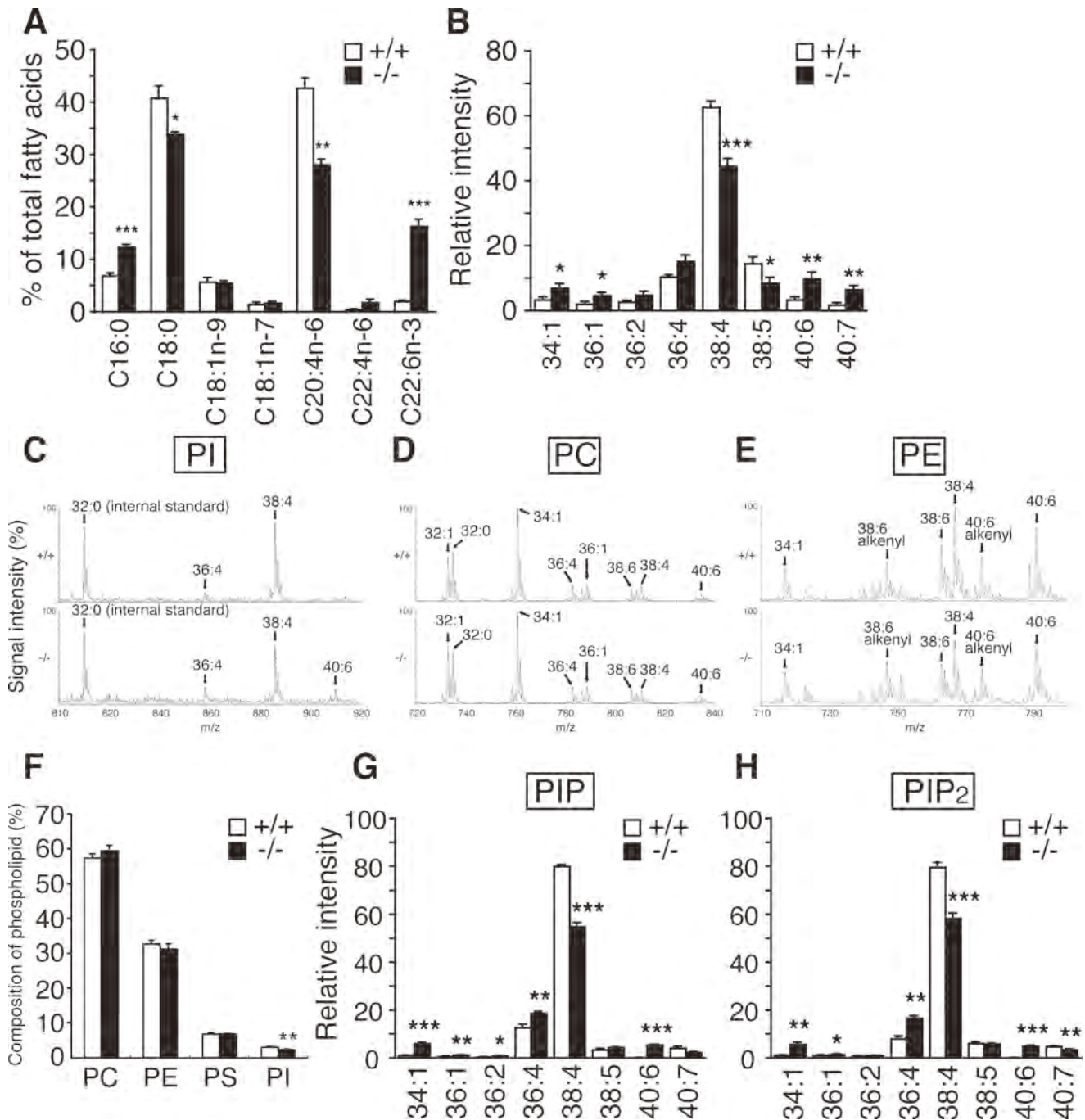


**FIGURE 2:** Lipid analysis of *Lpiat1*<sup>-/-</sup> mice. (A) Analysis of PI fatty acid composition of the brains by gas chromatography. C16:0, palmitic acid; C18:0, stearic acid; C18:1n-9, oleic acid; C18:1n-7, vaccenic acid; C20:4n-6, arachidonic acid; C22:4n-6, docosatetraenoic acid; C22:6n-3, docosahexaenoic acid. Data are means ± SEM (n = 3). \*p < 0.05; \*\*p < 0.01; \*\*\*p < 0.001. The unpaired, two-tailed t test was used. (B) LC-MS/MS analysis of PI. Negative-ionization LC-MS spectra of PI molecular species of the *Lpiat1*<sup>+/+</sup> and *Lpiat1*<sup>-/-</sup> brains. 34:1, 16:0/18:1; 36:1, 18:0/18:1; 36:2, 18:1/18:1; 36:4, 16:0/20:4; 38:4, 18:0/20:4; 38:5, 18:1/20:4; 40:6, 18:0/22:6; 40:7, 18:1/22:6. Data are means ± SEM (n = 5). \*p < 0.05; \*\*p < 0.01; \*\*\*p < 0.001. The unpaired, two-tailed t test was used. (C) Negative-ionization LC-MS spectra of PI molecular species of the *Lpiat1*<sup>+/+</sup> (top) and *Lpiat1*<sup>-/-</sup> (bottom) brains. 36:4, 16:0/20:4; 38:4, 18:0/20:4; 40:6, 18:0/22:6. (D) Positive-ionization LC-MS spectra of PC molecular species. 32:1, mainly 16:0/16:1; 32:0, 16:0/16:0; 34:1, 16:0/18:1; 36:4, mainly 16:0/20:4; 36:1, 18:0/18:1; 38:6, 16:0/22:6; 38:4, mainly 18:0/20:4; 40:6, 18:0/22:6. (E) Positive-ionization LC-MS spectra of PE molecular species. 34:1, 16:0/18:1; 38:6 alkenyl, 16:0 alkenyl/22:6; 38:6, mainly 16:0/22:6; 38:4, mainly 18:0/20:4; 40:6 alkenyl, 18:0 alkenyl/22:6; 40:6, 18:0/22:6. (F) The content of individual phospholipid of the brains. Data are means ± SEM (n = 4-5). \*p < 0.05. The unpaired, two-tailed t test was used. (G, H) LC/MS analysis of PIP (primarily PI4P; G) and PIP<sub>2</sub> (primarily PI(4,5)P<sub>2</sub>; H) of *Lpiat1*<sup>+/+</sup> and *Lpiat1*<sup>-/-</sup> mouse hippocampus. Data are means ± SEM (n = 3). \*p < 0.05; \*\*p < 0.01; \*\*\*p < 0.001. Unpaired, two-tailed t test was used.

and hippocampus were reduced in the *Lpiat1*<sup>-/-</sup> brain (Figure 4, E and F). The laminar structures of the cerebral cortex and hippocampus were disarranged in the *Lpiat1*<sup>-/-</sup> brain. These results indicate that LPIAT1 deficiency causes atrophy of the cerebral cortex and hippocampus and disordered lamination in the cortical layer.

The mammalian neocortex has a characteristic laminar structure composed of six layers of different cells. The cortical layer formation begins around E10–12 (Gleeson and Walsh, 2000). First, the earliest-born cells from cortical ventricular zone migrate toward the pial surface to form the preplate. Subsequently generated neurons arise from the ventricular zone and migrate into the preplate to form the cortical plate (layer 6), splitting the preplate into the marginal zone (layer 1) and the subplate below. Thereafter, newly born neurons migrate past the subplate and older cortical plate neurons to form more superficial layer, thereby making layers 2–6 in an inside-out pattern by E18.5 (Rakic, 1988; Tissir and Goffinet, 2003). We analyzed the layer formation in *Lpiat1*<sup>-/-</sup> mice with specific markers. *Tbr1* is a marker of early-born neurons. At E18.5, *Tbr1*-positive neurons were located mainly in the lower cortical plate (layer 6; Hevner et al., 2001) in wild-type mice (Figure 5A), whereas they were broadly scattered throughout the cortical plate in *Lpiat1*<sup>-/-</sup> mice (Figure 5B). *Brn1* is a marker of the late precursor cells of the ventricular and subventricular zones and the migrating neurons. By E18.5, *Brn1*-positive neurons in wild-type mice had migrated into the cortical plate (Figure 5C), as shown previously (McEvilly et al., 2002), whereas most of the *Brn1*-positive neurons were stacked in the intermediate zone in *Lpiat1*<sup>-/-</sup> mice (Figure 5D). Cells positive for Reelin, a marker of Cajal–Retzius neurons (Alcántara et al., 1998; D’Arcangelo et al., 1995, 1997; Ogawa et al., 1995), were normally distributed in the marginal zone of the *Lpiat1*<sup>-/-</sup> cortex (Figure 5, A and B). In the wild-type cortex, MAP2-positive neuronal processes were arranged radially and formed a tight, palisade-like structure (Figure 5E). In contrast, in *Lpiat1*<sup>-/-</sup> mice, the palisade-like neuronal processes were disordered in the cortex, and the subplate neurons, which are also stained by MAP2 (Luskin and Shatz, 1985), were dispersed (Figure 5F). Neuronal differentiation during early corticogenesis at E14.5 appeared normal in *Lpiat1*<sup>-/-</sup> mice as assessed by the expressions of  $\beta$ III-tubulin, *Tbr1*, and MAP2 (Figure 6). These data indicate that LPIAT1 is required for normal cortical lamination.

**Neuronal migration is delayed in *Lpiat1*<sup>-/-</sup> mice**

The disturbed laminar organization of the *Lpiat1*<sup>-/-</sup> cortex suggested that the migrations of cortical cells were abnormal. We injected pregnant females with 5-bromodeoxyuridine (BrdU) at E15.5, when neurogenesis of the middle and superficial layers is at a peak, and

AA metabolite	<i>Lpiat1</i> <sup>+/+</sup>	<i>Lpiat1</i> <sup>-/-</sup>
AA	1620 ± 307	971 ± 120
PGE <sub>2</sub>	0.581 ± 0.113	0.482 ± 0.121
PGD <sub>2</sub>	1.95 ± 0.64	0.873 ± 0.236
PGF <sub>2</sub> $\alpha$	0.447 ± 0.094	0.412 ± 0.080
6-keto-PGF <sub>1</sub> $\alpha$	1.02 ± 0.14	0.809 ± 0.204
TXB <sub>2</sub>	3.84 ± 0.94	4.74 ± 0.98
5-HETE	1.15 ± 0.30	0.424 ± 0.070
12-HETE	0.165 ± 0.043	0.069 ± 0.030
15-HETE	0.201 ± 0.052	0.168 ± 0.042

P0 brains were harvested, weighed, and frozen immediately in liquid nitrogen. Data are pg/mg wet weight expressed as means ± SEM (n = 6). TXB<sub>2</sub>, thromboxane B<sub>2</sub>.

**TABLE 1:** AA metabolites of *Lpiat1*<sup>+/+</sup> and *Lpiat1*<sup>-/-</sup> brains.

Stage		<i>Lpiat1</i> Genotype			
		+/+	+/-	-/-	Total
E16.5	Number of animals	28	52	28	108
	Percentage (%)	26.0	48.1	26.0	100
E18.5	Number of animals	27	43	23	93
	Percentage (%)	29.0	46.2	24.7	100
Birth (P0)	Number of animals	126	247	82	455
	Percentage (%)	27.7	54.3	18.0*	100

Neonates and embryos were harvested at the times indicated. Genomic DNA was extracted from the tail of each pup and subjected to PCR analysis to determine the genotype. Only live-born animals are counted at birth (P0). \*p = 0.0027. The p values were calculated using the chi-square test.

**TABLE 2:** Genotypes of litters from *Lpiat1*<sup>+/+</sup> intercrosses.

examined the localization of BrdU-positive cortical neurons at E18.5. Most of the BrdU-positive cells were superficially distributed in the *Lpiat1*<sup>+/+</sup> cortex (Figure 7A). In the *Lpiat1*<sup>-/-</sup> cortex, the number of BrdU-positive cells was comparable to that of the *Lpiat1*<sup>+/+</sup> cortex, suggesting that neurogenesis is not affected in *Lpiat1*<sup>-/-</sup> mice at E15.5. However, the proportion of cells in the superficial cortex was significantly reduced in the *Lpiat1*<sup>-/-</sup> cortex (Figure 7B). These results suggest that loss of LPIAT1 leads to a significant delay in neuronal

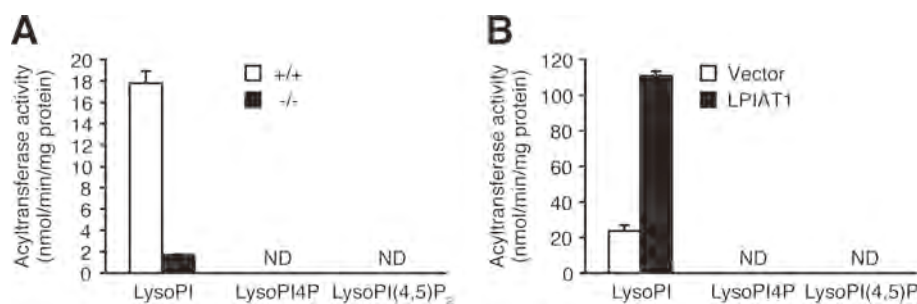


**FIGURE 3:** LPIAT1 does not use lysoPI4P or lysoPI(4,5)P<sub>2</sub> as acyl acceptors. (A) AA-CoA:acyltransferase activity toward lysoPI, lysoPI4P, or lysoPI(4,5)P<sub>2</sub> in the membrane fractions of the *Lpiat1*<sup>+/+</sup> and *Lpiat1*<sup>-/-</sup> brains at P0. Protein at 5  $\mu$ g was used. ND, not detected or present only in trace amounts. Data are means ± SD (n = 3). (B) AA-CoA:acyltransferase activity toward lysoPI, lysoPI4P, or lysoPI(4,5)P<sub>2</sub> in the membrane fractions of HEK 293A cells transfected with vector control or *Lpiat1* expression plasmid. ND, not detected or present only in trace amounts. Protein at 1  $\mu$ g was used. Data are means ± SD (n = 3).

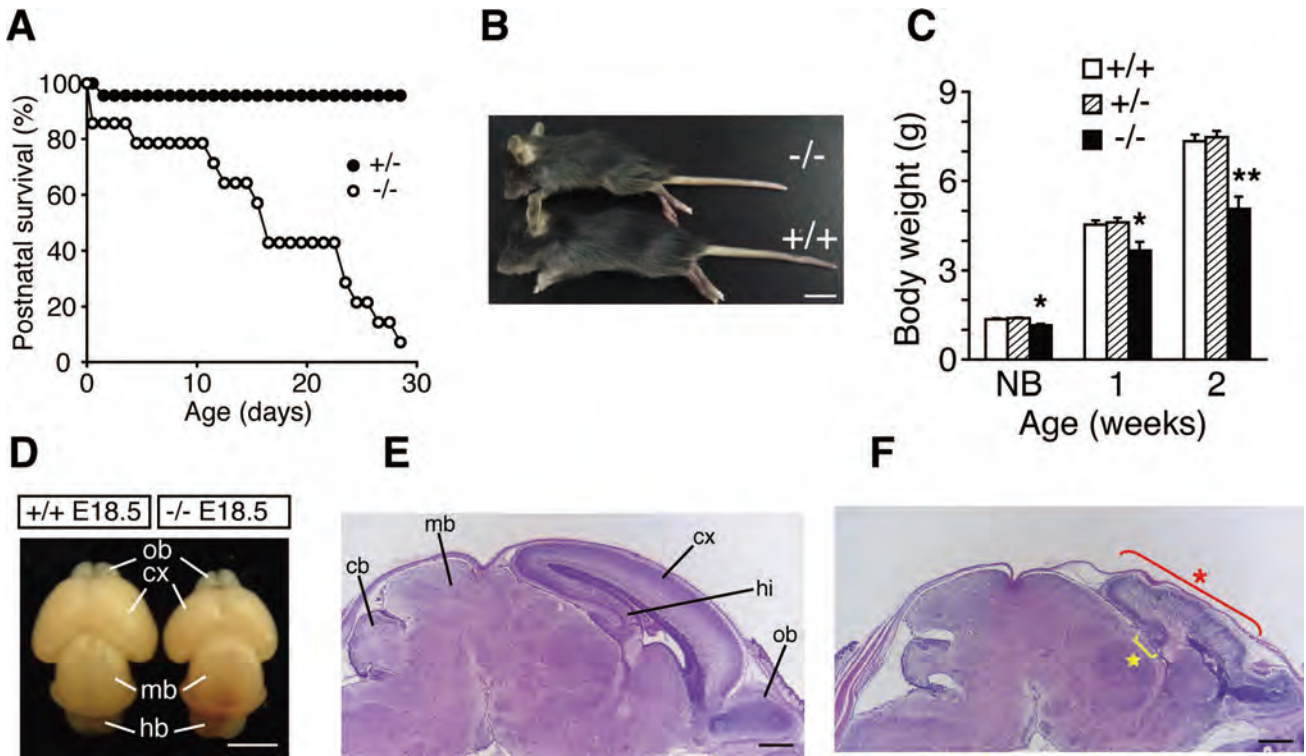


**FIGURE 4:** Abnormal morphology of the *Lpiat1*<sup>-/-</sup> brain. (A) Juvenile lethality of *Lpiat1*<sup>-/-</sup> mice (n = 14). (B) Representative photograph of *Lpiat1*<sup>-/-</sup> mouse compared with a wild-type littermate at 3 wk of age. Scale bar, 1 cm. (C) Body weights of *Lpiat1*<sup>+/+</sup>, *Lpiat1*<sup>+/-</sup>, and *Lpiat1*<sup>-/-</sup> mice at different points in time. Littermates of all genotypes (+/+, n = 29; +/-, n = 41; -/-, n = 14) were weighed at 1 and 2 wk of age. Newborn littermates (+/+, n = 6; +/-, n = 12; -/-, n = 4) were weighed before killing for primary hippocampal culture (see Figure 9). NB, newborn. Data are means ± SEM \*p < 0.05; \*\*p < 0.01. The analysis of variance with Tukey-Kramer post hoc test was used. (D) Brains from *Lpiat1*<sup>+/+</sup> and *Lpiat1*<sup>-/-</sup> littermates at E18.5. cx, cortex; hb, hindbrain; mb, midbrain; ob, olfactory bulb. Scale bar, 2.5 mm. (E, F) Sagittal sections of the brains from E18.5 *Lpiat1*<sup>+/+</sup> (E) and *Lpiat1*<sup>-/-</sup> (F) littermates were stained with hematoxylin and eosin (H&E). cb, cerebellum; cx, cortex; hi, hippocampus; mb, midbrain; ob, olfactory bulb. The red asterisk indicates the atrophic cortex, and the yellow star indicates the atrophic hippocampus. Scale bar, 500 μm.

migration. We also found that the number of apoptotic cells increased in the *Lpiat1*<sup>-/-</sup> cortex as judged by terminal deoxynucleotidyl transferase-mediated biotinylated UTP nick end labeling (TUNEL) assays (Figure 8), suggesting that atrophy of the cerebral cortex in *Lpiat1*<sup>-/-</sup> mice is caused by increased apoptosis of neuronal cells.

**Neurite outgrowth is reduced in *Lpiat1*<sup>-/-</sup> hippocampal neurons**

We then examined the role of LPIAT1 in neurite outgrowth of primary hippocampal neurons. Hippocampal neurons obtained from P0 brains were cultured for 72 h and immunostained with a βIII-tubulin antibody to visualize neuronal morphology. Hippocampal neurons from *Lpiat1*<sup>-/-</sup> mice had significantly fewer cells with neurites than did those from *Lpiat1*<sup>+/+</sup> mice (Figure 9, A and B). Moreover, the total neuritic length per cell and the length of the longest neurite in each cell were significantly reduced in *Lpiat1*<sup>-/-</sup> cells (Figure 9, C and D). Taken together, these results indicate that LPIAT1 deficiency causes defects in neuronal migration and neurite outgrowth, leading to cortical and hippocampal malformation.

**DISCUSSION**

In this article, we showed that *Lpiat1*<sup>-/-</sup> mice have reduced content of AA in PI and have defects in cortical lamination during brain development. Intensive efforts have been made to understand the

physiological roles of AA-derived metabolites such as prostaglandins and leukotrienes. However, little is known about the function of AA when attached to phospholipids other than serving as a source of free AA. Metabolites of AA have been reported to be involved in neuronal functions (Williams and Bliss, 1988; Chen et al., 2002; Shaw et al., 2003; Besana et al., 2005). As far as we know, mice with knockout of any AA-metabolizing enzyme, such as cPLA<sub>2</sub>α, MAGL, and 5-LOX, or knockout of the receptors for prostaglandins and leukotrienes, such as PGE<sub>2</sub> receptors, do not show phenotypes similar to those of *Lpiat1*<sup>-/-</sup> mice (Chen et al., 1994; Bonventre et al., 1997; Uozumi et al., 1997; Ushikubi et al., 1998). Moreover, the levels of major AA metabolites were not significantly changed in the *Lpiat1*<sup>-/-</sup> brain. Thus the defects in brain development seen in *Lpiat1*<sup>-/-</sup> mice are unlikely caused by the reduction or the impairment of the signaling pathways regulated by AA-derived metabolites.

In addition to PI, AA contents of PIP and PIP<sub>2</sub> were also reduced in the *Lpiat1*<sup>-/-</sup> brain. Previous in vitro studies demonstrated that whereas lysoPI was acylated with [<sup>3</sup>H]AA by the microsomes from rat liver and brain in the presence of ATP, CoA, and Mg<sup>2+</sup>, neither lysoPI4P nor lysoPI(4,5)P<sub>2</sub> was acylated with [<sup>3</sup>H]AA under the same assay conditions (Palmer, 1986). In the present study, we confirmed this observation and also showed that overexpression of LPIAT1 in cultured cells did not increase acyltransferase activity toward lysoPI4P or lysoPI(4,5)P<sub>2</sub>. These results indicate that LPIAT1 does not use lysoPI4P or lysoPI(4,5)P<sub>2</sub> as an acyl acceptor. Nevertheless, the

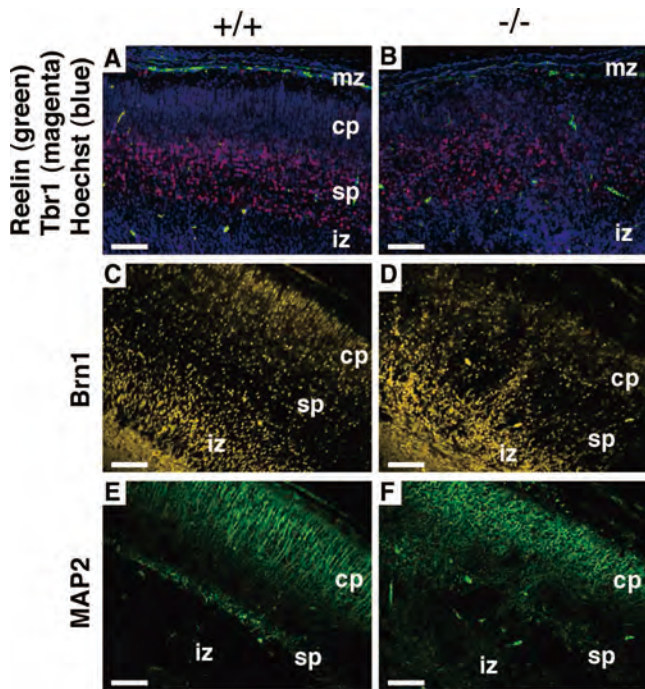


**FIGURE 5:** Abnormal cortical lamination in *Lpiat1*<sup>-/-</sup> mice. Sagittal sections of neocortices from E18.5 *Lpiat1*<sup>+/+</sup> (A, C, E) and *Lpiat1*<sup>-/-</sup> (B, D, F) littermates were stained with antibodies against Reelin and Tbr1, and DNA dye Hoechst 33342 (green, magenta, and blue, respectively; A, B), Brn1 (yellow; C, D), and MAP2 (green; E, F). cp, cortical plate; iz, intermediate zone; mz, maginal zone; sp, subplate. Scale bar, 100  $\mu$ m.

AA contents of PI phosphates and PI showed similar decreases in the *Lpiat1*<sup>-/-</sup> brain, suggesting that the reduction in the AA content in PI phosphates may result from the reduction of AA content in PI, a precursor of PI phosphates.

PI phosphates are synthesized by PI kinases and phosphatases and play crucial roles in the regulation of a wide variety of cellular processes via specific interactions of PIP-binding proteins (Di Paolo and De Camilli, 2006; Sasaki et al., 2009). Among PI phosphates, PI 3-phosphate (PI3P) regulates a variety of vesicular trafficking pathways, including endocytosis, endosome-to-Golgi retrograde transport, autophagy, and the target of rapamycin (TOR) signaling pathway (Backer, 2008). PI3P is synthesized from PI by a class III PI 3-kinase, Vps34 (Backer, 2008). Recently we showed that knock-down of *vps-34*, a *C. elegans* orthologue of Vps34, causes severe growth defects in *mboa-7* mutants (Lee et al., 2012). Moreover, PI3P signaling pathways such as autophagy and endosome morphology were impaired in *mboa-7* mutants. Of interest, Zhou (2010) recently showed that neuron-specific Vps34 conditional knockout mice exhibit defects in cortical lamination, which is very similar to that of *Lpiat1*<sup>-/-</sup> mice. On the basis of these observations, we hypothesize that reduction of AA content in PI3P impaired PI3P function(s), which leads to cortical lamination defects in *Lpiat1*<sup>-/-</sup> mice. The observation that the fatty acid compositions of PIP and PIP<sub>2</sub> were changed similarly to that of PI in *Lpiat1*<sup>-/-</sup> mice suggests that the enzymes involved in the synthesis of PIP and PIP<sub>2</sub> do not prefer AA-containing PI as a substrate. Change in the fatty acid composition in PI phosphates may affect the interaction with PI phosphate-binding proteins and/or the intramembrane localization of PI phosphates in subcellular organelles. We are testing this hypothesis.

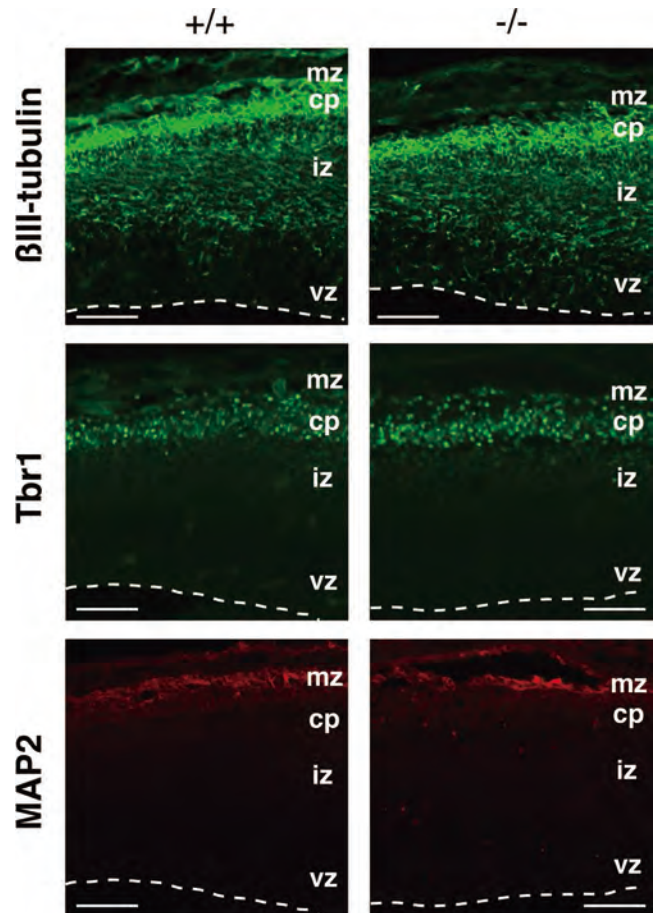


**FIGURE 6:** Loss of LPIAT1 does not affect neuronal differentiation. Coronal sections of the E14.5 neocortices were stained with antibodies against  $\beta$ III-tubulin, Tbr1, and MAP2. cp, cortical plate; iz, intermediate zone; mz, maginal zone; vz, ventricular zone. Scale bar, 50  $\mu$ m.

$\Delta 6$ -Fatty acid desaturase (FADS2) converts linoleic acid (18:2n-6) to  $\gamma$ -linolenic (18:3n-6), and  $\Delta 5$ -fatty acid desaturase (FADS1) converts dihomo- $\gamma$ -linolenic acid (20:3n-6) to AA. *Fads2*<sup>-/-</sup> mice show reduced content of PUFAs, including AA in tissues (Stoffel et al., 2008; Stroud et al., 2009). *Fads2*<sup>-/-</sup> mice exhibit a variety of symptoms, including sterility, ulceration, and dermatitis. PUFA supplementation restores the symptoms in *Fads2*<sup>-/-</sup> mice and in patients with  $\Delta 6$ -desaturase deficiency (Stoffel et al., 2008; Stroud et al., 2009; Roqueta-Rivera et al., 2010; Williard et al., 2001). *Fads1*<sup>-/-</sup> mice began to die gradually starting at 5–6 wk of age, with no survivors past 12 wk of age, although no overt physical differences between *Fads1*<sup>-/-</sup> and wild-type mice were observed (Fan et al., 2012). Thus *Fads1*<sup>-/-</sup> and *Fads2*<sup>-/-</sup> mice did not show any phenotypes similar to those of *Lpiat1*<sup>-/-</sup> mice. Although *Fads1*<sup>-/-</sup> and *Fads2*<sup>-/-</sup> mice are ideal for studying the function of AA and other PUFAs in vivo, PUFAs are supplied from the heterozygous mother through placental transfer in the homozygous embryos. Moreover, the content of PUFAs in the brain tends to remain stable even under PUFA-depleted conditions (García-Calatayud et al., 2002; Stroud et al., 2009). *Lpiat1*<sup>-/-</sup> embryos have a defect in the synthesis of AA-containing PI using AA derived from their heterozygous mother. Thus it is plausible that *Fads2*<sup>-/-</sup> mice and *Lpiat1*<sup>-/-</sup> mice show distinct brain phenotypes in the embryonic stage.

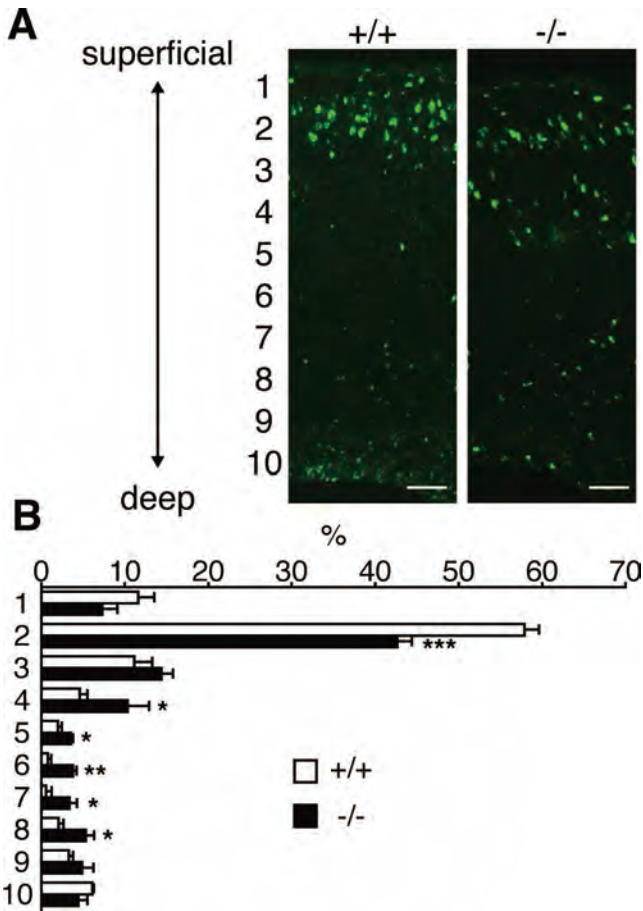


**FIGURE 7:** Neuronal migration is delayed in *Lpiat1*<sup>-/-</sup> mice. (A) Coronal sections of neocortices from E18.5 *Lpiat1*<sup>+/+</sup> and *Lpiat1*<sup>-/-</sup> littermates labeled with BrdU at E15.5. Scale bar, 50 μm. (B) The radial distribution of BrdU-labeled cells. Data are means ± SEM (n = 4). \*p < 0.05; \*\*p < 0.01; \*\*\*p < 0.001. Unpaired, two-tailed t test was used.

The fact that a considerable amount of AA remained in PI of *Lpiat1*<sup>-/-</sup> mice suggests that there are other pathways to enrich AA in PI. Lysophosphatidic acid acyltransferase (LPAAT) may catalyze the incorporation of PUFAs into the sn-2 position of lysophosphatidic acid (lysoPA) during de novo phospholipid synthesis. Mammalian LPAATs show relatively broad substrate specificity for acyl-CoAs and incorporate AA into lysoPA (Stamps *et al.*, 1997; Eberhardt *et al.*, 1997). Cytidine 5'-diphosphate-diacylglycerol synthase (CDS) catalyzes the biosynthesis of CDP-diacylglycerol, a direct precursor of PI, from phosphatidic acid (PA). CDS1, an isoform of CDS that is highly expressed in the brain, prefers AA-containing PA as a substrate (Saito *et al.*, 1997). Therefore it is possible that PI-containing AA can be synthesized once AA is incorporated into PA via the de novo pathway.

It has been recognized for decades that AA-containing PI is a major molecular species in PI in mammals. By knocking out LPIAT1—the enzyme responsible for incorporation of AA into PI—we showed for the first time that AA-containing PI is essential for brain development in mammals.

## MATERIALS AND METHODS

### Materials

[1-<sup>14</sup>C]-labeled fatty acids and fatty acyl-CoAs were purchased from American Radiolabeled Chemicals (St. Louis, MO). Arachidonoyl-

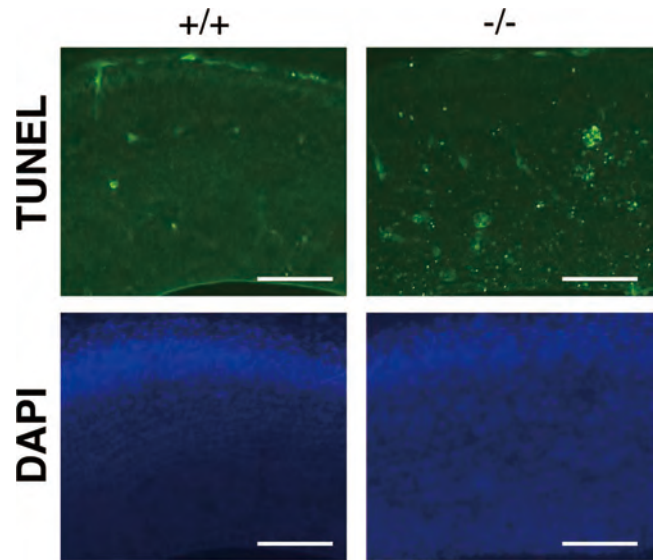


**FIGURE 8:** Loss of LPIAT1 causes increased apoptosis in early corticogenesis. Apoptotic cell death in coronal sections was examined by TUNEL staining at E14.5. Scale bar, 100 μm.

CoA was obtained from Sigma-Aldrich (St. Louis, MO). LysoPI from bovine liver, lysophosphatidylserine from porcine brain, lysoPE from porcine liver, lysoPC from egg yolk, sn-1-oleoyl-lysoPA, PI4P from porcine brain, and PI(4,5)P<sub>2</sub> from porcine brain were purchased from Avanti Polar Lipids (Alabaster, AL). Dipalmitoyl PI was purchased from Serdary Research Laboratories (London, Canada). PLA<sub>2</sub> from honey bee venom was purchased from Sigma-Aldrich. AA-d<sub>8</sub>, 15-HETE-d<sub>8</sub>, LTB<sub>4</sub>-d<sub>4</sub>, and PGE<sub>2</sub>-d<sub>4</sub> were purchased from Cayman Chemical (Ann Arbor, MI).

### Animals

Specific pathogen-free female C57BL/6 mice were obtained from CLEA Japan (Tokyo, Japan). We used *Lpiat1*-deficient mice backcrossed eight times to C57BL/6 background. Mice were maintained in our animal facility and treated in accordance with the guidelines of the Institutional Animal Care Committee (Graduate School of Pharmaceutical Sciences, University of Tokyo, Tokyo, Japan).

### Generation of LPIAT1-deficient mice

E14K murine embryonic stem (ES) cells heterozygous for a deletion mutation of the *Lpiat1* gene were generated. We replaced exons 2–4 of the murine *Lpiat1* gene with a PGK-Neo cassette because the putative translation initiation codons were identified in exons 2–4 but not in exon 1. The targeting vector contained a 5.5-kb genomic murine (129/Ola) *Lpiat1* fragment plus the PGK-Neo cassette inserted in antisense orientation to *Lpiat1* transcription. The linearized construct was electroporated into 1 × 10<sup>7</sup> E14K ES cells. ES cell colonies resistant to G418 (0.3 mg/ml) were screened for homologous recombination by PCR. Four different targeted ES cells derived from two independent electroporation experiments were injected into C57BL/6 blastocysts. Chimeric male mice were crossed with C57BL/6 females to achieve germline transmission. After heterozygous matings, *Lpiat1*<sup>-/-</sup> mice were distinguished from *Lpiat1*<sup>+/-</sup> and *Lpiat1*<sup>+/+</sup> mice by PCR. An oligo primer specific for the *Lpiat1*<sup>+</sup> allele (P1, 5'-CACGCCCTTCACCAATGCTG-3'), a primer common to the *Lpiat1*<sup>+</sup> and *Lpiat1*<sup>-</sup> alleles (P2, 5'-TGGAGGACGGTTTGCTACAGACTC-3'), and a primer specific for the *Lpiat1*<sup>-</sup> allele

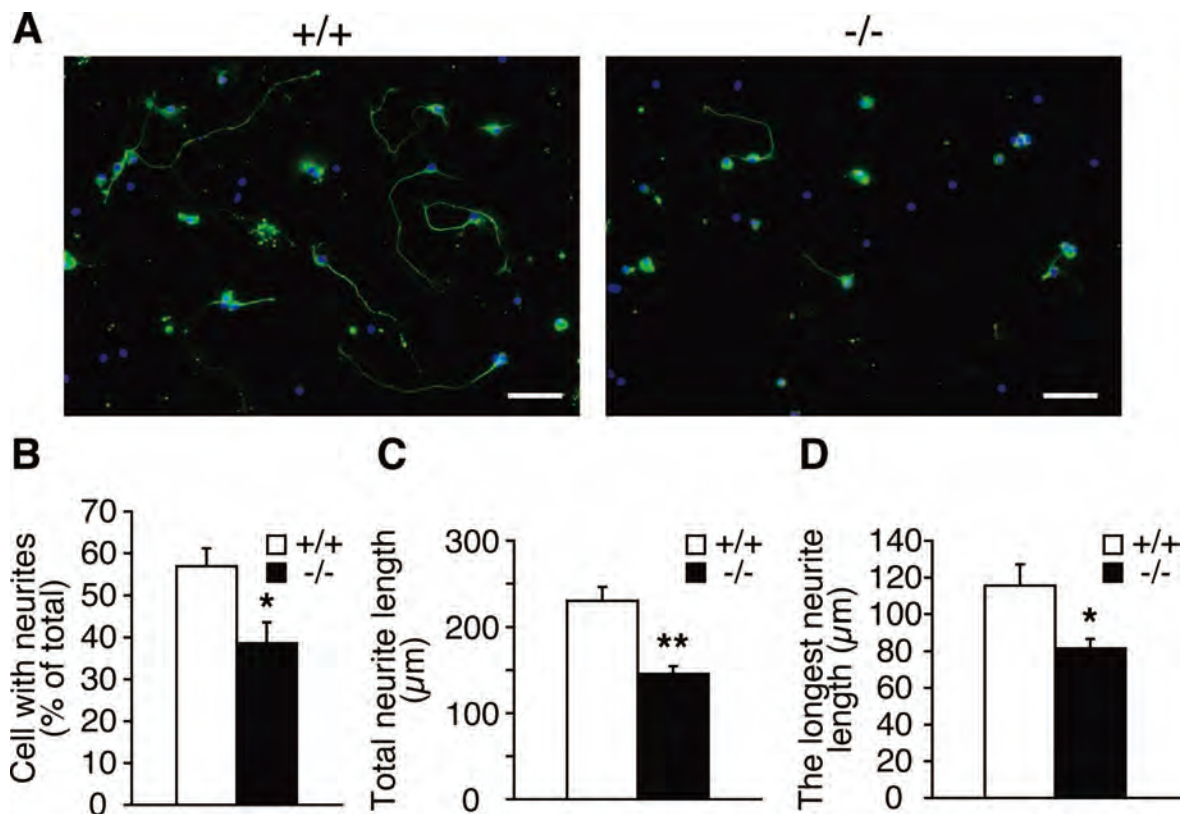


**FIGURE 9:** LPIAT1 deficiency causes defects in neurite elongation. (A) Cultured hippocampal neurons from P0 brains were stained with neuronal marker anti-βIII-tubulin antibody (green) and 4',6-diamidino-2-phenylindole (blue) at DIV3. Scale bar, 50 μm. Percentage of cells with neurites (B), total neurite length (C), and longest neurite length (D) of cultured hippocampal neurons from *Lpiat1<sup>+/+</sup>* and *Lpiat1<sup>-/-</sup>* mice. At least 50 neurons were measured for each group. Data are means ± SEM (n = 4). \*p < 0.05; \*\*p < 0.01. Unpaired, two-tailed t test was used.

(P3, 5'-AGACTGCCTTGGGAAAAGCG-3'), were combined in the same PCR.

**Generation of anti-mouse LPIAT1 antibody**

A recombinant mouse LPIAT1 (amino acids 274–334 of mouse LPIAT1, GenBank accession no. NM\_029934.3) that was expressed and purified by an *Escherichia coli* pCold TF expression system (TaKaRa, Otsu, Japan) was injected into the hind foot pads of WKY/Izm rat strain by using Freund's complete adjuvant. The enlarged medial iliac lymph nodes were used for cell fusion with mouse myeloma cells, PA1. In the present study, the established monoclonal antibody FT10 was used for immunoblotting and immunohistochemistry at dilutions of 1:1000 and 1:100, respectively.

**Western blot analysis**

Tissues from 2-wk-old mice were homogenized in 9x volume (wt/vol) of SET buffer (10 mM Tris-HCl, pH 7.4, 1 mM EDTA, 250 mM sucrose) with protease inhibitors (0.5 mM phenylmethylsulfonyl fluoride, 2 μg/ml pepstatin, 2 μg/ml leupeptin, 2 μg/ml aprotinin). After centrifugation at 1000 × g at 4°C, the supernatants were used as the total protein extracts. The protein concentrations of samples were determined by the bicinchoninic acid (BCA) assay (Pierce, Rockford, IL). Each total protein extract was separated by SDS-PAGE and transferred to either polyvinylidene difluoride (PVDF) or nitrocellulose membranes. The membranes were blocked with skim milk (Wako Pure Chemical Industries, Osaka, Japan) in TTBS buffer (10 mM Tris-HCl, pH 7.4, 150 mM NaCl, 0.05% [wt/vol] Tween 20)

and incubated with the specific monoclonal rat anti-mouse LPIAT1 antibody FT10 (see prior description). After incubation with horseradish peroxidase-conjugated goat anti-rat immunoglobulin G antibody (American Qualex, San Clemente, CA), LPIAT1 was detected by enhanced chemiluminescence (ECL Western blotting detection system; GE Healthcare, Piscataway, NJ). Anti-glyceraldehyde-3-phosphate dehydrogenase (GAPDH; 6C5) was purchased from Calbiochem (La Jolla, CA).

**Acyltransferase assay**

Murine tissues were pulverized under liquid nitrogen and homogenized in quadruple volumes (wt/vol) of SET buffer with protease inhibitors (0.5 mM phenylmethylsulfonyl fluoride, 2 μg/ml pepstatin, 2 μg/ml leupeptin, 2 μg/ml aprotinin). After centrifugation at 2330 × g for 20 min at 4°C, the resulting supernatant was further centrifuged at 105,000 × g for 60 min. The pellet was suspended in homogenizing buffer (without EDTA, phenylmethylsulfonyl fluoride, pepstatin, leupeptin, and aprotinin) and used for the enzyme assay. Acyl-CoA:1-acyl lysophospholipid acyltransferase assay was carried out as described before (Imae et al., 2010), except that the incubation temperature was 37°C and that 5 μg (Figure 1H) or 20 μg (Figure 1I) of microsomal protein was used. The protein concentrations of samples were determined by the BCA assay (Pierce).

**Acyltransferase assay toward lysoPI phosphates**

*sn*-1-acyl lysoPI4P and *sn*-1-acyl lysoPI(4,5)P<sub>2</sub> were prepared as described previously (Palmer, 1986). P0 brains and HEK 293A

cells were homogenized in phosphate buffer (pH 7.0) containing 0.15 M KCl, 0.25 M sucrose, 1 mM EDTA, 1 mM dithiothreitol, and 5 µg/ml pepstatin, leupeptin, and aprotinin (homogenizing buffer). After centrifugations at  $1000 \times g$  for 5 min and  $10,000 \times g$  for 30 min at 4°C, the supernatant was collected and centrifuged at  $105,000 \times g$  for 60 min at 4°C. The resulting pellet was resuspended in homogenizing buffer (without EDTA, dithiothreitol, and protease inhibitors) and used for the enzyme assay to be described. [ $^{14}C$ ]arachidonoyl-CoA (53 mCi/mmol) was diluted with the unlabeled arachidonoyl-CoA to 10 mCi/mmol before use. Reaction mixtures contained 10 µM of AA-CoA (10 mCi/mmol) and 10 µM of lysoPI(4,5)P<sub>2</sub> and 5 µg (for brains) or 1 µg (for cells) of microsomal protein in a total volume of 0.2-ml assay buffer (0.15 M KCl, 0.25 M sucrose, 50 mM potassium phosphate buffer, pH 6.8). After incubation at 37°C for 5 min, reactions were stopped by the addition of 1 ml of methanol. The lipids were extracted as described previously (Serunian et al., 1991) and separated by one-dimensional TLC on silica gel 60 plates (Merck, Darmstadt, Germany) in chloroform:methanol:concentrated NH<sub>4</sub>OH:water (45:45:4:11, vol/vol) (Tysnes et al., 1985). Acyltransferase activity toward lysoPI was also performed in the same assay condition to compare the acyl acceptor preference of LPIAT1.

### Histological analysis

Brains were embedded in paraffin wax, and serial sagittal sections were mounted on slides and stained with hematoxylin and eosin. For immunohistochemistry, brain sections were blocked for 30 min with 2% bovine serum albumin (BSA; Sigma-Aldrich) diluted in phosphate-buffered saline (PBS) containing 0.1% Tween 20 at room temperature and then incubated in primary antibody diluted in 2% BSA-PBS for 2 h. Primary antibodies and their dilutions used in this study were as follows: Reelin (CR50; 1:1000; Ogawa et al., 1995), Tbr1 (AB9616; 1:500; Millipore, Billerica, MA), Brn1 (SC-6028; 1:100; Santa Cruz Biotechnology, Santa Cruz, CA), MAP2 (M1406; 1:1000; Sigma-Aldrich), βIII-tubulin (GT431195; 1:500; Genzyme-Techne, Minneapolis, MN). Sections were incubated with fluorescent secondary antibodies (Alexa series; Molecular Probes, Eugene, OR) diluted at 1:400 in 2% BSA-PBS for 1 h at room temperature. Slides were washed for several hours in PBS and coverslips applied with Dako fluorescent mounting medium (Dako, Glostrup, Denmark). TUNEL analysis was performed using the Apop Tag Plus fluorescein In Situ Apoptosis Detection Kit (Millipore) according to the manufacturer's instructions.

### BrdU labeling and analysis

For BrdU experiments, pregnant mice were injected with BrdU (50 mg/g, intraperitoneally) at E15.5, and perinatal embryos were removed by cesarean section at E18.5. Embryo heads were fixed in 4% paraformaldehyde, and the brains were dissected out and soaked overnight in 20 and 30% sucrose and equilibrated and embedded in OCT on dry ice. Sections were stored frozen until use. After permeabilization with HCl, BrdU was detected by rat anti-BrdU antibodies (AB6326; 1:150; Abcam, Cambridge, MA). To determine the distribution of cells born at E15.5 in *Lpiat1*<sup>+/+</sup> and *Lpiat1*<sup>-/-</sup> cortex, sections were divided into the horizontal bins from superficial to deep, and the percentage of cells in each bin was calculated.

### Primary culture

The primary culture of neurons was prepared from hippocampi or cerebral cortices of E18.5 or P0 mice as described previously

(Bannai et al., 2004). The dissociated cells were plated on poly-L-lysine (Sigma-Aldrich)-coated dishes or coverslips and cultured in Neurobasal Medium (for expression analysis of LPIAT1, E18.5) or Neurobasal-A Medium (for morphometric analysis, P0; Invitrogen, Carlsbad, CA) supplemented with 2.5 mM L-glutamine (Nacalai Tesque, Kyoto, Japan), 2.5% (vol/vol) B-27 (Invitrogen), and antibiotics (250 U/ml penicillin and 250 mg/ml streptomycin). As for morphometric analysis, neurons were cultured at a density of  $2.5 \times 10^4$  cells/well in 24-well flat-bottom plates and fixed at 3 d in vitro (DIV) and then immunostained with the anti-TUJ1 antibody against the neuronal-specific βIII-tubulin (MAB1195; R&D Systems, Minneapolis, MN) at dilution of 1:5000. Cell images were captured by a fluorescence microscope (FSX100; Olympus, Tokyo, Japan), and then the length of neurites and the neurite number were determined.

### Lipid analysis

Lipids of each tissue were extracted by the method of Bligh and Dyer (1959). The fatty acid composition was determined by gas chromatography as described previously (Lee et al., 2008), except that the solvent used in the one-dimensional TLC was chloroform:methyl acetate:1-propanol:methanol:0.25% KCl (25:25:25:10:9, vol/vol; Imae et al., 2010). LC/ESI-MS analysis was performed as described previously (Ogiso and Taguchi, 2008; Imae et al., 2010). Lipid phosphorus was determined by Bartlett's method (Bartlett, 1959).

### Cell culture and transfection

Human embryonic kidney (HEK) 293A cells were maintained in DMEM supplemented with 10% fetal calf serum, penicillin (100 U/ml), streptomycin (100 mg/ml), and L-glutamine (2 mM). Transfection of the plasmid DNA into cells was performed using Lipofectamine 2000 (Invitrogen) according to the manufacturer's protocol.

### Plasmid construction

Full-length mouse *Lpiat1* was amplified by PCR from mouse cDNA with primers *Lpiat1* forward (5'-ACGGTTGAATTCATGACAC-CCGAAGAATGGAC-3') and reverse (5'-CAGCAGCTCGAGCTCT-TCCCGGAGCTTTTCCT-3') and was cloned into pCAGGS-myc vector (C-terminal Myc tag) at the *EcoRI* and *XhoI* sites.

### Metabolite extraction and analysis

Arachidonic acid metabolites were extracted from P0 mouse brains by solid-phase extraction using Sep-Pak C18 cartridges (Waters, Milford, MA) with deuterium-labeled internal standards (AA-d<sub>8</sub>, 15-HETE-d<sub>8</sub>, LTB<sub>4</sub>-d<sub>4</sub>, and PGE<sub>2</sub>-d<sub>4</sub>). LC-MS/MS-based lipidomic analyses were performed using a HPLC system (Waters UPLC) with a linear ion trap quadrupole mass spectrometer (QTRAP 5500; AB Sciex, Foster City, CA) equipped with an Acquity UPLC BEH C<sub>18</sub> column (1.0 mm × 150 mm × 1.7 µm; Waters). Samples were eluted with mobile phase composed of water/acetate (100:0.1, vol/vol) and acetonitrile/methanol (4:1, vol/vol) (73:27) for 5 min and ramped to 30:70 after 15 min, to 20:80 after 25 min and held for 8 min, ramped to 0:100 after 35 min, and held for 10 min with flow rates of 50 (0–30 min), 80 (30–33 min), and 100 µl/min (33–45 min). MS/MS analyses were conducted in negative-ion mode, and fatty acid metabolites were identified and quantified by multiple reaction monitoring. Quantitation was performed using calibration curves constructed for each compound, and recoveries were monitored using added deuterated internal standards.

## ACKNOWLEDGMENTS

We thank Tomohiko Taguchi for valuable discussion and Ryo Iwamoto for technical assistance in LC-MS/MS analysis. This work was supported by the Core Research for Evolutional Science and Technology, Japan Science and Technology Agency (to H.A.), the Program for Promotion of Basic and Applied Researches for Innovations in Bio-oriented Industry (to H.A.), grants-in-aid from the Japanese Ministry of Education, Culture, Sports, Science, and Technology (20370045 to H.A.), the Japanese Ministry of Health, Labor, and Welfare (to H. A.), and Research Fellowships of the Japan Society for the Promotion of Science for Young Scientists (to H.L. and S.M.).

## REFERENCES

- Abad-Jorge A (2008). The role of DHA and ARA in infant nutrition and neurodevelopmental outcomes. *Today's Dietician* 10, 66.
- Alcántara S, Ruiz M, D'Arcangelo G, Ezan F, de Lecea L, Curran T, Sotelo C, Soriano E (1998). Regional and cellular patterns of reelin mRNA expression in the forebrain of the developing and adult mouse. *J Neurosci* 18, 7779–7799.
- Backer JM (2008). The regulation and function of class III PI3Ks: novel roles for Vps34. *Biochem J* 410, 1–17.
- Baker RR, Thompson W (1973). Selective acylation of 1-acylglycerophosphorylinositol by rat brain microsomes. Comparison with 1-acylglycerophosphorylcholine. *J Biol Chem* 248, 7060–7065.
- Bannai H, Inoue T, Nakayama T, Hattori M, Mikoshiba K (2004). Kinesin dependent, rapid, bi-directional transport of ER sub-compartment in dendrites of hippocampal neurons. *J Cell Sci* 117, 163–175.
- Bartlett G (1959). Phosphorus assay in column chromatography. *J Biol Chem* 234, 466–468.
- Besana A, Robinson R, Feinmark S (2005). Lipids and two-pore domain K<sup>+</sup> channels in excitable cells. *Prostaglandins Other Lipid Mediat* 77, 103–110.
- Bligh E, Dyer W (1959). A rapid method of total lipid extraction and purification. *Can J Biochem Physiol* 37, 911–917.
- Bonventre JV, Huang Z, Taheri MR, O'Leary E, Li E, Moskowitz MA, Sapirstein A (1997). Reduced fertility and postischemic brain injury in mice deficient in cytosolic phospholipase A2. *Nature* 390, 622–625.
- Chen C, Magee J, Bazan N (2002). Cyclooxygenase-2 regulates prostaglandin E2 signaling in hippocampal long-term synaptic plasticity. *J Neurophysiol* 87, 2851–2857.
- Chen XS, Sheller JR, Johnson EN, Funk CD (1994). Role of leukotrienes revealed by targeted disruption of the 5-lipoxygenase gene. *Nature* 372, 179–182.
- Chyb S, Raghu P, Hardie RC (1999). Polyunsaturated fatty acids activate the *Drosophila* light-sensitive channels TRP and TRPL. *Nature* 397, 255–259.
- D'Arcangelo G, Miao GG, Chen SC, Soares HD, Morgan JI, Curran T (1995). A protein related to extracellular matrix proteins deleted in the mouse mutant reeler. *Nature* 374, 719–723.
- D'Arcangelo G, Nakajima K, Miyata T, Ogawa M, Mikoshiba K, Curran T (1997). Reelin is a secreted glycoprotein recognized by the CR-50 monoclonal antibody. *J Neurosci* 17, 23–31.
- Davis-Bruno K, Tassinari MS (2011). Essential fatty acid supplementation of DHA and ARA and effects on neurodevelopment across animal species: a review of the literature. *Birth Defects Res B Dev Reprod Toxicol* 92, 240–50.
- Di Paolo G, De Camilli P (2006). Phosphoinositides in cell regulation and membrane dynamics. *Nature* 443, 651–657.
- Dijk-Brouwer D, Hadders-Algra M, Bouwstra H, Decsi T, Boehm G, Martini I, Boersma E, Muskiet F (2005). Lower fetal status of docosahexaenoic acid, arachidonic acid and essential fatty acids is associated with less favorable neonatal neurological condition. *Prostaglandins Leukot Essent Fatty Acids* 72, 21–28.
- Eberhardt C, Gray PW, Tjoelker LW (1997). Human lysophosphatidic acid acyltransferase. cDNA cloning, expression, and localization to chromosome 9q34.3. *J Biol Chem* 272, 20299–20305.
- Fan YY, Monk JM, Hou TY, Callway E, Vincent L, Weeks B, Yang P, Chapkin RS (2012). Characterization of an arachidonic acid-deficient (*Fads1* knockout) mouse model. *J Lipid Res* 53, 1287–1295.
- García-Calatayud S, Ruiz JI, García-Fuentes M, Dierssen M, Flórez J, Crespo PS (2002). Long-chain polyunsaturated fatty acids in rat maternal milk, offspring brain and peripheral tissues in essential fatty acid deficiency. *Clin Chem Lab Med* 40, 278–284.
- Gijón MA, Riekhof WR, Zarini S, Murphy RC, Voelker DR (2008). Lysophospholipid acyltransferases and arachidonate recycling in human neutrophils. *J Biol Chem* 283, 30235–30245.
- Gleeson JG, Walsh CA (2000). Neuronal migration disorders: from genetic diseases to developmental mechanisms. *Trends Neurosci* 23, 352–359.
- Goldberg EM, Zidovetzki R (1997). Effects of dipalmitoylglycerol and fatty acids on membrane structure and protein kinase C activity. *Biophys J* 73, 2603–2614.
- Hevner R, Shi L, Justice N, Hsueh Y, Sheng M, Smiga S, Bulfone A, Goffinet A, Campagnoni A, Rubenstein J (2001). *Tbr1* regulates differentiation of the preplate and layer 6. *Neuron* 29, 353–366.
- Holub B, Kuksis A (1971). Differential distribution of orthophosphate-32 P and glycerol-14 C among molecular species of phosphatidylinositols of rat liver in vivo. *J Lipid Res* 12, 699–705.
- Imae R, Inoue T, Kimura M, Kanamori T, Tomioka N, Kage-Nakadai E, Mitani S, Arai H (2010). Intracellular phospholipase A1 and acyltransferase, which are involved in *Caenorhabditis elegans* stem cell divisions, determine the sn-1 fatty acyl chain of phosphatidylinositol. *Mol Biol Cell* 21, 3114–3124.
- Inoue M, Murase S, Okuyama H (1984). Acyl coenzyme a:phospholipid acyltransferases in porcine platelets discriminate between omega-3 and omega-6 unsaturated fatty acids. *Arch Biochem Biophys* 231, 29–37.
- Junglawala F, Evans J, McCluer R (1984). Compositional and molecular species analysis of phospholipids by high performance liquid chromatography coupled with chemical ionization mass spectrometry. *J Lipid Res* 25, 738–749.
- Kotani S, Nakazawa H, Tokimasa T, Akimoto K, Kawashima H, Toyoda-Ono Y, Kiso Y, Okaichi H, Sakakibara M (2003). Synaptic plasticity preserved with arachidonic acid diet in aged rats. *Neurosci Res* 46, 453–461.
- Lee H, Inoue T, Imae R, Kono N, Shirae S, Matsuda S, Gengyo-Ando K, Mitani S, Arai H (2008). *Caenorhabditis elegans* mboa-7, a member of the MBOAT family, is required for selective incorporation of polyunsaturated fatty acids into phosphatidylinositol. *Mol Biol Cell* 19, 1174–1184.
- Lee HC, Kubo T, Kono N, Kage-Nakadai E, Gengyo-Ando K, Mitani S, Inoue T, Arai H (2012). Depletion of mboa-7, an enzyme that incorporates polyunsaturated fatty acids into phosphatidylinositol (PI), impairs PI 3-phosphate signaling in *Caenorhabditis elegans*. *Genes Cells* 17, 748–757.
- Luskin M, Shatz C (1985). Studies of the earliest generated cells of the cat's visual cortex: cogeneration of subplate and marginal zones. *J Neurosci* 5, 1062–1075.
- Luthra M, Sheltawy A (1976). The metabolic turnover of molecular species of phosphatidylinositol and its precursor phosphatidic acid in guinea-pig cerebral hemispheres. *J Neurochem* 27, 1501–1511.
- Maekawa M et al. (2009). Arachidonic acid drives postnatal neurogenesis and elicits a beneficial effect on prepulse inhibition, a biological trait of psychiatric illnesses. *PLoS One* 4, 9.
- McEvilly R, de Diaz M, Schonemann M, Hooshmand F, Rosenfeld M (2002). Transcriptional regulation of cortical neuron migration by POU domain factors. *Science* 295, 1528–1532.
- Nakagawa Y, Sugiura T, Waku K (1985). The molecular species composition of diacyl-, alkylacyl- and alkenylacylglycerophospholipids in rabbit alveolar macrophages. High amounts of 1-O-hexadecyl-2-arachidonoyl molecular species in alkylacylglycerophosphocholine. *Biochim Biophys Acta* 833, 323–329.
- Ogawa M, Miyata T, Nakajima K, Yagyu K, Seike M, Ikenaka K, Yamamoto H, Mikoshiba K (1995). The reeler gene-associated antigen on Cajal-Retzus neurons is a crucial molecule for laminar organization of cortical neurons. *Neuron* 14, 899–912.
- Ogiso H, Taguchi R (2008). Reversed-phase LC/MS method for polyphosphoinositide analyses: changes in molecular species levels during epidermal growth factor activation in A431 cells. *Anal Chem* 80, 9226–9232.
- Okaichi Y, Ishikura Y, Akimoto K, Kawashima H, Toyoda-Ono Y, Kiso Y, Okaichi H (2005). Arachidonic acid improves aged rats' spatial cognition. *Physiol Behav* 84, 617–623.
- Palmer FB (1986). Metabolism of lysopolyphosphoinositides by rat brain and liver microsomes. *Biochem Cell Biol* 64, 117–125.
- Patton G, Fasulo J, Robins S (1982). Separation of phospholipids and individual molecular species of phospholipids by high-performance liquid chromatography. *J Lipid Res* 23, 190–196.
- Rakic P (1988). Specification of cerebral cortical areas. *Science* 241, 170–176.
- Roqueta-Rivera M, Stroud CK, Haschek WM, Akare SJ, Segre M, Brush RS, Agbaga MP, Anderson RE, Hess RA, Nakamura MT (2010).

- Docosahexaenoic acid supplementation fully restores fertility and spermatogenesis in male delta-6 desaturase-null mice. *J Lipid Res* 51, 360–367.
- Saito S, Goto K, Tonosaki A, Kondo H (1997). Gene cloning and characterization of CDP-diacylglycerol synthase from rat brain. *J Biol Chem* 272, 9503–9509.
- Sanjanwala M, Sun GY, MacQuarrie RA (1989). Purification and kinetic properties of lysophosphatidylinositol acyltransferase from bovine heart muscle microsomes and comparison with lysophosphatidylcholine acyltransferase. *Arch Biochem Biophys* 271, 407–413.
- Sasaki T, Takasuga S, Sasaki J, Kofuji S, Eguchi S, Yamazaki M, Suzuki A (2009). Mammalian phosphoinositide kinases and phosphatases. *Prog Lipid Res* 48, 307–343.
- Serunian LA, Auger KR, Cantley LC (1991). Identification and quantification of polyphosphoinositides produced in response to platelet-derived growth factor stimulation. *Methods Enzymol* 198, 78–87.
- Shaw K, Commins S, O'Mara S (2003). Deficits in spatial learning and synaptic plasticity induced by the rapid and competitive broad-spectrum cyclooxygenase inhibitor ibuprofen are reversed by increasing endogenous brain-derived neurotrophic factor. *Eur J Neurosci* 17, 2438–2446.
- Shindou H, Shimizu T (2009). Acyl-CoA:lysophospholipid acyltransferases. *J Biol Chem* 284, 1–5.
- Stamps AC, Elmore MA, Hill ME, Kelly K, Makda AA, Finnen MJ (1997). A human cDNA sequence with homology to non-mammalian lysophosphatidic acid acyltransferases. *Biochem J* 326, 455–461.
- Steinhauer J, Gijón MA, Riekhof WR, Voelker DR, Murphy RC, Treisman JE (2009). *Drosophila* lysophospholipid acyltransferases are specifically required for germ cell development. *Mol Biol Cell* 20, 5224–5235.
- Stoffel W *et al.* (2008). Delta6-desaturase (FADS2) deficiency unveils the role of omega3- and omega6-polyunsaturated fatty acids. *EMBO J* 27, 2281–2292.
- Stroud CK *et al.* (2009). Disruption of FADS2 gene in mice impairs male reproduction and causes dermal and intestinal ulceration. *J Lipid Res* 50, 1870–1880.
- Tanaka T, Iwawaki D, Sakamoto M, Takai Y, Morishige J, Murakami K, Satouchi K (2003). Mechanisms of accumulation of arachidonate in phosphatidylinositol in yellowtail. A comparative study of acylation systems of phospholipids in rat and the fish species *Seriola quinqueradiata*. *Eur J Biochem* 270, 1466–1473.
- Tissir F, Goffinet A (2003). Reelin and brain development. *Nat Rev Neurosci* 4, 496–505.
- Tysnes OB, Aarbakke GM, Verhoeven AJ, Holmsen H (1985). Thin-layer chromatography of polyphosphoinositides from platelet extracts: interference by an unknown phospholipid. *Thromb Res* 40, 329–338.
- Uozumi N *et al.* (1997). Role of cytosolic phospholipase A2 in allergic response and parturition. *Nature* 390, 618–622.
- Ushikubi F *et al.* (1998). Impaired febrile response in mice lacking the prostaglandin E receptor subtype EP3. *Nature* 395, 281–284.
- Williams J, Bliss T (1988). Induction but not maintenance of calcium-induced long-term potentiation in dentate gyrus and area CA1 of the hippocampal slice is blocked by nordihydroguaiaretic acid. *Neurosci Lett* 88, 81–85.
- Williard DE, Nwankwo JO, Kaduce TL, Harmon SD, Irons M, Moser HW, Raymond GV, Spector AA (2001). Identification of a fatty acid delta6-desaturase deficiency in human skin fibroblasts. *J Lipid Res* 42, 501–508.
- Xiao YF, Ke Q, Wang SY, Auktor K, Yang Y, Wang GK, Morgan JP, Leaf A (2001). Single point mutations affect fatty acid block of human myocardial sodium channel alpha subunit Na<sup>+</sup> channels. *Proc Natl Acad Sci USA* 98, 3606–3611.
- Yashiro K, Kameyama Y, Mizuno-Kamiya M, Shin SO, Fujita A (1995). Substrate specificity of microsomal 1-acyl-sn-glycero-3-phosphoinositol acyltransferase in rat submandibular gland for polyunsaturated long-chain acyl-CoAs. *Biochim Biophys Acta* 1258, 288–296.
- Zhao J, Del Bigio M, Weiler H (2009). Maternal arachidonic acid supplementation improves neurodevelopment of offspring from healthy and diabetic rats. *Prostaglandins Leukot Essent Fatty Acids* 81, 349–356.
- Zhou X (2010). Function of Phosphatidylinositol 3-Kinase Class III in the Nervous System. PhD Thesis, Durham, NC: Duke University.

# Mast cell maturation is driven via a group III phospholipase A<sub>2</sub>-prostaglandin D<sub>2</sub>-DP1 receptor paracrine axis

Yoshitaka Taketomi<sup>1,2</sup>, Noriko Ueno<sup>1</sup>, Takumi Kojima<sup>1</sup>, Hiroyasu Sato<sup>1,2</sup>, Remi Murase<sup>1,2</sup>, Kei Yamamoto<sup>1</sup>, Satoshi Tanaka<sup>3</sup>, Mariko Sakanaka<sup>4</sup>, Masanori Nakamura<sup>5</sup>, Yasumasa Nishito<sup>6</sup>, Momoko Kawana<sup>2</sup>, Naotomo Kambe<sup>7</sup>, Kazutaka Ikeda<sup>8</sup>, Ryo Taguchi<sup>9</sup>, Satoshi Nakamizo<sup>10</sup>, Kenji Kabashima<sup>10</sup>, Michael H Gelb<sup>11</sup>, Makoto Arita<sup>12</sup>, Takehiko Yokomizo<sup>13</sup>, Motonao Nakamura<sup>14</sup>, Kikuko Watanabe<sup>15</sup>, Hiroyuki Hirai<sup>16</sup>, Masataka Nakamura<sup>17</sup>, Yoshimichi Okayama<sup>18</sup>, Chisei Ra<sup>18</sup>, Kosuke Aritake<sup>19</sup>, Yoshihiro Urade<sup>19</sup>, Kazushi Morimoto<sup>20</sup>, Yukihiko Sugimoto<sup>20</sup>, Takao Shimizu<sup>14</sup>, Shuh Narumiya<sup>21</sup>, Shuntaro Hara<sup>2</sup> & Makoto Murakami<sup>1</sup>

Microenvironment-based alterations in phenotypes of mast cells influence the susceptibility to anaphylaxis, yet the mechanisms underlying proper maturation of mast cells toward an anaphylaxis-sensitive phenotype are incompletely understood. Here we report that PLA2G3, a mammalian homolog of anaphylactic bee venom phospholipase A<sub>2</sub>, regulates this process. PLA2G3 secreted from mast cells is coupled with fibroblastic lipocalin-type PGD<sub>2</sub> synthase (L-PGDS) to provide PGD<sub>2</sub>, which facilitates mast-cell maturation via PGD<sub>2</sub> receptor DP1. Mice lacking PLA2G3, L-PGDS or DP1, mast cell-deficient mice reconstituted with PLA2G3-null or DP1-null mast cells, or mast cells cultured with L-PGDS-ablated fibroblasts exhibited impaired maturation and anaphylaxis of mast cells. Thus, we describe a lipid-driven PLA2G3-L-PGDS-DP1 loop that drives mast cell maturation.

Anaphylaxis is a serious immediate allergic reaction that involves the activation of mast cells. Cross-linking of the high-affinity IgE receptor FcεRI on mast cells with IgE and antigen initiates signals leading to the release of allergic mediators that induce immediate hypersensitivity<sup>1</sup>. Anaphylaxis is triggered by allergens (for example, insect venom, food and medication) and damages multiple organs including the respiratory and circulatory systems, often leading to life-threatening episodes.

Environmentally induced alterations in phenotypes of mast cells could be one factor that influences the severity of anaphylaxis. Current evidence has established the essential role of stem cell factor (SCF) and its receptor c-Kit (CD117) for development of mast cells<sup>2</sup>. However, the SCF-c-Kit system alone is insufficient to drive the maturation of mast cells fully, as culture of immature mast cells with fibroblasts, but not with SCF alone, can induce differentiation

into mature mast cells<sup>2</sup>. Although several cytokines, chemokines and adhesion molecules have supporting roles in tissue-specific homing, growth or differentiation of mast cells<sup>3-7</sup>, precise mechanisms underlying mast cell-fibroblast communication leading to optimal maturation of mast cells still remain elusive.

Lipid mediators, such as prostaglandins, leukotrienes and lysophospholipids, have important roles in various biological processes, including allergy<sup>8-15</sup>. A given lipid mediator (for example, PGD<sub>2</sub>) aggravates, suppresses or resolves allergic responses<sup>11-13</sup>, and this functional variability may depend on the use of distinct biosynthetic enzyme and/or receptor subtypes in different cells. Eicosanoid biosynthesis is initiated by release of arachidonic acid from phospholipids by phospholipase A<sub>2</sub> (PLA<sub>2</sub>) enzymes<sup>16</sup>. PLA2G4A (cytosolic PLA<sub>2</sub>; cPLA<sub>2</sub>α) has an essential role in the generation of eicosanoids in various cells, and its deletion results in diminished airway hypersensitivity<sup>17</sup>.

<sup>1</sup>Lipid Metabolism Project, Tokyo Metropolitan Institute of Medical Science, Tokyo, Japan. <sup>2</sup>School of Pharmacy, Showa University, Tokyo, Japan. <sup>3</sup>Department of Immunobiology, Okayama University Graduate School of Medicine, Dentistry and Pharmaceutical Sciences, Okayama, Japan. <sup>4</sup>School of Pharmacy and Pharmaceutical Sciences, Mukogawa Women's University, Hyogo, Japan. <sup>5</sup>School of Dentistry, Showa University, Tokyo, Japan. <sup>6</sup>Core Technology and Research Center, Tokyo Metropolitan Institute of Medical Science, Tokyo, Japan. <sup>7</sup>Department of Dermatology, Chiba University Graduate School of Medicine, Chiba, Japan. <sup>8</sup>Institute for Advanced Biosciences, Keio University, Yamagata, Japan. <sup>9</sup>College of Life and Health Sciences, Chubu University, Aichi, Japan. <sup>10</sup>Department of Dermatology, Kyoto University Graduate School of Medicine, Kyoto, Japan. <sup>11</sup>Departments of Chemistry and Biochemistry, University of Washington, Washington, USA. <sup>12</sup>Graduate School of Pharmaceutical Sciences, The University of Tokyo, Tokyo, Japan. <sup>13</sup>Department of Biochemistry, Juntendo University School of Medicine, Tokyo, Japan. <sup>14</sup>Faculty of Medicine, The University of Tokyo, Tokyo, Japan. <sup>15</sup>Department of Nutrition, Koshien University, Hyogo, Japan. <sup>16</sup>Department of Advanced Medicine and Development, Bio Medical Laboratories, Saitama, Japan. <sup>17</sup>Human Gene Sciences Center, Tokyo Medical and Dental University, Tokyo, Japan. <sup>18</sup>Division of Molecular Cell Immunology and Allergology, Advanced Medical Research Center, Nihon University Graduate School of Medical Science, Tokyo, Japan. <sup>19</sup>Department of Molecular Behavioral Biology, Osaka Bioscience Institute, Osaka, Japan. <sup>20</sup>Department of Pharmaceutical Biochemistry, Graduate School of Medicine and Pharmaceutical Sciences, Kumamoto University, Kumamoto, Japan. <sup>21</sup>Department of Pharmacology, Kyoto University Graduate School of Medicine, Kyoto, Japan. Correspondence should be addressed to M.M. (murakami-mk@igakuken.or.jp).

Received 19 September 2012; accepted 11 March 2013; published online 28 April 2013; doi:10.1038/ni.2586

By contrast, the role of secreted PLA<sub>2</sub> (sPLA<sub>2</sub>) enzymes is still a subject of debate. Although the lower asthmatic responses in mice lacking two classical sPLA<sub>2</sub> enzymes (PLA2G5 and PLA2G10) have revealed their contribution to asthma<sup>18,19</sup>, the mechanisms underlying the actions of these enzymes remain poorly understood.

A major bee venom component responsible for anaphylaxis is an atypical form of sPLA<sub>2</sub> called BV-PLA<sub>2</sub><sup>20,21</sup>. The mammalian genome encodes group III sPLA<sub>2</sub> (PLA2G3), which is the sole homolog of BV-PLA<sub>2</sub><sup>16,22–26</sup>. Here we provide evidence that PLA2G3 is a major mast cell granule-associated sPLA<sub>2</sub> that facilitates the maturation of mast cells by driving a previously unrecognized lipid mediator circuit. PLA2G3 released from mast cells is coupled with fibroblast lipocalin-type PGD synthase (L-PGDS) to provide PGD<sub>2</sub>, which then acts on type-1 PGD receptor, DP1, induced on mast cells to promote their maturation.

## RESULTS

### PLA2G3 is expressed in mast cells and induces their activation

When injected intradermally into the mouse ear pinnae, BV-PLA<sub>2</sub> or human PLA2G3 alone induced a similar, dose-dependent vascular leak and augmented passive cutaneous anaphylaxis (PCA) induced by IgE and antigen in *Kit*<sup>+/+</sup> mice but not in mast cell-deficient *Kit*<sup>W<sup>sh</sup>/W<sup>sh</sup> mice, in which the SCF receptor c-Kit has a substitution (Fig. 1a,b). The edema induced by PLA2G3 was accompanied by ultrastructural degranulation of dermal mast cells (Fig. 1c). PLA2G3 induced the release of histamine (Fig. 1d), but not of lactate dehydrogenase (Supplementary Fig. 1a), from mouse peritoneal mast cells (pMCs) in a Ca<sup>2+</sup>-dependent manner, indicating that PLA2G3 elicits degranulation, not cell lysis.</sup>

Immunohistochemistry analysis revealed that PLA2G3 localized with toluidine blue<sup>+</sup> dermal mast cells in wild-type mice but not in *Pla2g3*<sup>-/-</sup> mice<sup>22</sup> (Fig. 1e). Punctate staining in resting mast cells and sparse staining in degranulated mast cells suggest that PLA2G3 is

released upon degranulation (Fig. 1e,f). In bone marrow-derived cell populations, *Pla2g3* mRNA was more highly enriched in IL-3-driven bone marrow-derived mast cells (BMMCs) and thymic stromal lymphopoietin (TSLP)-driven bone marrow-derived basophils (BM basophils) than in GM-CSF-driven bone marrow-derived dendritic cells (BMDCs) and M-CSF-driven bone marrow-derived macrophages (BMDMs), and was undetectable in Swiss 3T3 fibroblasts (Fig. 1g and Supplementary Fig. 1b). Of the mRNAs encoding sPLA<sub>2</sub> isoforms, *Pla2g3* mRNA was expressed most abundantly in BMMCs, followed by *Pla2g5* and *Pla2g2e*, whereas mRNAs encoding the other sPLA<sub>2</sub> isoforms were undetectable, and SCF-fibroblast-driven maturation of these cells toward connective tissue mast cells (CTMCs) did not affect the expression of these sPLA<sub>2</sub> enzymes (Supplementary Fig. 1c). When we transfected rat mastocytoma RBL-2H3 cells with cDNA encoding PLA2G3 or a catalytically inactive PLA2G3 variant, III-HQ, in which the catalytic-center histidine was replaced with asparagine<sup>23</sup>, release of β-hexosaminidase (β-HEX) and generation of PGD<sub>2</sub> induced by crosslinking of FcεRI by IgE and antigen (hereafter called IgE-Ag) was augmented in cells overexpressing native PLA2G3 but not catalytically inactive PLA2G3 (Supplementary Fig. 1d). Thus, PLA2G3 is the main sPLA<sub>2</sub> in mouse mast cells, is released by exocytosis and can augment activation of mast cells in a manner dependent upon its enzymatic activity.

### *Pla2g3* deletion ameliorates mast cell-associated anaphylaxis

Upon passive systemic anaphylaxis (PSA) induced by IgE-Ag, *Pla2g3*<sup>+/+</sup> and WBB6F1-*Kit*<sup>+/+</sup> mice, but not mast cell-deficient WBB6F1-*Kit*<sup>W<sup>sh</sup>/W<sup>sh</sup> mice, had much more plasma histamine and a temporary decrease in rectal temperature after systemic antigen challenge, whereas these responses were mild in *Pla2g3*<sup>-/-</sup> mice (Fig. 2a). Upon PCA induced by IgE-Ag (Fig. 2b and Supplementary Fig. 1e) or compound 48/80 (C48/80; Fig. 2c), edema was markedly lower in *Pla2g3*<sup>-/-</sup> mice than *Pla2g3*<sup>+/+</sup> mice. By contrast, transgenic overexpression of human</sup>

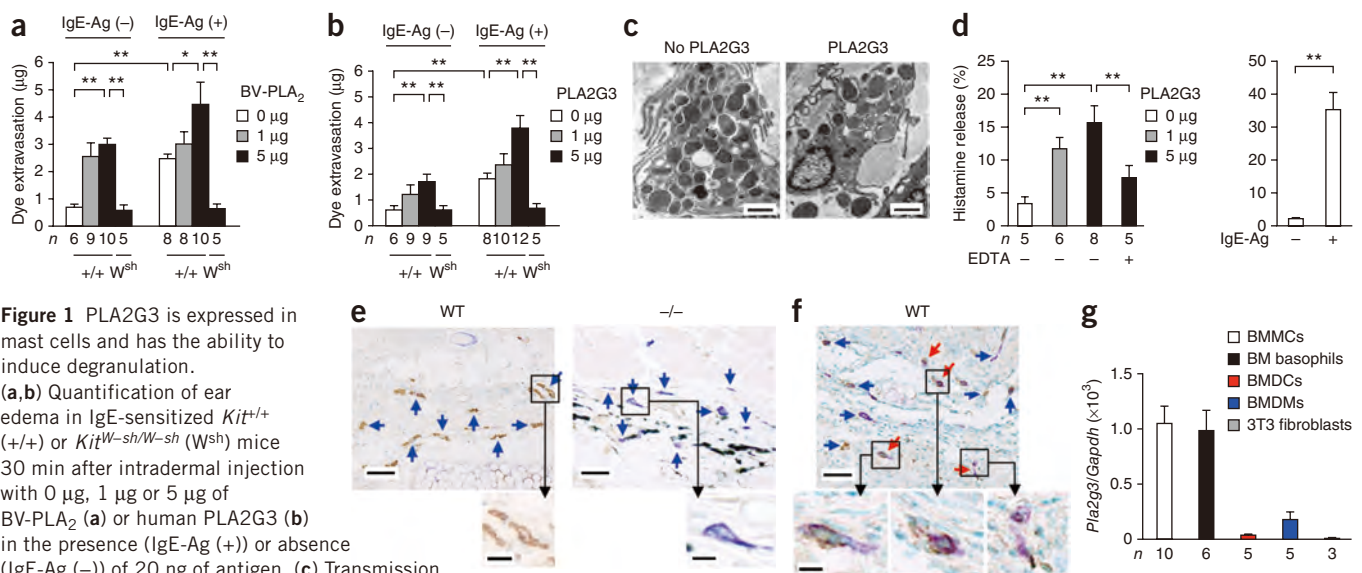


**Figure 1** PLA2G3 is expressed in mast cells and has the ability to induce degranulation.

(a,b) Quantification of ear edema in IgE-sensitized *Kit*<sup>+/+</sup> (+/+) or *Kit*<sup>W<sup>sh</sup>/W<sup>sh</sup> (*W*<sup>sh</sup>) mice 30 min after intradermal injection with 0 µg, 1 µg or 5 µg of BV-PLA<sub>2</sub> (a) or human PLA2G3 (b) in the presence (IgE-Ag (+)) or absence (IgE-Ag (-)) of 20 ng of antigen. (c) Transmission electron microscopy of ear mast cells in wild-type mice with (+) or without (-) administration of 5 µg of PLA2G3. Scale bars, 2 µm. (d) Histamine release from wild-type mouse peritoneal cells after treatment for 30 min with 0 µg, 1 µg or 5 µg of PLA2G3 in the presence or absence of 2 mM EDTA (left). Histamine release by IgE-Ag stimulation (positive control) is also shown (right). (e,f) Immunohistochemistry analysis of ear-skin sections of wild-type (WT) or *Pla2g3*<sup>-/-</sup> (-/-) mice before (e) and 2 min after (f) stimulation with IgE-Ag with anti-PLA2G3 (α-PLA2G3), followed by counterstaining with toluidine blue (scale bars, 50 µm). Boxed areas are magnified below (scale bars, 5 µm). Blue and red arrows indicate resting and degranulated mast cells, respectively. (g) Real-time PCR of *Pla2g3* relative to *Gapdh* in indicated bone marrow-derived cells from wild-type mice and Swiss 3T3 fibroblasts. Data are from one experiment (g), and compiled from two (d) and three (a,b) experiments (mean ± s.e.m.; \**P* < 0.05 and \*\**P* < 0.01). Data in c,e,f are representative of two experiments.</sup>

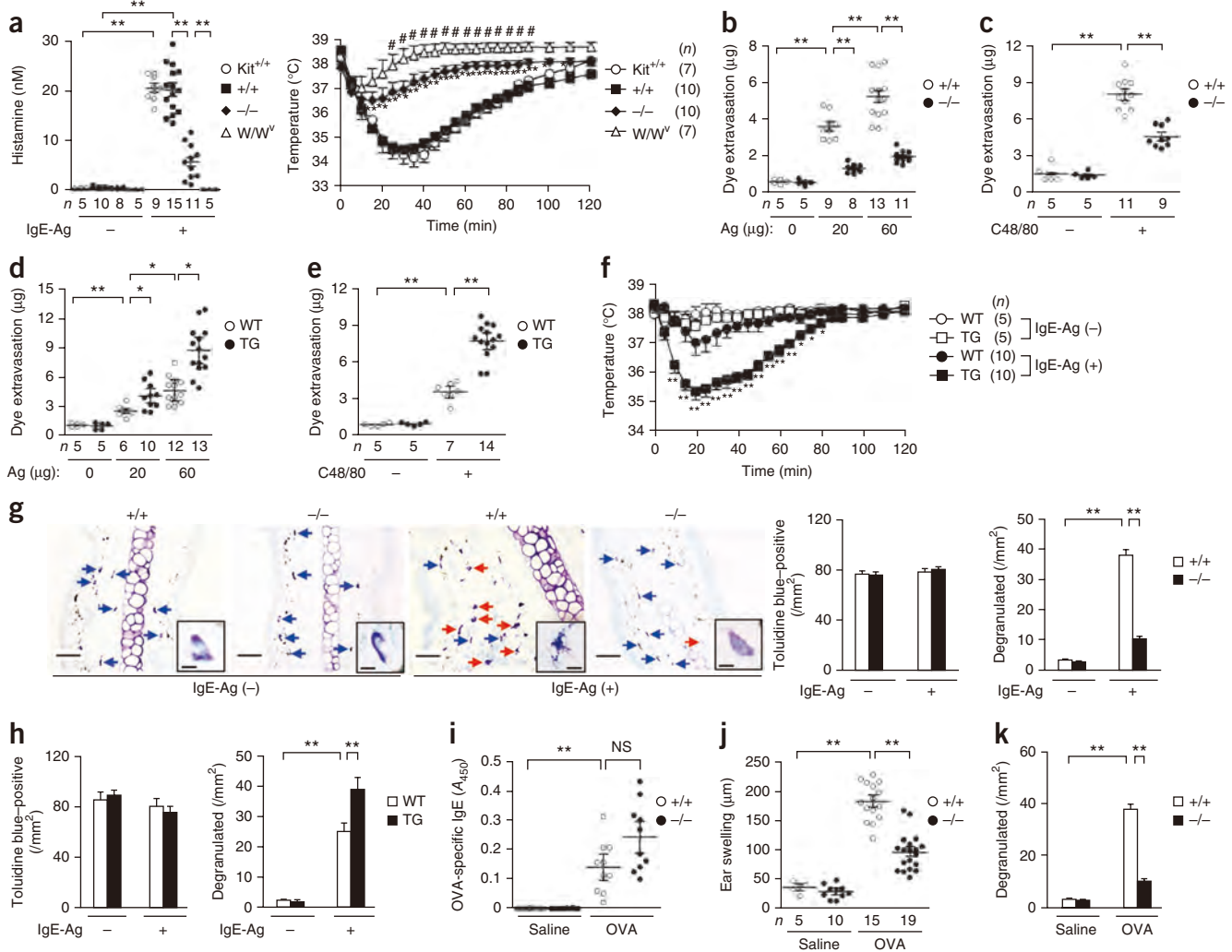


**Figure 2** Altered anaphylaxis in mice with deletion or overexpression of PLA2G3. (a) Serum histamine concentrations (left) and rectal temperatures (right) in IgE-Ag-dependent PSA in *Pla2g3<sup>+/+</sup>* (+/+), *Pla2g3<sup>-/-</sup>* (-/-), WBB6F1-*Kit<sup>+/+</sup>* (*Kit<sup>+/+</sup>*) and WBB6F1-*Kit<sup>W/W<sup>v</sup></sup>* (*W/W<sup>v</sup>*) mice after challenge with 500  $\mu$ g of antigen (Ag). \**P* < 0.05 and \*\**P* < 0.01, *Pla2g3<sup>-/-</sup>* versus *Pla2g3<sup>+/+</sup>* mice and #*P* < 0.05, *Kit<sup>W/W<sup>v</sup></sup>* versus *Pla2g3<sup>-/-</sup>* mice (right). (b–e) Analysis of ear edema in IgE-Ag-induced (b,d) or C48/80-induced (c,e) PCA in *Pla2g3<sup>+/+</sup>* (+/+) and *Pla2g3<sup>-/-</sup>* (-/-) mice (b,c) or wild-type (WT) and *PLA2G3<sup>tg/+</sup>* (TG) mice (d,e). (f) Rectal temperatures in IgE-Ag-dependent PSA in wild-type (WT) and *PLA2G3<sup>tg/+</sup>* (TG) mice after challenge with antigen (25  $\mu$ g). \**P* < 0.05 and \*\**P* < 0.01, WT versus TG after antigen challenge. (g,h) Toluidine blue staining of skin sections (left) and counts of toluidine blue<sup>+</sup> total and degranulated dermal mast cells (right) in *Pla2g3<sup>+/+</sup>* (+/+) and *Pla2g3<sup>-/-</sup>* (-/-) mice (g) or wild-type (WT) and *PLA2G3<sup>tg/+</sup>* (TG) mice (h) before (IgE-Ag (-)) and 2 min after (IgE-Ag (+)) IgE-Ag-mediated PCA (scale bars, 50  $\mu$ m) (*n* = 6). Blue and red arrows indicate resting and degranulated mast cells, respectively (g). Insets, magnified images (scale bars, 5  $\mu$ m) (g). (i–k) Serum levels of OVA-specific IgE (*n* = 10; i), ear swelling (j) and numbers of degranulated ear mast cells (*n* = 6; k) in OVA-induced active cutaneous anaphylaxis in *Pla2g3<sup>+/+</sup>* (+/+) and *Pla2g3<sup>-/-</sup>* (-/-) mice. Data are from one experiment (f–i,k) and compiled from three experiments (a–e,j) (mean  $\pm$  s.e.m., \**P* < 0.05; \*\**P* < 0.01; NS, not significant).

PLA2G3 (*PLA2G3<sup>tg/+</sup>*)<sup>26</sup> augmented both IgE-Ag-dependent (Fig. 2d and Supplementary Fig. 1e) and C48/80-induced (Fig. 2e) PCA as well as IgE-Ag-induced PSA (Fig. 2f). Although the ear skin of *Pla2g3<sup>-/-</sup>* and *Pla2g3<sup>+/+</sup>* mice contained an equivalent number of toluidine blue<sup>+</sup> mast cells, we detected fewer cells showing signs of IgE-Ag-induced degranulation in *Pla2g3<sup>-/-</sup>* mice than in *Pla2g3<sup>+/+</sup>* mice (Fig. 2g). Conversely, ears of IgE-Ag-treated *PLA2G3<sup>tg/+</sup>* mice had more degranulated mast cells than those of replicate control mice despite a similar total mast cell count (Fig. 2h). IgE-Ag-induced PCA in mice lacking other sPLA<sub>2</sub> enzymes (*Pla2g2d<sup>-/-</sup>*, *Pla2g2e<sup>-/-</sup>*, *Pla2g2f<sup>-/-</sup>*, *Pla2g5<sup>-/-</sup>* and *Pla2g10<sup>-/-</sup>*) was similar to that in respective wild-type littermates (Supplementary Fig. 1f).

We immunized *Pla2g3<sup>+/+</sup>* and *Pla2g3<sup>-/-</sup>* mice intraperitoneally with alum-adsorbed ovalbumin (OVA) and elicited active cutaneous

anaphylaxis by intradermal injection of OVA, which cross-links endogenous IgE-bound Fc $\epsilon$ R1 on mast cells. Under conditions in which serum anti-OVA IgE levels were similar in both genotypes, *Pla2g3<sup>-/-</sup>* mice exhibited lower local anaphylaxis than did *Pla2g3<sup>+/+</sup>* mice, as indicated by notable reductions in ear swelling and mast cell degranulation (Fig. 2i–k). Thus, PLA2G3 is the sole sPLA<sub>2</sub> isoform associated with mast cell-dependent anaphylaxis.

#### *Pla2g3* deletion impairs maturation of tissue mast cells

Transmission electron microscopy analysis revealed that resting mast cells in *Pla2g3<sup>+/+</sup>* mice were oval with regular short processes and had many secretory granules filled with electron-lucent and dense contents, whereas those in *Pla2g3<sup>-/-</sup>* mice had unusual granules that were small and irregular in size, suggesting the

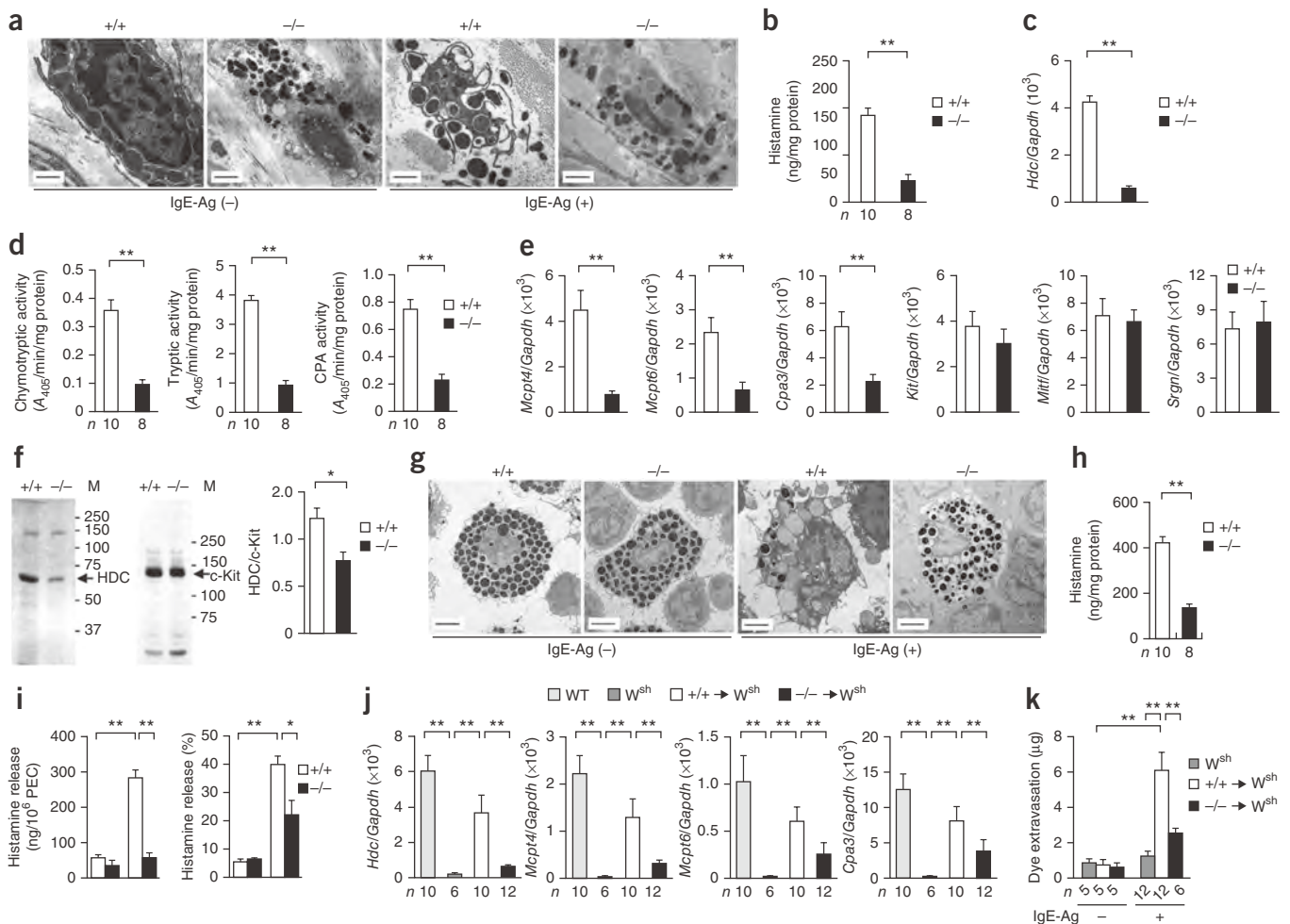


**Figure 3** Immature properties of tissue mast cells in *Pla2g3*-deficient mice. **(a)** Transmission electron micrographs of ear mast cells in *Pla2g3*<sup>+/+</sup> (+/+) and *Pla2g3*<sup>-/-</sup> (-/-) mice before (IgE-Ag (-)) and 2 min after (IgE-Ag (+)) antigen (Ag) challenge. Scale bars, 2  $\mu$ m. **(b,c)** Quantification of histamine amounts **(b)** and *Hdc* mRNA expression relative to that of *Gapdh* ( $n = 12$ ; **c**) in ears of *Pla2g3*<sup>+/+</sup> (+/+) and *Pla2g3*<sup>-/-</sup> (-/-) mice. **(d,e)** Quantification of protease activity **(d)** and mRNA expression of mast cell proteases ( $n = 12$ ) and other mast-cell markers ( $n = 7$ ) **(e)** in ears of *Pla2g3*<sup>+/+</sup> (+/+) and *Pla2g3*<sup>-/-</sup> (-/-) mice. **(f)** Immunoblotting of HDC and c-Kit in ears of *Pla2g3*<sup>+/+</sup> (+/+) and *Pla2g3*<sup>-/-</sup> (-/-) mice. M, molecular mass (kDa). The ratio of HDC/c-Kit was quantified by densitometric analysis ( $n = 4$ ). **(g)** Transmission electron micrographs of pMCs in *Pla2g3*<sup>+/+</sup> (+/+) and *Pla2g3*<sup>-/-</sup> (-/-) mice before (IgE-Ag (-)) and 2 min after (IgE-Ag (+)) stimulation with antigen. Scale bars, 2  $\mu$ m. **(h,i)** Quantification of histamine content **(h)** and IgE-Ag-induced histamine release (quantity and percentage; **i**) in *Pla2g3*<sup>+/+</sup> (+/+) and *Pla2g3*<sup>-/-</sup> (-/-) pMCs. PEC, peritoneal cells. **(j,k)** Expression of mast-cell marker mRNAs **(j)** and dye extravasation in IgE-Ag-dependent PCA **(k)** in ears of *Pla2g3*<sup>+/+</sup> (+/+) or *Pla2g3*<sup>-/-</sup> (-/-) BMMC-reconstituted or nonreconstituted *Kit*<sup>W<sup>sh</sup>/W<sup>sh</sup> (*W*<sup>sh</sup>) mice and wild-type (WT) *Kit*<sup>+/+</sup> mice. Data are compiled from two **(d,h,i)** or three **(b,c,e,j,k)** experiments (mean  $\pm$  s.e.m., \* $P < 0.05$ ; \*\* $P < 0.01$ ). Images are representative of one **(f)** or two **(a,g)** experiments.</sup>

immaturity of mast cells (**Fig. 3a** and **Supplementary Fig. 2a**). After challenge with antigen, *Pla2g3*<sup>+/+</sup> skin mast cells exhibited features typical of degranulation, whereas *Pla2g3*<sup>-/-</sup> mast cells were almost insensitive. In agreement, the amount of histamine (**Fig. 3b**) and the expression of *Hdc* (which encodes histidine decarboxylase, a histamine-biosynthetic enzyme; **Fig. 3c**) were lower in the ears of *Pla2g3*<sup>-/-</sup> mice than in those of *Pla2g3*<sup>+/+</sup> mice. Enzymatic activity (**Fig. 3d**) and expression (**Fig. 3e**) of mast cell proteases, including chymase (encoded by *Mcpt4*), tryptase (encoded by *Mcpt6*) and carboxypeptidase (encoded by *Cpa3*), were also notably lower in the ears of *Pla2g3*<sup>-/-</sup> mice relative to *Pla2g3*<sup>+/+</sup> mice. However, expression of *Kit*, *Mitf* (which encodes a transcription factor essential for mast cell differentiation) and *Srgn* (which encodes serglycin, a proteoglycan core protein) was unchanged in ears of *Pla2g3*<sup>-/-</sup> mice (**Fig. 3e**), indicating that not all mast cell markers were affected by PLA2G3 deficiency. We confirmed the lower expression of

HDC and the unaltered expression of c-Kit in the skin of *Pla2g3*<sup>-/-</sup> mice by immunoblotting (**Fig. 3f**).

*Pla2g3*<sup>-/-</sup> pMCs also had smaller and more irregular granules (**Fig. 3g** and **Supplementary Fig. 2b**), contained less histamine (**Fig. 3h**) and exhibited less IgE-Ag-induced histamine release (both amount and percentage; **Fig. 3i**) than *Pla2g3*<sup>+/+</sup> pMCs. Although the proportion of Kit<sup>+</sup>Fc $\epsilon$ RI $\alpha$ <sup>+</sup> skin mast cells or pMCs was similar in both genotypes, surface expression of Fc $\epsilon$ RI $\alpha$  was lower in *Pla2g3*<sup>-/-</sup> mice than in *Pla2g3*<sup>+/+</sup> mice (**Supplementary Fig. 2c,d**). A23187-induced histamine release by *Pla2g3*<sup>-/-</sup> pMCs was lower in terms of amount, but not percentage, compared to that by *Pla2g3*<sup>+/+</sup> pMCs (**Supplementary Fig. 2e**), suggesting that the attenuated IgE-Ag-induced degranulation and anaphylaxis in *Pla2g3*<sup>-/-</sup> mice was mainly due to the lower histamine content and surface Fc $\epsilon$ RI expression. Furthermore, intestinal expression of *Mcpt1* and *Mcpt2* (which encode mucosal mast-cell proteases) was markedly

lower in *Pla2g3*<sup>-/-</sup> mice than in *Pla2g3*<sup>+/+</sup> mice (Supplementary Fig. 2f). Thus, the lower anaphylaxis in *Pla2g3*<sup>-/-</sup> mice may result from abnormalities in the maturation and degranulation of mast cells in multiple anatomical sites. Other immune-cell populations in the skin and spleen were unaffected by PLA2G3 deficiency (Supplementary Fig. 2g,h).

To assess whether the aberrant features of mast cells in *Pla2g3*<sup>-/-</sup> mice relied on the absence of PLA2G3 in the mast cells themselves or in mast cell microenvironment, we transferred *Pla2g3*<sup>+/+</sup> or *Pla2g3*<sup>-/-</sup> BMMCs intradermally into mast cell-deficient *Kit*<sup>W-sh/W-sh</sup> mice. After 6 weeks, the distribution of mast cells in the ear dermis was comparable between mice reconstituted with *Pla2g3*<sup>+/+</sup> BMMCs and those reconstituted with *Pla2g3*<sup>-/-</sup> BMMCs (Supplementary Fig. 3a). Expression of mast-cell marker genes *Hdc*, *Mcpt4*, *Mcpt6* and *Cpa3* (Fig. 3j) and IgE-Ag-mediated PCA (Fig. 3k and Supplementary Fig. 3b) was much greater in the ears of mice that received *Pla2g3*<sup>+/+</sup> BMMCs over control *Kit*<sup>W-sh/W-sh</sup> mice, whereas these changes were scarcely seen in mice that received *Pla2g3*<sup>-/-</sup> BMMCs. We observed similar results when we transferred *Pla2g3*<sup>+/+</sup> or *Pla2g3*<sup>-/-</sup> BMMCs intravenously into *Kit*<sup>W-sh/W-sh</sup> mice. After 12 weeks of reconstitution, IgE-Ag-mediated PCA was restored in mice reconstituted with *Pla2g3*<sup>+/+</sup> BMMCs but remained poor in mice reconstituted with *Pla2g3*<sup>-/-</sup> BMMCs, although we observed similar numbers of reconstituted mast cells in the ear dermis (Supplementary Fig. 3c,d). In these experiments, low levels of mast-cell engraftment in the skin of *Kit*<sup>W-sh/W-sh</sup> mice relative to baseline amounts in the skin of wild-type mice restored PCA efficiently. *Kit*<sup>W-sh/W-sh</sup> mice transferred with *PLA2G3*<sup>tg/+</sup> BMMCs had a greater PCA response compared to those transferred with control BMMCs (Supplementary Fig. 3e). Altogether, the defective maturation and activation of mast cells in *Pla2g3*<sup>-/-</sup> mice are cell autonomous, even though the migration of mast cell progenitors into extravascular tissues is not profoundly impaired by PLA2G3 deficiency.

#### Impaired maturation of *Pla2g3*<sup>-/-</sup> mast cells in culture

*Pla2g3*<sup>-/-</sup> BMMCs grew normally in medium supplemented with IL-3 (Supplementary Fig. 4a) and, unlike tissue-resident mast cells, they had normal surface expression of FcεRIα (Supplementary Fig. 4b). Stimulation with IgE-Ag induced a robust release of sPLA<sub>2</sub> activity from wild-type BMMCs, whereas this release was ablated in *Pla2g3*<sup>-/-</sup> BMMCs and augmented in *PLA2G3*<sup>tg/+</sup> BMMCs (Supplementary Fig. 4c,d), confirming that PLA2G3 is released upon degranulation. IgE-Ag-stimulated *Pla2g3*<sup>-/-</sup> BMMCs released less histamine, PGD<sub>2</sub> and LTC<sub>4</sub> than *Pla2g3*<sup>+/+</sup> BMMCs, whereas these responses were greater in *PLA2G3*<sup>tg/+</sup> BMMCs than in control BMMCs (Supplementary Fig. 4e-j). IgE-Ag-induced influx of Ca<sup>2+</sup>, induction of cytokines (encoded by *Il4*, *Il6* and *Tnf*) and phosphorylation of phospholipase C (PLCγ2) and Akt were similar between the genotypes (Supplementary Fig. 4k-m), suggesting that FcεRI-dependent signaling was not profoundly perturbed by PLA2G3 deficiency. Generation of eicosanoids by mast cells depends on cPLA<sub>2</sub>α, which is regulated by Ca<sup>2+</sup>-dependent membrane translocation and MAP kinase-directed phosphorylation<sup>17</sup>. Consistent with the lower generation of eicosanoids (Supplementary Fig. 4f,g), FcεRI-dependent phosphorylation of ERK (not JNK and p38) and cPLA<sub>2</sub>α and decrease in arachidonic acid-containing phosphatidylcholine were partially impaired in *Pla2g3*<sup>-/-</sup> BMMCs compared to *Pla2g3*<sup>+/+</sup> BMMCs, despite the equivalent expression of total ERK and cPLA<sub>2</sub>α proteins in both cells (Supplementary Fig. 4m-o). Thus, PLA2G3 deficiency attenuates activation of ERK and cPLA<sub>2</sub>α in BMMCs.

We took advantage of an *in vitro* system in which immature BMMCs undergo maturation toward mature CTMC-like cells in coculture with Swiss 3T3 fibroblasts<sup>27</sup>. PLA2G3 deficiency did not affect the proliferation of BMMCs in coculture (Supplementary Fig. 5a). During coculture, sPLA<sub>2</sub> activity was secreted from wild-type BMMCs in response to SCF, whereas sPLA<sub>2</sub> secretion was absent in *Pla2g3*<sup>-/-</sup> BMMCs and augmented in *PLA2G3*<sup>tg/+</sup> BMMCs (Fig. 4a,b). Although the ultrastructure of *Pla2g3*<sup>-/-</sup> BMMCs appeared normal, *Pla2g3*<sup>-/-</sup> CTMC-like cells contained unusual granules with less electron-dense contents than did *Pla2g3*<sup>+/+</sup> CTMC-like cells (Fig. 4c and Supplementary Fig. 5b). After coculture, the expression of *Hdc* (Fig. 4d) and its product histamine (Fig. 4e) were markedly greater in *Pla2g3*<sup>+/+</sup> CTMC-like cells, whereas these changes were barely seen in *Pla2g3*<sup>-/-</sup> cells. Even before coculture, *Hdc* expression and histamine content were slightly lower in *Pla2g3*<sup>-/-</sup> BMMCs than in *Pla2g3*<sup>+/+</sup> BMMCs, indicating that some early developmental process had already been perturbed by PLA2G3 deficiency. IgE-Ag-induced histamine release was greater in *Pla2g3*<sup>+/+</sup> cells after coculture than before coculture, whereas this coculture-driven increase in histamine release was impaired in *Pla2g3*<sup>-/-</sup> cells (Fig. 4f). Conversely, coculture-induced *Hdc* expression was greater in *PLA2G3*<sup>tg/+</sup> CTMC-like cells than in control cells (Supplementary Fig. 5c). Supplementation with PLA2G3 in coculture significantly restored the histamine level in *Pla2g3*<sup>-/-</sup> CTMC-like cells and also elevated it in *Pla2g3*<sup>+/+</sup> cells (Fig. 4g). *Pla2g3*<sup>-/-</sup> BMMCs without coculture did not respond to PLA2G3 (Fig. 4g), suggesting that the action of PLA2G3 on histamine synthesis in mast cells depends on fibroblasts. Histamine content in *Pla2g3*<sup>+/+</sup> BMMCs without coculture was substantially lower in the presence of PLA2G3 than its absence (Fig. 4g), which might reflect that the enzyme elicits the release of prestored histamine by degranulation (Fig. 1b).

The maturation of wild-type BMMCs to CTMC-like cells increased FcεRI-dependent PGD<sub>2</sub> synthesis (Fig. 4h), with a concomitant increase in *Ptgds2* (hematopoietic PGD<sub>2</sub> synthase; H-PGDS) (Fig. 4i). However, these changes in the PGD<sub>2</sub> pathway occurred only weakly in *Pla2g3*<sup>-/-</sup> cells. Surface expression of FcεRIα was significantly elevated in *Pla2g3*<sup>+/+</sup> cells but not in *Pla2g3*<sup>-/-</sup> cells after coculture (Supplementary Fig. 5d), consistent with the lower surface FcεRIα expression on tissue-resident mast cells in *Pla2g3*<sup>-/-</sup> mice. The coculture-driven induction of *Mcpt4* and *Mcpt6* (which encode mast cell proteases) and *Ndr1* (which encodes a mast cell granule-associated protein<sup>27</sup>) was also impaired in *Pla2g3*<sup>-/-</sup> cells, whereas the constitutive expression of *Srgn* and *Kit* was unaffected (Supplementary Fig. 5e). We verified the attenuated induction of HDC and H-PGDS and the unaltered expression of c-Kit in *Pla2g3*<sup>-/-</sup> CTMC-like cells at the protein level (Fig. 4j). Although *Pla2g3*<sup>+/+</sup> CTMC-like cells acquired sensitivity to C48/80 after coculture<sup>27</sup>, C48/80-induced degranulation (Fig. 4k) and induction of the putative C48/80 receptors encoded by *Mrgprx1* and *Mrgprx2* (ref. 28; Supplementary Fig. 5e) after coculture were lower in *Pla2g3*<sup>-/-</sup> cells. The coculture-dependent decrease in *Iga5* (which encodes integrin α<sub>E</sub>) and increase in *Icam1* (which encodes integrin β<sub>7</sub>), which participates in tissue homing of mast-cell progenitors<sup>6</sup>, were unaffected by PLA2G3 deficiency (Supplementary Fig. 5e), consistent with the unaltered number of mast cells in *Pla2g3*<sup>-/-</sup> tissues. Microarray gene profiling using *Pla2g3*<sup>+/+</sup> and *Pla2g3*<sup>-/-</sup> BMMCs before and after coculture revealed that, of the ~41,000 genes examined, *Pla2g3*<sup>+/+</sup> cells expressed 3,632 coculture-inducible genes, of which 1,409 genes were barely or only partially induced in *Pla2g3*<sup>-/-</sup> cells. Genes affected by *Pla2g3* ablation included, for example, genes associated with secretory granules, genes related to biosynthesis or receptors for lipid mediators,



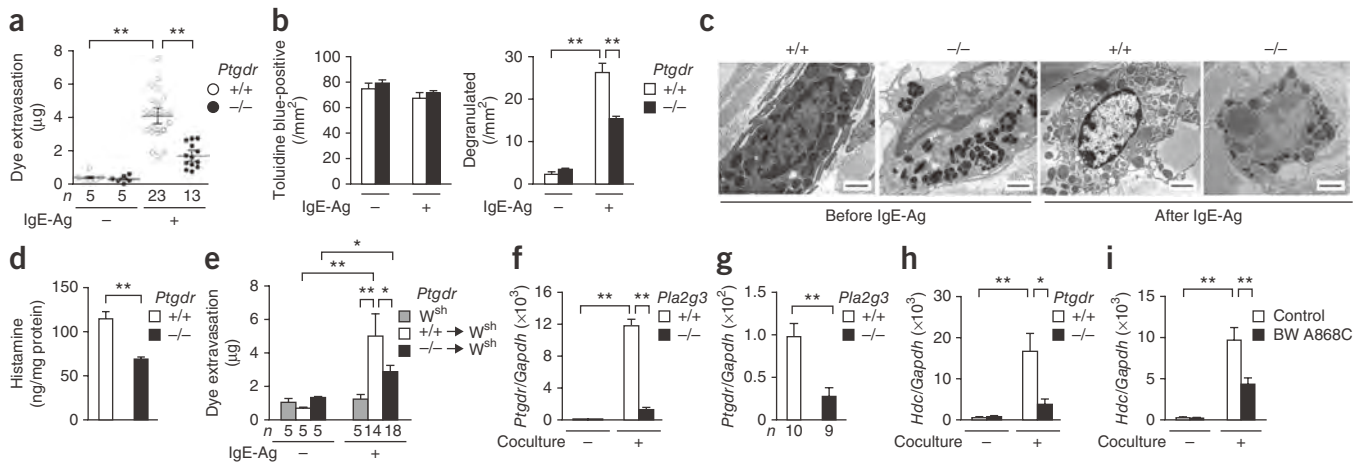


**Figure 5** Defective mast-cell maturation and anaphylaxis by DP1 deficiency.

(a) Quantification of ear edema in PCA in *Ptgdr*<sup>+/+</sup> (+/+) and *Ptgdr*<sup>-/-</sup> (-/-) mice with (IgE-Ag (+)) or without (IgE-Ag (-)) antigen challenge. (b) Counts of toluidine blue<sup>+</sup> dermal mast cells in *Ptgdr*<sup>+/+</sup> (+/+) and *Ptgdr*<sup>-/-</sup> (-/-) mice before and 2 min after IgE-Ag-mediated PCA (n = 6). Number of degranulated mast cells were evaluated by staining of skin sections from *Ptgdr*<sup>+/+</sup> and *Ptgdr*<sup>-/-</sup> mice with toluidine blue, as in **Figure 2g**. (c) Transmission electron microscopy of ear mast cells in *Ptgdr*<sup>+/+</sup> (+/+) and *Ptgdr*<sup>-/-</sup> (-/-) before (IgE-Ag (-)) and 2 min after (IgE-Ag (+)) antigen challenge. Scale bars, 2 µm. (d) Histamine levels in ears of *Ptgdr*<sup>+/+</sup> and *Ptgdr*<sup>-/-</sup> mice (n = 10). (e) Quantification of ear edema in IgE-Ag-dependent PCA in *Kit*<sup>W<sup>sh</sup>/W<sup>sh</sup> (*W<sup>sh</sup>*) mice with or without reconstitution with *Ptgdr*<sup>+/+</sup> (+/+) or *Ptgdr*<sup>-/-</sup> (-/-) BMMCs. (f,g) Expression of *Ptgdr* in *Pla2g3*<sup>+/+</sup> and *Pla2g3*<sup>-/-</sup> BMMCs before and on day 2 of coculture (n = 6; f) and in the ear of *Pla2g3*<sup>+/+</sup> and *Pla2g3*<sup>-/-</sup> mice (g). (h,i) Expression of *Hdc* relative to *Gapdh* in *Ptgdr*<sup>+/+</sup> and *Ptgdr*<sup>-/-</sup> BMMCs (n = 6; h) or in wild-type BMMCs with or without BW A868C (n = 7; i) before and on day 2 of coculture. (j,k) Expression of *Hdc* relative to *Gapdh* in *Pla2g3*<sup>+/+</sup> and *Pla2g3*<sup>-/-</sup> BMMCs before and on day 2 of coculture with or without BW 245C (n = 6; j) or forskolin (n = 6; k). Data are compiled from two (b,d,f-k) or three (a,e) experiments (mean ± s.e.m., \*P < 0.05; \*\*P < 0.01; NS, not significant). Images in **c** are representative of two experiments.</sup>

eicosanoid receptors or biosynthetic enzymes (*Ptgdr2*<sup>-/-</sup>, *Ptger1*<sup>-/-</sup>, *Ptger2*<sup>-/-</sup>, *Ptger3*<sup>-/-</sup>, *Ptger4*<sup>-/-</sup>, *Ptgifr*<sup>-/-</sup>, *Ptgir*<sup>-/-</sup>, *Tbxa2r*<sup>-/-</sup>, *Ltb4r1*<sup>-/-</sup>, *Ltb4r2*<sup>-/-</sup>, *Ptges*<sup>-/-</sup>, *Ptges2*<sup>-/-</sup> and *Alox15*<sup>-/-</sup>; **Supplementary Fig. 6a**). Although *Ltc4s*<sup>-/-</sup> mice exhibited a lower PCA response as reported<sup>10</sup>, their ear histamine content was unaffected (data not shown). Thus, abnormalities in mast cells observed in mice lacking PLA2G3 were phenocopied only in mice lacking DP1.

Next we examined the expression and function of DP1 in a mast cell–fibroblast coculture system<sup>27</sup>. Although we barely detected *Ptgdr* mRNA in BMMCs and Swiss 3T3 fibroblasts, *Ptgdr* mRNA was robustly induced in *Pla2g3*<sup>+/+</sup>, but not in *Pla2g3*<sup>-/-</sup>, CTMC-like cells after coculture (**Fig. 5f**). Consistently, *Ptgdr* expression in the ear was lower in *Pla2g3*<sup>-/-</sup> mice than in *Pla2g3*<sup>+/+</sup> mice (**Fig. 5g**). In agreement with the lower histamine amount in *Ptgdr*<sup>-/-</sup> dermal mast cells (**Fig. 5d**), the coculture-driven *Hdc* induction was severely impaired in *Ptgdr*<sup>-/-</sup> CTMC-like cells (**Fig. 5h**). In addition, the DP1 antagonist BW A868C prevented the coculture-induced upregulation of *Hdc* in wild-type CTMC-like cells (**Fig. 5i**). Conversely, the DP1 agonist BW 245C significantly enhanced *Hdc* induction in wild-type CTMC-like cells (**Fig. 5j**). However, the coculture-driven *Hdc* expression was barely restored by BW 245C in *Pla2g3*<sup>-/-</sup> mice (**Fig. 5j**), likely because DP1 induction was blunted by PLA2G3 deficiency (**Fig. 5f**). To circumvent this problem, we used the cAMP-elevating agent forskolin because DP1 is coupled with Gs-cAMP signaling<sup>9</sup>. The addition of forskolin to the coculture bypassed the requirement for DP1 in the induction of *Hdc* in *Pla2g3*<sup>-/-</sup> CTMC-like cells (**Fig. 5k**). By comparison, the expression of *Ptgdr2*, which encodes another PGD<sub>2</sub> receptor known as CRTH2, was high in BMMCs and lowered in accordance with their maturation into CTMC-like cells, without being affected by the *Pla2g3* genotypes (**Supplementary Fig. 6b**). Moreover, *Hdc*

induction in CTMC-like cells was unaffected by CRTH2 deficiency in coculture, and *Ptgdr2* expression was unaffected by PLA2G3 deficiency *in vivo* (**Supplementary Fig. 6c,d**). The coculture-driven production of other eicosanoids such as 15-HETE and PGI<sub>2</sub> was unaffected by PLA2G3 deficiency (**Supplementary Fig. 6e**). Thus, DP1-cAMP signaling is specifically required for the PLA2G3-dependent maturation of mast cells.

### L-PGDS supplies a PGD<sub>2</sub> pool for mast-cell maturation

We hypothesized that the absence of PGD<sub>2</sub> biosynthetic enzyme(s), acting downstream of PLA2G3 and upstream of DP1, would also influence maturation of mast cells. Of the two PGD<sub>2</sub> synthase-encoding genes, *Ptgs2* (which encodes H-PGDS) was expressed in BMMCs but not in Swiss 3T3 fibroblasts, whereas *Ptgs1* (which encodes lipocalin-type PGDS; L-PGDS) expression was higher in fibroblasts than in BMMCs (**Fig. 6a**) and was below the detection limit in pMCs (data not shown). L-PGDS immunoreactivity was associated with fibroblasts surrounding toluidine blue<sup>+</sup> mast cells in mouse skin (**Supplementary Fig. 7a**). PCA was exacerbated in *Ptgs2*<sup>-/-</sup> mice<sup>30</sup>, which lack H-PGDS (**Fig. 6b**), whereas it was suppressed in *Ptgs1*<sup>-/-</sup> mice<sup>31</sup>, which lack L-PGDS (**Fig. 6c**), in comparison with respective control mice. *Ptgs1*<sup>-/-</sup> mice had fewer degranulated ear mast cells than did *Ptgs1*<sup>+/+</sup> mice after antigen challenge, although the total mast cell count was unaffected (**Fig. 6d**). Dermal mast cells in *Ptgs1*<sup>-/-</sup> mice were ultrastructurally immature (that is, cytoplasmic granules were small and heterogeneous), comparatively resistant to antigen-induced degranulation, and contained less histamine than those in *Ptgs1*<sup>+/+</sup> mice (**Fig. 6e,f**). Thus, the notable similarity among *Pla2g3*<sup>-/-</sup>, *Ptgs1*<sup>-/-</sup> and *Ptgdr*<sup>-/-</sup> mice suggests that PLA2G3, L-PGDS and DP1 may lie in the same

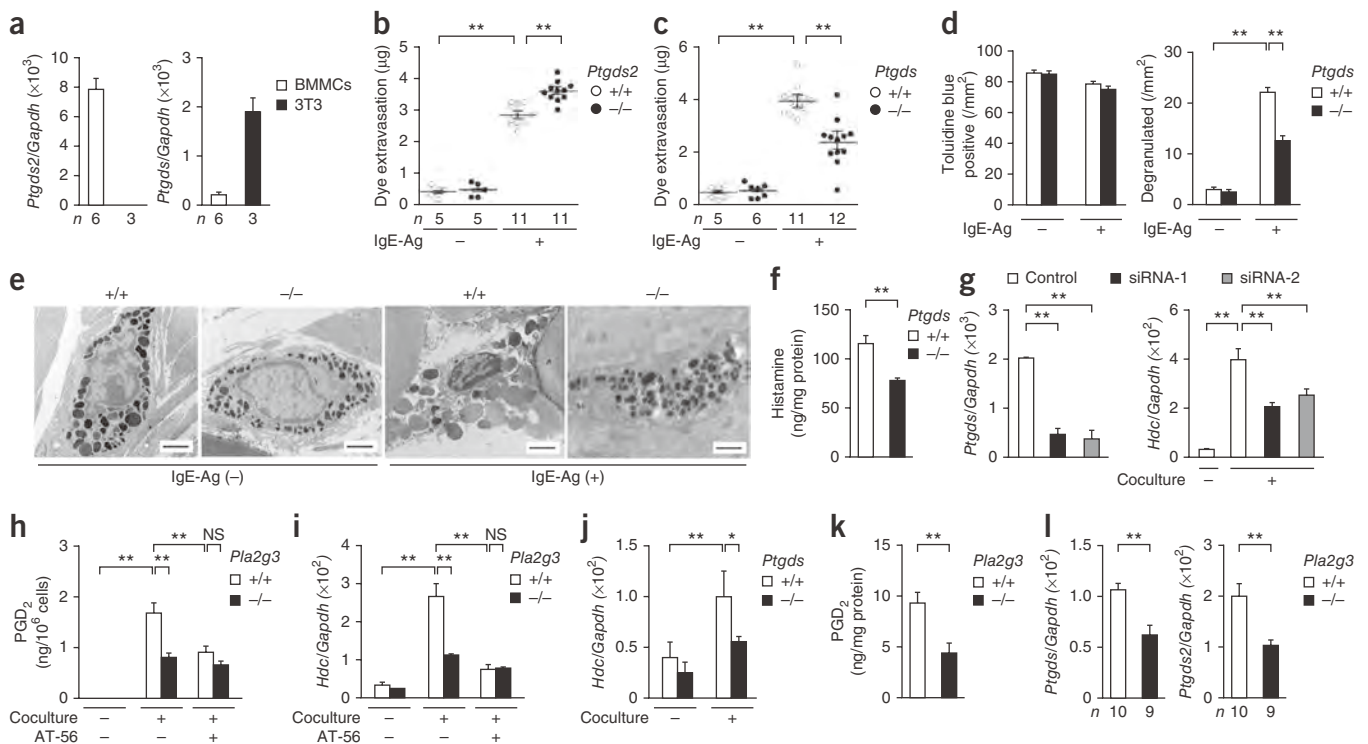


**Figure 6** Defective mast-cell maturation and anaphylaxis by L-PGDS deficiency. **(a)** Expression of *Ptgds* and *Ptgds2* relative to *Gapdh* in wild-type BMMCs and Swiss 3T3 fibroblasts. **(b,c)** Quantification of ear edema in PCA in *Ptgds*<sup>-/-</sup> **(b)**, *Ptgds2*<sup>-/-</sup> **(c)** mice (-/-) and littermate wild-type (+/+) mice with (IgE-Ag (+)) or without (IgE-Ag (-)) antigen challenge. **(d)** Dermal mast-cell counts in *Ptgds*<sup>+/+</sup> and *Ptgds*<sup>-/-</sup> mice before and 2 min after IgE-Ag-mediated PCA (*n* = 6). Number of degranulated mast cells were evaluated by staining of skin sections with toluidine blue, as in **Figure 2g**. **(e)** Transmission electron microscopy of *Ptgds*<sup>+/+</sup> (+/+) and *Ptgds*<sup>-/-</sup> (-/-) ear mast cells before (IgE-Ag (-)) and 2 min after (IgE-Ag (+)) antigen challenge. Scale bars, 2  $\mu$ m. **(f)** Histamine levels in ears of *Ptgds*<sup>+/+</sup> and *Ptgds*<sup>-/-</sup> mice (*n* = 10). **(g)** *Ptgds* expression in Swiss 3T3 fibroblasts after *Ptgds* or scrambled siRNA treatment and *Hdc* expression in wild-type BMMCs before and on day 2 of coculture with siRNA-treated fibroblasts (*n* = 7). **(h,i)** PGD<sub>2</sub> generation **(h)** and *Hdc* expression **(i)** before and on day 1 of coculture of *Pla2g3*<sup>+/+</sup> or *Pla2g3*<sup>-/-</sup> BMMCs with Swiss 3T3 fibroblasts with or without AT-56 (*n* = 6). **(j)** *Hdc* expression in wild-type BMMCs before and on day 4 of coculture with *Ptgds*<sup>+/+</sup> (+/+) or *Ptgds*<sup>-/-</sup> (-/-) skin fibroblasts (*n* = 6). **(k,l)** PGD<sub>2</sub> levels **(k)** and *Ptgds* and *Ptgds2* expression **(l)** in the ear skin of *Pla2g3*<sup>+/+</sup> and *Pla2g3*<sup>-/-</sup> mice. Data are compiled from two **(a,d,f,h-l)** or three **(b,c,g)** experiments (mean  $\pm$  s.e.m., \**P* < 0.05; \*\**P* < 0.01; NS, not significant). Images in **e** are representative of two experiments.

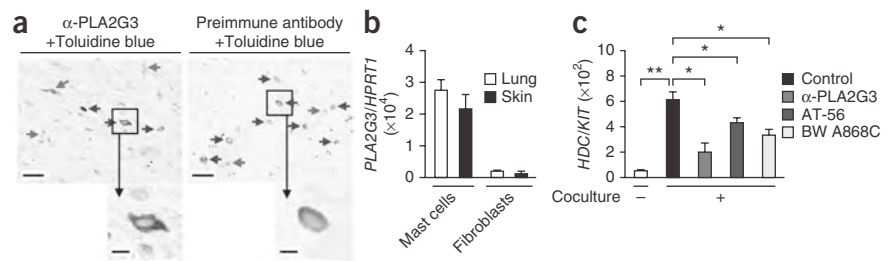
regulatory pathway driving maturation of mast cells. The transfer of *Ptgds*<sup>+/+</sup> or *Ptgds*<sup>-/-</sup> BMMCs into *Kit*<sup>W-sh/W-sh</sup> mice fully restored the PCA response (**Supplementary Fig. 7b**), and a similar induction of *Hdc* occurred when *Ptgds*<sup>+/+</sup> or *Ptgds*<sup>-/-</sup> BMMCs were cultured with fibroblasts (**Supplementary Fig. 7c**), indicating that L-PGDS in fibroblasts, not in mast cells, may be important for the regulation of mast cells.

Coculture with L-PGDS-silenced Swiss 3T3 fibroblasts by two distinct *Ptgds*-specific small interfering (si)RNAs resulted in less induction of *Hdc* in wild-type CTMC-like cells (**Fig. 6g**). PGD<sub>2</sub> generation after coculture of parent fibroblasts with *Pla2g3*<sup>-/-</sup> BMMCs was ~50% lower than with *Pla2g3*<sup>+/+</sup> BMMCs (**Fig. 6h**). The L-PGDS inhibitor AT-56 lowered PGD<sub>2</sub> generation and *Hdc* induction in *Pla2g3*<sup>+/+</sup> cocultures to amounts similar to those in *Pla2g3*<sup>-/-</sup> cocultures, although it did not affect these responses in *Pla2g3*<sup>-/-</sup> cocultures (**Fig. 6h,i** and **Supplementary Fig. 7d**). *Hdc* induction in wild-type BMMCs also occurred in coculture with primary skin fibroblasts from *Ptgds*<sup>+/+</sup> mice, whereas this response was impaired in coculture with those from *Ptgds*<sup>-/-</sup> mice (**Fig. 6j**). Thus, the augmentative effects of PLA2G3 on coculture-driven synthesis of PGD<sub>2</sub> and histamine were abrogated when L-PGDS in fibroblasts was ablated. L-PGDS-dependent production of PGD<sub>2</sub>, as revealed by coculture of *Ptgds2*<sup>-/-</sup> BMMCs with Swiss 3T3 fibroblasts, occurred

gradually over a long period, whereas H-PGDS-dependent production of PGD<sub>2</sub> was transient, albeit robust (**Supplementary Fig. 7e**), suggesting that the continuous supply of PGD<sub>2</sub> by L-PGDS is crucial for maturation of mast cells.

Additionally, we observed robust upregulation of *Ptgds2* in BMMCs and *Ptgds* in Swiss 3T3 fibroblasts or in primary mouse skin fibroblasts (and to a much lesser extent in BMMCs) in wild-type BMMC cocultures, whereas these responses occurred only partially in *Pla2g3*<sup>-/-</sup> BMMC cocultures (**Supplementary Fig. 7f-h**). Conversely, induction of *Ptgds* in Swiss 3T3 fibroblasts was enhanced in coculture with *PLA2G3*<sup>tg/+</sup> BMMCs relative to wild-type BMMCs (**Supplementary Fig. 7i**). Thus, not only did mast cell-derived PLA2G3 supply arachidonic acid to L-PGDS in fibroblasts, it also contributed to induced expression of L-PGDS for efficient biosynthesis of a pool of PGD<sub>2</sub> that promotes maturation of mast cells. However, addition of PLA2G3 or BV-PLA<sub>2</sub> alone did not increase *Ptgds* expression in fibroblasts (**Supplementary Fig. 7j**), suggesting that some additional mast cell-derived factor(s) may be required for the induction of L-PGDS in fibroblasts. In agreement with the *in vitro* studies, amounts of PGD<sub>2</sub> (**Fig. 6k**) and expression of two PGDSs (**Fig. 6l**) were significantly lower in the ear of *Pla2g3*<sup>-/-</sup> mice than that of *Pla2g3*<sup>+/+</sup> mice, confirming the coupling of PLA2G3 with PGD<sub>2</sub> synthesis *in vivo*. Thus, PLA2G3 secreted from mast cells is

**Figure 7** The PLA2G3–L-PGDS–DP1 axis facilitates maturation of human mast cells. (a) Immunohistochemistry analysis of human skin sections (atopic dermatitis) with anti-PLA2G3 ( $\alpha$ -PLA2G3) or a preimmune antibody, followed by counterstaining with toluidine blue (scale bars, 50  $\mu$ m). Blue and red arrows indicate resting and degranulated mast cells, respectively. Boxed areas are magnified below (scale bars, 5  $\mu$ m). (b) Expression of *PLA2G3* relative to *HRPT1* in primary mast cells and fibroblasts obtained from human skin and lung ( $n = 3$ ). (c) Expression of *HDC* relative to *KIT* in human lung mast cells before or on day 4 of coculture with human lung fibroblasts in the presence or absence of 5  $\mu$ g/ml anti-PLA2G3, 10  $\mu$ M AT-56 or 1  $\mu$ M BW A868C ( $n = 4$ ). Data are from one experiment (b,c; mean  $\pm$  s.e.m., \* $P < 0.05$ ; \*\* $P < 0.01$ ). Images in a are representative of two experiments.



linked to fibroblastic L-PGDS-dependent synthesis of PGD<sub>2</sub>, which in turn activates DP1 induced on mast cells to assist their terminal maturation toward a fully anaphylaxis-sensitive CTMC-like phenotype (Supplementary Fig. 7k).

**PLA2G3 PGD<sub>2</sub> axis induces maturation of human mast cells**

In human skin, toluidine blue<sup>+</sup> dermal mast cells showed PLA2G3 immunoreactivity, although some toluidine blue<sup>-</sup> cells also appeared PLA2G3<sup>+</sup> (Fig. 7a). We detected *PLA2G3* mRNA expression in mast cells in preference to fibroblasts obtained from human lung and skin (Fig. 7b). *HDC* mRNA expression was robustly induced in human lung mast cells after coculture with human lung fibroblasts, and this induction was suppressed either by anti-PLA2G3, by L-PGDS inhibitor (AT-56) or by DP1 antagonist (BW A868C) to a similar extent (Fig. 7c). Thus, the fibroblast-dependent *HDC* induction in human mast cells also depends on the PLA2G3–L-PGDS–DP1 pathway.

**DISCUSSION**

Here we showed that PLA2G3, a major sPLA<sub>2</sub> in mast cells, contributed to anaphylaxis by inducing maturation of mast cells in concert with adjacent fibroblasts through a unique pathway involving a cell-to-cell loop of the biosynthetic and receptor pathway for PGD<sub>2</sub>. Promotion of mast cell maturation by PGD<sub>2</sub>-DP1 signaling provides a mechanistic explanation for the protective effect of systemic DP1 ablation on asthma<sup>9</sup>. The paracrine PGD<sub>2</sub> circuit driven by PLA2G3, an ‘anaphylactic sPLA<sub>2</sub>’, is a previously unidentified lipid-orchestrated pathway linked to allergy and uncovers a missing microenvironmental cue underlying the proper maturation of mast cells.

The SCF–c-Kit system, in cooperation with transcription factors, integrins or accessory cytokines, is essential for the development, homing, proliferation and differentiation of mast cells<sup>3–7</sup>. However, SCF alone is insufficient to drive the full maturation of mast cells, leading to the hypothesis that some other stromal factor(s) may be additionally required. These signals may include, for instance, interleukin 33, nerve growth factor, the morphogen TGF- $\beta$ , hyaluronic acid and the adhesion molecule SgIGSF (spermatogenic immunoglobulin superfamily)<sup>3,4,7</sup>, although their *in vivo* relevancies have not yet been fully understood. As in mice lacking PLA2G3, mast cells in mice lacking histamine (*Hdc*<sup>-/-</sup>) or heparin (*Ndst2*<sup>-/-</sup> or *Srgn*<sup>-/-</sup>) are immature and have low histamine content<sup>32–34</sup>, suggesting that the lower amount of histamine may underlie, at least in part, the defective maturation of mast cells. We showed here that a signal driven by PGD<sub>2</sub>, a bioactive lipid, is a missing link required for the fibroblast-driven maturation of mast cells. The PLA2G3–L-PGDS–DP1 circuit revealed the paracrine action of sPLA<sub>2</sub> in the biosynthetic mobilization of PGD<sub>2</sub> by proximal cells, the functional segregation of the two PGDS enzymes in distinct cell populations and a new aspect of PGD<sub>2</sub>-DP1

signaling in promoting maturation of mast cells and thereby allergy. Moreover, our results revealed a previously unidentified aspect of the stromal cytokine SCF, which triggers this unique lipid-driven pathway by inducing PLA2G3 secretion from mast cells.

L-PGDS, a fibroblast-cell enzyme, acts downstream of PLA2G3 to supply PGD<sub>2</sub> to DP1 in mast cells to drive their terminal maturation. Contrary to our prediction, PGD<sub>2</sub> driven by H-PGDS, a mast cell enzyme, had an anti-allergy role, a view that is consistent with the exacerbated allergen-induced contact dermatitis in *Ptgds2*<sup>-/-</sup> mice<sup>11</sup>. Although it is unclear how the L-PGDS-driven extrinsic, but not the H-PGDS-driven intrinsic, pool of PGD<sub>2</sub> is preferentially used by DP1 on mast cells, we speculate that the prolonged supply of PGD<sub>2</sub> by L-PGDS, rather than its transient supply by H-PGDS, may be suitable for a long-lasting cell differentiation process. Alternatively, the PGD<sub>2</sub> captured by L-PGDS, a lipid carrier protein (lipocalin), may be stabilized or better presented to mast cell DP1. This idea is reminiscent of a finding that lysophosphatidic acid (LPA), another lipid mediator, is presented to its cognate receptor as a complex with autotaxin, an LPA-producing enzyme<sup>35</sup>. The spatiotemporal discrimination of distinct PGD<sub>2</sub> pools is also supported by the fact that although PGD<sub>2</sub> promotes Th2-based asthma<sup>9</sup>, it contributes to resolution of inflammation through limiting neutrophil infiltration, dendritic cell activation or other mechanisms<sup>11–13</sup>.

The paracrine PLA2G3–L-PGDS–DP1 circuit could not be compensated by other PLA<sub>2</sub> enzymes, implying a specific role of this atypical sPLA<sub>2</sub>. We observed no defects in maturation of mast cells or anaphylaxis even in mice lacking cPLA<sub>2</sub> $\alpha$ , although mild developmental changes in *Pla2g4a*<sup>-/-</sup> BMDCs have been reported, probably because of different culture conditions<sup>29</sup>. Presumably, ablation of only the specific and local lipid mediator pathway by PLA2G3 deficiency, in contrast to ablation of bulk eicosanoids in both mast cells and microenvironments by cPLA<sub>2</sub> $\alpha$  deficiency<sup>29</sup>, may have a different impact on mast cells. The phenotypes observed in *Pla2g3*<sup>-/-</sup> mice tend to be more severe than those observed in *Ptgdr*<sup>-/-</sup> or *Ptgds*<sup>-/-</sup> mice, suggesting that PLA2G3 might be also coupled with other lipid signal(s) that could act in concert with the L-PGDS–DP1 axis to promote full maturation of mast cells. Such lipid candidates include LPA and lysophosphatidylserine, which can affect mast cell development and activation<sup>36,37</sup>. Not only can lysophospholipids transmit signals through their specific receptors, but they can also facilitate the opening of Ca<sup>2+</sup> channels, which might explain the degranulation-promoting effect of PLA2G3 on mast cells.

Although it has been proposed that sPLA<sub>2</sub> enzymes, after being secreted, may act on neighboring cells or extracellular phospholipids to augment lipid mediator biosynthesis, this idea has yet to gain traction because *in vivo* evidence is largely lacking. Our study provides to our knowledge the first clear *in vivo* evidence that sPLA<sub>2</sub> acts in this

© 2013 Nature America, Inc. All rights reserved.



manner, thus providing a rationale for the long-standing question on the role of the secreted type of PLA<sub>2</sub>. This extracellular PLA<sub>2</sub> family, through a paracrine process, regulates homeostasis and pathology in response to a given microenvironmental cue. Given that PLA<sub>2</sub>G3 is insensitive to classical sPLA<sub>2</sub> inhibitors, a new agent that specifically inhibits this unique sPLA<sub>2</sub> may be useful for the treatment of patients with mast cell-associated allergic and other diseases.

## METHODS

Methods and any associated references are available in the online version of the paper.

**Accession code.** Gene Expression Omnibus: GSE44980 (microarray data).

Note: Supplementary information is available in the online version of the paper.

## ACKNOWLEDGMENTS

We thank Y. Tanoue, H. Ohkubo, K. Araki and K. Yamamura for generating *Ptges2<sup>-/-</sup>* mice. This work was supported by grants-in-aid for Scientific Research from the Ministry of Education, Culture, Sports, Science and Technology of Japan (22116005 and 24390021 to M.M. and 23790119 and 24117724 to Y.T.), Promoting Individual Research to Nurture the Seeds of Future Innovation and Organizing Unique Innovative Network (PRESTO) of Japan Science and Technology Agency (to M.M.), and the Uehara, Mitsubishi, Terumo, Mochida and Toray Science Foundations (to M.M.).

## AUTHOR CONTRIBUTIONS

Y.T. performed experiments and together with M.M. conceived and designed the study, interpreted the findings and wrote the manuscript; N.U., T.K., M.K., R.M. and H.S. performed experiments; S.T., M.S., Masanori Nakamura, Y.N., K.I., K.M., Satoshi Nakamizo, K.K., Y.O. and C.R. helped perform some experiments; K.Y., N.K., R.T., M.H.G. M.A., T.Y., Masataka Nakamura, K.W., H.H., Motono Nakamura, K.A., Y.U., Y.S., T.S., Shu Narumiya and S.H. contributed to experimental designs.

## COMPETING FINANCIAL INTERESTS

The authors declare no competing financial interests.

Reprints and permissions information is available online at <http://www.nature.com/reprints/index.html>.

- Galli, S.J. & Tsai, M. IgE and mast cells in allergic disease. *Nat. Med.* **18**, 693–704 (2012).
- Gurish, M.F. & Austen, K.F. Developmental origin and functional specialization of mast cell subsets. *Immunity* **37**, 25–33 (2012).
- Allakhverdi, Z., Smith, D.E., Comeau, M.R. & Deslespesse, G. Cutting edge: The ST2 ligand IL-33 potently activates and drives maturation of human mast cells. *J. Immunol.* **179**, 2051–2054 (2007).
- Matsuda, H. *et al.* Nerve growth factor induces development of connective tissue-type mast cells *in vitro* from murine bone marrow cells. *J. Exp. Med.* **174**, 7–14 (1991).
- Abonia, J.P. *et al.* Constitutive homing of mast cell progenitors to the intestine depends on autologous expression of the chemokine receptor CXCR2. *Blood* **105**, 4308–4313 (2005).
- Gurish, M.F. *et al.* Intestinal mast cell progenitors require CD49d $\beta$ 7 ( $\alpha$ 4 $\beta$ 7 integrin) for tissue-specific homing. *J. Exp. Med.* **194**, 1243–1252 (2001).
- Ito, A. *et al.* SgIGSF: a new mast-cell adhesion molecule used for attachment to fibroblasts and transcriptionally regulated by MITF. *Blood* **101**, 2601–2608 (2003).
- Shimizu, T. Lipid mediators in health and disease: enzymes and receptors as therapeutic targets for the regulation of immunity and inflammation. *Annu. Rev. Pharmacol. Toxicol.* **49**, 123–150 (2009).
- Matsuoka, T. *et al.* Prostaglandin D<sub>2</sub> as a mediator of allergic asthma. *Science* **287**, 2013–2017 (2000).
- Kanaoka, Y., Maekawa, A., Penrose, J.F., Austen, K.F. & Lam, B.K. Attenuated zymosan-induced peritoneal vascular permeability and IgE-dependent passive cutaneous anaphylaxis in mice lacking leukotriene C<sub>4</sub> synthase. *J. Biol. Chem.* **276**, 22608–22613 (2001).
- Trivedi, S.G. *et al.* Essential role for hematopoietic prostaglandin D<sub>2</sub> synthase in the control of delayed type hypersensitivity. *Proc. Natl. Acad. Sci. USA* **103**, 5179–5184 (2006).
- Hammad, H. *et al.* Activation of the D prostanoid 1 receptor suppresses asthma by modulation of lung dendritic cell function and induction of regulatory T cells. *J. Exp. Med.* **204**, 357–367 (2007).
- Levy, B.D., Clish, C.B., Schmidt, B., Gronert, K. & Serhan, C.N. Lipid mediator class switching during acute inflammation: signals in resolution. *Nat. Immunol.* **2**, 612–619 (2001).
- Kunikata, T. *et al.* Suppression of allergic inflammation by the prostaglandin E receptor subtype EP3. *Nat. Immunol.* **6**, 524–531 (2005).
- Serhan, C.N., Chiang, N. & Van Dyke, T.E. Resolving inflammation: dual anti-inflammatory and pro-resolution lipid mediators. *Nat. Rev. Immunol.* **8**, 349–361 (2008).
- Murakami, M. *et al.* Recent progress in phospholipase A<sub>2</sub> research: From cells to animals to humans. *Prog. Lipid Res.* **50**, 152–192 (2011).
- Uozumi, N. *et al.* Role of cytosolic phospholipase A<sub>2</sub> in allergic response and parturition. *Nature* **390**, 618–622 (1997).
- Munoz, N.M. *et al.* Deletion of secretory group V phospholipase A<sub>2</sub> attenuates cell migration and airway hyperresponsiveness in immunosensitized mice. *J. Immunol.* **179**, 4800–4807 (2007).
- Henderson, W.R. Jr. *et al.* Importance of group X-secreted phospholipase A<sub>2</sub> in allergen-induced airway inflammation and remodeling in a mouse asthma model. *J. Exp. Med.* **204**, 865–877 (2007).
- Bilo, B.M., Rueff, F., Mosbeck, H., Bonifazi, F. & Oude-Elberink, J.N. Diagnosis of Hymenoptera venom allergy. *Allergy* **60**, 1339–1349 (2005).
- Dudler, T. *et al.* A link between catalytic activity, IgE-independent mast cell activation, and allergenicity of bee venom phospholipase A<sub>2</sub>. *J. Immunol.* **155**, 2605–2613 (1995).
- Sato, H. *et al.* Group III secreted phospholipase A<sub>2</sub> regulates epididymal sperm maturation and fertility in mice. *J. Clin. Invest.* **120**, 1400–1414 (2010).
- Murakami, M. *et al.* Cellular distribution, post-translational modification, and tumorigenic potential of human group III secreted phospholipase A<sub>2</sub>. *J. Biol. Chem.* **280**, 24987–24998 (2005).
- Murakami, M. *et al.* Cellular arachidonate-releasing function of novel classes of secretory phospholipase A<sub>2</sub>s (groups III and XII). *J. Biol. Chem.* **278**, 10657–10667 (2003).
- Valentin, E., Ghomashchi, F., Gelb, M.H., Lazdunski, M. & Lambeau, G. Novel human secreted phospholipase A<sub>2</sub> with homology to the group III bee venom enzyme. *J. Biol. Chem.* **275**, 7492–7496 (2000).
- Sato, H. *et al.* Analyses of group III secreted phospholipase A<sub>2</sub> transgenic mice reveal potential participation of this enzyme in plasma lipoprotein modification, macrophage foam cell formation, and atherosclerosis. *J. Biol. Chem.* **283**, 33483–33497 (2008).
- Taketomi, Y. *et al.* Impaired mast cell maturation and degranulation and attenuated allergic responses in *Ndr1*-deficient mice. *J. Immunol.* **178**, 7042–7053 (2007).
- Kashem, S.W. *et al.* G protein coupled receptor specificity for C3a and compound 48/80-induced degranulation in human mast cells: roles of Mas-related genes MrgX1 and MrgX2. *Eur. J. Pharmacol.* **668**, 299–304 (2011).
- Nakatani, N. *et al.* Role of cytosolic phospholipase A<sub>2</sub> in the production of lipid mediators and histamine release in mouse bone-marrow-derived mast cells. *Biochem. J.* **352**, 311–317 (2000).
- Mohri, I. *et al.* Prostaglandin D<sub>2</sub>-mediated microglia/astrocyte interaction enhances astrogliosis and demyelination in twitcher. *J. Neurosci.* **26**, 4383–4393 (2006).
- Eguchi, N. *et al.* Lack of tactile pain (allodynia) in lipocalin-type prostaglandin D synthase-deficient mice. *Proc. Natl. Acad. Sci. USA* **96**, 726–730 (1999).
- Ohtsu, H. *et al.* Mice lacking histidine decarboxylase exhibit abnormal mast cells. *FEBS Lett.* **502**, 53–56 (2001).
- Forsberg, E. *et al.* Abnormal mast cells in mice deficient in a heparin-synthesizing enzyme. *Nature* **400**, 773–776 (1999).
- Humphries, D.E. *et al.* Heparin is essential for the storage of specific granule proteases in mast cells. *Nature* **400**, 769–772 (1999).
- Nishimasu, H. *et al.* Crystal structure of autotaxin and insight into GPCR activation by lipid mediators. *Nat. Struct. Mol. Biol.* **18**, 205–212 (2011).
- Bagga, S. *et al.* Lysophosphatidic acid accelerates the development of human mast cells. *Blood* **104**, 4080–4087 (2004).
- Iwashita, M. *et al.* Synthesis and evaluation of lysophosphatidylserine analogues as inducers of mast cell degranulation. Potent activities of lysophosphatidylthreonine and its 2-deoxy derivative. *J. Med. Chem.* **52**, 5837–5863 (2009).



Veritas) supplemented with human SCF (100 ng/ml; Peprotech) and human IL-6 (50 ng/ml; Peprotech). On day 42, methylcellulose was dissolved in PBS, and the cells were resuspended and cultured in IMDM medium (Invitrogen) containing 0.1% BSA, 100 ng/ml SCF and 50 ng/ml IL-6. The purity of human mast cells, as assessed with metachromatic staining, was more than 97%. Human skin and lung fibroblasts (CC-2511 and CC-2512, respectively) and their culture medium were purchased from Lonza. Human lung mast cells ( $5 \times 10^5$  cells) were seeded onto the human lung fibroblast monolayer and cocultured for 4 d in 500  $\mu$ l of IMDM medium plus 2% FBS in the presence of SCF and IL-6, with medium change at 2-d intervals. The cells were trypsinized and reseeded in culture dishes, and nonadherent cells were collected. The purity of mast cells was normalized based on the expression of *KIT*.

**Real-time PCR.** Total RNA was extracted from tissues and cells using TRIzol reagent (Invitrogen). First-strand cDNA synthesis was performed using the High-Capacity cDNA Reverse-Transcriptase Kit (Applied Biosystems). PCRs were carried out using the TaqMan Gene Expression System (Applied Biosystems) on an ABI7700 Real-Time PCR system (Applied Biosystems). The probe-primer sets are listed in **Supplementary Table 2**.

**Measurement of intracellular  $Ca^{2+}$  levels.** Intracellular  $Ca^{2+}$  levels were measured as described previously<sup>27</sup>. Briefly, IgE-sensitized BMMCs on coverslips were loaded for 60 min with the fluorescent  $Ca^{2+}$  indicator fura-2/AM (5  $\mu$ M; Invitrogen) in Tyrode-HEPES buffer (pH 7.4) containing 2.5 mM probenecid, 0.04% (v/v) pluronic acid and 1% (v/v) serum. Then, the cells were washed and stimulated with antigen. Fura-2 fluorescence images were obtained using an image analyzer (ARGUS-50; Hamamatsu Photonics) with excitation at 340 nm (F340) and 380 nm (F380) at 5-s intervals. The fluorescence ratio (F340/F380) was calculated using US National Institutes of Health ImageJ software.

**Western blotting.** Tissue homogenates (20  $\mu$ g protein equivalent) or BMMCs ( $2 \times 10^5$  cells) were lysed in SDS-PAGE sample buffer (63 mM Tris-HCl (pH 6.8), 2% (w/v) SDS, 10% (v/v) glycerol, and 0.08% (w/v) bromophenol blue) containing 5% (v/v) 2-mercaptoethanol, and then subjected to SDS-PAGE. Proteins were subsequently blotted onto PVDF membranes (Bio-Rad), followed by blocking with 5% (w/v) milk powder in PBS containing 0.05% (v/v) Tween 20 (PBS-T). The membranes were probed with rabbit polyclonal antibodies to HDC<sup>49</sup>, H-PGDS<sup>30</sup>, Kit (18101; IBL), PLC $\gamma$ 2 (3872; Cell Signaling), phospho-PLC $\gamma$ 2 Y1217 (3871; Cell Signaling), cPLA $_2\alpha$  (2832; Cell Signaling) or phospho-cPLA $_2\alpha$  S505 (2831; Cell Signaling) or mouse monoclonal antibodies against Akt (D9E; Cell Signaling), phospho-Akt S473 (C67E7; Cell Signaling), ERK1/2 (MK12; BD Transduction Laboratories), phospho-ERK1/2 T202/Y204 (20A; BD Transduction Laboratories), JNK (37; BD Transduction Laboratories), phospho-JNK T183/Y185 (41; BD Transduction Laboratories), p38 (27; BD Transduction Laboratories) or phospho-p38 MAPK T180/Y182 (30; BD Transduction Laboratories) at 1:500–1:2,000 dilutions in PBS-T containing 1% (w/v) milk powder or in Can Get Signal Solution 1 (Toyobo) for 1.5 h. After membranes were washed, the membranes were incubated for 1 h with horseradish peroxidase (HRP)-conjugated anti-rabbit (AP156P; Chemicon) or anti-mouse (21040; Molecular Probes) IgG at 1:5,000 dilution in PBS-T containing 1% milk powder or in Can Get Signal Solution 2 (Toyobo), and then visualized with ECL Prime western blotting detection reagent (GE Healthcare Life Science) on LAS-4000 (Fuji Film).

**Histological analysis.** Ears were fixed in 10% (v/v) neutral buffered formalin, embedded in paraffin and cut using a microtome. The sections (4  $\mu$ m thickness) were stained with 0.05% toluidine blue (pH 0.5) for the detection of mast cells. Degranulated mast cells were defined as those showing the release of cellular granules. For immunohistochemistry, sections were incubated in PBS containing 5% normal goat serum, 5% BSA and 0.025% Triton X-100 for 20 min and then immunostained with a rabbit polyclonal to human PLA2G3, which reacts with both mature human and mouse enzymes (whose homology is 83%)<sup>22–24</sup>, and mouse L-PGDS<sup>50</sup>, at dilutions of 1:200 and 1:1,000, respectively, in the same buffer at 4 °C overnight. These preparations were incubated with biotinylated goat anti-rabbit IgG (BA-1000; Vector Laboratories) in PBS containing 5% BSA, 0.025% Triton X-100 and 10% mouse serum for 30 min followed by incubation with avidin

DH and biotinylated HRP (Vectastain ABC kit; Vector Laboratories). These preparations were stained with 0.5 mg/ml 3,3'-diaminobenzidine and 0.1% (v/v) hydrogen peroxide solution. Human tissue sections were obtained from Chiba University following approval by the faculty ethical committee and informed consent from the patient. For transmission microscopy, tissues or cells were fixed with 0.1 M sodium cacodylate buffer (pH 7.2) containing 1% (v/v) glutaraldehyde and 4% (w/v) paraformaldehyde, post-fixed with 2% (w/v) OsO<sub>4</sub> in PBS, dehydrated by a graded ethanol series, passed through propylene oxide and embedded in Poly/Bed812 EPON (Polyscience). Ultrathin sections (0.08- $\mu$ m thickness) were stained with uranyl acetate and lead citrate and then examined using an electron microscope (H-7600; Hitachi).

**Adoptive transfer of BMMCs into mast cell-deficient mice.** BMMCs obtained from 8–12-week-old male mice were reconstituted by intradermal ( $10^6$  cells) or intravenous ( $10^7$  cells) injection into 6-week-old male *Kit<sup>W-sh/W-sh</sup>* mice. Six weeks after intradermal transfer or 12 weeks after intravenous transfer of BMMCs, the mice were subjected to IgE-Ag-induced PCA, as described above. Alternatively, mast cells from the base to the tip of the ears from these mice were evaluated by toluidine blue staining or by real-time PCR of mast cell marker genes.

**Flow cytometry.** Cells were stained with either a labeled monoclonal antibody or an isotype-matched control antibody (hamster IgG (HTK888), mouse IgG<sub>1</sub> (MOPC-21), rat IgG<sub>2a</sub> (RTK2758) or rat IgG<sub>2b</sub> (RTK4530); BioLegend) and analyzed by flow cytometry using FACSCalibur (BD Biosciences) or FACSAria III Cell Sorter (BD Biosciences) with FlowJo software (Tree Star). The antibodies used were specific for mouse Kit (2B8; BD Biosciences), Fc $\epsilon$ RI $\alpha$  (MAR-1; eBioscience), DX5 (DX5; eBioscience), CD200R3 (Ba13; BioLegend), CD45 (30-F11; eBioscience), CD11c (N418; eBioscience), MHC class II (M5/114.15.2; eBioscience), CD11b (M1/70; BioLegend), F4/80 (BM8; BioLegend), CD45R/B220 (RA3-6B2; BD Biosciences), CD3 $\epsilon$  (145-2X11; eBioscience), Gr-1 (RB-8C5; BioLegend), FOXP3 (150D; BioLegend) and FR4 (12A5; BioLegend).

**Microarray.** Total RNA was extracted from BMMCs derived from *Pla2g3<sup>-/-</sup>* and *Pla2g3<sup>+/+</sup>* mice before and after coculture and purified using the RNeasy Mini Kit (Qiagen). The quality of RNA was assessed with a 2100 Bioanalyzer (Agilent Technologies). Both cDNA and cRNA were synthesized with a Low Input Quick Amp Labeling Kit according to the manufacturer's protocol (Agilent Technologies). Samples were hybridized to the Whole Mouse Genome Microarray Kit (4  $\times$  44K; Agilent Technologies), washed and then scanned using a Laser Scanner GenePix 4000B (Molecular Devices). Microarray data were analyzed with Feature Extraction software (Agilent Technologies) and then imported into GeneSpringGX11.5 (Agilent Technologies). Probes were normalized by quantile normalization among all microarray data.

**RNA interference.** Swiss 3T3 fibroblasts were cultured in 12-well plates to 50% confluence and transfected with a Mission predesigned siRNA construct (20 nM) for *Ptgds* (SASI\_Mm01\_00116073 or 00116081; Sigma-Aldrich) or a scrambled control siRNA (Invitrogen) using oligofectamine (Invitrogen), according to the manufacturer's instructions. After 48 h, wild-type BMMCs were cocultured for 2 d with the transfected cells.

**Electrospray ionization mass spectrometry (ESI-MS).** ESI-MS lipidomics analysis using a 4000Q TRAP quadrupole-linear ion trap hybrid mass spectrometer (AB SCIEX) with an UltiMate 3000 nano/cap/micro-liquid chromatography system (Dionex Corporation) combined with an HTS PAL autosampler (CTC Analytics AG) was performed as described previously<sup>44</sup>. Briefly, phospholipids extracted from  $10^7$  BMMCs were subjected directly to ESI-MS analysis by flow injection; typically, 3  $\mu$ l (3 nmol phosphorous equivalent) of sample was applied. The mobile phase composition was acetonitrile/methanol/water (v/v/v = 6/7/2) plus 0.1% (v/v) ammonium formate (pH 6.8) at a flow rate of 10  $\mu$ l/min. The scan range of the instrument was set at *m/z* 200–1,000 at a scan speed of 1,000 Da/s. The trap fill-time was set at 3 ms in the positive ion mode and at 5 ms in the negative ion mode. The ion spray voltage was set at 5,500 V in the positive ion mode and at –4,500 V in the negative ion

mode. Nitrogen was used as a curtain gas (at a setting of 10 arbitrary units) and as a collision gas (set to 'high').

**Statistical analysis.** The Excel Statistical Program File ystat 2008 (Igaku Tosho Shuppan) was used to determine statistical significance evaluated by an unpaired Student's *t*-test for two groups or an analysis of variance (ANOVA) for multiple groups. *P* values of less than 0.05 and 0.01 were considered statistically significant. Data are presented as the mean ± s.e.m.

38. Satoh, T. *et al.* Prostaglandin D<sub>2</sub> plays an essential role in chronic allergic inflammation of the skin via CRTH2 receptor. *J. Immunol.* **177**, 2621–2629 (2006).
39. Segi, E. *et al.* Patent ductus arteriosus and neonatal death in prostaglandin receptor EP4-deficient mice. *Biochem. Biophys. Res. Commun.* **246**, 7–12 (1998).
40. Sugimoto, Y. *et al.* Failure of parturition in mice lacking the prostaglandin F receptor. *Science* **277**, 681–683 (1997).
41. Kobayashi, T. *et al.* Roles of thromboxane A<sub>2</sub> and prostacyclin in the development of atherosclerosis in *apoE*-deficient mice. *J. Clin. Invest.* **114**, 784–794 (2004).
42. Iizuka, Y. *et al.* Protective role of the leukotriene B<sub>4</sub> receptor BLT2 in murine inflammatory colitis. *FASEB J.* **24**, 4678–4690 (2010).
43. Sun, D. & Funk, C.D. Disruption of 12/15-lipoxygenase expression in peritoneal macrophages. Enhanced utilization of the 5-lipoxygenase pathway and diminished oxidation of low density lipoprotein. *J. Biol. Chem.* **271**, 24055–24062 (1996).
44. Ueno, N. *et al.* Analysis of two major intracellular phospholipases A<sub>2</sub> (PLA<sub>2</sub>) in mast cells reveals crucial contribution of cytosolic PLA<sub>2</sub>α, not Ca<sup>2+</sup>-independent PLA<sub>2</sub>β, to lipid mobilization in proximal mast cells and distal fibroblasts. *J. Biol. Chem.* **286**, 37249–37263 (2011).
45. Shore, P.A., Burkhalter, A. & Cohn, V.H. Jr. A method for the fluorometric assay of histamine in tissues. *J. Pharmacol. Exp. Ther.* **127**, 182–186 (1959).
46. Lutz, M.B. *et al.* An advanced culture method for generating large quantities of highly pure dendritic cells from mouse bone marrow. *J. Immunol. Methods* **223**, 77–92 (1999).
47. Siracusa, M.C. *et al.* TSLP promotes interleukin-3-independent basophil haematopoiesis and type 2 inflammation. *Nature* **477**, 229–233 (2011).
48. Kajiwara, N. *et al.* Activation of human mast cells through the platelet-activating factor receptor. *J. Allergy Clin. Immunol.* **125**, 1137–1145 (2010).
49. Tanaka, S. *et al.* Expression of l-histidine decarboxylase in granules of elicited mouse polymorphonuclear leukocytes. *Eur. J. Immunol.* **34**, 1472–1482 (2004).
50. Gerena, R.L., Eguchi, N., Urade, Y. & Killian, G.J. Stage and region-specific localization of lipocalin-type prostaglandin D synthase in the adult murine testis and epididymis. *J. Androl.* **21**, 848–854 (2000).

# Mutation for Nonsyndromic Mental Retardation in the *trans*-2-Enoyl-CoA Reductase *TER* Gene Involved in Fatty Acid Elongation Impairs the Enzyme Activity and Stability, Leading to Change in Sphingolipid Profile<sup>\*[5]</sup>

Received for publication, June 11, 2013, and in revised form, November 7, 2013. Published, JBC Papers in Press, November 12, 2013, DOI 10.1074/jbc.M113.493221

Kensuke Abe<sup>‡</sup>, Yusuke Ohno<sup>‡</sup>, Takayuki Sassa<sup>‡</sup>, Ryo Taguchi<sup>§</sup>, Minal Çalıřkan<sup>¶</sup>, Carole Ober<sup>¶</sup>, and Akio Kihara<sup>‡1</sup>

From the <sup>‡</sup>Laboratory of Biochemistry, Faculty of Pharmaceutical Sciences, Hokkaido University, Kita 12-jo, Nishi 6-chome, Kita-ku, Sapporo 060-0812, Japan, the <sup>§</sup>Department of Biomedical Sciences, College of Life and Health Sciences, Chubu University, 1200 Matsumoto-cho, Kasugai 487-8501, Japan, and the <sup>¶</sup>Department of Human Genetics, University of Chicago, Chicago, Illinois 60637

**Background:** The P182L mutation in the *trans*-2-enoil-CoA reductase (*TER*) gene required for very long-chain fatty acid (VLCFA) synthesis causes nonsyndromic mental retardation.

**Results:** This mutation reduces the activity and stability of the *TER* enzyme.

**Conclusion:** The impaired *TER* function affects VLCFA synthesis and thereby alters the cellular sphingolipid profile.

**Significance:** Maintenance of a proper VLCFA level may be important for neural function.

Very long-chain fatty acids (VLCFAs, chain length >C20) exist in tissues throughout the body and are synthesized by repetition of the fatty acid (FA) elongation cycle composed of four successive enzymatic reactions. In mammals, the *TER* gene is the only gene encoding *trans*-2-enoil-CoA reductase, which catalyzes the fourth reaction in the FA elongation cycle. The *TER*P182L mutation is the pathogenic mutation for nonsyndromic mental retardation. This mutation substitutes a leucine for a proline residue at amino acid 182 in the *TER* enzyme. Currently, the mechanism by which the *TER* P182L mutation causes nonsyndromic mental retardation is unknown. To understand the effect of this mutation on the *TER* enzyme and VLCFA synthesis, we have biochemically characterized the *TER* P182L mutant enzyme using yeast and mammalian cells transfected with the *TER* P182L mutant gene and analyzed the FA elongation cycle in the B-lymphoblastoid cell line with the homozygous *TER* P182L mutation (*TER*<sup>P182L/P182L</sup> B-lymphoblastoid cell line). We have found that *TER* P182L mutant enzyme exhibits reduced *trans*-2-enoil-CoA reductase activity and protein stability, thereby impairing VLCFA synthesis and, in turn, altering the sphingolipid profile (*i.e.* decreased level of C24 sphingomyelin and C24 ceramide) in the *TER*<sup>P182L/P182L</sup> B-lymphoblastoid cell line. We have also found that in addition to the *TER* enzyme-catalyzed fourth reaction, the third reaction in the FA elongation cycle is affected by the *TER* P182L mutation. These findings provide new insight into the biochemical defects associated with this genetic mutation.

Very long-chain fatty acids (VLCFAs)<sup>2</sup> are fatty acids (FAs) with a carbon chain greater than 20 carbons (>C20). A variety

of VLCFAs, differing in their chain lengths (up to C40) and degree of saturation (saturated, monounsaturated, *n*-3/*n*-6 polyunsaturated), have been reported in mammalian tissues (1–3). Although much less abundant than long-chain (C11–C20) FAs (LCFAs), VLCFAs are ubiquitous among tissues and play an important function that cannot be substituted for by LCFAs, including skin barrier formation, neural function, retina function, and resolution of inflammation (1–3).

VLCFAs are synthesized in the endoplasmic reticulum (ER) from dietary or endogenous LCFAs by the sequential addition of 2-carbon units from malonyl-CoA (Fig. 1A). Each elongation cycle is composed of four reactions catalyzed by distinct enzymes (2, 3): 1) condensation of an acyl-CoA substrate and malonyl-CoA by FA elongase to form 3-ketoacyl-CoA, which is the rate-limiting step of the elongation cycle (4); 2) reduction of the 3-keto group to a 3-hydroxyl group by NADPH-dependent 3-ketoacyl-CoA reductase; 3) dehydration of the resulting 3-hydroxyacyl-CoA to *trans*-2-enoil-CoA by 3-hydroxyacyl-CoA dehydratase; and 4) reduction of the *trans*-2 double bond by NADPH-dependent *trans*-2-enoil-CoA reductase yielding the elongated acyl-CoA. Currently, there are seven FA elongases with characteristic substrate specificities and tissue expression patterns (ELOVL1–7) (5), one 3-ketoacyl-CoA reductase (KAR) (6), four 3-hydroxyacyl-CoA dehydratases (HACD1–4) (7), and one *trans*-2-enoil-CoA reductase (*TER*/TECR/GPSN2) (6) known in mammals.

Most of the saturated and monounsaturated VLCFAs synthesized in the ER are used for sphingolipid synthesis (3). Sphingolipids are one of the major membrane lipids in eukaryotes and consist of a ceramide backbone (*i.e.* a long-chain base with an amide-linked FA) and a polar head group (8). The polar head group of mammalian sphingolipids is either phosphocholine in sphingomyelin or a sugar chain in glycosphingolipids (8, 9). The simplest glycosphingolipids are hexosylceramides, including

blastoid cell line; ER, endoplasmic reticulum; IAA, 3-indoleacetic acid; NSMR, nonsyndromic mental retardation; SC, synthetic complete.

\* This work was supported by Grant-in-Aid for Scientific Research (B) 23370057 (to A. K.) from the Japan Society for the Promotion of Science (JSPS).

[5] This article contains supplemental Fig. 1.

<sup>1</sup> To whom correspondence should be addressed. Tel.: 81-11-706-3754; Fax: 81-11-706-4900; E-mail: kihara@pharm.hokudai.ac.jp.

<sup>2</sup> The abbreviations used are: VLCFA, very long-chain fatty acid; FA, fatty acid; LCFA, long-chain fatty acid; AID, auxin-inducible degen; B-LCL, B-lympho-

## Reduced Activity and Stability of TER P182L Mutant Enzyme

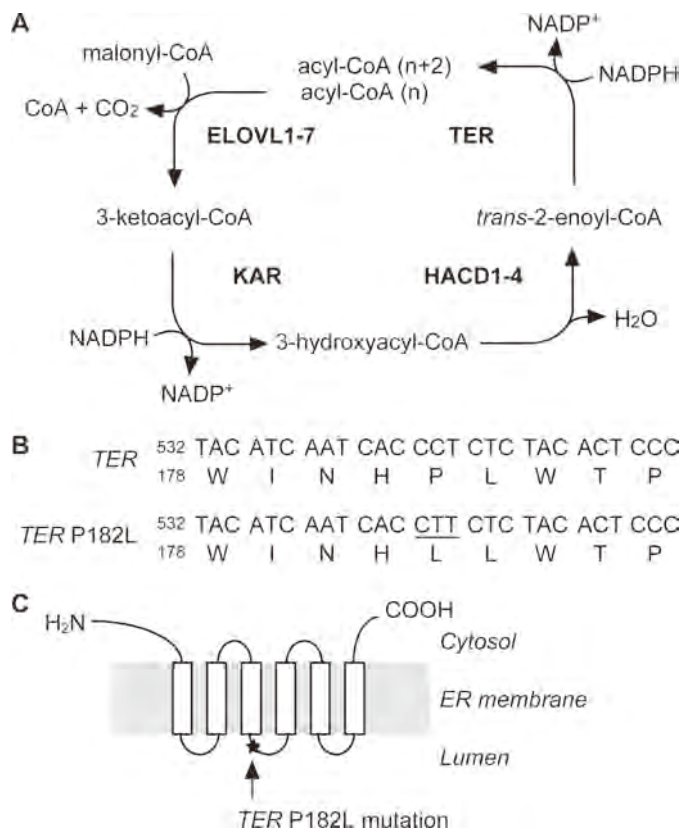


**FIGURE 1. The FA elongation cycle and the TER P182L mutation.** A, the FA elongation cycle consisting of four reactions (condensation, reduction, dehydration, and reduction) and the mammalian enzymes involved in each reaction are illustrated. Each elongation cycle adds two carbons from malonyl-CoA to a growing acyl-CoA chain. B, nucleotide and amino acid sequences of the TER enzyme and the TER P182L mutant enzyme around the mutation site are presented. C, the predicted membrane topology of the TER enzyme with the P182L mutation site (\*) is shown. The prediction was made based on the topology of the yeast and *Arabidopsis* homologs (20).

glucosylceramide and galactosylceramide, the latter of which and its sulfated derivative (sulfatide) are abundant in myelin (10). Sphingolipids containing VLCFAs (mainly C24:0 and C24:1) are ubiquitous among mammalian tissues and are especially abundant in the liver, kidney, and brain (3, 11, 12). For example, C24 sphingomyelin constitutes ~60% of the total sphingomyelin in the liver (11), and C24 galactosylceramide/sulfatide constitutes ~70% of the total galactosylceramide/sulfatide in the spinal cord (12).

Impairment of VLCFA synthesis is associated with several disorders and dysfunctions (3). For example, the dominant mutation in the *ELOVL4* gene causes Stargardt disease type 3, which is a juvenile onset macular dystrophy (13), whereas the recessive *ELOVL4* mutation leads to a neurocutaneous disorder of ichthyosis, seizures, mental retardation, and spasticity (14). A recessive mutation in the 3-hydroxyacyl-CoA dehydratase *HACD1/PTPLA* gene of the dog (15) and human (16) is known to cause myopathy. Moreover, VLCFAs have been shown to be essential for viability of yeast and mammals; for example, deletion of the *TSC13* gene (the only yeast *trans*-2-enoyl-CoA reductase gene, *i.e.* the yeast homolog of the *TER* gene) is lethal in yeast (17), and likewise the only 3-ketoacyl-CoA reductase *KAR* gene knock-out mice result in embryonic lethality due to disruption of organogenesis (18).

Recently, the P182L mutation in the *TER* gene (*TER* P182L mutation) has been identified in patients with nonsyndromic mental retardation (NSMR) (19). This mutation causes a substitution of a leucine for a proline residue at residue 182 in the *TER* enzyme (Fig. 1B). Although the membrane topology of the mammalian *TER* enzyme has not been determined, it is highly likely that this enzyme is an integral membrane protein with six membrane-spanning domains and cytosolic N and C termini (Fig. 1C) as deduced from the membrane topology of the yeast and *Arabidopsis* *TER* homologs (20). In this topology model, the Pro-182 residue is positioned in the second luminal loop.

Like the *KAR* enzyme, which is the only mammalian 3-ketoacyl-CoA reductase involved in VLCFA synthesis and is essential for embryonic viability (18), the *TER* enzyme is the only isozyme of mammalian *trans*-2-enoyl-CoA reductase for VLCFA synthesis; therefore, the *TER* null mutation should also be considered to be embryonically lethal. Because the *TER* P182L mutation affects only mental development (19), the *TER* P182L mutant enzyme appears to retain some residual function. The *TER* P182L mutation, not being a null mutation, must be useful for understanding the function of VLCFA in various tissues. In the present study, we have investigated the effect of the P182L mutation on the activity, stability, and intracellular localization of the *TER* enzyme using yeast and mammalian cells transfected with the *TER* P182L mutant gene. We have also analyzed the FA elongation cycle in the B-lymphoblastoid cell line (B-LCL) derived from NSMR patients (homozygous for the *TER* P182L mutation, *TER*<sup>P182L/P182L</sup>) to gain some insight into the pathogenesis of NSMR.

## EXPERIMENTAL PROCEDURES

**Cell Culture and Transfection**—HEK 293T and HeLa cells were grown in DMEM (D6429 for HEK 293T cells and D6046 for HeLa cells; Sigma) supplemented with 10% FBS, 100 units/ml penicillin, and 100 μg/ml streptomycin; HEK 293T cells were maintained in dishes coated with 0.3% collagen. Transfections were performed using Lipofectamine Plus<sup>TM</sup> reagent (Life Technologies) according to the manufacturer's instructions.

B-LCLs were generated at the University of Chicago from four NSMR patients, four carriers, and three noncarrier healthy controls. This study was approved by the Institutional Review Board at the University of Chicago. All unaffected subjects provided written informed consent; informed consents were obtained from the parents of the NSMR patients. Peripheral blood mononuclear cells were isolated from whole blood samples of each subject using Ficoll-Paque separation protocol (21). Peripheral blood mononuclear cells were then suspended in RPMI 1640 (Life Technologies) medium (supplemented with 20% fetal bovine serum and 50 μg/ml gentamicin) and incubated with Epstein-Barr virus at 37 °C and 5% CO<sub>2</sub> for 3–5 days to establish B-LCLs.

**Plasmids**—The pCE-puro 3×FLAG-1 plasmid is a mammalian expression vector designed to produce a protein tagged with an N-terminal 3×FLAG (7). The pCE-puro 3×FLAG-*TER* plasmid was described previously (5). The pCE-puro 3×FLAG-*TER* P182L plasmid was constructed using the QuikChange site-directed mutagenesis kit (Stratagene, Agilent Technolo-

## Reduced Activity and Stability of TER P182L Mutant Enzyme

gies, La Jolla, CA) with primers 5'-TATTACATCAATCAC-CTTCTCTACACTCCCCCT-3' and 5'-AGGGGAGTGT-AGAGAAGGTGATTGATGTAATA-3'. The pAKNF314 (*GAPDH* promoter, *TRP1* marker), pAKNF313 (*GAPDH* promoter, *HIS3* marker), and pAK1172 (*ADH* promoter, *HIS3* marker) plasmids are yeast expression vectors each designed to produce an N-terminal 3×FLAG-tagged protein. The pAB85 (pAKNF314-*TER*), pAB114 (pAK1172-*TER*), pAB95 (pAKNF314-*TER* P182L), or pAB110 (pAKNF313-*TER* P182L) plasmid was constructed by cloning the *TER* or *TER* P182L cDNA into each vector.

**Yeast Strains and Medium**—The yeast *Saccharomyces cerevisiae* strains used in this study were derived either from BY4741 (*MATa his3Δ1 leu2Δ0 met15Δ0 ura3Δ0*) (22) or from BY25598 (*MATa his3-11,15 leu2-3,112 ura3::P<sub>ADH</sub>-OsTIR1 (URA3) trp1-1 ade2-1 can1-100*) (23). YRF82 cells (*TSC13-HA-AID*) were constructed by chromosomal fusion of a coding sequence for tandemly oriented HA and auxin-inducible degron (AID) with the *TSC13* gene from BY25598 cells as described previously (24). For construction of ABY58 (BY4741, *tsc13Δ::LEU2/pAB110*) and ABY62 (BY4741, *tsc13Δ::LEU2/pAB114*) cells, the pAB110 (3×FLAG-*TER* P182L) and pAB114 (3×FLAG-*TER*) plasmids were respectively introduced into BY4741 cells. The *tsc13Δ::LEU2* mutation was then introduced into each of the resultant cells. Cells were grown in synthetic complete (SC) medium (0.67% yeast nitrogen base, 2% D-glucose, and nutritional supplements) without Trp (SC-Trp) or His (SC-His) at 30 °C.

**In Vitro trans-2-Enoyl-CoA Reductase Assay**—The yeast membrane fraction was prepared as follows. Yeast cells suspended in buffer I (50 mM HEPES-NaOH (pH 6.8), 150 mM NaCl, 10% glycerol, 1 mM DTT, 1 mM PMSF, and a 1× Complete<sup>TM</sup> protease inhibitor cocktail (EDTA-free; Roche Diagnostics)) were lysed by vigorous mixing with glass beads; unlysed cells were removed by centrifugation at 2,000 × *g* for 3 min; the supernatant was centrifuged at 100,000 × *g* and 4 °C for 30 min; and the resulting pellet (total membrane fraction) was suspended in buffer I.

The membrane fraction of B-LCLs was prepared as follows. Cells were washed with PBS, suspended in buffer I, and lysed by sonication; cell debris was removed by centrifugation at 300 × *g* for 5 min; the supernatant was centrifuged at 100,000 × *g* and 4 °C for 30 min; and the pellet (total membrane fraction) was suspended in buffer I.

The assay was performed by incubating the membrane fraction with 5 nCi of 3-hydroxy[1-<sup>14</sup>C]palmitoyl-CoA (55 mCi/mmol; American Radiolabeled Chemicals, St. Louis, MO) in 50 μl of reaction buffer (buffer I containing 2 mM MgCl<sub>2</sub>, 1 mM CaCl<sub>2</sub>, and 1 mM NADPH) at 37 °C for 30 min. The reaction was terminated by adding 25 μl of 75% (w/v) KOH-H<sub>2</sub>O and 50 μl of ethanol followed by heating at 70 °C for 1 h, and then the mixture was acidified with 100 μl of 5 M HCl in 50 μl of ethanol. Lipids were extracted with 700 μl of hexane and dried. The lipid residue was suspended in 20 μl of chloroform and separated by TLC on a Silica Gel 60 high performance TLC plate (Merck) with hexane/diethyl ether/acetic acid (30:70:1, v/v) as the solvent system. Radiolabeled lipids were detected by autoradiography and quantified by a bioimaging analyzer BAS-2500 (Fuji Photo Film, Tokyo, Japan).

**In Vitro FA Elongation Assay**—The assay was performed as described previously (5) using 20 μg of membrane fraction, 20 μM palmitoyl-CoA (Sigma), and [2-<sup>14</sup>C]malonyl-CoA (55 mCi/mmol, American Radiolabeled Chemicals).

**Immunological Assays**—Immunoblotting was performed as described previously (25) using the anti-FLAG antibody M2 (1 μg/ml; Stratagene), the anti-HA antibody 16B12 (1/1000 dilution; Covance, Princeton, NJ), the anti-Pma1 antibody yN-20 (0.4 μg/ml; Santa Cruz Biotechnology, Santa Cruz, CA), anti-Pgk1 antibody (1/2000 dilution; Life Technologies), or anti-α-tubulin antibody (1/1000, Sigma) as the primary antibody, together with HRP-conjugated anti-mouse or anti-goat IgG F(ab')<sub>2</sub> fragment (each at 1:7500 dilution; GE Healthcare Life Sciences, Buckinghamshire, UK) as the secondary antibody. The signal was detected with Pierce Western blotting substrate (Thermo Fisher Scientific).

Indirect immunofluorescence microscopy was performed as described previously (26) using the anti-FLAG antibody M2 (0.5 μg/ml, Stratagene), anti-calreticulin antibody (1/400 dilution; Alexis, Lausen, Switzerland), and DAPI stain (1 μg/ml; Roche Diagnostics). Fluorescence was observed under a DM5000B fluorescence microscope (Leica Microsystems, Wetzlar, Germany).

**RT-PCR**—The total RNA was isolated from B-LCLs using the NucleoSpin RNA II kit (MACHERY-NAGEL, Dueren, Germany). RT-PCR was performed using SuperScript One-Step RT-PCR with Platinum *Taq* (Life Technologies) and the following primers: for *TER*, 5'-TTCAGAGCAGGAAGGGGATGATGGGC-3' and 5'-GTCACTCATTCCACTACATCAAGCG-3', and for *GAPDH*, 5'-CCAAGGTCATCCATGACAACTTTGG-3' and 5'-GGTCCACCACCCTGTTGCTGTAGCC-3'.

**Pulse-Chase Experiment**—HEK 293T cells were transfected with the pCE-puro 3×FLAG-*TER* or pCE-puro 3×FLAG-*TER* P182L plasmid. Forty-eight hours after transfection, the medium was changed to Cys/Met- and serum-free DMEM (D0422, Sigma). Cells were treated with 55 μCi of [<sup>35</sup>S]Met/[<sup>35</sup>S]Cys (EXPRE<sup>35</sup>C<sup>35</sup>S protein labeling mix; PerkinElmer Life Sciences, Ontario, Canada) for 1 h. After changing the medium to normal DMEM medium (D6429, Sigma) containing 10% FCS, cells were incubated at 37 °C for 1, 2, 4, and 8 h. At the end of each incubation time, cells were washed with PBS, resuspended in 1 ml of radioimmune precipitation buffer prepared in-house (50 mM Tris-HCl (pH 8.0), 150 mM NaCl, 1 mM EDTA, 1% Triton X-100, 0.1% SDS, 0.1% sodium deoxycholate, 1 mM DTT, 1 mM PMSF, and 1× Complete<sup>TM</sup> protease inhibitor cocktail), and disrupted by five passages through a 21-gauge needle. Cell debris was removed by centrifugation at 20,000 × *g* and 4 °C for 5 min, and the supernatant was incubated at 4 °C overnight with anti-FLAG M2 agarose beads (Sigma). The beads were washed twice with 1 ml of radioimmune precipitation buffer and once with 1 ml of 10 mM Tris-HCl (pH 8.0), and the bound protein was eluted with 2× SDS sample buffer.

**Lipid Analysis Using Mass Spectrometry (MS)**—Cells were spiked with an internal standard, C17:0 sphingomyelin or C17:0 ceramide (500 pmol; Avanti Polar Lipids, Alabaster, AL), and homogenized in 250 μl of chloroform/methanol (1:2, v/v). Extracted lipids were recovered by centrifugation at 9,000 × *g*

## Reduced Activity and Stability of TER P182L Mutant Enzyme

and room temperature for 1 min and treated with 10  $\mu$ l of 4 M KOH in methanol. After incubation at 37 °C for 1 h, the mixture was neutralized with 10  $\mu$ l of 12 M formic acid and subjected to phase separation by adding 80  $\mu$ l of H<sub>2</sub>O and 80  $\mu$ l of chloroform followed by centrifugation. The organic phase was recovered and dried, and the lipid residue was suspended in chloroform/methanol (1:2, v/v). Lipids were analyzed as described previously (27), using a 4000 QTRAP MS/MS system (AB Sciex, Framingham, MA) equipped with the nanoflow ion source TriVersa NanoMate (Advion BioSystems, Ithaca, NY). Ions for ceramide, hexosylceramide, and sphingomyelin were identified by precursor ion scans of  $m/z$  264.4 (for ceramide and hexosylceramide) and  $m/z$  184.1 (for sphingomyelin) in the positive ion mode and analyzed by Analyst software (version 1.6; AB Sciex).

## RESULTS

**The TER P182L Mutant Enzyme Exhibits a Reduced Activity—** To investigate the effect of the P182L mutation on the *trans*-2-enoyl-CoA reductase activity of the TER enzyme, we first examined the ability of the TER P182L mutant enzyme to complement the growth defect of the yeast *TSC13* mutant deficient in *trans*-2-enoyl-CoA reductase. Because the *TSC13* gene is essential for the growth of yeast (17), we utilized the AID system (23) to generate a conditional yeast *TSC13* mutant. Thus, the chromosomal *TSC13* gene was replaced with the *TSC13* gene tagged with tandemly oriented HA and AID (*TSC13*-HA-AID). As expected, the *TSC13*-HA-AID cells harboring the vector only were not able to grow in the presence of the auxin 3-indolacetic acid (IAA) (Fig. 2A) due to the degradation of the Tsc13-HA-AID protein via the ubiquitin-proteasome pathway in response to IAA (Fig. 2B). The IAA-induced growth defect of the *TSC13*-HA-AID cells was complemented by the introduction of the plasmid encoding either the wild-type *TER* gene or the *TER* P182L mutant gene; however, the growth of cells expressing the mutant gene was slightly slower than those expressing the wild-type *TER* gene (Fig. 2A). In addition, the cellular level of the TER P182L mutant enzyme was found to be much lower (over 5-fold) than that of the wild-type TER enzyme (Fig. 2B).

We subsequently performed an *in vitro trans*-2-enoyl-CoA reductase assay using the total membrane fraction from the *TSC13* deletion mutant (*tsc13* $\Delta$ ) bearing the plasmid encoding either the wild-type *TER* gene or the *TER* P182L mutant gene. In an effort to obtain a similar expression level, each mRNA was transcribed under the control of the weaker *ADH* or strong *GAPDH* promoter, respectively. As a result, the level of the mutant enzyme was increased to about half of the wild-type enzyme level (Fig. 3A). An increasing amount of each membrane fraction (*i.e.* an increasing amount of the 3 $\times$ FLAG-tagged wild-type/mutant enzyme) was then subjected to the assay using 3-hydroxy[1-<sup>14</sup>C]palmitoyl-CoA, which is the substrate of 3-hydroxyacyl-CoA dehydratase in the third reaction of the FA elongation cycle (Fig. 1A), because the radiolabeled substrate of the TER enzyme, *trans*-2-enoyl-CoA, is not commercially available. The acyl-CoA products were analyzed after hydrolysis to the corresponding FAs. In the absence of the TER enzyme cofactor, NADPH, both membrane fractions accumulated *trans*-2-hexadecenoyl-CoA, some of which was however

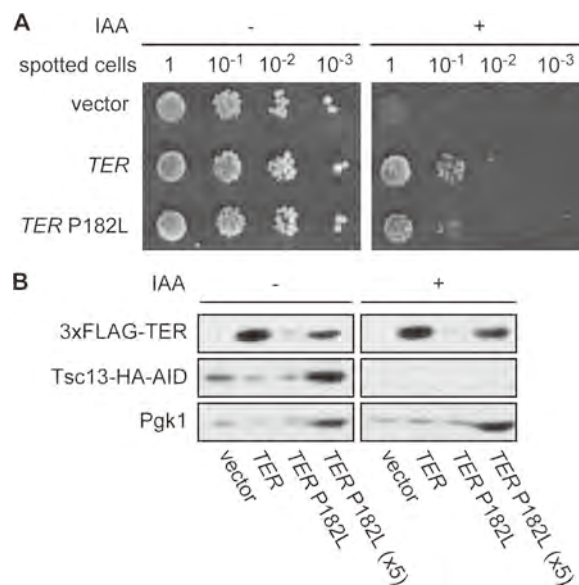


**FIGURE 2. The TER P182L mutant enzyme complements the IAA-induced growth defect of the yeast *TSC13*-HA-AID cells.** A and B, yeast YRF82 cells (*TSC13*-HA-AID) bearing the pAKNF314 (*vector*), pAB85 (3 $\times$ FLAG-*TER*), or pAB95 (3 $\times$ FLAG-*TER* P182L) plasmid were grown in SC-Trp medium at 30 °C to full growth. A, after 1:10 serial dilution, cells were spotted onto plates of SC-Trp and incubated with or without 150  $\mu$ M IAA (500 mM stock solution in ethanol) at 30 °C for 3 days. The dilution factors are indicated above the panel. B, cells were diluted with SC-Trp medium to  $A_{600} = 0.3$  and incubated at 30 °C for 2 h. Cells were then treated with 500  $\mu$ M IAA (500 mM stock solution in ethanol) or with its solvent ethanol and further incubated at 30 °C for 3 h. The total lysate was prepared from each transfected cell population, and the lysate equivalent to  $A_{600} = 0.2$  or 1.0 (5 $\times$ ) units of cells was separated by SDS-PAGE and immunoblotted with anti-FLAG antibody and anti-HA antibody or, to compare protein loading, with anti-Pgk1 antibody.

further converted to palmitoyl-CoA at the higher amount of the membrane fraction (Fig. 3B), probably due to the endogenous NADPH present in the membrane preparation. In both membrane fractions, a nearly identical amount of *trans*-2-enoyl-CoA was produced irrespective of the amount of the membrane fraction, suggesting either that the dehydration reaction by the endogenous yeast 3-hydroxyacyl-CoA dehydratase (Phs1) was saturated under the assay condition or that some 3-hydroxyacyl-CoA was not accessible to the yeast Phs1 enzyme for an unknown reason. In the presence of the cofactor NADPH, the membrane fraction from the yeast *tsc13* $\Delta$  mutant carrying the wild-type *TER* gene converted almost all *trans*-2-hexadecenoyl-CoA to palmitoyl-CoA, whereas, for the yeast *tsc13* $\Delta$  mutant carrying the *TER* P182L mutant gene, the degree of the conversion was proportional to the amount of the membrane fraction (Fig. 3, B and C). The *TER* P182L mutation appears to cause a reduction in the enzyme activity.

**The TER P182L Mutant Enzyme Is Unstable—**It is possible that the lower cellular level of the TER P182L mutant enzyme as compared with the wild-type TER enzyme may be due to its instability; therefore, we conducted a pulse-chase experiment using HEK 293T cells expressing either the 3 $\times$ FLAG-tagged wild-type *TER* mRNA or the 3 $\times$ FLAG-tagged *TER* P182L mutant mRNA from the elongation factor 1 $\alpha$  promoter. Like in yeast cells, the level of the mutant enzyme was lower than that of the wild-type enzyme (Fig. 4A). Cells were pulse-labeled with [<sup>35</sup>S]Met/Cys, and the fate of the labeled enzyme was monitored over time (Fig. 4B). The initial amount of the labeled TER

## Reduced Activity and Stability of TER P182L Mutant Enzyme

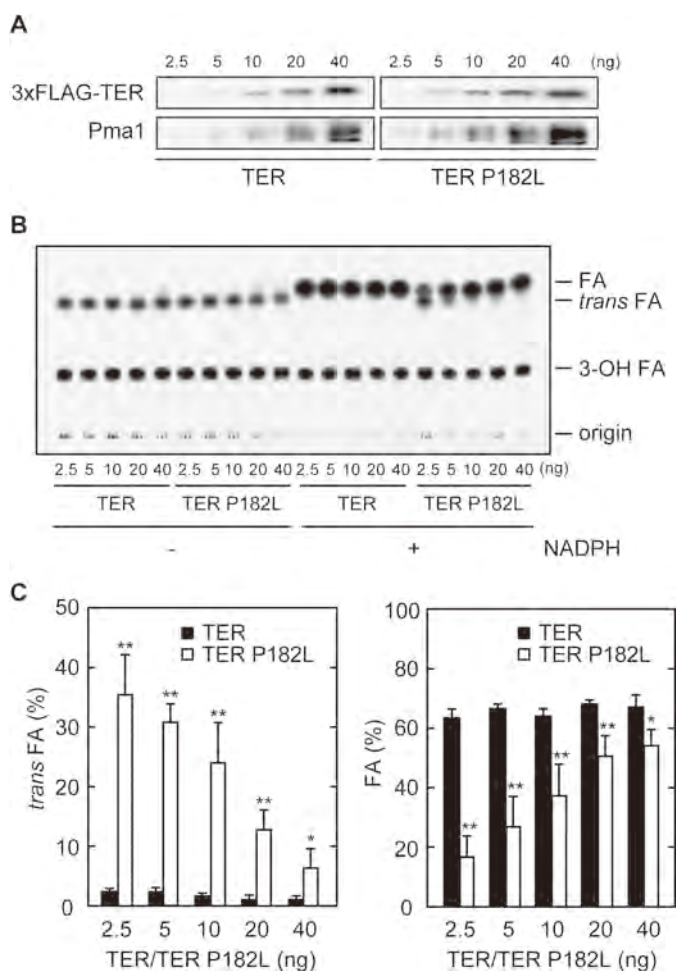


**FIGURE 3. The activity of the TER P182L mutant enzyme is lower than that of the wild-type TER enzyme.** A–C, yeast ABY62 cells (*tsc13Δ* mutant harboring the pAB114 ( $3\times$ FLAG-TER) plasmid) and ABY58 cells (*tsc13Δ* mutant harboring the pAB110 ( $3\times$ FLAG-TER P182L) plasmid) were grown in SC-His medium at 30 °C. An increasing amount of the total membrane fraction was subjected to immunoblotting (A) or *in vitro* *trans*-2-enoyl-CoA reductase assay (B and C): for cells expressing the  $3\times$ FLAG-TER enzyme, 0.625, 1.25, 2.5, 5, and 10  $\mu$ g, and for cells expressing the  $3\times$ FLAG-TER P182L mutant enzyme, 1.25, 2.5, 5, 10, and 20  $\mu$ g (corresponding respectively to 2.5, 5, 10, 20, and 40 ng of the  $3\times$ FLAG-TER enzyme as determined by comparison with the  $3\times$ FLAG-tagged maltose-binding protein standard, which are indicated in the figure). A, each total membrane fraction was separated by SDS-PAGE and immunoblotted with anti-FLAG antibody or, to compare protein loading, with anti-Pma1 (a plasma membrane protein) antibody. B, each total membrane fraction was incubated with 1.8  $\mu$ M 3-hydroxy[1- $^{14}$ C]palmitoyl-CoA (5 nCi) at 37 °C for 30 min. After a sequential work-up (see “Experimental Procedures”), lipids were separated by normal-phase TLC and detected by autoradiography. *trans* FA, *trans*-2-enoyl FA; 3-OH FA, 3-hydroxy FA. C, the radioactivities associated with 3-hydroxy-acyl FA, *trans*-2-enoyl FA, and FA in B were quantified by a bioimaging analyzer BAS-2500. Each bar represents the percentage of the radioactivity of *trans*-2-enoyl FA (left graph) or FA (right graph) relative to the total radioactivity and the mean  $\pm$  S.D. of three independent experiments. Statistically significant differences between the activities of the TER enzyme and the TER P182L mutant enzyme at the same protein amount are indicated (\*,  $p < 0.05$ , \*\*,  $p < 0.01$ ; Student's *t* test).

P182L mutant enzyme (1 h) was approximately equal to that of the labeled wild-type TER enzyme, indicating normal translation of the mutant enzyme. However, during the chase period of 8 h, the amount of the labeled mutant enzyme was reduced to  $\sim$ 20% of the initial level, whereas the amount of the labeled wild-type enzyme remained little changed (Fig. 4, B and C). Immunoblotting of each sample used for the pulse-chase experiment showed that the protein level (cold and radiolabeled) was

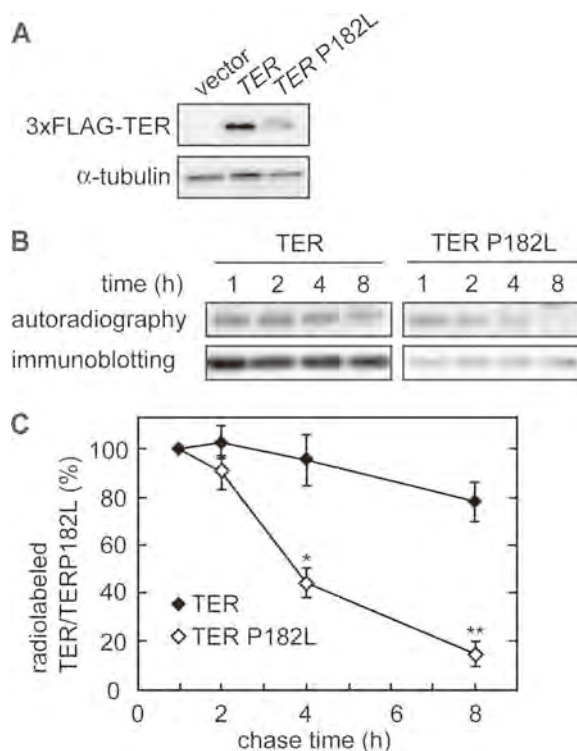


**FIGURE 4. The TER P182L mutant enzyme is unstable.** A, HEK 293T cells were transfected with the pCE-puro  $3\times$ FLAG-1 (vector), pCE-puro  $3\times$ FLAG-TER, or pCE-puro  $3\times$ FLAG-TER P182L plasmid. Forty-eight hours after transfection, the total lysate (5  $\mu$ g) prepared from each transfected cell population was separated by SDS-PAGE and subjected to immunoblotting with anti-FLAG antibody or, to demonstrate uniform protein loading, with anti- $\alpha$ -tubulin antibody. B, HEK 293T cells were transfected with the pCE-puro  $3\times$ FLAG-TER or pCE-puro  $3\times$ FLAG-TER P182L plasmid. Forty-eight hours after transfection, cells were labeled with [ $^{35}$ S]Met/Cys at 37 °C for 1 h. After changing the medium to remove [ $^{35}$ S]Met/Cys, cells were incubated for another 1, 2, 4, and 8 h. At the end of each incubation time, the total cell lysate was prepared and subjected to immunoprecipitation with anti-FLAG antibody. The precipitate was separated by SDS-PAGE and analyzed by autoradiography and by immunoblotting with anti-FLAG antibody. C, the radioactivities associated with the TER enzyme and the TER P182L mutant enzyme in B were quantified by a bioimaging analyzer BAS-2500. Each value represents the percentage of the radioactivity of the TER enzyme or the TER P182L mutant enzyme relative to its radioactivity at the 1-h chase point and the mean  $\pm$  S.D. of three independent experiments. Statistically significant differences between the radioactivities of the TER enzyme and the TER P182L mutant enzyme at the same chase point are indicated (\*,  $p < 0.05$ , \*\*,  $p < 0.01$ ; Student's *t* test).

fairly constant for both enzymes (Fig. 4B). These results suggest that the TER P182L mutation destabilizes the protein.

We also determined the intracellular localization of the TER P182L mutant enzyme using indirect immunofluorescence microscopy. Both the wild-type and the mutant enzymes tagged with  $3\times$ FLAG displayed a reticular pattern typical for the ER and were merged with the ER marker calreticulin (Fig. 5). The ER localization of the wild-type TER enzyme is consistent with the previous study (6); consequently, the TER P182L mutation does not affect the intracellular localization of the enzyme.

*The TER P182L Mutation Has an Indirect Influence on the Third Reaction (Dehydration of 3-Hydroxyacyl-CoA) in the FA Elongation Cycle*—We next analyzed the FA elongation cycle in B-LCLs derived from NSMR patients (homozygous for the TER P182L mutation, TER<sup>P182L/P182L</sup>) (19), asymptomatic carriers (heterozygous for the TER P182L mutation, TER<sup>+ /P182L</sup>), and

### Reduced Activity and Stability of TER P182L Mutant Enzyme

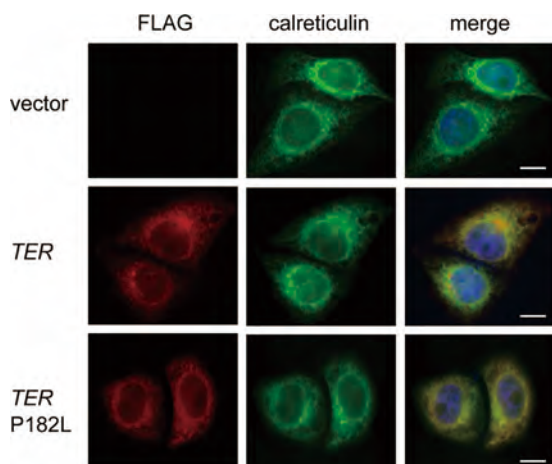


**FIGURE 5. The TER P182L mutant enzyme is localized in the ER.** HeLa cells were transfected with the pCE-puro 3×FLAG-1 (*vector*), pCE-puro 3×FLAG-TER, or pCE-puro 3×FLAG-TER P182L plasmid. Forty-eight hours after transfection, the transfected cells were fixed with formaldehyde and permeabilized with 0.1% Triton X-100. The cells were stained with anti-FLAG antibody (red, left panel), anti-calreticulin antibody (green, middle panel), and the DNA-staining reagent DAPI (blue, right panel). Calibration bar, 10  $\mu$ m.

healthy noncarrier controls ( $TER^{+/+}$ ). The RT-PCR indicated that the expression of the *TER* mRNA was comparable among these B-LCLs (Fig. 6A). The total membrane fraction of each B-LCL was incubated with 3-hydroxy[1- $^{14}$ C]palmitoyl-CoA, and the acyl-CoA products were analyzed after conversion to the corresponding FAs (Fig. 6, B and C). As expected, in the absence of the cofactor NADPH, all the membrane fractions yielded *trans*-2-enoyl-CoA as the only product in ~30% radiochemical yield. In the presence of the cofactor, the  $TER^{+/+}$  and  $TER^{+/P182L}$  membrane fractions consumed most of *trans*-2-enoyl-CoA, producing acyl-CoA in 72 and 61% radiochemical yield, respectively. The  $TER^{P182L/P182L}$  membrane fraction, on the other hand, generated only 28% radiochemical yield of acyl-CoA (39% of acyl-CoA produced by the  $TER^{+/+}$  membrane fraction) with a significant amount of unreacted *trans*-2-enoyl-CoA.

Because FA elongation is achieved by a repeated cycle of four successive enzyme-catalyzed reactions (Fig. 1A), we performed an *in vitro* FA elongation assay to investigate the effect of the *TER* P182L mutation on the overall FA elongation cycle. The total membrane fraction from each B-LCL was incubated with palmitoyl-CoA (the acyl-CoA substrate) and [2- $^{14}$ C]malonyl-CoA (the 2-carbon donor), and the radioactive acyl-CoA products were analyzed as the corresponding radioactive FAs (Fig. 7A). Because the first condensation reaction is the rate-limiting step in each round of the FA elongation cycle (4), acyl-CoA was the primary product in all the membrane fractions. In both the  $TER^{+/+}$  and the  $TER^{+/P182L}$  membrane fractions, 3-hydroxyacyl-CoA was also detected in a small amount, but neither 3-keetoacyl-CoA nor *trans*-2-enoyl-CoA was detected. Contrary to our expectation, the  $TER^{P182L/P182L}$  membrane fraction accumulated a substantial amount of 3-hydroxyacyl-CoA with only a small amount of *trans*-2-enoyl-CoA (the substrate of the *TER* enzyme). Similar results were also obtained using HeLa cells with *TER* knockdown (supplemental Fig. 1). The *TER* siRNA caused a reduction in the *TER* mRNA level (supplemental Fig. 1A), accompanied by a significant accumulation of 3-hydroxy-

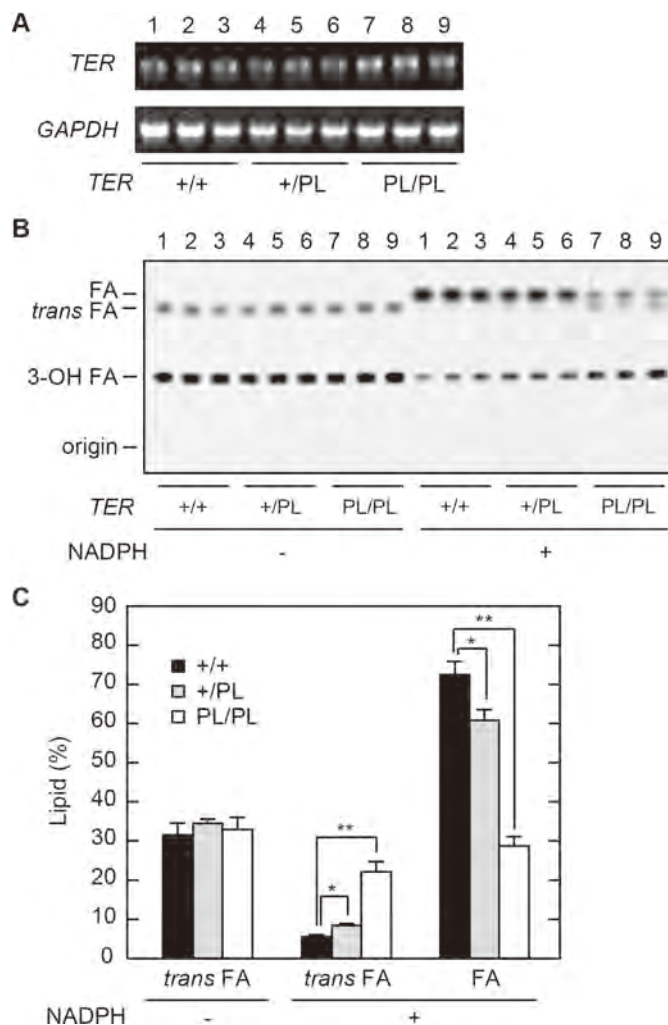


**FIGURE 6. The  $TER^{P182L/P182L}$  B-LCL exhibits lower *trans*-2-enoyl-CoA reductase activity as compared with the  $TER^{+/+}$  B-LCL.** A–C, three B-LCL clones were used for each *TER* genotype: for  $TER^{+/+}$ , clone CONT\_1 (lane 1 in A and B), clone CONT\_2 (lane 2 in A and B), and clone CONT\_3 (lane 3 in A and B); for  $TER^{+/P182L}$ , clone NSMRC\_1 (lane 4 in A and B), clone NSMRC\_2 (lane 5 in A and B), and clone NSMRC\_3 (lane 6 in A and B); and for  $TER^{P182L/P182L}$ , clone NSMR\_1 (lane 7 in A and B), clone NSMR\_2 (lane 8 in A and B), and clone NSMR\_3 (lane 9 in A and B). A, the *TER* and *GAPDH* cDNAs were amplified by RT-PCR from the total RNA prepared from each B-LCL clone using a specific primer. The amplified fragments were separated by agarose gel electrophoresis and stained with ethidium bromide. PL, P182L. B, the total membrane fraction (20  $\mu$ g) prepared from each B-LCL clone was incubated with 1.8  $\mu$ M 3-hydroxy[1- $^{14}$ C]palmitoyl-CoA (5 nCi) in the presence or absence of 1 mM NADPH at 37  $^{\circ}$ C for 30 min. After a sequential work-up (see “Experimental Procedures”), lipids were separated by normal-phase TLC and detected by autoradiography. *trans* FA, *trans*-2-enoyl FA; 3-OH FA, 3-hydroxy FA. C, the radioactivities associated with 3-hydroxy-acyl FA, *trans*-2-enoyl FA, and FA in B were quantified by a bioimaging analyzer BAS-2500. Each bar represents the percentage of the radioactivity of *trans*-2-enoyl FA or FA relative to the total radioactivity and the mean  $\pm$  S.D. of three clones. Statistically significant differences are indicated (\*,  $p < 0.05$ , \*\* $p < 0.01$ ; Student’s *t* test).

acyl-CoA and, to a lesser extent, *trans*-2-enoyl-CoA (supplemental Fig. 1, B and C). Therefore, it seems that the third reaction in the FA elongation cycle was indirectly affected by the impairment of the fourth reaction caused by the reduced enzymatic activity of the *TER* P182L mutant enzyme.

**The Levels of C24:1 Sphingomyelin and C24:1 Ceramide Are Decreased in the  $TER^{P182L/P182L}$  B-LCL**—Because VLCFAs are components of sphingolipids, the decreased activity of the *TER* P182L mutant enzyme leads to a reduction in VLCFA synthesis,

## Reduced Activity and Stability of TER P182L Mutant Enzyme

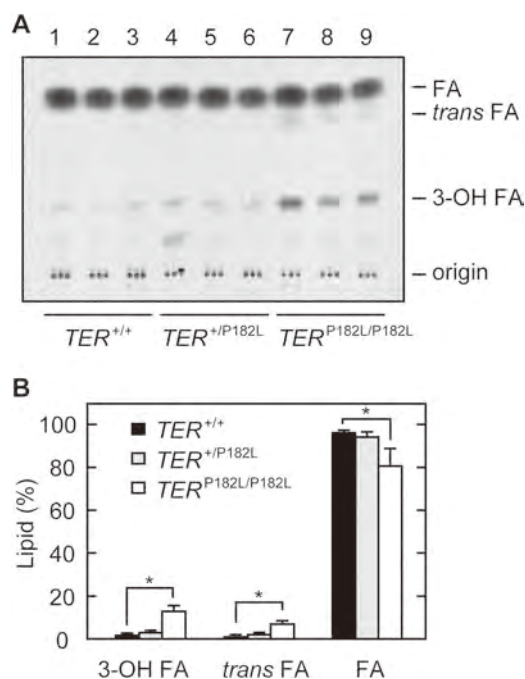


**FIGURE 7. 3-Hydroxyacyl-CoA is accumulated in the  $TER^{P182L/P182L}$  membrane in the FA elongation assay.** *A*, three B-LCL clones were used for each *TER* genotype: for  $TER^{+/+}$ , clone CONT\_1 (lane 1), clone CONT\_2 (lane 2), and clone CONT\_3 (lane 3); for  $TER^{+P182L}$ , clone NSMRC\_1 (lane 4), clone NSMRC\_2 (lane 5), and clone NSMRC\_3 (lane 6); and for  $TER^{P182L/P182L}$ , clone NSMR\_1 (lane 7), clone NSMR\_2 (lane 8), and clone NSMR\_3 (lane 9). The total membrane fraction (20  $\mu$ g) prepared from each B-LCL clone was incubated with 20  $\mu$ M palmitoyl-CoA and 27.3  $\mu$ M [ $^{14}$ C]malonyl-CoA (0.075  $\mu$ Ci) at 37  $^{\circ}$ C for 30 min. After a sequential work-up (see "Experimental Procedures"), lipids were separated by normal-phase TLC and detected by a bioimaging analyzer BAS-2500. *B*, the radioactivities associated with 3-hydroxy-acyl FA, *trans*-2-enoyl FA, and FA in *A* were quantified by a bioimaging analyzer BAS-2500. Each bar represents the percentage of the radioactivity of each lipid relative to the total radioactivity and the mean  $\pm$  S.D. of three independent experiments. Statistically significant differences are indicated (\*,  $p < 0.05$ ; Student's *t* test). *trans* FA, *trans*-2-enoyl FA; 3-OH FA, 3-hydroxy FA.

which may alter the sphingolipid profile in the cell. To test this possibility, we quantitatively analyzed sphingomyelin, ceramide, and hexosylceramide compositions in the  $TER^{+/+}$ ,  $TER^{+P182L}$ , and  $TER^{P182L/P182L}$  B-LCLs using MS/MS. In all the B-LCLs, C16:0 sphingolipids were the most abundant sphingolipid species followed by C24:1 and C24:0 sphingolipids (Fig. 8). However, in the  $TER^{P182L/P182L}$  B-LCL, the levels of C24:1 sphingomyelin and C24:1 ceramide were significantly reduced as compared with those in the  $TER^{+/+}$  and  $TER^{+P182L}$  B-LCLs (Fig. 8, *A* and *B*). In addition, the levels of C24:0 sphingomyelin and C24:0 ceramide also seemed to be decreased but not statistically significant. Interestingly, there was a concomitant increase in the levels of C16:0 sphingomyelin and C16:0 ceramide. In contrast to sphingomyelin and ceramide, although C16:0 hexosylceramide was significantly increased, no other hexosylceramide showed any noticeable changes in the  $TER^{P182L/P182L}$  B-LCL (Fig. 8C). Nevertheless, these findings indicated that the *TER* P182L mutation also has an influence on the synthesis of sphingolipids.

## DISCUSSION

Using yeast and mammalian cells transfected with the *TER* P182L mutant gene, we have revealed that the *TER* P182L

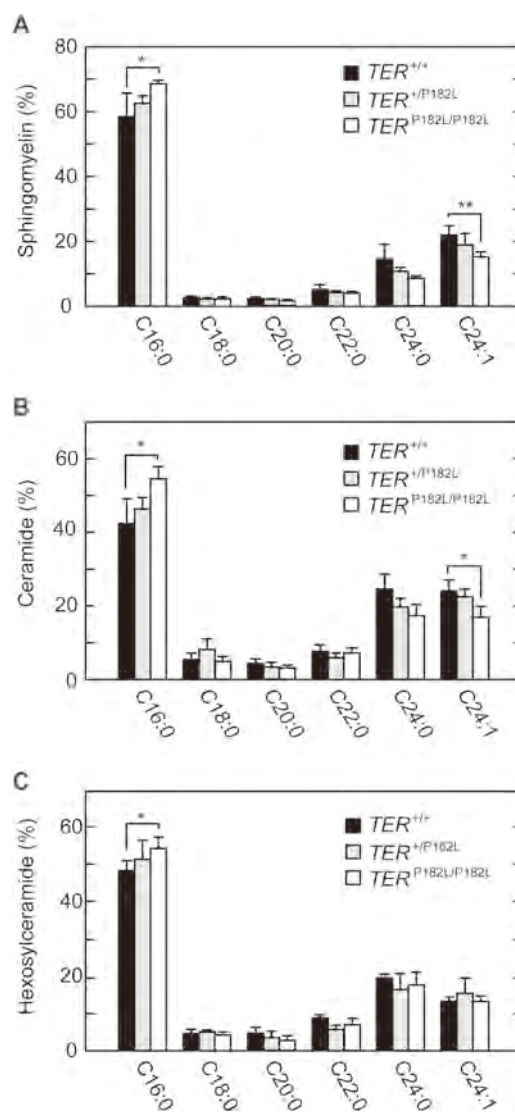


**FIGURE 8. C24:1 sphingomyelin and C24:1 ceramide are decreased in the  $TER^{P182L/P182L}$  B-LCL.** Lipids were extracted from multiple cells for each B-LCL clone: for  $TER^{+/+}$ , clones CONT\_1, CONT\_2, and CONT\_3; for  $TER^{+P182L}$ , clones NSMRC\_1, NSMRC\_2, NSMRC\_3, and NSMRC\_4; and for  $TER^{P182L/P182L}$ , clones NSMR\_1, NSMR\_2, NSMR\_3, and NSMR\_4. Sphingomyelin (*A*), ceramide (*B*), and hexosylceramide (*C*) compositions were identified by a 4000 QTRAP MS/MS system and analyzed by Analyst software. Each bar represents the percentage of the amount of each sphingolipid species relative to the total amount of the each corresponding sphingolipid and the mean  $\pm$  S.D. from three or four clones. Statistically significant differences are indicated (\*,  $p < 0.05$ , \*\*,  $p < 0.01$ ; Student's *t* test).

mutation reduces the activity and stability of the enzyme (Figs. 3 and 4), which seems to explain the decrease in the apparent *TER* activity observed in the  $TER^{P182L/P182L}$  B-LCL (Fig. 6, *B* and *C*). In the predicted membrane topology model of the *TER* enzyme (Fig. 1C), the Pro-182 residue is located in the second luminal loop. Due to its cyclic structure, a proline residue confers a local rigidity to the protein backbone and often plays an important role in protein architecture, producing turns and bends. Indeed, the Pro-182 residue is predicted to constitute a turn structure at the end of a  $\beta$ -strand by a protein secondary structure prediction algorithm (28); accordingly, its substitution with a leucine residue could impair the turn and dislocate the secondary structure, resulting in the reduced enzyme activity and stability.

## Reduced Activity and Stability of TER P182L Mutant Enzyme

Each FA elongation cycle is a four-reaction process (Fig. 1A) in which the first condensation reaction is the rate-limiting step (4). This is consistent with the results of the FA elongation assay on the B-LCLs showing that the major product was the substrate for the first reaction, acyl-CoA (Fig. 7). Interestingly, in the *TER*<sup>P182L/P182L</sup> B-LCL and the *TER* siRNA-treated HeLa cells, the substrate for the third reaction, 3-hydroxyacyl-CoA, was the second major product followed by the substrate for the fourth reaction (the *TER* enzyme-catalyzed reaction), *trans*-2-enoyl-CoA (Fig. 7 and supplemental Fig. 1). A small amount of 3-hydroxyacyl-CoA, but not *trans*-2-enoyl-CoA, was also detected in both the *TER*<sup>+/+</sup> and the *TER*<sup>+/P182L</sup> B-LCLs (Fig. 7A). The substrate for the second reaction, 3-ketoacyl-CoA, was not detected in any of the B-LCLs. This observation implies that the third reaction, dehydration of 3-hydroxyacyl-CoA to *trans*-2-enoyl-CoA, may be the secondary rate-limiting step in the FA elongation cycle and regulated by feedback inhibition of 3-hydroxyacyl-CoA dehydratase by its product accumulation due to the *TER* P182L mutation. It is noteworthy that, in mammals, multiple isozymes exist for both the first and the third reactions, in contrast to one enzyme each for the second and fourth reactions, suggesting the importance of the first and third reactions in the FA elongation cycle. Alternatively, because the enzymes involved in the FA elongation cycle are associated as a membrane-bound enzyme complex, any reduction in the *TER* enzyme level caused by either the P182L mutation or siRNA treatment could result in the disruption of the possible interaction of 3-hydroxyacyl-CoA dehydratase with the *TER* enzyme required for the dehydratase activity and thus the accumulation of its substrate 3-hydroxyacyl-CoA.

The levels of C24:1 sphingomyelin and C24:1 ceramide were significantly decreased in the *TER*<sup>P182L/P182L</sup> B-LCL as compared with the *TER*<sup>+/+</sup> B-LCL (Fig. 8, A and B). There was also a decrease in the levels of C24:0 sphingomyelin and C24:0 ceramide, but this was not statistically significant, probably due to the small sample size. Ceramide is the common precursor for hexosylceramide and sphingomyelin, and therefore, it was expected that, similar to C24:1 sphingomyelin, the level of C24:1 hexosylceramide would be decreased in the *TER*<sup>P182L/P182L</sup> B-LCL; however, it was found to remain virtually unchanged (Fig. 8C). This observation may be explained by the low hexosylceramide content in B-LCL (~0.1 of the sphingomyelin content; data not shown), which could cause measurement deviation. On the other hand, the levels of all three C16:0 sphingolipids were found to be similarly increased in the *TER*<sup>P182L/P182L</sup> B-LCL (Fig. 8). Because the *TER* enzyme is the only *trans*-2-enoyl-CoA reductase, the mutation in the *TER* gene must affect every FA elongation cycle; as a consequence, the effect of the *TER* P182L mutation may become more profound with a progression of the FA elongation cycle (e.g. synthesis of C24 VLCFAs). It is therefore conceivable that, in the *TER*<sup>P182L/P182L</sup> B-LCL, the mutation causes a reduction in the production of C24 VLCFAs, which in turn lowers the level of C24 sphingolipids.

In contrast to the *TER* null mutation, which probably leads to embryonic lethality as in the case of the knock-out mice for the only 3-ketoacyl-CoA reductase *KAR* gene (18), the *TER* P182L mutation appears to be a weak mutation and affects only neural function in the brain (19). This weak mutation could be con-

sistent with the relatively small changes observed in the level of C24 sphingolipids, which, however, may be enough to harm the nerve system without causing damage to other tissues/organ systems. Myelin plays an important role in the saltatory conduction of action potentials in the nervous system and is enriched in certain lipids, especially C24 sphingolipids (sphingomyelin, galactosylceramide, and sulfatide) (10, 12, 29). Indeed, mice deficient in C24 ceramide (and hence C24 sphingolipids) are known to exhibit neural defects (30). In this regard, it may be possible that the reduction in C24 sphingolipids as a result of the *TER* P182L mutation could affect neural development, contributing to the pathogenesis of NSMR.

In summary, we have identified that the *TER* P182L mutation reduces the activity and stability of the enzyme, leading to a decreased level of C24 sphingolipids, an essential component for proper myelin function, in the *TER*<sup>P182L/P182L</sup> B-LCL, which may be a part of the pathogenesis of NSMR. We have also found an indication that the third reaction (dehydration of 3-hydroxyacyl-CoA) is likely to be the secondary rate-limiting step in the FA elongation cycle. Future studies will be needed to determine the effect of the *TER* P182L mutation on brain lipid composition and brain function as well as to reveal the regulatory mechanism of the probable secondary rate-limiting step.

*Acknowledgments*—The yeast strain for the AID system (BY25598) was provided by the National Bio-Resource Project (NBRP) of the Ministry of Education, Culture, Sports, Science and Technology (MEXT), Japan. We are grateful to Dr. K. Obara for technical support and Dr. T. Toyokuni for scientific editing of the manuscript.

## REFERENCES

1. Agbaga, M. P., Mandal, M. N., and Anderson, R. E. (2010) Retinal very long-chain PUFAs: new insights from studies on ELOVL4 protein. *J. Lipid Res.* **51**, 1624–1642
2. Guillou, H., Zdravce, D., Martin, P. G., and Jacobsson, A. (2010) The key roles of elongases and desaturases in mammalian fatty acid metabolism: Insights from transgenic mice. *Prog. Lipid Res.* **49**, 186–199
3. Kihara, A. (2012) Very long-chain fatty acids: elongation, physiology and related disorders. *J. Biochem.* **152**, 387–395
4. Nugteren, D. H. (1965) The enzymic chain elongation of fatty acids by rat-liver microsomes. *Biochim. Biophys. Acta* **106**, 280–290
5. Ohno, Y., Suto, S., Yamanaka, M., Mizutani, Y., Mitsutake, S., Igarashi, Y., Sassa, T., and Kihara, A. (2010) ELOVL1 production of C24 acyl-CoAs is linked to C24 sphingolipid synthesis. *Proc. Natl. Acad. Sci. U.S.A.* **107**, 18439–18444
6. Moon, Y. A., and Horton, J. D. (2003) Identification of two mammalian reductases involved in the two-carbon fatty acyl elongation cascade. *J. Biol. Chem.* **278**, 7335–7343
7. Ikeda, M., Kanao, Y., Yamanaka, M., Sakuraba, H., Mizutani, Y., Igarashi, Y., and Kihara, A. (2008) Characterization of four mammalian 3-hydroxyacyl-CoA dehydratases involved in very long-chain fatty acid synthesis. *FEBS Lett.* **582**, 2435–2440
8. Kihara, A., Mitsutake, S., Mizutani, Y., and Igarashi, Y. (2007) Metabolism and biological functions of two phosphorylated sphingolipids, sphingosine 1-phosphate and ceramide 1-phosphate. *Prog. Lipid Res.* **46**, 126–144
9. Hakomori, S. (2000) Traveling for the glycosphingolipid path. *Glycoconj. J.* **17**, 627–647
10. Norton, W. T., and Cammer, W. (1984) Isolation and characterization of myelin. In *Myelin*, pp. 147–195, Plenum Press, New York, NY
11. Laviad, E. L., Albee, L., Pankova-Kholmyansky, I., Epstein, S., Park, H., Merrill, A. H., Jr., and Futerman, A. H. (2008) Characterization of ceramide synthase 2: tissue distribution, substrate specificity, and inhibition

## Reduced Activity and Stability of TER P182L Mutant Enzyme

- by sphingosine 1-phosphate. *J. Biol. Chem.* **283**, 5677–5684
12. Potter, K. A., Kern, M. J., Fullbright, G., Bielawski, J., Scherer, S. S., Yum, S. W., Li, J. J., Cheng, H., Han, X., Venkata, J. K., Khan, P. A., Rohrer, B., and Hama, H. (2011) Central nervous system dysfunction in a mouse model of FA2H deficiency. *Glia* **59**, 1009–1021
  13. Zhang, K., Kniazeva, M., Han, M., Li, W., Yu, Z., Yang, Z., Li, Y., Metzker, M. L., Allikmets, R., Zack, D. J., Kakuk, L. E., Lagali, P. S., Wong, P. W., MacDonald, I. M., Sieving, P. A., Figueroa, D. J., Austin, C. P., Gould, R. J., Ayyagari, R., and Petrukhin, K. (2001) A 5-bp deletion in *ELOVL4* is associated with two related forms of autosomal dominant macular dystrophy. *Nat. Genet.* **27**, 89–93
  14. Aldahmesh, M. A., Mohamed, J. Y., Alkuraya, H. S., Verma, I. C., Puri, R. D., Alaiya, A. A., Rizzo, W. B., and Alkuraya, F. S. (2011) Recessive mutations in *ELOVL4* cause ichthyosis, intellectual disability, and spastic quadriplegia. *Am. J. Hum. Genet.* **89**, 745–750
  15. Pelé, M., Tiret, L., Kessler, J. L., Blot, S., and Panthier, J. J. (2005) SINE exonic insertion in the *PTPLA* gene leads to multiple splicing defects and segregates with the autosomal recessive centronuclear myopathy in dogs. *Hum. Mol. Genet.* **14**, 1417–1427
  16. Muhammad, E., Reish, O., Ohno, Y., Scheetz, T., DeLuca, A., Searby, C., Regev, M., Benyamini, L., Fellig, Y., Kihara, A., Sheffield, V. C., and Parvari, R. (2013) Congenital myopathy is caused by mutation of *HACD1*. *Hum. Mol. Genet.*, in press
  17. Kohlwein, S. D., Eder, S., Oh, C. S., Martin, C. E., Gable, K., Bacikova, D., and Dunn, T. (2001) Tsc13p is required for fatty acid elongation and localizes to a novel structure at the nuclear-vacuolar interface in *Saccharomyces cerevisiae*. *Mol. Cell. Biol.* **21**, 109–125
  18. Rantakari, P., Lagerbohm, H., Kaimainen, M., Suomela, J. P., Strauss, L., Sainio, K., Pakarinen, P., and Poutanen, M. (2010) Hydroxysteroid (17 $\beta$ ) dehydrogenase 12 is essential for mouse organogenesis and embryonic survival. *Endocrinology* **151**, 1893–1901
  19. Çalışkan, M., Chong, J. X., Uricchio, L., Anderson, R., Chen, P., Sougnez, C., Garimella, K., Gabriel, S. B., dePristo, M. A., Shakir, K., Matern, D., Das, S., Waggoner, D., Nicolae, D. L., and Ober, C. (2011) Exome sequencing reveals a novel mutation for autosomal recessive non-syndromic mental retardation in the *TECR* gene on chromosome 19p13. *Hum. Mol. Genet.* **20**, 1285–1289
  20. Paul, S., Gable, K., and Dunn, T. M. (2007) A six-membrane-spanning topology for yeast and *Arabidopsis* Tsc13p, the enoyl reductases of the microsomal fatty acid elongating system. *J. Biol. Chem.* **282**, 19237–19246
  21. Fuss, I. J., Kanof, M. E., Smith, P. D., and Zola, H. (2009) Isolation of whole mononuclear cells from peripheral blood and cord blood. in *Current Protocols in Immunology*, Chapter 7, Unit 7.1, John Wiley & Sons, Inc., New York
  22. Brachmann, C. B., Davies, A., Cost, G. J., Caputo, E., Li, J., Hieter, P., and Boeke, J. D. (1998) Designer deletion strains derived from *Saccharomyces cerevisiae* S288C: a useful set of strains and plasmids for PCR-mediated gene disruption and other applications. *Yeast* **14**, 115–132
  23. Nishimura, K., Fukagawa, T., Takisawa, H., Kakimoto, T., and Kanemaki, M. (2009) An auxin-based degron system for the rapid depletion of proteins in nonplant cells. *Nat. Methods* **6**, 917–922
  24. Obara, K., Yamamoto, H., and Kihara, A. (2012) Membrane protein Rim21 plays a central role in sensing ambient pH in *Saccharomyces cerevisiae*. *J. Biol. Chem.* **287**, 38473–38481
  25. Kihara, A., and Igarashi, Y. (2002) Identification and characterization of a *Saccharomyces cerevisiae* gene, *RSB1*, involved in sphingoid long-chain base release. *J. Biol. Chem.* **277**, 30048–30054
  26. Ogawa, C., Kihara, A., Gokoh, M., and Igarashi, Y. (2003) Identification and characterization of a novel human sphingosine-1-phosphate phosphohydrolase, hSPP2. *J. Biol. Chem.* **278**, 1268–1272
  27. Sassa, T., Ohno, Y., Suzuki, S., Nomura, T., Nishioka, C., Kashiwagi, T., Hirayama, T., Akiyama, M., Taguchi, R., Shimizu, H., Itohara, S., and Kihara, A. (2013) Impaired epidermal permeability barrier in mice lacking the *Elovl1* gene responsible for very long-chain fatty acid production. *Mol. Cell. Biol.* **33**, 2787–2796
  28. Chou, P. Y., and Fasman, G. D. (1974) Prediction of protein conformation. *Biochemistry* **13**, 222–245
  29. Ben-David, O., Pewzner-Jung, Y., Brenner, O., Laviad, E. L., Kogot-Levin, A., Weissberg, I., Biton, I. E., Pienik, R., Wang, E., Kelly, S., Alroy, J., Raas-Rothschild, A., Friedman, A., Brügger, B., Merrill, A. H., Jr., and Futerman, A. H. (2011) Encephalopathy caused by ablation of very long acyl chain ceramide synthesis may be largely due to reduced galactosylceramide levels. *J. Biol. Chem.* **286**, 30022–30033
  30. Imgrund, S., Hartmann, D., Farwanah, H., Eckhardt, M., Sandhoff, R., Degen, J., Gieselmann, V., Sandhoff, K., and Willecke, K. (2009) Adult ceramide synthase 2 (CERS2)-deficient mice exhibit myelin sheath defects, cerebellar degeneration, and hepatocarcinomas. *J. Biol. Chem.* **284**, 33549–33560

# Sterylglucoside Catabolism in *Cryptococcus neoformans* with Endoglycoceramidase-related Protein 2 (EGCrP2), the First Steryl- $\beta$ -glucosidase Identified in Fungi\*

Received for publication, October 7, 2014, and in revised form, October 30, 2014. Published, JBC Papers in Press, October 31, 2014, DOI 10.1074/jbc.M114.616300

Takashi Watanabe<sup>†1</sup>, Tomoharu Ito<sup>†1</sup>, Hatsumi M. Goda<sup>‡</sup>, Yohei Ishibashi<sup>‡</sup>, Tomofumi Miyamoto<sup>§</sup>, Kazutaka Ikeda<sup>¶</sup>, Ryo Taguchi<sup>||</sup>, Nozomu Okino<sup>‡</sup>, and Makoto Ito<sup>‡2</sup>

From the <sup>†</sup>Department of Bioscience and Biotechnology, Graduate School of Bioresource and Bioenvironmental Sciences, Kyushu University, 6-10-1 Hakozaki, Higashi-ku, Fukuoka 812-8581, Japan, the <sup>§</sup>Graduate School of Pharmaceutical Sciences, Kyushu University, Maidashi 3-1-1, Higashi-ku, Fukuoka 812-8582, Japan, the <sup>¶</sup>Institute for Advanced Biosciences, Keio University, 246-2 Mizukami, Kakuganji, Tsuruoka, Yamagata 997-0052, Japan, and the <sup>||</sup>Department of Biomedical Sciences, College of Life and Health Sciences, Chubu University, 1200 Matsumoto-cho, Kasugai-shi, Aichi 487-8501, Japan

**Background:** Endoglycoceramidase-related protein 1 (EGCrP1) is a glucocerebrosidase in *Cryptococcus neoformans*; however, the functions of its paralogue, EGCrP2, remain unknown.

**Results:** EGCrP2, but not EGCrP1, hydrolyzed steryl- $\beta$ -glucosides. Disruption of *egcrp2* accumulated ergosteryl- $3\beta$ -glucoside in *C. neoformans*.

**Conclusion:** EGCrP2 degraded steryl- $\beta$ -glucosides both *in vivo* and *in vitro*.

**Significance:** EGCrP2 is a missing link in steryl- $\beta$ -glucoside metabolism in fungi. In addition, EGCrP2 is a potential target for antifungal drugs.

Cryptococcosis is an infectious disease caused by pathogenic fungi, such as *Cryptococcus neoformans* and *Cryptococcus gattii*. The ceramide structure (methyl-d18:2/h18:0) of *C. neoformans* glucosylceramide (GlcCer) is characteristic and strongly related to its pathogenicity. We recently identified endoglycoceramidase-related protein 1 (EGCrP1) as a glucocerebrosidase in *C. neoformans* and showed that it was involved in the quality control of GlcCer by eliminating immature GlcCer during the synthesis of GlcCer (Ishibashi, Y., Ikeda, K., Sakaguchi, K., Okino, N., Taguchi, R., and Ito, M. (2012) Quality control of fungus-specific glucosylceramide in *Cryptococcus neoformans* by endoglycoceramidase-related protein 1 (EGCrP1). *J. Biol. Chem.* 287, 368–381). We herein identified and characterized EGCrP2, a homologue of EGCrP1, as the enzyme responsible for sterylglucoside catabolism in *C. neoformans*. In contrast to EGCrP1, which is specific to GlcCer, EGCrP2 hydrolyzed various  $\beta$ -glucosides, including GlcCer, cholesteryl- $\beta$ -glucoside, ergosteryl- $\beta$ -glucoside, sitosteryl- $\beta$ -glucoside, and *para*-nitrophenyl- $\beta$ -glucoside, but not  $\alpha$ -glucosides or  $\beta$ -galactosides, under acidic conditions. Disruption of the EGCrP2 gene (*egcrp2*) resulted in the accumulation of a glycolipid, the structure of which was determined following purification to ergosteryl- $3\beta$ -glucoside, a major sterylglucoside in fungi, by mass spectrometric and two-dimensional nuclear magnetic resonance analyses. This glycolipid accumulated in vacuoles and EGCrP2 was detected in vacuole-enriched fraction. These results indicated that EGCrP2 was involved in the catabolism of ergosteryl- $\beta$ -glucoside in the vacuoles of *C. neoformans*. Dis-

tinct growth arrest, a dysfunction in cell budding, and an abnormal vacuole morphology were detected in the *egcrp2*-disrupted mutants, suggesting that EGCrP2 may be a promising target for anti-cryptococcal drugs. EGCrP2, classified into glycohydrolase family 5, is the first steryl- $\beta$ -glucosidase identified as well as a missing link in sterylglucoside metabolism in fungi.

Cryptococcosis is an infectious disease caused by pathogenic fungi, such as *Cryptococcus neoformans* and *Cryptococcus gattii*. The prevalence of cryptococcosis has increased over the past 20 years because of the increase in AIDS patients and expanded use of immunosuppressive drugs. More than 600,000 patients with immune deficiencies were reported to have died within 3 months of being infected with *C. neoformans* (1). The highly virulent *C. gattii*, a primary pathogen in healthy individuals and animals, was recently detected in the United States and Canada (2). Thus, the development of new drugs against cryptococcosis is urgently needed.

*C. neoformans* synthesizes a glucosylceramide (GlcCer)<sup>3</sup> composed of  $\beta$ -linked glucose and ceramide that possesses a characteristic sphingoid base, which has two double bonds at C4/C8 in the trans conformation and a methyl substitution at C9 (3). Previous studies reported that this fungus-specific GlcCer may be strongly associated with the pathogenicity of

\* This work was supported in part by Basic Research B Grant 24380058 from the Japanese Ministry of Education, Culture, Science, and Technology and the Japan Foundation for Applied Enzymology (to M. I.).

<sup>†</sup> These authors contributed equally to this work.

<sup>2</sup> To whom correspondence should be addressed. Tel.: 81-92-642-2898; Fax: 81-92-642-2907; E-mail: makotoi@agr.kyushu-u.ac.jp.

<sup>3</sup> The abbreviations used are: GlcCer, glucosylceramide; Cer, ceramide; EG, ergosteryl- $3\beta$ -glucoside; EGCase, endoglycoceramidase; EGCrP, endoglycoceramidase-related protein; rEGCrP, recombinant EGCrP; Glc, D-glucose; GSL, glycosphingolipid; LacCer, lactosylceramide; NBD, 7-nitro-2,1,3-benzoxadiazole; pNP, *para*-nitrophenyl; 4MU, 4-methylumbelliferyl; 1KO, *egcrp1*-knock-out mutant; 2KO, *egcrp2*-knock-out mutant; DKO, *egcrp1/egcrp2* double knock-out mutant; TOCSY, total correlation spectroscopy; HSQC, heteronuclear single quantum correlation; HMBC, heteronuclear multiple-bond correlation; carboxy-DCFDA, 5-(and 6)-carboxy-2',7'-dichlorofluorescein diacetate.

## Novel Steryl- $\beta$ -glucosidase in *C. neoformans*

*C. neoformans*; thus, the enzymes involved in the synthesis of GlcCer (e.g. UDP-glucose:ceramide glucosyltransferase (4, 5), sphingoid base C4/C8 desaturase (6, 7), and C9 methyltransferase (8, 9)) have been intensively studied, and the genes responsible for these enzyme activities have also been identified. However, how GlcCer is catabolized in fungi remains unclear because the enzyme(s) responsible for degrading GlcCer in fungi have not yet been identified.

Endoglycoceramidase-related protein 1 (EGCrP1) is a homologue of endoglycoceramidase (EGCase, ceramide glycanase; EC.3.2.1.123), which is an endo-type glycosidase capable of cleaving the  $\beta$ -glycosidic linkage between the ceramide (Cer) and oligosaccharide of various glycosphingolipids (GSLs) to release an intact oligosaccharide and Cer (10, 11). EGCase very weakly hydrolyzes GlcCer, whereas EGCrP1 specifically hydrolyzes GlcCer but not oligosaccharide-linked GSLs, such as LacCer, GM1a, and Gb3Cer, which are favorite substrates for EGCase. Thus, EGCrP1 was the first identified GlcCer-degrading enzyme (glucocerebrosidase) in fungi (12). Although the disruption of *egcrp1* in *C. neoformans* reduced glucocerebrosidase activity under neutral conditions, the activity remained almost unchanged under acidic conditions, suggesting the presence of other glucocerebrosidase(s) that function in *C. neoformans* under acidic conditions.

Fungi have two major glycolipids: GlcCer and sterylglucoside. The former is related to pathogenicity of fungi (6), and the latter is involved in stress-mediated signal transduction (13). Sterylglucoside synthase (UGT51) was identified in budding yeast (14). However, the enzyme(s) involved in sterylglucoside catabolism have not yet been identified in fungi or yeasts.

We herein report the molecular cloning, enzymatic characterization, and physiological relevance of EGCrP2, a homologue of EGCrP1, in *C. neoformans*. The specificity of EGCrP2 for aglycone moiety differed completely from that of EGCrP1; the former hydrolyzed not only GlcCer but also various  $\beta$ -glucosides, including steryl- $\beta$ -glucosides, *para*-nitrophenyl (*p*NP)- $\beta$ -glucoside, and 4-methylumbelliferyl (4MU)- $\beta$ -glucoside, whereas the latter specifically hydrolyzed GlcCer but not the other  $\beta$ -glucosides tested. Neither EGCrP1 nor EGCrP2 hydrolyzed  $\beta$ -galactosides or  $\alpha$ -glucosides, indicating that both enzymes were  $\beta$ -glucosidases with different aglycone specificities. The disruption of *egcrp2*, but not *egcrp1*, resulted in the accumulation of an unknown glycolipid, which was subsequently identified as an ergosteryl-3 $\beta$ -glucoside (EG) after purification. EG is a major molecular species of sterylglucoside in fungi and yeasts. These results indicated that EGCrP2 functioned *in vivo* as a steryl- $\beta$ -glucosidase, which is a missing link in sterylglucoside metabolism in fungi. This study also provided evidence to show that EGCrP2 may be a promising target for the development of anti-fungus drugs for *C. neoformans*.

### EXPERIMENTAL PROCEDURES

**Materials**—C6-7-nitro-2,1,3-benzoxadiazole (NBD)-Cer, C6-NBD-GlcCer, and C12-NBD-Gb3Cer were purchased from Matreya, and C6-NBD-LacCer, C6-NBD-GalCer, *p*NP glycosides, 4MU glycosides, and resorufin- $\beta$ -D-glucopyranoside were from Sigma-Aldrich. C12-NBD-GM1 and C12-NBD-sph-

ingomyelin were prepared using the sphingolipid Cer *N*-deacylase by the method described previously (15).

**Strain and Culture**—*C. neoformans* var. *grubii* serotype A strain H99 (ATCC 208821) was purchased from the American Type Culture Collection. *C. neoformans* was cultured at 30 °C in YPD medium (2% Glc, 2% peptone, 1% yeast extract).

**Construction of the Expression Vector**—Total RNA was obtained from fungus cells using Sepasol-RNA I Super G (Nacalai Tesque). First strand cDNA was synthesized from 1  $\mu$ g of total RNA using PrimeScript reverse transcriptase (Takara Bio Inc.). To insert the restriction sites, PCR was carried out using first strand cDNA as a template and the expression primers listed in Table 1. Amplification was performed using PrimeSTAR GXL DNA polymerase (Takara Bio Inc.). The amplified product was digested with appropriate restriction enzymes and inserted into the corresponding sites of pET23a (Novagen).

**Expression of Recombinant EGCrP2**—The EGCrP2 gene (*egcrp2*) of *C. neoformans* (CNAG\_05607) was expressed in *Escherichia coli* BL21 (DE3) by inserting a pET23a vector (Novagen) containing *egcrp2*. After incubating the transformants at 37 °C in Luria-Bertani (LB) medium containing 100  $\mu$ g/ml ampicillin until the  $A_{600\text{ nm}}$  reached  $\sim 0.6$ , isopropyl  $\beta$ -D-thiogalactopyranoside was then added to the culture at a final concentration of 1 mM. After cultivation for 24 h, the cells were harvested by centrifugation (8,000  $\times g$  for 15 min) and suspended in 50 mM Tris-HCl buffer, pH 7.5, containing 150 mM NaCl and 20 mM imidazole. The suspension was kept in a sonic bath for 30 s, this procedure was repeated four times to crush the cells, and cell debris was removed by centrifugation (18,000  $\times g$  for 15 min). The supernatant was applied to Ni Sepharose 6 Fast Flow resin (GE Healthcare) packed in a Muro-mac mini column M (Muromachi Technos), and the column was then washed with 50 mM Tris-HCl, pH 7.5, containing 150 mM NaCl and 40 mM imidazole. Recombinant EGCrP2 was eluted with 50 mM Tris-HCl, pH 7.5, containing 150 mM NaCl and 200 mM imidazole. The purified enzyme was dialyzed against 50 mM Tris-HCl, pH 7.5, containing 150 mM NaCl using an Amicon Ultra-4 30k device (Merck Millipore) and subjected to gel filtration chromatography on a Superdex 200 10/300 GL (GE Healthcare) column equilibrated with 25 mM MES, pH 6.0, containing 100 mM NaCl. EGCrP2 was eluted from the column with the same buffer at a flow rate of 0.5 ml/min, and each 0.5-ml fraction was collected using a fraction collector (GE Healthcare).

**Protein Assay**—Protein content was determined by Pierce 660 nm protein assay reagent (Thermo Fisher Scientific) with bovine serum albumin as a standard. SDS-PAGE was carried out according to the method of Laemmli (16) with prestained protein markers (Nacalai Tesque) as a standard. Proteins were stained with CBB Stain One (Nacalai Tesque).

**Enzyme Assay**—An aliquot of each substrate (NBD-labeled GSLs, *p*NP glycosides, 4MU- $\beta$ -glucosides, and resorufin- $\beta$ -D-glucoside) was incubated at 30 °C for an appropriate period with 100 ng of enzyme in 20  $\mu$ l of 50 mM MES buffer, pH 6.0, containing 0.025% cholic acid. The reaction mixture, dried using a SpeedVac concentrator, was dissolved in 10  $\mu$ l of chloroform/methanol (1:2, v/v) and applied to a Silica Gel 60 TLC plate (Merck Millipore), which was developed with chloro-

form/methanol/water (65:25:4 or 65:16:2, v/v/v). NBD-labeled GSLs were visualized using AE-6935B VISIRAYS-B and EZ-capture II (ATTO). The extent of the hydrolysis of NBD-labeled GSLs was calculated as follows: hydrolysis (%) = (peak area for the NBD-Cer generated)  $\times$  100/(peak area for the NBD-Cer generated + peak area for the remaining NBD-GSLs). GlcCer and glucose were visualized by spraying the TLC plate with orcinol- $\text{H}_2\text{SO}_4$  reagent. *p*-Nitrophenol released from *p*NP glycosides by the action of the enzyme was measured at 405 nm by Multiskan FC microplate reader (Thermo Fisher Scientific). 4-Methylumbelliferone and resorufin released from 4MU- $\beta$ -glucoside and resorufin- $\beta$ -D-glucoside, respectively, were measured at 355/460 nm and 544/590 nm of excitation/emission, respectively, by an ARVO MX 1420 fluorescence microplate reader (PerkinElmer Life Sciences).

**Characterization of Recombinant EGCrP2**—The pH dependence of EGCrP2 activity was determined in a pH range of 4–9 using the GTA buffer (3,3-dimethyl-glutaric acid, tris(hydroxymethyl) aminomethane, and 2-amino-2-methyl-1,3-ropenediol) at a final concentration of 150 mM. Temperature dependence was determined in the range between 15 and 40 °C. The effects of DMSO were examined in the range between 0 and 50%. The effects of detergents were examined using sodium cholate and Triton X-100 at the concentration indicated. The kinetic constants of EGCrP2 were measured using various glucosides (Table 2) at concentrations ranging between 0.08 and 10  $\mu\text{M}$ . The reaction product C6-NBD-Cer was separated from C6-NBD-GlcCer on a normal phase HPLC column (Inertsil SIL 150A-5, GL Science) and quantified according to the method described by Hayashi *et al.* (17).

**Generation of *egcrp1*-knock-out Mutant (1KO)**—1KO was generated from *C. neoformans* var. *grubii* H99 by a method described previously (12).

**Generation of *egcrp2*-knock-out Mutant (2KO) and *egcrp1/egcrp2* Double Knock-out Mutant (DKO)**—The *C. neoformans* EGCrP2 gene (*egcrp2*) (locus number CNAG\_05607 in the *C. neoformans* var. *grubii* H99 database) was disrupted with the NAT split marker according to the method described previously (12, 18). A gene-specific disruption cassette contained ~350 bp of the 5'- and 3'-flanking regions of *egcrp2*, an 860-bp fragment of the promoter sequence with the ATG start codon of the *C. neoformans* actin gene (19), a 310-bp fragment of the terminator sequence with the stop codon of *C. neoformans* TRP1 (20), and the selectable marker NAT gene (21) (Fig. 7). DNA fragments were amplified in the first round of PCR using the primers CN05607N-U and CN05607N-AP-D for the 5'-flanking region, CN05607C-U and CN05607C-D for the 3'-flanking region, ActinP-U and Act-Nat-Down for the actin promoter, and Ttrp-U and Ttrp-CN05607C-D for the TRP1 terminator with genome DNA as a template. Nat-Up and Nat-Ttrp-Down primers were used to amplify the NAT gene with pYL16 (WERNER BioAgents) as a template. The sequences of primers used in this study are summarized in Table 1. *C. neoformans* genome DNA was prepared using ISOPLANT II (NIPPON GENE). PCR products were separated on a 1% agarose gel and then extracted from the gel and used as a template in overlap PCR to combine DNA fragments. All PCR amplifications were performed using PrimeSTAR GXL DNA polym-

erase (Takara Bio Inc.). The combined overlap PCR product was then inserted into T-vector pGEM-T (Easy) to construct pGEM/EGCrP2-5' and pGEM/EGCrP2-3' after adding adenine overhang using 10 $\times$  A-attachment Mix (TOYOBO) and 2 $\times$  Ligation Mix (NIPPON GENE). A NAT split marker containing the 200-bp overlapping sequence was amplified by PCR using the primer sets of CN05607N-U and NSL-2 for the 5'-region of NAT and NSR-2 and CN05607C-D for the 3'-region of NAT with pGEM/EGCrP2-5' and pGEM/EGCrP2-3' as a template, respectively (18). The two PCR fragments were purified and then precipitated onto 500  $\mu\text{g}$  of gold microcarrier beads (0.6  $\mu\text{m}$ ; Bio-Rad), and introduced into *C. neoformans* H99 by biolistic transformation, as described previously (22), using a model PDS-1000/He Biolistic particle delivery system (Bio-Rad). Stable transformants were selected on a YPD-agarose plate containing 100  $\mu\text{g}/\text{ml}$  nourseothricin (WERNER BioAgents).

DKO was generated from 1KO using hygromycin-resistant split marker, according to the methods described previously (18). The gene-specific disruption cassette used was the same as that for the generation of 2KO except for the selectable maker. Hygromycin-resistant split marker was used instead of NAT split marker for the generation of DKO. The primers used are summarized in Table 1.

**Southern Blot Analysis**—It was conducted using 2  $\mu\text{g}$  of genomic DNA digested with BamHI-HindIII for *egcrp2* and HindIII for *egcrp1*. The gene-specific probes were amplified with primer sets of E2-5SENSE and E2-5ANTISENSE for *egcrp2* and 3Probe-S and 3Probe-A for *egcrp1* with genomic DNA as a template. The primers used are summarized in Table 1.

**Growth Curve**—The growth of *C. neoformans* was examined using a YPD liquid medium at 30 °C with shaking (150 rpm). *C. neoformans* ( $A_{600\text{ nm}}$ , 0.02) precultured for 2 days was transferred into fresh YPD medium, and growth was evaluated by measuring  $A_{600\text{ nm}}$  after the appropriate periods indicated.

**Extraction of Glycolipids**—Total lipids were extracted from *C. neoformans* by chloroform/methanol (1:2, v/v). Total lipids, dissolved in chloroform, were loaded onto a Sep-Pak plus silica cartridge (Waters) equilibrated with chloroform. The glycolipid fraction, which contained GlcCer and ergosterylglucoside, was eluted by acetone. The elution of the glycolipid fraction was monitored by TLC using chloroform/methanol/water (65:16:2, v/v/v) as a developing solution and stained with orcinol-sulfate reagent.

**Purification of the Glycolipid That Accumulated in *Egcrp2*-disrupted Mutants**—The glycolipid that accumulated in the *egcrp2*-disrupted mutants was extracted using the conventional Bligh and Dyer method (23). The lower phase was collected and dried using a SpeedVac concentrator. The dried lipid was dissolved in chloroform and loaded onto a Sep-Pak plus silica column cartridge equilibrated with chloroform. The glycolipid was eluted from the cartridge by a stepwise elution with chloroform/methanol (98:2, v/v), chloroform/methanol (95:5, v/v), and chloroform/methanol (2:1, v/v). The glycolipid was mainly recovered in the chloroform/methanol (95:5, v/v) fraction. The glycolipid was purified using an HPLC (EZChrom Elite, Hita-

Novel Steryl- $\beta$ -glucosidase in *C. neoformans*

TABLE 1

## Oligonucleotide primers used in this study

Restriction enzyme sites are underlined.

Oligonucleotide	Sequence (5'–3')	Aim
EGCrP-05607S-NotI	ATGGCGGCGGCATGCCTCCTCCACCAGAAGTCTCTCTGTCA	Expression
EGCrP-05607AS-XhoI	ATGCTCGCGAGCAATAACGCATTTCAGGACATC	
13CN005607seq-U	GACGGCAAGAACATTCAAGACT	Sequencing
14CN005607seq-D	CGTGAGGGTAGCTGAGGAGTT	
CN05607N-U	ATGCCTCCTCCACCAGAAGTCT	Gene disruption
CN05607N-AP-D	AATAGCGAGTCCATCGTCGAGATTCAAAGGT	
ActinP-U	ACTCGCTATTGTCCAGGCTGC	
Act-Nat-Down	CTTCTTCTCCATAGACATGTTGGGCGAG	
Actin-HygroR-D	CTCGACAGACGTCGCGGTGAGCATAGACATGTTGGGCGAGT	
Nat-Up	ATGGAAGAAGAAGTCACTCTTGACGACACGGCTTACC	
Hygro-U	CTCACCGCAGCTCTGTGCGAG	
NSL-2	AAGGTGTTCCCGACGACGAATCG	
NSR-2	AACTCCGTCGCGAGCCCATCAAC	
HSL	GGATGCCTCCGCTCGAAGTA	
HSR	CGTTGCAAGACCTGCCTGAA	
Nat-Trp-Down	TAACCCCTTACCGCCTTGGGGCAGGGCATGTCTCA	
Hygro-TrpT-D	GTATATATACACCCTTAAGGAAAACATTTCCTTTGCCCTCGGACG	
TTrp-Up	AAGGGCGTAAGGGGTTAATTTTCCTTAGAGGGTG	
Trp-U(hyg)	TTTTCCTTAGAGGGTGTATATATAC	
TrpT-CN05607C-D	GGATCGATACAGATGAGGGGTGCGACAGAAGAGA	
CN05607C-U	ACCCCTCATCTGTATCGATCC	
CN05607C-D	CTAAGCAATAACGCATTTCAGG	
E2-5SENSE	CGGTGACTTAATTAGAACGCTG	Southern blot
E2-5ANTISENSE	CCATCGTCGAGATTCAAAGGT	
3Probe-S	TCCGAAAAGAGTCCACAGAG	
3Probe-A	TTGTTCTGCGCTGGTTG	

chi, Japan) equipped with a Cosmosil 5SL-II column (4.6  $\times$  150 mm; particle size, 5  $\mu$ m), which was equilibrated and eluted with methanol at a flow rate of 1 ml/min and column temperature of 40  $^{\circ}$ C. The elution of glycolipid was monitored at 278 nm.

**MS Spectrometry**—An AXIMA-CFR instrument (Shimadzu) was used for the MALDI-TOF-MS analysis. Mass spectra were acquired in the positive mode, and 2,5-dihydroxybenzoic acid was used as the matrix.

**NMR Spectroscopy**—Spectra were recorded on a Varian INOVA600 spectrometer. The operating conditions were as follows:  $^1$ H: frequency, 600 MHz; sweep width, 8 kHz; sampling point, 44 K; accumulation, 128 pulses; temperature 30  $^{\circ}$ C.  $^{13}$ C: frequency, 150 MHz; sweep width, 32 kHz, sampling point 160 K; accumulation, 12,000 pulses; temperature 300 K. Chemical shifts were referenced to tetramethylsilane ( $\delta_{\text{H}}$ ,  $\delta_{\text{C}}$  0) in  $\text{CD}_3\text{OD}$  and  $\text{CDCl}_3$  (1:1, v/v). Conventional pulse sequences were used in the MQ-COSY, TOCSY, NOESY, HSQC, and HMBC experiments.

**Flow Cytometric Analysis**—Cells harvested from 3-day cultures were fixed with cold 70% EtOH for 3 h, washed with PBS, and then incubated for 5 min in Hoechst 33342 solution (50  $\mu$ g/ml in distilled water) at room temperature. The samples were placed on ice before the analysis and were then analyzed using an EC800 flow cytometer (Sony). Cell volumes were estimated by the flow cytometer according to the manufacturer's instructions. To eliminate the signals for aggregated cells, Hoechst 33342-based gating was performed in the analysis.

**Vacuole Analysis**—The vacuole-enriched fraction was isolated from *C. neoformans* cells by density gradient centrifugation in accordance with Cabrera and Ungermann (24). Typically, a 300-ml culture was subjected to centrifugation at 4,400  $\times$  g for 5 min at room temperature and washed twice with PBS. The pellet was resuspended with spheroplasting buffer containing with 14 ml of Mcllvain buffer, 6 ml of 1 M sodium

tartrate, and 250 mg of Westase (Takara Bio.) and incubated at 30  $^{\circ}$ C for 2 h with shaking at 60 rpm. After centrifuging at 5,300  $\times$  g, for 5 min at 4  $^{\circ}$ C, the supernatants were discarded. The pellet was dissolved in 2.5 ml of 15% Ficoll in PS buffer (15% (w/v) Ficoll 400, 20 mM PIPES/KOH, pH 6.8, 200 mM sorbitol), added to 200  $\mu$ l of 0.4 mg/ml DEAE-dextran in PS buffer, and incubated for 5 min on ice and at 30  $^{\circ}$ C for 90 s. Each 3 ml of the supernatant was transferred into centrifuge tubes, and 800  $\mu$ l of 8% Ficoll in PS buffer (8% (w/v) Ficoll 400, 20 mM PIPES/KOH, pH 6.8, 200 mM sorbitol) was carefully layered, followed by 800  $\mu$ l of 4% Ficoll in PS buffer (4% (w/v) Ficoll 400, 20 mM PIPES/KOH, pH 6.8, 200 mM sorbitol). Finally, 300  $\mu$ l of PS buffer without Ficoll (20 mM PIPES/KOH, pH 6.8, 200 mM sorbitol) was layered on the top. The tubes were centrifuged using a RPS65T Swing rotor (Hitachi) at 110,000  $\times$  g for 90 min at 4  $^{\circ}$ C. The vacuole and lipid droplet fractions were collected from the top to 0–4% interface using a 1-ml tip. Vacuoles and lipid droplets were separated according to the method described by Zinser *et al.* (25). Lipids were extracted from the lysate and vacuole vesicles (50  $\mu$ g of protein) by chloroform/methanol (1:2, v/v) and dried under a stream of  $\text{N}_2$ . The lipid was analyzed by TLC using chloroform/methanol/water (65:16:2, v/v/v) as a developing solvent. Vacuoles in cells were visualized with the incorporation of 5-(and 6)-carboxy-2',7'-dichlorofluorescein diacetate (carboxy-DCFDA; Molecular Probes) under microscopy (26).

## RESULTS

**Molecular Cloning and Characterization of EGCrP2**—EGCase, an enzyme capable of cleaving the  $\beta$ -glycosidic linkage between the oligosaccharide and Cer of various GSLs, is distributed in bacteria, actinomycetes, and some invertebrates, such as jellyfish and hydra (Fig. 1). We previously reported that the EGCase homologue, EGCrP1, was a glucocerebrosidase of *C. neoformans*, involved in the quality control of GlcCer, possibly asso-

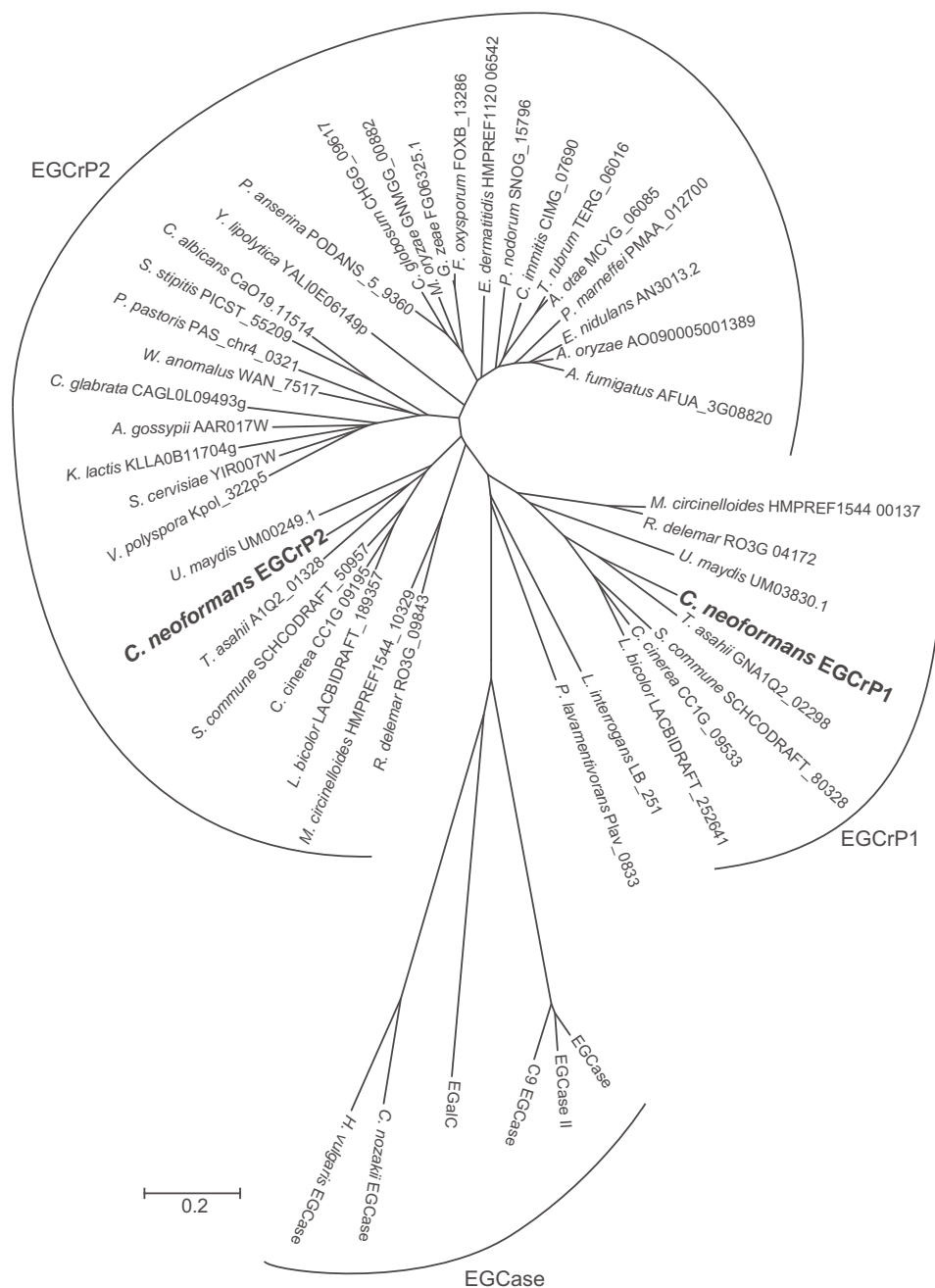


FIGURE 1. **Phylogenetic tree of EGCrP1, EGCrP2, and EGCase.** The amino acid sequences of EGCrPs and EGCases were reconstructed using the neighbor-joining method. The scale bar represents 0.2 amino acid substitutions/site.

ciated with the GlcCer synthesis pathway (12). In the present study, we identified another homologue of EGCase in *C. neoformans* and designated it as EGCrP2. It showed 28% identity to EGCrP1 and rhodococcal EGCase II. The alignment of the deduced amino acid sequence of EGCrP2 with those of EGCrP1 and EGCase II revealed that 8 residues, essential for the catalytic activity of glycoside hydrolase family 5 glycosidases (27), were completely conserved in these enzymes (Fig. 2, *open circles*). Of the 8 residues of EGCrP2, two catalytic glutamates, Glu-270 and Glu-520, at the end of  $\beta$ -strands 5 and 8, respectively, were thought to be an acid/base catalyst and nucleophile, respectively (Fig. 1, *closed circles*). EGCrP2-like homologues were widely distributed across the phyla/genera of fungi and

formed a gene family, which was independent of the EGCrP1 and EGCase families (Fig. 1).

To characterize EGCrP2, the *egcrp2* open reading frame encoding 851 amino acid residues was cloned from the complementary DNA of *C. neoformans* and expressed in *E. coli* BL21 (DE3) as a His tag-fused protein. Recombinant EGCrP2 (rEGCrP2) was purified by affinity chromatography using a nickel-conjugated Sepharose column and gel filtration using a Superdex 200 10/300 GL column. The purified enzyme showed a single protein band possessing a molecular mass of  $\sim$ 120 kDa on SDS-PAGE after staining with Coomassie Brilliant Blue (CBB Stain One) (Fig. 3A). Purified rEGCrP2 hydrolyzed C6-NBD-GlcCer to generate C6-NBD-Cer; however, it did not

### Novel Steryl- $\beta$ -glucosidase in *C. neoformans*

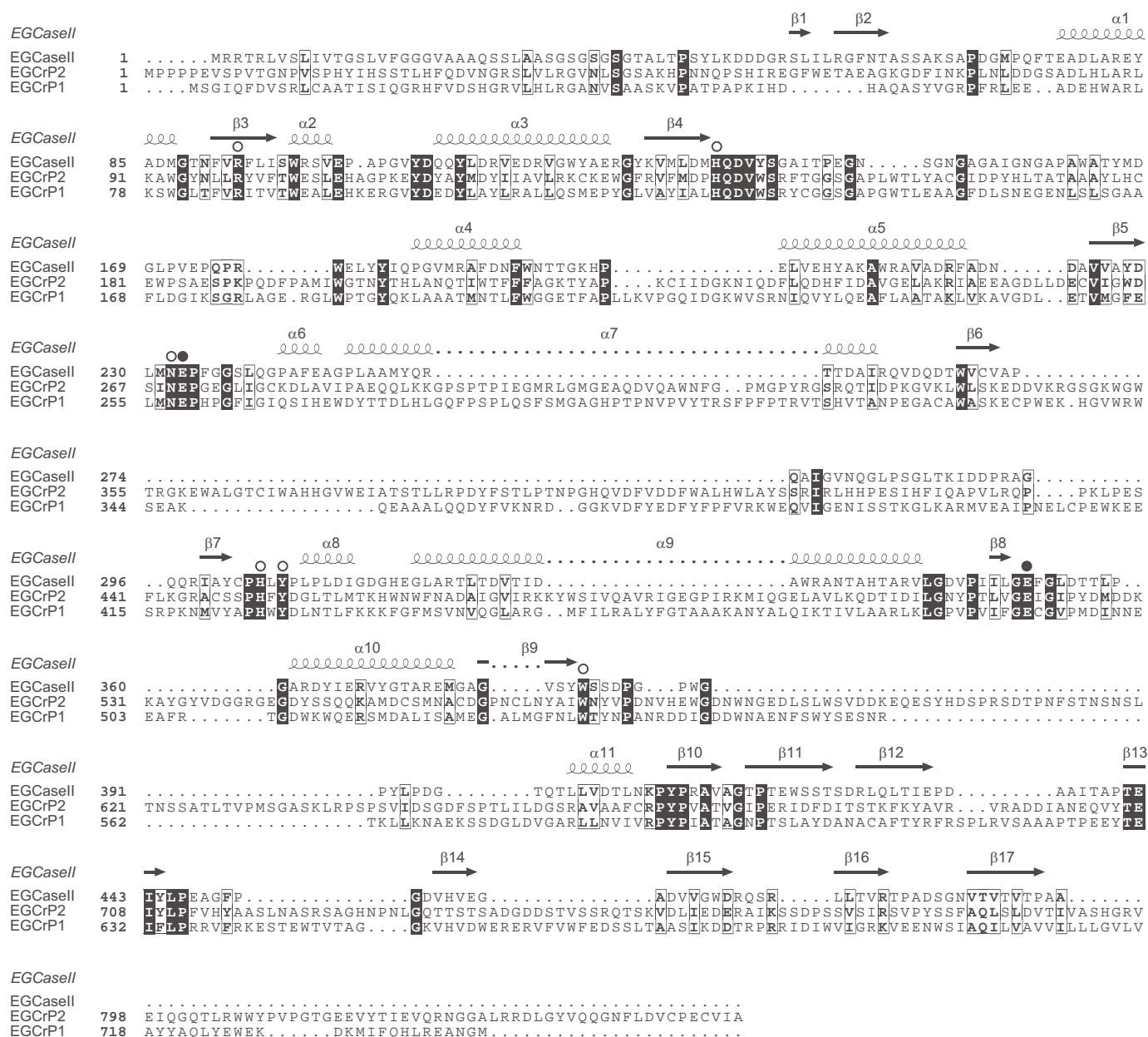
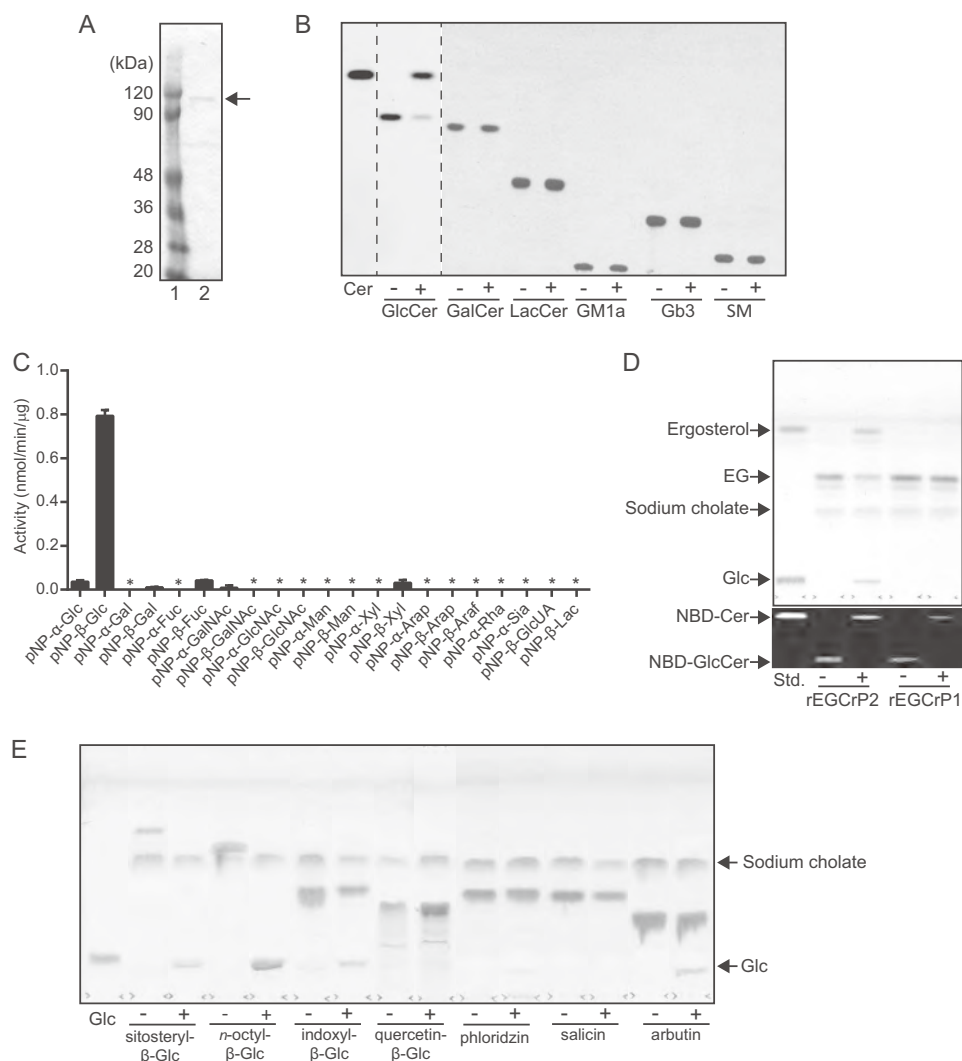


FIGURE 2. Alignments of EGCrP1 and EGCrP2 with EGCase II. The amino acid sequences of *Rhodococcus* EGCase (accession number AAB67050.1), *C. neoformans* EGCrP1 (accession number BAL46040.1), and *C. neoformans* EGCrP2 were aligned using ClustalW (42) and ESPript (43). White letters on a black background and black letters in an open box show identical and similar residues, respectively. Open circles indicate amino acid residues conserved in glycoside hydrolase family 5 glycosidase. Two glutamates, the Glu-258 and Glu-492 of EGCrP1 (12) and Glu-270 and Glu-520 of EGCrP2, are indicated by closed circles as possible acid/base catalyst and nucleophile, respectively. The secondary structural elements are shown above the amino acid sequence of EGCase II (44).

hydrolyze any of the other NBD-GSLs tested (Fig. 3B). rEGCrP2 was also found to hydrolyze native GlcCer, which was not labeled with NBD; however, it did not degrade any other native GSLs (data not shown). The specificity of rEGCrP2 toward GSLs appeared to be identical to that of EGCrP1 but was completely different from that of EGCase, which preferred oligosaccharide-linked GSLs such as LacCer and GM1a (10). Both EGCrP1 and EGCrP2 were  $\beta$ -glucosidases; however, the specificity of EGCrP2 was very broad for aglycone moieties (*i.e.* EGCrP2-hydrolyzed *p*NP- $\beta$ -glucoside (Fig. 3C) and 4MU- $\beta$ -glucoside (Table 2)), whereas these  $\beta$ -glucosides were completely resistant to hydrolysis by EGCrP1. Neither EGCrP1 nor

EGCrP2 hydrolyzed other *p*NP-glycosides, including *p*NP- $\beta$ -galactoside and *p*NP- $\alpha$ -glucoside (Fig. 3C). Differences in the aglycone specificities of the two EGCrPs were also shown with various  $\beta$ -glycosides (*i.e.* EGCrP2 hydrolyzed EG to generate ergosterol and glucose, but this glycolipid was not degraded by EGCrP1) (Fig. 3D). Furthermore, various  $\beta$ -glucosides, such as sitosteryl- $\beta$ -glucoside, *n*-octyl- $\beta$ -glucoside, indoxyl- $\beta$ -glucoside, and arbutin, were hydrolyzed by EGCrP2 under the conditions used (Fig. 3E). Salicin and phloridzin were hydrolyzed by EGCrP2 when the amount of the enzyme was increased 10-fold; however, quercetin- $\beta$ -glucoside was still resistant to hydrolysis by EGCrP2 under the same condition (data not



**FIGURE 3. Purification and characterization of the recombinant EGCrP2.** *A*, final preparation of rEGCrP2 on 10% SDS-PAGE. The protein eluted from the nickel-Sepharose column was purified using Superdex 200 10/300 GL. *Lane 1*, protein marker; *lane 2*, final preparation. *B*, TLC showing the specificity of EGCrP2 toward various NBD-GSLs. Each NBD-GSL (100 pmol) was incubated in 20  $\mu$ l of 50 mM MES buffer, pH 6.0, with 100 ng of rEGCrP2 (+) or heat-inactivated EGCrP2 (-) at 30  $^{\circ}$ C for 16 h, except for C6-NBD-GlcCer, which was incubated at 30  $^{\circ}$ C for 1 h. Samples were loaded onto a TLC plate, which was developed with chloroform/methanol/water (65:25:4, v/v/v). *C*, hydrolysis of *p*NP substrates by rEGCrP2. *Error bars*, S.D. of three experiments. An *asterisk* indicates no hydrolysis of *p*NP substrates. *D*, *top* TLC shows hydrolysis of EG by rEGCrP2. Fungal EG, purified from 2-mg dry cells of 2KO, was incubated at 30  $^{\circ}$ C for 18 h with 40  $\mu$ g of EGCrP1 or 20 ng of EGCrP2. TLC was developed with chloroform/methanol/water (65:16:2, v/v/v) and stained with orcinol sulfate reagent. The *bottom* TLC shows C6-NBD-Cer released from C6-NBD-GlcCer by rEGCrP1 and -2. 50 pmol of C6-NBD-GlcCer was incubated at 30  $^{\circ}$ C with 40  $\mu$ g of rEGCrP1 and 20 ng of rEGCrP2 for 18 h. +, with EGCrP2; -, without EGCrP2. *E*, TLC showing the hydrolysis of various  $\beta$ -glucosides by rEGCrP2. Each 100 nmol of substrate was incubated at 30  $^{\circ}$ C with 100  $\mu$ g of enzyme for 18 h. Samples were loaded onto a TLC plate, which was developed with chloroform/methanol/water (65:25:4, v/v/v) and visualized by orcinol sulfate reagent. *Glc*, glucose released from various  $\beta$ -glucosides by rEGCrP2. +, with EGCrP2; -, without EGCrP2.

**TABLE 2**  
Kinetic parameters of recombinant EGCrP2 and EGCrP1

Values are the mean  $\pm$  S.D. of three experiments. The values for EGCrP1 are from Ref. 12.

Substrate	Enzyme	$K_m$ $\mu$ M	$K_{cat}$ $s^{-1}$	$K_{cat}/K_m$ $M^{-1} s^{-1}$
C6-NBD-GlcCer	EGCrP2	38.4 $\pm$ 2.6	0.53 $\pm$ 0.03	(13.8 $\pm$ 0.05) $\times 10^3$
4MU- $\beta$ -Glc	EGCrP2	340 $\pm$ 13.4	8.8 $\pm$ 0.18	(25.7 $\pm$ 1.4) $\times 10^3$
Resorufin- $\beta$ -Glc	EGCrP2	43.6 $\pm$ 2.4	21.9 $\pm$ 0.36	(504 $\pm$ 24.2) $\times 10^3$
<i>p</i> NP- $\beta$ -Glc	EGCrP2	817 $\pm$ 37.4	13.8 $\pm$ 0.15	(16.9 $\pm$ 0.16) $\times 10^3$
C6-NBD-GlcCer	EGCrP1	5.80 $\pm$ 0.3	(38.3 $\pm$ 0.20) $\times 10^{-3}$	(6.6 $\pm$ 0.40) $\times 10^3$

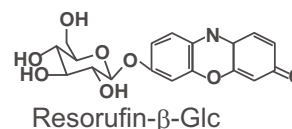
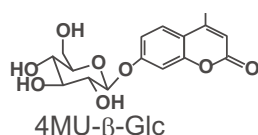
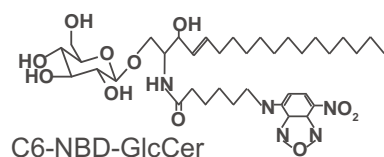
shown). The kinetic parameters of EGCrP2 for various  $\beta$ -glucosides and their structures are summarized in Table 2 and Fig. 4, respectively.

The maximal activity of EGCrP2 was observed at pH 5.0–5.5 when C6-NBD-GlcCer was used as a substrate, indicating that

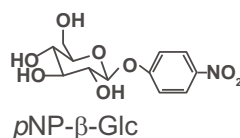
EGCrP2 was an acid  $\beta$ -glucosidase (Fig. 5A). In contrast, the pH optimum of EGCrP1 was previously shown to be  $\sim$ 7.5 (12). The optimal temperature of EGCrP2 was found between 32 and 37  $^{\circ}$ C (Fig. 5B), which was a suitable temperature for the growth of *C. neoformans*. The activity of EGCrP2 was enhanced by the

Novel Steryl- $\beta$ -glucosidase in *C. neoformans*

## Fluorescent substrates



## Color substrate



## Non-fluorescent substrates

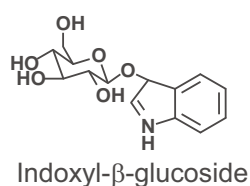
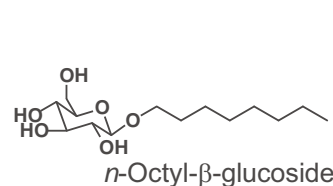
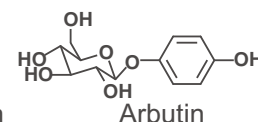
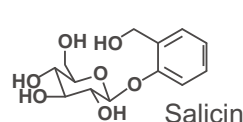
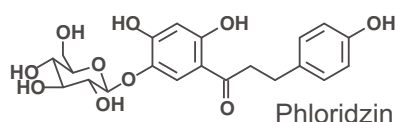
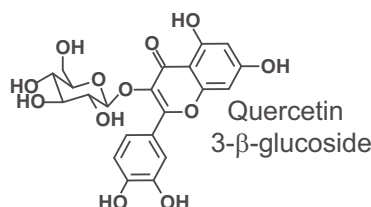
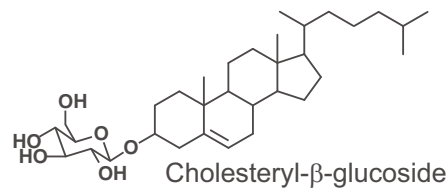
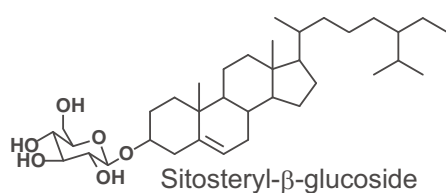


FIGURE 4. Structures of  $\beta$ -glucosides used to analyze the specificity of rEGCrP2. The specificity of EGCrP2 was examined using various  $\beta$ -glucosides, as indicated.

addition of sodium cholate at a concentration of 0.025% when C6-NBD-Cer was used as a substrate; however, higher concentrations of the detergent inhibited activity. Triton X-100 strongly inhibited the activity of EGCrP2 (Fig. 5C) and EGCrP1 (12). Although the addition of DMSO did not affect activity up to 30% of the reaction mixture, it inhibited activity at higher concentrations (Fig. 5D).

*Generation of 2KO and egcrp1/egcrp2 DKO*—To determine whether EGCrP2 was involved in the catabolism of  $\beta$ -glucosides *in vivo*, 2KO and DKO were generated from *C. neoformans* var. *grubii* serotype A strain H99 (WT) and 1KO (12) by gene-targeting homologous recombination using NAT and hygromycin (*hyg*)-resistant gene as a marker, respectively (Fig. 6A). Southern blot analysis using the BamHI-HindIII-digested genome DNA revealed that the *egcrp2* gene was disrupted by this method in 2KO and DKO, as expected (Fig. 6B, left), whereas the *egcrp1* gene was present in WT and 2KO but not in 1KO or DKO (Fig. 6B, right). The  $\beta$ -glucocerebrosidase activity decreased in the cell lysate of 1KO at pH 7.3 but not at pH 5.0

when the activity was measured using C6-NBD-GlcCer, as shown previously (12). On the other hand, the activity markedly decreased in the cell lysates of 2KO and DKO when it was measured using C6-NBD-GlcCer at pH 5.0, indicating that EGCrP2 possesses an acid  $\beta$ -glucocerebrosidase activity (Fig. 6C, left). However, the apparent decrease of  $\beta$ -glucosidase activity of 2KO and DKO was much lower when the activity was measured using 4MU- $\beta$ -Glc as a substrate at pH 5.0 (Fig. 6C, right), suggesting the presence of  $\beta$ -glucosidase(s) that may act on 4MU- $\beta$ -Glc but not C6-NBD-GlcCer under acidic conditions.

*Identification of the Lipid That Accumulated in 2KO*—TLC analysis of cell extracts showed that the accumulation of GlcCer was not significant in 2KO under the conditions used; alternatively, an unknown lipid, whose  $R_f$  corresponded to that of sitosteryl- $\beta$ -glucoside (SG), highly accumulated in both 2KO and DKO mutants (Fig. 7A, lanes 4 and 5). To clarify its structure, the accumulated lipid was extracted from 2KO, purified as described under "Experimental Procedures" (Fig. 7B, lane 7) and then analyzed by MALDI-TOF-MS in positive mode using

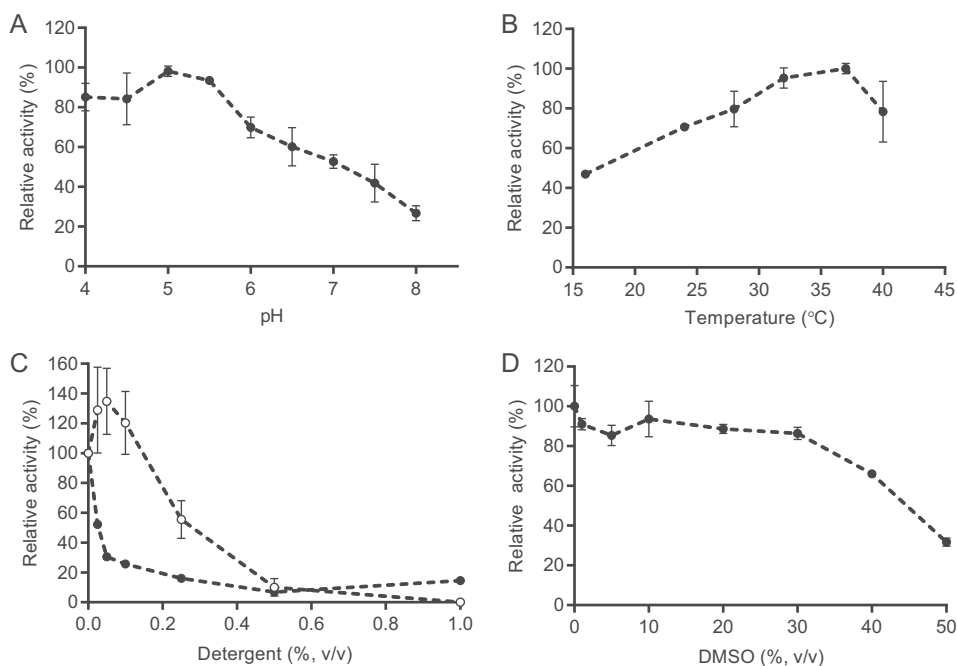


FIGURE 5. **General properties of rEGCrP2.** *A*, pH dependence of *C. neoformans* rEGCrP2. 150 mM of GTA buffer was used for the assay. *B*, effects of temperature on EGCrP2 activity. *C*, effects of detergents on EGCrP2 activity. Closed circles, Triton X-100; open circles, sodium cholate. *D*, effects of DMSO on EGCrP2 activity. Data represent the mean  $\pm$  S.D. (error bars) of three experiments. The assay was conducted using C6-NBD-ClcCer as the substrate.

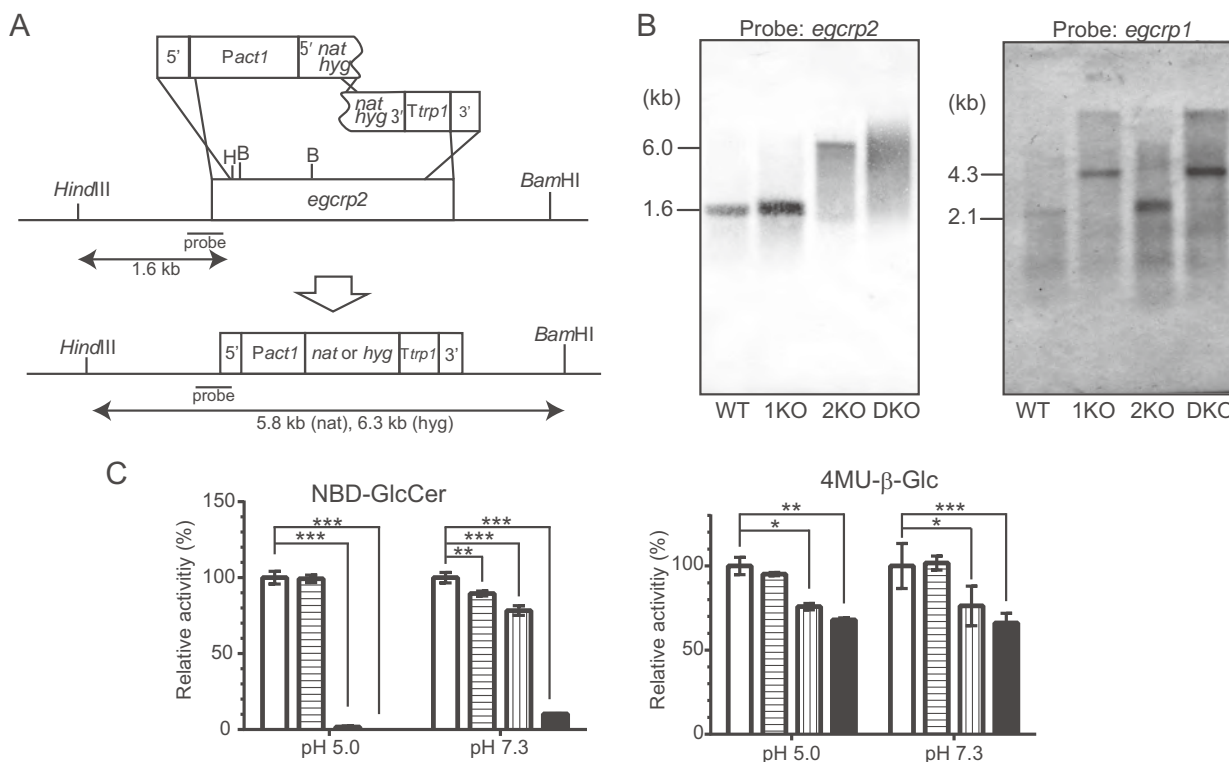
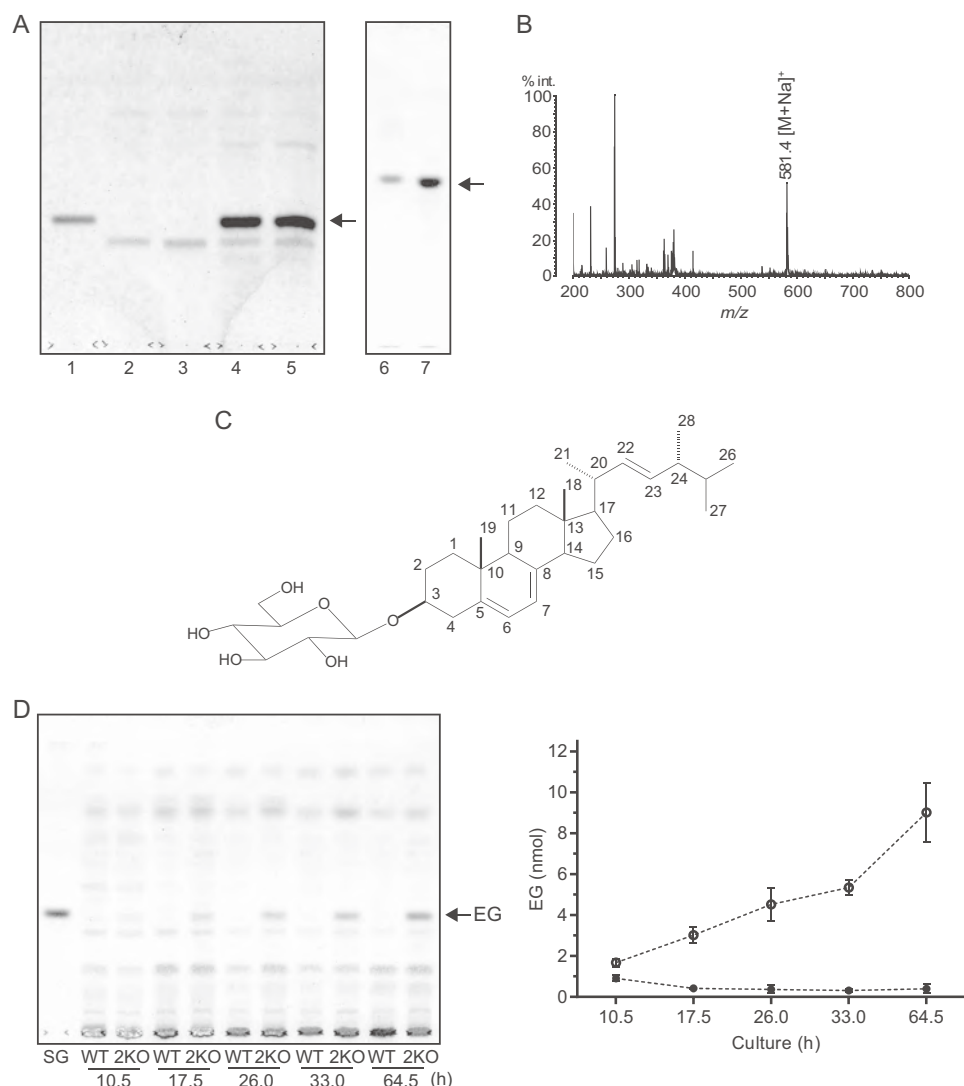


FIGURE 6. **Disruption of the *egcrp2* gene in *C. neoformans*.** *A*, strategy for the disruption of *C. neoformans* *egcrp2* using the split marker method. *B*, Southern blot analysis of BamHI-HindIII-digested genomic DNA for *egcrp2* (left) and HindIII-digested genomic DNA for *egcrp1* (right). The disruption of *egcrp1* and Southern blot analysis of HindIII-digested genomic DNA were performed by the method described previously (12). *C*, the activity of  $\beta$ -glucosidase was measured using NBD-GlcCer (left) and 4MU- $\beta$ -Glc (right). Activities were measured at 37 °C for 18 h using NBD-GlcCer and 2  $\mu$ g of protein for pH 5.0 or 10  $\mu$ g of protein for pH 7.3. When 4MU- $\beta$ -Glc was the substrate, 1  $\mu$ g of protein was incubated at 37 °C for 18 h for both pH values. The activity was expressed as a percentage of that of WT. \*, \*\*, and \*\*\*,  $p < 0.01$ ,  $p < 0.001$ , and  $p < 0.0001$ , respectively. Error bars, S.D.

2,5-dihydroxybenzoic acid as a matrix. The main molecular ion peak,  $[M + Na]^+$ , was observed at  $m/z$  581.4 for the lipid (Fig. 7B), which corresponded to the molecular mass of EG

( $C_{32}H_{54}O_6$ , 558.39). The NMR spectra of the lipid accumulated in 2KO are summarized in Table 3. The  $^1H$  NMR spectrum of the purified lipid showed the characteristic signals of a glyco-

Novel Steryl- $\beta$ -glucosidase in *C. neoformans*

**FIGURE 7. Identification of the lipid that accumulated in *egcrp2*-disrupted mutant (2KO) of *C. neoformans*.** *A*, TLC showing the glycolipid that accumulated in the mutants. Glycolipids were extracted by chloroform/methanol (1:2, v/v) from the cells after cultivation at 25 °C for 3 days and purified using a Sep-Pak plus silica column. Lipids corresponding to 4 mg of dry cells were loaded onto a TLC plate, which was developed with chloroform/methanol/water (65:16:2, v/v/v) for lanes 1–5 (left) and chloroform/methanol/water (65:25:4, v/v/v) for lanes 6 and 7 (right). Glycolipids were visualized by orcinol sulfate reagent. Lane 1, sitosteryl- $\beta$ -glucoside standard (5 nmol); lane 2, WT; lane 3, 1KO; lane 4, 2KO; lane 5, DKO; lane 6, sitosteryl- $\beta$ -glucoside standard; lane 7, purified glycolipid from 2KO. *B*, MALDI-TOF-MS of the glycolipid that accumulated in 2KO. *C*, the proposed structure of the glycolipid that accumulated in 2KO. *D*, TLC showing the accumulation of EG in 2KO during the course of cultivation. Total lipids were extracted by chloroform/methanol (1:2, v/v) from cells cultivated at 25 °C for the period indicated. SG, sitosteryl- $\beta$ -glucoside standard (10 nmol). EG contents on the TLC were calculated by a TLC chromatoscanner (right column). Open circle, 2KO; closed circle, WT. Data represent the mean  $\pm$  S.D. (error bars) of three experiments.

side structure composed by a sterol part and hexopyranose. The  $^1\text{H}$  NMR spectrum for the sterol moiety displayed signals for four secondary methyls as a doublet, two tertiary methyls as a singlet, four olefinic protons, and one oxygen-bearing methine proton. In the  $^{13}\text{C}$  NMR spectrum, 28 carbon signals (6 methyls, 7 methylenes, 6 methines, 4 quaternary carbons, 6 sp $^2$  carbons, and 1 oxygen-bearing methine) suggested that the sterol moiety could be an ergosterol (Table 3). Furthermore, the deshielded signal at  $\delta_{\text{C}}$  78.2 (C-3) in comparison with the ergosterol suggested a glycosidic linkage at C-3. The structure of the sugar moiety was assignable to  $\beta$ -glucopyranoside because of its chemical shift values and the correlation from the H-1 ( $\delta_{\text{H}}$  4.43 (d,  $J = 7.8$  Hz)) to H $_2$ -6 ( $\delta_{\text{H}}$  3.73 and 3.87) in the MQ-COSY and TOCSY spectra, and the glycosidic linkage at the C-3 of the ergosterol was also confirmed by the HMBC correlation

between the H-1 of Glc ( $\delta_{\text{H}}$  4.43) and C-3 of the ergosterol ( $\delta_{\text{C}}$  78.2). Collectively, the structure of the accumulated lipid was determined to be EG, a major sterylglucoside in fungi, as shown in Fig. 7C. EG accumulated in the 2KO in a time-dependent manner; however, the content of this glycolipid was very low and not increased in wild type during the course of cultivation (Fig. 7D). These results indicated that EGCrP2 is involved in the degradation of EG in *C. neoformans*, and disruption of *egcrp2* resulted in the accumulation of EG.

**Phenotype Analysis of 2KO and DKO**—To assess the physiological effects of the disruption of the *egcrp2* gene, we compared the cell growth of 2KO and DKO with that of WT and 1KO. The disruption of *egcrp2*, but not *egcrp1*, resulted in the arrest of cell growth from the middle log phase to the early stationary phase (Fig. 8A). Observations with differential interference-contrast

**TABLE 3**  
 **$^{13}\text{C}$  and  $^1\text{H}$  NMR spectral data of EG and ergosterol**

NMR chemical shifts of standard ergosterol were assigned by MQ-COSY, TOCSY, HSQC, and HMBC experimental data, which measured at the same condition of EG.

Carbon	$^{13}\text{C}$ NMR data			$^1\text{H}$ NMR data		
	EG	Ergosterol	Multiplicity	Proton	EG	Ergosterol
1	39.0	39.0	CH <sub>2</sub>	1 $\alpha$	1.32	1.30
				1 $\beta$	1.93	1.90
2	30.5	32.0	CH <sub>2</sub>	2 $\alpha$	2.00	1.86
				2 $\beta$	1.67	1.50
3	78.2	70.4	CH	3	3.72 (m)	3.54 (m)
4	37.8	40.9	CH <sub>2</sub>	4 $\alpha$	2.60 (brd, 14.7)	2.44
				4 $\beta$	2.33 (brt, 13.0)	2.27
5	140.1	140.6	C=			
6	120.5	120.1	CH=	6	5.57 (brs)	5.55
7	116.9	116.9	CH=	7	5.38 (brs)	5.38
8	141.8	141.6	C=			
9	46.9	46.9	CH	9	1.99	1.97
10	37.8	37.6	C			
11	21.6	21.7	CH <sub>2</sub>	11 $\alpha$	1.74	1.74
				11 $\beta$	1.62	1.62
12	39.7	39.7	CH <sub>2</sub>	12 $\alpha$	1.30	1.28
				12 $\beta$	2.09	2.09
13	43.4	43.4	C			
14	55.1	55.1	CH	14	1.92	1.90
15	23.5	23.5	CH <sub>2</sub>	15 $\alpha$	1.69	1.67
				15 $\beta$	1.32	1.38
16	28.8	28.8	CH <sub>2</sub>	16 $\alpha$	1.79	1.78
				16 $\beta$	1.36	1.34
17	56.4	56.4	CH	17	1.30	1.28
18	12.4	12.4	CH <sub>3</sub>	18	0.65 (3H, s)	0.65
19	16.5	16.5	CH <sub>3</sub>	19	0.96 (3H, s)	0.95
20	41.1	41.0	CH	20	2.06	2.06
21	21.4	21.4	CH <sub>3</sub>	21	1.05 (3H, d, 6.7)	1.05
22	136.3	136.2	CH=	22	5.20 (dd, 7.8, 15.3)	5.19
23	132.6	132.6	CH=	23	5.24 (dd, 7.3, 15.3)	5.24
24	43.6	43.5	CH	24	1.87	1.86
25	33.7	33.7	CH	25	1.48	1.48
26	19.9	19.9	CH <sub>3</sub>	26	0.84 (3H, d, 6.9)	0.84
27	20.2	20.2	CH <sub>3</sub>	27	0.85 (3H, d, 6.9)	0.85
28	17.9	18.0	CH <sub>3</sub>	28	0.93 (3H, d, 6.7)	0.93
$\beta$ -Glc						
C-1'	101.9		CH	H-1'	4.43 (d, 7.8)	
C-2'	74.3		CH	H-2'	3.22 (t, 8.4)	
C-3'	77.3		CH	H-3'	3.41 (t, 8.8)	
C-4'	80.0		CH	H-4'	3.38 (t, 9.0)	
C-5'	76.9		CH	H-5'	3.30 (m)	
C-6'	62.3		CH <sub>2</sub>	H-6a'	3.73 (dd, 5.2, 11.9)	
				H-6b'	3.87 (dd, 2.7, 11.9)	

microscopy revealed that 2KO and DKO cells were larger than WT and 1KO cells, possibly due to dysfunction of the budding process (Fig. 8B). In support of this observation, the flow cytometric analysis revealed that the average cell volumes of 2KO (173.82  $\mu\text{m}^3$ ) and DKO (191.49  $\mu\text{m}^3$ ) were 5–6-fold larger than those of WT (31.72  $\mu\text{m}^3$ ) and 1KO (44.27  $\mu\text{m}^3$ ). Small cells (cell volume,  $\sim 10 \mu\text{m}^3$ ) were found in WT and 1KO populations but not in 2KO and DKO populations (Fig. 8C). The vacuoles of 2KO were larger than those of WT and 1KO when carboxy-DCFDA was incorporated into these cells as an indicator to visualize vacuoles (Fig. 8D). The cell densities of 2KO and DKO were compared with those of WT and 1KO using Percoll cell gradient centrifugation. The distribution of cells in the Percoll gradient was markedly different (*i.e.* 2KO and DKO cells were mainly recovered in the 30% Percoll fraction (the specific gravity was estimated to be 1.039; *blue arrows*), whereas WT and 1KO cells were recovered in the 50% (specific gravity, 1.061; *yellow arrows*) and 80% Percoll fractions (specific gravity, 1.094; *red arrows*). Almost no 2KO and DKO cells were detected in the 80% Percoll fraction (Fig. 8E). These results indicated that

the specific gravities of 2KO and DKO cells were markedly lower than those of 1KO and WT cells.

**Vacuole Analysis of WT and 2KO**—The disruption of *egcrp2*, but not *egcrp1*, led to the accumulation of EG (Fig. 7, A and D) and hypertrophy of cell body (Fig. 8, B and C) and vacuoles (Fig. 8D). EGCrP2 degraded EG most efficiently at an acidic pH (Fig. 5A), and, thus, it was hypothesized that EG may be catabolized by EGCrP2 in acidic compartments in the cell, such as the vacuoles. Vacuoles were thus isolated from WT and 2KO cells using Ficoll gradient centrifugation as described under “Experimental Procedures.” The final fractions obtained from both WT and 2KO cells possessed high specific activity for the acid  $\alpha$ -mannosidase, which is a marker enzyme localized in the vacuole, indicating that vacuoles were enriched in these fractions as expected (Fig. 9A). The specific activity of the acid  $\alpha$ -mannosidase in the vacuole-enriched fraction of 2KO was markedly higher than that of WT (Fig. 9A); however, the specific activity of  $\beta$ -glucosidase was significantly lower in the same fraction of 2KO than that of WT when its activity was measured using C6-NBD-GlcCer (Fig. 9B, *left*) and 4MU- $\beta$ -glucoside (Fig. 9B, *right*) as substrates, indicating that EGCrP2 was present in the vacuole-enriched fraction. To determine whether EG accumulated in vacuoles, total lipids in the vacuole-enriched fraction were extracted and analyzed by TLC. As shown in Fig. 9C, EG was detected in the vacuole-enriched fraction of 2KO but not in that of WT. These results strongly suggested that EGCrP2 catabolizes EG in the vacuoles of *C. neoformans*.

## DISCUSSION

Because the activity of the glucocerebrosidase did not decrease under acidic conditions after the disruption of *egcrp1* in *C. neoformans* (12), we searched for glucocerebrosidase(s) capable of working under acidic conditions in this study. EGCrP2, a homologue of EGCrP1, was found to hydrolyze GlcCer *in vitro*, and the disruption of *egcrp2* greatly reduced glucocerebrosidase activity when C6-NBD-GlcCer was used as a substrate under acidic conditions (Fig. 6C, *left*). However, we found that DKO still exhibited glucocerebrosidase activity (Fig. 6C, *left*), suggesting that *C. neoformans* may possess glucocerebrosidase(s) other than EGCrP1 and EGCrP2.

The GlcCer of *C. neoformans* (WT) shows homogeneity in the sphingoid base, which possesses two double bonds at C4/C8 and a methyl substitution at C9 (methyl d18:2) (9, 12). However, the EGCrP1-knock-out mutant (1KO) accumulated GlcCer possessing several sphingoid bases without methyl substitution (d18:2, d18:1, and d18:0) that are intermediates generated from the pathway of GlcCer synthesis in *C. neoformans* (12). This indicates that EGCrP1 is involved in the quality control of GlcCer in *C. neoformans*. On the other hand, the sphingoid base of GlcCer in 2KO was exclusively methyl d18:2, as in WT (Fig. 10), indicating that EGCrP2 is unlikely to participate in the elimination of aberrant GlcCer found in 1KO. This discrepancy in the physiological role of EGCrPs may stem from the different localization of each EGCrP. The different pH optimum for each enzyme may support this hypothesis; however, the precise localization of EGCrPs in *C. neoformans* remains to be elucidated.

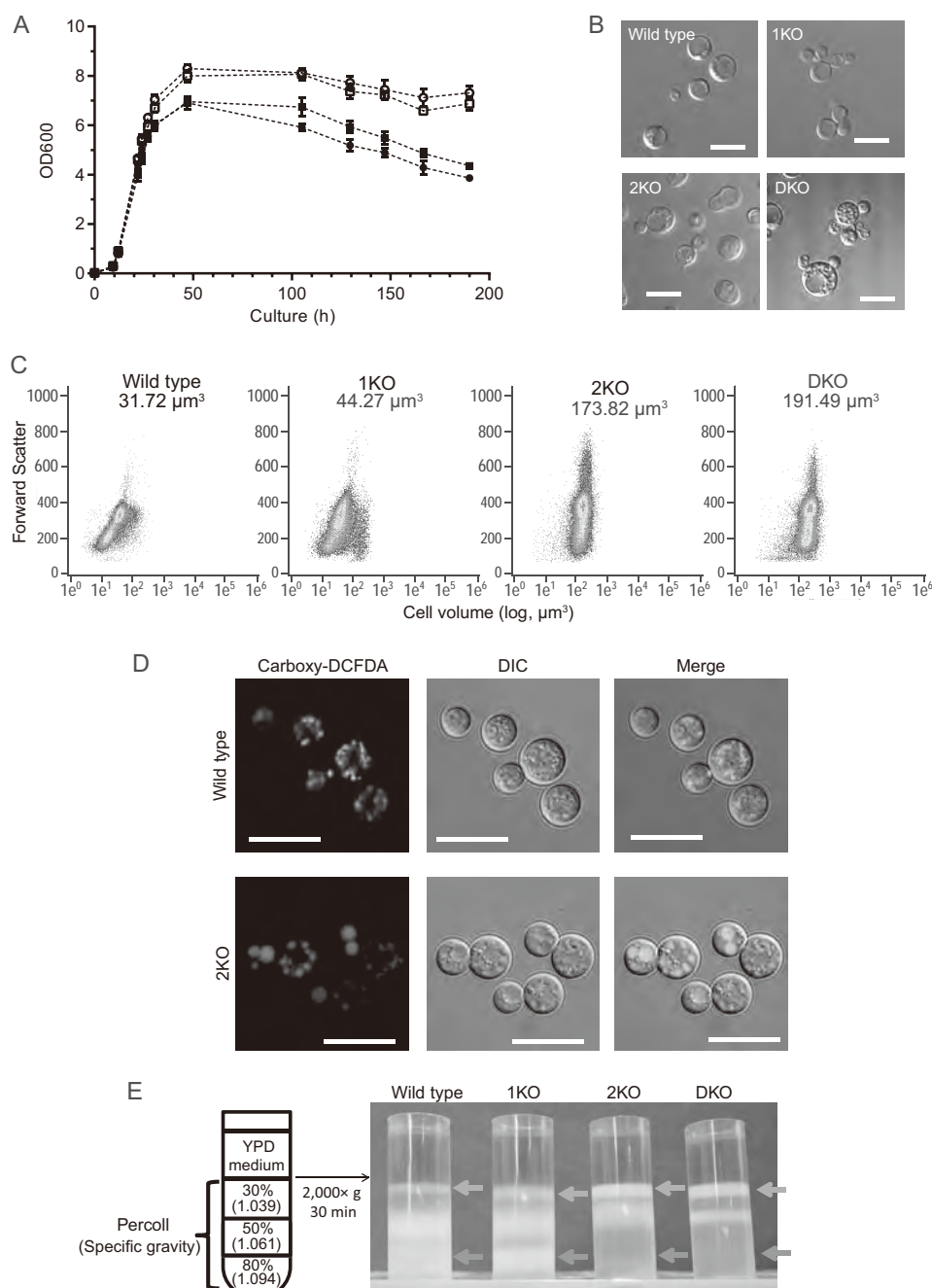
Novel Steryl- $\beta$ -glucosidase in *C. neoformans*

FIGURE 8. Analysis of the phenotype of *egcrp2*-disrupted mutants (2KO) of *C. neoformans*. *A*, growth curves of WT (open circles), 1KO (open squares), 2KO (closed circles), and DKO (closed squares). Data represent the mean  $\pm$  S.D. (error bars) of three experiments. *B*, cells observed under a differential interference-contrast microscope. 2KO and DKO cells exhibited cell-budding dysfunction, resulted in enlarged cells. Scale bars = 10  $\mu\text{m}$ . *C*, flow cytometric analysis. The average cell volumes of WT, 1KO, 2KO, and DKO are presented in each panel. *D*, vacuoles stained with carboxy-DCFDA of WT and 2KO. Scale bars = 10  $\mu\text{m}$ . Cells, cultured at 25  $^{\circ}\text{C}$  for 1 day, were incubated with 100  $\mu\text{M}$  carboxy-DCFDA at 25  $^{\circ}\text{C}$  for 20 min and observed with confocal microscopy. *E*, density gradient centrifugation of WT, 1KO, 2KO, and DKO cells by Percoll. Blue and red arrows indicate the layers, including cells with the lightest and heaviest specific gravities, respectively.

EGCrP2 seems to be a major EG-degrading enzyme in *C. neoformans* because *egcrp2*-disrupted mutants led to the significant accumulation of EG (Fig. 7, *A* and *D*), a major sterylglucoside in fungi and yeast (28). Sterylglucosides, sterol-containing glucosides, are a major class of glycolipids in fungi; however, they are also found in algae, plants, and animals (28). Sterol 3 $\beta$ -glucosyltransferase (EC 2.4.1.173), an enzyme that catalyzes the transfer of glucose from UDP-glucose to sterols, has been found in *Candida albicans* (14), *Colletotrichum gloeosporioides* (29), *Fusarium graminearum* (28), *Leptospha-*

*eria maculans* (30), *Saccharomyces cerevisiae* (14), and *Pichia pastoris* (14). The sterol 3 $\beta$ -glucosyltransferase-deficient mutants of *P. pastoris* were found to lack pexophagy, which is a process for the degradation of peroxisomes in vacuoles, whereas sterol 3 $\beta$ -glucosyltransferase did not appear to be essential for pexophagy in *S. cerevisiae* and *Yarrowia lipolytica* (31–33). It remains unclear whether the accumulation of EG affects pexophagy in *C. neoformans*. In the present study, the accumulation of EG due to a dysfunction in *egcrp2* may have led to the abnormal cell proliferation (Fig. 8, *A*–*C*) and vacuole

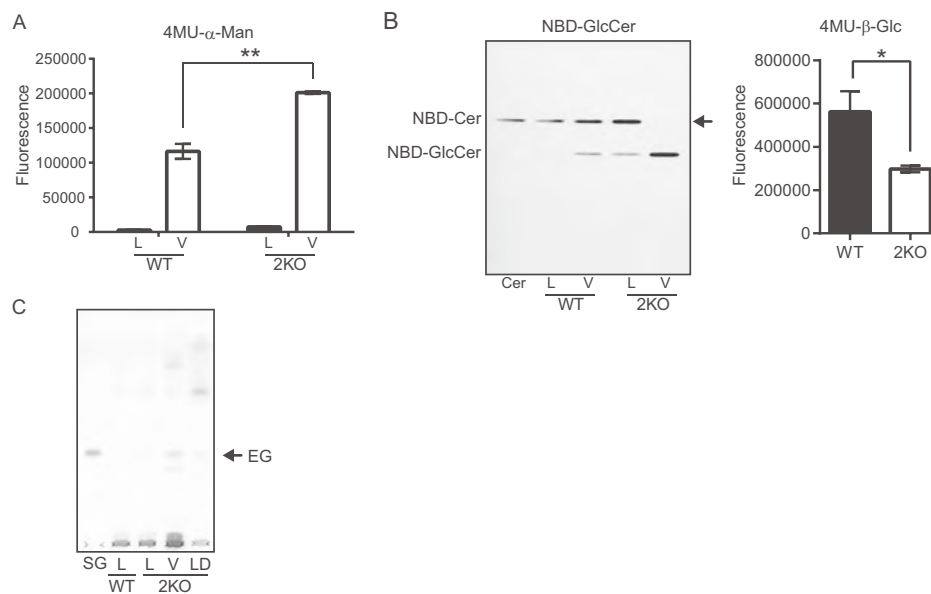


FIGURE 9. Cellular localization of EG that accumulated in *egcrp2*-disrupted mutants (2KO) of *C. neoformans*. A, the  $\alpha$ -mannosidase activity of the cell lysate and vacuole fractions. Activity was measured at 37 °C for 1 h using 0.5  $\mu$ g of protein from each fraction and 20 nmol of 4MU- $\alpha$ -mannoside as a substrate in 100  $\mu$ l of 50 mM phosphate buffer, pH 6.5. L, lysate; V, vacuole fraction. B, the  $\beta$ -glucosidase activity of the vacuole fraction of WT and 2KO. Activity was measured at 30 °C for 18 h by using 0.25  $\mu$ g of protein from vacuole fraction and 50 nmol of C6-NBD-GlcCer in 20  $\mu$ l or 30 nmol of 4MU- $\beta$ -glucoside as a substrate in 100  $\mu$ l of 50 mM sodium acetate buffer, pH 5.0. C, TLC showing EG that accumulated in 2KO. Glycolipids were extracted from the lysate and vacuole fractions of WT and 2KO (each 50  $\mu$ g as protein) and analyzed by TLC using the method described in the legend to Fig. 5A. L, lysate; V, vacuole fraction; LD, lipid droplet fraction. \* and \*\*,  $p < 0.05$  and  $p < 0.0001$ , respectively. Error bars, S.E.

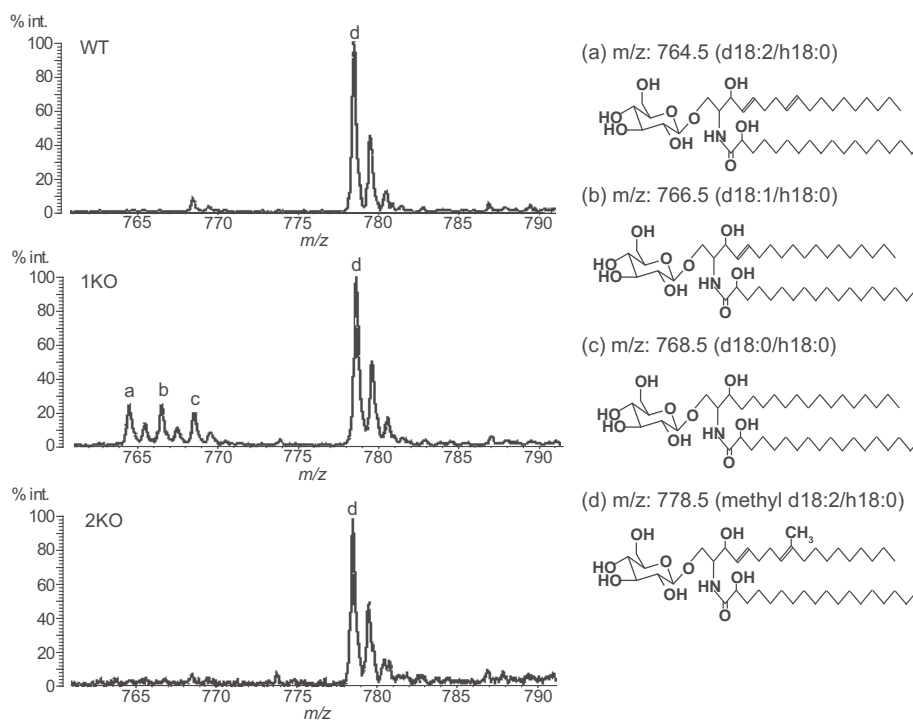


FIGURE 10. MALDI-TOF-MS analysis of GlcCer from WT, 1KO, and 2KO. GlcCer, purified from WT, 1KO, and 2KO, was analyzed by MALDI-TOF-MS in a positive ion mode using 2,5-dihydroxybenzoic acid as a matrix. The major ion peak at  $m/z$  778.5 (d), which corresponds to the molecular mass of mature GlcCer possessing Cer composed of methyl d18:2/h18:0, was detected in GlcCer from WT, 1KO, and 2KO. However, ion peaks at  $m/z$  764.5 (a), 766.5 (b), and 768.5 (c), which correspond to the molecular mass of immature GlcCer possessing Cer composed of d18:2/h18:0, d18:1/h18:0, and d18:0/h18:0, respectively, were detected in GlcCer from 1KO but not WT or 2KO.

morphology (Fig. 8D) in *C. neoformans*; however, the mechanism responsible remains unknown.

Although both EGCrP1 and EGCrP2 are  $\beta$ -glucohydrolases belonging to glycoside hydrolase family 5, the specificity of both enzymes completely differs for the aglycone moiety; EGCrP1

only cleaved the  $\beta$ -glucosidic linkage of GlcCer among the substrates tested (12), whereas EGCrP2 hydrolyzed various  $\beta$ -glucosides, including GlcCer, steryl- $\beta$ -glucosides, and artificial substrates, such as *p*NP- $\beta$ -glucoside and 4MU- $\beta$ -glucoside (Fig. 3 and Table 2). A comparison of the primary structure of

## Novel Steryl- $\beta$ -glucosidase in *C. neoformans*

EGCrP2 with EGCrP1 revealed the presence of several inserts in EGCrP2 between possible  $\beta$ -strands 6 and 7,  $\beta$ -strand 9, and  $\alpha$ -helix 11, and the carboxyl-terminal region (Fig. 2). Further studies are required to elucidate the relationship between the structures and aglycone specificities of EGCrPs. X-ray crystal analysis of EGCrP1 and EGCrP2 could provide valuable information on mutual relationships, and experiments are ongoing.

In the present study, we identified EGCrP2 as the first steryl- $\beta$ -glucosidase in fungi. Similar activity was found in *Sinapis alba* (34) and *Sulfolobus solfataricus* (35); however, these enzymes show no sequence homology with EGCrP1/EGCrP2. In addition, it remains unclear whether these plant and archaea enzymes are actually involved in sterylglucoside metabolism *in vivo* because knock-out of the corresponding genes in plants and archaea has not been reported.

EGCrP2 appeared to localize to the vacuole because  $\beta$ -glucosidase activity was detected in the vacuole-enriched fraction, and its activity was decreased in the fraction after the disruption of *egcrp2* in *C. neoformans* (Fig. 9B). The optimum pH of EGCrP2 was found to be 5.0–5.5 (Fig. 5A), which approximately corresponded to the vacuole pH determined in *C. neoformans* strain H99 (36). The expression of GFP-tagged EGCrP2 could help to estimate the intracellular localization of EGCrP2; however, the expression of GFP-EGCrP2 has yet to be successfully achieved in *C. neoformans*.

The abnormal morphology of vacuoles in *C. albicans* mutants led to a decrease in pathogenicity in a mouse model (37–40); thus, the vacuole proteins of this fungi are now being considered as targets for the development of antifungal drugs (41). In this context, EGCrP2 could be a promising candidate for the development of anti-*Cryptococcus* drugs because a dysfunction in EGCrP2 resulted in an abnormal morphology in the vacuoles (Fig. 8D). One of the reasons for this abnormality could stem from the accumulation of EG in the vacuoles; however, the molecular mechanism responsible remains unknown. Taken together, we herein uncovered the missing link in sterylglucoside metabolism in *C. neoformans* by identifying the enzyme responsible for degrading EG *in vivo* and *in vitro*.

**Acknowledgments**—We thank Dr. Kaoru Takegawa and Dr. Ken Matsuoka (Kyushu University) for valuable suggestions regarding vacuole morphology and physiology. Thanks also due to Emiko Matsunaga (Kyushu University) for MS analysis of EG.

## REFERENCES

- Park, B. J., Wannemuehler, K. A., Marston, B. J., Govender, N., Pappas, P. G., and Chiller, T. M. (2009) Estimation of the current global burden of cryptococcal meningitis among persons living with HIV/AIDS. *AIDS* **23**, 525–530
- Byrnes, E. J., 3rd, Bildfell, R. J., Frank, S. A., Mitchell, T. G., Marr, K. A., and Heitman, J. (2009) Molecular evidence that the range of the Vancouver Island outbreak of *Cryptococcus gattii* infection has expanded into the Pacific Northwest in the United States. *J. Infect. Dis.* **199**, 1081–1086
- Rhome, R., McQuiston, T., Kechichian, T., Bielawska, A., Hennig, M., Drago, M., Morace, G., Luberto, C., and Del Poeta, M. (2007) Biosynthesis and immunogenicity of glucosylceramide in *Cryptococcus neoformans* and other human pathogens. *Eukaryot. Cell* **6**, 1715–1726
- Leipelt, M., Warnecke, D., Zähringer, U., Ott, C., Müller, F., Hube, B., and Heinz, E. (2001) Glucosylceramide synthases, a gene family responsible for

- the biosynthesis of glucosylceramides in animals, plants, and fungi. *J. Biol. Chem.* **276**, 33621–33629
- Rittershaus, P. C., Kechichian, T. B., Allegood, J. C., Merrill, A. H., Jr., Hennig, M., Luberto, C., and Del Poeta, M. (2006) Glucosylceramide synthase is an essential regulator of pathogenicity of *Cryptococcus neoformans*. *J. Clin. Invest.* **116**, 1651–1659
  - Michaelson, L. V., Zäuner, S., Markham, J. E., Haslam, R. P., Desikan, R., Mugford, S., Albrecht, S., Warnecke, D., Sperling, P., Heinz, E., and Napier, J. A. (2009) Functional characterization of a higher plant sphingolipid Delta4-desaturase: defining the role of sphingosine and sphingosine-1-phosphate in Arabidopsis. *Plant Physiol.* **149**, 487–498
  - Oura, T., and Kajiwara, S. (2008) Disruption of the sphingolipid  $\Delta 8$ -desaturase gene causes a delay in morphological changes in *Candida albicans*. *Microbiology* **154**, 3795–3803
  - Ternes, P., Sperling, P., Albrecht, S., Franke, S., Cregg, J. M., Warnecke, D., and Heinz, E. (2006) Identification of fungal sphingolipid C9-methyltransferases by phylogenetic profiling. *J. Biol. Chem.* **281**, 5582–5592
  - Singh, A., Wang, H., Silva, L. C., Na, C., Prieto, M., Futerman, A. H., Luberto, C., and Del Poeta, M. (2012) Methylation of glycosylated sphingolipid modulates membrane lipid topography and pathogenicity of *Cryptococcus neoformans*. *Cell. Microbiol.* **14**, 500–516
  - Ito, M., and Yamagata, T. (1986) A novel glycosphingolipid-degrading enzyme cleaves the linkage between the oligosaccharide and ceramide of neutral and acidic glycosphingolipids. *J. Biol. Chem.* **261**, 14278–14282
  - Izu, H., Izumi, Y., Kurome, Y., Sano, M., Kondo, A., Kato, I., and Ito, M. (1997) Molecular cloning, expression of the endoglycosylceramidase II gene from *Rhodococcus* species strain M-777. *J. Biol. Chem.* **272**, 19846–19850
  - Ishibashi, Y., Ikeda, K., Sakaguchi, K., Okino, N., Taguchi, R., and Ito, M. (2012) Quality control of fungus-specific glucosylceramide in *Cryptococcus neoformans* by endoglycosylceramidase-related protein 1 (EGCrP1). *J. Biol. Chem.* **287**, 368–381
  - Kunimoto, S., Murofushi, W., Kai, H., Ishida, Y., Uchiyama, A., Kobayashi, T., Kobayashi, S., Murofushi, H., and Murakami-Murofushi, K. (2002) Steryl glucoside is a lipid mediator in stress-responsive signal transduction. *Cell Struct. Funct.* **27**, 157–162
  - Warnecke, D., Erdmann, R., Fahl, A., Hube, B., Müller, F., Zank, T., Zähringer, U., and Heinz, E. (1999) Cloning and functional expression of UGT genes encoding sterol glucosyltransferases from *Saccharomyces cerevisiae*, *Candida albicans*, *Pichia pastoris*, and *Dictyostelium discoideum*. *J. Biol. Chem.* **274**, 13048–13059
  - Nakagawa, T., Tani, M., Kita, K., and Ito, M. (1999) Preparation of fluorescence-labeled GM1 and sphingomyelin by the reverse hydrolysis reaction of sphingolipid ceramide *N*-deacylase as substrates for assay of sphingolipid-degrading enzymes and for detection of sphingolipid-binding proteins. *J. Biochem.* **126**, 604–611
  - Laemmli, U. K. (1970) Cleavage of structural proteins during the assembly of the head of bacteriophage T4. *Nature* **227**, 680–685
  - Hayashi, Y., Zama, K., Abe, E., Okino, N., Inoue, T., Ohno, K., and Ito, M. (2008) A sensitive and reproducible fluorescent-based HPLC assay to measure the activity of acid as well as neutral  $\beta$ -glucocerebrosidases. *Anal. Biochem.* **383**, 122–129
  - Kim, M. S., Kim, S. Y., Yoon, J. K., Lee, Y. W., and Bahn, Y. S. (2009) An efficient gene-disruption method in *Cryptococcus neoformans* by double-joint PCR with NAT-split markers. *Biochem. Biophys. Res. Commun.* **390**, 983–988
  - Cox, G. M., Rude, T. H., Dykstra, C. C., and Perfect, J. R. (1995) The actin gene from *Cryptococcus neoformans*: structure and phylogenetic analysis. *J. Med. Vet. Mycol.* **33**, 261–266
  - Perfect, J. R., Rude, T. H., Penning, L. M., and Johnson, S. A. (1992) Cloning the *Cryptococcus neoformans* *TRP1* gene by complementation in *Saccharomyces cerevisiae*. *Gene* **122**, 213–217
  - McDade, H. C., and Cox, G. M. (2001) A new dominant selectable marker for use in *Cryptococcus neoformans*. *Med. Mycol.* **39**, 151–154
  - Davidson, R. C., Cruz, M. C., Sia, R. A. L., Allen, B., Alspaugh, J. A., and Heitman, J. (2000) Gene disruption by biolistic transformation in serotype D strains of *Cryptococcus neoformans*. *Fungal Genet. Biol.* **29**, 38–48
  - Bligh, E. G., and Dyer, W. J. (1959) A rapid method of total lipid extraction and purification. *Can. J. Biochem. Physiol.* **37**, 911–917

24. Cabrera, M., and Ungermann, C. (2008) Purification and *in vitro* analysis of yeast vacuoles. *Methods Enzymol.* **451**, 177–196
25. Zinser, E., Paltauf, F., and Daum, G. (1993) Sterol composition of yeast organelle membranes and subcellular distribution of enzymes involved in sterol metabolism. *J. Bacteriol.* **175**, 2853–2858
26. Richards, A., Gow, N. A. R., and Veses, V. (2012) Identification of vacuole defects in fungi. *J. Microbiol. Methods* **91**, 155–163
27. Sakon, J., Adney, W. S., Himmel, M. E., Thomas, S. R., and Karplus, P. A. (1996) Crystal structure of thermostable family 5 endocellulase E1 from *Acidothermus cellulolyticus* in complex with cellotetraose. *Biochemistry* **35**, 10648–10660
28. Grille, S., Zaslowski, A., Thiele, S., Plat, J., and Warnecke, D. (2010) The functions of steryl glycosides come to those who wait: recent advances in plants, fungi, bacteria and animals. *Prog. Lipid Res.* **49**, 262–288
29. Kim, Y. K., Wang, Y., Liu, Z. M., and Kolattukudy, P. E. (2002) Identification of a hard surface contact-induced gene in *Colletotrichum gloeosporioides* conidia as a sterol glycosyl transferase, a novel fungal virulence factor. *Plant J.* **30**, 177–187
30. Idnurm, A., Warnecke, D. C., Heinz, E., and Howlett, B. J. (2003) Characterisation of neutral trehalase and UDP-glucose: sterol glucosyltransferase genes from the plant pathogenic fungus *Leptosphaeria maculans*. *Physiol. Mol. Plant Pathol.* **62**, 305–313
31. Oku, M., Warnecke, D., Noda, T., Müller, F., Heinz, E., Mukaiyama, H., Kato, N., and Sakai, Y. (2003) Peroxisome degradation requires catalytically active sterol glucosyltransferase with a GRAM domain. *EMBO J.* **22**, 3231–3241
32. Stasyk, O. V., Nazarko, T. Y., Stasyk, O. G., Krasovska, O. S., Warnecke, D., Nicaud, J. M., Cregg, J. M., and Sibirny, A. A. (2003) Sterol glucosyltransferases have different functional roles in *Pichia pastoris* and *Yarrowia lipolytica*. *Cell Biol. Int.* **27**, 947–952
33. Cao, Y., and Klionsky, D. J. (2007) Atg26 is not involved in autophagy-related pathways in *Saccharomyces cerevisiae*. *Autophagy* **3**, 17–20
34. Kalinowska, M., and Wojciechowski, Z. A. (1978) Purification and some properties of steryl  $\beta$ -D-glucoside hydrolase from *Sinapis alba* seedlings. *Phytochemistry* **17**, 1533–1537
35. Aguirre, A., Peiru, S., Eberhardt, F., Vetcher, L., Cabrera, R., and Menzella, H. G. (2014) Enzymatic hydrolysis of steryl glucosides, major contaminants of vegetable oil-derived biodiesel. *Appl. Microbiol. Biotechnol.* **98**, 4033–4040
36. Harrison, T. S., Chen, J., Simons, E., and Levitz, S. M. (2002) Determination of the pH of the *Cryptococcus neoformans* vacuole. *Med. Mycol.* **40**, 329–332
37. Cornet, M., Bidard, F., Schwarz, P., Da Costa, G., Blanchin-Roland, S., Dromer, F., and Gaillardin, C. (2005) Deletions of endocytic components VPS28 and VPS32 affect growth at alkaline pH and virulence through both RIM101-dependent and RIM101-independent pathways in *Candida albicans*. *Infect. Immun.* **73**, 7977–7987
38. Poltermann, S., Nguyen, M., Günther, J., Wendland, J., Härtl, A., Künkel, W., Zipfel, P. F., and Eck, R. (2005) The putative vacuolar ATPase subunit Vma7p of *Candida albicans* is involved in vacuole acidification, hyphal development and virulence. *Microbiology* **151**, 1645–1655
39. Franke, K., Nguyen, M., Härtl, A., Dahse, H. M., Vogl, G., Würzner, R., Zipfel, P. F., Künkel, W., and Eck, R. (2006) The vesicle transport protein Vac1p is required for virulence of *Candida albicans*. *Microbiology* **152**, 3111–3121
40. Johnston, D. A., Eberle, K. E., Sturtevant, J. E., and Palmer, G. E. (2009) Role for endosomal and vacuolar GTPases in *Candida albicans* pathogenesis. *Infect. Immun.* **77**, 2343–2355
41. Zhang, Y., and Rao, R. (2012) The V-ATPase as a target for antifungal drugs. *Curr. Protein Pept. Sci.* **13**, 134–140
42. Thompson, J. D., Higgins, D. G., and Gibson, T. J. (1994) CLUSTAL W: improving the sensitivity of progressive multiple sequence alignment through sequence weighting, position-specific gap penalties and weight matrix choice. *Nucleic Acids Res.* **22**, 4673–4680
43. Gouet, P., Robert, X., and Courcelle, E. (2003) ESPript/ENDscript: extracting and rendering sequence and 3D information from atomic structures of proteins. *Nucleic Acids Res.* **31**, 3320–3323
44. Caines, M. E. C., Vaughan, M. D., Tarling, C. A., Hancock, S. M., Warren, R. A. J., Withers, S. G., and Strynadka, N. C. J. (2007) Structural and mechanistic analyses of *endo*-glycoceramidase II, a membrane-associated family 5 glycosidase in the Apo and GM3 ganglioside-bound forms. *J. Biol. Chem.* **282**, 14300–14308

# The Adipocyte-Inducible Secreted Phospholipases PLA2G5 and PLA2G2E Play Distinct Roles in Obesity

Hiroyasu Sato,<sup>1,2</sup> Yoshitaka Taketomi,<sup>1,2</sup> Ayako Ushida,<sup>1,3</sup> Yuki Isogai,<sup>1,3</sup> Takumi Kojima,<sup>1</sup> Tetsuya Hirabayashi,<sup>1</sup> Yoshimi Miki,<sup>1,2</sup> Kei Yamamoto,<sup>1</sup> Yasumasa Nishito,<sup>4</sup> Tetsuyuki Kobayashi,<sup>3</sup> Kazutaka Ikeda,<sup>5</sup> Ryo Taguchi,<sup>6</sup> Shuntaro Hara,<sup>2</sup> Satoshi Ida,<sup>7</sup> Yuji Miyamoto,<sup>7</sup> Masayuki Watanabe,<sup>7</sup> Hideo Baba,<sup>7</sup> Keishi Miyata,<sup>8</sup> Yuichi Oike,<sup>8</sup> Michael H. Gelb,<sup>9</sup> and Makoto Murakami<sup>1,10,\*</sup>

<sup>1</sup>Lipid Metabolism Project, Tokyo Metropolitan Institute of Medical Science, 2-1-6 Kamikitazawa, Setagaya-ku, Tokyo 156-8506, Japan

<sup>2</sup>Department of Health Chemistry, Showa University, School of Pharmacy, 1-5-8 Hatanodai, Shinagawa-ku, Tokyo 142-8555, Japan

<sup>3</sup>Department of Biology, Faculty of Science, Ochanomizu University, 2-1-1 Otsuka, Bunkyo-ku, Tokyo 112-8610, Japan

<sup>4</sup>Core Technology and Research Center, Tokyo Metropolitan Institute of Medical Science, 2-1-6 Kamikitazawa, Setagaya-ku, Tokyo 156-8506, Japan

<sup>5</sup>Institute for Advanced Biosciences, Keio University, 246-2 Mizukami, Kakuganji, Tsuruoka, Yamagata 997-0052, Japan

<sup>6</sup>Department of Biomedical Sciences, College of Life and Health Sciences, Chubu University, 1200 Matsumoto-cho, Kasugai-shi, Aichi 487-8501, Japan

<sup>7</sup>Department of Gastroenterological Surgery, Kumamoto University, 1-1-1 Honjo, Chuo-ku, Kumamoto 860-8556, Japan

<sup>8</sup>Department of Molecular Genetics, Kumamoto University, 1-1-1 Honjo, Chuo-ku, Kumamoto 860-8556, Japan

<sup>9</sup>Departments of Chemistry and Biochemistry, University of Washington, Campus Box 351700, 36 Bagley Hall, Seattle, WA 98195, USA

<sup>10</sup>CREST, Japan Science and Technology Agency, 4-1-8 Honcho, Kawaguchi, Saitama 332-0012, Japan

\*Correspondence: murakami-mk@igakuken.or.jp

<http://dx.doi.org/10.1016/j.cmet.2014.05.002>

## SUMMARY

Metabolic disorders, including obesity and insulin resistance, have their basis in dysregulated lipid metabolism and low-grade inflammation. In a microarray search of unique lipase-related genes whose expressions are associated with obesity, we found that two secreted phospholipase A<sub>2</sub>s (sPLA<sub>2</sub>s), PLA2G5 and PLA2G2E, were robustly induced in adipocytes of obese mice. Analyses of *Pla2g5*<sup>-/-</sup> and *Pla2g2e*<sup>-/-</sup> mice revealed distinct roles of these sPLA<sub>2</sub>s in diet-induced obesity. PLA2G5 hydrolyzed phosphatidylcholine in fat-overladen low-density lipoprotein to release unsaturated fatty acids, which prevented palmitate-induced M1 macrophage polarization. As such, PLA2G5 tipped the immune balance toward an M2 state, thereby counteracting adipose tissue inflammation, insulin resistance, hyperlipidemia, and obesity. PLA2G2E altered minor lipoprotein phospholipids, phosphatidylserine and phosphatidylethanolamine, and moderately facilitated lipid accumulation in adipose tissue and liver. Collectively, the identification of “metabolic sPLA<sub>2</sub>s” adds this gene family to a growing list of lipolytic enzymes that act as metabolic coordinators.

## INTRODUCTION

Type 2 diabetes and metabolic syndrome are increasing at an explosive rate worldwide due to a pandemic of obesity associated with insulin resistance, nonalcoholic fatty liver disease, and hyperlipidemia (Després and Lemieux, 2006). The mecha-

nisms connecting obesity to insulin resistance include an elevation of circulating lipids, ectopic lipid deposition leading to lipotoxicity, and chronic inflammation in metabolically active tissues (Hotamisligil, 2006). Obesity relies on dysregulations of intracellular lipid metabolism or extracellular lipid partitioning among tissues, and perturbation of intracellular/extracellular lipases or related enzymes variably and often profoundly affect obesity and insulin resistance (Chen et al., 2008; Chiu et al., 2010; Haemmerle et al., 2006; Jaworski et al., 2009; Tian et al., 2010; Wang et al., 2011).

Among the phospholipase A<sub>2</sub> (PLA<sub>2</sub>) family, secreted PLA<sub>2</sub>s (sPLA<sub>2</sub>s) have been implicated in inflammation and atherosclerosis, since they can augment the production of proinflammatory lipid mediators and hydrolyze phospholipids in lipoproteins to generate proatherogenic particles in vitro (Murakami et al., 2011). Recent genetic studies have revealed that individual sPLA<sub>2</sub>s, which show distinct tissue distributions and substrate preferences, participate in diverse biological events in response to given microenvironmental cues (Sato et al., 2010; Taketomi et al., 2013). However, the regulatory roles of sPLA<sub>2</sub>s in metabolic disorders are not well understood. Except for studies using sPLA<sub>2</sub>-overexpressing transgenic mice (Ivancic et al., 1999; Sato et al., 2008), no reports have firmly established whether sPLA<sub>2</sub>s could affect lipoprotein metabolism in vivo. Moreover, although sPLA<sub>2</sub>s exert anti-inflammatory effects in certain situations (Ait-Oufella et al., 2013; Miki et al., 2013), except for PLA2G2D (group IID), a “resolving sPLA<sub>2</sub>” that ameliorates inflammation by mobilizing proresolving lipid mediators (Miki et al., 2013), the molecular mechanisms for the anti-inflammatory actions of sPLA<sub>2</sub>s remain elusive.

In our efforts to search for particular lipase-related genes whose roles in obesity have not been addressed before, we found that two particular sPLA<sub>2</sub>s, PLA2G5 (group V) and PLA2G2E (group IIE), were robustly induced in adipose tissue of obese mice. Reportedly, PLA2G5 deficiency exacerbates or



CrossMark

attenuates inflammation according to disease contexts in unknown ways (Murakami et al., 2011). Notably, *PLA2G5* gene polymorphisms correlate with low-density lipoprotein (LDL) levels in subjects with type 2 diabetes or obesity (Sergouniotis et al., 2011; Wootton et al., 2007), and in vitro *PLA2G5* susceptibility of LDL from patients with type 2 diabetes is greater than that of LDL from healthy subjects (Pettersson et al., 2008), suggesting a role of this sPLA<sub>2</sub> in metabolic regulation. After the identification of *PLA2G2E* (Suzuki et al., 2000; Valentin et al., 1999), its expression, target phospholipids, and biological roles in vivo have remained a mystery for more than a decade. We now provide evidence that the two diet-inducible, adipocyte-driven “metabolic sPLA<sub>2</sub>s” play distinct roles in obesity, hyperlipidemia, and insulin resistance, thus highlighting the importance of the sPLA<sub>2</sub> family in lipoprotein hydrolysis and immune regulation in the process of metabolic disorders.

## RESULTS

### PLA2G5 and PLA2G2E Are Induced in Adipocytes of Obese Mice

We performed gene profiling by microarray followed by quantitative RT-PCR of perigonadal white adipose tissue (WAT) from C57BL/6 mice fed a high-fat diet (HFD; 60% fat calorie) in comparison with those maintained on a low-fat diet (LFD; 4.8% fat calorie) to identify particular lipase-related genes whose expression levels were altered by diets and whose functions in obesity are currently unknown. We found that *Pla2g5* and *Pla2g2e*, two members of the sPLA<sub>2</sub> family, were highly induced in the WAT of HFD-fed mice compared with LFD-fed mice, ranking two of the top three among the diet-inducible lipase-related genes (Figure 1A; Table S1, available online). Marked induction of these two sPLA<sub>2</sub>s, but not other sPLA<sub>2</sub>s (Figure 1B) and intracellular PLA<sub>2</sub>s (Figure S1A), in the WAT of HFD-fed mice was confirmed by quantitative PCR. As in mice, the expression of *PLA2G5* was much higher than that of most other sPLA<sub>2</sub>s in human mesenteric WAT and fatty appendices, while that of *PLA2G2E* was very low (Figure 1C; Table S2). Note that *PLA2G2A*, which is highly homologous to *PLA2G2E* (Suzuki et al., 2000; Valentin et al., 1999) and absent in C57BL/6 mice due to a natural mutation (MacPhee et al., 1995), was highly expressed in human WAT, suggesting that *PLA2G2E* in mice might be compensated by *PLA2G2A* in humans.

Among the tissues with high lipid demand, constitutive *Pla2g5* expression in heart and skeletal muscle was unaffected by diet, and its expression in WAT of HFD-fed mice exceeded that in any other tissues examined so far and reached a level much higher than that in bone marrow (BM)-derived dendritic cells (BMDCs) and macrophages (BMDMs) (Figure 1D). HFD-induced expression of *Pla2g2e* occurred robustly in WAT and brown adipose tissue (BAT), while its expression in other tissues and cells was low (Figure 1E). Moreover, WAT expression of both sPLA<sub>2</sub>s was far greater in genetically obese *Lep<sup>ob/ob</sup>* mice than in control mice (Figure 1F). Kinetic experiments after HFD feeding revealed robust induction of *Pla2g5* and *Pla2g2e* in WAT by 8 weeks, thereafter reaching a maximal plateau level (Figure S1A). The kinetic induction of *Pla2g5* and *Pla2g2e* was similar to that of *Lep*, which encodes leptin (Pellemounter et al., 1995), but differed from that of adipogenic or immune cell markers (Figure S1A).

More detailed kinetic studies at an earlier period showed that the HFD induction of *Pla2g2e* preceded that of *Pla2g5* (Figure S1B). When the WAT was separated into adipocytes and stromal vascular fraction (SVF), both sPLA<sub>2</sub>s were located predominantly in adipocytes of HFD-fed mice (Figures 1G and S1C).

Expression of *Pla2g5* and *Pla2g2e* was increased markedly in mouse 3T3-L1 preadipocytes after culture for 14 days with an adipogenic cocktail (Figure S1D). Proinflammatory cytokines failed to affect their expression in 3T3-L1 cells (Figure S1E). Transwell culture of SVF cells and 3T3-L1 cells did not affect or even decreased the expression of *Pla2g5* and *Pla2g2e*, while it increased that of *Tnf* and *Ccl2*, in the latter cells (Figure S1F), ruling out the contribution of SVF-derived soluble factors to the induction of these sPLA<sub>2</sub>s in adipocytes. Notably, *Pla2g5*, not *Pla2g2e*, expression in differentiated 3T3-L1 cells was further increased by the endoplasmic reticulum (ER) stress inducer thapsigargin (Figure S1D) or tunicamycin (data not shown). These results suggest that the inducible expression of *Pla2g5* depends on the adipogenic program plus obesity-associated ER stress (Ozcan et al., 2006), while adipogenesis is sufficient to drive *Pla2g2e* expression. During adipogenesis, *Pla2g2e* expression started to increase on day 3, lagging behind the induction of the adipogenic marker *Pparg*, and continued to increase by day 12 (Figure S1G).

### Increased Diet-Induced Obesity in *Pla2g5*<sup>-/-</sup> Mice

To elucidate the role of *PLA2G5* in obesity, we placed *Pla2g5*<sup>-/-</sup> mice (Satake et al., 2004) and wild-type (WT) littermates on a HFD, along with a control group of each genotype on a LFD. HFD-induced obesity and weight gain were greater in *Pla2g5*<sup>-/-</sup> mice than in *Pla2g5*<sup>+/+</sup> mice (Figures 2A and 2B). Immunohistochemistry confirmed the location of *PLA2G5* protein in adipocytes of HFD-fed WT mice, whereas hardly any such reactivity was seen in those of *Pla2g5*<sup>-/-</sup> mice, which lacked *Pla2g5* expression (Figures S2A and S2B). Computed tomography (CT) showed significant increases in total, visceral, and subcutaneous fat depositions in HFD-fed *Pla2g5*<sup>-/-</sup> mice relative to *Pla2g5*<sup>+/+</sup> mice (Figure 2C). In agreement, the HFD-induced increase in plasma leptin, whose expression correlates with adiposity (Pellemounter et al., 1995), was higher in *Pla2g5*<sup>-/-</sup> mice than in *Pla2g5*<sup>+/+</sup> mice (Figure 2D). Although daily food intake was the same for both groups, locomotion and oxygen consumption were lower in *Pla2g5*<sup>-/-</sup> mice (Figures S2C–S2E), indicating decreased energy expenditure. The respiratory quotient was unchanged in *Pla2g5*<sup>-/-</sup> mice (Figure S2F).

HFD-induced elevation of plasma insulin was greater in *Pla2g5*<sup>-/-</sup> mice than in *Pla2g5*<sup>+/+</sup> mice (Figure 2E), despite comparable hyperglycemia in both genotypes (Figure S2G), suggesting exacerbated insulin resistance in *Pla2g5*<sup>-/-</sup> mice. Indeed, on an insulin tolerance test (ITT), HFD-fed *Pla2g5*<sup>-/-</sup> mice had greater insulin resistance than *Pla2g5*<sup>+/+</sup> mice (Figure 2F). Insulin-stimulated Akt phosphorylation was lower in WAT, but not in skeletal muscle and liver, of *Pla2g5*<sup>-/-</sup> mice than in that of *Pla2g5*<sup>+/+</sup> mice (Figures 2G and S2H), suggesting that *Pla2g5* ablation decreases insulin sensitivity mainly in WAT, where *PLA2G5* is induced. In a glucose tolerance test (GTT), the glucose disposal was similar in both genotypes (Figure 2H), probably because glucose-stimulated insulin secretion was greater in *Pla2g5*<sup>-/-</sup> mice than in *Pla2g5*<sup>+/+</sup> mice (Figure 2I).

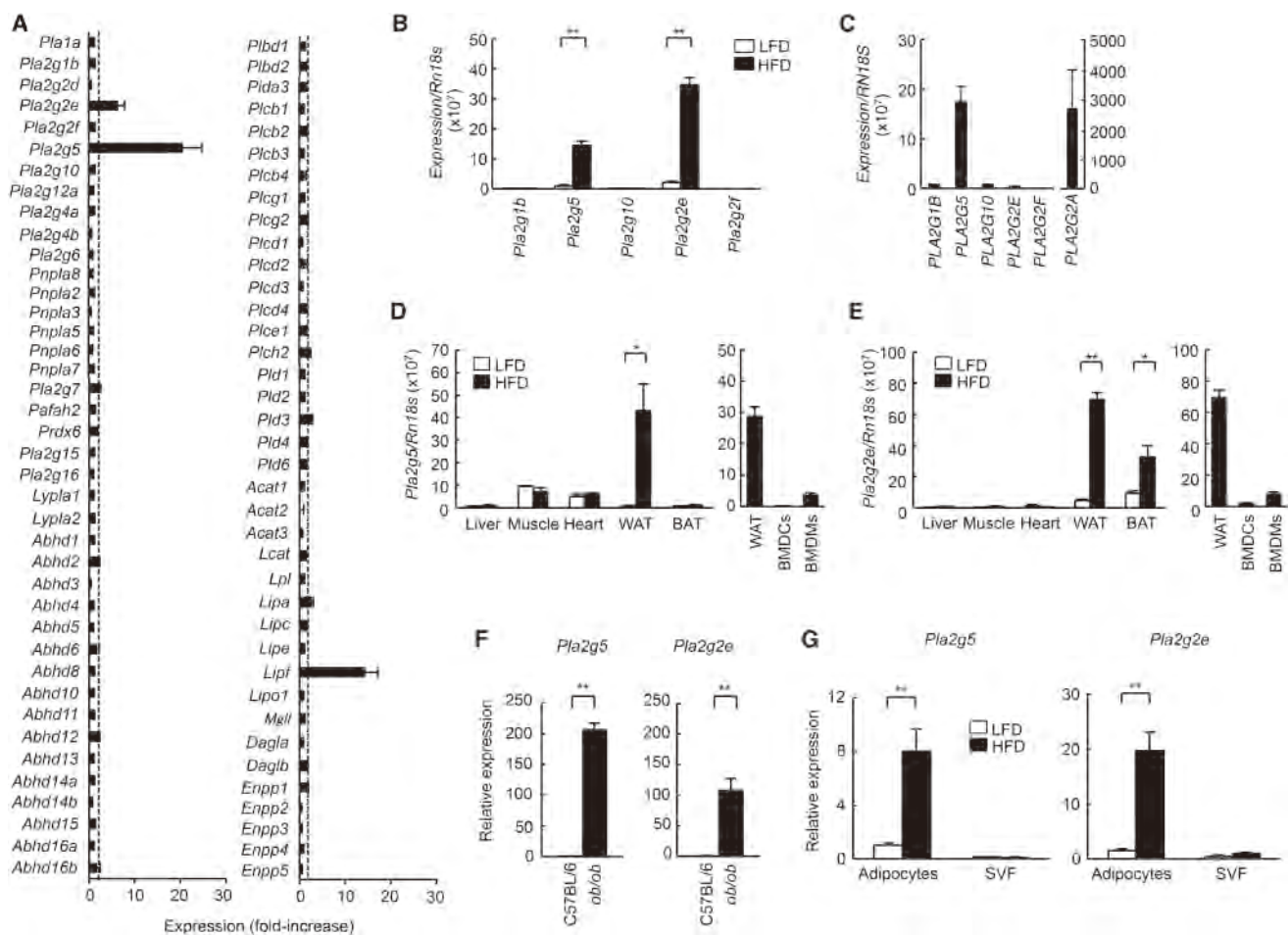


**Figure 1. Obesity-Induced Expression of *Pla2g5* and *Pla2g2e* in Hypertrophic Adipocytes**  
 (A) Microarray of lipase-related genes in the WAT of C57BL/6 mice fed a LFD or HFD for 18 weeks. Values indicate fold increases in the HFD group relative to the LFD group (n = 4; mean ± SD).  
 (B) Expression of sPLA<sub>2</sub> mRNAs relative to *Rn18s* in the WAT of C57BL/6 mice fed a LFD (n = 6) or HFD (n = 9).  
 (C) Expression of sPLA<sub>2</sub> mRNAs relative to *RN18S* in human visceral WAT (n = 18).  
 (D and E) Expression of *Pla2g5* (D) and *Pla2g2e* (E) in various tissues and cells of C57BL/6 mice (n = 5).  
 (F) Expression of *Pla2g5* and *Pla2g2e* in WAT of 12-week-old *Lep<sup>ob/ob</sup>* mice, the expression in age-matched C57BL/6 mice being regarded as 1 (n = 3).  
 (G) *Pla2g5* and *Pla2g2e* expression in adipocytes and SVF from WAT of LFD- or HFD-fed mice, the expression in adipocytes from LFD-fed mice being regarded as 1 (n = 8).  
 In (B), (D), (E), and (G), mice were fed a LFD or HFD for 26 weeks. Data are compiled from one (A, C, and F) or two (B, D, E, and G) experiments. Mean ± SEM (B–G), \*p < 0.05, \*\*p < 0.01.

Exacerbated insulin resistance was already evident, whereas oxygen consumption was unaffected, in *Pla2g5*<sup>-/-</sup> mice at 6 weeks after HFD feeding (Figures S2I and S2J), indicating that the metabolic dysfunction occurred prior to the decreased energy expenditure.

HFD feeding led to greater adipocyte hypertrophy in WAT (Figure 2J) and BAT (Figure S3A) of *Pla2g5*<sup>-/-</sup> mice compared to those of WT mice, although expression levels of adipogenic, lipogenic, lipid uptake, lipolytic, or thermogenic genes in WAT (Figure 2K) and BAT (Figure S3B) were similar between the genotypes. Expression of several other PLA<sub>2</sub>s, which have been implicated in adiposity (Su et al., 2004), in WAT was unaffected by PLA2G5 deficiency (Figure S3C). Thus, the increased obesity in *Pla2g5*<sup>-/-</sup> mice may not arise from intrinsic alterations in these

adipocyte programs but may involve other extrinsic mechanisms. HFD-increased plasma alanine aminotransferase (ALT) level (Figure 2L) and hepatic fat deposition (Figures 2M and 2N) were greater in *Pla2g5*<sup>-/-</sup> mice compared to *Pla2g5*<sup>+/+</sup> mice. Consistently, hepatic expression of genes for lipid synthesis or uptake and inflammation, but not for β-oxidation, was increased in HFD-fed *Pla2g5*<sup>-/-</sup> mice over *Pla2g5*<sup>+/+</sup> mice (Figures S3D and S3E), indicating exacerbated hepatic steatosis in *Pla2g5*<sup>-/-</sup> mice. Since the expression of *Pla2g5* in BAT and liver was low (Figure 1D), and since visceral adiposity and hepatic steatosis are etiologically intertwined (Després and Lemieux, 2006), the abnormalities in these tissues may reflect a secondary effect resulting from the increased obesity in *Pla2g5*<sup>-/-</sup> mice.

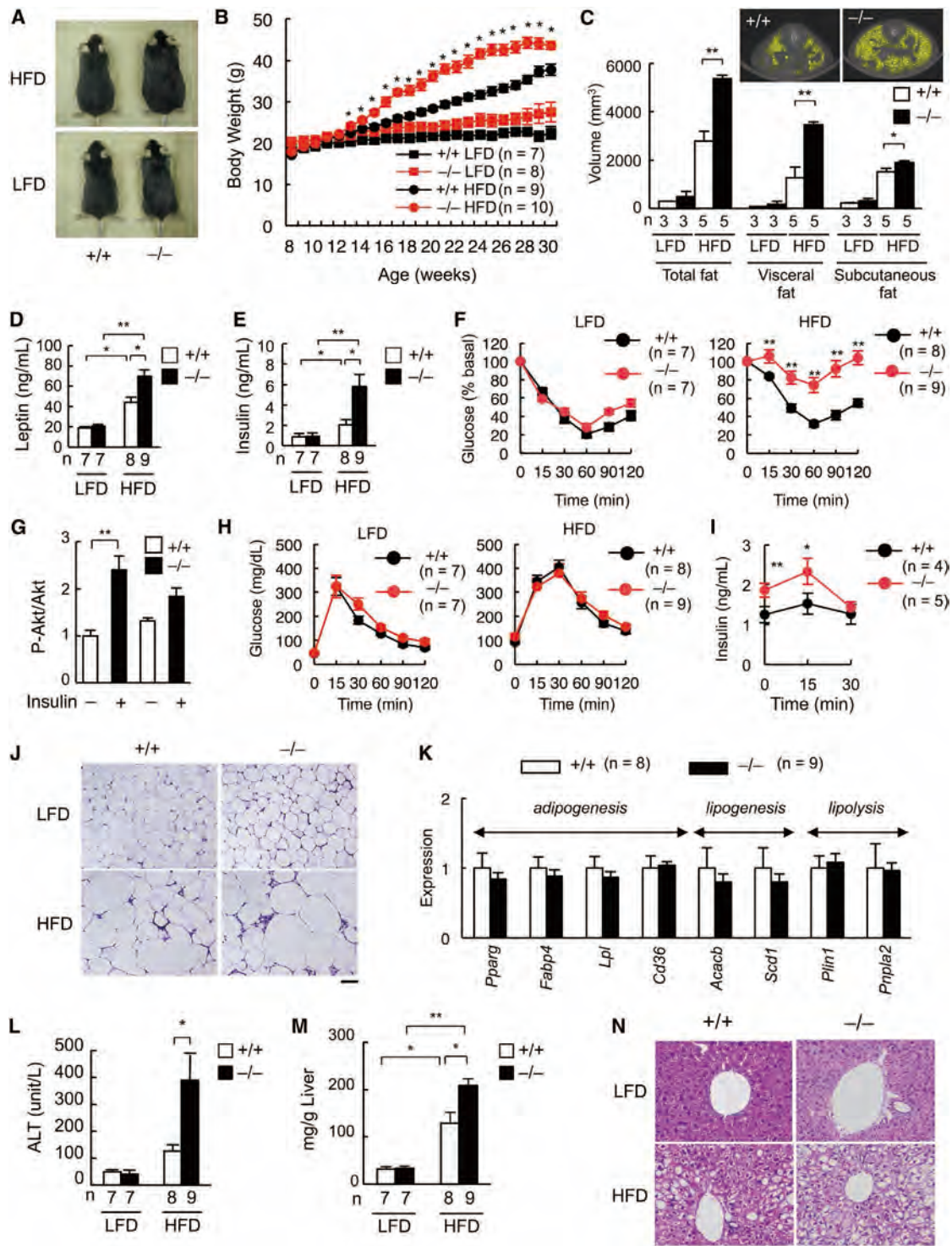


**Figure 2. Increased Diet-Induced Obesity in *Pla2g5<sup>-/-</sup>* Mice**

(A) Representative photos of *Pla2g5<sup>+/+</sup>* and *Pla2g5<sup>-/-</sup>* mice fed a LFD or HFD for 14 weeks. (B) Body weights of *Pla2g5<sup>+/+</sup>* and *Pla2g5<sup>-/-</sup>* mice placed on a LFD or HFD for the indicated periods. (C) CT analysis of fat volumes in *Pla2g5<sup>+/+</sup>* and *Pla2g5<sup>-/-</sup>* mice. Yellow areas indicate fat deposition in HFD-fed mice (inset). (D and E) Levels of fasting plasma leptin (D) and insulin (E) in *Pla2g5<sup>+/+</sup>* and *Pla2g5<sup>-/-</sup>* mice. (F) ITT using 6 hr fasted *Pla2g5<sup>+/+</sup>* and *Pla2g5<sup>-/-</sup>* mice. (G) Immunoblotting of phosphorylated (P-) and total Akt in WAT of HFD-fed *Pla2g5<sup>+/+</sup>* and *Pla2g5<sup>-/-</sup>* mice with (+) or without (-) 5 min treatment with insulin. The ratios of P-Akt to Akt were determined by densitometry, with the value of insulin-untreated *Pla2g5<sup>+/+</sup>* mice being regarded as 1 (n = 4).

(legend continued on next page)

**Altered Lipoprotein Profiles in HFD-Fed *Pla2g5*<sup>-/-</sup> Mice**

PLA2G5 hydrolyzes phosphatidylcholine (PC) in LDL and, to a lesser extent, in high-density lipoprotein (HDL) in vitro (Sato et al., 2008), yet in vivo evidence for this action was lacking. Kinetically, HFD feeding was accompanied by increases of phospholipids in plasma and in lipoproteins (Figure S4A), which preceded *Pla2g5* induction in WAT (Figure S1A). Plasma phospholipid and cholesterol levels were significantly greater in HFD-fed *Pla2g5*<sup>-/-</sup> mice than in *Pla2g5*<sup>+/+</sup> mice (Figure 3A). Moreover, phospholipid, cholesterol, and TG levels in LDL, but not chylomicron (CM), very-low-density lipoprotein (VLDL), and HDL, were significantly higher in HFD-fed *Pla2g5*<sup>-/-</sup> mice than in *Pla2g5*<sup>+/+</sup> mice (Figures 3B–3D, S4B, and S4C). These results suggest that diet-induced PLA2G5 acts on LDL phospholipids, eventually altering LDL lipid composition.

To explore the hydrolysis of LDL phospholipids by PLA2G5 further, phospholipids in LDL from HFD-fed mice were analyzed by electrospray ionization mass spectrometry (ESI-MS). LDL in HFD-fed *Pla2g5*<sup>-/-</sup> mice contained more PC34:1 (*sn*-1 palmitic acid [PA; 16:0] and *sn*-2 oleic acid [OA; 18:1])—and, to a lesser extent, other PC species containing polyunsaturated fatty acids (PUFAs), such as PC34:2 (16:0 and linoleic acid [LA; 18:2]), PC36:3 (18:1 and 18:2), PC36:4 (16:0 and arachidonic acid [AA; 20:4]), and PC38:6 (16:0 and docosahexaenoic acid [DHA; 22:6])—than that in *Pla2g5*<sup>+/+</sup> mice (Figures 3E and S4D). By contrast, PLA2G5 deficiency did not affect minor LDL phospholipids, phosphatidylethanolamine (PE), and phosphatidylserine (PS) (Figure 3E). These results imply that PLA2G5 preferentially hydrolyzes PC species (particularly those containing a fatty acid with a lower degree of unsaturation, such as OA in preference to LA [OA > LA]) in hyperlipidemic LDL in vivo, a view that agrees with its substrate preference in vitro (Przanski et al., 2005; Sato et al., 2008). Plasma levels of nonesterified fatty acids (NEFA) and lysophosphatidylcholine (LPC), which are PLA<sub>2</sub> reaction products, did not differ in both genotypes (Figure S4E), probably because the PLA2G5-driven NEFA and LPC pools were small relative to their high background levels or because they were produced locally in WAT. In support of the latter idea, the WAT level of OA was elevated in *Pla2g5*<sup>+/+</sup> mice after HFD feeding, whereas this increase was not seen in *Pla2g5*<sup>-/-</sup> mice (Figure 3F). PUFAs (LA > AA > DHA) also tended to be lower in HFD-fed *Pla2g5*<sup>-/-</sup> mice than in *Pla2g5*<sup>+/+</sup> mice, though to a lesser extent than OA. Overall, these lipid profiles agree with the fatty acid preference of PLA2G5. Thus, diet-induced PLA2G5 hydrolyzes PC in fat-overloaded LDL to provide OA in preference to PUFAs in WAT, which may eventually contribute to LDL lipid normalization. Notably, as in mice, WAT expression levels of PLA2G5 showed a significantly inverse correlation with plasma LDL levels in humans

(Figure 3G; Table S2), revealing an enzyme-substrate relationship across species.

**Exacerbated Adipose Tissue Inflammation in HFD-Fed *Pla2g5*<sup>-/-</sup> Mice**

Crown-like structures, an indication of macrophage infiltration, were histologically greater in the WAT of HFD-fed *Pla2g5*<sup>-/-</sup> than in that of *Pla2g5*<sup>+/+</sup> mice (Figure 2J). Consistently, HFD-induced WAT expression of M1 macrophage markers was increased, whereas M2 macrophage markers were unchanged or decreased, by *Pla2g5* deficiency, allowing the M1/M2 ratio to be greater in HFD-fed *Pla2g5*<sup>-/-</sup> mice (Figures 4A and 4B). Flow cytometry confirmed that the WAT of HFD-fed *Pla2g5*<sup>-/-</sup> mice contained a greater proportion of F40/80<sup>+</sup>CD11b<sup>+</sup> macrophages, with a greater number of CD11c<sup>+</sup> M1 and fewer CD206<sup>+</sup> M2 macrophages, compared to the WAT of *Pla2g5*<sup>+/+</sup> mice (Figures 4C and 4D). Thus, PLA2G5 plays an anti-inflammatory role in adipose tissue inflammation.

Recruitment of macrophages into obese WAT relies on several mechanisms, among which adipocyte death due to lipotoxicity represents a driving factor, attracting macrophages for phagocytic clearance of dead cells (Cinti et al., 2005). As *Pla2g5*<sup>-/-</sup> mice display lower macrophage phagocytosis (Balestrieri et al., 2009; Boilard et al., 2010), we evaluated dead cells in *Pla2g5*<sup>-/-</sup> or *Pla2g5*<sup>+/+</sup> WAT. TUNEL staining revealed a marked increase of dead cells in WAT of HFD-fed *Pla2g5*<sup>-/-</sup> mice over *Pla2g5*<sup>+/+</sup> mice (Figures 4E and 4F). Thus, the reduced clearance of dead cells by macrophages may account, at least partly, for the increased inflammation in *Pla2g5*<sup>-/-</sup> WAT.

**PLA2G5 Integrates Lipoprotein Metabolism and Anti-Inflammation**

Given that sPLA<sub>2</sub> acts in a paracrine fashion, we speculated that PLA2G5 secreted from adipocytes affected the properties of macrophages. Addition of PLA2G5 to lipopolysaccharide and interferon  $\gamma$  (LPS+IFN- $\gamma$ )-stimulated BMDMs augmented the expression of the M2 marker *Arg1* without affecting that of the M1 marker *Nos2* (Figure 5A), suggesting that PLA2G5 selectively upregulates the M2 gene. In a setting physiologically more relevant to sterile inflammation in obesity, exposure of BMDMs to PA, a saturated fatty acid that elicits proinflammatory responses through Toll-like receptor 4 (TLR4) or ER stress (Hotamisligil, 2006), increased *Nos2*, did not affect *Arg1*, and decreased *Cd206*, indicative of M1 skewing (Figures 5B and 5C). Further addition of PLA2G5 to PA-treated BMDMs reduced *Nos2*, upregulated *Arg1*, and partially restored *Cd206* expression (Figure 5B). *Pla2g5* expression was increased in PA-treated BMDMs (Figure 5D), in line with its induction by ER stress in adipocytes (Figure S1D). However, culture of *Pla2g5*<sup>+/+</sup> and *Pla2g5*<sup>-/-</sup>

(H) GTT using 16 hr fasted *Pla2g5*<sup>+/+</sup> and *Pla2g5*<sup>-/-</sup> mice.

(I) Glucose-stimulated insulin secretion under the conditions in (H).

(J) Hematoxylin and eosin staining of WAT in *Pla2g5*<sup>+/+</sup> and *Pla2g5*<sup>-/-</sup> mice (scale bar, 50  $\mu$ m).

(K) Expression of adipogenic, lipogenic, and lipolytic genes normalized by *Gapdh* in WAT of HFD-fed *Pla2g5*<sup>+/+</sup> and *Pla2g5*<sup>-/-</sup> mice, with the expression in *Pla2g5*<sup>+/+</sup> mice being regarded as 1.

(L and M) Levels of plasma ALT (L) and hepatic TG (M) in *Pla2g5*<sup>+/+</sup> and *Pla2g5*<sup>-/-</sup> mice.

(N) Hematoxylin and eosin staining of liver from *Pla2g5*<sup>+/+</sup> and *Pla2g5*<sup>-/-</sup> mice (scale bar, 50  $\mu$ m).

In (C)–(N), mice were fed a LFD or HFD for 26 weeks. Data are compiled from two (C, G, and I) or three (B, D–F, H, and K–M) experiments. Images in (A), (J), and (N) are representative of two experiments. Mean  $\pm$  SEM; \**p* < 0.05, \*\**p* < 0.01.

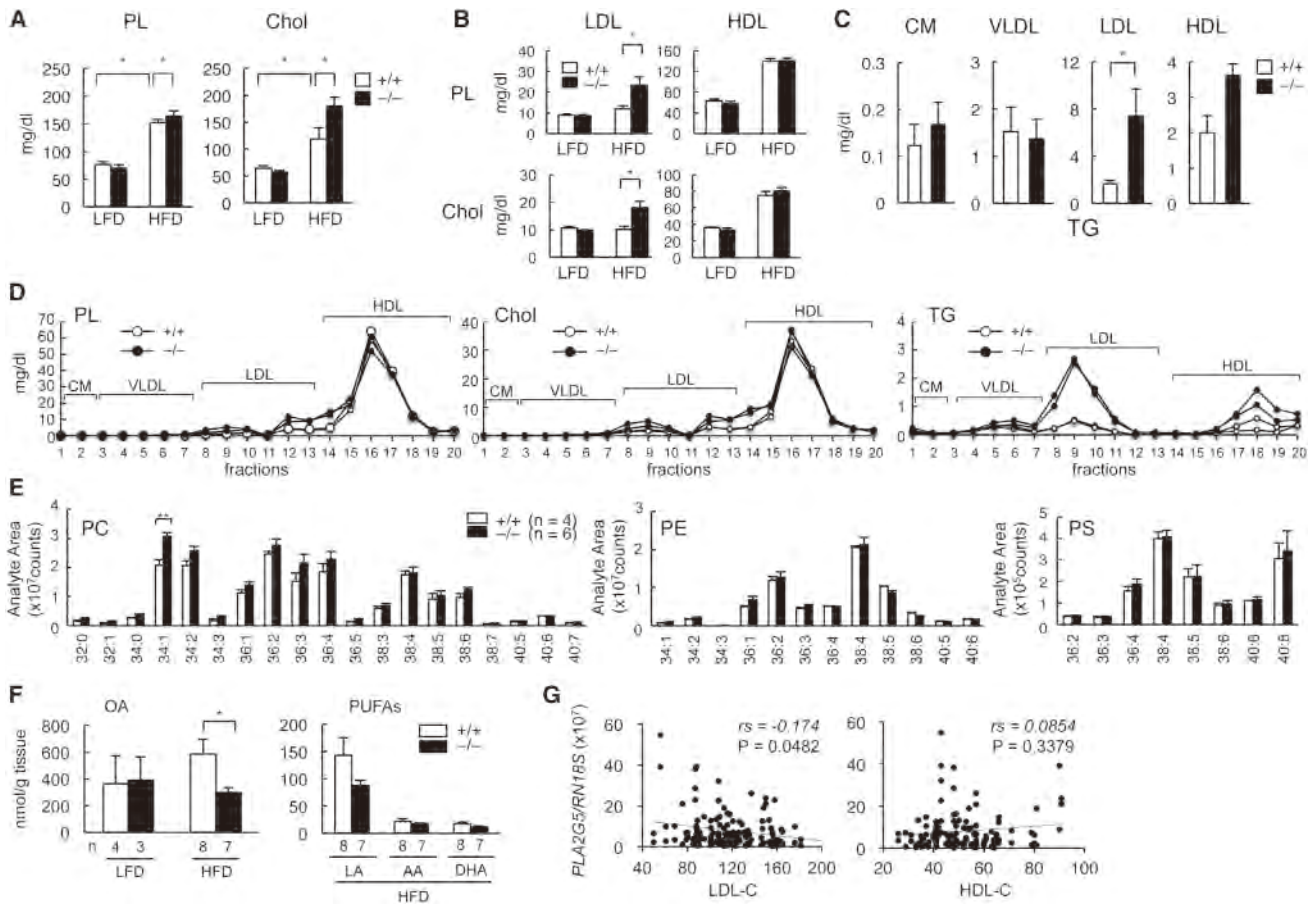


**Figure 3. Altered Lipoprotein Profiles in HFD-Fed *Pla2g5*<sup>-/-</sup> Mice**

(A) Plasma phospholipids (PL) and cholesterol (Chol) levels in *Pla2g5*<sup>+/+</sup> and *Pla2g5*<sup>-/-</sup> mice (n = 4).  
 (B) PL and Chol levels in LDL and HDL from *Pla2g5*<sup>+/+</sup> and *Pla2g5*<sup>-/-</sup> mice (n = 4).  
 (C) TG levels in individual lipoprotein particles from HFD-fed *Pla2g5*<sup>+/+</sup> and *Pla2g5*<sup>-/-</sup> mice (n = 4).  
 (D) High-performance liquid chromatography (HPLC) profiles of PL, Chol, and TG in plasma lipoproteins from HFD-fed *Pla2g5*<sup>+/+</sup> and *Pla2g5*<sup>-/-</sup> mice. Two examples from each genotype are shown.  
 (E) ESI-MS of PC, PE, and PS in LDL from HFD-fed *Pla2g5*<sup>+/+</sup> and *Pla2g5*<sup>-/-</sup> mice.  
 (F) ESI-MS of unsaturated fatty acids in WAT of *Pla2g5*<sup>+/+</sup> and *Pla2g5*<sup>-/-</sup> mice.  
 (G) Correlation of *PLA2G5* expression levels in human visceral WAT with LDL or HDL cholesterol (n = 128, 64 from mesenteric WAT and 64 from colorectal fat appendices).

In (A)–(F), mice were fed a LFD or HFD for 26 weeks. Data are representative of (A–C) or compiled from (D–G) two experiments. Mean ± SEM; \*p < 0.05, \*\*p < 0.01.

BMDMs under M1 or M2 skewing conditions led to a similar induction of respective macrophage subset markers (Figure S5A), suggesting that although *PLA2G5* expressed at a low level in macrophages is insufficient to affect their polarization, it can facilitate the conversion of M1 to M2 macrophages when supplied abundantly through a paracrine route. Indeed, when irradiated WT mice were adoptively transferred with *Pla2g5*<sup>-/-</sup> or *Pla2g5*<sup>+/+</sup> BM cells, HFD-induced obesity, insulin resistance, and hyperlipidemia were comparable in both groups (Figures S5B–S5D). Thus, *PLA2G5* in nonhematopoietic cells (likely adipocytes) appears to be mainly responsible for the amelioration of metabolic disorders.

Of the potential *PLA2G5*-driven lipid mediators tested, prostaglandin E<sub>2</sub> (PGE<sub>2</sub>), an AA metabolite, had the ability to induce *Arg1*, without affecting *Nos2*, in BMDMs stimulated with LPS+IFN-γ (Figure 5E) or PA (Figure 5F). Exogenous *PLA2G5*

augmented PGE<sub>2</sub> generation by PA-stimulated BMDMs (Figure 5G). In vivo, however, the WAT level of PGE<sub>2</sub> did not differ between HFD-fed *Pla2g5*<sup>-/-</sup> and *Pla2g5*<sup>+/+</sup> mice, while that of PGD<sub>2</sub> was higher in the null mice, likely due to upregulation of PGD<sub>2</sub> synthase (Figures S5E and S5F). Thus, it is more likely that *PLA2G5* action involves an alternative lipid-mediated process.

Proinflammatory ER stress induced by saturated fatty acids can be ameliorated by unsaturated fatty acids (Hotamisligil, 2006). As *PLA2G5* released OA > LA from LDL-PC (Figures 3D and 3E), we examined whether these unsaturated fatty acids affected PA-induced M1 macrophage polarization. Strikingly, OA or LA canceled out the induction of *Nos2* even at 2 μM and also restored the expression of *Cd206* dose dependently in PA-treated BMDMs (Figure 5H). The WAT level of the *PLA2G5*-sensitive OA pool was within a range enough to affect macrophage polarization (Figures 3E and 5H). Thus, OA, and possibly

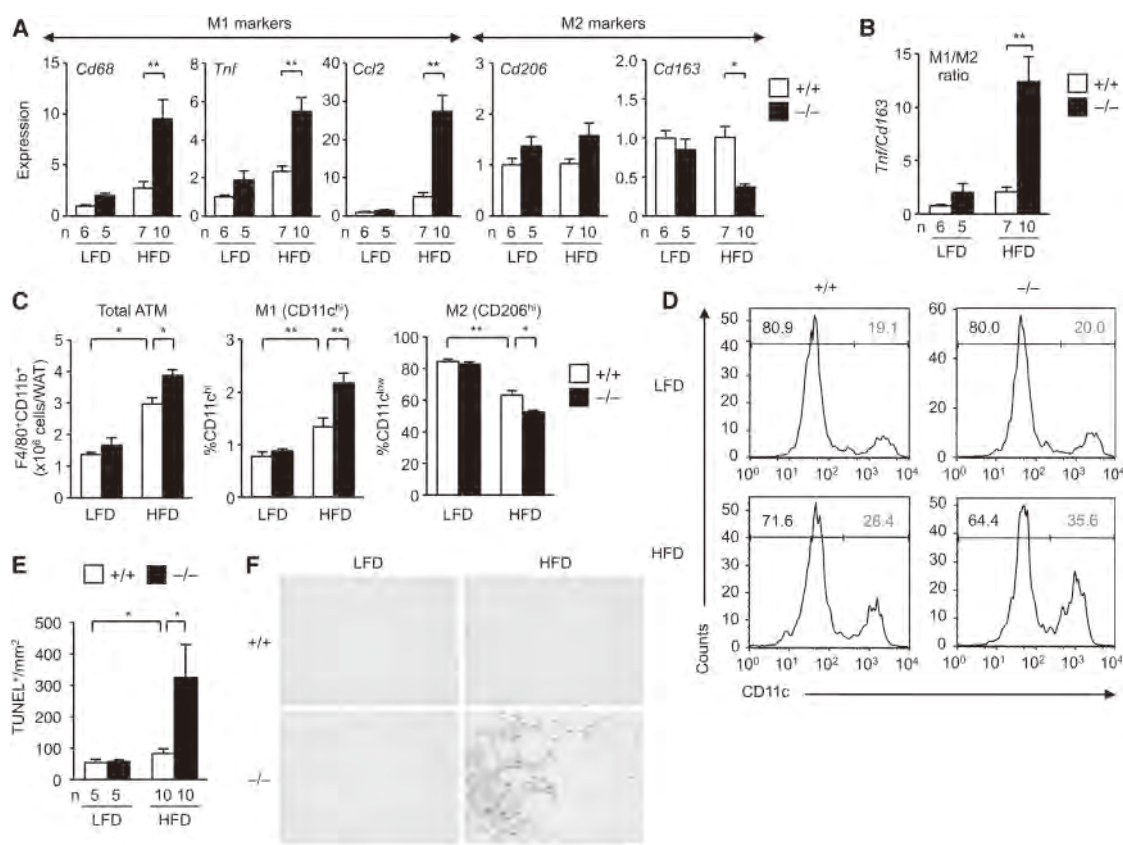


**Figure 4. Exacerbated Adipose Tissue Inflammation in HFD-Fed *Pla2g5*<sup>-/-</sup> Mice**

(A) Expression of M1 or M2 macrophage markers normalized by *Gapdh* in WAT of *Pla2g5*<sup>+/+</sup> and *Pla2g5*<sup>-/-</sup> mice, with their expression in *Pla2g5*<sup>+/+</sup> mice on a LFD being regarded as 1. (B) Ratios of M1 (*Tnf*) to M2 (*Cd163*) genes. (C) FACS analysis of adipose tissue macrophages (ATM) from *Pla2g5*<sup>+/+</sup> and *Pla2g5*<sup>-/-</sup> mice. Counts of F4/80<sup>+</sup>CD11b<sup>+</sup> ATM and proportions of CD11c<sup>hi</sup> (M1) and CD206<sup>hi</sup> (M2) macrophages in SVF from WAT (n = 4). (D) Representative FACS profiles of CD11c<sup>+</sup> cells in the SVF. (E and F) TUNEL staining of WAT in *Pla2g5*<sup>+/+</sup> and *Pla2g5*<sup>-/-</sup> mice. Average scores of TUNEL-positive cells (E) and representative images (scale bar, 50 μm) (F). Mice were fed a LFD or HFD for 26 weeks. Data are compiled from (A, B, and E) or representative of (C, D, and F) two experiments. Mean ± SEM; \*p < 0.05, \*\*p < 0.01.

PUFAs mobilized by PLA2G5 from LDL, may allow the polarization from M1 to M2 macrophages by attenuating the PA-induced stress response, which underscores a mechanistic link between PLA2G5-driven LDL hydrolysis and anti-inflammation in WAT.

### PLA2G5 Is a Th2/M2-Prone sPLA<sub>2</sub>

While T helper 2 (Th2) cytokines are proallergic, they facilitate M2 macrophage polarization, thereby counteracting adipose tissue inflammation and insulin resistance (Odegaard and Chawla, 2013). It has been shown that PLA2G5 from both hematopoietic and nonhematopoietic origins regulates the Th2 response and thereby asthma (Giannattasio et al., 2010; Henderson et al., 2013). Indeed, when WT mice were immunized intraperitoneally with ovalbumin (OVA), lymph node cells from *Pla2g5*<sup>-/-</sup> mice expressed levels of IL-4 and IL-13 lower than those from *Pla2g5*<sup>+/+</sup> mice upon OVA challenge ex vivo (Figure S5G). Serum levels of total or OVA-specific immunoglobulin E (IgE) were lower in *Pla2g5*<sup>-/-</sup> mice than in *Pla2g5*<sup>+/+</sup> mice (Figure S5H). Moreover, beyond the crucial role of adipocyte- rather than macrophage-derived PLA2G5 in obesity, *Pla2g5* expression in BMDMs was

markedly induced by M2-skewing Th2 cytokines (IL-4 and IL-13) and was unaffected or reduced by M1-skewing TLR agonists (LPS and zymozan) or Th1 cytokines (IFN-γ and granulocyte-macrophage colony-stimulating factor [GM-CSF]) among others (Figures S5I and S5J). In ex vivo skewing culture of splenic naive CD4<sup>+</sup> T cells, *Pla2g5* was induced preferentially in IL-4-driven Th2 cells (Figure S5K). In the context of obesity, the WAT expression of *I133*, a stromal Th2 cytokine that increases M2 macrophages and suppresses adipose tissue inflammation (Miller et al., 2010), was lower in HFD-fed *Pla2g5*<sup>-/-</sup> mice than in replicate *Pla2g5*<sup>+/+</sup> mice (Figure 5I). Thus, PLA2G5 is a unique sPLA<sub>2</sub> that is induced by Th2 cytokines and facilitates the Th2 and M2 responses. *Pla2g5*<sup>-/-</sup> mice are Th2/M2 insufficient, and this intrinsic immune balance shift may also underlie the exacerbated adipose tissue inflammation.

### Reduced Adiposity in Adipocyte-Specific *Pla2g5* Transgenic Mice

To explore whether the forced overexpression of PLA2G5 in the WAT would yield outcomes opposite to its deletion, we

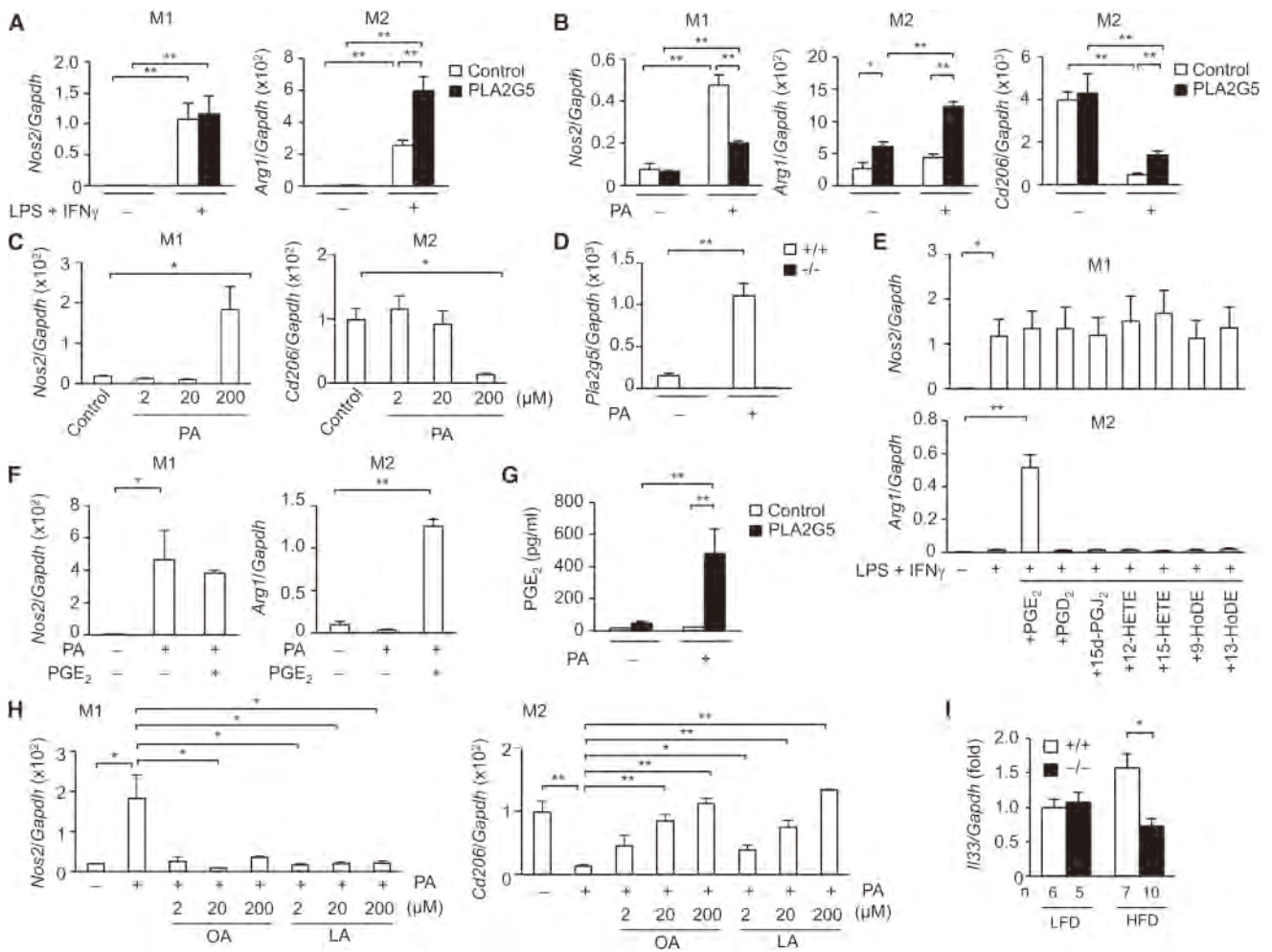


**Figure 5. PLA2G5 Promotes M2 Macrophage Polarization**

(A and B) Expression of M1 and M2 macrophage markers in WT BMDMs cultured for 24 hr with (+) or without (-) LPS+IFN- $\gamma$  (A) or 200  $\mu$ M PA (B) in the presence or absence of 70 nM PLA2G5 (n = 7).

(C) Expression of M1 and M2 macrophage markers in WT BMDMs after culture for 24 hr with various concentrations of PA (n = 6).

(D) Expression of *Pla2g5* in *Pla2g5*<sup>+/+</sup> and *Pla2g5*<sup>-/-</sup> BMDMs after culture for 24 hr with 200  $\mu$ M PA (n = 6).

(E and F) Expression of M1 and M2 markers in WT BMDMs cultured for 24 hr with (+) or without (-) LPS+IFN- $\gamma$  (E) or 200  $\mu$ M PA (F) in the presence or absence of 1  $\mu$ M lipid mediators (n = 6).

(G) PGE<sub>2</sub> generation by WT BMDMs treated for 6 hr with PLA2G5 in the presence (+) or absence (-) of 200  $\mu$ M PA (n = 3).

(H) Effects of OA or LA on the expression of M1 or M2 macrophage markers in WT BMDMs treated for 24 hr with 200  $\mu$ M PA (n = 3).

(I) Expression of *I133* relative to *Gapdh* in WAT of *Pla2g5*<sup>+/+</sup> and *Pla2g5*<sup>-/-</sup> mice fed a LFD or HFD for 26 weeks.

Data are compiled from (A–F and I) or representative of (G and H) two experiments. Mean  $\pm$  SEM; \*p < 0.05, \*\*p < 0.01.

generated adipocyte-specific *Pla2g5* transgenic mice (*Fabp4-Pla2g5*<sup>tg/+</sup>) by mating *LNL-Pla2g5*<sup>tg/+</sup> mice (Ohtsuki et al., 2006), in which the *Pla2g5* transgene was silent, with *Fabp4-Cre*<sup>tg/+</sup> mice, in which Cre recombinase is expressed under control of the adipocyte-specific *Fabp4* promoter (Figure S6A). *Fabp4-Pla2g5*<sup>tg/+</sup> mice were born normally and grew to adulthood. As expected, expression of *Pla2g5* was robustly increased in perigonadal WAT, but not in other tissues, in *Fabp4-Pla2g5*<sup>tg/+</sup> mice compared to control *LNL-Pla2g5*<sup>tg/+</sup> mice (Figure S6B). Even on a LFD, where the influence of diet-inducible endogenous PLA2G5 is negligible, *Fabp4-Pla2g5*<sup>tg/+</sup> mice had body weight significantly lower than that of age-matched control mice (Figure S6C). CT scanning re-

vealed a reduced adiposity in *Fabp4-Pla2g5*<sup>tg/+</sup> mice relative to control mice (Figure S6D). Phospholipid levels in plasma and LDL were significantly lower in *Fabp4-Pla2g5*<sup>tg/+</sup> mice than in control mice (Figure S6E). Moreover, WAT expression levels of proinflammatory genes, but not lipogenic genes, tended to be lower in *Pla2g5*<sup>tg/+</sup> mice than in control mice (Figure S6F). After 6 weeks of HFD feeding, when the induction of endogenous *Pla2g5* was still minimal (Figure S1B), *Fabp4-Pla2g5*<sup>tg/+</sup> mice displayed better insulin sensitivity and lower WAT expression of *Ccl2* compared to control mice (Figures S6G and S6H). Collectively, the data for adipocyte-specific PLA2G5 overexpression reciprocated those for PLA2G5 deficiency.

### Reduced Adiposity and Altered Lipoprotein Profiles in *Pla2g2e*<sup>-/-</sup> Mice

To address the roles of PLA2G2E, we generated *Pla2g2e*<sup>-/-</sup> mice (Figures S7A and S7B). Expression of mRNA and protein for PLA2G2E was absent in WAT of HFD-fed *Pla2g2e*<sup>-/-</sup> mice (Figure S7C). On a HFD, obesity and weight gain tended to be lower (though statistically insignificant) in *Pla2g2e*<sup>-/-</sup> mice than in *Pla2g2e*<sup>+/+</sup> mice (Figures 6A and 6B). Volumes of total, visceral, and subcutaneous fats (Figure 6C) and adipocyte size in perigonadal WAT (Figure 6D) were significantly reduced in HFD-fed *Pla2g2e*<sup>-/-</sup> mice relative to *Pla2g2e*<sup>+/+</sup> mice. Plasma leptin and insulin levels (Figures S7D and S7E), glucose and insulin tolerances (Figures S7F and S7G), food intake, locomotion and oxygen consumption (Figures S7H–S7J), and WAT expression of adipogenic, lipogenic, lipolytic, and inflammatory genes (Figure S7K) did not differ between HFD-fed *Pla2g2e*<sup>+/+</sup> and *Pla2g2e*<sup>-/-</sup> mice. HFD-induced fatty liver was mildly ameliorated by PLA2G2E deficiency, as revealed by reductions of hepatic lipid deposition (Figures 6E and 6F), plasma ALT, and aspartate amino transferase (AST) levels (Figure 6G), and hepatic expression of some genes for lipid storage and inflammation (Figure S7L) in HFD-fed *Pla2g2e*<sup>-/-</sup> mice compared to WT littermates. Lower hepatic *Lpl* expression in *Pla2g2e*<sup>-/-</sup> mice (Figure S7L) might partly contribute to the reduced fat uptake into the liver.

HFD-induced increases in plasma phospholipids and cholesterol were lower in *Pla2g2e*<sup>-/-</sup> mice than in *Pla2g2e*<sup>+/+</sup> mice (Figure 6H), suggesting that PLA2G2E alters lipoprotein composition. Indeed, phospholipids, TG, and cholesterol in VLDL, LDL, and HDL were significantly lower in HFD-fed *Pla2g2e*<sup>-/-</sup> mice than in *Pla2g2e*<sup>+/+</sup> mice (Figures 6I and S7M). ESI-MS revealed that LDL (Figure 6J) and HDL (data not shown) in *Pla2g2e*<sup>-/-</sup> mice contained more PE and PS species, with no apparent fatty acid selectivity, than those in *Pla2g2e*<sup>+/+</sup> mice, while PC species did not differ in both genotypes, suggesting that adipocyte-derived PLA2G2E acts on PE and PS in favor of PC in lipoproteins. The increase of these minor phospholipids by PLA2G2E deficiency may eventually decrease the relative proportion of PC and other lipids in lipoproteins, thereby affecting lipid partitioning among tissues.

Taken together, PLA2G5 is protective against metabolic disorders by hydrolyzing PC in hyperlipidemic LDL to release unsaturated fatty acids, which attenuate adipose tissue inflammation through M2 macrophage skewing, while PLA2G2E mildly promotes adiposity and fatty liver by altering the proportion of PE and PS in lipoproteins (Figure 7).

## DISCUSSION

Adipocyte hypertrophy results in secretion of bioactive factors such as adipokines, chemokines, and free fatty acids, which adversely affect inflammation and tissue remodeling while providing valuable protection against lipotoxic effects of excess lipid exposure (Després and Lemieux, 2006). We now show that two particular sPLA<sub>2</sub>s are induced in hypertrophic adipocytes and play distinct roles in metabolic control in the context of diet-induced obesity. Our results add the sPLA<sub>2</sub> family to a growing list of extracellular lipolytic enzymes that can control systemic metabolic states and give another insight into the paracrine role of sPLA<sub>2</sub> in response to a given microenvironmental cue.

The obesity-driven induction of PLA2G5 in hypertrophic adipocytes, along with its constitutive expression at relatively high levels in the heart and skeletal muscle, which have a high demand for lipid as an energy source, suggests that one of the primary roles of this sPLA<sub>2</sub> may be related to the regulation of energy metabolism. We show here that *Pla2g5* ablation exacerbates diet-induced obesity, hyperlipidemia, and insulin resistance, providing insight into the beneficial role of PLA2G5 in metabolic disorders. PLA2G5 can hydrolyze PC in lipoproteins in vitro (Sato et al., 2008), and our present results show that this reaction does occur in vivo in the context of obesity, where adipocyte-driven PLA2G5 hydrolyzes excess PC in lipid-overladen LDL, eventually protecting from hyperlipidemia. In this regard, the metabolic effects of PLA2G5 are similar to those of lipoprotein lipase, whose expression also shows a reciprocal relationship with obesity-related traits (Chen et al., 2008). Even though it has been thought that mice are not always good models to study LDL metabolism, as they use VLDL and HDL primarily, our results show that LDL metabolism by sPLA<sub>2</sub> can influence systemic metabolic states. The increased LDL-TG levels and the reduced physical activities in *Pla2g5*<sup>-/-</sup> mice could impact adipocyte hypertrophy, hepatic steatosis, and WAT inflammation. Importantly, PLA2G5 expression in human WAT inversely correlates with plasma LDL levels, implying a human relevance of our observations. Moreover, our findings are also compatible with the association of PLA2G5 mutations with LDL levels in subjects with type 2 diabetes or obesity (Sergouniotis et al., 2011; Wootton et al., 2007).

Importantly, PLA2G5 plays an anti-inflammatory role in obesity, which likely makes a major contribution to the exacerbated obesity, insulin resistance, and hyperlipidemia in *Pla2g5*<sup>-/-</sup> mice. This action of PLA2G5 depends on its capacity to hydrolyze phospholipids in LDL to release unsaturated fatty acids, which can allow the polarization shift of macrophages from the M1 to M2 state. Reportedly, fatty acids released from lipoproteins by venom sPLA<sub>2</sub> or lipoprotein lipase can facilitate anti-inflammatory responses in vitro (Ahmed et al., 2006; Duncan et al., 2010; Namgaladze et al., 2010). Herein, we demonstrate that unsaturated fatty acids including OA > LA, which are supplied by PLA2G5-driven hydrolysis of PC in hyperlipidemic LDL, prevent PA-induced M1 macrophage polarization, likely through attenuating the ER stress, revealing a functional link between lipoprotein metabolism and anti-inflammation by this sPLA<sub>2</sub>. This mechanism fits with the view that PLA2G5 displays an apparent (even if not strict) substrate preference for PC bearing a fatty acid with a low degree of unsaturation. Our study provides in vivo evidence that sPLA<sub>2</sub> acts in this manner, thus providing a rationale for the long-standing question on the physiological importance of lipoprotein hydrolysis by this enzyme family and revealing an anti-inflammatory mechanism exerted by a particular sPLA<sub>2</sub>. Nonetheless, it cannot be fully ruled out that the mobilization of PGE<sub>2</sub>, a  $\omega$ 6 AA-derived eicosanoid that promotes M2 macrophage skewing (Heusinkveld et al., 2011), or  $\omega$ 3 PUFA metabolites, which are protective against metabolic disorders (Oh and Olefsky, 2012; Spite et al., 2014), might also partly underlie the antiobese action of PLA2G5.

As another intriguing feature of PLA2G5, we show that it is a “Th2/M2-prone sPLA<sub>2</sub>” that allows the immune balance shift toward the Th2/M2 status. Given the increased metabolic

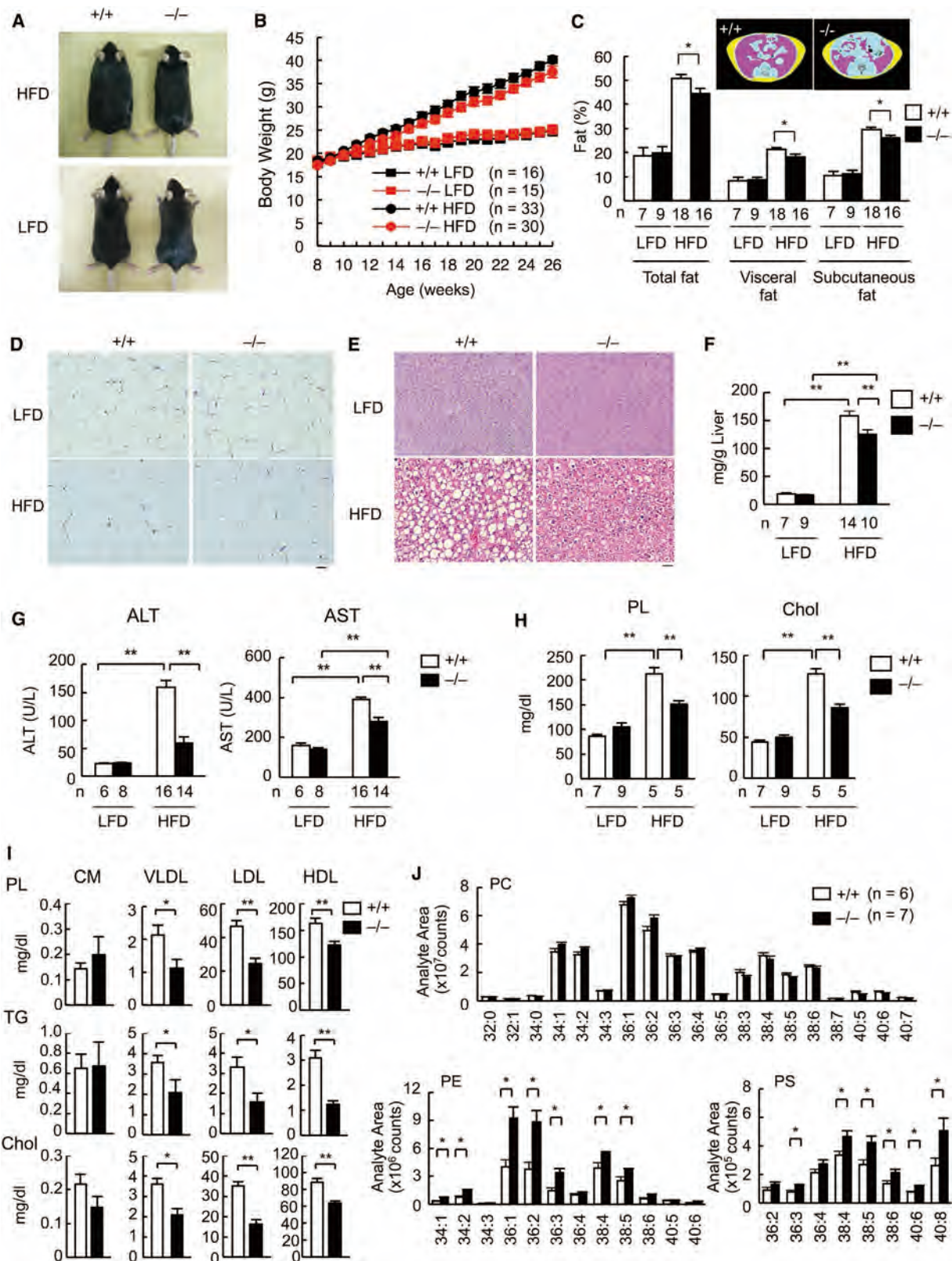


**Figure 6. Altered Diet-Induced Adiposity, Fatty Liver, and Lipoproteins in *Pla2g2e*<sup>-/-</sup> Mice**

(A) Representative photos of *Pla2g2e*<sup>+/+</sup> and *Pla2g2e*<sup>-/-</sup> mice fed a LFD or HFD.  
 (B) Body weights of *Pla2g2e*<sup>+/+</sup> and *Pla2g2e*<sup>-/-</sup> mice fed a LFD or HFD for the indicated periods.

(legend continued on next page)

Cell Metabolism

Metabolic sPLA<sub>2</sub>s in Obesity

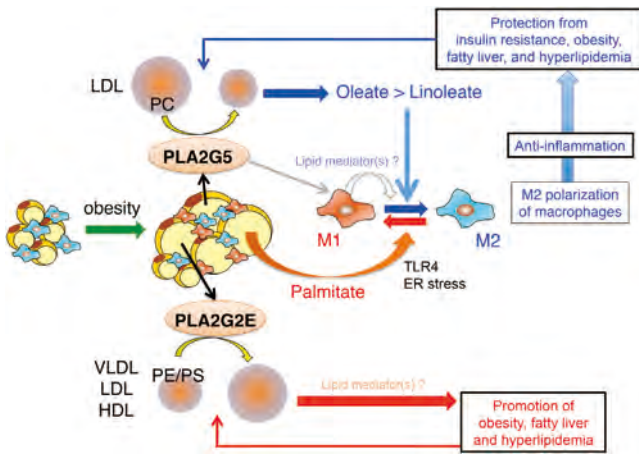


**Figure 7. Schematic Diagram of the Roles of Metabolic sPLA<sub>2</sub>s**

In obesity, PLA2G2E is induced in adipocytes in accordance with adipogenesis and hydrolyzes PE and PS in VLDL, LDL, and HDL, eventually promoting fat storage in WAT and liver. Subsequently, obesity-associated stress induces PLA2G5 in hypertrophic adipocytes. PLA2G5 hydrolyzes PC in hyperlipidemic LDL and facilitates the skewing of macrophages from M1 to M2 subsets, thereby playing protective roles against adipose tissue inflammation, insulin resistance, obesity, fatty liver, and hyperlipidemia. Saturated fatty acids (e.g., palmitate) supplied abundantly from adipocytes trigger M1 polarization of macrophages, which is ameliorated by PLA2G5-driven unsaturated fatty acids (oleate > linoleate) from LDL or possibly some lipid mediators from macrophages. It remains unknown whether particular PLA2G2E-produced lipid mediator(s) would participate in this process.

disorders by genetic deletion of Th2 or M2 inducers (e.g., *Il4*, *Il13*, *Il33*, *Stat6*, or *Pparg*) (Odegaard and Chawla, 2013), the lack of PLA2G5 may also decrease the whole-body Th2-M2 status, thereby aggravating obesity-related inflammation. This notion agrees with the fact that *Pla2g5*<sup>-/-</sup> mice are resistant to asthma (Giannattasio et al., 2010; Henderson et al., 2013), where Th2 cells and M2 macrophages promote allergy, while they suffer from exaggerated arthritis or infection (Balestrieri et al., 2009; Boilard et al., 2010), where Th2 immunity counteracts Th1/Th17-based inflammation, thus accounting for the pro- versus anti-inflammatory actions of PLA2G5 in distinct immunopathological settings. As the phagocytotic activities are distinct among macrophage subsets (Leidi et al., 2009; Titos et al., 2011), the altered M1/M2 ratio of macrophages in obese *Pla2g5*<sup>-/-</sup> WAT could explain the perturbed clearance of dead cells. This idea also accords with the finding that *Pla2g5* ablation decreases macrophage uptake of exogenous materials (Balestrieri et al., 2009; Boilard et al., 2010).

We also show the *in vivo* role of PLA2G2E as another obesity-induced, adipocyte-derived sPLA<sub>2</sub>. In contrast to PLA2G5 that

hydrolyzes PC in LDL, PLA2G2E acts on PE and PS in VLDL, LDL, and HDL. As such, PLA2G2E alters lipid composition in lipoprotein particles, eventually moderately facilitating fat deposition in tissues. Although little is known about the role of PE or PS in lipoproteins, our study has shed light on the importance of these minor lipoprotein phospholipids in the metabolic regulation and opened an opportunity to analyze this issue using *Pla2g2e*<sup>-/-</sup> mice as a tool. As the increase of negative charges in lipoproteins by oxidative modification renders the particles smaller (Hidaka et al., 2005), the increase of anionic phospholipids (e.g., PS) in lipoproteins may afford a similar effect. Lipoproteins with increased negative charges are more susceptible to hydrolysis by hepatic lipase, resulting in smaller particles (Boucher et al., 2007). Anionic phospholipids decrease the affinity of ApoE for its receptor, thereby reducing lipid transfer into tissues (Yamamoto and Ryan, 2007). Alternatively, Lyso-PE or Lyso-PS produced by PLA2G2E might have some metabolic effects, a possibility that needs to be addressed. Compatible with our present study, PLA2G2A in place of PLA2G2E is induced in obese rats in which the metabolic symptoms are blocked by a PLA2G2A inhibitor (Iyer et al., 2012).

In summary, our study underscores the physiological relevance of lipoprotein hydrolysis by sPLA<sub>2</sub>s, highlights metabolic sPLA<sub>2</sub>s as integrated regulators of immune and metabolic responses, and brings about a shift toward a better understanding of the biological roles of this extracellular lipolytic enzyme family as a metabolic coordinator. The contrasting metabolic effects of PLA2G5 and PLA2G2E are reminiscent of distinct roles of PLA2G5 and PLA2G2A in arthritis (Boilard et al., 2010), PLA2G5 and PLA2G10 in atherosclerosis (Ait-Oufella et al., 2013; Bostrom et al., 2007), or PLA2G2D and PLA2G5 in antigen-presenting cells (Giannattasio et al., 2010; Miki et al., 2013), warning about the use of pan-sPLA<sub>2</sub> inhibitors for therapy and pointing to an alternative strategy to use a sPLA<sub>2</sub> inhibitor specific for individual sPLA<sub>2</sub>s. Targeting the metabolic sPLA<sub>2</sub>s and their organ expression will be a challenge, since these enzymes appear to play highly selective roles in specific organs and disease states.

**EXPERIMENTAL PROCEDURES**

**Mice**

*Pla2g5*<sup>-/-</sup> (Satake et al., 2004), *Pla2g5*<sup>tg/tg</sup> (Ohtsuki et al., 2006), and their littermate control mice were backcrossed onto the C57BL/6 mice (Japan SLC) for >12 generations. Generation of *Pla2g2e*<sup>-/-</sup> mice is detailed in Supplemental Information. *Lep<sup>ob/ob</sup>* mice and *Fabp4-Cre* transgenic mice were obtained from Jackson Laboratory. All mice were housed in climate-controlled (23°C) pathogen-free facilities with a 12 hr light-dark cycle, with free access to standard LFD (CE2; CLEA Japan) and water. Knockout and littermate WT mice (8-week-old female) were placed on a HFD (High fat diet 32; CLEA Japan)

(C) CT analysis of fat volumes in *Pla2g2e*<sup>+/+</sup> and *Pla2g2e*<sup>-/-</sup> mice. Pink and yellow areas indicate visceral and subcutaneous fats in HFD-fed mice, respectively (inset).

(D and E) Hematoxylin and eosin staining of WAT (D) or liver (E) from *Pla2g2e*<sup>+/+</sup> and *Pla2g2e*<sup>-/-</sup> mice (scale bar, 50 μm).

(F and G) Levels of hepatic TG (F) and plasma ALT and AST (G) in *Pla2g2e*<sup>+/+</sup> and *Pla2g2e*<sup>-/-</sup> mice.

(H) Plasma levels of phospholipids (PL) and cholesterol (Chol) in *Pla2g2e*<sup>+/+</sup> and *Pla2g2e*<sup>-/-</sup> mice.

(I) PL, TG, and Chol levels in lipoproteins from HFD-fed *Pla2g2e*<sup>+/+</sup> and *Pla2g2e*<sup>-/-</sup> mice (n = 5).

(J) ESI-MS of PC, PE, and PS in LDL from HFD-fed *Pla2g2e*<sup>+/+</sup> and *Pla2g2e*<sup>-/-</sup> mice.

Mice were fed a LFD or HFD for 16 (A and C) or 18 (D–J) weeks. Data are compiled from two (H–J) or three (B, C, F, and G) experiments. Representative images of two experiments are shown (A, D, and E). Mean ± SEM; \*p < 0.05, \*\*p < 0.01.

or LFD for appropriate periods. All procedures were performed in accordance with approvals by the Institutional Animal Care and Use Committees of Tokyo Metropolitan Institute of Medical Science, Showa University, and the University of Washington.

#### Quantitative RT-PCR

Total RNA was extracted from tissues using TRIzol reagent (Invitrogen). First-strand cDNA synthesis was performed using a High Capacity cDNA Reverse Transcriptase Kit (Applied Biosystems). PCR reactions were carried out using a Power SYBR Green PCR system (Applied Biosystems) or a TaqMan Gene Expression System (Applied Biosystems) on the ABI7300 Real Time PCR system (Applied Biosystems). The probe/primer sets used are listed in Tables S3 and S4.

#### Microarray

Total RNA was extracted from WAT derived from female C57BL/6 mice fed a LFD or HFD for 18 weeks and purified using the RNeasy Mini Kit (QIAGEN). The quality of RNA was assessed with a 2100 Bioanalyzer (Agilent Technologies). Both cDNA and cRNA were synthesized with a Low Input QuickAmp Labeling Kit according to the manufacturer's protocol (Agilent Technologies). Samples were hybridized to the Whole Mouse Genome Microarray Kit (4 × 44K; Agilent Technologies), washed, and then scanned using a SureScan Microarray Scanner (Agilent Technologies). Microarray data were analyzed with Feature Extraction software (Agilent Technologies) and then imported into GeneSpring GX software (Agilent Technologies). Probes were normalized by quantile normalization among all microarray data.

#### Flow Cytometry

The isolated SVF cells were incubated with either labeled monoclonal antibody or isotype control antibody (hamster IgG [HTK888], rat IgG<sub>2a</sub> [RTK2758], or rat IgG<sub>2b</sub> [RTK4530]; BioLegend) and analyzed by flow cytometry with a FACS Aria III (BD Biosciences) and FlowJo (Tree Star) software. The antibodies used were specific for mouse F4/80 (BM8; BioLegend), CD11b (M1/70; BioLegend), CD11c (N418; eBioscience), and CD206 (C068C2; BioLegend).

#### Glucose and Insulin Tolerance Tests

Mice were fasted for 16 and 6 hr before intraperitoneal injection of glucose (2 mg glucose/g body weight) (Wako) and insulin (0.75 mIU/g body weight) (Eli Lilly) in saline, respectively. Blood glucose concentrations were monitored at various time intervals using a Medisafe-Mini blood glucose monitoring system (Terumo).

#### Measurement of Serum Biomedical Markers

Serum insulin and leptin levels were quantified by a mouse insulin ELISA kit (Mercodia) and a leptin immunoassay kit (R&D Systems), respectively. Serum ALT and AST levels were quantified using the transaminase CII-test Wako kit (Wako).

#### CT Analysis

Mice were anesthetized with nembutal (0.5 mg/g body weight) (Dainippon Sumitomo Pharma), and their adiposity was analyzed using the micro-CT systems eXplore Lucus Micro CT Scanner (GE Healthcare) or Latheta LCT-100 (Aloka).

#### Oxygen Consumption and Locomotor Activity

Oxygen consumption was measured every 3 min over 24 hr under resting conditions using an MK-5000RQ metabolism measuring system for small animals (Muromachi Kikai). For measurement of basal locomotor activity, mice were placed into chambers of an ACTIMO-S food intake, drinking, and locomotor activity monitoring system (Shintechno). Food and water were provided ad libitum. Mice were allowed to acclimatize in the chambers for 24 hr, and then their physical activities were measured over the next 24 hr.

#### Analyses of Plasma Lipids and Lipoproteins

Analysis of plasma lipoproteins was performed by LipoSearch (Skylight Biotech). Plasma cholesterol, phospholipid, LPC, TG, and NEFA levels were determined with a Determinar TC2 (Kyowa Medex), a Phospholipid C Test (Wako), a LPC Assay kit (AZWELL), a Determinar TG2 (Kyowa Medex), and a NEFA C Kit (Wako), respectively.

#### ESI-MS/MS

Lipid analysis was performed using a 4000 QTRAP quadrupole-linear ion trap hybrid MS (AB SCIEX) with liquid chromatography (LC-20AP; Shimadzu) combined with a HTS PAL autosampler (CTC Analytics AG), as detailed in Supplemental Information.

#### Cell Culture Studies

Studies using adipocytes and immune cells are detailed in Supplemental Information.

#### Human Samples

Mesenteric WAT and fatty appendices were obtained by curative resection from 64 patients with colorectal tumors, all of whom underwent elective surgical colectomy at the Kumamoto University Hospital (Kumamoto, Japan) from March 1, 2012 to August 31, 2013. The clinical characteristics are summarized in Table S2. The study was approved by the Ethics Committees of Kumamoto University, with written informed consent from all patients.

#### Statistical Analyses

All values are given as the mean ± SEM. Differences between two groups were assessed by using the unpaired two-tailed t test. Data involving more than two groups were assessed by ANOVA, and relationships between clinical and metabolic parameters were assessed by Spearman's rank correlation test. Correlation coefficients (R) and probability (P) values were calculated with the Excel Statistical Program File yStat 2008 (Igaku Tosho Shuppan).

#### ACCESSION NUMBERS

The GEO accession number for microarray data reported in this paper is GSE56038.

#### SUPPLEMENTAL INFORMATION

Supplemental Information includes Supplemental Experimental Procedures, seven figures, and four tables and can be found with this article online at <http://dx.doi.org/10.1016/j.cmet.2014.05.002>.

#### ACKNOWLEDGMENTS

We thank Dr. Jonathan P. Arm (Novartis Pharma) for providing us *Pla2g5<sup>-/-</sup>* mice and Dr. Osamu Kaminuma (Tokyo Metropolitan Institute of Medical Science) for providing us mRNAs from naive and polarized T cells. This work was supported by grants-in-aid for Scientific Research from the Ministry of Education, Culture, Sports, Science and Technology of Japan (22116005 and 24390021 to M.M.; 23790120 and 25860059 to H.S.; 24117724 and 23790119 to Y.T.), CREST from the Japan Science and Technology Agency (to M.M.), the Uehara, Mitsubishi, Terumo and Toray Science Foundations (to M.M.), and grant HL36235 (to M.H.G.) from the National Institutes of Health.

Received: August 23, 2013

Revised: February 19, 2014

Accepted: April 2, 2014

Published: June 5, 2014

#### REFERENCES

- Ahmed, W., Orasanu, G., Nehra, V., Asatryan, L., Rader, D.J., Ziouzenkova, O., and Plutzky, J. (2006). High-density lipoprotein hydrolysis by endothelial lipase activates PPARalpha: a candidate mechanism for high-density lipoprotein-mediated repression of leukocyte adhesion. *Circ. Res.* 98, 490–498.
- Ait-Oufella, H., Herbin, O., Lahoute, C., Coatrieux, C., Loyer, X., Joffre, J., Laurans, L., Ramkhalawon, B., Blanc-Brude, O., Karabina, S., et al. (2013). Group X secreted phospholipase A<sub>2</sub> limits the development of atherosclerosis in LDL receptor-null mice. *Arterioscler. Thromb. Vasc. Biol.* 33, 466–473.
- Balestrieri, B., Maekawa, A., Xing, W., Gelb, M.H., Katz, H.R., and Arm, J.P. (2009). Group V secretory phospholipase A<sub>2</sub> modulates phagosome maturation

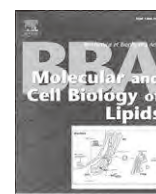
- and regulates the innate immune response against *Candida albicans*. *J. Immunol.* **182**, 4891–4898.
- Boilard, E., Lai, Y., Larabee, K., Balestrieri, B., Ghomashchi, F., Fujioka, D., Gobeze, R., Coblyn, J.S., Weinblatt, M.E., Massarotti, E.M., et al. (2010). A novel anti-inflammatory role for secretory phospholipase A<sub>2</sub> in immune complex-mediated arthritis. *EMBO Mol Med* **2**, 172–187.
- Bostrom, M.A., Boyanovsky, B.B., Jordan, C.T., Wadsworth, M.P., Taatjes, D.J., de Beer, F.C., and Webb, N.R. (2007). Group v secretory phospholipase A<sub>2</sub> promotes atherosclerosis: evidence from genetically altered mice. *Arterioscler. Thromb. Vasc. Biol.* **27**, 600–606.
- Boucher, J.G., Nguyen, T., and Sparks, D.L. (2007). Lipoprotein electrostatic properties regulate hepatic lipase association and activity. *Biochem. Cell Biol.* **85**, 696–708.
- Chen, Y., Zhu, J., Lum, P.Y., Yang, X., Pinto, S., MacNeil, D.J., Zhang, C., Lamb, J., Edwards, S., Sieberts, S.K., et al. (2008). Variations in DNA elucidate molecular networks that cause disease. *Nature* **452**, 429–435.
- Chiu, H.K., Qian, K., Ogimoto, K., Morton, G.J., Wisse, B.E., Agrawal, N., McDonald, T.O., Schwartz, M.W., and Dichek, H.L. (2010). Mice lacking hepatic lipase are lean and protected against diet-induced obesity and hepatic steatosis. *Endocrinology* **151**, 993–1001.
- Cinti, S., Mitchell, G., Barbatelli, G., Murano, I., Ceresi, E., Faloia, E., Wang, S., Fortier, M., Greenberg, A.S., and Obin, M.S. (2005). Adipocyte death defines macrophage localization and function in adipose tissue of obese mice and humans. *J. Lipid Res.* **46**, 2347–2355.
- Després, J.P., and Lemieux, I. (2006). Abdominal obesity and metabolic syndrome. *Nature* **444**, 881–887.
- Duncan, J.G., Bharadwaj, K.G., Fong, J.L., Mitra, R., Sambandam, N., Courtois, M.R., Lavine, K.J., Goldberg, I.J., and Kelly, D.P. (2010). Rescue of cardiomyopathy in peroxisome proliferator-activated receptor- $\alpha$  transgenic mice by deletion of lipoprotein lipase identifies sources of cardiac lipids and peroxisome proliferator-activated receptor- $\alpha$  activators. *Circulation* **121**, 426–435.
- Giannattasio, G., Fujioka, D., Xing, W., Katz, H.R., Boyce, J.A., and Balestrieri, B. (2010). Group V secretory phospholipase A<sub>2</sub> reveals its role in house dust mite-induced allergic pulmonary inflammation by regulation of dendritic cell function. *J. Immunol.* **185**, 4430–4438.
- Haemmerle, G., Lass, A., Zimmermann, R., Gorkiewicz, G., Meyer, C., Rozman, J., Heldmaier, G., Maier, R., Theussl, C., Eder, S., et al. (2006). Defective lipolysis and altered energy metabolism in mice lacking adipose triglyceride lipase. *Science* **312**, 734–737.
- Henderson, W.R., Jr., Ye, X., Lai, Y., Ni, Z., Bollinger, J.G., Tien, Y.T., Chi, E.Y., and Gelb, M.H. (2013). Key role of group v secreted phospholipase A<sub>2</sub> in Th2 cytokine and dendritic cell-driven airway hyperresponsiveness and remodeling. *PLoS ONE* **8**, e56172.
- Heusinkveld, M., de Vos van Steenwijk, P.J., Goedemans, R., Ramwadhoebe, T.H., Gorter, A., Welters, M.J., van Hall, T., and van der Burg, S.H. (2011). M2 macrophages induced by prostaglandin E<sub>2</sub> and IL-6 from cervical carcinoma are switched to activated M1 macrophages by CD4<sup>+</sup> Th1 cells. *J. Immunol.* **187**, 1157–1165.
- Hidaka, A., Inoue, K., Kutsukake, S., Adachi, M., Kakuta, Y., and Kojo, S. (2005). Decrease in the particle size of low-density lipoprotein (LDL) by oxidation. *Bioorg. Med. Chem. Lett.* **15**, 2781–2785.
- Hotamisligil, G.S. (2006). Inflammation and metabolic disorders. *Nature* **444**, 860–867.
- Ivandic, B., Castellani, L.W., Wang, X.P., Qiao, J.H., Mehrabian, M., Navab, M., Fogelman, A.M., Grass, D.S., Swanson, M.E., de Beer, M.C., et al. (1999). Role of group II secretory phospholipase A<sub>2</sub> in atherosclerosis: 1. Increased atherogenesis and altered lipoproteins in transgenic mice expressing group IIa phospholipase A<sub>2</sub>. *Arterioscler. Thromb. Vasc. Biol.* **19**, 1284–1290.
- Iyer, A., Lim, J., Poudyal, H., Reid, R.C., Suen, J.Y., Webster, J., Prins, J.B., Whitehead, J.P., Fairlie, D.P., and Brown, L. (2012). An inhibitor of phospholipase A<sub>2</sub> group IIA modulates adipocyte signaling and protects against diet-induced metabolic syndrome in rats. *Diabetes* **61**, 2320–2329.
- Jaworski, K., Ahmadian, M., Duncan, R.E., Sarkadi-Nagy, E., Varady, K.A., Hellerstein, M.K., Lee, H.Y., Samuel, V.T., Shulman, G.I., Kim, K.H., et al. (2009). AdPLA ablation increases lipolysis and prevents obesity induced by high-fat feeding or leptin deficiency. *Nat. Med.* **15**, 159–168.
- Leidi, M., Gotti, E., Bologna, L., Miranda, E., Rimoldi, M., Sica, A., Roncalli, M., Palumbo, G.A., Introna, M., and Golay, J. (2009). M2 macrophages phagocytose rituximab-opsonized leukemic targets more efficiently than m1 cells in vitro. *J. Immunol.* **182**, 4415–4422.
- MacPhee, M., Chepenik, K.P., Liddell, R.A., Nelson, K.K., Siracusa, L.D., and Buchberg, A.M. (1995). The secretory phospholipase A<sub>2</sub> gene is a candidate for the *Mom1* locus, a major modifier of *Apc*<sup>Min</sup>-induced intestinal neoplasia. *Cell* **81**, 957–966.
- Miki, Y., Yamamoto, K., Taketomi, Y., Sato, H., Shimo, K., Kobayashi, T., Ishikawa, Y., Ishii, T., Nakanishi, H., Ikeda, K., et al. (2013). Lymphoid tissue phospholipase A<sub>2</sub> group IID resolves contact hypersensitivity by driving antiinflammatory lipid mediators. *J. Exp. Med.* **210**, 1217–1234.
- Miller, A.M., Asquith, D.L., Hueber, A.J., Anderson, L.A., Holmes, W.M., McKenzie, A.N., Xu, D., Sattar, N., McInnes, I.B., and Liew, F.Y. (2010). Interleukin-33 induces protective effects in adipose tissue inflammation during obesity in mice. *Circ. Res.* **107**, 650–658.
- Murakami, M., Taketomi, Y., Miki, Y., Sato, H., Hirabayashi, T., and Yamamoto, K. (2011). Recent progress in phospholipase A<sub>2</sub> research: from cells to animals to humans. *Prog. Lipid Res.* **50**, 152–192.
- Namgaladze, D., Morbitzer, D., von Knethen, A., and Brüne, B. (2010). Phospholipase A<sub>2</sub>-modified low-density lipoprotein activates macrophage peroxisome proliferator-activated receptors. *Arterioscler. Thromb. Vasc. Biol.* **30**, 313–320.
- Odegaard, J.I., and Chawla, A. (2013). The immune system as a sensor of the metabolic state. *Immunity* **38**, 644–654.
- Oh, D.Y., and Olefsky, J.M. (2012).  $\omega$  3 fatty acids and GPR120. *Cell Metab.* **15**, 564–565.
- Ohtsuki, M., Taketomi, Y., Arata, S., Masuda, S., Ishikawa, Y., Ishii, T., Takanezawa, Y., Aoki, J., Arai, H., Yamamoto, K., et al. (2006). Transgenic expression of group V, but not group X, secreted phospholipase A<sub>2</sub> in mice leads to neonatal lethality because of lung dysfunction. *J. Biol. Chem.* **281**, 36420–36433.
- Ozcan, U., Yilmaz, E., Ozcan, L., Furuhashi, M., Vaillancourt, E., Smith, R.O., Görgün, C.Z., and Hotamisligil, G.S. (2006). Chemical chaperones reduce ER stress and restore glucose homeostasis in a mouse model of type 2 diabetes. *Science* **313**, 1137–1140.
- Pelleymounter, M.A., Cullen, M.J., Baker, M.B., Hecht, R., Winters, D., Boone, T., and Collins, F. (1995). Effects of the obese gene product on body weight regulation in *ob/ob* mice. *Science* **269**, 540–543.
- Pettersson, C., Fogelstrand, L., Rosengren, B., Ståhlman, S., Hurt-Camejo, E., Fagerberg, B., and Wiklund, O. (2008). Increased lipolysis by secretory phospholipase A<sub>2</sub>(s) group V of lipoproteins in diabetic dyslipidaemia. *J. Intern. Med.* **264**, 155–165.
- Pruzanski, W., Lambeau, L., Lazdunsky, M., Cho, W., Kopilov, J., and Kuksis, A. (2005). Differential hydrolysis of molecular species of lipoprotein phosphatidylcholine by groups IIA, V and X secretory phospholipases A<sub>2</sub>. *Biochim. Biophys. Acta* **1736**, 38–50.
- Satake, Y., Diaz, B.L., Balestrieri, B., Lam, B.K., Kanaoka, Y., Grusby, M.J., and Arm, J.P. (2004). Role of group V phospholipase A<sub>2</sub> in zymosan-induced eicosanoid generation and vascular permeability revealed by targeted gene disruption. *J. Biol. Chem.* **279**, 16488–16494.
- Sato, H., Kato, R., Isogai, Y., Saka, G., Ohtsuki, M., Taketomi, Y., Yamamoto, K., Tsutsumi, K., Yamada, J., Masuda, S., et al. (2008). Analyses of group III secreted phospholipase A<sub>2</sub> transgenic mice reveal potential participation of this enzyme in plasma lipoprotein modification, macrophage foam cell formation, and atherosclerosis. *J. Biol. Chem.* **283**, 33483–33497.
- Sato, H., Taketomi, Y., Isogai, Y., Miki, Y., Yamamoto, K., Masuda, S., Hosono, T., Arata, S., Ishikawa, Y., Ishii, T., et al. (2010). Group III secreted phospholipase A<sub>2</sub> regulates epididymal sperm maturation and fertility in mice. *J. Clin. Invest.* **120**, 1400–1414.

- Sergouniotis, P.I., Davidson, A.E., Mackay, D.S., Lenassi, E., Li, Z., Robson, A.G., Yang, X., Kam, J.H., Isaacs, T.W., Holder, G.E., et al. (2011). Biallelic mutations in PLA2G5, encoding group V phospholipase A<sub>2</sub>, cause benign fleck retina. *Am. J. Hum. Genet.* **89**, 782–791.
- Spite, M., Clària, J., and Serhan, C.N. (2014). Resolvins, specialized proresolving lipid mediators, and their potential roles in metabolic diseases. *Cell Metab.* **19**, 21–36.
- Su, X., Mancuso, D.J., Bickel, P.E., Jenkins, C.M., and Gross, R.W. (2004). Small interfering RNA knockdown of calcium-independent phospholipases A<sub>2</sub> β or γ inhibits the hormone-induced differentiation of 3T3-L1 preadipocytes. *J. Biol. Chem.* **279**, 21740–21748.
- Suzuki, N., Ishizaki, J., Yokota, Y., Higashino, K., Ono, T., Ikeda, M., Fujii, N., Kawamoto, K., and Hanasaki, K. (2000). Structures, enzymatic properties, and expression of novel human and mouse secretory phospholipase A<sub>2</sub>s. *J. Biol. Chem.* **275**, 5785–5793.
- Taketomi, Y., Ueno, N., Kojima, T., Sato, H., Murase, R., Yamamoto, K., Tanaka, S., Sakanaka, M., Nakamura, M., Nishito, Y., et al. (2013). Mast cell maturation is driven via a group III phospholipase A<sub>2</sub>-prostaglandin D<sub>2</sub>-DP1 receptor paracrine axis. *Nat. Immunol.* **14**, 554–563.
- Tian, C., Stokowski, R.P., Kershenovich, D., Ballinger, D.G., and Hinds, D.A. (2010). Variant in PNPLA3 is associated with alcoholic liver disease. *Nat. Genet.* **42**, 21–23.
- Titos, E., Rius, B., González-Pérez, A., López-Vicario, C., Morán-Salvador, E., Martínez-Clemente, M., Arroyo, V., and Clària, J. (2011). Resolvin D1 and its precursor docosahexaenoic acid promote resolution of adipose tissue inflammation by eliciting macrophage polarization toward an M2-like phenotype. *J. Immunol.* **187**, 5408–5418.
- Valentin, E., Ghomashchi, F., Gelb, M.H., Lazdunski, M., and Lambeau, G. (1999). On the diversity of secreted phospholipases A<sub>2</sub>. Cloning, tissue distribution, and functional expression of two novel mouse group II enzymes. *J. Biol. Chem.* **274**, 31195–31202.
- Wang, H., Astarita, G., Taussig, M.D., Bharadwaj, K.G., DiPatrizio, N.V., Nave, K.A., Piomelli, D., Goldberg, I.J., and Eckel, R.H. (2011). Deficiency of lipoprotein lipase in neurons modifies the regulation of energy balance and leads to obesity. *Cell Metab.* **13**, 105–113.
- Wootton, P.T., Arora, N.L., Drenos, F., Thompson, S.R., Cooper, J.A., Stephens, J.W., Hurel, S.J., Hurt-Camejo, E., Wiklund, O., Humphries, S.E., and Talmud, P.J. (2007). Tagging SNP haplotype analysis of the secretory PLA<sub>2</sub>-V gene, PLA2G5, shows strong association with LDL and oxLDL levels, suggesting functional distinction from sPLA<sub>2</sub>-IIA: results from the UDACS study. *Hum. Mol. Genet.* **16**, 1437–1444.
- Yamamoto, T., and Ryan, R.O. (2007). Anionic phospholipids inhibit apolipoprotein E—low-density lipoprotein receptor interactions. *Biochem. Biophys. Res. Commun.* **354**, 820–824.



Contents lists available at ScienceDirect

# Biochimica et Biophysica Acta

journal homepage: [www.elsevier.com/locate/bbalip](http://www.elsevier.com/locate/bbalip)

## Very-long-chain polyunsaturated fatty acids accumulate in phosphatidylcholine of fibroblasts from patients with Zellweger syndrome and acyl-CoA oxidase1 deficiency



Yuichi Abe <sup>a</sup>, Masanori Honsho <sup>a</sup>, Hiroki Nakanishi <sup>b</sup>, Ryo Taguchi <sup>c</sup>, Yukio Fujiki <sup>a,\*</sup>

<sup>a</sup> Department of Biology, Faculty of Sciences, Kyushu University Graduate School, Fukuoka 812-8581, Japan

<sup>b</sup> Department of Medical Biology, Akita University Graduate School of Medicine, Akita 010-8502, Japan

<sup>c</sup> Department of Biomedical Sciences, College of Life and Health Sciences, Chubu University, Aichi 487-8501, Japan

### ARTICLE INFO

#### Article history:

Received 4 September 2013

Received in revised form 19 December 2013

Accepted 2 January 2014

Available online 10 January 2014

#### Keywords:

Peroxisome

Zellweger syndrome

X-ALD

Peroxisomal  $\beta$ -oxidation

Very-long-chain fatty acid

Lipidomics

### ABSTRACT

Peroxisomes are subcellular organelles that function in multiple anabolic and catabolic processes, including  $\beta$ -oxidation of very-long-chain fatty acids (VLCFA) and biosynthesis of ether phospholipids. Peroxisomal disorders caused by defects in peroxisome biogenesis or peroxisomal  $\beta$ -oxidation manifest as severe neural disorders of the central nervous system. Abnormal peroxisomal metabolism is thought to be responsible for the clinical symptoms of these diseases, but their molecular pathogenesis remains to be elucidated. We performed lipidomic analysis to identify aberrant metabolites in fibroblasts from patients with Zellweger syndrome (ZS), acyl-CoA oxidase1 (AOx) deficiency, D-bifunctional protein (D-BP) and X-linked adrenoleukodystrophy (X-ALD), as well as in peroxisome-deficient Chinese hamster ovary cell mutants. In cells deficient in peroxisomal biogenesis, plasmalogen phospholipids were remarkably reduced and phosphatidylethanolamine was increased. Marked accumulation of very-long-chain saturated fatty acid and monounsaturated fatty acids in phosphatidylcholine was observed in all mutant cells. Very-long-chain polyunsaturated fatty acid (VLC-PUFA) levels were significantly elevated, whilst phospholipids containing docosahexaenoic acid (DHA, C22:6n-3) were reduced in fibroblasts from patients with ZS, AOx deficiency, and D-BP deficiency, but not in fibroblasts from an X-ALD patient. Because patients with AOx deficiency suffer from more severe symptoms than those with X-ALD, accumulation of VLC-PUFA and/or reduction of DHA may be associated with the severity of peroxisomal diseases.

© 2014 Elsevier B.V. All rights reserved.

### 1. Introduction

Peroxisomes are subcellular organelles that participate in various metabolic processes, such as  $\beta$ -oxidation of very-long-chain fatty acids (VLCFA) and the biosynthesis of ether phospholipids and bile acids [1,2]. The functional importance of peroxisome metabolism in humans is demonstrated by the symptoms of peroxisomal diseases,

including peroxisome biogenesis disorders (PBDs) and single peroxisomal enzyme deficiencies [3,4].

Generalized PBDs, including Zellweger syndrome (ZS), neonatal adrenoleukodystrophy (NALD), and infantile Refsum disease (IRD), are classified into thirteen complementation groups (CGs) by cell-fusion assay using skin fibroblasts [3]. The primary cause of PBDs is impaired biogenesis of peroxisomes, and genetic complementation analysis using peroxisome-deficient Chinese hamster ovary (CHO) cell mutants led to the identification of *PEX* genes essential for peroxisome biogenesis [3,5]. Patients with ZS, the most severe PBD, are characterized by seizures, facial dysmorphism, severe hypotonia, and brain dysfunction, and die before 1 year of age. Neural migration defects, dysmyelination, and neural heterotopia are observed in the central nervous system (CNS) of ZS patients [3], as are biochemical abnormalities, including VLCFA accumulation, marked depletion of ether phospholipids, and reduced levels of docosahexaenoic acid (DHA) [4]. Although deficiencies in peroxisomal metabolism are thought to be responsible for the pathology of ZS, the underlying pathogenic mechanism is still unclear.

Severe defects in the CNS are also observed in X-linked adrenoleukodystrophy (X-ALD) and peroxisomal  $\beta$ -oxidation-deficient diseases,

**Abbreviations:** AA, arachidonic acid; ABCD1, ATP-binding cassette transporter subfamily D member 1; AlkCho, plasmalogen; AOx, acyl-CoA oxidase 1; CG, complementation group; CHO, Chinese hamster ovary; CNS, central nervous system; D-BP, D-bifunctional protein; DHA, docosahexaenoic acid; DHAPLs, DHA-containing phospholipids; LC-ESI-MS/MS, liquid chromatography coupled with electrospray ionization tandem mass spectrometry; MUFA, monounsaturated fatty acid; OA, oleic acid; PBD, peroxisome biogenesis disorder; PlsEtn, plasmalogen; PtdCho, phosphatidylcholine; PtdEtn, phosphatidylethanolamine; PUFA, polyunsaturated fatty acid; SFA, saturated fatty acid; siRNA, short inhibitory RNAs; VLC, very-long-chain; VLCFA, very-long-chain fatty acid; X-ALD, X-linked adrenoleukodystrophy; ZS, Zellweger syndrome

\* Corresponding author at: Department of Biology, Faculty of Sciences, Kyushu University Graduate School, 6-10-1 Hakozaki, Higashi-ku, Fukuoka 812-8581, Japan. Tel.: +81 92 642 2635; fax: +81 92 642 4214.

E-mail address: [yfujiki@kyudai.jp](mailto:yfujiki@kyudai.jp) (Y. Fujiki).

1388-1981/\$ – see front matter © 2014 Elsevier B.V. All rights reserved.

<http://dx.doi.org/10.1016/j.bbalip.2014.01.001>

including acyl-CoA oxidase1 (AOx) deficiency and D-bifunctional protein (*D-BP*) deficiency [6,7]. These disorders are diagnosed by an elevated plasma VLCFA ratio, such as C26:0/C22:0 and C26:1/C22:0. Of these, X-ALD is the most common single peroxisome enzyme deficiency caused by mutations in the ATP-binding cassette transporter subfamily D member 1 (*ABCD1*), which is essential for the translocation for CoA-activated VLCFAs across the peroxisomal membrane [4,6,8]. AOx is the first step in and rate-limiting enzyme of peroxisomal fatty acid  $\beta$ -oxidation, while *D-BP* catalyzes in second and third steps [9]. The patients with AOx and *D-BP* deficiency exhibit more severe symptoms than patients with X-ALD [10–13]. Thus, peroxisomal fatty acid  $\beta$ -oxidation is of particular importance in the proper development and maintenance of the CNS.

The relationship between the biochemical and pathological abnormalities observed in patients with ZS and those with  $\beta$ -oxidation deficiencies remains to be defined. Since the majority of peroxisomal processes play a role in lipid metabolism, it is conceivable that aberrant peroxisomal lipid metabolites affect cellular function. Therefore, the identification of these aberrant lipid metabolites is essential for elucidating the pathogenesis of PBDs and  $\beta$ -oxidation disorders. Although the biochemical phenotypes of AOx deficiency and X-ALD are similar, their pathological severities are significantly different, indicating that additional metabolic abnormalities in patients with AOx deficiency may cause the severe dysfunction in the CNS.

To date, the phospholipid compositions of the brain [14–16] and skin fibroblasts [14,17,18] from ZS patients and in peroxisome-deficient CHO mutant cell lines [19–21] have been reported. Recently, liquid chromatography coupled with electrospray ionization tandem mass spectrometry (LC-ESI-MS/MS) was utilized to detect small amounts of lipid metabolites and discriminate the precise fatty acid composition of individual phospholipid classes. Thus, in the present study, we used LC-ESI-MS/MS to analyze the lipid composition of skin fibroblasts from patients with ZS and peroxisomal fatty acid  $\beta$ -oxidation deficiency diseases.

## 2. Material and methods

### 2.1. Materials

1-heptadecanoyl-*sn*-glycero-3-phosphocholine (LPC), 1, 2-didodecanoyl-*sn*-glycero-3-phosphocholine (DDPC), and 1, 2-didodecanoyl-*sn*-glycero-3-phosphoethanolamine (DDPE) were purchased from Avanti Polar Lipids (Alabaster, AL).

### 2.2. Cell culture and RNA interference

Human skin fibroblasts from the patients listed in Table 1 were obtained as described previously [22,23]. Fibroblast cell line from a patient with *D-BP* deficiency (GM13264) was purchased from Coriell Cell Repositories (Camden, NJ). Fibroblasts were cultured in Dulbecco's modified medium (DMEM; Invitrogen, Carlsbad, CA) supplemented with 10% fetal bovine serum (FBS) under 5% CO<sub>2</sub> at 37 °C. The CHO mutant cell lines used in this study are listed in Table 2.

CHO mutant cells were cultured in Ham's F-12 medium (Invitrogen) containing 10% FBS. Z65/Pex2p and ZP119/Pex19p cells were maintained as described previously [24,25].

The short inhibitory RNA (siRNA) against *ELOVL1* [26] was purchased from Sigma (St Louis, MO). The nucleotide sequence for *ELOVL5* RNAi was designed (Invitrogen). Fibroblasts were transfected twice with 40 nM double strand RNA, with a 48 h interval between transfections, using Lipofectamine 2000 (Invitrogen). Cells were harvested 72 h after the second transfection.

### 2.3. Lipid extraction

Cells were detached by incubation with trypsin and suspended in phosphate buffered saline (PBS). Protein concentration was determined by the bicinchonic acid (BCA) method (Thermo Fisher Scientific, Rockford, IL). Total lipids were extracted from 50 or 100  $\mu$ g of cellular protein by the Bligh and Dyer method [27]. Cells were dissolved in methanol/chloroform/water at 2:1:0.8 v/v/v and then 50 pmol of LPC, DDPC, and DDPE were added as internal standards. After incubation for 5 min at room temperature, 1 ml each of water and chloroform were added and the samples were then subjected to centrifugation to collect the lower organic phase. To re-extract the lipids from the water phase, 1 ml chloroform was added. The combined organic phase was evaporated under a nitrogen stream and the extracted lipids were dissolved in methanol.

### 2.4. LC-ESI-MS/MS

LC-ESI-MS/MS was performed using a 4000 Q-TRAP quadrupole linear ion trap hybrid mass spectrometer (AB Sciex, Framingham, MA) with a Shimadzu Prominence HPLC System (Shimadzu, Kyoto, Japan). Samples were injected into an X-Bridge C18 column (1.0  $\times$  150 mm; Waters, Milford, MA) and then directly subjected to ESI-MS/MS analysis. A 10  $\mu$ l sample volume was directly introduced by an autosampler injector and the samples were separated by step gradient elution with mobile phase A (acetonitrile:methanol:water at 2:2:1 v/v/v, 0.1% formic acid and 0.028% ammonia) and mobile phase B (isopropanol, 0.1% formic acid, and 0.028% ammonia) at the following ratios: 100:0 (for 0–5 min), 95:5 (5–20 min), 70:30 (20–21 min), 50:50 (21–45 min), 50:50 (45–100 min), and 100:0 (100–120 min). The flow rate was 70  $\mu$ l/min at 30 °C. The source temperature was 200 °C, the declustering potential (DP) was 60, and the collision cell exit potential (CXP) was 15. The methods used to detect phospholipids and DHA-containing phospholipids in multiple reaction monitoring (MRM) are listed in Tables 3 and 4, respectively.

Retention times of the individual fatty acid compositions of phosphatidylcholine (PtdCho) and phosphatidylethanolamine (PtdEtn) were assigned by the MS<sup>3</sup> methods of the 4000 Q-TRAP system, as described previously [28,29]. The data were analyzed and quantified using Analyst software (AB Sciex). The amounts of phospholipid were determined from the ratio of the peak area of each phospholipid species to that of internal standards and are represented as nmol/mg protein.

**Table 1**  
Human skin fibroblasts used in this study.

Cells	Mutated Gene	Phenotypes	Derivation	Reference
Control-1	–	Normal	Healthy subject	[22]
Control-2 (TIG-120)	–	Normal	Healthy subject	[23]
$\Delta$ PEX13	PEX13	Deficiency of matrix protein import	Zellweger syndrome patient	[30]
$\Delta$ PEX16 (GM06231)	PEX16	Deficiency of membrane biogenesis	Zellweger syndrome patient	[31]
$\Delta$ AOx (PDL30092)	acyl-CoA oxidase1	Deficiency of peroxisomal $\beta$ -oxidation	Acyl-CoA oxidase-deficient patient	[10,11]
$\Delta$ D-BP (GM13264)	D-bifunctional protein	Deficiency of peroxisomal $\beta$ -oxidation	D-bifunctional protein-deficient patient	[12,13]
X-ALD (PDL6886)	ABCD1	Accumulation of very long chain fatty acid	X-linked adrenoleukodystrophy patient	[23]

**Table 2**

Chinese hamster ovary cell lines used in this study.

Cell	Mutated gene	Derivation	Phenotypes	Reference
CHO-K1	–	–	Normal	
Z65	<i>PEX2</i>	CHO-K1 treated with mutagen	Deficiency of peroxisomal matrix protein import	[37]
Z65/Pex2p	<i>PEX2</i>	Z65 stably expressing Pex2p	Normal	[24]
ZP119	<i>PEX19</i>	TKa cell treated with mutagen	Deficiency of peroxisomal membrane biogenesis	[38]
ZP119/Pex19p	<i>PEX19</i>	ZP119 stably expressing Pex19p	Normal	[25]

### 2.5. Real-time PCR

Total RNA was extracted from cells using TRIzol reagent (Invitrogen) and first-strand cDNA was synthesized by the PrimeScript RT reagent Kit (Takara Bio, Shiga, Japan). Quantitative real-time PCR was performed using SYBR Premix Ex Taq II (Takara Bio) with an Mx3000P QPCR system (Agilent Technologies, Palo Alto, CA). The primer sets used are listed in Supplementary Table S1.

### 2.6. Statistical analysis

All data are shown as mean  $\pm$  S.D. of three independent experiments. Statistical analysis was performed by ANOVA with Dunnett's post hoc test or ANOVA with Tukey-Kramer post hoc test using R software (<http://www.r-project.org>).

## 3. Results

### 3.1. Changes in plasmylethanolamine and phosphatidylethanolamine levels in peroxisome-deficient skin fibroblasts

To investigate whether defective peroxisomal biogenesis influences lipid metabolism, we analyzed the lipid composition of fibroblasts derived from two patients with ZS, including one with a *PEX13*-deficiency causing peroxisomal matrix protein import dysfunction (CG-H,  $\Delta$ *PEX13*) [30] and one with a *PEX16*-deficiency resulting in impaired peroxisome membrane biogenesis (CG-D,  $\Delta$ *PEX16*) [31] (Table 1, Fig. S1A). In addition, fibroblasts from patients with three types of deficient peroxisomal fatty acid  $\beta$ -oxidation, *AOx* deficiency, *D-BP* deficiency, and X-ALD, were also analyzed (Table 1, Fig. S1A).

Plasmylethanolamine (PlsEtn) is abundant in myelin in the CNS [32]. The essential function of PlsEtn in CNS integrity is underscored by the symptoms of ether phospholipid-deficient diseases, such as rhizomelic chondrodysplasia punctata (RCDP) [32]. In mammals, the *sn*-1 position of PlsEtn typically contains C16:0, C18:0, or C18:1 fatty alcohols, and these three types of PlsEtn can be detected in an alkenyl chain-dependent manner by LC-ESI-MS/MS (Table 3) [33]. In the fibroblasts from a control patient, abundant oleic (OA), arachidonic (C20:4, AA), docosatetraenoic (C22:4, DTA), docosapentaenoic (C22:5, DPA),

**Table 3**

Detection methods for the phospholipids.

Phospholipid	Abbreviation	Detection methods	Collision energy
Plasmylethanolamine	PlsEtn	+ Prec 364 ( <i>sn</i> -1 16:0)	25–35
		+ Prec 392 ( <i>sn</i> -1 18:0)	25–35
		+ Prec 390 ( <i>sn</i> -1 18:1)	25–35
Phosphatidylethanolamine	PtdEtn	+ NL 141	25–35
Phosphatidylcholine	PtdCho	+ Prec 184	40–50
Plasmanylcholine	AlkCho	+ Prec 184	40–50
Very long chain fatty acid-containing phosphatidylcholine	VLC-PtdCho	+ Prec 184	40–50
Docosahexaenoic acid-containing phospholipids	DHAPL	-Prec 327 (MRM)	30

Prec: precursor ion scan, NL: neutral loss, MRM: multiple reaction monitoring.

and docosahexaenoic (C22:6, DHA) fatty acids at the *sn*-2 position were detected in all alkenyl types of PlsEtns (Fig. 1A, B, C, Supplementary Table S2), and PlsEtn with C16 alkenyl chains was the most abundant (Fig. 1D). In fibroblasts derived from PBD patients, the total amount of PlsEtn was markedly decreased (Fig. 1E). Conversely, PtdEtn was elevated (Fig. 1F, Supplementary Table S3), especially PtdEtns possessing OA and AA at the *sn*-2 position, including C36:1, C36:2, C38:4, and C38:5, which were significantly increased in the peroxisome-deficient cells (Supplementary Table S3). No statistically significant difference in the levels of PlsEtn and PtdEtn was observed in the fibroblasts from patients with  $\beta$ -oxidation deficiency and X-ALD, as compared to the control fibroblasts (Fig. 1E, F).

### 3.2. Species of phospholipids containing DHA in skin fibroblasts

DHA is an essential polyunsaturated fatty acid (PUFA) that is abundantly present in the CNS [34]. Synthesis of DHA from dietary linolenic acid (C18:3n-3) is initiated in the endoplasmic reticulum and completed by peroxisomal  $\beta$ -oxidation [35]. DHA levels have been reported to be severely reduced in the CNS of ZS patients [36], although phospholipid species containing DHA have not been precisely analyzed. Therefore, we performed LC-ESI-MS/MS analysis of DHA-containing phospholipids using MRM, as described previously [23]. As shown in control fibroblasts (Fig. 2B, C), DHA is present in PtdEtn, PlsEtn, and PtdCho. The total amount of DHA-containing phospholipids (DHAPLs) was decreased in peroxisome-, *AOx*-, and *D-BP*-deficient fibroblasts, but not in fibroblasts from an X-ALD patient (Fig. 2A). In the peroxisome-deficient cells, PlsEtn was the primary DHA-containing phospholipid affected. DHA-containing PtdCho was also reduced, whilst the level of DHA-containing PtdEtn was not significantly altered, in peroxisome-deficient cells (Fig. 2B, C). The levels of DHA-containing PlsEtn and PtdCho in *AOx*-deficient fibroblasts were reduced to about 50% of that in control cells (Fig. 2A, B). Similarly, significant decrease of DHA in PlsEtn and PtdCho was observed in *D-BP*-deficient fibroblasts (Fig. 2B, C). Taken together, these results

**Table 4**

m/z values of DHA-containing phospholipids in MRM methods at negative ion mode.

Phospholipid	Q1 m/z	Q3 m/z	Retention time (min)
PtdEtn 16:0/22:6	762.5	327.2	44.5
PtdEtn 16:1/22:6	760.5	327.2	41.0
PtdEtn 18:0/22:6	790.5	327.2	48.5
PtdEtn 18:1/22:6	788.5	327.2	44.6
PlsEtn 16:0/22:6	746.5	327.2	46.4
PlsEtn 18:0/22:6	774.5	327.2	50.5
PlsEtn 18:1/22:6	772.5	327.2	46.4
PtdCho 16:0/22:6	850.6	327.2	43.9
PtdCho 16:1/22:6	848.6	327.2	40.4
PtdCho 18:0/22:6	878.6	327.2	47.9
PtdCho 18:1/22:6	876.6	327.2	44.0
AlkCho 16:0/22:6	836.6	327.2	46.3
AlkCho 18:0/22:6	864.6	327.2	50.3
AlkCho 18:1/22:6	862.6	327.2	46.3
PtdSer 18:0/22:6	834.6	327.2	46.1

PtdEtn: phosphatidylethanolamine, PlsEtn: plasmylethanolamine.

PtdCho: phosphatidylcholine, AlkCho: plasmanylcholine.

PtdSer: phosphatidylserine.

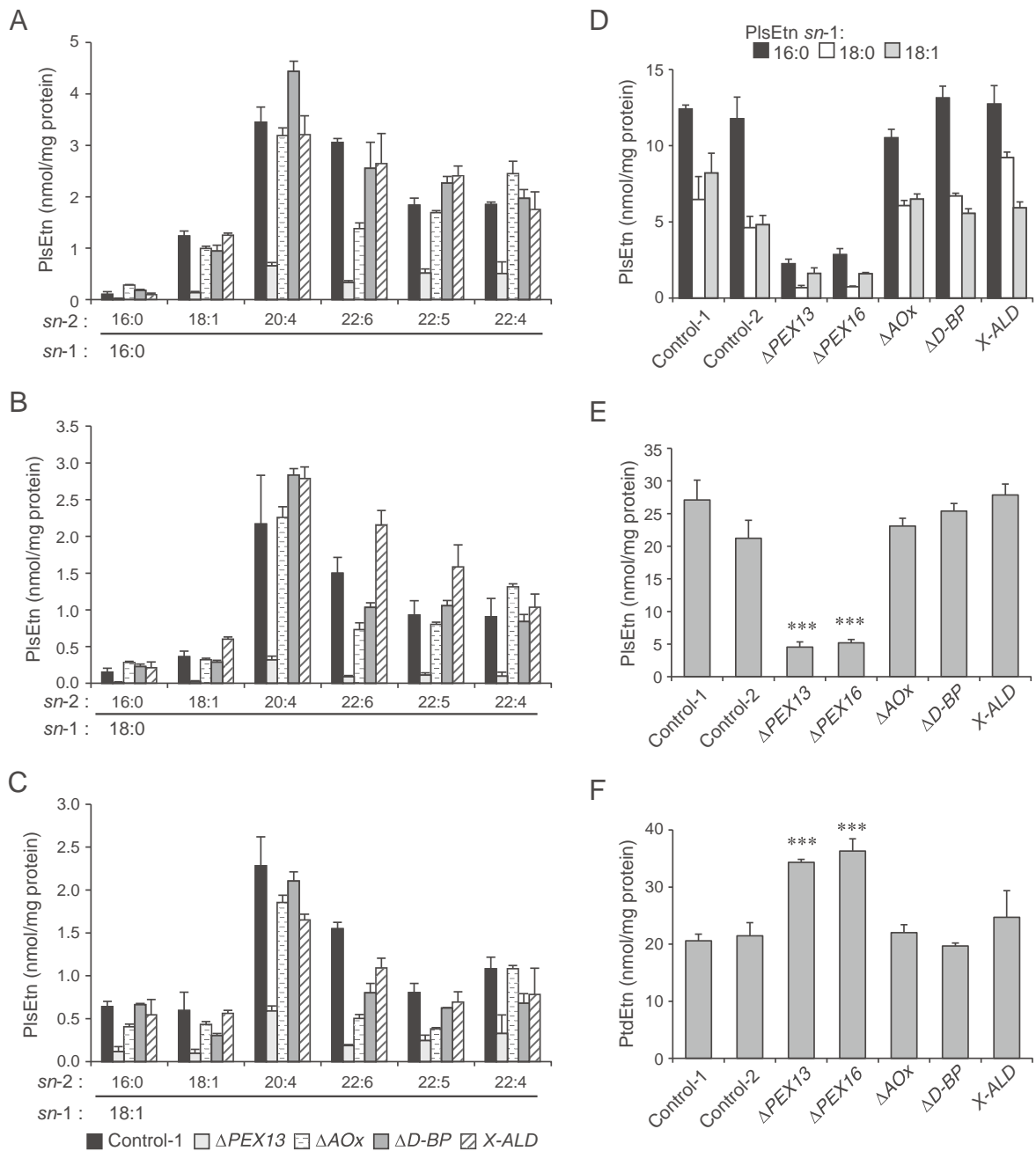


**Fig. 1.** LC-ESI-MS/MS analysis of PlsEtn and PtdEtn in fibroblasts from patients with PBDs and peroxisomal  $\beta$ -oxidation disorders. Lipids were extracted as described in Section 2.3 and analyzed by LC-ESI-MS/MS. PlsEtn with alkenyl 16:0 (A), 18:0 (B), and 18:1 (C) at the *sn*-1 position was detected by precursor ion scan of *m/z* 364, *m/z* 392, and *m/z* 390, respectively, in positive ion mode. Abundant subspecies (A-C), the sum of PlsEtn containing different alkenyl chains (D), and total amount (E) of PlsEtn are shown. PtdEtn was detected by neutral loss scan of *m/z* 141 in positive ion mode. Total amount (F) of PtdEtn is shown. Data represent the means  $\pm$  S.D. of three independent experiments (\*\*\*)  $p < 0.001$ ; ANOVA with Dunnett's post hoc test as compared with control fibroblasts).

suggest that peroxisomal fatty acid  $\beta$ -oxidation activity, not ABCD1 activity, contributes to the biosynthesis of DHA.

### 3.3. Accumulation of VLCFA in phosphatidylcholine in peroxisome-deficient and $\beta$ -oxidation-deficient skin fibroblasts

As shown in Fig. 3A, plasmalyncholine (AlkCho) possessing an ether bond at the *sn*-1 position was significantly decreased in fibroblasts from patients with PBDs, suggesting that the formation of ether bonds in peroxisomes is important for the synthesis of AlkCho. Therefore, we assessed the total amount of PtdChos in fibroblasts. In fibroblasts from a normal control or patients with peroxisomal defects, no differences were detected in the total amounts (Fig. 3B) or fatty acid

composition (data not shown) of PtdCho containing medium- and long-chain fatty acids with total carbon numbers of 30 to 40. However, the total amount of PtdCho containing VLCFA (VLC-PtdCho) with total carbon numbers from 42 to 48 was increased (Fig. 3D). Further analysis of VLC-PtdCho species revealed that almost all VLC-PtdChos were elevated in peroxisome-, *AOx*-, and *D-BP*-deficient fibroblasts (Fig. 3C). By contrast, PtdCho containing very-long-chain PUFA (VLC-PUFA) with more than three double bonds was not accumulated in X-ALD fibroblasts (Fig. 3C). When VLC-PtdChos was classified according to the number of double bonds, saturated, monounsaturated, and diunsaturated VLC-PtdChos species (C42:0, C42:1, C42:2, C44:0, C44:1, C44:2, C46:1, C46:2, and C48:2) were elevated in fibroblasts from all patients (Fig. 3E). However, no increase in VLC-PUFA-

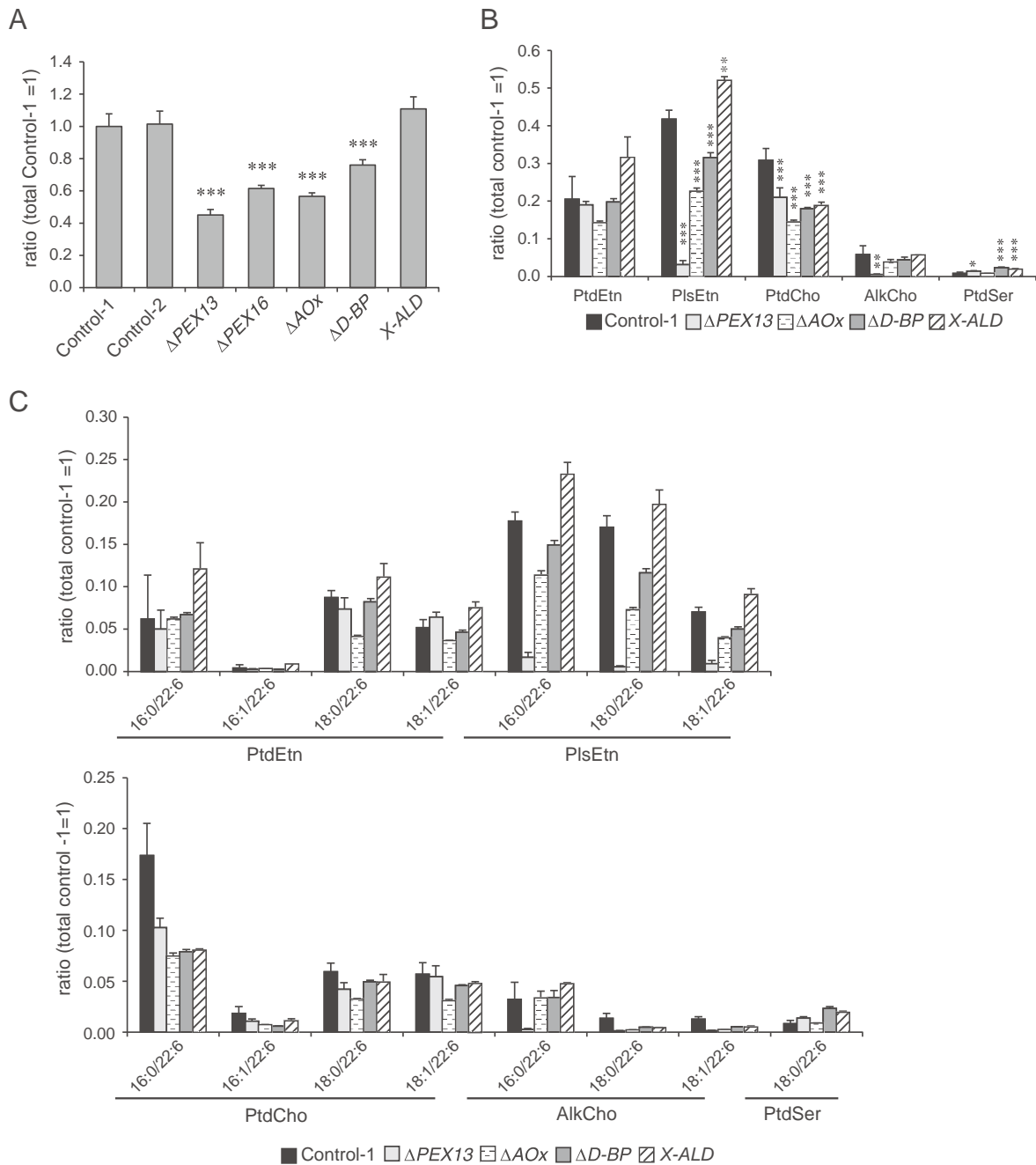


**Fig. 2.** LC-ESI-MS/MS analysis of DHAPLs in fibroblasts from patients with PBDs and peroxisomal  $\beta$ -oxidation disorders. DHAPLs were detected by MRM as described in Table 4. Total amount (A), phospholipid classes (B), and composition (C) of DHAPLs are presented relative to total DHAPLs in control fibroblasts. Data represent the means  $\pm$  S.D. of three independent experiments (\* $p$  < 0.05, \*\* $p$  < 0.01, \*\*\* $p$  < 0.001; ANOVA with Dunnett's post hoc test as compared with control fibroblasts).

containing PtdCho was observed in X-ALD fibroblasts (Fig. 3F). To determine which fatty acids were responsible for the increase in VLC-PtdCho, MS<sup>3</sup> analysis of VLC-PtdCho was performed [28]. Elevation of PtdCho C42:1 in the fibroblasts of patients with ZS, AOx deficiency, and X-ALD was due to increased levels of C24:0 and C26:1 (Supplementary Fig. S2A). VLC-PUFAs, such as C24:4, C24:5, and C26:5, were elevated in PtdCho C42:5 of the fibroblasts from patients with ZS and AOx deficiency, but not in those from the X-ALD patient (Supplementary Fig. S2B). Therefore, in fibroblasts from patients with ZS and AOx deficiency, VLC-saturated fatty acids (VLC-SFA), VLC-monounsaturated fatty acids (VLC-MUFA), and VLC-PUFA were accumulated in PtdCho (Supplementary Table S4). However, VLC-PUFA was not discernibly elevated in PtdCho in the X-ALD fibroblasts (Supplementary Table S4). MS<sup>3</sup> analysis revealed that the slight

increase in PUFA-containing PtdCho observed in X-ALD fibroblasts (Fig. 3C; C46:3, C46:4, C46:5, C48:3, C48:4, C48:5, and C48:6) was due to the elevation of VLC-SFA and VLC-MUFA, but not VLC-PUFA, where elevation of C46:4 was mainly composed of the elevation of 20:4/26:0 and 20:3/26:1, and C48:4 was of 20:4/28:0 and 20:3/28:1 (Supplementary Table S4). These results indicated that the accumulation of VLCFA in the patient with X-ALD was distinct from that observed in patients with ZS and AOx deficiency.

### 3.4. Lipidome of peroxisome biogenesis-defective CHO mutants

Next, the lipid composition in peroxisome biogenesis-defective cells was analyzed by LC-ESI-MS/MS in CHO cell mutants. The cell lines *pex2* Z65 [37] and *pex19* ZP119 [25,38] are defective in peroxisomal matrix

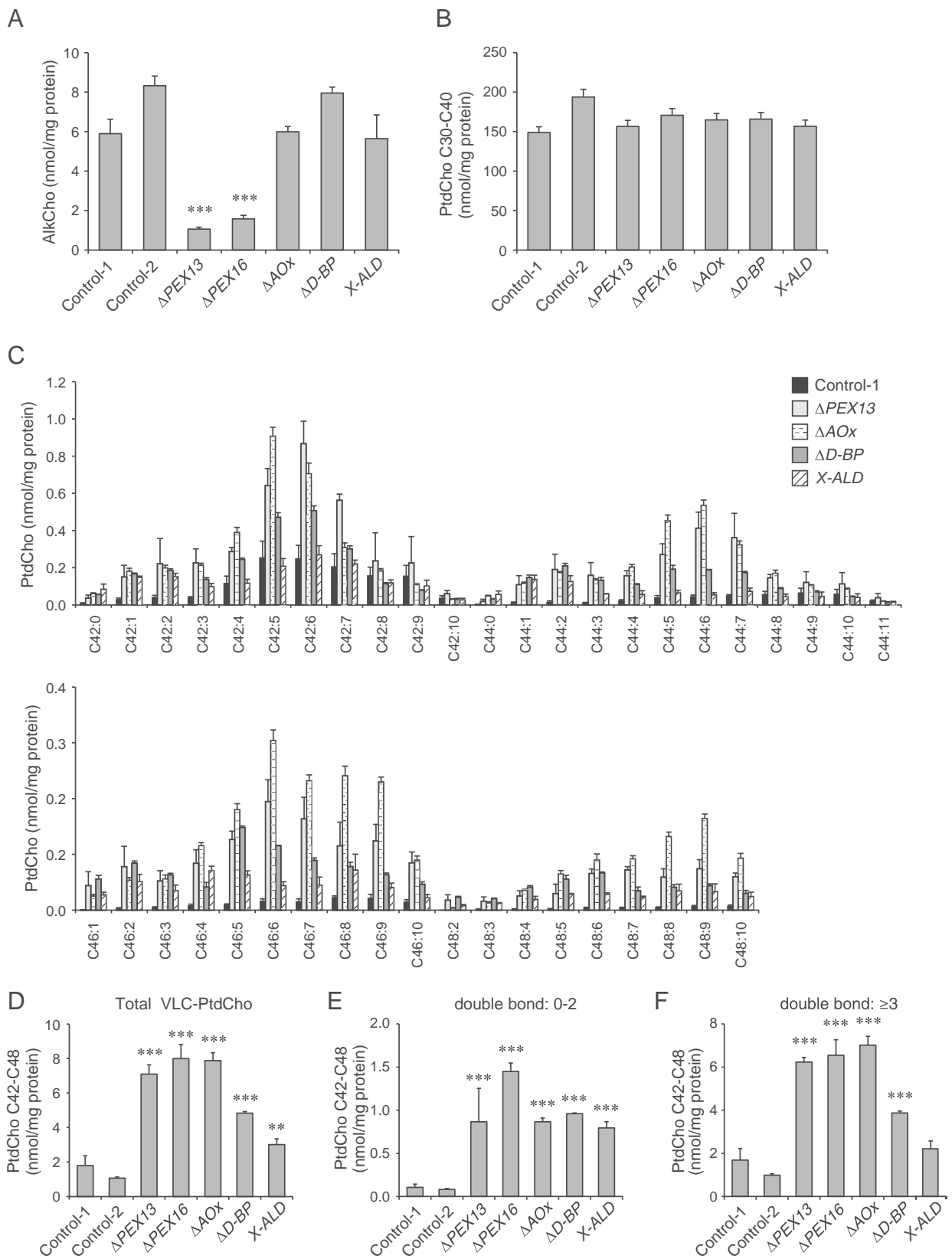


**Fig. 3.** LC-ESI-MS/MS analysis of AlkCho and PtdCho in fibroblasts from patients with PBDs and peroxisomal  $\beta$ -oxidation disorders. AlkCho (A), PtdCho containing 30 to 40 carbons of fatty acids (B), composition of VLC-PtdCho with carbon numbers from 42 to 48 (C), and total VLC-PtdCho (D) are shown. Total VLC-PtdCho was divided into two groups according to the number of double bonds. The amount of VLC-PtdCho with double bonds from zero to two (E) and VLC-PtdCho with three or more double bonds (F) are shown. Data represent the means  $\pm$  S.D. of three independent experiments (\*\* $p < 0.01$ , \*\*\* $p < 0.001$ ; ANOVA with Dunnett's post hoc test as compared with control fibroblasts).

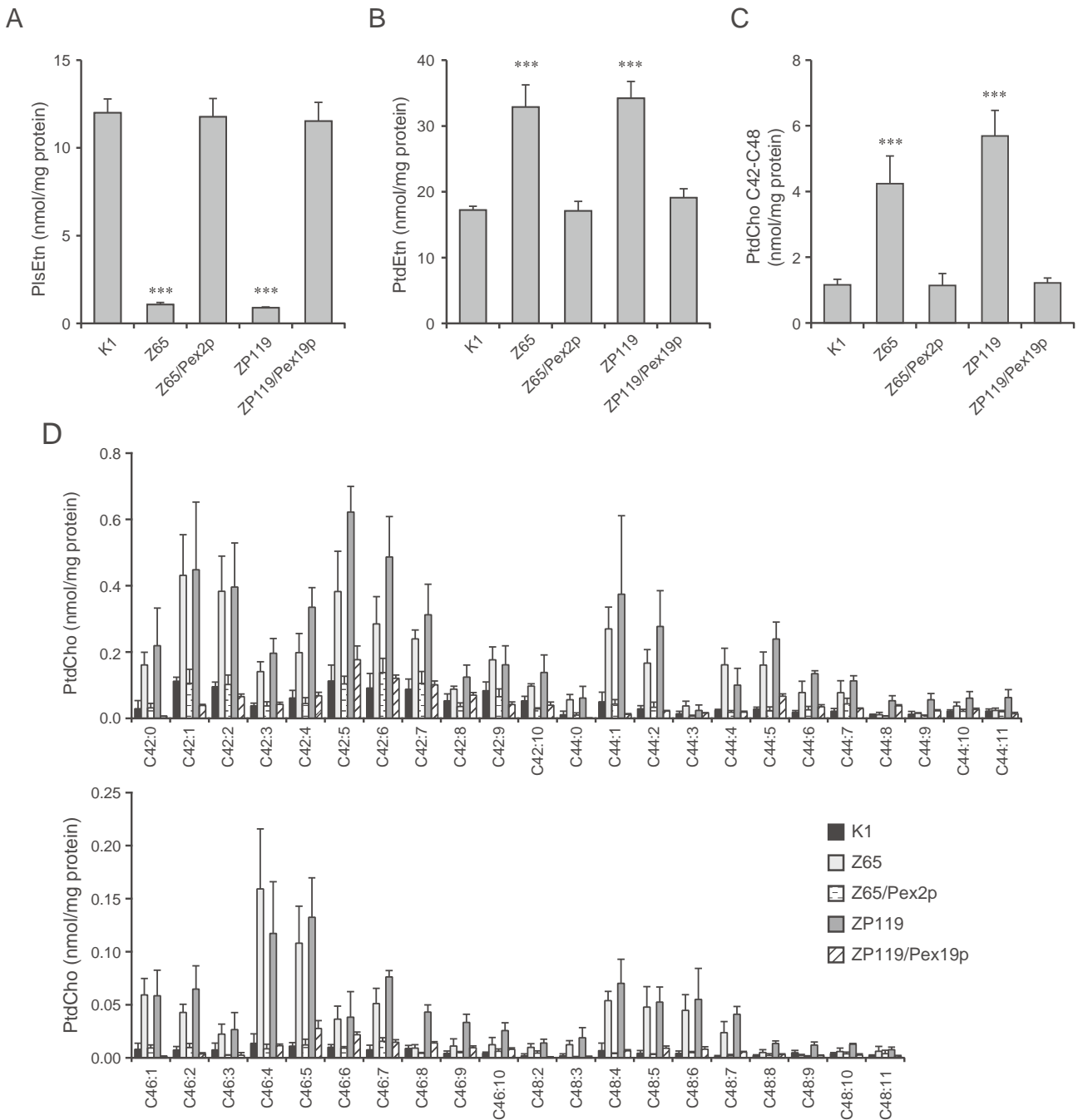


**Fig. 4.** LC-ESI-MS/MS analysis of peroxisome-deficient CHO cell mutants and cells expressing complementary genes. Lipids were extracted and analyzed by LC-ESI-MS/MS as described in Fig. 1. The amount of PlsEtn (A), PtdEtn (B), VLC-PtdCho (C), and the composition of VLC-PtdCho (D) are shown. Data represent the means  $\pm$  S.D. of three independent experiments (\*\*\*) $p < 0.001$ ; ANOVA with Dunnett's post hoc test as compared with CHO-K1 cells.

protein import and peroxisome membrane biogenesis, respectively (Fig. S1B). As shown in Fig. 4A, PlsEtn levels were decreased in both peroxisome-deficient mutants. To investigate the effect of restoration of peroxisome biogenesis on lipid metabolism in these mutant cells, we assessed the lipid composition of *pex2* Z65 cells complemented with CHO *PEX2*, termed Z65/Pex2p, and *pex19* ZP119 cells complemented with human *PEX19*, termed ZP119/Pex19p [24,25] (Table 2). Restoration of peroxisomal biogenesis in each mutant was confirmed by immunofluorescence microscopy (Fig. S1B). In Z65/Pex2p and ZP119/Pex19p cells, levels of PlsEtn were restored (Fig. 4A), and PtdEtn and VLCFA-containing PtdCho were reduced to the levels observed in wild-type CHO-K1 cells (Fig. 4B, C). Although VLC-PUFA-containing PtdCho was mainly elevated in fibroblasts (Fig. 3C), VLC-SFA- or VLC-MUFA-

containing PtdCho was markedly increased in the CHO mutant cells (Fig. 4D). This may be due to the distinct mechanism of VLCFA biosynthesis that occurs in CHO cells. These results demonstrate that deficient peroxisome biogenesis is responsible for the abnormal lipid metabolism observed in the mutant cells.

**3.5. Accumulation of PUFA in VLC-PtdCho in peroxisome-deficient cells is independent of Elov1 5**

Elov1 1-7 of the Elov1 family are the rate-limiting enzymes in the VLCFA elongation pathway [39]. Knockdown of *ELOVL 1* in X-ALD fibroblasts was reported to reduce the accumulation of VLC-SFA, including C26:0, as well as VLC-MUFA [40]. In this study, therefore, we

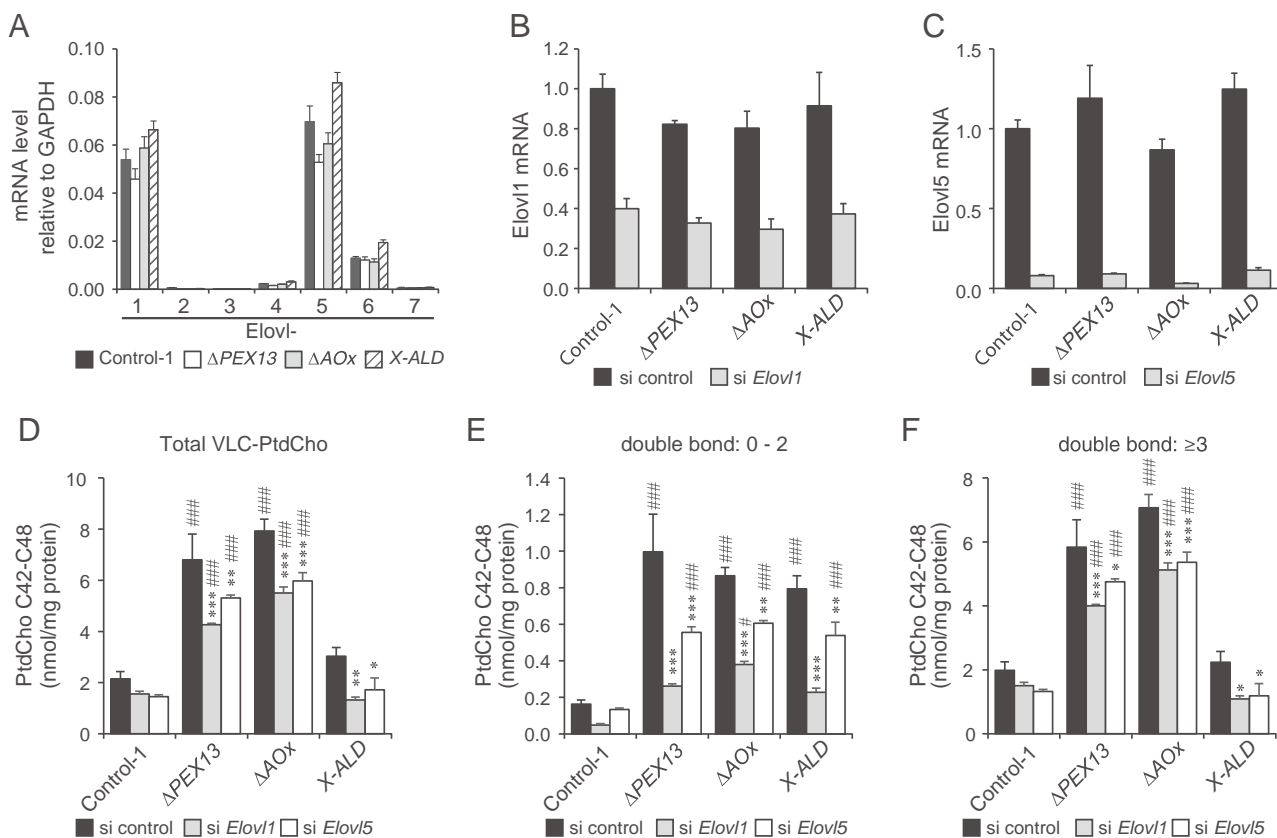


**Fig. 5.** Effect of Elovl activity on the accumulation of VLC-PtdCho in fibroblasts from patients with PBD and peroxisomal  $\beta$ -oxidation disorders. (A) Expression level of Elovl mRNA relative to that of GAPDH mRNA was determined by real-time PCR using total RNA. Fibroblasts were treated twice with control siRNA (solid bar) or siRNAs against *ELOVL1* or *ELOVL5* (gray bar), with a 48 h interval between treatments. *ELOVL1* (B) and *ELOVL5* (C) mRNA levels were determined by real-time PCR using total RNA. (D) VLC-PtdChos in fibroblasts treated with each siRNA were analyzed. Total VLC-PtdCho was separated into VLC-PtdCho with zero to two double bonds (E) or more than three double bonds (F). Data represent the means  $\pm$  S.D. of three independent siRNA transfections into fibroblasts indicated (# $p < 0.05$ , ### $p < 0.001$ ; ANOVA with Tukey–Kramer post hoc test as compared with control fibroblasts transfected with siRNA control, \* $p < 0.05$ , \*\* $p < 0.01$ , \*\*\* $p < 0.001$ ; ANOVA with Tukey–Kramer post hoc test as compared with respective fibroblasts transfected with siRNA control).

investigated whether Elovl activity is involved in the accumulation of VLC-PtdCho in the fibroblasts of patients with ZS, AOx deficiency, and X-ALD.

First, the expression levels of *ELOVL* family members were assessed by quantitative real-time PCR, and *ELOVL 1* and *ELOVL 5* were found to be highly expressed in all types of fibroblasts (Fig. 5A). Treatment of fibroblasts with siRNA targeting *ELOVL 1* and *ELOVL 5* resulted in a significant decrease in *ELOVL 1* and *ELOVL 5* mRNA, respectively (Fig. 5B, C). Knockdown of *ELOVL 1* significantly reduced the accumulation of VLC-SFA- and VLC-MUFA-containing PtdCho (0-2 double bonds) to nearly the same levels as observed in the control cells (Fig. 5E). Contrary to this, the accumulation of VLC-PUFA-containing PtdCho (double bonds  $\geq 3$ ) in peroxisome- and AOx-deficient fibroblasts was slightly lowered, not enough to restore it to control levels (Fig. 5F). Similarly, knockdown of *ELOVL 5* did not reduce the accumulation of VLC-PtdChos to the level of control cells (Fig. 5D, E, and F). These results suggest that accumulation of VLC-SFA- and VLC-MUFA-containing PtdCho in fibroblasts is most likely dependent on Elovl 1 activity, and that Elovl 1 and Elovl 5 are less likely to be involved in the accumulation of VLC-PUFA.

#### 4. Discussion

Abnormalities in peroxisomal metabolism that occur in PBDs and single peroxisomal enzyme deficiencies cause neurodegeneration and developmental defects in the CNS. Because the peroxisome participates in numerous lipid metabolic processes, including the biosynthesis of plasmalogen and bile acids and  $\beta$ -oxidation of VLCFA, it is conceivable that comprehensive analyses of aberrant lipid metabolites will lead to

elucidation of the pathogenic mechanisms of peroxisomal diseases. In the present study, we evaluated the lipid composition in peroxisome- and  $\beta$ -oxidation-deficient fibroblasts from patients and peroxisome-deficient CHO mutants using LC-ESI-MS/MS.

PlsEtn is significantly decreased in peroxisome-deficient fibroblasts and CHO mutants, as observed in patients with ZS [3,4], while the total amount of PtdEtn is increased in peroxisome-deficient cells. The increase in PtdEtn in peroxisome-deficient fibroblasts was mainly due to elevated levels of OA- and AA-containing PtdEtn, such as PtdEtn 16:0/18:1, PtdEtn 18:1/18:1, PtdEtn 18:1/20:4, and PtdEtn 18:0/20:4 (Supplementary Table S3). These results are consistent with the results of FAB-MS analysis of *pex2* CHO Z65 cells and brain tissue from a ZS patient [15,20]. PtdEtn is synthesized primarily through the CDP-ethanolamine pathway (Kennedy pathway) and the PtdSer decarboxylation (PSD) pathway in mitochondria. PtdEtn containing mono- or diunsaturated fatty acids at the sn-2 position (e.g. PtdEtn 16:0/18:1 and PtdEtn 18:1/18:2) is preferentially synthesized by the Kennedy pathway, whereas PUFA-containing PtdEtn is synthesized by both pathways [41]. As significant activation of the PSD pathway is not observed in *pex2* Z65 cells [21], the increase in OA- and AA-containing PtdEtn is most likely due to elevated PtdEtn synthesis via the Kennedy pathway. In addition, the remodeling pathway known as the Lands cycle [42] may also contribute to elevated levels of AA-containing PtdEtn in peroxisome-deficient cells, as well as incorporation of AA into PtdEtn catalyzed by lysophosphatidylcholine acyltransferase 3 (LPCAT3) [43].

DHA-containing phospholipids are reduced in the fibroblasts from patients with ZS and  $\beta$ -oxidation-deficiency [23], and DHA biosynthesis was shown to be reduced in fibroblasts from patients that were

deficient in *AOx* and *D-BP*, but not in *X-ALD* fibroblasts [44]. In the present study, we used LC-ESI-MS/MS analysis to determine the composition of phospholipids containing DHA. In fibroblasts from a control subject, DHA was abundantly incorporated into PlsEtn (Fig. 2B). The decrease in DHA-containing phospholipids observed in peroxisome-deficient fibroblasts was mainly due to the reduction of PlsEtn levels. During the developmental phase of myelination, the total amount of PlsEtn in the brain increases [45]. Correspondingly, DHA content increases in the brain [46]. Moreover, DHA incorporation into phospholipids is decreased in plasmalogen-deficient macrophages [47]. This suggests that PlsEtn serves as a storage mechanism for DHA in several types of cells. In *AOx*-deficient fibroblasts, DHA-PL levels were decreased by half in all phospholipid classes, while the rest of the DHA was most likely derived from serum in the culture medium: DHAPLs in fibroblasts cultured in serum-free medium were reduced to a half level of those in serum-plus medium (data not shown). These results suggest that the distribution of DHA in phospholipids is likely to be strictly regulated by the amount of free DHA, and that *de novo* synthesis of DHA by peroxisomal  $\beta$ -oxidation contributes significantly to the homeostasis of DHA.

DHA is also known as a precursor of anti-inflammatory bioactive lipid mediators, such as D-series resolvin and protectin D1 [48]. However, the source of these anti-inflammatory mediators is unclear. The secreted phospholipase A<sub>2</sub> group IID (PLA2G2D) was recently suggested to be involved in the production of resolvin D1 and 15-deoxy- $\Delta^{12,14}$ -prostaglandin J<sub>2</sub> via the deacylation of PtdEtn and PlsEtn [49]. It is noteworthy that inflammation is observed in the brain of oligodendrocyte-specific *PEX5* knockout mice [50]. The marked decrease in DHA levels observed in fibroblasts of patients with *ZS*, *AOx* deficiency, and *D-BP* deficiency may be linked to the inefficient synthesis of anti-inflammatory mediators.

To date, the levels of VLCFA and phytanic acid in serum or plasma as determined by GC/MS are utilized for the initial screening of peroxisomal disorders [51]. The accumulation of plasma VLCFA, especially elevation of the C26:0/C22:0 and C26:1/C22:0 ratios, is a common metabolic phenotype of peroxisomal disorders, including *ZS*, *X-ALD*, and  $\beta$ -oxidation deficiency. However, in addition to the accumulation of VLC-SFA and VLC-MUFA, VLC-PUFA is elevated in the brains of patients with *ZS* [52]. Furthermore, accumulation of VLC-PUFA in cholesterol esters and polar lipids has been shown by GC/MS [52]. Nonetheless, little attention has been paid to VLC-PUFA levels in patients with PBDs or peroxisomal  $\beta$ -oxidation deficiency. Here, we provide evidence by LC-ESI-MS/MS analysis that increased levels of VLC-SFA- and VLC-MUFA-containing PtdCho are common between *X-ALD* and  $\beta$ -oxidation-defective fibroblasts, while VLC-PUFA is elevated in peroxisome-, *AOx*-, and *D-BP*-deficient fibroblasts. These differences are most likely explained by the substrate specificity of the ABCD isoforms; ABCD1 specifically translocates VLC-SFA and VLC-MUFA, but not VLC-PUFA, whereas ABCD2 transports VLC-PUFA [53–56], which is indicative of normal  $\beta$ -oxidation activity of VLC-PUFA in *X-ALD* fibroblasts. By contrast, all types of VLCFAs are accumulated and incorporated into PtdCho in *AOx*- and *D-BP*-deficient cells due to the defective peroxisomal  $\beta$ -oxidation activity. *AOx*-deficient patients manifest more severe symptoms than *X-ALD* patients [4,11]. Therefore, in addition to VLC-SFA and VLC-MUFA, VLC-PUFA accumulation in PtdCho potentially contributes to the mechanism underlying the pathogenesis of fatty acid  $\beta$ -oxidation deficiency. Further profound pathology is observed in the patients with *D-BP* deficiency than those with *AOx* deficiency [12,13]. Since *D-BP* is also involved in oxidation of branched chain fatty acids, such as pristanic acids, and biosynthesis of bile acids, these aberrant metabolites may affect the pathology of *D-BP* deficiency.

The *Elovl* family is involved in the elongation of VLCFAs. Knockdown of *Elovl1* using siRNA decreases the accumulation of VLC-SFA and VLC-MUFA in PtdCho of *X-ALD* fibroblasts, consistent with an earlier report [40]. However, VLC-PUFA accumulation was slightly reduced by

knockdown of *ELOVL1* and *ELOVL5*. This may be because *Elovl5* is not believed to elongate PUFA beyond C22 [57]. Thus, other member(s) of the *Elovl* family are likely to be involved in the synthesis of VLC-PUFA, and could be potential targets of therapies designed to treat *AOx* deficiency and PBDs.

Supplementary data to this article can be found online at <http://dx.doi.org/10.1016/j.bbaliip.2014.01.001>.

## Acknowledgements

We thank K. Shimizu for preparing the figures and the other members of our laboratory for insightful discussion regarding this work. The work was supported in part by a CREST grant (to Y.F.) from the Science and Technology Agency of Japan, Grants-in-Aid for Scientific Research (numbers 19058011, 20370039, 24247038, and 25116717 to Y.F.; 23570236 to M.H.), Global COE Program, and Grants for Excellent Graduate Schools from The Ministry of Education, Culture, Sports, Science and Technology of Japan, Grants (to Y.A. and M.H.) from Kyushu University Interdisciplinary Programs in Education and Projects in Research Development, and grants (to Y.F.) from the Takeda Science Foundation and the Japanese Foundation for Applied Enzymology.

## References

- [1] R.J.A. Wanders, Peroxisomes, lipid metabolism, and peroxisomal disorders, *Mol. Genet. Metab.* 83 (2004) 16–27.
- [2] R.J.A. Wanders, H.R. Waterham, Biochemistry of mammalian peroxisomes revisited, *Annu. Rev. Biochem.* 75 (2006) 295–332.
- [3] S.J. Steinberg, G. Dodt, G.V. Raymond, N.E. Braverman, A.B. Moser, H.W. Moser, Peroxisome biogenesis disorders, *Biochim. Biophys. Acta, Mol. Cell Res.* 1763 (2006) 1733–1748.
- [4] R.J.A. Wanders, Metabolic and molecular basis of peroxisomal disorders: a review, *Am. J. Med. Genet. A* 126A (2004) 355–375.
- [5] Y. Fujiki, K. Okumoto, N. Kinoshita, K. Ghaedi, Lessons from peroxisome-deficient Chinese hamster ovary (CHO) cell mutants, *Biochim. Biophys. Acta, Mol. Cell Res.* 1763 (2006) 1374–1381.
- [6] J. Berger, J. Gärtner, X-linked adrenoleukodystrophy: clinical, biochemical and pathogenetic aspects, *Biochim. Biophys. Acta* 1763 (2006) 1721–1732.
- [7] R.J.A. Wanders, H.R. Waterham, Peroxisomal disorders: the single peroxisomal enzyme deficiencies, *Biochim. Biophys. Acta, Mol. Cell Res.* 1763 (2006) 1707–1720.
- [8] C. Wiesinger, M. Kunze, G. Regelsberger, S. Forss-Petter, J. Berger, Impaired Very Long-chain Acyl-CoA  $\beta$ -Oxidation in Human X-linked Adrenoleukodystrophy Fibroblasts Is a Direct Consequence of ABCD1 transporter Dysfunction, *J. Biol. Chem.* 288 (2013) 19269–19279.
- [9] Y. Poirier, V.D. Antonenkov, T. Glumoff, J.K. Hiltunen, Peroxisomal  $\beta$ -oxidation—a metabolic pathway with multiple functions, *Biochim. Biophys. Acta* 1763 (2006) 1413–1426.
- [10] S. Ferdinandusse, S. Denis, E.M. Hogenhout, J. Koster, C.W.T. van Roermund, L. IJlst, A.B. Moser, R.J.A. Wanders, H.R. Waterham, Clinical, biochemical, and mutational spectrum of peroxisomal acyl-coenzyme A oxidase deficiency, *Hum. Mutat.* 28 (2007) 904–912.
- [11] B.T. Poll-The, E. Roels, H. Ogier, J. Scotto, J. Vamecq, R.B.H. Schutgens, R.J.A. Wanders, C.W.T. van Roermund, M.J.A. van Wijland, A.W. Schram, J.M. Tager, J.M. Saudubray, A new peroxisomal disorder with enlarged peroxisomes and a specific deficiency of acyl-CoA oxidase (pseudo-neonatal adrenoleukodystrophy), *Am. J. Hum. Genet.* 42 (1988) 422–434.
- [12] Y. Suzuki, L.L. Jiang, M. Souri, S. Miyazawa, S. Fukuda, Z. Zhang, M. Ume, N. Shimozawa, N. Kondo, T. Orii, T. Hashimoto, D-3-hydroxyacyl-CoA dehydrogenase/D-3-hydroxyacyl-CoA dehydrogenase bifunctional protein deficiency: a newly identified peroxisomal disorder, *Am. J. Hum. Genet.* 61 (1997) 1153–1162.
- [13] S. Ferdinandusse, S. Denis, P.A. Mooyer, C. Dekker, M. Duran, R.J. Soorani-Lunsing, E. Boltshauser, A. Macaya, J. Gärtner, C.B. Majoie, P.G. Barth, R.J.A. Wanders, B.T. Poll-The, Clinical and biochemical spectrum of D-bifunctional protein deficiency, *Ann. Neurol.* 59 (2006) 92–104.
- [14] B.J. Pettus, M. Baes, M. Busman, Y.A. Hannun, P.P. Van Veldhoven, Mass spectrometric analysis of ceramide perturbations in brain and fibroblasts of mice and human patients with peroxisomal disorders, *Rapid Commun. Mass Spectrom.* 18 (2004) 1569–1574.
- [15] M. Saitoh, M. Itoh, S. Takashima, M. Mizuguchi, M. Iwamori, Phosphatidyl ethanolamine with increased polyunsaturated fatty acids in compensation for plasmalogen defect in the Zellweger syndrome brain, *Neurosci. Lett.* 449 (2009) 164–167.
- [16] M. Saitoh, Y. Sakakihara, M. Mizuguchi, M. Itoh, S. Takashima, M. Iwamori, S. Kamoshita, T. Igarashi, Increase of ceramide monohexoside and dipalmitoyl glycerophospholipids in the brain of Zellweger syndrome, *Neurosci. Lett.* 417 (2007) 165–170.
- [17] A. Petroni, B. Bertagnolio, P. La Spada, M. Blasevich, N. Papini, S. Govoni, M. Rimoldi, C. Galli, The  $\beta$ -oxidation of arachidonic acid and the synthesis of docosahexaenoic acid are selectively and consistently altered in skin fibroblasts from three Zellweger

- patients versus X-adrenoleukodystrophy, Alzheimer and control subjects, *Neurosci. Lett.* 250 (1998) 145–148.
- [18] K. Tatsumi, M. Saito, B. Lin, M. Iwamori, H. Ichiseki, N. Shimozawa, S. Kamoshita, T. Igarashi, Y. Sakakihara, Enhanced expression of  $\alpha$ -series gangliosides in fibroblasts of patients with peroxisome biogenesis disorders, *Biochim. Biophys. Acta* 1535 (2001) 285–293.
- [19] M. Nagura, M. Saito, M. Iwamori, Y. Sakakihara, T. Igarashi, Alterations of fatty acid metabolism and membrane fluidity in peroxisome-defective mutant ZP102 cells, *Lipids* 39 (2004) 43–50.
- [20] M. Saito, M. Horikawa, Y. Iwamori, Y. Sakakihara, M. Mizuguchi, T. Igarashi, Y. Fujiki, M. Iwamori, Alterations in the molecular species of plasmalogen phospholipids and glycolipids due to peroxisomal dysfunction in Chinese hamster ovary-mutant Z65 cells by FAB/MS method, *J. Chromatogr. B* 852 (2007) 367–373.
- [21] M. Saito, M. Iwamori, B. Lin, A. Oka, Y. Fujiki, N. Shimozawa, S. Kamoshita, M. Yanagisawa, Y. Sakakihara, Accumulation of glycolipids in mutant Chinese hamster ovary cells (Z65) with defective peroxisomal assembly and comparison of the metabolic rate of glycosphingolipids between Z65 cells and wild-type CHO-K1 cells, *Biochim. Biophys. Acta* 1438 (1999) 55–62.
- [22] R. Itoh, Y. Fujiki, Functional domains and dynamic assembly of the peroxin Pex14p, the entry site of matrix proteins, *J. Biol. Chem.* 281 (2006) 10196–10205.
- [23] A. Itoyama, M. Honsho, Y. Abe, A. Moser, Y. Yoshida, Y. Fujiki, Docosahexaenoic acid mediates peroxisomal elongation, a prerequisite for peroxisome division, *J. Cell Sci.* 125 (2012) 589–602.
- [24] K. Ghaedi, Y. Fujiki, Isolation and characterization of novel phenotype CHO cell mutants defective in peroxisome assembly, using ICR191 as a potent mutagenic agent, *Cell Biochem. Funct.* 26 (2008) 684–691.
- [25] Y. Matsuzono, N. Kinoshita, S. Tamura, N. Shimozawa, M. Hamasaki, K. Ghaedi, R.J.A. Wanders, Y. Suzuki, N. Kondo, Y. Fujiki, Human *PEX19*: cDNA cloning by functional complementation, mutation analysis in a patient with Zellweger syndrome and potential role in peroxisomal membrane assembly, *Proc. Natl. Acad. Sci. U. S. A.* 96 (1999) 2116–2121.
- [26] Y. Ohno, S. Suto, M. Yamanaka, Y. Mizutani, S. Mitsutake, Y. Igarashi, T. Sassa, A. Kihara, ELOVL1 production of C24 acyl-CoAs is linked to C24 sphingolipid synthesis, *Proc. Natl. Acad. Sci. U. S. A.* 107 (2010) 18439–18444.
- [27] E.G. Bligh, W.J. Dyer, A rapid method of total lipid extraction and purification, *Can. J. Med. Sci.* 37 (1959) 911–917.
- [28] T. Houjou, K. Yamatani, H. Nakanishi, M. Imagawa, T. Shimizu, R. Taguchi, Rapid and selective identification of molecular species in phosphatidylcholine and sphingomyelin by conditional neutral loss scanning and MS3, *Rapid Commun. Mass Spectrom.* 18 (2004) 3123–3130.
- [29] H. Nakanishi, Y. Iida, T. Shimizu, R. Taguchi, Separation and quantification of sn-1 and sn-2 fatty acid positional isomers in phosphatidylcholine by RPLC-ESIMS/MS, *J. Biochem.* 147 (2010) 245–256.
- [30] N. Shimozawa, Y. Suzuki, Z. Zhang, A. Imamura, R. Toyama, S. Mukai, Y. Fujiki, T. Tsukamoto, T. Osumi, T. Orii, R.J.A. Wanders, N. Kondo, Nonsense and temperature-sensitive mutations in *PEX13* are the cause of complementation group H of peroxisome biogenesis disorders, *Hum. Mol. Genet.* 8 (1999) 1077–1083.
- [31] M. Honsho, S. Tamura, N. Shimozawa, Y. Suzuki, N. Kondo, Y. Fujiki, Mutation in *PEX16* is causal in the peroxisome-deficient Zellweger syndrome of complementation group D, *Am. J. Hum. Genet.* 63 (1998) 1622–1630.
- [32] P. Brites, H.R. Waterham, R.J.A. Wanders, Functions and biosynthesis of plasmalogens in health and disease, *Biochim. Biophys. Acta* 1636 (2004) 219–231.
- [33] K.A. Zemski Berry, R.C. Murphy, Electrospray ionization tandem mass spectrometry of glycerophosphoethanolamine plasmalogen phospholipids, *J. Am. Soc. Mass Spectrom.* 15 (2004) 1499–1508.
- [34] S.M. Innis, Dietary omega 3 fatty acids and the developing brain, *Brain Res.* 1237 (2008) 35–43.
- [35] S. Ferdinandusse, S. Denis, P.A. Mooijer, Z. Zhang, J.K. Reddy, A.A. Spector, R.J.A. Wanders, Identification of the peroxisomal  $\beta$ -oxidation enzymes involved in the biosynthesis of docosahexaenoic acid, *J. Lipid Res.* 42 (2001) 1987–1995.
- [36] M. Martinez, Abnormal profiles of polyunsaturated fatty acids in the brain, liver, kidney and retina of patients with peroxisomal disorders, *Brain Res.* 583 (1992) 171–182.
- [37] T. Tsukamoto, S. Yokota, Y. Fujiki, Isolation and characterization of Chinese hamster ovary cell mutants defective in assembly of peroxisomes, *J. Cell Biol.* 110 (1990) 651–660.
- [38] N. Kinoshita, K. Ghaedi, N. Shimozawa, R.J.A. Wanders, Y. Matsuzono, T. Imanaka, K. Okumoto, Y. Suzuki, N. Kondo, Y. Fujiki, Newly identified Chinese hamster ovary cell mutants are defective in biogenesis of peroxisomal membrane vesicles (peroxisomal ghosts), representing a novel complementation group in mammals, *J. Biol. Chem.* 273 (1998) 24122–24130.
- [39] A. Jakobsson, R. Westerberg, A. Jakobsson, Fatty acid elongases in mammals: their regulation and roles in metabolism, *Prog. Lipid Res.* 45 (2006) 237–249.
- [40] R. Ofman, I.M. Dijkstra, C.W. van Roermund, N. Burger, M. Turkenburg, A. van Cruchten, C.E. van Engen, R.J.A. Wanders, S. Kemp, The role of ELOVL1 in very long-chain fatty acid homeostasis and X-linked adrenoleukodystrophy, *EMBO Mol. Med.* 2 (2010) 90–97.
- [41] O.B. Bleijerveld, J.F. Brouwers, A.B. Vaandrager, J.B. Helms, M. Houweling, The CDP-ethanolamine pathway and phosphatidylserine decarboxylation generate different phosphatidylethanolamine molecular species, *J. Biol. Chem.* 282 (2007) 28362–28372.
- [42] W.E. Lands, Metabolism of glycerolipides; a comparison of lecithin and triglyceride synthesis, *J. Biol. Chem.* 231 (1958) 883–888.
- [43] D. Hishikawa, H. Shindou, S. Kobayashi, H. Nakanishi, R. Taguchi, T. Shimizu, Discovery of a lysophospholipid acyltransferase family essential for membrane asymmetry and diversity, *Proc. Natl. Acad. Sci. U. S. A.* 105 (2008) 2830–2835.
- [44] H.M. Su, A.B. Moser, H.W. Moser, P.A. Watkins, Peroxisomal straight-chain Acyl-CoA oxidase and D-bifunctional protein are essential for the retroconversion step in docosahexaenoic acid synthesis, *J. Biol. Chem.* 276 (2001) 38115–38120.
- [45] N. Nagan, R.A. Zoeller, Plasmalogens: biosynthesis and functions, *Prog. Lipid Res.* 40 (2001) 199–229.
- [46] M. Martinez, Polyunsaturated fatty acids in the developing human brain, erythrocytes and plasma in peroxisomal disease: therapeutic implications, *J. Inher. Metab. Dis.* 18 (Suppl. 1) (1995) 61–75.
- [47] D.P. Gaposchkin, R.A. Zoeller, Plasmalogen status influences docosahexaenoic acid levels in a macrophage cell line. Insights using ether lipid-deficient variants, *J. Lipid Res.* 40 (1999) 495–503.
- [48] K.H. Weylandt, C.Y. Chiu, B. Gomolka, S.F. Waechter, B. Wiedenmann, Omega-3 fatty acids and their lipid mediators: towards an understanding of resolvin and protectin formation, *Prostaglandins Other Lipid Mediat.* 97 (2012) 73–82.
- [49] Y. Miki, K. Yamamoto, Y. Taketomi, H. Sato, K. Shimo, T. Kobayashi, Y. Ishikawa, T. Ishii, H. Nakanishi, K. Ikeda, R. Taguchi, K. Kabashima, M. Arita, H. Arai, G. Lambeau, J.M. Bollinger, S. Hara, M.H. Gelb, M. Murakami, Lymphoid tissue phospholipase A2 group IID resolves contact hypersensitivity by driving antiinflammatory lipid mediators, *J. Exp. Med.* 210 (2013) 1217–1234.
- [50] C.M. Kassmann, C. Lappe-Siefke, M. Baes, B. Brügger, A. Mildner, H.B. Werner, O. Natt, T. Michaelis, M. Prinz, J. Frahm, K.A. Nave, Axonal loss and neuroinflammation caused by peroxisome-deficient oligodendrocytes, *Nat. Genet.* 39 (2007) 969–976.
- [51] N. Shimozawa, Molecular and clinical findings and diagnostic flowchart of peroxisomal diseases, *Brain Dev.* 33 (2011) 770–776.
- [52] P. Sharp, A. Poulos, A. Fellenberg, D. Johnson, Structure and lipid distribution of polyenoic very-long-chain fatty acids in the brain of peroxisome-deficient patients (Zellweger syndrome), *Biochem. J.* 248 (1987) 61–67.
- [53] S. Fourcade, M. Ruiz, C. Camps, A. Schlüter, S.M. Houten, P.A. Mooyer, T. Pàmols, G. Dacremont, R.J.A. Wanders, M. Giròs, A. Pujol, A key role for the peroxisomal ABCD2 transporter in fatty acid homeostasis, *Am. J. Physiol. Endocrinol. Metab.* 296 (2009) E211–E221.
- [54] E.C. Genin, F. Geillon, C. Gondcaille, A. Athias, P. Gambert, D. Trompier, S. Savary, Substrate specificity overlap and interaction between adrenoleukodystrophy protein (ALDP/ABCD1) and adrenoleukodystrophy-related protein (ALDRP/ABCD2), *J. Biol. Chem.* 286 (2011) 8075–8084.
- [55] M. Morita, T. Imanaka, Peroxisomal ABC transporters: structure, function and role in disease, *Biochim. Biophys. Acta* 1822 (2012) 1387–1396.
- [56] C.W. van Roermund, W.F. Visser, L. Ijlst, H.R. Waterham, R.J.A. Wanders, Differential substrate specificities of human ABCD1 and ABCD2 in peroxisomal fatty acid  $\beta$ -oxidation, *Biochim. Biophys. Acta* 1811 (2011) 148–152.
- [57] A.E. Leonard, E.G. Bobik, J. Dorado, P.E. Kroeger, L.T. Chuang, J.M. Thurmond, J.M. Parker-Barnes, T. Das, Y.S. Huang, P. Mukerji, Cloning of a human cDNA encoding a novel enzyme involved in the elongation of long-chain polyunsaturated fatty acids, *Biochem. J.* 350 (2000) 765–770.

# The role of group IIF-secreted phospholipase A<sub>2</sub> in epidermal homeostasis and hyperplasia

Kei Yamamoto,<sup>1</sup> Yoshimi Miki,<sup>1</sup> Mariko Sato,<sup>1,2</sup> Yoshitaka Taketomi,<sup>1</sup> Yasumasa Nishito,<sup>3</sup> Choji Taya,<sup>3</sup> Kazuaki Muramatsu,<sup>2</sup> Kazutaka Ikeda,<sup>4</sup> Hiroki Nakanishi,<sup>5</sup> Ryo Taguchi,<sup>6</sup> Naotomo Kambe,<sup>7</sup> Kenji Kabashima,<sup>8</sup> Gérard Lambeau,<sup>9</sup> Michael H. Gelb,<sup>10</sup> and Makoto Murakami<sup>1,11</sup>

<sup>1</sup>Lipid Metabolism Project, Tokyo Metropolitan Institute of Medical Science, Tokyo 156-8506, Japan

<sup>2</sup>School of Science and Engineering, Tokyo Denki University, Saitama 350-0394, Japan

<sup>3</sup>Center for Basic Technology Research, Tokyo Metropolitan Institute of Medical Science, Tokyo 156-8506, Japan

<sup>4</sup>Laboratory for Metabolomics, Institute of Physical and Chemical Research (RIKEN) Center for Integrative Medical Sciences, Kanagawa 230-0045, Japan

<sup>5</sup>Research Center for Biosignal, Akita University, Akita 010-8543, Japan

<sup>6</sup>College of Bioscience and Biotechnology, Chubu University, Aichi 487-8501, Japan

<sup>7</sup>Department of Dermatology, Chiba University Graduate School of Medicine, Chiba 260-8677, Japan

<sup>8</sup>Department of Dermatology, Kyoto University Graduate School of Medicine, Kyoto 606-8507, Japan

<sup>9</sup>Institut de Pharmacologie Moléculaire et Cellulaire, UMR7275, Centre National de la Recherche Scientifique et Université de Nice-Sophia-Antipolis, 06560 Valbonne, France

<sup>10</sup>Departments of Chemistry and Biochemistry, University of Washington, Seattle, WA 98195

<sup>11</sup>CREST, Japan Agency for Medical Research and Development (AMED) and Japan Science and Technology Agency (JST), Tokyo 100-0004, Japan

**Epidermal lipids are important for skin homeostasis. However, the entire picture of the roles of lipids, particularly nonceramide lipid species, in epidermal biology still remains obscure. Here, we report that PLA2G2F, a functionally orphan-secreted phospholipase A<sub>2</sub> expressed in the suprabasal epidermis, regulates skin homeostasis and hyperplastic disorders. *Pla2g2f*<sup>-/-</sup> mice had a fragile stratum corneum and were strikingly protected from psoriasis, contact dermatitis, and skin cancer. Conversely, *Pla2g2f*-overexpressing transgenic mice displayed psoriasis-like epidermal hyperplasia. Primary keratinocytes from *Pla2g2f*<sup>-/-</sup> mice showed defective differentiation and activation. PLA2G2F was induced by calcium or IL-22 in keratinocytes and preferentially hydrolyzed ethanolamine plasmalogen-bearing docosahexaenoic acid secreted from keratinocytes to give rise to unique bioactive lipids (i.e., protectin D1 and 9S-hydroxyoctadecadienoic acid) that were distinct from canonical arachidonate metabolites (prostaglandins and leukotrienes). Ethanolamine lysoplasmalogen, a PLA2G2F-derived marker product, rescued defective activation of *Pla2g2f*<sup>-/-</sup> keratinocytes both in vitro and in vivo. Our results highlight PLA2G2F as a previously unrecognized regulator of skin pathophysiology and point to this enzyme as a novel drug target for epidermal-hyperplastic diseases.**

The epidermis is a highly organized stratified epithelium consisting of basal, spinous, granular, and cornified keratinocyte layers. Survival in a terrestrial dry environment requires an adapted permeability barrier for regulated permeation of water and electrolytes in the stratum corneum (SC). Corneocytes are embedded in a lipid-rich extracellular matrix that forms lamellar membranes composed of ceramides, cholesterol, and fatty acids in an acidic environment (Elias et al.,

2008). Perturbation of cutaneous lipid metabolism variably and often profoundly affects SC barrier or keratinocyte homeostasis, leading to skin disorders such as ichthyosis, psoriasis, atopic dermatitis, and cancer (Jobard et al., 2002; Vasireddy et al., 2007).

Linoleic acid (LA; C18:2), by far the most abundant polyunsaturated fatty acid (PUFA) in the SC, is esterified to the ω-hydroxyl group of

## CORRESPONDENCE

Makoto Murakami:  
murakami-mk@igakuken.or.jp

Abbreviations used: 10,17-diHDoHE, 10S, 17S-dihydroxy-DHA; AA, arachidonic acid; DHA, docosahexaenoic acid; DMBA, 9,10-dimethylbenz(a)anthracene; DNFB, dinitrofluorobenzene; EPA, eicosapentaenoic acid; ESI-MS, electrospray ionization mass spectrometry; HODE, hydroxyoctadecadienoic acid; IMQ, imiquimod; LA, linoleic acid; LOX, lipoxygenase; LPC, lysophosphatidylcholine; LPE, lysophosphatidylethanolamine; MRM, multiple reaction monitoring; P-LPE, plasmalogen forms of lysophosphatidylethanolamine; P-PE, plasmalogen form of phosphatidylethanolamine; PC, phosphatidylcholine; PD1, protectin D1 (10R, 17S-dihydroxy-DHA); PE, phosphatidylethanolamine; PG, prostaglandin; PLA<sub>2</sub>, phospholipase A<sub>2</sub>; PUFA, polyunsaturated fatty acid; RvD1, resolvin D1; SC, stratum corneum; sPLA<sub>2</sub>, secreted PLA<sub>2</sub>; TEWL, trans-epidermal water loss; TG, transgenic; TPA, 12-O-tetradecanoylphorbol-13-acetate.

K. Yamamoto's present address is Faculty of Bioscience and Bioindustry, Tokushima University, Tokushima 770-8506, Japan.

© 2015 Yamamoto et al. This article is distributed under the terms of an Attribution-Noncommercial-Share Alike-No Mirror Sites license for the first six months after the publication date (see <http://www.rupress.org/terms>). After six months it is available under a Creative Commons License (Attribution-Noncommercial-Share Alike 3.0 Unported license, as described at <http://creativecommons.org/licenses/by-nc-sa/3.0/>).

ceramides, which, along with ultra-long-chain fatty acids, are essential for formation of the cornified lipid envelope (Elias et al., 2014). Fatty acids are also important for SC acidification (Mao-Qiang et al., 1996; Fluhr et al., 2001, 2004). Dysregulated production of PUFA- or lysophospholipid-derived lipid mediators can be linked to skin disorders including alopecia, inflammation, and cancer (Nagamachi et al., 2007; Inoue et al., 2011). Release of fatty acids and lysophospholipids from phospholipids is catalyzed by phospholipase A<sub>2</sub> (PLA<sub>2</sub>) enzymes, which are classified into several families (Murakami et al., 2011). However, the roles of PLA<sub>2</sub>-driven lipid products in epidermal homeostasis and diseases are still not well understood.

The secreted PLA<sub>2</sub> (sPLA<sub>2</sub>) family consists of 11 members with distinct localizations and substrate specificities (Murakami et al., 2011, 2015). Recent gene targeting of sPLA<sub>2</sub>s has revealed their distinct roles in various biological events, such as immunity, host defense, atherosclerosis, metabolic disorders, and reproduction (Labonté et al., 2006; Henderson et al., 2007; Escoffier et al., 2010; Sato et al., 2010, 2014; Ait-Outfella et al., 2013; Miki et al., 2013; Taketomi et al., 2013; Boudreau et al., 2014; Pernet et al., 2014). In skin biology, sPLA<sub>2</sub>s have been suggested to supply bulk fatty acids for formation of the SC acid mantle (Fluhr et al., 2004; Hachem et al., 2005), an idea that stems primarily from the finding that SC acidity is perturbed by nonspecific sPLA<sub>2</sub> inhibitors (Mao-Qiang et al., 1996; Fluhr et al., 2001). Furthermore, transgenic (TG) mice overexpressing group IIA (PLA2G2A) or group X (PLA2G10) sPLA<sub>2</sub> develop skin abnormalities (Grass et al., 1996; Mulherkar et al., 2003; Yamamoto et al., 2011b). However, the findings that the C57BL/6 mouse strain lacks PLA2G2A due to a natural mutation (MacPhee et al., 1995) and that endogenous PLA2G10 is located in hair follicles (Yamamoto et al., 2011b) cast doubt on the intrinsic roles of these sPLA<sub>2</sub>s in the epidermis. Overall, it remains unclear whether sPLA<sub>2</sub> indeed regulates epidermal lipid processing, and if so, which sPLA<sub>2</sub> isoform is important, which lipid species serve as its substrates and products, and how sPLA<sub>2</sub>-driven lipid metabolism affects skin homeostasis and diseases.

It has recently been reported that group IIF sPLA<sub>2</sub> (PLA2G2F), a functionally orphan sPLA<sub>2</sub>, is expressed in the skin and that its genetic deletion perturbs SC acidification and delays barrier recovery (Ilic et al., 2014; Man et al., 2014). We now show that PLA2G2F is a bona fide epidermal sPLA<sub>2</sub> that controls keratinocyte differentiation, hyperproliferation, and function by mobilizing unique lipid products rather than by supplying fatty acids as a whole. Aberrant PLA2G2F expression is associated with epidermal hyperplasia in skin inflammation and cancer. Our results highlight a previously unrecognized sPLA<sub>2</sub>-driven lipid pathway underlying epidermal-hyperplastic diseases.

## RESULTS

### PLA2G2F is preferentially expressed in the suprabasal epidermis

We took advantage of epidermal-hyperplastic *PLA2G10<sup>tg/+</sup>* mice (Yamamoto et al., 2011b) to identify particular lipase-related

genes whose expression levels were altered in TG skin compared with control skin and whose *in vivo* functions are currently unknown. Microarray gene profiling revealed that several lipase-related genes showed increased expression in *PLA2G10<sup>tg/+</sup>* skin (Table S1). We were interested in *Pla2g2f*, as it was by far the most abundant sPLA<sub>2</sub> in control C57BL/6 skin and was increased in hyperplastic *PLA2G10<sup>tg/+</sup>* skin (Fig. 1 A), a finding that was verified by Northern blotting (Fig. 1 A, inset) and immunohistochemistry (Fig. 1 B). In control skin (P25), the outermost layer of the epidermis was stained with anti-PLA2G2F, but not the control antibody, whereas PLA2G2F staining in *PLA2G10<sup>tg/+</sup>* skin was more intense and distributed in the thickened epidermis and cysts (Fig. 1 B).

Quantitative RT-PCR demonstrated preferential expression of *Pla2g2f* in the skin (and only at trace levels in the small and large intestines) in C57BL/6 mice (Fig. 1 C). Developmental expression of *Pla2g2f* in mouse skin was far greater than that of other sPLA<sub>2</sub>s, gradually increasing before birth to reach a maximum level by postnatal day 5 (P5; Fig. 1 D). Separation of the epidermis and hair follicles (P8) by laser-capture microdissection followed by quantitative RT-PCR revealed the expression of *Pla2g2f* in the epidermis rather than in hair follicles, whereas that of other sPLA<sub>2</sub>s was low or undetectable in both compartments (Fig. 1 E). *In situ* hybridization confirmed the epidermal location of *Pla2g2f*, which was already detectable at embryonic day 14.5 (E14.5) when epidermal morphogenesis had started (Fig. 1 F). Confocal microscopy of mouse skin showed that PLA2G2F was colocalized with loricrin (a cornified and granular layer marker) and keratin 1 (a granular and spinous layer marker), but not with keratin 5 (a basal layer marker; Fig. 1 G), indicating that PLA2G2F is located in differentiated keratinocytes.

As in mouse skin, *PLA2G2F* was the most abundant sPLA<sub>2</sub> in normal human skin, although *PLA2G2A* was also expressed at a relatively low level (Fig. 1 H). Expression of *PLA2G2F*, but not that of *PLA2G2A*, tended to be higher in the psoriasis-form skin that expressed higher levels of the psoriasis-associated genes *S100A9*, *IL17A*, and *IL22* (Fig. 1 H). In humans, PLA2G2F immunoreactivity was distributed in the uppermost region of normal skin and increased in the thickened epidermis of psoriasis-form skin (Fig. 1 I). Thus, PLA2G2F is a major sPLA<sub>2</sub> expressed in the epidermis across species, and its expression increases during epidermal hyperplasia.

### *Pla2g2f<sup>tg/+</sup>* mice display alopecia and psoriasis-like epidermal hyperplasia

To assess the potential *in vivo* roles of PLA2G2F, we generated *Pla2g2f<sup>tg/+</sup>* mice on a C57BL/6 background (Fig. 2 A). *Pla2g2f* expression was elevated in various tissues of *Pla2g2f<sup>tg/+</sup>* mice relative to WT mice, with a ~5-fold increase in the TG skin (Fig. 2 B). *Pla2g2f<sup>tg/+</sup>* mice were born normally, showed no early mortality, were fertile, and had normal serum biomedical parameters (unpublished data).

*Pla2g2f<sup>tg/+</sup>* displayed robust skin abnormalities with apparent hair loss at 3–4 wk of age (Fig. 2 C), as seen in *PLA2G10<sup>tg/+</sup>* mice (Yamamoto et al., 2011b). The dorsal skin of *Pla2g2f<sup>tg/+</sup>*

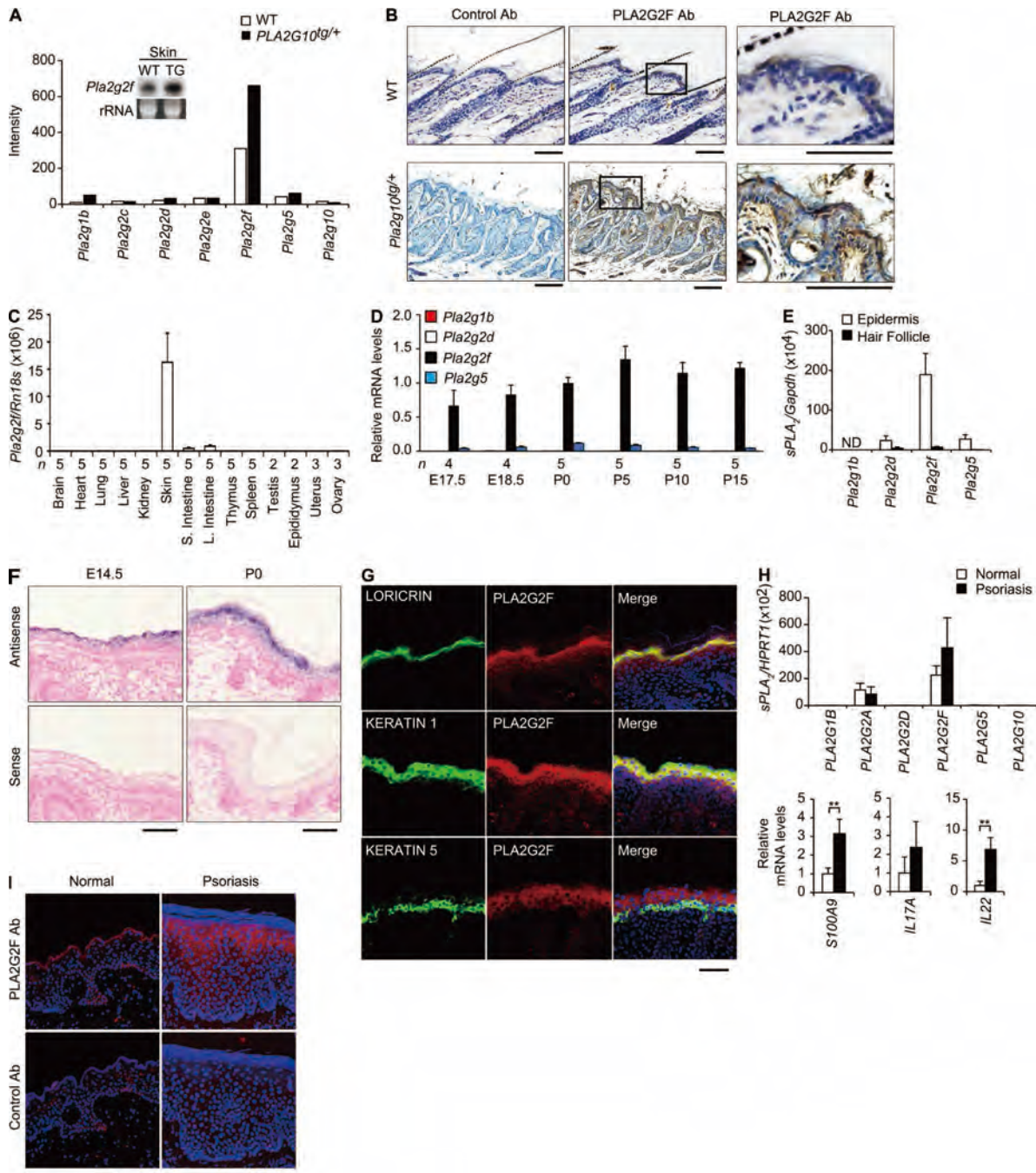


**Figure 1. PLA2G2F is expressed in the suprabasal epidermis.** (A) Expression of sPLA<sub>2</sub>s in PLA2G10<sup>tg/+</sup> (TG) and WT skins at P25, as evaluated by microarray. (inset) Northern blotting of *Pla2g2f*, with ribosomal RNA (rRNA) in an agarose gel with ethidium bromide as a control. (B) Immunohistochemistry of PLA2G2F in PLA2G10<sup>tg/+</sup> and WT skins at P25 (bars, 100 μm). Boxes (middle) are magnified on the right. (C) Quantitative RT-PCR of *Pla2g2f* in various tissues of 8-wk-old C57BL/6 mice. (D) Quantitative RT-PCR of sPLA<sub>2</sub>s in developmental skins of C57BL/6 mice, with expression of *Pla2g2f* at P0 as 1. (E) Microdissection followed by quantitative RT-PCR of sPLA<sub>2</sub>s in the epidermis (n = 5) and hair follicles (n = 6) of C57BL/6 mice at P8. (F) In situ hybridization of C57BL/6 skin with an antisense or sense probe for *Pla2g2f* (bar, 50 μm). (G) Confocal immunofluorescence microscopy of PLA2G2F (red), keratinocyte markers (green) and their merged images (yellow) in newborn C57BL/6 skin (bar, 100 μm). (H) Quantitative RT-PCR of sPLA<sub>2</sub>s and psoriasis markers in normal and psoriatic human skins, with expression in normal skin as 1 (n = 7). (I) Immunohistochemistry of PLA2G2F (red) in human normal and psoriatic skins, with DAPI counterstaining (blue; bar, 100 μm). Data are from one experiment (A, E, and H) or are representative of two experiments (C, D, and A [inset]); mean ± SEM; \*, P < 0.05; \*\*, P < 0.01). Images are representative of two experiments (B, F, G, and I). ND, not detected.

Downloaded from jem.rupress.org on January 6, 2016

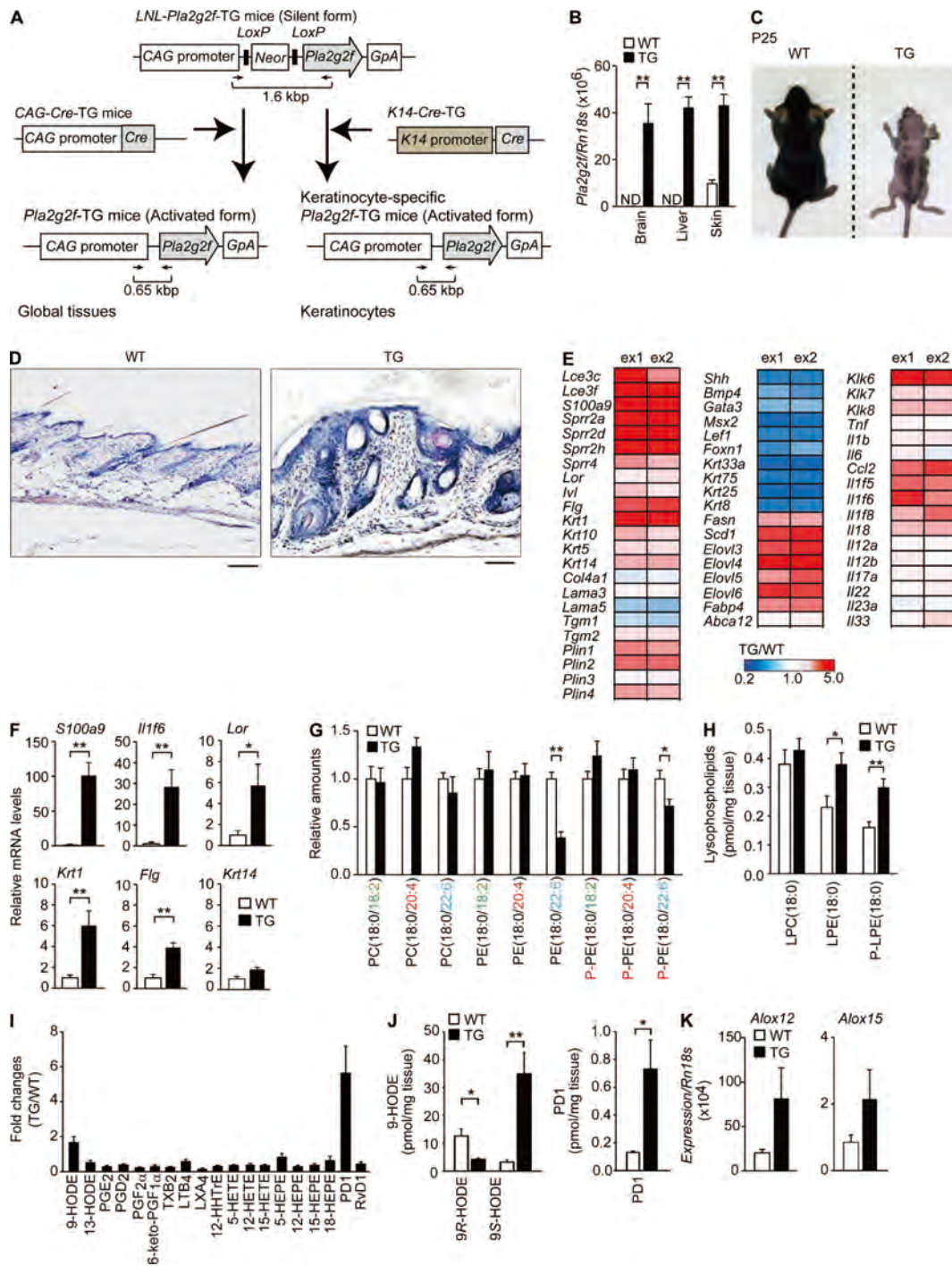


**Figure 2. Psoriasis-like epidermal hyperplasia in *Pla2g2f*<sup>tg/+</sup> mice.** (A) Generation of *Pla2g2f*<sup>tg/+</sup> mice. Mouse *Pla2g2f* cDNA was inserted into the pCALNL5 vector. The plasmid, containing the transgene downstream of a neomycin cassette (*Neor*) with *LoxP* sites at both ends, was excised at the *Hind*III and *Sall* sites to produce a 6-kb CAG-*LoxP*-*Neor*-*LoxP*-*Pla2g2f* (*LNL-Pla2g2f*) fragment. After removal of the *Neor* cassette by Cre recombinase, a 1.6-kb fragment amplified from the silent form (*LNL-Pla2g2f*<sup>tg/+</sup>) was shifted to a 0.65-kb fragment amplified from the active form (*Pla2g2f*<sup>tg/+</sup>). (B) Quantitative RT-PCR of *Pla2g2f* in *Pla2g2f*<sup>tg/+</sup> (TG) and WT tissues at P25 (*n* = 5). (C) Gross appearance of *Pla2g2f*<sup>tg/+</sup> (TG) and WT mice. (D) Hematoxylin-eosin staining of TG and WT skin sections at P25 (bar, 100 μm). (E) Microarray gene profiling of TG versus WT skins at P25. Results are from two experiments (ex1 and ex2). The heat maps are globally normalized for all genes shown in each panel, and the color code shows signal intensity. (F) Quantitative RT-PCR of keratinocyte marker genes in TG and WT skins at P25, with expression in WT skin as 1 (*n* = 6). (G–K) ESI-MS of phospholipids (*n* = 5; G), lysophospholipids (*n* = 5; H), PUFA metabolites (*n* = 6; I), and 9-HODEs and PD1 (*n* = 6; I and J) in WT and TG skins at P25. Relative amounts, with values for WT skin as 1

mice at P25 exhibited epidermal and sebaceous gland hyperplasia, hair follicle distortion and cyst formation, with the uppermost layer of the epidermis displaying hyperkeratosis with a highly thickened SC (Fig. 2 D). Microarray gene profiling (Fig. 2 E and Table S2) and quantitative RT-PCR (Fig. 2 F) supported the overall tendency for epidermal and sebaceous gland hyperplasia, as well as alopecia in *Pla2g2f<sup>tg/+</sup>* skin. A dramatic increase in the expression of *S100a9*, a marker of hyperproliferated and activated keratinocytes in psoriasis (Schonthaler et al., 2013), or *Il1f6*, which encodes the psoriasis-related keratinocyte cytokine IL-36 $\alpha$  (Tortola et al., 2012; Fig. 2, E and F), indicated that the epidermal hyperplasia in *Pla2g2f<sup>tg/+</sup>* mice has some features of psoriasis. We also generated skin-specific *K14-Pla2g2f<sup>tg/+</sup>* mice and obtained similar results (unpublished data), implying that PLA2G2F has a skin-intrinsic role. The smaller body size of *Pla2g2f<sup>tg/+</sup>* mice at P25 might be a result of up-regulation of thermogenic processes for temperature maintenance at the expense of fuel economy, an event often observed in hairless mice (Smith et al., 2000).

Although the phenotypes observed in sPLA<sub>2</sub> TG mice may not necessarily reflect the intrinsic functions of endogenous sPLA<sub>2</sub>s, they are useful for screening their potential in vivo substrates (phospholipids) and products (lysophospholipids, fatty acids, and their metabolites; Yamamoto et al., 2011a, b). Electrospray ionization mass spectrometry (ESI-MS) of skin lipids revealed that diacyl and plasmalogen (P-) forms of phosphatidylethanolamine (PE) with docosahexaenoic acid (DHA; C22:6), but not other phospholipids, were significantly reduced in *Pla2g2f<sup>tg/+</sup>* mice relative to WT mice (Fig. 2 G). Accordingly, there were concomitant increases in the acyl and plasmalogen forms of lysophosphatidylethanolamine (LPE and P-LPE, respectively), but not lysophosphatidylcholine (LPC), in TG skin (Fig. 2 H). These results suggest that the overexpressed PLA2G2F hydrolyzes PE and P-PE species with DHA as preferred substrates rather than acting on all phospholipids randomly. Of the oxygenated PUFA metabolites, the level of protectin D1 (PD1), a DHA metabolite that facilitates survival and renewal of epithelial cells (Serhan et al., 2006, 2014, 2015; Bazan et al., 2010), but not arachidonic acid (AA; C20:4)-derived or eicosapentaenoic acid (EPA; 20:5)-derived metabolites, was noticeably increased in *Pla2g2f<sup>tg/+</sup>* skin (Fig. 2, I and J). Although the levels of LA-containing phospholipids were similar in both genotypes (Fig. 2 G), the level of 9S-hydroxyoctadecadienoic acid (HODE), a LA metabolite that activates keratinocytes (Hattori et al., 2008), was increased in TG skin relative to control (Fig. 2, I and J). Cutaneous expression of *Alox12* and *Alox15*, which encode lipoxygenases (LOXs) that convert LA and DHA to 9S-HODE and PD1, respectively, was substantially higher in *Pla2g2f<sup>tg/+</sup>* mice than in WT mice (Fig. 2 K). These results suggest that the increases of these metabolites are caused by an increased supply of PUFA

precursors and/or the increased expression of PUFA-metabolizing LOXs in TG skin. Thus, among the potential PLA<sub>2</sub>-driven lipids detected so far, LPE, P-LPE, PD1, and 9S-HODE appear to be specific metabolites that are increased in *Pla2g2f<sup>tg/+</sup>* skin. We therefore focused on these lipid metabolites in subsequent studies.

### *Pla2g2f<sup>-/-</sup>* mice have fragile SC

To investigate the physiological roles of endogenous PLA2G2F in vivo, we generated *Pla2g2f<sup>-/-</sup>* mice (Fig. 3 A). Heterozygous mice carrying a mutated *Pla2g2f* allele (*Pla2g2f<sup>+/+</sup>*) were backcrossed onto a C57BL/6 background ( $n > 12$ ). Successful ablation of the *Pla2g2f* gene was confirmed by PCR genotyping from tail biopsy specimens (unpublished data) and by absence of its protein in the isolated SC (Fig. 3 B) and skin tissue (Fig. 3 C) of *Pla2g2f<sup>-/-</sup>* mice. Skin expression of other sPLA<sub>2</sub>s was unaffected by *Pla2g2f* ablation (unpublished data). The ratio of genotypes of heterozygous male and female offspring exhibited Mendelian proportions, and homozygous-null mice were indistinguishable from WT mice in terms of survival, fertility, behavior, and serum parameters (unpublished data).

A recent study has reported that PLA2G2F participates in formation of the SC barrier and acidity (Ilic et al., 2014). In our studies, *Pla2g2f<sup>-/-</sup>* mice from the embryonic to adult (8-wk-old) stages appeared grossly normal, and transmission electron microscopy revealed no ultrastructural abnormality in the dorsal skin of adult *Pla2g2f<sup>-/-</sup>* mice (unpublished data). Nonetheless, we noticed several unusual ultrastructural features in the SC of abdominal skin in *Pla2g2f<sup>-/-</sup>* mice. In contrast to the well-organized SC structure with 7–8 cornified layers interspaced by lipid matrices in the abdominal skin of *Pla2g2f<sup>+/+</sup>* mice, the SC of *Pla2g2f<sup>-/-</sup>* mice had only a few layers with signs of disorganized desmosomes, decreased stratification, accelerated desquamation, and edematous intercorneous spaces (Fig. 3 D). Trans-epidermal water loss (TEWL; Fig. 3 E) and cutaneous pH (Fig. 3 F) were higher in the abdominal, but not dorsal, skin of *Pla2g2f<sup>-/-</sup>* mice than that of *Pla2g2f<sup>+/+</sup>* mice, indicating that the mutant mice have perturbation of the SC barrier and acidification only in the abdominal skin. In comparison, deficiency of other sPLA<sub>2</sub>s did not affect TEWL significantly (Fig. 3 E). Although tape-stripped corneocytes from *Pla2g2f<sup>-/-</sup>* dorsal skin appeared normal in shape, short-term sonication resulted in more rapid collapse of *Pla2g2f<sup>-/-</sup>* cells than *Pla2g2f<sup>+/+</sup>* cells (Fig. 3 G), suggesting that *Pla2g2f<sup>-/-</sup>* mice have a fragile SC. Likely as a result of this SC fragility, epidermal layers beneath the SC of *Pla2g2f<sup>-/-</sup>* abdominal skin became thickened (Fig. 3 D), which may reflect a compensatory adaptation to the SC barrier defect, an event often seen in skin disorders characterized by SC abnormalities.

ESI-MS revealed that the levels of ceramides, which are prerequisite for the SC barrier, and fatty acids, which are

(G and I), or quantified amounts per milligram of tissue (H and J) are shown. (K) Quantitative RT-PCR of LOXs in TG and WT skins at P25 ( $n = 6$ ). Data are representative of two (B, F, J, and K) or three (G–I) experiments (mean  $\pm$  SEM; \*,  $P < 0.05$ ; \*\*,  $P < 0.01$ ). Images are representative of three experiments (C and D). ND, not detected. HETE, hydroxyeicosatetraenoic acid; HHTrE, hydroxyheptadecatrienoic acid; LT, leukotriene; LX, lipoxin; TX, thromboxane.

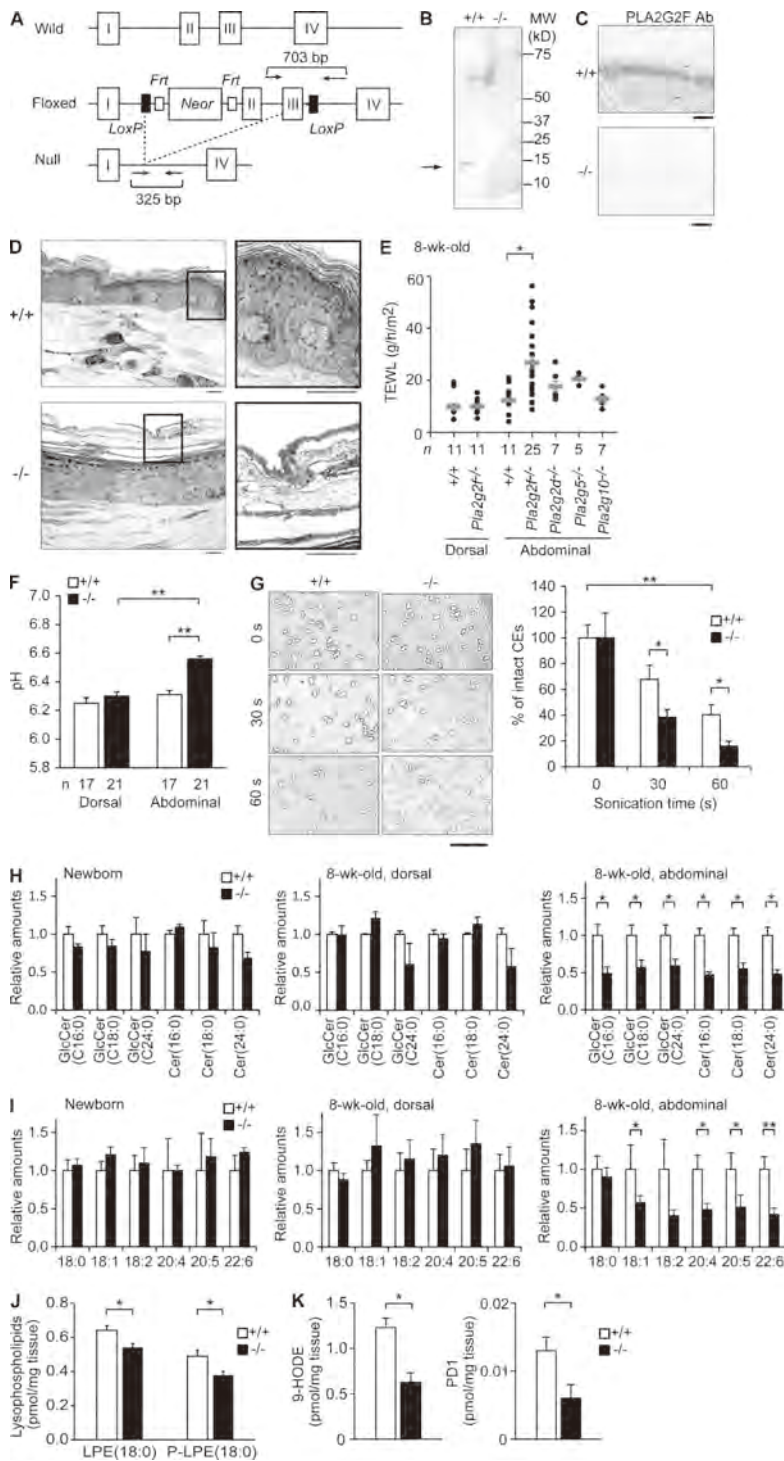


**Figure 3. SC abnormalities in *Pla2g2f<sup>-/-</sup>* mice.** (A) Generation of *Pla2g2f<sup>-/-</sup>* mice. The *Pla2g2f*-targeting vector was constructed with the *Neo<sup>r</sup>* gene that was inserted between exons 1 and 2 of the *Pla2g2f* gene. After mating with *CAG-Cre<sup>tg/tg</sup>* mice, the exons 2 and 3 plus the *Neo<sup>r</sup>* cassette were removed to generate *Pla2g2f*-null mice. Arrows indicate primer positions for genotyping. (B) Immunoblotting of PLA2G2F protein in the SC of adult *Pla2g2f<sup>+/+</sup>* and *Pla2g2f<sup>-/-</sup>* mice. (C) Immunohistochemistry of PLA2G2F in *Pla2g2f<sup>+/+</sup>* and *Pla2g2f<sup>-/-</sup>* skins at P0 (bars, 100 μm). (D) Transmission electron microscopy of abdominal skins of *Pla2g2f<sup>+/+</sup>* and *Pla2g2f<sup>-/-</sup>* mice (bar, 5 μm). Boxes are magnified on the right. (E) TEWL of dorsal and abdominal skins from various sPLA<sub>2</sub>-null or WT mice. (F) pH of dorsal and abdominal skins from *Pla2g2f<sup>+/+</sup>* and *Pla2g2f<sup>-/-</sup>* mice. (G) Microscopic images of corneocytes (CEs) after sonication for the indicated periods (bar, 50 μm). (right) Percentages of intact cells (n = 7). (H and I) ESI-MS of ceramides (n = 6; H) and fatty acids (n = 6; I) in newborn and adult (dorsal and abdominal) *Pla2g2f<sup>+/+</sup>* and *Pla2g2f<sup>-/-</sup>* skins, the values for WT skin being 1. (J and K) ESI-MS of LPE and P-LPE (J) or 9-HODE and PD1 (K) in abdominal *Pla2g2f<sup>+/+</sup>* and *Pla2g2f<sup>-/-</sup>* skins (n = 6). Data are representative from two experiments (G–K) or compiled from three experiments (E and F; mean ± SEM; \*, P < 0.05; \*\*, P < 0.01). Representative images of one or two experiments are shown (B, C, D, and G). Cer, ceramide; GlcCer, glucosylceramide.

Downloaded from jem.rupress.org on January 6, 2016

important for SC acidification, were not altered in newborn or adult dorsal skin, whereas most of them were significantly reduced in the adult abdominal skin of *Pla2g2f<sup>-/-</sup>* mice compared with *Pla2g2f<sup>+/+</sup>* mice (Fig. 3, H and I). Collectively, these data suggest that although epidermal differentiation and SC barrier formation occur almost normally in *Pla2g2f<sup>-/-</sup>*

mice under normal conditions, the SC of the null mice is vulnerable to mechanical or other environmental stresses (e.g., exposure to floor friction), leading to collapse of the abdominal SC and thereby perturbation of skin barrier and acidity, with concomitant decreases in multiple ceramide and fatty acid species. Notably, regardless of the distinct skin locations,

the levels of LPE, P-LPE, 9-HODE, and PD1, which were higher in *Pla2g2f<sup>tg/+</sup>* mice (Fig. 2, H–J), were reciprocally lower in *Pla2g2f<sup>-/-</sup>* mice than in controls (Fig. 3, J and K). Therefore, we speculated that the altered metabolism of particular lipid products, rather than the hydrolysis of skin phospholipids as a whole, may underlie the mechanistic actions of PLA2G2F.

#### Abnormal differentiation and activation of *Pla2g2f<sup>-/-</sup>* keratinocytes in culture

To explore the expression and function of PLA2G2F further, we used keratinocytes in primary culture. An epidermal  $\text{Ca}^{2+}$  gradient regulates keratinocyte differentiation and barrier function (Tu et al., 2012). Indeed,  $\text{Ca}^{2+}$  treatment of *Pla2g2f<sup>tg/+</sup>* keratinocytes resulted in marked induction of various markers of keratinocyte differentiation or activation (*Krt14*, *Krt1*, *Lor*, *Il1f6*, and *S100a9*), as well as *Pla2g2f* (Fig. 4 A). Importantly, this  $\text{Ca}^{2+}$ -induced response was markedly impaired in *Pla2g2f<sup>-/-</sup>* keratinocytes (Fig. 4 A). Microarray analysis using *Pla2g2f<sup>tg/+</sup>* and *Pla2g2f<sup>-/-</sup>* keratinocytes further supported this view, where the expression levels of many if not all  $\text{Ca}^{2+}$ -induced genes were down-regulated in *Pla2g2f<sup>-/-</sup>* cells (Fig. 4 B and Table S3). Consistent with these observations, treatment of WT keratinocytes with a sPLA<sub>2</sub> inhibitor (LY315920 derivative) that broadly inhibits sPLA<sub>2</sub>s (Oslund et al., 2008), but not its placebo, suppressed *S100a9* induction (Fig. 4 C). The impaired  $\text{Ca}^{2+}$ -driven keratinocyte activation in *Pla2g2f<sup>-/-</sup>* culture was restored by recombinant mouse PLA2G2F dose-dependently or by 9S-HODE, a potential PLA2G2F-driven product (Fig. 4 D). P-LPE also increased  $\text{Ca}^{2+}$ -induced *S100a9* and *Krt1* expression in *Pla2g2f<sup>tg/+</sup>* cells and restored it in *Pla2g2f<sup>-/-</sup>* cells, whereas 10S,17S-dihydroxy-DHA (10,17-diHDoHE, a commercially available PD1 stereoisomer) augmented the expression of these genes in *Pla2g2f<sup>tg/+</sup>*, but not in *Pla2g2f<sup>-/-</sup>* cells (Fig. 4 E).

It has been reported that differentiated keratinocytes secrete lipids (e.g., ceramides, cholesterol, and phospholipids) from lamellar granules for extracellular hydrolysis and that this extracellular phospholipid pool may serve as a substrate for sPLA<sub>2</sub> (Fluhr et al., 2004). Lipidomics studies of keratinocyte supernatants in serum-free culture revealed that WT keratinocytes did secrete phospholipids, particularly PE (Fig. 4 F), whereas the release of phosphatidylcholine (PC) was small (not depicted). The release of phospholipids was markedly lower in *Pla2g2f<sup>-/-</sup>* than in *Pla2g2f<sup>tg/+</sup>* cultures (Fig. 4 F), suggesting that this event relies on proper PLA2G2F-dependent keratinocyte differentiation. Probably because of the impaired substrate secretion or keratinocyte differentiation, the release of LPE, P-LPE, LA, DHA, and 9-HODE was also compromised in *Pla2g2f<sup>-/-</sup>* cells, whereas AA release was relatively low and LPC release was similar in both genotypes (Fig. 4 G). The failure to detect PD1 despite the robust release of DHA in WT culture suggests that the expression of LOXs responsible for the conversion of DHA to PD1 is low in keratinocytes or that its production requires the co-presence of other cell types in vivo. Thus, 9-HODE or LPE species may represent

particular lipid metabolites responsible for PLA2G2F-dependent keratinocyte differentiation or activation.

As in mouse keratinocytes, the expression of PLA2G2F, but not other sPLA<sub>2</sub>s, was induced in human keratinocytes after  $\text{Ca}^{2+}$  treatment (Fig. 4 H). A PLA2G2F-specific, but not a scramble, siRNA reduced the  $\text{Ca}^{2+}$ -induced expression of *KRT1*, *LOR*, and *S100A9*, as well as PLA2G2F (Fig. 4 I). Thus, the role of PLA2G2F in keratinocytes may also be relevant in human epidermis.

#### Substrate selectivity of PLA2G2F

To better address the substrate specificity of PLA2G2F, we performed in vitro enzymatic assays using recombinant mouse PLA2G2F (Singer et al., 2002). Given that sPLA<sub>2</sub>s act on extracellular phospholipids such as lipoproteins and microparticles (Boudreau et al., 2014; Sato et al., 2014), we incubated the serum-free culture medium of WT keratinocytes with PLA2G2F to examine the hydrolysis of phospholipids secreted from keratinocytes. After incubation, there was robust production of P-LPE species in comparison with other lysophospholipids (Fig. 5 A), indicating that PLA2G2F preferentially hydrolyzes P-PE secreted from the cells. Upon addition of a low dose of PLA2G2F to skin-extracted lipids, P-PE species containing DHA were preferentially hydrolyzed to yield P-LPE, whereas this substrate selectivity was apparently lost when a higher dose of PLA2G2F was added to the assay, with most species of PE with different fatty acid species being hydrolyzed to various degrees (Fig. 5, B–D). Taking the in vitro and in vivo results altogether, it appears that PLA2G2F has a substrate preference for DHA-containing P-PE secreted from keratinocytes under physiological conditions.

#### PLA2G2F promotes epidermal hyperplasia in psoriasis and contact dermatitis

Given the psoriasis-like phenotype in the skin of *Pla2g2f<sup>tg/+</sup>* mice (Fig. 2) and the impaired induction of psoriasis-associated genes in *Pla2g2f<sup>-/-</sup>* keratinocytes (Fig. 4), we next examined whether endogenous PLA2G2F participates in relevant skin pathologies. Psoriasis, one of the most common chronic inflammatory skin diseases, is characterized by epidermal hyperplasia (acanthosis) caused by aberrant proliferation and differentiation of keratinocytes, scaling, erythematous plaque formation, and infiltration of immune cells such as Th17 cytokine-producing lymphocytes (Lowe et al., 2014). In a model of imiquimod (IMQ)-induced psoriasis (Tortola et al., 2012), IMQ challenge onto the ears of WT mice elicited dermal swelling and acanthosis, accompanied by marked increases of *Pla2g2f* mRNA and its protein in the thickened epidermis, where PLA2G2F was colocalized with loricrin that was distributed diffusely throughout the suprabasal layers (Fig. 6, A and B). The IMQ-induced ear edema and epidermal thickening (Fig. 6, C–E) as well as IMQ-induced expression of various keratinocyte markers (*S100a9*, *Defb3*, *Lor*, *Tnf*, *Il6*, *Il1f6*, and *Il1f9*; Fig. 6 F) were significantly less marked in *Pla2g2f<sup>-/-</sup>* mice than in *Pla2g2f<sup>tg/+</sup>* mice. However, dermal migration of neutrophils, macrophages, and  $\gamma\delta\text{T}$  cells expressing IL-17A

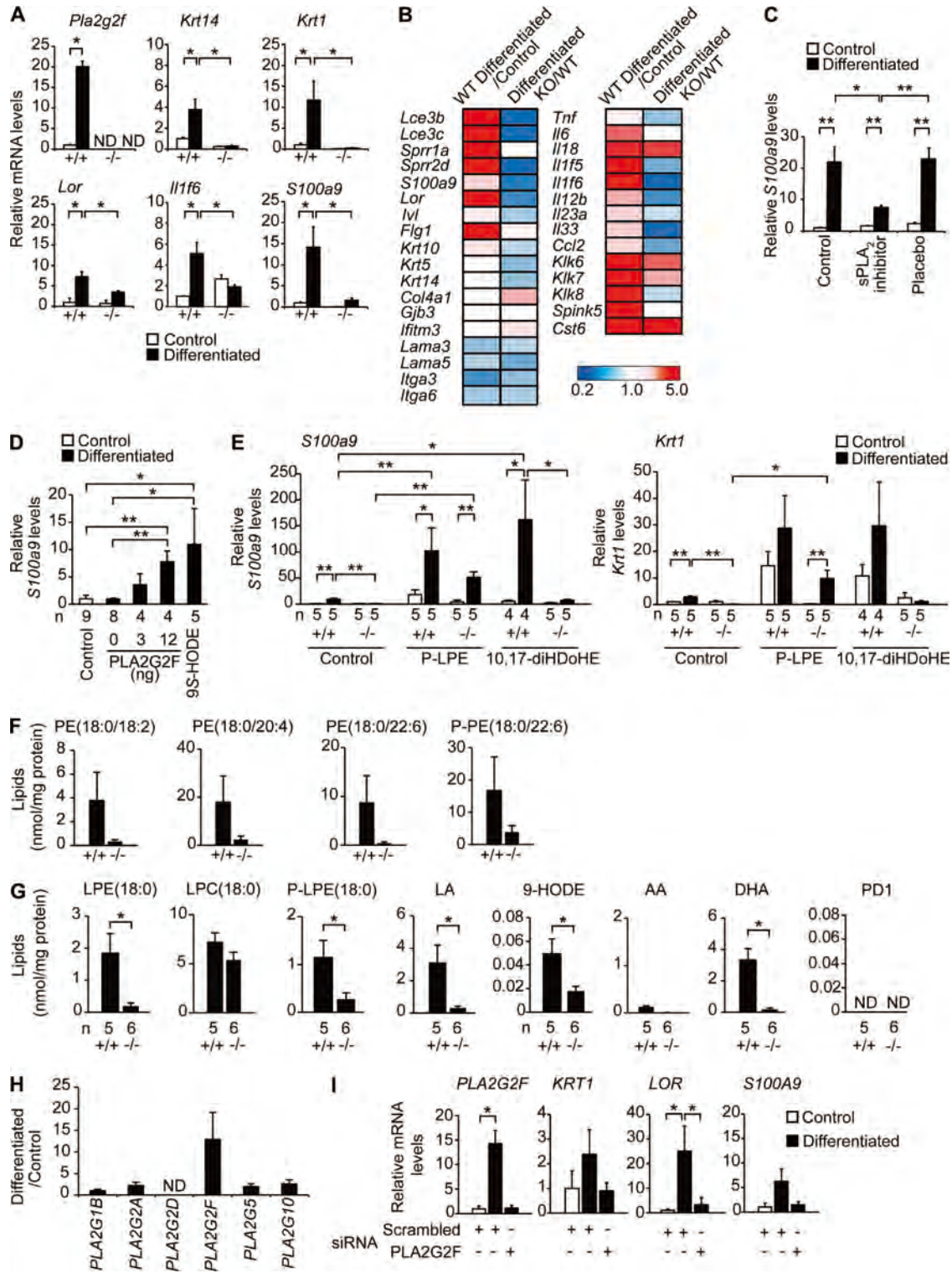


**Figure 4. Impaired differentiation and activation of *Pla2g2f*<sup>-/-</sup> keratinocytes.** (A) Quantitative RT-PCR of *Pla2g2f* and keratinocyte markers in *Pla2g2f*<sup>+/+</sup> and *Pla2g2f*<sup>-/-</sup> keratinocytes after culture for 2 d with (differentiated) or without (control) 1 mM CaCl<sub>2</sub> (*n* = 5). (B) Microarray gene profiling of *Pla2g2f*<sup>+/+</sup> (WT) and *Pla2g2f*<sup>-/-</sup> (KO) keratinocytes. Ratios of differentiated to control cultures in WT cells and those of KO to WT cells after differentiation are shown. The heat maps are globally normalized for all genes and the color code shows signal intensity. (C-E) Quantitative RT-PCR of *S100a9* or *Krt1* after 2-d culture of WT cells with 10 nM sPLA<sub>2</sub> inhibitor or placebo (*n* = 5; C), KO cells with various doses of PLA2G2F or 10 nM 9S-HODE (*n* = 5; D),

or IL-22 was not affected by *Pla2g2f* deficiency (unpublished data), implying that the primary defects caused by *Pla2g2f* ablation are specific for keratinocytes.

Lipidomics revealed that P-LPE was markedly increased after IMQ challenge and significantly more abundant in *Pla2g2f<sup>+/+</sup>* skin than in *Pla2g2f<sup>-/-</sup>* skin, whereas neither LPE nor LPC differed regardless of IMQ challenge or genotype (Fig. 6 G). 9-HODE and PD1 were also markedly elevated in IMQ-treated skin relative to vehicle-treated skin, yet unlike in normal skin (Fig. 3 K), their levels were not affected by *Pla2g2f* deficiency (Fig. 6 G), probably because *Alox15b* expression was equally elevated in the psoriatic skins of both genotypes (Fig. 6 F) or because other PLA<sub>2</sub>s in massively infiltrated leukocytes might be responsible for their production. AA-derived eicosanoids were also increased in IMQ-treated skin, with no influence by *Pla2g2f* deficiency (Fig. 6 G). Thus, P-LPE is the only metabolite that correlates with *Pla2g2f* expression in psoriatic skin.

To circumvent the bias arising from the presence of other cell types in the psoriatic skin in vivo, we again took advantage of primary keratinocytes. We found that IL-22, a psoriasis-associated Th17 cytokine (Lowes et al., 2014), induced *Pla2g2f* expression markedly (Fig. 7 A) and that the induction of *S100a9* and *Il1f6* by Th17 cytokines was abrogated by *Pla2g2f* deficiency (Fig. 7 B). Lipidomics of the culture supernatants revealed attenuated release of P-LPE and 9-HODE in IL-22-treated *Pla2g2f<sup>-/-</sup>* cells, whereas PD1 was undetectable even in WT cells (Fig. 7 C). The defective IL-22-induced *S100a9* expression in *Pla2g2f<sup>-/-</sup>* cells was partially restored by P-LPE, but not by 9S-HODE or the PD1 isomer 10,17-diHDoHE (Fig. 7 D). Moreover, topical application of P-LPE onto the *Pla2g2f<sup>-/-</sup>* skin rescued the defective IMQ-induced epidermal hyperplasia (Fig. 7, E and F) and keratinocyte activation (Fig. 7 G) in vivo, whereas LPE, 9-HODE, and 10,17-diHDoHE had no effect (Fig. 7 H). These results suggest that PLA2G2F is induced by IL-22 in keratinocytes and promotes keratinocyte activation by mobilizing P-LPE in psoriasis.

We also evaluated the effects of *Pla2g2f* ablation on hapten-induced contact dermatitis, in which application of dinitrofluorobenzene (DNFB) to abdominal skin followed by a second application of the same antigen to ear skin induced ear swelling (Miki et al., 2013). Expression of *Pla2g2f* mRNA and its protein was markedly elevated in the epidermis of DNFB-challenged WT skin relative to vehicle-treated skin, again being colocalized with loricrin (Fig. 8, A and B). The DNFB-induced ear thickening and epidermal hyperplasia were significantly milder in *Pla2g2f<sup>-/-</sup>* mice than in *Pla2g2f<sup>+/+</sup>*

mice (Fig. 8, C–E). DNFB-induced expression of markers for keratinocytes, but not those for immune cells, was significantly lower in *Pla2g2f<sup>-/-</sup>* mice than in *Pla2g2f<sup>+/+</sup>* mice (Fig. 8 F), again revealing the keratinocyte-specific effects of *Pla2g2f* ablation. Among the lipid products on which we focused, only P-LPE was increased in DNFB-treated *Pla2g2f<sup>+/+</sup>* skin, whereas this event occurred only partially in *Pla2g2f<sup>-/-</sup>* skin (Fig. 8 G). Collectively, we conclude that PLA2G2F promotes the aggravation of epidermal hyperplasia in psoriasis and contact dermatitis and that P-LPE represents a particular lipid product that mirrors the epidermal expression and function of PLA2G2F.

### PLA2G2F exacerbates skin carcinogenesis

Skin-specific TG mice for mouse PLA2G2A (*K14-Pla2g2a<sup>tg/tg</sup>*) are susceptible to a model of chemical carcinogenesis induced by 9,10-dimethylbenz(a)anthracene (DMBA) and 12-O-tetradecanoylphorbol-13-acetate (TPA; Mulherkar et al., 2003). Given that PLA2G2F is a major skin sPLA<sub>2</sub>, we applied DMBA/TPA to *Pla2g2f<sup>-/-</sup>* and *Pla2g2f<sup>+/+</sup>* mice on a BALB/c background, a strain that is more sensitive to this model of carcinogenesis. *Pla2g2f* expression was induced by TPA in WT keratinocytes (Fig. 9 A) and tended to increase in DMBA/TPA-treated WT skin relative to control skin at 4 wk (Fig. 9 B). At 24 wk, *Pla2g2f<sup>-/-</sup>* mice were highly protected from the development of skin tumors, in which epidermal thickening was markedly attenuated (Fig. 9, C and D). PLA2G2F staining in the WT tumor was distributed throughout the thickened epidermis (Fig. 9 E). Although tumor incidence and multiplicity were similar in both genotypes over time (Fig. 9 F), the tumors in *Pla2g2f<sup>-/-</sup>* mice were smaller than those in *Pla2g2f<sup>+/+</sup>* mice, large tumors (>50 mm<sup>3</sup>) being absent at 24 wk (Fig. 9 G), suggesting that *Pla2g2f* deficiency retarded tumor growth. Expression of keratinocyte differentiation, hyperproliferation, or activation markers was lower in *Pla2g2f<sup>-/-</sup>* than in *Pla2g2f<sup>+/+</sup>* tumors (Fig. 9 H). Moreover, expression of immune cell markers, indicative of tumor infiltration by immune cells, was reduced in *Pla2g2f<sup>-/-</sup>* mice (Fig. 9 H), possibly as a result of attenuated tumor progression. Indeed, the lower expression of *Cd206* (Fig. 9 H), a marker of tumor-associated macrophages that accelerate tumor growth (Condeelis and Pollard, 2006), and the reduced infiltration and degranulation of mast cells (Fig. 9 I), which diversely affect cancer (Marichal et al., 2013), may contribute to the reduced tumor size in *Pla2g2f<sup>-/-</sup>* mice.

Lipidomics revealed that P-LPE, 9-HODE, and PD1 were markedly increased in the *Pla2g2f<sup>+/+</sup>* tumors, whereas these changes were less evident in the *Pla2g2f<sup>-/-</sup>* tumors (Fig. 9 J).

or WT and KO cells with 10 nM P-LPE or 10,17-diHDoHE ( $n = 5$ ; E). (F and G) ESI-MS of phospholipids (F) and metabolites (G) in keratinocyte supernatants after differentiation culture for 2 d ( $n = 5$ ). (H) Quantitative RT-PCR of sPLA<sub>2</sub>s in human keratinocytes. Fold increases after culture for 2 d with 1 mM CaCl<sub>2</sub>, with that of *PLA2G1B* as 1, are shown ( $n = 6$ ). (I) Quantitative RT-PCR of keratinocyte genes in human keratinocytes that were pretreated with *PLA2G2F* or scrambled siRNA, and then cultured with or without 1 mM CaCl<sub>2</sub> for 2 d ( $n = 4$ ). In A, C–E, and I, expression was normalized with *Rn18s*, the values for the control culture being 1. Data are from one experiment (B and C) or are representative of two (H and I) or three (A and D–G) experiments (mean ± SEM; \*,  $P < 0.05$ ; \*\*,  $P < 0.01$ ). ND, not detected.

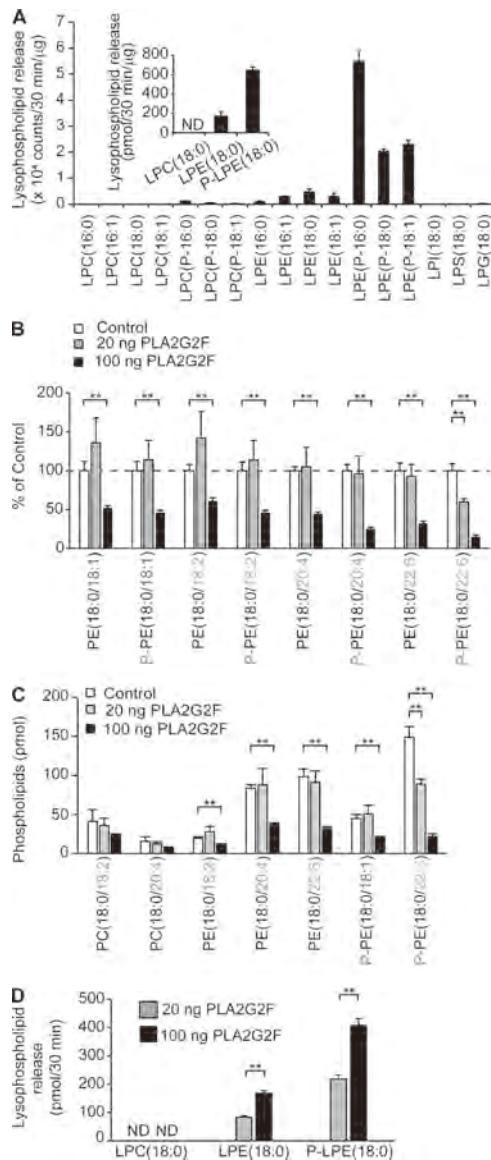


**Figure 5. Substrate selectivity of PLA2G2F in vitro.** (A) ESI-MS of lysophospholipids after incubation of keratinocyte supernatants with PLA2G2F (20 ng) for 30 min ( $n = 5$ ). (inset) Quantified data ( $n = 5$ ). (B–D) Evaluation of the substrate specificity of PLA2G2F toward phospholipids extracted from mouse skin. After incubation of skin-extracted lipids for 30 min with 20 or 100 ng of PLA2G2F, phospholipids (B and C) and lysophospholipids (D) were analyzed by ESI-MS ( $n = 5$ ). Values represent percentages with the control (no PLA2G2F) as 100% (B) or are quantified values (C and D). Data are representative of two experiments (mean  $\pm$  SEM; \*,  $P < 0.05$ ; \*\*,  $P < 0.01$ ). ND, not detected.

The tumor-associated increases of prostanoids were similar in the two genotypes (Fig. 9 J). Thus, the aforementioned studies show that several lipid metabolites can be affected by PLA2G2F in different experimental settings, with P-LPE appearing as a common PLA2G2F-related biomarker and bioactive metabolite. Collectively, our results suggest that

PLA2G2F is an intrinsic skin sPLA<sub>2</sub> that contributes to multiple epidermal disorders, including psoriasis, contact dermatitis, and cancer, by driving a unique lipid pathway.

**DISCUSSION**

Studies over the past decade have revealed the pathophysiological functions of various sPLA<sub>2</sub>s, as exemplified by group IB, IIA, IID, IIE, III, V, and X sPLA<sub>2</sub>s acting as digestive, inflammatory or bactericidal, resolving, metabolic, reproductive or anaphylactic, metabolic or Th2-prone, and reproductive or asthmatic sPLA<sub>2</sub>s, respectively (Labonté et al., 2006; Henderson et al., 2007; Escoffier et al., 2010; Sato et al., 2010, 2014; Ait-Oufella et al., 2013; Miki et al., 2013; Taketomi et al., 2013; Boudreau et al., 2014; Pernet et al., 2014). In this study, we have provided comprehensive insights into PLA2G2F, an orphan sPLA<sub>2</sub> whose expression, target substrates and products, and functions in vivo have remained largely unknown. Our results reveal a previously unrecognized role of PLA2G2F, an epidermal sPLA<sub>2</sub>, in skin homeostasis and diseases and point to this enzyme as a novel drug target for skin disorders characterized by epidermal hyperplasia such as psoriasis and cancer. Therefore, the skin phenotypes observed in TG mice for PLA2G2A (Grass et al., 1996; Mulherkar et al., 2003) or PLA2G10 (Yamamoto et al., 2011b) suggest that these enzymes mimic the intrinsic actions of PLA2G2F when artificially overexpressed in skin, or that endogenous PLA2G2F is up-regulated in the hyperplastic epidermis of these TG mice.

Previous pharmacological studies have suggested the potential role of sPLA<sub>2</sub>s in SC acidification (Mao-Qiang et al., 1996; Fluhr et al., 2001), and a recent preliminary study using *Pla2g2f*<sup>-/-</sup> mice showed that this sPLA<sub>2</sub> may be involved in this process (Ilic et al., 2014). In the present study, we confirmed that PLA2G2F is a major sPLA<sub>2</sub> expressed in the supra-basal epidermis of both mouse and human. In contrast to other sPLA<sub>2</sub>s that are active at neutral to alkaline pH, PLA2G2F exhibits nearly full activity within a pH range in line with skin acidity (Valentin et al., 1999). Notably, mice null for PLA2G2F, but not for other sPLA<sub>2</sub>s, have SC abnormalities with perturbed acidity and barrier function, although this phenotype is evident only in the abdominal (but not dorsal or newborn) skin of *Pla2g2f*<sup>-/-</sup> mice under normal conditions. It is therefore likely that PLA2G2F contributes to SC stability or recovery from SC perturbation in response to environmental stress (e.g., friction against the floor or prolonged exposure to microbiota) rather than to the central program of epidermal differentiation or basal SC barrier function and acidity.

Nevertheless, keratinocytes in culture fail to show proper differentiation and activation when PLA2G2F is ablated genetically or pharmacologically, a phenotype that is partially restored by PLA2G2F or its lipid metabolites. The more profound effects of *Pla2g2f* deficiency on keratinocytes in vitro than in vivo suggest that some mechanisms compensating for the lack of PLA2G2F might exist in vivo, as reported for mice null for several molecules crucial for skin homeostasis (Koch et al., 2000; Gareus et al., 2007). For instance, other (one or more) sPLA<sub>2</sub>s together with PLA2G2F might be

Downloaded from jem.rupress.org on January 6, 2016

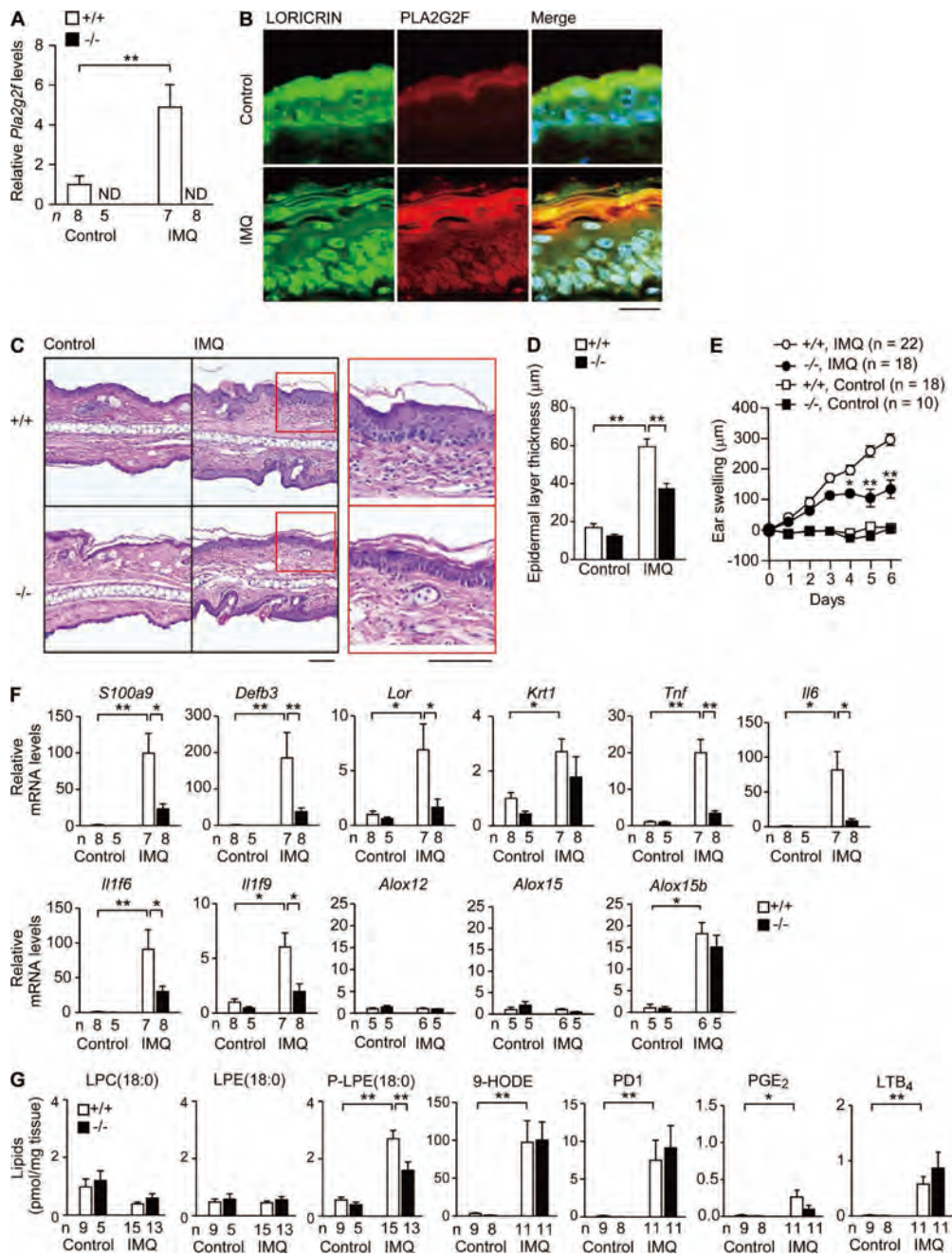


**Figure 6. Reduced psoriasis in *Pla2g2f*<sup>-/-</sup> mice.** (A) Quantitative RT-PCR of *Pla2g2f* in *Pla2g2f*<sup>+/+</sup> and *Pla2g2f*<sup>-/-</sup> ears with or without (control) IMQ treatment for 6 d. (B) Confocal microscopy of PLA2G2F (red), loricrin (green), and their merged images (yellow) in WT skin on day 6, with DAPI counter-staining (blue; bar, 20  $\mu$ m). (C) Hematoxylin-eosin staining of *Pla2g2f*<sup>+/+</sup> and *Pla2g2f*<sup>-/-</sup> ears on day 6 (bar, 50  $\mu$ m). Boxes are magnified on the right. (D and E) Epidermal thickness on day 6 (n = 6; D) or time-dependent ear swelling (E) of *Pla2g2f*<sup>+/+</sup> and *Pla2g2f*<sup>-/-</sup> mice. (F) Quantitative RT-PCR of keratinocyte and immune markers in *Pla2g2f*<sup>+/+</sup> and *Pla2g2f*<sup>-/-</sup> ears on day 6. (G) ESI-MS of lipid metabolites in *Pla2g2f*<sup>+/+</sup> and *Pla2g2f*<sup>-/-</sup> ears on day 6. In A and F, expression was normalized against *Gapdh*, the value for the control WT group being 1. Data are compiled from two experiments (A and D–G; mean  $\pm$  SEM; \*, P < 0.05; \*\*, P < 0.01). ND, not detected. Images are representative of two experiments (B and C).

involved in fatty acid release for SC acidification, and deficiency of PLA2G2F alone might not fully impair this process in vivo. Importantly, in several models of skin diseases, PLA2G2F expression is increased in the thickened epidermis

and its ablation attenuates epidermal hyperplasia in all of them. Thus, together with the findings that *Pla2g2f* is induced in keratinocytes by IL-22 and that *Pla2g2f*<sup>tg/+</sup> mice spontaneously develop psoriasis-like skin, it appears that aberrant PLA2G2F

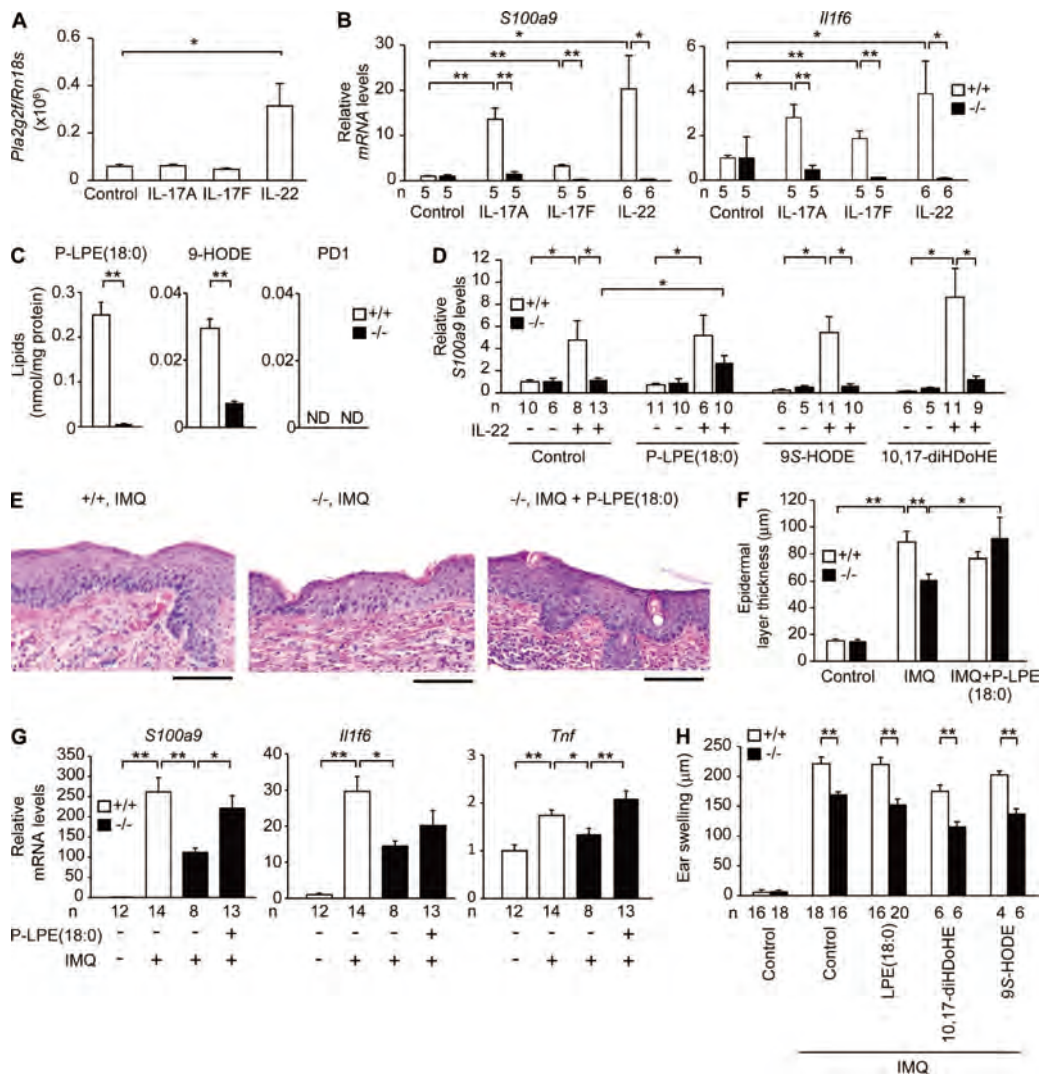


**Figure 7. P-LPE rescues defective skin phenotypes in *Pla2g2f*<sup>-/-</sup> mice.** (A and B) Quantitative RT-PCR of *Pla2g2f* (A) or *S100a9* and *Il1f6* (B) in keratinocytes after culture with or without Th17 cytokines (20 ng/ml) for 48 h (n = 5). (C) ESI-MS of lipid metabolites in culture medium of *Pla2g2f*<sup>+/+</sup> and *Pla2g2f*<sup>-/-</sup> keratinocytes after stimulation with IL-22 for 48 h (n = 6). (D) Quantitative RT-PCR of *S100a9* in *Pla2g2f*<sup>+/+</sup> and *Pla2g2f*<sup>-/-</sup> keratinocytes treated for 48 h with various lipids (10 nM) in the presence or absence of IL-22 (n = 5). (E) Hematoxylin-eosin staining of IMQ-treated *Pla2g2f*<sup>+/+</sup> and *Pla2g2f*<sup>-/-</sup> ears with or without P-LPE(18:0) at day 5 (bar, 100 μm). (F) Epidermal thickness of *Pla2g2f*<sup>+/+</sup> and *Pla2g2f*<sup>-/-</sup> ears treated with or without (control) IMQ or P-LPE(18:0) for 5 d (n = 8). (G) Quantitative RT-PCR of *Pla2g2f*<sup>+/+</sup> and *Pla2g2f*<sup>-/-</sup> ears treated with or without IMQ or P-LPE(18:0) for 5 d. (H) Effects of various lipids on IMQ-induced ear swelling in *Pla2g2f*<sup>+/+</sup> and *Pla2g2f*<sup>-/-</sup> mice at day 5. In B, D, and G, expression was normalized with *Rn18s* or *Gapdh*, the values for the control WT group being 1. Data are representative of two (A–C and E) or three (D) experiments, or are compiled from two experiments (F–H; mean ± SEM; \*, P < 0.05; \*\*, P < 0.01). ND, not detected.

expression, itself, can trigger keratinocyte hyperplasia and activation. Persistent abnormalities in keratinocyte activation and barrier function by the absence of PLA2G2F may stimulate downstream inflammation by secondary mechanisms (e.g., inflammatory cytokine production).

In one scenario, free fatty acids in the SC interfaces may be generated by sPLA<sub>2</sub>-catalyzed release from bulk phospholipids secreted from keratinocytes (Mao-Qiang et al., 1996; Fluhr et al., 2001, 2004; Ilic et al., 2014; Man et al., 2014). Our results, although partially supportive of this idea, rather

fit with the view that particular lipid metabolites driven by a given sPLA<sub>2</sub> influence keratinocyte functions, thereby affecting epidermal pathophysiology. We found that PLA2G2F preferentially cleaves a specific class of phospholipid, P-PE (plasmalogen), secreted from keratinocytes to yield P-LPE (lysoplasmalogen) and DHA, rather than hydrolyzing all phospholipid species nonselectively as has been previously thought. Moreover, the levels of its hydrolytic products, particularly P-LPE, are associated with those of *Pla2g2f* expression in distinct models. Thus, in line with our previous studies

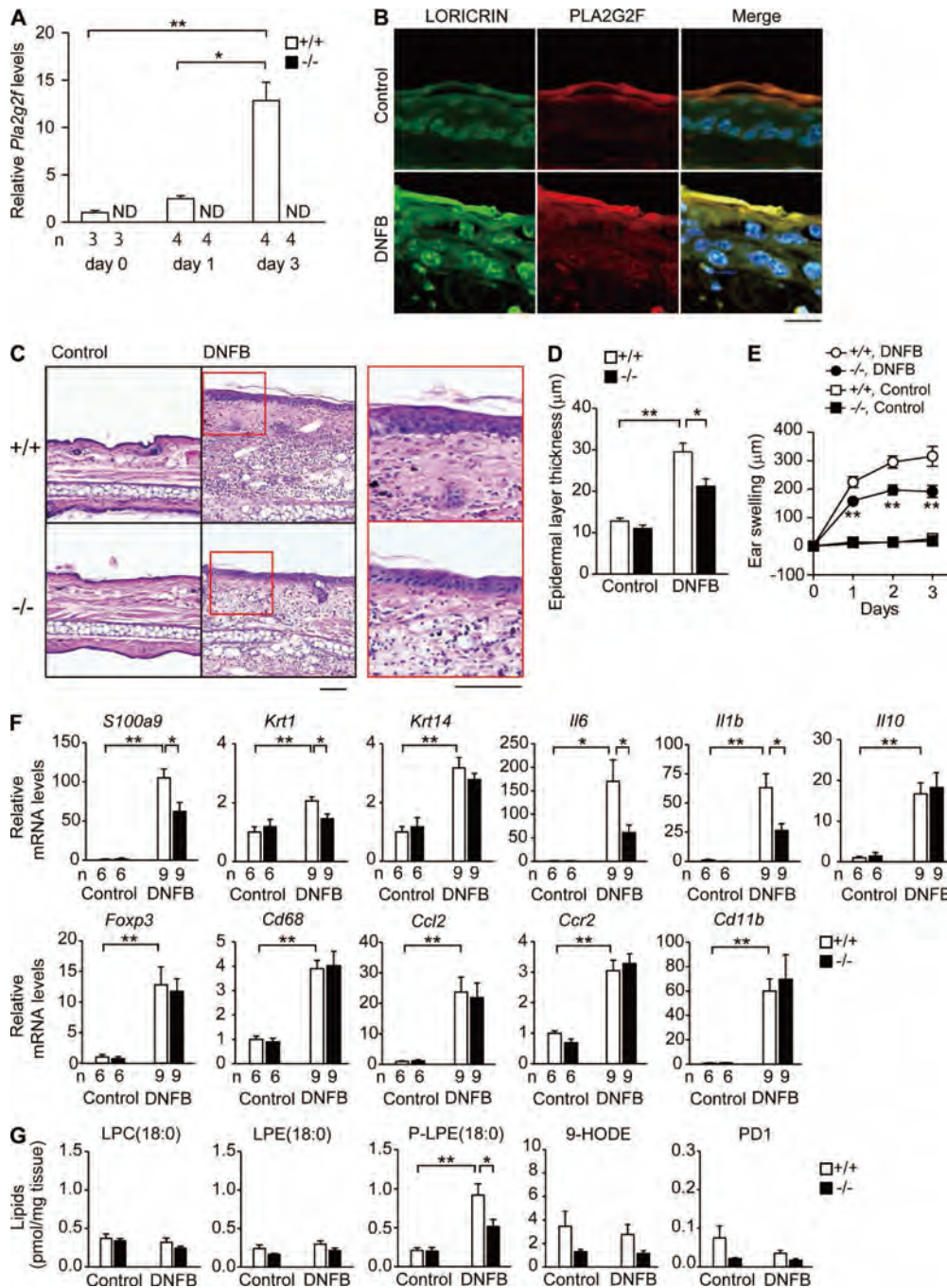


**Figure 8. Reduced contact dermatitis in *Pla2g2f*<sup>-/-</sup> mice.** (A) Quantitative RT-PCR of *Pla2g2f* in *Pla2g2f*<sup>+/+</sup> and *Pla2g2f*<sup>-/-</sup> ears after treatment with DNFB. (B) Confocal microscopy of PLA2G2F (red), loricrin (green), and their merged images (yellow) in WT skin on day 3, with DAPI counterstaining (blue; bar, 20 μm). (C) Hematoxylin-eosin staining of *Pla2g2f*<sup>+/+</sup> and *Pla2g2f*<sup>-/-</sup> skins on day 3 (bar, 50 μm). Boxes are magnified in right panels. (D and E) Epidermal thickness (n = 6; D) or time-dependent ear swelling (n = 8; E) of *Pla2g2f*<sup>+/+</sup> and *Pla2g2f*<sup>-/-</sup> mice on day 3. (F) Quantitative RT-PCR of keratinocyte or immune cell markers in *Pla2g2f*<sup>+/+</sup> and *Pla2g2f*<sup>-/-</sup> ears on day 3 (n = 6). (G) ESI-MS of lipid metabolites in *Pla2g2f*<sup>+/+</sup> and *Pla2g2f*<sup>-/-</sup> ears on day 3 (n = 6). In A and F, expression was normalized with *Gapdh*, the values for the control WT group being 1. Data are compiled from two experiments (D–F) or are representative of two experiments (A and G; mean ± SEM; \*, P < 0.05; \*\*, P < 0.01). Images are representative of two experiments (B and C). ND, not detected.

Downloaded from jem.rupress.org on January 6, 2016

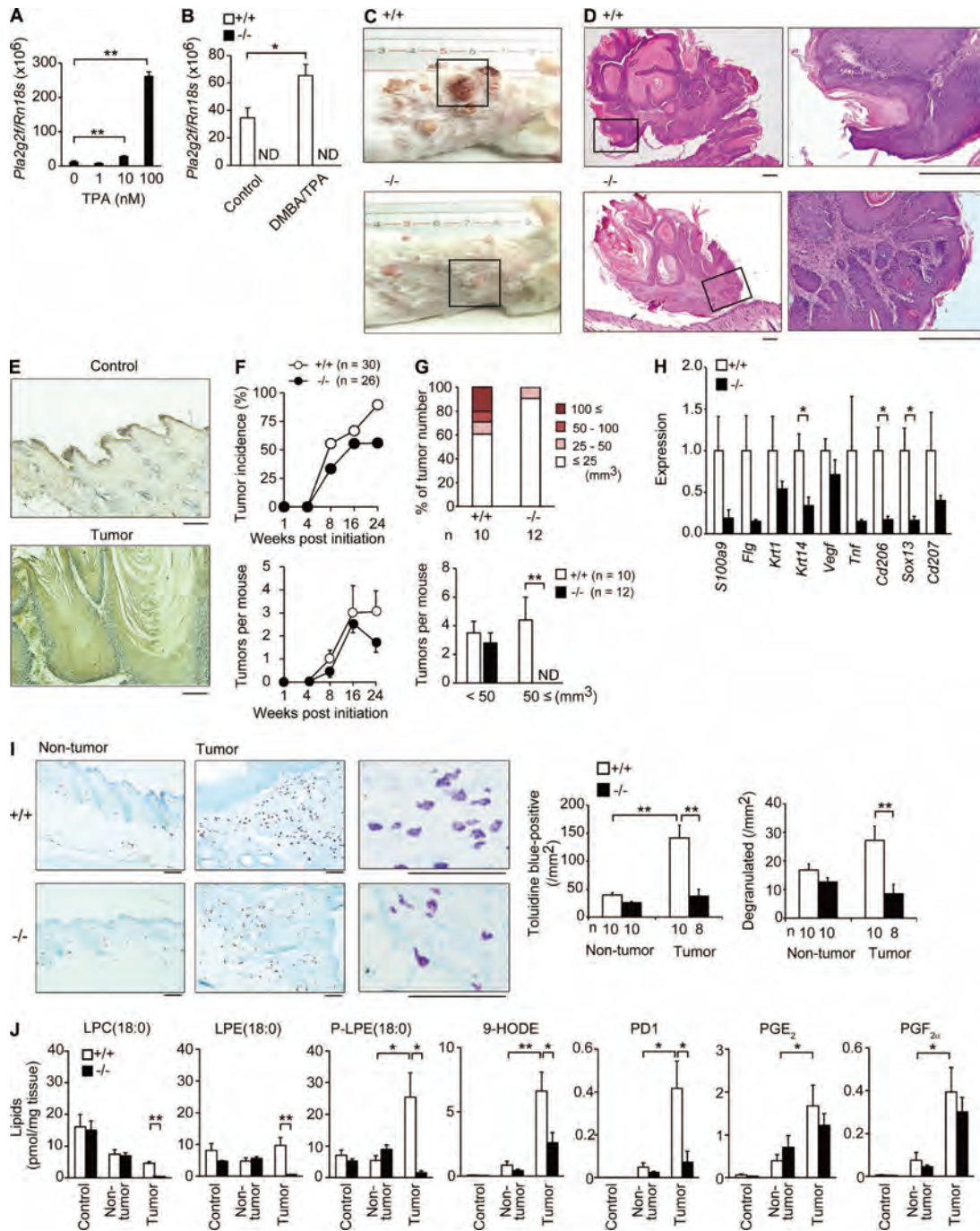


**Figure 9. Reduced skin carcinogenesis in *Pla2g2f*<sup>-/-</sup> mice.** (A and B) Quantitative RT-PCR of *Pla2g2f* in WT keratinocytes 48 h after treatment with TPA ( $n = 6$ ; A) or in *Pla2g2f*<sup>+/+</sup> and *Pla2g2f*<sup>-/-</sup> skins (BALB/c background) 4 wk after treatment with or without DMBA/TPA ( $n = 6$ ; B). (C and D) Gross appearances of *Pla2g2f*<sup>+/+</sup> and *Pla2g2f*<sup>-/-</sup> mice (C) and hematoxylin-eosin staining of skin tumors (D) at 24 wk (bar, 100  $\mu$ m). Boxes are magnified in the right panels (D). (E) Immunohistochemistry of PLA2G2F in tumor and nontumor areas of DMBA/TPA-treated WT skin at 24 wk. (F and G) Monitoring of tumor incidence, numbers (F), and sizes (G) in DMBA/TPA-treated *Pla2g2f*<sup>+/+</sup> and *Pla2g2f*<sup>-/-</sup> skins ( $n = 9$ ). (H) Quantitative RT-PCR of keratinocyte or immune cell genes in DMBA/TPA-treated *Pla2g2f*<sup>+/+</sup> and *Pla2g2f*<sup>-/-</sup> skins at 24 wk, the expression levels in WT being 1 ( $n = 6$ ). (I) Toluidine blue staining of skin mast cells at 24 wk. Right panels show magnified views, in which degranulated mast cells were frequently seen in *Pla2g2f*<sup>+/+</sup>, but not in *Pla2g2f*<sup>-/-</sup>, mice. Total and degranulated mast cells were counted (bar, 100  $\mu$ m). (J) ESI-MS of lipid metabolites in *Pla2g2f*<sup>+/+</sup> and *Pla2g2f*<sup>-/-</sup> skins 24 wk after treatment with (nontumor and tumor) or without (control) DMBA/TPA ( $n = 6$ ). Data are compiled from two (B) or three experiments (F–H and J) or from one (A) or two (I) experiments (mean  $\pm$  SEM; \*,  $P < 0.05$ ; \*\*,  $P < 0.01$ ). Representative images are shown (C–E and I). ND, not detected.

(Miki et al., 2013; Sato et al., 2014), several sPLA<sub>2</sub>s act selectively on particular phospholipids to generate specific products other than canonical AA metabolites, which may underlie their distinct functions.

Although little is known about the biological activity of P-LPE, we show here that it can rescue the hyperproliferation and activation defects of *Pla2g2f*<sup>-/-</sup> keratinocytes both ex vivo and in vivo. We therefore speculate that P-LPE itself, or after conversion to other lipid metabolites, may behave like a lipid mediator that regulates skin inflammation and cancer, as well as barrier homeostasis. It is also possible that PLA2G2F may affect skin pathophysiology through mobilization of some other unidentified lipid products, whose molecular identity awaits future studies. Nonetheless, our results have revealed P-LPE to be a novel biomarker and driver of skin diseases in which PLA2G2F is involved.

Hydrolysis of P-LPE by PLA2G2F gives rise to DHA and its metabolite PD1 in the skin in several if not all models. Because our MS analysis did not precisely discriminate PD1 (10R,17S-diHDoHE) and its stereoisomer (10S,17S-diHDoHE or protectin DX), the possibility that we measured the mixture of PD1 and 10S,17S-diHDoHE cannot be ruled out, although the latter is not the major product of human cells (Serhan et al., 2000; Hong et al., 2003). PD1 and its isomer have been shown to stop neutrophil recruitment, reduce inflammation, and stimulate resolution (Serhan, 2014; Serhan et al., 2015). Although PD1 or its isomer may not be involved in psoriatic epidermal hyperplasia, PD1 formation in the skin as discovered in the present work may be relevant in limiting acute inflammation and stimulating resolution of skin inflammation and the return to homeostasis. In this regard, our result showing an increase in Ca<sup>2+</sup>-induced *Krt1* expression by the PD1 isomer may reflect its role in adequate keratinocyte differentiation and barrier homeostasis.

As LA is crucial for skin homeostasis (Elias et al., 2014), some of the phenotypes observed in *Pla2g2f*<sup>-/-</sup> mice may be based on the disturbed LA metabolism. Indeed, one of the PLA2G2F-driven lipid products, 9S-HODE, increased Ca<sup>2+</sup>-dependent, but not IL-22-induced, *S100a9* expression in keratinocytes, underscoring the key and distinct roles of this LA metabolite in PLA2G2F-regulated epidermal biology. However, given the substrate selectivity of PLA2G2F, the PLA2G2F-dependent changes in LA metabolism may largely or even solely reflect an indirect consequence of altered keratinocyte differentiation or activation. From this viewpoint, other PLA<sub>2</sub>s or lipases may be responsible for the supply of a large pool of LA in association with keratinocyte differentiation. Candidate genes for this process include *ABHD5*, *PNPLA1*, and *LIPN*, which belong to the lipase family, are expressed in keratinocytes, and cause ichthyosis when mutated (Akiyama et al., 2003; Israeli et al., 2011; Grall et al., 2012).

Current therapies for psoriasis involve biologics that target cytokines, such as TNF, IL-17, or IL-23, and their efficacy has been proven in clinical trials (Lowes et al., 2014). However, inhibition of these cytokines may render individuals susceptible to infection due to undesirable immune defects, underlining

the need for tissue-specific targets. Nonsurgical management for skin cancer includes the use of chemotherapy, in which currently used agents may have survival benefits but also undesirable adverse effects. Given that PLA2G2F is expressed in the epidermis rather specifically, blocking PLA2G2F may be a novel approach for specific treatment of psoriasis, skin cancer, or other conditions characterized by epidermal hyperplasia.

## MATERIALS AND METHODS

**Mice.** All mice were housed in climate-controlled (23°C) specific pathogen-free facilities with a 12-h light/dark cycle, with free access to standard laboratory food (CE2; Laboratory Diet; CLEA Japan) and water. Male mice were used in most studies. All procedures involving animals were performed in accordance with protocols approved by the Institutional Animal Care and Use Committees of the Tokyo Metropolitan Institute of Medical Science, Showa University, and the University of Washington.

**Generation of *Pla2g2f*<sup>tg/+</sup> mice.** The strategy for the generation of TG mice for sPLA<sub>2</sub>s has been reported previously (Yamamoto et al., 2011b). In brief, the cDNA for mouse *Pla2g2f* was inserted into the EcoRI site (downstream of the *CAG* [cytomegalovirus immediate early enhancer-chicken β-actin hybrid] promoter) in the pCALNL5 vector (Kanegae et al., 1996; Fig. 2 A). The plasmid, containing the transgene downstream of a neomycin cassette (*Neo*) with *LoxP* sites at both ends, was excised at the HindIII and SalI sites to produce a 6-kb *CAG-LoxP-Neo-LoxP-Pla2g2f* (*LNL-Pla2g2f*) fragment. Then, the DNA was injected into fertilized eggs. Genotyping was performed on genomic DNA from tail biopsies by PCR using the primer pairs 5'-TGGTTATTGTGCTGTCTCATCATTT-3' and 5'-CACCATGGACTTCAGGTTTCAG-3' (Sigma-Aldrich), which amplified a 1,600-bp fragment specific for *LNL-Pla2g2f*. The reaction was 95°C for 10 s, and then 35 cycles of 95°C for 0 s and 65°C for 1 min on an Applied Biosystems 9800 Fast Thermal Cycler (Applied Biosystems). The PCR products were analyzed by 1.5% (wt/vol) agarose gel electrophoresis with ethidium bromide. Male founders were mated with female C57BL/6 mice (Japan SLC) to confirm germ line transmission by PCR genotyping, and those with successful germ line transmission (*LNL-Pla2g2f*<sup>tg/+</sup>) were then crossed with female *CAG-Cre*<sup>tg/+</sup> mice, which carry the Cre recombinase transgene under control of the *CAG* promoter (Kanegae et al., 1996). This step resulted in removal of the *Neo* cassette from the *LNL-Pla2g2f* transgene, thereby allowing activation of the *Pla2g2f* transgene in the whole body of the offspring (Fig. 2, A and B). All of the *Pla2g2f*<sup>tg/+</sup> mice were inbred with C57BL/6 mice. Phenotypes that appeared in *Pla2g2f*<sup>tg/+</sup> mice, which carried the active *Pla2g2f* transgene, but not in *LNL-Pla2g2f*<sup>tg/+</sup> mice, in which the *Pla2g2f* transgene remained silent, were regarded as events caused by the overexpressed PLA2G2F. For skin-specific TG overexpression, *LNL-Pla2g2f*<sup>tg/+</sup> mice were crossed with *K14-Cre*<sup>tg/+</sup> mice (Andl et al., 2004). *PLA2G10*<sup>tg/+</sup> mice were reported previously (Yamamoto et al., 2011b).

**Gene targeting of *Pla2g2f*.** The *Pla2g2f*-targeting vector was constructed with the *Neo* gene that was inserted between exons 1 and 2 of the *Pla2g2f* gene with *LoxP* sites at both ends (Fig. 3 A). ES cell transfection and embryo injections were performed by the Transgenic Resources Program (Department of Comparative Medicine, University of Washington). ES clones with homologous recombination were screened by PCR and Southern blotting. The founder heterozygous mice (129 x C57BL/6 background) with germ line transmission were crossed with *CAG-Cre*<sup>tg/+</sup> mice to delete exons 2 and 3 plus the *Neo* cassette in the offspring. Genotyping was performed on genomic DNA from tail biopsies by PCR using the primer pairs 5'-CAGTCAGCTGCCCTCTTTTAGAA-3' and 5'-GTGGGTCATCCTGGGTTTGT-3' (Sigma-Aldrich), which amplified a 490-bp fragment specific for the WT allele, and 5'-CATCCGGCTAAGGACAACAGA-3' and 5'-GTGGGTCATCCTGGGTTTGT-3', which amplified a 325-bp fragment specific for the mutant allele. *Pla2g2f*<sup>tg/-</sup> mice were backcrossed to

C57BL/6 or BALB/c mice (Japan SLC) for more than 12 generations and then intercrossed to obtain *Pla2g2f<sup>-/-</sup>* and *Pla2g2f<sup>+/+</sup>* mice. This *Pla2g2f<sup>-/-</sup>* mouse line was used in a previous study (Ilic et al., 2014). Knockout mice for other sPLA<sub>2</sub>s were described previously (Yamamoto et al., 2011b; Miki et al., 2013; Sato et al., 2014).

**Histological examination.** Histochemistry of mouse skin sections was performed as described previously (Yamamoto et al., 2011b). In brief, skin samples were fixed with 100 mM phosphate buffer (pH 7.2) containing 4% (wt/vol) paraformaldehyde, embedded in paraffin, sectioned, mounted on glass slides, deparaffinized in xylene, and rehydrated in ethanol with increasing concentrations of water. Hematoxylin and eosin staining was performed on the 5- $\mu$ m-thick cryosections. Paraffin-embedded tissue sections were incubated with Target Retrieval Solution (Dako), and then with rabbit anti-mouse PLA2G2F antibody (Degousee et al., 2002), which did not cross-react with other sPLA<sub>2</sub>s, or control antibody at 1:2,000 dilution in 10 mM Tris-HCl (pH 7.4) containing 0.15 M NaCl and 0.1% (wt/vol) BSA (TBS-BSA) overnight at 4°C. The sections were then treated with an EnVision+<sup>R</sup> System Staining kit (Dako) with diaminobenzidine substrate, followed by counterstaining with hematoxylin. The stained sections were analyzed with a BX61 microscope (Olympus). Epidermal layer thickness was measured using DP2-BSW software (Olympus).

**Immunofluorescence staining.** 5- $\mu$ m-thick mouse or human tissue sections were incubated with 1x Blockace (DS Pharma BioMedical) in PBS-T for 30 min, washed three times with PBS-T for 5 min each, and incubated with rabbit anti-mouse or -human PLA2G2F antibody (Degousee et al., 2002) at 1:500–1,000 dilution in a 10-fold-diluted Blockace for overnight at 4°C. The sections were then washed 3 times with PBS-T for 5 min each time and incubated with Alexa Fluor 647-labeled goat anti-rabbit IgG antibody (Molecular Probes; 1:1,000) at 20°C for 1 h. For double immunostaining, the sections were washed three times with PBS-T for 5 min each and incubated with rabbit antibodies against mouse loricrin, cytokeratin 1 and cytokeratin 5 (PRB-145P, PRB-165P and PRB-160P [Covance], respectively; 1:500) prelabeled with Alexa Fluor 555 (Zenon Labeling System; Molecular Probes) at 20°C for 1 h. Counterstaining was performed with 4,6-diamino-2-phenylindole (DAPI; Vector Laboratories). Stained sections were analyzed with a confocal laser-scanning microscope (LSM510 META, Carl Zeiss). Human skin sections were obtained by surgery at Chiba University (Chiba, Japan) after approval by the Faculty ethics committee and informed consents from patients.

**Immunoblotting.** The dorsal and abdominal skins of 10-mo-old mice were washed with 10 ml/mouse of a urea buffer comprising 5 M urea, 2 M thiourea, and 1 mM EDTA in PBS supplemented with a protease inhibitor cocktail (Roche). The washed skins were scrapped with the edge of a slide glass and continuously rinsed with 8 M urea solution. The buffer containing corneocytes was collected in a container placed below the mice. Corneocytes were removed by centrifugation at 3,000 *g* for 30 min at 4°C. The supernatants were concentrated using an Amicon-ultra 10K (EMD Millipore). Protein concentrations were determined with a BCA protein assay kit (Thermo Fisher Scientific). The extracts (50- $\mu$ g protein equivalents) were subjected to NuPAGE-PAGE on 4–12% (wt/vol) gels (Life Technologies) under reducing conditions and then electroblotted onto PVDF membranes (Bio-Rad Laboratories) with a semi-dry blotter (Transblot SD; Bio-Rad Laboratories). The membranes were blocked with 5% (wt/vol) skim milk in PBS containing 0.05% (vol/vol) Tween-20 (PBS-T), probed with rabbit anti-mouse PLA2G2F antibody (1:1,000) in PBS-T for 2 h, incubated with horseradish peroxidase-conjugated anti-rabbit IgG (Invitrogen) at 1:5,000 dilution in PBS-T for 2 h, and then visualized using ECL Prime Western blotting detection reagent (GE Healthcare Life Science) with LAS-4000 (Fuji Film).

**Corneocyte stability.** The SC samples were prepared by boiling of the epidermis for 30 min in a buffer consisting of 20 mM Tris-HCl, pH 7.5,

5 mM EDTA, 10 mM dithiothreitol (DTT), and 2% SDS. After centrifugation at 5,000 *g*, isolated corneocytes were washed twice at room temperature with a buffer consisting of 20 mM Tris-HCl, pH 7.5, 5 mM EDTA, 10 mM DTT, and 0.2% SDS. The corneocytes were suspended in 2% SDS solution and counted. The corneocyte suspensions were sonicated by an ultrasonic sonicator (EYEL4; Tokyo Rikakikai) for various time periods, and aliquots were taken for microscopic analyses.

**In situ hybridization.** *Pla2g2f* cDNA was subcloned into the pGEMT-Easy vector (Promega), and used for generation of sense or anti-sense RNA probes. Digoxigenin labeled-RNA probes were prepared with DIG RNA labeling Mix (Roche). 6- $\mu$ m-thick paraffin-embedded sections of mouse skin were hybridized with the digoxigenin-labeled RNA probes at 60°C for 16 h (Genostaff). The bound label was detected using the alkaline phosphate color substrates nitro-blue tetrazolium chloride and 5-bromo-4-chloro-3'-indolylphosphatase *p*-toluidine salt. The sections were counterstained with Kernechtrot (Muto Pure Chemicals).

**Transmission electron microscopy.** Tissues were fixed with 100 mM phosphate buffer (pH 7.2) containing 1% (vol/vol) glutaraldehyde and 4% (wt/vol) paraformaldehyde, post-fixed with 2% (wt/vol) OsO<sub>4</sub> in PBS, dehydrated through a graded ethanol series, passed through propylene oxide, and embedded in Poly/Bed 812 EPON (Polyscience). 0.08- $\mu$ m-thick ultrathin sections were stained with uranyl acetate and lead citrate, and then examined using an electron microscope (H-7600; Hitachi).

**Quantitative RT-PCR.** Total RNA was extracted from tissues and cells using TRIzol reagent (Invitrogen). First-strand cDNA synthesis was performed using a High Capacity cDNA Reverse transcription kit (Applied Biosystems). PCR reactions were performed using a Power SYBR Green PCR system (Applied Biosystems) or a TaqMan Gene Expression System (Applied Biosystems) on the ABI7300 Quantitative PCR system (Applied Biosystems). The probe/primer sets used are listed in Table S4.

**Microarray analysis.** Total RNA extracted from skins or keratinocytes were purified using the RNeasy Mini kit (QIAGEN). The quality of RNA was assessed with a 2100 Bioanalyzer (Agilent Technologies). cRNA targets were synthesized and hybridized with Whole Mouse Genome Microarray according to the manufacturer's instructions (G4122A or G4846A; Agilent Technologies). The array slides were scanned using a Laser Scanner GenePix 4000B (Molecular Devices) or a SureScan Microarray Scanner (Agilent Technologies). Microarray data were analyzed with GenePix Software (Molecular Devices) or Agilent's Feature Extraction Software. The Gene Expression Omnibus accession nos. for microarrays (Tables S1, S2, and S3) are GSE71827, GSE71829, and GSE71826, respectively.

**Lipid metabolome.** Samples for ESI-MS of phospholipids/ceramides and fatty acid derivatives were prepared separately and analyzed as described previously (Miki et al., 2013; Yamamoto et al., 2011b). In brief, for detection of phospholipids and ceramides, tissues were soaked in 10 volumes of 20 mM Tris-HCl (pH 7.4) and then homogenized with a Polytron homogenizer. Lipids were extracted from the homogenates by the method of Bligh and Dyer (Bligh and Dyer, 1959). As an internal standard for determination of recovery, 1 nmol LPC (17:0; Avanti) was added to each sample. The analysis was performed using a 4000Q-TRAP quadrupole-linear ion trap hybrid mass spectrometer (AB Sciex) with liquid chromatography (LC; NexeraX2 system; Shimadzu). The sample was applied to a Develosil C30-UG column (1  $\times$  150 mm i.d., 3- $\mu$ m particle; Nomura Chemical) coupled for ESI-MS/MS. The samples injected by an autosampler (10  $\mu$ l) were separated by a step gradient with mobile phase A (acetonitrile/methanol/water = 1:1:1 [vol/vol/vol]) containing 5  $\mu$ M phosphoric acid and 1 mM ammonium formate) and mobile phase B (2-propanol containing 5  $\mu$ M phosphoric acid and 1 mM ammonium formate) at a flow rate of 80  $\mu$ l/min at 50°C. Identification was conducted using multiple reaction monitoring (MRM) transition and retention times, and quantification was performed based on peak area of the

MRM transition and the calibration curve obtained with an authentic standard for each compound (Table S5).

For detection of fatty acids and their oxygenated metabolites, tissues were soaked in 10 volumes of methanol and then homogenized with a Polytron homogenizer. After overnight incubation at  $-20^{\circ}\text{C}$ , water was added to the mixture to give a final methanol concentration of 10% (vol/vol). As an internal standard, 1 nmol of *d5*-labeled EPA and *d4*-labeled PGE<sub>2</sub> (Cayman Chemicals) was added to each sample. The samples in 10% methanol were applied to Sep-Pak C18 cartridges (Waters), washed with 10 ml of hexane, eluted with 3 ml of methyl formate, dried up under N<sub>2</sub> gas, and dissolved in 60% methanol. The samples were then applied to a Develosil C30-UG column (1 × 150 mm i.d., 3- $\mu\text{m}$  particles; Nomura Chemical) coupled for ESI-MS/MS as described above. The samples injected by an autosampler (10  $\mu\text{l}$ ) were separated using a step gradient with mobile phase C (water containing 0.1% acetic acid) and mobile phase D (acetonitrile/methanol = 4:1; vol/vol) at a flow rate of 50  $\mu\text{l}/\text{min}$  at  $45^{\circ}\text{C}$ . Chiral HPLC analysis was performed using a Chiralpak IA-3 column (4.6 × 150 mm i.d., 3- $\mu\text{m}$  particles; Daicel) with mobile phase E (acetonitrile/methanol/H<sub>2</sub>O = 68:17:15 [vol/vol/vol] containing 0.1% acetic acid) at a flow rate of 0.2 ml/min at  $25^{\circ}\text{C}$ . Each lipid was detected and quantified as described above.

**Keratinocyte culture.** Keratinocytes were isolated from the whole skin of newborn mice using 0.05% (wt/vol) collagenase A (Roche) in KGM (–) medium (MCDB 153 medium [Sigma-Aldrich] supplemented with 0.5  $\mu\text{g}/\text{ml}$  hydrocortisone, 14.1  $\mu\text{g}/\text{ml}$  phosphorylethanolamine, 0.2% [vol/vol] Matrigel [BD], 100 U/ml penicillin, and 100 mg/ml streptomycin) overnight at  $4^{\circ}\text{C}$ . Then, the cells were cultured with KGM (+) medium (KGM [–] medium supplemented with 5 ng/ml insulin, 10 ng/ml EGF, and 40  $\mu\text{g}/\text{ml}$  bovine pituitary extract). After 3 d, the cells were treated with 1 mM CaCl<sub>2</sub> or the Th17 cytokines IL-17A, IL-17F or IL-22 (20 ng/ml; ProSpec) in KGM (+) medium. After appropriate periods, RNA was extracted from the cells and subjected to quantitative RT-PCR, and the supernatants were subjected to PLA<sub>2</sub> assay and lipid metabolome. As required for experiments, the sPLA<sub>2</sub> inhibitor LY315920 (2-(3-(2-amino-2-oxoacetyl)-1-benzyl-2-ethyl-1*H*-6,7-benzoindol-4-yloxy)acetic acid) or its placebo (2-(3-(2-N-methylamino-2-oxoacetyl)-1-benzyl-2-ethyl-1*H*-6,7-benzoindol-4-yloxy)acetic acid; Oslund et al., 2008), recombinant mouse PLA2G2F (Valentin et al., 1999; Singer et al., 2002), fatty acid derivatives (9*S*-HODE or 10,17-DiHDoHE; Cayman Chemical), and LPE species (LPE(18:0) or P-LPE(18:0); Avanti) were added to the culture.

Newborn human epidermal keratinocytes (NHEK; Kurabo) were cultured in HuMedia KG2 Medium (Kurabo) for 1 d. NHEK cells were transfected with 10 nM human PLA2G2F siRNA (FlexiTube siRNA, Hs\_PLA2G2F\_2; 5'-TACCAGGAAGCTCTTTGACCAA-3'; QIAGEN) or control siRNA (All Stars Negative Control siRNA; QIAGEN) using Lipofectamine RNAiMAX (Invitrogen), in accordance with the manufacturer's instructions. After 3 d, the medium was changed to Assay Medium (Japan Tissue Engineering) for cell differentiation. After 2 d, RNA was extracted from the cells and subjected to quantitative RT-PCR.

**IMQ-induced psoriasis.** Mice (BALB/c background; 8–12-wk-old males) received a daily topical application of 12.5  $\mu\text{g}$  of 5% IMQ or vehicle cream (Mochida Pharma) on the dorsal and ventral surfaces of the ears over 4 d (total 50  $\mu\text{g}$  of IMQ cream per mouse). As required for the experiments, 10 nM lipids were topically applied to the ears every day. Ear thickness was monitored at various time points with a micrometer. On day 6, the mice were sacrificed and subjected to quantitative RT-PCR, histochemistry and lipid metabolome analysis.

**Hapten-induced contact dermatitis.** On day –5, mice (C57BL/6 background; 8–12-wk-old, males) were sensitized with 50  $\mu\text{l}$  of 0.5% (wt/vol) DNFB in acetone/olive oil (4/1; vol/vol) on the shaved abdominal skin. On day 0, the dorsal and ventral surfaces of the ears were challenged with 20  $\mu\text{l}$  of 0.3% DNFB. Ear thickness was monitored at various time points with a micrometer. On day 3, the mice were sacrificed and subjected to quantitative RT-PCR, histochemistry, and lipidomics analysis.

**DMBA/TPA-induced skin carcinogenesis.** The back skin of mice (BALB/c background, 8-wk-old, female) was shaved with an electric clipper. 1 wk later, 200  $\mu\text{l}$  of 2 mM DMBA (Sigma-Aldrich) in acetone was applied to the shaved skin. After 1 wk, 200  $\mu\text{l}$  of 80  $\mu\text{M}$  TPA (Sigma-Aldrich) in acetone was applied to the skin twice a week over 24 wk. Cutaneous papillomas were counted and scored weekly. The mice were then sacrificed and subjected to quantitative RT-PCR, histochemistry, and lipidomics analysis.

**Flow cytometry.** Mouse ear skin was incubated in 0.25% (wt/vol) trypsin/EDTA solution (Sigma-Aldrich) for 1 h at  $37^{\circ}\text{C}$  for separation of the epidermis from the dermis. RPMI-1640 medium (Sigma-Aldrich) containing 1.6 mg/ml collagenase IV (Worthington) was used to obtain dermal cell suspensions, which were passed through a Cell Strainer 70- $\mu\text{m}$  Nylon (Falcon; BD) and then centrifuged at 300  $g$  for 5 min at  $4^{\circ}\text{C}$ . For surface staining, the cells were blocked with mouse BD Tc Block and incubated with various cell surface marker antibodies (listed in Table S6). For intracellular staining, the cells that had been stained with surface marker antibodies were fixed, permeabilized with 1  $\mu\text{g}/\text{ml}$  ionomycin, 25 ng/ml phorbol ester, and 0.5  $\mu\text{l}/\text{ml}$  GolgiStop (BD) for 4 h, and then stained with anti-cytokine antibodies (listed in Table S5). Flow cytometry was performed with a FACSAria III (BD) and FlowJo (Tree Star) software.

**Other procedures.** TEWL of mouse skin was determined using a Tewameter TM300 (Courage and Khazaka). Cutaneous pH was measured with a flat, glass surface electrode (Skin-pH-MeterPH 905; Courage and Khazaka). Serum biochemical markers were analyzed using the clinical chemistry analyzer VetScan with V-DPP rotors (Abaxis). Laser-capture microdissection of the epidermis and hair follicles from mouse skin and Northern blotting were performed as described previously (Yamamoto et al., 2011b).

**Statistical analyses.** All values are given as the mean  $\pm$  SEM. Differences between two groups were assessed by unpaired Student's *t*-test using the Excel Statistical Program File ystat 2008 (Igaku Tosho Shuppan). Differences at *p*-values of  $<0.05$  were considered statistically significant.

**Online supplemental material.** Table S1 shows microarray gene profiling of lipase-related genes in PLA2G10<sup>fl/fl</sup> and WT skins. Table S2 shows microarray gene profiling of *Pla2g2f*<sup>fl/fl</sup> and WT skins. Table S3 shows microarray gene profiling of *Pla2g2f*<sup>fl/fl</sup> and *Pla2g2f*<sup>fl/fl</sup> keratinocytes. Table S4 is a list of primers for quantitative RT-PCR. Table S5 indicates MRM transitions for the identification of lipids. Table S6 is a list of antibodies for flow cytometry. Online supplemental material is available at <http://www.jem.org/cgi/content/full/jem.20141904/DC1>.

We thank Dr. A. Brash (Vanderbilt University, Nashville, TN) for helpful discussion and Drs. S. Arata and A. Ohazama (Showa University, Tokyo, Japan) for providing *Cre-CAG* or *-K14 TG* mice.

This work was supported by grants-in aid for Scientific Research from the Ministry of Education, Culture, Sports, Science and Technology of Japan 22116005, 24390021, and 15H05905 (to M. Murakami), 23591665, 26461671 (to K. Yamamoto) and 26860051 (to Y. Miki), the JSPS-National Science Foundation Bilateral Joint Project FY2012 (to M. Murakami), Core Research for Evolutional Science and Technology from the Agency for Medical Research and Development (to M. Murakami), the Uehara, Mitsubishi, Terumo and Toray Science Foundations (to M. Murakami), and National Institutes of Health grant HL36235 (to M.H. Gelb).

The authors declare no competing financial interests.

Submitted: 5 October 2014

Accepted: 31 August 2015

## REFERENCES

Ait-Oufella, H., O. Herbin, C. Lahoute, C. Coatrieux, X. Loyer, J. Joffre, L. Laurans, B. Ramkhalawon, O. Blanc-Brude, S. Karabina, et al. 2013. Group X secreted phospholipase A<sub>2</sub> limits the development of atherosclerosis in LDL receptor-null mice. *Arterioscler. Thromb. Vasc. Biol.* 33:466–473. <http://dx.doi.org/10.1161/ATVBAHA.112.300309>

- Akiyama, M., D. Sawamura, Y. Nomura, M. Sugawara, and H. Shimizu. 2003. Truncation of CGI-58 protein causes malformation of lamellar granules resulting in ichthyosis in Dorfman-Chanarin syndrome. *J. Invest. Dermatol.* 121:1029–1034. <http://dx.doi.org/10.1046/j.1523-1747.2003.12520.x>
- Andl, T., K. Ahn, A. Kairo, E.Y. Chu, L. Wine-Lee, S.T. Reddy, N.J. Croft, J.A. Cebra-Thomas, D. Metzger, P. Chambon, et al. 2004. Epithelial Bmpr1a regulates differentiation and proliferation in post-natal hair follicles and is essential for tooth development. *Development.* 131:2257–2268. <http://dx.doi.org/10.1242/dev.01125>
- Bazan, N.G., J.M. Calandria, and C.N. Serhan. 2010. Rescue and repair during photoreceptor cell renewal mediated by docosahexaenoic acid-derived neuroprotectin D1. *J. Lipid Res.* 51:2018–2031. <http://dx.doi.org/10.1194/jlr.R001131>
- Bligh, E.G., and W.J. Dyer. 1959. A rapid method of total lipid extraction and purification. *Can. J. Biochem. Physiol.* 37:911–917. <http://dx.doi.org/10.1139/o59-099>
- Boudreau, L.H., A.C. Duchez, N. Cloutier, D. Soulet, N. Martin, J. Bollinger, A. Paré, M. Rousseau, G.S. Naika, T. Lévesque, et al. 2014. Platelets release mitochondria serving as substrate for bactericidal group IIA-secreted phospholipase A<sub>2</sub> to promote inflammation. *Blood.* 124:2173–2183. <http://dx.doi.org/10.1182/blood-2014-05-573543>
- Condeelis, J., and J.W. Pollard. 2006. Macrophages: obligate partners for tumor cell migration, invasion, and metastasis. *Cell.* 124:263–266. <http://dx.doi.org/10.1016/j.cell.2006.01.007>
- Degousee, N., F. Ghomashchi, E. Stefanski, A. Singer, B.P. Smart, N. Borregaard, R. Reithmeier, T.F. Lindsay, C. Lichtenberger, W. Reinisch, et al. 2002. Groups IV, V, and X phospholipases A<sub>2</sub> in human neutrophils: role in eicosanoid production and gram-negative bacterial phospholipid hydrolysis. *J. Biol. Chem.* 277:5061–5073. <http://dx.doi.org/10.1074/jbc.M109083200>
- Elias, P.M., M.L. Williams, W.M. Holleran, Y.J. Jiang, and M. Schmuth. 2008. Pathogenesis of permeability barrier abnormalities in the ichthyoses: inherited disorders of lipid metabolism. *J. Lipid Res.* 49:697–714. <http://dx.doi.org/10.1194/jlr.R800002-JLR200>
- Elias, P.M., R. Gruber, D. Crumrine, G. Menon, M.L. Williams, J.S. Wakefield, W.M. Holleran, and Y. Uchida. 2014. Formation and functions of the corneocyte lipid envelope (CLE). *Biochim. Biophys. Acta.* 314:318. <http://dx.doi.org/10.1016/j.bbali.2013.09.011>
- Escoffier, J., I. Jemel, A. Tanemoto, Y. Taketomi, C. Payre, C. Coatrieux, H. Sato, K. Yamamoto, S. Masuda, K. Pernet-Gallay, et al. 2010. Group X phospholipase A<sub>2</sub> is released during sperm acrosome reaction and controls fertility outcome in mice. *J. Clin. Invest.* 120:1415–1428. <http://dx.doi.org/10.1172/JCI40494>
- Fluhr, J.W., J. Kao, M. Jain, S.K. Ahn, K.R. Feingold, and P.M. Elias. 2001. Generation of free fatty acids from phospholipids regulates stratum corneum acidification and integrity. *J. Invest. Dermatol.* 117:44–51. <http://dx.doi.org/10.1046/j.0022-202x.2001.01399.x>
- Fluhr, J.W., M. Mao-Qiang, B.E. Brown, J.P. Hachem, D.G. Moskowitz, M. Demerjian, M. Haftek, G. Serre, D. Crumrine, T.M. Mauro, et al. 2004. Functional consequences of a neutral pH in neonatal rat stratum corneum. *J. Invest. Dermatol.* 123:140–151. <http://dx.doi.org/10.1111/j.0022-202x.2004.22726.x>
- Gareus, R., M. Huth, B. Breiden, A. Nenci, N. Rösch, I. Haase, W. Bloch, K. Sandhoff, and M. Pasparakis. 2007. Normal epidermal differentiation but impaired skin-barrier formation upon keratinocyte-restricted IKK1 ablation. *Nat. Cell Biol.* 9:461–469. <http://dx.doi.org/10.1038/ncb1560>
- Grall, A., E. Guaguère, S. Planchais, S. Grond, E. Bourrat, I. Hausser, C. Hitte, M. Le Gallo, C. Derbois, G.J. Kim, et al. 2012. PNPLA1 mutations cause autosomal recessive congenital ichthyosis in golden retriever dogs and humans. *Nat. Genet.* 44:140–147. <http://dx.doi.org/10.1038/ng.1056>
- Grass, D.S., R.H. Felkner, M.Y. Chiang, R.E. Wallace, T.J. Nevalainen, C.F. Bennett, and M.E. Swanson. 1996. Expression of human group II PLA<sub>2</sub> in transgenic mice results in epidermal hyperplasia in the absence of inflammatory infiltrate. *J. Clin. Invest.* 97:2233–2241. <http://dx.doi.org/10.1172/JCI118664>
- Hachem, J.P., M.Q. Man, D. Crumrine, Y. Uchida, B.E. Brown, V. Rogiers, D. Roseeuw, K.R. Feingold, and P.M. Elias. 2005. Sustained serine proteases activity by prolonged increase in pH leads to degradation of lipid processing enzymes and profound alterations of barrier function and stratum corneum integrity. *J. Invest. Dermatol.* 125:510–520. <http://dx.doi.org/10.1111/j.0022-202x.2005.23838.x>
- Hattori, T., H. Obinata, A. Ogawa, M. Kishi, K. Tatei, O. Ishikawa, and T. Izumi. 2008. G2A plays proinflammatory roles in human keratinocytes under oxidative stress as a receptor for 9-hydroxyoctadecadienoic acid. *J. Invest. Dermatol.* 128:1123–1133. <http://dx.doi.org/10.1038/sj.jid.5701172>
- Henderson, W.R. Jr., E.Y. Chi, J.G. Bollinger, Y.T. Tien, X. Ye, L. Castelli, Y.P. Rubtsov, A.G. Singer, G.K. Chiang, T. Nevalainen, et al. 2007. Importance of group X-secreted phospholipase A<sub>2</sub> in allergen-induced airway inflammation and remodeling in a mouse asthma model. *J. Exp. Med.* 204:865–877. <http://dx.doi.org/10.1084/jem.20070029>
- Hong, S., K. Gronert, P.R. Devchand, R.L. Moussignac, and C.N. Serhan. 2003. Novel docosatrienes and 17 $\alpha$ -resolvins generated from docosahexaenoic acid in murine brain, human blood, and glial cells. Autacoids in anti-inflammation. *J. Biol. Chem.* 278:14677–14687. <http://dx.doi.org/10.1074/jbc.M300218200>
- Ilic, D., J.M. Bollinger, M. Gelb, and T.M. Mauro. 2014. sPLA<sub>2</sub> and the epidermal barrier. *Biochim. Biophys. Acta.* 1841:416–421. <http://dx.doi.org/10.1016/j.bbali.2013.11.002>
- Inoue, A., N. Arima, J. Ishiguro, G.D. Prestwich, H. Arai, and J. Aoki. 2011. LPA-producing enzyme PA-PLA<sub>1</sub> $\alpha$  regulates hair follicle development by modulating EGFR signalling. *EMBO J.* 30:4248–4260. <http://dx.doi.org/10.1038/emboj.2011.296>
- Israeli, S., Z. Khamaysi, D. Fuchs-Telem, J. Nousebeck, R. Bergman, O. Sarig, and E. Sprecher. 2011. A mutation in LIPN, encoding epidermal lipase N, causes a late-onset form of autosomal-recessive congenital ichthyosis. *Am. J. Hum. Genet.* 88:482–487. <http://dx.doi.org/10.1016/j.ajhg.2011.02.011>
- Jobard, F., C. Lefèvre, A. Karaduman, C. Blanchet-Bardon, S. Emre, J. Weissenbach, M. Ozgüç, M. Lathrop, J.F. Prud'homme, and J. Fischer. 2002. Lipoxygenase-3 (ALOXE3) and 12(R)-lipoxygenase (ALOX12B) are mutated in non-bullous congenital ichthyosiform erythroderma (NCIE) linked to chromosome 17p13.1. *Hum. Mol. Genet.* 11:107–113. <http://dx.doi.org/10.1093/hmg/11.1.107>
- Kanegae, Y., K. Takamori, Y. Sato, G. Lee, M. Nakai, and I. Saito. 1996. Efficient gene activation system on mammalian cell chromosomes using recombinant adenovirus producing Cre recombinase. *Gene.* 181:207–212. [http://dx.doi.org/10.1016/S0378-1119\(96\)00516-1](http://dx.doi.org/10.1016/S0378-1119(96)00516-1)
- Koch, P.J., P.A. de Viragh, E. Scharer, D. Bundman, M.A. Longley, J. Bickenbach, Y. Kawachi, Y. Suga, Z. Zhou, M. Huber, et al. 2000. Lessons from loricrin-deficient mice: compensatory mechanisms maintaining skin barrier function in the absence of a major cornified envelope protein. *J. Cell Biol.* 151:389–400. <http://dx.doi.org/10.1083/jcb.151.2.389>
- Labonté, E.D., R.J. Kirby, N.M. Schildmeyer, A.M. Cannon, K.W. Huggins, and D.Y. Hui. 2006. Group 1B phospholipase A<sub>2</sub>-mediated lysophospholipid absorption directly contributes to postprandial hyperglycemia. *Diabetes.* 55:935–941. <http://dx.doi.org/10.2337/diabetes.55.04.06.db05-1286>
- Lowes, M.A., M. Suárez-Fariñas, and J.G. Krueger. 2014. Immunology of psoriasis. *Annu. Rev. Immunol.* 32:227–255. <http://dx.doi.org/10.1146/annurev-immunol-032713-120225>
- MacPhee, M., K.P. Chepenik, R.A. Liddell, K.K. Nelson, L.D. Siracusa, and A.M. Buchberg. 1995. The secretory phospholipase A<sub>2</sub> gene is a candidate for the Mom1 locus, a major modifier of ApcMin-induced intestinal neoplasia. *Cell.* 81:957–966. [http://dx.doi.org/10.1016/0092-8674\(95\)90015-2](http://dx.doi.org/10.1016/0092-8674(95)90015-2)
- Man, M.Q., T.K. Lin, J.L. Santiago, A. Celli, L. Zhong, Z.M. Huang, T. Roelandt, M. Hupe, J.P. Sundberg, K.A. Silva, et al. 2014. Basis for enhanced barrier function of pigmented skin. *J. Invest. Dermatol.* 134:2399–2407. <http://dx.doi.org/10.1038/jid.2014.187>
- Mao-Qiang, M., M. Jain, K.R. Feingold, and P.M. Elias. 1996. Secretory phospholipase A<sub>2</sub> activity is required for permeability barrier homeostasis. *J. Invest. Dermatol.* 106:57–63. <http://dx.doi.org/10.1111/1523-1747.ep12327246>
- Marichal, T., M. Tsai, and S.J. Galli. 2013. Mast cells: potential positive and negative roles in tumor biology. *Cancer Immunol Res.* 1:269–279. <http://dx.doi.org/10.1158/2326-6066.CIR-13-0119>

- Miki, Y., K. Yamamoto, Y. Taketomi, H. Sato, K. Shimo, T. Kobayashi, Y. Ishikawa, T. Ishii, H. Nakanishi, K. Ikeda, et al. 2013. Lymphoid tissue phospholipase A<sub>2</sub> group IID resolves contact hypersensitivity by driving antiinflammatory lipid mediators. *J. Exp. Med.* 210:1217–1234.
- Mulherkar, R., B.M. Kirtane, A. Ramchandani, N.P. Mansukhani, S. Kannan, and K.N. Naresh. 2003. Expression of enhancing factor/phospholipase A<sub>2</sub> in skin results in abnormal epidermis and increased sensitivity to chemical carcinogenesis. *Oncogene*. 22:1936–1944. <http://dx.doi.org/10.1038/sj.onc.1206229>
- Murakami, M., Y. Taketomi, Y. Miki, H. Sato, T. Hirabayashi, and K. Yamamoto. 2011. Recent progress in phospholipase A<sub>2</sub> research: from cells to animals to humans. *Prog. Lipid Res.* 50:152–192. <http://dx.doi.org/10.1016/j.plipres.2010.12.001>
- Murakami, M., H. Sato, Y. Miki, K. Yamamoto, and Y. Taketomi. 2015. A new era of secreted phospholipase A<sub>2</sub>. *J. Lipid Res.* 56:1248–1261. <http://dx.doi.org/10.1194/jlr.R058123>
- Nagamachi, M., D. Sakata, K. Kabashima, T. Furuyashiki, T. Murata, E. Segi-Nishida, K. Soontrapa, T. Matsuoka, Y. Miyachi, and S. Narumiya. 2007. Facilitation of Th1-mediated immune response by prostaglandin E receptor EP1. *J. Exp. Med.* 204:2865–2874. <http://dx.doi.org/10.1084/jem.20070773>
- Olund, R.C., N. Cermak, and M.H. Gelb. 2008. Highly specific and broadly potent inhibitors of mammalian secreted phospholipases A<sub>2</sub>. *J. Med. Chem.* 51:4708–4714. <http://dx.doi.org/10.1021/jm800422v>
- Pernet, E., L. Guillemot, P.R. Burgel, C. Martin, G. Lambeau, I. Sermet-Gaudelus, D. Sands, D. Leduc, P.C. Morand, L. Jeammet, et al. 2014. *Pseudomonas aeruginosa* eradicates *Staphylococcus aureus* by manipulating the host immunity. *Nat. Commun.* 5:5105. <http://dx.doi.org/10.1038/ncomms6105>
- Sato, H., Y. Taketomi, Y. Isogai, Y. Miki, K. Yamamoto, S. Masuda, T. Hosono, S. Arata, Y. Ishikawa, T. Ishii, et al. 2010. Group III secreted phospholipase A<sub>2</sub> regulates epididymal sperm maturation and fertility in mice. *J. Clin. Invest.* 120:1400–1414. <http://dx.doi.org/10.1172/JCI40493>
- Sato, H., Y. Taketomi, A. Ushida, Y. Isogai, T. Kojima, T. Hirabayashi, Y. Miki, K. Yamamoto, Y. Nishito, T. Kobayashi, et al. 2014. The adipocyte-inducible secreted phospholipases PLA2G5 and PLA2G2E play distinct roles in obesity. *Cell Metab.* 20:119–132. <http://dx.doi.org/10.1016/j.cmet.2014.05.002>
- Schonhaler, H.B., J. Guinea-Viniegra, S.K. Wculek, I. Ruppen, P. Ximénez-Embún, A. Guío-Carrión, R. Navarro, N. Hogg, K. Ashman, and E.F. Wagner. 2013. S100A8-S100A9 protein complex mediates psoriasis by regulating the expression of complement factor C3. *Immunity*. 39:1171–1181. <http://dx.doi.org/10.1016/j.immuni.2013.11.011>
- Serhan, C.N. 2014. Pro-resolving lipid mediators are leads for resolution physiology. *Nature*. 510:92–101. <http://dx.doi.org/10.1038/nature13479>
- Serhan, C.N., C.B. Clish, J. Brannon, S.P. Colgan, N. Chiang, and K. Gronert. 2000. Novel functional sets of lipid-derived mediators with antiinflammatory actions generated from omega-3 fatty acids via cyclooxygenase 2-nonsteroidal antiinflammatory drugs and transcellular processing. *J. Exp. Med.* 192:1197–1204. <http://dx.doi.org/10.1084/jem.192.8.1197>
- Serhan, C.N., K. Gotlinger, S. Hong, Y. Lu, J. Siegelman, T. Baer, R. Yang, S.P. Colgan, and N.A. Petasis. 2006. Anti-inflammatory actions of neuroprotectin D1/protectin D1 and its natural stereoisomers: assignments of dihydroxy-containing docosatrienes. *J. Immunol.* 176:1848–1859. <http://dx.doi.org/10.4049/jimmunol.176.3.1848>
- Serhan, C.N., J. Dalli, R.A. Colas, J.W. Winkler, and N. Chiang. 2015. Protectins and maresins: New pro-resolving families of mediators in acute inflammation and resolution bioactive metabolome. *Biochim. Biophys. Acta.* 1851:397–413. <http://dx.doi.org/10.1016/j.bbali.2014.08.006>
- Singer, A.G., F. Ghomashchi, C. Le Calvez, J. Bollinger, S. Bezzine, M. Rouault, M. Sadilek, E. Nguyen, M. Lazdunski, G. Lambeau, and M.H. Gelb. 2002. Interfacial kinetic and binding properties of the complete set of human and mouse groups I, II, V, X, and XII secreted phospholipases A<sub>2</sub>. *J. Biol. Chem.* 277:48535–48549. <http://dx.doi.org/10.1074/jbc.M205855200>
- Smith, S.J., S. Cases, D.R. Jensen, H.C. Chen, E. Sande, B. Tow, D.A. Sanan, J. Raber, R.H. Eckel, and R.V. Farese Jr. 2000. Obesity resistance and multiple mechanisms of triglyceride synthesis in mice lacking Dgat. *Nat. Genet.* 25:87–90. <http://dx.doi.org/10.1038/75651>
- Taketomi, Y., N. Ueno, T. Kojima, H. Sato, R. Murase, K. Yamamoto, S. Tanaka, M. Sakanaka, M. Nakamura, Y. Nishito, et al. 2013. Mast cell maturation is driven via a group III phospholipase A<sub>2</sub>-prostaglandin D<sub>2</sub>-DP1 receptor paracrine axis. *Nat. Immunol.* 14:554–563. <http://dx.doi.org/10.1038/ni.2586>
- Tortola, L., E. Rosenwald, B. Abel, H. Blumberg, M. Schäfer, A.J. Coyle, J.C. Renaud, S. Werner, J. Kisielow, and M. Kopf. 2012. Psoriasisiform dermatitis is driven by IL-36-mediated DC-keratinocyte crosstalk. *J. Clin. Invest.* 122:3965–3976. <http://dx.doi.org/10.1172/JCI63451>
- Tu, C.L., D.A. Crumrine, M.Q. Man, W. Chang, H. Elalieh, M. You, P.M. Elias, and D.D. Bikle. 2012. Ablation of the calcium-sensing receptor in keratinocytes impairs epidermal differentiation and barrier function. *J. Invest. Dermatol.* 132:2350–2359. <http://dx.doi.org/10.1038/jid.2012.159>
- Valentini, E., F. Ghomashchi, M.H. Gelb, M. Lazdunski, and G. Lambeau. 1999. On the diversity of secreted phospholipases A<sub>2</sub>. Cloning, tissue distribution, and functional expression of two novel mouse group II enzymes. *J. Biol. Chem.* 274:31195–31202. <http://dx.doi.org/10.1074/jbc.274.44.31195>
- Vasireddy, V., Y. Uchida, N. Salem Jr., S.Y. Kim, M.N. Mandal, G.B. Reddy, R. Bodepudi, N.L. Alderson, J.C. Brown, H. Hama, et al. 2007. Loss of functional ELOVL4 depletes very long-chain fatty acids (> or =C28) and the unique omega-O-acylceramides in skin leading to neonatal death. *Hum. Mol. Genet.* 16:471–482. <http://dx.doi.org/10.1093/hmg/ddl480>
- Yamamoto, K., Y. Isogai, H. Sato, Y. Taketomi, and M. Murakami. 2011a. Secreted phospholipase A<sub>2</sub>, lipoprotein hydrolysis, and atherosclerosis: integration with lipidomics. *Anal. Bioanal. Chem.* 400:1829–1842. <http://dx.doi.org/10.1007/s00216-011-4864-z>
- Yamamoto, K., Y. Taketomi, Y. Isogai, Y. Miki, H. Sato, S. Masuda, Y. Nishito, K. Morioka, Y. Ishimoto, N. Suzuki, et al. 2011b. Hair follicular expression and function of group X secreted phospholipase A<sub>2</sub> in mouse skin. *J. Biol. Chem.* 286:11616–11631. <http://dx.doi.org/10.1074/jbc.M110.206714>

# SCIENTIFIC REPORTS

OPEN

## Characterization of hepatic lipid profiles in a mouse model with nonalcoholic steatohepatitis and subsequent fibrosis

Received: 25 February 2015

Accepted: 18 June 2015

Published: 20 August 2015

Kosuke Saito<sup>1,\*</sup>, Takashi Uebanso<sup>2,\*</sup>, Keiko Maekawa<sup>1</sup>, Masaki Ishikawa<sup>1</sup>, Ryo Taguchi<sup>1</sup>, Takao Nammo<sup>2</sup>, Tomoko Nishimaki-Mogami<sup>3</sup>, Haruhide Udagawa<sup>2</sup>, Masato Fujii<sup>4</sup>, Yuichiro Shibazaki<sup>4</sup>, Hiroyuki Yoneyama<sup>4</sup>, Kazuki Yasuda<sup>2</sup> & Yoshiro Saito<sup>1</sup>

Nonalcoholic steatohepatitis (NASH) is a major health problem since it often leads to hepatocellular carcinoma. However, the underlying mechanisms of NASH development and subsequent fibrosis have yet to be clarified. We compared comprehensive lipidomic profiles between mice with high fat diet (HFD)-induced steatosis and STAM mice with NASH and subsequent fibrosis. The STAM mouse is a model that demonstrates NASH progression resembling the disease in humans: STAM mice manifest NASH at 8 weeks, which progresses to fibrosis at 12 weeks, and finally develop hepatocellular carcinoma. Overall, 250 lipid molecules were detected in the liver using liquid chromatography-mass spectrometry. We found that STAM mice with NASH presented a significantly higher abundance of sphingolipids and lower levels of triacylglycerols than the HFD-fed control mice. The abundance of certain fatty acids in phospholipid side chains was also significantly different between STAM and control mice, although global levels of phosphatidylcholines and phosphatidylethanolamines were comparable. Finally, increase in levels of acylcarnitines and some diacylglycerols was observed in STAM mice toward the fibrosis stage, but not in age-matched control mice. Our study provides insights into the lipid status of the steatotic, NASH, and fibrotic liver that would help elucidate the molecular pathophysiology of NASH progression.

Nonalcoholic fatty liver disease (NAFLD) is one of the major hepatic health problems in the world<sup>1–4</sup>. About 10% of NAFLD patients are reported to develop nonalcoholic steatohepatitis (NASH), in which hepatic steatosis is accompanied by inflammation and hepatocyte apoptosis<sup>4–6</sup>. NASH can lead to fibrosis, liver cirrhosis and eventually hepatocellular carcinoma. According to the “two-hit hypothesis” of NASH progression, the “first hit” is lipid accumulation in hepatocytes<sup>6,7</sup>. The “second hit” is more complicated, and is probably a combination of multiple factors including genetics, insulin resistance, oxidative stress, mitochondrial dysfunction, and inflammation.

However, the precise mechanisms of progression from steatosis to NASH have yet to be elucidated. In addition, mechanisms underlying progression from NASH to liver fibrosis and cirrhosis also remain unclear. In humans with NAFLD, free fatty acids, which undergo esterification into triglycerides,

<sup>1</sup>Division of Medical Safety Science, National Institute of Health Sciences, 1-18-1 Kamiyoga, Setagaya, Tokyo 158-8501, Japan. <sup>2</sup>Department of Metabolic Disorder, Diabetes Research Center, Research Institute, National Center for Global Health and Medicine, 1-21-1 Toyama, Shinjuku, Tokyo 162-8655, Japan. <sup>3</sup>Division of Biochemistry, National Institute of Health Sciences, 1-18-1 Kamiyoga, Setagaya, Tokyo 158-8501, Japan. <sup>4</sup>Stelic Institute & Co., Inc., 1-9-15 Higashi Azabu, Minato, Tokyo 106-0044, Japan. \*These authors contributed equally to this work. Correspondence and requests for materials should be addressed to K.M. (email: maekawa@nihs.go.jp) or K.Y. (email: kyasuda@ri.ncgm.go.jp)

	8 weeks		12 weeks	
	HFD	STAM	HFD	STAM
Body weight (g)	25.4 ± 0.8 <sup>a</sup>	16.7 ± 0.9 <sup>b</sup>	34.9 ± 1.4 <sup>c</sup>	19.2 ± 0.7 <sup>d</sup>
Fasting blood glucose (mg/dl)	53.8 ± 2.8 <sup>a</sup>	354.7 ± 53.3 <sup>b</sup>	104.4 ± 9.1 <sup>c</sup>	501.4 ± 44.7 <sup>d</sup>
Fasting serum insulin (ng/ml)	0.222 ± 0.242	0.160 ± 0.004	0.484 ± 0.120	0.226 ± 0.041
Relative liver weight (g/kg BW)	38.5 ± 0.8 <sup>a</sup>	56.9 ± 1.6 <sup>b</sup>	37.2 ± 2.0 <sup>a</sup>	73.0 ± 5.1 <sup>c</sup>
NAFLD activity score	0.0 ± 0 <sup>a</sup>	2.5 ± 0.3 <sup>b</sup>	2.2 ± 0.7 <sup>b</sup>	5.0 ± 0.4 <sup>c</sup>

**Table 1. Physiological and histological characteristics of STAM mice.** Data represent mean ± S.E. (n = 5 or 6). Significant differences were observed among groups marked with different letters,  $p < 0.05$ .

circulate at higher levels in the blood, leading to fat accumulation in the liver<sup>8,9</sup>. Another report has demonstrated that stearoyl-CoA desaturase (SCD1), an enzyme that synthesizes monounsaturated fatty acids from saturated fatty acids, plays an important role in hepatic lipid accumulation and NASH progression<sup>10</sup>. Moreover, depletion of the palmitate elongase, Elov16, attenuated NASH progression in mice, and expression of Elov16 was positively correlated with severity of steatosis and liver injury in human NASH patients<sup>11</sup>. However, these observations focused only on free fatty acids, and detailed differences in overall lipid profiles at different stages of the disease have not been characterized.

Lipidomics overviews a broad range of lipid metabolites, including phospholipids, sphingolipids and neutral lipids<sup>12,13</sup>. This approach is useful to identify novel biomarkers as well as to understand changes in lipid status in clinically important diseases, such as diabetes mellitus<sup>14,15</sup>. Recently, we have demonstrated the progressive change in lipid profiles in mouse and hamster models of Alzheimer's disease and dilated cardiomyopathy<sup>16,17</sup>. We hypothesized that characterization of lipid status using lipidomics would help illuminate the mechanism of NASH progression.

The STAM mouse develops NASH, fibrosis and finally hepatocellular carcinoma<sup>18</sup>. This model demonstrates the pathological progression that is very similar to the human disease, in particular the rapid and step-wise progression from steatosis to NASH to fibrosis. STAM mice also suffer from very high incidence of tumour development, at a rate of nearly 100% in males. Hence, the STAM mouse is the best available model of human NASH. In the present study, we used this model to examine changes in the lipid status in NASH. Because our primary focus is the mechanism of NASH progression from simple steatosis, we compared the lipid status of STAM mice with those of HFD-fed mice that only developed 'benign' steatosis. Overall, we detected 250 lipid molecules from liver tissue, including 103 phospholipids, 16 sphingolipids, 112 neutral lipids, 11 free fatty acids and 8 acylcarnitines (Cars). These metabolites were categorized into seven, three, and four classes within phospholipids, sphingolipids, and neutral lipids, respectively. In addition, we also investigated temporal lipid changes in STAM mice between 8 (NASH stage) and 12 weeks (fibrosis stage) of age. Our results show the differences in the lipid profiles between steatosis and NASH and the changes in lipid status during disease progression from NASH to fibrosis. This would help clarify the underlying molecular mechanisms.

## Results

**Biological and histological characteristics of STAM mice.** STAM mice exhibited hyperglycemia and hepatomegaly as observed in previous reports (Table 1)<sup>18</sup>. Histological examination revealed hepatocellular ballooning and steatosis at 8 weeks (Supplemental Fig. 1a-b), the age we defined to be the NASH stage. Subsequently, lobular inflammation and fibrosis in the liver were observed at 12 weeks (Supplemental Fig. 1a-c), at which we deemed the mice to be in fibrosis stage. In contrast, HFD mice did not exhibit hepatocellular ballooning or lobular inflammation (Supplemental Fig. 1a). NAFLD activity scores of both 8- and 12-week old STAM mice were significantly higher than those of age-matched HFD mice (Table 1). Our findings were consistent with those reported in our previous paper<sup>18</sup> describing this NASH model in more detail, where we also reported elevated serum ALT and AST levels, and infiltration of F4/80 positive cells by immunohistochemistry.

**Lipid profile in the NASH stage.** Using ultraperformance liquid chromatography-time of flight mass spectrometry (UPLC-TOFMS), we identified 250 lipid molecules overall from liver tissues (Supplemental Table 1), including 103 phospholipids, 16 sphingolipids, 112 neutral lipids, 11 free fatty acids and 8 Cars. The number of lipid molecules in each class is listed in Table 2. The relative abundance of each lipid molecules in 8- and 12-week old HFD and STAM mice are summarized in Supplemental Table 2. Levels were normalized by internal standards (see Materials and Methods).

To examine differences in lipid profiles between steatotic and NASH mice, we first compared the sum of the peak heights of all lipid molecules within each class. As shown in Fig. 1, no phospholipid class was significantly different in abundance between HFD and STAM mice. However, sphingomyelin (SM), ceramide (Cer) and coenzyme Q (CoQ) were significantly higher in STAM mice. In contrast, diacylglycerol (DG) and triacylglycerol (TG) were significantly lower.

Lipid class	Ion mode	Lipid classes	Number of species
Phospholipid	Negative	lysophosphatidylcholine (LPC)	3
		phosphatidylcholine (PC)	33
		phosphatidylethanolamine (PE)	29
		phosphatidylglycerol (PG)	3
		phosphatidylinositol (PI)	9
	bis(monoacylglycerol)phosphate (BMP)	9	
	Positive	cardiolipin (CL)	17
Sphingolipid	Negative	sphingomyelin (SM)	7
		ceramide (Cer)	5
		hexosylceramide (HexCer)	4
Neutral lipid	Positive	coenzyme Q (CoQ)	3
		cholesterol/cholesterolester (Ch/ChE)	6
		diacylglycerol (DG)	14
		triacylglycerol (TG)	89
Free fatty acid	Negative	free saturated fatty acid (fSFA)	3
		free monounsaturated fatty acid (fMUFA)	2
		free polyunsaturated fatty acid (fPUFA)	6
Acylcarnitine	Positive	acylcarnitine (Car)	8
		total	250

**Table 2. Lipid classes detected in the liver, and number of individual lipid species within each class.**

On the other hand, analysis of individual molecules revealed bi-directional changes in phospholipid molecules (*i.e.*, the number of phospholipids in significantly higher levels in STAM mice was similar to the number that was significantly lower in abundance) (Fig. 2 and Supplemental Table 2). Further, sphingolipid molecules (42:1SM, 38:1Cer, 42:1Cer and 42:1HexCer) were either significantly elevated or unchanged in STAM mice, in agreement with the increased class total. Determination of fatty acid side chain revealed that 38:1Cer is C16 Cer (d18:1/16:0Cer) (Supplemental Table 2). On the other hand, most neutral lipids such as 32:1DG and 48:0TG were found to be significantly lower in STAM mice.

These results suggest that even though phospholipid class totals are comparable, the composition of each class differed between the livers of HFD and STAM mice. To further explore this phenomenon, we determined the composition of fatty acid side chains within phosphatidylcholines (PC) and phosphatidylethanolamines (PE), the two largest phospholipid classes comprising about 30 lipids each, which are sufficient to detect differences in composition. Table 3 presents the percentage of individual phospholipids in each class, along with their fatty acid side chains. In each class, seven molecules presented a difference in abundance of more than 1% between HFD and STAM mice. It is noteworthy that these molecules contain either palmitate (16:0) or stearate (18:0) as a side chain. All phospholipid molecules containing palmitate, except 16:0/22:6PC, were less abundant in STAM mice, while those containing stearate were more so.

For a systemic comparison, we also calculated the abundance of each fatty acid as a percentage of all side chains within PC or PE (Fig. 3a). Among PCs, palmitate and oleate (18:1) side chains were significantly lower in STAM mice, stearate side chains were significantly higher, while all other side chains were unchanged in abundance. On the other hand, palmitate and stearate side chains were significantly lower and higher, respectively, among PE in STAM mice. Notably, the abundance of free palmitate and free stearate was not statistically different between HFD and STAM mice (Fig. 3b).

Since inflammation is an important NASH symptom, we determined levels of free arachidonate (20:4) and its metabolites. Arachidonate and its lipoxygenase (LOX) metabolite, 5-hydroxyicosatetraenoate (HETE), as well as its cytochrome P450 (CYP) metabolite, 18-HETE, were significantly diminished in STAM mice (Supplemental Fig. 2a). On the other hand, the cyclooxygenase (COX) metabolites prostaglandin D<sub>2</sub> (PGD<sub>2</sub>), thromboxane B<sub>2</sub> (TXB<sub>2</sub>) and 12-hydroxyheptadecatrienoate (12-HHT) were unchanged. However, when levels of metabolites were normalized to arachidonate, all COX metabolites were significantly elevated in STAM mice, but LOX and CYP metabolites were unchanged, suggesting a possible relative amplification of the COX pathway (Supplemental Fig. 2b).

**Lipid profiles in subsequent fibrosis.** STAM mice exhibit progression from NASH to fibrosis in a manner similar to disease development in humans<sup>18</sup>. Thus, to examine changes in lipid profile during disease progression, we compared STAM mice at 8 weeks (NASH stage) and 12 weeks (fibrosis

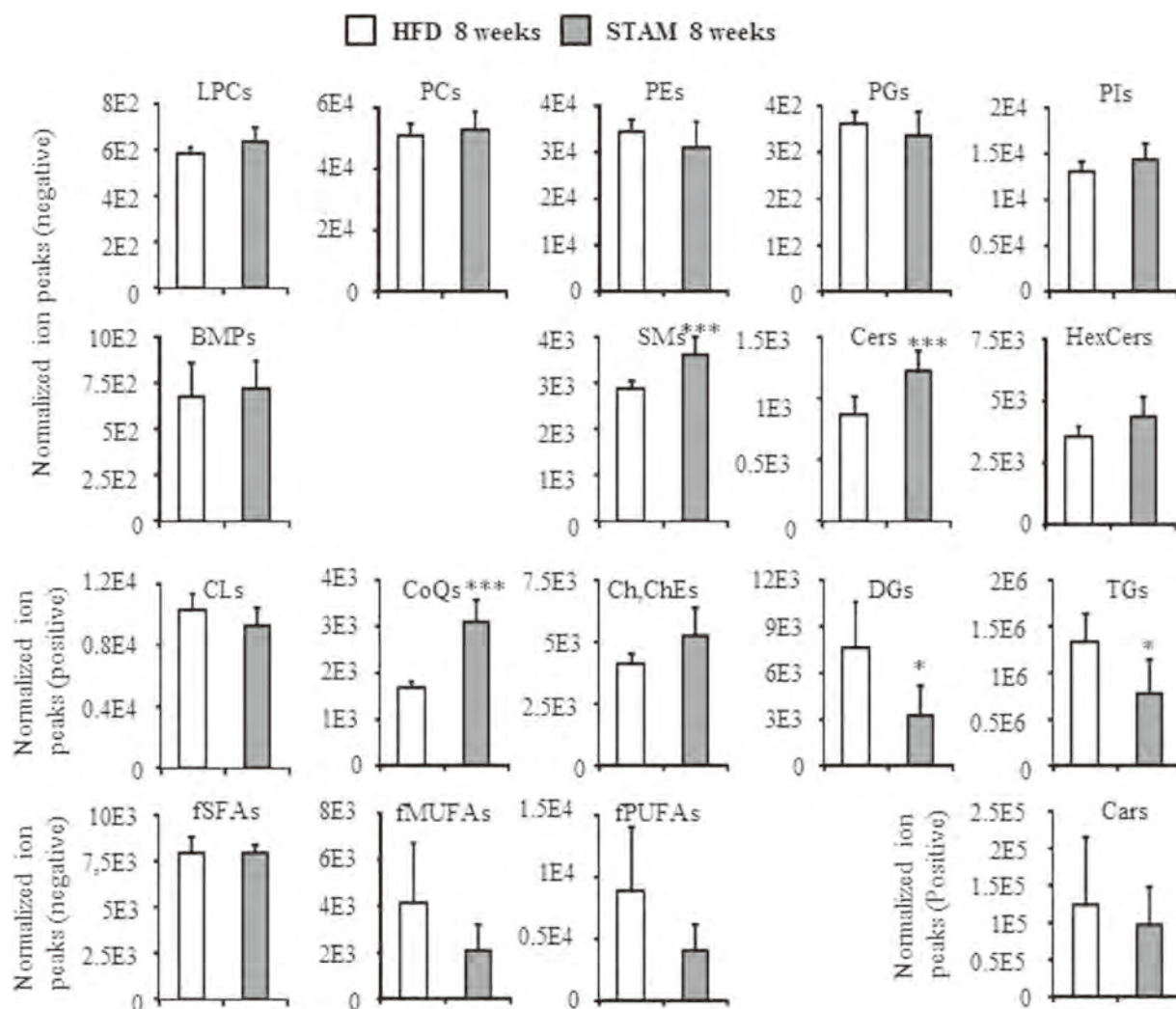


**Figure 1. Global abundance of hepatic lipid classes in STAM and control HFD mice at 8 weeks.**

Lipid extracts were prepared from mouse livers as described in Materials and Methods, and abundance of lipid molecules was measured individually. Data are sum of ion peak heights of all lipid molecules within each class and shown as mean  $\pm$  SD ( $n = 5$  in each group). \* $p < 0.05$ ; \*\*\* $p < 0.005$  in statistical tests comparing control HFD mice and STAM mice. LPCs, lysophosphatidylcholines; PCs, phosphatidylcholines; PEs, phosphatidylethanolamines; PGs, phosphatidylglycerols; PIs, phosphatidylinositols; BMPs, bis(monoacylglycerol)phosphates; SMs, sphingomyelins; Cers, ceramides; HexCers, hexosylceramides; CLs, cardiolipins; CoQs, coenzyme Qs; Ch/ChEs, cholesterol and cholesteroles; DGs, diacylglycerols; TGs, triacylglycerols; fSFAs, free saturated fatty acids; fMUFAs, free monounsaturated fatty acids; fPUFAs, free polyunsaturated fatty acids; Cars, acylcarnitines.

stage) (Fig. 4). We also examined changes in lipid status of age-matched control HFD mice (Fig. 4b and Supplemental Fig. 3).

As shown in Fig. 4a, total Cars was significantly elevated in fibrosis-stage STAM mice, a change that was not observed in HFD mice (Supplemental Fig. 3). In contrast, a temporal increase in total phosphatidylinositol (PI) was observed in HFD mice but not in STAM mice, an observation that could be attributed to an increase in 38:4PI, the major PI molecule (Supplementary Table 2). Moreover, we observed elevated DG in STAM mice, and although this rise was not statistically significant, it was not observed in control HFD mice. As shown in Supplemental Table 2, the major DG molecules 34:1DG-a and 36:2DG significantly increased between 8 and 12 weeks in STAM mice only. On the other hand, phosphatidylglycerol (PG), cholesterol (Ch) and cholesteroles (ChE) significantly diminished, and TG significantly increased, in both HFD and STAM mice. In addition, pattern of changes in CoQ and free polyunsaturated fatty acids (fPUFAs) were similar between HFD and STAM mice, although these changes were not statistically significant in the latter.

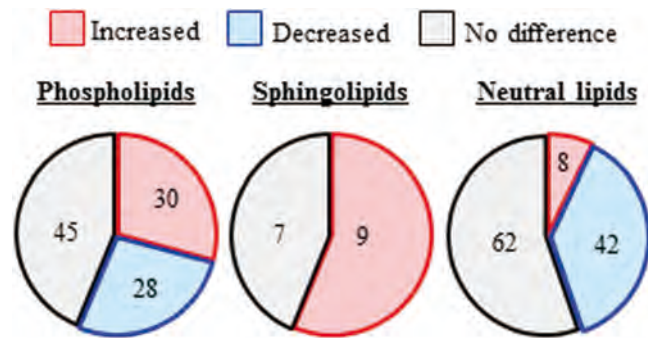


**Figure 2.** Venn diagrams of the number of lipid molecules within phospholipids, sphingolipids and neutral lipids that were significantly different in abundance between STAM and control HFD mice at 8 weeks. Increased: STAM > control, decreased; STAM < control.

There were 31 molecules of phospholipids in HFD mice, and five in STAM mice, with levels that significantly increased in 12 weeks compared to 8 weeks (Fig. 5 and Supplemental Table 2). Of these, 13 molecules were PC, and two of these molecules increased in abundance in both HFD and STAM mice (17:0/20:4PC and 18:0/18:1PC, Supplemental Fig. 5). The increase in the other 11 molecules, which include 18:1/20:4PC and 18:0/22:6PC, was observed only in HFD mice.

On the other hand, seven PC molecules in HFD mice, and 12 in STAM mice, significantly decreased between 8 and 12 weeks. Of these, six molecules, including 18:2/20:4PC, 18:2/22:6PC and 20:4/20:4 PC, diminished in STAM mice only.

As for arachidonate and its metabolites, all five molecules detected were unchanged between 8 week- and 12 week-old STAM mice (Supplemental Fig. 4a), while they diminished in age-matched HFD mice (Supplemental Fig. 4b).

## Discussion

In the present study, we compared overall lipid profiles of mice at different stages of NASH progression. We used the STAM mouse, a unique diabetic mouse model with NASH that resembles the human disease in various aspects. We analysed STAM mice at the NASH (8 weeks) and fibrosis (12 weeks) stage, and compared them with control HFD mice, which only developed simple steatosis. The notable features of NASH included (1) elevated sphingolipids; (2) decreased DGs and TGs; (3) relative decrease and increase in the levels of palmitate and stearate as phospholipid side chains, respectively; and (4) increased relative abundance of COX metabolites from arachidonate. On the other hand, we observed the following characteristics in fibrosis compared with NASH: (1) increase in Cars and major DG molecules; and (2) unchanged PI, which is increased in HFD control mice.

We demonstrated that sphingolipids, including Cers, were elevated in the liver of STAM mice exhibiting NASH, while palmitate was less abundant as acyl side chains in their phospholipids. It is possible that in NASH, palmitate might be funnelled away from the synthesis of phospholipids and toward the synthesis of sphingolipids. Whether the increase in sphingolipids plays a pivotal role in NASH is presently unclear. However, it has been reported that the sphingolipid Cers have cell signalling properties relevant to inflammation, apoptosis and insulin resistance<sup>19–21</sup>, and may also be involved in cystic fibrosis in the lung<sup>22,23</sup>. Thus, it may be reasonable to speculate that increased Cers in the NASH liver could contribute to inflammation and trigger pathological fibrosis.

Esterification of fatty acids into TG is currently thought to quench excess free fatty acids, and to prevent lipotoxicity<sup>24</sup>. In our NASH model, levels of TG and DG decreased in the liver. Relative insulin deficiency compared to hyperglycemic conditions was observed in STAM mice which had been treated with streptozotocin, and this may have suppressed DG and TG synthesis through down-regulation of the sterol regulatory element binding transcription factor 1 (SREBP1), because SREBP1 responds to insulin and activates DG and TG synthesis through lipogenesis and esterification of fatty acids into glycerol<sup>25</sup>. In fact, a report using a different model demonstrated that SREBP1 was also down-regulated in diet-induced NASH<sup>26</sup>, supporting the idea that suppression of TG synthesis might be involved in NASH progression.

On the other hand, phospholipids are important not only as components of the plasma membrane, but also as cell signalling messengers. For example, 16:0/18:1 PC activates peroxisome proliferator-activated receptor  $\alpha$  (PPAR $\alpha$ ) in the liver<sup>27</sup>, while 18:0/18:1 PC activates it in the muscle<sup>28</sup>. These observations suggest that the nature of acyl side chains modulates cell signalling. In the present study, we found that palmitate-containing PC, such as 16:0/18:1 PC, decreased in abundance in NASH, but those containing stearate, such as 18:0/18:2 PC, increased. Thus, these changes might regulate hepatic function through altered cell signalling, possibly via PPAR $\alpha$ . For example, decreased 16:0/18:1 PC may lead to insufficient PPAR $\alpha$  activity in NASH and impair  $\beta$ -oxidation, which is enhanced through induction of PPAR $\alpha$ -responsive genes<sup>29</sup>. This might also explain, at least in part, the accumulation of Cars in subsequent fibrosis.

PC	Side chains	% of all PC		% change	PE	Side chains	% of all PE		% change
		HFD	STAM				HFD	STAM	
32:0PC	16:0/16:0	1.06	1.09	+0.03	34:1PE	16:0/18:1	0.74	0.34	-0.40
32:1PC	16:0/16:1	1.02	0.24	-0.78	34:2PE	<b>16:0/18:2</b>	4.15	2.25	-1.90
32:2PC	14:0/18:2 16:1/16:1	0.17	0.13	-0.04	36:1PE	18:0/18:1	0.24	0.26	+0.03
34:0PC	16:0/18:0	0.14	0.24	+0.09	36:2PE	<b>18:0/18:2</b>	2.44	3.81	+1.37
34:1PC	<b>16:0/18:1</b>	16.64	8.71	-7.93	36:3PE	18:1/18:2	2.16	2.00	-0.17
34:2PC	<b>16:0/18:2</b>	23.37	19.91	-3.46	36:4PE-a	<b>16:0/20:4</b>	8.22	5.52	-2.70
34:3PC-a	16:1/18:2	1.40	1.01	-0.39	36:4PE-b	18:2/18:2	0.15	0.31	+0.16
34:3PC-b	16:0/18:3	1.11	0.57	-0.54	36:5PE	16:1/20:4	0.48	0.13	-0.36
35:2PC	17:0/18:2	0.18	0.35	+0.17	37:4PE	17:0/20:4	0.31	0.44	+0.13
36:1PC	18:0/18:1	1.05	1.37	+0.32	38:3PE	18:0/20:3	0.30	0.70	+0.40
36:2PC	<b>18:0/18:2</b>	3.97	7.56	+3.59	38:4PE	<b>18:0/20:4</b>	30.82	35.41	+4.59
36:3PC	16:0/20:3	2.21	3.09	+0.89	38:5PE-a	18:1/20:4	5.72	5.71	-0.02
36:4PC-a	<b>16:0/20:4</b>	19.80	15.38	-4.42	38:5PE-b	<b>16:0/22:5</b>	2.41	1.35	-1.06
36:4PC-b	18:2/18:2	0.50	1.27	+0.77	38:6PE-a	<b>16:0/22:6</b>	25.48	21.28	-4.19
36:5PC	16:1/20:4	0.57	0.20	-0.36	38:6PE-b	18:2/20:4	0.22	0.38	+0.17
37:4PC	17:0/20:4	0.14	0.29	+0.15	38:7PE	16:1/22:6	0.55	0.16	-0.39
38:3PC-a	18:0/20:3	0.36	1.01	+0.65	39:4PE-a	19:0/20:4	0.20	0.25	+0.05
38:3PC-b	n.d.	0.14	0.19	+0.05	39:4PE-b	19:0/20:4	0.19	0.10	-0.09
38:4PC-a	<b>18:0/20:4</b>	6.07	13.54	+7.47	39:6PE	17:0/22:6	0.17	0.30	+0.13
38:4PC-b	18:1/20:3	0.15	0.26	+0.11	40:4PE	18:0/22:4	0.32	0.43	+0.11
38:5PC-a	18:1/20:4	2.76	3.10	+0.34	40:5PE-a	18:0/22:5	1.16	1.00	-0.16
38:5PC-b	16:0/22:5	1.27	0.69	-0.57	40:5PE-b	18:0/22:5 20:1/20:4	0.34	0.32	-0.02
38:6PC-a	<b>16:0/22:6</b>	10.50	12.07	+1.58	40:6PE-a	<b>18:0/22:6</b>	5.93	9.15	+3.22
38:6PC-b	18:2/20:4	0.49	0.74	+0.25	40:6PE-b	18:1/22:5	0.91	0.73	-0.18
38:7PC	16:1/22:6	0.33	0.20	-0.13	40:7PE	18:1/22:6	4.67	5.21	+0.54
39:6PC	n.d.	0.06	0.14	+0.08	40:8PE	18:2/22:6	0.17	0.38	+0.21
40:5PC-a	18:0/22:5	0.48	0.46	-0.02	36:5e/pPE	16:0p/20:4	0.74	0.84	+0.10
40:5PC-b	20:1/20:4	0.17	0.18	+0.01	38:5e/pPE	18:0p/20:4	0.54	0.84	+0.29
40:6PC-a	<b>18:0/22:6</b>	2.11	3.92	+1.82	38:6e/pPE	18:1p/20:4	0.27	0.37	+0.10
40:6PC-b	n.d.	0.22	0.15	-0.07					
40:7PC	18:1/22:6	1.22	1.35	+0.13					
40:8PC	18:2/22:6 20:4/20:4	0.21	0.41	+0.20					
38:5e/pPC	16:0e/22:5 18:1e/20:4	0.13	0.15	+0.02					

**Table 3. The acyl side chains and abundance of individual phospholipids in PC or PE from HFD and STAM mice at 8 weeks.** % change = percent in STAM control mice - percent in HFD mice. Numbers in bold are changes larger than 1% Lipid species of the same formula are distinguished by letters. Abbreviation of lipid classes are listed in Table 2.

In the present study, arachidonate was depleted in STAM mice at 8 weeks. Alternatively, our results further suggest that relative production of COX metabolites, but not LOX and P450 metabolites, increased in NASH. COX2 metabolites, such as PGD<sub>2</sub> and TXB<sub>2</sub>, modulate liver injury and inflammation<sup>30,31</sup>. For example, PGD<sub>2</sub> exacerbated dicloxacillin-induced liver injury by enhancing IL-4 production, and anti-TXB<sub>2</sub> antibodies protect against acetaminophen-induced liver injury. It has also been reported that hepatic COX2 was elevated in mouse steatohepatitis<sup>32</sup>. In addition, COX2 is up-regulated in patients with cirrhosis and hepatocellular carcinoma<sup>33,34</sup>. Thus, elevated COX2 activity might be a key feature of the NASH liver. Indeed, depleted arachidonate levels in NASH may be partly due to its consumption during synthesis of PGD<sub>2</sub>, TXB<sub>2</sub>, and 12-HHT. Another possibility is that signaling molecules other than arachidonate are mainly involved in inflammatory response in our NASH model.

Major molecules of DG, 34:1DG-a and 36:2DG, increased during the progression of NASH to fibrosis, although the change in total DG did not reach statistically significant levels. In response to various cell signals, DG is synthesized by phospholipase C from phosphatidylinositol (4,5)-biphosphate, and the

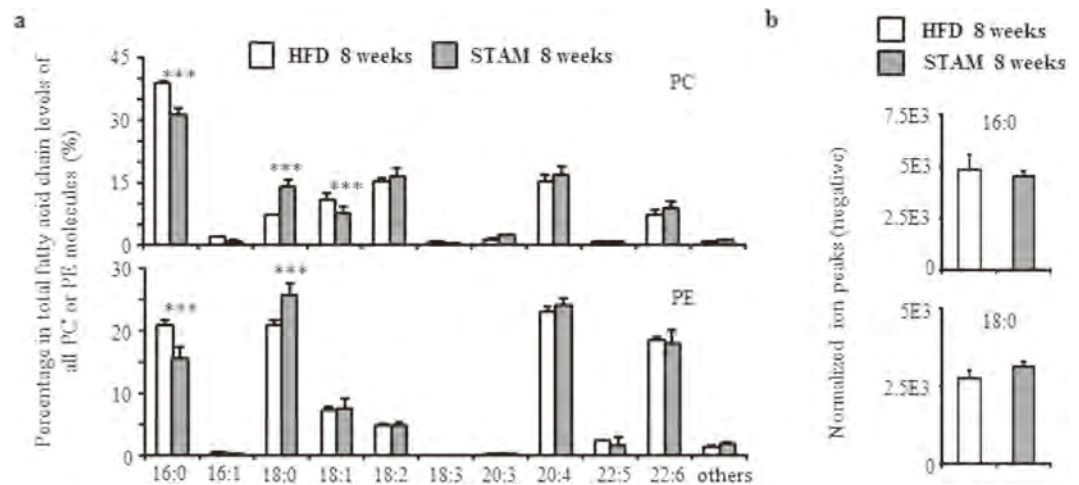


**Figure 3. Fatty acid levels between 8-week old HFD and STAM mice. a,** Abundance of each fatty acid as percentage of all side chains, calculated as the ratio of the sum of ion peak heights containing the fatty acid to  $2 \times$  the sum of peak heights of all PC or PE (one PC or PE contains two fatty acid chains). Data are mean  $\pm$  SD ( $n = 5$  in each group).  $***p < 0.005$  when comparing control HFD vs. STAM mice. 16:0, palmitate; 16:1, palmitoleate; 18:0, stearate; 18:1, oleate; 18:2 linoleate; 18:3, linolenate; 20:3, eicosatrienoate; 20:4, arachidonate; 22:5, docosapentaenoate; 22:6, docosahexaenoate. **b,** Levels of free palmitate (16:0) and stearate (18:0) expressed as mean  $\pm$  SD ( $n = 5$  in each group).

molecule acts as a secondary messenger to activate protein kinase C (PKC)<sup>35</sup>. Indeed, it has been reported that PKC activation by DG contributes to the development of hepatic cirrhosis<sup>36,37</sup>. Notably, PI, which is a precursor to phosphatidylinositol (4,5)-bisphosphate, increased between 8 and 12 weeks in control HFD mice, but not in STAM mice. Hence, it is possible that DG synthesis from PI is enhanced during progression from NASH to fibrosis, and thus an increase in DG may be a key step in this progression.

Our analysis also detected changes in polyunsaturated PC in STAM mice that were distinct from changes in HFD control mice over the same time frame (from NASH to fibrosis). It has been reported that supplementation with soybean polyunsaturated PC such as 18:2/18:2 PC attenuate hepatic fibrosis<sup>38</sup>. Although the mechanism by which the altered PC levels could induce fibrosis remains to be investigated, polyunsaturated PC could be a novel target for intervention to prevent the fibrosis that follows NASH.

Our present study showed the notable features of hepatic lipidomic status in NASH and fibrosis using STAM mice as a model, in which pathological progression is very similar to that in humans. However, there are still several concerns as to whether the lipidomic status in our model ideally mimics that in human NASH. For example, we used chemical intervention by streptozotocin in the neonatal period of the mice to develop the model. It may be also pointed out that HFD32 contains about 60 kcal% fat, which would be considered very high for humans. However, neonatal streptozotocin treatment is commonly used for generating a model of type 2, but not type 1, diabetes mellitus, and indeed our STAM mice did not show ‘absolute’ insulin deficiency, but ‘relative’ insulin deficiency compared with hyperglycemia. In addition, C16 Cer accumulation in STAM mice may reflect insulin resistance<sup>19</sup>. Therefore, we believe that our model shared common features with human NASH, which is often accompanied by type 2 diabetes mellitus characterized by insulin resistance and relative insulin deficiency. Thus, the lipidomic status in our NASH model, at least in part, would also be relevant for human NASH, although further studies using human subjects will be required.

## Conclusion

In conclusion, our comprehensive lipidomics approach in a mouse model of NASH revealed, for the first time, changes in lipid profile between steatosis and NASH, and between NASH and subsequent fibrosis. Understanding the molecular basis of these changes would be useful to develop novel drugs to prevent or treat NASH and fibrosis.

## Materials and Methods

**Animals.** The NASH model, a STAM mouse, was generated as previously described<sup>18</sup>. Briefly, C57BL/6J mice were purchased from Charles River (Kanagawa, Japan) at 15 days post pregnancy. On the second day after birth, male mice were subjected to a single subcutaneous injection of 200  $\mu$ g streptozotocin (Sigma, MO, USA). Four weeks after injection, mice were fed high fat diet (HFD32, CLEA JAPAN, Tokyo, Japan) *ad libitum* until sacrifice at 8 or 12 weeks. Male mice fed HFD32 without an initial streptozotocin injection were used as control HFD animals. Blood glucose and serum insulin levels were measured by a blood glucose meter (Glutest Ace, Sanwa Chemical, Nagoya, Japan) and Morinaga Ultra Sensitive Mouse/

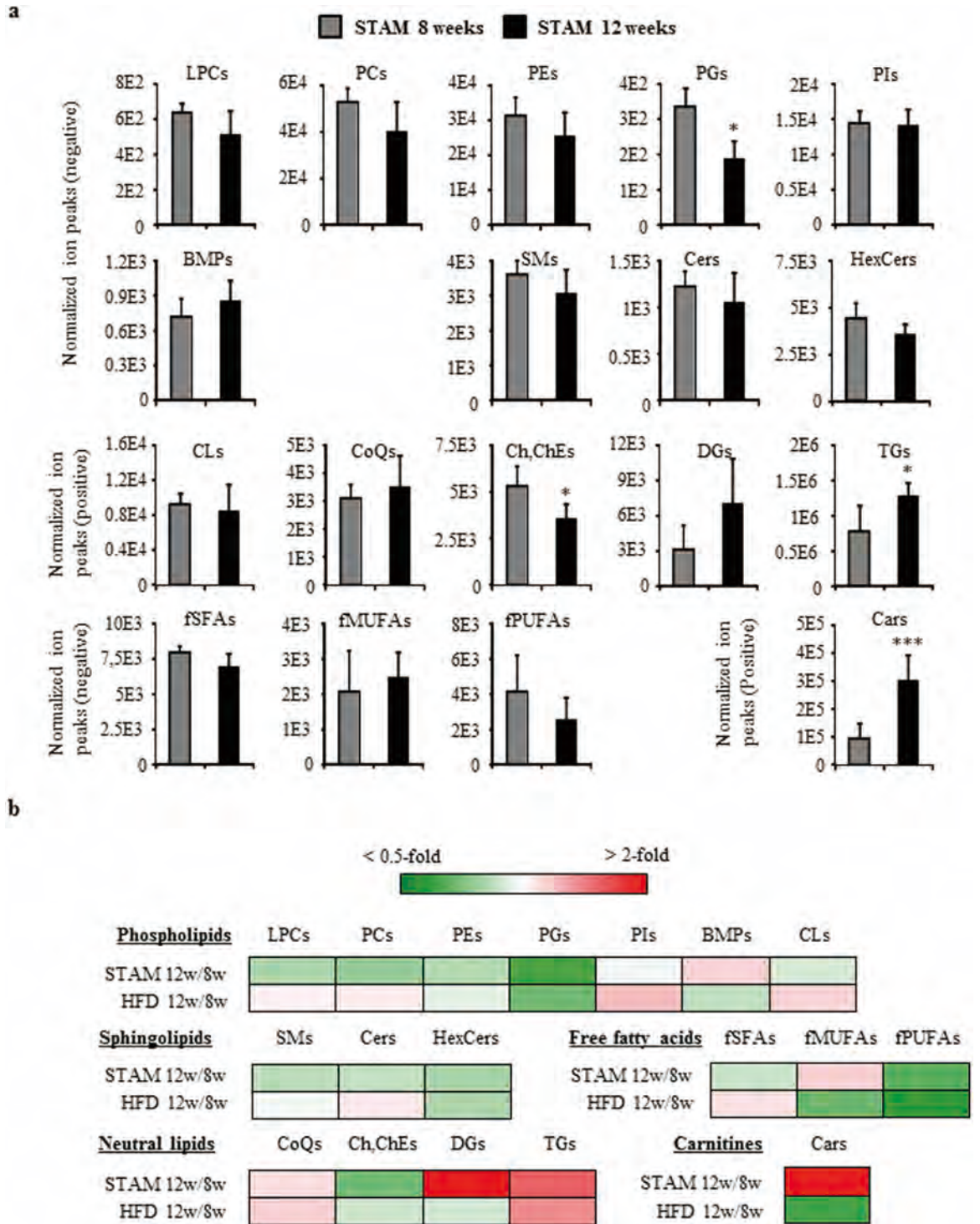


**Figure 4. Global changes in hepatic lipid classes between STAM mice at 8 weeks and 12 weeks. a** Lipid extracts were prepared from mouse livers as described in Materials and Methods, and abundance of individual lipid molecules were measured. Data are sum of ion peak heights of all molecules within each class, and shown as mean  $\pm$  SD ( $n = 5$  in each group).  $*p < 0.05$ ;  $***p < 0.005$  when comparing between STAM mice at 8 weeks and 12 weeks. LPCs, lysophosphatidylcholines; PCs, phosphatidylcholines; PEs, phosphatidylethanolamines; PGs, phosphatidylglycerols; PIs, phosphatidylinositols; BMPs, bis(monoacylglycerol)phosphates; SMs, sphingomyelins; Cers, ceramides; HexCers, hexosylceramides; CLs, cardiolipins; CoQs, coenzyme Qs; Ch/ChEs, cholesterol and cholesterolesters; DGs, diacylglycerols; TGs, triacylglycerols; fSFAs, free saturated fatty acids; fMUFAs, free monounsaturated fatty acids; fPUFAs, free polyunsaturated fatty acids; Cars, acylcarnitines. **b** Heatmap showing fold change in each lipid class between age-matched control HFD and STAM mice. 8 w, mice at 8 weeks; 12 w, mice at 12 weeks.

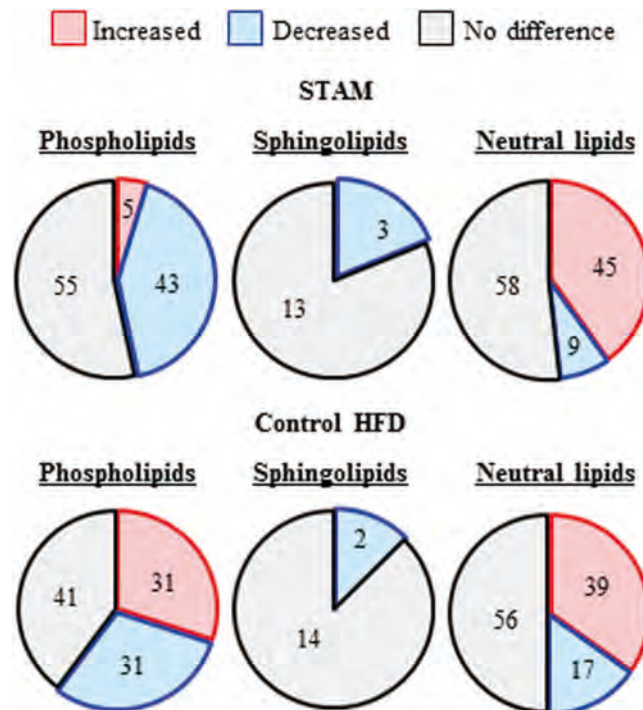


**Figure 5.** Venn diagrams of the number of phospholipids, sphingolipids and neutral lipid molecules that were statistically significantly different in abundance between STAM (upper panel) and HFD (lower panel) mice at 8 and 12 weeks. Increased: 12 weeks > 8 weeks, decreased; 12 weeks < 8 weeks.

Rat Insulin ELISA Kit (Morinaga Institute of Biological Science, Yokohama, Japan), respectively. Animal experiments were conducted according to protocols approved by the Animal Research Committee at Research Institute, National Center for Global Health and Medicine. Mice were maintained according to National Institutes of Health guidelines for care and use of laboratory animals.

**Histology.** Liver samples were fixed in 4% buffered paraformaldehyde, embedded in paraffin, stained with hematoxylin and eosin or Masson's trichrome, and examined by light microscopy as previously described<sup>18</sup>. NAFLD activity score was calculated according to Kleiner *et al.* (2005)<sup>39</sup>. Results were determined as means of three different fields in each section.

**Analysis of global lipid metabolites.** Lipid extraction from 10 mg liver tissue was performed as described previously<sup>16</sup>. Lipid extracts were loaded into UPLC-TOFMS (Waters, Milford, MA) to measure phospholipids, sphingolipids and neutral lipids as described previously<sup>16</sup>, and free fatty acids and Cars as follows. Free fatty acids and Cars from 5  $\mu$ L lipid extracts were separated on an ACQUITY UPLC HSS T3 (2.1  $\times$  100 mm, 1.8  $\mu$ m) column (Waters). Solvent A and B were acetonitrile-water (2:3) and acetonitrile-isopropanol (1:9), respectively, with 0.1% formic acid and 0.1% of 28% ammonium hydroxide. The initial mobile phase was 27% solvent B at a flow rate of 70  $\mu$ L min<sup>-1</sup>. A linear gradient to solvent B was run initially to 60% over 10 min, then to 80% over the next 10 min, then to 90% over another 10 min, and finally 100% solvent B over 10 min. The column was held in 100% solvent B for 15 min before re-equilibration to the initial mobile phase. The MS was operated in V-optic mode with setting scan range at 100–600 m/z from 5 to 25 min, and two functions, negative and positive ion modes, were simultaneously recorded. The MS parameters for free fatty acids and Cars were consistent with those for phospholipids, sphingolipids and neutral lipids.

UPLC-TOFMS raw data were processed using 2DICAL software (Mitsui Knowledge Industry, Tokyo, Japan), which allows detection and alignment of ion peaks of every biomolecule obtained at specific m/z and column retention time. The main parameters in 2DICAL were set as described previously<sup>16</sup> with mass range from 250 to 500 m/z. Identification of ion peaks was performed as described previously<sup>16</sup>. Intensities of ion peaks (heights) were normalized to the following internal standards: 16:0/16:0 PC-d6 (Loradan, Malmo, Sweden) for phospholipids and sphingolipids in negative ion mode; 12:0/12:0 PE (Avanti Polar Lipid, Alabaster, AL) for Cars in positive ion mode; 16:0 lysophosphatidylcholine-d3 (Loradan) for free fatty acids in negative ion mode; and 8:0/8:0/18:2 TG (Loradan) for cardiolipin and neutral lipids in positive ion mode. Standards were added to liver homogenate prior to lipid extraction.

**Determination of fatty acid side chains in phospholipids and ceramides.** Determination of fatty acid side chains in phospholipids was performed by LC-Fourier Transform Mass Spectrometry (LC-FTMS, LTQ Orbitrap XL, Thermo Fisher Scientific, Waltham, MA) as described previously<sup>40</sup>.

**Analysis of arachidonate metabolites.** Extraction of arachidonate metabolites was performed as described previously<sup>16</sup>. Subsequently, metabolites were subjected to targeted analysis as described previously<sup>17</sup> using a UPLC-5500QTRAP triple quadrupole-linear ion trap hybrid mass spectrometer (AB SCIEX, Framingham, MA). Intensities of ion peaks (areas) were normalized to internal standards (Leukotriene B<sub>4</sub>-d<sub>4</sub>, Cayman Chemical, Ann Arbor, MI), which were added to liver homogenate before metabolite extraction.

**Statistics.** Body weight, liver weight, fasting blood glucose, and NAFLD activity scores are expressed as mean ± SE. To compare metabolite levels, statistical analyses of lipidomics data were performed using the Mann-Whitney U-test. Analyses were carried out using R statistical environment software (<http://r-project.org/>). In our analyses,  $p < 0.05$  represents statistical significance.

## References

- Browning, J. D. *et al.* Prevalence of hepatic steatosis in an urban population in the United States: impact of ethnicity. *Hepatology* **40**, 1387–1395 (2004).
- Yoshiike, N. & Lwin, H. Epidemiological aspects of obesity and NASH/NAFLD in Japan. *Hepatol. Res.* **33**, 77–82 (2005).
- Zelber-Sagi, S., Nitzan-Kaluski, D., Halpern, Z. & Oren, R. Prevalence of primary non-alcoholic fatty liver disease in a population-based study and its association with biochemical and anthropometric measures. *Liver Int.* **26**, 856–863 (2006).
- Clark, J. M. The epidemiology of nonalcoholic fatty liver disease in adults. *J. Clin. Gastroenterol.* **40**, S5–S10 (2006).
- Bugianesi, E. *et al.* Expanding the natural history of nonalcoholic steatohepatitis: from cryptogenic cirrhosis to hepatocellular carcinoma. *Gastroenterology* **123**, 134–140 (2002).
- Day, C. P. & James, O. F. Steatohepatitis: a tale of two “hits”? *Gastroenterology* **114**, 842–845 (1998).
- Dowman, J. K., Tomlinson, J. W. & Newsome, P. N. Pathogenesis of non-alcoholic fatty liver disease. *QJM* **103**, 71–83 (2010).
- Nehra, V., Angulo, P., Buchman, A. L. & Lindor, K. D. Nutritional and metabolic considerations in the etiology of nonalcoholic steatohepatitis. *Dig. Dis. Sci.* **46**, 2347–2352 (2001).
- Puri, P. *et al.* The plasma lipidomic signature of nonalcoholic steatohepatitis. *Hepatology* **50**, 1827–1838 (2009).
- Kurikawa, N. *et al.* A novel inhibitor of stearoyl-CoA desaturase-1 attenuates hepatic lipid accumulation, liver injury and inflammation in model of nonalcoholic steatohepatitis. *Biol. Pharm. Bull.* **36**, 259–267 (2013).
- Matsuzaka, T. *et al.* Elovl6 promotes nonalcoholic steatohepatitis. *Hepatology* **56**, 2199–2208 (2012).
- Han, X. & Gross, R. W. Shotgun lipidomics: electrospray ionization mass spectrometric analysis and quantitation of cellular lipidomes directly from crude extracts of biological samples. *Mass Spectrom. Rev.* **24**, 367–412 (2005).
- Taguchi, R., Nishijima, M. & Shimizu, T. Basic analytical systems for lipidomics by mass spectrometry in Japan. *Methods Enzymol.* **432**, 185–211 (2007).
- Hu, C. *et al.* Analytical strategies in lipidomics and applications in disease biomarker discovery. *J. Chromatogr. B* **877**, 2836–2846 (2009).
- Zhao, C. *et al.* Integrated lipidomics and transcriptomic analysis of peripheral blood reveals significantly enriched pathways in type 2 diabetes mellitus. *BMC Med. Genomics* **6**, S12 (2013).
- Maekawa, K. *et al.* Global metabolomic analysis of heart tissue in a hamster model for dilated cardiomyopathy. *J. Mol. Cell Cardiol.* **59**, 76–85 (2013).
- Tajima, Y. *et al.* Lipidomic analysis of brain tissues and plasma in a mouse model expressing mutated human amyloid precursor protein/tau for Alzheimer’s disease. *Lipids Health Dis.* **12**, 68 (2013).
- Fujii, M. *et al.* A murine model for non-alcoholic steatohepatitis showing evidence of association between diabetes and hepatocellular carcinoma. *Med. Mol. Morphol.* **46**, 141–152 (2013).
- Summers, S. A. Ceramides in insulin resistance and lipotoxicity. *Prog. Lipid Res.* **45**, 42–72 (2006).
- Teichgräber, V. *et al.* Ceramide accumulation mediates inflammation, cell death and infection susceptibility in cystic fibrosis. *Nat. Med.* **14**, 382–391 (2008).
- Colombini, M. Ceramide channels and their role in mitochondria-mediated apoptosis. *Biochim. Biophys. Acta.* **1797**, 1239–1244 (2010).
- Shea, B. S. & Tager, A. M. Sphingolipid regulation of tissue fibrosis. *Open Rheumatol. J.* **6**, 123–129 (2012).
- Ziobro, R., Henry, B., Edwards, M. J., Lentsch, A. B. & Gulbins, E. Ceramide mediates lung fibrosis in cystic fibrosis. *Biochem. Biophys. Res. Commun.* **434**, 705–709 (2013).
- Listenberger, L. L. *et al.* Triglyceride accumulation protects against fatty acid-induced lipotoxicity. *Proc. Natl. Acad. Sci. USA* **100**, 3077–3082 (2003).
- Zammit, V. A. Hepatic triacylglycerol synthesis and secretion: DGAT2 as the link between glycaemia and triglyceridaemia. *Biochem. J.* **451**, 1–12 (2013).
- Dorn, C. *et al.* Expression of fatty acid synthase in nonalcoholic fatty liver disease. *Int. J. Clin. Exp. Pathol.* **3**, 505–514 (2010).
- Chakravarthy, M. V. *et al.* Identification of a physiologically relevant endogenous ligand for PPAR $\alpha$  in liver. *Cell* **138**, 476–488 (2009).
- Liu, S. *et al.* A diurnal serum lipid integrates hepatic lipogenesis and peripheral fatty acid use. *Nature* **502**, 550–554 (2013).
- Dreyer, C. *et al.* Positive regulation of the peroxisomal  $\beta$ -oxidation pathway by fatty acids through activation of peroxisome proliferator-activated receptors (PPAR). *Biol. Cell* **77**, 67–76 (1993).
- Higuchi, S. *et al.* IL-4 mediates dicloxacillin-induced liver injury in mice. *Toxicol. Lett.* **200**, 139–145 (2011).
- Čavar, I., Kelava, T., Pravdić, D. & Čulo, F. Anti-thromboxane B<sub>2</sub> antibodies protect against acetaminophen-induced liver injury in mice. *J. Xenobiotics* **1**, e8 (2011).
- Yu, J. *et al.* COX-2 induction in mice with experimental nutritional steatohepatitis: Role as pro-inflammatory mediator. *Hepatology* **43**, 826–836 (2006).
- Williams, C. S., Mann, M. & DuBois, R. N. The role of cyclooxygenases in inflammation, cancer, and development. *Oncogene* **18**, 7908–7916 (1999).
- Cheng, A. S. *et al.* Expression of HBx and COX-2 in chronic hepatitis B, cirrhosis and hepatocellular carcinoma: implication of HBx in upregulation of COX-2. *Mod. Pathol.* **17**, 1169–1179 (2004).
- Berridge, M. J. Inositol trisphosphate and diacylglycerol as second messengers. *Biochem. J.* **220**, 345–360 (1984).

36. Jeong, D. H. *et al.* Subcellular redistribution of protein kinase C isozymes is associated with rat liver cirrhotic changes induced by carbon tetrachloride or thioacetamide. *J. Gastroenterol. Hepatol.* **16**, 34–40 (2001).
37. Di Sario, A. *et al.* Selective Na<sup>+</sup>/H<sup>+</sup> exchange inhibition by cariporide reduces liver fibrosis in the rat. *Hepatology* **37**, 256–266 (2003).
38. Lieber, C. S., DeCarli, L. M., Mak, K. M., Kim, C. I. & Leo, M. A. Attenuation of alcohol-induced hepatic fibrosis by polyunsaturated lecithin. *Hepatology* **12**, 1390–1398 (1990).
39. Kleiner, D. E. *et al.* Design and validation of a histological scoring system for nonalcoholic fatty liver disease. *Hepatology* **41**, 1313–1321 (2005).
40. Taguchi, R. & Ishikawa, M. Precise and global identification of phospholipid molecular species by an Orbitrap mass spectrometer and automated search engine Lipid Search. *J. Chromatogr. A* **1217**, 4229–4239 (2010).

### Acknowledgements

The authors thank Ms. C. Sudo (NIHS) for secretarial assistance; Dr. K. Ikeda (RIKEN), Dr. H. Nakanishi (Akita University) and Dr. M. Arita (RIKEN) for LC-MS technical support; Ms. Y. Tajima, Ms. M. Inoue and Mr. Y. Senoo (NIHS) for experimental and analytical support; and Dr. M. Hiramoto, and Dr. W. Nishimura (NCGM) for suggestions and helpful discussion. This work was supported by Advanced Research for Products Mining Program (Grant number 10–44 and 10–45) from the National Institute of Biomedical Innovation of Japan; the Health Labour Sciences Research Grants (H26-SOUYAKU-IPPAN-008) from the Ministry of Health, Labour and Welfare of Japan; a grant from the Japan Society for the Promotion of Sciences (JSPS) Grants-in-Aid for Scientific Research (KAKENHI), and a grant from National Center for Global Health and Medicine.

### Author Contributions

K.M., R.T., T.N.-M., K.Y. and Y.Sa. designed experiments. K.S., T.U., K.M., M.I., H.U. and H.Y. performed experiments. K.S., T.U., K.M., M.I., T.N., M.F., Y.Sh., H.Y. and KY. performed data analysis. K.S. and K.Y. wrote the paper. All authors reviewed and critically revised the paper.

### Additional Information

**Supplementary information** accompanies this paper at <http://www.nature.com/srep>

**Competing financial interests:** The authors declare no competing financial interests.

**How to cite this article:** Saito, K. *et al.* Characterization of hepatic lipid profiles in a mouse model with nonalcoholic steatohepatitis and subsequent fibrosis. *Sci. Rep.* **5**, 12466; doi: 10.1038/srep12466 (2015).

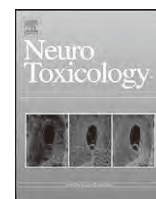


This work is licensed under a Creative Commons Attribution 4.0 International License. The images or other third party material in this article are included in the article's Creative Commons license, unless indicated otherwise in the credit line; if the material is not included under the Creative Commons license, users will need to obtain permission from the license holder to reproduce the material. To view a copy of this license, visit <http://creativecommons.org/licenses/by/4.0/>



Contents lists available at SciVerse ScienceDirect

## NeuroToxicology



## Exposure to low-dose barium by drinking water causes hearing loss in mice

Nobutaka Ohgami<sup>a</sup>, Sohjiro Hori<sup>a</sup>, Kyoko Ohgami<sup>a</sup>, Haruka Tamura<sup>a</sup>, Toyonori Tsuzuki<sup>b</sup>, Shoko Ohnuma<sup>a</sup>, Masashi Kato<sup>a,\*</sup><sup>a</sup> Unit of Environmental Health Sciences, Department of Biomedical Sciences, College of Life and Health Sciences, Chubu University, 1200 Matsumoto, Kasugai, Aichi 487-8501, Japan<sup>b</sup> Department of Pathology, Nagoya Daini Red Cross Hospital, Nagoya, Japan

## ARTICLE INFO

## Article history:

Received 4 April 2012

Accepted 26 July 2012

Available online 3 August 2012

## Keywords:

Barium  
Oral exposure  
Hearing loss  
Inner ears  
Degeneration

## ABSTRACT

**Purpose:** We continuously ingest barium as a general element by drinking water and foods in our daily life. Exposure to high-dose barium (>100 mg/kg/day) has been shown to cause physiological impairments. Direct administration of barium to inner ears by vascular perfusion has been shown to cause physiological impairments in inner ears. However, the toxic influence of oral exposure to low-dose barium on hearing levels has not been clarified *in vivo*. We analyzed the toxic influence of oral exposure to low-dose barium on hearing levels and inner ears in mice.

**Experimental design:** We orally administered barium at low doses of 0.14 and 1.4 mg/kg/day to wild-type ICR mice by drinking water. The doses are equivalent to and 10-fold higher than the limit level (0.7 mg/l) of WHO health-based guidelines for drinking water, respectively. After 2-week exposure, hearing levels were measured by auditory brain stem responses and inner ears were morphologically analyzed. After 2-month exposure, tissue distribution of barium was measured by inductively coupled plasma mass spectrometry.

**Results:** Low-dose barium in drinking water caused severe hearing loss in mice. Inner ears including inner and outer hair cells, stria vascularis and spiral ganglion neurons showed severe degeneration. The Barium-administered group showed significantly higher levels of barium in inner ears than those in the control group, while barium levels in bone did not show a significant difference between the two groups. Barium levels in other tissues including the cerebrum, cerebellum, heart, liver and kidney were undetectably low in both groups.

**Conclusions:** Our results demonstrate for the first time that low-dose barium administered by drinking water specifically distributes to inner ears resulting in severe ototoxicity with degeneration of inner ears in mice.

© 2012 Elsevier Inc. All rights reserved.

## 1. Introduction

Barium has been detected in raw surface waters and public drinking water supplies at levels ranging from  $\leq 5$  to 15,000  $\mu\text{g/l}$  (ATSDR, 2005; Calabrese, 1977; EPA, 2002, 2005). Barium has also been found in soil and foods such as Brazil nuts, seaweed, fish and some plants. Thus, barium is one of the general elements found in drinking water and foods. However, it has been thought that the

amounts of barium found in food and water are not a health concern.

The toxic influence of exposure to barium has been investigated in previous studies. Oral exposure to barium had no neurotoxic influence on weight or histopathology of the brain in rats or mice in the following studies: acute exposure of rats for several days to barium at 198 mg/kg/day as barium chloride (Borzelleca et al., 1988), oral exposure of rats to barium at 115 mg/kg/day in drinking water (McCauley et al., 1985; NTP, 1994; Tardiff et al., 1980), oral exposure of mice to barium at less than 450 mg/kg/day as barium chloride in drinking water (NTP, 1994) and chronic exposure of rats and mice to barium at more than 60 or 160 mg/kg/day as barium chloride in drinking water (NTP, 1994). Furthermore, after oral exposure to barium chloride at 70 or 110 mg barium/kg/day for 15 or 90 days, no abnormal changes in neurobehavioral performances including spontaneous motor activity, grip strength and tail flick were observed in rats and mice (NTP, 1994). On the other hand,

**Abbreviations:** ABR, auditory brainstem response; ICP-MS, inductively coupled plasma-mass spectrometry.

\* Corresponding author at: Unit of Environmental Health Sciences, Department of Biomedical Sciences, College of Life and Health Sciences, Chubu University, Chubu University (No. 50 Building, 11F), 1200 Matsumoto, Kasugai, Aichi 487-8501, Japan. Tel.: +81 568 51 7364; fax: +81 568 51 9635.

E-mail address: katomasa@isc.chubu.ac.jp (M. Kato).

0161-813X/\$ – see front matter © 2012 Elsevier Inc. All rights reserved.  
http://dx.doi.org/10.1016/j.neuro.2012.07.008

exposure to barium at 180 mg/kg/day and 495 mg/kg/day had significant effects on spontaneous motor activity in female rats and mice, respectively (NTP, 1994). Other than neurotoxic effects, previous *in vivo* studies showed increase in blood pressure in mice treated with 100 mg/l of barium for 16 months (Perry et al., 1983) and significant increases in kidney weights in female rats exposed to 115 or 180 mg barium/kg/day and in males exposed to 200 mg barium/kg/day (NTP, 1994). A significant decrease in survival rate with lymphoid depletions in the spleen, thymus and lymph nodes has been reported in mice treated with 2500 mg/l of barium for 15 months (NTP, 1994). Thus, these previous studies suggest that oral exposure to high-dose barium (>100 mg/kg/day) affects physiological functions in experimental animals. However, the toxic influence of oral exposure to low-dose barium has not been clarified in an *in vivo* study.

The inner ears containing the organ of Corti and stria vascularis (SV) play an important role in hearing. The organ of Corti in inner ears, which consists of two kinds of sensory cells [inner hair cells (IHCs) and outer hair cells (OHCs)], is responsible for mechanotransduction, by which sound impulses are converted into neural impulses. Auditory information from the sensory cells is transmitted to spiral ganglion neurons (SGNs) as the primary carrier, followed by eventual transmission to the auditory cortex (Lalwani and Gürtler, 2008). In electrophysiological studies, barium has been used as an analytic tool for potassium channels, and direct administration of barium to inner ears by vascular perfusion has been shown to inhibit potassium channels expressed in inner ears (Takeuchi and Ando, 1999; Takeuchi et al., 2000). Since potassium channels expressed in inner ears are crucial for hearing (Rozengurt et al., 2003), it is possible that barium affects hearing levels if barium administered by drinking water is distributed to inner ears. However, there is no information *in vivo* about the toxic influence of oral exposure to barium administered by drinking water on hearing levels.

Previous studies on the tissue distribution of barium in humans have shown that barium is distributed mainly in the bone with small amounts in muscle, adipose, skin and connective tissue (Bauer et al., 1957; Losee et al., 1974; Miller et al., 1985; Schroeder et al., 1972; Sowden, 1958; Sowden and Pirie, 1958; Sowden and Stitch, 1957). The tissue distribution of barium after oral administration has also been investigated. Ingestion of diets with equivalent doses of barium chloride or barium from Brazil nuts for about 1 month significantly increased the levels of barium in bone in rats. The barium concentration in Brazil nuts can be as high as 4000 mg/kg (Stoewsand et al., 1988). In addition, acute exposure to radiolabeled barium chloride and barium carbonate in drinking water for 24 h resulted in significant distribution of barium to the heart, eyes, skeletal muscle, kidney, blood and liver in rats (McCaughey and Washington, 1983). Thus, these previous studies suggest that chronic oral exposure to high-dose barium results in distribution of barium mainly to bone, while acute exposure to radiolabeled barium results in distribution to tissues ubiquitously. However, there is no information about accumulation levels of barium in inner ears after oral exposure to low-dose barium.

In this study, in order to determine the toxic influence of exposure to low-dose barium on hearing levels in mice, we orally administered barium to mice at 0.14 and 1.4 mg/kg/day, based on results of previous studies on barium in drinking water, and analyzed hearing levels, morphological influence on inner ears and tissue distribution of barium to inner ears in mice.

## 2. Materials and methods

### 2.1. Mice and exposure to barium

Randomly bred wild-type female mice (ICR) at 3 weeks of age were used for exposure experiments. Mice were exposed for 2

weeks or for 2 months to barium chloride (Wako) at 0.14 and 1.4 mg/kg/day by drinking water. We performed hearing measurements and morphological analyses at 5 weeks of age and determination of barium contents at 11 weeks of age. These doses are equivalent to and 10-fold higher than the limit level (0.7 mg/l) of World Health Organization (WHO) health-based guidelines for drinking water, respectively. Our regular monitoring of intake of drinking water and food by the mice and body weights during exposure showed that a mouse (20–25 g in body weight) ingests about 4–5 ml water per day and that mice treated with barium and those not treated with barium showed no significant difference in intake of both food and water and body weights. Mice were housed under specific pathogen-free (SPF) conditions at a constant temperature ( $23 \pm 2$  °C) and a 12-h light/dark cycle. All experiments were authorized by the Institutional Animal Care and Use Committee in Chubu University (approval number: 2210038) and followed the Japanese Government Regulations for Animal Experiments.

### 2.2. Determination of barium contents

Measurements of barium concentrations were performed as described previously (Kato et al., 2010; Thang et al., 2011). In brief, various tissues (100–300 mg, wet weight) collected from mice were minced using a Multi-bead shocker with zirconia beads (Yasui Kikai, Japan). Homogenized tissues were placed in a 15 ml polyethylene tube in the presence of 3 ml of nitric acid (61%). The tubes were capped and incubated at 80 °C for 3 h, followed by cooling for 1 h to room temperature. After cooling, 3 ml of hydrogen peroxide (30%) was added to each tube, followed by incubation at 80 °C for 3 h. After suitable dilution of the digested materials with Milli-Q water, barium level was determined by inductively coupled plasma mass spectrometry (ICP-MS, Agilent 7500cx). In our measurements with ICP-MS, barium level in drinking water of a breeding room in our facility was 4.29 µg/l.

### 2.3. Measurement of hearing

Auditory brainstem response (ABR) measurements (AD Instruments Pty. Ltd.) were performed as described previously (Ida-Eto et al., 2011; Ohgami et al., 2010, 2012). Tone burst stimuli were measured 5 dB-stepwise from 0 dB sound pressure level (SPL) to 90 dB SPL. The threshold was obtained by identifying the lowest level of the I wave of ABR recognized. Data are presented as means  $\pm$  SD.

### 2.4. Morphological analyses with a light microscope

Morphological analyses were performed as described previously (Ida-Eto et al., 2011; Ohgami et al., 2010, 2012). In brief, after perfusion fixation by Bouin's solution, inner ears from mice were immersed in the same solution for 3 days to 1 week at 4 °C. Kluver–Barrera's staining was performed with paraffin serial sections. Estimation of the cell density of SGNs with Kluver–Barrera's staining basically followed the previous method (Lang et al., 2006; Ohgami et al., 2010; Shimada et al., 1992). In brief, the area of Rosenthal's canal in 5 sections from each mouse was measured with the software program WinROOF (ver. 6.5, Mitani, Japan). The cell density of SGNs from 3 or 4 mice was calculated by dividing the cell number of SGNs in the measured Rosenthal's canal by the area. A total of 160–200 SGNs in 5 sections from each mouse were examined.

### 2.5. Morphological analyses by electron microscopy

Preparation of tissues for transmission electron microscopy basically followed the previous method (Ida-Eto et al., 2011; Ohgami et al., 2010, 2012). In brief, after perfusion fixation with a

mixture of 2% paraformaldehyde and 2% glutaraldehyde in 0.3 M HEPES-buffer (pH 7.4), dissected murine cochleae were immersed in the same fixative solution overnight at 4 °C. The cochleae were then fixed with 2% osmium tetroxide in 0.3 M HEPES-buffer (pH 7.4) at 4 °C for 3 h. After rinsing off the fixative solution, the cochleae were dehydrated with a graded series of ethanol and embedded in epoxy resin (Quetol 651, Nisshin EM, Japan). Ultrathin sections (thickness = 70 nm) were observed under an electron microscope at 80 kV (JEOL JEM1200EX, Tokyo, Japan). For scanning electron microscopy, 2% glutaraldehyde and 2% paraformaldehyde-fixed inner ears were microdissected, stepwise dehydrated in ethanol solutions, and eventually dried up to a critical point. Prepared inner ears were then mounted on aluminum stubs with colloidal silver adhesive and sputter-coated with gold palladium before imaging in a Hitachi S-800s scanning electron microscope.

2.6. Statistics

Significant difference (\*\**P* < 0.01; \**P* < 0.05) from the control was analyzed by the Mann–Whitney *U* test (Figs. 1, 3 and 5) (Ohgami et al., 2011).

3. Results

3.1. Influence of barium administered by drinking water on hearing levels

We first analyzed the influence of barium administered by drinking water on hearing levels in mice. Before administration, all of 3-week-old mice showed comparable hearing levels (Fig. 1A). Corresponding to the results of a previous study in

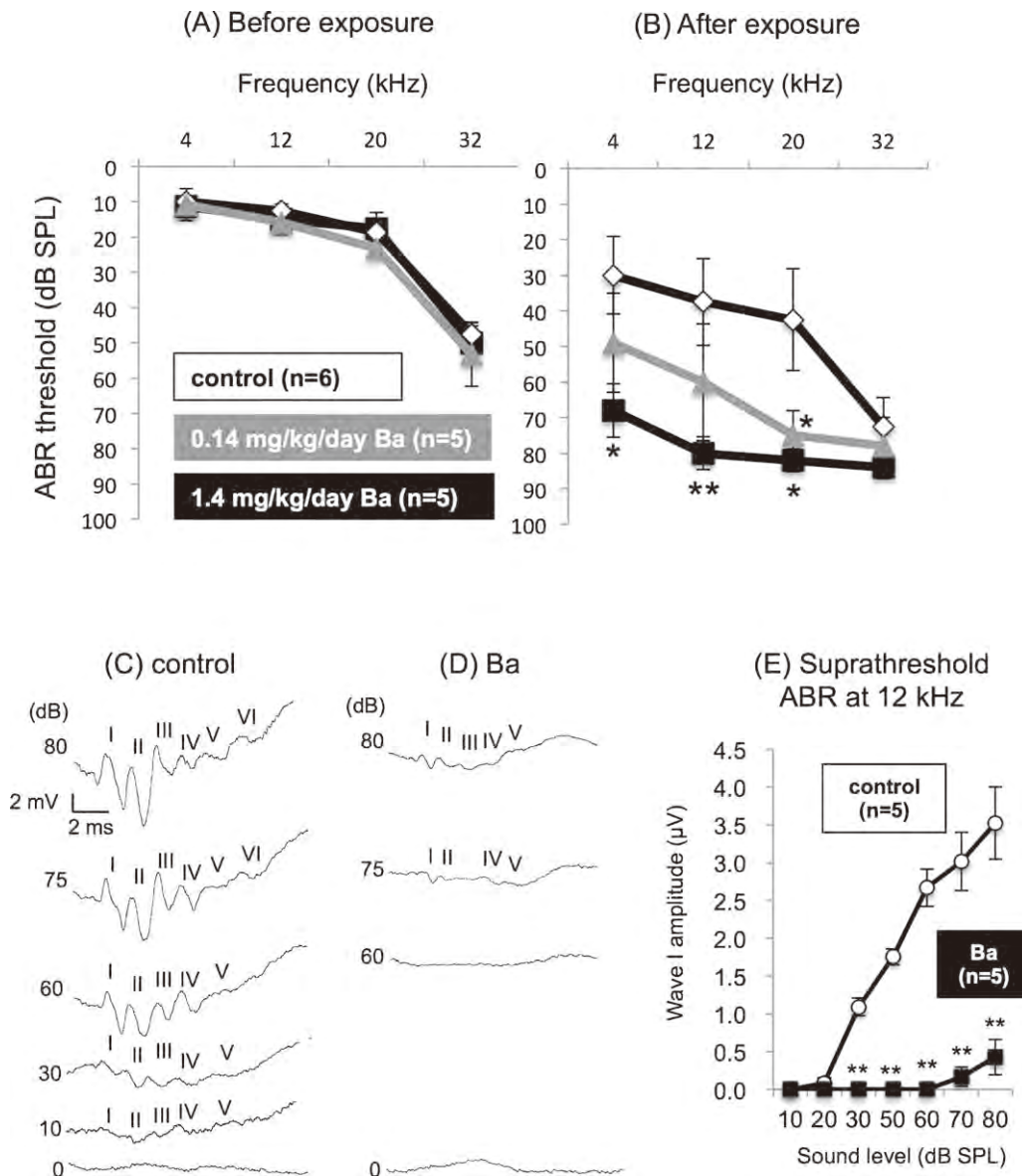


**Fig. 1.** Influence of barium administered by drinking water on hearing levels. (A, B) Hearing levels (mean ± SD) of mice before (A) and after (B) administration of drinking water only (shown as control; white diamonds; *n* = 6), barium at 0.14 mg/kg/day (shown as 0.14 mg/kg/day Ba; gray triangles; *n* = 5) and barium at 1.4 mg/kg/day (shown as 1.4 mg/kg/day Ba; black squares; *n* = 5) for 2 weeks. Hearing levels were measured by auditory brainstem response (ABR). (C, D) ABR waveforms at 0–80 dB SPL of 12 kHz sound after administration of (C) drinking water only (shown as control) and (D) barium at 1.4 mg/kg/day (shown as Ba) for 2 weeks. 10 dB SPL of 12 kHz sound showed ABR waves (I–V) in control mice (C), while ABR waves in barium-treated mice were undetectable up to 60 dB SPL (D). (E) Suprathreshold ABR analysis after administration of drinking water only (shown as control; white circles, *n* = 5) and barium at 1.4 mg/kg/day (shown as Ba; black squares; *n* = 5) to mice for 2 weeks. The amplitude versus sound level relationship (means ± SD) of the 12 kHz wave I obtained during ABR analysis was plotted. Significant difference (\*\**P* < 0.01; \**P* < 0.05) from the control was analyzed by the Mann–Whitney *U* test.

which hearing levels of ICR mice were measured (Drayton and Noben-Trauth, 2006), progressive hearing loss was observed in the control group ( $n = 6$ ) (Fig. 1A–C). Mice in the control group started to suffer from progressive hearing loss especially at a high-pitch sound (20–32 kHz) at 5 weeks of age (Fig. 1B). Administration of barium at 0.14 mg/kg/day for 2 weeks to mice ( $n = 5$ ) worsened hearing loss especially at 20 kHz compared to that in the control group ( $n = 6$ ) (Fig. 1B). Mice administered barium at 1.4 mg/kg/day ( $n = 5$ ) showed severe hearing loss at 1–20 kHz compared to that in the control group ( $n = 6$ ) and 0.14 mg/kg/day barium-treated group ( $n = 5$ ) (Fig. 1B–D), while hearing levels at 32 kHz were comparable among the groups (Fig. 1B). The suprathreshold ABR, which has been shown to reflect auditory nerve activity (Ida-Eto et al., 2011), showed significantly impaired amplitudes *versus* sound levels in 1.4 mg/kg/day barium-treated group (Fig. 1E).

### 3.2. Barium administered by drinking water causes degeneration of inner ears

We next examined the morphological influence of barium on the inner ears including IHCs, OHCs, SGNs and SV in order to analyze the pathogenesis of hearing loss caused by barium administered by drinking water. Barium-administered mice clearly showed deleted hair bundles in OHCs by scanning electron microscopy (SEM) (Fig. 2A, lower panel, arrows and dotted squares). Transmission electron microscopy (TEM) further showed degenerated morphology of intracellular organelles in IHCs and OHCs in the barium-administered group compared to that in the control group (Fig. 2B). Barium-administered mice also showed decreased cell density of SGNs with impaired morphology (Fig. 3A, right panel, arrows and B) compared to those in control mice (Fig. 3A, left panel, arrows and B). TEM analysis further showed gaps between SGNs and Schwann cells (SCs) (Fig. 3C, right panel, arrow) and vacuole degeneration in barium-administered mice (Fig. 3C, right panel, arrowheads), while control mice showed intact cellular membranes (Fig. 3C, left panel, arrow) and mitochondria (Fig. 3C, left panel, arrowheads). The nuclei of SGNs from barium-administered mice exhibited discontinuous nuclear membranes (Fig. 3C, right panel, white arrow), while those from control mice had intact bilayer membranes of nuclei (Fig. 3C, left panel, white arrow). TEM analysis of the SV in barium-administered mice showed impaired morphology (Fig. 4B, right panel, arrow) compared to the equivalent area in control mice (Fig. 4B, left panel).

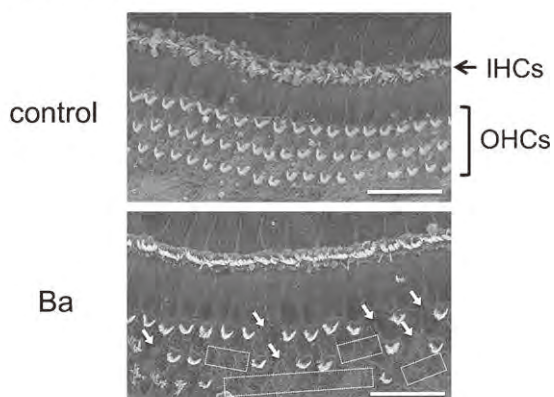
### 3.3. Tissue distribution of barium administered by drinking water

In order to evaluate the relevance between tissue accumulation levels of barium and affected physiological functions (*i.e.*, hearing loss), we finally analyzed tissue distribution of barium administered by drinking water in mice. After administration for 2 months, mice ( $n = 5$ ) showed significantly higher levels of barium in inner ears than those in the control group ( $n = 5$ ), while barium levels in bone did not show a significant difference between the two groups (Fig. 5A). Barium levels in other tissues including the cerebrum, cerebellum, heart, liver and kidney were undetectably low in both groups (Fig. 5A). Mice administered barium at 1.4 mg/kg/day showed increased levels of barium in inner ears compared to the levels in the control group ( $n = 5$ ) and 0.14 mg/kg/day barium-treated group ( $n = 5$ ) (Fig. 5B). We further analyzed the influence of barium on coordinate movement regulated by the cerebellum, in which barium levels were undetectably low. Mice administered barium for 4 weeks at 1.4 mg/kg/day ( $n = 5$ ) showed performance comparable to that of mice in the control group ( $n = 5$ ) (see Supplementary Fig. 1.).

## 4. Discussion

Hearing loss afflicts about 110 million people worldwide. Furthermore, a large number of elderly people worldwide suffer from age-related (late-onset) hearing loss (Lalwani and Gürtler, 2008). Hearing losses develop intricately due to genetic, aging and environmental factors (Lalwani and Gürtler, 2008) and lead to negative impacts on quality of life (QOL) in all generations. As environmental factors causing hearing loss, exposure to heavy metals including mercury, cadmium and arsenic has been shown to affect hearing levels in humans and experimental animals (Ozcaglar et al., 2001; Rice and Gilbert, 1990; Shargorodsky et al., 2011), while exposure to noise is generally known as one of the major environmental factors causing hearing loss in humans and mice (Lalwani and Gürtler, 2008). However, there is limited information about the number of heavy metals affecting hearing

#### (A) SEM of hair cells



#### (B) TEM of hair cells

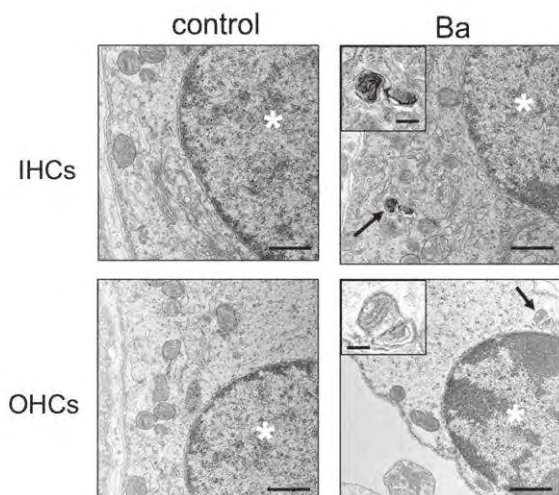


**Fig. 2.** Morphological influence of barium administered by drinking water on hair cells. (A) Scanning electron microscopy (SEM) showed no morphological differences of inner hair cells (IHCs) and outer hair cells (OHCs) at equivalent positions between mice administered barium at 1.4 mg/kg/day (Ba; lower panel) and control mice (control; upper panel). Barium-administered mice showed hair bundle losses in OHCs (lower panel, arrows and dotted squares). Scale bars: 20  $\mu\text{m}$ . (B) Transmission electron microscopy (TEM) for IHCs (upper panels) and OHCs (lower panels) at equivalent positions between mice administered with barium at 1.4 mg/kg/day (Ba; right panels) and control mice (control; left panels). Barium-administered mice showed vacuolar degeneration in IHCs (upper right panel, arrow and inset) and OHCs (lower right panel, arrow and inset), while control mice showed intact morphology in IHCs and OHCs (left panels). Asterisks indicate nuclei. Scale bars: 1  $\mu\text{m}$  and 0.25  $\mu\text{m}$  in insets.

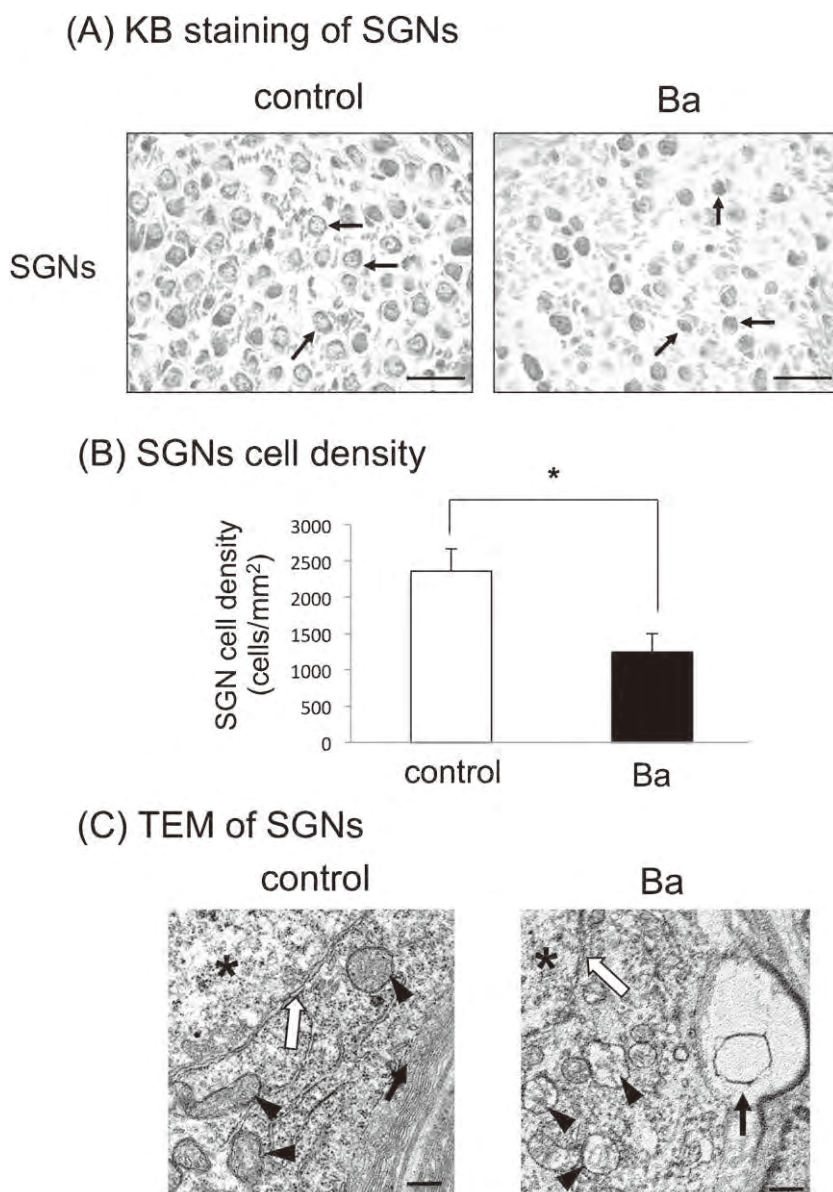
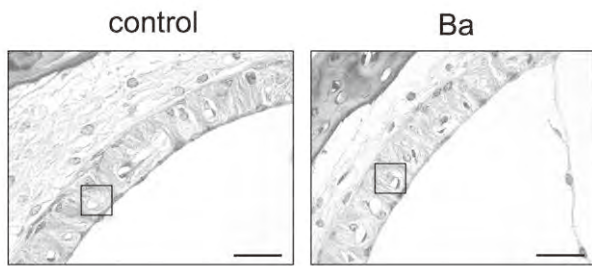


**Fig. 3.** Morphological influence of barium administered by drinking water on spiral ganglion neurons. (A) Morphological analysis for spiral ganglion neurons (SGNs) in the mid turn from mice administered barium at 1.4 mg/kg/day (Ba; right panel) and control mice (control; left panel) by Kluver–Barrera's (KB) staining. Arrows indicate SGNs with normal morphology in control mice (left panel) and with impaired morphology in barium-administered mice (right panel). Scale bars: 20  $\mu$ m. (B) Cell density (mean  $\pm$  SD) of SGNs in the mid turn from barium-administered mice (Ba, black bars,  $n = 3$ ) and control mice (control, white bars,  $n = 3$ ) is presented. The method for staining and estimating the percentage and cell density is described in detail in Section 2. Significant difference ( $*P < 0.05$ ) from the control was analyzed by the Mann–Whitney  $U$  test. (C) Transmission electron microscopy (TEM) for SGNs in the mid turn from barium-administered mice (Ba; right panel) and control mice (control; left panel). Gap areas between SGNs and Schwann cells were observed in barium-administered mice (right panel, black arrow) but not in control mice (left panel, black arrow). Discontinuous nuclear membranes in SGNs from barium-administered mice (right panel, white arrow) and intact nuclear membranes of SGNs from control mice (left panel, white arrow) were observed. Barium-administered mice showed vacuolar degeneration in SGNs (right panel, arrowheads) compared to intact mitochondria in control mice (left panel, arrowheads). Asterisks indicate nucleus. Scale bars: 500 nm.

levels, especially the relevance between exposure to low doses of heavy metals and hearing loss. The doses used in this study were set on the basis of information obtained in previous studies on barium in drinking water (ATSDR, 2005; Calabrese, 1977; EPA, 2002, 2005; Thang et al., 2011), while previous *in vivo* studies showed that administration of barium chloride at more than 100-times higher than the doses used in this study affected physiological functions besides hearing in mice and rats (Dietz et al., 1992; NTP, 1994; Perry et al., 1983). This study demonstrated for the first time that barium at low doses of 0.14 and 1.4 mg/kg/day administered by drinking water is specifically distributed to inner ears and results in hearing loss in mice.

There has been no report about the direct relevance between barium and hearing levels in humans, although this study showed that exposure to low-dose barium caused severe ototoxicity in mice. In this study, we exposed mice to only barium because there is no information about the influence of barium on hearing levels *in vivo*. On the other hand, drinking water and foods contain not only barium but also other elements (Thang et al., 2011). A previous study showed that co-exposure to methylmercury and polychlorinated biphenyls (PCBs) appeared to attenuate PCB-related hearing impairments (Powers et al., 2009). Thus, it is possible that hearing loss caused by exposure to barium can be intricately affected by the presence of other environmental factors. Further investigation is needed to determine the influence of co-exposure

(A) KB staining of SV



(B) TEM of SV

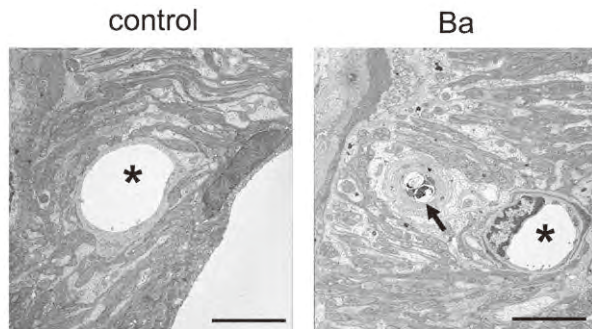
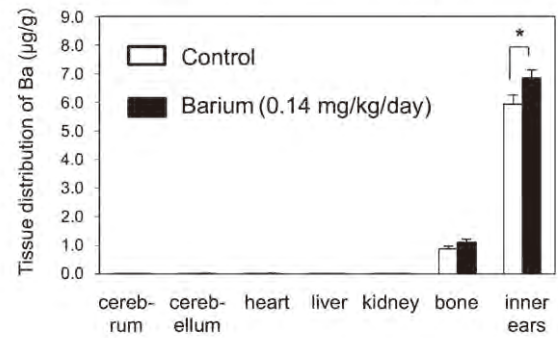


**Fig. 4.** Morphological influence of barium administered by drinking water on stria vascularis. (A) Morphological analysis for the stria vascularis (SV) in the mid turn from mice administered barium at 1.4 mg/kg/day (Ba; right panel) and control mice (control; left panel) by Kluver–Barrera's (KB) staining. Equivalent positions marked with squares were analyzed by transmission electron microscopy (TEM) in (B). Scale bars: 20  $\mu$ m. (B) TEM for the SV in the mid turn from barium-administered mice (Ba; right panel) and control mice (control; left panel). Barium-administered mice showed vacuolar degeneration in intermediate cells of the SV (right panel, arrow) compared to intact mitochondria in the equivalent area from control mice (right panel). Asterisks indicate blood vessel. Scale bars: 5  $\mu$ m.

to barium and other factors on hearing levels in mice and humans. In this study, we used ICR mice, which have been shown to suffer progressive hearing loss (Drayton and Noben-Trauth, 2006), although a hereditary cause has not been clarified. A previous study suggested that exposure to ototoxic factors can affect the rate of progression of hereditary hearing loss (Johnson, 1993). Thus, it is possible that ICR mice have higher sensitivity to ototoxic factors. The rate of progressive hearing loss has been shown to vary in several lines of mice (Drayton and Noben-Trauth, 2006; Noben-Trauth et al., 2003). Differences in susceptibility to ototoxic factors have been shown in different mouse lines and animal species (Johnson, 1993; Poirrier et al., 2010). Therefore, additional investigation is needed to determine the influence of exposure to low-dose barium on hearing levels in other experimental animals.

Tissue distribution analysis in this study demonstrated that low-dose barium administered by drinking water specifically distributed to inner ears. Similar distributions to inner ears of heavy metals known to have ototoxicity including an arsenic-related compound, cadmium and methyl mercury have been shown (Anniko and Plantin, 1977; Konishi and Hamrick, 1979; Ozcaglar et al., 2001). In previous studies, ion channels including an epithelial calcium channel, TRPV6, have been shown to mediate cellular uptake of calcium and barium (Bolanz et al., 2009). In addition, PMCA2 and TRPV6, which mediate cellular uptake of calcium, have been shown to be expressed in inner ears including the SV, OHCs, and support cells (Deiters' cells) for OHCs and SGNs (Lang et al., 2007). These transporters also play important roles in maintenance of hearing levels (Lang et al., 2007). An *in vitro* study showed that TRPV6 mediates cellular uptake of barium and

(A) Tissue distribution of barium administered by drinking water



(B) Tissue distribution of barium to inner ears

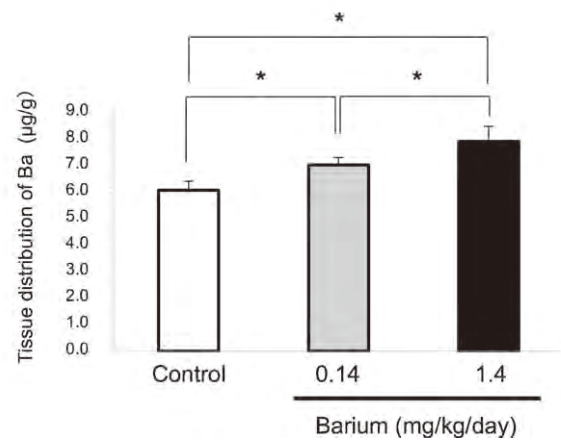


**Fig. 5.** Tissue distribution of barium administered by drinking water. (A) After administration of barium at 0.14 mg/kg/day for 2 months, barium levels (mean  $\pm$  SD) in tissues including the cerebrum, cerebellum, heart, bone and inner ears from mice administered barium (black bars;  $n = 5$ ) and control mice (white bars;  $n = 5$ ) were measured by inductively coupled plasma-mass spectrometry (ICP-MS). (B) After administration of barium for 2 months, barium levels (mean  $\pm$  SD) in inner ears from mice administered barium at 0.14 (gray bars;  $n = 5$ ) and 1.4 mg/kg/day (black bars;  $n = 5$ ) and control mice (white bars;  $n = 5$ ) were measured by ICP-MS. Y-axis stands for barium (Ba) levels calculated by amount of barium (ng) divided by wet tissue weight (g). Significant difference ( $*P < 0.05$ ) from the control was analyzed by the Mann-Whitney  $U$  test.

calcium in MCF7 cells (Bolanz et al., 2009). Meanwhile, barium has been used as an analytical tool for potassium ( $K^+$ ) channels in electrophysiological studies, since barium specifically inhibits  $K^+$  channels. As a matter of fact, an inward rectifier  $K^+$  channel, Kir4.1 (KCNJ10), has been shown to be expressed in intermediate cells of the SV in inner ears (Takeuchi and Ando, 1999; Takeuchi et al., 2000). Kir4.1 has also been shown to be expressed in SGNs and support cells (Deiters' cells) for OHCs as well as intermediate cells of the SV in inner ears (Rozengurt et al., 2003). Thus, it is possible that channels for calcium or  $K^+$  expressed in inner ears contribute to the tissue distribution of barium to inner ears. On the other hand, oral administration of low-dose barium for 2 months did not result in significantly increased levels of barium in bone compared to the levels in inner ears, although the levels in bone in both groups were higher than those in the cerebrum, cerebellum, heart, liver and kidney in mice. A previous study showed that oral administration of high-dose barium for 1 month resulted in distribution of barium to bone in rats (Stoewsand et al., 1988). Therefore, it is possible that longer exposure to low-dose barium could allow bone to accumulate a larger amount of barium. In contrast to inner ears and bone, barium levels in the cerebellum were undetectably low. Correspondingly, influence of barium on

coordinate movement regulated by the cerebellum was not observed in treated mice. Thus, the results of this study indicate the need for further evaluation of the tissue distribution of barium administered by drinking water in order to determine the relevance between accumulation levels of barium in tissues and toxic influence on physiological functions mediated by the tissues.

This study demonstrated for the first time that barium at low doses of 0.14 and 1.4 mg/kg/day administered by drinking water results in development of hearing loss. Exposure to barium at 1.4 mg/kg/day also resulted in degeneration of inner ears including IHCs, OHCs, SV and SGNs, while SEM and TEM showed that morphology of inner ears was comparable between the control group and 2-week exposed group at 0.14 mg/kg/day (data not shown). Further investigation with other approaches including an electrophysiological technique is needed to analyze the etiology of the ototoxicity of barium at 0.14 mg/kg/day. On the other hand, hearing loss caused by barium administered by drinking water partially correspond to results of previous studies showing that direct administration of barium to the SV by vascular perfusion inhibited physiological functions mediated by potassium channel Kir4.1 expressed in inner ears (Takeuchi and Ando, 1999; Takeuchi et al., 2000). Importantly, Kir4.1(–/–) knockout mice have been shown to develop hearing loss with severe degeneration of inner ears including support cells (Deiters' cells) for OHCs, SV and SGNs (Rozengurt et al., 2003). Mice deficient in PMCA2 have also been shown to develop congenital deafness with severe degeneration of similar sites in inner ears (Kozel et al., 1998) as those in Kir4.1(–/–) knockout mice. Thus, it is possible that barium that has accumulated in inner ears leads to degeneration of IHCs, OHCs, SV and SGNs in inner ears by the inhibition of channels or pumps including Kir4.1 or PMCA2 expressed in similar sites of inner ears, resulting in hearing loss.

In summary, this study demonstrated that exposure to barium by drinking water can be one of the environmental factors leading to severe ototoxicity in mice. In previous studies, childhood exposure to heavy metals has been shown to sensitively affect hearing development in humans (Prasher, 2009; Ramirez et al., 2003; Rothenberg et al., 1994). Aging has also been shown to change susceptibility to ototoxic factors in mice (Prieve and Yan, 1984). On the other hand, there is no information about the relevance between age and ototoxicity caused by oral exposure to barium, while previous studies suggested that infants and young children have a higher barium absorption rate than that in adults (ICRP, 1993; Taylor et al., 1962). Therefore, further studies are needed to determine the age-specific sensitivities to low-dose barium in terms of ototoxicity in mice and humans.

## 5. Conclusions

In this study, we demonstrated that barium at low doses of 0.14 and 1.4 mg/kg/day administered orally by drinking water specifically distributed to inner ears resulting in severe hearing loss. Exposure to barium at 1.4 mg/kg/day also resulted in degeneration of inner ears in mice. The doses administered in this study are equivalent to and 10-fold higher than the limit level (0.7 mg/l) of WHO health-based guidelines for drinking water, respectively. Our results indicate for the first time that oral exposure to low-dose barium can cause ototoxicity.

## Conflict of interest statement

The authors declare that there are no conflicts of interest.

## Acknowledgements

We thank Harumi Ohno, Kohichi Nakamura, Midori Yamaguchi and Nozomi Kato for their technical assistance. This study was

supported in part by Grants-in-Aid for Scientific Research (B) (No. 20406003, No. 24390157 and No. 24406002) and (C) (No. 23592479), Grant-in-Aid for Challenging Exploratory Research (No. 23650241) and Grants-in-Aid for Young Scientists (B) (No. 23790160) from the Ministry of Education, Culture, Sports, Science and Technology (MEXT), AA Science Platform Program from the Japan Society for the Promotion of Science (JSPS), Adaptable and Seamless Technology Transfer Program through Target-driven R&D, Japan Science and Technology Agency, COE Project (Health Science Hills) for Private Universities from MEXT and Chubu University (No. S0801055), Mitsui & Co., Ltd. Environment Fund (R08-C097), Research Grant from the Tokyo Biochemical Research Foundation (TBRF), the Naito Foundation Natural Science Scholarship, Research Foundation from the Institute of Science and Technology Research in Chubu University and Chubu University Grants A, B and CG.

## Appendix A. Supplementary data

Supplementary data associated with this article can be found, in the online version, at doi:10.1016/j.neuro.2012.07.008.

## References

- ATSDR (Agency for Toxic Substances and Disease Registry). Toxicological profile for barium. Atlanta, GA: U.S. Department of Health and Human Services, Public Health Service; 2005 [draft for public comment].
- Anniko M, Plantin LO. Delayed elimination of the ototoxic compound atoxyl from the inner ear. *Arch Otorhinolaryngol* 1977;215(1):81–9.
- Bauer GCH, Carlsson A, Lindquist B. Metabolism of <sup>140</sup>Ba in man. *Acta Orthop Scand* 1957;26:241–54.
- Bolanz KA, Kovacs GG, Landowski CP, Hediger MA. Tamoxifen inhibits TRPV6 activity via estrogen receptor-independent pathways in TRPV6-expressing MCF-7 breast cancer cells. *Mol Cancer Res* 2009;7(12):2000–10.
- Borzelleca JF, Condie LW Jr, Egle JL Jr. Short-term toxicity (one- and ten-day gavage) of barium chloride in male and female rats. *J Am Coll Toxicol* 1988;7:675–85.
- Calabrese EJ. Excessive barium and radium-226 in Illinois drinking water. *J Environ Health* 1977;39:366–9.
- Dietz DD, Elwell MR, Davis WE Jr, Meirhenry EF. Subchronic toxicity of barium chloride dihydrate administered to rats and mice in the drinking water. *Fundam Appl Toxicol* 1992;19(4):527–37.
- Drayton M, Noben-Trauth K. Mapping quantitative trait loci for hearing loss in Black Swiss mice. *Hear Res* 2006;212(1–2):128–39.
- EPA (Environmental Protection Agency). National primary drinking water regulations., Washington, DC: Office of Ground Water and Drinking Water; 2002 U.S. EPA816F02013 [accessed 15.02.05] <http://www.epa.gov/safewater/mcl.html>.
- EPA (Environmental Protection Agency). Technical factsheet on: barium. Ground water and drinking water. Washington, DC: U.S. Environmental Protection Agency; 2005 ICRP (International Commission on Radiological Protection). Age-dependent doses to members of the public from intake of radionuclides: part 2. Ingestion dose coefficients. ICRP Publication 67.23 (3/4). New York, NY: Pergamon Press; 1993.
- Ida-Eto M, Ohgami N, Iida M, Yajima I, Kumasaka MY, Takaawa K, et al. Partial requirement of endothelin receptor B in spiral ganglion neurons for postnatal development of hearing. *J Biol Chem* 2011;286(34):29621–6.
- Johnson AC. The ototoxic effect of toluene and the influence of noise, acetyl salicylic acid, or genotype. A study in rats and mice. *Scand Audiol Suppl* 1993;39:1–40.
- Kato M, Onuma S, Kato Y, Thang ND, Yajima I, et al. Toxic elements in well water from Malaysia. *Toxicol Environ Chem* 2010;92:1609–12.
- Konishi T, Hamrick PE. The uptake of methyl mercury in guinea pig cochlea in relation to its ototoxic effect. *Acta Otolaryngol* 1979;88(3–4):203–10.
- Kozel PJ, Friedman RA, Erway LC, Yamoah EN, Liu LH, Riddle T, et al. Balance and hearing deficits in mice with a null mutation in the gene encoding plasma membrane Ca<sup>2+</sup>-ATPase isoform 2. *J Biol Chem* 1998;273(30):18693–6.
- Lalwani AK, Gürtler N. Sensorineural hearing loss, the aging inner ear, and hereditary hearing impairment. In: Lalwani AK, editor. *Current diagnosis & treatment in otolaryngology-head & neck surgery* 2nd ed. McGraw-Hill: New York; 2008, pp. 683–704.
- Lang F, Vallon V, Knipper M, Wangemann P. Functional significance of channels and transporters expressed in the inner ear and kidney. *Am J Physiol Cell Physiol* 2007;293(4):C1187–208.
- Lang H, Schulte BA, Zhou D, Smythe N, Spicer SS, Schmiedt RA. Nuclear factor kappaB deficiency is associated with auditory nerve degeneration and increased noise-induced hearing loss. *J Neurosci* 2006;26(13):3541–50.
- Losee FL, Cutress TW, Brown R. Natural elements of the periodic table in human dental enamel. *Caries Res* 1974;8:123–34.
- McCaughey PT, Douglas BH, Laurie RD, Bull RJ. Investigations into the effect of drinking water barium on rats. *Advances in modern environmental toxicology*, vol. IX. Princeton, NJ: Princeton Publishing Co.; 1985 p. 197–210.

- McCauley PT, Washington IS. Barium bioavailability as the chloride, sulfate or carbonate salt in the rat. *Drug Chem Toxicol* 1983;6:209–17.
- Miller RG, Featherstone JDB, Curzon MEJ, Mills TS, Shields CP. Barium in teeth as indicator of body burden. *Advances in modern environmental toxicology*, vol. IX. Princeton, NJ: Princeton Publishing Co.; 1985 p. 211–9.
- Noben-Trauth K, Zheng QY, Johnson KR. Association of cadherin 23 with polygenic inheritance and genetic modification of sensorineural hearing loss. *Nat Genet* 2003;35(1):21–3.
- NTP (National Toxicology Program). NTP toxicology and carcinogenesis studies of barium chloride dihydrate (CAS No. 10326-27-9) in F344/N rats and B6C3F1 mice (drinking water studies). *Natl Toxicol Program Tech Rep Ser* 1994;432:1–285.
- Ohgami N, Ida-Eto M, Sakashita N, Sone M, Nakashima T, Tabuchi KET AL. Partial impairment of c-Ret at tyrosine 1062 accelerates age-related hearing loss in mice. *Neurobiol Aging* 2012;33(3) 626.e25–626.e34.
- Ohgami N, Ida-Eto M, Shimotake T, Sakashita N, Sone M, Nakashima TET AL. c-Ret-mediated hearing loss in mice with Hirschsprung disease. *Proc Natl Acad Sci U S A* 2010;107(29):13051–6.
- Ohgami N, Kondo T, Kato M. Effects of light smoking on extra-high-frequency auditory thresholds in young adults. *Toxicol Ind Health* 2011;27(2):143–7.
- Ozcaglar HU, Agirdir B, Dinc O, Turhan M, Kilincarslan S, Oner G. Effects of cadmium on the hearing system. *Acta Otolaryngol* 2001;121(3):393–7.
- Perry HM Jr, Kopp SJ, Erlanger MW, Perry EF. Cardiovascular effects of chronic barium ingestion. *Trace Subst Environ Health* 1983;16:155–64.
- Poirrier AL, Van den Ackerveken P, Kim TS, Vandenbosch R, Nguyen L, Lefebvre PP, Malgrange B. Ototoxic drugs: difference in sensitivity between mice and guinea pigs. *Toxicol Lett* 2010;193(1):41–9.
- Powers BE, Poon E, Sable HJ, Schantz SL. Developmental exposure to PCBs, MeHg, or both: long-term effects on auditory function *Environ Health Perspect* 2009;117(7): 1101–7.
- Prasher D. Heavy metals and noise exposure: health effects. *Noise Health* 2009;11(44): 141–4.
- Prieve BA, Yanz JL. Age-dependent changes in susceptibility to ototoxic hearing loss. *Acta Otolaryngol* 1984;98(5–6):428–38.
- Ramirez GB, Pagulayan O, Akagi H, Francisco Rivera A, Lee LV, Berroya A, et al. Tagum study II: follow-up study at two years of age after prenatal exposure to mercury. *Pediatrics* 2003;111(3):e289–95.
- Rice DC, Gilbert SG. Effects of developmental exposure to methyl mercury on spatial and temporal visual function in monkeys. *Toxicol Appl Pharmacol* 1990;102: 151–63.
- Rothenberg SJ, Poblano A, Garza-Morales S. Prenatal and perinatal low level lead exposure alters brainstem auditory evoked responses in infants. *Neurotoxicology* 1994;15(3):695–9.
- Rozengurt N, Lopez I, Chiu CS, Kofuji P, Lester HA, Neusch C. Time course of inner ear degeneration and deafness in mice lacking the Kir4.1 potassium channel subunit. *Hear Res* 2003;177(1–2):71–80.
- Schroeder HA, Tipton IH, Nason AP. Trace metals in man: strontium and barium. *J Chronic Dis* 1972;25:491–517.
- Shargorodsky J, Curhan SG, Henderson E, Eavey R, Curhan GC. Heavy metals exposure and hearing loss in US adolescents. *Arch Otolaryngol Head Neck Surg* 2011;137(12):1183–9.
- Shimada A, Ohta A, Akguchi I, Takeda T. Inbred SAM-P/10 as a mouse model of spontaneous, inherited brain atrophy. *J Neuropathol Exp Neurol* 1992;51(4): 440–50.
- Sowden EM. Trace elements in human tissue: 3. Strontium and barium in non-skeletal tissue. *Biochem J* 1958;70:712–5.
- Sowden EM, Pirie A. Barium and strontium concentrations in eye tissue. *Biochem J* 1958;70:716–7.
- Sowden EM, Stinch SR. Trace elements in human tissue: 2. Estimation of the concentrations of stable strontium and barium in human bone. *Biochem J* 1957;67:104–9.
- Stoewsand GS, Anderson JL, Rutzke M, Lisk DJ. Deposition of barium in the skeleton of rats fed Brazil nuts. *Nutr Rep Int* 1988;38:259–62.
- Takeuchi S, Ando M. Voltage-dependent outward K(+) current in intermediate cell of stria vascularis of gerbil cochlea. *Am J Physiol* 1999;277(1 Pt 1):C91–9.
- Takeuchi S, Ando M, Kakigi A. Mechanism generating endocochlear potential: role played by intermediate cells in stria vascularis. *Biophys J* 2000;79(5):2572–82.
- Tardiff RG, Robinson M, Ulmer NS. Subchronic oral toxicity of BaCl<sub>2</sub> in rats. *J Environ Pathol Toxicol* 1980;4:267–75.
- Taylor DM, Bligh PH, Duggan MH. The absorption of calcium, strontium, barium and radium from the gastrointestinal tract of the rat. *Biochem J* 1962;83:25–9.
- Thang ND, Yajima I, Kumasaka MY, Ohnuma S, Yanagishita T, Hayashi RET AL. Barium promotes anchorage-independent growth and invasion of human HaCaT keratinocytes via activation of c-SRC kinase. *PLoS One* 2011;6(10):e25636.

# Chronic Exposure to Low Frequency Noise at Moderate Levels Causes Impaired Balance in Mice

Haruka Tamura<sup>1</sup>, Nobutaka Ohgami<sup>1</sup>, Ichiro Yajima<sup>1</sup>, Machiko Iida<sup>1</sup>, Kyoko Ohgami<sup>1</sup>, Noriko Fujii<sup>2</sup>, Hiroyuki Itabe<sup>3</sup>, Tastuya Kusudo<sup>4</sup>, Hitoshi Yamashita<sup>4</sup>, Masashi Kato<sup>1\*</sup>

**1** Unit of Environmental Health Sciences, Department of Biomedical Sciences, College of Life and Health Sciences, Chubu University, Kasugai, Aichi, Japan, **2** Research Reactor Institute, Kyoto University, Kumatori-cho, Sennan, Osaka, Japan, **3** Department of Biological Chemistry, Showa University School of Pharmacy, Hatanodai, Shinagawa-ku, Tokyo, Japan, **4** Unit of Molecular Biology, Department of Biomedical Sciences, College of Life and Health Sciences, Chubu University, Kasugai, Aichi, Japan

## Abstract

We are routinely exposed to low frequency noise (LFN; below 0.5 kHz) at moderate levels of 60–70 dB sound pressure level (SPL) generated from various sources in occupational and daily environments. LFN has been reported to affect balance in humans. However, there is limited information about the influence of chronic exposure to LFN at moderate levels for balance. In this study, we investigated whether chronic exposure to LFN at a moderate level of 70 dB SPL affects the vestibule, which is one of the organs responsible for balance in mice. Wild-type ICR mice were exposed for 1 month to LFN (0.1 kHz) and high frequency noise (HFN; 16 kHz) at 70 dB SPL at a distance of approximately 10–20 cm. Behavior analyses including rotarod, beam-crossing and footprint analyses showed impairments of balance in LFN-exposed mice but not in non-exposed mice or HFN-exposed mice. Immunohistochemical analysis showed a decreased number of vestibular hair cells and increased levels of oxidative stress in LFN-exposed mice compared to those in non-exposed mice. Our results suggest that chronic exposure to LFN at moderate levels causes impaired balance involving morphological impairments of the vestibule with enhanced levels of oxidative stress. Thus, the results of this study indicate the importance of considering the risk of chronic exposure to LFN at a moderate level for imbalance.

**Citation:** Tamura H, Ohgami N, Yajima I, Iida M, Ohgami K, et al. (2012) Chronic Exposure to Low Frequency Noise at Moderate Levels Causes Impaired Balance in Mice. *PLoS ONE* 7(6): e39807. doi:10.1371/journal.pone.0039807

**Editor:** Georges Chapouthier, Université Pierre et Marie Curie, France

**Received:** April 20, 2012; **Accepted:** May 26, 2012; **Published:** June 29, 2012

**Copyright:** © 2012 Tamura et al. This is an open-access article distributed under the terms of the Creative Commons Attribution License, which permits unrestricted use, distribution, and reproduction in any medium, provided the original author and source are credited.

**Funding:** This study was supported in part by Grants-in-Aid for Scientific Research (B) (No. 19390168 and 20406003), Grant-in-Aid for Challenging Exploratory Research (No. 23650241), Grants-in-Aid for Young Scientists (B) (No. 18790738) from the Ministry of Education, Culture, Sports, Science and Technology (MEXT), Center of Excellence (COE) Project (Health Science Hills) for Private Universities from MEXT and Chubu University (No. S0801055), Adaptable and Seamless Technology Transfer Program through Target-driven R&D, Japan Science and Technology Agency, AA Science Platform Program from the Japan Society for the Promotion of Science (JSPS), Mitsui & Co., Ltd. Environment Fund (No. R08-C097), Research Grant from the Tokyo Biochemical Research Foundation (TBRF), Research Foundation from the Institute of Science and Technology Research in Chubu University and Chubu University grants A, B and CG. The authors also declare that the funders had no role in study design, data collection and analysis, decision to publish, or preparation of the manuscript.

**Competing Interests:** Mitsui & Co., Ltd. was a commercial funder of this study. This does not alter the authors' adherence to all the PLoS ONE policies on sharing data and materials.

\* E-mail: katomasa@isc.chubu.ac.jp

## Introduction

Exposure to noise generated in occupational and daily environments is one of the community hazards in our society [1,2]. Noise consists of sound with broad frequencies, but there is limited information about the frequency-dependent influence of noise on health. Low frequency noise (LFN) is constantly generated from natural and artificial sources. The frequency range of LFN is usually defined as being below 100 Hz, while that of infrasound is usually below 20 Hz [3]. LFN is ubiquitously detected in our modern society and is generated from many occupational and daily sources including transportation systems, industrial devices, air movement devices (e.g., wind turbines, compressors, ventilation and air-conditioning units) and household appliances (e.g., washing machines, refrigerators and freezers). Thus, we are routinely exposed to LFN generated from various devices in the daily environment. In fact, our measurements showed LFN at moderate levels of about 70 dB sound pressure level (SPL) generated from various ordinary devices (Table 1).

Previous studies have indicated that LFN at below 0.5 kHz can be an environmental factor threatening health [4]. In humans, effects of LFN on several physiological functions including the cardiovascular and nervous systems, visual system, auditory system and the endocrine system have been shown [3]. Effects of LFN on the central nervous system including annoyance, sleep and wakefulness, perception, evoked potentials, electroencephalographic changes and cognition have also been shown [5,6]. Chronic exposure to environmental infrasound has been shown to affect blood pressure, resulting in hypertension in humans [7]. Furthermore, exposure to moderate levels of LFN (70 dB SPL) at the frequency region of 31.5 Hz to 125 Hz for 2 hours has been shown to affect neuroendocrine activity in humans [8]. On the other hand, audible frequencies for humans and mice are known to be approximately 0.02–20 kHz and 1–40 kHz, respectively [9]. Therefore, it is basically difficult for people and mice even without hearing loss to recognize LFN in a noisy environment [3]. Thus, it is important to further analyze the potential risk of occupational and daily exposure to LFN at moderate levels on our health, even if we hardly recognize LFN in daily or occupational environments.

Balance is coordinately regulated by several organs including the vestibule, skeletal muscle and cerebellum [10]. A previous study showed that aging, injuries and other genetic factors can cause abnormal physiological functions in these crucial organs that result in impairments of balance in mice and humans [11], which have a negative impact on quality of life in an aging society. On the other hand, exposure to infrasound (5 Hz and 16 Hz, 95 dB, 5 minutes) has been shown to affect the control of upright standing posture in humans [12]. Also, occupational exposure to LFN has been shown to lead to impairments of vestibular functions [13]. Thus, these previous studies suggest that exposure to LFN can affect balance regulated by vestibular functions in humans. In previous studies with experimental animals, behavior analyses including rotarod, beam-crossing and footprint tests have been used to determine balance [14–16]. However, there is very limited information about how chronic exposure to LFN affects balance in mice.

Inner ears contain the vestibule in the vicinity of the organ of Corti. Vestibular hair cells covered with otoconia play an important role in mechanotransduction, by which gravity impulses are converted into neural impulses. Impairments of vestibular hair cells have been shown to cause abnormal behaviors including balance [16]. Thus, the vestibule containing hair cells and an otolith is one of the organs responsible for balance. On the other hand, exposure to a broadband noise (at 1–20 kHz) has been shown to induce ototoxic damage of hair cells with enhanced oxidative stress in the organ of Corti in the inner ear, resulting in noise-induced hearing loss in rodent animal models and humans [17]. In addition, exposure to broadband noise has been shown to enhance oxidative stress in the brain [18,19]. Thus, it is possible that exposure to noise causes damage of hair cells with increased oxidative stress in inner ears, although those previous studies used broadband noise without consideration of specific frequencies. At present, however, there is no information about whether exposure to LFN enhances oxidative stress in vestibular hair cells, which play a crucial role in regulation of balance.

In this study, we used LFN (0.1 kHz) and high frequency noise (HFN; 16 kHz) at a moderate level of 70 dB SPL [20] for exposure of mice to noise (Fig. 1) in order to determine the pathogenesis of impaired balance caused by LFN stress. Our results show for the first time that chronic exposure to LFN at a moderate level can cause impaired balance involving partial loss of hair cells with increased levels of oxidative stress in the vestibule.

## Results

### Chronic Exposure to LFN at a Moderate Level Affects Balance in Mice

We started to expose ICR mice to 70 dB SPL of LFN (0.1 kHz, Fig. 1B) and HFN (16 kHz, Fig. 1A) from 6 weeks of age in order to determine how exposure to noise affects balance in a frequency-dependent manner. After noise exposure, we performed behavior analyses to determine whether exposure to LFN affects balance in mice. Comparable rotarod performance was observed in non-exposed and exposed mice before noise exposure (Fig. 2A). LFN-exposed mice showed significantly worse rotarod performance than that of non-exposed mice (Fig. 2B). In contrast, mice exposed to HFN and non-exposed mice showed comparable rotarod performances (Fig. 2B). The beam-crossing test also showed imbalance behaviors in LFN-exposed mice compared to those in non-exposed mice and HFN-exposed mice (Table 2). Footprint analysis further showed winding gait patterns and short strides in LFN-exposed mice (Fig. 3A, center panel) compared to those in non-exposed mice and HFN-exposed mice (Fig. 3B). These results suggest that LFN-exposed mice had impaired balance. An abrupt change of body weight was not observed during noise exposure (Fig. S1).

### Chronic Exposure to LFN at a Moderate Level Causes Partial Loss of Vestibular Hair Cells

We then performed morphological analyses of the vestibule in inner ears from ICR mice after LFN exposure (Fig. 4). Immunohistochemical analyses with anti-calbindin D28k antibody, a marker for vestibular hair cells [21], showed a significant decrease in the number of vestibular hair cells in LFN-exposed mice (Fig. 4B) compared to that in non-exposed mice (Fig. 4A, arrows, 4G). Furthermore, we histologically determined oxidative stress levels of the vestibule in LFN-exposed mice. Immunohistochemistry with anti-oxidized phospholipid (Ox-PC) antibody [22,23] and anti-D-beta-aspartic acid (D-beta-Asp) antibody [24] showed much stronger signals in marginal zones of the vestibule in LFN-exposed mice than in non-exposed mice (Fig. 4C-F, H, I).

## Discussion

In previous studies, exposure to LFN has been shown to lead to impairments of balance in humans [4,12]. However, there is very limited information about the etiology of imbalance caused by LFN and the influence of a moderate level of LFN on balance since it is basically difficult to reveal the pathogenesis of impaired balance caused by LFN stress in humans. This study showed for the first time that chronic exposure to LFN at a moderate level causes imbalance involving morphological impairments in the vestibule in mice.

This study showed that exposure to LFN caused impairments of balance in mice, whereas mice exposed to HFN for 1 month and non-exposed mice showed comparable performances related to balance. A previous study showed that energy of LFN (~ 0.5 kHz) can penetrate our body, whereas HFN is easily attenuated [25]. Therefore, we assume that LFN stress causes damage to the vestibule due to its higher energy than that of HFN. On the other hand, there has been no study showing the influence of noise on behavior and morphology of the responsible tissues in mice or humans by consideration of both frequency (Hz) and intensity (dB). A previous study in which the influence of LFN on sleep in humans was investigated showed that 1 kHz noise only at 30 dB increased wakefulness, while 42 Hz LFN even at 70 dB had little effect [5]. Since audible frequencies for humans are known to be

**Table 1.** Typical low frequency noise levels of electric devices in experimental rooms.

Electric devices	Noise levels (dB SPL) at 100 Hz
4°C freezers	65.3±4.8
−30°C freezers	66.1±4.5
−80°C freezers	69.9±2.9
Ice makers	61.8±1.0
Draft chambers	75.5±0.7

Noise levels (means ± SD) were measured by a noise level meter and calculated as an average of five repeated measurements. Noise levels were measured at a distance of approximately 20 cm from the devices shown in Table 1. Background level (mean ± SD) of low frequency noise at 100 Hz was 35.7±2.7 dB SPL in 5 experimental rooms without noise-generating devices shown in Table 1.

doi:10.1371/journal.pone.0039807.t001

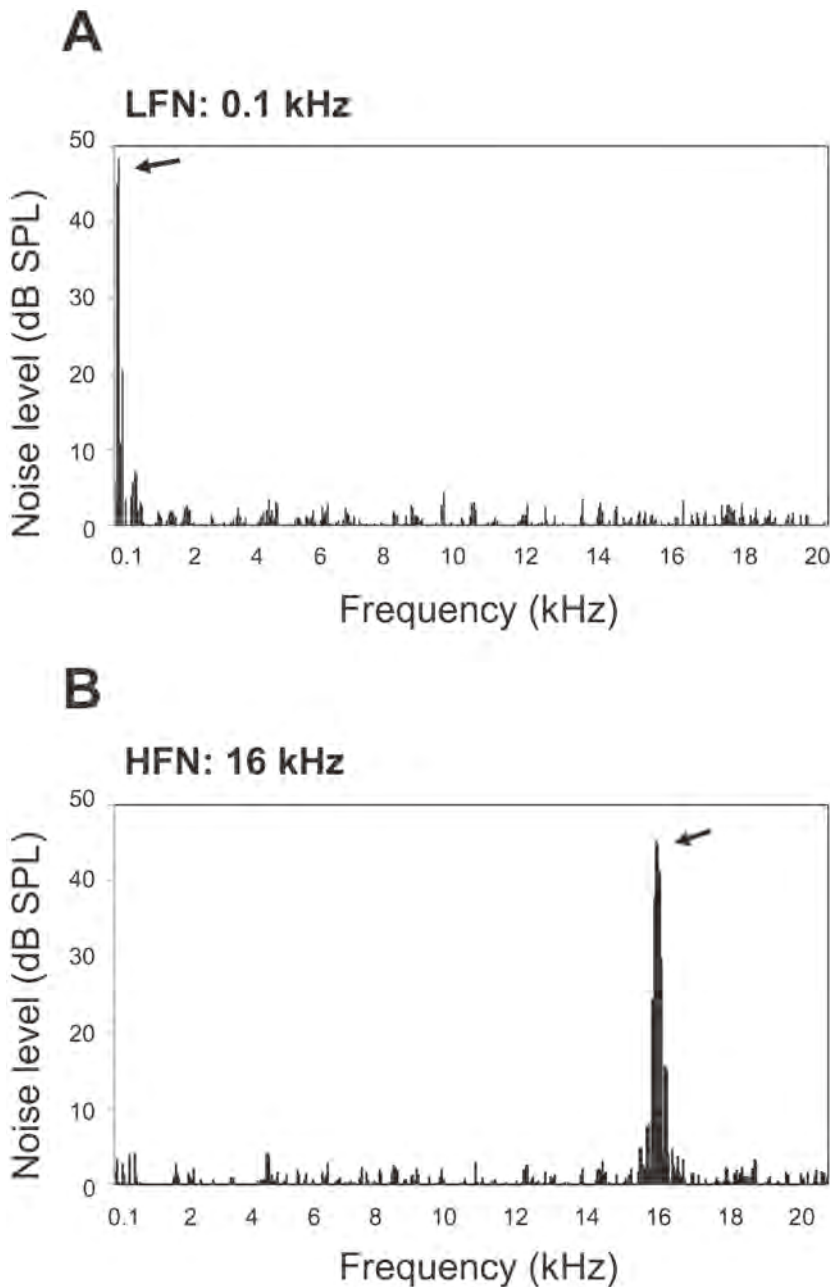


**Figure 1. Frequency distributions of noise used in this study.** Frequency distributions (means  $\pm$  SD) of (A) low frequency noise (LFN; 0.1 kHz) and (B) high frequency noise (HFN; 16 kHz) are presented. Noise levels from a speaker at a distance of 10 cm in a soundproof room were measured by a noise level meter and calculated as average of five repeated measurements. Background levels measured in a soundproof room without noise-generating devices were subtracted from noise levels from the speaker. Whole noise levels of (A) LFN and (B) HFN measured by the noise level meter without FFT analyzing software were almost the same (70 dB SPL). doi:10.1371/journal.pone.0039807.g001

approximately 0.02–20 kHz, it is basically harder for people even without hearing loss to recognize noise at 42 Hz than that at 1 kHz. Thus, it is possible that not only frequency and intensity of noise but also the range of audible frequencies of the recipient affect physiological functions including balance. Therefore, it is also important to measure changes in auditory responses to noise by auditory brain stem responses (ABR) in frequency- and intensity-dependent manners. Further study is needed to determine the influence of noise on balance and morphology of the

responsible tissues in mice and humans by consideration of frequency (Hz), intensity (dB) and the range of audible frequencies of mice and humans.

In a previous study, several organs including muscles, the cerebellum and the vestibule were shown to coordinately regulate balance [10]. Our results obtained with light microscopy showed comparable morphologies of soleus muscle fibers and the cerebellum in exposed and non-exposed mice (Fig. S2, Method S1). Body weights of LFN-exposed and non-exposed mice were

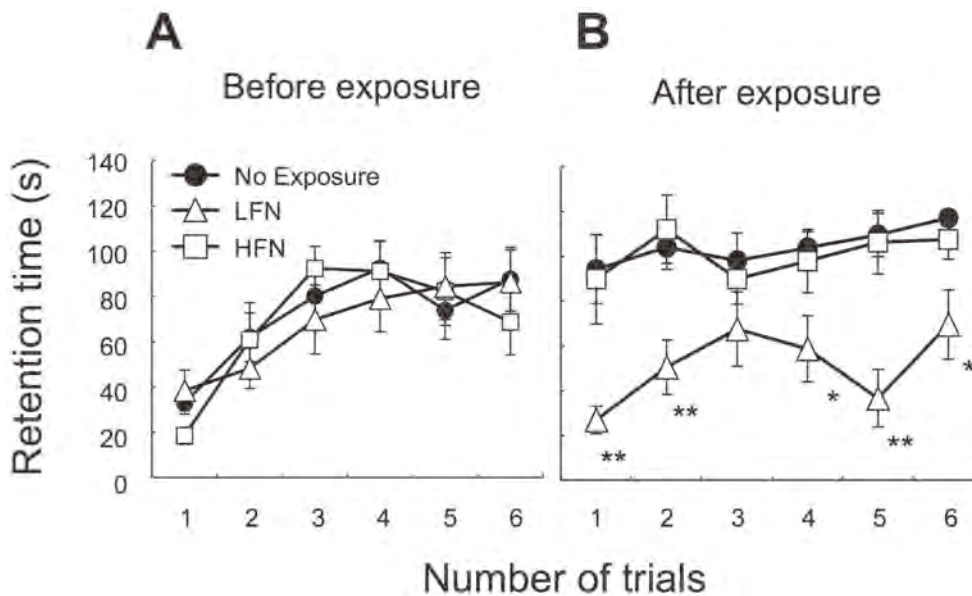


**Figure 2. Exposure to LFN affects rotarod performance of ICR mice.** Before (A) and after (B) exposure to LFN (open triangles) and HFN (open squares), retention times (seconds, mean ± SD, n=7) on the rotarod (at 30 rpm) were measured. Results for non-exposed mice (closed circles) are also plotted (mean ± SD, n=7). Mice were allowed a maximum retention time of 120 seconds per trial. Significant difference (\*\*,  $p < 0.01$ ; \*,  $p < 0.05$ ) from the non-exposure group was analyzed by the Mann-Whitney *U* test. doi:10.1371/journal.pone.0039807.g002

not different (Fig. S1). Thus, our results suggest that LFN causes morphological impairment of the vestibule rather than the soleus muscle and cerebellum. In previous studies, exposure to LFN has been suggested to ubiquitously affect several organs in our body [3]. Also, exposure to a moderate level of LFN (70 dB SPL) for 2 hours has been shown to influence neuroendocrine activity related to emotional stress in humans [8]. Therefore, it would be interesting to determine whether chronic exposure to LFN stress affects psychological functions relevant to balance. One the other hand, female mice were used for exposure experiments in this study. It has been reported that hormonal changes during the menstrual cycle in females affect behaviors including depression symptoms in humans and mice [26,27]. As far as we measured behavior in female and male mice, the two sexes showed similar susceptibility to the influence of LFN exposure on balance (data not shown). Our results partially correspond to the results of a previous study showing that performance of a visual inspection task was not affected by any combinational effect or interaction between menstrual cycle and exposure to broadband noise in humans [28]. It would be of interest to further investigate whether chronic exposure to LFN stress affects hormonal functions including physiological functions relevant to balance.

The inner ears contain the organ of Corti in the vicinity of the vestibule. The organ of Corti, which consists of two kinds of sensory cells [inner hair cells (IHCs) and outer hair cells (OHCs)], is a sound receptor by which sound impulses are converted into neural impulses. Auditory information from sensory cells is eventually transmitted to the auditory cortex [29], where auditory stimuli activate other parts of the cortex including the amygdala and thalamus. Thus, exposure to LFN can simultaneously stimulate not only the vestibule, directly causing impairment of balance, but also the organ of Corti, affecting behavior indirectly via the central nervous system through the auditory system. Additional experiments are required to determine whether exposure to LFN affects vestibular functions separately from the auditory system.

In this study, we showed that impairment of balance involved partial loss of calbindin-positive hair cells in the vestibule with enhanced oxidative stress in LFN-exposed mice. Our results partially correspond to results of previous studies showing that behavioral impairments induced by antibiotics were accompanied by degeneration of vestibular cells and oxidative stress [30,31]. Also, a previous study has shown that antioxidant compounds have preventive effects on noise-induced hearing loss [17]. Ototoxicity caused by oxidative stress in inner ears usually has been shown to involve impairments of antioxidant enzymes [17]. Thus, those previous studies indicate the necessity for further investigation of a causal molecule related to oxidative stress in vestibular hair cells affected by LFN and a preventive effect of antioxidants on impaired balance caused by LFN exposure. On the other hand, a previous study showed that calbindin D28k serves as a calcium buffering protein to maintain a low endolymphatic calcium  $[Ca^{2+}]$  level in inner ears [32]. In addition, a low luminal calcium concentration ( $[Ca^{2+}]$ ) as well as a high endolymphatic potassium concentration ( $[K^+]$ ) of the mammalian endolymph in the inner ear are required for normal balance [32,33]. Endolymphatic levels of these ions are maintained by channels, transporters and buffering proteins expressed in inner

**Table 2. Beam crossing test for LFN-exposed mice.**

	No exposure	HFN	LFN
Success	12	10	2
Failure	0	0	10**

ICR mice that had been exposed to LFN (n = 12) and to HFN (n = 10) and non-exposed mice (n = 12) were examined by a beam crossing test. The number of mice that fell from the beam (i.e., imbalance behavior) is shown as "Failure" in Table 2. The number of mice crossing the beam without falling is shown as "Success" in Table 2. P values were obtained by chi square analysis. \*\* $p < 0.01$ . doi:10.1371/journal.pone.0039807.t002

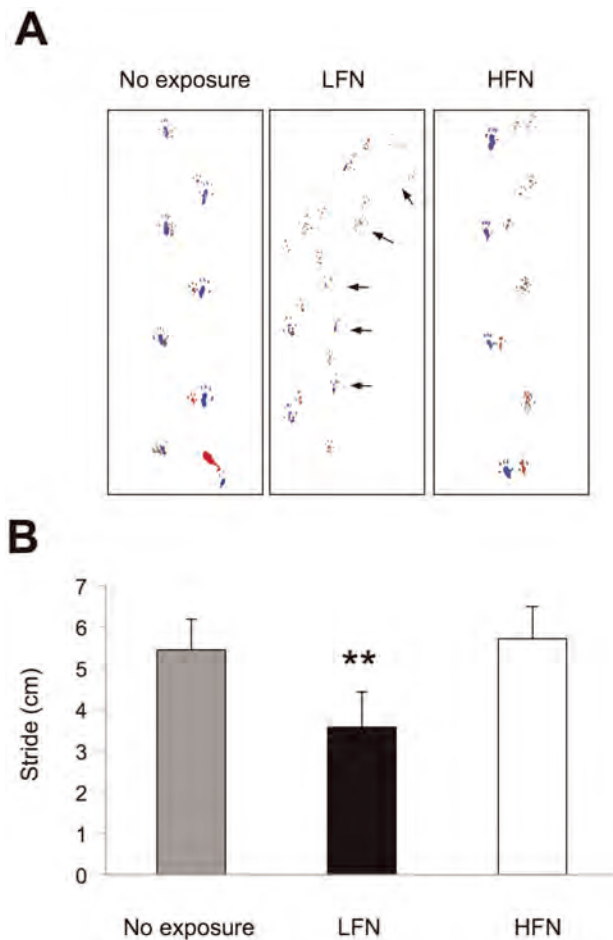


**Figure 3. Exposure to LFN affects gait pattern of ICR mice.** (A) After exposure to LFN (center panel) and HFN (right panel), front and back paws of mice were dipped in red or green paint, and mice walked across a box lined with paper. Non-exposed mice (left panel) are also shown. LFN-exposed mice display shorter stride length and winding gait patterns (center panel, arrows). (B) Quantification of stride length. Strides (mean  $\pm$  SD) for seven mice (each group) were assessed. A total of 40–50 steps for each group were determined. Significant difference (\*\*,  $p < 0.01$ ) from the non-exposure group was analyzed by the Mann-Whitney  $U$  test. doi:10.1371/journal.pone.0039807.g003

ears [33]. Rats exposed to a toxic compound have been shown to have a decreased number of calbindin D28k-positive neurons with enhanced oxidative stress in the cerebellum [34]. Interestingly, infrasound has been shown to cause impairments of  $[Ca^{2+}]$  levels in rat cardiac tissues resulting in cardiac dysfunction [35]. Based on our results and the results obtained in previous studies, we hypothesize that partial loss of calbindin-positive hair cells in the vestibule caused by LFN exposure may involve impairments of endolymphatic  $[Ca^{2+}]$  levels resulting in imbalance.

Exposure of children to environmental factors has been shown in previous studies to sensitively affect auditory development [36,37]. Aging has also been shown to change susceptibility to ototoxic factors in mice [38]. On the other hand, there is very limited information about the relevance between age and imbalance caused by exposure to LFN, while a previous study suggested that young children have a high susceptibility to LFN [39]. Therefore, our results indicate the necessity for further

investigation of the age-specific susceptibility of imbalance to LFN in mice and humans.

In conclusion, our results demonstrate for the first time that chronic exposure of ICR mice to LFN at 70 dB SPL for 1 month results in a decreased number of vestibular hair cells with enhanced levels of oxidative stress, leading to impairment of balance.

## Materials and Methods

### Mice

Randomly bred wild-type female mice (ICR) at 6 weeks of age were used for exposure experiments. Mice were purchased from Japan SLC (Hamamatsu, Japan). All experiments were authorized by the Institutional Animal Care and Use Committee in Chubu University (approval number: 2410030) and followed the Japanese Government Regulations for Animal Experiments.

### Noise Exposure

Mice were continuously exposed for 1 month to noise at 70 dB SPL from a speaker (Sound Stimulator DPS-725, Diya Medical System CO., LTD, Japan) with the mice being located at a distance of approximately 10–20 cm from the speaker in a soundproof room (Yamaha Co., Japan). The acoustic output was regularly monitored using a noise level meter (Type 6224 with an FFT analyzer, ACO CO., LTD, Japan). Mice were housed under specific pathogen-free (SPF) conditions at a constant temperature ( $23 \pm 2^\circ\text{C}$ ) and a 12-h light/dark cycle. The mice were weighed weekly on a gram scale.

### Behavior Analyses

Measurement of balance was performed according to previous studies [14–16]. Before and after noise exposure for 4 weeks, mice were examined using a rotating rod treadmill (Ugo Basile; Stoelting Co., Chicago, IL). Mice with similar body weights were used. The rotating rod was set in motion at a constant speed (30 rpm) and the mice were placed into individual sections of the rotating rod. Each time an animal fell, it was noted whether the fall had occurred when it sat still or when it walked. Each animal's performance score in seconds was recorded when the mouse was unable to stay on the rotating rod, tripped a plate and stopped the timer. Six successive trials separated by 5-min pauses were performed. For the beam-crossing test, a round wooden bar of 2 cm in diameter was attached to two Styrofoam platforms at the ends, and the length of the bar to be crossed was adjustable at the ends. Pre-training of mice on the bar at 5 cm in length was performed first, followed by three consecutive trials of crossing the bar at 30 cm in length. Mice were allowed up to 60 sec to traverse each beam. A gait assay was performed as previously reported [14]. Briefly, the front paws were dipped in red paint and the back paws were dipped in blue paint, and mice were placed on Whatman paper at one end of a  $14 \times 44$  cm box. The distance between the back edge of each same-side paw print was used to determine stride length.

### Morphological Analyses of the Vestibule

After perfusion fixation by Bouin's solution, inner ears with semicircular canals from mice were immersed in the same solution for 3 days to 1 week at  $4^\circ\text{C}$ . Immunohistochemistry with rabbit anti-calbindin D28k antibody (1:150; Chemicon) [40] and rabbit anti-D-beta-aspartic acid (D-beta-Asp) antibody (1:100) [24] was performed with 5- $\mu\text{m}$ -thick serial paraffin sections. A VECTASTAIN ABC kit (Vector) and an Envision kit/HRP (diaminobenzidine; DAB) (DAKO) were used in each immunohistochemical analysis

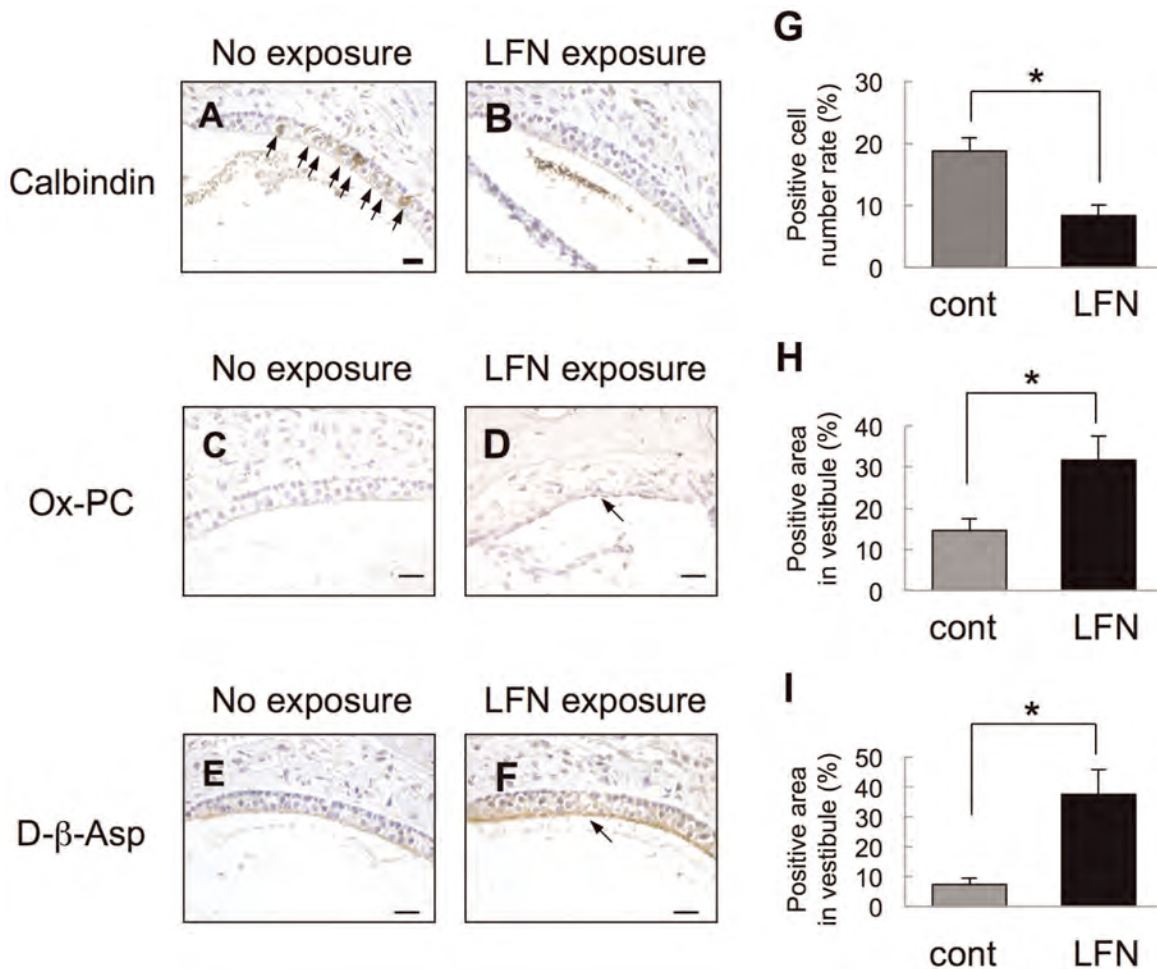


**Figure 4. Decreased number of vestibular hair cells with increased levels of oxidative stress in LFN-exposed mice.** (A, B) Immunohistochemical analysis with anti-calbindin D28k for vestibules in LFN-exposed (B) and non-exposed mice (A). (C-F) Enhanced oxidative stress levels in vestibules of LFN-exposed mice. Vestibules of LFN-exposed (D, F) and non-exposed mice (C, E) were immunohistochemically stained by an anti-Ox-PC antibody (DLH3) (C, D) and anti-D-beta-Asp antibody (E, F). Vestibules of LFN-exposed mice showed stronger signals (D, F, arrows) than those of non-exposed mice (C, E). Scale bars: 20 μm. (G-I) Percentage (means ± SD) of calbindin-positive hair cells (G) and positive areas of anti-Ox-PC antibody (H) and anti-D-beta-Asp antibody (I) in vestibules from LFN-exposed mice (LFN, black bar, n=7) and non-exposed mice (Cont, gray bar, n=7). Significant difference (\*,  $p < 0.05$ ) from non-exposed mice was analyzed by the Mann-Whitney *U* test. doi:10.1371/journal.pone.0039807.g004

with hematoxylin counterstaining. Immunohistochemical analyses with a monoclonal antibody against oxidized phospholipids (Ox-PC; 20 μg/ml; DLH3) [22] were performed for frozen sections [23]. Briefly, after treatment with 0.3% hydrogen peroxide for 20 min at room temperature, the frozen sections were incubated in blocking buffers (20 μg/ml of goat IgG (DAKO) in PBS for 1 h at room temp, followed by 20 μg/ml of Goat Fab-anti mouse IgG (Jackson ImmunoResearch)). After incubation with the primary antibody, the frozen sections were further incubated in an alkaline phosphatase-labeled goat anti-mouse IgM (1:200 in 2% skim milk in PBS; AbD serotec). The DAKO New Fuchsin substrate system (DAKO) was used to develop a signal with hematoxylin counterstaining. About 5 sections were observed in seven exposed and seven non-exposed mice, respectively. The percentage of positive signals histochemically detected by antibodies was estimated with Win-ROOF (version 6.2) as previously reported [40,41]. Briefly, the number of positive hair cells was divided by the total number of hair cells in the vestibule. A total of 100–150 cells in 5 sections from each mouse were examined. In the case of oxidative stress markers

including Ox-PC and D-beta-Asp, positive areas in the measured vestibule were divided by the areas of the section measured. Vestibules from seven mice for each group were measured for each estimation.

**Statistics**

Statistical analysis was performed as previously reported [42]. Significant difference (\*\*,  $p < 0.01$ ; \*,  $p < 0.05$ ) from the control (no exposure) was analyzed by the Mann-Whitney *U* test (Figs. 2, 3, and 4 and Fig. S1) and chi square analysis (Table 2).

**Supporting Information**

**Figure S1 Exposure to low frequency noise does not affect body weight of ICR mice.** Body weights (mean ± SD) were monitored at 1 week (1W), 2 weeks (2W), and 4 weeks (4W) during exposure to LFN. No significant difference (n.s.) of body weight was observed in LFN-exposed and non-exposed mice. (TIFF)

**Figure S2 Morphological analysis of cerebellum and soleus muscle in LFN-exposed and non-exposed mice.** (A, B) Hematoxylin-eosin (HE) staining of the cerebellum in LFN-exposed (B) and non-exposed mice (A) was performed with 5- $\mu$ m-thick serial paraffin sections. (C, D) NADH-TR staining for the soleus muscle in exposed (D) and non-exposed mice (C) was performed. Scale bars: 20  $\mu$ m (A, B), 50  $\mu$ m (C, D). (TIFF)

**Methods S1 NADH-tetrazolium (NADH-TR) staining.** (DOC)

## References

- Dougherty JD, Welsh OL (1966) Environmental hazards. Community noise and hearing loss. *N Engl J Med* 275: 759–765.
- Wallenius M (2004) The interaction of noise stress and personal project stress on subjective health. *J Environ Psych* 24: 167–177.
- Leventhall G (2003) A Review of Published Research on Low Frequency Noise and its Effects, Department of Environment, Food, and Rural Affairs (DEFRA), United Kingdom. Accessed 2003 May.
- Schust M (2004) Effects of low frequency noise up to 100 Hz. *Noise Health* 6: 73–85.
- Landstroem U, Lundstroem R, Bystroem M (1983) Exposure to infrasound - perception and changes in wakefulness. *J Low Frequency Noise and Vibration* 2: 1–11.
- Karpova NI, Alekseev SV, Erokhin VN, Kadyskina EN, Reutov OV (1970) Early response of the organism to low-frequency acoustical oscillations. *Noise and Vibration Bulletin* 11: 100–103.
- Danielsson A, Landström U (1985) Blood pressure changes in man during infrasonic exposure. An experimental study. *Acta Med Scand* 217: 531–535.
- Waye KP, Bengtsson J, Ryländer R, Hucklebridge F, Evans P, et al. (2002) Low frequency noise enhances cortisol among noise sensitive subjects during work performance. *Life Sci* 70: 745–758.
- Heffner HE, Heffner RS (2007) Hearing ranges of laboratory animals. *J Am Assoc Lab Anim Sci* 46: 20–22.
- Matsumura BA, Ambrose AF (2006) Balance in the elderly. *Clin Geriatr Med* 22: 395–412.
- Kuo AD, Donelan JM (2010) Dynamic principles of gait and their clinical implications. *Phys Ther* 90: 157–174.
- Takigawa H, Hayashi F, Sugiura S, Sakamoto H (1988) Effects of infrasound on human body sway. *Journal of Low Frequency Noise and Vibration* 7: 66–73.
- Doroshenko PN, Stepchuk ID (1983) Health related assessment of combined effect of infrasound and low-frequency noise on the acoustic and vestibular analyser of compressor operators. *Noise and Vibration Bulletin Nov.* 1983: 192–194.
- Ko DC, Milenkovic L, Beier SM, Manuel H, Buchanan J, et al. (2005) Cell-autonomous death of cerebellar purkinje neurons with autophagy in Niemann-Pick type C disease. *PLoS Genet* 1: 81–95.
- Mariño G, Fernández AF, Cabrera S, Lundberg YW, Cabanillas R, et al. (2010) Autophagy is essential for mouse sense of balance. *J Clin Invest* 120: 2331–2344.
- Zhao X, Jones SM, Yamoah EN, Lundberg YW (2008) Otoconin-90 deletion leads to imbalance but normal hearing: a comparison with other otoconia mutants. *Neuroscience* 153: 289–299.
- Henderson D, Bielefeld EC, Harris KC, Hu BH (2006) The role of oxidative stress in noise-induced hearing loss. *Ear Hear* 27: 1–19.
- Samson J, Shecladevi R, Ravindran R (2007) Oxidative stress in brain and antioxidant activity of *Ocimum sanctum* in noise exposure. *Neurotoxicology* 28: 679–685.
- Samson J, Shecladevi R, Ravindran R, Senthilvelan M (2007) Stress response in rat brain after different durations of noise exposure. *Neurosci Res* 57: 143–147.
- Pienkowski M, Eggermont JJ (2012) Reversible Long-Term Changes in Auditory Processing in Mature Auditory Cortex in the Absence of Hearing Loss Induced by Passive, Moderate-Level Sound Exposure. *Ear Hear In press.*
- Zakon H, Lu Y, Weisleder P (1998) Sensory cells determine afferent terminal morphology in cross-innervated electroreceptor organs: implications for hair cells. *J Neurosci* 18: 2581–2591.
- Itabe H, Takeshima E, Iwasaki H, Kimura J, Yoshida Y, et al. (1994) A monoclonal antibody against oxidized lipoprotein recognizes foam cells in atherosclerotic lesions. Complex formation of oxidized phosphatidylcholines and polypeptides. *J Biol Chem* 269: 15274–15279.

## Acknowledgments

We thank Tadashi Shimo-Oka for preparing the anti-D-beta-aspartic acid antibody. We thank Harumi Ohno, Sohjiro Hori, Kohichi Nakamura and Seina Ito for their technical assistance.

## Author Contributions

Conceived and designed the experiments: NO HT MK. Performed the experiments: HT NO KO. Analyzed the data: HT NO MK. Contributed reagents/materials/analysis tools: IY MI NF HI TK HY. Wrote the paper: HT NO MK.

- Akishima Y, Akasaka Y, Ishikawa Y, Lijun Z, Kiguchi H, et al. (2005) Role of macrophage and smooth muscle cell apoptosis in association with oxidized low-density lipoprotein in the atherosclerotic development. *Mod Pathol* 18: 365–373.
- Fujii N, Tajima S, Tanaka N, Fujimoto N, Takata T, et al. (2002) The presence of D-beta-aspartic acid-containing peptides in elastic fibers of sun-damaged skin: a potent marker for ultraviolet-induced skin aging. *Biochem Biophys Res Commun* 294: 1047–1051.
- Gerhardt KJ, Abrams RM (1996) Fetal hearing: characterization of the stimulus and response. *Semin Perinatol* 20: 11–20.
- Kaur G, Kulkarni SK (2002) Evidence for serotonergic modulation of progesterone-induced hyperphagia, depression and algesia in female mice. *Brain Res* 943: 206–15.
- Miller LJ, Girgis C, Gupta R (2009) Depression and related disorders during the female reproductive cycle. *Womens Health (Lond Engl)* 5: 577–87.
- Wijayanto T, Tochiyama Y, Wijaya AR, Hermawati S (2009) Combined factors effect of menstrual cycle and background noise on visual inspection task performance: a simulation-based task. *J Physiol Anthropol* 28: 253–9.
- Lalwani AK, Gürtler N (2008) Sensorineural Hearing Loss, The Aging Inner Ear, and Hereditary Hearing Impairment. In: Lalwani AK, editor. *CURRENT Diagnosis & Treatment in Otolaryngology-Head & Neck Surgery*, second edition. New York: McGraw-Hill. 683–704.
- Al Deeb S, Al Moutaery K, Khan HA, Tariq M (2000) Exacerbation of iminodipropionitrile-induced behavioral toxicity, oxidative stress, and vestibular hair cell degeneration by gentamicin in rats. *Neurotoxicol Teratol* 22: 213–220.
- Guthrie OW (2008) Aminoglycoside induced ototoxicity. *Toxicology* 249: 91–96.
- Yamauchi D, Nakaya K, Raveendran NN, Harbidge DG, Singh R, et al. (2010) Expression of epithelial calcium transport system in rat cochlea and vestibular labyrinth. *BMC Physiol* 10: 1.
- Bartolami S, Gaboyard S, Quentin J, Travo C, Cavalier M, et al. (2011) Critical roles of transitional cells and Na/K-ATPase in the formation of vestibular endolymph. *J Neurosci* 31: 16541–16549.
- Patel RS, Rachamalla M, Chary NR, Shera FY, Tikoo K, et al. (2012) Cytarabine induced cerebellar neuronal damage in juvenile rat: correlating neurobehavioral performance with cellular and genetic alterations. *Toxicology* 293: 41–52.
- Pei Z, Sang H, Li R, Xiao P, He J, et al. (2007) Infrasound-induced hemodynamics, ultrastructure, and molecular changes in the rat myocardium. *Environ Toxicol* 22: 169–175.
- Prasher D (2009) Heavy metals and noise exposure: health effects. *Noise Health* 11: 141–144.
- Rothenberg SJ, Poblano A, Garza-Morales S (1994) Prenatal and perinatal low level lead exposure alters brainstem auditory evoked responses in infants. *Neurotoxicology* 15: 695–699.
- Prieve BA, Yanz JL (1984) Age-dependent changes in susceptibility to ototoxic hearing loss. *Acta Otolaryngol* 98: 428–438.
- Ising H, Ising M (2002) Chronic Cortisol Increases in the First Half of the Night Caused by Road Traffic Noise. *Noise Health* 4: 13–21.
- Ohgami N, Ida-Eto M, Shimotake T, Sakashita N, Sone M, et al. (2010) c-Ret-mediated hearing loss in mice with Hirschsprung disease. *Proc Natl Acad Sci USA* 107: 13051–13056.
- Ohgami N, Ida-Eto M, Sakashita N, Sone M, Nakashima T, et al. (2012) Partial impairment of c-Ret at tyrosine 1062 accelerates age-related hearing loss in mice. *Neurobiol Aging* 33: 626.e25–626.e34.
- Ohgami N, Kondo T, Kato M (2011) Effects of light smoking on extra-high-frequency auditory thresholds in young adults. *Toxicol Ind Health* 27: 143–147.

# Hearing impairments caused by genetic and environmental factors

Nobutaka Ohgami · Machiko Iida · Ichiro Yajima ·  
Haruka Tamura · Kyoko Ohgami · Masashi Kato

Received: 28 June 2012 / Accepted: 26 July 2012 / Published online: 17 August 2012  
© The Author(s) 2012. This article is published with open access at Springerlink.com

**Abstract** Impairments of hearing and balance are major problems in the field of occupational and environmental health. Such impairments have previously been reported to be caused by genetic and environmental factors. However, their mechanisms have not been fully clarified. On the other hand, the inner ear contains spiral ganglion neurons (SGNs) in the organ of Corti, which serve as the primary carriers of auditory information from sensory cells to the auditory cortex in the cerebrum. Inner ears also contain a vestibule in the vicinity of the organ of Corti—one of the organs responsible for balance. Thus, inner ears could be a good target to clarify the pathogenesis of sensorineural hearing losses and impaired balance. In our previous studies with *c-Ret* knock-in mice and *Endothelin receptor B (Ednrb)* knock-out mice, it was found that syndromic hearing losses involved postnatal neurodegeneration of SGNs caused by impairments of *c-Ret* and *Ednrb*, which play important roles in neuronal development and maintenance of the enteric nervous system. The organ of Corti and the vestibule in inner ears also suffer from degeneration caused by environmental stresses including noise and heavy metals, resulting in impairments of hearing and balance. In this review, we introduce impairments of hearing and balance caused by genetic and environmental

factors and focus on impairments of SGNs and the vestibule in inner ears as the pathogenesis caused by these factors.

**Keywords** Hearing loss · *c-Ret* · *Ednrb* · Spiral ganglion neuron · Neurodegeneration · Balance · Noise

## Introduction

It has been reported that about 250 million people worldwide suffer from hearing losses. About 30 % of people with congenital hearing loss are syndromic and the remaining 70 % are non-syndromic. In addition, most elderly people develop age-related (late-onset) hearing loss [1–3]. In general, these hearing losses have been classified as different diseases due to distinct pathogenesis [1, 2]. Sensorineural hearing losses are caused by impairments of inner ears and are difficult to cure due to the location and complex morphology of inner ears [1, 2]. Sensorineural hearing loss is a clinically heterogeneous disease leading to negative impacts on quality of life (QOL) in all generations. Sensorineural hearing loss involves different onset, severity and pathological sites.

Inner ears have been analyzed in order to clarify the pathogenesis of sensorineural hearing losses. The inner ears contain the organ of Corti and stria vascularis (SV). The SV is essential for maintenance of endolymph potential. The organ of Corti contains two kinds of sensory cells [inner hair cells (IHCs) and outer hair cells (OHCs)] and plays an important role in mechanotransduction, by which sound stimuli are converted into electric stimuli. Auditory information from the sensory cells is transferred to spiral ganglion neurons (SGNs) as the primary carriers and is eventually transferred to the auditory cortex in the

---

This review is based on research that was given an encouragement award at the 82nd annual meeting of the Japanese Society for Hygiene held in Kyoto, Japan on 24–26 March 2012.

---

N. Ohgami · M. Iida · I. Yajima · H. Tamura · K. Ohgami ·  
M. Kato (✉)  
Unit of Environmental Health Sciences,  
Department of Biomedical Sciences, College of Life and Health  
Sciences, Chubu University, No. 50 Building 11 floor,  
1200 Matsumoto, Kasugai, Aichi 487-8501, Japan  
e-mail: katomasa@isc.chubu.ac.jp

cerebrum [1, 2]. The SV consists of marginal cells, melanocytes (also known as intermediate cells) and basal cells, and has been shown to maintain high levels of potassium ion for endocochlear potential (EP) [4, 5]. Melanocytes in the inner ear are located specifically in the SV, and defects in melanocytes lead to impaired EP levels resulting in hearing loss [6]. Thus, disturbance of these constituent cells in inner ears has been shown to cause hearing losses [7]. Inner ears also contain a vestibule in the vicinity of the organ of Corti. Vestibular hair cells covered with otoconia play an important role in mechanotransduction, by which gravity impulses are converted into neural impulses. Impairments of vestibular hair cells have been shown to cause abnormal behaviors including balance [8]. Thus, the vestibule containing hair cells and an otolith is one of the organs responsible for balance.

Impairments of hearing and balance—both major problems in the field of occupational and environmental health—are caused by the intricate interplay of genetic, aging and environmental factors [1–3]. However, there is limited information about the pathogenesis of hearing loss and imbalance. This review focuses on hearing impairments caused by neurodegeneration of SGNs due to impairments of hearing-related genes (*c-Ret* and *Ednrb*) and by environmental stresses [low frequency noise (LFN) and heavy metals].

### **c-Ret-mediated hearing losses**

c-RET is a receptor-tyrosine kinase [9]. Glial cell line-derived neurotrophic factor (GDNF)—one of the ligands for c-RET—exerts its effect on target cells by binding to a glycosyl phosphatidylinositol (GPI)-anchored cell surface protein (GFR $\alpha$ 1). This binding facilitates the formation of a complex with the receptor tyrosine kinase c-RET. Formation of this complex activates c-RET autophosphorylation as a trigger for c-RET-mediated signaling pathways to give positive signals for cell survival [9–12]. Previous studies have also indicated that GDNF stimulates a Ret-independent signaling pathway [10, 13, 14]. Tyrosine 1062 (Y1062) in c-Ret plays an important role in kinase activation as one of the autophosphorylation sites, and is also a multi-docking site for several signaling molecules including SHC, a transmitter for c-Ret-mediated signaling pathways [13, 15, 16]. In both mice and humans, *c-RET* has been shown to be essential for the development and maintenance of the enteric nervous system (ENS) [13, 15] and to be the most frequent causal gene of Hirschsprung disease (HSCR; megacolon disease) (in 20–25 % of cases) in humans [17, 18]. In fact, severe HSCR (e.g., total intestinal agangliosis and impaired development of the kidney) has been shown to develop in homozygous knock-

in mice in which Y1062 in c-Ret was replaced with phenylalanine (*c-Ret-KI*<sup>Y1062F/Y1062F</sup>-mice), while heterozygous *c-Ret* Y1062F knock-in mice (*c-Ret-KI*<sup>Y1062F/+</sup>-mice) are reported to have no HSCR-linked phenotypes [11]. Thus, the results of previous studies indicate that HSCR in mice develops recessively [11], while HSCR in humans has been shown to develop dominantly due to RET mutations [19]. As described above, *c-Ret* and *c-RET* are crucial genes for HSCR; however, there had been no direct evidence to link *c-Ret* and *c-RET* to hearing impairments in mice or humans. Our recent studies have shown that complete unphosphorylated Y1062 in c-Ret, with no change in expression level, caused congenital hearing loss in *c-Ret-KI*<sup>Y1062F/Y1062F</sup>-mice [20], while partially unphosphorylated c-Ret led to normal hearing development until 1 month of age but then accelerated age-related hearing loss in *c-Ret-KI*<sup>Y1062F/+</sup>-mice [21]. Thus, impairments of *c-Ret* phosphorylation monogenetically result in early-onset syndromic hearing loss as well as late-onset non-syndromic hearing loss. Our results correspond in part to the results of previous studies demonstrating that c-Ret, GFR $\alpha$ 1 and GDNF are expressed in auditory neurons [22, 23] and that GDNF has a protective effect on antibiotic-mediated ototoxicities [24–27].

### **Ednrb-mediated hearing loss**

Waardenburg-Shah syndrome (WS type IV, WS-IV), which is caused by mutations in the transcription factor Sox10 [28], cytokine endothelin (ET)-3 [29] and its receptor endothelin receptor B (*Ednrb*) [30], is characterized by hypopigmentation, megacolon disease and hearing loss. The incidence of WS is 1 per 10,000 to 20,000 people [31]. Endothelin receptor B (*Ednrb/EDNRB*) belongs to the G-protein-coupled receptor family that mediates the multifaceted actions of endothelins [32, 33]. Mutations of *Ednrb/EDNRB* have been shown to cause embryonic defects in melanocytes and enteric ganglion neurons derived from the neural crest, resulting in hypopigmentation, megacolon disease and congenital hearing loss. In previous studies with animal models, both piebald-lethal rats in which *Ednrb* is spontaneously mutated [34] and *Ednrb* homozygous knock-out [*Ednrb*(-/-)] mice [35] have been shown to have typical WS-IV phenotypes. Thus, previous studies indicate that *Ednrb* is a key regulatory molecule for embryonic development of melanocytes and peripheral neurons, including neurons in the ENS. Previous studies also demonstrated that impairments of *Ednrb/EDNRB* cause syndromic hearing loss due to congenital defects of melanocytes in the stria vascularis of the inner ear [30, 32–35]. In our previous study, *Ednrb* protein was expressed in SGNs from wild-type (WT)-mice on postnatal

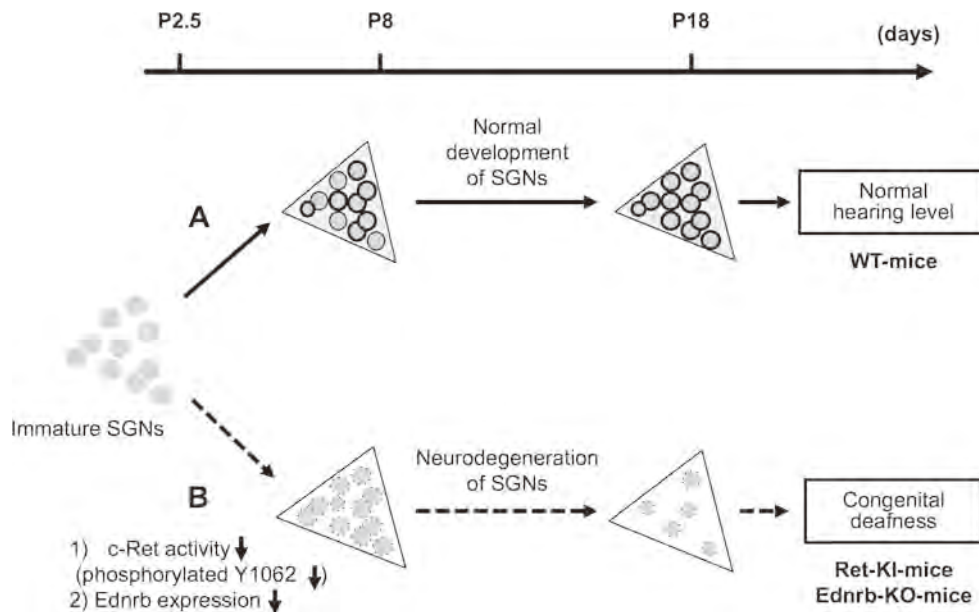


**Fig. 1** Schematic summary of congenital deafness caused by neurodegeneration of spiral ganglion neurons (SGNs) in *c-Ret*-knock-in-mice and *Ednrb*-knock-out-mice. The *x*-axis indicates age (days after birth) of mice. Triangles Rosenthal’s canals in wild-type (WT) (light gray background), or homozygous *c-Ret*-knock-in<sup>Y1062F/Y1062F</sup> (Ret-KI) [20] and homozygous *Ednrb*-knock-out-mice (Ednrb-KO) (white background) [36]; gray circles/no outline immature SGNs; gray circles/thin outline SGNs; gray circles/bold outline SGNs with “phosphorylated Y1062 in *c-Ret*” or “expression of *Ednrb*”. Dark

gray circles/dotted outline SGNs with “decreased phosphorylation of Y1062 in *c-Ret*” or “decreased expression of *Ednrb*”. **a** *c-Ret*-KI- and *Ednrb*-KO-mice suffer from congenital deafness with neurodegeneration of SGNs. **b** *c-Ret*-KI<sup>Y1062F/Y1062F</sup>-mice showed no Y1062-phosphorylated SGNs even on P8, although Y1062-phosphorylated SGNs began to appear in WT mice from P8 [20]. *Ednrb*-KO-mice also showed undetectably low expression level of *Ednrb* in SGNs on P8, although *Ednrb*-positive SGNs began to appear in WT mice from P8 [36]

day 19 (P19), while it was undetectable in SGNs from WT-mice on P3. Correspondingly, *Ednrb* homozygously deleted mice [*Ednrb*(-/-)-mice] developed congenital hearing loss (Fig. 1) [36]. Thus, expression of *Ednrb* expressed in SGNs in the inner ears is required for post-natal development of hearing in mice. A therapeutic strategy for congenital hearing loss in WS-IV patients has not been established. EDNRB expressed in SGNs could be a novel potential therapeutic strategy for congenital hearing loss in WS-IV patients.

### Neurodegeneration of SGNs caused by impairments of *c-Ret* and *Ednrb*

Phosphorylation of Y1062 in *c-Ret* has been shown to mediate several biological responses, including development and survival of neuronal cells [13, 37]. In our recent studies, *c-Ret*-KI<sup>Y1062F/Y1062F</sup>-mice developed severe congenital deafness with neurodegeneration of SGNs on postnatal day (P) 8–18, while *c-Ret*-KI<sup>Y1062F/Y1062F</sup>-mice showed morphology of SGNs comparable to that in WT mice on P2–3 [20]. Phosphorylation of Y1062 in *c-Ret* of SGNs from WT mice on P2–3 was below the limit of detection, while that on P8–18 was clearly detectable [20]. Thus, it is thought that SGNs from *c-Ret*-KI<sup>Y1062F/Y1062F</sup>-

mice developed normally at least until P3 after birth, when Y1062 in *c-Ret* of SGNs from WT mice is unphosphorylated. However, in *c-Ret*-KI<sup>Y1062F/Y1062F</sup>-mice, phosphorylation of Y1062 is no longer maintained by P8–P18, when Y1062 in *c-Ret* of SGNs from WT mice exhibits significant phosphorylation [20]. Furthermore, partially unphosphorylated Y1062 in *c-Ret* of SGNs accelerated age-related hearing loss with accelerated reduction of SGNs from 4 months of age, while normal hearing and normal density of SGNs were observed at least until 1 month of age, when hearing has matured [21]. On the other hand, *Ednrb* protein was expressed in SGNs from WT-mice on postnatal day 19 (P19), while it was undetectable in SGNs from WT-mice on P3. Correspondingly, *Ednrb*(-/-)-mice with congenital hearing loss showed a decreased number of SGNs (Fig. 1) and degeneration of SGNs on P19 but not on P3 [36]. Thus, our results show that *Ednrb* expression in SGNs in inner ears is required for postnatal survival of SGNs in mice. The neurodegeneration of SGNs from *c-Ret*-KI<sup>Y1062F/Y1062F</sup>-mice and *Ednrb*(-/-)-mice did not show typical apoptotic signals and did not involve disturbance of hair bundles of IHCs and OHCs [20, 36]. The congenital hearing loss involving neurodegeneration of SGNs as well as megacolon disease in *Ednrb*(-/-)-mice were improved markedly by introducing an *Ednrb* transgene under the control of the dopamine beta-hydroxylase promoter (*Ednrb*(-/-);

*DBH-Ednrb*-mice). Neurodegeneration of SGNs was restored by introducing constitutively activated RET also in the case of c-Ret-mediated hearing loss. Thus, our results indicate that c-RET and EDNRB expressed in SGNs could be molecular targets in the prevention of hearing impairments.

### Environmental stress-related impairments of hearing and balance

Exposure to noise is recognized as one of the major environmental factors causing hearing loss [1]. Noise consists of sound with broad frequencies, but there is limited information about the frequency-dependent influence of noise on health. Low frequency noise (LFN) is constantly generated from natural and artificial sources. The frequency range of LFN is usually defined as being below 100 Hz, while that of infrasound is usually below 20 Hz [38]. In our recent study, we found that chronic exposure to LFN at moderate levels of 70 dB sound pressure level (SPL) causes impaired balance involving morphological abnormalities of the vestibule with increased levels of oxidative stress (Fig. 2) [39]. Previous studies have shown that behavioral impairments induced by antibiotics involved degeneration of vestibular cells and oxidative stress [40, 41]. In addition, a previous study has shown that antioxidant compounds prevent noise-induced hearing loss [42]. Ototoxicity caused by oxidative stress in inner ears has been shown to accompany impairment of antioxidant enzymes [42]. Thus, existing studies indicate the necessity for further

investigation of a causal molecule related to oxidative stress in vestibular hair cells affected by LFN, and of the preventive effect of antioxidants on impaired balance caused by LFN exposure. On the other hand, exposure to heavy metals including mercury, cadmium and arsenic has been suggested to cause impairments in balance [43] and hearing [44–46] in humans and experimental animals. Smoking has also been shown to affect hearing in humans [47]. In previous studies, childhood exposure to heavy metals has been shown to sensitively affect hearing development in humans [48–50]. Aging has also been shown to affect sensitivities to ototoxic factors in mice [51]. Therefore, further studies are needed to determine the age-specific susceptibilities to environmental stresses, including heavy metals, in terms of ototoxicity in mice and humans.

### Conclusions

Our studies provide direct evidence that c-RET and EDNRB expressed in SGNs are novel targets for hearing loss. These studies underline the importance of considering the activity as well as the expression of the target molecule in order to elucidate the etiologies of hereditary deafness. In addition, environmental stresses, including exposure to noise and heavy metals, can cause impairments of hearing and balance that are affected intricately by aging and genetic factors. Information obtained in previous studies prompts further investigation of the influence of environmental stresses on the impairment of hearing and balance with consideration of aging and genetic factors to develop new diagnostic, preventive and therapeutic strategies against impairment of hearing and balance.

**Acknowledgments** This review is based on research that was given an encouragement award at the 82nd annual meeting of the Japanese Society for Hygiene held in Kyoto, Japan on 24–26 March 2012. We thank Yoko Kato and Harumi Ohno for their technical assistance. This study was supported in part by Grants-in-Aid for Scientific Research (B) (No. 20406003, No. 24390157 and No. 24406002) and (C) (No. 23592479), Grant-in-Aid for Challenging Exploratory Research (No. 23650241) and Grants-in-Aid for Young Scientists (B) (No. 23790160) from the Ministry of Education, Culture, Sports, Science and Technology (MEXT), AA Science Platform Program from the Japan Society for the Promotion of Science (JSPS), Adaptable and Seamless Technology Transfer Program through Target-driven R&D, Japan Science and Technology Agency, COE Project (Health Science Hills) for Private Universities from MEXT and Chubu University (No. S0801055), Research Grant from the Tokyo Biochemical Research Foundation (TBRF), the Naito Foundation Natural Science Scholarship, Research Foundation from the Institute of Science and Technology Research in Chubu University and Chubu University grants A, B and CG.

**Conflict of interest** We have no financial conflict of interest in relation to this submission.

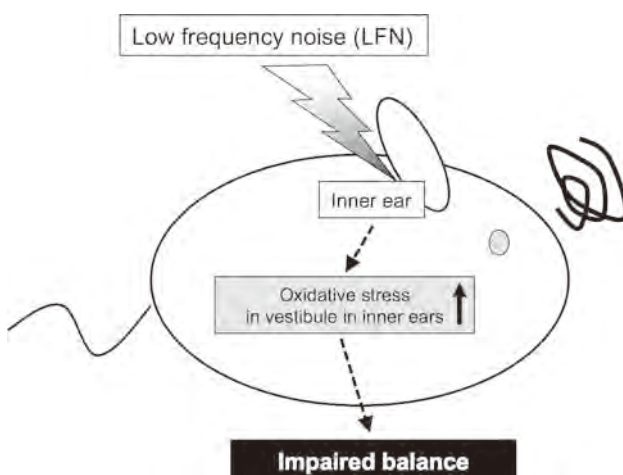


**Fig. 2** Schematic summary of impaired balance in mice caused by exposure to low frequency noise (LFN). Chronic exposure to low frequency noise (LFN, 0.1 kHz) at moderate levels of 70 dB sound pressure level (SPL) causes impaired balance involving morphological impairments of the vestibule with enhanced levels of oxidative stress [39]

**Open Access** This article is distributed under the terms of the Creative Commons Attribution License which permits any use, distribution, and reproduction in any medium, provided the original author(s) and the source are credited.

## References

- Lalwani AK, Gürtler N. Sensorineural hearing loss, the aging inner ear, and hereditary hearing impairment. In: Lalwani AK, editor. *CURRENT diagnosis & treatment in otolaryngology—head & neck surgery*. 2nd edn. New York: McGraw-Hill; 2008. pp. 683–704.
- Brown SD, Hardisty-Hughes RE, Mburu P. Quiet as a mouse: dissecting the molecular and genetic basis of hearing. *Nat Rev Genet*. 2008;9:277–90.
- Gratton MA, Vázquez AE. Age-related hearing loss: current research. *Curr Opin Otolaryngol Head Neck Surg*. 2003;11:367–71.
- Salt AN, Melichar I, Thalmann R. Mechanisms of endocochlear potential generation by stria vascularis. *Laryngoscope*. 1987;97:984–91.
- Steel KP, Barkway C. Another role for melanocytes: their importance for normal stria vascularis development in the mammalian inner ear. *Development*. 1989;107:453–63.
- Nin F, Hibino H, Doi K, Suzuki T, Hisa Y, Kurachi Y. The endocochlear potential depends on two K<sup>+</sup> diffusion potentials and an electrical barrier in the stria vascularis of the inner ear. *Proc Natl Acad Sci USA*. 2008;105:1751–6.
- Gürtler N, Lalwani AK. Etiology of syndromic and nonsyndromic sensorineural hearing loss. *Otolaryngol Clin North Am*. 2002;35:891–908.
- Zhao X, Jones SM, Yamoah EN, Lundberg YW. Otoconin-90 deletion leads to imbalance but normal hearing: a comparison with other otoconia mutants. *Neuroscience*. 2008;153:289–99.
- Kato M, Iwashita T, Takeda K, Akhand AA, Liu W, Yoshihara M, et al. Ultraviolet light induces redox reaction-mediated dimerization and superactivation of oncogenic Ret tyrosine kinases. *Mol Biol Cell*. 2000;11:93–101.
- Trupp M, Scott R, Whittemore SR, Ibáñez CF. Ret-dependent and -independent mechanisms of glial cell line-derived neurotrophic factor signaling in neuronal cells. *J Biol Chem*. 1999;274:20885–94.
- Jijwa M, Fukuda T, Kawai K, Nakamura A, Kurokawa K, Murakumo Y, et al. A targeting mutation of tyrosine 1062 in Ret causes a marked decrease of enteric neurons and renal hypoplasia. *Mol Cell Biol*. 2004;24:8026–36.
- Drosten M, Pützer BM. Mechanisms of disease: cancer targeting and the impact of oncogenic RET for medullary thyroid carcinoma therapy. *Nat Clin Pract Oncol*. 2006;3:564–74.
- Airaksinen MS, Saarma M. The GDNF family: signalling, biological functions and therapeutic value. *Nat Rev Neurosci*. 2002;3:383–94.
- Poteryaev D, Titievsky A, Sun YF, Thomas-Crusells J, Lindahl M, Billaud M, et al. GDNF triggers a novel ret-independent Src kinase family-coupled signaling via a GPI-linked GDNF receptor alpha1. *FEBS Lett*. 1999;463:63–6.
- Heanue TA, Pachnis V. Enteric nervous system development and Hirschsprung's disease: advances in genetic and stem cell studies. *Nat Rev Neurosci*. 2007;8:466–79.
- Kato M, Takeda K, Kawamoto Y, Iwashita T, Akhand AA, Senga T, et al. Repair by Src kinase of function-impaired RET with multiple endocrine neoplasia type 2A mutation with substitutions of tyrosines in the COOH-terminal kinase domain for phenylalanine. *Cancer Res*. 2002;62:2414–22.
- Moore SW, Johnson AG. Hirschsprung's disease: genetic and functional associations of Down's and Waardenburg syndromes. *Semin Pediatr Surg*. 1998;7:156–61.
- Moore SW. The contribution of associated congenital anomalies in understanding Hirschsprung's disease. *Pediatr Surg Int*. 2006;22:305–15.
- Inoue K, Shimotake T, Iwai N. Mutational analysis of RET/GDNF/NTN genes in children with total colonic aganglionosis with small bowel involvement. *Am J Med Genet*. 2000;93:278–84.
- Ohgami N, Ida M, Shimotake T, Sakashita N, Sone M, Nakashima T, et al. c-Ret-mediated hearing loss in mice with Hirschsprung disease. *Proc Natl Acad Sci USA*. 2010;107:13051–6.
- Ohgami N, Ida-Eto M, Sakashita N, Sone M, Nakashima N, Tabuchi K, et al. Partial impairment of c-Ret at tyrosine 1062 accelerates age-related hearing loss in mice. *Neurobiol Aging*. 2012;33:626.e25–34.
- Stöver T, Gong TL, Cho Y, Altschuler RA, Lomax MI. Expression of the GDNF family members and their receptors in the mature rat cochlea. *Brain Res Mol Brain Res*. 2000;76:25–35.
- Stöver T, Nam Y, Gong TL, Lomax MI, Altschuler RA. Glial cell line-derived neurotrophic factor (GDNF) and its receptor complex are expressed in the auditory nerve of the mature rat cochlea. *Hear Res*. 2001;155:143–51.
- Suzuki M, Yagi M, Brown JN, Miller AL, Miller JM, Raphael Y. Effect of transgenic GDNF expression on gentamicin-induced cochlear and vestibular toxicity. *Gene Ther*. 2000;7:1046–54.
- Yagi M, Kanzaki S, Kawamoto K, Shin B, Shah PP, Magal E, et al. Spiral ganglion neurons are protected from degeneration by GDNF gene therapy. *J Assoc Res Otolaryngol*. 2000;1:315–25.
- Liu Y, Okada T, Shimazaki K, Sheykhloeslami K, Nomoto T, Muramatsu S, et al. Protection against aminoglycoside-induced ototoxicity by regulated AAV vector-mediated GDNF gene transfer into the cochlea. *Mol Ther*. 2008;16:474–80.
- Scheper V, Paasche G, Miller JM, Warnecke A, Berkingali N, Lenarz T, et al. Effects of delayed treatment with combined GDNF and continuous electrical stimulation on spiral ganglion cell survival in deafened guinea pigs. *J Neurosci Res*. 2009;87:1389–99.
- Pingault V, Bondurand N, Kuhlbrodt K, Goerich DE, Prehu MO, Puliti A, et al. SOX10 mutations in patients with Waardenburg-Hirschsprung disease. *Nat Genet*. 1998;18:171–3.
- Edey P, Attie T, Amiel J, Pelet A, Eng C, Hofstra RMW, et al. Mutation of the endothelin-3 gene in the Waardenburg-Hirschsprung disease (Shah-Waardenburg syndrome). *Nat Genet*. 1996;12:442–4.
- Puffenberger EG, Hosoda K, Washington SS, Nakao K, deWit D, Yanagisawa M, et al. A missense mutation of the endothelin-B receptor gene in multigenic Hirschsprung's disease. *Cell*. 1994;79:1257–66.
- Pardono E, van Bever Y, van den Ende J, Havrenne PC, Iughetti P, Maestrelli SRP, et al. Waardenburg syndrome: clinical differentiation between types I and II. *Am J Med Genet A*. 2003;117A:223–35.
- Hosoda K, Hammer RE, Richardson JA, Baynash AG, Cheung JC, Giaid A, et al. Targeted and natural (piebald-lethal) mutations of endothelin-B receptor gene produce megacolon associated with spotted coat color in mice. *Cell*. 1994;79:1267–76.
- Bagnato A, Spinella F, Rosanò L. Emerging role of the endothelin axis in ovarian tumor progression. *Endocr Relat Cancer*. 2005;12:761–72.
- Garipey CE, Cass DT, Yanagisawa M. Null mutation of endothelin receptor type B gene in spotting lethal rats causes

- aganglionic megacolon and white coat color. *Proc Natl Acad Sci USA*. 1996;93:867–72.
35. Matsushima Y, Shinkai Y, Kobayashi Y, Sakamoto M, Kunieda T, Tachibana M. A mouse model of Waardenburg syndrome type 4 with a new spontaneous mutation of the endothelin-B receptor gene. *Mamm Genome*. 2002;13:30–5.
  36. Ida-Eto M, Ohgami N, Iida M, Yajima I, Kumasaka MY, Takaiwa K, et al. Partial requirement of endothelin receptor B in spiral ganglion neurons for postnatal development of hearing. *J Biol Chem*. 2011;286:29621–6.
  37. Hayashi H, Ichihara M, Iwashita T, Murakami H, Shimono Y, Kawai K, et al. Characterization of intracellular signals via tyrosine 1062 in RET activated by glial cell line-derived neurotrophic factor. *Oncogene*. 2000;19:4469–75.
  38. Leventhall G. A review of published research on low frequency noise and its effects, Department of Environment, Food, and Rural Affairs (DEFRA), UK. 2003. <http://archive.defra.gov.uk/environment/quality/noise/research/lowfrequency/documents/lowfreqnoise.pdf>. Accessed 20 June 2012.
  39. Tamura H, Ohgami N, Yajima I, Iida M, Ohgami K, Fujii N, et al. Chronic exposure to low frequency noise at moderate levels causes impaired balance in mice. *PLoS ONE*. 2012;7:e39807.
  40. Al Deeb S, Al Moutaery K, Khan HA, Tariq M. Exacerbation of iminodipropionitrile-induced behavioral toxicity, oxidative stress, and vestibular hair cell degeneration by gentamicin in rats. *Neurotoxicol Teratol*. 2000;22:213–20.
  41. Guthrie OW. Aminoglycoside induced ototoxicity. *Toxicology*. 2008;249:91–6.
  42. Henderson D, Bielefeld EC, Harris KC, Hu BH. The role of oxidative stress in noise-induced hearing loss. *Ear Hear*. 2006; 27:1–19.
  43. Bhattacharya A, Shukla R, Auyang ED, Dietrich KN, Bornschein R. Effect of succimer chelation therapy on postural balance and gait outcomes in children with early exposure to environmental lead. *Neurotoxicology*. 2007;28:686–95.
  44. Ozcaglar HU, Agirdir B, Dinc O, Turhan M, Kilinçarslan S, Oner G. Effects of cadmium on the hearing system. *Acta Otolaryngol*. 2001;121:393–7.
  45. Rice DC, Gilbert SG. Effects of developmental exposure to methyl mercury on spatial and temporal visual function in monkeys. *Toxicol Appl Pharmacol*. 1990;102:151–63.
  46. Shargorodsky J, Curhan SG, Henderson E, Eavey R, Curhan GC. Heavy metals exposure and hearing loss in US adolescents. *Arch Otolaryngol Head Neck Surg*. 2011;137:1183–9.
  47. Ohgami N, Kondo T, Kato M. Effects of light smoking on extra-high-frequency auditory thresholds in young adults. *Toxicol Ind Health*. 2011;27:143–7.
  48. Prasher D. Heavy metals and noise exposure: health effects. *Noise Health*. 2009;11:141–4.
  49. Ramirez GB, Pagulayan O, Akagi H, Francisco Rivera A, Lee LV, Berroya A, et al. Tagum study II: follow-up study at two years of age after prenatal exposure to mercury. *Pediatrics*. 2003; 111:289–95.
  50. Rothenberg SJ, Poblano A, Garza-Morales S. Prenatal and perinatal low level lead exposure alters brainstem auditory evoked responses in infants. *Neurotoxicology*. 1994;15:695–9.
  51. Prieve BA, Yanz JL. Age-dependent changes in susceptibility to ototoxic hearing loss. *Acta Otolaryngol*. 1984;98:428–38.

## RESEARCH ARTICLE

# Cigarette Smoking Causes Hearing Impairment among Bangladeshi Population

Ahmed Faisal Sumit<sup>1</sup>, Anindya Das<sup>1</sup>, Zinat Sharmin<sup>1</sup>, Nazmul Ahsan<sup>1</sup>, Nobutaka Ohgami<sup>2,3</sup>, Masashi Kato<sup>3</sup>, Anwarul Azim Akhand<sup>1\*</sup>

**1** Department of Genetic Engineering and Biotechnology, University of Dhaka, Dhaka, Bangladesh, **2** Nutritional Health Science Research Center, Chubu University, Kasugai, Japan, **3** Department of Occupational and Environmental Health, Nagoya University Graduate School of Medicine, Nagoya, Japan

\* akhand66@yahoo.com


 OPEN ACCESS

**Citation:** Sumit AF, Das A, Sharmin Z, Ahsan N, Ohgami N, Kato M, et al. (2015) Cigarette Smoking Causes Hearing Impairment among Bangladeshi Population. PLoS ONE 10(3): e0118960. doi:10.1371/journal.pone.0118960

**Academic Editor:** Ming Yang, Beijing University of Chemical Technology, CHINA

**Received:** August 13, 2014

**Accepted:** January 7, 2015

**Published:** March 17, 2015

**Copyright:** © 2015 Sumit et al. This is an open access article distributed under the terms of the [Creative Commons Attribution License](https://creativecommons.org/licenses/by/4.0/), which permits unrestricted use, distribution, and reproduction in any medium, provided the original author and source are credited.

**Data Availability Statement:** All relevant data are within the paper and its Supporting Information files.

**Funding:** These authors have no support or funding to report.

**Competing Interests:** Co-author Anwarul Azim Akhand of this manuscript is a PLOS ONE Editorial Board Member. This does not alter the authors' adherence to PLOS ONE Editorial policies.

## Abstract

Lifestyle including smoking, noise exposure with MP3 player and drinking alcohol are considered as risk factors for affecting hearing synergistically. However, little is known about the association of cigarette smoking with hearing impairment among subjects who carry a lifestyle without using MP3 player and drinking alcohol. We showed here the influence of smoking on hearing among Bangladeshi subjects who maintain a lifestyle devoid of using MP3 player and drinking alcohol. A total of 184 subjects (smokers: 90; non-smokers: 94) were included considering their duration and frequency of smoking for conducting this study. The mean hearing thresholds of non-smoker subjects at 1, 4, 8 and 12 kHz frequencies were 5.63±2.10, 8.56±5.75, 21.06±11.06, 40.79±20.36 decibel (dB), respectively and that of the smokers were 7±3.8, 13.27±8.4, 30.66±12.50 and 56.88±21.58 dB, respectively. The hearing thresholds of the smokers at 4, 8 and 12 kHz frequencies were significantly ( $p < 0.05$ ) higher than those of the non-smokers, while no significant differences were observed at 1 kHz frequency. We also observed no significant difference in auditory thresholds among smoker subgroups based on smoking frequency. In contrast, subjects smoked for longer duration (>5 years) showed higher level of auditory threshold (62.16±19.87 dB) at 12 kHz frequency compared with that (41.52±19.21 dB) of the subjects smoked for 1-5 years and the difference in auditory thresholds was statistically significant ( $p < 0.0002$ ). In this study, the Brinkman Index (BI) of smokers was from 6 to 440 and the adjusted odds ratio showed a positive correlation between hearing loss and smoking when adjusted for age and body mass index (BMI). In addition, age, but not BMI, also played positive role on hearing impairment at all frequencies. Thus, these findings suggested that cigarette smoking affects hearing level at all the frequencies tested but most significantly at extra higher frequencies.

## Introduction

Hearing is one of the most important tools of social communication. Hearing is known to be deteriorated gradually during the ageing process [1]. In addition to ageing, a variety of environmental factors may also cause hearing impairment. Noise exposure has been proven to be the most important environmental factor for weakening hearing level [2]. In the United States 14% of workers work in an environment where the noise level exceeds 90 decibels (dB) according to a report of the National Institute for Occupational Safety and Health [3]. In Korea, workers with noise-induced hearing loss account for more than 90% of total workers with occupational diseases according to an earlier report [4]. In addition to the work-related exposure to noise, previous studies have shown that a modern lifestyle generally using MP3 player with an earphone is becoming a serious risk for hearing loss [5, 6]. On the other hand, smoking is also considered as one of the risk factors for hearing loss. A previous study has shown that light smoking classified by the Brinkman Index (BI; cigarettes/day multiplied by number of years) affects extra-high-frequency (12 kHz) auditory thresholds in young adults who have a lifestyle using portable MP3 player and drinking alcohol [7]. Other studies further examined the relationship between smoking and noise-induced hearing loss and showed that the incidence of noise-induced hearing loss is significantly higher in smokers [8–10] or that there is a synergistic effect between the two factors [11, 12]. Moreover, some studies showed a dose-response relationship between the amount of smoking and impairment of noise-induced hearing acuity [13]. Meanwhile, there is a previous study showing the absence of a significant correlation between the two factors [14]. Thus, the synergistic influence on hearing by smoking and noise-induced hearing loss remains controversial.

On the other hand, smoking cigarettes is considered as a potential risk factor for the most life-threatening chronic diseases including cancers (lung, throat, blood etc.), cardiovascular and respiratory diseases [15, 16]. In spite of these consequences, prevalence of smoking is very widespread around the world. In Bangladesh, more than 20% of populations are addicted to some form of smoking [17]. Prevalence of hearing impairment among South Asian population is also known to be quite high. However, the direct relationship between hearing impairment and smoking cigarettes remained mostly unfocused. Only few studies have been shown to cause hearing loss linking with cigarette smoking [7, 18–20]. Meanwhile, some studies failed to find any direct correlation between them [21, 22]. Most of the earlier studies have investigated the correlation of hearing impairment among subjects who have used MP3 player and have drunk alcohol. This study was therefore attempted to investigate whether cigarette smoking affects hearing among subjects in Bangladesh who maintain a lifestyle without using MP3 player and drinking alcohol. For this purpose, the study was conducted among 184 subjects of different ages, among them 90 subjects smoked cigarettes on daily basis. The audiometric measurement was taken at 1, 4, 8 and 12 kHz frequencies. The mean  $\pm$  S.D values of auditory thresholds were measured followed by analysis of the correlation between hearing impairment and smoking cigarettes. Furthermore, the study was attempted to find out any association of hearing impairment with frequency and duration of cigarettes smoked.

## Methods

### Study Subjects

The study was conducted among 184 male subjects aged between 18–60 years who agreed in written to participate in audiometric testing. In this study, we did not include those subjects who had a habit of drinking alcohol and using portable music player with earphones. We also excluded those participants who had a previous history of ear diseases and suffered from illness

at the time of survey. In addition, no subject was included in this study from other ethnic group or race. The body mass index (BMI) was calculated by using the formula: Weight in kg/(Height in metre<sup>2</sup>). All the experiments were undertaken considering the ethical issues and the study was approved by the Faculty of Biological Science, University of Dhaka (Ref. no. 5509/Bio.Sc). A survey was performed using a self-reporting questionnaire on smoking habit including duration of smoking, frequency of cigarette smoking/day, age, previous history of disease, weight and height of the participants.

## Measurement of Hearing Level

Measurement of hearing level at 1, 4, 8 and 12 kHz frequencies were performed in all the participating subjects. Audiometric examination was conducted in a sound-proof room using an iPod with earphones as described previously [23, 24]. Sound signals at 1, 4, 8 and 12 kHz frequencies were presented to each subject until the threshold of sound that the subjects were just able to perceive was identified. Hearing levels of all the subjects were measured by providing an initial 5 dB stimulus followed by stepwise increase in sound level by 5 dB. Examination of hearing was duplicated in each subject to confirm the repeatability of the values. The subjects were classified as having low/mild frequency hearing loss if the average of the pure-tone thresholds at 1 and 4 kHz frequencies were exceeded 20 dB. High frequency hearing loss was considered if the average of the pure-tone thresholds at 8 and 12 kHz frequencies were exceeded 40 dB. As described earlier, of the 184 subjects, 90 were smokers and the rest 94 were non-smokers control. The relationship between cigarette smoking and hearing level was evaluated using Brinkman index (BI) which was defined by the number of cigarettes smoked/day multiplied by the number of years [25]. According to BI, subjects were classified as a non-smoking group (BI = 0) and a smoking group ( $6 \leq BI \leq 440$ ). Since the highest BI (e.g. 440) in this study was less than the BI (e.g. > 600) of defined heavy smokers in a previous report [26], we included all the smokers in smoking group rather than classifying them as heavy or light smoking groups.

## Data analysis

Data were statistically analyzed using SPSS program version 22 software (SPSS Inc., Chicago, USA). As the data did not show normal distribution, the difference between each group was analyzed using Pearson's  $\chi^2$  (chi-square) method. The descriptive statistics were also presented in the result. For each characteristics of the subjects, *p*-value and odds ratio were measured. For further confirmation, binary logistic regression analysis was performed to determine adjusted odds ratio and 95% confidence interval (CI). The regression analysis made use of the different predictor variables in the numerical form. Hearing level was taken as dependent variable, and smoking habit, age and BMI were considered as independent variables. The significance of the results was set at  $p < 0.05$ .

## Results

### Characteristics of the study population

Among 184 subjects analyzed, 90 (48.91%) were smokers and 94 (51.08%) were non-smokers. Of the smokers ( $n = 90$ ), 49 (54.4%) were aged  $\leq 40$  years and the rest 41 (45.6%) were aged  $> 40$  years (Table 1). The mean age for the smokers was  $39.07 \pm 11.6$  years and that for the non-smokers was  $36.34 \pm 12.2$  years. BMI of the smokers and nonsmokers were  $23.26 \pm 3.3$  and  $23.78 \pm 2.7$  kg/m<sup>2</sup>, respectively. The subjects were further categorized as underweight, normal weight and overweight based on their BMI  $< 18.5$ ,  $18.5$ – $25$  and  $> 25$  kg/m<sup>2</sup>, respectively. The number of subjects under normal weight of smokers and nonsmokers were 63 (70% of total

**Table 1. Characteristics of the participants according to smoking status.**

	Smoker	Nonsmoker	p-value
<b>Total No.</b>	90	94	
<b>Mean age (years)</b>	39.07±11.6	36.34±12.2	0.122
<b>Age category</b>			
≤40 years old: n (%)	49 (54.4%)	55 (58.5%)	0.07
>40 years old: n (%)	41 (45.6%)	39 (41.5%)	0.28
<b>BMI (kg/m<sup>2</sup>)</b>	23.26 ± 3.3	23.78 ± 2.7	0.241
<b>BMI category<sup>†</sup></b>			
Under weight: n (%)	4 (4.4%)	3 (3.2%)	0.002
Normal weight: n (%)	63 (70%)	62 (66%)	0.003
Over weight: n (%)	23 (25.6%)	29 (30.9%)	0.007
<b>Duration of smoking</b>			
1–5 years: n	23		
>5 years: n	67		
<b>Frequency of smoking/day</b>			
1–10 cigarettes/day: n	35		
11–20 cigarettes/day: n	45		
>20 cigarettes/day: n	10		

<sup>†</sup>The subjects were categorized underweight, normal weight and overweight when the BMI was found <18.5, 18.5–25 and >25 kg/m<sup>2</sup>, respectively.

doi:10.1371/journal.pone.0118960.t001

smokers) and 62 (66% of total nonsmokers), respectively (Table 1), denoting the major portion of the subjects. The number of subjects under overweight category in both the smokers and nonsmokers were relatively low (smoker: 23, 25.6%; nonsmoker: 29, 30.9%). Least numbers of subjects were underweight in both of the smokers (4, 4.4%) and nonsmokers (3, 3.2%). *P*-values for comparing the mean age, age category, BMI and BMI category between smoker and nonsmoker are also shown in Table 1.

### Cigarette smoking caused hearing impairment

In case of control (non-smoker) subjects (*n* = 94), the average auditory thresholds observed at 1, 4, 8 and 12 kHz frequencies were 5.63±2.10, 8.56±5.75, 21.06±11.06, 40.79±20.36 dB, respectively (Fig. 1). When the average auditory thresholds for smokers (*n* = 90) were measured at all of the frequencies above, we found the values as 7±3.8, 13.27±8.4, 30.66±12.50 and 56.88±21.58 dB, respectively. The hearing level is quantified relative to 'normal' hearing in dB, with higher values of dB indicating worse hearing. The average auditory thresholds for smokers were found significantly (*p* = 0.0001) higher than non-smokers at 8 and 12 kHz frequencies. The differences which might be attributed to smoking that smoking with BI≤440 caused impairment of hearing level at all the frequencies and that the hearing impairment was most evident at the higher frequency (12 kHz). Since the mean ± S.D of BI in this experiment was 129.25 ± 124.80, smoking group (*n* = 90) with an average BI of ~130 might cause hearing impairment at all frequencies compared to non-smokers.

### Correlation between age and smoking

The prevalence of hearing impairment was found higher among smokers of both age groups (≤40 and >40 years) compared with those of the nonsmokers at all the frequencies tested (Table 2). At 1, 4, 8 and 12 kHz frequencies, the percentage of the older smokers (>40 years) who experienced

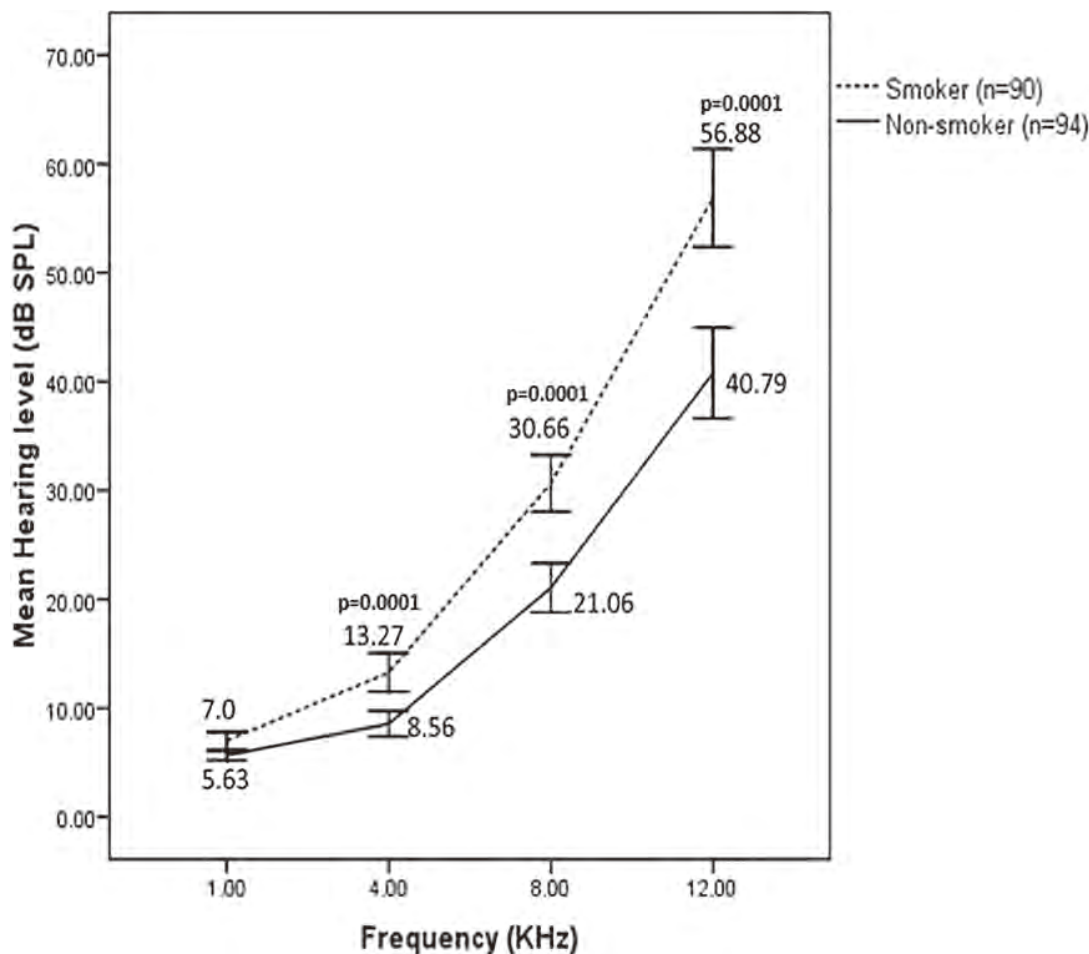


**Fig 1. Effect of smoking on hearing level.** Auditory thresholds (mean  $\pm$  S.D) from 1 to 12 kHz frequencies in non-smoker 'control' (Brinkman index [BI = 0];  $n = 94$ ) and smokers ( $6 \leq BI \leq 440$ ;  $n = 90$ ) are shown. Smokers showed significantly ( $p = 0.0001$ ) higher auditory thresholds than non-smokers at 4, 8 and 12 kHz frequencies.

doi:10.1371/journal.pone.0118960.g001

hearing loss was 14.6, 39.0, 68.3 and 92.7%, however, the values for those of the nonsmokers was 5.1, 10.3, 35.9 and 76.9%. In case of younger smokers ( $\leq 40$  years), smoking also caused hearing loss compared with younger nonsmokers, however, the effect was relatively less than the older age groups at all the frequencies. The above results indicated a possible role of smoking in decreasing hearing level of the subjects regardless of their age. Moreover, the most profound effect of smoking on hearing for both age groups was observed at the extra high frequency (12 kHz). For both smokers and nonsmokers of older and younger groups, there was a significant difference ( $p < 0.05$ ) in hearing impairment at almost all of the higher frequencies. However, the difference was not found significant ( $p = 0.06$ ) between smoker and nonsmoker older than 40 years at the extra higher frequency (12 kHz). As hearing loss was more profound for the older age group (nonsmoker: 76.9%, smoker: 92.7%) at that frequency, significant difference probably was not obtained.

### Correlation between smoking frequency and hearing impairment

We divided the smokers into 3 subgroups depending on their frequency of smoking per day (Table 1) to examine whether this frequency could influence hearing level. Although the

**Table 2. Association between smoking and age on hearing impairment.**

Frequency	Age & smoking status	Subjects undergoing hearing impairment		p-value	Odds ratio (95% CI)
		No.	%		
12 kHz	<b>≤40 years</b>				
	Smoker (n = 49)	26	53.1	0.0003*	5.08 (2.09–12.33)
	Non-smoker (n = 55)	10	18.2		
	<b>&gt;40 years</b>				
	Smoker (n = 41)	38	92.7	0.06	3.80 (0.94–15.20)
	Non-smoker (n = 39)	30	76.9		
8 kHz	<b>≤40 years</b>				
	Smoker (n = 49)	18	36.7	0.002*	5.80 (1.95–17.22)
	Non-smoker (n = 55)	5	9.1		
	<b>&gt;40 years</b>				
	Smoker (n = 41)	28	68.3	0.004*	3.84 (1.52–9.72)
	Non-smoker (n = 39)	14	35.9		
4kHz	<b>≤40 years</b>				
	Smoker (n = 49)	10	20.4	0.03*	4.44 (1.14–17.23)
	Non-smoker (n = 55)	3	5.5		
	<b>&gt;40 years</b>				
	Smoker (n = 41)	16	39.0	0.005*	5.60 (1.67–18.77)
	Non-smoker (n = 39)	4	10.3		
1kHz	<b>≤40 years</b>				
	Smoker (n = 49)	2	4.1	0.05	2.2 (0.20–26.15)
	Non-smoker (n = 55)	1	1.8		
	<b>&gt;40 years</b>				
	Smoker (n = 41)	6	14.6	0.17	3.1 (0.59–16.77)
	Non-smoker (n = 39)	2	5.1		

\*Statistically significant.

Abbreviation: CI: confidence interval; OR: odds ratio.

doi:10.1371/journal.pone.0118960.t002

average auditory thresholds were slightly increased with increasing smoking frequency, however; the difference in hearing thresholds among the smoker subgroups at all the frequencies (1, 4, 8 and 12 kHz) tested was not statistically significant ( $p > 0.05$ ; Fig. 2). Though smoking generally affects hearing level, frequency of smoking (1 to >20 cigarette ranges/day) did not show significant additional impairment of hearing with increasing smoking amount.

### Duration of smoking impaired hearing level at high frequencies

The effect of smoking duration on hearing level was also examined. Smokers were divided into two subgroups (Table 1): smoking for 1–5 years and smoking for >5 years. Smoking duration was classified into 1–5 years and >5 years to denote smoking for shorter and longer period of time based on an earlier study that examined the influence of intensity and duration of smoking on recurrent aphthous stomatitis lesions [27]. The auditory thresholds at 8 and 12 kHz frequencies for smokers who smoked for 1–5 years (n = 23) were 24.13±10.15 and 41.52±19.21 dB, respectively, whereas the values for smokers who smoked for more than 5 years (n = 67)

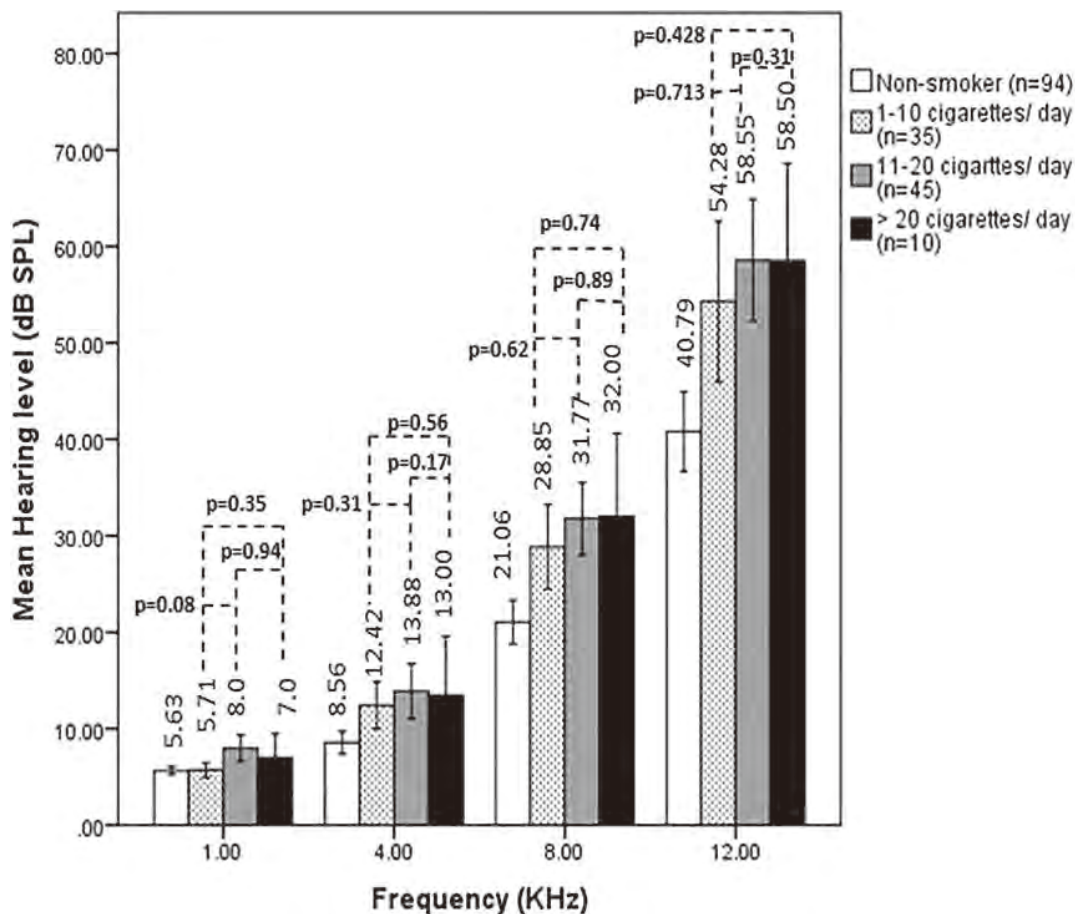


**Fig 2. Effects of smoking frequency on hearing level.** Auditory thresholds (mean± S.D) from 1 kHz to 12 kHz frequencies in non-smoker ‘control’ (n = 94) and smokers are shown. According to the frequency of smoking, smokers were divided into 3 subgroups as 1–10 cigarettes/day (n = 35), 11–20 cigarettes/day (n = 45) and >20 cigarettes/day (n = 10). The p-values for the difference in hearing thresholds among the smoker subgroups at all the frequencies tested were shown. P-values were calculated comparing between smoker subgroups 1–10 cigarettes/day and 11–20 cigarettes/day; 1–10 cigarettes/day and >20 cigarettes/day; and 11–20 cigarettes/day and >20 cigarettes/day.

doi:10.1371/journal.pone.0118960.g002

were 32.91±12.40 and 62.16±19.87 dB, respectively (Fig. 3). The difference in auditory threshold at 12 kHz frequency between smokers smoked for 1–5 years and more than 5 years was statistically significant ( $p = 0.005$ ). However, at lower frequencies such as 1, 4 and 8 kHz, the results were not found significant ( $p$ -value 0.293, 0.451 and 0.07, respectively). As the auditory threshold (62.16±19.87 dB) for smokers who smoked for more than 5 years exceeded far from the normal value of 40 dB at 12 kHz extra high frequency, it might be concluded that smoking cigarettes for long time chronically affect hearing levels.

### Binary logistic regression analysis

Association of hearing loss with smoking was further examined by logistic regression. The hearing loss (>40 dB for 12 and 8 kHz frequencies and >20 dB for 4 and 1 kHz frequencies) was taken as dependent variable and smoking habit, age, BMI of the participants were considered as independent variables. The independent variables were categorized considering non-smoker, age ≤40 years and BMI (normal weight) as reference group. Smoking and age were found to affect the hearing level more profoundly than the control groups after adjusting these

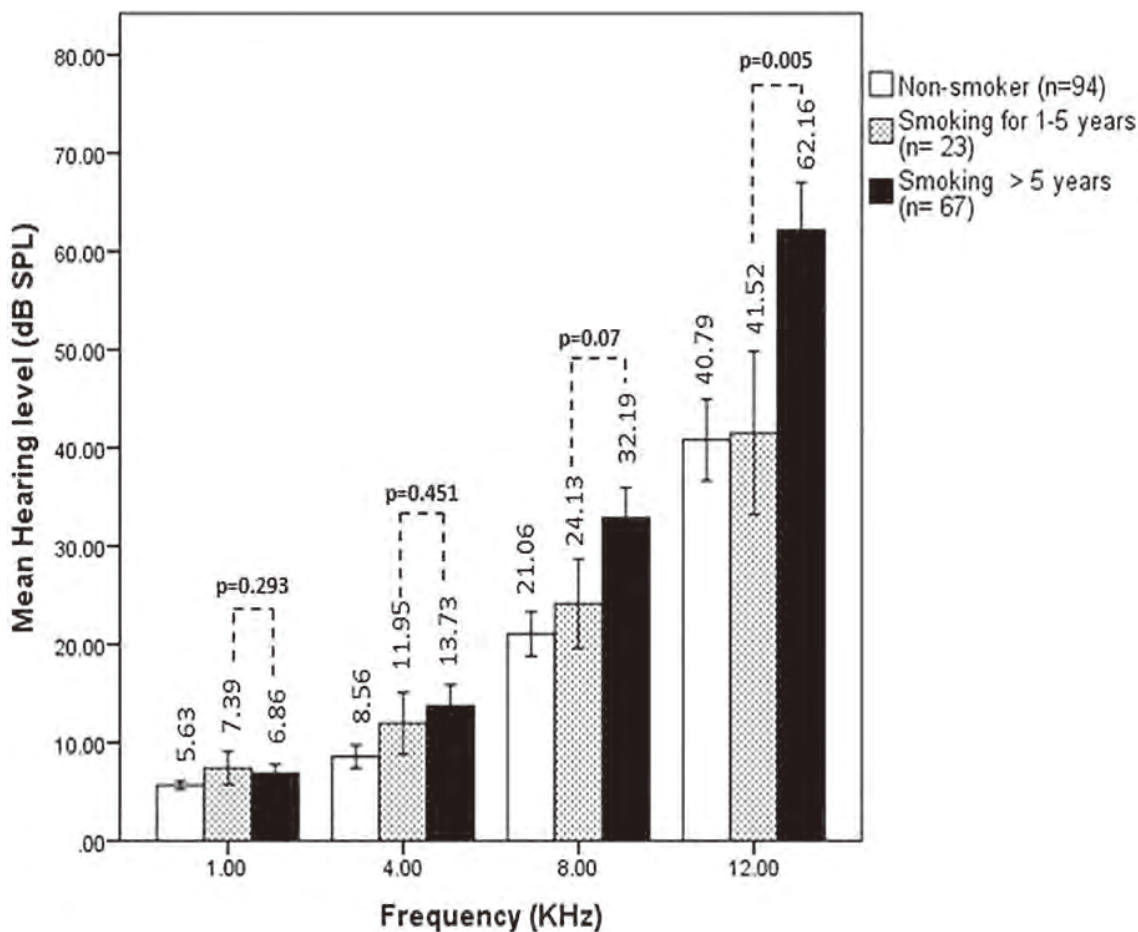


**Fig 3. Effects of duration of smoking on hearing level.** Auditory thresholds (mean±S.D) from 1 kHz to 12 kHz frequencies in non-smoker 'control' (n = 94) and smokers are shown. Based on duration of smoking, smokers were divided into 2 subgroups as smoked for 1–5 years (n = 23), and for more than 5 years (n = 67). The difference in auditory threshold between smokers smoked for 1–5 years and >5 years was statistically significant ( $p = 0.005$ ) at 12 kHz frequency, however, the values were not found significant at all other frequencies ( $p > 0.05$ ).

doi:10.1371/journal.pone.0118960.g003

factors (Table 3). The results suggested that controlling for differences in age and BMI of the participants, smoking increased the likelihood of hearing loss 4.90, 4.74, 5.04 and 2.85 times at 12, 8, 4 and 1 kHz frequencies respectively than non-smokers. Age also played positive role on hearing impairment at all frequencies. On the other hand, there were minor correlations of hearing loss with BMI (Table 3).

## Discussion

This study showed that smoking cigarettes significantly increased the risk of hearing impairment especially at higher frequencies. Among the smokers, 35% found to be smoked 1–10, 45% smoked 11–20 and 10% smoked more than 20 cigarettes daily. As compared with the non-smoker group, the smoker group was found at higher risk of developing hearing loss due to showing higher hearing thresholds at various frequencies tested. According to our results, the smokers with higher hearing thresholds at 4, 8 and 12 kHz might be more vulnerable for developing hearing loss due to showing significant difference in hearing levels in those

**Table 3. Adjusted odds ratio for hearing level<sup>†</sup> at all frequencies.**

Hearing level (n = 184)	1kHz		4kHz		8kHz		12kHz	
	Adjusted OR (95% CI)	p-value						
<b>Smoking habit</b>								
Non-smoker	1.0	0.14	1.0	0.0001*	1.0	0.0001*	1.0	0.0001*
Smoker	2.85 (0.7–11.3)		5.04 (2–12.5)		4.74 (2.3–9.6)		4.9 (2.3–10.5)	
<b>Age</b>								
≤40 years old	1.0	0.06	1.0	0.03*	1.0	0.0001*	1.0	0.0001*
>40 years old	3.71 (0.9–14.9)		2.38 (1.1–5.4)		4.14 (2.1–8.3)		12.75 (5.7–28.7)	
<b>BMI</b>								
Normal weight	1.0	0.99	1.0	0.78	1.0	0.86	1.0	0.30
Underweight	0.0		0.73 (0.7–7.0)		0.84 (0.13–5.2)		0.66 (0.1–4.0)	
Overweight	0.75 (0.2–3.0)	0.18	0.86 (0.35–2.1)	0.74	1.38 (0.64–2.9)	0.41	1.55 (0.7–3.6)	0.65

Abbreviation: CI: confidence interval; OR: odds ratio.

<sup>†</sup>Adjusted for smoking, age and BMI.

\*Statistically significant.

doi:10.1371/journal.pone.0118960.t003

frequencies. Our study correlates with some previous reports showing smoking mediated hearing loss at extra-high frequencies [7, 21, 28].

The association between smoking or alcohol consumption/exposure to occupational noise/ use of MP3 player and hearing loss have been shown in earlier studies [3–11]. Ohgami et al. [7] demonstrated the effects of life style (with smoking, drinking, noise exposure and sleeping time) on hearing level in young adults with narrow age range of 21–23 years. This study was so far the first attempted to determine the relationship of smoking alone with hearing impairment in Bangladeshi population with a wider age range of 18–60 years. Therefore, we mainly included those subjects in this study who maintained a lifestyle devoid of using music player and alcohol drinking to exclude a possible synergistic role of these factors with smoking. Apart from the earlier report that smoking, but not noise exposure or sleeping time, significantly affects hearing level at extra high frequency (12 kHz) in young adults [7], our results demonstrated that smoking affected the hearing level more profoundly in subjects of a wider age range at all higher frequencies (Table 3). The duration and frequency of smoking were also considered as risk factors for evaluating hearing loss at higher frequency. We found that the average auditory thresholds were slightly increased with increasing smoking amount but the difference in hearing thresholds among the smoker subgroups at all the frequencies tested was not statistically significant ( $p > 0.05$ ; Fig. 2). However, some earlier studies have demonstrated that there is a significant correlation between the severity of hearing loss and smoking amount [3, 10]. In addition, a dose-response relationship between the amount of smoking and the impairment of hearing acuity has been reported in the presence [13] or absence of exposure to noise [18].

Some previous studies have been carried out to distinguish the synergistic effect on hearing impairment between smoking and aging or other related factors [12, 19, 29]. In accordance with the results of these previous studies, the present study also showed subjects that smoke with aged >40 years had a greater risk of hearing impairment compared to nonsmokers.

Although hearing loss was observed in older nonsmokers as a function of age, the combined effects of smoking and age on hearing in smokers were more intense. When differences in age and BMI of the subjects were controlled, logistic regression analysis showed several fold increase in hearing loss by smoking compared to nonsmokers (OR: 4.90, 4.74, 5.04 and 2.85 at 12, 8, 4 and 1 kHz frequencies). Although the present study showed minor correlation of hearing loss with BMI, however, it was reported that BMI correlated well with higher hearing threshold across the whole frequency range in a large population-based study [30].

There are some limitations associated with the present study. The study was conducted using a self-reporting questionnaire on smoking habit, age and previous disease history of the participants. Data obtained through self-reporting were adopted directly without testing their authenticity by any other means. This limitation was probably minimized by guaranteeing the participants that their answers would be kept confidential. Apart from their smoking habit, the subjects with an earlier history of diseases were excluded and therefore the influence of this important risk factor on hearing could not be analyzed due to incompleteness of the data. No female subjects were included in this study mainly because female smokers are relatively rare in urban areas of Bangladesh. For this reason, we could not compare the effect of smoking on hearing level between male and female smokers. Nonetheless, based on the findings of the current study these limitations do not prevent to conclude that smoking impaired hearing level on the subjects with a wider range of age group (18–60 years).

Although the exact mechanism by which smoking affects the auditory organ is still unclear, several studies pointed out some mechanisms including direct ototoxicity of nicotine, cochlear ischemia due to increased levels of carboxyhemoglobin, and smoking-mediated increased blood viscosity [31–33]. Therefore, the involvement of these mechanisms collectively or individually might cause the smokers more vulnerable to hearing loss as compared with non-smokers. Further studies are needed to determine the molecular mechanism of smoking-mediated hearing impairment.

## Supporting Information

**S1 Fig. Similar frequency distributions of sound output between pure tone audiometry (PTA) and iPod.** Frequency distributions (means  $\pm$  SD) of tone burst sound (1–12 kHz) output by (A) PTA system and (B) iPod are presented. Both devices used earphone-type headphone (Panasonic RP-HJE150). The PTA system consists of PR2.1 Enhanced Real Time Processor, PA5 Programmable Attenuator and HB7 Headphone driver (Tucker-Davis Technologies, Inc). Sound levels from an earphone in a soundproof room were measured by a noise level meter (Type 6224 with an FFT analyzer, ACO CO., LTD, Japan) for 30 seconds and calculated as average of three repeated measurements. Background levels measured in a soundproof room without sound-generating devices were subtracted from sound levels from the earphone. Whole sound levels of (A) PTA and (B) iPod measured by the noise level meter without FFT analyzing software were almost the same (70 dB SPL).

(TIF)

**S2 Fig. Comparable hearing measurements between PTA and iPod.** Hearing levels (1–12 kHz) of eight subjects (21 years old) measured by PTA (closed square) and iPod (open diamond) are presented.

(TIF)

## Acknowledgments

We are thankful to Shamal Chandra Karmaker of the Department of Statistics, Biostatistics and Informatics of the University of Dhaka for his kind help in statistical analysis of our data.

## Author Contributions

Conceived and designed the experiments: NA AAA. Performed the experiments: AFS AD ZS. Analyzed the data: AFS. Contributed reagents/materials/analysis tools: NO MK. Wrote the paper: AFS NA AAA.

## References

1. Brant LJ, Fozard JL. Age changes in pure-tone hearing thresholds in a longitudinal study of normal human aging. *J Acoust Soc Am*. 1990; 88: 813–820. PMID: [2212307](#)
2. Lusk SL. Noise exposures. Effects on hearing and prevention of noise induced hearing loss. *AAOHN J*. 1997; 45(8): 397–408. PMID: [9341314](#)
3. Mohammadi S, Mazhari MM, Mehrparvar AH, Attarchi MS. Effect of simultaneous exposure to occupational noise and cigarette smoke on binaural hearing impairment. *Noise Health*. 2010; 12: 187–190. doi: [10.4103/1463-1741.64975](#) PMID: [20603575](#)
4. Kim KS. Occupational hearing loss in Korea. *J Korean Med Sci*. 2010; 25: 62–69.
5. Kim MG, Hong SM, Shim HJ, Kim YD, Cha CI, Yeo SG. Hearing threshold of Korean adolescents associated with the use of personal music players. *Yonsei Med J*. 2009; 50: 771–776. doi: [10.3349/ymj.2009.50.6.771](#) PMID: [20046416](#)
6. Vogel I, Verschuure H, van der Ploeg CP, Brug J, Raat H. Adolescents and MP3 players: too many risks, too few precautions. *Pediatrics*. 2009; 123: 953–958.
7. Ohgami N, Kondo T, Kato M. The effects of light smoking on extra-high-frequency auditory thresholds in young adults. *Toxicol Ind Health*. 2011; 27(2): 143–147. doi: [10.1177/0748233710382539](#) PMID: [20858647](#)
8. Palmer KT, Griffin MJ, Syddall HE, Coggon D. Cigarette smoking, occupational exposure to noise, and self-reported hearing difficulties. *Occup Environ Med*. 2004; 61: 340–344. PMID: [15031392](#)
9. Wild DC, Brewster MJ, Banerjee AR. Noise-induced hearing loss is exacerbated by long-term smoking. *Clin Otolaryngol*. 2005; 30: 517–520. PMID: [16402976](#)
10. Pouryaghoub G, Mehrdad R, Mohammadi S. Interaction of smoking and occupational noise exposure on hearing loss: a cross-sectional study. *BMC Publ Health*. 2007; 7: 137.
11. Mizoue T, Miyamoto T, Shimizu T. Combined effect of smoking and occupational exposure to noise on hearing loss in steel factory workers. *Occup Environ Med*. 2003; 60: 56–59. PMID: [12499458](#)
12. Ferrite S, Santana V. Joint effects of smoking, noise exposure and age on hearing loss. *Occup Med (Lond)*. 2005; 55: 48–53. PMID: [15699090](#)
13. Virokannas H, Anttonen H. Dose–response relationship between smoking and impairment of hearing acuity in workers exposed to noise. *Scand Audiol Suppl*. 1995; 24:211–216.
14. Starck J, Toppila E, Pyykko I. Smoking as a risk factor in sensory neural hearing loss among workers exposed to occupational noise. *Acta Otolaryngol*. 1999; 119, 302–305. PMID: [10380732](#)
15. Bartecchi CE, MacKenzie TD, Schrier RW. The human costs of tobacco use. *N Engl J Med*. 1994; 330(13): 907–12. PMID: [8114863](#)
16. Pope CA, Burnett RT, Turner MC, Cohen A, Krewski D, Jerrett M et al. Lung cancer and cardiovascular disease mortality associated with ambient air pollution and cigarette smoke: shape of the exposure-response relationships. *Environ Health Perspect*. 2011; 119(11): 1616–1621. doi: [10.1289/ehp.1103639](#) PMID: [21768054](#)
17. Flora MS, Mascie-Taylor CG, Rahman M. Gender and locality differences in tobacco prevalence among adult Bangladeshis. *Tob Control*. 2009; 18(6), 445–450. doi: [10.1136/tc.2008.028142](#) PMID: [19679888](#)
18. Nakanishi N, Okamoto M, Nakamura K, Suzuki K, Tatara K. Cigarette smoking and risk for hearing impairment: a longitudinal study in Japanese male office workers. *J Occup Environ Med*. 2000; 42(11): 1045–1049. PMID: [11094781](#)
19. Baur M, Fransen E, Tropitzsch A, van Laer L, Mauz PS, Van Camp G, et al. Influence of exogenic factors on age-related hearing impairment. *HNO*. 2009; 57(10): 1023–1028. doi: [10.1007/s00106-009-1900-9](#) PMID: [19730805](#)
20. De Oliveira DC, de Lima MA. Low and high frequency tonal threshold audiometry: comparing hearing thresholds between smokers and non-smokers. *Braz J Otorhinolaryngol*. 2009; 75(5): 738–744. PMID: [19893945](#)

21. Brant LJ, Gordon-Salant S, Pearson JD, Klein LL, Morrell CH, Metter EJ, et al. Risk factors related to age-associated hearing loss in the speech frequencies. *J Am Acad Audiol*. 1996; 7(3): 152–160. PMID: [8780987](#)
22. Karlsmose B, Lauritzen T, Engberg M, Parving A. A five-year longitudinal study of hearing in a Danish rural population aged 31–50 years. *Br J Audiol*. 2000; 34(1): 47–55. PMID: [10759077](#)
23. Szudek J, Ostevik A, Dziegielewska P, Robinson-Anagor J, Gomma N, Hodgetts B, et al. Can Uhear me now? Validation of an iPod-based hearing loss screening test. *J Otolaryngol Head Neck Surg*. 2012; 1:78–84.
24. VanTasell DJ, Folkeard P. Reliability and accuracy of a method of adjustment for self-measurement of auditory thresholds. *Otol Neurotol*. 2013; 34(1): 9–15.
25. Brinkman GL, Coates EO Jr. The effect of bronchitis, smoking, and occupation on ventilation. *Am Rev Respir Dis*. 1963; 87:684–93. PMID: [14015517](#)
26. Nomura K, Nakao M, Yano E (2005) Hearing loss associated with smoking and occupational noise exposure in a Japanese metal working company. *Int Arch Occup Environ Health*. 2005; 78(3):178–84. PMID: [15761747](#)
27. Sawair FA. Does smoking really protect from recurrent aphthous stomatitis? *Ther Clin Risk Manag*. 2010; 6: 573–577. doi: [10.2147/TCRM.S15145](#) PMID: [21151626](#)
28. Uy J, Forcica MA. Hearing Loss. *Ann Intern Med*. 2013; 158(7):505–514. doi: [10.7326/0003-4819-158-7-201304020-00002](#) PMID: [23546562](#)
29. Nasir HM, Rampal KG. Hearing loss and contributing factors among airport workers in Malaysia. *Med J Malaysia*. 2012; 67(1):81–86. PMID: [22582554](#)
30. Franssen E, Topsakal V, Hendrickx JJ, Laer LV, Huyghe JR, Eyken EV, et al. Occupational noise, smoking, and a high body mass index are risk factors for age-related hearing impairment and moderate alcohol consumption is protective: A European population-based multicenter study. *J Assoc Res Otolaryngol*. 2008; 9: 264–276. doi: [10.1007/s10162-008-0123-1](#) PMID: [18543032](#)
31. Shimada S, Hasegawa K, Wada H, Terashima S, Satoh-Asahara N, Yamakage H, et al. High blood viscosity is closely associated with cigarette smoking and markedly reduced by smoking cessation. *Circ J*. 2011; 75: 185–89. PMID: [21071876](#)
32. Unverdorben M, Von Holt K, Winkelmann BR. Smoking and atherosclerotic cardiovascular disease: part II: role of cigarette smoking in cardiovascular disease development. *Biomark Med*. 2009; 3: 617–653. doi: [10.2217/bmm.09.51](#) PMID: [20477529](#)
33. Oliveira DC, Lima MA. Low and high frequency tonal threshold audiometry: comparing hearing thresholds between smokers and non-smokers. *Braz J Otorhinolaryngol*. 2009; 75: 738–744. PMID: [19893945](#)

increases in the fluence might have affected hair counts but were not tried, to avoid complications. The increase in pulse duration did not significantly affect the onset of hair regrowth ( $P = 0.345$ ).

The anagen/telogen ratio and hair shaft thickness were significantly more reduced on the left side ( $P = 0.033$  and  $P = 0.045$  respectively) (figure 1C). One year later, four cases showed hair shaft thickness on the left side still less than on the right side.

Apart from immediate transient side effects; perifollicular erythema, edema and pain, no chronic adverse side effects developed. High overall satisfaction with the results was reported by 20 patients (83.33%).

To the best of our knowledge, this is the first split chin controlled trial to study the effects of increasing the pulse duration of long pulsed Nd:YAG and to evaluate the A/T ratio and hair shaft thickness following laser hair removal. It appears that increasing the pulse duration of long pulsed Nd:YAG significantly decreases hair thickness and induces more telogen hair but does not affect the percentage of hair reduction or the onset of hair re-growth. Various manipulations in the pulse duration and fluence are recommended until reaching the best parameters to achieve permanent hair loss. ■

**Disclosure.** Financial support: none. Conflict of interest: none.

<sup>1</sup>Department of Dermatology,  
Cairo University,  
Kasr Al Ainy Hospital  
Kasr Al Ainy St  
Cairo, 11562, Egypt  
<sup>2</sup>Department of Dermatology,  
<sup>3</sup>Department of Pathology,  
Medical Research Division,  
National Research Centre, Egypt  
<abdelhalimmona@gmail.com>

Samia ESMAT<sup>1</sup>  
Mona R.E.  
ABDEL-HALIM<sup>1</sup>  
Amira EL-TAWDY<sup>1</sup>  
Marwa M. FAWZY<sup>2</sup>  
Asmaa RAGHEB<sup>2</sup>  
Nabila HASAN<sup>3</sup>

1. Gan SD, Graber EM. Laser hair removal: a review. *Dermatol Surg* 2013; 39: 823-38.
2. Rogachefsky AS, Becker K, Weiss G, Goldberg DJ. Evaluation of a long-pulsed Nd:YAG laser at different parameters: an analysis of both fluence and pulse duration. *Dermatol Surg* 2002; 28: 932-5.
3. Raff K, Landthaler M, Hohenleutner U. Optimizing treatment parameters for hair removal using long-pulsed Nd:YAG-lasers. *Lasers Med Sci* 2004; 18: 219-22.

doi:10.1684/ejd.2014.2324

## The effects of non-thermal atmospheric pressure plasma irradiation on expression levels of matrix metalloproteinases in benign melanocytic tumors in *RET*-transgenic mice

Large congenital melanocytic nevi (LCMN) have been defined as congenital melanocytic nevi having a projected adult size exceeding 20 cm in diameter and they are benign

melanocytic tumors [1]. Previous studies have shown a high risk of development of melanoma from LCMN [1].

Tumor formation by inoculation of malignant cells into mice provides a useful model for studying the effects of *in vivo* anti-melanoma treatment. However, formation of a benign tumor by inoculation of cells is impossible, because benign cells have no ability for anchorage-independent growth. We previously developed a hairless mouse line of 304-hr/hr (HL-RET-mice) carrying constitutively activated *RET*, in which benign melanocytic tumor and melanoma spontaneously develop stepwise [2, 3]. Since the process of tumor development and malignant transformation in HL-RET-mice resembles that of LCMN of humans [2, 3], the mouse model could be a strong tool to establish therapies for preventing the development of melanoma from benign melanocytic tumors.

Matrix metalloproteinase (MMP) -2, -9 and -14 and their regulators (tissue inhibitor of metalloproteinases-2 (TIMP-2) and reversion-inducing cysteine-rich protein with Kazal motifs (RECK)) have been reported to be associated with melanoma formation in humans and mice [4-6]. Since MMPs have been suggested to be involved in the conversion of a benign tumor to a malignant tumor [4, 7], MMPs are possible candidate targets of melanoma therapies.

Plasma is an ionized gas that has been defined as the fourth state of matter. Recently, non-thermal atmospheric pressure plasma has received attention in the medical field. Previous studies have shown anti-tumor effects of plasma on various tumor cells, including lung carcinoma cells, glioma cells and melanoma cells *in vitro* [8]. However, there have been few studies showing the effects of plasma irradiation on melanoma *in vivo*. More importantly, to our knowledge, there is no information about the preventive effect of plasma irradiation on the development of melanoma from a benign melanocytic tumor *in vivo*.

In this study, we performed a molecular-based analysis of non-thermal, atmospheric pressure, plasma irradiation-mediated effects in benign melanocytic tumors which spontaneously developed in HL-RET-mice, with focus on the expression levels of MMPs and their regulators. Twelve mice, each with a solitary melanocytic tumor that was clinically and histologically diagnosed as benign, were used. Six mice were treated with plasma and the other six mice were not. Interestingly, expression levels of *MMP-2*, -9 and -14 transcripts in plasma-treated tumors ( $n = 6$ ) were 75%, 56% and 51% lower, respectively, than those in untreated tumors ( $n = 6$ ) (figure 1A). The differences in expression levels of *MMP-2*, -9 and -14 transcripts were statistically significant (Fig. 1A). Expression levels of *TIMP-2* transcript in plasma-treated and untreated tumors were comparable (figure 1A). The expression level of *RECK* transcript in plasma-treated tumors was 50% higher than that in untreated tumors (figure 1A).

We then examined the biological meaning of our results showing decreased expression levels of *MMP-2*, -9 and -14 transcripts and increased expression level of *RECK* transcript by the plasma irradiation. Clinically and histologically diagnosed solitary benign melanocytic tumors ( $n = 6$ ) from six mice and solitary melanomas ( $n = 6$ ) from six mice were used. Expression levels of *MMP-2*, -9 and -14 transcripts in melanomas were 9.6-fold, 6.3-fold and 1.7-fold higher, respectively, than those in benign tumors, and the differences were statistically significant (figure 1B).

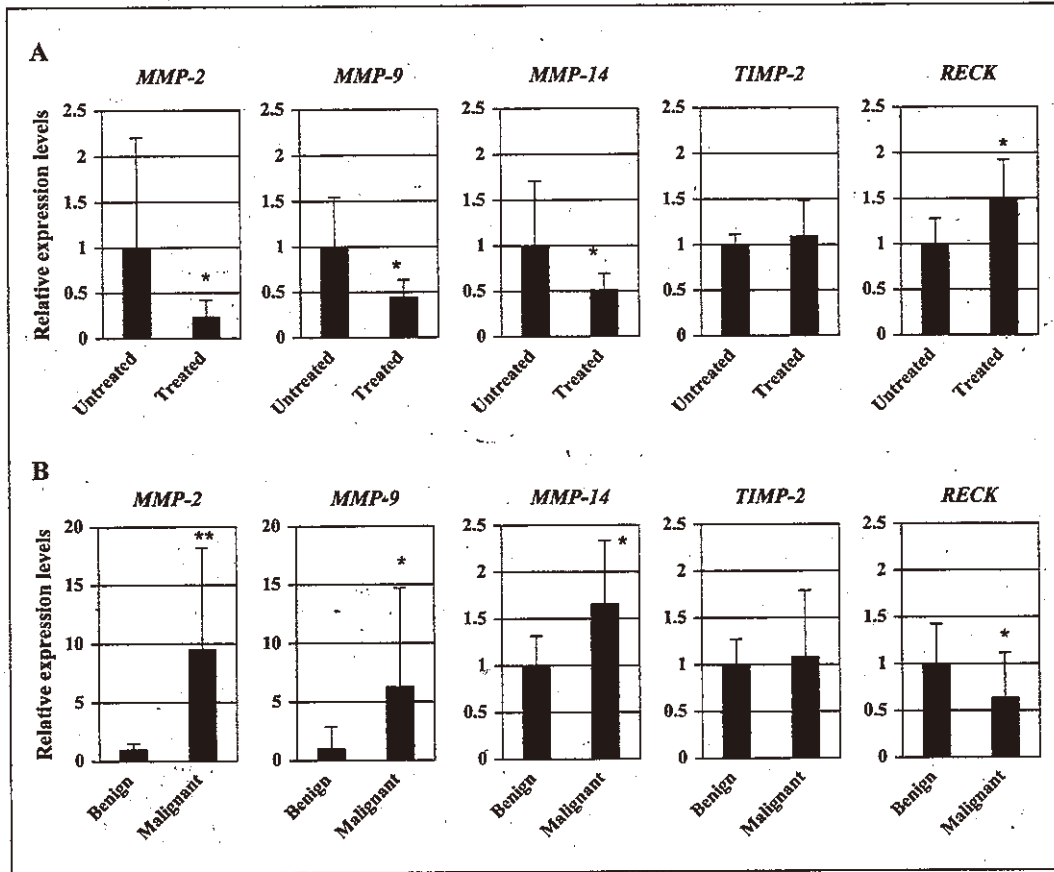


**Figure 1. A)** Transcript expression levels (means  $\pm$  SD) of matrix metalloproteinases (MMPs)-2, -9 and -14, tissue inhibitor of metalloproteinases-2 (TIMP-2) and reversion-inducing cysteine-rich protein with Kazal motifs (RECK), in non-thermal, atmospheric pressure plasma-treated and -untreated benign melanocytic tumors from HL-RET-mice are presented. The plasma-untreated tumors were exposed to argon gas as a control of the plasma treatment because argon gas was used for production of the plasma. The device of non-thermal atmospheric pressure plasma used in this study was previously reported [9]. Non-thermal atmospheric pressure plasma with ultra-high density (approximately  $2 \times 10^{16} \text{ cm}^{-3}$ ) was produced with an estimated O density of approximately  $4 \times 10^{15} \text{ cm}^{-3}$  [9]. Plasma in the main discharge region was excited by applying 10 kV from a 60-Hz commercial power supply to two electrodes. The distance between the two electrodes was 2 cm. The flow rate of argon gas was set at 2 standard liters/min [9]. The distance between the plasma source and the skin surface was fixed at 13 mm. The plasma or argon gas was applied on the skin surface over benign tumors for one minute, using the robot arm so that all of the tumor area was equally treated [8]. The plasma source was moved with reciprocating motion by 3.5 cm in the Y-axis direction (speed: 5mm/sec). Treatment with the plasma or argon gas was performed once a week for 11 weeks. Tumors were collected at one week after the last exposure. **B)** Transcript expression levels (means  $\pm$  SD) of MMP-2, -9 and -14, TIMP-2 and RECK in benign melanocytic tumors (n = 6) and melanomas (n = 6) from HL-RET-mice are presented. The expression levels of MMPs, TIMP-2 and RECK transcripts were measured by quantitative PCR and adjusted by the transcript expression level of hypoxanthine ribosyltransferase (Hprt) as previously described [10]. Sequences of primers used in this study are as follow: 5'-TATGTCCCCGTTGACTGAT-3' and 5'-CTTTGCTGACCTGCTGGATT-3' for Hprt, 5'-CGCCCCTAAAACAGACAAAG-3' and 5'-GGTCTCGATGGTGTCTGGT-3' for MMP-2, 5'-CATTTCGCGTGATAAGGAGT-3' and 5'-TCACACGCCAGAAGAATTTG-3' for MMP-9, 5'-GACTGTCCAAAATGAGGATC-3' and 5'-TCTTTGTGGGTGACCCTGAC-3' for MMP-14, 5'-GCATCACCCAGAAGAAGAGC-3' and 5'-GTCCATCCAGAGGCACTCAT-3' for TIMP-2, 5'-AGGTCTCCAGCAGTCTCC-3' and 5'-GCAGTTCCTCCAGTTGTG-3' for RECK. Statistical significance was analyzed by the Mann-Whitney U test (\* $p < 0.05$ , \*\* $p < 0.01$ ). All experiments were performed in Chubu University. The experiments using animals and recombinant DNA were approved by the Animal Care and Use Committee of Chubu University (approval no. 2510052) and Recombination DNA Advisory Committee (approval no. 12-04) in Chubu University, respectively.

Expression levels of TIMP-2 transcript in benign tumors and melanomas were comparable (figure 1B). Expression levels of RECK transcript in melanomas were 60% lower than in benign tumors (figure 1B). MMP-14, promotes MMP-2 activation [4], and RECK inhibits MMP-2, -9, and -14 activities [6]. Increased expression levels of MMPs and decreased expression levels of RECK have also been observed in the process of con-

version from benign melanocytic tumors to melanoma in humans [4, 6]. Therefore, our results suggest that the malignant property of benign melanocytic tumors is potentially decreased by irradiation of non-thermal atmospheric pressure plasma. Constant TIMP-2 expression, regardless of plasma irradiation and histological types of benign and malignancy, is possible, because TIMP-2 can bidirectionally regulate MMP-2 activity [7].

In summary, plasma irradiation is a potential candidate for preventive therapies for malignant transformation of LCMN. ■

**Disclosure.** Financial support: Grant-in-Aid for Scientific Research on Innovative Areas (No. 24108001) from the Ministry of Education, Culture, Sports, Science and Technology (MEXT) and TOYOAKI Scholarship Foundation. Conflict of interest: none.

<sup>1</sup> Department of Biomedical Sciences,  
<sup>2</sup> Graduate School of Bioscience and Biotechnology, Chubu University, Kasugai, Aichi, Japan  
<sup>3</sup> Department of Occupational and Environmental Health,  
<sup>4</sup> Graduate School of Regional Innovation Studies, Mie University, Tsu, Japan  
<sup>5</sup> Department of Electrical Engineering and Computer Science, Nagoya University Graduate School of Medicine, 65 Tsurumai-cho, Showa-ku, Nagoya, Aichi 466-8550, Japan  
<katomasa@med.nagoya-u.ac.jp>

Machiko IIDA<sup>1,3</sup>  
Ichiro YAJIMA<sup>1,3</sup>  
Nobutaka OHGAMI<sup>1</sup>  
Haruka TAMURA<sup>1,2</sup>  
Kozue TAKEDA<sup>1</sup>  
Sahoko ICHIHARA<sup>4</sup>  
Masaru HORI<sup>5</sup>  
Masashi KATO<sup>1,3</sup>

1. Marghoob AA. Congenital melanocytic nevi. Evaluation and management. *Dermatol Clin* 2002; 20: 607-16.
2. Thang ND, Yajima I, Nakagawa K, et al. A novel hairless mouse model for malignant melanoma. *J Dermatol Sci* 2012; 65: 207-12.
3. Kato M, Takahashi M, Akhand AA, et al. Transgenic mouse model for skin malignant melanoma. *Oncogene* 1998; 17: 1885-8.
4. Overall CM, López-Otin C. Strategies for MMP inhibition in cancer: innovations for the post-trial era. *Nat Rev Cancer* 2002; 2: 657-72.
5. Candrea E, Senila S, Tatomir C, Cosgarea R. Active and inactive forms of matrix metalloproteinases 2 and 9 in cutaneous melanoma. *Int J Dermatol* 2012 Oct 5. doi: 10.1111/j.1365-4632.2012.05772.x. [Epub ahead of print].
6. Oh J, Takahashi R, Kondo S, et al. The membrane-anchored MMP inhibitor RECK is a key regulator of extracellular matrix integrity and angiogenesis. *Cell* 2001; 107: 789-800.
7. Egeblad M, Werb Z. New functions for the matrix metalloproteinases in cancer progression. *Nat Rev Cancer* 2002; 2: 161-74.
8. Iseki S, Nakamura K, Hayashi M, et al. Selective killing of ovarian cancer cells through induction of apoptosis by nonequilibrium atmospheric pressure plasma. *Appl Phys Lett* 2012; 100: 113702-4.
9. Tanaka H, Mizuno M, Ishikawa K, et al. Plasma-activated medium selectively kills glioblastoma brain tumor cells by downregulating a survival signaling molecule, AKT kinase. *Plasma Med* 2011; 1: 265-77.
10. Ohshima Y, Yajima I, Takeda K, et al. c-RET molecule in malignant melanoma from oncogenic RET-carrying transgenic mice and human cell lines. *PLoS One* 2010; 5: e10279.

doi:10.1684/ejd.2014.2330

## Generalized eruptive xanthomas associated with diabetic dyslipidemia

A 39-year-old, obese male, (body mass index 41.3 kg/m<sup>2</sup>) presented to the Department of Dermatology with gen-

eralized, diffuse, pruritic skin lesion patient, the first skin lesions had been years before, on the extensor side of shoulders. Two months before dermatological examination, new skin lesions appeared in the trunk and extremities, with a tendency to generalize. Physical examination showed small, generalized, pruritic, yellowish papules on an erythematous base. Koebner phenomenon was observed as a reaction to scratching (figures 1A-B). Microscopic examination of a biopsy taken from a skin lesion showed grouped foamy cells, with extracellular lipid between collagen bundles dominantly present in the reticular dermis, and a moderate inflammatory infiltrate throughout the dermis (figures 1C-D). Endocrinological examinations revealed metabolic syndrome with increased serum glucose levels (147.6 mg/dL) and highly increased tChol (1,055.68 mg/dL) and TAG (4,844.99 mg/dL). Chylomicrons were present in serum incubated overnight. Furthermore, an oral glucose tolerance test showed diabetes mellitus (DM) with compensatory hyperinsulinemia as a consequence of the insulin resistance. Parathyroid hormone, thyroid-stimulating hormone, free thyroxin, antithyroid antibodies, calcitonin, serum cortisol and prolactin were absent/normal. Abdominal ultrasound examination showed hepatic steatosis. A diagnosis of generalized eruptive xanthomas associated with diabetic dyslipidemia was made.

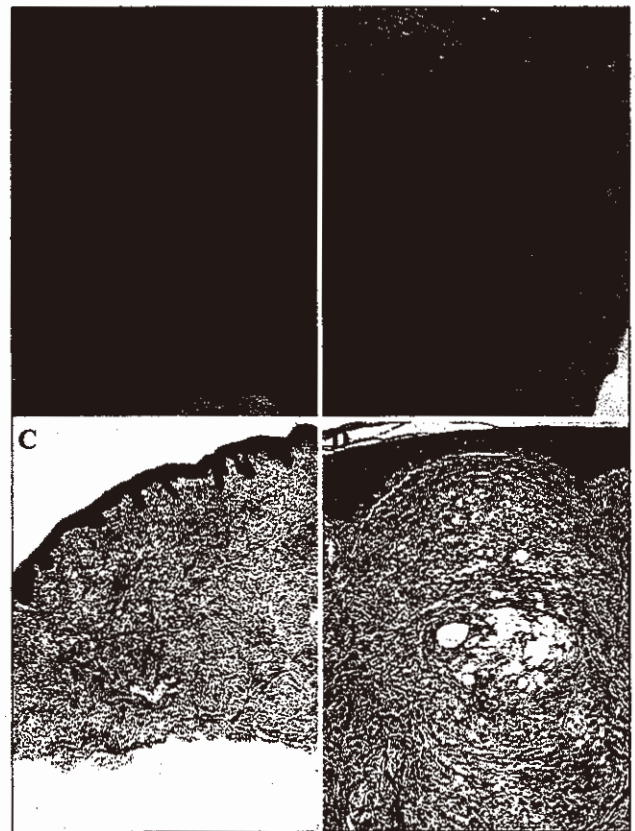


**Figure 1.** Generalized eruptive xanthomas with Koebner phenomenon (A). Typical clinical presentation of eruptive xanthomas: small, yellowish papules on an erythematous base (B). Histopathological examination of the skin biopsy shows foamy cells with extracellular lipid between collagen bundles, and a moderate inflammatory infiltrate in the reticular dermis (C: ×100, D: ×200).



Contents lists available at ScienceDirect

# Environmental Pollution

journal homepage: [www.elsevier.com/locate/envpol](http://www.elsevier.com/locate/envpol)

Short communication

## Carcinogenic risk of chromium, copper and arsenic in CCA-treated wood



Nobutaka Ohgami<sup>a, c, d, 2</sup>, Osamu Yamanoshita<sup>b, d, 2</sup>, Nguyen Dinh Thang<sup>b, 1, 2</sup>,  
 Ichiro Yajima<sup>a, b, d</sup>, Chihiro Nakano<sup>a</sup>, Wu Wenting<sup>a</sup>, Shoko Ohnuma<sup>d</sup>,  
 Masashi Kato<sup>a, b, d, \*</sup>

<sup>a</sup> Department of Occupational and Environmental Health, Nagoya University Graduate School of Medicine, 65 Tsurumai-cho, Showa-ku, Nagoya, Aichi 466-8550, Japan

<sup>b</sup> Unit of Environmental Health Sciences, Department of Biomedical Sciences, College of Life and Health Sciences, Chubu University, 1200 Matsumoto, Kasugai, Aichi 487-8501, Japan

<sup>c</sup> Nutritional Health Science Research Center, Chubu University, 1200 Matsumoto, Kasugai, Aichi 487-8501, Japan

<sup>d</sup> Voluntary Body for International Health Care in Universities, 65 Tsurumai-cho, Showa-ku, Nagoya, Aichi 466-8550, Japan

### ARTICLE INFO

#### Article history:

Received 22 June 2015

Received in revised form

23 July 2015

Accepted 25 July 2015

Available online xxx

#### Keywords:

Great East Japan Earthquake

CCA-treated wood

Debris

Chromium

Copper

Arsenic

### ABSTRACT

We showed that 2.1% of 233 pieces of lumber debris after the Great East Japan Earthquake was chromated copper arsenate (CCA)-treated wood. Since hexavalent chromium (Cr), copper (Cu) and pentavalent arsenic (As) in the debris may be diffused in the air via incineration, we exposed human lung normal (BEAS-2B) and carcinoma (A549) cells to Cr, Cu and As at the molar ratio in a representative CCA-treated wood. Co-exposure to 0.10  $\mu$ M Cr and 0.06  $\mu$ M As, which solely had no effect on colony formation, synergistically promoted colony formation in BEAS-2B cells, but not A549 cells, with activation of the PI3K/AKT pathway. Sole exposure and co-exposure to Cu showed limited effects. Since previous reports showed Cr and As concentrations to which human lungs might be exposed, our results suggest the importance to avoid diffusion of Cr and As in the air via incineration of debris including CCA-treated wood after the disaster.

© 2015 Elsevier Ltd. All rights reserved.

### 1. Introduction

The Great East Japan Earthquake and following tsunami on March 11, 2011 destroyed cities on the east coast of Japan including Tohoku, resulting in about 20,000 casualties. This disaster generated about 20 million tons of debris mainly from destroyed wooden houses. Some of the debris was recycled and some was burned as shown in the information from the Japanese Ministry of the Environment (2014).

Chromated copper arsenate (CCA)-treated wood is an architectural material that is pressure-treated with hexavalent chromium

(Cr), copper (Cu) and pentavalent arsenic (As). CCA-treated wood is classified into 3 types (Types A, B and C) based on the contents of Cr, Cu and As. The relative contents of Cr, Cu and As are as follows: 65.5%, 18.1% and 16.4% in Type A, 35.3%, 19.6% and 45.1% in Type B, and 47.5%, 18.5% and 34.0% in Type C, respectively (AWPA, 1991). These values are also valid in Japan (Saitoh et al., 2005). CCA was shown to be toxic (EPA, 2008), and there has been no production of CCA-treated wood for the past 20 years in Japan, though it had generally been used for foundations of houses until 1996 (Saitoh et al., 2005). Debris derived from the Great East Japan Earthquake may contain high levels of Cr, Cu and As due to the previously used CCA-treated wood. Since CCA is a water-soluble inorganic pesticide, soil and ground water may be contaminated due to the harmful elements eluted from CCA-treated wood by exposure to rainwater (Aceto and Fedele, 1994).

If debris including CCA-treated wood is incinerated after the disaster, Cr, Cu and As would be diffused in the air, and lungs in humans would be exposed to Cr, Cu and As through inhalation. Inhalation of inorganic As has been reported to increase the risk of

\* Corresponding author. Department of Occupational and Environmental Health, Nagoya University Graduate School of Medicine, 65 Tsurumai-cho, Showa-ku, Nagoya, Aichi 466-8550, Japan.

E-mail address: [katomasa@med.nagoya-u.ac.jp](mailto:katomasa@med.nagoya-u.ac.jp) (M. Kato).

<sup>1</sup> Present address: Department of Biochemistry and Plant Physiology, VNU University of Science, Vietnam National University of Science, Hanoi, Vietnam.

<sup>2</sup> These authors equally contributed to this study.

lung cancer in humans (Taylor et al., 1989). Exposure to hexavalent Cr has also been reported to increase the risk of lung cancer (Gibb et al., 2000; Luippold et al., 2003), while there is limited information about carcinogenicity by sole exposure to Cu (EPA, 2008). To our knowledge, however, there is no information about the risk for lung cancer through co-exposure to Cr, Cu and As, despite the possibility of co-exposure to these elements by incineration of CCA-treated wood.

About 75% of the debris derived from the Great East Japan Earthquake consisted of wood according to the Ministry of Land, Infrastructure, Transport and Tourism of Japan (2014). In this study, we first performed a fieldwork study to examine the percentage of CCA-treated wood and also levels of Cr, Cu and As in the debris. We next examined effects of co-exposure to Cr, Cu and As on malignant transformation in human normal lung cells and on malignant progression of human lung carcinoma cells *in vitro*.

## 2. Methods

### 2.1. Fieldwork study

We collected 233 pieces of lumber debris along a coastline in Miyagi Prefecture in Tohoku, Japan after the Great East Japan Earthquake. Ashing of the debris and measurement with an inductively coupled plasma-mass spectrophotometer (ICP-MS) partially followed procedures described in previous reports (Wallinga, 2006; Kato et al., 2013). Detailed information is provided in Supplementary methods.

### 2.2. Experimental research

A human normal lung epithelial cell line (BEAS-2B) (Health Science Research Resources Bank, Japan) and a human lung epithelial carcinoma cell line (A549) (RIKEN BRC CELL BANK) were used. A colony formation assay and immunoblotting were performed according to the methods described previously (Thang et al., 2011, 2015; Ohgami et al., 2010). Detailed information including antibodies used in this study is provided in Supplementary methods.

### 2.3. Statistical analysis

We performed statistical analysis following the method described in a previous report (Yajima et al., 2015).

## 3. Results and discussion

### 3.1. Levels of Cr, Cu and As in lumber debris

We performed fieldwork research to collect lumber debris after the Great East Japan Earthquake and tsunami in order to investigate the levels of Cr, Cu and As in the debris (Fig. 1 A, B). Measurements of elements in 233 pieces of the debris revealed that 5 pieces were CCA-treated wood containing  $10,000 \pm 8869$  mg/kg of Cr,  $2064 \pm 1319$  mg/kg of Cu and  $3380 \pm 2328$  mg/kg of As (Fig. 1C, Table 1 and Table S1) and that 6 pieces were Cu-preservative wood containing high levels of Cu ( $2700 \pm 3000$  mg/kg) with  $1.3 \pm 1.0$  mg/kg As and  $1.4 \pm 0.6$  mg/kg Cr (Fig. 1C and Table 1). In addition,  $2.0 \pm 2.0$  mg/kg of Cr,  $4.0 \pm 7.2$  mg/kg of Cu and  $0.4 \pm 0.7$  mg/kg of As were detected in 222 pieces of untreated wood (Fig. 1C and Table 1). Our data showed that 2.1% of 233 pieces of the debris after the Great East Japan Earthquake were CCA-treated wood. Although the number of samples is limited, our results indicate that the concentrations of Cr, Cu and As in only 2.1% of CCA-treated wood contribute to increases in the concentrations of these elements in

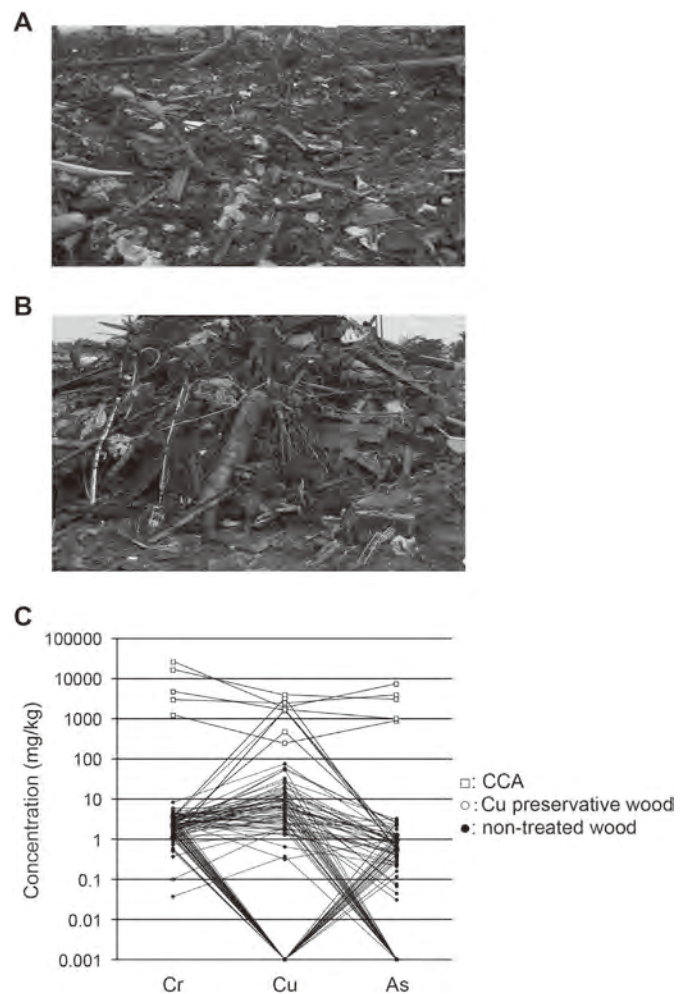


**Fig. 1.** Debris generated in Tohoku, Japan in June 2011. (A, B) Photographs of debris produced by the Great East Japan Earthquake and/or following tsunami are presented. A large proportion of wood in the debris can be seen. (C) Concentrations of chromium (Cr), copper (Cu) and arsenic (As) in lumber debris are presented with frequency plot of CCA-treated wood (open square), Cu-preservative wood (open circle) and untreated wood (closed circle). Concentrations of CCA are presented as log scale in the Y-axis.

total debris by 110 fold, 35 fold and 300 fold, respectively, compared to those in untreated wood, which accounts for 95.3% of the total debris. We assume that 94,500 tons of the debris in Tohoku was CCA-treated wood based on our results, if 75% of the debris (about 6,000,000 tons) was lumber.

### 3.2. Biological effects of co-exposure to Cr, Cu and As on human lung cells

We experimentally examined the effects of co-exposure to Cr, Cu and As on activities of transformation and progression in BEAS-2B cells and A549 cells. Since the levels of Cr, Cu and As in our fieldwork research (Table 1) were too high to perform a colony formation assay, we first examined the effects of sole exposure to hexavalent Cr, Cu and pentavalent As on survival of BEAS-2B cells. Sole exposure to less than  $1 \mu\text{M}$  of hexavalent Cr, to less than  $25 \mu\text{M}$  of Cu and to less than  $5 \mu\text{M}$  of As statistically had no effect of the ratio of surviving BEAS-2B cells, although the survival cell ratio showed a tendency to be reduced by  $0.5 \mu\text{M}$  and  $1.0 \mu\text{M}$  of Cr and by  $2.5 \mu\text{M}$  and  $5.0 \mu\text{M}$  of As (Fig. S1).

We next performed a colony formation assay using BEAS-2B cells solely exposed to  $0.1$ – $1 \mu\text{M}$  hexavalent Cr (Fig. S2A and B),

**Table 1**

**Classification of lumber debris in Tohoku after the Great East Japan Earthquake.** Means  $\pm$  standard deviations for percentages and concentrations (mg/kg) of CCA-treated wood, Cu-preservative wood and untreated wood in lumber debris collected in Tohoku after the Great East Japan Earthquake are presented.

	Total	Untreated wood	CCA-treated wood	Cu-preservative wood
Number of debris samples (%)	233 (100%)	222 (95.3%)	5 (2.1%)	6 (2.6%)
Cr (mg/kg)	220 $\pm$ 1900	2.0 $\pm$ 2.0	10,000 $\pm$ 8869	1.4 $\pm$ 0.6
Cu (mg/kg)	140 $\pm$ 780	4.0 $\pm$ 7.2	2064 $\pm$ 1319	2700 $\pm$ 3000
As (mg/kg)	120 $\pm$ 1100	0.4 $\pm$ 0.7	3380 $\pm$ 2328	1.3 $\pm$ 1.0

1–25  $\mu$ M Cu (Fig. S2C and D) and 0.5–5  $\mu$ M As (Fig. S2E and F). Sole exposure to 0.25  $\mu$ M and 0.5  $\mu$ M hexavalent Cr (Fig. S2A and B) and to 2.5  $\mu$ M and 5  $\mu$ M As (Fig. S2E and F) increased the number of colonies in BEAS-2B cells. Exposure to 1  $\mu$ M of Cr suddenly decreased the colony formation to the control level (Fig. S2A and B) despite comparable survival ratios of cells exposed to 0.5  $\mu$ M and 1.0  $\mu$ M of Cr. Sole exposure to 1–25  $\mu$ M Cu had no effect on the number of colonies (Fig. S2C and D). Based on the exposure levels without affecting colony formation (Fig. S2) and the molar ratio of 1:0.7:0.6 (=Cr:Cu:As) contained in a representative CCA-treated wood of type B (AWPA, 1991), 0.10  $\mu$ M Cr, 0.07  $\mu$ M Cu and 0.06  $\mu$ M As were used for the following experiments. Co-exposure to Cr, Cu and As significantly increased the number of colonies in BEAS-2B cells compared to that in the case of sole exposure to each element, while both the effects of sole exposure to Cu and co-exposure to Cu in addition to Cr and/or As on colony formation were undetectably low in BEAS-2B normal lung cells (Fig. 2 A, B), indicating that the effect of Cu on transforming activity in BEAS-2B cells is limited. Sole exposure and co-exposure to Cr, Cu and As did not affect the number of colonies in A549 lung carcinoma cells (Fig. 2C and D). Thus, our experimental research demonstrated the health risk of co-exposure to Cr, Cu and As, although the concentrations that we examined *in vitro* are not based on the actual concentrations in the air through incineration of debris in the study area. These results suggest that co-exposure to low doses of Cr and As, but not Cu, promotes transformation in normal lung cells but not progression in transformed lung cells. Exposure to 5  $\mu$ M of As has been shown to induce angiogenesis in A549 lung carcinoma cells (Liu et al., 2011), suggesting promoted progression in transformed cells (A549) by sole exposure to As, which is more than 80-fold higher than the concentration used in this study. Our previous study showed synergistic promotion of transforming activity in non-tumorigenic human HaCaT keratinocytes by co-exposure to 10  $\mu$ M of iron and 1  $\mu$ M of As (Kumasaka et al., 2013). These results suggest the necessity for health risk assessment considering the synergistic effect by co-exposure to heavy metals.

Previous studies showed mean concentrations of 46.5  $\mu$ M of Cr and 7.5  $\mu$ M of As in dried lung tissues and mean concentrations of 4.8  $\mu$ M of Cr and 1.9  $\mu$ M of As in wet lung tissues (Mari et al., 2014). These results suggest that 0.10  $\mu$ M of Cr and 0.06  $\mu$ M of As are concentrations to which human lung cells might be exposed, while we understand the difficulty in comparing the results for concentrations of Cr and As in human lung tissue *in vivo* and the results for promoted transforming activity by co-exposure to Cr and As in our experimental research *in vitro*. A previous study also showed that Cr level in wet lung tissue from subjects living near a hazardous waste incinerator in 2013 (12.3  $\mu$ M) was about 2-fold higher ( $p < 0.001$ ) than that in 1998 (6.6  $\mu$ M) (Mari et al., 2014), suggesting the concentrations of heavy metals diffused from the incinerator increase in human lungs. Taken together, our results suggest that measures should be taken to prevent diffusion, especially of Cr and As, in the air through incineration of lumber debris including CCA-treated wood after the disaster. Co-combustion of CCA-treated

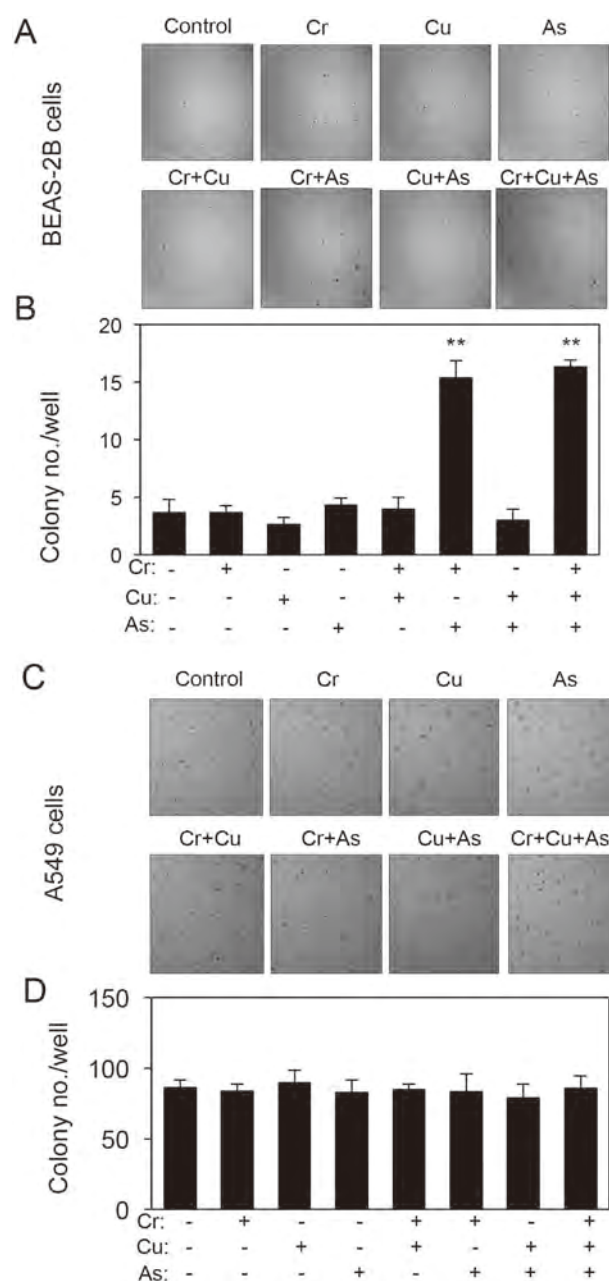


**Fig. 2. Synergistically increased transforming activity in human untransformed lung cells by co-exposure to Cr, Cu and As.** (A–D) Photographs of colonies (A, C) and graphs (mean  $\pm$  standard deviation) showing colony number per well (B, D) in BEAS-2B human normal lung epithelial cells (A, B) and A549 human lung epithelial carcinoma cells (C, D) in the presence or absence of 0.10  $\mu$ M of Cr, 0.07  $\mu$ M of Cu and 0.06  $\mu$ M of As are presented. \*\*, Significant difference ( $p < 0.01$ ) from the control was analyzed by Student's t-test.

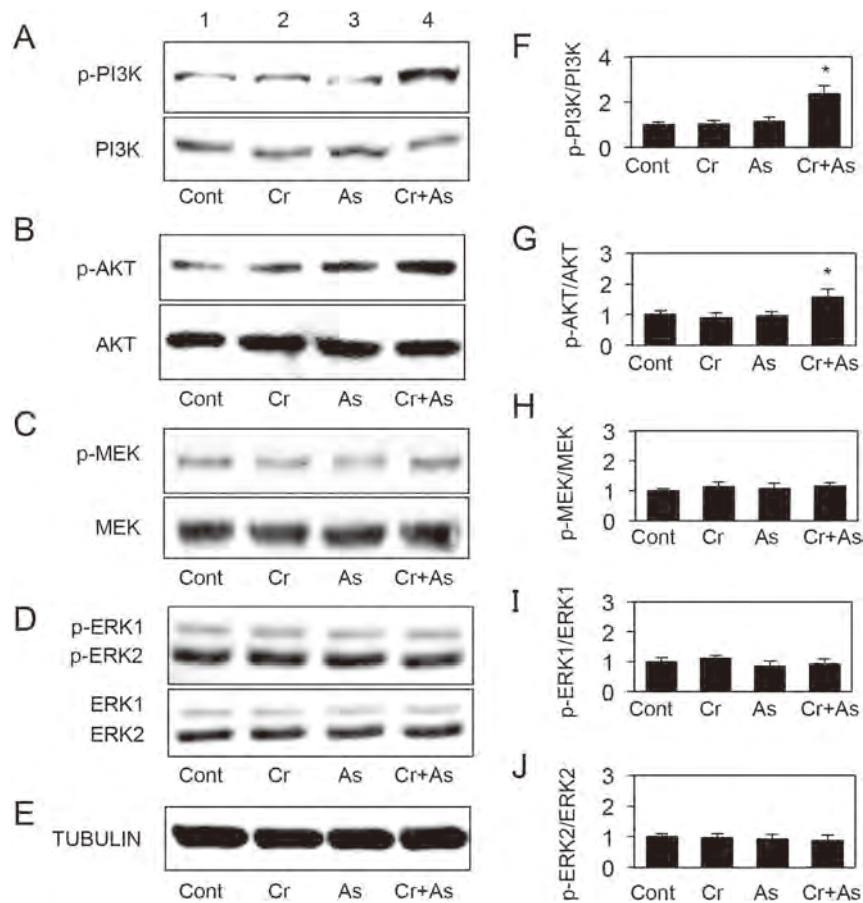


**Fig. 3. Synergistically activated PI3K/AKT, but not MEK/ERK, signaling pathway by co-exposure to Cr and As.** (A–J) Results of immunoblot analysis in human normal lung epithelial cells (BEAS-2B) with no exposure (lane 1; Cont), sole exposure to 0.10  $\mu$ M of Cr (lane 2; Cr) and 0.06  $\mu$ M of As (lane 3; As) and co-exposure to 0.10  $\mu$ M of Cr and 0.06  $\mu$ M of As (lane 4; Cr + As) are presented. Photographs (A–E) show the levels of phosphorylation (top panels in A–D) and expression (bottom panels in A–D) for PI3K (A), AKT (B), MEK (C), ERK1/2 (D) and TUBULIN (E). Graphs (mean  $\pm$  standard deviation) show the ratios of phosphorylation levels of PI3K (F), AKT (G), MEK (H), ERK1 (I) and ERK2 (J), respectively. The values were obtained by dividing the levels of phosphorylation (top panels in A–D) by the expression (bottom panels in A–D) for PI3K (A), AKT (B), MEK (C) and ERK1/2 (D), respectively. \*, Significant difference ( $p < 0.05$ ) from the control was analyzed by Student's t-test.

wood with peat additive, as performed in previous studies (Lundholm et al., 2007, 2008) may be an effective method for reducing diffusion of harmful elements in air.

### 3.3. Activation of the PI3K/AKT signaling pathway by co-exposure to Cr and As

We finally examined the effects of sole exposure and co-exposure to Cr and As on PI3K/AKT and MEK/ERK signaling pathways in BEAS-2B cells. Sole exposure to Cr and As did not affect phosphorylation and expression levels of PI3K/AKT and MEK/ERK (Fig. 3). Phosphorylated levels of PI3K/AKT, but not those of MEK/ERK, with co-exposure to Cr and As were significantly higher than those with sole exposure to Cr or As and a nil control (Fig. 3). Thus, our experimental research further revealed the molecular mechanism for the synergistic increase of transforming activity by co-exposure to Cr and As. Since the PI3K/AKT signaling pathway has been reported to be involved in the transformation of various cancers including lung carcinoma (Kikuchi et al., 2008; Patek et al., 2008; Molina-Arcas et al., 2013; Thang et al., 2015), synergistic activation of the PI3K/AKT signaling pathway by co-exposure to Cr and As may be involved in the increased transforming activity of BEAS-2B human lung epithelial cells.

In conclusion, the results of this study combining fieldwork research and molecular biology research suggest increased

carcinogenic risk by co-exposure to Cr and As in the process of incineration of debris including CCA-treated wood after the disaster.

### Conflict of interest

The authors declare that there are no conflicts of interest.

### Acknowledgments

This study was supported in part by Grants-in-Aid for Scientific Research (A) (15H01743 and 15H02588), (B) (24390157 and 24406002) and (C) (No. 25460178, 25340052), Grant-in-Aid for Challenging Exploratory Research (26670525), Grant-in-Aid for Scientific Research on Innovative Areas (24108001), Grants-in-Aid for Young Scientists (B) (22770008) and COE Project for Private Universities (Nutritional Health Science Research Center; No. S12010072) from the Ministry of Education, Culture, Sports, Science and Technology (MEXT), Mitsui & Co., Ltd. Environment Fund, Foundation from Center for Advanced Medical and Clinical Research Nagoya University Hospital, Toyoaki Scholarship Foundation, the Mitsubishi Foundation, AEON Environmental Foundation and the JKA and its promotion funds from KEIRIN RACE.

## Appendix A. Supplementary data

Supplementary data related to this article can be found at <http://dx.doi.org/10.1016/j.envpol.2015.07.041>.

## References

- Aceto, M., Fedele, A., 1994. Rain water effect on the release of arsenic, chromium and copper from treated Wood. *Fresenius Environ. Bull.* 3, 389–394.
- American Wood-preservers' Association (AWPA), 1991. P5–91 Standards for Waterborne Preservatives. In: American Wood Preservers' Association (AWPA) Book of Standards. Granbury, TX.
- Environmental Protection Agency (EPA), 2008. Reregistration Eligibility Decision for Chromated Arsenicals List a Case No. 0132. Office of Prevention, Pesticides EPA 739-R-08-006 and Toxic Substances.
- Gibb, H.J., Lees, P.S.J., Pinsky, P.F., Rooney, B.C., 2000. Lung cancer among workers in chromium chemical production. *Am. J. Ind. Med.* 38, 115–126.
- Kato, M., Kumasaka, M.Y., Ohnuma, S., Furuta, A., Kato, Y., Shekhar, H.U., Kojima, M., Koike, Y., Dinh Thang, N., Ohgami, N., Ly, T.B., Jia, X., Yetti, H., Naito, H., Ichihara, G., Yajima, I., 2013. Comparison of barium and arsenic concentrations in well drinking water and in human body samples and a novel remediation system for these elements in well drinking water. *PLoS One* 8, e66681.
- Kikuchi, J., Kinoshita, I., Shimizu, Y., Oizumi, S., Nishimura, M., Birrer, M.J., Dosaka-Akita, H., 2008. Simultaneous blockade of AP-1 and phosphatidylinositol 3-kinase pathway in non-small cell lung cancer cells. *Br. J. Cancer* 99, 2013–2019.
- Kumasaka, M.Y., Yamanoshita, O., Shimizu, S., Ohnuma, S., Furuta, A., Yajima, I., Nizam, S., Khalequzzaman, M., Shekhar, H.U., Nakajima, T., Kato, M., 2013. Enhanced carcinogenicity by coexposure to arsenic and iron and a novel remediation system for the elements in well drinking water. *Arch. Toxicol.* 87 (3), 439–447.
- Liu, L.Z., Jiang, Y., Carpenter, R.L., Jing, Y., Peiper, S.C., Jiang, B.H., 2011. Role and mechanism of arsenic in regulating angiogenesis. *PLoS One* 6 (6), e20858.
- Luippold, R.S., Mundt, K.A., Austin, R.P., Liebig, E., Panko, J., Crump, C., Crump, K., Proctor, D., 2003. Lung cancer mortality among chromate production workers. *Occup. Environ. Med.* 60, 451–457.
- Lundholm, K., Boström, D., Nordin, A., Shchukarev, A., 2007. Fate of Cu, Cr, and As during combustion of impregnated wood with and without peat additive. *Environ. Sci. Technol.* 41 (18), 6534–6540.
- Lundholm, K., Rogers, J.M., Haynes, B.S., Boström, D., Nordin, A., 2008. Fate of Cu, Cr, and As during the combustion stages of CCA-treated Wood fuel particles. *Energy Fuels* 22 (3), 1589–1597.
- Mari, M., Nadal, M., Schuhmacher, M., Barbería, E., García, F., Domingo, J.L., 2014. Human exposure to metals: levels in autopsy tissues of individuals living near a hazardous waste incinerator. *Biol. Trace Elem. Res.* 159, 15–21.
- Ministry of the Environment Government of Japan, 2014. Progress on Treatment of Debris from the Great East Japan Earthquake. <https://www.env.go.jp/en/focus/recycle/eq/ptd20140326.pdf> (accessed 26.08.2014).
- Ministry of Land, Infrastructure, Transport and Tourism of Japan, 2014. Status of Wooden House. <http://www.mlit.go.jp/common/000023402.pdf> (in Japanese) (accessed 26.08.2014).
- Molina-Arcas, M., Hancock, D.C., Sheridan, C., Kumar, M.S., Downward, J., 2013. Coordinate direct input of both KRAS and IGF1 receptor to activation of PI 3-kinase in KRAS mutant lung cancer. *Cancer Discov.* 3 (5), 548–563.
- Ohgami, N., Ida-Eto, M., Shimotake, T., Sakashita, N., Sone, M., Nakashima, T., Tabuchi, K., Hoshino, T., Shimada, A., Tsuzuki, T., Yamamoto, M., Sobue, G., Jijiwa, M., Asai, N., Hara, A., Takahashi, M., Kato, M., 2010. c-Ret-mediated hearing loss in mice with Hirschsprung disease. *Proc. Natl. Acad. Sci. U. S. A.* 107, 13051–13056.
- Patek, C.E., Arends, M.J., Wallace, W.A., Luo, F., Hagan, S., Brownstein, D.G., Rose, L., Devenney, P.S., Walker, M., Plowman, S.J., Berry, R.L., Kolch, W., Sansom, O.J., Harrison, D.J., Hooper, M.L., 2008. Mutationally activated K-ras 4A and 4B both mediate lung carcinogenesis. *Exp. Cell Res.* 314 (5), 1105–1114.
- Saitoh, K., Sakamoto, H., Watanabe, H., Yoshino, H., 2005. Heavy metals in unused and used CCA treated wood. *Bull. Kanagawa Environ. Res. Cent.* 28, 66–72 (in Japanese).
- Taylor, P.R., Qiao, Y.L., Schatzkin, A., Yao, S.X., Lubin, J., Mao, B.L., Rao, J.Y., McAdams, M., Xuan, X.Z., Li, J.Y., 1989. Relation of arsenic exposure to lung cancer among tin miners in Yunnan Province, China. *Br. J. Ind. Med.* 46, 881–886.
- Thang, N.D., Yajima, I., Kumasaka, M., Iida, M., Suzuki, T., Kato, M., 2015. Deltex-3-like (DTX3L) stimulates metastasis of melanoma through FAK/PI3K/AKT but not MEK/ERK pathway. *Oncotarget* 6 (16), 14290–14299.
- Thang, N.D., Yajima, I., Kumasaka, M.Y., Ohnuma, S., Yanagishita, T., Hayashi, R., Shekhar, H.U., Watanabe, D., Kato, M., 2011. Barium promotes anchorage-independent growth and invasion of human HaCaT keratinocytes via activation of c-SRC kinase. *PLoS One* 6, e25636.
- Wallinga, D., 2006. Playing Chicken: Avoiding Arsenic in Your Meat. The Institute for Agriculture and Trade Policy, Minneapolis. [http://www.iatp.org/files/421\\_2\\_80529.pdf](http://www.iatp.org/files/421_2_80529.pdf) (accessed 26.08.2014).
- Yajima, I., Kumasaka, M.Y., Ohnuma, S., Ohgami, N., Naito, H., Shekhar, H.U., Omata, Y., Kato, M., 2015. Arsenite-mediated promotion of anchorage-independent growth of HaCaT cells through placental growth factor. *J. Invest. Dermatol.* 135, 1147–1156.



## Prevention of allergic rhinitis by ginger and the molecular basis of immunosuppression by 6-gingerol through T cell inactivation☆

Yoshiyuki Kawamoto<sup>a,\*</sup>, Yuki Ueno<sup>b</sup>, Emiko Nakahashi<sup>a</sup>, Momoko Obayashi<sup>a</sup>, Kento Sugihara<sup>a</sup>, Shanlou Qiao<sup>a</sup>, Machiko Iida<sup>c</sup>, Mayuko Y. Kumasaka<sup>c</sup>, Ichiro Yajima<sup>c</sup>, Yuji Goto<sup>d</sup>, Nobutaka Ohgami<sup>c</sup>, Masashi Kato<sup>c</sup>, Kozue Takeda<sup>a</sup>

<sup>a</sup>College of Life and Health Sciences, Chubu University, Kasugai, Aichi, Japan

<sup>b</sup>Department of Health and Nutrition, Faculty of Psychological and Physical Science, Aichi Gakuin University, Nisshin, Aichi, Japan

<sup>c</sup>Department of Occupational and Environmental Health, Nagoya University Graduate School of Medicine, Nagoya, Japan

<sup>d</sup>Department of Biology, Faculty of Science, Toho University, Funabashi, Chiba, Japan

Received 6 March 2015; received in revised form 20 August 2015; accepted 20 August 2015

### Abstract

The incidence of allergies has recently been increasing worldwide. Immunoglobulin E (IgE)-mediated hypersensitivity is central to the pathogenesis of asthma, hay fever and other allergic diseases. Ginger (*Zingiber officinale* Roscoe) and its extracts have been valued for their medical properties including anti-nausea, antiinflammation, antipyresis and analgesia properties. In this study, we investigated the antiallergic effects of ginger and 6-gingerol, a major compound of ginger, using a mouse allergy model and primary/cell line culture system. In mice with ovalbumin (OVA)-induced allergic rhinitis, oral administration of 2% ginger diet reduced the severity of sneezing and nasal rubbing by nasal sensitization of OVA and suppressed infiltration of mast cells in nasal mucosa and secretion of OVA-specific IgE in serum. 6-Gingerol inhibited the expression of not only Th2 cytokines but also Th1 cytokines in OVA-sensitized spleen cells. Accordingly, 6-gingerol suppressed *in vitro* differentiation of both Th1 cells and Th2 cells from naïve T cells. In addition, 6-gingerol suppressed both superantigen staphylococcal enterotoxin B (SEB)- and anti-CD3-induced T cell proliferation. 6-Gingerol also abrogated PMA plus ionomycin- and SEB-induced IL-2 production in T cells, suggesting that 6-gingerol affected T cell receptor-mediated signal transduction rather than the antigen-presentation process. Indeed, 6-gingerol inhibited the phosphorylation of MAP kinases, calcium release and nuclear localization of c-fos and NF-κB by PMA and ionomycin stimulation. Thus, our results demonstrate that 6-gingerol suppresses cytokine production for T cell activation and proliferation, thereby not causing B cell and mast cell activation and resulting in prevention or alleviation of allergic rhinitis symptoms.

© 2015 Elsevier Inc. All rights reserved.

**Keywords:** Allergy; Cytokine; Immunoglobulin E (IgE); T helper cells; Ginger; 6-gingerol

### 1. Introduction

Allergies are an immunological diseases, and the number of patients with allergies in industrialized countries has recently been increasing [1,2]. IgE-mediated Type I hypersensitivities, including food allergies, asthma, atopic dermatitis, hives, eczema and hay fever, are associated with mast cell degranulation with release of histamine, serotonin and other biologically active mediators. Based on the knowledge of mediators involved in Type I reactions and the mechanism of mast cell degranulation, several drugs for allergies

have been developed (e.g., antihistamines, calcium influx blocker, phosphodiesterase inhibitor, cAMP stimulator, thromboxane inhibitor, leukotriene antagonist and Th2 cytokine inhibitor). However, these drugs have not been developed not for cure but for palliative care for hypersensitivity symptoms [3]. Recently, allergen-specific immunotherapy as a desensitization therapy for allergic diseases has been improved and is a potentially curative approach for allergies [4]. Although the development of further efficacious palliative and curative therapies is needed, a method for prevention of allergic diseases is more desirable.

Because chemical synthetic drugs for allergy prophylaxis not only require high development costs, but also have the risk of adverse reactions, the search for safer food-derived ingredients with antiallergic effects is promising. Results of recent studies suggest that there are some bioactive chemicals in food that have antiallergic effects. Catechins, epigallocatechin-3-O-(3-O-methyl) gallate and strictinin in green tea inhibit histamine release, FcεRI expression and IgE production [5–7]. Resveratrol, a polyphenolic stilbene in the skin of grapes, inhibits the production of Th2 cytokines in plasma and bronchoalveolar lavage

**Abbreviations:** SEB, staphylococcal enterotoxin B; HPRT, hypoxanthine-guanine phosphoribosyltransferase; io, ionomycin.

\* Funding: This work was supported by Chubu University Grants A (22IM22A) and B (25IM06B).

\* Corresponding author. College of Life and Health Sciences, Chubu University, 1200 Matsumotocho, Kasugai, Aichi, Japan 487-8501. Tel./fax: +81-568-51-7329.

E-mail address: [ykawa@isc.chubu.ac.jp](mailto:ykawa@isc.chubu.ac.jp) (Y. Kawamoto).

<http://dx.doi.org/10.1016/j.jnutbio.2015.08.025>  
0955-2863/© 2015 Elsevier Inc. All rights reserved.

fluid [8]. Luteolin, which is a flavone contained in vegetables and spices, inhibits CD40 ligand expression in human basophils [9]. Thus, an evidence-based approach for preventing allergies by such bioactive chemicals in food has been actively developed.

Ginger (*Zingiber officinale* Roscoe) is one of the most popular spices cultivated in temperate and tropical zones. In traditional Chinese and Indian medicine, ginger has been used for a wide range of diseases including nausea, asthma, diarrhea, gingivitis and arthritis [10]. Ginger extracts, in which more than four hundred chemicals have been identified, are multicomponent mixtures of biologically active constituents including the structurally related compounds gingerols, shogaols, paradol, gingerdiol and zingerone. Some studies using sensitive analytical methods such as HPLC or LC-mass spectrometry have demonstrated that 6-gingerol (5-hydroxy-1-(4-hydroxy-3-methoxyphenyl)-3-decanone) is a major constituent of ginger [11–13]. 6-Gingerol has been shown to have a variety of pharmacological activities including antiinflammatory, analgesic, anticancer, antiangiogenesis, antiplatelet and antioxidant effects [14–17]. Ginger and its bioactive components can be effectively used to prevent allergies. However, there has been no report scientifically demonstrating a preventative effect of ginger against allergies, and the mechanism of the antiallergy actions of 6-gingerol has not been fully elucidated.

In this study, we investigated the antiallergic effect of ginger diet administration in Type I allergy model mice and the activation or proliferation of T cells by 6-gingerol *in vitro*. Our results suggest that ginger might be able to be used as a prophylactic agent for allergic rhinitis, as 6-gingerol inhibits the activation of T cells and shows no significant cytotoxicity, therefore playing an important role in the inhibition of Type 1 hypersensitivity.

## 2. Materials and methods

### 2.1. Materials and reagents

Ginger powder was purchased from Asaoka Spices, Japan. 6-Gingerol, phorbol 12-myristate 13-acetate (PMA) and ionomycin were obtained from Wako Pure Chemical Industries, Japan. Staphylococcal enterotoxin B was purchased from Toxin Technology, USA. Interleukin-2, interleukin-4, interleukin-12, anti-IL-4 and anti-IL-12 antibodies were obtained from R&D Systems Inc., USA. Anti-CD3/CD28 antibody-bound beads were purchased from Life Technologies Inc., USA. Protease inhibitor cocktails were obtained from Sigma-Aldrich Co., LLC, USA.

### 2.2. Mice

Female Balb/c mice at 8 weeks of age were purchased from Charles River Laboratories Inc., Japan, and maintained in a humidity (50±10%), 12-h light/dark cycle, temperature (22±2°C)-controlled pathogen-free animal facility. Three to five mice were housed in each cage and fed a standard or 2% ginger-containing chow diet (CRF-1; 8.2% moisture, 21.9% proteins, 5.4% crude fats, 6.3% crude ash, 2.9% crude fiber and 55.3% nitrogen free extract, 3.57 kcal/g; Oriental Yeast Co., Ltd., Japan) provided with tap water filtered by a polypropylene string wound cartridge (Organo Co., Ltd., Japan). The Animal Care and Use Committee (approval no. 2410025) in Chubu University approved this study.

### 2.3. Cell lines and culture

Human T cell line Jurkat cells (clone E6-1) and human B cell line Raji cells were purchased from the American Type Culture Collection and maintained in RPMI 1640 medium containing 10% heat-inactivated FBS, 100-units/ml penicillin, and 100-µg/ml streptomycin. All cell cultures were processed at 37°C and 5% CO<sub>2</sub> in a humidified atmosphere.

### 2.4. OVA sensitization and challenge

Mice were sensitized with 50 µg of OVA along with 1 mg of Alum (LSL, Japan) in PBS by ip injection twice at a 2-week interval. The mice were fed a diet containing 2% ginger or a control diet from 2 weeks before the first injection of OVA and until the end of the experiment. Two weeks after the second injection, sensitization was followed by intranasal challenges daily for 6 days with OVA in all groups.

### 2.5. ELISA

Concentrations of OVA-specific IgE in mice sera and IL-4 in culture media were measured by using an ELISA kit (Shibayagi Co., Ltd., Japan and R&D Systems, respectively) according to the instructions of the manufacturers.

### 2.6. Histology and mast cell staining

To obtain transverse sections through tips of the noses of the mice, nasal cavity tissues were fixed overnight in 4% paraformaldehyde at 4°C and then processed for paraffin embedding. Four-µm-thick paraffin sections were deparaffinized and stained with Toluidine blue solution (0.05%, pH 4.1, Wako Pure Chemical Industries, Japan). Cells were examined by light microscopy.

### 2.7. Quantitative RT-PCR

Total RNA was isolated from spleen cells or Jurkat T cells using a Nucleospin RNA II isolation kit (Macherey-Nagel, Germany) according to the manufacturer's instructions. cDNA was synthesized from total RNA (200 ng from spleen cells and 1 µg from Jurkat T cells, respectively) using a ReverTra Ace kit (TOYOBO, Japan). For quantitative RT-PCR reaction, 2 µl of cDNA was used in combination with 10 µl of THUNDERBIRD SYBR qPCR Mix (TOYOBO, Japan), 1 µl of each primer (10 µM), 0.04 µl of 50×ROX reference dye, and 5.96 µl of H<sub>2</sub>O with the following two-step PCR conditions using 7500 Real-Time PCR system (Life Technologies): initial denaturation at 95°C for 1 min followed by 50 cycles of denaturation and extension (95°C for 15 s and 60°C for 1 min). A melting curve was then generated to check for the specificity of the primers. The primers used were as follows: mouse HPRT, 5'-ACG GAG ATG GAT GTG CCA AAC-3' (forward) and 5'-AGC ACC TTG GAA GCC CTA CAG A-3' (reverse); mouse IL-4, 5'-ACG GAG ATG GAT GTG CCA AAC-3' (forward) and 5'-AGC ACC TTG GAA GCC CTA CAG A-3' (reverse); mouse IL-10, 5'-GCC AGA GCC ACA TGC TCC TA-3' (forward) and 5'-GAT AAG GCT TGG CAA CCC AAG TAA-3' (reverse); mouse IL-13, 5'-CAA TTG CAA TGC CAT CTA CAG GAC-3' (reverse); mouse IFN-γ, 5'-CGG CAC AGT CAT TGA AAG CCT A-3' (forward) and 5'-GTT GCT GAT GGC CTG ATT GTC-3' (reverse); human GAPDH, 5'-CAA CTA CAT GGT TTA CAT GTT CC-3' (forward) and 5'-GGA CTG TGG TCA TGA GTC CT-3' (reverse); human interleukin 2 (IL-2), 5'-CAA CTG GAG CAT TTA CTG CTG G-3' (forward) and 5'-TCA GTT CTG TGG CCT TCT TGG-3' (reverse).

### 2.8. T-cell primary cultures

Mice were sacrificed, and the spleens were surgically excised. Each organ was forced through a nylon screen to make a single-cell suspension, and cells were washed and resuspended in RPMI medium. To remove erythrocytes, the spleen cells were treated with 0.83% ammonium chloride for 10 min and resuspended in RPMI medium. Mouse pan T cells were isolated by using anti-Thy1.2 antibody-bound Dynabeads (Life Technologies) according to the manufacturer's instructions. The T cells were then treated with anti-CD4 (FITC) antibody, anti-CD62L antibody (PE) and anti-CD44 antibody (APC) and subjected to cell sorter analysis. Naïve T lymphocytes defined as CD4<sup>+</sup> CD62L<sup>high</sup> CD44<sup>low</sup> cells were isolated, and 2.5×10<sup>5</sup> cells were plated in an anti-CD3 antibody-bound plate (24-well plate, 1 ml). T cells were cultured under Th1 or Th2 polarizing conditions by the addition of murine IL-2 (20 ng/ml, R&D Systems), murine IL-12 (10 ng/ml, R&D Systems) and anti-IL-4 neutralizing antibody (10 µg/ml, R&D Systems) or murine IL-2 (20 ng/ml, R&D Systems), murine IL-4 (20 ng/ml, R&D Systems) and anti-IL-12 neutralizing antibody (10 µg/ml, R&D Systems).

### 2.9. Cell viability assay

Cell proliferation/viability was determined by reduction of the tetrazolium salt WST-8 through mitochondrial dehydrogenases using Cell Counting Kit-8 (Dojindo, Japan) according to the manufacturer's instructions.

### 2.10. Isolation of cytosolic and nuclear proteins (NPs)

Jurkat cells were washed twice with PBS and lysed with cytoplasmic lysis buffer (20-mM HEPES, 20% glycerol, 10-mM NaCl, 1.5-mM MgCl<sub>2</sub>, 0.2-mM EDTA pH 8.0, 1-mM DTT, 0.1% NP-40, PMSF and protease inhibitor cocktail) for 15 min on ice. After centrifugation at 500×g for 5 min, the supernatant was used as a cytosolic protein sample. The pellet was resuspended with nuclear lysis buffer (20-mM HEPES, 20% glycerol, 500-mM NaCl, 1.5-mM MgCl<sub>2</sub>, 0.2-mM EDTA pH 8.0, 1-mM DTT, 0.1% NP-40, PMSF and protease inhibitor cocktail), mixed vigorously and incubated for 30 min on ice. After centrifugation at 23,000×g for 15 min, the supernatant was used as a NP sample.

### 2.11. Immunoblotting and antibodies

Western blotting was performed according to the method described previously [18]. Briefly, lysates of Jurkat cells were subjected to SDS-PAGE using 8% polyacrylamide gel and transferred to a polyvinylidene difluoride membrane (Merck Millipore, Billerica, MA, USA). The membrane was blocked with 5% nonfat milk or 2% BSA for 1 h at room temperature and then reacted with a first antibody for 18 h at 4°C followed by reaction

with a corresponding second horseradish peroxidase-conjugated antibody for 1 h at room temperature. The levels of phosphorylation or protein signal were detected by Western Lightning Plus-ECL (PerkinElmer, Inc., MA, USA). Anti-phospho-ERK p44/42, anti-phospho-JNK, anti-phospho-p38 and anti-GAPDH antibodies were purchased from Cell Signaling Technology Inc (Danvers, MA, USA). Anti-NF- $\kappa$ B, anti-c-fos and anti-Histone H1 antibodies were obtained from Santa Cruz Biotechnology Inc (Dallas, TX, USA). Anti- $\beta$ -actin antibody was purchased from BioVision (Milpitas, CA, USA).

2.12. Ethics statement

This study was performed in Chubu University, Japan. The study was approved by the Animal Care and Use Committee (approval no.2210048 and 2310009) at Chubu University.

3. Results

3.1. Suppression of OVA-induced allergy was suppressed in ginger-fed mice

To study the antiallergic effect of ginger, we made use of a model of OVA-induced allergic rhinitis. In this model, three groups of Balb/c mice were prepared ( $n=8-10$ /group). Two groups of Balb/c mice were fed a control diet, and one group of mice was fed a diet containing 2% ginger. Two weeks later, one group of control diet mice and the group of ginger diet mice were sensitized by two intraperitoneal

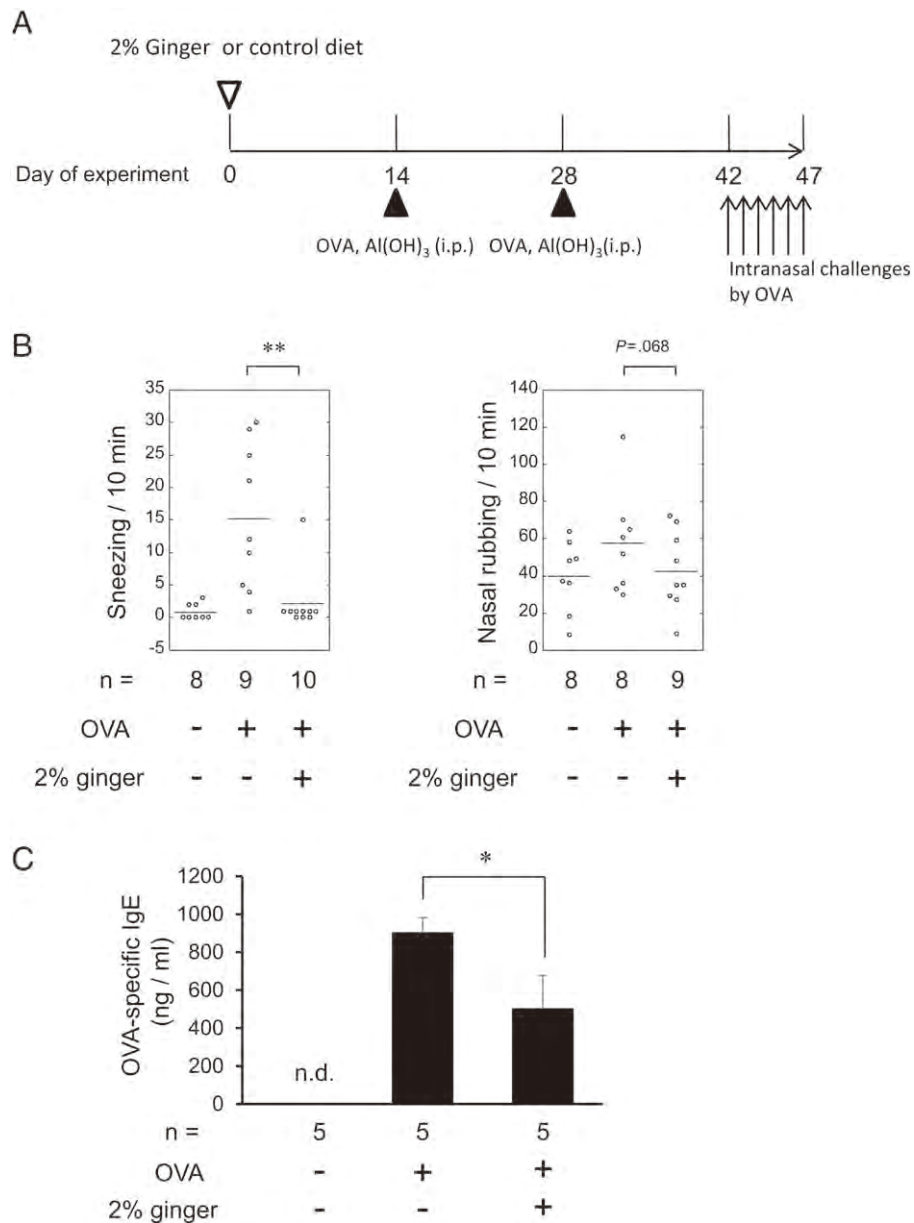


Fig. 1. (A) Experimental design. Groups of female Balb/c mice (8 weeks old) were fed a diet containing 2% ginger from 2 weeks before the first OVA sensitization until the end of the experiment. Mice received 50  $\mu$ g of OVA adsorbed onto 1-mg Alum at day 14 (first sensitization). After that, mice were immunized with OVA at day 28 (second sensitization). Sensitization was followed by intranasal challenges daily for 6 days with OVA in all groups from day 42. (B) Effect of 2% ginger feeding on allergic rhinitis symptoms. The numbers of sneezes and nasal rubbing movements were counted for 10 min after the nasal drop of OVA (10 mg/ml) ( $n=8-10$ /group). Small horizontal lines indicate means. \*\*Mann-Whitney  $U$  test,  $P<0.01$ . (C) Comparison of OVA-specific IgE levels in serum among the three groups of mice ( $n=5$ /group). Values are mean  $\pm$  S.D. \*Mann-Whitney  $U$  test,  $P<0.05$ . (D) Analysis of mast cells accumulation in the nasal mucosa. Nasal mucosal sections of the three groups of mice were stained with toluidine blue for detection of mast cells (upper panel); mast cells were stained red-purple (metachromatic staining against a blue background). Number of mast cells, indicated by arrows, was counted in six randomly selected fields at a power of  $\times 400$  within a section, and relative number of cells is shown (lower panel). The data shown are from a single representative experiment from five or six animals. The data are expressed as relative values, with the OVA-sensitized control diet group being 100%. \*Mann-Whitney  $U$  test,  $P<0.05$ .

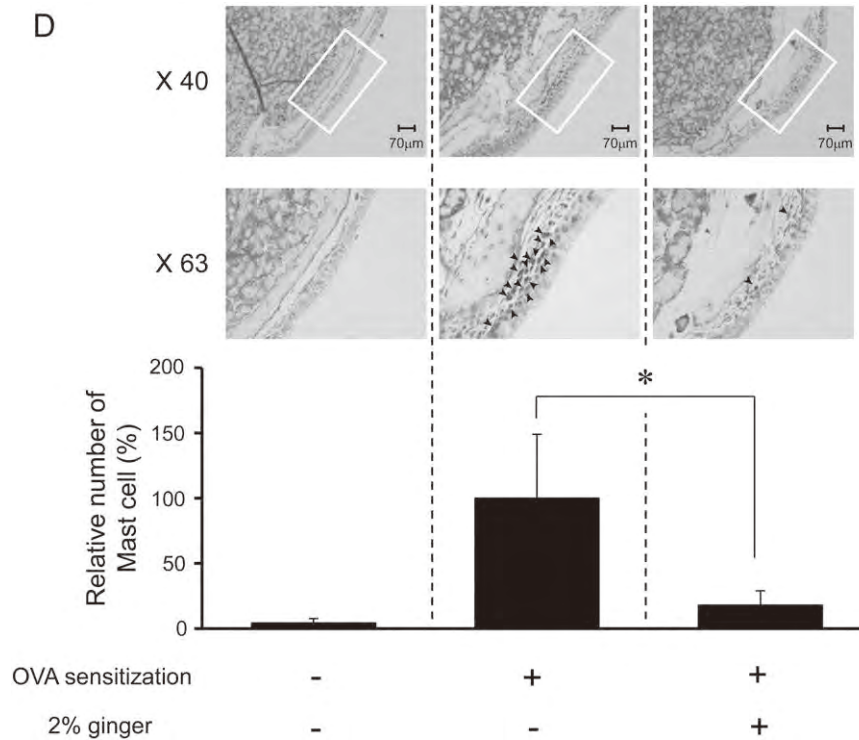


Fig. 1. (continued)

injections (at days 14 and 28) of 50 µg of OVA adsorbed onto 1 mg of alum. The other group of control mice was injected with PBS as a negative control (NC). From days 42 to 47, all mice were intranasally challenged daily with 10 mg/ml of OVA (Fig. 1A). Every 6 or 7 days, the body weights of all mice were measured, and it was confirmed that there was no significant difference in body weights among the mouse groups during the experimental period ( $n=5-6$ /group) (Table 1).

At day 47, the numbers of sneezes ( $n=8-10$ ) and nasal rubbing movements ( $n=8-9$ ) were counted for 10 min after the nasal sensitization. Fig. 1B shows that the number of sneezes was significantly decreased in the ginger-fed group. The number of nasal rubbing movements showed a strong tendency for suppression of allergic responses in the ginger-fed mice ( $P=0.068$ ). Then we evaluated OVA-specific IgE concentrations in serum in the three groups of mice ( $n=5$ /group). As shown in Fig. 1C, in the OVA-immunized groups, the level of IgE in the ginger-fed mice was significantly lower than that in the control diet mice.

To further investigate the effect of ginger in the OVA-induced allergy model, we counted the number of mast cells that had

infiltrated nasal mucosa by toluidine blue staining. As shown in Fig. 1D, the number of mast cells in ginger-fed mice was significantly smaller than that in control mice. Hematoxylin–Eosin staining also showed a decrease in the number of infiltrating inflammatory leukocytes in nasal mucosa (data not shown). These results suggest that OVA-induced allergy was potently suppressed by 2% ginger diet.

### 3.2. Inhibition of antigen-induced cytokine expression by 6-gingerol

It is well known that Th2 cytokines (referred to also as type 2 cytokines), including IL-4, IL-5, IL-6, IL-10 and IL-13, play important roles in establishing Type I allergies. During the production process of antigen-specific IgG or IgE, Th2 cytokines are necessary, and Th1 cytokines (referred to also as Type 1 cytokines), including IL-12, IFN-γ and tumor necrosis factor alpha, are relatively suppressed and vice versa.

Since 6-gingerol (Fig. 2A) is a major bioactive phenolic compound derived from ginger, we assumed that this compound plays a role in the anti-allergic effect. To examine whether 6-gingerol can suppress Th2 cytokine expression, spleen cells from a Balb/c mouse that had been sensitized with OVA were re-stimulated with or without 6-gingerol *in-vitro*. One day and 7 days after re-stimulation with OVA, the production of IL-4, one of the major Th2 cytokines, was determined by ELISA. As shown in Fig. 2B, there was a slight increase in IL-4 production by OVA stimulation at 1 day after stimulation, but no significant difference by 6-gingerol was observed. However, 7 days after stimulation, 6-gingerol significantly inhibited the production of IL-4 in a dose-dependent manner. To further examine the inhibitory effect of 6-gingerol on Th2 cytokines, we then performed quantitative PCR to assess the gene expression of IL-4, IL-10 and IL-13. We confirmed that the gene expression of all of these Th2 cytokines was clearly inhibited by 6-gingerol. The gene expression of IFN-γ, however, was also significantly suppressed by 6-gingerol (Fig. 2C). To examine whether 6-gingerol can suppress cytokine production from unprimed spleen cells, we used superantigen staphylococcal

Table 1  
Food intake, ginger intake and weight gain of mice-fed control or 2% ginger diet for 42 days

Group	Food intake	Ginger intake*	Body weight gain
	g/d	g/d/kg	g/42 d
Control diet/PBS ( $n=5$ )	2.98±0.076	–	4.6±0.89
Control diet/OVA ( $n=5$ )	2.92±0.077	–	3.2±0.84
2% ginger diet/OVA ( $n=5$ )	2.81±0.089	2.68±0.13	3.3±0.82

\* Conversion of food weight into ginger weight. Five mice were housed per cage (control diet group for PBS injection, control diet group for OVA injection and 2% ginger diet group for OVA injection). Every 6 or 7 days, the amount of remaining food and body weight of all mice were measured to calculate food intake per day and body weight gain during the period of the experiment (42 days). On each occasion, mice were placed in a new cage, and fresh control or 2% ginger diets from the same batch were produced. Values are mean±S.D. There were no significant difference in food intake or body weight gain between the groups (ANOVA followed by Dunnet's post-hoc test).

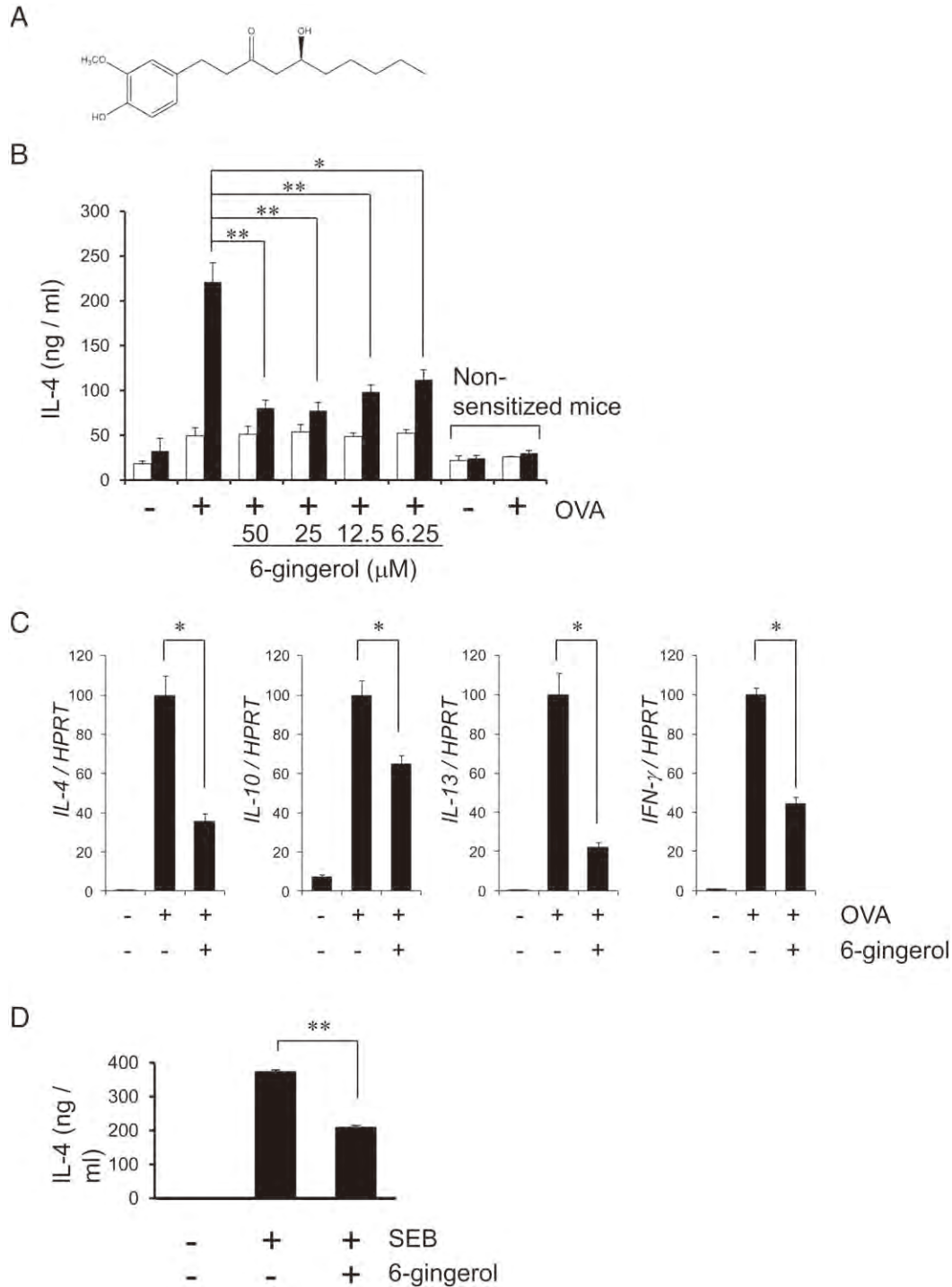


Fig. 2. Effect of 6-gingerol on OVA-induced expression of cytokines. (A) Chemical structure of 6-gingerol. (B) IL-4 secretion by *in vitro* antigen stimulation. Spleen cells from an OVA-sensitized mouse fed a normal diet were stimulated by OVA (1 mg/ml) with 6-gingerol at various concentrations (0–50 μM) for 1 day (open bar) or 7 days (closed bar). The concentration of IL-4 was determined by ELISA. Values are mean±S.D. calculated from three independent experiments. The asterisk indicates a significant difference from the OVA-stimulated control value (\**P*<0.05, \*\**P*<0.01, Student's *t* test). (C) Expression of interleukins by *in vitro* antigen stimulation. Spleen cells from an OVA-sensitized mouse fed a normal diet were stimulated by OVA (1 mg/ml) with or without 6-gingerol (50 μM). RNA samples were extracted, and the mRNA expression levels were measured by quantitative PCR. HPRT was used as a control for normalization. The data are expressed as relative values, with the OVA-stimulated group being 100%. Values are mean±S.D. calculated from three independent experiments. The asterisk indicates a significant difference from the OVA-stimulated control value (\**P*<0.05, Student's *t* test). (D) Spleen cells from a Balb/c mouse were stimulated by superantigen (SEB, 5 μg/ml) with or without 6-gingerol (50 μM) for 3 days, and IL-4 production was measured by ELISA. Values are mean±S.D. calculated from three independent experiments. The asterisk indicates a significant difference from the SEB-stimulated control value (\*\**P*<0.01, Student's *t* test).

enterotoxin B (SEB). This can be used to induce the production of cytokines, including IL-4, from T cells without an antigen when co-cultured with major histocompatibility complex (MHC) Class II

expressing cells to stimulate spleen cells from a Balb/c mouse. 6-Gingerol suppressed SEB-induced IL-4 production (Fig. 2D), indicating that 6-gingerol possibly affected T cell receptor-mediated signal

transduction rather than the antigen presentation process. These results suggest that ginger or 6-gingerol may interfere with a variety of cytokines, not only Th2 cytokines but also Th1 cytokines, and consequently suppress the Th2-dominant phenotype of Type I allergy.

### 3.3. Inhibition of helper T cell polarization by 6-gingerol

6-Gingerol may not suppress Th2 cytokines by promoting Th1 cytokines but may prevent Type I allergy by inhibiting excess production of cytokines including Th2 cytokines. To investigate this hypothesis, we carried out an experiment on *in vitro* induction of helper T cell polarization of naïve CD4-positive ( $CD4^+$ ) T cells. Naïve T lymphocytes defined as  $CD4^+CD62L^{high}CD44^{dull}$  cells were cultured under Th1 or Th2 polarizing conditions with or without 6-gingerol. It is well known that Th1 cytokines including IL-2, TNF- $\alpha$  and IFN- $\gamma$  are expressed in Th1 cells under Th1 polarizing conditions. On the other hand, IL-4, IL-5, IL-6, IL-10 and IL-13 are expressed in Th2 cells under Th2 polarizing conditions. Because Th1 and Th2 responses are known to cross-inhibit each other, there was a possibility that 6-gingerol up-regulates the production of Th1 cytokines, thereby down-regulating the production of Th2 cytokines. We analyzed the gene expression of IFN- $\gamma$  and IL-4 as representative cytokines of Th1 and Th2 cells, respectively. Fig. 3A and B shows that 6-gingerol significantly inhibited not only IFN- $\gamma$  gene expression but also IL-4 gene expression in a dose-dependent manner. These findings suggest that suppression of the expression of Th2 cytokines by 6-gingerol does not mediate the promotion of Th1 cytokine expression.

### 3.4. Inhibition of cell proliferation by 6-gingerol

To test the effect of 6-gingerol on lymphocyte proliferation in response to immune stimulation, we counted the number of living cells after various stimuli. Firstly, we checked proliferation of total spleen cells by antigen stimulation. Total spleen cells from an OVA-sensitized mouse or PBS control mouse were subjected to *in vitro* stimulation with OVA with/without 6-gingerol for 7 days. As shown in Fig. 4A (left panel), 6-gingerol significantly suppressed proliferation of OVA-stimulated spleen cells in a dose-dependent manner. To count the number of T cells, we isolated pan T cells by using anti-Thy1.2 antibody-bound magnetic beads from total spleen cells at day 7 after OVA stimulation. Fig. 4A (right panel) shows that proliferation of T cells was significantly suppressed by treatment with 6-gingerol in a dose-dependent manner. These results suggest that 6-gingerol can inhibit activation of primed T cells.

We then examined whether 6-gingerol suppress proliferation of unprimed T cells. To assess this possibility, we used SEB to stimulate spleen cells from a Balb/c mouse. Fig. 4B shows that 6-gingerol suppressed SEB-induced cell proliferation in a dose-dependent manner. Furthermore, it is possible to induce strong T cell expansion by culturing with anti-CD3/CD28 antibody-bound beads and recombinant murine IL-2. We then used a Jurkat T cell line and cultured the cells with the antibody beads and the cytokine with or without 6-gingerol. Fig. 4C shows that 6-gingerol significantly suppressed the expansion of Jurkat T cells even in such a strong stimulation system. These results suggest that the site of action of 6-gingerol against T cell proliferation exists in the T cell receptor-mediated signal transduction pathway rather than during the antigen-processing event in antigen-presenting cells.

### 3.5. Effect of 6-gingerol on cytokine expression

Our results indicated that 6-gingerol strongly affects proliferation and cytokine expression of T cells. To elucidate the mechanism by which 6-gingerol suppresses the expression of cytokines induced by T cell receptor stimulation, we used a Jurkat T cell line. Initially, we

confirmed that cell viability was not influenced by 6-gingerol treatment (Fig. 5A) and cytotoxicity of 6-gingerol is therefore not the reason for suppression of the expression of cytokines. To mimic a physiologic response, Jurkat T cells were co-cultured with SEB-pulsed Raji B cells. IL-2 expression was then analyzed by quantitative PCR after 24 h of incubation in the presence or absence of 6-gingerol. As shown in Fig. 5B, 6-gingerol significantly inhibited IL-2 expression in Jurkat T cells with SEB-pulsed Raji B cells. Furthermore, expression of the IL-2 gene was robustly induced by treatment with PMA and ionomycin. Pretreatment with 6-gingerol significantly inhibited IL-2 expression induced by PMA and ionomycin (Fig. 5C). These results suggest that 6-gingerol suppresses cytokine expression or proliferation of T cells not by inhibiting IL-2-mediated cell proliferation but by inhibiting the expression of cytokines including IL-2.

### 3.6. Inhibition of MAPK phosphorylation and calcium release by 6-gingerol

We next investigated whether 6-gingerol suppresses PMA and ionomycin-induced phosphorylation of MAPKs (Fig. 6A). ERK1/2, JNK

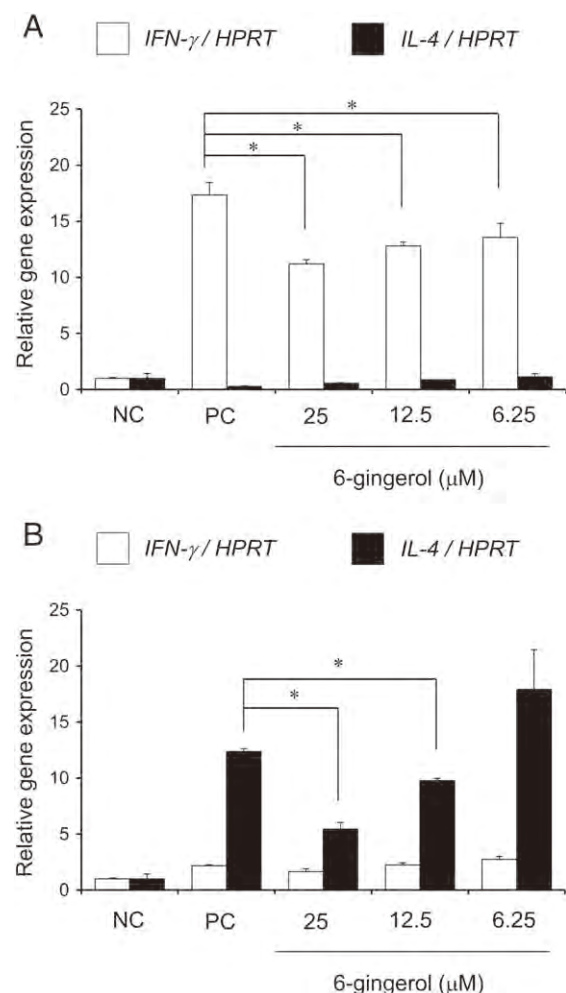


Fig. 3. Effect of 6-gingerol on gene expression of Th1 or Th2 cytokines. Spleen cells from a Balb/c mouse were cultured with IL-12 and anti-IL-4 antibodies (Th1 culture condition, A) or with IL-4 and anti-IL-12 antibodies (Th2 culture condition, B) for 7 days. 6-Gingerol was added at various concentrations (0–25  $\mu$ M) during the culture. At the end of culture, cells were collected, and total RNA was purified, and then the gene expression of IL-4 and IFN- $\gamma$  was measured by quantitative PCR. HPRT was used as a control for normalization. Data are shown as relative gene expression levels compared to the NC. Open bar ( $\square$ ) and closed bar ( $\blacksquare$ ) indicate IFN- $\gamma$  and IL-4, respectively. Values are mean  $\pm$  S.D. calculated from three independent experiments. The asterisk indicates a significant difference from the positive control value (\* $P$ <0.05, Student's  $t$  test).

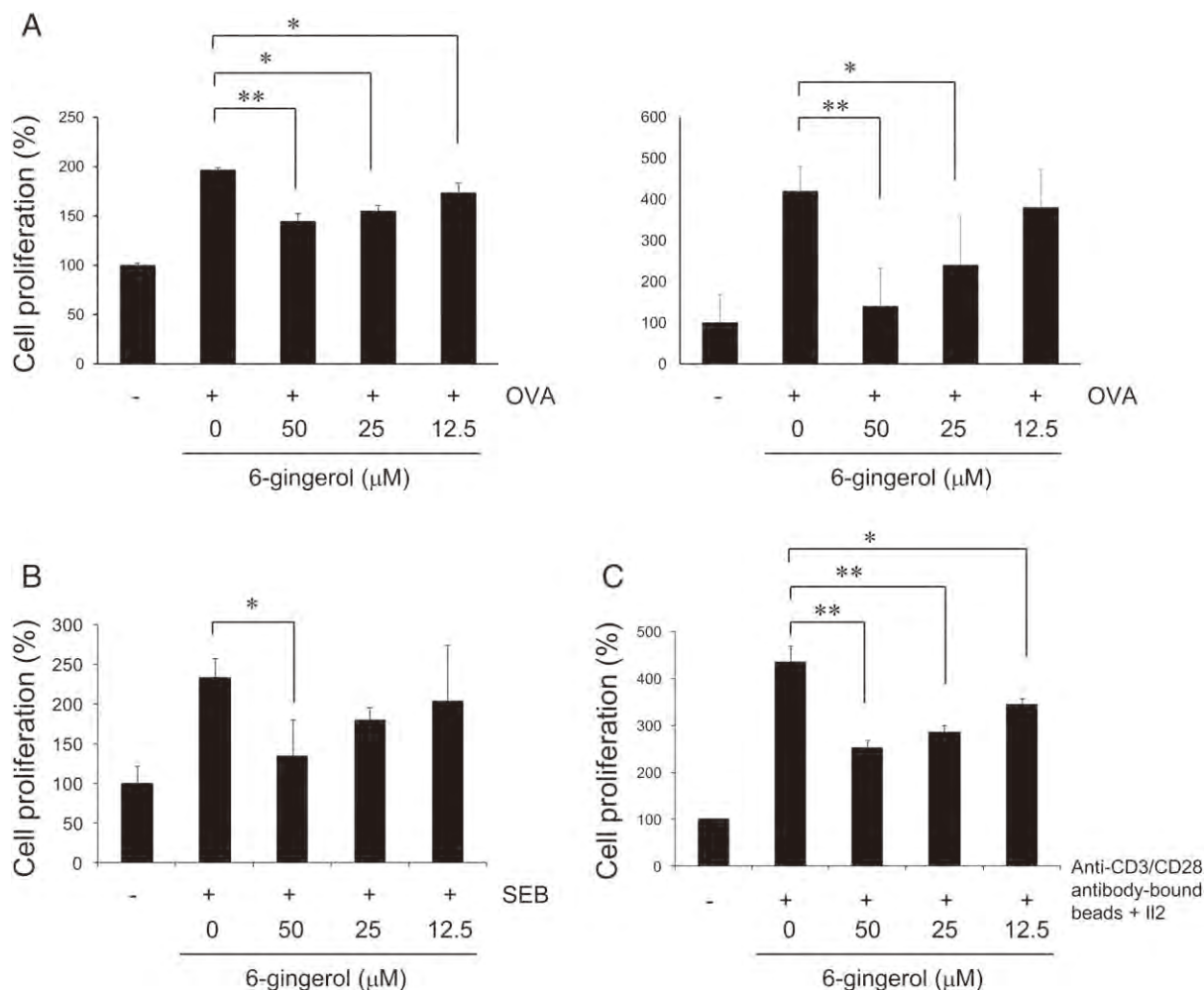


Fig. 4. Effect of 6-gingerol on proliferation of stimulated spleen cells or Jurkat T cells. The absolute number of live spleen cells (A, B) in each sample was counted by the trypan blue exclusion assay, and the relative cell proliferation compared with control (no stimulation) was calculated. (A)  $1 \times 10^7$  cells/sample of total spleen cells (left panel) or purified pan-T cells by Thy1.2 antibody-bound magnetic beads (right panel) from an OVA-sensitized mouse were cultured without or with OVA (1 mg/ml) in culture media containing various concentrations of 6-gingerol (0–50 μM) for 7 days. (B)  $1 \times 10^7$  cells/sample of total spleen cells from a normal Balb/c mouse were cultured with superantigen (SEB, 5 μg/ml) in culture media containing various concentrations of 6-gingerol (0–50 μM) for 3 days. Live Jurkat cells (C) were determined using Cell Counting Kit-8, and the relative cell proliferation compared with control (no stimulation) was calculated. (C)  $5 \times 10^5$  cells/sample of Jurkat T cells were cultured with anti-CD3/CD28 antibody-bound beads and recombinant human IL-2 (2 ng/ml) in culture media containing various concentrations of 6-gingerol (0–50 μM) for 3 days. Values are mean  $\pm$  S.D. calculated from three independent experiments. The asterisk indicates a significant difference (\* $P < 0.05$ , \*\* $P < 0.01$ , Student's *t* test).

and p38 were transiently phosphorylated during a period of 60 min after the treatment. Pretreatment with 6-gingerol suppressed phosphorylation of all MAPKs. As was expected, 6-gingerol also significantly inhibited intracellular calcium release (Fig. 6B).

### 3.7. Inhibition of nuclear localization of transcription factors by 6-gingerol

We further investigated the effect of 6-gingerol on nuclear translocation of transcription factors, which are required for cytokine expression. Among some transcription factors that play a critical role in IL-2 expression when T cells are stimulated by PMA and ionomycin, we chose NF-κB (p65/RelA) and c-fos as representative transcription factors and analyzed the translocation of them from the cytosol to nucleus. Jurkat T cells were pretreated with 6-gingerol for 2 h before PMA and ionomycin stimulation for 18 h. Subsequently, cytosolic and NPs were prepared and analyzed using Western blotting. As shown in Fig. 7, pretreatment with 6-gingerol effectively suppressed the nuclear localization of NF-κB and c-fos in a dose-dependent manner. The inhibitory effect of 6-gingerol on the translocation of NF-κB and c-fos was confirmed by immunofluorescence staining using

specific antibodies (data not shown). These results demonstrate that 6-gingerol suppresses cytokine expression by inhibiting NF-κB and AP1 activation.

## 4. Discussion

In this study, we investigated whether ginger and its major compound 6-gingerol exert an antiallergic effect by employing a widely used OVA-induced allergic rhinitis model. In an *in vivo* study, we confirmed that administration of a ginger diet significantly reduced production of antigen-specific IgE and alleviated sneezing and nasal rubbing behavior. To elucidate the molecular basis for these observations, we chose 6-gingerol and investigated its effect on primary culture cells or lymphocytic cell lines. Because OVA-specific IgE was reduced by ginger feeding, we first hypothesized that ginger components suppressed the production of Th2 cytokines rather than inhibiting degranulation of mast cells. It has been reported that ginger prevented Th2-mediate immune responses and that 6-gingerol was sufficient to suppress eosinophilia in a mouse model of airway inflammation [19]. Therefore, we predicted that its mechanism of action is the

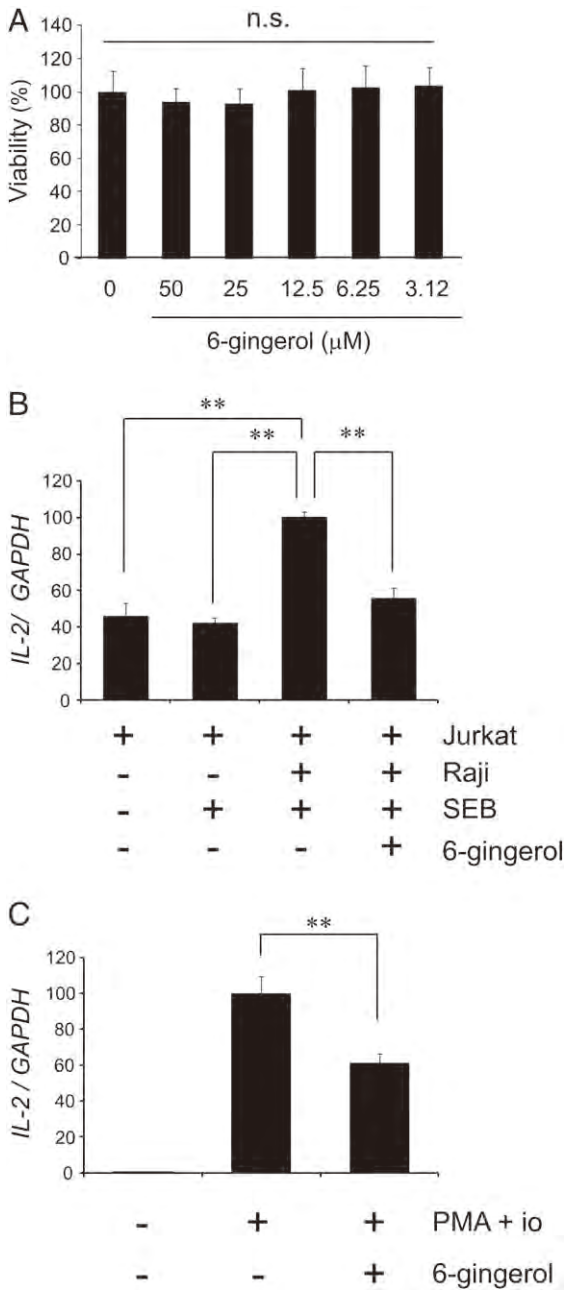


Fig. 5. Effect of 6-gingerol on cytokine production in T cells. (A) Jurkat T cells were cultured with various concentrations of 6-gingerol (0–50  $\mu\text{M}$ ) for 2 days. Cell viability was determined by using a Cell Counting Kit-8. Values are mean  $\pm$  S.D. calculated from three independent experiments. (B) Jurkat cells and Raji cells were co-cultured and stimulated by SEB with or without 6-gingerol (50  $\mu\text{M}$ ) for 24 h. Then *IL-2* gene expression was measured by quantitative PCR. The *GAPDH* gene was used as a control for normalization. Values are mean  $\pm$  S.D. calculated from three independent experiments. (C) Jurkat cells were stimulated by PMA and ionomycin with or without 6-gingerol (50  $\mu\text{M}$ ) for 24 h, and *IL-2* gene expression was measured by quantitative PCR. Values are mean  $\pm$  S.D. calculated from three independent experiments. The asterisk indicates a significant difference (\*\*\*)  $P < 0.01$ , Student's *t* test).

downgrading of Th2 cell-dependent allergic reactions. Indeed, administration of ginger resulted in a marked decrease in infiltration of mast cells in nasal mucosa, and 6-gingerol potently suppressed the expression of IL-4, one of the key cytokines secreted by Th2 cells.

Since the expression of Th2 cytokines including IL-4, IL-5 and IL-13 was suppressed by Th1 cytokines including IL-12 and IFN- $\gamma$  and vice versa [20], our next question was whether 6-gingerol enhances the

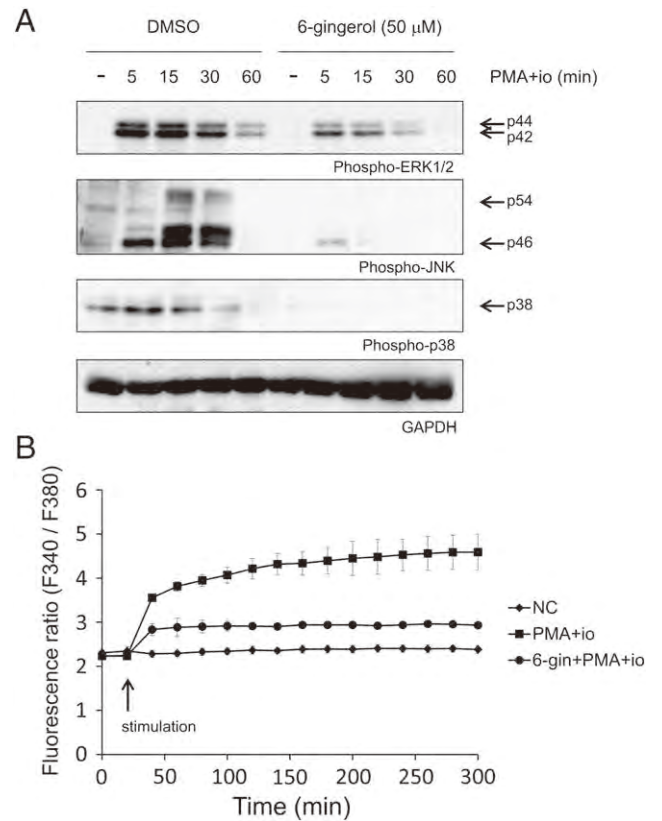


Fig. 6. Effect of 6-gingerol on cell-signaling molecules. (A) Western blot analysis of the phosphorylation of MAP kinases. Jurkat cells were pretreated with 6-gingerol (50  $\mu\text{M}$ ) 2 h before stimulation by PMA and ionomycin. Time-dependent changes in the phosphorylation of ERK p44/p42, JNK and p38 were analyzed by Western blotting. GAPDH is shown as a loading control. The resulting blots were cropped to show the bands of interest. (B) Calcium-signaling analysis. Jurkat cells were stained with Fura-2AM and then stimulated with PMA and ionomycin. Fluorescence was monitored in a fluorescence spectrophotometer as described in "Materials and Methods."

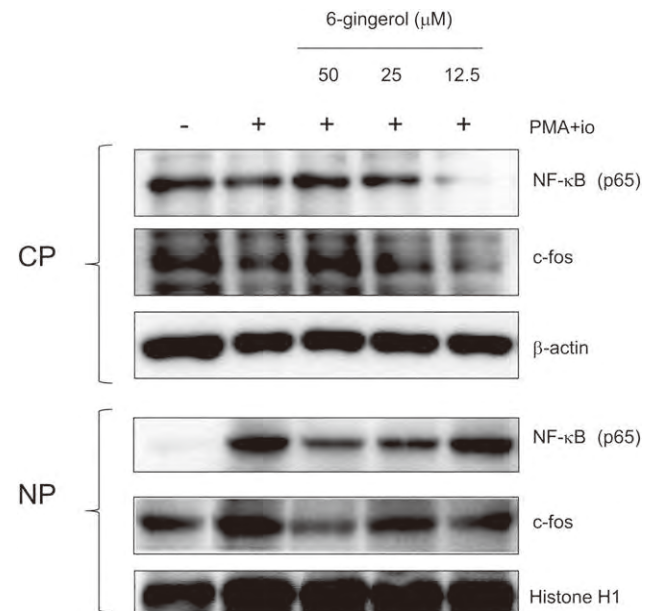


Fig. 7. Effect of 6-gingerol on the localization of transcription factors induced by PMA and ionomycin. Jurkat cells were pretreated with 6-gingerol for 2 h before stimulation with PMA+ionomycin. After 18 h, cells were collected, and NPs were extracted. The proteins were measured and were subjected with an equal amount of NPs to SDS-PAGE followed by Western blotting.  $\beta$ -actin and Histone H1 are shown as loading controls.

expression of Th1 cytokines. Our results showed that 6-gingerol also suppressed the expression of Th1 cytokines even in strong Th1-polarizing conditions *in vitro*. These findings are in agreement with results of previous studies showing that ginger extracts can inhibit the production of several Th1 cytokines [19,21]. Superantigen SEB binds to and cross-links variable regions of certain  $\beta$ -chains of T cell receptors in addition to either one or both of the  $\alpha$ - or  $\beta$ -chains of MHC Class II molecules on antigen-presenting cells such as dendritic cells, macrophages or B cells [22,23]. Interestingly, 6-gingerol suppressed SEB-induced IL-4 production in spleen cells and cell proliferation of Jurkat T cells. These results suggest that 6-gingerol affected TCR-mediated signal transduction rather than antigen presentation processes. Hence, we proposed that suppression of the expression of Th2 cytokines by 6-gingerol was due not to enhancement of Th1 cytokine production but to inhibition of the general pathway for cytokine expression.

Ginger or its extracts was known to possess a range of biological functions as mentioned in the introduction section. It is very recently demonstrated that intraperitoneal administration of ethanol and/or aqueous extract of ginger ameliorated allergic asthma [24]. However, it has not been clarified whether oral administration of ginger can prevent allergic rhinitis. In this study, we used ginger powder that is widely used for cooking and demonstrated for the first time that 2% ginger-containing diet prevented exacerbation of allergic rhinitis in mice. In ginger powder, 6-gingerol, 6-shogaol, 8-gingerol and 10-gingerol have been identified as the major pungent compounds. The compositions of fresh and dry ginger have been analyzed in detail in several studies using HPLC or LC-TOF/MS, and it has been shown that 6-gingerol is the most abundant compound among the gingerol-related compounds in fresh and dry ginger [11–13]. In studies investigating mice receiving 6-gingerol orally, significant physiological effects have been observed using doses ranging from approximately 10 to 30 mg/day/kg [25–28]. According to the previous studies [11–13], ginger powder contains approximately 0.5% 6-gingerol. To receive 10 mg/day/kg of 6-gingerol by oral ingestion of a ginger powder-containing diet, mice must theoretically consume 2-g/day/kg ginger powder. An 8–12-week-old mouse (body weight, ~20 g) consumes approximately 2–3-g food a day (100–150 g/day/kg). Accordingly, we selected a weight-based ginger content of 2% (corresponding to an approximate 6-gingerol dose of 10–15 mg/kg) for diets used in this study. Thus, we found that 6-gingerol significantly inhibited T cell proliferation/activation because of the down-regulation of mitogen-activated protein kinases and calcium release-mediated IL-2 expression. Here, we found that 6-gingerol significantly inhibited T cell proliferation/activation due to down-regulation of mitogen-activated protein kinases and calcium release-mediated IL-2 expression. Helper T cells play essential roles in establishing and maximizing the capabilities of the immune system, and suppression of T cell proliferation/activation is therefore one of the possible reasons for the alleviation of allergic symptoms by ginger.

We proved that 6-gingerol not only inhibits the activation of T cells caused by the activation of T cell receptors by anti-CD3/CD28 antibodies but also inhibits T cell activation by PKC stimulation by PMA and ionomycin. We did not examine the effects of 6-gingerol on the antigen-processing pathway in antigen-presenting cells, but these results clearly suggest that one of the important molecular sites of action of 6-gingerol is onset of T cell activation. It has been reported that 8-gingerol, another component of ginger, suppressed OVA, lipopolysaccharide and concanavalin A-stimulated spleen cell proliferation [29]. According to a previous report, 8-gingerol content in ginger powder is about one fourth of that of 6-gingerol [13], and the antiallergic effect of ginger in OVA-immunized mice in this study may therefore be simultaneous effects of gingerols and other unknown components. That said, our data using 6-gingerol *in vitro* that can explain a part of the mechanism of antiallergic effects suggest that 6-gingerol greatly contributes to the antiallergic effects in our model.

It has already been demonstrated that ginger prevents Th2-mediated airway inflammation in a mouse model [19]; that ginger inhibits the synthesis of proinflammatory cytokines including IL-1, IL-8 and TNF- $\alpha$  [10]; and that ginger extracts and simultaneous addition of a green tea that is rich in epigallocatechin-3-O-(3-O-methyl) gallate significantly suppress delay-type allergy [30]. Mounting evidence suggests that ginger is useful for prevention of allergic symptoms. However, it has not been reported whether ginger diet can prevent allergic rhinitis using a Type I allergy model. This study, for the first time, demonstrated that 2% ginger diet significantly prevented OVA-induced allergic rhinitis via inhibition of T-cell activation.

Ginger is used globally and is routinely used for food or drinks. It has been reported that oral administration of ethanol extract of ginger to mice at 2.5 g/kg is not associated with mortality [31]. We also confirmed that 2% ginger (about 2.6 g/kg) diet did not induce weight loss (Table 1) or any morbid events and showed significant effects against intentional induction of Type I allergy. Although we demonstrated that ginger has a preventive effect against the establishment of allergic rhinitis, the optimal content of ginger for this experimental system remains to be investigated. Importantly, an antiallergic effect of oral administration of 6-gingerol has yet to be demonstrated. Kim *et al.* reported a pharmacokinetics study in mice after the intravenous administration of 6-gingerol [32]. To our knowledge, however, there has been no report demonstrating the pharmacokinetics of 6-gingerol following the oral administration of 6-gingerol or ginger extract in mice. However, it has been reported that after a single oral dose of 240-mg/kg ginger extract (containing 53% of 6-gingerol) in rats, 6-gingerol was found to be rapidly absorbed into the plasma with maximal concentration (4.23  $\mu$ g/ml, approximately 14.4  $\mu$ M) reached after 10-min postadministration and well distributed to the tissues, including the spleen [33]. Another group reported that the  $C_{max}$  of glucuronide of 6-gingerol, the major metabolite of 6-gingerol, in rat plasma was 15.14  $\mu$ g/ml (30.8  $\mu$ M) after a single oral administration of 30-mg/kg 6-gingerol [34]. Thus, although the ingestion of 6-gingerol may result in its dispersion to organs containing T cells after oral administration, 6-gingerol is rapidly cleared from the body. In this study, 2% ginger diet mice ingested approximately 2.68 g/day/kg of ginger, which approximates to 13.4-mg/day/kg 6-gingerol. According to the previous reference using rats, the maximal concentration of 6-gingerol in plasma is assumed to be at most 1.5  $\mu$ M. However, the method of oral administration in the present study was set at *ad libitum* feeding for 47 days as opposed to a single dose by direct stomach intubation. Therefore, although the concentration of 6-gingerol in our mice did not reach 50  $\mu$ M, we suggest that a long-term administration of ginger gradually exerts T cell inactivation as qualitatively demonstrated in our *in vitro* experiment. However, the actual pharmacokinetics of 6-gingerol in plasma and organs in mice during long-term oral administration should be clarified.

It is intriguing whether administration of ginger or ginger extracts can ameliorate an allergic rhinitis once it has been established. It should be noted that some undesirable effects of ginger have been reported; inhalation of dust from ginger may cause IgG-mediated allergy [35], large intake of ginger may act as a gastric irritant [36] and 6-gingerol induces genotoxicity by oxidative stress in human cancer cells [37,38].

In this study, we demonstrated that 6-gingerol inhibited the signal transduction of cytokine production by not only T cell receptor stimulation but also by PMA and ionomycin stimulation. This interaction synergistically enhances the activation of protein kinase C and strongly induces IL-2 gene expression through Ras- and Raf-dependent activation of MAPKs and calcium release in T cells [39–42]. We consider that abrogation of T cell activation is the mechanism of immunosuppression by ginger or 6-gingerol, but the precise mechanism(s) has yet to be elucidated. We showed that 6-gingerol inhibited the phosphorylation of MAP kinases, nuclear import of transcription

factors including c-fos and NF- $\kappa$ B and calcium release by PMA and ionomycin in Jurkat T cells. These results do not conflict with the results of a previous study in which the inhibitory effects of 6-gingerol on PMA-induced activation of NF- $\kappa$ B and p38 MAP kinase were investigated in mouse skin [43]. Our findings indicated that 6-gingerol may affect protein kinase C or its downstream molecules. It has also been reported that a ginger extract inhibits airway contraction and associated calcium signaling [44]. Therefore, other possible targets of 6-gingerol are calcium channels including the voltage-sensitive calcium channel or N-methyl-D-aspartate receptor, but to our knowledge, there has been no report showing that 6-gingerol is associated with calcium channels. 6-Gingerol is thought to interact with various proteins including vanilloid receptor 1 or its homologs [45], leukotriene A<sub>4</sub> hydrolase [46], angiotensin II Type 1 receptor [47] and cyclooxygenase-2 [48]. The molecule directly binding with 6-gingerol in T cells, however, remains to be identified in order to explain the precise mechanisms of down-regulation of cytokine expression. In addition, we cannot exclude the possibility of compounds in ginger other than 6-gingerol having antiallergic effects because more than 19 gingerol-related compounds have been identified in ginger products [13]. Including the potential of an additive or synergistic protective effect on Type 1 allergy by ginger compounds, examination of combination treatment with gingerol-related compounds *in vivo* and *in vitro* will be biologically and clinically meaningful. Although we demonstrated a preventive effect of a 2% ginger diet against allergic rhinitis using a mouse model, a separate clinical study is necessary to determine when and how much ginger powder or 6-gingerol should be ingested daily to produce an antiallergic effect in humans because humans and mice differ in food intake and the clearance of ginger per body weight. Previous studies in humans show that the daily oral ingestion of 1–50 g of ginger favorably influences physical conditions such as nausea, motion sickness and rheumatoid arthritis [31].

In conclusion, we proposed that ginger can be used for prevention of IgE-mediated allergic disorders including allergic rhinitis and that 6-gingerol is a potential immunosuppressive agent that contributes to “calming down” of cytokine-mediated immune responses.

## Disclosure statements

The authors have nothing to disclose.

## Acknowledgments

This work was supported by Chubu University Grants A (22IM22A) and B (25IM06B). We thank Ms. Taeko Kawai for technical assistance. We thank Crimson Interactive Pvt. Ltd. and SES Translation and Proofreading Services for their assistance in manuscript translation and editing. All authors read and approved the final manuscript.

## References

- Holgate ST. The epidemic of allergy and asthma. *Nature* 1999;402:B2–4.
- Haahtela T, Holgate S, Pawankar R, Akdis CA, Benjaponpitak S, Caraballo L, et al. The biodiversity hypothesis and allergic disease: world allergy organization position statement. *World Allergy Organ J* 2013;6:3.
- Soyer OU, Akdis M, Akdis CA. Mechanisms of subcutaneous allergen immunotherapy. *Immunol Allergy Clin North Am* 2011;31:175–90 [vii–viii].
- Akdis CA, Akdis M. Mechanisms of allergen-specific immunotherapy. *J Allergy Clin Immunol* 2011;127:18–27 [quiz 8–9].
- Matsuo N, Yamada K, Shoji K, Mori M, Sugano M. Effect of tea polyphenols on histamine release from rat basophilic leukemia (RBL-2H3) cells: the structure-inhibitory activity relationship. *Allergy* 1997;52:58–64.
- Fujimura Y, Tachibana H, Maeda-Yamamoto M, Miyase T, Sano M, Yamada K. Antiallergic tea catechin, (-)-epigallocatechin-3-O-(3-O-methyl)-gallate, suppresses Fc $\epsilon$ RI expression in human basophilic KU812 cells. *J Agric Food Chem* 2002;50:5729–34.
- Tachibana H, Kubo T, Miyase T, Tanino S, Yoshimoto M, Sano M, et al. Identification of an inhibitor for interleukin 4-induced epsilon germline transcription and antigen-specific IgE production *in vivo*. *Biochem Biophys Res Commun* 2001;280:53–60.
- Lee M, Kim S, Kwon OK, Oh SR, Lee HK, Ahn K. Anti-inflammatory and anti-asthmatic effects of resveratrol, a polyphenolic stilbene, in a mouse model of allergic asthma. *Int Immunopharmacol* 2009;9:418–24.
- Hirano T, Arimitsu J, Higa S, Naka T, Ogata A, Shima Y, et al. Luteolin, a flavonoid, inhibits CD40 ligand expression by activated human basophils. *Int Arch Allergy Immunol* 2006;140:150–6.
- Grzanna R, Lindmark L, Frondoza CG. Ginger—an herbal medicinal product with broad anti-inflammatory actions. *J Med Food* 2005;8:125–32.
- Hiserodt RD, Franzblau SG, Rosen RT. Isolation of 6-, 8-, and 10-Gingerol from Ginger Rhizome by HPLC and preliminary evaluation of inhibition of Mycobacterium avium and Mycobacterium tuberculosis. *J Agric Food Chem* 1998;46:2504–8.
- Schwertner HA, Rios DC. High-performance liquid chromatographic analysis of 6-gingerol, 8-gingerol, 10-gingerol, and 6-shogaol in ginger-containing dietary supplements, spices, teas, and beverages. *J Chromatogr B Analyt Technol Biomed Life Sci* 2007;856:41–7.
- Park JS, Jung MY. Development of high-performance liquid chromatography-time-of-flight mass spectrometry for the simultaneous characterization and quantitative analysis of gingerol-related compounds in ginger products. *J Agric Food Chem* 2012;60:10015–26.
- Young HY, Luo YL, Cheng HY, Hsieh WC, Liao JC, Peng WH. Analgesic and anti-inflammatory activities of [6]-gingerol. *J Ethnopharmacol* 2005;96:207–10.
- Kim EC, Min JK, Kim TY, Lee SJ, Yang HO, Han S, et al. [6]-Gingerol, a pungent ingredient of ginger, inhibits angiogenesis *in vitro* and *in vivo*. *Biochem Biophys Res Commun* 2005;335:300–8.
- Lee HS, Seo EY, Kang NE, Kim WK. [6]-Gingerol inhibits metastasis of MDA-MB-231 human breast cancer cells. *J Nutr Biochem* 2008;19:313–9.
- Surh Y. Molecular mechanisms of chemopreventive effects of selected dietary and medicinal phenolic substances. *Mutat Res* 1999;428:305–27.
- Kawamoto Y, Takeda K, Okuno Y, Yamakawa Y, Ito Y, Taguchi R, et al. Identification of RET autophosphorylation sites by mass spectrometry. *J Biol Chem* 2004;279:14213–24.
- Ahui ML, Champy P, Ramadan A, Pham Van L, Araujo L, Brou Andre K, et al. Ginger prevents Th2-mediated immune responses in a mouse model of airway inflammation. *Int Immunopharmacol* 2008;8:1626–32.
- Morel PA, Oriss TB. Crossregulation between Th1 and Th2 cells. *Crit Rev Immunol* 1998;18:275–303.
- Shen CL, Hong KJ, Kim SW. Effects of ginger (*Zingiber officinale* Rosc.) on decreasing the production of inflammatory mediators in sow osteoarthrotic cartilage explants. *J Med Food* 2003;6:323–8.
- Wang L, Zhao Y, Li Z, Guo Y, Jones LL, Kranz DM, et al. Crystal structure of a complete ternary complex of TCR, superantigen and peptide-MHC. *Nat Struct Mol Biol* 2007;14:169–71.
- Marrack P, Kappler J. The staphylococcal enterotoxins and their relatives. *Science* 1990;248:705–11.
- Khan AM, Shahzad M, Raza Asim MB, Imran M, Shabbir A. *Zingiber officinale* ameliorates allergic asthma via suppression of Th2-mediated immune response. *Pharm Biol* 2015;53:359–67.
- Shukla Y, Prasad S, Tripathi C, Singh M, George J, Kalra N. *In vitro* and *in vivo* modulation of testosterone mediated alterations in apoptosis related proteins by [6]-gingerol. *Mol Nutr Food Res* 2007;51:1492–502.
- Sabina EP, Pragasam SJ, Kumar S, Rasool M. 6-gingerol, an active ingredient of ginger, protects acetaminophen-induced hepatotoxicity in mice. *Zhong Xi Yi Jie He Xue Bao* 2011;9:1264–9.
- Okumi H, Tashima K, Matsumoto K, Namiki T, Terasawa K, Horie S. Dietary agonists of TRPV1 inhibit gastric acid secretion in mice. *Planta Med* 2012;78:1801–6.
- El-Bakly WM, Louka ML, El-Halwany AM, Schaaln MF. 6-gingerol ameliorated doxorubicin-induced cardiotoxicity: role of nuclear factor kappa B and protein glycation. *Cancer Chemother Pharmacol* 2012;70:833–41.
- Lu J, Guan S, Shen X, Qian W, Huang G, Deng X, et al. Immunosuppressive activity of 8-gingerol on immune responses in mice. *Molecules* 2011;16:2636–45.
- Maeda-Yamamoto M, Ema K, Shibuichi I. *In vitro* and *in vivo* anti-allergic effects of 'benifuuki' green tea containing O-methylated catechin and ginger extract enhancement. *Cytotechnology* 2007;55:135–42.
- Chrubasik S, Pittler MH, Roufogalis BD. *Zingiberis rhizoma*: a comprehensive review on the ginger effect and efficacy profiles. *Phytomedicine* 2005;12:684–701.
- Kim MG, Shin BS, Choi Y, Ryu JK, Shin SW, Choo HW, et al. Determination and pharmacokinetics of [6]-gingerol in mouse plasma by liquid chromatography-tandem mass spectrometry. *Biomed Chromatogr* 2012;26:660–5.
- Jiang SZ, Wang NS, Mi SQ. Plasma pharmacokinetics and tissue distribution of [6]-gingerol in rats. *Biopharm Drug Dispos* 2008;29:529–37.
- Wang W, Li CY, Wen XD, Li P, Qi LW. Plasma pharmacokinetics, tissue distribution and excretion study of 6-gingerol in rat by liquid chromatography-electrospray ionization time-of-flight mass spectrometry. *J Pharm Biomed Anal* 2009;49:1070–4.
- van Toorenbergen AW, Dieges PH. Immunoglobulin E antibodies against coriander and other spices. *J Allergy Clin Immunol* 1985;76:477–81.
- Desai HG, Kalro RH, Choksi AP. Effect of ginger & garlic on DNA content of gastric aspirate. *Indian J Med Res* 1990;92:139–41.
- Nigam N, Bhui K, Prasad S, George J, Shukla Y. [6]-Gingerol induces reactive oxygen species regulated mitochondrial cell death pathway in human epidermoid carcinoma A431 cells. *Chem Biol Interact* 2009;181:77–84.

- [38] Yang G, Zhong L, Jiang L, Geng C, Cao J, Sun X, et al. Genotoxic effect of 6-gingerol on human hepatoma G2 cells. *Chem Biol Interact* 2010;185:12–7.
- [39] Whitehurst CE, Geppert TD. MEK1 and the extracellular signal-regulated kinases are required for the stimulation of IL-2 gene transcription in T cells. *J Immunol* 1996;156:1020–9.
- [40] Robbins DJ, Zhen E, Cheng M, Xu S, Ebert D, Cobb MH. MAP kinases ERK1 and ERK2: pleiotropic enzymes in a ubiquitous signaling network. *Adv Cancer Res* 1994;63:93–116.
- [41] Chatila T, Silverman L, Miller R, Geha R. Mechanisms of T cell activation by the calcium ionophore ionomycin. *J Immunol* 1989;143:1283–9.
- [42] Blumberg PM. Protein kinase C as the receptor for the phorbol ester tumor promoters: sixth Rhoads memorial award lecture. *Cancer Res* 1988;48:1–8.
- [43] Kim SO, Chun KS, Kundu JK, Surh YJ. Inhibitory effects of [6]-gingerol on PMA-induced COX-2 expression and activation of NF-kappaB and p38 MAPK in mouse skin. *Biofactors* 2004;21:27–31.
- [44] Ghayur MN, Gilani AH, Janssen LJ. Ginger attenuates acetylcholine-induced contraction and Ca<sup>2+</sup> signalling in murine airway smooth muscle cells. *Can J Physiol Pharmacol* 2008;86:264–71.
- [45] Someya A, Horie S, Yamamoto H, Murayama T. Modifications of capsaicin-sensitive neurons in isolated guinea pig ileum by [6]-gingerol and lafutidine. *J Pharmacol Sci* 2003;92:359–66.
- [46] Jeong CH, Bode AM, Pugliese A, Cho YY, Kim HG, Shim JH, et al. [6]-Gingerol suppresses colon cancer growth by targeting leukotriene A4 hydrolase. *Cancer Res* 2009;69:5584–91.
- [47] Liu Q, Liu J, Guo H, Sun S, Wang S, Zhang Y, et al. [6]-Gingerol: a novel AT1 antagonist for the treatment of cardiovascular disease. *Planta Med* 2013;79:322–6.
- [48] Saptarini NM, Sitorus EY, Levita J. Structure-based in silico study of 6-Gingerol, 6-Ghogaol, and 6-Paradol, active compounds of ginger (*Zingiber officinale*) as COX-2 inhibitors. *Int J Chem* 2013;5:p12.

## ORIGINAL ARTICLE

## Epidemiological analysis of the association between hearing and barium in humans

Nobutaka Ohgami<sup>1,2,3,6</sup>, Yuji Mitsumatsu<sup>1,6</sup>, Nazmul Ahsan<sup>4</sup>, Anwarul Azim Akhand<sup>4</sup>, Xiang Li<sup>1</sup>, Machiko Iida<sup>1,2,3</sup>, Ichiro Yajima<sup>1,3</sup>, Mariko Naito<sup>5</sup>, Kenji Wakai<sup>5</sup>, Shoko Ohnuma<sup>3</sup> and Masashi Kato<sup>1,3</sup>

Our previous study experimentally showed barium (Ba)-mediated hearing loss in mice. To our knowledge, however, it remains unknown whether Ba affects hearing in humans. This epidemiological study aimed at investigating ototoxicity of Ba in humans. Associations of Ba levels in hair, toenails and urine with hearing levels (1, 4, 8 and 12 kHz) were analyzed in 145 Bangladeshi subjects. Binary logistic regression analysis with adjustment for age, sex, BMI and smoking showed that Ba levels in hair had significant associations with hearing loss at 8 kHz (OR = 4.75; 95% CI: 1.44, 17.68) and 12 kHz (OR = 15.48; 95% CI: 4.04, 79.45). Ba levels in toenails were also associated with hearing loss at 8 kHz (OR = 3.20; 95% CI: 1.35, 7.85) and 12 kHz (OR = 3.63; 95% CI: 1.58, 8.55), whereas there was no correlation between Ba level in urinary samples and hearing. There was a significant correlation between hearing loss and Ba levels in hair and toenails in the model adjusted with arsenic levels as the confounder. In conclusion, this study suggested that Ba levels could be a new risk factor for hearing loss, especially at high frequencies of 8 and 12 kHz, in humans.

*Journal of Exposure Science and Environmental Epidemiology* (2015) **00**, 1–6. doi:10.1038/jes.2015.62

**Keywords:** barium; hair; hearing loss; ICP-MS; ototoxicity; toenail

## INTRODUCTION

Hearing loss is one of the most common disorders affecting quality of life (QOL).<sup>1</sup> The number of patients with hearing loss is estimated to be 360 million worldwide, which is equivalent to 5.3% of the world's population. It is estimated that the 360 million patients include 328 million adults and 32 million children.<sup>2</sup> In addition, it is estimated that one third of people over 65 years of age worldwide have age-related hearing loss.<sup>2</sup> Genetic, aging and environmental factors intricately affect the onset of hearing losses, which lowers the QOL.<sup>1</sup> However, information about the environmental factors affecting hearing and the number of patients is limited.

Barium (Ba) has been shown to be included in raw surface water, tap water supplies and tube wells at concentrations ranging from  $\leq 5$  to 15 mg/l.<sup>3–5</sup> In addition, seaweed, fish and some foods have been shown to contain Ba.<sup>6,7</sup> In a diet investigation in Canada, Ba levels in nuts including peanuts and peanut butter were shown to be relatively high (2919.11  $\mu\text{g}/\text{kg}$ ). Fruits and vegetables contain Ba levels at concentrations ranging from 57.62 to 3750.03  $\mu\text{g}/\text{kg}$  and from 47.99 to 2282.23  $\mu\text{g}/\text{kg}$ , respectively, while Ba levels in meats and fish are relatively low (ranging from 12.06 to 237.57 and from 36.17 to 481.34  $\mu\text{g}/\text{kg}$ , respectively). The average Ba intake in humans from diets has been shown to be 8.817  $\mu\text{g}/\text{kg}/\text{day}$ .<sup>8</sup> An investigation in Canary Islands, Spain showed that Ba levels ranged from  $5.210 \pm 2.117$  mg/kg in nuts to  $0.035 \pm 0.043$  mg/l in water and that total intake of Ba was

0.685 mg/day, mainly from cereals.<sup>9</sup> Thus, diets that we ingest in daily life contain Ba as one of the general elements. However, Ba is not regarded as one of the elements affecting our health.

The possible association between exposure to Ba and health problems in humans was investigated in previous epidemiological studies. Residents living in communities in Illinois, USA where tap water contains high levels of Ba (2–10 mg/l) have been shown to have significantly high mortality rates associated with arteriosclerosis and cardiovascular disease.<sup>10–12</sup> However, the relevance was not analyzed with potential confounders (e.g., population mobility, water softeners, duration of exposure and actual barium intake). Also, the prevalence's of cardiovascular disease in two Illinois communities were compared in a follow-up cross-sectional study. The two communities had similar demographic and socioeconomic characteristics, but Ba levels in drinking water were different. However, no significant differences were found between the two communities in mean systolic or diastolic blood pressure or in history of hypertension, heart disease, stroke or kidney disease for men or women when many of the possible confounding factors not considered in earlier studies were accounted for.<sup>13</sup> In previous studies performed in India and the Kingdom of Saudi Arabia, prevalence rates of cancer and autism have been shown to be associated with Ba levels in biological samples and drinking water.<sup>14–16</sup> However, there is very limited information about a correlation between exposure to Ba and other health problems in humans.

Q1  
Q2

<sup>1</sup>Departments of Occupational and Environmental Health, Nagoya University Graduate School of Medicine, Nagoya, Japan; <sup>2</sup>Nutritional Health Science Research Center, Chubu University, Matsumoto, Kasugai, Aichi, Japan; <sup>3</sup>Voluntary Body for International Health Care in Universities, Nagoya, Japan; <sup>4</sup>Department of Genetic Engineering and Biotechnology, University of Dhaka, Dhaka, Bangladesh and <sup>5</sup>Departments of Preventive Medicine, Nagoya University Graduate School of Medicine, Nagoya, Japan. Correspondence: Masashi Kato, Department of Occupational and Environmental Health, Nagoya University Graduate School of Medicine, 65 Tsurumai-cho, Showa-ku, Nagoya, Aichi 466-8550, Japan.

Tel.: +81 52 744 2122. Fax: +81 52 744 2124.

E-mail: katomasa@med.nagoya-u.ac.jp

<sup>6</sup>These authors equally contributed to this work.

Received 1 June 2015; revised 10 August 2015; accepted 21 August 2015

In our experimental study, oral exposure of mice to Ba by drinking water was shown to cause severe hearing loss with degeneration of the organ of Corti in mice. Ba-exposed mice showed high levels of Ba in inner ears compared with the levels in mice not exposed to Ba.<sup>17</sup> However, there is no information about the correlation between Ba levels in biological samples and health problems in humans. In this pilot study, we performed hearing examinations and measurements of Ba levels in human biological samples to determine whether Ba levels in biological samples are associated with hearing loss.

## METHODS

### Study Subjects

The study was performed for 145 subjects in Bangladesh aged from 12 to 55 years (mean  $\pm$  SD, 29.58  $\pm$  10.92 years) who agreed in written form to participate in hearing examinations. In this study, we did not include subjects who had a previous history of ear diseases and suffered from illness at the time of investigation. We also did not include subjects who had a habit of drinking alcohol or using a portable music player (e.g., MP3 player) with earphones. In addition, another ethnic group or race was not included as subjects in this study. This investigation was performed using a self-reporting questionnaire on smoking, age, clinical history, weight and height of subjects. Body mass index (BMI; mean  $\pm$  SD = 21.99  $\pm$  3.42) was obtained by using the following formula: weight in kg/height in meter squares. The procedures were explained and informed consent was obtained from all of the subjects. This study was ethically approved by Nagoya University International Bioethics Committee following the regulations of the Japanese government (approval number 2013-0070) and the Faculty of Biological Science, University of Dhaka (Ref. no. 5509/Bio.Sc).

### Measurement of Auditory Thresholds

Auditory thresholds at frequencies of 1, 4, 8 and 12 kHz were measured by pure tone audiometry (PTA). We measured hearing level at an extra-high frequency (12 kHz) because hearing level of the frequency is sensitive to environmental factors including smoking.<sup>18,19</sup> The sound data of PTA were installed into an iPod. The sound stimuli were output by the iPod with an earphone-type headphone (Panasonic RP-HJE150) in a sound-proof room as described previously.<sup>19–21</sup> Sound signals at frequencies of 1, 4, 8 and 12 kHz were output to each subject until the thresholds of sound were identified. Hearing levels of the subjects were all measured by providing an initial stimulus of 5 decibels (dB) followed by a stepwise increase in sound level by 5 dB. Duplicated measurement of hearing was performed in each subject to verify the repeatability of values.

### Measurement of Barium Levels in Biological Samples

We measured Ba levels in biological samples by the method previously described.<sup>17,22,23</sup> In short, biological samples were put into a 15 ml polypropylene tube with 3 ml of HNO<sub>3</sub> (61%). The sample tubes were incubated at 80 °C for 48 h and then allowed to cool to room temperature for 1 h. Then, 3 ml of H<sub>2</sub>O<sub>2</sub> (30%) was added to each tube and the tubes were incubated at 80 °C for 3 h. After the samples had been diluted with ultrapure water, the Ba level in each sample was measured by using an inductively coupled plasma mass spectrometer (ICP-MS; 7500cx, Agilent Technologies) with a reaction cell for absence of ArCl ion interference. Total Ba levels in urinary samples were corrected by specific gravity expressed as  $\mu\text{g/l}$ .<sup>24,25</sup>

### Statistical Analysis

Statistical analyses were performed following the method previously reported.<sup>18,26</sup> No randomization was used and the investigators were not blinded to the group allocation during the experiments or when assessing the outcomes. For univariate analyses, Spearman correlation coefficients were used to determine a significant association between nonparametric variables, since the Shapiro–Wilks normality test showed that Ba levels in biological samples were not normally distributed. The two-tailed Mann–Whitney *U*-test (equivalent to the Wilcoxon rank sum test) and Steel–Dwass test were also used for nonparametric data to determine a significant difference of hearing levels between two groups and among three groups, respectively, since hearing levels are discontinuous variables. Steel–Dwass test was performed with set the alpha level to 0.05. Levene's test and

Bartlett's test for equality of variances were conducted. Difference with  $P < 0.05$  was considered significant, and the actual *P*-value for each test was displayed except for the *P*-values below 0.0001. For multivariate analysis, we categorized subjects into two or three groups according to sex, age, BMI, smoking and Ba concentration in biological samples and compared the average auditory thresholds at frequencies of 1, 4, 8 and 12 kHz. We performed binary logistic regression analysis with auditory thresholds at 1 kHz ( $> 10$  dB),<sup>27</sup> 4 kHz ( $> 10$  dB),<sup>28</sup> 8 kHz ( $> 25$  dB)<sup>29,30</sup> and 12 kHz ( $> 40$  dB)<sup>18</sup> of hearing levels as dependent variables and Ba levels in hair, toenail and urine samples as independent variables. Models were adjusted for age,<sup>31</sup> sex,<sup>32</sup> smoking<sup>33</sup> and BMI<sup>34</sup> because associations between hearing loss and these factors have been shown. All statistical analyses were performed using JMP Pro (version 11.0.0; SAS Institute, Cary, NC, USA).

## RESULTS

### Correlation between Hearing Levels and Confounding Factors Including Age, BMI, Sex and Smoking

Characteristics of subjects and cut-off values of confounders analyzed in this study are shown in Table 1. We set the mean age of the subjects (i.e., 30-years-old) as the cut-off value for age. The average auditory thresholds at 1, 4, 8 and 12 kHz in the older group ( $n = 68$ ) were significantly higher (1 kHz,  $P = 0.0098$ ; 4, 8 and 12 kHz,  $P < 0.0001$ ) than those in the younger group ( $n = 77$ ; Figure 1a). We also categorized the subjects into three groups based on BMI set by the WHO category (underweight,  $< 18.5$ ; normal range, 18.5–25; overweight,  $25 \leq$ ) as shown in Table 2. There were no significant differences in average auditory thresholds among the three groups (Figure 1b). The average auditory thresholds at 4, 8 and 12 kHz in females ( $n = 76$ ) were significantly higher (4 kHz;  $P = 0.0257$ , 8 kHz;  $P = 0.0004$ , 12 kHz;  $P = 0.0066$ ) than those in males ( $n = 69$ ; Figure 1c). We next compared the auditory thresholds in smokers ( $n = 31$ ) and non-smokers ( $n = 114$ ) since smoking has been shown to be one of the risk factors for hearing loss.<sup>18,19,33</sup> The average auditory thresholds at 1, 4, 8 and 12 kHz in the smoking group were significantly higher than those in the non-smoking group (1 kHz;  $P = 0.0057$ , 4 kHz;  $P < 0.0001$ , 8 kHz;  $P = 0.0002$ , 12 kHz;  $P < 0.0001$ ; Figure 1d). Hearing level on average at extra-high frequency (12 kHz) was more affected compared with those at lower frequencies (Figure 1d).

### Correlation between Hearing Levels and Ba Levels in Human Biological Samples

Barium levels (mean  $\pm$  SD) in hair, toenail and urine samples from all subjects were 3.21  $\pm$  2.87  $\mu\text{g/g}$ , 7.08  $\pm$  5.54  $\mu\text{g/g}$  and

**Table 1.** Variables for each factor.

Variables	Participants	Percentage (%)
Sex		
Male	69	47.59
Female	76	52.41
Age		
< 30	77	53.1
$\geq 30$	68	46.9
BMI		
18.5 <	23	15.86
18.5–25	94	64.83
$\geq 25$	28	19.31
Smoking		
Yes	31	21.38
No	114	78.62

Abbreviation: BMI, body mass index.

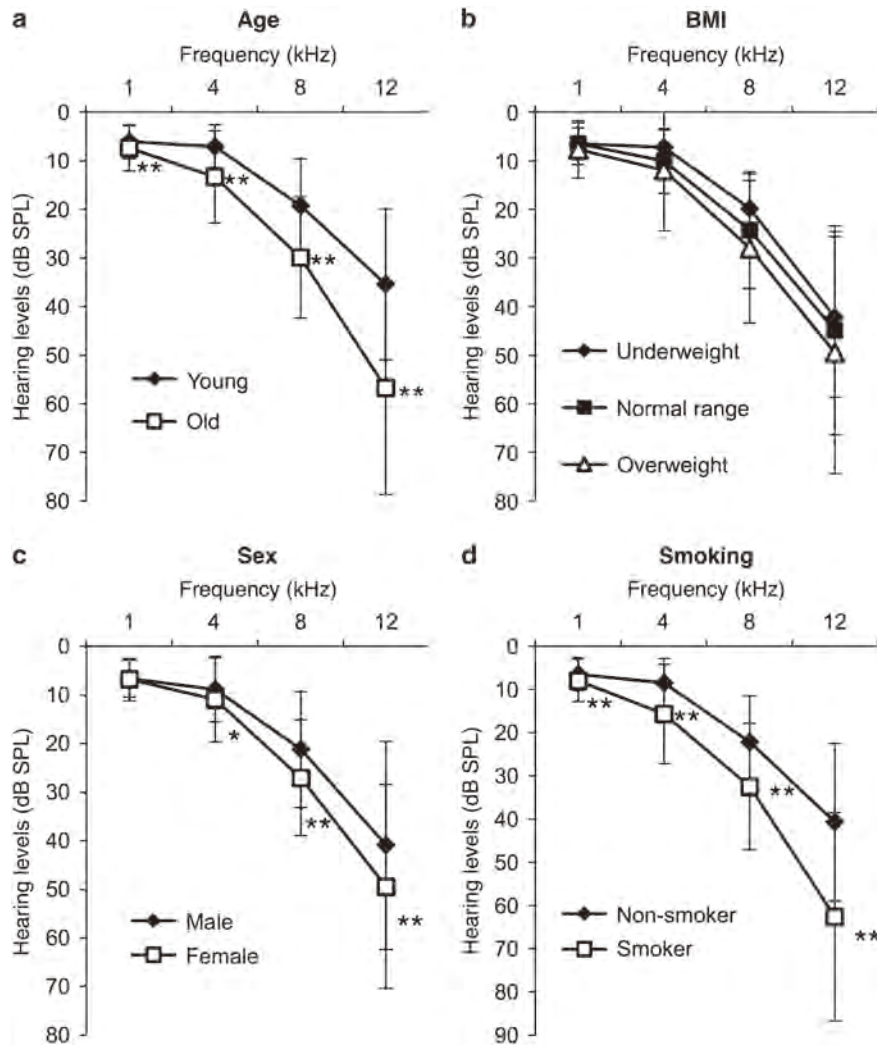


**Figure 1.** Correlations between hearing levels and confounding factors including age, BMI, sex and smoking. (a) Auditory thresholds (mean  $\pm$  SD) at 1, 4, 8 and 12 kHz in the young group (< 30-years-old;  $n=77$ , diamonds) and the old group ( $\geq 30$ -years-old;  $n=68$ , squares) are displayed. (b) Auditory thresholds (mean  $\pm$  SD) from frequencies of 1–12 kHz in the underweight group (BMI < 18.5;  $n=23$ , diamonds), normal range group ( $18.5 \leq \text{BMI} < 25$ ;  $n=94$ , squares) and overweight group ( $25 \leq \text{BMI}$ ;  $n=28$ , triangles) are displayed. (c) Auditory thresholds (mean  $\pm$  SD) from frequencies of 1–12 kHz in males ( $n=69$ , diamonds) and females ( $n=76$ , squares) are presented. (d) Auditory thresholds (mean  $\pm$  SD) from frequencies of 1–12 kHz in smokers ( $n=31$ , diamonds) and non-smokers ( $n=114$ , squares) are displayed. Smokers include people using tobacco powder. Significant differences (\* $P < 0.05$ , \*\* $P < 0.01$ ) were analyzed by the Mann–Whitney  $U$ -test (a, c and d) and Steel–Dwass test (b). BMI, body mass index.

**Table 2.** Barium levels in biological samples.

	Barium level ( $\mu\text{g/g}$ )		
	Mean $\pm$ SD	Minimum	Maximum
Hair	7.08 $\pm$ 5.54	0.33	23.96
Toenail	3.21 $\pm$ 2.87	0.2	16.56
Urine <sup>a</sup>	3.87 $\pm$ 4.85	0.13	36.72

<sup>a</sup>Barium concentration in urine was corrected by specific gravity ( $\mu\text{g/l}$ ).

3.87  $\pm$  4.85  $\mu\text{g/l}$ , respectively (Table 2). A significant correlation of Ba levels was observed in toenail and hair samples ( $r=0.3370$ ,  $P < 0.0001$ ) or in urine and toenail samples ( $r=0.1668$ ,  $P=0.0449$ ), while no correlation was found in urine and hair samples

( $r=0.0665$ ,  $P=0.4269$ ). In addition, Ba levels (mean  $\pm$  SD) in female subjects were 3.859  $\pm$  3.226  $\mu\text{g/g}$  in toenail samples and 11.155  $\pm$  4.504  $\mu\text{g/g}$  in hair samples, while those in male subjects were 2.489  $\pm$  2.215  $\mu\text{g/g}$  in toenail samples and 2.582  $\pm$  1.907  $\mu\text{g/g}$  in hair samples. There is no information about the correlation between Ba levels in biological samples and hearing loss in humans. Based on the determination of Ba levels significantly associated with hearing loss, we categorized the subjects into two groups at 12.62  $\mu\text{g/g}$  in hair and 1.88  $\mu\text{g/g}$  in toenails (Table 3). On the other hand, we used the median (2.55  $\mu\text{g/l}$ ) for urine samples (Table 3) since there was no correlation between Ba levels in urine samples and hearing levels. We then compared the auditory thresholds at 1, 4, 8 and 12 kHz between the two groups (Figure 2). The group with high Ba level in hair ( $n=26$ ) showed significantly (8 kHz;  $P=0.0027$ , 12 kHz;  $P=0.0045$ ) higher auditory thresholds at 8 kHz and 12 kHz than those in the group with low Ba level in hair ( $n=119$ ; Figure 2a). The average auditory

**Table 3.** Classification according to barium levels in biological samples.

Barium level ( $\mu\text{g/g}$ )	Participants	Percentage (%)
<i>Hair</i>		
Low ( $< 12.62$ )	119	82.07
High ( $\geq 12.62$ )	26	17.93
<i>Toenail</i>		
Low ( $< 1.88$ )	55	37.93
High ( $\geq 1.88$ )	90	62.07
<i>Urine<sup>a</sup></i>		
Low ( $< 2.55$ )	73	50.34
High ( $\geq 2.55$ )	72	49.66

<sup>a</sup>Barium concentration in urine was corrected by specific gravity ( $\mu\text{g/l}$ ).

thresholds at 4 kHz, 8 kHz and 12 kHz in the group with high Ba level in toenails ( $n=90$ ) were significantly higher ( $P < 0.0001$ ) than those in the group with low Ba level in toenails ( $n=55$ ; Figure 2b). On the other hand, there were no significant differences in average auditory thresholds at all of the frequencies between the groups with the high and low Ba levels in urine samples (Figure 2c).

**Binary Logistic Regression Analysis**

Binary logistic regression analysis with adjustment for age, sex, BMI and smoking showed that Ba levels in hair were significantly associated with hearing loss at 8 kHz (odds ratio (OR) = 4.75; 95% confidence interval (CI): 1.44, 17.68;  $P=0.0096$ ) and 12 kHz (OR = 15.48; 95% CI: 4.04, 79.45;  $P < 0.0001$ ) (Table 4). Ba levels in toenails also showed significant associations with hearing loss at 4 kHz (OR = 2.76; 95% CI: 1.15, 6.85,  $P=0.0230$ ), 8 kHz (OR = 3.20; 95% CI: 1.35, 7.85;  $P=0.0083$ ) and 12 kHz (OR = 3.63; 95% CI: 1.58, 8.55;  $P=0.0023$ ) in the adjusted model (Table 4). The model adjusted with continuous variable of arsenic as the additional confounder also showed a significant correlation between hearing loss and Ba levels in hair and toenails (Table 5). On the other hand, we did not find any relationship between Ba level in urine and hearing levels at all frequencies in the adjusted models (Tables 4 and 5). To verify the appropriateness of our model, we shifted the cut-off values of the dependent variable dichotomizing hearing levels from 10 to 15 dB at 4 kHz, from 25 to 30 dB at 8 kHz and from 40 to 45 dB at 12 kHz. In addition, we shifted the cut-off values of the independent valuable dichotomizing Ba levels from 10.62 to 13.62  $\mu\text{g/g}$  in hair and from 1.88 to 2.38  $\mu\text{g/g}$  in toenails. The results showed significant correlations between Ba levels in toenails and hair and hearing loss remained except for the correlation between Ba levels in toenails and hearing loss at 4 kHz. Thus, these results obtained in different classifications indicate that Ba levels in toenails and hair are associated with hearing loss at higher frequencies.

**DISCUSSION**

In our previous study, exposure of mice to Ba by drinking water resulted in accumulation of Ba in inner ears that led to hearing loss.<sup>17</sup> However, there is no information about a correlation between ototoxicity and Ba in humans. This pilot study epidemiologically demonstrated a significant correlation between Ba levels in toenail and hair samples and hearing loss in humans. On the other hand, it has been shown that food is one of the major sources of Ba exposure in general,<sup>3</sup> although the major source of Ba that accumulated in subjects in this study remains unclear. In our previous study, Ba levels in inner ears of mice not

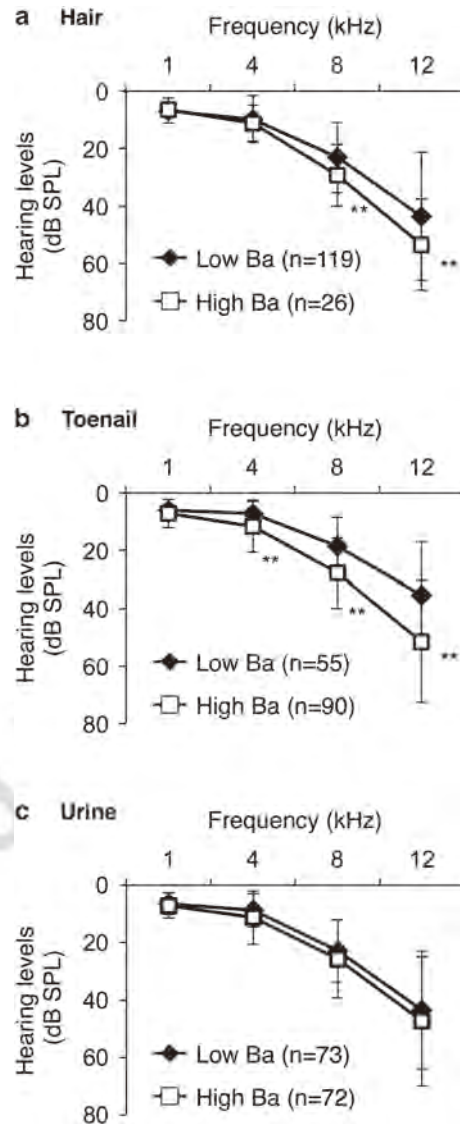


**Figure 2.** Correlations between barium levels in biological samples and hearing levels. (a) Auditory thresholds (mean  $\pm$  SD) from frequencies of 1–12 kHz in the high Ba level group ( $\geq 12.62 \mu\text{g/g}$ ;  $n=26$ , squares) and the low Ba level group ( $< 12.62 \mu\text{g/g}$ ;  $n=119$ , diamonds) in hair are displayed. (b) Auditory thresholds (mean  $\pm$  SD) from frequencies of 1–12 kHz in the high Ba level group ( $\geq 1.88 \mu\text{g/g}$ ;  $n=90$ , squares) and the low Ba level group ( $< 1.88 \mu\text{g/g}$ ;  $n=55$ , diamonds) in toenails are displayed. (c) Auditory thresholds (mean  $\pm$  SD) from frequencies of 1–12 kHz in the high Ba level group ( $\geq 2.55 \mu\text{g/l}$ ;  $n=72$ , squares) and the low Ba level group ( $< 2.55 \mu\text{g/l}$ ;  $n=73$ , diamonds) in urine are displayed. Ba level in urine was corrected by specific gravity. Significant differences ( $*P < 0.05$ ,  $**P < 0.01$ ) were analyzed by the Mann–Whitney *U*-test.

exposed to Ba were higher than those in other tissues including the liver, kidney and heart, in which Ba levels were undetectably low, while mice exposed to Ba by drinking water showed significantly increased Ba levels by about 10% in inner ears.<sup>17</sup> Our measurements of Ba levels in foods and drinking water for normal mouse breeding showed that Ba level in food was about 35 mg/kg and that in water was about 4  $\mu\text{g/l}$ . Thus, it is possible that the accumulation of Ba in inner ears of mice bred under normal conditions is mainly derived from food and it could be accelerated in mice exposed to Ba by drinking water. Therefore, it

**Table 4.** Adjusted odds ratio (95% CI) for hearing levels and barium (Ba) levels in biological samples ( $n = 145$ ).<sup>a</sup>

	1 kHz ( $\geq 10$ dB)	4 kHz ( $\geq 10$ dB)	8 kHz ( $\geq 25$ dB)	12 kHz ( $\geq 40$ dB)
Ba in hair	1.63 (0.50, 5.19)	2.60 (0.85, 8.41)	4.75** (1.44, 17.68)	15.48** (4.04, 79.45)
Ba in toenail	0.82 (0.32, 2.10)	2.76* (1.15, 6.85)	3.20** (1.35, 7.85)	3.63** (1.58, 8.55)
Ba in urine	1.23 (0.54, 2.85)	1.16 (0.52, 2.56)	1.01 (0.45, 2.23)	0.93 (0.43, 1.99)

Abbreviation: CI, confidence interval. <sup>a</sup>Models were adjusted for sex,<sup>26</sup> age,<sup>43</sup> BMI<sup>44</sup> and smoking,<sup>15</sup> which were previously reported to affect hearing levels. \* $P < 0.05$ , \*\* $P < 0.01$ .

**Table 5.** Adjusted odds ratio (95% CI) for hearing levels and barium (Ba) levels in biological samples ( $n = 145$ ).<sup>a</sup>

	1 kHz ( $\geq 10$ dB)	4 kHz ( $\geq 10$ dB)	8 kHz ( $\geq 25$ dB)	12 kHz ( $\geq 40$ dB)
Ba in hair	1.56 (0.47, 4.98)	2.34 (0.75, 7.70)	4.46* (1.32, 17.24)	21.72** (4.95, 129.53)
Ba in toenail	0.84 (0.32, 2.21)	3.04* (1.23, 7.72)	3.10* (1.26, 7.79)	2.72* (1.10, 6.76)
Ba in urine	1.29 (0.56, 3.01)	1.18 (0.53, 2.62)	1.03 (0.46, 2.28)	0.90 (0.41, 1.95)

Abbreviation: CI, confidence interval. <sup>a</sup>Models were adjusted for sex,<sup>26</sup> age,<sup>43</sup> BMI,<sup>44</sup> smoking<sup>15</sup> and arsenic,<sup>29,30</sup> which were previously reported to affect hearing levels. \* $P < 0.05$ , \*\* $P < 0.01$ .

is important to monitor Ba levels in food and drinking water worldwide to further analyze the correlation between ingestion of Ba and hearing loss in humans.

In this study, hearing levels at higher frequencies (8 and 12 kHz) were affected in groups with high Ba levels in hair and toenails, whereas our previous study with ICR mice showed that hearing levels at lower frequencies (4, 12 and 20 kHz) were affected in the Ba exposure group.<sup>17</sup> On the other hand, hearing levels at high frequency (32 kHz) in the non-exposed group and Ba-exposed group were comparable at the end of the exposure period, because ICR mice have been shown to progressively suffer from hearing loss,<sup>35</sup> although a genetic reason has not been demonstrated. Therefore, it is possible that people who potentially have a genetic factor for hearing loss also suffer from hearing loss at lower frequency by exposure to Ba, although we could not find such a case in this study. On the other hand, there is no information about a correlation of Ba levels among inner ears, hair and toenails. It is crucial to analyze an association of Ba levels among those tissues in an experimental animals exposed to Ba to determine the threshold of Ba levels in hair and toenails associated with hearing loss.

This study showed that there was a significant correlation between hearing levels and Ba levels in hair and toenails, while there was no significant correlation between hearing levels and Ba level in urine. Major excretion routes of Ba ingested from daily diets (750  $\mu\text{g}$ ) have been shown to be feces (690  $\mu\text{g}$ ), hair (75  $\mu\text{g}$ ), urine (50  $\mu\text{g}$ ) and sweat (10  $\mu\text{g}$ ).<sup>3</sup> Meanwhile, the growth cycle of a fingernail is generally known to be about 6 months<sup>36</sup> and that of a toenail has been shown to be about 10 months.<sup>37</sup> Also, the growth cycle of hair has shown to be several years,<sup>38,39</sup> while detection of an element level in urine is generally regarded as being associated with daily exposure. Measurements of trace element levels in toenails and hair have been considered as reliable biomarkers that can reflect chronic exposure status.<sup>40–43</sup> Therefore, our results suggest that Ba levels in toenails and hair can reflect levels after chronic exposure to Ba. Thus, our results raise the possibility that chronic exposure to Ba causes hearing loss, although our experimental study showed sub-acute exposure to Ba by drinking water caused hearing loss in ICR mice.<sup>17</sup> Additional study is needed to analyze a correlation between duration of exposure to Ba and hearing loss with consideration for exposure conditions in humans and mice.

This study showed that hearing levels in female subjects were significantly worse than those in male subjects. In addition, Ba

levels in female subjects were significantly higher than those in male subjects (hair;  $P < 0.0001$ , nail;  $P = 0.0018$ ). Therefore, it is possible that higher Ba levels in female subjects cause higher auditory thresholds than those in male subjects, although the reason for the gender difference in Ba levels is not clear. On the other hand, hearing levels in males are generally known to be worse than those in females,<sup>32</sup> while a previous study showed that females with depression tend to have hearing loss compared with males.<sup>44</sup> Hence, it is important for an understanding of the gender difference in hearing levels to compare Ba levels in biological samples from males and females and to consider other confounders including mental status. Meanwhile, since this study showed that the smoking group had greater hearing loss than did the non-smoking group as was previously reported,<sup>33</sup> we compared Ba levels in the two groups. The results showed that there was no significant difference in Ba levels between the smoking group and the non-smoking group, although it has been shown that tobacco leaves contain barium hydroxide.<sup>45</sup> In this study, we found that there was a significant correlation between hearing loss and Ba levels in hair and toenails in binary logistic regression analysis adjusted with arsenic as the confounder, though univariate analyses have shown that arsenic levels in hair samples and in nail samples affect hearing in humans.<sup>46,47</sup> Thus, this study suggests that Ba could be an independent risk factor for hearing loss.

In conclusion, the present pilot study further provided epidemiological evidence that there is a correlation between Ba and hearing loss in humans in addition to our previous experimental study in mice.<sup>17</sup> Our study also suggested possible thresholds in hair and toenails that increase the risk for hearing loss in humans.

#### CONFLICT OF INTEREST

The authors declare no conflict of interest.

#### ACKNOWLEDGEMENTS

This work was supported in part by Grants-in-Aid for Scientific Research (A) (No. 15H01743 and 15H02588), (B) (No. 24390157 and 24406002) and (C) (No. 25460178, 25340052, 25461717), Grant-in-Aid for Challenging Exploratory Research (No. 23650241 and No. 26670525), Grant-in-Aid for Scientific Research on Innovative Areas (No. 24108001) and COE Project for Private Universities (Nutritional Health Science Research Center; No. S1201007) from the Ministry of Education, Culture, Sports, Science and Technology (MEXT); the Mitsubishi Foundation; Toyoaki

Scholarship Foundation; the Mitsui & Co., Ltd. Environment Fund; Aichi Health Promotion Foundation, Foundation from Center for Advanced Medical and Clinical Research Nagoya University Hospital and AEON Environmental Foundation.

## REFERENCES

- Lalwani AK, Gürtler N. Sensorineural hearing loss, the aging inner ear, and hereditary hearing impairment. In: Lalwani AK (ed), *CURRENT Diagnosis & Treatment in Otolaryngology—Head & Neck Surgery*, 2nd edn. McGraw-Hill: New York, USA, 2008, pp 683–704.
- WHO (World Health Organization). *Global Estimates on Prevalence of Hearing Loss*, 2012. Available at [http://www.who.int/entity/pbd/deafness/WHO\\_GE\\_HL.pdf?ua=1](http://www.who.int/entity/pbd/deafness/WHO_GE_HL.pdf?ua=1) (accessed on 7 January 2015).
- ATSDR (Agency for Toxic Substances and Disease Registry). *Toxicological Profile for Barium*, 2007. Available at <http://www.atsdr.cdc.gov/toxprofiles/tp24.pdf> (accessed on 12 December 2014).
- Calabrese EJ. Excessive barium and radium-226 in Illinois drinking water. *J Environ Health* 1977; **39**: 366–369.
- EPA (Environmental Protection Agency). *Technical Factsheet on: Barium*, 2005. Available at <http://www.epa.gov/ogwdw/pdfs/factsheets/ioc/tech/barium.pdf> (accessed on 12 December 2014).
- Robinson WO, Whetstone RR, Edgington G. The occurrence of barium in soils and plants. *US Department of Agriculture Technical Bulletin* 1950; **1013**: 1–36.
- Smith KA. The comparative uptake and translocation by plants of calcium, strontium, barium and radium. I. *Bertholletia excelsa* (Brazil nut tree). *Plant Soil* 1971; **34**: 369–379.
- Health Canada. *Canadian Total Diet Study*, 2005. Available at [http://www.hc-sc.gc.ca/food-aliment/cs-ipc/fr-ra/e\\_tds.html](http://www.hc-sc.gc.ca/food-aliment/cs-ipc/fr-ra/e_tds.html) (accessed on 12 December 2014).
- González-Weller D, Rubio C, Gutiérrez AJ, González GL, Mesa JM, Gironés CR *et al*. Dietary intake of barium, bismuth, chromium, lithium, and strontium in a Spanish population (Canary Islands, Spain). *Food Chem Toxicol* 2013; **62**: 856–868.
- Brenniman GR, Kojola WH, Levy PS, Carnow BW, Namekata TI. *Health Effects of Human Exposure to Barium in Drinking Water*, 1979. Available at <http://nepis.epa.gov/Exe/ZyPURL.cgi?Dockkey=2000Z0BX.txt> (accessed on 12 December 2014).
- Brenniman GR, Namekata T, Kojola WH, Carnow BW, Levy PS. Cardiovascular disease death rates in communities with elevated levels of barium in drinking water. *Environ Res* 1979; **20**: 318–324.
- Brenniman GR, Kojola WH, Levy PS, Carnow BW, Namekata T. High barium levels in public drinking water and its association with elevated blood pressure. *Arch Environ Health* 1981; **36**: 28–32.
- Brenniman GR, Levy PS. Epidemiological study of barium in Illinois drinking water supplies. In: Calabrese EJ, Tuthill RW, Condie L (eds), *Inorganics in Water and Cardiovascular Disease*. Princeton Scientific Publishing Co: Princeton, Texas, USA, 1985, pp 231–240.
- Blaurock-Busch E, Busch YM, Friedle A, Buerner H, Parkash C, Kaur A. Comparing the metal concentration in the hair of cancer patients and healthy people living in the malwa region of punjab, India. *Clin Med Insights Oncol* 2014; **8**: 1–13.
- Blaurock-Busch E, Friedle A, Godfrey M, Schulte-Uebbing CE. Metal exposure in the physically and mentally challenged children of Punjab, India. *Maedica (Buchar)* 2010; **5**: 102–110.
- Blaurock-Busch E, Amin OR, Rabah T. Heavy metals and trace elements in hair and urine of a sample of arab children with autistic spectrum disorder. *Maedica (Buchar)* 2011; **6**: 247–257.
- Ohgami N, Hori S, Ohgami K, Tamura H, Tsuzuki T, Ohnuma S *et al*. Exposure to low-dose barium by drinking water causes hearing loss in mice. *Neurotoxicology* 2012; **33**: 1276–1283.
- Ohgami N, Kondo T, Kato M. Effects of light smoking on extra-high-frequency auditory thresholds in young adults. *Toxicol Ind Health* 2011; **27**: 143–147.
- Sumit AF, Das A, Sharmin Z, Ahsan N, Ohgami N, Kato M *et al*. Cigarette smoking causes hearing impairment among Bangladeshi population. *PLoS One* 2015; **10**: e0118960.
- Szudek J, Ostevik A, Dziegielewski P, Robinson-Anagor J, Goma N, Hodgetts B *et al*. Can U hear me now? Validation of an iPod-based hearing loss screening test. *J Otolaryngol Head Neck Surg* 2012; **Suppl 1**: S78–S84.
- Van Tasell DJ, Folkeard P. Reliability and accuracy of a method of adjustment for self-measurement of auditory thresholds. *Otol Neurotol* 2013; **34**: 9–15.
- Seow WJ, Pan WC, Kile ML, Baccarelli AA, Quamruzzaman Q, Rahman M *et al*. Arsenic reduction in drinking water and improvement in skin lesions: a follow-up study in Bangladesh. *Environ Health Perspect* 2012; **120**: 1733–1738.
- Kato M, Kumasaka MY, Ohnuma S, Furuta A, Kato Y, Shekhar HU *et al*. Comparison of barium and arsenic concentrations in well drinking water and in human body samples and a novel remediation system for these elements in well drinking water. *PLoS One* 2013; **8**: e66681.
- Miller RC, Brindle E, Holman DJ, Shofer J, Klein NA, Soules MR *et al*. Comparison of specific gravity and creatinine for normalizing urinary reproductive hormone concentrations. *Clin Chem* 2004; **50**: 924–932.
- Hauser R, Meeker JD, Park S, Silva MJ, Calafat AM. Temporal variability of urinary phthalate metabolite levels in men of reproductive age. *Environ Health Perspect* 2004; **112**: 1734–1740.
- Kato M, Iida M, Goto Y, Kondo T, Yajima I. Sunlight exposure-mediated DNA damage in young adults. *Cancer Epidemiol Biomarkers Prev* 2011; **20**: 1622–1628.
- Cantley LF, Galusha D, Cullen MR, Dixon-Ernst C, Rabinowitz PM, Neitzel RL. Association between ambient noise exposure, hearing acuity, and risk of acute occupational injury. *Scand J Work Environ Health* 2015; **41**: 75–83.
- Job A, Raynal M, Kossowski M, Studler M, Ghernaoui C, Baffioni-Venturi A *et al*. Otoacoustic detection of risk of early hearing loss in ears with normal audiograms: a 3-year follow-up study. *Hear Res* 2009; **251**: 1–2.
- Bainbridge KE, Hoffman HJ, Cowie CC. Risk factors for hearing impairment among U.S. adults with diabetes. *Diabetes Care* 2011; **34**: 1540–1545.
- Fabry DA, Davila EP, Arheart KL, Serdar B, Dietz NA, Bandiera FC *et al*. Secondhand smoke exposure and the risk of hearing loss. *Tob Control* 2011; **20**: 82–85.
- CDC (Centers for Disease Control and Prevention). *Hearing Levels of Adults, by Age and Sex, United States, 1960–1962, 1965*. Available at <http://stacks.cdc.gov/view/cdc/12597> (accessed on 12 December 2014).
- Jun HJ, Hwang SY, Lee SH, Lee JE, Song JJ, Chae S. The prevalence of hearing loss in South Korea: data from a population-based study. *Laryngoscope* 2015; **125**: 690–694.
- Dawes P, Cruickshanks KJ, Moore DR, Edmondson-Jones M, McCormack A, Fortnum H *et al*. Cigarette smoking, passive smoking, alcohol consumption, and hearing loss. *J Assoc Res Otolaryngol* 2014; **15**: 663–674.
- Dąbrowski M, Mielnik-Niedzielska G, Nowakowski A. Impact of different modifiable factors on hearing function in type 1 and type 2 diabetic subjects. A preliminary study. *Ann Agric Environ Med* 2013; **20**: 773–778.
- Drayton M, Noben-Trauth K. Mapping quantitative trait loci for hearing loss in Black Swiss mice. *Hear Res* 2006; **212**: 128–139.
- Williams DD, Short R, Bowden DM. Fingernail growth rate as a biomarker of aging in the pigtailed macaque (*Macaca nemestrina*). *Exp Gerontol* 1990; **25**: 423–432.
- Yaemsiri S, Hou N, Slining MM, He K. Growth rate of human fingernails and toenails in healthy American young adults. *J Eur Acad Dermatol Venereol* 2010; **24**: 420–423.
- Lynfield YL. Effect of pregnancy on the human hair cycle. *J Invest Dermatol* 1960; **35**: 323–327.
- Lyle S, Christofidou-Solomidou M, Liu Y, Elder DE, Albelda S, Cotsarelis G. The C8/144B monoclonal antibody recognizes cytokeratin 15 and defines the location of human hair follicle stem cells. *J Cell Sci* 1998; **111**: 3179–3188.
- Airey D. Mercury in human hair due to environment and diet: a review. *Environ Health Perspect* 1983; **52**: 303–316.
- Longnecker MP, Stampfer MJ, Morris JS, Spate V, Baskett C, Mason M *et al*. A 1-y trial of the effect of high-selenium bread on selenium concentrations in blood and toenails. *Am J Clin Nutr* 1993; **57**: 408–413.
- Garland M, Morris JS, Rosner BA, Stampfer MJ, Spate VL, Baskett CJ *et al*. Toenail trace element levels as biomarkers: reproducibility over a 6-year period. *Cancer Epidemiol Biomarkers Prev* 1993; **2**: 493–497.
- He K. Trace elements in nails as bio-markers in clinical research. *Eur J Clin Invest* 2011; **41**: 98–102.
- Li CM, Zhang X, Hoffman HJ, Cotch MF, Themann CL, Wilson MR. Hearing impairment associated with depression in US adults, National Health and Nutrition Examination Survey 2005–2010. *JAMA Otolaryngol Head Neck Surg* 2014; **140**: 293–302.
- Van Duuren BL, Sivak A, Langseth L, Goldschmidt BM, Segal A. Initiators and promoters in tobacco carcinogenesis. World conference on smoking and health: toward a less harmful cigarette. *Natl Cancer Inst Monogr* 1968; **28**: 173–180.
- Bencko V, Symon K. Test of environmental exposure to arsenic and hearing changes in exposed children. *Environ Health Perspect* 1977; **19**: 95–101.
- Saunders JE, Jastrzembski BG, Buckley JC, Enriquez D, MacKenzie TA, Karagas MR. Hearing loss and heavy metal toxicity in a Nicaraguan mining community: audiological results and case reports. *Audiol Neurootol* 2013; **18**: 101–113.

# SCIENTIFIC REPORTS

OPEN

## Manganese-mediated acceleration of age-related hearing loss in mice

Nobutaka Ohgami<sup>1,2,3</sup>, Ichiro Yajima<sup>1,3</sup>, Machiko Iida<sup>1</sup>, Xiang Li<sup>1</sup>, Reina Oshino<sup>1,3</sup>, Mayuko Y. Kumasaka<sup>1</sup> & Masashi Kato<sup>1,3</sup>

Received: 28 July 2016

Accepted: 13 October 2016

Published: 08 November 2016

Despite the fact that manganese (Mn) is known to be a neurotoxic element relevant to age-related disorders, the risk of oral exposure to Mn for age-related hearing loss remains unclear. In this study, we orally exposed wild-type young adult mice to Mn (Mn-exposed WT-mice) at 1.65 and 16.50 mg/L for 4 weeks. Mn-exposed WT-mice showed acceleration of age-related hearing loss. Mn-exposed WT-mice had neurodegeneration of spiral ganglion neurons (SGNs) with increased number of lipofuscin granules. Mn-exposed WT-mice also had increased hypoxia-inducible factor-1 alpha (Hif-1 $\alpha$ ) protein with less hydroxylation at proline 564 and decreased c-Ret protein in SGNs. Mn-mediated acceleration of age-related hearing loss involving neurodegeneration of SGNs was rescued in *RET*-transgenic mice carrying constitutively activated *RET*. Thus, oral exposure to Mn accelerates age-related hearing loss in mice with Ret-mediated neurodegeneration of SGNs.

Hearing loss is one of the sensory diseases that have a negative impact on the quality of life (QOL). It is estimated that about 360 million people in the world suffer from hearing loss and about one third of people over the age of 65 years suffer from age-related (late onset) hearing loss<sup>1</sup>. Genetic and aging factors have been shown to cause onset of hearing loss in humans and mice based on evaluations by pure tone audiometry (PTA) and auditory brainstem response (ABR)<sup>2,3</sup>. On the other hand, previous studies indicated risks of hearing impairments in young adult humans exposed to environmental factors including noise and heavy metals<sup>4–6</sup>. In an experimental study, exposure to audible noise at excessive levels was shown to cause acceleration of age-related hearing loss in young adult mice at 4–8 weeks of age<sup>7</sup>. Thus, young adults have a potential risk of age-related hearing loss, though there is limited information about environmental factors other than exposure to noise that accelerate age-related hearing loss in young adult humans and mice.

Manganese (Mn) is known to be a neurotoxic element relevant to age-related disorders. In humans, excessive exposure to Mn via inhalation causes neurodegeneration of the substantia nigra that has pathological similarities to Parkinsonism<sup>8,9</sup>. High levels of Mn up to 34,000  $\mu$ g/L in well drinking water have been reported in various developing countries<sup>10–14</sup>. Excessive exposure to Mn by drinking well water is also a risk for neural diseases<sup>10,15</sup>. In experimental studies, exposure to Mn by inhalation resulted in Parkinsonism in mice<sup>16</sup>. C57BL/6 mice (4–5 months old) orally exposed to Mn at 400 mg/L via drinking water for 5–6 weeks showed increased Mn levels in the brain including the substantia nigra, resulting in neurobehavioral defects<sup>17,18</sup>. Oral exposure to Mn also had effects on brain dopamine levels and neurocognitive functions in neonatal rats<sup>19</sup>. On the other hand, C57BL/6 mice are known to suffer from acceleration of age-related hearing loss at a high-frequency sound (20–40 kHz) from 4 months of age<sup>20</sup>. Subcutaneous injection of a high concentration of Mn (100 mg/kg) into C57BL/6 mice was shown to increase Mn levels in the inner ears<sup>21</sup>. The inner ears contain the organ of Corti and stria vascularis (SV). The SV maintains endolymph potential. The organ of Corti, which contains inner hair cells (IHCs) and outer hair cells (OHCs), plays an important role in conversion of sound stimulations to neural impulses, followed by transmission to spiral ganglion neurons (SGNs), which serve as the primary carrier of auditory information<sup>22,23</sup>. In a previous study, *ex vivo* exposure of SGNs to Mn at levels as low as 50  $\mu$ M (6.29 mg/L) was shown to cause neurodegeneration of SGNs<sup>24</sup>. However, there has been no study showing an association between oral exposure to Mn via drinking water and hearing loss as well as onset of age-related hearing loss determined by ABR in experimental animals.

c-Ret is a tyrosine kinase and a receptor for neurotrophic factors including glial cell line-derived neurotrophic factor (GDNF)<sup>25</sup>. In our previous studies, impairment of c-RET was shown to be involved in hearing loss in

<sup>1</sup>Department of Occupational and Environmental Health, Nagoya University Graduate School of Medicine, Nagoya, Japan. <sup>2</sup>Nutritional Health Science Research Center, Chubu University, 1200 Matsumoto, Kasugai, Aichi 487-8501, Japan. <sup>3</sup>Voluntary Body for International Health Care in Universities, Nagoya, Japan. Correspondence and requests for materials should be addressed to M.K. (email: katomasa@med.nagoya-u.ac.jp)

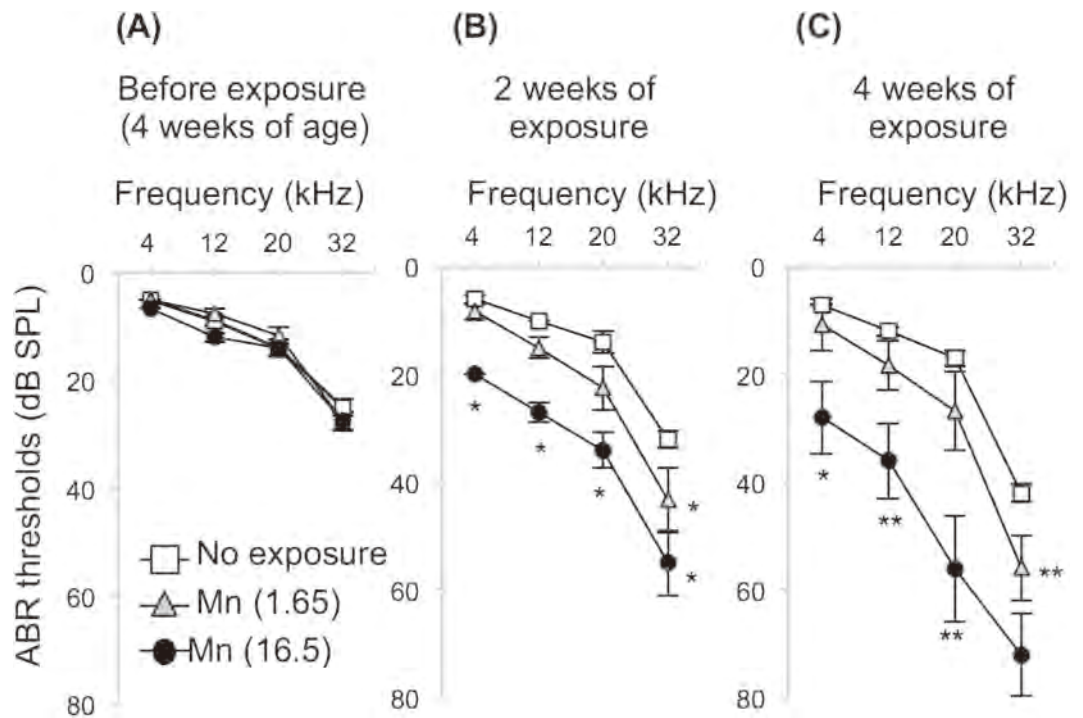


**Figure 1. WT mice exposed to Mn showed acceleration of age-related hearing loss.** (A–C) Hearing levels (means  $\pm$  SE) of mice before exposure (A) and at 2 weeks (B) and 4 weeks after exposure (C) to Mn at 1.65 mg/L [Mn (1.65), gray triangles;  $n = 6$ ] and at 16.50 mg/L [Mn (16.50), black circles;  $n = 6$ ] and of mice in the non-exposure group (open squares;  $n = 10$ ). Significant differences (\* $p < 0.05$ , \*\* $p < 0.01$ ) were analyzed by the Steel–Dwass test.

humans<sup>26</sup>. The phosphorylation level of tyrosine 1062 (Y1062) in c-Ret directly affects kinase activity of c-Ret<sup>25</sup>. Partial impairment of Y1062 phosphorylation in c-Ret was shown to accelerate age-related hearing loss with neurodegeneration of SGNs with impairment of NF- $\kappa$ B, which is a downstream molecule of c-Ret<sup>26</sup> in the inner ears of c-Ret-knock-in mice<sup>20</sup>. Thus, c-Ret kinase is an age-related hearing loss-related molecule. On the other hand, hypoxia-inducible factor-1 alpha (HIF-1 $\alpha$ ) is known to be a transcriptional factor and to form a heterodimer with HIF-1 $\beta$  under the condition of environmental stress. A previous study showed that age-related hearing loss is associated to HIF-1 $\alpha$  protein in SGNs<sup>27</sup>. Exposure to transitional elements including cobalt and Mn has been shown to stabilize HIF-1 $\alpha$  protein with less hydroxylation at proline 564 *in vitro*<sup>28,29</sup>. Furthermore, a previous *in vitro* study showed that stabilization of HIF-1 $\alpha$  protein is required for decrease of RET protein in neural cells exposed to cobalt<sup>30</sup>. Thus, the results of previous studies raise the possibility that exposure to Mn affects the onset of age-related hearing loss caused by impairment of c-Ret via HIF-1 $\alpha$  in SGNs, though it remains unknown whether there is a correlation between HIF-1 $\alpha$  protein and c-Ret in SGNs.

We therefore performed an experimental study to examine the correlation between Mn and age-related hearing level in humans and to clarify the mechanism of age-related hearing loss in mice exposed to Mn at possible levels ingested from drinking water.

## Results

**Oral exposure of young adult mice to Mn accelerated age-related hearing loss.** We performed an experimental study with wild-type young adult C57BL/6J mice (WT mice) at 1 month of age exposed to Mn at 1.65 and 16.50 mg/L for 4 weeks. Before exposure, hearing levels in all groups were comparable (Fig. 1A). The non-exposure group ( $n = 10$ ) showed age-related hearing loss at a high-frequency sound (32 kHz) (Fig. 1C), corresponding to results of previous studies<sup>20,31</sup>. WT mice exposed to Mn at 1.65 mg/L showed an increased threshold of ABR at 32 kHz compared with that in the non-exposure group (Fig. 1B,C). WT mice exposed to Mn at 16.50 mg/L for 2 weeks and 4 weeks showed severe hearing loss at 1–32 kHz compared to the hearing level in the non-exposure group (Fig. 1B,C).

**Mn-mediated acceleration of age-related hearing loss in mice involved neurodegeneration of SGNs.** We then performed morphological analysis of the inner ears from WT mice exposed to Mn in order to determine the pathogenesis of age-related hearing loss caused by Mn administered by drinking water. Nissl staining revealed that WT mice exposed to Mn had a decreased density of SGNs without an impaired staining pattern of nuclei (Fig. 2A, right panel, inset and B) compared to the morphology and density of SGNs in non-exposed mice (Fig. 2A, left panel, inset and B). We further performed detailed morphological analyses of SGNs from WT mice exposed to Mn by transmission electron microscopy (TEM) (Fig. 2C). Gaps between SGNs and Schwann cells (SCs) (Fig. 2C, right upper panel, arrows), increased number of lipofuscin granules (Fig. 2C, right upper

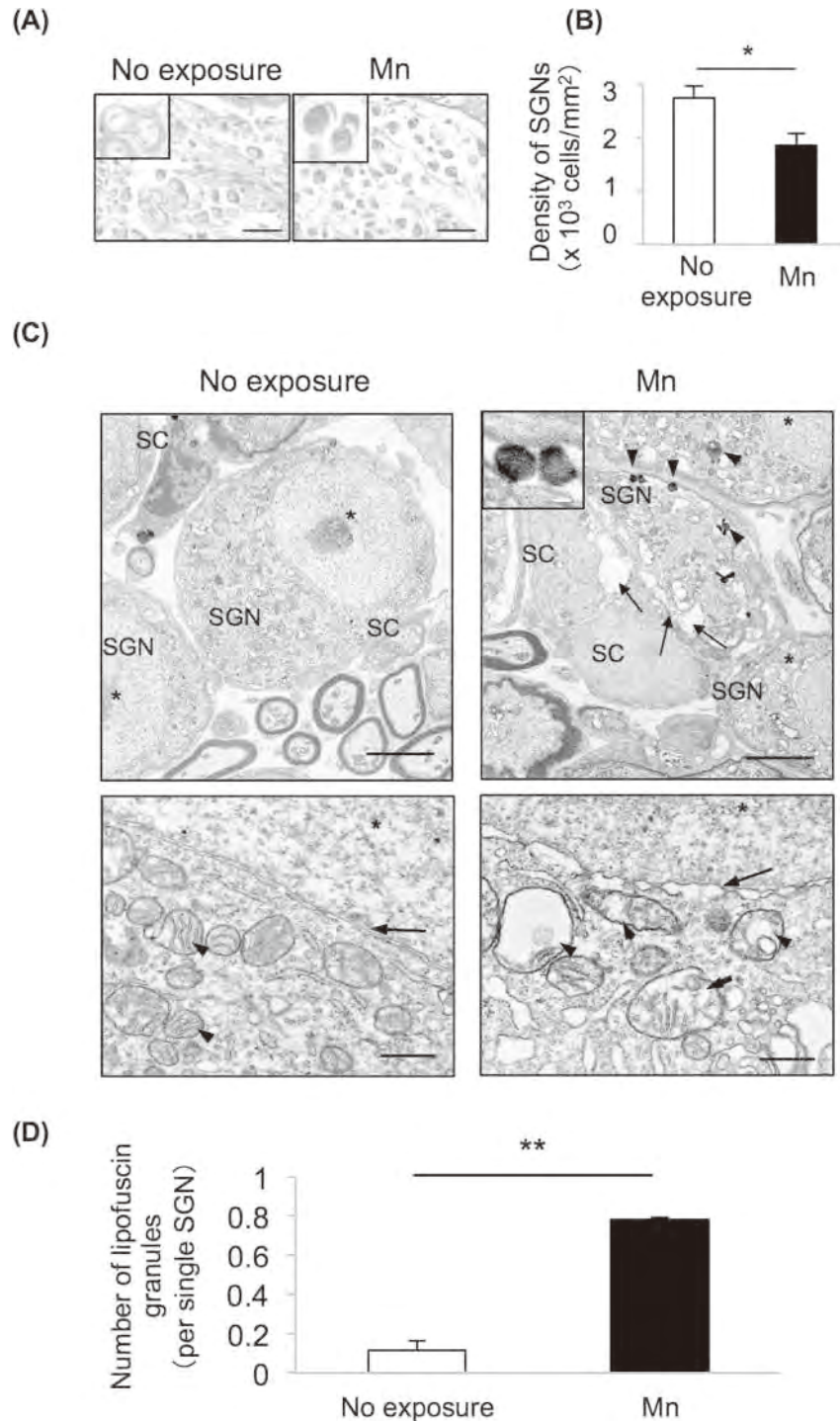


**Figure 2. Oral exposure of WT mice to Mn caused neurodegeneration in SGNs.** (A) Nissl staining of SGNs in the mid turn from mice administered Mn at 16.50 mg/L (Mn; right panels) and non-exposed mice (left panels). The inset in the left panel shows a typical example of SGNs with normal morphology in the non-exposure group, while the inset in the right panel shows an impaired staining pattern of nuclei of SGNs in the Mn exposure group. Scale bars: 20  $\mu\text{m}$ . (B) Densities of SGNs (mean  $\pm$  SD) without an impaired staining pattern of nuclei in the mid turn from WT mice exposed to Mn (Mn, black bars,  $n = 3$ ) and non-exposed mice (white bars,  $n = 3$ ) are presented. Significant difference ( $*p < 0.05$ ) from the control mice was analyzed by the unpaired t-test. (C,D) Transmission electron microscopy (TEM) for SGNs in the mid turn from Mn-administered mice (Mn; right panels) and non-exposed mice (left panels). Asterisks indicate the nucleus. Gaps between SGNs and SCs (right upper panel, arrows) and lipofuscin granules (right upper panel, arrowheads; inset in the right upper panel) were observed in WT mice exposed to Mn. Scale bars: 5  $\mu\text{m}$  (upper panels), 500 nm (lower panels) and 200 nm (inset). (D) The number of lipofuscin granules per single SGN (mean  $\pm$  SD) was counted. Significant difference ( $**p < 0.01$ ;  $*p < 0.05$ ) from the control mice was analyzed by the unpaired t-test.

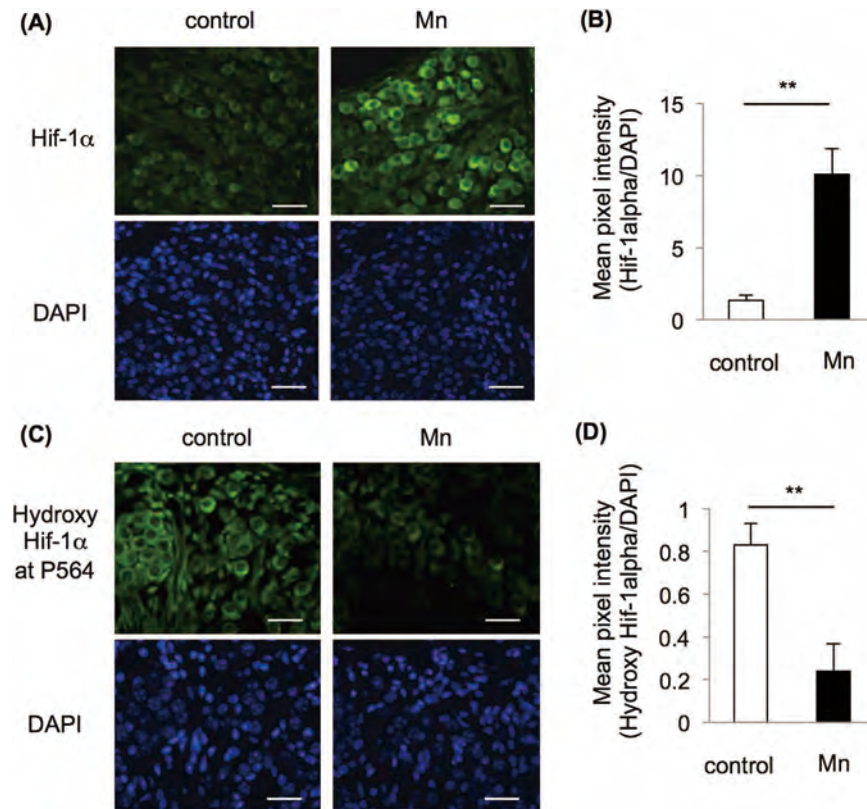


**Figure 3.** Oral exposure of WT mice to Mn increased Hif-1 $\alpha$  protein with less hydroxylation at proline 564 in SGNs. Immunohistochemistry with anti-Hif-1 $\alpha$  (A) and anti-hydroxy Hif-1 $\alpha$  at proline 564 of SGNs in the mid turn from mice administered Mn at 16.50 mg/L (Mn; right panels) and non-exposed mice (left panels). Scale bars: 20  $\mu$ m. Mean pixel intensities (means  $\pm$  SD) of Hif-1 $\alpha$  (B) and hydroxyl Hif-1 $\alpha$  at proline 564 (D) of SGNs in the mid turn from WT mice exposed to Mn (Mn, black bars,  $n = 3$ ) and non-exposed WT mice (white bars,  $n = 3$ ) are presented. All positive signals were normalized by DAPI. Significant difference ( $*p < 0.05$ ,  $**p < 0.01$ ) from the control was analyzed by the unpaired t-test.

panel, arrowheads and D) and vacuole degeneration were observed in WT mice exposed to Mn (Fig. 2C, right lower panel, arrowheads), in contrast to intact cellular membranes (Fig. 2C, left upper panel) and mitochondria (Fig. 2C, left lower panel, arrowheads) in non-exposed mice. The nuclei of SGNs from WT mice exposed to Mn showed discontinuous nuclear membranes (Fig. 2C, right lower panel, arrow), in contrast to the intact nuclear membranes observed in non-exposed mice (Fig. 2C, left lower panel, arrow).

**Mn-mediated acceleration of age-related hearing loss in mice involved impairment of Hif-1 $\alpha$  and c-Ret in SGNs.** We finally analyzed the mechanism of Mn-mediated hearing loss in mice. Immunofluorescent staining showed an increased level of Hif-1 $\alpha$  and a decreased level of hydroxyl Hif-1 $\alpha$  at proline 564 in SGNs from WT mice exposed to Mn (Fig. 3). Next, we used *RET-transgenic mice carrying constitutively activated RET (RFP-RET) (RET-Tg mice)* of line 242, in which no tumor develops without exception<sup>20,26,32</sup>, and litter WT mice in order to determine whether Mn-mediated hearing loss involves impairment of c-Ret in SGNs *in vivo*. WT mice exposed to Mn showed decreased levels of c-Ret protein and phosphorylation in SGNs compared to those in the non-exposed groups and *RET-Tg* mice exposed to Mn (Fig. 4A–C). WT mice exposed to Mn also showed a decreased density of SGNs without abnormal morphology, while the density and morphology of SGNs in *RET-Tg* mice exposed to Mn were comparable to those in non-exposed WT mice and non-exposed *RET-Tg* mice (Fig. 4A,D). WT mice exposed to Mn also showed decreased phosphorylation of NF- $\kappa$ B in SGNs compared to those in the non-exposed groups and *RET-Tg* mice exposed to Mn (Fig. 4A,E). Correspondingly, hearing levels in *RET-Tg* mice exposed to Mn were comparable to those in the non-exposed groups, while WT mice exposed to Mn showed hearing loss (Fig. 5B). All of the groups showed comparable hearing levels before exposure (Fig. 5A).

## Discussion

This study showed acceleration of age-related hearing loss in young adult mice orally exposed to Mn. Correspondingly, the WT mice orally exposed to Mn showed significantly higher levels of Mn in inner ears than those in the non-exposed mice, while the two groups of mice showed comparable Mn levels in the cerebrum, cerebellum, heart, kidney, muscle and bone (Table S1). Thus, the results suggest that oral exposure to Mn during young adulthood increases Mn levels in inner ears, resulting in acceleration of age-related hearing loss in mice.

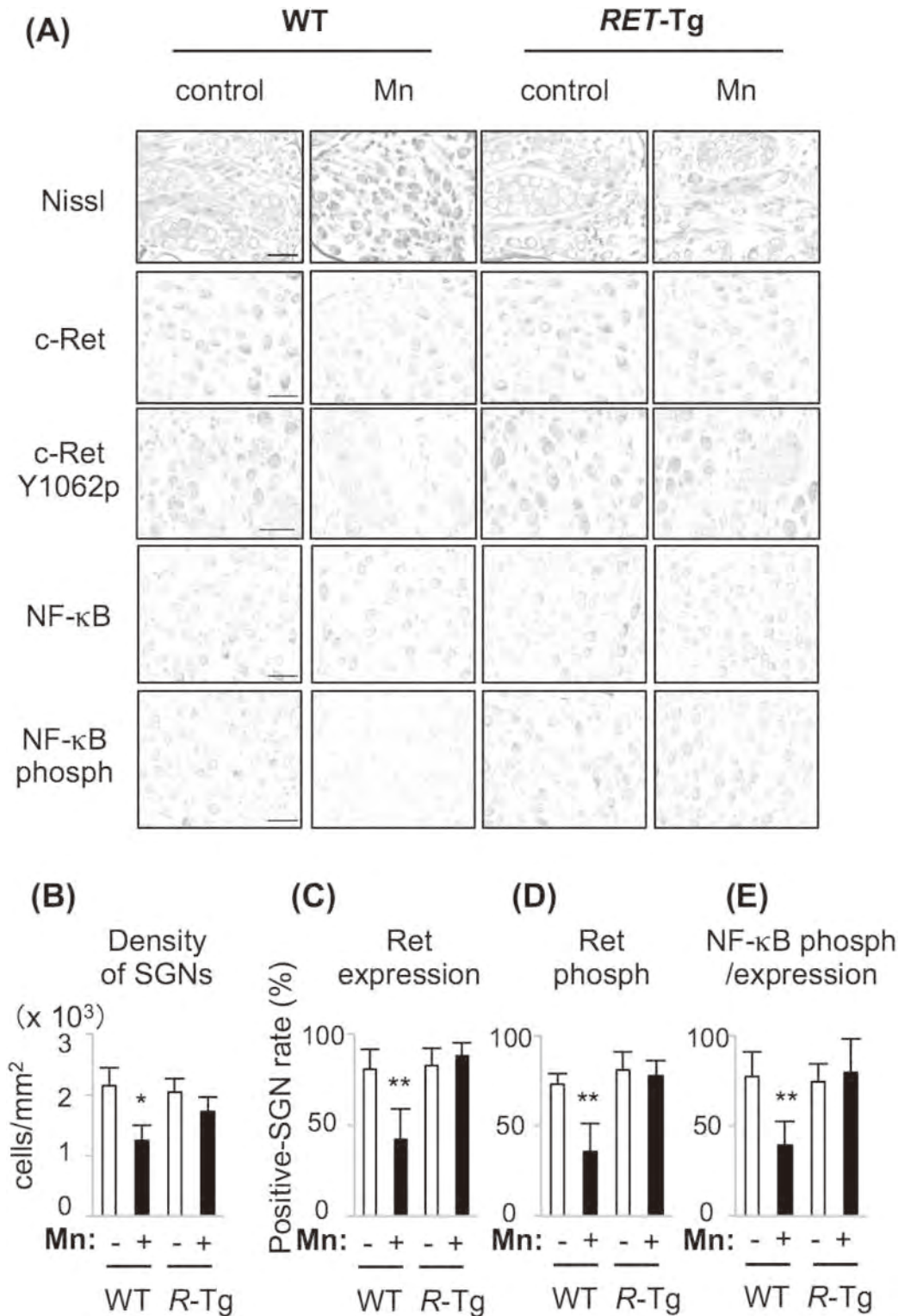


**Figure 4. Mn-mediated impairment of c-Ret in SGNs.** (A) Nissl staining (top panels) and results of immunohistochemical analyses with polyclonal antibodies against c-Ret, phosphorylated c-Ret at Y1062 (c-Ret Y1062p), NF-κB and phosphorylated NF-κB (NF-κB phosph) are presented. All specimens were SGNs from wild-type (WT) and littermate *RET-Tg* (*R-Tg*) mice without (control) or with exposure to Mn at 16.50 mg/L for 4 weeks (Mn). All immunohistochemical analyses were performed with diaminobenzidine followed by counterstaining with hematoxylin. Scale bars: 20 μm. (B–D) Densities (means ± SD) of SGNs without an impaired staining pattern of nuclei (B) and percentages of positive SGN numbers (means ± SE) of c-Ret expression (C), phosphorylated c-Ret (D) and phosphorylated NF-κB normalized by NF-κB expression (E) in the mid turn from 2-month-old WT and littermate *R-Tg* mice with (+) or without (–) exposure to Mn. Significant differences (\**p* < 0.05, \*\**p* < 0.01) were analyzed by the Tukey test.

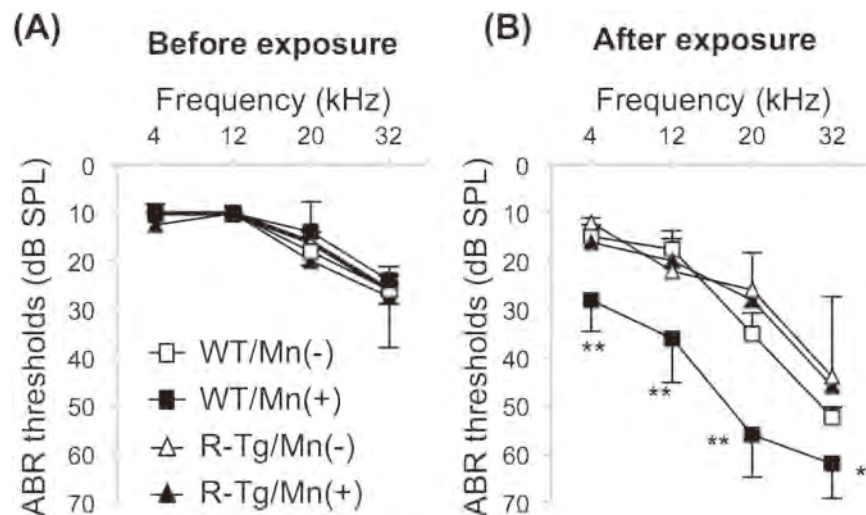


**Figure 5. Mn-mediated age-related hearing loss in mice was rescued by introducing constitutively activated *RET*.** (A,B) Hearing levels (means  $\pm$  SE) of WT (squares) and littermate R-Tg mice (triangles) before exposure (A) and after exposure (B) with [Mn(+)] or without [Mn(-)] exposure to Mn at 16.50 mg/L for 4 weeks ( $n = 5$ , each group). Significant differences ( $*p < 0.05$ ,  $**p < 0.01$ ) were analyzed by the Steel-Dwass test.

Our results showed Mn-mediated neurodegeneration of SGNs with increased lipofuscin granules. Lipofuscin granules are known to be undegradable protein aggregates and to be involved in age-related degeneration<sup>33</sup>. Our results partially correspond to results of a previous study showing that age-related hearing loss involved neurodegeneration of SGNs with accumulation of lipofuscin granules in SAMP8 mice<sup>34</sup>, while a previous study has shown Mn-mediated aggregation of alpha-synuclein in the frontal cortex in non-human primates injected with manganese sulfate ( $MnSO_4$ ) at 3.3–10.0 mg/kg/week for maximum 52 weeks<sup>35</sup>. Thus, it is possible that oral exposure to Mn accelerates age-related neurodegeneration of SGNs with protein aggregates.

Morphological abnormalities in the organ of Corti including IHCs, OHCs and the SV were undetectable in WT mice exposed to Mn in this study (Figure S1). These results correspond to results of our previous studies showing that *c-Ret*-mediated neurodegeneration of SGNs occurred in *c-Ret*-knock-in mice, while morphological abnormalities in IHCs, OHCs and the SV were undetectable<sup>20,26</sup>. Thus, our morphological analyses suggest that Mn-mediated degeneration occurs in SGNs but not in hair cells and the SV under the exposure conditions.

Our results showed that Mn-mediated age-related hearing loss involved an increased level of Hif-1 $\alpha$  protein with less hydroxylation at proline 564 and decreased expression and phosphorylation levels of *c-Ret* in SGNs. In previous studies, *in vitro* exposure to Mn increased HIF-1 $\alpha$  protein in HepG2 cells<sup>36</sup> and stabilized HIF-1 $\alpha$  protein by direct inhibition of HIF-prolyl hydroxylase in a cell free experiment<sup>29</sup>. A previous study also showed that exposure to audible noise resulted in stabilization of Hif-1 $\alpha$  protein in inner ears including SGNs<sup>37</sup>. Thus, it is possible that Hif-1 $\alpha$  protein is one of the molecular targets in inner ears for environmental factors including Mn. Since stabilization of HIF-1 $\alpha$  protein has been shown to decrease *c-RET* mRNA in a human lung cell line<sup>38</sup> and to decrease *c-RET* protein in a human neuroblastoma cell line<sup>30</sup>, we hypothesized that the mechanism of Mn-mediated decrease of *c-Ret* protein occurs at the transcriptional level mediated by stabilization of Hif-1 $\alpha$  protein in SGNs (Figure S2).

In conclusion, our study provides novel evidence of Mn-mediated ototoxicity showing acceleration of age-related hearing loss in young adult mice. Our results further showed that Mn-mediated age-related hearing loss as well as decreased cell density of SGNs with impairment of *c-Ret* and NF- $\kappa$ B were restored by introducing constitutively activated *RET*. Our results partially correspond to results of our previous study showing that partial impairment of *c-Ret* accelerated age-related hearing loss with neurodegeneration of SGNs with impairment of NF- $\kappa$ B in *c-Ret*-knock-in mice<sup>20</sup>. Thus, our results suggest the mechanism of neurodegeneration of SGNs caused by impairment of *c-Ret* in young adult mice orally exposed to Mn.

## Materials and Methods

**Mice.** *RET*-Tg mice of line 242<sup>32</sup> and littermate WT mice were previously reported. WT mice showed age-related hearing loss due to the C57BL/6 genetic background as previously reported<sup>39</sup>. Hearing levels in 10-week-old *RET*-Tg mice and littermate WT mice have been shown to be comparable<sup>40</sup>. All experiments were approved by the Institutional Animal Care and Use Committee in Nagoya University (approval number: 28251) and Chubu University (approval number: 2810030) and the Institutional Recombinant DNA Experiment Committee in Nagoya University (approval number: 14–88, 13–35) and Chubu University (approval number: 13–03) and followed the Japanese Government Regulations for Animal Experiments.

**Oral exposure to Mn.** Manganese (II) chloride ( $MnCl_2 \cdot 4H_2O$ ) purchased from Nacalai Tesque was dissolved in distilled water. Mice were exposed to Mn at 1.65 and 16.50 mg Mn/L via drinking water. The drinking water containing Mn was freshly prepared and changed every week. The non-exposure group was given distilled water. The exposure was started at 1 month of age. We regularly monitored the amounts of drinking water and

food ingested by the mice and the body weights of mice during exposure as described previously<sup>41</sup>. The monitoring showed that one mouse (20–30 g in body weight) consumes about 4–6 ml water per day and that mice exposed to Mn and those not exposed to Mn showed no significant difference in the intake of either food or water or in body weight. Mice were maintained under specific pathogen-free (SPF) conditions at a fixed temperature ( $23 \pm 2^\circ\text{C}$ ) and a 12-h light/dark cycle.

**Measurement of hearing.** ABR measurements (AD Instruments Pty. Ltd.) were performed as described previously<sup>20,26</sup>. Tone burst stimuli were measured 5 dB-stepwise from 0 dB SPL to 90 dB SPL. The measurements were performed by researchers who were blinded to the experimental groups. The threshold was judged by an appearance of the lowest level of the I wave of ABR. Data are presented as means  $\pm$  SE.

**Morphological analysis with a light microscope and a fluorescent microscope.** Morphological analyses were performed as described previously<sup>20,26</sup>. The morphological analyses were performed by researchers who were blinded to the experimental groups. Nissl staining was performed with paraffin sections. Stained cells with round and palely stained nuclei were considered to be surviving cells, whereas shrunken cells with pyknotic nuclei were considered to be non-surviving cells as described previously<sup>42</sup>. Immunohistochemistries with polyclonal antibodies against c-Ret protein (1:100; Immuno Biological Laboratories), phosphorylated c-Ret Y1062 (1:100; Abcam) and phosphorylated NF- $\kappa$ B p50 (1:50; Santa Cruz) were performed for frozen sections with Can Get Signal immunostaining solution (TOYOBO). We used a VECTASTAIN ABC Rabbit IgG kit (Vector) and 3, 3'-diaminobenzidine (DAB) kit (DAKO) to detect the primary antibodies. Specimens were observed under a light microscope (Leica DM1000LED). Immunohistochemical analysis with polyclonal antibodies against Hif-1 $\alpha$  (1:100; Abcam), Hif-1 $\alpha$  hydroxyl proline 564 (1:30; Novus Biologicals) and NF- $\kappa$ B p50 (1:100; Santa Cruz) was performed for paraffin sections. Antigen retrieval was performed with a citrate buffer (pH 6.0) at 90–92  $^\circ\text{C}$  for 10 minutes for the detection of Hif-1 $\alpha$  and NF- $\kappa$ B p50. We used Alexa Fluor 488-labeled donkey anti-rabbit IgG (1:1000, Invitrogen) as a secondary antibody followed by counterstaining with 4',6-diamidino-2-phenylindole (DAPI) to detect Hif-1 $\alpha$  and Hif-1 $\alpha$  hydroxyl proline 564 under the fluorescent microscope (Leica DMI6000B). We used the software program WinROOF (Mitani Corp., Fukui, Japan) to estimate the percentage of positive SGNs detected by antibodies as previously reported<sup>20,26</sup>.

**Morphological analysis by electron microscopy.** Preparation of tissues for TEM basically followed the previous method<sup>20,26</sup>. In brief, we performed perfusion fixation with a mixture of 2% paraformaldehyde (PFA) and 2% glutaraldehyde in 0.3 M HEPES-buffer (pH 7.4) and then dissected murine cochleas. The cochleas were immersed in the same fixative solution overnight at 4  $^\circ\text{C}$ . The cochleas were further fixed with 2% osmium tetroxide in 0.3 M HEPES-buffer (pH 7.4) at 4  $^\circ\text{C}$  for 3 hours. After dehydrating the cochleas with a graded series of ethanol, we embedded the cochleas in epoxy resin (Quetol 651). We observed ultrathin sections ( $t = 70$  nm) under an electron microscope at 80 kV (JEOL JEM1200EX, Tokyo, Japan). The number of lipofuscin granules in SGNs from the mid turn was counted. A total of 60 cells per area were counted. For scanning electron microscopy, we performed perfusion fixation with the same mixture of 2% PFA and 2% glutaraldehyde. After dissection of inner ears under a stereomicroscope, stepwise dehydration in ethanol solutions and dry up with a critical point dryer (Hitachi HCP-2) were performed. Prepared inner ears were eventually mounted on aluminum stubs with colloidal silver adhesive and sputter-coated with gold palladium before imaging by a scanning electron microscope (Hitachi S-800s).

**Statistical analysis.** Statistical analyses were performed by the method previously reported<sup>43–46</sup>. We used the two-tailed Mann-Whitney *U* test (equivalent to the Wilcoxon rank sum test) and Steel-Dwass test for non-parametric data to determine a significant difference of hearing levels between two groups and among three groups, respectively, since hearing levels are discontinuous variables. We used the unpaired *t*-test for parametric data to determine a significant difference of the morphological analyses between two groups. We also performed one-way ANOVA followed by Tukey's post-hoc multiple comparison tests to determine significant differences among four groups. The Steel-Dwass test was also performed with the alpha level set to 0.05. A difference with  $p < 0.05$  was considered significant. All statistical analyses were performed using JMP Pro (version 11.0.0; SAS Institute Inc., Cary, NC, USA).

## References

1. World Health Organization (WHO). Deafness and hearing loss. Available: <http://www.who.int/mediacentre/factsheets/fs300/en/>. [Accessed 12 July 2016] (2015).
2. Gates, G. A., Couropmitree, N. N. & Myers, R. H. Genetic associations in age-related hearing thresholds. *Arch Otolaryngol Head Neck Surg* **125**, 654–659 (1999).
3. Gates, G. A. & Mills, J. H. Presbycusis. *Lancet* **366**, 1111–1120, doi: 10.1016/S0140-6736(05)67423-5 (2005).
4. Lees, R. E. M., Roberts, J. H. & Wald, Z. Noise induced hearing loss and leisure activities of young people: a pilot study. *Can J Public Health* **76**, 171–173 (1985).
5. Sadhra, S., Jackson, C. A., Ryder, T. & Brown, M. J. Noise exposure and hearing loss among student employees working in university entertainment venues. *Ann Occup Hyg* **46**, 455–463 (2002).
6. Shargorodsky, J. *et al.* Heavy metals exposure and hearing loss in US adolescents. *Arch Otolaryngol Head Neck Surg* **137**, 1183–1189, doi: 10.1001/archoto.2011.202 (2011).
7. Kujawa, S. G. & Liberman, M. C. Acceleration of Age-Related Hearing Loss by Early Noise Exposure: Evidence of a Misspent Youth. *J Neurosci* **26**, 2115–2123, doi: 10.1523/JNEUROSCI.4985-05.2006 (2006).
8. Bowler, R. M. *et al.* Prospective study on neurotoxic effects in manganese-exposed bridge construction welders. *Neurotoxicology* **32**, 596–605, doi: 10.1016/j.neuro.2011.06.004 (2011).
9. Racette, B. A. *et al.* Increased risk of parkinsonism associated with welding exposure. *Neurotoxicology* **33**, 1356–1361, doi: 10.1016/j.neuro.2012.08.011 (2012).

10. Wasserman, G. A. *et al.* Water manganese exposure and children's intellectual function in Arahazar, Bangladesh. *Environ Health Perspect* **114**, 124–129 (2006).
11. Hafeman, D. *et al.* Association between manganese exposure through drinking water and infant mortality in Bangladesh. *Environ Health Perspect* **115**, 1107–1112, doi: 10.1289/ehp.10051 (2007).
12. Agusa, T. *et al.* Contamination by arsenic and other trace elements in tube-well water and its risk assessment to humans in Hanoi, Vietnam. *Environ Pollut* **139**, 95–106, doi: 10.1016/j.envpol.2005.04.033 (2006).
13. Buschmann, J. *et al.* Contamination of drinking water resources in the Mekong delta floodplains: arsenic and other trace metals pose serious health risks to population. *Environ Int* **34**, 756–764, doi: 10.1016/j.envint.2007.12.025 (2008).
14. Kato, M. *et al.* Toxic Elements in Well Water from Malaysia. *Toxicol Environ Chem* **92**, 1609–1612, doi: 10.1080/02772241003707454 (2010).
15. Bouchard, M. F. *et al.* Intellectual impairment in school-age children exposed to manganese from drinking water. *Environ Health Perspect* **119**, 138–143, doi: 10.1289/ehp.1002321 (2011).
16. Ordoñez-Librado, J. L. *et al.* Inhalation of divalent and trivalent manganese mixture induces a Parkinson's disease model: immunocytochemical and behavioral evidences. *Neuroscience* **155**, 7–16, doi: 10.1016/j.neuroscience.2008.05.012 (2008).
17. Krishna, S., Dodd, C. A., Hekmatyar, S. K. & Filipov, N. M. Brain deposition and neurotoxicity of manganese in adult mice exposed via the drinking water. *Arch Toxicol* **88**, 47–64, doi: 10.1007/s00204-014-1221-y (2014).
18. Kumasaka, M. Y. *et al.* Commentary to Krishna *et al.* brain deposition and neurotoxicity of manganese in adult mice exposed via the drinking water. *Arch Toxicol* **88**, 1185–1186, doi: 10.1007/s00204-014-1221-y (2014).
19. Tran, T. T. *et al.* Effects of neonatal dietary manganese exposure on brain dopamine levels and neurocognitive functions. *Neurotoxicology* **23**, 645–651 (2002).
20. Ohgami, N. *et al.* Partial impairment of c-Ret at tyrosine 1062 accelerates age-related hearing loss in mice. *Neurobiol Aging* **33**, 626.e25–e34, doi: 10.1016/j.neurobiolaging.2011.04.002 (2012).
21. Ma, C. *et al.* Manganese accumulation in the mouse ear following systemic exposure. *J Biochem Mol Toxicol* **22**, 305–310, doi: 10.1002/jbt.20241 (2008).
22. Lalwani, A. K. & Guertler, N. Sensorineural hearing loss, the aging inner ear, and hereditary hearing impairment. In *CURRENT diagnosis & treatment in otolaryngology—head & neck surgery*. 2nd edn (eds Lalwani, A. K.) 683–704 (McGraw-Hill, 2008).
23. Brown, S. D., Hardisty-Hughes, R. E. & Mburu, P. Quiet as a mouse: dissecting the molecular and genetic basis of hearing. *Nat Rev Genet* **9**, 277–290, doi: 10.1038/nrg2309 (2008).
24. Ding, D., Roth, J. & Salvi, R. Manganese is toxic to spiral ganglion neurons and hair cells *in vitro*. *Neurotoxicology* **32**, 233–241, doi: 10.1016/j.neuro.2010.12.003 (2011).
25. Kato, M. *et al.* Repair by Src kinase of function-impaired RET with multiple endocrine neoplasia type 2A mutation with substitutions of tyrosines in the COOH-terminal kinase domain for phenylalanine. *Cancer Res* **62**, 2414–2422 (2002).
26. Ohgami, N. *et al.* c-Ret-mediated hearing loss in mice with Hirschsprung disease. *Proc Natl Acad Sci USA* **107**, 13051–13056, doi: 10.1073/pnas.1004520107 (2010).
27. Riva, C., Donadieu, E., Magnan, J. & Lavieille, J. P. Age-related hearing loss in CD/1 mice is associated to ROS formation and HIF target proteins up-regulation in the cochlea. *Exp Gerontol* **42**, 327–336, doi: 10.1016/j.exger.2006.10.014 (2007).
28. Yuan, Y., Hilliard, G., Ferguson, T. & Millhorn, D. E. Cobalt inhibits the interaction between hypoxia-inducible factor- $\alpha$  and von Hippel-Lindau protein by direct binding to hypoxia-inducible factor- $\alpha$ . *J Biol Chem* **278**, 15911–15916, doi: 10.1074/jbc.M300463200 (2003).
29. Han, J. *et al.* Manganese (II) induces chemical hypoxia by inhibiting HIF-prolyl hydroxylase: implication in manganese-induced pulmonary inflammation. *Toxicol Appl Pharmacol* **235**, 261–267, doi: 10.1016/j.taap.2009.01.003 (2009).
30. Foti, R. *et al.* Parkinson disease-associated DJ-1 is required for the expression of the glial cell line-derived neurotrophic factor receptor RET in human neuroblastoma cells. *J Biol Chem* **285**, 18565–18574, doi: 10.1074/jbc.M109.088294 (2010).
31. Lang, H. *et al.* Nuclear factor kappaB deficiency is associated with auditory nerve degeneration and increased noise-induced hearing loss. *J Neurosci* **26**, 3541–3550, doi: 10.1523/JNEUROSCI.2488-05.2006 (2006).
32. Kato, M. *et al.* Linkage between melanocytic tumor development and early burst of Ret protein expression for tolerance induction in metalloproteinase-1/ret transgenic mouse lines. *Oncogene* **18**, 837–842, doi: 10.1038/sj.onc.1202329 (1999).
33. Brunk, U. T. & Terman, A. Lipofuscin: mechanisms of age-related accumulation and influence on cell function. *Free Radic Biol Med* **33**, 611–619 (2002).
34. Menardo, J. *et al.* Oxidative stress, inflammation, and autophagic stress as the key mechanisms of premature age-related hearing loss in SAMP8 mouse Cochlea. *Antioxid Redox Signal* **16**, 263–274, doi: 10.1089/ars.2011.4037 (2012).
35. Verina, T., Schneider, J. S. & Guilarte, T. R. Manganese exposure induces  $\alpha$ -synuclein aggregation in the frontal cortex of non-human primates. *Toxicol Lett* **217**, 177–183, doi: 10.1016/j.toxlet.2012.12.006 (2013).
36. Shin, H. J. *et al.* Manganese-mediated up-regulation of HIF-1 $\alpha$  protein in Hep2 human laryngeal epithelial cells via activation of the family of MAPKs. *Toxicol In Vitro* **24**, 1208–1214, doi: 10.1016/j.tiv.2010.02.008 (2010).
37. Chung, J. W., Kang, H. H., Shin, J. E. & Kim, J. U. Accumulation of hypoxia-inducible factor-1 $\alpha$  in mouse inner ear by noise stimulation. *Neuroreport* **15**, 2353–2356 (2004).
38. Elvidge, G. P. *et al.* Concordant regulation of gene expression by hypoxia and 2-oxoglutarate-dependent dioxygenase inhibition: the role of HIF-1 $\alpha$ , HIF-2 $\alpha$ , and other pathways. *J Biol Chem* **281**, 15215–15226, doi: 10.1074/jbc.M511408200 (2006).
39. Noben-Trauth, K., Zheng, Q. Y. & Johnson, K. R. Association of cadherin 23 with polygenic inheritance and genetic modification of sensorineural hearing loss. *Nat Genet* **35**, 21–23, doi: 10.1038/ng1226 (2003).
40. Hayashi, H. *et al.* A novel RFP-RET transgenic mouse model with abundant eumelanin in the cochlea. *Hear Res* **195**, 35–40, doi: 10.1016/j.heares.2004.01.020 (2004).
41. Ohgami, N. *et al.* Exposure to low-dose barium by drinking water causes hearing loss in mice. *Neurotoxicology* **33**, 1276–1283, doi: 10.1016/j.neuro.2012.07.008 (2012).
42. Wang, Y. *et al.* Developmental iodine deficiency and hypothyroidism impair neural development, upregulate caveolin-1, and downregulate synaptotagmin-1 in the rat cerebellum. *Biol Trace Elem Res* **144**, 1039–1049, doi: 10.1007/s12011-011-9089-7 (2011).
43. Ohgami, N., Kondo, T. & Kato, M. Effects of light smoking on extra-high-frequency auditory thresholds in young adults. *Toxicol Ind Health* **27**, 143–147, doi: 10.1177/0748233710382539 (2011).
44. Ohgami, N. *et al.* Carcinogenic risk of chromium, copper and arsenic in CCA-treated wood. *Environ Pollut* **206**, 456–460, doi: 10.1016/j.envpol.2015.07.041 (2015).
45. Ohgami, N. *et al.* Epidemiological analysis of the association between hearing and barium in humans. *J Expo Sci Environ Epidemiol* in press, doi: 10.1038/jes.2015.62 (2015).
46. Wang, J. *et al.* Overexpression of Xa-linked inhibitor of apoptosis protein protects against noise-induced hearing loss in mice. *Gene Ther* **18**, 560–568; doi: 10.1038/gt.2010.172 (2011).

## Acknowledgements

This study was supported in part by Grants-in-Aid for Scientific Research on Innovative Areas (24108001, 16H01639), Scientific Research (A) (15H01743 and 15H02588), (B) (16H02962) and (C) (25460178, 16K08343), Grant-in-Aid for Challenging Exploratory Research (26670525) and center of excellence (COE) Project for

Private Universities (Nutritional Health Science Research Center; No. S1201007) from the Ministry of Education, Culture, Sports, Science and Technology (MEXT), Matching Planner Program (MP27115658214) from the Japan Science and Technology Agency (JST), the Japan Health Foundation, the Mitsui & Co., Ltd. Environment Fund, Foundation from Center for Advanced Medical and Clinical Research Nagoya University Hospital, the Mitsubishi Foundation, and the Research Foundation for Health Sciences (The KENKO-KAGAKU Zaidan). The funders had no role in study design, data collection and analysis, decision to publish, or preparation of the manuscript.

### Author Contributions

The project was conceived by N.O. Experimental studies were designed by N.O. and performed by N.O., I.Y., M.I., X.L., R.O. and M.Y.K. N.O. and M.K. wrote the paper.

### Additional Information

**Supplementary information** accompanies this paper at <http://www.nature.com/srep>

**Competing financial interests:** The authors declare no competing financial interests.

**How to cite this article:** Ohgami, N. *et al.* Manganese-mediated acceleration of age-related hearing loss in mice. *Sci. Rep.* **6**, 36306; doi: 10.1038/srep36306 (2016).

**Publisher's note:** Springer Nature remains neutral with regard to jurisdictional claims in published maps and institutional affiliations.



This work is licensed under a Creative Commons Attribution 4.0 International License. The images or other third party material in this article are included in the article's Creative Commons license, unless indicated otherwise in the credit line; if the material is not included under the Creative Commons license, users will need to obtain permission from the license holder to reproduce the material. To view a copy of this license, visit <http://creativecommons.org/licenses/by/4.0/>

© The Author(s) 2016

## 第 17 章

## 皮膚以外に存在するメラノサイトの機能

矢崎伊知朗・大神信孝・山本博章・加藤昌志

メラノサイトが皮膚以外の種々の器官にも存在することはよく知られている。たとえば、メラノサイトは中間細胞として内耳血管系にも存在し、皮膚に存在するメラノサイトが紫外線に反応してメラニンを産生して皮膚を防御するがごとく、騒音刺激に対してメラニンを産生することにより難聴の発症を防御する機能をもつ可能性が提案されている。しかし、皮膚以外の種々の器官に存在するメラノサイトの機能についてはいまだ不明な点も多い。本章では、眼、耳、心臓などのその他の器官に存在するメラノサイトに焦点をあて、最新の知見を紹介しながら皮膚以外の器官に存在するメラノサイトの機能を考察する。

## 17.1 耳に存在するメラノサイトの機能

## 17.1.1 内耳に存在するメラノサイト

われわれ哺乳動物の内耳は、蝸牛とよばれる特徴的な構造を有している。内耳は頭頭骨に存在し、その外側の殻は骨包とよばれ、「カタツムリ」の殻と同様、硬組織からなっている。内耳の内側には管状の構造をもつ蝸牛管がうずまき状に配置されている。蝸牛管の内側は、基底板とライズネル膜によって、前庭階、中央階、鼓室階とよばれる3つの空洞(管)に隔てられている(図17.1)。これら3つの階はそれぞれリンパ液が充填されており、蝸牛の頂回転部でつながっている前庭階と鼓室階には外リンパ液が、中央階には内リンパ液が充填されている。このような特殊な構造が、内耳の形態解析を難しくさせる一因だと思われる。内リンパ液はカリウムレベルが高い特徴をもち、血管系はその維持に重要な役割を担っている。いわゆる聴覚に重要な役割を担うコルチ器は、有毛細

胞、ラセン神経節、血管系などにより構成されていることが知られているが、血管系は基底膜、中間細胞、辺縁細胞の3種の細胞から構成される<sup>1)</sup>。

有色動物の中間細胞の細胞内にはメラニン顆粒が観察され(図17.2)、この中間細胞が内耳のメラノサイトであることが知られている。中間細胞の由来は神経冠(neural crest)だと報告されている<sup>2)</sup>。中間細胞にはカリウムチャンネルなど豊富な発現しており、中間細胞が先天的に欠損しているマウスでは、血管系の層構造も薄く、内リンパ電位の異常をきたすため、先天性難聴を発症する(図17.3)。一方、内耳には平衡感覚に重要な前庭とよばれる感覚器も存在する。前庭の卵形囊と球形囊には平衡斑とよばれる部位があり、その部位にも暗細胞とよばれるメラノサイトが存在し、ギャップ結合を形成していることが報告されている<sup>3)</sup>。

## 17.1.2 血管系に存在する中間細胞の機能

内耳の中央階の内リンパ電位は細胞外液である

García, A., González-Sánchez, B., Körf, B. R., Kuster, W., Moss, C., et al.: *Am. J. Med. Genet. A*, 122A, 125-132, 2003.

Losada, J., Sagraera, A., Read, A. P., Sánchez-García, I.: *Hum. Mol. Genet.*, 11, 3231-3236, 2002.

66) Sánchez-Martín, M., Pérez-Losada, J., Rodríguez-

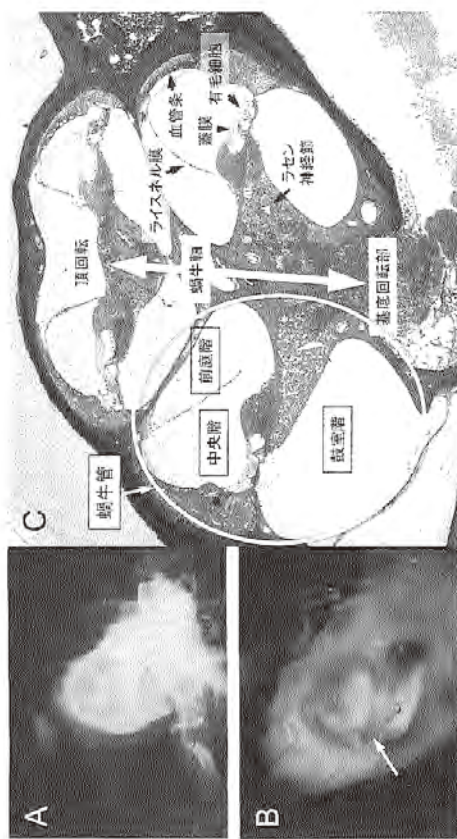


図 17.1 マウス内耳の構造 (A) マウスから抽出した内耳。(B) 骨包除去後の内耳標本の内部構造。(矢印) らせん状に連なったコルチ器の露出像が観察される。(C) 内耳切片のトルイジンブルー染色像。蝸牛管は中央階、前庭階、鼓室階からなる (白丸部分)。中央階はライスイスネル膜より前庭階と隔たれており、その中に有毛細胞、莖毛、および色素細胞 (中間細胞) が存在する血管系などが存在する。

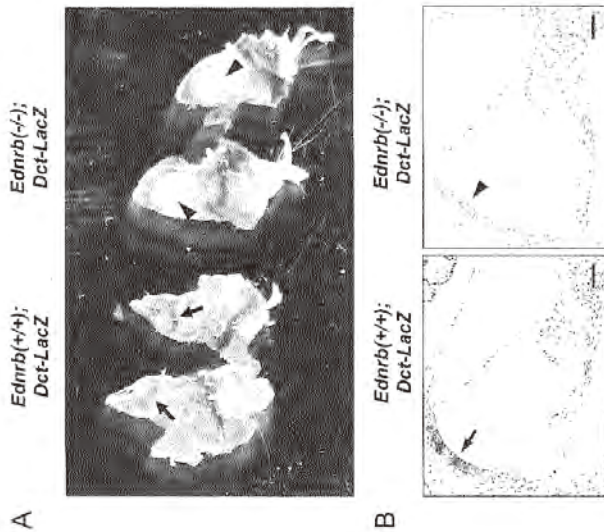


図 17.3 LacZ 染色による内耳色素細胞の検出

(A) *Ednrb*(+/+) マウス。LacZ トランスジェニックマウスの内耳の LacZ 染色。帯状に観察される LacZ 陽性の色素細胞は (左, arrows), *Ednrb* を欠損させると観察されず、先天性に色素細胞が欠損していることがわかる (右, arrowheads)。(B) 内耳切片の LacZ 陽性の色素細胞像。血管系に隣接細胞が観察されるが (左, arrow), *Ednrb* を欠損させると観察されない (右, arrowhead)。対比染色はヘマトキシリン。スケールバー = 20  $\mu$ m。[文献 12 より一部改変]

先天性難聴で血管系のタイロジジャンクシオンの形態異常および内リンパ電位異常が報告されている。中間細胞は血管系の中で毛細血管の周皮・内皮、基底細胞などとギャップ結合でつながっている一方、辺縁細胞とはギャップ結合は形成していないことが知られている。つまり、血管系の間細胞 (メラノサイト) は、メラニン生成よりむしろ、中間細胞に発現するイオンチャンネルや細胞間のタイロジジャンクシオン形成により、内リンパ電位、そして聴覚機能の維持に貢献していると考えられている。一方、従来血管系には前述した 3 種類の細胞から構成されていると考えられてきたが、これらの他にも血管周囲にマクロファージ様のメラノサイトが存在することがわかってきた。この細胞は分子重 50 kDa の糖タンパク質である pigment epithelium growth factor (PEDF) を分

泌し、タイロジジャンクシオンの安定化と内リンパ電位の維持に重要な役割を担っていることが明らかにになっている<sup>5)</sup>。遺伝子改変マウスを用いて、血管系に発現するこの細胞を後に除去すると、内リンパ電位および聴力レベルの著しい低下がみられたことから、この細胞は聴覚系に必須の細胞のひとつであることが示唆されている<sup>6)</sup>。また、PEDF をマウスに静脈内投与すると、聴覚性難聴の予防効果を示すことが報告されている<sup>6)</sup>。この細胞が皮膚に存在するマクロファージやメラノサイトと同様の機能を有するか今後の研究の進展に期待される。

17.1.3 先天性色素異常症と聴覚障害

チャールズ・ダーウィンの代表的著書『種の起源』の中で、眼の虹彩の色が左右で異なる猫が種

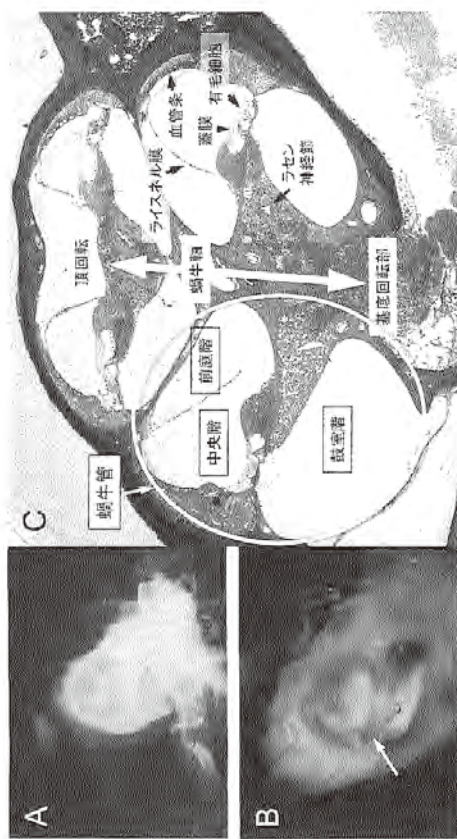
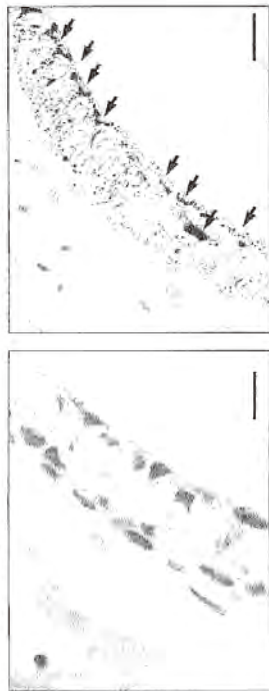


図 17.2 マウスの内耳血管系のメラニン顆粒

(A) ニッセル染色。ニッセル染色や H&E 染色した 3 週齢のマウスの内耳標本を光学顕微鏡で観察しても、メラニン顆粒はほとんど観察できない。(B) フォンタナマッソン染色。メラニンの特殊染色により、多くのメラニン顆粒が観察される (矢印)。同染色とも、3 週齢の野生型マウス (C57/BL6 系統) の内耳パラフィン切片を用いた。スケールバー = 20  $\mu$ m。

A ニッセル染色 B フォンタナマッソン染色



にもかわかず、カリウム濃度が高く維持されている。また、内リンパ直流電位とよばれる陽性電位を有しており、これらが蝸牛マイクログフォン電位を増幅し聴覚に寄与していると考えられている。血管系の間細胞には  $K_{ir4.1}$  などのカリウムチャンネルが発現しており、辺縁細胞の基底脚に供給し、辺縁細胞は  $Na^+/K^+-ATPase$  などに

B 12ヶ月齢



A 1ヶ月齢



図 17.4 加齢に伴い増加する内耳メラニン像

(A) 1ヶ月齢のマウス (C57/BL6系統) の内耳ではメラニン顆粒はほとんど観察できないが、(B) 12ヶ月齢では、メラニンの特殊染色をしながらも、光学顕微鏡下で多数のメラニン顆粒を観察できる (矢印)。両標本ともにニッソル染色を

ラニン量が増加することが知られている (図 17.4)。一方、遺伝子改変マウスを用いた解析により L-DOPA などメラニン前駆体が加齢性難聴や騒音性難聴に予防効果を示す報告もあるが<sup>18)</sup>、加齢あるいは環境因子により増加する内耳メラニンの生理的意義は依然として不明な点が多い。内耳のメラニンは、環状因子を担荷した際の内耳機能「保護因子」として内耳機能の維持に貢献しているのかもしれない。

17.1.5 まとめ

聴覚と平衡感覚を担う重要な感覚器官である内耳にもメラノサイトが存在する。前庭に存在するメラノサイトはギャップジャンクション形成に寄与していることが知られているが、その機能については不明な点が多い。蝸牛の血管条に存在するメラノサイトは、カリウムチャネルによる内リンパ電位の維持と細胞間のタイトジャンクション形成により聴覚に寄与する。

17.2 心臓その他の器官に存在するメラノサイトの機能

17.2.1 心臓その他の器官に存在するメラノサイトの分布
皮膚以外に存在するメラノサイトの分布について

ウス [Ednrb(-/-)] が報告されている。これらの共通する表現型として、先天性難聴を含む WS の主症状に加えて、先天性巨大結腸症 (ヒルシュシュブルグ病) も伴い、典型的な WS4 型の表現型を示すことが報告されている。ヒトにおいても、EDNRB のエキソン 3 に変異をもつ患者は WS4 を発症し、先天性難聴も伴うことが報告されている。一方、われわれの解析によると、Ednrb タンパク質は血管条のメラノサイトだけではなくラセン神経節にも発現しており、Ednrb (-/-) マウスでは、血管条のメラノサイトの先天的欠損だけではなく、ラセン神経節の神経変性も伴うことが明らかになった。さらに、ラセン神経節を標的にして Ednrb を発現させると、Ednrb (-/-) マウスの先天性難聴を部分的にレスキューできることがわかった<sup>20)</sup>。つまり、内耳蝸牛に発現する Ednrb は血管条の中間細胞の発達だけではなく、ラセン神経節の維持にも関与していると考えられる。

17.1.4 環境因子と内耳のメラニン

内耳機能に影響する代表的な環境因子は騒音であるが、その曝露により内耳の血管条に蓄積するメラニン顆粒が増加することが報告されている<sup>19)</sup>。皮膚のメラノサイトは、紫外線に曝露されるとメラニン合成を亢進し、紫外線などの環境因子に対して防御的に機能することにより生体の恒常性維持に貢献している。その防御機構には、メラニンの活性酸素を除去する作用が関与していると考えられている。一方、騒音曝露も内耳の酸化ストレスレベル上昇を招くことが示唆されていることから、騒音曝露により誘導されるメラニンは、内耳で発生する活性酸素の軽減に貢献している可能性もある。過去の報告によると、アルビノラットと有色ラットのあいだに聴性脳幹反応の測定値に有意な差はないと報告されている。また、有色と白色ラットやマウスを用いた検討では、内耳におけるメラニンの有無は少なくとも生理的条件下での経時的聴力変化には影響がないという報告もあるが、有色マウスでは加齢に伴い内耳のメ

226 第 17 章 皮膚以外に存在するメラノサイトの機能
覚障害を伴うことが記述されており、古くからその関連は認識されていた。その後、1951 年にオランダ人医師ワーデンブルグが虹彩・皮膚色素異常症と難聴を伴うヒトの症例を初めて報告した。この症候群はワーデンブルグ症候群 (Waardenburg syndrome: WS) とよばれ、先天性色素異常症と先天性難聴を伴い、その発症率は 10,000 ~ 20,000 人に 1 人の割合で発症すると報告されている<sup>7,8)</sup>。WS は、原因遺伝子や WS のおもな症状 (皮膚白斑、虹彩異色、先天性難聴) に随伴する症状により、おもに 4 つのタイプに分類されている。顔面形態形成異常も伴う WS1 型は PAX3 遺伝子の異常により、WS2 型は microphthalmia-associated transcription factor (MITF) 遺伝子の変異により発症する。また、上肢の形成不全も伴う WS3 型 (別名、Klein-Waardenburg 症候群) は PAX3 遺伝子の変異により誘発することが知られている。PAX3、MITF ともにメラノサイト分化を制御する転写因子で、PAX3 は paired box と homeobox 構造を、MITF は basic-helix-loop-helix-leucine zipper (bHLHZip) 構造をもつことが報告されている。Waardenburg-Shah syndrome (WS 4 型、WS-IV) は転写因子 SOX10<sup>9)</sup>、エンドセリン 3 (endothelin: ET-3)<sup>10)</sup>、あるいはエンドセリン受容体 B (endothelin receptor B: EDNRB)<sup>10)</sup> などの変異により発症し、先天性色素異常症、先天性難聴と巨大結腸症を伴う。Ednrb は G タンパク質共役型受容体ファミリーに属し、エンドセリンによる多様な生理機能に重要な役割を担う<sup>10,11)</sup>。Ednrb/EDNRB の先天的異常は神経由来のメラノサイトおよび腸管神経への発達に重大な障害をきたし、先天性の色素異常症、巨大結腸症、先天性難聴を引き起こす。WS4 型の動物モデルとして、Ednrb 遺伝子に変異をもつイントロン 1 に自然発症的な欠損をもつ sl マウス、エキソン 2 ~ 3 に自然発症的な欠損をもつ WS-IV マウス、あるいは遺伝子改変技術によりエキソン 3 を欠損させた Ednrb ノックアウトマ

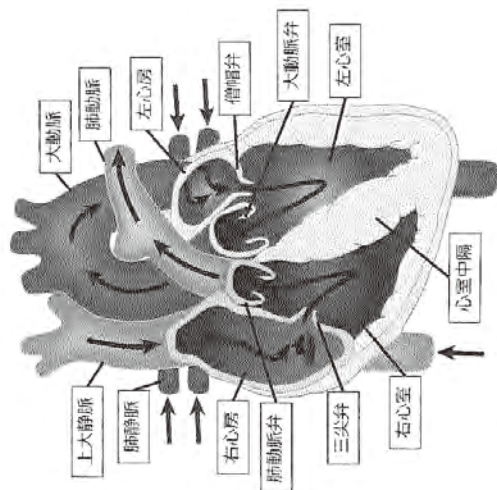


図 17.5 ヒト心臓の構造と名称  
矢印は血流を示す。

あるいはメラノサイト関連マーカー分子である *Det*, *Tyrpl*, *Mif* などに対する抗体を利用してメラノサイト特異的免疫染色によって心臓メラノサイトを同定している<sup>16-19, 21, 23</sup>。ヒトを含む哺乳類の多くは4つの部屋と4つの弁からなる心臓をもち、血流を循環させている(図17.5)。心臓メラノサイトは、マウスではおもに僧帽弁と三尖弁に存在し(図17.6)、他に大動脈弁、肺動脈弁、心室中隔、心房内部表面での存在が報告されている<sup>16-20, 21, 23</sup>。ヒト心臓におけるメラノサイトの組織学的解析はほとんど報告がないが、2009年、Levinらはヒト肺動脈弁に存在するメラノサイトについて報告している<sup>17</sup>。8つのヒトの肺動脈弁検体について抗DCT抗体を用いた免疫組織学的解析を行ない、すべての検体でDCT陽性メラノサイトを検出している。ただし、これらのDCT陽性細胞ではメラニン沈着は認められず、TYRP1陰性である<sup>17</sup>。

### 17.2.2 心臓メラノサイトの起源

心臓メラノサイトについて、これまでに遺伝子改変マウスを用いた研究がいくつ報告されている。メラノサイトの異常増殖やメラノーマ発症に関与する活性化型NRASをメラノサイト特異的に過剰発現するマウス(*Tyr::NRas<sup>G60S</sup>*)<sup>27</sup>や、メラノサイトの増殖、分化、メラニン合成などに関与する *endothelin 3* (*EDN3*), *hepatocyte growth factor* (*HGF*) を皮膚メラノサイトで特異的に過剰発現するマウス (*hK14::EDN3*, *hK14::HGF*)<sup>28, 29</sup> は、皮膚がメラノサイトに覆われた *hyperpigmentation* を呈するが、これらのマウスの心臓の僧帽弁と三尖弁でも同様に過剰なメラニン沈着が観察されている<sup>23</sup>。安定型  $\beta$ -catenin をメラノサイト特異的に発現するマウス (*bcnl<sup>tm</sup>*) は体毛の *hyperpigmentation* を呈するが、心臓のメラノサイトも同様にメラニン沈着レベルが減少する<sup>23</sup>。メラノサイトで発現し、増殖、分化、生存、メラニン合成などに関与するタンパク質である *Mitf* や *Ednrb*, *Kit* の突然変異マウス (*Mitf<sup>cre/cre</sup>*, *Ednrb<sup>cre/cre</sup>*, *Kit<sup>cre/cre</sup>*) は毛包内を含む皮膚メラ

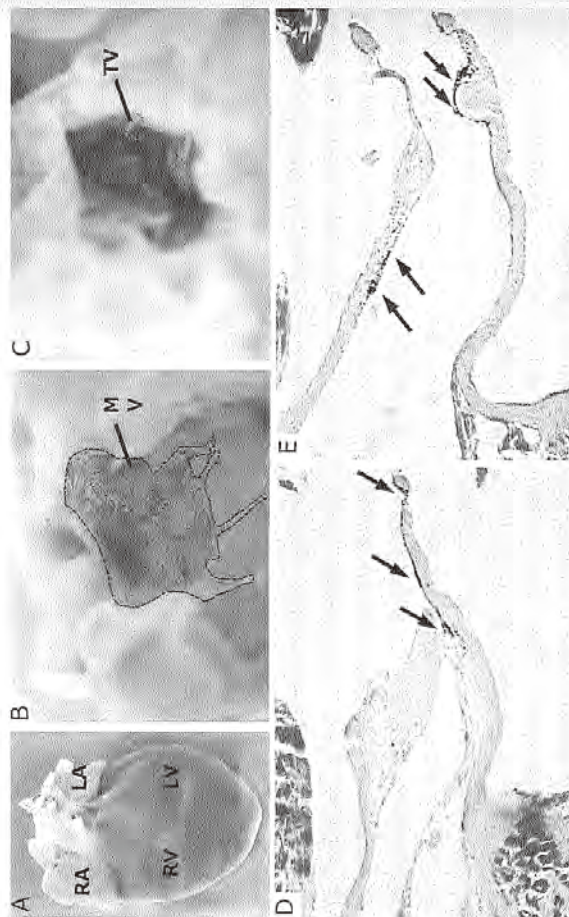


図 17.6 マウス心臓メラノサイトの分布

心臓メラノサイトはさまざまな場所に存在するが、とくに心臓弁で多くみられる。(A) 生後28日のマウス心臓の外観。僧帽弁(B, D) および三尖弁(C, E) のメラノサイトを。切片(D, E) の矢印がメラニン沈着を示す。LA: 左心房, LV: 左心室, MV: 僧帽弁, RA: 右心房, RV: 右心室, TV: 三尖弁。

ノサイトの多く、あるいはすべてが欠損するが、これらのマウスの心臓においてもメラノサイトは失われる<sup>16, 20</sup>。このように、心臓メラノサイトの分化、増殖、メラニン合成は、皮膚メラノサイトと同様の分子機構で制御されており、皮膚メラノサイトに類似した表現型を示している。

皮膚メラノサイトは *neural crest* (神経冠) 細胞を起源として移動・増殖のあと分化するが、心臓には *neural crest* 細胞を起源とした細胞が存在する。この *cardiac neural crest* 細胞はおもに *outflow tract* (OFT, 心臓流出路) の発生に寄与し、流出路中隔を形成することで大動脈および肺動脈が形成される<sup>30</sup>。この *neural tube* (神経管) から心臓への *cardiac neural crest* の「大移動」において、*melanoblast* (メラノブラスト) も同様に心臓へと移動する。*Def::LacZ* マウスを利用して胚発生中の *melanoblast* の位置を確認すると、胎生期11.5日(E11.5)では *cardiac neural crest* の移動先である OFT に *melanoblast* が集団で確認できる(図17.7A)。E13.5, E16.5では *melanoblast* の一部は心臓弁の一部侵入し<sup>17</sup>, E18.5では心臓弁および卵円孔 (*foramen ovale*) に多くの *melanoblast* が存在するようになる(図17.7B, C)。また、*neural crest* で発現する *Wnt1* (*Wnt1::Cre*) と、*CAG-CAT-EGFP* レポーターマウスを交配により *cardiac neural crest* を GFP ラベルすると、大動脈弁、肺動脈弁において GFP 陽性細胞は *Tyrpl* 陽性であり、メラノサイトであることを示している<sup>19</sup>。上記のようなさまざまな解析から、心臓メラノサイトは *neural crest* 由来であり、皮膚メラノサイトと同質の表現型を保ちつつ、*cardiac neural crest* の移動とともに心臓で分化することが明らかとなっている。

### 17.2.3 心臓メラノサイトの機能

心臓メラノサイトの機能については、これまでほとんど報告がないが、近年になって興味深い2

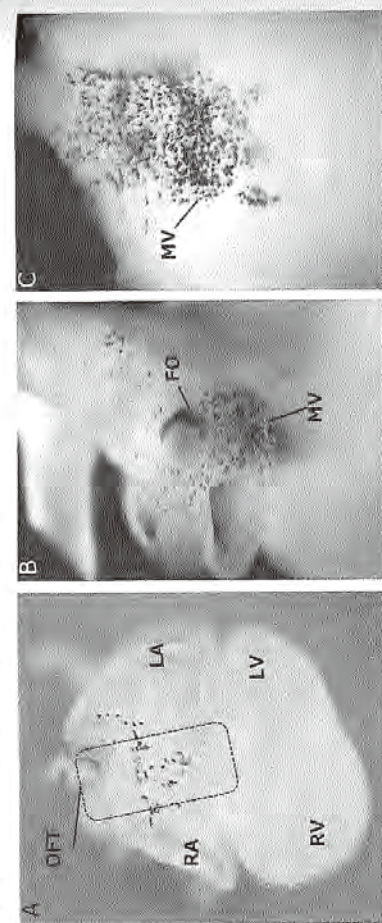


図 17.7 胎生期の心臓に存在するメラノプラスト  
 心臓形成期に outflow tract (OFT, 心臓流出路) が neural crest によって形成する際にメラノプラストも移動する。  
 $\beta$ -galactosidase 発色による *Def::LacZ* マウス心臓におけるメラノプラストの分布。(A) E11.5 のメラノプラスト。おもに  
 OFT に分布する。E18.5 の卵巣 (B) および卵巣弁 (C) では多くのメラノプラストが存在している。FO: 卵巣孔  
 (foramen ovale), LA: 左心房, LV: 左心室, MV: 卵巣弁, RA: 右心房, RV: 右心室。

つの研究が報告されている。2009年, Levinらは、  
 心臓メラノサイトがメラニン産生酵素の一つであ  
 る *Def* (*dopachrome tautomerase*) を介して心  
 房細胞由来の不整脈発症と関係していることを報  
 告している<sup>17)</sup>。*Def* ノックアウトマウス (*Def<sup>-/-</sup>*)  
 に対し心房へのパルスをベータシグナルとして用いた *Def*  
 誘導を行なうと、コントロールとして用いた *Def*  
 ヘテロマウス (*Def<sup>+/-</sup>*) では心房性不整脈が誘導  
 されたマウスは8%であったが、*Def<sup>-/-</sup>* マウスで  
 は80%以上の個体で不整脈が発生する。また、  
 定常状態の *Def<sup>+/-</sup>* マウスでは50%の個体に心房  
 性頻脈が観察される。一方、心房性不整脈の発症  
 頻度やその他の心機能に差はなく、心臓に構造的  
 欠陥も認められない。Levinらはさらに、メラノ  
 サイトの発生・分化・増殖に関与する *Klf* 変異体  
 マウス (*W/W<sup>fl</sup>*) が心臓メラノサイトを消失して  
 いる点を利用して、上記の心房不整脈誘導を行  
 なった。興味深いことに、コントロールマウス  
 (*Def<sup>+/-</sup>*)、*Klf* 変異体マウス (*W/W<sup>fl</sup>*)、*Def<sup>-/-</sup>* およ  
 び *Klf* 変異体マウス (*W/W<sup>fl</sup>*) マウス (*Def<sup>-/-</sup>*; *W/  
 W<sup>fl</sup>*) のあいだで心房不整脈の発生率に有意な差  
 は認められず、正常なメラノサイトの存在の有無  
 は心房性不整脈の発生率に影響しないことを示し  
 ている。つまり、*Def* を発現しない「異常な」メ  
 ラノサイトの存在が心房不整脈の発生率を上昇さ  
 せている原因であると考えられる。心臓メラノサ  
 イトはメラノサイト特異的タンパク質を発現する  
 だけでなく、アドレナリン受容体やムスカリン受  
 容体を発現し、かつ交感神経および副交感神経と  
 隣接しているという、きわめてユニークな配置・  
 性質をもっている。ムスカリンアンゴニストであ  
 るプロプラノロール投与による心房不整脈誘導・  
 拮抗実験が行なわれ、正常な心臓メラノサイトを  
 もつ野生型マウスと心臓メラノサイトを欠失して  
 いる *W/W<sup>fl</sup>* マウスでは、野生型マウスのほうが  
 より心房性不整脈が発生しやすいことが明らかと  
 なっている。また、心臓メラノサイトは皮膚メラ  
 ノサイトと同様<sup>18)</sup>、電位依存性イオンチャネル  
 をもつが、*Def<sup>-/-</sup>* マウスの心臓メラノサイトは活  
 動電位異常を示し、その異常は隣接する心筋の活  
 動電位にも影響を与える。このように、心臓メラ  
 ノサイトに心臓にも影響を及ぼしており、*Def* の機能  
 が欠損したメラノサイトはその制御に異常をきたし、結果と  
 して心房性不整脈を誘発する。それでは、心臓機

能における心臓メラノサイトが発現する *Def* の  
 役割とは何だろうか。Levinらはその答えとし  
 て *Def* の抗酸化機能について言及している。メ  
 ラニン合成経路の中間産物である DOPAchrome  
 は自発的反応により DHICA へと変換する。DHICA は  
 DHI よりも酸化毒性が低く、このため *Def* には  
 抗酸化機能をもつことが報告されている<sup>16)</sup>。  
 Levinらは抗酸化剤 *tempol* を *Def<sup>-/-</sup>* マウスに1  
 週間事前投与したのちに心房性不整脈誘導実験を  
 行なうと、不整脈発生率が劇的に減少することを  
 示し、*Def<sup>-/-</sup>* マウスでは *Def* による抗酸化機能  
 が失われたために不整脈発生率が増加すること  
 がある。*Def* による DOPAchrome の DHICA への  
 変換は DHI の毒性を減少することで抗酸化機能  
 を発揮するとしているが、それ以外の抗酸化機能  
 は不明であり、*Def* の心臓メラノサイトにおける  
 機能については今後より詳細な研究が必要であ  
 る。

上記の報告は元来存在する心臓メラノサイトの  
 機能に關するものであるが、2013年, Yajimaらは、  
 $\beta$ -catenin のメラノサイト系特異的活性化に  
 よって異所的に分化した心臓メラノサイトが心臓  
 機能に影響することを報告している<sup>20)</sup>。メラノ  
 サイト特異的に *Cre ricombinase* を発現するマウ  
 ス (*Tyr::Cre*)<sup>21)</sup> と、*Cre ricombinase* によって  
 安定化した  $\beta$ -catenin を発現し、*Wnt* シグナルを  
 活性化するマウス (*cnnb1Δex3<sup>+/+</sup>*)<sup>22)</sup> の交配によっ  
 て生じたマウス (*Tyr::Cre; cnnb1Δex3<sup>+/+</sup>*) は、  
 動脈管閉塞 (patent ductus arteriosus; PDA)  
 および左心房・左心室肥大を発症し生後3カ月以  
 内に死亡する。動脈管 (ductus arteriosus; DA)  
 は胎児期にのみ機能する血管で、大動脈と肺動脈  
 をバイパスしている。左心房と左心室をバイパス  
 する卵円孔とともに機能し、肺呼吸のできない胎  
 児が肺の緒を通じて母体から酸素などを取り込ん  
 だ際に、新鮮な血液を速やかに体中に行き渡らせ  
 るためのバイパス路となる (図17.8A)。出生後、  
 肺呼吸開始とともに血中酸素濃度が上昇し、それ  
 がシグナルとなって動脈管はきわめて短時間で閉

鎖する。閉鎖は筋収縮と細胞移動によって行なわ  
 れ、肺呼吸に適應した血流を生み出す (図  
 17.8B)。動脈管閉塞は出生時の動脈管閉鎖不全  
 によって大動脈から肺動脈へ血液の流入 (左右  
 シャント) が生じ、肺動脈の血圧上昇、左心房・  
 左心室肥大を呈する (図17.8C)。ヒトの動脈管閉  
 塞症は未熟児に多く、1500グラム以下の極低出  
 生体重児では40%以上が発症するという報告も  
 ある<sup>23)</sup>。*Tyr::Cre; cnnb1Δex3<sup>+/+</sup>* マウス (以降、  
*PDA* マウス) は、動脈管閉塞と共に左心房・左  
 心室肥大も観察され (図17.9B)、ヒトの動脈管閉  
 塞症と類似した形態であることを示している。生  
 後直後の野生型マウスの動脈管は閉鎖している  
 (図17.9C) が、*PDA* マウスの動脈管は閉鎖が不  
 十分であり、多くの異所的なメラニン沈着が見ら  
 れる (図17.9D)。*Def::LacZ* マウスの交配により、  
 発生中のメラノプラストを可視化すると、野生型  
 マウスではメラノプラストは観察されない (図  
 17.9E) が、*PDA* マウスでは異所的なメラノプラ  
 ストが多数観察される (図17.9F)。動脈管の平滑  
 筋細胞は出生後の閉鎖に必須であり、その起源は  
 neural crest 細胞に由来する。*PDA* マウスの動  
 脈管における平滑筋細胞数と異所的に存在するメ  
 ラノサイトの数を測定すると、野生型に比べて平  
 滑筋細胞数は減少し、その分をメラノサイトが埋  
 めていることが判明しており、動脈管におけるメ  
 ラノサイトの異所的な分化が動脈管閉塞を引き  
 起こしている可能性が示唆されている。Yajima  
 らはさらに、メラノサイトを欠失する *Mif* 変異  
 体マウス (*Mif<sup>neo</sup>/Mif<sup>neo</sup>*) と *PDA* マウスとの  
 交配により作成したマウス (*Tyr::Cre; cnnb1  
 Δex3<sup>+/+</sup>; Mif<sup>neo</sup>/Mif<sup>neo</sup>*) もまた動脈管閉塞症  
 を発症することを示している。*PDA* マウスにお  
 ける動脈管閉塞症の発症は、動脈管における異所  
 的なメラノサイトの分化が動脈管の平滑筋細胞数  
 を減少させることが原因であると考えられる。動  
 脈管の平滑筋細胞 (SMC) にはその発生段階に  
 おいて tyrosinase プロモーターが活性化しない  
 細胞集団 (SMCI) と、活性化し、*PDA* マウス  
 では異所的なメラノサイトに分化可能な細胞集団

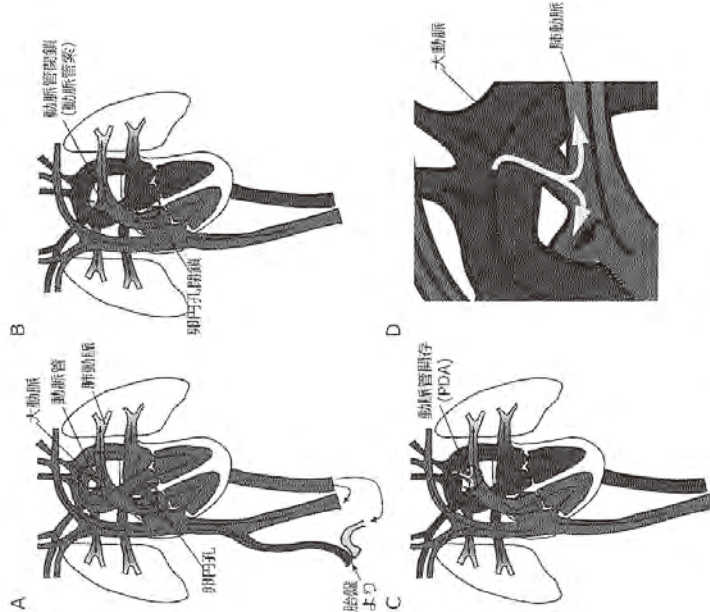


図 17.8 胎生期および出生後の心臓における血液の流れと動脈管閉鎖  
詳しくは本文を参照のこと。

(SMC2)が存在する。SMC2の起源となる neural crest 細胞集団は平滑筋細胞とメラノサイトに分化可能な bipotent な細胞であり、PDA マウスでは  $\beta$ -catenin の安定化により Wnt シグナルが活性化することでメラノサイトが分化し、結果として SMC2 は失われる。この SMC2 の存在あるいは機能が正常な動脈管の閉鎖に必須ではないかと考えられる。

心臓その他の器官に存在するメラノサイトに関する知見はいまだ少ない。心臓メラノサイトについては近年、その存在がクロームズアップされつつあるが、特定の動物種に限定された情報であり、その機能についてはユニークな機能をもつことが示唆されているものの、不明な点も多い。しかし、今後も注目し、より多くの研究を行なうことでこ

れまで知られていなかった新たなメラノサイトの機能が明らかになるのではないかと期待している。

### 17.3 眼に存在するメラノサイトの機能

胚発生時に高い移動能をもつメラノブラスト (メラノサイト) は、眼球の外縁部に位置する (網膜の外側を構成する) 脈絡膜にも多く定着する (第7章図 7.3 参照)。ぶどう膜の後部を構成する脈絡膜は、網膜と強膜のあいだの層で、豊かな脈管系構造をもつ組織であり、メラノサイトは脈管系の周囲を幾重にも覆うように分布する。

Nickla と Wallman は彼らの最近のレビューで、脈絡膜の機能として、網膜周囲への脈管機能の提

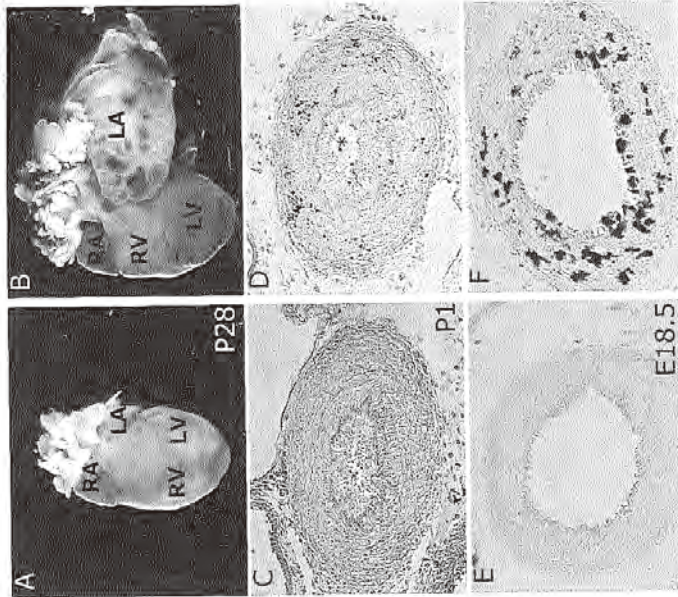


図 17.9 Tyr::Cre: *ctnmb1aex3* / + マウスの動脈管閉鎖による左心房・左心室肥大と異所的なメラノサイトの分布

生後 28 日の Tyr::Cre: *ctnmb1aex3* / + マウス (PDA マウス, B) は、野生型マウス (A) と比較して左心房、左心室の肥大が観察される。生後 1 日のマウスでは野生型マウスの動脈管は閉鎖している (C) が、PDA マウスでは閉鎖し (アスタリスタ in D)、異所的なメラニン沈着が観察される (D)。PDA マウスと *Dox::LacZ* マウスの交配によって作成されたマウスの胎生期 E18.5 の心臓では異所的なメラノブララスト ( $\beta$ -galactosidase 染色による) が観察される (F)。野生型マウスでは動脈管にメラノブララストは観察されない (E)。LA: 左心房, LV: 左心室, RA: 右心房, RV: 右心室。

供が大きく、この機能欠損による酸素供給不足は加齢 (性) 黄斑変性症を引き起こす可能性があること、さらには、他のどの臓器に比べても勝ることも劣らない血流量が、網膜を冷やし、また温める機能を発揮する可能性があることについて述べている<sup>36)</sup>。さらに彼らは、脈絡膜が血管新生や、脈絡膜の外側に位置する強膜の成長を調節する可能性のある分泌細胞を産すること、また、脈絡膜の「厚さ」を変化させることで、網膜を前後に動かす、視細胞を焦点面に位置させる働きもあることも紹介している。

脈絡膜の脈管系領域は、外側には大きな血管系

が、内側には中規模また小規模の動脈や細動脈が走っている。この脈管系の周囲の間質には、コラーゲンや elastic な繊維、繊維芽細胞、非脈管系の平滑筋細胞、それに多数の巨大なメラノサイトが血管に密着して配置されている。これらメラノサイトの機能は、メラニン合成以外によくわかっていない。しかしながら、メラノサイトに発現するエンドセリン B レセプターが、エンドセリン 1 に誘導されたカルシウムイオンの流入を伸介する可能性を紹介している。この機能的な意義も現時点においては不明ではある<sup>36)</sup>。

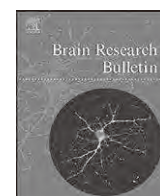
なお、メラノサイトによって、脈絡膜は暗い色

を呈する。組織観察の際に抽出した眼球を光にかざしてみると、たとえばC57BL/6と、同じ遺伝的背景に*Mitf<sup>cre/+</sup>*のアレルをホモにもちメラノサイトを欠損する黒眼白毛色マウス(第7章図7.3参照)由来の眼球を、それぞれ視神経側から見る。通常では、発生中の細胞に由来する一層の網膜色素上皮と、その外側に位置する神経冠(莖)由来のメラノサイトの2種類の色素細胞層が、外光を強力にブロックしていることになり、両系統では、眼球の外側(奥側)に到達する光量も大きく異なるはずである。これをみても、脈絡膜メラノサイトは「何か」役割をもっているにちがいないと「感じる」のである。ちなみに、この層の「色の濃さ:明るさ」は種によって異なるようだ<sup>8)</sup>。色素細胞を研究対象とする立場からすると、これほど多くのメラノサイトが、多機能な脈絡膜の機能に寄与しないとはとうてい思えない。解明が待たれるところである。

## 参考文献

- 1) 小林俊光・重野浩一郎・中尾善亮・柳山幸彦・NEW耳鼻咽喉科・頭頸部外科学(改訂第2版)(著者村勉・森山寛 編) 1-9, 南江堂, 2007.
- 2) Hilding D. A., Günsberg, R. D.: *Acta Otolaryngol.* 84, 24-37, 1977.
- 3) Masuda, M., Yamazaki, K., Toyama, Y., Kanazaki, J., Hosoda, Y.: *Anat. Rec.* 246, 8-14, 1996.
- 4) Nim, F., Hibino, H., Doi, K., Suzuki, T., Hisa, Y., Kurachi, Y.: *Proc. Natl. Acad. Sci. USA*, 105, 1751-1755, 2008.
- 5) Zhang, W., Dai, M., Fridberger, A., Hassan, A., Degagne, J., Neng, L., Zhang, F. et al.: *Proc. Natl. Acad. Sci. USA*, 109, 10388-10393, 2012.
- 6) Zhang, F., Dai, M., Neng, L., Zhang, J. H., Zhi, Z., Fridberger, A., Shi, X.: *FASEB J.* 27, 3730-3740, 2013.
- 7) Pardono, E., van Bever, Y., van den Ende, J., Havrenne, P. C., Iughetti, P., Maestrelli, S. R. P., Costa, F. O. et al.: *Am. J. Med. Genet. A* 117A, 223-235, 2003.
- 8) Pingault, V., Bondurand, N., Kuhlbrodt, K., Goerich, D. E., Prehn, M. O., Püschel, A., Herbarth, B. et al.: *Nat. Genet.* 18, 171-173, 1998.
- 9) Edery, P., Attie, T., Amiel, J., Pelet, A., Eug. C., Hoisra, R. M. W., Martelli, E. et al.: *Nat. Genet.* 12, 442-444, 1995.
- 10) Hosoda, K., Hammer, R. E., Richardson, J. A., Baynash, A. G., Cheung, J. C., Gaid, A., Yanagisawa, M.: *Cell* 79, 1267-1276, 1994.
- 11) Bagnato, A., Spinella, F., Rossato, L.: *Endocr. Relat. Cancer*, 12, 761-772, 2005.
- 12) Ida-Eto, M., Ohgami, N., Iida, M., Yajima, I., Kamatsuka, M. Y., Takaie, K., Kimitsuki, T. et al.: *J. Biol. Chem.* 286, 28621-28626, 2011.
- 13) Tachibana, M.: *Pigment Cell Res.* 12, 344-354, 1999.
- 14) Murillo-Cuesta, S., Contreras, J., Zurita, E., Cediel, R., Cantero, M., Varela-Nieto, I., Montoliu, L.: *Pigment Cell Melanoma Res.* 23, 72-83, 2010.
- 15) Bardot, H. and Levine, S.: *Brain Res. Bull.* 10, 847-851, 1983.
- 16) Brito, F. C., Kos, L.: *Pigment Cell Melanoma Res.* 21, 464-470, 2008.
- 17) Levin, M. D., Lu, M. M., Petrenko, N. E., Hawkins, B. J., Gupta, T. H., Lang, D., Buckley, P. T. et al.: *J. Clin. Invest.* 119, 3420-3426, 2009.
- 18) Mjatsvedt, C. H., Kern, C. B., Norris, R. A., Fahey, S., Cave, C. L.: *Anat. Rec. A Discov. Mol. Cell Evol. Biol.* 285, 748-757, 2005.
- 19) Nakamura, T., Colbert, M. C., Robbins, J.: *Chr. Res.* 98, 1547-1554, 2006.
- 20) Nichols, S. E., Jr., Reams, W. M., Jr.: *J. Embryol. Exp. Morphol.* 8, 24-32, 1960.
- 21) Puig, I., Yajima, I., Bonaventure, J., Delmas, V., Larue, L.: *Pigment Cell Melanoma Res.* 22, 331-334, 2009.
- 22) Yajima, I., Colombo, S., Puig, I., Champeval, D., Kumasaka, M., Belloir, E., Bonaventure, J. et al.: *PLoS One* 8, e53183, 2013.
- 23) Yajima, I., Larue, L.: *Pigment Cell Melanoma Res.* 21, 471-476, 2008.
- 24) Gebarski, S. S., Blaiwas, M. A.: *AJNR Am. J. Neuroradiol.* 17, 55-60, 1996.
- 25) Elchevers H. C., Couly, G., Vincent, C., Le Douarin, N. M.: *Development*, 126, 3533-3543, 1999.
- 26) Kadonaga, J. N., Fritsch, I. J.: *J. Am. Acad. Dermatol.* 24, 747-755, 1991.
- 27) Ackermann, J., Fritsch, M., Kaloupek, K., McKee, T., Trunpp, A., Beermann, F.: *Cancer Res.* 65, 4005-4011, 2005.
- 28) Kanisada, T., Yamazaki, H., Hirobe, T., Kamei, S., Omotono, M., Tagaya, H., Henmi, H. et al.: *Mech. Dev.* 94, 67-78, 2000.
- 29) Kanisada, T., Yoshida, H., Yamazaki, H., Miyamoto, A., Henmi, H., Nishimura, E., Shultz, L. D. et al.: *Development*, 125, 2915-2923, 1998.
- 30) Kirby, M. L., Gale, T. F., Stewart, D. E.: *Science* 220, 1059-1061, 1983.
- 31) Elmehag, B., Persson, B., Rorsman, P., Rorsman, H.: *Pigment Cell Res.* 7, 333-338, 1994.

- 32) Salinas, C., Garcia-Borrón, J. C., Solano, F., Lozano, J. A.: *Biochim. Biophys. Acta* 1204, 53-60, 1991.
- 33) Delmas, V., Martinuzzi, S., Bourgeois, Y., Holzenberger, M., Larue, L.: *Genesis* 36, 75-80, 2003.
- 34) Harada, N., Tamai, Y., Ishikawa, T., Sauter, B., Takake, K., Oshima, M., Takeito, M. M.: *EMBO J.* 18, 5931-5942, 1999.
- 35) Cotton, R. B., Stahlman, M. T., Kovar, L., Callerton, W. Z.: *J. Pediatr.* 92, 467-473, 1978.
- 36) Debora L. Nickla, Josh Wallman.: *Prog. Retin. Eye Res.* 29, 144-168, 2010.



## Research report

## Preventive effect of theanine intake on stress-induced impairments of hippocampal long-term potentiation and recognition memory



Haruna Tamano<sup>a</sup>, Kotaro Fukura<sup>b</sup>, Miki Suzuki<sup>a</sup>, Kazuhiro Sakamoto<sup>b</sup>,  
Hidehiko Yokogoshi<sup>b</sup>, Atsushi Takeda<sup>a,\*</sup>

<sup>a</sup> Graduate School of Pharmaceutical Sciences, University of Shizuoka, Global COE, Japan

<sup>b</sup> Graduate School of Nutritional and Environmental Sciences, University of Shizuoka, Global COE, Japan

## ARTICLE INFO

## Article history:

Received 3 August 2012

Received in revised form 24 January 2013

Accepted 20 February 2013

Available online xxx

## Keywords:

Theanine

Green tea

Recognition memory

Stress

LTP

Corticosterone

## ABSTRACT

Theanine,  $\gamma$ -glutamylethylamide, is one of the major amino acid components in green tea. On the basis of the preventive effect of theanine intake after birth on mild stress-induced attenuation of hippocampal CA1 long-term potentiation (LTP), the present study evaluated the effect of theanine intake after weaning on stress-induced impairments of LTP and recognition memory. Young rats were fed water containing 0.3% theanine for 3 weeks after weaning and subjected to water immersion stress for 30 min, which was more severe than tail suspension stress for 30 s used previously. Serum corticosterone levels were lower in theanine-administered rats than in the control rats even after exposure to stress. CA1 LTP induced by a 100-Hz tetanus for 1 s was inhibited in the presence of 2-amino-5-phosphonovalerate (APV), an N-methyl-D-aspartate (NMDA) receptor antagonist, in hippocampal slices from the control rats and was attenuated by water immersion stress. In contrast, CA1 LTP was not significantly inhibited in the presence of APV in hippocampal slices from the theanine-administered rats and was not attenuated by the stress. Furthermore, object recognition memory was impaired in the control rats, but not in theanine-administered rats. The present study indicates the preventive effect of theanine intake after weaning on stress-induced impairments of hippocampal LTP and recognition memory. It is likely that the modification of corticosterone secretion after theanine intake is involved in the preventive effect.

© 2013 Elsevier Inc. All rights reserved.

## 1. Introduction

Humans and animals are constantly exposed to environmental stress. Stressful life events are one of the causes of psychiatric disorders and are associated with suicidal behavior (Mann et al., 2005; Abreu et al., 2009). The hypothalamic–pituitary–adrenal (HPA) axis serves to respond to stress and controls glucocorticoid secretion from the adrenal gland (Keller-Wood and Dallman, 1984; Jacobson and Sapolsky, 1991; Linthorst and Reul, 2008). The HPA axis activation increases glucocorticoid secretion to maintain homeostasis in the living body through energy mobilization or to restore it (Chrousos and Gold, 1992; Chrousos, 2009). The hippocampus is enriched with glucocorticoid receptors, plays an important role in stress response in addition to cognitive function, and negatively modulates HPA axis activity (Kim and Yoon, 1998). However, the hippocampus is vulnerable to stress (McEwen, 1999; Garcia, 2001). Stress and glucocorticoids have diverse effects on cognitive behavior and synaptic plasticity such as long-term potentiation (LTP)

that is thought to be a potential cellular mechanism of memory (Howland and Wang, 2008). Studies on how acute stress and the stress-related hormones affect learning and memory have shown inconsistent findings, which might be due to some variables such as the properties of stressors, the nature of memory, the protocols for behavioral tasks, and the characteristics of the subjects (Cazakoff et al., 2010).

Tea is one of the most widely consumed beverages worldwide (Graham, 1992). The interest in green tea has grown for human health. Green tea has the putative benefits to brain function (Bolling et al., 2009; Gonzalez de Mejia et al., 2009). Theanine,  $\gamma$ -glutamylethylamide, is one of the major amino acid components in green tea and is synthesized from ethylamine and glutamate in green tea leaves (Terashima et al., 1999). It has been reported that theanine has an impact on brain function (Haskell et al., 2008; Kelly et al., 2008; Einöther et al., 2010; Kakuda, 2011). It can counteract excitotoxicity and/or mitochondrial radical formation. Theanine intake might lead to neuroprotective effects (Egashira et al., 2004; Cho et al., 2008; Di et al., 2010). Furthermore, theanine may improve cognitive function; an experimental study indicates that 0.3% theanine administration facilitates hippocampal neurogenesis in the developing rats, followed by enhanced recognition memory (Takeda et al., 2011b). It is likely that theanine

\* Corresponding author. Tel.: +81 54 264 5700; fax: +81 54 264 5705.  
E-mail address: [takedaa@u-shizuoka-ken.ac.jp](mailto:takedaa@u-shizuoka-ken.ac.jp) (A. Takeda).

intake has benefits to the postnatal development of hippocampal function.

Theanine has been used historically as a relaxing agent (McKay and Blumberg, 2002; Shimbo et al., 2005). Kobayashi et al. (1998) report that theanine (200 mg) increases alpha waves when administered to resting participants. Theanine potentially reduces stress in humans (Kimura et al., 2007). However, the effect of theanine intake on acute stress and its mechanism remains to be solved. On the basis of the preventive effect of theanine intake after birth on mild stress (tail suspension for 30 s)-induced attenuation of hippocampal CA1 LTP (Takeda et al., 2012), the present study evaluated the effect of theanine intake after weaning on acute stress-induced impairments of LTP and recognition memory. It is unknown whether theanine intake prevents stress-induced impairment of memory. Neuronal circuits are shaped by experience during critical periods of early postnatal life (Hensch, 2004). Dietary environment in the critical periods is important for the shaping and can irreversibly influence brain functions. Therefore, it is important to know whether theanine intake after weaning rescues the impairment of learning and memory after acute stress.

## 2. Materials and methods

### 2.1. Animals and chemicals

Male Wistar rats (3 weeks old) were purchased from Japan SLC (Hamamatsu, Japan). They were housed under the standard laboratory conditions ( $23 \pm 1^\circ\text{C}$ ,  $55 \pm 5\%$  humidity) and had access to tap water containing 0.3% theanine and food (CE-2, CLEA JAPAN, Tokyo, Japan) for 3 weeks ad libitum. Six-week-old rats were used for the experiments. In the preliminary experiment, the increase in body weight after weaning was significantly suppressed in rats fed water containing 1–2% theanine (70–80% of the control). Thus, we used water containing 0.3% theanine, which is estimated to be approximately 10 times higher than theanine concentration in green tea usually prepared in Japan. Because water intake of a rat was 22 ml, an averaged amount per day, theanine intake was 66 mg/rat/day. All experiments were performed in accordance with the Guidelines for the Care and Use of Laboratory Animals of the University of Shizuoka that refer to American Association for Laboratory Animals Science and the guidelines laid down by the NIH (NIH Guide for the Care and Use of Laboratory Animals) in the USA.

L-Theanine was obtained from Taiyo Kagaku Co., Ltd. (Yokkaichi, Japan).

### 2.2. Exposure to acute stress

Rats (3 weeks old) were fed water containing 0.3% theanine for 3 weeks and then subjected to water immersion stress. Rats were placed into a plastic tank (diameter, 19.2 cm; height, 45 cm) containing water (400 ml,  $23\text{--}24^\circ\text{C}$ ) for 30 min. They moved around to explore the tank and to avoid water. A few minutes later, they stopped moving and kept the same posture against water in the tank.

### 2.3. Theanine concentration in the hippocampus

The hippocampus was excised from the brain of ether-anesthetized rats after feeding water containing 0.3% theanine for 3 weeks. The hippocampi were homogenized with 3-fold volume (v/w) of 3% sulfosalicylic acid solution to the weight of the hippocampi by using an ultrasonic homogenizer and centrifuged at  $12,000 \times g$  for 10 min ( $4^\circ\text{C}$ ) to obtain the supernatant. The supernatant was filtered with a  $0.45 \mu\text{m}$  cellulose acetate membrane filter and analyzed for theanine concentration (detection limit, 100 pM) in an automatic amino acid analyzer (L-8500, Hitachi Co. Ltd., Tokyo, Japan).

### 2.4. Serum corticosterone concentration

Blood samples were collected from the common carotid arteries of the control and theanine-administered rats under diethyl ether anesthesia. Because the peak of serum corticosterone level usually reaches 30–60 min after the start of acute stress, blood samples were also collected in the same manner from the control and theanine-administered rats immediately after exposure to water immersion stress for 30 min. The collection from each group was performed in the morning (10–11 O'clock) and quickly finished within 2 min. Blood samples were kept on ice and centrifuged for 10 min (6000 rpm,  $4^\circ\text{C}$ ). Corticosterone concentration in the serum obtained was determined by a corticosterone EIA kit (detection limit (80% B/B<sub>0</sub>), 30 pg/ml; Cayman Chemical Company, Ann Arbor, MI).

### 2.5. Hippocampal slice preparation

The control and theanine-administered rats were anesthetized with ether and decapitated. In another experiment, the control and theanine-administered rats were anesthetized with ether 1 h after exposure to water immersion stress for 30 min and decapitated. The brain was quickly removed and immersed in ice-cold artificial cerebrospinal fluid (ACSF) containing 119 mM NaCl, 2.5 mM KCl, 1.3 mM MgSO<sub>4</sub>, 1.0 mM NaH<sub>2</sub>PO<sub>4</sub>, 2.5 mM CaCl<sub>2</sub>, 26.2 mM NaHCO<sub>3</sub>, and 11 mM D-glucose (pH 7.3). Transverse hippocampal slices (400  $\mu\text{m}$ ) were prepared in an ice-cold ACSF using a vibratome ZERO-1 (Dosaka Kyoto, Japan). Slices were then maintained in a holding chamber at room temperature for at least 1 h. All solutions used in the experiments were continuously bubbled with 95% O<sub>2</sub> and 5% CO<sub>2</sub>.

### 2.6. CA1 LTP induction

The hippocampal slices were transferred to a recording chamber and submerged beneath continuously superfusing ACSF, which was maintained at  $26\text{--}27^\circ\text{C}$ . The Schaffer collateral/commissural-CA1 pyramidal neuron responses were induced by stimulation of the Schaffer collateral/commissural pathway with a bipolar tungsten electrode. Extracellular recording was obtained by using a glass micropipette filled with 3 M NaCl (2–10 M $\Omega$ ). The recording electrode was placed along the trajectory of Schaffer collateral/commissural pathway. An Axopatch-200B amplifier was used. The signal was filtered at 300 Hz, digitized with a 12 bit analog-to-digital converter (Digidata 1322 A; Axon instruments, Foster City, CA) and acquired at 50 kHz by using pClamp10.2 software (Axon Instruments). Before each experiment, we determined the stimulus intensities that elicited threshold and maximum field excitatory postsynaptic potentials (fEPSPs) by gradually increasing stimulus intensity until the fEPSP amplitude reached a saturated level. The stimulus intensity was then set to produce approximately 40% (around 100  $\mu\text{A}$ , 200  $\mu\text{s}$ /pulse) of the maximum fEPSPs and responses were elicited every 30 s (test stimulation, 0.033 Hz). The stimulus intensity is varied even in slices prepared from the control rats. However, the averaged stimulus intensity was almost the same (around 100  $\mu\text{A}$ ) in slices prepared from four groups; the unstressed and stressed control rats, and unstressed and stressed theanine-administered rats. CA1 LTP was induced by tetanic stimuli at 100 Hz for 1 s. At the beginning of the experiments, the physiological state of the slices was tested by verifying the existence of paired-pulse facilitation, which was induced by application of paired pulses separated by 40 ms.

Field EPSP amplitudes were averaged over 180 s intervals. Each point and line (the mean  $\pm$  SEM) in the figures shows the mean of 180 s (6 points) and expressed as percentages of the mean fEPSP amplitude measured during the 30 min baseline period perfused with ACSF prior to LTP induction. Grouped data are expressed as the mean  $\pm$  SEM. An averaged fEPSP amplitude 45–60 min after tetanic stimulation was taken as a LTP magnitude; in the result section, the values in parentheses represent the mean  $\pm$  SEM.

### 2.7. Open field

Behavior and locomotor activity of the control and theanine-administered rats were assessed in the open-field test for 10 min. In another experiment, the control and theanine-administered rats were subjected to water immersion stress for 30 min. One hour later, behavior and locomotor activity of rats were assessed in the open-field test for 10 min. Each rat was placed in an arena (70 cm  $\times$  70 cm  $\times$  40 cm) made of a black-colored polyvinyl chloride box where it has never been placed. Behavior of each rat in the arena was recorded with a camera and analyzed using software made from the NIH Image.

### 2.8. Object recognition memory

The control and theanine-administered rats were placed for 10 min into an open field, which was a 70 cm  $\times$  60 cm arena surrounded by 70 cm high walls, made of a black-colored plastic, once a day for 2 days. Twenty-four hours later, the rats were subjected to water immersion stress for 30 min. One hour later, the rats were trained and tested in a novel object recognition task. Training in the object recognition task took place in the same area used for the open field exploration. The open field exploration was thus used as a context habituation trial for the recognition memory task. The object recognition test requires that rats recall which of two earthenware objects they had been previously familiarized with. Training was conducted by placing individual rats into the field, in which two identical objects (objects A1 and A2; sake bottle) were positioned in two adjacent corners, 15 cm from the walls. Rats were left to explore the objects for 5 min. Rats were not used for the test when the total of the object exploration time was less than 20 s. Twenty-four hours after training, the rats explored the open field for 3 min in the presence of one familiar (A) and one novel object (B; cup). The familiar and novel objects were counterbalanced between rats in the object recognition task and the position of the novel object was also counterbalanced. All objects presented similar textures, colors and sizes, but distinctive shapes. Behavior of rats was recorded with a video camera during the training and the test. Two persons independently measured exploratory time and the averaged time was used. A recognition index calculated for each rat was expressed by the ratio (%)  $T_B/(T_A + T_B) \times 100$  [ $T_A$  = time spent to explore the familiar object A;  $T_B$  = time spent to explore the novel object B]. In the training trial,  $T_B$  is the

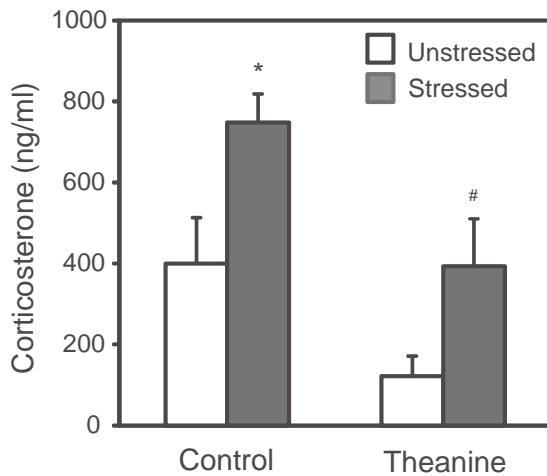


**Fig. 1.** Serum corticosterone concentration after theanine intake. Blood samples were quickly collected from the control and theanine-administered rats ( $n=6$ ). Blood samples were also quickly collected from the control and theanine-administered rats after exposure to water immersion stress for 30 min ( $n=6$ ). Each bar and line represent the mean  $\pm$  SEM. \* $p < 0.05$ , vs. unstressed control; # $p < 0.05$ , vs. stressed control.

time spent to explore the other familiar object A. Between trials the objects were washed with 70% ethanol solution. Exploration was defined as sniffing or touching the object with the nose and/or forepaws. Sitting on the object was not considered as exploration.

### 2.9. Statistical analysis

For statistical analysis, Student's paired *t*-test was used for comparison of the means of paired data. For multiple comparisons, differences between treatments were assessed by two-way ANOVA followed by post hoc testing using the Bonferroni multiple comparisons test (the statistical software, GraphPad Prism 5). A value of  $p < 0.05$  was considered significant.

## 3. Results

### 3.1. Serum corticosterone level after theanine intake

Serum corticosterone level was measured 3 weeks after the start of theanine administration (Fig. 1). Two-way ANOVA demonstrated that there was no significant interaction between the effects of theanine intake and water immersion stress on serum corticosterone level ( $F_{1,19} = 0.165$ ,  $p = 0.689$ ) but significant effects of theanine intake ( $F_{1,19} = 11.09$ ,  $p = 0.0035$ ) and water immersion stress ( $F_{1,19} = 10.61$ ,  $p = 0.0041$ ). Serum corticosterone level was lower in theanine-administered rats (body weight,  $155 \pm 1$  g) than in the control rats (body weight,  $153 \pm 3$  g). There was only a trend toward a reduction but the difference did not reach the statistical significance (control,  $400 \pm 113$  ng/ml; theanine,  $122 \pm 49$  ng/ml, post hoc test). When rats were subjected to water immersion stress for 30 min, serum corticosterone level was significantly increased in the control rats ( $748 \pm 70$  ng/ml,  $p < 0.05$  vs. unstressed, post hoc test), but not in theanine-administered rats ( $393 \pm 118$  ng/ml). Serum corticosterone level was significantly lower in theanine-administered rats than in the control rats after exposure to water immersion stress ( $p < 0.05$ , post hoc test).

Theanine level in the hippocampus was under the detectable limit in theanine-administered (6-week-old) rats.

### 3.2. CA1 LTP induction after theanine intake

CA1 LTP consists of NMDA receptor-dependent and NMDA receptor-independent components (Grover and Teyler, 1990; Shankar et al., 1998). To examine the effects of theanine intake

on CA1 LTP induction, CA1 LTP was induced in the hippocampal slices prepared from theanine-administered and control rats in the presence of 2-amino-5-phosphonovalerate (APV), an N-methyl-D-aspartate (NMDA) receptor antagonist. Two-way ANOVA analysis revealed that there was a significant interaction between the effects of theanine intake and APV on CA1 LTP induction ( $F_{1,34} = 7.245$ ,  $p = 0.011$ ), and that there was a significant effect of APV ( $F_{1,34} = 29.63$ ,  $p < 0.0001$ ) but no significant effect of theanine intake ( $F_{1,34} = 1.268$ ,  $p = 0.268$ ).

There was no significant difference in the magnitude of CA1 LTP induced by a 100-Hz tetanus for 1 s between the control and theanine-administered rats (control,  $155.1 \pm 5.6\%$ ; theanine,  $142.5 \pm 9.4\%$ ) (Fig. 2). When CA1 LTP was induced in the presence of  $50 \mu\text{M}$  2-amino-5-phosphonovalerate (APV), an N-methyl-D-aspartate (NMDA) receptor antagonist in ACSF, CA1 LTP induced by a 100-Hz tetanus for 1 s was completely inhibited in the control rats as reported previously (APV,  $99.7 \pm 8.1\%$ ,  $p < 0.001$ , vs. control (ACSF), post hoc test) (Fig. 2A and C) (Takeda et al., 2012). In contrast, CA1 LTP induced by a 100-Hz tetanus for 1 s was not significantly inhibited in theanine-administered rats (APV,  $120.6 \pm 6.6\%$ ) (Fig. 2B and C). There was a significant rise in the magnitude of CA1 LTP in the presence of APV in theanine-administered rats ( $p < 0.05$  vs. APV-perfused control, post hoc test; Fig. 2C).

The effect of water immersion stress on CA1 LTP induction was compared between the theanine-administered and control rats. Two-way ANOVA analysis revealed that there was a significant interaction between the effects of theanine intake and water immersion stress on the magnitude of CA1 LTP ( $F_{1,32} = 5.103$ ,  $p = 0.0031$ ). There was a significant effect of stress ( $F_{1,32} = 7.541$ ,  $p = 0.0098$ ) but no significant effect of theanine intake on the magnitude of CA1 LTP ( $F_{1,32} = 0.635$ ,  $p = 0.432$ ). The post hoc test demonstrated that CA1 LTP induced by a 100-Hz tetanus for 1 s was significantly attenuated in the control rats after water immersion stress (unstressed,  $154.9 \pm 5.8\%$ ; stressed,  $113.9 \pm 3.6\%$ ,  $p < 0.001$  vs. unstressed control), but not in theanine-administered rats (unstressed,  $142.5 \pm 9.4\%$ ; stressed,  $138.9 \pm 12.1\%$ ) (Fig. 3). The magnitude of CA1 LTP was greater in theanine-administered rats than in the control rats after water immersion stress. There was only a trend toward a rise in the magnitude of CA1 LTP by theanine intake but the difference did not reach the statistical significance.

### 3.3. Behavior and object recognition memory after theanine intake

The open-field test was performed to assess the basal behavior and locomotor activity after theanine intake. Two-way ANOVA revealed that there were no significant interactions in locomotor activity (distance) ( $F_{1,35} = 0.047$ ,  $p = 0.830$ ), grooming behavior (time) ( $F_{1,28} = 0.870$ ,  $p = 0.359$ ) and the number of times of rearing (standing) ( $F_{1,30} = 0.542$ ,  $p = 0.467$ ) between the effects of theanine intake and water immersion stress. In locomotor activity, there was no significant effect of theanine intake ( $F_{1,30} = 0.258$ ,  $p = 0.614$ ) in both the unstressed and stressed rats (Fig. 4A). After water immersion stress, however, locomotor activity was significantly decreased in the both control rats ( $F_{1,35} = 21.3$ ,  $p < 0.0001$ , two-way ANOVA;  $p < 0.01$ , vs. unstressed control, post hoc test) and theanine-treated rats ( $p < 0.01$  vs. unstressed theanine-administered, post hoc test). In the number of times of rearing, there was a significant effect of theanine intake in the unstressed rats ( $F_{1,30} = 16.54$ ,  $p = 0.0003$ , two-way ANOVA;  $p < 0.01$ , vs. control, post hoc test) but no significant effect of theanine intake in the stressed rats (Fig. 4B). Grooming behavior was not significantly different between the control and theanine-administered rats before and after water immersion stress (Fig. 4C).

In the object recognition task, there was no significant difference in the time spent to explore the two identical objects in the training

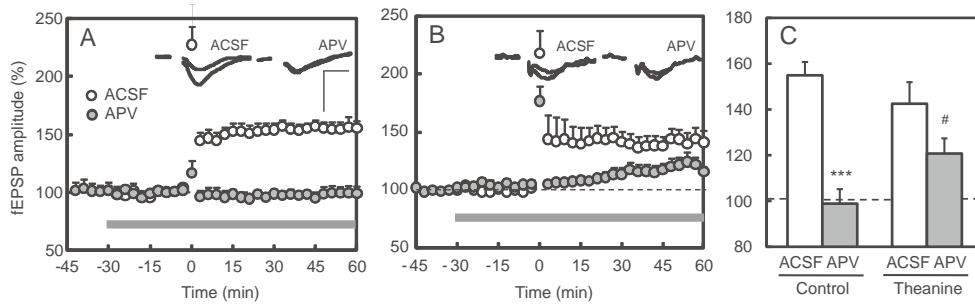


**Fig. 2.** Change in CA1 LTP components after theanine intake. Hippocampal slices were prepared from the control (A) and theanine-administered (B) rats, perfused with ACSF for 30 min, perfused with ACSF ( $n = 10$ ) or  $50 \mu\text{M}$  APV in ACSF ( $n = 7$ ) for 30 min, tetanized at 100 Hz for 1 s, and perfused under the same condition. The shaded bar indicates the period of perfusion with APV. Tetanic stimulation was delivered at time 0 min. Each point and line represents the mean  $\pm$  SEM (left side). Representative fEPSP recordings at time  $-10$  and  $50$  min are shown in the left side. Calibration;  $0.5$  mV,  $10$  ms. Each bar and line (mean  $\pm$  SEM) represents the averaged fEPSP amplitude of the last 15 min (time  $45$ – $60$  min) (C). \*\*\* $p < 0.001$ , vs. ACSF; # $p < 0.05$ , vs. APV-perfused control.

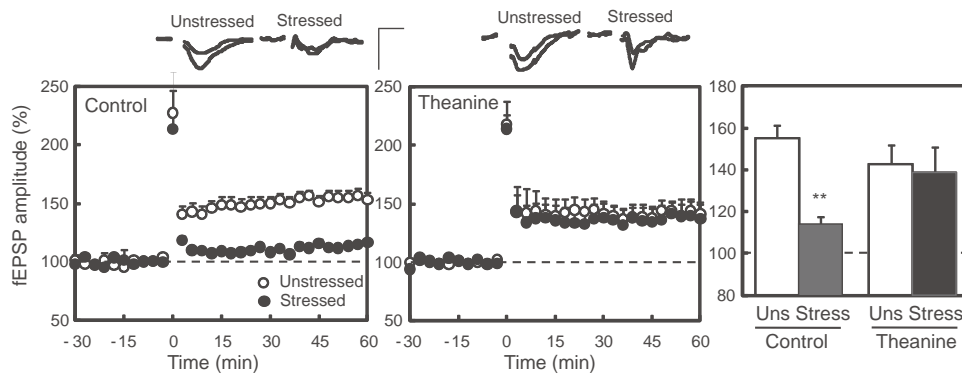


**Fig. 3.** Effect of theanine intake on CA1 LTP induction after exposure to water immersion stress. The control and theanine-administered rats were subjected to water immersion stress for 30 min. One hour later, hippocampal slices were prepared from the rats. Hippocampal slices were also prepared from the unstressed control and theanine-administered rats. Hippocampal slices were perfused with ACSF for 60 min, tetanized at 100 Hz for 1 s, and perfused under the same condition (control/unstressed,  $n = 13$ , control/stressed,  $n = 8$ , theanine/unstressed,  $n = 10$ , theanine/stressed,  $n = 6$ ). Tetanic stimulation was delivered at time 0 min. Each point and line represents the mean  $\pm$  SEM (left side). Representative fEPSP recordings at time  $-10$  and  $50$  min are shown in the left-upper side. Calibration;  $0.5$  mV,  $10$  ms. Each bar and line (mean  $\pm$  SEM) represents the averaged fEPSP amplitude of the last 15 min (time  $45$ – $60$  min) (right side). \*\* $p < 0.01$ , vs. unstressed control.

trial and the recognition index of the two groups was around 50% (Fig. 5). The recognition index is elevated in the test trial if rats remember the familiarized object. In the test trial 24 h after the training, the recognition index was significantly elevated in both the control ( $65.5 \pm 1.9\%$ ,  $p < 0.001$ , vs. training, paired  $t$ -test) and theanine-administered ( $68.1 \pm 3.3\%$ ,  $p < 0.05$ , vs. training, paired  $t$ -test) rats.

In the test trial, two-way ANOVA revealed that there was no significant interaction between the effects of theanine intake and water immersion stress on the recognition index ( $F_{1,41} = 3.702$ ,

$p = 0.085$ ). There was a significant effect of theanine intake on the recognition index ( $F_{1,41} = 7.024$ ,  $p = 0.011$ ) but not significant effect of water immersion stress ( $F_{1,41} = 3.114$ ,  $p = 0.061$ ). There was no significant difference in the recognition index in the test trial between the control and theanine-administered rats. When the control and theanine-administered rats were subjected to the training 1 h after water immersion stress, there was also no significant difference in the time spent to explore the two identical objects in the training trial and the recognition index of the two groups was around 50% (Fig. 5). In the test trial 24 h

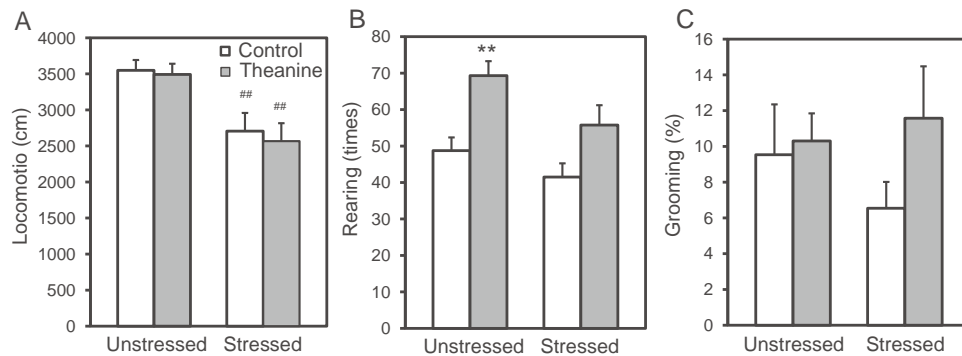


**Fig. 4.** Open-field test after theanine intake. The control ( $n = 8$ ) and theanine-administered ( $n = 8$ ) rats were subjected to the open-field test (A). In another experiment, the control ( $n = 8$ ) and theanine-administered ( $n = 8$ ) rats were subjected to the open-field test 1 h after exposure to water immersion stress for 30 min (B). Locomotor activity (distance) (A), rearing (frequency) (B), and grooming (percentage of grooming time to the test period) (C) were measured. Each bar and line represents the mean  $\pm$  SEM. \*\* $p < 0.001$ , vs. control; ## $p < 0.01$ , vs. unstressed.

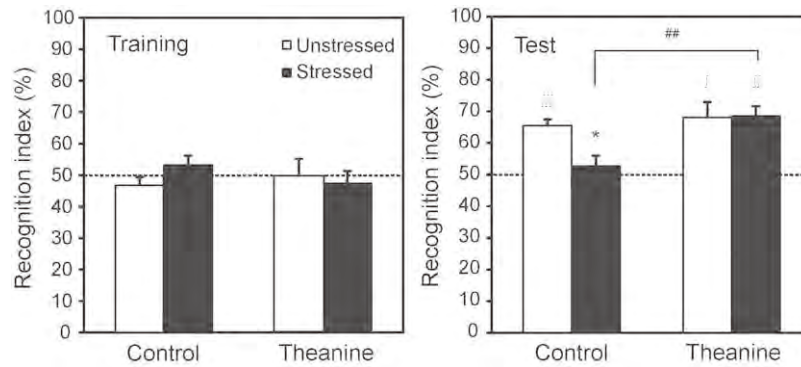


**Fig. 5.** Effect of theanine intake on object recognition memory after exposure to water immersion stress. The control ( $n=14$ ) and theanine-administered ( $n=10$ ) rats were subjected to the novel object recognition task. In another experiment, the control ( $n=12$ ) and theanine-administered ( $n=10$ ) rats were subjected to the novel object recognition task 1 h after exposure to water immersion stress for 30 min. The recognition index was calculated as described in the method. There was no significant difference in the time spent to explore the two identical objects in the training trial and the recognition index was around 50% (unstressed control rats, 46.7% and 53.3%; unstressed theanine-administered rats, 50.0 and 50.0; stressed control rats, 53.3% and 46.7%; stressed theanine-administered rats, 47.3% and 52.7). The former values of four groups were used as the recognition index in the training. Each bar and line represents the mean  $\pm$  SEM. \* $p < 0.05$ , vs. unstressed control; ## $p < 0.01$ , vs. stressed theanine;  $\int p < 0.05$ ,  $\iint p < 0.01$ ,  $\iiint p < 0.001$ , vs. training.

after the training, the recognition index was significantly elevated in theanine-administered rats ( $68.6 \pm 3.0\%$ ,  $p < 0.01$ , vs. training, paired  $t$ -test), but not in the control rats ( $52.7 \pm 4.9\%$ ). The recognition index in the test was not elevated in the control rats ( $p < 0.05$ , vs. unstressed control, two-way ANOVA with post hoc test) after water immersion stress. However, the lack of this elevation was rescued by theanine intake ( $p < 0.01$ , vs. stressed theanine-administered, two-way ANOVA with post hoc test).

#### 4. Discussion

The increase in serum corticosterone level after exposure to stress is involved in the impairment of LTP induction and the information processing of memory (Joëls et al., 2008; Sandi, 2011). In regard to LTP induction after exposure to stress, hippocampal LTP is attenuated in hippocampal slices prepared 1–24 h after acute stress (Garcia, 2001). The peak of serum corticosterone level usually reaches 30–60 min after exposure to acute stress (Joëls and Krugers, 2007). The nongenomic stress response of corticosterone is induced 30–60 min after exposure to stress and the genomic stress response of corticosterone is induced after that (60 min). It is likely that both the nongenomic and genomic responses of corticosterone are involved in the attenuation of hippocampal LTP. In the present study, the effect of theanine intake on the induction of hippocampal CA1 LTP was examined in hippocampal slices of rats prepared 1 h after exposure to water immersion stress for 30 min. CA1 LTP was attenuated in hippocampal slices prepared from the control rats, but not in hippocampal slices prepared from theanine-administered rats. The basal level of serum corticosterone was lower in theanine-administered rats than in the control rats and serum corticosterone level was also lower in theanine-administered rats after water immersion stress. In theanine-administered rats, the lack of the significant increase in serum corticosterone seems to be linked to the rescue of stress-induced attenuation of CA1 LTP.

On the other hand, CA1 LTP was not significantly inhibited in the presence of APV, an NMDA receptor antagonist, in hippocampal slices prepared from theanine-administered rats, unlike the control rats. There was a significant rise in the magnitude of CA1 LTP in the presence of APV in theanine-administered rats, suggesting that NMDA receptor-independent CA1 LTP is induced by theanine intake. The rate of NMDA receptor-dependent CA1 LTP,

is almost 100% in control (6-week-old) rats and is 36.9% in rats fed water containing 0.3% theanine for 6 weeks after birth (Takeda et al., 2012). In the present study, the rate of NMDA receptor-dependent CA1 LTP was 51.2% in theanine-administered rats. Thus, it is likely that the rate of NMDA receptor-dependent CA1 LTP is decreased with the period of theanine intake. Glucocorticoid receptor activation, which is induced by stress, selectively hampers NMDA receptor-dependent CA1 LTP (Wiegert et al., 2005). Behavioral stress modifies LTP and LTD in the hippocampal CA1 through NMDA receptor activation (Kim et al., 1996). It is generally agreed that NMDA receptor-dependent LTP is impaired by stress. However, such impairment is not always seen for NMDA receptor-independent LTP (Joëls and Krugers, 2007). Therefore, the decrease in NMDA receptor-dependent CA1 LTP component by theanine intake may partially participate in the rescue of stress-induced attenuation of CA1 LTP. On the other hand, the mechanisms of NMDA receptor-independent LTP are poorly understood. It is reported that voltage-dependent calcium channels play an important role for the rise in postsynaptic calcium to be required for LTP (Grover and Teyler, 1990). Because glucocorticoid is closely related with calcium metabolism (Tamano et al., 2009; Takeda and Tamano, 2009), it might be important that the mechanisms of LTP induction after theanine intake is examined focused on the decrease in glucocorticoid secretion.

It has been reported that the increase in glucocorticoid secretion by stress has diverse effects on not only synaptic plasticity but also learning and memory (Howland and Wang, 2008; Joëls and Krugers, 2007; Wong et al., 2007). The hippocampus plays a role in the object recognition task (Barker and Warburton, 2011), and the perirhinal and/or prefrontal cortex are also involved in the task. When CA1 LTP is attenuated, object recognition memory is impaired (Takeda et al., 2011b). In the present study, object recognition memory was impaired in the control rats after water immersion stress, but not in theanine-administered rats. In theanine-administered rats, the prevention of stress-induced impairment of recognition memory seems to be linked to the modification of corticosterone secretion and the rescue of stress-induced attenuation of CA1 LTP.

Theanine is absorbed from the gut and transported into the brain through the leucine-preferring transport system of the blood–brain barrier (Yokogoshi et al., 1998). Theanine is readily metabolized in tissues including the brain; theanine is not detected in tissues 24 h after oral administration of theanine (Terashima et al., 1999). In the present study, theanine level in the hippocampus was

under the detectable limit in theanine-administered rats. In the case of intragastrical administration of theanine (4 g/kg) to rats, theanine concentration in the brain reaches  $1.52 \pm 0.10 \mu\text{mol/g}$  tissue 5 h after administration and is almost under the detectable limit 24 h after administration (Terashima et al., 1999). Although theanine concentration can transiently increase in the hippocampus of theanine-administered rats, it is estimated that theanine concentration is much lower in the hippocampus than glutamate concentration. Because the  $\text{IC}_{50}$  of theanine to glutamate receptors is considerably high (Kakuda et al., 2002), the effect of theanine on glutamate receptors seems to be negligible. On the other hand, orally administered theanine is hydrolyzed to glutamic acid and ethylamine in the kidney (Unno et al., 1999). An ethylamine derivative, N-[2-(3,4-dichlorophenyl)ethyl]-N-methyl-2-(dimethylamino) ethylamine is bound to  $\sigma_1$  receptor (Zambon et al., 1997) that is involved in the facilitation of cortical dopaminergic transmission in the rat brain (Kobayashi et al., 1997). If ethylamine is transported into the brain, it is possible that ethylamine partially participate in the effect of theanine intake. The effect of theanine intake on brain function indicates that brain function is changed by theanine in spite of the metabolic speed (Takeda et al., 2011a, 2012).

In conclusion, the present study indicates the preventive effect of theanine intake after weaning on stress-induced impairments of hippocampal LTP and recognition memory. It is likely that the modification of the HPA axis activity, i.e., glucocorticoid secretion, by theanine intake is involved in the preventive effect.

## References

- Abreu, L.N., Lafer, B., Baca-Garcia, E., Oquendo, M.A., 2009. Suicidal ideation and suicide attempts in bipolar disorder type I: an update for the clinician. *Revista Brasileira de Psiquiatria* 31, 271–280.
- Barker, G.R., Warburton, E.C., 2011. When is the hippocampus involved in recognition memory? *Journal of Neuroscience* 31, 10721–10731.
- Bolling, B.W., Chen, C.Y., Blumberg, J.B., 2009. Tea and health: preventive and therapeutic usefulness in the elderly? *Current Opinion in Clinical Nutrition and Metabolic Care* 12, 42–48.
- Cazakoff, B.N., Johnson, K.J., Howland, J.G., 2010. Converging effects of acute stress on spatial and recognition memory in rodents: a review of recent behavioural and pharmacological findings. *Progress in Neuro-Psychopharmacology and Biological Psychiatry* 34, 733–741.
- Cho, H.S., Kim, S., Lee, S.Y., Park, J.A., Kim, S.J., Chun, H.S., 2008. Protective effect of the green tea component, L-theanine on environmental toxins-induced neuronal cell death. *Neurotoxicology* 29, 656–662.
- Chrousos, G.P., 2009. Stress and disorders of the stress system. *Nature Reviews Endocrinology* 5, 374–381.
- Chrousos, G.P., Gold, P.W., 1992. The concepts of stress and stress system disorders: overview of physical and behavioral homeostasis. *Journal of the American Medical Association* 267, 1244–1252.
- Di, X., Yan, J., Zhao, Y., Zhang, J., Shi, Z., Chang, Y., Zhao, B., 2010. L-Theanine protects the APP (Swedish mutation) transgenic SH-SY5Y cell against glutamate-induced excitotoxicity via inhibition of the NMDA receptor pathway. *Neuroscience* 168, 778–786.
- Egashira, N., Hayakawa, K., Mishima, K., Kimura, H., Iwasaki, K., Fujiwara, M., 2004. Neuroprotective effect of gamma-glutamylethylamide (theanine) on cerebral infarction in mice. *Neuroscience Letters* 363, 58–61.
- Einöther, S.J., Martens, V.E., Rycroft, J.A., De Bruin, E.A., 2010. L-Theanine and caffeine improve task switching but not intersensory attention or subjective alertness. *Appetite* 54, 406–409.
- Garcia, R., 2001. Stress, hippocampal plasticity, and spatial learning. *Synapse* 40, 180–183.
- Gonzalez de Mejia, E., Ramirez-Mares, M.V., Puangraphant, S., 2009. Bioactive components of tea: cancer, inflammation and behavior. *Brain, Behavior, and Immunity* 23, 721–732.
- Graham, H.N., 1992. Green tea composition, consumption, and polyphenol chemistry. *Preventive Medicine* 21, 334–350.
- Grover, L.M., Teyler, T.J., 1990. Two components of long-term potentiation induced by different patterns of afferent activation. *Nature* 347, 477–479.
- Haskell, C.F., Kennedy, D.O., Milne, A.L., Wesnes, K.A., Scholey, A.B., 2008. The effects of L-theanine, caffeine and their combination on cognition and mood. *Biological Psychology* 77, 113–122.
- Hensch, T.K., 2004. Critical period regulation. *Annual Review of Neuroscience* 27, 549–579.
- Howland, J.G., Wang, Y.T., 2008. Synaptic plasticity in learning and memory: stress effects in the hippocampus. *Progress in Brain Research* 169, 145–158.
- Jacobson, L., Sapolsky, R., 1991. The role of the hippocampus in feedback regulation of the hypothalamic–pituitary–adrenocortical axis. *Endocrine Reviews* 12, 118–134.
- Joëls, M., Krugers, H.L., 2007. LTP after stress: up or down? *Neural Plasticity* 2007, 93202.
- Joëls, M., Karst, H., DeRijk, R., de Kloet, E.R., 2008. The coming out of the brain mineralocorticoid receptor. *Trends in Neurosciences* 31, 1–7.
- Kakuda, T., 2011. Neuroprotective effects of theanine and its preventive effects on cognitive dysfunction. *Pharmacological Research* 64, 162–168.
- Kakuda, T., Nozawa, A., Sugimoto, A., Niino, H., 2002. Inhibition by theanine of binding of [ $^3\text{H}$ ]AMPA, [ $^3\text{H}$ ]kainate, and [ $^3\text{H}$ ]MDL 105,519 to glutamate receptors. *Bioscience, Biotechnology, and Biochemistry* 66, 2683–2686.
- Keller-Wood, M.E., Dallman, M.F., 1984. Corticosteroid inhibition of ACTH secretion. *Endocrine Reviews* 5, 1–24.
- Kelly, S.P., Gomez-Ramirez, M., Montesi, J.L., Foxe, J.J., 2008. L-Theanine and caffeine in combination affect human cognition as evidenced by oscillatory alpha-band activity and attention task performance. *Journal of Nutrition* 138, 1572S–1577S.
- Kim, J.J., Yoon, K.S., 1998. Stress: metaplastic effects in the hippocampus. *Trends in Neurosciences* 21, 505–509.
- Kim, J.J., Foy, M.R., Thompson, R.F., 1996. Behavioral stress modifies hippocampal plasticity through N-methyl-D-aspartate receptor activation. *Proceedings of the National Academy of Sciences of the United States of America* 93, 4750–4753.
- Kimura, K., Ozeki, M., Juneja, L.R., Ohira, H., 2007. L-Theanine reduces psychological and physiological stress responses. *Biological Psychology* 74, 39–45.
- Kobayashi, T., Matsuno, K., Murai, M., Mita, S., 1997. Sigma 1 receptor subtype is involved in the facilitation of cortical dopaminergic transmission in the rat brain. *Neurochemical Research* 22, 1105–1109.
- Kobayashi, K., Nagato, Y., Aoi, N., Juneja, L.R., Kim, M., Yamamoto, T., Sugimoto, S., 1998. Effects of L-theanine on the release of  $\alpha$ -brain waves in human volunteers. *Nippon Noeigakagaku Kaishi* 72, 153–157.
- Linthorst, A.C., Reul, J.M., 2008. Stress and the brain: solving the puzzle using microdialysis. *Pharmacology Biochemistry and Behavior* 90, 163–173.
- Mann, J.J., Apter, A., Bertolote, J., Beautrais, A., Currier, D., Haas, A., Hegerl, U., Lonqvist, J., Malone, K., Marusic, A., Mehlum, L., Patton, G., Phillips, M., Rutz, W., Rihmer, Z., Schmidtke, A., Shaffer, D., Silverman, M., Takahashi, Y., Varnik, A., Wasserman, D., Yip, P., Hendin, H., 2005. Suicide prevention strategies: a systematic review. *JAMA* 294, 2064–2074.
- McEwen, B.S., 1999. Stress and hippocampal plasticity. *Annual Review of Neuroscience* 22, 105–122.
- McKay, D.L., Blumberg, H.R., 2002. The role of tea in human health: an update. *Journal of the American College of Nutrition* 21, 1013.
- Sandi, C., 2011. Glucocorticoids act on glutamatergic pathways to affect memory processes. *Trends in Neurosciences* 34, 165–176.
- Shankar, S., Teyler, T.J., Robbins, N., 1998. Aging differentially alters forms of long-term potentiation in rat hippocampal area CA1. *Journal of Neurophysiology* 79, 334–341.
- Shimbo, M., Nakamura, K., Shi, H.J., Kizuki, M., Seino, K., Inose, T., Takano, T., 2005. Green tea consumption in everyday life and mental health. *Public Health Nutrition* 8, 1300–1306.
- Takeda, A., Tamano, H., 2009. Insight into zinc signaling from dietary zinc deficiency. *Brain Research Reviews* 62, 33–44.
- Takeda, A., Sakamoto, K., Tamano, H., Fukura, K., Inui, N., Suh, S.W., Won, S.J., Yokogoshi, H., 2011a. Facilitated neurogenesis in the developing hippocampus after intake of theanine, an amino acid in tea leaves, and object recognition memory. *Cellular and Molecular Neurobiology* 31, 1079–1088.
- Takeda, A., Takada, S., Nakamura, M., Suzuki, M., Tamano, H., Ando, M., Oku, N., 2011b. Transient increase in  $\text{Zn}^{2+}$  in hippocampal CA1 pyramidal neurons causes reversible memory deficit. *PLoS ONE* 6, e28615.
- Takeda, A., Tamano, H., Suzuki, M., Sakamoto, K., Oku, N., Yokogoshi, H., 2012. H Unique induction of CA1 LTP components after intake of theanine an amino acid in tea leaves and its effect on stress response. *Cellular and Molecular Neurobiology* 32, 41–48.
- Tamano, H., Kan, F., Kawamura, M., Oku, N., Takeda, A., 2009. Behavior in the forced swim test and neurochemical changes in the hippocampus in young rats after 2-week zinc deprivation. *Neurochemistry International* 55, 536–541.
- Terashima, T., Takido, J., Yokogoshi, H., 1999. Time-dependent changes of amino acids in the serum, liver, brain and urine of rats administered with theanine. *Bioscience, Biotechnology, and Biochemistry* 63, 615–618.
- Unno, T., Suzuki, Y., Kakuda, T., Hayakawa, T., Tsuge, H., 1999. Metabolism of theanine, gamma-glutamylethylamide, in rats. *Journal of Agricultural and Food Chemistry* 47, 1593–1596.
- Wiegert, O., Pu, Z., Shor, S., Joëls, M., Krugers, H., 2005. Glucocorticoid receptor activation selectively hampers N-methyl-D-aspartate receptor dependent hippocampal synaptic plasticity in vitro. *Neuroscience* 135, 403–411.
- Wong, T.P., Howland, J.G., Robillard, J.M., Ge, Y., Yu, W., Titterness, A.K., Brebner, K., Liu, L., Weinberg, J., Christie, B.R., Phillips, A.G., Wang, Y.T., 2007. Hippocampal long-term depression mediates acute stress-induced spatial memory retrieval impairment. *Proceedings of the National Academy of Sciences of the United States of America* 104, 11471–11476.
- Yokogoshi, H., Kobayashi, M., Mochizuki, M., Terashima, T., 1998. Effect of theanine,  $\gamma$ -glutamylethylamide, on brain monoamines and striatal dopamine release in conscious rats. *Neurochemical Research* 23, 667–673.
- Zambon, A.C., De Costa, B.R., Kanthasamy, A.G., Nguyen, B.Q., Matsumoto, R.R., 1997. Subchronic administration of N-[2-(3,4-dichlorophenyl) ethyl]-N-methyl-2-(dimethylamino) ethylamine (BD1047) alters sigma 1 receptor binding. *European Journal of Pharmacology* 324, 39–47.

# EFFECT OF SMELLING GREEN TEA RICH IN AROMA COMPONENTS ON EEG ACTIVITY AND MEMORY TASK PERFORMANCE

Ai YOTO

Shizuoka Industrial Foundation,  
Shizuoka, Japan  
ai\_yoto@hotmail.com

Hidehiko YOKOGOSHI

Dept. of Food & Nutritional Sciences  
Chubu University  
Aichi, Japan  
yokogoshi@isc.chubu.ac.jp

Tsuyoshi MORIYAMA

Dept. of Media and Image Technology,  
Tokyo Polytechnic University  
Kanagawa, Japan  
moriyama@mega.t-kougei.ac.jp

Yoriyuki NAKAMURA

School of Food and Nutritional Sciences  
The University of Shizuoka  
Shizuoka, Japan  
yori.naka222@u-shizuoka-ken.ac.jp

Tsuyoshi KATSUNO

Shizuoka Tea Research Center  
Shizuoka, Japan  
tsuyoshi1\_katsuno@pref.shizuoka.lg.jp

Tsutomu NAKAYAMA

School of Food and Nutritional Sciences  
The University of Shizuoka  
Shizuoka, Japan  
nkymttm@u-shizuoka-ken.ac.jp

**Abstract**— In this study, we investigated the memory task performance and the central nervous activity after smelling two kinds of pan-fired Japanese green tea to examine the differences of their physical and psychological effects. Twenty eight subjects (14 male and 14 female) participated in this study. We used Koushun and Kouju for test samples, which were made by different manufacturing processes. After smelling each odor sample, a memory task and an arithmetic task were used to test mental stress. Electroencephalogram (EEG) was recorded before and after smelling the test samples, and EEG activity was estimated for 4 frequency bands (alpha 1, alpha 2, beta 1 and beta 2). The profiles of mood states (POMS) and the visual analog scale (VAS) after mental stress task were completed for subjective assessments. The results showed that the odor of Kouju may induce a positive emotion such as a more familiar and a less hate feeling. It may also affect the EEG band power of beta 1 at right frontal region and improve memory task performance as well.

**Keywords**- *electroencephalogram (EEG); memory task; green tea; odor*

## I. INTRODUCTION

A growing literature demonstrates several health benefits of green tea based on its chemical composition, including prevention and/or control of different types of cancer, heart disease, liver disease, atherosclerosis, hypertension, diabetes, metabolic syndrome and obesity, as well as antibacterial, antiviral and antifungal activities [1, 2, 3, 4]. Some odor components of green tea, such as green odor and linalool, have also been shown to have an anti-stress effect in animal and human studies [5, 6, 7, 8, 9, 10]. In our previous paper,

smelling green tea showed an increase of the subjective rating about relaxed feeling and a less decrease in vigor score after stress loads, and electroencephalographic (EEG) activities changed after smelling green tea, suggesting that smelling green tea may have anti-stress effects. The more, different types of green tea, depending on how they are processed, not only showed their different effects on the mood, but also on EEG activity and task performance [8]. We found that smelling the Shaded white tea induced a more positive emotion, and affected EEG activity and task performance more than the normal green tea did.

Meanwhile, a growing attention has been paid to the pan-fired green tea by its rich flavor. It does not undergo the usual steam treatments of usual Japanese tea but processed by roast and roll method. This process develops flower-like sweet, mildly roasted flavors. Using different cultivar and/or manufacturing by different process can produce a large variety of its aromatic character. We hypothesize that smelling different kinds of this richly flavored green tea might affect people in different way physically and psychologically depending on their special odor characters. However, to our knowledge, no other research has been conducted on the influence of smelling different kinds of pan-fired Japanese green tea.

In this study, we assessed the anti-stress effects of two kinds of pan-fired green tea, i.e. Koushun and Kouju, together with the warm water as a control sample, on central nervous activities in healthy people by measuring EEG and mental task performance. We also evaluated subjects' Profile of Mood States (POMS) scores and the Visual Analogue Scales (VAS) scores as subjective ratings on mental state.

## II. MATERIALS AND METHOD

The experiment conducted in this study was approved by the research ethics committee of the University of Shizuoka and was carried out in accordance with the Declaration of Helsinki.

### A. Participants

Twenty-eight healthy and right-handed volunteers (14 males, 14 females, ages:  $22.5 \pm 1.5$  years old) participated in the experiment individually. All participants were requested to avoid eating or drinking except for water intake beginning 3 hours before the start of the experiment.

### B. Treatment

Koushun and Kouju, the tea leaves used as test samples were manufactured from a collaboration of Shizuoka Tea Research Center and Honyama research group. The concentrations of caffeine in the two samples were analyzed by HPLC (High Performance Liquid Chromatography) with UV detection at 280nm, and the samples' odor components were analyzed by FEDHS (Full Evaporation Dynamic Head Space) method, results are shown in Table 1.

Odor samples were extracted in paper cups with 50 ml of hot water at 70 degrees C from 3 g of each type of tea leaf or without tea leaf for totally 3 test samples, i.e. Koushun, Kouju and warm water. Then, we covered the cup with a silicon cover for about 2 min until it was served to the subjects under their nose and let the subjects smell the odor from the cup for 1 minute with their eyes closed.

### C. Stress load mental tasks

A memory task and an arithmetic task were imposed as mental stress load.

The memory task was a computer-based task formulated by the authors. The subjects were asked to remember the combinations of randomly showed human face figures and names consisting of 4 Japanese characters or 9 English characters. There were 3, 4, 6, or 12 combinations of the face

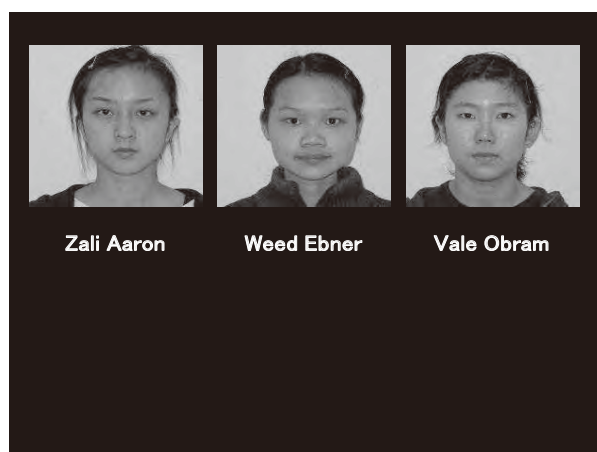


Figure 1. Example of a level 1 presentation for the memory task

TABLE I. CONCENTRATION OF CAFFEINE AND ODOR COMPONENTS IN TEA SAMPLES (PEAK AREA DIVIDED BY INTERNAL STANDARD)

components	Koushun	Kouju
caffeine	0.82	1.11
1,2-Benzenedicarboxylic acid, bis(2-methylpropyl) ester	1.45	0.83
1-Dodecanol	1.42	1.38
1-Hexanol, 2-ethyl-	0.79	1.06
1H-Pyrrole-2,5-dione, 3-ethyl-4-methyl-	1.38	1.13
2(3H)-Furanone, 5-ethylidihydro-	6.36	5.18
2H-1-Benzopyran-2-one	6.28	5.53
2H-Pyran-2-one, tetrahydro-6-(2-pentenyl)-, (Z)-	24.99	22.46
2-Propanol, 1-(2-methoxypropoxy)-	1.46	1.08
Benzoic acid, 2-ethylhexyl ester	0.89	1.09
Benzyl Alcohol	1.36	1.68
Benzyl nitrile	1.82	5.03
Butanoic acid, 3-hexenyl ester, (Z)-	2.33	1.71
Dimethyl Sulfoxide	0.89	0.69
Ethanol, 2-(2-ethoxyethoxy)-	1.43	1.14
Indole	1.53	1.29
Methyl jasmonate	3.89	2.42
Pentanoic acid, 2,2,4-trimethyl-3-carboxyisopropyl, isobutyl ester	1.13	1.09
Phenol	0.99	1.00
Phenylethyl Alcohol	3.76	3.34
Propanoic acid, 2-methyl-, 2,2-dimethyl-1-(2-hydroxy-1-methylethyl)propyl ester	1.09	1.22
Propanoic acid, 2-methyl-, 2-ethyl-3-hydroxyhexyl ester	1.08	1.16

※odor components were estimated from MS data

and the name simultaneously presented on a PC monitor for 15 sec each. After each presentation, subjects were asked to input the answers about the presented information from the keyboard within 60 sec. Therefore, the memory task consisted of 4 levels in difficulty, while level 1 presenting 3 combinations was the easiest and the level 4 presenting 12 combinations was the most difficult memory task. The order of the combinations sets was from level 1 to level 4 for each trial. Fig. 1 shows a sample screen of the level 1 presentation.

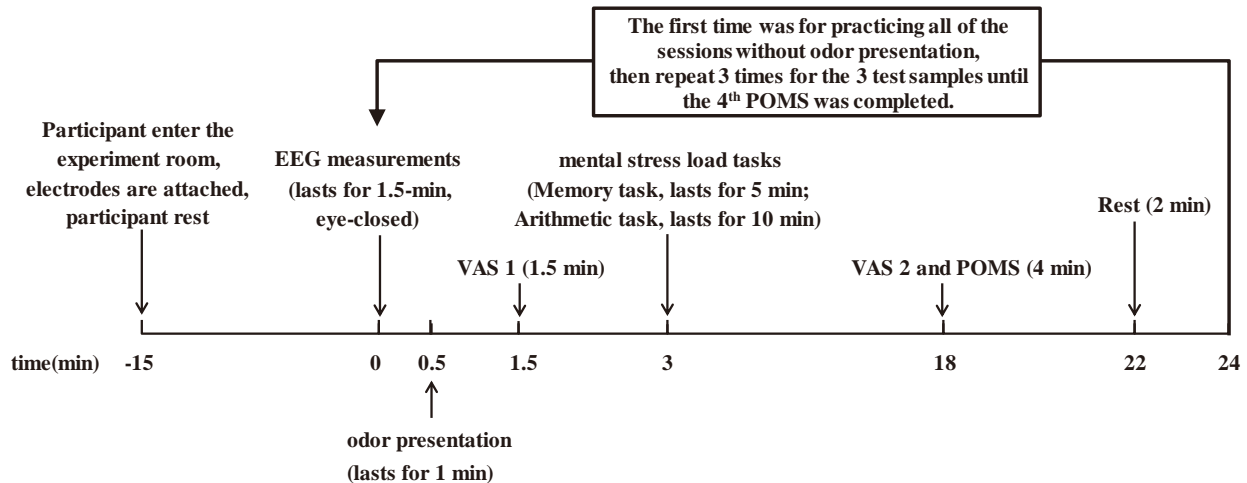


Figure 2. Procedure of the experiment

In the 10-min arithmetic task, subjects were asked to add/subtract a number to/from another which were randomly and continuously displayed on the PC monitor and type the answer in the answer column with a numerical keypad as quickly and accurately as possible.

The accuracy rates of all of the answers were calculated for further analysis about the task performance.

#### D. Subjective assessment

The VAS used in this experiment was a 10-cm line, with the end point 0 for “not feel” and 10 for “strongly feel”. Subjects were asked to make a mark on the line that represented their mood at the time. The first VAS was used for subjective ratings on their feelings about the odor right after smelling each sample. It comprises 5 scales including the level of how they feel “familiar”, “strong”, “tasty”, “hate”, and “not stinky” about the odor. The ratings about the two tea samples were used for the analysis.

Another VAS was used for the ratings on the mood after mental stress load sessions. This VAS comprises 8 scales on the feelings with regard to pressure, drowsiness, stress, relaxation, fatigue, security, tension and difficulty of the memory task, and all ratings in the 3 odor samples’ conditions were used for further analysis.

Following the second VAS, a short version of POMS was held to assess distinct affective mood states. POMS is a popular tool used widely among psychologists and scientists from many other fields. Six identifiable mood or affective states: Tension-Anxiety (T-A), Depression-Dejection (D), Anger-Hostility (A-H), Vigor-Activity (V), Fatigue-Inertia (F), and Confusion-Bewilderment (C) can be measured and were used for analysis in this study.

#### E. Measurement

Active electrodes were attached for EEG recording at 5 locations: F3, F4, Pz, O1 and O2 according to the international 10/20 system. The two locations at frontal

region (F3 and F4) were selected to detect the left and right frontal cortical activities relating to affective responses, while O1 and O2 were used for monitoring the left and right posterior cortical activities. Pz was chosen for the possibility of further study on analyzing the event-related potential (ERP) during memory task. Electrooculogram (EOG) was recorded at the left eye supra- and infra-orbitally for monitoring the ocular movements. EEG and EOG data were amplified and A/D converted by a versatile amplification unit (polymate AP1132, TEAC Corporation), and FFT was transferred offline using VitalTracer and ATAMAP II (KISSEI COMTEC CO. LTD). Filters were set for EEG at High Pass of 0.016 Hz and Low Pass of 60 Hz, for EOG at High Pass of 0.16 Hz and Low Pass of 15 Hz. The sampling rate was 1000 Hz. Absolute EEG band power was calculated in the alpha1 ( $\geq 8$ ,  $< 10$  Hz), alpha2 ( $\geq 10$ ,  $< 13$  Hz), beta1 ( $\geq 13$ ,  $< 20$  Hz), and beta2 ( $\geq 20$ ,  $< 30$  Hz) bands. Data with artifacts such as ocular or body movements were excluded from further processing. The mean band power of the alpha 1, alpha 2, beta 1 and beta2 calculated from the first 10-sec, second 10-sec, and the third 10-sec of each EEG measurement with the participant’s eyes closed were used for the analysis.

#### F. Procedure

Prior to the start of the experiment, all participants were given the opportunity to familiarize themselves with all of the stress load tasks. Experiments took place in a quiet room. The room temperature was  $24.5 \pm 1.3$  degrees C, and the humidity was  $36.2 \pm 6.3\%$ . On the experiment day, as shown in Fig. 2, the participant entered the room, was seated and rested for 15 minutes. During the resting time, electrodes were attached. After the rest, a 90-second EEG measurement session took place, followed by the first VAS for the ratings on how they feel about the smell during the EEG session, even though they were under normal status of not having smelled either test odor in the first EEG measurement

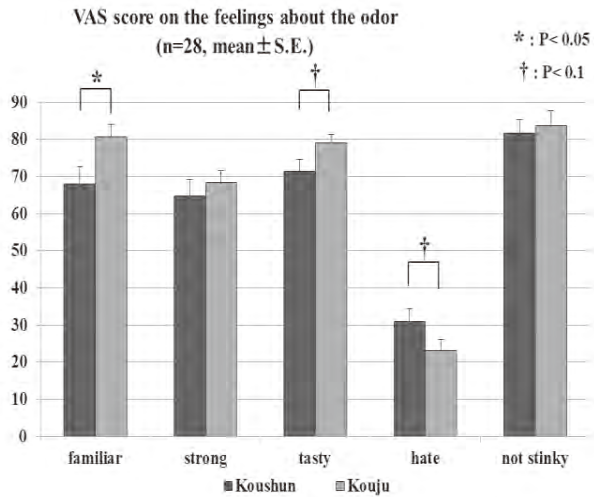


Figure 3. Results of VAS on the feelings about the tea odor samples

session. Next, the mental stress load tasks including the memory task and arithmetic task were performed. Then the second VAS and POMS were filled out. This regimen was repeated 3 times for the 3 odor samples served in random order, and the subjects smelled either of the samples keeping their eyes closed during the last 1 minute of the EEG measurement. After the 4th session of POMS was completed, the electrodes were taken off, and the participant left the experiment room.

G. *Statistic analysis*

Data were analyzed using IBM SPSS Statistics version 19. Nonparametric Friedman tests were performed to detect differences of VAS and POMS scores and task performance among the 3 order samples. Wilcoxon Signed Ranks tests with Bonferroni correction were then carried out for the comparisons between sample treatments.

Kruskal Wallis tests were also performed to detect differences of the EEG data among the 3 odor samples compared with the baseline, which was measured at the beginning of each EEG measurement for 0.5 minutes before odor sample's presentations. Mann-Whitney's U-test with Bonferroni correction was performed for the comparisons between sample treatments.

III. RESULTS AND DISCUSSION

A. *VAS*

Fig. 3 shows the result of the first VAS on feelings about the odor of the tea samples. The odor of Kouju was significantly more familiar than that of Koushun ( $p < 0.05$ ), and showed that it smelled slightly tastier ( $p < 0.1$ ) and had less feeling of hate compared with Koushun ( $p < 0.1$ ).

Fig 4 shows the score of the second VAS which were completed after mental tasks. The feeling of difficulty toward performing the memory task was slightly lower after smelling Kouju than smelling warm water ( $p < 0.1/3$ ).

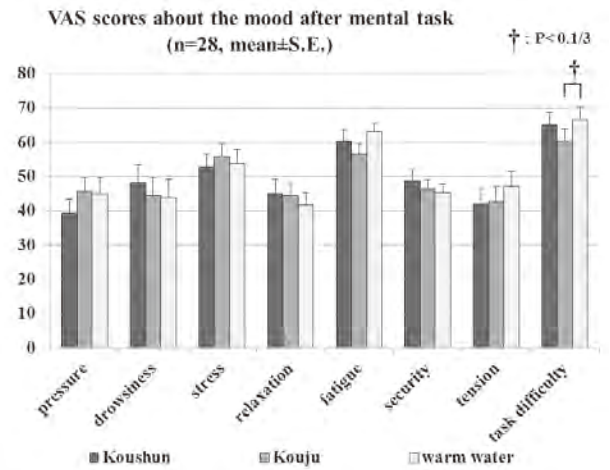


Figure 4. Results of VAS on the feelings about mood under each tea odor sample condition

From these results, the odor of Kouju showed the best score at the subjective assessments, which indicated that Kouju might be a familiar and better favorite odor than Koushun, even though it had been the first time for all the subjects to smell either of the test tea samples in this study.

B. *POMS*

All measurements in POMS were analyzed by Friedman test but no significant difference between sample treatments could be found (data not shown). That is to say, the samples used in this study showed no different effects on subjective rating about their mood after mental tasks.

C. *Task performance*

Fig. 5 shows the accuracy rates of the memory tasks. After smelling Kouju, the average accuracy rate of all of the 4 levels was slightly higher than after smelling warm water ( $p < 0.1/3$ ). This corresponded exactly to the subjective

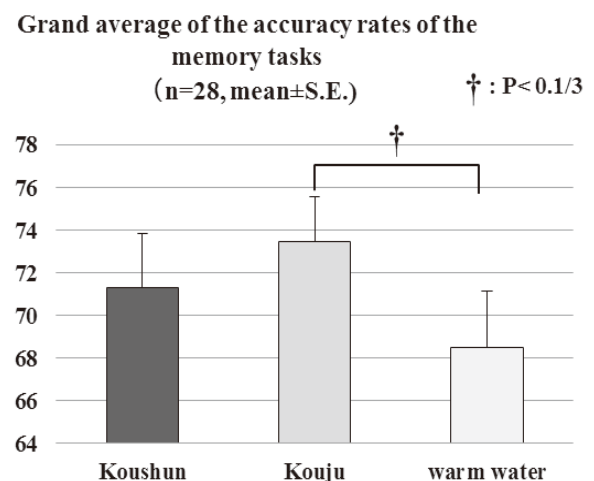


Figure 5. Results of the accuracy rates of the memory task including 4 levels all together.

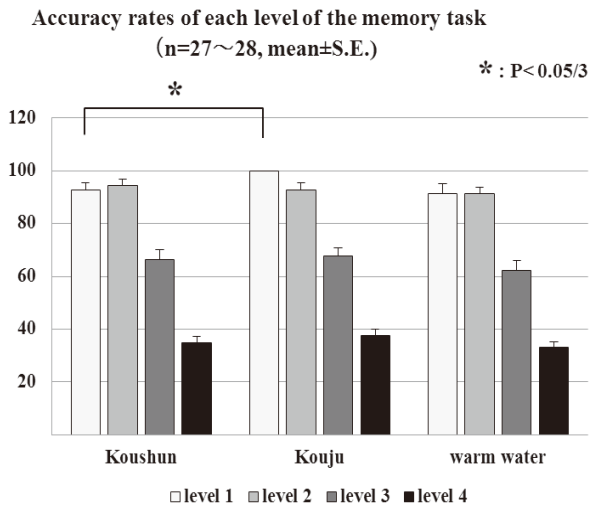


Figure 6. Results of the accuracy rates of each level of the memory tasks

ratings about the feeling of memory task’s difficulty in the second VAS.

Fig. 6 shows the accuracy rates of each level of the memory tasks. A significant difference was found among the 3 test samples ( $p < 0.05$ ). At level 1, which was the easiest and was performed right after the smelling session, the subjects performed a better accuracy rate in the memory task after smelling Kouju than the condition of after smelling Koushun ( $p < 0.05/3$ ). This might have been caused by the different affective effects between the two kinds of pan-fired green tea shown in the results of the first VAS. That is to say, the less favorite feelings about the odor of Koushun than Kouju, such as the lower score of feeling “familiar” or the higher score of feeling “hate”, might have lowered the easiest memory task performance right after smelling the odor.

D. EEG

Fig 7 shows the percentage of the EEG beta 1 power during smelling the odor samples to the baseline value calculated from the EEG power during the prior 30-minute measurements before the smelling session. During the first and the second 10-second measurements, percentage of the beta1 power at right frontal region were significantly lower when smelling the odor of Kouju than the condition of smelling Koushun ( $p < 0.05/3$ ). That means, Kouju showed a different effect on EEG beta 1 activity during the first 20 second of smelling its odor.

The beta band is suggested to play an important role in attention or higher cognitive functions [12] and to be related to good performance [13]. Gross et al. (2004) indicated that changes in synchronization in the beta band reflect changes in the attentional demands of the task and are directly related to behavioral performance [14]. However, in our study, the memory task performance of level 1 was higher with decreased band power of beta 1 at right frontal region by

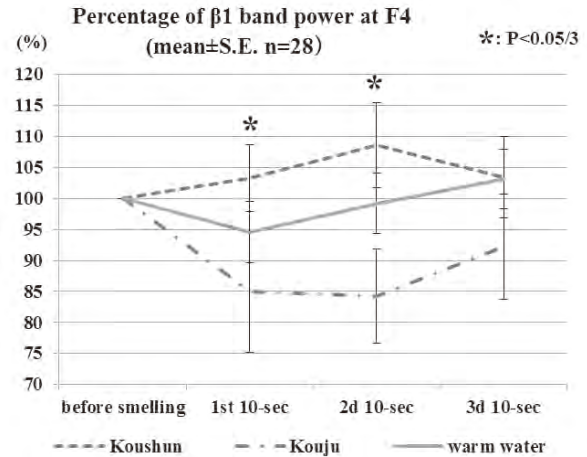


Figure 7. Results of EEG percentage of beta 1 band power at right frontal region

smelling Kouju right before completing the level 1 memory task. This might have corresponded with the different affective effect between the two kinds of tea odor showed in the results of the first VAS.

According to the frontal activation asymmetry theory, the left frontal region is associated with approach-related emotions such as happiness, joy and interest, whereas the right frontal region is associated with avoidance-related emotions, including fear, sadness and disgust [15, 16, 17, 18]. At the same time, it is considered that the more intense the emotional experience, the greater the level of absolute frontal cortical activity [19, 20, 21, 22]. From the VAS result in our study (Fig 3), the odor of Kouju was more familiar and had less feeling of hate compared with Koushun. This may have caused a less anxious emotional state with a decline of right frontal cortical activity when smelling the odor of Kouju, and this positive emotional state might have then led to the better task performance, i.e. better accuracy rate at the memory task level 1.

On the other hand, both tea odor samples had low feelings of hate as Figure 3 indicated their scores of "hate" were roughly 20-30%, the above anxiety might have due to the emotional state when the subjects were asked to wait for the odor stimulus with their eyes closed from the beginning of the EEG measurements, without knowing what kind of smell the coming odor stimulus would be like. Thus, when a more preferable odor, i.e. Kouju compared with Koushun, was presented, this anxious feeling might then somewhat relieved relatively.

The above different effects between the two kinds of pan-fired green tea may come from their different amount or the sensitivity threshold of odor components. On the other hand, it is difficult to define which component had contributed to this difference from our study. Noted that most of the aromatic components in Koushun had slightly larger amount than in Kouju (table 1), it is more likely that not one or some of the specific components, but the combination of the total

components had play an important role of the beneficial effect.

#### IV. CONCLUSION

We investigated the difference of smelling two kinds of pan-fired green tea on their physical and psychological effects using EEG, subjective assessment and task performance in this study.

The results are summarized as follows:

1. The odor of Kouju was significantly more familiar than that of Koushun, and it smelled slightly tastier and had less feeling of hate from results of the subjective assessments.

2. After smelling Kouju, the average accuracy rate of the entire memory task was slightly higher than after smelling warm water, and showed a significantly higher accuracy rate than after smelling Koushun at the easiest level of the memory task.

3. The band power of the beta 1 at right frontal region decreased with smelling Kouju.

These results indicated that the odor of Kouju may induce a positive emotion including the familiar feeling even though it was smelled for the first time; it also tended to smell tastier and slightly induce a less hate feeling. At the same time, it may also affect EEG activity and improve task performance compared with the odor of Koushun.

#### ACKNOWLEDGMENT

This study was partly supported by a project of Shizuoka Prefecture and Shizuoka City Collaboration of Regional Entities for the Advancement of Technological Excellence, Japan Science and Technology Agency (JST).

#### REFERENCES

- [1] R.L. Pastore, and P. Fratellone, "Potential health benefits of green tea (*Camellia sinensis*): a narrative review", *Explore (NY)*, vol.2, 2006, pp.531-539.
- [2] N. Khan and H. Mukhar, Tea polyphenols for health promotion. *Life Sci.*, vol. 81, 2007, pp519-533
- [3] E.G. De Mejla, M.V. Ramirez-Mares and S. Puangphaphant, "Bioactive components of tea: cancer, inflammation and behaviour", *Brain Behav Immun*, vol. 23, 2009, pp721-731.
- [4] A.B. Sharangi, "Medicinal and therapeutic potentialities of tea (*Camellia sinensis* L.)—a review", *Food Res Int*, vol. 42, 2009, pp529-535
- [5] H.Kako, S.Fukumoto, Y.Kobayashi, & H. Yokogoshi, "Effects of direct exposure of green odour components on dopamine release from rat brain striatal slices and PC12 cells", *Brain Research Bulletin*, vol. 75, (5), 2008, pp706-712.
- [6] T. Watanabe, M. Fujihara, E. Murakami, M. Miyoshi, Y. Tanaka, S. Koba, & H. Tachibana, "Green odor and depressive-like state in rats: toward an evidence-based alternative medicine?", *Behavioural Brain Research*, vol. 224, (2), 2011, pp 290-296.
- [7] K. Sano, Y. Tsuda, H. Sugano, S. Aou, & A. Hatanaka, "Concentration effects of green odor on event-related potential (P-300) and pleasantness", *Chem Senses*, vol. 27, 2002, pp225-230.
- [8] F.N. Souto-Maior, F.L. de Carvalho, L.C. de Morais, S.M. Netto, D.P. de Sousa & R.N. de Almeida, "Anxiolytic-like effects of inhaled linalool oxide in experimental mouse anxiety models", *Pharmacology Biochemistry and Behavior*, vol. 100, (2), 2011, pp259-263
- [9] V.M. Linck, A.L. da Silva, M. Figueiró, E.B. Caramão, P.R. Moreno & E. Elisabetsky, "Effects of inhaled Linalool in anxiety, social interaction and aggressive behavior in mice", *Phytomedicine*, vol. 17, (8-9), 2010, pp679-683
- [10] M. Hoferl, S. Krist, & G. Buchbauer, "Chirality influences the effects of linalool on physiological parameters of stress", *Planta*, vol. 72, 2006, pp1188-1192
- [11] S. Murao, A. Yoto, and H. Yokogoshi, "Effect of smelling green tea on mental status and EEG activity", *International Journal of Affective Engineering*, vol.12, in press.
- [12] P. Sauseng, & W. Klimesch, "What does phase information of oscillatory brain activity tell us about cognitive processes?", *Neurosci Biobehav*, vol. 32, (5), 2008, pp1001-13.
- [13] O.M. Razoumnikova, "Functional organization of different brain areas during convergent and divergent thinking: an EEG investigation", *Cogn Brain Res*, vol. 10, 2000, pp11-18.
- [14] J. Gross, F. Schmitz, I. Schnitzler, K. Kessler, K. Shapiro, B. Hommel, & A. Schnitzler, "Modulation of long-range neural synchrony reflects temporal limitations of visual attention in humans", *Proc Natl Acad Sci U.S.A.*, vol. 101, 2004, pp13050-13055.
- [15] R.J. Davidson, "The neuropsychology of emotion and affective style", *Handbook of Emotion* (eds M. Lewis & J. M. Haviland), Guilford, Press, NewYork, 1993, pp. 143-54.
- [16] R. J. Davidson, "Affective style, psychopathology and resilience: brain mechanisms and plasticity", *American Psychologist*, vol. 55, 2000, pp 1196-214.
- [17] R. J.Davidson, K.R. Scherer & H.H.Goldsmith (eds), "Handbook of Affective Science", Oxford University Press, NewYork. (2003)
- [18] J. A. Coan & J. J. B. Allen, "Frontal EEG asymmetry as a moderator and mediator of emotion", *Biological Psychology*, vol. 67, 2004, pp 7-49.
- [19] J.B.Henriques & R.J. Davidson, "Left frontal hypoactivation in depression", *Journal of Abnormal Psychology*, vol. 100, 1991, pp535-45.
- [20] G.Dawson, "Frontal electroencephalographic correlates of individual differences in emotion expression in infants: a brain systems perspective on emotion", *Monographs of the Society for Research in Child Development*, vol. 59, 1994, pp135-51.
- [21] L. A.Schmidt, "Frontal brain electrical activity (EEG) in shyness and sociability", *Psychological Science*, vol. 10, 1999, pp 316-20.
- [22] L. A.Schmidt & N. A.Fox, "Conceptual, biological, and behavioral distinctions among different categories of shy children.", *Extreme Fear, Shyness, and Social Phobia: Origins, Biological Mechanisms, and Clinical Outcomes* (eds L. A. Schmidt & J. Schulkin), Oxford University Press, NewYork.1999, pp. 47-66.

# Advantageous effect of theanine intake on cognition

Haruna Tamano<sup>1</sup>, Kotaro Fukura<sup>2</sup>, Miki Suzuki<sup>1</sup>, Kazuhiro Sakamoto<sup>2</sup>, Hidehiko Yokogoshi<sup>2</sup>, Atsushi Takeda<sup>1</sup>

<sup>1</sup>Graduate School of Pharmaceutical Sciences, University of Shizuoka, 52-1 Yada, Suruga-ku, Shizuoka 422-8526, Japan, <sup>2</sup>Graduate School of Nutritional and Environmental Sciences, University of Shizuoka, 52-1 Yada, Suruga-ku, Shizuoka 422-8526, Japan

Theanine,  $\gamma$ -glutamylethylamide, is one of the major amino acid components in green tea. On the basis of the preventive effect of theanine intake after weaning on stress-induced impairment of recognition memory, the advantageous effect of theanine intake on recognition memory was examined in young rats, which were fed water containing 0.3% theanine for 3 weeks after weaning. The rats were subjected to object recognition test. Object recognition memory was maintained in theanine-administered rats 48 hours after the training, but not in the control rats. When *in vivo* dentate gyrus long-term potentiation (LTP) was induced, it was more greatly induced in theanine-administered rats than in the control rats. The levels of brain-derived neurotrophic factor and nerve growth factor in the hippocampus were significantly higher in theanine-administered rats than in the control rats. The present study indicates the advantageous effect of theanine intake after weaning on recognition memory. It is likely that theanine intake is of advantage to the development of hippocampal function after weaning.

**Keywords:** Theanine, Green tea, Recognition memory, Hippocampus

## Introduction

The hippocampal formation receives major input from the entorhinal cortex via the perforant pathway. The dentate granule cells project to the CA3 pyramidal cells via the mossy fibers. The CA3 pyramidal cells project to the CA1 pyramidal cells via the Schaffer collaterals. The hippocampal formation is required for memory storage for a limited period of time after learning.<sup>1</sup> Acquisition and consolidation of new information are neuroplastic processes. Memory consolidation is commonly viewed to be a process lasting several hours through which the memories are transformed from a labile to a more stable state.<sup>2–5</sup> Functional integrity of the medial temporal lobe including the hippocampus proper (Ammon's horn), the dentate gyrus, and parahippocampal cortices are essential for object recognition memory processing.<sup>6–8</sup>

Tea is one of the most widely consumed beverages worldwide.<sup>9</sup> The interest in green tea has grown for human health. Green tea has putative benefits for brain function.<sup>10,11</sup> Theanine,  $\gamma$ -glutamylethylamide, is one of the major amino acid components in green tea and is synthesized from ethylamine and glutamate in green tea leaves.<sup>12</sup> It has been reported that theanine has an impact on brain function.<sup>13–16</sup> It can counteract

excitotoxicity and/or mitochondrial radical formation. Theanine intake might lead to neuroprotective effects.<sup>17–19</sup> Furthermore, theanine may improve cognitive function; an experimental study indicates that 0.3% theanine administration facilitates hippocampal neurogenesis in the developing rats, followed by enhanced recognition memory.<sup>20</sup> It is likely that theanine intake has advantages for the postnatal development of hippocampal function.

On the basis of the preventive effect of theanine intake after weaning on stress-induced impairment of recognition memory,<sup>21</sup> the advantageous effect of theanine intake on recognition memory was examined in young rats, which were fed water containing 0.3% theanine for 3 weeks after weaning. Neuronal circuits are shaped by experience during critical periods of early postnatal life.<sup>22</sup> Dietary environment in the critical periods is important for the shaping and can irreversibly modify brain functions.

## Materials and methods

### *Animals and chemicals*

Male Wistar rats (3 weeks old) were purchased from Japan SLC (Hamamatsu, Japan). They were housed under the standard laboratory conditions ( $23 \pm 1^\circ\text{C}$ ,  $55 \pm 5\%$  humidity) and had access to tap water containing 0.3% theanine and food (CE-2, CLEA

Correspondence to: Atsushi Takeda, Graduate School of Pharmaceutical Sciences, University of Shizuoka, 52-1 Yada, Suruga-ku, Shizuoka 422-8526, Japan. Email: takedaa@u-shizuoka-ken.ac.jp

JAPAN, Tokyo, Japan) for 3 weeks ad libitum. Six-week-old rats were used for the experiments. Water containing 0.3% theanine is estimated to be approximately 10 times higher than theanine concentration in green tea usually prepared in Japan. All the experiments were performed in accordance with the Guidelines for the Care and Use of Laboratory Animals of the University of Shizuoka that refer to the American Association for Laboratory Animals Science and the guidelines laid down by the NIH (NIH Guide for the Care and Use of Laboratory Animals) in the USA. This work was approved by the Ethics Committee for Experimental Animals at the University of Shizuoka. Also, every effort was made to avoid unnecessary stress and pain to the animals.

L-Theanine was obtained from Taiyo Kagaku Co., Ltd (Yokkaichi, Japan).

### *Object recognition memory*

The control and theanine-administered rats were placed for 10 minutes into an open field, which was a 70 × 60 cm arena surrounded by 70-cm high walls, made of a black-colored plastic, once a day for 2 days. Twenty-four hours later, training in the object recognition task took place in the same area used for the open field exploration. The open field exploration was thus used as a context habituation trial for the recognition memory task. The object recognition test requires that the rats recall which of the two earthenware objects they had been previously familiarized with. Training was conducted by placing individual rats into the field, in which two identical objects (objects A1 and A2; sake bottle) were positioned in two adjacent corners, 15 cm from the walls. The rats were left to explore the objects for 5 minutes. The rats were not used for the test when the total of the object exploration time was less than 20 seconds. Forty-eight hours after training, the rats explored the open field for 3 minutes in the presence of one familiar (A) and one novel object (B; cup). The familiar and novel objects were counterbalanced between the rats in the object recognition task and the position of the novel object was also counterbalanced. All the objects presented similar textures, colors and sizes, but distinctive shapes. The behavior of rats was recorded with a video camera during the training and the test. Two persons independently measured the exploratory time and the averaged time was used. A recognition index calculated for each rat was expressed by the ratio (%)  $T_B/(T_A + T_B) \times 100$  [ $T_A$  = time spent to explore the familiar object A;  $T_B$  = time spent to explore the novel object B]. In the training trial,  $T_B$  is the time spent to explore the other familiar object A. Between trials, the objects were washed with 70% ethanol solution. Exploration was defined as sniffing or touching the object with

the nose and/or forepaws. Sitting on the object was not considered as exploration.

### *Dentate gyrus long-term potentiation*

Male rats were anesthetized with chloral hydrate (400 mg/kg) and placed in a stereotaxic apparatus. A bipolar stimulating electrode and a monopolar recording electrode made of tungsten wire were positioned stereotaxically so as to selectively stimulate the perforant pathway while recording in the dentate gyrus. The electrode stimulating the perforant pathway fibers was implanted 8.0 mm posterior to the bregma, 4.5 mm lateral, 3.0–3.5 mm inferior to the dura. A recording electrode was implanted ipsilaterally 4.0 mm posterior to the bregma, 2.3 mm lateral and 3.0–3.5 mm inferior to the dura. All the stimuli were biphasic square wave pulses (200  $\mu$ s width) and their intensities were set at the current that evoked 40% of the maximum population spike (PS) amplitude. Test stimuli (0.05 Hz) were delivered at 20 seconds intervals to monitor PS.

At the beginning of the experiments, input/output curves were generated by systematic variation of the stimulus current (0.1–1.0 mA) to evaluate synaptic potency. After stable baseline recording for at least 30 minutes, long-term potentiation (LTP) was induced by delivery of high-frequency stimulation (HFS; 10 trains of 20 pulses at 200 Hz separated by 1 second). PS amplitudes (test frequency: 0.05 Hz) were averaged over 120-second intervals and expressed as percentages of the mean PS amplitude measured during the 30-minute baseline period perfused with artificial cerebrospinal fluid (ACSF) prior to LTP induction.

### *Brain-derived neurotrophic factor and nerve growth factor concentrations in the hippocampal formation*

The brain was excised from the ether-anesthetized rats. The hippocampal formation dissected from the brain was homogenized with 100-fold volume of tissue sample diluent by using an ultrasonic homogenizer. The homogenate was centrifuged at 14 000g for 30 minutes (4°C) to obtain the supernatant for the analysis of brain-derived neurotrophic factor (BDNF) and nerve growth factor (NGF). The supernatant was filtered with a cellulose acetate membrane filter (0.45  $\mu$ m). The concentrations of BDNF and NGF in the supernatant were measured by using a BDNF Sandwich ELISA kit and an NGF Sandwich ELISA kit (Chemicon International Inc., Temecula, California, USA), respectively.

### *Statistical analysis*

The data were analyzed with GraphPad Prism 5 software and all the data were parametric. Student's paired *t*-test was used for comparison of the means of paired data.

**Results**

There was no significant difference in the amount of water intake between the control and theanine-administered rats (Table 1). On the basis of the data on water intake, theanine intake of 6-week-old rats was approximately 66 mg/day. Theanine intake did not influence the increase in body weight after weaning (Control, 155.3 ± 0.1 g; Theanine, 153.0 ± 2.6 g). In the object recognition memory, there was no significant difference in learning behavior between the control and theanine-administered rats in the training trial. The time spent to explore the two identical

objects was almost the same between the control (52.0 ± 8.1 seconds) and theanine-administered (65.7 ± 9.9 seconds) rats and both rats equally explored the two identical objects. The recognition index is elevated in the test trial if the rats remember the familiarized object. The recognition index of theanine-administered rats (65.3 ± 2.9%) was significantly higher than that of the control rats (54.7 ± 4.0%) 48 hours after the training (Fig. 1).

When in vivo dentate gyrus LTP was induced, it was more greatly induced in theanine-administered rats than in the control rats (Control, 180.3 ± 7.9%; Theanine, 220.0 ± 12.2%; Fig. 2). The levels of BDNF (Control, 406.4 ± 13.9 ng/g; Theanine, 493.4 ± 30.2 ng/g) and NGF (Control, 29.8 ± 9.4 ng/g; Theanine, 60.0 ± 7.9 ng/g) in the hippocampal formation were significantly higher in theanine-administered rats than in the control rats (Fig. 3).

**Table 1 Water intake**

	Day 2	Day 8	Day 16	Day 20
Control	7.7 ± 0.4	13.1 ± 1.3	18.3 ± 2.2	19.6 ± 2.1
Theanine	8.1 ± 1.7	13.3 ± 1.5	18.4 ± 1.6	22.2 ± 2.1

Averaged water intake (ml/rat/day). n = 7.

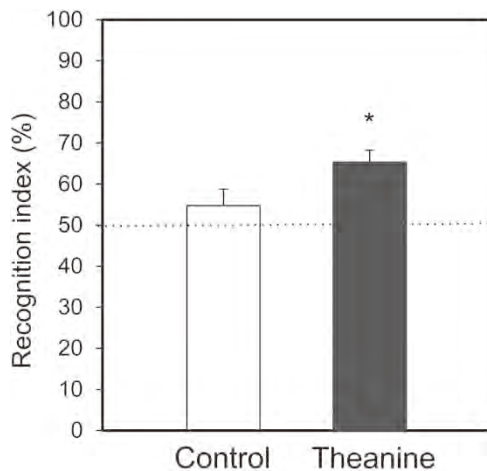


**Figure 1 Object recognition test.** The recognition index was calculated as described in the Materials and methods section. Each bar and line represents the mean ± SEM (n = 12). \*P < 0.05 vs. control.

**Discussion**

When the rats are fed water containing 0.3% theanine after birth, hippocampal neurogenesis and object recognition memory are significantly elevated in theanine-administered rats (6-week-old), indicating that theanine intake is of advantage to the postnatal development of the hippocampal function.<sup>20</sup> Furthermore, we found the preventive effect of theanine intake on stress-mediated impairment of object recognition memory in 6-week-old rats, which were fed water containing 0.3% theanine for 3 weeks after weaning.<sup>21</sup> It is possible that the advantageous effect on recognition memory is observed in theanine intake after weaning. In the present study, the effect of theanine intake on recognition memory was examined in young rats, which were fed water containing 0.3% theanine for 3 weeks after weaning. Object recognition memory was maintained in theanine-administered rats

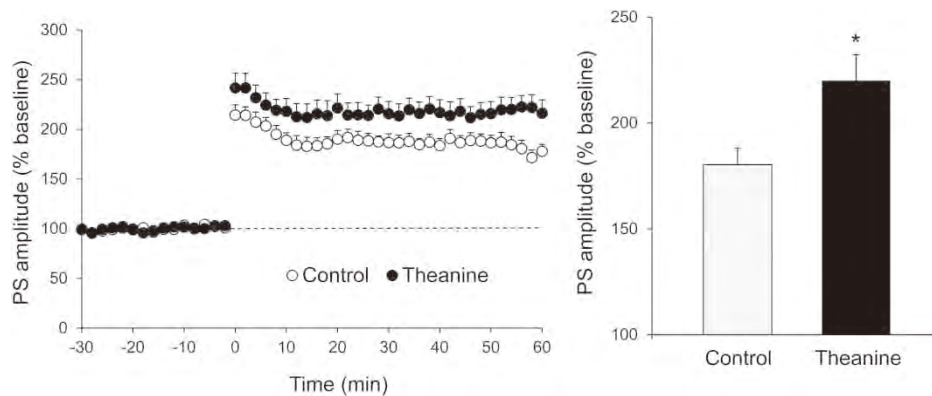


**Figure 2 Dentate gyrus LTP.** A stimulating electrode and a recording electrode were implanted stereotaxically so as to selectively stimulate the perforant pathway of the anesthetized rats while recording in the dentate gyrus. To deliver high-frequency stimulation (HFS; 10 trains of 20 pulses at 200 Hz separated by 1 second), test stimuli (0.05 Hz) were delivered to the perforant pathway of the anesthetized rats and PS was recorded in the dentate gyrus. HFS was delivered at time 0 minutes. Each point and line (the mean ± SEM) shows the mean of 120 seconds (6 points) (left, n = 13). Each bar and line (mean ± SEM) represents the averaged PS amplitude of the last 10 minutes (time 50–60 minutes) (right). \*P < 0.05 vs. control.

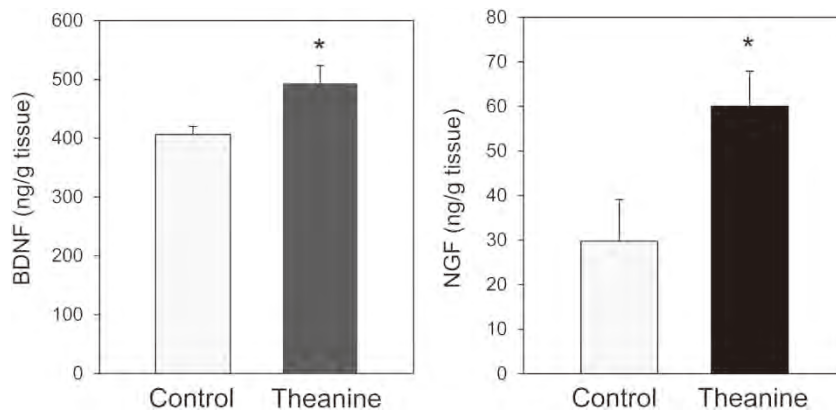


**Figure 3** BDNF and NGF concentrations in the hippocampus. Each bar and line represents mean  $\pm$  SEM ( $n = 12$ ). \* $P < 0.05$  vs. control.

48 hours after the training, but not in the control rats. Object recognition memory is usually maintained 24 hours after the training in the control rats.<sup>21,23</sup> These data suggest that theanine intake consolidates object recognition memory.

In healthy participants after ingestion of theanine (capsule) and theanine in green tea, theanine increases in plasma, erythrocytes, and urine with comparable results after both treatments. The maximum plasma concentration of theanine occurs 0.8 hours after the intake of 100 mg theanine via capsules ( $24.3 \pm 5.7 \mu\text{mol/l}$ ) and tea ( $26.5 \pm 5.2 \mu\text{mol/l}$ ), respectively.<sup>24</sup> The plasma concentration of theanine returns to baseline 24 hours after intake. The AUC, area under the concentration–time curve, of theanine in the plasma increases dose-dependently after an intake of 50–200 mg theanine. Moreover, ethylamine and glutamic acid increase in the plasma and are excreted by urine after intake. Theanine is rapidly absorbed and seems to be hydrolyzed to ethylamine and glutamic acid. It is likely that the functional effects of theanine intake result from theanine, ethylamine, or glutamic acid.<sup>24</sup>

Theanine is transported into the brain through the leucine-preferring transport system of the blood–brain barrier.<sup>25</sup> Since theanine is readily metabolized in tissues including the brain, theanine is not detected in tissues 24 hours after oral administration of theanine.<sup>12</sup> In the case of intragastrical administration of theanine (4 g/kg) to the rats, theanine concentration in the brain reaches  $1.52 \pm 0.10 \mu\text{mol/g}$  tissue 5 hours after administration and is almost under the detectable limit 24 hours after administration.<sup>12</sup> Although theanine concentration can transiently increase in the hippocampal formation of theanine-administered rats, it is estimated that theanine concentration is much lower in the hippocampal formation than glutamate concentration. Theanine level in the hippocampal formation is under the detectable limit in 0.3% theanine-administered rats.<sup>21</sup> Since the  $\text{IC}_{50}$  of theanine to glutamate receptors is considerably high,<sup>26</sup> the effect of theanine on glutamate receptors seems to be negligible. On the

other hand, theanine intake lowers the serum corticosterone level.<sup>21</sup> Corticosterone secretion increases after exposure to stress and corticosterone potentiates glutamatergic neuron activity. Thus, it is likely that theanine intake has a neuroprotective effect through the suppression of stress-mediated increase in glutamatergic neuron activity, which is associated with the dysfunctions after exposure to stress.

In the hippocampal slices prepared from the control rats, CA1 LTP induction is not significantly influenced under perfusion with  $10 \mu\text{M}$  theanine,<sup>27</sup> suggesting that theanine itself does not directly modify hippocampal LTP induction. In the present study, *in vivo* dentate gyrus LTP was more greatly induced in theanine-administered rats than in the control rats. The effect of theanine intake on recognition memory and LTP expression indicates that hippocampal function is changed by theanine intake in spite of the metabolic speed.<sup>20,27</sup>

The role of neurotrophins in various forms of synaptic plasticity, including expression of LTP and memory acquisition and consolidation, has been reported.<sup>28–31</sup> Neurotrophins activate two different receptor classes, the tropomyosin-related kinase (Trk) family of receptor tyrosine kinases and the p75 receptor, a member of the tumor necrosis factor (TNF) receptor superfamily.<sup>32</sup> The evidence supports a specific role for the TrkA ligand NGF and the TrkB ligands BDNF in expression of LTP and learning and memory. These neurotrophins play a pivotal role for recognition memory.<sup>33</sup> BDNF-stimulated signaling pathways in both dentate gyrus and perirhinal cortex contribute to long-term recognition memory.<sup>34</sup> When the levels of BDNF and NGF were checked in the hippocampal formation, both levels were significantly higher in theanine-administered rats than in the control rats. BDNF is stored at glutamatergic synapses and released during LTP induction.<sup>35–39</sup> BDNF has emerged as a regulator of late phase LTP (L-LTP) at excitatory glutamatergic synapses in the adult brain. It has been indicated that synaptic consolidation at excitatory medial perforant path-granule cell synapses requires BDNF signaling and the induction of the

immediate early gene activity-regulated cytoskeleton-associated protein (Arc).<sup>40,41</sup> The increased BDNF may be linked to the consolidation of recognition memory in theanine-administered rats.

In conclusion, the present study indicates the advantageous effect of theanine intake after weaning on recognition memory. It is likely that theanine intake is of advantage to the development of the hippocampal function after weaning. The increased expression of neurotrophins, i.e., BDNF and NGF, may play a pivotal role in recognition memory after theanine intake.

## References

- Zola-Morgan SM, Squire LR. The primate hippocampal formation: evidence for a time-limited role in memory storage. *Science* 1990;250:288–90.
- Bliss TV, Collingridge GL. A synaptic model of memory: long-term potentiation in the hippocampus. *Nature* 1993;361:31–9.
- Kandel ER. The molecular biology of memory storage: a dialogue between genes and synapses. *Brain Res* 2001;294:1030–8.
- Riedel G, Platt B, Micheau J. Glutamate receptor function in learning and memory. *Behav Brain Res* 2003;140:1–47.
- Izquierdo I, Bevilacqua LR, Rossato JI, Bonini JS, Medina JH, Cammarota M. Different molecular cascades in different sites of the brain control memory consolidation. *Trends Neurosci* 2006;29:496–505.
- Brown MW, Aggleton JP. Recognition memory: what are the roles of the perirhinal cortex and hippocampus? *Nat Rev Neurosci* 2001;2:51–61.
- de Lima MN, Luft T, Roesler R, Schroder N. Temporary inactivation reveals an essential role of the dorsal hippocampus in consolidation of object recognition memory. *Neurosci Lett* 2006;405:142–6.
- Malleret G, Alarcon JM, Martel G, Takizawa S, Vronskaya S, Yin D. Bidirectional regulation of hippocampal long-term synaptic plasticity and its influence on opposing forms of memory. *J Neurosci* 2010;30:3813–25.
- Graham HN. Green tea composition, consumption, and polyphenol chemistry. *Prev Med* 1992;21:334–50.
- Bolling BW, Chen CY, Blumberg JB. Tea and health: preventive and therapeutic usefulness in the elderly? *Curr Opin Clin Nutr Metab Care* 2009;12:42–8.
- Gonzalez de Mejia E, Ramirez-Mares MV, Puangphaphant S. Bioactive components of tea: cancer, inflammation and behavior. *Brain Behav Immun* 2009;23:721–32.
- Terashima T, Takido J, Yokogoshi H. Time-dependent changes of amino acids in the serum, liver, brain and urine of rats administered with theanine. *Biosci Biotechnol Biochem* 1999;63:615–8.
- Haskell CF, Kennedy DO, Milne AL, Wesnes KA, Scholey AB. The effects of L-theanine, caffeine and their combination on cognition and mood. *Biol Psychol* 2008;77:113–22.
- Kelly SP, Gomez-Ramirez M, Montesi JL, Foxe JJ. L-theanine and caffeine in combination affect human cognition as evidenced by oscillatory alpha-band activity and attention task performance. *J Nutr* 2008;138:1572S–7S.
- Einöther SJ, Martens VE, Rycroft JA, De Bruin EA. L-theanine and caffeine improve task switching but not intersensory attention or subjective alertness. *Appetite* 2010;54:406–9.
- Kakuda T. Neuroprotective effects of theanine and its preventive effects on cognitive dysfunction. *Pharmacol Res* 2011;64:162–8.
- Egashira N, Hayakawa K, Mishima K, Kimura H, Iwasaki K, Fujiwara M. Neuroprotective effect of gamma-glutamylethylamide (theanine) on cerebral infarction in mice. *Neurosci Lett* 2004;363:58–61.
- Cho HS, Kim S, Lee SY, Park JA, Kim SJ, Chun HS. Protective effect of the green tea component, L-theanine on environmental toxins-induced neuronal cell death. *Neurotoxicology* 2008;29:656–62.
- Di X, Yan J, Zhao Y, Zhang J, Shi Z, Chang Y, et al. L-theanine protects the APP (Swedish mutation) transgenic SH-SY5Y cell against glutamate-induced excitotoxicity via inhibition of the NMDA receptor pathway. *Neuroscience* 2010;168:778–86.
- Takeda A, Sakamoto K, Tamano H, Fukura K, Inui N, Suh SW, et al. Facilitated neurogenesis in the developing hippocampus after intake of theanine, an amino acid in tea leaves, and object recognition memory. *Cell Mol Neurobiol* 2011;31:1079–88.
- Tamano H, Fukura K, Suzuki M, Sakamoto K, Yokogoshi H, Takeda A. Preventive effect of theanine intake on stress-induced impairments of hippocampal long-term potentiation and recognition memory. *Brain Res Bull* 2013;95:1–6.
- Hensch TK. Critical period regulation. *Annu Rev Neurosci* 2004;27:549–79.
- Takeda A, Takada S, Ando M, Itagaki K, Tamano H, Suzuki M, et al. Impairment of recognition memory and hippocampal long-term potentiation after acute exposure to cloquinol. *Neuroscience* 2010;171:443–50.
- Scheid L, Ellinger S, Alteheld B, Herholz H, Ellinger J, Henn T, et al. Kinetics of L-theanine uptake and metabolism in healthy participants are comparable after ingestion of L-theanine via capsules and green tea. *J Nutr* 2012;142:2091–6.
- Yokogoshi H, Kobayashi M, Mochizuki M, Terashima T. Effect of theanine, r-glutamylethylamide, on brain monoamines and striatal dopamine release in conscious rats. *Neurochem Res* 1998;23:667–73.
- Kakuda T, Nozawa A, Sugimoto A, Niino H. Inhibition by theanine of binding of [3H]AMPA, [3H]kainate, and [3H]MDL 105,519 to glutamate receptors. *Biosci Biotechnol Biochem* 2002;66:2683–6.
- Takeda A, Tamano H, Suzuki M, Sakamoto K, Oku N, Yokogoshi H. Unique induction of CA1 LTP components after intake of theanine, an amino acid in tea leaves and its effect on stress response. *Cell Mol Neurobiol* 2012;32:41–8.
- Alonso M, Bekinschtein P, Cammarota M, Vianna MR, Izquierdo I, Medina JH. Endogenous BDNF is required for long-term memory formation in the rat parietal cortex. *Learn Mem* 2005;12:504–10.
- Bekinschtein P, Cammarota M, Igaz LM, Bevilacqua LR, Izquierdo I, Medina JH. Persistence of long-term memory storage requires a late protein synthesis- and BDNF-dependent phase in the hippocampus. *Neuron* 2007;53:261–77.
- Chen J, Kitanishi T, Ikeda T, Matsuki N, Yamada MK. Contextual learning induces an increase in the number of hippocampal CA1 neurons expressing high levels of BDNF. *Neurobiol Learn Mem* 2007;88:409–15.
- Hennigan A, Callaghan CK, Kealy J, Rouine J, Kelly AM. Deficits in LTP and recognition memory in the genetically hypertensive rat are associated with decreased expression of neurotrophic factors and their receptors in the dentate gyrus. *Behav Brain Res* 2009;197:371–7.
- Patapoutian A, Reichardt LF. Trk receptors: mediators of neurotrophin action. *Curr Opin Neurobiol* 2001;11:272–80.
- Callaghan CK, Kelly AM. Neurotrophins play differential roles in short and long-term recognition memory. *Neurobiol Learn Mem* 2013. doi: pii: S1074-7427(13)00069-5.
- Callaghan CK, Kelly AM. Differential BDNF signaling in dentate gyrus and perirhinal cortex during consolidation of recognition memory in the rat. *Hippocampus* 2012;22:2127–35.
- Wibrand K, Messaoudi E, Hävik B, Steenslid V, Løvlie R, Steen VM, et al. Identification of genes co-upregulated with Arc during BDNF-induced long-term potentiation in adult rat dentate gyrus in vivo. *Eur J Neurosci* 2006;23:1501–11.
- Hartmann M, Heumann R, Lessmann V. Synaptic secretion of BDNF after high-frequency stimulation of glutamatergic synapses. *EMBO J* 2001;20:5887–97.
- Aicardi G, Argilli E, Cappello S, Santi S, Riccio M, Thoenen H, et al. Induction of long-term potentiation and depression is reflected by corresponding changes in secretion of endogenous brain-derived neurotrophic factor. *PNAS* 2004;101:15788–92.
- Matsuda N, Lu H, Fukata Y, Noritake J, Gao H, Mukherjee S, et al. Differential activity-dependent secretion of brain-derived neurotrophic factor from axon and dendrite. *J Neurosci* 2009;29:14185–98.
- Panja D, Bramham CR. BDNF mechanisms in late LTP formation: a synthesis and breakdown. *Neuropharmacology* 2013. doi: pii: S0028-3908(13)00292-X
- Kang H, Welcher AA, Shelton D, Schuman EM. Neurotrophins and time: different roles for TrkB signaling in hippocampal long-term potentiation. *Neuron* 1997;19:653–64.
- Messaoudi E, Ying SW, Kanhema T, Croll SD, Bramham CR. BDNF triggers transcription-dependent, late phase LTP *in vivo*. *J Neurosci* 2002;22:7453–61.

## Note

## Effect of Dietary $\gamma$ -Aminobutyric Acid on the Nerve Growth Factor and the Choline Acetyltransferase in the Cerebral Cortex and Hippocampus of Ovariectomized Female Rats

Kazuho TUJIOKA<sup>1</sup>, Panicha THANAPREEDAWAT<sup>2</sup>, Takashi YAMADA<sup>3</sup>, Hidehiko YOKOGOSHI<sup>3</sup>, Kenji HORIE<sup>4</sup>, Mujo KIM<sup>4</sup>, Kazumi TSUTSUI<sup>5</sup> and Kazutoshi HAYASE<sup>5,\*</sup>

<sup>1</sup>Faculty of Early Childhood Care and Education, Ohkagakuen University, Toyoake, Aichi 470–1163, Japan

<sup>2</sup>Laboratory of Nutritional Biochemistry, School of Food and Nutritional Sciences, The University of Shizuoka, Yada, Shizuoka 422–8526, Japan

<sup>3</sup>Department of Food and Nutritional Sciences, College of Bioscience and Biotechnology, Chubu University, Matsumoto-cho, Kasugai, Aichi 487–8501, Japan

<sup>4</sup>Research Department, Pharma Foods International Company Ltd., Kyoto 615–8245, Japan

<sup>5</sup>Department of Home Economics, Aichi University of Education, Kariya, Aichi 448–8542, Japan

(Received July 1, 2013)

**Summary** The brain protein synthesis and the plasma concentration of growth hormone (GH) is sensitive to the dietary  $\gamma$ -aminobutyric acid (GABA) in ovariectomized female rats; however, the role of dietary GABA on biomarkers including nerve growth factor (NGF) and choline acetyltransferase for the function of cholinergic neurons remains unknown in ovariectomized female rats. The purpose of this study was to determine whether the dietary GABA affects the concentration and mRNA level of NGF, and the activity of choline acetyltransferase in the brains of ovariectomized female rats. Experiments were done on two groups of 24-wk-old ovariectomized female rats given 0 or 0.5% GABA added to a 20% casein diet. The concentrations of NGF and activities of choline acetyltransferase in the cerebral cortex and hippocampus, and mRNA level of NGF in the hippocampus increased significantly with the 20% casein+0.5% GABA compared with the 20% casein diet alone. In the hippocampus, the mRNA level of NGF significantly correlated with the NGF concentration ( $r=0.714$ ,  $p<0.01$ ). These results suggest that the administration of GABA to ovariectomized female rats is likely to control the mRNA level and concentration of NGF and cause an increase in the activity of choline acetyltransferase in the brains.

**Key Words**  $\gamma$ -aminobutyric acid, choline acetyltransferase, nerve growth factor, brain, rats

Nerve growth factor (NGF) is one of the neurotrophic factors and stimulates differentiation and growth of basal forebrain cholinergic neurons (1, 2). The highest concentrations of NGF mRNA were found in the cortex and hippocampus, which are the major targets of the NGF-responsive cholinergic neurons of the basal forebrain (3). Choline acetyltransferase, the biomarker for the function of cholinergic neurons, is induced by NGF (4) and the concentration and mRNA level in hippocampal NGF are correlated with the density of cholinergic innervation (5). NGF was able to affect survival of central cholinergic neurons after axonal transections in adult rats (6). Alzheimer's disease is associated loss of cholinergic neurons (7), which are essential for learning and memory processes, notwithstanding the exact mechanism of response. Sherwin (8) reported that there was a beneficial effect of estrogen on memory tasks in

postmenopausal women. Data in ovariectomized rats indicated that soy isoflavones and estrogen increased the activity of choline acetyltransferase and NGF mRNAs in the brain (9). We also reported that estrogen and dietary genistein increased the brain protein synthesis in ovariectomized female rats (10, 11). These data suggest the possibility that the concentration and mRNA level of NGF may play a role in determining the choline acetyltransferase activity in the brain regions and brain function.

On the other hand, several investigations have demonstrated that estrogen stimulated the release of  $\gamma$ -aminobutyric acid (GABA) in the brain (12). GABA is a kind of the amino acid widely distributed in nature, and is an inhibitory transmitter compound in vertebrates (13, 14). Recently, GABA has been attracting attention as a food with functions such as improvement of memory and study capability and relaxation (12, 15). In a previous study, the plasma concentration of growth hormone (GH) and the protein synthesis in the brain were also shown to be sensitive to the dietary GABA in ovariectomized female rats, and a positive correlation existed

\*To whom correspondence should be addressed.

E-mail: khayase@aeu.ac.jp

Abbreviations: GABA,  $\gamma$ -aminobutyric acid; NGF, nerve growth factor.

between the protein synthesis rate in the brain and the plasma concentration of GH (16). The biomarkers including NGF and choline acetyltransferase have been shown to be important for the function of cholinergic neurons (17). However, the role of dietary GABA in maintaining the concentration and mRNA level of NGF in the brains of ovariectomized female rats remains unknown. Therefore, the possible effects of the dietary GABA on the concentration and mRNA level of NGF and the activity of choline acetyltransferase in the brains of ovariectomized female rats are of nutritional importance in understanding the role of nutrition in the brain function in mammals.

The purpose of our study was to determine whether the GABA affects the NGF concentration and the mRNA level, and choline acetyltransferase activity in the brains of the ovariectomized female rats. Two questions were considered in the present study: 1) whether the dietary GABA might affect the concentration of NGF and the activity of choline acetyltransferase in the brains of ovariectomized female rats, and 2) whether the increased mRNA level of NGF in ovariectomized female rats given the GABA resulted in a higher NGF concentration in the brain regions than that in rats fed the basal diet, and increased the choline acetyltransferase activity in the brain. Therefore, we examined the concentration of NGF and the mRNA level, and the activity of choline acetyltransferase in the cerebral cortex and hippocampus. We have already reported that the plasma concentration of GH and the protein synthesis rate in the brain depended on the level of dietary addition of GABA, and the rate of protein synthesis in the brain was the highest in rats administered 0.5% GABA added to a 20% casein diet compared with control rats (18). Thus, in this study, we used a 20% casein+0.5% GABA diet as the experimental diet. The effects of GABA treatment on the GH concentration in plasma were also investigated.

### Materials and Methods

**Chemicals.** All reagents were purchased from Wako Pure Chemical Industries, Ltd. (Osaka, Japan).

**Animals and diets.** Ovariectomized female rats (24 wk, Japan SLC, Inc., Hamamatsu, Japan) were individually housed at 24°C in a room with a 12-h light-dark cycle. The rats were transferred to the experimental diets after being fed a 20% casein diet for 10 d. The experimental diets contained 0 or 0.5% GABA added to the 20% casein diet (Table 1). All rats were individually housed and given free access to food and water. The approval of Aichi University of Education Animal Care and Use Committee was given for our animal experiments.

**Experimental design.** Three experiments was conducted on two groups of rats. In Experiments 1 and 2, all rats were fed the experimental diets for 10 d. After the 10-d feeding period, the rats were decapitated, and the cerebral cortex and hippocampus (19) were quickly removed. The blood was collected into heparinized tubes, and the plasma was separated by centrifugation at 2,500 rpm for 15 min. For measuring the concentration of GABA, the plasma was treated with ethyl alcohol

Table 1. Composition (g/100 g of diet) of experimental diets.

	20% Casein	20% Casein+ 0.5% GABA <sup>1</sup>
Casein	20.0	20.0
GABA	0.0	0.5
Cystine	0.3	0.3
Cornstarch <sup>2</sup>	43.3	43.0
Sucrose <sup>2</sup>	21.7	21.5
Corn oil	5.0	5.0
AIN-93M mineral mix <sup>3</sup>	3.5	3.5
AIN-93VX vitamin mix <sup>3</sup>	1.0	1.0
Cellulose <sup>2</sup>	5.0	5.0
Choline chloride	0.2	0.2

<sup>1</sup>  $\gamma$ -Aminobutyric acid.

<sup>2</sup> Supplied by Oriental Yeast Co., Ltd., Tokyo, Japan.

<sup>3</sup> Supplied by CLEA Japan, Inc., Tokyo, Japan (39).

to precipitate the protein (20). The GABA concentration was measured by high pressure liquid chromatography. The effects of dietary GABA on the concentrations and mRNA levels of NGF (Experiment 1), and activities of choline acetyltransferase (Experiment 2) in the brains were investigated. The plasma concentration of GH rose very rapidly after GABA treatment. Therefore, in Experiment 3, the plasma concentration of GH was measured after only one 3-h feeding period of the test diet. After feeding on the 20% casein diet for 10 d (one 3-h feeding period per day, from 9:00–12:00), the rats were given the experimental diets for 1 d (only one 3-h period). After the 3-h feeding period, rats were decapitated. The concentration of plasma GH was measured by the method of EIA (SPI bio, Massy, Cedex, France).

**Determination of choline acetyltransferase activity.** The activity of choline acetyltransferase in the brains was measured according to the method of Fonnum (21). The tissue samples were homogenized with 20 volumes of cold 50 mmol/L sodium phosphate buffer (pH 7.4) containing 0.01 mol/L EDTA and 0.5% Triton X100. The homogenate was incubated with 50 mmol/L sodium phosphate (pH 7.4), 0.2 mmol/L acetylCoA, 14.8 MBq/L  $1$ -<sup>14</sup>C-acetylCoA, 0.8 mmol/L choline chloride, 20 mmol/L EDTA, and 0.1 mmol/L physostigmine sulphate at 37°C in 300  $\mu$ L. After 15 min, all reaction mixtures were quickly transferred to the scintillation vial by cold 10 mmol/L sodium phosphate (pH 7.4). The radioactivity was determined by adding a toluene scintillation mixture containing 0.05% diphenyloxazole and 0.02% 1,4-bis-(5-phenyloxazole-2yl)benzene, and acetonitrile containing 0.5% Kalignost (Accuflex LSC 7400, Hitachi Aloka Co., Tokyo, Japan).

**Determination of NGF by enzyme immunoassay (EIA).** The tissue samples were homogenized with 20 volumes of cold 20 mmol/L Tris-HCl buffer (pH 8.0) containing 137 mmol/L NaCl, 1% Triton X100, 10% glycerol, 1 mmol/L phenylmethylsulfonyl fluoride, 10  $\mu$ g/mL aprotinin, 1  $\mu$ g/mL leupeptin and 0.5 mmol/L sodium vanadate. Homogenates were centrifuged at 15,000  $\times$ g

Table 2. Effects of the addition of GABA<sup>1</sup> to a basal diet on the concentrations and relative mRNA levels of NGF in ovariectomized female rats (Exp. 1).<sup>2</sup>

	Control	GABA
Initial body weight (g)	195.6±2.2	195.6±2.1
Changes in body weight (g/10 d)	27.8±2.9	30.6±2.2
Food intake (g/d)	17.1±0.3	17.5±0.4
Tissue weight (g/100 g body weight)		
Cerebral cortex	0.121±0.005	0.125±0.003
Hippocampus	0.054±0.003	0.053±0.002
NGF <sup>3</sup> (ng/g tissue)		
Cerebral cortex	4.08±0.37	5.22±0.29*
Hippocampus	9.46±0.40	11.30±0.31*
NGF mRNA <sup>4</sup>		
Cerebral cortex	1.000±0.040	0.854±0.130
Hippocampus	1.000±0.142	1.698±0.119*

<sup>1</sup>  $\gamma$ -Aminobutyric acid.

<sup>2</sup> Values are means and SE,  $n=6$ . \* Significantly different from the control value ( $p<0.05$ ).

<sup>3</sup> Nerve growth factor.

<sup>4</sup> The relative mRNA levels are shown as the ratio to the value of control group.

for 15 min at 4°C. The supernatant was used for the measurements of NGF.

The NGF protein was measured by EIA (NGF E<sub>max</sub> System, Promega Co., Madison, WI).

**RT-PCR analysis.** Brain cerebral cortex and hippocampus tissues were homogenized and total RNA was extracted using the RNeasy Mini Kit (Qiagen Japan, Tokyo) (22). First-strand cDNA was synthesized from total RNA using first-strand synthesis system (Life Technologies Japan, Tokyo). NGF mRNA was measured by a light cycler real time PCR system and real time PCR kit for light cycler (Roche, Mannheim, Germany). Primer sequences for amplification were 5'-CAACAGGACTCAGGAGCA-3' and 5'-GTCCGTGGCTGTGGTCTTAT-3' for NGF and 5'-TGACGGTCAGGTCATCACTATC-3' and 5'-GGCATAGAGGTCTTTACGGATG-3' for  $\beta$ -actin. The RNA preparation and real time PCR in the present study were performed in duplicate. We used the  $\beta$ -actin mRNA level to normalize the NGF mRNA level.

**Statistical analysis.** The means and SE are reported. Student's *t*-test was used to compare means (23). Differences were considered significant at  $p<0.05$ . A linear regression analysis was used to assess the relationship between the concentration and mRNA level of NGF (23).

### Results and Discussion

Cholinergic neurons are essential for learning and memory processes (7, 24). Biomarkers including choline acetyltransferase and NGF have been shown to be important for the function of cholinergic neurons (17). In previous studies, we reported that the administration of GABA to ovariectomized female rats increased the rate of protein synthesis in the brain, and that the brain

Table 3. Effects of the addition of GABA<sup>1</sup> to a basal diet on the activities of choline acetyltransferase in ovariectomized female rats (Exp. 2).<sup>2</sup>

	Control	GABA
Initial body weight (g)	189.8±2.7	190.2±1.9
Changes in body weight (g/10 d)	28.8±1.6	31.0±2.1
Food intake (g/d)	18.9±0.4	18.8±0.7
Plasma GABA ( $\mu$ mol/L)	0.11±0.01	3.53±0.22*
Tissue weight (g/100 g body weight)		
Cerebral cortex	0.119±0.004	0.120±0.004
Hippocampus	0.053±0.003	0.052±0.002
Choline acetyltransferase (units <sup>3</sup> /g tissue)		
Cerebral cortex	2,105±81	2,468±40*
Hippocampus	2,490±132	2,888±52*

<sup>1</sup>  $\gamma$ -Aminobutyric acid.

<sup>2</sup> Values are means and SE,  $n=6$ . \* Significantly different from the control value ( $p<0.05$ ).

<sup>3</sup> Unit of enzyme activity: nmoles of acetylcholine produced per hour.

function may be affected by the dietary GABA (16). However, little information is available on the effects of dietary GABA on the concentrations and mRNA levels of NGF in ovariectomized female rats. Therefore, we determined whether dietary GABA increased the concentrations and mRNA levels of NGF in the brain.

The body weight gain and food intake did not differ among experimental groups (Table 2). The relative weights of the cerebral cortex and hippocampus did not differ among experimental groups.

In the brain regions of the cerebral cortex and hippocampus, GABA supplementation to the basal diet elevated the concentration of NGF (Table 2). The changes in NGF concentration in the cerebral cortex and hippocampus were likely attributable to the dietary GABA. In the function of cholinergic neurons is partly related to the concentration of NGF in the cerebral cortex and hippocampus. In the present study, the mRNA level of NGF in the group fed the 20% casein+0.5% GABA diet was higher than in the group fed the 20% casein diet alone (Table 2). Correlations between the concentration and mRNA level of NGF were significant in the hippocampus ( $r=0.704$ ,  $p<0.01$ ). However, the mRNA level of NGF in the cerebral cortex did not differ between the two groups (Table 2). The higher concentrations and higher mRNA level in NGF were found in the hippocampus, which is a major targets of the cholinergic neurons of the basal forebrain (3, 25). Therefore, the dietary addition of GABA may have controlled the NGF mRNA level only in the hippocampus and increased the NGF concentration in ovariectomized female rats. The effects of GABA treatment on the NGF concentration in the cerebral cortex should be determined in detail in further studies.

In the present experiment, the activity of choline acetyltransferase in the cerebral cortex and hippocampus, and the plasma concentration of GABA increased with the treatment with GABA (Table 3). It is well

Table 4. Effects of the addition of GABA<sup>1</sup> to a basal diet on the plasma concentration of growth hormone in ovariectomized female rats (Exp 3).<sup>2</sup>

	Control	GABA
Final body weight (g)	218 $\pm$ 4	221 $\pm$ 5
Food intake (g)	11.3 $\pm$ 0.3	11.1 $\pm$ 0.3
Plasma GH <sup>3</sup> ( $\mu$ g/L)	17.6 $\pm$ 2.5	50.9 $\pm$ 6.9*

<sup>1</sup>  $\gamma$ -Aminobutyric acid.

<sup>2</sup> Values are means and SE,  $n=6$ . \* Significantly different from the control value ( $p<0.05$ ). The plasma concentration of growth hormone was measured after only one 3-h feeding period of the test diet. After feeding on the 20% casein diet for 10 d (one 3-h feeding period per day), the rats were given the experimental diets for 1 d (only one 3-h period).

<sup>3</sup> Growth hormone.

known that NGF protects cholinergic neurons against cell death and that an elevated survival of cholinergic neurons correlates with enhanced choline acetyltransferase activity (26). Korsching et al. (5) indicated that the concentration and mRNA level of hippocampal NGF are correlated with the density of cholinergic innervation. Gnahn et al. (4) reported that the NGF treatment increased the activity of choline acetyltransferase *in vivo* in the hippocampus and cortex of newborn rats. The higher mRNA level NGF in the hippocampus of ovariectomized female rats fed the GABA may have regulated the NGF concentration in the hippocampus and increased the activity of choline acetyltransferase in the brain. However, in the present study, we did not determine the mRNA level of choline acetyltransferase in the brain. The effect of dietary GABA on the choline acetyltransferase mRNA level in the brains of ovariectomized female rats is another question to consider in a future study.

A deficiency of growth hormone (GH) also affects brain function. Treatment of adult GH-deficient patients with human GH is reported to improve the cognitive efficiency and memory function (27, 28). GH has been found to facilitate the long-term memory and the extinction response as recorded in a behavioral assay in rats (29). Le Greves et al. (30) suggested that GH induced the gene expression of hippocampal *N*-methyl-D-aspartate receptor in rats, coinciding with improved learning and memory capabilities. The possibility that the hormone itself may pass the blood-brain barrier is supported by several studies (31). The GH-binding receptor has been identified in the brains of humans and rats (32). Recently, we (33) reported that dietary GABA increased the rate of brain protein synthesis in sham-operated rats, and did not affect the rate of brain protein synthesis in hypophysectomized rats. Thus, the GABA-induced increase in the concentration of GH may be primarily responsible for changes in the brain protein synthesis (33). In Experiment 3, a transiently higher plasma concentration of GH was observed after feed-

ing GABA diet; however, the food intake did not differ between the experimental groups (Table 4). Therefore, the results suggested that the dietary GABA affected the gene expression of brain protein, and that the regulation of NGF by GABA treatment was mediated through changes in the concentration of GH. However, the role of GH treatment in maintaining NGF in the brains of rats given GABA remains unknown. Measurement of the role of GABA and GH on the mRNA of NGF in the hippocampus of hypophysectomized rats should be included in further studies of the effect of GABA treatment on the brain function of aged rats.

Several investigators reported that GABA did not pass the blood-brain barrier (34, 35). Recently, in the pituitaries of young rats, the GH stimulatory effect of GABA has been shown to involve enhanced calcium-flux (36) and increased intracellular calcium (37). Mergl et al. (38) suggested that GABA directly stimulated GH secretion in the pituitary. However, little documentation of the effect of GABA treatment on the GH secretion has been reported in ovariectomized female rats. The regulatory mechanism for the effect of GABA on the plasma concentration of GH of ovariectomized female rats is another question to consider in a future study.

Sherwin (8) reported that there was a beneficial effect of estrogen on memory tasks in postmenopausal women, and that estrogen deficiency may be partly responsible for the neurodegeneration of Alzheimer's disease. Data in ovariectomized rats demonstrated that treatment with estrogen increased the mRNA of NGF and choline acetyltransferase in the brain, which are important for learning and memory processes (9). In the present study, we found a higher concentration and mRNA level of NGF, and higher activity of choline acetyltransferase in the hippocampus of GABA-treated ovariectomized female rats. The results strongly suggested that the ingestion of dietary GABA reversed the effect of ovariectomy on the brain function in the female aged rats. On the other hand, little documentation of the effect of GABA treatment on the brain function or content of choline acetyltransferase and NGF has been reported in young or male rats. Therefore, for future study, the effects of dietary GABA on the NGF concentration and choline acetyltransferase activity in the brains of young rats or male rats is another question.

These results suggest that the administration of GABA to ovariectomized female rats is likely to control the mRNA level and concentration of NGF and cause an increase in the activity of choline acetyltransferase in the brains. The mRNA level is at least partly related to the mechanism by which the dietary GABA affects the NGF concentration in the brains of rats. These findings are also of importance nutritionally in understanding the role of GABA in the brain function in mammals.

#### Acknowledgments

The authors are grateful to K. Takahashi and R. Horioka for their valuable technical assistance. This study is supported in part by a grant from the Pharma Foods International Company Ltd.

## REFERENCES

- 1) Hefti F. 1986. Nerve growth factor promotes survival of septal cholinergic neurons after fimbrial transections. *J Neurosci* **6**: 2155–2162.
- 2) Lindsay RM, Wiegand SJ, Altar A, Distefano PS. 1994. Neurotrophic factors: from molecule to man. *Trends Neurosci* **17**: 182–192.
- 3) Shelton DL, Reichardt LF. 1986. Studies on the expression of the  $\beta$ -nerve growth factor (NGF) gene in the central nervous system: level and regional distribution of NGF mRNA suggest that NGF functions as a trophic factor for several distinct populations of neurons. *Proc Natl Acad Sci USA* **83**: 2714–2718.
- 4) Gnahn H, Hefti F, Heumann R, Schwab ME, Thoenen H. 1983. NGF-mediated increase of choline acetyltransferase in the neonatal rat forebrain: evidence for a physiological role of NGF in the brain. *Dev Brain Res* **9**: 45–52.
- 5) Korsching S, Auburger G, Heumann R, Scott J, Thoenen H. 1985. Levels of nerve growth factor and its mRNA in the central nervous system of the rat correlate with cholinergic innervation. *EMBO J* **4**: 1389–1393.
- 6) Hefti F, Hartikka J, Knusel B. 1989. Function of neurotrophic factors in the adult and aging brain and their possible use in the treatment of neurodegenerative diseases. *Neurobiol Aging* **10**: 515–533.
- 7) Kosik KS. 1992. Alzheimer's disease: a cell biological perspective. *Science* **256**: 780–783.
- 8) Sherwin BB. 1994. Estrogenic effects on memory in women. *Ann NY Acad Sci* **743**: 213–231.
- 9) Pan Y, Anthony M, Clarkson TB. 1999. Effect of estradiol and soy phytoestrogens on choline acetyltransferase and nerve growth factor mRNAs in the frontal cortex and hippocampus of female rats. *Proc Soc Exp Biol Med* **221**: 118–125.
- 10) Hayase K, Tanaka M, Tujioka K, Hirano E, Habuchi O, Yokogoshi H. 2001. 17- $\beta$ -Estradiol affects brain protein synthesis rate in ovariectomized female rats. *J Nutr* **131**: 123–126.
- 11) Lyou S, Hirano E, Tujioka K, Mawatari Y, Hayase K, Okuyama S, Yokogoshi H. 2002. Dietary genistein affects brain protein synthesis rates in ovariectomized female rats. *J Nutr* **132**: 2055–2058.
- 12) Mitsushima D, Shwe T-T-W, Funabashi T, Shinohara K, Kimura F. 2002. GABA release in the medial preoptic area of cyclic female rats. *Neuroscience* **113**: 109–114.
- 13) Roberts E, Frankel S. 1950.  $\gamma$ -Aminobutyric acid in brain: its formation glutamic acid. *J Biol Chem* **187**: 55–63.
- 14) Otsuka M, Kravitz EA, Potter DD. 1966. Physiological and chemical architecture of a lobster ganglion with particular reference to gamma-aminobutyrate and glutamate. *J Neurophysiol* **30**: 725–752.
- 15) Lyou S, Yokogoshi H. 2004. Hormones and brain function. In: Brain Function and Nutrition (Yokogoshi H, ed), p 359–372. Saiwaishobo, Tokyo.
- 16) Tujioka K, Ohsumi M, Horie K, Kim M, Hayase K, Yokogoshi H. 2009. Dietary  $\gamma$ -aminobutyric acid affects the brain protein synthesis rate in ovariectomized female rats. *J Nutr Sci Vitaminol* **55**: 75–80.
- 17) Gibbs RB, Wu D, Hersh LB, Pfaff DW. 1994. Effects of estrogen replacement on the relative levels of choline acetyltransferase, trk A and nerve growth factor messenger RNAs in the basal forebrain and hippocampal formation of adult rats. *Exp Neurol* **129**: 70–80.
- 18) Tujioka K, Okuyama S, Yokogoshi H, Fukaya Y, Hayase K, Horie K, Kim M. 2007. Dietary  $\gamma$ -aminobutyric acid affects the brain protein synthesis rate in young rats. *Amino Acids* **32**: 255–260.
- 19) Reinstein DK, Isaacson RI, Dunn AJ. 1979. Regional change in 2-deoxyglucose uptake after neocortical and hippocampal destruction. *Brain Res* **175**: 392–397.
- 20) Bianchi L, Della Corte L, Tipton KF. 1999. Simultaneous determination of basal and evoked output levels of aspartate, glutamate, taurine and 4-aminobutyric acid during microdialysis and from superfused brain slices. *J Chromatogr* **723**: 47–59.
- 21) Fonnum F. 1975. A rapid radiochemical method of the determination of choline acetyltransferase. *J Neurochem* **24**: 407–409.
- 22) Yamada T, Terashima T, Wada K, Ueda S, Ito M, Okubo T, Juneja LR, Yokogoshi H. 2007. Theanine,  $\gamma$ -glutamyl-ethylamide, increases neurotransmission concentrations and neurotrophin mRNA levels in the brain during lactation. *Life Sci* **81**: 1247–1255.
- 23) Snedecor GW, Cochran WG. 1967. Statistical Methods, 6th ed, p 135–171. Iowa State University Press, Ames.
- 24) Singh M, Meyer EM, Millard WL, Simpkins JW. 1994. Ovarian steroid deprivation results in a reversible learning impairment and compromised cholinergic function in female Sprague-Dawley rats. *Brain Res* **644**: 305–312.
- 25) Tujioka K, Shi X, Ohsumi M, Tuchiya T, Hayase K, Uchida T, Ikeda S, Morishita A, Yokogoshi H. 2009. Effect of quantity and quality of dietary protein on choline acetyltransferase and nerve growth factor, and their mRNAs in the cerebral cortex and hippocampus of rats. *Amino Acids* **36**: 13–19.
- 26) Deckwerth TL, Johnson EM Jr. 1993. Temporal analysis of events associated with programmed cell death (apoptosis) of sympathetic neurons deprived of nerve growth factor. *J Cell Biol* **123**: 1207–1222.
- 27) Deijien JB, de Boer H, van der Veen EA. 1998. Cognitive changes during growth hormone replacement in adult men. *Psychoneuroendocrinology* **23**: 45–55.
- 28) Gibney J, Wallace JD, Spinks T, Schnorr L, Ranicar A, Cueno RC, Lockhart S, Burnand KG, Salomon F, Sonken PH, Russel-Jones D. 1999. The effects of 10 years of recombinant human growth hormone (GH) in adult GH-deficient patients. *J Clin Endocrinol Metab* **84**: 2596–2602.
- 29) Schneider-Rivas S, Rivas-Arancibia S, Vazquez-Pereyra F, Vezquez-Sandval R, Borgonio-Perez G. 1995. Modulation of long-term memory and extinction responses induced by growth hormone (GH) and growth hormone releasing hormone (GHRH) in rats. *Life Sci* **56**: PL433–441.
- 30) Le Greves M, Steensland P, Le Greves P, Nyberg F. 2002. Growth hormone induces age-dependent alteration in the expression of hippocampal growth hormone receptor and N-methyl-D-aspartate receptor subunits gene transcripts in male rats. *Proc Natl Acad Sci USA* **99**: 7119–7123.
- 31) Burman P, Hetta J, Wide L, Mansson JE, Ekman R, Karlsson EA. 1996. Growth hormone treatment affects brain neurotransmitters and thyroxine. *Clin Endocrinol* **44**: 319–324.
- 32) Lai Z, Roos P, Zhai Q, Olsson Y, Fholenhag K, Larsson C, Nyberg F. 1993. Age-related reduction of human growth hormone-binding sites in the human brain.

- Brain Res* **621**: 260–266.
- 33) Tujioka K, Ohsumi M, Sakamoto K, Thanapreedawat P, Akao M, Kim M, Hayase K, Yokogoshi H. 2011. Effect of dietary  $\gamma$ -aminobutyric acid on the brain protein synthesis rate in hypophysectomized aged rats. *J Nutr Sci Vitaminol* **57**: 285–291.
- 34) Van Gelder NM, Elliot KAC. 1958. Disposition of  $\gamma$ -aminobutyric acid administered to mammals. *J Neurochem* **3**: 139–143.
- 35) Takemoto M, Murayama S. 1967. The effects of gamma aminobutyric acid and gamma hydroxybutyrate upon responses of cat cerebral cortex to direct stimulation. *J Chiba Med Soc* **43**: 260–262.
- 36) Acs Z, Zsom L, Makara GB. 1992. Possible mediation of GABA induced growth hormone secretion by increased calcium-flux in neonatal pituitaries. *Life Sci* **50**: 273–279.
- 37) Horvath G, Acs Z, Mergl Z, Nagy I, Makara GB. 1993. Gamma-aminobutyric acid-induced elevation of intracellular calcium concentration in pituitary cells of neonatal rats. *Neuroendocrinology* **57**: 1028–1034.
- 38) Mergl Z, Acs Z, Makara GB. 1995. Growth hormone secretion and activation of cyclic AMP by growth hormone releasing hormone and gamma-aminobutyric acid in the neonatal rat pituitary. *Life Sci* **56**: 579–585.
- 39) American Institute of Nutrition. 1993. AIN purified diets for laboratory rodents: final report of the American Institute of Nutrition Ad Hoc Writing Committee on the reformulation of the AIN 76A rodent diet. *J Nutr* **123**: 1939–1951.

Original research paper

# *Lactobacillus helveticus*–fermented milk improves learning and memory in mice

Kazuhito Ohsawa<sup>1</sup>, Naoto Uchida<sup>1</sup>, Kohji Ohki<sup>1</sup>, Yasunori Nakamura<sup>1</sup>, Hidehiko Yokogoshi<sup>2</sup>

<sup>1</sup>Microbiology & Fermentation Laboratory, CALPIS Co., Ltd, Chuo-ku, Sagamihara-shi Kanagawa, Japan,

<sup>2</sup>Department of Food & Nutritional Sciences, College of Bioscience and Biotechnology, Chubu University, Kasugai-shi, Aichi, Japan

**Objectives:** To investigate the effects of Calpis sour milk whey, a *Lactobacillus helveticus*–fermented milk product, on learning and memory.

**Methods:** We evaluated improvement in scopolamine-induced memory impairment using the spontaneous alternation behaviour test, a measure of short-term memory. We also evaluated learning and working memory in mice using the novel object recognition test, which does not involve primary reinforcement (food or electric shocks). A total of 195 male ddY mice were used in the spontaneous alternation behaviour test and 60 in the novel object recognition test.

**Results:** Forced orally administered Calpis sour milk whey powder (200 and 2000 mg/kg) significantly improved scopolamine-induced cognitive impairments ( $P < 0.05$  and  $P < 0.01$ , respectively) and object recognition memory (2000 mg/kg;  $P < 0.05$ ).

**Discussion:** These results suggest that Calpis sour milk whey may be useful for the prevention of neurodegenerative disorders, such as Alzheimer's disease, and enhancing learning and memory in healthy human subjects; however, human clinical studies are necessary.

**Keywords:** Fermented milk, *Lactobacillus helveticus*, Learning, Memory, Scopolamine

## Introduction

Fermented milks have been widely produced in many countries for thousands of years.<sup>1</sup> Extensive efforts have been made to demonstrate the beneficial effects of fermented milks on health, such as their hypotensive properties, antimicrobial activities, prevention of acute diarrhoea, and hypocholesterolemic effects.<sup>2</sup> For example, Calpis sour milk has several physiological effects, including life-extending effects, inhibition of chemically induced tumorigenesis, and antihypertensive effects.<sup>3,4</sup> Calpis sour milk (Calpis, Tokyo, Japan) is cultured milk prepared by fermenting skim milk with a natural starter culture containing *Lactobacillus helveticus* and *Saccharomyces cerevisiae* as the predominant microorganisms, and has been used for many years.<sup>4</sup>

Alzheimer's disease is a progressive neurodegenerative disorder common among elderly people. Alzheimer's disease is characterized by alterations of

various neurotransmitters and related markers and receptors.<sup>5</sup> Of these, the most severely affected by far is the cholinergic system.<sup>6</sup> A large number of studies have shown that the cholinergic system plays an important role in learning and memory.<sup>7</sup> Moreover, reductions in cholineacetyltransferase activity and acetylcholine synthesis are strongly correlated with the degree of cognitive impairment in patients with Alzheimer's disease.<sup>8</sup> Cognitive enhancers, such as choline esterase inhibitors (donepezil, rivastigmine, and galantamine), are being used to improve cognitive deficits related to Alzheimer's disease and other neurodegenerative disorders.<sup>9</sup> Although most of the enhancers are therapeutics their improving effects are mild, and they have adverse effects, such as nausea, vomiting, diarrhoea, dizziness, and weight loss.<sup>9</sup> Therefore, it is worthwhile exploring the therapeutic effects of functional foods which prevent various cognitive disorders without adverse effects.

With raised awareness of the effects of nutrition on physical and mental health, there has increasing research into the effect of omega-3 polyunsaturated fatty acids on health and the brain. Although few

Correspondence to: Kazuhito Ohsawa, Microbiology & Fermentation Laboratory, CALPIS Co., Ltd, 11-10, 5-chome, Fuchinobe, Chuo-ku, Sagamihara-shi Kanagawa 252-0206, Japan.  
Email: kazuhito.oosawa@calpis.co.jp

studies have examined the cognitive effects of omega-3 polyunsaturated fatty acids through childhood, young adulthood, and middle-age, multiple studies have suggested omega-3 polyunsaturated fatty acids can protect against neurodegeneration and possibly reduce the chance of developing cognitive impairment at later ages.<sup>10</sup> Polyphenols, which are abundant in fruits, vegetables, herbs and various drinks (tea, wine, and juices), have proven to be effective in alleviating and protecting against the general mechanisms of neurodegenerative diseases in various cell cultures and animal models. However, as investigations into the benefits of polyphenols in human health have only recently begun, further study is necessary.<sup>11</sup> Recently, interest in the use of dairy products in the prevention or amelioration of normal age-related cognitive decline and dementia has grown.<sup>12</sup> Current evidence suggests that regular consumption of low-fat dairy products as part of a balanced diet may have a number of positive effects on neurocognitive health in ageing.<sup>13</sup> A form of dairy product, Colostrin<sup>®</sup>, a proline-rich polypeptide complex from ovine colostrums, has shown potential in the treatment of patients with mild Alzheimer's disease.<sup>14</sup> To examine the effects of *L. helveticus* fermented milk whey on neurocognitive health, we investigated the effects of Calpis sour milk whey on memory impairment induced by scopolamine in mice using a spontaneous alternation behaviour test. We chose scopolamine-treated mice as an amnesic model because spontaneous alternation performance is significantly impaired by scopolamine, and this model is widely used in learning and memory studies.<sup>15</sup> As scopolamine has been used as a model in screening anti-amnesic drugs,<sup>16</sup> it is hypothesized that substances effective in reversing scopolamine-induced cognitive deficits in mice might improve cognitive function. In addition, we investigated the effects of Calpis sour milk whey on learning and memory in mice using a novel object recognition test. We chose the novel object recognition test as a measure of working memory. As the test does not involve primary reinforcement, such as food or electric shocks, it is comparable with memory tests used in humans.<sup>17</sup> The performance of mice depends on their innate tendency to investigate a novel object more than a familiar object and may be less dependent on the strain,<sup>18</sup> suggesting the novel object recognition test has several advantages in assessing the effects of substance treatment on memory processes.

## Methods

### Animals

A total of 255 male ddY mice (Japan SLC Inc., Shizuoka, Japan), aged 7 weeks, were used to perform all the memory tasks. The ddY strain is an outbred one, has been maintained as a closed colony and is

often used for behavioural experiments.<sup>19</sup> The animals were housed 3–5 per cage, maintained under standard conditions (23 ± 3°C, 55 ± 15% humidity, 12 hours light–dark cycle with the light on between 07:00 and 19:00 hours), and allowed access to water and food *ad libitum*. The mice were used in the experiments following at least 1 week's adaptation to the laboratory conditions and were naive to each of the tests used in the present study. All experiments were conducted between 09:00 and 18:00 hours and the time of the behavioural test was designed at random to avoid treating the control group or the test group only at certain times. Before and during the behavioural tests, mice were handled to minimize stress. All experiments were performed in compliance with the Guidelines for Animal Experiments of Japan Bioscience Center or Intelligence & Technology Lab, based on the Guidelines for Proper Conduct of Animal Experiments (Science Council of Japan, 2006), Act on Welfare and Management of Animals (Act No. 68 of 2005, Japanese Law) and the Standards Relating to the Care and Management of Laboratory Animals and Relief of Pain (Notice no. 88, Ministry of the Environment, Government of Japan).

### Materials

Calpis sour milk was prepared by fermenting skim milk with a starter culture containing *L. helveticus* and *S. cerevisiae*, as previously described.<sup>3</sup> In brief, pasteurized skim milk was inoculated with a 3% starter culture, fermented at 37°C for 24 hours and pasteurized. Calpis sour milk was separated into the supernatant and precipitate fractions by centrifugation at 8000 g for 30 minutes. The supernatant whey fraction was then freeze dried into Calpis sour milk whey powder which was dissolved in distilled water at the indicated concentrations for the animal experiments. Forced oral administration was performed for all substances using an injection volume of 10 ml/kg body weight. Scopolamine hydrobromide (Tocris Bioscience, MO, USA) was dissolved in saline at a concentration of 0.5 mg/ml and subcutaneously administered using an injection volume of 2 ml/kg body weight.

### Spontaneous alternation behaviour test

#### The effects of Calpis sour milk whey on spontaneous alternation behaviour in mice

The testing procedure was based on that of Itoh *et al.*<sup>19</sup> The experimental apparatus consisted of a black-painted Y-maze made of plywood. Each of the three arms of the Y-maze were 40 cm long, 12 cm high, 3 cm wide at the bottom, and 10 cm wide at the top and positioned at equal angles around the centre. Mice were brought to the experimental room more than 1 hour before the behavioural experiment to

habituate them to the environment. During testing, white light of 220–240 lx intensity was used to evenly illuminate the Y-maze. The Y-maze was cleaned with fragrance free paper in between test subjects. Following random assignment to experimental groups, mice were forcibly orally administered Calpis sour milk whey powder (20, 200, and 2000 mg/kg;  $n = 15$  mice per group) or distilled water (control; 10 ml/kg,  $n = 15$  mice per group) 60 minutes before the start of the spontaneous alternation behaviour test. After 30 minutes, the entire group (60 mice) received saline subcutaneously. The spontaneous alternation behaviour test was conducted 30 minutes after saline administration. The sequence and number of arm entries were recorded manually during the session by a person unaware of the administered substance. The entry of mice was defined as whole body into each arm. Alternation was defined as entry into all three arms on consecutive choices. The percentage alternation was determined by dividing the total number of alternations by the total number of choices minus 2. For example, if the arms (A, B, C) were entered in the order ABCBABAC, there would be three alternations (ABC, CBA, BAC) out of a possible six (8 minus 2), resulting in a percentage alternation score of 50. Mice that exhibited arm entries less than eight times during the test were eliminated because the data obtained from these mice were not considered to reflect precise alternation.

#### **The effects of Calpis sour milk whey on scopolamine-induced impairment of spontaneous alternation behaviour in mice**

In this study, three different sets of mice ( $n = 15$  mice per group) were used to test behaviour after scopolamine treatment. The testing procedure was as described in the Introduction. Following random assignment to experimental groups, mice were forcibly orally administered Calpis sour milk whey powder (20, 200, 2000 mg/kg;  $n = 15$  mice per group) or distilled water (control and vehicle; 10 ml/kg,  $n = 45$  mice per group) 60 minutes before the start of the spontaneous alternation behaviour test. After 30 minutes, memory impairment was induced by subcutaneous administration of scopolamine (1 mg/kg); the control group (45 mice) received saline. The spontaneous alternation behaviour test was conducted 30 minutes after scopolamine administration. The sequence and number of arm entries were recorded manually during the session by a person unaware of the administered substance. Analysis was performed as described in the Introduction.

#### **Novel object recognition test**

The testing procedure was a modified version of that reported by Sik *et al.* (2003)<sup>18</sup>. The apparatus was an

open clear box made of vinyl chloride with 30 cm × 30 cm × 30 cm dimensions. A ceramic cat ornament, a wooden column-shaped pen stand, and a resin block were used as objects in the experiment. Mice were brought to the experimental room more than 1 hour before the behavioural experiment to habituate them to the environment. During testing, white light of 220–240 lx intensity was used to evenly illuminate the open clear box. Mice showed no significant preference for the three objects and the objects used for each test were randomized. The objects were positioned 8 cm along the centre line of the floor. The box was cleaned with fragrance free paper in between test subjects. The objects were cleaned with ethanol to get rid of odours in between test subjects. During the training session, two novel objects, A and B, were placed in an open-field box, and each mouse was allowed to explore for 5 minutes. Before each test, the time between a training session and a retention test was evaluated. The exploratory preference of non-treated ddY mice in a training session was  $47.0 \pm 2.5\%$  ( $n = 15$ , retention time: 1 day) and  $51.4 \pm 2.0\%$  ( $n = 20$ , retention time: 2 days). The exploratory preference of non-treated ddY mice in a retention test was  $59.1 \pm 3.6\%$  ( $n = 15$ , retention time: 1 day time difference) and  $53.9 \pm 2.7\%$  ( $n = 20$ , retention time: 2-day time difference). As non-treated ddY mice remembered objects 1 day after a training session ( $P < 0.05$ ) and forgot objects 2 days after a training session ( $P = 0.46$ ), the interval between the training session and the retention test was 2 days. In this study, two different sets ( $n = 15$  mice per group) of mice were used for behavioural testing. Following random assignment to experimental groups, mice were forcibly orally administered Calpis sour milk whey powder (200, 2000 mg/kg, po;  $n = 15$  mice per group) 60 minutes before the training session of the novel object recognition test. The control group (30 mice) was forcibly orally administered distilled water. The behaviour of mice was recorded by video and the length of time that the mouse explored each object was measured by a person unaware of the administered substance. Object exploration was defined as directing the nose to the object at a distance less than 1 cm. Mice turning around or sitting on the object were not considered as displaying exploratory behaviour. Two days after the training session, the retention test was conducted. During the retention test, each mouse was placed in the same box, in which the familiar object B was replaced with a novel object C, and was allowed to explore for 5 minutes. The behaviour of mice was recorded by video and the length of time that the mouse explored each object was measured during the retention test. The length of time that the mouse explored each object was measured by a person unaware of the administered substance. A

1

preference index, the ratio of time spent exploring the familiar object B (training session) or the novel object C (retention test) to the total time spent exploring both objects, was used to measure recognition memory. Mice that explored the two objects for less than 10 seconds during the training session or the retention test were excluded from the sample.

### Statistical analysis

All of the results are expressed as means  $\pm$  standard error of the mean (SEM). In all of the analyses, the assumption of normality was tested using the Shapiro and Wilk test. The assumption of homogeneity of variances was tested using the Bartlett test. When both assumptions of normality and homogeneity of variances were satisfied, parametric testing was performed. When the assumption of normality or homogeneity of variances was rejected, non-parametric testing was performed. All statistical analyses were performed using EZR (Saitama Medical Center, Jichi Medical University), which is a graphical user interface for R (The R Foundation for Statistical Computing). More precisely, it is a modified version of R commander designed to add statistical functions frequently used in biostatistics.<sup>20</sup>

In the spontaneous alternation behaviour test without scopolamine, all data were analysed using one-way analysis of variance (ANOVA), followed by the Dunnett test. Differences in values were considered significant when the *P* value was less than 0.05. In the spontaneous alternation behaviour test using scopolamine, since three different sets of tests were conducted, the data from the control groups and the scopolamine + vehicle groups were analysed to verify differences between batches. As there were no differences between batches, all data were analysed together. Data were analysed using a Kruskal–Wallis non-parametric one-way ANOVA, followed by the *post hoc* Steel–Dwass test. Differences in values were considered significant when the *P* value was less than 0.05.

In the novel object recognition test, two different sets of test were conducted and data from the control groups were analysed using Student's *t*-test. As there were no differences between batches, all data were analysed together. Data from the novel object recognition test were analysed using one-way ANOVA, followed by the Dunnett test. Differences in values were considered significant when the *P* value was less than 0.05.

## Results

### Spontaneous alternation behaviour test

#### The effects of Calpis sour milk whey on spontaneous alternation behaviour in mice

No mice were excluded from the analysis. Data from the percentage of alternations and total arm entries were analysed by parametric testing, as assumptions

of normality and homogeneity of variances were satisfied. As shown in Fig. 1A and B, there were no significant differences in the percentage of alternations ( $F(3, 56) = 0.24, P = 0.87$ ) and in the total arm entries ( $F(3, 56) = 0.51, P = 0.67$ ).

#### The effects of Calpis sour milk whey on scopolamine-induced impairment of spontaneous alternation behaviour in mice

No mice were excluded from the analysis. In the three different sets of spontaneous alternation behaviour testing, the percentage of alternations (Kruskal–Wallis analysis:  $H = 0.48, df = 2, P = 0.79$ ) and total arm entries of the control groups ( $F(2, 42) = 0.80, P = 0.46$ ) did not differ between batches. In addition, the percentage of alternations (Kruskal–Wallis analysis:  $H = 0.35, df = 2, P = 0.84$ ) and total arm entries of the scopolamine + vehicle groups ( $F(2, 42) = 0.11, P = 0.90$ ) did not differ between batches. The three different sets of spontaneous alternation behaviour testing were therefore analysed together. As assumptions of normality and homogeneity of variances were rejected, a non-parametric test was used for the analyses of the spontaneous alternation behaviour test. The mean percentage of alternations and total arm entries are presented in Fig. 2A and B, respectively. There were statistically significant differences in the percentage of alternations among groups (Kruskal–Wallis analysis:  $H = 91.4, df = 4, P < 0.01$ ). The mean percentage of alternations in the scopolamine + vehicle group (50.1%) was significantly lower than in the control group (73.6%;  $P < 0.01$ , Fig. 2A). The mean percentage of alternations in the scopolamine + Calpis sour milk whey powder (200 and 2000 mg/kg) groups were significantly higher than in the scopolamine + vehicle group (58.0 and 67.1%;  $P < 0.05$  and  $P < 0.01$ , Fig. 2A), while lower concentrations of Calpis sour milk whey powder (20 mg/kg) group did not significantly affect scopolamine impairment (50.9%;  $P = 1.00$ , Fig. 2A). There were statistically significant differences in total arm entries among groups (Kruskal–Wallis analysis:  $H = 18.1, df = 4, P < 0.01$ ). The total arm entries of the scopolamine + vehicle group were significantly higher than those of the control group ( $P < 0.01$ , Fig. 2B). The total arm entries of the scopolamine + Calpis sour milk whey powder (20, 200, and 2000 mg/kg) groups were not significantly different from those of the scopolamine + vehicle group ( $P = 0.12, 0.51, \text{ and } 0.72$ ).

### Novel object recognition test

One mouse of the Calpis sour milk whey powder (2000 mg/kg) group explored two objects for less than 10 seconds during the training session, and this mouse was excluded from the sample. As assumptions of normality and homogeneity of variances were

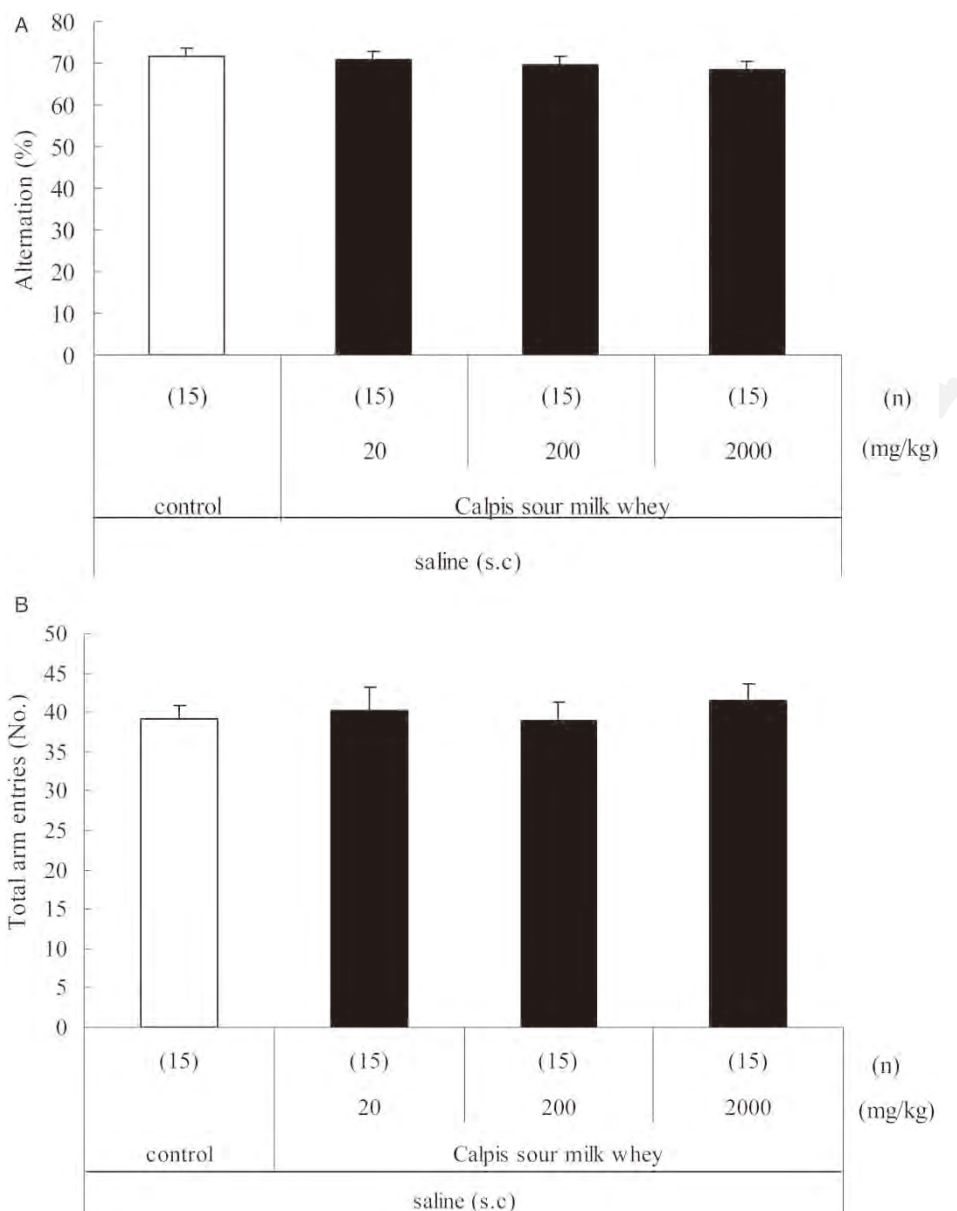


**Figure 1** Effect of Calpis sour milk whey powder on per cent alternation (A) and total number of arm entries (B) in a spontaneous alternation behaviour test. Calpis sour milk whey powder (20, 200, and 2000 mg/kg) or distilled water was forcibly orally administered to mice 60 minutes before testing. Saline was subcutaneously administered 30 minutes before testing. Data are expressed as means  $\pm$  SEM. The number of mice used are shown in parentheses ( $n = 15$  per each group).

satisfied, parametric testing was used in the analyses of the novel object recognition test. In the two different sets of the spontaneous alternation behaviour test, there were no significant differences in the total exploratory time (Student's *t*-test:  $P = 0.41$ ) and in the exploratory preference (Student's *t*-test:  $P = 0.82$ ) during the training session. There were also no significant differences in the total exploratory time (Student's *t*-test:  $P = 0.60$ ) and in the exploratory preference (Student's *t*-test:  $P = 0.96$ ) during the retention test. The two different sets of spontaneous alternation behaviour testing were therefore analysed together. As shown in Fig. 3A and B, during the training session there were no significant differences in the total exploratory time ( $F(2, 56) = 1.01, P = 0.37$ ) or in the exploratory preference between the two objects ( $F(2,$

$56) = 0.36, P = 0.70$ ). In the retention test, as shown in Fig. 3C, there was also no significant difference in the total exploratory time among the groups ( $F(2, 56) = 2.51, P = 0.09$ ). As shown in Fig. 3D, there was a significant difference in the exploratory preference among the groups ( $F(2, 56) = 4.40, P < 0.05$ ). The exploratory preference of the Calpis sour milk whey powder (2000 mg/kg) group was significantly higher than the control group.

**Discussion**

*Summary of main findings*

In the present study, a single administration of Calpis sour milk whey powder (200 or 2000 mg/kg) to mice improved memory impairment induced by scopolamine during the spontaneous alternation behaviour

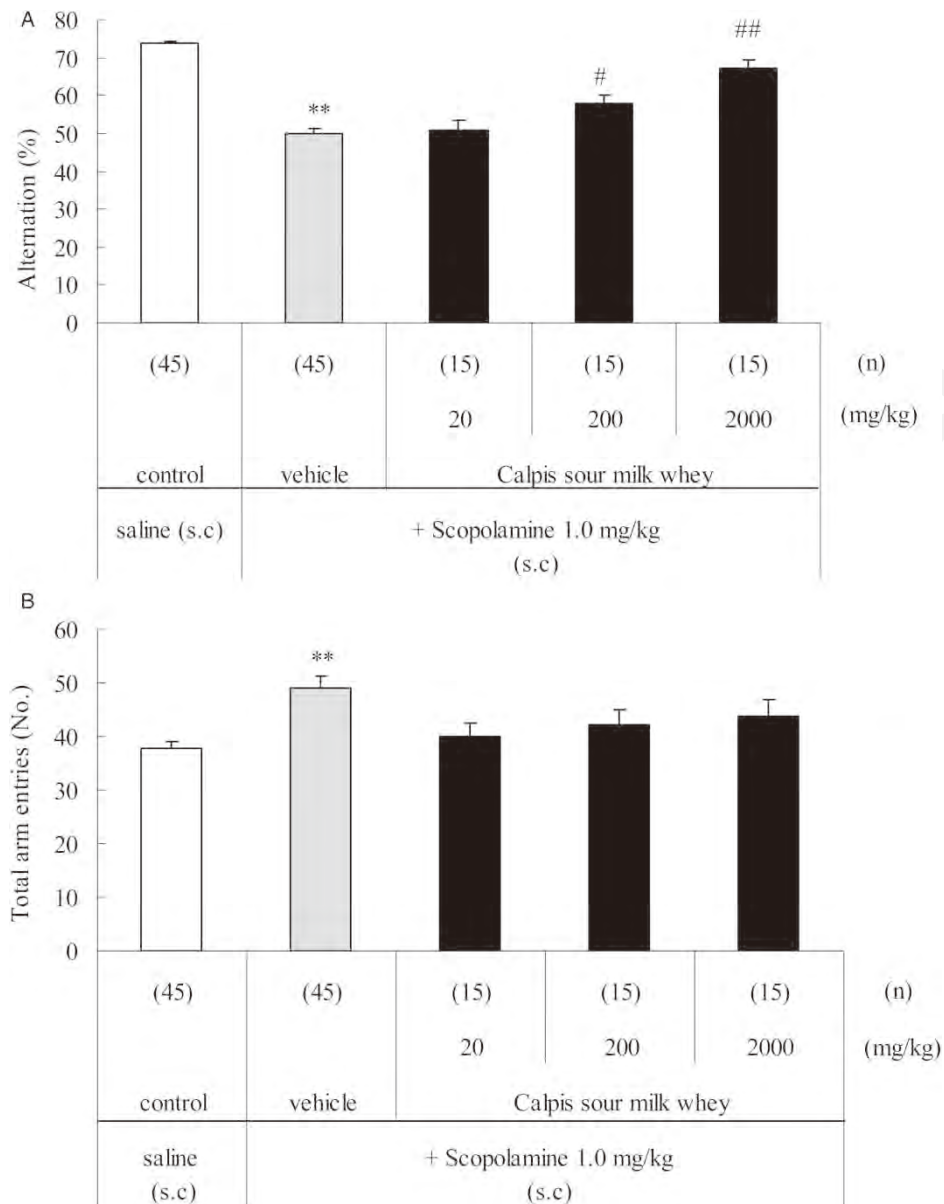


**Figure 2** Effect of Calpis sour milk whey powder on scopolamine-induced impairment of per cent alternation (A) and total number of arm entries (B) in a spontaneous alternation behaviour test. Calpis sour milk whey powder (20, 200, and 2000 mg/kg) or distilled water was forcibly orally administered to mice 60 minutes before testing. Scopolamine (1 mg/kg) or saline was subcutaneously administered 30 minutes before testing. Data are expressed as means  $\pm$  SEM. The number of mice used are shown in parentheses (control group;  $n = 45$ , scopolamine + vehicle group;  $n = 45$  and scopolamine + Calpis sour milk whey powder group;  $n = 15$  per each dose). \*\* $P < 0.01$  vs. control group, # $P < 0.05$  and ## $P < 0.01$  vs. scopolamine + vehicle group.

test, which is used as a measure of immediate spatial working memory, a form of short-term memory.<sup>15</sup> A single administration of Calpis sour milk whey powder (2000 mg/kg) was also effective in the improvement of object recognition memory in the novel object recognition test, a measure of working memory which exploits the tendency of rodents to explore a novel object in their environment more than a familiar one.

*Spontaneous alternation behaviour test*

Scopolamine, an antagonist of muscarinic acetylcholine receptors, causes memory deficits and decreases cholinergic activity during behavioural

performance. The scopolamine model is often used as it provides a simple and quick test of the cognition-enhancing properties of new drugs.<sup>16</sup> Recent studies using the currently prescribed Alzheimer’s drugs, donepezil, galantamine and rivastigmine, have reported similar scopolamine reversal properties in rats.<sup>21</sup> Therefore, Calpis sour milk whey powder, which was effective in reversing scopolamine-induced cognitive deficits in mice, might improve cognitive function in patients with neurodegenerative disorders, such as vascular dementia and Alzheimer’s disease. To date, there have been no reports that a single oral administration of milk, or its ingredients, has a positive effect on cognition, however, some reports

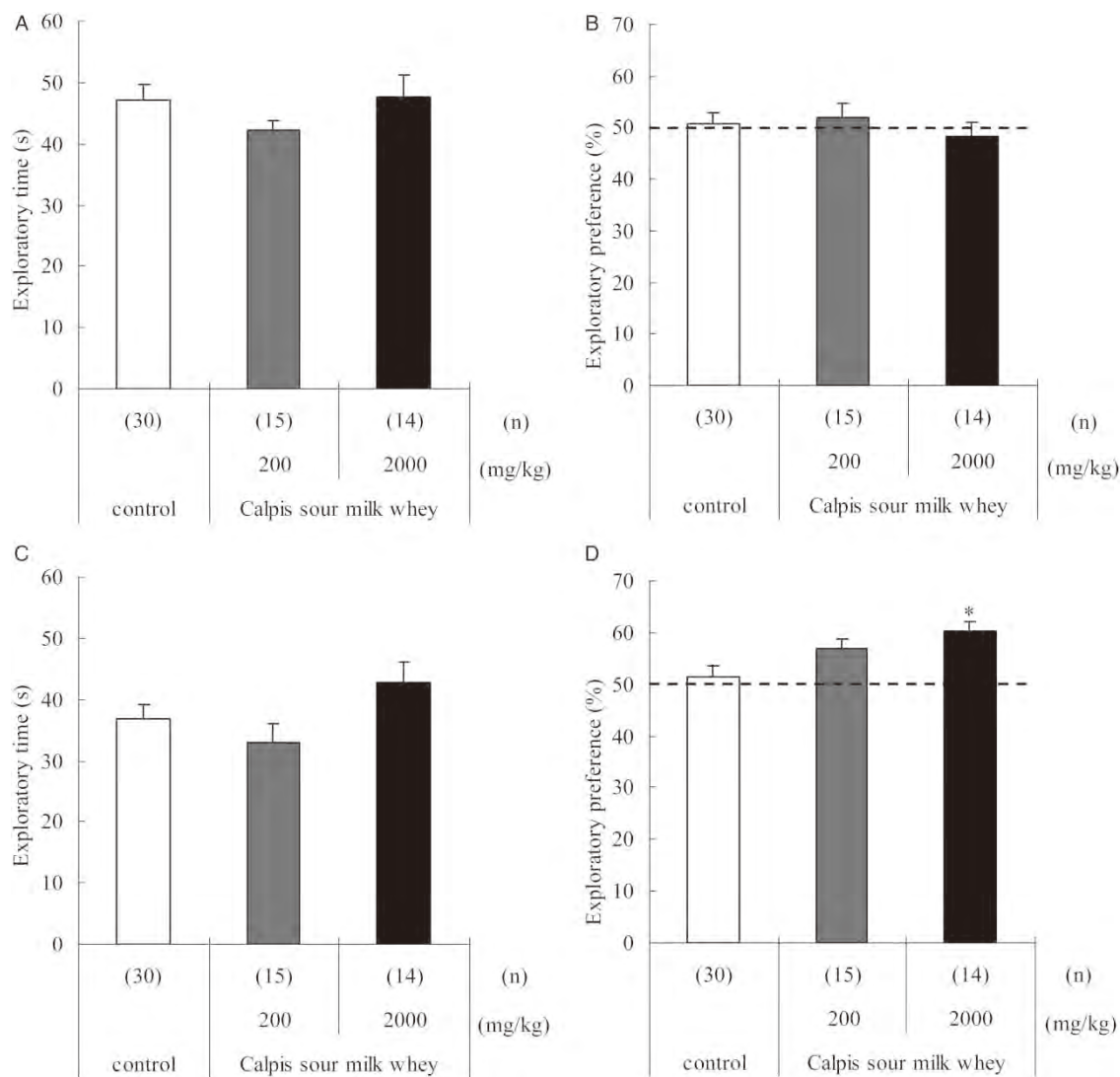


**Figure 3** Effect of Calpis sour milk whey powder on exploratory time (A) and exploratory preference (B) during the training session, and on exploratory time (C) and exploratory preference (D) during the retention test in a novel object recognition test. Calpis sour milk whey or distilled water was forcibly orally administered to mice 60 minutes before the training session. Data are expressed as means  $\pm$  SEM. The number of mice used are shown in parentheses (control group;  $n = 30$ , Calpis sour milk whey powder (200 mg/kg) group;  $n = 15$  and Calpis sour milk whey powder (2000 mg/kg) group;  $n = 14$ ). \* $P < 0.05$  vs. control group.

indicate that continuous administration does have a positive effect. For example, it is reported that the consumption of some low fat dairy products (yogurt and cheese) as part of a balanced diet may be positively associated with some measures of cognitive and psychological health (memory, social functioning, and stress) in middle-aged men and women.<sup>13</sup> It is also reported that milk whey ingredients, such as whey protein, calcium and vitamin B<sub>12</sub>, might have positive effects on cognition in humans when consumed regularly as part of a balanced diet.<sup>12</sup> In particular, alpha-lactalbumin from whey protein has been found to be beneficial in increasing the levels of serotonin: preliminary data suggested potentially beneficial effects on sleep in rats and humans, mood in stress-vulnerable subjects, and cognition in women who display serotonergic hypofunction.<sup>12</sup> Calpis sour milk whey is prepared by fermenting skim milk with

a starter culture containing *L. helveticus* and *S. cerevisiae*. As it is reported that cell counts of *L. helveticus* were more than 100 times higher than *S. cerevisiae* after 24 hours fermentation, skim milk was mainly fermented by *L. helveticus*.<sup>4</sup> The breakdown of milk proteins with lactic acid bacteria (LAB) plays an important role in generating lactic acid, peptides, and amino acids for bacterial growth and in the formation of metabolites that contribute to flavour formation of fermented products.<sup>22</sup> In particular, *L. helveticus* is recognized as a thermophilic LAB, possessing efficient protease and peptidase activities with respect to milk proteins.<sup>22</sup> It was reported that the hydrolysis of milk proteins by *L. helveticus* produces many peptides, including angiotensin I-converting enzyme inhibitory peptides, Val-Pro-Pro and Ile-Pro-Pro, and that the peptide contents of Calpis sour milk increases during the log phase, from 4 to 10

hours.<sup>23</sup> In our study, as a single oral administration of Calpis sour milk whey showed positive effects on cognition, it was hypothesized that lactic acid, peptides, amino acids, or flavour might be effective in improving memory. Further study is necessary to clarify the effective components.

The total arm entries of the scopolamine + vehicle group were significantly higher than those of the control group. It is reported that the role of scopolamine in locomotor behaviour (i.e., an increase or decrease in activity) appears to be dependent on various experimental factors, such as strain, test, type of reinforcement, and drug doses.<sup>18</sup> In this study, scopolamine increased locomotor activities, however, Calpis sour milk whey powder (20, 200, and 2000 mg/kg) did not significantly alter total arm entries.

### Novel object recognition test

The novel object recognition test is used as a measure of working memory that exploits the tendency of rodents to explore a novel object in their environment more than a familiar one. The test does not involve primary reinforcement, such as food or electric shocks, making it comparable to memory tests used in humans.<sup>17</sup>

In this study, the control group mice forgot the familiar object and explored both familiar and novel objects with the same level of interest after a 48 hours retention interval. The Calpis sour milk whey powder (2000 mg/kg) group, however, explored the novel object significantly longer than the control group. Although 200 mg/kg Calpis sour milk whey powder was enough to see an effect on memory in the spontaneous alternation behaviour test, this dose was not enough in the novel object recognition test. It was suggested that the difference in the effective dose depended on the individual difference. Scopolamine might lower the individual difference in the spontaneous alternation behaviour test. However, as the exploratory preference of Calpis sour milk whey powder (200 mg/kg) group (57.0%) was higher than the control group (51.4%), an effect on memory of Calpis sour milk whey powder (200 mg/kg) might be detected using different conditions, such as using a different sample size or animal.

It is necessary for us to examine the mechanism of why a single administration of Calpis sour milk whey improved memory impairment induced by scopolamine and object recognition memory in only 60 minutes. Oral administration of donepezil hydrochloride 60 minutes before a radial maze task improved the scopolamine-induced memory deficit in rats by inhibiting AChE and increasing acetylcholine content in the hippocampus.<sup>24</sup> Intracerebroventricular administration of dynorphin

A-(1-13) 60 minutes before the spontaneous alternation behaviour test improved scopolamine-induced memory deficits in mice by inhibition of dopaminergic activity, through the mediation of kappa-opioid receptors.<sup>25</sup> Intraperitoneal administration of glucose 24 minutes before the spontaneous alternation behavioural test in a four-arm cross maze improved memory by increasing acetylcholine release.<sup>26</sup> Various neurotransmitters, such as glutamate, GABA, dopamine, acetylcholine, serotonin and norepinephrine, are reported to be differently involved in learning and memory.<sup>27</sup> So, it is hypothesized that the release of neurotransmitters after oral administration of *L. helveticus* fermented milk might rapidly improve memory.

The results of two behavioural tests suggest that Calpis sour milk whey powder (200–2000 mg/kg) might be effective in amelioration of memory impairment and enhancement of object recognition memory in humans. The amount of Calpis sour milk whey powder (200–2000 mg/kg) required to produce an effect in mice corresponds to 200–2000 ml/60 kg in humans which is a possible volume for humans to drink.

### Conclusion

Calpis sour milk whey powder improved both scopolamine-induced memory impairment and object recognition memory in mice. These results suggest that Calpis sour milk whey may be useful for the prevention of Alzheimer's disease and for enhancing learning and memory in healthy humans.

### Implications for future research

Alzheimer's drugs are able to stabilize or slow the decline in cognition, but they have adverse events.<sup>9</sup> Therefore, cognition-enhancing foods without adverse events would be advantageous for the prevention of various cognitive disorders. To find such cognition-enhancing foods, many food ingredients, such as arachidonic and docosahexaenoic acids,<sup>28</sup> astaxanthin,<sup>29</sup> and Colostrinin<sup>®</sup>,<sup>14</sup> have been examined and shown to improve cognition in human volunteers. After supplementation with 240 mg/day arachidonic and docosahexaenoic acids for 90 days, patients diagnosed with mild cognitive impairment showed a significant improvement in immediate memory and attention score in the RBANS test.<sup>28</sup> After 12 weeks of 12 mg astaxanthin dialcohol treatment, the response time for tasks in subjects with age-related forgetfulness was reduced and the accuracy of working memory tasks was significantly improved using CogHealth tasks.<sup>29</sup> After supplementation of Colostrinin<sup>®</sup> for 12 months, 8 of 15 Alzheimer's disease patients showed improvement and the disease had stabilized in the remaining 7.<sup>14</sup> It is necessary for us to further examine *L. helveticus* fermented

milk, not only in animals but also in humans, to clarify its potential for cognition enhancement.

## Disclaimer statements

### Contributors

Kazuhito Ohsawa was responsible for study design; preparation of materials; data analysis and interpretation; drafting, critical revision, and final approval of the article. Naoto Uchida was responsible for study design; preparation of materials; data interpretation; critical revision, and final approval of the article. Kohji Ohki was responsible for study design; logistic, administrative and technical support; critical revision and final approval of the article. Yasunori Nakamura was responsible for study design; logistic, administrative and technical support; critical revision and final approval of the article. Hidehiko Yokogoshi was responsible for logistic and technical support; critical revision and final approval of the article. Kazuhito Ohsawa is the guarantor.

### Conflicts of interest

None.

### Ethics approval

All animal experiments in our paper were approved by Japan Bioscience Center Animal Experiments Committee. And all animal experiments in our paper were performed in compliance with the Guidelines for Animal Experiments of Japan Bioscience Center, based on the Guidelines for Proper Conduct of Animal Experiments (Science Council of Japan, 2006), Act on Welfare and Management of Animals (Act No. 68 of 2005, Japanese Law) and the Standards Relating to the Care and Management of Laboratory Animals and Relief of Pain (Notice no. 88, Ministry of the Environment, Government of Japan).

## References

- Tamime AY. Fermented milks: a historical food with modern applications – a review. *Eur J Clin Nutr* 2002;56(Suppl. 4): S2–15.
- Ebringer L, Ferencik M, Krajcovic J. Beneficial health effects of milk and fermented dairy products – review. *Folia Microbiol (Praha)* 2008;53:378–94.
- Takano T, Arai S, Murota I, Hayakawa K, Mizutani T, Mituoka T. Effects of feeding sour milk on longevity and tumorigenesis in mice and rats. *Bifidobacteria Microflora* 1985;4:31–7.
- Hata Y, Yamamoto M, Ohni M, Nakajima K, Nakamura Y, Takano T. A placebo-controlled study of the effect of sour milk on blood pressure in hypertensive subjects. *Am J Clin Nutr* 1996;64:767–71.
- Carr DB, Goate A, Phill D, Morris JC. Current concepts in the pathogenesis of Alzheimer's disease. *Am J Med* 1997;103(3A): 3S–10S.
- Dumas JA, Newhouse PA. The cholinergic hypothesis of cognitive aging revisited again: cholinergic functional compensation. *Pharmacol Biochem Behav* 2011;99:254–61.
- Blockland A. Acetylcholine: a neurotransmitter for learning and memory? *Brain Res Rev* 1995;21:285–300.
- Francis PT, Palmer AM, Snape M, Wilcock GK. The cholinergic hypothesis of Alzheimer's disease: a review of progress. *J Neurol Neurosurg Psychiatry* 1999;66:137–47.
- Hansen RA, Gartlehner G, Webb AP, Morgan LC, Moore CG, Jonas DE. Efficacy and safety of donepezil, galantamine and rivastigmine for the treatment of Alzheimer's disease: a systematic review and meta-analysis. *Clin Interv Aging* 2008;3:211–25.
- Karr JE, Alexander JE, Winningham RG. Omega-3 polyunsaturated fatty acids and cognition throughout the lifespan: a review. *Nutr Neurosci* 2011;14:216–25.
- Albarracin SL, Stab B, Casas Z, Sutachan JJ, Samudio I, Gonzalez J, et al. Effects of natural antioxidants in neurodegenerative disease. *Nutr Neurosci* 2012;15:1–9.
- Camfield DA, Owen L, Scholey AB, Pipingas A, Stough C. Dairy constituents and neurocognitive health in aging. *Br J Nutr* 2011;106:159–74.
- Crichton GE, Murphy KJ, Bryan J. Dairy intake and cognitive health in middle-aged South Australians. *Asia Pac J Clin Nutr* 2010;19:161–71.
- Leszek J, Inglot AD, Janusz M, Lisowski J, Krukowska K, Georgiades JA. Colostrinin<sup>®</sup>, a proline-rich polypeptide (PRP) complex isolated from ovine colostrum for treatment of Alzheimer's disease. A double-blind, placebo-controlled study. *Arch Immunol Ther Exp (Warsz)* 1999;47:377–85.
- Sarter M, Bodewitz G, Stephens DN. Attenuation of scopolamine-induced impairment of spontaneous alternation behavior by antagonist but not inverse agonist and antagonist  $\beta$ -carbolines. *Psychopharmacology (Berl)* 1988;94:491–5.
- Sik A, Nieuwehuizen P, Prickaerts J, Blockland A. Performance of different mouse strains in an object recognition task. *Behav Brain Res* 2003;147:49–54.
- Klinkenberg I, Blockland A. The validity of scopolamine as a pharmacological model for cognitive impairment: a review of animal behavioral studies. *Neurosci Biobehav Rev* 2010;34: 1307–50.
- Ennaceur A, Delacour J. A new one-trial test for neurobiological studies of memory in rats. 1: behavioral data. *Behav Brain Res* 1988;31:47–59.
- Itoh J, Ukai M, Kameyama T. Dynorphin A-(1-13) markedly improves scopolamine-induced impairment of spontaneous alternation performance in mice. *Eur J Pharmacol* 1993;236: 341–5.
- Kanda Y. Investigation of the freely-available easy-to-use software 'EZ' (Easy R) for medical statistics. *Bone Marrow Transplant* 2013;48:452–8.
- Buccafusco JJ. The revival of scopolamine reversal for the assessment of cognition-enhancing drugs. In: Buccafusco JJ, (ed.) *Methods of behavior analysis in neuroscience*. 2nd ed. Boca Raton, FL: CRC Press; 2009. Chapter 17. 2
- Sadat-Mekmene L, Genay M, Atlan D, Lortal S, Gagnaire V. Original features of cell-envelope proteinases of *Lactobacillus helveticus*. A review. *Int J Food Microbiol* 2011;146:1–13.
- Nakamura Y, Yamamoto N, Sakai K, Okubo A, Yamazaki S, Takano T. Purification and characterization of angiotensin I-converting enzyme inhibitors from sour milk. *J Dairy Sci* 1995; 78:777–83.
- Sugimoto H, Ogura H, Arai Y, Iimura Y, Yamanishi Y. Research and development of donepezil hydrochloride, a new type of acetylcholinesterase inhibitor. *Jpn J Pharmacol* 2002;89:7–20.
- Itoh J, Ukai M, Kameyama T. Dopaminergic involvement in the improving effects of dynorphin A-(1-13) on scopolamine-induced impairment of alternation performance. *Eur J Pharmacol* 1993;241:99–104.
- Ragozzino M, Unick K, Gold P. Hippocampal acetylcholine release during memory testing in rats: augmentation by glucose. *Proc Natl Acad Sci* 1996;93:4693–8.
- Myhrer T. Neurotransmitter systems involved in learning and memory in the rat: a meta-analysis based on studies of four behavioural tasks. *Brain Res Rev* 2003;41:268–87.
- Kotani S, Sakaguchi E, Warashina S, Matsukawa N, Ishikura Y, Kiso Y, et al. Dietary supplementation of arachidonic and docosahexaenoic acids improves cognitive dysfunction. *Neurosci Res* 2006;56:159–64.
- Satoh A, Tsuji S, Okada Y, Murakami N, Urami M, Nakagawa K, et al. Preliminary clinical evaluation of toxicity and efficacy of a new astaxanthin-rich *Haematococcus pluvialis* extract. *J Clin Biochem Nutr* 2009;44:280–4.

## Authors Queries

Journal: **Nutritional Neuroscience**

Paper: **NNS207**

Article title: ***Lactobacillus helveticus*–fermented milk improves learning and memory in mice**

Dear Author

During the preparation of your manuscript for publication, the questions listed below have arisen.

Please attend to these matters and return this form with your proof. Many thanks for your assistance

Query Reference	Query	Remarks
1	Please check Sik et al. (2003) is not matching with reference 18 in the ref. list.	
2	Please provide the page numbers in reference 21.	

## 大脳半球優位性による色刺激の情動効果の検討

陽東 藍\*<sup>1</sup>・中村 順行\*<sup>1</sup>・横越 英彦\*<sup>2</sup>

A STUDY OF AFFECTIVE EFFECTS OF COLOR STIMULI IN RELATION TO BRAIN ASYMMETRY

Ai YOTO, Yoriyuki NAKAMURA, Hidehiko YOKOGOSHI

### Abstract

Red-, green-, and blue-colored paper stimuli were used to investigate the positive/negative emotions caused by looking at these colors in relation to the simultaneously recorded brain activity. The left lateral activity on electroencephalography (EEG), mental task performance, and the evaluation of color preference by the eight adult subjects were used as indexes. The results showed greater left lateral activity in the alpha band during the closed-eye resting period right after the subjects looked at red compared to the corresponding blue and green conditions. A significant positive correlation was revealed between the color preference evaluations and the left lateral activities, and a significant negative correlation was observed between the color preference evaluations and the activity at occipital regions during the closed-eye resting period.

キーワード: 色, 脳波, 大脳半球優位性, 情動

Key words: Color, Electroencepharogram, Brain asymmetry, Emotion

### 1 はじめに

茶の官能評価で香りや味と共に、茶の浸出液も水色と称して色が検討されることから分かるように、色は食品への嗜好に影響する重要な要素であり、ヒトの情動にも作用する。こうした色と情動との関連についての基礎研究として、筆者らは先行研究の結果から、青などに比べ、赤は情動的不安や内的注意が促進される可能性を示した<sup>1)2)</sup>。色の好き嫌いの度合いの違いや、その色の注視によってもたらされる快、不快などの情動変化がいかに生理測定に反映され、又は影響するかを明らかにすることも、色の情動効果を多側面から考察する上で必要であると考えられる。

情動の指標となる生理測定についての研究から、Herrington らは快、中性、不快な言語刺激が何色で書かれているかを判断させるタスク遂行時の fMRI データを分析した。その結果、快言語刺激時の前頭前野後外側部が活性化し、右より左側の前頭前野後外側部が

活性化すると報告している<sup>3)</sup>。Ekman らは被験者らに喜び、嫌悪を誘発する映像刺激を見せた時の脳波を記録した。その結果、喜び感情を伴う笑顔の時に比べ、喜びの度合いが低い場合の右前頭部 (F4)  $\alpha$  波帯域密度が左 (F3) より低減しており、 $\alpha$  波帯域パワーは脳活動亢進と負の関連を持つことに基づき、右前頭部  $\alpha$  波帯域密度の低減は右半球の活性化を示したと考察している<sup>4)</sup>。同様に Wheeler らも映像刺激提示時の前頭部脳半球活動の非対称性を観察した。右脳側  $\alpha$  帯域のパワー密度の自然対数値から左脳側の数値を引いたものを左脳半球優位性評価値として解析した。つまり、評価値が大きければ大きいほど左脳半球が活性化することを反映するとした。結果として、ポジティブ感情時 (positive affect) は左前頭部の活性化を伴い、ネガティブ感情時 (negative affect) は右前頭部の活性化を伴うと報告した<sup>5)</sup>。綿貫らは不快誘発の香り刺激により右側頭部 (T4, T6) および右頭頂部 (C4, P4) で  $\alpha$  波が減少するなど、種々の物理刺激を与えた状況で、快・不快という情動が生じた時の背景脳波の特徴を検討した。そして、快では左前頭頭部で、不快では左右の前頭部および主に右脳において広範囲に脳活動が増加すると考察した<sup>6)</sup>。

Davidson は脳半球のそれぞれの情動プロセスにつ

\*<sup>1</sup> 静岡県立大学食品栄養環境科学研究院  
School of Food and Nutritional Sciences, the University of Shizuoka

\*<sup>2</sup> 中部大学応用生物学部  
College of Bioscience and Biotechnology, Chubu University

いて、左前頭、前側頭部は楽しい、嬉しいなどの接近行動 (behavioral approach) を引き起こす情動反応、右前頭、前側頭部は嫌悪感などの回避行動 (behavioral withdrawal) を引き起こす情動反応に関連するとまとめている<sup>7)</sup>。更に、Harmon-Jones は、怒りなどのようなネガティブだが接近的な動機傾向を持つ情動に反応して、左前頭部が活性化すると報告している<sup>8)</sup>。このように怒り情動など一部一致しない場合があるものの、31 の研究のメタ解析において、うつや不安障害患者で有意に半球優位差が認められることが報告されており、快情動では主に左前頭部で、不快情動では主に右前頭部において脳活動が増加することが推察されている<sup>9)</sup>。この特徴は鬱患者の不安や抑圧症状を予言するマーカーになりうるとの報告が出ているほど<sup>10) 11) 12)</sup>、多くの研究データによって支持されている説である<sup>13) 14) 15)</sup>。

また、 $\alpha$  波帯域をさらに  $\alpha 1$  と  $\alpha 2$  に分けて情動反応との関連についての報告も散見される。Davidson らは  $\alpha 1$  (8-10Hz) 帯域において、右脳半球優位性 ( $\alpha 1$  パワーの低減) が恐怖情動との正の相関を示唆した<sup>16)</sup>。一方、Pizzagalli らは左脳半球  $\alpha 2$  (10.5-12Hz) 活動はタスクの報酬意識と負の相関を持ち、左脳半球活性化は接近的な動機傾向を持つ情動反応に関連すると考察した<sup>17)</sup>。これらの報告のように、 $\alpha$  波全帯域よりも高い感度が得られる場合があることが予想される。よって、 $\alpha$  波帯域を細分して情動反応との関わりを検討する必要が生じる可能性が示された。

以上のことから、映像などの視覚刺激による快、不快などの情動効果と脳波に関する研究で、肯定的感情は左前頭部の脳活動に関連し、否定的情動は主に右前頭部に関連するが、接近型ネガティブ情動の場合は左前頭部の脳活動に関連することが推察される。さらに、綿貫らの研究においては、匂い刺激などによる不快情動を感じた際に、右頭頂部を含む広範囲に活性化が見られたことが報告されており<sup>6)</sup>、前頭部以外の部位の半球優位性も検討する必要があると考えられる。

しかし、色の好き嫌いなどによる情動変化と脳半球活動の特徴との関連についての研究はまだ少ない。本論文は物体色刺激を注視することにより引き起こされる不安、緊張、または色の好き嫌いによりもたらされるポジティブ感情とネガティブ感情を、大脳半球優位性との関連から明らかにすること、同時にこれらの情動効果が集中力を必要とする単純計算などのような精神作業に与える影響を検証することを目的とした。

## 2 実験方法

### 2-1 被験者

20-23歳の大学生 8 名 (平均  $21.38 \pm 1.19$  歳、男性 4 名、女性 4 名) に実験の趣旨、方法、そしてこの実験の参加による身体の危険性がなく、被験者の意思により途中でやめることによるデメリットがないなどについて口頭で説明し、被験者の同意を得て、実験に参加してもらった。

### 2-2 実験環境

人工気象室 (室温  $24-25^{\circ}\text{C}$ 、相対湿度 50%) 内に背もたれ付きの椅子と机を設置し、刺激色となる色紙を机の上に置いた。照明は昼光色蛍光灯 (FLR 40S-D/M Matsushita Electric Industrial Co. Ltd.) を用い、天井から照らした。色紙の表面における照度を  $500 \text{ lx}$  とした。色刺激は明度と彩度をできる限り同一にした市販の A2 判の色紙 ( $594\text{mm} \times 420\text{mm}$ ) を提示した。色票を用いた目測による各色紙のマンセル値の測定結果はそれぞれ青 (9B5/9)、緑 (5G5/8)、赤 (4/R5/12) 及びベース色の灰 (N5.5) であった。

### 2-3 実験手順

まず被験者を人工気象室内のブースに入室させ、座位安静にしてもらった。タスクの説明、計算タスクの練習、電極装着を行い、実験を開始した。

実験手順は図 1 で示したように、被験者それぞれの色に対する好き嫌いのレベルを評価するため、上記 4 色の他、市販されている色紙で、色相環上でできる限り均等に離れているものを選び、黄 (6Y9/9)、紫 (5P5/6)、黒 (N2)、薄い灰 (N7)、紺 (4PB3/4)、薄ピンク (2R8/5)、肌 (2Y9/5)、黄緑 (8GY7/9)、赤紫 (3RP6/10)、茶 (9YR7/4)、橙 (5YR7/12)、濃い茶 (6YR6/6)、水色 (3B7/7)、青紫 (1P5/8)、濃ピンク (7RP6/11)、白 (N9) の 16 色の参考色を加え、計 20 色を嗜好度評価に用いた。20 枚の色紙を好み順に並べた後、30 秒間閉眼安静し、計測セッションを開始した。15 秒間のコントロール刺激 (灰色) 提示と 15 秒間の閉眼安静後、刺激色提示状態で脳波 (開、閉眼状態で 1 分ずつ計 2 分間) を記録し、加算タスクを課した。加算タスクは最初の 10 秒間は色紙注視してから、加算タスク用紙に暗算及び奇数偶数判別の結果を記入してもらった。

加算タスクについて、暗算は与えられた 1 桁の数字列を、隣り合う数字同士を足した和の下 1 桁目をマスに記入するようにさせた。奇数偶数判別は更に足した和が偶数なら“0”、奇数なら“1”をマスに記入させた。暗算と加算後奇偶判別タスクをそれぞれ 1 分ずつ交互に、計 4 分間遂行してもらった。被験者に、出来るだけ早く、かつ正確に作業を進めるように要求した。1

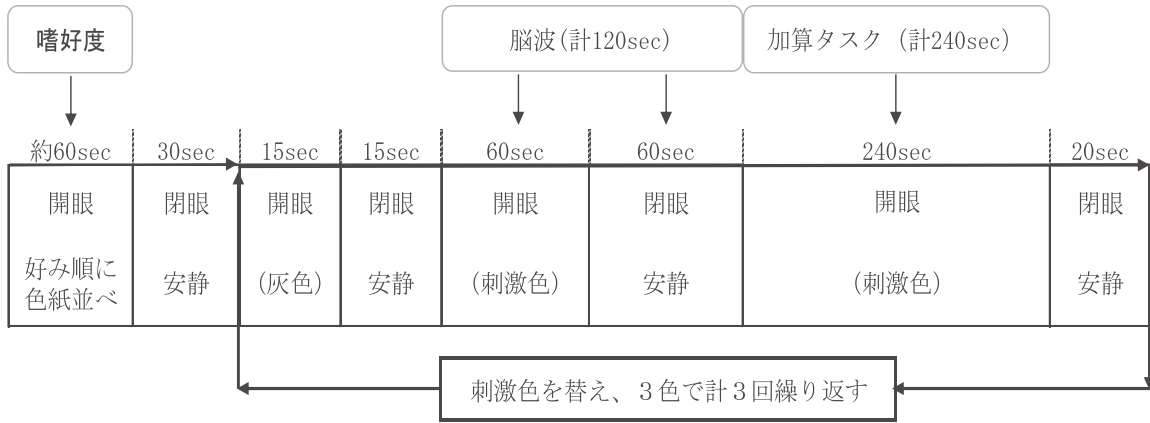


図1 実験プロトコール

分間毎タスクの正解数及び全タスクの平均正解数を解析に用いた。

セッションの最後に20秒間の閉眼安静を経て、刺激色を替えて次のセッションへと繰り返した。3色の刺激色提示で計3セッションが連続で実施され、刺激色の提示順はランダムとした。

2-4 測定項目

a. 色の嗜好度

実験開始時に計20色の色紙(刺激色を含める)を好み順に並べさせた順位評価値(1から20まで)を20で割った数値を更に1で引いた値を嗜好度として解析に用いた。つまり、1に近いほど好き、0に近いほど好きでないことを表す。

b. 脳波

国際10-20法に基づき、Fp1、Fp2、F7、F8、C3、C4、O1、O2、T5、T6、Fz、Cz、Pz、A1、A2の15箇所 Ag/AgCl 皿電極を装着し、脳波を導出した。なお、A1とA2は結合し、基準電極とした。眼球運動監視のため右目上下に Ag/AgCl 小型電極を装着し、眼球電図も導出した。脳波と眼球電図は生体電気用増幅ユニット(Bio-Top 6R12-4、NEC 三栄製)により、脳波は Low-Cut 0.016Hz、Hi-Cut 30Hz、眼球電図は Low-Cut 0.16Hz、Hi-Cut 15Hz で増幅した。パーソナルコンピュータ(ThinkPad A21e、IBM Japan Ltd)で脳波計測・解析ソフト AcqKnowledgeIII for the MP100WS (BIOPAC Systems、Inc.)を用いて、サンプリング周波数200HzでA/D変換を行い、記録した後、100Hzでリサンプルした。また、実験終了後、開、閉眼時の脳波サンプルを眼球運動などのアーチファクトを含まない5.12秒分のデータ毎に高速フーリエ変換を行った。各色条件のそれぞれの電極部位において2つの帯域に分割した a1 (8-10Hz)、a2 (10-13Hz) と、a 帯域 (8-13Hz) のパワー密度の自然対数値をそれぞれ算

出し、色条件ごとに左脳半球優位性の指標として、前頭極(Fp2-Fp1)、前頭部(F8-F7)、中心部(C4-C3)、後頭部(O2-O1)、側頭後部(T6-T5)の5部位でそれぞれの式の計算結果を解析に用いた<sup>16)17)</sup>。a波帯域パワーは脳活動亢進と負の関連を持つことから<sup>4)5)7)8)</sup>、指標値が大きければ、左脳半球の活動が右脳半球に比べ相対的により活性化することを示す。

2-5 統計解析

データ解析については、脳波のそれぞれの指標と嗜好度、加算タスクの成績を用いて、反復測定分散分析を行い、主効果が有意だった場合、色刺激間の効果の差をさらに Bonferroni の多重比較検定を行い、検討した。また、嗜好度と各生理的指標との Spearman の相関係数を求めた。

3 結果

精神作業については、単純加算と加算後奇偶判別タスク正解数(各2回分)および全タスクの平均正解数のいずれも色刺激条件間で有意な違いはなかった(F(2,14)=0.924, 3.713, 0.638, 0.287, p>0.05、図2)。

脳波については赤・青・緑の三条件間で統計的有意な結果が認められたのは、閉眼時で、a1波は側頭後部((T6-T5)、F(2,14)=5.211, p=0.020)、a2波は中心部(C4-C3、F(2,14)=6.372, p=0.008)、a波も左脳半球優位性指標値は中心部((C4-C3)、F(2,14)=4.430, p=0.032)で色の有意な主効果が認められた。三色間の多重比較で有意差が示された結果として、①a1波で赤注視後の閉眼時に側頭後部で指標値が青のそれより有意に小さかった(p=0.021、図3); ②a2波では赤の閉眼時に中心部で指標値が緑の閉眼時より著しく小さかった(p=0.009、図4); ③a波では中心部で指標値は赤条件閉眼時が緑より小さかった(p=0.030、

図5)。

色刺激の嗜好度についての採点を解析した結果、本実験の被験者間で各色刺激についての好き嫌いレベルに色間で有意な差がなかった ( $F(2,14)=0.409$ ,  $p=0.672$ , 図6)。

すべての色刺激をまとめた嗜好度と各生理測定との相関をもとめた結果、有意な相関が認められた項目は、閉眼時、 $\alpha 1$ 波で前頭部左脳半球優位性指標値と負の相関(図7左上、 $r=-0.437$ ,  $n=24$ ,  $p=0.033$ )、後頭部指標値と正の相関(図7右下、 $r=0.515$ ,  $n=24$ ,  $p=0.010$ )、 $\alpha 2$ 波で前頭部指標値と強い負の相関(図7右上、 $r=0.605$ ,  $n=24$ ,  $p=0.002$ )、 $\alpha$ 波では前頭部指標値と負の相関(図5左下、 $r=-0.618$ ,  $n=24$ ,  $p=0.001$ )が観察された。また、開眼時は各生理的指標と嗜好度との相関は認められなかった。

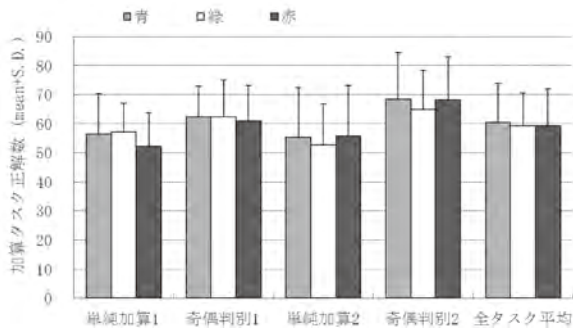


図2 各色紙注視時の精神作業成績。  
図の値は、加算タスクの暗算及び奇数偶数判別の正解数及び全タスクの平均値である。

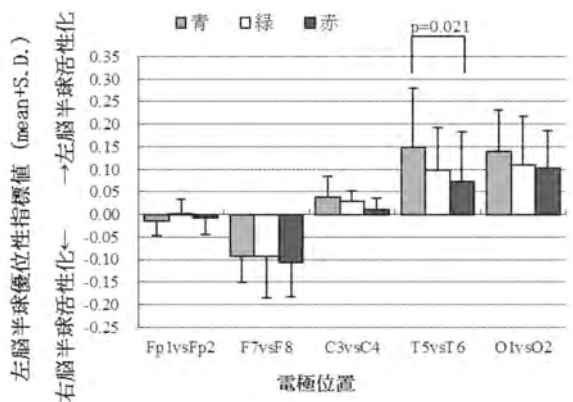


図3 各色紙注視直後の閉眼時の $\alpha 1$ 波における左脳半球優位性指標値。  
図の値は、 $\alpha 1$ 波パワー密度の自然対数値について右脳から左脳を減じた差である。指標値が大きければ、左脳半球の活動が右側半球の活動に比べ相対的により活性化することを示す。

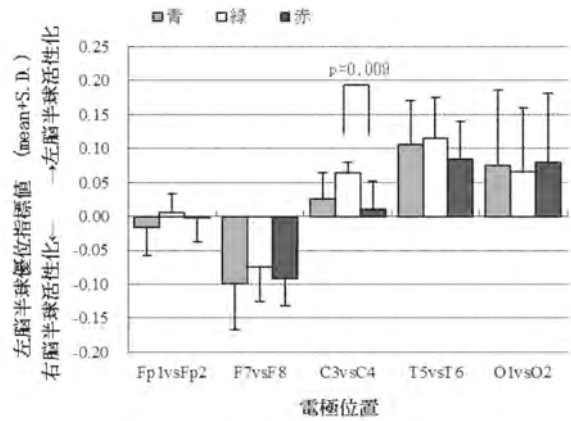


図4 各色紙注視直後の閉眼時の $\alpha 2$ 波における左脳半球優位性指標値。  
図の値は、 $\alpha 2$ 波パワー密度の自然対数値について右脳から左脳を減じた差である。指標値が大きければ、左脳半球の活動が右側半球の活動に比べ相対的により活性化することを示す。

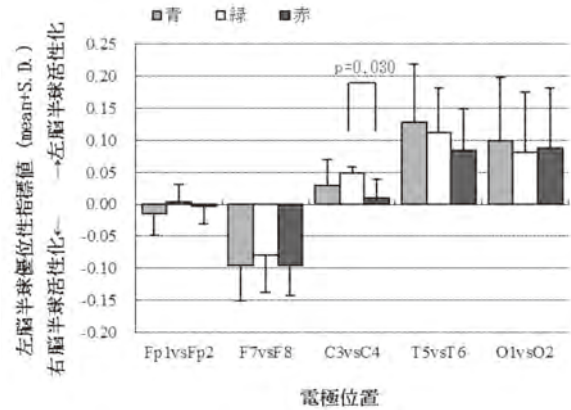


図5 各色紙注視直後の閉眼時の $\alpha$ 波における左脳半球優位性指標値。  
図の値は、 $\alpha$ 波パワー密度の自然対数値について右脳から左脳を減じた差である。指標値が大きければ、左脳半球の活動が右側半球の活動に比べ相対的により活性化することを示す。

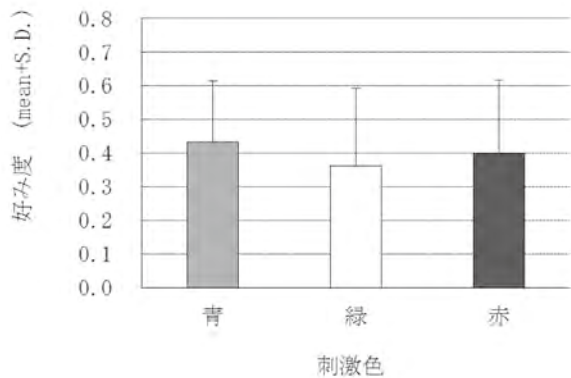


図6 各色刺激に対する嗜好度。  
図の値は、実験開始時に計20色の色紙(刺激色を含める)を好み順に並べさせた順位評価値(1から20まで)を20で割った数値を更に1で引いて嗜好度として集計した平均値。1に近いほど好き、0に近いほど好きでないことを表す主観評価値である。

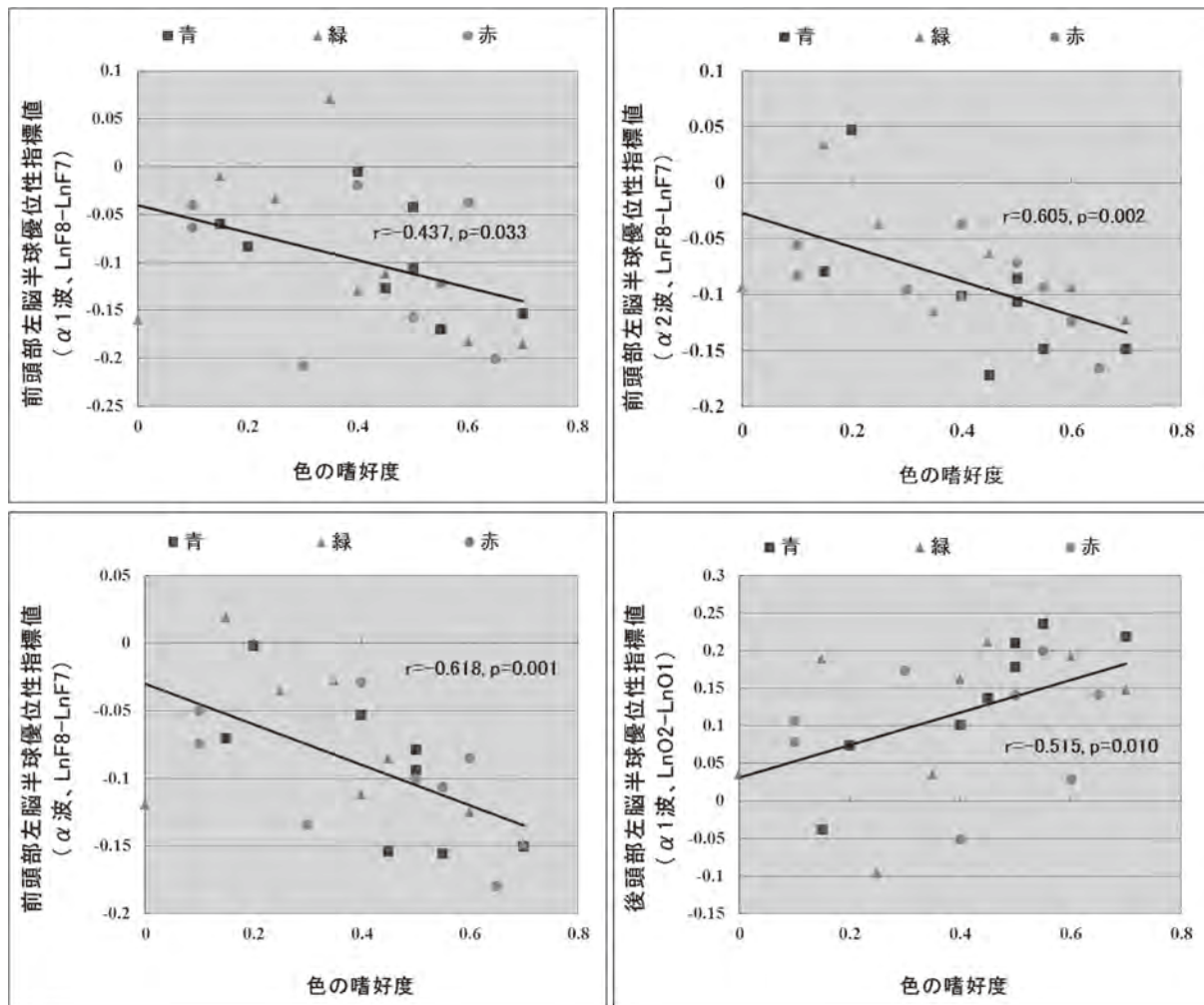


図7 色の嗜好度とすべての色紙注視直後の閉眼時左脳半球優位性指標値との相関。

左上は前頭部α1波、右上は前頭部α2波、左下は前頭部α波、右下は後頭部α1波における左脳半球優位性指標値と色の嗜好度の相関結果。

横軸の値は色の嗜好度で、1に近いほど好き、0に近いほど好きでないことを表す主観評価値である。

縦軸の左脳半球優位性指標値はα1、α2、α波のパワー密度の自然対数値について右脳から左脳を減じた差である。指標値が大きければ、左脳半球の活動が右脳半球の活動に比べ相対的に活性化することを示す。

#### 4 考 察

赤注視後の閉眼時のα1波で側頭後部の左脳半球優位性指標値が青のそれより有意に小さかったとの結果から、赤条件は青条件より相対的に左半球活動が抑制され、右脳半球活動がより亢進することが示された。快情動では主に左前頭部で、不快情動では主に右前頭部において脳活動が増加することが推察されている<sup>9)</sup>ことや、不快では主に右脳において広範囲に脳活動が増加するとの考察<sup>6)</sup>から、赤条件の閉眼時が青より不快情動を引き起こす可能性を示唆した。これは、先行研究で示唆された赤の不安、内的注意を引き起こす効果に一致した<sup>1)2)</sup>。緑の閉眼時のα2やα波全帯域の中心部で左脳半球優位性指標値は赤の閉眼時より著しく大きかった結果から、緑条件は赤条件より左脳半球の活動がより活性化することが示された。逆に言う

と、左脳半球優位性指標値は中心部で赤条件閉眼時が緑より小さく、赤色紙を見た直後の閉眼時は、緑より右脳半球が活性化するとのこと、α1波の結果と同様に赤条件で不快情動が引き起こされた可能性を示唆した。これも、先行研究で示唆された赤の不安、内的注意を引き起こす効果に一致した<sup>1)2)</sup>。しかし、こうした結果は開眼時では得られなかったことから、赤刺激の不安、内的注意効果は、色注視時に比べ、直後の閉眼時により強く現れることが示唆された。

以上の分析をまとめると、赤刺激は青、緑より不快情動を引き起こす可能性が大きいと判断できる。これは、先行研究との結果に一致している<sup>1)2)</sup>。また、赤刺激による情動効果は、色注視時よりも、直後の閉眼時に顕著に現れた。さらに、色刺激の嗜好度についての採点結果から、本実験の被験者間で各色刺激についての好き嫌いレベルに色間で有意な差がなかったこと

で、上記の脳波活動は色の好き嫌いによる影響ではないことも示唆された。

すべての色刺激をまとめた嗜好度と各生理測定との相関で、 $a1$ 波、 $a2$ 波、 $a$ 波全帯域は前頭部で左脳半球優位性指標値と負の相関、 $a1$ 波は後頭部左脳半球優位性と正の相関が示された。嫌いな色ほど、色を見た後の閉眼時に、前頭部の左脳半球優位性が大きく、後頭部では逆に左脳半球優位性が小さくなることが示唆された。つまり、嫌いな色を見た後の閉眼時に、前頭部で左脳半球的活動がより活性化し、後頭部では右半球的活動が相対的に活性化すると解釈できる。

前頭部と後頭部で逆な脳半球優位性という結果の解釈は難しいが、綿貫らは香り、触刺激、全身振動など種々の物理刺激を与えた状況で生じる快・不快情動に伴い、快では左前頭部で、不快では左右の前頭部および主に右脳において広範囲に脳活動が増加すると考察している<sup>6)</sup>。本研究で示された嫌いな色ほど左前頭部と右後頭部の脳活動が活性化するのは、綿貫らの研究と同様に、不快情動の増加を反映する脳波活動である可能性が考えられる。そして、嫌いな色を見ている時は不快になり、逆に好きな色ほど、注視している時はより快情動を引き起こすことは容易に想像できる。一方、この不快情動は色注視時ではなく、その直後の閉眼時により顕著に現れることが本研究の結果から示唆された。

## 5 まとめ

本実験で用いた赤、緑、青に色紙刺激によって、左脳半球優位性に異なる影響をもつことが認められた。赤刺激は青、緑より不快情動を反映する脳活動を誘発する可能性があり、この情動効果は刺激直後の閉眼時に顕著に現れた。また、色に対する好き嫌いに関して、色への嗜好度が低いほど、色刺激を遮断した直後の閉眼時に不快情動を示す脳波活動を誘発することが示唆された。よって、色刺激の情動効果を左脳半球優位性による評価が可能であることが分かった。その際、色の好き嫌いなどの感情的要素を除いた色刺激が引き起こす生理的反応と、色に対する嗜好度による影響との総合的な考察が必要であることも明らかとなった。

## 《謝 辞》

本研究の実施にあたり、実験の遂行に大いなるご協力頂いた千葉大学工学部人間生活工学研究室及びデザイン心理学研究室の学生のみなさんに心より感謝を致します。

## 《引用文献》

- 1) 陽東藍, 下村義弘, 岩永光一, 勝浦哲夫. 随伴陰性変動と気分に対する物体色の効果. 日本生理人類学会誌, 11: 1-6, 2006
- 2) Yoto A, Katsuura T, Iwanaga K, Shimomura Y. Effects of object color stimuli on human brain activities in perception and attention referred to EEG alpha band response. *J Physiol Anthropol*, 26: 373-379, 2007
- 3) Herrington JD, Mohanty A, Koven NS, Fisher JE, Stewart JL, Banich MT, Webb AG, Miller GA, Heller W. Emotion-modulated performance and activity in left dorsolateral prefrontal cortex. *Emotion*, 5: 200-207, 2005
- 4) Ekman P, Davidson RJ, Friesen WV. The Duchenne smile: emotional expression and brain physiology. *J Pers Soc Psychol*, 58: 342-353, 1990
- 5) Wheeler RE, Davidson RJ, Tomarken AJ. Frontal brain asymmetry and emotional reactivity: A biological substrate of affective style. *Psychophysiology*, 30: 82-89, 1993
- 6) 綿貫茂喜, キムヨンキュ, 李 貞美. 快・不快という情動が生じた時の背景脳波およびその他の生理反応の特徴. *臨床神経生理学*, 33(1): 21-26, 2005
- 7) Davidson RJ. Anterior cerebral asymmetry and the nature of emotion. *Brain Cogn*, 20: 125-151, 1992
- 8) Harmon-Jones E. Contributions from research on anger and cognitive dissonance to understanding the motivational functions of asymmetrical frontal brain activity. *Biol Psychol*, 67: 51-76, 2004
- 9) Thibodeau R, Jorgensen RS, Kim S. Depression, anxiety, and resting frontal EEG asymmetry: a meta-analytic review. *J Abnorm Psychol*, 115(4): 715-29, 2006
- 10) Gotlib IH, Ranganath C, Rosenfeld JP. Frontal EEG alpha asymmetry, depression, and cognitive functioning. *Cognition and Emotion*, 12: 449-478, 1998
- 11) Schmidt B, Hanslmayr S. Resting frontal EEG alpha-asymmetry predicts the evaluation of affective musical stimuli. *Neurosci Lett*, 460: 237-240, 2009
- 12) Blackhart GC, Minnix JA, Kline JP. Can EEG asymmetry patterns predict future development of anxiety and depression? A preliminary study. *Biol Psychol*, 72: 46-50, 2006
- 13) Hagemann D, Naumann E, Lurken A, Becker G, Maier S, Bartussek D. EEG asymmetry, disposi-

- tional mood and personality. *Pers Individ Dif*, 27: 541-568, 1999
- 14) Jackson DC, Mueller CJ, Dolski I, Dalton KM, Nitschke JB, Urry HL, Rosenkranz MA, Ryff CD, Singer BH, and Davidson RJ. Now you feel it, now you don't: frontal brain electrical asymmetry and individual differences in emotion regulation. *Psychol Sci*, 14: 612-617, 2003
- 15) Sutton SK, Davidson RJ. Prefrontal brain electrical asymmetry predicts the evaluation of affective stimuli. *Neuropsychologia*, 38: 1723-1733, 2000
- 16) Davidson RJ, Marshall JR, Tomarken AJ, Henriques JB. While a phobic waits: regional brain electrical and autonomic activity in social phobics during anticipation of public speaking. *Biol Psychiatry*, 47: 85-95, 2000
- 17) Pizzagalli DA, Sherwood RJ, Henriques JB, Davidson RJ. Frontal brain asymmetry and reward responsiveness. *Psychol Sci*, 16(10): 805-813, 2005

《連絡先》

陽東 藍

〒422-8526 静岡市駿河区谷田52-1

E-mail : ai\_yoto@hotmail.com

(2016年2月8日受付, 2016年8月9日採用決定, 討論受付期限2017年11月末日)

# Scalable Solution-Phase Synthesis of the Biologically Active Cyclodepsipeptide Destruxin E, a Potent Negative Regulator of Osteoclast Morphology

Masahito Yoshida,<sup>†</sup> Hiroshi Sato,<sup>†,‡</sup> Yoshitaka Ishida,<sup>†</sup> Hiroshi Nakagawa,<sup>§</sup> and Takayuki Doi<sup>\*,†</sup>

<sup>†</sup>Graduate School of Pharmaceutical Sciences, Tohoku University 6-3 Aza-Aoba, Aramaki, Aoba-ku, Sendai 980-8578, Japan

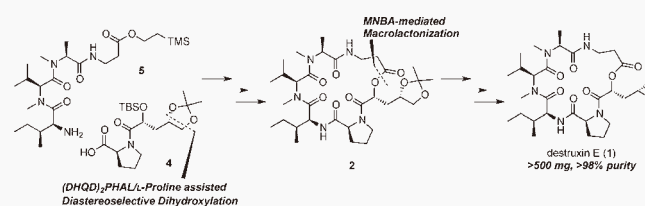
<sup>‡</sup>Mitsubishi Tanabe Pharma Corporation 1000 Kamoshida-cho, Aoba-ku, Yokohama 227-0033, Japan

<sup>§</sup>Department of Applied Biological Chemistry, Chubu University 1200 Matsumoto-cho, Kasugai, Aichi 487-8501, Japan

## Supporting Information

**ABSTRACT:** The scalable solution-phase synthesis of the cyclodepsipeptide destruxin E (**1**) has been achieved. Diastereoselective dihydroxylation of the terminal alkene in a 2-alkoxy-4-pentenoic amide, **7**, was successfully accomplished utilizing (DHQD)<sub>2</sub>PHAL as the chiral ligand, and it was found that the use of the L-proline moiety in the substrate as a chiral auxiliary was essential for the induction of high diastereoselectivity to afford the key compound **4** on a gram scale.

MNBA-mediated macrolactonization of **3** was also performed without formation of the dimerized product even under higher-dilution conditions, and it is noteworthy that the internal hydrogen bonds and *s-cis* configuration of the amide bond between *N*-methylalanine and *N*-methylvaline in the cyclization precursor **3** would assist in the macrolactonization to provide the macrolactone **2** without forming a dimerized product. Finally, epoxide formation in the side chain afforded destruxin E (**1**) on a gram scale in high purity (>98%).



## INTRODUCTION

Osteoporosis, characterized by the loss of bone mass and bone mineral density, is a worldwide health problem, particularly among postmenopausal women and elderly people.<sup>1</sup> Osteoporosis is caused by disorders of bone homeostasis including excessive bone resorption by osteoclasts, and thus, several antiresorptive agents such as bisphosphonate and denosumab have been developed and are widely used for osteoporosis treatment.<sup>2</sup> The antiresorptive agents currently in use efficiently inhibit osteoclastic bone resorption by reducing the number of osteoclasts. However, it is difficult for patients to completely recover their bone health because bone remodeling is regulated by a balance between osteoblasts and osteoclasts and is occasionally hampered during treatment with antiresorptive agents. Thus, a therapy for osteoporosis that inhibits bone resorption without affecting osteoclast viability is desired. Recently, a vacuolar-type H<sup>+</sup>-ATPase (V-ATPase) in osteoclasts was postulated as an attractive and a potential drug target for osteoporosis therapeutics.<sup>3</sup> The pumping of protons by the osteoclastic V-ATPase is a prerequisite for promoting bone resorption; therefore, specific inhibition of the osteoclastic V-ATPase without affecting the viability of osteoclasts would be a desirable mode of action in the treatment of osteolytic diseases.

Destruxin E (**1**), isolated from *Metarhizium anisopliae* by País et al. in 1981, is a 19-membered cyclodepsipeptide consisting of five amino acids (L-proline, L-isoleucine, *N*-methyl-L-valine, *N*-methyl-L-alanine, and  $\beta$ -alanine) and an epoxide-containing hydroxy acid derivative.<sup>4</sup> It has recently been reported that

destruxin derivatives exhibit potent V-ATPase inhibitory activity, and **1** in particular strongly inhibits the activity of V-ATPase.<sup>5</sup> To date, the synthesis of destruxin and its derivatives has been reported by several research groups.<sup>6</sup> We have recently achieved the first total synthesis and structural determination of **1** and also reported that the stereochemistry of the epoxide is crucial for potent V-ATPase inhibitory activity.<sup>7</sup> In addition, destruxin E (**1**) intriguingly induces morphological changes in osteoclast-like multinuclear cells (OCLs) at low concentration without affecting the V-ATPase activity of the OCLs.<sup>8</sup> Therefore, **1** is consequently considered as a new type of antiresorptive agent. We are thus interested in the elucidation of the mode of action of destruxin E (**1**) in OCLs and its effect on bone metabolism in vivo. However, the limited production of **1** from fungi such as *M. anisopliae* has prevented a detailed study of its in vivo mechanism. Hence, the development of an efficient synthetic route to **1** is essential for obtaining sufficient quantities of **1** for in vivo studies. We herein report the scalable solution-phase synthesis of the naturally occurring cyclodepsipeptide destruxin E (**1**) via a 2-methyl-6-nitrobenzoic anhydride (MNBA)-mediated macrolactonization<sup>9</sup> and a diastereoselective dihydroxylation<sup>10</sup> of the terminal alkene in a 2-alkoxy-4-pentenoic amide using (DHQD)<sub>2</sub>PHAL as the chiral ligand and the L-proline moiety in the substrate as a chiral auxiliary.

Received: November 1, 2013

Published: November 19, 2013

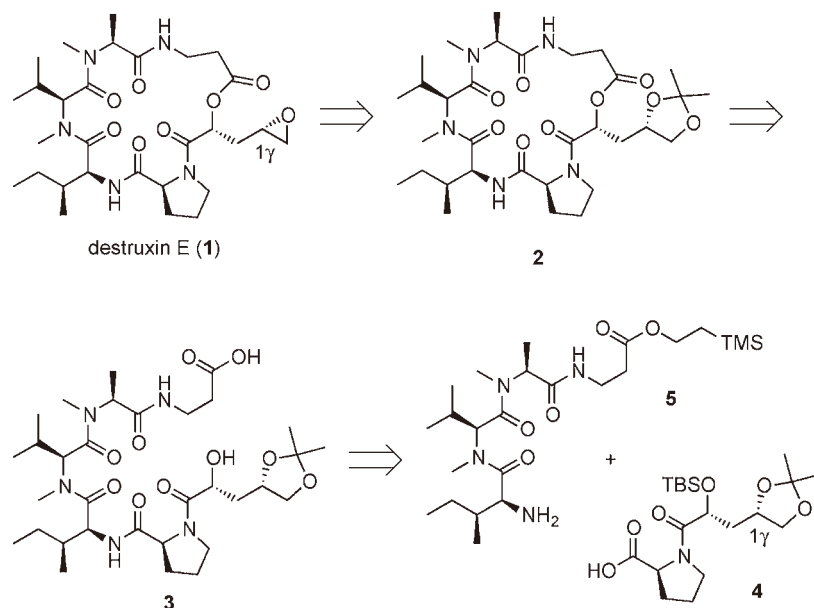


Figure 1. Retrosynthesis of destruxin E (1).

## RESULTS AND DISCUSSION

To achieve the preparation of destruxin E (1) on a gram scale, we planned a solution-phase synthesis of 1, and the synthetic outline is illustrated in Figure 1. The unstable epoxide side chain would be synthesized from macro lactone 2 in the final step. The selection of the cyclization site was important for obtaining the desired macro lactone 2, and thus, the macrolactonization at the  $\beta$ -Ala- $\alpha$ -hydroxy acid site was chosen in accordance with our previous synthesis.<sup>6a,b,7</sup> The cyclization precursor 3 would be obtained via coupling of acid 4 and tetrapeptide 5 followed by simultaneous deprotection of the N- and C-termini. A TBS group was chosen to protect the hydroxyl group at the N-terminus of 3 and a 2-(trimethylsilyl)ethyl (TMSEt) group was selected as the protecting group at the C-terminus of 5 because both the TBS and TMSEt groups can be readily removed by treatment with TBAF under ambient conditions without decomposition of the peptide sequence.<sup>11</sup>

The efficient preparation of 4 is a key issue for achieving the gram-scale synthesis of destruxin E (1). The secondary alcohol at the 1 $\gamma$  position should be diastereoselectively prepared because the stereochemistry at the 1 $\gamma$  position is important for the inhibition of V-ATPase activity.<sup>7</sup> We previously reported the synthesis of compound 4 from 8 through lactone 6; however, the total yield of 4 was not reproducible on a gram scale because of the high polarity of the resulting acid after hydrolysis of lactone 6a (Figure 2). Moreover, the overall yield of the desired lactone 6a was less than 50% because of the non-stereoselective dihydroxylation of alkene 8, which was utilized to prepare both lactones 6a and 6b for structural determination of destruxin E (1). Therefore, preparation of the key compound 4 utilizing lactone 6a is problematic on a gram scale. Thus, an alternative route to 4 involving diastereoselective dihydroxylation of alkene 7 followed by acetal formation and removal of the benzyl group was anticipated to provide a higher yield. In general, it is known that dihydroxylation of terminal alkenes proceeds with lower enantioselectivity than that of internal alkenes.<sup>12</sup> Therefore, we expected that the proline moiety in 7 might act as a chiral auxiliary in the diastereoselective dihydroxylation of the terminal alkene moiety. Compound 7

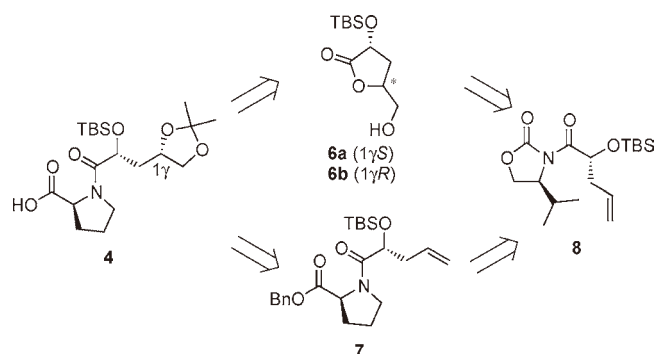


Figure 2. Retrosynthesis of key compound 4.

can be readily synthesized via the coupling of L-proline benzyl ester and the acid obtained by hydrolysis of the previously synthesized compound 8.

Compound 7 was initially synthesized from the previously reported<sup>7</sup> TBS ether 9 (Scheme 1). In our previous report, the asymmetric allylation of 9 was performed using allyl bromide/lithium hexamethyldisilazide (LiHMDS) at  $-30$  °C for 16 h to achieve reproducible yield and diastereoselectivity. To improve on these results, highly reactive allyl iodide was used as the electrophile.<sup>13</sup> Expectedly, the allylation with NaHMDS at  $-45$  °C was smoothly completed within 1.5 h, affording the desired product 8 in 94% yield with >95% diastereoselectivity. However, acid 11 was not formed by direct hydrolysis of 8 under basic conditions because the cyclic carbamate was readily hydrolyzed under the reaction conditions. The stepwise modification to give 11 through methyl ester 10 was then attempted via methanolysis of 8 utilizing samarium trifluoromethanesulfonate.<sup>14</sup> However, this reaction took over 48 h to go to completion, and the TBS group in 11 was easily removed under the acidic workup. Thus, the nucleophilic cleavage of 8 with MeOMgBr was investigated,<sup>15</sup> this reaction proceeded successfully at room temperature to provide 10 in 94% yield without removal of the TBS group. Hydrolysis of the methyl ester followed by amidation of the resulting acid 11 with L-Pro-OBn using bromotripyrrolidinophosphonium hexafluorophos-

Scheme 1. Synthesis of 7

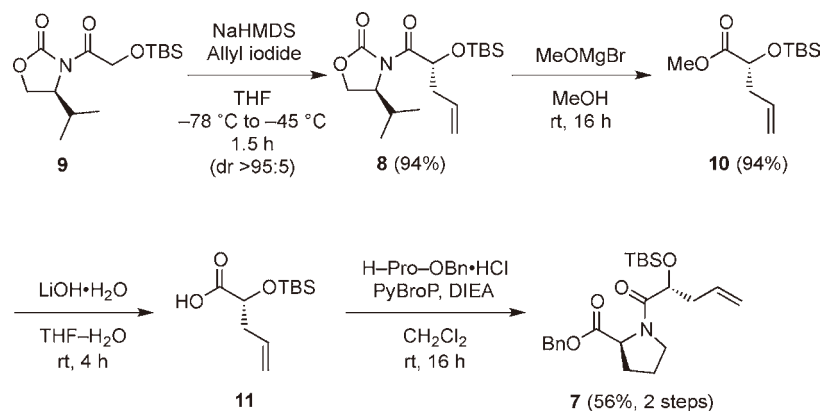
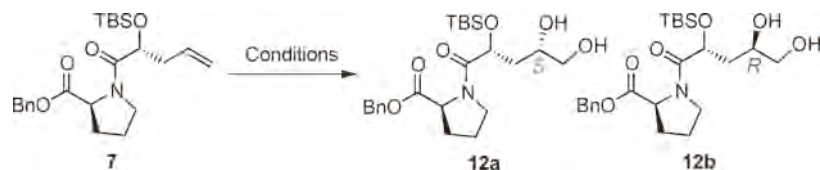


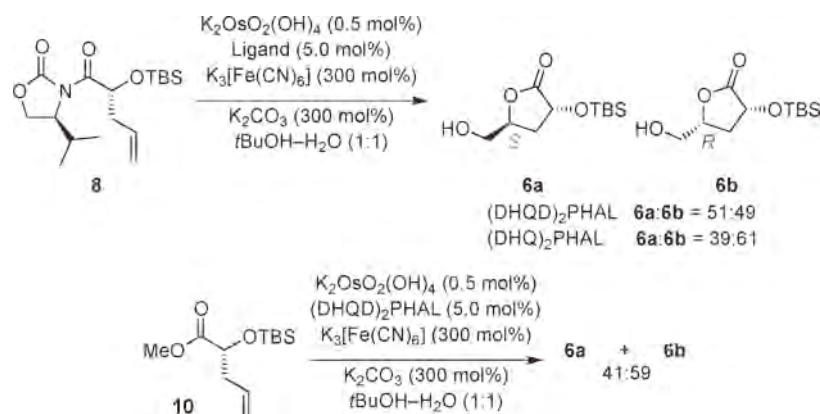
Table 1. Investigation of the Reaction Conditions for Diastereoselective Dihydroxylation of 7



entry	conditions <sup>a</sup>	S:R ratio <sup>b</sup>	yield (%) <sup>c</sup>
1	AD-mix- $\beta$ (1.4 g/mmol)	67:33	51
2	AD-mix $\alpha$ (1.4 g/mmol)	50:50	43
3	OsO <sub>4</sub> (1.0 mol %), (DHQD) <sub>2</sub> PHAL (5.0 mol %)	77:23	71
4	K <sub>2</sub> OsO <sub>2</sub> (OH) <sub>4</sub> (1.0 mol %), (DHQD) <sub>2</sub> PHAL (5.0 mol %)	86:14	97
5	K <sub>2</sub> OsO <sub>2</sub> (OH) <sub>4</sub> (0.5 mol %), (DHQD) <sub>2</sub> PHAL (5.0 mol %)	86:14	quant
6	K <sub>2</sub> OsO <sub>2</sub> (OH) <sub>4</sub> (1.0 mol %), (DHQD) <sub>2</sub> AQN (5.0 mol %)	84:16	90
7	K <sub>2</sub> OsO <sub>2</sub> (OH) <sub>4</sub> (1.0 mol %), (DHQD) <sub>2</sub> PYR (5.0 mol %)	31:69	92

<sup>a</sup>K<sub>3</sub>[Fe(CN)<sub>6</sub>] (300 mol %), K<sub>2</sub>CO<sub>3</sub> (300 mol %), *t*BuOH–H<sub>2</sub>O (1:1), rt, 18–24 h. <sup>b</sup>Determined by <sup>1</sup>H NMR analysis of the crude mixtures. <sup>c</sup>Combined yields.

Scheme 2. Attempts at Diastereoselective Dihydroxylation of 8



phate (PyBroP)<sup>16</sup> then afforded the desired product 7 in 56% yield.

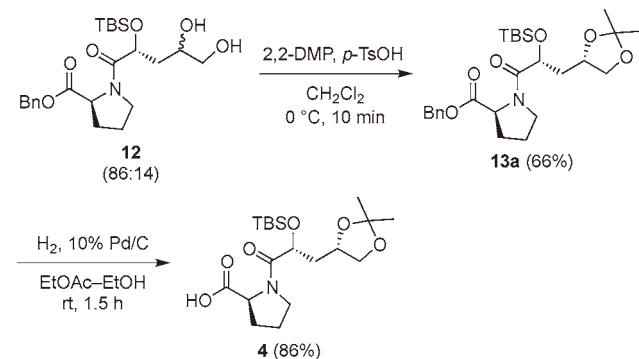
Once the gram-scale synthesis of the desired 7 was achieved, we next investigated the diastereoselective dihydroxylation of the terminal alkene in 7. It is known that the asymmetric dihydroxylation of terminal alkenes generally proceeds with poor enantioselectivity. Thus, extensive studies of the asymmetric dihydroxylation of terminal alkenes have been conducted, and bis(cinchona alkaloid) ligands with 1,4-phthalazine (PHAL) or pyrimidine (PYR) spacers have been shown to be effective for obtaining the corresponding diols with

high enantioselectivity.<sup>12</sup> As an initial attempt at the synthesis of the desired diol 12a, the dihydroxylation of 7 utilizing AD-mix- $\beta$  was examined (Table 1). This reaction provided the desired diol 12a and its diastereomer 12b in a ratio of 67:33 (entry 1).<sup>17</sup> By contrast, dihydroxylation utilizing AD-mix- $\alpha$  provided a 50:50 mixture of diastereomers (entry 2). Thus, the dihydroxylation was further investigated using cinchonidine-based chiral ligands. When the reaction was performed using (DHQD)<sub>2</sub>PHAL (5 mol %) in the presence of OsO<sub>4</sub> (1 mol %), the diols 12 were formed in a 77:23 ratio (entry 3). After extensive investigations, it was found that the dihydroxylation

of **7** utilizing  $K_2OsO_2(OH)_4$ -(DHQD)<sub>2</sub>PHAL quantitatively afforded **12a** with 86% diastereoselectivity and that reduction of the osmium catalyst loading to 0.5 mol % did not affect the diastereoselectivity (entry 5). On the other hand, it was found that with other chiral ligands, such as (DHQD)<sub>2</sub>AQN<sup>18</sup> or (DHQD)<sub>2</sub>PYR,<sup>12a</sup> the yield or diastereoselectivity was decreased (entries 6 and 7). Therefore, (DHQD)<sub>2</sub>PHAL was selected as the chiral ligand for the diastereoselective dihydroxylation of the terminal alkene in **7**. In contrast to the dihydroxylation of **7**, the dihydroxylation of **8** under the optimized conditions utilizing (DHQD)<sub>2</sub>PHAL and (DHQ)<sub>2</sub>PHAL resulted in poor stereoselectivity (**6a:6b** = 51:49 and 39:61, respectively; Scheme 2). In addition, the dihydroxylation of methyl ester **10** in the presence of  $K_2OsO_2(OH)_4$ -(DHQD)<sub>2</sub>PHAL afforded a mixture of lactones **6a** and **6b** in a 41:59 ratio. Thus, it seemed that the chirality at the  $\alpha$ -position in the hydroxyl acid derivative was mismatched in the dihydroxylation utilizing (DHQD)<sub>2</sub>PHAL for the induction of the desired stereochemistry at the 1 $\gamma$  position. Therefore, the chirality of the proline moiety in **7** also would assist in the induction of the high diastereoselectivity obtained for **12a**.

Because it was difficult to separate the resulting diols **12** using conventional column chromatography, acetal formation with 2,2-dimethoxypropane was performed on the mixture of diastereomers **12**, and this was followed by isolation of the resulting acetal **13a** via flash column chromatography in 66% overall yield. Finally, removal of the benzyl group by hydrogenolysis furnished the desired compound **4** in 86% yield (Scheme 3).

### Scheme 3. Synthesis of Compound 4



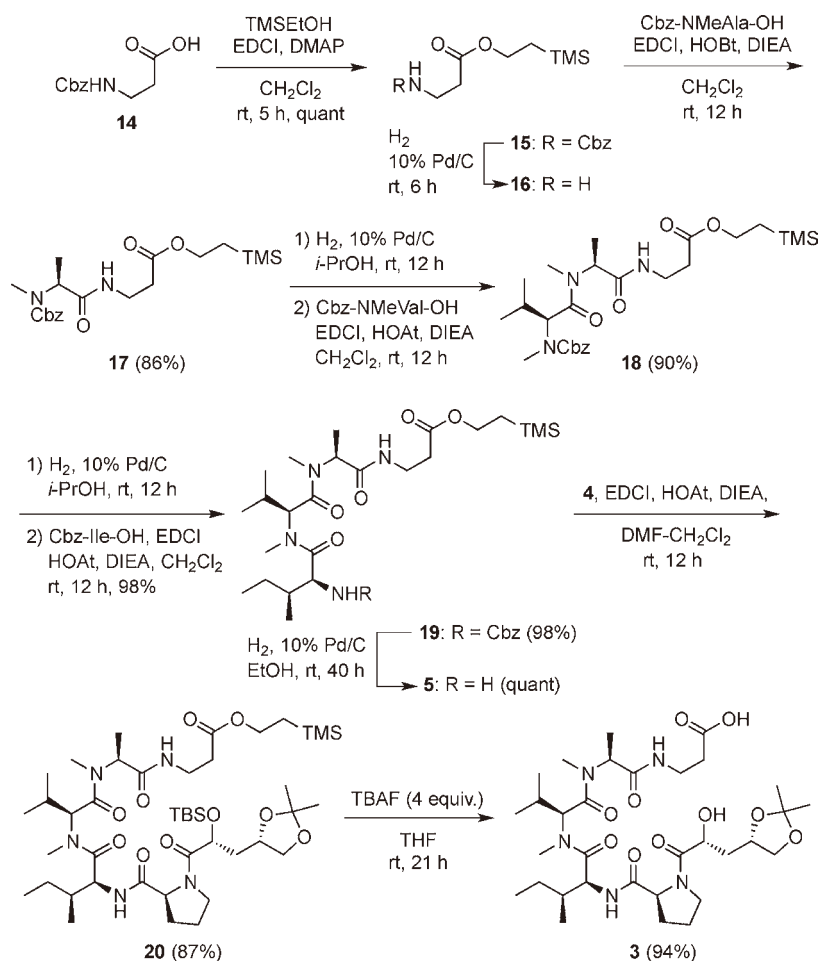
With the desired **4** in hand, the gram-scale synthesis of the cyclization precursor **3** was then investigated. Although we have reported the solid-phase synthesis of cyclization precursor **3** using an Fmoc method, we considered performing the gram-scale synthesis of **3** in solution because of facile scale-up and yield. As it is well-known that peptide sequences including *N*-methylamide are readily hydrolyzed at the *N*-methylamide bond under acidic conditions,<sup>19</sup> peptide elongation utilizing the Boc strategy had to be avoided for the synthesis of **5**. Instead, the benzyloxycarbonyl (Cbz) group was selected as the protecting group.<sup>6a,c-h</sup> The Cbz group can be removed by hydrogenolysis under ambient conditions without cleavage of *N*-methylamide bonds, and Cbz-protected *N*-methylamino acids can be readily prepared in one step from the corresponding amino acids on a large scale.<sup>20</sup> The starting material Cbz- $\beta$ -Ala-OH (**14**) was thus converted to the corresponding TMSEt ester **15**<sup>11b</sup> via condensation with 2-

(trimethylsilyl)ethanol. Hydrogenolysis of **15** in isopropanol provided amine **16** without transesterification at the C-terminus. The resulting amine **16** was then coupled with Cbz-NMeAla-OH using EDCI-HOBt, and dipeptide **17** was obtained in 86% yield. However, when the preparation of **18** from **17** and Cbz-NMeVal-OH was carried out in the same manner as for the preparation of **17**, the yield of **18** was moderate (56%). After several attempts at the tripeptide synthesis, it was found that the use of HOAt instead of HOBt enabled efficient amidation to provide the desired product **18** in 90% yield without formation of the diketopiperazine through displacement of the C-terminal  $\beta$ -Ala residue.<sup>6c,21</sup> Next, tetrapeptide **5** was prepared through **19** in the same manner as used for **18**, and then hexapeptide **20** was obtained via coupling of **5** with **4** using EDCI-HOAt. Concomitant removal of the TBS and TMSEt groups with TBAF furnished the desired cyclization precursor **3** on a multigram scale (Scheme 4).

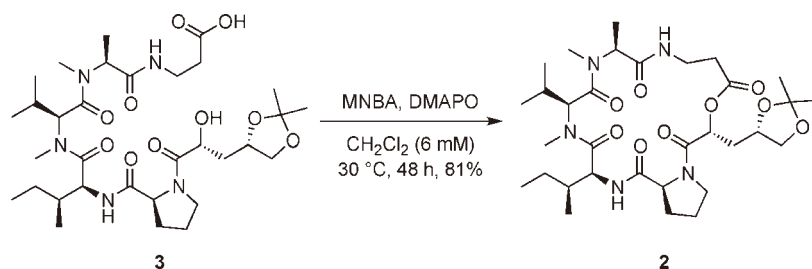
Next, we investigated the MNBA-mediated macrolactonization of **3** (Scheme 5).<sup>8</sup> Previously, we performed the macrolactonization of **3** at 3 mM. However, in the present study it was found that the macrocyclization of **3** could be achieved at 6 mM on a gram scale, providing the corresponding product **2** in 81% yield without formation of the dimerized byproduct (Scheme 5). On the other hand, we also attempted the macrolactamization of L-Pro and L-Ile residues of **21** based on the previous reports.<sup>6c,f,g</sup> Although the macrolactamization of **21**<sup>22</sup> at 1 mM utilizing EDCI-HOAt proceeded smoothly at room temperature, a mixture of **2** and its dimer **22** in a 53:47 ratio was obtained (Scheme 6). On the basis of previously reported conformational studies of destruxin A and roseotoxin B using NMR and X-ray crystallographic analyses, it has been suggested that the amide bond between *N*-MeAla and *N*-MeVal adopts the *s-cis* configuration, leading to a  $\beta$ -turn-shaped structure stabilized by two internal hydrogen bonds.<sup>23</sup> Therefore, we believe that the cyclization precursor **3** forms a similar conformation as **A**, which is proper for the macrolactonization (Figure 3). Wang et al.<sup>24</sup> recently reported that the destruxins are produced via nonribosomal peptide synthesis of a linear peptide, which undergoes macrolactonization in the biosynthesis. Thus, the macrolactonization between  $\beta$ -Ala and the hydroxy acid would be structurally suitable for the ring construction of destruxins, rather than the macrolactamization between the proline and isoleucine residues.

With the desired macrolactone **2** on a gram scale, removal of the acetonide in **2** was performed [3 M aqueous HCl/dioxane (1:2), 10 °C, 10 min] in accordance with our previous report. However, the yield of **26** was moderate because the *N*-methylamide bond was partially cleaved under the acidic conditions. After further investigation, it was found that the ratio of water and dioxane was crucial for removal of the acetonide without cleavage of the peptide bond. The reaction was complete under milder conditions [1.5 M aqueous HCl/dioxane (2:1), 0 °C, 2 h], providing diol **26** in 87% yield. For completion of the scalable synthesis of **1**, selective tosylation of the primary alcohol in **26** was carefully performed via treatment with 2 equiv of TsCl at room temperature to afford the desired tosylate **27** in 81% yield. Finally, formation of the epoxide under basic conditions furnished destruxin E (**1**) in several hundred milligram yield with high purity (>98%) after silica gel column chromatography (Scheme 7).

Scheme 4. Synthesis of Cyclization Precursor 3



Scheme 5. Synthesis of Macrolactone 2 via Macrolactonization



## CONCLUSION

In conclusion, we have accomplished the improved solution-phase synthesis of destruxin E (**1**) and established an efficient synthetic process for the production of a sufficient quantity of **1** in high purity for use in vivo experiments. Diastereoselective dihydroxylation of the terminal alkene in **7** was successfully performed utilizing (DHQD)<sub>2</sub>PHAL, and the L-proline moiety in the substrate was essential for inducing the high diastereoselectivity in this reaction. It is also noteworthy that the  $\beta$ -turn-shaped structure stabilized by internal hydrogen bonds and the *s-cis* configuration of the NMe amido bonds assisted in the efficient macrolactonization of **3** without high-dilution conditions, leading to macrolactone **2** without formation of the dimerized byproduct. These improved synthetic processes made it possible to access a sufficient quantity of destruxin E (**1**) in high purity (>98%), and in vivo

experiments on **1** to study its effect on bone metabolism are currently underway in our laboratories.

## EXPERIMENTAL SECTION

**General Techniques.** Chemicals and solvents were all purchased from commercial suppliers and used without further purification. All reactions in the solution phase were monitored by thin-layer chromatography carried out on glass-packed silica gel plates (60F-254) with UV light and visualized by *p*-anisaldehyde H<sub>2</sub>SO<sub>4</sub>-ethanol solution or phosphomolybdic acid ethanol solution. Flash column chromatography was carried out with silica gel (40–100  $\mu\text{m}$ ) with the indicated solvent system. <sup>1</sup>H NMR spectra (400 MHz, 600 MHz) and <sup>13</sup>C NMR spectra (100 MHz) were recorded in the indicated solvents. Chemical shifts ( $\delta$ ) are reported in units of parts per million (ppm) relative to the signal for internal tetramethylsilane (0.00 ppm for <sup>1</sup>H) for solutions in chloroform-*d*. NMR spectral data are reported as follows: chloroform-*d* (77.0 ppm for <sup>13</sup>C), methanol-*d*<sub>3</sub> (3.30 ppm for

## Scheme 6. Alternative Synthesis of Macrolactone 2 via Macrolactamization

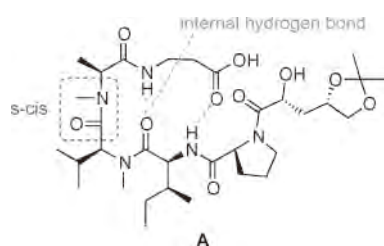
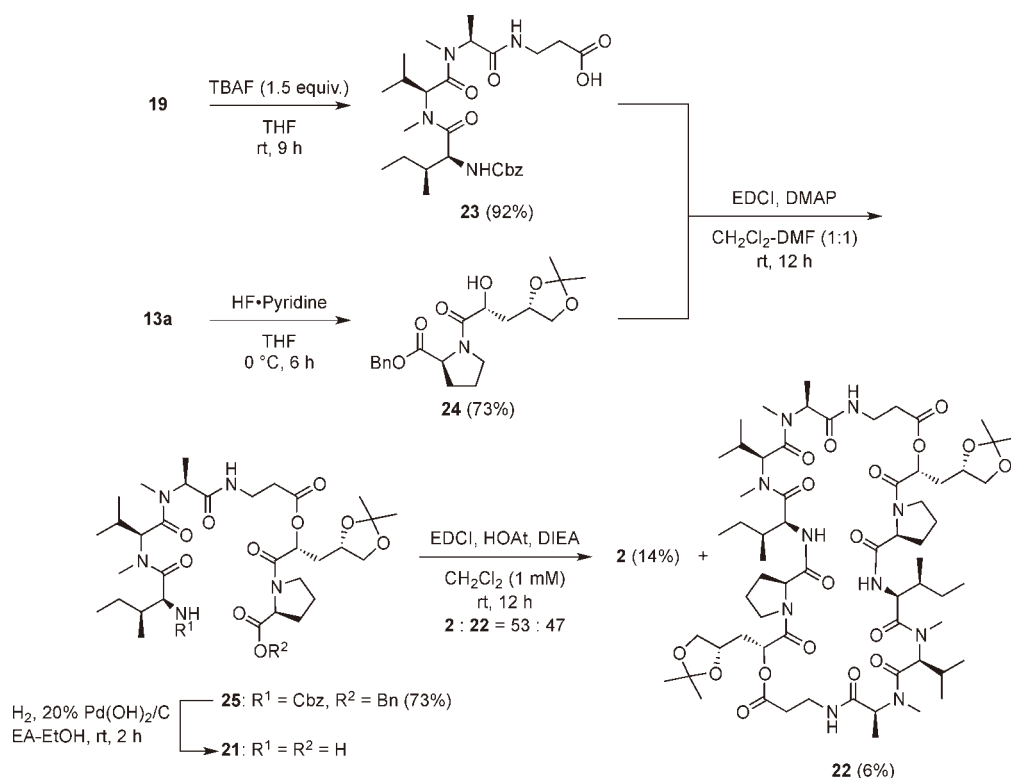
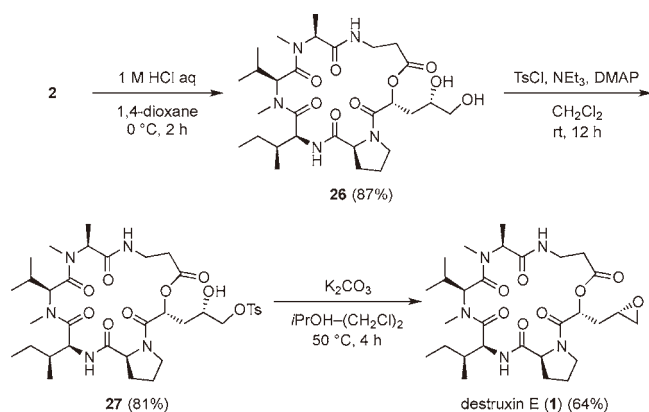


Figure 3. Plausible conformation of cyclization precursor 3.

## Scheme 7. Achievement of the Scalable Synthesis of 1



<sup>1</sup>H), dimethyl sulfoxide-*d*<sub>4</sub> (2.49 ppm for <sup>1</sup>H and 39.5 ppm for <sup>13</sup>C) when an internal standard is not indicated. Multiplicities are reported using the following abbreviations: s (singlet), d (doublet), t (triplet), m (multiplet), dd (doublet of doublets), dt (doublet of triplets), dq (doublet of quartets), ddd (doublet of doublets of doublets), ddt (doublet of doublets of triplets). Coupling constants (*J*) are reported in hertz (Hz). High-resolution mass spectra were measured on TOF-MS with ESI or FAB probe. Infrared spectra are reported in reciprocal

centimeters (cm<sup>-1</sup>). Melting points were measured on a melting point apparatus and are not corrected. Optical rotations were measured with a polarimeter at 589 nm. HPLC analysis was performed on an HPLC system with a photodiode array detector and an analytical C<sub>18</sub> column (3.5 mm, 4.6 × 100 mm i.d.) at a flow rate of 1.1 mL/min with a gradient solvent (0 min, 10% MeOH/H<sub>2</sub>O; 4 min, 95% MeOH/H<sub>2</sub>O; 11 min, 95% MeOH/H<sub>2</sub>O; 11.1 min, 10% MeOH/H<sub>2</sub>O; 15 min, 10% MeOH/H<sub>2</sub>O). HPLC solvents (MeOH and H<sub>2</sub>O) were buffered with 0.1% LC-MS-grade formic acid. Purity was measured with the peak area at UV (214 nm).

**Syntheses.** (*R*)-2-(*tert*-Butyldimethylsilyloxy)pentenoyl Oxazolidinone (**8**). To a solution of TBS ether **9**<sup>7</sup> (17.5 g, 58.1 mmol, 1 equiv) in dry THF (200 mL, 3.4 mL/mmol) was added a solution of NaHMDS in THF (1.00 M, 116 mL, 116 mmol, 2 equiv) dropwise at -78 °C under an argon atmosphere. After the reaction mixture was stirred at -78 °C for 30 min, a solution of allyl iodide (15.9 mL, 174 mmol, 3 equiv) in dry THF (50 mL, 0.29 mL/mmol) was added dropwise at -78 °C. After being stirred at -45 °C for 1 h, the reaction mixture was poured into saturated aqueous NH<sub>4</sub>Cl, and then the aqueous layer was extracted with ethyl acetate. The organic layer was washed with saturated aqueous NaHCO<sub>3</sub> and brine, dried over MgSO<sub>4</sub>, and filtered. The filtrate was concentrated in vacuo, and the resulting residue was purified by silica gel column chromatography (eluted with hexane/AcOEt = 20:1) to afford the allylated product **8** (18.7 g, 54.8 mmol, 94%, >95% ds) as a yellow oil. <sup>1</sup>H NMR (400 MHz, CDCl<sub>3</sub>) δ 5.84–5.95 (1H, ddt, *J* = 6.4, 8.4, 16.0 Hz), 5.41 (1H, dd, *J* = 4.0, 7.2 Hz), 5.13 (1H, d, *J* = 16.0 Hz), 5.10 (1H, d, *J* = 8.4 Hz), 4.51 (1H, dt, *J* = 3.6, 8.4 Hz), 4.34 (1H, t, *J* = 8.8 Hz), 4.23 (1H, dd, *J* = 3.6, 8.8 Hz), 2.56–2.63 (1H, m), 2.38–2.46 (1H, m), 2.31 (1H, dq, *J* = 3.6, 7.2 Hz), 0.90 (9H, s), 0.90 (3H, d, *J* = 6.8 Hz), 0.87 (3H, d, *J* = 6.8 Hz), 0.07 (3H, s), 0.05 (3H, s); <sup>13</sup>C NMR (100 MHz, CDCl<sub>3</sub>) δ 173.5, 153.6, 133.4, 118.1, 71.0, 63.9, 58.2, 40.0, 28.2, 25.7, 18.3, 17.8, 14.7, -4.9, -5.2; IR (CHCl<sub>3</sub>) 2958, 2931, 1781, 1717, 1389, 1249, 1209, 1116, 837 cm<sup>-1</sup>; [α]<sub>D</sub><sup>25</sup> +63.5 (*c* 1.03, CHCl<sub>3</sub>); HRFABMS calcd for C<sub>17</sub>H<sub>31</sub>NO<sub>4</sub>Si [M + H]<sup>+</sup> 342.2101, found 342.2086.

(*R*)-2-(*tert*-Butyldimethylsilyloxy)pent-4-enoic Acid Methyl Ester (**10**). Dry MeOH (30 mL, 0.83 mL/mmol) was added to a solution of

methylmagnesium bromide in THF (0.97 M, 74 mL, 72 mmol, 2 equiv) dropwise at 0 °C under an argon atmosphere. After the reaction mixture was stirred at 0 °C for 15 min, a solution of **8** (12.3 g, 36.0 mmol, 1 equiv) in dry MeOH (90 mL, 2.5 mL/mmol) was added dropwise at 0 °C. After being stirred at room temperature for 16 h, the reaction mixture was poured into saturated aqueous NH<sub>4</sub>Cl, and then the aqueous layer was extracted with ether. The organic layer was washed with brine, and its organic layer was dried over MgSO<sub>4</sub> and filtered. The filtrate was concentrated in vacuo, and the resulting residue was purified by silica gel column chromatography (eluted with hexane/AcOEt = 20:1) to afford methyl ester **10** (8.26 g, 33.8 mmol, 94%) as a colorless oil. <sup>1</sup>H NMR (400 MHz, CDCl<sub>3</sub>) δ 5.82 (1H, ddt, *J* = 7.2, 10.4, 17.0 Hz), 5.06–5.15 (2H, m), 4.26 (1H, dd, *J* = 4.8, 7.2 Hz), 3.72 (3H, s), 2.40–2.53 (2H, m), 0.90 (9H, s), 0.08 (3H, s), 0.06 (3H, s); <sup>13</sup>C NMR (100 MHz, CDCl<sub>3</sub>) δ 173.4, 133.4, 117.9, 72.2, 51.8, 39.8, 25.8, 18.4, –4.9, –5.2; IR (CHCl<sub>3</sub>) 2953, 2935, 1760, 1473, 1257, 1143, 837, 779 cm<sup>-1</sup>; [α]<sub>D</sub><sup>25</sup> +11.6 (c 0.900, CHCl<sub>3</sub>); HRFABMS calcd for C<sub>12</sub>H<sub>24</sub>O<sub>3</sub>Si [M + H]<sup>+</sup> 245.1573, found 245.1587.

*N*-[(2*R*)-*tert*-Butyldimethylsilyloxyprop-4-enyl]-*L*-proline Benzyl Ester (**7**). To a solution of methyl ester **10** (8.02 g, 32.8 mmol, 1 equiv) in THF (126 mL, 3.8 mL/mmol) and H<sub>2</sub>O (126 mL, 3.8 mL/mmol) was added lithium hydroxide monohydrate (2.75 g, 65.6 mmol, 2 equiv) at 0 °C. After the reaction mixture was stirred at room temperature for 4 h, 2 M sodium dihydrogen phosphate (pH 3, 70 mL, 140 mmol, 4.3 equiv) was added at 0 °C, and the aqueous layer was extracted with ether. The organic layer was washed with brine, and its organic layer was dried over MgSO<sub>4</sub> and filtered. The filtrate was concentrated in vacuo, and the resulting residue was used for the next reaction without further purification.

To a solution of the crude carboxylic acid **11**, *L*-proline benzyl ester hydrochloride (8.73 g, 36.1 mmol, 1.1 equiv), and *N,N*-diisopropylethylamine (17.1 mL, 98.4 mmol, 3 equiv) in dry CH<sub>2</sub>Cl<sub>2</sub> (164 mL, 5.00 mL/mmol) was added PyBroP (23.0 g, 49.2 mmol, 1.5 equiv) at 0 °C under an argon atmosphere. After the reaction mixture was stirred at room temperature for 16 h, H<sub>2</sub>O was added, and the aqueous layer was extracted with CH<sub>2</sub>Cl<sub>2</sub>. The organic layer was washed with brine, and its organic layer was dried over MgSO<sub>4</sub> and filtered. The filtrate was concentrated in vacuo, and the resulting residue was purified by silica gel column chromatography (eluted with hexane/AcOEt = 7:1) to afford amide **7** (7.67 g, 18.4 mmol, 56%) as a pale-yellow oil. <sup>1</sup>H NMR (400 MHz, CDCl<sub>3</sub>) δ 7.26–7.40 (5H, m), 5.81 (1H, ddt, *J* = 7.2, 10.0, 17.2 Hz), 5.16 (2H, s), 5.10 (1H, d, *J* = 17.2 Hz), 5.06 (1H, d, *J* = 10.0 Hz), 4.52 (1H, dd, *J* = 3.6, 8.8 Hz), 4.32, (1H, t, *J* = 6.8 Hz), 3.87 (1H, dt, *J* = 6.8, 10.4 Hz), 3.68–3.74 (1H, m), 2.39–2.48 (2H, m), 2.10–2.17 (1H, m), 1.99–2.05 (1H, m), 1.88–1.94 (2H, m), 0.89 (9H, s), 0.07 (3H, s), 0.05 (3H, s); <sup>13</sup>C NMR (100 MHz, CDCl<sub>3</sub>) δ 172.0, 171.3, 135.8, 133.7, 128.4, 128.1, 128.0, 117.8, 74.9, 66.6, 59.6, 46.7, 39.2, 28.4, 25.9, 25.3, 18.3, –4.7, –5.1; IR (CHCl<sub>3</sub>) 2954, 2928, 2856, 1746, 1641, 1430, 1258, 1169, 837, 779 cm<sup>-1</sup>; [α]<sub>D</sub><sup>25</sup> –34.4 (c 0.450, CHCl<sub>3</sub>); HRFABMS calcd for C<sub>23</sub>H<sub>35</sub>NO<sub>4</sub>Si [M + H]<sup>+</sup> 418.2414, found 418.2412.

**Benzyl Ester 13a**. To a solution of alkene **7** (7.67 g, 18.4 mmol, 1 equiv) in *t*-BuOH (90 mL, 4.89 mL/mmol) and H<sub>2</sub>O (90 mL, 4.89 mL/mmol) were added (DHQD)<sub>2</sub>PHAL (717 mg, 0.92 mmol, 5.0 mol %), K<sub>2</sub>CO<sub>3</sub> (7.63 g, 55.2 mmol, 3 equiv), K<sub>3</sub>[Fe(CN)<sub>6</sub>] (18.2 g, 55.2 mmol, 3 equiv), and a solution of K<sub>2</sub>OsO<sub>2</sub>(OH)<sub>4</sub> in H<sub>2</sub>O (0.05 M, 1.84 mL, 0.092 mmol, 0.5 mol %) at 0 °C. After the reaction mixture was stirred at room temperature for 8 h, saturated aqueous Na<sub>2</sub>S<sub>2</sub>O<sub>3</sub> was added, and the aqueous layer was extracted with ethyl acetate. The organic layer was washed with brine, and its organic layer was dried over MgSO<sub>4</sub> and filtered. The filtrate was concentrated in vacuo, and the resulting residue was filtered through a short pad of silica gel (eluted with AcOEt/MeOH = 10:1) to afford diol **12** (86:14 diastereomeric mixture, 8.26 g, 18.4 mmol, quant) as a colorless oil.

To a solution of diol **12** (8.26 g, 18.4 mmol, 1 equiv) and 2,2-dimethoxypropane (12.1 mL, 92.0 mmol, 5.00 equiv) in dry CH<sub>2</sub>Cl<sub>2</sub> (123 mL, 6.7 mL/mmol) was added *p*-TsOH (317 mg, 1.78 mmol, 0.10 equiv) at 0 °C under an argon atmosphere. After being stirred at the same temperature for 10 min, the reaction mixture was quenched with *N,N*-diisopropylethylamine. The reaction mixture was concen-

trated in vacuo, and the resulting residue was purified by silica gel column chromatography (eluted with hexane/AcOEt = 6:1) to afford **13a** (5.82 g, 11.8 mmol, 66% over two steps) as a colorless oil. <sup>1</sup>H NMR (400 MHz, CDCl<sub>3</sub>) δ 7.25–7.37 (5H, m), 5.18 (1H, d, *J* = 12.0 Hz), 5.13 (1H, d, *J* = 12.0 Hz), 4.52 (1H, dd, *J* = 3.6, 8.4 Hz), 4.45 (1H, t, *J* = 6.4 Hz), 4.11 (1H, q, *J* = 6.4 Hz), 4.04 (1H, dd, app. dt, *J* = 6.8 Hz), 3.81–3.88 (1H, m), 3.63–3.70 (1H, m), 3.57 (1H, dd, app. dt, *J* = 7.2 Hz), 1.88–2.20 (6H, m), 1.40 (3H, s), 1.32 (3H, s), 0.89 (9H, s), 0.08 (3H, s), 0.07 (3H, s); <sup>13</sup>C NMR (100 MHz, CDCl<sub>3</sub>) δ 172.0, 170.9, 135.8, 128.5, 128.1, 128.0, 108.5, 72.8, 71.4, 69.5, 66.6, 59.4, 46.6, 38.7, 28.4, 27.0, 25.7, 25.6, 25.1, 18.1, –4.8, –5.3; IR (CHCl<sub>3</sub>) 2956, 2934, 1755, 1666, 1643, 1442, 1256, 1157, 835 cm<sup>-1</sup>; [α]<sub>D</sub><sup>28</sup> –32.9 (c 1.00, CHCl<sub>3</sub>); HRFABMS calcd for C<sub>26</sub>H<sub>41</sub>NO<sub>6</sub>Si [M + H]<sup>+</sup> 492.2781, found 492.2787.

**Acid 4**. To a solution of benzyl ester **13a** (5.82 g, 11.8 mmol, 1 equiv) in AcOEt (23.6 mL, 2.00 mL/mmol) and EtOH (23.6 mL, 2.00 mL/mmol) was added 10% Pd/C (580 mg, 10 wt %) at room temperature under an argon atmosphere, and the flask was purged with hydrogen three times. After being stirred at room temperature for 1 h, the reaction mixture was filtered through a pad of Celite, and the filtrate was concentrated in vacuo. The resulting residue was recrystallized from hexane to afford carboxylic acid **4** (4.06 g, 10.1 mmol, 86%) as a white solid. <sup>1</sup>H NMR (400 MHz, CDCl<sub>3</sub>) δ 4.62 (1H, dd, *J* = 2.4, 8.4 Hz), 4.55 (1H, dd, app. dt, *J* = 6.0 Hz), 4.10–4.18 (1H, m), 4.07 (1H, dd, app. dt, *J* = 6.8 Hz), 3.80–3.90 (1H, m), 3.60–3.68 (1H, m), 3.58 (1H, dd, app. dt, *J* = 7.6 Hz), 2.43–2.53 (1H, m), 1.85–2.10, (5H, m), 1.40 (3H, s), 1.32 (3H, s), 0.90 (9H, s), 0.09 (3H, s), 0.08 (3H, s); <sup>13</sup>C NMR (100 MHz, CDCl<sub>3</sub>) δ 173.6, 173.1, 109.0, 72.3, 71.2, 69.4, 60.4, 47.2, 38.8, 28.8, 27.2, 26.9, 25.7, 25.6, 25.1, 18.1, –4.8, –5.2; IR (CHCl<sub>3</sub>) 2928, 2857, 1741, 1616, 1462, 1369, 1255, 1159, 1063 cm<sup>-1</sup>; mp 84–87 °C; [α]<sub>D</sub><sup>26</sup> –75.9 (c 1.03, CHCl<sub>3</sub>); HRFABMS calcd for C<sub>19</sub>H<sub>35</sub>NO<sub>6</sub>Si [M + H]<sup>+</sup> 402.2312, found 402.2325.

**Cbz-β-Ala-OTMSEt (15)**. To a solution of Cbz-β-Ala-OH (**14**) (3.00 g, 13.4 mmol, 1 equiv), 2-(trimethylsilyl)ethanol (2.12 mL, 14.8 mmol, 1.1 equiv), and DMAP (164 mg, 1.34 mmol, 0.1 equiv) in dry CH<sub>2</sub>Cl<sub>2</sub> (54 mL, 4 mL/mmol) was added EDCI (2.84 g, 14.8 mmol, 1.1 equiv) at 0 °C under an argon atmosphere. After being stirred at room temperature for 5 h, the reaction mixture was quenched with 3 M HCl at 0 °C. The aqueous layer was extracted with ethyl acetate. The organic layer was washed with saturated aqueous NaHCO<sub>3</sub> and brine. The organic layer was dried over MgSO<sub>4</sub> and filtered. The filtrate was concentrated in vacuo to afford TMSEt ester **15** (4.34 g, 13.4 mmol, quant) as a colorless oil. <sup>1</sup>H NMR (400 MHz, CDCl<sub>3</sub>) δ 7.26–7.36 (5H, m), 5.29 (1H, br s), 5.09 (2H, s), 4.18 (2H, t, *J* = 8.6 Hz), 3.46 (2H, dt, *J* = 5.6, 6.0 Hz), 2.52 (2H, t, *J* = 6.0 Hz), 0.98 (2H, t, *J* = 8.6 Hz), 0.04 (9H, s); <sup>13</sup>C NMR (100 MHz, CDCl<sub>3</sub>) δ 172.5, 156.2, 136.5, 128.5, 128.05, 128.05, 66.7, 63.0, 36.6, 34.6, 17.3, –1.52; IR (CHCl<sub>3</sub>) 3353, 2954, 1729, 1523, 1250, 1175, 860, 837, 697 cm<sup>-1</sup>; HRFABMS calcd for C<sub>16</sub>H<sub>26</sub>NO<sub>4</sub>Si [M + H]<sup>+</sup> 324.1631, found 324.1641; HPLC retention time 8.73 min, purity >97%.

**Cbz-MeAla-β-Ala-OTMSEt (17)**. To a solution of **15** (1.36 g, 4.21 mmol, 1 equiv) in *i*-PrOH (14 mL, 3.3 mL/mmol) was added 10% Pd/C (140 mg, 10 wt %) at room temperature under an argon atmosphere, and the flask was purged with hydrogen three times. After being stirred at room temperature for 6 h, the reaction mixture was filtered through a pad of Celite, and the filtrate was concentrated in vacuo. The crude residue was used for the next reaction without further purification.

To a solution of the crude amine **16** (0.781 g, 4.13 mmol, 1 equiv), Cbz-MeAla-OH (1.00 g, 4.21 mmol, 1.0 equiv), HOBT (0.670 g, 4.96 mmol, 1.2 equiv), and DIEA (1.08 mL, 6.20 mmol, 1.5 equiv) in dry CH<sub>2</sub>Cl<sub>2</sub> (16.5 mL, 4 mL/mmol) was added EDCI (0.951 g, 4.96 mmol, 1.2 equiv) at 0 °C under an argon atmosphere. After being stirred at room temperature for 12 h, the reaction mixture was quenched with saturated aqueous NH<sub>4</sub>Cl at 0 °C. The aqueous layer was extracted with CHCl<sub>3</sub>. The organic layer was washed with saturated aqueous NaHCO<sub>3</sub> and brine. The organic layer was dried over MgSO<sub>4</sub> and filtered. The filtrate was concentrated in vacuo, and the resulting residue was purified by silica gel column chromatography

(eluted with hexane/AcOEt = 1:1) to afford dipeptide **17** (1.46 g, 3.57 mmol, 86%) as a colorless oil.  $^1\text{H}$  NMR (400 MHz,  $\text{CDCl}_3$ )  $\delta$  7.33–7.23 (5H, m), 6.50 (1H, br s), 5.13 (2H, s), 4.72 (1H, br s), 4.13 (2H, t,  $J = 8.6$  Hz), 3.46 (2H, dt,  $J = 5.2, 6.4$  Hz), 2.81 (3H, s), 2.44 (2H, t,  $J = 5.2$  Hz), 1.32 (3H, d,  $J = 7.2$  Hz), 0.94 (2H, t,  $J = 8.6$  Hz), 0.03 (9H, s);  $^{13}\text{C}$  NMR (100 MHz,  $\text{CDCl}_3$ )  $\delta$  172.4, 171.0, 136.4, 128.5, 128.1, 127.9, 67.6, 63.0, 35.0, 34.1, 17.3, –1.54; IR ( $\text{CHCl}_3$ ) 3340, 2953, 2898, 1732, 1703, 1683, 1527, 1455, 1400, 1313, 1250, 1218, 1172, 1061, 860, 838  $\text{cm}^{-1}$ ;  $[\alpha]_{\text{D}}^{26} -44$  ( $c$  0.66,  $\text{CHCl}_3$ ); HRFABMS calcd for  $\text{C}_{20}\text{H}_{33}\text{N}_2\text{O}_5\text{Si}$   $[\text{M} + \text{H}]^+$  409.2159, found 409.2158; HPLC retention time 8.75 min, purity 94%.

**Cbz-MeVal-MeAla- $\beta$ -Ala-OTMSEt (18).** To a solution of **17** (1.45 g, 3.55 mmol, 1 equiv) in *i*-PrOH (14 mL, 3.9 mL/mmol) was added 10% Pd/C (145 mg, 10 wt %) at room temperature under an argon atmosphere, and the flask was purged with hydrogen three times. After being stirred at room temperature for 12 h, the reaction mixture was filtered through a pad of Celite, and the filtrate was concentrated in vacuo. The crude residue was used for the next reaction without further purification.

To a solution of the crude amine (0.931 g, 3.39 mmol, 1 equiv), Cbz-MeVal-OH (1.08 g, 4.07 mmol, 1.2 equiv), HOAt (0.693 g, 5.09 mmol, 1.5 equiv), and DIEA (1.78 mL, 10.2 mmol, 3 equiv) in dry  $\text{CH}_2\text{Cl}_2$  (14 mL, 4 mL/mmol) was added EDCI (0.975 g, 5.09 mmol, 1.5 equiv) at 0 °C under an argon atmosphere. After being stirred at room temperature for 12 h, the reaction mixture was quenched with saturated aqueous  $\text{NH}_4\text{Cl}$  at 0 °C. The aqueous layer was extracted with ethyl acetate. The organic layer was washed with saturated aqueous  $\text{NaHCO}_3$  and brine. The organic layer was dried over  $\text{MgSO}_4$  and filtered. The filtrate was concentrated in vacuo, and the resulting residue was purified by silica gel column chromatography (eluted with hexane/AcOEt = 1:1) to afford tripeptide **18** (1.67 g, 3.21 mmol, 90%) as a colorless oil.  $^1\text{H}$  NMR (600 MHz,  $\text{DMSO}-d_6$ , 80 °C)  $\delta$  7.15–7.50 (6H, m), 5.00–5.14 (2H, m), 4.86 (1H, d,  $J = 6.6$  Hz), 4.48–4.58 (1H, m), 4.09 (2H, t,  $J = 7.8$  Hz), 3.20–3.30 (2H, m), 2.66–2.83 (6H, m), 2.38 (2H, t,  $J = 7.2$  Hz), 2.15–2.25 (1H, m), 1.13–1.30 (3H, m), 0.76–0.91 (8H, m), 0.00 (9H, s);  $^{13}\text{C}$  NMR (100 MHz,  $\text{DMSO}-d_6$ , mixture of rotamers)  $\delta$  171.23, 171.19, 170.5, 169.7, 169.6, 169.5, 156.2, 156.0, 155.2, 136.9, 136.7, 136.5, 128.37, 128.34, 128.0, 127.8, 127.6, 127.25, 127.23, 79.1, 66.8, 66.7, 66.5, 61.9, 60.0, 59.3, 54.6, 52.0, 51.9, 35.0, 34.84, 34.81, 33.8, 33.7, 30.5, 30.3, 29.3, 29.0, 28.9, 28.8, 27.1, 26.96, 26.92, 19.42, 19.35, 19.32, 18.3, 18.09, 18.05, 16.75, 16.73, 15.7, 14.4, –1.55, –1.58; IR ( $\text{CHCl}_3$ ) 3334, 2958, 2898, 1731, 1692, 1646, 1522, 1498, 1472, 1456, 1396, 1370, 1303, 1250, 1224, 1174, 1133, 1111, 860, 838  $\text{cm}^{-1}$ ;  $[\alpha]_{\text{D}}^{27} -117$  ( $c$  1.00,  $\text{CHCl}_3$ ); HRFABMS calcd for  $\text{C}_{26}\text{H}_{44}\text{N}_3\text{O}_6\text{Si}$   $[\text{M} + \text{H}]^+$  522.2999, found 522.3011; HPLC retention time 9.18 min, purity >98%

**Cbz-Ile-MeVal-MeAla- $\beta$ -Ala-OTMSEt (19).** To a solution of **18** (1.67 g, 3.21 mmol, 1 equiv) in *i*-PrOH (17 mL, 5.3 mL/mmol) was added 10% Pd/C (167 mg, 10 wt %) at room temperature under an argon atmosphere, and the flask was purged with hydrogen three times. After being stirred at room temperature for 12 h, the reaction mixture was filtered through a pad of Celite, and the filtrate was concentrated in vacuo. The crude residue was used for the next reaction without further purification.

To a solution of the crude amine (1.24 g, 3.21 mmol, 1 equiv), Cbz-Ile-OH (1.30 g, 4.91 mmol, 1.5 equiv), HOAt (0.668 g, 4.91 mmol, 1.5 equiv), and DIEA (1.71 mL, 9.84 mmol, 3 equiv) in dry  $\text{CH}_2\text{Cl}_2$  (13 mL, 4 mL/mmol) was added EDCI (0.941 g, 4.91 mmol, 1.5 equiv) at 0 °C under an argon atmosphere. After being stirred at room temperature for 12 h, the reaction mixture was quenched with saturated aqueous  $\text{NH}_4\text{Cl}$  at 0 °C. The aqueous layer was extracted with ethyl acetate. The organic layer was washed with saturated aqueous  $\text{NaHCO}_3$  and brine. The organic layer was dried over  $\text{MgSO}_4$  and filtered. The filtrate was concentrated in vacuo, and the resulting residue was purified by silica gel column chromatography (eluted with hexane/AcOEt = 1:1) to afford tetrapeptide **19** (1.99 g, 3.13 mmol, 98%) as a colorless oil.  $^1\text{H}$  NMR (400 MHz,  $\text{DMSO}-d_6$ , 80 °C)  $\delta$  7.35–7.45 (1H, br), 7.23–7.33 (5H, m), 6.95–7.15 (1H, br), 4.93–5.10 (3H, m), 4.89 (1H, q,  $J = 7.2$  Hz), 4.30 (1H, dd, app. dt,  $J = 8.4$  Hz), 4.09 (2H, t,  $J = 8.2$  Hz), 3.23–3.35 (1H, m), 2.93 (3H, s), 2.85

(3H, s), 2.39 (2H, t), 2.10–2.26 (1H, m), 1.68–1.75 (1H, m), 1.40–1.52 (1H, m), 1.05–1.25 (1H, m), 1.13 (3H, d,  $J = 7.2$  Hz), 0.92 (2H, t,  $J = 8.4$  Hz), 0.83 (3H, d,  $J = 6.8$  Hz), 0.79 (3H, t,  $J = 7.6$  Hz), 0.78 (3H, d,  $J = 6.8$  Hz), 0.68 (3H, d,  $J = 6.8$  Hz), 0.00 (9H, s);  $^{13}\text{C}$  NMR (100 MHz,  $\text{DMSO}-d_6$ , mixture of rotamers)  $\delta$  172.4, 171.3, 170.3, 169.6, 156.2, 137.2, 128.3, 127.7, 127.5, 79.2, 65.3, 61.9, 57.4, 54.9, 51.8, 35.6, 34.9, 33.8, 30.4, 30.0, 26.6, 24.2, 19.5, 17.9, 16.8, 15.4, 14.7, 14.3, 10.6, –1.51; IR ( $\text{CHCl}_3$ ) 3314, 2961, 2876, 1720, 1685, 1629, 1527, 1467, 1455, 1408, 1388, 1293, 1250, 1226, 1173, 1038, 860, 838  $\text{cm}^{-1}$ ;  $[\alpha]_{\text{D}}^{28} -100$  ( $c$  1.01,  $\text{CHCl}_3$ ); HRFABMS calcd for  $\text{C}_{32}\text{H}_{55}\text{N}_4\text{O}_7\text{Si}$   $[\text{M} + \text{H}]^+$  635.3840, found 635.3810; HPLC retention time 9.25 min, purity >97%.

**TBS-HA-Pro-Ile-MeVal-MeAla- $\beta$ -Ala-OTMSEt (20).** To a solution of **19** (5.00 g, 7.88 mmol, 1 equiv) in EtOH (50 mL, 6.3 mL/mmol) was added 10% Pd/C (500 mg, 10 wt %) at room temperature under an argon atmosphere, and the flask was purged with hydrogen three times. After being stirred at room temperature for 40 h, the reaction mixture was filtered through a pad of Celite, and the filtrate was concentrated in vacuo. The crude residue was used for the next reaction without further purification.

To a solution of the crude amine **5** (3.73 g, 7.45 mmol, 1 equiv), acid **4** (2.99 g, 7.45 mmol, 1 equiv), HOAt (1.52 g, 11.2 mmol, 1.5 equiv), and DIEA (3.89 mL, 22.4 mmol, 3 equiv) in dry DMF– $\text{CH}_2\text{Cl}_2$  (1:1, 30 mL, 4 mL/mmol) was added EDCI (2.15 g, 11.2 mmol, 1.5 equiv) at 0 °C under an argon atmosphere. After being stirred at room temperature for 12 h, the reaction mixture was quenched with saturated aqueous  $\text{NH}_4\text{Cl}$  at 0 °C. The aqueous layer was extracted with ethyl acetate. The organic layer was washed with saturated aqueous  $\text{NaHCO}_3$  and brine. The organic layer was dried over  $\text{MgSO}_4$  and filtered. The filtrate was concentrated in vacuo, and the resulting residue was purified by silica gel column chromatography (eluted with  $\text{CHCl}_3/\text{MeOH} = 50:1$ ) to afford hexapeptide **20** (5.71 g, 6.46 mmol, 87%) as a colorless oil.  $^1\text{H}$  NMR (400 MHz,  $\text{DMSO}-d_6$ , 80 °C)  $\delta$  7.75–7.85 (1H, br), 7.43 (1H, br t,  $J = 5.2$  Hz), 5.09 (1H, d,  $J = 10.4$  Hz), 4.91 (1H, q,  $J = 7.2$  Hz), 4.52–4.62 (1H, m), 4.30–4.50 (2H, m), 4.12 (2H, t,  $J = 8.4$  Hz), 4.00–4.15 (1H, m), 3.97 (1H, dd, app. dt,  $J = 7.0$  Hz), 3.40–3.75 (3H, m), 3.25–3.35 (2H, m), 2.94 (3H, s), 2.88 (3H, s), 2.42 (2H, t,  $J = 6.6$  Hz), 2.15–2.30 (1H, m), 1.65–2.00 (7H, m), 1.50–1.58 (1H, m), 1.31 (3H, s), 1.24 (3H, s), 1.16 (3H, d,  $J = 7.2$  Hz), 1.05–1.15 (1H, m), 0.95 (2H, t,  $J = 8.4$  Hz), 0.86 (9H, s), 0.75–0.90 (9H, m), 0.72 (3H, d,  $J = 6.4$  Hz), 0.04 (3H, s), 0.038 (3H, s), 0.03 (9H, s);  $^{13}\text{C}$  NMR (100 MHz,  $\text{DMSO}-d_6$ , mixture of rotamers)  $\delta$  172.0, 171.4, 171.3, 170.4, 169.6, 169.5, 107.6, 79.2, 72.5, 72.4, 70.1, 68.9, 68.7, 61.9, 59.2, 57.5, 55.0, 52.5, 51.9, 46.3, 38.0, 35.9, 34.9, 33.8, 30.4, 29.9, 28.6, 26.83, 26.80, 26.6, 25.7, 25.57, 25.55, 24.4, 23.8, 19.6, 17.9, 17.7, 16.8, 14.9, 14.3, 10.7, –1.52, –4.78, –5.49; IR ( $\text{CHCl}_3$ ) 3320, 2958, 2931, 2877, 2858, 1733, 1683, 1634, 1538, 1471, 1463, 1446, 1410, 1379, 1369, 1314, 1251, 1174, 1118, 1098, 860, 838  $\text{cm}^{-1}$ ;  $[\alpha]_{\text{D}}^{27} -101$  ( $c$  1.00,  $\text{CHCl}_3$ ); HRFABMS calcd for  $\text{C}_{43}\text{H}_{82}\text{O}_{10}\text{N}_5\text{Si}_2$   $[\text{M} + \text{H}]^+$  884.5595, found 884.5569; HPLC retention time 10.23 min, purity >98%.

**Cyclization Precursor 3.** To a solution of **20** (5.71 g, 6.46 mmol, 1 equiv) in dry THF (32 mL, 5 mL/mmol) was slowly added TBAF (1.0 M solution in THF, 19.4 mL, 19.4 mmol, 3 equiv) at 0 °C under an argon atmosphere. After the reaction mixture was stirred at room temperature for 9 h, TBAF (1.0 M solution in THF, 6.5 mL, 6.5 mmol, 1 equiv) was added at 0 °C. After the resulting mixture was stirred at room temperature for 12 h, DOWEX 50WX8-400 (7.0 g) was added at 0 °C, and the reaction mixture was filtered through a pad of Celite. The filtrate was concentrated in vacuo, and the resulting residue was purified by silica gel column chromatography (eluted with  $\text{CHCl}_3/\text{MeOH} = 30:1$ ) to afford cyclization precursor **3** (4.2 g, 6.40 mmol, 94%) as a colorless oil.  $^1\text{H}$  NMR (600 MHz,  $\text{DMSO}-d_6$ , 80 °C)  $\delta$  7.75–7.90 (1H, br), 7.35–7.45 (1H, br), 5.10 (1H, d,  $J = 9.6$  Hz), 4.93 (1H, q,  $J = 6.6$  Hz), 4.48–4.58 (1H, m), 4.35–4.45 (1H, m), 4.18–4.30 (1H, m), 4.02–4.13 (1H, m), 3.88–4.00 (1H, m), 3.35–3.70 (3H, m), 3.20–3.35 (2H, m), 2.95 (3H, s), 2.88 (3H, s), 2.33–2.41 (2H, m), 2.18–2.40 (1H, m), 1.60–2.00 (7H, m), 1.50–1.60 (1H, m), 1.31 (3H, s), 1.24 (3H, s), 1.16 (3H, d,  $J = 7.2$  Hz), 1.05–1.15 (1H, m), 0.75–0.90 (9H, m), 0.72 (3H, d,  $J = 6.0$  Hz);  $^{13}\text{C}$  NMR (100

MHz, DMSO-*d*<sub>6</sub>, mixture of rotamers)  $\delta$  172.9, 172.4, 172.2, 171.9, 171.4, 171.0, 170.8, 170.3, 169.58, 169.55, 169.1, 107.6, 107.4, 79.1, 72.7, 72.6, 68.7, 68.5, 66.8, 66.7, 59.0, 58.5, 57.4, 57.4, 56.8, 54.9, 53.1, 52.9, 51.8, 51.8, 46.6, 46.3, 37.6, 37.3, 35.9, 35.7, 35.2, 34.9, 33.7, 33.6, 31.7, 30.4, 30.1, 29.94, 29.90, 28.96, 28.93, 28.8, 27.0, 26.79, 26.77, 26.60, 26.56, 25.7, 25.6, 24.3, 24.2, 24.12, 24.07, 24.04, 21.4, 19.5, 19.4, 17.7, 15.4, 15.0, 14.86, 14.68, 14.3, 10.9, 10.7; IR (neat) 3311, 2966, 2938, 2877, 1725, 1624, 1540, 1457, 1409, 1380, 1241, 1221, 1159, 1098, 1065, 754 cm<sup>-1</sup>; [ $\alpha$ ]<sub>D</sub><sup>27</sup> -158 (c 0.80, CHCl<sub>3</sub>); HRFABMS calcd for C<sub>32</sub>H<sub>55</sub>N<sub>5</sub>O<sub>10</sub>Na [M + Na]<sup>+</sup> 692.3841, found 692.3808; HPLC retention time 7.18 min, purity 94%.

**Macrolactone 2.** To a solution of cyclization precursor **3** (4.20 g, 6.40 mmol, 1 equiv) and DMAP (1.77 g, 12.8 mmol, 2 equiv) in dry CH<sub>2</sub>Cl<sub>2</sub> (1060 mL, 166 mL/mmol) was added MNBA (6.61 g, 19.2 mmol, 3 equiv) at room temperature under an argon atmosphere. After the reaction mixture was stirred at 30 °C for 48 h, saturated aqueous NaHCO<sub>3</sub> was added at 0 °C, and the aqueous layer was extracted with CHCl<sub>3</sub>. The organic layer was washed with brine, dried over MgSO<sub>4</sub>, and filtered. The filtrate was concentrated in vacuo, and the resulting residue was purified by silica gel column chromatography (eluted with CHCl<sub>3</sub>/MeOH = 30:1) to afford macrolactone **2** (3.32 g, 5.21 mmol, 81%) as a colorless amorphous solid. <sup>1</sup>H NMR (400 MHz, CDCl<sub>3</sub>)  $\delta$  8.19 (1H, d, *J* = 8.0 Hz), 7.15 (1H, d, *J* = 9.2 Hz), 5.15 (1H, q, *J* = 6.8 Hz), 5.06 (1H, dd, *J* = 5.8, 7.6 Hz), 4.97 (1H, d, *J* = 11.2 Hz), 4.90 (1H, dd, *J* = 6.8, 9.0 Hz), 4.69 (1H, d, *J* = 6.8 Hz), 4.00–4.15 (3H, m), 3.86–3.94 (1H, m), 3.73–3.80 (1H, m), 3.62 (1H, dd, app. dt, *J* = 6.8 Hz), 3.23 (3H, s), 3.08 (1H, dd, *J* = 11.6, 13.4 Hz), 2.72 (3H, s), 2.45–2.75 (3H, m), 2.26–2.39 (1H, m), 1.83–2.20 (6H, m), 1.24–1.46 (2H, m), 1.49 (3H, s), 1.33 (3H, s), 1.29 (3H, d, *J* = 6.8 Hz), 0.93 (3H, d, *J* = 6.8 Hz), 0.89 (3H, d, *J* = 6.8 Hz), 0.87 (3H, d, *J* = 7.2 Hz), 0.86 (3H, t, *J* = 7.2 Hz); <sup>13</sup>C NMR (100 MHz, CDCl<sub>3</sub>)  $\delta$  173.5, 173.4, 171.0, 170.8, 169.6, 168.8, 109.2, 71.5, 70.8, 69.1, 60.8, 58.0, 55.5, 53.5, 46.4, 37.4, 34.5, 34.4, 33.2, 30.8, 29.2, 28.1, 27.2, 26.8, 25.5, 24.3, 23.9, 20.0, 19.6, 15.4, 15.1, 11.3; IR (CHCl<sub>3</sub>) 3853, 3744, 3385, 3308, 2965, 2928, 2879, 2360, 2341, 1733, 1683, 1669, 1653, 1635, 1628, 1539, 1521, 1441, 1381, 1183, 1101 cm<sup>-1</sup>; [ $\alpha$ ]<sub>D</sub><sup>28</sup> -199 (c 1.00, CHCl<sub>3</sub>); HRESIMS calcd for C<sub>32</sub>H<sub>53</sub>N<sub>5</sub>O<sub>9</sub>Na [M + Na]<sup>+</sup> 674.3735, found 674.3714.

**Cbz-Ile-MeVal-MeAla- $\beta$ -Ala-OH (23).** To a solution of ester **19** (0.100 g, 0.158 mmol, 1 equiv) in dry THF (1.2 mL, 7.6 mL/mmol) was slowly added TBAF (0.237 mL, 0.237 mmol, 1.5 equiv) at 0 °C under an argon atmosphere. After the reaction mixture was stirred at room temperature for 9 h, DOWEX 50WX8-400 (0.200 g) was added at 0 °C, and the resulting mixture was filtered through a pad of Celite. The filtrate was concentrated in vacuo, and the resulting residue was purified by silica gel column chromatography (eluted with CHCl<sub>3</sub>/MeOH = 30:1) to afford carboxylic acid **23** (0.0779 g, 0.146 mmol, 92%) as a colorless oil. <sup>1</sup>H NMR (600 MHz, DMSO-*d*<sub>6</sub>, 80 °C)  $\delta$  7.35–7.45 (1H, br), 7.20–7.35 (5H, m), 7.00–7.25 (1H, br), 5.10 (1H, d, *J* = 10.2 Hz), 4.95–5.18 (2H, m), 4.92 (1H, q, *J* = 6.6 Hz), 4.33 (1H, dd, app. dt, *J* = 8.7 Hz), 3.20–3.35 (2H, m), 2.96 (3H, s), 2.88 (3H, s), 2.37 (2H, t, *J* = 6.6 Hz), 2.15–2.26 (1H, m), 1.74–1.82 (1H, m), 1.45–1.54 (1H, m), 1.15 (3H, d, *J* = 6.6 Hz), 1.10–1.20 (1H, m), 0.86 (3H, d, *J* = 6.6 Hz), 0.82 (3H, d, *J* = 7.8 Hz), 0.80 (3H, t, *J* = 7.8 Hz), 0.71 (3H, d, *J* = 6.6 Hz); <sup>13</sup>C NMR (100 MHz, DMSO-*d*<sub>6</sub>)  $\delta$  172.9, 172.4, 170.3, 169.7, 156.2, 137.1, 128.3, 127.7, 127.5, 65.3, 57.4, 54.9, 51.8, 35.6, 34.9, 33.7, 30.4, 30.0, 26.6, 24.2, 19.4, 17.9, 14.7, 14.3, 10.6; IR (CHCl<sub>3</sub>) 3310, 2965, 2938, 2876, 1716, 1681, 1628, 1530, 1456, 1408, 1344, 1293, 1251, 1123, 1099, 1027, 755, 698 cm<sup>-1</sup>; [ $\alpha$ ]<sub>D</sub><sup>25</sup> -152 (c 1.04, CHCl<sub>3</sub>); HRESIMS calcd for C<sub>27</sub>H<sub>42</sub>N<sub>4</sub>O<sub>7</sub>Na [M + Na]<sup>+</sup> 557.2946, found 557.2927; HPLC retention time 8.05 min, purity >98%.

**Alcohol 24.** To a solution of TBS ether **13a** (0.500 g, 1.02 mmol, 1 equiv) in THF (4.0 mL, 3.9 mL/mmol) was added HF-pyridine (~70% HF, 1.0 mL) at 0 °C under an argon atmosphere. After being stirred at same temperature for 6 h, the reaction mixture was poured into saturated aqueous NaHCO<sub>3</sub> at 0 °C. The aqueous layer was extracted with ethyl acetate, and the organic layer was washed with brine, dried over MgSO<sub>4</sub>, and filtered. The filtrate was concentrated in vacuo, and the resulting residue was purified by silica gel column

chromatography (eluted with hexane/AcOEt = 1:1) to afford alcohol **24** (0.281 g, 0.745 mmol, 73%) as a colorless solid. <sup>1</sup>H NMR (400 MHz, CDCl<sub>3</sub>)  $\delta$  7.30–7.45 (5H, m), 5.18 (2H, d, *J* = 11.2 Hz), 4.53 (1H, dd, *J* = 2.8, 8.8 Hz), 4.41 (1H, dd, *J* = 6.4, 10.8 Hz), 4.18–4.25 (1H, m), 4.10 (1H, dd, *J* = 5.8, 8.2 Hz), 3.70 (1H, dd, *J* = 7.2, 8.2 Hz), 3.60–3.70 (1H, m), 3.58 (1H, d, *J* = 6.4 Hz), 1.80–2.25 (6H, m), 1.39 (3H, s), 1.34 (3H, s); <sup>13</sup>C NMR (100 MHz, CDCl<sub>3</sub>)  $\delta$  172.4, 171.6, 135.6, 128.5, 128.3, 128.1, 108.6, 72.7, 69.2, 67.2, 66.9, 59.6, 46.5, 37.5, 28.8, 26.8, 25.6, 24.6; IR (neat) 3422, 2983, 2956, 2935, 2880, 1744, 1645, 1456, 1380, 1212, 1170, 1051 cm<sup>-1</sup>; mp 105–106 °C; [ $\alpha$ ]<sub>D</sub><sup>27</sup> -54.5 (c 1.03, CHCl<sub>3</sub>); HRESIMS calcd for C<sub>20</sub>H<sub>27</sub>NO<sub>6</sub>Na [M + Na]<sup>+</sup> 400.1731, found 400.1717.

**Cbz-Ile-MeVal-MeAla- $\beta$ -Ala-HA-Pro-OBn (25).** To a solution of acid **23** (20.7 mg, 0.0346 mmol, 1 equiv) in CH<sub>2</sub>Cl<sub>2</sub>/DMF (1:1, 1 mL, 23 mL/mmol) were added alcohol **24** (17.0 mg, 0.0450 mmol, 1.3 equiv), DMAP (1.3 mg, 0.0104 mmol, 0.3 equiv), and EDCI (9.9 mg, 0.0519 mmol, 1.5 equiv) at 0 °C under an argon atmosphere. After being stirred at room temperature for 12 h, the reaction mixture was quenched with saturated aqueous NH<sub>4</sub>Cl, and the aqueous layer was extracted with ethyl acetate. The organic layer was washed with saturated aqueous NaHCO<sub>3</sub> and brine, dried over MgSO<sub>4</sub>, and filtered. The filtrate was concentrated in vacuo, and the resulting residue was purified by silica gel column chromatography (eluted with hexane/AcOEt = 1:3) to afford amide **25** (28.8 mg, 0.0322 mmol, 73%) as an amorphous solid. <sup>1</sup>H NMR (600 MHz, DMSO-*d*<sub>6</sub>, mixture of rotamers)  $\delta$  7.60–7.85 (2H, m), 7.31–7.50 (10H, m), 4.80–5.42 (7H, m), 3.80–4.45 (4H, m), 3.60–3.75 (2H, m), 3.30–3.65 (2H, m), 2.80–3.14 (6H, m), 2.50–2.65 (2H, m), 1.70–2.30 (8H, m), 1.10–1.60 (11H, m), 0.60–1.00 (12H, m); <sup>13</sup>C NMR (100 MHz, DMSO-*d*<sub>6</sub>, mixture of rotamers)  $\delta$  172.4, 171.2, 170.4, 170.2, 169.7, 166.99, 166.95, 156.2, 137.2, 136.0, 128.5, 128.4, 128.3, 127.9, 127.7, 127.6, 127.5, 108.1, 108.1, 79.2, 72.0, 69.0, 68.5, 68.1, 66.7, 65.7, 65.3, 59.7, 59.1, 58.9, 58.7, 57.4, 54.9, 51.8, 46.3, 35.6, 34.7, 34.2, 33.5, 30.5, 30.0, 28.4, 26.71, 26.66, 26.62, 25.5, 24.4, 24.1, 20.7, 19.4, 17.9, 14.7, 14.31, 14.27, 14.1, 10.6, 10.5; IR (neat) 3309, 2963, 2936, 2877, 1740, 1721, 1639, 1527, 1455, 1407, 1380, 1341, 1249, 1226, 1170, 1095, 1040, 751 cm<sup>-1</sup>; [ $\alpha$ ]<sub>D</sub><sup>27</sup> -120 (c 1.00, CHCl<sub>3</sub>); HRESIMS calcd for C<sub>47</sub>H<sub>67</sub>N<sub>5</sub>O<sub>12</sub>Na [M + Na]<sup>+</sup> 916.4678, found 916.4650; HPLC retention time 8.95 min, purity 97%.

**Dimer 22.** To a solution of benzyl ester **25** (20.0 mg, 0.0224 mmol, 1 equiv) in AcOEt/EtOH (1:1, 1.0 mL, 45 mL/mmol) was added 20% Pd(OH)<sub>2</sub>/C (3.1 mg, 4.48  $\mu$ mol, 0.2 equiv) under an argon atmosphere, and the flask was purged with hydrogen three times. After being stirred at room temperature for 2 h, the reaction mixture was filtered through a pad of Celite. The filtrate was concentrated in vacuo, and the resulting residue was used without further purification.

To a solution of amino acid **21** (10.5 mg, 0.0157 mmol, 1 equiv) in CH<sub>2</sub>Cl<sub>2</sub> (15.7 mL, 1 mM) were added DIEA (13.7  $\mu$ L, 0.0785 mmol, 5.0 equiv), HOAt (8.5 mg, 0.0628 mmol, 4.0 equiv), and EDCI (9.0 mg, 0.0471 mmol, 3 equiv) at 0 °C under an argon atmosphere. After being stirred at room temperature for 12 h, the reaction mixture was quenched with saturated aqueous NH<sub>4</sub>Cl, and the aqueous layer was extracted with CHCl<sub>3</sub>. The organic layer was washed with saturated aqueous NaHCO<sub>3</sub> and brine, dried over MgSO<sub>4</sub>, and filtered. The filtrate was concentrated in vacuo, and the resulting residue was purified by reversed-phase HPLC (eluted with CH<sub>3</sub>CN/H<sub>2</sub>O) to afford macrolactone **2** (1.4 mg, 0.00215 mmol, 14%) and dimer **22** (1.3 mg, 0.997  $\mu$ mol, 6%). <sup>1</sup>H NMR (400 MHz, CDCl<sub>3</sub>)  $\delta$  7.00–7.80 (4H, m), 1.80–5.50 (54H, m), 0.70–1.55 (46H, m); <sup>13</sup>C NMR (100 MHz, CDCl<sub>3</sub>, mixture of rotamers)  $\delta$  173.4, 170.85, 170.83, 170.2, 168.7, 109.3, 71.5, 70.7, 69.2, 60.4, 57.3, 56.0, 53.6, 46.5, 36.4, 36.0, 34.5, 33.7, 31.9, 31.0, 29.7, 29.5, 29.4, 28.9, 27.8, 26.9, 25.6, 25.2, 23.9, 22.7, 19.7, 18.7, 15.1, 14.9, 14.1, 10.5; HRESIMS calcd for C<sub>64</sub>H<sub>106</sub>N<sub>10</sub>O<sub>18</sub>Na [M + Na]<sup>+</sup> 1325.7579, found 1325.7548; HPLC retention time 8.65 min, purity >98%.

**Diol 26.** To a solution of macrolactone **2** (1.33 g, 2.04 mmol, 1 equiv) in 1,4-dioxane (6.7 mL, 3.3 mL/mmol) was slowly added 1.5 M HCl(aq) (13.3 mL, 6.5 mmol) at 0 °C. After the reaction mixture was stirred at 0 °C for 2 h, saturated aqueous NaHCO<sub>3</sub> was added, and the aqueous layer was extracted with ethyl acetate. The organic layer was

washed with brine, dried over  $\text{MgSO}_4$ , and filtered. The filtrate was concentrated in vacuo, and the resulting residue was purified by silica gel column chromatography (eluted with  $\text{CHCl}_3/\text{MeOH} = 30:1$ ) to afford diol **26** (1.08 g, 1.77 mmol, 87%) as a colorless amorphous solid.  $^1\text{H}$  NMR (400 MHz,  $\text{CDCl}_3$ )  $\delta$  8.15 (1H, d,  $J = 10.4$  Hz), 7.13 (1H, d,  $J = 9.2$  Hz), 5.19 (1H, q,  $J = 6.8$  Hz), 5.12 (1H, dd,  $J = 5.2, 6.4$  Hz), 4.98 (1H, d,  $J = 11.2$  Hz), 4.89 (1H, dd,  $J = 6.4, 9.2$  Hz), 4.68 (1H, d,  $J = 6.0$  Hz), 3.96–4.10 (2H, m), 3.85–3.95 (1H, m), 3.63–3.73 (2H, m), 3.45–3.55 (1H, m), 3.23 (3H, s), 3.05–3.15 (1H, m), 2.73 (3H, s), 2.45–2.70 (3H, m), 2.28–2.38 (1H, m), 1.85–2.10 (5H, m), 1.25–1.45 (2H, m), 1.31 (3H, d,  $J = 6.8$  Hz), 0.93 (3H, d,  $J = 6.8$  Hz), 0.89 (3H, d,  $J = 6.8$  Hz), 0.86 (3H, d,  $J = 6.8$  Hz), 0.86 (3H, t,  $J = 7.6$  Hz);  $^{13}\text{C}$  NMR (100 MHz,  $\text{CDCl}_3$ )  $\delta$  173.6, 173.5, 171.1, 171.0, 169.9, 70.8, 67.7, 66.4, 60.9, 58.1, 55.5, 53.7, 46.7, 37.3, 34.5, 33.9, 33.3, 30.8, 29.3, 28.1, 27.2, 24.4, 23.9, 19.9, 19.5, 15.4, 15.1, 11.3; IR ( $\text{CHCl}_3$ ) 3345, 3301, 2961, 2886, 2360, 1734, 1720, 1652, 1634, 1630, 1622, 1538, 1455, 1414, 1262, 1179, 1025  $\text{cm}^{-1}$ ;  $[\alpha]_{\text{D}}^{28} -230.4$  (c 1.00,  $\text{CHCl}_3$ ); HRESIMS calcd for  $\text{C}_{29}\text{H}_{49}\text{N}_5\text{O}_8\text{Na}$   $[\text{M} + \text{Na}]^+$  634.3422, found 634.3397.

**Tosylate 27.** To a solution of diol **26** (1.08 g, 1.77 mmol, 1 equiv), triethylamine (0.371 mL, 2.12 mmol, 1.5 equiv), and DMAP (21.6 mg, 0.177 mmol, 0.1 equiv) in dry  $\text{CH}_2\text{Cl}_2$  (18 mL, 10 mL/mmol) was added *p*-toluenesulfonyl chloride (0.405 g, 2.12 mmol, 1.2 equiv) at 0 °C under an argon atmosphere. After the reaction mixture was stirred at room temperature for 6 h, additional triethylamine (0.246 mL, 1.77 mmol, 1.0 equiv) and *p*-toluenesulfonyl chloride (0.270 g, 1.416 mmol, 0.8 equiv) were added at 0 °C. After the reaction mixture was stirred at room temperature for 6 h, saturated aqueous  $\text{NH}_4\text{Cl}$  was added, and the aqueous layer was extracted with  $\text{CHCl}_3$ . The organic layer was washed with brine, dried over  $\text{MgSO}_4$ , and filtered. The filtrate was concentrated in vacuo, and the resulting residue was purified by silica gel flash column chromatography (eluted with  $\text{CHCl}_3/\text{MeOH} = 30:1$ ) to afford tosylate **27** (1.10 g, 1.44 mmol, 81%) as a colorless amorphous solid.  $^1\text{H}$  NMR (400 MHz,  $\text{CDCl}_3$ )  $\delta$  8.12 (1H, d,  $J = 8.4$  Hz), 7.79 (2H, d,  $J = 8.2$  Hz), 7.37 (2H, d,  $J = 8.2$  Hz), 7.09 (1H, d,  $J = 9.2$  Hz), 5.16 (1H, q,  $J = 6.8$  Hz), 5.10 (1H, dd, app. dt,  $J = 5.8$  Hz), 4.96 (1H, d,  $J = 11.2$  Hz), 4.89 (1H, dd,  $J = 6.2, 9.4$  Hz), 4.65 (1H, d,  $J = 6.8$  Hz), 4.10–4.16 (1H, m), 3.95–4.09 (3H, m), 3.87–3.94 (1H, m), 3.57–3.67 (1H, m), 3.22 (3H, s), 3.00–3.10 (1H, m), 2.72 (3H, s), 2.48–2.68 (2H, m), 2.47 (3H, s), 2.28–2.38 (1H, m), 1.85–2.15 (5H, m), 1.23–1.48 (2H, m), 1.30 (3H, d,  $J = 6.8$  Hz), 1.28–1.33 (1H, m), 0.92 (3H, d,  $J = 6.8$  Hz), 0.88 (3H, d,  $J = 6.8$  Hz), 0.86 (3H, d,  $J = 7.2$  Hz), 0.85 (3H, t,  $J = 7.2$  Hz);  $^{13}\text{C}$  NMR (100 MHz,  $\text{CDCl}_3$ )  $\delta$  173.6, 173.3, 171.0, 170.7, 169.7, 169.5, 145.3, 132.3, 130.0, 127.9, 73.2, 70.0, 65.2, 60.9, 58.0, 55.4, 53.6, 46.7, 37.3, 34.4, 33.6, 33.1, 30.8, 29.1, 28.1, 27.2, 24.3, 23.9, 21.6, 19.9, 19.5, 15.4, 15.1, 11.3; IR ( $\text{CHCl}_3$ ) 3387, 3301, 2962, 2922, 2852, 1733, 1673, 1632, 1630, 1627, 1622, 1520, 1464, 1362, 1265, 1177, 1098  $\text{cm}^{-1}$ ;  $[\alpha]_{\text{D}}^{28} -202$  (c 1.00,  $\text{CHCl}_3$ ); HRESIMS calcd for  $\text{C}_{36}\text{H}_{55}\text{N}_5\text{O}_{11}\text{SNa}$   $[\text{M} + \text{Na}]^+$  788.3511, found 788.3485.

**Destruxin E (1).** To a solution of tosylate **27** (1.10 g, 1.44 mmol, 1 equiv) in *i*-PrOH/ $(\text{CH}_2\text{Cl}_2)$  (10:1, 15 mL, 10 mL/mmol) was added  $\text{K}_2\text{CO}_3$  (0.793 g, 5.74 mmol, 4 equiv) at 0 °C under an argon atmosphere. After the reaction mixture was stirred at 50 °C for 4 h, saturated aqueous  $\text{NH}_4\text{Cl}$  was added at 0 °C, and the aqueous layer was extracted with  $\text{CHCl}_3$ . The organic layer was washed with brine, dried over  $\text{MgSO}_4$ , and filtered. The filtrate was concentrated in vacuo, and the resulting residue was purified by silica gel flash column chromatography twice (eluted with  $\text{CHCl}_3/\text{MeOH} = 50:1$ , ethyl acetate/ $\text{MeOH} = 20:1$ ) to afford destruxin E (**1**) (0.547 g, 0.921 mmol, 64%) as a colorless amorphous solid.  $^1\text{H}$  NMR (400 MHz,  $\text{CDCl}_3$ )  $\delta$  8.21 (1H, d,  $J = 10.0$  Hz), 7.16 (1H, d,  $J = 9.2$  Hz), 5.16 (1H, q,  $J = 6.8$  Hz), 4.99 (1H, dd, app. dt,  $J = 7.2$  Hz), 4.97 (1H, d,  $J = 10.8$  Hz), 4.89 (1H, dd,  $J = 6.8, 9.2$  Hz), 4.70 (1H, d,  $J = 7.2$  Hz), 4.00–4.10 (1H, m), 3.92–3.99 (1H, m), 3.23 (3H, s), 3.08 (1H, br t,  $J = 12.0$  Hz), 2.95–3.00 (1H, m), 2.83 (1H, dd, app. dt,  $J = 4.4$  Hz), 2.72 (3H, s), 2.62–2.72 (1H, m), 2.45–2.59 (3H, m), 2.24–2.40 (2H, m), 2.02–2.12 (1H, m), 1.85–2.01 (4H, m), 1.38–1.46 (1H, m), 1.31 (3H, d,  $J = 6.8$  Hz), 1.28–1.33 (1H, m), 0.93 (3H, d,  $J = 6.8$  Hz), 0.89 (3H, d,  $J = 6.8$  Hz), 0.87 (3H, d,  $J = 7.2$  Hz), 0.86 (3H, t,  $J = 7.6$  Hz);

$^{13}\text{C}$  NMR (100 MHz,  $\text{CDCl}_3$ )  $\delta$  173.5, 173.4, 171.0, 170.8, 169.7, 168.6, 70.6, 60.9, 58.0, 55.5, 53.6, 47.8, 47.1, 46.6, 37.5, 34.5, 33.6, 33.2, 30.8, 29.2, 28.1, 27.2, 24.4, 24.0, 20.0, 19.6, 15.4, 15.2, 11.4; IR ( $\text{CHCl}_3$ ) 3385, 3298, 2960, 2923, 2851, 1731, 1673, 1670, 1636, 1631, 1622, 1519, 1445, 1413, 1378, 1278, 1178, 1100  $\text{cm}^{-1}$ ;  $[\alpha]_{\text{D}}^{28} -247$  (c 1.00,  $\text{CHCl}_3$ ) {lit<sup>4b</sup>  $[\alpha]_{\text{D}}^{25} -253$  (c 1.00,  $\text{CHCl}_3$ )}; HRESIMS calcd for  $\text{C}_{29}\text{H}_{47}\text{N}_5\text{O}_8\text{Na}$   $[\text{M} + \text{Na}]^+$  616.3317, found 616.3297.

## ■ ASSOCIATED CONTENT

### ● Supporting Information

Copies of  $^1\text{H}$  and  $^{13}\text{C}$  NMR spectra for **1–4**, **7**, **8**, **13a**, **15**, **17–20**, **22–27**; copy of the  $^1\text{H}$  spectrum for **21**; and HPLC chromatograms for **1**, **3**, **15**, **17–23**, and **25**. This material is available free of charge via the Internet at <http://pubs.acs.org>.

## ■ AUTHOR INFORMATION

### Corresponding Author

\*E-mail: doi\_taka@mail.pharm.tohoku.ac.jp.

### Notes

The authors declare no competing financial interest.

## ■ ACKNOWLEDGMENTS

This work was supported by a Grant-in-Aid for Young Scientists (B) (M.Y.) from JSPS and the Japan Science and Technology Agency (A-STEP, AS242Z00980Q). We thank Mr. Hisayuki Takeuchi for initial investigations on the synthesis of destruxin E.

## ■ REFERENCES

- (1) (a) Seeman, E. *J. Appl. Physiol.* **2003**, *95*, 2142–2151. (b) Sambrook, P.; Cooper, C. *Lancet* **2006**, *367*, 2010–2018.
- (2) (a) Karsdal, M. A.; Qvist, P.; Christiansen, C.; Tankó, L. B. *Drugs* **2006**, *66*, 1909–1918. (b) Rachner, T. D.; Khosla, S.; Hofbauer, L. C. *Lancet* **2011**, *377*, 1276–1287. (c) Henriksen, K.; Bollerslev, J.; Everts, V.; Karsdal, M. A. *Endocr. Rev.* **2011**, *32*, 31–63.
- (3) (a) Farina, C.; Gagliardi, S. *Drug Discovery Today* **1999**, *4*, 163–172. (b) Farina, C.; Gagliardi, S. *Curr. Pharm. Des.* **2002**, *8*, 2033–2048. (c) Bowman, E. J.; Bowman, B. J. *J. Bioenerg. Biomembr.* **2005**, *37*, 431–435. (d) Yuan, F.-L.; Li, X.; Lu, W.-G.; Li, C.-W.; Li, J.-P.; Wang, Y. *Mol. Biol. Rep.* **2010**, *37*, 3561–3566. (e) Katner, N.; Yao, Y.; Crasto, G. J.; Datti, A.; Manolson, M. F. *J. Biol. Chem.* **2010**, *285*, 37476–37490. (f) Thudium, C. S.; Jensen, V. K.; Karsdal, M. A.; Henriksen, K. *Curr. Protein Pept. Sci.* **2012**, *13*, 141–151.
- (4) (a) País, M.; Das, B. C.; Ferron, P. *Phytochemistry* **1981**, *20*, 715–723. (b) Gupta, S.; Roberts, D. W.; Renwick, J. A. A. *J. Chem. Soc., Perkin Trans. 1* **1989**, 2347–2357.
- (5) Vázquez, M. J.; Albarrán, M. L.; Espada, A.; Rivera-Sagredo, A.; Díaz, E.; Hueso-Rodríguez, J. A. *Chem. Biodiversity* **2005**, *2*, 123–130.
- (6) (a) Kuyama, S.; Tamura, S. *Agric. Biol. Chem.* **1965**, *29*, 168–190. (b) Lee, S.; Izumiya, N.; Suzuki, A.; Tamura, S. *Tetrahedron Lett.* **1975**, *16*, 883–886. (c) Calmes, M.; Cavelier-Frontin, F.; Jacquier, R.; Mercadier, J.-L.; Sabil, S.; Verducci, J.; Qciot, J.-M.; Vey, A. *Int. J. Pept. Protein Res.* **1993**, *41*, 528–535. (d) Cavelier, F.; Jacquier, R.; Mercadier, J.-L.; Verducci, J. *Tetrahedron* **1996**, *52*, 6173–6186. (e) Ward, D. E.; Lazny, R.; Pedras, M. S. C. *Tetrahedron Lett.* **1997**, *38*, 339–342. (f) Cavelier, F.; Jacquier, R.; Mercadier, J.-L.; Verducci, J.; Traris, M.; Vey, A. *J. Pept. Res.* **1997**, *50*, 94–101. (g) Cavelier, F.; Verducci, J.; André, F.; Haraux, F.; Sigalat, C.; Traris, M.; Vey, A. *Pestic. Sci.* **1998**, *52*, 81–89. (h) Ward, D. E.; Gai, Y.; Lazny, R.; Pedras, M. S. C. *J. Org. Chem.* **2001**, *66*, 7832–7840. (i) Ast, T.; Barron, E.; Kinne, L.; Schmidt, M.; Germeroth, L.; Simmons, K.; Wenschuh, H. *J. Pept. Res.* **2001**, *58*, 1–11.
- (7) Yoshida, M.; Takeuchi, H.; Ishida, Y.; Yashiroda, M.; Takagi, M.; Shin-ya, K.; Doi, T. *Org. Lett.* **2010**, *12*, 3792–3795.

(8) Nakagawa, H.; Takami, M.; Udagawa, N.; Sawae, Y.; Suda, K.; Sasaki, T.; Takahashi, N.; Wachi, M.; Nagai, K.; Woo, J. T. *Bone* **2003**, *33*, 443–455.

(9) (a) Shiina, I.; Ibuka, R.; Kubota, M. *Chem. Lett.* **2002**, 286–287. (b) Shiina, I.; Kubota, M.; Ibuka, R. *Tetrahedron Lett.* **2002**, *43*, 7535–7539. (c) Shiina, I.; Kubota, M.; Oshiumi, H.; Hashizume, M. *J. Org. Chem.* **2004**, *69*, 1822–1830. (d) Shiina, I.; Hashizume, M.; Yamai, Y.; Oshiumi, H.; Shimazaki, T.; Takasuna, Y.; Ibuka, R. *Chem.—Eur. J.* **2005**, *11*, 6601–6608.

(10) (a) Jacobsen, E. N.; Marko, I.; Mungall, W. S.; Schroder, G.; Sharpless, K. B. *J. Am. Chem. Soc.* **1988**, *110*, 1968–1970. (b) Kolb, H. C.; VanNieuwenhze, M. S.; Sharpless, K. B. *Chem. Rev.* **1994**, *94*, 2483–2547.

(11) (a) Roth, G. A. *J. Org. Chem.* **1995**, *60*, 8105–8109. (b) Kobayashi, M.; Kurosu, M.; Wang, W.; Kitagawa, I. *Chem. Pharm. Bull.* **1994**, *42*, 2394–2396.

(12) (a) Crispino, G. A.; Jeong, K.-S.; Kolb, H.-C.; Wang, Z.-M.; Xu, D.; Sharpless, K. B. *J. Org. Chem.* **1993**, *58*, 3785–3786. (b) Arrington, M. P.; Bennani, Y. L.; Göbel, T.; Walsh, P.; Zhao, S.-H.; Sharpless, K. B. *Tetrahedron Lett.* **1993**, *34*, 7375–7378. (c) Becker, H.; King, S. B.; Taniguchi, M.; Vanhessche, K. P. M.; Sharpless, K. B. *J. Org. Chem.* **1995**, *60*, 3940–3941. (d) Corey, E. J.; Guzman-Perez, A.; Noe, M. C. *J. Am. Chem. Soc.* **1995**, *117*, 10806–10816.

(13) Crimmins et al. have reported that allyl iodide is effective for the alkylation of glycolate derivatives. See: Crimmins, M. T.; Emmitte, K. A.; Katz, J. D. *Org. Lett.* **2000**, *2*, 2165–2167.

(14) Evans, D. A.; Trotter, B. W.; Côté, B.; Colman, P. J.; Dias, L. C.; Tyler, A. N. *Angew. Chem., Int. Ed. Engl.* **1997**, *36*, 2744–2748.

(15) Evans, D. A.; Morrissey, M. M.; Dorow, R. L. *J. Am. Chem. Soc.* **1985**, *107*, 4346–4348.

(16) Frérot, E.; Coste, J.; Pantaloni, A.; Dufour, M.-N.; Jouin, P. *Tetrahedron* **1991**, *47*, 259–270.

(17) Structure determinations of **12a** and **12b** were carried out after partial separation by column chromatography. Acetal formation of the partially obtained **12a** and **12b** led to **13a** and its diastereomer, whose spectra were identical to those of the corresponding isomers of **13** prepared from optically active known **6S** and **6R**, respectively.

(18) Becker, H.; Sharpless, K. B. *Angew. Chem., Int. Ed. Engl.* **1996**, *35*, 448–451.

(19) Anteunis, M. J. O.; Van Der Auwera, C. *Int. J. Pept. Protein Res.* **1988**, *31*, 301–310.

(20) Hughes, A. B.; Sleebs, B. E. *Helv. Chim. Acta* **2006**, *89*, 2611–2637.

(21) Mauger, A. B.; Desai, R. B.; Rittner, I.; Rzeszotarski, W. J. *J. Chem. Soc., Perkin Trans. 1* **1972**, 2146–2148.

(22) The cyclization precursor **21** was immediately used for next macrolactamization because of decomposition during the purification by silica gel column chromatography.

(23) Conformational studies of destruxin and related molecules have been performed. See: (a) Springer, J. P.; Cole, R. J.; Dorner, J. W.; Cox, R. H.; Richard, J. L.; Barnes, C. L.; van der Helm, D. *J. Am. Chem. Soc.* **1984**, *106*, 2388–2392. (b) Snyder, J. P. *J. Am. Chem. Soc.* **1984**, *106*, 2393–2400. (c) Gupta, S.; Roberts, D. W.; Renwick, J. A. A.; Ni, C.-Z.; Clardy, J. *Tetrahedron Lett.* **1989**, *30*, 4189–4192.

(24) Wang, B.; Kang, Q.; Lu, Y.; Bai, L.; Wang, C. *Proc. Natl. Acad. Sci. U.S.A.* **2012**, *109*, 1287–1292.



Contents lists available at ScienceDirect

## Phytomedicine

journal homepage: [www.elsevier.de/phymed](http://www.elsevier.de/phymed)

## Nitensidine A, a guanidine alkaloid from *Pterogyne nitens*, is a novel substrate for human ABC transporter ABCB1



Yasuhiro Tajima<sup>a,1</sup>, Hiroshi Nakagawa<sup>a,b,c,1</sup>, Ai Tamura<sup>b,c</sup>, Onat Kadioglu<sup>d</sup>, Kazuhiro Satake<sup>a</sup>, Yuji Mitani<sup>a</sup>, Hayato Murase<sup>a</sup>, Luis Octavio Regasini<sup>e</sup>, Vanderlan da Silva Bolzani<sup>e</sup>, Toshihisa Ishikawa<sup>b,f</sup>, Gert Fricker<sup>c</sup>, Thomas Efferth<sup>d,\*</sup>

<sup>a</sup> Department of Applied Biological Chemistry, College of Bioscience and Biotechnology, Chubu University, 1200 Matsumoto-cho, Kasugai 487-8501, Japan

<sup>b</sup> Department of Biomolecular Engineering, Graduate School of Bioscience and Biotechnology, Tokyo Institute of Technology, 4259 Nagatsuta-cho, Midori-ku, Yokohama 226-8501, Japan

<sup>c</sup> Institute of Pharmacy and Molecular Biotechnology, University of Heidelberg, Im Neuenheimer Feld 366, 69120 Heidelberg, Germany

<sup>d</sup> Department of Pharmaceutical Biology, Institute of Pharmacy and Biochemistry, University of Mainz, Staudinger Weg 5, 55128 Mainz, Germany

<sup>e</sup> Department of Organic Chemistry, Institute of Chemistry, São Paulo State University, 355, 14800-900 Araraquara, Brazil

<sup>f</sup> Omics Science Center, RIKEN Yokohama Institute, 1-7-22 Suehiro-cho, Tsurumi-ku, Yokohama 230-0045, Japan

## ARTICLE INFO

## Article history:

Received 18 March 2013

Received in revised form 20 July 2013

Accepted 23 August 2013

## Keywords:

ATP-binding cassette (ABC) transporter ABCB1

P-glycoprotein

*Pterogyne nitens*

Guanidine alkaloid

## ABSTRACT

The *Pterogyne nitens* (Fabaceae) tree, native to South America, has been found to produce guanidine alkaloids as well as bioactive flavonols such as kaempferol, quercetin, and rutin. In the present study, we examined the possibility of interaction between human ATP-binding cassette (ABC) transporter ABCB1 and four guanidine alkaloids isolated from *P. nitens* (i.e., galegine, nitensidine A, pterogynidine, and pterogynine) using human T cell lymphoblast-like leukemia cell line CCRF-CEM and its multi-drug resistant (MDR) counterpart CEM/ADR5000. In XTT assays, CEM/ADR5000 cells were resistant to the four guanidine alkaloids compared to CCRF-CEM cells, although the four guanidine alkaloids exhibited some level of cytotoxicity against both CCRF-CEM and CEM/ADR5000 cells. In ATPase assays, three of the four guanidine alkaloids were found to stimulate the ATPase activity of ABCB1. Notably, nitensidine A was clearly found to stimulate the ATPase activity of ABCB1 as strongly as the control drug, verapamil. Furthermore, the cytotoxic effect of nitensidine A on CEM/ADR5000 cells was synergistically enhanced by verapamil. Nitensidine A inhibited the extrusion of calcein by ABCB1. In the present study, the possibility of interaction between ABCB1 and two synthetic nitensidine A analogs (nitensidine AT and AU) were examined to gain insight into the mechanism by which nitensidine A stimulates the ATPase activity of ABCB1. The ABCB1-dependent ATPase activity stimulated by nitensidine A was greatly reduced by substituting sulfur (S) or oxygen (O) for the imino nitrogen atom (N) in nitensidine A. Molecular docking studies on human ABCB1 showed that, guanidine alkaloids from *P. nitens* dock to the same binding pocket as verapamil. Nitensidine A and its analogs exhibit similar binding energies to verapamil. Taken together, this research clearly indicates that nitensidine A is a novel substrate for ABCB1. The present results also suggest that the number, binding site, and polymerization degree of the isoprenyl moiety in the guanidine alkaloids and the imino nitrogen atom cooperatively contribute to their stimulation of ABCB1's ATPase activity.

© 2013 Elsevier GmbH. All rights reserved.

## Introduction

Human ABCB1 (P-gp; P-glycoprotein) is a transmembrane efflux pump that belongs to ATP-binding cassette (ABC) transporter superfamily. It was cloned as the multidrug resistance 1 (*MDR1*)

gene from cancer cells exhibiting cross-resistance to a large number of structurally diverse and mechanistically unrelated anticancer drugs (Chen et al., 1986; de Jong et al., 2006; Juliano and Ling, 1976; Ueda et al., 1986). Since the enzymatic activity of ABCB1 plays a crucial role in regulating the pharmacokinetics of many drug types and protecting the human body from attack by xenobiotics (Lin, 2003; Schinkel et al., 1994), it is generally recognized as a drug/xenobiotic transporter. As a drug/xenobiotic transporter, ABCB1 regulates the intracellular concentration of various substrates by extruding them from the cells. In fact, overexpression of ABCB1 reportedly confers cancer cells with resistance to anti-cancer drugs such as doxorubicin, vincristine and paclitaxel (Gribar et al., 2000; Ishikawa, 2003;

Abbreviations: ABC, ATP-binding cassette; MDR, multi-drug resistance; P-gp, P-glycoprotein.

\* Corresponding author. Tel.: +49 6131 3924322; fax: +49 6131 3923752.

E-mail address: [efferth@uni-mainz.de](mailto:efferth@uni-mainz.de) (T. Efferth).

<sup>1</sup> These authors contributed equally to this work.

Ling, 1997). Thus, the enzymatic activity of ABCB1 can contribute to multi-drug resistance (MDR) in cancer cells, and sometimes becomes an obstacle to successful cancer chemotherapy.

The molecular mechanisms by which ABCB1 recognizes the drugs/xenobiotics have been extensively studied, as well as the regulatory mechanism of its function and expression. In particular, ABCB1 inhibitors, modulators and chemosensitizers have been extensively screened to understand the details of how ABCB1 recognizes and transports substrates and to circumvent MDR. The calcium channel blocker verapamil was the first compound reported to inhibit the activity of ABCB1, and various compounds such as cyclosporin A and valspodar (PSC-833) have also been shown to prevent MDR (Adachi et al., 2007; Ford, 1996; Tsuruo et al., 1981). Extensive structure–activity relationship (SAR) and quantitative SAR (QSAR) analyses have been performed to better understand the structural features of ABCB1 inhibitors, modulators and chemosensitizers. Our previous QSAR analysis with 41 structurally-different compounds revealed that two carbocyclic systems with at least one aromatic ring and ring-linking groups containing one carbon atom were important for stimulating ABCB1-dependent ATPase activity (Sakurai et al., 2007). On the other hand, other investigations have indicated important structural features of molecules that modulate the function of ABCB1, namely two planar aromatic domains and a basic nitrogen atom within an extended aliphatic chain, a bulky aromatic ring system with a heteroatom in the third position toward the anthranilamide nucleus at the opposite end of the tetrahydroquinoline group, hydrophobicity, and nitrogen or hydrogen bond acceptor groups (Chiba et al., 1996; Ecker et al., 1999; Globisch et al., 2006; Klopman et al., 1997; Pearce et al., 1989, 1990; Zamora et al., 1988). Furthermore, previous studies of pharmacophore identification of ABCB1-related drugs have pointed to hydrophobic and hydrogen bond-acceptor interactions as the most likely to be involved in ligand binding to ABCB1 (Ekins et al., 2002; Garrigues et al., 2002; Pajeva and Wiese, 2002; Penzotti et al., 2002). Although ABCB1 inhibitors, modulators and chemosensitizers have been extensively screened and analyzed via SAR for many years, the structural features important for ABCB1 inhibition, modulation and chemosensitization are not completely understood at present. Therefore, it is important to find novel substrates for ABCB1 and understand the molecular mechanisms by which it recognizes its substrates.

The *Pterogyne nitens* (Fabaceae), a tree native to South America, has been found to produce flavonols and guanidine alkaloids (Aller et al., 2009; Duarte et al., 2010; Fernandes et al., 2008; Noguchi et al., 2009; Regasini et al., 2009, 2010). Among the known products from *P. nitens*, kaempferol, quercetin, and rutin have been reported to interact with ABCB1 (Kitagawa et al., 2005). In contrast, no interaction between ABCB1 and the guanidine alkaloids has yet been found. However, the guanidine alkaloids have demonstrated cytotoxicity against the human infiltrating ductal carcinoma ZR-7531 cell line, human myeloblastic leukemia HL-60, and human glioblastoma SF-295 cells (Duarte et al., 2010; Regasini et al., 2009). Taking into account the biological and chemical features of the four guanidine alkaloids isolated from *P. nitens* (i.e., galegine, nitensidine A, pterogynidine, and pterogynine), in the present study we examined the possibility of interaction between ABCB1 and the guanidine alkaloids using the human T cell lymphoblast-like cell line, CCRF-CEM, and its multi-drug resistance (MDR) counterpart, CEM/ADR5000.

## Materials and methods

### Plant materials

The four guanidine alkaloids tested in the present study were obtained from *Pterogyne nitens* leaves or branches; their isolation

and identification have been previously described (Regasini et al., 2009, 2010).

### Synthesis of nitensidine A analogs

Synthetic nitensindines AT and AU were prepared as described previously, with minor modifications (Venkatachalam et al., 2003). A solution of 1,1'-carbonyldiimidazole (1.0 mmol) or 1,1'-thiocarbonyldiimidazole (1.0 mmol) in dried *p*-dioxane (15 ml) was added to a solution of geranylamine (2.2 mmol) in dried *p*-dioxane (3.0 ml), at 5 °C. This mixture was stirred for two hours at room temperature. The solvent was removed under reduced pressure. The residue was partitioned three times in ethyl acetate and then filtered. The filtrate was partitioned three times: first with saturated aqueous citric acid solution (two times), next with saturated aqueous sodium bicarbonate (two times), and third with water (two times), and then dried over magnesium sulphate. The crude products were purified over a silica gel column using an isocratic system of hexane–ethyl acetate (3:2) to obtain nitensindines AT and AU. The structures of these compounds were established by <sup>1</sup>H and <sup>13</sup>C NMR spectral analysis. Chemical shifts ( $\delta$ ) were expressed in ppm, coupling constants ( $J$ ) were expressed in Hz, and splitting patterns are described as follows: s = singlet, br s = broad singlet, t = triplet, m = multiplet.

**Nitensidine AT:** This yellow oil was obtained in 55% yield. <sup>1</sup>H NMR (500 MHz, CDCl<sub>3</sub>)  $\delta$  5.93 (br s; 3-NH, 4-NH), 5.17 (t;  $J$  = 7.0 Hz, H-2'), 4.99 (t;  $J$  = 7.0 Hz, H-6'), 3.93 (br s; H-1'), 2.01 (m; H-5'), 1.96 (m; H-4'), 1.61 (s; H-9' and H-10'), 1.52 (s; H-8'). <sup>13</sup>C NMR (125 MHz, CDCl<sub>3</sub>)  $\delta$  181.2 (C-2), 140.7 (C-3'), 131.6 (C-7'), 123.4 (C-6'), 118.8 (C-2'), 42.3 (C-1'), 39.2 (C-4'), 26.1 (C-5'), 25.4 (C-9'), 17.4 (C-8'), 16.2 (C-10').

**Nitensidine AU:** This white solid was obtained in 21% yield. <sup>1</sup>H NMR (500 MHz, CDCl<sub>3</sub>)  $\delta$  5.17 (t;  $J$  = 6.0 Hz, H-2'), 4.97 (t;  $J$  = 6.0 Hz, H-6'), 4.52 (br s; 3-NH, 4-NH), 3.65 (t;  $J$  = 6.0 Hz, H-1'), 1.96 (m; H-5'), 1.89 (m; H-4'), 1.58 (s; H-10'), 1.56 (s; H-10'), 1.50 (s; H-8'). <sup>13</sup>C NMR (125 MHz, CDCl<sub>3</sub>)  $\delta$  158.5 (C-2), 139.0 (C-3'), 134.6 (C-7'), 123.8 (C-6'), 121.0 (C-2'), 39.4 (C-1'), 38.4 (C-4'), 26.4 (C-5'), 25.5 (C-9'), 17.5 (C-8'), 16.1 (C-10').

### Cell culture

CCRF-CEM and CEM/ADR5000 cells were kindly provided by Dr. Axel Sauerbrey (Department of Pediatrics, University of Jena, Jena, Germany). CEM/ADR5000 cells are an ABCB1 over-expressing, multidrug-resistant subline of CCRF-CEM cells. All cells were maintained in RPMI1640 medium (Biochrom AG, Berlin, Germany) supplemented with 10% (v/v) fetal bovine serum (Biochrom AG, Berlin, Germany), 0.8 mM L-glutamine, 50  $\mu$ g/ml kanamycin, 100 U/ml penicillin, and 100  $\mu$ g/ml streptomycin at 37 °C in a humidified atmosphere of 5% (v/v) CO<sub>2</sub> in air. CEM/ADR5000 cells were cultured with 2.5  $\mu$ g/ml doxorubicin for 24 h once per week to maintain the expression of ABCB1 in the cells.

### XTT assay

The cytotoxicity of nitensidine A against CCRF-CEM and CEM/ADR5000 cells was examined using the Cell Proliferation Kit II (XTT assay) (Roche, Mannheim, Germany). In brief, the cells were seeded into 96-well culture plates at  $2 \times 10^4$  cells/well and cultured with test compounds for 72 h. After incubation, cells were treated with XTT for 5 h according to manufacturer protocols for the kit. Absorbance at 490 nm and 655 nm was measured as test and reference wavelengths, respectively. Data are the mean  $\pm$  SEM of triplicate determinations.

### ATPase assay

The effects of the guanidine alkaloids on the ATPase activities of plasma membrane fractions prepared from the cells were measured according to the following procedure with plasma membrane fractions prepared from ABCB1-expressing Sf9 cells (Sakurai et al., 2007). In brief, cell membranes (1 µg of protein per well) were incubated with 10 µM verapamil or guanidine alkaloids in 96-well plates with 40 µl of the incubation medium [50 mM Tris–Mes (pH 6.8), 2 mM EGTA, 2 mM dithiothreitol, 50 mM potassium chloride, 5 mM sodium azide, 2 mM ouabain, and 2 mM ATP/Mg] at 37 °C for 30 min. The reaction was stopped by the addition of 20 µl of 5% trichloroacetic acid followed by 42 µl of solution A [2 N hydrochloric acid:0.1 M sodium molybdate = 4:3] and 18 µl of solution B [0.084% (w/v) malachite green in 1% (w/v) polyvinyl alcohol]. Thereafter, 120 µl of solution C [7.8% (v/v) sulfuric acid] was added to the mixture in the well plates. One hour after incubation at room temperature, the absorbance of the reaction mixture in each well was measured at a wavelength of 655 nm using a Bio-Rad Model 680 Absorbance Microplate Reader (Bio-Rad Laboratories, Inc.). The amount of liberated phosphate was quantified on the basis of the calibration line established with inorganic phosphate standards. Data are expressed as the means ± SEM of triplicate determinations.  $K_m$  and  $V_{max}$  values for test compounds were calculated from the Hanes–Wolf plots of (compound concentration) × (compound-stimulated ATPase activity)<sup>-1</sup> vs (compound concentration).

Plasma membranes of CCRF–CEM and CEM/ADR5000 cells were prepared according to a previously described method (Sakurai et al., 2007).

### Calcein assay

The effects of the guanidine alkaloids on the transporter activity of ABCB1 were examined by fluorescence-activated cell sorting. In brief, CEM/ADR5000 cells ( $3 \times 10^6$  cells) were incubated with or without 20 µM nitensidine A or 5 µM verapamil for 15 min on 24-well culture plates and further incubated with 1 µM calcein acetoxymethyl ester (calcein-AM) for 30 min at 37 °C in a humidified atmosphere of 5% (v/v) CO<sub>2</sub> in air. After the incubation, CEM/ADR5000 cells were mixed with 700 µl of RPMI1640 medium with 1 µg/ml propidium iodide, washed with RPMI1640 medium, and analyzed with BD a FACSCanto™ II Flow Cytometry System (Becton, Dickinson and Company, Franklin Lakes, NJ). In the analysis, ten thousand cells were analyzed using CellQuest software (Franklin Lakes, NJ, USA). Any dead cells, as identified by their scatter characteristics, were gated out.

### Calculation for chemical structures

In order to obtain the 3D structures of nitensidines and verapamil, their 2D structures drawn by CS ChemDraw Ultra 6.0 software (CambridgeSoft Corp., MA, USA) were applied to CS Chem3D Pro 5.0 software (CambridgeSoft Corp., MA, USA). The 3D structures of nitensidines and verapamil were optimized according to MM2 procedure based on molecular mechanics method (MM2 in Table 4) or AM1 parameters based on semi-empirical molecular orbital method (AM1 in Table 4) by using CS Chem3D Pro 5.0 software in order to perform Molecular Docking studies considering the existence of electron (Dewar et al., 1985).

### Molecular docking studies

Human ABCB1 structure was created by homology modeling using mouse ABCB1 as a template structure (PDB code: 3G60). Human and mouse ABCB1 protein sequences were aligned with EMBOSS Needle (<http://www.ebi.ac.uk/Tools/psa/>

**Table 1**

Cytotoxicity of guanidine alkaloids in CCRF–CEM and CEM/ADR5000 cells.

Compounds	IC <sub>50</sub> (µM)	
	CCRF–CEM cells	CEM/ADR5000 cells
Galegine	>100	>100
Nitensidine A	4.9 ± 0.03	23 ± 2
Pterogynidine	16 ± 0.8	>100
Pterogynine	37 ± 3	>100

Data are expressed as the mean ± SEM of triplicate determinations.

emboss\_needle/), then the alignment file was used to create homology models with MODELLER 9.11 (Fiser and Sali, 2003; Venkatachalam et al., 2003) and Swiss-MODEL Alignment Mode (Kiefer et al., 2009; Noguchi et al., 2009). The best homology model was determined with Swiss-MODEL structure assessment tool for the molecular docking studies.

AutoDock4 (Morris et al., 2009) was used for the defined molecular docking calculations. Drug binding residues of ABCB1 were identified as His61, Gly64, Leu65, Met69, Ser222, Leu304, Ile306, Tyr307, Phe336, Leu339, Ile340, Ala342, Phe343, Gln725, Phe728, Phe732, Leu762, Thr837, Ile868, Gly872, Phe942, Thr945, Tyr953, Leu975, Phe978, Ser979, Val982, Gly984, Ala985, Met986, Gly989, Gln990, and Ser993 (Aller et al., 2009). A grid map was chosen to cover these residues and verapamil was selected as the control ligand. For the docking calculations, the number of evaluations was set to 2,500,000 and the number of runs was set to 100. Lamarckian Genetic Algorithm was chosen for the docking calculations. For visualization of the docking results, AutoDock Tools and Visual Molecular Dynamics were used. The surface representation image showing the binding pocket of human ABCB1 was made with VMD software developed with NIH support by the Theoretical and Computational Biophysics group at the Beckman Institute, University of Illinois at Urbana-Champaign.

### Statistical analysis

Statistical analyses were performed using Microsoft Excel 2003 software (Microsoft Co., Redmond, WA, USA). The statistical significance of differences was determined according to Student's *t*-test. *P* values <0.05 were considered statistically significant.

### Results

#### *The effects of guanidine alkaloids on the activity of ABCB1 expressed in CEM/ADR5000 cells*

Firstly, we performed XTT assays to evaluate the possibility of interactions between ABCB1 and the guanidine alkaloids isolated from *P. nitens* (i.e., galegine, nitensidine A, pterogynidine, and pterogynine) (Fig. 1). As shown in Fig. 2, all of the four guanidine alkaloids reduced the viability of CCRF–CEM and CEM/ADR5000 cells in a concentration-dependent manner, where CEM/ADR5000 cells showed resistance to all of the cytotoxic guanidine alkaloids compared to CCRF–CEM cells (Fig. 2). The IC<sub>50</sub> values of the compounds were calculated on the basis of the results shown in Fig. 2 and are summarized in Table 1. Among the four guanidine alkaloids, nitensidine A showed the strongest cytotoxicity on both the CCRF–CEM and the CEM/ADR5000 cells. These results suggest that guanidine alkaloids can be extruded by ABCB1 and that nitensidine A is more easily extruded by ABCB1 than the others.

To evaluate the possibility of interactions between ABCB1 and the four guanidine alkaloids in detail, we examined the effect of the four compounds on ABCB1-dependent ATPase activity. As shown in Fig. 3, we measured guanidine alkaloid-stimulated ATPase activity by incubating different concentrations of guanidine alkaloids

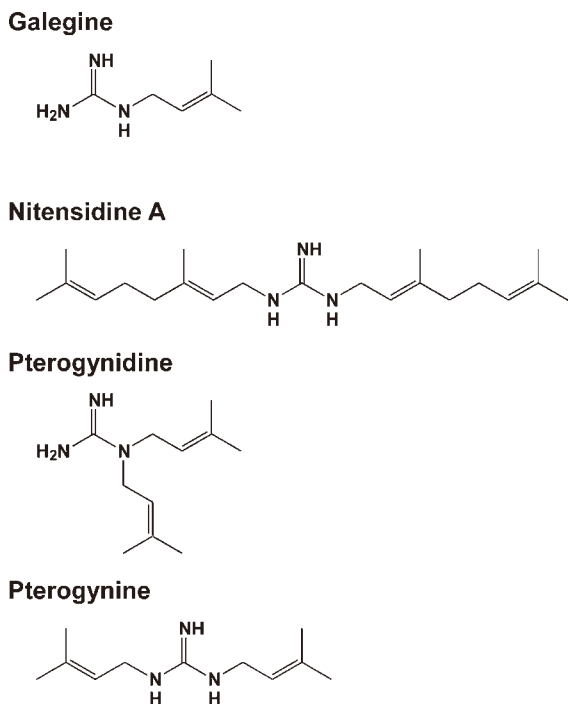


Fig. 1. Structures of the guanidine alkaloids.

(0–100  $\mu\text{M}$ ) with plasma membranes prepared from CCRF-CEM or CEM/ADR5000 cells. Among the four guanidine alkaloids, nitensidine A showed saturation kinetics in the relationship between the compound-stimulated ATPase activity and the compound concentration, suggesting Michaelis–Menten kinetics. Thus,  $K_m$  and  $V_{max}$  values were calculated from Hanes–Woolf plots of (compound concentration)  $\times$  (compound-stimulated ATPase activity) $^{-1}$  vs (compound concentration); these are summarized in Fig. 3. The plots in Fig. 3 indicated that the  $K_m$  and  $V_{max}$  values of nitensidine A were higher than and comparable to, respectively, those of verapamil. These results indicate that some of the guanidine alkaloids can stimulate ABCB1-dependent ATPase activity.

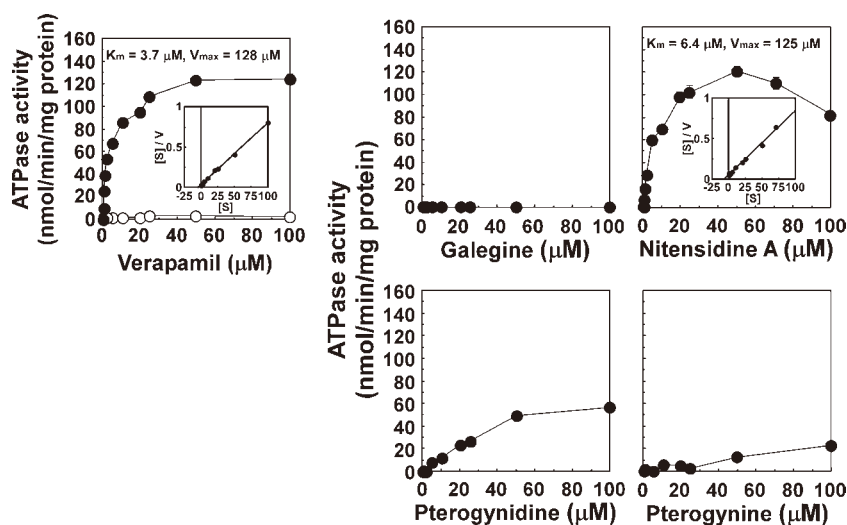


Fig. 3. Concentration-dependent stimulation of ABCB1 ATPase activity by the guanidine. ATPase activity in the plasma membranes of CCRF-CEM cells (open circles) and CEM/ADR5000 cells (closed circles) was measured in the presence of different concentrations of each of verapamil or the guanidine alkaloids as described in Materials and methods. Similar results were obtained in at least three other experiments. Data are expressed as the means  $\pm$  SEM of triplicate determinations. [S], compound concentration; [V], ATPase activity (nmol/min/mg protein).

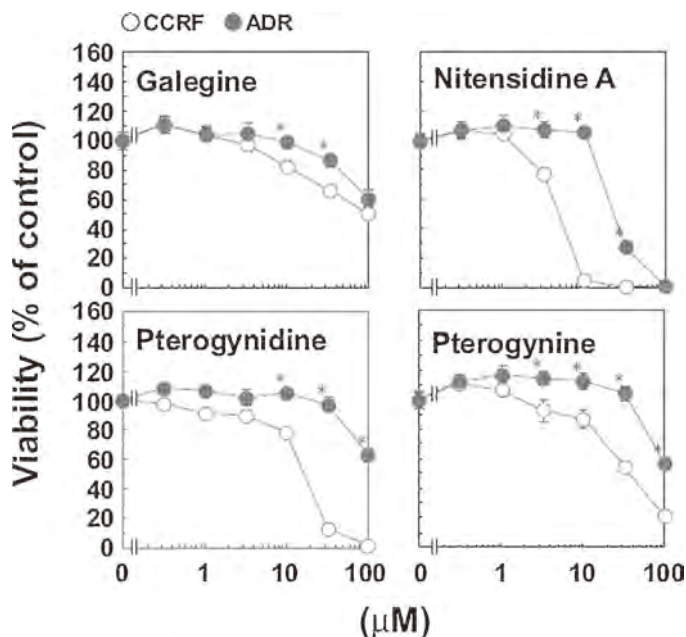
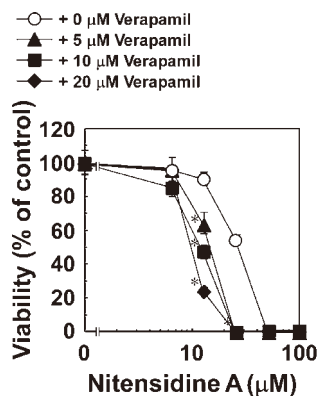


Fig. 2. Effect of the guanidine alkaloids on the viability of CCRF-CEM and CEM/ADR5000. CCRF-CEM (open circles) and CEM/ADR5000 cells (closed circles) were cultured with or without the guanidine alkaloids for 72 h. After the culture, viability of the cells was determined by XIT assay as described in Materials and methods. Similar results were obtained in at least three other experiments. Data are expressed as the mean  $\pm$  SEM of triplicate determinations. \*,  $P < 0.05$  compared with the result from CCRF-CEM cells.

The biological activities of nitensidine A and its analogs

Since it was found that nitensidine A stimulated ABCB1-dependent ATPase activity and CEM/ADR5000 cells were resistant to nitensidine A, the biological activity of ABCB1 was examined in the presence or absence of the combination of nitensidine A and two substrates for ABCB1 (verapamil and calcein). As shown in Fig. 4, the cytotoxic effect of nitensidine A on CEM/ADR5000 cells was synergistically enhanced in a verapamil-concentration-dependent manner when the cells were treated with non-cytotoxic concentrations of verapamil (0, 5, 10, 20  $\mu\text{M}$ ). Histograms of the



**Fig. 4.** Effect of combined treatment of nitensidine A and verapamil on the viability of CEM/ADR5000. CEM/ADR5000 cells were cultured with different concentrations of nitensidine A in the presence of verapamil (0, 5, 10, or 20  $\mu\text{M}$ ), after which the viability of the cells was determined by XTT assay as described in Materials and methods. Similar results were obtained in at least three other experiments. Data are expressed as the mean  $\pm$  SEM of triplicate determinations. \*,  $P < 0.05$  compared with the result from open circle.

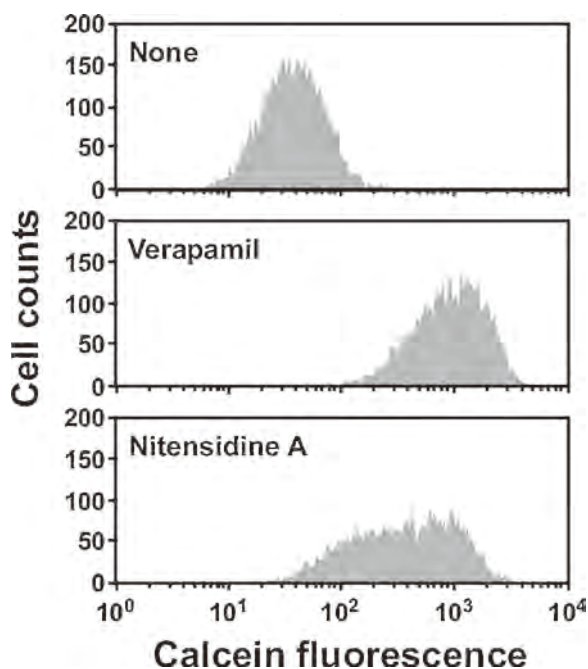


**Fig. 5.** Effect of the guanidine alkaloids on calcein extrusion by CEM/ADR5000. CEM/ADR5000 cells were incubated in suspension with 5  $\mu\text{M}$  verapamil or 20  $\mu\text{M}$  guanidine alkaloids for 15 min at 37  $^{\circ}\text{C}$  and further incubated with 1  $\mu\text{M}$  calcein acetoxyethyl ester for 30 min at 37  $^{\circ}\text{C}$ . After incubation, the amount of accumulated calcein in the cells was measured as described in Materials and methods. Histograms depict the cellular fluorescence intensity of calcein. Similar results were obtained in at least three other experiments.

fluorescence intensity derived from intracellular calcein were created for the calcein assays with CEM/ADR5000 cells (Fig. 5). The peak of the histogram was dramatically shifted to the right when CEM/ADR5000 cells were treated with verapamil at 5  $\mu\text{M}$ . Treatment with 20  $\mu\text{M}$  nitensidine A also caused a rightward shift in the histogram's peak, indicating that nitensidine A inhibited extrusion of calcein by ABCB1. These results indicate that nitensidine A can behave as a substrate for ABCB1.

To gain more insight into which structural features of nitensidine A contribute to its ability to serve as a substrate for ABCB1, the role of the imino nitrogen atom was examined with a focus on its biological activities. To this end, the nitensidine A

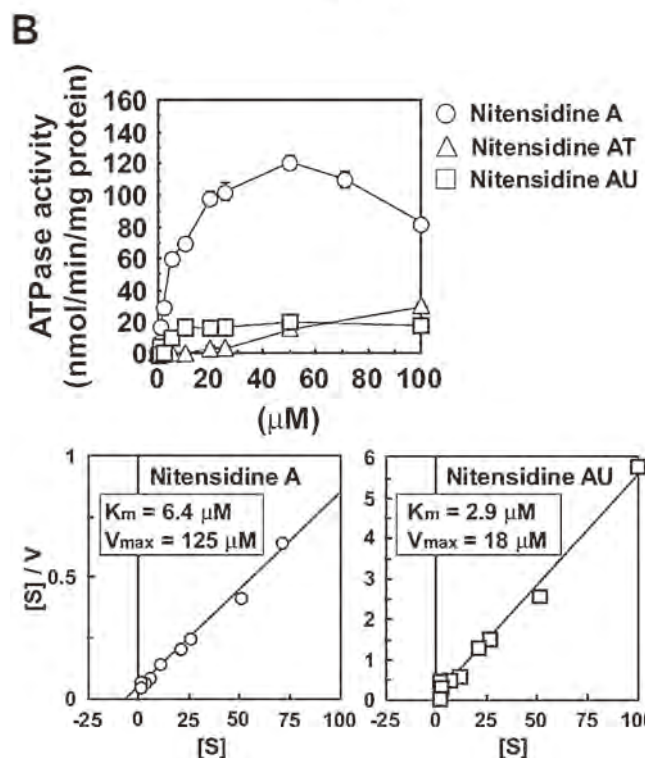
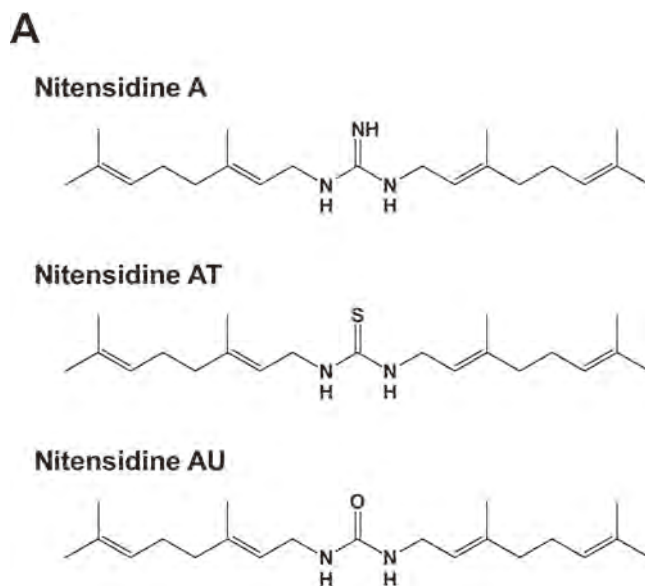


**Fig. 6.** Effects of nitensidine A and its analogs on P-glycoprotein ATPase. (A) Structures of nitensidine A and its thiourea and urea analogs (nitensidine AT and AU). (B) ATPase activity in the plasma membranes of CEM/ADR5000 cells was measured in the presence of different concentrations of nitensidine A (open circles), nitensidine AT (open triangles) and nitensidine AU (open squares) as described in the Materials and methods. Similar results were obtained in at least three other experiments. Data are expressed as the means  $\pm$  SEM of triplicate determinations. [S], compound concentration; [V], ATPase activity (nmol/min/mg protein).

analogs were synthesized by substituting sulfur (nitensidine AT) or oxygen (nitensidine AU) atoms for the imino nitrogen atom in nitensidine A, and ATPase and XTT assays were performed (Fig. 6B and Table 2). The analog-stimulated ATPase activities were measured by incubating the plasma membranes prepared from CEM/ADR5000 cells with different concentrations of the analogs (0–100  $\mu\text{M}$ ) (Fig. 6B). For nitensidine AU, but not for nitensidine AT, saturation kinetics was observed in the relationship between the compound-stimulated ATPase activity and the compounds'

**Table 2**  
Characterization of the chemical features and biological activities of nitensidine A and its synthetic analogs (nitensidines AT and AU).

Compounds	Log <i>P</i>	Dipole moment	<i>K<sub>m</sub></i> (μM)	<i>V<sub>max</sub></i> (nmol/min/mg protein)	IC <sub>50</sub> (μM)	
					CCRF-CEM cells	CEM/ADR5000 cells
Nitensidine A	5.761	2.272	6.4	125	4.9 ± 0.03	23 ± 2
Nitensidine AT	6.324	5.260	ND	ND	22 ± 2	35 ± 2
Nitensidine AU	4.636	3.169	2.9	18	>100	>100

Data are expressed as the mean ± SEM of triplicate determinations. ND, not determined.

**Table 3**  
Grid map parameters for molecular docking on human ABCB1.

Spacing	0.436		
	<i>x</i>	<i>y</i>	<i>z</i>
Number of points	92	100	90
Grid center	23.500	57.355	26.166

concentration, suggesting Michaelis–Menten kinetics. Thus, *K<sub>m</sub>* and *V<sub>max</sub>* values were calculated from Hanes–Wolf plots of (compound concentration) × (compound-stimulated ATPase activity)<sup>-1</sup> vs (compound concentration); these are summarized in Fig. 6B. The values of *K<sub>m</sub>* for each compound were related as follows: nitensidine AT > nitensidine A > nitensidine AU. The values of *V<sub>max</sub>* showed the following relationship: nitensidine A > nitensidine AU, while the relative cytotoxicities were: nitensidine A > nitensidine AT > nitensidine AU (Fig. 6 and Table 2). These results indicate that the part of nitensidine A's structure important for the stimulation of ABCB1-dependent ATPase activity is likely different from the part of its structure that mediates its cytotoxicity.

#### The chemical features of nitensidine A and its analogs

The role of the imino nitrogen atom was also examined with a focus on its chemical features to gain more insight into which structural features of nitensidine A contribute to its ability to behave as a substrate for ABCB1. To this end, a molecular docking study was performed with AutoDock4 on human ABCB1 targeting its drug-binding site. The grid map was arranged as shown in Table 3 to cover the drug binding residues of human ABCB1. A typical substrate for ABCB1, verapamil, was employed as a control compound to compare the docking results of guanidine alkaloids. As shown in Fig. 7A, B and Table 4, nitensidine A and its analogs docked to the same binding pocket in ABCB1 as verapamil with similar binding energies. The number and site of amino acid residues in ABCB1

**Table 4**  
Binding of nitensidine A, nitensidine analogs, and verapamil to human ABCB1.

Compound	Mean binding energy <sup>a</sup> (kcal/mol)	Residues involved in hydrogen bond interactions	Number of residues involved in hydrophobic interactions
MM2 <sup>b</sup>			
Verapamil	-7.38		15
Nitensidine A	-7.12	Tyr953	10
Nitensidine AT	-7.23		14
Nitensidine AU	-7.18		12
AM1 <sup>c</sup>			
Verapamil	-6.30	<b>Ser222</b>	13
Nitensidine A	-7.61		11
Nitensidine AT	-7.42		13
Nitensidine AU	-7.72	<b>Ser222</b>	11

Residues that reside in the drug binding site are indicated in bold.

<sup>a</sup> Data are expressed as the mean of quadruplicate determinations.

<sup>b</sup> Structure optimized according to MM2 procedures.

<sup>c</sup> Structure optimized according to AM1 parameters.

involved in hydrophobic interactions and hydrogen bond formations with nitensidine A and its analogs were also similar to that of verapamil. Among the amino acid residues in drug-binding site of ABCB1, Tyr953 and Ser222 were shown to be involved in the hydrogen bond formation with nitensidine A and nitensidine AU respectively (Fig. 7E and J), while Ser222 was shown to be involved in that with verapamil (Fig. 7J and Table 4).

The conformations of nitensidine A and its analogs were optimized according to MM2 procedure (Fig. 8A) and AM1 parameters (Fig. 8B), and their structures observed from three different view-points (X, Y, and Z) were displayed in Fig. 8. The substitution in the imino nitrogen atom has been shown to change the optimal conformation of each analog. The optimal conformations, Log *P* values, and dipole moment of nitensidine A and its analogs were also analyzed based on quantum chemical calculations (Fig. 8 and Table 2). The magnitudes of the Log *P* values and dipole moments were ordered as follows: nitensidine AT > nitensidine A > nitensidine AU and nitensidine AT > nitensidine AU > nitensidine A, respectively (Table 2). These results indicate that the imino nitrogen atom of nitensidine A plays a significant role in the regulation of its conformation.

## Discussion

### Nitensidine A can behave as a substrate for ABCB1

In the present study, we performed ATPase assays, XTT assays, calcein assays, molecular docking studies, and calculation for chemical structures to investigate the interaction between ABCB1 and four guanidine alkaloids isolated from *P. nitens* (i.e., galegine, nitensidine A, pterogynidine, and pterogynine). We first found that nitensidine A behaved as a substrate for ABCB1. In XTT assays, it was found that CEM/ADR5000 cells were more resistant to the four guanidine alkaloids than their parental CCRF-CEM cell line, suggesting that ABCB1 is involved in the resistance of CEM/ADR5000

cells. In ATPase assays, all of the guanidine alkaloids except for galegine stimulated ABCB1-dependent ATPase activity. Among the three guanidine alkaloids, nitensidine A stimulated ABCB1-dependent ATPase activity most strongly. The results from the ATPase assay support the hypothesis that the guanidine alkaloids may be recognized as a substrate by ABCB1, since ABCB1 utilizes energy derived from ATP hydrolysis to transport its substrates. The hypothesis is further supported by the results from XTT and calcein assays, where the cytotoxicity of nitensidine A was modulated by a typical substrate of the transporter (verapamil) and the ABCB1-dependent transport of calcein was inhibited by nitensidine A. Furthermore, molecular docking studies showed that nitensidine A docked to the same binding pocket of ABCB1 as verapamil with similar binding energies. Therefore, we can say with confidence that nitensidine A, at least, can behave as a substrate for ABCB1. Based on the results of the XTT assay, pterogynidine and pterogynine can also behave as a substrate for ABCB1, although saturation kinetics were not observed in the relationship between these compounds' stimulated ATPase activities and these compounds' concentrations.

*The number, binding site, and polymerization degree of the isoprenyl moiety and the imino nitrogen atom in the guanidine alkaloids cooperatively determine the levels required to stimulate ABCB1-dependent ATPase activity*

The results from the ATPase assay with the four guanidine alkaloids (galegine, nitensidine A, pterogynidine, and pterogynine) suggest that ABCB1 recognized more than one isoprenyl unit of the guanidine alkaloids. In addition, ABCB1 might favor tertiary amines over primary and secondary ones, since pterogynidine stimulated the ATPase activity more strongly than did galegine or pterogynine. Comparison of the structures and the ABCB1 stimulating ability of nitensidine A and pterogynine further suggests that the polymerization degree of the isoprenyl moiety may modulate

the ability of guanidine alkaloids to stimulate ABCB1-dependent ATPase activity. Although extensive SAR analysis with other guanidine alkaloids is required to determine the optimal number, binding site, and polymerization degree of isoprenyl moieties in guanidine alkaloids, these factors can affect stimulation of ABCB1-dependent ATPase activity.

The ATPase assay was also performed using two synthetic analogs of nitensidine A (nitensidine AT and AU) to gain further insight into which structural features of nitensidine A contribute to its behavior as a substrate for ABCB1. Although nitensidine AT did not show saturation kinetics in its compound-stimulated ATPase activity, nitensidine AU did. Therefore, the values of  $V_{max}$  and  $K_m$  are ordered as follows: nitensidine A > nitensidine AT and nitensidine AU > nitensidine A > nitensidine AT, respectively. In contrast, we also performed docking study using the structures optimized by MM2 procedure or AM1 parameter in the present study. Among the predicted amino acid residues in ABCB1 where drugs bind (His61, Gly64, Leu65, Met69, Ser222, Leu304, Ile306, Tyr307, Phe336, Leu339, Ile340, Ala342, Phe343, Gln725, Phe728, Phe732, Leu762, Thr837, Ile868, Gly872, Phe942, Thr945, Tyr953, Leu975, Phe978, Ser979, Val982, Gly984, Ala985, Met986, Gly989, Gln990, and Ser993) (Aller et al., 2009), Tyr953, Ser222, and Ser222 were found to be involved in hydrogen bond formation with nitensidine A, nitensidine AU, and verapamil, respectively. Comparing the amino acid residues in ABCB1 (Tyr953 and Ser222) where nitensidine A, nitensidine AU and verapamil form hydrogen bonds to  $K_m$  values of them for ABCB1 (6.4, not determined, and 3.7  $\mu\text{M}$ ), neither Tyr953 nor Ser222 may play a crucial role in the interaction between compounds and ABCB1. Since the order of binding energy was correlated with the  $K_m$  values when the structures were optimized by AM1 parameters, the electron should affect the affinity of nitensidine A for ABCB1. Therefore, the different biological activities of nitensidine A and its analogs can be partially explained by differences in their conformation. As shown by optimal conformations

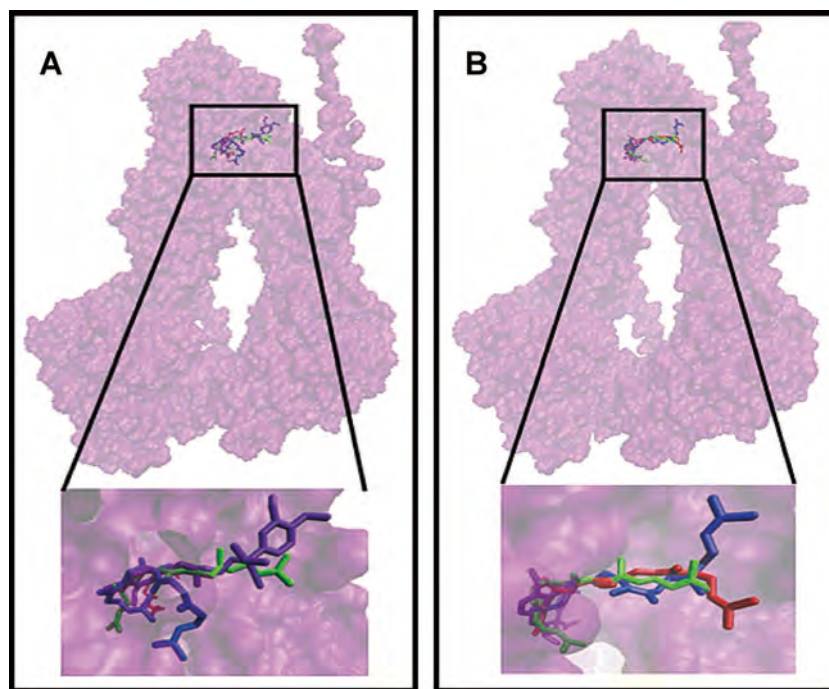


**Fig. 7.** Docking studies of nitensidine A and its analogs. The structures of nitensidine A (red), nitensidine AT (blue), nitensidine AU (green), and verapamil (violet) were optimized according to MM2 procedure (A, C, E, G, and I) or AM1 parameters (B, D, F, H, and J) and docked to the drug binding site of human ABCB1 (reddish violet surface representation). Homology modeled human ABCB1 was created using the mouse ABCB1, PDB code: 3G60. The compounds occupy the same binding site as verapamil, a typical substrate for ABCB1 (violet). Docked structure of verapamil (C and D), nitensidine A (E and F), nitensidine AT (G and H), and nitensidine AU (I and J) in ABCB1 binding pocket. The hydrogen bonds are shown as green dots.

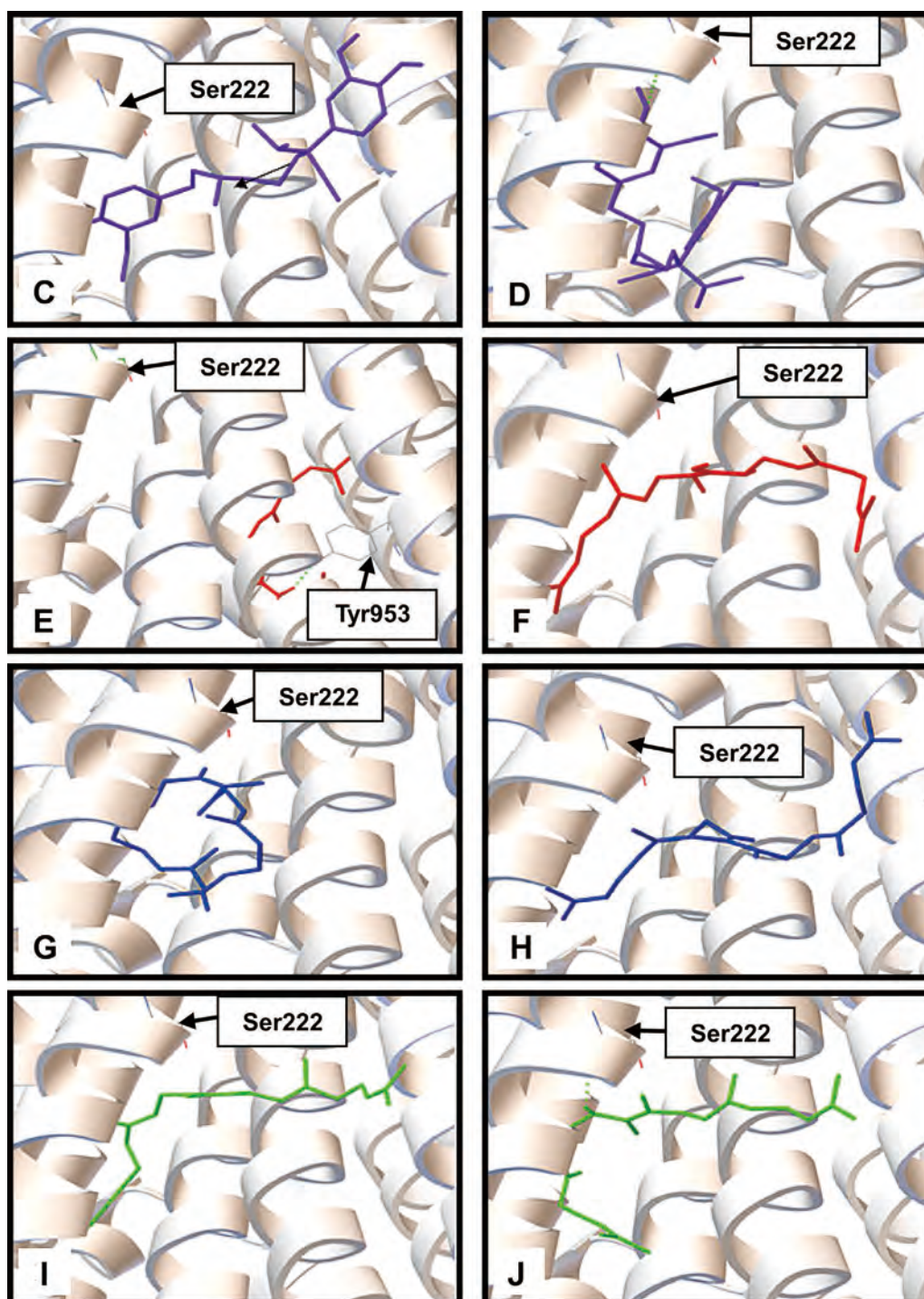


Fig. 7. (continued).

of nitensidine A and its analogs calculated in the absence of the electron, the calculated optimal conformations of them look similar. In contrast, their conformations are quite different as shown by their optimal conformations calculated in the presence of the electron, indicating that the electrons on the imino nitrogen atom in nitensidine A play a crucial role in determining its conformation and its affinity for ABCB1. Among nitensidine A and its analogs, the  $K_m$  and the  $V_{max}$  values calculated from the Hanes–Wolf plots were correlated with the  $\log P$  and dipole moment values, respectively. Thus, these values may be utilized as index values to estimate the ability of nitensidine A to stimulate ABCB1-dependent activity and

to estimate the binding energy with ABCB1. In order to demonstrate the relationship between biological and chemical features of nitensidine A and to fully understand how ABCB1 recognizes and transports nitensidine A, however, extensive SAR analysis of other nitensidine A analogs would be required.

#### Concluding remarks

The enzymatic activity of ABCB1 can contribute to multi-drug resistance (MDR) in cancer cells, and sometimes becomes an obstacle to successful cancer chemotherapy. In order to overcome

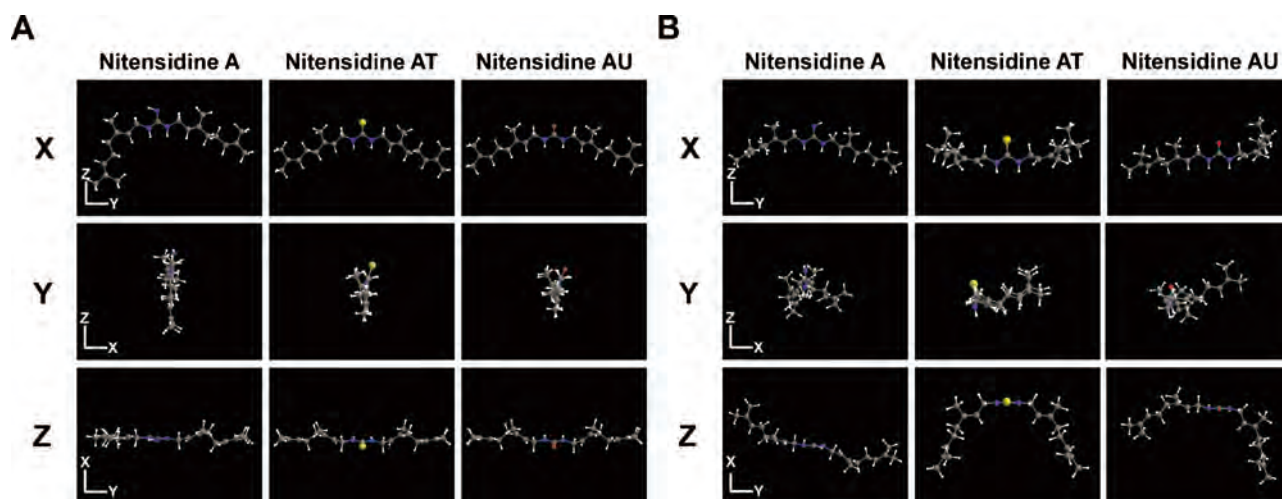


**Fig. 8.** Calculated three-dimensional chemical structures of nitensidine A and its analogs. The 3D structures optimized according to MM2 procedure (A) or AM1 parameters (B) were shown. The structures shown in Y and Z resulted from 90 degree rotation of X around the Z and Y axes, respectively. The colors in the figure signify elements as follows: gray, carbon; white, hydrogen; blue, nitrogen, yellow, sulfur; and red, oxygen.

MDR, therefore, it is important to find novel substrates for ABCB1 and understand the molecular mechanisms by which it recognizes the substrates. In the present study, nitensidine A was found to be a novel substrate for ABCB1. Although extensive SAR analysis with other nitensidine A analogs would be required to fully understand how nitensidine A stimulates ABCB1-dependent ATPase activity, the number, binding site, and polymerization degree of isoprenyl moieties, and the kind of atoms residing at the site of the imino nitrogen atom in the guanidine alkaloids cooperatively contribute to their ability to stimulate ABCB1-dependent ATPase activity. Since *P. nitens* produces several guanidine alkaloids that are similar in structure (Regasini et al., 2009, 2010), SAR analysis with those guanidine alkaloids produced by *P. nitens* may shed light on the molecular mechanisms by which ABCB1 recognizes its substrates.

#### Acknowledgments

This study was supported by the international training program of the Japanese Society for the Promotion of Science (JSPS), Grant-in-Aid for Scientific Research (C) (JSPS KAKENHI Grant Number 24592822) from the Ministry of Education, Culture, Sports, Science and Technology (MEXT), Chubu University Grant A (23IM04A) and B (24M01B) from Chubu University, and an intramural grant from the German Cancer Research Center, Heidelberg, Germany. The phytochemistry studies were supported by a grant from the Fundação de Amparo à Pesquisa do Estado de São Paulo (FAPESP) as part of the Biota-FAPESP-The Biodiversity Virtual Institute Program ([www.biotasp.org.br](http://www.biotasp.org.br)), grant no. 03/02176-7, awarded to V.S.B.

#### References

- Adachi, T., Nakagawa, H., Chung, I., Hagiya, Y., Hoshijima, K., Noguchi, N., Kuo, M.T., Ishikawa, T., 2007. Nrf2-dependent and -independent induction of ABC transporters ABC1, ABC2, and ABCG2 in HepG2 cells under oxidative stress. *J. Exp. Ther. Oncol.* 6, 335–348.
- Aller, S.G., Yu, J., Ward, A., Weng, Y., Chittaboina, S., Zhuo, R., Harrell, P.M., Trinh, Y.T., Zhang, Q., Urbatsch, I.L., Chang, G., 2009. Structure of P-glycoprotein reveals a molecular basis for poly-specific drug binding. *Science* 323, 1718–1722.
- Chen, C.J., Chin, J.E., Ueda, K., Clark, D.P., Pastan, I., Gottesman, M.M., Roninson, I.B., 1986. Internal duplication and homology with bacterial transport proteins in the *mdr1* (P-glycoprotein) gene from multidrug-resistant human cells. *Cell* 47, 381–389.
- Chiba, P., Ecker, G., Schmid, D., Drach, J., Tell, B., Goldenberg, S., Gekeler, V., 1996. Structural requirements for activity of propafenone-type modulators in P-glycoprotein-mediated multidrug resistance. *Mol. Pharmacol.* 49, 1122–1130.

- de Jong, F.A., de Jonge, M.J., Verweij, J., Mathijssen, R.H., 2006. Role of pharmacogenetics in irinotecan therapy. *Cancer Lett.* 234, 90–106.
- Dewar, M.J.S., Zeobisch, E.G., Healy, E.F., Stewart, J.P., 1985. Development and use of quantum mechanical molecular models. 76. AM1: a new general purpose quantum mechanical molecular model. *J. Am. Chem. Soc.* 107, 3902–3909.
- Duarte, R.A., Mello, E.R., Araki, C., Bolzani Vda, S., Siqueira e Silva, D.H., Regasini, L.O., Silva, T.G., de Moraes, M.C., Ximenes, V.F., Soares, C.P., 2010. Alkaloids extracted from *Pterogyne nitens* induce apoptosis in malignant breast cell line. *Tumour Biol.* 31, 513–522.
- Ecker, G., Huber, M., Schmid, D., Chiba, P., 1999. The importance of a nitrogen atom in modulators of multidrug resistance. *Mol. Pharmacol.* 56, 791–796.
- Ekins, S., Kim, R.B., Leake, B.F., Dantzig, A.H., Schuetz, E.G., Lan, L.B., Yasuda, K., Shepard, R.L., Winter, M.A., Schuetz, J.D., Wikel, J.H., Wrighton, S.A., 2002. Application of three-dimensional quantitative structure–activity relationships of P-glycoprotein inhibitors and substrates. *Mol. Pharmacol.* 61, 974–981.
- Fernandes, D.C., Regasini, L.O., Velloso, J.C., Pauletti, P.M., Castro-Gamboa, I., Bolzani, V.S., Oliveira, O.M., Silva, D.H., 2008. Myeloperoxidase inhibitory and radical scavenging activities of flavones from *Pterogyne nitens*. *Chem. Pharm. Bull. (Tokyo)* 56, 723–726.
- Fiser, A., Sali, A., 2003. Modeller: generation and refinement of homology-based protein structure models. *Methods Enzymol.* 374, 461–491.
- Ford, J.M., 1996. Experimental reversal of P-glycoprotein-mediated multidrug resistance by pharmacological chemosensitizers. *Eur. J. Cancer* 32A, 991–1001.
- Garrigues, A., Loiseau, N., Delaforge, M., Ferte, J., Garrigos, M., Andre, F., Orłowski, S., 2002. Characterization of two pharmacophores on the multidrug transporter P-glycoprotein. *Mol. Pharmacol.* 62, 1288–1298.
- Globisch, C., Pajeva, I.K., Wiese, M., 2006. Structure–activity relationships of a series of tariquidar analogues as multidrug resistance modulators. *Bioorg. Med. Chem.* 14, 1588–1598.
- Gribar, J.J., Ramachandra, M., Hrycyna, C.A., Dey, S., Ambudkar, S.V., 2000. Functional characterization of glycosylation-deficient human P-glycoprotein using a vaccinia virus expression system. *J. Membr. Biol.* 173, 203–214.
- Ishikawa, T., 2003. Multidrug resistance: genomics of ABC transporters. In: Cooper, D.N. (Ed.), *Nature Encyclopedia of the Human Genome*, Vol. 4. Nature Publishing Group, London, UK, pp. 154–160.
- Juliano, R.L., Ling, V., 1976. A surface glycoprotein modulating drug permeability in Chinese hamster ovary cell mutants. *Biochim. Biophys. Acta* 455, 152–162.
- Kiefer, F., Arnold, K., Kunzli, M., Bordoli, L., Schwede, T., 2009. The SWISS-MODEL repository and associated resources. *Nucleic Acids Res.* 37, D387–D392.
- Kitagawa, S., Nabekura, T., Takahashi, T., Nakamura, Y., Sakamoto, H., Tano, H., Hirai, M., Tsukahara, G., 2005. Structure–activity relationships of the inhibitory effects of flavonoids on P-glycoprotein-mediated transport in KB-C2 cells. *Biol. Pharmaceut. Bull.* 28, 2274–2278.
- Klopman, G., Shi, L.M., Ramu, A., 1997. Quantitative structure–activity relationship of multidrug resistance reversal agents. *Mol. Pharmacol.* 52, 323–334.
- Lin, J.H., 2003. Drug–drug interaction mediated by inhibition and induction of P-glycoprotein. *Adv. Drug Deliv. Rev.* 55, 53–81.
- Ling, V., 1997. Multidrug resistance: molecular mechanisms and clinical relevance. *Cancer Chemother. Pharmacol.* 40, S3–S8.
- Morris, G.M., Huey, R., Lindstrom, W., Sanner, M.F., Belew, R.K., Goodsell, D.S., Olson, A.J., 2009. Autodock4 and autodocktools4: automated docking with selective receptor flexibility. *J. Comput. Chem.* 30, 2785–2791.

- Noguchi, K., Katayama, K., Mitsuhashi, J., Sugimoto, Y., 2009. Functions of the breast cancer resistance protein (BCRP/ABCG2) in chemotherapy. *Adv. Drug Deliv. Rev.* 61, 26–33.
- Pajeva, I.K., Wiese, M., 2002. Pharmacophore model of drugs involved in P-glycoprotein multidrug resistance: explanation of structural variety (hypothesis). *J. Med. Chem.* 45, 5671–5686.
- Pearce, H.L., Safa, A.R., Bach, N.J., Winter, M.A., Cirtain, M.C., Beck, W.T., 1989. Essential features of the P-glycoprotein pharmacophore as defined by a series of reserpine analogues that modulate multidrug resistance. *Proc. Natl. Acad. Sci. U.S.A.* 86, 5128–5132.
- Pearce, H.L., Winter, M.A., Beck, W.T., 1990. Structural characteristics of compounds that modulate P-glycoprotein-associated multidrug resistance. *Adv. Enzyme Regul.* 30, 357–373.
- Penzotti, J.E., Lamb, M.L., Evensen, E., Grootenhuis, P.D., 2002. A computational ensemble pharmacophore model for identifying substrates of P-glycoprotein. *J. Med. Chem.* 45, 1737–1740.
- Regasini, L.O., Castro-Gamboa, I., Silva, D.H., Furlan, M., Barreiro, E.J., Ferreira, P.M., Pessoa, C., Lotufo, L.V., de Moraes, M.O., Young, M.C., Bolzani Vda, S., 2009. Cytotoxic guanidine alkaloids from *Pterogyne nitens*. *J. Nat. Prod.* 72, 473–476.
- Regasini, L.O., Pivatto, M., Scorzoni, L., Benaducci, T., Fusco-Almeida, A., Giannini, M., Barreiro, E.J., Silva, D., Bolzani Vda, S., 2010. Antimicrobial activity of *Pterogyne nitens* Tul., Fabaceae, against opportunistic fungi. *Rev. Bras. Farmacogn.* 20, 706–711.
- Sakurai, A., Onishi, Y., Hirano, H., Seigneuret, M., Obayama, K., Kim, G., Liew, E.L., Sakaeda, T., Yoshiura, K., Niikawa, N., Sakurai, M., Ishikawa, T., 2007. Quantitative structure–activity relationship analysis and molecular dynamics simulation to functionally validate nonsynonymous polymorphisms of human ABC transporter ABCB1 (P-glycoprotein/MDR1). *Biochemistry* 46, 7678–7693.
- Schinkel, A.H., Smit, J.J., van Tellingen, O., Beijnen, J.H., Wagenaar, E., van Deemter, L., Mol, C.A., van der Valk, M.A., Robanus-Maandag, E.C., te Riele, H.P., et al., 1994. Disruption of the mouse *mdr1a* P-glycoprotein gene leads to a deficiency in the blood-brain barrier and to increased sensitivity to drugs. *Cell* 77, 491–502.
- Tsuruo, T., Iida, H., Tsukagoshi, S., Sakurai, Y., 1981. Overcoming of vincristine resistance in P388 leukemia in vivo and in vitro through enhanced cytotoxicity of vincristine and vinblastine by verapamil. *Cancer Res.* 41, 1967–1972.
- Ueda, K., Cornwell, M.M., Gottesman, M.M., Pastan, I., Roninson, I.B., Ling, V., Riordan, J.R., 1986. The *mdr1* gene, responsible for multidrug-resistance, codes for P-glycoprotein. *Biochem. Biophys. Res. Commun.* 141, 956–962.
- Venkatachalam, T.K., Qazi, S., Samuel, P., Uckun, F.M., 2003. Inhibition of mast cell leukotriene release by thiourea derivatives. *Bioorg. Med. Chem. Lett.* 13, 485–488.
- Zamora, J.M., Pearce, H.L., Beck, W.T., 1988. Physical–chemical properties shared by compounds that modulate multidrug resistance in human leukemic cells. *Mol. Pharmacol.* 33, 454–462.

# Nitensidine A, a guanidine alkaloid from *Pterogyne nitens*, induces osteoclastic cell death

Yasuhiro Tajima · Hayato Murase · Kazuhiro Satake · Yuji Mitani · Luis Octavio Regasini · Vanderlan da Silva Bolzani · Thomas Efferth · Hiroshi Nakagawa

Received: 14 January 2013 / Accepted: 21 May 2013  
© Springer Science+Business Media Dordrecht 2013

**Abstract** Nitensidine A is a guanidine alkaloid isolated from *Pterogyne nitens*, a common plant in South America. To gain insight into the biological activity of *P. nitens*-produced compounds, we examined herein their biological effects on osteoclasts, multinucleated giant cells that regulate bone metabolism by resorbing bone. Among four guanidine alkaloids (i.e., galegine, nitensidine A, pterogynidine, and pterogynine), nitensidine A and pterogynine exhibited anti-osteoclastic effects at 10  $\mu\text{M}$  by reducing the number of osteoclasts on the culture plate whereas galegine and pterogynidine did not. The anti-osteoclastic activities of nitensidine A and pterogynine were exerted in a concentration-dependent manner, whereas nitensidine A exhibited an approximate threefold stronger effect than pterogynine ( $\text{IC}_{50}$  values: nitensidine A,  $0.93 \pm 0.024 \mu\text{M}$ ; pterogynine,

$2.7 \pm 0.40 \mu\text{M}$ ). In the present study, the anti-osteoclastic effects of two synthetic nitensidine A derivatives (nitensidine AT and AU) were also examined to gain insight into the structural features of nitensidine A that exert an anti-osteoclastic effect. The anti-osteoclastic effect of nitensidine A was greatly reduced by substituting the imino nitrogen atom in nitensidine A with sulfur or oxygen. According to the differences in chemical structures and anti-osteoclastic effects of the four guanidine alkaloids and the two synthetic nitensidine A derivatives, it is suggested that the number, binding site, and polymerization degree of isoprenyl moiety in the guanidine alkaloids and the imino nitrogen atom cooperatively contribute to their anti-osteoclastic effects.

**Keywords** *Pterogyne nitens* · Guanidine alkaloids · Osteoclast · Cytotoxicity · Structure and activity relationship

Y. Tajima · H. Murase · K. Satake · Y. Mitani · H. Nakagawa (✉)  
Department of Applied Biological Chemistry, College of Bioscience and Biotechnology, Chubu University, 1200 Matsumoto-cho, Kasugai, Aichi 487-8501, Japan  
e-mail: hnakagaw@isc.chubu.ac.jp

L. O. Regasini · V. da Silva Bolzani  
Department of Organic Chemistry, Institute of Chemistry, São Paulo State University, Araraquara 14800-900, Brazil

T. Efferth  
Department of Pharmaceutical Biology, Institute of Pharmacy and Biochemistry, University of Mainz, 55128 Mainz, Germany

## Introduction

Osteoclasts are multinucleated primary bone-resorbing cells that differentiate from hematopoietic stem cells (Edwards and Mundy 2011). Hematopoietic stem cells are differentiated into mononuclear osteoclasts in the presence of cytokines, macrophage-colony stimulating factor (M-CSF) (Felix et al. 1990; Yoshida et al. 1990), and receptor activator of nuclear factor- $\kappa\text{B}$

(NF- $\kappa$ B) ligand (RANKL) (Yasuda et al. 1998; Lacey et al. 1998), which are produced by osteoblasts. Under the control of these cytokines, mononuclear osteoclasts are multinucleated and actively resorb bone. Although bone resorption is an essential physiological event for bone remodeling and tooth eruption, excessive bone resorption by osteoclasts causes several metabolic bone disorders including osteoporosis, arthritis, periodontitis, bone metastasis, corticosteroid-induced bone loss, and Paget's disease (Rodan and Martin 2000; Chambers 2000; Teitelbaum 2000; Boyle et al. 2003). Therefore, compounds that specifically induce osteoclastic cell death could be developed as anti-osteoclastic drugs for the treatment of the above-mentioned metabolic bone disorders.

A native tree *Pterogyne nitens*, common in South America (Bolzani et al. 1995; Regasini et al. 2008; Fernandes et al. 2008; Regasini et al. 2009, 2010; Duarte et al. 2010) has been found to produce flavonoids, such as kaempferol, quercetin, and rutin, which have been reportedly found to exert anti-osteoclastic effects (Wattel et al. 2003; Woo et al. 2004). In addition to the flavonoids, we have also revealed that *Pterogyne nitens* produced cytotoxic guanidine alkaloids (Regasini et al. 2009; Duarte et al. 2010), whose biological activities against osteoclasts have not been reported. In the present study, therefore, we examined the anti-osteoclastic effects of four guanidine alkaloids isolated from *Pterogyne nitens* (i.e., galegine, nitensidine A, pterogynidine, and pterogynine) to gain insight into the biological activity of *Pterogyne nitens*-produced compounds and understand the various possibilities of the plant for ethno-medicinal use. Among the four guanidine alkaloids, the anti-osteoclastic effect of nitensidine A was the most effective. Therefore, the effects of synthesized nitensidine A derivatives were also examined in this study to gain insight into the structural features of nitensidine A that exert an anti-osteoclastic effect.

## Materials and methods

### Guanidine alkaloids

The guanidine alkaloids tested in the present study were obtained from *Pterogyne nitens* leaves or branches. Briefly, the *Pterogyne nitens* leaves or branches were macerated in ethanol at room temperature and the

extract was separated by gel permeation chromatography, reversed-phase silica gel column chromatography and reversed-phase HPLC according to the procedure previously reported (Regasini et al. 2009, 2010).

### Synthesis of nitensidine A derivatives

Synthetic nitensindines AT and AU were prepared as described previously, with minor modifications (Venkatachalam et al. 2003). A solution of 1,1'-carbonyldiimidazole (1.0 mmol) or 1,1'-thiocarbonyldiimidazole (1.0 mmol) in dried *p*-dioxane (15 ml) was added to a solution of geranylamine (2.2 mmol) in dried *p*-dioxane (3.0 ml), at 5 °C. This mixture was stirred for 2 h, at room temperature. The solvent was removed under reduced pressure. The residue was partitioned three times in ethyl acetate and then filtered. The filtrate was partitioned three times with saturated aqueous citric acid solution (two times), saturated aqueous sodium bicarbonate (two times), water (two times), dried over magnesium sulphate. The crude products were purified over a silica gel column using isocratic system of hexane–ethyl acetate (3:2) to afford nitensindines AT and AU. Structures of these compounds were established by  $^1\text{H}$  and  $^{13}\text{C}$  NMR spectral analysis. Chemical shifts ( $\delta$ ) were expressed in ppm. Coupling constants (J) were expressed in Hz, and splitting patterns are described as follows: s = singlet, br s = broad singlet, t = triplet, m = multiplet.

### Nitensidine AT

This yellow oil was obtained in 55 % yield.  $^1\text{H}$  NMR (500 MHz,  $\text{CDCl}_3$ )  $\delta$  5.93 (br s; 3-NH, 4-NH), 5.17 (t; J = 7.0 Hz, H-2'), 4.99 (t; J = 7.0 Hz, H-6'), 3.93 (br s; H-1'), 2.01 (m; H-5'), 1.96 (m; H-4'), 1.61 (s; H-9' and H-10'), 1.52 (s; H-8').  $^{13}\text{C}$  NMR (125 MHz,  $\text{CDCl}_3$ )  $\delta$  181.2 (C-2), 140.7 (C-3'), 131.6 (C-7'), 123.4 (C-6'), 118.8 (C-2'), 42.3 (C-1'), 39.2 (C-4'), 26.1 (C-5'), 25.4 (C-9'), 17.4 (C-8'), 16.2 (C-10').

### Nitensidine AU

This white solid was obtained in 21 % yield.  $^1\text{H}$  NMR (500 MHz,  $\text{CDCl}_3$ )  $\delta$  5.17 (t; J = 6.0 Hz, H-2'), 4.97 (t; J = 6.0 Hz, H-6'), 4.52 (br s; 3-NH, 4-NH), 3.65 (t; J = 6.0 Hz, H-1'), 1.96 (m; H-5'), 1.89 (m; H-4'), 1.58 (s; H-10'), 1.56 (s; H-10'), 1.50 (s; H-8').  $^{13}\text{C}$  NMR (125 MHz,  $\text{CDCl}_3$ )  $\delta$  158.5 (C-2), 139.0 (C-3'), 134.6

(C-7'), 123.8 (C-6'), 121.0 (C-2'), 39.4 (C-1'), 38.4 (C-4'), 26.4 (C-5'), 25.5 (C-9'), 17.5 (C-8'), 16.1 (C-10').

### Biochemicals

Leukoprol (recombinant human M-CSF) was purchased from Kyowa Hakko Kogyo Co., Ltd. (Tokyo, Japan). GST-human sRANKL (GST-RANKL) was purchased from Oriental Yeast Co., Ltd. (Tokyo, Japan). Recombinant human TGF- $\beta_1$  (TGF- $\beta_1$ ) was purchased from R&D Systems, Inc. (Minneapolis, MN, USA). Minimum essential medium Eagle ( $\alpha$ -MEM) and 3-[4,5-dimethylthiazol-2-yl]-2,5-diphenyltetrazolium bromide (MTT reagent) were purchased from Sigma-Aldrich Co. (St. Louis, MO, USA). Dulbecco's modified Eagle's medium (4.5 g/l glucose) (DMEM), Antibiotic–Antimycotic Mixed Stock Solution (100 $\times$ ) (Stabilized), Fast red violet LB salt, naphthol AS-MX phosphate, and 2.5 g/l trypsin-1 mM EDTA were purchased from Nacalai Tesque, Inc. (Kyoto, Japan). All other chemicals used were of analytical grade.

### Preparation of mouse osteoclasts from bone marrow cells

For the preparation and culture of mouse osteoclasts,  $\alpha$ -MEM supplemented with 10 % (v/v) heat-inactivated fetal calf serum (ICN Biomedicals, Inc., Aurora, OH, USA), 4 mM L-glutamine, 100 U/ml penicillin, 100  $\mu$ g/ml streptomycin, and 250 ng/ml amphotericin B was used in the present study, and the cells were cultured at 37 °C in a humidified atmosphere of 5 % (v/v) CO<sub>2</sub> in air.

Mouse osteoclasts were prepared from mouse bone marrow cells of 6- to 9-week-old male ddY mice (SLC Inc., Shizuoka, Japan). In brief, mouse bone marrow cells (1.0–1.5  $\times$  10<sup>7</sup> cells/dish/6 ml) were cultured for the first 3 days in the presence of 4,000 U/ml recombinant human M-CSF (M-CSF), 1 ng/ml recombinant human TGF- $\beta_1$  (TGF- $\beta_1$ ), and 100 ng/ml GST-human sRANKL (GST-RANKL) in 100-mm diameter type I collagen-coated culture dishes (AGC Techno Glass Co., Ltd., Chiba, Japan), where GST-RANKL and Leukoprol were used for preparation of mouse osteoclasts instead of RANKL and M-CSF, respectively, according to previous reports (Mochizuki et al. 2006; Zhao et al. 2009; Tomimori et al. 2009). TGF- $\beta_1$  was added to the culture medium together with M-CSF and GST-RANKL according to previous reports to

promote the efficiency of osteoclast differentiation (Sells Galvin et al. 1999; Kaneda et al. 2000; Fuller et al. 2000; Yan et al. 2001). After 3 days of culture, adherent cells were harvested by treatment with trypsin–EDTA, and the resulting harvested cells (3  $\times$  10<sup>4</sup> cells/well/100  $\mu$ l) were placed on 96-well half area culture plates (Corning Inc., Corning, NY, USA). After culture on the plates for 24 h, the culture medium was replaced with fresh medium that contained 4,000 U/ml M-CSF and 100 ng/ml sRANKL, and the cells were further cultured with 0.5 % (v/v) vehicle [dimethyl sulfoxide (DMSO) (Nacalai Tesque, Inc., (Kyoto, Japan))] or test compounds for 24 h.

The present study with experimental animals was approved by and conducted in accordance with the guidelines of the Animal Experiment Committee of Chubu University.

### TRAP staining

Osteoclasts cultured with 0.5 % (v/v) vehicle (DMSO) or test compounds for 24 h were stained for tartrate-resistant acid phosphatase (TRAP), a typical marker enzyme of osteoclasts, as previously described (Nakagawa et al. 2002, 2003, 2007) to visualize osteoclasts. In brief, the cells were fixed with 3.7 % formaldehyde in phosphate buffered saline (PBS)(–) for 15 min. After treatment with ethanol/acetone (1:1) for 1 min, the well surface was dried and treated with the TRAP staining solution [0.1 M sodium acetate buffer (pH 5.0) containing 50 mM sodium tartrate, 0.1 mg/ml naphthol AS-MX phosphate, and 1 mg/ml fast red violet LB salt] for 30 min at room temperature. The resulting visualized osteoclasts were detected under an All-in-One Fluorescence Microscope, the BZ-8100 BIOZERO (KEYENCE Corp., Osaka, Japan), where the number of osteoclasts having more than five nuclei was also counted. Data are expressed as the mean values  $\pm$  SD of six replicate cultures in one of three experiments.

### MTT assay

The MTT assay was performed to evaluate cellular sensitivity to nitensidine A as previously described (Nakagawa et al. 2009). In brief, the cells (osteoblasts, Caco-2 (generously provided by Dr. Shinji Yamashita (Setsunan University)), KB-3-1 (generously provided by Dr. Kazumitsu Ueda (Kyoto University)), MCF-7

(generously provided by Prof. Hideki Enokida (Kagoshima University)) and HepG2 cells (obtained from the Riken Cell Bank (Tsukuba, Japan)) were seeded at  $3 \times 10^4$  cells/well/100  $\mu$ l into 96-well culture plates and pre-cultured in  $\alpha$ -MEM (osteoblasts) or DMEM (Caco-2, HepG2, KB3-1, and MCF-7 cells) supplemented with 10 % (v/v) heat-inactivated fetal calf serum, 4 mM L-glutamine, 100 U/ml penicillin, 100  $\mu$ g/ml streptomycin, and 250 ng/ml amphotericin B for 24 h at 37 °C in a humidified atmosphere of 5 % (v/v) CO<sub>2</sub> in air. The cells were further cultured with nitensidine A for 72 h, treated with 500  $\mu$ g/ml MTT reagent for 4 h, and then 10 % (w/v) SDS in PBS(–) (100  $\mu$ l/well) was added to solubilize MTT-formazan produced by enzyme within the cell. After overnight incubation, absorbances at 570 and 630 nm were measured as test and reference wavelengths, respectively. Data are expressed as the mean values  $\pm$  SD of four replicate cultures in one of three experiments.

#### Statistical analysis

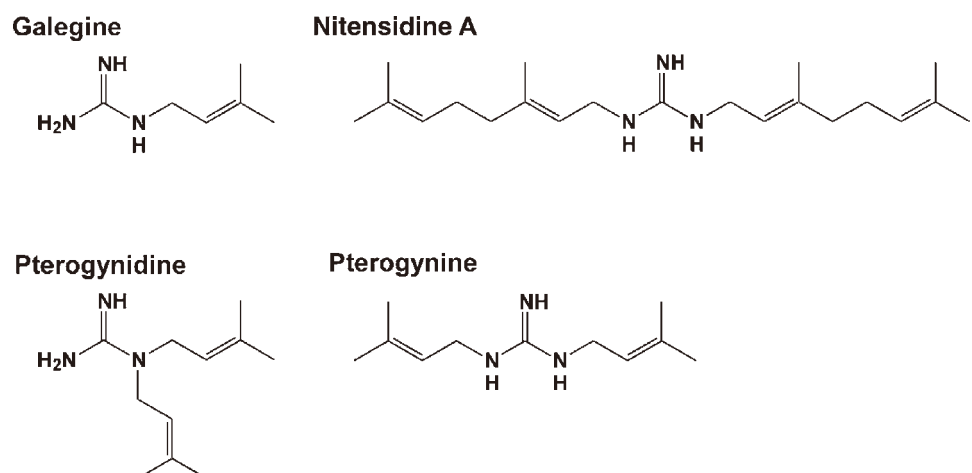
Statistical analyses were performed using Microsoft Excel 2010 software (Microsoft Co., Redmond, WA, USA). The statistical significance of differences was determined using the Student's *t* test. *P* values <0.01 were considered statistically significant.

## Results

To gain insight into the biological activity of *Pterogyne nitens*-produced compounds, we examined the anti-osteoclastic effects of four *Pterogyne nitens*-produced

guanidine alkaloids (i.e., galegine, nitensidine A, pterogynidine, and pterogynine), which are guanidine derivatives that have different numbers of isoprenyl moieties at their amino nitrogens (Fig. 1). To assess the anti-osteoclastic effects of the four alkaloids, osteoclasts were cultured with each of them at 10  $\mu$ M for 24 h. As shown in Fig. 2a, galegine, whose amino nitrogen has one isoprenyl moiety, and pterogynidine, whose amino nitrogen has two isoprenyl moieties, appeared to exert no cytotoxic effects on osteoclasts as well as the 0.5 % (v/v) vehicle (DMSO). In contrast, nitensidine A, whose two amino nitrogens have one geranyl moiety, and pterogynine, whose two amino nitrogens have one isoprenyl moiety, appeared to exert cytotoxic effects against osteoclasts because they markedly reduced the number of cells. To elucidate the anti-osteoclastic effects of the four guanidine alkaloids in detail, the number of multinucleated osteoclasts (>5 nuclei) was counted as shown in Fig. 2b. The number of multinucleated cells in the culture wells was not significantly reduced by either 10  $\mu$ M galegine or 10  $\mu$ M pterogynidine. In contrast, the number of multinucleated cells was significantly reduced by 10  $\mu$ M nitensidine A or pterogynine because few multinucleated osteoclasts were observed in the culture wells, suggesting that these guanidine alkaloids induced osteoclastic cell death. Thus, osteoclasts were cultured with different concentrations of nitensidine A or pterogynine for 24 h to elucidate how they reduced the number of multinucleated cells. As shown in Fig. 3, both of the guanidine alkaloids reduced the number of multinucleated osteoclasts in a concentration-dependent manner. Upon comparing the IC<sub>50</sub> value of nitensidine A with that of pterogynine, which were calculated from the

**Fig. 1** Structures of the guanidine alkaloids



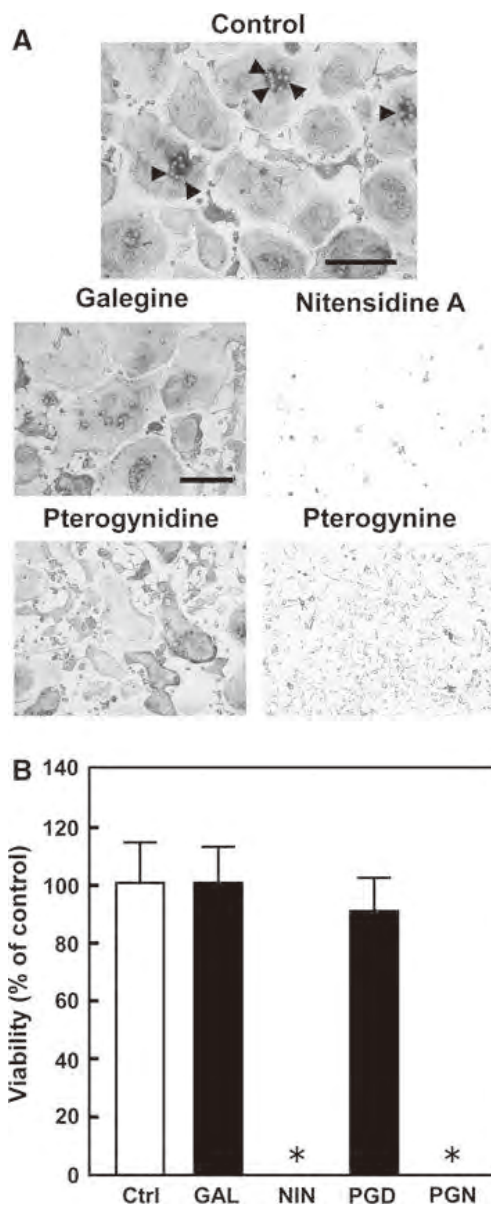


**Fig. 2** Anti-osteoclastic effect of guanidine alkaloids. Mononuclear osteoclasts were placed on 96-well half area culture plates. After culture for 24 h, the resulting multinucleated osteoclasts were cultured with or without 10  $\mu$ M guanidine alkaloids for 24 h. After culture, the cells were stained for TRAP (a), and then multinucleated osteoclasts (>5 nuclei) were counted (b). *Bar* = 200  $\mu$ m. Similar results were obtained in at least two other experiments. Data are expressed as the mean values  $\pm$  SD of six replicate cultures in one of three experiments. *Ctrl* control, *GAL* galegine, *NIN* nitensidine A, *PGD* pterogynidine, *PGN* pterogynine. *Asterisks*,  $P < 0.01$  compared with control

concentration–viability curve shown in Fig. 3, the value of nitensidine A was approximately threefold lower than that of pterogynine (IC<sub>50</sub> value: nitensidine A, 0.93  $\pm$  0.024  $\mu$ M; pterogynine, 2.7  $\pm$  0.40  $\mu$ M), indicating that

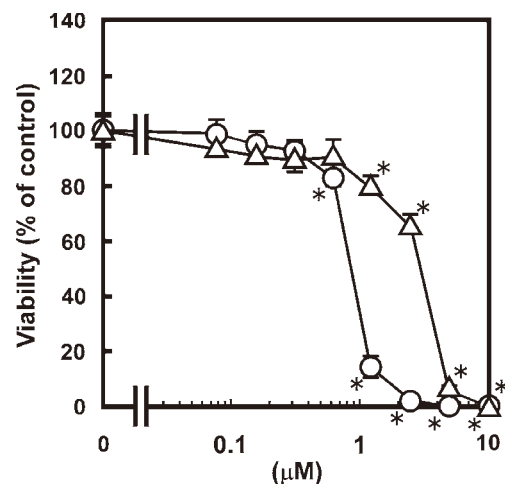


**Fig. 3** Concentration-dependent anti-osteoclastic effects of nitensidine A and pterogynine. Mononuclear osteoclasts were placed on 96-well half area culture plates. After culture for 24 h, they were cultured with nitensidine A (*circles*) and pterogynine (*triangles*) at different concentrations for 24 h. After culture, the cells were stained for TRAP, and then multinucleated osteoclasts (>5 nuclei) were counted. Similar results were obtained in at least two other experiments. Data are expressed as the mean values  $\pm$  SD of six replicate cultures in one of three experiments. *Asterisks*,  $P < 0.01$  compared with the control

nitensidine A is approximately threefold more effective than pterogynine. In the present study, the cytotoxicities of nitensidine A against osteoblasts and 4 cell lines were also examined to judge whether the cytotoxic effect of nitensidine A is specific to osteoclasts or not. As shown in Table 1, nitensidine A exerted cytotoxicities against osteoblasts and the 4 cell lines at approximately 10- to 40-fold higher concentration than its cytotoxicity against osteoclasts.

In the present study, we also examined the anti-osteoclastic effects of synthetic nitensidine A derivatives (nitensidine AT and AU) to begin structure–activity relationship (SAR) analysis and obtain insight into the structural features of nitensidine A that exert an anti-osteoclastic effect. To this end, the imino nitrogen atom (N) in nitensidine A was substituted with sulfur (S) (nitensidine AT) or oxygen (O) (nitensidine AU) at the beginning of SAR analysis (Fig. 4a). As shown in Fig. 4b, c, more than 75 % of the multinucleated osteoclasts remained in the culture wells when the cells were treated with nitensidine AT or AU at 10  $\mu$ M for 24 h, indicating that the substitution of the imino nitrogen atom in nitensidine A with sulfur or oxygen substantially reduced the anti-osteoclastic effect.

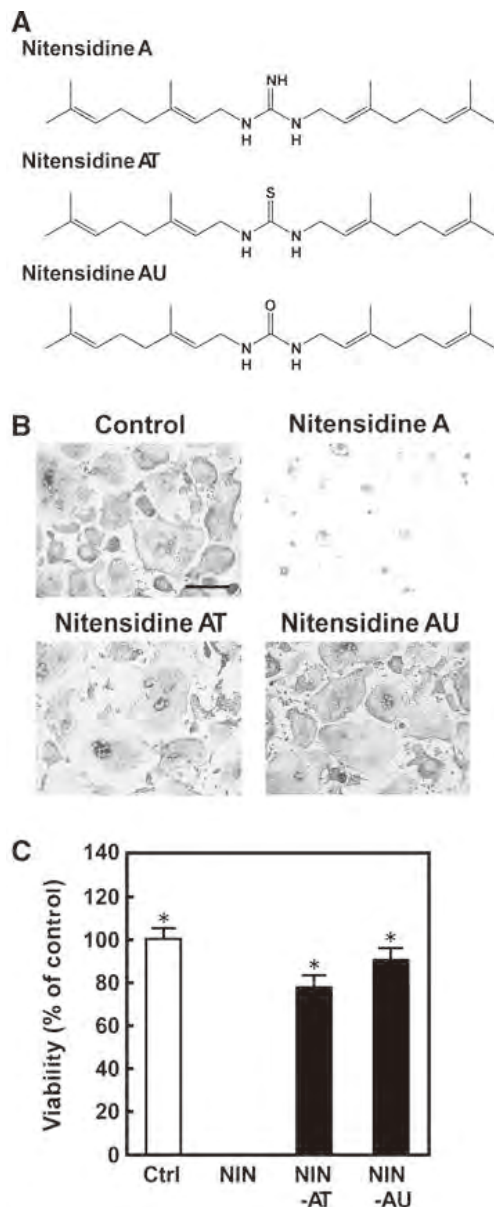


**Fig. 4** Anti-osteoclastic effects of synthetic nitensidine A derivatives. **a** Structures of nitensidine A and its synthetic derivatives. **b, c** Mononuclear osteoclasts were placed on 96-well half area culture plates. After culture for 24 h, they were cultured with or without 10  $\mu$ M nitensidine A or its derivatives for 24 h. After culture, the cells were stained for TRAP, and then multinucleated osteoclasts (>5 nuclei) were counted. Bar = 200  $\mu$ m. Similar results were obtained in at least two other experiments. Data are expressed as the mean values  $\pm$  SD of six replicate cultures in one of three experiments. Ctrl control, NIN nitensidine A, NIN-AT nitensidine AT, NIN-AU nitensidine AU. Asterisks,  $P < 0.01$  compared with nitensidine A

## Discussion

In the present study, we examined the anti-osteoclastic effects of guanidine alkaloids isolated from *Pterogyne*

**Table 1** Cytotoxicity of nitensidine A against osteoclasts and four cell lines

Cells	IC <sub>50</sub> ( $\mu$ M)
Osteoclasts	0.93 $\pm$ 0.042
Osteoblasts	19 $\pm$ 0.39
Caco-2 cells	28 $\pm$ 0.63
HepG2 cells	11 $\pm$ 0.57
KB3-1 cells	36 $\pm$ 0.35
MCF-7 cells	14 $\pm$ 0.0

Data are expressed as the mean values  $\pm$  SD of four replicate cultures in one of three experiments

*nitens*, a common plant in South America, and first found that nitensidine A and pterogynine exert anti-osteoclastic effects via reducing the number of multinucleated osteoclasts in culture wells by focusing on the cytotoxicity of guanidine alkaloids against osteoclasts. In contrast, the studies to elucidate the effects of guanidine alkaloids on osteoclastogenesis and expression of the genes regulated by M-CSF and RANKL are currently in progress since osteoclasts differentiate from hematopoietic stem cells in the presence of these cytokines (Felix et al. 1990; Yoshida et al. 1990; Yasuda et al. 1998; Lacey et al. 1998).

Although the mechanism for how nitensidine A and pterogynine reduce the number of osteoclasts is unclear, both apoptosis and necrosis must be involved in the anti-osteoclastic effect as previous reports have described using other cell types (Bolzani et al. 1995; Regasini et al. 2009; Duarte et al. 2010). Instead, four guanidine alkaloids and two nitensidine A derivatives were prepared in the present study and used in preliminary SAR analysis to obtain insight into the structural features of nitensidine A that exert an anti-osteoclastic effect. Based on the relationship between the structures and anti-osteoclastic effects of the four guanidine alkaloids tested (galegine, nitensidine A, pterogynidine, and pterogynine), it is suggested that the number and position of the isoprenyl moiety binding to guanidine could determine the anti-osteoclastic effect. The present study at least indicated that the isoprenyl moiety could confer anti-osteoclastic effects onto guanidine. Based on the relationship between the structures and anti-osteoclastic effects of nitensidine A and pterogynine, it is suggested that the polymerization degree of isoprenyl moiety could enhance the anti-osteoclastic effect of guanidine alkaloid. In addition to the importance of the number,

binding site, and polymerization degree of isoprenyl moiety in the guanidine alkaloids, synthetic nitensidine A derivatives clearly indicated the importance of the imino nitrogen atom in the guanidine core unit. Although extensive SAR analysis with other nitensidine A analogs would be required to fully understand how nitensidine A exerts anti-osteoclastic effects, the generation of imino tautomeric forms of guanidine may play a crucial role in their anti-osteoclastic effects as mentioned in our previous study (Regasini et al. 2009).

Excessive bone resorption by osteoclasts is strongly implicated in the pathogenesis of several bone disorders, such as osteoporosis, arthritis, periodontitis, bone metastasis, corticosteroid-induced bone loss and Paget's disease (Rodan and Martin 2000; Chambers 2000; Teitelbaum 2000; Boyle et al. 2003). Although nitensidine A was the most effective among the six compounds tested, nitensidine A seems to develop side effects in vivo since nitensidine A exerted cytotoxicity against HepG2 cells at about only 10-fold higher concentrations than that against osteoclasts. Nitensidine A seems to have substantial cytotoxic off-target effects in vivo and does not so specifically exert cytotoxicity against osteoclasts among normal cells since the cytotoxicity of nitensidine A against osteoclasts was exerted at about 20-fold lower concentrations than that against osteoblasts as shown in Table 1. However, nitensidine A could be a promising lead compound for the development of an anti-osteoclastic drug for the treatment of above-mentioned metabolic bone disorders.

Collectively, the number, binding site, and polymerization degree of isoprenyl moiety in the guanidine alkaloids and the imino nitrogen atom in the guanidine core unit would cooperatively contribute to the anti-osteoclastic effects of guanidine alkaloids.

**Acknowledgments** This study was supported by a Grant-in-Aid for Young Scientists (B) (JSPS KAKENHI Grant Number 22791786) and Grant-in-Aid for Scientific Research (C) (JSPS KAKENHI Grant Number 24592822) from the Ministry of Education, Culture, Sports, Science and Technology (MEXT), and Chubu University Grant A (23IM04A) and B (23IM02B and 24M01B) from Chubu University. The isolation of the guanidine alkaloids and synthesis of the nitensidine A derivatives were supported by a grant from the Fundação de Amparo à Pesquisa do Estado de São Paulo (FAPESP) as part of the Biota-FAPESP-The Biodiversity Virtual Institute Program ([www.biotasp.org.br](http://www.biotasp.org.br)), Grant No. 03/02176-7, awarded to V.S.B.

## References

- Bolzani VS, Gunatilaka AA, Kingston DG (1995) Bioactive guanidine alkaloids from *Pterogyne nitens*. *J Nat Prod* 58:1638–1688
- Boyle WJ, Simonet WS, Lacey DL (2003) Osteoclast differentiation and activation. *Nature* 423:337–342
- Chambers TJ (2000) Regulation of the differentiation and function of osteoclasts. *J Pathol* 192:4–13
- Duarte RA, Mello ER, Araki C, Bolzani Vda S, Siqueira e Silva DH, Regasini LO, Silva TG, de Moraes MC, Ximenes VF, Soares CP (2010) Alkaloids extracted from *Pterogyne nitens* induce apoptosis in malignant breast cell line. *Tumour Biol* 31:513–522
- Edwards JR, Mundy GR (2011) Advances in osteoclast biology: old findings and new insights from mouse models. *Nat Rev Rheumatol* 7:235–243
- Felix R, Cecchini MG, Hofstetter W, Elford PR, Stutzer A, Fleisch H (1990) Impairment of macrophage colony-stimulating factor production and lack of resident bone marrow macrophages in the osteopetrotic op/op mouse. *J Bone Miner Res* 5:781–789
- Fernandes DC, Regasini LO, Velloso JC, Pauletti PM, Castro-Gamboa I, Bolzani VS, Oliveira OM, Silva DH (2008) Myeloperoxidase inhibitory and radical scavenging activities of flavones from *Pterogyne nitens*. *Chem Pharm Bull (Tokyo)* 56:723–726
- Fuller K, Lean JM, Bayley KE, Wani MR, Chambers TJ (2000) A role for TGF $\beta$ <sub>1</sub> in osteoclast differentiation and survival. *J Cell Sci* 113:2445–2453
- Kaneda T, Nojima T, Nakagawa M, Ogasawara A, Kaneko H, Sato T, Mano H, Kumegawa M, Hakeda Y (2000) Endogenous production of TGF-beta is essential for osteoclastogenesis induced by a combination of receptor activator of NF-kappa B ligand and macrophage-colony-stimulating factor. *J Immunol* 165:4254–4263
- Lacey DL, Timms E, Tan HL, Kelley MJ, Dunstan CR, Burgess T, Elliott R, Colombero A, Elliott G, Scully S, Hsu H, Sullivan J, Hawkins N, Davy E, Capparelli C, Eli A, Qian YX, Kaufman S, Sarosi I, Shalhoub V, Senaldi G, Guo J, Delaney J, Boyle WJ (1998) Osteoprotegerin ligand is a cytokine that regulates osteoclast differentiation and activation. *Cell* 93:165–176
- Mochizuki A, Takami M, Kawawa T, Suzumoto R, Sasaki T, Shiba A, Tsukasaki H, Zhao B, Yasuhara R, Suzawa T, Miyamoto Y, Choi Y, Kamijo R (2006) Identification and characterization of the precursors committed to osteoclasts induced by TNF-related activation-induced cytokine/receptor activator of NF-kappa B ligand. *J Immunol* 177:4360–4368
- Nakagawa H, Wachi M, Woo JT, Kato M, Kasai S, Takahashi F, Lee IS, Nagai K (2002) Fenton reaction is primarily involved in a mechanism of (–)-epigallocatechin-3-gallate to induce osteoclastic cell death. *Biochem Biophys Res Commun* 292:94–101
- Nakagawa H, Takami M, Udagawa N, Sawae Y, Suda K, Sasaki T, Takahashi N, Wachi M, Nagai K, Woo JT (2003) Destruixins, cyclodepsipeptides, block the formation of actin rings and prominent clear zones and ruffled borders in osteoclasts. *Bone* 33:443–455

- Nakagawa H, Hasumi K, Takami M, Aida-Hyugaji S, Woo JT, Nagai K, Ishikawa T, Wachi M (2007) Identification of two biologically crucial hydroxyl groups of (–)-epigallocatechin gallate in osteoclast culture. *Biochem Pharmacol* 73:34–43
- Nakagawa H, Wakabayashi-Nakao K, Tamura A, Toyoda Y, Koshiba S, Ishikawa T (2009) Disruption of N-linked glycosylation enhances ubiquitin-mediated proteasomal degradation of the human ATP-binding cassette transporter ABCG2. *FEBS J* 276:7237–7252
- Regasini LO, Velloso JC, Silva DH, Furlan M, de Oliveira OM, Khalil NM, Brunetti IL, Young MC, Barreiro EJ, Bolzani VS (2008) Flavonols from *Pterogyne nitens* and their evaluation as myeloperoxidase inhibitors. *Phytochemistry* 69:1739–1744
- Regasini LO, Castro-Gamboa I, Silva DH, Furlan M, Barreiro EJ, Ferreira PM, Pessoa C, Lotufo LV, de Moraes MO, Young MC, Bolzani Vda S (2009) Cytotoxic guanidine alkaloids from *Pterogyne nitens*. *J Nat Prod* 72:473–476
- Regasini LO, Pivatto M, Scorzoni L, Benaducci T, Fusco-Almeida A, Giannini M, Barreiro EJ, Silva D, Bolzani Vda S (2010) Antimicrobial activity of *Pterogyne nitens* Tul., Fabaceae, against opportunistic fungi. *Rev Bras Farmacogn* 20:706–711
- Rodan GA, Martin TJ (2000) Therapeutic approaches to bone diseases. *Science* 289:1508–1514
- Sells Galvin RJ, Gatlin CL, Horn JW, Fuson TR (1999) TGF-beta enhances osteoclast differentiation in hematopoietic cell cultures stimulated with RANKL and M-CSF. *Biochem Biophys Res Commun* 265:233–239
- Teitelbaum SL (2000) Bone resorption by osteoclasts. *Science* 289:1504–1508
- Tomimori Y, Mori K, Koide M, Nakamichi Y, Ninomiya T, Udagawa N, Yasuda H (2009) Evaluation of pharmaceuticals with a novel 50-h animal model of bone loss. *J Bone Miner Res* 24:1194–1205
- Venkatachalam TK, Qazi S, Samuel P, Uckun FM (2003) Inhibition of mast cell leukotriene release by thiourea derivatives. *Bioorg Med Chem Lett* 13:485–488
- Wattel A, Kamel S, Mentaverri R, Lorget F, Prouillet C, Petit JP, Fardelonne P, Brazier M (2003) Potent inhibitory effect of naturally occurring flavonoids quercetin and kaempferol on in vitro osteoclastic bone resorption. *Biochem Pharmacol* 65:35–42
- Woo JT, Nakagawa H, Notoya M, Yonezawa T, Udagawa N, Lee IS, Ohnishi M, Hagiwara H, Nagai K (2004) Quercetin suppresses bone resorption by inhibiting the differentiation and activation of osteoclasts. *Biol Pharm Bull* 27:504–509
- Yan T, Riggs BL, Boyle WJ, Khosla S (2001) Regulation of osteoclastogenesis and RANK expression by TGF-beta1. *J Cell Biochem* 83:320–325
- Yasuda H, Shima N, Nakagawa N, Yamaguchi K, Kinosaki M, Mochizuki S, Tomoyasu A, Yano K, Goto M, Murakami A, Tsuda E, Morinaga T, Higashio K, Udagawa N, Takahashi N, Suda T (1998) Osteoclast differentiation factor is a ligand for osteoprotegerin/osteoclastogenesis-inhibitory factor and is identical to TRANCE/RANKL. *Proc Natl Acad Sci USA* 95:3597–3602
- Yoshida H, Hayashi S, Kunisada T, Ogawa M, Nishikawa S, Okamura H, Sudo T, Shultz LD, Nishikawa S (1990) The murine mutation osteopetrosis is in the coding region of the macrophage colony stimulating factor gene. *Nature* 345:442–444
- Zhao B, Takami M, Yamada A, Wang X, Koga T, Hu X, Tamura T, Ozato K, Choi Y, Ivashkiv LB, Takayanagi H, Kamijo R (2009) Interferon regulatory factor-8 regulates bone metabolism by suppressing osteoclastogenesis. *Nat Med* 15:1066–1071

# Human ABCB1 confers cells resistance to cytotoxic guanidine alkaloids from *Pterogyne nitens*

Kazuhiro Satake<sup>a</sup>, Megumi Tsukamoto<sup>a</sup>, Yuji Mitani<sup>a</sup>, Luis Octavio Regasini<sup>b</sup>, Vanderlan da Silva Bolzani<sup>b</sup>, Thomas Efferth<sup>c</sup> and Hiroshi Nakagawa<sup>a,d,\*</sup>

<sup>a</sup> Department of Applied Biological Chemistry, Graduate School of Bioscience and Biotechnology, Chubu University, Kasugai, Japan

<sup>b</sup> Department of Organic Chemistry, Institute of Chemistry, São Paulo State University, Araraquara, Brazil

<sup>c</sup> Department of Pharmaceutical Biology, Institute of Pharmacy and Biochemistry, University of Mainz, Mainz, Germany

<sup>d</sup> Department of Applied Biological Chemistry, College of Bioscience and Biotechnology, Chubu University, Kasugai, Japan

Received 22 September 2014

Accepted 14 November 2014

**Abstract.** Multidrug resistance (MDR) caused by human ABCB1 (P-glycoprotein/MDR1) is one of the major obstacles in chemotherapy. To understand the mechanism of MDR by ABCB1 and circumvent the MDR, in the present study, we established human ABCB1-expressing cells (Flp-In-293/ABCB1 cells) and examined the cytotoxic effects of four guanidine alkaloids from *Pterogyne nitens* (galegine, nitensidine A, pterogynidine and pterogynine) using Flp-In-293/Mock and Flp-In-293/ABCB1 cells. The activity of ABCB1 in Flp-In-293/ABCB1 cells were confirmed by typical substrates for ABCB1 (taxol and vinblastine) in MTT assay. Flp-In-293/ABCB1 cells were also resistant to the four guanidine alkaloids as well as taxol and vinblastine compared to Flp-In-293/Mock cells although the four guanidine alkaloids exhibited cytotoxicity against the two Flp-In-293 cells. Furthermore, the four guanidine alkaloids were also found to stimulate the ATPase activity of ABCB1 in ATPase assays. These results suggest that ABCB1 can confer the resistance to the cytotoxic guanidine alkaloids by transporting them.

Keywords: ABCB1, P-glycoprotein, ATP-binding cassette (ABC) transporter, guanidine alkaloids

## 1. Background

Human ABCB1 (P-glycoprotein/MDR1) is a transmembrane efflux pump that belongs to the ATP-binding cassette (ABC) transporter superfamily. It has been cloned as the multidrug resistance 1 (MDR1) gene from cancer cells exerting cross-resistance to several structurally diverse and mechanistically unrelated anti-cancer drugs [1–4]. As a drug transporter, ABCB1 regulates the intracellular concentration of

---

\* Address for correspondence: Hiroshi Nakagawa, PhD, Lecturer, Department of Applied Biological Chemistry, College of Bioscience and Biotechnology, Chubu University, 1200 Matsumoto-cho, Kasugai, Aichi 487-8501, Japan. Tel.: +81 568 51 9606; Fax: +81 568 52 6594; E-mail: hnakagaw@isc.chubu.ac.jp.

various substrates by extruding them from cells. Overexpression of ABCB1 reportedly confers cancer cells with resistance to anti-cancer drugs such as doxorubicin, vincristine and paclitaxel [5–8]. Thus, the enzymatic activity of ABCB1 can contribute to multidrug resistance (MDR) in cancer cells, and can be an obstacle to successful cancer chemotherapy. Inhibitors, modulators and chemosensitizers of ABCB1 have been screened extensively to circumvent MDR. However, the structural features important for the inhibition, modulation and chemosensitization of ABCB1 are incompletely understood. Thus, screening for inhibitors, modulators and chemosensitizers of ABCB1 with novel structures, and subsequent structure–activity relationship analyses of these structures, would be helpful for understanding the detailed mechanisms by which ABCB1 recognizes and transports its substrates.

## 2. Objective

The ultimate goal of this work is to discover ways to circumvent ABCB1-mediated MDR. In the present study, we provide evidence that ABCB1-expressing cells can exert resistance to cytotoxic guanidine alkaloids isolated from a plant species found in Brazil: *Pterogyne nitens*.

## 3. Materials and methods

### 3.1. Guanidine alkaloids

The guanidine alkaloids tested in the present study were obtained from *Pterogyne nitens* leaves or branches; their isolation and identification have been previously described [9,10].

### 3.2. Cell culture

CCRF-CEM and CEM/ADR5000 cells were kindly provided by Dr. Axel Sauerbrey (Department of Pediatrics, University of Jena, Jena, Germany). CEM/ADR5000 cells are an ABCB1 overexpressing, multidrug-resistant subline of CCRF-CEM cells. All cells were maintained in RPMI 1640 medium (Biochrom AG, Berlin, Germany) supplemented with 10% (v/v) fetal bovine serum (FBS) (ICN Biomedicals, Aurora, OH, USA), 0.8 mM L-glutamine, 50 µg/ml kanamycin, 100 U/ml penicillin and 100 µg/ml streptomycin at 37°C in a humidified atmosphere of 5% (v/v) CO<sub>2</sub> in air. CEM/ADR5000 cells were cultured with 2.5 µg/ml doxorubicin for 24 h once a week to maintain ABCB1 expression in the cells.

We prepared Flp-In-293/ABCB1 cells from Flp-In-293 cells (Invitrogen, Carlsbad, CA, USA) having the Flp recombination target (FRT) site at the telomeric region of only one of the pair of chromosomes 12 [11,12] to examine the effect of ABCB1 on the cytotoxicity of guanidine alkaloids. For this purpose, Flp-In-293 cells were transfected with the pcDNA5/FRT/ABCB1 vector, the Flp recombinase expression plasmid pOG44 [13–15], and Lipofectamine™-2000 (Invitrogen) according to manufacturer instructions. Single colonies resistant to hygromycin B (Invitrogen) were selected and subcultured. Selection of positive colonies was undertaken by immunoblotting with ABCB1-specific monoclonal antibody C219 (EMD Biosciences, Darmstadt, Germany). Mock (Flp-In-293/Mock) cells used in the present study had been established in our previous studies [11]. Parental Flp-In-293 cells were maintained in Dulbecco's Modified Eagle's Medium (DMEM) supplemented with 10% (v/v) heat-inactivated FBS, 2 mM L-glutamine, 100 U/ml penicillin, 100 µg/ml streptomycin, 250 ng/ml amphotericin B and 100 µg/ml Zeocin™ at 37°C in a humidified atmosphere of 5% (v/v) CO<sub>2</sub> in air. Flp-In-293/ABCB1 and

Flp-In-293/Mock cells were maintained in DMEM supplemented with the agents shown above except that 100 µg/ml hygromycin B was used instead of Zeocin.

### 3.3. 2,3-bis-(2-methoxy-4-nitro-5-sulfophenyl)-2H-tetrazolium-5-carboxanilide (XTT) assay

CCRF-CEM and CEM/ADR5000 cells were seeded ( $2 \times 10^4$  cells/well) into 96-well culture plates and cultured with compounds for 72 h. After incubation, cells were treated with XTT for 5 h using Cell Proliferation Kit II (XTT assay) (Roche, Mannheim, Germany) according to manufacturer protocols. Absorbance at 490 nm and 655 nm was measured as test and reference wavelengths, respectively. Data are the mean  $\pm$  SEM of two experiments.

### 3.4. 3-(4,5-dimethyl-2-thiazolyl)-2,5-diphenyl-2H-tetrazolium bromide (MTT) assay

Flp-In-293/Mock and Flp-In-293/ABCB1 cells were seeded ( $5 \times 10^3$  cells/well) into 96-well culture plates and pre-cultured for 24 h. After pre-culture, compounds were added into the cell cultures and cells were incubated for 72 h. After incubation, cells were treated with 500 µg/ml MTT (Sigma-Aldrich, St. Louis, MO, USA) for 3 h. And then 20% (w/v) sodium dodecyl sulfate in phosphate-buffered saline (100 µl/well) was added to solubilize MTT-formazan, followed by overnight incubation. After the incubation, absorbance at 570 nm and 630 nm was measured as a test and reference wavelengths, respectively. Data are the mean  $\pm$  SEM of two experiments.

### 3.5. ATPase assay

The ATPase activities of ABCB1 in the presence of various test compounds were measured in 96-well plates by using plasma membrane fractions prepared from ABCB1-expressing Sf9 cells [16]. In brief, cell membranes (1 µg of protein per well) were suspended in 10 µl of the incubation medium containing 50 mM Tris-Mes (pH 6.8), 2 mM EGTA, 2 mM dithiothreitol, 50 mM potassium chloride, 5 mM sodium azide and 2 mM ouabain. This medium was mixed with 10 µl of a test compound solution in 96-well plates. The ATPase reaction was started by adding 20 µl of 4 mM ATP/Mg solution to the reaction mixture in the plates, and the incubation was maintained at 37°C for 30 min. The reaction was stopped by the addition of 20 µl of 5% trichloroacetic acid followed by 42 µl of solution A (2 N hydrochloric acid: 0.1 M sodium molybdate = 4 : 3) and 18 µl of solution B (0.084% (w/v) malachite green in 1% (w/v) polyvinyl alcohol). Thereafter, 120 µl of solution C (7.8% (v/v) sulfuric acid) was added to the mixture in the well plates. After one hour of incubation at room temperature, the absorbance of the reaction mixture in each well was measured at a wavelength of 655 nm by using Bio-Rad Model 680 Absorbance Microplate Reader (Bio-Rad Laboratories, Inc.). The amount of liberated phosphate was quantified on the basis of the calibration line established with inorganic phosphate standards.

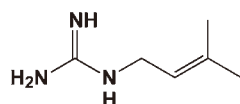
### 3.6. Statistical analyses

The results were statistically analyzed using Microsoft Excel 2010 software (Microsoft, Redmond, WA, USA). The statistical significance of differences was determined using the Student's *t*-test.  $P < 0.05$  compared with the results from CCRF-CEM cells or Flp-In-293/Mock cells was considered significant.

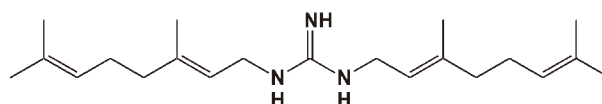
#### 4. Results

We evaluated the cytotoxic effects of four guanidine alkaloids isolated from *Pterogyne nitens* on CCRF-CEM and its MDR counterpart (CEM/ADR5000 cells) (Fig. 1 and Table 1). CCRF-CEM and CEM/ADR5000 cells were cultured with or without guanidine alkaloids for 72 h. After the culture, cell viability was determined using the XTT assay. All four guanidine alkaloids exhibited toxicity against CCRF-CEM cells as shown in Table 1. The order of cytotoxic activity was nitensidine A > pterogynidine > pterogynine > galegine. Compared with CCRF-CEM cells, CEM/ADR5000 cells were resistant to the toxic effects of all four guanidine alkaloids. To elucidate the involvement of ABCB1 in the resistance of CEM/ADR5000 cells against the four guanidine alkaloids, the cytotoxic effects of the four compounds were examined using Flp-In-293/ABCB1 cells stably expressing wild-type human ABCB1 and its counterpart Flp-In-293/Mock cells. For this purpose, Flp-In-293/ABCB1 cells were established

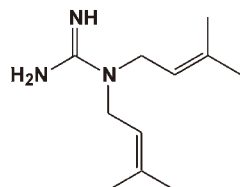
Galegine



Nitensidine A



Pterogynidine



Pterogynine

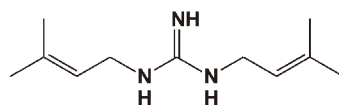


Fig. 1. Structures of guanidine alkaloids.

Table 1

Cytotoxicity of guanidine alkaloids against CCRF-CEM, CEM/ADR5000, Flp-In-293/Mock, Flp-In-293/ABCB1 cells

Guanidine alkaloids	IC <sub>50</sub> (μM)			
	CCRF-CEM cells	CEM/ADR5000 cells	Flp-In-293/Mock cells	Flp-In-293/ABCB1 cells
Galegine	>100	>100	79 ± 4.1	90 ± 9.7
Nitensidine A	4.9 ± 0.030	23 ± 2.0	40 ± 4.1	74 ± 8.2
Pterogynidine	16 ± 0.80	>100	22 ± 1.8	53 ± 11
Pterogynine	37 ± 3.0	>100	60 ± 3.6	85 ± 13

Note: Data are expressed as the means ± SEM of triplicate determinations.

and their drug-resistance activities were examined using taxol and vinblastine (typical substrates for ABCB1). Flp-In-293/Mock (open circles in Fig. 2) and Flp-In-293/ABCB1 cells (closed circles in Fig. 2) were cultured with or without the typical ABCB1 substrates for 72 h. After the culture, cell viability was determined by the MTT assay. Compared with Flp-In-293/Mock cells, Flp-In-293/ABCB1 cells showed resistance to both ABCB1 substrates (Fig. 2). Flp-In-293/Mock (open circles in Fig. 2) and Flp-In-293/ABCB1 cells (closed circles in Fig. 3) were also cultured with or without the guanidine al-

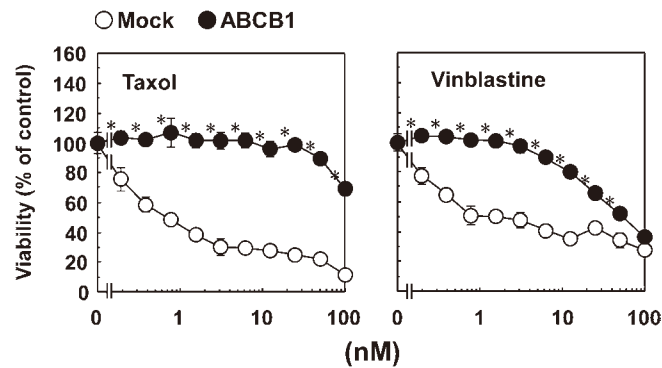


Fig. 2. Drug resistance ability of Flp-In-293/ABCB1 cells. Flp-In-293/Mock (*open circles*) and Flp-In-293/ABCB1 cells (*closed circles*) were cultured with or without the taxol and vinblastine for 72 h. After the culture, viability of the cells was determined by MTT assay as described in Section 3. Similar results were obtained in more than two other experiments. Data are expressed as the mean  $\pm$  SEM of triplicate determinations. \*  $P < 0.05$  compared with the result from Flp-In-293/Mock cells.

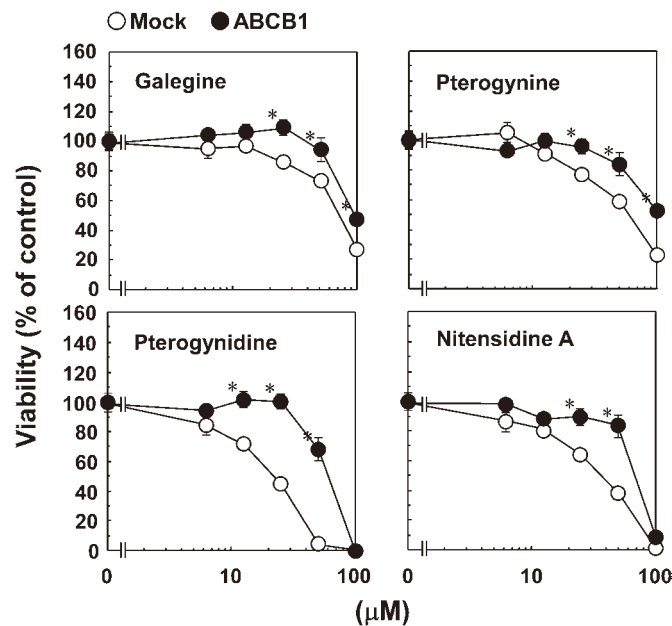


Fig. 3. Effect of the guanidine alkaloids on the viability of Flp-In-293/Mock and Flp-In-293/ABCB1 cells. Flp-In-293/Mock (*open circles*) and Flp-In-293/ABCB1 cells (*closed circles*) were cultured with or without the guanidine alkaloids for 72 h. After the culture, viability of the cells was determined by MTT assay as described in Section 3. Similar results were obtained in more than two other experiments. Data are expressed as the mean  $\pm$  SEM of triplicate determinations. \*  $P < 0.05$  compared with the result from Flp-In-293/Mock cells.

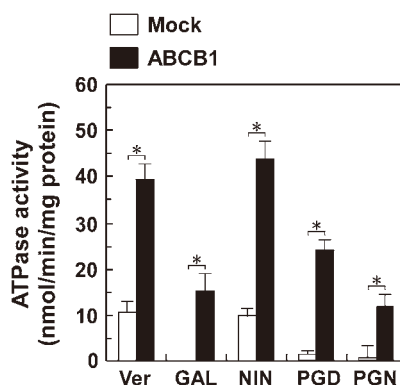


Fig. 4. Effect of the guanidine alkaloids on ATPase activity of ABCB1. The ATPase activity in the plasma membrane from Sf9 cells expressing ABCB1 (closed bars) or not expressing ABCB1 (open bars) was measured in the presence of 10  $\mu$ M guanidine alkaloids as described in Section 3. Similar results were obtained in more than two other experiments. Data is expressed as the mean  $\pm$  SEM of triplicate determinations. Ver – verapamil, GAL – galegine, NIN – nitsensidine A, PGD – pterogynidine, PGN – pterogynine. \* $P < 0.05$  as compared between the indicated groups.

kaloids for 72 h. All four guanidine alkaloids showed toxicity against Flp-In-293/Mock cells (Fig. 3). The order of cytotoxic activity was pterogynidine > nitsensidine A > pterogynine > galegine. As well as CEM/ADR5000 cells, Flp-In-293/ABCB1 cells were resistant to four guanidine alkaloids compared with Flp-In-293/Mock cells.

As shown in Fig. 4, four guanidine alkaloids were each found to cause an ABCB1-dependent hydrolysis of ATP when incubated with plasma membranes from Sf9 cells expressing wild-type ABCB1. Furthermore, the hydrolysis levels of ATP by nitsensidine A were comparable to those by verapamil. These results suggest that the guanidine alkaloids were recognized as substrates by ABCB1.

## 5. Conclusions

We carried out XTT and MTT assays to investigate the cytotoxic effects of guanidine alkaloids on cells expressing human ABCB1 and their counterpart cells. Guanidine alkaloids have been reported to be cytotoxic against the human infiltrating ductal carcinoma ZR-7531 cell line but not against human myeloblastic leukemia HL-60, human colon carcinoma HCT-8, human melanoma MDA-MB-435 and human glioblastoma SF-295 cells [9,10]. In the present study, four guanidine alkaloids were found to be cytotoxic against four cell lines (CCRF-CEM, CEM/ADR5000, Flp-In-293/Mock and Flp-In-293/ABCB1 cells). Although the current number of the compounds is not sufficient for structure–activity relationship analysis, based on the structural differences among the four guanidine alkaloids, the number, length and binding site of aliphatic side chains of the four guanidine alkaloids seem to determine their levels of cytotoxicity.

The sensitivities of CCR-CEM and Flp-In-293 cells to the four guanidine alkaloids were slightly different; CCR-CEM and Flp-In-293 cells were the most sensitive to nitsensidine A and pterogynidine, respectively. As well as the chemical features of the four guanidine alkaloids, the present study clearly showed that the cytotoxic activities of the four compounds were dependent upon ABCB1 expression. In the XTT and MTT assays, cells expressing ABCB1 were resistant to all of the guanidine alkaloids tested. These results suggest that ABCB1 confers the cells resistance to the four guanidine alkaloids.

A study to ascertain if the four guanidine alkaloids are substrates for ABCB1 is in progress although they were shown to stimulate ATPase activity of ABCB1 in Fig. 4.

In the present study, ABCB1-expressing cells showed resistance to the four cytotoxic guanidine alkaloids, suggesting that several guanidine alkaloids can serve as substrates for ABCB1. Among the guanidine alkaloid test compounds, pterogynidine and pterogynine (which both have a molecular weight of 195) may be the smallest molecules transported by ABCB1 because these guanidine alkaloids are smaller than phenytoin (molecular weight = 252), which was reported to be the smallest substrate for ABCB1 by Schinkel et al. [17]. Further studies are required to circumvent MDR, but the present study has shed light on the molecular mechanisms by which ABCB1 recognizes its substrates.

### Acknowledgements

This study was supported by the Grant-in-Aid for Scientific Research (C) (JSPS KAKENHI Grant Number 24592822) from the Ministry of Education, Culture, Sports, Science and Technology (MEXT) and intramural grants from Chubu University (Grant A (23IM04A) and B (23IM02B and 24M01B)) and the German Cancer Research Center (Heidelberg, Germany). The phytochemical studies were supported by a grant from the Fundação de Amparo à Pesquisa do Estado de São Paulo (FAPESP) as part of the Biota-FAPESP-Biodiversity Virtual Institute Program ([www.biota.org.br](http://www.biota.org.br)), grant number 03/02176-7, awarded to V.S.B. We thank Karen Duffy (Cornell University, Ithaca, NY, USA) for her critique of the manuscript.

### References

- [1] R.L. Juliano and V. Ling, A surface glycoprotein modulating drug permeability in Chinese hamster ovary cell mutants, *Biochimica et Biophysica Acta* **455** (1976), 152–162.
- [2] K. Ueda, M.M. Cornwell, M.M. Gottesman, I. Pastan, I.B. Roninson, J.R. Riordan et al., The *mdr1* gene, responsible for multidrug-resistance, codes for P-glycoprotein, *Biochemical and Biophysical Research Communications* **141** (1986), 956–962.
- [3] C.J. Chen, J.E. Chin, K. Ueda, D.P. Clark, I. Pastan, M.M. Gottesman et al., Internal duplication and homology with bacterial transport proteins in the *mdr1* (P-glycoprotein) gene from multidrug-resistant human cells, *Cell* **47** (1986), 381–389.
- [4] F.A. de Jong, M.J. de Jonge, J. Verweij and R.H. Mathijssen, Role of pharmacogenetics in irinotecan therapy, *Cancer Letters* **234** (2006), 90–106.
- [5] T. Ishikawa, Multidrug resistance: Genomics of ABC transporters, in: *Nature Encyclopedia of the Human Genome*, Nature Publishing Group, D.N. Cooper, ed., 2003, pp. 154–160.
- [6] J.J. Gribar, M. Ramachandra, C.A. Hrycyna, S. Dey and S.V. Ambudkar, Functional characterization of glycosylation-deficient human P-glycoprotein using a vaccinia virus expression system, *J. Membr. Biol.* **173** (2000), 203–214.
- [7] V. Ling, Multidrug resistance: Molecular mechanisms and clinical relevance, *Cancer Chemotherapy and Pharmacology* **40** Suppl. (1997), S3–S8.
- [8] A.H. Schinkel, J.J. Smit, O. van Tellingen, J.H. Beijnen, E. Wagenaar, H.P. te Riele et al., Disruption of the mouse *mdr1a* P-glycoprotein gene leads to a deficiency in the blood–brain barrier and to increased sensitivity to drugs, *Cell* **77** (1994), 491–502.
- [9] L.O. Regasini, I. Castro-Gamboa, D.H. Silva, M. Furlan, E.J. Barreiro and S. Bolzani Vda, Cytotoxic guanidine alkaloids from *Pterogyne nitens*, *J. Nat. Prod.* **72** (2009), 473–476.
- [10] R.A. Duarte, E.R. Mello, C. Araki, S. Bolzani Vda, D.H. Siqueira e Silva, C.P. Soares et al., Alkaloids extracted from *Pterogyne nitens* induce apoptosis in malignant breast cell line, *Tumour Biology: The Journal of the International Society for Oncodevelopmental Biology and Medicine* **31** (2010), 513–522.
- [11] K. Wakabayashi, H. Nakagawa, T. Adachi, I. Kii, E. Kobatake, T. Ishikawa et al., Identification of cysteine residues critically involved in homodimer formation and protein expression of human ATP-binding cassette transporter ABCG2: A new approach using the flp recombinase system, *J. Exp. Ther. Oncol.* **5** (2006), 205–222.

- [12] A. Tamura, K. Wakabayashi, Y. Onishi, H. Nakagawa, M. Tsuji, T. Ishikawa et al., Genetic polymorphisms of human ABC transporter ABCG2: Development of the standard method for functional validation of SNPs by using the Flp recombinase system, *J. Exp. Ther. Oncol.* **6** (2006), 1–11.
- [13] S. O’Gorman, D.T. Fox and G.M. Wahl, Recombinase-mediated gene activation and site-specific integration in mammalian cells, *Science* **251** (1991), 1351–1355.
- [14] B. Sauer, Site-specific recombination: Developments and applications, *Curr. Opin. Biotechnol.* **5** (1994), 521–527.
- [15] D. Wirth and H. Hauser, Flp-mediated integration of expression cassettes into FRT-tagged chromosomal loci in mammalian cells, *Methods in Molecular Biology* **267** (2004), 467–476.
- [16] A. Sakurai, Y. Onishi, H. Hirano, M. Seigneuret, K. Obayama, T. Ishikawa et al., Quantitative structure–activity relationship analysis and molecular dynamics simulation to functionally validate nonsynonymous polymorphisms of human ABC transporter ABCB1 (P-glycoprotein/MDR1), *Biochemistry* **46** (2007), 7678–7693.
- [17] A.H. Schinkel, E. Wagenaar, C.A. Mol and L. van Deemter, P-glycoprotein in the blood–brain barrier of mice influences the brain penetration and pharmacological activity of many drugs, *The Journal of Clinical Investigation* **97** (1996), 2517–2524.

## Review Article

# Diagnosis of Human Axillary Osmidrosis by Genotyping of the Human *ABCC11* Gene: Clinical Practice and Basic Scientific Evidence

Yu Toyoda,<sup>1</sup> Tsuneaki Gomi,<sup>2</sup> Hiroshi Nakagawa,<sup>3</sup>  
 Makoto Nagakura,<sup>4</sup> and Toshihisa Ishikawa<sup>5,6</sup>

<sup>1</sup>Department of Pharmacy, The University of Tokyo Hospital, 7-3-1 Hongo, Bunkyo-ku, Tokyo 113-8655, Japan

<sup>2</sup>Gomi Clinic, 1-10-12 Hyakunin-cho, Shinjyuku-ku, Tokyo 169-0073, Japan

<sup>3</sup>Department of Applied Biological Chemistry, Graduate School of Bioscience and Biotechnology, Chubu University, 1200 Matsumoto-cho, Kasugai 487-8501, Japan

<sup>4</sup>BioTec Co., Ltd., 2-29-4 Yushima, Bunkyo-ku, Tokyo 113-0034, Japan

<sup>5</sup>RIKEN Center for Life Science Technology, 1-7-22 Suehiro-cho, Tsurumi-ku, Yokohama 230-0045, Japan

<sup>6</sup>NGO Personalized Medicine & Healthcare, Yokohama 226-0016, Japan

Correspondence should be addressed to Yu Toyoda; [ytoyoda-tky@umin.ac.jp](mailto:ytoyoda-tky@umin.ac.jp)

Received 26 December 2015; Revised 25 January 2016; Accepted 28 January 2016

Academic Editor: Stephen H. Safe

Copyright © 2016 Yu Toyoda et al. This is an open access article distributed under the Creative Commons Attribution License, which permits unrestricted use, distribution, and reproduction in any medium, provided the original work is properly cited.

The importance of personalized medicine and healthcare is becoming increasingly recognized. Genetic polymorphisms associated with potential risks of various human genetic diseases as well as drug-induced adverse reactions have recently been well studied, and their underlying molecular mechanisms are being uncovered by functional genomics as well as genome-wide association studies. Knowledge of certain genetic polymorphisms is clinically important for our understanding of interindividual differences in drug response and/or disease risk. As such evidence accumulates, new clinical applications and practices are needed. In this context, the development of new technologies for simple, fast, accurate, and cost-effective genotyping is imperative. Here, we describe a simple isothermal genotyping method capable of detecting single nucleotide polymorphisms (SNPs) in the human ATP-binding cassette (ABC) transporter *ABCC11* gene and its application to the clinical diagnosis of axillary osmidrosis. We have recently reported that axillary osmidrosis is linked with one SNP 538G>A in the *ABCC11* gene. Our molecular biological and biochemical studies have revealed that this SNP greatly affects the protein expression level and the function of *ABCC11*. In this review, we highlight the clinical relevance and importance of this diagnostic strategy in axillary osmidrosis therapy.

## 1. Introduction

Body odor production is a physiological characteristic of animals, including humans. In humans, however, strong or specific body odors are sometimes considered to be unpleasant. Axillary osmidrosis is known as a phenomenon characterized by strong body odor and profuse sweating from the armpits resulting from an excessive secretion of the body's metabolites from well-developed apocrine glands in the axillae.

Recently, we have reported that axillary osmidrosis is linked with one single nucleotide polymorphism (SNP) 538G>A in exon 4 of the human *ABCC11* gene, a member of

the human ABC transporter gene family. This SNP 538G>A (rs17822931) in the *ABCC11* gene is a nonsynonymous polymorphism that alters one amino acid at position 180 from Glycine (Gly180) to Arginine (Arg180) in the *ABCC11* protein. As discussed later, this amino acid substitution enhances proteasomal degradation of the SNP variant (Arg180) of *de novo* synthesized *ABCC11* protein and disruption of its transport function [1]. Human subjects carrying homozygous alleles of 538G/G or heterozygous alleles of 538G/A have a higher risk of axillary osmidrosis, whereas those who are carrying the homozygous allele of 538A/A have no risk [1–3]. This association has also been confirmed within various ethnic groups [4, 5].

The *ABCC11* gene is located on human chromosome 16q12.1 [6–8]. *ABCC11*, also known as multidrug resistance-associated protein 8 (MRP8), is a full ABC transporter with a total of 12 putative transmembrane domains and two ATP-binding cassettes [9]. The predicted amino acid sequence of *ABCC11* shows high similarity to those of *ABCC4* and *ABCC5* among the C family of human ABC transporters [6]. Functional assays have demonstrated that *ABCC11* WT (Gly180) is able to transport a variety of lipophilic organic anions including cyclic nucleotides, glutathione conjugates such as leukotriene C<sub>4</sub> (LTC<sub>4</sub>) and S-(2,4-dinitrophenyl)-glutathione (DNP-SG), steroid sulfates such as dehydroepiandrosterone 3-sulfate (DHEAS) and estrone 3-sulfate (E<sub>1</sub>3S), glucuronides such as estradiol 17-β-D-glucuronide (E<sub>2</sub>17βG), and the monoanionic bile acids glycocholate and taurocholate, as well as folic acid and its analog methotrexate [10, 11]. Interestingly, there is no putative mouse or rat orthologous gene corresponding to human *ABCC11* [12], indicating that *ABCC11* is not an orthologous gene but rather a paralogous gene generated by gene duplication within the human genome.

The SNP 538G>A in the *ABCC11* gene was originally identified as a determinant of human earwax type [13]. Human earwax, a secretory product of the ceruminous apocrine glands, is classified into wet and dry types. Both *ABCC11* 538G/G and 538G/A correspond to the wet type, and 538A/A corresponds to the dry type. The latter is the recessive phenotype and is commonly found within the Asian population (Korean, Chinese, and Japanese populations), whereas the former is the dominant phenotype and is found majorly in Africans and Caucasians. Accordingly, the frequency of the 538A allele is predominantly high among the Mongoloid populations in Asia but low among Africans and Caucasians. Thus, humans with the wet type of earwax naturally have a strong axillary odor, whereas those with dry earwax have little odor. Interestingly, this association had already been pointed out in the middle of the 20th century [14, 15]. In this context, wet earwax is regarded as an apocrine gland-related phenotype. The family history of axillary osmidrosis and its autosomal dominant pattern has also been recognized [16], and the wet type of earwax has been used as one of the phenotype-based diagnostic criteria for axillary osmidrosis [17].

## 2. A New Method for Genotype-Based Diagnosis

**2.1. Rapid Genotyping of *ABCC11* 538G>A to Assess the Risk of Axillary Osmidrosis.** The association between the *ABCC11* genotype (538G>A) and axillary osmidrosis has enabled us to perform genotyping-based diagnosis of axillary osmidrosis, which is considered to be more objective than the phenotype-based diagnosis. Therefore, in the clinical setting, rapid, simple, and cost-effective methods are required for on-demand genotyping. To achieve this objective, we have recently developed a simple method targeting the SNP 538G>A in the human *ABCC11* gene based on an isothermal DNA amplification technique [18] (Figures 1(a)–1(c)). The new method enabled the determination of the genotype

TABLE 1: Primers sets for the detection of WT and SNP alleles in the human *ABCC11* gene.

WT (538G) detection primers set (5' to 3')	
TP	<u>C</u> GAGTACACTGGTTGATTTTCGATGCACTTC
FP	agcgatgcgttcgagcatcgctGTCTGCCACTTACTGGCC
BP	AGAAGCAGATGCCAGAA
OP1	TGATGCTGAGGTTCCAG
OP2	TAGAGTCCCCCAAACCT
CP	TACTGGCC <u>T</u> GAGTACAC-NH <sub>2</sub>
SNP (538A) detection primers set (5' to 3')	
TP	<u>C</u> TGAGTACACTGGTTGATTTTCGATGCACTTC
FP	agcgatgcgttcgagcatcgctGTCTGCCACTTACTGGCC
BP	AGAAGCAGATGCCAGAA
OP1	TGATGCTGAGGTTCCAG
OP2	TAGAGTCCCCCAAACCT
CP	TACTGGCC <u>C</u> GAGTACAC-NH <sub>2</sub>

TP: turn-back primer; FP: forward primer; BP: boost primer; OP: outer primer; CP: competitive probe.

within 30 min under isothermal reaction conditions without necessitating the isolation of genomic DNA and sequential PCR steps [1, 2].

**2.2. Genotyping Procedure.** In the method we developed, the entire DNA amplification process is achieved by designing a total of five primers, namely, turn-back primer (TP), forward primer (FP), boost primer (BP), and outer primers 1 and 2 (OP1 and OP2) (Table 1). In addition, to inhibit the background amplification from mismatch sequence pairs, a competitive probe (CP) was constructed for effective genotyping at the SNP 538G>A in the *ABCC11* gene.

Since this method requires only a small volume (1–2 μL) of peripheral blood, genotyping is easy [19]. Each SNP typing reaction is performed in a 25 μL reaction mixture under an isothermal condition at 60°C. The mixture contains 2.0 μM FP, 2.0 μM TP, 1.0 μM BP, 0.25 μM each of the OPs, 20 μM CP, 1.4 mM dNTPs, 5% DMSO, 20 mM Tris-HCl (pH 8.0), 10 mM KCl, 10 mM (NH<sub>4</sub>)<sub>2</sub>SO<sub>4</sub>, 8 mM MgSO<sub>4</sub>, 0.1% (v/v) Tween\*20, 1/100,000 diluted SYBR® Green I (Takara Bio Inc., Shiga, Japan), and 0.24 U/μL Aac DNA polymerase (K.K. DNAFORM, Yokohama, Japan). The polymorphism 538G>A is distinguished by TPs. DNA amplification and subsequent self-priming elongation (larger DNA production) are induced by the allele-specific TP and FP.

A multiple end-point determination of the SNP-dependent DNA amplification signal, an increase in the fluorescence of SYBR Green I, can be achieved by introducing a CCD camera and computational data acquisition, resulting in a simpler and more cost-effective detection (Figure 1(d)) [20].

**2.3. DNA Amplification Process in the SmartAmp-Based Method.** In the first step of the isothermal SmartAmp-based DNA amplification, FP and TP hybridize the template genomic DNA. Next, amplification products primed by each primer are detached from template genomic DNA. This

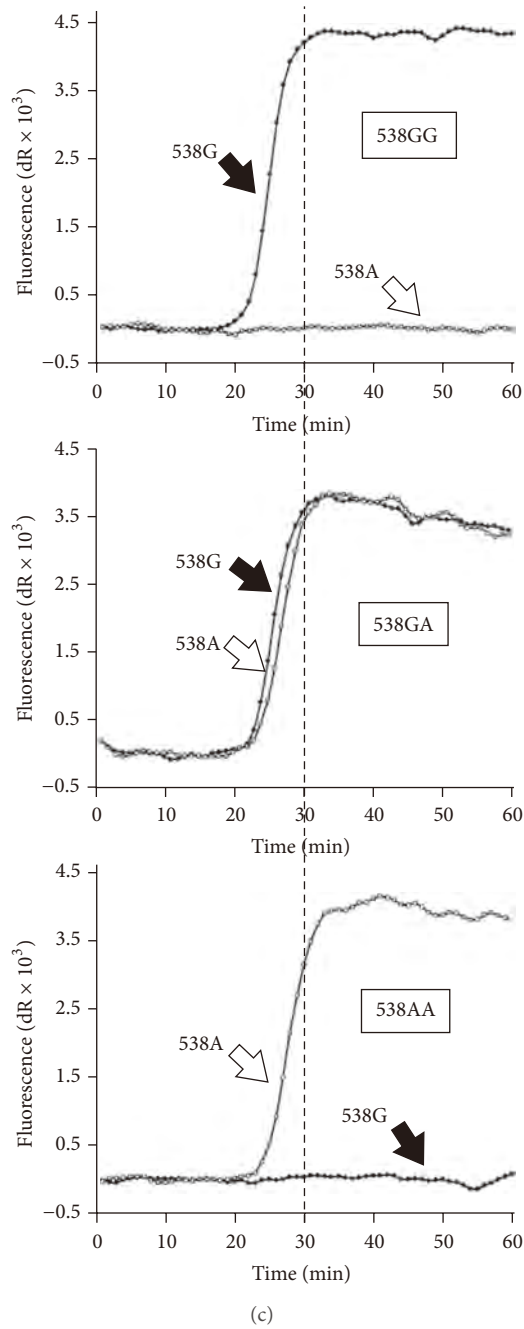
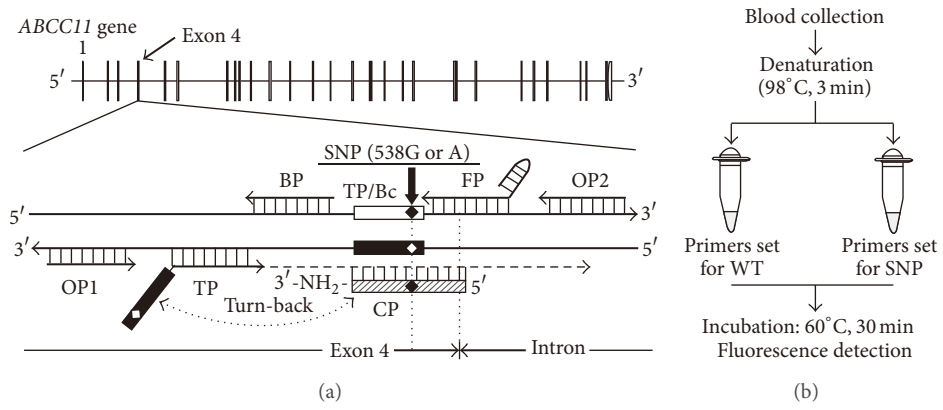


FIGURE 1: Continued.

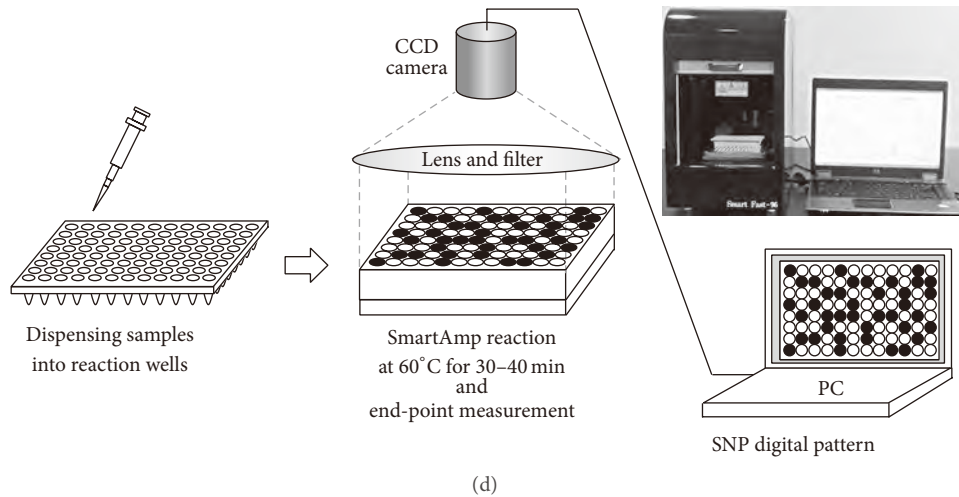


FIGURE 1: Genotyping at *ABCC11* 538G>A by the SmartAmp method. (a) Flowchart of the SmartAmp-based genotyping. After a simple heat treatment to degrade RNA and denature proteins, blood samples were added to the reaction mixture (total 25  $\mu$ L) and subjected to isothermal incubation at 60°C for 30 min while the fluorescence intensity was monitored. (b) Detection of the SNP 538G>A in *ABCC11* by the SmartAmp method. Time-dependent increases in fluorescence intensity produced by the SmartAmp reaction with *ABCC11* allele-specific primers carrying 538G (WT) or 538A (SNP) alleles were monitored by a real-time PCR system (Mx3000P; Stratagene). (c) Schematic illustration of the human *ABCC11* gene and relative positions of each primer for SmartAmp-based genotyping. The details of the DNA amplification process were described in Aw et al. [19]. (d) Schematic illustration for multiple end-point detection of SmartAmp-based SNP typing with a CCD camera-linked digital processor.

process is induced by strand-displacing DNA polymerase, whose extensions are primed by OP1 and OP2, respectively. Subsequently, single-stranded amplification products become new templates in the second amplification step for opposing FP and TP. Due to the special features of the FP and TP, those amplicons will refold at their 3' and 5' ends to form new priming sites that maintain self-amplification in the further self-primed DNA elongation. The formation of concatenated DNA products in the SmartAmp reaction was schematically illustrated in our previous report [19].

The CPs inhibit the background amplification from mismatch sequence pairs. For example, the CP for the detection of WT (538G) allele is designed as a complementary sequence around the alternative (538A) allele and its 3' end is modified by amination (Figure 1(a)). Therefore, this CP (538G) inhibits the misannealing of FP for WT allele and the following SmartAmp-based amplification from the genomic DNA carrying SNP (538A) allele. The CP (538A) enhances the assay specificity of allele-specific amplification in the similar manner.

**2.4. Clinical Decision and Treatments of Axillary Osmidrosis.** The genetic test for a SNP in the *ABCC11* gene is one of the clinical factors that underlies a doctor's decision. Patients carrying genotypes of 538G/G or 538G/A may be subjected to a surgical operation of excising apocrine glands, whereas such surgery is not indicated for those who are carrying the genotype of 538A/A (Figure 2).

Epidemiologic surveys indicate that subjects with *ABCC11* 538A/A have little risk of axillary osmidrosis, unlike 538GG/GA subjects. This SNP has been reported to correlate with deodorant usage, at least within the

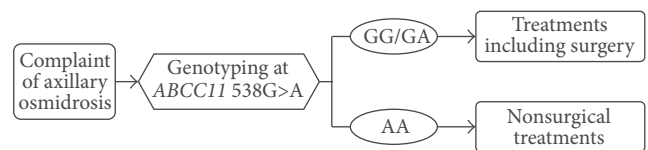


FIGURE 2: Gene-targeted strategy for the diagnosis and treatment of axillary osmidrosis. This strategy would be useful for the objective diagnosis of axillary osmidrosis, especially in ORS patients who have subjective olfactory delusion.

European population [21], while subjects with the 538A/A genotype are not directly affected by axillary osmidrosis. In particular, for the management of patients with olfactory reference syndrome (ORS) who tend to opt for aggressive surgical treatment simply due to the delusion of body odor, genetic evidence would be a powerful tool for diagnosis and nonsurgical treatment. Therefore, we proposed the clinical decision tree shown in Figure 2 [2].

**2.5. Distinguishing Olfactory Reference Syndrome and Axillary Osmidrosis.** The genotype-based diagnosis would be useful especially for olfactory reference syndrome (ORS) patients. Many ORS patients, also referred to as “jiko-syu-kyofu” in the Japanese medical literature, are characterized by having a preoccupation with the idea that their body emits a foul body odor that may be strong and/or offensive to others [22, 23]. These patients are convinced that they are the source of a strong smell, even if the people around them deny it. This kind of olfactory delusion, the main feature of ORS, is sometimes recognized by medical doctors during

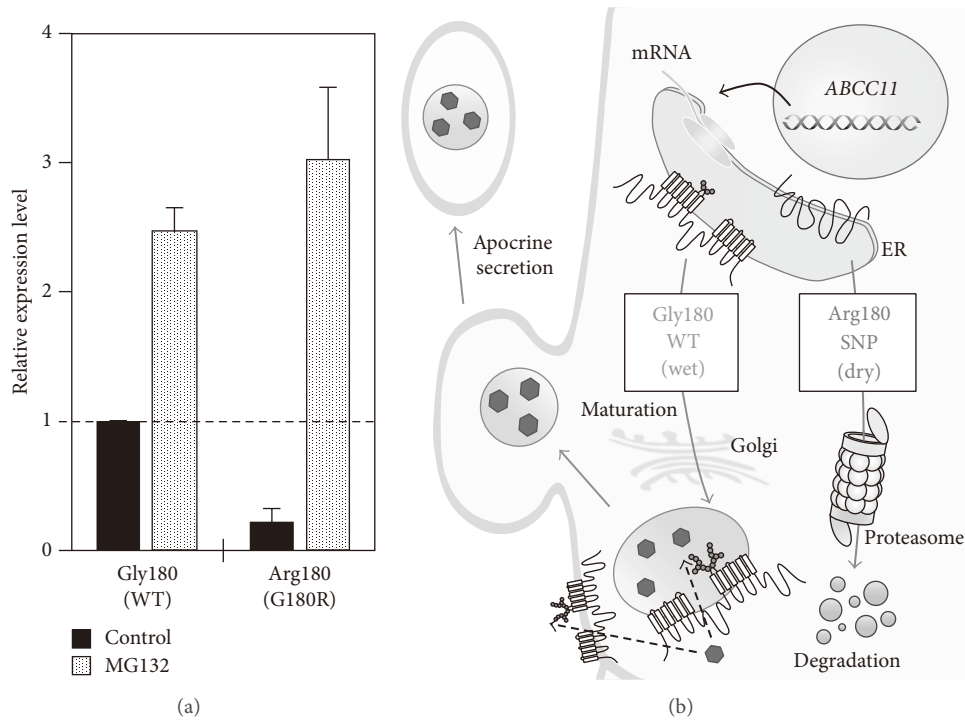


FIGURE 3: Effects of the SNP variant (Arg180) on the protein level and intracellular degradation of ABCC11. (a) To assess the effect of the Arg180 variant on the protein level of ABCC11, Flp-In-293 cells expressing the WT or Arg180 variant of ABCC11 were cultivated in the presence of MG132, a proteasome inhibitor, for 24 h. ABCC11 WT and Arg180 variant proteins were analyzed by immunoblotting with ABCC11-specific antibody after treatment with PNGase F, a glycosidase. The signal intensity ratio (ABCC11/GAPDH, internal control) was normalized to the control and expressed as mean ± SD. (b) Schematic illustration of the posttranslational modification of ABCC11 WT and proteasomal degradation of the Arg180 variant.

diagnosis of axillary osmidrosis. ORS patients tend to hope that surgical resection of the axillary apocrine glands will fundamentally resolve their problem, even if this is contrary to the clinical judgment of the doctor. Since the subjective diagnosis of this odor-producing disease by a doctor is psychologically difficult for these patients to accept, objective evidence indicating that they have no risk is important for dissuasion from surgery. Moreover, it would be unfortunate if the distress of body odor was not alleviated despite having undergone surgery, leading such patients to become even more nervous regarding their odor. Hence, an unnecessary surgery based solely on a request from patients or their family should be avoided, even if they are anxious about it. Therefore, genotyping the *ABCC11* SNP 538G>A can provide scientific evidence in an objective manner as an alternative approach to subjective/experienced assessment by clinicians.

### 3. More Insight into *ABCC11* 538G>A

While more than 10 nonsynonymous SNPs are found in the human *ABCC11* gene, only 538G>A (Gly180Arg) is directly related to the phenotypes above described. The SNP 538G>A is located in exon 4 where Gly180 is substituted by Arg180 in the putative first transmembrane domain of the ABCC11 protein. This amino acid substitution results in constitutional instability of the nascent ABCC11 protein. The SNP variant ABCC11 Arg180 undergoes proteasomal

degradation and loses its intracellular function (Figure 3). This molecular mechanism is consistent with the fact that apocrine gland-related phenotypes such as human earwax and axillary osmidrosis are Mendelian traits [1]. In fact, fluorescence immunohistochemistry analyses of the human apocrine gland show that ABCC11 Gly180 (wild type: WT) is expressed in the gland, and the nonsynonymous SNP 538G>A greatly affects the cellular localization of the ABCC11 protein in apocrine secretory cells [1].

Although the endogenous substrate of ABCC11 determining the dominant phenotype has not been elucidated to date, recent findings suggest that ABCC11 WT contributes to development and/or regulation of the secretion activity of human apocrine glands [24, 25]. For instance, during surgical resection, large and extensive apocrine glands are usually observed in the axillae of patients with axillary osmidrosis [26]. The wet type of earwax is derived from the secretion product of the apocrine gland in the external auditory canal, whereas this apocrine secretion is lacking in the dry-type phenotype. Furthermore, according to our preliminary analyses of tissue sections from ceruminous apocrine glands, the luminal area of the apocrine glands of a 538G/A subject was larger than that of a 538A/A subject (Figure 4). Since the total secretion activity of apocrine glands depends on tissue development and intracellular mechanisms regulating apocrine secretion, ABCC11 WT would be responsible for the development of human apocrine glands, resulting in the

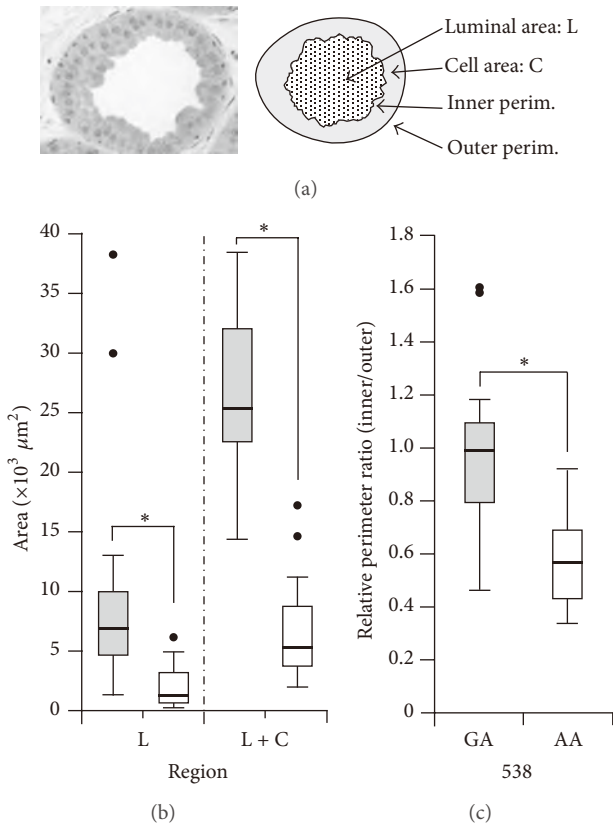


FIGURE 4: Image analysis of human apocrine glands with *ABCC11* 538GA and 538AA. (a) Typical image of human apocrine glands in the external auditory canal (left). Schematic illustration of measurement parameters for image analysis (right). (b and c) Well-developed apocrine glands in a subject with *ABCC11* 538GA (grey) as compared with a subject with 538AA (white). Histological images of human apocrine glands [1] were analyzed by the ImageJ program (v1.46d). Calculated data are expressed as box plots. Differences were considered significant when  $p < 0.01$  (\*).

excess production of apocrine sweat, including the precursor compounds of axillary odor. Recently, Harker et al. demonstrated that the *ABCC11* 538A/A genotype did not result in the complete absence of precursors and produced significantly lower levels of precursor compounds as compared with the 538G/G or G/A genotype [27]. These findings suggest that apocrine glands with the *ABCC11* 538A/A genotype have little secretory activity. They surmised that their results were due to the extremely low level of *ABCC11* activity in the Arg180 variant. A more rational explanation of this minimal secretion, however, might be that other contributors regulating the total secretory activity of apocrine glands besides *ABCC11* also contribute to the promotion of apocrine secretion. To clarify this, we need to further address the issue of how *ABCC11* proteins are involved in the regulation of apocrine glands.

Interestingly, as shown in Figure 5, the allele frequency of the SNP 538G>A in the human *ABCC11* gene exhibits wide differences across different ethnic groups [13], reflecting the genetic diversity of the human genome that occurred

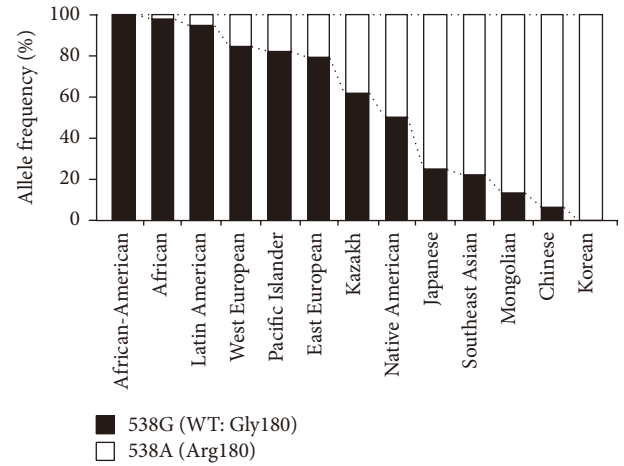


FIGURE 5: Allele frequencies of *ABCC11* 538G (WT; Gly180) and 538A (Arg180) among different ethnic populations. Data are calculated from Yoshiura et al. [13].

during the history of intercontinental migrations of *Homo sapiens* [9, 24]. According to the popular theory of *out of Africa*, ancient humans should have had the *ABCC11* 538G allele which corresponds to the high secretory phenotype of apocrine glands. Considering the production of pheromone-like compounds in human armpits probably originating from their axillary apocrine glands [17, 28], axillary odor directly or indirectly regulated by *ABCC11* might have been important for nonverbal communication among ancient *Homo sapiens* and our ancestors.

#### 4. Nature of Body Odor

**4.1. Characteristics of Axillary Osmidrosis.** Humans tend to emit peculiar body odors, but each individual might have a chronic body odor or little odor. Across most cultures, body odor is often perceived as being unpleasant by other persons, whereas it also affects the confidence and self-esteem of the person emitting the odor. To address this problem, mankind has developed ways and means to manage body odor, for example, by the use of deodorants, refreshing sprays, and perfumes. In modern society, elimination of body odor is part of daily grooming, like hand-washing, hair styling, and other similar activities. Nevertheless, the genetic and/or environmental factors that give rise to individual differences in body odor and the molecular mechanisms thereof remain unclear.

Axillary osmidrosis is a condition characterized by strong odors and profuse sweating from the axillae [29]. The symptoms of axillary osmidrosis generally develop around the time of puberty when the apocrine glands existing from birth become active for the first time [30]. The yellow staining in the armpits of clothing also impacts the affected individual's quality of life. Thus, axillary osmidrosis is often perceived as an undesired problem, particularly by young women. Especially in Asian countries where persons with strong body odor comprise a minor population, axillary osmidrosis tends

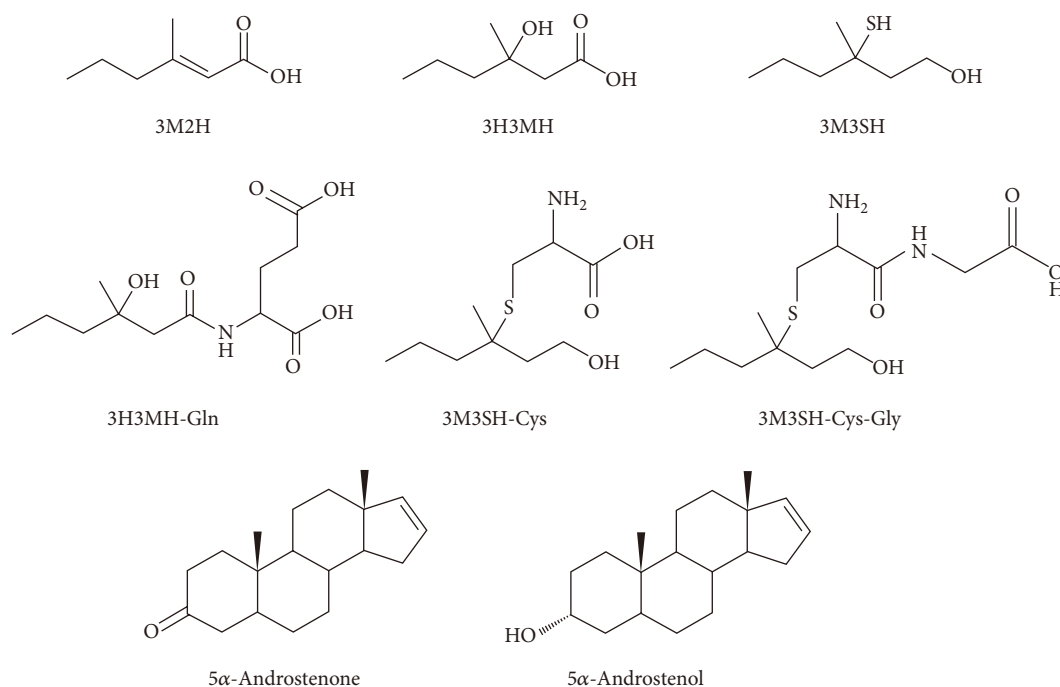


FIGURE 6: Chemical structures of compounds underlying human axillary odor.

to be even more strongly disliked. In particular, it is true that axillary osmidrosis is recognized as a disease in Japan, and its clinical treatments are covered by the national health insurance system.

The major contributors to axillary odor are unsaturated fatty acids, hydroxylated branched fatty acids, sulfanylalkanoles, and some steroids represented by (E)-3-methyl-2-hexenoic acid (3M2H) [31], 3-hydroxy-3-methyl-hexanoic acid (3H3MH), 3-methyl-3-sulfanylhexan-1-ol (3M3SH) [32, 33], 5α-androstenone, and 5α-androst-16-en-3α-ol [34, 35], respectively (Figure 6). In addition, an *in vitro* transport experiment showed that the glutathione conjugate of 3M3SH, a putative precursor of 3M3SH, was transported by ABCC11 WT [36], suggesting the involvement of ABCC11 in the formation of axillary odor. Some precursors of those odorous components have been found to be secreted from axillary apocrine glands [5, 37, 38], which suggests that the inhibition of secretion and/or development of axillary apocrine glands would contribute to the prevention or treatment of axillary osmidrosis.

## 5. Future Perspectives

Apart from axillary osmidrosis, *ABCC11* genotypes might be associated with the risk of breast cancer or drug-induced toxicity [25, 39–41]. According to recent studies, women in the Japanese population with the 538G allele in *ABCC11* had a higher risk of breast cancer than those with the 538A allele [41], whereas this association was not found in the Caucasian population [42, 43]. It has also been shown by a Japanese research group that the expression of *ABCC11* in women with breast cancer is associated with aggressive phenotypes

and poor disease-free survival [44]. Since some anticancer agents and metabolites thereof are substrates of *ABCC11*, a patient's response to nucleoside-based chemotherapy could be affected by the *ABCC11* genotype [25]. A recent Caucasian human liver cohort study has shown an association between *ABCC11* SNP 1637C>T (Trp546Met) and the risk of toxicity of 5-fluorouracil, which is a widely used antipyrimidine anticancer drug [40]. There is no finding, however, on the relationship between the *ABCC11* 538A allele and the risk of toxicity of 5-fluorouracil in this European case study. Further studies, preferably in Asia, where the 538A allele is predominant, are warranted to shed light on this question. In addition, it remains to be clarified how *ABCC11* affects breast cancer or its origin. Interestingly, an evolutionary derivation of mammary glands from apocrine glands has been suggested based on their biological similarities [45]. Since the functional form of *ABCC11* might contribute to the development and/or activity control of both mammary glands, as well as apocrine glands, further verifications would be required from various aspects including not only chemoresistance but also the physiological function and regulation of *ABCC11*.

## 6. Conclusions

In this review article, we have addressed the clinical importance of human *ABCC11* 538G>A as a risk factor of axillary osmidrosis by using an efficient genotyping method. This genotyping-based strategy would be helpful in making the diagnosis of axillary osmidrosis, since the objective evidence acquired would relieve ORS patients of their odor delusion. Although the molecular mechanisms regulating the secretory process in apocrine glands have not been clearly

understood, accumulating evidence strongly suggests that ABCC11 contributes to the function of apocrine glands and ABCC11 538G>A reflects their activity. Further studies are needed to elucidate the physiological function of ABCC11 and its endogenous substrates secreted from apocrine glands. Therefore, the validation of clinically relevant genetic factors and the development of systems to be used for personalized medicine would be the next important steps.

## Conflict of Interests

The authors have no conflict of interests to declare.

## Acknowledgments

The authors thank Drs. Norio Niikawa (Health Sciences University of Hokkaido) and Koh-ichiro Yoshiura (Nagasaki University), as well as Dr. Yasuo Sakai (Osaka University) for their helpful discussions about the relationship between ABCC11 genotype and axillary osmidrosis risk. Furthermore, the authors' thanks go to Drs. Hiroshi Suzuki and Tappei Takada (The University of Tokyo Hospital) for their generous support. In addition, they acknowledge collaboration with Drs. Yoshihide Hayashizaki, Alexander Lezhava, Aki Sakurai, and Wanping Aw (RIKEN Omics Science Center).

## References

- [1] Y. Toyoda, A. Sakurai, Y. Mitani et al., "Earwax, osmidrosis, and breast cancer: why does one SNP (538G>A) in the human ABC transporter ABCC11 gene determine earwax type?" *The FASEB Journal*, vol. 23, no. 6, pp. 2001–2013, 2009.
- [2] Y. Inoue, T. Mori, Y. Toyoda et al., "Correlation of axillary osmidrosis to a SNP in the ABCC11 gene determined by the Smart Amplification Process (SmartAmp) method," *Journal of Plastic, Reconstructive & Aesthetic Surgery*, vol. 63, no. 8, pp. 1369–1374, 2010.
- [3] M. Nakano, N. Miwa, A. Hirano, K.-I. Yoshiura, and N. Niikawa, "A strong association of axillary osmidrosis with the wet earwax type determined by genotyping of the ABCC11 gene," *BMC Genetics*, vol. 10, article 42, 2009.
- [4] Y. Sun, J. Long, and Y. Wang, "Correlation between ABCC11 gene single nucleotide polymorphism and the incidence of axillary osmidrosis in Chinese Han population," *Zhong Nan Da Xue Xue Bao Yi Xue Ban*, vol. 38, no. 11, pp. 1141–1145, 2013.
- [5] A. Martin, M. Saathoff, F. Kuhn, H. Max, L. Terstegen, and A. Natsch, "A functional ABCC11 allele is essential in the biochemical formation of human axillary odor," *The Journal of Investigative Dermatology*, vol. 130, no. 2, pp. 529–540, 2010.
- [6] H. Yabuuchi, H. Shimizu, S.-I. Takayanagi, and T. Ishikawa, "Multiple splicing variants of two new human ATP-binding cassette transporters, ABCC11 and ABCC12," *Biochemical and Biophysical Research Communications*, vol. 288, no. 4, pp. 933–939, 2001.
- [7] J. Tammur, C. Prades, I. Arnould et al., "Two new genes from the human ATP-binding cassette transporter superfamily, ABCC11 and ABCC12, tandemly duplicated on chromosome 16q12," *Gene*, vol. 273, no. 1, pp. 89–96, 2001.
- [8] T. K. Bera, S. Lee, G. Salvatore, B. Lee, and I. Pastan, "MRP8, a new member of ABC transporter superfamily, identified by EST database mining and gene prediction program, is highly expressed in breast cancer," *Molecular Medicine*, vol. 7, no. 8, pp. 509–516, 2001.
- [9] Y. Toyoda, Y. Hagiya, T. Adachi, K. Hoshijima, M. T. Kuo, and T. Ishikawa, "MRP class of human ATP binding cassette (ABC) transporters: historical background and new research directions," *Xenobiotica*, vol. 38, no. 7-8, pp. 833–862, 2008.
- [10] M. Bortfeld, M. Rius, J. König, C. Herold-Mende, A. T. Nies, and D. Keppler, "Human multidrug resistance protein 8 (MRP8/ABCC11), an apical efflux pump for steroid sulfates, is an axonal protein of the CNS and peripheral nervous system," *Neuroscience*, vol. 137, no. 4, pp. 1247–1257, 2006.
- [11] Z.-S. Chen, Y. Guo, M. G. Belinsky, E. Kotova, and G. D. Kruh, "Transport of bile acids, sulfated steroids, estradiol 17- $\beta$ -D-glucuronide, and leukotriene C4 by human multidrug resistance protein 8 (ABCC11)," *Molecular Pharmacology*, vol. 67, no. 2, pp. 545–557, 2005.
- [12] H. Shimizu, H. Taniguchi, Y. Hippo, Y. Hayashizaki, H. Aburatani, and T. Ishikawa, "Characterization of the mouse Abcc12 gene and its transcript encoding an ATP-binding cassette transporter, an orthologue of human ABCC12," *Gene*, vol. 310, no. 1-2, pp. 17–28, 2003.
- [13] K.-I. Yoshiura, A. Kinoshita, T. Ishida et al., "A SNP in the ABCC11 gene is the determinant of human earwax type," *Nature Genetics*, vol. 38, no. 3, pp. 324–330, 2006.
- [14] B. Adachi, "Das ohrenschmalz als rassenmerkmal und der rassengeruch ("Achselgeruch") nebst dem rassenunterschied der schweissdrüsen," *Zeitschrift für Rassenkunde und die Gesamte Forschung*, vol. 6, pp. 273–307, 1937.
- [15] E. Matsunaga, "The dimorphism in human normal cerumen," *Annals of Human Genetics*, vol. 25, pp. 273–286, 1962.
- [16] W. M. Yoo, N. S. Pae, S. J. Lee, T. S. Roh, S. Chung, and K. C. Tark, "Endoscopy-assisted ultrasonic surgical aspiration of axillary osmidrosis: a retrospective review of 896 consecutive patients from 1998 to 2004," *Journal of Plastic, Reconstructive & Aesthetic Surgery*, vol. 59, no. 9, pp. 978–982, 2006.
- [17] G. Rothardt and K. Beier, "Peroxisomes in the apocrine sweat glands of the human axilla and their putative role in pheromone production," *Cellular and Molecular Life Sciences*, vol. 58, no. 9, pp. 1344–1349, 2001.
- [18] Y. Mitani, A. Lezhava, Y. Kawai et al., "Rapid SNP diagnostics using asymmetric isothermal amplification and a new mismatch-suppression technology," *Nature Methods*, vol. 4, no. 3, pp. 257–262, 2007.
- [19] W. Aw, I. Ota, Y. Toyoda et al., "Pharmacogenomics of human ABC transporters: detection of clinically important SNPs by SmartAmp2 method," *Current Pharmaceutical Biotechnology*, vol. 12, no. 4, pp. 693–704, 2011.
- [20] T. Ishikawa and Y. Toyoda, "Human ABC transporter ABCC11: looking back pioneers' odyssey and creating a new path toward clinical application," in *ABC Transporters—40 Years on*, T. George, Ed., pp. 297–318, Springer, Basel, Switzerland, 2016.
- [21] S. Rodriguez, C. D. Steer, A. Farrow, J. Golding, and I. N. M. Day, "Dependence of deodorant usage on ABCC11 genotype: scope for personalized genetics in personal hygiene," *The Journal of Investigative Dermatology*, vol. 133, no. 7, pp. 1760–1767, 2013.
- [22] K. A. Phillips and W. Menard, "Olfactory reference syndrome: demographic and clinical features of imagined body odor," *General Hospital Psychiatry*, vol. 33, no. 4, pp. 398–406, 2011.
- [23] K. Suzuki, N. Takei, Y. Iwata et al., "Do olfactory reference syndrome and jiko-shu-kyofu (a subtype of Taijin-kyofu) share

- a common entity?" *Acta Psychiatrica Scandinavica*, vol. 109, no. 2, pp. 150–155, 2004.
- [24] T. Ishikawa, Y. Toyoda, K.-I. Yoshiura, and N. Niikawa, "Pharmacogenetics of human ABC transporter ABCC11: new insights into apocrine gland growth and metabolite secretion," *Frontiers in Genetics*, vol. 3, article 306, 2013.
- [25] Y. Toyoda and T. Ishikawa, "Pharmacogenomics of human ABC transporter ABCC11 (MRP8): potential risk of breast cancer and chemotherapy failure," *Anti-Cancer Agents in Medicinal Chemistry*, vol. 10, no. 8, pp. 617–624, 2010.
- [26] Y. H. Bang, J. H. Kim, S. W. Paik, S. H. Park, I. T. Jackson, and R. Lebeda, "Histopathology of apocrine bromhidrosis," *Plastic and Reconstructive Surgery*, vol. 98, no. 2, pp. 288–292, 1996.
- [27] M. Harker, A.-M. Carvell, V. P. J. Marti et al., "Functional characterisation of a SNP in the ABCC11 allele—effects on axillary skin metabolism, odour generation and associated behaviours," *Journal of Dermatological Science*, vol. 73, no. 1, pp. 23–30, 2014.
- [28] K. Stern and M. K. McClintock, "Regulation of ovulation by human pheromones," *Nature*, vol. 392, no. 6672, pp. 177–179, 1998.
- [29] W.-H. Wu, S. Ma, J.-T. Lin, Y.-W. Tang, R.-H. Fang, and F.-L. Yeh, "Surgical treatment of axillary osmidrosis: an analysis of 343 cases," *Plastic and Reconstructive Surgery*, vol. 94, no. 2, pp. 288–294, 1994.
- [30] K. Wilke, A. Martin, L. Terstegen, and S. S. Biel, "A short history of sweat gland biology," *International Journal of Cosmetic Science*, vol. 29, no. 3, pp. 169–179, 2007.
- [31] X.-N. Zeng, J. J. Leyden, H. J. Lawley, K. Sawano, I. Nohara, and G. Preti, "Analysis of characteristic odors from human male axillae," *Journal of Chemical Ecology*, vol. 17, no. 7, pp. 1469–1492, 1991.
- [32] A. Natsch, J. Schmid, and F. Flachsmann, "Identification of odoriferous sulfanylalkanols in human axilla secretions and their formation through cleavage of cysteine precursors by a C-S lyase isolated from axilla bacteria," *Chemistry & Biodiversity*, vol. 1, no. 7, pp. 1058–1072, 2004.
- [33] Y. Hasegawa, M. Yabuki, and M. Matsukane, "Identification of new odoriferous compounds in human axillary sweat," *Chemistry & Biodiversity*, vol. 1, no. 12, pp. 2042–2050, 2004.
- [34] S. Bird and D. B. Gower, "The validation and use of a radioimmunoassay for 5 $\alpha$ -androst-16-en-3-one in human axillary collections," *Journal of Steroid Biochemistry*, vol. 14, no. 2, pp. 213–219, 1981.
- [35] D. B. Gower, "16-Unsaturated C19 steroids. A review of their chemistry, biochemistry and possible physiological role," *Journal of Steroid Biochemistry*, vol. 3, no. 1, pp. 45–103, 1972.
- [36] T. Baumann, S. Bergmann, T. Schmidt-Rose et al., "Glutathione-conjugated sulfanylalkanols are substrates for ABCC11 and  $\gamma$ -glutamyl transferase 1: a potential new pathway for the formation of odorant precursors in the apocrine sweat gland," *Experimental Dermatology*, vol. 23, no. 4, pp. 247–252, 2014.
- [37] C. Starkenmann, Y. Niclass, M. Troccaz, and A. J. Clark, "Identification of the precursor of (S)-3-methyl-3-sulfanylhexan-1-ol, the sulfury malodour of human axilla sweat," *Chemistry & Biodiversity*, vol. 2, no. 6, pp. 705–716, 2005.
- [38] R. Emter and A. Natsch, "The sequential action of a dipeptidase and a  $\beta$ -lyase is required for the release of the human body odorant 3-methyl-3-sulfanylhexan-1-ol from a secreted Cys-Gly-(S) conjugate by *Corynebacteria*," *The Journal of Biological Chemistry*, vol. 283, no. 30, pp. 20645–20652, 2008.
- [39] A. T. Nies, T. Magdy, M. Schwab, and U. M. Zanger, "Role of ABC transporters in fluoropyrimidine-based chemotherapy response," *Advances in Cancer Research*, vol. 125, pp. 217–243, 2015.
- [40] T. Magdy, R. Arlanov, S. Winter et al., "ABCC11/MRP8 polymorphisms affect 5-fluorouracil-induced severe toxicity and hepatic expression," *Pharmacogenomics*, vol. 14, no. 12, pp. 1433–1448, 2013.
- [41] I. Ota, A. Sakurai, Y. Toyoda et al., "Association between breast cancer risk and the wild-type allele of human ABC transporter ABCC11," *Anticancer Research*, vol. 30, no. 12, pp. 5189–5194, 2010.
- [42] T. Lang, C. Justenhoven, S. Winter et al., "The earwax-associated SNP c.538G>A (G180R) in ABCC11 is not associated with breast cancer risk in Europeans," *Breast Cancer Research and Treatment*, vol. 129, no. 3, pp. 993–999, 2011.
- [43] J. Beesley, S. E. Johnatty, X. Chen et al., "No evidence for an association between the earwax-associated polymorphism in ABCC11 and breast cancer risk in Caucasian women," *Breast Cancer Research and Treatment*, vol. 126, no. 1, pp. 235–239, 2011.
- [44] A. Yamada, T. Ishikawa, I. Ota et al., "High expression of ATP-binding cassette transporter ABCC11 in breast tumors is associated with aggressive subtypes and low disease-free survival," *Breast Cancer Research and Treatment*, vol. 137, no. 3, pp. 773–782, 2013.
- [45] O. T. Oftedal, "The mammary gland and its origin during synapsid evolution," *Journal of Mammary Gland Biology and Neoplasia*, vol. 7, no. 3, pp. 225–252, 2002.

## RESEARCH ARTICLE

## Open Access



# *ABCB1* polymorphism is associated with atorvastatin-induced liver injury in Japanese population

Koya Fukunaga<sup>1</sup>, Hiroshi Nakagawa<sup>2</sup>, Toshihisa Ishikawa<sup>3</sup>, Michiaki Kubo<sup>4</sup> and Taisei Mushiroda<sup>1\*</sup>

## Abstract

**Background:** To investigate the associations between atorvastatin-induced liver injury (AILI) and polymorphisms in eight genes possibly involved in the hepatic metabolism (*CYP2C9*, *CYP2C19*, *CYP3A4*, *CYP3A5* and *UGT1A1*) and membrane transport (*ABCB1*, *ABCG2* and *SLCO1B1*) of atorvastatin, we genotyped 30 AILI and 414 non-AILI patients recruited at BioBank Japan for 15 single nucleotide polymorphisms (SNPs).

**Results:** An SNP in *ABCB1* (rs2032582: 2677G > T/A) was significantly associated with AILI ( $P = 0.00068$ , odds ratio (OR) = 2.59 with 95 % confidence interval (CI) of 1.49–4.50, G allele versus T and A alleles), indicating that the G allele might be a risk factor for AILI. The cytotoxicity test demonstrated that  $IC_{50}$  value of atorvastatin to inhibit the growth and/or viability of Flp-In-293/*ABCB1* (2677G) cells was  $5.44 \pm 0.10$  mM, which was significantly lower than those in Flp-In-293/*ABCB1* (2677 T) ( $6.02 \pm 0.07$  mM) and Flp-In-293/*ABCB1* (2677A) cells ( $5.95 \pm 0.08$  mM).

**Conclusions:** These results indicate that *ABCB1* rs2032582 may predict the risk of AILI in Japanese population.

**Keywords:** Atorvastatin-induced adverse reaction, Genetic association, Hepatotoxicity, MDR1 Ala893Ser/Thr/

## Background

Atorvastatin (atorvastatin calcium; Lipitor®) is widely used in the treatment of dyslipidemia of low- and high-density lipoproteins in patients with or without heart disease [1]. However, atorvastatin-induced liver injury (AILI) can be caused after atorvastatin treatment [1, 2]. In Japanese post-marketing surveillance of atorvastatin, 1.42 % of patients who received atorvastatin treatment suffered from liver injury. In general, drug-induced liver injury (DILI) can be divided into 3 types (hepatocellular injury, cholestatic liver injury and mixed liver injury) based on potential liver toxicity symptoms (e.g., anorexia, nausea, vomiting or jaundice), the presence or absence of risk factors (e.g., viral infection and alcohol consumption) and serum levels of alanine aminotransferase (ALT) and alkaline phosphatase (ALP) as well as the ALT/ALP ratio [3]. AILI falls within the hepatocellular injury category because ALT level of two patients treated with atorvastatin reportedly raised three-fold

higher than that of the upper limit of normal but ALP and bilirubin levels did not change [4].

Atorvastatin is orally administered in the active acid form and undergoes marked first-pass metabolism by uptake into hepatocytes via passive diffusion and *SLCO1B1* (encoding OATP1B1 [5–7]). Atorvastatin is metabolized mainly by *CYP3A4*, with minor contributions from *CYP2C9*, *CYP2C19*, *CYP3A5*, and *UGT1A1* [8–12]. Subsequently, atorvastatin and the metabolites are predominantly eliminated by *ABCB1* (encoding P-glycoprotein or MDR1)- and *ABCG2* (encoding BCRP)-mediated transport from liver into bile [7, 13–15]. Single nucleotide polymorphisms (SNPs) identified in *ABCB1* rs1128503 (1236C > T), rs2032582 (2677G > T/A), and rs1045642 (3435C > T) markedly affected area under the plasma concentration versus time curve (AUC) of atorvastatin and the lipid-lowering effects of atorvastatin therapy [16–18]. Therefore, we hypothesized that the genetic variability of eight candidate genes associated with the hepatic metabolism and membrane transport of atorvastatin may affect the risk of AILI because higher concentrations of atorvastatin can cause hepatocellular injury, even at appropriate atorvastatin dosages. However, to our knowledge, there

\* Correspondence: mushiroda@riken.jp

<sup>1</sup>Laboratory for Pharmacogenomics, RIKEN Center for Integrative Medical Sciences, Yokohama, Japan

Full list of author information is available at the end of the article



© 2016 The Author(s). **Open Access** This article is distributed under the terms of the Creative Commons Attribution 4.0 International License (<http://creativecommons.org/licenses/by/4.0/>), which permits unrestricted use, distribution, and reproduction in any medium, provided you give appropriate credit to the original author(s) and the source, provide a link to the Creative Commons license, and indicate if changes were made. The Creative Commons Public Domain Dedication waiver (<http://creativecommons.org/publicdomain/zero/1.0/>) applies to the data made available in this article, unless otherwise stated.

are no reports on an association of the functional SNPs of the candidate genes with AILI.

In this study, we investigated whether 15 functional SNPs in eight candidate genes that are possibly involved in the pharmacokinetics of atorvastatin were associated with AILI in Japanese population. We found that *ABCB1* rs2032582 was significantly associated with AILI. In addition, the cytotoxicity of atorvastatin was investigated using the Flp-In-293 cells stably expressing ABCB1 proteins encoded by *ABCB1* rs2032582 [19]. We clarified that the *ABCB1* rs2032582 G allele was a significant AILI risk factor *in vivo* and *in vitro*.

## Methods

### Subjects

The BioBank Japan project (<https://biobankjp.org/>) started in 2003 for the collection of genomic DNA, serum and clinical information from about 300,000 Japanese patients diagnosed with either of 47 diseases by a collaborative network of 66 hospitals in Japan. We diagnosed AILI based on symptoms, such as nausea, vomiting, loss of appetite, and jaundice, and results of a physical examination and blood tests after atorvastatin administration. From the registered samples in the BioBank Japan, we selected individuals that were clinically diagnosed as having AILI (AILI group,  $N = 30$ ) and individuals that showed no liver injury during atorvastatin therapy (non-AILI group,  $N = 414$ ).

### Selection of SNPs and genotyping

A total of 15 functional SNPs in eight candidate genes (*ABCB1*, *ABCG2*, *CYP2C9*, *CYP2C19*, *CYP3A4*, *CYP3A5*, *SLCO1B1* and *UGT1A1*) reportedly-altering pharmacokinetics of atorvastatin were genotyped by a multiplex polymerase chain reaction (PCR)-based invader assay as described previously [20] and direct sequencing using ABI 3730xl DNA analyzer (Applied Biosystems, Foster City, CA) for rs8175347 and rs2032582, according to the manufacturer's protocol of the Big Dye Terminator v3.1 cycle sequencing kit (Applied Biosystems). HLA-A, -B and -C genotyping was carried out using a WAKFlow HLA Typing kit (Wakunaga, Osaka, Japan), which is based on PCR-sequence-specific oligonucleotide probes coupled with multiple analyte profiling (xMAP) technology (Luminex System; Luminex Corporation, Austin, TX). The data analysis was performed using the WAKFlow Typing software (Wakunaga).

### Cell culture

HepaRG cells (KAC, Kyoto, Japan) were maintained in HepaRG Thawing and Seeding Medium 670 (KAC) and HepaRG Maintenance and Metabolism medium 620 (KAC) at 37 °C under 5 % CO<sub>2</sub> and 95 % air according to the manufacturer's instructions. Flp-In-293 cells (Life

Technologies, Foster City, CA) were maintained in Dulbecco's modified Eagle's medium (Life Technologies) supplemented with 10 % heat-inactivated fetal bovine serum (Life Technologies) and Antibiotic-Antimycotic (100×) liquid (Life Technologies) at 37 °C under 5 % CO<sub>2</sub> and 95 % air, where 100 µg/ml Zeocin (Life Technologies) and 100 µg/ml hygromycin B (Life Technologies) were also supplemented for the maintenance for parental and ABCB1-expressed Flp-In-293 cells, respectively.

### Generation of *ABCB1* 2677G/T/A variant forms

The pcDNA5/FRT/*ABCB1* (2677G) vector was generated by inserting *ABCB1* (2677G) in pFastBac1/*ABCB1* (2677G) into the pcDNA5/FRT vector (Life Technologies) between the restriction enzyme sites of *Bam*HI and *Xho*I. *ABCB1* 2677 T/A variant forms were generated by using the QuikChange Site-directed Mutagenesis Kit (Agilent Technologies, Santa Clara, CA) according to the manufacturer's protocol, where pcDNA5/FRT/*ABCB1* (2677G) vector was used as the template [21]. The PCR reaction consisted of 94 °C for 2 min and then followed by 12 cycles of reactions at 94 °C for 30 sec, 55 °C for 30 sec and at 68 °C for 18 min, where Pfu Turbo DNA polymerase (Agilent Technologies) and the following PCR primers were used: 5'-GAAAGAAGTACTAGAAGGTTCTGGGAA GATCGCTAC-3' and 5'-GTAGCGATCTTCCCAGAAC CTTCTAGTTCTTTC-3' for *ABCB1* 2677 T, and 5'-GAAAGAAGTACTAGAAGGTACTGGGAAGATCGCTAC-3' and 5'-GTAGCGATCTTCCCAGTACCTTCTAGTTC TTTC-3' for *ABCB1* 2677A. After the PCR, the reaction mixture was incubated with *Dpn*I endonuclease at 37 °C for 1 h to digest the original template pcDNA5/FRT/*ABCB1* (2677G) vector. The resulting sequence was examined to confirm the generation of the pcDNA5/FRT/*ABCB1* (2677G/T/A) vectors.

### Establishment of *ABCB1* 2677G/T/A variant forms-expressing cells

Flp-In-293 cells having the Flp Recombination Target (FRT) site at the telomeric region of only one of the pair of chromosomes 12 were transfected with the pcDNA5/FRT/*ABCB1* (2677G/T/A) and the Flp recombinase expression plasmid pOG44 vectors as previously reported [19]. Single colonies resistant to hygromycin B (Life Technologies) were picked and sub-cultured as Flp-In-293/*ABCB1* (2677G), Flp-In-293/*ABCB1* (2677 T) and Flp-In-293/*ABCB1* (2677A) cells. Protein expression levels of ABCB1 in these cells ( $2 \times 10^7$  cells) were determined using Membrane Protein Extraction Kit (BioVision, Milpitas, CA) and Human permeability glycoprotein (P-gp/*ABCB1*) ELISA kit (Cusabio Biotech, Wuhan, China) by a microplate reader (ARVomx, PerkinElmer, Waltham, MA).

**Cytotoxicity studies**

In atorvastatin (Sigma-Aldrich, St Louis, Mo) cytotoxicity experiment, HepaRG ( $5 \times 10^5$  cells/well), Flp-In-293/ABCB1 (2677G), Flp-In-293/ABCB1 (2677 T) and Flp-In-293/ABCB1 (2677A) cells were cultured in monolayers at 37 °C for 24 h in 24-well collagen type I-coated plates (Iwaki Glass, Chiba, Japan). After the preculture, cells were cultured in the presence of different concentrations of atorvastatin 0, 0.3, 1, 3, 10, 30, 100 and 300 μM for HepaRG cells, 0, 0.6, 1, 2, 3, 4, 5, 6, 7, 8, 9 and 10 mM for Flp-In-293/ABCB1 (2677G/T/A) cells for 24 h. After the culture, 50 μl of WST-8 working solution (Cell Counting Kit-8, Dojindo Laboratories, Kumamoto, Japan) was added to each well and the plates were incubated at 37 °C for 1 h under 5 % CO<sub>2</sub> and 95 % air. Optical density at 450 nm was measured by a microplate reader (ARVomx, PerkinElmer, Waltham, MA). Lactate dehydrogenase (LDH), aspartate aminotransferase (AST) and ALT releases from HepaRG cells into the medium were determined according to the manufacturers' protocol of LDH, AST and ALT activity assay kits (Biovision, Milpitas, CA).

**Statistical analysis**

Association studies were conducted by using Fisher's exact test under an allelic model. P values were corrected according to Bonferroni correction. A significance

level was set at 0.0029 (0.05/17) in Table 1. In case of *ABCB1* rs2032582, the patients were divided into two groups (T/A versus G, G/A versus T or G/T versus A) to evaluate the association of the three alleles by using the Fisher's exact test (Table 1). The haplotype analysis was performed using SNPalyze software (version. 8.0.1, Dynacom, Chiba, Japan). Statistical analysis of cytotoxicity test of HepaRG and ABCB1 protein expression levels in Flp-In-293 cells was performed by using one-way analysis of variance with Dunnett's and Tukey's post-hoc test using GraphPad Prism software (version 6, San Diego, CA). Cell viability was analyzed based on four independent experiments performed in duplicate to accurately estimate IC<sub>50</sub> and statistical analysis of IC<sub>50</sub> among three groups (2677G wild-type, 2677 T and 2677A alleles) was performed by using one-way analysis of variance with Dunnett's post-hoc test using GraphPad Prism software.

**Results**

No significant association of disease background was observed between AILI and non-AILI patients (Additional file 1: Table S1). The median age values were 61 years (range 27–82) and 66 years (32–89) in AILI and non-AILI groups, respectively. The 60.0 and 53.9 % were male in AILI and non-AILI groups, respectively. All

**Table 1** Association of 15 functional SNPs in eight candidate genes with atorvastatin-induced liver injury

Gene	SNP	Allele (1/2)	Amino acid change	Other name	AILI <sup>a</sup>			Non-AILI <sup>a</sup>			RAF		P value <sup>b</sup>			HWE	
					11	12	22	11	12	22	AILI	Non-AILI	ALLELIC	DOM	REC	AILI	Non-AILI
<i>ABCB1</i>	rs1045642	C/T	I1145I	C3435T	12	15	3	151	196	67	0.65	0.60	0.50	0.70	0.60	0.59	0.80
	rs2032582	T, A/G	S,T893A	G2677 T/A	2	16	12	138	191	85	0.67	0.44	<b>0.00068</b>	0.0017	0.020	0.27	0.21
		G, A/T	A,T893S		15	14	1	158	193	63	0.73	0.61	0.073	0.24	0.10	0.29	0.75
		G, T/A	A,S893T		26	4	0	283	114	17	0.93	0.82	0.031	0.039	0.62	0.70	0.21
	rs1128503	T/C	G412G	C1236T	15	12	3	146	197	71	0.70	0.59	0.10	0.12	0.45	0.79	0.74
<i>ABCG2</i>	rs2231142	C/A	Q141K	C421A	12	15	3	195	180	39	0.35	0.31	0.57	0.57	0.76	0.59	0.78
<i>CYP2C9</i>	rs1799853	C/T	R144C	<i>CYP2C9</i> *2	30	0	0	412	0	0	1.00	1.00	1.00	1.00	1.00	1.00	1.00
	rs1057910	A/C	I359L	<i>CYP2C9</i> *3	28	2	0	393	20	0	0.03	0.02	0.66	0.65	1.00	0.85	0.61
<i>CYP2C19</i>	rs4244285	G/A	P227P	<i>CYP2C19</i> *2	16	9	5	197	180	36	0.32	0.31	0.88	0.58	0.18	0.09	0.57
	rs4986893	G/A	W212X	<i>CYP2C19</i> *3	27	3	0	321	86	6	0.95	0.88	0.14	0.16	1.00	0.77	0.93
<i>CYP3A4</i>	rs12721627	C/G	T185S	<i>CYP3A4</i> *16	29	1	0	405	8	0	0.02	0.01	0.47	0.47	1.00	0.93	0.84
	rs28371759	T/C	L292P	<i>CYP3A4</i> *18	29	1	0	399	14	0	0.98	0.98	1.00	1.00	1.00	0.93	0.73
<i>CYP3A5</i>	rs776746	G/A	–	<i>CYP3A5</i> *3	18	11	1	223	165	26	0.78	0.74	0.54	0.57	1.00	0.66	0.54
<i>SLCO1B1</i>	rs2306283	G/A	N130D	<i>SLCO1B1</i> *1B	14	12	4	185	179	50	0.67	0.66	1.00	0.85	0.77	0.58	0.51
	rs4149056	T/C	V174A	<i>SLCO1B1</i> *5	18	11	1	306	95	13	0.22	0.15	0.14	0.13	1.00	0.66	0.10
<i>UGT1A1</i>	rs4148323	G/A	G71R	<i>UGT1A1</i> *6	25	5	0	281	118	15	0.92	0.82	0.075	0.10	0.61	0.62	0.55
	rs8175347	(TA) <sub>6</sub> /(TA) <sub>7</sub>	–	<i>UGT1A1</i> *28	23	7	0	332	76	6	0.12	0.11	0.83	0.64	1.00	0.47	0.49

Abbreviation: *AILI* atorvastatin-induced liver injury, *RAF* risk allele frequency, *ALLELIC* Allelic model, *Dom* Dominant model, *REC* Recessive model, *HWE* Hardy-Weinberg equilibrium

<sup>a</sup>AILI, N = 30; Non-AILI, N = 414

<sup>b</sup>The lowest significant P value after Bonferroni correction among three models is shown in bold (P < 0.0011)

SNPs met quality control criteria (call rate > 95 %, Hardy–Weinberg equilibrium P value > 10<sup>-3</sup> and minor allele frequency > 1 %). *ABCB1* rs2032582 was found to be associated with an increased risk of AILI (*P* = 0.00068, odds ratio (OR) = 2.59 with 95 % confidence interval (CI) of 1.49–4.50, G allele versus T and A alleles) by genotyping 444 Japanese subjects for 15 functional SNPs in eight candidate genes that reportedly affect the pharmacokinetics of atorvastatin (Table 1). No other polymorphisms showed a significant association with AILI. The frequency for *ABCB1* rs2032582 G allele in AILI patients was significantly higher than that in non-AILI patients whereas the frequencies of *ABCB1* rs2032582 T and A alleles were not significantly different between AILI and non-AILI groups, indicating that the G allele might be a risk factor for AILI (Table 1 and Additional file 1: Table S2). Although we performed haplotype analysis using three SNPs of *ABCB1* (rs1128503, rs2032582 and rs1045642), no haplotype constructed from the SNPs showed an extremely smaller P value than a single marker association of the *ABCB1* rs2032582 (Table 2). No association of HLA-A, -B and -C genotypes with AILI was shown (Additional file 1: Table S3, Additional file 1: Table S4 and Additional file 1: Table S5).

The cytotoxicity study using HepaRG cells demonstrated concentration-dependent effects of atorvastatin on cell viability as well as on LDH, AST and ALT release from the cells (Additional file 1: Figure S1). To estimate the effects of *ABCB1* rs2032582 on cytotoxicity induced by atorvastatin, we conducted cytotoxicity study using Flp-In-293 cells stably expressing *ABCB1* proteins encoded by 2677G wild-type [Flp-In-293/*ABCB1* (2677G) cells], 2677A [Flp-In-293/*ABCB1* (2677A) cells] and 2677 T [Flp-In-293/*ABCB1* (2677 T) cells] alleles. No

**Table 2** Association of haplotypes consisting of three SNPs of *ABCB1* with atorvastatin-induced liver injury

rs1128503	rs2032582	rs1045642	Number of carriers		P value <sup>b</sup>
			AILI <sup>a</sup> (%)	Non-AILI <sup>a</sup> (%)	
T	T	T	15 (50.0)	237 (57.2)	0.45
C	G	C	11 (36.7)	158 (38.2)	1.00
T	G	C	16 (53.3)	126 (30.4)	0.014
C	A	C	4 (13.3)	128 (30.9)	0.060
T	G	T	3 (10.0)	25 (6.0)	0.45
T	T	C	0 (0.0)	24 (5.8)	0.39
C	G	T	2 (6.7)	11 (2.7)	0.22
T	A	C	0 (0.0)	5 (1.2)	1.00
C	T	T	0 (0.0)	2 (0.5)	1.00
C	T	C	0 (0.0)	2 (0.5)	1.00

Abbreviation: AILI atorvastatin-induced liver injury

<sup>a</sup>AILI, *N* = 30; Non-AILI, *N* = 414

<sup>b</sup>The significant P value after Bonferroni correction is less than 0.005

significant differences were observed in *ABCB1* protein expression levels in Flp-In-293/*ABCB1* (2677G/T/A) cells (Additional file 1: Figure S2). The IC<sub>50</sub> value in Flp-In-293/Mock cells was about two-fold lower than those in Flp-In-293/*ABCB1* (2677G/T/A) cells, indicating higher accumulation of atorvastatin in the Flp-In-293/Mock cells compared to that in Flp-In-293/*ABCB1* (2677G/T/A) cells. The IC<sub>50</sub> value in Flp-In-293/*ABCB1* (2677G) cells was significantly lower than those in Flp-In-293/*ABCB1* (2677 T) and Flp-In-293/*ABCB1* (2677A) cells (Table 3, Additional file 1: Figure S3).

### Discussion

To identify the genetic markers associated with AILI, we genotyped 15 functional SNPs in eight genes that are possibly involved in the hepatic metabolism (*CYP2C9*, *CYP2C19*, *CYP3A4*, *CYP3A5* and *UGT1A1*) and membrane transport (*ABCB1*, *ABCG2* and *SLCO1B1*) of atorvastatin. *ABCB1* rs2032582 was significantly associated with AILI. *ABCB1* rs2032582 changes *ABCB1* amino acid 893 from alanine to serine or threonine, respectively. These variants did not appear to affect *ABCB1* protein expression levels in Flp-In-293/*ABCB1* (2677G/T/A) cells, but gave a lower IC<sub>50</sub> in Flp-In-293/*ABCB1* (2677G) cells than those in Flp-In-293/*ABCB1* (2677 T/A) cells. ATP-dependent uptake of [<sup>3</sup>H]-vincristine into membrane vesicles is also reportedly slower in cells expressing the *ABCB1* rs2032582 G allele than those expressing the *ABCB1* rs2032582 T/A alleles [22]. Therefore, we speculate that patients carrying the *ABCB1* rs2032582 G allele experience lower atorvastatin efflux activity from the hepatocytes into bile and higher hepatocellular concentrations of atorvastatin than carriers of the *ABCB1* rs2032582 T/A alleles. The higher hepatocellular concentration of atorvastatin can increase the risk of hepatotoxicity because atorvastatin induced concentration-dependent cytotoxicity in HepaRG cells (Additional file 1: Figure S1).

The *ABCB1* rs2032582 allele frequencies in our 444 patients (45.2 %, 37.7 % and 17.1 % for G, T and A alleles, respectively) are consistent with the previous

**Table 3** Atorvastatin-dependent cytotoxicity in Flp-In-293 cells stably expressing different *ABCB1* proteins

Cell name	<i>ABCB1</i>		IC <sub>50</sub> (mM)	P value
	Allele	Amino acid		
Mock	–	–	2.74 ± 0.04	–
2677G wild-type	G	Alanine	5.44 ± 0.10	–
2677 T	T	Serine	6.02 ± 0.07	<b>0.009</b>
2677A	A	Threonine	5.95 ± 0.08	<b>0.026</b>

Abbreviation: SE standard error, CI confidence interval

Experiments were performed in duplicate wells and repeated four times. The significant P value is shown in bold (*P* < 0.05, versus 2677G wild-type, one-way analysis of variance with Dunnett's post-hoc test)

report of 154 Japanese subjects (42.9 %, 40.6 % and 16.6 % for G, T and A alleles, respectively) [23]. The above report revealed that the *ABCB1* rs2032582 G and T/A allele frequencies in a Japanese population were comparable with those in a Caucasian population (42.9 % vs. 50.0 % and 57.2 % vs. 50.0 % for G and T/A alleles, respectively) [23]. Taking into account that no differences were reported in the systemic exposure to atorvastatin between Asian and Caucasian subjects [24], the *ABCB1* rs2032582 allele might be also associated with the risk of AILI in the Caucasian population.

Of the atorvastatin-induced adverse reactions, myopathy is one of the most fatal adverse reactions [25, 26]. No statistically significant difference in AUC and the maximum plasma concentrations was observed between 14 patients with atorvastatin-induced myopathy and 15 healthy controls [27]. However, patients with atorvastatin-induced myopathy showed 2.4- and 3.1-fold higher AUC to atorvastatin lactone and *p*-hydroxy atorvastatin, respectively, compared to controls [27]. Atorvastatin is converted to its corresponding lactone form spontaneously or via glucuronidation mediated by UGT1A1, 1A3 and 1A4 and is metabolized to *p*-hydroxy atorvastatin by CYP3A4/5 [11, 28]. The present association studies showed that known functional SNPs of UGT1A1 and CYP3A4/5 were not associated with AILI. The higher accumulation of atorvastatin in the liver of patients carrying the *ABCB1* rs2032582 G allele may cause hepatotoxicity, rather than those of atorvastatin lactone and *p*-hydroxy atorvastatin, the atorvastatin metabolites generated by UGT1A1 and CYP3A4/5. Therefore, the genetic markers might differ between liver injury and myopathy induced by atorvastatin.

In general, DILI can be divided into dose-dependent and idiosyncratic types [29]. The former is related to the pharmacokinetics and/or pharmacological actions of the drug and the latter is related to immune systems, such as human leukocyte antigen (HLA) in a dose-independent manner. In fact, several HLA alleles showed drug-specific associations with DILI, such as HLA-A\*33:03 for ticlopidine and HLA-B\*57:01 for flucloxacillin [30]. Therefore, we examined association of HLA alleles with AILI. However, no significant association was observed for HLA-A, -B and -C alleles with AILI (Additional file 1: Table S3, Additional file 1: Table S4 and Additional file 1: Table S5).

## Conclusions

Our results showed that *ABCB1* rs2032582 was associated with an increased risk of AILI in the Japanese population. A genetic test of *ABCB1* rs2032582 may provide useful information for predicting individuals at higher risk of AILI. However, additional studies with

larger sample size are needed before applying this genetic marker in clinical practice.

## Additional file

**Additional file 1:** Fig. S1 Atorvastatin concentration-dependent cytotoxicity on HepaRG cells. Fig. S2 Expression levels of ABCB1 protein in Flp-In-293 cells stably expressing ABCB1 proteins encoded by 2677G wild-type, 2677 T and 2677A alleles. Fig. S3 Cell viability curve for IC50 determination in Flp-In-293 cells stably expressing ABCB1 proteins encoded by 2677G wild-type, 2677 T and 2677A alleles. Table S1 Distribution of disease status in 30 AILI and 414 non-AILI patients registered in BioBank Japan. Table S2 Frequency of rs2032582 in 30 AILI and 414 non-AILI patients. Table S3 Association of HLA-A alleles with atorvastatin-induced liver injury. Table S4 Association of HLA-B alleles with atorvastatin-induced liver injury. Table S5 Association of HLA-C alleles with atorvastatin-induced liver injury. (DOCX 147 kb)

## Acknowledgments

We thank all the patients who participated in the BioBank Japan project. We thank all members of BioBank Japan, Institute of Medical Science, The University of Tokyo and RIKEN Center for Integrative Medical Sciences, for their contribution to the completion of our study. We also express our gratitude to Dr. Siew-Keen Low and Dr. Atsushi Takahashi of RIKEN Center for Integrative Medical Sciences for their helpful comments and discussion.

## Funding

This study was supported by grants from the BioBank Japan project.

## Availability of data and materials

The data sets supporting the results of this article are included within the article and its additional files.

## Authors' contributions

Conceived and designed the experiments: KF, MK, TM. Performed the experiments: KF, HN. Analyzed the data: KF, TM. Contributed reagents/materials/analysis tools: HN, TI. Wrote the paper: KF, HN, TI, MK, TM. All authors approved the final manuscript.

## Competing interests

The authors declare that they have no competing interests.

## Consent for publication

Not applicable.

## Ethical approval and consent to participate

All individuals who participated in this study provided written informed consent. This project was approved by the ethical committees at the RIKEN Yokohama Branch, Japan and The Institute of Medical Science, The University of Tokyo, Tokyo, Japan.

## Author details

<sup>1</sup>Laboratory for Pharmacogenomics, RIKEN Center for Integrative Medical Sciences, Yokohama, Japan. <sup>2</sup>Department of Biological Chemistry, College of Bioscience and Biotechnology, Chubu University, Aichi, Japan. <sup>3</sup>NPO Personalized Medicine & Healthcare, Yokohama, Japan. <sup>4</sup>Laboratory for Genotyping Development, RIKEN Center for Integrative Medical Sciences, Yokohama, Japan.

Received: 8 October 2015 Accepted: 7 June 2016

Published online: 13 June 2016

## References

1. Saku K, Zhang B, Noda K, Investigators PT. Randomized head-to-head comparison of pitavastatin, atorvastatin, and rosuvastatin for safety and efficacy (quantity and quality of LDL): the PATROL trial. *Circ J*. 2011;75(6):1493–505.
2. Ooba N, Sato T, Wakana A, Orii T, Kitamura M, Kokan A, Kurata H, Shimodozono Y, Matsui K, Yoshida H, et al. A prospective stratified case-

- cohort study on statins and multiple adverse events in Japan. *PLoS One*. 2014;9(5):e96919.
3. Chalasani NP, Hayashi PH, Bonkovsky HL, Navarro VJ, Lee WM, Fontana RJ, Practice Parameters Committee of the American College of G. ACG Clinical Guideline: the diagnosis and management of idiosyncratic drug-induced liver injury. *Am J Gastroenterol*. 2014;109(7):950–66. quiz 967.
  4. Liu Y, Cheng Z, Ding L, Fang F, Cheng KA, Fang Q, Shi GP. Atorvastatin-induced acute elevation of hepatic enzymes and the absence of cross-toxicity of pravastatin. *Int J Clin Pharmacol Ther*. 2010;48(12):798–802.
  5. Pasanen MK, Fredrikson H, Neuvonen PJ, Niemi M. Different effects of SLCO1B1 polymorphism on the pharmacokinetics of atorvastatin and rosuvastatin. *Clin Pharmacol Ther*. 2007;82(6):726–33.
  6. Nies AT, Niemi M, Burk O, Winter S, Zanger UM, Stieger B, Schwab M, Schaeffeler E. Genetics is a major determinant of expression of the human hepatic uptake transporter OATP1B1, but not of OATP1B3 and OATP2B1. *Genome Med*. 2013;5(1):1.
  7. Lee YJ, Lee MG, Lim LA, Jang SB, Chung JY. Effects of SLCO1B1 and ABCB1 genotypes on the pharmacokinetics of atorvastatin and 2-hydroxyatorvastatin in healthy Korean subjects. *Int J Clin Pharmacol Ther*. 2010;48(1):36–45.
  8. Yasar U, Sain-Guven G, Yardimci Y, Kilicaslan A, Babaoglu MO, Bozkurt A. Effect of atorvastatin on CYP2C9 metabolic activity as measured by the formation rate of losartan metabolite in hypercholesterolaemic patients. *Basic Clin Pharmacol Toxicol*. 2011;109(2):73–7.
  9. Stormo C, Bogsrud MP, Hermann M, Asberg A, Piehler AP, Retterstol K, Kringen MK. UGT1A1\*28 is associated with decreased systemic exposure of atorvastatin lactone. *Mol Diagn Ther*. 2013;17(4):233–7.
  10. Riedmaier S, Klein K, Hofmann U, Keskitalo JE, Neuvonen PJ, Schwab M, Niemi M, Zanger UM. UDP-glucuronosyltransferase (UGT) polymorphisms affect atorvastatin lactonization in vitro and in vivo. *Clin Pharmacol Ther*. 2010;87(1):65–73.
  11. Park JE, Kim KB, Bae SK, Moon BS, Liu KH, Shin JG. Contribution of cytochrome P450 3A4 and 3A5 to the metabolism of atorvastatin. *Xenobiotica*. 2008;38(9):1240–51.
  12. Leoncini M, Toso A, Maioli M, Angiolillo DJ, Giusti B, Marcucci R, Abbate R, Bellandi F. High-dose atorvastatin on the pharmacodynamic effects of double-dose clopidogrel in patients undergoing percutaneous coronary interventions: The ACHIDO (Atorvastatin and Clopidogrel High DOse in stable patients with residual high platelet activity) study. *JACC Cardiovasc Interv*. 2013;6(2):169–79.
  13. Kokudai M, Inui N, Takeuchi K, Sakaeda T, Kagawa Y, Watanabe H. Effects of statins on the pharmacokinetics of midazolam in healthy volunteers. *J Clin Pharmacol*. 2009;49(5):568–73.
  14. Keskitalo JE, Zolk O, Fromm MF, Kurkinen KJ, Neuvonen PJ, Niemi M. ABCG2 polymorphism markedly affects the pharmacokinetics of atorvastatin and rosuvastatin. *Clin Pharmacol Ther*. 2009;86(2):197–203.
  15. Black AE, Hayes RN, Roth BD, Woo P, Woolf TF. Metabolism and excretion of atorvastatin in rats and dogs. *Drug Metab Dispos*. 1999;27(8):916–23.
  16. Rosales A, Alvear M, Cuevas A, Saavedra N, Zambrano T, Salazar LA. Identification of pharmacogenetic predictors of lipid-lowering response to atorvastatin in Chilean subjects with hypercholesterolemia. *Clin Chim Acta*. 2012;413(3–4):495–501.
  17. Poduri A, Khullar M, Bahl A, Sehrawat BS, Sharma Y, Talwar KK. Common variants of HMGCR, CETP, APOAI, ABCB1, CYP3A4, and CYP7A1 genes as predictors of lipid-lowering response to atorvastatin therapy. *DNA Cell Biol*. 2010;29(10):629–37.
  18. Keskitalo JE, Kurkinen KJ, Neuvonen PJ, Niemi M. ABCB1 haplotypes differentially affect the pharmacokinetics of the acid and lactone forms of simvastatin and atorvastatin. *Clin Pharmacol Ther*. 2008;84(4):457–61.
  19. Ishikawa T, Wakabayashi-Nakao K, Nakagawa H. Methods to examine the impact of nonsynonymous SNPs on protein degradation and function of human ABC transporter. *Methods Mol Biol*. 2013;1015:225–50.
  20. Ohnishi Y, Tanaka T, Ozaki K, Yamada R, Suzuki H, Nakamura Y. A high-throughput SNP typing system for genome-wide association studies. *J Hum Genet*. 2001;46(8):471–7.
  21. Sakurai A, Onishi Y, Hirano H, Seigneuret M, Obanayama K, Kim G, Liew EL, Sakaeda T, Yoshiura K, Niikawa N, et al. Quantitative structure–activity relationship analysis and molecular dynamics simulation to functionally validate nonsynonymous polymorphisms of human ABC transporter ABCB1 (P-glycoprotein/MDR1). *Biochemistry (Mosc)*. 2007;46(26):7678–93.
  22. Schaefer M, Roots I, Gerloff T. In-vitro transport characteristics discriminate wild-type ABCB1 (MDR1) from ALA893SER and ALA893THR polymorphisms. *Pharmacogenet Genomics*. 2006;16(12):855–61.
  23. Komoto C, Nakamura T, Sakaeda T, Kroetz DL, Yamada T, Omatsu H, Koyama T, Okamura N, Miki I, Tamura T, et al. MDR1 haplotype frequencies in Japanese and Caucasian, and in Japanese patients with colorectal cancer and esophageal cancer. *Drug Metab Pharmacokinet*. 2006;21(2):126–32.
  24. Gandelman K, Fung GL, Messig M, Laskey R. Systemic exposure to atorvastatin between Asian and Caucasian subjects: a combined analysis of 22 studies. *Am J Ther*. 2012;19(3):164–73.
  25. Sakaeda T, Kadoyama K, Okuno Y. Statin-associated muscular and renal adverse events: data mining of the public version of the FDA adverse event reporting system. *PLoS One*. 2011;6(12):e28124.
  26. Chang CH, Kusama M, Ono S, Sugiyama Y, Orii T, Akazawa M. Assessment of statin-associated muscle toxicity in Japan: a cohort study conducted using claims database and laboratory information. *BMJ open*. 2013;3(4):e002040.
  27. Hermann M, Bogsrud MP, Molden E, Asberg A, Mohebi BU, Ose L, Retterstol K. Exposure of atorvastatin is unchanged but lactone and acid metabolites are increased several-fold in patients with atorvastatin-induced myopathy. *Clin Pharmacol Ther*. 2006;79(6):532–9.
  28. Goosen TC, Bauman JN, Davis JA, Yu C, Hurst SI, Williams JA, Loi CM. Atorvastatin glucuronidation is minimally and nonselectively inhibited by the fibrates gemfibrozil, fenofibrate, and fenofibric acid. *Drug Metab Dispos*. 2007;35(8):1315–24.
  29. Pirmohamed M, Breckenridge AM, Kitteringham NR, Park BK. Adverse drug reactions. *BMJ*. 1998;316(7140):1295–8.
  30. Kaniwa N, Saito Y. Pharmacogenomics of severe cutaneous adverse reactions. *Pharmacogenomics*. 2013;14(6):595–8.

Submit your next manuscript to BioMed Central and we will help you at every step:

- We accept pre-submission inquiries
- Our selector tool helps you to find the most relevant journal
- We provide round the clock customer support
- Convenient online submission
- Thorough peer review
- Inclusion in PubMed and all major indexing services
- Maximum visibility for your research

Submit your manuscript at  
[www.biomedcentral.com/submit](http://www.biomedcentral.com/submit)



# TRPV4 deficiency increases skeletal muscle metabolic capacity and resistance against diet-induced obesity

Tatsuya Kusudo,<sup>1</sup> Zhonghua Wang,<sup>1</sup> Atsuko Mizuno,<sup>2</sup> Makoto Suzuki,<sup>2</sup> and Hitoshi Yamashita<sup>1</sup>

<sup>1</sup>Department of Biomedical Sciences, College of Life and Health Sciences, Chubu University, Kasugai; and <sup>2</sup>Department of Pharmacology, Division of Molecular Pharmacology, Jichi Medical University, Shimotsuke, Japan

Submitted 24 August 2011; accepted in final form 23 December 2011

**Kusudo T, Wang Z, Mizuno A, Suzuki M, Yamashita H.** TRPV4 deficiency increases skeletal muscle metabolic capacity and resistance against diet-induced obesity. *J Appl Physiol* 112: 1223–1232, 2012. First published December 29, 2011; doi:10.1152/jappphysiol.01070.2011.— Transient receptor potential channel V4 (TRPV4) functions as a nonselective cation channel in various cells and plays physiological roles in osmotic and thermal sensation. However, the function of TRPV4 in energy metabolism is unknown. Here, we report that TRPV4 deficiency results in increased muscle oxidative capacity and resistance to diet-induced obesity in mice. Although no difference in body weight was observed between wild-type and *Trpv4*<sup>-/-</sup> mice when fed a standard chow diet, obesity phenotypes induced by a high-fat diet were significantly improved in *Trpv4*<sup>-/-</sup> mice, without any change in food intake. Quantitative analysis of mRNA revealed the constitutive upregulation of many genes, including those for transcription factors such as peroxisome proliferator-activated receptor  $\alpha$  and for metabolic enzymes such as phosphoenolpyruvate carboxykinase. These upregulated genes were especially prominent in oxidative skeletal muscle, in which the activity of  $\text{Ca}^{2+}$ -dependent phosphatase calcineurin was elevated, suggesting that other  $\text{Ca}^{2+}$  channels function in the skeletal muscle of *Trpv4*<sup>-/-</sup> mice. Indeed, gene expressions for TRPC3 and TRPC6 increased in the muscles of *Trpv4*<sup>-/-</sup> mice compared with those of wild-type mice. The number of oxidative type I fiber also increased in the mutant muscles following myogenin gene induction. These results strongly suggested that inactivation of *Trpv4* induces compensatory increases in TRPC3 and TRPC6 production, and elevation of calcineurin activity, affecting energy metabolism through increased expression of genes involved in fuel oxidation in skeletal muscle and thereby contributing to increased energy expenditure and protection from diet-induced obesity in mice.

energy metabolism; oxidative fiber; transient receptor potential channels; gene expression; obesity

IN BOTH DEVELOPED AND DEVELOPING COUNTRIES, the number of people with metabolic syndrome is increasing rapidly and has become a serious worldwide problem. Metabolic syndrome is a major risk factor for cardiovascular disease and Type 2 diabetes mellitus. The syndrome is marked by abdominal obesity, hypertension, insulin resistance, and dyslipidemia. Obesity is a major risk factor for developing metabolic syndrome (15, 19). It arises from dysfunctional energy metabolism, and therefore it is important to understand the molecular mechanisms of energy homeostasis. Their identification will help elucidate the etiology of obesity and might provide new treatment paradigms for patients with obesity and metabolic syndrome.

The transient receptor potential (TRP) channels are nonselective cation channels found in many animals, both vertebrate

and invertebrate. TRP channels are implicated in diverse cellular functions and sensing that include store-operated  $\text{Ca}^{2+}$  entry,  $\text{Ca}^{2+}$  transport, cell survival and growth, temperature, osmolality, touch, pain, and taste (6, 7, 51). The TRP channels are divided into three major subfamilies according to DNA sequences. The major subfamilies include the classical or canonical-like TRP channels (TRPC), the vanilloid receptor channels (TRPV), and the melastatin-like channels (TRPM). TRPV1, first cloned as the capsaicin receptor, senses unpleasant heat above 43°C (4). After the discovery of TRPV1, a series of other thermoreceptors sensing different temperature ranges were identified (3, 12, 28, 36, 37, 43, 44, 57, 59). Temperature-sensitive TRP channels transduce changes in ambient temperature to the central nervous system and elicit thermoregulatory responses, such as heat production and body temperature control (54, 60). Thermosensation appears to be closely linked with energy metabolism. Indeed, capsaicin induces heat loss via vasodilation and stimulates heat production by increasing metabolism in brown adipose tissue (BAT) (63). Several TRP channel members were reported to be associated with various diseases including cardiovascular diseases and metabolic disorders (17, 33). TRPV1 is related to the development of diabetes and obesity (31, 46). TRPV1, M2, M3, M4, C3, and C4 are also involved in insulin secretion and/or pancreatic islet inflammation (5, 38, 39, 50, 53).

TRPV4, which belongs to the TRPV family, shares ~40% amino acid homology with TRPV1. It is expressed in a variety of tissues, including the lung, spleen, kidney, heart, liver, brain, and white adipose tissue (WAT) (23, 45, 58). TRPV4 is also expressed in the most important thermogenic organ, BAT (56). TRPV4 is activated by osmolarity (42), heat (12), phorbol derivatives (57), and arachidonic acid metabolites (52). By those means, TRPV4 increases intracellular  $\text{Ca}^{2+}$  and plays important roles in regulating cell volume and water permeability or thermosensation. A number of studies using *Trpv4* gene-deficient (*Trpv4*<sup>-/-</sup>) mice, engineered by Dr. Suzuki's group (30), have also confirmed or revealed the physiological roles of TRPV4 in pressure and osmotic sensations (30, 47), thermal hyperalgesia (49), normal thermal responsiveness (22), hippocampal neural excitability (40), and the terminal differentiation of osteoclasts (61). Moreover, Yin et al. (27) reported a pathological relevance of TRPV4 to the formation of hydrostatic lung edema through the regulation of endothelial  $\text{Ca}^{2+}$  concentrations. However, no studies have reported the involvement of TRPV4 in energy metabolism, although TRPV4 is expressed in metabolic tissues such as liver, skeletal muscle, WAT, and BAT.

In this study, we addressed whether TRPV4 deficiency affects energy metabolism and susceptibility to diet-induced obesity. We demonstrated that *Trpv4*<sup>-/-</sup> mice showed in-

Address for reprint requests and other correspondence: H. Yamashita, Dept. of Biomed. Sci., College of Life and Health Sci., Chubu Univ., Kasugai 487-8501, Japan.

creased muscle oxidative capacity and resistance to diet-induced obesity, mainly by increased expression of genes involved in energy metabolism in skeletal muscles, in which the induction of TRPC3 and TRPC6 genes was stimulated. To our knowledge, this is the first report that implies a connection between TRPV4 and energy metabolism.

## METHODS

**Animals.** *Trpv4*<sup>-/-</sup> mice were generated with a C57BL/6 background as described (30). Adult mice from generations N8–N10 were used in this study. The *Trpv4*<sup>-/-</sup> and wild-type (WT) mice were bred and maintained at 23°C under artificial lighting for 12 h/day. They were given a standard chow diet (diet no. CE-2, 344 kcal/100 g, 11.6% kcal from fat; CLEA Japan, Higashiyama, Japan) and tap water ad libitum in our animal facility. Some mice were fed a high-fat diet [HF; diet no. B15040, 423 kcal/100 g, 41.9% kcal from fat; CLEA (55)] starting at 4 mo of age. Body weight and food intake were measured weekly for 3 mo after starting the HF diet. At 7 mo of age, the mice were anesthetized with ether, then blood and various tissues were isolated and stored at -80°C until analysis. Tissues for histological analysis were fixed immediately in 10% formaldehyde neutral buffer solution. Adiposity index was calculated using the depot weight data of inguinal, gonadal, retroperitoneal, and mesenteric WATs and BATs. We performed five independent experiments (twice for the standard chow and three times for HF diets) using male and/or female mice. Unless otherwise noted, the data shown are for male mice. All experiments were performed in accordance with our institutional guidelines for the care and use of research animals.

**Biochemical analyses.** Blood glucose level was determined with a glucometer (NovoAssist Plus, Novo Nordisk, Tokyo, Japan) just before death. The serum levels of insulin, leptin, and adiponectin were measured using enzyme-linked immunosorbent assay kits (insulin: Lebis-insulin-mouse, Sibayagi, Gunma, Japan; leptin: Lebis-leptin-mouse, Sibayagi, Gunma, Japan; and adiponectin: Quantikine adiponectin, R&D systems, Minneapolis, MN). Serum triglycerides, free fatty acid, and total cholesterol levels were measured using TG E-test, NEFA C-test, and T-Cho E-test kits (Wako Pure Chemical, Osaka, Japan), respectively. Calcineurin phosphatase activity was analyzed using Biomol Green Calcineurin Assay Kit Plus (BIOMOL Research Laboratories, Plymouth Meeting, PA), in accordance with the manufacturer's instructions. In brief, the soleus muscle was homogenized in 0.12 ml of lysis buffer and centrifuged at 150,000 g for 45 min. To remove free phosphates and nucleotides, the supernatants were desalted using Bio-Spin 6 columns (Bio-Rad Laboratories, Hercules, CA). Desalted samples were added to assay buffer containing RII phosphopeptide as a substrate for calcineurin. After the samples had been incubated at 25°C for 20 min, reactions were stopped by adding BIOMOL GREEN reagent. The samples were then incubated at room temperature for 30 min to allow color development, and the absorbance at 630 nm (A630) was determined. Calcineurin-specific phosphatase activity was determined by subtracting the A630 value of samples with total phosphatase activity from that of samples in the presence of EGTA.

**Histological analysis.** Fixed tissues were embedded in paraffin wax, sectioned at 6 µm, and stained with hematoxylin and eosin. For lipid staining, tissues were fixed in 4% paraformaldehyde/PBS, embedded in a Tissue-Tek optimal cutting temperature compound (Sakura Finetek, Tokyo, Japan), sectioned at 8 µm, and stained with Oil Red O.

**Liver lipid measurement.** Total liver lipids were extracted according to a method modified from Blish and Dyer (2). Briefly, frozen liver tissue samples (100 mg) were homogenized in 1 ml of chloroform/methanol (vol/vol = 2:1) and extracted twice with chloroform and once with water/chloroform/methanol (vol/vol/vol = 47:48:3). The organic layer was dried and resolubilized in 1 ml of isopropyl

alcohol containing 10% Triton X-100. The triglyceride levels were assayed using TG E-test kits (Wako Chemicals, Osaka, Japan).

**Indirect calorimetry studies.** Mice fed a standard chow or HF diet for 8 wk were housed individually in a four-chamber Oxymax laboratory animal monitoring system (Columbus Instruments, Columbus, OH) and acclimated to this before any experiment. The oxygen consumption rate ( $\dot{V}O_2$ ), carbon dioxide production rate ( $\dot{V}CO_2$ ), and respiratory exchange ratio (RER) of individual mice were measured every 5 min for 22 h. During this study, mice had ad libitum access to food and water.

**Biotelemetry studies.** Core body temperature and physical activity were continuously monitored in conscious, unrestrained mice with a VitalView Data Acquisition System (Mini Mitter, Sunriver, OR). Briefly, each mouse was anesthetized, and a transmitter (PDT-4000, Mini Mitter) was implanted intra-abdominally. Mice were allowed to recover for a minimum of 7 days after implantation. The signals emitted by the transmitter were received and converted into temperature and activity by VitalView software. Core body temperature and physical activity were monitored at a rate of 60 measurements/h for 3 days.

**Quantitative real-time RT-PCR.** Total RNA was extracted using Trizol reagent (Invitrogen, Carlsbad, CA), according to the manufacturer's protocol. RNA was reverse-transcribed using high-capacity cDNA reverse transcription kits (Applied Biosystems, Foster City, CA), according to the manufacturer's instructions. To quantify mRNA expression levels, real-time RT-PCR analysis was performed using Light-Cycler and FastStart DNA Master<sup>PLUS</sup> SYBR GREEN I (Roche Diagnostics, Mannheim, Germany). All gene expression data were normalized to 36B4. The oligonucleotide primer sets used are shown in Table 1.

**Western blot analysis.** Tissue lysates were prepared from soleus muscles by homogenizing in RIPA buffer (50 mM Tris-HCl, pH 7.5, 150 mM NaCl, 1 mM EDTA, 0.1% SDS, 1% NP-40, 0.5% sodium deoxycholate, 1 mM Na<sub>3</sub>VO<sub>4</sub>, and 1 mM NaF) containing protease inhibitor cocktail (Nakalai Tesque, Kyoto, Japan). The homogenate was then centrifuged at 12,000 g at 4°C for 5 min, and the supernatant was collected. The protein concentration of each sample was measured using the BCA protein assay (Pierce, Rockford, IL). Protein samples (30 µg) were subjected to SDS-PAGE and transferred onto PVDF membranes (Millipore, Bedford, MA). The membrane was blocked with 5% nonfat dry milk in TBS containing 0.1% Tween-20 (TBS-T) for 1–2 h at room temperature and then incubated with specific antibodies against TRPV4 (Alomone Lab, Jerusalem, Israel), phosphoenolpyruvate carboxykinase (Cayman Chemicals, Ann Arbor, MI), myogenin (Thermo Scientific, Fremont, CA), or  $\alpha/\beta$ -tubulin (Cell Signaling Technology, Danvers, MA) overnight at 4°C. The blots were then washed in TBS-T three times and incubated with horseradish peroxidase-conjugated secondary antibody at 1:2,000 dilution for 1 h at room temperature. After washing in TBS-T three times, the protein band was detected using ECL Western blotting detection reagents (GE Healthcare, Little Chalfont, Buckinghamshire, UK).

**Staining for NADH-tetrazolium reductase.** Muscles were dissected and rapidly frozen in cooled isopentane (-150°C). Frozen muscles were cut into 8-µm sections using a cryostat. Muscle sections were incubated for 30 min at 37°C in a solution of 50 mM Tris-HCl (pH 7.4), 1.5 mM  $\beta$ -NADH, and 1.5 mM nitrotetrazolium blue. Sections were then serially incubated in 30%, 60%, 90%, 60%, and 30% acetone/deionized water solutions and mounted with glycerin/gelatin solution. To determine the composition of the muscle fiber types, 100–200 fibers from five sections per mouse were characterized.

**Measurement of exercise capacity.** Treadmill exercise was performed according to the exercise protocol described by Hakimi et al. (13). Briefly, 8-mo-old WT and *Trpv4*<sup>-/-</sup> male mice were acclimated to the treadmill for 30 min. After the acclimation, the mice ran at 12 m/min for 30 min as a warm-up. Then, the treadmill speed was

Table 1. Real-time PCR primer sequences

Gene	Sense	Antisense
<i>PEPCK</i>	5'-GTGGGCGATGACATTGCC-3'	5'-ACTGAGGTGCCAGGAGCAAC-3'
<i>LXR<math>\alpha</math></i>	5'-TCTGGAGACGTCACGGAGGTA-3'	5'-CCCGGTTGTAAGTGAAGTCCTT-3'
<i>HSL</i>	5'-GCTCTTCTTCGAGGGTGATG-3'	5'-ACACTGAGGCCTGTCTCGTT-3'
<i>LPL</i>	5'-GGGCTCTGCCTGAGTTGTAG-3'	5'-CCACTGTGCCGTACAGAGAA-3'
<i>ACO</i>	5'-CAGCACTGGTCTCCGTCATG-3'	5'-CTCGGACTACCATCCAAGATG-3'
<i>CPT-1</i>	5'-ACTCCTGGAAGAAGAAGTTCA-3'	5'-GTATCTTTGACAGCTGGGAC-3'
<i>UCP-1</i>	5'-GTGAAGGTCAGAATGCAAGC-3'	5'-AGGGCCCCCTTCATGAGGTC-3'
<i>UCP-2</i>	5'-GGCTGGTGGTGGTCCGAGAT-3'	5'-CCGAAGGCAGAAGTGAAGTG-3'
<i>UCP-3</i>	5'-GAGCGGACCACTCCAGCGTC-3'	5'-TGAGACTCCAGCAACTTCTC-3'
<i>PPAR<math>\alpha</math></i>	5'-GGCAAGAGAATCCACGAA-3'	5'-GTTGTTGCTGCTTTTCCCG-3'
<i>PPAR<math>\gamma</math></i>	5'-TTTTCAAGGGTGCCAGTTTC-3'	5'-AATCCTTGGCCCTCTGAGAT-3'
<i>PPAR<math>\delta</math></i>	5'-CGGCAGCCTCAACATGG-3'	5'-AGATCCGATCCGACTTCTCATA-3'
<i>AdipoR1</i>	5'-ACGTTGGAGAGTCATCCCGTAT-3'	5'-CTCTGTGTGGATGCGGAAGAT-3'
<i>AdipoR2</i>	5'-TCCAGGAAGATGAAGGGTTTAT-3'	5'-TTCATTGCTTCGATAGCATGA-3'
<i>MyoG</i>	5'-CTGGGGACCCCTGAGCATTG-3'	5'-ATCGCGCTCCTCCTGGTTGA-3'
<i>TRPC3</i>	5'-GGAGAGCGATCTGAGCGAAGT-3'	5'-GGAGCCATTGTTCTCTAGCA-3'
<i>TRPC6</i>	5'-ACTACATTGGCCGAAAAACAGAA-3'	5'-AGAAAGACCAAAGATAGCCAGAA-3'
<i>36B4</i>	5'-TCATCCAGCAGGTGTTTGACA-3'	5'-CCCATTGATGATGGAGTGTGG-3'

increased to 24 m/min until mice reached exhaustion. Exhaustion was defined as the point when the mouse stops running for 10 s despite electrical stimulation (0.2 mA).

**Statistical analysis.** Data are expressed as means  $\pm$  SE. Significant differences between groups were assessed using ANOVA or repeated-measures ANOVA. *P* values of  $<0.05$  were considered statistically significant.

## RESULTS

**Effects of TRPV4 deficiency on phenotypes of energy metabolism.** To study the physiological role of TRPV4 in energy metabolism in mice, we first examined their basal phenotypes under standard chow diet condition for 10 wk, starting from the age of 4 mo. As shown in Fig. 1, there was minimal change and no significant difference in body weight for both *Trpv4*<sup>-/-</sup> and WT mice, although the body weight of WT mice tended to be higher than that of the mutant mice. There was also no significant difference in food intake between

*Trpv4*<sup>-/-</sup> and WT mice fed on the standard chow diet (Fig. 1B). When various parameters such as tissue mass were examined in the 7-mo-old mice, we found significant decreases in the brown and mesenteric fat tissue weight of *Trpv4*<sup>-/-</sup> mice compared with those of WT mice. However, there were no differences in other tissues or in blood parameters including insulin, leptin, total cholesterol, triglyceride, and free fatty acid between genotypes (data not shown).

We next challenged 4-mo-old mice with a HF diet for 10 wk. As expected, WT mice body weight increased steadily with the HF diet, whereas body weight gain was considerably suppressed in *Trpv4*<sup>-/-</sup> mice (Fig. 1C). This difference in weight gain between genotypes was observed from the first week of HF feeding. No significant difference was detected in food intake between *Trpv4*<sup>-/-</sup> and WT mice (Fig. 1D). Similar results in body weight gain were obtained in experiments using female mice fed the HF diet (data not shown). To examine

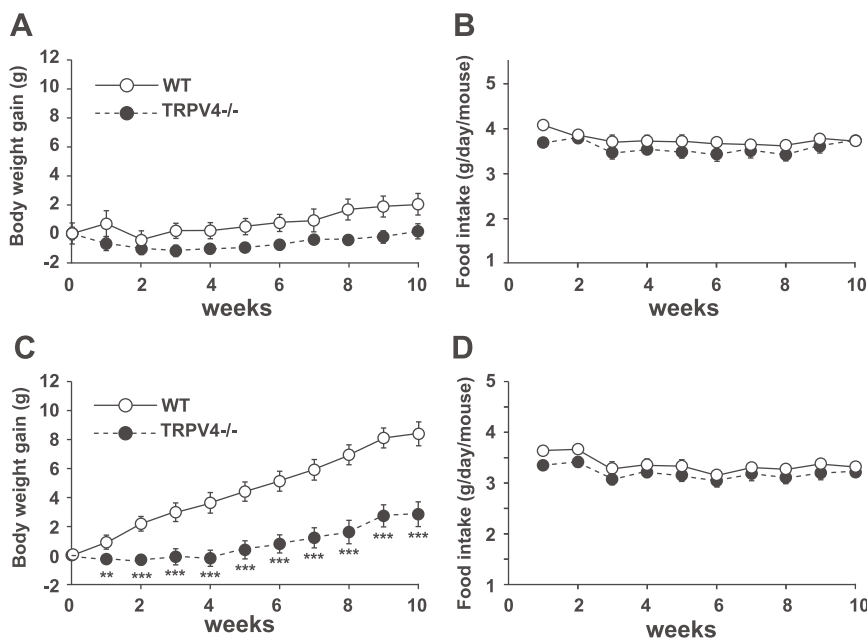


Fig. 1. Changes in body weight and food intake in TRPV4-deficient mice under standard chow or high-fat (HF) diet condition. Male wild-type (WT) and *Trpv4*<sup>-/-</sup> mice were fed a standard chow or a HF diet from 16 wk of age for 10 wk (*n* = 6 per group). A and B: body weight gain and food intake in mice fed a standard chow. C and D: body weight gain and food intake in mice fed a HF diet. Data are expressed as means  $\pm$  SE. Significant difference vs. WT mice: \*\**P* < 0.01; \*\*\**P* < 0.001.

whether *Trpv4*<sup>-/-</sup> mice resistance to HF diet-induced obesity was caused by altered energy expenditure, we performed indirect calorimetry. As shown in Fig. 2, we found a significant increase in  $\dot{V}O_2$  (ml·h<sup>-1</sup>·kg body wt<sup>0.75</sup>) of *Trpv4*<sup>-/-</sup> mice compared with WT mice under the HF diet condition, whereas there was no difference between genotypes with the standard chow diet. There was no significant difference in the respiratory exchange ratio (RER) between genotypes (data not shown). Moreover, we performed biotelemetry to measure core body temperature and physical activity in the mice. No significant difference was detected in body temperature or physical activity between WT and *Trpv4*<sup>-/-</sup> mice (Fig. 3). The average body temperatures were  $36.28 \pm 0.05$  and  $36.06 \pm 0.10^\circ\text{C}$  during light phase and  $37.54 \pm 0.16$  and  $37.28 \pm 0.07^\circ\text{C}$  during dark phase in WT and *Trpv4*<sup>-/-</sup> mice, respectively. The average physical activity values were  $791 \pm 42$  and  $702 \pm 126$  counts/h during light phase and  $2,252 \pm 679$  and  $1,363 \pm 248$  counts/h during dark phase in WT and *Trpv4*<sup>-/-</sup> mice, respectively.

We then measured various parameters such as tissue mass in the 7-mo-old mice fed with HF diet (Table 2). There were no significant differences in the weights of the heart, the kidney, the pancreas, the gastrocnemius muscle (GM), or the soleus muscle (SM) between genotypes. Although the difference in liver mass between genotypes did not reach a significant level, a decreased trend was observed in the *Trpv4*<sup>-/-</sup> mice ( $P = 0.056$  vs. WT mice). The weights of all the fat depots, including BAT, were significantly reduced in *Trpv4*<sup>-/-</sup> mice compared with those in WT mice, leading to an ~40% reduction in adiposity in the mutant mice. There was no significant difference in blood glucose levels consumed between *Trpv4*<sup>-/-</sup> and WT mice, whereas the insulin levels in serum were significantly lower in *Trpv4*<sup>-/-</sup> mice than in WT mice. As expected from the adiposity data, the serum leptin level was significantly lower in *Trpv4*<sup>-/-</sup> mice than in WT mice. There was no difference in the serum adiponectin level between genotypes. For lipid parameters, we also found a significant decrease in total cholesterol level but not in triglyceride (TG) or nonesterified fatty acids (NEFA) levels in the serum of *Trpv4*<sup>-/-</sup> mice compared with those of WT mice.

Histology showed that the adipocytes in BAT and WAT were smaller in *Trpv4*<sup>-/-</sup> mice than in WT mice (Fig. 4A), suggesting lower lipid accumulation in the adipose tissues of

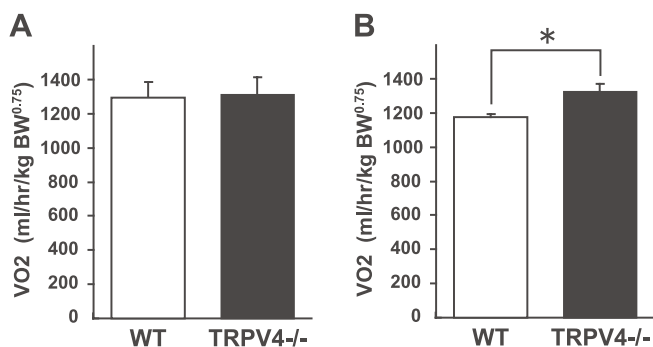


Fig. 2. Whole body oxygen consumption ( $\dot{V}O_2$ ) in TRPV4-deficient mice.  $\dot{V}O_2$  of mice fed a standard chow (A) or a HF (B) diet was measured using indirect calorimetry ( $n = 6$  each genotype). Mice were monitored continuously for 22 h (1900–1700). Data are expressed as means  $\pm$  SE. \*Significant difference vs. WT mice ( $P < 0.05$ ).

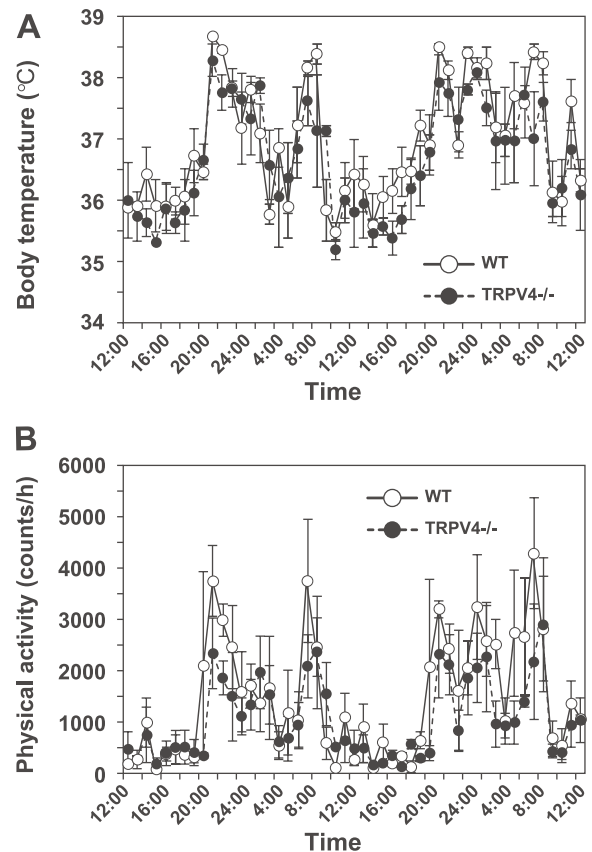


Fig. 3. Body temperature and physical activity in TRPV4-deficient mice. Core body temperature and physical activity were measured in 6-mo-old female WT and *Trpv4*<sup>-/-</sup> mice fed a standard chow by telemetry using VitalView Data Acquisition System, as described in METHODS. Body temperature and activity values are shown as means  $\pm$  SE at each hour ( $n = 3$  per group).

mutant mice under a HF diet condition. Likewise, lower lipid accumulation was observed in the livers of *Trpv4*<sup>-/-</sup> mice compared with WT mice, as assessed by Oil Red O staining (Fig. 4B). This difference in lipid accumulation was confirmed by total TG content measurement in the livers of *Trpv4*<sup>-/-</sup> and WT mice ( $2.9 \pm 0.9$  vs.  $5.29 \pm 0.7$  mg/g tissue, respectively;  $P = 0.03$ ).

*Upregulation of genes related to energy metabolism in Trpv4*<sup>-/-</sup> mice. To clarify the molecular mechanisms responsible for protection against HF diet-induced obesity in *Trpv4*<sup>-/-</sup> mice, we analyzed tissues for the expression of genes for uncoupling proteins (UCPs) and other genes involved in energy metabolism using real-time RT-PCR. Compared with the WT mice, significant increases in gene expression for phosphoenolpyruvate carboxykinase (*Pepck*) and lipoprotein lipase (*Lpl*) were found in the BAT of *Trpv4*<sup>-/-</sup> mice; however, we could not detect any differences in the expression of UCPs or other genes at significant levels in this tissue (Fig. 5A). We also failed to detect differences in gene expression from epididymal WAT of *Trpv4*<sup>-/-</sup> mice (Fig. 5B). Only one gene, the peroxisome proliferator-activated receptor  $\alpha$  (PPAR $\alpha$ ), was significantly increased (1.5-fold of control) in the liver of *Trpv4*<sup>-/-</sup> mice, although the expression of PPAR $\alpha$  target genes such as carnitine palmitoyl-

Table 2. Phenotypic characteristics of WT and TRPV4-deficient mice fed a HF diet

Parameter	WT	TRPV4 <sup>-/-</sup>	P Value
Body weight, g	38.5 ± 2.6	33.6 ± 5.7	0.041
Adiposity, % of body wt	12.0 ± 1.3	7.2 ± 2.7	0.002
WAT, mg			
Epididymal WAT	2035 ± 120	1197 ± 263	0.008
Retroperitoneal WAT	525 ± 41	313 ± 86	0.025
Mesenteric WAT	749 ± 52	413 ± 96	0.006
Inguinal WAT	1321 ± 107	621 ± 133	0.001
BAT, mg	142 ± 10	104 ± 16	0.038
Liver, mg	1667 ± 78	1381 ± 145	0.057
Heart, mg	147 ± 5	152 ± 7	0.268
Kidney, mg	196 ± 9	211 ± 22	0.267
Pancreas, mg	325 ± 7	350 ± 32	0.234
Gastrocnemius muscle, mg	161 ± 4	156 ± 8	0.307
Soleus muscle, mg	9.59 ± 0.72	9.23 ± 0.76	0.371
Glucose, mg/dl	140 ± 4	147 ± 5	0.110
Insulin, ng/ml	2.24 ± 0.59	1.06 ± 0.42	0.010
Leptin, ng/ml	26.0 ± 6.3	8.44 ± 2.41	0.020
Adiponectin, mg/dl	14.4 ± 0.8	16.0 ± 1.4	0.331
Triglyceride, mg/dl	96.3 ± 8.5	85.2 ± 6.5	0.166
NEFA, mEq/l	1.45 ± 0.13	1.42 ± 0.26	0.459
Total cholesterol, mg/dl	223 ± 13	181 ± 22	0.030

Sixteen-week-old male mice were fed a high-fat (HF) diet for 12 wk. Tissue and blood samples were collected at nonfasted state. Adiposity index was calculated by using the data of white adipose tissue (WAT) and brown adipose tissue (BAT). Blood biochemistry parameters, except glucose level, were measured by using the serum as described in METHODS. Values are means ± SE ( $n = 6$  per group). WT, wild-type mice; NEFA, nonesterified fatty acids.

transferase (CPT1) and acyl-CoA oxidase (ACO) did not reach significant levels (Fig. 5C).

We next examined gene expression in skeletal muscles, in which TRPV4 protein production had been confirmed, as shown in Fig. 6. We found notable gene expression changes in the skeletal muscle of *Trpv4*<sup>-/-</sup> mice. In addition to increased expression of the liver X receptor  $\alpha$  (LXR $\alpha$ ) gene, Pepck mRNA levels in the GM of *Trpv4*<sup>-/-</sup> mice were ~300% above the WT control (Fig. 5D). Many other genes also tended to increase in the glycolytic muscle types of *Trpv4*<sup>-/-</sup> mice compared with WT mice. Interestingly, most of the genes examined in the SM were stably upregulated in the mutant mice (Fig. 5E). These included genes encoding transcriptional factors such as LXR $\alpha$ , PPAR $\alpha$ , PPAR $\delta$ , and myogenin, a muscle-specific transcription factor. In parallel with the transcriptional stimulation of these nuclear factor genes, a number of genes related to glucose and lipid metabolism [PEPCK, LPL, ACO, CPT1, and adiponectin receptor 1 (AdipoR1)] were induced in the oxidative muscle types of *Trpv4*<sup>-/-</sup> mice. The increased expression of PEPCK and myogenin in the SM of mutant mice was confirmed at the protein level, which were 1.5- and 2.2-fold higher, respectively, in *Trpv4*<sup>-/-</sup> mice than in WT mice (Fig. 6). Increases in the mRNA level of most of these genes were also detected in the SM of *Trpv4*<sup>-/-</sup> mice that were fed a standard chow diet (data not shown).

**Induction of TRPC3 and TRPC6 gene expression and elevation of calcineurin activity in skeletal muscle of *Trpv4*<sup>-/-</sup> mice.** The extensive gene expression induction suggested that there was increased signaling pathway activity to stimulate gene transcription in skeletal muscles. Despite the lack of TRPV4, the activity of calcineurin, a Ca<sup>2+</sup>-dependent phosphatase, was elevated in the SM of *Trpv4*<sup>-/-</sup> mice compared

with that of WT mice (Fig. 7A). We also found significant increases in TRPC3 and TRPC6 gene expression in the muscles of *Trpv4*<sup>-/-</sup> mice compared with those of WT mice (Fig. 7, B and C). The mRNA levels for TRPC3 in the SM increased to 141% of controls in *Trpv4*<sup>-/-</sup> mice (Fig. 7B). The mRNA levels for TRPC6 in the SM also increased to 148% of controls in those mice (Fig. 7C).

**Changes in the fiber-type composition and oxidative capacity in skeletal muscle of *Trpv4*<sup>-/-</sup> mice.** We evaluated the fiber-type composition in SM using enzyme histochemistry for NADH-tetrazolium reductase, a mitochondrial enzyme in complex I, because of significant increases in myogenin expression and calcineurin activity in the muscle of *Trpv4*<sup>-/-</sup> mice (Figs. 5E, 6, and 7A). As shown in Fig. 8, a significant increase in the number of oxidative type I fiber was found in the muscles of *Trpv4*<sup>-/-</sup> mice compared with those of WT mice. In addition, *Trpv4*<sup>-/-</sup> mice showed a higher exercise capacity on a treadmill compared with WT mice (Fig. 9). The running time and distance on a treadmill at 24 m/min were significantly longer (1.42-fold) for *Trpv4*<sup>-/-</sup> mice than for WT mice.

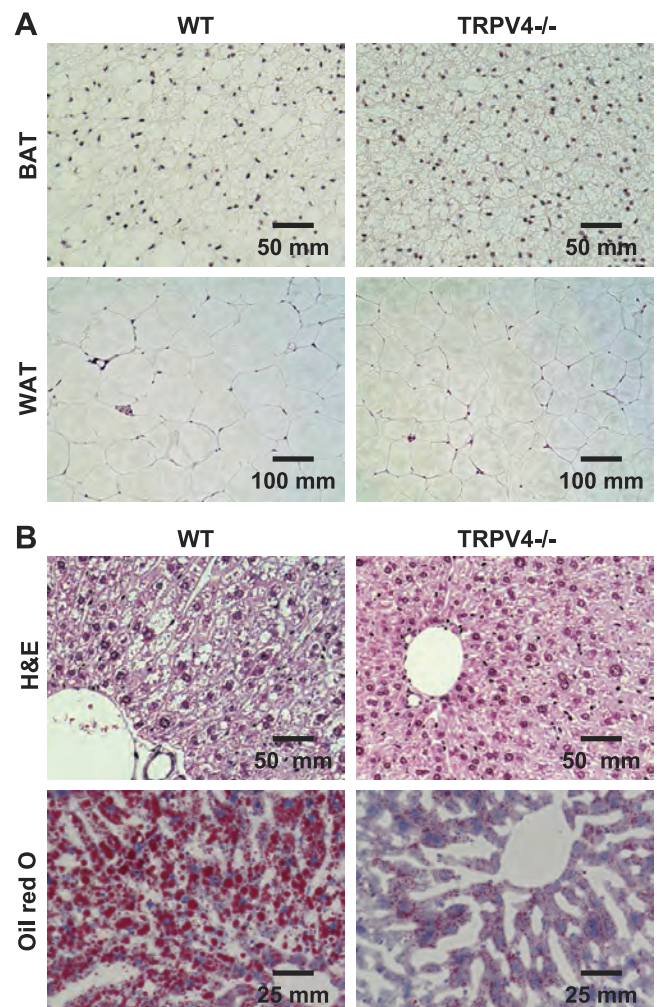


Fig. 4. Histology of TRPV4-deficient mice fed a HF diet. A: tissue sections of BAT and epididymal WAT were stained with hematoxylin and eosin (H&E). B: liver sections were stained with Oil Red O and counterstained with hematoxylin.

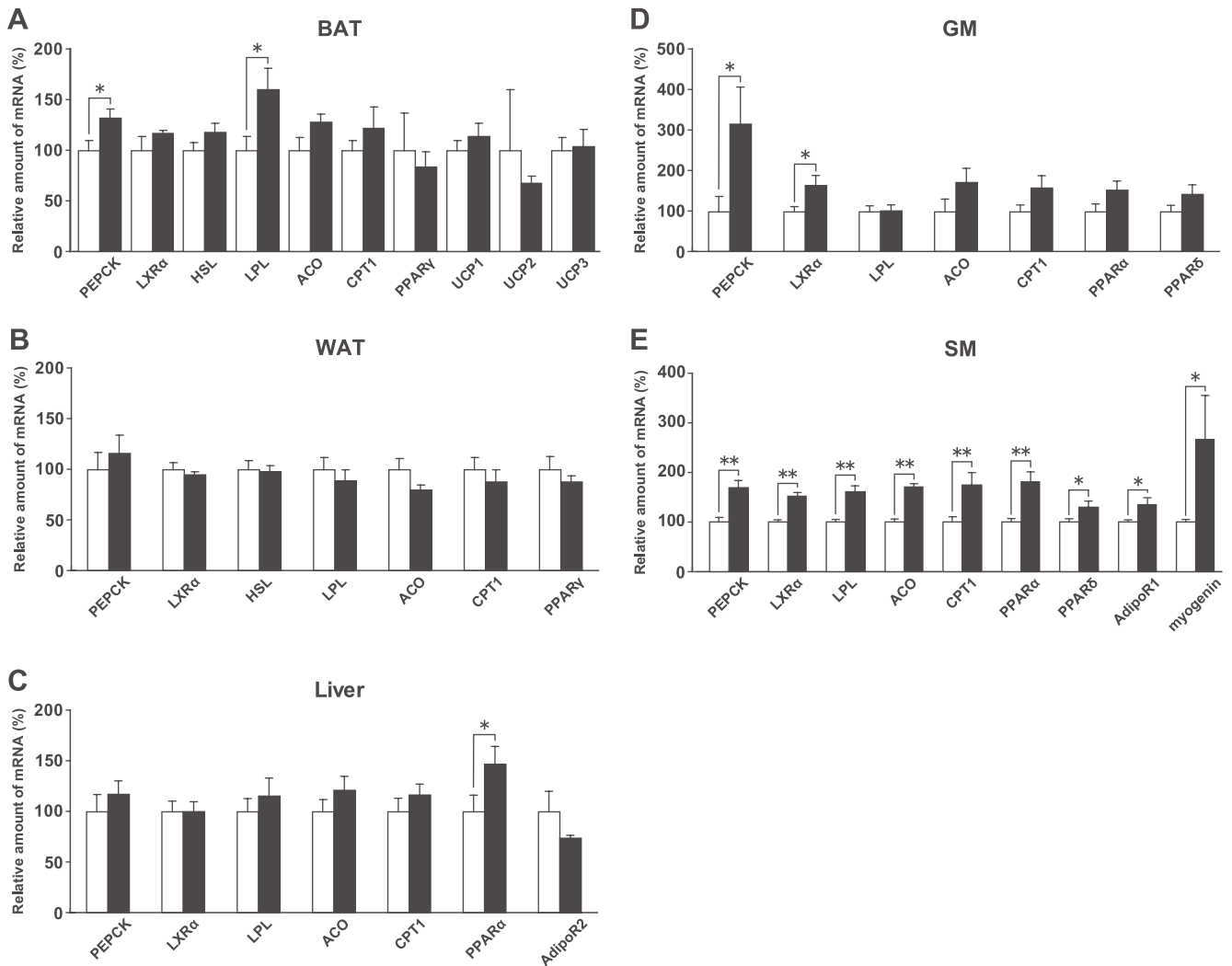


Fig. 5. Expression of genes related to energy metabolism in TRPV4-deficient mice fed a HF diet. Real-time quantitative RT-PCR analysis of mRNAs was performed on total RNA samples from BAT (A), epididymal WAT (B), liver (C), gastrocnemius muscle (GM) (D), and soleus muscle (SM) (E) of WT and *Trpv4*<sup>-/-</sup> mice fed a HF diet, as described in METHODS. Primer sequences used are shown in Table 1. PEPCK, phosphoenolpyruvate carboxykinase; LXRα, liver X receptor α; HSL, hormone-sensitive lipase; LPL, lipoprotein lipase; ACO, acyl-CoA oxidase; CPT1, carnitine palmitoyl transferase 1; PPAR, peroxisome proliferator-activated receptor; AdipoR, adiponectin receptor. Quantitative data for each gene were normalized to 36B4 gene as internal control. Data (means ± SE) are presented as percentages of the WT control ( $n = 6$  per group). Significant difference vs. WT mice: \* $P < 0.05$ ; \*\* $P < 0.01$ .

## DISCUSSION

Previous studies using TRPV4-deficient mice showed that TRPV4 plays important roles for sensing osmolarity (30), temperature (22, 41, 49), and/or mechanical stress (48). In this study, we have demonstrated for the first time that lack of TRPV4 protects mice from HF diet-induced obesity. Histological analysis of adipose tissues indicated that adipocytes were smaller in mutant mice than in WT mice under HF diet condition, suggesting that adipocyte hypertrophy associated with obesity development was suppressed in the adipose tissues of mutant mice. Observation of low adiposity and hepatic steatosis in *Trpv4*<sup>-/-</sup> mice also indicated a resistance to obesity development compared with WT mice. The anti-obesity phenotype induced by TRPV4 deficiency appeared to be caused by increased energy expenditure because we observed an increase in  $\dot{V}O_2$ , but not in food intake, for *Trpv4*<sup>-/-</sup> mice compared with WT mice. Although physical activity and body

temperature of *Trpv4*<sup>-/-</sup> mice were similar to those of WT mice, which are consistent with a previous report (22), the exercise capacity and/or muscle contractile performance of *Trpv4*<sup>-/-</sup> mice were not determined in their study. Therefore, the primary mechanism underlying the anti-obesity property of *Trpv4*<sup>-/-</sup> mice is assumed to be associated with energy metabolism enhancement and not due to increased physical activity. This mechanism could be diet-induced thermogenesis, one of the adaptive thermogenic mechanisms, which is stimulated to maintain energy homeostasis in mammals (26). Adaptive thermogenesis is also induced as a response to cold for maintaining homeothermy (referred to as cold-induced thermogenesis).

To identify the tissue responsible for increased energy expenditure in *Trpv4*<sup>-/-</sup> mice, we examined gene expression in various tissues important for energy metabolism. BAT plays crucial roles in cold-induced thermogenesis for the mainte-

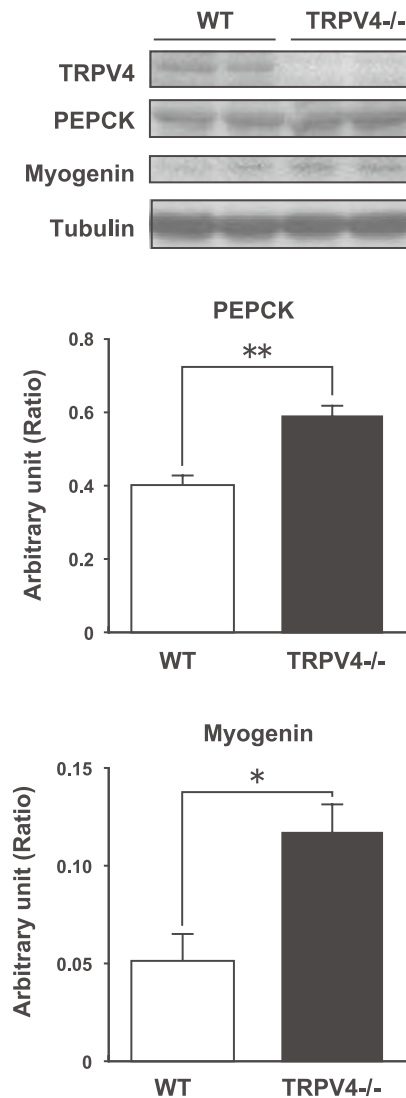


Fig. 6. Protein expression of TRPV4, PEPCK, and myogenin in soleus muscles (SM) of TRPV4-deficient mice. Tissue lysates (30  $\mu$ g) of SM from WT and *Trpv4*<sup>-/-</sup> mice were analyzed by Western blotting for TRPV4, PEPCK, and myogenin, as described in METHODS. Protein signal was quantified and normalized to  $\alpha/\beta$ -tubulin level. Data are expressed as means  $\pm$  SE ( $n = 5$  per group). \*Significant difference vs. WT mice ( $P < 0.05$ ).

nance of body temperature in cold conditions (10) and also in diet-induced thermogenesis for body weight regulation during excessive caloric intake (11, 18). This function is mediated by UCP1, which dissipates caloric energy as heat. Because TRPV4 is also consistently produced in the BAT and WAT of mice as reported (23, 56), TRPV4 deficiency might affect the cellular functions of adipose tissues. However, the gene expression levels of UCPs, including UCP1, in adipose tissues of *Trpv4*<sup>-/-</sup> mice were not different from those of WT mice, although we detected significant increases in PEPCK and LPL mRNA levels in the BAT of mutant mice. In addition, the lack of TRPV4 did not affect adipocyte differentiation in primary cell culture from the WAT of *Trpv4*<sup>-/-</sup> mice (56). These results suggested that TRPV4 does not play major roles in the regulation of BAT thermogenesis or adipogenesis. Similarly, the expression levels of genes related to energy metabolism in

the liver were similar between *Trpv4*<sup>-/-</sup> and WT mice, except for an increase in PPAR $\alpha$  mRNA level in mutant mice. PPAR $\alpha$  and PPAR $\delta$  regulate the transcription of genes implicated in fatty acid oxidation and glucose utilization, thus stimulating energy metabolism (9, 32). Although the expression levels of PPAR $\alpha$  target genes were not increased significantly in the liver of *Trpv4*<sup>-/-</sup> mice, increased PPAR $\alpha$  production might have contributed to the stimulation of fatty acid oxidation and protection against hepatic steatosis in mutant mice fed a HF diet, as observed by reduced lipid accumulation in histological analysis.

Skeletal muscle comprises one of the largest organ systems in the body and plays a critical role in glucose and fatty acid metabolism. Skeletal muscle is not only essential for physical activity but also for adaptive thermogenesis (26). TRPV4 protein expression was detected in the skeletal muscle of normal mice, which was consistent with a recent report that TRPV4 protein exists in a fraction of muscle fibers beneath the sarcolemma and around the myonuclei in mice (20). Therefore, we examined gene expression changes in *Trpv4*<sup>-/-</sup> mouse skeletal muscle. Interestingly, gene expression for PPAR $\alpha$  and  $\delta$  and their target genes such as CPT1 and ACO, which are key players in fatty acid  $\beta$ -oxidation, were constitutively increased in *Trpv4*<sup>-/-</sup> mice skeletal muscles, especially in the SM. Since the SM is composed predominantly of oxidative fibers whose energy is provided mainly by oxidative phosphorylation of fatty acids, the induction of CPT1 and ACO genes

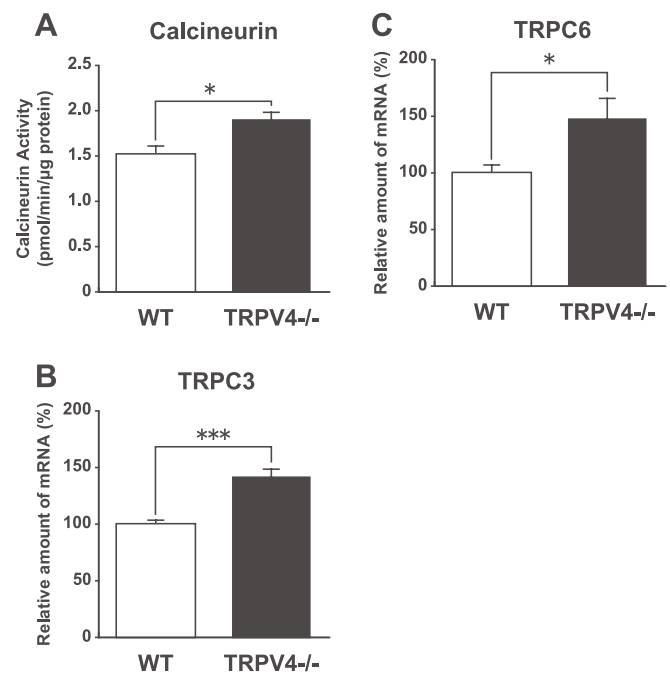


Fig. 7. Calcineurin activity and gene expression levels of TRPC3 and TRPC6 in soleus muscles (SM) of TRPV4-deficient mice. A: phosphatase activity of calcineurin in the SM of mice was measured using Biomol Green Calcineurin Assay kits, as described in METHODS. The activity was normalized to protein content. Data are expressed as means  $\pm$  SE ( $n = 5$  per group). B and C: mRNA expression of TRPC3 (B) and TRPC6 (C) in SM of WT and *Trpv4*<sup>-/-</sup> mice fed a HF diet. Real-time quantitative RT-PCR analyses of the mRNA levels were performed on total RNA samples from the SM of the mice, as described in METHODS. Primer sequences used are shown in Table 1. Data are expressed as means  $\pm$  SE ( $n = 8$  per group). Significant difference vs. WT mice: \* $P < 0.05$ ; \*\*\* $P < 0.001$ .

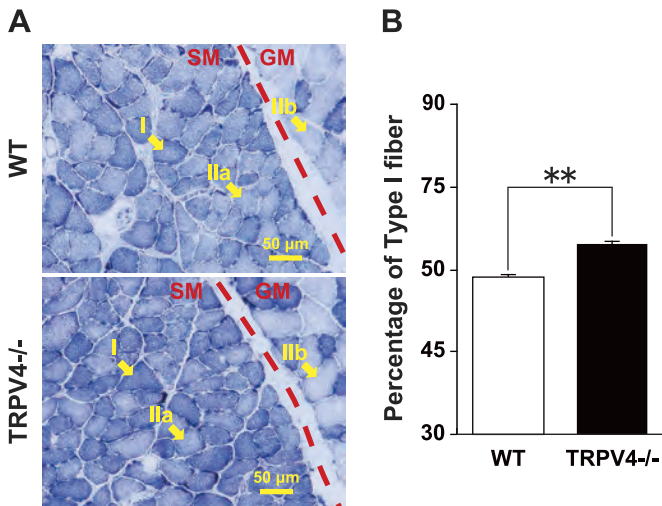


Fig. 8. Muscle fiber composition of SM in TRPV4-deficient mice. *A*: staining for NADH-tetrazolium reductase in muscle sections from WT (*top*) and *Trpv4*<sup>-/-</sup> mice (*bottom*). The right area of each picture is the GM, and the left area is the SM. The deeply stained fibers are the most oxidative (type I; I), the moderately stained fibers are intermediate oxidative/glycolytic (type IIa; IIa), and the unstained fibers are glycolytic (type IIb; IIb). *B*: type I fiber percentage in SM. The composition of muscle fiber types in the SM were determined by counting 100–200 fibers in five sections per mouse (*n* = 4 per group). \*\*Significant difference vs. WT mice (*P* < 0.01).

might contribute to the enhancement of fatty acid oxidation in SM. We also found increased expression level of adiponectin receptor 1 in the SM of *Trpv4*<sup>-/-</sup> mice. Adiponectin functions by increasing fatty acid oxidation in skeletal muscle via AMP-activated protein kinase (AMPK) activation, which produces beneficial effects for metabolic disorders (62). Nevertheless, the serum adiponectin levels and AMPK phosphorylation in muscles were similar for both *Trpv4*<sup>-/-</sup> mice and WT mice in our study (data not shown). Therefore, any possible contribution of adiponectin-AMPK signaling to increased metabolism in *Trpv4*<sup>-/-</sup> mice is likely minor.

One of the notable changes in gene expression for *Trpv4*<sup>-/-</sup> mice was a significant induction of the *Pepck* gene in skeletal muscles. This is a rate-limiting enzyme for gluconeogenesis and is also involved in glyceroneogenesis (14). Although the PEPCK content in muscle is basically low, Hakimi et al. (13) used skeletal muscle-specific *Pepck*-transgenic mice to demonstrate that PEPCK stimulates glyceroneogenesis and the production of triglyceride, which results in increased fatty acid oxidation and the subsequent stimulation of mitochondrial biogenesis in skeletal muscle, and the mice showed enhanced exercise capacity and extended longevity (14). They also suggested that increased PEPCK activity in skeletal muscle could enhance citric acid cycle flux and alter energy metabolism in the whole body, including increased fuel oxidation. Novak et al. (34) recently reported that PEPCK levels were significantly higher in skeletal muscle of obesity-resistant rats than that of diet-induced obese rats, suggesting that PEPCK contributes to leanness by altering skeletal muscle energetics. Similar to *Pepck* transgenic mice, *Trpv4*<sup>-/-</sup> mice showed a higher exercise capacity in endurance training compared with WT mice, suggesting an augmented oxidative capacity in the mutant mice. Therefore, it is likely that increased PEPCK

levels in the BAT and skeletal muscles contribute to the enhancement of energy metabolism in *Trpv4*<sup>-/-</sup> mice.

Ca<sup>2+</sup> is a second messenger that transmits physiological signals in a variety of cells. In skeletal muscles, this ion plays crucial roles in various cellular responses such as muscle contraction and fiber differentiation. One important signaling pathway is Ca<sup>2+</sup>-dependent activation of calcineurin (25). Previous reports have highlighted the roles of calcineurin signaling in muscle metabolism (24) and myogenesis (1) by regulating the transcription factor nuclear factor of activated T cells (NFAT) (35). In the present study, we initially thought that TRPV4 ablation would reduce Ca<sup>2+</sup> influx into skeletal muscle, which would attenuate calcium signaling in the cells. Unexpectedly, calcineurin activity increased in the skeletal muscle of *Trpv4*<sup>-/-</sup> mice compared with that of WT mice, suggesting an increase rather than a decrease in Ca<sup>2+</sup> influx in the mutant muscles. This result also implied that other Ca<sup>2+</sup> channels might compensate for the lack of TRPV4 and contribute to increased calcium signaling in the skeletal muscle of *Trpv4*<sup>-/-</sup> mice. Indeed, we found that TRPC3 and TRPC6 gene expression levels increased in the muscles of *Trpv4*<sup>-/-</sup> mice compared with WT mice. The two TRPC family members are expressed in mouse skeletal muscle (20) and have been proposed to play a role as store-operated channels. Therefore, the enhanced induction of TRPC3 and TRPC6 could be a reasonable response when TRPV4 deficiency causes a decrease in intracellular Ca<sup>2+</sup> stores. A similar enhancement of TRPC3 gene expression has been observed in the arteries of TRPC6-deficient mice, which showed an unexpected phenotype of vascular smooth muscle contractility (8). Moreover, TRPC3 gene expression was reported to be upregulated by neuromuscular activity in a calcineurin-dependent manner in skeletal myocytes (40). The report proposed that increased TRPC3 production enhances calcineurin-NFAT signaling that persists for subsequent periods of neuromuscular activity, thereby conferring cellular memory that stabilizes the slow oxidative phenotype. Kuwahara et al. (21) have also reported that TRPC6 positively regulates calcineurin-NFAT signaling and contributes to cardiac remodeling. In our study, we detected a significant increase in myogenin mRNA and protein levels, which is

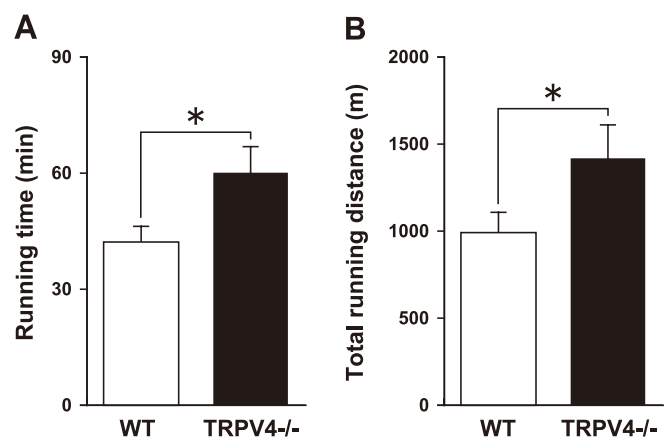


Fig. 9. Exercise capacity of TRPV4-deficient mice. Eight-month-old WT and *Trpv4*<sup>-/-</sup> male mice were subjected to treadmill exercise. After acclimation, mice ran on a treadmill at 24 m/min until exhaustion. *A*: running time (min). *B*: total running distance (m). Data are expressed as means  $\pm$  SE (*n* = 6). \*Significant difference vs. WT mice (*P* < 0.05).

a key regulator of oxidative metabolism in skeletal muscle (16) and is regulated by the calcineurin-NFAT signaling pathway (1). The number of oxidative type I fiber increased in the SM of *Trpv4*<sup>-/-</sup> mice compared with WT mice, as expected from myogenin gene induction. This phenotypic change in muscle fiber types might contribute to the higher exercise ability and increased energy expenditure under HF diet condition in *Trpv4*<sup>-/-</sup> mice. Other calcineurin-regulated genes such as LPL, CPT1, PPAR $\alpha$ , and PPAR $\delta$  were observed to be upregulated in TRPV4-deficient muscles. Taken together, our data suggested that calcineurin signaling activation via TRPC3 and TRPC6 stimulates the expression of genes involved in energy metabolism in skeletal muscles, thus contributing to the altered metabolism phenotype of *Trpv4*<sup>-/-</sup> mice. There might also be redundant roles for TRPV4, TRPC3, and TRPC6 as intracellular Ca<sup>2+</sup> regulators in skeletal muscle.

In conclusion, inactivation of the *Trpv4* gene induced TRPC3 and TRPC6 expression and calcineurin activity elevation, which affected energy metabolism mainly by increasing expression of genes involved in fuel oxidation in skeletal muscle and thereby protected mice from diet-induced obesity. The present data might provide us with a better understanding of energy regulation in skeletal muscle. The expression levels of TRP channels in skeletal muscle may be the traits that underlie both skeletal muscle energetics and resistance to obesity. TRP channels are thought to play a pivotal role in regulating Ca<sup>2+</sup> level in skeletal muscle cells. Therefore, activation of these channels could affect various cellular responses, including muscle contraction, and changing skeletal muscle energetics. Although hyperactivation of calcineurin can cause muscle degeneration (29), the regulation of TRP channels, including TRPV4, TRPC3, and TRPC6, expressed in skeletal muscles could be new therapeutic targets to prevent the development of obesity and metabolic syndrome.

#### ACKNOWLEDGMENTS

We are grateful to Drs. M. Tominaga and R. A. Koza for critical reading of the manuscript, and to K. Ito, Y. Yamashita, S. Takeda, and Y. Nakagami for technical assistance.

#### GRANTS

This study was supported by a grant from the MEXT COE project for private universities.

#### DISCLOSURES

No conflicts of interest, financial or otherwise, are declared by the author(s).

#### AUTHOR CONTRIBUTIONS

Author contributions: T.K., Z.W., A.M., and H.Y. performed experiments; T.K., Z.W., A.M., and H.Y. analyzed data; T.K., M.S., and H.Y. interpreted results of experiments; T.K. and H.Y. prepared figures; T.K., M.S., and H.Y. edited and revised the manuscript; T.K., Z.W., A.M., M.S., and H.Y. approved the final version of the manuscript; H.Y. conception and design of research; H.Y. drafted the manuscript.

#### REFERENCES

- Armand AS, Bourajjaj M, Martínez-Martínez S, el Azzouzi H, da Costa Martins PA, Hatzis P, Seidler T, Redondo JM, De Windt LJ. Cooperative synergy between NFAT and MyoD regulates myogenin expression and myogenesis. *J Biol Chem* 283: 29004–29010, 2008.
- Bligh EG, Dyer WJ. A rapid method of total lipid extraction and purification. *Can J Biochem Physiol* 37: 911–917, 1959.
- Caterina MJ, Rosen TA, Tominaga M, Brake AJ, Julius D. A capsaicin-receptor homologue with a high threshold for noxious heat. *Nature* 398: 436–441, 1999.
- Caterina MJ, Schumacher MA, Tominaga M, Rosen TA, Levine JD, Julius D. The capsaicin receptor: a heat-activated ion channel in the pain pathway. *Nature* 389: 816–824, 1997.
- Cheng H, Beck A, Launay P, Gross SA, Stokes AJ, Kinet JP, Fleig A, Penner R. TRPM4 controls insulin secretion in pancreatic beta-cells. *Cell Calcium* 41: 51–61, 2007.
- Clapham DE. TRP channels as cellular sensors. *Nature* 426: 517–524, 2003.
- Damann N, Voets T, Nilius B. TRPs in our senses. *Curr Biol* 18: R880–R889, 2008.
- Dietrich A, Mederos Y, Schnitzler M, Gollasch M, Gross V, Storch U, Dubrovskaja G, Obst M, Yildirim E, Salanova B, Kalwa H, Essin K, Pinkenburg O, Luft FC, Gudermann T, Birnbaumer L. Increased vascular smooth muscle contractility in TRPC6<sup>-/-</sup> mice. *Mol Cell Biol* 25: 6980–6989, 2005.
- Dressel U, Allen TL, Pippal JB, Rohde PR, Lau P, Muscat GE. The peroxisome proliferator-activated receptor beta/delta agonist, GW501516, regulates the expression of genes involved in lipid catabolism and energy uncoupling in skeletal muscle cells. *Mol Endocrinol* 17: 2477–2493, 2003.
- Enerbäck S, Jacobsson A, Simpson EM, Guerra C, Yamashita H, Harper ME, Kozak LP. Mice lacking mitochondrial uncoupling protein are cold-sensitive but not obese. *Nature* 387: 90–94, 1997.
- Guerra C, Koza RA, Yamashita H, Walsh K, Kozak LP. Emergence of brown adipocytes in white fat in mice is under genetic control. Effects on body weight and adiposity. *J Clin Invest* 102: 412–420, 1998.
- Güler AD, Lee H, Iida T, Shimizu I, Tominaga M, Caterina M. Heat-evoked activation of the ion channel, TRPV4. *J Neurosci* 22: 6408–6414, 2002.
- Hakimi P, Yang J, Casadesus G, Massillon D, Tolentino-Silva F, Nye CK, Cabrera ME, Hagen DR, Utter CB, Baghdy Y, Johnson DH, Wilson DL, Kirwan JP, Kalhan SC, Hanson RW. Overexpression of the cytosolic form of phosphoenolpyruvate carboxykinase (GTP) in skeletal muscle repatterns energy metabolism in the mouse. *J Biol Chem* 282: 32844–32855, 2007.
- Hanson RW, Hakimi P. Born to run; the story of the PEPCCK-C<sup>mus</sup> mouse. *Biochimie* 90: 838–842, 2008.
- Hill JO, Wyatt HR, Reed GW, Peters JC. Obesity and the environment: where do we go from here? *Science* 299: 853–855, 2003.
- Hughes SM, Chi MM, Lowry OH, Gundersen K. Myogenin induces a shift of enzyme activity from glycolytic to oxidative metabolism in muscles of transgenic mice. *J Cell Biol* 145: 633–642, 1999.
- Inoue R, Jensen LJ, Jian Z, Shi J, Hai L, Lurie AI, Henriksen FH, Salomonsson M, Morita H, Kawarabayashi Y, Mori M, Mori Y, Ito Y. Synergistic activation of vascular TRPC6 channel by receptor and mechanical stimulation via phospholipase C/diacylglycerol and phospholipase A2/omega-hydroxylase/20-HETE pathways. *Circ Res* 99: 119–131, 2006.
- Kontani Y, Wang Y, Kimura K, Inokuma KI, Saito M, Suzuki-Miura T, Wang Z, Sato Y, Mori N, Yamashita H. UCP1 deficiency increases susceptibility to diet-induced obesity with age. *Aging Cell* 4: 147–155, 2005.
- Kopelman PG. Obesity as a medical problem. *Nature* 404: 635–643, 2000.
- Krüger J, Kunert-Keil C, Bisping F, Brinkmeier H. Transient receptor potential cation channels in normal and dystrophic mdx muscle. *Neuromuscul Disord* 18: 501–513, 2008.
- Kuwahara K, Wang Y, McAnally J, Richardson JA, Bassel-Duby R, Hill JA, Olson EN. TRPC6 fulfills a calcineurin signaling circuit during pathologic cardiac remodeling. *J Clin Invest* 116: 3114–3126, 2006.
- Lee H, Iida T, Mizuno A, Suzuki M, Caterina MJ. Altered thermal selection behavior in mice lacking transient receptor potential vanilloid 4. *J Neurosci* 25: 1304–1310, 2005.
- Liedtke W, Choe Y, Martí-Renom MA, Bell AM, Denis CS, Sali A, Hudspeth AJ, Friedman JM, Heller S. Vanilloid receptor-related osmotically activated channel (VR-OAC), a candidate vertebrate osmoreceptor. *Cell* 103: 525–535, 2000.
- Long YC, Glund S, Garcia-Roves PM, Zierath JR. Calcineurin regulates skeletal muscle metabolism via coordinated changes in gene expression. *J Biol Chem* 282: 1607–1614, 2007.

25. Long YC, Zierath JR. Influence of AMP-activated protein kinase and calcineurin on metabolic networks in skeletal muscle. *Am J Physiol Endocrinol Metab* 295: E545–E552, 2008.
26. Lowell BB, Spiegelman BM. Towards a molecular understanding of adaptive thermogenesis. *Nature* 404: 652–660, 2000.
27. Masuyama R, Vriens J, Voets T, Karashima Y, Owsianik G, Vennekens R, Lieben L, Torrekens S, Moermans K, Vanden Bosch A, Bouillon R, Nilius B, Carmeliet G. TRPV4-mediated calcium influx regulates terminal differentiation of osteoclasts. *Cell Metab* 8: 257–265, 2008.
28. McKemy DD, Neuhausser WM, Julius D. Identification of a cold receptor reveals a general role for TRP channels in thermosensation. *Nature* 416: 52–58, 2002.
29. Millay DP, Goonasekera SA, Sargent MA, Maillet M, Aronow BJ, Molkenstin JD. Calcium influx is sufficient to induce muscular dystrophy through a TRPC-dependent mechanism. *Proc Natl Acad Sci USA* 106: 19023–19028, 2009.
30. Mizuno A, Matsumoto N, Imai M, Suzuki M. Impaired osmotic sensation in mice lacking TRPV4. *Am J Physiol Cell Physiol* 285: C96–C101, 2003.
31. Motter AL, Ahern GP. RPV1-null mice are protected from diet-induced obesity. *FEBS Lett* 582: 2257–2262, 2008.
32. Muoio DM, MacLean PS, Lang DB, Li S, Houmard JA, Way JM, Winegar DA, Corton JC, Dohm GL, Kraus WE. Fatty acid homeostasis and induction of lipid regulatory genes in skeletal muscles of peroxisome proliferator-activated receptor (PPAR) alpha knock-out mice. Evidence for compensatory regulation by PPAR delta. *J Biol Chem* 277: 26089–26097, 2002.
33. Nilius B, Owsianik G, Voets T, Peters JA. Transient receptor potential cation channels in disease. *Physiol Rev* 87: 165–217, 2007.
34. Novak CM, Escande C, Gerber SM, Chini EN, Zhang M, Britton SL, Koch LG, Levine JA. Endurance capacity, not body size, determines physical activity levels: role of skeletal muscle PEPCK. *PLoS One* 4: e5869, 2009.
35. Olson EN, Williams RS. Remodeling muscles with calcineurin. *Bioessays* 22: 510–519, 2000.
36. Peier AM, Moqrich A, Hergarden AC, Reeve AJ, Andersson DA, Story GM, Earley TJ, Dragoni I, McIntyre P, Bevan S, Patapoutian A. A TRP channel that senses cold stimuli and menthol. *Cell* 108: 705–715, 2002.
37. Peier AM, Reeve AJ, Andersson DA, Moqrich A, Earley TJ, Hergarden AC, Story GM, Colley S, Hogenesch JB, McIntyre P, Bevan S, Patapoutian A. A heat-sensitive TRP channel expressed in keratinocytes. *Science* 296: 2046–2049, 2002.
38. Qian F, Huang P, Ma L, Kuznetsov A, Tamarina N, Philipson LH. TRP genes: candidates for nonselective cation channels and store-operated channels in insulin-secreting cells. *Diabetes* 51, Suppl 1: S183–S189, 2002.
39. Razavi R, Chan Y, Afifyan FN, Liu XJ, Wan X, Yantha J, Tsui H, Tang L, Tsai S, Santamaria P, Driver JP, Serreze D, Salter MW, Dosch HM. TRPV1+ sensory neurons control beta cell stress and islet inflammation in autoimmune diabetes. *Cell* 127: 1123–1135, 2006.
40. Rosenberg P, Hawkins A, Stiber J, Shelton JM, Hutcheson K, Bassel-Duby R, Shin DM, Yan Z, Williams RS. TRPC3 channels confer cellular memory of recent neuromuscular activity. *Proc Natl Acad Sci USA* 101: 9387–9392, 2004.
41. Shibasaki K, Suzuki M, Mizuno A, Tominaga M. Effects of body temperature on neural activity in the hippocampus: regulation of resting membrane potentials by transient receptor potential vanilloid 4. *J Neurosci* 27: 1566–1575, 2007.
42. Sidhaye VK, Güler AD, Schweitzer KS, D'Alessio F, Caterina MJ, King LS. Transient receptor potential vanilloid 4 regulates aquaporin-5 abundance under hypotonic conditions. *Proc Natl Acad Sci USA* 103: 4747–4752, 2006.
43. Smith GD, Gunthorpe MJ, Kelsell RE, Hayes PD, Reilly P, Facer P, Wright JE, Jerman JC, Walhin JP, Ooi L, Egerton J, Charles KJ, Smart D, Randall AD, Anand P, Davis JB. TRPV3 is a temperature-sensitive vanilloid receptor-like protein. *Nature* 418: 186–190, 2002.
44. Story GM, Peier AM, Reeve AJ, Eid SR, Mosbacher J, Hricik TR, Earley TJ, Hergarden AC, Andersson DA, Hwang SW, McIntyre P, Jegla T, Bevan S, Patapoutian A. ANKTM1, a TRP-like channel expressed in nociceptive neurons, is activated by cold temperatures. *Cell* 112: 819–829, 2003.
45. Strotmann R, Harteneck C, Nunnenmacher K, Schultz G, Plant TD. OTRPC4, a nonselective cation channel that confers sensitivity to extracellular osmolarity. *Nat Cell Biol* 2: 695–702, 2000.
46. Suri A, Szallasi A. The emerging role of TRPV1 in diabetes and obesity. *Trends Pharmacol Sci* 29: 29–36, 2008.
47. Suzuki M, Hirao A, Mizuno A. Microtubule-associated protein 7 increases the membrane expression of transient receptor potential vanilloid 4 (TRPV4). *J Biol Chem* 278: 51448–51453, 2003.
48. Suzuki M, Mizuno A, Kodaira K, Imai M. Impaired pressure sensation in mice lacking TRPV4. *J Biol Chem* 278: 22664–22668, 2003.
49. Todaka H, Taniguchi J, Satoh J, Mizuno A, Suzuki M. Warm temperature-sensitive transient receptor potential vanilloid 4 (TRPV4) plays an essential role in thermal hyperalgesia. *J Biol Chem* 279: 35133–35138, 2004.
50. Togashi K, Hara Y, Tominaga T, Higashi T, Konishi Y, Mori Y, Tominaga M. TRPM2 activation by cyclic ADP-ribose at body temperature is involved in insulin secretion. *EMBO J* 25: 1804–1815, 2006.
51. Venkatchalam K, Montell C. TRP channels. *Annu Rev Biochem* 76: 387–417, 2007.
52. Vriens J, Watanabe H, Janssens A, Droogmans G, Voets T, Nilius B. Cell swelling, heat, and chemical agonists use distinct pathways for the activation of the cation channel TRPV4. *Proc Natl Acad Sci USA* 101: 396–401, 2004.
53. Wagner TF, Loch S, Lambert S, Straub I, Mannebach S, Mathar I, Düfer M, Lis A, Flockerzi V, Philipp SE, Oberwinkler J. Transient receptor potential M3 channels are ionotropic steroid receptors in pancreatic beta cells. *Nat Cell Biol* 10: 1421–1430, 2008.
54. Wang Y, Kimura K, Inokuma K, Saito M, Kontani Y, Kobayashi Y, Mori N, Yamashita H. Potential contribution of vasoconstriction to suppression of heat loss and homeothermic regulation in UCPI-deficient mice. *Pflügers Arch* 452: 363–369, 2006.
55. Wang T, Wang Y, Kontani Y, Kobayashi Y, Sato Y, Mori N, Yamashita H. Evodiamine improves diet-induced obesity in a uncoupling protein-1-independent manner: involvement of antiadipogenic mechanism and extracellularly regulated kinase/mitogen-activated protein kinase signaling. *Endocrinology* 149: 358–366, 2008.
56. Wang T, Wang Y, Yamashita H. Evodiamine inhibits adipogenesis via the EGFR-PKCa/alpha-ERK signaling pathway. *FEBS Lett* 583: 3655–3659, 2009.
57. Watanabe H, Vriens J, Suh SH, Benham CD, Droogmans G, Nilius B. Heat-evoked activation of TRPV4 channels in a HEK293 cell expression system and in native mouse aorta endothelial cells. *J Biol Chem* 277: 47044–47051, 2002.
58. Wissenbach U, Bödding M, Freichel M, Flockerzi V. Trp12, a novel Trp related protein from kidney. *FEBS Lett* 485: 127–134, 2000.
59. Xu H, Ramsey IS, Kotecha SA, Moran MM, Chong JA, Lawson D, Ge P, Lilly J, Silos-Santiago I, Xie Y, DiStefano PS, Curtis R, Clapham DE. TRPV3 is a calcium-permeable temperature-sensitive cation channel. *Nature* 418: 181–186, 2002.
60. Yamashita H, Wang Z, Wang Y, Furuyama T, Kontani Y, Sato Y, Mori N. Impaired basal thermal homeostasis in rats lacking capsaicin-sensitive peripheral small sensory neurons. *J Biochem* 143: 385–393, 2008.
61. Yin J, Hoffmann J, Kaestle SM, Neye N, Wang L, Baeurle J, Liedtke W, Wu S, Kuppe H, Pries AR, Kuebler WM. Negative-feedback loop attenuates hydrostatic lung edema via a cGMP-dependent regulation of transient receptor potential vanilloid 4. *Circ Res* 102: 966–974, 2008.
62. Yoon MJ, Lee GY, Chung JJ, Ahn YH, Hong SH, Kim JB. Adiponectin increases fatty acid oxidation in skeletal muscle cells by sequential activation of AMP-activated protein kinase, p38 mitogen-activated protein kinase, and peroxisome proliferator-activated receptor alpha. *Diabetes* 55: 2562–2570, 2006.
63. Yoshida T, Yoshioka K, Wakabayashi Y, Nishioka H, Kondo M. Effects of capsaicin and isothiocyanate on thermogenesis of interscapular brown adipose tissue in rats. *J Nutr Sci Vitaminol (Tokyo)* 34: 587–594, 1988.

# Evodiamine Inhibits Insulin-Stimulated mTOR-S6K Activation and IRS1 Serine Phosphorylation in Adipocytes and Improves Glucose Tolerance in Obese/Diabetic Mice

Ting Wang<sup>1‡</sup>, Tatsuya Kusudo<sup>1</sup>, Tamaki Takeuchi<sup>1</sup>, Yukari Yamashita<sup>1,2</sup>, Yasuhide Kontani<sup>3</sup>, Yuko Okamatsu<sup>4</sup>, Masayuki Saito<sup>5</sup>, Nozomu Mori<sup>6</sup>, Hitoshi Yamashita<sup>1,2\*</sup>

**1** Department of Biomedical Sciences, College of Life and Health Sciences, Chubu University, Kasugai, Japan, **2** Nutritional Health Science Research Center, Chubu University, Kasugai, Japan, **3** Department of Food Science for Health, Minami-Kyushu University, Miyazaki, Japan, **4** Department of Biomedical Sciences, Graduate School of Veterinary Medicine, Hokkaido University, Sapporo, Japan, **5** Department of Nutrition, School of Nursing and Nutrition, Tenshi College, Sapporo, Japan, **6** Department of Anatomy and Neurobiology, Nagasaki University School of Medicine, Nagasaki, Japan

## Abstract

Evodiamine, an alkaloid extracted from the dried unripe fruit of the tree *Evodia rutaecarpa* Benth (Rutaceae), reduces obesity and insulin resistance in obese/diabetic mice; however, the mechanism underlying the effect of evodiamine on insulin resistance is unknown. This study investigated the effect of evodiamine on signal transduction relating to insulin resistance using obese/diabetic KK-Ay mice and an *in vitro* adipocyte culture. There is a significant decrease in the mammalian target of rapamycin (mTOR) and ribosomal S6 protein kinase (S6K) signaling in white adipose tissue (WAT) in KK-Ay mice treated with evodiamine, in which glucose tolerance is improved. In addition, reduction of insulin receptor substrate 1 (IRS1) serine phosphorylation, an indicator of insulin resistance, was detected in their WAT, suggesting suppression of the negative feedback loop from S6K to IRS1. As well as the stimulation of IRS1 and Akt serine phosphorylation, insulin-stimulated phosphorylation of mTOR and S6K is time-dependent in 3T3-L1 adipocytes, whereas evodiamine does not affect their phosphorylation except for an inhibitory effect on mTOR phosphorylation. Moreover, evodiamine inhibits the insulin-stimulated phosphorylation of mTOR and S6K, leading to down-regulation of IRS1 serine phosphorylation in the adipocytes. Evodiamine also stimulates phosphorylation of AMP-activated protein kinase (AMPK), an important regulator of energy metabolism, which may cause down-regulation of mTOR signaling in adipocytes. A similar effect on AMPK, mTOR and IRS1 phosphorylation was found in adipocytes treated with rosiglitazone. These results suggest evodiamine improves glucose tolerance and prevents the progress of insulin resistance associated with obese/diabetic states, at least in part, through inhibition of mTOR-S6K signaling and IRS1 serine phosphorylation in adipocytes.

**Citation:** Wang T, Kusudo T, Takeuchi T, Yamashita Y, Kontani Y, et al. (2013) Evodiamine Inhibits Insulin-Stimulated mTOR-S6K Activation and IRS1 Serine Phosphorylation in Adipocytes and Improves Glucose Tolerance in Obese/Diabetic Mice. PLoS ONE 8(12): e83264. doi:10.1371/journal.pone.0083264

**Editor:** Krisztian Stadler, Pennington Biomedical Research Center, United States of America

**Received:** April 22, 2013; **Accepted:** November 1, 2013; **Published:** December 31, 2013

**Copyright:** © 2013 Wang et al. This is an open-access article distributed under the terms of the Creative Commons Attribution License, which permits unrestricted use, distribution, and reproduction in any medium, provided the original author and source are credited.

**Funding:** This work was supported by a grant from MEXT-Supported program for Strategic Research Foundation at Private Universities (to H.Y.). The funders had no role in study design, data collection and analysis, decision to publish, or preparation of the manuscript.

**Competing Interests:** The authors have declared that no competing interests exist.

\* E-mail: hyamashi@isc.chubu.ac.jp

‡ Current address: Division of Gastroenterology and Hepatology, Department of Internal Medicine, Iwate Medical University, Morioka, Japan

## Introduction

The increased availability of food in Western countries and in Japan has augmented the prevalence of obesity and insulin resistance, which are central in the development of metabolic syndrome [1]. High fat intake is considered to be the major cause of metabolic abnormalities due to overnutrition. Adipose tissue is responsible for the majority of fat metabolism affecting largely glucose metabolism and insulin sensitivity under the control of various hormones and cytokines [2]. Nutrient overload increases serum insulin levels, which stimulates uptake of free fatty acids (FFAs) and glucose into adipocytes mainly in white adipose tissue (WAT), where excess energy is stored in the form of triglycerides. When this energy storage system is active, increases in the number and size of adipocytes are required for additional fat deposition in

WAT, causing excessive growth of adipose tissue leading to obesity [3]. Elevated levels of serum insulin as well as non-esterified FFAs in the obese state decrease insulin sensitivity and increase insulin resistance in metabolic tissues, including liver, muscle and adipose tissue, leading to type 2 diabetes mellitus. Regulation of WAT is a potential strategy for the treatment of obesity and for improvement of insulin resistance. Brown adipose tissue (BAT) is specialized for thermogenesis through the function of uncoupling protein 1 (UCP1) located in the mitochondria [4,5]. Because of UCP1, which dissipates caloric energy as heat, BAT has an important role in preventing obesity, as shown in our earlier study using UCP1-knockout mice [6]. It was found recently that functional BAT, despite its reduction with age, exists in adult humans and its level is correlated inversely to the degree of adiposity [7,8]. These findings have accelerated basic and clinical

studies on the stimulation of BAT formation and activity as a potential therapeutic target against obesity and insulin resistance [9]; however, an alternative strategy independent of UCP1 thermogenesis is needed for BAT-negative individuals.

Insulin signaling is implicated in the regulation of adipocyte biology. Many of the metabolic and anti-apoptotic effects of insulin are mediated by the signaling pathway beginning from phosphorylation and activation of insulin/insulin-like growth factor I receptors, which results in tyrosine phosphorylation of the insulin receptor substrate 1 (IRS1) [10]. Activation of phosphatidylinositol 3-kinase (PI3K) and protein kinase B/Akt by the IRS1 protein appears to be important in the mechanism of glucose uptake in adipocytes and muscle cells. In addition, insulin signaling is intimately linked to the nutrient-responsive mammalian target of rapamycin (mTOR) signaling pathway via activation of Akt [11,12]. The activation of mTOR phosphorylates its downstream protein ribosomal S6 protein kinase (S6K), participating in several processes including protein synthesis and proliferation [12,13]. It became apparent that serine phosphorylation of IRS1 reduces the ability of IRS1 to activate PI3K [10–12]. In diet-induced obesity, overactivation of mTOR-S6K signaling favors expansion of the WAT mass, leading to insulin resistance of adipocytes through elevated serine phosphorylation of IRS1. Mice deficient of S6K are protected against diet-induced obesity and show enhanced insulin sensitivity owing to the loss of the negative feedback loop from S6K to IRS1 [14,15]. These findings suggest further development of interventions targeting mTOR-S6K signaling for the treatment and prevention of obesity and insulin resistance.

Evodiamine, an alkaloid extracted from the dried unripe fruit of *Evodia rutaecarpa* Benth (Rutaceae), has been used for many years as a traditional Chinese herbal medicine for the treatment of pain, vomiting and pyresis. Evodiamine has a wide variety of bioactivity with antinociceptive, anti-obesity, vasodilatory, anti-tumor and anti-inflammatory effects [16–20]. We found evodiamine decreases diet-induced obesity and glucose intolerance in a UCP1-independent manner in mice [21]. We showed that evodiamine increases phosphorylation of extracellular signal-regulated kinase (ERK) and reduces the expression of transcription factors such as PPAR $\gamma$  in pre-adipocytes, strongly inhibiting their differentiation into mature adipocytes. It was shown recently that evodiamine improves insulin resistance and fat accumulation in obese/diabetic db/db mice [22]. However, the mechanisms underlying the effects of evodiamine on glucose tolerance and insulin resistance are not known. This study used obese/diabetic mice and adipocyte culture *in vitro* to investigate how evodiamine affects glucose tolerance and insulin resistance, especially from the viewpoint of signal transduction, including the mTOR-S6K signaling pathway.

## Results

### Effects of evodiamine on metabolic phenotypes in obese/diabetic KK-Ay mice

We examined the effects of evodiamine on the metabolic phenotypes associated with obese/diabetic states in KK-Ay mice. When mice were treated daily with evodiamine or vehicle (control) for one week, a significant decrease in body weight (BW) gain, but not in food intake, was found in the evodiamine group compared to the control group (Figs. 1A, B). As shown in Table 1, there was a significant reduction in tissue mass in several white fat depots, including inguinal white adipose tissue (IWAT) and retroperitoneal WAT (RWAT), in evodiamine-treated mice. There was no difference in liver weight between the two groups (Table 1). The

same amount of glucose was fed to each group (Fig. 1C) but insulin levels were significantly lower in the evodiamine group compared to the control group (Fig. 1D), suggesting increased insulin sensitivity. Moreover, glucose intolerance (measured by an intraperitoneal (i.p.) glucose tolerance test) decreased in the evodiamine group compared to the control group (Fig. 1E). Histological analysis showed decreased trends of adipocyte size in WATs of the evodiamine group compared to the control group (RWAT,  $3737 \pm 226 \mu\text{m}^2$  and  $3503 \pm 303 \mu\text{m}^2$ ; gonadal WAT (GWAT),  $1845 \pm 205 \mu\text{m}^2$  and  $1403 \pm 152 \mu\text{m}^2$ ; IWAT,  $4112 \pm 592 \mu\text{m}^2$  and  $3844 \pm 308 \mu\text{m}^2$  in the control and evodiamine group, respectively; Fig. 2).

### Evodiamine attenuates mTOR-S6K signaling and down-regulates IRS1 serine phosphorylation in WAT of obese/diabetic KK-Ay mice

We examined the effects of evodiamine on the signaling of mTOR and IRS1 in the obese/diabetic mice because attenuated phosphorylation of Akt, an upstream kinase for mTOR, is present in the WAT of the evodiamine-treated mice, as reported [21]. There was no difference in mTOR Ser2448 phosphorylation in RWAT between the evodiamine and control groups (Fig. S1A in File S1) but there was a significant reduction of its level in IWAT of KK-Ay mice treated with evodiamine compared to the control group (Fig. 3A). There was a reduction in mTOR phosphorylation also in the WAT of UCP1-KO mice treated with evodiamine compared to the control group (Fig. S2A in File S1). There was no effect of evodiamine on mTOR phosphorylation or UCP1 protein level in the BAT of KK-Ay mice (Fig. S3 in File S1). Moreover, there were decreases in S6K Thr389 phosphorylation in IWAT and RWAT of evodiamine-treated mice (Fig. 3B and Fig. S1B in File S1). Similar to the results for the WAT of UCP1-KO mice treated with evodiamine (Figs. S2B, C in File S1), phosphorylation of Akt Ser473 and IRS1 Ser636/639 in the IWAT of KK-Ay mice was significantly lower (54% and 12% of the control, respectively) in the evodiamine group compared to the vehicle group (Figs. 3C, D) and phosphorylation of IRS1 Tyr612 and PDK1 Ser241 was not different between the two groups (Figs. 3D, E). There were significant decreases in the Akt and IRS1 serine phosphorylation in the RWAT of mice treated with evodiamine compared to the vehicle control (Figs. S1C, D in File S1). Although evodiamine administration reduces mTOR phosphorylation in liver, the phosphorylation levels of S6K, Akt and IRS1 were not different between the evodiamine and control groups (Fig. 4). Likewise, there were no differences in the phosphorylation levels of mTOR, S6K, Akt and IRS1 in gastrocnemius muscle (GM) between the evodiamine and control groups (Figs. S4A–D in File S1).

### Evodiamine inhibits insulin-stimulated phosphorylation of mTOR and S6K, reducing IRS1 serine phosphorylation in 3T3-L1 adipocytes

To assess the direct effects of evodiamine on adipocytes, we examined the effects of insulin and evodiamine on stimulation of the mTOR-S6K signaling pathway using differentiated 3T3-L1 adipocytes. As well as the stimulation of IRS1 and Akt phosphorylation, insulin-stimulated phosphorylation of mTOR and S6K was time-dependent; however, evodiamine had little effect on their phosphorylation (Fig. 5). Insulin, but not evodiamine, stimulated ERK phosphorylation transiently in mature adipocytes. This was in contrast to the effect of evodiamine in 3T3-L1 pre-adipocytes, in which this compound markedly increased ERK phosphorylation (Fig. S5 in File S1). In the presence of insulin stimulation, evodiamine seemed to suppress the

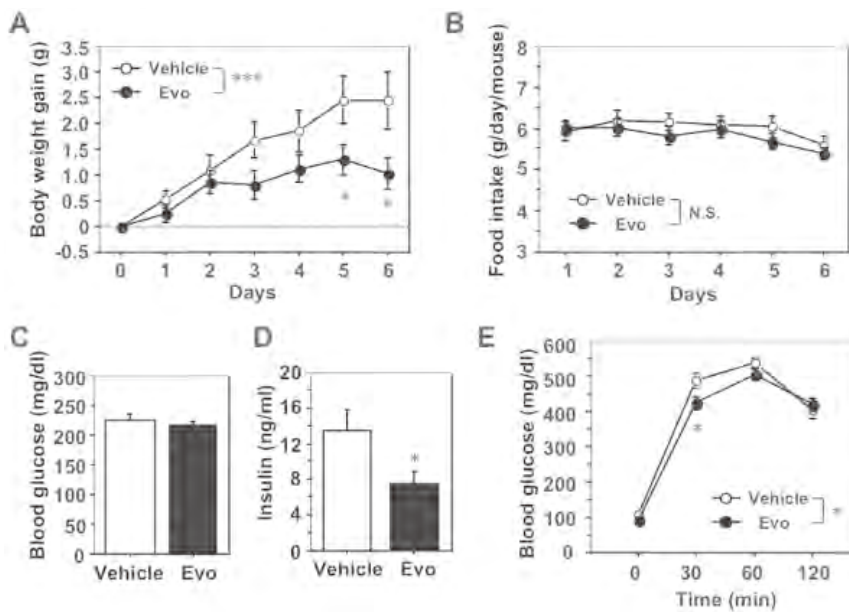


**Figure 1. Effects of evodiamine on body weight, food intake, blood parameters and glucose tolerance in KK-Ay mice.** Eight-weeks old female KK-Ay mice were injected i.p. daily with evodiamine (3 mg/kg body weight) or vehicle for 1 week. A, Body weight gain; B, food intake; C, fed glucose level; D, insulin level; E, IPGTT. After starvation for 17 h, mice were injected i.p. with glucose (1.5 mg/g body weight). Data are expressed as mean  $\pm$  SEM;  $n = 14$  and  $13$  for body weight gain and food intake;  $n = 8$  each for glucose and insulin levels;  $n = 9$  and  $8$  for IPGTT, in vehicle and evodiamine groups, respectively. \* $p < 0.05$ , \*\*\* $p < 0.001$  vs. vehicle group. doi:10.1371/journal.pone.0083264.g001

phosphorylation of mTOR, S6K, IRS1 and Akt, except for ERK phosphorylation in adipocytes (Fig. 6), although evodiamine did not affect glucose uptake in adipocytes (Fig. 7). Insulin-induced serine phosphorylation of Akt and IRS1 was suppressed by evodiamine in pre-adipocytes (Fig. S5 in File S1). We evaluated the effects of insulin and evodiamine on phosphorylation of these molecules in adipocytes. As shown in Figures 8A–E, insulin markedly increased phosphorylation of mTOR (1.8-fold), S6K (10.3-fold), IRS1 (26.1-fold), Akt (7.3-fold) and ERK (5.6-fold) in 3T3-L1 adipocytes compared to the control, whereas evodiamine had no significant effect on phosphorylation of these signaling molecules, except for an inhibitory effect on mTOR phosphorylation. By contrast, evodiamine suppressed insulin-stimulated phosphorylation of mTOR, S6K and IRS1 in adipocytes significantly (Figs. 8A–C). Evodiamine did not significantly affect the levels of insulin-stimulated Akt or ERK phosphorylation in adipocytes (Figs. 8D, E), although their phosphorylation was affected considerably by evodiamine in pre-adipocytes; i.e. Akt phosphorylation was inhibited but ERK phosphorylation was enhanced (Fig. S5 in File S1) [21].

We examined the effects of rosiglitazone, an anti-diabetic compound, on the phosphorylation of these signaling molecules compared to the effects of insulin and evodiamine in adipocytes. Similar to evodiamine, rosiglitazone alone did not affect phosphorylation of S6K, IRS1, Akt and ERK (except mTOR) in the cells but, like evodiamine, rosiglitazone suppressed insulin-stimulated phosphorylation of mTOR and IRS1 in adipocytes significantly (Figs. 8A, C), although its effect on S6K phosphorylation in insulin-stimulated cells did not reach significance (Fig. 8B). There was no significant effect of rosiglitazone on insulin-stimulated Akt or ERK phosphorylation in adipocytes (Figs. 8D, E).

### Evodiamine stimulates phosphorylation of AMP-activated protein kinase (AMPK) in 3T3-L1 adipocytes and WAT

From the results in Figures 8D–E, Akt and ERK may not be the upstream effectors for mTOR-S6K signaling in mature adipocytes stimulated by evodiamine. So, we finally examined an involvement of AMPK in the mechanism by which evodiamine affects mTOR signaling pathway, because its phosphorylation is negatively regulated by the activity of AMPK, which regulates various cellular processes including glucose and lipid metabolism [22,23]. As well as rosiglitazone, evodiamine significantly stimulated AMPK Thr172 phosphorylation (1.9-fold) in 3T3-L1 adipocytes compared to the control, whereas insulin had no effect on its phosphorylation (Fig. 8F). Significant increases in AMPK phosphorylation were also detected in the WAT and liver, but not in gastrocnemius muscle (GM), of KK-Ay mice treated with evodiamine compared to the vehicle control (Figs. 9A–C), supporting the decreases of mTOR phosphorylation in these tissues (Figs. 3A and 4A).

### Discussion

Evodiamine is a multipotent compound that has a wide variety of bioactivities, such as anti-obesity and anti-tumor effects [17,19]. Earlier, we reported that a dietary supplementation of evodiamine inhibited adipocyte differentiation and several obesity-associated phenotypes, such as insulin resistance in mice lacking UCP1 thermogenesis, indicating that UCP1-independent roles of this compound improve health under conditions of excess caloric intake [21]. Although indirect calorimetric analysis did not detect the effect of evodiamine on energy expenditure, a precise analysis of respiratory quotient (RQ) values indicated that a higher frequency of higher RQ values was present in evodiamine-injected mice compared to vehicle-injected animals. This indicates that

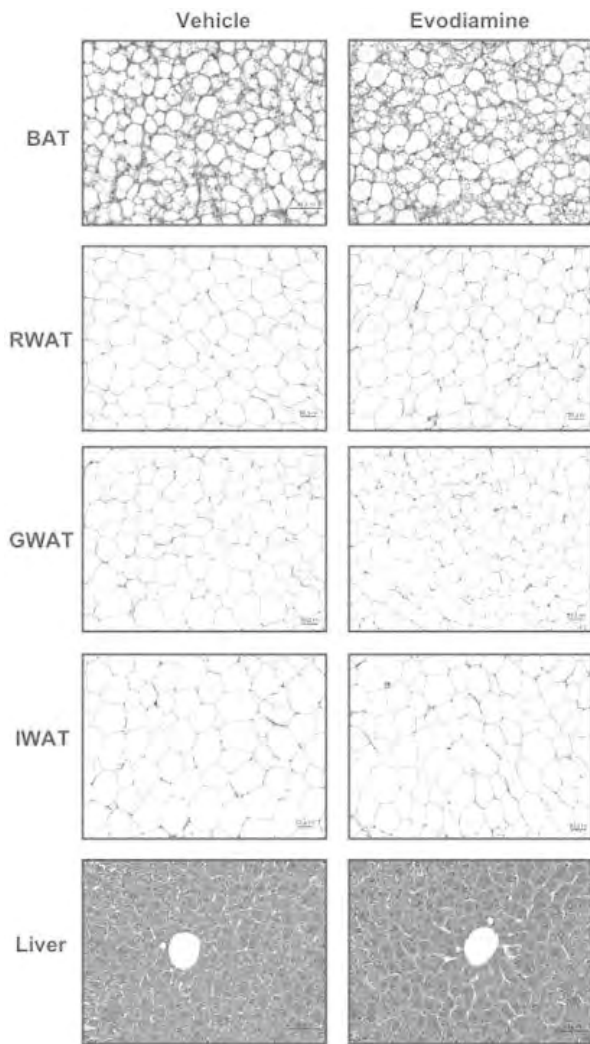


**Figure 2. Histological analysis of BAT, RWAT, GWAT, IWAT and liver in KK-Ay mice treated with evodiamine.** Tissue samples were collected from the mice treated with evodiamine for 7 days. Tissue sections of brown adipose tissue (BAT), retroperitoneal (RWAT), gonadal (GWAT), inguinal white adipose tissues (IWAT) and liver were stained with hematoxylin and eosin.  
doi:10.1371/journal.pone.0083264.g002

evodiamine affects glucose homeostasis in the whole body (Fig. S6 in File S1). We also detected the effect of evodiamine on glucose tolerance and insulin sensitivity in obese/diabetic KK-Ay mice, in which decreases in BW gain and WAT mass were observed in the evodiamine-treated KK-Ay mice compared to the vehicle control. These results were consistent with the Bak's study that evodiamine prevented BW gain and insulin resistance in db/db mice [24]. Reduced fat accumulation in several depots of WAT might contribute to the improvement of insulin sensitivity in the obese/diabetic mice treated with evodiamine, because hypertrophy of WATs is known to cause the decrease in insulin sensitivity in animals.

The recent advance in understanding the role of the mTOR-S6K signaling pathway is of great interest in relation to the effects of evodiamine, because this signaling pathway is activated in response to growth factors, insulin or nutrients such as glucose and amino acids [12,14] and its increased activity leads to serine phosphorylation of IRS1, creating a negative feedback loop to

**Table 1. Effect of evodiamine on tissue weight in KK-Ay mice.**

	Vehicle (n=5)	Evodiamine (n=5)	p
Body weight (g)	38.0±1.2	37.3±0.5	0.6001
Tissue weight (mg)			
BAT	251±25	236±16	0.6305
IWAT	598±29	467±40	0.0300
GWAT	1584±145	1283±34	0.0786
RWAT	175±10	133±13	0.0372
MWAT	1017±122	911±23	0.4196
Kidney	174±7	179±6	0.5901
Liver	1901±54	1862±80	0.6979
Pancreas	330±21	362±17	0.2740
Heart	146±2	161±8	0.1163
Spleen	101±9	84±7	0.1722

Female 8-weeks old KK-Ay mice were injected i.p. daily with evodiamine (3 mg/kg body weight) or vehicle control. After 1 week, non-fasting samples of tissues and blood were collected. The left pads of inguinal (IWAT), gonadal (GWAT) and retroperitoneal (RWAT) white adipose tissues were used to measure tissue weight.  
BAT, brown adipose tissue; MWAT, mesenteric WAT.  
doi:10.1371/journal.pone.0083264.t001

insulin signaling that attenuates insulin sensitivity [14,15]. As expected, there is a significant decrease in phosphorylation of S6K in the WATs of evodiamine-treated KK-Ay mice. This down-regulation of S6K activity appears to lead to reduced serine phosphorylation of IRS1 in tissues, contributing to the improvement of insulin sensitivity in KK-Ay mice treated with evodiamine. Akt is also a key molecule for the intracellular signal cascade in the regulation of many cellular activities, including growth, glucose metabolism and adipogenesis [25,26]. Akt activity is regulated by various pathways and insulin signaling via IRS1 and PDK1 [11,12]. IRS1 protein contains multiple sites for tyrosine phosphorylation and both Tyr612 and Tyr632 are important for IRS1 to fully activate PI3K and mediate translocation of GLUT4 in response to insulin in adipocytes [27]. PDK1 may also stimulate GLUT4 translocation via atypical protein kinase C (PKC) activation without Akt activation, because PDK1 phosphorylates the PKC isoforms in a PI3K-dependent manner [28] and glucose uptake can be regulated through the Akt-independent PI3K-PKC pathway in adipocytes [29,30]. In the present study, there was a significant decrease in Akt phosphorylation in WATs of evodiamine-treated KK-Ay mice compared to the vehicle control, which is similar to the result in mice fed an evodiamine diet [21]. Nevertheless, glucose metabolism was improved in these evodiamine-treated mice. Moreover, evodiamine did not significantly affect Akt phosphorylation or glucose uptake in adipocytes *in vitro*. So, the contribution of decreased Akt phosphorylation in WATs to the regulation of glucose uptake may be little in the evodiamine-treated mice. Because phosphorylation of IRS1 Tyr612 and PDK1 Ser241 in the WAT was not changed by treatment with evodiamine (Fig. 3), the decrease in Akt phosphorylation could have been induced by signaling pathways other than the main pathway of insulin signaling.

mTOR is the catalytic subunit of complexes mTORC1 and mTORC2. Akt stimulates mTORC1 activity but, at the same time, is a target of mTORC2 signaling [12]. So, the decrease in Akt phosphorylation could be mediated by reduction of mTORC2 activity. The meaning of this down-regulation of Akt phosphorylation in WATs is not clear, but its reduction might have contributed to suppression of adipocyte differentiation, because

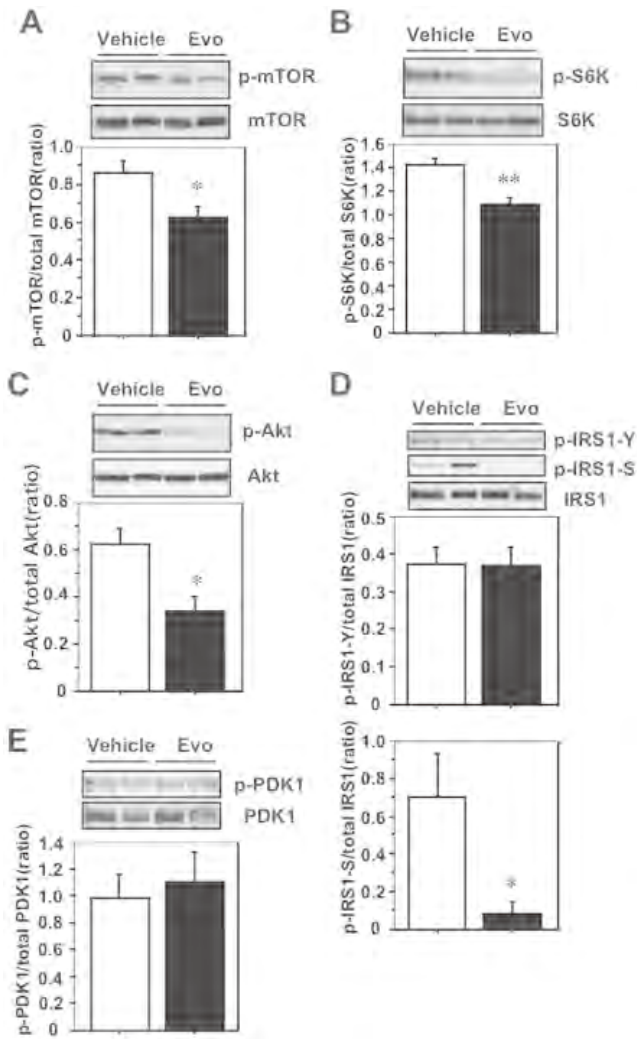


**Figure 3. Effect of evodiamine on the mTOR-S6K signaling in the inguinal WAT (IWAT) of mice treated with evodiamine.** Western blot analysis for mTOR (A), S6K (B), Akt (C), IRS1 (D) and PDK1 (E) were done with tissue lysates (30 µg protein) of IWAT from the KK-Ay mice treated with evodiamine for 7 days. Phosphorylation levels of mTOR Ser2448, S6K Thr389, Akt Ser473, IRS1 Tyr612 and Ser636/639, and PDK1 Ser241 were normalized to the total level of each protein. Data are expressed as mean ± SEM (n = 5). \*p < 0.05, \*\*p < 0.01 vs. vehicle group. doi:10.1371/journal.pone.0083264.g003

adipogenesis is blocked in cultured cells or mice lacking Akt [26]. The insulin-stimulated Akt phosphorylation is attenuated by evodiamine in pre-adipocytes but not in mature adipocytes. Because the basal phosphorylation level of Akt is much higher in pre-adipocytes than in mature adipocytes, it is possible that the decreased level of Akt phosphorylation in WATs of mice treated with evodiamine was owing to its reduction in pre-adipocytes, rather than in mature adipocytes, existing in the depots. It is also possible that reduction of mTORC2 activity might contribute to the improvement of glucose tolerance in the evodiamine-treated KK-Ay mice, as glucose uptake into WAT is increased in mice with whole-body deletion of Rictor, the mTORC2 subunit, whereas disruption of mTORC2 in liver causes glucose intolerance [31]. Chronic treatment (2–4 weeks) with rapamycin, the mTOR inhibitor, causes glucose intolerance and insulin resistance in mice [31,32] but evodiamine appears not to be included,

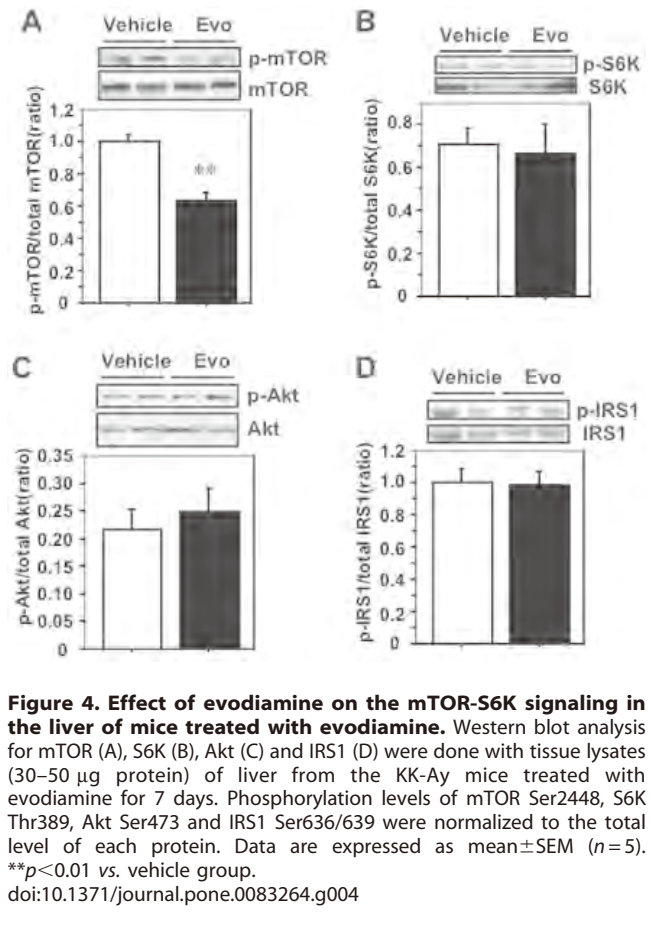


**Figure 4. Effect of evodiamine on the mTOR-S6K signaling in the liver of mice treated with evodiamine.** Western blot analysis for mTOR (A), S6K (B), Akt (C) and IRS1 (D) were done with tissue lysates (30–50 µg protein) of liver from the KK-Ay mice treated with evodiamine for 7 days. Phosphorylation levels of mTOR Ser2448, S6K Thr389, Akt Ser473 and IRS1 Ser636/639 were normalized to the total level of each protein. Data are expressed as mean ± SEM (n = 5). \*\*p < 0.01 vs. vehicle group. doi:10.1371/journal.pone.0083264.g004

because administration of this compound for 2 months improved glucose tolerance and insulin resistance associated with diet-induced obesity in mice [21], in which phosphorylation levels of

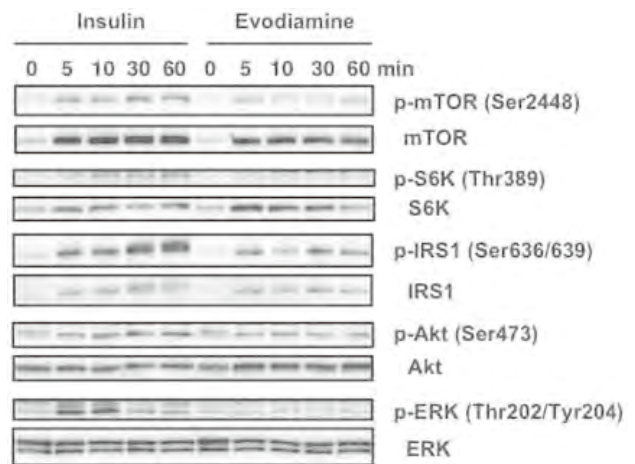


**Figure 5. Effect of evodiamine and insulin on the mTOR-S6K signaling in differentiated adipocytes.** After 3T3-L1 pre-adipocytes were differentiated into mature adipocytes, the cells were maintained in DMEM for 4 h and then stimulated by 20 nM insulin or 20 µM evodiamine for the indicated length of time. The cell lysates (15–30 µg protein) were analyzed for phosphorylation of mTOR Ser2448, S6K Thr389, IRS1 Ser636/639, Akt Ser473 and ERK Thr202/Tyr204 by Western blot analysis. Representative images of two independent experiments are shown. doi:10.1371/journal.pone.0083264.g005

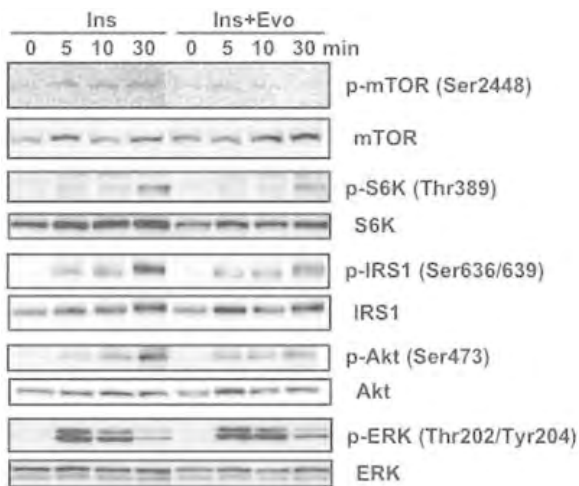


**Figure 6. Effect of evodiamine on the insulin-stimulated activation of mTOR-S6K signaling in differentiated adipocytes.** After 3T3-L1 pre-adipocytes were differentiated into mature adipocytes, the cells were maintained in DMEM for 4 h and then stimulated by 20 nM insulin with or without 20 μM evodiamine for the indicated length of time. The cell lysates (15–30 μg protein) were analyzed for phosphorylation of mTOR Ser2448, S6K Thr389, IRS1 Ser636/639, Akt Ser473 and ERK Thr202/Tyr204 by Western blot analysis. Representative images of two independent experiments are shown. doi:10.1371/journal.pone.0083264.g006

mTOR and IRS1 were decreased in evodiamine-treated WAT (Fig. S2 in File S1). Likewise, mTORC1 activity appears to be attenuated in the WATs of KK-Ay mice treated with evodiamine, because the phosphorylation of S6K, a target of mTORC1 signaling, is reduced considerably in adipose tissues, which blocks serine phosphorylation of IRS1. Similar effects of evodiamine on mTOR-S6K signaling were confirmed in adipocytes *in vitro*. In contrast to the insulin effects that stimulated serine phosphorylation of IRS1 and Akt as well as activation of mTOR-S6K signaling, evodiamine alone does not affect these molecules except for the inhibitory effect on mTOR phosphorylation in adipocytes. However, evodiamine inhibited insulin-stimulated phosphorylation of mTOR and S6K, leading to suppression of IRS1 serine phosphorylation in adipocytes, suggesting evodiamine acts to improve insulin resistance by repressing activation of mTOR-S6K signaling by insulin.

AMPK is a major cellular energy sensor controlling glucose and lipid metabolism [22,23]. AMPK is activated in response to a variety of stimuli, including metabolic stress that generates an increase in the AMP/ATP ratio. Genetic and pharmacologic studies demonstrated that AMPK is required for maintaining glucose homeostasis [33]. Therefore, AMPK is now considered to be a potential pharmacologic target for improving insulin resistance, diabetes and metabolic syndrome. Ching et al. have recently reported that evodiamine increased AMPK phosphorylation in endothelial cells [34]. In the present study, we found that evodiamine significantly stimulated AMPK phosphorylation in mature adipocyte culture and in WAT of KK-Ay mice. The increased phosphorylation of AMPK was also detected in liver to a lesser extent, but not in skeletal muscle, in the evodiamine-treated KK-Ay mice compared to the vehicle control. AMPK down-regulates mTOR signaling pathway via phosphorylation of tuberous sclerosis complex 2, which inhibits cell growth [12,35]. Therefore, it is plausible that evodiamine inhibits mTOR-S6K signaling through AMPK phosphorylation in adipocytes. Because increased AMPK phosphorylation and decreased mTOR phos-

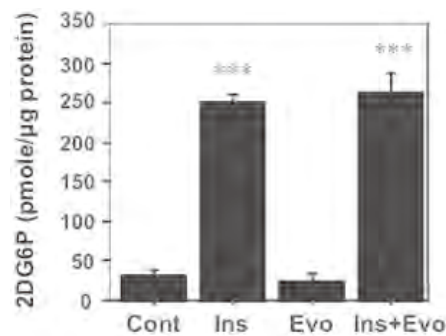


**Figure 7. Effect of evodiamine and insulin on glucose uptake in differentiated adipocytes.** After 3T3-L1 pre-adipocytes were differentiated into mature adipocytes, the cells were maintained in DMEM for 6 h and then stimulated by 20 nM insulin or 20 μM evodiamine alone, or in combination with insulin and evodiamine for 40 min and with 1 μM 2DG for the last 20 min. The 2DG6P content in each cell sample was measured by using glucose uptake colorimetric assay kit. Data are expressed as mean ± SEM (n=3–4). \*\*\**p*<0.001 vs. control group without stimulation. doi:10.1371/journal.pone.0083264.g007

phorylation were also detected in liver, but not in skeletal muscle, of the evodiamine-treated mice, evodiamine might affect glucose metabolism and insulin sensitivity in various tissues including WAT and liver.

The anti-diabetic compound rosiglitazone has effects similar to those of evodiamine on AMPK phosphorylation and insulin-stimulated phosphorylation of mTOR and IRS1 in adipocytes, although the effects of these two compounds on adipogenesis are opposite; i.e. evodiamine inhibits but rosiglitazone stimulates the cellular process [21,22]. It is noteworthy that the difference between adipocytes and pre-adipocytes in responsiveness to evodiamine, as indicated from the results of ERK and Akt phosphorylation, suggests a change in the mode of evodiamine action corresponding to the differentiation of pre-adipocytes into mature adipocytes. So, evodiamine might exhibit its improved effects against obesity and insulin resistance in different modes of action in pre-adipocytes and adipocytes.

Our data suggest evodiamine improves glucose tolerance and prevents progress of insulin resistance associated with obese/diabetic states, at least in part, through AMPK activation followed by inhibition of mTOR-S6K signaling and IRS1 serine phosphorylation in adipocytes. The anti-obesity effect of evodiamine may also contribute indirectly to prevention against insulin resistance. Considering that inhibition of mTOR-S6K signaling has attracted a great deal of attention in connection with health and longevity [12,36,37], evodiamine might be a unique compound able to combat obesity and age-related diseases; however, the effects of evodiamine on energy metabolism in other metabolic tissues remain to be clarified.

## Methods

### Ethics statement

This study was performed in strict accordance with the recommendations in Fundamental Guidelines for Proper Conduct of Animal Experiment and Related Activities in Academic Research Institutions under the jurisdiction of the Ministry of Education, Culture, Sports, Science and Technology, Japan. The protocol was approved by the Institutional Animal Care and Use Committee in Chubu University (approval number: 2310039 and 2410003).

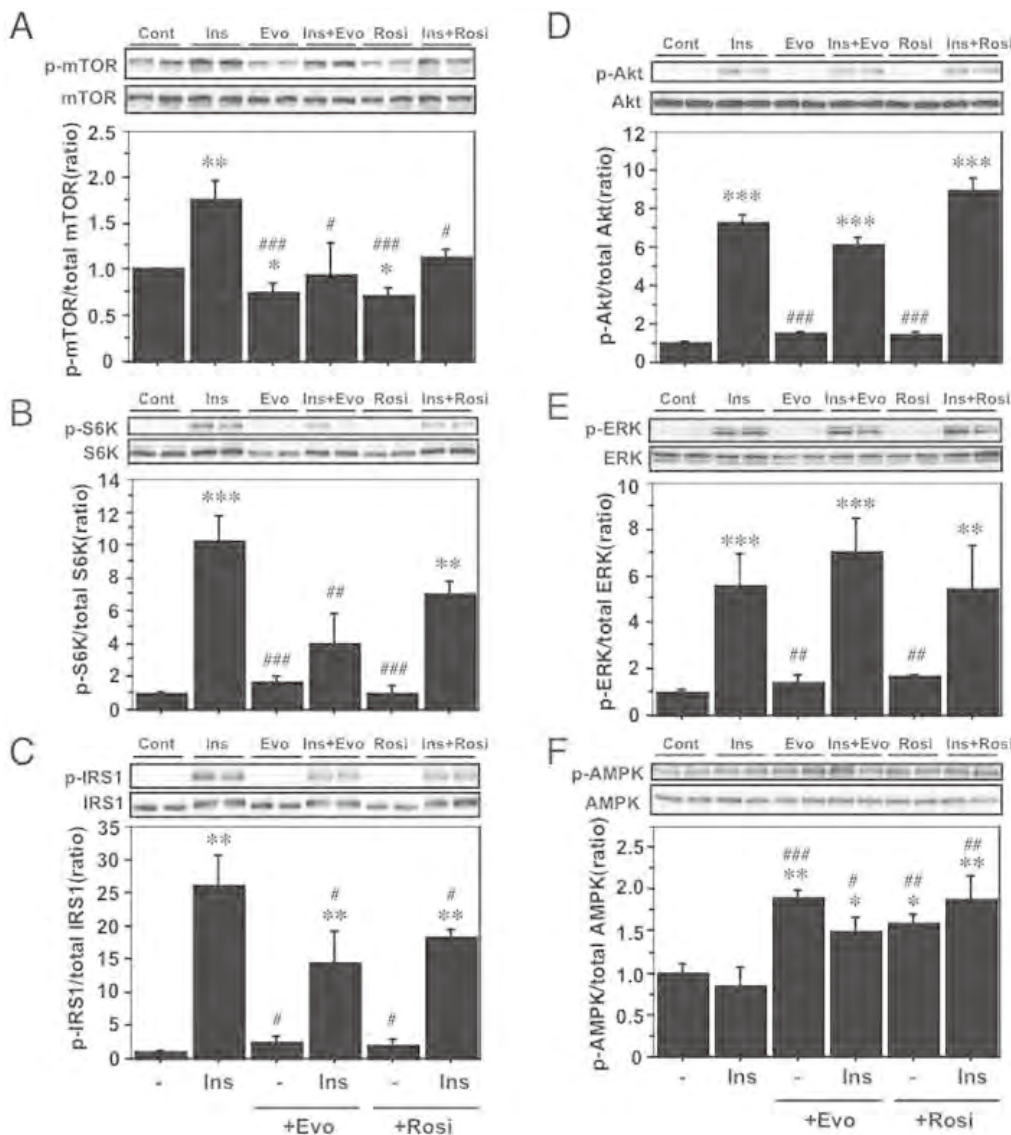


**Figure 8. Effect of evodiamine and rosiglitazone on the mTOR-S6K signaling in adipocytes with or without insulin stimulation.** After 3T3-L1 pre-adipocytes were differentiated into mature adipocytes, the cells were maintained in DMEM for 4 h and then stimulated by 20 nM insulin, 20 μM evodiamine or 20 μM rosiglitazone alone, or in combination with insulin and evodiamine or rosiglitazone for 30 min. The cell lysates (15–30 μg protein) were analyzed for phosphorylation of mTOR Ser2448, S6K Thr389, IRS1 Ser636/639, Akt Ser473, ERK Thr202/Tyr204 and AMPK Thr172 by Western blot analysis. Phosphorylation levels were normalized to the total level of each protein. Data are expressed as mean±SEM (n=3–5). \*p<0.05, \*\*p<0.01, \*\*\*p<0.001 vs. control group without stimulation. #p<0.05, ##p<0.01, ###p<0.001 vs. insulin stimulation. doi:10.1371/journal.pone.0083264.g008

**Experimental animals**

KK-Ay mice were obtained from CLEA Japan, Inc. and maintained at 23±1°C under artificial lighting for 12 h/day and provided a standard chow (11.6% kcal from fat; Diet no. CE-2, CLEA Japan, Inc.) and tap water *ad libitum*. Eight-weeks old female mice were administered evodiamine by i.p. injection (3 mg/kg BW, KISIDA CHEMICAL CO., LTD, Japan) or vehicle (10% (v/v) DMSO, 10% (v/v) Tween80, 80% (w/v) NaCl) once a day for 7 days. Compound solutions were kept at ~35°C and injected i.p. at a dose of 100 μl/g BW (3 mg/ml). BW and food intake were recorded each day. After 1 week, ten mice for tissue analyses were euthanized by cervical dislocation; their blood and tissue samples were recovered and stored at -80°C. Total seventeen mice in two independent experiments for glucose tolerance test were fasted for 17 h after the final injection of evodiamine or vehicle.

**Biochemical analysis**

Blood samples were collected from a tail vein and used immediately to determine the glucose level with a glucometer (OneTouch Ultra, Johnson & Johnson K.K., Tokyo, Japan). Insulin levels were measured with serum and commercial assay kits (Ultrasensitive insulin ELISA, Mercodia, Winston Salem NC, USA). An i.p. glucose tolerance test (IPGTT) using 1.5 mg glucose/g BW was done after starvation for 17 h. The blood glucose level was measured before the injection of glucose at time zero and at 30, 60 and 120 min later.

**Cell culture**

3T3-L1 cells (ATCC, CL173, DS Pharma Biomedical Co., Osaka, Japan) were grown in Dulbecco's modified Eagle medium (DMEM; Wako Pure Chemical, Osaka, Japan) containing 10%

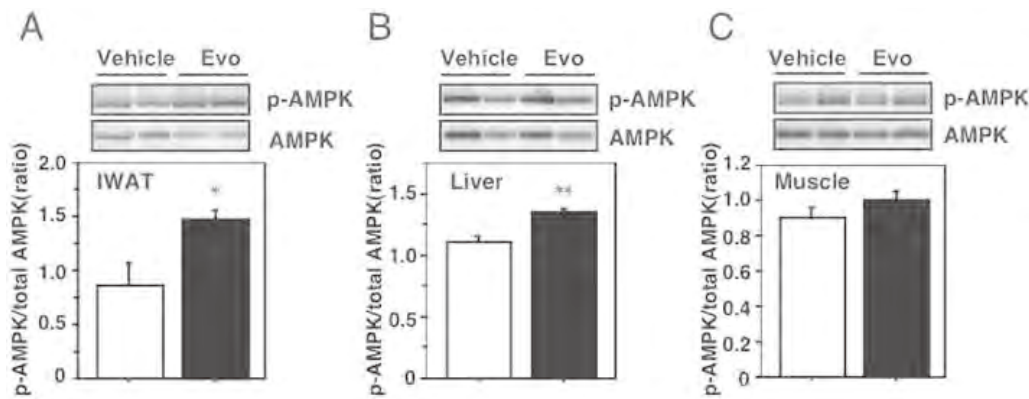


**Figure 9. Effect of evodiamine on AMPK phosphorylation in the WAT, liver and skeletal muscle of mice treated with evodiamine.** Western blot analysis for AMPK were done with tissue lysates (30  $\mu$ g protein) of IWAT (A), liver (B) and gastrocnemius muscle (C) from the KK-Ay mice treated with evodiamine for 7 days. Phosphorylation levels of AMPK Thr172 were normalized to its total level. Data are expressed as mean  $\pm$  SEM ( $n=5$ ). \* $p<0.05$ , \*\* $p<0.01$  vs. vehicle group. doi:10.1371/journal.pone.0083264.g009

(v/v) calf serum (BioWest). Adipocyte differentiation was done essentially as described but with minor modifications [38]. Briefly, 2 days post confluence, the medium was changed to DMEM containing 10% (v/v) fetal bovine serum (ICN Biomedicals, Aurora, OH, USA), 10  $\mu$ g/ml insulin, 1  $\mu$ M dexamethasone, 0.5 mM 3-isobutyl-1-methylxanthine and 10  $\mu$ M pioglitazone. Dexamethasone, 3-isobutyl-1-methylxanthine and pioglitazone were withdrawn after 2 days of exposure and insulin was withdrawn after 4 days. On day 6, most of the pre-adipocytes were differentiated into adipocytes. The cells were maintained in DMEM for 4 h and then stimulated by 20 nM insulin, 20  $\mu$ M evodiamine or 20  $\mu$ M rosiglitazone (Wako).

### Protein analysis

Western blot analysis was done as described with the total tissue lysates or whole-cell lysates recovered from the WAT or 3T3-L1 adipocytes [39]. The concentration of protein in the lysates was measured with the BCA protein assay (Pierce Biotechnology, Rockford, IL, USA). Equal amounts of protein (15–50  $\mu$ g) were separated by electrophoresis in SDS/4–20% (w/v) polyacrylamide gels (Daiichi Pure Chemicals, Tokyo, Japan) and transferred electrophoretically onto Immobilon polyvinylidene difluoride membranes (Millipore, Bedford, MA, USA). The membranes were incubated with specific antibodies against Akt, phospho-Ser473 Akt, mTOR, phospho-Ser2448 mTOR, IRS1, phospho-Ser636/639 IRS1, p70S6 kinase, phospho-Thr389 p70S6 kinase, PDK1, phospho-Ser241 PDK1, Erk1/2, phospho-Thr202/Tyr204 Erk1/2, AMPK, phospho-Thr172 AMPK (Cell Signaling Technology, Danvers, MA, USA) or phospho-Tyr612 IRS1/2 (Santa Cruz). After the secondary antibody reaction at 4°C overnight, specific signals were detected using Immobilon Western Detection Reagents (Merck Japan, Tokyo). The resulting images were quantified with NIH Image (version 1.63) software.

### Glucose uptake analysis

Glucose uptake into 3T3-L1 adipocytes was evaluated according to the method of Saito et al. [40] with minor modification. After the adipocytes were maintained in DMEM for 6 h, cells were washed with Krebs Ringer Phosphate Hepes (KRPH) buffer (20 mM HEPES, 5 mM KH<sub>2</sub>PO<sub>4</sub>, 1 mM MgSO<sub>4</sub>, 1 mM CaCl<sub>2</sub>, 136 mM NaCl, 4.7 mM KCl, pH 7.4) containing 2% bovine albumin (fatty acid-free, NACALAI TESQUE, INC. KYOTO, JAPAN) three times and incubated in the KRPH buffer for

40 min. The cells were then stimulated by 20 nM insulin with or without 20  $\mu$ M evodiamine for 40 min and with 1  $\mu$ M 2-Deoxy-D-glucose (2DG, Sigma-Aldrich, St. Louis, MO, USA) for the last 20 min. Cells were washed with ice-cold phosphate buffered saline containing 5  $\mu$ M cytochalasin B (Sigma-Aldrich) three times and collected in 1 ml of 10 mM Tris-HCl (pH 8.0). After sonication, the homogenates were heated at 80°C for 15 min and centrifuged at 15,000 g for 20 min at 4°C. A portion of the resulting supernatant was diluted 10 times with 10 mM Tris-HCl (pH 8.0) and analyzed for 2DG6P content by using glucose uptake colorimetric assay kit (BioVision, Milpitas, CA, USA). The 2DG6P content in each sample was corrected by subtracting the value derived from the untreated cells without 2DG addition.

### Histological analysis

Immediately after removal, tissue pieces were fixed by immersion at 4°C in 10% (v/v) formaldehyde in neutral buffer solution (Kishida Chemical), dehydrated, cleared and embedded in paraffin. Paraffin sections (4- $\mu$ m thick) were stained with hematoxylin and eosin. All observations were done with a fluorescence microscope (Biorevo BZ-9000; Keyence, Tokyo, Japan). The average cell size of adipocytes in WAT was calculated by dividing the chosen microscopic area by the total cell number in the area.

### Statistical analysis

Data were expressed as mean  $\pm$  SEM. Differences between groups were assessed by analysis of variance (ANOVA) or repeated measure ANOVA. The level of statistically significant difference was set at  $p\leq 0.05$ .

### Supporting Information

**File S1** Methods S1, Animal experiments using UCP1-knockout (KO) mice and cell culture experiments using 3T3-L1 pre-adipocytes. References S1, References for supplementary methods. Figure S1, Effect of evodiamine on mTOR-S6K signaling in the RWAT of KK-Ay mice treated with evodiamine. Western blot analysis of mTOR (A), S6K (B), Akt (C) and IRS1 (D) was done with tissue lysates (30  $\mu$ g protein) of retroperitoneal WAT from KK-Ay mice treated with evodiamine for 7 days. Phosphorylation levels of mTOR Ser2448, S6K Thr389, Akt Ser473 and IRS1 Ser636/639 were normalized to the total level of each protein.

Data are expressed as mean $\pm$ SEM ( $n=5$ ). \* $p<0.05$  vs. vehicle group. Figure S2, Effect of evodiamine on phosphorylation of mTOR, Akt and IRS1 in the WAT of obese UCPI-KO mice. Western blot analysis for mTOR (A), Akt (B) and IRS1 (C) was done with tissue lysates (50  $\mu$ g protein) of epididymal WAT from the UCPI-KO mice fed a high-fat diet with or without evodiamine for 2 months as described in Supplemental Methods. Phosphorylation levels of mTOR Ser2448, Akt Ser473 and IRS1 Ser636/639 were normalized to the total level of each protein. Data are expressed as mean $\pm$ SEM ( $n=4$ ). \* $p<0.05$  vs. control group. Figure S3, Effect of evodiamine on phosphorylation of mTOR and UCP1 in the BAT of KK-Ay mice treated with evodiamine. Western blot analysis for mTOR (A) and UCP1 (B) was done with tissue lysates (30  $\mu$ g protein) of BAT from KK-Ay mice treated with evodiamine for 7 days. Levels of mTOR Ser2448 phosphorylation and UCP1 protein were normalized to the total mTOR and tubulin levels, respectively. Data are expressed as mean $\pm$ SEM ( $n=5$ ). Figure S4, Effect of evodiamine on phosphorylation of mTOR, S6K, Akt and IRS1 in the gastrocnemius muscle (GM) of KK-Ay mice treated with evodiamine. Western blot analysis for mTOR (A), S6K (B), Akt (C) and IRS1 (D) was done with tissue lysates (30  $\mu$ g protein) of GM from KK-Ay mice treated with evodiamine for 7 days. Phosphorylation levels of mTOR Ser2448, S6K Thr389, Akt Ser473 and IRS1 Ser636/639 were normalized to the total level of each protein. Data are expressed as mean $\pm$ SEM ( $n=5$ ). Figure S5, Effect of evodiamine

on phosphorylation of ERK, Akt and IRS1 in pre-adipocytes. 3T3-L1 pre-adipocytes were serum-deprived for 4 h and then treated with 20  $\mu$ M evodiamine for 1 h and with 20 nM insulin for the last 10 min. Western blot analysis for ERK, Akt and IRS1 were done with cell lysates (30  $\mu$ g protein). Figure S6, Measurement of oxygen consumption ( $VO_2$ ) and respiratory quotient (RQ) in UCPI-KO mice with or without treatment with evodiamine.  $VO_2$  (A) and RQ (B) were measured for 24 h in male mice injected with vehicle or evodiamine (3 mg/kg BW) at 14:00 h. C, Data on RQs were analyzed as relative cumulative frequency (PRCF). Each curve represents 1365 measurements of RQ from three mice for each group as described in Supplemental Methods. Data are expressed as mean $\pm$ SEM ( $n=3$  for each group). \*\*\* $p<0.001$  vs. vehicle group. (DOCX)

## Acknowledgments

We thank Dr. L.P. Kozak for critical review of the manuscript.

## Author Contributions

Conceived and designed the experiments: HY. Performed the experiments: TW YY TT TK YK YO HY. Analyzed the data: YY TT TW YO MS NM HY. Contributed reagents/materials/analysis tools: MS. Wrote the paper: HY.

## References

- Kopelman PG (2000) Obesity as a medical problem. *Nature* 404: 635–643.
- Rosen ED, Spiegelman BM (2006) Adipocytes as regulators of energy balance and glucose homeostasis. *Nature* 444: 847–853.
- Kolonin MG, Saha PK, Chan L, Pasqualini R, Arap W (2004) Reversal of obesity by targeted ablation of adipose tissue. *Nat Med* 10: 625–632.
- Enerback S, Jacobsson A, Simpson EM, Guerra C, Yamashita H, et al. (1997) Mice lacking mitochondrial uncoupling protein are cold-sensitive but not obese. *Nature* 387: 90–94.
- Cannon B, Nedergaard J (2004) Brown adipose tissue: function and physiological significance. *Physiol Rev* 84: 277–359.
- Kontani Y, Wang Y, Kimura K, Inokuma KI, Saito M, et al. (2005) UCP1 deficiency increases susceptibility to diet-induced obesity with age. *Aging Cell* 4: 147–155.
- Cypess AM, Lehman S, Williams G, Tal I, Rodman D, et al. (2009) Identification and importance of brown adipose tissue in adult humans. *N Engl J Med* 360: 1509–1517.
- Saito M, Okamatsu-Ogura Y, Matsushita M, Watanabe K, Yoneshiro T, et al. (2009) High incidence of metabolically active brown adipose tissue in healthy adult humans: effects of cold exposure and adiposity. *Diabetes* 58: 1526–1531.
- Cannon B, Nedergaard J (2012) Yes, even human brown fat is on fire! *J Clin Invest* 122: 486–489.
- Draznin B (2006) Molecular mechanisms of insulin resistance: serine phosphorylation of insulin receptor substrate-1 and increased expression of p85alpha: the two sides of a coin. *Diabetes* 55: 2392–2397.
- White MF (2002) IRS proteins and the common path to diabetes. *Am J Physiol Endocrinol Metab* 283: E413–E422.
- Zoncu R, Efeyan A, Sabatini DM (2011) mTOR: from growth signal integration to cancer, diabetes and ageing. *Nat Rev Mol Cell Biol* 12: 21–35.
- Shima H, Pende M, Chen Y, Fumagalli S, Thomas G, et al. (1998) Disruption of the p70(s6k)/p85(s6k) gene reveals a small mouse phenotype and a new functional S6 kinase. *EMBO J* 17: 6649–6659.
- Um SH, Frigerio F, Watanabe M, Picard F, Joaquin M, et al. (2004) Absence of S6K1 protects against age- and diet-induced obesity while enhancing insulin sensitivity. *Nature* 431: 200–205.
- Um SH, D'Alessio D, Thomas G (2006) Nutrient overload, insulin resistance, and ribosomal protein S6 kinase 1, S6K1. *Cell Metab* 3: 393–402.
- Chiou WF, Chou CJ, Shum AY, Chen CF (1992) The vasorelaxant effect of evodiamine in rat isolated mesenteric arteries: mode of action. *Eur J Pharmacol* 215: 277–283.
- Kobayashi Y, Nakano Y, Kizaki M, Hoshikuma K, Yokoo Y, et al. (2001) Capsaicin-like anti-obese activities of evodiamine from fruits of *Evodia rutaecarpa*, a vanilloid receptor agonist. *Planta Med* 67: 628–633.
- Wang Y, Kimura K, Inokuma K, Saito M, Kontani Y, et al. (2006) Potential contribution of vasoconstriction to suppression of heat loss and homeothermic regulation in UCP1-deficient mice. *Pflugers Arch* 452: 363–369.
- Takada Y, Kobayashi Y, Aggarwal BB (2005) Evodiamine abolishes constitutive and inducible NF-kappaB activation by inhibiting IkkappaBalpha kinase activation, thereby suppressing NF-kappaB-regulated antiapoptotic and metastatic gene expression, up-regulating apoptosis, and inhibiting invasion. *J Biol Chem* 280: 17203–17212.
- Heo SK, Yun HJ, Yi HS, Noh EK, Park SD (2009) Evodiamine and rutaecarpine inhibit migration by LIGHT via suppression of NADPH oxidase activation. *J Cell Biochem* 107: 123–133.
- Wang T, Wang Y, Kontani Y, Kobayashi Y, Sato Y, et al. (2008) Evodiamine improves diet-induced obesity in a uncoupling protein-1-independent manner: involvement of antiadipogenic mechanism and extracellularly regulated kinase/mitogen-activated protein kinase signaling. *Endocrinol* 149: 358–366.
- Kahn BB, Alquier T, Carling D, Hardie DG (2005) AMP-activated protein kinase: ancient energy gauge provides clues to modern understanding of metabolism. *Cell Metab* 1: 15–25.
- Hardie DG (2007) AMP-activated/SNF1 protein kinases: conserved guardians of cellular energy. *Nat Rev Mol Cell Biol* 8: 774–785.
- Bak EJ, Park HG, Kim JM, Kim JM, Yoo YJ, et al. (2010) Inhibitory effect of evodiamine alone and in combination with rosiglitazone on in vitro adipocyte differentiation and in vivo obesity related to diabetes. *Int J Obes (Lond)* 34: 250–260.
- Cho H, Thorvaldsen JL, Chu Q, Feng F, Birnbaum MJ (2001) Akt/PKB $\alpha$  is required for normal growth but dispensable for maintenance of glucose homeostasis in mice. *J Biol Chem* 276: 38349–38352.
- Peng XD, Xu PZ, Chen ML, Hahn-Windgassen A, Skeen J, et al. (2003) Dwarfism, impaired skin development, skeletal muscle atrophy, delayed bone development, and impeded adipogenesis in mice lacking Akt1 and Akt2. *Genes Dev* 17: 1352–1365.
- Esposito DL, Li Y, Cama A, Quon MJ (2001) Tyr612 and Tyr632 in human insulin receptor substrate-1 are important for full activation of insulin-stimulated phosphatidylinositol 3-kinase activity and translocation of GLUT4 in adipose cells. *Endocrinol* 142: 2833–2840.
- Le Good JA, Ziegler WH, Parekh DB, Alessi DR, Cohen P, et al. (1998) Protein kinase C isotypes controlled by phosphoinositide 3-kinase through the protein kinase PDK1. *Science* 281: 2042–2045.
- Standaert MJ, Galloway L, Karnam P, Bandyopadhyay G, Moscat J, et al. (1997) Protein kinase C- $\zeta$  as a downstream effector of phosphatidylinositol 3-kinase during insulin stimulation in rat adipocytes. Potential role in glucose transport. *J Biol Chem* 272: 30075–30082.
- Kotani K, Ogawa W, Matsumoto M, Kitamura T, Sakaue H, et al. (1998) Requirement of atypical protein kinase lambda for insulin stimulation of glucose uptake but not for Akt activation in 3T3-L1 adipocytes. *Mol Cell Biol* 18: 6971–6982.
- Lamming DW, Ye L, Katajisto P, Goncalves MD, Saitoh M, et al. (2012) Rapamycin-induced insulin resistance is mediated by mTORC2 loss and uncoupled from longevity. *Science* 335: 1638–1643.

32. Cunningham JT, Rodgers JT, Arlow DH, Vazquez F, Mootha VK, et al. (2007) mTOR controls mitochondrial oxidative function through a YY1-PGC-1alpha transcriptional complex. *Nature* 450: 736–740.
33. Shaw RJ, Lamia KA, Vasquez D, Koo SH, Bardeesy N, et al. (2005) The kinase LKB1 mediates glucose homeostasis in liver and therapeutic effects of metformin. *Science* 310: 1642–1446.
34. Ching LC, Chen CY, Su KH, Hou HH, Shyue SK, et al. (2012) Implication of AMP-activated protein kinase in transient receptor potential vanilloid type1-mediated activation of endothelial nitric oxide synthase. *Mol Med* 18: 805–815.
35. Inoki K, Ouyang H, Zhu T, Lindvall C, Wang Y, et al. (2006) TSC2 integrates Wnt and energy signals via a coordinated phosphorylation by AMPK and GSK3 to regulate cell growth. *Cell* 126: 955–968.
36. Kennedy BK, Steffen KK, Kaeberlein M (2007) Ruminations on dietary restriction and aging. *Cell Mol Life Sci* 64: 1323–1328.
37. Harrison DE, Strong R, Sharp ZD, Nelson JF, Astle CM, et al. (2009) Rapamycin fed late in life extends lifespan in genetically heterogeneous mice. *Nature* 460: 392–395.
38. Hemati N, Ross SE, Erickson RL, Groblewski GE, MacDougald OA (1997) Signaling pathways through which insulin regulates CCAAT/enhancer binding protein alpha (C/EBPalpha) phosphorylation and gene expression in 3T3-L1 adipocytes. Correlation with GLUT4 gene expression. *J Biol Chem* 272: 25913–25919.
39. Summers SA, Lipfert L, Birnbaum MJ (1998) Polyoma middle T antigen activates the Ser/Thr kinase Akt in a PI3-kinase-dependent manner. *Biochem Biophys Res Commun* 246: 76–81.
40. Saito K, Lee S, Shiuchi T, Toda C, Kamijo M, et al. (2011) An enzymatic photometric assay for 2-deoxyglucose uptake in insulin-responsive tissues and 3T3-L1 adipocytes. *Anal Biochem* 412: 9–17.

## Supporting Information

### Supplementary Methods

*Experimental animals.* Congenic UCPI-knockout (KO) mice on a C57BL/6J background were prepared as previously described [1]. The mice were maintained under artificial lighting for 12 h per day and provided a standard chow (11.6% kcal from fat; Diet No. CE-2, CLEA Japan, Inc.) and tap water *ad libitum* in our animal facility at 23±1°C. The experiment of evodiamine diet using UCPI-KO mice was performed as previously described [2]. Briefly, the 4-month-old mice were fed a high-fat diet (HF: 41.9% kcal from fat, Diet No. B15040, CLEA Japan, Inc) with or without 300 mg evodiamine per kg food (Kishida Chemical, Osaka, Japan) for 2 months. The 6-month-old mice were sampled and the tissues were stored at -80°C until use. All experiments were performed in accordance with our institutional guidelines for the care and use of research animals.

*Indirect calorimetry.* Whole body oxygen consumption (VO<sub>2</sub>) and respiratory quotient (RQ) were measured by using an O<sub>2</sub> analyzer (MM-102R; Muromachi Kikai, Ltd., Tokyo, Japan). Adult male UCPI-KO mouse was housed in an airflow chamber at a room temperature of 24°C with standard chow and tap water *ad libitum* for 72 h, and the air samples were taken every 3 minutes for analysis except once per hour for calibration (228 data points per 12 h in each light and dark phase). After the basal oxygen consumption in each mouse was determined during the first 24 h, the measurement was continued to obtain the data on vehicle and evodiamine treatment during the second and last 24 h, respectively. The mice were intraperitoneally administered vehicle (10% Tween80, 10% DMSO and 80% saline) or evodiamine (3 mg/kg BW, Kishida Chemical, Osaka, Japan) at 14:00. Data on RQs

was also analyzed as percent relative cumulative frequency (PRCF) to address the slight differences in the number of data points collected between mouse groups and to facilitate comparison of data sets from experiment to experiment as previously described [3]. The resulting curves, which were derived from 1365 measurements from an experimental group of 3 mice, provided a sensitive indicator of slight shifts to lower or higher RQ.

*Cell culture.* 3T3-L1 pre-adipocytes, which are mouse embryonic fibroblasts capable of differentiating into adipocytes, were grown in Dulbecco's modified Eagle's medium (DMEM; Invitrogen, Grand Island, NY, USA) containing 10% calf serum (CS; ICN Biomedicals, Aurora, OH, USA). Two days postconfluence, the pre-adipocytes were washed with serum-free DMEM once and cultured in the fresh DMEM for 4 h. The cells were then treated with 20µM evodiamine for 1 h and with 20nM insulin for the last 10 min.

*Protein analysis.* Western blot analyses were carried out using the total tissue lysates or whole cell lysates recovered from adipose tissues or 3T3-L1 pre-adipocytes, as described previously [4]. The concentrations of protein in the lysates were measured by using a BCA protein assay (Pierce Biotechnology, Rockford, IL). Equal amounts of protein (15~50 µg) were separated on 4~20% SDS-polyacrylamide gels (Daichi Pure Chemicals, Tokyo, Japan) and transferred onto Immobilon polyvinylidene difluoride membranes (Millipore, Bedford, MA, USA). The membranes were incubated with specific antibodies against Akt, phospho-Ser473 Akt, mTOR, phospho-Ser2448 mTOR, IRS1, phospho-Ser307 IRS1, phospho-Ser636/639 IRS1, p70S6 kinase, phospho-Thr389 p70S6 kinase, Erk1/2, phospho-Thr202/Tyr204 Erk1/2, α/β-tubulin (Cell Signaling Technology, Danvers, MA, USA) or UCPI (Abnova, Taipei City, Taiwan). After performing the secondary antibody reaction at 4°C overnight, specific signals were detected using Immobilon Western Detection

## Supplementary Figure Legends

Figure S1.

Effect of evodiamine on mTOR-S6K signaling in the RWAT of KK-Ay mice treated with evodiamine. Western blot analysis of mTOR (A), S6K (B), Akt (C) and IRS1 (D) was done with tissue lysates (30  $\mu$ g protein) of retroperitoneal WAT from KK-Ay mice treated with evodiamine for 7 days. Phosphorylation levels of mTOR Ser2448, S6K Thr389, Akt Ser473 and IRS1 Ser636/639 were normalized to the total level of each protein. Data are expressed as mean $\pm$ SEM ( $n = 5$ ). \* $p < 0.05$  vs. vehicle group.

Figure S2.

Effect of evodiamine on phosphorylation of mTOR, Akt and IRS1 in the WAT of obese UCPI-KO mice. Western blot analysis for mTOR (A), Akt (B) and IRS1 (C) was done with tissue lysates (50  $\mu$ g protein) of epididymal WAT from the UCPI-KO mice fed a high-fat diet with or without evodiamine for 2 months as described in Supplemental Methods. Phosphorylation levels of mTOR Ser2448, Akt Ser473 and IRS1 Ser636/639 were normalized to the total level of each protein. Data are expressed as mean $\pm$ SEM ( $n = 4$ ). \* $p < 0.05$  vs. control group.

Figure S3.

Effect of evodiamine on phosphorylation of mTOR and UCPI in the BAT of KK-Ay mice treated with evodiamine. Western blot analysis for mTOR (A) and UCPI (B) was done with tissue lysates (30  $\mu$ g protein) of BAT from KK-Ay mice treated with evodiamine for 7 days. Levels of mTOR Ser2448 phosphorylation and UCPI protein were normalized to the total mTOR and tubulin levels, respectively. Data are expressed as mean $\pm$ SEM ( $n = 5$ ).

Figure S4.

Effect of evodiamine on phosphorylation of mTOR, S6K, Akt and IRS1 in the gastrocnemius muscle (GM) of KK-Ay mice treated with evodiamine. Western blot analysis for mTOR (A), S6K (B), Akt (C) and IRS1 (D) was done with tissue lysates (30  $\mu$ g protein) of GM from KK-Ay mice treated with evodiamine for 7 days. Phosphorylation levels of mTOR Ser2448, S6K Thr389, Akt Ser473 and IRS1 Ser636/639 were normalized to the total level of each

Reagents (Merck Japan, Tokyo). The resulting images were quantified with NIH Image (version 1.63).

## Supplementary References

1. Enerback S, Jacobsson A, Simpson EM, Guerra C, Yamashita H, Harper ME, Kozak LP (1997) Mice lacking mitochondrial uncoupling protein are cold-sensitive but not obese. *Nature* 387, 90-94.
2. Wang T, Wang Y, Kontani Y, Kobayashi Y, Sato Y, Mori N, Yamashita H (2008) Evodiamine improves diet-induced obesity in a uncoupling protein-1-independent manner: involvement of antiadipogenic mechanism and extracellularly regulated kinase/mitogen-activated protein kinase signaling. *Endocrinol.* 149, 358-366.
3. Liu X, Rossmeis M, McClaine J, Riachi M, Harper ME, Kozak LP (2003) Paradoxical resistance to diet-induced obesity in UCPI-deficient mice. *J. Clin. Invest.* 111, 399-407.
4. Summers SA, Lipfert L, Birnbaum MJ (1998) Polyoma middle T antigen activates the Ser/Thr kinase Akt in a PI3-kinase-dependent manner. *Biochem. Biophys. Res. Commun.* 246, 76-81.

protein. Data are expressed as mean±SEM (*n* = 5).

Figure S5.

Effect of evodiamine on phosphorylation of ERK, Akt and IRS1 in pre-adipocytes. 3T3-L1 pre-adipocytes were serum-deprived for 4 h and then treated with 20 μM evodiamine for 1 h and with 20 nM insulin for the last 10 min. Western blot analysis for ERK, Akt and IRS1 were done with cell lysates (30 μg protein).

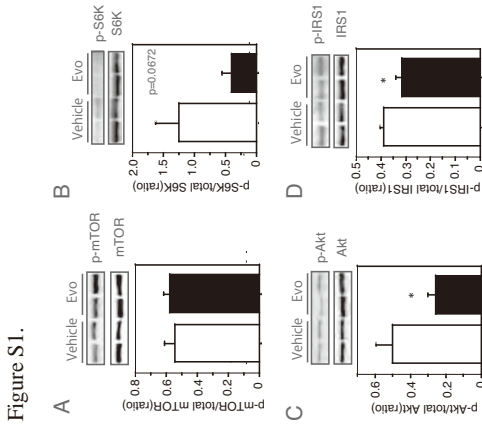


Figure S1.

Figure S6.

Measurement of oxygen consumption (VO<sub>2</sub>) and respiratory quotient (RQ) in UCPI-KO mice with or without treatment with evodiamine. VO<sub>2</sub> (A) and RQ (B) were measured for 24 h in male mice injected with vehicle or evodiamine (3 mg/kg BW) at 14:00 h. C, Data on RQs were analyzed as relative cumulative frequency (PRCF). Each curve represents 1365 measurements of RQ from three mice for each group as described in Supplemental Methods. Data are expressed as mean±SEM (*n* = 3 for each group). \*\*\**p* < 0.001 vs. vehicle group.

Figure S2.

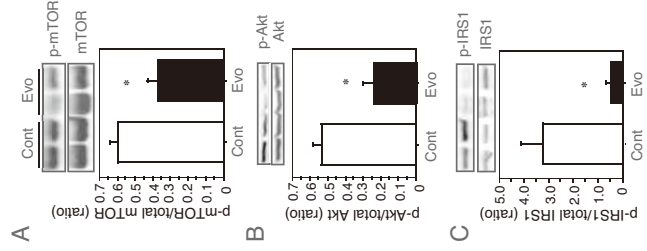


Figure S3.

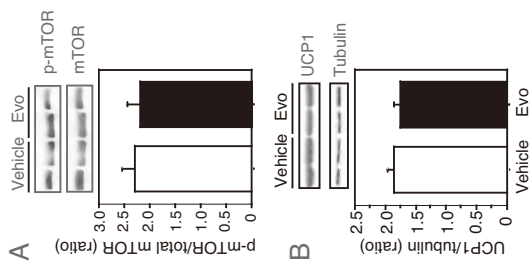


Figure S4.

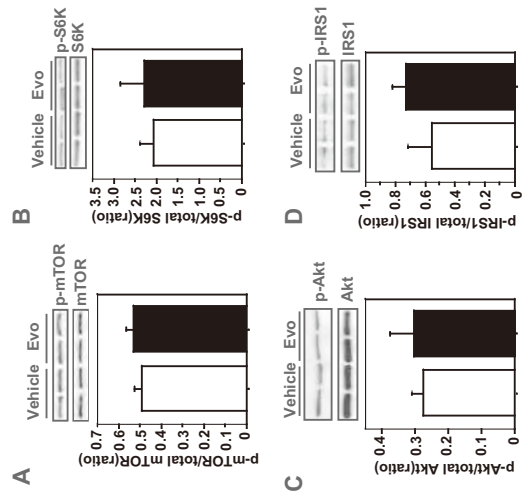


Figure S5.

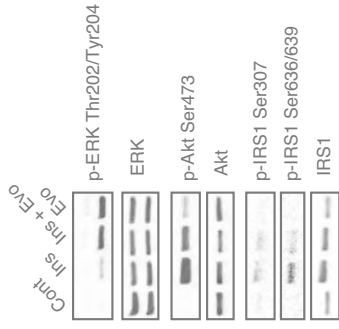
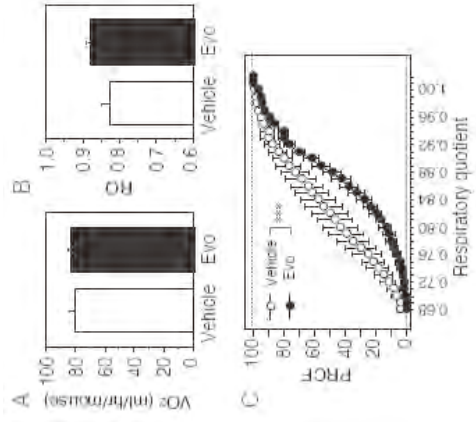


Figure S6.



## 【トピックス】

## 脂肪組織特異的 CREG1 トランスジェニックマウスを利用した

## 褐色脂肪化促進と生活習慣病改善の検討

橋本 理尋、楠堂 達也、竹内 環、遠藤 優貴、山下 均

中部大学 生命健康科学部 生命医科学科

キーワード：CREG1、UCP1、褐色脂肪、生活習慣病

## 1. はじめに

我が国を筆頭とした先進国では、医療技術の進歩により平均寿命が大幅に延長した結果、超高齢化社会を迎えるに至っている。この中にあり、多くの国民の興味が単なる寿命の延長から、如何に元気に老後を過ごせるかという、いわゆる健康寿命の延長に移っている。健康寿命の延長を達成するためには加齢性疾患の予防が不可欠であることから、現在さまざまな老化研究が推進されている。我々の研究グループは、加齢/老化と密接に係る生活習慣病の基盤となる肥満という切り口から健康寿命の延長に貢献しようと考え、基礎研究を重ねてきた。

## 2. 褐色脂肪化促進による生活習慣病の改善

脂肪細胞に中性脂肪が過剰に蓄積した肥満は、それ単独では病気とは言い難いが、高脂血症、高血圧、糖尿病、悪性新生物、心疾患、脳血管疾患などの様々な生活習慣病の発症リスクを大幅に上昇させる要因となる。哺乳動物の脂肪細胞は多様であり、中性脂肪としてエネルギーを貯蔵する白色脂肪細胞以外にも、中性脂肪を燃焼させることにより熱産生を行う褐色脂肪細胞も存在している。最近の研究では、従来から知られている筋前駆細胞由来の褐色脂肪細胞（クラシカルタイプ）とは別に、中胚葉由来前駆細胞から分化誘導される褐色様脂肪細胞（ベージュ細胞あるいはブライト細胞と呼ばれる）が存在することが明らかとなっているが、どちらも熱産生によりエネルギーを消費し、抗肥満効果やインスリン抵抗性の改善作用を示すと考えられている [1]。従って、褐色脂肪細胞の数が増加すれば、肥満に悩む中年男性に光明が差すわけだが、そう都合のよいことばかりではない。実は、褐色脂肪細胞は加齢に伴い減少していくことがわ

かっており、この減少が肥満や糖尿病、メタボリックシンドローム発症の一因であることが明らかになっているのである [2]。つまり褐色脂肪細胞の分化誘導を促進すること（褐色脂肪化）が可能となれば、先進国で深刻な社会問題となっている加齢に伴うメタボ発症やその悪化を抑制する有効な手段になるものと期待されるわけである。

## 3. 褐色脂肪細胞分化誘導剤の探索

未分化脂肪細胞の褐色脂肪細胞への分化は、熱産生の中心的な役割を果たすミトコンドリア脱共役タンパク質 1 (UCP1) の発現上昇で特徴づけられる (図 1)。古くから知られている褐色脂肪細胞への分化誘導機構は、ノルエピネフリンや甲状腺ホルモン T3 などの内分泌因子を介するものである。ノルエピネフリンは脂肪細胞膜上の  $\beta$  3 アドレナリン受容体を介して PKA や CREB を活性化することにより UCP1 の転写を促進している。一方で、T3 は甲状腺ホルモン核内受容体を介して UCP1 の転写を促進する。加えて、BMP7、Irisin、FGF21、Natriuretic peptides などの内分泌因子が褐色脂肪細胞

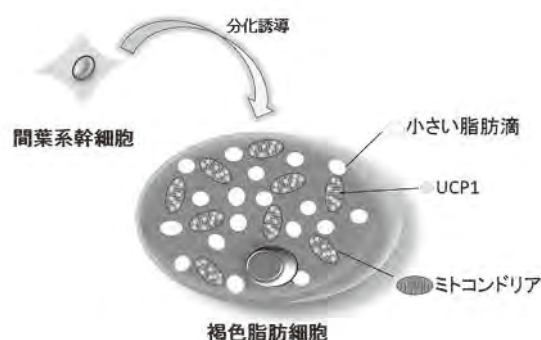


図 1 褐色脂肪細胞の特徴

褐色脂肪細胞は多数のミトコンドリアと UCP1 の発現で特徴づけられる。脂肪滴は白色脂肪細胞と比較して小さい。

連絡先：橋本理尋 〒 487-8501

愛知県春日井市松本町 1200

TEL : 0568-51-1111 (内線 8135)

FAX : 0568-51-6017

E-mail : mhashimoto@isc.chubu.ac.jp

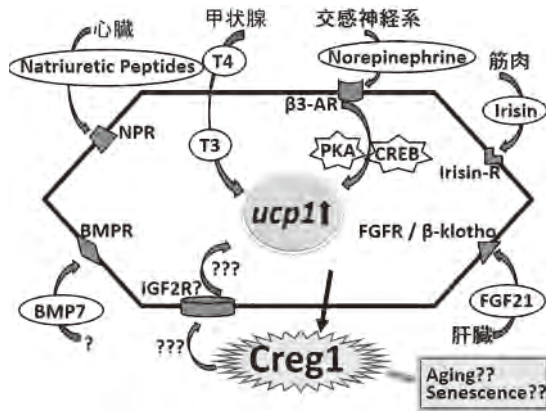


図2 褐色脂肪細胞の分化促進因子

褐色脂肪化の促進に関わることが報告されている内分泌因子とCREG1の関係性を模式的に示した。

への分化誘導に関与していることも報告されている (図2)。最近の研究では、PRDM16やEHMT1などの転写制御因子が関わっていることも報告されている [3]。これらの知見を利用して、様々な角度から褐色脂肪化への分化誘導促進剤開発が進められてきたが、現在のところヒトへ応用された分化誘導剤はない。

#### 4. CREG1 の褐色脂肪化及び抗肥満作用

我々は先行研究においてUCP1欠損マウスが加齢に伴い食餌誘導性肥満になることなどを報告してきた [4, 5]。また、UCP1欠損マウスを用いて白色脂肪組織の褐色脂肪化に関連する遺伝子群を探索する中で、褐色脂肪化の促進に伴い発現量が上昇する遺伝子の1つとしてCellular Repressor of E1A-stimulated genes 1 (CREG1)を同定した。CREG1は分子量が約24,000の分泌糖タンパク質であり、細胞の増殖や分化に関与するRbやE2Fなどの転写因子と相互作用すること [6] やM6P/IGF2Rに結合すること [7] などが報告されているが、その生理的機能についてはほとんど分かっていなかった。我々はUCP1欠損マウスの研究から得られた知見をもとに、褐色脂肪組織や鼠蹊部白色脂肪組織から調製した初代培養細胞を用いた分化誘導実験を行い、褐色脂肪化マーカーであるUCP1の発現上昇に先行してCREG1の発現が誘導されることを見出した。さらに、培養細胞へのCREG1遺伝子の導入によりUCP1のmRNAレベルが上昇することを確認した。

続いて、生体におけるCREG1の生理機能を検証するために、食餌誘導性肥満条件下のC57BL/6マウスに精製したCREG1タンパク質を浸透圧ポンプにより投与する実験を行い、実際にCREG1投与群ではPBSを投与した対照群と比較して有意な体重抑制効果が認められ、白色脂肪組織では脂肪サイズの減少や褐色脂肪細胞の出現も確認された。加えて、CREG1投与群では肝中脂質レベルにおける有意な改善効果も認められた。これらの成績は、生体レベルでもCREG1が褐色脂肪化に関与しており、抗肥満において重要な役割を果たすことを強く示唆するものと考えられた (論文投稿中)。

#### 5. 脂肪組織特異的CREG1-Tgマウスの樹立と表現型の解析

我々は、生体レベルにおけるCREG1の役割や抗肥満作用をさらに検討するため、 $\alpha$ P2プロモーターを用いて脂肪組織特異的にCREG1の発現が誘導されるトランスジェニックマウス (CREG1-Tgマウス) を作製した。得られた複数のCREG1-TgマウスラインについてC57BL/6マウスへの戻し交配を進め、脂肪細胞で誘導されるCREG1の発現レベルの異なる低発現ラインと高発現ラインを樹立した。これら両ラインのマウスでは、通常の飼育条件下でも複数の脂肪組織で褐色脂肪化の促進が認められた。次に、これらのTgマウスに高脂肪食を投与する実験を行った結果、野生型のWTマウスと比較して、Tgマウスでは体重増加が顕著に抑制され、血糖値や血清脂質レベルも改善する傾向が認められた。さらに組織学的検討から、Tgマウスでは各脂肪組織の脂肪細胞のサイズが小さくなり、UCP1の発現量も増加しているという褐色脂肪化の特徴を有していることが明らかとなった。これらの結果はCREG1が生体内においても脂肪組織の褐色脂肪化を促進する生理機能を有しており、褐色脂肪化促進により抗肥満作用を発揮する新規内分泌因子であることを証明するものと考えられた (図2)。

#### 6. おわりに

CREG1に関する報告は少ないが、Moolmuangらは、CREG1が癌抑制遺伝子であるp16により誘導される細胞老化を促進することを報告している [8]。最近では、糖尿病患者のアテローム動脈粥状硬化症部位から採取した内皮細胞では、正常な内皮細胞と比較してCREG1の発現量が減少しており、アポトーシスが促進されていることが報告された [9]。この研究では、CREG1が高グルコース条件下で誘導される内皮細胞のアポトーシスを抑制することも示された。これらの報告は、我々の研究成果と同様に、CREG1の働きが老化や生活習慣病と密接な関わりを持っていることを示唆しており大変興味深い。未だ十分明らかとなっていない新規内分泌因子としてのCREG1の作用メカニズムの解明が待たれるところである。

#### 参考文献

1. Inagaki, T, Sakai, J, and Kajimura, S. Transcriptional and epigenetic control of brown and beige adipose cell fate and function. *Nat Rev Mol Cell Biol* 17 (8) :480-495, 2016.
2. Cypess, A M, Lehman, S, Williams, G, *et al.* Identification and Importance of Brown Adipose Tissue in Adult Humans. *N Engl J Med* 360 (15) :1509-1517, 2009.
3. Harms, M J, Ishibashi, J, Wang, W, *et al.* Prdm16 is required for the maintenance of brown adipocyte identity and function in adult mice. *Cell Metab* 19 (4) :593-604, 2014.

4. Enerbäck, S, Jacobsson, A, Simpson, E M, *et al.* Mice lacking mitochondrial uncoupling protein are cold-sensitive but not obese. *Nature* 387 (6628) :90-94, 1997.
5. Kontani, Y, Wang, Y, Kimura, K, *et al.* UCP1 deficiency increases susceptibility to diet-induced obesity with age. *Aging Cell* 4 (3) :147-155, 2005.
6. Veal, E, Eisenstein, M, Tseng, Z H, *et al.* A cellular repressor of E1A-stimulated genes that inhibits activation by E2F. *Mol Cell Biol* 18 (9) :5032-5041, 1998.
7. Di Bacco, A and Gill, G. The secreted glycoprotein CREG inhibits cell growth dependent on the mannose-6-phosphate/insulin-like growth factor II receptor. *Oncogene* 22 (35) :5436-5445, 2003.
8. Moolmuang, B and Tainsky, M A. CREG1 enhances p16 (INK4a) -induced cellular senescence. *Cell Cycle* 10 (3) :518-530, 2011.
9. Liu, Y, Tian, X, Li, Y, *et al.* Up-regulation of CREG expression by the transcription factor GATA1 inhibits high glucose- and high palmitate-induced apoptosis in human umbilical vein endothelial cells. *PLoS One* 11 (5) :e0154861, 2016.

## 【トピックス】

### エボジアミンは肥満とインスリン抵抗性を改善する

山下 均<sup>1</sup>、王 挺<sup>2</sup>、楠堂 達也<sup>1</sup>、竹内 環<sup>1</sup>、李 勇学<sup>1</sup>、喬 善楼<sup>1</sup>、紺谷 靖英<sup>3</sup>、森 望<sup>4</sup>

<sup>1</sup>中部大・生命健康、<sup>2</sup>岩手医大・消化器肝臓内科、<sup>3</sup>南九州大・健康栄養、<sup>4</sup>長崎大・医・解剖

#### 1. はじめに

現在、内臓肥満をベースとするメタボリックシンドロームはその予備軍を含めて2,000万人を超え、男女ともに40歳以上でその割合が高くなる。肥満によるインスリン抵抗性はⅡ型糖尿病の最も重要な成因と考えられ、加齢と共に発症率が上昇する。従って、肥満の治療はⅡ型糖尿病の予防と治療につながるばかりでなく、他の生活習慣病の予防および健康寿命の延長に寄与するものと考えられる。

肥満はエネルギー収支の結果余ったエネルギーが白色脂肪細胞に過剰に蓄積した状態である。肥満は様々な要因により進行するが、体温調節に係わる分子群がエネルギー代謝の中でも極めて重要な役割を担い、その機能低下が肥満など老化の過程で生ずる種々の病態と関連することが近年明らかとなってきた。また最近、熱産生によりエネルギー消費に寄与する褐色脂肪細胞が加齢と共に減少していくことが肥満の原因の1つと考えられ、褐色脂肪細胞をターゲットとした肥満予防法の開発に注目が集まっている[1]。我々は、褐色脂肪熱産生の中心分子であるミトコンドリア脱共役蛋白質-1 (UCP1) を欠損するマウスが、ヒトと同様に加齢と共にインスリン抵抗性を伴う肥満を呈すること[2]、生薬ゴシュユの主要成分であるエボジアミン (Evodiamine) がUCP1欠損型肥満に対しても予防効果を示すこと[3,4]を報告している。

エボジアミンは、温度受容体TRPV1のリガンドであるカプサイシンと類似の薬理作用を有することが古くから知られてきた。しかし、我々の研究からエボジアミンはカプサイシンにはみられない白色脂肪細胞の分化阻害やインスリン抵抗性の改善などの新規作用も有することが明らかとなっている。本稿では、肥満およびインスリン抵抗性に対するエボジアミンの作用について紹介する。

#### 2. エボジアミンの抗肥満メカニズム

カプサイシンやエボジアミンは血管拡張作用により体表からの熱放散を促進する[5]。続いて、交感神経系が活性化されて褐色脂肪細胞による熱産生が起こる際に、エネルギーが消費され抗肥満につながると考えられる。そこで我々は、実際にエボジアミンが褐色脂肪細胞にお

けるUCP1機能依存的に抗肥満作用を発揮するかどうかをUCP1欠損マウスを用いて検討した。その結果、予想に反してエボジアミンは、野生型マウスに対してと同様に、UCP1欠損マウスの食事誘導性肥満を強く抑制し耐糖能を改善することが明らかとなった[3]。すなわち、エボジアミン (300mg/kg飼料) を添加した高脂肪食を2ヶ月間摂取したマウスでは、高脂肪食のみを摂取したマウスに比べて、摂取量に差はみられなかったが、体重、脂肪組織量、血中レプチンおよびインスリン量などの有意な低下が観察された。また、肥満に伴う脂肪肝の改善なども認められ、エボジアミンが褐色脂肪細胞のUCP1機能に依存しないユニークな抗肥満作用を有することが明らかとなった。

それでは、エボジアミンはどのような作用メカニズムで抗肥満作用を発揮するのであろうか？肥満が進行する過程では、白色脂肪細胞は過剰なエネルギーを中性脂肪としてより多く蓄えるために肥大化するが、それと同時に、成熟白色脂肪細胞の数の増加が肥満の進展における重要な要素となる。脂肪細胞の分化は様々なシグナル伝達分子や転写因子により制御される。特に、白色脂肪前駆細胞が増殖から分化に移行する初期過程において、増殖期に高いERK/MAPK活性が低下することが白色脂肪細胞への分化のトリガーとして重要である[6]。3T3-L1脂肪前駆細胞の培養系を用いてエボジアミンの白色脂肪細胞に対する直接作用を検討した結果、エボジアミンは脂肪前駆細胞の初期分化においてERK/MAPK活性の低下を阻害することが明らかとなった[7]。3T3-L1脂肪前駆細胞はTRPV1をほとんど発現せず、実際にカプサイシンにはエボジアミンと同様の作用は認められないことから、TRPV1以外のターゲットとなる受容体の関与を検討した。その結果、エボジアミンはEGF受容体のリン酸化を介してPKC $\alpha$ -MEK経路を経てERK/MAPKを活性化することが明らかとなった(図1)。このERK/MAPKの活性化により、脂肪細胞分化に重要な役割を果たす転写因子C/EBP $\beta$ およびPPAR $\gamma$ 蛋白質の発現が強く阻害されて白色脂肪前駆細胞の分化が阻害されることが判明した。また、ERK/MAPKの活性化はPPAR $\gamma$ をリン酸化(不活性化)することも報告されている[8]。

#### 3. エボジアミンの抗インスリン抵抗性メカニズム

エボジアミンはERK/MAPKの活性化を介して白色脂肪細胞分化を強く阻害することが明らかとなったが、インスリン抵抗性に対する作用は明らかではない。組織におけるインスリン抵抗性のメカニズムとしては、インス

連絡先：〒487-8501

愛知県春日井市松本町1200

Tel: 0568-51-1111

Fax: 0568-51-6017

E-mail: hyamashi@isc.chubu.ac.jp

リン受容体基質1 (IRS-1) のSerリン酸化が重要である。また、IRS-1のSerリン酸化はラパマイシン標的蛋白質 (mTOR) を介してp70S6キナーゼ (S6K) により活性化される[9]。肥満によりインスリンレベルが上昇すると、Aktのリン酸化を介してmTOR-S6K経路が活性化され、IRS-1のSerリン酸化によるインスリン抵抗性が亢進することが予想される。そこで、エボジアミン添加高脂肪食を摂取したUCP1欠損マウスの白色脂肪組織についてこれらのシグナル分子を解析した結果、コントロール群に比べて、エボジアミン摂取群においてAkt、mTORおよびIRS-1のSerリン酸化レベルが低いことが見出された (図2)。同様の結果は、肥満糖尿病モデルKK-Ayマ

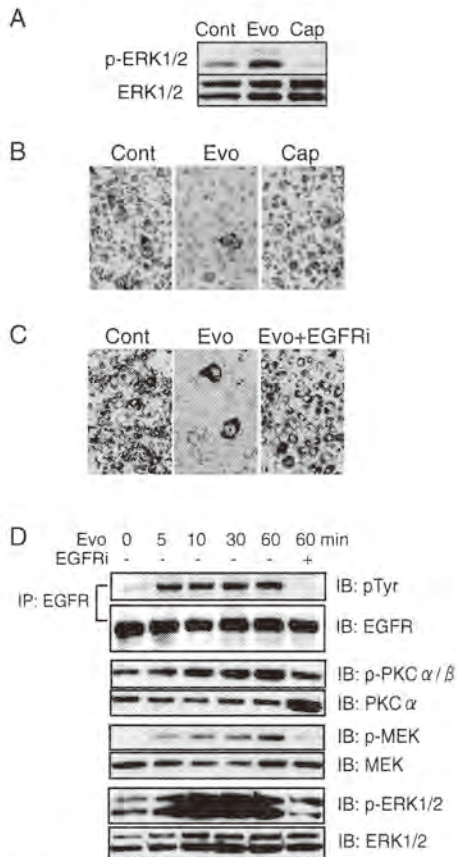


図1 エボジアミンの脂肪細胞分化阻害メカニズム  
A, B. 3T3-L1脂肪前駆細胞におけるERKリン酸化 (A) 及び分化 (B) に対するエボジアミン (Evo) とカプサイジン (Cap) の効果。C. EGF受容体阻害剤 (EGFi) によるエボジアミンの抗脂肪細胞分化作用の阻害。D. 脂肪前駆細胞のエボジアミン刺激によるEGFR, PKC $\alpha$ , MEK及びERKリン酸化の経時変化とEGFiの作用。(文献3, 7より引用改変)

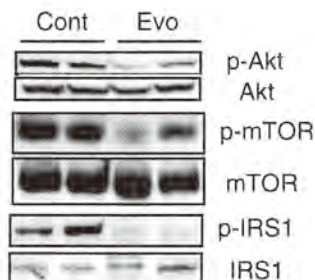


図2 エボジアミン添加 (300mg/kg) 高脂肪食を2ヶ月間摂取したUCP1欠損マウスの白色脂肪組織におけるAkt, mTOR及びIRS-1 Serリン酸化レベル

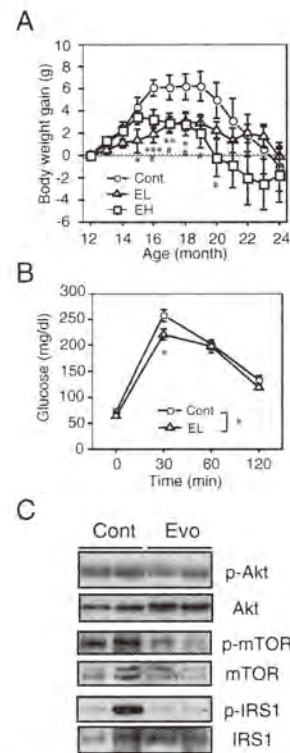


図3 加齢性肥満及びインスリン抵抗性に対するエボジアミンの効果

A. 12ヶ月齢からエボジアミンを1 mg/kg (EL群) 又は10mg/kg (EH群) 添加した標準食を摂取したC57BL/6Jマウス体重の経時変化。B, C. 18ヶ月齢における耐糖能試験 (B) 及び白色脂肪組織におけるAkt, mTOR及びIRS-1 Serリン酸化レベル (C)。\* $P < 0.05$ , \*\* $P < 0.01$  and \*\*\* $P < 0.001$  Cont vs. EL group. #  $P < 0.05$  Cont vs. EH group.

ウスにエボジアミンを1週間腹腔内投与した実験においても観察された。従って、エボジアミンはmTOR-S6K経路の活性化を阻害することにより過剰なインスリンシグナル経路の活性化とIRS-1のSerリン酸化を抑制しインスリン抵抗性の改善に寄与するものと考えられた。

#### 4. 加齢性肥満とインスリン抵抗性に対するエボジアミンの効果

カロリー制限による寿命延長においてmTOR経路の重要性が最近明らかとなってきた。実際に、マウス実験においてmTOR-S6K経路を阻害すると高脂肪食下でも肥満にならずインスリン抵抗性が改善すること[9]、mTOR阻害薬のラパマイシンの長期投与により寿命が延びること[10]が報告された。エボジアミンが細胞および組織レベルにおいてmTOR経路を阻害し抗肥満/抗インスリン抵抗性作用を示すことから、エボジアミンの長期摂取による加齢性肥満とインスリン抵抗性に対する効果について検討した。C57BL/6Jマウスの体重は低脂肪の標準食摂取によっても自由摂食下において加齢とともに増加し、18ヶ月齢頃にピークとなる。しかし、12ヶ月齢からエボジアミン添加飼料 (1又は10mg/kg標準食) を摂取したマウスでは、コントロール群に比べて摂食量はむしろ高い傾向がみられたが体重増加は有意に抑制され、18ヶ月齢ではインスリンレベルの低値と耐糖能の改善も認められた (図3A,B)。また、白色脂肪組織のシグナ

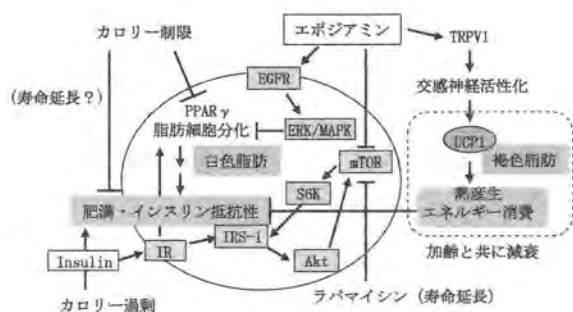


図4 エボジアミンによる脂肪細胞機能の制御

ル解析を行った結果、コントロール群に比べて、エボジアミン摂取群においてAkt、mTORおよびIRS-1のSerリン酸化が低下していることが観察された。一方、寿命に対する効果については、エボジアミン群とコントロール群の間に有意差はみられなかった。

## 5. おわりに

最近、Mattisonらはアカゲザルの研究からカロリー制限は疾患発症リスクを軽減して健康を増進する効果はあるが寿命延長効果については否定する結果を報告した[11]。一方、我々が直面するカロリー過剰状態により加齢とともに進行する肥満は、糖尿病や動脈硬化発症を助長して心血管系疾患を招き寿命短縮につながる。現在、加齢に伴う褐色脂肪細胞の減少を抑えることにより肥満を予防する方法の開発に注目が集まっているが[1]、エボジアミンは褐色脂肪細胞の活性化作用と白色脂肪細胞の分化阻害作用を併せもつ極めてユニークな機能性分子であり、褐色脂肪細胞の減衰したヒトに対しても摂取量を減らすことなく、加齢性肥満及びインスリン抵抗性を改善する新しい予防/治療法を提供する可能性が明らかとなった(図4)。エボジアミンはラパマイシンと同様に抗ガン作用を有することも報告されている。健康寿命を延長する画期的なアンチエイジング剤として、エボジアミン研究のさらなる進展が期待される。

## 参考文献

1. 文部科学省科学技術政策研究所. 肥満解消に期待される褐色脂肪細胞における新知見. 科学技術動向 99(6):4, 2009.
2. Kontani Y, Wang Z, Kimura K, Inokuma K, Saito M, Suzuki-Miura T, Wang Z, Sato Y, Mori N and Yamashita H. UCP1 deficiency increases susceptibility to diet-induced obesity with age. *Aging Cell* 4:147-155, 2005.
3. Wang T, Wang Y, Kontani Y, Kobayashi Y,

Sato Y, Mori N and Yamashita H. Evodiamine improves diet-induced obesity in a UCP1-independent manner: Involvement of anti-adipogenic mechanism and ERK/MAPK signaling. *Endocrinol* 149: 358-366, 2008.

4. 山下 均. 脂肪細胞の役割からみる肥満-新しい肥満予防法開発の試み-. 中部大学生命健康科学研究所紀要 4:47-53, 2008.
5. Wang Y, Kimura K, Inokuma K, Saito M, Kontani Y, Kobayashi Y, Mori M and Yamashita H. Potential contribution of vasoconstriction to suppression of heat loss and homeothermic regulation in UCP1-deficient mice. *Pflugers Arch - Eur J Physiol* 452: 363-369, 2006.
6. Sakaue H, Ogawa W, Nakamura T, Mori T, Nakamura K and Kasuga M. Role of MAPK phosphatase-1 (MKP-1) in adipocyte differentiation. *J Biol Chem* 279:39951-39957, 2004.
7. Wang T, Wang Y and Yamashita H. Evodiamine inhibits adipogenesis via EGFR-PCK $\alpha$ -ERK signaling pathway. *FEBS Lett* 583:3655-3659, 2009.
8. Hu E, Kim JB, Sarraf P and Spiegelman BM. Inhibition of adipogenesis through MAP kinase-mediated phosphorylation of PPARgamma. *Science* 274:2100-2103, 1996.
9. Um SH, Frigerio F, Watanabe M, Picard F, Joaquin M, Sticker M, Fumagalli S, Allegri PR, Kozma SC, Auwerx J and Thomas G. Absence of S6K1 protects against age- and diet-induced obesity while enhancing insulin sensitivity. *Nature* 431:200-205, 2004.
10. Harrison DE, Strong R, Sharp ZD, Nelson JF, Astle CM, Flurkey K, Nadon NL, Wilkinson JE, Frenkel K, Carter CS, Pahor M, Javors MA, Fernandez E and Miller RA. Rapamycin fed late in life extends lifespan in genetically heterogeneous mice. *Nature* 460:392-395, 2009.
11. Mattison JA, Roth GS, Beasley TM, Tilmont EM, Handy AM, Herbert RL, Longo DL, Allison DB, Young JE, Bryant M, Barnard D, Ward WF, Qi W, Ingram DK and de Cabo R. Impact of caloric restriction on health and survival in rhesus monkeys from the NIA study. *Nature* 489:318-321, 2012.



OPEN

# A key role for neuropeptide Y in lifespan extension and cancer suppression via dietary restriction

SUBJECT AREAS:

AGEING

EXPERIMENTAL MODELS OF  
DISEASE

Received

25 September 2013

Accepted

13 March 2014

Published

31 March 2014

Correspondence and requests for materials should be addressed to I.S. (shimo@nagasaki-u.ac.jp)

\* Current address: Biomedical Gerontology Laboratory, Faculty of Human Sciences, and Institute of Applied Brain Sciences, Waseda University, Tokorozawa 359-1192, Japan.

Takuya Chiba<sup>1,2\*</sup>, Yukari Tamashiro<sup>2</sup>, Daeui Park<sup>3</sup>, Tatsuya Kusudo<sup>4</sup>, Ryoko Fujie<sup>2</sup>, Toshimitsu Komatsu<sup>1,2</sup>, Sang Eun Kim<sup>1,2</sup>, Seongjoon Park<sup>1,2</sup>, Hiroko Hayashi<sup>1,2</sup>, Ryoichi Mori<sup>1,2</sup>, Hitoshi Yamashita<sup>4</sup>, Hae Young Chung<sup>3</sup> & Isao Shimokawa<sup>1,2</sup>

<sup>1</sup>Department of Investigative Pathology, Unit of Basic Medical Science, Graduate School of Biomedical Sciences, Nagasaki University, Nagasaki 852-8523, Japan, <sup>2</sup>Department of Pathology, Nagasaki University School of Medicine, Nagasaki 852-8523, Japan, <sup>3</sup>Department of Pharmacy, College of Pharmacy, and Molecular Inflammation Research Center for Aging Intervention, Pusan National University, Busan 609-735, Korea, <sup>4</sup>Department of Biomedical Sciences, College of Life and Health Sciences, Chubu University, Kasugai 487-8501, Japan.

**Knowledge of genes essential for the life-extending effect of dietary restriction (DR) in mammals is incomplete. In this study, we found that neuropeptide Y (Npy), which mediates physiological adaptations to energy deficits, is an essential link between DR and longevity in mice. The lifespan-prolonging effect of lifelong 30% DR was attenuated in Npy-null mice, as was the effect on the occurrence of spontaneous tumors and oxidative stress responses in comparison to wild-type mice. In contrast, the physiological processes activated during adaptation to DR, including inhibition of anabolic signaling molecules (insulin and insulin-like growth factor-1), modulation of adipokine and corticosterone levels, and preferential fatty acid oxidation, were unaffected by the absence of Npy. These results suggest a key role for Npy in mediating the effects of DR. We also provide evidence that most of the physiological adaptations to DR could be achieved in mice without Npy.**

Moderate restriction of dietary calories while providing essential nutrients, known as dietary restriction (DR), inhibits ageing-dependent disorders and increases the lifespan in many organisms, including yeast, invertebrates, and mammals<sup>1,2</sup>. DR also extends the disease-free lifespan of non-human primates<sup>3,4</sup>, although it may not increase overall survival<sup>4</sup>. These findings suggest that the DR paradigm may extend the healthy lifespans of humans by preventing age-related disorders. Accordingly, it is essential to identify the genes encoding the key proteins that mediate the effects of DR. Epistasis analyses using genetic mutations have led to the identification of several genes critical for the effects of DR in invertebrates, including sirtuins, DAF-16, SKN-1, and the target of rapamycin (TOR)<sup>1</sup>. However, similar studies in mammals have been limited.

An evolutionary view predicts that the effects of DR are due to the processes used by animals to adapt to harsh environmental conditions, especially famine<sup>5,6</sup>. In mammals, neurons in the hypothalamic arcuate nuclei (ARC) sense the states of energy intake and storage through the levels of circulating hormones<sup>7</sup>. A negative energy balance and a subsequent decrease in adipose tissue reduce the circulating levels of leptin, insulin, and insulin-like growth factor (IGF)-1 but increase the levels of ghrelin and adiponectin. These hormonal changes subsequently activate neuropeptide Y (Npy) neurons in the ARC. Many of these neurons co-express agouti-related protein (Agrp), which attenuates the activity of proopiomelanocortin (Pomc) neurons in the ARC. Changes in the activities of these first-order neurons inhibit the second-order hypothalamic neurons, including those secreting growth hormone-releasing hormone (Ghrh), gonadotropin-releasing hormone (Gnrh), and thyrotropin-releasing hormone (Trh), but activate corticotropin-releasing hormone (Crh) neurons<sup>7,8</sup>. These hypothalamic changes ultimately suppress the somatotrophic, reproductive, and thyroid axes, and activate the adrenal glucocorticoid axis<sup>7,8</sup>. In fact, many of these neuroendocrinological changes occur in rodents subjected to DR<sup>8</sup>. The neuroendocrine equilibrium maintained during DR is believed to favor longevity over growth and reproduction. By contrast, genetic inhibition of the Ghrh–GH axis and the subsequent reduction in plasma IGF-1 levels extends the lifespan of rodents without restricted food intake. This suggests that inhibition of anabolic signaling pathways mediates the effects of DR.

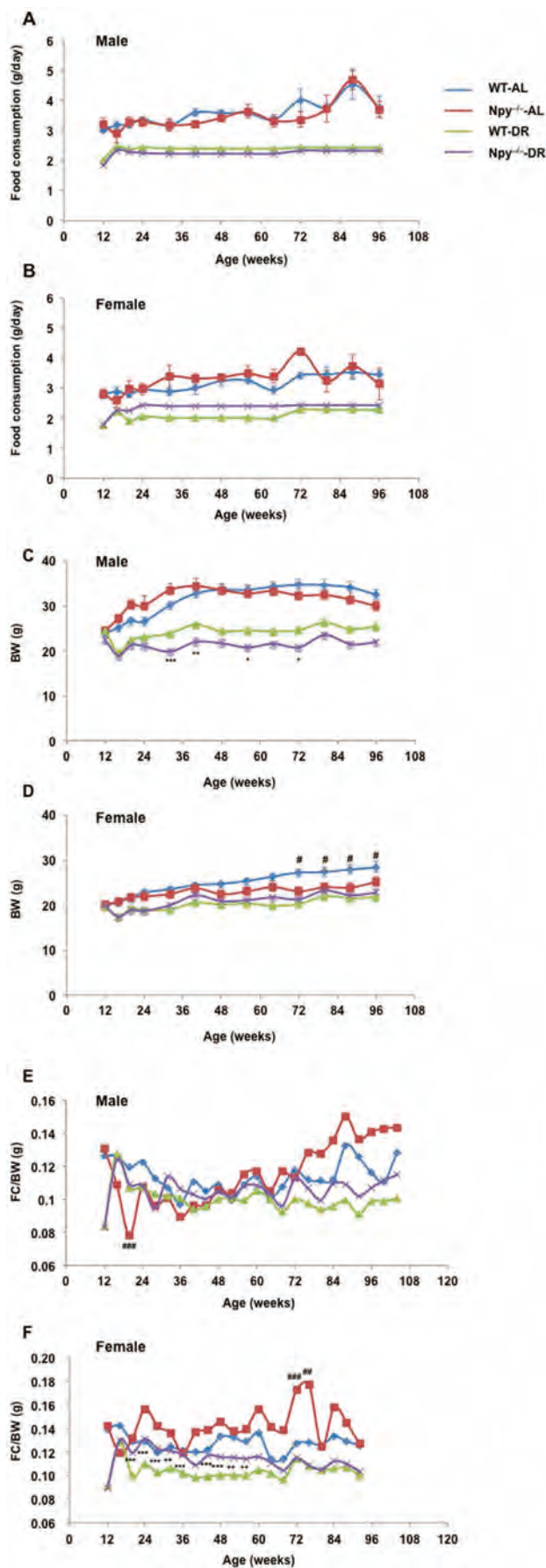


**Figure 1 | Food consumption (FC, g/day/mouse), body weight (BW), and food efficiency (FC/BW) in male and female mice.** (A, B) The FC in male and female *Npy*<sup>-/-</sup>-AL and WT-AL mice. The data for the control mice fed ad libitum (AL) are presented as the mean  $\pm$  SE ( $n = 3$  to 9 cages). The food allotments for the 30% dietary restricted (DR) groups were adjusted every 2 weeks between 12 and 32 weeks; the allotments were fixed between 32 and 72 weeks and from 72 weeks and onward. (C) The BW in the male mice. \*, \*\*, \*\*\*,  $p < 0.05$ ,  $p < 0.01$ ,  $p < 0.001$  vs WT-DR at each age point by Bonferroni post hoc test. The data are presented as the mean  $\pm$  SE. The initial numbers of mice as follows;  $n = 23$ , 21, 13, and 12 for the WT-AL, WT-DR, *Npy*<sup>-/-</sup>-AL, and *Npy*<sup>-/-</sup>-DR groups, respectively. (D) The BW in female mice. #,  $p < 0.05$  vs. WT-AL at each age point by Bonferroni post hoc test. Data are presented as the mean  $\pm$  SE. The initial numbers of mice were as follows;  $n = 25$ , 21, 12, 12 for the WT-AL, WT-DR, *Npy*<sup>-/-</sup>-AL, and *Npy*<sup>-/-</sup>-DR groups, respectively. (E) The FC/BW in male mice. Data represent means; the SEs are not drawn ( $n = 17$ , 16, 6, and 5 for the WT-AL, WT-DR, *Npy*<sup>-/-</sup>-AL, and *Npy*<sup>-/-</sup>-DR groups, respectively) (F) The FC/BW in female mice. ##, ###,  $p < 0.01$ ,  $p < 0.0001$  vs. WT-AL mice by Bonferroni post hoc test. \*\*, \*\*\*,  $p < 0.01$ ,  $p < 0.001$ , respectively, vs. WT-DR by Bonferroni post hoc test. The data represent the means; the SEs are not drawn ( $n = 10$ , 17, 5, and 9 for the WT-AL, WT-DR, *Npy*<sup>-/-</sup>-AL, and *Npy*<sup>-/-</sup>-DR groups, respectively).

In this study, we focused on the role of Npy in mediating the effects of DR because of its unique properties that differ from those of other hypothalamic neuropeptides. Npy is required to inhibit Ghrh neurons and GH secretion into the circulation in fasted rats<sup>9,10</sup>, whereas *Agrp* did not inhibit GH secretion<sup>11</sup>. Thus, DR may exert some of its effects via Npy-induced inhibition of the Ghrh-GH axis. Overexpression of Npy gene tended to increase the lifespan of rats, even in the absence of DR<sup>12</sup>. Activation of specific Npy receptors protects hippocampal neurons from kainate-induced excitotoxicity and ischemia<sup>13</sup>. Extended lifespan and resistance to harmful stresses are hallmarks of DR<sup>14</sup>. Additionally, Npy was recently reported to be involved in the antineoplastic effects of DR in mice<sup>15</sup>. Therefore, we hypothesized that Npy plays a key role in the effects of DR. We tested this hypothesis by comparing the effects of DR on lifespan, pathology, oxidative stress resistance, neuroendocrine systems, energy metabolism, and gene expression between Npy-null (*Npy*<sup>-/-</sup>) and wild-type (WT) mice. We suspected that the absence of Npy may compromise the neuroendocrine equilibrium induced by DR and thus minimize the effects of DR in mice.

## Results

**The effects of DR on food intake, body weight and energy metabolism in *Npy*<sup>-/-</sup> mice.** Npy is a potent orexigenic and energy-conserving neuropeptide<sup>7</sup>. Genetic disruption of Npy signaling, however, exerts subtle effects on feeding and weight gain in young mice<sup>16,17</sup>, most likely due to compensatory changes in the neuroendocrine system that normalizes feeding and energy expenditure in the absence of Npy. In the longevity groups in this study, male *Npy*<sup>-/-</sup>-AL mice consumed 5% less food, whereas female *Npy*<sup>-/-</sup>-AL mice had approximately 10% greater amounts of food during the lifespan study, although these differences were statistically insignificant ( $p = 0.1182$  in males and  $p = 0.0624$  in females by 2-f ANOVA (Genotype); FC data collected from 3 to 9 cages; Figure 1A and B). Accordingly, the male *Npy*<sup>-/-</sup>-DR mice received 5% less food, whereas the female *Npy*<sup>-/-</sup>-DR mice ate on average 10% more food than mice in the corresponding WT-DR groups. However, dietary restriction was generally maintained at 30% of AL intake in each group.

Body weight (BW) did not statistically differ between male WT-AL and *Npy*<sup>-/-</sup>-AL mice ( $p = 0.0845$  by 2-f ANOVA (Genotype); initial numbers were 23 male WT-AL and 13 *Npy*<sup>-/-</sup>-AL mice); BW was greater in male *Npy*<sup>-/-</sup>-AL than in WT-AL mice between 12 and 36 weeks, but tended to be lower in male *Npy*<sup>-/-</sup>-AL mice beyond 36

weeks ( $p = 0.0287$  by 2-f ANOVA (Genotype  $\times$  Age interaction); Figure 1C). BW was lower in female  $Npy^{-/-}$ -AL mice than in WT-AL mice ( $p < 0.0001$  by 2-f ANOVA (Genotype); initial numbers were 25 female WT-AL and 12  $Npy^{-/-}$ -AL; Figure 1D). BW was 8 to 16% lower in male  $Npy^{-/-}$ -DR mice than in WT-DR mice ( $p < 0.0001$  by 2-f ANOVA (Genotype); initial numbers were 21 male WT-DR and 12  $Npy^{-/-}$ -DR; Figure 1C); BW in female  $Npy^{-/-}$ -DR and WT-DR mice did not differ (initial numbers were 21 female WT-DR and 12  $Npy^{-/-}$ -DR; Figure 1D).

Although the absolute values of FC and BW in  $Npy^{-/-}$  and WT mice were similar or slightly different under AL or DR conditions (Figure 1A, B, C and D), FC normalized to BW was significantly less in WT-DR than in WT-AL males and females ( $p < 0.0001$  in males and  $p < 0.0001$  in females by 2-f ANOVA (Genotype); Figure 1E and F), indicating that DR increases food efficiency, as an index of how efficiently body weight (i.e., the lean body and fat mass) is maintained by food utilization. Weindruch and Wolford<sup>18</sup> proposed a model of metabolic efficiency, in which DR retards aging by reducing mitochondrial proton leakage, which in turn increases ATP production efficiency and reduces body temperature and the generation of reactive oxygen species. In fact, recent studies in recombinant inbred strains of mice support the model<sup>19,20</sup>. Therefore, food efficiency as defined here could be used as a predictor of DR efficacy. The FC/BW was also lower in  $Npy^{-/-}$ -DR than in  $Npy^{-/-}$ -AL males and females ( $p < 0.0001$  in males and  $p < 0.0001$  in females by 2-f ANOVA (Genotype); Figure 1E and F). Therefore, the metabolic trait of DR was maintained in  $Npy^{-/-}$  mice, although the FC/BW in male  $Npy^{-/-}$ -AL mice was greater than in male WT-AL mice at 76 weeks of age and later ( $p < 0.0001$  by 2-f ANOVA (Genotype  $\times$  Age); Figure 1E). The FC/BW was 6% greater in male  $Npy^{-/-}$ -DR versus WT-DR mice, particularly at 72 weeks of age and later ( $p < 0.0001$  by 2-f ANOVA (Genotype);  $p = 0.0544$  by 2-f ANOVA (Genotype  $\times$  Age); Figure 1E). FC/BW was greater in female  $Npy^{-/-}$ -AL mice than in WT-AL females at many, but not all, age points ( $p < 0.0001$  by 2-f ANOVA (Genotype, Genotype  $\times$  Age respectively; Figure 1F). The FC/BW was 10% greater  $Npy^{-/-}$ -DR females than in WT-DR females between 16 and 68 weeks of age; thereafter, FC/BW was similar ( $p < 0.0001$  by 2-f ANOVA (Genotype, Genotype  $\times$  Age respectively); Figure 1F). Thus, by this measure, food efficiency was slightly reduced in  $Npy^{-/-}$  versus WT mice in the lifelong, but not entire, period under AL and DR conditions, although the aging-related changes were sexually dimorphic in the DR groups.

The FC and BW data prompted us to analyze energy homeostasis under DR conditions. In the daily DR regimen, DR mice finish food allotments within a few hours and remain without food for approximately 20 hours thereafter. A metabolic shift from carbohydrate to fatty acid oxidation in the fed-and-fasted feeding cycle characterizes DR rodents<sup>21</sup>. In contrast, AL animals constantly oxidize carbohydrates according to the composition of standard chow. Due to bypassing complex I by electrons into the electron transport chain, the DR-specific preference for fatty acid oxidation to produce ATP contributes to the extension of lifespan through reduced generation of reactive oxygen species<sup>22</sup>. Npy enhances the utilization of carbohydrates as an energy source when food is supplied<sup>23</sup>. Npy also inhibits an excess loss of body energy, such as by heat and physical activity, under conditions of negative energy balance<sup>7</sup>. To eliminate the possibility that energy metabolism was compromised in the  $Npy^{-/-}$ -DR mice, we analyzed the respiratory quotient (RQ) and energy expenditure (EE) in 7-month-old male mice in a metabolic cage with an indirect open-circuit calorimeter (Columbus Instruments, Columbus, OH). We suspected that the fraction of adaptive thermogenesis in the total EE might be increased in  $Npy^{-/-}$  versus WT mice, given that Npy competes with  $\beta$ -adrenergic-induced thermogenesis in the brown adipose tissue (BAT)<sup>24</sup>.

The findings can be summarized as follows; 1) the diurnal variation in RQ was comparable in WT-DR and  $Npy^{-/-}$ -DR mice (the

number of mice in each group was 6; Fig. 2A), although the RQ was lower in  $Npy^{-/-}$ -AL mice than in WT-AL mice; 2) the EE per unit body mass did not differ, particularly between male  $Npy^{-/-}$ -DR and WT-DR mice (Fig. 2B); 3) there were no differences in body temperature (BT) between WT-DR and  $Npy^{-/-}$ -DR mice (Fig. 2C), although the preprandial BT was lower in the DR groups than in the AL groups; 4) Consistently, mRNA expression of Ucp1, 2, and 3 in the BAT did not significantly differ between  $Npy^{-/-}$ -DR and WT-DR mice (see Supplementary Table S1). The BAT weight was also comparable in the  $Npy^{-/-}$ -DR and WT-DR mice (see Supplementary Table S2). Considering our results on energy metabolism, we concluded that  *$Npy^{-/-}$  mice were not metabolically impaired in comparison to WT mice when treated with long-term 30% DR, although food efficiency was slightly lower in  $Npy^{-/-}$ -DR mice.*

**The effects of DR on lifespan, cancer, and stress resistance in  $Npy^{-/-}$  mice.** Lifespans in male and female  $Npy^{-/-}$ -AL mice did not significantly differ from those in WT-AL groups (the initial number of mice for the longevity study ( $n =$  male/female): WT-AL (23/25),  $Npy^{-/-}$ -AL (13/12); Fig. 3A, B). DR significantly extended lifespan in WT mice ( $p = 0.0028$  in male and  $p = 0.0004$  in female WT-DR vs. WT-AL mice by log-rank test; Fig. 3A, B) but not in  $Npy^{-/-}$  mice ( $p = 0.7151$  in male and 0.3852 in female  $Npy^{-/-}$ -DR vs.  $Npy^{-/-}$ -AL mice by log-rank test; WT-DR (21/21),  $Npy^{-/-}$ -DR (12/12)).

The lifespan data are summarized in Table 1. In male WT mice, DR extended lifespan by 20.3% and 14.8% at the 50th and 25th percentile survival points; in male  $Npy^{-/-}$  mice, these were  $-1.9\%$  and  $7.1\%$ , respectively. In female WT mice, DR increased lifespan by 36.0% and 33.6% at the 50th and 25th percentile survival points; in female  $Npy^{-/-}$  mice, DR increased lifespan by  $-1.0\%$  and  $19.5\%$ . Female  $Npy^{-/-}$ -DR mice received 10% more food compared to female WT-DR mice, this might cause the diminution of life-extending effect of DR, when compared to the extent of lifespan extension by DR in WT mice. However, daily allotments for male  $Npy^{-/-}$ -DR mice were 5% less than those for male WT-DR mice; nonetheless, the life-extending effect was diminished in  $Npy^{-/-}$ -DR mice. Thus, it is reasonable to conclude that the loss of Npy could minimize the effect of DR.

Five of twelve male  $Npy^{-/-}$ -DR mice died before reaching the age of 52 weeks of life; in contrast, only a few WT mice died during this period (Fig. 3A). Post-mortem examination found no specific causes of death in these males. To eliminate bias resulting from these early deaths, we reanalyzed the lifespan data by censoring the deaths of these mice. In the reanalysis, we used a Cox hazards model with covariates, Genotype (WT vs.  $Npy^{-/-}$ ), Diet (AL vs. DR), and Sex (male vs. female). The results indicated that 1) WT mice lived longer than  $Npy^{-/-}$  mice ( $p = 0.0004$  [Genotype: Risk ratio (RR) = 0.418 (lower 95%: 0.262 ~ upper 95%: 0.671)], 2) the DR group also lived longer than the AL group ( $p < 0.0001$  [Diet: RR = 0.339 (0.206 ~ 0.671)], and 3) the lifespan of male mice did not differ from that of female male ( $p = 0.5045$  [Sex: RR = 0.864 (0.560 ~ 1.329)]). As suspected from the survival curves, WT and  $Npy^{-/-}$  mice seemed to respond differently to the DR diet in terms of lifespan extension ( $p = 0.0578$  [Genotype  $\times$  Diet]). Then, we analyzed the lifespan data separately by the genotype. In WT mice, the DR group lived significantly longer than the AL group [ $p < 0.0001$  [Diet: RR = 0.240 (0.126 ~ 0.440)]. In  $Npy^{-/-}$  mice, DR mice also lived longer than AL mice ( $p = 0.0167$  [Diet: RR = 0.329 (0.119 ~ 0.821)]). However, the RR seemed to be greater in  $Npy^{-/-}$  mice than in WT mice. Based on the lifespan data, we concluded that the life-prolonging effect of DR was significantly diminished, if not completely abolished, in  $Npy^{-/-}$  mice.

Post-mortem examination of the 72-week survivors revealed that 64.3% of the WT-AL mice had evidence of tumors at death, primarily malignant lymphoma, hepatocellular carcinoma, or lung adenocarci-

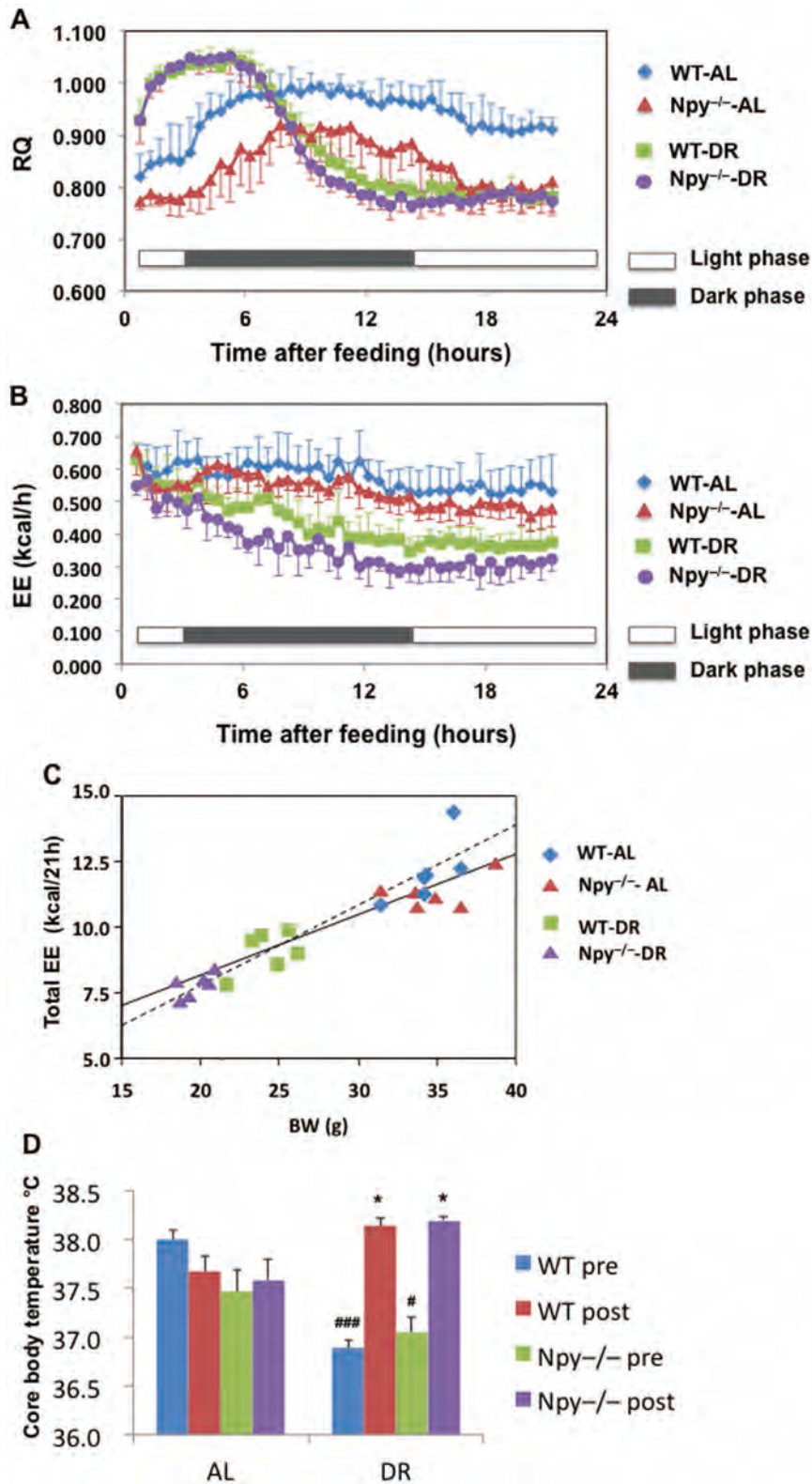


**Figure 2 | DR regulates fuel utilization and energy expenditure in *Npy<sup>-/-</sup>* mice in a manner similar to that in WT mice. (A) Respiratory quotient (RQ) and (B) Energy expenditure (EE) in male mice at 7 months of age. The values represent the mean  $\pm$  SE (n = 6). (C) Scatterplots of body weight and total EE within 21 h after feeding.  $R^2 = 0.240$  for WT-DR (solid line) and  $R^2 = 0.468$  for *Npy<sup>-/-</sup>*-DR (dotted line). (D) Body temperature during the pre- and post-prandial phases of feeding in male mice at 7 months of age. Values represent the means  $\pm$  SE (n = 6). \*, p < 0.05 vs. the preprandial phase in each group. #, p < 0.05, ###, p < 0.001, vs. the AL group during the preprandial phase.**

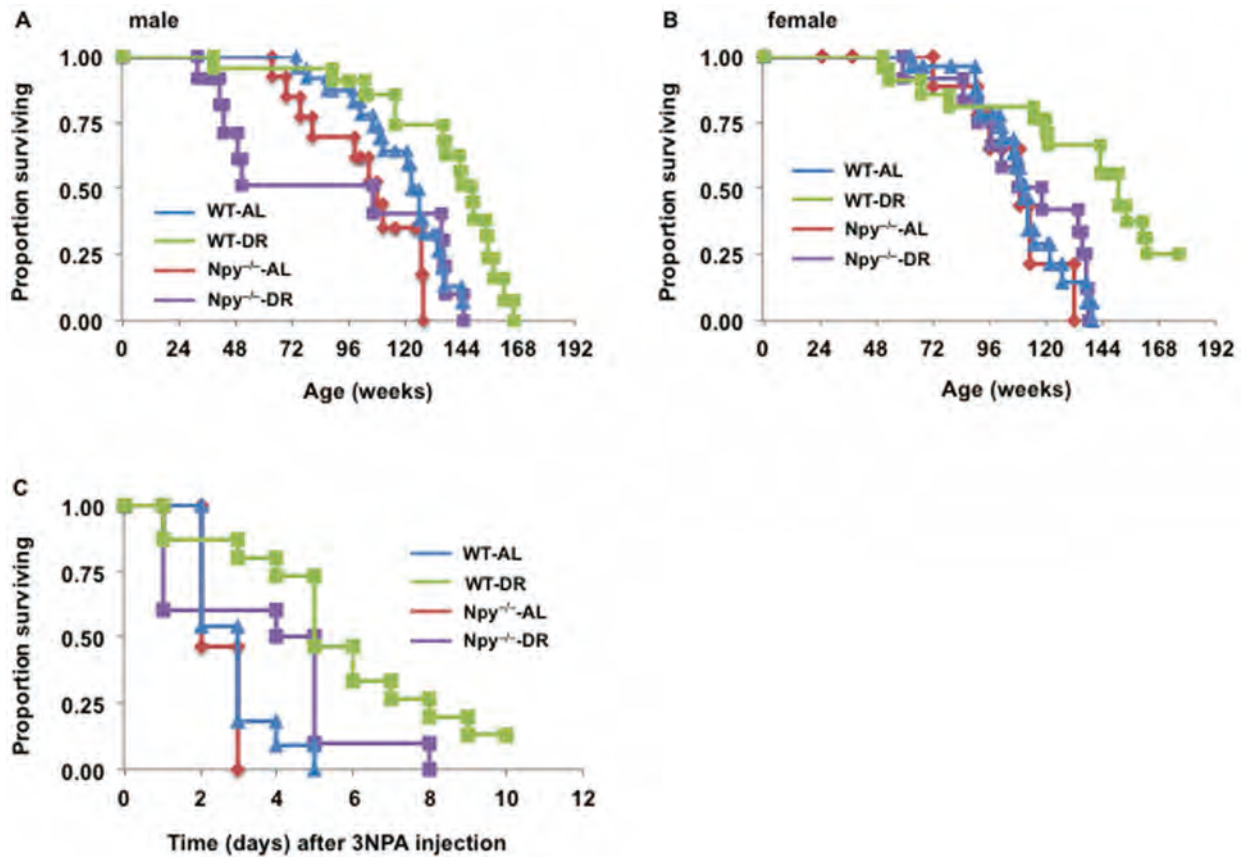


**Figure 3 | The effects of dietary restriction (DR) on lifespan and stress response are diminished in *Npy*<sup>-/-</sup> mice.** Kaplan-Meier survival curves of WT and *Npy*<sup>-/-</sup> mice fed AL or the 30% DR diets, beginning at 12 weeks of age. (A) Survival curves in male mice. The initial numbers of mice as follows; n = 23, 21, 13, and 12 for the WT-AL, WT-DR, *Npy*<sup>-/-</sup>-AL, and *Npy*<sup>-/-</sup>-DR groups, respectively. Comparisons of survival curves by log-rank test; *Npy*<sup>-/-</sup>-AL vs. WT-AL, p = 0.0736; WT-DR vs. WT-AL, p = 0.0028; *Npy*<sup>-/-</sup>-DR vs. *Npy*<sup>-/-</sup>-AL, p = 0.7151. (B) Survival curves in female mice. The initial numbers of mice as follows; n = 25, 21, 12, 12 for the WT-AL, WT-DR, *Npy*<sup>-/-</sup>-AL, and *Npy*<sup>-/-</sup>-DR groups, respectively. The longevity study was concluded at 176 weeks of age because only the female WT-DR group survived between 163 and 176 weeks of age and the proportion of surviving mice in the female WT-DR group decreased to below the 25th percentile survival point at 163 weeks. Comparisons of survival curves by log-rank test; *Npy*<sup>-/-</sup>-AL vs. WT-AL, p = 0.7648; WT-DR vs. WT-AL, p = 0.0004; *Npy*<sup>-/-</sup>-DR vs. *Npy*<sup>-/-</sup>-AL, p = 0.3852. (C) The proportion of surviving mice after lethal oxidative stress induced by daily injection of 3-nitropropionic acid (75 mg/kg BW) in 6-month-old male mice [the numbers of mice examined (n): WT-AL (11), WT-DR (15), *Npy*<sup>-/-</sup>-AL (15), *Npy*<sup>-/-</sup>-DR (10)]. Comparisons of survival curves by log-rank test; *Npy*<sup>-/-</sup>-AL vs. WT-AL, p = 0.2772; WT-AL vs. WT-DR, p < 0.0001; *Npy*<sup>-/-</sup>-AL vs. *Npy*<sup>-/-</sup>-DR, p = 0.0612.

noma (Table 2). The proportion of mice bearing tumors in the *Npy*<sup>-/-</sup>-AL group (55.6%) did not statistically differ in WT-AL mice (64.3%). The proportion was significantly reduced in WT-DR (35.1%) vs. WT-AL mice (Table 2), but did not differ between *Npy*<sup>-/-</sup>-DR (66.7%) and *Npy*<sup>-/-</sup>-AL mice.

Experimental animals subjected to DR are resistant to a range of stressors, such as oxidative and chemically toxic stresses<sup>14</sup>. This trait

has been linked to the longevity induced by DR. We therefore assessed survival rates of 6-month-old male mice from different experimental groups subjected to oxidative stress induced by administration of 3-nitropropionic acid, an inhibitor of mitochondrial respiratory complex II<sup>25</sup> [the numbers of mice examined (n): WT-AL (11), WT-DR (15), *Npy*<sup>-/-</sup>-AL (15), *Npy*<sup>-/-</sup>-DR (10)]. Most WT-AL and *Npy*<sup>-/-</sup>-AL mice died within the first 3 days (Fig. 3C). In

**Table 1 | Summary of lifespan data in wild type (WT) and neuropeptide Y (Npy)-knockout (-/-) mice**

	Initial number of mice	50th percentile survival point	% increase relative to each AL	25th percentile survival point	% increase relative to each AL	Maximum lifespan
<b>Male</b>						
WT-AL	23	123 (2.6)	–	135 (1.5)	–	145
WT-DR	21	148 (4.7)	20.3%	155 (2.8)	14.8%	166
<i>Npy</i> <sup>-/-</sup> -AL	13	108 (4.9)	–	127 (6.9)	–	128
<i>Npy</i> <sup>-/-</sup> -DR	12	106 (64.3)	-1.9%	136 (1.3)	7.1%	145
<b>Female</b>						
WT-AL	25	111 (8.7)	–	122 (8.4)	–	140
WT-DR	21	151 (6.8)	36.0%	163 (3.4)	33.6%	176<
<i>Npy</i> <sup>-/-</sup> -AL	12	109 (8.2)	–	113 (9.8)	–	128
<i>Npy</i> <sup>-/-</sup> -DR	12	108 (14.7)	-0.9%	135 (1.8)	19.5%	145

Lifespan data represent the mean (SE). At 176 weeks of age, the longevity study was concluded; at 176 weeks of age, 4 mice of the female WT-DR group remained alive.

Table 2 | Summary of longevity and pathology in survivors at 72 weeks of age

	WT-AL	WT-DR	Npy <sup>-/-</sup> -AL	Npy <sup>-/-</sup> -DR
Numbers of survivors at 72 weeks of age <sup>†</sup>	42	37	18	15
No. of mice bearing tumors	27	13	10	10
No. of tumor-free mice	15	24	8	5
%Tumor (+)	64.3%	35.1%*	55.6%	66.7%
No. of mice bearing HCC	8	1 <sup>#</sup>	2	1
No. of mice bearing LT	6	7	1	3
No. of mice bearing ML	14	6	5	3

<sup>†</sup>, male and female data were combined.

HCC: Hepatocellular carcinoma, LT: Lung tumor (mostly adenocarcinoma), ML: Malignant lymphoma. \* p < 0.05, # p = 0.0732 vs. WT-AL. The sum totals of mice bearing HCC, LT, and ML exceeded the number of mice with tumors because some of the mice had multiple tumors at the time of death.

contrast, the WT-DR mice exhibited notable stress resistance in comparison to WT-AL mice, as indicated by the significantly increased survival rate (p = 0.0009 by log-rank test; Fig. 3C). The DR effect was diminished in Npy<sup>-/-</sup> mice (p = 0.0612 by log-rank test; Fig. 3C); therefore, Npy may also be involved in the stress resistance induced by DR.

A limitation of this study is the fact that the genetic backgrounds of the Npy<sup>-/-</sup> (Npy<sup>tm1Rpa/J</sup>, approximate to 129S1/SvImJ) and WT (129S6/SvEvTac) mice differed; the genetic background approximated those of the Npy-knockout mice originally generated by Erickson et al<sup>16</sup>. The responses to DR in RQ, neuropeptide mRNA expression, and circulating hormones (as described below) were similar between WT and Npy<sup>-/-</sup> mice in this study, suggesting minimal effect of this difference in this respect. However, it is possible that the diminished salutary effects of DR were derived from the difference in the genetic backgrounds of the WT and Npy<sup>-/-</sup> mice. The small numbers of mice in the longevity study also limit our conclusions.

**The effects of DR on hormonal and neuroendocrine systems.** The loss of Npy signaling might compromise hormonal and neuroendocrine processes recruited to adapt to DR. We evaluated circulating insulin and IGF-1 concentrations, given that DR suppresses these hormones in mammals<sup>1</sup>. In contrast, inhibition of IGF-1-related signaling extends lifespan in mice, even if fed AL<sup>1</sup>; interference in insulin signaling also slightly extends lifespan in male but not female mice<sup>26</sup>. By definition, AL mice have free access to food. The DR mice ate quickly, fully consuming their food within 6 hours, and then

fasted until the next feeding. Blood samples were collected from the retro-orbital veins in the preprandial (4 hours prior to feeding in the DR groups) and postprandial phases (1.5 hours after feeding, the number of mice examined in each phase was 4 or 5). Plasma insulin concentrations did not show statistically significant differences between the preprandial and postprandial phases in the AL groups (Table 3); however, insulin concentrations remained low in the DR groups in the preprandial phase (Table 3) and significantly increased in the postprandial phase. Plasma insulin concentrations did not differ between WT-DR and Npy<sup>-/-</sup>-DR mice at 6 and 24 months of age (Table 3, see Supplementary Fig. S1). Blood glucose levels also did not significantly differ between WT and Npy<sup>-/-</sup> groups under AL or DR conditions at 6 and 24 months of age (see Supplementary Fig. S1).

Plasma IGF-1 concentrations, evaluated in the preprandial phase, did not significantly differ between WT-AL and Npy<sup>-/-</sup>-AL mice (9 mice per group; Table 3). DR reduced plasma IGF-1 by approximately 25% in WT and Npy<sup>-/-</sup> mice, and there was no difference between WT-DR and Npy<sup>-/-</sup>-DR mice.

Anabolic signals including insulin and IGF-1 activate mammalian mTOR pathways<sup>1</sup>. The mTOR pathway plays a central role in the effects of DR in invertebrates<sup>27,28</sup> and mammals<sup>29</sup>. We also investigated the levels of ribosomal protein S6 kinase polypeptide 1 (Rps6kb1), a component of the mTOR pathway, in the liver. The levels of phosphorylated (active) Rps6kb1 were significantly reduced by DR in WT and Npy<sup>-/-</sup> mice (the number of mice examined in each group was 3, 4, or 5 respectively; Table 3, see Supplementary

Table 3 | Effects of DR on plasma hormone concentrations, hepatic ribosomal protein S6 kinase polypeptide 1 (Rps6kb1) levels, and hypothalamic neuropeptide mRNA expression in 6-month-old male mice

	WT-AL	WT-DR	Npy <sup>-/-</sup> -AL	Npy <sup>-/-</sup> -DR
Insulin (ng/mL)				
Preprandial	1.82 (0.26)	0.70 (0.15) <sup>#</sup>	2.42 (0.41)	0.55 (0.14) <sup>#</sup>
Postprandial	2.75 (1.05)	7.19 (1.37) <sup>***</sup>	3.84 (0.98)	6.06 (1.42) <sup>***</sup>
IGF-1 (ng/mL)	423.9 (13.7)	314.2 (8.6) <sup>###</sup>	434.1 (14.9)	268.7 (19.2) <sup>###</sup>
p-Rps6kb1	1.00 (0.14)	0.41 (0.14) <sup>#</sup>	0.98 (0.12)	0.24 (0.06) <sup>##</sup>
Leptin (ng/mL)	1.48 (0.12)	0.22 (0.08) <sup>###</sup>	1.36 (0.16)	0.07 (0.03) <sup>###</sup>
Adiponectin (ng/mL)	15.4 (0.6)	18.3 (0.9) <sup>#</sup>	14.6 (0.7)	18.2 (0.5) <sup>##</sup>
Corticosterone (ng/mL)	70.0 (6.8)	148.6 (13.6) <sup>##</sup>	89.2 (9.5)	154.8 (22.0) <sup>#</sup>
Neuropeptide Y (ng/mL)	0.250 (0.016)	0.271 (0.055)	ND	ND
Rn18s-mRNA	1.00 (0.07)	0.88 (0.22)	1.12 (0.05)	0.93 (0.11)
Npy-mRNA	1.00 (0.09)	1.94 (0.09) <sup>###</sup>	ND	ND
AgRP-mRNA	1.00 (0.15)	1.37 (0.18)	1.94 (0.35) <sup>*</sup>	2.23 (0.59)
Pomc-mRNA	1.00 (0.12)	0.35 (0.07) <sup>##</sup>	1.42 (0.09)	0.49 (0.15) <sup>###</sup>
Ghrh-mRNA	1.00 (0.30)	0.61 (0.09)	1.64 (0.46)	0.64 (0.14) <sup>#</sup>
CRH-mRNA	1.00 (0.17)	0.80 (0.06)	1.44 (0.25)	0.99 (0.23)

All values represent means (SE). Plasma insulin was measured in the 4 h prior to (preprandial) and 1.5 h after feeding (postprandial) in the DR groups. Plasma samples were also collected from AL mice at the same time points, although the AL mice were allowed free access to food; n = 5, #, p < 0.05 ##, p < 0.01 vs. each AL group. \*\*\*, p < 0.001 vs. each preprandial phase. The other hormones, Rps6kb1, and mRNA levels were evaluated during the preprandial phase (n = 9 for plasma IGF-1, leptin, adiponectin, corticosterone, and neuropeptide Y). The levels of phosphorylated (active) Rps6kb1 in the liver were quantified by western blotting (n = 3 ~ 5). The values are relevant to those in the WT-AL groups. Hypothalamic mRNA levels, normalized to 18S ribosomal RNA (Rn18s), are also relevant to those in the WT-AL group (n = 4 ~ 6). Npy-mRNA levels in Npy<sup>-/-</sup> mice were below the detection limit (ND). #, p < 0.05; ##, p < 0.01; ###, p < 0.001 vs. each AL group. \* p < 0.05, vs. WT-AL.

Fig. S2); total protein abundance of Rps6kb1 did not differ between groups. We conclude that the insulin-, IGF-1-, and mTOR-associated anabolic pathways are down-regulated by DR in the absence of Npy in mice.

DR may extend lifespan in part by reducing fat mass and altering adipokines<sup>30</sup>. Indeed, increased plasma adiponectin is associated with insulin-sensitizing, anti-diabetic, and anti-atherosclerotic effects<sup>31</sup>. Transgenic overexpression of adiponectin genes extends lifespan in mice<sup>32</sup>. In this study, white adipose tissue (WAT) weight (the sum of inguinal and epididymal WAT weights) and WAT normalized to body weight (BW) were lower in the DR groups than in the AL groups (see Supplementary Table S2); the WAT/BW was even lower in *Npy*<sup>-/-</sup>-DR than in WT-DR mice at 6 months of age. The Plasma leptin and adiponectin concentrations were down- and up-regulated by DR in *Npy*<sup>-/-</sup> mice in a manner similar to that in WT mice (9 mice per group; Table 3).

Plasma corticosterone levels are increased by DR, particularly in the preprandial phase in rats<sup>33</sup>, and has been correlated with DR-induced stress resistance<sup>6</sup>. The present study also confirmed the modest increase in plasma corticosterone by DR in WT and *Npy*<sup>-/-</sup> mice (9 mice per group; Table 3); there was no difference between WT and *Npy*<sup>-/-</sup> mice.

Loss of Npy may alter hypothalamic neuropeptide expression to facilitate adaptation to DR. Therefore, we analyzed expression of hypothalamic neuropeptides by quantitative real-time PCR (qRT-PCR) in tissues collected during the preprandial phase in male mice at 6 months of age. The findings can be summarized as follows (4, 5 or 6 mice per group; Table 3): 1) loss of Npy significantly or marginally increased *Agrp*, *Pomc*, *Ghrh*, and *Crh* transcript levels under AL feeding; 2) DR reduced *Pomc* and *Ghrh* levels in the absence of Npy. Loss of Npy had no influence on DR inhibition of *Pomc* and *Ghrh* transcript expression.

**DR and gene expression profiles in the liver.** Our results suggest that Npy-linked pathways mediating the effect of DR do not overlap with the insulin/IGF-1/mTOR, adipokine, and corticosterone-associated pathways, which are thought to represent mechanisms of action of DR<sup>1,6,8,33</sup>. To characterize the putative Npy-linked pathways, we performed whole-genome microarray and pathway analyses in the liver with a gene set enrichment analysis (GSEA)<sup>34</sup> using the Molecular Signatures Database (MsigDB) and NCBI BioSystems Database (n = 2 mice per group). Initially, we identified genes that were differentially expressed between 2 groups of mice, such as WT-DR vs. WT-AL or *Npy*<sup>-/-</sup>-DR vs. WT-DR, with filtering criteria set for the present study.

Based on the MsigDB, the GSEA delineated pathways involving differentially regulated genes that were significantly altered in WT-DR versus WT-AL mice (see Supplementary Tables S3 and S4). We focused on pathways that were down-regulated in *Npy*<sup>-/-</sup>-DR versus WT-DR mice (see Supplementary Table S5). These pathways might mediate the effects of DR and depend on Npy signaling. These procedures helped to identify four pathways (Fig. 4A). The gene sets of three of the pathways in this category reflect the gene expression profile of a superior survival group (versus poor survival of human hepatocellular carcinoma<sup>35</sup>) and that of relatively well-differentiated (versus poorly differentiated) states of head and neck cancers<sup>36</sup>. The remaining single gene set “MICROSOME” includes genes encoding the metabolism of drugs and xenobiotics. The pathways enriched in genes up-regulated in WT-DR (versus the WT-AL) but down-regulated in *Npy*<sup>-/-</sup>-DR mice likely reflect mechanisms underlying the inhibition or retardation of neoplastic processes by DR.

In contrast, the GSEA delineated 10 pathways associated with DR-down-regulated genes in WT mice (see Supplementary Table S6). One of these pathways was identified in the context of Npy deletion and its cancellation of the inhibitory effect of DR (Fig. 4A). This was the gene set “ICHIBA GRAFT VERSUS HOST DISEASE 35D DN”,

which represents down-regulated genes associated with metabolic and endocrine functions in the liver where hepatic graft-versus-host diseases manifest and where genes related to inflammation were up-regulated<sup>37</sup>. Gene expression profiling in long-lived dwarf mice, mice subjected to DR, and premature aging models has suggested that the down-regulation of metabolic and endocrine functions represents a protective mechanism against inflammatory and/or genotoxic stress during the aging process<sup>38</sup>. Therefore, loss of Npy might abolish some protections against cellular stresses.

Pathway analysis in the NCBI BioSystems Database identified pathways signified by up-regulated genes in WT-DR versus WT-AL mice (see Supplementary Table S7). These were mostly related to detoxification or degradation of chemical compounds. In contrast, pathways enriched in genes down-regulated by DR in WT mice included pathways relevant to lipid, cholesterol, and steroid metabolism or biosynthesis (see Supplementary Table S8).

Comparison of gene expression profiles in *Npy*<sup>-/-</sup>-DR and WT-DR mice revealed that many of the pathways signified by DR-up-regulated genes in WT mice, i.e., pathways associated with detoxification, were enriched among the down-regulated genes in *Npy*<sup>-/-</sup>-DR mice (Fig. 4B, see Supplementary Table S9). Pathways enriched in up-regulated genes in *Npy*<sup>-/-</sup>-DR versus WT-DR mice included steroid biosynthesis and complement cascade (Fig. 4B, see Supplementary Table S10). The NCBI BioSystems pathway analysis suggests that detoxification or degradation of chemical compounds, which may be up-regulated by DR, is not activated properly in the absence of Npy. Up-regulation of the complement cascade also implies that Npy inhibits inflammatory processes.

Although our microarray analysis was limited to the liver, our analysis of hepatic gene expression profiles suggests Npy plays a key role in inhibiting the occurrence and/or progression of cancers through detoxification or degradation of potentially carcinogenic chemical compounds. The analysis also indicates Npy-linked pathways protect cells from inflammation.

## Discussion

This study clearly showed that Npy is a neuropeptide that links DR to longevity in mammals. However, Npy is not required for many of the physiological adaptations to DR, as demonstrated by the changes in hypothalamic neuropeptide transcript levels, hormone concentrations, and energy metabolism.

Among the neuroendocrine changes induced by DR, inhibition of anabolic signaling molecules, including insulin, GH/IGF-1, and mTOR, and upregulation of adiponectin were found to extend lifespan in rodents without restricted food intake<sup>1,8,26,29,32</sup>. Thus, the effects of DR were attributed to these molecules or related signaling pathways based on the observed physiological adaptations. However, in the present study, the salutary effects of DR were significantly reduced in *Npy*<sup>-/-</sup> mice, even though they showed normal physiological adaptations to DR. Therefore, these neuroendocrine adaptations to DR may not be essential for longevity or cancer and stress resistance. Although the present findings do not directly support the evolutionary view of the mechanisms of DR<sup>3,6</sup>, they reveal new roles of Npy as a lifespan and aging regulator.

Food efficiency was elevated by DR in WT and *Npy*<sup>-/-</sup> mice, although it was 6% and 10% lower in male and female *Npy*<sup>-/-</sup>-DR mice than in their respective WT-DR groups. Negative energy balance provokes adaptive responses to prevent an excess loss of body fat by decreasing energy expenditure, i.e., reducing thermogenesis and/or physical activity<sup>7</sup>. This adaptive response leads to elevated food efficiency and is induced by activation of hypothalamic Npy- and *Agrp*-synthesizing neurons and inhibition of signalling of  $\alpha$ -melanocyte stimulating hormone or its precursor POMC by *Agrp*<sup>7</sup>. A recent study using the ILSXISS series of recombinant inbred strains of mice indicate a correlation between DR-induced longevity and greater fuel efficiency, defined by measures of weight maintenance

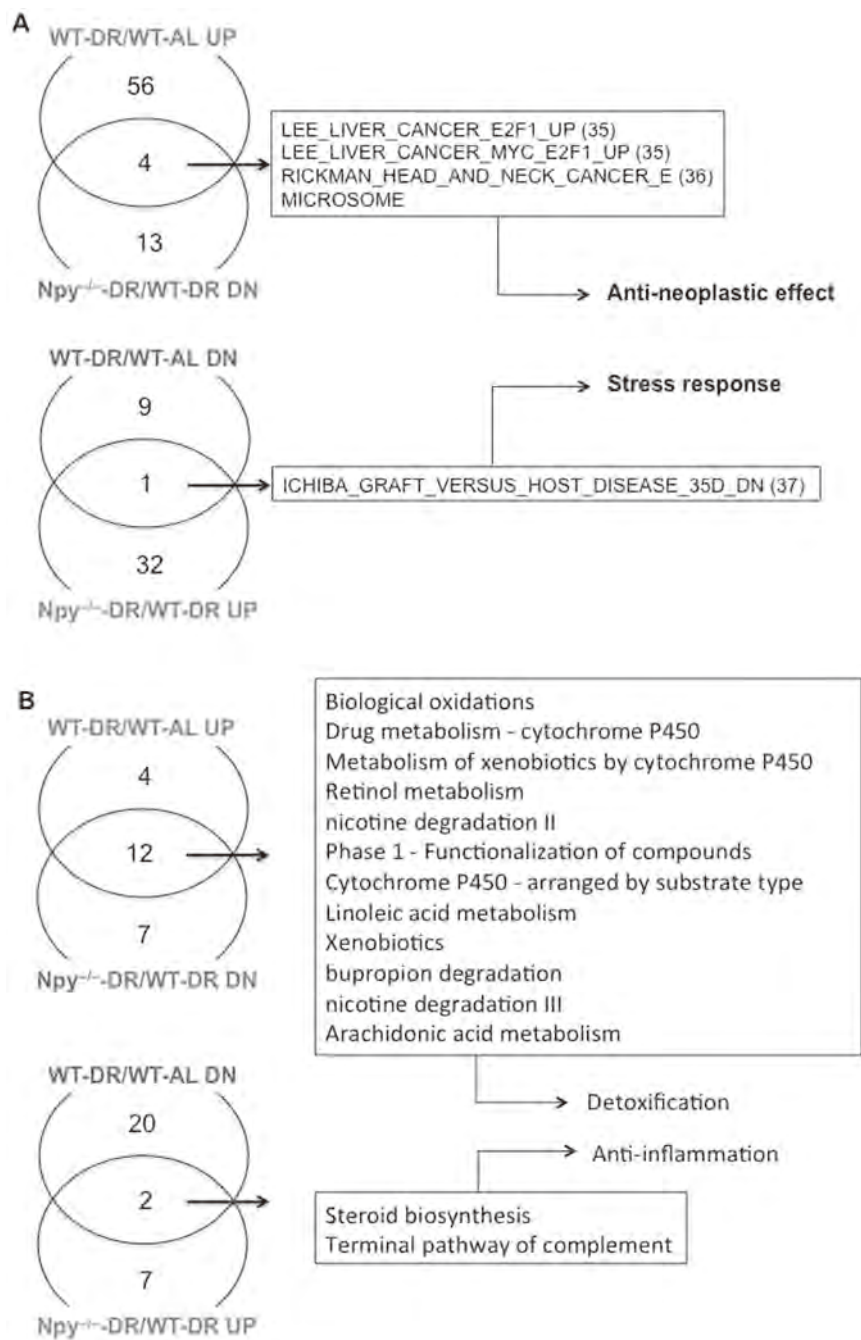


**Figure 4 | Summary of microarray data for the liver.** A) Gene set enrichment analysis (GSEA) identified 60 pathways enriched in the up-regulated (UP) genes of the WT-DR vs. WT-AL groups. Four of these pathways overlapped with pathways enriched in the down-regulated (DN) genes in the *Npy*<sup>-/-</sup>-DR vs. WT-DR groups. The pathway names of 4 gene sets are described in the rectangle and the references<sup>35,36</sup> are noted in parentheses. These pathways reflect the anti-neoplastic effect of DR. In contrast, 10 pathways were enriched among the DN genes in WT-DR vs. WT-AL groups; one of these pathways overlapped with pathways enriched in the UP genes in *Npy*<sup>-/-</sup>-DR vs. WT-DR groups. The pathway<sup>37</sup> reflects a stress response. B) The pathway analysis with NCBI BioSystems identified 16 pathways enriched in the UP genes of WT-DR vs. WT-AL mice. Twelve of these pathways overlapped with pathways enriched in the DN genes in *Npy*<sup>-/-</sup>-DR vs. WT-DR mice. Most of these are related to detoxification of chemical compounds. In contrast, 22 pathways were enriched in the DN genes of WT-DR vs. WT-AL groups; two of these pathways overlapped with pathways enriched in the UP genes in *Npy*<sup>-/-</sup>-DR vs. WT-DR groups. One pathway “Terminal pathway of complement” reflects activation of inflammation.

and ability of maintaining hair and tail growth<sup>19</sup>. The life-extending effect of DR correlated inversely with fat reduction<sup>20</sup>. Therefore, the net reduction of food efficiency or a concomitant signal pathway might diminish the effects of DR.

The *Npy* pathways that induce the effects of DR remain elusive. Regarding the cancer-suppressing effects of DR, we speculate that *Npy* inhibits tumors by enhancing the detoxification or degradation of chemical compounds or xenobiotics (i.e., carcinogens and

promoters) and inhibiting inflammatory processes (promoters), based on the hepatic gene expression profiles, because *Npy* could act in the liver via the sympathetic nerves and the circulation.

In *Npy*-overexpressing rats, it is thought that the sympatholytic and hypotensive effects of *Npy* protect the cardiovascular system from sympathetic hyperexcitation<sup>12</sup>. In this study, there were few cardiac lesions and they were not increased in *Npy*<sup>-/-</sup> mice. Thus, it seems unlikely that cardiac lesions affected the lifespan in *Npy*<sup>-/-</sup>

mice. However, the potential role of Npy in the regulation of lifespan and ageing, via the sympathetic nervous system and/or circulation, remains to be elucidated.

Dysregulation of the hypothalamic-pituitary adrenal axis and increased noradrenergic activity causes neuropsychiatric disorders such as post-traumatic stress disorder<sup>39</sup>. In contrast, increased Npy levels in the brain and plasma are associated with resilience or improved recovery from the harmful effects of traumatic stress<sup>40</sup>. Thus, *Npy*<sup>-/-</sup> mice might remain under stressed conditions to an extent that diminishes the life-prolonging effect of DR. However, we observed no signs to indicate this kind of stress in *Npy*<sup>-/-</sup> mice. In fact, the plasma corticosterone level did not differ between *Npy*<sup>-/-</sup> and WT mice.

In the present study, the genetic backgrounds of the *Npy*<sup>-/-</sup> and WT (129S6/SvEvTac) mice were not identical. However, it should be emphasized that the life-extending and cancer-suppressing effects of DR are considerably diminished in *Npy*<sup>-/-</sup> mice when compared to the published data in a number of inbred strains as well as WT mice in the present study. Although a recent study indicated that some recombinant inbred strains do not respond to DR with lifespan extension<sup>41</sup>, to our knowledge, there has been no indication that the 129S substrains of mice are unresponsive to DR. In fact, the 129S1/SvImJ substrain, an approximate genetic match to *Npy*<sup>tm1Rpa/J</sup>, is reported to respond to DR via physical fitness and antineoplastic effects<sup>15,42</sup>. Therefore, it is unlikely that genetic factors other than Npy confounded the present outcomes, although we cannot rule out this possibility.

## Methods

**Experimental animals and husbandry.** The animal care and all experiments were performed in accordance with the guidelines approved by the Ethics Review Committee for Animal Experimentation at Nagasaki University. Male *Npy*<sup>-/-</sup> mice (129S-Npy<sup>tm1Rpa/J</sup>) and female wild-type (WT) mice (129S6/SvEvTac), the strain used to derive the ES cell lines<sup>16</sup>, were obtained from Jackson Laboratory (Bar Harbor, ME, USA) and Taconic Farms, Inc. (Germantown, NY, USA). They were bred in a barrier facility at the Center for Frontier Life Sciences at Nagasaki University. After 2 generations of crossing male and female *Npy*<sup>-/-</sup> mice, offspring born between December 2006 and February 2007 were genotyped and set as longevity groups of *Npy*<sup>-/-</sup> and WT mice. Thus, *Npy*<sup>-/-</sup> and wild type (WT) control mice in this study were on a mixed 129S-Npy<sup>tm1Rpa/J</sup> and 129S6/SvEvTac background.

Two or 3 mice (typically 3) were housed in individual cages in the barrier facility (temperature, 22–25°C; 12 h light/dark cycle) under specific pathogen-free conditions, which were maintained for the entire study. Sentinel animals were sent for bacterial and viral testing every 3 months<sup>43</sup>.

All mice were fed ad libitum (AL) with Charles River-LPF diet (Oriental Yeast Co. Ltd., Tsukuba, Japan). At 12 weeks of age, mice were divided into AL and DR groups. The DR groups received a food allotment consisting of 70% of the mean daily food intake of the AL groups of male and female *Npy*<sup>-/-</sup> and WT mice every day, 30 min before lights were turned off. The food allotments for the DR groups were adjusted every 2 weeks between 12 and 32 weeks; the allotments were fixed between 32 and 72 weeks and from 72 weeks and onward. Details of the feeding procedure have been described elsewhere<sup>44</sup>. Body weight was monitored every 2 weeks between 6 and 20 weeks of age and every 4 weeks thereafter. Dead mice were subjected to post-mortem examination.

**Indirect calorimetry.** In male 7-month-old mice, the respiratory quotient (RQ) and energy expenditure (EE) were measured in metabolic cages equipped with an indirect open-circuit calorimeter (Columbus Instruments, Columbus, OH). Experiments were initiated at 17:30, when an allotment was provided for each mouse in the DR group. Gas content was recorded for 10 seconds every 5 minutes between 18:00 and 15:00 on the following day, that is, for 21 hours. Data were averaged every 30 minutes. Lights were turned off at 20:00 and turned on at 8:00. The EE was calculated as the product of calorific value of oxygen and VO<sub>2</sub> per kilogram body weight, where the calorific value of oxygen = 3.815 + 1.232 × RQ. The EE was normalized to body weight<sup>45</sup>.

**Body temperature.** Body temperature was measured with rectal thermometers (TERUMO CTM-303; Terumo Corporation: Tokyo) following the procedure reported elsewhere<sup>46</sup>. The rectal probe (ME-PDK061; Terumo Corporation: Tokyo) was lubricated with glycerol and inserted ~3 cm into the rectum. The rectal temperature measurement procedure took 1 minute.

**Enzyme-Linked Immunosorbent Assay (ELISA) for circulating hormone concentrations.** Plasma samples collected from orbital blood were stored at -80°C. Plasma leptin and insulin concentrations were measured with ELISA kits (Shibayagi

Co. Ltd., Gunma, Japan). Plasma adiponectin, IGF-1, Npy, and corticosterone concentrations were measured by ELISA (adiponectin: Otsuka Pharmaceutical Co. Ltd., Tokyo, Japan, IGF-1 and Npy: Millipore, Billerica, MA, USA, corticosterone: Yanaiharu Institute Inc., Fujinomiya, Shizuoka, Japan). All samples were tested in duplicate. All ELISA methods were performed according to manufacturer protocols.

**Western blotting of ribosomal protein S6 kinase polypeptide 1 (Rps6kb1).** About 40 mg frozen liver tissues were homogenized in 800 μL T-PER buffer (PIERCE Biotechnology, Rockford, IL, USA) with a protease-inhibitor cocktail (P8340 Sigma-Aldrich, St. Louis, MO, USA) and a phosphatase-inhibitor cocktail (Nacalai Tesque Inc., Kyoto, Japan). The homogenates were centrifuged at 10000 × g for 5 min at 4°C, and the supernatant was collected. Protein concentrations were measured using the BCA assay kit (PIERCE Biotechnology). All samples were mixed with Laemmli sample buffer and heated at 95°C for 5 min. Proteins (8 μg) were separated by 12.5% SDS-PAGE and transferred to PVDF membranes. The membranes were immediately placed in blocking solution (Blocking One-P for p-S6K or 3% non-fat dried milk in TBS-T buffer for Rps6kb1) for 60 min. The membranes were incubated with anti-phosphorylated Rps6kb1 (#2215; Cell Signaling Technology, Beverly, USA) or Rps6kb1 (#2217; Cell Signaling Technology) antibody diluted 1 : 1000 in TBS-T for 16 h at 4°C with gentle shaking and washed 3 times in TBS-T. Then, the membranes were incubated for 1 h with HRP-conjugated anti-rabbit IgG (Amersham Pharmacia Biotech, Little Chalfont, UK) diluted 1 : 10,000 in TBS-T. Immunoreactive proteins were visualized using ImmunoStar LD (Wako, Osaka, Japan) and quantitated using a densitometer (LAS-3000: Fuji Film, Tokyo, Japan) and MultiGauge software (Fuji Film). To minimize variations in signal intensity, a standard sample of p-Rps6kb1 was prepared from a WT-CR mouse liver and included in each blot.

**Quantitative real-time (qRT) PCR for mRNA expression in tissues.** Total RNA was purified from the hypothalamus, liver, and brown adipose tissues<sup>47</sup>. The quality of extracted RNA was evaluated as the densitometric ratio of 28S and 16S ribosomal RNA. The extracted RNA was reverse-transcribed using a Bio-Rad reverse transcriptase reagent kit (Hercules, CA, USA) according to the manufacturer's instructions. Primers and probes were purchased from Applied Biosystems with reference to the TaqMan Gene Expression Assay library (Applied Biosystems, Tokyo, Japan) and TAKARA with reference to the Perfect Real Time support system (TAKARA BIO INC., Shiga, Japan) (see Supplementary Table S11). In PCR reactions with Takara primers, SYBR Green (ThunderBird SYBR qPCR Mix: TOYOBO Co. Ltd., Osaka, Japan) was used up to a final volume of 10 μL, and reactions were performed according to the manufacturer's protocol. Control housekeeping genes [beta-actin (Actb), 18S ribosomal RNA (Rn18sc)] were also analyzed using TaqMan or SYBR Green primers and probes. All samples and standard curves were tested in triplicate. Amplification, data quantification, and analysis were performed on an ABI PRISM 7900HT Sequence Detector (Applied Biosystems).

**Gene expression profiling.** RNA that was extracted from live tissues and that passed the Agilent Technologies 2100 Bioanalyzer quality control test was used to generate biotin-labelled cRNA with a MessageAmp™ II-Biotin Enhanced Kit (Ambion, Inc., Austin, TX). Labelled cRNA was applied to the CodeLink Mouse Whole Mouse Genome Bioarrays (Applied Microarrays, Inc., Tempe, AZ) for 18 hours at 37°C. Individual samples from 2 mice of each group were run on separate microarrays. After incubation, slides were washed, stained with Cy5-streptavidin (GE Healthcare Bio-Science Corp., Piscataway, NJ), and scanned by GenePix4000B (Molecular Devices LLC., Sunnyvale, CA). Array images were processed using CodeLink™ Expression Analysis v5.0 (Applied Microarray Inc.), and each slide was subjected to quantile normalization. To identify genes differentially expressed between 2 groups of mice, the following filtering criteria were used: Quality flag, G (signal intensity was above noise levels), p-value less than 0.100, ratio of expression levels between 2 groups, over ±1.5-fold. With differential regulated genes, pathway analyses were performed with a gene set enrichment analysis (GSEA)<sup>32</sup> using MsigDB [a nominal p < 0.01 and false discovery rate (FDR) q < 0.25; see Supplementary Tables S3, S4, S5, S6] and the NCBI BioSystems Database (nominal p < 0.01; see Supplementary Tables S7, S8, S9, S10).

The data set for these DNA microarrays has been deposited at the National Center of Biotechnology Information Gene Expression Omnibus (GEO; <http://www.ncbi.nlm.nih.gov/geo/>) and is accessible through GEO Series accession number GSE42761.

Microarray data were verified by qRT-PCR of 19 selected genes using RNA samples extracted from mice in the same groups used for the microarray analysis (see Supplementary Table S11). A scatter plot between the fold changes (*Npy*<sup>-/-</sup>-DR versus WT-DR) calculated by the microarray data and qRT-PCR data was drawn and analysed with a linear regression model (Supplementary Fig. S3).

**Statistical analysis.** Data were expressed as the mean and standard error (SE). Food consumption (FC), body weight (BW), and FC/BW, and RQ were analyzed by 2-factor (2-f) analysis of variance (ANOVA) for the effects of genotype and age and their interaction (Genotype, Age, Genotype × Age). The Bonferroni post hoc test was performed to compare data between groups at each age point. Survival curves were estimated using the Kaplan-Meier method and were compared with the Log-rank test. A multivariate analysis with the Cox proportional-hazards model was also used to estimate the hazard ratios for mortality as variables: Genotype (*Npy*<sup>-/-</sup> vs. WT), Diet (DR vs. AL) and Sex (male and female). The proportion of mice bearing tumors and the prevalence of selected lesions were analyzed using chi-square or Fisher's exact

tests. The levels of mRNA expression, circulating hormones, and protein abundance were analyzed by one-factor ANOVA and the post hoc (Newman-Keuls multiple comparison) test when needed. Regression analysis of the scatter plot of EE and body weight and analysis of covariance (ANCOVA) were performed to determine the relationship of EE and body mass within each group and to test whether this relationship differs between groups<sup>44</sup>. All statistical analyses were performed using Prism 5 for Mac OS X (Graphpad Software, Inc.) and STATVIEW 5.0 software (SAS Institute Inc., Cary, NC). P values < 0.05 were considered statistically significant.

- Mair, W. & Dillin, A. Aging and survival: the genetics of life span extension by dietary restriction. *Annu. Rev. Biochem.* **77**, 727–754 (2008).
- Weindruch, R. & Walford, R. L. [Dietary restriction: Effects on survivorship] [31–72] *The Retardation of Aging and Disease by Dietary Restriction*. (Charles C Thomas Pub. Ltd., Springfield, 1988).
- Colman, R. J. *et al.* Caloric restriction delays disease onset and mortality in rhesus monkeys. *Science* **325**, 201–204 (2009).
- Mattison, J. A. *et al.* Impact of caloric restriction on health and survival in rhesus monkeys from the NIA study. *Nature* **489**, 318–322 (2012).
- Holliday, R. Food, reproduction and longevity: is the extended lifespan of calorie-restricted animals an evolutionary adaptation? *Bioessays* **10**, 125–127 (1989).
- Masoro, E. J. & Austad, S. N. The evolution of the antiaging action of dietary restriction: a hypothesis. *J. Gerontol. A Biol. Sci. Med. Sci.* **51**, B387–91 (1996).
- Sainsbury, A. & Zhang, L. Role of the hypothalamus in the neuroendocrine regulation of body weight and composition during energy deficit. *Obes. Rev.* **12**, 234–257 (2011).
- Shimokawa, I., Chiba, T., Yamaza, H. & Komatsu, T. Longevity genes: insights from calorie restriction and genetic longevity models. *Mol. Cells* **26**, 427–435 (2008).
- Luque, R. M., Park, S. & Kineman, R. D. Severity of the catabolic condition differentially modulates hypothalamic expression of growth hormone-releasing hormone in the fasted mouse: potential role of neuropeptide Y and corticotropin-releasing hormone. *Endocrinology* **148**, 300–309 (2007).
- Okada, K., Sugihara, H., Minami, S. & Wakabayashi, I. Effect of parenteral administration of selected nutrients and central injection of gamma-globulin from antiserum to neuropeptide Y on growth hormone secretory pattern in food-deprived rats. *Neuroendocrinology* **57**, 678–686 (1993).
- Tamura, H. *et al.* The effect of agouti-related protein on growth hormone secretion in adult male rats. *Regul. Pept.* **125**, 145–149 (2005).
- Michalkiewicz, M., Knestaut, K. M., Bytchkova, E. Y. & Michalkiewicz, T. Hypotension and reduced catecholamines in neuropeptide Y transgenic rats. *Hypertension* **41**, 1056–1062 (2003).
- Smiałowska, M. *et al.* Neuroprotective effects of neuropeptide Y-Y2 and Y5 receptor agonists in vitro and in vivo. *Neuropeptides* **43**, 235–249 (2009).
- Masoro, E. J. Influence of caloric intake on aging and on the response to stressors. *J. Toxicol. Environ. Health B Crit. Rev.* **1**, 243–257 (1998).
- Minor, R. K. *et al.* The arcuate nucleus and neuropeptide Y contribute to the antitumorigenic effect of calorie restriction. *Aging Cell* **10**, 483–492 (2011).
- Erickson, J. C., Holoopeter, G. & Palmiter, R. D. Attenuation of the obesity syndrome of ob/ob mice by the loss of neuropeptide Y. *Science* **274**, 1704–1707 (1996).
- Gunapala, K. M., Gallardo, C. M., Hsu, C. T. & Steele, A. D. Single gene deletions of orexin, leptin, neuropeptide Y, and ghrelin do not appreciably alter food anticipatory activity in mice. *PLoS ONE* **6**, e18377 (2011).
- Weindruch, R. & Walford, R. L. [Mechanisms: How does dietary restriction retard aging?] [231–294] *The Retardation of Aging and Disease by Dietary Restriction*. (Charles C Thomas Pub. Ltd., Springfield, 1988).
- Rikk, B. A. *et al.* Genetic dissection of dietary restriction in mice supports the metabolic efficiency model of life extension. *Exp. Gerontol.* **45**, 691–701 (2010).
- Liao, C. Y. fat maintenance is a predictor of the murine lifespan response to dietary restriction. *Aging Cell* **10**, 629–639 (2010).
- Bruss, M., Khambatta, C., Ruby, M., Aggarwal, I. & Hellerstein, M. Calorie restriction increases fatty acid synthesis and whole body fat oxidation rates. *Am. J. Physiol. Endocrinol. Metab.* **298**, E108 (2010).
- Guarente, L. Mitochondria—a nexus for aging, calorie restriction, and sirtuins? *Cell* **132**, 171–176 (2008).
- Currie, P. J., Mirza, A., Fuld, R., Park, D. & Vasselli, J. R. Ghrelin is an orexigenic and metabolic signaling peptide in the arcuate and paraventricular nuclei. *Am. J. Physiol. Regul. Integr. Comp. Physiol.* **289**, R353–R358 (2005).
- Granneman, J. G., Li, P., Zhu, Z. & Lu, Y. Metabolic and cellular plasticity in white adipose tissue I: effects of beta3-adrenergic receptor activation. *Am. J. Physiol. Endocrinol. Metab.* **289**, E608–16 (2005).
- Fu, Y. T., He, F. S., Zhang, S. L. & Zhang, J. S. Lipid peroxidation in rats intoxicated with 3-nitropropionic acid. *Toxicol.* **33**, 327–331 (1995).
- Nelson, J. F., Strong, R., Bokov, A., Diaz, V. & Ward, W. Probing the relationship between insulin sensitivity and longevity using genetically modified mice. *J. Gerontol. A Biol. Sci. Med. Sci.* **67**, 1332–1338 (2012).
- Walker, G., Houthoofd, K., Vanfleteren, J. R. & Gems, D. Dietary restriction in *C. elegans*: from rate-of-living effects to nutrient sensing pathways. *Mech. Ageing Dev.* **126**, 929–937 (2005).
- Kapahi, P. *et al.* Regulation of lifespan in *Drosophila* by modulation of genes in the TOR signaling pathway. *Curr. Biol.* **14**, 885–890 (2004).
- Selman, C. *et al.* Ribosomal protein S6 kinase 1 signaling regulates mammalian life span. *Science* **326**, 140–144 (2009).
- Yamaza, H. *et al.* Involvement of insulin-like growth factor-1 in the effect of caloric restriction: regulation of plasma adiponectin and leptin. *J. Gerontol. A Biol. Sci. Med. Sci.* **62**, 27–33 (2007).
- Hui, X., Lam, K. S. L., Vanhoutte, P. M. & Xu, A. Adiponectin and cardiovascular health: an update. *Br. J. Pharmacol.* **165**, 574–590 (2012).
- Otabe, S. *et al.* Overexpression of human adiponectin in transgenic mice results in suppression of fat accumulation and prevention of premature death by high-calorie diet. *Am. J. Physiol. Endocrinol. Metab.* **293**, E210–8 (2007).
- Sabatino, F., Masoro, E. J., McMahan, C. A. & Kuhn, R. W. Assessment of the Role of the Glucocorticoid System in Aging Processes and in the Action of Food Restriction. *J. Gerontol.* **46**, B171–B179 (1991).
- Subramanian, A. *et al.* Gene set enrichment analysis: a knowledge-based approach for interpreting genome-wide expression profiles. *Proc. Natl. Acad. Sci. USA* **102**, 15545–15550 (2005).
- Lee, J.-S. *et al.* Application of comparative functional genomics to identify best-fit mouse models to study human cancer. *Nat. Genet.* **36**, 1306–1311 (2004).
- Rickman, D. S. *et al.* Prediction of future metastasis and molecular characterization of head and neck squamous-cell carcinoma based on transcriptome and genome analysis by microarrays. *Oncogene* **27**, 6607–6622 (2008).
- Ichiba, T. *et al.* Early changes in gene expression profiles of hepatic GVHD uncovered by oligonucleotide microarrays. *Blood* **102**, 763–771 (2003).
- Schumacher, B. *et al.* Delayed and accelerated aging share common longevity assurance mechanisms. *PLoS Genet.* **4**, e1000161 (2008).
- Skelton, K. *et al.* PTSD and gene variants: New pathways and new thinking. *Neuropharmacology* **62**, 628–637 (2012).
- Sah, R. & Geraciotti, T. D. Neuropeptide Y and posttraumatic stress disorder. *Mol. Psychiatry* **18**, 646–655 (2013).
- Liao, C. Y. *et al.* Genetic variation in the murine lifespan response to dietary restriction: from life extension to life shortening. *Aging Cell* **9**, 92–95 (2010).
- Minor, R. K. *et al.* Calorie restriction alters physiological performance but not cognition in two models of altered neuroendocrine signaling. *Behav. Brain Res.* **189**, 202–211 (2008).
- Shimokawa, I. *et al.* Life span extension by reduction in growth hormone-insulin-like growth factor-1 axis in a transgenic rat model. *Am. J. Pathol.* **160**, 2259–2265 (2002).
- Yamaza, H. *et al.* FoxO1 is involved in the antineoplastic effect of calorie restriction. *Aging Cell* **9**, 372–382 (2010).
- Arch, J. R. S., Hislop, D., Wang, S. J. Y. & Speakman, J. R. Some mathematical and technical issues in the measurement and interpretation of open-circuit indirect calorimetry in small animals. *Int. J. Obes. Relat. Metab. Disord.* **30**, 1322–1331 (2006).
- Saegusa, Y. & Tabata, H. Usefulness of infrared thermometry in determining body temperature in mice. *J. Vet. Med. Sci.* **65**, 1365–7 (2003).
- Chiba, T. *et al.* Similar metabolic responses to calorie restriction in lean and obese Zucker rats. *Mol. Cell. Endocrinol.* **309**, 17–25 (2009).

## Acknowledgments

We are grateful to the staff at the Laboratory Animal Center for Biomedical Research at the Center for Frontier Life Sciences, Nagasaki University for their animal care and technical assistance. We also thank Yutaka Araki, Yuko Moriyama, and Rieko Tahara for their excellent technical assistance. The study was supported by Grants-in-Aid for Scientific Research from the Japan Society for the Promotion of Science (I.S., nos. 19590227; T.C., nos. 24659181 and 25282027), the 2012 Danone Institute of Japan Foundation Research Grant (T.C.), and the JSPS Asian CORE Program (I.S., nos. FY2010-5).

## Author contributions

T.C. and T. Komatsu performed most of the experiments. Y.T. and R.F. performed most of the RT-PCR analysis. D.P. and H.Y.C. analyzed the microarray data. T. Kusudo and H.Y. conducted the indirect calorimetry experiment. S.J.P. measured the rectal temperature and served as advisor for the qRT-PCR in fat tissues. S.E.K., H.H. and R.M. served as advisors for the pathological analysis, animal care and provide knowledge of genotyping and western blots. I.S. was the overall director of the research, provided funds for the research (T.C., H.H. and R.M. also provided some funds), and contributed to the statistical analysis, and writing and editing of the manuscript.

## Additional information

Supplementary information accompanies this paper at <http://www.nature.com/scientificreports>

**Competing financial interests:** The authors declare no competing financial interests.

**How to cite this article:** Chiba, T. *et al.* A key role for neuropeptide Y in lifespan extension and cancer suppression via dietary restriction. *Sci. Rep.* **4**, 4517; DOI:10.1038/srep04517 (2014).

 This work is licensed under a Creative Commons Attribution-NonCommercial-ShareAlike 3.0 Unported License. To view a copy of this license, visit <http://creativecommons.org/licenses/by-nc-sa/3.0>

A key role for neuropeptide Y in lifespan extension and cancer suppression via dietary restriction

Authors: Takuya Chiba<sup>1,2,4</sup>, Yukari Tamashiro<sup>2</sup>, Daegu Park<sup>3</sup>, Tatsuya Kusudo<sup>4</sup>, Ryoko Fujie<sup>2</sup>, Toshimitsu Komatsu<sup>1,2</sup>, Sang Eun Kim<sup>1,2</sup>, Seungjoon Park<sup>1,2</sup>, Hiroko Hayashi<sup>1,2</sup>, Ryotchi Mori<sup>1,2</sup>, Hiroshi Yamashita<sup>1</sup>, Hae Young Chung<sup>5</sup>, Isao Shimokawa<sup>1,2</sup>

Supplemental figures S1-S5 and supplemental table S1-S11

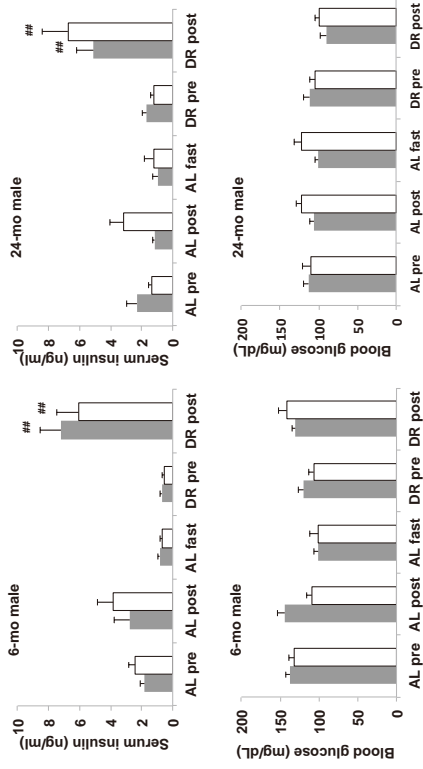


Fig. S1. Plasma insulin and blood glucose concentrations at 6 and 24 months of age. The values represent means  $\pm$  SE (n = 4 to 7). Dark gray bars represent the WT mice; white bars represent the Npy<sup>-/-</sup> mice. "pre" and "post" represent preprandial and postprandial phases of a feeding cycle respectively. The AL groups were also subjected to overnight fasting to compare the insulin and glucose levels with

those in the DR pre groups. ##, p < 0.01 vs the respective the DR pre groups.

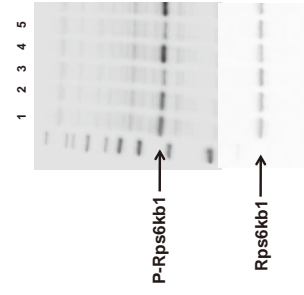
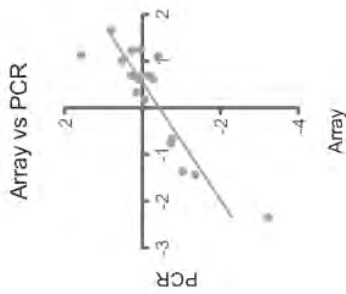


Fig. S2. Western blots of phosphorylated (an active form) and total ribosomal protein S6 kinase polypeptide 1 (Rps6kb1). Representative western blots. Lane 1, positive control; lane 2, WT-AL; lane 3, WT-DR; lane 4, Npy<sup>-/-</sup>-AL; lane 5, Npy<sup>-/-</sup>-DR.

**Table S1.** The mRNA expression levels of uncoupling protein (Ucp) 1, 2, and 3 in the brown adipose tissue in the 6-month-old male mice.

	WT-AL	WT-DR	Npy <sup>-/-</sup> -AL	Npy <sup>-/-</sup> -DR
Actb	1.00 (0.08)	1.05 (0.04)	0.92 (0.05)	1.23 (0.12)
Ucp1/Actb	1.00 (0.10)	0.94 (0.08)	0.77 (0.13)	1.01 (0.14)
Ucp2/Actb	1.00 (0.07)	1.10 (0.13)	1.15 (0.10)	1.15 (0.06)
Ucp3/Actb	1.00 (0.12)	0.93 (0.06)	0.82 (0.13)	1.04 (0.10)

Values represent the means (S.E., n = 4 - 6) of mRNA expression levels normalized by the level in the WT-AL. Actb, b-actin.



**Fig. S3.** A scatter plot between the fold changes (Npy<sup>-/-</sup>-DR/ WT-DR) calculated by the microarray data and qRT-PCR data. A linear regression model; R = 0.7717; p < 0.0001.

**Table S2.** The weights of white adipose and brown adipose tissues in 6-month-old male mice

	WT-AL	WT-DR	Npy <sup>-/-</sup> -AL	Npy <sup>-/-</sup> -DR
WAT (mg)	161.2 (324)	908 (84) <sup>†</sup>	2481 (171)**	474 (104) <sup>###</sup>
WAT (mg/g BW)	48.5 (7.0)	34.3 (2.4) <sup>†</sup>	61.9 (2.3)**	20.1 (3.7) <sup>###</sup>
BAT (mg)	116 (13)	99 (7)	183 (25)**	63 (9) <sup>###</sup>
BAT (mg/g BW)	3.6 (0.4)	3.8 (0.3)	4.5 (0.4)	2.7 (0.2) <sup>##</sup>

Values represent the means (S.E., n = 4-6). WAT, white adipose tissue; the sum of weights of peri-renal and epididymal white adipose tissues. BAT, brown adipose tissue. <sup>†</sup>, p < 0.05 and <sup>\*\*</sup>, p < 0.01 versus (vs) WT-AL. <sup>##</sup>, p < 0.05, <sup>###</sup>, p < 0.01, <sup>###</sup>, p < 0.001 vs respective AL-groups. <sup>\*</sup>, p < 0.05 vs WT-DR

**Table S3.** List of pathways enriched in genes upregulated in the WT-DR compared to the WT-AL mouse liver. Gene set enrichment analysis (GSEA) using Molecular Signatures Database (MsigDB).

Pathway Name	P-value	Q-value	Gene	Pathway Description
GNF2_TST	0.0000	0.0036	AFCS HSD17B6 ALDH1L1 CES1 ORM2 SLC22A7 DCXR	http://www.broadinstitute.org/gsea/msigdb/ncats/gnf2_tst.html
GNF2_GSTM1	0.0000	0.0036	AFCS HSD17B6 ALDH1L1 CES1 ORM2 SLC22A7 DCXR	http://www.broadinstitute.org/gsea/msigdb/ncats/gnf2_gstm1.html
CHIANG_LIVER_CANCER_SUBCLASS PROLIFERATION_DN	0.0000	0.0036	MYO1B ALDH1L1 DCXR SULT1B1 SLC2A2 GPT HSD17B6 FMG3	http://www.broadinstitute.org/gsea/msigdb/ncats/chiang_liver_cancer_subclass_proliferation_dn.html
WOO_LIVER_CANCER_RECURREN _DN	0.0000	0.0036	CPS1 SLC2A2 GPT ALDH1L1 DCXR SULT1B1	http://www.broadinstitute.org/gsea/msigdb/ncats/woo_liver_cancer_recurrence_dn.html
GNF2_CYP2B6	0.0000	0.0036	AFCS DCXR HSD17B6 CES1 ORM2	http://www.broadinstitute.org/gsea/msigdb/ncats/gnf2_cyp2b6.html
GNF2_LCAT	0.0000	0.0036	AFCS HSD17B6 ALDH1L1 CES1 ORM2 SLC22A7 DCXR	http://www.broadinstitute.org/gsea/msigdb/ncats/gnf2_lcat.html
LEE_LIVER_CANCER_MYC_EEF1L1P	0.0000	0.0038	FMG3 RAD51L1PL CYP39A1 PTGS2	http://www.broadinstitute.org/gsea/msigdb/ncats/lee_liver_cancer_myc_eeef1l1p.html
GNF2_HFN	0.0000	0.0038	ALDH1L1 DCXR HSD17B6 CES1 SLC22A7	http://www.broadinstitute.org/gsea/msigdb/ncats/gnf2_hfn.html

GNF2_HPX	ALDH1L1 DCXR APCS HSD17B6 CES1 ORM2 SLC22A7	0.0038	0.0000	<a href="http://www.broadinstitute.org/gsea/msigdb/cancer/gnf2_hp_x.html">http://www.broadinstitute.org/gsea/msigdb/cancer/gnf2_hp_x.html</a>
WU_CELL_MIGRATION	ARHGAP29 WNTFR1 TNFAIP2 SORDL GJAI BST2 GSTM3 HMGGA2	0.0038	0.0000	<a href="http://www.broadinstitute.org/gsea/msigdb/cancer/wu_cell_migration.html">http://www.broadinstitute.org/gsea/msigdb/cancer/wu_cell_migration.html</a>
GNF2_CEBPA	APCS HSD17B6 CES1 ORM2 DCXR	0.0064	0.0001	<a href="http://www.broadinstitute.org/gsea/msigdb/cancer/gnf2_cebpa.html">http://www.broadinstitute.org/gsea/msigdb/cancer/gnf2_cebpa.html</a>
HOSHIDA_LIVER_CANCER_SUBCLAS S_S3	CPS1 SLC2A2 ALDH1B1 PTGR1 SREBF1 ASCL1 APCS GPT CES1	0.0076	0.0001	<a href="http://www.broadinstitute.org/gsea/msigdb/cancer/hoshida_liver_cancer_subclass_s3.html">http://www.broadinstitute.org/gsea/msigdb/cancer/hoshida_liver_cancer_subclass_s3.html</a>
CAIRO_LIVER_DEVELOPMENT_DN	PLA1A ALDH1L1 DCXR SORDL STAB2 ALDH1B1 RDH5	0.0104	0.0002	<a href="http://www.broadinstitute.org/gsea/msigdb/cancer/cairo_liver_development_dn.html">http://www.broadinstitute.org/gsea/msigdb/cancer/cairo_liver_development_dn.html</a>
NAKAYAMA_SOFT_TISSUE_TUMORS PCA2_DN	NTRK2 CES1 PLA2G16 LPL BST2	0.0145	0.0003	<a href="http://www.broadinstitute.org/gsea/msigdb/cancer/nakayama_soft_tissue_tumors_pca2_dn.html">http://www.broadinstitute.org/gsea/msigdb/cancer/nakayama_soft_tissue_tumors_pca2_dn.html</a>

LEE_LIVER_CANCER_SURVIVAL_UP	DCXR SLC2A2 APCS CES1 FMO3 RDH5	0.0177	0.0003	<a href="http://www.broadinstitute.org/gsea/msigdb/cancer/lee_liver_cancer_survival_up.html">http://www.broadinstitute.org/gsea/msigdb/cancer/lee_liver_cancer_survival_up.html</a>
WILLERT_WNT_SIGNALING	GSTM3 GYPC GJAI	0.0177	0.0004	<a href="http://www.broadinstitute.org/gsea/msigdb/cancer/willert_wnt_signaling.html">http://www.broadinstitute.org/gsea/msigdb/cancer/willert_wnt_signaling.html</a>
SUL_LIVER	FMO3 CPS1 APCS GPT	0.0305	0.0007	<a href="http://www.broadinstitute.org/gsea/msigdb/cancer/sul_liver.html">http://www.broadinstitute.org/gsea/msigdb/cancer/sul_liver.html</a>
GNF2_IGF1	HSD17B6 APCS ORM2	0.0341	0.0008	<a href="http://www.broadinstitute.org/gsea/msigdb/cancer/gnf2_igf1.html">http://www.broadinstitute.org/gsea/msigdb/cancer/gnf2_igf1.html</a>
LEE_LIVER_CANCER_EFPI_UP	FMO3 RAD51L1 LPL CYP39A1	0.0341	0.0009	<a href="http://www.broadinstitute.org/gsea/msigdb/cancer/lee_liver_cancer_efpi_up.html">http://www.broadinstitute.org/gsea/msigdb/cancer/lee_liver_cancer_efpi_up.html</a>
REACTOME_REGULATION_OF_LIPID_METABOLISM_BY_PEROXISOME_PROLIFERATOR_ACTIVATED_RECEPTOR_ALPHA	SLC2A2 SREBF1 LPL FASN	0.0341	0.0009	<a href="http://www.broadinstitute.org/gsea/msigdb/cancer/reactome_regulation_of_lipid_metabolism_by_peroxisome_proliferator_activated_receptor_alpha.html">http://www.broadinstitute.org/gsea/msigdb/cancer/reactome_regulation_of_lipid_metabolism_by_peroxisome_proliferator_activated_receptor_alpha.html</a>

CHARADONNA_NEOPLASTIC_TRANSFORMATION_KRAS_CDC25_UP	WNTFR1 HMGGA2 VAMP5 GJAI	0.0341	0.0009	<a href="http://www.broadinstitute.org/gsea/msigdb/cancer/charadonna_neoplastic_transformation_kras_cdc25_up.html">http://www.broadinstitute.org/gsea/msigdb/cancer/charadonna_neoplastic_transformation_kras_cdc25_up.html</a>
HORMONE_METABOLIC_PROCESS	HSD17B6 BMP6 SULT1B1	0.0502	0.0015	<a href="http://www.broadinstitute.org/gsea/msigdb/cancer/hormone_metabolic_process.html">http://www.broadinstitute.org/gsea/msigdb/cancer/hormone_metabolic_process.html</a>
CARBOXYLESTERASE_ACTIVITY	LPL PLA1A CES1	0.0502	0.0015	<a href="http://www.broadinstitute.org/gsea/msigdb/cancer/carboxylesterase_activity.html">http://www.broadinstitute.org/gsea/msigdb/cancer/carboxylesterase_activity.html</a>
HSIAO_LIVER_SPECIFIC_GENES	CPS1 SLC2A2 FMO3 PTGR1 APCS GPT CES1	0.0503	0.0016	<a href="http://www.broadinstitute.org/gsea/msigdb/cancer/hsiao_liver_specific_genes.html">http://www.broadinstitute.org/gsea/msigdb/cancer/hsiao_liver_specific_genes.html</a>
CAR_HPX	CPS1 APCS HSD17B6 FMO3 BMP6 CYP39A1 PLA1A LPL PTGDS MGST3 SREBF1 HSD17B6	0.0550	0.0018	<a href="http://www.broadinstitute.org/gsea/msigdb/cancer/car_hp_x.html">http://www.broadinstitute.org/gsea/msigdb/cancer/car_hp_x.html</a>
LIPID_METABOLIC_PROCESS		0.0550	0.0019	<a href="http://www.broadinstitute.org/gsea/msigdb/cancer/lipid_metabolic_process.html">http://www.broadinstitute.org/gsea/msigdb/cancer/lipid_metabolic_process.html</a>

YAMASHITA_LIVER_CANCER_STEM_CELL_DN	APCS ALDH1L1 CES1 FMO3	0.0550	0.0020	<a href="http://www.broadinstitute.org/gsea/msigdb/cancer/yamashita_liver_cancer_stem_cell_dn.html">http://www.broadinstitute.org/gsea/msigdb/cancer/yamashita_liver_cancer_stem_cell_dn.html</a>
REACTOME_BIOLOGICAL_OXIDATION	MGST3 CYP26A1 CYP39A1 FMO3 SULT1B1	0.0550	0.0022	<a href="http://www.broadinstitute.org/gsea/msigdb/cancer/reactome_biological_oxidation.html">http://www.broadinstitute.org/gsea/msigdb/cancer/reactome_biological_oxidation.html</a>
OSAWA_TNF_TARGETS	TNFAIP2 COL3A1	0.0550	0.0022	<a href="http://www.broadinstitute.org/gsea/msigdb/cancer/osawa_tnf_targets.html">http://www.broadinstitute.org/gsea/msigdb/cancer/osawa_tnf_targets.html</a>
GARGALOVIC_RESPONSE_TO_OXIDIZED_PHOSPHOLIPIDS_LIGHTYELLOW_DN	RARB CIRBP	0.0550	0.0022	<a href="http://www.broadinstitute.org/gsea/msigdb/cancer/gargalovic_response_to_oxidized_phospholipids_lightyellow_dn.html">http://www.broadinstitute.org/gsea/msigdb/cancer/gargalovic_response_to_oxidized_phospholipids_lightyellow_dn.html</a>
CHARADONNA_NEOPLASTIC_TRANSFORMATION_KRAS_UP	GREM2 MYO1B TNFAIP2 GJAI HMGGA2	0.0550	0.0022	<a href="http://www.broadinstitute.org/gsea/msigdb/cancer/charadonna_neoplastic_transformation_kras_up.html">http://www.broadinstitute.org/gsea/msigdb/cancer/charadonna_neoplastic_transformation_kras_up.html</a>
ACUTE_INFLAMMATORY_RESPONSE	APCS ORM2	0.0637	0.0027	<a href="http://www.broadinstitute.org/gsea/msigdb/cancer/acute_inflammatory_response.html">http://www.broadinstitute.org/gsea/msigdb/cancer/acute_inflammatory_response.html</a>

LEE_TARGETS_OF_PTCH1_AND_SUF U_UP	0.0036	0.0698	ALDH1L1 CNP GIA1 PTGDS	<a href="http://www.broadinstitute.org/gsea/msigdb/cancer/lee_targets_of_ptch1_and_suf_up.html">http://www.broadinstitute.org/gsea/msigdb/cancer/lee_targets_of_ptch1_and_suf_up.html</a>
CHANDRAN_METASTASIS_TOP50_DN	0.0037	0.0698	ETHE1 CIRBP	<a href="http://www.broadinstitute.org/gsea/msigdb/cancer/chandran_metastasis_top50_dn.html">http://www.broadinstitute.org/gsea/msigdb/cancer/chandran_metastasis_top50_dn.html</a>
NIKOLSKY_BREAST_CANCER_IQ32_AMP_LICON	0.0037	0.0698	FCAMR IKBKE	<a href="http://www.broadinstitute.org/gsea/msigdb/cancer/nikolsky_breast_cancer_iq32_amp_licon.html">http://www.broadinstitute.org/gsea/msigdb/cancer/nikolsky_breast_cancer_iq32_amp_licon.html</a>
ONSKEN_UVEAL_MELANOMA_DN	0.0042	0.0739	ALDH1L1 GYPC ETHE1 RPL3 RARB GSTM3 PDE4B PLALA CFS1 CIRBP	<a href="http://www.broadinstitute.org/gsea/msigdb/cancer/onsken_uveal_melanoma_dn.html">http://www.broadinstitute.org/gsea/msigdb/cancer/onsken_uveal_melanoma_dn.html</a>
SWEET_LUNG_CANCER_KRAS_DN	0.0043	0.0739	GREM2 BMP6 COL3A1 MYO1B WWTR1 FMO3 MFAP5 INMT COX7A1	<a href="http://www.broadinstitute.org/gsea/msigdb/cancer/sweet_lung_cancer_kras_dn.html">http://www.broadinstitute.org/gsea/msigdb/cancer/sweet_lung_cancer_kras_dn.html</a>
CYCLIC_NUCLEOTIDE_PHOSPHODIESTERASE_ACTIVITY	0.0043	0.0739	PDE4B CNP	<a href="http://www.broadinstitute.org/gsea/msigdb/cancer/cyclic_nucleotide_phosphodiesterase_activity.html">http://www.broadinstitute.org/gsea/msigdb/cancer/cyclic_nucleotide_phosphodiesterase_activity.html</a>

REACTOME_METABOLISM_OF_LIPIDS_AND_LIPOPROTEINS	0.0059	0.0878	SREBF1 CYP9A1 FASN PPM1L SLC2A2	<a href="http://www.broadinstitute.org/gsea/msigdb/cancer/reactome_metabolism_of_lipids_and_lipoproteins.html">http://www.broadinstitute.org/gsea/msigdb/cancer/reactome_metabolism_of_lipids_and_lipoproteins.html</a>
LE_EGR2_TARGETS_DN	0.0075	0.1097	MGST3 MYO1B LPL PTGDS	<a href="http://www.broadinstitute.org/gsea/msigdb/cancer/le_egr2_targets_dn.html">http://www.broadinstitute.org/gsea/msigdb/cancer/le_egr2_targets_dn.html</a>
LEE_LIVER_CANCER_CIPROFIBRATE_UP	0.0082	0.1125	APCS RAD51L1 LPL	<a href="http://www.broadinstitute.org/gsea/msigdb/cancer/lee_liver_cancer_ciprofibrate_up.html">http://www.broadinstitute.org/gsea/msigdb/cancer/lee_liver_cancer_ciprofibrate_up.html</a>
BROWNE_HCMV_INFECTION_18HR_DN	0.0084	0.1125	CACNA1A COL3A1 VAMP5 CIRBP RDH5	<a href="http://www.broadinstitute.org/gsea/msigdb/cancer/browne_hcmv_infection_18hr_dn.html">http://www.broadinstitute.org/gsea/msigdb/cancer/browne_hcmv_infection_18hr_dn.html</a>
LEE_LIVER_CANCER_MYC_TGFA_UP	0.0086	0.1125	RAD51L1 LPL CYP9A1	<a href="http://www.broadinstitute.org/gsea/msigdb/cancer/lee_liver_cancer_myc_tgfa_up.html">http://www.broadinstitute.org/gsea/msigdb/cancer/lee_liver_cancer_myc_tgfa_up.html</a>
LEE_LIVER_CANCER_DENA_UP	0.0086	0.1125	APCS RAD51L1 LPL	<a href="http://www.broadinstitute.org/gsea/msigdb/cancer/lee_liver_cancer_dena_up.html">http://www.broadinstitute.org/gsea/msigdb/cancer/lee_liver_cancer_dena_up.html</a>

CAIRO_HEPATOBLASTOMA_DN	0.0030	0.0685	GREM2 CYP26A1 CYP9A1 PLA2G16 SLC22A7 STAB2 HSD17B6	<a href="http://www.broadinstitute.org/gsea/msigdb/cancer/cairo_hepatoblastoma_dn.html">http://www.broadinstitute.org/gsea/msigdb/cancer/cairo_hepatoblastoma_dn.html</a>
MICROSOME	0.0031	0.0697	FMO3 MGST3 CYP9A1	<a href="http://www.broadinstitute.org/gsea/msigdb/cancer/microsome.html">http://www.broadinstitute.org/gsea/msigdb/cancer/microsome.html</a>
PICCALUGA_ANGIOIMMUNOBLASTIC_LYMPHOMA_UP	0.0033	0.0698	COL3A1 ARHGAP29 WWTR1 GIA1 PTGDS COX7A1	<a href="http://www.broadinstitute.org/gsea/msigdb/cancer/piccaluga_angioimmunoblastic_lymphoma_up.html">http://www.broadinstitute.org/gsea/msigdb/cancer/piccaluga_angioimmunoblastic_lymphoma_up.html</a>
VARELA_ZMPSTE24_TARGETS_UP	0.0033	0.0698	CYP26A1 CIRBP CYP2C39	<a href="http://www.broadinstitute.org/gsea/msigdb/cancer/varela_zmpste24_targets_up.html">http://www.broadinstitute.org/gsea/msigdb/cancer/varela_zmpste24_targets_up.html</a>
RICKMAN_HEAD_AND_NECK_CANCER_E	0.0035	0.0698	NTRK2 CYP26A1 CES1 FMO3	<a href="http://www.broadinstitute.org/gsea/msigdb/cancer/rickman_head_and_neck_cancer_e.html">http://www.broadinstitute.org/gsea/msigdb/cancer/rickman_head_and_neck_cancer_e.html</a>
VESICULAR_FRACTION	0.0036	0.0698	FMO3 MGST3 CYP9A1	<a href="http://www.broadinstitute.org/gsea/msigdb/cancer/vesicular_fraction.html">http://www.broadinstitute.org/gsea/msigdb/cancer/vesicular_fraction.html</a>

YAMASHITA_LIVER_CANCER_WITH_EPCAM_DN	0.0043	0.0739	ALDH1L1 CES1	<a href="http://www.broadinstitute.org/gsea/msigdb/cancer/yamashita_liver_cancer_with_epcam_dn.html">http://www.broadinstitute.org/gsea/msigdb/cancer/yamashita_liver_cancer_with_epcam_dn.html</a>
GLUTATHIONE_TRANSFERASE_ACTIVITY	0.0050	0.0812	MGST3 GSTM3	<a href="http://www.broadinstitute.org/gsea/msigdb/cancer/glutathione_transferase_activity.html">http://www.broadinstitute.org/gsea/msigdb/cancer/glutathione_transferase_activity.html</a>
CHANG_IMMORTALIZED_BY_HPV31_UP	0.0050	0.0812	SLC2A2 LTBPI	<a href="http://www.broadinstitute.org/gsea/msigdb/cancer/chang_immortalized_by_hpv31_up.html">http://www.broadinstitute.org/gsea/msigdb/cancer/chang_immortalized_by_hpv31_up.html</a>
YAO_TEMPORAL_RESPONSE_TO_GESTERONE_CLUSTER_8	0.0051	0.0819	CYP26A1 CAPRIN2 PNKD	<a href="http://www.broadinstitute.org/gsea/msigdb/cancer/yao_temporal_response_to_gestosterone_cluster_8.html">http://www.broadinstitute.org/gsea/msigdb/cancer/yao_temporal_response_to_gestosterone_cluster_8.html</a>
PETRETTO_HEART_MASS_QTL_CIS_DN	0.0057	0.0878	GIA1 SORDL	<a href="http://www.broadinstitute.org/gsea/msigdb/cancer/petretto_heart_mass_qtl_cis_dn.html">http://www.broadinstitute.org/gsea/msigdb/cancer/petretto_heart_mass_qtl_cis_dn.html</a>
LEE_LIVER_CANCER_MYC_UP	0.0057	0.0878	MGST3 CYP26A1 LPL	<a href="http://www.broadinstitute.org/gsea/msigdb/cancer/lee_liver_cancer_myc_up.html">http://www.broadinstitute.org/gsea/msigdb/cancer/lee_liver_cancer_myc_up.html</a>

Table S4. List of pathways enriched in genes down-regulated in the WT-DR compared to the WT-AL mouse liver.

Pathway Name	P-value	Q-value	Gene	Pathway Description
ICHBA_GRAFT_VERSUS_HOST_DISEASE_35_DN.html	0.0000	0.0572	CYP8B1 CYP7B1 MUP4 ACSL1 RETSAT VNN1 MLP3	<a href="http://www.broadinstitute.org/genes/msigdb/cards/41">http://www.broadinstitute.org/genes/msigdb/cards/41</a>
LEE_LIVER_CANCER_DENA_DN.html	0.0001	0.0758	PEX11A EHHAADH CYP7B1 EPHX2 CSAD ACSL1 MEI	<a href="http://www.broadinstitute.org/genes/msigdb/cards/1">http://www.broadinstitute.org/genes/msigdb/cards/1</a>
REACTOME_METABOLISM_OF_LIPIDS_AND_LIPOPROTEINS.html	0.0001	0.0769	TMTSE2 CYP8B1 HSD17B7 CRAT ACSL1 MEI ACOT8 PEX11A EACTOME_FARMER_BREAST_CANCER_CLUSTERS_AND_LIPOPROTEINS.html	<a href="http://www.broadinstitute.org/genes/msigdb/cards/R">http://www.broadinstitute.org/genes/msigdb/cards/R</a>
OXIDOREDUCTASE_ACTIVITY_GO.html	0.0002	0.0798	LDHA NSDHL UGDH EHHAADH MEI HSD17B7	<a href="http://www.broadinstitute.org/genes/msigdb/cards/O">http://www.broadinstitute.org/genes/msigdb/cards/O</a>
LEE_LIVER_CANCER_MYC_E2F1_DN.html	0.0002	0.0798	EPHX2 ACSL1 CYP7B1 MEI	<a href="http://www.broadinstitute.org/genes/msigdb/cards/L">http://www.broadinstitute.org/genes/msigdb/cards/L</a>
REACTOME_STEROID_METABOLISM.html	0.0003	0.0798	ACOT8 TMTSE2 NSDHL CYP8B1 M	<a href="http://www.broadinstitute.org/genes/msigdb/cards/R">http://www.broadinstitute.org/genes/msigdb/cards/R</a>
OXIDOREDUCTASE_ACTIVITY_OF_TING_ON_CH_OH_GROUP_OF_DO.html	0.0003	0.0798	LDHA UGDH EHHAADH HSD17B7 NSDHL MEI	<a href="http://www.broadinstitute.org/genes/msigdb/cards/O">http://www.broadinstitute.org/genes/msigdb/cards/O</a>
REACTOME_TRANSMFORMATION_OF_LIPIDS.html	0.0003	0.0798	HSD17B7 TMTSE2 NSDHL ACOT8 PEX11A EHHAADH CRAT	<a href="http://www.broadinstitute.org/genes/msigdb/cards/R">http://www.broadinstitute.org/genes/msigdb/cards/R</a>
KEGG_PEROXISOME.html	0.0009	0.1855	EPHX2 ACSL1 TMEH56 FDP5 CLTB GNAI	<a href="http://www.broadinstitute.org/genes/msigdb/cards/K">http://www.broadinstitute.org/genes/msigdb/cards/K</a>
LEE_EGR2_TARGETS_DN.html	0.0010	0.1855	NSDHL CYP51 MEI	<a href="http://www.broadinstitute.org/genes/msigdb/cards/L">http://www.broadinstitute.org/genes/msigdb/cards/L</a>

The pathway delineated by genes up-regulated in the Npy-/-DR compared to the WT-DR are noted by red letters.

Pathway Name	P-value	Q-value	Gene	Pathway Description
LEE_LIVER_CANCER_ACOX1_UP.html	0.0086	0.1125	AFCS RAD51L1 LPL	<a href="http://www.broadinstitute.org/genes/msigdb/cards/LEE_LIVER_CANCER_ACOX1_UP.html">http://www.broadinstitute.org/genes/msigdb/cards/LEE_LIVER_CANCER_ACOX1_UP.html</a>
CELLULAR_LIPID_METABOLIC_PROCESS.html	0.0087	0.1125	BMP6 CYP9A1 PLA1A LPL PTGD5 HSD17B6	<a href="http://www.broadinstitute.org/genes/msigdb/cards/CELLULAR_LIPID_METABOLIC_PROCESS.html">http://www.broadinstitute.org/genes/msigdb/cards/CELLULAR_LIPID_METABOLIC_PROCESS.html</a>
FARMER_BREAST_CANCER_CLUSTER_R_7.html	0.0088	0.1125	SREBF1 FASN	<a href="http://www.broadinstitute.org/genes/msigdb/cards/FARMER_BREAST_CANCER_CLUSTER_R_7.html">http://www.broadinstitute.org/genes/msigdb/cards/FARMER_BREAST_CANCER_CLUSTER_R_7.html</a>
LIANG_SILENCED_BY_METHYLATION_UP.html	0.0088	0.1125	COX7A1 MEAP5	<a href="http://www.broadinstitute.org/genes/msigdb/cards/LIANG_SILENCED_BY_METHYLATION_UP.html">http://www.broadinstitute.org/genes/msigdb/cards/LIANG_SILENCED_BY_METHYLATION_UP.html</a>

The pathways delineated by genes down-regulated in the Npy-/-DR compared to the WT-DR are noted by red letters.

Table S5. The list of pathways enriched in genes downregulated in the Npy-/-DR compared to the WT-DR mice.

Pathway Name	P-value	Q-value	Gene	Pathway Description
SEBMA_FHT_TARGETS_UP.html	0.0007	0.0740	COL27A1 COL1A1	<a href="http://www.broadinstitute.org/genes/msigdb/cards/SEBMA_FHT_TARGETS_UP.html">http://www.broadinstitute.org/genes/msigdb/cards/SEBMA_FHT_TARGETS_UP.html</a>
LEE_LIVER_CANCER_MYC_E2F1_UP.html	0.0009	0.0740	FMO3 CYP9A1 COL1A1	<a href="http://www.broadinstitute.org/genes/msigdb/cards/LEE_LIVER_CANCER_MYC_E2F1_UP.html">http://www.broadinstitute.org/genes/msigdb/cards/LEE_LIVER_CANCER_MYC_E2F1_UP.html</a>
LEE_LIVER_CANCER_E2F1_UP.html	0.0013	0.0740	FMO3 CYP9A1 COL1A1	<a href="http://www.broadinstitute.org/genes/msigdb/cards/LEE_LIVER_CANCER_E2F1_UP.html">http://www.broadinstitute.org/genes/msigdb/cards/LEE_LIVER_CANCER_E2F1_UP.html</a>
DENDRITE.html	0.0015	0.0740	ACTN2 BNIP3	<a href="http://www.broadinstitute.org/genes/msigdb/cards/DENDRITE.html">http://www.broadinstitute.org/genes/msigdb/cards/DENDRITE.html</a>
REACTOME_PHASE_I_FUNCTIONALIZATION_OF_COMPOUNDS.html	0.0018	0.0740	FMO2 CYP9A1 FMO3	<a href="http://www.broadinstitute.org/genes/msigdb/cards/REACTOME_PHASE_I_FUNCTIONALIZATION_OF_COMPOUNDS.html">http://www.broadinstitute.org/genes/msigdb/cards/REACTOME_PHASE_I_FUNCTIONALIZATION_OF_COMPOUNDS.html</a>
GRABARCATK_BCL11B_TARGETS_UP.html	0.0028	0.0740	PIK3R1 BNIP3 CAMSAP1L1	<a href="http://www.broadinstitute.org/genes/msigdb/cards/GRABARCATK_BCL11B_TARGETS_UP.html">http://www.broadinstitute.org/genes/msigdb/cards/GRABARCATK_BCL11B_TARGETS_UP.html</a>
NIKOLSKY_BREAST_CANCER_15Q2_6_AMPLICON.html	0.0028	0.0740	LRRC28 TTC23	<a href="http://www.broadinstitute.org/genes/msigdb/cards/NIKOLSKY_BREAST_CANCER_15Q2_6_AMPLICON.html">http://www.broadinstitute.org/genes/msigdb/cards/NIKOLSKY_BREAST_CANCER_15Q2_6_AMPLICON.html</a>
YAO_TEMPORAL_RESPONSE_TO_PROGESTERONE_CLUSTER_16.html	0.0029	0.0740	COL1A1 STRA6 PCP4L1	<a href="http://www.broadinstitute.org/genes/msigdb/cards/YAO_TEMPORAL_RESPONSE_TO_PROGESTERONE_CLUSTER_16.html">http://www.broadinstitute.org/genes/msigdb/cards/YAO_TEMPORAL_RESPONSE_TO_PROGESTERONE_CLUSTER_16.html</a>
RADMACHER_AML_PROGNOSIS.html	0.0029	0.0740	COL1A1 NPB GYPC	<a href="http://www.broadinstitute.org/genes/msigdb/cards/RADMACHER_AML_PROGNOSIS.html">http://www.broadinstitute.org/genes/msigdb/cards/RADMACHER_AML_PROGNOSIS.html</a>
REACTOME_COLLAGEN_MEDIATED_ACTIVATION_CASCADE.html	0.0031	0.0740	COL1A1 PIK3R1	<a href="http://www.broadinstitute.org/genes/msigdb/cards/REACTOME_COLLAGEN_MEDIATED_ACTIVATION_CASCADE.html">http://www.broadinstitute.org/genes/msigdb/cards/REACTOME_COLLAGEN_MEDIATED_ACTIVATION_CASCADE.html</a>
SHL_SPARC_TARGETS_UP.html	0.0033	0.0740	PIK3R1 ANKRD11	<a href="http://www.broadinstitute.org/genes/msigdb/cards/SHL_SPARC_TARGETS_UP.html">http://www.broadinstitute.org/genes/msigdb/cards/SHL_SPARC_TARGETS_UP.html</a>
RICKMAN_HEAD_AND_NECK_CANCER.html	0.0038	0.0740	FMO2 CES1 FMO3	<a href="http://www.broadinstitute.org/genes/msigdb/cards/RICKMAN_HEAD_AND_NECK_CANCER.html">http://www.broadinstitute.org/genes/msigdb/cards/RICKMAN_HEAD_AND_NECK_CANCER.html</a>
NAKAMURA_CANCER_MICROENVIRONMENT_UP.html	0.0039	0.0740	LRRC28 COL1A1	<a href="http://www.broadinstitute.org/genes/msigdb/cards/NAKAMURA_CANCER_MICROENVIRONMENT_UP.html">http://www.broadinstitute.org/genes/msigdb/cards/NAKAMURA_CANCER_MICROENVIRONMENT_UP.html</a>

MONOOXYGENASE_ACTIVITY.html	0.0049	0.0852	CYP9A1 FMO2	<a href="http://www.broadinstitute.org/genes/msigdb/cards/MONOOXYGENASE_ACTIVITY.html">http://www.broadinstitute.org/genes/msigdb/cards/MONOOXYGENASE_ACTIVITY.html</a>
MARTORIATI_MDM4_TARGETS_NEUROEPITHELIUM_UP.html	0.0061	0.0992	BNIP3 241000N99RIK MTI	<a href="http://www.broadinstitute.org/genes/msigdb/cards/MARTORIATI_MDM4_TARGETS_NEUROEPITHELIUM_UP.html">http://www.broadinstitute.org/genes/msigdb/cards/MARTORIATI_MDM4_TARGETS_NEUROEPITHELIUM_UP.html</a>
HOO1_S77_TARGETS_DN.html	0.0082	0.1019	MCOLN3 COL1A1 PPP1 R3B	<a href="http://www.broadinstitute.org/genes/msigdb/cards/HOO1_S77_TARGETS_DN.html">http://www.broadinstitute.org/genes/msigdb/cards/HOO1_S77_TARGETS_DN.html</a>
MICROSOME.html	0.0096	0.1019	FMO3 CYP9A1	<a href="http://www.broadinstitute.org/genes/msigdb/cards/MICROSOME.html">http://www.broadinstitute.org/genes/msigdb/cards/MICROSOME.html</a>
VESICULAR_FRACTION.html	0.0105	0.1019	FMO3 CYP9A1	<a href="http://www.broadinstitute.org/genes/msigdb/cards/VESICULAR_FRACTION.html">http://www.broadinstitute.org/genes/msigdb/cards/VESICULAR_FRACTION.html</a>
REACTOME_BIOLOGICAL_OXIDATIONS.html	0.0108	0.1019	FMO2 CYP9A1 FMO3	<a href="http://www.broadinstitute.org/genes/msigdb/cards/REACTOME_BIOLOGICAL_OXIDATIONS.html">http://www.broadinstitute.org/genes/msigdb/cards/REACTOME_BIOLOGICAL_OXIDATIONS.html</a>
LIANG_HEMATOPOIESIS_STEM_CELL_NUMBER_LARGE_VS_TINY_DN.html	0.0110	0.1019	NPTX1 KLHL7	<a href="http://www.broadinstitute.org/genes/msigdb/cards/REACTOME_HEMATOPOIESIS_STEM_CELL_NUMBER_LARGE_VS_TINY_DN.html">http://www.broadinstitute.org/genes/msigdb/cards/REACTOME_HEMATOPOIESIS_STEM_CELL_NUMBER_LARGE_VS_TINY_DN.html</a>
SENSE_HDAC2_TARGETS_DN.html	0.0112	0.1019	COL1A1 ZBTB20 NFBF	<a href="http://www.broadinstitute.org/genes/msigdb/cards/SENSE_HDAC2_TARGETS_DN.html">http://www.broadinstitute.org/genes/msigdb/cards/SENSE_HDAC2_TARGETS_DN.html</a>
REACTOME_SIGNALING_BY_EGFR.html	0.0129	0.1019	PIK3R1 ADAM17	<a href="http://www.broadinstitute.org/genes/msigdb/cards/REACTOME_SIGNALING_BY_EGFR.html">http://www.broadinstitute.org/genes/msigdb/cards/REACTOME_SIGNALING_BY_EGFR.html</a>
INTEGRAL_TO_ORGANELLE_MEMB_RANE.html	0.0135	0.1019	PEX11A BNIP3	<a href="http://www.broadinstitute.org/genes/msigdb/cards/INTEGRAL_TO_ORGANELLE_MEMB_RANE.html">http://www.broadinstitute.org/genes/msigdb/cards/INTEGRAL_TO_ORGANELLE_MEMB_RANE.html</a>
BOYAUT_LIVER_CANCER_SUBCLASS_G3_DN.html	0.0140	0.1019	NFB1 ILEF3	<a href="http://www.broadinstitute.org/genes/msigdb/cards/BOYAUT_LIVER_CANCER_SUBCLASS_G3_DN.html">http://www.broadinstitute.org/genes/msigdb/cards/BOYAUT_LIVER_CANCER_SUBCLASS_G3_DN.html</a>
INTRINSIC_TO_ORGANELLE_MEMB_RANE.html	0.0145	0.1019	PIK3R1 ACAT1	<a href="http://www.broadinstitute.org/genes/msigdb/cards/INTRINSIC_TO_ORGANELLE_MEMB_RANE.html">http://www.broadinstitute.org/genes/msigdb/cards/INTRINSIC_TO_ORGANELLE_MEMB_RANE.html</a>
PROTEIN_COMPLEX_BINDING.html	0.0162	0.1019	PEX11A BNIP3	<a href="http://www.broadinstitute.org/genes/msigdb/cards/PROTEIN_COMPLEX_BINDING.html">http://www.broadinstitute.org/genes/msigdb/cards/PROTEIN_COMPLEX_BINDING.html</a>
BOQUEST_STEM_CELL_CULTURED_VS_FRESH_UP.html	0.0179	0.1019	FMO3	<a href="http://www.broadinstitute.org/genes/msigdb/cards/BOQUEST_STEM_CELL_CULTURED_VS_FRESH_UP.html">http://www.broadinstitute.org/genes/msigdb/cards/BOQUEST_STEM_CELL_CULTURED_VS_FRESH_UP.html</a>
REACTOME_PLATELET_ACTIVATION_TRIGGERS.html	0.0191	0.1019	PIK3R1 COL1A1	<a href="http://www.broadinstitute.org/genes/msigdb/cards/REACTOME_PLATELET_ACTIVATION_TRIGGERS.html">http://www.broadinstitute.org/genes/msigdb/cards/REACTOME_PLATELET_ACTIVATION_TRIGGERS.html</a>



Table S6. The list of pathways enriched in genes upregulated in the Npy-/-DR compared to the WT-DR mice.

Pathway Name	P-value	Q-value	Gene	Pathway Description
UEIDA_PERIPHERAL_CLOCK	0.0060	0.0010	ETHE1 AQPR CRIP2 FDRS GLDC HSD3B5 ID2 S100A10 GABARAPL1	<a href="http://www.broadinstitute.org/genes/msigdb/cards/UEIDA_PERIPHERAL_CLOCK.html">http://www.broadinstitute.org/genes/msigdb/cards/UEIDA_PERIPHERAL_CLOCK.html</a>
ICHHBA_GRAFT_VERSUS_HOST_DISEASE_3SD_DN	0.0001	0.0213	CYP7B1 HSD3B2 LIFR MUP4	<a href="http://www.broadinstitute.org/genes/msigdb/cards/ICHHBA_GRAFT_VERSUS_HOST_DISEASE_3SD_DN.html">http://www.broadinstitute.org/genes/msigdb/cards/ICHHBA_GRAFT_VERSUS_HOST_DISEASE_3SD_DN.html</a>
ICHHBA_GRAFT_VERSUS_HOST_DISEASE_D7_DN	0.0004	0.1003	LIFR MUP4 HSD17B2 NRIP1	<a href="http://www.broadinstitute.org/genes/msigdb/cards/ICHHBA_GRAFT_VERSUS_HOST_DISEASE_D7_DN.html">http://www.broadinstitute.org/genes/msigdb/cards/ICHHBA_GRAFT_VERSUS_HOST_DISEASE_D7_DN.html</a>
LEE_LIVER_CANCER_DENA_UP	0.0006	0.1221	ANXA5 FBLN2 LPL SPP1	<a href="http://www.broadinstitute.org/genes/msigdb/cards/LEE_LIVER_CANCER_DENA_UP.html">http://www.broadinstitute.org/genes/msigdb/cards/LEE_LIVER_CANCER_DENA_UP.html</a>
CUI_TCTE1_TARGETS_UP	0.0016	0.2331	MEG3 COL3A1 CYP7B1	<a href="http://www.broadinstitute.org/genes/msigdb/cards/CUI_TCTE1_TARGETS_UP.html">http://www.broadinstitute.org/genes/msigdb/cards/CUI_TCTE1_TARGETS_UP.html</a>
CAIRO_LIVER_DEVELOPMENT_DN	0.0031	0.2331	HSD17B2 MORC4 FKBP11	<a href="http://www.broadinstitute.org/genes/msigdb/cards/CAIRO_LIVER_DEVELOPMENT_DN.html">http://www.broadinstitute.org/genes/msigdb/cards/CAIRO_LIVER_DEVELOPMENT_DN.html</a>
PARENT_MTOR_SIGNALING_UP	0.0035	0.2331	GLDC C9 F11 ETHE1 HSD17B2 TOP3A ETH1 TSHZ2 F11 RTEL1 CTH	<a href="http://www.broadinstitute.org/genes/msigdb/cards/PARENT_MTOR_SIGNALING_UP.html">http://www.broadinstitute.org/genes/msigdb/cards/PARENT_MTOR_SIGNALING_UP.html</a>
BIOCARTA_CLASSIC_PATHWAY	0.0036	0.2331	GABARAPL1 FDRS FLOD1	<a href="http://www.broadinstitute.org/genes/msigdb/cards/BIOCARTA_CLASSIC_PATHWAY.html">http://www.broadinstitute.org/genes/msigdb/cards/BIOCARTA_CLASSIC_PATHWAY.html</a>
RODRIGUES_THYROID_CARCINOMA_UP	0.0042	0.2331	FKBP11 SDF2L1	<a href="http://www.broadinstitute.org/genes/msigdb/cards/RODRIGUES_THYROID_CARCINOMA_UP.html">http://www.broadinstitute.org/genes/msigdb/cards/RODRIGUES_THYROID_CARCINOMA_UP.html</a>

YAMASHITA_LIVER_CANCER_WITH_EPCAM_DN	0.0493	0.1019	CES1	<a href="http://www.broadinstitute.org/genes/msigdb/cards/YAMASHITA_LIVER_CANCER_WITH_EPCAM_DN.html">http://www.broadinstitute.org/genes/msigdb/cards/YAMASHITA_LIVER_CANCER_WITH_EPCAM_DN.html</a>
BIOCARTA_PSI_PATHWAY	0.0493	0.1019	ADAM17	<a href="http://www.broadinstitute.org/genes/msigdb/cards/BIOCARTA_PSI_PATHWAY.html">http://www.broadinstitute.org/genes/msigdb/cards/BIOCARTA_PSI_PATHWAY.html</a>
PROTEIN_TETRAMERIZATION	0.0493	0.1019	ACTN2	<a href="http://www.broadinstitute.org/genes/msigdb/cards/PROTEIN_TETRAMERIZATION.html">http://www.broadinstitute.org/genes/msigdb/cards/PROTEIN_TETRAMERIZATION.html</a>
BIOCARTA_CELL_CYCLE_PATHWAY	0.0493	0.1019	ACTN2	<a href="http://www.broadinstitute.org/genes/msigdb/cards/BIOCARTA_CELL_CYCLE_PATHWAY.html">http://www.broadinstitute.org/genes/msigdb/cards/BIOCARTA_CELL_CYCLE_PATHWAY.html</a>

The pathways delineated by genes upregulated in the WT-AL mouse liver are noted by red letters.

SETLUR_PROSTATE_CANCER_TWPRS_S2_ERG_FUSION_UP	0.0080	0.2331	PEX10 ERG EIF4G3	<a href="http://www.broadinstitute.org/genes/msigdb/cards/SETLUR_PROSTATE_CANCER_TWPRS_S2_ERG_FUSION_UP.html">http://www.broadinstitute.org/genes/msigdb/cards/SETLUR_PROSTATE_CANCER_TWPRS_S2_ERG_FUSION_UP.html</a>
SHAFER_IRF1_TARGETS_IN_ACTIVATED_DENDRITIC_CELL	0.0084	0.2331	FKBP11 GLDC GIT2IRD1	<a href="http://www.broadinstitute.org/genes/msigdb/cards/SHAFER_IRF1_TARGETS_IN_ACTIVATED_DENDRITIC_CELL.html">http://www.broadinstitute.org/genes/msigdb/cards/SHAFER_IRF1_TARGETS_IN_ACTIVATED_DENDRITIC_CELL.html</a>
REACTION_SIGNALING_BY_PDGF_LIVER_CANCER_CIPROFIBRATE_DN	0.0084	0.2331	RAPGEF1 COL3A1 SPP1	<a href="http://www.broadinstitute.org/genes/msigdb/cards/REACTION_SIGNALING_BY_PDGF_LIVER_CANCER_CIPROFIBRATE_DN.html">http://www.broadinstitute.org/genes/msigdb/cards/REACTION_SIGNALING_BY_PDGF_LIVER_CANCER_CIPROFIBRATE_DN.html</a>
RODWELL_AGING_KIDNEY_NO_BLOOD_D_DN	0.0088	0.2354	CYP7B1 HSD3B2 OAT	<a href="http://www.broadinstitute.org/genes/msigdb/cards/RODWELL_AGING_KIDNEY_NO_BLOOD_D_DN.html">http://www.broadinstitute.org/genes/msigdb/cards/RODWELL_AGING_KIDNEY_NO_BLOOD_D_DN.html</a>
STERIOD_BIOSYNTHETIC_PROCESS	0.0095	0.2458	LPL CTH GABARAPL1 OAT	<a href="http://www.broadinstitute.org/genes/msigdb/cards/STERIOD_BIOSYNTHETIC_PROCESS.html">http://www.broadinstitute.org/genes/msigdb/cards/STERIOD_BIOSYNTHETIC_PROCESS.html</a>

The pathway delineated by genes down-regulated in the WT-DR compared to the WT-AL mouse liver is noted by red letters.

LEE_LIVER_CANCER_MYC_E2F1_UP	0.0050	0.2331	ANXA5 LPL SPP1	<a href="http://www.broadinstitute.org/genes/msigdb/cards/LEE_LIVER_CANCER_MYC_E2F1_UP.html">http://www.broadinstitute.org/genes/msigdb/cards/LEE_LIVER_CANCER_MYC_E2F1_UP.html</a>
ZHU_CMV_24_HR_DN	0.0052	0.2331	COL3A1 HSD17B2 ID2	<a href="http://www.broadinstitute.org/genes/msigdb/cards/ZHU_CMV_24_HR_DN.html">http://www.broadinstitute.org/genes/msigdb/cards/ZHU_CMV_24_HR_DN.html</a>
KEGG_STEROID_HORMONE_BIOSYNTHESIS	0.0055	0.2331	HSD17B2 CYP7B1 HSD3B2	<a href="http://www.broadinstitute.org/genes/msigdb/cards/KEGG_STEROID_HORMONE_BIOSYNTHESIS.html">http://www.broadinstitute.org/genes/msigdb/cards/KEGG_STEROID_HORMONE_BIOSYNTHESIS.html</a>
GEN_SMAD6_TARGETS_DN	0.0060	0.2331	CTH DDC	<a href="http://www.broadinstitute.org/genes/msigdb/cards/GEN_SMAD6_TARGETS_DN.html">http://www.broadinstitute.org/genes/msigdb/cards/GEN_SMAD6_TARGETS_DN.html</a>
S1H_COEXPRESSED_WITH_ID1_AND_ID2_UP	0.0060	0.2331	GABARAPL1 ID2	<a href="http://www.broadinstitute.org/genes/msigdb/cards/S1H_COEXPRESSED_WITH_ID1_AND_ID2_UP.html">http://www.broadinstitute.org/genes/msigdb/cards/S1H_COEXPRESSED_WITH_ID1_AND_ID2_UP.html</a>
TONG_INTERACT_WITH_PTTG1	0.0061	0.2331	GSTM3 NOB1 GABARAPL1	<a href="http://www.broadinstitute.org/genes/msigdb/cards/TONG_INTERACT_WITH_PTTG1.html">http://www.broadinstitute.org/genes/msigdb/cards/TONG_INTERACT_WITH_PTTG1.html</a>
RODWELL_AGING_KIDNEY_DN	0.0063	0.2331	LPL CTH GABARAPL1 OAT	<a href="http://www.broadinstitute.org/genes/msigdb/cards/RODWELL_AGING_KIDNEY_DN.html">http://www.broadinstitute.org/genes/msigdb/cards/RODWELL_AGING_KIDNEY_DN.html</a>
DIKZ_CHRONIC_MEYLOGENOUS_LEU_KEMIA_DN	0.0065	0.2331	ANXA5 EEF1A1 GAST LPL	<a href="http://www.broadinstitute.org/genes/msigdb/cards/DIKZ_CHRONIC_MEYLOGENOUS_LEU_KEMIA_DN.html">http://www.broadinstitute.org/genes/msigdb/cards/DIKZ_CHRONIC_MEYLOGENOUS_LEU_KEMIA_DN.html</a>
BIOCARTA_COMP_PATHWAY	0.0067	0.2331	C9C6	<a href="http://www.broadinstitute.org/genes/msigdb/cards/BIOCARTA_COMP_PATHWAY.html">http://www.broadinstitute.org/genes/msigdb/cards/BIOCARTA_COMP_PATHWAY.html</a>
MARTINEZ_RESPONSE_TO TRABECTEDIN_UP	0.0073	0.2331	ANXA5 S100A10 ID2	<a href="http://www.broadinstitute.org/genes/msigdb/cards/MARTINEZ_RESPONSE_TO TRABECTEDIN_UP.html">http://www.broadinstitute.org/genes/msigdb/cards/MARTINEZ_RESPONSE_TO TRABECTEDIN_UP.html</a>
WILLERT_WNT_SIGNALING	0.0074	0.2331	GSTM3 ID2	<a href="http://www.broadinstitute.org/genes/msigdb/cards/WILLERT_WNT_SIGNALING.html">http://www.broadinstitute.org/genes/msigdb/cards/WILLERT_WNT_SIGNALING.html</a>
GRUETZMANN_PANCREATIC_CANCER_UP	0.0074	0.2331	CKS1B CE2N2 EIF4G3 FBLN2 CRIP2 ANXA5 S100A10	<a href="http://www.broadinstitute.org/genes/msigdb/cards/GRUETZMANN_PANCREATIC_CANCER_UP.html">http://www.broadinstitute.org/genes/msigdb/cards/GRUETZMANN_PANCREATIC_CANCER_UP.html</a>
LEE_LIVER_CANCER_MYC_TGFA_DN	0.0077	0.2331	AQPR CYP7B1 OAT	<a href="http://www.broadinstitute.org/genes/msigdb/cards/LEE_LIVER_CANCER_MYC_TGFA_DN.html">http://www.broadinstitute.org/genes/msigdb/cards/LEE_LIVER_CANCER_MYC_TGFA_DN.html</a>
KAN_RESPONSE_TO_ARSENIC_TRIOXIDE	0.0078	0.2331	ID2 GSTM3 CTH GABARAPL1	<a href="http://www.broadinstitute.org/genes/msigdb/cards/KAN_RESPONSE_TO_ARSENIC_TRIOXIDE.html">http://www.broadinstitute.org/genes/msigdb/cards/KAN_RESPONSE_TO_ARSENIC_TRIOXIDE.html</a>
CAIRO_HEPATOBLASTOMA_DN	0.0078	0.2331	FAM134B CTH ID2 C6 C9 F11	<a href="http://www.broadinstitute.org/genes/msigdb/cards/CAIRO_HEPATOBLASTOMA_DN.html">http://www.broadinstitute.org/genes/msigdb/cards/CAIRO_HEPATOBLASTOMA_DN.html</a>

**Table S7.** The list of pathways enriched in up-regulated genes in the WT-DR compared to the WT-AL. Analysis with NCBI BioSystems Database.

Pathway/Name	Changed Genes	Total Genes	Z score	P-value	Gene ID
Biological oxidations	10	107	9.884	2.E-08	Entrez_Gene:13082,Entrez_Gene:13096,Entrez_Gene:13097,Entrez_Gene:13098,Entrez_Gene:14262,Entrez_Gene:14864,Entrez_Gene:14867,Entrez_Gene:56050,Entrez_Gene:56362,Entrez_Gene:66447
Drug metabolism: cyclochrome P450	8	59	10.961	4.E-08	Entrez_Gene:13096,Entrez_Gene:13097,Entrez_Gene:13098,Entrez_Gene:14262,Entrez_Gene:14864,Entrez_Gene:14867,Entrez_Gene:56050,Entrez_Gene:56362,Entrez_Gene:66447
Metabolism of xenobiotics by cytochrome P450	7	51	10.323	3.E-07	Entrez_Gene:13096,Entrez_Gene:13097,Entrez_Gene:13098,Entrez_Gene:14262,Entrez_Gene:14864,Entrez_Gene:14867,Entrez_Gene:56050,Entrez_Gene:56362,Entrez_Gene:66447
Retinol metabolism	6	47	9.174	3.E-06	Entrez_Gene:13082,Entrez_Gene:13096,Entrez_Gene:13097,Entrez_Gene:13098,Entrez_Gene:14262,Entrez_Gene:14864,Entrez_Gene:14867,Entrez_Gene:56050,Entrez_Gene:56362,Entrez_Gene:66447
nicotine degradation II	5	30	9.72	7.E-06	Entrez_Gene:13096,Entrez_Gene:13097,Entrez_Gene:13098,Entrez_Gene:14262,Entrez_Gene:14864,Entrez_Gene:14867,Entrez_Gene:56050,Entrez_Gene:56362,Entrez_Gene:66447
Phase I - Functionalization of compounds	6	68	7.398	2.E-05	Entrez_Gene:13082,Entrez_Gene:13096,Entrez_Gene:13097,Entrez_Gene:13098,Entrez_Gene:14262,Entrez_Gene:14864,Entrez_Gene:14867,Entrez_Gene:56050
Cytochrome P450 - arranged by substrate type	5	53	7.028	9.E-05	Entrez_Gene:13096,Entrez_Gene:13097,Entrez_Gene:13098,Entrez_Gene:14262,Entrez_Gene:14864,Entrez_Gene:14867,Entrez_Gene:56050
Linoleic acid metabolism	4	36	6.918	3.E-04	Entrez_Gene:13096,Entrez_Gene:13097,Entrez_Gene:13098,Entrez_Gene:14262,Entrez_Gene:14864,Entrez_Gene:14867,Entrez_Gene:56050
Glutathione conjugation	3	15	8.318	4.E-04	Entrez_Gene:13096,Entrez_Gene:13097,Entrez_Gene:13098,Entrez_Gene:14262,Entrez_Gene:14864,Entrez_Gene:14867,Entrez_Gene:56050
Phase II conjugation	4	40	6.506	4.E-04	Entrez_Gene:13096,Entrez_Gene:13097,Entrez_Gene:13098,Entrez_Gene:14262,Entrez_Gene:14864,Entrez_Gene:14867,Entrez_Gene:56050
glutathione-mediated detoxification	3	20	7.103	8.E-04	Entrez_Gene:13096,Entrez_Gene:13097,Entrez_Gene:13098,Entrez_Gene:14262,Entrez_Gene:14864,Entrez_Gene:14867,Entrez_Gene:56050
hormonal degradation	3	22	6.734	1.E-03	Entrez_Gene:13096,Entrez_Gene:13097,Entrez_Gene:13098,Entrez_Gene:14262,Entrez_Gene:14864,Entrez_Gene:14867,Entrez_Gene:56050
nicotine degradation III	3	24	6.41	1.E-03	Entrez_Gene:13096,Entrez_Gene:13097,Entrez_Gene:13098,Entrez_Gene:14262,Entrez_Gene:14864,Entrez_Gene:14867,Entrez_Gene:56050
Arachidonic acid metabolism	4	67	4.73	2.E-03	Entrez_Gene:13096,Entrez_Gene:13097,Entrez_Gene:13098,Entrez_Gene:14262,Entrez_Gene:14864,Entrez_Gene:14867,Entrez_Gene:56050

**Table S8.** The list of pathways enriched in down-regulated genes in the Npy<sup>-/-</sup>DR compared to the WT-DR. The pathways with p < 0.01 are listed.

Pathway/Name	Changed Genes	Total Genes	Z score	P-value	Gene ID
Endogenous steroids	3	12	7.283	8.0783E-04	Entrez_Gene:13121,Entrez_Gene:13123,Entrez_Gene:13124
Bile acid and bile salt metabolism	4	34	5.416	1.2933E-03	Entrez_Gene:105387,Entrez_Gene:13123,Entrez_Gene:13124,Entrez_Gene:170789
Phase I - Functionalization of compounds	5	68	4.434	2.2442E-03	Entrez_Gene:13121,Entrez_Gene:13123,Entrez_Gene:13124,Entrez_Gene:170789
Synthesis of bile acids and bile salts via 7alpha-hydroxysterol	6	104	4.051	2.6267E-03	Entrez_Gene:1472,Entrez_Gene:12279,Entrez_Gene:18751,Entrez_Gene:20706,Entrez_Gene:226519,Entrez_Gene:381286
Biological oxidations	6	107	3.961	2.9222E-03	Entrez_Gene:105387,Entrez_Gene:13124,Entrez_Gene:170789
Beta-oxidation of very long chain fatty acids	2	5	7.675	3.0966E-03	Entrez_Gene:13121,Entrez_Gene:13123,Entrez_Gene:13124,Entrez_Gene:22335,Entrez_Gene:71519,Entrez_Gene:72034
Terminal pathways of complement	2	6	6.960	4.2578E-04	Entrez_Gene:12274,Entrez_Gene:12279
Miscellaneous substrates	2	7	6.401	5.4293E-03	Entrez_Gene:71519,Entrez_Gene:2084
Beta-oxidation of pristanoyl-CoA	2	8	5.947	6.7390E-03	Entrez_Gene:12908,Entrez_Gene:170789
PPAR signaling pathway	4	61	3.649	9.1566E-03	Entrez_Gene:13124,Entrez_Gene:4081,Entrez_Gene:17436,Entrez_Gene:71419

The pathways delineated by genes up-regulated in the Npy<sup>-/-</sup>DR compared to the WT-DR are noted by blue letters. The pathways with p < 0.01 are listed.

**Table S8.** The list of pathways enriched in down-regulated genes in WT-DR compared to WT-AL. Analysis with NCBI BioSystems Database.

Pathway/Name	Changed Genes	Total Genes	Z score	P-value	Gene ID
Metabolism of lipids and lipoproteins	13	243	5.612	1.7100E-05	Entrez_Gene:105387,Entrez_Gene:10196,Entrez_Gene:12908,Entrez_Gene:13121,Entrez_Gene:13123,Entrez_Gene:13124,Entrez_Gene:18194,Entrez_Gene:18631,Entrez_Gene:18670,Entrez_Gene:73166
Metabolic pathways	27	983	4.050	8.3200E-05	Entrez_Gene:10196,Entrez_Gene:11656,Entrez_Gene:11761,Entrez_Gene:13121,Entrez_Gene:13124,Entrez_Gene:13850,Entrez_Gene:14864,Entrez_Gene:14867,Entrez_Gene:18194,Entrez_Gene:18263,Entrez_Gene:20019,Entrez_Gene:20441,Entrez_Gene:21990,Entrez_Gene:22018,Entrez_Gene:22335,Entrez_Gene:24627,Entrez_Gene:26938,Entrez_Gene:27402,Entrez_Gene:54447,Entrez_Gene:71519,Entrez_Gene:72034,Entrez_Gene:73166,Entrez_Gene:73167,Entrez_Gene:78390
Steroid biosynthesis	4	17	8.131	1.2327E-04	Entrez_Gene:13121,Entrez_Gene:13121,Entrez_Gene:18194,Entrez_Gene:73166
Cholesterol biosynthesis	4	20	7.420	2.1260E-04	Entrez_Gene:10196,Entrez_Gene:13121,Entrez_Gene:18194,Entrez_Gene:73166
suprapathway of cholesterol biosynthesis	4	23	6.848	3.4109E-04	Entrez_Gene:10196,Entrez_Gene:13123,Entrez_Gene:18194,Entrez_Gene:73166
Synthesis of bile acids and bile salts	4	24	6.680	3.9412E-04	Entrez_Gene:105387,Entrez_Gene:13123,Entrez_Gene:13124,Entrez_Gene:170789
cholesterol biosynthesis III (via desmosterol)	3	9	8.524	4.0151E-04	Entrez_Gene:15900,Entrez_Gene:18194,Entrez_Gene:73166
Peroxisome	6	73	5.250	4.6562E-04	Entrez_Gene:12908,Entrez_Gene:13850,Entrez_Gene:14081,Entrez_Gene:170789,Entrez_Gene:18631,Entrez_Gene:74147
cholesterol biosynthesis I	3	10	8.051	5.1719E-04	Entrez_Gene:15900,Entrez_Gene:18194,Entrez_Gene:73166
Synthesis of bile acid and bile salts via 27-hydroxysterol	3	11	7.642	6.5722E-04	Entrez_Gene:105387,Entrez_Gene:13123,Entrez_Gene:13124
Cytochrome P450 - arranged by substrate type	5	53	5.238	7.9410E-04	Entrez_Gene:13121,Entrez_Gene:13123,Entrez_Gene:13124,Entrez_Gene:170789,Entrez_Gene:72054

**Table S9.** The list of pathways enriched in genes down-regulated in the Npy-/-DR compared to the WT-DR. Analysis with NCBI BioSystems Database.

Pathway/Name	Changed Genes	Total Genes	Z score	P-value	Gene ID
Phase 1 - Functionalization of compounds	7	68	14.512	2.E-09	Entrez_Gene:13096,Entrez_Gene:13097,Entrez_Gene:13098,Entrez_Gene:13119,Entrez_Gene:14262,Entrez_Gene:55990,Entrez_Gene:56080,Entrez_Gene:13096,Entrez_Gene:13097,Entrez_Gene:13098,Entrez_Gene:13119,Entrez_Gene:14262,Entrez_Gene:55990,Entrez_Gene:56080
Biological oxidations	7	107	11.554	4.E-08	Entrez_Gene:13096,Entrez_Gene:13097,Entrez_Gene:13098,Entrez_Gene:13119,Entrez_Gene:14262,Entrez_Gene:55990,Entrez_Gene:56080
nicotine formation II	5	30	15.799	6.E-08	Entrez_Gene:13096,Entrez_Gene:13097,Entrez_Gene:13098,Entrez_Gene:13119,Entrez_Gene:14262,Entrez_Gene:55990,Entrez_Gene:56080
Cytochrome P450 - araneby substrate type	5	53	11.707	8.E-07	Entrez_Gene:13096,Entrez_Gene:13097,Entrez_Gene:13098,Entrez_Gene:14262,Entrez_Gene:55990
Drug metabolism - cytochrome P450	5	59	11.051	1.E-06	Entrez_Gene:13096,Entrez_Gene:13097,Entrez_Gene:13098,Entrez_Gene:13119
Retinol metabolism	4	47	9.907	2.E-05	Entrez_Gene:13096,Entrez_Gene:13097,Entrez_Gene:13098
Xenobiotics biotransformation	3	20	11.584	5.E-05	Entrez_Gene:13096,Entrez_Gene:13097,Entrez_Gene:13098
hupropion degradation	3	22	11.021	6.E-05	Entrez_Gene:13096,Entrez_Gene:13097,Entrez_Gene:13098,Entrez_Gene:13119
Atenolol metabolism	4	67	8.159	7.E-05	Entrez_Gene:13096,Entrez_Gene:13097,Entrez_Gene:13098,Entrez_Gene:13119,Entrez_Gene:14262,Entrez_Gene:55990,Entrez_Gene:56080
nicotine degradation III	3	24	10.529	8.E-05	Entrez_Gene:13096,Entrez_Gene:13097,Entrez_Gene:13098
PMO oxidizes nucleobases	2	3	20.28	1.E-04	Entrez_Gene:14262,Entrez_Gene:55990
Linkolic acid metabolism	3	36	8.483	2.E-04	Entrez_Gene:13096,Entrez_Gene:13097,Entrez_Gene:13098
Metabolism of xenobiotics by cytochrome P450	3	51	7.008	6.E-04	Entrez_Gene:13096,Entrez_Gene:13097,Entrez_Gene:13098
Fatty acid, triacylglycerol, and ketone body metabolism	3	86	5.182	3.E-03	Entrez_Gene:10446,Entrez_Gene:13119,Entrez_Gene:18631
GPVI-mediated activation cascade	2	27	6.497	4.E-03	Entrez_Gene:12842,Entrez_Gene:18708
Amoebiasis	3	104	4.612	5.E-03	Entrez_Gene:10446,Entrez_Gene:13119,Entrez_Gene:18631,Entrez_Gene:56080
Fatty acid metabolism	2	36	5.542	6.E-03	Entrez_Gene:10446,Entrez_Gene:13119,Entrez_Gene:18631,Entrez_Gene:56080
Metabolism of lipids and lipoproteins	4	243	3.642	7.E-03	Entrez_Gene:10446,Entrez_Gene:13119,Entrez_Gene:18631,Entrez_Gene:56080

**Table S10.** The list of pathways enriched in genes upregulated in the Npy-/-DR compared to the WT-DR. Analysis with NCBI BioSystems Database.

Pathway/Name	Changed Genes	Total Genes	Z score	P-value	Gene ID
Steroid hormone biosynthesis	4	42	7.297	2.E-04	Entrez_Gene:13123,Entrez_Gene:15486,Entrez_Gene:15493,Entrez_Gene:15496
Mineralocorticoid biosynthesis	2	6	10.14	1.E-03	Entrez_Gene:15493,Entrez_Gene:15496
Terminal pathway of complement	2	6	10.14	1.E-03	Entrez_Gene:12274,Entrez_Gene:12279
Androgen biosynthesis	2	7	9.558	1.E-03	Entrez_Gene:15493,Entrez_Gene:15496
Glucocorticoid biosynthesis	2	8	8.725	2.E-03	Entrez_Gene:10746,Entrez_Gene:15493,Entrez_Gene:15496
Signaling by PDGF	3	69	4.286	7.E-03	Entrez_Gene:10746,Entrez_Gene:15493,Entrez_Gene:20750
Complement cascade	2	19	5.461	3.E-03	Entrez_Gene:12274,Entrez_Gene:12279
Complement cascade	3	65	4.069	9.E-03	Entrez_Gene:10981,Entrez_Gene:12274,Entrez_Gene:12279
Metabolism of steroid hormones and vitamins A and D	2	21	5.16	9.E-03	Entrez_Gene:15493,Entrez_Gene:15496

The pathways with p < 0.01 are listed.

**Table S11.** Primer set ID of quantitative RT-PCR

Gene symbol	Gene name	Taqman Expression Assays ID	Gene	Takara primer set ID
Primers for hypothalamic neuropeptides				
Npy	neuropeptide Y	Mm03048253_m1		/
Agrp	agouti-related peptide	Mm00475829_g1		/
Pome	proopiomelanocortin	Mm00435874_m1		/
Ghrh	growth hormone-releasing hormone	Mm01250745_m1		/
Sst	Somatostatin	Mm00436671_m1		/
Primers for Ucp in the brown adipose tissue				
Ucp1	uncoupling protein 1	Mm01244860_m1		/
Ucp2	uncoupling protein 2	Mm00627588_m1		/
Ucp3	uncoupling protein 3	Mm01163394_m1		/
Rn 18s	TaqMan® Ribosomal RNA Control Reagents			/
Primers for selected genes in the liver				
Actb	actin, beta			MA050368
Col27a1	collagen, type XXVII, alpha 1			MA111474

Type	glycophorin C	MA113198
Had3b2	hydroxy-delta-5-steroid dehydrogenase, 3 beta- and steroid delta-isomerase 2	MA103166
Had3b5	hydroxy-delta-5-steroid dehydrogenase, 3 beta- and steroid delta-isomerase 5	MA126618
Id2	inhibitor of DNA binding 2	MA106141
Mup4	major urinary protein 4	MA124794
Rn 18s	18S ribosomal RNA	MA050364
Gapdh	glyceraldehyde-3-phosphate dehydrogenase	MA050371
Lpl	lipoprotein lipase	MA120682
Anxa5	annexin A5	MA114909
Lifr	leukemia inhibitory factor receptor	MA120383
Ninj1	ninjurin 1	MA119502
Ror	RAR-related orphan receptor gamma	MA097596
Fno3	flavin containing monooxygenase 3	MA108600
St10a10	ST100 calcium binding protein A10 (calpactin)	MA108600
Spp1a	secreted phosphoprotein 1	MA130294

Spp1B	secreted phosphoprotein 1	MA114392
Eef1a	eukaryotic translation elongation factor 1 alpha 1	MA080227
Fbln2	fibulin 2	MA128665
Pex11a	peroxisomal biogenesis factor 11 alpha	MA117235

# A natural compound Evo(kes) signaling for fat regulation

Hitoshi Yamashita\*

Department of Biomedical Sciences; College of Life and Health Sciences; Chubu University; Kasugai, Japan

Regulation of body fat is critical to prevent progression of metabolic syndrome and extend lifespan. Adipose tissue is largely responsible for fat metabolism, affecting glucose metabolism and insulin sensitivity under the control of various hormones and cytokines. Indeed, obesity, characterized by excess fat deposition mainly in white adipose tissue (WAT), is a serious health risk in industrialized societies. Since obesity is the result of an energy imbalance when intake exceeds expenditure, intervention to reduce caloric intake through hormonal regulation and/or to increase energy expenditure by increasing thermogenic functions such as uncoupling protein 1 (UCP1) activity in brown adipose tissue (BAT) could be reasonable ways of preventing obesity. The recent rediscovery of functional BAT in humans, despite its reduction with age, has accelerated basic and clinical studies on the stimulation of BAT formation and activity as a potential therapeutic target in the battle against obesity and insulin resistance; however, an alternative strategy independent of UCP1 thermogenesis is needed for BAT-negative individuals.

Evodiamine (Evo), an alkaloid extracted from the dried unripe fruit of *Evodia rutaecarpa* Benth (Rutaceae), has long been used in traditional Chinese herbal medicine to treat pain, vomiting and pyresis. Similar to capsaicin, Evo has wide-ranging bioactivity with anti-nociceptive, anti-tumor and anti-obesity effects. In earlier studies, the anti-obesity effect of Evo was attributed to BAT activation, because this compound may stimulate the sympathetic nervous system by acting as a capsaicin receptor agonist, inducing UCP1 thermogenesis. However,

we found that Evo unexpectedly decreased diet-induced obesity and glucose intolerance in a UCP1-independent manner.<sup>1</sup> In that report, we revealed that Evo, but not capsaicin, increased phosphorylation of extracellular signal-regulated kinase (ERK) and reduced expression of peroxisome proliferator-activated receptor- $\gamma$  (PPAR $\gamma$ ) in preadipocytes, strongly inhibiting their differentiation into mature adipocytes. Evo also inhibited adipogenesis by activating the EGFR-PKC $\alpha$ -ERK signaling pathway.<sup>2</sup> These findings, based on Evo signaling in preadipocytes, suggest that this compound may offer a useful treatment for obesity by preventing the expansion of WAT.

In a recent paper, we further reported an unidentified mechanism whereby Evo improves insulin resistance by signaling through mammalian target of rapamycin (mTOR) and ribosomal S6 protein kinase (S6K) in mature adipocytes.<sup>3</sup> Recent advances in understanding of mTOR signaling unveiled the crucial role of this pathway in nutrient metabolism, cell growth and aging.<sup>4</sup> We first found significant decreases in mTOR and Akt phosphorylation in WAT, but not BAT, of obese/diabetic KK-Ay mice treated with Evo, in which various obesity phenotypes including glucose tolerance were improved without any change in food intake. Evo treatment also reduced mTOR (not Akt) phosphorylation in liver, whereas its effect on mTOR-S6K signaling appeared more potent in WAT. In particular, down-regulation of insulin receptor substrate 1 (IRS1) serine phosphorylation (an indicator of insulin resistance) was remarkable, while its tyrosine phosphorylation (indicating insulin

sensitivity) was intact in Evo-treated WAT, suggesting suppression of the negative feedback loop from S6K to IRS1, as reported by Um et al.<sup>5</sup> These results led us to examine the effect of Evo on nutrient signaling in mature adipocytes, which are central to the physiological and pathological function of WAT, although our previous studies revealed anti-adipogenic ERK signaling by Evo in preadipocytes. In cultures of 3T3-L1 adipocytes, we confirmed that Evo inhibited the insulin-stimulated phosphorylation of mTOR and S6K, leading to downregulation of IRS1 serine phosphorylation. Evo alone did not affect ERK and Akt phosphorylation, contradicting the results observed in preadipocytes. In addition, this compound was found to stimulate phosphorylation of AMP-activated protein kinase (AMPK), a cellular energy sensor, in adipocyte cultures and in Evo-treated WAT. The anti-diabetic compound rosiglitazone showed similar effects to those of Evo on AMPK, mTOR and IRS1 phosphorylation in adipocytes, although rosiglitazone stimulates adipogenesis. We also detected activation of tuberous sclerosis complex 2, a regulator of mTOR activity, through AMPK activation in Evo-treated adipocytes (our unpublished data). Taken together, these findings suggest that Evo might be a unique compound able to combat obesity and insulin resistance through activation of AMPK and inhibition of mTOR-S6K signaling in white adipocytes, thus contributing to preventing progression of metabolic syndrome and extending the healthy lifespan (Fig. 1).

In conclusion, we demonstrate that evodiamine evokes several signaling pathways controlling fat regulation in WAT.

\*Correspondence to: Hitoshi Yamashita; Email: hyamashi@isc.chubu.ac.jp

Submitted: 07/31/2014; Accepted: 08/04/2014

<http://dx.doi.org/10.4161/15384101.2014.954213>

Comment on: Wang T, et al. *PLoS One* 2013; 8(12):e83264; <http://dx.doi.org/10.1371/journal.pone.0083264>

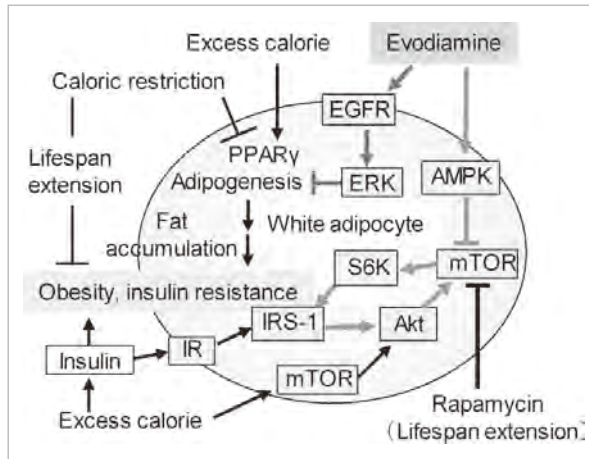


**Figure 1.** Proposed mechanisms of evodiamine signaling in white adipocytes. Excess caloric intake stimulates insulin and mTOR signaling, increases adipogenesis, and causes obesity and insulin resistance. Evodiamine stimulates EGFR-ERK signaling in preadipocytes to inhibit adipogenesis (blue pathway) but also activates AMPK and inhibits insulin-stimulated mTOR-S6K signaling (red pathway) in mature adipocytes, leading to improvements of obesity and insulin resistance.

Because modulation of the mTOR pathway is intimately linked with age-related

diseases and longevity,<sup>6</sup> the Evo effect on longevity is of great interest and a long-

**References**

1. Wang T, et al. *Endocrinol* 2008; 149:358-66.; <http://dx.doi.org/10.1210/en.2007-0467>
2. Wang T, et al. *FEBS Lett* 2009; 583:3655-59.; PMID:19854188; <http://dx.doi.org/10.1016/j.febslet.2009.10.046>
3. Wang T, et al. *PLoS ONE* 2013; 8:e83264; PMID:24391749; <http://dx.doi.org/10.1371/journal.pone.0083264>
4. Zoncu R, et al. *Nat Rev Mol Cell Biol* 2011; 12:21-35.; PMID:21157483; <http://dx.doi.org/10.1038/nrm3025>
5. Um SH, et al. *Nature* 2004; 431:200-5.; PMID:15306821; <http://dx.doi.org/10.1038/nature02866>
6. Johnson SC, et al. *Nature* 2013; 493:338-45.; PMID:23325216; <http://dx.doi.org/10.1038/nature11861>

term feeding study involving Evo is under investigation in mice. The impact of rapamycin intervention on lifespan extension emphasizes the importance of the mTOR signaling pathway in the regulation of longevity in small animals. It is also interesting that Evo stimulates AMPK phosphorylation in mice without affecting food intake, even though its phosphorylation is generally increased under conditions of caloric restriction or starvation when the cellular AMP:ATP ratio increases. Because mTOR and AMPK are involved in autophagy signaling, Evo could induce so-called lipophagy to reduce excess fat deposition in adipocytes. This mechanism may also explain the Evo effect, which significantly improved hepatic steatosis in our mouse models; however this mechanism remains to be clarified as does as the question of how Evo activates AMPK.



## Asp3Gly polymorphism affects fatty acid-binding protein 3 intracellular stability and subcellular localization



Tatsuya Kusudo<sup>a,\*</sup>, Yasuhiko Hashida<sup>b</sup>, Fujiko Ando<sup>c</sup>, Hiroshi Shimokata<sup>d</sup>, Hitoshi Yamashita<sup>a</sup>

<sup>a</sup> Department of Biomedical Sciences, College of Life and Health Sciences, Chubu University, Kasugai 487-8501, Japan

<sup>b</sup> Institute for Integrated Cell-Material Sciences (iCeMS), Kyoto University, Kyoto, Japan

<sup>c</sup> Department of Health and Medical Sciences, Aichi Shukutoku University, Nagakute 480-1197, Japan

<sup>d</sup> Graduate School of Nutritional Sciences, Nagoya University of Arts and Sciences, Nisshin 470-0196, Japan

### ARTICLE INFO

#### Article history:

Received 8 June 2015

Revised 30 June 2015

Accepted 6 July 2015

Available online 20 July 2015

Edited by Sandro Sonnino

#### Keywords:

Fatty acid binding protein

Polymorphism

Single-nucleotide polymorphism

Protein stability

Subcellular localization

### ABSTRACT

**Fatty acid-binding proteins (FABP) play a crucial role in intracellular fatty acid transportation and metabolism. In this study, we investigate the effects of the FABP3 Asp3Gly (D3G) polymorphism on protein structure and function. Although the mutation did not alter protein secondary structure or the ability to bind 1-anilinonaphthalene-8-sulfonic acid and palmitate, the intracellular stability of the D3G mutant was significantly decreased. Immunocytochemical analysis reveals that the mutation alters FABP3 subcellular localization. Our results suggest that the D3G polymorphism may impact energy metabolism and physiological functions.**

© 2015 Federation of European Biochemical Societies. Published by Elsevier B.V. All rights reserved.

### 1. Introduction

Fatty acids are physiologically important energy sources, biological components, and metabolic regulators. Because fatty acids cannot diffuse freely in the cytosol, intracellular diffusion is dependent on specific carrier proteins such as fatty acid-binding proteins (FABP). FABPs are low molecular weight (~15kDa) intracellular proteins that bind long-chain fatty acids and other hydrophobic ligands with high affinity. At least ten FABP-family molecules are found in humans, exhibit tissue-specific expression in almost all tissues [1], and are responsible for lipid uptake, transport, and metabolism.

In addition to the regulation of fatty acid transport and metabolism, FABPs control ligand trafficking to modulate the activity of ligand-dependent transcription factors, enzyme activity, and signaling pathways in cells [2–5]. FABPs have been implicated in various diseases including obesity, diabetes, atherosclerosis, and diverse aspects of brain function [1,6,7].

*Author contributions:* T.K., F.A., H.S. and H.Y. conceived and designed the experiments. T.K. and Y.H. performed the experiments and analyzed data. T.K. and H.Y. wrote the paper.

\* Corresponding author. Fax: +81 568 51 1111.

E-mail address: [kusudo@isc.chubu.ac.jp](mailto:kusudo@isc.chubu.ac.jp) (T. Kusudo).

<http://dx.doi.org/10.1016/j.febslet.2015.07.007>

0014-5793/© 2015 Federation of European Biochemical Societies. Published by Elsevier B.V. All rights reserved.

Many single-nucleotide polymorphisms (SNPs) have been identified in FABPs, with some associated with metabolic syndrome [8]. The FABP2 polymorphism, Ala54Thr, expressed in the small intestine was reported to be associated with insulin resistance and increased cardiovascular risk in a patient with diabetes [9]. The Thr94Ala variant of FABP1, predominantly expressed in the liver, is associated with plasma lipid levels, atherothrombotic cerebral infarction, and non-alcoholic fatty-liver disease [10].

FABP3 is expressed predominantly in heart, skeletal muscle, and brown adipose tissue and is involved in lipid and glucose metabolism [11–14]. We have previously shown that increased FABP3 expression in muscle and brown adipose tissue correlates with obesity in mice [13,14] and that FABP3 expression improves palmitate-induced insulin resistance in myotubes [13], establishing FABP3 importance in the development of obesity. FABP3 is also expressed in the adult brain and regulates polysaturated fatty acid uptake and metabolism in neurons, implicating FABP3 involvement in neurological functions and diseases such as Down syndrome, Alzheimer's disease, schizophrenia, and autism spectrum disorder [15,16]. Therefore, studying the consequences of FABP3 polymorphisms on protein function is essential to understanding the causes of metabolic disorders and cerebropathy.

Over 400 FABP3 SNPs are registered in the National Center of Biotechnology information (NCBI) dbSNP database (<http://www.ncbi.nlm.nih.gov/snp/>). Although most SNPs are located in either

the intronic or untranslated regions of the FABP3 gene, some have been identified in the coding regions (referred to as a coding SNP or cSNP). A cSNP resulting in an amino-acid alteration in the FABP3 protein could influence protein function leading to disease development. Although *in silico* analysis using the PolyPhen algorithm (<http://coot.embl.de/PolyPhen/>) revealed that an FABP3 cSNP resulting in an Asp3Gly mutation (D3G; rs17848124) is predicted to be “probably damaging” [17], there have been no structure–function analyses of this FABP3 mutant. Here, we investigate the effects of the D3G mutation on FABP3 and its ability to bind fatty acids. Furthermore, we examine intracellular protein stability and localization of FABP3 D3G in skeletal muscle cells.

## 2. Materials and methods

### 2.1. Materials

The fluorescent dye, 1-anilinonaphthalene-8-sulfonic acid (1,8-ANS), was purchased from Molecular Probes (Eugene, OR, USA). Palmitic acid (PA) was purchased from Kanto Chemical Co., Inc. (Tokyo, Japan). The C2C12 myoblast cell line was purchased from American Type Culture Collection (Manassas, VA, USA). Plat-E cells were provided by Dr. Kamei (Kyoto Prefectural University, Kyoto, Japan). All other chemicals were of reagent grade and commercially available. The *Escherichia coli* strains DH5 $\alpha$  and BL21 (DE3) were used as a cloning host and for protein expression, respectively.

### 2.2. Cell culture

C2C12 myoblasts were maintained in Dulbecco's Modified Eagle's Medium (DMEM; Nacalai Tesque, Kyoto, Japan) containing 10% fetal bovine serum (FBS; JRH Biosciences, Lenexa, IA, USA) at 37 °C in 5% CO<sub>2</sub>. Plat-E cells were maintained in DMEM supplemented with 10% FBS, 1  $\mu$ g/ml puromycin, and 10  $\mu$ g/ml blasticidin, 100 U/ml penicillin, and streptomycin.

### 2.3. Construction of recombinant FABP3 expression vector

The cDNA encoding human FABP3 was amplified by using cDNA from HeLa cells with primers 5'-TAGCCACCATGGCGGACGCCTTTG T-3' and 5'-CTTATGTGTTGGTGGCGTGACCTGG-3'. The amplified cDNA fragment was subcloned into a pTA-2 vector (TOYOBO Co., Osaka, Japan) and the sequence was confirmed by DNA sequencing. The FABP3 D3G mutant was generated by using the QuikChange site-directed mutagenesis kit (Stratagene, La Jolla, CA, USA). The primers used for mutagenesis are as follows: sense 5'-CAGCATCA CTATGGTGGCGCTTTCCT-3'; antisense 5'-AGGAAAGCGCCACCAT AGTGATGCTG-3'. Successful incorporation of the mutation was confirmed by DNA sequencing. The FABP3 wild-type (WT) and D3G mutant cDNAs were inserted into modified pET-21b (lacking the His-Tag) to create pET-hFABP3 and pET-hFABP3-D3G.

### 2.4. Expression of FABP3 proteins in *E. coli*

The *E. coli* strain BL21 (DE3) was transformed with each of the pET-FABP3 vectors. Recombinant *E. coli* cells were grown in LB broth containing 50  $\mu$ g/ml ampicillin at 37 °C. Protein expression was induced by the addition of isopropyl-thio- $\beta$ -D-galactopyranoside at a final concentration of 1 mM followed by incubation at 37 °C for 16 h. Cells were harvested by centrifugation at 8000 $\times$ g for 20 min and stored at –80 °C until use.

### 2.5. Purification of FABP3 proteins

Cells were suspended in 50 mM Tris–HCl (pH 7.5) and disrupted by sonication at 200 W for 20 min (Kubota Insonator 200 M,

Kubota Co., Tokyo, Japan). Following centrifugation at 15000 rpm for 20 min, the supernatant was fractionated with 40–70% ammonium sulfate and the precipitate dissolved in 50 mM Tris–HCl (pH 7.5) and dialyzed against the same buffer overnight. The dialyzed solution was applied to a HiLoad 16/10 Q Sepharose HP column (GE Healthcare UK Ltd) equilibrated with 50 mM Tris–HCl (pH 7.5) and eluted with a linear gradient of NaCl (0–0.5 M). The eluted proteins were concentrated using a YM-10 ultrafiltration membrane (Millipore, Bedford, MA). The concentrated proteins were applied to a HiLoad 16/60 Superdex 75 pg column (GE Healthcare UK Ltd) equilibrated with 50 mM Tris–HCl, 0.5 M NaCl (pH 7.5) and eluted with the same buffer. To remove any fatty acids bound to the FABP3 proteins, purified proteins were applied to a Lipidex 1000 column (14.5 mm i.d.  $\times$  50 mm) equilibrated with 50 mM Tris–HCl, 0.5 M NaCl (pH 7.5). The purity of FABP3 proteins was confirmed by polyacrylamide gel electrophoresis. Purified FABP3 (1  $\mu$ g) were separated on 12.5% gels and stained with Coomassie Brilliant Blue (Nacalai tesque, Kyoto, Japan) (CBB) and protein concentrations calculated using extinction coefficients of 14105 cm M<sup>–1</sup> at 280 nm [18].

### 2.6. Isoelectric focusing

Isoelectric focusing was performed using Novex IEF Gels (pH 3–7) (Life Technologies, Paisley, UK) according to manufacturer protocol. Protein bands were stained with CBB.

### 2.7. Circular dichroism measurement of FABP3

Circular dichroism (CD) measurements were performed using a Jasco J-820 spectropolarimeter. The spectrometer conditions were as follows: spectral range 190–260 nm; 100 mdeg sensitivity; 0.1 nm resolution; 1 s response time; 100 nm/min scan rate. Measurements were performed in 50 mM Tris–HCl, 0.5 M NaCl (pH 7.5) at 25 °C using a 2-mm light-pass-length quartz cuvette. The protein concentrations were adjusted to 0.5  $\mu$ M.

### 2.8. Kinetic analysis of interaction between FABP3 and 1, 8-ANS

The interaction between FABP3 and 1, 8-ANS (ANS) was evaluated from fluorescence change of ANS associated with its interaction with FABP3. ANS was dissolved in ethanol and its concentration was determined spectrophotometrically ( $\epsilon_{372} = 8000$  cm<sup>–1</sup> M<sup>–1</sup>). Final ethanol concentrations were kept below 1% (v/v). The fluorescent intensity of ANS solution (0–50  $\mu$ M) in the presence of 1  $\mu$ M FABP3 was measured at  $\lambda_{ex} = 390$  nm and  $\lambda_{em} = 435$  nm with a fluorescence spectrophotometer, and the fluorescence difference ( $\Delta F$ ) between in the presence and absence of FABP3 was analyzed with following equation:

$$\Delta F = \Delta F_{max} \cdot [ANS]_0 / (K_{d,ANS} + [ANS]_0) \quad (1)$$

where  $\Delta F_{max}$  and  $K_{d,ANS}$  were maximum fluorescence change and dissociation constant of FABP3 for ANS, respectively. The values of  $\Delta F_{max}$  and  $K_{d,ANS}$  were calculated by direct fitting of Eq. (1) to the data with a least-squares method performed by Gnuplot software (ver. 4.6, <http://www.gnuplot.info/>).

### 2.9. Kinetic analysis of PA binding

FABP3 binding of PA was evaluated by changes in fluorescence associated with competitive replacement of ANS with PA. The fluorescent intensity of solution containing 1  $\mu$ M FABP3 and 50  $\mu$ M ANS was measured at  $\lambda_{ex} = 390$  nm and  $\lambda_{em} = 435$  nm in the presence of PA at several concentrations (0–50  $\mu$ M) and the data were analyzed by the competitive binding model described below (Scheme 1).



**Scheme 1.** Competitive binding of ANS and PA to FABP3.

The initial concentrations of FABP3 ( $[\text{FABP3}]_0$ ), ANS ( $[\text{ANS}]_0$ ), and PA ( $[\text{PA}]_0$ ), and the dissociation constants of FABP3 for ANS ( $K_{d,\text{ANS}}$ ) and PA ( $K_{d,\text{PA}}$ ) are given by the following equations:

$$[\text{FABP3}]_0 = [\text{FABP3}] + [\text{FABP3} \cdot \text{ANS}] + [\text{FABP3} \cdot \text{PA}] \quad (2)$$

$$[\text{ANS}]_0 = [\text{ANS}] + [\text{FABP3} \cdot \text{ANS}] \quad (3)$$

$$[\text{PA}]_0 = [\text{PA}] + [\text{FABP3} \cdot \text{PA}] \quad (4)$$

$$K_{d,\text{ANS}} = [\text{FABP3}][\text{ANS}]/[\text{FABP3} \cdot \text{ANS}] \quad (5)$$

$$K_{d,\text{PA}} = [\text{FABP3}][\text{PA}]/[\text{FABP3} \cdot \text{PA}] \quad (6)$$

$[\text{FABP3}]_0$  and  $[\text{ANS}]_0$  were 1  $\mu\text{M}$  and 50  $\mu\text{M}$ , respectively. Under this condition,  $[\text{ANS}]_0 \gg [\text{FABP3} \cdot \text{ANS}]$  and, therefore, Eq. (3) is approximated as  $[\text{ANS}]_0 \approx [\text{ANS}]$ . Solving these equations,  $[\text{FABP3} \cdot \text{ANS}]$  is described as:

$$[\text{FABP3} \cdot \text{ANS}] = \{-\beta + \sqrt{\beta^2 - 4\alpha\gamma}\}/2\alpha \quad (7)$$

where  $\alpha$ ,  $\beta$ , and  $\gamma$  are given as,

$$\alpha = [\text{ANS}]_0 + K_{d,\text{ANS}},$$

$$\beta = [\text{ANS}]_0(K_{d,\text{PA}} + [\text{ANS}]_0 \cdot K_{d,\text{PA}}/K_{d,\text{ANS}} + [\text{PA}]_0) - [\text{FABP3}]_0,$$

$$\gamma = -[\text{ANS}]_0^2[\text{FABP3}]_0 \cdot K_{d,\text{PA}}/K_{d,\text{ANS}}$$

The fluorescent intensity is proportional to  $[\text{FABP3} \cdot \text{ANS}]$ , thus:

$$\Delta F/\Delta F_{\text{max}} = [\text{FABP3} \cdot \text{ANS}]/[\text{FABP3}]_0 \quad (8)$$

The value of  $K_{d,\text{PA}}$  was estimated by directly fitting Eq. (8) to the fluorescent data using the previously determined values of  $K_{d,\text{ANS}}$  and  $\Delta F_{\text{max}}$ .

### 2.10. HaloTag pulse-chase experiment

A HaloTag (Promega, Madison, WI, USA) was genetically fused to the C-terminus of FABP3 WT and D3G to create FABP3-Halo proteins. The FABP3-Halos DNA fragments were inserted into the

retroviral expression vector pMXs-Puro (pMX-WT-Halo and pMX-D3G-Halo). Plat-E cells were transfected with pMX-WT-Halo and pMX-D3G-Halo and the culture media was collected after 48 h. C2C12 cells were infected with the WT-Halo and D3G-Halo retroviral vectors and selected with 1  $\mu\text{g}/\text{ml}$  puromycin for 3 days. C2C12 myoblast cells stably expressing WT-Halo and D3G-Halo were pulse-labeled with 1  $\mu\text{M}$  HaloTag TMR Ligand (Promega, Madison, WI, USA) for 15 min. After washing four times with DMEM, cells were incubated in DMEM with 10% FBS for 72 h, washed twice with PBS, lysed in 150  $\mu\text{l}$  of SDS sample buffer, and subjected to SDS-PAGE. The HaloTag TMR Ligand-labeled FABP3 WT and D3G were visualized using a fluorescence image analyzer, LAS4000 (GE healthcare), and analyzed using ImageJ (Rasband, W.S., ImageJ, U.S. National Institutes of Health, Bethesda, Maryland, USA, <http://imagej.nih.gov/ij/>, 1997–2014). Half-life ( $t_{1/2}$ ) was calculated by direct fitting of the theoretical equation (Eq. (9)) to the data of three independent experiments:

$$\text{FABP3 Remaining (\%)} = 100 \times (1/2)^{t/(t_{1/2})} \quad (9)$$

### 2.11. Analysis of subcellular localization

C2C12 cells were infected with adenovirus-expressing FABP3 WT and D3G at a multiplicity of infection of 200 for 24 h. After 48 h, cells were subcultured on ibidi  $\mu$ -Slides (Integrated BioDiagnostics), then after an additional 24 h, fixed with 4% paraformaldehyde in PBS for 30 min at room temperature and washed twice with PBS. Fixed cells were permeabilized with 0.4% Triton X-100 in PBS for 10 min and blocked with Blocking One Histo (Nacalai Tesque, Kyoto, Japan). Cells were then incubated with Mouse anti-human FABP3 monoclonal antibody (Hycult, Netherland) at a dilution of 1:100 in 5% Blocking One Histo at 4  $^{\circ}\text{C}$  overnight and incubated with the secondary antibody, Goat anti-Rabbit IgG Alexa Fluor 488 (Molecular Probes, Leiden, Netherlands) at a dilution of 1:1000 in 5% Blocking One Histo for 1 h at room temperature. Nuclei were stained with DAPI (Dojindo, Kumamoto, Japan) and examined using a BIOREVO BZ-9000 fluorescence microscope (Keyence, Osaka, Japan).

### 2.12. Statistical analysis

Data were expressed as means  $\pm$  standard error of the mean (S.E.M.). Significant differences between groups were assessed by Student's *t*-test.

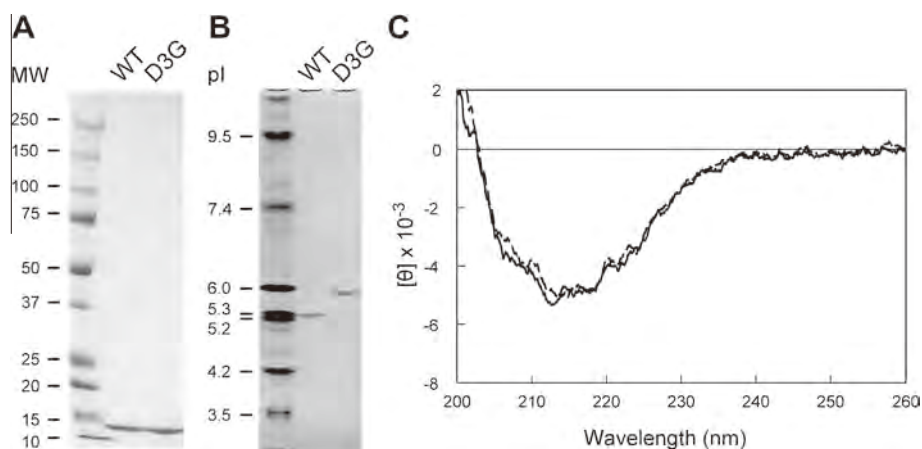


**Fig. 1.** Purification of FABP3 WT and D3G variants and secondary-structure analysis. (A) Molecular weight determination using SDS-PAGE. Size markers (left), FABP3 WT (middle), and FABP3 D3G (right). (B) Measurement of isoelectric point (pI). Markers (left), FABP3 WT (middle), and FABP3 D3G (right). (C) CD-spectra of 0.5  $\mu\text{M}$  FABP3 WT and FABP3 D3G.

### 3. Results

#### 3.1. Purification of FABP3 proteins from *E. coli*

Expression and purification of recombinant human FABP3 WT and D3G was undertaken as described in Materials and Methods. To ensure that the purified FABP3 variants were devoid of residual bound fatty acids, proteins were delipidated prior to binding experiments [19]. Purified FABP3 variants are shown in Fig. 1A. Aspartate is a polar amino acid and has a negative charge at physiological pH, while glycine is a non-polar amino acid with no charge. Therefore, the D3G Asp-Gly substitution may result in a more positively-charged protein as compared to WT. Isoelectric focusing experiments to examine the impact of this mutation on surface charge were performed, resulting in estimated pI values for WT and D3G of 5.2 and 6.0, respectively (Fig. 1B). CD spectra were then measured to investigate the presence of secondary-structure differences between FABP3 WT and D3G, revealing no measurable differences observed between the two variants (Fig. 1C). These results indicate that the Asp-Gly substitution does not significantly impact secondary structure or the overall conformation of FABP3, but does contribute to an alteration in surface charge.

#### 3.2. Binding properties of recombinant FABP3 variants

To elucidate the impact of mutations on ligand binding, we performed binding assays using FABP3 WT and D3G in the presence of

1,8-ANS, a fluorescent probe with affinity for the FABP3 ligand-binding pocket [20,21]. The apparent dissociation constants ( $K_d$ ) associated with 1,8-ANS binding to FABP3 WT and D3G are  $5.69 \pm 0.36 \mu\text{M}$  and  $6.24 \pm 0.19 \mu\text{M}$ , respectively, indicating no significant difference in binding affinity for 1, 8-ANS between the two variants (Fig. 2A). To investigate differences in affinity between FABP3 WT and D3G for fatty acid, PA binding was measured using a competitive-displacement assay. Competition curves indicate that 1,8-ANS fluorescence decreased relative to increasing concentrations of PA (Fig. 2A). The  $K_d$  values associated with PA binding are  $1.16 \pm 0.08 \mu\text{M}$  and  $1.28 \pm 0.10 \mu\text{M}$  for FABP3 WT and D3G, respectively, and are in agreement with those previously published [22]. These results indicate that the Asp-Gly mutation does not significantly impact FABP3 ligand binding.

#### 3.3. D3G mutation decreases FABP3 stability in C2C12 myoblast cells

To investigate whether the Asp-Gly mutation contributes to FABP3 intracellular stability in mammalian cells, we performed HaloTag-mediated pulse-chase experiments [23]. Since FABP3 is expressed mainly in cardiac and skeletal muscle cells, we used mouse myoblast C2C12 cells for this experiment. Our results revealed increased degradation of the FABP3 D3G mutants as compared to WT in C2C12 myoblast cells (Fig. 3). The half-lives of FABP3 WT and D3G were calculated to be  $45.0 \pm 1.9 \text{ h}$  and  $37.2 \pm 1.9 \text{ h}$ , respectively, indicating that the Asp-Gly mutation reduces FABP3 intracellular stability.

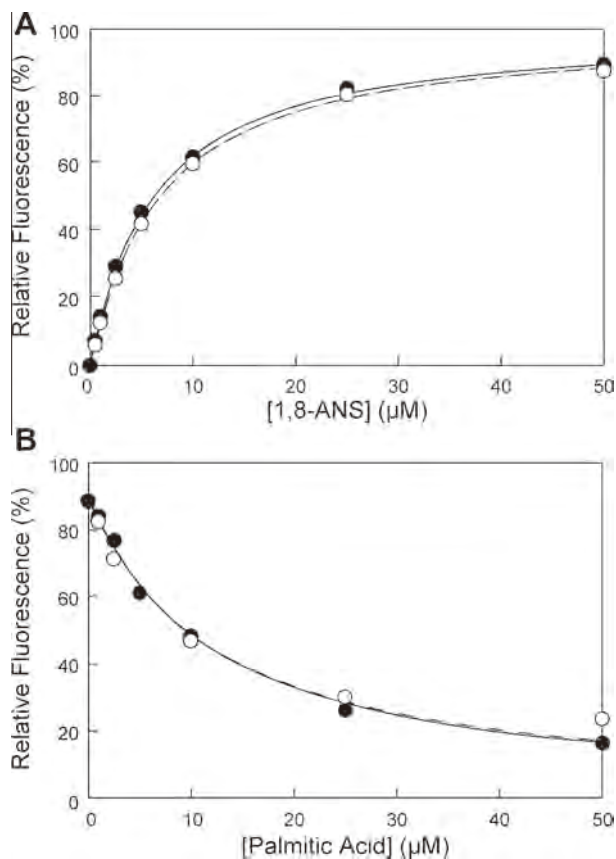


**Fig. 2.** Lipid-binding capability of FABP3 WT and D3G variants. (A) 1,8-ANS binding to FABP3 WT and FABP3 D3G. (B) Displacement of 1,8-ANS from FABP3 WT and FABP3 D3G by palmitate. FABP3 WT and FABP3 D3G are shown as closed and open circles, respectively.  $K_d$  values were calculated from at least four independent experiments.

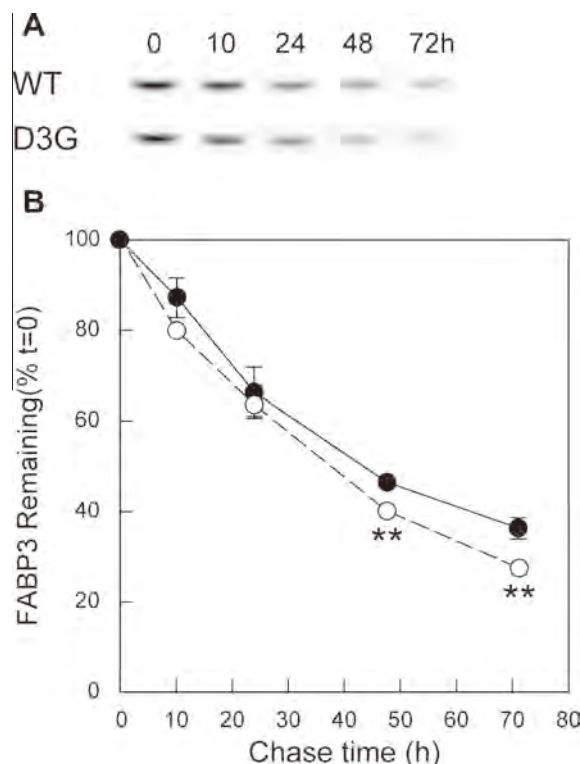


**Fig. 3.** Protein stability of FABP3 WT and D3G variants in C2C12 myoblast cells. Pulse-chase experiments were performed using C2C12 cells expressing HaloTag FABP3 variants. (A) FABP3 WT-Halo and FABP3 D3G-Halo were labeled with HaloTag TMR Ligand and chased for indicated time. (B) Time courses for clearance of labeled FABP3 WT-Halo and FABP3 D3G-Halo are shown as closed and open circles, respectively. Results represent the mean  $\pm$  S.E.M. of three independent experiments, \*\* $P < 0.01$  vs. WT.

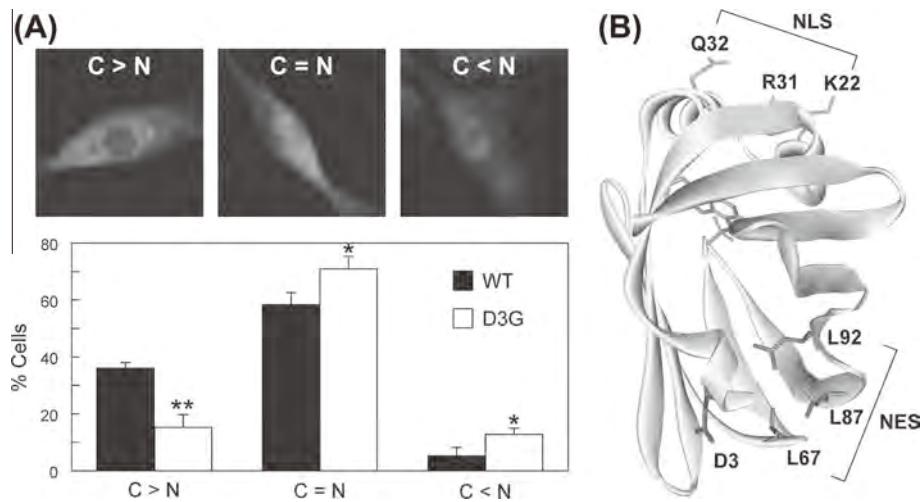


**Fig. 4.** Subcellular localization of FABP3 WT and D3G variants in C2C12 myoblast cells. C2C12 cells were infected with adenoviral vectors expressing FABP3 WT and FABP3 D3G. (A) Subcellular localization of FABP3. Cells were classified as follows; C > N, FABP3 concentration is higher in the cytosol than that observed in the nucleus; C = N, FABP3 concentration in the cytosol is similar to that observed in the nucleus; C < N, FABP3 concentration is lower in the cytosol than that observed in the nucleus. Cell images and percentages of the classified cells are shown. At least 100 cells in 4–6 different images were quantified. Results represent the mean  $\pm$  S.E.M., \* $P < 0.05$ , \*\* $P < 0.01$  vs. WT. (B) Putative structure of the FABP3 protein shown as ribbon model (Protein Data Bank ID, 3WBG). Asp3 (red), putative NES (L67, L97, L92, blue) and NLS (K22, R31, Q32, green) residues and 1,8-ANS (orange) are shown as sticks. The structure was generated using Discovery Studio 4.1 (Accelrys, San Diego, CA).

### 3.4. Subcellular localization of FABP3

Finally, we examined the subcellular localization of FABP3 WT and D3G in C2C12 myoblast cells. To evaluate localization to either the cytosol or the nucleus, stained cells were classified into three groups according to their fluorescence intensity: C > N, the fluorescence intensity of FABP3 is higher in the cytosol than that observed in the nucleus; C = N, the fluorescence intensity of FABP3 in the cytosol is equal to that observed in the nucleus; C < N, the fluorescence intensity of FABP3 in the cytosol is lower than that observed in the nucleus (Fig. 4A). The Asp-Gly mutation resulted in a decrease in the percentage of cells classified as C > N from 36.3% to 15.7%, while the percentage of cells classified as C < N and C = N increased from 5.2% to 13% and 58.5% to 72.0%, respectively. These results indicate that the Asp-Gly mutation influences FABP3 subcellular localization.

## 4. Discussion

The amino-acid alterations in FABPs impact their physiological functions. The Ala54Thr mutant of FABP2 shows a 2-fold greater affinity for fatty acid than FABP2 WT [24,23]. The increased affinity for fatty acid results in higher levels of fatty-acid uptake and lower peripheral insulin sensitivity [25]. In the case of FABP1, a Thr94Ala mutation alters protein secondary structure, stability, and ligand activation of PPAR $\alpha$  transcriptional activity in human hepatocytes [10]. Here, we have examined the impact of an Asp3Gly mutation on FABP3 structure and function.

Although the mutation resulted in changes to FABP3 surface charge, no difference was observed in secondary structure between the FABP3 WT and D3G variants, indicating that Asp3 does not contribute to the FABP3 structure. This mutation also did not alter the ability of FABP3 to bind 1,8-ANS and PA, which may be explained by the location of Asp3 relative to the ligand-binding pocket and its evident minimal impact on overall structure.

The results of in silico analysis of FABP3 D3G were not corresponded. Shimamoto et al. analyzed the impact of the D3G mutation on FABP3 biological function using the in silico tools SIFT (<http://blocks.fhcrc.org/sift/SIFT.html>), PolyPhen-2 (<http://genetics.bwh.harvard.edu/pph2/>), and Pmut (<http://mmb2.pcb.ub.es:8080/PMut/>) [15]. The analyses indicated that the effects of the mutation were 'tolerable' according to SIFT, 'benign' according to PolyPhen-2, and 'neutral' according to Pmut, and that the overall impact on FABP3 structure and function was minimal. However, using the PolyPhen algorithm, Maekawa et al. predicted that the FABP3 D3G mutation results in elimination of a salt bridge between Asp3 and Lys45 that might adversely impact protein stability [17]. Our results revealed that the intracellular stability of FABP3 D3G was decreased relative to WT in C2C12 myoblast cells, suggesting that Asp3 may contribute to protein stability.

Additionally, variations in intracellular localization between FABP3 WT and D3G were observed. Amino acid sequences identifying nuclear export signal (NES) or nuclear localization signal (NLS) have not been identified in FABP3. Although neither NES nor NLS sequences have been detected in the primary sequence of FABP [21], residues L66, L86, L91, and K21, R30, K31 qualify as NES and NLS sequences, respectively. Similarly, FABP3 residues L67, L87 and L92 mimic NES sequences and, while the typical NLS sequence is not fully conserved in FABP3, the residues K22, R31 and Q32 share similar properties with NLS sequences (Fig. 4B). In our analysis, the FABP3 D3G exhibited twofold higher levels of nuclear localization relative to FABP3 WT. Also, FABP3 D3G localized to the cytosol 50% less often than FABP3 WT. Given the proximity of Asp3 relative to the putative NES sequence (Fig. 4B), the Asp-Gly mutation may inhibit interactions between FABP3 and exportins such as CRM1, which transports FABP4 from the nucleus to the cytosol [21]. These results suggest that increased FABP3 D3G nuclear localization may be caused by a reduction in the capability of FABP3 to be exported from the nucleus rather than increases in cytosol-to-nucleus translocation. Likewise, decreased FABP3 stability observed in the cytosol could impact differences in subcellular localization between FABP3 variants.

In summary, the FABP3 D3G mutation resulted in altered protein stability and localization in myoblast cells. Although there were minimal differences in ligand-binding capability between FABP3 D3G and WT, this mutation could influence other FABP3 functions including ligand transport to target organelles, enzyme regulation, or ligand-dependent transcription-factor activation. Given the importance of FABP3 in lipid metabolism, the FABP3 D3G polymorphism may also impact energy metabolism and brain

function, however, the specific association of this mutation with disease remains unclear. A large cohort study would be required to clarify connections between the FABP3 D3G polymorphism and certain disorders.

### Disclosures

No conflicts of interest, financial or otherwise, are declared by the authors.

### Acknowledgements

We thank Dr. Yasutomi Kamei for providing pMXs-puro vector and Plat-E. This study was supported by Grant-in-Aid for Young Scientists (B) (to T.K.), and by a grant from the MEXT-Supported program for Strategic Research Foundation at private universities (to H.Y.).

### References

- [1] Furuhashi, M. and Hotamisligil, G.S. (2008) Fatty acid-binding proteins: role in metabolic diseases and potential as drug targets. *Nat. Rev. Drug Discov.* 7, 489–503.
- [2] Tan, N.S., Shaw, N.S., Vinckenbosch, N., Liu, P., Yasmin, R., Desvergne, B., Wahli, W. and Noy, N. (2002) Selective cooperation between fatty acid binding proteins and peroxisome proliferator-activated receptors in regulating transcription. *Mol. Cell. Biol.* 22, 5114–5127.
- [3] Adida, A. and Spener, F. (2006) Adipocyte-type fatty acid-binding protein as inter-compartmental shuttle for peroxisome proliferator activated receptor gamma agonists in cultured cell. *Biochim. Biophys. Acta* 1761, 172–181.
- [4] Hui, X., Li, H., Zhou, Z., Lam, K.S., Xiao, Y., Wu, D., Ding, K., Wang, Y., Vanhoutte, P.M. and Xu, A. (2010) Adipocyte fatty acid-binding protein modulates inflammatory responses in macrophages through a positive feedback loop involving c-Jun NH2-terminal kinases and activator protein-1. *J. Biol. Chem.* 285, 10273–10280.
- [5] Makowski, L., Brittingham, K.C., Reynolds, J.M., Suttles, J. and Hotamisligil, G.S. (2005) The fatty acid-binding protein, aP2, coordinates macrophage cholesterol trafficking and inflammatory activity. Macrophage expression of aP2 impacts peroxisome proliferator-activated receptor gamma and IkkappaB kinase activities. *J. Biol. Chem.* 280, 12888–12895.
- [6] Matsumata, M., Inada, H. and Osumi, N. (2014) Fatty acid binding proteins and the nervous system: their impact on mental conditions. *Neurosci. Res.*
- [7] Liu, R.Z., Mita, R., Beaulieu, M., Gao, Z. and Godbout, R. (2010) Fatty acid binding proteins in brain development and disease. *Int. J. Dev. Biol.* 54, 1229–1239.
- [8] Smathers, R.L. and Petersen, D.R. (2011) The human fatty acid-binding protein family: evolutionary divergences and functions. *Hum. Genomics* 5, 170–191.
- [9] Baier, L.J., Sacchettini, J.C., Knowler, W.C., Eads, J., Paolisso, G., Tataranni, P.A., Mochizuki, H., Bennett, P.H., Bogardus, C. and Prochazka, M. (1995) An amino acid substitution in the human intestinal fatty acid binding protein is associated with increased fatty acid binding, increased fat oxidation, and insulin resistance. *J. Clin. Invest.* 95, 1281–1287.
- [10] Martin, G.G., McIntosh, A.L., Huang, H., Gupta, S., Atshaves, B.P., Landrock, K.K., Landrock, D., Kier, A.B. and Schroeder, F. (2013) The human liver fatty acid binding protein T94A variant alters the structure, stability, and interaction with fibrates. *Biochemistry* 52, 9347–9357.
- [11] Claffey, K.P., Herrera, V.L., Brecher, P. and Ruiz-Opazo, N. (1987) Cloning and tissue distribution of rat heart fatty acid binding protein mRNA: identical forms in heart and skeletal muscle. *Biochemistry* 26, 7900–7904.
- [12] Adhikari, S., Erol, E. and Binas, B. (2007) Increased glucose oxidation in H-FABP null soleus muscle is associated with defective triacylglycerol accumulation and mobilization, but not with the defect of exogenous fatty acid oxidation. *Mol. Cell. Biochem.* 296, 59–67.
- [13] Kusudo, T., Kontani, Y., Kataoka, N., Ando, F., Shimokata, H. and Yamashita, H. (2011) Fatty acid-binding protein 3 stimulates glucose uptake by facilitating AS160 phosphorylation in mouse muscle cells. *Genes Cells* 16, 681–691.
- [14] Yamashita, H., Wang, Z., Wang, Y., Segawa, M., Kusudo, T. and Kontani, Y. (2008) Induction of fatty acid-binding protein 3 in brown adipose tissue correlates with increased demand for adaptive thermogenesis in rodents. *Biochem. Biophys. Res. Commun.* 377, 632–635.
- [15] Shimamoto, C., Ohnishi, T., Maekawa, M., Watanabe, A., Ohba, H., Arai, R., Iwayama, Y., Hisano, Y., Toyota, T., Toyoshima, M., Suzuki, K., Shirayama, Y., Nakamura, K., Mori, N., Owada, Y., Kobayashi, T. and Yoshikawa, T. (2014) Functional characterization of FABP3, 5 and 7 gene variants identified in schizophrenia and autism spectrum disorder and mouse behavioral studies. *Hum. Mol. Genet.*
- [16] Cheon, M.S., Kim, S.H., Fountoulakis, M. and Lubec, G. (2003) Heart type fatty acid binding protein (H-FABP) is decreased in brains of patients with Down syndrome and Alzheimer's disease. *J. Neural Transm. Suppl.*, 225–234.
- [17] Maekawa, M., Iwayama, Y., Arai, R., Nakamura, K., Ohnishi, T., Toyota, T., Tsujii, M., Okazaki, Y., Osumi, N., Owada, Y., Mori, N. and Yoshikawa, T. (2010) Polymorphism screening of brain-expressed FABP7, 5 and 3 genes and association studies in autism and schizophrenia in Japanese subjects. *J. Hum. Genet.* 55, 127–130.
- [18] Gill, S.C. and von Hippel, P.H. (1989) Calculation of protein extinction coefficients from amino acid sequence data. *Anal. Biochem.* 182, 319–326.
- [19] Lowe, J.B., Sacchettini, J.C., Laposata, M., McQuillan, J.J. and Gordon, J.I. (1987) Expression of rat intestinal fatty acid-binding protein in *Escherichia coli*. Purification and comparison of ligand binding characteristics with that of *Escherichia coli*-derived rat liver fatty acid-binding protein. *J. Biol. Chem.* 262, 5931–5937.
- [20] Hirose, M., Sugiyama, S., Ishida, H., Niiyama, M., Matsuoka, D., Hara, T., Mizohata, E., Murakami, S., Inoue, T., Matsuoka, S. and Murata, M. (2013) Structure of the human-heart fatty-acid-binding protein 3 in complex with the fluorescent probe 1-anilino-8-naphthalene-sulphonic acid. *J. Synchrotron Radiat.* 20, 923–928.
- [21] Ayers, S.D., Nedrow, K.L., Gillilan, R.E. and Noy, N. (2007) Continuous nucleocytoplasmic shuttling underlies transcriptional activation of PPARgamma by FABP4. *Biochemistry* 46, 6744–6752.
- [22] Veerkamp, J.H., van Moerkerk, H.T., Prinsen, C.F. and van Kuppevelt, T.H. (1999) Structural and functional studies on different human FABP types. *Mol. Cell. Biochem.* 192, 137–142.
- [23] Los, G.V., Encell, L.P., McDougall, M.G., Hartzell, D.D., Karassina, N., Zimprich, C., Wood, M.G., Learish, R., Ohana, R.F., Urh, M., Simpson, D., Mendez, J., Zimmerman, K., Otto, P., Vidugiris, G., Zhu, J., Darzins, A., Klauert, D.H., Bulleit, R.F. and Wood, K.V. (2008) HaloTag: a novel protein labeling technology for cell imaging and protein analysis. *ACS Chem. Biol.* 3, 373–382.
- [24] Agren, J.J., Vidgren, H.M., Valve, R.S., Laakso, M. and Uusitupa, M.I. (2001) Postprandial responses of individual fatty acids in subjects homozygous for the threonine- or alanine-encoding allele in codon 54 of the intestinal fatty acid binding protein 2 gene. *Am. J. Clin. Nutr.* 73, 31–35.
- [25] Marín, C., Pérez-Jiménez, F., Gómez, P., Delgado, J., Paniagua, J.A., Lozano, A., Cortés, B., Jiménez-Gómez, Y., Gómez, M.J. and López-Miranda, J. (2005) The Ala54Thr polymorphism of the fatty acid-binding protein 2 gene is associated with a change in insulin sensitivity after a change in the type of dietary fat. *Am. J. Clin. Nutr.* 82, 196–200.

Available online at [www.sciencedirect.com](http://www.sciencedirect.com)

ScienceDirect

journal homepage: [www.elsevier.com/locate/jff](http://www.elsevier.com/locate/jff)

# Dietary supplementation with evodiamine prevents obesity and improves insulin resistance in ageing mice

Hitoshi Yamashita <sup>a,\*</sup>, Tatsuya Kusudo <sup>a</sup>, Tamaki Takeuchi <sup>a</sup>,  
Shanlou Qiao <sup>a</sup>, Kaname Tsutsumiuchi <sup>b</sup>, Ting Wang <sup>c</sup>, Youxue Wang <sup>d,\*\*</sup>

<sup>a</sup> Department of Biomedical Sciences, College of Life and Health Sciences, Chubu University, Kasugai 487-8501, Japan

<sup>b</sup> Department of Biological Chemistry, College of Bioscience and Biotechnology, Chubu University, Kasugai 487-8501, Japan

<sup>c</sup> Division of Gastroenterology and Hepatology, Department of Internal Medicine, Iwate Medical University, Morioka 020-8505, Japan

<sup>d</sup> Department of Physiology, The University of Texas Southwestern Medical Center at Dallas, 5323 Harry Hines Boulevard, Dallas, TX 75390-9040, USA

## ARTICLE INFO

### Article history:

Received 15 June 2015

Received in revised form 5

September 2015

Accepted 11 September 2015

Available online

### Keywords:

Evodiamine

Ageing

Obesity

Insulin resistance

Adipose tissue

## ABSTRACT

Evodiamine is a major alkaloid extracted from the fruit of *Evodia fructus*, which reduces diet-induced obesity in young animals. We investigated the effects of long-term dietary supplementation with evodiamine on obesity, insulin resistance and longevity in normal ageing mice. Twelve-month-old C57BL/6J male mice were fed with standard chow with or without 1 or 10 mg evodiamine per kg food and maintained until death. Supplementation with low dose evodiamine prevented body weight gain and improved glucose tolerance in the mice, in which increased AMPK phosphorylation and down-regulation of mTOR signaling responsible for regulating energy metabolism were detected in white adipose tissue. However, evodiamine supplementation did not increase lifespan, and the high dose evodiamine caused excessive reduction in body weight, which could have side effects in aged animals. Thus, evodiamine at a low dose (1 mg/kg food) prevents obesity and insulin resistance even when ingestion begins in middle age.

© 2015 Elsevier Ltd. All rights reserved.

## 1. Introduction

Excess caloric intake, in contrast to caloric restriction, induces obesity and type-2 diabetes mellitus, accelerating the progression of cardiovascular diseases and cancers, and

reducing longevity. Indeed, obesity, characterized by excessive fat deposition mainly in white adipose tissue (WAT) but also leading to fat accumulation in the liver, skeletal muscle and pancreas, is a serious health risk in industrialized societies (Kolonin, Saha, Chan, Pasqualini, & Arap, 2004). Ageing is an important factor that increases susceptibility to obesity

\* Corresponding authors. Department of Biomedical Sciences, College of Life and Health Sciences, Chubu University, Kasugai 487-8501, Japan. Tel.: +81 568 51 6017.

E-mail address: [hyamashi@isc.chubu.ac.jp](mailto:hyamashi@isc.chubu.ac.jp) (H. Yamashita).

\*\* Corresponding authors. Department of Physiology, The University of Texas Southwestern Medical Center at Dallas, 5323 Harry Hines Boulevard, Dallas, TX 75390-9040, USA. Tel.: +1 214 645 6045.

E-mail address: [youxue.wang@utsouthwestern.edu](mailto:youxue.wang@utsouthwestern.edu) (Y. Wang).

Abbreviation: WAT, white adipose tissue; BAT, brown adipose tissue; IPGTT, intraperitoneal glucose tolerance test; mTOR, serine/threonine protein kinase mammalian target of rapamycin; S6K, ribosomal S6 protein kinase; AMPK, AMP-activated protein kinase; UCP, uncoupling protein

<http://dx.doi.org/10.1016/j.jff.2015.09.032>

1756-4646/© 2015 Elsevier Ltd. All rights reserved.

because the basal metabolic rate and activity generally decline with age, although there are individual variations in the degree of their attenuation. Indeed, the prevalence of overweight and obesity increases with age until 50–60 years in humans (Kopelman, 2000). Since obesity develops as the result of energy imbalance when energy intake exceeds energy expenditure, interventions to reduce caloric intake through hormonal regulation and/or to increase energy expenditure by increasing thermogenic function such as uncoupling protein 1 (UCP1) in brown adipose tissue (BAT) would be reasonable ways to prevent or cure obesity (Bray & Tartaglia, 2000; Guerra, Koza, Yamashita, Walsh, & Kozak, 1998). Although UCP1 is not essential for longevity under conditions of standard diet and normal housing temperature, deficiency increases susceptibility to obesity with age in combination with a high-fat (HF) diet (Kontani et al., 2005). Recent findings that functional BAT, despite its reduction with age, exists even in adult humans have accelerated basic and clinical studies on the stimulation of BAT formation and activity as a potential therapeutic target against age-related diseases (Mattson, 2010; Yoneshiro et al., 2011); however, an alternative strategy independent of UCP1 thermogenesis is needed for BAT-negative individuals.

Previous studies involving calorie restriction have revealed several putative molecular bases underlying the regulation of age-related diseases and longevity. In particular, recent advances towards understanding the molecular mechanisms of longevity have been made by the study of signalling pathways such as insulin/insulin-like growth factor I (IGF-1) and serine/threonine protein kinase mammalian target of rapamycin (mTOR) in multiple model organisms (Kennedy, Steffen, & Kaerberlein, 2007; Kenyon, 2010; Zoncu, Efeyan, & Sabatini, 2011). Insulin signalling is intimately linked to the nutrient-responsive mTOR signalling pathway via activation of Akt (White, 2002; Zoncu et al., 2011). The activation of mTOR phosphorylates its downstream protein ribosomal S6 protein kinase (S6K), which participates in several processes including protein synthesis and proliferation (Shima et al., 1998; Zoncu et al., 2011). mTOR activation is also negatively regulated by AMP-activated protein kinase (AMPK), which regulates various cellular processes including glucose and lipid metabolism (Hardie, 2007; Kahn, Alquier, Carling, & Hardie, 2005). Hyperactivation of mTOR by nutrients, Akt, or hyperinsulinaemia results in serine phosphorylation of insulin receptor substrate 1 (IRS1) by S6K, which is involved in insulin resistance (Draznin, 2006). On the other hand, mice deficient in S6K are protected against age- and diet-induced obesity while exhibiting enhanced insulin sensitivity owing to the loss of the negative feedback loop from S6K to IRS1 (Selman et al., 2009; Um et al., 2004). Rapamycin is a macrolide antibiotic and is used as an anti-tumour drug because it prevents cell growth and proliferation by inhibiting mTOR activation (Zoncu et al., 2011). Harrison et al. (2009) in a large-scale mouse study reported the striking results that dietary supplementation with rapamycin extends lifespan in mice even when initiated at 600 days of age. This impact of rapamycin intervention on lifespan extension emphasizes the importance of the mTOR signalling pathway in preventing age-related diseases and regulating longevity.

Evodiamine is a major alkaloidal compound extracted from the fruit of *Evodia fructus* (*Evodia rutaecarpa* Benth., Rutaceae), which has been used for many years as a traditional Chinese

herbal medicine for the treatment of pain, vomiting, and pyrexia. Studies have demonstrated that evodiamine exhibits anti-nociceptive, anti-obesity, vasodilatory, anti-tumour and anti-inflammatory effects (Chiou, Chou, Shum, & Chen, 1992; Heo, Yun, Yi, Noh, & Park, 2009; Kobayashi et al., 2001; Takada, Kobayashi, & Aggarwal, 2005; Wang et al., 2006). We have also demonstrated that evodiamine improves diet-induced obesity and glucose tolerance in a UCP1-independent manner in UCP1-knockout mice, which were given an HF diet supplemented with 300 mg evodiamine/kg food for two months (Wang et al., 2008; Wang, Wang, & Yamashita, 2009). Supplementation of evodiamine (300 mg/kg food, approximately 30 mg/kg body weight per day) inhibited body weight gain by 52% in the control mice in the UCP1-knockout mice fed with HF diet. Our studies showed that evodiamine increased phosphorylation of extracellular signal-regulated kinase (ERK) and reduced the expression of peroxisome proliferator-activated receptor- $\gamma$  in preadipocytes, strongly inhibiting their differentiation into mature adipocytes. Bak et al. (2010) reported that daily injection of evodiamine (10 mg evodiamine/kg body weight) for 2 weeks improved insulin resistance and the undesirable effect of rosiglitazone on body weight gain in db/db mice. More recently, we reported that daily injection of evodiamine (3 mg evodiamine/kg body weight) for one week improved obesity and insulin resistance in obese/diabetic KK-Ay mice via inhibition of insulin-stimulated mTOR-S6K activation and stimulation of AMPK phosphorylation in mature adipocytes (Wang et al., 2013). Thus, evodiamine shows great potential for the prevention of metabolic diseases including obesity and diabetes (Yamashita, 2014). However, the effects of long-term supplementation of low dose evodiamine on age-related pathophysiology and longevity are not clear. In the present study we carried out longitudinal experiments to clarify the effects of evodiamine at low dosages (1 and 10 mg evodiamine/kg food, equivalent to approximately 0.1 and 1 mg/kg body weight per day, respectively) on obesity, insulin resistance and lifespan in normal ageing mice.

## 2. Materials and methods

### 2.1. Experimental animals

Twelve-month-old male C57BL/6J mice were provided by the ageing farm at the National Institute for Longevity Sciences. Mice which did not show overt signs of diseases were used in the diet study. The mice were maintained under artificial lighting for 12 h per day and provided with standard chow (11.6% kcal from fat; Diet No. CE-2, CLEA Japan, Inc.) and tap water *ad libitum* in our animal facility at 23 °C. Mice were divided randomly into three groups and were fed with the standard chow without or with 1 or 10 mg evodiamine (Kishida Chemical, Osaka, Japan) per kg food (referred to as EL or EH, respectively, 10 mice per group). Evodiamine dose of supplementation was estimated on the assumption that the 12-month-old male mouse weighing 35 g consumes approximately 3.5 g of standard chow per day; that is, 10 and 1 mg evodiamine/kg food supply, 1 and 0.1 mg evodiamine/kg body weight per day, respectively. One mg evodiamine per kg food was the lowest concentration that could be prepared in a compound diet. These mice were housed in groups of 3 and 4 and maintained until

death to examine the effects of evodiamine on lifespan. The survival of mice was confirmed by daily inspections. Body weight and food intake were examined every month and blood samples were collected from a tail vein at 18 months of age. Six months after the start of the first cohort, studies were repeated using a second cohort (9 mice per group). Further six months after the start of the second cohort, studies were repeated using a third cohort (12 and 11 mice for control and EL groups, respectively), of which six mice of each group were used for intraperitoneal glucose tolerance test (IPGTT) at 18 months of age and sampled two weeks later. Tissues and blood were recovered and stored at  $-80^{\circ}\text{C}$  until further use. This study was performed in strict accordance with the recommendations of the Fundamental Guidelines for Proper Conduct of Animal Experiments and Related Activities in Academic Research Institutions under the jurisdiction of the Ministry of Education, Culture, Sports, Science and Technology, Japan. The protocol was approved by the Institutional Animal Care and Use Committee of the National Institute for Longevity Sciences and Chubu University.

## 2.2. Biochemical analysis

Blood samples were collected from a tail vein and immediately used to determine the glucose level by using a glucometer (NovoAssist Plus, Novo Nordisk, Tokyo, Japan). Serum levels of insulin, leptin, and adiponectin were measured using enzyme-linked immunosorbent assay kits (insulin: ultrasensitive insulin ELISA, Mercodia, Winston Salem, NC, USA; or lebis-insulin-mouse, Sibayagi, Gunma, Japan; leptin: enzyme immunoassay kit, Cayman, Ann Arbor, MI, USA; and adiponectin: quantikine adiponectin, R&D systems, Minneapolis, MN, USA). IPGTT was performed using 1.5 mg of glucose/g body weight after 17 h of starvation. Blood glucose level was measured using a glucometer before glucose injection (0 min) and at 30, 60, and 120 min after injection.

## 2.3. Protein analysis

Western blot analyses were performed on total tissue lysates of WAT, BAT, liver and gastrocnemius muscle (GM), as described previously (Summers, Lipfert, & Birnbaum, 1998). The concentrations of protein in the lysates were measured using a BCA protein assay (Pierce Biotechnology, Rockford, IL, USA). Equal amounts of protein (30  $\mu\text{g}$ ) were separated on 4–20% SDS-polyacrylamide gels (Daiichi Pure Chemicals, Tokyo, Japan) and transferred onto Immobilon polyvinylidene difluoride membranes (Millipore, Bedford, MA, USA). The membranes were incubated with specific antibodies against AMPK, phospho-Thr172 AMPK, mTOR, phospho-Ser2448 mTOR, p70S6 kinase, phospho-Thr389 p70S6 kinase, IRS1, phospho-Ser636/639 IRS1, Akt, phospho-Ser473 Akt, ribosomal protein S6 (rpS6), phospho-Ser235/236 rpS6, phospho-Thr197 cAMP-dependent protein kinase catalytic subunit (PKAc), cAMP response element binding protein (CREB), phospho-Ser133 CREB,  $\alpha/\beta$ -tubulin (all from Cell Signaling Technology, Danvers, MA, USA), PKAc (BD Biosciences, CA, USA), or UCP1 (Abnova, Taipei City, Taiwan). After reacting with the appropriate secondary antibody for 1 h at room temperature, specific signals were detected using ECL western blotting detection reagents (GE Healthcare, Little

Chalfont, Buckinghamshire, UK). The resulting images were quantified with NIH Image (version 1.63).

## 2.4. Histological analysis

Immediately after removal, tissue samples were fixed by immersion at  $4^{\circ}\text{C}$  in 10% formaldehyde in neutral buffer solution (Kishida Chemical, Osaka, Japan). They were then dehydrated, cleared, and paraffin-embedded. Paraffin sections (4  $\mu\text{m}$ ) were stained with haematoxylin and eosin. All observations were performed with a BIOREVO BZ-9000 microscope (Keyence, Tokyo, Japan). The average cell size of adipocytes in WAT was calculated by dividing the chosen microscopic area by the total cell number in the area.

## 2.5. Statistical analysis

All data are expressed as the mean  $\pm$  SE. The significance of differences between groups was assessed by analysis of variance (ANOVA) using Fisher's PLSD test. Values of  $P < 0.05$  were considered statistically significant.

# 3. Results

## 3.1. Effects of evodiamine on obesity, insulin resistance and lifespan

Longitudinal ageing experiments were initiated with 12-month-old C57BL/6J mice to determine the effects of evodiamine (1 and 10 mg evodiamine/kg food) on body weight gain and insulin resistance, which become prominent in both middle-aged mice and humans. In our previous study, 4-month-old young mice were fed with an HF diet supplemented with 300 mg evodiamine/kg food for two months (Wang et al., 2008). In the present study, much lower dosages considering daily intake for the long term throughout life were set for the normal middle-aged mice from the aspect of physiological relevance. We performed three independent experiments using different cohorts and their combined data are shown in Fig. 1, because the results of these experiments were reproducible. The body weight of the control mice peaked between 16 and 19 months of age and thereafter declined with age (Fig. 1A). Some mice maintained their body weight at a consistently higher level, but other mice lost body weight quickly after 19 months of age, thereby increasing variation for the group. At 24 months of age, the average body weight of the control group was lower than that at the beginning of the study (12 months of age). Interestingly, the increase in body weight observed in the control group was effectively prevented in the EL and EH groups ( $P < 0.01$  and  $P < 0.001$  respectively, vs. control group); however, continuous feeding with high-dose evodiamine (EH group) caused unexpected further reduction in body weight at approximately 19 months of age. In contrast, many mice in the EL group maintained their body weight within a constant range up to 23 months of age. Irrespective of the body weight change, food intake remained quite constant within each group up to 18 months of age (Fig. 1B). However, significant differences in food intake were observed between groups and the amounts were

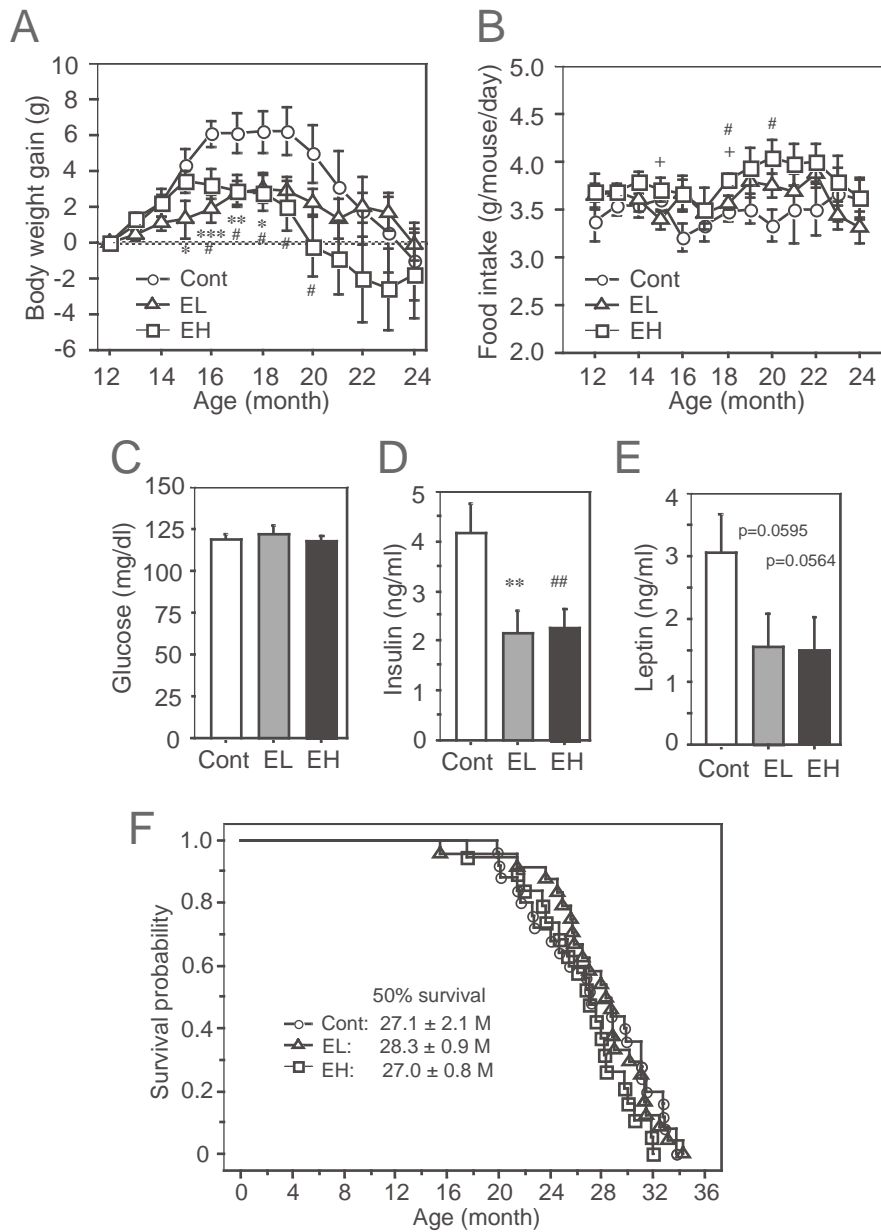


**Fig. 1 – Effects of evodiamine on age-associated obesity and lifespan. Twelve-month-old male C57BL/6J mice were fed the standard chow diet without (Cont) or supplemented with 1 mg evodiamine per kg food (EL) or 10 mg evodiamine per kg food (EH) until death. (A) Body weight gain. Data of mice which survived until 24 months of age were used (Cont: n = 15, EL: n = 16, EH: n = 14). (B) Food intake. (C–E) Fed glucose level (C), insulin level (D) and leptin level (E) at 18 months of age. Data are expressed as the mean ± SE (n = 17–19). (F) Lifespan of mice fed with the evodiamine diet. Kaplan–Meier analysis of survival was performed (Cont: n = 25, EL: n = 24, EH: n = 19). \*P < 0.05, \*\*P < 0.01 and \*\*\*P < 0.001 Cont group vs. EL group. #P < 0.05 and ##P < 0.01 Cont group vs. EH group. +P < 0.05 EL group vs. EH group.**

EH > EL > control groups (control vs. EL group, P < 0.05; control vs. EH group, P < 0.001; EL vs. EH group, P < 0.05). The variations in food intake levels increased with age from 19 months onwards in each group, with large differences among individual mice, reflecting their state of health. At 18 months old, after dietary intervention for 6 months, there was no difference in fed glucose levels among the groups (Fig. 1C), whereas insulin and leptin levels were considerably lower (~50%) in the EL and EH groups compared to the control group (Fig. 1D and E). Despite the protective effect of the evodiamine diets against

body weight gain, no significant difference in lifespan was observed among the three groups (Fig. 1F). In the parameters of longevity, the 50% survivals were 27.1, 28.3 and 27.0 months old in the control, EL and EH groups, respectively. The longest lifespan was 33.8, 34.3 and 32.0 months old in the control, EL and EH groups, respectively. To examine whether the spectrum of lesions was altered by dietary evodiamine, gross diagnosis was performed on the dead mice (Table 1). Although increased incidences of cardiac hypertrophy and chronic nephritis were noted in the EH group, evodiamine did not

**Table 1 – Gross evaluation of mice fed with the control and evodiamine diets at the time of death.**

Lesions		Cont (n = 25)	EL (n = 24)	EH (n = 19)
Cardiovascular system	Cardiac hypertrophy		1	3
	Lung tumour	1		
Respiratory system	Lung haemorrhage		1	
	Pneumonia		1	
	Pleural effusion	1	1	2
Haemolymphatic system	Splenoma	5	7	5
	Lymph node enlargement	2		
	Haemothorax or/and haemoperitoneum	2	2	1
Genitourinary system	Kidney tumour	1	1	
	Renal atrophy		1	
	Chronic nephritis	1	1	3
Gastrointestinal system	Tumours	2	2	2
	Fatty liver		2	2
	Intussusception	1		
	Ileus	1		
	Gastrointestinal haemorrhage	2	1	1
	Ascites fluid		1	
Hepatobiliary system	Lipoma	1	2	
	Hepatoma	7	6	5

The mean ages at death were 27.1 ± 2.1, 28.3 ± 0.9 and 27.0 ± 0.8 months in the control, EL and EH groups, respectively. The gross evaluation of dead mice for diagnosis was performed by an experienced pathologist.

change the distribution of presumptive causes of death compared with that of the control group.

In precise analyses of the evodiamine effect on middle-aged mice, we focused on the mice given low-dose evodiamine (EL group), because an excessive effect of high-dose evodiamine on body weight control in aged mice was found in the longitudinal experiments (EH group) as shown in Fig. 1A. Although no significant differences in body and WAT weights were detected between the two groups (Supplementary Table S1), body weight gain was significantly lower in the EL group compared to the control group (Fig. 2A), which was consistent with the result shown in Fig. 1A. Significantly lower tissue weights were also observed in kidney and GM in the EL group compared to the control group (Supplementary Table S1). In these mice, IPGTT indicated improved glucose tolerance in the EL group compared to the control group (Fig. 2B). The fasting glucose level (at the 0 time-point in the IPGTT) was lower in the EL group than in the control group (EL: 65 ± 3 mg/dL; control: 73 ± 3 mg/dL,  $P = 0.0937$ ). In addition, a trend towards a reduced adiponectin level was detected in the EL group compared to the control group (9.212 ± 0.815 and 7.797 ± 0.450 mg/L, respectively,  $P = 0.0929$ ). Histological analysis suggested a decrease in adipocyte size in EWAT and IWAT (EWAT, 1894 ± 169  $\mu\text{m}^2$  and 1433 ± 206  $\mu\text{m}^2$ ,  $P = 0.0792$ ; IWAT, 2046 ± 142  $\mu\text{m}^2$  and 1515 ± 254  $\mu\text{m}^2$ ,  $P = 0.0711$  in the control and EL groups,

respectively), as well as reduced lipid accumulation in the liver, in the EL group compared to the control group (Fig. 2C). Collectively, these results suggested that the evodiamine diet improved overweight, obesity and insulin resistance in ageing mice.

### 3.2. Effects of dietary evodiamine on the expression of metabolic genes in adipose tissues of middle-aged mice

To examine the molecular mechanisms underlying the effects of long-term evodiamine treatment on obesity and insulin resistance, we next examined the gene expression of UCP1, UCP2 and UCP3 in WAT and BAT in the control and EL groups, because a previous study suggested that evodiamine stimulates sympathetic nervous activity by increasing catecholamine release in bovine adrenal medulla (Yoshizumi et al., 1997). However, qRT-PCR analyses of UCP expression showed no significant difference in gene expression in EWAT or BAT between the two groups (Supplementary Table S3). The mRNA levels of genes involved in energy metabolism such as acyl-CoA oxidase (ACO), carnitine palmitoyltransferase 1 (CPT1) and phosphoenolpyruvate carboxykinase (PEPCK) were also similar in EWAT and BAT among the groups (Supplementary Table S3). Moreover, the UCP1 protein level as well as the phosphorylation levels of cAMP-dependent protein kinase catalytic subunit (PKAc) and cAMP response element binding protein (CREB) in BAT did not differ between the control and EL groups (Fig. 3), suggesting that BAT thermogenesis was not centred on the effect of dietary evodiamine in protecting against body weight gain in the normal middle-aged mice.

### 3.3. Effects of dietary evodiamine on signal transduction in the tissues of middle-aged mice

We next examined the changes in signal transduction responsible for regulating energy metabolism. Protein analysis of EWAT identified differences in the phosphorylation levels of AMPK and in the mTOR signalling pathway between the EL and control groups (Fig. 4), which were similar to the results obtained in the experiments of obese/diabetic KK-Ay mice (Wang et al., 2013). A significant increase in AMPK phosphorylation was detected in WAT of the EL group compared to the control group (Fig. 4A), whereas the phosphorylation of mTOR and S6K showed decreased trends in WAT of the EL group compared to the control group (Fig. 4B and C). There were no significant differences in serine phosphorylation of IRS1 or Akt between the EL and control groups (Fig. 4D and E). A significant decrease in the Ser235/236 phosphorylation of rpS6, a target molecule of S6K, was also found in the WAT of the EL group compared to the control (Fig. 4F). Next, we determined phosphorylation levels in the liver and GM in the mice administered with long-term evodiamine. Unlike the results in WAT, there were no significant differences in the phosphorylation levels of AMPK, mTOR, S6K or IRS1 in the liver (Fig. 5A–D) or the GM (Supplementary Fig. S1A–D) between the control and EL groups. On the other hand, the phosphorylation levels of Akt and rpS6 were significantly higher in the liver (Fig. 5E and F), but not in the GM (Supplementary Fig. S1E and F), in the EL group compared to the control.

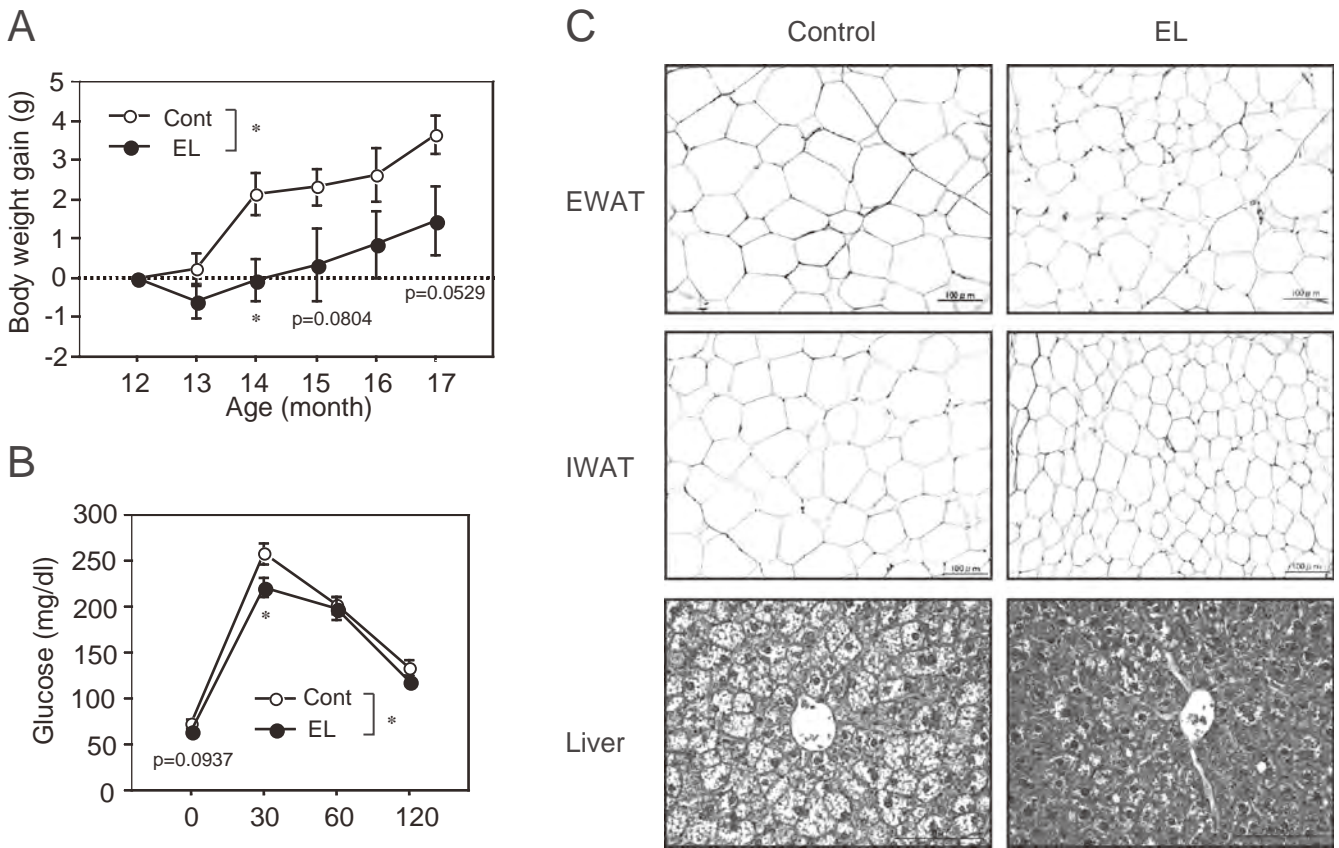


Fig. 2 – Glucose tolerance test and histological analysis in middle-aged mice. Twelve-month-old male C57BL/6J mice were fed with the standard chow for 6.5 months without (Cont) or with 1 mg evodiamine per kg food (EL). (A) Body weight gain. (B) IPGTT at 18 months of age. Data are expressed as the mean  $\pm$  SE (n = 6). (C) Histology of EWAT, IWAT and liver at 18.5 months of age. Tissue sections were stained with haematoxylin and eosin.

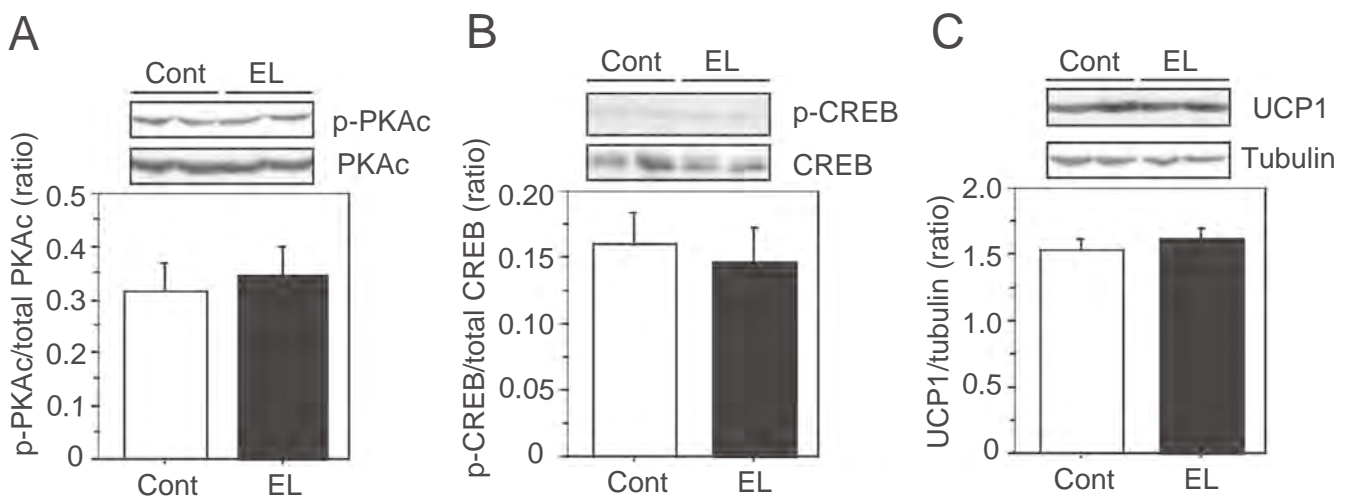
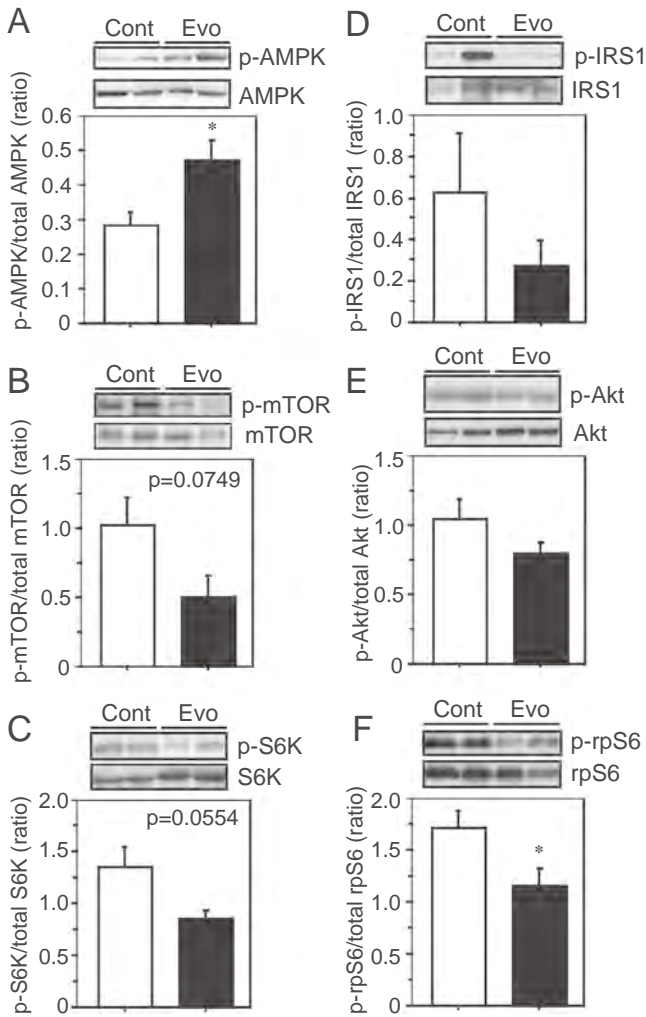
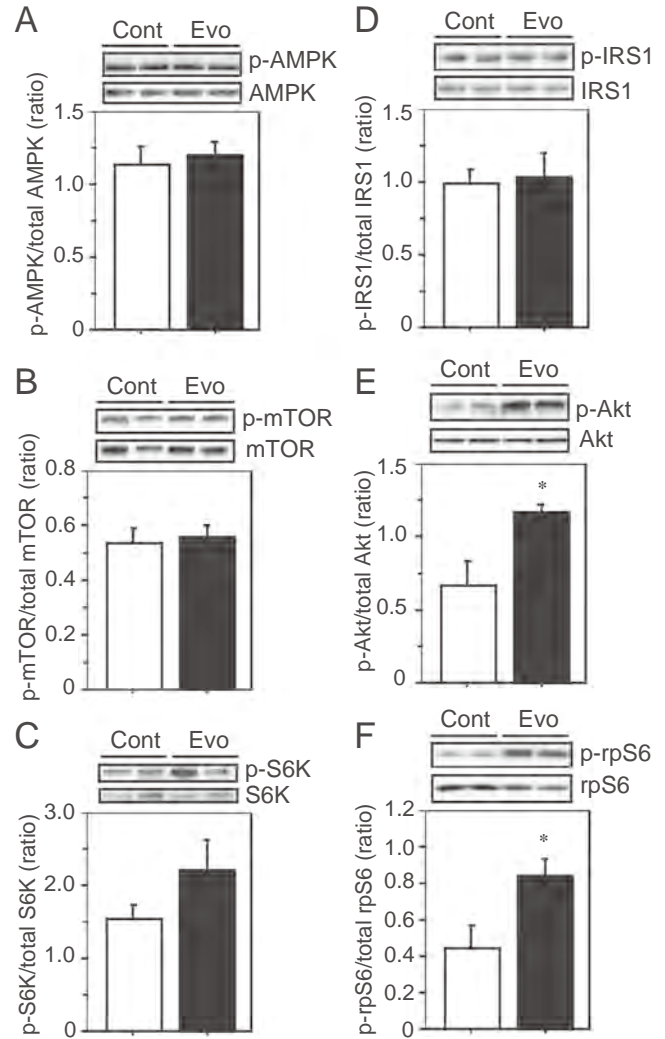


Fig. 3 – Effects of evodiamine on PKA signalling and UCP1 expression in BAT of mice fed with dietary evodiamine. Western blot analyses of PKAc (A), CREB (B) and UCP1 (C) were performed on tissue lysates (30  $\mu$ g protein) of BAT from male 18.5-month-old C57BL/6J mice fed with standard chow for 6.5 months without (Cont) or with 1 mg evodiamine per kg food (EL). Phosphorylation levels of PKAc Thr197 and CREB Ser133 were normalized to the total level of each protein. UCP1 level was normalized to  $\alpha$ / $\beta$ -tubulin level. Data are expressed as the mean  $\pm$  SE (n = 5-6).



**Fig. 4 – Effects of evodiamine on AMPK and mTOR–S6K signalling in the WAT of mice fed with dietary evodiamine.** Western blot analyses of AMPK (A), mTOR (B), S6K (C), IRS1 (D), Akt (E) and rpS6 (F) were performed using tissue lysates (30 µg protein) of epididymal WAT from male 18.5-month-old C57BL/6J mice fed with standard chow for 6.5 months without (Cont) or with 1 mg evodiamine per kg food (EL). Phosphorylation levels of AMPK Thr172, mTOR Ser2448, S6K Thr389, IRS1 Ser636/639, Akt Ser473 and rpS6 Ser235/236 were normalized to the total level of each protein. Data are expressed as mean ± SE (n = 5–6). \*P < 0.05 vs. control group.



**Fig. 5 – Effects of evodiamine on AMPK and mTOR–S6K signalling in the liver of mice fed with dietary evodiamine.** Western blot analyses of AMPK (A), mTOR (B), S6K (C), IRS1 (D), Akt (E) and rpS6 (F) were performed using tissue lysates (30 µg protein) of liver from male 18.5-month-old C57BL/6J mice fed with standard chow for 6.5 months without (Cont) or with 1 mg evodiamine per kg food (EL group). Phosphorylation levels of AMPK Thr172, mTOR Ser2448, S6K Thr389, IRS1 Ser636/639, Akt Ser473 and rpS6 Ser235/236 were normalized to the total level of each protein. Data are expressed as the mean ± SE (n = 5–6). \*P < 0.05 vs. control group.

#### 4. Discussion

There is accumulating evidence that evodiamine exerts a powerful anti-obesity effect in rodents. Evodiamine strongly inhibits adipogenesis via stimulation of ERK phosphorylation in preadipocytes (Wang et al., 2008, 2009). Wei et al. (2013) suggested in the experiments using apolipoprotein E and transient receptor potential vanilloid type 1 (TRPV1) double-knockout mice that evodiamine confers novel TRPV1-dependent atheroprotection and TRPV1-independent anti-obesity action

(2013). We also recently demonstrated that this compound improves glucose tolerance and insulin resistance associated with obese/diabetic status through inhibition of mTOR–S6K signalling mainly in WAT in KK-Ay and UCP1-knockout mice without causing any change in food intake (Wang et al., 2013). Although a number of beneficial effects, including anti-tumour (Takada et al., 2005) and anti-inflammatory actions (Heo et al., 2009), of evodiamine have been reported from studies on various animal models, to date no studies have investigated the effects of chronic evodiamine supplementation on age-related pathophysiology and longevity.

To clarify the effects of evodiamine on age-associated body weight change, obesity and insulin resistance and on lifespan, we carried out longitudinal experiments involving dietary supplementation of evodiamine using normal C57BL6/J mice. Similar to the study of Harrison et al. (2009), we designed experiments in which we used 12-month-old middle-aged mice and fed them standard chow diets containing relatively low doses of evodiamine (1 and 10 mg/kg food). The normal laboratory mice fed with the standard chow (control group) gained a significant amount of weight with age even under standard dietary conditions. Their body weights reached a peak between 16 and 19 months of age in the housing conditions of our animal facilities. However, the increase in body weight with age was significantly prevented in both the low (EL) and the high (EH) dose evodiamine groups in spite of higher food intake in the evodiamine diet groups, suggesting that energy expenditure was higher in these groups compared with the control group. The result on food intake was unexpected because we did not detect any stimulating effect in our previous study (Wang et al., 2008) in which mice were given an HF-diet supplemented with a very high dose of evodiamine (300 mg/kg diet). In addition, we were unable to detect any acute effect of evodiamine on stimulating energy expenditure in mice injected with 3 mg evodiamine/kg body weight in an indirect calorimetric analysis (Wang et al., 2013). Moreover, no stimulation of the PKA-CREB-UCP1 pathway nor increased expression of any metabolic genes examined was detected in the BAT of the EL group (Fig. 3 and Supplementary Table S3), suggesting that the contribution of thermogenic tissue to the inhibitory effect of evodiamine on body weight gain may be low. Schwarz et al. (2013) have reported that acute ingestion of 500 mg evodiamine is not effective at inducing thermogenesis and increasing fat oxidation at rest or during exercise in men (2013). Therefore, there remain several possibilities as follows: 1) if there is any increase in energy expenditure as a result of long-term supplementation with evodiamine, this must occur gradually by a UCP1-independent mechanism, as suggested by previous studies (Liu et al., 2003; Wang et al., 2008), and 2) evodiamine increases excretion of diet due to decreased digestion and/or absorption in older mice. Further studies are required to address these questions and to ascertain whether evodiamine affects appetite.

Body weight in mice begins to decline after reaching a plateau as a natural part of the ageing process. Although we successfully identified the effects of evodiamine in improving obesity and glucose tolerance even at its lowest dose (EL group) at 18 months of age, we also found an unexpected reduction in body weight in the EH group after the later phase of ageing, which was distinguishable from the body weight changes in the control and EL groups. This sharp reduction in body weight might be a sign of the deterioration of health, although the 50% survival and longest lifespan in the EH group were not significantly different from those in the control group. Our previous study also did not reveal any deteriorative signs by pathological analysis of tissues in young 6-month-old mice fed with an HF diet containing 30 times higher evodiamine concentration than the EH group for 2 months (data not shown; Wang et al., 2008). In this longitudinal experiment, the increased incidence of cardiac hypertrophy and nephritis in the EH group revealed by pathological evaluation may suggest that long-term supplementation with evodiamine at 10 mg/kg food throughout life produces

harmful side effects on the heart and kidney in mice. In contrast, in the EL group supplemented with 1 mg/kg food this was not the case. Many metabolic phenotypes in the EL group were better than those in the control group (Figs. 1 and 2) and no apparent difference was observed between the two groups by pathological evaluation (Table 1); however we failed to detect a significant increase in lifespan in the evodiamine-treated mice compared to the control mice. The effect of evodiamine on lifespan in female mice remains to be determined, because gender effects on longevity have been reported in heterozygous IGF-1 receptor-knockout (Holzenberger et al., 2003) and S6K-null mice (Selman et al., 2009), in which a significantly extended lifespan was observed only in female mice. It is also noted that the effective dose of evodiamine (1 mg/kg food) used in our study appears to be quite low compared to those of rapamycin (14 mg/kg food) and caffeic acid phenethyl ester (30 mg/kg food) used in the studies of the National Institute on Aging Interventions Testing Program (Harrison et al., 2009).

To further evaluate the potential of evodiamine as an anti-ageing compound, we examined the effects of dietary evodiamine on mTOR–S6K signalling in the tissues from 18.5-month-old mice in the EL group, because reduced activation of mTOR signalling is believed to mediate a major beneficial effect of caloric restriction (Kenyon, 2010; Zoncu et al., 2011). In agreement with the results of experiments using KK-Ay mice and 3T3-L1 adipocytes (Wang et al., 2013), attenuated signalling of the mTOR–S6K pathway in WAT, but not in the liver or GM, was identified in the EL group compared with the control group, although we failed to detect any significant decrease in IRS1 serine phosphorylation in the WAT of the EL group. Because S6K phosphorylated by mTOR promotes mRNA translation by phosphorylating multiple proteins such as eukaryotic translation initiation factor 4B and rpS6 (Zoncu et al., 2011), the decrease in rpS6 phosphorylation suggests attenuation of protein synthesis and cell growth in the WAT of mice fed with the evodiamine diet. This inhibitory effect of evodiamine on the mTOR–S6K–rpS6 signalling pathway might prevent the expansion of WAT and the associated increase in lipid accumulation, thereby improving the degraded function of adipocytes and increasing adiponectin production. Adiponectin is known to activate AMPK (Kadowaki et al., 2006), which downregulates the mTOR signalling pathway via phosphorylation of tuberous sclerosis complex 2 (Inoki et al., 2006; Zoncu et al., 2011). Because genetic and pharmacologic studies have demonstrated that AMPK is required to maintain glucose homeostasis (Shaw et al., 2005), AMPK is now considered to be a potential pharmacologic target for improving insulin resistance, diabetes and metabolic syndrome. Likewise, recent findings that several compounds such as esculetin, a coumarin derivative, and theaflavin-3,3'-digallate, a black tea polyphenol, exhibit anti-adiposity activity via AMPK phosphorylation in 3T3-L1 adipocytes suggest their potential application in nutraceuticals for preventing the development of obesity (Kim & Lee, 2015; Ko, Lo, Wang, Chiou, & Lin, 2015). Consistent with the previous findings that evodiamine significantly stimulates AMPK phosphorylation in cultured endothelial cells and mature adipocytes and in the WAT of KK-Ay mice (Ching et al., 2012; Wang et al., 2013), increased phosphorylation of AMPK was confirmed in the WAT of the EL group compared to controls. Consequently, it is plausible that inhibition of the mTOR–S6K–rpS6 pathway

and AMPK activation in WAT might contribute to the improvement of glucose tolerance and insulin resistance in the evodiamine-treated group. In hepatic insulin signalling, activation of phosphatidylinositol 3-kinase and Akt plays an important role in the regulation of gluconeogenesis in the liver (Perry, Samuel, Petersen, & Shulman, 2014). An increase in hepatic lipids results in inhibition of insulin signalling and reduced Akt activity. This suggests that increased phosphorylation of Akt in the liver of the EL group is associated with a decrease in hepatic lipid accumulation, which may contribute to the improvement of insulin resistance in mice fed with the evodiamine diet.

Thus, our results indicate that long-term dietary supplementation with evodiamine prevents obesity and improves glucose tolerance and insulin resistance in normal ageing mice. These beneficial effects of evodiamine supplementation appear to be mediated at least in part through its action on the AMPK and mTOR-S6K signalling pathways in WAT. An appropriate supplementation of evodiamine at a low dose (such as 0.1 mg/kg body weight per day) beginning in middle age may reduce mid-life mortality risk by preventing obesity and insulin resistance, but additional data including the minimum effective dose as a food supplement are needed to provide an accurate estimate of effect size to improve longevity. Although the roles of UCP1 in thermoregulation and body weight control have been established, the present data provide an important insight that a supplementary intervention prevents the development of obesity and its related phenotypes irrespective of UCP1 function in the general population.

### Conflict of interest

The authors declare no conflict of interest.

### Acknowledgements

We thank Ms. Y. Yamashita, Y. Kadokawa and Dr. J. Yao for technical assistance. This work was supported by a Research Grant (15C-8) for Longevity Sciences from the Ministry of Health, Labour and Welfare (to H.Y.), and by a grant (S1201007) from the MEXT-Supported program for the Strategic Research Foundation at private universities (to H.Y.). The early phase of this study was performed at the Department of Molecular Genetics in the National Institute for Longevity Sciences.

### Appendix: Supplementary material

Supplementary data to this article can be found online at doi:10.1016/j.jff.2015.09.032.

### REFERENCES

- Bak, E. J., Park, H. G., Kim, J. M., Kim, J. M., Yoo, Y. J., & Cha, J. H. (2010). Inhibitory effect of evodiamine alone and in combination with rosiglitazone on in vitro adipocyte differentiation and in vivo obesity related to diabetes. *International Journal of Obesity*, 163, 250–260.
- Bray, G. A., & Tartaglia, L. A. (2000). Medicinal strategies in the treatment of obesity. *Nature*, 404, 672–677.
- Ching, L. C., Chen, C. Y., Su, K. H., Hou, H. H., Shyue, S. K., Kou, Y. R., & Lee, T. S. (2012). Implication of AMP-activated protein kinase in transient receptor potential vanilloid type 1-mediated activation of endothelial nitric oxide synthase. *Molecular Medicine*, 18, 805–815.
- Chiou, W. F., Chou, C. J., Shum, A. Y., & Chen, C. F. (1992). The vasorelaxant effect of evodiamine in rat isolated mesenteric arteries: Mode of action. *European Journal of Pharmacology*, 215, 277–283.
- Draznin, B. (2006). Molecular mechanisms of insulin resistance: Serine phosphorylation of insulin receptor substrate-1 and increased expression of p85alpha: The two sides of a coin. *Diabetes*, 55, 2392–2397.
- Guerra, C., Koza, R. A., Yamashita, H., Walsh, K., & Kozak, L. P. (1998). Emergence of brown adipocytes in white fat in mice is under genetic control. Effects on body weight and adiposity. *Journal of Clinical Investigation*, 102, 412–420.
- Hardie, D. G. (2007). AMP-activated/SNF1 protein kinases: Conserved guardians of cellular energy. *Nature Review Molecular Cell Biology*, 8, 774–785.
- Harrison, D. E., Strong, R., Sharp, Z. D., Nelson, J. F., Astle, C. M., Flurkey, K., Carter, C. S., Pahor, M., Javors, M., Fernandez, E., & Miller, R. A. (2009). Rapamycin fed late in life extends lifespan in genetically heterogeneous mice. *Nature*, 460, 392–395.
- Heo, S. K., Yun, H. J., Yi, H. S., Noh, E. K., & Park, S. D. (2009). Evodiamine and rutaecarpine inhibit migration by LIGHT via suppression of NADPH oxidase activation. *Journal of Cellular Biochemistry*, 107, 123–133.
- Holzenberger, M., Dupont, J., Ducos, B., Leneuve, P., Géoïen, A., Even, P. C., Cervera, P., & Bouc, Y. L. (2003). IGF-1 receptor regulates lifespan and resistance to oxidative stress in mice. *Nature*, 421, 182–187.
- Inoki, K., Ouyang, H., Zhu, T., Lindvall, C., Wang, Y., Zhang, X., Yang, Q., Bennett, C., Harada, Y., Stankunas, K., Wang, C. Y., He, X., MacDougald, O. A., You, M., Williams, B. O., & Guan, K. L. (2006). TSC2 integrates Wnt and energy signals via a coordinated phosphorylation by AMPK and GSK3 to regulate cell growth. *Cell*, 126, 955–968.
- Kadowaki, T., Yamauchi, T., Kubota, N., Hara, K., Ueki, K., & Tobe, K. (2006). Adiponectin and adiponectin receptors in insulin resistance, diabetes, and the metabolic syndrome. *Journal of Clinical Investigation*, 116, 1784–1792.
- Kahn, B. B., Alquier, T., Carling, D., & Hardie, D. G. (2005). AMP-activated protein kinase: Ancient energy gauge provides clues to modern understanding of metabolism. *Cell Metabolism*, 1, 15–25.
- Kennedy, B. K., Steffen, K. K., & Kaeberlein, M. (2007). Ruminations on dietary restriction and aging. *Cellular and Molecular Life Sciences*, 64, 1323–1328.
- Kenyon, C. J. (2010). The genetics of ageing. *Nature*, 464, 504–512.
- Kim, Y., & Lee, J. (2015). Esculetin, a coumarin derivative, suppresses adipogenesis through modulation of the AMPK pathway in 3T3-L1 adipocytes. *Journal of Functional Foods*, 12, 509–515.
- Ko, H.-J., Lo, C.-Y., Wang, B.-J., Chiou, R. Y.-Y., & Lin, S.-M. (2015). Theaflavin-3,3'-digallate, a black tea polyphenol, stimulates lipolysis associated with the induction of mitochondrial uncoupling proteins and AMPK-FoxO3A-MnSOD pathway in 3T3-L1 adipocytes. *Journal of Functional Foods*, 17, 271–282.
- Kobayashi, Y., Nakano, Y., Kizaki, M., Hoshikuma, K., Yokoo, Y., & Kamiya, T. (2001). Capsaicin-like anti-obese activities of evodiamine from fruits of *Evodia rutaecarpa*, a vanilloid receptor agonist. *Planta Medica*, 67, 628–633.

- Kolonin, M. G., Saha, P. K., Chan, L., Pasqualini, R., & Arap, W. (2004). Reversal of obesity by targeted ablation of adipose tissue. *Nature Medicine*, 10, 625–632.
- Kontani, Y., Wang, Y., Kimura, K., Inokuma, K. I., Saito, M., Suzuki-Miura, T., Wang, Z., Sato, Y., Mori, N., & Yamashita, H. (2005). UCP1 deficiency increases susceptibility to diet-induced obesity with age. *Aging Cell*, 4, 147–155.
- Kopelman, P. G. (2000). Obesity as a medical problem. *Nature*, 404, 635–643.
- Liu, X., Rossmeisl, M., McClaine, J., Riachi, M., Harper, M. E., & Kozak, L. P. (2003). Paradoxical resistance to diet-induced obesity in UCP1-deficient mice. *Journal of Clinical Investigation*, 111, 399–407.
- Mattson, M. P. (2010). Perspective: Does brown fat protect against diseases of aging? *Ageing Research Reviews*, 9, 69–76.
- Perry, R. J., Samuel, V. T., Petersen, K. F., & Shulman, G. I. (2014). The role of hepatic lipids in hepatic insulin resistance and type 2 diabetes. *Nature*, 510, 84–91.
- Schwarz, N. A., Spillane, M., La Bounty, P., Grandjean, P. W., Leutholtz, B., & Willoughby, D. S. (2013). Capsaicin and evodiamine ingestion does not augment energy expenditure and fat oxidation at rest or after moderately-intense exercise. *Nutrition Research*, 33, 1034–1042.
- Selman, C., Tullet, J. M., Wieser, D., Irvine, E., Lingard, S. J., Choudhury, A. I., Claret, M., Al-Qassab, H., Carmignac, D., Ramadani, F., Woods, A., Robinson, I. C. A., Schuster, E., Batterham, R. L., Kozma, S. C., Thomas, G., Carling, D., Okkenhaug, K., Thornton, J. M., Partridge, L., Gems, D., & Withers, D. J. (2009). Ribosomal protein S6 kinase 1 signaling regulates mammalian life span. *Science*, 326, 140–144.
- Shaw, R. J., Lamia, K. A., Vasquez, D., Koo, S. H., Bardeesy, N., Depinho, R. A., Montminy, M., & Cantley, L. C. (2005). The kinase LKB1 mediates glucose homeostasis in liver and therapeutic effects of metformin. *Science*, 310, 1642–1646.
- Shima, H., Pende, M., Chen, Y., Fumagalli, S., Thomas, G., & Kozma, S. C. (1998). Disruption of the p70(s6k)/p85(s6k) gene reveals a small mouse phenotype and a new functional S6 kinase. *The EMBO Journal*, 17, 6649–6659.
- Summers, S. A., Lipfert, L., & Birnbaum, M. J. (1998). Polyoma middle T antigen activates the Ser/Thr kinase Akt in a PI3-kinase-dependent manner. *Biochemical and Biophysical Research Communications*, 246, 76–81.
- Takada, Y., Kobayashi, Y., & Aggarwal, B. B. (2005). Evodiamine abolishes constitutive and inducible NF- $\kappa$ B activation by inhibiting I $\kappa$ B kinase activation, thereby suppressing NF- $\kappa$ B-regulated antiapoptotic and metastatic gene expression, up-regulating apoptosis, and inhibiting invasion. *Journal of Biological Chemistry*, 280, 17203–17212.
- Um, S. H., Frigerio, F., Watanabe, M., Picard, F., Joaquin, M., Sticker, M., Fumagalli, S., Allegrini, P. R., Kozma, S. C., Auwerx, J., & Thomas, G. (2004). Absence of S6K1 protects against age- and diet-induced obesity while enhancing insulin sensitivity. *Nature*, 431, 200–205.
- Wang, T., Kusudo, T., Takeuchi, T., Yamashita, Y., Kontani, Y., Okamoto, Y., Saito, M., Mori, N., & Yamashita, H. (2013). Evodiamine inhibits insulin-stimulated mTOR-S6K activation and IRS1 serine phosphorylation in adipocytes and improves glucose tolerance in obese/diabetic mice. *PLoS ONE*, 8, e83264.
- Wang, T., Wang, Y., Kontani, Y., Kobayashi, Y., Sato, Y., Mori, N., & Yamashita, H. (2008). Evodiamine improves diet-induced obesity in a uncoupling protein-1-independent manner: Involvement of antiadipogenic mechanism and extracellularly regulated kinase/mitogen-activated protein kinase signaling. *Endocrinology*, 149, 358–366.
- Wang, T., Wang, Y., & Yamashita, H. (2009). Evodiamine inhibits adipogenesis via the EGFR-PKC $\alpha$ -ERK signaling pathway. *FEBS Letters*, 583, 3655–3659.
- Wang, Y., Kimura, K., Inokuma, K., Saito, M., Kontani, Y., Kobayashi, Y., Mori, N., & Yamashita, H. (2006). Potential contribution of vasoconstriction to suppression of heat loss and homeothermic regulation in UCP1-deficient mice. *Pflügers Archiv – European Journal of Physiology*, 452, 363–369.
- Wei, J., Ching, L. C., Zhao, J. F., Shyue, S. K., Lee, H. F., Kou, Y. R., & Lee, T. S. (2013). Essential role of transient receptor potential vanilloid type 1 in evodiamine-mediated protection against atherosclerosis. *Acta Physiologica*, 207, 299–307.
- White, M. F. (2002). IRS proteins and the common path to diabetes. *American Journal of Physiology. Endocrinology and Metabolism*, 283, E413–E422.
- Yamashita, H. (2014). A natural compound Evo(ke)s signaling for fat regulation. *Cell Cycle (Georgetown, Tex.)*, 13, 2801–2802.
- Yoneshiro, T., Aita, S., Matsushita, M., Okamoto-Ogura, Y., Kameya, T., Kawai, Y., Miyagawa, M., Tsujisaki, M., & Saito, M. (2011). Age-related decrease in cold-activated brown adipose tissue and accumulation of body fat in healthy humans. *Obesity*, 19, 1755–1760.
- Yoshizumi, M., Houchi, H., Ishimura, Y., Hirose, M., Kitagawa, T., Tsuchiya, K., Minakuchi, K., & Tamaki, T. (1997). Effect of evodiamine on catecholamine secretion from bovine adrenal medulla. *The Journal of Medical Investigation*, 44, 79–82.
- Zoncu, R., Efeyan, A., & Sabatini, D. M. (2011). mTOR: From growth signal integration to cancer, diabetes and ageing. *Nature Review Molecular Cell Biology*, 12, 21–35.

**Supplementary Information**

**Supplementary Methods**

Protein analysis

Western blot analyses were carried out using total tissue lysates recovered from the gastrocnemius muscle (GM) of mice, as described previously.<sup>1</sup> The concentrations of protein in the lysates were measured using a BCA protein assay (Pierce Biotechnology, Rockford, IL, USA). Equal amounts of protein (30 µg) were separated on 4–20% SDS-polyacrylamide gels (Daiichi Pure Chemicals, Tokyo, Japan) and transferred onto Immobilon polyvinylidene difluoride membranes (Millipore, Bedford, MA, USA). The membranes were incubated with specific antibodies against AMPK, phospho-Thr172 AMPK, mTOR, phospho-Ser2448 mTOR, p70S6 kinase, phospho-Thr389 p70S6 kinase, IRS1, phospho-Ser636/639 IRS1, Akt, phospho-Ser473 Akt, ribosomal protein S6 (rpS6), and phospho-Ser235/236 rpS6 (all from Cell Signaling Technology, Danvers, MA, USA). After incubating with an appropriate secondary antibody for 1 h at room temperature, specific signals were detected using ECL Western Blotting Detection Reagents (GE Healthcare, Little Chalfont, Buckinghamshire, UK). The resulting images were quantified with NIH Image (version 1.63).

Quantitative real-time reverse transcription polymerase chain reaction (qRT-PCR)

Total RNA was extracted using Trizol reagent (Invitrogen, Carlsbad, CA, USA) according to the manufacturer's protocol. RNA was reverse-transcribed using High Capacity cDNA Reverse Transcription kits (Applied Biosystems, Foster City, CA, USA) according to the manufacturer's instructions. To quantify mRNA expression levels, real-time RT-PCR analysis was performed using Light-Cycler and FastStart DNA Master<sup>PLUS</sup> SYBR Green I (Roche Diagnostics GmbH, Mannheim, Germany). All gene expression data were normalized to 36B4. The oligonucleotide primer sets used are shown in Table S1.

**Supplementary References**

- Summers SA, Lipfert L, Birnbaum MJ. Polyoma middle T antigen activates the Ser/Thr kinase Akt in a PI3-kinase-dependent manner. *Biochem Biophys Res Commun* 1998; **246**: 76–81.

**Supplementary Tables**

Table S1. Effects of dietary evodiamine on the tissue mass of middle-aged mice

	Control (n = 6)	EL (n = 6)	P value
Body weight (g)	46.6 ± 3.8	40.6 ± 2.3	0.1997
Tissue weight (mg)			
BAT	146 ± 20	149 ± 14	0.9043
IWAT	1145 ± 274	892 ± 135	0.4254
EWAT	1262 ± 205	1080 ± 135	0.4759
RWAT	453 ± 93	359 ± 68	0.4327
Kidney	236 ± 8	205 ± 10	0.0380
Liver	2328 ± 273	1792 ± 182	0.1328
Pancreas	202 ± 15	188 ± 9	0.4501
GM	159 ± 3	147 ± 4	0.0362
SM	8.8 ± 0.3	8.8 ± 0.2	0.8891
Heart	168 ± 11	171 ± 19	0.8867
Spleen	95 ± 12	74 ± 5	0.1587

Male 12-month-old C57BL/6J mice were fed standard chow without (control) or with 1 mg evodiamine per kg food (EL). After 6.5 months, tissue samples were collected without fasting. The left pads of inguinal, epididymal, and retroperitoneal white adipose tissues (IWAT, EWAT and RWAT, respectively) and gastrocnemius and soleus muscles (GM and SM, respectively) were used for the analysis of tissue mass. BAT: brown adipose tissue.

Table S2. Sequences of the primers used for quantitative RT-PCR

Gene	Sense	Antisense
UCP1	5'-GTGAAGGTCAGAAATGCAAGC-3'	5'-AGGGCCCCCTTCATGAGGTC-3'
UCP2	5'-GGCTGGTGGTGGTCCGGAGAT-3'	5'-CCGAAGGCAGAAAGTGAAGTG-3'
UCP3	5'-GAGGGGACCACCTCCAGCGTC-3'	5'-TGAGACTCCAGCAACTTCTC-3'
ACO	5'-CAGCACTGGTCTCCGTCAATG-3'	5'-CTCCGGACTACCATCCAAAGATG-3'
CPT1	5'-ACTCTCTGGAAGAAGAAGTTCA-3'	5'-GTATCTTTTGACACAGCTGGGAC-3'
PEPCK	5'-GTGGGGCGATGACATTGGC-3'	5'-ACTGAGGTGCCAGGAGCAAC-3'

Table S3. Effect of dietary evodiamine on the expression of genes related to energy metabolism in middle-aged mice

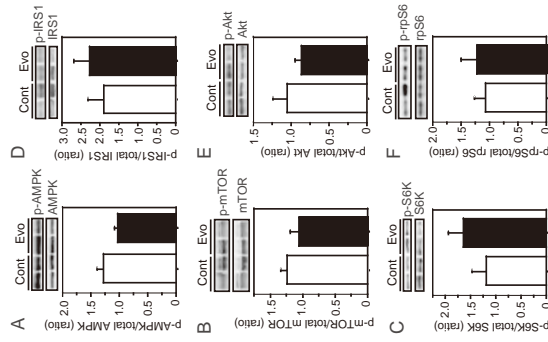
Gene	WAT		BAT		P value
	fold increase	P value	fold increase	P value	
UCP1	0.39	0.1702	0.8	0.1236	
UCP2	0.87	0.7294	1.11	0.6558	
UCP3	-	-	0.91	0.3677	
ACO	1.13	0.6541	1.14	0.3734	
CPT1	1.02	0.9371	1.14	0.4930	
PEPCK	1.41	0.5132	0.72	0.2077	

qRT-PCR was performed using total RNA from epididymal white adipose tissues (WAT) and brown adipose tissues (BAT) of male 18.5-month-old C57BL/6J mice fed standard chow for 6.5 months without (control) or with 1 mg evodiamine per kg food (EL). The data are presented as fold-increase compared to the levels in the control group (n = 4-6).

Legend of Supplementary Figure

Figure S1. Effect of evodiamine on signal transduction in the skeletal muscle of mice fed dietary evodiamine. Western blot analyses of AMPK (A), mTOR (B), S6K (C), IRS1 (D), Akt (E) and rpS6 (F) were performed using tissue lysates (30 µg protein) of gastrocnemius muscle from male 18.5-month-old C57BL/6J mice fed the standard chow for 6.5 months without (control) or with 1 mg evodiamine per kg food (EL group). Phosphorylation levels of AMPK Thr172, mTOR Ser2448, S6K Thr389, IRS1 Ser636/639, Akt Ser473 and rpS6 Ser235/236 were normalized to total level of each protein. Data are expressed as the mean ± SE (n = 5-6).

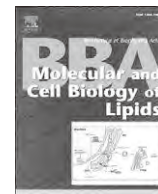
Supplemental Figure S1





Contents lists available at ScienceDirect

Biochimica et Biophysica Acta

journal homepage: [www.elsevier.com/locate/bbalip](http://www.elsevier.com/locate/bbalip)

## Calpain-mediated ABCA1 degradation: Post-translational regulation of ABCA1 for HDL biogenesis<sup>☆</sup>

Shinji Yokoyama<sup>a,\*</sup>, Reijiro Arakawa<sup>b</sup>, Cheng-ai Wu<sup>b</sup>, Noriyuki Iwamoto<sup>b</sup>,  
Rui Lu<sup>a</sup>, Maki Tsujita<sup>b</sup>, Sumiko Abe-Dohmae<sup>b</sup>

<sup>a</sup> Food and Nutritional Sciences, College of Bioscience and Biotechnology, Chubu University, Matsumoto-cho 1200, Kasugai 487-8501, Japan

<sup>b</sup> Biochemistry, Graduate School of Medical Sciences, Nagoya City University, Kawasumi 1, Mizuho-cho, Mizuho-ku, Nagoya 467-8601, Japan

### ARTICLE INFO

#### Article history:

Received 28 May 2011

Received in revised form 20 July 2011

Accepted 26 July 2011

Available online 31 July 2011

#### Keywords:

ABCA1

Calpain

HDL

Cholesterol

Atherosclerosis

### ABSTRACT

Helical apolipoproteins remove cellular phospholipid and cholesterol to generate nascent HDL and this reaction is the major source of plasma HDL. ABCA1 is mandatory and rate-limiting for this reaction. Besides regulation of the gene expression by transcriptional factors including LXR, AP2 and SREBP, the ABCA1 activity is regulated post-translationally by calpain-mediated proteolytic degradation of ABCA1 protein that occurs in the early endosome after its endocytosis. When the HDL biogenesis reaction is ongoing as helical apolipoproteins interact with ABCA1, ABCA1 becomes resistant to calpain and is recycled to cell surface after endocytosis. Biogenesis of HDL is most likely to take place on cell surface. Clearance rate of ABCA1 by this mechanism is also retarded by various factors that interact with ABCA1, such as  $\alpha$ 1-syntrophin, LXR $\beta$  and calmodulin. Physiological relevance of the retardation by these factors is not entirely clear. Pharmacological inhibition of the calpain-mediated ABCA1 degradation results in the increase of the ABCA1 activity and HDL biogenesis in vitro and in vivo, and potentially suppresses atherogenesis. This article is part of a Special Issue entitled Advances in High Density Lipoprotein Formation and Metabolism: A Tribute to John F. Oram (1945–2010).

© 2011 Elsevier B.V. All rights reserved.

### 1. Introduction

Generation of high density lipoprotein (HDL) particles by interaction of helical apolipoprotein with cells was first described by Hara and Yokoyama in 1991 [1]. When mouse peritoneal macrophages are exposed to helical apolipoproteins such as apoA-I, apoA-II and apoE, lipoprotein particles are generated by removing cellular phospholipid and cholesterol to meet the criteria of HDL with respect to density, electrophoretic mobility [1] and reactivity to lecithin: cholesterol acyltransferase [2]. The reaction was found lacking in the fibroblasts from the patients of Tangier disease [3], genetic deficiency of HDL, and in the cells given probucol [4] that is known to reduce plasma HDL, and was predicted by Oram and Yokoyama as the major source of plasma HDL [5]. ATP-binding cassette transporter (ABC) A1 was identified responsible for this reaction, as mutations of its gene in Tangier patients [6–8].

The major up-regulatory factor for the ABCA1 gene expression is the liver X-receptor (LXR) [9–11] to sense oxysterol as a marker of cell

cholesterol increase. This mechanism indicates that primary function of the ABCA1/apolipoprotein system is to reduce cell cholesterol by exporting it generating HDL particles, although the particles are assembled primarily with cell phospholipid and incorporation of cholesterol into the particles is a secondary reaction [12]. On the other hand, expression of the ABCA1 gene is negatively regulated by such factors as AP2 [13,14] and SREBP [15]. The latter was found specific in the liver of the rodents, perhaps to function to maintain cholesterol homeostasis for the whole body by retaining cholesterol recovered by the liver from the peripheral tissues against the ABCA1/apolipoprotein system. Thus, ABCA1 is one of the very important players for cholesterol homeostasis in cells and in the whole body.

Post-translational regulation of ABCA1 expression seems also important for modulation of its activity. Oram et al. first pointed out that clearance of ABCA1 is one of the important factors for regulation of HDL biogenesis [16]. Like many other membrane proteins, ABCA1 also undergoes lysosomal degradation [17] or ubiquitin-mediated proteolytic degradation [18]. However, it is not very clear how these systems are involved in turnover of ABCA1 for regulation of its activity and HDL metabolism. On the other hand, calpain was found to degrade ABCA1 in a more specific manner [19,20]. It is perhaps more clearly involved in regulation of the activity of ABCA1 for biogenesis of HDL and accordingly in HDL metabolism and cholesterol homeostasis than other proteolytic systems.

<sup>☆</sup> This article is part of a Special Issue entitled Advances in High Density Lipoprotein Formation and Metabolism: A Tribute to John F. Oram (1945–2010).

\* Corresponding author. Tel.: +81 568 1712x5581; fax: +81 52 853 8304.

E-mail address: [syokoyam@med.nagoya-cu.ac.jp](mailto:syokoyam@med.nagoya-cu.ac.jp) (S. Yokoyama).

### 1.1. Calpain-mediated degradation of ABCA1 and its stabilization by helical peptides

Wang and Oram reported that HDL biogenesis is down-regulated by the increase of cellular unsaturated free fatty acids, and ABCA1 degradation was found enhanced in such a condition [21]. Natural degradation rate of ABCA1 is with a half-life of less than an hour [19,21], and this rapid clearance is effectively inhibited by cysteine protease inhibitors [19], and more specifically by a calpain inhibitor [20,22]. A calpain-specific cleavage site Pro-Glu-Ser-Tyr (PEST) sequence is identified in the cytosolic region in the middle of the ABCA1 molecule and deletion of this sequence results in its stabilization [20].

Interestingly, ABCA1 increased when HDL apoproteins such as apoA-I or apoA-II were added to the culture medium to induce HDL biogenesis [19]. This increase was found not due to the increase of either transcriptional or translational stage of ABCA1, but to the decrease of the clearance rate of ABCA1. However, when HDL was added as a whole particle, decrease of the ABCA1 clearance rate was much less on the basis of standardized protein mass [19]. Therefore, apoA-I/apoA-II must act in their free forms for this reaction, similarly to their reaction to generate HDL particles [23–25]. Thus, HDL apolipoproteins were shown to stabilize ABCA1 against the degradation by calpain. This finding implicates that half-life of ABCA1 may not be so rapid *in vivo* as observed with the cells in culture since most of the cells including somatic and floating cells are likely exposed to free apolipoproteins, especially apoA-I, in the concentration near or higher than  $K_m$  for the reaction of HDL biogenesis (a few microgram/ml) by interacting with ABCA1. Clearance rate of ABCA1 is indeed retarded in the hepatic cells in culture that secrete substantial amount of apoA-I to generate HDL in an autocrine reaction [25]. ABCA1 is stabilized not only by most of helical apolipoproteins such as apoA-I, A-II, E and Cs but also by amphiphilic helical peptides of 37 residues, as was demonstrated for HDL biogenesis reaction [22]. ABCA1 stabilization was also achieved both by L and D peptides [22], showing that physicochemical property is more essential than biological properties of the peptides. Similar findings were with ABCA7, a homologue of ABCA1 that is involved in cellular phagocytotic function. ABCA7 is stabilized against calpain-mediated degradation by helical apolipoproteins, resulting in enhancement of phagocytosis [26].

Phosphorylation of a PEST sequence in ABCA1 seems to enhance its degradation by calpain and apoA-I modulates this process in stabilization [27]. Enhancement of ABCA1 degradation by unsaturated fatty acids is also reported to be mediated by phosphorylation at the PEST sequence [21]. On the other hand, overall phosphorylation of ABCA1 is shown proportional to its stabilization by various helical apolipoproteins and peptides [22], which is apparently protein kinase C- $\alpha$  dependent [28]. Roles of this modification are unknown in regulation of ABCA1 activity.

### 1.2. Endocytosis and recycle of ABCA1 in HDL biogenesis

It has been reported that during the HDL biogenesis reaction, apoA-I is internalized and secreted by exocytosis [29,30]. To investigate this process, surface ABCA1 was traced by using a biotin-labeling technique [31]. ABCA1 is internalized rapidly, and degraded by calpain after this internalization perhaps in the endosomes. Small portion of ABCA1 escapes the degradations and is recycled to cell surface. Inhibition of calpain does not influence the endocytosis process, and apoA-I does not influence this rapid ABCA1 endocytosis either. ABCA1 becomes resistant against calpain-mediated proteolysis when it is pre-exposed to extracellular apoA-I before the endocytosis. When ABCA1 becomes resistant to calpain by apoA-I, a large portion of the internalized ABCA1 is recycled to the surface (Fig. 1). Thus, in the presence of extracellular free apolipoproteins, ABCA1 is stabilized and recycled between the cell surface and the endosomes as HDL

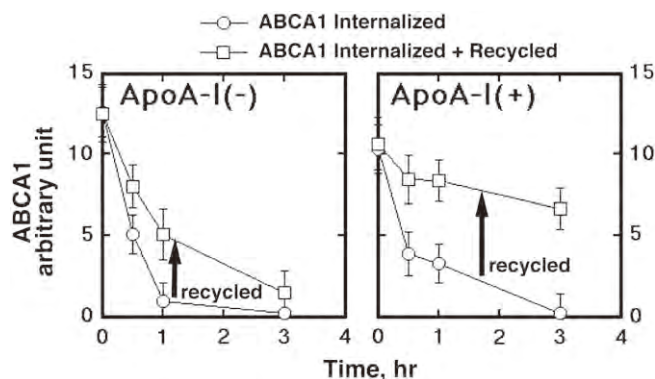


Fig. 1. Recycle of ABCA1 to the cell surface of BALB3/3T3 (modified from the figure in reference [31]). ABCA1 was pre-labeled by biotinylation of surface protein at 4 °C for 30 min, incubated for 1 h at 37 °C, and remaining surface biotinylation was cleaved to detect internalized ABCA1 as biotinylated molecules (zero time). After further incubation, surface biotinylation was cleaved again and the biotinylated ABCA1 was analyzed. “Circles”; intracellular ABCA1 after the second cleavage. “Squares”; intracellular plus surface, without the second cleavage. The results of digital scanning are demonstrated.

biogenesis reaction is ongoing [31]. It is therefore likely that apoA-I, and perhaps other helical apolipoproteins and amphiphilic peptides physically interact with ABCA1 to stabilize it against calpain (Fig. 2).

When the endocytosis of ABCA1 is inhibited by cytochalasin D, ABCA1 accumulates in the cell surface even in the presence of apoA-I and the biogenesis of HDL increased proportionally to the surface ABCA1 [31]. This finding strongly indicates that HDL biogenesis reaction with the membrane lipid takes place on cell surface [32]. It is however reported that assembly of the HDL particles may take place intracellularly when cholesterol over-accumulates in the cells [33]. As calpain inhibitors increases HDL biogenesis, calpain is likely to attack ABCA1 at the early endosomes.

### 1.3. Factors to modulate ABCA1 degradation

Some intracellular factors are found to interact with ABCA1, modulate its degradation and are accordingly involved in regulation of ABCA1 activity. A PDZ protein,  $\alpha$ 1-syntrophin, interacts with ABCA1

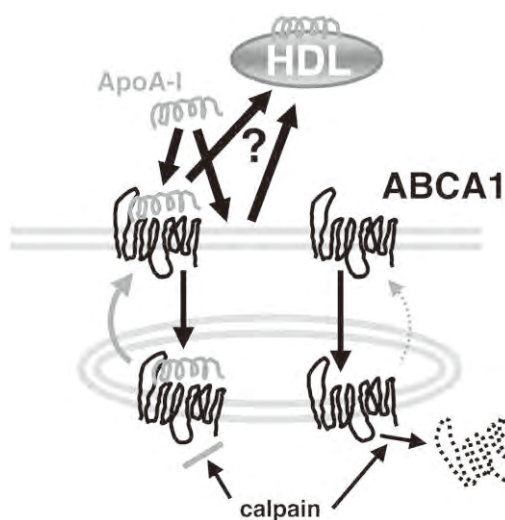
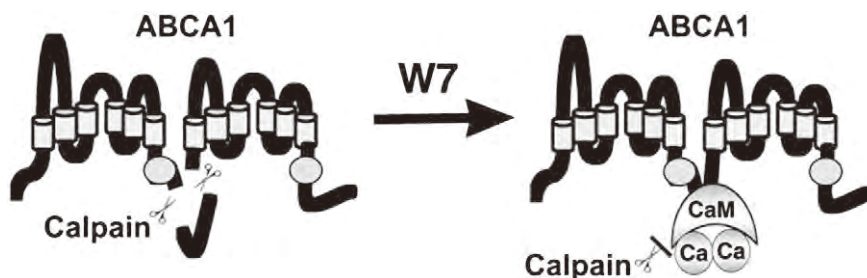


Fig. 2. A model diagram for calpain-mediated degradation. ABCA1 is internalized and degraded in the early endosome. When apoA-I or any other helical apolipoproteins interact with ABCA1, it becomes resistant to calpain and recycles to the cell surface. HDL biogenesis takes place at the cell surface, but it is yet unknown exactly how. HDL biogenesis mechanism is still controversial whether the ABCA1-bound apoA-I is responsible or apoA-I interacts with membrane lipids “destabilized” by ABCA1.



**Fig. 3.** Model diagram for stabilization of ABCA1 by calmodulin (CaM) and its modulation by W7. (modified from the figure in reference [37]). ABCA1 is cleaved by calpain presumably at the two positions in the cytoplasmic loop domain. One is within PEST sequence, and the other is the N terminus domain of the 1-5-8-14 motif. Calmodulin interacts with ABCA1 by the cytoplasmic loop in a  $Ca^{2+}$ -dependent manner and protects it from proteolysis by calpain. W7 increases calmodulin binding to ABCA1 to protect it from calpain.

at the C-terminal [34]. Clearance rate of ABCA1 is markedly retarded when the two proteins were co-expressed [34]. A nuclear transcriptional factor LXR $\beta$  directly interacts with ABCA1 also at the C-terminal, and retards its degradation [35]. Cellular cholesterol level apparently regulates this interaction, showing that this may be an extra-nuclear function of this factor for regulation of cellular cholesterol homeostasis [36]. Calmodulin binds ABCA1 at the specific interacting site nearby PEST sequence and retards its degradation [37]. Interestingly, a calmodulin inhibitor W7 increases this interaction and accordingly stabilizes ABCA1 [37] (Fig. 3). This is consistent with our previous finding that W7 increases HDL biogenesis by apoA-I-cell interaction [38].

1.4. ABCA1 degradation as a potential target of antiatherogenic treatment

As mentioned in the sections above, calpain-mediated degradation is one of the major mechanisms to regulate the function of ABCA1 to mediate biogenesis or assembly of HDL particles with apolipoproteins

and membrane lipid. We previously observed that probucol, a lipid lowering drug once popular before statins appear in the market, inactivates ABCA1 for HDL biogenesis and this should be considered as a cause of severe reduction of HDL by this drug [4,39]. However, probucol was also found to stabilize ABCA1 against calpain at the same time [40]. We therefore explored probucol derivatives to find out whether any of them may retain only the activity to stabilize ABCA1 but not to inhibit HDL biogenesis. Since probucol is a strong antioxidant molecule, its oxidative products were examined for these activities [41]. Among the stable oxidative products, spiroquinone and diphenoquinone were shown to increase HDL biogenesis by the ABCA1/apoA-I pathway [41]. As expected, ABCA1 degradation was retarded by both of these compounds (Fig. 4) without changing its message and without impairing its HDL biogenesis activity [41]. When the compounds were given to mice, plasma HDL significantly increased without changing ABCA1 mRNA in the liver. By using a biotin-labeling technique for surface ABCA1, spiroquinone and diphenoquinone both were shown to interfere with ABCA1 internalization [41] (Fig. 5). Those compounds increase HDL biogenesis even in cholesterol-laden macrophages [41], supporting the idea that HDL biogenesis takes place at cell surface even in such cells.

Cholesterol-fed rabbits were used as a model for atherogenesis. Spiroquinone or diphenoquinone was given for 8 weeks by monitoring plasma lipoproteins and various signs of potential side effects including the liver functions [41]. Plasma HDL increased by both of these compounds throughout the experimental periods, without significant changes in the liver functions and other vital signs. At the end of the period, lipid deposits in the aorta were examined. Both

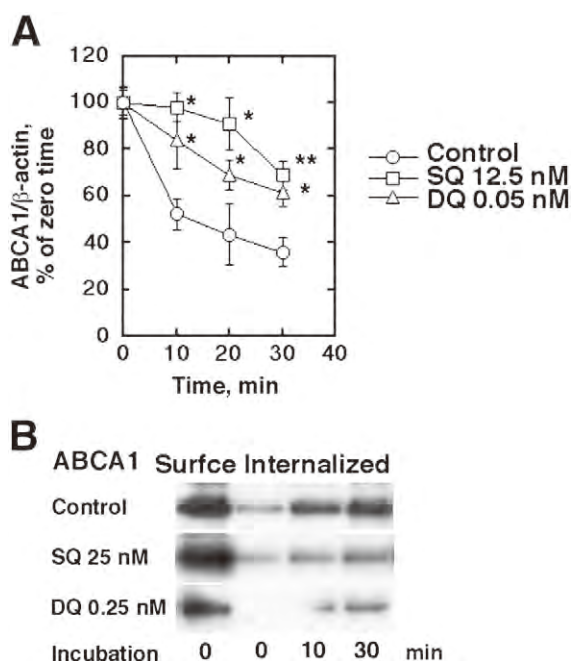


**Fig. 4.** Stabilization of ABCA1 by SQ and DQ in THP-1 macrophages (modified from the figure in reference [41]). A. Retarded degradation of ABCA1 in the presence of SQ and DQ. Error bars indicate SE for three measurements. Significant difference from control at each time point is indicated as \*  $p < 0.05$  and \*\*  $p < 0.01$ . B. Internalization of ABCA1. Left panel: cells were pre-incubated with SQ (25 nM) and DQ (0.25 nM) for 16 h to equilibrate the cells with the compounds. The surface ABCA1 was then labeled by biotinylation and the cells were incubated for time indicated. The surface biotinylation was cleaved and the remaining biotinylated ABCA1 was analyzed as the protein internalized.

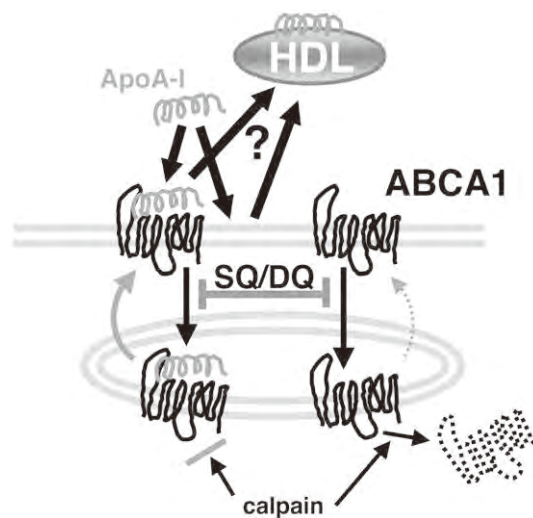


**Fig. 5.** A model diagram for the action of spiroquinone and diphenoquinone. Both compounds interfere with internalization of ABCA1 and consequently reduce its degradation by calpain.

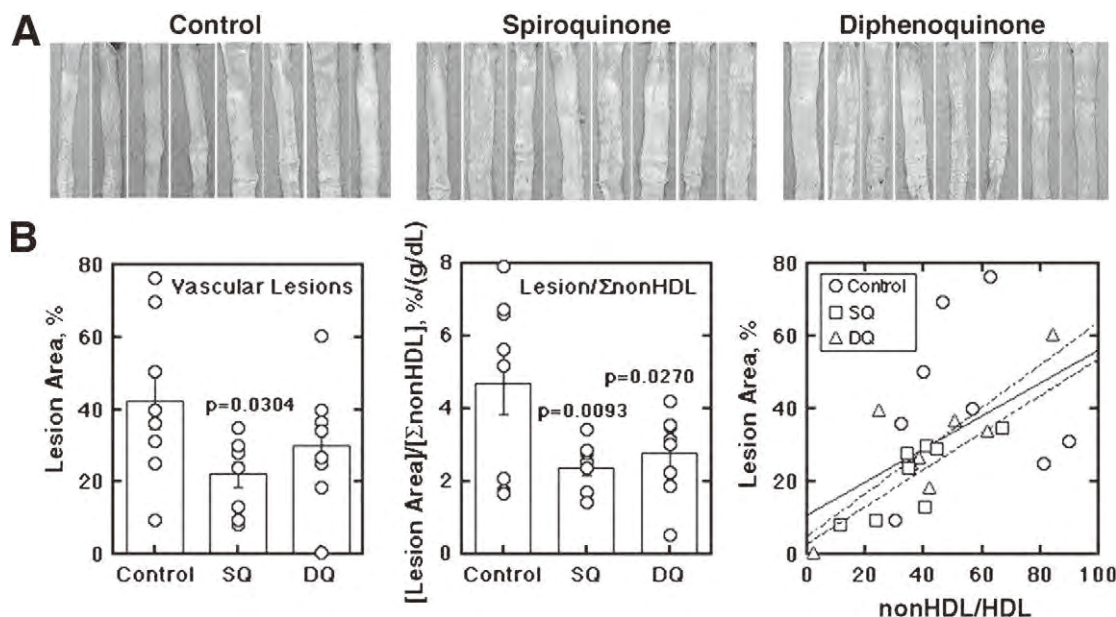


**Fig. 6.** Effects of SQ and DQ on vascular lipid deposit in cholesterol-fed rabbits. (taken from reference [41]). After 8 weeks of the experiments described in Fig. 4, lipid deposit in the aortic wall was evaluated by Oil Red-O staining. A. Lipid deposit in the thoracic and abdominal aorta. B. Digitalized images were analyzed by an image processing software. Left panel, the lesion relative area (%). Middle panel, the relative lesion area standardized by the integrated non-HDL-cholesterol in each animal. Right panel, plot of the relative lesion area (%) against the index of (integrated non-HDL-cholesterol)/(integrated HDL-cholesterol). Solid line represents fitting for all the groups ( $y = 0.46x + 11.2$ ,  $r = 0.528$ ); Even-broken line for the SQ-fed group ( $y = 0.51x + 3.3$ ,  $r = 0.81$ ); and uneven-broken line for the DQ group ( $y = 0.59x + 5.2$ ,  $r = 0.83$ ).

spiroquinone and diphenylquinone significantly reduced lipid deposit in the aorta [41] (Fig. 6).

In summary, calpain-mediated proteolytic degradation is one of the important regulatory mechanisms of physiological relevance for the ABCA1 activity of HDL biogenesis. The degradation takes place at the early endosomes after ABCA1 is internalized. When ABCA1 interacts with helical apolipoproteins, ABCA1 becomes resistant to calpain and is recycled to cell surface. Calpain apparently cleaves ABCA1 at the PEST sequence in the cytosolic loop in the middle of the molecule. The proteolysis seems enhanced by phosphorylation at this region, which is suppressed by apolipoprotein and increased by unsaturated fatty acids in the membrane. Helical apolipoproteins induce overall phosphorylation of ABCA1 as stabilizing ABCA1, but its physiological relevance is unknown. HDL biogenesis largely takes place at cell surface, but intracellular assembly of HDL in the cholesterol-laden cells remains controversial. ABCA1 degradation is modulated by various intracellular factors that interact with ABCA1. Inhibition of calpain-mediated degradation of ABCA1 results in the increase of HDL biogenesis and may lead to prevention or regression of atherosclerosis.

## References

- [1] H. Hara, S. Yokoyama, Interaction of free apolipoprotein with macrophages: formation of high density lipoprotein-like lipoproteins and reduction of cellular cholesterol, *J. Biol. Chem.* 266 (1991) 3080–3086.
- [2] H. Czarnecka, S. Yokoyama, Lecithin: cholesterol acyltransferase reaction on cellular lipid released by free apolipoprotein-mediated efflux, *Biochemistry* 34 (1995) 4385–4392.
- [3] G.A. Francis, R.H. Knopp, J.F. Oram, Defective removal of cellular cholesterol and phospholipids by apolipoprotein A-I in Tangier disease, *J. Clin. Invest.* 96 (1995) 78–87.
- [4] M. Tsujita, S. Yokoyama, Selective inhibition of free apolipoprotein-mediated cellular lipid efflux by probucol, *Biochemistry* 35 (1996) 13011–13020.
- [5] J.F. Oram, S. Yokoyama, Apolipoprotein-mediated removal of cellular cholesterol and phospholipids, *J. Lipid Res.* 37 (1996) 2473–2491.
- [6] M. Bodzioch, E. Orso, J. Klucken, T. Langmann, A. Bottcher, W. Dierich, W. Drobnic, S. Barlage, C. Buchler, M. Porsch-Ozucurumez, W.E. Kaminski, H.W. Hahmann, K. Oette, G. Rothe, C. Aslanidis, K.J. Lackner, G. Schmitz, The gene encoding ATP-binding cassette transporter 1 is mutated in Tangier disease, *Nat. Genet.* 22 (1999) 347–351.
- [7] A. Brooks-Wilson, M. Marcil, S.M. Clee, L.-H. Zhang, K. Roomp, M.v. Dam, C. Brewer, J.A. Collins, H.O.F. Molhuizen, D. Loubser, B.F.F. Ouellette, K. Fechter, K.J.D. Asbourne-Excoffon, C. Sensen, S. Scherer, S. Mott, M. Denis, D. Martindale, J. Frohlich, K. Morgan, B. Koop, S. Pimstone, J.J.P. Kastelein, J.J. Genest, M.R. Hayden, Mutations in ABC1 in tangier disease and familial high-density lipoprotein deficiency, *Nat. Genet.* 22 (1999) 336–345.
- [8] S. Rust, M. Rosier, H. Funke, J. Real, Z. Amoura, J.-C. Piette, J.-F. Deleuze, H.B. Brewer, N. Duverger, P. Deneffe, G. Assmann, Tangier disease is caused by mutations in the gene encoding ATP-binding-cassette transporter 1, *Nat. Genet.* 22 (1999) 352–355.
- [9] K. Schwartz, R.M. Lawn, D.P. Wade, ABC1 gene expression and ApoA-I-mediated cholesterol efflux are regulated by LXR, *Biochem. Biophys. Res. Commun.* 274 (2000) 794–802.
- [10] P. Costet, Y. Luo, N. Wang, A.R. Tall, Sterol-dependent transactivation of the ABC1 promoter by the liver X receptor/retinoid X receptor, *J. Biol. Chem.* 275 (2000) 28240–28245.
- [11] A. Venkateswaran, B.A. Laffitte, S.B. Joseph, P.A. Mak, D.C. Wilpitz, P.A. Edwards, P. Tontonoz, Control of cellular cholesterol efflux by the nuclear oxysterol receptor LXR alpha, *Proc. Natl. Acad. Sci. U.S.A.* 97 (2000) 12097–12102.
- [12] Y. Yamauchi, S. Abe-Dohmae, S. Yokoyama, Differential regulation of apolipoprotein A-I/ATP binding cassette transporter A1-mediated cholesterol and phospholipid release, *Biochim. Biophys. Acta* 1585 (2002) 1–10.
- [13] N. Iwamoto, S. Abe-Dohmae, M. Ayaori, N. Tanaka, M. Kusuhara, F. Ohsuzu, S. Yokoyama, ATP-binding cassette transporter A1 gene transcription is down-regulated by activator protein 2alpha. Doxazosin inhibits activator protein 2alpha and increases high-density lipoprotein biogenesis independent of alpha1-adrenoceptor blockade, *Circ. Res.* 101 (2007) 156–165.
- [14] N. Iwamoto, S. Abe-Dohmae, R. Lu, S. Yokoyama, Involvement of protein kinase D in phosphorylation and increase of DNA binding of activator protein 2 alpha to downregulate ATP-binding cassette transporter A1, *Arterioscler. Thromb. Vasc. Biol.* 28 (2008) 2282–2287.
- [15] N. Tamehiro, Y. Shigemoto-Mogami, T. Takeya, K. Okuhira, K. Suzuki, R. Sato, K. Nagao, T. Nishimaki-Mogami, Sterol regulatory element-binding protein-2 and liver X receptor-driven dual promoter regulation of hepatic ABC transporter A1 gene expression: mechanism underlying the unique response to cellular cholesterol status, *J. Biol. Chem.* 282 (2007) 21090–21099.
- [16] Y. Wang, J.F. Oram, Unsaturated fatty acids inhibit cholesterol efflux from macrophages by increasing degradation of ATP-binding cassette transporter A1, *J. Biol. Chem.* 277 (2002) 5692–5697.
- [17] B. Haidar, R.S. Kiss, L. Sarov-Blat, R. Brunrt, C. Harder, R. McPherson, Y.L. Marcel, Cathepsin D, a lysosomal protease, reduces ABCA1-mediated lipid efflux, *J. Biol. Chem.* 281 (2006) 3997–3981.
- [18] M. Ogura, M. Ayaori, Y. Terao, T. Hisada, M. Iizuka, S. Takiguchi, H. Uto-Kondo, E. Yakushiji, K. Nakaya, M. Sasaki, T. Komatsu, H. Ozasa, F. Ohsuzu, K. Ikewaki, Proteasomal Inhibition Promotes ATP-Binding Cassette Transporter A1 (ABCA1) and ABCG1 Expression and Cholesterol Efflux From Macrophages In Vitro and In Vivo, *Arterioscler. Thromb. Vasc. Biol.* 31 (2011) 1980–1987.
- [19] R. Arakawa, S. Yokoyama, Helical apolipoproteins stabilize ATP-binding cassette transporter A1 by protecting it from thiol protease-mediated degradation, *J. Biol. Chem.* 277 (2002) 22426–22429.

- [20] N. Wang, W. Chen, P. Linsel-Nitschke, L.O. Martinez, B. Agerholm-Larsen, D.L. Silver, A.R. Tall, A PEST sequence in ABCA1 regulates degradation by calpain protease and stabilization of ABCA1 by apoA-I, *J. Clin. Invest.* 111 (2003) 99–107.
- [21] Y. Wang, J.F. Oram, Unsaturated fatty acids phosphorylate and destabilize ABCA1 through a phospholipase D2 pathway, *J. Biol. Chem.* 280 (2005) 35896–35903.
- [22] R. Arakawa, M. Hayashi, A.T. Remaley, B.H. Brewer Jr., Y. Yamauchi, S. Yokoyama, Phosphorylation and stabilization of ATP binding cassette transporter A1 by synthetic amphiphilic helical peptides, *J. Biol. Chem.* 279 (2004) 6217–6220.
- [23] H. Hara, S. Yokoyama, Role of apolipoproteins in cholesterol efflux from macrophages to lipid microemulsion: proposal of a putative model for the pre- $\beta$  high-density lipoprotein pathway, *Biochemistry* 31 (1992) 2040–2046.
- [24] K. Okuhira, M. Tsujita, Y. Yamauchi, S. Abe-Dohmae, K. Kato, T. Handa, S. Yokoyama, Potential involvement of dissociated apoA-I in the ABCA1-dependent cellular lipid release by HDL, *J. Lipid Res.* 45 (2004) 645–652.
- [25] M. Tsujita, C.-A. Wu, S. Abe-Dohmae, S. Usui, M. Okazaki, S. Yokoyama, On the hepatic mechanism of HDL assembly by the ABCA1/apoA-I pathway, *J. Lipid Res.* 46 (2005) 154–162.
- [26] N. Tanaka, S. Abe-Dohmae, N. Iwamoto, M.L. Fitzgerald, S. Yokoyama, Helical apolipoproteins of high-density lipoprotein enhance phagocytosis by stabilizing ATP-binding cassette transporter A7, *J. Lipid Res.* 51 (2010) 2591–2599.
- [27] L.O. Martinez, B. Agerholm-Larsen, N. Wang, W. Chen, A.R. Tall, Phosphorylation of a pest sequence in ABCA1 promotes calpain degradation and is reversed by ApoA-I, *J. Biol. Chem.* 278 (2003) 37368–37374.
- [28] Y. Yamauchi, M. Hayashi, S. Abe-Dohmae, S. Yokoyama, Apolipoprotein A-I activates protein kinase C $\alpha$  signaling to phosphorylate and stabilize ATP binding cassette transporter A1 for the high density lipoprotein assembly, *J. Biol. Chem.* 278 (2003) 47890–47897.
- [29] Y. Takahashi, J.D. Smith, Cholesterol efflux to apolipoprotein A-I involves endocytosis and resecretion in a calcium-dependent pathway, *Proc. Natl. Acad. Sci. U.S.A.* 96 (1999) 11358–11363.
- [30] L.E. Faulkner, S.E. Panagotopoulos, J.D. Johnson, L.A. Woollet, D.Y. Hui, S.R. Witting, J.N. Maiorano, W.S. Davidson, An analysis of the role of a retroendocytosis pathway in ABCA1-mediated cholesterol efflux from macrophages, *J. Lipid Res.* 49 (2008) 1322–1332.
- [31] R. Lu, R. Arakawa, C. Ito-Osumi, N. Iwamoto, S. Yokoyama, ApoA-I facilitates ABCA1 recycle/accumulation to cell surface by inhibiting its intracellular degradation and increases HDL generation, *Arterioscler. Thromb. Vasc. Biol.* 28 (2008) 1820–1824.
- [32] M. Denis, Y.D. Landry, X. Zha, ATP-binding cassette A1-mediated lipidation of apolipoprotein A-I occurs at the plasma membrane and not in the endocytic compartments, *J. Biol. Chem.* 283 (2008) 16178–16186.
- [33] Y. Azuma, M. Takada, H.W. Shin, N. Kioka, K. Nakayama, K. Ueda, Retroendocytosis pathway of ABCA1/apoA-I contributes to HDL formation, *Genes Cells* 14 (2009) 191–204.
- [34] Y. Munehira, T. Ohnishi, S. Kawamoto, A. Furuya, K. Shitara, M. Imamura, T. Yokota, S. Takeda, T. Amachi, M. Matsuo, N. Kioka, K. Ueda,  $\alpha$ 1-syntrophin modulates turnover of ABCA1, *J. Biol. Chem.* 279 (2004) 15091–15095.
- [35] M. Hozoji, Y. Munehira, Y. Ikeda, M. Makishima, M. Matsuo, N. Kioka, K. Ueda, Direct interaction of nuclear liver X receptor-beta with ABCA1 modulates cholesterol efflux, *J. Biol. Chem.* 283 (2008) 30057–30063.
- [36] M. Hozoji-Inada, Y. Munehira, K. Nagao, N. Kioka, K. Ueda, LXRBeta directly interacts with ABCA1 to promote HDL formation during acute cholesterol accumulation, *J. Biol. Chem.* 286 (2011) 20117–20124.
- [37] N. Iwamoto, R. Lu, N. Tanaka, S. Abe-Dohmae, S. Yokoyama, Calmodulin interacts with ATP binding cassette transporter A1 to protect from calpain-mediated degradation and upregulates high-density lipoprotein generation, *Arterioscler. Thromb. Vasc. Biol.* 30 (2010) 1446–1452.
- [38] S. Suzuki, S. Abe-Dohmae, T. Fukutomi, S. Ito, M. Itoh, S. Yokoyama, Enhancement of the cAMP-induced apolipoprotein-mediated cellular lipid release by calmodulin inhibitors W7 and W5 from RAW 264 mouse macrophage cell line cells, *J. Cardiovasc. Pharmacol.* 36 (2000) 609–616.
- [39] M. Tsujita, S. Tomimoto, K. Okumura-Noji, M. Okazaki, S. Yokoyama, Apolipoprotein-mediated cellular cholesterol/phospholipid efflux and plasma high density lipoprotein level in mice, *Biochim. Biophys. Acta* 1485 (2000) 199–213.
- [40] C. Wu, M. Tsujita, M. Hayashi, S. Yokoyama, Probuco inactivates ABCA1 in plasma membrane for its function to mediate apolipoprotein binding and HDL assembly and for its Proteolytic Degradation, *J. Biol. Chem.* 279 (2004) 30168–30174.
- [41] R. Arakawa, M. Tsujita, N. Iwamoto, C. Ito-Osumi, R. Lu, C. Wu, K. Shimizu, T. Aotsuka, H. Kanazawa, S. Abe-Dohmae, S. Yokoyama, Pharmacological inhibition of ABCA1 degradation increases HDL biogenesis and exhibits antiatherogenesis, *J. Lipid Res.* 50 (2009) 2299–2305.

## CD36-related protein in *Schistosoma japonicum*: candidate mediator of selective cholesteryl ester uptake from high-density lipoprotein for egg maturation

Kuniko Okumura-Noji,<sup>\*,†,‡</sup> Yutaka Miura,<sup>§</sup> Rui Lu,<sup>\*,†</sup> Kiyofumi Asai,<sup>§</sup> Nobuo Ohta,<sup>||,¶</sup>  
Paul J. Brindley,<sup>#</sup> and Shinji Yokoyama<sup>\*,†,‡,¶,1</sup>

\*Nutritional Health Science Research Centre and <sup>†</sup>Department of Food and Nutritional Sciences, Chubu University, Kasugai, Japan; <sup>‡</sup>Department of Biochemistry, <sup>§</sup>Department of Neurosciences, and <sup>||</sup>Department of Parasitology, Nagoya City University Graduate School of Medical Sciences, Nagoya, Japan; <sup>¶</sup>Department of Environmental Parasitology, Tokyo Medical and Dental University, Tokyo, Japan; and <sup>#</sup>Department of Microbiology, Immunology, and Tropical Medicine, School of Medicine and Health Sciences, George Washington University, Washington, District of Columbia, USA

**ABSTRACT** Familial cholesteryl ester transfer protein (CETP) deficiency is more common in some East Asian populations than elsewhere, suggesting the possibility of a selective advantage of this genetic defect against regional infectious diseases. Historically, infection with the Asian blood fluke *Schistosoma japonicum* has been endemic in these regions, including Japan. We previously reported that eggs of *S. japonicum* require cholesteryl ester uptake from normal high-density lipoprotein (HDL) but not from CETP-deficient HDL for their maturation to miracidia, a critical step of the hepatic pathogenesis of schistosomiasis. Herein we show that cholesteryl ester uptake is selective from HDL, and identified CD36-related protein (CD36RP) as a candidate to mediate the reaction. CD36RP was cloned from the adult and the egg developmental stages of *S. japonicum*, with 1880 bp encoding 506 amino acid residues exhibiting the CD36 domains and two transmembrane regions. Using antibodies against recombinant peptides representing the potential extracellular domains of CD36RP, Western blotting detected a protein with a molecular mass of 82 kDa in the particulate fraction of the adult parasite cells, which was reduced to 62 kDa after N-glycanase treatment. The extracellular domain peptide bound human HDL, as established by immunoblots following nondenaturing gel electrophoresis. Antibodies against the extracellular domain suppressed HDL cholesteryl ester uptake and maturation of the eggs *in vitro*. CD36RP is a candidate receptor on eggs of *S. japonicum* that facilitates uptake

of HDL cholesteryl ester necessary for egg embryonation and maturation.—Okumura-Noji, K., Miura, Y., Lu, R., Asai, K., Ohta, N., Brindley, P. J., Yokoyama, S. CD36-related protein in *Schistosoma japonicum*: candidate mediator of selective cholesteryl ester uptake from high-density lipoprotein for egg maturation. *FASEB J.* 27, 1236–1244 (2013). [www.fasebj.org](http://www.fasebj.org)

**Key Words:** CETP deficiency • miracidium • CETP • embryonation • hepatic granulomatosis • HDL

THE MAJOR AND FATAL PATHOGENESIS of schistosomiasis due to infection with *Schistosoma japonicum* or *Schistosoma mansoni* is ectopic implant of the eggs in the liver via the portal blood flow and their intrahepatic maturation to miracidia to cause hepatic granulomatogenesis and, accordingly, hepatic cirrhosis (1–5). Schistosomes take up lipids as their nutrient sources from the host blood plasma lipoproteins, and the receptors for low-density and very low density lipoproteins (LDLs and VLDLs) that mediate this interaction have been identified on their surfaces (6–9). On the other hand, it is not yet clear whether or not schistosomes use high-density lipoprotein (HDL) lipids as a nutrient source. In this regard, we previously showed that eggs of *S. japonicum* in culture require the presence of HDL to grow and develop to miracidia. Notably, maturation of schistosome eggs was significantly retarded when they were incubated with HDL from homozygous cholesteryl ester transfer protein (CETP)-deficient patients (10). In addition, expression of the CETP transgene significantly enhanced this process in mice that lack endog-

Abbreviations: apoA-I, apolipoprotein A-I; apoB-LP, apoB-containing lipoprotein; CD36RP, CD36-related protein; CETP, cholesteryl ester transfer protein; EndoH, endoglycosidase H; GSH, reduced glutathione; GST, glutathione S-transferase; HDL, high-density lipoprotein; LDL, low-density lipoprotein; N-acetylglucosaminidase, N-acetyl-β-D-glycosaminide-N-acetylglucosamino-hydrolase; N-glycanase, peptide-N-glycosidase F; PBS, phosphate buffered saline; SR-BI, scavenger receptor BI; VLDL, very low density lipoprotein

<sup>1</sup> Correspondence: Nutritional Health Science Research Centre and Food and Nutritional Sciences, Chubu University, Kasugai 487-8501, Japan. E-mail: [syokoyam@med.nagoya-cu.ac.jp](mailto:syokoyam@med.nagoya-cu.ac.jp)  
doi: 10.1096/fj.12-219816

This article includes supplemental data. Please visit <http://www.fasebj.org> to obtain this information.

enous CETP activity in plasma (10). These findings indicate that there is a specific pathway available to eggs of *S. japonicum* to utilize mammalian HDL lipid, including cholesterol or cholesteryl ester, to grow to miracidia. The abnormal HDL generated in the CETP-deficient plasma, large and cholesteryl ester-rich HDL, may not be a good substrate for such reactions. Thus, CETP deficiency may render humans resistant to hepatic maturation of eggs of *S. japonicum*, a phenomenon central to liver pathology characteristic of schistosomiasis japonica. We proposed that this could be a background behind the high prevalence of CETP deficiency in Far Eastern Asia (10–14).

Accordingly, we have undertaken an investigation to locate specific mediators of the schistosome parasite involved in interaction with human HDL lipids. We cloned a cDNA composed of 1880 bp encoding 506 aa that includes the CD36 domains and two transmembrane domains. Whereas functional expression of this protein remains to be accomplished, we now demonstrate binding of the proposed extracellular domain of a schistosome CD36-like glycoprotein to HDL, and suppression of cholesteryl uptake and maturation of the eggs by the antibody against this domain.

## MATERIALS AND METHODS

### Reagents commercially purchased or previously established

Anti-scavenger receptor BI (SR-BI) rabbit antisera (NB 400-101) was purchased from Novus Biologicals, Inc. (Littleton, CO, USA). Anti-apolipoprotein A-I (apoA-I) antibody was raised with rabbit against human apoA-I. Peptide-*N*-glycosidase F (*N*-glycanase) was purchased from PROzyme, Inc. (Hayward, CA, USA), endoglycosidase H (EndoH) was from Seikagaku Corp. (Tokyo, Japan), and *N*-acetyl- $\beta$ -D-glycosaminide-*N*-acetylglucosamino-hydrolase (*N*-acetylglucosaminidase) was from Calbiochem (Berlin, Germany). Anti-glutathione *S*-transferase (GST) antibodies were purchased from GE Healthcare (Piscataway, NJ, USA), and anti-RGS-His antibodies were from Qiagen (Valencia, CA, USA).

### Parasites and egg embryonation *in vitro*

*S. japonicum* (Yamanashi strain) was maintained by passage through *Oncomelania nosophora* and BALB/C mice (15,16). The pairs of adult worms were recovered from the portal vein of the infected mice and cultured as 1 pair/well of 12-well culture plates in RPMI 1640 medium supplemented with 5 or 10% human serum in 5% CO<sub>2</sub> atmosphere, as described previously (10). C57Black/6J mouse serum or lipoprotein-depleted serum was also used as a supplement in some experiments. For egg culture, the adult worms were removed from the wells after 2 d; eggs left in the wells were incubated further for 8 d in the same medium with or without 10% serum. After incubation for 10 d, the eggs were collected, the numbers of miracidia were counted microscopically, and the percentage of maturation was estimated as a maturation/embryonation rate.

### Cholesterol uptake from [<sup>3</sup>H], [<sup>14</sup>C] double-labeled HDL and binding of [<sup>3</sup>H]- or [<sup>125</sup>I]-HDL by *S. japonicum* eggs

HDL and apoB-containing lipoprotein (apoB-LP, including LDL and VLDL) fractions were prepared from fresh human

serum as density fractions at 1.063–1.21 g/ml and <1.063 g/ml, respectively, by sequential ultracentrifugation and labeled differentially with [<sup>1</sup> $\alpha$ ,2 $\alpha$ -<sup>3</sup>H]cholesteryl ester and [4-<sup>14</sup>C]cholesterol (Amersham, Piscataway, NJ, USA) as described previously (10). No [<sup>14</sup>C]cholesteryl ester was detected in lipoproteins after labeling. [<sup>125</sup>I]-labeled HDL was prepared as described previously (17), using [<sup>125</sup>I] (Amersham) and iodine chloride. Total and free cholesterol in the labeled lipoproteins were measured by Determiner L reagents (Kyowa Medex Co. Ltd., Tokyo, Japan). *S. japonicum* eggs were collected from the homogenates of the liver and the intestine of the *S. japonicum*-infected BALB/C mice by the digestion method (18), and incubated with [<sup>3</sup>H], [<sup>14</sup>C] double-labeled lipoproteins (70–280  $\mu$ g cholesterol/ml) in 0.5 ml RPMI 1640 in 12-well plates for 24 h at 37 or 4°C in 5% CO<sub>2</sub> atmosphere. The eggs were collected by centrifugation and washed with phosphate buffered saline (PBS), and the radioactivity of [<sup>14</sup>C] and [<sup>3</sup>H] in the egg pellet was analyzed. Uptake of free and esterified cholesterol was estimated by counting uptake of [<sup>14</sup>C] and [<sup>3</sup>H] radioactivity, respectively (10). Active uptake was determined by the difference between the results at 37 and 4°C. To observe selectivity of the lipid uptake, 10 vol of cold HDL or apoB-LP was added before adding the labeled HDL. HDL binding was also studied in parallel with [<sup>3</sup>H]cholesteryl ester-labeled HDL and [<sup>125</sup>I]-labeled HDL. Use of human plasma lipoprotein was justified by institutional guidelines and approval of Nagoya City University.

### RNA isolation, cDNA synthesis, and PCR amplification

Total RNA was extracted from the adult *S. japonicum* by using Isogen (Nippon Gene, Toyama, Japan). From 1 or 2  $\mu$ g of total RNA, first-strand cDNA was synthesized by a SuperScriptII RT-PCR system (Invitrogen, Carlsbad, CA, USA) with random hexamer primers, according to the manufacturer's instruction. To search a new CD36 family protein in *S. japonicum*, the sequence of coding region of Sj-Ts2 protein consisting of 671 bp (Genbank AF291715), which appeared to have one of the CD36 domains defined by Prodom (release 2001.3; <http://prodom.prabi.fr>) analysis of the U.S. National Center for Biotechnology Information (NCBI) database, was used for preparation of the hybridization probes for Northern blot analysis and for screening of the *S. japonicum* adult cDNA library. First-strand cDNA was amplified by PCR using the specific primers for Sj-Ts2 protein: sense, 5'-TAATGAAATG-AATACAGTC-3'; antisense, 5'-AACAAACATATAATGACAAT-3'; and for GAPDH: sense, 5'-TGTACTCCGTGCAGCTTTTC-3'; antisense, 5'-AATGGATCCCTCTCGCAGTA-3' (synthesized by Hokkaido System Science, Sapporo, Japan). The PCR products (488 and 198 bp) were purified by gel extraction and ligated in pGEM-T Easy vector (Promega, Madison, WI, USA). Ligation products were transformed into DH10B competent cells, and the sequences of inserts of positive clones were analyzed with T7 primer by using Applied Biosystems 3100 DNA sequencer (Applied Biosystems, Foster City, CA, USA). The 488-bp PCR product corresponded to nucleotide positions 5–492, consisting of coding region of Sj-Ts2 protein mRNA. For screening of the *S. japonicum* egg cDNA library, another probe was obtained by PCR using the specific primers for CD36-related protein (CD36RP): sense, 5'-CCGT-GAAAAACGTTTGAAGC-3'; antisense, 5'-AACATCATTGGATT-GATGGCTA-3'. The resulting PCR product size was 1177 bp. To analyze the size of the coding region of egg CD36RP, first-strand cDNA from *S. japonicum* adults or eggs was amplified by PCR using the 5' primer with *Kpn*I site addition (5'-GCGTGGTACCTCTTGTACACCGATGATATCTCG-3') and GSP2 primer (below). PCR analysis with the center-region primer was also carried out: sense (L1), 5'-CCGTGAAAAACGT-

TTGAAGC-3'; antisense (R3), 5'-GTGCACCAGGTTGACATGA-3'. The PCR product corresponds to positions 321–1060 of CD36RP. Quantitative RT-PCR analysis was performed in a 7300 Realtime PCR System (Applied Bioscience) by using probe sets of 5'-primer GSP2 and L1-GSP2.

#### Northern blot analysis

Total RNA (10 µg) from mixed-sex adult *S. japonicum* worms was electrophoresed in 1.0% agarose-formaldehyde gel and transferred to nylon membranes. The 489-bp fragment of Sj-Ts2 cDNA and 198-bp fragment of *S. japonicum* GAPDH cDNA were purified by SigmaSpin column (Sigma-Aldrich, St. Louis, MO, USA) and labeled with [ $\alpha$ -<sup>32</sup>P]dCTP by using Klenow fragment, *Escherichia coli* DNA polymerase I (Takara Bio, Otsu, Japan), and hybridized to the membrane in a 5× SSPE hybridization solution containing 20% formamide at 42°C for 16 h. After washing, hybridization signals were detected by autoradiography on X-Omat film (Eastman Kodak, Rochester, NY, USA).

#### Screening and sequencing of CD36-related protein

Two cDNA-libraries (2×10<sup>4</sup> pfu) derived from *S. japonicum* adult (China) and eggs (Philippine) (19) were amplified using *E. coli* XL1-blue host cells (Stratagene, La Jolla, CA, USA) followed by plating and incubating at 37°C overnight. Plates were transferred to nylon membrane (Hybond-N+; Amersham), after which membranes were hybridized to the <sup>32</sup>P-labeled 488-bp probe (for *S. japonicum* adult) or 1177-bp probe (for *S. japonicum* eggs) in similar fashion as for the Northern blot analysis (above), except that 6× SSC solution containing 15% formamide was employed. Secondary screening was carried out after selection of positive phage plaques, and the final positive plaques were excised into SOLR cells by using the pBluescript II phagemid vector kit (Stratagene). Sequence analysis of the inserts was performed by using T3, T7, and the specific primer Sj-Ts2. For determination of 5' end sequencing, 5' RACE was carried out by the Gibco 5'RACE system, ver.2 kit (Gibco, Carlsbad, CA, USA), using two primers: GSP1, 5'-ATTGAATCCATGCGTTGACA-3'; GSP2, 5'-AGAAACCATGGCATTGAATTG-3'. The nucleotide sequence (1892 bp) and amino acid sequence (506 aa) of the product have been assigned Genbank accession no. AY496973 and termed CD36RP of *S. japonicum* (Supplemental Fig. S1).

#### Recombinant CD36RP

To prepare the antigens for anti-CD36RP antibodies, cDNA from *S. japonicum* adults was amplified by PCR with specific primers: sense, 5'-ATGGTAGTGTGGAACATT-3'; antisense, 5'-ATTGGTAGAAGAGTAGTTGA-3'. This PCR product, corresponding to the positions 797–1280 and coding the predicted extracellular half region, Ex160 (aa G249-P408, 160 residues) of CD36RP (see Fig. 7), was ligated first into pGEM-T Easy and then into the bacterial expression vector, pQE30 (Qiagen). For analysis of lipoprotein binding, a shorter discrete extracellular fragment of CD36RP, Ex121 (aa G249-Y369, 121 residues; see Fig. 7) was expressed as a GST-fusion protein in *E. coli*, BL21 with pGEX-6p vector (Amersham). GST-fusion proteins of full size CD36RP and Ex121 in the lysates of BL21 cells were adsorbed to reduced glutathione (GSH)-Sepharose gels, and the GST-free proteins were obtained in the supernatant in 50 mM TBS, 1 mM DTT, and 1 mM EDTA from GSH-Sepharose gels by treatment with PreScission Protease (GE Healthcare), according to the protocol of the kit.

#### Raising antibodies against CD36RP

The expression and purification of this His-tagged protein product (Ex160), as well as immunization of rabbits with Ex160, were carried out by Medical and Biological Laboratory. Co. Ltd. (MBL; Nagoya, Japan). An IgG fraction was affinity purified from polyclonal antiserum against Ex160 for Western blotting. Peptides 331-348, CQPGAPIVVSQPHFLNAN, amino acid residues 331-348 of CD36RP were synthesized and used by MBL to immunize rabbits.

#### Homology search

Homology and structural analysis of predicted polypeptides was carried out by using BLAST-X (20), BLOCKS (21), PROSITE motif analysis (22), and PHD searching (23) from the NCBI database.

#### Western blotting analysis

*S. japonicum* adult worms and mouse liver were sonicated for 5 s in hypotonic 50 mM phosphate buffer (pH7.4), containing protease inhibitor cocktail (Sigma-Aldrich). For preparation of the particulate fraction of *S. japonicum* eggs, freeze-thawing and sonication were repeated 10 times. After removing cell debris and nuclei by centrifugation at 1000 rpm for 5 min, the supernatant was further treated by centrifugation at 90,000 rpm for 30 min (Himac model CS120GX centrifuge; Hitachi, Tokyo, Japan). Both the pelleted particulate fraction and the supernatant cytosol fraction were solubilized in 1% SDS sample buffer and subjected to 10% SDS-PAGE, after which gel contents were transferred to polyvinylidene fluoride membrane (Bio-Rad). Western blotting analysis was carried out using 1:1,000 dilution of the rabbit anti-Ex160 IgG or anti-SR-BI antiserum and 1:10,000 horseradish peroxidase-conjugated goat anti-rabbit IgG secondary antibody. For detection of recombinant protein Ex121, a 1:500 dilution of rabbit anti-peptide 331-348 (anti-P) antibody was used. A 1:200,000 dilution of the anti-human apoA-I rabbit serum was used for detection of apoA-I in HDL.

#### Deglycosylation of particulate fractions

The particulate fractions of *S. japonicum* adults (48 µg protein) and mouse liver particulate fractions (100 µg protein) were suspended and heated at 100°C in the denaturing solution containing 0.1% SDS and 50 mM β-mercaptoethanol, and after addition of 0.75% Nonidet P-40 detergent, reacted with 10 mU N-glycanase in 50 µl for overnight at 37°C or room temperature, according to the manufacturer's protocol. In some cases, 35 mU N-acetyl-glucosaminidase was added to the reaction mixtures. The particulate fraction of *S. japonicum* eggs was incubated with 10 mU EndoH at 37°C for 1 h. Subsequently, reaction mixtures were solubilized with SDS sample buffer and subjected to SDS-PAGE for Western blot analysis.

#### Lipoprotein binding of recombinant Ex121

Ex121 preparation (1 or 2 µl) was incubated with 5–30 µg (protein) of human HDL or LDL in 8–12 µl PBS at room temperature for 30 min, and then mixed with native sample buffer (62 mM Tris-HCl, pH 6.8; 10% sucrose; and 0.1% bromphenol blue), followed by application to nondenaturing PAGE with 4%–20% gradient Tris-Gly gel (Invitrogen). Two parallel samples were run; one was analyzed with the anti-P antibody and the other with the anti-apoA-I antibody. The

reference positions of lipoproteins were identified by staining with Coomassie Brilliant Blue and prestaining with Sudan black.

## RESULTS

### Dependence on HDL of *S. japonicum* egg embryonation

Maturation and embryonation of *S. japonicum* eggs was investigated during the culture by counting formation of miracidia. The eggs were cultured with or without 10% pooled human serum for 8 d after separation from the parent adults precultured for 2 d in medium containing 5 or 10% serum. Embryonation significantly decreased without serum supplementation when the eggs were laid by parents precultured in 5% serum, while the maturation proceeded even without serum when the parent flukes were precultured in 10% serum (15.8 vs. 38.0%; Fig. 1A). When the apoB-LP-deficient serum (bottom fraction of  $d=1.063$  g/ml) was used for culture of the eggs, the eggs from the 5% serum-treated parents achieved the similar level of embryonation (Fig. 1B). Egg embryonation was estimated in the medium after pairs of *S. japonicum* worms were incubated for 10 d with and without HDL fraction ( $1.063 < d < 1.21$ ) in addition to the lipoprotein-deficient serum ( $d > 1.21$ ) at the equivalent concentration of 10% serum. Egg embryonation by HDL reached a similar level to that by 10% serum, but lipoprotein deficient serum alone showed little or no maturation (Fig. 1C).

The results indicated that the egg maturation requires serum nutrients. Preconditioning of the parents or the eggs in the early stage by exposure to well-supplemented nourishment overcomes insufficient nourishment in the later stage. Nutritional support for the adults is perhaps primarily essential to deposit egg yolk/vitelline materials for embryonation, but the eggs also are able to take up nutrients from serum to grow even when they were laid in an insufficiently nourished condition. ApoB-LPs were shown not to be functional, but a normal HDL fraction is essential for egg maturation. Interestingly, minimal embryonation of the eggs was seen in culture medium containing 10% serum from wild-type mice, which is deficient in CETP,

whereas the maturation proceeded well in medium containing serum from CETP-transgenic mice or wild-type mouse serum presupplemented with human CETP (ref. 24 and Fig. 1D), supporting our previous findings (10).

### Uptake of cholesterol and cholesteryl ester from HDL *S. japonicum* eggs

To characterize association of HDL with the *S. japonicum* eggs, HDL was labeled with [<sup>3</sup>H]cholesteryl ester or <sup>125</sup>I on the HDL protein, and association of their radioactivity with *S. japonicum* eggs was determined. Apparent association of HDL was estimated as its protein based on specific radioactivity of HDL. As shown in Fig. 2A, [<sup>3</sup>H]-based association, assessed as increment from 4 to 37°C, was markedly higher than that of <sup>125</sup>I binding, which showed no difference between 37 and 4°C, indicating that no active HDL protein processing was involved, suggesting that cholesteryl ester is selectively taken up by the eggs. As the concentration of HDL increased, the <sup>125</sup>I binding seemed saturated at lower concentrations of HDL (100 µg/ml) than the [<sup>3</sup>H]-based association ( $>>600$  µg/ml). The egg takes up cholesteryl ester also from apoB-LP, but the rate seems saturated at lower concentrations (150 µg/ml) with less maximum uptake than HDL, based on cholesteryl ester (Fig. 2A, right panel). Uptake by schistosome eggs of free and esterified cholesterol was examined by using double-labeled HDL and apoB-LP with [<sup>14</sup>C]cholesterol and [<sup>3</sup>H]cholesteryl ester. Uptake of [<sup>14</sup>C]cholesterol was impeded by excess apoB-LP and HDL, but the uptake of [<sup>3</sup>H]cholesteryl ester was suppressed only by HDL and not by apoB-LP (Fig. 2B). This profile indicated a specific pathway for selective uptake of cholesteryl ester from HDL, at least different from a pathway for the uptake of apoB-LP cholesteryl ester (25), while free cholesterol uptake is nonspecific from LDL and HDL, including its exchange among lipoproteins and cell membranes.

### Northern blot analysis

Assuming that selective uptake is mediated by SR-BI-like protein or CD36 family protein, expression of

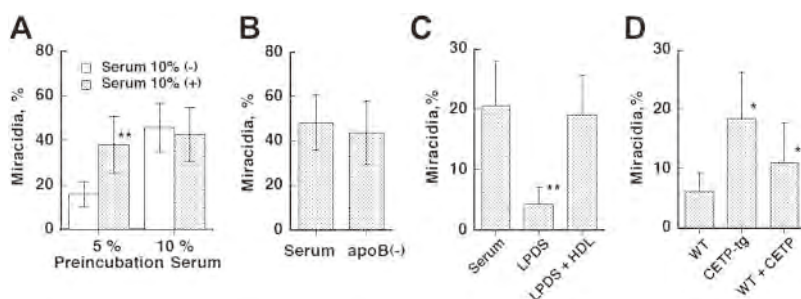


**Figure 1.** Embryonation and maturation of the *S. japonicum* eggs in culture. The percentage of miracidia in total eggs per pair of adult parasites cultured for 10 d was counted and estimated as efficiency of embryonation. A) Eggs were separated from the adult worms after 2 d of culture in RPMI 1640 medium supplemented with 5 or 10% human pooled serum, and cultured further in fresh medium supplemented with or without 10% serum for 8 d. B) Eggs were separated from the parents cultured

in the same condition as in A with 5% serum, and the eggs were further cultured in 5% CO<sub>2</sub> atmosphere with 10% of whole serum and its  $d = 1.063$  bottom fraction (apoB(-)). C) A pair of parent adults was cultured for 10 d in the medium with lipoprotein-depleted serum (LPDS; 4 mg protein/ml) with or without isolated HDL fraction (150 µg cholesterol/ml). D) A pair of *S. japonicum* adults was cultured with mouse sera (4 mg protein/ml) of wild-type, CETP transgenic, and wild-type presupplemented with purified human CETP (24) to make it equivalent activity in human serum. Numbers of adult pairs assayed were: 6 (A), 8 (B, C), and 5 (D). Data represent average and SE. \* $P < 0.05$ , \*\* $P < 0.005$ .

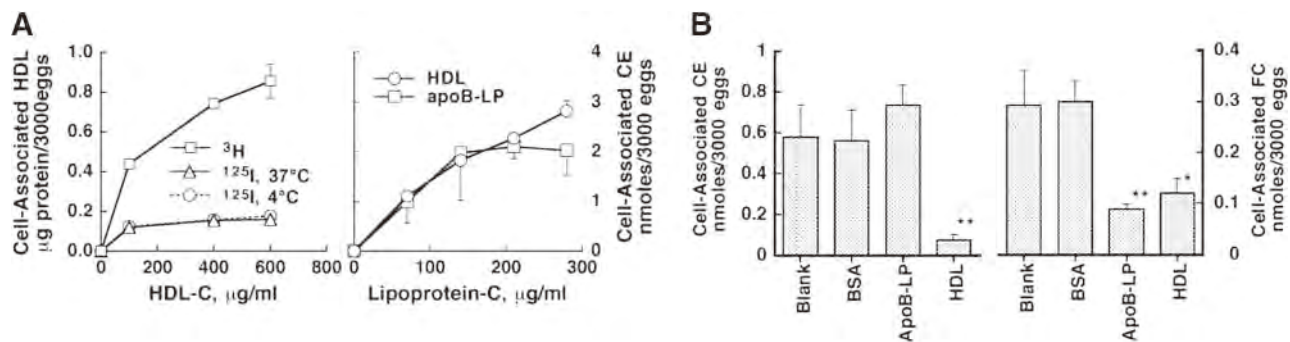


**Figure 2.** Specific cholesterol uptake from lipoproteins by *S. japonicum* eggs. **A)** Left panel: human HDL was labeled with [<sup>3</sup>H]cholesteryl ester ([<sup>3</sup>H]-CE) or [<sup>125</sup>I]. *S. japonicum* eggs (8400/well) were incubated with indicated concentrations of [<sup>3</sup>H]-CE-HDL (<sup>3</sup>H; squares) or [<sup>125</sup>I]-HDL (<sup>125</sup>I; triangles and circles) at 37°C and 4°C, in 0.5 ml/well RPMI 1640 for 20 h. Association of HDL with the eggs was estimated as HDL protein calculated from each specific activity (694.2 dpm/µg protein for [<sup>3</sup>H], 53,380 cpm/µg protein for [<sup>125</sup>I]). Specific association was estimated by displacement with a 10× amount of nonlabeled HDL. Specific association of [<sup>3</sup>H] was assessed as difference between the results at 37 and 4°C. Right panel: human HDL and apoB-lipoprotein (apoB-LP, as *d*>1.063) were double-labeled with [<sup>3</sup>H]-CE [<sup>14</sup>C]cholesterol as described in Materials and Methods. *S. japonicum* eggs (3000/well) were incubated as in left panel, with the labeled HDL (circles) or apoB-LP (squares). Specific active uptake of CE (cell-associated CE) was determined as difference between the specific uptake values at 37 and 4°C. Horizontal axes indicate lipoprotein cholesterol (C). **B)** Selective uptake of cholesterol by *S. japonicum* eggs from HDL. HDL was double-labeled with [<sup>3</sup>H]-CE and [<sup>14</sup>C]cholesterol, and incubated with the *S. japonicum* eggs (58 µg HDL cholesterol for 3000 eggs/ml medium/well) in the presence of 10 vol of nonlabeled HDL, nonlabeled LDL, or 1 µg/ml BSA. Uptake of CE (cell-associated CE, right panel) or cholesterol (cell-associated FC, right panel) was calculated as the difference between the specific values at 37 and 4°C. Data represent average and SE of the triplicate assay. \**P* < 0.05, \*\**P* < 0.01 vs. blank.

mRNA was searched by using the 489-bp probe derived from the cDNA of Sj-Ts2 protein that has one of the CD36 domains (671 bp was submitted to Genbank; see above). The mRNA representing a CD36 family protein was identified in *S. japonicum* adult (Fig. 3A). The approximate size was 1.8 kb, longer than that previously reported for Sj-Ts2 (671 bp). GAPDH mRNA was detected as a 1.2-kb band, consistent with the size of 1148 bp reported for *S. japonicum*.

#### Screening of a CD36-related gene from the cDNA libraries of *S. japonicum* adults and eggs

From the *S. japonicum* adult cDNA library, Sj-Ts2-containing cDNAs of variable sizes longer than 1 kb were obtained as inserts of <sup>32</sup>P<sup>+</sup> clones. These cDNA fragments all seemed to be derived by single transcription, including the sequence of the reported Sj-Ts2 protein. Inserts of 8 clones showed >1068 bp elongated from the 5' terminus, and one showed ~100 bp elongated from the 3' terminus of Sj-Ts2 protein. By 5'-RACE analysis, the start codon downstream of a stop codon was detected, and the sequence of the final full-length (1880-bp) original mRNA was determined and deduced to 506 amino acid residues (Supplemental Fig. S1). On the other hand, more than half of 26 inserts of positive clones derived from the egg cDNA library had a deletion of 68-bp nucleotides at positions 98–165 within the coding region. However, the inserts of remaining clones had no deletion and identical sequences with the nucleotide, beginning at position 14 of adult mRNA. These findings indicate that alternative splicing of this mRNA may occur. The size of the PCR product of 5' fragment with 5' primer and GSP2 with the first-strand cDNA derived from total RNA as template was similar (467 bp) between eggs and adults (Fig.

3B), so that the CD36RP mRNA is likely to be expressed in eggs, though the level seems lower (Fig. 3C).

The amino acid sequence indicated that the protein sequence belongs to the CD36 family. It had two transmembrane regions by PHD analysis (23), 15 *N*-glycosylation sites by PROSITE motif analysis, and CD36 domains by conserved domain (CD) search analysis (Supplemental Figs. S1 and S2). Blastp analysis revealed identity with high score to SRC1\_RAT (SR-B1) (48%; *E* score 8e-51) and with CD36\_RAT (49%; *E* score 5e-45) and SRC\_HUMAN (CLA-1) (49%; *E* score 2e-52). By multialignment (pfam01130) of 32 CD36 family proteins from a variety of organisms by CDD, the highly conserved 4 Cys and 4 Pro residues were demonstrated in domains from IPB002159D to IPB002159F in CD36 family proteins, including this CD36RP (Supplemental Fig. S2, boxed). Three *N*-glycosylation sites (aa 97, 205, and 248) identified among the 15 candidate glutamines in CD36RP were conserved in mammalian SR-B1 and CD36 (not shown). It had 15 nucleotide polymorphism sites in the coding region identified during screening, resulting in 11 amino acid substitutions.

#### Expression of recombinant CD36RP

Recombinant GST-fused full size CD36RP (rCD36RP) expressed in *E. coli* and isolated as GSH-Sepharose gel-bound protein was shown as an 82-kDa band by Western blotting, by using anti-GST and anti-Ex160 antibodies (Fig. 4). His-tagged extracellular half size CD36RP (Ex160) was expressed and shown as a 25 kDa polypeptide by Western blotting with anti-RGS-His antibody and antibody was raised against this peptide. After treatment of the GSH-gel-bound rCD36RP with protease, the anti-Ex160<sup>+</sup> band of the apparent molec-

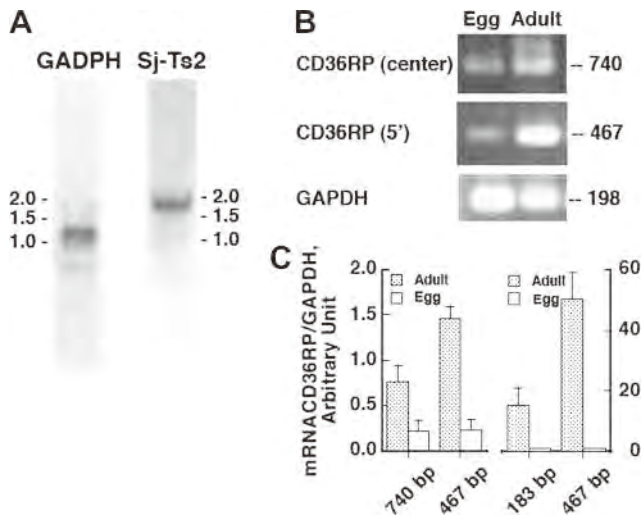


**Figure 3.** Expression of a CD36-like gene in *S. japonicum*. A) Northern blot hybridization of total RNA isolated from adult *S. japonicum*. Total RNA was subjected to electrophoresis in 1.0% agarose-formaldehyde gel, transferred to nylon membrane, and hybridized with the <sup>32</sup>P-labeled 489- and 198-bp oligonucleotide probes corresponding to S<sub>j</sub>-Ts2 and *S. japonicum* GAPDH cDNA, respectively, as described in Materials and Methods. B) Expression of CD36RP mRNA in the eggs and adults of *S. japonicum*. RT-PCR of total RNA was performed for both in the same concentration by using the 5' primer and GSP2 primer for CD36RP (5'), 467 bp; the center primers (L1 and R3) for CD36RP (center), 740 bp; and primers for glyceraldehyde-3-phosphate dehydrogenase (GAPDH). Size of the PCR products is shown. C) Quantitative data of conventional RT-PCR (left panel) and results of quantitative RT-PCR (right panel) performed by using primers L1 and GSP2 (183 bp) and the same primers for CD36RP (5') (467 bp).

ular mass of ~60 kDa (Fig. 4, arrow) was detected in the supernatant, which had no reactivity to anti-GST antibody, indicating the cleavage of GST of 22 kDa. The anti-Ex160 antibody showed stronger reactivity for recognition of CD36RP in *S. japonicum* adults and *S. japonicum* eggs than anti-P 331–348. Ex160 peptide was, however, hardly soluble in aqueous solution without detergents to perform lipoprotein-binding experiments in nondenaturing PAGE. Therefore, a shorter recombinant peptide Ex121, trimmed at the C terminus of Ex160, was expressed in *E. coli* as a GST-fusion protein. Free Ex121 released from GSH Sepharose gel after cleavage of GST (Fig. 4) was able to enter the gel in nondenaturing PAGE. This solution was used for binding to lipoproteins.

### Characterization of *S. japonicum* CD36RP

The particulate and cytosol fractions were prepared from *S. japonicum* adults and mouse liver, and Western blotting analysis was carried out in 10% SDS-PAGE. CD36RP and SR-BI were detected as 82- and 85-kDa bands, respectively, only in the particulate fraction (Fig. 5) and not in the cytosol fraction. After treatment with N-glycanase, the size of CD36RP in the *S. japonicum* adult particulate fractions decreased from 82 to 62 kDa, probed by anti-Ex160 antibody, indicating CD36RP

glycosylation (Fig. 5). By similar treatment of the mouse liver particulate fractions, deglycosylated SR-BI appeared as a 60-kDa band by anti-SR-BI antibody. Murine SR-BI was reported to have 11 N-linked glycosylation sites, 2 of which were important for expression in plasma membrane (26). Additional treatment with N-acetylglucosaminidase resulted in no further reduction of the size of CD36RP. The EndoH treatment showed similar results. The main band in the *S. japonicum* egg particulate fractions was broader around 82 kDa, with a minor band of 62 kDa. Treatment with EndoH seemed to cause no apparent change of the bands, giving inconclusive results as to whether CD36RP is glycosylated and the experimental condition is good for deglycosylation in the eggs.

### Lipoprotein binding of the recombinant peptide, Ex121

The water-soluble extracellular domain peptide Ex121 was incubated with HDL and LDL and subsequently analyzed by density-gradient nondenaturing PAGE. The Ex121 peptide was detected by immunoblotting with anti-P 331–348. The position of Ex121 was shifted from that of free Ex121 to the position corresponding to HDL, assured by anti-apoA-I antibody and by HDL samples prestained with Sudan black B (not shown and Fig. 6A). Binding of Ex121 to HDL increased and free Ex121 decreased as the concentration of HDL increased. HDL isolated from the CETP-deficient human serum showed less binding of Ex121 than normal HDL (Fig. 6B, left panel). Ex121 also seemed to bind to LDL but to a much lesser extent, and the Ex121<sup>+</sup> band was at the position a little smaller than regular LDL parti-

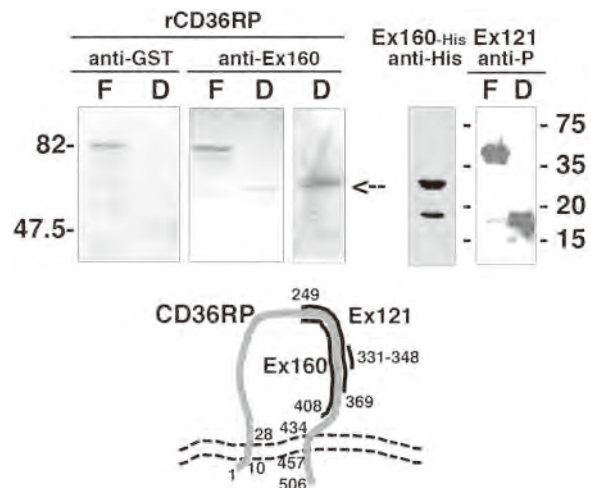


**Figure 4.** SDS-PAGE of recombinant CD36RP. Full-length CD36RP (rCD36RP) and the extracellular region peptide, Ex121, Gly249-Tyr369, were expressed in *E. coli* as the GST-fusion proteins. Digested product (D) was obtained after treatment of the GST-fusion protein (F) by precision protease, as described in Materials and Methods (arrow). Anti-Ex160 and anti-GST antibodies were used for detection of GST-free rCD36RP (D) and GST-fusion protein (F), and anti-peptide 331-348 (anti-P) for Ex121. Ex160-His peptide was detected by anti-His antibody. Bottom panel: predicted topology of CD36RP and positions of the peptides used.

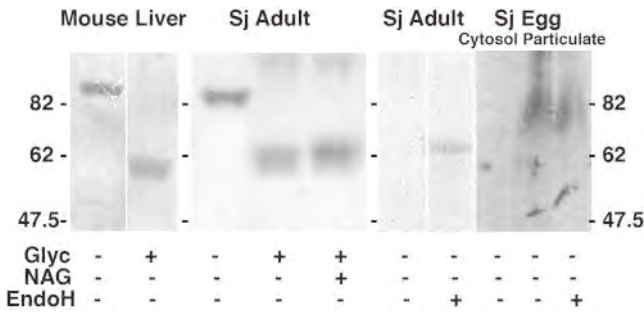


**Figure 5.** Deglycosylation of Sj CD36RP in the particulate fractions from *S. japonicum* adults. Particulate fractions (48 μg protein of *S. japonicum* or 100 μg protein of mouse liver) were treated with or without 10 mU N-glycanase in 50 μl reaction mixture overnight at 37°C, as described in Materials and Methods. Reaction mixtures without enzyme (-), with glycanase (Glyc), or with glycanase plus 35 mU N-acetyl glucosaminidase (Glyc, NAG) were analyzed in SDS-PAGE and Western blotting carried out by using anti-Ex160 or anti-SR-BI antibody. Particulate fraction of *S. japonicum* eggs was similarly treated with (+) or without (-) 10 mU EndoH, and CD36RP was detected with anti-P.

cles. When HDL is added, EX121 interacted with LDL is likely to be transferred to HDL, but the Ex121-HDL complex seemed shifted to a position of higher molecular mass (Fig. 6B, right panel). These results suggest that an extracellular fragment containing the conserved Cys and Prorich domain of *S. japonicum* CD36RP binds to HDL particles (27). This association seems to be selective.

**Effect of the anti-Ex160 antibody on HDL-cholesteryl ester uptake and maturation of the eggs**

The antibody against the extracellular domain peptide Ex160 was examined for CD36RP activity for HDL cholesteryl ester uptake and egg maturation (Fig. 7). The effect of the antibody was observed on HDL-cholesteryl ester uptake by the eggs. The antibody suppressed the cholesteryl ester uptake at 37°C but not at 4°C, so that significant suppression was for the active uptake shown as NET uptake in Fig. 7A. The antibody was added to the egg maturation assay system of Fig. 1, except that a pair of the parent adults was cultured for 10 d in the presence of 10% serum in the presence of

**Figure 6.** Association of recombinant protein Ex121 with HDL. A) Ex121 (35 ng) was incubated with 1–5 μg protein of HDL in 8 μl PBS at room temperature for 30 min and at 4°C for 3 h, and then mixed with 6 μl native sample buffer (62 mM Tris-HCl, pH 6.8; 10% sucrose; and 0.1% BPB). The double samples were subjected to nondenaturing PAGE with 4–20% gradient Tris-Gly gel and detected with anti-P parallel with anti-apoA-I. B) Ex121 (70 ng) was incubated with 30 μg protein of HDLs obtained from normal subjects (normal 1, normal 2) or CETP-deficient subject (CETP-d), or LDL in 7 μl PBS (left panel), or with 15 μg protein of HDL or LDL or mixture of HDL and LDL (right panel) in 12 μl PBS, at room temperature for 30 min. Western blotting was carried out using anti-P. Arrows indicate positions of HDL prestained by Sudan black.

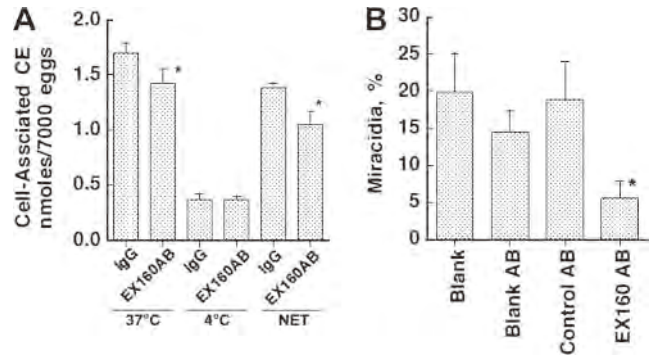
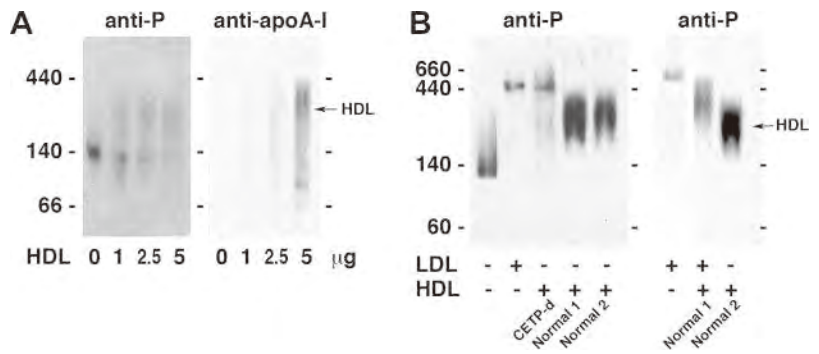


**Figure 7.** Suppression of HDL-cholesteryl ester (CE) uptake and maturation of the eggs by the antibody against EX160. A) Uptake of HDL-CE was measured in the same system as used in Fig. 2, in the presence of the antibody. B) Maturation of *S. japonicum* eggs was estimated in the same condition as Fig. 1, except for using 5% serum, in the presence of the antibodies. IgG, nonimmune rabbit IgG; EX160AB, antibody against Ex160; blank, with no additional antibody/antisera; blank AB, with 1:100 vol of nonimmune rabbit serum; control AB, with 1:100 vol of rabbit antisera against the intracellular domain peptide of CD36RP (anti-P 331–348). Titer of Ex160 was adjusted to <1/25 of the anti-P antisera. Data represent means ± SE of n = 6/group. \*P < 0.05 vs. IgG (A) or all other treatments (B).

the antibody. Maturation of the eggs to miracidia was significantly reduced in the presence of the anti-Ex160 antibody in comparison to control antibody, anti-P 331–348, or blank (Fig. 7B).

**DISCUSSION**

Schistosomes are the parasites that finally reside in the blood vessels of the host patients, and in the case of *S. japonicum*, the adult flukes locate to the portal vein and its draining venules. Chronic schistosomiasis causes various pathological problems in the body, not only from the parasites themselves but also the eggs laid in the body. The adult worms lay eggs in the portal vein to be released to the intestinal tract, but many are flushed back to the liver, where they embolize and develop into miracidia, a phenomenon that deals with the morbidity and mortality of hepatic granulomatosis (1–5).

We previously reported that maturation of *S. japonicum* eggs to miracidia requires normal HDL, presumably as a nutrient supplier, but it is insufficient in culture in the presence of the HDL recovered from CETP-deficient patients (10). We confirmed this process in more detail, as presented in Fig. 1. This was consistent with the *in vivo* findings that the egg maturation in the liver and hepatic granulomatosis were less in wild-type mice, which lack endogenous CETP activity, than in the CETP transgenic mice (10). We therefore investigated potential candidate factors to catalyze this reaction. Both schistosome eggs and adults were found to selectively take up cholesteryl ester from HDL particles. As this type of reaction is known to be carried out by CD36-like proteins, including SR-BI, in many animals (25–27), we searched for schistosome genes homologous to CD36. We used probes with the sequence consisting of coding region of Sj-Ts2 protein (Genbank AF291715), which appeared to have one of the CD36 domains by Prodom analysis, for Northern blot analysis screening of the *S. japonicum* adult cDNA library, and an identified positive band of mRNA of ~1.8 kb in length. Based on this information, we cloned from the *S. japonicum* adult cDNA library a cDNA of 1880 bp that was deduced to encode 506 aa, and have termed this CD36RP. The transcript encoding this protein was also expressed by eggs of *S. japonicum*. Sequence and structural analyses showed clear relatedness to other CD36 family proteins. The extracellular domain peptide of CD36RP demonstrated selective binding to normal HDL but markedly reduced interaction with HDL from CETP-deficient patients. Finally, the antibody against the extracellular domain of CD36RP suppressed HDL-cholesteryl ester uptake and maturation of the eggs *in vitro*.

Based on these new findings, we now propose that CD36RP is a lead candidate for a mediator of selective uptake of cholesteryl ester from HDL by *S. japonicum* necessary for egg maturation to miracidia. It is instructive that preexposure of the adult schistosomes to standard (wild-type) HDL is sufficient for the eggs to mature, perhaps because the vitelline of the egg were preformed adequately in such a condition. In contrast, even the eggs with inadequate vitelline (yolk) provisions may mature provided that normal HDL is supplied after the eggs are laid (*i.e.*, released from the female schistosome into the culture medium). The data we present here support the view that absence of normal HDL retards maturation of the *S. japonicum* eggs in the host liver and, accordingly, prevents hepatic granulomatosis, in a situation such as CETP deficiency where abnormal large HDL does not efficiently bind CD36RP (Fig. 6B). This may be one of the reasons why the prevalence of CETP deficiency is so high in the Far East (11–14) where schistosomiasis japonica has been and/or remains common in rural or underdeveloped areas. If this hypothesis were valid, CETP inhibitors could be useful to prevent hepatic granulomatosis in schistosomiasis. This would be reminiscent of the selective advantage that hemoglobinopathies confer against malaria (*e.g.*, see ref. 28 and references therein).

The question may remain whether cholesterol is a specific nutrient for this reaction. Although triglyceride

is a minor component of HDL core, it may still contribute to maturation of the *S. japonicum* eggs and HDL in CETP deficiency is characterized as low content of triglyceride (29,30). The particular CETP-deficient HDL used in the experiment, however, contained triglyceride as 1.6% of cholesteryl ester and 3.3% of phospholipid as mass, while normal HDL contained it as 0.5–4% and 1–6%, respectively, depending on plasma VLDL concentration. Therefore, contribution of triglyceride is less likely.

We have attempted at length to demonstrate functional alteration of cholesteryl ester uptake by adults or eggs of *S. japonicum* by manipulating expression of the whole CD36RP protein. However, neither functional expression by transfection of full-length CD36RP nor knockdown/knockout of the gene in the parasite cells was successful so far, seemingly because of various profound technical problems, including expressing the parasite genes in cells or cell lines from other species. Therefore, we do not have direct evidence that CD36RP mediates the selective uptake of cholesteryl ester by schistosome adults or eggs. However, structural similarity of CD36RP to CLA1 or SR-BI that mediate cholesteryl ester uptake from HDL in the cells of human and rodents, respectively, can be extrapolated to the functional similarity. Furthermore, the extracellular domain of CD36RP indeed demonstrated selective binding to HDL, and its antibody suppressed HDL cholesteryl uptake and maturation of the eggs in culture. Thus, it is not unreasonable to speculate that CD36RP is a strong candidate for a mediator of HDL cholesteryl ester uptake by the adults and eggs of *S. japonicum*, and therefore a key molecule for maturation of the egg to the miracidium. This means that CD36RP, as well as host plasma HDL, is a key protein for hepatic granulomatosis in *S. japonicum* infection that can represent a fatal pathological process in infected persons.

Clearly it will be necessary to demonstrate more direct evidence for CD36RP to catalyze selective cholesteryl ester uptake before this schistosome glycoprotein can be definitively ascribed a role as the mediator of the reaction. Technical difficulties remain to be overcome in order to accomplish the necessary manipulations, such as functional transfection and expression of the gene or knockdown of the gene to down-regulate the reaction. However, given recent advances with transgenesis approaches in schistosomes and other parasitic helminths (31–33), it is feasible that informative functional genetics approaches may soon allow definitive assignment or not of a physiological role for schistosome CD36RP in selective uptake of cholesteryl ester from host HDL. FJ

This work was supported in part by the MEXT-Supported Program for the Strategic Research Foundation at Private Universities (Japan).

## REFERENCES

1. Ross, A. G. P., Bartley, P. B., Sleight, A. C., Olds, G. R., Li, Y., Williams, G. M., and McManus, D. P. (2002) Schistosomiasis. *New Eng. J. Med.* **346**, 1212–1220

2. Wynn, T. A., Thompson, R. W., Cheever, A. W., and Mentink-Kane, M. M. (2004) Immunopathogenesis of schistosomiasis. *Immunol. Rev.* **201**, 156–167
3. King, C. H., Dickman, K., and Tisch, D. J. (2005) Reassessment of the cost of chronic helminthic infection: a meta-analysis of disability-related outcomes in endemic schistosomiasis. *Lancet* **365**, 1561–1569
4. Gryseels, B., Polman, K., Clerinx, J., and Kestens, L. (2006) Human schistosomiasis. *Lancet* **368**, 1106–1118
5. Gray, D. J., Ross, A. G., Li, Y. S., and McManus, D. P. (2011) Diagnosis and management of schistosomiasis. *Br. Med. J.* **342**, d2651
6. Furlong, S. T., Thibault, K. S., Morbelli, L. M., Guinn, J. J., and Rogers, R. A. (1995) Uptake and compartmentalization of fluorescent lipid analogs in larval *Schistosoma mansoni*. *J. Lipid Res.* **36**, 1–12
7. Rogers, M. V., Quilici, D., Mitchell, G. F., and Fidge, N. H. (1990) Purification of a putative lipoprotein receptor from *Schistosoma japonicum* adult worms. *Mol. Biochem. Parasitol.* **41**, 93–100
8. Xu, X., and Caulfield, J. P. (1992) Characterization of human low density lipoprotein binding proteins on the surface of *Schistosoma mansoni*. *Eur. J. Cell Biol.* **57**, 229–235
9. Fan, J., Xiaoxian, G., Yang, W., Shen, L., McManus, D. P., and Brindley, P. J. (2003) A *Schistosoma japonicum* very low-density lipoprotein-binding protein. *Int. J. Biochem. Cell Biol.* **1507**, 1–16
10. Okumura-Noji, K., Sasai, K., Zhan, R., Kawaguchi, H., Maruyama, H., Tada, T., Takahashi, H., Okazaki, M., Miida, T., Sakuma, N., Kimura, G., Ohta, N., and Yokoyama, S. (2001) Cholesteryl ester transfer protein deficiency causes slow egg embryonation of *Schistosoma japonicum*. *Biochem. Biophys. Res. Com.* **286**, 305–310
11. Hirano, K., Yamashita, S., Funahashi, T., Sakai, N., Menju, M., Ishigami, M., Hiraoka, H., Kameda-Takemura, K., Tokunaga, K., Hoshino, T., Kumasaka, K., Kawano, K., and Matsuzawa, Y. (1993) Frequency of intron 14 splicing defect of cholesteryl ester transfer protein gene in the Japanese general population—relation between the mutation and hyperalphalipoproteinemia. *Atheroscler* **100**, 85–90
12. Hirano, K., Yamashita, S., Nakajima, N., Arai, T., Maruyama, T., Yoshida, Y., Ishigami, M., Sakai, N., Kameda-Takemura, K., and Matsuzawa, Y. (1997) Genetic cholesteryl ester transfer protein deficiency is extremely frequent in the Omagari area of Japan. Marked hyperalphalipoproteinemia caused by CETP gene mutation is not associated with longevity. *Arterioscler Thromb. Vasc. Biol.* **17**, 1053–1059
13. Hui, S.-P. (1997) Frequency and effect on plasma lipoprotein metabolism of a mutation in the cholesteryl ester transfer protein gene in the Chinese. *Hokkaido J. Med. Sci.* **72**, 319–327
14. Song, G.-J., Han, G.-H., Chae, J.-J., Namkoong, Y., Lee, H.-K., Park, Y.-B., and Lee, C.-C. (1997) The effect of the cholesterol ester transfer protein gene and environmental factors on the plasma high density lipoprotein cholesterol levels in the Korean population. *Mol. Cells* **7**, 615–619
15. Zhang, R., Yoshida, A., Kumagai, T., Kawaguchi, H., Maruyama, H., Suzuki, T., Itoh, M., El-Malky, M., and Ohta, N. (2001) Vaccination with calpain induces a Th1-biased protective immune response against *Schistosoma japonicum*. *Infect. Immun.* **69**, 386–391
16. Zhang, R., Suzuki, T., Takahashi, S., Yoshida, A., Kawaguchi, H., Maruyama, H., Yabu, Y., Fu, J., Shirai, T., and Ohta, N. (2000) Cloning and molecular characterization of calpain, a calcium-activated neutral proteinase, from different strains of *Schistosoma japonicum*. *Parasitol. Int.* **48**, 232–242
17. Bilheimer, D. W., Eisenberg, S., and Levy, R. I. (1972) The metabolism of very low density lipoprotein proteins. I. Preliminary in vitro and in vivo observations. *Biochim. Biophys. Acta* **260**, 329–323
18. Owhashi, M., and Ishii, A. (1981) Fractionation and characterization of allergens extracted from eggs of *Schistosoma japonicum*. *Int. Arch. Allergy Appl. Immunol.* **64**, 146–156
19. Fan, J., Minchella, D. J., Day, S. R., McManus, D. P., Tiu, W. U., and Brindley, P. J. (1998) Generation, identification, and evaluation of expressed sequence tags from different developmental stages of the Asian blood fluke *Schistosoma japonicum*. *Biochem. Biophys. Res. Com.* **252**, 348–356
20. Altschul, S. F., Madden, T. L., Schaffer, A. A., Zhang, J., Zhang, Z., Miller, W., and Lipman, D. J. (1997) Gapped BLAST and PSI-BLAST: a new generation of protein database search programs. *Nucleic Acids Res.* **25**, 3389–3402
21. Henikoff, S., and Henikoff, J. G. (1994) Protein family classification based on searching a database of blocks. *Genomics* **19**, 97–107
22. Bairoch, A., Bucher, P., and Hofmann, K. (1997) The PROSITE database, its status in 1997. *Nucleic Acids Res.* **25**, 217–221
23. Rost, B. (1996) Predicting one-dimensional protein structure by profile-based neural networks. *Methods Enzymol.* **266**, 525–539
24. Ohnishi, T., Yokoyama, S., and Yamamoto, A. (1990) Rapid purification of human plasma lipid transfer proteins. *J. Lipid Res.* **31**, 397–406
25. Acton, S., Gigotti, A., Landschulz, T., Xu, S., Hobbs, H. H., and Krieger, M. (1996) Identification of scavenger receptor SR-BI as a high density lipoprotein receptor. *Science* **271**, 518–520
26. Vinals, M., Xu, S., Vasile, E., and Krieger, M. (2003) Identification of N-linked glycosylation sites on the high density lipoprotein (HDL) receptor SR-BI and assessment of their effects on HDL binding and selective lipid uptake. *J. Biol. Chem.* **278**, 5325–5332
27. Gu, X., Trigatti, B., Xu, S., Acton, S., Babitt, J., and Krieger, M. (1998) The efficient cellular uptake of high density lipoprotein lipids via scavenger receptor class B type I requires not only receptor-mediated surface binding but also receptor-specific lipid transfer mediated by its extracellular domain. *J. Biol. Chem.* **273**, 26338–26348
28. Taylor, S. M., Parobek, C. M., and Fairhurst, R. M. (2012) Haemoglobinopathies and the clinical epidemiology of malaria: a systematic review and meta-analysis. *Lancet Infect. Dis.* **12**, 457–468
29. Bisgaier, C. L., Siebenkas, M. V., Brown, M. L., Inazu, A., Koizumi, J., Mabuchi, H., and Tall, A. R. (1991) Familial cholesteryl ester transfer protein deficiency is associated with triglyceride-rich low density lipoproteins containing cholesteryl esters of probable intracellular origin. *J. Lipid Res.* **32**, 21–33
30. Chiba, H., Akita, H., Tsuchihashi, K., Hui, S. P., Takahashi, Y., Fuda, H., Suzuki, H., Shibuya, H., Tsuji, M., and Kobayashi, K. (1997) Quantitative and compositional changes in high density lipoprotein subclasses in patients with various genotypes of cholesteryl ester transfer protein deficiency. *J. Lipid Res.* **38**, 1204–1216
31. Yang, S., Brindley, P. J., Zeng, Q., Li, Y., Zhou, J., Liu, Y., Liu, B., Cai, L., Zeng, T., Wei, Q., Lan, L., and McManus, D. P. (2010) Transduction of *Schistosoma japonicum* schistosomules with vesicular stomatitis virus glycoprotein pseudotyped murine leukemia retrovirus and expression of reporter human telomerase reverse transcriptase in the transgenic schistosomes. *Mol. Biochem. Parasitol.* **174**, 109–116
32. Rinaldi, G., Eckert, S. E., Tsai, I. J., Suttiprapa, S., Kines, K. J., Tort, J. F., Mann, V. H., Turner, D. J., Berriman, M., and Brindley, P. J. (2012) Germline transgenesis and insertional mutagenesis in *Schistosoma mansoni* mediated by murine leukemia virus. *PLoS Pathogens* **8**, e1002820
33. Shao, H., Li, X., Nolan, T. J., Massey, H. C., Pearce, E. J., and Lok, J. B. (2012) Transposon-mediated chromosomal integration of transgenes in the parasitic nematode *strongyloides ratti* and establishment of stable transgenic lines. *PLoS Pathogens* **8**, e1002871

Received for publication August 27, 2012.  
Accepted for publication November 13, 2012.

Supplementary Figure 1. Okumura-Noji, et al.

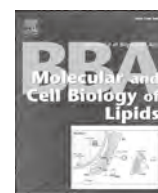
1 acatatttataacagcgttttaaaataaacagacaacagctttcaacttctgtaacagatgata M I  
61 TCCTCGTGTGGTTAAGTGTACAGTTTATTAATTCATCTGATATGATTTGATATATCAATTA 120  
S R V W L S A T V L F T V L I C I S L L  
121 TCFTTATGCGTATTAACAACCGTTTCFTTGGTTCTTAATATAGGAAAACACGTTTAACT 180  
S L C V L Q P L W F L I N R Q T R L I  
181 CCAGGAAATPAACGTATTCAGAAATGTTAGAGCCATCAGTACCTGTTTAAACAACAATC 240  
P G T K L Y S E A E L E P S (L) P V L T Q F  
241 TATTTTTCAATTAACAATCCAAATGAAATTCAAATCTGCTGATGAACCTCATGTTCAA 300  
Y F F N L T N P I E F Q S G H K P H V Q  
301 CAATTAGGACCAATATACATACCGTGAACCGTTTGAAGCTTAATATACACATAGTAAT 360  
O L G P Y T Y R E K R L K L N I T H S N  
361 GGAACAATPACGTATAAGAAATGAATGGTATTAATTTTGGATGAAATTTATCTAAATGT 420  
G T I T Y K E M K W Y Y F D Q N L S N G  
421 ATGGTGAATGATTCATCACTAGTCAATCTTGTTCATATCGATTCGATTCGAAATC 480  
M V N D S I T S V N L V F I S I A L R I  
481 AATTCATAGCCATGGTTTCTCAAAACAATAATTAATTAATGAAATCCCGCTTCAATGA 540  
N S M P W F L K Q I E L I E S R F H E  
541 TATCTATTATACAAAACACTGCAATGAATTAATATGGGGTATATGATGAATTA 600  
Y L F I T K T V N E L L W G Y N D E L L  
601 ACATATCTGTCACGCAATGATTCATCACTCAAGTAACTCATATATGGTCTATCAAT 660  
T Y (L) S (T) H G F N M S T V T H I G L F I  
661 AATAAAAATAATACACTAGTATATGTAACAATAATTAATGATGGTGCATAATAATAA 720  
N K N N T I S D Y V T I N D G L H N N K  
721 ATGATGGACAATTAATCTGATATCATGGTAATAACAATTAATCCATTCATGGAATGTTCA 780  
M I G Q I (T) R) Y H G N T T L S Y W N S S  
781 ACAGCCAATATGATGATGATGGAACATTTTTTCATTCATTCATTCATTCATTCATTCAT 840  
T A N M I N G S D G L F F H S F L T K Y  
841 GATAACCGTATGTTTGGATCAGATATTTGCTGTTTCATTCGGAATTTACATGATCA 900  
D K P Y V F A S D I C R S L Q F Y T E S  
901 ATGTAATAATTAATTAATTAATTAATTAATTAATTAATTAATTAATTAATTAATTAAT 960  
I D K L H N L P V L K L T P M L D T F K  
961 TCACCGAATATGTAAGAAATGAGGATTTGTTTAAATGGCCTAATGTTATGAG 1020  
S P K Y Y E K N R G F C L N W P (N) C Y E  
1021 GATGGTATTAGACATGTCATGTCACCTGGTGCACCGATGTTGTTATCAACCA 1080  
D G V L D M S S C Q P G A P I V V S Q P  
1081 CATTTTTTAAAGCTAATAAACAATCAAGATGCTGTTGATGGAAATGATCCAACTAAT 1140  
H F L N A N K T Y Q D A V D G M Y P T N  
1141 GAAATGAATACAGTCTCTATGAGAACCAAACTGTTGATGATAATAAAGCACAGAAA 1200  
E M N T V I Y V E P N T G S I I K A Q K  
1201 AAAATCAAATTAACATTTTATGTTAAATGATACAAATTAACCACTTGGCCAAAT 1260  
K I Q I N I L V K N D T T F K Q L A N I  
1261 TCAACTACTCTTCCAAATGATCAATTAATCAATTCAGTCAATTCGAATGATACATTA 1320  
S L T (L) L P I V F I N E S V Q L N D T (L)  
1321 ATGACAATGATGATGATTAATTAATTAATTAATTAATTAATTAATTAATTAATTAAT 1380  
I E Q L T N A L I Q P F I V Q I I L V  
1381 TGATTAATCACTTTGCAATAATTAATTAATTAATTAATTAATTAATTAATTAATTAAT 1440  
C I I L S I S L G S L I S I H F Y Q  
1441 AATAGACAATCACTTATGATGATTAATTAATTAATTAATTAATTAATTAATTAATTAAT 1500  
N R O H T T Y (M) (H) F I D S H O S N D V I  
1501 CCTCAGAAATACATGAGGTTAATACACAACACAGACAATCAATCAATGATTTACAAGAA 1560  
P Q N (S) L E V N I Q Q I I S N D L E  
1561 AATCCAAATTTGTTAATGTTAATGTTAATGTTAATGTTAATGTTAATGTTAATGTTAAT 1620  
N P I V  
1621 tgttattgttct 1680  
1681 tctgt 1740  
1741 tgt 1800  
1801 taacaattgagatgagatgagatgagatgagatgagatgagatgagatgagatgagatgag 1860  
1861 attgaaact 1892

Supplementary Figure 2. Okumura-Noji, et al.

ESIDK 285 DKYVFAADICRSLSQRYT  
SRIFVFPDHCSEHSDA.[3].ATATH 289  
DLQSFSPDLCSEKAWH  
SSEFFSPDLCSEKIMY KESGV 292  
QKTS 309  
EVM.[4].EQC NMI NGTAGOMWAPF.[2].PE SLEFFSPDLCSEKIMY QESRV 292  
IPB002159F  
235 TLS.[4].GTA NMI NGDGTFFHSP.[2].KY DKYVFAADICRSLSQRYT  
Sm SRB 236 SLN.[4].DVA NMI NGDGSVIRBG.[2].MS SRIFVFPDHCSEHSDA.[3].ATATH 289  
P.moth SNMPL 260 QID.[3].DHC NEF QDGTLVFBF.[2].YK DLQSFSPDLCSEKAWH  
GLA1 242 KVD.[4].DQC NMI NGTAGOMWAPF.[2].PE SLEFFSPDLCSEKIMY KESGV 292  
Rat SRB2 242 EVM.[4].EQC NMI NGTAGOMWAPF.[2].PE SLEFFSPDLCSEKIMY QESRV 292  
IPB002159F  
286 .[1].H NLPVLKLP.[4].RK.[11].Q.[4]. NGY EDVLDMSG.[2].GAP LVSQPHHL 345  
Sm SRB 290 .[1].S GVHLRFAS.[4].SQ.[11].Q.[7]. DCP PTGMPLSHC.[5].AVP LFAQPHHL 355  
P.moth SNMPL 310 .[1].K GKTNRYTA.[4].FA.[8].Q.[11].Q.[4]. HCL PKGIMDIRKQ.[1].KVP MVLSPHHL 365  
GLA1 293 .[1].E GPTYRFVA.[4].FA.[11].Q.[11].Q.[11]. HCL ESIGNVSTG.[2].SAP LFAHPHHL 348  
Rat SRB2 293 .[1].E GPTYRFVA.[4].FA.[11].Q.[11].Q.[11]. HCL ESIGNVSTG.[2].GAP LFLSQPHHL 348  
IPB002159F  
346 NANKTQDAVD GMY NEMNTLYVEBNTGSIKAKQIINILKNDTT.[3].LANIS 403  
Sj CD36RP 346 NANKTQDAVD GMY NEMNTLYVEBNTGSIKAKQIINILKNDTT.[3].LANIS 403  
Sm SRB 356 GADPSRAAMD GTR.[1].BD.[1].KHDSTILLLEBNTGFLFAFKKQIINAVIENRAS.[4].YKDMA.[1].417  
P.moth SNMPL 366 EFDTSVTNOVK GLT NEMNTLYVEBNTGFLFAFKKQIINAVIENRAS.[4].YKDMA.[1].417  
GLA1 349 NADPVAEAVT GLH B.N.[1].EASHLFLDHLBNTGFLFAFKKQIINAVIENRAS.[4].YKDMA.[1].417  
Rat SRB2 349 NADPVAEAVT GLH B.N.[1].EASHLFLDHLBNTGFLFAFKKQIINAVIENRAS.[4].YKDMA.[1].417  
IPB002159F  
346 NANKTQDAVD GMY NEMNTLYVEBNTGSIKAKQIINILKNDTT.[3].LANIS 403  
Sj CD36RP 346 NANKTQDAVD GMY NEMNTLYVEBNTGSIKAKQIINILKNDTT.[3].LANIS 403  
Sm SRB 356 GADPSRAAMD GTR.[1].BD.[1].KHDSTILLLEBNTGFLFAFKKQIINAVIENRAS.[4].YKDMA.[1].417  
P.moth SNMPL 366 EFDTSVTNOVK GLT NEMNTLYVEBNTGFLFAFKKQIINAVIENRAS.[4].YKDMA.[1].417  
GLA1 349 NADPVAEAVT GLH B.N.[1].EASHLFLDHLBNTGFLFAFKKQIINAVIENRAS.[4].YKDMA.[1].417  
Rat SRB2 349 NADPVAEAVT GLH B.N.[1].EASHLFLDHLBNTGFLFAFKKQIINAVIENRAS.[4].YKDMA.[1].417

**Supplementary Figure 1.** The nucleotide sequence of *S. japonicum* CD36RP mRNA the predicted amino acid sequence. The position of transmembrane regions are indicated as underlined italics. The potential N-linked glycosylation sites are indicated as bold and underlined letters. Eleven amino acid substitutions, indicated in parentheses, are by the polymorphism among 15 nucleotides cloned in coding region, position 55 to

**Supplementary Figure 2.** Multi-alignment of the amino acid sequences of CD36 proteins. The amino acid residues expressed in bold and underlined letters are conserved in 32 proteins from a variety of organisms. Conserved Cys and Pro residues in CD36 blocks IPB0021.59D to F regions are indicated as boxed.



## Apolipoprotein A-I induces tubulin phosphorylation in association with cholesterol release in fetal rat astrocytes



Jin-ichi Ito <sup>a,1</sup>, Rui Lu <sup>b,c,1</sup>, Yuko Nagayasu <sup>a</sup>, Shinji Yokoyama <sup>b,c,\*</sup>

<sup>a</sup> Biochemistry, Nagoya City University Graduate School of Medical Sciences, Nagoya 467-8601, Japan

<sup>b</sup> Nutritional Health Science Research Center, Chubu University, Kasugai 487-8501, Japan

<sup>c</sup> Department of Applied Bioscience and Biotechnology, Chubu University, Kasugai 487-8501, Japan

### ARTICLE INFO

#### Article history:

Received 16 January 2014

Received in revised form 20 March 2014

Accepted 29 April 2014

Available online 9 May 2014

#### Keywords:

ApoA-I

Astrocyte

Microtubule

Tubulin

Protein kinase C

Caveolin-1

### ABSTRACT

We previously identified cytosolic lipid–protein particles (CLPP) having size and density of HDL in rat astrocytes, to which apoA-I induces translocation of cholesterol, caveolin-1 and protein kinase C $\alpha$  (PKC $\alpha$ ) following its association with microtubules prior to cholesterol release/biogenesis of HDL (JBC 277: 7929, 2002; JLR 45: 2269, 2004). To further understand the physiological relevance of these findings, we investigated the CLPP/microtubule association and its role in intracellular cholesterol trafficking by using a technique of reconstituted microtubule-like filaments (rMT) in rat astrocyte cytosol. When the cells were pretreated with apoA-I,  $\alpha$ -tubulin as a 52-kDa protein in rMT was found phosphorylated while  $\alpha$ -tubulin in a soluble monomeric form was little phosphorylated. The phosphorylation took place coincidentally to apoA-I-induced association with rMT of CLPP, a complex containing PKC $\alpha$ , and was suppressed by a PKC inhibitor, Bis indolylmaleimide 1 (BIM).  $\alpha$ -Tubulin dissociated from CLPP when phosphorylated, and it poorly bound to CLPP once dissociated. BIM did not influence association of PKC $\alpha$  with rMT but suppressed apoA-I-induced cholesterol translocation to the cytosol from the ER/Golgi apparatus and apoA-I-mediated cholesterol release. We thereby concluded that  $\alpha$ -tubulin phosphorylation by PKC $\alpha$  on CLPP is involved in reversible CLPP association with the microtubules and intracellular cholesterol trafficking for apoA-I-dependent HDL biogenesis/cholesterol release in rat astrocytes.

© 2014 Elsevier B.V. All rights reserved.

### 1. Introduction

The central nervous system (CNS) is segregated from plasma lipoproteins by the blood brain barrier so that its cholesterol homeostasis is maintained by the brain-specific lipid transport system [1–4]. It is likely dependent on high-density lipoprotein (HDL) in cerebrospinal fluid mainly composed of apolipoprotein (apo) E and A-I [4,5]. ApoD, A-IV and J are also identified as its minor components. ApoA-I seems either to originate from or transcytosed through capillary endothelial cells [6,7] while apoE is produced and secreted mainly by astrocytes and partly by microglia [8]. ApoA-I therefore exogenously stimulates astrocytes to release cholesterol to form HDL [4]. We found that apoA-I generates phospholipid-rich and cholesterol-poor HDL while endogenous apoE produces cholesterol-rich HDL from rat astrocytes in culture [4]. The mechanism underlying apoA-I-mediated HDL biogenesis in astrocytes is thus important to understand the CNS-specific extracellular cholesterol transport system.

We previously reported a unique finding that in rat astrocytes in culture apoA-I induces translocation of newly synthesized cholesterol

to the cytosolic lipid–protein particle (CLPP) fraction from the endoplasmic reticulum/Golgi apparatus [9] along with generation of extracellular HDL. CLPP appears as a lipid–protein complex in the cytosol of astrocytes having density of 1.09–1.16 g/mL and diameter of 17–18 nm, similarly to plasma HDL. This particle is recovered with phospholipid and unesterified cholesterol as main lipid components and with caveolin-1, protein kinase C $\alpha$  (PKC $\alpha$ ) and cyclophilin A as protein components [10]. Cyclosporin A, a cyclophilin A inhibitor, was found to suppress apoA-I-mediated cholesterol release as well as these intracellular cholesterol trafficking events in rat astrocytes [11]. On the other hand, caveolin-1 has been described as a factor to influence intracellular cholesterol transport linked to the apoA-I/ATP-binding cassette transporter protein A1 (ABCA1)-dependent HDL biogenesis [9,12,13]. We therefore speculate that CLPP is involved in cholesterol transport for apoA-I/ABCA1-dependent HDL biogenesis.

In rat astrocytes, apoA-I induces translocation of phospholipase C $\gamma$  to the CLPP fraction and therefore production of diacylglyceride in there, which causes translocation of PKC $\alpha$  to CLPP from the membrane fraction [10,14]. ApoA-I then enhances association of CLPP with reconstituted microtubule-like filaments (rMT) in the cytosol fraction [14]. As a peptide representing a scaffolding domain of caveolin-1 suppresses association of caveolin-1 with PKC $\alpha$  and  $\alpha$ -tubulin, caveolin-1 in the CLPP seems to be involved in regulation of the interaction

\* Corresponding author. Tel./fax: +81 568 51 9698.

E-mail address: [syokoyam@isc.chubu.ac.jp](mailto:syokoyam@isc.chubu.ac.jp) (S. Yokoyama).

<sup>1</sup> The first two authors (JI and RL) equally contributed to this work.

between CLPP and rMT [14]. The findings implicate that CLPP transports cholesterol by interacting with microtubules.

We here examined protein phosphorylation along with CLPP-related reactions induced by stimulation of rat astrocytes with apoA-I. It was found that 52 K protein in microtubules,  $\alpha$ -tubulin, is phosphorylated by CLPP-bound PKC $\alpha$ , seemingly being involved in intracellular transport of cholesterol for apoA-I/ABCA1-dependent HDL biogenesis.

## 2. Materials and methods

### 2.1. Materials

ApoA-I was prepared by delipidation of human HDL followed by anion-exchange chromatography [15]. Mouse anti- $\alpha$ -tubulin and mouse anti- $\beta$ -actin antibodies and phorbol 12-myristate 13-acetate (PMA) were purchased from Sigma-Aldrich. Rabbit anti-caveolin-1 and mouse anti-PKC $\alpha$  antibodies were purchased from Santa Cruz Biotechnology Inc. and Wako Pure Chemical Ind., respectively. Bisindolylmaleimide 1 (BIM) was purchased from Calbiochem. Bovine brain tubulin was purchased from Cytoskeleton, Inc.

### 2.2. Cell culture and preparation of cytosol and membrane fractions

Astrocytes were prepared from the cerebrum of 17-day fetal Wistar rat as previously described [16]. After removal of the meninges, the cerebral hemisphere was treated with 0.1% trypsin solution in Dulbecco's phosphate buffered saline (DPBS) containing 0.15% glucose (0.1% trypsin/DPBS/G) for 3 min at room temperature. The cells pelleted by centrifugation at 300  $\times$ g for 3 min were cultured in F-10 medium containing 10% fetal calf serum (10% FCS/F-10) at 37 °C for 1 week. The cells were treated with 0.1% trypsin/DPBS/G containing 1 mM EDTA again and cultured in 10% FCS/F-10 using a 6-well multiple tray (Coning Costar 3516) or 10-cm-diameter culture dish (TPP tissue culture dish) for 1 week. The preparation contains 95% astrocytes, 0.3% microglia and 3% oligodendroglia, defined by respective specific staining [17]. The cells were stimulated by apoA-I (5 mg) for 5 min in 0.02% bovine serum albumin (BSA)/F-10 medium. Cytosol and membrane fractions of astrocytes were prepared according to the method of Thom et al. [18]. The cell pellet was obtained by centrifugation at 300  $\times$ g for 10 min and treated with cold 0.02 M Tris-HCl buffer, pH 7.5, containing a protease inhibitors cocktail (Sigma) (0.02 M Tris/protease inhibitor) for 15 min with strong agitation for 10 s at every 5 min for 25 times. The cell suspension was centrifuged at 1000  $\times$ g for 20 min for the preparation of denuclearized-supernatant fraction as a supernatant. The denuclearized-supernatant was centrifuged at 367,000  $\times$ g for 30 min at 4 °C with Hitachi S100AT6 rotor to obtain a cytosol fraction containing depolymerized cytoskeletal components as supernatant and a membrane fraction as pellet. The animal experiment protocol was approved by the Animal Welfare Committee at Nagoya City University Medical School.

### 2.3. Immunoprecipitation and Western blotting

Immunoprecipitation of caveolin-1 was carried out by incubation of the cytosol fraction with rabbit anti-caveolin-1 antibody and protein G-Sepharose (Amersham Bioscience Corp.) at room temperature for 2 h. The Sepharose fraction was washed 5 times with 0.02 M Tris buffered saline containing protease inhibitors cocktail and analyzed by 0.5% SDS/12.5% polyacrylamide gel electrophoresis (SDS-PAGE) and Western blotting by using mouse anti- $\alpha$ -tubulin, mouse anti- $\beta$ -actin, rabbit anti-caveolin-1 and mouse anti-PKC $\alpha$  antibodies.

### 2.4. Reconstitution of microtubule-like filaments

Microtubule-like filaments were reconstituted as previously described [14]. The cytosol fraction prepared from rat astrocytes by

treatment with cold 0.02 M Tris/protease inhibitors and centrifugation was incubated with 100  $\mu$ M GTP and 2 mM MgCl<sub>2</sub> at room temperature for 20 min to induce "polymerization" of  $\alpha$ -tubulin to form microfilaments. After centrifugation at 290,000  $\times$ g at 20 °C for 30 min, the reconstituted microtubule-like filaments (rMT) was obtained as a pellet and used for analysis by SDS-PAGE and Western blotting.

Immobilized rMT was constructed on Affi-Gel 10. The gel was equilibrated with 0.02 M phosphate buffer, pH 7.5, and incubated with bovine tubulin (125  $\mu$ g, 1st tubulin) in 500  $\mu$ L of 0.02 M phosphate buffer at room temperature for 3 h. After washing 3 times with cold 0.02 M Tris-HCl buffer, pH 7.5 (Tris buffer), the bovine tubulin-conjugated Affi-Gel 10 was incubated with 1 M Glycine at 4 °C overnight and washed with Tris buffer. The Gel was then incubated with bovine tubulin (60  $\mu$ g in 500  $\mu$ L of 0.02 M phosphate buffer, 2nd tubulin) or the cytosol fraction (100  $\mu$ g protein in 500  $\mu$ L) of rat astrocytes in the presence of 100  $\mu$ M GTP and 2 mM MgCl<sub>2</sub> at room temperature for 30 min in order to construct immobilized rMT on the gel (rMT-Affi-Gel).

### 2.5. Phosphorylation

Specific phosphorylation of cytosolic proteins associated with caveolin-1 was examined by incubation of cytosolic proteins with 5  $\mu$ Ci of [ $\gamma$ -<sup>32</sup>P]ATP (PerkinElmer) in the presence of 1 mM CaCl<sub>2</sub>, 1 mM MgCl<sub>2</sub> and protease inhibitors at 30 °C for 10 min and immunoprecipitation with anti-caveolin-1 antibody-Protein G. The phosphorylated proteins were analyzed by autoradiography after SDS-PAGE. For homogeneous phospholabeling of cell proteins, rat astrocytes were incubated with [<sup>32</sup>P]orthophosphate (0.2 mCi/mL) in a fresh 0.1% BSA/F-10 for 3 h, followed by washing with DPBS and replacement with 0.02% BSA/F-10.

### 2.6. Biosynthesis, translocation and release of cholesterol

After washing with DPBS four times and incubation in 0.1% BSA/F-10 for 24 h, rat astrocytes at a confluent cell density were incubated with [<sup>3</sup>H]acetate (20  $\mu$ Ci/mL, PerkinElmer) in a fresh 0.02% BSA/F-10. For cholesterol biosynthesis, the cells were incubated with [<sup>3</sup>H]acetate for 3 h in the presence and absence of apoA-I (5  $\mu$ g/mL) and incorporation of radioactivity into cholesterol was counted. For cholesterol translocation to the cytosol fraction and its release from the cell, the cells were pre-labeled with [<sup>3</sup>H]acetate for 16 h, and thoroughly washed three times with cold DPBS to remove the [<sup>3</sup>H]acetate. The labeled cells were incubated in 0.02% BSA/F-10 with and without apoA-I (5  $\mu$ g/mL), for 90 min to evaluate cholesterol translocation to the cytosol, and for 6 h to measure cell cholesterol release. After the incubation, lipid was extracted from the cells, the cytosol fraction and the conditioned medium, respectively, with chloroform:methanol (2:1, v/v) mixture, and analyzed by thin layer chromatography on Silica Gel-60 plates (Merck Millipore). Radioactivity was counted in unesterified cholesterol fraction according to the method previously described [12].

### 2.7. Others

Experiments were repeated in precise combination of each data set shown at least twice in addition to repeating them in various different conditions to confirm reproducibility of the findings. The data were statistically analyzed if necessary by Student *t* test.

## 3. Results

### 3.1. Phosphorylation of $\alpha$ -tubulin by conditioning with apoA-I

It was previously shown that apoA-I induces association with microtubules of PKC $\alpha$ -containing CLPP, so that phosphorylation of  $\alpha$ -tubulin was examined by conditioning of the cells with apoA-I [10]. The cytosol

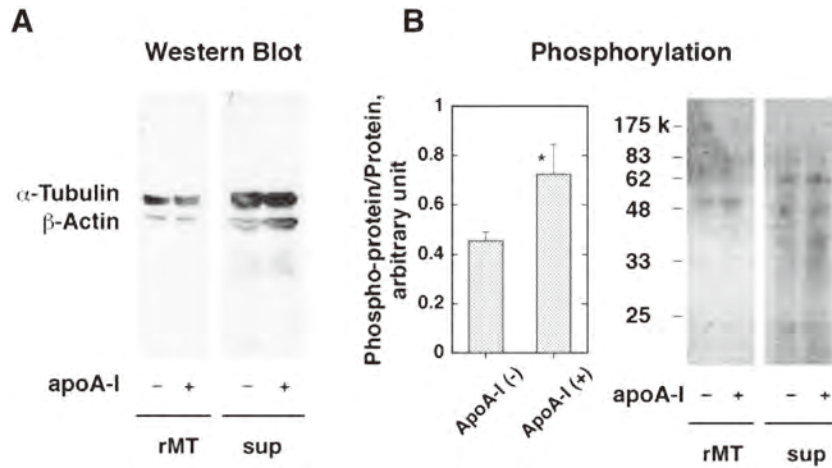


**Fig. 1.** Phosphorylation of  $\alpha$ -tubulin in rMT reconstituted in the cytosol fraction of rat astrocytes treated with apoA-I. A: After the treatment of rat astrocytes with apoA-I, the cytosol fraction (100  $\mu$ g proteins) was incubated with 5  $\mu$ Ci of [ $\gamma$ - $^{32}$ P]ATP at 30  $^{\circ}$ C for 10 min. The cytosol was then incubated with 100  $\mu$ M GTP and 2 mM MgCl<sub>2</sub> at 30  $^{\circ}$ C for 20 min. The rMT fraction and the supernatant were analyzed in SDS-PAGE and by autoradiography. The graph represents the quantitative results of three measurements of the rMT fraction (asterisk  $p < 0.05$ ). B: Western blotting was performed using mouse anti- $\alpha$ -tubulin and mouse anti- $\beta$ -actin antibodies.

fraction of the astrocytes pretreated with apoA-I was incubated with  $^{32}$ P-ATP, and microtubule-like filaments (rMT) were reconstituted as described in the method section.  $\alpha$ -Tubulin and  $\beta$ -actin were both recovered in the rMT fraction (Fig. 1A). When the cells were pretreated with apoA-I,  $\alpha$ -tubulin in the rMT fraction was found phosphorylated in autoradiogram (Fig. 1B). We examined whether this phosphorylation of  $\alpha$ -tubulin in rMT takes place along with PKC $\alpha$  translocation to CLPP and CLPP binding to rMT. rMT was constructed as an immobilized form by conjugating bovine  $\alpha$ -tubulin with Affi-Gel (1st tubulin), incubating the tubulin-Affi-Gel with bovine  $\alpha$ -tubulin (2nd tubulin) or with the cytosol of rat astrocyte, for elongation of microtubule-like filaments. The Affi-Gel fraction was analyzed by immunoblotting to show the presence of  $\alpha$ -tubulin, indicating formation of rMT even when the cytosol

was incubated instead of the “2nd tubulin” (Fig. 2A). When the apoA-I-preconditioned cytosol was used for filament elongation, PKC $\alpha$  was detected in the rMT fraction (Fig. 2B). Phosphorylation of  $\alpha$ -tubulin took place in rMT but not apparently in soluble phase, and this was inhibited by a PKC inhibitor, BIM (Fig. 2C). Both rat and bovine tubulins were well detected by anti-rat tubulin antibody and showed similar biochemical behaviors.

Selectivity of phosphorylation was examined for  $\alpha$ -tubulin molecules in the microtubules rather than the ones monomeric in the solution. When bovine  $\alpha$ -tubulin was added to the incubation mixture of Affi-Gel-rMT, a substantial amount of  $\alpha$ -tubulin was found in the soluble fraction in the mixture (Fig. 3A). By incubating with the apoA-I-preconditioned cytosol, phosphorylation of  $\alpha$ -tubulin was induced in

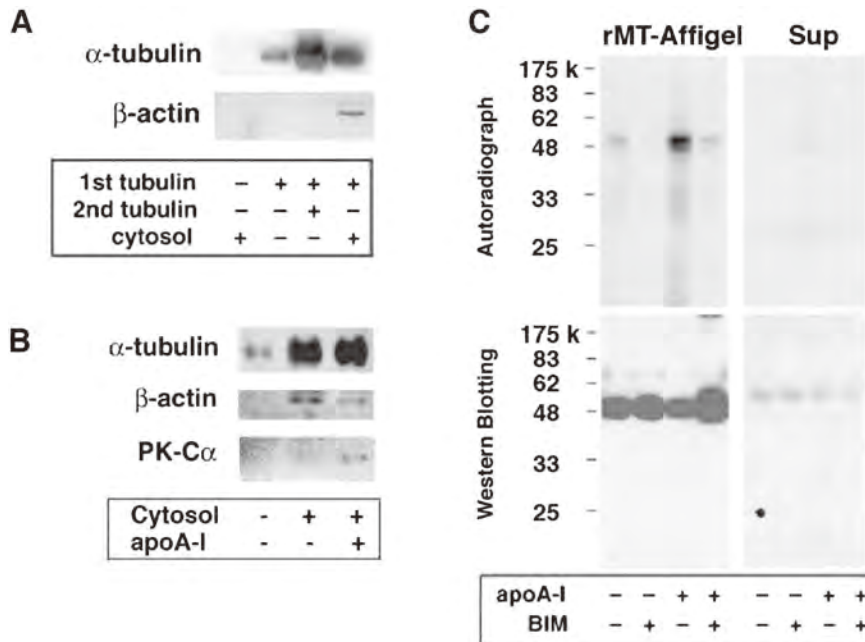


**Fig. 2.** Suppression of  $\alpha$ -tubulin phosphorylation in rMT by BIM. A: Immobilized rMT was constructed on Affi-Gel 10. The gel was conjugated with bovine tubulin (1st tubulin), and the bovine tubulin-Affi-Gel 10 was then incubated with bovine tubulin solution (2nd tubulin) or the cytosol fraction of apoA-I treatment-free rat astrocytes. The gel-bound protein was analyzed by Western blotting for  $\alpha$ -tubulin and  $\beta$ -actin. B: Association of PKC $\alpha$  with rMT. The bovine tubulin-conjugated Gel (1st tubulin) was incubated at room temperature for 30 min with 100  $\mu$ M GTP and 2 mM MgCl<sub>2</sub> in the presence of the cytosol (100  $\mu$ g proteins/mL) of rat astrocytes conditioned with/without apoA-I. The rMT-Affi-Gel was analyzed by Western blotting for  $\alpha$ -tubulin,  $\beta$ -actin and PKC $\alpha$ . C: Inhibition of  $\alpha$ -tubulin phosphorylation by a PKC inhibitor. rMT-Affi-Gel was prepared with the cytosol fraction (150  $\mu$ g protein) of rat astrocytes treated with or without apoA-I. The Gel fraction was incubated with 5  $\mu$ Ci of [ $\gamma$ - $^{32}$ P]ATP, 100  $\mu$ M GTP and 1 mM MgCl<sub>2</sub> in the presence or absence of 10  $\mu$ M BIM at 30  $^{\circ}$ C for 10 min. After washing, the Gel and the supernatant were analyzed in SDS-PAGE and by autoradiography (the upper panels) and Western blotting for  $\alpha$ -tubulin (the lower panels).

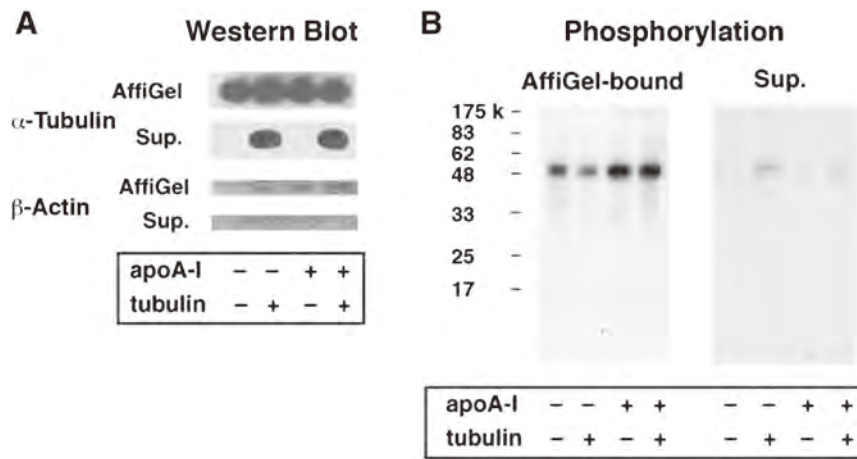


**Fig. 3.** Phosphorylation of tubulin. rMT-Affi-Gel prepared by incubating Affi-Gel 10 with bovine tubulin and subsequently with cytosol fraction (150  $\mu$ g) of rat astrocytes treated with or without apoA-I as described in Fig. 2. The rMT-Affi-Gel was further incubated with or without 10  $\mu$ g of bovine tubulin in 500  $\mu$ L of Tris buffer containing 5  $\mu$ Ci of [ $\gamma$ - $^{32}$ P]ATP, 100  $\mu$ M GTP and 1 mM MgCl<sub>2</sub> at 30 °C for 10 min. An aliquot of the supernatant fraction (50  $\mu$ L) and the Gel fraction were analyzed for Western blotting by using mouse anti- $\alpha$ -tubulin and mouse anti- $\beta$ -actin antibodies (A) and for autoradiography (B).

the Affi-Gel-rMT fraction but only very slightly in the soluble phase (Fig. 3B). The findings were consistent with the view that apoA-I induced translocation of PKC $\alpha$  to CLPP and PKC $\alpha$ -containing CLPP to rMT [10] to cause selective phosphorylation in the microtubules.

3.2. Interaction of  $\alpha$ -tubulin with caveolin-1-containing particles

Protein kinase activity responsible for phosphorylation of  $\alpha$ -tubulin was examined. We previously showed that CLPP physically interacts with  $\alpha$ -tubulin in a non-polymerized form regardless of the apoA-I treatment while apoA-I induces translocation of PKC $\alpha$  to CLPP [11]. Immunoprecipitation was carried out from the cytosol by using an anti-caveolin-1 antibody conjugated with protein G-Sepharose, and demonstrated co-precipitation of  $\alpha$ -tubulin to show CLPP- $\alpha$ -tubulin interaction (Fig. 4). No increase of this association was observed by the apoA-I treatment. Phosphorylation of  $\alpha$ -tubulin however markedly increased by the apoA-I-treatment and it was inhibited by BIM (Fig. 4). The finding was consistent with the view that increase of PKC $\alpha$  in CLPP by apoA-I is responsible for the phosphorylation.

To examine the stability of the CLPP- $\alpha$ -tubulin interaction, release of  $\alpha$ -tubulin from the Sepharose-bound caveolin-1 was observed in the presence of Triton X100. While association of  $\alpha$ -tubulin with the

Affi-Gel was uninfluenced by the apoA-I treatment, the phosphorylated  $\alpha$ -tubulin was released from the complex indicating its readiness for dissociation (Fig. 5). To find the interaction with CLPP of phosphorylated proteins not-forming microtubules, the cells were universally prephospholabeled, treated with apoA-I, and the cytosol was prepared. Alternatively, apoA-I-preconditioned cytosolic proteins were phosphorylated. The cytosol was analyzed by co-precipitation with caveolin-1 containing complex, presumably CLPP. Almost no phosphorylated protein was found associated with CLPP suggesting that CLPP does not associate with phosphorylated  $\alpha$ -tubulin (Fig. 6). The cytosolic proteins were phosphorylated in the apoA-I-stimulated astrocytes, predominantly a 42 kDa protein, and it was suppressed by BIM. These findings suggest that the caveolin-1-associated PKC $\alpha$  (on CLPP) phosphorylates  $\alpha$ -tubulin, a 52 K protein, only when CLPP, a complex carrying both caveolin-1-and PKC $\alpha$ , associates with  $\alpha$ -tubulin-dominant microtubules after the apoA-I pretreatment.

3.3. Phosphorylation of  $\alpha$ -tubulin and cell cholesterol release by apoA-I/ABCA1

In order to find a role of  $\alpha$ -tubulin phosphorylation in cell cholesterol transport and its release as HDL by the apoA-I/ABCA1 pathway, the

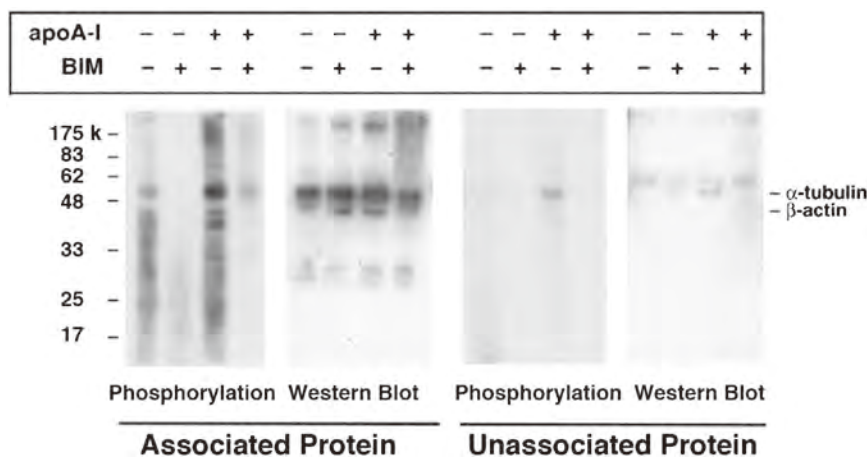


**Fig. 4.** Suppression by BIM of apoA-I-induced phosphorylation of cytosolic caveolin-1-associated proteins. Rat astrocytes were treated with or without 10  $\mu$ M BIM for 1 h, and were incubated with and without apoA-I. The cytosol (150  $\mu$ g protein/mL) was prepared and incubated with rabbit anti-caveolin-1 antibody bound to protein G-conjugated Sepharose at room temperature for 2 h. The Sepharose fraction was washed 3 times with Tris-saline containing protease inhibitors cocktail (SIGMA) and incubated with [ $\gamma$ - $^{32}$ P]ATP (5  $\mu$ Ci) in the presence of 1 mM CaCl<sub>2</sub> and 1 mM MgCl<sub>2</sub> at 30 °C for 10 min. The Sepharose fraction (associated proteins) and the supernatant (unassociated proteins) were analyzed in 10% SDS-PAGE after pelleting with 10% trichloroacetic acid for autoradiography and Western blotting by using mouse anti- $\alpha$ -tubulin and mouse anti- $\beta$ -actin antibodies.

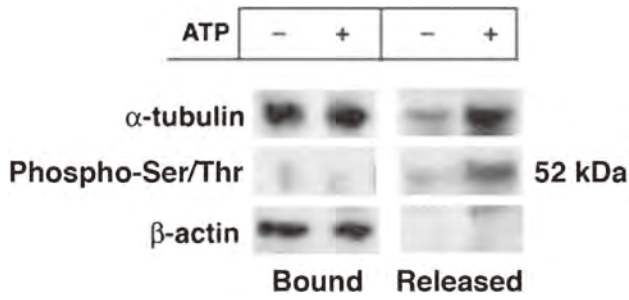


**Fig. 5.** Dissociation of phosphorylated  $\alpha$ -tubulin from caveolin-1-containing complex. The cytosol fraction (141  $\mu$ g protein/mL  $\times$  5 mL) was incubated with rabbit anti-caveolin-1 antibody-conjugated Protein G-Sepharose 4 °C for 2 h. The gel was washed with DPBS containing 0.05% Triton X-100 and then with Tris-saline. The Sepharose fraction was incubated with 50 nM PMA, 0.1 mM MgCl<sub>2</sub>, 0.1 mM CaCl<sub>2</sub> and protease inhibitors cocktail in the presence or absence of 0.1 mM ATP at 30 °C for 10 min. After adding 0.01% BSA to the reaction mixture, the Sepharose fraction (Bound) and supernatant fraction (Released) were obtained by centrifugation at 300  $\times$ g for 5 min. The proteins were analyzed in SDS-PAGE and Western blotting by using anti- $\alpha$ -tubulin, anti- $\beta$ -actin and mouse anti-phosphoserine/threonine (BD Transduction Laboratories) antibodies to detect phosphorylated proteins including  $\alpha$ -tubulin.

effect of inhibition of PKC $\alpha$  was observed. A BIM did not influence association of CLPP with rMT as far as monitored as co-precipitation of the CLPP-related proteins, PKC $\alpha$  and caveolin-1 (Fig. 7) indicating no effect on association of CLPP with rMT. In contrast, BIM significantly suppressed the apoA-I-induced reactions in the cells, de novo biosynthesis of cholesterol, cholesterol translocation to the cytosol from the ER/Golgi and release of cholesterol in rat astrocytes (Fig. 8). The increase of cholesterol biosynthesis and its translocation by apoA-I stimulation were completely canceled by BIM (Fig. 8AB). Small increase of the background translocation was observed by the BIM treatment, indicating potential involvement of PKC in the negative regulation. The cholesterol release was partially inhibited (Fig. 8C) perhaps due to the presence of the labeled cholesterol already in the plasma membrane and other sources for HDL biogenesis. These findings are consistent with our previous findings that PKC inhibition suppresses cholesterol release in

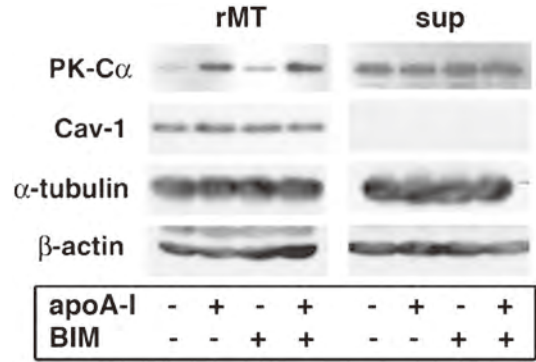


**Fig. 7.** Effect of a protein kinase C inhibitor on association of CLPP with rMT. After pretreatment with or without BIM (10  $\mu$ M) for 1 h, rat astrocytes were treated with or without apoA-I (5  $\mu$ g/mL) for 5 min. The cytosol (145  $\mu$ g protein/mL) was incubated with 100  $\mu$ M GTP and 2 mM MgCl<sub>2</sub> at room temperature for 20 min and centrifuged at 290,000  $\times$ g for 30 min. The precipitant (rMT) and supernatant (sup) were analyzed in SDS-PAGE and Western blotting by using anti-protein kinase C $\alpha$ , anti-caveolin-1, anti- $\alpha$ -tubulin and anti- $\beta$ -actin antibodies.

apoA-I-mediated HDL biogenesis reactions [19–21]. The results suggest that phosphorylation of  $\alpha$ -tubulin in the microtubules contributes to intracellular cholesterol trafficking for cell cholesterol release by the apoA-I/ABCA1 pathway in rat astrocytes.

**4. Discussion**

We previously reported unique intracellular reactions in association with apoA-I/ABCA1-mediated generation of HDL in rat astrocytes. We have used human apoA-I, which has high homology in primary structure [22] and similarity in functional structure [23] and function to generate nascent HDL [24] to the rat counterpart. ApoA-I induces translocation of cholesterol and phospholipid to cytosolic lipid-protein complex having HDL-like physicochemical properties, CLPP, prior to their incorporation into extracellular HDL generated with apoA-I [9]. Along with this reaction, apoA-I induces tyrosine phosphorylation and

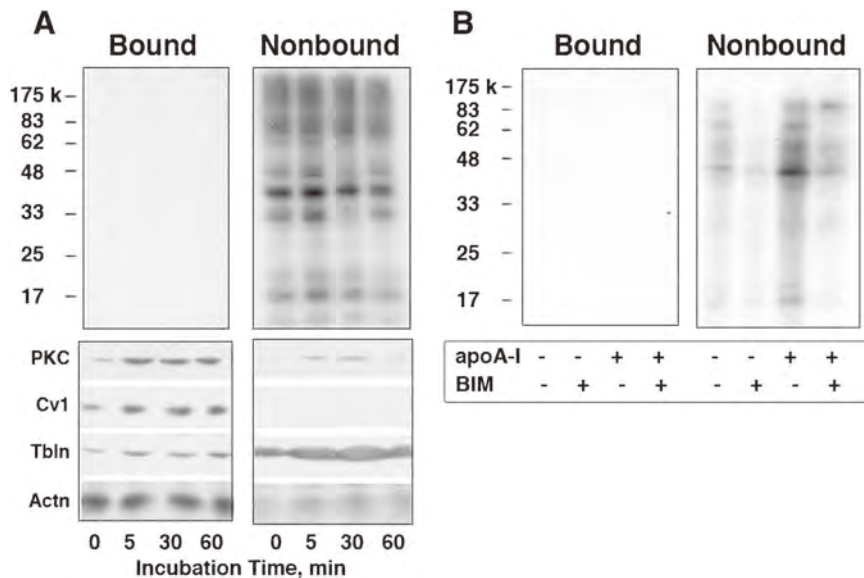


**Fig. 6.** Interaction of phosphorylated cytosolic proteins with caveolin-1-containing complex. Rat astrocytes were incubated with [<sup>32</sup>P]orthophosphate (0.2 mCi/mL) in a fresh 0.1% BSA/F-10 for 3 h, followed by washing with DPBS and replacement with 0.02% BSA/F-10. **A:** The cells were incubated with apoA-I (5  $\mu$ g/mL) for 0, 5, 30 and 60 min. The cytosol from the cells (150  $\mu$ g proteins/mL) was incubated with anti-caveolin-1-Protein G-conjugated Sepharose as described in Fig. 4. The Sepharose-bound fraction (Bound) and non-bound fraction (Non-bound) were analyzed by autoradiography (the upper panels) and Western blotting for PKC $\alpha$  (PKC), caveolin-1 (Cv1),  $\alpha$ -tubulin (Tbln) and  $\beta$ -actin (Actin), after 10% SDS-PAGE. **B:** The cytosol (150  $\mu$ g protein) prepared from the rat astrocytes pretreated with or without apoA-I (0 or 5  $\mu$ g/mL) was incubated with 5  $\mu$ Ci of [ $\gamma$ -<sup>32</sup>P]ATP, 1 mM CaCl<sub>2</sub> and 1 mM MgCl<sub>2</sub> in the presence or absence of 10  $\mu$ M BIM at 30 °C for 10 min. After incubation of the cytosol with anti-caveolin-1 antibody-Protein G-conjugated Sepharose, the gel-bound fraction (Bound) and the non-bound fraction (Non-bound) were analyzed in SDS-PAGE and autoradiography.

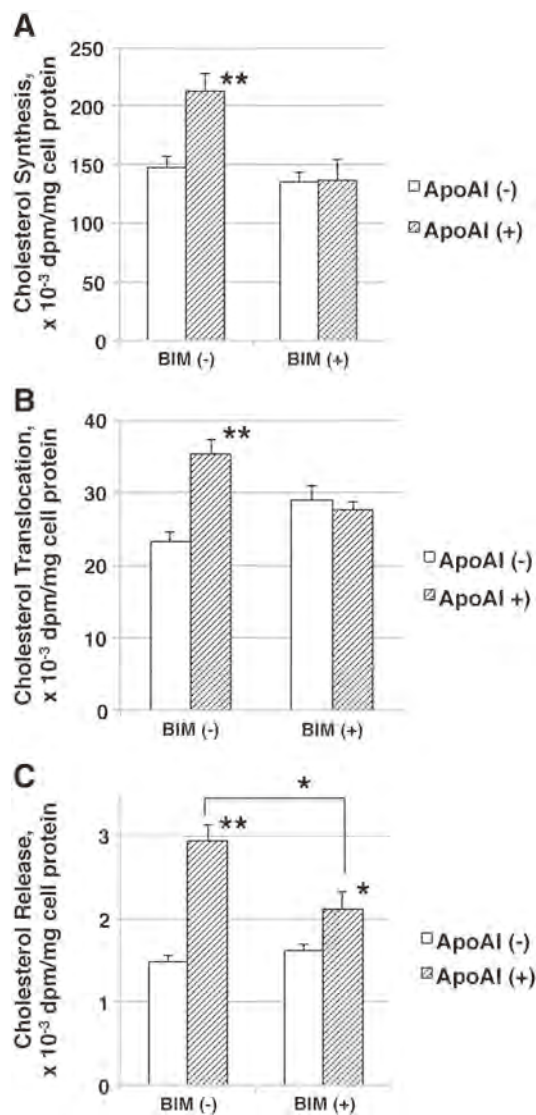


**Fig. 8.** Effects of a protein kinase C inhibitor BIM on apoA-I-induced cholesterol biosynthesis, its translocation to cytosol and its release from cells. Rat astrocytes at a confluent cell density were incubated with [ $^3$ H]acetate (20  $\mu$ Ci/mL, PerkinElmer) in a fresh 0.02% BSA/F-10. A. For cholesterol biosynthesis, the cells were incubated with [ $^3$ H]acetate for 3 h in the presence and absence of apoA-I (5  $\mu$ g/mL) with and without BIM (25  $\mu$ M), and incorporation of radioactivity into cholesterol was counted. B. For cholesterol translocation to the cytosol fraction, the cells were uniformly pre-labeled with [ $^3$ H]acetate for 16 h, and thoroughly washed. The labeled cells were incubated with and without apoA-I (5  $\mu$ g/mL) for 90 min and radioactive cholesterol was analyzed in the cytosol. C. For cellular cholesterol release, the uniformly pre-labeled cells were incubated with and without apoA-I (5  $\mu$ g/mL) for 6 h, and the radioactive cholesterol in the medium was counted. Data represent the average and SE of the measurements using three cell plates. Statistical significance of the effect of apoA-I indicated as asterisk; \*,  $P < 0.05$ ; \*\*,  $P < 0.01$  by Student's  $t$  test. Cell cholesterol release by apoA-I was decreased by BIM with  $p < 0.05$ .

translocation to CLPP of phospholipase C $\gamma$ , increases diacylglycerol production in the CLPP fraction, and translocation of PKC $\alpha$  to CLPP and its activation there [9,10,12]. Phospholipase C inhibitor, U73122, suppressed both apoA-I-induced reactions of PKC $\alpha$  translocation to and diacylglycerol production in CLPP, as well as cholesterol translocation to cytosol and its release as HDL biogenesis [12]. In addition, apoA-I provokes translocation of newly synthesized cholesterol to CLPP rather than the cholesterol molecules already in the membranes, and enhances association of caveolin-1 and PKC $\alpha$  with CLPP [9,14]. Thus, apoA-I induces complex signal transduction for intracellular cholesterol trafficking, including PKC $\alpha$  translocation to and its activation in CLPP in association with activation of phospholipase C $\gamma$ . Moreover, apoA-I induces association of CLPP with microtubules being regulated by

caveolin-1 through its scaffolding domain [14]. These findings allow us to speculate that CLPP is one of the sites for apoA-I-induced signal transductions and plays a role of a vehicle for intracellular cholesterol transport. In this context, we reported that apoA-I enhances association of CLPP with rMT and promotes intracellular cholesterol transport for generation of apoA-I-HDL in rat astrocytes [11,14].

To understand the underlying molecular mechanism, we investigated phosphorylation of an rMT component  $\alpha$ -tubulin by CLPP-associated PKC in relation to intracellular cholesterol trafficking and cholesterol release mediated by exogenous apoA-I in fetal rat astrocytes. The experimental results are summarized as follows. 1) Phosphorylation of  $\alpha$ -tubulin of molecular weight of 52 kDa is intensified in the rMT prepared from the cytosol of rat astrocytes treated with apoA-I. It is suppressed by protein kinase C inhibitor, BIM. 2) rMT-associated PKC $\alpha$  phosphorylates endogenous  $\alpha$ -tubulin as well as exogenously added bovine tubulin in rMT. 3) Activation of caveolin-1-associated (presumably CLPP-associated) PKC $\alpha$  induces phosphorylation of  $\alpha$ -tubulin in the caveolin-1-containing complex, but CLPP tends to dissociate from the phosphorylated  $\alpha$ -tubulin. 4) Inhibition of PKC by BIM suppresses cholesterol translocation to the cytosol from the ER/Golgi and accordingly inhibits the increase of de novo biosynthesis of cholesterol by apoA-I and apoA-I-mediated cholesterol release in rat astrocytes.

These findings are consistent with the view that phosphorylation of  $\alpha$ -tubulin is catalyzed by the CLPP-associated PKC $\alpha$  when apoA-I induces translocation of caveolin-1, phospholipase C $\gamma$  and PKC $\alpha$  to CLPP, activation of PKC $\alpha$ , and association of CLPP with microtubules. This phosphorylation likely takes place locally in the site of the microtubule where the CLPP binds. It is interesting that  $\alpha$ -tubulin once phosphorylated no longer remains in tight association with CLPP and easily dissociates. CLPP may therefore change the position for the interaction on the microtubules, as it keeps phosphorylating new  $\alpha$ -tubulin molecules.

It has been known that tubulin phosphorylation by calmodulin-dependent protein kinase II or casein kinase II in the presence of Ca $^{2+}$  induces depolymerization of microtubules [25–27]. Tau factor, microtubule-associated protein-2 (MAP2) and MAP4 among microtubule components are phosphorylated by PKC [28]. There is a report that PKC $\alpha$  phosphorylates  $\alpha$ 6-tubulin at Ser $^{165}$  in human breast cells and enhances the motility of the cells [29] at least suggesting that  $\alpha$ 6-tubulin is a PKC $\alpha$  substrate, although the underlying mechanism remains unknown. Biochemical significance of phosphorylation of tubulin or components of microtubules by PKC is little known at present in comparison to other types of tubulin modifications [30,31]. More recent reports may suggest that phosphorylation of tubulins is associated with various functional reactions of cells to extracellular stimulus [32–35]. In the current experiments, phosphorylation of  $\alpha$ -tubulin in rMT by CLPP-associated PKC $\alpha$  did not cause depolymerization of rMT.

Unstable interaction of CLPP with microtubules seems caused by  $\alpha$ -tubulin phosphorylation and may result in continuous translocation of CLPP on microtubules. Inhibition of this phosphorylation is associated with decrease of apoA-I-mediated cholesterol translocation to the cytosol and cholesterol release presumably as HDL in rat astrocytes.  $\alpha$ -Tubulin phosphorylation mediated by CLPP-associated PKC $\alpha$  thus may activate intracellular cholesterol trafficking for cholesterol release/biogenesis of HDL through the CLPP-microtubules interaction in rat astrocytes. Physiological relevance of these findings, such as roles of apoA-I-HDL and the CLPP system in biogenesis of brain HDL is still to be determined. Further investigation is required to confirm this view.

#### Acknowledgement

This work was supported in part by MEXT (Ministry of Education, Culture, Sports, Science and Technology of Japan)-Supported Program for the Strategic Research Foundation at Private Universities (Japan) S1201007, and Grant-in-aid from MEXT 24614018.

The authors declare that no conflict of interest exists.

## References

- [1] R.B. DeMattos, R.P. Brendza, J.E. Heuser, M. Kierson, J.R. Cirrito, J. Fryer, P.M. Sullivan, A.M. Fagan, X. Han, D.M. Holtzman, Purification and characterization of astrocyte-secreted apolipoprotein E and J-containing lipoproteins from wild-type and human apoE transgenic mice, *Neurochem. Int.* 39 (2001) 415–425.
- [2] H. Chiba, T. Mitamura, S.-i. Fujisawa, A. Ogata, Y. Aimoto, K. Tashiro, K. Kobayashi, Apolipoproteins in rat cerebrospinal fluid: a comparison with plasma lipoprotein metabolism and effect of aging, *Neurosci. Lett.* 133 (1991) 207–210.
- [3] I. Borghini, F. Barja, D. Pometta, R.W. James, Characterization of subpopulations of lipoprotein particles isolated from human cerebrospinal fluid, *Biochim. Biophys. Acta* 1255 (1995) 192–200.
- [4] J. Ito, L.-Y. Zhang, M. Asai, S. Yokoyama, Differential generation of high-density lipoprotein by endogenous and exogenous apolipoproteins in cultured fetal rat astrocytes, *J. Neurochem.* 72 (1999) 2362–2369.
- [5] E.S. Krul, J. Tang, Secretion of apolipoprotein E by an astrocytoma cell line, *J. Neurosci. Res.* 32 (1992) 227–238.
- [6] B. Mockel, H. Zinke, R. Flach, B. Weis, H. Weiler-Guttler, H.G. Gassen, Expression of apolipoprotein A-I in porcine brain endothelium in vitro, *J. Neurochem.* 62 (1994) 788–798.
- [7] Z. Balazs, U. Panzenboeck, A. Hammer, A. Sovic, O. Quehenberger, E. Malle, W. Sattler, Uptake and transport of high-density lipoprotein (HDL) and HDL-associated alpha-tocopherol by an in vitro blood-brain barrier model, *J. Neurochem.* 89 (2004) 939–950.
- [8] S.C. Fujita, K. Sakuta, R. Tsuchiya, H. Hamanaka, Apolipoprotein E is found in astrocytes but not in microglia in the normal mouse brain, *Neurosci. Res.* 35 (1999) 123–133.
- [9] J. Ito, Y. Nagayasu, K. Kato, R. Sato, S. Yokoyama, Apolipoprotein A-I induces translocation of cholesterol, phospholipid, and caveolin-1 to cytosol in rat astrocytes, *J. Biol. Chem.*, vol. 277, 2002, pp. 7929–7935.
- [10] J. Ito, H. Li, Y. Nagayasu, A. Kheirollah, S. Yokoyama, Apolipoprotein A-I induces translocation of protein kinase Calpha to a cytosolic lipid-protein particle in astrocytes, *J. Lipid Res.* 45 (2004) 2269–2276.
- [11] A. Kheirollah, J.-i. Ito, Y. Nagayasu, R. Lu, S. Yokoyama, Cyclosporin A inhibits apolipoprotein A-I-induced early events in cellular cholesterol homeostasis in rat astrocytes, *Neuropharmacology* 51 (2006) 693–700.
- [12] J. Ito, Y. Nagayasu, S. Ueno, S. Yokoyama, Apolipoprotein-mediated cellular lipid release requires replenishment of sphingomyelin in a phosphatidylcholine-specific phospholipase C-dependent manner, *J. Biol. Chem.* 277 (2002) 44709–44714.
- [13] R. Arakawa, S. Abe-Dohmae, M. Asai, J.-i. Ito, S. Yokoyama, Involvement of caveolin-1 in cholesterol enrichment of high density lipoprotein during its assembly by apolipoprotein and THP-1 cells, *J. Lipid Res.* 41 (2000) 1952–1962.
- [14] J. Ito, A. Kheirollah, Y. Nagayasu, R. Lu, K. Kato, S. Yokoyama, Apolipoprotein A-I increases association of cytosolic cholesterol and caveolin-1 with microtubule cytoskeletons in rat astrocytes, *J. Neurochem.* 97 (2006) 1034–1043.
- [15] S. Yokoyama, S. Tajima, A. Yamamoto, The process of dissolving apolipoprotein A-I in an aqueous buffer, *J. Biochem.* 91 (1982) 1267–1272.
- [16] J. Ito, T. Kato, S. Wakabayashi, F. Hara, R. Tanaka, K. Kato, Autocrine regulation of glial proliferation and differentiation: The induction of cytodifferentiation of postmitotic normal glioblast by growth-promoting factor from astrocytoma cell, *Brain Res.* 374 (1986) 335–341.
- [17] J. Ito, Y. Nagayasu, R. Lu, A. Kheirollah, M. Hayashi, S. Yokoyama, Astrocytes produce and secrete FGF-1, which promotes the production of apoE-HDL in a manner of autocrine action, *J. Lipid Res.* 46 (2005) 679–686.
- [18] D. Thom, A.J. Powell, C.W. Lloyd, D.A. Rees, Rapid isolation of plasma membranes in high yield from cultured fibroblasts, *Biochem. J.* 168 (1977) 187–194.
- [19] Q. Li, M. Tsujita, S. Yokoyama, Selective down-regulation by protein kinase C inhibitors of apolipoprotein-mediated cellular cholesterol efflux in macrophages, *Biochemistry* 36 (1997) 12045–12052.
- [20] Y. Yamauchi, M. Hayashi, S. Abe-Dohmae, S. Yokoyama, Apolipoprotein A-I activates protein kinase C alpha signaling to phosphorylate and stabilize ATP binding cassette transporter A1 for the high density lipoprotein assembly, *J. Biol. Chem.* 278 (2003) 47890–47897.
- [21] Y. Yamauchi, C.C. Chang, M. Hayashi, S. Abe-Dohmae, P.C. Reid, T.Y. Chang, S. Yokoyama, Intracellular cholesterol mobilization involved in the ABCA1/apolipoprotein-mediated assembly of high density lipoprotein in fibroblasts, *J. Lipid Res.* 45 (2004) 1943–1951.
- [22] J.E. Poncin, J.A. Martial, J.E. Gielen, Cloning and structure analysis of the rat apolipoprotein A-I cDNA, *Eur. J. Biochem.* 140 (1984) 493–498.
- [23] X. Collet, Y.L. Marcel, N. Tremblay, C. Lazure, R.W. Milne, B. Perret, P.K. Weech, Evolution of mammalian apolipoprotein A-I and conservation of antigenicity: correlation with primary and secondary structure, *J. Lipid Res.* 38 (1997) 634–644.
- [24] J.B. Marsh, M.R. Diffenderfer, Isolation of nascent high-density lipoprotein from rat liver perfusates by immunoaffinity chromatography: effects of oleic acid infusion, *Metabolism* 40 (1991) 26–30.
- [25] F. Wandosell, L. Serrano, M.A. Hernandez, J. Avila, Phosphorylation of tubulin by a calmodulin-dependent protein kinase, *J. Biol. Chem.* 261 (1986) 10332–10339.
- [26] M.L. Vallano, J.R. Goldenring, R.S. Lasher, R.J. Delorenzo, Association of calcium/calmodulin-dependent kinase with cytoskeletal preparations: phosphorylation of tubulin, neurofilament, and microtubule-associated proteins, *Ann. N. Y. Acad. Sci.* 466 (1986) 357–374.
- [27] L. Serrano, J. Diaz-Nido, F. Wandosell, J. Avila, Tubulin phosphorylation by casein kinase II is similar to that found in vivo, *J. Cell Biol.* 105 (1987) 1731–1739.
- [28] T. Akiyama, E. Nishida, J. Ishida, N. Saji, H. Ogawara, M. Hoshi, Y. Miyata, H. Sakai, Purified protein kinase C phosphorylates microtubule-associated protein 2, *J. Biol. Chem.* 261 (1986) 15648–15651.
- [29] T.P. Abeyweera, X. Chen, S.A. Rotenberg, Phosphorylation of alpha6-tubulin by protein kinase Calpha activates motility of human breast cells, *J. Biol. Chem.* 284 (2009) 17648–17656.
- [30] S. Westermann, K. Weber, Post-translational modifications regulate microtubule function, *Nat. Rev. Mol. Cell Biol.* 4 (2003) 938–947.
- [31] N. Fukushima, D. Furuta, Y. Hidaka, R. Moriyama, T. Tsujiuchi, Post-translational modifications of tubulin in the nervous system, *J. Neurochem.* 109 (2009) 683–693.
- [32] F. Caudron, E. Denarier, J.C. Thibout-Quintana, J. Brocard, A. Andrieux, A. Fourest-Lievin, Mutation of Ser172 in yeast beta tubulin induces defects in microtubule dynamics and cell division, *PLoS ONE* 5 (2010) e13553.
- [33] T.C. Lin, L. Gombos, A. Neuner, D. Sebastian, J.V. Olsen, A. Hrlle, C. Benda, E. Schiebel, Phosphorylation of the yeast gamma-tubulin Tub4 regulates microtubule function, *PLoS ONE* 6 (2011) e19700.
- [34] E.C. Mattos, R.I. Schumacher, W. Colli, M.J. Alves, Adhesion of *Trypanosoma cruzi* trypomastigotes to fibronectin or laminin modifies tubulin and paraflagellar rod protein phosphorylation, *PLoS ONE* 7 (2012) e46767.
- [35] Y. Ban, Y. Kobayashi, T. Hara, T. Hamada, T. Hashimoto, S. Takeda, T. Hattori, alpha-tubulin is rapidly phosphorylated in response to hyperosmotic stress in rice and arabidopsis, *Plant Cell Physiol.* 54 (2013) 848–858.



## Prevention of fatal hepatic complication in schistosomiasis by inhibition of CETP

Shinji Yokoyama, Kuniko Okumura-Noji, Rui Lu

Nutritional Health Science Research Center, Chubu University, Kasugai 487-8501, Japan.

### Abstract

*Schistosoma japonicum*, once endemic all the East Asia, remains as a serious public health problem in certain regions. Ectopic egg embryonation in the liver causes granulomatosis and eventually fatal cirrhosis, so that prevention of this process is one of the keys to reduce its mortality. The embryonation requires cholesteryl ester from HDL of the host blood for egg yolk formation, and this reaction is impaired from the abnormal large HDL in genetic cholesteryl ester transfer protein (CETP) deficiency. When CETP was expressed in mice that otherwise lack this protein, granulomatosis of the liver was shown increased compared to the wild type upon infection of *Schistosoma japonicum*. The CETP deficiencies accumulated exclusively in East Asia, from Indochina to Siberia, so that Schistosomiasis can be a screening factor for this accumulation. CD36 related protein (CD36RP) was identified as a protein for this reaction, cloned from the cDNA library of *Schistosoma japonicum* with 1880-bp encoding 506 amino acids. The antibody against the extracellular loop of CD36RP inhibited cholesteryl ester uptake from HDL and suppressed egg embryonation in culture. Therefore, inhibition of CETP is a potential approach to prevent liver granulomatosis and thereby fatal liver cirrhosis in the infection of *Schistosoma japonicum*.

**Keywords:** *Schistosoma japonicum*, liver cirrhosis, granulomatosis, CETP deficiency, HDL, cholesteryl ester

### *Schistosoma japonicum* in Asia

*Schistosoma (S.) japonicum*, an Asian specific blood fluke parasite, was endemic in East Asia including Indonesia, Philippines, China, and Japan as far as traced in recorded history. Its Mekong strain or *S. mekongi* is also found around the Mekong basin in Indochina peninsula. The parasite was first identified in Japan early 20<sup>th</sup> century when a few intensively infected regions were known, which is basically eliminated in these days<sup>[1]</sup>. It used to infect as many as 12 million people in China until the modern public health

effort was initiated<sup>[2]</sup>. Although the number of the patients has dramatically decreased, it is still active at least in China<sup>[2-3]</sup>, Philippines<sup>[4-5]</sup>, Cambodia, Laos, Thailand, Malaysia, and Indonesia<sup>[6]</sup>, perhaps accounting for some 2-million patients, and remains as the world second major Schistosomiasis next to the African blood fluke, *S. mansoni*.

The life cycle of this parasite includes an intermediate host of specific fresh water snails such as *Oncomelania nosophora*. The adults reside in the portal or intestinal veins of the host animals including humans, and lay eggs to be excreted with feces. The eggs embryonate

Corresponding author: Shinji Yokoyama, Ph.D, Nutritional Health Science Research Center, Chubu University, 1200 Matsumoto-cho, Kasugai 487-8501, Japan, Tel: +81-568-51-9698, E-mail: syokoyam@isc.chubu.ac.jp.

Received 08 January 2015, Accepted 26 January 2015, Epub 15 April 2015

CLC number: R532.21, Document code: A

The authors reported no conflict of interests.

in environmental fresh water and are hatched to release miracidia that penetrate into the snails to infect. They further grow there to sporocysts and then to cercariae, and are released into the water again to swim and penetrate the skin of the terminal hosts. Thus, endemic of *S. japonicum* is closely associated with intensive contact with natural fresh water reserve in everyday life. The historical geographic distribution of *S. japonicum* overlaps the regions with the culture of water farming of rice grain. This might have caused intensive endemic of *S. japonicum* in East Asia.

One of the most life threatening clinical manifestations is liver cirrhosis, which is caused by ectopic egg embryonation. The adult pairs of the parasite locate in the portal and its draining venules and lay eggs to be released to the intestinal tract. However, many of them are flushed back via the portal blood flow to the liver where they embolize and develop into miracidia, a phenomenon that leads to the morbidity and mortality of hepatic granulomatosis and cirrhosis<sup>[7]</sup>. Thus, egg embryonation is one of targets to prevent fatal development of schistosomiasis. The active mechanism to induce this lesion is unknown. Specific antibodies against various egg antigens have been identified as indicators of the infection, but their relationship with granulomatogenesis is unclear<sup>[8]</sup>. A potential pathogenesis factor is egg embryonation to the stage of miracidium, as the eggs only after this stage seem to cause the liver lesion when transplanted<sup>[9]</sup>. *L*-Selectin of the host binds the eggs only in the stage of miracidium<sup>[10]</sup>. Vaccination to stabilize the embryonation process has been proposed for an anti-Schistosomiasis therapy<sup>[11]</sup>.

Schistosomes use the host plasma lipoproteins as lipid nutrient sources. *S. mansoni* express the low density

lipoprotein (LDL) receptor-like protein<sup>[12-13]</sup>. The receptors for LDL and very low density lipoprotein (VLDL) were shown to mediate uptake of the lipoproteins in *S. mansoni*<sup>[14-15]</sup>, as well as in *S. japonicum*<sup>[16-17]</sup>. However, there has not been much information whether and how high density lipoprotein (HDL) interacts with Schistosomes. We investigated a role of HDL in life-cycle of *S. japonicum*<sup>[18-20]</sup>.

### HDL for embryonation of *S. japonicum* eggs and CETP deficiency

Embryonation of *S. japonicum* eggs to miracidia was investigated *in vitro*<sup>[19]</sup>. The paired adult parent parasites removed from the infected mouse portal vein were pre-incubated for laying eggs in the presence of 5% and 10% normal human serum for 2 days. The eggs were isolated and cultured for another 8 days for embryonation in the absence and presence of 10% human serum. When the eggs were laid in the presence of adequate serum source (10%), they did not require serum for their embryonation. When they were laid in the poor nutritional condition (5% serum), the eggs needed the serum for embryonation (**Fig. 1A**). The finding indicates that the egg yolk is established for embryonation before they are laid but the eggs themselves also uptake nutrients from the serum, to grow. The latter effect was not reduced even when apoB lipoprotein was removed from the serum, indicating that LDL/VLDL are not major nutrient sources for the embryonation. Finally, HDL was shown as a requirement for embryonation (**Fig. 1B** and **C**). The results lead us to wonder how alteration of HDL metabolism influences the egg embryonation and accordingly development of the hepatic lesions.

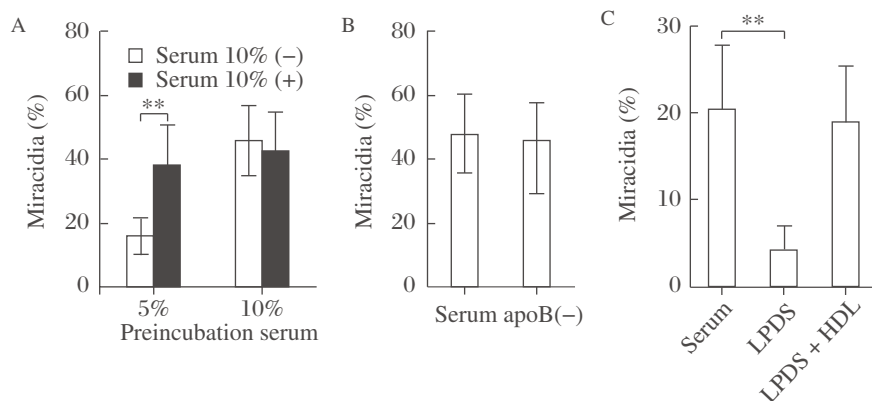


**Fig. 1** Embryonation of *S. japonicum* eggs in culture, monitored as miracidia formation (%), modified from the reference<sup>[19]</sup> A: incubation of the eggs with and without human serum (10%) for 8 days after pre-exposure to 5 and 10% human serum of the parents laying the eggs. B: Normal embryonation after the preincubation with 5% serum, even with apoB-lipoprotein-deficient human serum (apoB (-)). C: Requirement of HDL for embryonation. LPDS; lipoprotein deficient serum. Asterisks \*\* indicate statistical difference at  $P < 0.01$  from serum (-) (A) or serum (C).

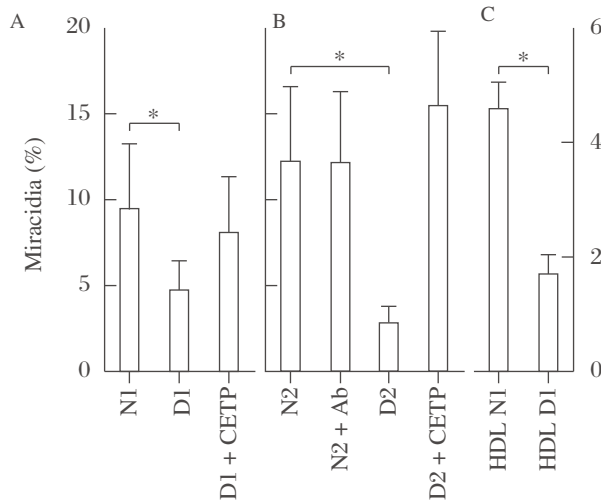


**Fig. 2 Embryonation (% Miracidia) of *S. japonicum* eggs in culture with CETP-deficient human serum in 10% normal human sera (N1 and N2) and that of CETP-deficient subjects (D1 and D2), modified from the reference<sup>[18]</sup>.** Embryonation is retarded in CETP-deficient serum (A) and adding CETP recovers this (B). Normal HDL is adequate for the embryonation but not HDL from CETP-deficiency (C). Asterisk indicates statistical difference at  $P < 0.05$  from normal HDL.

Some genetic mutations are known to manifest abnormal HDL metabolism. Deficiencies in HDL is seen in dysfunctional mutations in ATP-binding cassette transporter A1, lecithin: cholesterol acyltransferase and apolipoprotein A1, while deficiency of cholesteryl ester transfer protein (CETP) causes very high HDL cholesterol level as it generates a large abnormal HDL particle. While the former diseases are rare anywhere in the world except for the very limited regions with the founders' effect, CETP deficiency is found with very high prevalence widely in East Asia as discussed later in this text. Therefore, the *in vitro* experiments for egg embryonation were carried out with the serum from human subjects of genetic CETP deficiency<sup>[18]</sup>.

The egg embryonation was significantly low when incubated with the serum of CETP deficient subjects, and this was substantially recovered in the presence of purified human CETP (**Fig. 2A**). However, the presence of the anti-CETP inhibitory antibody in the normal serum did not attenuate embryonation (**Fig. 2B**). Finally, normal HDL gave the eggs normal embryonation without other serum components, but HDL of CETP deficient subjects showed inadequate embryonation (**Fig. 2C**). Selective cholesteryl ester (CE) uptake was slower from HDL from CETP deficient subjects while free cholesterol exchange showed no difference between the normal and CETP-deficiency HDL (**Fig. 3**)<sup>[18]</sup>. Wild type mouse serum that lacks CETP activity did not induce adequate embryonation and

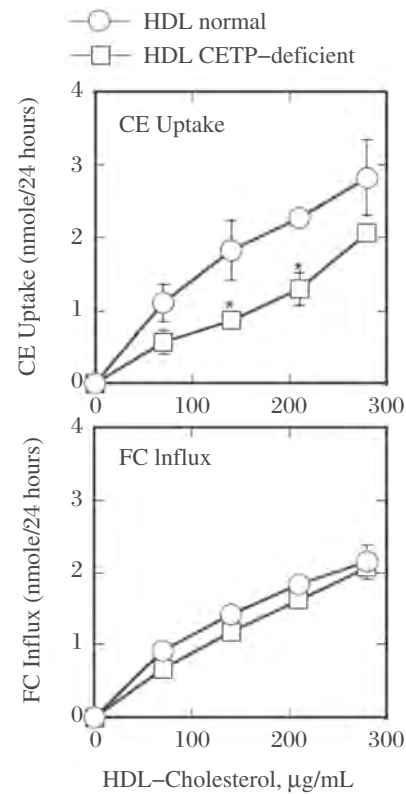


**Fig. 3 Uptake of cholesteryl ester (CE) and free cholesterol (FC) from HDL by *S. japonicum* eggs, modified from reference<sup>[18]</sup>.** The eggs were incubated with normal and CETP-deficient HDL with radiolabeled CE or FC.

the serum of the *CETP*-transgenic mouse enhanced it. Adding purified CETP to the mouse serum partially recovered the rate of embryonation (**Fig. 4**). Thus the findings with human blood serum were reproduced with mouse serum with and without CETP activity *in vitro*.

Accordingly, *in-vivo* studies were carried out in mice, using wildtype mice as a model for CETP-deficiency and the *CETP*-transgenic mice for normal human subject<sup>[18]</sup>. Number of the eggs plugged into the liver and the rate of their embryonation were counted microscopically in the liver specimens. While the number of the eggs was similar between the models, their embryonation was significantly higher in the transgenic mouse liver (**Fig. 5**). The average granulomatous lesion per egg was larger in the transgenic mice (**Table 1**). Absence of CETP thus seems to reduce ectopic embryonation of *S. japonicum* eggs in the host liver, making the host resistant to its hepatic complication.

### Endemics of CETP deficiency

CETP is present in the plasma of certain species of mammals including humans<sup>[21-24]</sup>. Human CETP is composed of 476 amino acid residues<sup>[25]</sup> with a glycosi-

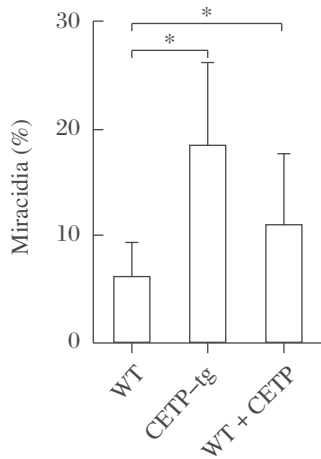


**Fig. 4** The effect of mouse serum on egg embryonation (% miracidia), modified from the reference<sup>[18]</sup>. Embryonation is poor with wildtype mouse serum that lacks CETP and proceeds with CETP-transgenic mouse serum (CETP-tg). Adding human CETP to the wildtype serum partially restored embryonation. Asterisk indicates statistical difference at  $P<0.05$  from WT.

lated molecular weight of 74,000. It catalyzes non-directional equimolar exchange of CE and triglyceride (TG) among lipoproteins with low substrate specificity<sup>[26-29]</sup>. The reaction equalizes distribution of the core lipids among lipoproteins, and consequently causes the net move of CE from HDL to TG-rich lipoproteins such as VLDL and TG from TG-rich lipoproteins to HDL and LDL<sup>[26]</sup>. CE is generated in plasma on HDL and plasma TG is present in VLDL and chylomicron originating from the liver and the intestinal cells, so that the CETP reaction results in decrease of CE in HDL and increase of TG both in HDL and LDL. TG is hydrolyzed by hepatic lipase in any lipoprotein subfraction so that the size of HDL and LDL gets

**Table 1.** Granulomatous lesion in the liver.

	CETP transgenic	Wildtype
Granuloma area (%)	10.5 ± 5.5	14.4 ± 5.4
Area per egg ( $\mu\text{m}^2$ ) × 10 <sup>-3</sup>	86.7 ± 26.5	66.1 ± 19.3*

\* $P<0.05$ . Taken from the reference<sup>[18]</sup>. The eggs and granulomatous lesion were microscopically identified in the liver specimens of the wildtype and CETP transgenic mice, infected by *S. japonicum*. The total area of the lesion per egg was calculated for each section. The area per egg was calculated as a mean ± SE of the 12 mice, for each of which 12 random liver sections were examined.

smaller by the CETP reaction to produce HDL3 particles and so-to-speak small dense LDL. Increase in plasma TG indeed decreases plasma HDL and increases small dense LDL in the presence of CETP. In turn, HDL-CE increases when CETP reaction decreases<sup>[30]</sup>.

Since generation of CE in HDL is one of the driving force for the removal of cell cholesterol<sup>[31]</sup>, playing an important part of cholesterol transport for catabolism from peripheral somatic cells to the liver as its catabolic site, the CETP reaction may facilitate this transport by sending HDL-CE to LDL for the pathway of recovery of LDL through the hepatic LDL receptor<sup>[32]</sup>. On the other hand, the increase in the HDL surface area in low CETP activity may provide more capacity to accept cell cholesterol.

CETP became a popular topic of lipoprotein study since discovery of the genetic defect of CETP. The patients were first described in Japan in 1985 as cases with hyperalphalipoproteinemia with the lack of CE transfer reaction between lipoproteins<sup>[33-34]</sup>. Its genetic background was soon established<sup>[35]</sup>, and many cases were found thereafter in Japan. Two major mutations have been identified as major disorders, intron 14 G(+1)-to-A (Int14A) and exon 15 missense mutation

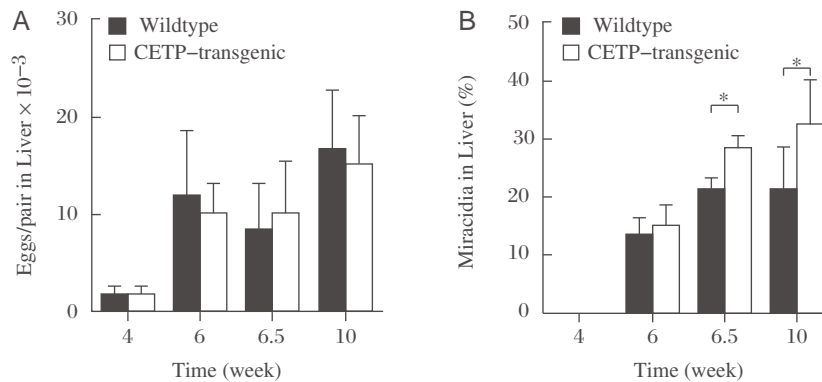


**Fig. 5** Number of eggs embolizing in the liver and their ectopic embryonation in the mice infected with *S. japonica*, modified from the reference<sup>[18]</sup>. Wildtype and CETP-transgenic mice are infected by *S. japonica*. The ectopic embryonation is accelerated in the transgenic mice. A: Egg count in liver. B: Egg maturation in liver. Asterisk indicates statistical difference at  $P<0.05$  from wildtype.

(D442G)<sup>[36-38]</sup>. Prevalence of these two mutants was found very high in Japanese general population, as int14A 1% to 2% and D442G 6% to 7%. In addition, sporadic cases with 10 or more other types of mutations were also identified among Japanese<sup>[39-41]</sup>. Accordingly, the estimated number of the heterozygotes can be around 10 millions in Japan and the homozygotes would be as many as 150,000 to 250,000. CETP deficiency may account for 27.6 % of the people with HDL cholesterol  $\geq 60$  mg/dL and 31.4%–32.5% of those with HDL  $\geq 80$  mg/dL in Japan<sup>[36,42]</sup>. Above all, Omagari of Akita district in Northern Japan was discovered as the region with high accumulation of the Int14A mutant, with the prevalence of the heterozygote of 27%<sup>[38]</sup>. Thus, genetic CETP deficiency was found highly common among Japanese.

The first non-Japanese patient was reported from Switzerland as a Chinese descent<sup>[43]</sup>. Several reports thereafter described CETP deficiency among other Asians.

Genetic prevalence of D442G mutant heterozygote case was found to be 3.3%–10.8% in the main-land Chinese population<sup>[44-46]</sup>, and 4.5%–7.7% in the population of Taiwan<sup>[42,47-49]</sup>. It could be estimated up to 12% among Koreans based on its allele frequency of 6%<sup>[50]</sup>. Vietnamese D442G mutants were estimated to be 6.9% in the general population<sup>[51]</sup>. Nine cases were identified to be D442G heterozygotes out of the 35 individuals with hyperalphalipoproteinemias in Thailand<sup>[52]</sup>, accounting for 26%, similar to the ratio among Japanese<sup>[36,42]</sup> strongly indicating CETP mutants common in Thailand. Further detailed information is available in the previous review article<sup>[53]</sup>. More recent result for elderly Siberian Yakuts indicates the prevalence of D442G mutant 16.2% in the native Yakuts and 5.2% among the non-indigenous<sup>[54]</sup>, mostly Russians and Ukrainians, whose intermarriage rate with Yakuts may be 10 to 20% (Ariev AL, personal communication). Not much reliable information is available for the Int14A mutation, except for two out of the



**Fig. 6 Endemics map of *S. japonicum* and CETP deficiency (D442G).** Red spots show the regions where the cases were found since the parasite was identified in the early 20<sup>th</sup> Century. The regions spread over Japan, China including Taiwan, Mekong valleys, Thailand, Philippines, and Indonesia. The endemic was eliminated in many of these regions in the 21<sup>st</sup> Century. Data of the prevalence of G442G available in literature till today are listed as percentage in each ethnic general population unless otherwise indicated.

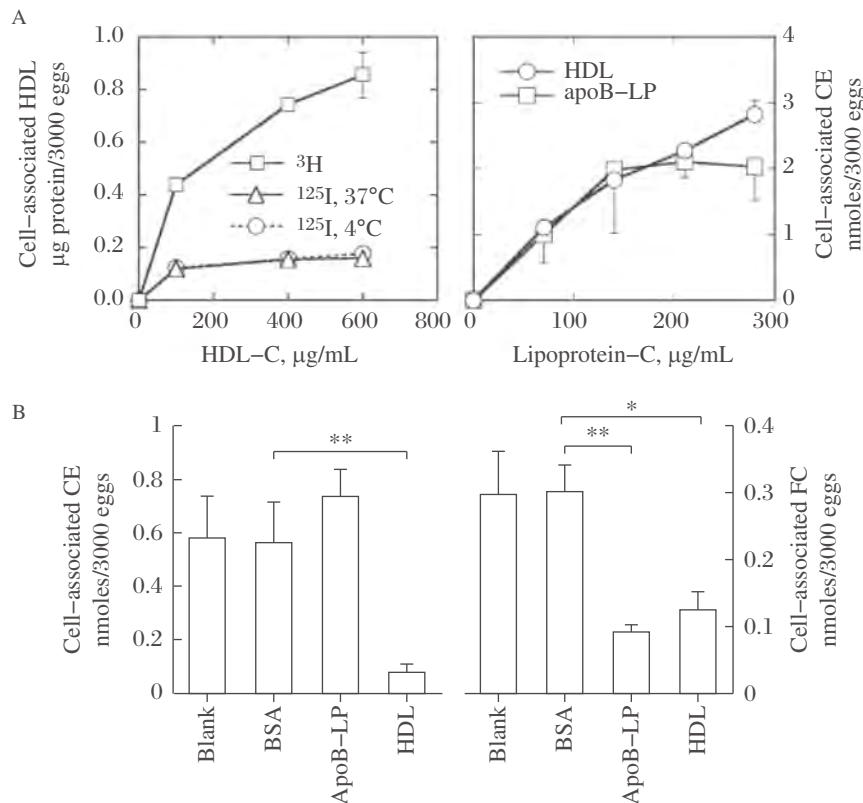


**Fig. 7** Selective uptake of CE from HDL by the eggs of *S. japonicum* modified from the reference<sup>[19]</sup>. A: The labeled HDL with <sup>125</sup>I for protein and with <sup>3</sup>H for CE was incubated with the eggs and the uptake of each radioactivity was measured and standardized for HDL protein (left). The CE uptake was also measured from HDL and LDL (right). B: CE (left) and FC (right) uptake from HDL in the presence of each plasma component indicated (BSA, ApoB lipoprotein, and HDL). Asterisks indicate statistical difference at  $P < 0.05$  (\*) and  $P < 0.01$  (\*\*) from BSA.

145 subjects (1.4%) in Hong Kong Chinese<sup>[18,47,55-59]</sup> and none of the 346 Vietnamese<sup>[51]</sup>. In a unique spot, Omagari of Akita district in Northern Japan, accumulation of Int14A mutant was found with the prevalence of the heterozygote 27.0%<sup>[33]</sup>.

In contrast, CETP deficiency is rare in other ethnic groups. The first Caucasian case was reported in 1997<sup>[60]</sup>, and one case of Int14A was reported in 1998 in Canada without ethnic background identification<sup>[61]</sup>. It was thus concluded that CETP deficiency is rare among North American Caucasians<sup>[62]</sup>. Nevertheless, a few studies reported sporadic cases of CETP deficiency in The United States<sup>[63]</sup>, Italy<sup>[64-65]</sup>, and the Netherlands<sup>[62,66]</sup>. There was an estimate of D442G mutant as "less than 1%"<sup>[67]</sup>, but the ground for this estimation, as well as how "less", is unclear.

Clinical manifestation of CETP deficiency is limited to abnormal plasma lipoprotein profile represented by very high HDL cholesterol and moderately reduced LDL cholesterol. In the lack of CETP activity, CE generated in HDL is detained there, so that the core CE compartment expands and HDL particles become larger in their size, as large as LDL, and rich in apoE<sup>[68-71]</sup>. The

patients in general do not exhibit any serious clinical symptoms. It has been wondered whether this large HDL is protective against atherosclerosis. The answer has been controversial for the genetic CETP deficiency<sup>[38,72-73]</sup> and the attempts of pharmacological inhibition of CETP were also inconclusive so far<sup>[74-75]</sup>.

In summary, CETP deficiency is highly prevalent in East Asia, at least among Japanese, Chinese both in mainland and Taiwan, and Koreans, predominantly with the D442G mutant. It is likely similarly high in Thailand. The Int14A mutant may be the second common, but it is not clearly demonstrated except for Japan. Other types of mutation have also been found frequently in Japan. It may also be so in other East Asian regions, but the information is not adequate. In contrast, this disease is rare in other ethnic groups.

For geographic or ethnic accumulation of a genetic abnormality, two potential hypotheses may be considered, "founders' effect" or screening by a regional fatal disease(s). The former cases are normally found in limited communities of the descendants of earlier settlers. Typical examples are accumulation of familial hypercholesterolemia in French Canadians<sup>[76]</sup>,

Afrikaners in South Africa<sup>[77]</sup> and perhaps in Lebanon<sup>[78]</sup>. In this case, the accumulated mutations may not be highly diverse as originating in a few carrier families. The latter is represented by sickle cell anemia that is resistant to malaria infection, as a believed reason for high prevalence of this genetic anemia among African ethnic groups<sup>[79–81]</sup>. This case may affect large populations historically exposed to such diseases, mostly infectious diseases.

Accumulation of CETP deficiency can also be discussed from such points of view. Majority of the patients of the region may be limited to one or two type(s) of mutations although further diversity of the mutation is also observed in the region, being not inconsistent with founders' effect. However, the region where this disease is found with high prevalence seems a large portion of East Asia, far beyond founder's effect. No specific settler family can be conceivable to account for such large descending population affected. However, extreme accumulation of *int14A* in Omagari may be the case of local "founders' effect"<sup>[33]</sup>. It should be noted that its only significant clinical phenotype is abnormal plasma lipoprotein metabolism. Very few infectious diseases are found with any relation to or dependency on plasma lipoproteins. Schistosomes may be one of the few to meet such criteria. The regions of historic endemics of *S. japonicum* and of high prevalence of CETP deficiency in fact largely overlap (**Fig. 6**).

### Identification and characterization of CD36-related protein in *S. japonicum*

In order to investigate a specific role of HDL for egg embryonation, uptake by the *S. japonicum* eggs of cholesterol, the most specific nutrient carried by lipoproteins, was observed. Uptake of lipoprotein CE by the eggs is shown in **Fig. 7**<sup>[19]</sup>. CE is selectively taken up from HDL. The uptake also seems to occur from apoB-lipoprotein, but it is saturated at much lower level and the pathways are independent of each other. In contrast, free cholesterol (FC) exchange between the eggs and lipoproteins is by a common pathway for HDL and apoB-lipoproteins (**Fig. 7**).

Selective cellular uptake of CE has been shown to be mediated by CD36-like proteins, such as scavenger receptor-B1 (SR-B1) in rodent<sup>[82]</sup> or CLA1 in human<sup>[83]</sup>. Assuming a similar protein mediates the reaction, expression of mRNA was searched in *S. japonicum* by using the 489-bp probe derived from the cDNA of Sj-Ts2 protein that has one of the CD36 domains (671-bp submitted and registered as Genbank AF291715). From the *S. japonicum* adult cDNA library, Sj-Ts2-containing cDNAs of variable sizes longer than 1-kb

were obtained all seemingly derived by single transcription, including the sequence of the reported Sj-Ts2 protein. The sequence of the full length (1880-bp) original mRNA was determined and deduced to 506 amino acid residues (**Fig. 8**) (GenBank accession no. AY496973)<sup>[19]</sup>. Though there is an indication of alternative splicing of this mRNA, the size of the PCR product, with the first-strand cDNA derived from total RNA as template, was similar (467-bp) between eggs and adults (**Fig. 9**). Therefore, the message is likely to be expressed in eggs though the level seems lower.

The amino acid sequence indicated that it has two transmembrane regions and at least three CD36 domains that are conserved in 32 CD36 proteins from variety of organism according to Conserved Domain search analysis (**Fig. 8**), having high homology with rat SR-B1, rat CD36 and human CLA-1. The protein was thus thought to be of the CD36 family and termed CD36-related protein (CD36RP)<sup>[19]</sup>. It had 15 nucleotide polymorphism sites in the coding region identified during screening, resulting in 11 amino acid substitutions. Three *N*-glycosylation sites (aa97, 205, 248) identified among the 15 candidates asparagine in CD36RP were conserved in mammalian SR-B1 and CD36 (**Fig. 8**). In fact, the size of CD36RP in the *S. japonicum* adult decreased from 82 kDa to 62 kDa after *N*-glycanase treatment<sup>[19]</sup>.

A recombinant peptide representing the extracellular domain containing the conserved Cys and Pro-rich domain of CD36RP was used for binding to lipoproteins<sup>[19]</sup>. The water-soluble extracellular domain peptide was shown to strongly bind to normal HDL, but neither to LDL nor to the HDL from a CETP deficient subject as poorly as to LDL (**Fig. 10**)<sup>[19]</sup>. The antibody against the extracellular domain peptide of CD36RP significantly suppressed the active CE uptake at 37°C, as well as the egg embryonation to miracidia (**Fig. 11**)<sup>[19]</sup>.

### Proposal of the hypothesis

Available information can be summarized as follows. 1) CETP deficiency is a unique inborn error to manifest very high HDL cholesterol due to extreme enlargement of HDL particles, without other apparent clinical features. CETP deficiency was shown highly prevalent among East Asians, at least shown with those in Japan, mainland China, Taiwan, Vietnam, Korea, Siberia and probably Thailand, while it seems rare among other ethnic groups. 2) One of the regional endemic diseases having any relation to plasma lipoproteins is schistosomiasis where the parasites use plasma lipoproteins as nutrient sources. *S. japonicum* has been known evidently endemic at least in Japan, China, Philippine, Indonesia, and its close

Prevention of fatal hepatic complication in schistosomiasis

1	aca ttt tat tta aca gct ttt aaa aat taa cag aca acg ttt cac ttg tac acg	ATG ATA	60
		M I	
61	TCT CGT GTT TGG TTA AGT GCT ACA GTT TTA TTT ACT TTG TTG ATT TGT ATA TCA TTA TTA	L L	120
	S R V W L S A T <b>V L F T V L I C I S L L</b>		
121	TCT TTA TGC GTA TTA CAA CCG TTT CTT TGG TTT CTA ATC AAT AGG CAA ACA CGT TTA ACT	L T	180
	<b>S L C V L</b> Q P F L W F L I N R Q T R L T		
181	CCA GGA ACT AAA CTG TAT TCA GAA TGG TTA GAG CCA TCA CTA CCT GTT TTA ACA CAA TTC	T F	240
	P G T K L Y S E W L E P S (L) P V L T Q F		
241	TAT TTT TTC AAT TTA ACA AAT CCA ATT GAA TTT CAA TCT GGT CAT AAA CCT CAT GIT CAA	Q	300
	Y F F N L T N P I E F Q S G H K P H V Q		
301	CAA TTA GGA CCA TAT ACA TAC CGT GAA AAA CGT TTG AAG CTT AAT ATT ACA CAT AGT AAT	N	360
	Q L G P Y T Y R E K R L K L <b>N</b> I T H S N		
361	GGA ACA ATT ACG TAT AAA GAA ATG AAA TGG TAT TAT TTT GAT CAA AAT TTA TCT AAT GGT	G	420
	G T I T Y Y A A M K W Y T Y F D Q N L T S A T G G T		
421	ATG GTG AAT GAT TCA ATC ACT AGT GTC AAT CTT GTT TTC ATA TCG ATT GCA TTG AGA ATC	I	480
	M V N D S I T S V N L V F I S I A L R I		
481	AAT TCA ATG CCA TGG TTT CTC AAA CAA ATA ATT GAA TTA ATT GAA TCC CGC TTT CAT GAA	E	540
	N S M P W F L K Q I I E L I E S R F H E		
541	TAT CTA TTT ATA ACA AAA ACT GTC AAT GAA TTA TTA TGG GGT TAT AAT GAT GAA TTA TTA	L L	600
	Y L F I T K T V N E L L W G Y N D E L L		
601	ACA TAC TTG TCA ACG CAT GGA TTC AAT ATG TCA ACA GTA ACT CAT ATT GGT CTA TTC ATT	I	660
	T Y (L) S (T) H G F N M S T V T H I G L F I		
661	AAT AAA AAT AAT ACA CTT AGT GAT TAT GTA ACA ATT AAT GAT GGT CTG CAT AAT AAT AAA	K	720
	N K N N T L S D Y V T I <b>N</b> D G L H N N K		
721	ATG ATT GGA CAA ATT ACT CGA TAT CAT GGT AAT ACA ACA TTA TCC TAT TGG AAT AGT TCA	S	780
	M I G Q I (T) (R) Y H G N T T L S Y W N S <u>S</u>		
781	ACA GCC AAT ATG ATA AAT GGT AGT GAT GGA ACA TTT TTT CAT TCA TTT CTA ACT AAA TAT	Y	840
	<u>T A N M I <b>N</b> G S D G T F F H S F L T K Y</u>		
841	GAT AAA CCG TAT GTT TTT GCA TCA GAT ATT TGT CGT TCA TTG CAA TTT TAC ACT GAA TCA	S	900
	<u>D K P Y V F A S D I C R S L Q F Y T E S</u>		
901	ATT GAT AAA TTA CAT AAT TTA CCA GTT TTA AAA TTA ACT CCA ATG TTG GAT ACA TTT AAA	K	960
	I D K L H N L P V L K L T P M L D T F K		
961	TCA CCG AAA TAT TAT GAA AAG AAT AGA GGA TTT TGT TTA AAT TGG CCT AAT TGT TAT GAG	E	1020
	S P K Y Y G A K N R G F C L N W P (N) <u>C Y E</u>		
1021	GAT GGT GTA TTA GAC ATG TCA TCA TGT CAA CCT GGT GCA CCG ATA GTT GTA CAA CCA	P	1080
	<u>D G V L D M S S C Q P G A P I V V S Q P</u>		
1081	CAT TTT TTA AAT GCT AAT AAA ACA TAT CAA GAT GCT GTT GAT GGA ATG TAT CCA ACT AAT	N	1140
	<u>H F L N A N K T Y Q D A V D G M Y P T N</u>		
1141	GAA ATG AAT ACA GTC ATC TAT GTA GAA CCA AAT ACT GGT AGT ATA ATA AAA GCA CAG AAA	K	1200
	E M <u>N T V I Y V E P N T G S I I K A O K</u>		
1201	AAA ATT CAA ATT AAC ATT TTA GTT AAA AAT GAT ACA ACA TTT AAA CAA CTT GCC AAT ATT	I	1260
	<u>K I Q I N I L V K N D T T F K Q L A N I</u>		
1261	TCA ACT ACT CTT CTA CCA ATT GTA TTC ATT AAT GAA TCA GTT CAA TTG AAT GAT ACA TTA	(L)	1320
	S T T (L) L P I V F I N E S V Q L N D T T (L)		
1321	ATT GAA CAA TTG ACT AAT GCA TTA ATT CAA CAA P TTC ATT GTT CAA ACA ATT TTA GTT	V	1380
	I E Q L T N A L I Q Q P <b>F I V Q T I L V</b>		
1381	TGT ATT ATC ACT TTG TCA ATA ATT TCA CTA GGT TCA CTT ATT TCA ATA CAT TTT TAT CAG	Q	1440
	<b>C I I T L S I I S L G S L I</b> S I H F Y Q		
1441	AAT AGA CAA CAT ACT ACT TAT ATG CAT TTT ATT GAT AGC CAT CAA TCC AAT GAT GTT ATA	I	1500
	N R Q H T T Y (M) (H) F I D S H Q S N D V I		
1501	CCT CAG AAT ACA TTA GAG GTT AAT ACA CAA CAA CAG ACA ATA TCA AAT GAT TTA CAA GAA	E	1560
	P Q N (S) L E V N T Q Q Q T I S N D L Q E		
1561	AAT CCA ATT GTT TAA * ttg tta att aac atg att caa ttg aca ata ttg tca tta tat gtt	1620	
	N P I V		
1621	tgt tat tgt tat tgt tct ata ttt gca tct gac tat cga tta gac att gat tag tga aag	1680	
1681	tct gtg tgt gag tgt gtg taa ttt tca att gtc aat ttt ttg taa ctt aga tgt ttt act	1740	
1741	tgt gaa tta ttt aat tta cct tca agg aga ata atc act gat tat ttg atg aat tgt gca	1800	
1801	taa caa ttg aat aaa tga caa aat atc tac agt taa gat gaa tga aat acc att gag ttt	1860	
1861	att gaa ctc tct atg agg taa aaa aaa aaa aa	1892	

Fig. 8 Nucleotide sequence and the deduced amino acid residue sequence of CD36RP cloned from *S. japonicum*, modified from the reference<sup>[19]</sup>. Shadowed portions are predicted membrane spanning regions. Bald letters of N indicate potential glycosylation sites. The sequences double underline portions are potential CD36-related regions (IPB 002159D, 002159E, and 002159F).

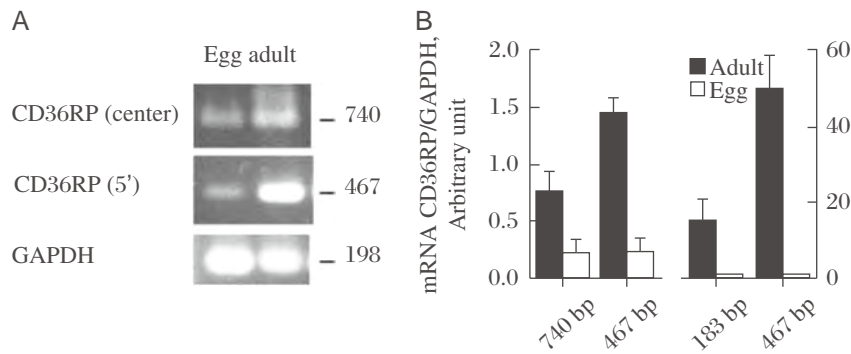


**Fig. 9** Expression of CD36RP in *S. japonicum*, the adults and the eggs, modified from the reference<sup>[19]</sup>. Two different probes (near the center and 5' region) were used to yield PCR products of 740 bp and 467 bp, respectively. A: The results of conventional PCR. B: The results of real-time PCR.

strain in the Mekong basin, substantially overlapping with the regions of high prevalence of the CETP deficiency (Fig. 6). 3) The ectopic egg embryonation to miracidia of *S. japonicum* in the liver requires normal plasma HDL, and it is impaired with the HDL of CETP deficiency. 4) CD36RP, a membrane protein of the CD36 family, was identified in *S. japonicum*. The antibodies against the extracellular domain of this protein suppressed selective uptake of CE by the eggs as well as the embryonation of the eggs.

Based on these findings and insights into them, we propose that CD36RP is a candidate for a mediator of selective uptake of CE from HDL by *S. japonicum* necessary for the egg embryonation to miracidia<sup>[19-20]</sup>. Pre-exposure of the adult schistosomes to wildtype HDL is sufficient for the eggs to mature, perhaps because the yolk of the egg was preformed adequately in such a condition. The eggs laid with inadequate yolk may still mature provided that normal HDL is supplied after they are laid. Absence of normal HDL retards

embryonation of the *S. japonicum* eggs in the host liver and, accordingly, prevents hepatic granulomatosis, in a situation such as CETP deficiency where abnormal large HDL does not efficiently bind CD36RP. Therefore, it is not unreasonable to speculate that CD36RP is a strong candidate for a mediator of HDL-CE uptake by the adults and eggs of *S. japonicum* as a key molecule for embryonation of the egg to the miracidium, based on structural similarity of CD36RP to CD36 or SR-BI, selective binding of the extracellular domain of CD36RP to HDL, and suppression of the HDL-CE uptake and embryonation of the eggs in culture by the antibody against CD36RP. CD36RP and host plasma HDL are both key elements for hepatic granulomatosis in *S. japonicum* infection, a fatal pathological process in infected patients.

If this hypothesis is valid, inhibition of CETP could be useful to prevent hepatic granulomatosis in schistosomiasis. CETP inhibitors have been developed hoping to raise HDL cholesterol to prevent athero-

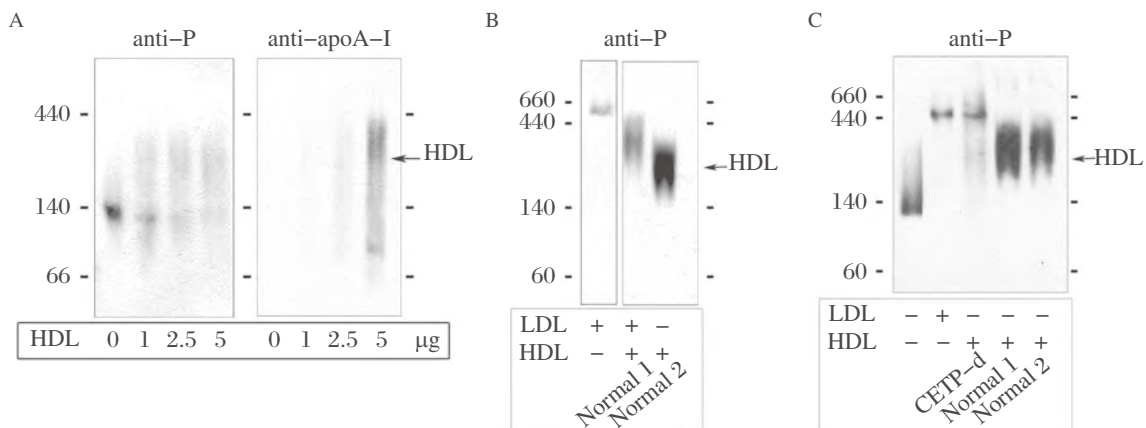


**Fig. 10** Interaction of the peptide representing the extracellular domain of CD36RP (residues 249–369) with lipoproteins, modified from the reference<sup>[19]</sup>. HDL was visualized by immunoblotting with anti-apoA-I antibody and the peptide was visualized by the antibody against the shorter peptide (331–348)(anti-P). A: Binding of the peptide with human HDL. B: Interaction of the peptide with HDL and LDL. C: Binding of the peptide with HDL from the normal and the CETP-deficient subjects.

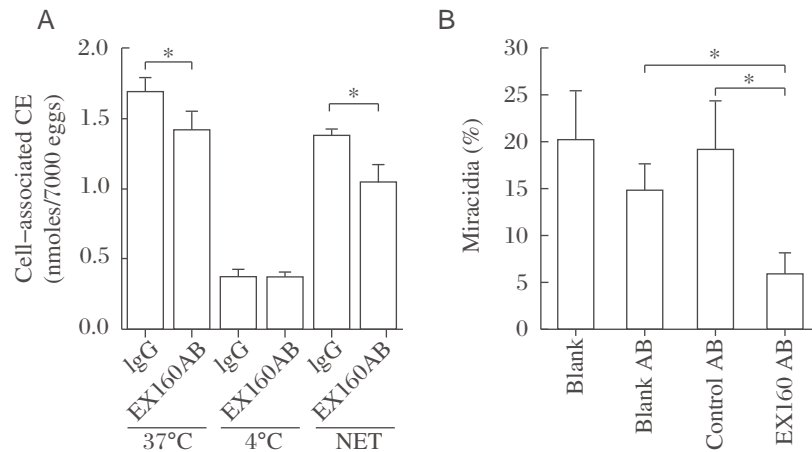


**Fig. 11** Suppression of CE uptake by and embryonation of the *S. japonicum* eggs in culture, by the antibody raised against the extracellular domain peptide of CD36RP representing the residues 249–408, modified from the reference<sup>[19]</sup>. Blank AB, nonimmunized rabbit antibody, Control AB, antibody against the intracellular domain of CD36RP (residues 331–348). Asterisk indicates statistical difference at  $P < 0.05$  from IgG or Blank AB/Control AB.

sclerotic vascular diseases such as coronary heart disease. The hypothesis has been proven valid in an animal experiment<sup>[8,4]</sup>, but has not been successful to demonstrate clinical outcome yet<sup>[74–75]</sup>. The inhibitors, however, can be useful to intend the off-target effect on other serious public health problem, prevention of the fatal liver cirrhosis in Schistosomiasis<sup>[20]</sup>.

### Acknowledgements

This work was supported in part by MEXT-Supported Program for the Strategic Research Foundation at Private Universities (S1201007) and by Grant-in-aid from MEXT Japan (24614018).

### References

- [1] Iida F, Iida R, Kamijo H, et al. Chronic Japanese schistosomiasis and hepatocellular carcinoma: ten years of follow-up in Yamanashi Prefecture, Japan[J]. *Bull World Health Organ*, 1999,77(7):573–581.
- [2] McManus DP, Gray DJ, Li Y, et al. Schistosomiasis in the People's Republic of China: the era of the Three Gorges Dam[J]. *Clin Microbiol Rev*, 2010,23(2):442–466.
- [3] Wang LD, Chen HG, Guo JG, et al. A strategy to control transmission of *Schistosoma japonicum* in China[J]. *N Engl J Med*, 2009,360(2):121–128.
- [4] Bergquist R, Tanner M. Controlling schistosomiasis in Southeast Asia: a tale of two countries[J]. *Adv Parasitol*, 2010,72:109–144.
- [5] Gordon CA, Acosta LP, Gray DJ, et al. High prevalence of *Schistosoma japonicum* infection in Carabao from Samar Province, the Philippines: implications for transmission and control[J]. *PLoS Negl Trop Dis*, 2012,6(9):e1778.
- [6] Harinasuta C. Epidemiology and control of schistosomiasis in Southeast Asia[J]. *Southeast Asian J Trop Med Public Health*, 1984,15(4):431–438.
- [7] Ross AGP, Bartley PB, Sleight AC, et al. Schistosomiasis[J]. *New Eng J Med*, 2002,346(16):1212–1220.
- [8] Mohda J, Redman CA, Thormhill JA, et al. Schistosomes: Unanswered questions on the basic biology of the host-parasite relationship[J]. *Parasitol Today*, 1998,14(10):396–401.
- [9] Hirata M, Takushima M, Kaga M, et al. Induction of experimental murine granuloma formation against *Schistosoma japonicum* eggs produced by in vitro ova deposition, in vitro tissue extraction, or lyophilization[J]. *Parasitol Res*, 1991,77(4):315–319.
- [10] El Ridi R, Velupillai P, Harn DA. Regulation of Schistosome egg granuloma formation: Host-soluble I-selectin enters tissue-trapped eggs and binds to carbohydrate antigens on surface membrane of miracidia[J]. *Infect Immun*, 1996,64(11):4700–4705.
- [11] Mitchell G, Garcia EG, Rivera PT, et al. Evidence for and implications of anti-embryonation immunity in Schistosomiasis[J]. *Exper Parasitol*, 1994,79(4):546–549.
- [12] Rumjanek FD, Campos EG, Afonso LC. Evidence for the occurrence of LDL receptors in extracts of schistosomula of *Schistosoma mansoni*[J]. *Mol Biochem Parasitol*, 1988,28(2):145–152.
- [13] Rumjanek FD, McLaren DJ, Smithers SR. Serum-induced expression of a surface protein in schistosomula of *Schistosoma mansoni*: a possible receptor for lipid uptake[J]. *Mol Biochem Parasitol*, 1983,9(4):337–350.
- [14] Xu X, Caulfield JP. Characterization of human low density lipoprotein binding proteins on the surface of Schistosomula of *Schistosoma mansoni*[J]. *Eur J Cell Biol*, 1992,57(2):229–235.
- [15] Furlong ST, Thibault KS, Morbelli LM, et al. Uptake and compartmentalization of fluorescent lipid analogs in larval *Schistosoma mansoni*[J]. *J Lipid Res*, 1995,36(1):1–12.

- [16] Rogers MV, Quilici D, Mitchell GF, et al. Purification of a putative lipoprotein receptor from *Schistosoma japonicum* adult worms[J]. *Mol Biochem Parasitol*, 1990,41(1):93–100.
- [17] Fan J, Xiaoxian G, Yang W, et al. A *Schistosoma japonicum* very low-density lipoprotein-binding protein[J]. *Int J Biochem Cell Biol*, 2003,35(10):1436–1451.
- [18] Okumura-Noji K, Sasai K, Zhan R, et al. Cholesteryl ester transfer protein deficiency causes slow egg embryonation of *Schistosoma japonicum*[J]. *Biochem Biophys Res Com*, 2001,286(2):305–310.
- [19] Okumura-Noji K, Miura Y, Lu R, et al. CD36-related protein in *Schistosoma japonicum*: candidate mediator of selective cholesteryl ester uptake from high-density lipoprotein for egg maturation[J]. *FASEB J*, 2013, 27(3):1236–1244.
- [20] Yokoyama S. A potential screening factor for accumulation of cholesteryl ester transfer protein deficiency in East Asia: *Schistosoma japonicum*[J]. *Biochim Biophys Acta*, 2014,1841(4):495–504.
- [21] Bruce C, Davidson WS, Kussie P, et al. Molecular determinants of plasma cholesteryl ester transfer protein binding to high density lipoproteins[J]. *J Biol Chem*, 1995,270(19): 11532–11542.
- [22] Jiang XC, Bruce C, Cocke T, et al. Point mutagenesis of positively charged amino acids of cholesteryl ester transfer protein: conserved residues within the lipid transfer/lipopolysaccharide binding protein gene family essential for function[J]. *Biochemistry*, 1995,34(21):7258–7263.
- [23] Tall A. Plasma lipid transfer proteins[J]. *Ann Rev Biochem*, 1995,64:235–257.
- [24] Wang S, Kussie P, Deng L, et al. Defective binding of neutral lipids by carboxyl-terminal deletion mutant of cholesteryl ester transfer protein[J]. *J Biol Chem*, 1995, 270(2):612–618.
- [25] Drayna D, Jarnagin AS, McLean J, et al. Cloning and sequencing of human cholesteryl ester transfer protein cDNA[J]. *Nature*, 1987,327(6123):632–634.
- [26] Ko KW, Ohnishi T, Yokoyama S. Triglyceride transfer is required for net cholesteryl ester transfer between lipoproteins in plasma by lipid transfer protein. Evidence for a hetero-exchange transfer mechanism demonstrated by using novel monoclonal antibodies[J]. *J Biol Chem*, 1994,269(45):28206–28213.
- [27] Ohnishi T, Hicks LD, Oikawa K, et al. Properties of human plasma lipid transfer protein in aqueous solution and at interfaces[J]. *Biochemistry*, 1994,33(20):6093–6099.
- [28] Ohnishi T, Tan C, Yokoyama S. Selective transfer of cholesteryl ester over triglyceride by human plasma lipid transfer protein between apolipoprotein-activated lipid microemulsion[J]. *Biochemistry*, 1994,33:4533–4542.
- [29] Qiu X, Mistry A, Ammirati MJ, et al. Crystal structure of cholesteryl ester transfer protein reveals a long tunnel and four bound lipid molecules[J]. *Nat Struct Mol Biol*, 2007, 14(2):106–113.
- [30] Foger B, Ritsch A, Doblinger A, et al. Relationship of plasma cholesteryl ester transfer protein to HDL cholesterol. Studies in normotriglyceridemia and moderate hypertriglyceridemia[J]. *Arterioscler Thromb Vasc Biol*, 1996,16(12):1430–1436.
- [31] Czamecka H, Yokoyama S. Regulation of lecithin-cholesterol acyltransferase reaction by acyl acceptors and demonstration of its “idling” reaction[J]. *J Biol Chem*, 1993,268(26):19334–19340.
- [32] Francis GA, Ko KW, Hara H, et al. Regulation of the uptake of high-density lipoprotein-originated cholesteryl ester by HepG2 cells: role of low-density lipoprotein and plasma lipid transfer protein[J]. *Biochim Biophys Acta*, 1991,1084(2):159–166.
- [33] Kurasawa T, Yokoyama S, Miyake Y, et al. Rate of cholesteryl ester transfer between high and low density lipoproteins in human serum and a case with decreased transfer rate in association with hyperalphalipoproteinemia[J]. *J Biochem*, 1985,98(6):1499–1508.
- [34] Koizumi J, Mabuchi H, Yoshimura A, et al. Deficiency of serum cholesteryl-ester transfer activity in patients with familial hyperalphalipoproteinemia[J]. *Atheroscler*, 1985,58(1–3):175–186.
- [35] Brown ML, Inazu A, Hesler CB, et al. Molecular basis of lipid transfer protein deficiency in a family with increased high-density lipoproteins[J]. *Nature*, 1989,342(6248): 448–451.
- [36] Inazu A, Jiang XC, Haraki T, et al. Genetic cholesteryl ester transfer protein deficiency caused by two prevalent mutations as a major determinant of increased levels of high density lipoprotein cholesterol[J]. *J Clin Invest*, 1994,94(5):1872–1882.
- [37] Sakai N, Yamashita S, Hirano K, et al. Frequency of exon 15 missense mutation (442D:G) in cholesteryl ester transfer protein gene in hyperalphalipoproteinemic Japanese subjects[J]. *Atherosclerosis*, 1995,114(2):139–145.
- [38] Hirano K, Yamashita S, Nakajima N, et al. Genetic cholesteryl ester transfer protein deficiency is extremely frequent in the Omagari area of Japan. Marked hyperalphalipoproteinemia caused by CETP gene mutation is not associated with longevity[J]. *Arterioscler Thromb Vasc Biol*, 1997, 17(6):1053–1059.
- [39] Maruyama T, Yamashita S, Matsuzawa Y, et al. Mutations in Japanese subjects with primary hyperlipidemia—results from the Research Committee of the Ministry of Health and Welfare of Japan since 1996[J]. *J Atheroscler Thromb*, 2004,11(3):131–145.
- [40] Yamashita S, Hirano K, Sakai N, et al. Molecular biology and pathophysiological aspects of plasma cholesteryl ester transfer protein[J]. *Biochim Biophys Acta*, 2000, 1529(1–3):257–275.
- [41] Nagano M, Yamashita S, Hirano K, et al. Molecular mechanisms of cholesteryl ester transfer protein deficiency in Japanese[J]. *J Atheroscler Thromb*, 2004, 11(3):110–121.
- [42] Nagano M, Yamashita S, Hirano K, et al. Two novel missense mutations in the CETP gene in Japanese hyperalphalipoproteinemic subjects: high-throughput assay by Invader assay[J]. *J Lipid Res*, 2002,43(7):1011–1018.
- [43] Ritsch A, Drexel H, Amann FW, et al. Deficiency of cholesteryl ester transfer protein: Description of molecular defect and the dissociation of cholesteryl ester and triglyceride transfer in plasma[J]. *Arterioscler Thromb Vasc Biol*, 1997,17(16):3433–3441.
- [44] Chen DW, Yang JF, Tang Z, et al. Cholesteryl ester transfer protein polymorphism D442G associated with a potential decreased risk for Alzheimer’s disease as a modifier for APOE epsilon4 in Chinese[J]. *Brain Res*, 2008,1187:52–57.

- [45] Chiba H, Akita H, Tsuchihashi K, et al. Quantitative and compositional changes in high density lipoprotein subclasses in patients with various genotypes of cholesteryl ester transfer protein deficiency[J]. *J Lipid Res*, 1997,38(6):1204-1216.
- [46] Hui S-P. Frequency and effect on plasma lipoprotein metabolism of a mutation in the cholesteryl ester transfer protein gene in the Chinese[J]. *Hokkaido J Med Sci*, 1997,72(3):319-327.
- [47] Hsu LA, Ko YL, Hsu KH, et al. Genetic variations in the cholesteryl ester transfer protein gene and high density lipoprotein cholesterol levels in Taiwanese Chinese[J]. *Hum Genet*, 2002,110(1):57-63.
- [48] Jap TS, Wu YC, Tso YC, et al. A novel mutation in the intron 1 splice donor site of the cholesterol ester transfer protein (CETP) gene as a cause of hyperalphalipoproteinemia[J]. *Metabolism*, 2002,51(3):394-397.
- [49] Yang GJ, Gemperli A, Vounatsou P, et al. A growing degree-days based time-series analysis for prediction of *Schistosoma japonicum* transmission in Jiangsu province, China[J]. *Am J Trop Med Hyg*, 2006,75(3):549-555.
- [50] Song G-J, Han G-H, Chae J-J, et al. The effect of the cholesterol ester transfer protein gene and environmental factors on the plasma high density lipoprotein cholesterol levels in the Korean population[J]. *Molecules & Cells*, 1997,7(5):615-619.
- [51] Thu NN, Mai TT, Ohmori R, et al. Effect of the cholesteryl ester transfer protein genotypes on plasma lipid and lipoprotein levels in Vietnamese children[J]. *Pediatr Res*, 2005,58(6):1249-1253.
- [52] Plengpanich W, Siri Wong S, Khovichunkit W. Two novel mutations and functional analyses of the CETP and LIPC genes underlying severe hyperalphalipoproteinemia[J]. *Metabolism*, 2009,58(8):1178-1184.
- [53] Thompson JF, Reynolds JM, Williams SP, et al. Frequency and function of CETP variants among individuals of Asian ancestry[J]. *Atherosclerosis*, 2009,202(1):241-247.
- [54] Arkhipova NS, Ar'ev AL, Popova EK, et al. Association of polymorphism of angiotensin-converting enzyme gene I/D and D442G cholesteryl ester transfer protein gene with risk factors for atherosclerosis among elderly and senile patients with coronary heart disease in the Republic Sakha (Yakutia)[J]. *Adv Gerontol*, 2013,3(4):277-281.
- [55] Finkelstein JL, Schleinitz MD, Carabin H, et al. Decision-model estimation of the age-specific disability weight for schistosomiasis japonica: a systematic review of the literature[J]. *PLoS Negl Trop Dis*, 2008,2(3):e158.
- [56] Ma YQ, Thomas GN, Critchley JA, et al. Identification of the intron 14 splicing defect of the cholesteryl ester transfer protein gene in Hong Kong Chinese[J]. *Clin Genet*, 2001,59(4):287-289.
- [57] Nihei N, Kajihara N, Kirinoki M, et al. Establishment of a GIS monitoring system for schistosomiasis japonica in Kofu, Japan[J]. *Ann Trop Med Parasitol*, 2006,100(2):143-153.
- [58] Takahashi H, Takahashi A, Maki M, et al. Effect of CETP on the plasma lipoprotein profile in four strains of transgenic mouse[J]. *Biochem Biophys Res Commun*, 2001,283(1):118-123.
- [59] Zhang R, Yoshida A, Kumagai T, et al. Vaccination with calpain induces a Th1-biased protective immune response against *Schistosoma japonicum*[J]. *Infect Immun*, 2001,69(1):386-391.
- [60] Teh EM, Dolphin PJ, Breckenridge WC, et al. Human plasma CETP deficiency: identification of a novel mutation in exon 9 of the CETP gene in a Caucasian subject from North America[J]. *J Lipid Res*, 1998,39:442-456.
- [61] Hill SA, Nazir DJ, Jayaratne P, et al. Mutations in cholesteryl ester transfer protein and hepatic lipase in a North American population[J]. *Clin Biochem*, 1997,30(5):413-418.
- [62] van der Steeg WA, Hovingh GK, Klerkx AH, et al. Cholesteryl ester transfer protein and hyperalphalipoproteinemia in Caucasians[J]. *J Lipid Res*, 2007,48(3):674-682.
- [63] Rhyne J, Ryan MJ, White C, et al. The two novel CETP mutations Gln87X and Gln165X in a compound heterozygous state are associated with marked hyperalphalipoproteinemia and absence of significant coronary artery disease[J]. *J Mol Med (Berl)*, 2006,84(8):647-650.
- [64] Cefalu AB, Noto D, Magnolo L, et al. Novel mutations of CETP gene in Italian subjects with hyperalphalipoproteinemia[J]. *Atherosclerosis*, 2009,204(1):202-207.
- [65] Calabresi L, Nilsson P, Pinotti E, et al. A novel homozygous mutation in CETP gene as a cause of CETP deficiency in a Caucasian kindred[J]. *Atherosclerosis*, 2009,205(2):506-511.
- [66] Chantepie S, Bochem AE, Chapman MJ, et al. High-density lipoprotein (HDL) particle subpopulations in heterozygous cholesteryl ester transfer protein (CETP) deficiency: maintenance of antioxidative activity[J]. *PLoS One*, 2012,7(11):e49336.
- [67] Thompson A, Di Angelantonio E, Sarwar N, et al. Association of cholesteryl ester transfer protein genotypes with CETP mass and activity, lipid levels, and coronary risk[J]. *JAMA*, 2008,299(23):2777-2788.
- [68] Inazu A, Brown ML, Hesler CB, et al. Increased high-density lipoprotein levels caused by a common cholesteryl-ester transfer protein gene mutation[J]. *N Engl J Med*, 1990,323(18):1234-1238.
- [69] Yamashita S, Sprecher DL, Sakai N, et al. Accumulation of apolipoprotein E-rich high density lipoproteins in hyperalphalipoproteinemic human subjects with plasma cholesteryl ester transfer protein deficiency[J]. *J Clin Invest*, 1990,86(3):688-695.
- [70] Sakai N, Matsuzawa Y, Hirano K, et al. Detection of two species of low density lipoprotein particles in cholesteryl ester transfer protein deficiency[J]. *Arterioscler Thromb*, 1991,11(1):71-79.
- [71] Yamashita S, Hui DY, Wetterau JR, et al. Characterization of plasma lipoproteins in patients heterozygous for human plasma cholesteryl ester transfer protein (CETP) deficiency: Plasma CETP regulated high-density lipoprotein concentration and composition[J]. *Metabolism*, 1991,40(7):756-763.
- [72] Moriyama Y, Okamura T, Inazu A, et al. A low prevalence of coronary heart disease among subjects with increased high-density lipoprotein cholesterol levels, including those with plasma cholesteryl ester transfer protein deficiency[J]. *Prev Med*, 1998,27(5 Pt 1):659-667.
- [73] Curb JD, Abbott RD, Rodriguez BL, et al. A prospective study of HDL-C and cholesteryl ester transfer protein gene mutations and the risk of coronary heart disease in the elderly[J]. *J Lipid Res*, 2004,45(5):948-953.

- [74] Nissen SE, Tardif JC, Nicholls SJ, et al. Effect of torcetrapib on the progression of coronary atherosclerosis[J]. *N Engl J Med*, 2007,356(13):1304–1316.
- [75] Schwartz GG, Olsson AG, Abt M, et al. Effects of dalcetrapib in patients with a recent acute coronary syndrome[J]. *N Engl J Med*, 2012,367(22):2089–2099.
- [76] Betard C, Kessler AM, Roy M, et al. Molecular genetic evidence for a founder effect in familial hypercholesterolemia among French Canadians[J]. *Hum Genet*, 1992,88(5): 529–536.
- [77] Torrington M, Botha JL, Pilcher GJ, et al. Association between familial hypercholesterolaemia and church affiliation. Is this the result of sociocultural isolation of migrant farmers in 19th-century South Africa?[J]. *S Afr Med J*, 1984,65(19):762–767.
- [78] Abifadel M, Rabes JP, Jambart S, et al. The molecular basis of familial hypercholesterolemia in Lebanon: spectrum of LDLR mutations and role of PCSK9 as a modifier gene[J]. *Hum Mutat*, 2009,30(7):E682–691.
- [79] Allison AC. Protection afforded by sickle-cell trait against subtertian malarial infection[J]. *Br Med J*, 1954,1(4857): 290–294.
- [80] Hedrick PW. Resistance to malaria in humans: the impact of strong, recent selection[J]. *Malar J*, 2012,11:349.
- [81] Taylor SM, Parobek CM, Fairhurst RM. Haemoglobinopathies and the clinical epidemiology of malaria: a systematic review and meta-analysis[J]. *The Lancet Infectious Diseases*, 2012,12(6):457–468.
- [82] Acton S, Gigotti A, Landschulz T, et al. Identification of scavenger receptor SR-BI as a high density lipoprotein receptor[J]. *Science*, 1996,271(5248):518–520.
- [83] Muraio K, Terpstra V, Green SR, et al. Characterization of CLA-1, a human homologue of rodent scavenger receptor BI, as a receptor for high density lipoprotein and apoptotic thymocytes[J]. *J Biol Chem*, 1997,272(28):17551–17557.
- [84] Okamoto H, Yonemori F, Wakitani K, et al. A cholesteryl ester transfer protein inhibitor attenuates atherosclerosis in rabbits[J]. *Nature*, 2000,406(6792):203–207.

#### CLINICAL TRIAL REGISTRATION

The *Journal* requires investigators to register their clinical trials in a public trials registry for publication of reports of clinical trials in the *Journal*. Information on requirements and acceptable registries is available at [www.icmje.org/faq\\_clinical.html](http://www.icmje.org/faq_clinical.html).

## Basic Sciences

# Probucol-Oxidized Products, Spiroquinone and Diphenquinone, Promote Reverse Cholesterol Transport in Mice

Emi Yakushiji, Makoto Ayaori, Takafumi Nishida, Kazusa Shiotani, Shunichi Takiguchi, Kazuhiro Nakaya, Harumi Uto-Kondo, Masatsune Ogura, Makoto Sasaki, Makiko Yogo, Tomohiro Komatsu, Rui Lu, Shinji Yokoyama, Katsunori Ikewaki

**Objective**—Oxidized products of probucol, spiroquinone and diphenquinone, were shown to increase cell cholesterol release and plasma high-density lipoprotein (HDL) by inhibiting degradation of ATP-binding cassette transporter A1. We investigated whether these compounds enhance reverse cholesterol transport in mice.

**Approach and Results**—Spiroquinone and diphenquinone increased ATP-binding cassette transporter A1 protein (2.8- and 2.6-fold, respectively,  $P < 0.01$ ) and apolipoprotein A-I-mediated cholesterol release (1.4- and 1.4-fold,  $P < 0.01$  and  $P < 0.05$ , respectively) in RAW264.7 cells. However, diphenquinone, but not spiroquinone, enhanced cholesterol efflux to HDL (+12%,  $P < 0.05$ ), whereas both increased ATP-binding cassette transporter G1 protein, by 1.8- and 1.6-fold, respectively. When given orally to mice, both compounds significantly increased plasma HDL-cholesterol, by 19% and 20%, respectively ( $P < 0.05$ ), accompanied by an increase in hepatic and macrophage ATP-binding cassette transporter A1 but not ATP-binding cassette transporter G1. We next evaluated in vivo reverse cholesterol transport by injecting RAW264.7 cells labeled with  $^3\text{H}$ -cholesterol intraperitoneally into mice. Both spiroquinone and diphenquinone increased fecal excretion of the macrophage-derived  $^3\text{H}$ -tracer, by 25% and 28% ( $P < 0.01$  and  $P < 0.05$ ), respectively. Spiroquinone/diphenquinone did not affect fecal excretion of HDL-derived  $^3\text{H}$ -cholesterol, implying that macrophage-to-plasma was the most important step in spiroquinone/diphenquinone-mediated promotion of in vivo reverse cholesterol transport. Finally, spiroquinone significantly reduced aortic atherosclerosis in apolipoprotein E null mice when compared with the vehicle.

**Conclusions**—Spiroquinone and diphenquinone increase functional ATP-binding cassette transporter A1 in both the macrophages and the liver, elevate plasma HDL-cholesterol, and promote overall reverse cholesterol transport in vivo. These compounds are promising as therapeutic reagents against atherosclerosis. (*Arterioscler Thromb Vasc Biol.* 2016;36:591-597. DOI: 10.1161/ATVBAHA.115.306376.)

**Key Words:** apolipoprotein A-I ■ diphenquinone ■ HDL-cholesterol ■ macrophage ■ probucol

Reverse cholesterol transport (RCT) is an important part of cholesterol homeostasis in which body cholesterol is transported back to the liver for conversion to bile acids and excretion into bile and eventually feces.<sup>1,2</sup> High-density lipoprotein (HDL) plays a major role in this. RCT is thus believed to protect against atherogenesis by preventing cholesterol accumulation in vascular lesions. The first step of RCT is removal of cell cholesterol as helical apolipoproteins of HDL, such as apolipoprotein A-I (apoA-I), generation of HDL particles by removing cellular lipids, which is mediated by ATP-binding transporter A1 and acceptance of cell cholesterol by HDL particles, which is mediated by ATP-binding cassette transporter G1 (ABCG1) and perhaps scavenger receptor BI (SR-BI) as well. These reactions occur in a

sequential manner with ATP-binding cassette transporter A1 (ABCA1)-mediating generation of disc-like nascent HDL particles from cellular lipids and lipid-free apoA-I,<sup>3,4</sup> and such HDL particles act as efficient acceptors of effluxed cholesterol, which is mediated by ABCG1 and SR-BI, to form mature spherical HDL particles.<sup>5</sup> Manipulation of ABCA1 or ABCG1 modulates development of atherosclerotic lesions in vivo, with deletion accelerating development<sup>6</sup> and overexpression retarding development,<sup>7</sup> indicating their synergistic roles in antiatherogenesis.

Transcriptions of ABCA1 and ABCG1 are upregulated by the liver X receptor<sup>8</sup> in extrahepatic cells, sensing oxidized cholesterol as a signal of an increase in cell cholesterol. ABCA1 and ABCG1 have thus emerged as targets of novel

Received on: August 20, 2015; final version accepted on: January 21, 2015.

From the Division of Anti-Aging and Vascular Medicine, Department of Internal Medicine, National Defense Medical College, Tokorozawa, Japan (E.Y., M.A., T.N., K.S., S.T., K.N., H.U.-K., M.O., M.S., M.Y., T.K., K.I.); and Nutritional Health Science Research Center, Chubu University, Kasugai, Japan (R.L., S.Y.).

The online-only Data Supplement is available with this article at <http://atvb.ahajournals.org/lookup/suppl/doi:10.1161/ATVBAHA.115.306376/-DC1>.

Correspondence to Makoto Ayaori, MD, PhD, Division of Anti-Aging, Department of Internal Medicine, National Defense Medical College, 3-2 Namiki, Tokorozawa, Japan. E-mail ayaori@ba2.so-net.ne.jp

© 2016 American Heart Association, Inc.

*Arterioscler Thromb Vasc Biol* is available at <http://atvb.ahajournals.org>

DOI: 10.1161/ATVBAHA.115.306376

Downloaded from <http://atvb.ahajournals.org/> by SHINJI YOKOYAMA on March 23, 2016

Nonstandard Abbreviations and Acronyms	
<b>ABCA1</b>	ATP-binding cassette transporter A1
<b>ABCG1</b>	ATP-binding cassette transporter G1
<b>RCT</b>	reverse cholesterol transport
<b>HDL</b>	high-density lipoprotein
<b>apoA-I</b>	apolipoprotein A-I
<b>SR-BI</b>	scavenger receptor BI

therapeutic strategies against atherosclerosis. However, liver X receptor agonists have major drawbacks, including development of fatty liver and dyslipidemia, as they inevitably activate sterol regulatory element-binding protein-1c and thereby upregulate the genes for lipogenesis.<sup>9</sup>

An alternative approach would be to modulate post-translational regulation of ABCA1 and ABCG1 expression. We have previously shown that oxidized products of probucol, spiroquinone and diphenquinone, enhance apoA-I-mediated cell cholesterol release by increasing ABCA1 protein through inhibition of its calpain-mediated degradation,<sup>10</sup> whereas their parent compound, probucol, not only retards ABCA1 degradation but also inhibits HDL biogenesis by inhibiting ABCA1 function.<sup>10,11</sup> Spiroquinone and diphenquinone increased HDL-cholesterol (HDL-C) levels and reduced development of atherosclerosis in rabbits.<sup>10</sup> We have also demonstrated that ABCA1 and ABCG1 undergo proteasomal degradation, and proteasome inhibitors enhanced cholesterol efflux by increasing ABCA1 and ABCG1, translating into promotion of macrophage-to-feces RCT in vivo,<sup>12</sup> using a validated murine assay.<sup>13</sup> We therefore decided to investigate how spiroquinone and diphenquinone exert beneficial effects with respect to promotion of RCT in vivo and in this study demonstrated that spiroquinone and diphenquinone enhance overall RCT in mice.

## Materials and Methods

Materials and Methods are available in the online-only Data Supplement.

## Results

### Effects of Spiroquinone/Diphenquinone in RAW264.7 Cells

The effects of spiroquinone/diphenquinone on ABCA1, ABCG1, and SR-BI were assessed in RAW264.7 cells. Figure 1A and 1B shows that probucol induced an increase in ABCA1 that was consistent with the previous finding.<sup>11</sup> Spiroquinone and diphenquinone significantly increased ABCA1, by 2.8- and 2.6-fold, respectively, as previously demonstrated in THP-1 and murine fibroblasts.<sup>10</sup> Spiroquinone and diphenquinone induced a 1.8- and 1.6-fold increase in ABCG1 expression, respectively, whereas probucol increased it only slightly. Conversely, both spiroquinone and diphenquinone reduced SR-BI expression, by 365 and 32%, respectively. Reflecting the increase in ABCA1, spiroquinone and diphenquinone promoted apoA-I-mediated cell cholesterol release 1.4-fold. Probucol, as expected, completely inhibited the apoA-I-mediated cholesterol release. However, HDL-mediated cell cholesterol release was significantly enhanced

only by diphenquinone, by 12%, but not by spiroquinone. No effect was seen for probucol in this regard.

### Spiroquinone and Diphenquinone Increased Plasma HDL-C in Mice

To investigate whether the in vitro findings were translated into the in vivo setting, we administered spiroquinone and diphenquinone to mice and evaluated plasma lipid profiles. Oral administration of spiroquinone and diphenquinone for 7 days did not affect body weight, food intake, or biochemical parameters, such as plasma aspartate aminotransferase, alanine aminotransferase, and creatine phosphokinase, when compared with the vehicle. We also performed a long-term experiment, which confirmed the above results in the short-term experiments. Spiroquinone/diphenquinone seemed to increase plasma total cholesterol levels, though the changes did not reach statistical significance (Figure 2A and 2B). HDL-C was significantly increased by both spiroquinone and diphenquinone (19% and 20% compared with the vehicle and 27% and 18% compared with baseline, respectively; Figure 2C and 2D), being consistent with observations in rabbits.<sup>10</sup> Lipoprotein analyses using fast protein liquid chromatography revealed an increase in the HDL fractions, consistent with the stimulatory effects of spiroquinone and diphenquinone on HDL-C, and showed that these compounds did not influence the HDL size (Figure 3A and 3B). Diphenquinone, but not spiroquinone, increased cholesterol in the low-density lipoprotein fractions. This was minimal but reproducible. We also evaluated other lipids in fast protein liquid chromatography fractions. Spiroquinone/diphenquinone increased CE (Figure 3C), FC (Figure 3D), and PL (Figure 3E), similar to total cholesterol. There were no significant changes in TG (Figure 3F) among the treatments.

### Spiroquinone and Diphenquinone Increased ABCA1 Protein in Livers and Peritoneal Macrophages in Mice

ABCA1 protein expression was examined in mice livers and peritoneal macrophages. Figure 4A and 4B shows that oral administration of spiroquinone and diphenquinone for 7 days increased expression of hepatic ABCA1, by 1.4- and 1.5-fold, respectively, but caused no change in ABCG1 or SR-BI, neither in *N*-glycosylated ( $\approx 80$  kD) nor native forms ( $\approx 50$  kD). Spiroquinone and diphenquinone also increased ABCA1 in the peritoneal macrophages, by 1.5- and 1.6-fold, respectively, but induced no change in ABCG1 or SR-BI. These results were somewhat inconsistent with the in vitro findings for ABCG1 and SR-BI as shown in Figure 1. We previously observed that cholesterol absorption contributed to in vivo RCT using ezetimibe, an inhibitor of Niemann–Pick C1-Like 1, a cholesterol transporter in the intestine.<sup>14</sup> Therefore, we checked mRNA levels of the cholesterol transporters, Niemann–Pick C1-Like 1 and ABCG5/8. The results revealed that spiroquinone/diphenquinone did not affect their expression (data not shown).

### Spiroquinone and Diphenquinone Promoted Macrophage-to-Feces RCT in Mice

To further investigate whether the in vivo effects of these compounds with respect to ABCA1 in the liver and peripheral

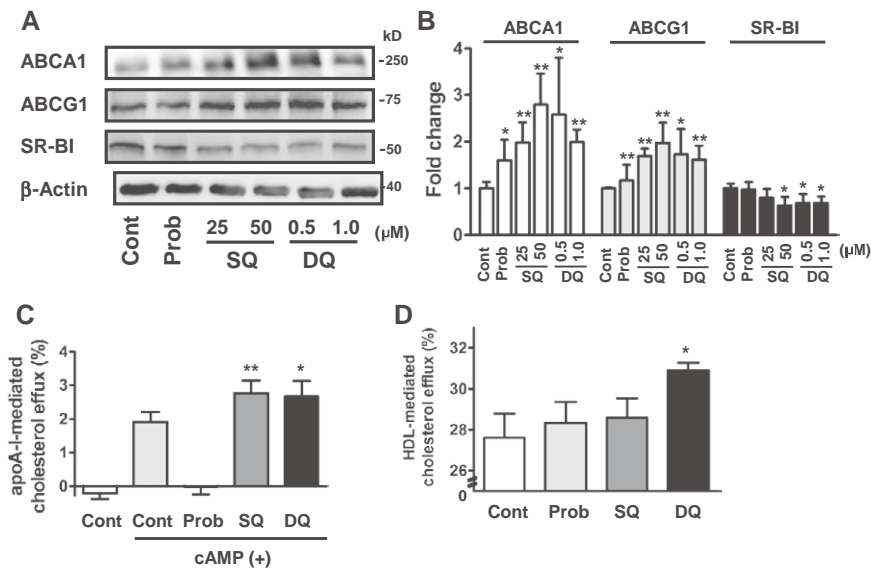


**Figure 1.** Spiroquinone (SQ)/diphenylquinone (DQ) increased ATP-binding cassette transporter A1 (ABCA1) and ATP-binding cassette transporter G1 (ABCG1) and enhanced apolipoprotein A-I (apoA-I)-mediated cholesterol release in RAW264.7 cells stimulated by 0.3 mmol/L dB-cAMP. **A**, RAW264.7 cells were lysed and subjected to a Western blot analysis 24 hours after treatment with 1  $\mu$ mol/L of probucol and the indicated doses of SQ/DQ and the vehicle. **B**, Quantitation of the proteins from 3 separate experiments. **C** and **D**, RAW264.7 cells were labeled with  $^3$ H-cholesterol (1.0  $\mu$ Ci/mL) for 24 hours. The cells were washed with PBS and incubated in the presence of probucol (1  $\mu$ mol/L), SQ (50  $\mu$ mol/L) or DQ (1  $\mu$ mol/L) for 24 hours in the presence of apoA-I (**C**, 10  $\mu$ g/mL) or 4 hours in the presence of high-density lipoprotein (**D**, 50  $\mu$ g/mL protein). The percentage cholesterol efflux was calculated as described in Materials and Methods section of this article. The results are representative of  $\geq 3$  experiments and are presented as mean  $\pm$  SD. \* $P < 0.05$ , \*\* $P < 0.01$  vs the vehicle (**C**, vs vehicle in the presence of dB-cAMP).

macrophages and plasma HDL-C elevation translate into promotion of RCT, overall transport of cholesterol from macrophages to feces was assessed. Appearance of  $^3$ H-tracer was not increased in the plasma, the liver, or the bile, by spiroquinone or diphenylquinone. However, fecal  $^3$ H-tracer excretion was increased by spiroquinone and diphenylquinone, by 25% and 28%, respectively. Thus, both compounds promoted macrophage-to-feces RCT in vivo. To further investigate which step contributed to the enhanced RCT by spiroquinone/diphenylquinone, we performed additional experiments using  $^3$ H-CEs-labeled HDL, whereby the initial step of RCT, namely macrophage-to-plasma, was not taken into consideration. Figure 5E demonstrates that spiroquinone/diphenylquinone did not affect fecal excretion of HDL-derived cholesterol, implying that macrophage-to-plasma was the most important step in the stimulatory effects of spiroquinone/diphenylquinone on in vivo RCT. We also investigated the cholesterol efflux capacity of HDL treated with spiroquinone/diphenylquinone to assess whether the enhanced RCT resulted from alteration of HDL particles by spiroquinone/diphenylquinone that favored an increase in efflux capacity. As shown in Figure 5F, HDL cholesterol efflux capacity was not affected by spiroquinone/diphenylquinone, suggesting that HDL biogenesis on the macrophage cell surface associated with promoted ABCA1 functionality by spiroquinone/diphenylquinone might contribute to enhanced RCT.

### Spiroquinone Inhibited Atherosclerotic Plaque Development in apoE Null Mice

Finally, we investigated whether spiroquinone exerted an inhibitory effect on atherosclerotic development using apoE null mice. Figure 6 shows that 12-week treatment with

spiroquinone significantly reduced atherosclerotic lesion area when compared with the vehicle.

## Discussion

The great burden of atherosclerotic diseases remains despite currently available optimum therapies. Elevation of plasma low-density lipoprotein has been recognized as one of the

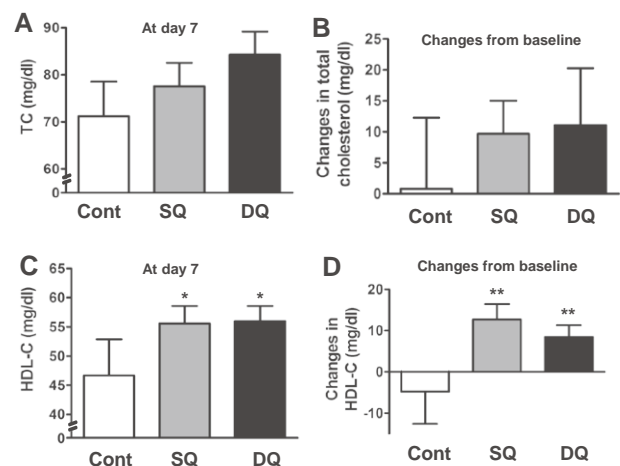


**Figure 2.** Spiroquinone (SQ) and diphenylquinone (DQ) increased plasma high-density lipoprotein-cholesterol (HDL-C) in mice. Mice were given 500 mg/kg of SQ, DQ, or the vehicle by oral administration. Before and 7 days after administration, blood samples were taken and analyzed for lipid and lipoprotein. **A–D**, Plasma total cholesterol (TC) and HDL-C were determined as described in Materials and Methods section of this article. The results are representative of 3 experiments and presented as mean  $\pm$  SD of  $n = 6$ . \* $P < 0.05$ , \*\* $P < 0.01$  vs the vehicle.

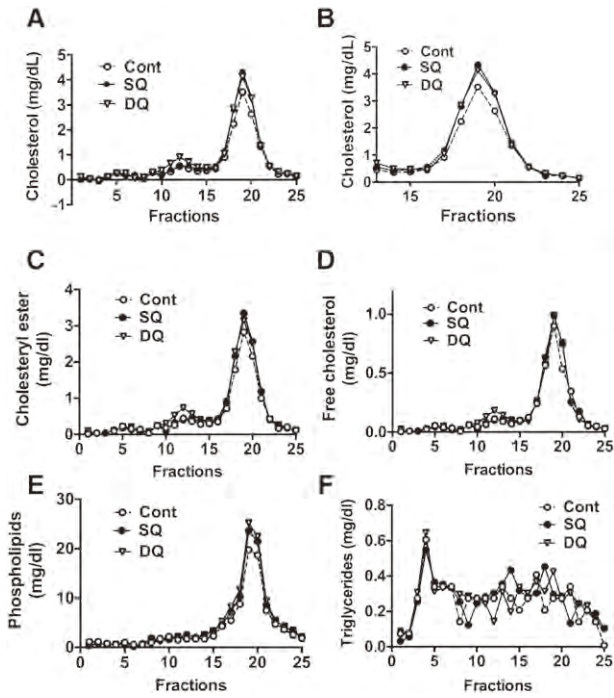


**Figure 3.** Spiroquinone (SQ) and diphenquinone (DQ) increased plasma high-density lipoprotein-cholesterol in mice. Mice were given 500 mg/kg of SQ, DQ, or the vehicle by oral administration. Before and 7 days after administration, blood samples were taken and analyzed for lipid and lipoprotein. Pooled plasma samples for each treatment group were fractionated using fast protein liquid chromatography and total cholesterol (A), free cholesterol (D), phospholipids (E), and triglycerides (F) in each fraction were determined. B, Close-up of fractions 13 to 25 of total cholesterol. Cholesteryl ester concentrations (C) were calculated by subtracting free cholesterol levels from total cholesterol levels.

primary risks and its reduction has been established as a standard approach to preventing atherosclerotic diseases. Low HDL is also a strong risk for atherosclerotic vascular diseases and has been investigated as one of the next strategic targets for interventions to prevent and treat atherosclerosis. However, attempts to increase HDL have not yet been proven

to decrease the risk. In this regard, inhibition of cholesteryl ester transfer protein has been unsuccessful to date in achieving a beneficial clinical outcome.<sup>15,16</sup>

One might raise the argument that functional aspects of HDL should be targeted rather than merely increasing HDL-cholesterol to achieve clinical benefits, specifically focusing on enhancement of RCT. A recent study showed that the ability of serum HDL to promote cholesterol release from macrophages in culture is a better negative risk predictor for coronary artery disease than HDL-C.<sup>17</sup> In this context, increasing cellular cholesterol release should be a primary target for enhancing overall RCT. Stimulation of ABCA1 activity to generate HDL and ABCG1 activity to enhance outflow of cell cholesterol to HDL would be a rational therapeutic strategy in this regard.

Probucol, a hypolipemic drug, is a strong inhibitor of ABCA1 and reduces plasma HDL<sup>18,19</sup> but it also inhibits calpain-mediated degradation of ABCA1 causing an increase in inactive ABCA1 in cells.<sup>11</sup> Interestingly, the oxidative products of probucol, spiroquinone and diphenquinone, were shown to inhibit ABCA1 degradation without inhibiting its activity, bringing about an increase active in ABCA1, which had antiatherogenic effects in rabbit.<sup>10</sup> Our previous study found that attenuating proteasomal degradation increased ABCA1 and ABCG1, which promoted cholesterol release from macrophages and enhanced RCT in mice.<sup>12</sup>

In this study, we demonstrated that spiroquinone and diphenquinone increased ABCA1 in a mouse macrophage cell line and promoted apoA-I-mediated cell cholesterol release in vitro, whereas probucol inhibited ABCA1 activity. Although spiroquinone, diphenquinone, and probucol all increased ABCG1 protein (Figure 1A and 1B), only diphenquinone increased HDL-mediated cholesterol efflux (Figure 1D). The specific mechanism for these findings remains to be investigated. Similar to the case of ABCA1, we could speculate that these compounds would all inhibit degradation of ABCG1, whereas probucol and spiroquinone would suppress ABCG1 activity. As diphenquinone is downstream of spiroquinone in the oxidative

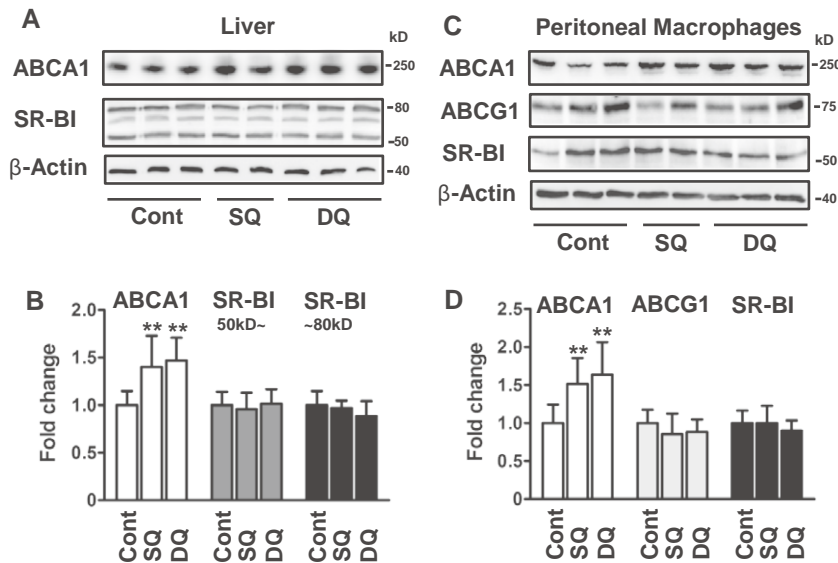


**Figure 4.** Spiroquinone (SQ) and diphenquinone (DQ) increased ATP-binding cassette transporter A1 (ABCA1) in liver and peritoneal macrophages in mice. Mice were treated with 500 mg/kg of SQ, DQ, or the vehicle by oral administration. Seven days after administration, peritoneal macrophages (A) and liver (B) samples were obtained as described in Materials and Methods section of this article. They were analyzed by Western blotting. B and D, Quantitation of the data in A and C as described in Materials and Methods section of this article. Results are representative of 3 experiments and presented as mean±SD; n=6 for each group. \*\*P<0.01 vs the vehicle. SR-BI indicates scavenger receptor BI.

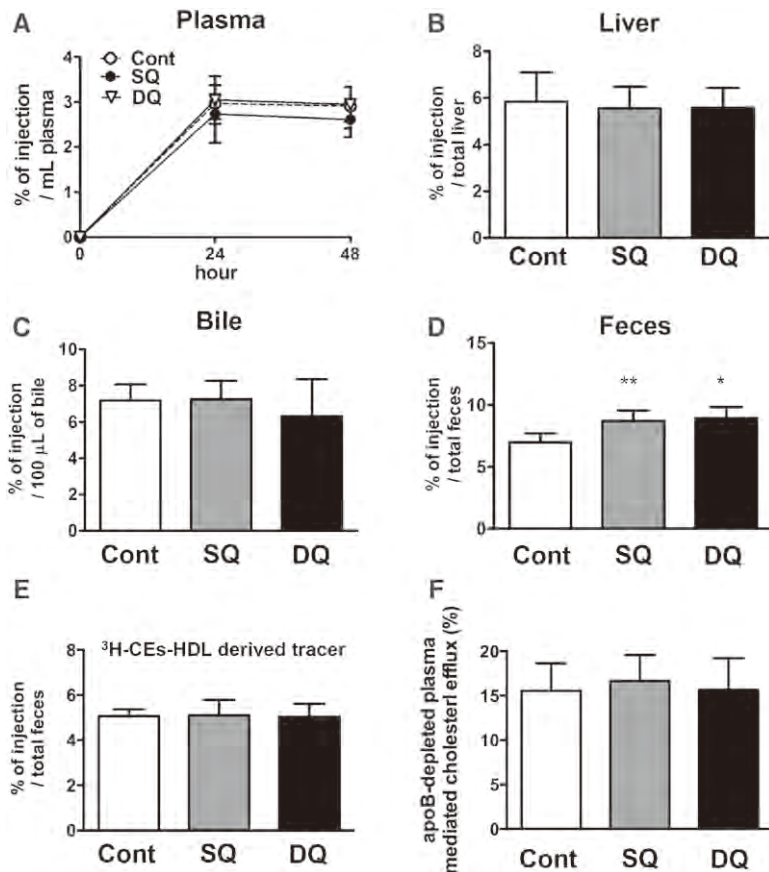


**Figure 5.** Spiroquinone (SQ) and diphenylquinone (DQ) promoted macrophage-to-feces reverse cholesterol transport in mice. Mice were treated with 500 mg/kg of SQ, DQ, or the vehicle by oral administration. Seven days after administration, <sup>3</sup>H-cholesterol-labeled RAW264.7 cells were injected intraperitoneally. **A**, Blood samples obtained from mice 24 and 48 hours after injection were counted for <sup>3</sup>H-tracer radioactivity. **B** and **C**, Tracer radioactivity in the liver (**B**) and in the bile (**C**) were determined as described in Materials and Methods section of this article. **D**, Tracer radioactivity in the feces. Feces collected continuously from 0 to 48 hours were prepared as described in Materials and Methods section of this article, and then analyzed for tracer radioactivity. **E**, <sup>3</sup>H-cholesteryl oleate (CEs)-labeled high-density lipoprotein (HDL) were intravenously injected into mice treated with SQ/DQ or the vehicle for 7 days. Feces were collected continuously ≤48 hours and then analyzed for tracer radioactivity. Data are expressed as percent counts to total injected tracer, mean±SD; n=6 for each group. **F**, Using apoB-depleted plasma obtained from mice treated with SQ/DQ or the vehicle for 7 days, HDL cholesterol efflux capacity was assayed as described in Materials and Methods section of this article. \**P*<0.05, \*\**P*<0.01 vs the vehicle.

pathway of probucol, it might not be inhibitory toward ABCG1. An alternative interpretation is that attenuation of SR-BI expression by probucol, spiroquinone and diphenylquinone (Figure 1A and 1B) would counteract an increase in ABCG1.

Regulation of cholesterol homeostasis would be different between liver cells and extrahepatic cells in operating RCT. In fact, regulation of ABCA1 gene expression by the cell cholesterol level in the liver seems to be in the opposite direction to that in peripheral cells unless cholesterol is overloaded, perhaps to retain cholesterol recruited from the peripheral cells to the liver.<sup>20,21</sup> Although liver ABCA1 mainly contributes to the plasma HDL concentration,<sup>22–24</sup> it is controversial whether liver-specific modulation of ABCA1 expression has an effect on atherogenesis,<sup>25,26</sup> and the findings for macrophage-specific manipulation have also been inconclusive.<sup>26,27</sup> A recent study demonstrated that hepatic ABCA1 expression did not contribute to RCT,<sup>28</sup> while we observed that hepatic ABCA1 knock-down resulted in attenuated RCT in mice (E. Yakushiji and M. Ayaori, unpublished data, 2013). In contrast, Yamamoto et al<sup>29</sup> demonstrated that pharmacological inhibition of hepatic ABCA1 activity with probucol reduced HDL-C levels but promoted RCT through diversion of HDL-derived cholesterol from efflux back into plasma from excretion into the bile. In this study, spiroquinone and diphenylquinone significantly increased both hepatic and macrophage ABCA1 expression, accounting for the increase in HDL-C levels (Figure 2C–2F). Overall RCT from the macrophages to the feces was accordingly enhanced (Figure 4D). However, no apparent change

was seen in the appearance of the macrophage cholesterol in the serum, the liver, or the bile (Figure 4A–4C). Moreover, spiroquinone/diphenylquinone did not affect fecal excretion of

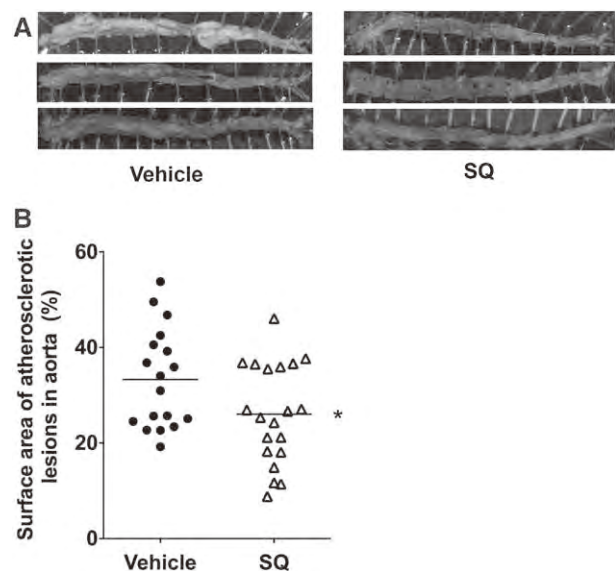


**Figure 6.** Effect of spiroquinone (SQ) on atherosclerotic lesions of the aorta in apolipoprotein E (apoE) null mice. The 6- to 8-week-old apoE null mice were fed with a high-cholesterol diet (1.25%) with or without SQ (0.1%) for 12 weeks. The excised aorta was opened longitudinally, followed by Sudan IV staining (**A**, representative pictures of the aorta). **B**, Percentage areas of intimal atherosclerotic lesions of the aortic wall were calculated as described in Materials and Methods section of this article. \**P*<0.05 vs the vehicle).

HDL-derived cholesterol. Taken together, these observations suggest that contribution of hepatic ABCA1 to RCT is dependent on the status of cholesterol homeostasis in hepatocytes. In the stage that hepatic ABCA1 is upregulated by liver X receptor, increase in HDL seems to be because of regurgitation of cholesterol to plasma and, therefore, may not enhance RCT even though HDL/ABCG1-mediated cholesterol efflux is increased in the peripheral tissues.

There was no apparent change in SR-BI or ABCG1 either in the liver (Figure 3A–3B) or in the macrophages (Figure 3C–3D), being inconsistent with the *in vitro* results in RAW26437 cells. The reason for this is unknown.

In conclusion, this study demonstrated that the probucol-derived oxidative products spiroquinone and diphenoquinone increase ABCA1 expression and enhance cell cholesterol release *in vitro*, and increase HDL-C by increasing ABCA1 in the liver and macrophages in mice. Enhancement of overall RCT by spiroquinone/diphenoquinone *in vivo* might be part of one of the mechanisms of their antiatherosclerotic property. These findings provide the basis of a novel therapeutic strategy for atherosclerotic diseases.

### Acknowledgments

We thank Dr Tomoji Aotsuka of Asuka Pharmaceutical Co Ltd for synthesizing spiroquinone and diphenoquinone.

### Sources of Funding

This work was supported by Foundation for Promotion of Defense Medicine.

### Disclosures

There is no relationship with industry, except that Dr Yokoyama is involved in the foundation of a venture organization, HYKES Laboratories.

### References

- Duffy D, Rader DJ. Update on strategies to increase HDL quantity and function. *Nat Rev Cardiol*. 2009;6:455–463. doi: 10.1038/nrcardio.2009.94.
- Lewis GF, Rader DJ. New insights into the regulation of HDL metabolism and reverse cholesterol transport. *Circ Res*. 2005;96:1221–1232. doi: 10.1161/01.RES.0000170946.56981.5c.
- Wang N, Silver DL, Thiele C, Tall AR. ATP-binding cassette transporter A1 (ABCA1) functions as a cholesterol efflux regulatory protein. *J Biol Chem*. 2001;276:23742–23747. doi: 10.1074/jbc.M102348200.
- Yokoyama S. Assembly of high-density lipoprotein. *Arterioscler Thromb Vasc Biol*. 2006;26:20–27. doi: 10.1161/01.ATV.0000195789.39418.e8.
- Wang N, Lan D, Chen W, Matsuura F, Tall AR. ATP-binding cassette transporters G1 and G4 mediate cellular cholesterol efflux to high-density lipoproteins. *Proc Natl Acad Sci U S A*. 2004;101:9774–9779. doi: 10.1073/pnas.0403506101.
- Yvan-Charvet L, Ranalletta M, Wang N, Han S, Terasaka N, Li R, Welch C, Tall AR. Combined deficiency of ABCA1 and ABCG1 promotes foam cell accumulation and accelerates atherosclerosis in mice. *J Clin Invest*. 2007;117:3900–3908. doi: 10.1172/JCI33372.
- Wang F, Jia J. Polymorphisms of cholesterol metabolism genes CYP46 and ABCA1 and the risk of sporadic Alzheimer's disease in Chinese. *Brain Res*. 2007;1147:34–38. doi: 10.1016/j.brainres.2007.02.005.
- Costet P, Luo Y, Wang N, Tall AR. Sterol-dependent transactivation of the ABC1 promoter by the liver X receptor/retinoid X receptor. *J Biol Chem*. 2000;275:28240–28245. doi: 10.1074/jbc.M003337200.
- Schultz JR, Tu H, Luk A, Repa JJ, Medina JC, Li L, Schwendner S, Wang S, Thoolen M, Mangelsdorf DJ, Lustig KD, Shan B. Role of LXRs in control of lipogenesis. *Genes Dev*. 2000;14:2831–2838.
- Arakawa R, Tsujita M, Iwamoto N, Ito-Ohsumi C, Lu R, Wu CA, Shimizu K, Aotsuka T, Kanazawa H, Abe-Dohmae S, Yokoyama S. Pharmacological inhibition of ABCA1 degradation increases HDL biogenesis and exhibits antiatherogenesis. *J Lipid Res*. 2009;50:2299–2305. doi: 10.1194/jlr.M900122-JLR200.
- Wu CA, Tsujita M, Hayashi M, Yokoyama S. Probucol inactivates ABCA1 in the plasma membrane with respect to its mediation of apolipoprotein binding and high density lipoprotein assembly and to its proteolytic degradation. *J Biol Chem*. 2004;279:30168–30174. doi: 10.1074/jbc.M403765200.
- Ogura M, Ayaori M, Terao Y, Hisada T, Iizuka M, Takiguchi S, Uto-Kondo H, Yakushiji E, Nakaya K, Sasaki M, Komatsu T, Ozasa H, Ohsuzu F, Ikewaki K. Proteasomal inhibition promotes ATP-binding cassette transporter A1 (ABCA1) and ABCG1 expression and cholesterol efflux from macrophages *in vitro* and *in vivo*. *Arterioscler Thromb Vasc Biol*. 2011;31:1980–1987. doi: 10.1161/ATVBAHA.111.228478.
- Rader DJ, Alexander ET, Weibel GL, Billheimer J, Rothblat GH. The role of reverse cholesterol transport in animals and humans and relationship to atherosclerosis. *J Lipid Res*. 2009;suppl 50:S189–S194. doi: 10.1194/jlr.R800088-JLR200.
- Uto-Kondo H, Ayaori M, Sotherden GM, Nakaya K, Sasaki M, Yogo M, Komatsu T, Takiguchi S, Yakushiji E, Ogura M, Nishida T, Endo Y, Ikewaki K. Ezetimibe enhances macrophage reverse cholesterol transport in hamsters: contribution of hepato-biliary pathway. *Biochim Biophys Acta*. 2014;1841:1247–1255. doi: 10.1016/j.bbali.2014.05.009.
- Schwartz GG, Olsson AG, Abt M, et al; dal-OUTCOMES Investigators. Effects of dalcetrapib in patients with a recent acute coronary syndrome. *N Engl J Med*. 2012;367:2089–2099. doi: 10.1056/NEJMoa1206797.
- Barter PJ, Rye KA. Cholesteryl ester transfer protein inhibition as a strategy to reduce cardiovascular risk. *J Lipid Res*. 2012;53:1755–1766. doi: 10.1194/jlr.R024075.
- Khera AV, Cuchel M, de la Llera-Moya M, Rodrigues A, Burke MF, Jafri K, French BC, Phillips JA, Mucksavage ML, Wilensky RL, Mohler ER, Rothblat GH, Rader DJ. Cholesterol efflux capacity, high-density lipoprotein function, and atherosclerosis. *N Engl J Med*. 2011;364:127–135. doi: 10.1056/NEJMoa1001689.
- Tsujita M, Yokoyama S. Selective inhibition of free apolipoprotein-mediated cellular lipid efflux by probucol. *Biochemistry*. 1996;35:13011–13020. doi: 10.1021/bi960734h.
- Tsujita M, Tomimoto S, Okumura-Noji K, Okazaki M, Yokoyama S. Apolipoprotein-mediated cellular cholesterol/phospholipid efflux and plasma high density lipoprotein level in mice. *Biochim Biophys Acta*. 2000;1485:199–213.
- Tamehiro N, Shigemoto-Mogami Y, Kakeya T, Okuhira K, Suzuki K, Sato R, Nagao T, Nishimaki-Mogami T. Sterol regulatory element-binding protein-2- and liver X receptor-driven dual promoter regulation of hepatic ABC transporter A1 gene expression: mechanism underlying the unique response to cellular cholesterol status. *J Biol Chem*. 2007;282:21090–21099. doi: 10.1074/jbc.M701228200.
- Ohoka N, Okuhira K, Cui H, Wu W, Sato R, Naito M, Nishimaki-Mogami T. HNF4 $\alpha$  increases liver-specific human ATP-binding cassette transporter A1 expression and cholesterol efflux to apolipoprotein A-I in response to cholesterol depletion. *Arterioscler Thromb Vasc Biol*. 2012;32:1005–1014. doi: 10.1161/ATVBAHA.111.238360.
- Aiello RJ, Brees D, Francone OL. ABCA1-deficient mice: insights into the role of monocyte lipid efflux in HDL formation and inflammation. *Arterioscler Thromb Vasc Biol*. 2003;23:972–980. doi: 10.1161/01.ATV.0000054661.21499.FB.
- Haghighat M, Bourassa PA, Francone OL, Aiello RJ. Monocyte/macrophage expression of ABCA1 has minimal contribution to plasma HDL levels. *J Clin Invest*. 2001;108:1315–1320. doi: 10.1172/JCI12810.
- Timmins JM, Lee JY, Boudyguina E, Kluckman KD, Brunham LR, Mulya A, Gebre AK, Coutinho JM, Colvin PL, Smith TL, Hayden MR, Maeda N, Parks JS. Targeted inactivation of hepatic Abca1 causes profound hypoalphalipoproteinemia and kidney hypercatabolism of apoA-I. *J Clin Invest*. 2005;115:1333–1342. doi: 10.1172/JCI23915.
- Joyce CW, Wagner EM, Basso F, et al. ABCA1 overexpression in the liver of LDLR-KO mice leads to accumulation of pro-atherogenic lipoproteins and enhanced atherosclerosis. *J Biol Chem*. 2006;281:33053–33065. doi: 10.1074/jbc.M604526200.
- Brunham LR, Singaraja RR, Duong M, Timmins JM, Fievat C, Bissada N, Kang MH, Samra A, Fruchart JC, McManus B, Staels B, Parks JS, Hayden MR. Tissue-specific roles of ABCA1 influence susceptibility to atherosclerosis. *Arterioscler Thromb Vasc Biol*. 2009;29:548–554. doi: 10.1161/ATVBAHA.108.182303.

27. Westerterp M, Murphy AJ, Wang M, et al. Deficiency of ATP-binding cassette transporters A1 and G1 in macrophages increases inflammation and accelerates atherosclerosis in mice. *Circ Res*. 2013;112:1456–1465. doi: 10.1161/CIRCRESAHA.113.301086.
28. Bi X, Zhu X, Duong M, Boudyguina EY, Wilson MD, Gebre AK, Parks JS. Liver ABCA1 deletion in LDLrKO mice does not impair macrophage reverse cholesterol transport or exacerbate atherogenesis. *Arterioscler Thromb Vasc Biol*. 2013;33:2288–2296. doi: 10.1161/ATVBAHA.112.301110.
29. Yamamoto S, Tanigawa H, Li X, Komaru Y, Billheimer JT, Rader DJ. Pharmacologic suppression of hepatic ATP-binding cassette transporter 1 activity in mice reduces high-density lipoprotein cholesterol levels but promotes reverse cholesterol transport. *Circulation*. 2011;124:1382–1390. doi: 10.1161/CIRCULATIONAHA.110.009704.

### Significance

An increase in plasma HDL should reduce the risk of atherosclerotic vascular diseases but no efficient strategy for this has been established. ABCA1 is a membrane protein that mediates the generation of HDL particles with cellular lipids and extracellular helical apolipoproteins and is thus a good candidate target for such a strategy. Probucol, a hypolipidemic drug, markedly reduces HDL by inhibiting ABCA1 but is also known to inhibit the proteolytic degradation of ABCA1, resulting in an increase in inactive ABCA1. On the other hand, oxidized products of probucol, spiroquinone and diphenoquinone, increase active ABCA1 by inhibiting its degradation, and enhance apolipoprotein A-I-mediated cell cholesterol release. Here, these compounds were shown to increase plasma HDL-C in mice, accompanied by an increase in hepatic and macrophage ABCA1. Overall reverse cholesterol transport from peripheral macrophages to feces was also increased. Thus, inhibiting ABCA1 degradation was shown to be a promising antiatherogenic strategy.

## Methods and Materials

### Materials

Probucol was purchased from WAKO Pure Chemical (Osaka, Japan). SQ and DQ were synthesized as previously described<sup>1</sup>. Human apoA-I was purchased from Sigma (St. Louis, MO, USA). HDL was isolated by sequential ultracentrifugation from human plasma. Acetylated human low-density lipoprotein (AcLDL) was prepared according to the methods previously described<sup>2</sup>.

### Cell Culture

RAW264.7 cells (Riken Cell Bank, Tsukuba, Japan), a murine macrophage cell line, were maintained in Dulbecco's modified Eagle's medium (DMEM) containing 10% fetal bovine serum (FBS). The cells were stimulated in 0.3 mmol/L 8-bromoadenosine 3',5'-cyclic monophosphate (8-Br-cAMP) to induce expression of ABCA1 and ABCG1<sup>3</sup>. All cultures were in a humidified atmosphere of 5% CO<sub>2</sub> and 95% air at 37°C.

### Cell Cholesterol Release

Release of cell cholesterol was determined as previously described<sup>4,5</sup>. RAW264.7 cells were labeled with <sup>3</sup>H-cholesterol (1.0 μCi/mL) in DMEM containing 0.2% bovine serum albumin (BSA) for 24 hr. The cells were washed with phosphate buffered saline (PBS) and incubated in the same medium in the presence or absence of apoA-I (10 μg/mL) or HDL (50 μg/mL as protein) for 4 hr and 24 hr. Probucol, SQ or DQ was added to the incubation mixture with apoA-I or HDL. After the incubation, radioactivity in the medium and cells was counted in a liquid scintillation counter (LSC). Cholesterol release was calculated as percentage of the initial cell cholesterol count, by dividing the media radioactivity by the sum of that in the media and the cells.

### Western Blot Analyses

Cells were harvested and protein extracts prepared as previously described<sup>5,6</sup> for analysis by Western blotting (10% SDS-PAGE; 15 μg protein per lane), using anti-human ABCA1 rat monoclonal antibodies<sup>7,8</sup> and rabbit antibodies against ABCG1 (Novus Biologicals), SR-BI (Novus Biologicals) and β-actin (Santa Cruz). The proteins were visualized and quantified using a chemiluminescence method (ECL Plus Western Blotting Detection System; GE Healthcare UK Ltd) and the NIH image analysis software program.

### Animals

C57BL/6J and apolipoprotein E (apoE) null mice were obtained from Clea Japan

(Tokyo, Japan) and Jackson Laboratory (West Grove, PA), and fed a standard chow and high cholesterol (1/25%) diet, respectively. The experiments were performed using mice aged 6-8 weeks. The animal experiment protocol was approved by the National Defense Medical College Institutional Animal Care and Use Committee, and the mice were treated according to its guidelines.

### Effects of SQ and DQ on ABC Proteins, Plasma Lipids and Other Biochemical

#### Parameters in Mice

SQ, DQ, 500 mg/kg, or the vehicle was orally administered to six-week-old male C57BL/6 mice. Immediately before and 7 days after the administration, blood samples were taken from the tail vein. Total cholesterol, HDL-C, free cholesterol (FC), triglycerides (TG), phospholipids (PL), aspartate aminotransferase (AST), alanine aminotransferase (ALT) and creatine phosphokinase (CPK) in plasma were determined by enzymatic methods (WAKO, Osaka, Japan). For lipoprotein analysis, 400 μL of plasma from each mouse were pooled for each treatment group, and each pooled plasma was fractionated using a Superose 6 10/300 GL fast protein liquid chromatography (FPLC) column (Amersham Biosciences, Piscataway, NJ). Fractions of 500 μL were collected for lipid measurement. The mice were sacrificed after seven days of the treatment. Peritoneal macrophages were collected by peritoneal lavage with ice-cold PBS and centrifugation at 3000 rpm. Cells obtained as a pellet were re-suspended in DMEM and plated onto 6-well cell culture plates for 1 hr (mouse peritoneal macrophages; MPM). Livers were recovered and perfused with PBS before the analyses. Protein extracts from the liver and MPM were prepared with T-PER (Pierce Chemical Co., Rockford, IL) in the presence of protease inhibitors (Roche Applied Science, Barcelona, Spain), and analyzed by Western blotting as described above.

#### Real-time Quantitative RT-PCR

Total RNA was extracted from the livers, and first-strand cDNA was synthesized from the total RNA (250 ng) by placing in a Reverse Transcription Reagent (Applied Biosystems, Foster City, CA). Quantitative PCR was performed with a Perkin-Elmer 7900 PCR machine, TaqMan PCR master mix and FAM-labeled TaqMan probes (Assays-on-Demand, Applied Biosystems) for mouse ABCG5, ABCG8, Niemann-Pick C1-Like 1 (NPC1L1) and glyceraldehyde-3-phosphate dehydrogenase (GAPDH). Expression data were normalized for GAPDH levels.

#### In Vivo Macrophage RCT Studies

RAW264.7 cells were cultured under RPMI 1640 supplemented with 10% FBS, and then radiolabeled with 5  $\mu\text{Ci/mL}$   $^3\text{H}$ -cholesterol and enriched with cholesterol by incubating with 100  $\mu\text{g/mL}$  of AcLDL for 48 hr. The cells were washed, equilibrated, detached with cell scrapers, resuspended in RPMI 1640, and pooled. Seven-week-old male C57BL/6 mice (Clea Japan, Tokyo, Japan) were divided into 3 groups (6 mice per group) and caged individually with unlimited access to food and water. The mice were preconditioned by daily administration of 500 mg/kg of SQ, DQ or the vehicle by oral gavage for 7 days. The AcLDL-loaded and  $^3\text{H}$ -cholesterol-labeled RAW264.7 cells (typically  $5.0 \times 10^6$  cells containing  $7.5 \times 10^6$  counts per minute (cpm) in 0.5 mL RPMI 1640) were intraperitoneally injected into the mice as described previously<sup>9</sup>. Blood was taken at 24 and 48 hr after the injection, and radioactivity in plasma was counted in an LSC. Feces were collected continuously from 0 to 48 hr and stored at 4°C until counting for radioactivity. At 48 hr after the injection, mice were exsanguinated and livers and bile were collected.

#### **Liver, Bile and Fecal Analyses**

Liver lipid was extracted as described previously<sup>9</sup>. Briefly, a 50-mg piece of tissue was homogenized in water, and lipid was extracted with a 2:1 (vol/vol) mixture of chloroform/methanol. The organic layer was collected, evaporated, resuspended in a 3:2 (vol/vol) mixture of hexane/isopropanol, and counted for radioactivity. Radioactivity in bile was directly counted in an LSC. The total feces collected from 0 to 48 hr were weighed and soaked in distilled water (1 mL water per 100 mg feces) overnight at 4°C. An equal volume of ethanol was added the next day, and the samples were homogenized. In a 200  $\mu\text{L}$  aliquot of each homogenized sample was counted for radioactivity. Results were expressed as percentage of the cpm injected.

#### **HDL Metabolic Studies**

Human HDL was isolated from pooled human plasma by sequential ultracentrifugation (density 1.063 < density 1.21 g/ml). Dialyzed human HDL was labeled with  $^3\text{H}$ -cholesteryl oleate (CEs). Fifty  $\mu\text{Ci}$  of cholesteryl ether or oleate in toluene were dried down under nitrogen. Ethanol was then added, and the solution taken up by a pipette. This was added to the HDL<sub>3</sub> solution (1.07 ml of dialyzed HDL containing 10 mg of protein) over a period of 5 min while gently shaking with short interruptions for a brief vortex. The HDL solution was incubated for 24 hr at 37°C. The HDL<sub>3</sub> from the solution was re-isolated by ultracentrifugation (40,000 rpm, 48 hr) at the original

density and the  $^3\text{H}$ -HDL was dialyzed overnight against PBS containing 0.01% EDTA. Finally, the  $^3\text{H}$ -HDL was filter-sterilized and stored at 4°C until injection.

For the metabolic study, 1 million dpm of HDL labeled with  $^3\text{H}$ -CEs were injected intravenously via tail veins into the mice at day 7 after administration of SQ/DQ or the vehicle. Feces were collected continuously up to 48 hr and then analyzed for tracer radioactivity. Results were expressed as a percentage of the injected dose.

#### **HDL Cholesterol Efflux Capacity Assay**

J774 macrophages were purchased from RIKEN (Tsukuba, Japan) and cultured in RPMI 1640 medium containing 10% FBS and kept under constant conditions of 5% CO<sub>2</sub> and 37°C. J774 cells were plated in 24-well plates and grown until 80% confluency, and radiolabeled with 2  $\mu\text{Ci/mL}$  of  $^3\text{H}$ -cholesterol. Apolipoprotein B-depleted sera were prepared by incubating with 13% polyethylene glycol 6000 solution (Wako Pure Chemicals). We confirmed depletion of apolipoprotein B by fast protein liquid chromatography and western blot analysis. Subsequently, efflux mediums containing 2.8% apolipoprotein B (apoB)-depleted sera obtained from the mice treated with SQ/DQ or the vehicle were added and incubation conducted for 4 hr. All procedures were performed in the presence of the acyl-coenzyme A: cholesterol acyltransferase inhibitor; Sandoz 58-035 (2  $\mu\text{g/mL}$ ) (Sigma) and 8-bromoadenocine 3',5'-cyclic monophosphate (0.3 mmol/L) (Sigma). An LSC was used to quantify the efflux of radioactive cholesterol from the cells. The quantity of radioactive cholesterol incorporated into cellular lipids was calculated by means of hexane: isopropanol (v:v:1) extraction of control wells not exposed to the serum (blank). For each 24-wells in the culture plate, 3 were used for the blank. Percent efflux was calculated by the following formula [(cpm of  $^3\text{H}$ -cholesterol in media containing 2.8% apoB-depleted plasma - cpm of  $^3\text{H}$ -cholesterol in plasma-free media)/cpm of  $^3\text{H}$ -cholesterol in cells extracted before the efflux step]  $\times 100$ .

#### **Atherosclerotic Lesion Analysis**

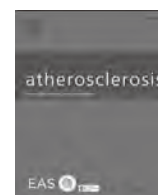
Forty apoE mice were fed with a high cholesterol diet (containing 1.25% cholesterol) with or without SQ (0.1%) for 12 weeks. Two mice in the control group died due to unknown reasons. The entire aorta was dissected, opened longitudinally, and stained with Sudan IV. Total areas of the aorta and intimal atherosclerotic plaques were measured from NIH images. The areas of atherosclerotic lesions as percentages of the aortic wall were calculated by dividing atherosclerotic area by total area of the aorta.

### Statistical Analysis

The Student's t-test was performed as appropriate. A p value of less than 0.05 was considered to be statistically significant. Values are expressed as mean  $\pm$  SD.

### References

- Arakawa R, Tsujita M, Iwamoto N, Ito-Ohsumi C, Lu R, Wu CA, Shimizu K, Aotsuka T, Kanazawa H, Abe-Dohmae S, Yokoyama S. Pharmacological inhibition of abca1 degradation increases hdl biogenesis and exhibits antiatherogenesis. *J Lipid Res.* 2009;50:2299-2305
- Basu SK, Goldstein JL, Brown MS. Characterization of the low density lipoprotein receptor in membranes prepared from human fibroblasts. *J Biol Chem.* 1978;253:3852-3856
- Abe-Dohmae S, Suzuki S, Wada Y, Aburatani H, Vance DE, Yokoyama S. Characterization of apolipoprotein-mediated hdl generation induced by camp in a murine macrophage cell line. *Biochemistry.* 2000;39:11092-11099
- Ayaori M, Sawada S, Yonemura A, Iwamoto N, Ogura M, Tanaka N, Nakaya K, Kusuhara M, Nakamura H, Ohsuzu F. Glucocorticoid receptor regulates atp-binding cassette transporter-1 expression and apolipoprotein-mediated cholesterol efflux from macrophages. *Arterioscler Thromb Vasc Biol.* 2006;26:163-168
- Terao Y, Ayaori M, Ogura M, et al. Effect of sulfonylurea agents on reverse cholesterol transport in vitro and vivo. *J Atheroscler Thromb.* 2011;18:513-530
- Ayaori M, Yakushiji E, Ogura M, et al. Retinoic acid receptor agonists regulate expression of atp-binding cassette transporter g1 in macrophages. *Biochim Biophys Acta.* 2012;1821:561-572
- Iwamoto N, Abe-Dohmae S, Ayaori M, Tanaka N, Kusuhara M, Ohsuzu F, Yokoyama S. Atp-binding cassette transporter 1 gene transcription is downregulated by activator protein 2alpha. Doxazosin inhibits activator protein 2alpha and increases high-density lipoprotein biogenesis independent of alpha1-adrenoceptor blockade. *Circ Res.* 2007;101:156-165
- Abe-Dohmae S, Kato KH, Kumon Y, Hu W, Ishigami H, Iwamoto N, Okazaki M, Wu CA, Tsujita M, Ueda K, Yokoyama S. Serum amyloid a generates high density lipoprotein with cellular lipid in an abca1- or abca7-dependent manner. *J Lipid Res.* 2006;47:1542-1550
- Tamigawa H, Billheimer JT, Tohyama J, Fuki IV, Ng DS, Rothblat GH, Rader DJ. Lecithin: Cholesterol acyltransferase expression has minimal effects on macrophage reverse cholesterol transport in vivo. *Circulation.* 2009;120:160-169



# Caveolin-1 facilitates internalization and degradation of ABCA1 and probucol oxidative products interfere with this reaction to increase HDL biogenesis



Rui Lu, Tomoe Tsuboi, Kuniko Okumura-Noji, Noriyuki Iwamoto<sup>1</sup>, Shinji Yokoyama\*

Nutritional Health Science Research Center and College of Bioscience and Biotechnology, Chubu University, Kasugai 487-8501, Japan

## ARTICLE INFO

### Article history:

Received 4 February 2016  
Received in revised form  
1 August 2016  
Accepted 23 August 2016  
Available online 24 August 2016

### Keywords:

Cholesterol  
HDL  
ABCA1  
Caveolin-1  
Probucol

## ABSTRACT

**Background and aims:** Expression of ATP binding cassette transporter (ABC) A1, a key membrane protein for biogenesis of high-density lipoprotein (HDL), is regulated not only by its gene transcription but also by its intracellular degradation to modulate plasma HDL concentration. We previously showed that inhibition of ABCA1 degradation by probucol oxidative products, spiroquinone (SQ) and diphenylquinone (DQ), increased HDL biogenesis and reverse cholesterol transport, and achieved reduction of atherosclerosis in animal models. The background mechanism has thus been investigated.

**Methods:** Involvement of caveolin-1, a protein of multiple functions in cell biology, particularly in cholesterol trafficking, has been examined for its roles in ABCA1 degradation as well as the effects of SQ and DQ on the reaction.

**Results:** ABCA1 protein was increased in caveolin-1-deficient mouse embryonic fibroblasts, not by increase of transcription but by decrease in its internalization and degradation. Transfection and expression of caveolin-1 normalized the protein level and the rate of degradation of ABCA1. Immunoprecipitation experiments demonstrated association between ABCA1 and caveolin-1 and SQ and DQ disrupted this interaction. The effects of SQ and DQ to increase ABCA1 and cell cholesterol release induced by apolipoprotein A-I were dependent on expression of caveolin-1. Fluorescence imaging of ABCA1 and caveolin-1 in cultured cells demonstrated their co-localization as well as its disruption by SQ and DQ, being consistent with the biochemical findings.

**Conclusions:** Caveolin-1 enhances internalization and degradation of ABCA1 by its association with ABCA1. Interference of this interaction by probucol oxidative products suppresses ABCA1 degradation and increase HDL biogenesis.

© 2016 Elsevier Ireland Ltd. All rights reserved.

## 1. Introduction

High-density lipoprotein (HDL) plays a central role in the pathway of cholesterol transport from peripheral tissues to the liver for its catabolism to bile acids as an essential part of cholesterol homeostasis. Release of cell cholesterol to HDL is the initial step of this pathway that is composed of two reactions: generation of new discoidal “nascent” HDL particles from cell membrane phospholipid and cholesterol by extracellular helical apolipoprotein (apo) such as apoA-I [1], and non-specific passive flow of cholesterol from the cell membrane to extracellular cholesterol acceptors, particularly HDL

[2]. The former reaction is almost the exclusive source of plasma HDL, mediated by the cell membrane protein ATP binding cassette transporter (ABC) A1 [3–5]. The latter reaction is actively promoted by another ABC transporter ABCG1 [6] and by acyl esterification of cholesterol on HDL that shifts esterified cholesterol to the core of HDL and creates more room on the HDL surface for further cell cholesterol release [7]. These two reactions take place in sequence to generate spherical HDL; the ABCA1/apoA-I reaction generates discoidal HDL particles with phospholipid and cholesterol. Subsequent cholesterol esterification on HDL and further transfer of cholesterol from cells and other lipoproteins generate the hydrophobic core of spherical particles. Inhibition of ABCA1 activity decreases plasma HDL [8,9], and overexpression of ABCA1 increases the plasma HDL level at least in animal experiments [10].

The level of ABCA1 protein on the cell surface is regulated not

\* Corresponding author.

E-mail address: [syokoyam@isc.chubu.ac.jp](mailto:syokoyam@isc.chubu.ac.jp) (S. Yokoyama).

<sup>1</sup> Present address: Eli Lilly and Company Japan, Kobe 651-0086, Japan.

only by transcription of the gene but also posttranslational proteolytic degradation. ABCA1 is rapidly degraded intracellularly by calpain after its endocytotic internalization [11–13]. When HDL is generated with extracellular helical apolipoproteins, internalization of ABCA1 is unaffected but the associated apolipoproteins protect ABCA1 from proteolytic degradation, perhaps by making it resistant to calpain [14,15], and therefore allowing recycling of ABCA1 to the cell surface [13]. The HDL biogenesis reaction therefore positively feeds back ABCA1 activity by recycling ABCA1. HDL biogenesis is further enhanced by inhibition of the ABCA1 degradation [13].

Interestingly, a strong inhibitor of ABCA1 activity, probucol, also inhibits ABCA1 degradation [8,9,16,17], while oxidative products of probucol, spiroquinone (SQ) and diphenylquinone (DQ), inhibit ABCA1 degradation without inhibiting its activity for HDL biogenesis [18]. SQ and DQ were shown to decrease ABCA1 internalization, increase HDL biogenesis, elevate plasma HDL, and prevent atherosclerosis in a rabbit model [18]. These compounds were further demonstrated to facilitate “reverse transport” of cholesterol from peritoneal macrophages to excreted feces and to reduce atherosclerosis in a mouse model [19]. Thus, reducing ABCA1 degradation is a potential target to prevent atherosclerotic vascular diseases.

Production of “nascent” discoidal HDL particles has been demonstrated in liver perfusion experiments [20], by direct interaction of helical apolipoproteins and phospholipids in vitro [21] and by ABCA1-dependent HDL biogenesis from the cells in culture [22]. Cholesterol is not essential to form nascent HDL, not only in in-vitro reactions [23] but also in the ABCA1-mediated reaction with cellular lipids [24]. Enrichment of cholesterol in HDL is dependent on various cellular factors including a type of ABCA transporters to mediate the reaction [22,25] and intracellular signalling [26]. Another factor may be caveolin-1 [27], which is involved in many cellular activities including transcytosis, potocytosis, and signal transduction [28], and most of all intracellular trafficking of cholesterol [29,30].

Previous findings linking caveolin-1 and HDL metabolism are, however, controversial. Cell cholesterol release to HDL shows apparently positive correlation with caveolin-1 expression and the ABCA1/apoA-1 or ABCG1/HDL pathways [27,31–33]. ABCA1 has been shown to interact with caveolin-1, though it is not clear whether the interaction regulates HDL biogenesis [34–36]. On the other hand, plasma HDL levels were shown to increase in caveolin-1 deficient mice [30,37,38] and these animals were resistant to atherogenesis [37,39]. ABCA1 is largely recovered in the non-raft fraction of plasma membrane [40–42], seemingly consistent with

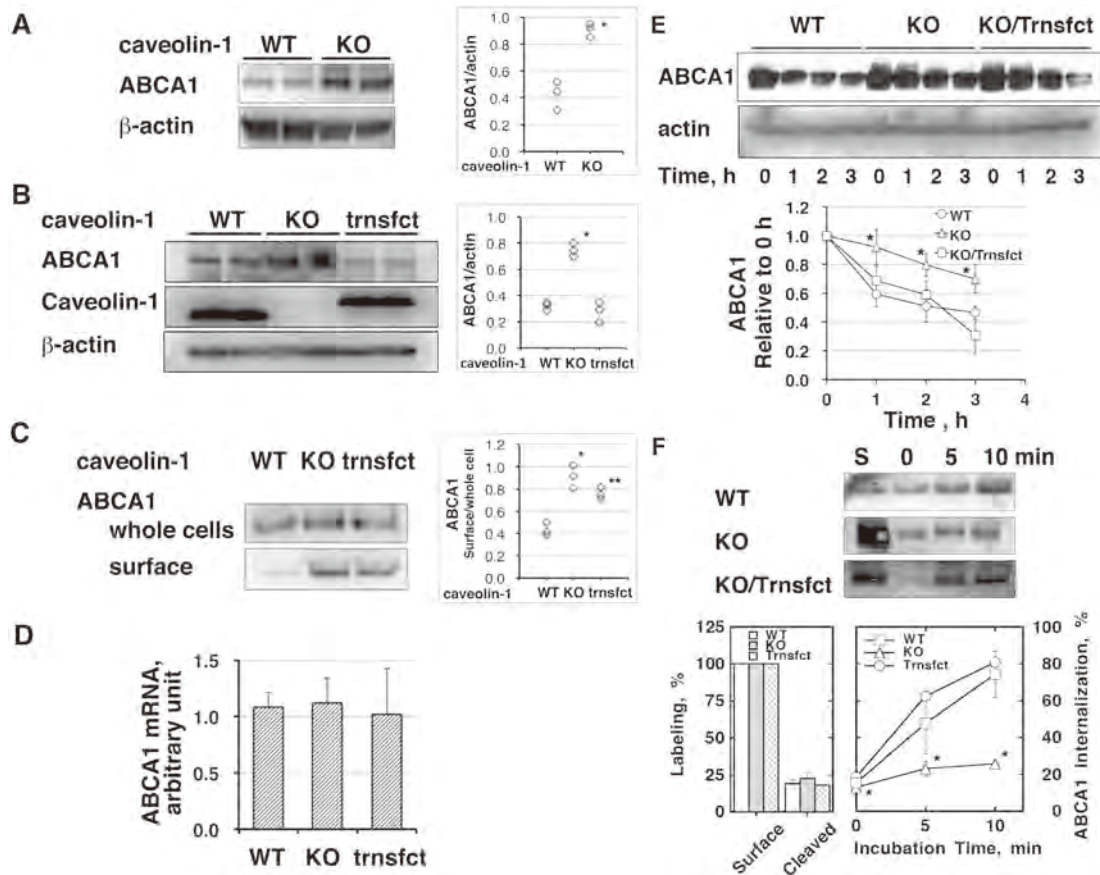


**Fig. 1.** ABCA1 protein levels in response to the presence or absence of caveolin-1. (A) ABCA1 protein was analyzed by immunoblotting in MEFs of wild-type (WT) and caveolin-1-deficient (KO) mice. (B) ABCA1 protein was analyzed by immunoblotting in MEFs of wild-type and caveolin-1-deficient mice, and KO cells to which caveolin-1 was transfected and expressed (trnsfct). (C) Cell surface ABCA1 was probed using biotinylation, as described in the text. (D) ABCA1 mRNA levels in WT, KO and trnsfct cells analyzed by real-time PCR. Graphs in panels A, B, and C represent the results of quantitative analyses of each series of experiments (n = 3). \*p < 0.05 versus WT, and \*\*p < 0.05 versus KO. (E) Degradation of ABCA1 in WT, KO and KO-trnsfct cells. Decay of ABCA1 was analyzed as time course in the presence of cycloheximide to inhibit synthesis of the protein, as described in the text. The graph represents results of the quantitative analysis (n = 3). (F) Internalization of ABCA1 in WT, KO and KO-trnsfct cells. Surface ABCA1 was labeled by biotinylation and its internalization was monitored, as described in the text. Graphs represent results of the quantification of bands (n = 3). The left-hand graph represents biotin labeling remaining after cleavage of biotin immediately after labeling (Cleaved) expressed as percentage of initial labeling (Surface). The right-hand graph represents the time course of ABCA1 internalization. Asterisks in the graph indicate p < 0.05 in comparison to WT and trnsfct.

the findings that it disrupts cholesterol/sphingomyelin-rich, raft microdomains [43]. More recently we demonstrated that ABCA1 destabilizes/disintegrates membrane conformation to mobilize membrane lipids for HDL biogenesis and intracellular regulation of cholesterol metabolism [44]. In contrast, caveolin-1 strongly associates with raft to create invaginated microdomains, caveolae [28]. It is thus puzzling how caveolin-1 plays a role in the ABCA1-mediated HDL biogenesis reaction. We therefore undertook investigation to look into the interaction between ABCA1 and caveolin-1 in relation to the regulation of HDL biogenesis.

**2. Materials and methods**

Embryonic fibroblasts prepared from a caveolin-1-deficient mouse (STOCK *Cav1<sup>tm1Mls</sup>/J*) and a control wild type control mouse (B6<sub>129</sub>SF<sub>2</sub>/J) (MEFs) were used for analysis of the ABCA1/caveolin-1 interaction. The effects of the probucol and its oxidized metabolites known to increase ABCA1 were examined in this interaction. Further details of the Materials and methods used are described in *Supplementary Materials*.

**3. Results**

**3.1. Regulation of ABCA1 level by caveolin-1**

MEFs were prepared from wild type and caveolin-1 null mice and expression of ABCA1 was examined by immunoblot analysis (Fig. 1A). ABCA1 protein level increased in the caveolin-1 null mice cells. When full-length caveolin-1 was transfected and expressed in the caveolin-1 null cells, the increase of ABCA1 was partially reversed (Fig. 1B). The increase of ABCA1 in the caveolin-1 deficient cells was mainly in the cell surface, which was also reversed by transfection of caveolin-1 (Fig. 1C). Expression of the *ABCA1* mRNA was not altered in caveolin-1-deficient cells or by transfection of caveolin-1 (Fig. 1D).

The rate of degradation of ABCA1 was examined as decay of the protein in the presence of cycloheximide by immunoblotting (Fig. 1E). The half-life of ABCA1 was around 2 h in the wild type cells, consistent with our previous observation, while this rate was substantially slower in the caveolin-1-null cells. Transfection of caveolin-1 increased the rate of degradation back to the half-life of 2–3 h, almost similar to that of the wild type mice cells.

Since degradation of ABCA1 is initiated by its endocytotic internalization, this reaction was examined by monitoring the fate of the cell surface ABCA1 labeled with biotin as described in the experimental methods (Fig. 1F). The rate of ABCA1 internalization is retarded in the caveolin-1 null cells and it was restored by transfection and expression of full-length caveolin-1. We therefore concluded that ABCA1 protein increased in the absence of caveolin-1 because its degradation is retarded due to slow internalization.

**3.2. Influence of ABCA1 on caveolin-1 metabolism**

Expression of caveolin-1 protein was examined in the presence and absence of ABCA1. The overall expression levels of caveolin-1 protein were not influenced by the lack of ABCA1 (Fig. 2A). The degradation rate of caveolin-1 was slow and uninfluenced by the absence of ABCA1 (Fig. 2B). On the other hand, cell surface caveolin-1 was internalized at a rate similar to ABCA1 in the wild type MEFs, and this rate was slower in the absence of ABCA1 (Fig. 2C and D). These results suggest that internalization of caveolin-1 does not significantly correlate with the overall rate of its degradation, either because internalization is a part of its recycling or due to a small contribution of this portion to the entire cellular pool size of caveolin-1. This is in contrast to ABCA1 whose internalization

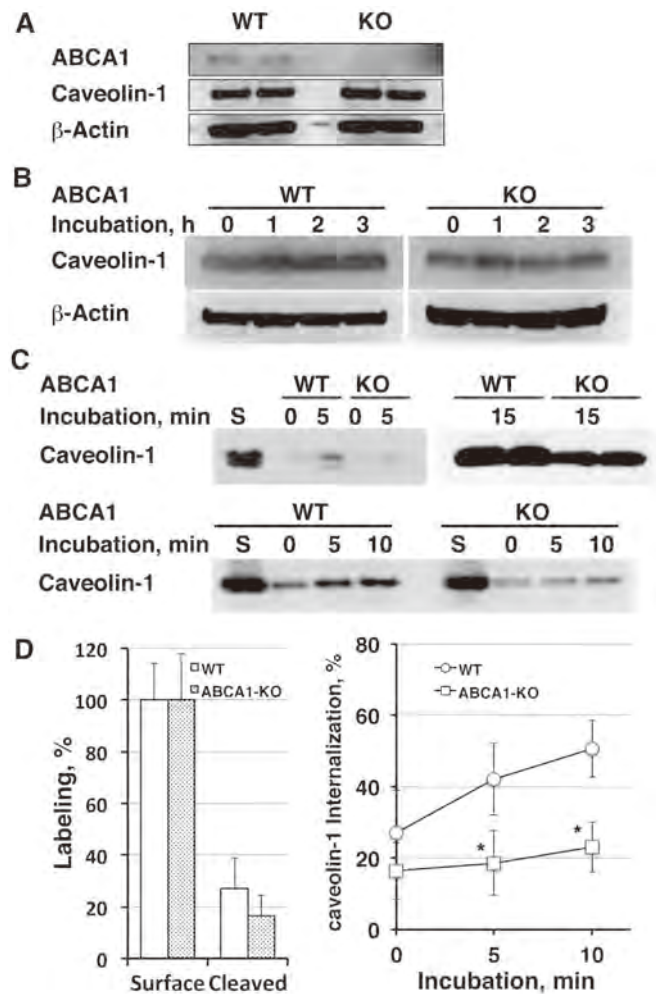


**Fig. 2. Metabolic analysis of caveolin-1.** (A) Caveolin-1 protein in MEFs of wild-type (WT) and ABCA1-deficient (KO) mice. Caveolin-1 was analyzed by immunoblotting. (B) Degradation of caveolin-1 in WT and KO cells. Change in caveolin-1 was monitored as time course in the presence of cycloheximide. (C) Internalization of caveolin-1, monitored in WT and KO cells after labeling surface caveolin-1 by biotinylation, as described in the text. (D) Quantification of caveolin-1 internalization (n = 3). The left-hand graph represents cleavage of biotinylation label immediately after labeling (Cleared), expressed as percentage of initial labeling (Surface). The right-hand graph shows the time course of internalization of surface caveolin-1. Asterisks indicate *p* < 0.05 in comparison to WT.

regulates its degradation.

**3.3. Interaction of ABCA1 and caveolin-1**

The interaction of caveolin-1 with ABCA1 was probed by using apoA-I, which inhibits ABCA1 degradation by rendering ABCA1 resistant to calpain and recycles it to the cell surface, and by using the compounds SQ and DQ, which interfere with proteolytic degradation of ABCA1 by inhibiting endocytotic internalization of ABCA1 (Fig. 3A and B). ABCA1 was increased by apoA-I and SQ in wild type MEFs, consistent with our previous findings. In contrast, neither apoA-I nor SQ influenced the expression of ABCA1 in the caveolin-1 deficient MEFs. The increase of ABCA1 by apoA-I, probucol, SQ and DQ was demonstrated in the wild type MEFs, but all disappeared in caveolin-1-deficient MEFs (Fig. 3B). Transfection and expression of caveolin-1 in the caveolin-1 null cells recovered the effects of apoA-I, SQ and DQ (Fig. 3B). The results of the cell cholesterol release experiments by apoA-I also showed cancellation

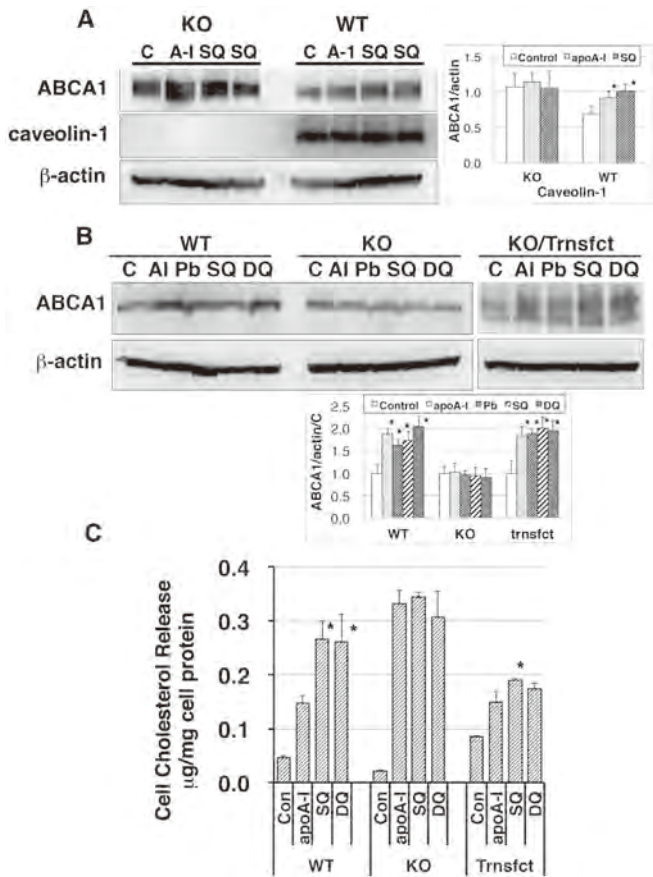


**Fig. 3. Effects of ABCA1 modulators in the presence and absence of caveolin-1.** (A) Increase in ABCA1 protein by apoA-I and SQ. ABCA1 levels were analyzed by immunoblotting in MEF prepared from wild-type (WT) and caveolin-1-deficient (KO) mice. (B) Change in ABCA1 protein in WT and KO cells and in KO cells where caveolin-1 was transfected and expressed (KO/Trnsfct). Cells were treated with apoA-I (A-I), probucol (Pb), SQ and DQ. Graphs in panel A and B represent the results of quantitative analyses (n = 3) as \* p < 0.05 versus control in each set. (C) Cholesterol release from WT, KO and Trnsfct cells into control culture medium (Con), in the presence of apoA-I and the additional presence of SQ and DQ (n = 3). Asterisks indicate p < 0.05 in comparison to the apoA-I-mediated reaction.

of the effects of SQ and DQ by caveolin-1 deficiency and their restoration by transfection of caveolin-1, consistent with the findings above (Fig. 3C).

The interaction was examined by co-precipitation with anti-ABCA1 and anticaveolin-1 antibodies. ABCA1 and caveolin-1 were precipitated with anticaveolin-1 antibody and anti-ABCA1 antibody, respectively, in the wild type MEFs, and these reactions were cancelled in the cells deficient in these proteins (Fig. 4A). Co-precipitation of ABCA1 with anticaveolin-1 antibody in the wild type cells increased in the presence of apoA-I but decreased with SQ and DQ. The results demonstrated that apoA-I increases surface ABCA1 to increase the interaction with caveolin-1, while SQ and DQ decreased it in the wild type MEFs (Fig. 4B). Similar findings were obtained with immunoprecipitation experiments using anti-ABCA1 antibody. ApoA-I increased the co-precipitation of caveolin-1 while SQ and DQ decreased it in the wild type MEFs (Fig. 4C).

The results demonstrated that the increase of surface ABCA1 by apoA-I increases its interaction with caveolin-1 [13], while SQ and DQ rather disrupt this interaction. These data are consistent with the findings that ABCA1 internalization and degradation are retarded in the caveolin-1-deficient cells and in the wild type cells

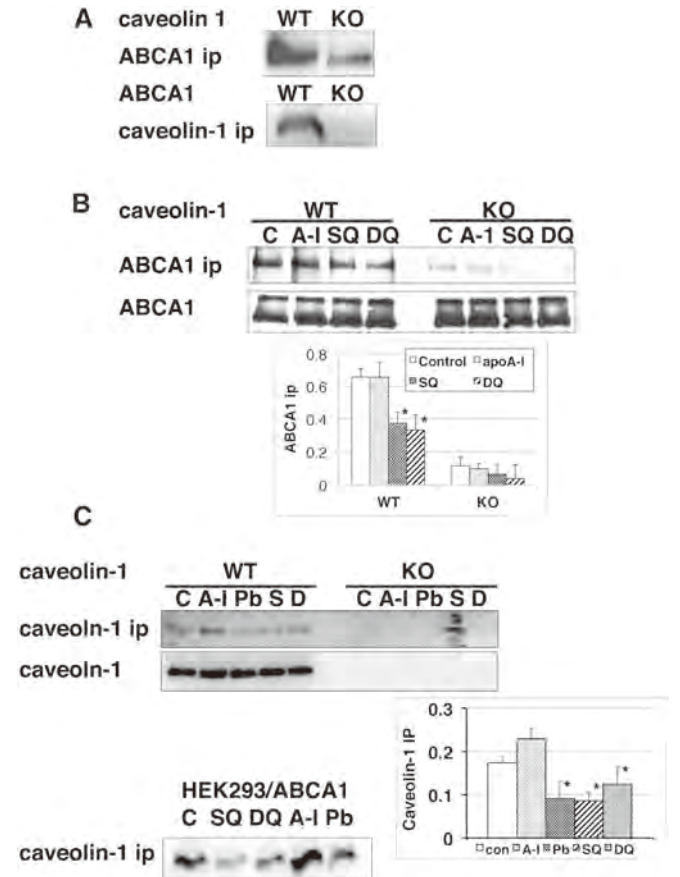


**Fig. 4. Immunoprecipitation experiments of ABCA1 and caveolin-1.** (A) Immunoprecipitation of ABCA1 (ABCA1 ip) with anticaveolin-1 antibody in WT and caveolin-1 deficient MEFs (KO), and that of caveolin-1 (caveolin-1 ip) with anti-ABCA1 antibody in WT and ABCA1-deficient MEFs (KO). (B) ABCA1 was analyzed in the immunoprecipitate with anticaveolin-1 antibody (caveolin-1 ip) in MEFs prepared from wild-type (WT) and caveolin-1-deficient (KO) mice, after the treatment of cells with apoA-I, SQ and DQ. ABCA1 represents ABCA1 protein in the whole cell lysate. (C) Immunoprecipitated caveolin-1 with anti-ABCA1 antibody (caveolin-1 ip) in wild-type (WT) and caveolin-1-deficient cells (KO); caveolin-1 represents caveolin-1 in the whole cell lysate. The bottom panel represents the results of a similar experiment in HEK293 cells, where ABCA1 was transfected and expressed (HEK293/ABCA1). Cells were pretreated with apoA-I (A-I), Pb, SQ or DQ. Graphs in panels B and C represent the results of quantitative analyses (n = 3) as \* p < 0.05 versus control in each set.

where SQ and DQ interfere with ABCA1 internalization and therefore degradation [18].

### 3.4. Imaging of colocalization of ABCA1 and caveolin-1

The interaction of ABCA1 with caveolin-1 was examined in fluorescent microscopy. Wild type MEFs were stained for ABCA1 and caveolin-1 and visualized with fluorescein FITC and TR, for green and red emission colors, respectively (Fig. 5 and Supplementary Fig. II). When the two color channels were merged, co-localization of the two molecules in the cell membrane was visualized as orange color. In the presence of SQ, DQ and probucol, co-localization of ABCA1 and caveolin-1 was shown diminished by quantitation of the imaging data. The graph attached to Fig. 5 demonstrates the average photointensity of the red/orange color areas relatively to the background green area, showing marked decrease of the co-localization of ABCA1 and caveolin-1 by these three compounds. Supplementary Fig. II represents the results of the quantitative line profile analyses for green and red color elements. The intensity of red and green elements along with the cell

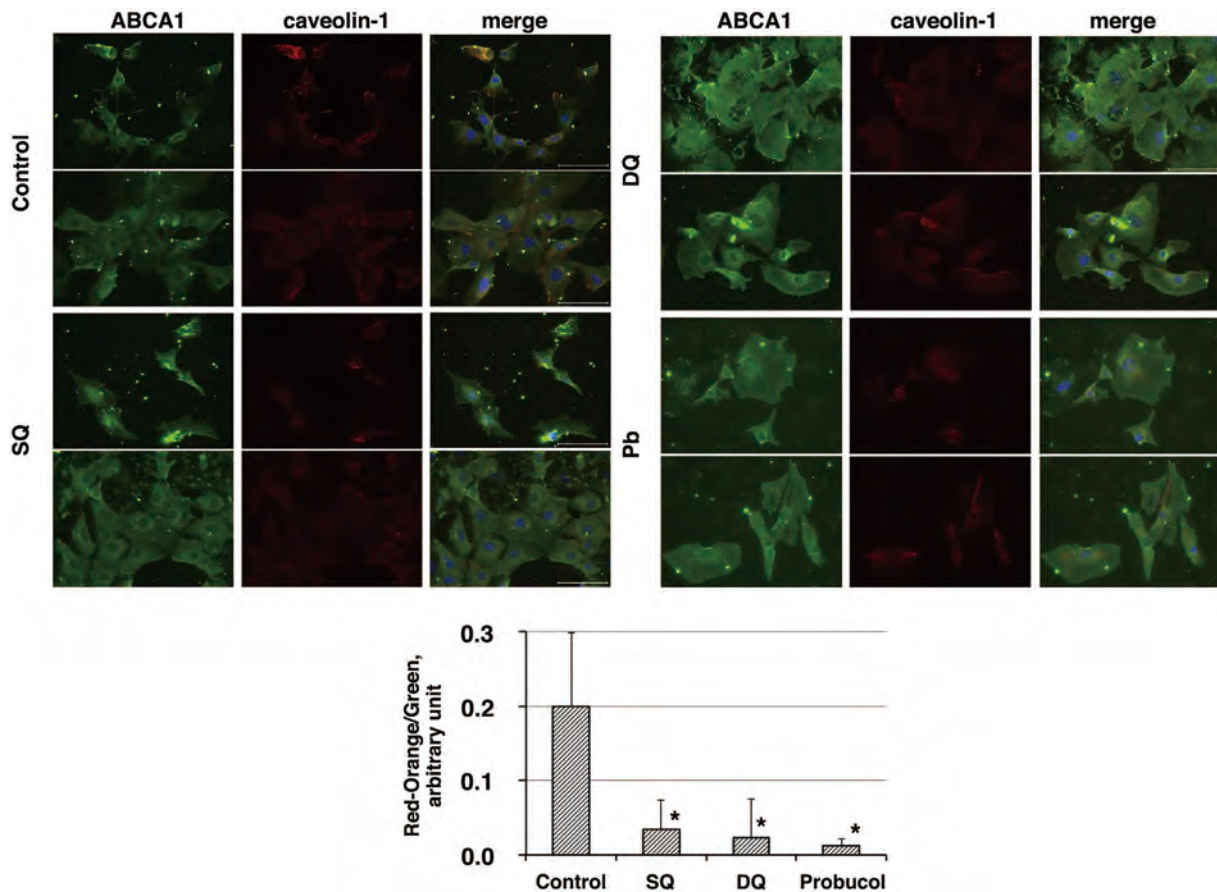


**Fig. 5. Fluorescent staining of ABCA1 and caveolin-1 in MEF prepared from wild-type mice.** ABCA1 and caveolin-1 were immuno-stained with fluorescein isothiocyanate (FITC) and Texas Red (TR), for green and red emission colors, respectively, and examined in a KEYENCE BZ90000 immunofluorescence microscope (KEYENCE). ABCA1 was visualized in green (ABCA1) and caveolin-1 in red (caveolin-1), so that co-localization of the two proteins appeared in orange when the two staining images were merged (merge). Cells were pre-treated with probucol (Pb), SQ and DQ. The graph represents the values of [area x photo-intensity] of the orange/red region in the merged images, analyzed by Photoshop software, relatively to the background green (n = 7 fields, each including average 12 cells), as \*  $p < 0.01$  versus control.

perimeter lines indicated in the photos is shown in the graphs in the middle column. The graphs in the right column show the plot of green against red intensity of each pixel to indicate the extent of synchronization of the two colors. Correlation coefficient, an indicator of the co-localization, showed decrease of the co-localization of ABCA1 and caveolin-1 by SQ, DQ and probucol. The imaging experiments thus strongly supported the findings in the biochemical experiments reported above.

#### 4. Discussion

We have demonstrated that 1) ABCA1 protein increases in caveolin-1 deficient cells, 2) this increase is not due to an increase in the ABCA1 gene transcription but a decrease in internalization and degradation of ABCA1 protein, 3) the retarded rates of ABCA1 internalization and degradation are recovered by transfection and expression of caveolin-1, 4) ABCA1 and caveolin-1 are co-precipitated by the alternate protein antibody and shown to be co-localized in immunostaining images, 5) the caveolin-1/ABCA1 interaction is disrupted by the oxidative products of probucol which thus retard ABCA1 internalization/degradation. We conclude that caveolin-1 interacts with ABCA1 to enhance the internalization of the complex and degradation of ABCA1. Deficiency of caveolin-1 or disruption of the caveolin-1/ABCA1 interaction results in an increase in surface ABCA1 protein levels.

Helical apolipoproteins such as apoA-I interact with cells to

generate HDL in the form of nascent discoid particle primarily with membrane phospholipids and secondarily cholesterol: this only occurs in the presence of ABCA1 [22,24]. This reaction is an essential part of cholesterol homeostasis in the cells and in the whole body [45,46], and is almost the exclusive source of plasma HDL [47]. Accordingly, expression of ABCA1 is the major rate-limiting factor determining plasma HDL concentration [48].

Transcription of the ABCA1 gene is upregulated by sensing increased cell cholesterol levels, as a mean of maintaining intracellular cholesterol homeostasis [49]. However, expression of the ABCA1 gene is further fine-tuned, such as down-regulation by cholesterol in the hepatocytes [50,51] probably to prevent cholesterol recovered by HDL from peripheral cells to hepatocytes from being rereleased into blood and to convert it to bile acids for excretion. ABCA1 is also regulated positively by other transcriptional factors [52–54] and negatively by activator protein A2 [55–57].

ABCA1 activity is also regulated by specific protein degradation, by calpain [11,58], the ubiquitin proteasome system [59], and eventually by the lysosomal system [60], which are associated with endocytotic internalization of the protein [13]. Such post-translational regulation of ABCA1 activity can also be a pharmacological target for prevention or treating atherosclerotic vascular diseases. We demonstrated that the hypolipidemic drug, probucol, inhibits the HDL biogenesis activity of ABCA1, but also interferes with ABCA1 degradation [17] and that oxidative products of

probuco, SQ and DQ, inhibit ABCA1 degradation without interfering with ABCA1 activity for HDL biogenesis [18]. SQ and DQ in fact raise HDL, enhance cholesterol transport from peripheral cells to feces and prevent atherogenesis in experimental animals [18,19].

Caveolin-1 is one potential key co-player in cell cholesterol release and atherogenesis. However, previous *in vitro* data were somewhat controversial. Caveolin-1 expression positively correlated with cell cholesterol release [32,33], and overexpression of caveolin-1 may increase plasma HDL [31]. We also showed that suppression of caveolin-1 expression decreased cholesterol content in the HDL generated by ABCA1/apoA-I pathway [27] and that caveolin-1 is specifically involved in intracellular trafficking of cholesterol for the ABCA1/apoA-I-mediated HDL biogenesis in rat astrocytes [61,62]. Yang and her colleagues demonstrated the interaction between caveolin-1 and ABCA1 in rat aortic endothelial cells [34–36,63,64]. However, “HDL-mediated” cell cholesterol release, rather than cholesterol release by apoA-I, was shown to be associated with this interaction, which is more consistent with the view that caveolin-1 is associated with ABCG1 activity [65]. On the other hand, caveolin-1-deficient mice showed the increase of plasma HDL cholesterol levels [32,37,38,66] and nitrogen oxide synthase activity [67–70] as well as resistance to atherogenesis [37,39]. ABCA1 protein expression was seemingly suppressed by overexpression of caveolin-1 in hepatocytes, in spite of the authors' claim that it was unchanged [33]. Thus, the reported data and their interpretation on association of ABCA1 with caveolin-1 are still controversial, in terms of the physical interaction and functional regulation. We therefore intended to investigate a role of caveolin-1 in posttranslational regulation of the ABCA1 expression for HDL biogenesis.

The data reported here are consistent with the findings in caveolin-1-deficient animal models showing increased HDL and reduced atherosclerosis [30,32,37–39], as well as our previous data showing inhibition of ABCA1 degradation by SQ and DQ [18,19]. The findings also relate to our recent observation that ABCA1 may disrupt raft conformation to destabilize the membrane and make lipid molecules more available for removal [44], while caveolin-1 may protect raft integrity by enhancing degradation of ABCA1. The findings here also increase understanding of the mixed effects of the lipid-lowering drug probuconol, including regression of xanthomas despite severe HDL reduction. We reported that probuconol inhibits ABCA1 activity for HDL biogenesis [8,9,17] despite retarding ABCA1 degradation [17]. We also found that the oxidative metabolites of probuconol only retard the degradation of ABCA1, without inhibiting its activity [18,19]. The data here provide mechanistic insight for these effects. Disruption of the ABCA1/caveolin-1 interaction by compounds such as SQ and DQ is thus a good candidate for increasing HDL biogenesis in peripheral cells and prevention of atherosclerotic vascular diseases. Further investigation is required to elucidate the roles of caveolin-1 in regulation of other membrane proteins especially other ABC transporters and the organ-specific relevance of this reaction.

#### Conflict of interest

The authors declared they do not have anything to disclose regarding conflict of interest with respect to this manuscript.

#### Financial support

This work was supported by the MEXT-Supported Program for Strategic Founding of Research in Private Universities (S1201007) and by Grants-in-aid from MEXT Japan (24614018, 26461370, 15H02903).

#### Author contributions

Rui Lu initiated and conducted the project doing most of the experiments, Tomoe Tsuboi was responsible for performing imaging experiments, Kuniko Okumura-Noji was supportive for biochemical experiments, Noriyuki Iwamoto provided a part of the experimental data and Shinji Yokoyama supervised the project.

#### Acknowledgements

The authors are grateful to Dr. Giorgio Cavigliolo, Children's Hospital of Oakland Research Institute, for his helpful critical reading the manuscript and for many valuable comments and suggestions.

#### Appendix A. Supplementary data

Supplementary data related to this article can be found at <http://dx.doi.org/10.1016/j.atherosclerosis.2016.08.025>.

#### References

- [1] H. Hara, S. Yokoyama, Interaction of free apolipoproteins with macrophages. Formation of high density lipoprotein-like lipoproteins and reduction of cellular cholesterol, *J. Biol. Chem.* 266 (1991) 3080–3086.
- [2] J.B. Karlin, W.J. Johnson, C.R. Benedict, et al., Cholesterol flux between cells and high density lipoprotein. Lack of relationship to specific binding of the lipoprotein to the cell surface, *J. Biol. Chem.* 262 (1987) 12557–12564.
- [3] M. Bodzioch, E. Orso, J. Klucken, et al., The gene encoding ATP-binding cassette transporter 1 is mutated in Tangier disease, *Nat. Genet.* 22 (1999) 347–351.
- [4] A. Brooks-Wilson, M. Marcil, S.M. Clee, et al., Mutations in ABC1 in Tangier disease and familial high-density lipoprotein deficiency, *Nat. Genet.* 22 (1999) 336–345.
- [5] S. Rust, M. Rosier, H. Funke, et al., Tangier disease is caused by mutations in the gene encoding ATP-binding cassette transporter 1, *Nat. Genet.* 22 (1999) 352–355.
- [6] N. Wang, D. Lan, W. Chen, et al., ATP-binding cassette transporters G1 and G4 mediate cellular cholesterol efflux to high-density lipoproteins, *Proc. Natl. Acad. Sci. U. S. A.* 101 (2004) 9774–9779.
- [7] H. Czarnecka, S. Yokoyama, Regulation of cellular cholesterol efflux by lecithin:cholesterol acyltransferase reaction through nonspecific lipid exchange, *J. Biol. Chem.* 271 (1996) 2023–2028.
- [8] M. Tsujita, S. Yokoyama, Selective inhibition of free apolipoprotein-mediated cellular lipid efflux by probuconol, *Biochemistry* 35 (1996) 13011–13020.
- [9] M. Tsujita, S. Tomimoto, K. Okumura-Noji, et al., Apolipoprotein-mediated cellular cholesterol/phospholipid efflux and plasma high density lipoprotein level in mice, *Biochim. Biophys. Acta* 1485 (2000) 199–213.
- [10] J. McNeish, R.J. Aiello, D. Guyot, et al., High density lipoprotein deficiency and foam cell accumulation in mice with targeted disruption of ATP-binding cassette transporter-1, *Proc. Natl. Acad. Sci. U. S. A.* 97 (2000) 4245–4250.
- [11] R. Arakawa, S. Yokoyama, Helical apolipoproteins stabilize ATP-binding cassette transporter A1 by protecting it from thiol protease-mediated degradation, *J. Biol. Chem.* 277 (2002) 22426–22429.
- [12] R. Arakawa, M. Hayashi, A.T. Remaley, et al., Phosphorylation and stabilization of ATP binding cassette transporter A1 by synthetic amphiphilic helical peptides, *J. Biol. Chem.* 279 (2004) 6217–6220.
- [13] R. Lu, R. Arakawa, C. Ito-Osumi, et al., ApoA-I facilitates ABCA1 recycle/accumulation to cell surface by inhibiting its intracellular degradation and increases HDL generation, *Arterioscler. Thromb. Vasc. Biol.* 28 (2008) 1820–1824.
- [14] L.O. Martinez, B. Agerholm-Larsen, N. Wang, et al., Phosphorylation of a pest sequence in ABCA1 promotes calpain degradation and is reversed by ApoA-I, *J. Biol. Chem.* 278 (2003) 37368–37374.
- [15] N. Wang, W. Chen, P. Linsel-Nitschke, et al., A PEST sequence in ABCA1 regulates degradation by calpain protease and stabilization of ABCA1 by apoA-I, *J. Clin. Investig.* 111 (2003) 99–107.
- [16] M. Tsujita, C.A. Wu, S. Abe-Dohmae, et al., On the hepatic mechanism of HDL assembly by the ABCA1/apoA-I pathway, *J. Lipid Res.* 46 (2005) 154–162.
- [17] C.A. Wu, M. Tsujita, M. Hayashi, et al., Probuconol inactivates ABCA1 in the plasma membrane with respect to its mediation of apolipoprotein binding and high density lipoprotein assembly and to its proteolytic degradation, *J. Biol. Chem.* 279 (2004) 30168–30174.
- [18] R. Arakawa, M. Tsujita, N. Iwamoto, et al., Pharmacological inhibition of ABCA1 degradation increases HDL biogenesis and exhibits antiatherogenesis, *J. Lipid Res.* 50 (2009) 2299–2305.
- [19] E. Yakushiji, M. Ayaori, T. Nishida, et al., Probuconol oxidized products, spiroquinone and diphenoquinone, promote reverse cholesterol transport in mice, *Arter. Thromb. Vasc. Biol.* 36 (2016) 591–597.

- [20] R.L. Hamilton, M.C. Williams, C.J. Fielding, et al., Discoidal bilayer structure of nascent high density lipoproteins from perfused rat liver, *J. Clin. Investig.* 58 (1976) 667–680.
- [21] H.F. Hoff, J.D. Morrisett, A.M. Gotto Jr., Interaction of phosphatidylcholine and apolipoprotein-alanine: electron microscopic studies, *Biochim. Biophys. Acta* 296 (1973) 653–660.
- [22] M. Hayashi, S. Abe-Dohmae, M. Okazaki, et al., Heterogeneity of high density lipoprotein generated by ABCA1 and ABCA7, *J. Lipid Res.* 46 (2005) 1703–1711.
- [23] M. Fukuda, M. Nakano, M. Miyazaki, et al., Thermodynamic and kinetic stability of discoidal high-density lipoprotein formation from phosphatidylcholine/apolipoprotein A-I mixture, *J. Phys. Chem. B* 114 (2010) 8228–8234.
- [24] Y. Yamauchi, S. Abe-Dohmae, S. Yokoyama, et al., Differential regulation of apolipoprotein A-I/ATP binding cassette transporter A1-mediated cholesterol and phospholipid release, *Biochim. Biophys. Acta* 1585 (2002) 1–10.
- [25] S. Abe-Dohmae, Y. Ikeda, M. Matsuo, et al., Human ABCA7 supports apolipoprotein-mediated release of cellular cholesterol and phospholipid to generate high density lipoprotein, *J. Biol. Chem.* 279 (2004) 604–611.
- [26] Y. Yamauchi, C.C. Chang, M. Hayashi, et al., Intracellular cholesterol mobilization involved in the ABCA1/apolipoprotein-mediated assembly of high density lipoprotein in fibroblasts, *J. Lipid Res.* 45 (2004) 1943–1951.
- [27] R. Arakawa, S. Abe-Dohmae, M. Asai, et al., Involvement of caveolin-1 in cholesterol enrichment of high density lipoprotein during its assembly by apolipoprotein and THP-1 cells, *J. Lipid Res.* 41 (2000) 1952–1962.
- [28] H.N. Fridolfsson, D.M. Roth, P.A. Insel, et al., Regulation of intracellular signaling and function by caveolin, *FASEB J.* 28 (2014) 3823–3831.
- [29] P.G. Frank, M.W. Cheung, S. Pavlides, et al., Caveolin-1 and regulation of cellular cholesterol homeostasis, *Am. J. Physiol. Heart Circ. Physiol.* 291 (2006) H677–H686.
- [30] P.G. Frank, S. Pavlides, M.W. Cheung, et al., Role of caveolin-1 in the regulation of lipoprotein metabolism, *Am. J. Physiol. Cell Physiol.* 295 (2008) C242–C248.
- [31] P.G. Frank, A. Pedraza, D.E. Cohen, et al., Adenovirus-mediated expression of caveolin-1 in mouse liver increases plasma high-density lipoprotein levels, *Biochemistry* 40 (2001) 10892–10900.
- [32] P.G. Frank, F. Galbiati, D. Volonte, et al., Influence of caveolin-1 on cellular cholesterol efflux mediated by high-density lipoproteins, *Am. J. Physiol. Cell Physiol.* 280 (2001) C1204–C1214.
- [33] Y. Fu, A. Hoang, G. Escher, et al., Expression of caveolin-1 enhances cholesterol efflux in hepatic cells, *J. Biol. Chem.* 279 (2004) 14140–14146.
- [34] W.T. Chao, S.H. Tsai, Y.C. Lin, et al., Cellular localization and interaction of ABCA1 and caveolin-1 in aortic endothelial cells after HDL incubation, *Biochem. Biophys. Res. Commun.* 332 (2005) 743–749.
- [35] Y.C. Lin, C.H. Lin, C.Y. Kuo, et al., ABCA1 modulates the oligomerization and Golgi exit of caveolin-1 during HDL-mediated cholesterol efflux in aortic endothelial cells, *Biochem. Biophys. Res. Commun.* 382 (2009) 189–195.
- [36] C.Y. Kuo, Y.C. Lin, J.J. Yang, et al., Interaction abolishment between mutant caveolin-1(Delta62-100) and ABCA1 reduces HDL-mediated cellular cholesterol efflux, *Biochem. Biophys. Res. Commun.* 414 (2011) 337–343.
- [37] P.G. Frank, H. Lee, D.S. Park, et al., Genetic ablation of caveolin-1 confers protection against atherosclerosis, *Arterioscler. Thromb. Vasc. Biol.* 24 (2004) 98–105.
- [38] S. Heimerl, G. Liebisch, S. Le Lay, et al., Caveolin-1 deficiency alters plasma lipid and lipoprotein profiles in mice, *Biochem. Biophys. Res. Commun.* 367 (2008) 826–833.
- [39] D. Engel, L. Beckers, E. Wijnands, et al., Caveolin-1 deficiency decreases atherosclerosis by hampering leukocyte influx into the arterial wall and generating a regulatory T-cell response, *FASEB J.* 25 (2011) 3838–3848.
- [40] A.J. Mendez, G. Lin, D.P. Wade, et al., Membrane lipid domains distinct from cholesterol/sphingomyelin-rich rafts are involved in the ABCA1-mediated lipid secretory pathway, *J. Biol. Chem.* 276 (2001) 3158–3166.
- [41] H.H. Hassan, M. Denis, D.Y. Lee, et al., Identification of an ABCA1-dependent phospholipid-rich plasma membrane apolipoprotein A-I binding site for nascent HDL formation: implications for current models of HDL biogenesis, *J. Lipid Res.* 48 (2007) 2428–2442.
- [42] O. Sano, S. Ito, R. Kato, et al., ABCA1, ABCG1, and ABCG4 are distributed to distinct membrane meso-domains and disturb detergent-resistant domains on the plasma membrane, *PLoS One* 9 (2014) e109886.
- [43] Y.D. Landry, M. Denis, S. Nandi, et al., ATP-binding cassette transporter A1 expression disrupts raft membrane microdomains through its ATPase-related functions, *J. Biol. Chem.* 281 (2006) 36091–36101.
- [44] Y. Yamauchi, N. Iwamoto, M.A. Rogers, et al., Deficiency in the lipid exporter ABCA1 impairs retrograde sterol movement and disrupts sterol sensing at the endoplasmic reticulum, *J. Biol. Chem.* 290 (2015) 23464–23477.
- [45] S. Yokoyama, ABCA1 and biogenesis of HDL, *J. Atheroscler. Thromb.* 13 (2006) 1–15.
- [46] S. Yokoyama, Assembly of high-density lipoprotein, *Arterioscler. Thromb. Vasc. Biol.* 26 (2006) 20–27.
- [47] G.A. Francis, R.H. Knopp, J.F. Oram, Defective removal of cellular cholesterol and phospholipids by apolipoprotein A-I in Tangier Disease, *J. Clin. Investig.* 96 (1995) 78–87.
- [48] A.D. Attie, J.P. Kastelein, M.R. Hayden, Pivotal role of ABCA1 in reverse cholesterol transport influencing HDL levels and susceptibility to atherosclerosis, *J. Lipid Res.* 42 (2001) 1717–1726.
- [49] P. Costet, Y. Luo, N. Wang, et al., Sterol-dependent transactivation of the ABC1 promoter by the liver X receptor/retinoid X receptor, *J. Biol. Chem.* 275 (2000) 28240–28245.
- [50] N. Tamehiro, Y. Shigemoto-Mogami, T. Takeya, et al., Sterol regulatory element-binding protein-2- and liver X receptor-driven dual promoter regulation of hepatic ABC transporter A1 gene expression: mechanism underlying the unique response to cellular cholesterol status, *J. Biol. Chem.* 282 (2007) 21090–21099.
- [51] N. Ohoka, K. Okuhira, H. Cui, et al., HNF4alpha increases liver-specific human ATP-binding cassette transporter A1 expression and cholesterol efflux to apolipoprotein A-I in response to cholesterol depletion, *Arterioscler. Thromb. Vasc. Biol.* 32 (2012) 1005–1014.
- [52] R. Arakawa, N. Tamehiro, T. Nishimaki-Mogami, et al., Fenofibrate acid, an active form of fenofibrate, increases apolipoprotein A-I-mediated high-density lipoprotein biogenesis by enhancing transcription of ATP-binding cassette transporter A1 gene in a liver X receptor-dependent manner, *Arterioscler. Thromb. Vasc. Biol.* 25 (2005) 1193–1197.
- [53] M.A. Hossain, M. Tsujita, F.J. Gonzalez, et al., Effects of fibrates drugs on expression of ABCA1 and HDL biogenesis in hepatocytes, *J. Cardiovasc. Pharmacol.* 51 (2008) 258–266.
- [54] M. Ogata, M. Tsujita, M.A. Hossain, et al., On the mechanism for PPAR agonists to enhance ABCA1 gene expression, *Atherosclerosis* 205 (2009) 413–419.
- [55] N. Iwamoto, S. Abe-Dohmae, M. Ayaori, et al., ATP-binding cassette transporter A1 gene transcription is downregulated by activator protein 2alpha. Doxazosin inhibits activator protein 2alpha and increases high-density lipoprotein biogenesis independent of alpha1-adrenoceptor blockade, *Circ. Res.* 101 (2007) 156–165.
- [56] N. Iwamoto, S. Abe-Dohmae, R. Lu, et al., Involvement of protein kinase D in phosphorylation and increase of DNA binding of activator protein 2 alpha to downregulate ATP-binding cassette transporter A1, *Arterioscler. Thromb. Vasc. Biol.* 28 (2008) 2282–2287.
- [57] N. Iwamoto, S. Yokoyama, Protein kinase D regulates the adiponectin gene expression through phosphorylation of AP-2: a common pathway to the ABCA1 gene regulation, *Atherosclerosis* 216 (2011) 90–96.
- [58] S. Yokoyama, R. Arakawa, C.A. Wu, et al., Calpain-mediated ABCA1 degradation: post-translational regulation of ABCA1 for HDL biogenesis, *Biochim. Biophys. Acta* 1821 (2012) 547–551.
- [59] M. Ogura, M. Ayaori, Y. Terao, et al., Proteasomal inhibition promotes ATP-binding cassette transporter A1 (ABCA1) and ABCG1 expression and cholesterol efflux from macrophages in vitro and in vivo, *Arterioscler. Thromb. Vasc. Biol.* 31 (2011) 1980–1987.
- [60] T. Mizuno, H. Hayashi, S. Naoi, et al., Ubiquitination is associated with lysosomal degradation of cell surface-resident ATP-binding cassette transporter A1 (ABCA1) through the endosomal sorting complex required for transport (ESCRT) pathway, *Hepatology* 54 (2011) 631–643.
- [61] J. Ito, Y. Nagayasu, K. Kato, et al., Apolipoprotein A-I induces translocation of cholesterol, phospholipid, and caveolin-1 to cytosol in rat astrocytes, *J. Biol. Chem.* 277 (2002) 7929–7935.
- [62] J. Ito, A. Kheirollah, Y. Nagayasu, et al., Apolipoprotein A-I increases association of cytosolic cholesterol and caveolin-1 with microtubule cytoskeletons in rat astrocytes, *J. Neurochem.* 97 (2006) 1034–1043.
- [63] W.T. Chao, S.S. Fan, J.K. Chen, et al., Visualizing caveolin-1 and HDL in cholesterol-loaded aortic endothelial cells, *J. Lipid Res.* 44 (2003) 1094–1099.
- [64] Y.C. Lin, C. Ma, W.C. Hsu, et al., Molecular interaction between caveolin-1 and ABCA1 on high-density lipoprotein-mediated cholesterol efflux in aortic endothelial cells, *Cardiovasc Res.* 75 (2007) 575–583.
- [65] H.M. Gu, F.Q. Wang, D.W. Zhang, Caveolin-1 interacts with ATP binding cassette transporter G1 (ABCG1) and regulates ABCG1-mediated cholesterol efflux, *Biochim. Biophys. Acta* 1841 (2014) 847–858.
- [66] B. Razani, J.A. Engelman, X.B. Wang, et al., Caveolin-1 null mice are viable but show evidence of hyperproliferative and vascular abnormalities, *J. Biol. Chem.* 276 (2001) 38121–38138.
- [67] E. Felley-Bosco, F.C. Bender, F. Courjault-Gautier, et al., Caveolin-1 downregulates inducible nitric oxide synthase via the proteasome pathway in human colon carcinoma cells, *Proc. Natl. Acad. Sci. U. S. A.* 97 (2000) 14334–14339.
- [68] N. Terasaka, M. Westerterp, J. Koetsveld, et al., ATP-binding cassette transporter G1 and high-density lipoprotein promote endothelial NO synthesis through a decrease in the interaction of caveolin-1 and endothelial NO synthase, *Arterioscler. Thromb. Vasc. Biol.* 30 (2010) 2219–2225.
- [69] I. Lobysheva, G. Rath, B. Sekkali, et al., Moderate caveolin-1 downregulation prevents NADPH oxidase-dependent endothelial nitric oxide synthase uncoupling by angiotensin II in endothelial cells, *Arterioscler. Thromb. Vasc. Biol.* 31 (2011) 2098–2105.
- [70] A.E. Trane, D. Pavlov, A. Sharma, et al., Deciphering the binding of caveolin-1 to client protein endothelial nitric-oxide synthase (eNOS): scaffolding subdomain identification, interaction modeling, and biological significance, *J. Biol. Chem.* 289 (2014) 13273–13283.

### Supplementary Materials for

## Caveolin-1 Facilitates Internalization and Degradation of ABCA1 and Probucol Oxidative Products Interfere with this Reaction to Increase HDL Biogenesis

Rui Lu, Tomoe Tsuboi, Kumiko Okumura-Noji, Noriyuki Iwamoto\*\*, and Shinji Yokoyama\*

Nutritional Health Science Research Center and College of Bioscience and Biotechnology, Chubu University, Kasugai 487-8501, Japan

### Methods

#### 1. *Proteins and chemicals*

ApoA-I was isolated from human plasma HDL as described previously [1]. It was used at 10 µg/mL in the medium. Probucol was purchased from Tokyo Chemical Industry, and SQ and DQ were synthesized and isolated as previously described [2]. These compounds were added to the cell culture medium as 0.1, 50 and 0.5 nM, respectively, as previously described [2].

#### 2. *Cell culture*

Mouse embryonic fibroblasts (MEFs) were prepared from the caveolin-1-deficient mouse (STOCK *Cav1<sup>tm1MlsJ</sup>*) [3] and its control wild type control mouse (B6129SF2/J) both obtained from The Jackson Laboratory, according to the procedure described elsewhere [4], by Toyoshi Fujimoto, Anatomy and Molecular Cell Biology, Nagoya University Graduate School of Medicine, Nagoya 466-8550, Japan and kindly provided for the experiments. MEFs were also prepared from the ABCA1-deficient mouse and its wild type control as previously described [5]. Cells were incubated in the 1 : 1 mixture of Dulbecco's modified Eagle medium and Ham F12 medium containing 10 % fetal bovine serum at 37°C in 5 % CO<sub>2</sub>.

#### 3. *Immunological analyses of cell proteins*

The cell pellets were harvested by sonication in the 50 mM Tris-hydrochloride buffer (pH 7.5) containing 150 mM NaCl, 1 % Triton X-100, 1 % sodium dodecylcholate, 10

mM EDTA, 1 % SDS and protease inhibitor cocktail (Sigma). Insoluble debris was removed by centrifugation at 12,000 x g for 10 minutes at 4° C and the supernatant was collected as cell lysate. Protein concentration was measured using a bicinchoninic acid protein assay system (Pierce). For immunoblotting analysis, proteins were separated by polyacrylamide electrophoresis in SDS and transferred to a polyvinylidene fluoride membrane (Millipore). Blots were probed with rabbit antihuman caveolin-1 antibody (1 : 1000, v/v) (Cell signal) or rat antihuman ABCA1 antibody[6] (1 : 50, v/v) followed by goat anti-rat IgG (1 : 2500, v/v) or goat anti-rabbit IgG (1 : 1000, v/v) conjugated with horse radish peroxidase (R & D Systems). After washing with phosphate-buffered saline (PBS) containing 0.5 % Tween 20, peroxidase activity was visualized by using enhanced chemiluminescence (PerkinElmer Life Science). Densitometric quantitation of the immunoblot bands by using Photoshop software yielded linear relationship to the dose for the range of the experiments (Supplementary Figure D). ABCA1 in some occasions appeared as double bands for unknown reason, perhaps due to potential molecular heterogeneity resulting in slightly different electrophoretic mobility. For immunoprecipitation, 500 µg cell protein was rotated with the anti-ABCA1 antibody (1 : 10, v/v) or anticaveolin-1 antibody (1 : 200) overnight at 4° C and incubated with agarose G beads. Proteins bound to the beads were eluted by the SDS sample buffer and analyzed by immunoblotting using specific antibodies as described above.

#### 4. *Metabolic Analysis of ABCA1 and caveolin-1*

To examine degradation rate of ABCA1 or caveolin-1, the cells were incubated in RPMI1640 containing 0.2 % bovine serum albumin 140 mM cycloheximide (Sigma) for the indicated periods of time, and the proteins were analyzed by immunoblotting as described above[7]. To trace internalization of the surface proteins, cell surface proteins were labeled with sulfosuccinimidyl 2-(biotinamido)-ethyl-1, 3-dithiopropionate (sulfo-SS-biotin) (Pierce), 0.8 mM, for 1 hour at 4° C as previously reported[7]. After quenching the reaction, cells were washed and lysed, and the biotinylated membrane proteins were isolated by coprecipitation with streptavidin-agarose beads (Sigma) at 4° C for 1 hour. Proteins bound to the beads were eluted with the SDS sample buffer, and analyzed in immunoblotting by using a specific antibody against ABCA1 or caveolin-1. After certain time periods of incubation, biotinylation remaining in the cell surface proteins was cleaved by incubating the cells with 50 mmol/L reduced glutathione

(Sigma) in pH 7.8 three times for 20 minutes at 4°C, and the uncleaved protein was regarded as internalized portion, quantified as percentage to the initial surface protein indicated as the biotinylated protein at zero-time incubation [7].

5. *Construction of recombinant plasmid for caveolin-1 and its transient transfection*

The cDNA of the full length caveolin-1 domain was generated and amplified using the primer sets of 5'-TCT AGA ATG TCT GGG GGC AAA TAC G-3' and 5'-GGT ACC TAT TTC TTT CTG CAA G-3'. The primer set anchored at the EcoRI and XhoI restriction sites was used to construct the recombinant expression plasmid. The gene fragment was cloned into the EcoRI- and XhoI-digested pCDNA 3.1-c-myc-His-tagged plasmid (Invitrogen), which yields the product with additional 6 histidine of molecular weight 870 Dal. The sequence and orientations of the inserts were confirmed by auto-sequencing. The cells were grown in 6 cm plastic dishes until they reached 70 – 80% confluence before inducing the expression of full length constructs by transfection with Lipofectamine™ 2000 (Invitrogen, CA, USA) according to the manufacturer's instructions.

6. *Real time polymerase chain reaction (PCR)*

Total RNA was isolated from MEFs with ISOGEN reagent (NIPONJIN) according to the manufacturer's instruction. The cDNA was prepared by using High-Capacity cDNA Reverse Transcription Kits (Applied Biosystems). Real time PCR was performed by using a SYBR Premix Ex Taq (Til RNaseH Plus) Kits (TaKaRa). The primers used were; mouse ABCA1 forward 5'-AAC AGT TTG TGG CCC TTT TG-3' and the reverse 5'-AGT TCC AGG CTG GGG TAC TT-3', and mouse b-actin forward 5'-GGA CTT CGA GCA AGA GAT GG-3', and the reverse 5'-AGC ACT GTG TTG GCG TAC AG-3'.

7. *Immunofluorescent staining of cells*

MEFs grown on a chamber slide were incubated with SQ, DQ and probucol overnight at 37°C. The cells were washed 2 times with cold PBS, fixed in 2 % paraformaldehyde at 4°C for 20 min and treated with 0.1 % Tween-20 for 5 min x 2 at room temperature. After fixation, the cells were blocked with PBS containing 1 % bovine serum albumin and 0.05 % Tween-20. After washing with PBS, the chamber slide cultures were

incubated with rabbit anti-human caveolin-1 antibody (1 : 400, Cell signal) or rat anti-human ABCA1 (1 : 30, v/v) for 48 h, washed 3 times with PBS, and incubated for 30 min with goat anti-rat IgG-fluorescein isothiocyanate (FITC) (1 : 100 SANTA CRUS) and goat anti-rabbit IgG-Texas Red (TR). (1:200 SANTA CRUS) to visualize each protein with green and red emission colors, respectively. After washing 3 times with PBS, the chamber slides were enclosed with Dapi- Fluoromount-G (SouthernBiotech) for examining in a KEYENCE BZ90000 immunofluorescence microscope (KEYENCE). BZ-II Measurement Module v1.01 BZ-H1M was used to obtain line profiles of RGB photointensity. Co-localization of ABCA1 and caveolin-1 was analyzed by quantitation of the imaging data using two different methods. The average photointensity of the areas of red/orange color to indicated co-localization of ABCA1 and caveolin-1 were calculated relatively to that as the background green area by using Photoshop software. Alternatively, the quantitative line profile for green and red color elements was analyzed by using BZ-II Measurement Module provided with KEYENCE BZ9000. The cells showing only minimum or not-apparent co-localization were chosen and indicated in the merged photos were analyzed. The intensity of red and green elements along with the perimeters of those cells was measured and the plot of green against red intensity of each pixel indicated the extent of synchronization of the two colors as a correlation coefficient, an indicator for the co-localization.

8. *Cell lipid release assay*

Cellular lipid release by apoA-I was measured as described elsewhere [6]. After incubation of the cells with apoA-I for the indicated time, concentration of cholesterol and choline-phospholipid in the medium were evaluated by enzymatic measurement.

9. *Other remarks*

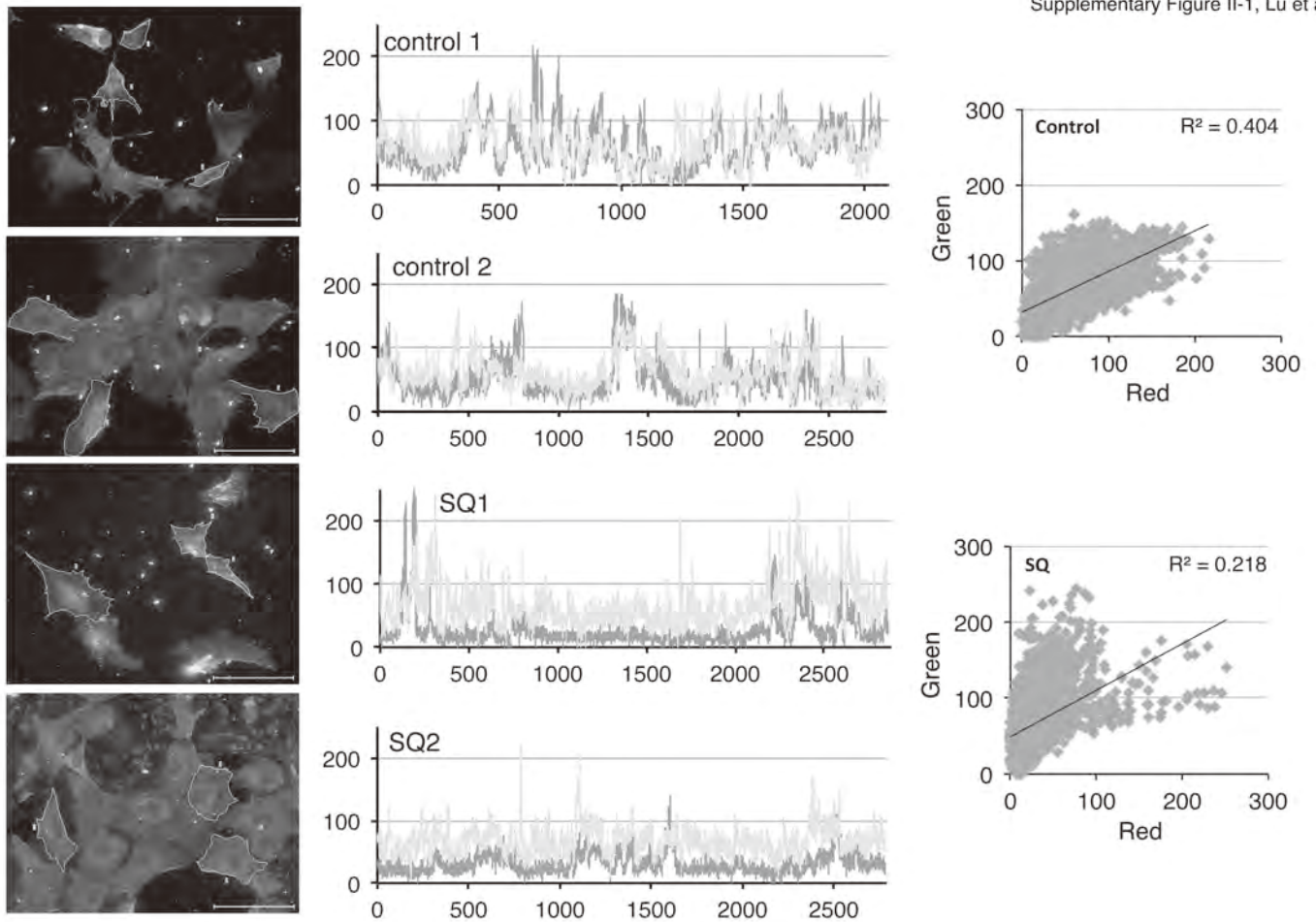
All the experiments for measurements and analysis were performed independently n times (at least three). Immuno-stained bands were quantified by densitometric measurement as described above. The data were analyzed statistically by either Student t test if n > 3 or non-parametric test if necessary.

## References

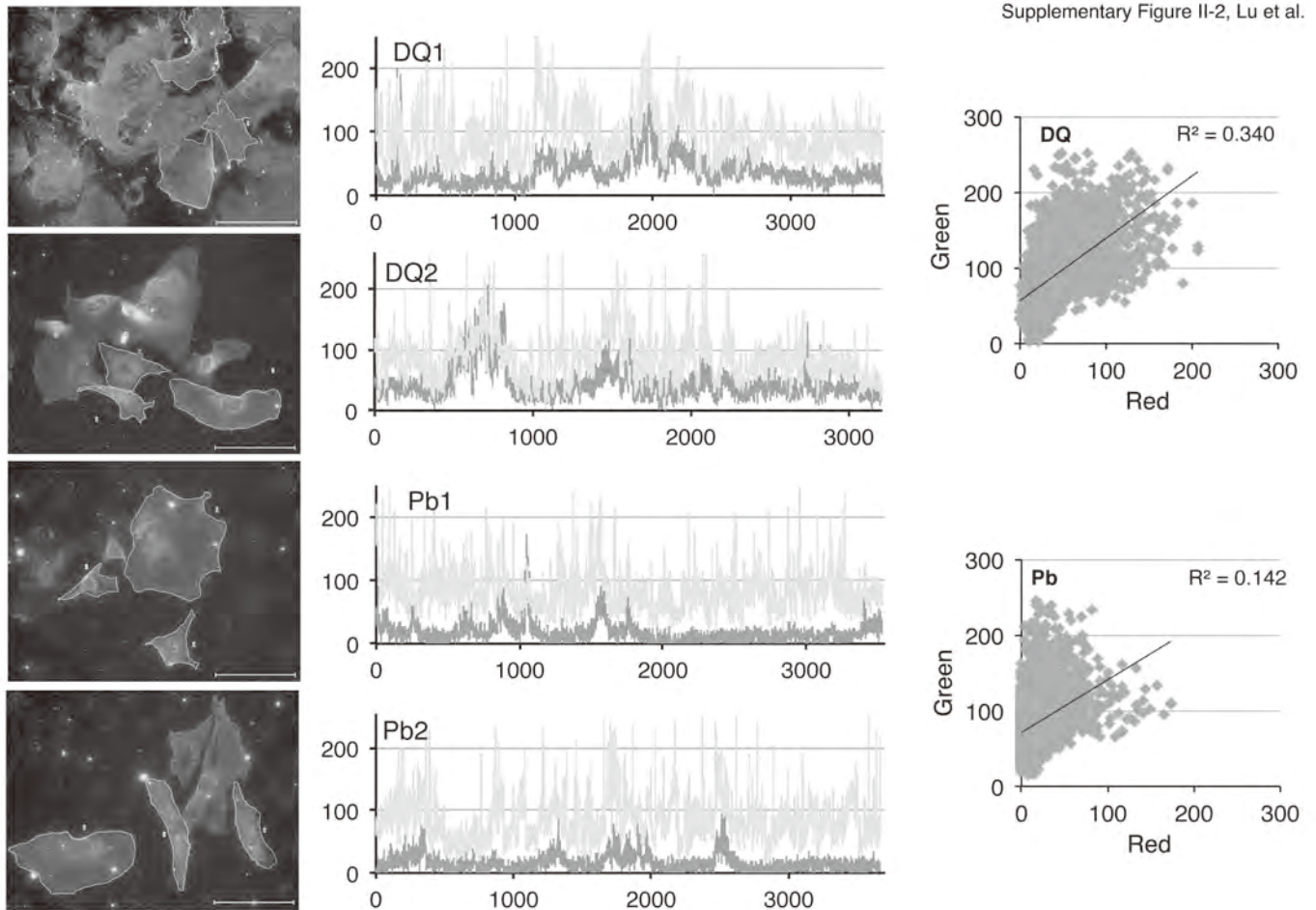
- [1] Yokoyama, S, Tajima, S and Yamamoto, A, The process of dissolving apolipoprotein A-I in an aqueous buffer, *J. Biochem.*, 1982;91:1267-1272.
- [2] Arakawa, R, Tsujita, M, Iwamoto, N, et al., Pharmacological inhibition of ABCA1 degradation increases HDL biogenesis and exhibits antiatherogenesis, *J Lipid Res*, 2009;50:2299-2305.
- [3] Razani, B, Engelman, JA, Wang, XB, et al., Caveolin-1 null mice are viable but show evidence of hyperproliferative and vascular abnormalities, *J Biol Chem*, 2001;276:38121-38138.
- [4] Xu, J, Preparation, culture, and immortalization of mouse embryonic fibroblasts, *Curr Protoc Mol Biol*, 2005;Chapter 28:Unit 28 21.
- [5] Hu, W, Abe-Dohmae, S, Tsujita, M, et al., Biogenesis of HDL by SAA is dependent on ABCA1 in the liver in vivo, *J. Lipid Res.*, 2008;49:386-393.
- [6] Abe-Dohmae, S, Ikeda, Y, Matsuo, M, et al., Human ABCA7 supports apolipoprotein-mediated release of cellular cholesterol and phospholipid to generate high density lipoprotein, *J. Biol. Chem.*, 2004;279:604-611.
- [7] Lu, R, Arakawa, R, Ito-Osumi, C, et al., ApoA-I facilitates ABCA1 recycle/accumulation to cell surface by inhibiting its intracellular degradation and increases HDL generation, *Arterioscler. Thromb. Vasc. Biol.*, 2008;28:1820-1824.



Supplementary Figure II-1, Lu et al.



Supplementary Figure II-2, Lu et al.



## Special Report

## Background to Discuss Guidelines for Control of Plasma HDL-Cholesterol in Japan\*

Shinji Yokoyama<sup>1</sup>, Shizuya Yamashita<sup>2</sup>, Shun Ishibashi<sup>3</sup>, Hirohito Sone<sup>4</sup>, Shinichi Oikawa<sup>5</sup>, Kohji Shirai<sup>6</sup>, Takao Ohta<sup>7</sup>, Hideaki Bujo<sup>8</sup>, Junji Kobayashi<sup>9</sup>, Hidenori Arai<sup>10</sup>, Mariko Harada-Shiba<sup>11</sup>, Masaaki Eto<sup>12</sup>, Toshio Hayashi<sup>13</sup>, Takanari Gotoda<sup>14</sup>, Hiroaki Suzuki<sup>15</sup> and Nobuhiro Yamada<sup>16</sup>

<sup>1</sup>Food and Nutritional Sciences, College of Bioscience and Biotechnology, Chubu University, Kasugai, Japan

<sup>2</sup>Department of Cardiovascular Medicine, Osaka University Graduate School of Medicine, Suita, Japan

<sup>3</sup>Division of Endocrinology and Metabolism, Diabetes Center, Department of Medicine, Jichi Medical University Graduate School of Medicine, Shimotsuke, Japan

<sup>4</sup>Department of Endocrinology and Metabolism, Graduate School of Comprehensive Human Sciences, University of Tsukuba, Tsukuba, Japan

<sup>5</sup>Division of Endocrinology and Metabolism, Department of Medicine, Nippon Medical School, Tokyo, Japan

<sup>6</sup>Internal Medicine, Sakura Hospital, School of Medicine, Toho University, Sakura, Japan

<sup>7</sup>Department of Child Health and Welfare (Pediatrics), Faculty of Medicine, University of the Ryukyus, Nishihara, Japan

<sup>8</sup>Department of Genome Research and Clinical Application, Chiba University Graduate School of Medicine, Chiba, Japan

<sup>9</sup>Department of Lipidology, Kanazawa University Graduate School of Medical Science, Kanazawa, Japan

<sup>10</sup>Department of Human Health Sciences, Kyoto University Graduate School of Medicine, Kyoto, Japan

<sup>11</sup>Department of Molecular Innovation in Lipidology, National Cerebral and Cardiovascular Center Research Institute, Osaka, Japan

<sup>12</sup>School of Pharmaceutical Sciences, Ohu University and Department of Medicine, Ohu University Hospital, Kohriyama, Japan

<sup>13</sup>Department of Geriatrics, Nagoya University Graduate School of Medicine, Nagoya, Japan

<sup>14</sup>Department of Clinical and Molecular Epidemiology, 22nd Century Medical and Research Center, University of Tokyo Hospital, Tokyo, Japan

<sup>15</sup>Department of Endocrinology and Metabolism, Graduate School of Comprehensive Human Sciences, University of Tsukuba, Tsukuba, Japan

<sup>16</sup>University of Tsukuba, Tsukuba, Japan

A decrease in high density lipoprotein-cholesterol (HDL-C) is a strong risk factor for atherosclerotic disorders in Japan, probably more important than an increase in low density lipoprotein-cholesterol (LDL-C). While there are rational grounds for the argument that elevation of HDL-C leads to decreased risk, there has as yet been no direct evidence of such an effect. If elevation of HDL-C decreases the risk, this effect is expected throughout the normal range of HDL-C or perhaps even higher than that. Simulation based on epidemiological data indicated that it may eventually reduce the incidence of ischemic heart disease by 60-70% in Japan. In the risk management guideline, "low" HDL-C is presently defined as 40 mg/dL or below. While there is no evidence that strongly urges a change in this definition, the results of epidemiological studies support "The higher the HDL-C level, the lower the risk," even in the "normal range". Elevation of the HDL-C level may reduce the risk, probably at least up to 70 mg/dL; however, there are no supportive data for this effect still being obtained over 80 mg/dL. Patients with homozygous CETP deficiency should be followed-up while controlling other risk factors, so as not to dismiss the possibility of a risk increase with an extremely elevated HDL-C level.

*J Atheroscler Thromb, 2012; 19:207-212.*

**Key words;** HDL, LDL, Guidelines, NNT, Prevention

\* Revised Edition (May 2, 2009) of the Report on the Meeting of the Research Group for the Management of Primary Hyperlipidemia (January 30, 2009)

Address for correspondence: Shinji Yokoyama, Food and Nutritional Sciences, College of Bioscience and Biotechnology, Chubu University, 1200 Matsumoto-cho, Kasugai, Japan  
E-mail: syokoyam@med.nagoya-cu.ac.jp  
Received: August 17, 2011  
Accepted for publication: September 29, 2011

### Clinical Relevance of HDL-C Management

Numbers of epidemiological studies have established that the risk of coronary artery disease increases as plasma HDL-C decreases, and decreases as it increases. In addition, many experimental approaches

have demonstrated that cholesterol is extracted by HDL particles in the culture medium from cultured cells, including macrophages overloaded with cholesterol.

From these two lines of evidence, HDL is believed to be a “preventive factor” against atherosclerosis. This view is strongly associated with the hypothesis that HDL plays a central role in the recovery of cholesterol molecules from tissues and organs, which cannot be catabolized in peripheral cells, and in their transport to the liver for conversion to bile acids. From the viewpoint of public health, many research results suggest that a decrease in HDL-C contributes more than an increase in LDL-C to the development of ischemic heart disease in Japan. In studies conducted at Nagoya City University, for example, narrowing of the coronary artery was more closely related to triglycerides (TG) and HDL-C than to total cholesterol (TC) or LDL-C<sup>1, 2)</sup>, and this tendency is commonly observed in many other reports. HDL-C is thus suggested to be a strong determinant of atherosclerosis in Japan and perhaps a more important risk factor than LDL-C from a public health point of view.

HDL is smaller (12 nm or less in diameter) than other lipoproteins, abundant in protein and does not contain much TG, so it has a greater hydrated density than other lipoproteins ( $d=1.063-1.21$ ). Similarly to other plasma lipoproteins, however, HDL functions to transport cholesterol among cells or organs using the flow of blood or extracellular fluid. Cholesterol, an essential molecule for the life of animals, requires a number of steps and plenty of energy for synthesis, and its dietary intake is not always guaranteed; therefore, the animal body has developed systems to use cholesterol sparingly as a precious material. As a result, little cholesterol is converted to energy in its catabolism, and, with the exception of a very small amount used for the production of steroid hormones, most cholesterol is transported to the liver for conversion to bile acids and is recycled and reused in the intestine before excretion. Its steroid backbone is not degraded in the metabolism in the animal body and finally broken down by microorganisms in the environment. Therefore, cholesterol molecules must be released from most somatic cells for metabolic homeostasis, and HDL receives these cholesterol molecules for their transport. Cholesterol is converted to cholesteryl acyl-ester (CE) as a fatty acyl chain and transferred from phosphatidylcholine to its hydroxyl group to form an ester bond, for packing cholesterol molecules into the core of HDL. CE is recovered by the liver directly from HDL by a selective uptake reaction, or as LDL particles after being transferred to apolipoprotein

B-containing lipoproteins by CE transfer protein (CETP). As a result of these activities, HDL is considered to exert a preventive effect against atherosclerosis as it interferes with the excessive accumulation of cholesterol in cells from LDL, etc., by extracting it.

No drug has been marketed yet to independently increase HDL-C; therefore, the question of whether increasing HDL-C is effective for preventing and treating atherosclerotic disorders has not been answered. However, researchers have recently directed more attention to HDL and, accordingly, more research results on HDL metabolism have recently accumulated. Much effort to develop drugs targeting HDL has been initiated. On the other hand, some existing drugs are known to increase plasma HDL-C. Drugs that reduce TG generally increase HDL-C, primarily because these drugs reverse low HDL-C induced by high TG through CETP<sup>3)</sup>. In addition, fibrates have been suggested to directly increase HDL production<sup>4)</sup>. Many clinical studies have also shown that statins elevate HDL-C as well as decreasing LDL-C. Concerning their mechanism, statins have recently been reported to increase HDL synthesis in the liver, unlike their effects in peripheral tissues<sup>5)</sup>. The mechanism of the increase in HDL through exercise and alcohol intake has not been sufficiently elucidated. As mentioned below, the question of whether HDL-C increase by inhibiting CETP prevents atherogenesis has been shelved because of the failure to develop a CETP-inhibiting drug, perhaps due to a business-oriented strategy<sup>6)</sup>.

### Position of HDL in Risk-Reducing Strategies

Large-scale clinical studies targeted to high LDL-C and high TG, major risk factors of atherosclerotic diseases, such as ischemic heart disease, have indicated that ischemic heart disease can be prevented by reducing LDL-C and TG and, particularly, that mortality due to the disease can be lowered by controlling the LDL-C level, with a consequent reduction in the total number of deaths in the high-risk group. In addition, based on stratified analysis of the results of many clinical trials, the conclusion has been reached that an increase in HDL-C contributes to the prevention of diseases as a “statistically independent factor”. In consideration of the above-stated marked epidemiological contribution of HDL-C as a “negative risk factor” and the significant “indirect evidence” of an increase in HDL-C in the prevention of atherogenesis, the argument that a standard should be set for the control of HDL-C appears to be well grounded. However, it is also true that a consensus concerning

HDL-C management, similar to that in evidence-based quantitative guidelines for the control of LDL-C and the management and treatment of high TG, is difficult to reach at present, when no therapeutic technique specifically targeted to increase HDL-C has reached a practical level and there is no direct evidence concerning the prevention and treatment of atherosclerotic disorders using such a technique. Thus, any therapeutic guideline regarding HDL-C is merely a “proposal” based on indirect circumstantial evidence until the results of a large-scale clinical trial of a technique to specifically increase HDL-C become available.

Recently, some negative implications have been spread regarding the anti-atherosclerotic effect of an increase in HDL-C, inviting some confusion in the discussion. One is the discontinuation of a large-scale clinical study on the prevention of ischemic heart disease by increasing HDL-C, carried out to develop the CETP inhibitor torcetrapib, due to an increase in the mortality rate in the treated group<sup>6)</sup>. Another is a large-scale epidemiological study reporting that a mutation to cause dysfunction of ABCA1, a rate-regulating protein of HDL biogenesis, is not likely to be a risk factor of ischemic heart disease<sup>7)</sup>. The first report appears to support the contention of researchers arguing that “an increase in HDL-C by CETP inhibition has no anti-atherosclerotic effect,” and allowed the generalized assertion that “the HDL-C increasing strategy is a mistake” to emerge; however, these reports do not necessarily mean the failure of CETP inhibitors themselves, and the pressor effect of a particular drug, torcetrapib, is likely to have led to such results. This incidence postponed an answer to the question of whether increasing HDL-C with a CETP inhibitor is a good idea, the most important medical issue, and markedly complicated the strategy for developing HDL-C elevating agents in general. Also, studies on ABCA1 mutation have shown that the maximum decrease in HDL is about 20%, suggesting that this does not necessarily reject the benefit of high HDL-C.

Under these circumstances, the position has not changed that an elevation of HDL-C is an important part of the anti-atherosclerotic strategy, including CETP inhibition. The above discussion may be summarized as follows: 1) a decrease in HDL-C is a strong risk factor for atherosclerotic disorders, 2) there are rational grounds for the supposition that this risk can be reduced by correcting low HDL-C (increasing HDL-C), but 3) no direct evidence has been obtained that increasing HDL-C is effective for the prevention and treatment of atherosclerotic disorders, 4) changes in HDL-C may include changes in the number and

size of HDL particles, and the difference in their clinical significance may become a problem in the future.

### Simulation of Atherosclerosis Prevention by Increasing HDL-C

There are qualitative scientific grounds for lowering the LDL-C level to reduce the risk of atherosclerotic disorders or, more specifically from an evidence-based viewpoint, to reduce the probability of the occurrence of ischemic heart disease; however, to prepare specific guidelines for diagnosis and treatment, quantitative criteria are considered indispensable. This is a problem with the concept in setting therapeutic goals for target groups. A quantitative profile of increases in the risk associated with elevations of the LDL-C level is necessary, and, if possible, results directly showing that the treatment reverses this curve of increasing risk must be presented. It is not impossible to set medical goals according to this parameter alone, but how criteria are set markedly affects the cost-effectiveness of treatment depending on the distribution of the HDL-C level and demographic composition of the target population; therefore, simulation involving these factors is one of the tasks that must be implemented to devise guidelines.

**Fig. 1B** shows the relationship between the LDL-C level and incidence (per 1,000 people) of myocardial infarction (lethal/non-lethal) in the JLIT, a cohort study that followed up a simvastatin-treated group for 5 years<sup>8)</sup>. From this graph, the distribution of the HDL-C level in Japanese of corresponding ages (**Fig. 1A**)<sup>9)</sup>, and the population composition of the Japanese by age, the number of people needed to treat (NNT) and number of patients in whom the disease is prevented can be calculated when the control target is fulfilled 100% by reducing LDL-C (**Fig. 1C**). According to this calculation, the primary prevention efficacy, expressed as the inverse of NNT, is high at a target LDL-C level of 140 mg/dL but begins to fall rapidly as it is reduced to 120 mg/dL. Reflecting this, the incidence of myocardial infarction shows no further decrease when the target control level is set lower than 140 mg/dL. According to this analysis, roughly 140 mg/dL is considered to be medically and medico-economically appropriate as the target control level of LDL-C for primary prevention, at least on the basis of the results of the JLIT. In this case, the maximum preventive effect is 30-35% for myocardial infarction, which is in close agreement with the results of the MEGA study, the only large-scale interventional study of ischemic heart disease conducted in Japan using a statin<sup>10)</sup>.

**Fig. 2B** shows the decreases in the risk of ischemic heart disease associated with elevations of the HDL-C level in 3 epidemiological studies with prospective risk evaluation carried out in Japan including the JLIT<sup>8, 11, 12</sup>). While it is difficult to directly compare the incidences because the clinical definition of the endpoint varied among the studies, the peak decrease of the risk associated with increased HDL-C is less notable than that associated with the change of LDL-C in all studies. In other words, HDL-C-dependent decreases in the risk were observed even at HDL-C exceeding 60 mg/dL in all 3 studies. **Fig. 2C** shows the results of simulation similar to that of LDL-C performed using the results of the JLIT, which analyzed the therapeutic outcomes, on the basis of the HDL-C distribution curve in Japanese (**Fig. 2A**)<sup>9</sup>) and the population composition. Since decreases in the risk associated with increases in HDL-C have not been directly demonstrated, the simulation was based on the hypothesis that increases in the risk associated with decreases in HDL can be reversed by increasing HDL-C. In contrast with the results concerning LDL, little decrease or peaking of the preventive efficacy associated with increased HDL-C was observed with an HDL-C level over 60 mg/dL. Reflecting this, the preventive effect against myocardial infarction could still be increased by raising the HDL-C level beyond 60 mg/dL. These results suggest that, under the hypothesis that the risk of myocardial infarction is reversibly reduced by elevating HDL-C, myocardial infarction can be prevented in 60-70% of the Japanese population at risk.

As far as these results are concerned, it can be concluded that the criterion of a “low HDL-C level” is unnecessary in guidelines for the control of HDL-C, and that the higher the HDL-C the better; however, according to the results in **Fig. 2A**, some studies have shown relatively large increases in the risk associated with decreases in HDL-C at about 50 mg/dL or below and, particularly, below 40 mg/dL; therefore, it may be reasonable to set a “caution level” around here. On the other hand, views on high HDL-C are divided. First, there is no epidemiological evidence indicating that higher HDL-C is better, even when it exceeds 60 mg/dL. This is probably because the population falling in this category is small (even though high HDL-C is relatively frequent in Japan) and cardiovascular incidence is low, making it difficult to obtain significant results.

In addition, the controversy is further complicated by the inclusion in this category of cases of homozygous CETP-deficient patients, in which elevations of HDL may not be considered to decrease the

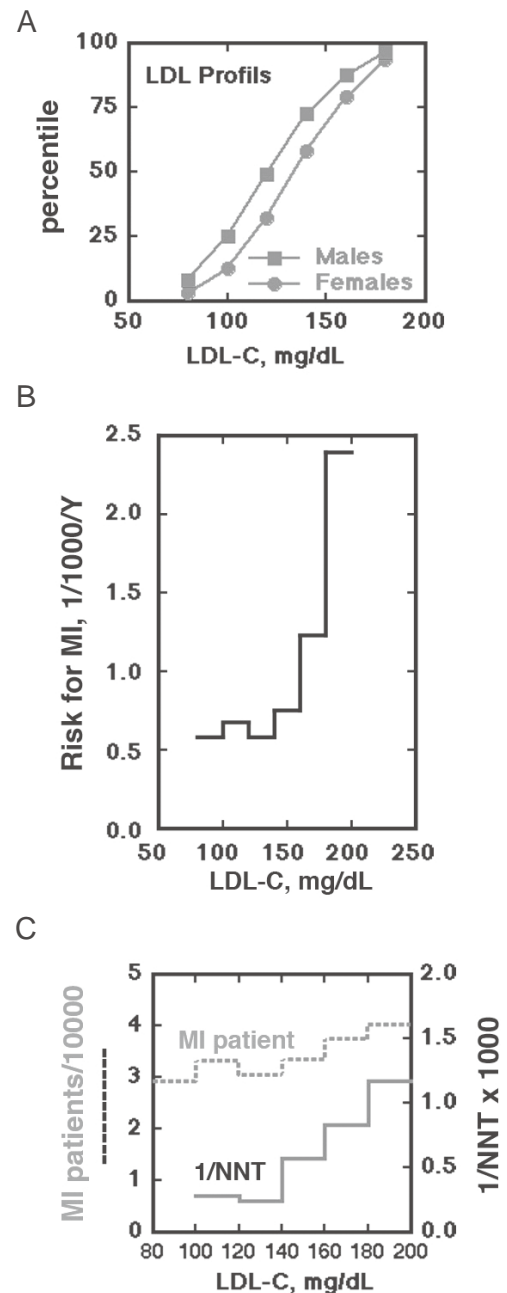


**Fig. 1.** Prevention of ischemic heart disease in Japanese by reducing LDL.

A: Distribution curve of the plasma LDL-C level in Japanese<sup>9</sup>). B: Relationship between the plasma LDL-C level and risk of “myocardial infarction” observed in the JLIT<sup>8</sup>). C: Simulation of the prevention of “myocardial infarction” based on Graphs A and B and demographic data for Japanese. Solid lines represent the inverse of NNT ( $\cdot 1,000$ ) as an indicator of the treatment efficacy for managing lipoproteins to a target. The value of each horizontal segment is the efficacy when reaching a target LDL-C value at the left end of the segment in all Japanese at ages covered by the JLIT. Each horizontal segment of broken lines represents the number of MI patients when LDL is reduced to or lower than the level of the right end of the segment.

risk. The argument that increased HDL does not necessarily contribute to decreased risk is supported by the absence of a further decrease in the risk when the HDL-C increases above 70 mg/dL and the increased risk in patients with a homozygous CETP defect<sup>13</sup>; however, HDL-C is usually 80 mg/dL or higher and often reaches 100-200 mg/dL or even higher in patients with a homozygous CETP defect<sup>13-16</sup>, and such high HDL-C should be considered separately from regular high HDL-C. Still, researchers are not in agreement concerning the increase in risk. In this sense, the differentiation of homozygous CETP deficiency is necessary in patients showing HDL-C exceeding 80 mg/dL, and there is no clinical or experimental evidence pointing to any conclusion about whether HDL-C should be maintained above this level. Nevertheless, the high prevalence of CETP deficiency among Japanese (1/20 for D442G and 1/100 for I14A) may have a limited but significant impact on the association between high HDL and atherogenesis in Japanese.

### Proposal of Standards for Management of the HDL-C Level

On the basis of the above discussion, this article summarizes a proposal for the management of the HDL-C level as follows:

1) The evidence status is summarized as (1) A decrease in HDL-C is a strong risk factor for atherosclerotic disorders, particularly in Japan and, from the viewpoint of public health, it may be a more important risk factor than an increase in LDL-C; (2) While there are rational grounds for the argument that elevated HDL-C leads to a decreased risk, (3) there is as yet no direct evidence that elevating HDL-C is effective for the prevention and treatment of atherosclerotic disorders.

2) If elevations of HDL-C through interventional measures cause reversible decreases in the risk, this effect is expected, at least, up to 60 mg/dL or higher, and a simulation indicated that it eventually reduce the incidence of ischemic heart disease in Japan by 60-70%.

3) In risk management, high HDL-C is presently defined as 40 mg/dL or below. While there is no evidence that strongly urges a change in this definition, the results of epidemiological studies support “the higher the HDL-C level, the lower the risk,” even in the “normal range” so that elevation of HDL-C may reduce the risk probably at least up to 70 mg/dL; however, there are no supportive data for this effect still being obtained over 80 mg/dL. Patients with a

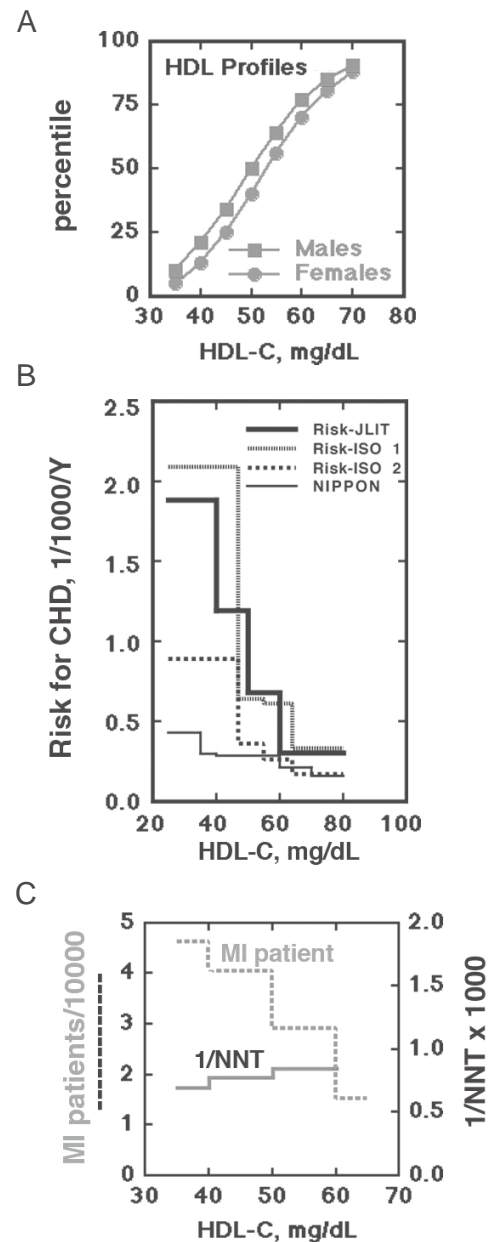


**Fig. 2.** Prevention of ischemic heart disease in Japanese by increasing HDL-C.

A: Distribution curve of the plasma HDL-C level in Japanese<sup>9)</sup>. B: Relationship between the plasma HDL-CH level and risk of ischemic heart disease in Japanese. “Myocardial infarction” in the JLIT<sup>8)</sup>, “coronary artery disease” and “definitive diagnosis of myocardial infarction” by Kitamura, Iso, *et al.*<sup>11)</sup>, and “deaths due to cardiovascular diseases” according to NIPPON DATA<sup>12)</sup>. C: Simulation for prevention of “myocardial infarction” based on Graphs A and B and demographic data of Japanese. Solid lines represent the inverse of NNT (x 1000) as an indicator of the treatment efficacy for managing lipoproteins to a target. The value of each horizontal segment is the efficacy when reaching a target HDL level at the right end of the horizontal segment in all Japanese at ages covered by the JLIT. Each horizontal segment of broken lines represents the number of MI patients when HDL is raised to the left end of the segment.

homozygous CETP deficiency should be followed-up while controlling other risk factors, not to dismiss the possibility of the risk increase with an extremely elevated HDL-C level. A gender-dependent strategy for HDL-C management should be discussed when further epidemiological and clinical evidence becomes available.

### References

- 1) Sasai K, Okuyama-Noji K, Hibino T, Ikeuchi R, Sakuma N, Fujinami T, Yokoyama S: Human cholesteryl ester transfer protein (CETP) measured by enzyme-linked immunosorbent assay with two monoclonal antibodies against rabbit CETP: Plasma CETP and lipoproteins among Japanese hypercholesterolemic patients. *Clin Chem*, 1998; 44: 1466-1473
- 2) Goto A, Sasai K, Suzuki S, Fukutomi T, Ito S, Matsushita T, Okamoto M, Suzuki T, Itoh M, Okuyama-Noji K, Yokoyama S: Cholesteryl ester transfer protein and atherosclerosis in Japanese subjects: A study based on coronary angiography. *Atheroscler*, 2001; 159: 153-163
- 3) Foger B, Ritsch A, Doblinger A, Wessels H, Patsch JR: Relationship of plasma cholesteryl ester transfer protein to HDL cholesterol. Studies in normotriglyceridemia and moderate hypertriglyceridemia. *Arterioscler Thromb Vasc Biol*, 1996; 16: 1430-1436
- 4) Arakawa R, Tamehiro N, Nishimaki-Mogami T, Ueda K, Yokoyama S: Fenofibric acid, an active form of fenofibrate, increases apolipoprotein A-I-mediated high-density lipoprotein biogenesis by enhancing transcription of ATP-binding cassette transporter A1 gene in a liver X receptor-dependent manner. *Arterioscler Thromb Vasc Biol*, 2005; 25: 1193-1197
- 5) Tamehiro N, Shigemoto-Mogami Y, Kakeya T, Okuhira K, Suzuki K, Sato R, Nagao T, Nishimaki-Mogami T: Sterol regulatory element-binding protein-2- and liver X receptor-driven dual promoter regulation of hepatic ABC transporter A1 gene expression: mechanism underlying the unique response to cellular cholesterol status. *J Biol Chem*, 2007; 282: 21090-21099
- 6) Barter PJ, Caulfield M, Eriksson M, Grundy SM, Kastelein JJ, Komajda M, Lopez-Sendon J, Mosca L, Tardif JC, Waters DD, Shear CL, Revkin JH, Buhr KA, Fisher MR, Tall AR, Brewer B: ILLUMINATE Investigators, Effects of torcetrapib in patients at high risk for coronary events. *New Engl J Med*, 2007; 357: 2109-2122
- 7) Frikke-Schmidt R., Nordestgaard BG, Stene MC, Sethi AA, Remaley AT, Schnohr P, Grande P, Tybjaerg-Hansen A: Association of loss-of-function mutations in the ABCA1 gene with high-density lipoprotein cholesterol levels and risk of ischemic heart disease. *JAMA*, 2008; 299: 2524-2532
- 8) Matsuzaki M, Kita T, Mabuchi H, Matsuzawa Y, Nakaya N, Oikawa S, Saito Y, Sasaki J, Shimamoto K, Itakura H: J.-L.S. Group, Large scale cohort study of the relationship between serum cholesterol concentration and coronary events with low-dose simvastatin therapy in Japanese patients with hypercholesterolemia. *Circ J*, 2002; 66: 1087-1095
- 9) Research Committee on Serum Lipid Level Survey 1990 in Japan: Current state of and recent trends in serum lipid levels in the general Japanese population. *J Atheroscler Thromb*, 1996; 2: 122-132
- 10) Nakamura H, Arakawa K, Itakura H, Kitabatake A, Goto Y, Toyota T, Nakaya N, Nishimoto S, Muranaka M, Yamamoto A, Mizuno K, Ohashi Y: MEGA Study Group, Primary prevention of cardiovascular disease with pravastatin in Japan (MEGA Study): a prospective randomised controlled trial. *Lancet*, 2006; 368: 1155-1163
- 11) Kitamura A, Iso H, Naito Y, Iida M, Konishi M, Folsom AR, Sato S, Kiyama M, Nakamura M, Sankai T, Shimamoto T, Komachi Y: High-density lipoprotein cholesterol and premature coronary heart disease in urban Japanese men. *Circulation*, 1994; 89: 2533-2539
- 12) Okamura T, Hayakawa T, Kadowaki T, Kita Y, Okayama A, Ueshima H: NIPPON DATA90 Research Group, The inverse relationship between serum high-density lipoprotein cholesterol level and all-cause mortality in a 9.6-year follow-up study in the Japanese general population. *Atherosclerosis*, 2006; 184: 143-150
- 13) Hirano K, Yamashita S, Nakajima N, Arai T, Maruyama T, Yoshida Y, Ishigami M, Sakai N, Kameda-Takemura K, Matsuzawa Y: Genetic cholesteryl ester transfer protein deficiency is extremely frequent in the Omagari area of Japan. Marked hyperalphalipoproteinemia caused by CETP gene mutation is not associated with longevity. *Arterioscler Thromb Vasc Biol*, 1997; 17: 1053-1059
- 14) Inazu A, Brown ML, Hesler CB, Agellon LB, Koizumi J, Takata K, Maruhama Y, Mabuchi H, Tall AR: Increased high-density lipoprotein levels caused by a common cholesteryl-ester transfer protein gene mutation. *New Eng J Med*, 1990; 323: 1234-1238
- 15) Inazu A, Jiang XC, Haraki T, Yagi K, Kamon N, Koizumi J, Mabuchi H, Takeda R, Takata K, Moriyama Y, Doi M, Tall AR: Genetic cholesteryl ester transfer protein deficiency caused by two prevalent mutations as a major determinant of increased levels of high density lipoprotein cholesterol. *J Clin Invest*, 1994; 94: 1872-1882
- 16) Maruyama T, Sakai N, Ishigami M, Hirano K, Arai T, Okada S, Okuda E, Ohya A, Nakajima N, Kadowaki K, Fushimi E, Yamashita S, Matsuzawa Y: Prevalence and phenotypic spectrum of cholesteryl ester transfer protein gene mutations in Japanese hyperalphalipoproteinemia. *Atherosclerosis*, 2003; 166: 177-185

## Original Article

# High-Density Lipoprotein Levels Have Markedly Increased Over the Past Twenty Years in Japan

Shinji Yokoyama<sup>1</sup>, Hirotsugu Ueshima<sup>2</sup>, Takashi Miida<sup>3</sup>, Masakazu Nakamura<sup>4</sup>, Koki Takata<sup>5</sup>, Tatsuyuki Fukukawa<sup>6</sup>, Takaaki Goto<sup>7</sup>, Mariko Harada-Shiba<sup>8</sup>, Michitaka Sano<sup>9</sup>, Kiminori Kato<sup>10</sup> and Kazuhiro Matsuda<sup>10</sup>

Shinji Yokoyama and Hirotsugu Ueshima contributed equally to this work.

<sup>1</sup>Nutritional Health Science Research Center, Chubu University, Kasugai, Japan

<sup>2</sup>Health Science, Shiga University of Medical Science, Otsu, Japan

<sup>3</sup>Clinical Laboratory Medicine, Juntendo University Graduate school of Medicine, Tokyo, Japan

<sup>4</sup>Lipid Reference Laboratory at National Cerebral and Cardiovascular Center under The Cholesterol Reference Method Laboratory Network of CDC, Suita, Japan

<sup>5</sup>Preventive Medicine Center, Chugoku Rosai Hospital, Hiroshima, Japan

<sup>6</sup>Quality Assurance Department, SRL Inc., Hachioji, Japan

<sup>7</sup>Clinical Chemistry Laboratory, Nagoya City University Hospital, Nagoya, Japan

<sup>8</sup>Molecular Innovation in Lipidology, National Cerebral and Cardiovascular Center Research Institute, Suita, Japan

<sup>9</sup>Clinical Chemistry of National Cerebral and Cardiovascular Center Hospital, Suita, Japan

<sup>10</sup>Niigata Association of Occupational Health, Niigata, Japan

**Aim:** The high-density lipoprotein cholesterol (HDL-C) level is a major negative risk factor for atherosclerotic diseases dependent on various lifestyle parameters. Changes in the lifestyle of Japanese individuals over the past several decades is believed to have increased their total cholesterol levels and the incidence of cardiovascular disease in Japan. It is therefore important to assess the long-term trends in the HDL-C levels with respect to public health in the community.

**Methods:** In this study, accumulated data for the serum/plasma HDL-C levels published in cohort studies and obtained during health checkup programs in Japan were analyzed with respect to time-dependent changes.

**Results:** The levels of HDL-C have continuously and significantly increased over the past 20 years by 12-15% according to the National Health and Nutrition Study, other cohort studies and commercially available data. On the other hand, the non-HDL-cholesterol levels demonstrated no changes or only a slight decrease during the same period. This finding is consistent with several sets of data obtained from health checkup programs. The commercially measured levels of serum apoA-I, an independent parameter of serum HDL, also showed a similar long-term increase, supporting the above findings.

**Conclusion:** We concluded that the serum/plasma HDL concentrations in Japanese individuals, selectively, have increased continuously and significantly over the past 20 years or more. The reasons for this phenomenon and the consequent public health outcomes have yet to be investigated.

*J Atheroscler Thromb, 2014; 21:151-160.*

**Key words:** HDL, HDL cholesterol, ApoA-I, Non-HDL cholesterol, Japanese

## Introduction

The serum/plasma high-density lipoprotein cholesterol (HDL-C) level is a strong negative risk factor

for atherosclerotic vascular diseases, such as coronary heart disease (CHD), as demonstrated by most epidemiological studies historically worldwide. It is therefore important to assess and monitor the HDL-C lev-

els in the community in order to improve public health. A recent report by Huxley *et al.*<sup>1)</sup> found that isolated low HDL levels are more common in Asians with a high risk of CHD. This finding appears to be somewhat controversial, as the prevalence of CHD is traditionally low in Japan, while the HDL-C levels are generally considered to be high. The data used in this meta-analysis indeed showed relatively high levels among other Asian ethnic groups. We therefore evaluated the historic trend of the Japanese HDL-C levels.

## Methods

### Sources of Data for the Analysis

The data used in this analysis were available for public use or obtained in previous cohort studies. The National Health and Nutrition Survey (NHNS) conducted by the Ministry of Health, Labour and Welfare of Japan (MHLWJ) maintains files of serum HDL-C data collected since 1989<sup>2, 3)</sup>. The data were obtained in the laboratory of SRL, Inc., a commercial clinical chemistry laboratory in Tokyo, based on the standardization and validation protocols issued for nearly 20 years by The Lipid Reference Laboratory in Osaka under the Cholesterol Reference Method Laboratory Network of the CDC (CDC/CRMLN). The SRL has also maintained their own data obtained using commercially ordered laboratory tests, including the serum HDL-C levels, since 1984. In addition, lipid surveys were conducted by the Research Groups on Serum Lipid Level Survey under the MHLWJ in 1990<sup>4)</sup> and 2000<sup>5)</sup> (measured by SRL and BML, Inc., respectively). Cohort study data have also been accumulated in the Circulatory Risk in Communities Study (CIRCS) at the Kyowa site in Ibaraki<sup>6)</sup> and in the Occupational Health Check Program conducted by the Niigata Association of Occupational Health; in both of these studies, the HDL-C assays were standardized according to the criteria of the CDC/CRMLN. Follow-up data obtained in the health checkup program are available at Chugoku Rosai (Labor Welfare) Hospital in Hiroshima, without standardization by the CDC/CRMLN. The HDL-C data obtained in the beta quantification procedure conducted in the CDC/CRMLN Lipid Reference Laboratory in 2011 were also used<sup>7)</sup>. Historic data are also available in the clinical laboratories of a few other

Address for correspondence: Shinji Yokoyama, Nutritional Health Research Center, Chubu University, Matsumoto-cho 1200, Kasugai 487-8501, Japan  
E-mail: syokoyam@med.nagoya-cu.ac.jp  
Received: August 5, 2013  
Accepted for publication: August 30, 2013

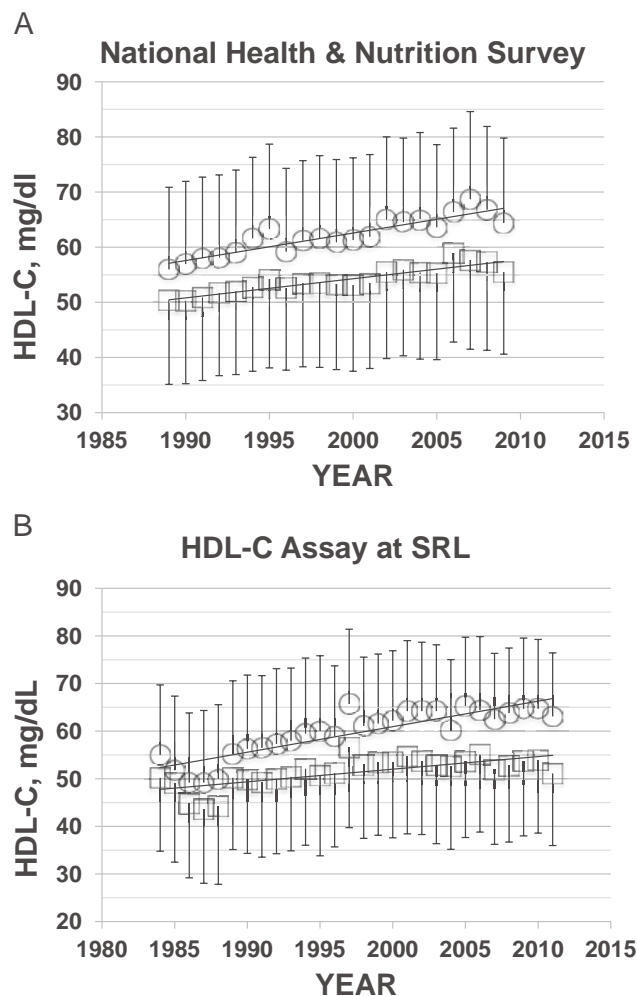


**Fig. 1.** A. HDL-C data obtained in the National Health and Nutrition Study, mean  $\pm$  SD, for men (squares) and women (circles). The slopes are 0.35 mg/dL/year and 0.5 mg/dL/year for men and women, respectively, with  $p < 0.001$  for both. B. HDL-C data commercially measured in the SRL laboratory, mean  $\pm$  SD, for men (squares) and women (circles). The slopes are 0.27 mg/dL/year and 0.5 mg/dL/year for men and women, respectively, with  $p < 0.001$  for both.

institutions. In addition, the SRL maintains assay data for the levels of serum apolipoprotein A-I (apoA-I), an independent parameter of HDL-C, for determining the HDL concentrations. The assay system was based on standardization by the International Federation of Clinical Chemistry Standardization Project for Measurement of Apolipoproteins A-I and B<sup>8)</sup>. The numbers of case samples in each study are listed in **Supplementary Tables 1 and 2**. The assay reagents and systems are listed in **Supplementary Table 3**, with as much detail as possible. The NHNS, CIRCS and

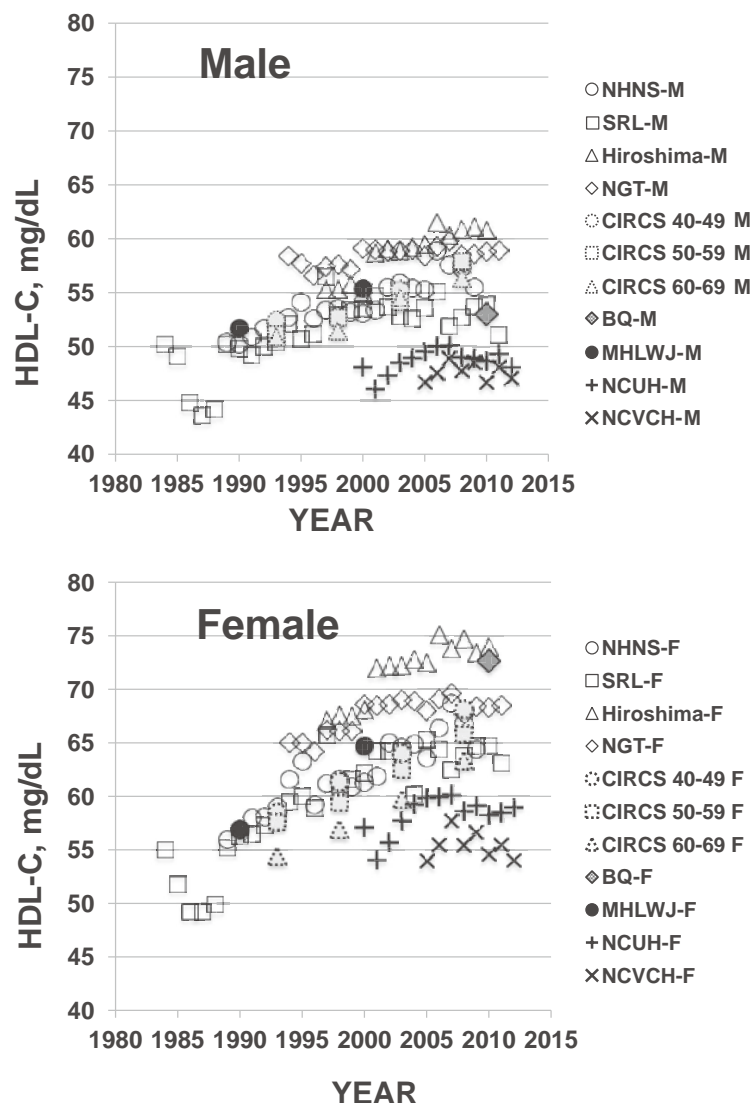


**Fig. 2.** HDL-C data for men (M) and women (F) obtained from cohort studies, health checkup programs and other sources in Japan. NHNS, National Health and Nutrition Study; SRL, data commercially measured in the SRL laboratory; Hiroshima, health checkup data program at Chugoku Rosai Hospital; NGT, Niigata, health checkup program data for the Niigata Association of Occupational Health; CIRCS, data obtained from CIRCS at the Kyowa site in each age group indicated for every 5-year average represented as each center year time point; BQ, beta-quantification data obtained at the CDC/CRMLN Lipid Laboratory at the National Cerebral and Cardiovascular Research Center for the evaluation of homogeneous LDL measurement<sup>7)</sup>; MHLWJ, data obtained from the Serum Lipid Survey conducted by the Ministry of Health, Labour and Welfare of Japan in 1990 and 2000<sup>4, 5)</sup>; NCUH and NCVCH, patient data obtained from the Clinical Laboratories of Nagoya City University Hospital and National Cerebral and Cardiovascular Center Hospital.

MHLWJ are cohort studies of the general population. The Hiroshima and Niigata studies are occupational health surveys that include actively working groups. The data obtained from the NCUH and NCVCH studies represent patients who visited the respective hospitals. The SRL samples include those submitted from clinics and hospitals nationwide.

### Statistical Analysis

A multivariate regression analysis and the *t*-test were applied to the serially collected data in order to determine the historical trend.

### Results

The HDL-C data obtained in the NHNS study

are shown in **Fig. 1**. The HDL-C levels steadily increased in both men and women over 20 years from 50 to 58 mg/dL and 55 to 67 mg/dL, respectively, (0.35 and 0.50 mg/dL/year with  $p < 0.001$  for both) (**Fig. 1A**). The commercially measured HDL-C SRL data were very similar to those of the NHNS, also showing an increase with statistical significance (0.27 and 0.50 mg/dL/year, for men and women, both with  $p < 0.001$ ) (**Fig. 1B**). This trend did not change among the SRL data samples for the age range of 30-59 years (0.40 and 0.69 mg/dL/year, for men and women). The cohort data obtained from the CIRCIS Kyowa study in every age group and those obtained from the Niigata health checkup program both coincided with the NHNS data (**Fig. 2**). The increase in the CIRCIS data was statistically significant<sup>6)</sup>. The follow-up study conducted at Chugoku Rosai Hospital also showed a statistically significant increase in the levels of HDL-C since 1997, with apparently higher values than those discussed above in both men and women (**Fig. 2**). The HDL-C data obtained using beta-quantification in 2011<sup>7)</sup> yielded “elevated values” in the blood samples of patients without lipid disorders (serum total cholesterol  $< 250$  mg/dL and triglycerides  $< 150$  mg/dL) consistent with a long-term increasing trend (**Fig. 2**).

It is notable that the non-HDL-C ([total cholesterol] - [HDL-C]) levels showed no or only marginally significant decreases in the NHNS data ( $-0.33$  mg/dL/year with  $p = 0.01$  and  $-0.29$  mg/dL/year with  $p = 0.07$  for men and women) (**Fig. 3**).

Supporting these trends, the data obtained by MHLWJ Research Group showed a comparable increase in the levels of HDL-C from 1990 to 2000 in every age group (**Fig. 4**). The non-HDL-C levels calculated using the MHLWJ Research Group data were very similar between 1990 and 2000 for both men and women with respect to age distribution (**Fig. 4**).

The increase in the levels of HDL-C reaches a plateau in the most recent several years. This is also indicated by the data obtained from the Clinical Laboratories at Nagoya City University Hospital (NCUH) and National Cerebral and Cardiovascular Center Hospital (NCVCH), which showed almost no tendency toward an increase over a relatively short period comprising the immediate past few years for which reliable data are available (**Fig. 2**). The levels of HDL-C in these institutions are much lower than those observed in the general population, perhaps representing high-risk patients, especially in the NCVCH study.

The levels of serum apoA-I, an independent parameter of serum HDL, have been commercially measured at SRL for years. The accumulated data showed a similar increasing trend in the levels of

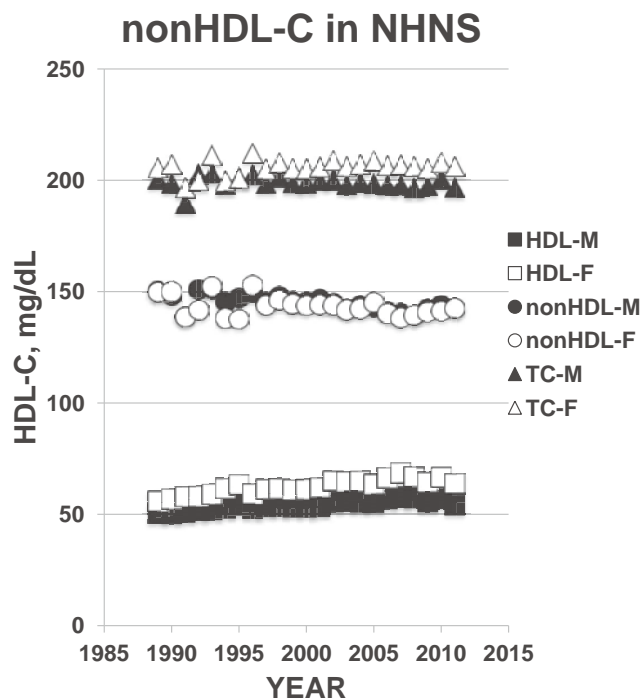


**Fig. 3.** Non-HDL-C data obtained in the NHNS study presented as [total cholesterol] - [HDL-C] for men (M) and women (F). The slopes and p values are:  $-0.330$  mg/dL/year and 0.010 for men and  $-0.294$  mg/dL/year and 0.070 for women, respectively.

HDL-C (0.49 and 1.06 mg/dL/year for men and women, both with  $p < 0.001$ ) (**Fig. 5**).

From these data, we may conclude that the serum/plasma HDL concentrations of Japanese patients have increased by 12-15% in both men and women over the past two to three decades.

## Discussion

The data analyzed in this study were obtained from mixed sources, collected in epidemiological studies in a somewhat controlled manner and including arbitrarily collected data from patients seen at ordinary regular clinics. It should also be noted that the procedures for measuring the HDL-C levels have varied over the past two decades included in the study period. Routine statistical approaches, such as standardization and adjustment, may therefore not be appropriate or valid for analyzing these sets of data.

The most troublesome concern we have is whether this trend is the result of methodological bias. A variety of methods for measuring the HDL-C levels have been historically applied, including ultracentrifugation, precipitation with polysaccharide sulfate with

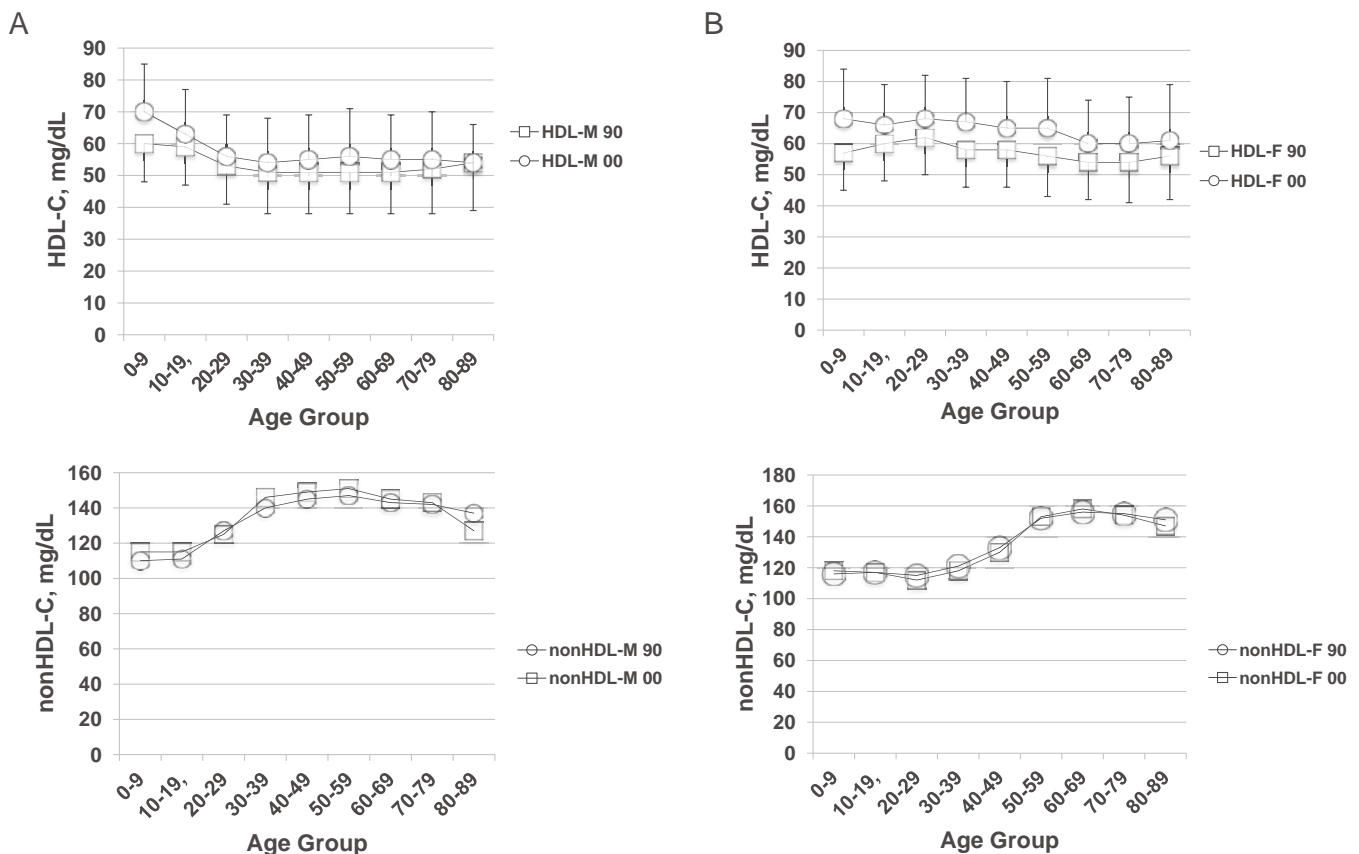


**Fig. 4.** Analysis of the data obtained in the Serum Lipid Survey conducted by the Ministry of Health, Labour and Welfare of Japan in 1990 and 2000<sup>4, 5)</sup> for men (A) and women (B). The levels of HDL-C and non-HDL-C are plotted against age. The HDL-C levels increased significantly in both men and women, with  $p < 0.001$  according to the  $t$ -test, while no changes were observed in the non-HDL levels.

divalent cations and, more recently, homogeneous assay systems<sup>9, 10)</sup> developed based on the principles of precipitation methods. The SRL used the heparin-calcium precipitation method until 1995, after which the homogeneous method was employed. Many other clinical laboratories rapidly switched to this method around that time. However, the HDL-C data appear to have continuously increased over this transition time; therefore the change in method is unlikely a major cause of the increase. Nevertheless, continuous efforts by industries to standardize and adjust the calibration of assay systems may ironically have caused a gradual shift in values over the years, inadvertently showing a great and continuous change.

Three lines of evidence may exclude this possibility. First, the results of the apoA-I measurements also showed an increasing trend very similar to that of the HDL-C levels (**Fig. 4**). This assay employs the enzyme immunoassay system<sup>11)</sup>, which has been based on international standardization since it was established

in the mid 1980's; therefore, there have been no changes in the assay environment during this historical data collection period. This finding supports the view that the HDL concentrations in fact increased. Second, all methods of HDL-C measurement used by the SRL were validated using reference methods based on strictly standardized beta-quantification by the CDC/CRMLN Lipid Reference Laboratory. The beta-quantification HDL-C data obtained in the CDC/CRMLN Lipid Reference Laboratory in 2011<sup>7)</sup> are consistent with the "elevated values" observed in the long-term increasing trend (**Fig. 2**); therefore, the HDL-C levels appear to be currently high in Japan. Third, the analysis of the data performed by the MHLWJ Research Group revealed interesting results. While the HDL-C levels measured in 1990 and 2000 were consistent with the increasing trend that observed in other sets of data, as a whole and with respect to age distribution, the non-HDL-C data were remarkably similar in the age distribution profiles of both

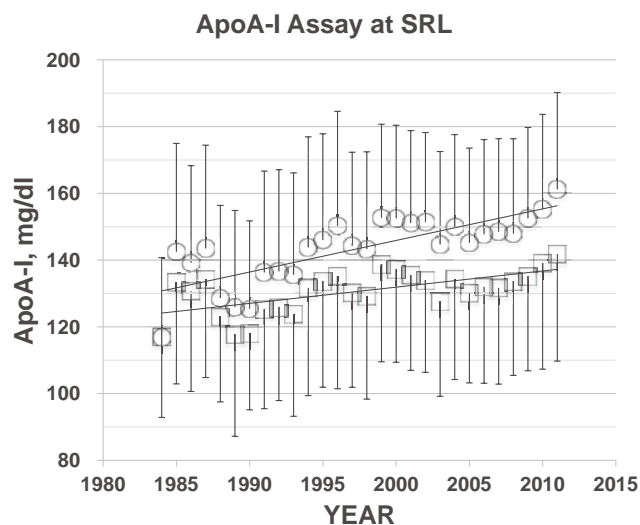


**Fig. 5.** The apoA-I levels commercially measured in the SRL laboratory, mean  $\pm$  SD, for men (squares) and women (circles). The slopes are 0.485 mg/dL/year and 1.064 mg/dL/year for men and women, respectively, with  $p < 0.001$  for both.

men and women between the two measurements (Fig. 4). This finding is consistent with the trend observed in the non-HDL-C levels obtained in the NHNS study (Fig. 3). These findings indicate that the long-term increasing trend in the HDL-C levels is less likely to be an artifact and is instead a real phenomenon. It is remarkable that the magnitude of increase (12-15%) is greater than that achieved in most interventional trials using statins or fibrates. The increasing trend in the HDL levels was apparent regardless of the type of data background, such as cohort studies, commercially measured samples or health checkup programs, or regional factors, such as nationwide or local data. Little information is available in the literature regarding the long-term trends in serum lipoprotein profiles. Carroll *et al.* reported that the HDL-C levels showed no changes in the period of 1966-2002, while a slight and significant increase was observed during the time period of 1988-2010 (45.6 to 47 mg/dL by 3% and 55.4 to 57.6 mg/dL by 4% in men and women) in the United States National Health and Nutritional Examination Survey<sup>12, 13</sup>. The current findings indicate that the levels and magnitude of the increase are both much higher among Japanese individuals.

Various factors are known to influence the serum/plasma HDL levels. Nutritional changes may influence the HDL-C level<sup>14</sup>, as an increase in calories or fat or cholesterol intake generally increases both the LDL and HDL levels, unless accompanied by eleva-

tion of the serum/plasma triglyceride (TG) levels. An increase in physical activity also increases the HDL level by decreasing the TG level. A decrease in the smoking rate should also increase the HDL levels. Moderate habitual alcohol intake is known to result in increased HDL levels. Hypolipidemic drugs, such as fibrates and statins increase the HDL levels, while bile acid sequestering resins and probucol decrease this parameter.

Drastic changes in the eating habits of Japanese individuals took place in the post-WWII period<sup>15</sup>). A marked increase in fat and protein intake was observed until the mid-1970's and stabilized thereafter, while a decrease in carbohydrate intake has continued throughout the postwar period. Interestingly, the total energy intake increased until the mid-1970's then began to gradually decrease thereafter. Therefore, it is not apparent whether there are any specific nutritional causes of the increase in HDL-C observed over the past two to three decades. There may be some prolonged effects of the drastic nutritional changes that occurred in the early postwar period.

More people may currently make an effort to engage in physical exercise; however, overall, the physical activity of Japanese individuals decreased during the period of this survey. The plasma/serum TG levels showed no change, not to account for the increase in HDL-C observed in the NHNS data. Statins were introduced into the market in 1989. However, the proportion of NHNS subjects prescribed these drugs has remain between 10% and 12% over the past 10 years, and the average HDL-C levels observed after excluding these people showed very little changes. The rate of smoking among Japanese men was high and decreased during this period; however, the rate of smoking among women was low and instead increased. The rate of alcohol consumption in Japan has not changed enough to account for such a large increase in the levels of HDL-C. The body mass index has decreased over the past few decades among young Japanese women according to the NHNS data, which may partly account for the increase in the HDL levels observed in women.

From these facts, it can be concluded that the serum/plasma HDL concentrations have increased for at least two decades, from the late 1980's to the mid 2000's. The magnitude in the increase is as large as 10% to 15%. At this point, no apparent reasons accounting for this change can be identified. On the other hand, there were no significant changes in the levels of the atherogenic lipoprotein indicator, non-HDL-C, during this period. Both the mortality and incidence of heart disease and myocardial infarction

may have decreased in Japan throughout the period surveyed in this study<sup>16)</sup>. Improvements in blood pressure control during this period are a possible reason for this reduction<sup>16)</sup>; however, the increase in HDL demonstrated in this study may be an additional factor causing this change. If there is a prolonged effect of HDL elevation in reducing CHD, further effects of this trend may become apparent in the near future. It is important to confirm whether this increasing trend is a reality in Japan, determine what caused this large change and identify the possible consequences for Japanese public health.

### Acknowledgment

The authors are grateful to Dr. Kazumasa Yamagishi at the University of Tsukuba and Dr. Hiroyasu Iso at Osaka University for their helpful discussion. They also thank Dr. Kunihiko Nishimura at NCVS and Dr. Hidenori Arai at Kyoto University for kindly providing background information for the data analysis.

### Funding Sources

MEXT-Supported Program for the Strategic Research Foundation at Private Universities (Japan), Grant-in-aid from MEXT Japan.

### Conflict of Interest Disclosure

None.

### References

- Huxley RR, Barzi F, Lam TH, Czernichow S, Fang X, Welborn T, Shaw J, Ueshima H, Zimmet P, Jee SH, Patel JV, Caterson I, Perkovic V, Woodward M: Isolated low levels of high-density lipoprotein cholesterol are associated with an increased risk of coronary heart disease: an individual participant data meta-analysis of 23 studies in the Asia-Pacific region. *Circulation*, 2011; 124: 2056-2064
- Katanoda K, Matsumura Y: National Nutrition Survey in Japan--its methodological transition and current findings. *J Nutr Sci Vitaminol (Tokyo)*, 2002; 48: 423-432
- Katanoda K, Nitta H, Hayashi K, Matsumura Y: Is the national nutrition survey in Japan representative of the entire Japanese population? *Nutrition*, 2005; 21: 964-966
- Yamamoto A, Nakamura H, Yasugi T, Mabuchi H, Kita T, Matsuzawa Y, Nakaya N, Saito S, Horibe H: Current state of and recent trends in serum lipid levels in the general Japanese population. Research Committee on Serum Lipid Level Survey 1990 in Japan. *J Atheroscler Thromb*, 1996; 2: 122-132
- Arai H, Yamamoto A, Matsuzawa Y, Saito Y, Yamada N, Oikawa S, Mabuchi H, Teramoto T, Sasaki J, Nakaya N, Itakura H, Ishikawa Y, Ouchi Y, Horibe H, Kita T: Serum lipid survey and its recent trend in the general Japanese population in 2000. *J Atheroscler Thromb*, 2005; 12: 98-106
- Kadono A, Yamagishi K, Sankai T, Umesawa M, Cui R, Imano H, Ohira T, Kiyama M, Kitamura A, Wakabayashi Y, Nakamura M, Iso H: A 20-year trends in serum HDL-cholesterol in a community: The CIRCS Kyowa Study (abstract) [in Japanese] *J Epidemiol* 2013; 23 (suppl 1): 96
- Miida T, Nishimura K, Okamura T, Hirayama S, Ohmura H, Yoshida H, Miyashita Y, Ai M, Tanaka A, Sumino H, Murakami M, Inoue I, Kayamori Y, Nakamura M, Nobori T, Miyazawa Y, Teramoto T, Yokoyama S: A multicenter study on the precision and accuracy of homogeneous assays for LDL-cholesterol: Comparison with a beta-quantification method using fresh serum obtained from non-diseased and diseased subjects. *Atherosclerosis*, 2012; 225: 208-215
- Dati F, Tate J: Reference Materials for the Standardization of the Apolipoproteins A-I and B, and Lipoprotein(a). *eJ Int Fed Clin Chem*, 2002; 13: <http://www.ifcc.org/ifcc-files/docs/1303200103.pdf>
- Sugiuchi H, Uji Y, Okabe H, Irie T, Uekama K, Kayahara N, Miyauchi K: Direct measurement of high-density lipoprotein cholesterol in serum with polyethylene glycol-modified enzymes and sulfated alpha-cyclodextrin. *Clin Chem*, 1995; 41: 717-723
- Huang YC, Kao JT, Tsai KS: Evaluation of two homogeneous methods for measuring high-density lipoprotein cholesterol. *Clin Chem*, 1997; 43: 1048-1055
- Sakai Y, Itakura K, Kanada T, Ebata N, Suga K, Aikawa H, Nakamura K, Sata T: Quantitation of apolipoprotein A-I in pooled human serum by single radial immunodiffusion and sodium dodecyl sulfate-polyacrylamide gel electrophoresis. *Anal Biochem*, 1984; 137: 1-7
- Carroll MD, Kit BK, Lacher DA, Shero ST, Mussolino ME: Trends in lipids and lipoproteins in US adults, 1988-2010. *JAMA*, 2012; 308: 1545-1554
- Carroll MD, Lacher DA, Sorlie PD, Cleeman JI, Gordon DJ, Wolz M, Grundy SM, Johnson CL: Trends in serum lipids and lipoproteins of adults, 1960-2002. *JAMA*, 2005; 294: 1773-1781
- Schaefer EJ: Lipoproteins, nutrition, and heart disease. *Am J Clin Nutr*, 2002; 75: 191-212
- Matsumura Y: Nutrition trends in Japan. *Asia Pac J Clin Nutr*, 2001; 10 Suppl: S40-47
- Ueshima H: Explanation for the Japanese paradox: prevention of increase in coronary heart disease and reduction in stroke. *J Atheroscler Thromb*, 2007; 14: 278-286

**Supplementary Table 1.** Number of case samples (n) for HDL-C in each study

Year	NHNS		SRL		Hiroshima		Niigata		BQ		NCUH		NCVCH		CIRCS		MHLWJ Ref. 4 and 5
	Male	Female	Male	Female	Male	Female	Male	Female	Male	Female	Male	Female	Male	Female	Male	Female	
1984			983	983													
1985			1205	1071													
1986			1168	935													
1987			1242	980													
1988			848	882													
1989	2750	4167	4056	5393													
1990	3371	4745	6352	7215													
1991	3521	5033	8062	8512													
1992	2940	4303	10960	11274													
1993	2618	3917	10321	10632													
1994	2083	3279	11597	11180			181782	86779			23492	27772					
1995	1823	2975	7080	7980			178522	85308			24007	27857					
1996	2209	3431	5461	6006			181103	88378			22372	26210					
1997	2503	3797	5444	6999	1337	660	185679	88719			9194	9169					
1998	2691	4029	6401	9142	1360	598	176125	86221			9142	7827					
1999	2293	3591	7767	9449	1525	749	170871	82774			7845	7446					
2000	2316	3326	3584	3199	1444	653	168874	83892			7813	7483					
2001	2126	3357	2324	1802	1490	703	169774	82827			7820	7671					
2002	2124	3183	2708	2640	1473	681	162309	78926			8514	8647					
2003	2078	3151	2041	2375	1505	704	146517	72089			8967	9153					
2004	1220	1912	1629	1384	1577	751	145241	71123			11874	13171					
2005	1521	2273	1447	1280	1523	711	146498	69303			9396	10154					
2006	1703	2504	1184	941	1687	714	143343	69010			9952	10199	20833	13451			
2007	1602	2368	918	952	1560	777	144260	71409			14187	14575	21264	14629			
2008	1817	2630	1192	952	1368	547	150931	79452			17417	18000	13934	10447			
2009	1738	2558	905	727	1130	415	145893	79337			19652	19806	32969	20856			
2010			1097	824	1102	411	142370	78465	36	26	26149	26095	35307	20378			
2011			869	614			141558	79224			26749	26369	39423	22589			
2012											28980	27858	27696	16261			

**Supplementary Table 2.** Number of case samples (n) in the apoA-I study

Year	SRL apoA-I	
	Male	Female
1984	286	227
1985	512	525
1986	650	723
1987	983	1185
1988	1203	1339
1989	1568	1881
1990	2363	2890
1991	3226	3472
1992	3458	4005
1993	3130	3439
1994	3152	3519
1995	3563	3500
1996	3355	3402
1997	2562	2376
1998	2902	2904
1999	2625	2615
2000	2748	2618
2001	1994	2114
2002	2008	2021
2003	1554	1541
2004	1727	1589
2005	1932	1595
2006	1699	1514
2007	2103	1888
2008	2078	1681
2009	2411	1931
2010	2619	1870
2011	2772	1866

**Supplementary Table 3.** Assay systems, Reagents and CDC or other Standardization

Year	SRL							Niigata	NCUH
	HDL-C (CDC)				ApoA-I (International Standardization)			HDL-C (CDC)	HDL-C (CDC)
	Reagent	System	Standard	Correlation *	Reagent	System	Correlation	Reagent	Reagent
1984	W-MnCL	Techni-con AA			SRID				
1985					ApoA-I Auto Daiichi	Cobas	$y=0.96x+1.13,$ $r=0.974$		
1986	Heparin-Ca		Preiset Cholestrin	$y=0.96x+1.02,$ $r=0.992$					
1987		H705		$y=1.04x-1.37,$ $r=0.995$					
1988						H7150	$y=0.98x+1.0,$ $r=0.974$		
1989									
1990									
1991		H7150		$y=0.97x+2.06,$ $r=0.998$					
1992									
1993									
1994									
1995						H7170	$y=0.99x+2.5,$ $r=0.988$		
1996	HDL-C Auto Daiichi	H7170	HDL-C Auto CAL	$y=0.95x+4.9,$ $r=0.994$					
1997	Choles Test HDL		Choles Test HDL CAL	$y=0.99x-0.1,$ $r=0.992$	ApoA-I AutoN Daiichi		$y=0.82x-0.55,$ $r=0.998$	Choles Test HDL	
1998						BM12	$y=1.01x-0.554,$ $r=0.998$		
1999									
2000			ColesTest Calibrater	$y=1.01x-0.0,$ $r=0.992$					Choles Test N HDL
2001	Choles Test N HDL			$y=0.98x+1.18,$ $r=0.997$				Choles-Test N HDL	
2002									Determi-ner LHDL
2003									
2004									Denka EX-N
2005									
2006									
2007		BM8060		$y=1.003x+1.18,$ $r=0.998$					
2008						BM8040	$y=1.03x-3.87,$ $r=0.999$		
2009									
2010									
2011									
2012									

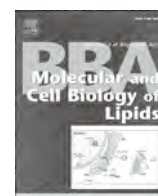
The NCVCH and CIRCS data are qualified by CDC standardization.

\*Validation for changing assay systems/reagents.



Contents lists available at ScienceDirect

Biochimica et Biophysica Acta

journal homepage: [www.elsevier.com/locate/bbalip](http://www.elsevier.com/locate/bbalip)

## Review

A potential screening factor for accumulation of cholesteryl ester transfer protein deficiency in East Asia: *Schistosoma japonicum*

Shinji Yokoyama\*

Nutritional Health Science Research Center, Chubu University, Matsumoto-cho 1200, Kasugai 487–8501, Japan

## ARTICLE INFO

## Article history:

Received 20 October 2013

Received in revised form 12 December 2013

Accepted 24 December 2013

Available online 3 January 2014

## Keywords:

CETP

CETP deficiency

HDL

Schistosoma

Egg embryonation

Liver

## ABSTRACT

Cholesteryl ester transfer protein (CETP)-deficiency manifests a unique plasma lipoprotein profile without other apparent symptoms. It is highly common in East Asia while rather rare anywhere else. A potential environmental screening factor(s) may therefore contribute to this eccentric distribution, such as its selective advantage against a regional illness, most likely an infectious disease, in relation to plasma lipoproteins. Blood flukes use the host plasma lipoproteins as nutrient sources through the lipoprotein receptor-like systems. Its Asian-specific species, *Schistosoma (S) japonicum*, which has been endemic in East Asia, takes up cholesteryl ester (CE) from high-density lipoprotein (HDL) for the embryonation of their eggs to miracidia, a critical step of the hepatic pathogenesis of this parasite, but poorly from HDL of CETP-deficiency. CD36-related protein (CD36RP) was cloned from the adults and the eggs of *S. japonicum*, with 1880-bp encoding 506 amino-acid residues exhibiting the CD36 domains and two transmembrane regions. Its extracellular domain selectively bound human HDL but neither LDL nor CETP-deficiency HDL, and the antibody against the extracellular domain suppressed the selective HDL-CE uptake and embryonation of the eggs. When infected with *S. japonicum*, wild-type mice developed less hepatic granulomatosis than CETP-transgenic mice by the ectopic egg embryonation. CD36RP is thus a candidate receptor of *S. japonicum* to facilitate uptake of HDL-CE necessary for egg embryonation. Abnormal HDL caused by CETP-deficiency retards this process and thereby protects the patients from development of hepatic lesions. *S. japonicum* infection is a potential screening factor for high prevalence of CETP deficiency in East Asia.

© 2013 Elsevier B.V. All rights reserved.

## 1. Geographic profile of genetic CETP deficiency

Cholesteryl ester transfer protein (CETP), a plasma protein of 476 amino acid residues in a case of human [1] with a glycosylated molecular weight of 74,000, catalyzes non-directional equimolar exchange of non-polar lipids represented by cholesteryl acylester (CE) and triglyceride (TG) among lipoprotein subfractions with low substrate specificity [2–4], being present in certain species of mammals such as rabbits, hamsters and some primates including humans [5]. The reaction as its nature equalizes distribution of the core lipids among lipoproteins. CE is actively generated in plasma high-density lipoprotein (HDL) by lecithin: cholesterol acyltransferase (LCAT) reaction, and the source of plasma TG is secretion of very-low-density lipoproteins (VLDL) and chylomicron by the liver and the intestinal cells, respectively. Consequently, CETP mediates the net move of CE from HDL to VLDL/chylomicron and TG from VLDL/chylomicron to HDL and low-density lipoproteins (LDL) [2], to function as a regulator of HDL cholesterol [6]. Increase of plasma TG thus decreases HDL cholesterol and reduces the size of LDL, both complying cardiovascular risks of hypertriglyceridemia, as TG is hydrolyzed in any lipoprotein subfraction. In turn, HDL-CE increases when CETP reaction decreases.

However, physiological roles of CETP reaction are not clearly understood. Generation of CE by LCAT in HDL is one of the driving force for the removal of cell cholesterol [7] as an important component of cholesterol transport for catabolism from peripheral somatic cells to its catabolic site, the liver, and the CETP reaction may facilitate this transport by sending CE from HDL to the LDL pathway dependent on the recovery of LDL through the hepatic LDL receptor [5].

Investigation of CETP was much helped and facilitated by the discovery of the genetic defect of CETP, who were primarily characterized by marked increase of HDL. The CETP deficiency patients was first described in Japan in 1985 as cases with hyperalphalipoproteinemia and the lack of cholesteryl ester transfer reaction between lipoprotein subfractions [8,9], and its genetic background was later identified [10]. Many cases were found thereafter in Japan among those with hyperalphalipoproteinemia. The two major mutations have been found to account for majority of the patients, intron 14 G(+1)-to-A (Int14A) and exon 15 missense mutation (D442G) [11–13]. Prevalence of the heterozygous patients with these two major mutants has been reported very high in Japanese general population, as 1 to 2% for Int14A and 6 to 7% for D442G. In addition, sporadic cases with many other types of mutations have also been identified among Japanese [14–16]. Accordingly, the estimated numbers of the heterozygotes can be around 10 millions in Japan and even the homozygotes would be as many as 150,000 to 250,000. Above all, Omagari of Akita district

\* Tel.: +81 568 51 9698.

E-mail address: [syokoyam@isc.chubu.ac.jp](mailto:syokoyam@isc.chubu.ac.jp).

in Northern Japan was discovered as the region with high accumulation of the Int14A mutant, with the prevalence of the heterozygote of 27% [13]. Thus, the prevalence of genetic CETP deficiency is extremely high among Japanese.

The first non-Japanese patient was found in Switzerland but as a Chinese descendant [17]. Several reports thereafter described CETP deficiency among other Asians. Genetic prevalence of D442G mutant heterozygote case was found 2.1 – 3.8% in the mainland Chinese population [18,19], and 4.5 – 6.7% in the population of Taiwan [20,21]. On the other hand, the prevalence of D442G patients could be estimated as some 2% among Koreans based on its allele frequency of 0.94% [22]. No other population study data is available for other Asian countries and regions. However, 9 cases were identified to be D442G heterozygotes out of 35 individuals with hyperalphalipoproteinemias in Thailand [23], accounting for 26% in comparison to 21–32% in similar surveys in Japan [11,24] as a strong indication that CETP mutants are not uncommon in Thailand. No reliable information is available for the Int14A mutation except for the report for Hong Kong Chinese, two out of 145 subjects (1.4%) [25].

In contrast, genetic CETP deficiency seems rare among other ethnic groups. The first Caucasian case of the disease was reported in 1997 [26], and the presence of one case of Int14A was recognized in 1998 in Canada without ethnic background information [27]. It was thus concluded that CETP deficiency is rare among North American Caucasians [28]. Nevertheless, a few studies reported sporadic cases of CETP deficiency from The United States [29], Italy [30,31], and the Netherlands [28,32]. There was an estimation of the frequency of D442G mutant as “less than 1%” [33], but the ground for this estimation, as well as how “less”, is unclear.

Clinical manifestation of CETP deficiency is limited to abnormal plasma lipoprotein profile characterized as very high HDL cholesterol and moderately reduced LDL cholesterol. In the lack of the CETP activity, CE generated by LCAT is detained in HDL while the substrate molecules

of free cholesterol and glycerophospholipid are continuously supplied to HDL by non-specific exchange or other transfer reaction from other lipoproteins and cells including erythrocytes [7]. Accordingly, HDL particles become larger in their size as the core CE compartment expands. Therefore, the apparent increase of HDL cholesterol is not by the increase of HDL particle number but because of the enlargement of HDL particles, to a diameter as large as LDL and containing a large amount of apoE [34–36]. LDL particles in turn get somewhat smaller and contain increased amount of TG in their core, resulting in overall reduction of LDL-cholesterol [37,38]. The patients generally do not exhibit any serious clinical symptoms, and it has been wondered whether this increase of HDL is protective against atherosclerotic vascular diseases. The answer has been controversial in epidemiological cohort studies [13,39,40], and the attempts of pharmacological inhibition of CETP have yielded inconclusive outcomes so far [41,42].

In summary, CETP deficiency is highly prevalent in East Asia, at least among Japanese, Chinese both in mainland and Taiwan, and Koreans, predominantly with the D442G mutant. It is likely to be similarly high in Thailand. Int14A mutant may be the second common but it is not clearly evident except for Japan. Other types of mutation have also been found frequently in Japan, but the information is not available so far in other Asian countries and regions. In contrast, this disease is rare in other ethnic groups in other regions. The two common mutations are not commonly identified even among the sporadic cases from other areas on the earth. Any potential reason for this unique accumulation has never been given insight to except for an extreme case in Omagari, Japan, as a possibility of a founders' effect [13].

## 2. Background of East Asia-specific hypothesis

The geographic distribution of genetic CETP deficiency is thus very unique. For geographic or ethnic accumulation of a genetic abnormality, two potential backgrounds may be considered in general, “founders’

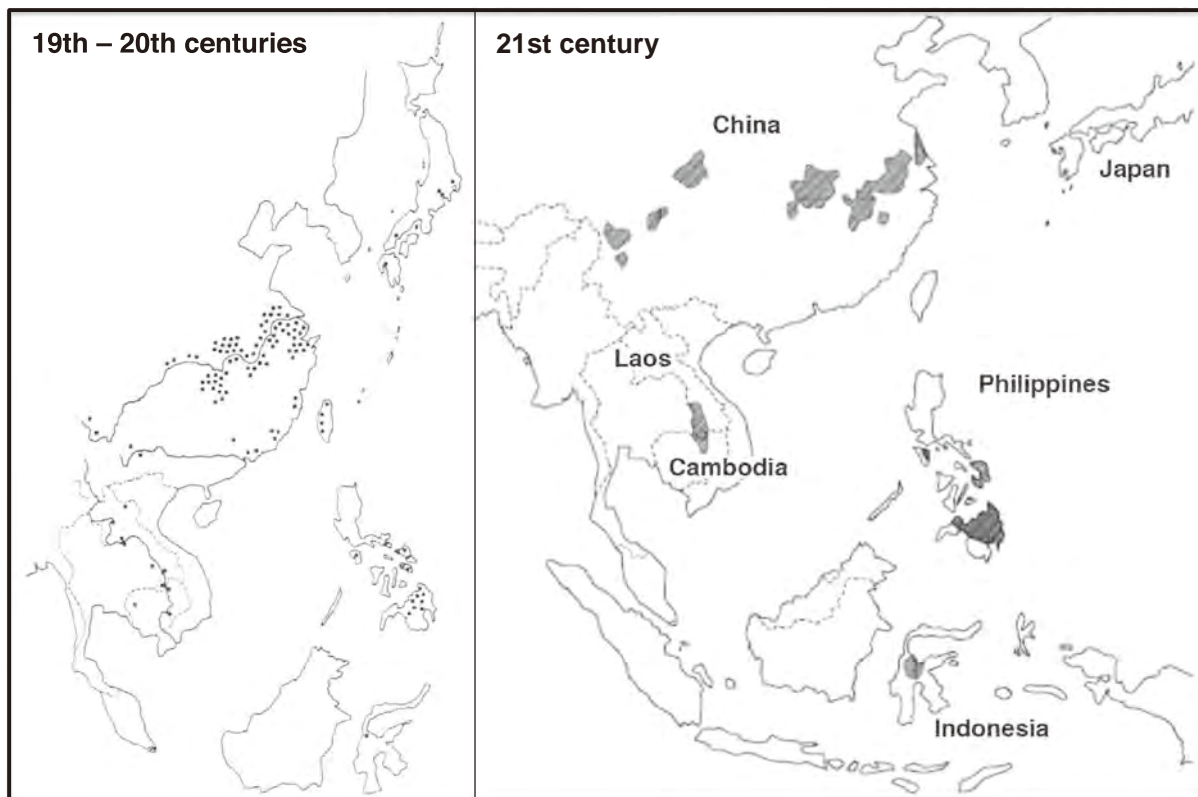


**Fig. 1.** Endemic maps of *S. japonicum*. The left map shows by spots the regions where the cases were found since the parasite was identified in the early 20th century. The regions included Japan, the southeast coast of China including Taiwan and wide area of Mekong valleys and Thailand. The endemic was eliminated in many of these regions as shown in the right panel in the 21st century.

effect” or screening by a regional fatal disease(s). The former cases are normally found in limited communities considered as descendants of the earlier settlers. Typical examples are accumulation of familial

hypercholesterolemia in French Canadians in Quebec [43], Afrikaners in South Africa [44] and perhaps in Lebanon [45]. In this case, the accumulated mutation may not be highly diverse as originating in a few carrier families even though not just in a single family. The latter is represented by sickle cell anemia that is resistant to tropical parasitic protozoans malaria infection due to deformation and vulnerability

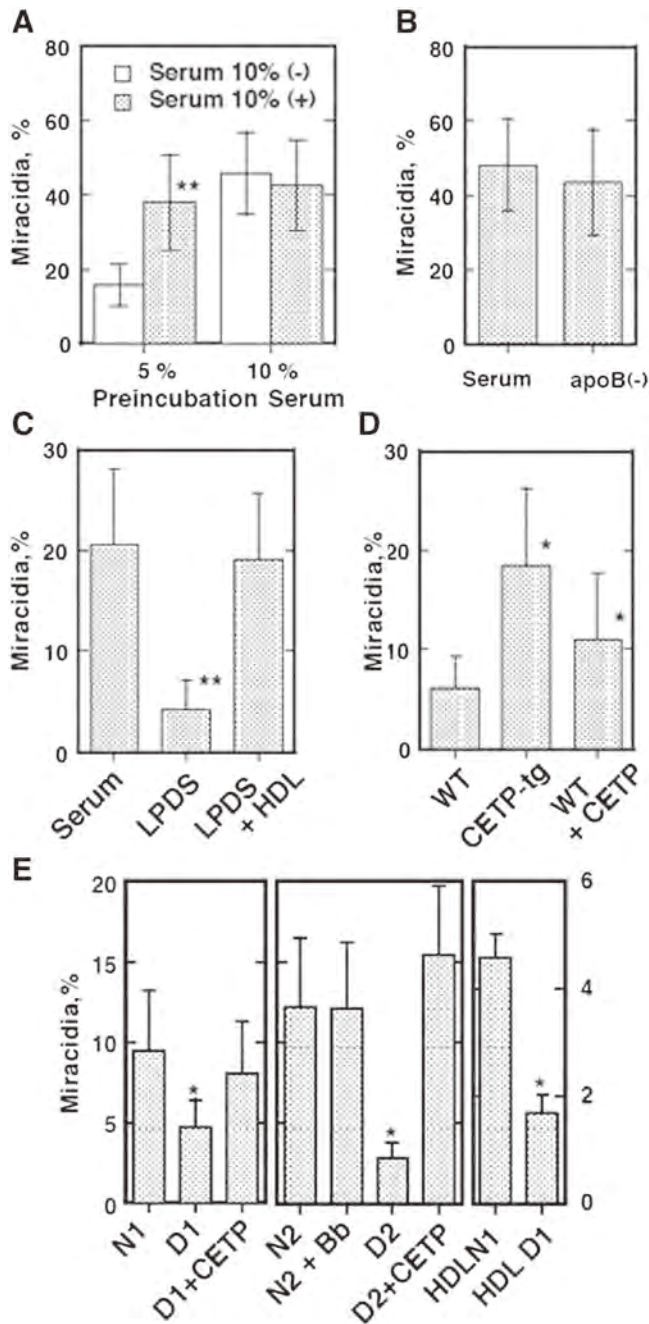


**Fig. 2.** Lipoprotein requirement for embryonation of the *S. japonicum* eggs in 8 days in culture, taken from the reference [66] the experimental details should be referred to. A: incubation of the eggs with and without human serum (10%) after pre-exposure of the parents while laying the eggs to 5 and 10% of human serum. Embryonation proceeds when the parents or eggs have access to adequate human serum. Preincubation with 5% serum is applied hereafter. B: Embryonation is not influenced even when apoB-lipoprotein is removed from human serum (apoB (-)). C: Embryonation requires HDL fraction of human serum. LPDS; lipoprotein deficient serum. D: The effect of mouse serum on the egg embryonation. Embryonation is poor with wild-type mouse serum that lacks CETP and proceeds with CETP-transgenic mouse serum (CETP-tg). Adding human CETP to the wild-type serum partially restored embryonation. E: Embryonation of the *S. japonicum* eggs in 8 days in culture with CETP-deficient human sera, taken from the reference [67]. Embryonation is estimated in the culture of the eggs in 10% normal human sera (N1 and N2) and that of CETP-deficient subjects (D1 and D2). Embryonation is retarded in CETP-deficient serum (A) and adding CETP recovers this (B). Normal HDL is adequate for the embryonation but not HDL from CETP-deficiency (C). \*\*  $p < 0.01$  and \*  $p < 0.05$  from serum (-) (A), serum (C), WT (D), and normal HDL (E).

**A** ■ Wild □ CETP-Transgenic

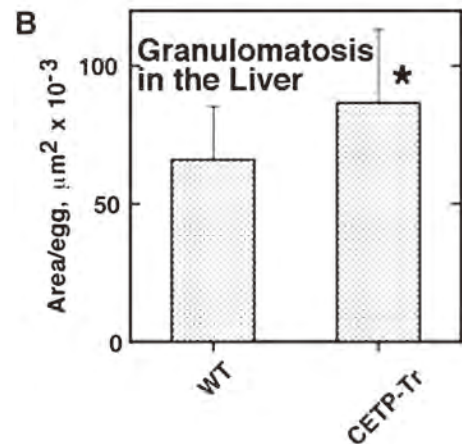
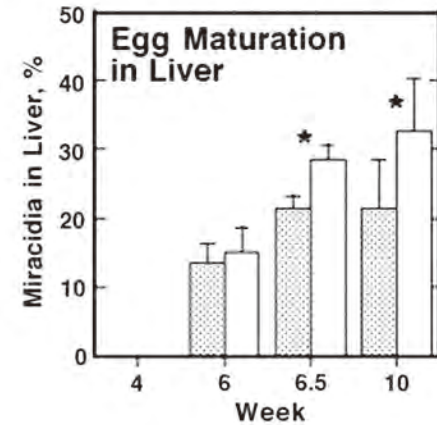
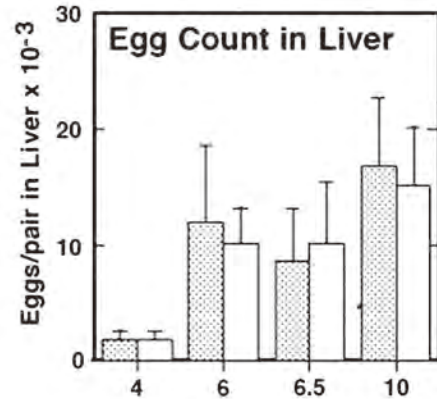


**Fig. 3.** The egg embryonation and the liver lesion development in the wild-type and CETP-transgenic mice infected with *S. japonicum*, taken from the reference [67] the experimental details should be referred to. A: Number of the eggs embolizing in the liver. B: Ectopic embryonation of the eggs counted microscopically. C: Granulomatous lesion in the liver. The eggs and granulomatous lesion was microscopically identified in the liver specimens. The total area of the lesion per egg was calculated for each section. The area per egg was calculated as an average  $\pm$  SE of the 12 mice, for each of which 12 random liver sections were examined. Asterisks indicate difference at  $p < 0.05$  from the wild type.

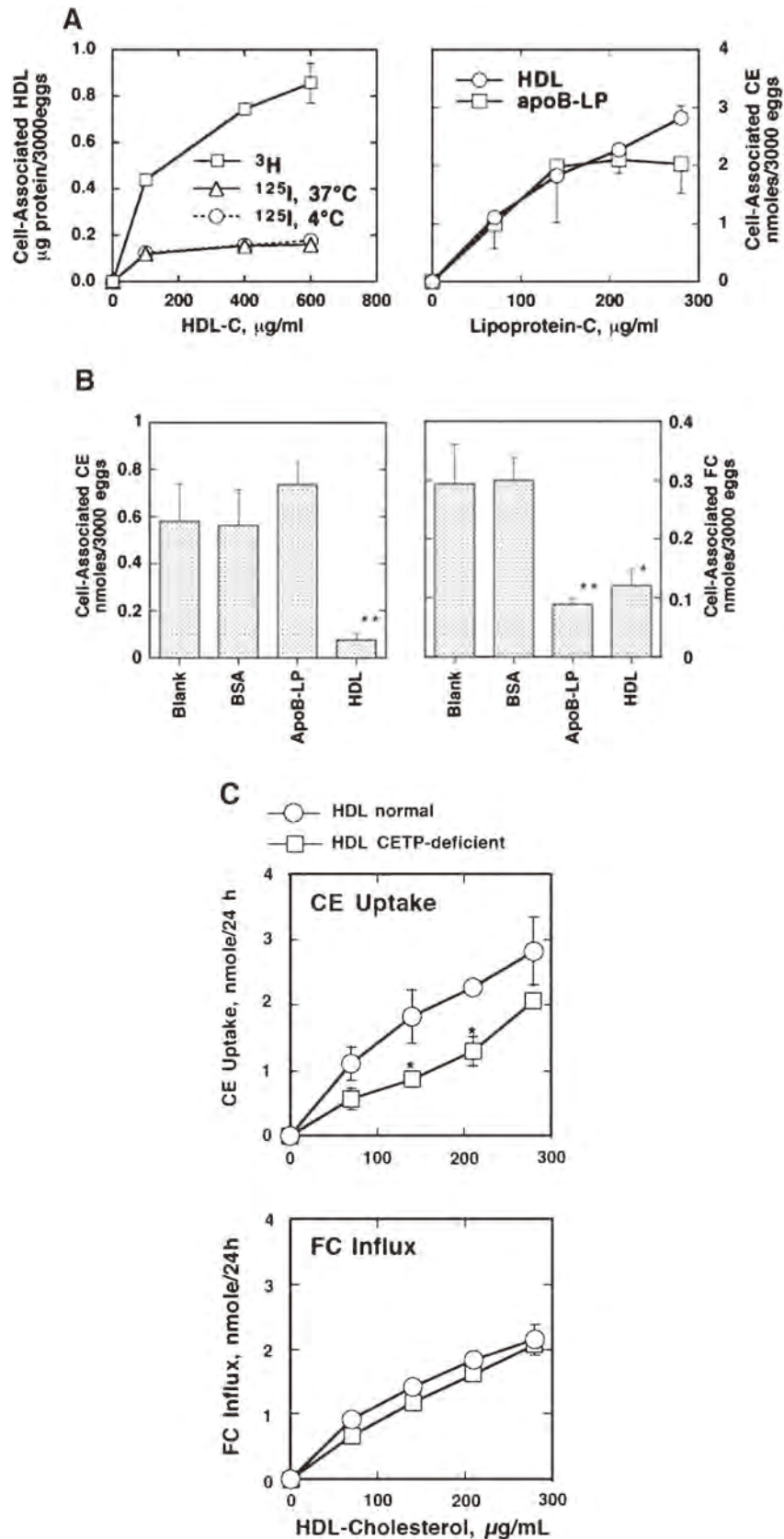


**Fig. 4.** Selective uptake of CE from HDL by the eggs of *S. japonicum*, taken from the reference [66] the experimental details should be referred to. A: HDL was labeled with 125I for protein and with 3H for CE. The uptake of each radioactivity was measured and standardized for HDL protein (left). The CE uptake from HDL and LDL was measured as dependency on lipoprotein concentration (right). B: CE (left) and FC (right) uptake from HDL in the presence of each plasma component indicated (BSA, ApoB lipoprotein, and HDL). C: Uptake of CE and free cholesterol (FC) from HDL by the eggs of *S. japonicum*, taken from the reference [67]. The eggs are incubated with normal and CETP-deficient HDL incorporated with radio-labeled CE or FC and uptake of the radioactivity is measured. CE-uptake from the CETP-deficient HDL is retarded.

of erythrocyte in this disease, as a believed reason for high prevalence of this genetic anemia among African ethnic groups [46–48]. This type of gene selection may affect large populations historically exposed to such diseases, most likely infectious diseases.

Accumulation of CETP deficiency can also be discussed from such points of view. Majority of the patients of the region may be limited to one or two type(s) of mutations though diversity of the mutant genotype in the region is also observed, being not inconsistent with founder's effect from the limited numbers of the origin family. However, the region where this disease is found with high prevalence seems a large portion of East Asia, which is likely far beyond considering founder's effect. No specific settler family can be conceivable to account for such large descending population affected. However, extreme accumulation of int14A in Omagari may be the case of "founder's effect" [13].

For searching potential screening infectious diseases for CETP deficiency, one should take into account its only significant clinical phenotype of abnormal plasma lipoprotein metabolism. Very few infectious diseases are found with any relation to or dependency on plasma lipoproteins. A significant relation with plasma lipoproteins was found in African blood fluke, *Schistosoma (S) mansoni*, which expresses the LDL receptor-like protein [49,50]. The receptors for LDL and VLDL were shown to mediate the uptake of the host lipoproteins in *S. mansoni* [51,52], as well as in East Asian blood fluke, *S. japonicum*, the second major type endemic in the world [53,54]. Therefore, the parasites seem to take up lipids from the host blood plasma lipoproteins as their nutrient sources.

While *S. mansoni* is endemic worldwide mainly through Africa to South America, *S. japonicum* shows limited distribution to East and Southeast Asian countries but perhaps intensively endemic with as many as 12 million people infected in the limited area in China until the modern public health effort initiated some 60 years ago [55]. Although the number of the patients has dramatically decreased, it is still active in China [55,56], Philippines [57,58], Cambodia, Laos, Thailand, Malaysia, and Indonesia [59] perhaps accounting for some 2-million patients. Endemic was historically more widespread including Japan where the infection is basically eliminated in these days [60] (Fig. 1). Life cycle of schistosoma includes releasing the eggs from the host to grow to miracidium and hatch in fresh water in the environment, growing to cercaria in fresh water snails as the intermediate hosts, and its infection to and growing to adult in the host including human. The historical geographic distribution of *S. japonicum* more or less overlaps the regions with the culture of water farming of rice grain, which goes with intensive contact of the people with natural fresh water reserve in everyday life. This might have caused intensive endemic of *S. japonicum* in East Asia.

Besides acute and massive infectious reactions, chronic schistosomiasis causes various pathological problems in the body, not only the parasites themselves but also the eggs laid in the body. One of the most life threatening clinical manifestations is the liver cirrhosis, which is caused by ectopic egg embryonation. The adult pairs of the parasite locate in the portal and its draining venules and lay eggs in the portal vein to be released to the intestinal tract to initialize their life cycle. However, many are flushed back via the portal blood flow to the liver where they embolize, develop to embryogenesis and form miracidia, a phenomenon that deals to the morbidity and mortality of hepatic granulomatosis [61]. Thus, the egg embryonation is one of the targets to prevent fatal development of the schistosomiasis. The active mechanism to induce this lesion is unknown. Specific antibodies against various egg antigens have been identified as indicators of the infection, but their relationship with the granulomatogenesis is unclear [62]. A potential pathogenesis factor is egg embryonation to the stage of miracidium. The eggs only after this stage seem to cause the liver lesion when transplanted [63]. L-Selectin of the host binds the eggs only the stage of miracidium [64]. Vaccination to stabilize the embryonation process has been proposed for an anti-Schistosomiasis therapy [65].

### 3. HDL-CE as a nutrient source for the egg embryonation of *S. japonicum*

The effect of human serum on embryonation of the *S. japonicum* eggs to miracidia was investigated in vitro [66]. The paired adult parent parasites are removed from the infected mouse portal vein, and pre-incubated in culture in the presence of 5% and 10% normal human serum for 2 days for laying eggs. The eggs were isolated and cultured in the absence and presence of 10% human serum for another 8 days, and evaluated for their embryonation to miracidia. When the eggs were laid in the presence of adequate serum source (10%), they do not require serum for embryonation (Fig. 2A). When they were laid in the poor nutritional environment (5% serum), the eggs needed the presence of serum to grow (Fig. 2A). This finding indicates that the egg yolk may be established for the embryonation before they are laid but the egg or embryonic cells themselves can still uptake the nutrients from the host serum after being laid to grow. The latter effect was not reduced even when apoB lipoprotein was removed from the serum, and the presence of HDL was demonstrated as an essential requirement for the embryonation (Fig. 2BC). In contrast, mouse serum that lacks CETP activity did not provide adequate embryonation of the eggs and that of the CETP transgenic mouse enhanced the embryonation. Adding purified CETP to the mouse serum partially recovered the embryonation (Fig. 2D). Similar experiments were conducted by incubating the parents-pair worms for 8 to 10 days with the serum from normal human subjects and those of the CETP deficiency [67]. The egg embryonation was significantly low with the serum from the CETP deficiency, and this was substantially recovered in the presence of the purified human CETP (Fig. 2E). However, the presence of the anti-CETP inhibitory antibody in the normal serum did not alter the embryonation rate (Fig. 2E). Finally the presence of normal HDL achieved the normal embryonation rate even without serum but HDL isolated from the CETP deficiency subject gave lower rate of embryonation (Fig. 2E).

In vivo studies were carried out in mice, using wild type mice (C57BL/6) as a model for CETP-deficiency and the CETP-transgenic mice for normal subjects [67]. Number of the eggs plugged into the liver and the rate of their embryonation were counted microscopically in the liver specimens (Fig. 3)[67]. While the number of the eggs was similar between the models, the rate of its embryonation was significantly higher in the transgenic mice liver. The average granulomatous lesion per egg was larger in the transgenic mice [67].

Uptake by the *S. japonicum* eggs of cholesterol, the most specific nutrient carried by lipoproteins, was investigated focusing on specificity of HDL. Uptake of lipoprotein CE by the eggs is shown in Fig. 4. CE is selectively taken up from HDL particles. The uptake also seems to occur from apoB-lipoprotein, but it is saturated at much lower level and the pathways are independent of each other [66]. In contrast, free cholesterol exchange between the eggs and lipoproteins is by a common pathway for HDL and apoB-lipoproteins [66]. Selective CE uptake was slower from the HDL of the CETP deficiency subject while free cholesterol exchange shows no difference between normal and CETP-deficient HDL [67]. It is still unclear specific reason for impair of the CE uptake to cause low efficiency of the embryonation though it is perhaps due to insufficiency in establishment of egg yolk.

### 4. Identification and characterization of CD36-related protein in *S. japonicum*

Selective cellular uptake of CE is mediated by CD36-like proteins, such as scavenger receptor-B1 (SR-B1) in rodent [68] or CLA1 in human [69]. Assuming a similar protein to mediate the reaction, expression of mRNA was searched in *S. japonicum* by using the 489-bp probe derived from the cDNA of Sj-Ts2, *S. japonicum* protein previously submitted as 671-bp and registered as Genbank AF291715, having one of the CD36 domains. The mRNA representing a CD36 family protein was identified in the adult with the size of 1.8-kb. From the *S. japonicum*

**A**

1 aca ttt tat tta aca gct ttt aaa aat taa cag aca acg ttt cac ttg tac acg ATG ATA 60  
M I

61 TCT CGT GTT TGG TTA AGT GCT ACA GTT TTA TTT ACT TTG TTG ATT TGT ATA TCA TTA TTA 120  
S R V W L S A T **V L F T V L I C I S L L**

121 TCT TTA TGC GTA TTA CAA CCG TTT CTT TGG TTT CTA ATC AAT AGG CAA ACA CGT TTA ACT 180  
**S L C V L** Q P F L W F L I N R Q T R L T

181 CCA GGA ACT AAA CTG TAT TCA GAA TGG TTA GAG CCA TCA CTA CCT GTT TTA ACA CAA TTC 240  
P G T K L Y S E W L E P S (L) P V L T Q F

241 TAT TTT TTC AAT TTA ACA AAT CCA ATT GAA TTT CAA TCT GGT CAT AAA CCT CAT GTT CAA 300  
Y F F N L T N P I E F Q S G H K A P C H V Q

301 CAA TTA GGA CCA TAT ACA TAC CGT GAA AAA CGT TTG AAG CTT AAT ATT ACA CAT AGT AAT 360  
Q L G P Y T Y R E K R L K L **N** I T H S N

361 GGA ACA ATT ACG TAT AAA GAA ATG AAA TGG TAT TAT TTT GAT CAA AAT TTA TCT AAT GGT 420  
G T I T Y K E M K W Y Y F D Q N L S N G

421 ATG GTG AAT GAT TCA ATC ACT AGT GTC AAT CTT GTT TTC ATA TCG ATT GCA TTG AGA ATC 480  
M V N D S I T S V N L V F I S I A L R I

481 AAT TCA ATG CCA TGG TTT CTC AAA CAA ATA ATT GAA TTA ATT GAA TCC CGC TTT CAT GAA 540  
N S M P W F L I E S R F H E

541 TAT CTA TTT ATA ACA AAA ACT GTC AAT GAA TTA TTA TGG GGT TAT AAT GAT GAA TTA TTA 600  
Y L F I T K T V N E L L W G Y N D E L L

601 ACA TAC TTG TCA ACG CAT GGA TTC AAT ATG TCA ACA GTA ACT CAT ATT GGT CTA TTC ATT 660  
T Y (L) S (T) H G F N M S T V T H I G L F I

661 AAT AAA AAT AAT ACA CTT AGT GAT TAT GTA ACA ATT AAT GAT GGT CTG CAT AAT AAT AAA 720  
N K N N T L S D Y V T I **N** D G L H N N K

721 ATG ATT GGA CAA ATT ACT CGA TAT CAT GGT AAT ACA ACA TTA TCC TAT TGG AAT AGT TCA 780  
M I G Q I (T) (R) Y H G N T T L S Y W N S S

781 ACA GCC AAT ATG ATA AAT GGT AGT GAT GGA ACA TTT TTT CAT TCA TTT CTA ACT AAA TAT 840  
T A N M L I **N** G S D G T F F H S F L T K Y

841 GAT AAA CCG TAT GTT TTT GCA TCA GAT ATT TGT CGT TCA TTG CAA TTT TAC ACT GAA TCA 900  
D K P Y V F A S D I C R S L Q F Y T E S

901 ATT GAT AAA TTA CAT AAT TTA CCA GTT TTA AAA TTA ACT CCA ATG TTG GAT ACA TTT AAA 960  
I D K L H N L P V L K L T P M L D T F K

961 TCA CCG AAA TAT TAT GAA AAG AAT AGA GGA TTT TGT TTA AAT TGG CCT AAT TGT TAT GAG 1020  
S P K Y Y E K N R G F C L N W P (N) C Y E

1021 GAT GGT GTA TTA GAC ATG TCA TCA TGT CAA CCT GGT GCA CCG ATA GTT GTA TCA CAA CCA 1080  
D G V L D M S S C Q P G A P I V V S Q P

1081 CAT TTT TTA AAT GCT AAT AAA ACA TAT CAA GAT GCT GTT GAT GGA ATG TAT CCA ACT AAT 1140  
H L N A N K T Y Q D A V D G M Y P T N

1141 GAA ATG AAT ACA GTC ATC TAT GTA GAA CCA AAT ACT GGT AGT ATA ATA AAA GCA CAG AAA 1200  
E M N T V I Y V E P N T G S I I K A Q K

1201 AAA ATT CAA ATT AAC ATT TTA GTT AAA AAT GAT ACA TTT AAA CAA CTT GCC AAT ATT 1260  
K I Q I N I L V K N D T T F K Q L A N I

1261 TCA ACT ACT CTT CTA CCA ATT GTA TTC ATT AAT GAA TCA GTT CAA TTG AAT GAT ACA TTA 1320  
S T T (L) L P I V F I N E S V Q L N D T (L)

1321 ATT GAA CAA TTG ACT AAT GCA TTA ATT CAA CAA CCA **TTC ATT GTT CAA ACA ATT TTA GTT 1380**  
I E Q L T N A L I Q Q P **F I V Q T I L V**

1381 TGT ATT ATC ACT TTG TCA ATA ATT TCA CTA GGT TCA CTT ATT TCA ATA CAT TTT TAT CAG 1440  
**C I I T L S I I S L G S L I** S I H F Y Q

1441 AAT AGA CAA CAT ACT ACT TAT ATG CAT TTT ATT GAT AGC CAT CAA TCC AAT GAT GTT ATA 1500  
N R Q H T T Y (M) (H) F I D S H Q S N D V I

1501 CCT CAG AAT ACA TTA GAG GTT AAT ACA CAA CAA CAG ACA ATA TCA AAT GAT TTA CAA GAA 1560  
P Q N (S) L E V N T Q Q Q T I S N D L Q E

1561 AAT CCA ATT GTT TAA ttg tta att aac atg att caa ttg aca ata ttg tca tta tat gtt 1620  
N P I V \*

1621 tgt tat tgt tat tgt tct ata ttt gca tct gac tat cga tta gac att gat tag tga aag 1680  
1681 tct gtg tgt gag tgt gtg taa ttt tca att gtc aat ttt ttg taa ctt aga tgt ttt act 1740  
1741 tgt gaa tta ttt aat tta cct tca agg aga ata atc act gat tat ttg atg aat tgt gca 1800  
1801 taa caa ttg aat aaa tga caa aat atc tac agt taa gat gaa tga aat acc att gag ttt 1860  
1861 att gaa ctc tct atg agg taa aaa aaa aa 1892

**Fig. 5.** Cloning of CD36RP from the reference [66]. A: Nucleotide sequence and the deduced amino acid residue sequence of CD36RP cloned from *S. japonicum*. Shadowed portions are predicted membrane spanning regions. Bald Ns indicate potential glycosylation sites. The sequences double underline portions are potential CD36-related regions (IPB 002159D, 002159E, 002159 F). B: Expression of CD36RP in *S. japonicum*, the adults and the eggs. Two different probes (near the center and 5' region to yield PCR products of 740 bp and 467 bp, respectively). The left and right panels show the results of conventional and real-time PCR.

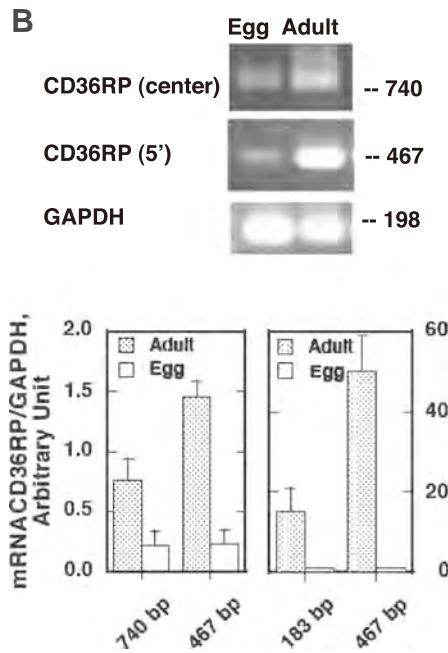


Fig. 5 (continued).

adult cDNA library, S<sub>j</sub>-Ts2-containing cDNAs of variable sizes longer than 1-kb were obtained, all seemingly derived by single transcription, including the sequence of the reported S<sub>j</sub>-Ts2 protein. The sequence of

the full length (1880-bp) original mRNA was determined and deduced to 506 amino acid residues, as CD36-related protein (CD36-RP) (Fig. 5A) [66]. Although there is an indication of alternative splicing of this mRNA, the size of the PCR product, with the first-strand cDNA derived from total RNA as template, was similar (467-bp) between eggs and adults (Fig. 5B). Therefore, the CD36RP mRNA is likely to be expressed in eggs though the level seems lower.

The amino acid sequence indicated that the protein belongs to the CD36 family [66]. It has two transmembrane regions and at least three CD36 domains by Conserved Domain search analysis (Fig. 5A), having high homology with rat SR-B1, rat CD36 and human CLA-1. It had 15 nucleotide polymorphism sites in the coding region identified during screening, resulting in 11 amino acid substitutions. Three N-glycosylation sites (aa97, 205, 248) identified among the 15 candidate glutamines in CD36RP were conserved in mammalian SR-B1 and CD36 (Fig. 5A). In fact, the size of CD36RP in the *S. japonicum* adult decreased from 82 kDa to 62 kDa after treatment with N-Glycanase, probed by the antibody against its extracellular domain [66].

A recombinant peptide representing the extracellular domain containing the conserved Cys and Pro-rich domain of CD36RP was used for binding to lipoproteins [66]. The water-soluble extracellular domain peptide was incubated with HDL and LDL and analysed by density-gradient non-denaturing PAGE and immunoblotting with the anti-peptide antibody (Fig. 6AB). The position of the peptide was shifted from to the position of HDL. The peptide bound much less to LDL and the HDL isolated from the CETP-deficient human serum.

The effect of the antibody against the extracellular domain peptide was examined for CD36RP activity for HDL cholesteryl ester uptake and egg embryonation [66] (Fig. 6CD). The antibody suppressed the

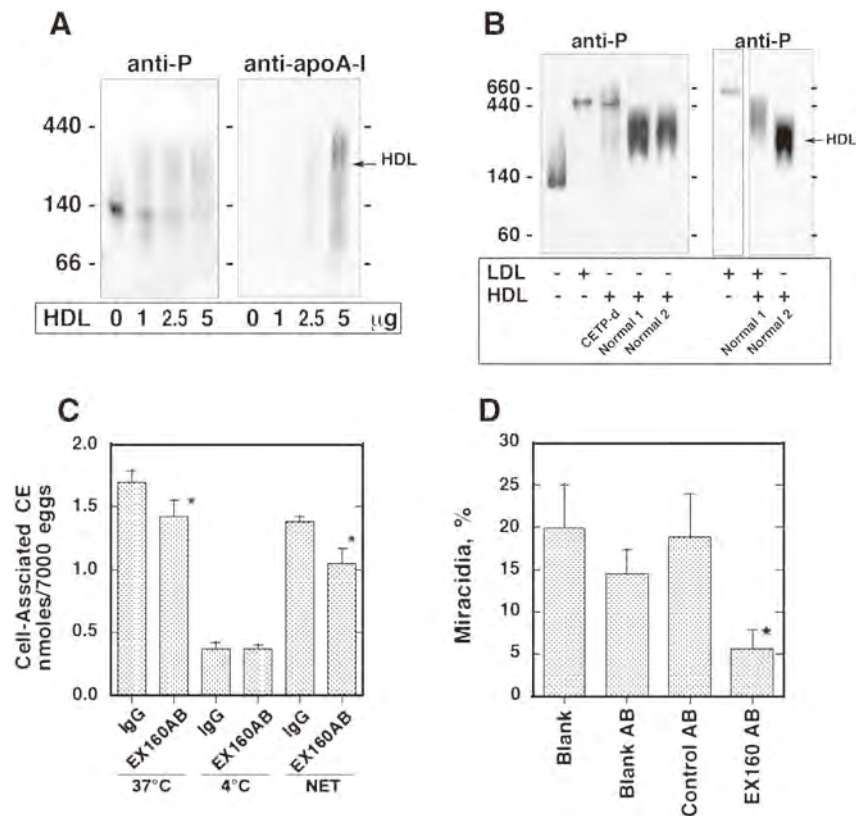


**Fig. 6.** Interaction of the peptide representing the extracellular domain of CD36RP, taken from the reference [66] the experimental details should be referred to. A: Binding of the peptide representing the residues 249–369 with human HDL. HDL is visualized by immunoblotting with anti-apoA-I antibody and the peptide is visualized by using the antibody against the shorter peptide (331–348) (anti-P). B: interaction of the peptide with lipoprotein subfractions, visualized with anti-P. Binding with CETP-deficient HDL is as weak as LDL. C and D: Suppression of CE uptake by and embryonation of the *S. japonicum* eggs, by the antibody raised against the extracellular domain peptide of CD36RP representing the residues 249–408. Blank AB, nonimmunized rabbit antibody, Control AB, antibody against the intracellular domain of CD36RP (residues 331–348).

cholesteryl ester uptake at 37 °C but not at 4 °C, so that significant suppression was for the active uptake shown as NET uptake. Embryonation of the eggs to miracidia was significantly suppressed.

### 5. Proposal of hypothesis and further investigation

The information to date can be summarized as follows. 1) CETP deficiency is a unique inborn error to manifest abnormal lipoprotein profile characterized as very high HDL cholesterol due to extreme enlargement of HDL particles, without other apparent clinical features. CETP deficiency was shown highly prevalent in East Asia, in Japan, China including mainland and Taiwan, and probably in Korea and Thailand, as far as the cohort studies data available, while it seems rare among other ethnic or regional groups. 2) One of the regional endemic diseases that have any relation to plasma lipoproteins is schistosomiasis, blood flukes infection, in which the parasites use the lipoproteins as nutrient sources. Its Asian species *S. japonicum* has a historic evidence of distribution in Japan, China, Philippine and the Mekong river valleys, largely overlap with the region where CETP deficiency is found with high prevalence. 3) The ectopic egg embryonation to miracidia in the liver develops liver cirrhosis, a major fatal pathogenic event in Schistosomiasis. The egg embryonation of *S. japonicum* requires normal plasma HDL and it is not efficient with the HDL of CETP deficiency. 4) CD36RP, a membrane protein of the CD36 family, was identified in the adults and eggs of *S. japonicum*. Its extracellular domain selectively binds to HDL but not the CETP-deficient HDL. The antibodies against the extracellular domain of this protein suppress selective uptake of CE by the eggs as well as the embryonation of the eggs.

Based on these findings and insights, we here propose that CD36RP is a lead candidate for a mediator of selective uptake of cholesteryl ester from HDL by *S. japonicum* necessary for the egg embryonation to form miracidia. It is instructive that pre-exposure of the adult schistosomes to wild-type HDL is sufficient for the eggs to mature, perhaps because the vitelline (yolk) of the egg was preformed adequately in such a condition. In contrast, even the eggs with inadequate vitelline provisions may mature provided that normal HDL is supplied after the eggs are laid. Absence of normal HDL results in inefficient embryonation of the *S. japonicum* eggs in the host liver and, accordingly, less hepatic granulomatosis. This is the case in CETP deficiency where HDL is abnormal large and does not efficiently bind CD36RP. This may be one of the reasons for why the prevalence of CETP deficiency is so high in the East Asia where the infection of *S. japonicum* has been and/or remains common in rural or underdeveloped areas. If this hypothesis were valid, CETP inhibitors could be useful to prevent hepatic granulomatosis in schistosomiasis. This would be reminiscent of the selective advantage that hemoglobinopathies confer against malaria.

We have attempted at length to demonstrate functional alteration of CE uptake by adults or eggs of *S. japonicum* by manipulating expression of the whole CD36RP protein. However, neither functional expression by transfection of full length CD36RP nor knockdown/knockout of the gene in the parasite cells was successful so far, seemingly because of various profound technical problems including expressing the parasite genes in cells or cell lines from other species. Therefore, direct evidence remains waited, that CD36RP mediates the selective uptake of CE by schistosome adults or eggs. However, it is not unreasonable to speculate that CD36RP is a strong candidate for a mediator of HDL-CE uptake by the adults and eggs of *S. japonicum* and therefore a key molecule for embryonation of the egg to the miracidium, because of structural similarity of CD36RP to CD36 or SR-BI, selective binding of the extracellular domain of CD36RP to HDL, and suppression of the HDL-CE uptake and embryonation of the eggs in culture by the antibody against CD36RP. This means that CD36RP is, as well as host plasma HDL, a key protein for hepatic granulomatosis in *S. japonicum* infection that can represent a fatal pathological process in infected persons.

Technical difficulties remain to be overcome in order to accomplish the necessary manipulations such as functional transfection and expression of the gene or knock down of the gene to down regulate the reaction. Given recent advances with transgenesis approaches in schistosomes and other parasitic helminths [70–72], it is feasible that informative functional genetics approaches may soon allow definitive assignment or not of a physiological role for schistosome CD36RP in selective uptake of cholesteryl ester from host high density lipoprotein. It is also important to conduct further epidemiological research focusing more specifically on coincidence of endemic of *S. japonicum* and local prevalence of the CETP deficiency. However, the attempt may not be so simple and easy due to historic shift and dilution of such coincidence.

This work has been supported in part by MEXT-Supported Program for the Strategic Research Foundation at Private Universities, and by a Grant-in-Aid by MEXT.

### References

- [1] D. Drayna, A.S. Jarnagin, J. McLean, W. Henzel, W. Kohr, C. Fielding, R. Lawn, Cloning and sequencing of human cholesteryl ester transfer protein cDNA, *Nature* 327 (1987) 632–634.
- [2] K.W. Ko, T. Ohnishi, S. Yokoyama, Triglyceride transfer is required for net cholesteryl ester transfer between lipoproteins in plasma by lipid transfer protein. Evidence for a hetero-exchange transfer mechanism demonstrated by using novel monoclonal antibodies, *J. Biol. Chem.* 269 (1994) 28206–28213.
- [3] T. Ohnishi, C. Tan, S. Yokoyama, Selective transfer of cholesteryl ester over triglyceride by human plasma lipid transfer protein between apolipoprotein-activated lipid microemulsion, *Biochemistry* 33 (1994) 4533–4542.
- [4] X. Qiu, A. Mistry, M.J. Ammirati, B.A. Chrnyk, R.W. Clark, Y. Cong, J.S. Culp, D.E. Danley, T.B. Freeman, K.F. Geoghegan, M.C. Griffor, S.J. Hawrylik, C.M. Hayward, P. Hensley, L.R. Hoth, G.A. Karam, M.E. Lira, D.B. Lloyd, K.M. McGrath, K.J. Stutzman-Engwall, A.K. Subashi, T.A. Subashi, J.F. Thompson, I.K. Wang, H. Zhao, A.P. Seddon, Crystal structure of cholesteryl ester transfer protein reveals a long tunnel and four bound lipid molecules, *Nat. Struct. Mol. Biol.* 14 (2007) 106–113.
- [5] A. Tall, Plasma lipid transfer proteins, *Annu. Rev. Biochem.* 64 (1995) 235–257.
- [6] B. Foger, A. Ritsch, A. Doblinger, H. Wessels, J.R. Patsch, Relationship of plasma cholesteryl ester transfer protein to HDL cholesterol. Studies in normotriglyceridemia and moderate hypertriglyceridemia, *Arterioscler. Thromb. Vasc. Biol.* 16 (1996) 1430–1436.
- [7] H. Czarnecka, S. Yokoyama, Regulation of cellular cholesterol efflux by lecithin:cholesterol acyltransferase reaction through nonspecific lipid exchange, *J. Biol. Chem.* 271 (1996) 2023–2028.
- [8] T. Kurasawa, S. Yokoyama, Y. Miyake, T. Yamamura, S. Yokoyama, Rate of cholesteryl ester transfer between high and low density lipoproteins in human serum and a case with decreased transfer rate in association with hyperalphalipoproteinemia, *J. Biochem.* 98 (1985) 1499–1508.
- [9] J. Koizumi, H. Mabuchi, A. Yoshimura, I. Michishita, M. Takeda, H. Itoh, Y. Sakai, T. Sakai, K. Ueda, R. Takeda, Deficiency of serum cholesteryl-ester transfer activity in patients with familial hyperalphalipoproteinemia, *Atherosclerosis* 58 (1985) 175–186.
- [10] M.L. Brown, A. Inazu, C.B. Hesler, L.B. Agellon, C. Mann, M.E. Whitlock, Y.L. Marcel, R.W. Milne, J. Koizumi, H. Mabuchi, et al., Molecular basis of lipid transfer protein deficiency in a family with increased high-density lipoproteins, *Nature* 342 (1989) 448–451.
- [11] A. Inazu, X.C. Jiang, T. Haraki, K. Yagi, N. Kamon, J. Koizumi, H. Mabuchi, R. Takeda, K. Takata, Y. Moriyama, et al., Genetic cholesteryl ester transfer protein deficiency caused by two prevalent mutations as a major determinant of increased levels of high density lipoprotein cholesterol, *J. Clin. Invest.* 94 (1994) 1872–1882.
- [12] N. Sakai, S. Yamashita, K. Hirano, M. Menju, T. Arai, K. Kobayashi, M. Ishigami, Y. Yoshida, T. Hoshino, N. Nakajima, et al., Frequency of exon 15 missense mutation (442D:G) in cholesteryl ester transfer protein gene in hyperalphalipoproteinemic Japanese subjects, *Atherosclerosis* 114 (1995) 139–145.
- [13] K. Hirano, S. Yamashita, N. Nakajima, T. Arai, T. Maruyama, Y. Yoshida, M. Ishigami, N. Sakai, K. Kameda-Takemura, Y. Matsuzawa, Genetic cholesteryl ester transfer protein deficiency is extremely frequent in the Omagari area of Japan. Marked hyperalphalipoproteinemia caused by CETP gene mutation is not associated with longevity, *Arterioscler. Thromb. Vasc. Biol.* 17 (1997) 1053–1059.
- [14] T. Maruyama, S. Yamashita, Y. Matsuzawa, H. Bujo, K. Takahashi, Y. Saito, S. Ishibashi, K. Ohashi, F. Shionoiri, T. Gotoda, N. Yamada, T. Kita, Mutations in Japanese subjects with primary hyperlipidemia—results from the Research Committee of the Ministry of Health and Welfare of Japan since 1996, *J. Atheroscler. Thromb.* 11 (2004) 131–145.
- [15] S. Yamashita, K. Hirano, N. Sakai, Y. Matsuzawa, Molecular biology and pathophysiological aspects of plasma cholesteryl ester transfer protein, *Biochim. Biophys. Acta* 1529 (2000) 257–275.
- [16] M. Nagano, S. Yamashita, K. Hirano, M. Takano, T. Maruyama, M. Ishihara, Y. Sagehashi, T. Kujiraoka, K. Tanaka, H. Hattori, N. Sakai, N. Nakajima, T. Egashira, Y. Matsuzawa, Molecular mechanisms of cholesteryl ester transfer protein deficiency in Japanese, *J. Atheroscler. Thromb.* 11 (2004) 110–121.

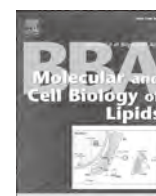
- [17] A. Ritsch, H. Drexel, F.W. Amann, C. Pfeifhofer, J.R. Patsch, Deficiency of cholesteryl ester transfer protein: description of molecular defect and the dissociation of cholesteryl ester and triglyceride transfer in plasma, *Arterioscler. Thromb. Vasc. Biol.* 17 (1997) 3433–3441.
- [18] S.-P. Hui, Frequency and effect on plasma lipoprotein metabolism of a mutation in the cholesteryl ester transfer protein gene in the Chinese, *Hokkaido J. Med. Sci.* 72 (1997) 319–327.
- [19] D.W. Chen, J.F. Yang, Z. Tang, X.M. Dong, X.L. Feng, S. Yu, P. Chan, Cholesteryl ester transfer protein polymorphism D442G associated with a potential decreased risk for Alzheimer's disease as a modifier for APOE epsilon4 in Chinese, *Brain Res.* 1187 (2008) 52–57.
- [20] T.S. Jap, Y.C. Wu, Y.C. Tso, C.Y. Chiu, A novel mutation in the intron 1 splice donor site of the cholesterol ester transfer protein (CETP) gene as a cause of hyperalphalipoproteinemia, *Metabolism* 51 (2002) 394–397.
- [21] L.A. Hsu, Y.L. Ko, K.H. Hsu, Y.H. Ko, Y.S. Lee, Genetic variations in the cholesteryl ester transfer protein gene and high density lipoprotein cholesterol levels in Taiwanese Chinese, *Hum. Genet.* 110 (2002) 57–63.
- [22] G.-J. Song, G.-H. Han, J.-J. Chae, Y. Namkoong, H.-K. Lee, Y.-B. Park, C.-C. Lee, The effect of the cholesterol ester transfer protein gene and environmental factors on the plasma high density lipoprotein cholesterol levels in the Korean population, *Mol. Cells* 7 (1997) 615–619.
- [23] W. Plengpanich, S. Siri Wong, W. Khovichunkit, Two novel mutations and functional analyses of the CETP and LIPC genes underlying severe hyperalphalipoproteinemia, *Metabolism* 58 (2009) 1178–1184.
- [24] M. Nagano, S. Yamashita, K. Hirano, M. Ito, T. Maruyama, M. Ishihara, Y. Sagehashi, T. Oka, T. Kujiraoka, H. Hattori, N. Nakajima, T. Egashira, M. Kondo, N. Sakai, Y. Matsuzawa, Two novel missense mutations in the CETP gene in Japanese hyperalphalipoproteinemic subjects: high-throughput assay by Invader assay, *J. Lipid Res.* 43 (2002) 1011–1018.
- [25] Y.Q. Ma, G.N. Thomas, J.A. Critchley, J.C. Chan, Z.S. Lee, B. Tomlinson, Identification of the intron 14 splicing defect of the cholesteryl ester transfer protein gene in Hong Kong Chinese, *Clin. Genet.* 59 (2001) 287–289.
- [26] E.M. Teh, P.J. Dolphin, W.C. Breckenridge, M.H. Tan, Human plasma CETP deficiency: identification of a novel mutation in exon 9 of the CETP gene in a Caucasian subject from North America, *J. Lipid Res.* 39 (1998) 442–456.
- [27] S.A. Hill, D.J. Nazir, P. Jayaratne, K.S. Bamford, M.J. McQueen, Mutations in cholesteryl ester transfer protein and hepatic lipase in a North American population, *Clin. Biochem.* 30 (1997) 413–418.
- [28] W.A. van der Steeg, G.K. Hovingh, A.H. Klerkx, B.A. Hutten, I.C. Nootenboom, J.H. Levels, A. van Tol, G.M. Dallinga-Thie, A.H. Zwinderman, J.J. Kastelein, J.A. Kuivenhoven, Cholesteryl ester transfer protein and hyperalphalipoproteinemia in Caucasians, *J. Lipid Res.* 48 (2007) 674–682.
- [29] J. Rhyne, M.J. Ryan, C. White, T. Chimonas, M. Miller, The two novel CETP mutations Gln87X and Gln165X in a compound heterozygous state are associated with marked hyperalphalipoproteinemia and absence of significant coronary artery disease, *J. Mol. Med. (Berl)* 84 (2006) 647–650.
- [30] A.B. Cefalu, D. Noto, L. Magnolo, E. Pinotti, M. Gomarasci, S. Martini, G.B. Vigna, L. Calabresi, P. Tarugi, M.R. Averna, Novel mutations of CETP gene in Italian subjects with hyperalphalipoproteinemia, *Atherosclerosis* 204 (2009) 202–207.
- [31] L. Calabresi, P. Nilsson, E. Pinotti, M. Gomarasci, E. Favari, M.P. Adorni, F. Bernini, C.R. Sirtori, S. Calandra, G. Franceschini, P. Tarugi, A novel homozygous mutation in CETP gene as a cause of CETP deficiency in a Caucasian kindred, *Atherosclerosis* 205 (2009) 506–511.
- [32] S. Chantepie, A.E. Bochem, M.J. Chapman, G.K. Hovingh, A. Kontush, High-density lipoprotein (HDL) particle subpopulations in heterozygous cholesteryl ester transfer protein (CETP) deficiency: maintenance of antioxidative activity, *PLoS One* 7 (2012) e49336.
- [33] A. Thompson, E. Di Angelantonio, N. Sarwar, S. Erqou, D. Saleheen, R.P. Dullaart, B. Keavney, Z. Ye, J. Danesh, Association of cholesteryl ester transfer protein genotypes with CETP mass and activity, lipid levels, and coronary risk, *JAMA* 299 (2008) 2777–2788.
- [34] A. Inazu, M.L. Brown, C.B. Hesler, L.B. Agellon, J. Koizumi, K. Takata, Y. Maruhama, H. Mabuchi, A.R. Tall, Increased high-density lipoprotein levels caused by a common cholesteryl-ester transfer protein gene mutation, *N. Engl. J. Med.* 323 (1990) 1234–1238.
- [35] S. Yamashita, D.L. Sprecher, N. Sakai, Y. Matsuzawa, S. Tarui, D.Y. Hui, Accumulation of apolipoprotein E-rich high density lipoproteins in hyperalphalipoproteinemic human subjects with plasma cholesteryl ester transfer protein deficiency, *J. Clin. Invest.* 86 (1990) 688–695.
- [36] S. Yamashita, D.Y. Hui, J.R. Wetterau, D.L. Sprecher, J.A.K. Harmony, N. Sakai, Y. Matsuzawa, S. Tarui, Characterization of plasma lipoproteins in patients heterozygous for human plasma cholesteryl ester transfer protein (CETP) deficiency: plasma CETP regulated high-density lipoprotein concentration and composition, *Metabolism* 40 (1991) 756–763.
- [37] N. Sakai, Y. Matsuzawa, K. Hirano, S. Yamashita, S. Nozaki, Y. Ueyama, M. Kubo, S. Tarui, Detection of two species of low density lipoprotein particles in cholesteryl ester transfer protein deficiency, *Arterioscler. Thromb.* 11 (1991) 71–79.
- [38] C.L. Bisgaier, M.V. Siebenkas, M.L. Brown, A. Inazu, J. Koizumi, H. Mabuchi, A.R. Tall, Familial cholesteryl ester transfer protein deficiency is associated with triglyceride-rich low density lipoproteins containing cholesteryl esters of probable intracellular origin, *J. Lipid Res.* 32 (1991) 21–33.
- [39] Y. Moriyama, T. Okamura, A. Inazu, M. Doi, H. Iso, Y. Mouri, Y. Ishikawa, H. Suzuki, M. Iida, J. Koizumi, H. Mabuchi, Y. Komachi, A low prevalence of coronary heart disease among subjects with increased high-density lipoprotein cholesterol levels, including those with plasma cholesteryl ester transfer protein deficiency, *Prev. Med.* 27 (1998) 659–667.
- [40] J.D. Curb, R.D. Abbott, B.L. Rodriguez, K. Masaki, R. Chen, D.S. Sharp, A.R. Tall, A prospective study of HDL-C and cholesteryl ester transfer protein gene mutations and the risk of coronary heart disease in the elderly, *J. Lipid Res.* 45 (2004) 948–953.
- [41] S.E. Nissen, J.C. Tardif, S.J. Nicholls, J.H. Revkin, C.L. Shear, W.T. Duggan, W. Ruzylo, W.B. Bachinsky, G.P. Lasala, E.M. Tuzcu, Effect of torcetrapib on the progression of coronary atherosclerosis, *N. Engl. J. Med.* 356 (2007) 1304–1316.
- [42] G.G. Schwartz, A.G. Olsson, M. Abt, C.M. Ballantyne, P.J. Barter, J. Brumm, B.R. Chaitman, I.M. Holme, D. Kallend, L.A. Leiter, E. Leitersdorf, J.J. McMurray, H. Mundl, S.J. Nicholls, P.K. Shah, J.C. Tardif, R.S. Wright, Effects of dalcetrapib in patients with a recent acute coronary syndrome, *N. Engl. J. Med.* 367 (2012) 2089–2099.
- [43] C. Betard, A.M. Kessling, M. Roy, A. Chamberland, S. Lussier-Cacan, J. Davignon, Molecular genetic evidence for a founder effect in familial hypercholesterolemia among French Canadians, *Hum. Genet.* 88 (1992) 529–536.
- [44] M. Torrington, J.L. Botha, G.J. Pilcher, S.G. Baker, Association between familial hypercholesterolemia and church affiliation. Is this the result of sociocultural isolation of migrant farmers in 19th-century South Africa? *S. Afr. Med. J.* 65 (1984) 762–767.
- [45] M. Abifadel, J.P. Rabes, S. Jambart, G. Halaby, M.H. Gannage-Yared, A. Sarkis, G. Beaino, M. Varret, N. Salem, S. Corbani, H. Aydenian, C. Junien, A. Munnich, C. Boileau, The molecular basis of familial hypercholesterolemia in Lebanon: spectrum of LDLR mutations and role of PCSK9 as a modifier gene, *Hum. Mutat.* 30 (2009) E682–E691.
- [46] A.C. Allison, Protection afforded by sickle-cell trait against subtertian malareal infection, *Br. Med. J.* 1 (1954) 290–294.
- [47] P.W. Hedrick, Resistance to malaria in humans: the impact of strong, recent selection, *Malar. J.* 11 (2012) 349.
- [48] S.M. Taylor, C.M. Parobek, R.M. Fairhurst, Haemoglobinopathies and the clinical epidemiology of malaria: a systematic review and meta-analysis, *Lancet Infect. Dis.* 12 (2012) 457–468.
- [49] F.D. Rumjanek, E.G. Campos, L.C. Afonso, Evidence for the occurrence of LDL receptors in extracts of schistosomula of *Schistosoma mansoni*, *Mol. Biochem. Parasitol.* 28 (1988) 145–152.
- [50] F.D. Rumjanek, D.J. McLaren, S.R. Smithers, Serum-induced expression of a surface protein in schistosomula of *Schistosoma mansoni*: a possible receptor for lipid uptake, *Mol. Biochem. Parasitol.* 9 (1983) 337–350.
- [51] X. Xu, J.P. Caulfield, Characterization of human low density lipoprotein binding proteins on the surface of *Schistosoma mansoni*, *Eur. J. Cell Biol.* 57 (1992) 229–235.
- [52] S.T. Furlong, K.S. Thibault, L.M. Morbelli, J.J. Guinn, R.A. Rogers, Uptake and compartmentalization of fluorescent lipid analogs in larval *Schistosoma mansoni*, *J. Lipid Res.* 36 (1995) 1–12.
- [53] M.V. Rogers, D. Quilici, G.F. Mitchell, N.H. Fidge, Purification of a putative lipoprotein receptor from *Schistosoma japonicum* adult worms, *Mol. Biochem. Parasitol.* 41 (1990) 93–100.
- [54] J. Fan, G. Xiaoxian, W. Yang, L. Shen, D.P. McManus, P.J. Brindley, A *Schistosoma japonicum* very low-density lipoprotein-binding protein, *Int. J. Biochem. Cell Biol.* 1507 (2003) 1–16.
- [55] D.P. McManus, D.J. Gray, Y. Li, Z. Feng, G.M. Williams, D. Stewart, J. Rey-Ladino, A.G. Ross, Schistosomiasis in the People's Republic of China: the era of the Three Gorges Dam, *Clin. Microbiol. Rev.* 23 (2010) 442–466.
- [56] L.D. Wang, H.G. Chen, J.G. Guo, X.J. Zeng, X.L. Hong, J.J. Xiong, X.H. Wu, X.H. Wang, L.Y. Wang, G. Xia, Y. Hao, D.P. Chin, X.N. Zhou, A strategy to control transmission of *Schistosoma japonicum* in China, *N. Engl. J. Med.* 360 (2009) 121–128.
- [57] R. Bergquist, M. Tanner, Controlling schistosomiasis in Southeast Asia: a tale of two countries, *Adv. Parasitol.* 72 (2010) 109–144.
- [58] C.A. Gordon, L.P. Acosta, D.J. Gray, R.M. Olveda, B. Jarilla, G.N. Gobert, A.G. Ross, D.P. McManus, High prevalence of *Schistosoma japonicum* infection in Carabao from Samar Province, the Philippines: implications for transmission and control, *PLoS Negl. Trop. Dis.* 6 (2012) e1778.
- [59] C. Harinasuta, Epidemiology and control of schistosomiasis in Southeast Asia, *Southeast Asian J. Trop. Med. Public Health* 15 (1984) 431–438.
- [60] F. Iida, R. Iida, H. Kamijo, K. Takaso, Y. Miyazaki, W. Funabashi, K. Tsuchiya, Y. Matsumoto, Chronic Japanese schistosomiasis and hepatocellular carcinoma: ten years of follow-up in Yamanashi Prefecture, Japan, *Bull. World Health Organ.* 77 (1999) 573–581.
- [61] A.G.P. Ross, P.B. Bartley, A.C. Sleight, G.R. Olds, Y. Li, G.M. Williams, D.P. McManus, Schistosomiasis, *N. Engl. J. Med.* 346 (2002) 1212–1220.
- [62] J. Mohda, C.A. Redman, J.A. Thormhill, J.R. Kusel, Schistosomes: unanswered questions on the basic biology of the host-parasite relationship, *Parasitol. Today* 14 (1998) 396–401.
- [63] M. Hirata, M. Takushima, M. Kaga, T. Fukuma, Induction of experimental murine granuloma formation against *Schistosoma japonicum* eggs produced by in vitro ova deposition, in vitro tissue extraction, or lyophilization, *Parasitol. Res.* 77 (1991) 315–319.
- [64] R. El Ridi, P. Velupillai, D.A. Harn, Regulation of Schistosoma egg granuloma formation: host-soluble I-selectin enters tissue-trapped eggs and binds to carbohydrate antigens on surface membrane of miracidia, *Infect. Immun.* 64 (1996) 4700–4705.
- [65] G. Mitchell, E.G. Garcia, P.T. Rivera, W.U. Tiu, K.M. Davern, Evidence for and implications of anti-embryonation immunity in *Schistosomiasis*, *Exp. Parasitol.* 79 (1994) 546–549.
- [66] K. Okumura-Noji, Y. Miura, R. Lu, K. Asai, N. Ohta, P.J. Brindley, S. Yokoyama, CD36-related protein in *Schistosoma japonicum*: candidate mediator of selective cholesteryl ester uptake from high-density lipoprotein for egg maturation, *FASEB J.* 27 (2013) 1236–1244.
- [67] K. Okumura-Noji, K. Sasai, R. Zhan, H. Kawaguchi, H. Maruyama, T. Tada, H. Takahashi, M. Okazaki, T. Miida, N. Sakuma, G. Kimura, N. Ohta, S. Yokoyama, Cholesteryl ester transfer protein deficiency causes slow egg embryonation of *Schistosoma japonicum*, *Biochem. Biophys. Res. Commun.* 286 (2001) 305–310.

- [68] S. Acton, A. Gigotti, T. Landschulz, S. Xu, H.H. Hobbs, M. Krieger, Identification of scavenger receptor SR-BI as a high density lipoprotein receptor, *Science* 271 (1996) 518–520.
- [69] K. Murao, V. Terpstra, S.R. Green, N. Kondratenko, D. Steinberg, O. Quehenberger, Characterization of CLA-1, a human homologue of rodent scavenger receptor BI, as a receptor for high density lipoprotein and apoptotic thymocytes, *J. Biol. Chem.* 272 (1997) 17551–17557.
- [70] S. Yang, P.J. Brindley, Q. Zeng, Y. Li, J. Zhou, Y. Liu, B. Liu, L. Cai, T. Zeng, Q. Wei, L. Lan, D.P. McManus, Transduction of *Schistosoma japonicum* schistosomules with vesicular stomatitis virus glycoprotein pseudotyped murine leukemia retrovirus and expression of reporter human telomerase reverse transcriptase in the transgenic schistosomes, *Mol. Biochem. Parasitol.* 174 (2010) 109–116.
- [71] G. Rinaldi, S.E. Eckert, I.J. Tsai, S. Suttiprapa, K.J. Kines, J.F. Tort, V.H. Mann, D.J. Turner, M. Berriman, P.J. Brindley, Germline transgenesis and insertional mutagenesis in *Schistosoma mansoni* mediated by murine leukemia virus, *PLoS Pathog.* 8 (2012) e1002820.
- [72] H. Shao, X. Li, T.J. Nolan, H.C. Massey, E.J. Pearce, J.B. Lok, Transposon-mediated chromosomal integration of transgenes in the parasitic nematode *strongyloides ratti* and establishment of stable transgenic lines, *PLoS Pathog.* 8 (2012) e1002871.



Contents lists available at ScienceDirect

# Biochimica et Biophysica Acta

journal homepage: [www.elsevier.com/locate/bbalip](http://www.elsevier.com/locate/bbalip)

## Corrigendum

### Corrigendum to “A potential screening factor for accumulation of cholesteryl ester transfer protein deficiency in East Asia: *Schistosoma japonicum*” [Biochim. Biophys. Acta 1841 (2014) 495–504]



Shinji Yokoyama\*

Nutritional Health Science Research Center, Chubu University, Matsumoto-cho 1200, Kasugai 487-8501, Japan

Due to the further completion of the literature survey and to the miscalculation found for the mutant prevalence among Koreans, background information for prevalence and distribution of CETP deficiency in East Asia described in the second paragraph of page 496 should be revised as below. The references are in alphabetical order of the primary author.

The first non-Japanese patient was found in Switzerland but of Chinese descent [11]. Several reports thereafter described CETP deficiency among other Asians. Genetic prevalence of D442G mutant heterozygote case was found to be 2.1–3.8% in the mainland Chinese population [2,5], and 4.5–6.7% in the population of Taiwan [4,7]. The prevalence of D442G patients could be estimated as some 12% among Koreans based on its allele frequency of 6% [12]. Vietnamese D442G mutants were estimated to be 6.9% in the general population [14]. Nine cases were identified to be D442G heterozygotes out of the 35 individuals with hyperalphalipoproteinemias in Thailand [10], accounting for 26% in comparison to the 21–32% in the similar surveys in Japan [6,9] as a strong indication that CETP mutants are not uncommon in Thailand. However, no D442G mutant was found among the 400 individuals examined in North India [3]. Further detailed information is available in the previous review article [13]. More recently, the results from Siberian Yakuts became available, saying that the prevalence of D442G mutant is 16.3% in the native Yakuts and 5.2% among the non-indigenous [1] whose intermarriage rate with Yakuts may be 10 to 20% (Ariev AL, personal communication). A few reliable information is available for the Int14A mutation such as two out of the 145 subjects (1.4%) in Hong Kong Chinese [8] and none of the 346 Vietnamese [14].

## References

- [1] N.S. Arkhipova, A.L. Ariev, et al., Association of polymorphism of angiotensin-converting enzyme gene I/D and D442G cholesteryl ester transfer protein gene with risk factors for atherosclerosis among elderly and senile patients with coronary heart disease in the Republic Sakha (Yakutia) (Original Russian text is published in Uspekhi Gerontologii Vol 26: 76–81 in 2013), *Adv. Gerontol.* 3 (4) (2013) 277–281.
- [2] D.W. Chen, J.F. Yang, et al., Cholesteryl ester transfer protein polymorphism D442G associated with a potential decreased risk for Alzheimer's disease as a modifier for APOE epsilon4 in Chinese, *Brain Res.* 1187 (2008) 52–57.
- [3] M. Dixit, S. Bhattacharya, et al., Association of CETP TaqI and APOE polymorphisms with type II diabetes mellitus in North Indians: a case control study, *BMC Endocr. Disord.* 5 (2005) 7.
- [4] L.A. Hsu, Y.L. Ko, et al., Genetic variations in the cholesteryl ester transfer protein gene and high density lipoprotein cholesterol levels in Taiwanese Chinese, *Hum. Genet.* 110 (1) (2002) 57–63.
- [5] S.-P. Hui, Frequency and effect on plasma lipoprotein metabolism of a mutation in the cholesteryl ester transfer protein gene in the Chinese, *Hokkaido J. Med. Sci.* 72 (3) (1997) 319–327.
- [6] A. Inazu, X.C. Jiang, et al., Genetic cholesteryl ester transfer protein deficiency caused by two prevalent mutations as a major determinant of increased levels of high density lipoprotein cholesterol, *J. Clin. Invest.* 94 (5) (1994) 1872–1882.
- [7] T.S. Jap, Y.C. Wu, et al., A novel mutation in the intron 1 splice donor site of the cholesteryl ester transfer protein (CETP) gene as a cause of hyperalphalipoproteinemia, *Metabolism* 51 (3) (2002) 394–397.
- [8] Y.Q. Ma, G.N. Thomas, et al., Identification of the intron 14 splicing defect of the cholesteryl ester transfer protein gene in Hong Kong Chinese, *Clin. Genet.* 59 (4) (2001) 287–289.
- [9] M. Nagano, S. Yamashita, et al., Two novel missense mutations in the CETP gene in Japanese hyperalphalipoproteinemic subjects: high-throughput assay by Invader assay, *J. Lipid Res.* 43 (7) (2002) 1011–1018.
- [10] W. Plengpanich, S. Siri Wong, et al., Two novel mutations and functional analyses of the CETP and LIPC genes underlying severe hyperalphalipoproteinemia, *Metabolism* 58 (8) (2009) 1178–1184.
- [11] A. Ritsch, H. Drexel, et al., Deficiency of cholesteryl ester transfer protein: description of molecular defect and the dissociation of cholesteryl ester and triglyceride transfer in plasma, *Arterioscler. Thromb. Vasc. Biol.* 17 (1997) 3433–3441.
- [12] G.-J. Song, G.-H. Han, et al., The effect of the cholesteryl ester transfer protein gene and environmental factors on the plasma high density lipoprotein cholesterol levels in the Korean population, *Mol. Cells* 7 (1997) 615–619.
- [13] J.F. Thompson, J.M. Reynolds, et al., Frequency and function of CETP variants among individuals of Asian ancestry, *Atherosclerosis* 202 (1) (2009) 241–247.
- [14] N.N. Thu, T.T. Mai, et al., Effect of the cholesteryl ester transfer protein genotypes on plasma lipid and lipoprotein levels in Vietnamese children, *Pediatr. Res.* 58 (6) (2005) 1249–1253.

DOI of original article: <http://dx.doi.org/10.1016/j.bbalip.2013.12.014>.

\* Tel.: +81 568 51 9698.

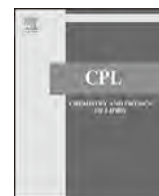
E-mail address: [syokoyam@isc.chubu.ac.jp](mailto:syokoyam@isc.chubu.ac.jp).<http://dx.doi.org/10.1016/j.bbalip.2014.03.006>

1388-1981/© 2014 Elsevier B.V. All rights reserved.



Contents lists available at ScienceDirect

## Chemistry and Physics of Lipids

journal homepage: [www.elsevier.com/locate/chemphyslip](http://www.elsevier.com/locate/chemphyslip)

# Preferential incorporation of shorter and less unsaturated acyl phospholipids into high density lipoprotein-like particles in the ABCA1- and ABCA7-mediated biogenesis with apoA-I

Noriko Hotta<sup>a,b,1,2</sup>, Sumiko Abe-Dohmae<sup>b,1</sup>, Ryo Taguchi<sup>a,c</sup>, Shinji Yokoyama<sup>c,\*</sup>

<sup>a</sup> Graduate Schools of Pharmaceutical Sciences, Nagoya, Japan

<sup>b</sup> Medical Sciences, Nagoya City University, Nagoya, Japan

<sup>c</sup> Nutritional Health Science Research Center, Chubu University, Kasugai, Japan

## ARTICLE INFO

## Article history:

Received 25 November 2014

Received in revised form 24 January 2015

Accepted 27 January 2015

Available online 7 February 2015

## Keywords:

HDL  
Lipidomics  
Global analysis  
Phosphatidylcholine  
Sphingomyelin  
ABCA1  
ABCA7

## ABSTRACT

Molecular species of phosphatidylcholine (PC) and sphingomyelin (SPM) were globally analyzed for lipidomics in the nascent high-density lipoprotein (HDL)-like particles generated with human apolipoprotein A-I (apoA-I) from HEK293 cells where either human ATP binding cassette transporter (ABC) A1 or ABCA7 was transfected and overexpressed. SPM/PC ratio was higher in the ABCA1-mediated HDL than ABCA7-mediated HDL likely being related to their cholesterol content, while it was less than the ratio in the cell membrane in either case. Molecular species composition of hydrocarbon chain moiety in each phospholipid in the HDL largely reflected that in the cells the lipoprotein originated in, without remarkable difference between ABCA1 and ABCA7. Further analysis, however, revealed apparent preference for the molecules with shorter hydrocarbon chain length for both PC and SPM in their relative incorporation into HDL by ABCA1 and ABCA7. Likewise, it was in favor for less-unsaturated hydrocarbon chains of PC while this preference was not apparent for SPM. The results are consistent with the view that assembly of HDL particles with extracellular apoA-I is primarily with the cellular phospholipid molecules being regulated in part by their physicochemical nature.

© 2015 Elsevier Ireland Ltd. All rights reserved.

## 1. Introduction

Plasma high density lipoprotein (HDL) is primarily generated through the interaction of helical apolipoproteins (apo) such as apoA-I with the cell membrane lipids (Hara and Yokoyama, 1991) in the presence of a membrane protein ATP-binding cassette transporter (ABC) A1 (Bodzioch et al., 1999; Brooks-Wilson et al., 1999; Rust et al., 1999). The lipoprotein is initially assembled as a disk-like particle with phospholipid and cholesterol (Hayashi et al., 2005) and acylesterification of cholesterol by lecithin: cholesterol acyltransferase generates a core lipid, cholesteryl acylester, to

render the particles spherical (McCall et al., 1989, 1993). Disk-like particles can be generated as a physicochemical reaction between helical apolipoprotein and phospholipid with the help of sonication, presence of detergent or even spontaneously (Guo et al., 1980; Hoff et al., 1973; Jonas, 1986). Cholesterol is not essential for constructing such particles (Fukuda et al., 2010). The initial biogenesis/assembly of the discoidal HDL thus includes two components: formation of the disk-like particles of apolipoprotein/phospholipid, and incorporation of cholesterol into the particles. ABCA1 mediates the former process, formation of a disk-like apolipoprotein–phospholipid complex, and it does not always accompany incorporation of cholesterol into the particles (Yamauchi et al., 2002). It is not clear whether these two components of the reaction occur as sequential steps, parallel independent reactions or simply depending on cholesterol availability from that reaction. It is also unknown whether ABCA1 catalyzes “transport” of lipid molecules from the membrane to their “acceptor” apolipoproteins (Tall, 2008), or mediates direct interaction of apolipoproteins with membrane lipid to form the disk-like complex which otherwise is prevented by tight structure of cell membrane (Hassan et al., 2007; Vedhachalam et al., 2007). It is therefore important to know how membrane

**Abbreviations:** HDL, high density lipoprotein; ABC, ATP-binding cassette transporter; PC, phosphatidylcholine; SPM, sphingomyelin; LPC, lysophosphatidylcholine; LC/ESI-MS, capillary liquid chromatography/electrospray mass spectroscopy; GFP, green fluorescence protein; FCS, fetal calf serum; HPLC, high performance liquid chromatography.

\* Corresponding author. Tel.: +81 568 51 9698; fax: +81 568 51 9698.

E-mail address: [syokoyam@isc.chubu.ac.jp](mailto:syokoyam@isc.chubu.ac.jp) (S. Yokoyama).

<sup>1</sup> Noriko Hotta and Sumiko Abe-Dohmae contributed equally to this work.

<sup>2</sup> Present address: CMIC Co. Ltd., 2-8-1 Nishi-Gotanda, Shinagawa, Tokyo 114-0031, Japan.

<http://dx.doi.org/10.1016/j.chemphyslip.2015.01.005>

0009-3084/© 2015 Elsevier Ireland Ltd. All rights reserved.

phospholipids are removed from the cells to form the disk-like HDL particles (Yokoyama, 2005, 2006a,b). To gain an insight into the reaction mechanism, incorporation of specific molecular species of phospholipid into the HDL particles should be one of the essential basic information. We therefore intended to carry out global analysis of phospholipid lipidomics in the generation of HDL by apoA-I-cell interaction. The lipid released by apoA-I from cells into the culture medium is almost exclusively in the HDL-like particles except for lysophospholipid (Hara and Yokoyama, 1991), so that lipid in the medium was analyzed for the amount of phosphatidylcholine (PC) and sphingomyelin (SPM) as the HDL phospholipid, as well as lysophosphatidylcholine (LPC). Molecular species compositions of PC and SPM were analyzed by using capillary liquid chromatography/electrospray ionization mass spectrometry (LC/ESI-MS) (Taguchi et al., 2000).

In order to obtain an adequate amount of the HDL to analyze phospholipid molecular species by mass spectrometry, model systems of HEK293 cell were used, in which either human ABCA1 or ABCA7 was transfected and overexpressed (Abe-Dohmae et al., 2004). The ABCA1-transfected cells were shown to generate cholesterol-rich discoidal HDL with extracellular apoA-I (Hayashi et al., 2005). The cells transfected by ABCA7, a membrane protein highly homologous to ABCA1, were also shown to produce discoidal HDL-like lipoprotein particles but containing much less cholesterol than those generated by ABCA1 (Abe-Dohmae et al., 2004; Hayashi et al., 2005; Wang et al., 2003). It is known however that endogenous ABCA7 does not mediate HDL biogenesis and is rather strongly associates with phagocytic function of cells being regulated in an opposite direction to ABCA1 with respect to cell cholesterol via the SREBP system (Iwamoto et al., 2006; Tanaka et al., 2010). So, this artificial model should be considered just as a reference to physiological model of the ABCA1-transfected cells.

## 2. Materials and methods

### 2.1. Cell culture

Human ABCA1 and ABCA7 were cloned and overexpressed as described previously. Full-length cDNAs for ABCA1 and ABCA7 were cloned and introduced to pcDNA3.1/Hygro (Invitrogen), pCMV6c, and pEGFP-N1 (Clontech) to obtain constructs for the proteins with green fluorescent protein (GFP) at their C terminus (Abe-Dohmae et al., 2004; Tanaka et al., 2001). The cDNA constructs were transfected to HEK293 cells to establish the clones 293/2c and 293/6c stably expressing high level of human ABCA1-GFP and ABCA7-GFP, respectively (Abe-Dohmae et al., 2004). The cells were maintained in 1:1 mixture of Dulbecco's modified Eagle's medium and Ham's F12 medium (DF) supplemented with 10% (v/v) of fetal calf serum (FCS, Invitrogen) under a humidified atmosphere of 5% CO<sub>2</sub>, 95% air at 37 °C as described previously.

### 2.2. Apolipoprotein A-I

ApoA-I was isolated from human plasma HDL fraction (density 1.09–1.21) and stored at –80 °C until use as described previously (Yokoyama et al., 1982). Stock solutions (1 mg/ml) were prepared and stored at 4 °C as described previously (Abe-Dohmae et al., 2004).

293/2c and 293/6c cells were subcultured in 100-mm dishes (TPP catalog number 93100) at a density of  $6.0 \times 10^6$  cells/dish with 10% FCS-DF medium. After 48-h incubation, the cells were washed once with buffer H (Hank's balanced salt solution containing 20 mM HEPES-KOH (pH 7.5) and 14 mM glucose), and incubated in 5 ml/dish of DF medium containing 0.02% bovine serum albumin (BSA) with apoA-I (10 µg/ml) for 24 h. The medium was

centrifuged to remove cell debris and concentrated to 75 µl by spinning through an Ultrafree-15 filter unit with a Biomax-10 membrane (Millipore). Lipoproteins were separated by 0.5% agarose gel electrophoresis and stained by sudan black B (Paragon lipoprotein electrophoresis, Beckman Coulter).

### 2.3. Choline-phospholipids mass assay

293/2c and 293/6c cells were subcultured in 100-mm dishes as described above. HEK293 cells were subcultured in 6-well trays (TPP catalog number 92406) at a density of  $1.0 \times 10^6$  cells/well with 10% FCS-DF medium. After 48-h incubation, the cells were washed once with buffer H, and incubated in 1 ml/well of 0.02% BSA-DF medium with or without apoA-I (10 µg/ml) for 24 h. For lipid mass analysis, lipid in the medium of one dish or well, and in the cells (1/2 of dish or well), was extracted by the method of Bligh and Dyer (1959). The extract was divided into 1/2, 1/3, and 1/6, for the assay of SPM, LPC, and total choline-phospholipid, respectively. Choline-phospholipid was measured as described previously (Takayama et al., 1977). For the SPM assay, glycerolipid was pre-removed by mild alkaline hydrolysis in 0.5 M methanolic NaOH at 37 °C for 1 h and by mild acidic hydrolysis in 2.6 M methanolic HCl at 37 °C for 15 min. The amounts of LPC were measured as described previously (Kishimoto et al., 2002). The amount of PC was calculated by subtracting SPM and LPC from total choline-phospholipid. Remaining a half of the cells was used for measuring cell protein by BCA protein assay reagent (PIERCE).

### 2.4. LC/ESI-MS

Phospholipid molecular species was analyzed by LC/ESI-MS as described elsewhere with some modification (Taguchi et al., 2000). The cells, 293/2c, 293/6c and HEK293, were subcultured in 100-mm dishes and incubated with apoA-I (10 µg/ml) and lipid in the medium and cells was extracted as described above. For PC sample, the medium extracts from 80 ml medium were resolved in 50 µl of 2:1 CHCl<sub>3</sub>/MeOH mixture, and the cell extract of 2 dishes were resolved in 200 µl of the same mixture. The extracted phospholipids were directly subjected to LC/ESI-MS analysis. For SPM sample, the extract was pretreated by the hydrolysis procedure as described above. The medium extract equivalent to 70 ml medium was resolved in 25 µl of the CHCl<sub>3</sub>/MeOH mixture and the cell extracts from 2 dishes were resolved in 200 µl of the same mixture. A 5 µl of the aliquot was applied for each LC/ESI-MS assay. The LC/ESI-MS analysis was performed on an HP 1100HPLC system (Hewlett-Packard) and a Quattro II triple-stage quadrupole mass spectrometer (Micromass) equipped with an electrospray ion source. Solvent systems were used at a flow-rate of 60 µl/min. The flow from the HPLC pump was split at a ratio of 20:1 using an accurate flow splitter (LC packings) by using a flow rate for elution ~5 µl/min. The HPLC system was equipped with a 5 µl sample loop. For both positive and negative ionization, the mobile phase consisted of acetonitrile-methanol (2:1) containing 0.1% ammonium formate (pH 6.4) (solvent A) and methanol-H<sub>2</sub>O (2:1) containing 0.1% ammonium formate (pH 6.4) (solvent B). In both solvent A and B, the pH of the solvent containing 0.1% formic acid was adjusted to 6.4 with aqueous ammonia. The mass spectrometer was operated in both positive and negative ion modes. The nitrogen drying gas flow-rate was ~12 l/min at temperature of 60 °C. The tuning parameters for the positive ion mode were capillary voltage 3.70 kV, HV lens, 0.05 kV, skimmer offset 5 V, skimmer 1.5 V and r.f. lens 0.2 V. In the detection process of the quadrupole mass spectrometer, positive molecular ions and negative molecular ions were analyzed under different functions. For monitoring the positive molecular ions, the cone voltage was set at 30 V in the positive ion mode and the mass range was within

**Table 1**  
Molecular composition of phosphatidylcholine (PC).

PC[M+1]	Possible pair(s) of sn-1 and sn-2 acyl chains	PC composition											
		293/2c (ABCA1)					293/6c (ABCA7)					HEK293	
		PC in medium		Cell PC (%)		HDL mass <sup>a</sup>	PC in medium		Cell PC (%)		HDL mass <sup>a</sup>	Cell PC (%)	
		apoA-I (-)	apoA-I (+)	HDL (%)	apoA-I (-)		apoA-I (+)	HDL (%)	apoA-I (-)	apoA-I (+)		HDL (%)	apoA-I (-)
PC[706.5]	(14:0-16:0)	4.9±0.2	5.0±0.5	3.9±0.3	5.1±0.4	3.1±0.3	4.22±0.4	4.0±0.3	9.6±0.9	4.0±0.4	2.7±0.4	3.5±0.2	2.0±0.2
PC[718.6]	(16:0-16:1)-alkyl/(16:0-16:0)-alkenyl	3.7±0.3	3.8±0.2	2.9±0.2	3.8±0.3	3.7±0.3	3.47±0.7	2.7±0.2	6.3±0.8	2.6±0.3	3.1±0.3	2.7±0.3	2.9±0.2
PC[720.6]	(16:0-16:0)-alkyl	2.2±0.3	2.0±0.2	1.5±0.2	2.0±0.2	1.9±0.5	2.60±0.5	2.1±0.4	4.9±1.0	2.0±0.4	1.3±0.1	1.3±0.1	0.9±0.1
PC[730.6]	(16:1-16:1)	1.8±0.2	1.7±0.1	1.3±0.1	1.7±0.1	2.8±0.2	1.85±0.3	2.0±0.4	5.0±0.9	2.1±0.4	3.2±0.4	2.6±0.2	3.0±0.1
PC[732.6]	(16:0-16:1)	1.78±0.5	2.0±0.2	1.58±0.3	2.0±0.4	1.91±0.5	19.07±1.2	18.0±0.7	43.0±2.2	17.9±0.9	17.7±1.7	19.4±0.3	16.9±0.3
PC[734.6]	(16:0-16:0)	2.8±0.2	2.0±0.2	1.3±0.1	1.7±0.1	0.6±0.1	3.45±0.9	3.0±0.4	7.1±1.4	2.9±0.6	1.6±0.2	1.7±0.5	0.7±0.1
PC[744.6]	(16:0-18:2)-alkyl/(16:0-18:1)-alkenyl	1.5±0.2	1.5±0.2	1.2±0.2	1.5±0.2	3.5±0.6	1.73±0.2	1.8±0.5	4.4±0.7	1.8±0.3	3.8±0.6	2.2±0.7	3.7±0.2
PC[746.6]	(16:0-18:1)-alkyl/(16:0-18:0)-alkenyl	5.1±0.2	5.4±0.3	4.2±0.2	5.6±0.3	4.7±0.3	4.89±0.8	4.7±0.6	11.2±1.7	4.7±0.7	3.8±0.2	3.7±0.3	4.1±0.2
PC[758.6]	(16:0-18:2)	6.2±0.4	7.5±0.2	6.0±0.3	7.9±0.4	10.2±0.1	6.36±1.1	8.2±0.8	20.0±2.6	8.3±1.1	8.5±0.3	9.1±0.6	9.6±0.3
PC[760.6]	(16:0-18:1)	3.13±1.3	3.25±0.8	2.5±0.8	3.3±0.1	3.05±0.5	29.49±0.5	33.3±0.5	80.7±1.3	33.6±0.5	31.5±0.2	31.6±1.7	34.0±0.2
PC[782.6]	(16:0-20:4)	4.0±0.5	3.2±0.8	2.2±0.4	2.9±0.5	3.1±1.5	5.13±1.8	2.2±0.3	4.7±1.1	1.9±0.5	2.0±0.4	3.4±1.7	1.7±0.1
PC[784.6]	(16:0-20:3)	2.2±0.2	1.8±0.1	1.2±0.1	1.6±0.1	2.9±0.1	2.07±0.3	2.2±0.3	5.4±0.7	2.3±0.3	2.9±0.4	2.6±0.5	2.4±0.1
PC[786.6]	(16:0-20:2,18:0-18:2, 18:1-18:1)	8.6±0.3	8.7±0.2	6.6±0.2	8.7±0.3	11.4±0.4	8.16±1.0	10.1±0.7	24.6±2.4	10.2±1.0	11.4±0.5	10.7±0.7	12.5±0.3
PC[788.6]	(16:0-20:1,18:0-18:1)	7.6±0.1	4.7±0.3	2.7±0.1	3.6±0.1	4.0±0.4	7.50±1.2	5.8±0.5	13.7±1.7	5.7±0.7	6.5±0.5	5.3±0.6	5.6±0.5
Total				75.8			240.5						

<sup>a</sup> : increase; : decrease. Increase/decrease: more than 10% change from the cell data of either apoA-I (-) or apoA-I (+), with  $p$  value < 0.05.  
 pg/mg cell protein. Calculated from total PC (Fig. 2) and percentage of each molecule, and difference between apoA-I (-) and apoA-I (+).

$m/z$  50–1200, with scan time 3 s. For monitoring the negative molecular ions, the cone voltage was set at 30 V in the negative ion mode and the mass range was within  $m/z$  50–1200, with scan time 3 s. These different conditions were successively monitored in 10 s cycles. Typical patterns are shown in Supplementary Fig. 1, with identification of the peaks as described below.

### 2.5. Identification of individual molecular species from LC/MS-ESI data

Individual molecular species of PC was identified by using the theoretical mass data as described previously (Taguchi et al., 2000). PC was designated as follows: diacyl 34:1 PC ( $m/z$  760.6) (protonated molecular weight in the positive ion mode), where 34: means the summed number of carbon atoms at both the sn-1 and sn-2 positions and :1 means the summed number of unsaturated bonds at both the sn-1 and sn-2 positions. Possible major species are indicated as diacyl 16:0–18:1 PC or diacyl 16:1–18:0 PC, where 16:0 and 18:0 are the number of carbon atoms in the fatty acyl chains at sn-1 and sn-2 positions, respectively, and :0 and :1 are the number of double bonds of the sn-1 and sn-2 fatty acyl chains, respectively (Taguchi et al., 2000). A cluster of diacyl group pairs was observed in slightly higher peaks at each mass difference of 28. An intervening lower cluster of peaks represented an alkyl- or alkenylacyl group, which has a mass difference of 14 or 16 from the corresponding diacyl groups. Consequently, the  $m/z$  718.6 peak was categorized as (16:0–16:1) alkyl/(16:0–16:0) alkenyl PC and likewise those of 744.6 and 746.6 defined in Table 1. *D-erythro*-sphingomyelin, was designated as follow: 16:0 SPM ( $m/z$  703.6), where 16: means the number of carbon atoms of the *N*-acyl chain and :0 means the number of double bonds of the *N*-acyl chain. From the spectrums, 14 peaks of PC sample and 10 peaks of SPM samples were considered as major PC and SPM molecule peaks and the relative composition of each major peak was calculated, respectively (Taguchi et al., 2000).

### 2.6. Statistical analysis

Statistical significance of differences in three groups was estimated using Scheffe's test after one-way analysis of variance. The statistical significance of difference between two groups was determined using paired *t*-tests. Significant difference was defined as  $p < 0.05$ .

## 3. Results

### 3.1. Cellular lipid release by apoA-I

HEK293 cells do not exhibit apoA-I-dependent cell lipid release. However, the cells where ABCA1 or ABCA7 transfected and expressed released choline-phospholipid and cholesterol into the medium when incubated with apoA-I in a dose dependent manner, indicating that HDL particles are generated in the medium (Fig. 1A and B). We previously characterized these reactions extensively to demonstrate that two distinguished discoidal particles are generated; large cholesterol-rich and small cholesterol-poor particles. The ABCA1-transfected cells generate the former more and the ABCA7 cells generates almost exclusively the latter (Hayashi et al., 2005). Being consistent with these previous findings, the cells expressing ABCA1 release relatively more cholesterol to phospholipid than those expressing ABCA7. Agarose gel electrophoresis confirmed generation of alpha-lipoprotein (HDL) in the medium by this incubation (Supplementary Fig. 2). The very front band is considered as lysophospholipid bound to albumin, so that the bands with alpha and prebeta mobilities may represent the two HDL-like particles. Due to the technical limit,

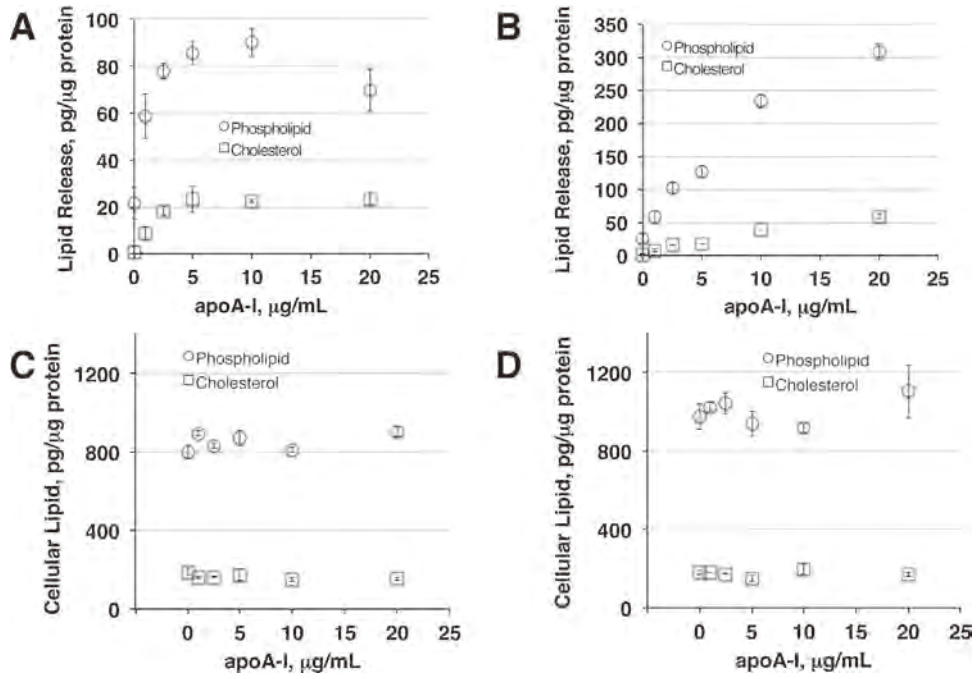


**Fig. 1.** Release of cholesterol and choline-phospholipid from HEK293 cells transfected with human ABCA1 or ABCA7 (293/2c or 293/6c). A: release of cholesterol and phospholipid from 293/2c cells (ABCA1) by apoA-I. B: release of cholesterol and phospholipid from 293/6c cells (ABCA7) by apoA-I. C: change of cell cholesterol and phospholipid in 293/2c cells (ABCA1) as lipid release by apoA-I is carried out. D: change of cell cholesterol and phospholipid in 293/6c cells (ABCA7) as lipid release by apoA-I is carried out. Experimental conditions are described in the text. The data represent  $M \pm SD$  for three measurements.

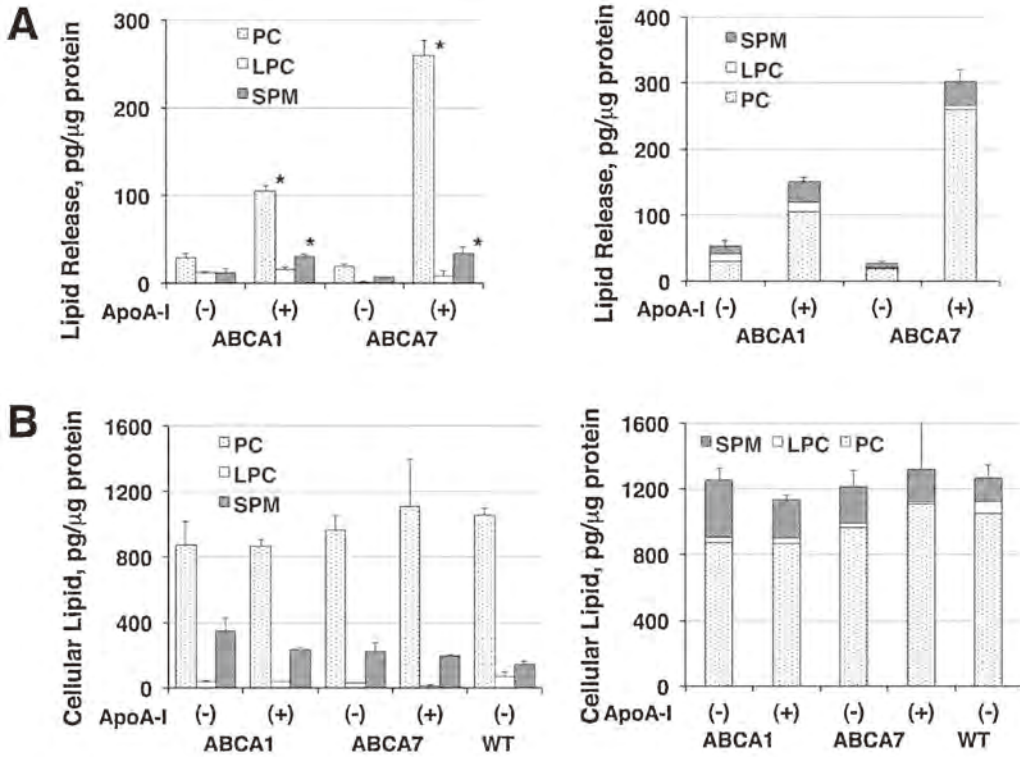


**Fig. 2.** Choline-phospholipid composition in the apoA-I (10  $\mu\text{g/ml}$ )-dependent release of choline-phospholipid (HDL) into the medium. A (left): the composition in the medium with 263/2c cells (ABCA1) and 263/6c cells (ABCA7). A (right): the same data in the left panel are shown in compiled columns. B (left): changes in cellular phospholipid in 263/2c cells (ABCA1) and 263/6c cells (ABCA7). B (right): the same data in the left panel are shown in compiled columns. ApoA-I (+) and (-) indicate incubation with and without apoA-I. Asterisks indicate  $p < 0.05$  for apoA-I (+) from apoA-I (-).

**Table 2**  
Molecular composition of sphingomyelins (SPM).

SPM molecular species	HEK293											
	293/2c (ABCA1)						293/6c (ABCA7)					
	SPM in medium			Cell SPM (%)			SPM in medium			Cell SPM (%)		
	N-acyl chain	apoA-I (-), (%)	apoA-I (+), (%)	HDL mass <sup>a</sup>	HDL (%)	apoA-I (-), (%)	apoA-I (+), (%)	HDL mass <sup>a</sup>	HDL (%)	apoA-I (-), (%)	apoA-I (+), (%)	apoA-I (-), (%)
SM[675.6]	(14:0)	3.6 ± 1.5	6.5 ± 0.7	1.5 ± 0.4	8.4 ± 2.2	4.0 ± 0.1	3.9 ± 0.5	2.0 ± 0.3	7.1 ± 1.2	3.2 ± 0.3	3.3 ± 0.3	2.8 ± 0.4
SM[701.6]	(16:1)	6.1 ± 0.4	6.7 ± 0.1	1.3 ± 0.1	7.2 ± 0.3	2.4 ± 0.2	2.3 ± 0.2	0.9 ± 0.3	3.1 ± 0.9	2.8 ± 0.3	1.6 ± 0.4	3.7 ± 0.3
SM[703.6]	(16:0)	39.3 ± 0.5	47.3 ± 0.7	9.4 ± 0.1	52.7 ± 0.7	55.9 ± 1.1	54.7 ± 2.2	17.4 ± 1.0	62.8 ± 3.5	53.8 ± 0.5	51.3 ± 1.2	57.7 ± 2.0
SM[729.6]	(18:1)	3.8 ± 0.4	4.2 ± 0.2	0.8 ± 0.1	4.5 ± 0.3	1.3 ± 0.1	1.4 ± 0.3	0.7 ± 0.2	2.6 ± 0.2	0.9 ± 0.2	1.4 ± 0.4	2.0 ± 0.2
SM[731.6]	(18:0)	6.2 ± 0.2	6.0 ± 0.5	1.1 ± 0.1	5.9 ± 0.4	6.7 ± 0.2	6.5 ± 0.2	1.1 ± 0.1	3.9 ± 0.2	5.9 ± 1.1	6.7 ± 0.8	6.1 ± 0.3
SM[759.6]	(20:0)	3.0 ± 0.6	1.8 ± 0.2	0.2 ± 0.0	0.9 ± 0.1	1.6 ± 0.1	1.9 ± 0.2	0.2 ± 0.0	0.9 ± 0.1	1.7 ± 0.5	2.1 ± 0.2	1.2 ± 0.1
SM[785.6]	(22:1)	5.8 ± 0.5	5.0 ± 0.1	0.8 ± 0.0	4.5 ± 0.2	3.16 ± 0.1	3.2 ± 0.3	0.9 ± 0.1	3.3 ± 0.4	2.5 ± 0.3	3.4 ± 0.7	2.3 ± 0.1
SM[787.6]	(22:0)	9.7 ± 0.5	6.2 ± 0.6	0.7 ± 0.1	3.8 ± 0.3	5.7 ± 0.5	6.3 ± 0.5	0.7 ± 0.1	2.7 ± 0.2	7.0 ± 0.5	6.4 ± 0.9	4.7 ± 0.5
SM[815.7]	(24:1)	16.2 ± 1.3	12.7 ± 0.1	1.9 ± 0.1	10.4 ± 0.4	13.2 ± 0.4	14.5 ± 1.8	3.0 ± 0.1	10.8 ± 0.5	14.4 ± 0.9	16.7 ± 1.4	12.6 ± 1.2
SM[817.7]	(24:0)	6.3 ± 0.9	3.6 ± 0.2	0.3 ± 0.0	1.7 ± 0.2	6.1 ± 0.9	5.4 ± 0.7	0.8 ± 0.1	2.9 ± 0.3	7.8 ± 0.3	7.1 ± 0.7	7.0 ± 0.8
Total												

Legend: **↑**: increase; **↓**: decrease; Increase/decrease: more than 10% change from the cell data of either apoA-I (-) or apoA-I (+), with *p* value < 0.05.  
<sup>a</sup> pg/mg cell protein. Calculated from total SPM (Fig. 2) and percentage of each molecule, and difference between apoA-I (-) and apoA-I (+).

lipid mass was analyzed for the two types of HDL particles as a single pool.

Mass ratio of cholesterol to choline-phospholipid released into the medium by apoA-I (in HDL) was estimated as 0.33–1 and 0.19–1 from the ABCA1- and ABCA7-expressing cells, respectively. There was no significant change in cellular phospholipid and cholesterol during these incubations (Fig. 1C and D), indicating substantial compensatory biosynthesis (Ito et al., 2002) as some 11 and 22% of cell phospholipid and cholesterol were released from ABCA1-transfected cells and 27 and 34% from ABCA7-transfected cells, at maximum. The mass ratio of SPM to PC in the lipid released by apoA-I was also higher from the ABCA1-transfected cells than the ABCA7-transfected cells, indicated as 0.24–1 and 0.11–1, seemingly reflecting the cholesterol/phospholipid ratio in the HDL particles generated (Fig. 2A, left). However, this ratio was lower than the SPM/PC ratio in the cells even with the ABCA1-expressing cells. Although overall cellular choline-phospholipid mass has not changed, decrease of SPM and therefore relative increase of PC were found by the incubation with apoA-I (Fig. 2B, left). Accordingly, lipid mass compositional ratios of cholesterol, SPM and PC were, 0.41: 0.24: 1 in the ABCA1-mediated HDL and 0.21: 0.12: 1 in the ABCA7-mediated HDL. Total phospholipid and its composition are shown in the left graphs of each panel of Fig. 2 for convenience to readers.

### 3.2. Lipidomics analysis of phospholipids

The results of analysis by LC/ESI-MS are listed for PC and SPM in Tables 1 and 2 with respect to their acyl/alkyl/alkenyl chains. Spectrum of molecular species of each phospholipid in HDL largely reflected those of the cells the HDL generated from, either mediated by ABCA1 or ABCA7. However, there was a trend of the relative increase of certain molecular species. Overall tendency was that the phospholipid molecules with shorter hydrocarbon chain length are incorporated relatively more into the HDL either by ABCA1- or ABCA7-mediated reactions. PC molecules with saturated hydrocarbon chains in both ABCA1- and ABCA7-mediated HDL, such as (14:0–16:0), (16:0–16:0), (16:0–16:0)-alkyl, and some of those potentially with monounsaturated chains like (16:0–16:1)-alkyl/(16:0–16:0)-alkenyl (16:0–18:1)-alkyl/(16:0–18:0)-alkenyl. However, this trend was unclear for SPM molecules as the *N*-acyl chains of SPM were all unsaturated or monounsaturated.

Such trends are graphically displayed in Figs. 3 and 4. Fig. 3A and B compares compositions of PC and SPM molecular species, respectively, between the HDL and the cells as to the length of acyl/alkyl chains. As demonstrated in Fig. 3B for PC and 3D for SPM, the molecules with shorter hydrocarbon chain length were more preferentially incorporated into the HDL mediated either by ABCA1 or ABCA7. Similar analysis was carried out with respect to hydrocarbon chain saturation levels in Fig. 4. Differential incorporation of each phospholipid molecule from the cell to HDL is shown in Fig. 4B, expressed as HDL/cell ratio of the composition of each molecule, indicating more incorporation of the less-unsaturated molecules into HDL both in ABCA1- and ABCA7-mediated reactions. No preference was observed between the saturated and monounsaturated *N*-acyl chains of SPM in incorporation into HDL (Fig. 4C).

## 4. Discussion

Molecular species of choline-phospholipid compositions were analyzed in the HDL generated from cellular lipid by extracellular apoA-I in the presence of ABCA1 or ABCA7, to investigate selectivity/preference of the reactions over those molecular species. The results are summarized as below. (1) Cholesterol

content was higher in the HDL generated from the ABCA1 transfected cells than those transfected with ABCA7, being consistent with our previous findings (Abe-Dohmae et al., 2004, 2006; Hayashi et al., 2005). (2) SPM content in the HDL was lower relatively to PC than that in the cell membrane and seemed associated with its cholesterol content. (3) Species composition of the phospholipid in the HDL largely reflects the composition in the cell membrane. (4) Preferential incorporation was yet observed for the molecules with shorter hydrocarbon chain length of PC and SPM, and less unsaturated chains for PC.

Generation of HDL-like particles was discovered upon the interaction of helical apolipoproteins with the cells in culture (Abe-Dohmae et al., 2006; Hara and Yokoyama, 1991; Hayashi et al., 2005), and this reaction was identified as a major source of plasma HDL as the lack of this reaction was found to cause genetic defect of plasma HDL, Tangier disease, (Francis et al., 1995), and probucol, a drug that strongly reduces plasma HDL, inhibits the reaction (Tsujita and Yokoyama, 1996; Wu et al., 2004). Dysfunctional mutation ABCA1 was later identified as a genetic background for Tangier disease (Bodzioch et al., 1999; Brooks-Wilson et al., 1999; Rust et al., 1999). As HDL biogenesis reaction is an essential part of cholesterol homeostasis in the body and cells, the ABCA1 gene is regulated through the transcription systems related to cholesterol and lipid metabolism (Costet et al., 2003). HDL-like particle is assembled as a disk particle composed of phospholipid and unesterified cholesterol by ABCA1-helical apolipoprotein interaction (Abe-Dohmae et al., 2006; Jayaraman et al., 2011). However, cholesterol by itself does not form lipid-protein complex particles with apolipoprotein, though it may directly bind to some proteins such as serum albumin (Ha et al., 2003; Peng et al., 2008). To the contrary, physicochemical assembly of the HDL-like particles, similarly to those produced by the ABCA1-mediated cell-apolipoprotein interaction may not essentially require

cholesterol (Fukuda et al., 2010; Jayaraman et al., 2010). Also, HDL-like particles can be generated even without cholesterol upon the ABCA1-mediated cell-apolipoprotein interaction (Yamauchi et al., 2002). Therefore, biogenesis of HDL particles is primarily with cellular phospholipid, and cholesterol is secondarily included in the particles, whether sequentially, all at once or else. Accordingly, it is one of the important and essential information for the mechanism of the ABCA1-mediated biogenesis of HDL how molecular preference of phospholipid is involved in the assembly of the particles.

ABCA7, a molecule highly homologues to ABCA1, also mediates the HDL biogenesis when transfected (Abe-Dohmae et al., 2004). The HDL thus generated however contains much less cholesterol than that generated by ABCA1. More detailed analyses showed that the HDL particle generated by ABC-transporters are composed of large cholesterol-rich and small cholesterol-poor fractions. ABCA7-generated HDL is mostly composed of the latter while ABCA1-generated HDL includes predominantly the former (Hayashi et al., 2005). However, HDL biogenesis by transfected ABCA7 is a kind of artifact since endogenous ABCA7 does not seem involved in production of HDL but rather associated strongly with phagocytic function of the cells being regulated by SREBP (Iwamoto et al., 2006; Tanaka et al., 2011). Nevertheless, the ABCA7-transfected model can still be useful as a reference system to the ABCA1-mediated HDL biogenesis system because of apparent similarity of the reaction and difference of the reaction product. ABCA7 did not show significant difference from ABCA1 in preference for molecular species for incorporation into HDL, indicating that the basic mechanism for the HDL biogenesis to construct phospholipid-apolipoprotein disk complex is similar between ABCA1 and ABCA7 as far as when transfected.

SPM and cholesterol form clusters as so-called raft domains in the plasma membrane predominantly composed of PC. This

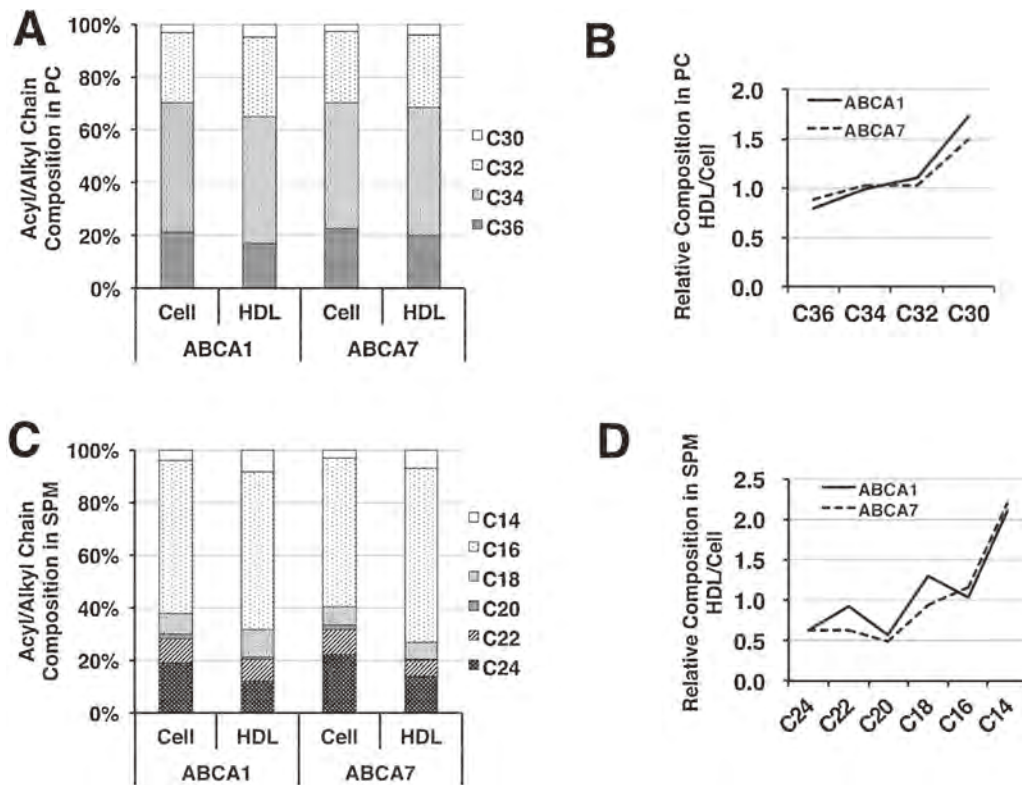


**Fig. 3.** Molecular species composition of choline-phospholipid with respect to chain length of hydrocarbon mieties in the apoA-I-dependent release (HDL) of choline-phospholipid and that in the cells. The data are calculated from those listed in Tables 1 and 2. A, PC; C, SPM. Ratio of relative compositions of each molecular species as HDL/cell is graphically shown in B (PC) and D (SPM). C[number] indicates the number of total carbon atoms in acyl/alkyl/alkenyl chains of PC and in acyl chains of SPM.

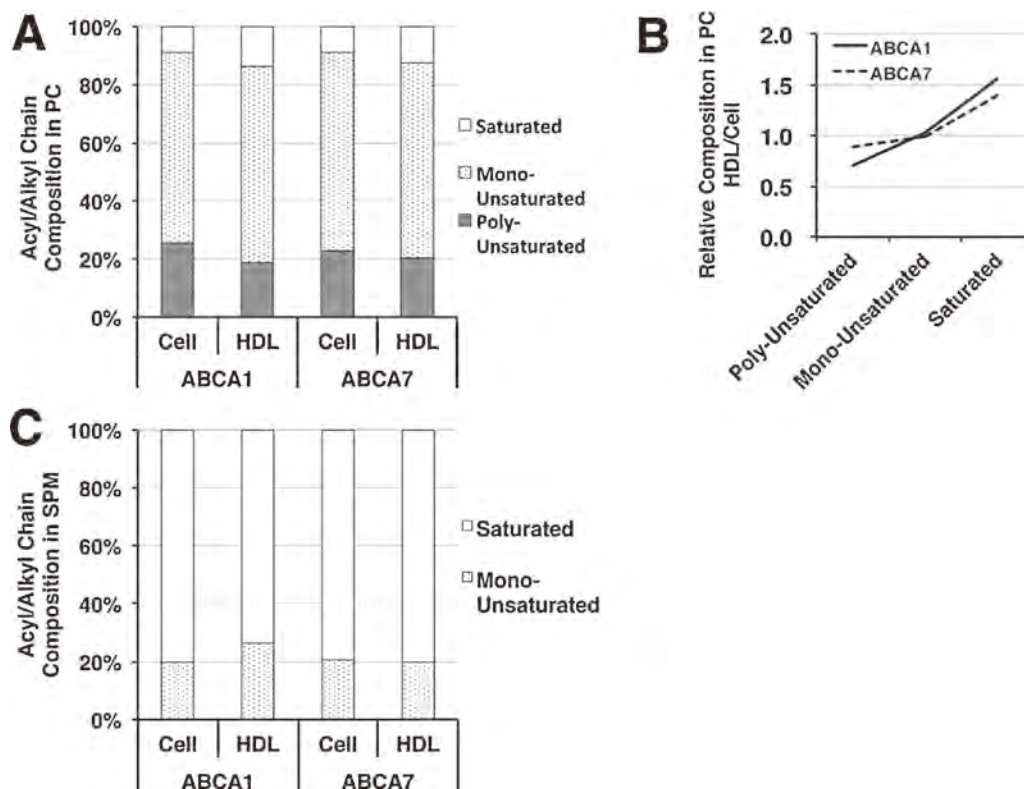


**Fig. 4.** Molecular species composition of choline-phospholipid with respect to unsaturation levels of hydrocarbon moieties in the apoA-I-dependent release (HDL) and that in the cells. The data are calculated from those listed in Tables 1 and 2. A, PC; C, SPM. Ratio of relative compositions of each molecular species as HDL/cells is graphically shown in B (PC). Mono-unsaturated, molecules with one or both mono-unsaturated acyl/alkyl/alkenyl chain(s) in PC and acyl chain in SPM; poly-unsaturated, molecules with at least one poly-unsaturated hydrocarbon chain(s). For the peaks of PC (718.6, 744.6, 746.6, 786.6), equal molecular mass of each candidate molecule was arbitrarily assumed for calculation. The calculation by “all or none” assumption gave essentially similar results (not shown).

domain provides distinct physicochemical microenvironment to accumulate certain types of membrane proteins to construct molecular machineries such as signal transduction systems. SPM accordingly restricts mobility of cholesterol molecule in this domain and its degradation releases cholesterol towards intracellular compartments or HDL biogenesis (Ito et al., 2000). Parallel release of cholesterol and SPM in the current work seems consistent with this view.

Preference or selectivity of phospholipid molecular species in their use for the HDL biogenesis were investigated for chain length and saturation levels of acyl/alkyl chains. In the similar studies previously carried out for fibroblasts and macrophages, the authors concluded preferential use specific molecules such as monounsaturated PC or medium chain SPM (Schifferer et al., 2007). The current observation showed more general tendency in preferential use of phospholipid molecular species rather than selectivity for specific types of molecules. While composition of molecular species was largely reflection of that in the cell membrane the HDL originated from both for PC and SPM, more preferential incorporation to HDL was apparent for shorter and less unsaturated hydrocarbon chains. Although the nature of the data do not exactly match statistical analysis, the curve against carbon number was consistent with exponential functions as  $y = 64 \times \exp(-0.12x)$  and  $y = 15 \times \exp(-0.08x)$  for ABCA1 and ABCA7 in phosphatidylcholine and  $y = 7.0 \times \exp(-0.10x)$  and  $9.5 \times \exp(-0.13x)$  for sphingomyelin, indicating that the trend is similar between the ABCA1- and ABCA7- mediated reactions. Hydrophobicity can be a factor considered from the chain-length preference in the case of SPM, but it is unlikely for the preference of PC with less-unsaturated chains. Molecular fluidity may more likely be an alternative interpretation.

Mechanism to assemble the disk-like HDL particle by ABCA1 has not been elucidated. It seems to require the ATPase activity of ABCA1 and its dimeric form is proposed to be active, and two major streams of the hypothesis are discussed. The one is to assume that ABCA1 works as a lipid transporter within or across the membrane to “load” lipid molecules to lipid-free or “lipid-poor” helical apolipoproteins to construct the lipoprotein particle (Smith et al., 2004), and the other is to conceive that ABCA1 disorganizes the membrane lipid conformation to make apolipoproteins to access and “solubilize” a part of the membrane lipid to form a disk-like HDL (Gillotte et al., 1999). In the former model, assembly of an HDL particle would be a consequence of transporting phospholipid and cholesterol may be loaded to the particles by a discrete mechanism unless ABCA1 transport both. In the latter model, it rather rational to assume that solubilization of the membrane takes place with cholesterol even though a sequential model may not completely be excluded (Wang et al., 2003, 2001).

Preference among the incorporation phospholipid molecules into HDL can be interpreted in either model. For a transporter model, phospholipid can be transported by ABCA1 with certain selectivity for molecular species. In a “microsolubilization” model, difference of physicochemical nature among phospholipid molecular species may result in their selective incorporation. Alternatively, potential unequal distribution of phospholipid molecular species in the plasma membrane may result in their differential incorporation into HDL. This view can be applied to either model. However, preference for shorter and less-unsaturated acyl/alkyl chains is at least consistent with the observation in physicochemical reconstitution of disk-like particles with helical apolipoproteins and phospholipid in vitro that the molecules more unstable and

mobile in the membrane are preferably incorporated into HDL (Jayaraman et al., 2005).

The data here demonstrated that phospholipid is incorporated into HDL from cell membrane with a trend of preference for the molecules with less unsaturated and shorter acyl chain moieties. Thus, the trends may not be interpreted by fluidity or hydrophobicity but may be perhaps be instability of membrane. The results would help further understanding of the mechanism of HDL biogenesis.

### Conflict of interest

The authors declare that there are no conflicts of interest.

### Transparency document

The Transparency document associated with this article can be found in the online version.

### Acknowledgments

This work was supported in part by MEXT-Supported Program for the Strategic Research Foundation at Private Universities (S1201007) and by Grant-in-aid from MEXT Japan (24614018).

### Appendix A. Supplementary data

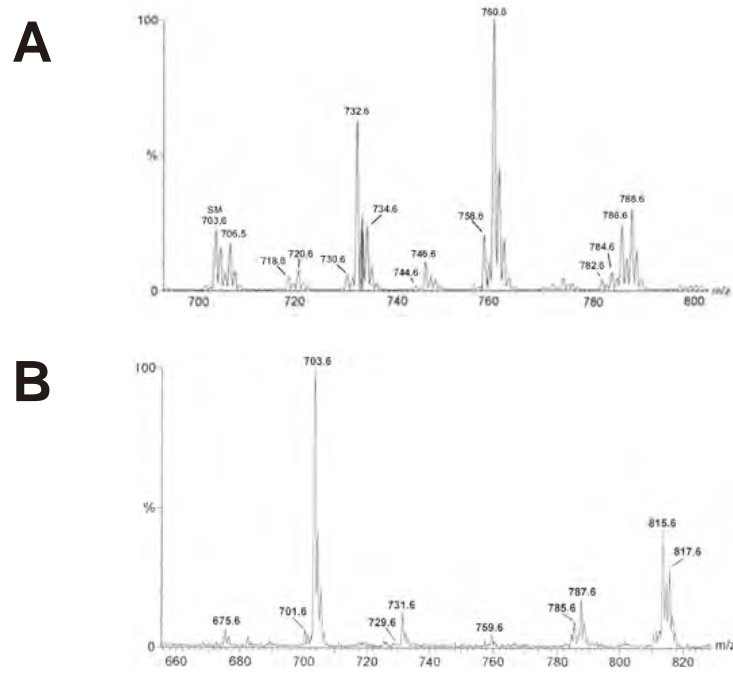
Supplementary data associated with this article can be found, in the online version, at <http://dx.doi.org/10.1016/j.chemphyslip.2015.01.005>.

### References

- Abe-Dohmae, S., Ikeda, Y., Matsuo, M., Hayashi, M., Okuhira, K., Ueda, K., Yokoyama, S., 2004. Human ABCA7 supports apolipoprotein-mediated release of cellular cholesterol and phospholipid to generate high density lipoprotein. *J. Biol. Chem.* 279, 604–611.
- Abe-Dohmae, S., Kato, K.H., Kumon, Y., Hu, W., Ishigami, H., Iwamoto, N., Okazaki, M., Wu, C.A., Tsujita, M., Ueda, K., Yokoyama, S., 2006. Serum amyloid A generates high density lipoprotein with cellular lipid in an ABCA1- or ABCA7-dependent manner. *J. Lipid Res.* 47, 1542–1550.
- Bligh, E.G., Dyer, W.J., 1959. A rapid method of total lipid extraction and purification. *Can. J. Biochem. Physiol.* 37, 911–917.
- Bodzioch, M., Orso, E., Klucken, J., Langmann, T., Bottcher, A., Diederich, W., Drobnik, W., Barlage, S., Buchler, C., Porsch-Ozcurumez, M., Kaminski, W.E., Hahmann, H. W., Oette, K., Rothe, G., Aslanidis, C., Lackner, K.J., Schmitz, G., 1999. The gene encoding ATP-binding cassette transporter 1 is mutated in Tangier disease. *Nat. Genet.* 22, 347–351.
- Brooks-Wilson, A., Marcil, M., Clee, S.M., Zhang, L.H., Roomp, K., van Dam, M., Yu, L., Brewer, C., Collins, J.A., Molhuizen, H.O., Loubser, O., Ouellette, B.F., Fichter, K., Ashbourne-Excoffon, K.J., Sensen, C.W., Scherer, S., Mott, S., Denis, M., Martindale, D., Frohlich, J., Morgan, K., Koop, B., Pimstone, S., Kastelein, J.J., Genest Jr., J., Hayden, M.R., 1999. Mutations in ABC1 in Tangier disease and familial high-density lipoprotein deficiency. *Nat. Genet.* 22, 336–345.
- Costet, P., Lalanne, F., Gerbod-Giannone, M.C., Molina, J.R., Fu, X., Lund, E.G., Gudas, L. J., Tall, A.R., 2003. Retinoic acid receptor-mediated induction of ABCA1 in macrophages. *Mol. Cell. Biol.* 23, 7756–7766.
- Francis, G.A., Knopp, R.H., Oram, J.F., 1995. Defective removal of cellular cholesterol and phospholipids by apolipoprotein A-I in Tangier Disease. *J. Clin. Invest.* 96, 78–87.
- Fukuda, M., Nakano, M., Miyazaki, M., Handa, T., 2010. Thermodynamic and kinetic stability of discoidal high-density lipoprotein formation from phosphatidylcholine/apolipoprotein A-I mixture. *J. Phys. Chem. B* 114, 8228–8234.
- Gillotte, K.L., Zaiou, M., Lund-Katz, S., Anantharamaiah, G.M., Holvoet, P., Dhoest, A., Palgunachari, M.N., Segrest, J.P., Weisgraber, K.H., Rothblat, G.H., Phillips, M.C., 1999. Apolipoprotein-mediated plasma membrane microsolubilization: role of lipid affinity and membrane penetration in the efflux of cellular cholesterol and phospholipid. *J. Biol. Chem.* 274, 2021–2028.
- Guo, L.S., Hamilton, R.L., Goerke, J., Weinstein, J.N., Havel, R.J., 1980. Interaction of unilamellar liposomes with serum lipoproteins and apolipoproteins. *J. Lipid Res.* 21, 993–1003.
- Ha, J.S., Ha, C.E., Chao, J.T., Petersen, C.E., Theriault, A., Bhagavan, N.V., 2003. Human serum albumin and its structural variants mediate cholesterol efflux from cultured endothelial cells. *Biochim. Biophys. Acta* 1640, 119–128.
- Hara, H., Yokoyama, S., 1991. Interaction of free apolipoproteins with macrophages. Formation of high density lipoprotein-like lipoproteins and reduction of cellular cholesterol. *J. Biol. Chem.* 266, 3080–3086.
- Hassan, H.H., Denis, M., Lee, D.Y., Iatan, I., Nyholt, D., Ruel, I., Krimbou, L., Genest, J., 2007. Identification of an ABCA1-dependent phospholipid-rich plasma membrane apolipoprotein A-I binding site for nascent HDL formation: implications for current models of HDL biogenesis. *J. Lipid Res.* 48, 2428–2442.
- Hayashi, M., Abe-Dohmae, S., Okazaki, M., Ueda, K., Yokoyama, S., 2005. Heterogeneity of high density lipoprotein generated by ABCA1 and ABCA7. *J. Lipid Res.* 46, 1703–1711.
- Hoff, H.F., Morrisett, J.D., Gotto Jr., A.M., 1973. Interaction of phosphatidylcholine and apolipoprotein-alanine: electron microscopic studies. *Biochim. Biophys. Acta* 296, 653–660.
- Ito, J., Nagayasu, Y., Yokoyama, S., 2000. Cholesterol-sphingomyelin interaction in membrane and apolipoprotein-mediated cellular cholesterol efflux. *J. Lipid Res.* 41, 894–904.
- Ito, J., Nagayasu, Y., Ueno, S., Yokoyama, S., 2002. Apolipoprotein-mediated cellular lipid release requires replenishment of sphingomyelin in a phosphatidylcholine-specific phospholipase C-dependent manner. *J. Biol. Chem.* 277, 44709–44714.
- Iwamoto, N., Abe-Dohmae, S., Sato, R., Yokoyama, S., 2006. ABCA7 expression is regulated by cellular cholesterol through the SREBP2 pathway and associated with phagocytosis. *J. Lipid Res.* 47, 1915–1927.
- Jayaraman, S., Gantz, D.L., Gursky, O., 2005. Kinetic stabilization and fusion of apolipoprotein A-2:DMPC disks: comparison with apoA-1 and apoC-1. *Biophys. J.* 88, 2907–2918.
- Jayaraman, S., Benjwal, S., Gantz, D.L., Gursky, O., 2010. Effects of cholesterol on thermal stability of discoidal high density lipoproteins. *J. Lipid Res.* 51, 324–333.
- Jayaraman, S., Abe-Dohmae, S., Yokoyama, S., Cavigliolo, G., 2011. Impact of self-association on function of apolipoprotein A-I. *J. Biol. Chem.* 286, 35610–35623.
- Jonas, A., 1986. Reconstitution of high-density lipoproteins. *Methods Enzymol.* 128, 553–582.
- Kishimoto, T., Soda, Y., Matsuyama, Y., Mizuno, K., 2002. An enzymatic assay for lysophosphatidylcholine concentration in human serum and plasma. *Clin. Biochem.* 35, 411–416.
- McCall, M.R., Nichols, A.V., Blanche, P.J., Shore, V.G., Forte, T.M., 1989. Lecithin: cholesterol acyltransferase-induced transformation of HepG2 lipoproteins. *J. Lipid Res.* 30, 1579–1589.
- McCall, M.R., Nichols, A.V., Morton, R.E., Blanche, P.J., Shore, V.G., Hara, S., Forte, T.M., 1993. Transformation of HepG2 nascent lipoproteins by LCAT: modulation by HepG2 *d* > 1.235 g/ml fraction. *J. Lipid Res.* 34, 37–48.
- Peng, L., Minbo, H., Fang, C., Xi, L., Chaocan, Z., 2008. The interaction between cholesterol and human serum albumin. *Protein Pept. Lett.* 15, 360–364.
- Rust, S., Rosier, M., Funke, H., Real, J., Amoura, Z., Piette, J.C., Deleuze, J.F., Brewer, H. B., Duverger, N., Deneffe, P., Assmann, G., 1999. Tangier disease is caused by mutations in the gene encoding ATP-binding cassette transporter 1. *Nat. Genet.* 22, 352–355.
- Schifferer, R., Liebisch, G., Bandulik, S., Langmann, T., Dada, A., Schmitz, G., 2007. ApoA-I induces a preferential efflux of monounsaturated phosphatidylcholine and medium chain sphingomyelin species from a cellular pool distinct from HDL(3) mediated phospholipid efflux. *Biochim. Biophys. Acta* 1771, 853–863.
- Smith, J.D., Le Goff, W., Settle, M., Brubaker, G., Waelde, C., Horwitz, A., Oda, M.N., 2004. ABCA1 mediates concurrent cholesterol and phospholipid efflux to apolipoprotein A-I. *J. Lipid Res.* 45, 635–644.
- Taguchi, R., Hayakawa, J., Takeuchi, Y., Ishida, M., 2000. Two-dimensional analysis of phospholipids by capillary liquid chromatography/electrospray ionization mass spectrometry. *J. Mass Spectrom.* 35, 953–966.
- Takayama, M., Itoh, S., Nagasaki, T., Tanimizu, I., 1977. A new enzymatic method for determination of serum choline-containing phospholipids. *Clin. Chim. Acta* 79, 93–98.
- Tall, A.R., 2008. Cholesterol efflux pathways and other potential mechanisms involved in the athero-protective effect of high density lipoproteins. *J. Intern. Med.* 263, 256–273.
- Tanaka, A.R., Ikeda, Y., Abe-Dohmae, S., Arakawa, R., Sadanami, K., Kidera, A., Nakagawa, S., Nagase, T., Aoki, R., Kioka, N., Amachi, T., Yokoyama, S., Ueda, K., 2001. Human ABCA1 contains a large amino-terminal extracellular domain homologous to an epitope of Sjogren's Syndrome. *Biochem. Biophys. Res. Commun.* 283, 1019–1025.
- Tanaka, N., Abe-Dohmae, S., Iwamoto, N., Fitzgerald, M.L., Yokoyama, S., 2010. Helical apolipoproteins of high-density lipoprotein enhance phagocytosis by stabilizing ATP-binding cassette transporter A7. *J. Lipid Res.* 51, 2591–2599.
- Tanaka, N., Abe-Dohmae, S., Iwamoto, N., Yokoyama, S., 2011. Roles of ATP-binding cassette transporter A7 in cholesterol homeostasis and host defense system. *J. Atheroscler. Thromb.* 18, 274–281.
- Tsujita, M., Yokoyama, S., 1996. Selective inhibition of free apolipoprotein-mediated cellular lipid efflux by probucol. *Biochemistry* 35, 13011–13020.
- Vedhachalam, C., Duong, P.T., Nickel, M., Nguyen, D., Dhanasekaran, P., Saito, H., Rothblat, G.H., Lund-Katz, S., Phillips, M.C., 2007. Mechanism of ATP-binding cassette transporter A1-mediated cellular lipid efflux to apolipoprotein A-I and formation of high density lipoprotein particles. *J. Biol. Chem.* 282, 25123–25130.
- Wang, N., Silver, D.L., Thiele, C., Tall, A.R., 2001. ATP-binding cassette transporter A1 (ABCA1) functions as a cholesterol efflux regulatory protein. *J. Biol. Chem.* 276, 23742–23747.
- Wang, N., Lan, D., Gerbod-Giannone, M., Linsel-Nitschke, P., Jehle, A.W., Chen, W., Martinez, L.O., Tall, A.R., 2003. ATP-binding cassette transporter A7 (ABCA7)

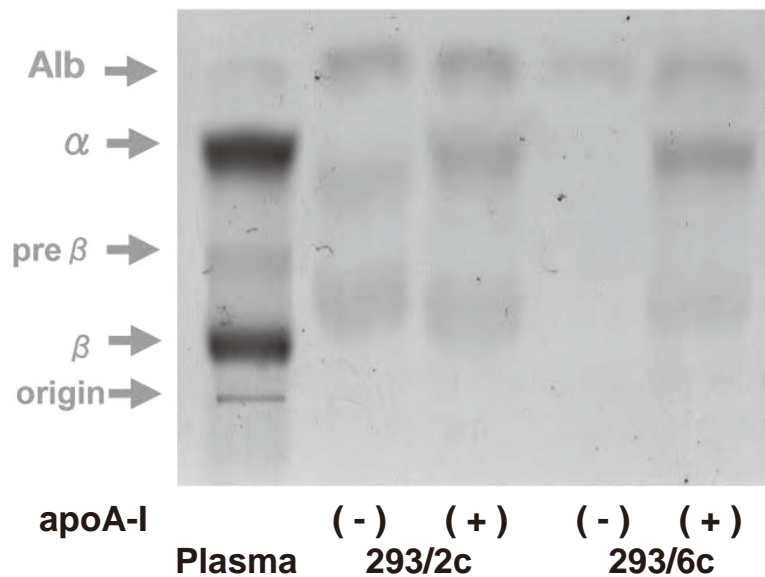
- binds apolipoprotein A-I and mediates cellular phospholipid but not cholesterol efflux. *J. Biol. Chem.* 278, 42906–42912.
- Wu, C.A., Tsujita, M., Hayashi, M., Yokoyama, S., 2004. Probucol inactivates ABCA1 in the plasma membrane with respect to its mediation of apolipoprotein binding and high density lipoprotein assembly and to its proteolytic degradation. *J. Biol. Chem.* 279, 30168–30174.
- Yamauchi, Y., Abe-Dohmae, S., Yokoyama, S., 2002. Differential regulation of apolipoprotein A-I/ATP binding cassette transporter A1-mediated cholesterol and phospholipid release. *Biochim. Biophys. Acta* 1585, 1–10.
- Yokoyama, S., 2005. Assembly of high density lipoprotein by the ABCA1/apolipoprotein pathway. *Curr. Opin. Lipidol.* 16, 269–279.
- Yokoyama, S., 2006a. ABCA1 and biogenesis of HDL. *J. Atheroscler. Thromb.* 13, 1–15.
- Yokoyama, S., 2006b. Assembly of high-density lipoprotein. *Arterioscler. Thromb. Vasc. Biol.* 26, 20–27.
- Yokoyama, S., Tajima, S., Yamamoto, A., 1982. The process of dissolving apolipoprotein A-I in an aqueous buffer. *J. Biochem.* 91, 1267–1272.

Supplementary Figure I, Hotta et al.



Supplementary Figure I. Typical LC/ESI-MS patterns in a positive ion mode of PC (A) and SPM (B) in the media of the cells expressing ABCA1 after incubation with apoA-I. Each molecular weight represents the original plus one (protonated).

Supplementary Figure II, Hotta et al.



Supplementary Figure II. Agarose gel electrophoresis of the medium after incubation with (+) and without (-) apoA-I (10 µg/mL). The medium (5mL) was concentrated by using a centrifuge filtration (ULTRAFREE-15, Millipore) to 75 µL. An aliquot of 5 µL was analyzed in a Paragon Lipoprotein Electrophoresis System (Beckman Coulter) with Sudan Black staining. Reference positions are indicated with normal human plasma as  $\alpha$ , pre $\beta$ ,  $\beta$  and the origin.

OPEN ACCESS

nutrients

ISSN 2072-6643

www.mdpi.com/journal/nutrients

Review

## Unique Features of High-Density Lipoproteins in the Japanese: In Population and in Genetic Factors

Shinji Yokoyama

Nutritional Health Science Research Centre and Bioscience and Biotechnology, Chubu University, Kasugai 487-8501, Japan; E-Mail: [syokoyam@isc.chubu.ac.jp](mailto:syokoyam@isc.chubu.ac.jp); Tel./Fax: +81-568-51-9698

Received: 23 December 2014 / Accepted: 25 February 2015 / Published: 2 April 2015

**Abstract:** Despite its gradual increase in the past several decades, the prevalence of atherosclerotic vascular disease is low in Japan. This is largely attributed to difference in lifestyle, especially food and dietary habits, and it may be reflected in certain clinical parameters. Plasma high-density lipoprotein (HDL) levels, a strong counter risk for atherosclerosis, are indeed high among the Japanese. Accordingly, lower HDL seems to contribute more to the development of coronary heart disease (CHD) than an increase in non-HDL lipoproteins at a population level in Japan. Interestingly, average HDL levels in Japan have increased further in the past two decades, and are markedly higher than in Western populations. The reasons and consequences for public health of this increase are still unknown. Simulation for the efficacy of raising HDL cholesterol predicts a decrease in CHD of 70% in Japan, greater than the extent by reducing low-density lipoprotein cholesterol predicted by simulation or achieved in a statin trial. On the other hand, a substantial portion of hyperalphalipoproteinemic population in Japan is accounted for by genetic deficiency of cholesteryl ester transfer protein (CETP), which is also commonly unique in East Asian populations. It is still controversial whether CETP mutations are antiatherogenic. Hepatic Schistosomiasis is proposed as a potential screening factor for historic accumulation of CETP deficiency in East Asia.

**Keywords:** keyword; HDL; atherosclerosis; Japan; CETP; schistosoma; cholesterol

### 1. Introduction

Coronary heart disease (CHD) is one of the leading causes of death in most of the industrialized countries of the world. While it is still the number one cause of death in North America and Europe, its prevalence in Japan is one-third or less of that in the Western world in spite of its heavy

industrialization, even after the gradual increase in CHD in Japan in the decades post World War II [1]. The major reasons for this difference are largely considered to be environmental factors such as the differences in Japanese life style. That is supported by such findings that Japanese immigrants to the United States show a similar risk of CHD to other Americans [2,3].

In addition, plasma high-density lipoprotein (HDL) concentration, often represented by its cholesterol and a strong epidemiological protective factor against atherosclerotic vascular diseases, is high among the Japanese. It is therefore important to investigate whether this contributes to the lower prevalence of atherosclerotic vascular diseases in Japan, and what environmental and/or genetic factors are responsible for this high HDL. Because of this very population background, low HDL cholesterol can be a stronger risk factor for CHD in Japan than is elevation of non-HDL cholesterol (cholesterol in all other lipoproteins than HDL) [4,5]. This article reviews some unique findings recently unveiled about HDL in the Japanese; its recent remarkable increase in comparison to other parts of the world [6], strong contribution of HDL to CHD risk and therefore its high potential as a target of risk reduction treatment [7], and the particular genetic backgrounds for high HDL in East Asia, including Japan [8–10].

### 2. HDL Levels of Japanese

Measurement of HDL cholesterol has been a standard clinical parameter since early 1980s. The technology for its determination has been well developed and established in the past twenty years [11], so that the HDL cholesterol assay is now adequately standardized and the values are reasonably reliable for international comparisons [12,13]. HDL cholesterol has been shown to be a strong inverse predictor of risk for atherosclerosis in almost all epidemiological and interventional studies worldwide [14–17]. This is also the case in Japan based on many studies, including those of ourselves [3,4], and the prevalence of CHDs is still substantially lower in Japan than Western countries.

Plasma lipoprotein profiles have been determined in National Health and Nutrition Survey (NHNS), a nationwide survey conducted in Japan by the Ministry of Health, Welfare and Labor, in which HDL cholesterol data are available since 1988 [1]. As demonstrated in Figure 1, a trend of prominent and continuous increase in HDL cholesterol has been seen for the time period of 1988 to 2010 [6]. Linear regression of the plot yielded the slope of the increase to be 0.35 and 0.50 mg/dL/year for both men and women ( $p < 0.001$ ). These values stayed the same even after the subjects taking lipid-related medications were excluded. The same trend was also confirmed in HDL cholesterol data obtained from one of the major commercial clinical laboratories in Japan, SRL, as well as many other cohort studies throughout Japan during this period [6].

On the other hand, the United States National Health and Nutritional Examination Survey demonstrated no significant change in HDL cholesterol for the period of 1966 to 2002 [18], but significant increase between 1988–1994 and 2007–2010 [19]. The increase was significant in both sexes and the total population, but differences were apparent among different ethnic groups; significant changes were only seen in “non-Hispanic white” and this seemed a main factor to cause overall significant increase in the total population. Significant increase was also seen in “non-Hispanic black women” group when the subgroup taking lipid-lowering drugs was excluded. The increase of HDL cholesterol was 4.9% and 5.6% for men and women, respectively, of the non-Hispanic white group and 4.3% and 5.0% for men and women of the entire population surveyed, respectively [19] (The copyright policy of AMA does not allow

reusing part of the Tables/Figures from AMA publication to create a new table, so that the readers are advised to refer directly to the reference).

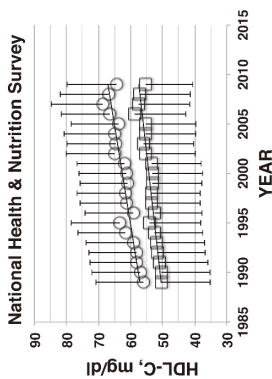


**Figure 1.** HDL-cholesterol (HDL-C) data in the National Health and Nutrition Survey, mean  $\pm$  SD, for male (squares) and female (circles). The slopes are 0.35 mg/dL/year and 0.5 mg/dL/year for male and female, respectively, with  $p < 0.001$  for both [6].

The Japanese population data were analyzed in the same manner to compare with the results of the United States and summarized in Table 1. Both NHNS and SRL data showed the percentage increase of 7%–10% and by 14% for men and women, respectively, between the comparable time periods, more than double the increase in the United States. HDL cholesterol values were higher in Japan than the United States already in the 1988–1994 period by 12.3% and 6.3% in men and women, respectively, of the entire population and 14% and 5.7% in non-Hispanic white men and women, respectively, and the gaps were widened to 19.1% and 14.2% for the former and 20.4% and 13.1% in the latter by the 2010s.

**Table 1.** Change of HDL and non-HDL in mg/dL, Mean  $\pm$  SE, in the National Health and Nutrition Survey (NHNS) and SRL data.

		1988–1994	2007–2010	% Change	p value
NHNS	Men	51.3 $\pm$ 14.9	56.8 $\pm$ 15.4	10.6	<0.001
	Women	59.0 $\pm$ 15.1	66.6 $\pm$ 15.5	14.2	<0.001
HDL-Cholesterol	SRL Men	49.4 $\pm$ 15.5	53.1 $\pm$ 14.2	7.3	<0.001
	SRL Women	56.1 $\pm$ 15.7	63.9 $\pm$ 15.7	13.9	<0.001
Apolipoprotein A-I	Men	123.6 $\pm$ 30.1	134.9 $\pm$ 29.0	9.1	0.01
	Women	133.2 $\pm$ 28.0	151.0 $\pm$ 29.3	13.4	0.02
non HDL-Cholesterol	Men	148	142	-4.0	
	Women	145	140	-3.2	

The possibility remained that this trend was caused by technical errors, such as drifting of standardization for the assay systems, as the methodology for HDL cholesterol measurement has been shifted during the periods the surveys covered, from precipitation of apoB lipoproteins to homogeneous and automated assay systems. In order to exclude the possibility of such artifacts, independent parameters for HDL have been explored. Apolipoprotein A-I (apoA-I) has been measured in SRL by using an enzyme-linked immune assay system, which followed international standardization and stayed

with the same technology throughout the period. As demonstrated in Figure 2 and Table 1, apoA-I data obtained from SRL showed a similar trend of increase to that observed with HDL cholesterol [6]. The increase was also confirmed in the data obtained in the Serum Lipid Survey by the Research Group for Primary Hyperlipidemia under the Ministry of Health, Welfare and Labor of Japan, conducted in 1990 and 2000 independently of NHNS [6,20,21]. HDL cholesterol increased in all age groups of both men and women by 10.3% and 12.6%, respectively, being consistent with other results. In contrast, non-HDL cholesterol values decreased in the both countries, but seemed more in the United States than in Japan [6,19]. The age distribution profile of non-HDL cholesterol was almost superimposable between 1990 and 2000 in Serum Lipid Survey [6,20,21].

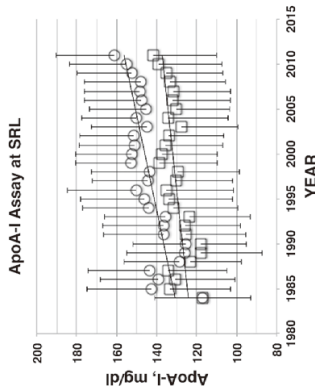


**Figure 2.** Apolipoprotein A-I (ApoA-I) measured commercially in the SRL laboratory, mean  $\pm$  SD, for male (squares) and female (circles). The slopes are 0.485 mg/dL/year and 1.064 mg/dL/year for male and female, respectively, with  $p < 0.001$  for both [6].

We thus conclude that the increase of HDL is very likely a real phenomenon, both in the United States and Japan. Average HDL level among Japanese is apparently higher than that of Americans of most ethnic groups. It was already higher 25 years ago and the difference became much greater in the past 20 years, reaching almost 20% in men and 13%–14% in women (Table 1).

### 3. Simulation of the Effect of Raising HDL on CHD in Japan

It is an important question to what extent the change in plasma concentration of each lipoprotein subfraction would contribute to the risk of atherosclerotic vascular diseases in the Japanese population. The prevalence of stroke and CHD is roughly similar in Japan but lipoprotein risks for the former are not apparently detected, perhaps because the aging risk masks them. On the other hand, many cohort or observational trial studies in Japan, including those of ourselves, demonstrated that plasma HDL cholesterol is the strongest risk predictor for CHD among lipoprotein-related parameters, including low density lipoprotein (LDL) cholesterol [4,5]. Pharmacological reduction of LDL-cholesterol did demonstrate reduction of the risk of CHD by some 30% in Japan even though LDL is not the leading risk factor [22]. Therefore, it is not irrational to conceive that HDL cholesterol could be a better target to

The numbers of new MI patients a year were predicted for each segment group of LDL or HDL in Table 2 from the population in each LDL or HDL concentration segment group and the risk-adjusted MI prevalence in the J-LIT study as MI/1000/year (MI/K/Y). The numbers in each line of LDL/HDL segment (I–VI) in Table 2 indicate MI/K/Y when the people in the respective segment are treated to reduce LDL cholesterol (2A) or increase HDL cholesterol (2B) to the segment (I–VI) represented by each column. Therefore, the sum of each column (the bottom line, total) indicates MI/K/Y when the segment level of the column was reached by the treatment of the entire population. For example, the population with LDL above 180 mg/dL is 854,000 and the number of MI is predicted as 5449 per year (Table 2A). If the LDL level of this entire population group can be reduced to the 160–180 mg/dL segment, the number of MI in this original group decreases to 2178, and then it becomes 1554 when LDL is reduced further to the 140–160 mg/dL segment. A similar assumption was followed for the effect of raising HDL in Table 2B. Parameters for the “treatment efficacy” were calculated as NNT in Table 3. Overall decreases of the MI patients by LDL reduction/HDL elevation were taken from the values in Table 2. The population needed to treat to accomplish the particular lipoprotein level segment was calculated (to reach the 120–140 mg/dL of LDL cholesterol segment, add 854K, 2196K and 3660K in Table 2A, for example). The NNT can be thus calculated for each LDL target segment. For graphical illustration of NNT for each sextile as the efficacy of the treatment, the inverse of the value ( $\times 1000$ ) was used.

prevent CHD, assuming that raising HDL reverses the risk similarly to reduction of LDL. We therefore attempted to conduct such a simulation [7].

The age-adjusted prevalence of myocardial infarction was obtained as events per year per population of 1000 for every segment of serum LDL-cholesterol and HDL-cholesterol concentration, from the cohort study Japan Lipid Intervention Trial (J-LIT), six-year follow-up study of 47,294 patients treated with low-dose simvastatin, carried out between 1992 and 1999 [23]. Serum lipoprotein cholesterol concentration profiles among Japanese were taken from the study by the Research Committee on Serum Lipid Levels Survey 1990 in Japan [20]. Population statistics of Japan were taken from the Census Japan 1995 [24] for the age group of 50–70 to match the age range of the subjects monitored in J-LIT and population profiles of serum LDL-cholesterol and HDL-cholesterol were calculated for this age group. We concluded that raising HDL cholesterol is more efficient than reduction of LDL cholesterol for prevention of myocardial infarction (MI) in Japan based on the assumption that the former approach is valid to reverse the risk, although, sex difference has not been taken into consideration [7].

As the further detail of J-LIT data became available for male and female subjects separately [25] (Figure 3), the same simulation was conducted for each sex for this review. The treatment efficacy was empirically calculated by the method previously described [7]. The process of the calculation can be followed as the data in Table 2 for male. The population in each lipoprotein concentration sextile was determined from its distribution statistics [20]. The number of new patients a year was predicted for each segment by using the primary risk estimates of MI for each lipoprotein segment group in J-LIT study [23,25]. Reduction of MI in the population segments by reducing LDL to the next lower segment was estimated by the difference of the primary risk between these segments, assuming that the risk is reversible by reducing LDL concentration. This calculation was sequentially performed to simulate reduction of the numbers of the patients by reducing LDL of the entire population from one segment to the next towards the lowest LDL segment. For HDL, the same procedure was applied, except that the calculation starts with the lowest HDL group to shift to the higher segment. The efficacy of the treatment (assuming it is “effective”) was calculated as the number needed to treat (NNT) for each level of lipoprotein target.

prevalence in the J-LIT study as MI/1000/year (MI/K/Y). The numbers in each line of LDL/HDL segment (I–VI) in Table 2 indicate MI/K/Y when the people in the respective segment are treated to reduce LDL cholesterol (2A) or increase HDL cholesterol (2B) to the segment (I–VI) represented by each column. Therefore, the sum of each column (the bottom line, total) indicates MI/K/Y when the segment level of the column was reached by the treatment of the entire population. For example, the population with LDL above 180 mg/dL is 854,000 and the number of MI is predicted as 5449 per year (Table 2A). If the LDL level of this entire population group can be reduced to the 160–180 mg/dL segment, the number of MI in this original group decreases to 2178, and then it becomes 1554 when LDL is reduced further to the 140–160 mg/dL segment. A similar assumption was followed for the effect of raising HDL in Table 2B. Parameters for the “treatment efficacy” were calculated as NNT in Table 3. Overall decreases of the MI patients by LDL reduction/HDL elevation were taken from the values in Table 2. The population needed to treat to accomplish the particular lipoprotein level segment was calculated (to reach the 120–140 mg/dL of LDL cholesterol segment, add 854K, 2196K and 3660K in Table 2A, for example). The NNT can be thus calculated for each LDL target segment. For graphical illustration of NNT for each sextile as the efficacy of the treatment, the inverse of the value ( $\times 1000$ ) was used.

**Table 2.** (A) Decrease of myocardial infarction (MI) by reducing LDL cholesterol (LDL-C; male), according to the method in ref. [7]; (B) Decrease of MI by increasing HDL cholesterol (HDL-C; male).

(A)							(B)											
Segment	LDL-C mg/dL	Population (K)	MI/K/Y	Number of MI/Y when the Segment Targeted														
				VI	V	IV	III	II	I				Number of MI/Y when the Segment Targeted					
													VI	V	IV	III	II	I
I	-100	6100	0.67	4087	4087	4087	4087	4087	4087				2974	2974	2974	2974	2974	2974
II	100	5856	1.18	6910	6910	6910	6910	6910	6910				3426	3426	3426	3426	3426	3426
III	120	5734	1.22	6995	6995	6995	6995	6995	6995				4270	4270	4270	4270	4270	4270
IV	140	3660	1.82	6661	6661	6661	6661	6661	6661				5583	5583	5583	5583	5583	5583
V	160	2196	1.82	5600	5600	5600	5600	5600	5600				6566	6566	6566	6566	6566	6566
VI	180	854	6.38	5449	2178	1554	1042	1008	572				16397	10607	7327	6405	5534	2716
Total	-	24,400	-	35,702	32,431	30,204	26,178	25,691	16,348				39,216	33,426	28,116	25,920	23,265	12,931

Each line represent the group of the subjects of lipoprotein cholesterol level (LDL-C or HDL-C) defined as I to VI with population of the age between 50 and 70 (J-LIT age) and risk of myocardial

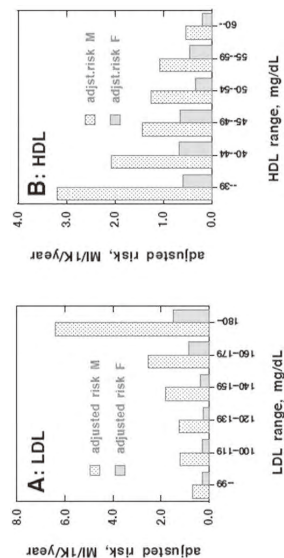


**Figure 3.** Age-adjusted risk of myocardial infarction (MI) dependent of plasma lipoprotein-cholesterol for each sex. The risk is expressed as events per 1000 population per year (MI/1K/Y) in J-LIT trial [25].

infarction (MI/K/Y), and predicted numbers when lipoprotein-C is managed towards the target segment as VI to I. Total indicates the sum of the column, i.e., the numbers of MI when each lipoprotein-C target is achieved. When no treatment is done, the number of MI is predicted as 35,702 while it is down to 30,204 if the goal of the segment IV is achieved for the entire population.

**Table 3.** (A) Number needed to treat (NNT) in prevention of myocardial infarction (MI) by increasing LDL cholesterol (male); (B) NNT in prevention of MI by increasing HDL cholesterol (male).

HDL Segment Targeted	(A)					
	I (-100)	II (100-120)	III (120-140)	IV (140-160)	V (160-180)	VI (180-)
Total MI	16,348	25,691	26,178	30,204	32,431	35,702
% reduction	46	72	73	85	91	100
MI Overall Decreased	19,354	10,011	9527	5498	3271	
Population to Treat (K)	18,300	12,444	6710	3050	854	
NNT	946	1242	704	555	261	
1/NNT × 1000	1.5	0.805	1.42	1.8	3.83	

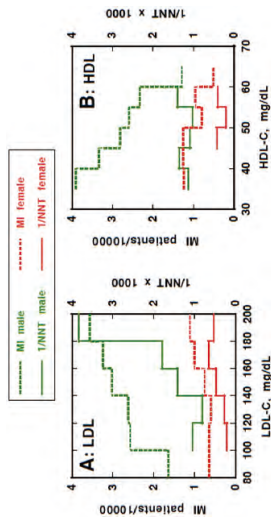
  

HDL Segment Targeted	(B)					
	I (60-)	II (55-60)	III (50-55)	IV (45-50)	V (40-45)	VI (-40)
Total MI	12,931	23,265	25,920	28,116	33,426	39,216
% reduction	33	59	66	72	85	100
MI Overall Decreased	26,285	15,951	13,296	11,100	5790	
Population to Treat (K)	18,788	15,616	12,200	8296	5125	
NNT	714	979	918	737	885	
1/NNT × 1000	1.401	1.021	1.089	1.451	1.134	

Parameters for treatment efficacy as each lipoprotein cholesterol target (I to VI) is achieved, based on the date in Table 2. NNT: number needed to treat ((decreased MI)/(Population to treat)). Calculation was, according to the method in ref. [7].

As demonstrated in Table 3, the estimated reduction of MI prevalence using this simulation is greater by raising HDL than reducing LDL in Japanese male subjects aged 50 to 70, assuming that the risk is reversible based on changes in the plasma concentration of each lipoprotein.

Figure 4 represents a graphical view of the results of the simulation for decrease of MI by reduction of LDL (4A) and raising HDL (4B) both in males and females. The data shown are for the number of patients per year as the lipoprotein treatment target is achieved for all those to be treated, and for NNT to reach this goal, calculated for each lipoprotein target levels (the values for male are listed in Table 3). For LDL reduction in males, the treatment efficacy (1/NNT) sharply dropped when the treatment goal is lowered from 180 to 160 mg/dL, and then gradually decreased to the level that NNT is a little higher than 1000. The final potential prevention of MI is estimated at about 50% by reducing LDL to 100 mg/dL. In females, the same tendency was demonstrated but with much lower incidence of CHD, but the data might not be qualified for conclusive analysis, since the number of the events was so low.



**Figure 4.** Prevention of ischemic heart disease in Japanese by decreasing LDL-cholesterol (LDL-C) and increasing HDL-cholesterol (HDL-C). Simulation for prevention of myocardial infarction (MI) based on the graphs in Figure 3 and demographic data of Japanese, for males and females, according to the data represented in Tables 2 and 3. Solid lines represent the inverse of NNT (×1000) as an indicator of the treatment efficacy for managing lipoproteins to a target. The value of each horizontal segment is the efficacy when reaching a target LDL or HDL level at the left or right end of the segment, respectively, in all Japanese at ages covered by the JLLT. Each horizontal segment of broken lines represents the number of MI patients when LDL is decreased or HDL is raised to the left end of the segment.

In the simulation of increasing HDL, the treatment efficacy did not diminish as much as the lowering of LDL when HDL cholesterol increased from below 40 mg/dL to over 60 mg/dL. The NNT stayed at around the level somewhat less than 1000 throughout the range of change in HDL. The reduction of MI is linear and would reach approximately 30% of the original level by raising HDL cholesterol to the segment over 60 mg/dL. In females, the results were essentially similar to those in males but not highly conclusive because of low incidence of events.

Our simulation model predicted that MI among Japanese could be prevented by at most 50% by aggressive reduction of LDL, but could reach as much as 70% by interventions raising HDL, granted it is feasible. LDL reduction, however, may have an advantage over raising HDL with respect to the treatment effectiveness (NNT) as far as setting a target higher than 160 mg/dL. These results indicate that elevation of LDL is not as great a risk factor for CHD in the Japanese as is low HDL, and low HDL should be considered as a more important target to reduce the overall risk.

**4. A Genetic Factor that Increases HDL among the Japanese**

Plasma HDL concentration, typically represented by HDL cholesterol content, is likely more important for Japanese public health than in the Western world. This is suggested by the higher average HDL concentration in Japan, the fact that CHD events are lower in Japan, and based on the simulation model presented here predicting the potential of more efficient reduction of atherosclerotic cardiac diseases by raising HDL than by reducing LDL. It is quite conceivable that some genetic factors may also contribute to the higher plasma HDL concentration in Japan. One genetic factor resulting in higher

**Table 4.** Allele Frequency identified as prevalence of mutants, summarized by Thompson *et al.* \* [50], unless otherwise referred to \*\*.

	D442G	Int14	Number Genotyped
Japanese Americans	5.1	0.49	3469
Japanese not on meds	8.1	0.60	2267
Osaka controls	6.0	1.00	514
Japanese children	6.0	0.00	500
Japanese hemodialysis	6.5	--	414
Japanese FH	3.5	0.69	288
Japanese centenarians	6.3	0.78	256
Japanese controls	6.8	1.69	236
Japanese normal HDL	13.7	4.42	226
Japanese controls	6.8	1.58	190
Ohmagari controls	4.0	27.0	173
Chinese controls	4.2	--	379
Chinese controls	5.0	1.00	335
Chinese controls	3.3	--	209
Chinese CHD	10.8	--	203
Chinese CHD	3.5	0.00	200
Chinese stroke	3.6	0.91	110
Chinese Healthy elderly	3.0	--	103
Chinese MI	3.5	1.05	94
Hong Kong Chinese **	--	1.4	145
			(Thu <i>et al.</i> [48])
Taiwanese controls	6.7	718	278
Taiwanese controls	4.7	--	224
Taiwanese controls	4.5	--	196
Taiwanese CHD	7.7	--	270
Korean **	12	--	(Song <i>et al.</i> [47])
Korean post menopausal	9.2	--	228
Vietnamese	6.9	0.00	
Yakuts **	16.3	--	144
			(Arkhipova <i>et al.</i> [51])

HDL cholesterol and higher frequency in Japan are dysfunctional mutations of cholesteryl ester transfer protein (CETP).

CETP is a glycosylated plasma protein with a molecular weight of 74,000 that catalyzes the non-directional equimolar exchange of non-polar lipids, mainly cholesteryl acylester (CE) and triglyceride (TG), among lipoprotein particles core [26–28]. CETP is present in the plasma of some animals, such as rabbits, hamsters and some primates including humans [29]. The reaction equalizes distribution of the core lipids among lipoproteins. CE is actively generated in plasma HDL by the lecithin: cholesterol acyltransferase (LCAT) reaction and TG originates in secretion of very-low-density lipoproteins (VLDL) and chylomicrons by the liver and the intestinal cells, respectively. Accordingly, CETP mediates the net movement of CE from HDL to VLDL/chylomicrons and TG from VLDL/chylomicron to HDL and low-density lipoproteins (LDL) [26], and consequently regulates the HDL cholesterol level in plasma [30]. Increase of the plasma TG therefore results in decrease of HDL cholesterol, which may partially explain the cardiovascular risk of hypertriglyceridemia. In turn, HDL-CE increases when the CETP reaction decreases. Generation of CE by LCAT in HDL is one of the driving forces for the removal of cell cholesterol [31], and is an important part of cholesterol transport from somatic cells to its catabolic site, the liver. The CETP reaction may facilitate this transport by sending CE from HDL to the LDL pathway for removal from plasma through the hepatic LDL receptor [29].

The patients with CETP deficiency patients were first discovered in Japan in 1985 in individuals with extremely high HDL cholesterol [32,33] and CETP mutations were subsequently identified [34]. This was found to be a frequent cause of hyperalphalipoproteinemia among Japanese. The two major mutations account for the majority of the cases are intron 14 G(+1)-to-A (Int14A) and exon 15 missense mutation (D442G) [35–37]. These two mutants are present in 1% to 2% and 6% to 7% of the Japanese population, respectively. Sporadic cases of other CETP mutations have also been identified among Japanese [36–40]. Accordingly, the estimated numbers of CETP mutation heterozygotes in Japan is around 10 million, with 150,000 to 250,000 having mutations in both CETP alleles. Based on this frequency, CETP deficiency may account for 27.6% of the people with HDL cholesterol  $\geq 60$  mg/dL and 31.4%–32.5% of those with HDL  $\geq 80$  mg/dL in Japan [35,41].

The first non-Japanese patient with CETP deficiency was of Chinese descent, reported from Switzerland [42]. Several reports thereafter described CETP deficiency among other Asians. The prevalence of CETP D442G was found to be 2.1%–3.8% in the Mainland Chinese population [43,44], and 4.5%–6.7% in the population of Taiwan [45,46]. The prevalence of D442G was estimated to be 12% among Koreans based on an allele frequency of 6% [47] and 6.9% in the Vietnamese population [48]. D442G heterozygosity was found to be the cause of nine out of the 35 individuals with hyperalphalipoproteinemias in a study in Thailand [49], accounting for 26% of cases, similar to the ratio among the Japanese [35,41] and strongly indicating that CETP mutants are common in Thailand. Further detailed information is available in the previous review article [50]. More recent result for Siberian Yakuts indicates the prevalence of D442G mutant is 16.3% in the native Yakuts, compared to 5.2% among the non-indigenous Siberians [51], whose intermarriage rate with Yakuts is estimated at 10% to 20% (Ariev AL, personal communication). Not much reliable information is available for the Int14A CETP mutation, except for two out of the 145 subjects (1.4%) in Hong Kong Chinese [52] and none of 346 Vietnamese [48]. In the Omagari of Akita district in Northern Japan, accumulation of Int14A has a heterozygote prevalence of 27% [37]. These up-to-date data are summarized in Table 4.

Table 4. Cont.

	D442G	In14	Number Genotyped
Russians/Ukrainians ** (10%–20% cross-marriage with Yakuts)	5.2	--	116 (Arkipova <i>et al.</i> [51])
North Indian controls	0.0	0.0	
French healthy controls	0.0		
Scottish case/controls	0.0		
	(<1.0)		
Caucasians ** (Thompson <i>et al.</i> [50])			

In contrast, genetic CETP deficiency is rare in ethnic groups other than East Asians. No D442G mutations were found among the 400 individuals examined in North India [53]. The first Caucasian case was reported in 1997 [54], and the presence of one case of Int14A was recognized in 1998 in Canada without ethnic background information [55]. It was concluded that CETP deficiency is rare among North American Caucasians [56]. Nevertheless, a few studies reported sporadic cases of CETP deficiency from the United States [57], Italy [58,59], and the Netherlands [56,60]. There was a statement for the frequency of D442G mutant as “less than 1%” in US without providing the data [61].

In summary, CETP deficiency is highly prevalent in East Asia, at least among the Japanese, Chinese both in Mainland and Taiwan, and Koreans, predominantly with the D442G mutant. It is likely be similarly as frequent in Thailand, Vietnam and Siberian native people. Int14A mutant may be a second common mutation, but it is not clearly evident except in Japan. Many other less-frequent types of mutation have also been found in Japan, but such information is not available so far from other Asian regions. In contrast, it is rare in any other ethnic groups in other parts of the world. The two common Asian mutations are not commonly identified even among the sporadic cases from other continents. Thus, geographic or ethnic distribution of CETP mutations is extremely unique. It can be hypothesized that there is a unique environmental reason(s) for this peculiar accumulation of CETP mutants, other than Omagari, Japan, that is potentially due to a founders' effect [37].

Clinical manifestations of CETP deficiency are limited to the abnormal plasma lipoprotein profile, including markedly elevated HDL cholesterol and moderately reduced LDL cholesterol. With reduced CETP activity, CE generated by LCAT is retained in HDL while its substrate molecules of free cholesterol and glycerophospholipids are continuously supplied to HDL from other lipoproteins and cells, including erythrocytes by non-specific exchange or other transfer reactions [31]. Thus, HDL particles become larger as the core CE compartment expands. Therefore, the apparent increase of HDL cholesterol is not due to an increase in HDL particle number but because of the enlargement of the particles, to the extent of reaching diameters as large as LDL [62–64]. LDL particles in turn get somewhat smaller and contain an increased amount of TG in their core and resulting in overall reduction of LDL-cholesterol [65,66]. No obvious clinical symptoms are present in CETP-deficient individuals.

We thus investigated region-specific and potentially fatal diseases that might be associated with plasma lipoprotein metabolism to explore a screening factor for accumulation of CETP mutations in

East Asia, and focused on *Schistosoma japonicum*, an Asian-specific blood fluke [8–10]. Parasitic blood flukes reside as a pair in the host portal and intestinal veins and use plasma lipoproteins as nutrient sources through the lipoprotein receptor-like systems. A portion of the eggs laid for excretion through the gastrointestinal tract go into the liver via the portal circulation and undergo ectopic embryonation to cause hepatic granulomatosis and fatal cirrhosis. Accordingly, we examined *Schistosoma japonicum*, with respect to dependency of its pathogenesis on plasma lipoproteins. The parasites were shown to take up CE from HDL for the embryonation of their eggs to miracidia, which is a critical step of the hepatic pathogenesis of this parasite, but this reaction was shown to be impaired from the HDL of CETP-deficiency (Figure 5). Due to similarity of the reaction to those by scavenger receptor B1 or CLA-1 of selective CE uptake from HDL in rodents or humans, we searched for a factor responsible for this reaction as a CD-36 family protein(s). A new protein, CD36-related protein (CD36RP), was cloned from the adults and the eggs of *Schistosoma japonicum*, with 1880-bp encoding 506 amino-acid residues exhibiting the CD36 domains and two transmembrane regions. The extracellular domain of this protein selectively bound normal human HDL but neither LDL nor CETP-deficiency HDL, and the antibody against the extracellular domain suppressed the selective HDL-CE uptake from normal HDL and embryonation of the eggs (Figure 6). When infected with *Schistosoma japonicum*, wild-type mice developed less hepatic granulomatosis than CETP-transgenic mice by the ectopic egg embryonation (Figure 7). CD36RP is thus a candidate receptor of *Schistosoma japonicum* to facilitate uptake of HDL-CE necessary for egg embryonation. Abnormal HDL caused by CETP-deficiency retards this process and thereby protects the patients from development of hepatic lesions in this infection.

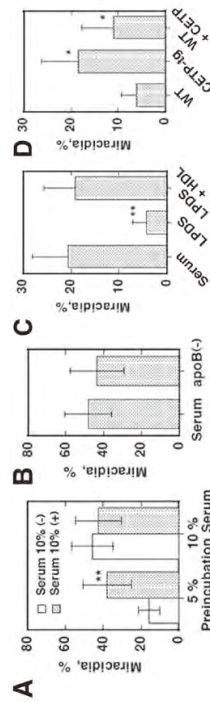
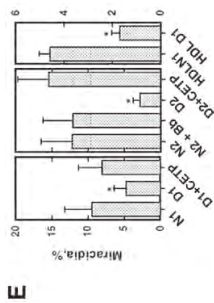
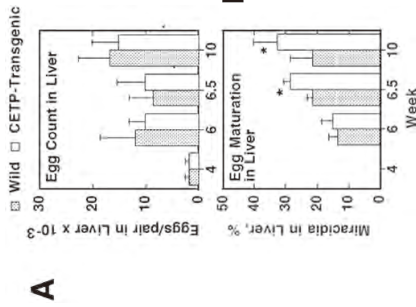


Figure 5. Cont.



**Figure 5.** Lipoprotein requirement for embryonation of the *S. japonicum* eggs after eight days in culture [7–10]. (A): incubation of the eggs with and without human serum (10%) after pre-exposure of the parents while laying the eggs to 5% and 10% of human serum. Embryonation proceeds when the parents or eggs have access to adequate human serum. Preincubation with 5% serum is applied hereafter; (B): Embryonation is not influenced even when apoB-lipoprotein is removed from human serum (apoB (-)); (C): Embryonation requires the HDL fraction of human serum. LPDS; lipoprotein deficient serum; (D): The effect of mouse serum on the egg embryonation. Embryonation is poor with wild-type mouse serum that lacks CETP and proceeds with CETP-transgenic mouse serum (CETP-tg). Adding human CETP to the wild-type serum partially restored embryonation; (E): Embryonation of the *S. japonicum* eggs after eight days in culture with CETP-deficient human serum, taken from the reference [8]. Embryonation is estimated in the culture of the eggs in 10% normal human sera (N1 and N2) and that of CETP-deficient subjects (D1 and D2). Embryonation is retarded in CETP-deficient serum (A) and adding CETP recovers this (B). Normal HDL is adequate for the embryonation but not HDL from CETP-deficiency (C). \*\*  $p < 0.01$  and \*  $p < 0.05$  from serum (-) (A), serum (C), WT (D), normal HDL (E).



**Figure 7.** Egg embryonation and the liver lesion development in the wild-type and CETP-transgenic mice infected with *S. japonicum*. (A): Number of the eggs embryonizing in the liver and ectopic embryonation of the eggs counted microscopically; (B): Granulomatosis lesion in the liver. The eggs and granulomatous lesions were identified microscopically in the liver specimens. The total area of the lesion per egg was calculated for each section. The area per egg was calculated as an average  $\pm$  SE of the 12 mice, for each of which 12 random liver sections were examined. Asterisks indicate difference at  $p < 0.05$  from the wild type [8,10].

**5. Discussion**

Plasma HDL levels of the Japanese were shown to be high based on HDL cholesterol content and apoA-I levels, and have gradually but substantially increased even further during the past 20 years to reach the levels 15%–20% higher than the average in the United States (Table 1) [6,19]. This may contribute at least in part to low incidence of CHD, including myocardial infarction in Japan [4,5]. Conversely, low HDL is a strong epidemiological risk for CHD in Japan. Raising HDL (cholesterol, at least in simulations) may potentially prevent the CHD more efficiently than reduction of LDL, assuming that correcting plasma lipoprotein concentrations can reverse the risk (Table 3, Figure 4) [7]. One of the genetic causes for high HDL in Japan is a high prevalence of mutation in the CETP gene, which is uniquely common in East Asia, at least from the Indochina Peninsula to Siberia. The two major mutations are present in 6%–10% of general population and may account for 25%–30% of high HDL populations in these regions. Homozygotes of CETP deficiency seem to be resistant to development of fatal hepatic Schistosomiasis providing survival advantage for development of these mutations in this region [8–10]. Further analysis will be required to determine whether the increase of HDL over time or the specific genetic background, *i.e.*, CETP mutation, is responsible for low prevalence of CHD in Japan.

There is no doubt that CETP deficiency contributes to the average high HDL concentration in Japan [35,40]. However, it is unknown whether the increase of abnormal HDL caused by CETP

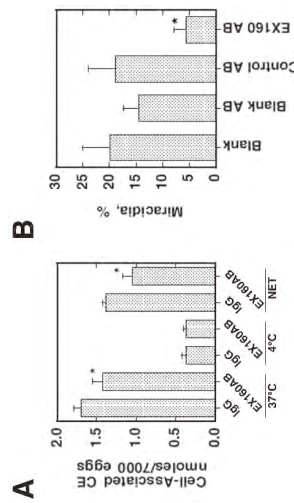


**Figure 6.** Suppression of cholesteryl acylester (CE) uptake (A) and embryonation of the *S. japonicum* eggs (B) by the antibody raised against the extracellular domain peptide representing the residues 249–408 of CD36GRP. Blank AB, nonimmunized rabbit antibody, Control AB, antibody against the intracellular domain of CD36GRP (residues 331–348) [9,10].

mutations plays an anti-atherogenic role as suggested by the reduced CHD with high HDL in population studies. HDL particles become as large as LDL with substantial accumulation of apolipoprotein E in homozygous deficiency of CETP [67]. It has been wondered whether CETP deficiency is protective against atherosclerotic vascular diseases, and the answer has been controversial and inconclusive in epidemiological cohort studies on heterozygotes [37,68,69]. Abnormal HDLs present in the homozygotes may not be as anti-atherogenic as normal HDL, since they show apparently impaired capacity for removal of cell cholesterol [70]; in addition, the homozygotes patients do not show resistance to atherosclerosis [37].

Pharmacological inhibition of CETP has been attempted in the past decade, and has demonstrated very positive results in a rabbit model of diet-induced hyperlipoproteinemia [68]. However, clinical trials have so far failed to prove the positive effect of CETP inhibitors [71,72]. The trials are ethically obliged to demonstrate additional effect of raising HDL on a background of statin treatment so that a part of the beneficial effect of raising HDL may have been masked. Furthermore, the doses of statins used in these trials were relatively high because the subjects of the trials were those at high risk. On the other hand, it is argued that inhibition of CETP may not be beneficial as it blocks the routing cholesterol esters from HDL to LDL/VLDL for its more efficient flow to the liver and causes accumulation of cholesterol ester in HDL. In addition, consequent enlargement of the particle may diminish the ability of HDL to remove cell cholesterol [70]. It is thus inconclusive whether inhibition of CETP is beneficial in spite of it being an efficient way to increase HDL. When considering these backgrounds, we cannot answer the question yet whether high prevalence of CETP deficiency contributes to low incidence of CHD in Japan. Alternatively, CETP inhibitors can potentially be useful to prevent development of fatal hepatic schistosomiasis.

An increase in average HDL levels over the past 20 years has occurred both in Japan and in the United States [6,19] (Table 1). The magnitude of the increase was much greater in Japan and it made the gap in HDL levels between the two countries much wider. It is conceivable that extensive health education and an intentional trend in lifestyle changes were major factors to lead to such results in both countries. An increase of average HDL cholesterol by around 5% of general population in the United States is significant when compared to the increase of HDL in many clinical trials using statins or even fibrates. A decrease in plasma triglycerides is associated with increases in HDL cholesterol as the CETP reaction causes reciprocal changes of these parameters [26,30], and decreases of triglyceride were indeed observed in the same survey [19]. However, such a relationship is not maintained throughout different ethnic groups in the United States, so that this is unlikely the major reason for HDL cholesterol increase [19]. As the change is more prominent in Adults than youths in the United States, lifestyle change seems more likely the cause [73].

The magnitude of increase in HDL cholesterol in Japan for the same period of time was almost 10% to 15%, much greater than that in the United States. Changes in plasma triglycerides were not significant at all during this period [1], so that the reason for this change is presumed to be other factors related to the environment, including lifestyle change.

Most of the fundamental changes in lifestyle in Japan took place during the immediate postwar time, 1946–1975, along with rapid economic growth, drastic shifting in the energy source of power and great changes in the fundamentals of society, such as large increase in car and telephone ownership and changing food quantity and quality. Total calorie intake increased by 20% with the increase of protein by 1.5% and fat by 3.5 fold, and the decrease in carbohydrate by 15% from the peak intake in 1955.

These changes all must have pushed plasma lipid parameters towards an atherogenic direction. However, such trends were more or less stabilized after the mid seventies, and total caloric intake gradually decreased by 20% after the peak time of 1977, along with further substantial decreases in carbohydrate intake by 23%. In the same period of time, alcoholic consumption remained the same, smoking rates decreased in males but increased a little in females, and intentional exercise may have increased a bit. The most remarkable change in lifestyle in Japan is perhaps as anywhere else, the rapid spread of intellectual technology, and lives became greatly dependent on the use of cell phones and the Internet. However, by any of those or even altogether, it is difficult to explain the increase of HDL by 10% to 15%.

Interesting changes are found in Japanese food intake by looking into detail at trends after World War II (NHNS, [1]). While seafood intake has shown only mild increase from 65 to 90 g/capita/day by 1975 and slightly declined to 70 g/capita/day again after 2000, sharp increases were seen in the intake of animal meat products from 5 to 75 g/capita/day by 1980 and reaching 80 g/capita/day in 1990s, milk products from 1 to 100 g/capita/day by 1975, hitting a peak of 140 g/capita/day in 1995 and declining thereafter to 120 g/capita/day, and egg and egg products from 2 to 40 g/capita/day by 1975. These nutritional changes were apparently one of the driving forces for extending average lifespan of the Japanese to one of the highest in the world. According to the United Nations Food and Agricultural Organization (UNFAO) [74], Japan is one of the top consumers of fish per capita, along with Portugal, Norway and Korea. However, the ratios of seafood to meat in calorie intake per capita basis are 0.16, 0.29 and 0.45, respectively, in these countries while that of Japan was 0.99 in 2010. The ratios were 0.16, 0.13 and 0.08 in France, Italy and the United States, respectively. Thus, even after such a tremendous change in food intake pattern, Japanese are still the highest fish eaters in the world.

This background, however, may not be likely to account for the increase of HDL in the past 20 years unless the drastic change in the time more immediately after the war had some distant or prolonged effects. On the other hand, a more recent important trend in food intake of Japanese is found in NHNS data (Figure 8). From 2001 to 2011, the ratio of fish intake to meat may have only slightly decreased for the overall population mainly by shrinking fish consumption. However, the ratio dropped to almost half in the age groups from 20 to 50 during these 10 years. It will be very important to monitor this trend in relation with various risk factors for lifestyle-related diseases, including HDL-related parameters and CHD incidence.

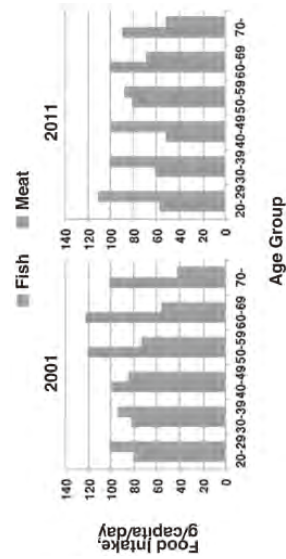


**Figure 8.** Source of food intake by the age groups of Japanese, according to the National Health and Nutrition Survey [1].

## 6. Conclusions

The situations related to HDL are thus quite unique in Japan in comparison to other part of the world, with respect to both environmental and genetic factors of Japanese, in association with long historic backgrounds. The questions have to be set to address whether any of these factors may be involved in the lower incidence of CHD in Japan. The attempt to draw answers even partially should contribute to solving worldwide public health problems of prevention and cure of atherosclerotic vascular diseases. There is no direct evidence yet, however, that these unique findings are associated with any public health problem of Japan. Extensive investigation is required.

## Acknowledgments

This work was supported by the MEXT-Supported Program for Strategic Founding of Research in Private Universities (S1201007) and by Grant-in-aid from MEXT Japan (24614018).

## Conflicts of Interest

The author declares no conflict of interest.

## References

- Ministry of Health, Labor and Welfare of Japan, National Health and Nutritional Survey. Available online: <http://www.mhlw.go.jp/toukei/tiran/gaiyo/k-eisei.html> (accessed on 1 January 2012). (In Japanese)
- Worth, R.M.; Kato, H.; Rhoads, G.G.; Kagan, K.; Syme, S.L. Epidemiologic studies of coronary heart disease and stroke in Japanese men living in Japan, Hawaii and California: Mortality. *Amer. J. Epidemiol.* **1975**, *102*, 481–490.
- Sekikawa, A.; Curb, J.D.; Ueshima, H.; El-Saed, A.; Kadowaki, T.; Abbott, R.D.; Evans, R.W.; Rodriguez, B.L.; Okamura, T.; Sutton-Tyrrell, K.; et al. Marine-derived *n*-3 fatty acids and atherosclerosis in Japanese, Japanese-American, and white men: A cross-sectional study. *J. Am. Coll. Cardiol.* **2008**, *52*, 417–424.
- Sasai, K.; Okuyama-Noji, K.; Hibino, T.; Ikeuchi, R.; Sakuma, N.; Fujinami, T.; Yokoyama, S. Human cholesteryl ester transfer protein (CETP) measured by enzyme-linked immunosorbent assay with two monoclonal antibodies against rabbit cept: Plasma CETP and lipoproteins among Japanese hypercholesterolemic patients. *Clin. Chem.* **1998**, *44*, 1466–1473.
- Goto, A.; Sasai, K.; Suzuki, S.; Fukutomi, T.; Ito, S.; Matsushita, T.; Okamoto, M.; Suzuki, T.; Itoh, M.; Okuyama-Noji, K.; et al. Cholesteryl ester transfer protein and atherosclerosis in Japanese subjects: A study based on coronary angiography. *Atherosclerosis* **2001**, *159*, 153–163.
- Yokoyama, S.; Ueshima, H.; Miida, T.; Nakamura, M.; Takata, K.; Fukukawa, T.; Goto, T.; Harada-Shiba, M.; Sano, M.; Kato, K.; et al. High-density lipoprotein levels have markedly increased over the past twenty years in Japan. *J. Atheroscler. Thromb.* **2014**, *21*, 151–160.
- Yokoyama, S.; Yamashita, S.; Ishibashi, S.; Sone, H.; Oikawa, S.; Shirai, K.; Ohta, T.; Bujo, H.; Kobayashi, J.; Arai, H.; et al. Background to discuss guidelines for control of plasma HDL-cholesterol in Japan. *J. Atheroscler. Thromb.* **2012**, *19*, 207–212.
- Okumura-Noji, K.; Sasai, K.; Zhan, R.; Kawaguchi, H.; Maruyama, H.; Tada, T.; Takahashi, H.; Okazaki, M.; Miida, T.; Sakuma, N.; et al. Cholesteryl ester transfer protein deficiency causes slow egg embryonation of *Schistosoma japonicum*. *Biochem. Biophys. Res. Com.* **2001**, *286*, 305–310.
- Okumura-Noji, K.; Miura, Y.; Lu, R.; Asai, K.; Ohta, N.; Brindley, P.J.; Yokoyama, S. Cd36-related protein in *Schistosoma japonicum*: Candidate mediator of selective cholesteryl ester uptake from high-density lipoprotein for egg maturation. *FASEB J.* **2013**, *27*, 1236–1244.
- Yokoyama, S. A potential screening factor for accumulation of cholesteryl ester transfer protein deficiency in East Asia: *Schistosoma japonicum*. *Biochim. Biophys. Acta* **2014**, *1841*, 495–504.
- Sugiuchi, H.; Uji, Y.; Okabe, H.; Irie, T.; Uekama, K.; Kayahara, N.; Miyauchi, K. Direct measurement of high-density lipoprotein cholesterol in serum with polyethylene glycol-modified enzymes and sulfated alpha-cyclodextrin. *Clin. Chem.* **1995**, *41*, 717–723.
- Miida, T.; Nishimura, K.; Okamura, T.; Hirayama, S.; Ohmura, H.; Yoshida, H.; Miyashita, Y.; Ai, M.; Tanaka, A.; Sumino, H.; et al. Validation of homogeneous assays for HDL-cholesterol using fresh samples from healthy and diseased subjects. *Atherosclerosis* **2014**, *233*, 253–259.
- Nakamura, M.; Yokoyama, S.; Kayamori, Y.; Iso, H.; Kitamura, A.; Okamura, T.; Kiyama, M.; Noda, H.; Nishimura, K.; Nakai, M.; et al. HDL cholesterol performance using an ultracentrifugation reference measurement procedure and the designated comparison method. *Clin. Chim. Acta* **2015**, *439*, 185–190.
- Andersson, C.; Lyass, A.; Vasan, R.S.; Massaro, J.M.; D'Agostino, R.B., Sr.; Robins, S.J. Long-term risk of cardiovascular events across a spectrum of adverse major plasma lipid combinations in the framingham heart study. *Am. Heart J.* **2014**, *168*, 878–883.
- Gordon, T.; Kannel, W.B.; Castelli, W.P.; Dawber, T.R. Lipoproteins, cardiovascular disease, and death. The framingham study. *Arch. Intern. Med.* **1981**, *141*, 1128–1131.
- Preis, S.R.; Pencina, M.J.; Mann, D.M.; D'Agostino, R.B., Sr.; Savage, P.J.; Fox, C.S. Early-adulthood cardiovascular disease risk factor profiles among individuals with and without diabetes in the framingham heart study. *Diabetes Care* **2013**, *36*, 1590–1596.
- Wilson, M.D.; Abbott, R.D.; Castelli, W.P. High density lipoprotein cholesterol and mortality. The framingham heart study. *Arteriosclerosis* **1988**, *8*, 737–741.
- Carroll, M.D.; Lacher, D.A.; Sorlie, P.D.; Cleeman, J.I.; Gordon, D.J.; Wolz, M.; Grundy, S.M.; Johnson, C.L. Trends in serum lipids and lipoproteins of adults, 1960–2002. *JAMA* **2005**, *294*, 1773–1781.
- Carroll, M.D.; Kit, B.K.; Lacher, D.A.; Shero, S.T.; Mussolino, M.E. Trends in lipids and lipoproteins in us adults, 1988–2010. *JAMA* **2012**, *308*, 1545–1554.
- Yamamoto, A.; Nakamura, H.; Yasugi, T.; Mabuchi, H.; Kita, T.; Matsuzawa, Y.; Nakaya, N.; Saito, S.; Horibe, H. Current state of and recent trends in serum lipid levels in the general Japanese population. Research committee on serum lipid level survey 1990 in Japan. *J. Atheroscler. Thromb.* **1996**, *2*, 122–132.
- Arai, H.; Yamamoto, A.; Matsuzawa, Y.; Saito, Y.; Yamada, N.; Oikawa, S.; Mabuchi, H.; Teramoto, T.; Sasaki, J.; Nakaya, N.; et al. Serum lipid survey and its recent trend in the general Japanese population in 2000. *J. Atheroscler. Thromb.* **2005**, *12*, 98–106.

22. Nakamura, H.; Arakawa, K.; Itakura, H.; Kitabatake, A.; Goto, Y.; Toyota, T.; Nakaya, N.; Nishimoto, S.; Muranaka, M.; Yamamoto, A.; *et al.* Primary prevention of cardiovascular disease with pravastatin in Japan (mega study): A prospective randomised controlled trial. *Lancet* **2006**, *368*, 1155–1163.
23. Matsuzaki, M.; Kita, T.; Mabuchi, H.; Matsuzawa, Y.; Nakaya, N.; Oikawa, S.; Saito, Y.; Sasaki, J.; Shimamoto, K.; Itakura, H.; *et al.* Large scale cohort study of the relationship between serum cholesterol concentration and coronary events with low-dose simvastatin therapy in Japanese patients with hypercholesterolemia. *Circ. J.* **2002**, *66*, 1087–1095.
24. National Sensus 1995. Available online: <http://www.stat.go.jp/data/kokusei/1995/zuiyou/06273.xls> (accessed on 1 January 2012). (In Japanese)
25. Sasaki, J.; Kita, T.; Mabuchi, H.; Matsuzaki, M.; Matsuzawa, Y.; Nakaya, N.; Oikawa, S.; Saito, Y.; Shimamoto, K.; Kono, S.; *et al.* Gender difference in coronary events in relation to risk factors in Japanese hypercholesterolemic patients treated with low-dose simvastatin. *Circ. J.* **2006**, *70*, 810–814.
26. Ko, K.W.; Ohnishi, T.; Yokoyama, S. Triglyceride transfer is required for net cholesteryl ester transfer between lipoproteins in plasma by lipid transfer protein. Evidence for a hetero-exchange transfer mechanism demonstrated by using novel monoclonal antibodies. *J. Biol. Chem.* **1994**, *269*, 28206–28213.
27. Ohnishi, T.; Tan, C.; Yokoyama, S. Selective transfer of cholesteryl ester over triglyceride by human plasma lipid transfer protein between apolipoprotein-activated lipid microemulsion. *Biochemistry* **1994**, *33*, 4533–4542.
28. Qiu, X.; Mistry, A.; Ammirati, M.J.; Chrunyk, B.A.; Clark, R.W.; Cong, Y.; Culp, J.S.; Danley, D.E.; Freeman, T.B.; Geoghegan, K.F.; *et al.* Crystal structure of cholesteryl ester transfer protein reveals a long tunnel and four bound lipid molecules. *Nat. Struct. Mol. Biol.* **2007**, *14*, 106–113.
29. Tall, A. Plasma lipid transfer proteins. *Ann. Rev. Biochem.* **1995**, *64*, 235–257.
30. Foger, B.; Ritsch, A.; Doblinger, A.; Wessels, H.; Patsch, J.R. Relationship of plasma cholesteryl ester transfer protein to HDL cholesterol. Studies in normotriglyceridemia and moderate hypertriglyceridemia. *Arterioscler. Thromb. Vasc. Biol.* **1996**, *16*, 1430–1436.
31. Czarnecka, H.; Yokoyama, S. Regulation of cellular cholesterol efflux by lecithin: Cholesterol acyltransferase reaction through nonspecific lipid exchange. *J. Biol. Chem.* **1996**, *271*, 2023–2028.
32. Kurasawa, T.; Yokoyama, S.; Miyake, Y.; Yamamura, T.; Yokoyama, S. Rate of cholesteryl ester transfer between high and low density lipoproteins in human serum and a case with decreased transfer rate in association with hyperalphalipoproteinemia. *J. Biochem.* **1985**, *98*, 1499–1508.
33. Koizumi, J.; Mabuchi, H.; Yoshimura, A.; Michishita, I.; Takeda, M.; Itoh, H.; Sakai, Y.; Sakai, T.; Ueda, K.; Takeda, R. Deficiency of serum cholesteryl-ester transfer activity in patients with familial hyperalphalipoproteinemia. *Atherosclerosis* **1985**, *58*, 175–186.
34. Brown, M.L.; Inazu, A.; Hesler, C.B.; Agellon, L.B.; Mann, C.; Whitlock, M.E.; Marcel, Y.L.; Milne, R.W.; Koizumi, J.; Mabuchi, H.; *et al.* Molecular basis of lipid transfer protein deficiency in a family with increased high-density lipoproteins. *Nature* **1989**, *342*, 448–451.

35. Inazu, A.; Jiang, X.C.; Haraki, T.; Yagi, K.; Kamon, N.; Koizumi, J.; Mabuchi, H.; Takeda, R.; Takata, K.; Moriyama, Y.; *et al.* Genetic cholesteryl ester transfer protein deficiency caused by two prevalent mutations as a major determinant of increased levels of high density lipoprotein cholesterol. *J. Clin. Invest.* **1994**, *94*, 1872–1882.
36. Sakai, N.; Yamashita, S.; Hirano, K.; Menju, M.; Arai, T.; Kobayashi, K.; Ishigami, M.; Yoshida, Y.; Hoshino, T.; Nakajima, N.; *et al.* Frequency of exon 15 missense mutation (442D>G) in cholesteryl ester transfer protein gene in hyperalphalipoproteinemic Japanese subjects. *Atherosclerosis* **1995**, *114*, 139–145.
37. Hirano, K.; Yamashita, S.; Nakajima, N.; Arai, T.; Maruyama, T.; Yoshida, Y.; Ishigami, M.; Sakai, N.; Kameda-Takemura, K.; Matsuzawa, Y. Genetic cholesteryl ester transfer protein deficiency is extremely frequent in the omagari area of Japan. Marked hyperalphalipoproteinemia caused by CETP gene mutation is not associated with longevity. *Arterioscler. Thromb. Vasc. Biol.* **1997**, *17*, 1053–1059.
38. Maruyama, T.; Yamashita, S.; Matsuzawa, Y.; Bujo, H.; Takahashi, K.; Saito, Y.; Ishibashi, S.; Ohashi, K.; Shionoiri, F.; Gotoda, T.; *et al.* Mutations in Japanese subjects with primary hyperlipidemia—Results from the research committee of the ministry of health and welfare of Japan since 1996. *J. Atheroscler. Thromb.* **2004**, *11*, 131–145.
39. Yamashita, S.; Hirano, K.; Sakai, N.; Matsuzawa, Y. Molecular biology and pathophysiological aspects of plasma cholesteryl ester transfer protein. *Biochim. Biophys. Acta* **2000**, *1529*, 257–275.
40. Nagano, M.; Yamashita, S.; Hirano, K.; Takano, M.; Maruyama, T.; Ishihara, M.; Sagehashi, Y.; Kujiraoka, T.; Tanaka, K.; Hattori, H.; *et al.* Molecular mechanisms of cholesteryl ester transfer protein deficiency in Japanese. *J. Atheroscler. Thromb.* **2004**, *11*, 110–121.
41. Nagano, M.; Yamashita, S.; Hirano, K.; Ito, M.; Maruyama, T.; Ishihara, M.; Sagehashi, Y.; Oka, T.; Kujiraoka, T.; Hattori, H.; *et al.* Two novel missense mutations in the cebp gene in Japanese hyperalphalipoproteinemic subjects: High-throughput assay by invader assay. *J. Lipid Res.* **2002**, *43*, 1011–1018.
42. Ritsch, A.; Drexel, H.; Amann, F.W.; Pfeifferhofer, C.; Patsch, J.R. Deficiency of cholesteryl ester transfer protein: Description of molecular defect and the dissociation of cholesteryl ester and triglyceride transfer in plasma. *Arterioscler. Thromb. Vasc. Biol.* **1997**, *17*, 3433–3441.
43. Hui, S.P. Frequency and effect on plasma lipoprotein metabolism of a mutation in the cholesteryl ester transfer protein gene in the Chinese. *Hokkaido J. Med. Sci.* **1997**, *72*, 319–327.
44. Chen, D.W.; Yang, J.F.; Tang, Z.; Dong, X.M.; Feng, X.L.; Yu, S.; Chan, P. Cholesteryl ester transfer protein polymorphism D442G associated with a potential decreased risk for Alzheimer's disease as a modifier for APOE epsilon4 in Chinese. *Brain Res.* **2008**, *1187*, 52–57.
45. Hsu, L.A.; Ko, Y.L.; Hsu, K.H.; Ko, Y.H.; Lee, Y.S. Genetic variations in the cholesteryl ester transfer protein gene and high density lipoprotein cholesterol levels in Taiwanese Chinese. *Hum. Genet* **2002**, *110*, 57–63.
46. Jap, T.S.; Wu, Y.C.; Tso, Y.C.; Chiu, C.Y. A novel mutation in the intron 1 splice donor site of the cholesteryl ester transfer protein (CETP) gene as a cause of hyperalphalipoproteinemia. *Metabolism* **2002**, *51*, 394–397.

47. Song, G.J.; Han, G.-H.; Chae, J.J.; Namkoong, Y.; Lee, H.K.; Park, Y.B.; Lee, C.C. The effect of the cholesterol ester transfer protein gene and environmental factors on the plasma high density lipoprotein cholesterol levels in the Korean population. *Mol. Cells* **1997**, *7*, 615–619.
48. Thu, N.N.; Mai, T.T.; Ohmori, R.; Kuroki, M.; Van Chuyen, N.; Hung, N.T.; Kawakami, M.; Kondo, K. Effect of the cholesteryl ester transfer protein genotypes on plasma lipid and lipoprotein levels in Vietnamese children. *Pediatr. Res.* **2005**, *58*, 1249–1253.
49. Plengpanich, W.; Siriwong, S.; Khovidhunkit, W. Two novel mutations and functional analyses of the CETP and LIPC genes underlying severe hyperalphalipoproteinemia. *Metabolism* **2009**, *58*, 1178–1184.
50. Thompson, J.F.; Reynolds, J.M.; Williams, S.P.; Wood, L.S.; Paciga, S.A.; Lloyd, D.B. Frequency and function of CETP variants among individuals of Asian ancestry. *Atherosclerosis* **2009**, *202*, 241–247.
51. Arkhipova, N.S.; Ar'ev, A.L.; Popova, E.K.; Grigoreva, L.V.; Kozina, L.S. Association of polymorphism of angiotensin-converting enzyme gene I/D and D442G cholesteryl ester transfer protein gene with risk factors for atherosclerosis among elderly and senile patients with coronary heart disease in the Republic Sakha (Yakutia) (original Russian text is published in *Uspekhi gerontologii* vol 26: 76–81 in 2013). *Adv. Gerontol.* **2013**, *3*, 277–281.
52. Ma, Y.Q.; Thomas, G.N.; Critchley, J.A.; Chan, J.C.; Lee, Z.S.; Tomlinson, B. Identification of the intron 14 splicing defect of the cholesteryl ester transfer protein gene in Hong Kong Chinese. *Clin. Genet.* **2001**, *59*, 287–289.
53. Dixit, M.; Bhattacharya, S.; Mittal, B. Association of CETP TaqI and APOE polymorphisms with type II diabetes mellitus in North Indians: A case control study. *BMC Endocr. Disord.* **2005**, *5*, doi:10.1186/1472-6823-5-7.
54. Teh, E.M.; Dolphin, P.J.; Breckenridge, W.C.; Tan, M.H. Human plasma CETP deficiency: Identification of a novel mutation in exon 9 of the CETP gene in a Caucasian subject from North America. *J. Lipid Res.* **1998**, *39*, 442–456.
55. Hill, S.A.; Nazir, D.J.; Jayaratne, P.; Bamford, K.S.; McQueen, M.J. Mutations in cholesteryl ester transfer protein and hepatic lipase in a North American population. *Clin. Biochem.* **1997**, *30*, 413–418.
56. van der Steeg, W.A.; Hovingh, G.K.; Klerkx, A.H.; Hutten, B.A.; Nootenboom, I.C.; Levels, J.H.; van Tol, A.; Dallinga-Thie, G.M.; Zwinderman, A.H.; Kastelein, J.J.; et al. Cholesteryl ester transfer protein and hyperalphalipoproteinemia in Caucasians. *J. Lipid Res.* **2007**, *48*, 674–682.
57. Rhyné, J.; Ryan, M.J.; White, C.; Chimonas, T.; Miller, M. The two novel CETP mutations Gln87X and Gln165X in a compound heterozygous state are associated with marked hyperalphalipoproteinemia and absence of significant coronary artery disease. *J. Mol. Med. (Berl)* **2006**, *84*, 647–650.
58. Cefalu, A.B.; Noto, D.; Magnolo, L.; Pinotti, E.; Gomasrachi, M.; Martini, S.; Vigna, G.B.; Calabresi, L.; Tarugi, P.; Averna, M.R. Novel mutations of CETP gene in Italian subjects with hyperalphalipoproteinemia. *Atherosclerosis* **2009**, *204*, 202–207.
59. Calabresi, L.; Nilsson, P.; Pinotti, E.; Gomasrachi, M.; Favari, E.; Adorni, M.P.; Bernini, F.; Sirtori, C.R.; Calandra, S.; Franceschini, G.; et al. A novel homozygous mutation in CETP gene as a cause of CETP deficiency in a Caucasian kindred. *Atherosclerosis* **2009**, *205*, 506–511.

60. Chantepie, S.; Bochem, A.E.; Chapman, M.J.; Hovingh, G.K.; Kontush, A. High-density lipoprotein (HDL) particle subpopulations in heterozygous cholesteryl ester transfer protein (CETP) deficiency: Maintenance of antioxidant activity. *PLoS ONE* **2012**, *7*, e49336.
61. Thompson, A.; Di Angelantonio, E.; Sarwar, N.; Erqou, S.; Saleheen, D.; Dullaart, R.P.; Keavney, B.; Ye, Z.; Danesh, J. Association of cholesteryl ester transfer protein genotypes with CETP mass and activity, lipid levels, and coronary risk. *JAMA* **2008**, *299*, 2777–2788.
62. Inazu, A.; Brown, M.L.; Hesler, C.B.; Agellon, L.B.; Koizumi, J.; Takata, K.; Maruhamma, Y.; Mabuchi, H.; Tall, A.R. Increased high-density lipoprotein levels caused by a common cholesteryl-ester transfer protein gene mutation. *New Eng. J. Med.* **1990**, *323*, 1234–1238.
63. Yamashita, S.; Hui, D.Y.; Sprecher, D.L.; Matsuzawa, Y.; Sakai, N.; Tarui, S.; Kaplan, D.; Wetterau, J.R.; Harmony, J.A. Total deficiency of plasma cholesteryl ester transfer protein in subjects homozygous and heterozygous for the intron 14 splicing defect. *Biochem. Biophys. Res. Commun.* **1990**, *170*, 1346–1351.
64. Yamashita, S.; Hui, D.Y.; Wetterau, J.R.; Sprecher, D.L.; Harmony, J.A.K.; Sakai, N.; Matsuzawa, Y.; Tarui, S. Characterization of plasma lipoproteins in patients heterozygous for human plasma cholesteryl ester transfer protein (CETP) deficiency: Plasma CETP regulated high-density lipoprotein concentration and composition. *Metabolism* **1991**, *40*, 756–763.
65. Sakai, N.; Matsuzawa, Y.; Hirano, K.; Yamashita, S.; Nozaki, S.; Ueyama, Y.; Kubo, M.; Tarui, S. Detection of two species of low density lipoprotein particles in cholesteryl ester transfer protein deficiency. *Arterioscler. Thromb.* **1991**, *11*, 71–79.
66. Bisgaier, C.L.; Siebenkas, M.V.; Brown, M.L.; Inazu, A.; Koizumi, J.; Mabuchi, H.; Tall, A.R. Familial cholesteryl ester transfer protein deficiency is associated with triglyceride-rich low density lipoproteins containing cholesteryl esters of probable intracellular origin. *J. Lipid Res.* **1991**, *32*, 21–33.
67. Yamashita, S.; Sprecher, D.L.; Sakai, N.; Matsuzawa, Y.; Tarui, S.; Hui, D.Y. Accumulation of apolipoprotein E-rich high density lipoproteins in hyperalphalipoproteinemic human subjects with plasma cholesteryl ester transfer protein deficiency. *J. Clin. Invest.* **1990**, *86*, 688–695.
68. Moriyma, Y.; Okamura, T.; Inazu, A.; Doi, M.; Iso, H.; Mouri, Y.; Ishikawa, Y.; Suzuki, H.; Iida, M.; Koizumi, J.; et al. A low prevalence of coronary heart disease among subjects with increased high-density lipoprotein cholesterol levels, including those with plasma cholesteryl ester transfer protein deficiency. *Prev. Med.* **1998**, *27*, 659–667.
69. Curb, J.D.; Abbott, R.D.; Rodriguez, B.L.; Masaki, K.; Chen, R.; Sharp, D.S.; Tall, A.R. A prospective study of HDL-C and cholesteryl ester transfer protein gene mutations and the risk of coronary heart disease in the elderly. *J. Lipid Res.* **2004**, *45*, 948–953.
70. Yamashita, S.; Sakai, N.; Hirano, K.; Arai, T.; Ishigami, M.; Maruyama, T.; Matsuzawa, Y. Molecular genetics of plasma cholesteryl ester transfer protein. *Curr. Opin. Lipidol.* **1997**, *8*, 101–110.
71. Nissen, S.E.; Tardif, J.C.; Nicholls, S.J.; Revkin, J.H.; Shear, C.L.; Duggan, W.T.; Ruzyllo, W.; Bachinsky, W.B.; Lasala, G.P.; Tuzcu, E.M. Effect of torcetrapib on the progression of coronary atherosclerosis. *N. Engl. J. Med.* **2007**, *356*, 1304–1316.

72. Schwartz, G.G.; Olsson, A.G.; Abt, M.; Ballantyne, C.M.; Barter, P.J.; Brumm, J.; Chaitman, B.R.; Holme, I.M.; Kallend, D.; Leiter, L.A.; *et al.* Effects of dalcetrapib in patients with a recent acute coronary syndrome. *N. Engl. J. Med.* **2012**, *367*, 2089–2099.
73. Kit, B.K.; Carroll, M.D.; Lacher, D.A.; Sorlie, P.D.; DeJesus, J.M.; Ogden, C. Trends in serum lipids among us youths aged 6 to 19 years, 1988–2010. *JAMA* **2012**, *308*, 591–600.
74. FAOSTAT (Food and Agriculture Organization of The United Nations, Statistics Division). Available online: [http://faostat3.fao.org/download/FB/\\*E](http://faostat3.fao.org/download/FB/*E) (accessed on 1 January 2012).

© 2015 by the author; licensee MDPI, Basel, Switzerland. This article is an open access article distributed under the terms and conditions of the Creative Commons Attribution license (<http://creativecommons.org/licenses/by/4.0/>).

# Deficiency in the Lipid Exporter ABCA1 Impairs Retrograde Sterol Movement and Disrupts Sterol Sensing at the Endoplasmic Reticulum<sup>\*♦</sup>

Received for publication, May 1, 2015, and in revised form, July 10, 2015. Published, JBC Papers in Press, July 20, 2015, DOI 10.1074/jbc.M115.662668

Yoshio Yamauchi<sup>†1,2</sup>, Noriyuki Iwamoto<sup>§1</sup>, Maximillian A. Rogers<sup>¶1,3</sup>, Sumiko Abe-Dohmae<sup>§</sup>, Toyoshi Fujimoto<sup>||</sup>, Catherine C. Y. Chang<sup>¶</sup>, Masato Ishigami<sup>\*\*</sup>, Takuma Kishimoto<sup>††</sup>, Toshihide Kobayashi<sup>††</sup>, Kazumitsu Ueda<sup>\*\*</sup>, Koichi Furukawa<sup>‡</sup>, Ta-Yuan Chang<sup>¶4</sup>, and Shinji Yokoyama<sup>§§</sup>

From the <sup>†</sup>Department of Biochemistry II, Nagoya University Graduate School of Medicine, Nagoya 466-8550, Japan, the <sup>¶</sup>Department of Biochemistry, Geisel School of Medicine at Dartmouth, Hanover, New Hampshire 03755, the <sup>§</sup>Department of Biochemistry, Nagoya City University Graduate School of Medical Sciences, Nagoya 467-8601, Japan, the <sup>||</sup>Department of Anatomy and Molecular Cell Biology, Nagoya University Graduate School of Medicine, Nagoya 466-8550, Japan, the <sup>\*\*</sup>Institute for Integrated Cell-Material Sciences and Division of Applied Life Sciences, Graduate School of Agriculture, Kyoto University, Kyoto 606-8502, Japan, the <sup>††</sup>Lipid Biology Laboratory, RIKEN, Wako, Saitama 351-0198, Japan, and the <sup>§§</sup>Nutritional Health Science Research Center and Department of Food and Nutritional Sciences, Chubu University, Kasugai 487-8501, Japan

**Background:** Little is known about how mammalian cells modulate retrograde sterol transport for cellular cholesterol homeostasis.

**Results:** ABCA1 deficiency impairs endocytic retrograde sterol transport to the endoplasmic reticulum and activates the SREBP-2 pathway.

**Conclusion:** ABCA1 participates in bidirectional sterol movement at the plasma membrane to regulate cellular cholesterol homeostasis.

**Significance:** A novel function of ABCA1 is identified.

Cellular cholesterol homeostasis involves sterol sensing at the endoplasmic reticulum (ER) and sterol export from the plasma membrane (PM). Sterol sensing at the ER requires efficient sterol delivery from the PM; however, the macromolecules that facilitate retrograde sterol transport at the PM have not been identified. ATP-binding cassette transporter A1 (ABCA1) mediates cholesterol and phospholipid export to apolipoprotein A-I for the assembly of high density lipoprotein (HDL). Mutations in *ABCA1* cause Tangier disease, a familial HDL deficiency. Several lines of clinical and experimental evidence suggest a second function of ABCA1 in cellular cholesterol homeostasis in addition to mediating cholesterol efflux. Here, we report the unexpected finding that ABCA1 also plays a key

role in facilitating retrograde sterol transport from the PM to the ER for sterol sensing. Deficiency in ABCA1 delays sterol esterification at the ER and activates the SREBP-2 cleavage pathway. The intrinsic ATPase activity in ABCA1 is required to facilitate retrograde sterol transport. ABCA1 deficiency causes alternation of PM composition and hampers a clathrin-independent endocytic activity that is required for ER sterol sensing. Our finding identifies ABCA1 as a key macromolecule facilitating bidirectional sterol movement at the PM and shows that ABCA1 controls retrograde sterol transport by modulating a certain clathrin-independent endocytic process.

Cellular cholesterol homeostasis is maintained by the sterol-sensing system in the endoplasmic reticulum (ER)<sup>5</sup> for its biosynthesis and uptake and by the sterol export system in the plasma membrane (PM) (1–3). Most cellular cholesterol is located in the PM, which forms a functional regulatory network with other intracellular compartments, particularly the ER (4).

\* This work was supported, in whole or in part, by National Institutes of Health Grants AG037609 and HL060306 (to T. Y. C. and C. C. Y. C.). This work was also supported by a grant-in-aid for young scientists from the Japan Society for the Promotion of Sciences (to Y. Y.), grants-in-aid for scientific research from the Ministry of Education, Sciences, Technology, Culture, and Sports of Japan (to Y. Y., to S. A.-D., to T. F., to K. U., and to S. Y.), and a MEXT-supported program for the Strategic Research Foundation at Private Universities (to S. Y.). The authors declare that they have no conflicts of interest with the contents of this article.

♦ This article was selected as a Paper of the Week.

<sup>1</sup> These authors contributed equally to this work.

<sup>2</sup> To whom correspondence may be addressed: Dept. of Biochemistry II, Nagoya University Graduate School of Medicine, 65 Tsurumai, Showa-ku, Nagoya 466-8550, Japan. Tel.: 81-52-744-2068; Fax 81-52-744-2069; E-mail: yyoshio@med.nagoya-u.ac.jp.

<sup>3</sup> Recipient of NRSA Institutional Postdoctoral Training Grant T32 from National Institutes of Health.

<sup>4</sup> To whom correspondence may be addressed: Dept. of Biochemistry, Geisel School of Medicine at Dartmouth, 7200 Vail Bldg. Rm. 304, Hanover, NH 03755. Tel.: 603-650-1622; Fax: 603-650-1128; E-mail: Ta.Yuan.Chang@Dartmouth.edu.

<sup>5</sup> The abbreviations used are: ER, endoplasmic reticulum; ACAT, acylCoA: cholesterol acyltransferase; apoA-I, apolipoprotein A-I; Cav1, caveolin-1; CIE, clathrin-independent endocytosis; CME, clathrin-mediated endocytosis; CTxB, cholera toxin B subunit; CE, cholesteryl ester; HMGR, HMG-CoA reductase; LDLR, LDL receptor; MEF, mouse embryonic fibroblast; mTORC1, mechanistic target of rapamycin complex 1; PL, phospholipid; PM, plasma membrane; SM, sphingomyelin; SMase, sphingomyelinase; Scap, SREBP cleavage activating protein; SREBP, sterol regulatory element-binding protein; TD, Tangier disease; qRT quantitative RT; MCD, methyl- $\beta$ -cyclodextrin; ANOVA, analysis of variance; ACIE, ABCA1-regulated, clathrin-independent endocytosis; CE, cholesteryl ester; LDL-Chol, LDL-derived cholesterol; DF, DMEM/F-12; DRM, detergent-resistant membrane; BHK, baby hamster kidney; SRE, sterol regulatory element; 25HC, 25-hydroxycholesterol.

**ABCA1 Regulates Bidirectional Sterol Transport**

Upon cholesterol supply, ER cholesterol down-regulates sterol regulatory element-binding protein-2 (SREBP-2) through binding to the SREBP cleavage-activating protein (Scap) to suppress cholesterol synthesis and low density lipoprotein (LDL) receptor (LDLR) expression (1). The sterol removal is regulated by cholesterol release from the PM mainly to high density lipoprotein (HDL). It involves the ATP-binding cassette transporters, ABCA1 and ABCG1 (3); ABCA1 plays a predominant role in cholesterol efflux (5). It mediates formation of new HDL particles at the PM with cellular cholesterol, phospholipid (PL), and  $\alpha$ -helical apolipoproteins such as apolipoprotein A-I (apoA-I) (6, 7). Excessive PM cholesterol is also esterified in the ER by acyl-CoA:cholesterol acyltransferase 1 (ACAT1) for storage (2). Retrograde sterol transport from the PM to the ER is thus an important part of cellular cholesterol homeostasis; aside from its independence from Niemann-Pick C proteins (8, 9), the mechanisms of this process are largely unknown. Specifically, the macromolecules located at the PM that modulate retrograde sterol transport have not been identified.

In whole body cholesterol homeostasis, sterol must be transported from peripheral cells to the liver for conversion to bile acids, and HDL plays a central role in this “reverse cholesterol transport.” This is perhaps why plasma HDL levels inversely correlate with the incidence of cardiovascular disease. Loss-of-function mutations in *ABCA1* cause HDL deficiency known as Tangier disease (TD) (3, 6). *ABCA1* deficiency in humans or animals exhibits a risk for premature atherosclerosis. TD patients display cholesterol deposition in various tissues, despite reduced plasma LDL levels (10). In *Abca1*<sup>-/-</sup> mice, free cholesterol accumulates in macrophages (11). In addition, deletion of hepatic *Abca1* in mice resulted in increases of LDLR expression and of LDL clearance in the liver (12). In a mouse model of hypoxic advanced atherosclerotic plaques, *ABCA1* expression and cell cholesterol release are decreased, but HMG-CoA reductase (HMGR) expression and sterol synthesis are increased, resulting in the accumulation of free sterol in macrophages (13). These puzzling observations cannot be satisfactorily explained by the assumption that *ABCA1* functions only in cellular sterol release, suggesting that *ABCA1* may have additional functions.

*ABCA1* is expressed in various tissues and cell types, including hepatocytes, macrophages, and fibroblasts. Since defective apoA-I-mediated cholesterol efflux was first described in fibroblasts isolated from TD patients (14), fibroblasts are widely accepted as a model system to study *ABCA1*-dependent HDL formation. In this study, we examine cellular sterol trafficking and ER sterol sensing in *Abca1*<sup>+/+</sup> and *Abca1*<sup>-/-</sup> mouse embryonic fibroblasts (MEFs) and other mammalian cell models. We report an undisclosed, novel function of *ABCA1* in regulation of cellular cholesterol homeostasis.

**Experimental Procedures**

**Materials**—ApoA-I was prepared as described previously (15, 16). [<sup>3</sup>H]Acetic acid was from American Radiochemicals. [1,2-<sup>3</sup>H]Cholesterol and [<sup>14</sup>C]oleate were from PerkinElmer Life Sciences. [<sup>3</sup>H]Cholesteryl oleate was from GE Healthcare. [<sup>3</sup>H]Cholesteryl oleate-containing LDL was prepared as described (17). [<sup>3</sup>H]Lanosterol was prepared and purified as

described (18). Dynasore was from Cayman Chemical. Dynole 34-2 and dynole 31-2 were from Abcam. Other chemical compounds were described previously (8).

**Cell Culture**—MEFs from *Abca1*<sup>+/+</sup> and *Abca1*<sup>-/-</sup> mice were isolated as described previously (19). MEFs isolated were expanded and stored as stocks at an early passage stage. MEFs less than 15 passages were used in experiments reported here. Wild-type (WT) and 25RA CHO cells were employed as described previously (16). A mouse fibroblast cell line, BALB/3T3, was obtained from Riken Cell Bank. Baby hamster kidney (BHK) cells harboring WT-*ABCA1* expression plasmid or empty plasmid were the kind gift of Dr. Oram (20). BHK cells harboring *ABCA1*-MM were generated using the mifepristone-inducible GeneSwitch system (Invitrogen) as described previously (20). Human *ABCA1*-MM cDNA was inserted into pGene/V5-HisA (blasticidin), in which the original Zeocin resistance gene was replaced by the blasticidin resistance gene. BHK cells harboring pSwitch plasmid (20) were transfected with pGene/V5-HisA (blasticidin)/*ABCA1*-MM; stable transfects were selected with hygromycin (350  $\mu$ g/ml) and blasticidin (5  $\mu$ g/ml). After the selection, a clone in which *ABCA1*-MM expression was highly induced by mifepristone was isolated. Mouse and hamster cells were maintained in Dulbecco's modified Eagle's medium (DMEM) supplemented with 10% fetal bovine serum (FBS) and in DMEM/F-12 (DF) supplemented with 7.5% FBS, respectively. All cells were grown in humidified CO<sub>2</sub> incubators at 37 °C. Media used were designated as follows: medium A contains 10 or 7.5% FBS as described above; medium B contains 0.1% BSA; medium D contains 5% delipidated FBS; medium F contains no supplements. Incubation of MEFs in medium F for up to 24 h did not cause significant cell death, as demonstrated by flow cytometric measurement of the incorporation of 7-amino-actinomycin D (BD Biosciences) into cells (viability  $\geq$ 97%).

**Intracellular Sterol Transport Assays**—Five different assays were employed to study retrograde transport of sterol from PM. Cells were seeded in 6-well plates at  $2.5 \times 10^5$  cells/well for MEFs or at  $2.0 \times 10^5$  cells/well for CHO and BHK cells and were treated as indicated in the figure legends before labeling. First, cells were pulse-labeled with [<sup>3</sup>H]acetate for 1 h at 37 °C and then chased in medium F for various times as indicated to monitor the conversion of precursor sterols to cholesterol by a method employed previously (8). Second, the conversion of [<sup>3</sup>H]lanosterol to [<sup>3</sup>H]cholesterol was monitored. Cells were pulse-labeled with 0.1  $\mu$ Ci/ml [<sup>3</sup>H]lanosterol (added to medium B as 0.1% ethanolic solution) in medium B for 30 min at 37 °C, followed by washing cells with medium B twice and chasing in medium F for various times as indicated. Sterols were extracted, saponified, and analyzed by TLC as above. Third, to monitor retrograde movement of cholesterol, the conversion of [<sup>3</sup>H]cholesterol to [<sup>3</sup>H]cholesteryl ester was monitored; cells were pulse-labeled with 0.1  $\mu$ Ci/ml [<sup>3</sup>H]cholesterol (added to medium B as 0.1% ethanolic solution without adding unlabeled cholesterol as carrier) in medium B for 30 min at 37 °C, followed by chasing as above. Alternatively, cells were incubated with [<sup>3</sup>H]cholesterol for 8 h in medium A and further incubated for 16 h in medium A in the absence of [<sup>3</sup>H]cholesterol to reach cellular [<sup>3</sup>H]cholesterol distribution at the steady-state level.

## ABCA1 Regulates Bidirectional Sterol Transport

Cellular lipids were separated by TLC; radioactivities in cholesterol and cholesteryl oleate fractions were counted. In certain experiments as indicated, agents were included in medium during the chase period. When using mifepristone-induced ABCA1 expression system, cells were either treated or untreated with mifepristone and then used to perform the pulse/chase experiments; counts in [<sup>3</sup>H]cholesteryl ester formed in untreated cells were subtracted from those formed in mifepristone-treated cells, to calculate ABCA1-dependent esterification. Fourth, ACAT1 activity in intact cells was monitored by feeding cells with [<sup>14</sup>C]oleate for 3 h and determined the incorporation of [<sup>14</sup>C]oleate into CE according to procedures described previously (16). Fifth, intracellular transport of LDL-derived cholesterol (LDL-Chol) was monitored by using [<sup>3</sup>H]cholesteryl oleate-containing LDL; cells were incubated with [<sup>3</sup>H]cholesteryl oleate-containing LDL for 4 h at 18 °C and chased in medium D at 37 °C for various times. After the chase period, cells were treated with 4% methyl- $\beta$ -cyclodextrin (MCD) for 10 min at 4 °C to determine PM-associated [<sup>3</sup>H]cholesterol. LDL uptake was determined by measuring the sum of <sup>3</sup>H counts present in cells and in medium.

**Antibodies and Immunoblot**—Rabbit anti-human ABCA1 antiserum was described previously (15). The anti-ACAT1 rabbit polyclonal antibodies (DM102) were as described previously (21). Hybridoma cells producing anti-HMG-CoA reductase (IgG-A9), anti-SREBP-1 (IgG-2A4), or anti-SREBP-2 (IgG-7D4) antibodies were obtained from ATCC, and supernatants of hybridoma cell cultured media were used for immunoblotting. Other antibodies were obtained from commercial sources as follows: anti-caveolin-1 polyclonal antibodies (N-20) and anti-Insig-1 polyclonal antibodies from Santa Cruz Biotechnology; monoclonal antibodies to flotillin-1 and calnexin from BD Biosciences; anti-SREBP-2 polyclonal antibodies from Cayman Chemical; anti- $\beta$ -actin monoclonal antibody (AC74) from Sigma; anti-transferrin receptor monoclonal antibody from Zymed Laboratories Inc.; and anti-p70 S6 kinase (numbers 2708 and 9206) and anti-4E-BP1 (numbers 9644 and 2855) monoclonal antibodies from Cell Signaling Technology. Whole cell lysate was prepared by lysing cells with urea buffer (8 M urea, 50 mM sodium phosphate, pH 8.0, 10 mM Tris-HCl, pH 8.0, 100 mM NaCl, 0.2% protease inhibitor mixture (Sigma)) as described previously (22). To detect mouse SREBP-2, polyclonal anti-SREBP-2 antibodies from Cayman Chemical were employed. Protein concentration was determined by BCA protein assay (Pierce). Equal amounts of proteins were subjected to SDS-PAGE and immunoblot analysis. Expression of a protein was analyzed by using ImageJ software and was normalized to a loading control.

**Cell Fractionation**—Cells grown in 100-mm dishes were treated with 1% Triton X-100 (Sigma) in TNE buffer (25 mM Tris-HCl, pH 7.5, 150 mM NaCl, 5 mM EDTA) containing protease inhibitor mixture (Sigma) for 30 min at 4 °C. Afterward, cells were homogenized with a stainless homogenizer for 10 strokes. Post-nuclear supernatant was then subjected to density gradient centrifugation as described (22). Eight 0.5-ml fractions were collected from the top. Lipids were extracted from equal amounts of each fraction by chloroform/methanol (2:1, v/v).

**Small Interfering RNA (siRNA)**—Small interfering RNA experiments were performed as described previously (23). siRNA duplexes specific for mouse *Abca1* (5'-AUUUCUUCUGUCAGAUUCUGAAGG-3') or control (5'-UAGUGAAGACAGUCACUCGGGAAGC-3') were obtained from Invitrogen and transfected into BALB/3T3 mouse fibroblast cells using Lipofectamine 2000 (Invitrogen). Seventy two hours after transfection, cells were subjected to further analyses.

**RNA Isolation, mRNA Expression Analysis, and Luciferase Reporter Assay**—Total RNA was isolated with TRIzol reagent (Invitrogen). mRNA levels of various genes were determined by quantitative real time PCR (qRT-PCR) and quantified by using the  $\Delta\Delta CT$  method; *Hprt* expression was used as an internal control as described previously (24). SRE promoter activity was assessed by a luciferase reporter assay. The 4 $\times$ SRE tandem repeat region was amplified by the *Hmgcs*-specific primers using DNA isolated from mouse liver. The resultant fragment was inserted into a pGL4 basic vector (Promega). The sequence was verified. On day 0, cells were plated into 24-well plates and grown for 24 h in medium A. On day 1, the reporter luciferase plasmid (1  $\mu$ g) and the pRL-TK (Promega) encoding *Renilla* luciferase (for normalization; 30 ng) were transfected with the indicated siRNA by using Lipofectamine 2000 (Invitrogen). Cells were then incubated in medium D for 2 days. On day 3, the cells were lysed, and the luciferase activity was measured by the Dual-Luciferase Reporter Assay System (Promega).

**Lipid Analyses and Visualization**—To estimate cell surface cholesterol levels, cells were incubated either with 4% 2-hydroxypropyl- $\beta$ -cyclodextrin for 10 min at 37 °C (25) or with 3 mM MCD for 5 min at 37 °C (26). Afterward, cholesterol contents in medium were determined as described (16). Alternatively, cell surface cholesterol in living cells was visualized by using mCherry-fused domain 4 of perfringolysin O (also known as  $\theta$ -toxin) (27) (mCherry-D4), which specifically binds to the cholesterol-rich membrane domain. mCherry-D4 was prepared as described (27) except enhanced GFP was replaced by mCherry. Cells cultured on glass-bottom dishes in medium A for 2 days were washed with phenol red-free DF. Cells were then incubated with mCherry-D4 (16  $\mu$ g/ml) in phenol red-free DF at room temperature for 10 min. After several washes with phenol red-free DF, cell were further incubated in phenol red-free DF at room temperature. Cell images were acquired within 15 min without fixation by using a Zeiss LSM 700 confocal microscope equipped with PLAN-NEOFLUAR  $\times 20$  (0.5 NA) objective (Zeiss). Images were then processed with LSM 700 software Zen (Zeiss) and ImageJ software. Cell surface GM1 levels were examined by flow cytometry. Cells were detached by trypsin and incubated with 1  $\mu$ g/ml biotin-conjugated cholera toxin B subunit (biotin-CTxB) (List Biological Laboratories) for 60 min at 4 °C. After washing cells with ice-cold PBS, they were incubated with FITC-conjugated avidin for 60 min and washed extensively, followed by fluorescence measurement using a FACSCalibur (BD Biosciences). Gated 10,000 cells were analyzed for each sample, and mean fluorescence intensity was determined. Total cholesterol, free cholesterol, and cholesterols were measured by colorimetric enzymatic assay systems as described (16). Cholesteryl ester (CE) was determined by subtracting free cholesterol from total cholesterol.

## ABCA1 Regulates Bidirectional Sterol Transport

**Immunofluorescence Microscopy**—Cells were seeded on glass coverslips in 6-well plates and grown for 2 days in medium A. After incubation of the cells in medium F overnight, they were fixed with 4% paraformaldehyde for 10 min and blocked with 5% FBS in PBS for 1 h. Specimens were incubated with biotin-conjugated CTxB (1  $\mu$ g/ml) and anti-caveolin-1 antibody or with biotin-conjugated CTxB (1  $\mu$ g/ml) and anti-flotillin-1 antibody for 1 h at room temperature. Specimens were then stained with FITC-conjugated avidin (for biotin-CTxB detection) and Alexa Fluor 555-conjugated anti-rabbit IgG antibody (for caveolin-1) or with Alexa Fluor 555-conjugated anti-mouse IgG antibody (for flotillin-1), respectively. The nuclei were stained with Hoechst 33342. After extensive washes, they were mounted with ProLong Gold Antifade Reagent (Invitrogen). Cell images were acquired by using a confocal laser microscopy FV500 (Olympus) or FV10i (Olympus). Images were processed by a Fluoview software (Olympus).

**CTxB Internalization**—To analyze internalization of CTxB, cells were seeded into glass-bottom 35-mm dishes at a density of  $1 \times 10^5$  cells/well and grown for 2–3 days. The cells were then washed twice with ice-cold medium F and incubated with 2  $\mu$ g/ml Alexa Fluor 555-CTxB (Molecular Probe) either at 4 or 37  $^{\circ}$ C for the indicated times. The cells incubated at 37  $^{\circ}$ C were washed three times for 30 s with 0.5 M glycine, pH 2.2, to remove cell surface Alexa Fluor 555-CTxB (28). Cells were then fixed with 4% paraformaldehyde, and nuclei were stained with Hoechst 33342. After extensive washing with PBS, images were acquired by using a confocal laser microscope FV10i (Olympus). Cellular mean fluorescence intensity was analyzed by MetaMorph software (Molecular Devices).

**Electron Microscopy**—Cells were seeded on glass coverslips and grown for 1 day in medium A. After incubation in medium F for 18 h, they were fixed with 2.5% glutaraldehyde and 2% formaldehyde in 0.1 M sodium cacodylate buffer, pH 7.4, added with 1 mM  $\text{CaCl}_2$  for 2 h. After rinses, samples were postfixed with 1% osmium tetroxide and 0.1% potassium ferrocyanide in the same buffer, dehydrated in ethanol series, and embedded in Quetol 812. Ultrathin sections cut perpendicular to the substrate were stained with lead citrate and observed under a JEM-1011 electron microscope (JEOL).

**Statistical Analysis**—Data are presented as means  $\pm$  S.D. or S.E. as indicated in the figure legends. Statistical analyses of results were performed using the two-tailed, unpaired Student's *t* test, using Mann-Whitney *U* test or using one-way ANOVA followed by Tukey-Kramer post hoc test for multiple comparisons.

## Results

**ABCA1 Deficiency Leads to Hyperactivation of SREBP-2 Pathway**—We hypothesize that ABCA1 may have an additional role in cholesterol homeostasis that does not require extracellular cholesterol acceptors. To test this possibility, we incubated *Abca1*<sup>+/+</sup> (wild type, WT) and *Abca1*<sup>-/-</sup> MEFs in serum-free medium (medium F), which does not contain any extracellular cholesterol acceptors. Lipid analysis of these cells showed that lack of ABCA1 caused a substantial increase of free (unesterified) cholesterol in cells (Fig. 1A). In contrast, the CE contents in these two cell types did not differ significantly

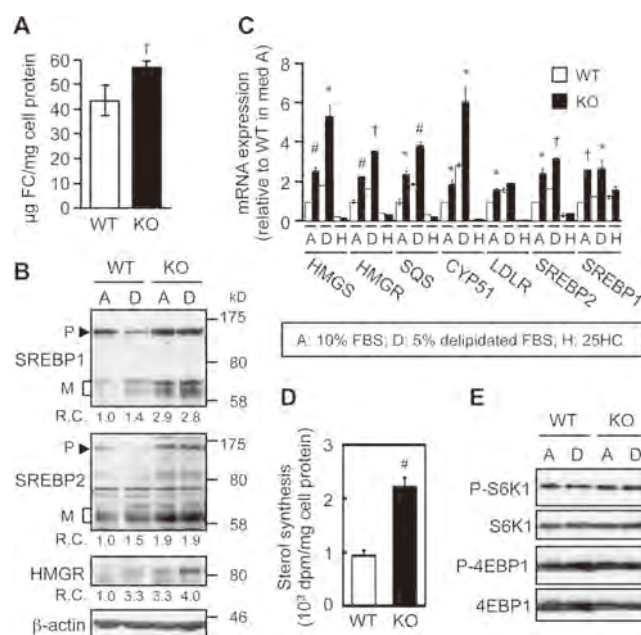


**FIGURE 1. ABCA1 deficiency causes elevated SREBP-2 pathway.** *A*, cellular free cholesterol contents. On day 0, WT and *Abca1*<sup>-/-</sup> (KO) MEFs were seeded and grown in medium A (medium containing FBS). On day 3, cells were switched to medium F (serum-free medium) and incubated for 1 day. †,  $p = 0.00001$  ( $n = 8$  for WT,  $n = 10$  for KO). *B*, SREBP processing. MEFs were set up as in *A*. On day 2, cells were replaced with medium A (medium with FBS) or D (medium with delipidated-serum) and incubated for 2 days. SREBP-1, SREBP-2, and HMGR expression was examined by immunoblot.  $\beta$ -Actin serves as a loading control. Average relative changes (R.C.) of three to five experiments are shown at the bottom of each blot image. P, precursor form; M, mature form. *C*, mRNA expression. MEFs were set up as in *B*. Cells grown in medium D were further treated without or with 10  $\mu$ M 25-HC (H) for 7 h. mRNA levels of HMG-CoA synthase (HMGS), HMGR, squalene synthase (SQS), CYP51, LDLR, SREBP-2, and SREBP-1 were analyzed by qRT-PCR. Values reported were relative to values in WT MEFs grown in medium A. \*,  $p < 0.05$ ; #,  $p < 0.01$ ; †,  $p < 0.005$  ( $n = 3$  except 25-HC was  $n = 2$ ). *D*, cholesterol synthesis. After incubation in medium D for 24 h, MEFs were incubated with [<sup>3</sup>H]acetate for 2 h to determine sterol synthesis. #,  $p < 0.01$  ( $n = 3$ ). *E*, mTORC1 signaling. MEFs were incubated in medium A or medium D as in *B*. Phosphorylation of S6K1 and 4E-BP1 was examined by immunoblot. Phospho(P)-S6K1 and phospho-4E-BP1 were detected first. After stripping, membranes were probed with anti-S6K1 and anti-4E-BP1 antibodies. Error bars represent S.D. Statistical analyses were performed by Student's *t* test.

( $1.5 \pm 0.9$   $\mu$ g/mg cell protein in WT MEFs;  $n = 8$ , and  $2.0 \pm 0.6$   $\mu$ g/mg cell protein in *Abca1*<sup>-/-</sup> MEFs;  $n = 10$ , means  $\pm$  S.D.;  $p = 0.167$ ). As a control experiment, we determined cholesterol release to serum-free medium, after cells were labeled with [<sup>3</sup>H]cholesterol and its distribution in cells reached steady state. The result of this experiment showed that in both WT and *Abca1*<sup>-/-</sup> cells, cholesterol release to serum-free medium in 6 h was at a minimal level ( $0.85 \pm 0.02$  and  $0.93 \pm 0.11\%$ , respectively). Together, these results suggest that ABCA1 may play an undisclosed role in cellular cholesterol homeostasis, independent of extracellular sterol acceptors. Additional results showed that despite an increase in cellular cholesterol content, cleavages of both SREBP-1 and -2, which are known to be sensitive to feedback inhibition by cholesterol (29), were activated in *Abca1*<sup>-/-</sup> MEFs (Fig. 1B). Consistent with this finding, mRNA levels of various cholesterol biosynthetic enzymes were elevated in both cholesterol-rich (medium A) and cholesterol-poor (medium D) conditions in *Abca1*<sup>-/-</sup> cells (Fig. 1C). Additionally, the sterol biosynthesis rate was also increased in these cells (Fig. 1D). Mechanistic target of rapamycin complex 1

## ABCA1 Regulates Bidirectional Sterol Transport

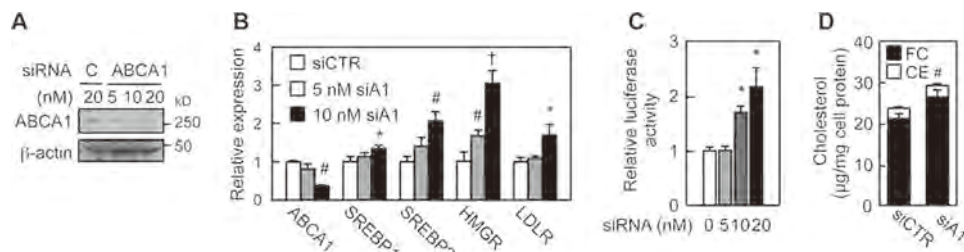


**FIGURE 2. ABCA1 knockdown activates SREBP-2 pathway.** A, ABCA1 expression. The indicated amounts of control (C) or ABCA1 siRNA were transfected in BALB/3T3 cells. ABCA1 expression was examined by immunoblot. B, mRNA expression. BALB/3T3 cells were transfected with control (siCTR) or ABCA1 (siA1) siRNA. mRNA levels of the indicated genes were analyzed by qRT-PCR. \*,  $p < 0.05$ ; #,  $p < 0.01$ ; †,  $p < 0.001$  ( $n = 3$ ). C, SRE promoter activity. BALB/3T3 cells were transfected with luciferase reporter vector harboring SRE and control or ABCA1 siRNA as indicated. Luciferase activity was measured. \*,  $p < 0.05$  ( $n = 3$ ). D, cellular cholesterol contents in BALB/3T3 cells transfected with 10 nM control (siCTR) or ABCA1 (siA1) siRNA were determined. #,  $p < 0.01$  ( $n = 3$ ). FC, free cholesterol. Error bars represent S.D. Statistical analyses were performed by Student's *t* test.

(mTORC1) signaling has been implicated in SREBP regulation (30). We tested the possibility that altered mTORC1 signaling activity might occur in *Abca1*<sup>-/-</sup> MEFs, but we did not observe a difference in phosphorylation of the two mTOR substrates p70-S6K1 and 4E-BP1 (Fig. 1E). The results of an additional control experiment showed that when 25-hydroxycholesterol (25HC), a membrane-permeable regulatory oxysterol that enters the cell interior rapidly, was added to the growth medium, it caused efficient down-regulation of various SREBP-2 response genes in both WT and *Abca1*<sup>-/-</sup> MEFs, demonstrating that the ER sterol-sensing machinery in the *Abca1*<sup>-/-</sup> cells is not impaired (Fig. 1C). These data suggest that ABCA1 deficiency decreases the ER cholesterol levels despite a substantial increase in total cellular cholesterol. We noted that a significant increase in cholesterol content occurred in *Abca1*<sup>-/-</sup> cells; this result could in part be due to the consequence of a significant increase in cholesterol synthesis in these cells (Fig. 1D).

To validate these results, we silenced ABCA1 expression in a mouse fibroblast cell line BALB/3T3 using siRNA (Fig. 2A). The result showed that knockdown of ABCA1 markedly increased the expression of various SREBP target genes (Fig. 2B) and the SRE promoter activity (Fig. 2C). ABCA1 knockdown in BALB/3T3 cells also led to a significant increase in unesterified cholesterol content (Fig. 2D). Together, these results demonstrate a crucial role of ABCA1 in the regulation of the SREBP-2 pathway.

**ABCA1 Facilitates PM-to-ER Retrograde Sterol Movement—** To further test whether the ER cholesterol level is reduced in *Abca1*<sup>-/-</sup> MEFs, we labeled WT and *Abca1*<sup>-/-</sup> MEFs with [<sup>3</sup>H]cholesterol for 8 h, removed the [<sup>3</sup>H]cholesterol present in the medium, and allowed the cellular [<sup>3</sup>H]cholesterol to equilibrate within cells for 16 h and then measured percent esterification of [<sup>3</sup>H]cholesterol. Under this condition, we found a marked reduction in esterification of [<sup>3</sup>H]cholesterol in the *Abca1*<sup>-/-</sup> MEFs (Fig. 3A), which supports the notion that under this condition the ER cholesterol level is reduced in *Abca1*<sup>-/-</sup> MEFs. The majority of cellular cholesterol is located at the PM. Partial defects in PM-to-ER cholesterol transport are known to increase cholesterol synthesis (31). To directly explore whether aberrant activation of the SREBP-2 pathway in *Abca1*<sup>-/-</sup> cells is due to impaired sterol delivery to the ER, we assessed PM-to-ER sterol movement by using multiple intracellular sterol trafficking assays. We pulse-labeled the WT and *Abca1*<sup>-/-</sup> cells with trace amounts of [<sup>3</sup>H]cholesterol (with

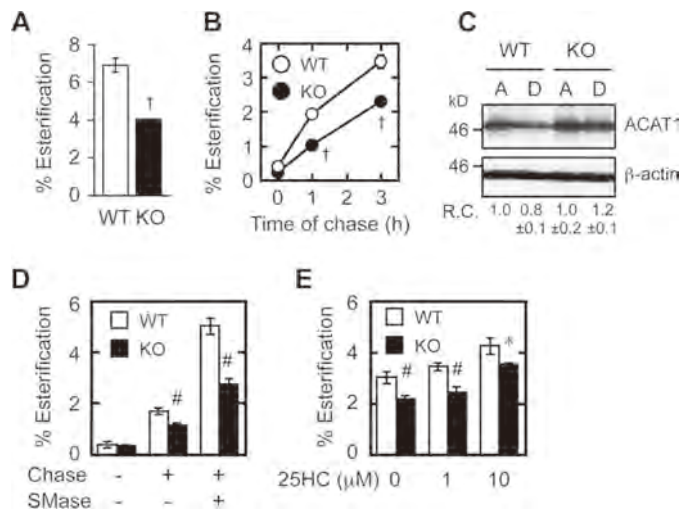


**FIGURE 3. Retrograde cholesterol transport is impaired in *Abca1*<sup>-/-</sup> cells.** A, esterification of [<sup>3</sup>H]cholesterol at steady-state level. MEFs were set up as described in Fig. 1. On day 2, cells were labeled with [<sup>3</sup>H]cholesterol for 8 h in medium A. After washing [<sup>3</sup>H]cholesterol present in the medium, cells were incubated in medium A for 16 h for equilibration, and further incubated for 6 h in medium F. [<sup>3</sup>H]cholesterol and [<sup>3</sup>H]CE in cells were analyzed. †,  $p < 0.001$  ( $n = 3$ ). B, esterification of cell surface cholesterol. MEFs were set up as described in Fig. 1. On day 3, cells were pulse-labeled with [<sup>3</sup>H]cholesterol for 30 min in medium B (medium containing 0.1% BSA) at 37 °C, washed twice, and chased in medium F (serum-free medium) for various times as indicated. [<sup>3</sup>H]cholesterol and [<sup>3</sup>H]CE in cells were analyzed. †,  $p \leq 0.001$  ( $n = 3$ ). C, ACAT1 protein expression. MEFs were incubated in medium A or D for 2 days. ACAT1 and  $\beta$ -actin expressions were analyzed by immunoblots. Relative changes in ACAT1 expression (ACAT1/ $\beta$ -actin) (R.C.) are indicated at the bottom. D, effect of SMase on retrograde cholesterol transport. MEFs were set up and pulse-labeled with [<sup>3</sup>H]cholesterol as in B and chased or not chased for 1 h with or without SMase (0.1 unit/ml). Cellular [<sup>3</sup>H]cholesterol and [<sup>3</sup>H]CE were analyzed. #,  $p < 0.003$  ( $n = 3$ ). E, effect of 25HC on the esterification of PM cholesterol. MEFs were set up and pulse-labeled with [<sup>3</sup>H]cholesterol as in B and chased or not chased for 3 h with or without 25HC (1 or 10  $\mu$ M as indicated). Cellular [<sup>3</sup>H]cholesterol and [<sup>3</sup>H]CE were analyzed. \*,  $p < 0.05$ ; #,  $p < 0.01$  ( $n = 3$ ). Error bars represent S.D. Statistical analyses were performed by one-way ANOVA with Tukey-Kramer post hoc test.

high specific radioactivity but without unlabeled cholesterol as carrier, to prevent minimal membrane disturbance), and we monitored its esterification by the ER resident enzyme ACAT1 at the ER. In WT MEFs, about 3.5% of the cellular surface [<sup>3</sup>H]cholesterol was esterified within 3 h (Fig. 3B). In contrast, this esterification was substantially attenuated in *Abca1*<sup>-/-</sup> MEFs. Despite the differences in esterification efficiency, ACAT1 protein levels were found to be the same between the two cells (Fig. 3C). Treatment of cells with sphingomyelinase (SMase) causes hydrolysis of PM sphingomyelin and acceler-

## ABCA1 Regulates Bidirectional Sterol Transport

ates cholesterol movement from the PM to the ER (32). We utilized this method to further examine retrograde cholesterol transport. In WT MEFs, adding exogenous SMase enhanced esterification of PM-derived cholesterol 3.5-fold. In contrast, in *Abca1*<sup>-/-</sup> MEFs, the SMase-enhanced esterification was reduced by ~50% of values found in treated WT cells (Fig. 3D). A previous work showed that the SMase treatment increases the PM cholesterol pool available for ABCA1-dependent cholesterol efflux to apoA-I (33). The results presented in Fig. 3D show that the SMase treatment also increases the PM cholesterol pool, which is available for ABCA1-dependent inward movement of cholesterol. Similar to SMase, 25HC is also known to facilitate PM-to-ER cholesterol transport, in part by altering PM composition (34). However, the action of 25HC on cholesterol esterification in intact cells may be complicated because, in addition to its ability to mobilize cholesterol from the PM, it may disrupt composition of internal membranes; 25HC can also serve as an allosteric activator for ACAT1, when cholesterol is used as the ACAT1 substrate (35). To serve as a control experiment for the SMase treatment, we assessed the effect of 25HC on esterification of PM cholesterol in WT and *Abca1*<sup>-/-</sup> MEFs. The result showed that when used at 1  $\mu$ M, 25HC failed to significantly affect the esterification of PM cholesterol in either WT or *Abca1*<sup>-/-</sup> MEFs; at a very high concentration (10  $\mu$ M), 25HC caused a modest increase in esterification; the increase occurred more in the *Abca1*<sup>-/-</sup> cells than in the WT cells (Fig. 3E). In the presence of 10  $\mu$ M 25HC, retardation in the esterification of PM cholesterol was observed in *Abca1*<sup>-/-</sup> cells. These results implicate the 25HC-dependent activation of cholesterol esterification is not a sensitive assay to monitor the cholesterol movement from the PM to the ER in intact cells.

We next looked at whether retrograde movement of biosynthetic precursor sterols was also retarded in *Abca1*<sup>-/-</sup> cells. Lanosterol, the first sterol synthesized in the cholesterol biosynthetic pathway, is immediately transported to the PM upon its synthesis at the ER. After arriving at the PM, it is rapidly transported back to and converted to cholesterol at the ER (8), where the enzymes involved in the conversion of lanosterol to cholesterol are located. One of the key enzymes involved in converting lanosterol to cholesterol is CYP51 (lanosterol 14-demethylase); CYP51 is transcriptionally up-regulated by SREBP-2; in our cell system, *Cyp51* gene expression is higher in *Abca1*<sup>-/-</sup> MEFs than in WT MEFs (Fig. 1C). If the retrograde movement of lanosterol was normal in *Abca1*<sup>-/-</sup> MEFs, one would predict a more rapid conversion of lanosterol to cholesterol in *Abca1*<sup>-/-</sup> MEFs. We monitored the conversion of [<sup>3</sup>H]lanosterol biosynthesized *de novo* to [<sup>3</sup>H]cholesterol, and we found that in contrast, the rate of conversion of lanosterol to cholesterol is clearly impaired in *Abca1*<sup>-/-</sup> MEFs (Fig. 4A). As an additional approach, the same assay was used to monitor the conversion of [<sup>3</sup>H]lanosterol added directly to the growth medium of cells (without adding unlabeled lanosterol as carrier). The results showed that the conversion of [<sup>3</sup>H]lanosterol to [<sup>3</sup>H]cholesterol was also markedly retarded in *Abca1*<sup>-/-</sup> MEFs (Fig. 4B). Together, these results demonstrated an important role of ABCA1 in the PM-to-ER transport of both cholesterol and lanosterol. A previous study suggested that

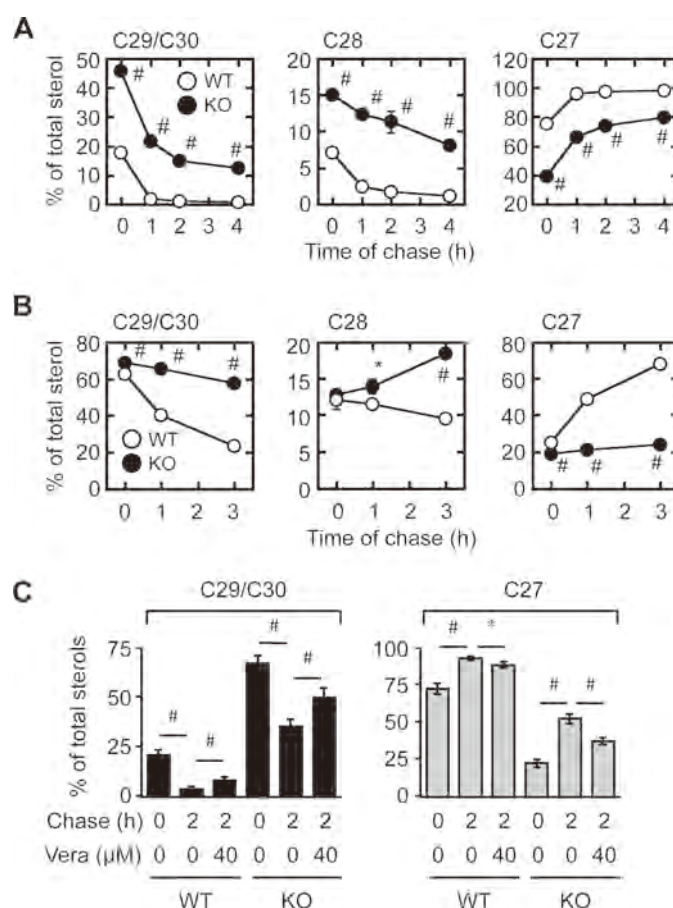


**FIGURE 4. Retrograde transport of precursor sterols is retarded in *Abca1*<sup>-/-</sup> cells.** A and B, conversion of lanosterol to cholesterol. MEFs incubated in medium D for 2 days were pulse-labeled with [<sup>3</sup>H]acetate for 1 h in medium F (A), or with [<sup>3</sup>H]lanosterol for 30 min in medium B (B). Afterward, cells were chased in medium F for various times. Cellular radioactive sterols were analyzed. Lanosterol and cholesterol are major components of C29/C30 sterols and C27 sterols, respectively. \*,  $p < 0.03$ ; #,  $p < 0.005$  ( $n = 3$ ). C, effect of verapamil on retrograde sterol transport. WT and KO MEFs were incubated in medium D for 2 days. Cells were pretreated with or without 40  $\mu$ M verapamil (*Vera*) for 60 min and pulse-labeled with [<sup>3</sup>H]acetate for 60 min. The cells were then chased for 2 h in medium F. Verapamil was present throughout the experiments where indicated. Results of C29/C30 sterols (left) and C27 sterols (right) are shown. \*,  $p < 0.05$ ; #,  $p < 0.01$  ( $n = 3$ ). Error bars represent S.D. Statistical analyses were performed by Student's *t* test.

ABCB1 (also known as multidrug-resistant protein or P-glycoprotein) might be involved in the retrograde movement of precursor sterols (36). Verapamil inhibits ABCB1 but not ABCA1 (37). We found that verapamil only partially inhibited the conversion of lanosterol to cholesterol in both WT and *Abca1*<sup>-/-</sup> cells and that ABCA1 deficiency caused a much more significant retardation in the conversion than verapamil did (Fig. 4C), indicating that ABCA1 plays the predominant role in retrograde lanosterol transport.

We next tested whether ABCA1 is involved in the retrograde movement of LDL-Chol. Cells were incubated with [<sup>3</sup>H]cholesteryl oleate-containing LDL at 18  $^{\circ}$ C for 4 h and then chased with the label at 37  $^{\circ}$ C. At the indicated chase time, cells were briefly incubated with the soluble cholesterol acceptor MCD. As expected, uptake of [<sup>3</sup>H]cholesteryl oleate-labeled LDL was significantly increased in *Abca1*<sup>-/-</sup> cells (Fig. 5A). After a 30-min chase, the MCD extractable counts (considered as [<sup>3</sup>H]cholesterol associated with the PM) were the same in these

## ABCA1 Regulates Bidirectional Sterol Transport

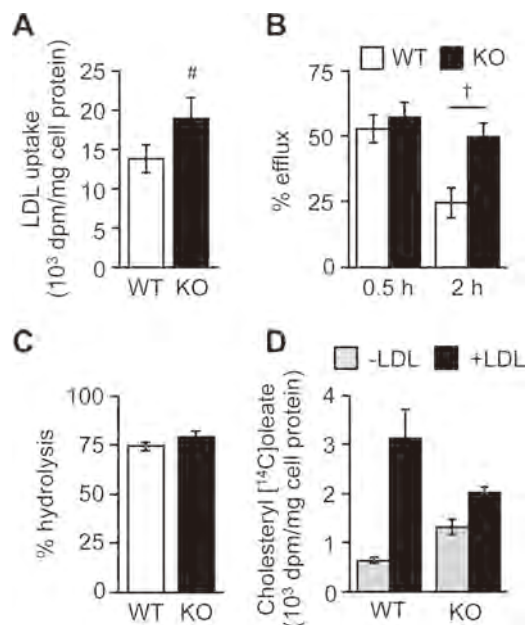


**FIGURE 5. Retrograde transport of LDL-derived cholesterol is retarded in *Abca1*<sup>-/-</sup> cells.** A–C, LDL uptake and retrograde movement of LDL-Chol. MEFs set up as in Fig. 4A were fed with [<sup>3</sup>H]cholesteryl oleate-containing LDL (100 μg/ml) for 4 h at 18 °C. Cells were then chased in medium D for 0.5 or 2 h at 37 °C. Afterward, LDL uptake (A), PM-associated [<sup>3</sup>H]cholesterol (B), and hydrolysis of [<sup>3</sup>H]cholesteryl oleate (C) were determined. #, *p* = 0.003; †, *p* < 0.001 (*n* = 6). D, cholesterol esterification. MEFs were incubated with or without LDL (150 μg/ml) for 5 h in medium D. Afterward, cells were incubated with [<sup>14</sup>C]oleate for 3 h (*n* = 3). Error bars represent S.D. Statistical analyses were performed by Student's *t* test.

two cell types (Fig. 5B). However, after 2 h of chase, the MCD extractable counts decreased much less in *Abca1*<sup>-/-</sup> MEFs than in WT MEFs, indicating that the disappearance of PM-arrived [<sup>3</sup>H]cholesterol from the PM to cell interior is slower in *Abca1*<sup>-/-</sup> cells. A control experiment showed that the hydrolysis of LDL-derived [<sup>3</sup>H]cholesteryl oleate was the same between these two cell types (Fig. 5C). Consequently, an increase in [<sup>14</sup>C]oleate incorporation into CE upon LDL addition was markedly attenuated in *Abca1*<sup>-/-</sup> cells (Fig. 5D). Together, these results indicate that although the transport of LDL-Chol to the PM is not impaired in *Abca1*<sup>-/-</sup> cells, its delivery from the PM to the ER is. The results described in Figs. 3–5 show that, in addition to mediating lipid efflux, ABCA1 expresses influx-like activity for sterols located at the PM.

**ABCA1 Deficiency Impairs Sterol Sensing at the ER**—Both cholesterol and lanosterol are biologically important regulatory sterols; but they differ in mode of action. Lanosterol is first converted to dihydrolanosterol by the enzyme 3β-hydroxysterol Δ24-reductase located at the ER; dihydrolanosterol enhances ubiquitination of HMGR, causing HMGR to be rapidly degraded (38, 39). Instead, cholesterol interacts with Scap and inhibits the ER exit of the precursor form of SREBP-2 and subsequently its proteolytic cleavage, thus preventing it from acting as an active transcription factor (1). In *Abca1*<sup>-/-</sup> MEFs, the impaired retrograde transport of the two regulatory sterols may lead to a sluggish response to regulatory sterols at the ER. To test this possibility, we first showed that in WT CHO cells, SMase treatment caused a rapid reduction in the mature form of SREBP-2, as reported previously (40), but not in a mutant

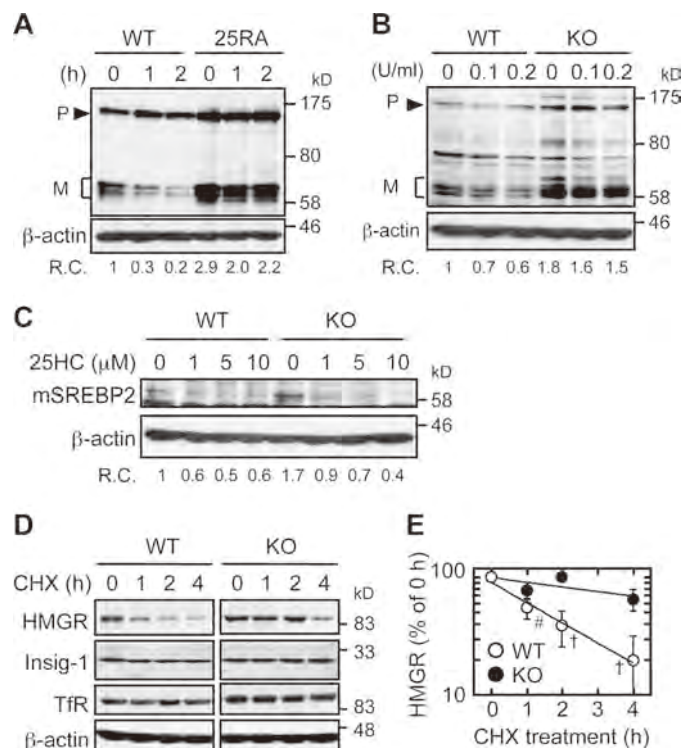


**FIGURE 6. Sterol sensing at the ER is impaired in *Abca1*<sup>-/-</sup> cells.** A, SREBP-2 cleavage in response to SMase treatment in WT CHO cells and in the sterol-resistant mutant CHO cells 25RA (containing a gain-of-function mutation in Scap). On day 0, cells ( $2 \times 10^5$  cells/well) were set up in medium A in 6-well plates. On day 1, cells were switched to medium D. On day 3, cells were treated with or without SMase (0.1 unit/ml) in medium F for 1 or 2 h. Afterward, whole cell lysates were subjected to immunoblot analysis with anti-SREBP-2 antibody (IgG-7D4). Relative changes (R.C.) in mature form/ $\beta$ -actin ratios are indicated at the bottom (*n* = 2). B, SREBP-2 cleavage in response to SMase treatment in WT and KO MEFs. Cells were seeded as described in Fig. 1. On day 2, cells were switched to medium D for 2 days. Cells were then treated with the indicated concentration of SMase for 2 h in medium F. Whole cell lysates were subjected to immunoblot analysis with the indicated antibodies. Relative changes (R.C.) in mature form/ $\beta$ -actin ratio are indicated at the bottom (*n* = 2). C, SREBP-2 cleavage in response to 25HC treatment in WT and KO MEFs. MEFs set up as above were treated without or with 1, 5, or 10 μM 25HC for 2 h. Whole cell lysates were subjected to immunoblot analysis with the indicated antibodies. Relative changes (R.C.) in mature form/ $\beta$ -actin ratio are indicated at the bottom (*n* = 2). D and E, half-lives of HMGR in WT and KO MEFs. MEFs were set up as described in B. Cells were then treated with cycloheximide (CHX) (20 μg/ml) for various times as indicated. Afterward, whole cell lysates were subjected to immunoblot analysis with antibodies as indicated. Transferrin receptor (*TfR*) and  $\beta$ -actin were used as controls. A representative result was shown (C). The results of three experiments were plotted (D). Data represent means  $\pm$  S.D. #, *p* = 0.0017; †, *p* < 0.0001 by Student's *t* test.

CHO cell line 25RA that is resistant to cholesterol-dependent regulation due to a mutation (D443N) within the sterol-sensing domain of Scap (Fig. 6A) (41, 42). These results demonstrate the specificity of the SMase assay to assess cholesterol sensing at the ER. We next showed that in cells maintained without sterol acceptors, SMase treatment resulted in an efficient reduction of SREBP-2 cleavage in WT MEFs; in contrast, in *Abca1*<sup>-/-</sup> MEFs, the cleavage of SREBP-2 was highly resistant to the SMase treatment (Fig. 6B). As a control experiment, we treated these cells with various concentrations of 25HC and examined SREBP-2 processing. As expected, 25HC suppressed SREBP-2 cleavage in both cell types at various concentrations (from 1 to 10 μM) (Fig. 6C), indicating that the impaired cholesterol delivery to the ER is a major cause of the resistance to the SMase treatment observed in *Abca1*<sup>-/-</sup> cells. To test whether ABCA1

## ABCA1 Regulates Bidirectional Sterol Transport

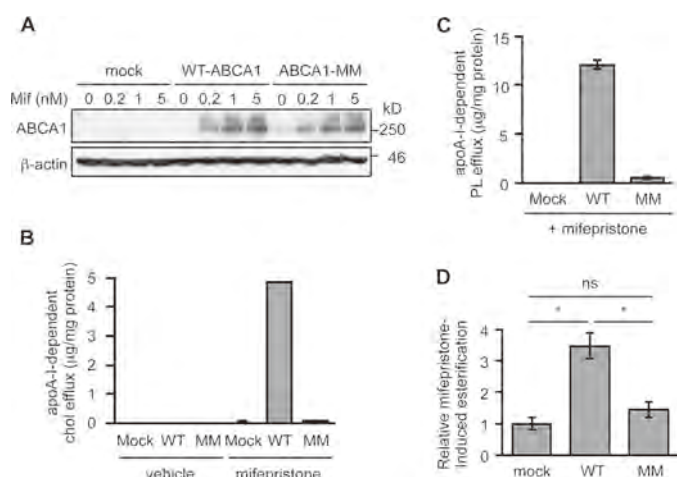


**FIGURE 7. ATPase activity of ABCA1 is required for its ability to facilitate retrograde cholesterol transport.** *A*, induction of ABCA1 expression by mifepristone. BHK cells stably transfected with vector or vector harboring WT-ABCA1 or ABCA1-MM cDNA (BHK/mock, BHK/WT-ABCA1, and BHK/ABCA1-MM respectively) cells were incubated with the indicated concentrations of mifepristone for 18 h. ABCA1 expression was examined by immunoblot. *B* and *C*, apoA-I-dependent cholesterol and PL efflux. BHK/mock, BHK/WT-ABCA1, and BHK/ABCA1-MM cells were incubated with or without apoA-I (5  $\mu$ g/ml) in the absence or presence of 5 nM mifepristone for 18 h, as indicated. Amounts of cholesterol (*B*) and PL (*C*) released into medium were measured. Subtracted values are shown. Data represent means  $\pm$  S.D. ( $n = 3$ ). *D*, PM-to-ER cholesterol transport. BHK cells treated without or with 5 nM mifepristone were pulse-labeled with [ $^3$ H]cholesterol and then chased for 3 h. ABCA1-specific esterification was calculated by subtracting counts of mifepristone-untreated cells. Data represent means  $\pm$  S.D. ( $n = 3$ ). #,  $p < 0.01$  by one-way ANOVA with Tukey-Kramer post hoc test. ns, not significant.

also plays important roles in delivering lanosterol as a regulatory sterol, we monitored the turnover rates of HMGR in the WT and *Abca1*<sup>-/-</sup> MEFs, by treating these cells with cycloheximide, an inhibitor of protein synthesis. The results showed that the apparent half-life of HMGR in the WT cells was  $\sim$ 1 h (Fig. 6, *D* and *E*), similar to the value reported previously (43). In contrast, its half-life was markedly prolonged to more than 4 h in *Abca1*<sup>-/-</sup> cells. These results show that ABCA1 mediates sterol sensing at the ER.

**Intrinsic ATPase Activity of ABCA1 Is Required to Facilitate Retrograde Cholesterol Transport**—ABCA1 possesses intrinsic ATPase activity, which is essential for its role in lipid efflux (44). We sought to determine whether this activity is also required for the ABCA1-dependent retrograde sterol movement. We used cells that express WT ABCA1 or mutant ABCA1 (ABCA1-MM) lacking ATPase activity by replacement of the two lysine residues (Lys-939 and Lys-1952) crucial for ATP hydrolysis by methionine (45), under the control of mifepristone (Fig. 7*A*). The results showed that, in the absence of mifepristone, neither WT-ABCA1 nor ABCA1-MM cells exported cholesterol to apoA-I (Fig. 7*B*). When mifepristone was added to the medium, only cells expressing WT-ABCA1 but not cells expressing ABCA1-MM exported cholesterol and PL to apoA-I (Fig. 7, *B* and *C*). We next used the same cell systems to perform the retrograde cholesterol transport assay. Cells were treated with or without mifepristone for 18 h and then were labeled with [ $^3$ H]cholesterol. The arrival of [ $^3$ H]cholesterol at the ER was monitored by measuring the amount of [ $^3$ H]CE formed. The results showed that WT-ABCA1 markedly increased PM-to-ER cholesterol transport but ABCA1-MM did not exhibit an

increase (Fig. 7*D*). These results indicate that the ATPase activity intrinsically associated with ABCA1 is required to facilitate retrograde cholesterol transport.

**ABCA1 Deficiency Alters PM Composition**—To explain how ABCA1 acts to control retrograde sterol movement at the PM, we examined possible changes in PM caused by lack of ABCA1. We found that in live cells, PM from *Abca1*<sup>-/-</sup> MEFs contained elevated levels of cholesterol as probed by using 2-hydroxypropyl- $\beta$ -cyclodextrin- or MCD-mediated removal of cell surface cholesterol (Fig. 8, *A* and *B*). Similarly, an increase of PM cholesterol in *Abca1*<sup>-/-</sup> cells was observed (Fig. 8*C*) when cell surface cholesterol was assessed by using mCherry-D4, a nontoxic, cholesterol-binding domain of perfringolysin O that recognizes cholesterol-rich membrane domains but has no pore-forming activity (27). We also found an increase in cell surface ganglioside GM1, as detected by using the specific GM1 probe CTxB, in *Abca1*<sup>-/-</sup> MEFs (Fig. 8*D*). Cholesterol content in detergent-resistant membrane (DRM, fraction 2) domains, where caveolin-1 (Cav1) and flotillin-1 were enriched, was markedly increased in *Abca1*<sup>-/-</sup> cells (Fig. 8, *E* and *F*). In addition to DRM, however, a modest increase of cholesterol content in non-DRM (fractions 4–8) was also observed in *Abca1*<sup>-/-</sup> cells, suggesting an overall increase in PM cholesterol. Furthermore, Cav1 expression was increased (Fig. 9*A*), and the cell surface colocalization between Cav1 and GM1 was more frequent in *Abca1*<sup>-/-</sup> MEFs (Fig. 9*B*). The difference in flotillin-1 expression between the two cell types was less significant (Fig. 9*A*). Cav1, cholesterol, and ganglioside are essential components to form caveolae (46). We looked for possible changes in caveolae in *Abca1*<sup>-/-</sup> cells and found that the number of cell surface-associated caveolae is increased in *Abca1*<sup>-/-</sup> cells (Fig. 9*C*). Overall, our results suggest that ABCA1 regulates membrane composition at the PM. This interpretation is in agreement with previous observations made in macrophages (11, 47).

**ABCA1 Is Involved in Certain Clathrin-independent Endocytoses**—Changes in PM composition are expected to affect PM functionality. Endocytosis is a cellular process that internalizes extracellular and membrane-associated molecules into the cell interior and requires dynamic membrane reorganization. Endocytosis is largely categorized into two pathways as follows: clathrin-dependent and clathrin-independent. Clathrin-independent endocytosis (CIE) plays an important role in internalization of proteins and lipid molecules located to lipid rafts. It has been reported that Cav1 acts as a negative regulator of CIE (28, 48). We asked whether ABCA1 deficiency alters CIE, and we tested this possibility by assessing internalization of CTxB, an established marker of CIE (49). Our results showed that when compared with WT cells, CTxB internalization was significantly retarded in *Abca1*<sup>-/-</sup> MEFs, despite significant increases in cell surface binding of CTxB in these cells (Fig. 10, *A* and *B*, see also Fig. 8*D*). The decrease in CTxB internalization in *Abca1*<sup>-/-</sup> cells was observed as early as 10 min after incubation with CTxB (Fig. 10, *C* and *D*). These results show that ABCA1 deficiency causes a reduction in a certain CIE activity that internalizes CTxB.

**CIE Inhibitors and Dynamin Inhibitors Abolish Retrograde Cholesterol Movement**—Next, we used various small molecule inhibitors to further test whether the CIE activity is involved in

## ABCA1 Regulates Bidirectional Sterol Transport

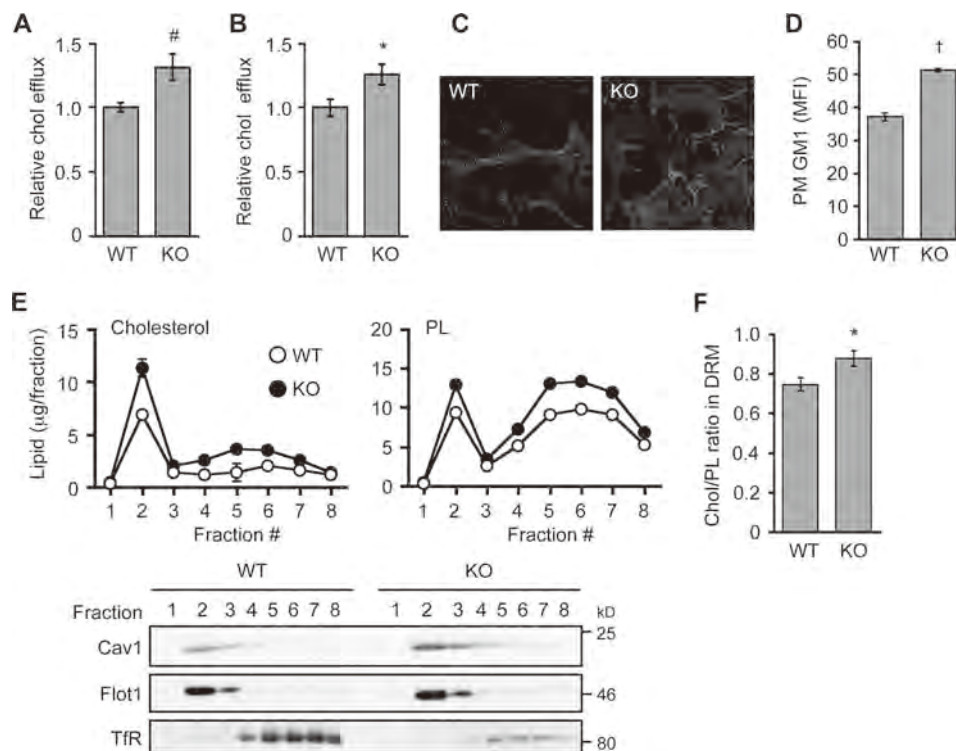


**FIGURE 8. ABCA1 deficiency causes cholesterol accumulation at the PM.** A and B, cell surface cholesterol levels. WT and KO MEFs were seeded as described in Fig. 1. On day 2, cells were switched to medium F (medium with no supplement). After incubation for 18 h, cells were washed twice with ice-cold PBS and incubated with 4% 2-hydroxypropyl- $\beta$ -cyclodextrin for 10 min at 37 °C (A) or 3 mM (~0.4%) MCD for 5 min at 37 °C (B). Afterward, medium was collected to determine cholesterol released from cells. \*,  $p = 0.013$ ; #,  $p = 0.007$  ( $n = 3$ ). C, cell surface cholesterol staining in live cells. WT and KO MEFs were treated with mCherry-D4 to visualize cell surface cholesterol in live cells. D, cell surface GM1 levels. Cells were set up as described in A. Binding of the GM1 probe CTxB to the cell surface was measured by FACS. Mean fluorescent intensity (MFI) was plotted. †,  $p < 0.0001$  ( $n = 3$ ). E and F, DRM analysis. WT and KO MEFs were treated with 1% Triton X-100 for 30 min at 4 °C. Post-nuclear supernatant was subjected to density gradient ultracentrifugation. Amounts of cholesterol and phospholipid in each fraction were determined and normalized to cellular protein (upper panels). Equal amount of each fraction was subjected to immunoblot analysis to determine the distribution of caveolin-1 (Cav1), flotillin-1 (Flot1), and transferrin receptor (TfR) (lower panels). Fraction 2 contained the majority of DRM domains. Cholesterol/phospholipid ratio in DRM fraction (fraction 2) is shown in F. Data represent means  $\pm$  S.D. ( $n = 3$ ). \*,  $p = 0.016$ . Error bars represent S.D. Statistical analyses were performed by Student's  $t$  test.

PM-to-ER cholesterol transport. First, we performed pulse labeling of cells with [ $^3$ H]cholesterol and chased the cells with-out or with chlorpromazine, a clathrin-mediated endocytosis (CME) inhibitor, or with genistein and nystatin, the CIE inhibitors. Genistein and nystatin are known to block cholesterol-dependent endocytic internalization such as caveolar endocytosis, without affecting CME (50). The result showed that genistein and nystatin significantly suppressed the delivery of [ $^3$ H]cholesterol to the ER (Fig. 11A), whereas chlorpromazine only had little effect, suggesting that CIE but not CME may play a major role in delivering PM cholesterol to the ER. This result is consistent with our previous work reporting that genistein or nystatin suppressed PM-to-ER transport of precursor sterols (8). It is also important to point out that LDLR-mediated LDL uptake, which requires CME, was not impaired in *Abca1*<sup>-/-</sup> MEFs (Fig. 5A), indicating that CME is not disrupted in *Abca1*<sup>-/-</sup> cells. The CIE activity can mainly be classified into two categories based on its dependence on dynamin, a GTPase that plays a key role in scission of endocytic vesicles from the PM (51). CTxB is internalized by a CIE pathway that requires dynamin and endophilin (49). To test whether dynamin is involved in retrograde cholesterol transport, we used two structurally distinct specific dynamin inhibitors, dynasore (52) and dynole 34-2 (53), with dynole 34-2 being more potent than dynasore. The results showed that both dynole 34-2 and dyna-

sore markedly retarded PM-to-ER cholesterol transport within 1 h of treatment in both CHO cells and WT MEFs (Fig. 11, B and C). The results of a control experiment showed that dynole 31-2, an inactive analog of dynole 34-2, only slightly affected retrograde cholesterol transport. Additional results showed that dynole 34-2, but not its inactive analog, rapidly activated SREBP-2 processing and up-regulated HMGCR expression in CHO cells (Fig. 11, D and E) and WT MEFs (Fig. 11F). To further test the potential role of dynamin in ER sterol sensing, we examined the effect of dynole 34-2 in the mutant CHO cell line 25RA that expresses sterol-resistant Scap<sup>D443</sup> (41, 42), and we showed that the dynamin inhibitor had no effect on SREBP-2 processing in this mutant cell (Fig. 11, G and H). Together, these results are consistent with the interpretation that a dynamin-mediated endocytic pathway may play a key role in the delivery of PM cholesterol to the ER for sterol sensing.

### Discussion

Our current work reveals a new function of ABCA1; in addition to the well established role in mediating cellular cholesterol release, it plays a crucial role in the retrograde movements of both biosynthesized sterols and LDL-Chol arriving at the PM, to be sensed by regulatory enzymes/proteins located at the ER. We propose a model to depict how ABCA1 acts at the PM

## ABCA1 Regulates Bidirectional Sterol Transport

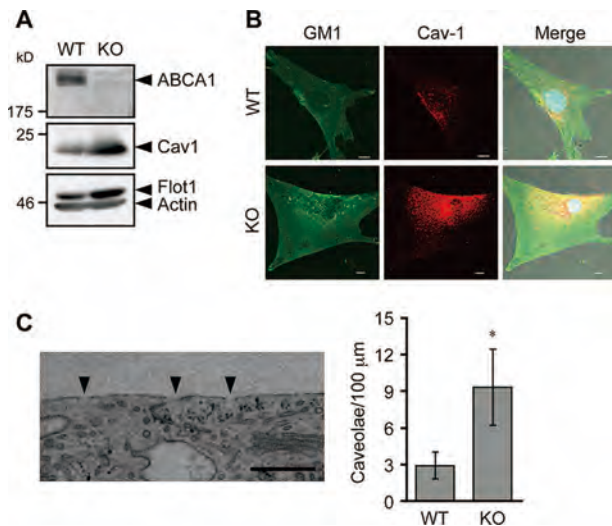


**FIGURE 9. ABCA1 deficiency increases caveolae.** *A*, expression of caveolin-1. MEFs were set up as described in *A*, and whole cell lysates were prepared. Expressions of ABCA1, caveolin-1 (*Cav1*), Flotillin-1 (*Flot1*), and  $\beta$ -actin were analyzed by immunoblot. *B*, colocalization of GM1 and Cav1. MEFs set up as in *A* were fixed. Cells were incubated with biotin-CTxB and with anti-Cav1 antibody followed by appropriate secondary antibodies (FITC-avidin for biotin-CTxB and Alexa Fluor 555-anti-rabbit IgG for anti-Cav1). Images were taken under a confocal laser microscope. Nuclei were stained with Hoechst 33342. Bar, 10  $\mu$ m. *C*, number of caveolae. MEFs set up as described in *A* were subjected to EM analysis, and cell surface-associated caveolae were counted. Left panel shows typical picture of caveolae in KO MEFs. Arrowheads indicate caveolae. Right panel shows the number of cell surface-associated caveolae per 100- $\mu$ m cell surface length. Data represent mean  $\pm$  S.E. (WT;  $n = 29$ ; KO;  $n = 36$ ). \*,  $p = 0.036$  by Mann-Whitney *U* test. Bar, 0.5  $\mu$ m.

to regulate cellular cholesterol homeostasis (Fig. 12A); the increase in cellular cholesterol induces *ABCA1* gene expression by the liver X receptor-mediated mechanism (54). Elevated *ABCA1* expression leads to the increase in sterol release from the PM and also leads to the increase in retrograde sterol movement from the PM. The retrograde sterol movement results in an increase in cholesterol esterification and decreases in LDL uptake and sterol synthesis by inhibiting SREBP-2 processing. The net effect of induced *ABCA1* expression is to reduce toxic accumulation of free cholesterol in cells. Through its ability to facilitate bidirectional sterol flux at the PM, *ABCA1* participates in controlling cholesterol homeostasis.

How does *ABCA1* participate in both cholesterol efflux and retrograde sterol transport? Most ATP-binding cassette transporters act as substrate exporters (55), and only a few of them show substrate influx activity (56, 57). *ABCA1*, as reported here, is the first ATP-binding cassette transporter to be shown to mediate substrate flux bidirectionally. It has previously been shown that overexpression of *ABCA1* in cells alters lipid packing at PM (58, 59) and creates outward membrane curvatures where apoA-I binds (7). Here we show that in the absence of sterol acceptors, *ABCA1* deficiency causes cholesterol accumulation at the PM. Cholesterol forms stoichiometric complexes with PLs, including SM at the PM; the cholesterol pool that exceeds the binding capacity of PLs can be described as "active cholesterol" (60, 61). Based on the active cholesterol hypothesis, *ABCA1* may act by producing local lipid packing deformations at the PM, which in turn generates more active cholesterol. The active cholesterol at the membrane deformation sites created by *ABCA1* may serve as a source for sterol release for

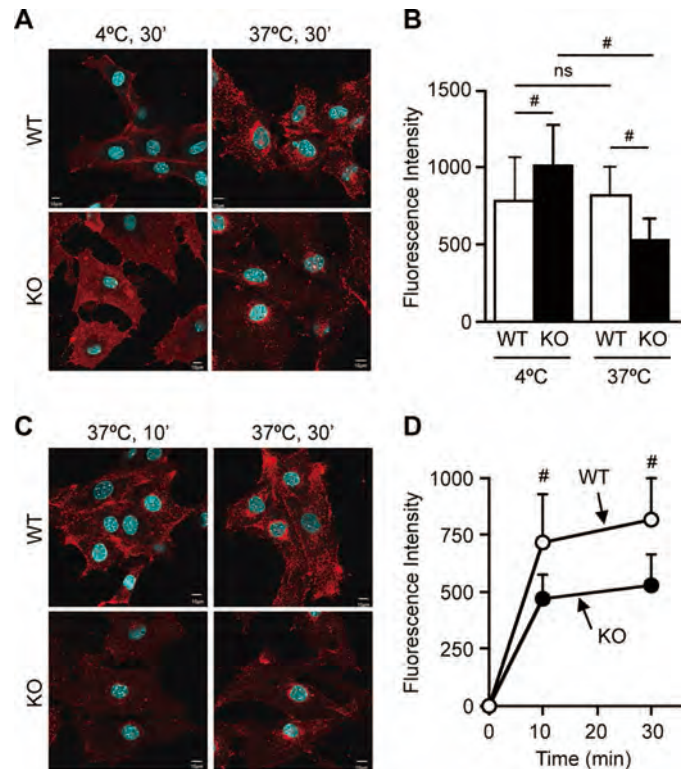


**FIGURE 10. CTxB internalization is impaired in *Abca1*<sup>-/-</sup> cells.** Internalization of CTxB is shown. WT and KO MEFs were incubated with AF555-CTxB for 30 min either at 4 or at 37  $^{\circ}$ C (*A* and *B*) or for 10 or 30 min at 37  $^{\circ}$ C (*C* and *D*). Cellular mean fluorescent intensity of 30–60 cells was plotted in *B* and *D*. CTxB was found at cell periphery at 10 min, but at a later time (30 min) it was localized to peri-nuclear regions, most likely Golgi. Data represent means  $\pm$  S.D. Statistical analyses were performed by one-way ANOVA with Tukey-Kramer post hoc test. #,  $p < 0.01$ ; ns, not significant. Bar, 10  $\mu$ m.

apoA-I-mediated HDL biogenesis or may undergo retrograde movement to exert regulatory actions at the ER (Fig. 12B). "Activation" of cholesterol can therefore be considered as local destabilization of PM. Depletion of SM by SMase also generates more active cholesterol to become readily accessible for sterol sensing at the ER (32, 40) and for *ABCA1*-dependent efflux out of cells (33). A recent proteoliposome study showed that *ABCA1* directly exports select PLs, including phosphatidylcholine, phosphatidylserine, and SM, across the membrane and suggested that cholesterol efflux occurs in an indirect manner (62). Through its PL floppase activity, *ABCA1* may change PL composition in the PM, which causes alterations in membrane-cholesterol interaction and cholesterol activation threshold; these changes lead to an increase in the availability of cholesterol in membranes (63). Consistent with this view, a study with a mammalian cell mutant suggested that altered PL composition at the PM affects PM-to-ER cholesterol transport (31). Thus, it is conceivable that in the absence of *ABCA1*, reduced PL movement within the PM leads to stabilization of cholesterol-membrane complexes, causing a decrease in cholesterol movement at the PM. Caveolae are highly stable, immobile membrane domains, and they may serve as cholesterol storage sites at the PM (46). Consistent with this view, we found that *ABCA1* deficiency causes increases in Cav1 expression and in caveola number, in addition to increases in PM cholesterol. Cholesterol associated with caveolae may not be capable of act-

**ABCA1 Regulates Bidirectional Sterol Transport**

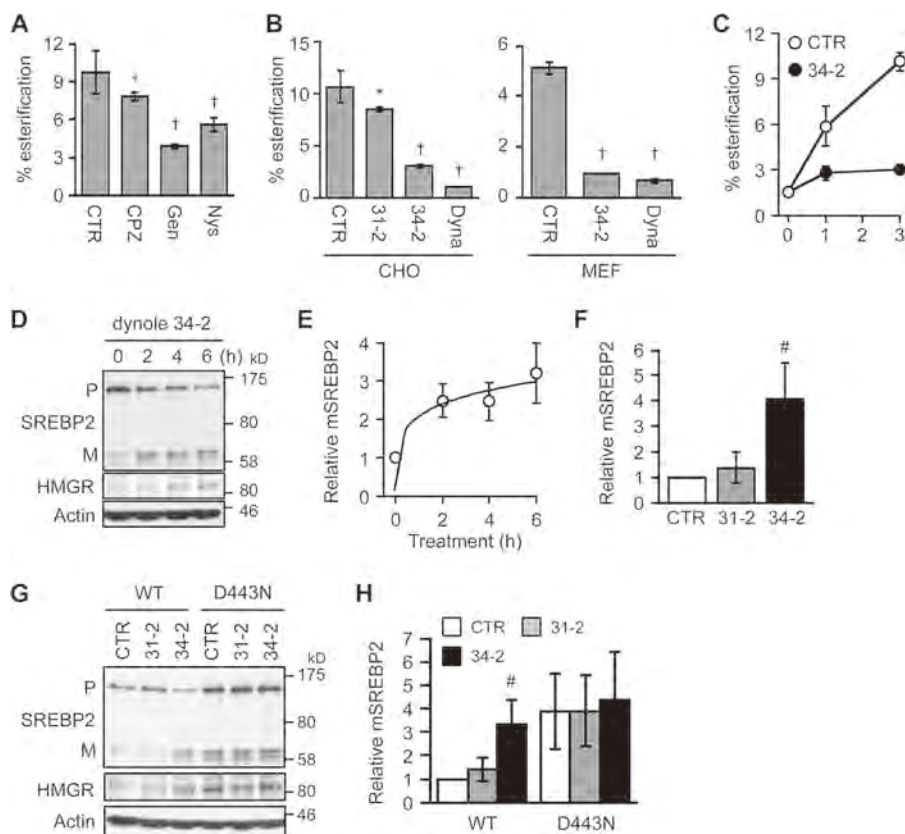


**FIGURE 11. Effects of small molecule inhibitors for endocytosis on PM-to-ER cholesterol transport and ER sterol sensing.** A and B, effects of inhibitors for CIE and for dynamin in PM-to-ER cholesterol transport. CHO cells (A and B, left) or WT MEFs (B, right) were pulse-labeled with [<sup>3</sup>H]cholesterol for 30 min. Afterward, cells were incubated for 3 h with vehicle (CTR), 10 μM chlorpromazine (CPZ), 50 μM genistein (Gen), 50 μM nystatin (Nys), 10 μM dynole 31-2 (31-2), 10 μM dynole 34-2 (34-2), or 50 μM dynasore (Dyna). Esterification of [<sup>3</sup>H]cholesterol was assessed to determine its delivery to the ER (n = 3). C, CHO cells were pulse-labeled as above and chased for 0, 1, or 3 h in the presence of vehicle (CTR) or 10 μM dynole 34-2. Esterification of [<sup>3</sup>H]cholesterol was determined (n = 3). D–F, effect of dynole 34-2 on SREBP-2 processing. D and E, CHO cells grown in medium A were switched to medium F for 6 h. Dynole 34-2 (10 μM) was added to medium 2, 4, or 6 h before harvesting cells. F, WT MEFs were treated with vehicle (CTR), dynole 31-2 (10 μM), and dynole 34-2 (10 μM) for 6 h (n = 3). SREBP-2 processing and HMGR expression were analyzed by immunoblot. Relative changes in mature form presented in D are shown in E (n = 3). G and H, effects of dynamin inhibitors on cholesterol sensing by Scap. CHO cells expressing WT and gain-of-function (D443N) Scap were treated with vehicle (CTR), dynole 31-2 (10 μM), or dynole 34-2 (10 μM) for 6 h in medium F. SREBP-2 processing and HMGR expression were assessed. Relative changes in mature form are shown in H (n = 3–5). Error bars represent S.D. Statistical analyses were performed by Student's t test. \*, p < 0.05; #, p < 0.01; †, p < 0.001 (versus respective control).

ing as active cholesterol. In this study, by assessing CTxB internalization and retrograde cholesterol transport, we show that a certain endocytic activity, likely CIE, becomes defective in ABCA1-deficient cells. We designate this endocytic pathway as ABCA1-regulated, clathrin-independent endocytosis (ACIE). We also showed that this pathway is probably dynamin-dependent. Caveolar endocytosis is known to be a dynamin-mediated CIE process; this process internalizes PM glycosphingolipids (50, 64). We speculate that the caveolar endocytosis pathway may play an important role in internalization of PM cholesterol in a dynamin-dependent manner, and this pathway may be controlled by ABCA1. Further studies are required to determine the functional significance and molecular nature of ACIE. Endocytic internalization involves recognition of membrane deformation sites by membrane curvature-sensing proteins, which is a key endocytic process (51, 65). Endophilin was recently identified as a membrane curvature-sensing protein for dynamin-mediated CIE (49, 66). Interestingly, intracellular curvature-sensing proteins and extracellular apolipoproteins (lipid acceptors) such as apoA-I share a similar structural feature, namely amphipathic α-helices. As such, certain membrane curvature-sensing proteins may be involved in ABCA1-

mediated retrograde sterol transport. In addition to its effect on ACIE, ABCA1 deficiency may also affect nonvesicular retrograde sterol transport in a certain manner.

Several lines of clinical and experimental observations in TD patients and *Abca1*<sup>-/-</sup> mice (10–13) are not fully explained by assuming that ABCA1 functions only in sterol release. Our current findings provide a plausible mechanism to explain these paradoxical observations. ABCA1 deficiency causes abnormal cholesterol accumulation at the PM and a deficiency in the delivery of regulatory sterols to the ER. Abnormalities at the PM disrupt PM function, including ACIE, whereas the lack of regulatory sterols at the ER causes enhanced SREBP cleavage. It is therefore conceivable that in local tissues and in macrophages, the enhanced SREBP cleavage leads to elevated LDLR expression and higher cholesterol biosynthesis, which accelerates tissue cholesterol deposition, despite concomitant plasma LDL reduction. In addition to TD, HDL levels are often associated with rare mutant alleles in the *ABCA1* gene (67, 68). Patients with low HDL have a higher risk of coronary heart disease (68, 69). The bidirectional sterol movement driven by ABCA1 demonstrated in this work may provide a plausible explanation for the higher risk of coronary heart disease



## ABCA1 Regulates Bidirectional Sterol Transport

10. Assmann, G., von Eckardstein, A., and Brewer, H. B. (2001) in *The Metabolic & Molecular Bases of Inherited Disease* (Scriver, R. C., Beaudet, L. A., Sly, S. W., and Valle, D., eds) pp. 2937–2960, 8th Ed., McGraw-Hill, New York
11. Zhu, X., Lee, J. Y., Timmins, J. M., Brown, J. M., Boudyguina, E., Mulya, A., Gebre, A. K., Willingham, M. C., Hiltbold, E. M., Mishra, N., Maeda, N., and Parks, J. S. (2008) Increased cellular free cholesterol in macrophage-specific Abca1 knock-out mice enhances pro-inflammatory response of macrophages. *J. Biol. Chem.* **283**, 22930–22941
12. Chung, S., Timmins, J. M., Duong, M., Degirolamo, C., Rong, S., Sawyer, J. K., Singaraja, R. R., Hayden, M. R., Maeda, N., Rudel, L. L., Shelness, G. S., and Parks, J. S. (2010) Targeted deletion of hepatocyte ABCA1 leads to very low density lipoprotein triglyceride overproduction and low density lipoprotein hypercatabolism. *J. Biol. Chem.* **285**, 12197–12209
13. Parathath, S., Mick, S. L., Feig, J. E., Joaquin, V., Grauer, L., Habel, D. M., Gassmann, M., Gardner, L. B., and Fisher, E. A. (2011) Hypoxia is present in murine atherosclerotic plaques and has multiple adverse effects on macrophage lipid metabolism. *Circ. Res.* **109**, 1141–1152
14. Francis, G. A., Knopp, R. H., and Oram, J. F. (1995) Defective removal of cellular cholesterol and phospholipids by apolipoprotein A-I in Tangier disease. *J. Clin. Invest.* **96**, 78–87
15. Arakawa, R., and Yokoyama, S. (2002) Helical apolipoproteins stabilize ATP-binding cassette transporter A1 by protecting it from thiol protease-mediated degradation. *J. Biol. Chem.* **277**, 22426–22429
16. Yamauchi, Y., Chang, C. C., Hayashi, M., Abe-Dohmae, S., Reid, P. C., Chang, T. Y., and Yokoyama, S. (2004) Intracellular cholesterol mobilization involved in the ABCA1/apolipoprotein-mediated assembly of high density lipoprotein in fibroblasts. *J. Lipid Res.* **45**, 1943–1951
17. Nishikawa, O., Yokoyama, S., Kurasawa, T., and Yamamoto, A. (1986) A method for direct incorporation of radiolabeled cholesteryl ester into human plasma low-density-lipoproteins: preparation of tracer substrate for cholesteryl ester transfer reaction between lipoproteins. *J. Biochem.* **99**, 295–301
18. Moller, M. L., and Tchen, T. T. (1961) Inhibition of cholesterol biogenesis by arsenite: preparation of labeled lanosterol. *J. Lipid Res.* **2**, 342–343
19. Hu, W., Abe-Dohmae, S., Tsujita, M., Iwamoto, N., Ogikubo, O., Otsuka, T., Kumon, Y., and Yokoyama, S. (2008) Biogenesis of HDL by SAA is dependent on ABCA1 in the liver *in vivo*. *J. Lipid Res.* **49**, 386–393
20. Oram, J. F., Vaughan, A. M., and Stocker, R. (2001) ATP-binding cassette transporter A1 mediates cellular secretion of  $\alpha$ -tocopherol. *J. Biol. Chem.* **276**, 39898–39902
21. Chang, C. C., Miyazaki, A., Dong, R., Kheirollah, A., Yu, C., Geng, Y., Higgs, H. N., and Chang, T. Y. (2010) Purification of recombinant acyl-coenzyme A:cholesterol acyltransferase 1 (ACAT1) from H293 cells and binding studies between the enzyme and substrates using difference intrinsic fluorescence spectroscopy. *Biochemistry* **49**, 9957–9963
22. Yamauchi, Y., Furukawa, K., Hamamura, K., and Furukawa, K. (2011) Positive feedback loop between PI3K-Akt-mTORC1 signaling and the lipogenic pathway boosts Akt signaling: induction of the lipogenic pathway by a melanoma antigen. *Cancer Res.* **71**, 4989–4997
23. Tanaka, N., Abe-Dohmae, S., Iwamoto, N., Fitzgerald, M. L., and Yokoyama, S. (2010) Helical apolipoproteins of high density lipoprotein enhance phagocytosis by stabilizing ATP-binding cassette transporter A7. *J. Lipid Res.* **51**, 2591–2599
24. Bryleva, E. Y., Rogers, M. A., Chang, C. C., Buen, F., Harris, B. T., Rousselet, E., Seidah, N. G., Oddo, S., LaFerla, F. M., Spencer, T. A., Hickey, W. F., and Chang, T. Y. (2010) ACAT1 gene ablation increases 24(S)-hydroxycholesterol content in the brain and ameliorates amyloid pathology in mice with AD. *Proc. Natl. Acad. Sci. U.S.A.* **107**, 3081–3086
25. Sugii, S., Reid, P. C., Ohgami, N., Du, H., and Chang, T. (2003) Distinct endosomal compartments in early trafficking of low density lipoprotein-derived cholesterol. *J. Biol. Chem.* **278**, 27180–27189
26. Heino, S., Lusa, S., Somerharju, P., Ehnholm, C., Olkkonen, V. M., and Ikonen, E. (2000) Dissecting the role of the Golgi complex and lipid rafts in biosynthetic transport of cholesterol to the cell surface. *Proc. Natl. Acad. Sci. U.S.A.* **97**, 8375–8380
27. Abe, M., Makino, A., Hullah-Matsuda, F., Kamijo, K., Ohno-Iwashita, Y., Hanada, K., Mizuno, H., Miyawaki, A., and Kobayashi, T. (2012) A role for sphingomyelin-rich lipid domains in the accumulation of phosphatidylinositol-4,5-bisphosphate to the cleavage furrow during cytokinesis. *Mol. Cell. Biol.* **32**, 1396–1407
28. Chaudhary, N., Gomez, G. A., Howes, M. T., Lo, H. P., McMahon, K. A., Rae, J. A., Schieber, N. L., Hill, M. M., Gaus, K., Yap, A. S., and Parton, R. G. (2014) Endocytic crosstalk: caveins, caveolins, and caveolae regulate clathrin-independent endocytosis. *PLoS Biol.* **12**, e1001832
29. Adams, C. M., Reitz, J., De Brabander, J. K., Feramisco, J. D., Li, L., Brown, M. S., and Goldstein, J. L. (2004) Cholesterol and 25-hydroxycholesterol inhibit activation of SREBPs by different mechanisms, both involving SCAP and Insigs. *J. Biol. Chem.* **279**, 52772–52780
30. Düvel, K., Yecies, J. L., Menon, S., Raman, P., Lipovsky, A. I., Souza, A. L., Triantafellow, E., Ma, Q., Gorski, R., Cleaver, S., Vander Heiden, M. G., MacKeigan, J. P., Finan, P. M., Clish, C. B., Murphy, L. O., and Manning, B. D. (2010) Activation of a metabolic gene regulatory network downstream of mTOR complex 1. *Mol. Cell* **39**, 171–183
31. Brandis, K. A., Gale, S., Jinn, S., Langmade, S. J., Dudley-Rucker, N., Jiang, H., Sidhu, R., Ren, A., Goldberg, A., Schaffer, J. E., and Ory, D. S. (2013) Box C/D small nucleolar RNA (snoRNA) U60 regulates intracellular cholesterol trafficking. *J. Biol. Chem.* **288**, 35703–35713
32. Slotte, J. P., and Bierman, E. L. (1988) Depletion of plasma-membrane sphingomyelin rapidly alters the distribution of cholesterol between plasma membranes and intracellular cholesterol pools in cultured fibroblasts. *Biochem. J.* **250**, 653–658
33. Ito, J., Nagayasu, Y., and Yokoyama, S. (2000) Cholesterol-sphingomyelin interaction in membrane and apolipoprotein-mediated cellular cholesterol efflux. *J. Lipid Res.* **41**, 894–904
34. Gale, S. E., Westover, E. J., Dudley, N., Krishnan, K., Merlin, S., Scherrer, D. E., Han, X., Zhai, X., Brockman, H. L., Brown, R. E., Covey, D. F., Schaffer, J. E., Schlesinger, P., and Ory, D. S. (2009) Side chain oxygenated cholesterol regulates cellular cholesterol homeostasis through direct sterol-membrane interactions. *J. Biol. Chem.* **284**, 1755–1764
35. Cheng, D., Chang, C. C., Qu, X., and Chang, T. Y. (1995) Activation of acyl-coenzyme A:cholesterol acyltransferase by cholesterol or by oxysterol in a cell-free system. *J. Biol. Chem.* **270**, 685–695
36. Metherall, J. E., Li, H., and Waugh, K. (1996) Role of multidrug resistance P-glycoproteins in cholesterol biosynthesis. *J. Biol. Chem.* **271**, 2634–2640
37. Suzuki, S., Nishimaki-Mogami, T., Tamemiro, N., Inoue, K., Arakawa, R., Abe-Dohmae, S., Tanaka, A. R., Ueda, K., and Yokoyama, S. (2004) Verapamil increases the apolipoprotein-mediated release of cellular cholesterol by induction of ABCA1 expression via liver X receptor-independent mechanism. *Arterioscler. Thromb. Vasc. Biol.* **24**, 519–525
38. Lange, Y., Ory, D. S., Ye, J., Lanier, M. H., Hsu, F. F., and Steck, T. L. (2008) Effectors of rapid homeostatic responses of endoplasmic reticulum cholesterol and 3-hydroxy-3-methylglutaryl-CoA reductase. *J. Biol. Chem.* **283**, 1445–1455
39. Song, B. L., Javitt, N. B., and DeBose-Boyd, R. A. (2005) Insig-mediated degradation of HM-CoA reductase stimulated by lanosterol, an intermediate in the synthesis of cholesterol. *Cell Metab.* **1**, 179–189
40. Scheek, S., Brown, M. S., and Goldstein, J. L. (1997) Sphingomyelin depletion in cultured cells blocks proteolysis of sterol regulatory element binding proteins at site 1. *Proc. Natl. Acad. Sci. U.S.A.* **94**, 11179–11183
41. Chang, T. Y., and Limanek, J. S. (1980) Regulation of cytosolic acetoacetyl coenzyme A thiolase, 3-hydroxy-3-methylglutaryl coenzyme A synthase, 3-hydroxy-3-methylglutaryl coenzyme A reductase, and mevalonate kinase by low density lipoprotein and by 25-hydroxycholesterol in Chinese hamster ovary cells. *J. Biol. Chem.* **255**, 7787–7795
42. Hua, X., Nothurfft, A., Goldstein, J. L., and Brown, M. S. (1996) Sterol resistance in CHO cells traced to point mutation in SREBP cleavage-activating protein. *Cell* **87**, 415–426
43. Gil, G., Faust, J. R., Chin, D. J., Goldstein, J. L., and Brown, M. S. (1985) Membrane-bound domain of HMG CoA reductase is required for sterol-enhanced degradation of the enzyme. *Cell* **41**, 249–258
44. Hamon, Y., Broccardo, C., Chambenoit, O., Luciani, M. F., Toti, F., Chaslin, S., Freyssinet, J. M., Devaux, P. F., McNeish, J., Marguet, D., and Chimini, G. (2000) ABC1 promotes engulfment of apoptotic cells and transbilayer redistribution of phosphatidylserine. *Nat. Cell Biol.* **2**, 399–406
45. Takahashi, K., Kimura, Y., Kioka, N., Matsuo, M., and Ueda, K. (2006)

**ABCA1 Regulates Bidirectional Sterol Transport**

- Purification and ATPase activity of human ABCA1. *J. Biol. Chem.* **281**, 10760–10768
46. Parton, R. G., and Simons, K. (2007) The multiple faces of caveolae. *Nat. Rev. Mol. Cell Biol.* **8**, 185–194
  47. Koseki, M., Hirano, K., Masuda, D., Ikegami, C., Tanaka, M., Ota, A., Sandoval, J. C., Nakagawa-Toyama, Y., Sato, S. B., Kobayashi, T., Shimada, Y., Ohno-Iwashita, Y., Matsuura, F., Shimomura, I., and Yamashita, S. (2007) Increased lipid rafts and accelerated lipopolysaccharide-induced tumor necrosis factor- $\alpha$  secretion in Abca1-deficient macrophages. *J. Lipid Res.* **48**, 299–306
  48. Le, P. U., Guay, G., Altschuler, Y., and Nabi, I. R. (2002) Caveolin-1 is a negative regulator of caveolae-mediated endocytosis to the endoplasmic reticulum. *J. Biol. Chem.* **277**, 3371–3379
  49. Renard, H. F., Simunovic, M., Lemièrre, J., Boucrot, E., Garcia-Castillo, M. D., Arumugam, S., Chambon, V., Lamaze, C., Wunder, C., Kenworthy, A. K., Schmidt, A. A., McMahon, H. T., Sykes, C., Bassereau, P., and Johannes, L. (2015) Endophilin-A2 functions in membrane scission in clathrin-independent endocytosis. *Nature* **517**, 493–496
  50. Puri, V., Watanabe, R., Singh, R. D., Dominguez, M., Brown, J. C., Wheatley, C. L., Marks, D. L., and Pagano, R. E. (2001) Clathrin-dependent and -independent internalization of plasma membrane sphingolipids initiates two Golgi targeting pathways. *J. Cell Biol.* **154**, 535–547
  51. Doherty, G. J., and McMahon, H. T. (2009) Mechanisms of endocytosis. *Annu. Rev. Biochem.* **78**, 857–902
  52. Macia, E., Ehrlich, M., Massol, R., Boucrot, E., Brunner, C., and Kirchhausen, T. (2006) Dynasore, a cell-permeable inhibitor of dynamin. *Dev. Cell* **10**, 839–850
  53. Hill, T. A., Gordon, C. P., McGeachie, A. B., Venn-Brown, B., Odell, L. R., Chau, N., Quan, A., Mariana, A., Sakoff, J. A., Chircop, M., Robinson, P. J., and McCluskey, A. (2009) Inhibition of dynamin mediated endocytosis by the dynoles—synthesis and functional activity of a family of indoles. *J. Med. Chem.* **52**, 3762–3773
  54. Beaven, S. W., and Tontonoz, P. (2006) Nuclear receptors in lipid metabolism: targeting the heart of dyslipidemia. *Annu. Rev. Med.* **57**, 313–329
  55. van Meer, G., Voelker, D. R., and Feigenson, G. W. (2008) Membrane lipids: where they are and how they behave. *Nat. Rev. Mol. Cell Biol.* **9**, 112–124
  56. Quazi, F., Lenevich, S., and Molday, R. S. (2012) ABCA4 is an *N*-retinylidene-phosphatidylethanolamine and phosphatidylethanolamine importer. *Nat. Commun.* **3**, 925
  57. Li, Y., and Prinz, W. (2004) ATP-binding cassette (ABC) transporters mediate nonvesicular, raft-modulated sterol movement from the plasma membrane to the endoplasmic reticulum. *J. Biol. Chem.* **279**, 45226–45234
  58. Landry, Y. D., Denis, M., Nandi, S., Bell, S., Vaughan, A. M., and Zha, X. (2006) ATP-binding cassette transporter A1 expression disrupts raft membrane microdomains through its ATPase-related functions. *J. Biol. Chem.* **281**, 36091–36101
  59. Zarubica, A., Plazzo, A. P., Stöckl, M., Trombik, T., Hamon, Y., Müller, P., Pomorski, T., Herrmann, A., and Chimini, G. (2009) Functional implications of the influence of ABCA1 on lipid microenvironment at the plasma membrane: a biophysical study. *FASEB J.* **23**, 1775–1785
  60. Radhakrishnan, A., Anderson, T. G., and McConnell, H. M. (2000) Condensed complexes, rafts, and the chemical activity of cholesterol in membranes. *Proc. Natl. Acad. Sci. U.S.A.* **97**, 12422–12427
  61. Steck, T. L., and Lange, Y. (2010) Cell cholesterol homeostasis: mediation by active cholesterol. *Trends Cell Biol.* **20**, 680–687
  62. Quazi, F., and Molday, R. S. (2013) Differential phospholipid substrates and directional transport by ATP-binding cassette proteins ABCA1, ABCA7, and ABCA4 and disease-causing mutants. *J. Biol. Chem.* **288**, 34414–34426
  63. Olsen, B. N., Bielska, A. A., Lee, T., Daily, M. D., Covey, D. F., Schlesinger, P. H., Baker, N. A., and Ory, D. S. (2013) The structural basis of cholesterol accessibility in membranes. *Biophys. J.* **105**, 1838–1847
  64. Shvets, E., Bitsikas, V., Howard, G., Hansen, C. G., and Nichols, B. J. (2015) Dynamic caveolae exclude bulk membrane proteins and are required for sorting of excess glycosphingolipids. *Nat. Commun.* **6**, 6867
  65. Antony, B. (2011) Mechanisms of membrane curvature sensing. *Annu. Rev. Biochem.* **80**, 101–123
  66. Boucrot, E., Ferreira, A. P., Almeida-Souza, L., Debard, S., Vallis, Y., Howard, G., Bertot, L., Sauvonnnet, N., and McMahon, H. T. (2015) Endophilin marks and controls a clathrin-independent endocytic pathway. *Nature* **517**, 460–465
  67. Cohen, J. C., Kiss, R. S., Pertsemlidis, A., Marcel, Y. L., McPherson, R., and Hobbs, H. H. (2004) Multiple rare alleles contribute to low plasma levels of HDL cholesterol. *Science* **305**, 869–872
  68. Clee, S. M., Kastelein, J. J., van Dam, M., Marcil, M., Roomp, K., Zwarts, K. Y., Collins, J. A., Roelants, R., Tamasawa, N., Stulc, T., Suda, T., Ceska, R., Boucher, B., Rondeau, C., DeSouich, C., et al. (2000) Age and residual cholesterol efflux affect HDL cholesterol levels and coronary artery disease in ABCA1 heterozygotes. *J. Clin. Invest.* **106**, 1263–1270
  69. Schaefer, E. J., Zech, L. A., Schwartz, D. E., and Brewer, H. B. (1980) Coronary heart disease prevalence and other clinical features in familial high density lipoprotein deficiency (Tangier disease). *Ann. Intern. Med.* **93**, 261–266
  70. Frechin, M., Stoeger, T., Daetwyler, S., Gehin, C., Battich, N., Damm, E. M., Stergiou, L., Riezman, H., and Pelkmans, L. (2015) Cell-intrinsic adaptation of lipid composition to local crowding drives social behaviour. *Nature* **523**, 88–91

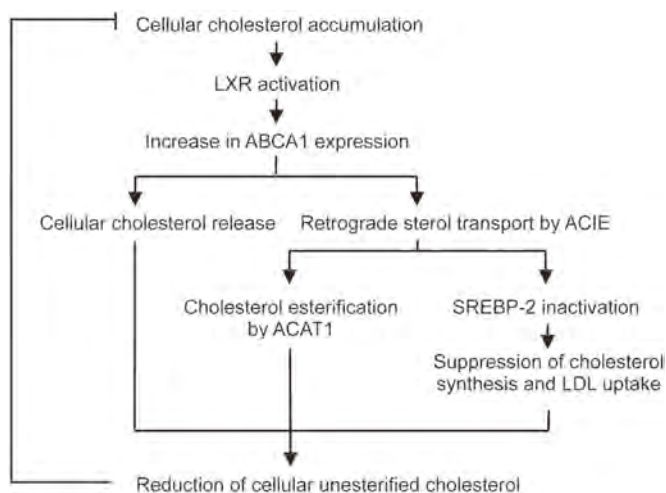
## Papers of the Week

### Discovering an Unexpected Function of the Lipid Carrier ATP-binding Cassette Transporter A1 ♦

♦ See referenced article, *J. Biol. Chem.* 2015, **290**, 23464–23477

#### Deficiency in the Lipid Exporter ABCA1 Impairs Retrograde Sterol Movement and Disrupts Sterol Sensing at the Endoplasmic Reticulum

Maintaining the correct level of cholesterol in the cell relies partly on sterol delivery from the plasma membrane to the endoplasmic reticulum. But the details of how this retrograde transport happens are unclear. A protein called ATP-binding cassette transporter A1 (ABCA1) exports cholesterol and phospholipids out of cells. In this Paper of the Week, a team led by Yoshio Yamachi at the Nagoya University Graduate School of Medicine in Japan and Ta-Yuan Chang at the Geisel School of Medicine at Dartmouth showed that ABCA1 also is capable of carrying sterols from the plasma membrane to the endoplasmic reticulum. The investigators showed that a deficiency in ABCA1 altered the plasma membrane composition and affected an endocytic mechanism. The authors say, “Our finding identifies ABCA1 as a key macromolecule facilitating bidirectional sterol movement at the (plasma membrane) and shows that ABCA1 controls retrograde sterol transport by modulating a certain clathrin-independent endocytic process.”



ABCA1 participates in bidirectional sterol movement at the plasma membrane to prevent excess cholesterol accumulation in cells.

DOI 10.1074/jbc.P115.662668

# Discovering an Unexpected Function of the Lipid Carrier ATP-binding Cassette Transporter A1<sup>◆</sup>

Yoshio Yamauchi



**Current position:** Assistant Professor/Lecturer,  
Department of Biochemistry II, Nagoya University Graduate  
School of Medicine, Nagoya, Japan

**Education:** Ph.D. in Biochemistry, 2003, Nagoya City  
University Graduate School of Medical Sciences, Nagoya,  
Japan

**Nonscientific interests:** Hiking, soccer (used to play, but  
only watch now), and listening to classical music

---

I have a longstanding research interest in membrane lipids, particularly the vital lipid cholesterol. After completing my Ph.D. work on HDL assembly at Nagoya City University (with Professor Shinji Yokoyama as mentor), I was trained in the laboratory of Professor T. Y. Chang, Department of Biochemistry, Geisel School of Medicine at Dartmouth (Hanover, NH), with a postdoctoral fellowship support from the American Heart Association. Since 2007, I have been working as an assistant professor in the Department of Biochemistry II of Nagoya University Graduate School of Medicine, with Professor Koichi Furukawa, who is an expert scientist in ganglioside research, as well as the department chair. My current research interests include studying cholesterol and glycosphingolipids in various human diseases, including cancer, metabolic disorders, and lysosomal diseases. These two lipids are critical components of lipid rafts and work cooperatively in membranes. The current work is the fruit of close collaboration between the three laboratories (two labs in Nagoya, Japan, and one lab in Hanover, NH). Here, we made some interesting and unexpected findings; the ABC transporter ABCA1 plays a crucial role in both outward and inward movement of cholesterol at the plasma membrane. Deficiency in this transporter, therefore, impairs the integrity of plasma membrane. Our findings may help to understand how membrane lipid composition regulates membrane functionality and how cellular cholesterol homeostasis is linked to cellular functions.

Read Yamauchi's article on page 23464.

Advertisement

# ATP-binding Cassette Transporter A7 (ABCA7) Loss of Function Alters Alzheimer Amyloid Processing\*

Received for publication, March 27, 2015, and in revised form, July 30, 2015. Published, JBC Papers in Press, August 10, 2015, DOI 10.1074/jbc.M115.655076

Kanayo Satoh<sup>†1</sup>, Sumiko Abe-Dohmae<sup>§</sup>, Shinji Yokoyama<sup>¶</sup>, Peter St George-Hyslop<sup>‡||\*\*</sup>, and Paul E. Fraser<sup>‡||</sup>

From the <sup>†</sup>Tanz Centre for Research in Neurodegenerative Diseases, University of Toronto, Toronto, Ontario M5T 2S8, Canada, <sup>§</sup>Biochemistry, Nagoya City University Graduate School of Medical Sciences, Nagoya 467-8601, Japan, <sup>¶</sup>Nutritional Health Science Research Center, Chubu University, Matsumoto-cho 1200, Kasugai 487-8501, Japan, <sup>||</sup>Departments of Medicine (Neurology) and Medical Biophysics, University of Toronto, Toronto, Ontario M5G 1L7, Canada, and <sup>\*\*</sup>Cambridge Institute for Medical Research, University of Cambridge, Cambridge CB2 0XY, United Kingdom

**Background:** The ATP-binding cassette transporter A7 (ABCA7) is a risk factor for sporadic Alzheimer disease (AD).

**Results:** Loss of ABCA7 promoted A $\beta$  processing and pathology in cell culture and AD mouse models.

**Conclusion:** Altered ABCA7 function may contribute to AD by impacting A $\beta$  production in addition to clearance.

**Significance:** AD-related risk factors may contribute to disease progression through multiple pathways.

The ATP-binding cassette transporter A7 (ABCA7) has been identified as a susceptibility factor of late onset Alzheimer disease in genome-wide association studies. ABCA7 has been shown to mediate phagocytosis and affect membrane trafficking. The current study examined the impact of ABCA7 loss of function on amyloid precursor protein (APP) processing and generation of amyloid- $\beta$  (A $\beta$ ). Suppression of endogenous ABCA7 in several different cell lines resulted in increased  $\beta$ -secretase cleavage and elevated A $\beta$ . ABCA7 knock-out mice displayed an increased production of endogenous murine amyloid A $\beta$ 42 species. Crossing ABCA7-deficient animals to an APP transgenic model resulted in significant increases in the soluble A $\beta$  as compared with mice expressing normal levels of ABCA7. Only modest changes in the amount of insoluble A $\beta$  and amyloid plaque densities were observed once the amyloid pathology was well developed, whereas A $\beta$  deposition was enhanced in younger animals. *In vitro* studies indicated a more rapid endocytosis of APP in ABCA7 knock-out cells that is mechanistically consistent with the increased A $\beta$  production. These *in vitro* and *in vivo* findings indicate a direct role of ABCA7 in amyloid processing that may be associated with its primary biological function to regulate endocytic pathways. Several potential loss-of-function ABCA7 mutations and deletions linked to Alzheimer disease that in some instances have a greater impact than apoE allelic variants have recently been identified. A reduction in ABCA7 expression or loss of function would be predicted to increase amyloid production and that may be a contributing factor in the associated Alzheimer disease susceptibility.

\* This work was supported by Canadian Institute of Health Research Grant MOP-115056 (to P.E.F.), the Ontario Alzheimer's Society, the Ontario Research Fund, Japan Society for the Promotion of Science KAKENHI Grants 21591164 and 25461375, the Japan Health Sciences Foundation, and the Ministry of Education, Culture, Sports, Science and Technology-supported program for the Strategic Research Foundation at Private Universities (Japan). The authors declare no competing financial interests.

<sup>†</sup> To whom correspondence should be addressed: Tanz CRND, University of Toronto, 60 Leonard Ave., Toronto, Ontario M5T 2S8, Canada. E-mail: kanayo.sato@utoronto.ca.

Genome-wide association studies have identified the ATP-binding cassette transporter A7 (ABCA7)<sup>2</sup> as a susceptibility locus for late onset Alzheimer disease (LOAD) (1, 2). The single nucleotide polymorphisms (SNPs) associated with LOAD are distributed in various domains of the ABCA7 gene and include intronic SNPs and a coding sequence causing G1527A substitution. Studies have identified loci in different clusters, suggesting multiple sites within the ABCA7 gene associated with increased risk for AD (3). However, there is no indication that individuals with at-risk alleles display any differences in ABCA7 expression.

ABCA7 is a member of the ATP-binding cassette transporter family largely involved in lipid transport and homeostasis (4). Its highly homologous member ABCA1 has also been linked to LOAD through cholesterol and processing of the amyloid precursor protein (5–7). Overexpression of ABCA7 resulted in a significant decrease in amyloid- $\beta$  (A $\beta$ ) processing (8). It was therefore suggested that ABCA7 directly impacts amyloid pathology by altering APP trafficking and substrate availability.

Human ABCA7 overexpressed in HEK293 cells mediated generation of HDL containing less cholesterol as compared with ABCA1 (9, 10). Mouse ABCA7 under the same conditions generated HDL almost exclusively composed of phospholipid (11). However, loss or reduction of ABCA7 demonstrated no change in cell lipid release, indicating that it is unlikely to be redundant with ABCA1 in HDL biogenesis (12–14). Transcription of ABCA7 is regulated by sterol regulatory element/sterol regulatory element-binding protein in an opposite direction to the liver X receptor-mediated regulation of ABCA1, suggesting that it is unlikely to mediate cell cholesterol release (14). Subsequent studies demonstrated that endogenous ABCA7 is primarily associated with endocytic pathways, including phagocytosis (14). Thus, endogenous ABCA7 is speculated to link sterol

<sup>2</sup> The abbreviations used are: ABCA7, ATP-binding cassette transporter A7; AD, Alzheimer disease; LOAD, late onset Alzheimer disease; APP, amyloid precursor protein; A $\beta$ , amyloid- $\beta$ ; ABCA1, ATP-binding cassette transporter A1; sAPP, secreted APP; APP-FL, full-length APP; CTF, C-terminal fragment; APPSw, APP Swedish mutation; PICALM, phosphatidylinositol clathrin assembly lymphoid-myeloid leukemia; Tg, transgenic.

metabolism to host defense pathways rather than lipoprotein generation (15–17).

Similar studies found that ABCA7 suppression reduced clearance of apoptotic cell debris and that endogenous ABCA7 co-localized with LRP1 in stimulated macrophages (18). Exposure of apoptotic cells facilitated enrichment in cell surface ABCA7 and LRP1, and this was attenuated in ABCA7-hemizygous deficient mice (18). It is therefore conceivable that ABCA7 is linked to AD through a diminished ability to remove neuronal debris and/or amyloid aggregates. Our findings indicate that ABCA7 may also contribute to APP processing and A $\beta$  production possibly by modulating LRP1 function. LRP1 associates with APP in the presence of a cytoplasmic adaptor protein, FE65, to internalize APP and produce A $\beta$  in endosomal-lysosomal compartments (19, 20). The exact role of ABCA7 in LOAD is under debate, and it may contribute to Alzheimer pathology by altering A $\beta$  production and/or clearance. The current study focused on ABCA7 loss of function and its involvement in amyloid processing in an effort to reconcile these two possible mechanisms.

### Experimental Procedures

**Antibodies**—ABCA7 expression levels of cell and brain lysate were detected by Western blotting using rat monoclonal antibodies for human ABCA7 (KM3096) and mouse ABCA7 (KM3097). Samples were separated on 4–20% Mini-PROTEAN Tris-glycine extended precast gels (Bio-Rad). Anti-ABCA7 antibodies were provided by Kyowa Hakko Kirin Co. Ltd. Mouse monoclonal antibody 6E10 (Covance) was used for the APP internalization assay, and rabbit polyclonal anti-EEA1 antibody (ab2900, Abcam), an early endosome marker, was used for endosome immunostaining.

**Plasmids and RNAi**—Full-length cDNAs for human ABCA7 were cloned as described previously (21). ABCA7 cDNA within pEGFP-N3 was digested by EcoRI and subcloned into pcDNA3 (Life Technologies). The vector has an immediate early promoter of cytomegalovirus promoter for expression of cDNA. Three sets of Stealth RNAi<sup>TM</sup> small interfering RNA (siRNA) duplexes specific for ABCA7 (5'-GGAACCUGUCUGACUCC UGGUCA-3', 5'-CCGCACUGCUGGUU-CUGGUGCUCAA-3', and 5'-CGGAUCUUGAA-ACAGGUCUCCUUA-3') were designed and purchased from Life Technologies. High GC duplex was used as a negative control.

**Cell Culture and Transfection**—HEK293, KNS-42, SH-SY5Y, and HeLa cells were maintained in Dulbecco's modified Eagle's medium (DMEM; Life Technologies) supplemented with 10% (v/v) fetal calf serum in a humidified incubator with 5% CO<sub>2</sub> at 37 °C. The cells were grown on 35-mm glass-bottomed dishes. cDNA and Stealth RNAi siRNAs were transfected with Lipofectamine LTX and PLUS Reagent (Life Technologies) according to the manufacturer's protocols. Cells were examined 48 h after transfection. For primary cells, ABCA7-deficient mice (ABCA7<sup>-/-</sup>) were cross-bred with TgCRND8 (ABCA7<sup>+/+</sup>) mice. Primary cultures were prepared from brain of either embryonic 16-day-old (cortical neurons) or postnatal 1-day-old (astrocytes and microglia) mice according to the method of Cole and de Vellis (22), and mixed glial cells were cultured as described previously (23, 24). After 20–24 days of culturing,

microglia were harvested by mild trypsinization (25). Briefly, cortical neurons were maintained in Neurobasal medium (Life Technologies) supplemented with B27 (Life Technologies), GlutaMAX (Life Technologies), sodium pyruvate (Life Technologies), and penicillin/streptomycin (Life Technologies) by a twice weekly half-volume medium change. Astrocyte and microglia cultures were maintained in DMEM supplemented with GlutaMAX, minimum essential medium amino acids (Life Technologies), minimum essential medium vitamin solution (pH 7.2; Life Technologies), and 10% (v/v) fetal calf serum by a twice weekly complete medium change in a humidified incubator with 5% CO<sub>2</sub> at 37 °C. All experiments were performed according to the Canadian Council on Animal Care guidelines.

**Preparation of Cell and Brain Lysates**—HEK293, KNS-42, SH-SY5Y, and HeLa cells and mouse primary microglia were cultivated and solubilized with radioimmune precipitation assay buffer (150 mM NaCl, 50 mM Tris, 1% Triton X-100, 0.5% deoxycholate, 0.1% SDS, 1 mM EDTA, pH 7.6). Protein quantitation was performed using the method of Bradford (64). Mouse hemibrain or dissected samples were homogenized in a buffered sucrose solution (20 mM HEPES, pH 7.4, 0.25 M sucrose, 1 mM EDTA, 1 mM EGTA) and a protease inhibitor mixture followed by 1.0% Nonidet P-40 lysis buffer to examine the endogenous APP/A $\beta$  level. To isolate soluble/insoluble A $\beta$ , hemibrain or dissected samples were homogenized in a buffered sucrose solution followed by either a mixture of 0.4% diethylamine and 100 mM NaCl for soluble A $\beta$  or cold formic acid for the isolation of total A $\beta$ . After neutralization, samples were diluted and analyzed for A $\beta$ 40 and A $\beta$ 42 levels.

**APP Processing Analysis**—Approximately 48 h after transfection, conditioned medium was collected and analyzed for A $\beta$ 40, A $\beta$ 42, secreted APP (sAPP)  $\beta$ /Sw, and sAPP $\beta$ /WT levels using commercially available ELISA kits (human A $\beta$ 40 and human A $\beta$ 42 from Life Technologies and mouse A $\beta$ 40, mouse A $\beta$ 42, human sAPP $\beta$ /Sw, and human sAPP $\beta$ /WT from IBL International). Levels of full-length APP and C-terminal fragment of APP in cell lysate and brain lysate were analyzed by Western blotting using the monoclonal antibody C1/6.1 as described previously (26). The conditioned medium or brain lysate was used to analyze secreted APPs, sAPP $\beta$ /Sw, sAPP $\beta$ /WT, and A $\beta$  levels by Western blotting using monoclonal antibody 22C11 for secreted APPs (Chemicon), monoclonal antibody 6A1 for human sAPP $\beta$ /Sw (IBL International), polyclonal antibody for human sAPP $\beta$ /WT (IBL International), and monoclonal antibody 6E10 for sAPP $\alpha$  and A $\beta$  (Signet/Covance).

**Knock-out and Transgenic Mice**—The TgCRND8 transgenic mice express APP695 on a prion cos-tet vector on a C57BL/6/C3H mixed background as described previously (27). The ABCA7 knock-out mice were generated as described previously (28) and maintained on a C57BL/6 background. An equal mix of age-matched male and female mice was examined in this investigation. The TgCRND8-ABCA7<sup>+/+</sup> and TgCRND8-ABCA7<sup>-/-</sup> crosses were maintained on the same C57BL/6/C3H mixed background to avoid any background-related variations in APP expression and amyloid pathology.

**Analysis of A $\beta$  Plaque Densities**—Animals were perfused, and brains were fixed in 4% paraformaldehyde and prepared for immunostaining as described previously (29). Plaques were

## ABCA7 and Amyloid Pathology

identified using an HRP-conjugated primary A $\beta$ -specific antibody (6E10-HRP, Signet) and visualized with 3,3'-diaminobenzidine following pretreatment with 70% formic acid. Dense and diffuse plaque stainings were assessed by measuring the amyloid-positive area over total area as described previously (30). Briefly, immunostained sections (5  $\mu$ m) were scanned with Mirax Scan (Zeiss) and assessed using ImageScope (Aperio). Slides were scanned using the Mirax Scan v.1.11 software and Zeiss Mirax Slide Scanner at 20 $\times$  magnification with a Zeiss 20 $\times$ /0.8 objective lens and a Marlin F146-C charge-coupled device camera. The rendered digital images were analyzed using the color deconvolution algorithm in the ImageScope software as described previously (31). RGB values were determined for both the applied hematoxylin and 3,3'-diaminobenzidine stains. 3,3'-Diaminobenzidine was chosen as the positive color channel for identifying and quantifying A $\beta$ -stained plaques within different areas of the brain (cortex and hippocampus). Furthermore, recognition and measurement of dense and diffuse plaque stained areas were achieved by setting the threshold values of color intensity. The strong positive threshold was set to 80, correlating with dense staining; the medium positive threshold was set to 160, correlating with medium/diffuse staining; and the weak positive threshold was set to 0. In this way, the amyloid-positive area as well as the intensity of A $\beta$  staining was quantified in different brain regions, allowing for quick, objective comparison between brains from different animals.

**APP Endocytosis and ABCA7/Endosome Localization**—The primary microglia from P1 C57BL/6 or ABCA7 knock-out mice were cultured for 3 weeks on 35-mm dishes (Nunc), then washed with cold PBS, and incubated at 4  $^{\circ}$ C with 6E10 antibody (1:200 in PBS) for 30 min to label surface APP. Cells were carefully rinsed with ice-cold PBS and incubated at 37  $^{\circ}$ C for 0, 5, 10, and 20 min to permit internalization. Cells were fixed in 4% paraformaldehyde in PBS for 10 min at room temperature, permeabilized in 0.1% Triton X-100, washed in 0.1% Tween 20 in PBS, and blocked in 5% normal goat serum in PBS-Tween 20. Cells were then incubated with anti-ABCA7 antibody (KM3097) or anti-EEA1 primary antibody, washed, and then incubated with goat Cy3-conjugated anti-mouse IgG and goat FITC-conjugated anti-rat or -rabbit IgG (Jackson ImmunoResearch Laboratories). Cells were mounted with fluorescent mounting medium (Dako) or Prolong Gold antifade reagent with DAPI (Life Technologies). Fluorescence images were observed using an Axioplan 2 imaging microscope (Zeiss) and AxioVision software (Zeiss) equipped with a laser-scanning confocal (LSM-510, Zeiss) or an AxioObserverZ1 inverted microscope (Zeiss) equipped with a spinning disk confocal scanner (CSU-XI, Yokogawa), an AxioCam 506 camera (Zeiss), an Evolve 512 electron-multiplying charge-coupled device camera (Photometrics), and a 63 $\times$  (oil; numerical aperture, 1.40) objective lens (Zeiss). Imaging data were analyzed using Volocity version 6.3.0 (PerkinElmer Life Sciences).

**Statistical Analysis**—All data were analyzed by Prism 5 (GraphPad Software), Igor Pro 6.02 (WaveMetrics), or Excel (Microsoft) using either a two-tailed Student's *t* test or Tukey-Kramer test. Data were expressed as mean  $\pm$  S.D. Differences

were deemed significant at  $p < 0.05$  (\*),  $p < 0.01$  (\*\*), and  $p < 0.001$  (\*\*\*)

## Results

**In Vitro Suppression of Endogenous ABCA7 and A $\beta$  Generation**—Endogenous ABCA7 in a number of different cell lines was examined using human-specific monoclonal anti-ABCA7 antibody (KM3096), which revealed variability in the level of expression. The neuroblastoma SH-SY5Y and HEK293 cells did not express any detectable ABCA7 (Fig. 1A). In contrast, HeLa cells expressed moderate levels of ABCA7, and higher levels were expressed in the glioma KNS-42 cells. All cell lines had equivalent levels of endogenous APP (Fig. 1A).

Transient overexpression of mouse ABCA7 was previously demonstrated to result in significant reductions in A $\beta$  levels for cells co-expressing human APP (8). Our investigations of cells transfected with human ABCA7 and APP have supported the link to altered APP processing resulting in a significant decrease in secreted A $\beta$  (data not shown). However, comparable studies examining lipid efflux suggest that the cellular effects of transfected ABCA7 do not reflect the function of the endogenous protein (16). Because of the potentially confounding issues associated with artificially high expression levels of ABCA7, the current study focused on loss-of-function conditions and the consequences these have for amyloid processing and deposition within the brain.

For knockdown studies, KNS-42 cells have the highest ABCA7 expression, but this line has low transfection efficiency, and despite repeated attempts, it was not possible to obtain sufficient knockdown of ABCA7. We therefore examined suppression of ABCA7 in HeLa cells using three independent siRNA duplex constructs. Endogenous HeLa ABCA7 was assessed with a human-specific monoclonal antibody. All three RNAi constructs were found to virtually eliminate expression when compared with a negative control or untransfected cells (Fig. 1B). Examination of endogenous APP processing in the HeLa cells revealed a small but detectable increase in the sAPP $\beta$  species as determined by immunoblotting (Fig. 1C). This effect was confirmed by ELISA quantification of the HeLa endogenous sAPP $\beta$ /WT (Fig. 1C). To ascertain the effects on A $\beta$  generation, cells were transfected with APP<sup>Sw</sup> with and without ABCA7 knockdown. The levels of full-length APP (APP-FL) and C-terminal fragments (APP-CTFs) were not significantly different (Fig. 1D). Total levels of secreted APP (sAPP) were not significantly altered by ABCA7 suppression (Fig. 1E). An ELISA assessment confirmed the elevated levels of secreted APP $\beta$ /Sw (Fig. 1F). In addition to the increase in  $\beta$ -cleavage, elevations in A $\beta$ 40 and A $\beta$ 42 peptides for cells lacking endogenous ABCA7 expression were seen as compared with the negative control or APP-only expression (Fig. 1, G and H). Greater variation was observed for cells transfected with the RNAi control as compared with untransfected cells, which reduced the statistical significance of the ABCA7 knockdown cells. This may reflect the low levels of endogenous HeLa ABCA7, which reduces the impact of ABCA7 loss on APP processing and A $\beta$  production. The reduction is therefore modest, but cumulatively, these observations are consistent with a direct action of ABCA7 on

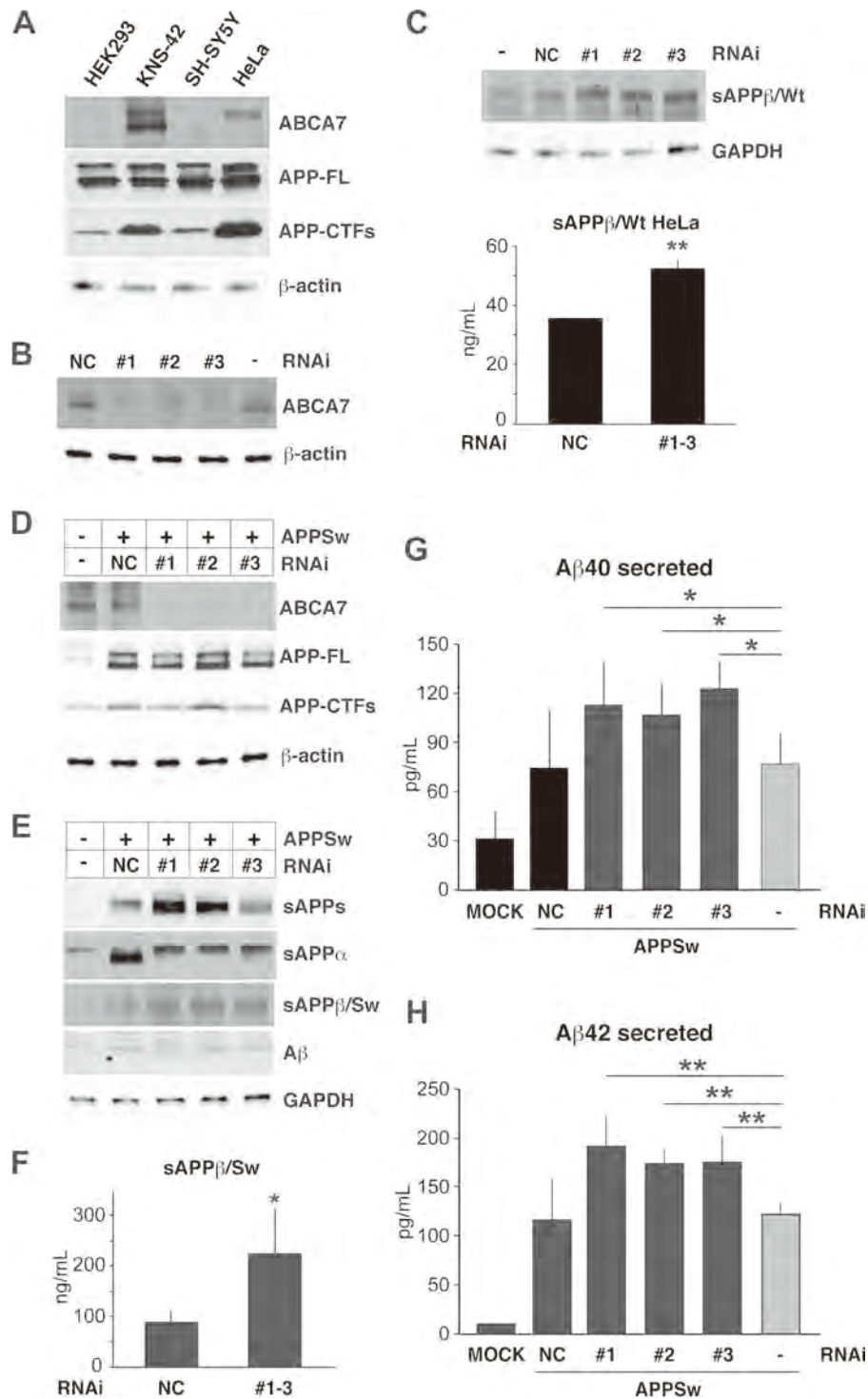


**FIGURE 1. ABCA7 knockdown effects on APP processing and A $\beta$  production in HeLa cells.** *A*, Western blot analysis of endogenous ABCA7 in different cell lines indicated the highest levels in the glioma KNS-42 cells and modest levels in HeLa cells, whereas ABCA7 was undetectable in HEK293 and SH-SY5Y cells (15  $\mu$ g of total protein/lane). Levels of full-length endogenous APP were comparable among the different cell lines, and increases in APP-CTF were observed in cells expressing ABCA7. *B*, suppression of endogenous ABCA7 in HeLa cells by three independent RNAi constructs (#1–3) as compared with a negative control (NC) was validated by Western blotting using a human-specific ABCA7 monoclonal antibody (15  $\mu$ g of total protein/lane). *C*, effect of ABCA7 knockdown on endogenous APP as assessed by Western blotting revealed a modest increase in sAPP $\beta$ /WT. Quantification of sAPP $\beta$ /WT by ELISA confirmed the increased levels possibly due to preferential  $\beta$ -secretase cleavage in the absence of ABCA7. The data represent means  $\pm$  S.D. (error bars) of six independent measurements. \*\*,  $p < 0.01$  by Student's  $t$  test. *D*, Western blotting of HeLa cells transiently transfected with APPSw with and without ABCA7 suppression revealed no detectable changes in APP-FL or APP-CTF. *E*, immunoblotting of HeLa cells transiently transfected with APPSw to examine total sAPP and the specific sAPP $\alpha$  and sAPP $\beta$ /Sw species demonstrated a slight increase in sAPP $\beta$ /Sw for cells with reduced ABCA7 levels. No immediately obvious differences were observed for total A $\beta$  by Western blotting. *F*, ELISA analysis for sAPP $\beta$ /Sw confirmed the increased levels possibly due to preferential  $\beta$ -secretase cleavage in the absence of ABCA7. The data represent means  $\pm$  S.D. (error bars) of four independent measurements. \*,  $p < 0.05$  by Student's  $t$  test. *G* and *H*, knockdown of endogenous ABCA7 was accompanied by significant increases in A $\beta$ 40 and particularly A $\beta$ 42 as compared with those transfected with APPSw alone as determined by ELISA. The data represent means  $\pm$  S.D. (error bars) of eight independent measurements. \*,  $p < 0.05$ ; \*\*,  $p < 0.01$  as determined by Tukey-Kramer test.

Downloaded from <http://www.jbc.org/> by Shinji Yokoyama on October 2, 2015

## ABCA7 and Amyloid Pathology

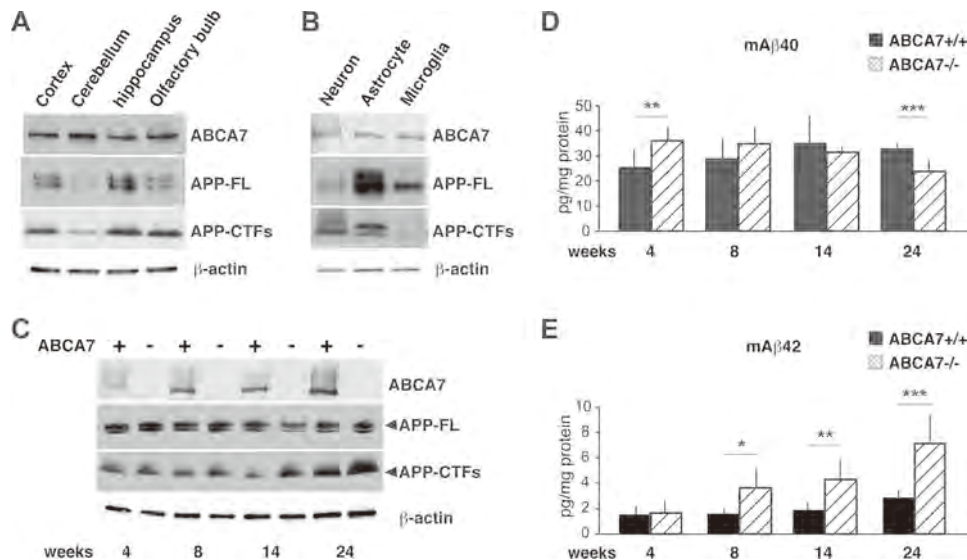


FIGURE 2. **ABCA7 knock-out increases endogenous murine A $\beta$ 42.** *A*, levels of endogenous ABCA7 in different regions of mouse brain examined with a murine-specific monoclonal antibody indicated no major variations in expression levels. Western blotting for APP-FL and -CTF did not reveal any correlations with ABCA7 within the same brain areas. *B*, immunoblotting of endogenous ABCA7 in primary cells from non-transgenic mice displayed comparable expression levels in all cell types, and no consistent changes in APP-FL or -CTF were observed. *C*, Western blot analysis for endogenous ABCA7, APP-FL and APP-CTF for wild-type (+) and ABCA7 knock-out (-) mice over the course of 4–24 weeks of age. Total brain lysates of wild-type ABCA7 and ABCA7 knock-out mice confirmed the expected absence in the knock-outs and a progressive increase in wild-type mice over the course of 4–24 weeks of age (40  $\mu$ g of total protein/lane). No differences were observed in any of the APP species as a result of ABCA7 knockdown. *D* and *E*, ELISA analysis for endogenous murine A $\beta$ 40 indicated a decline in levels with age (*D*). ELISA analysis for endogenous murine A $\beta$ 42 revealed a significant elevation with age in animals lacking ABCA7 (ABCA7 $^{-/-}$ ) as compared with wild-type mice (ABCA7 $^{+/+}$ ) (*E*). The data represent means  $\pm$  S.D. (error bars) of six to eight individual mice. \*,  $p < 0.05$ ; \*\*,  $p < 0.01$ ; \*\*\*,  $p < 0.001$  by Student's *t* test.

APP processing leading to A $\beta$  production possibly by modulating the efficiency of  $\beta$ -secretase cleavage.

**Endogenous Murine A $\beta$ 42 Increases in ABCA7 Knock-outs—**Loss of function was explored further in a physiological setting using an ABCA7 knock-out mouse model (28). Expression of ABCA7 in the wild-type mice was examined using murine-specific monoclonal antibodies, and comparable levels were found in all brain regions (Fig. 2*A*). Nearly identical levels of ABCA7 expression were observed in primary neurons and glia from wild-type mice (Fig. 2*B*). These findings indicate that ABCA7 is found throughout the brain and is expressed by all major cell types.

ABCA7 levels were also examined in total brain extracts from wild-type and knock-out animals over different time points after weaning until 6 months of age. The expected lack of ABCA7 was observed in the ABCA7 knock-out mice (ABCA7 $^{-/-}$ ), and a modest increase in ABCA7 levels was observed in wild-type mice (ABCA7 $^{+/+}$ ) from 4 to 24 weeks of age (Fig. 2*C*). No significant differences in APP-FL or APP-CTF were seen between ABCA7 $^{+/+}$  and ABCA7 $^{-/-}$  mice at comparable ages (Fig. 2*C*). Quantification of endogenous mouse A $\beta$ 40 revealed a higher concentration in 4–8-week-old ABCA7 $^{-/-}$  mice that gradually diminished to culminate in slightly lower levels than those of wild-type animals (ABCA7 $^{+/+}$ ) at 14–24 weeks of age (Fig. 2*D*). In contrast, a specific increase in A $\beta$ 42 during aging was observed with the loss of ABCA7. Endogenous murine A $\beta$ 42 was roughly equivalent in the 4-week-old animals, progressively increased in the ABCA7 $^{-/-}$  mice, and was significantly higher than in ABCA7 $^{+/+}$  mice at 8–24 weeks of age (Fig. 2*E*). A comparison of genders indicated a slight elevation in A $\beta$ 42 levels in male ABCA7 $^{-/-}$  mice ( $8.63 \pm 1.62$  pg/mg of protein) as compared

with females ( $5.57 \pm 1.79$  pg/mg of protein), although these were not statistically significant ( $n = 3$  in both groups). Total brain A $\beta$ 42 in the ABCA7 $^{+/+}$  mice was also slightly higher at 24 weeks of age, but this did not reach statistical significance when compared with younger mice (Fig. 2*E*). These findings, particularly the specific A $\beta$ 42 elevation, are consistent with ABCA7-mediated changes in both  $\beta$ - and  $\gamma$ -secretases.

Links between A $\beta$  production and cholesterol have been extensively reported where high fat diets lead to increased amyloid processing (for a review see, Ref. 32). To determine whether changes in putative ABCA7-mediated cholesterol and lipid pathways had any impact on endogenous A $\beta$  generation, ABCA7 knock-outs were compared with wild types that were placed on fat-enriched diets postweaning until 14 weeks of age. Expression of ABCA7 decreased slightly in the wild-type animals, which is consistent with the sterol regulatory element-binding protein 2 regulation and effects of sterols on ABCA7 (14). Substantial increases in APP-FL and APP-CTFs were observed for animals on a high fat diet (Fig. 3*A*). However, total brain A $\beta$ 40 and A $\beta$ 42 were nearly identical in the wild-type and knock-out mice under these conditions, and the differences in A $\beta$ 42 seen for animals on normal diet were eliminated (Fig. 3, *B* and *C*). The mice on a high fat diet were compared with the same animals on a normal diet that were used to determine the endogenous A $\beta$ 40 and A $\beta$ 42 levels (see Fig. 2). These observations indicate that increased cholesterol and lipid did not have an additive effect on amyloid processing in the ABCA7-ablated mice.

**Loss of ABCA7 Increases Soluble A $\beta$  in APP Transgenic Mice—**The changes in endogenous mouse A $\beta$ 42 for mice lacking ABCA7 indicate that ABCA7 affects pathways related to secretase cleavages of APP. To examine these pathways in more

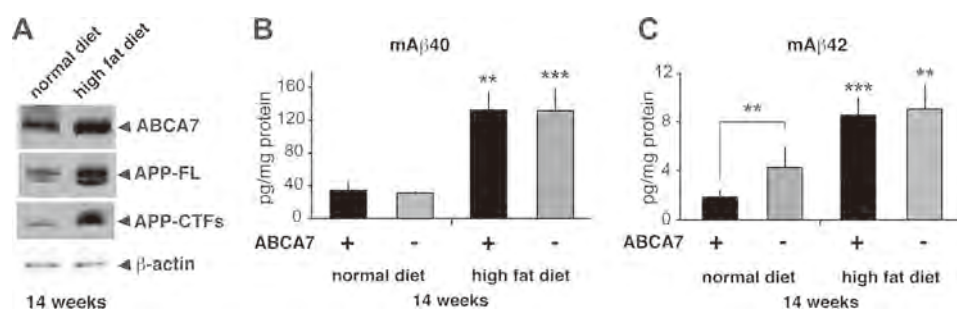


FIGURE 3. **APP expression in ABCA7 knock-out mice and effects of high fat diet.** *A*, Western blotting for wild-type mice on normal and high fat diets indicated no significant changes in ABCA7 levels, but an increase in APP-FL and APP-CTF was observed for animals on the high fat diet (40  $\mu$ g of total protein/lane). *B* and *C*, levels of endogenous murine A $\beta$ 40 and A $\beta$ 42 in wild-type (+) and ABCA7 knock-out (-) mice at 14 weeks of age were increased in both groups, and the differences in A $\beta$ 42 were eliminated on the high fat diet. The A $\beta$ 40 and A $\beta$ 42 data shown for mice on the normal diet are from the same group of animals used to determine endogenous A $\beta$  levels as shown in Fig. 2. The data represent means  $\pm$  S.D. (error bars) of eight individual mice. \*\*,  $p < 0.01$ ; \*\*\*,  $p < 0.001$ , by Student's *t* test.

detail and determine the effects on amyloid pathology, ABCA7 knock-out mice were crossed with a mutant APP transgenic mouse model (TgCRND8). The TgCRND8 model has been widely used and is an aggressive model with AD-related amyloid plaques and oligomers forming within 3–4 months of age (27, 29). The TgCRND8-ABCA7 $^{-/-}$  cross was compared with TgCRND8 on a wild-type ABCA7 background at 18 weeks of age when extensive amyloid pathology is observed in this particular model. ABCA7 levels in TgCRND8 mice were comparable with non-transgenic animals, indicating that the APP transgene does not have any appreciable impact on ABCA7 expression (data not shown).

Western blotting for APP revealed the expected high levels of APP-FL, which were equivalent in both TgCRND8-ABCA7 $^{-/-}$  and TgCRND8-ABCA7 $^{+/+}$  (Fig. 4A). However, a slight increase in APP-CTF $\alpha/\beta$  was observed in the TgCRND8-ABCA7 $^{-/-}$  mice as compared with TgCRND8 alone. Secreted APP $\beta$  was also increased in TgCRND8-ABCA7 $^{-/-}$  mice as determined by ELISA (Fig. 4B). A statistically significant elevation in soluble A $\beta$ 40 was observed in whole brain extracts from TgCRND8-ABCA7 $^{-/-}$  mice (Fig. 4, C). The soluble A $\beta$ 42 and insoluble A $\beta$ 40 or A $\beta$ 42 tended to be higher in the ABCA7-deficient mice, but these values did not achieve statistical significance (Fig. 4, C and D). These findings indicate that the loss of ABCA7 has a direct impact by altering APP processing, leading to increased A $\beta$  production similar to that observed for endogenous mouse amyloid.

Assessment of soluble and insoluble A $\beta$  was conducted in specific brain regions associated with AD-related pathology to determine whether similar trends were observed as compared with whole brain extracts. Soluble A $\beta$ 40 and A $\beta$ 42 were found to be the highest in the cortex, and significant increases in both species were observed in the APP transgenic mice (TgCRND8) on the ABCA7 knock-out background (Fig. 5, A and C). Similar trends were observed for soluble A $\beta$ 40 and A $\beta$ 42 in the hippocampus, cerebellum, and olfactory bulb of TgCRND8-ABCA7 $^{-/-}$  mice as compared with TgCRND8-ABCA7 $^{+/+}$  animals (Fig. 5, A and C). The most pronounced changes in soluble A $\beta$ 42 were in the cortex and olfactory bulb where an  $\sim$ 4-fold increase was detected (Fig. 5C). The olfactory bulb is an area of extensive pathology in the TgCRND8 model due to the prion cos-tet promoter that drives high expression in this region (33). In contrast, insoluble A $\beta$ 40 and A $\beta$ 42 in the cortex

and hippocampus did not exhibit statistically significant differences between TgCRND8-ABCA7 $^{-/-}$  and TgCRND8-ABCA7 $^{+/+}$  mice (Fig. 5, B and D). In the olfactory bulb, increased amounts of insoluble A $\beta$  were found in the transgenic mice lacking ABCA7, likely reflecting the high level of APP expression and A $\beta$  production. No significant differences in soluble A $\beta$  levels were observed between males and females in this study. These findings are in keeping with the whole brain extracts and demonstrated that A $\beta$  generation is increased and accumulates as plaques.

*Amyloid Plaque Density in ABCA7 Knock-outs Crossed with APP Transgenic Mouse Model*—Amyloid deposition in the mouse models at 18 weeks of age was examined by immunohistochemistry to quantify plaque density. Serial sections from successive regions of the brain were stained for total A $\beta$ , and typical amyloid plaques were observed in the cortex and hippocampus of the APP transgenic mice on the ABCA7 wild-type and knock-out backgrounds (Fig. 6, A and B). Image analysis of dense and diffuse plaque areas was conducted with sampling over the entire cortex and hippocampus. Quantification of the staining revealed a statistically significant increase in TgCRND8-ABCA7 $^{-/-}$  mice in dense core plaques area, but no detectable change in the diffuse plaque area was observed (Fig. 6C). The total number of plaques, as opposed to average size, showed a slight trend to higher amounts in the ABCA7 knock-out mice, but this did not achieve statistical significance when compared with the TgCRND8 on an ABCA7 wild-type background (Fig. 6D). The increase in the area of dense plaques is likely a reflection of the increased production of A $\beta$  in the TgCRND8-ABCA7 $^{-/-}$  mice.

*Amyloid Deposition at Early Stages of Pathology Development*—Given the observed elevations in soluble A $\beta$  displayed by the TgCRND8-ABCA7 $^{-/-}$  mice, it could have been expected that this would translate into increased plaque loads for these animals as compared with TgCRND8 transgenic mice on an ABCA7 $^{+/+}$  background. A likely explanation is that aggregation and deposition of the insoluble A $\beta$  have plateaued in the older animals (18 weeks), and to investigate this possibility in more detail, comparable mice were examined at 10 weeks of age. Previous studies have indicated that at  $\sim$ 10 weeks of age the TgCRND8 mouse model undergoes a transition where the total amount of A $\beta$ 42 generated by the transgenic mice

ABCA7 and Amyloid Pathology

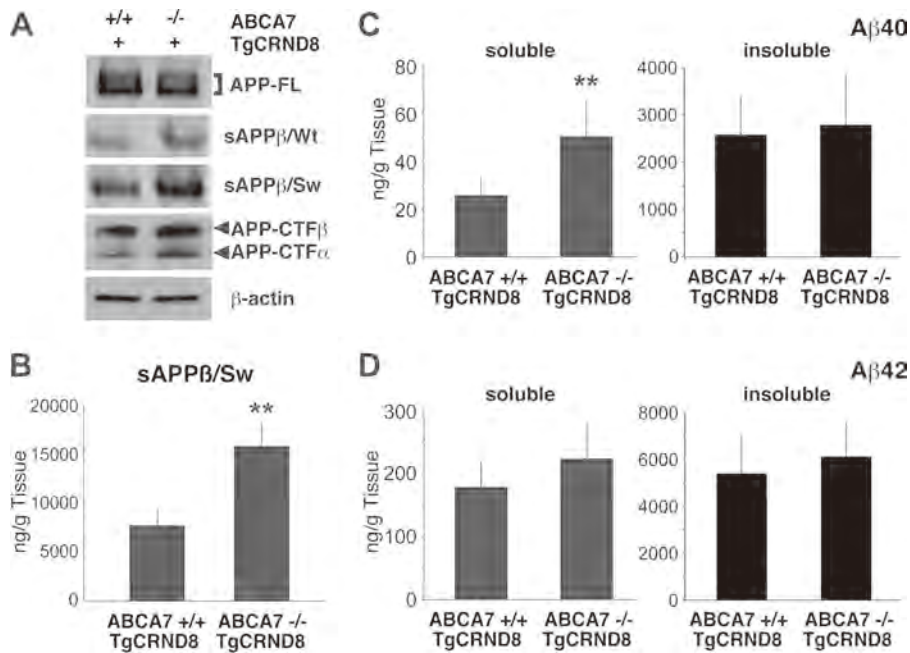


FIGURE 4. **Amyloid processing in APP transgenic mice lacking ABCA7.** *A*, the levels of APP-FL and -CTFs in TgCRND8 mice (18 weeks) and ABCA7 knock-out and TgCRND8 double transgenic mice (TgCRND8-ABCA7<sup>-/-</sup>; 18 weeks). *B*, total brain sAPPβ/Sw levels were increased by ~60% in the APP transgenic mice on the ABCA7 knock-out background as determined by ELISA. The data represent means ± S.D. (error bars) of six independent measurements. \*\*, *p* < 0.01 by Student's *t* test. *C* and *D*, soluble Aβ40 from total brain lysates was significantly increased in ABCA7 knock-out mice, whereas no changes in the insoluble form were observed (*C*). Comparable ELISA analysis indicated an increase in soluble Aβ42 and the plaque-associated insoluble species in the mice lacking ABCA7 but no significant differences (*D*). The data represent means ± S.D. (error bars) of 10–12 individual mice. \*, *p* < 0.01 by Student's *t* test.

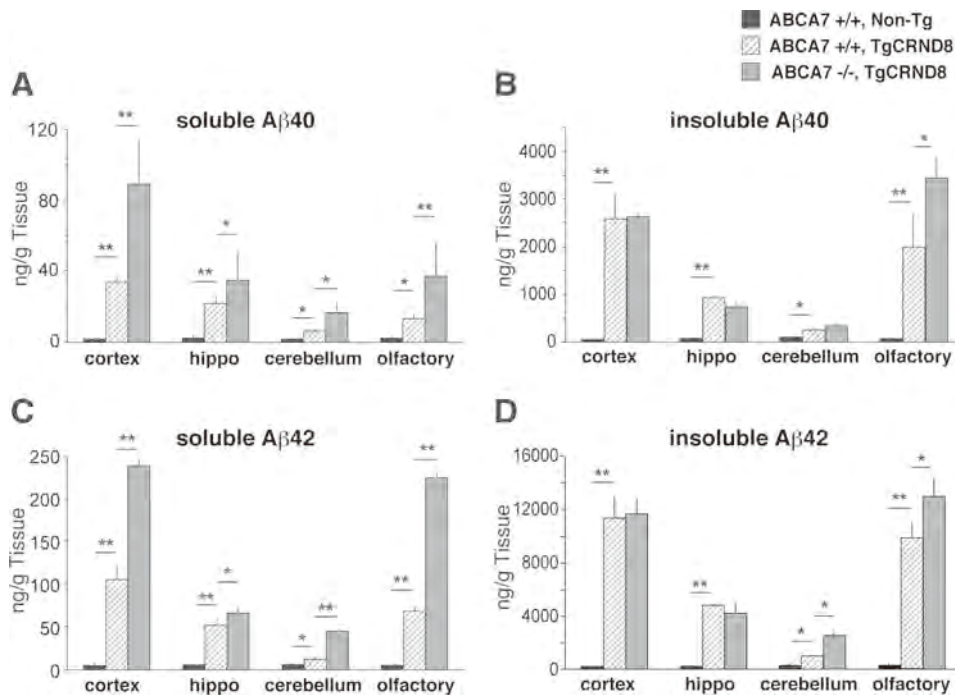


FIGURE 5. **Loss of ABCA7 increases soluble Aβ in all brain regions.** The levels of soluble and insoluble Aβ40 and Aβ42 were assessed in cerebral cortex (*cortex*), hippocampus (*hippo*), cerebellum, and the olfactory bulb (*olfactory*) for mice at 18 weeks of age by ELISA. The absolute amount of Aβ40 or Aβ42 varied in the different brain areas, but a consistent increase in the soluble species was observed. Similar to total brain extracts, the quantity of insoluble Aβ40 and Aβ42 was generally comparable between APP transgenic mice expressing endogenous ABCA7 and those on the knock-out background. However, increases in the insoluble Aβ40 and Aβ42 were observed in the olfactory bulb. The data represent means ± S.D. (error bars) of four individual mice. \*, *p* < 0.05; \*\*, *p* < 0.01 as determined by Tukey-Kramer test.

increases ~3-fold, and this is closely followed by the appearance of amyloid plaques (27).

Western blotting for APP indicated similar levels in TgCRND8 mice on both the ABCA7 wild-type and knock-out

backgrounds and models elevations in the β-secretase-cleaved protein (Fig. 7A). The increase in the secreted APPβ fragments was confirmed by ELISA, which is consistent with the observations in the older animals (Fig. 7B). As expected, quantification

ABCA7 and Amyloid Pathology

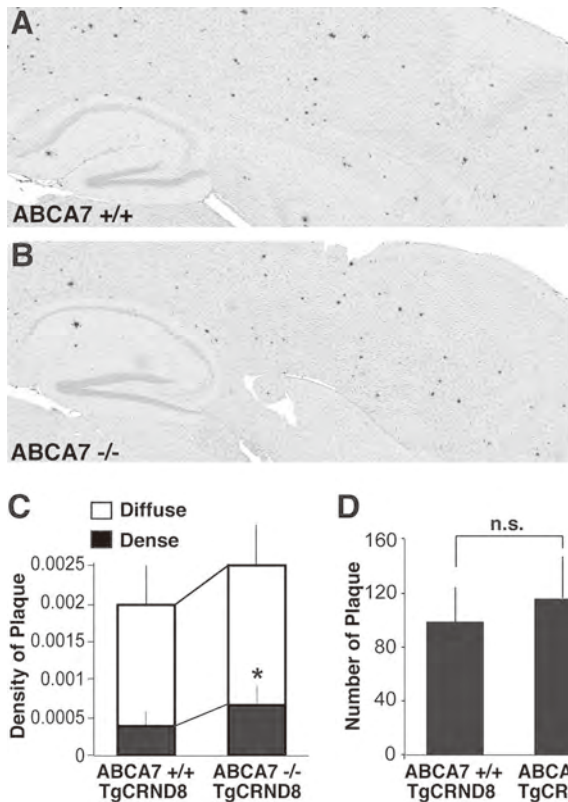


**FIGURE 6. Amyloid plaque density in APP transgenic mice lacking ABCA7.** Immunohistochemistry for total amyloid in APP transgenic mice (TgCRND8) on wild-type (+/+) and ablated ABCA7 (-/-) backgrounds. Representative images of diffuse and dense plaques in the cortex and hippocampus in TgCRND8 APP transgenic mice (A) and TgCRND8 mice deficient for ABCA7 (B) are shown. Amyloid plaques were quantified in scanned slides by deconvolution image analysis algorithms (ImageScope). C, the total area of dense plaques was found to be higher in the APP transgenic mice lacking ABCA7, but no significant differences were observed for diffuse plaques. D, total plaque numbers were not significantly different in the two mouse models at 18 weeks of age. The data represent means  $\pm$  S.D. (error bars) of six individual mice. \*,  $p < 0.05$ ; n.s., not significant by Student's *t* test.

of the A $\beta$  in whole brain extracts indicated that the levels were lower in the 10-week-old animals as compared with those at 18 weeks of age. However, soluble A $\beta$ 40 and A $\beta$ 42 were both lower in the TgCRND8-ABCA7<sup>-/-</sup> animals as compared with those expressing normal levels of ABCA7 (Fig. 7, C and E). In contrast, insoluble A $\beta$ 40 and particularly A $\beta$ 42 were significantly higher in the TgCRND8 transgenic mice lacking ABCA7 (Fig. 7, D and F). The level of insoluble A $\beta$ 42 in the TgCRND8-ABCA7<sup>+/+</sup> animals is consistent with previous reports where levels are ~300 ng/g of tissue (27). Transgenic mice lacking ABCA7 display greater than 600 ng/g insoluble A $\beta$ 42 (Fig. 7F). Immunohistochemistry for A $\beta$  was performed on serial sections from both groups of mice, and image analysis revealed a substantial increase in the density of both diffuse and dense plaques in the ABCA7 knock-out mice, which is consistent with the observed elevations in the insoluble A $\beta$  (Fig. 7G). In addition, increases in the total number of cortical and hippocampal plaques were found in TgCRND8-ABCA7<sup>-/-</sup> animals (Fig. 7H). The higher amounts of soluble A $\beta$  in the older animals indicated that ABCA7 loss of function results in enhanced APP cleavage and the generation of A $\beta$  peptides but not increased amyloid deposition. At the earlier 10-week stage, it appeared

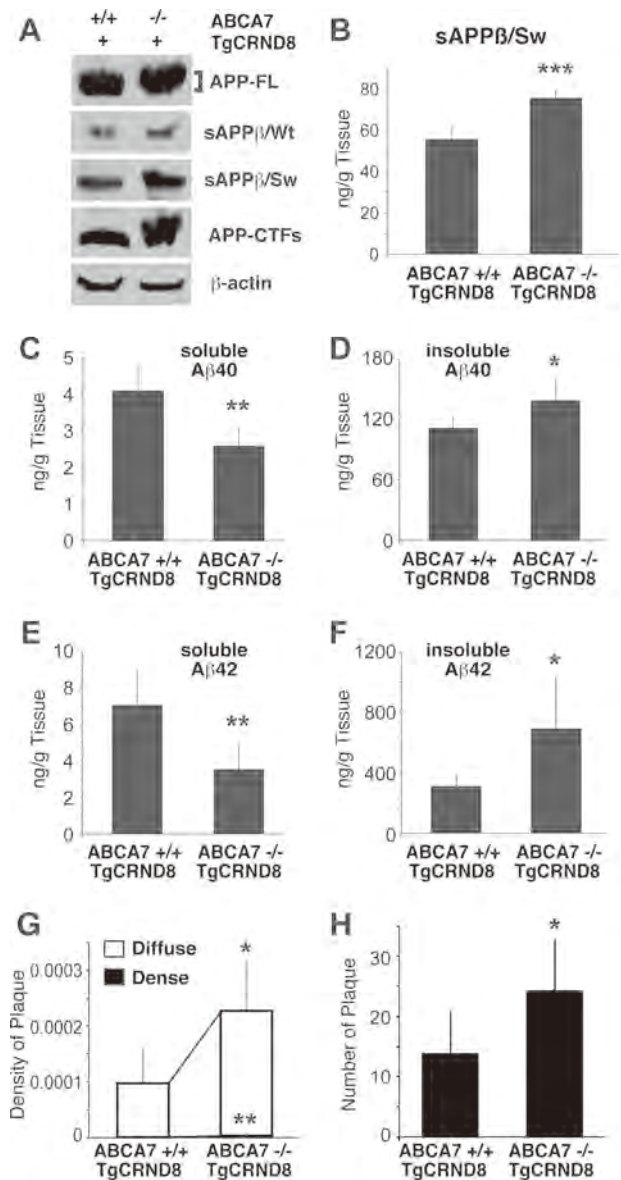


**FIGURE 7. Amyloid plaque density during early stages of pathology.** Quantitative analyses of APP species and A $\beta$  levels in 10-week-old APP transgenic mice (TgCRND8) on an ABCA7 knock-out (-/-) or wild-type (ABCA7<sup>+/+</sup>) background. A, Western blotting of total brain extracts for APP-FL,  $\beta$ -secretase-cleaved secreted APP for the endogenous mouse protein (sAPP $\beta$ /WT) and transgenic protein (sAPP $\beta$ /Sw), and APP-CTFs. B, increased  $\beta$ -cleavage of transgenic APP in ABCA7 knock-out mice was confirmed by ELISA. Total A $\beta$  levels were reduced as compared with 18-week-old mice, soluble A $\beta$ 40 was found to be lower in mice on the ABCA7<sup>-/-</sup> background (C), and insoluble A $\beta$ 40 was elevated in the same animals (D). Soluble A $\beta$ 42 was also decreased (E), and a comparable increase in insoluble deposited A $\beta$ 42 in ABCA7 knock-out animals (F) was seen. G, image analysis of A $\beta$  immunohistochemistry indicated a substantial increase in the density of diffuse plaques and detection of dense plaques in APP transgenic mice lacking ABCA7. H, increases in the total number of plaques were also observed in ABCA7<sup>-/-</sup> mice. The data represent means  $\pm$  S.D. (error bars) of six to 14 individual mice. \*,  $p < 0.05$ ; \*\*,  $p < 0.01$ ; \*\*\*,  $p < 0.001$  by Student's *t* test.

that the increased A $\beta$ 42 was aggregating rapidly and accumulating as amyloid plaques, which would account for the reduction in the soluble peptide. However, we cannot rule out the possibility that loss of ABCA7 in these animals may also have an impact on amyloid clearance.

*APP Endocytosis Is Enhanced in ABCA7 Knock-outs*—To explore potential mechanisms by which ABCA7 contributes to

## ABCA7 and Amyloid Pathology

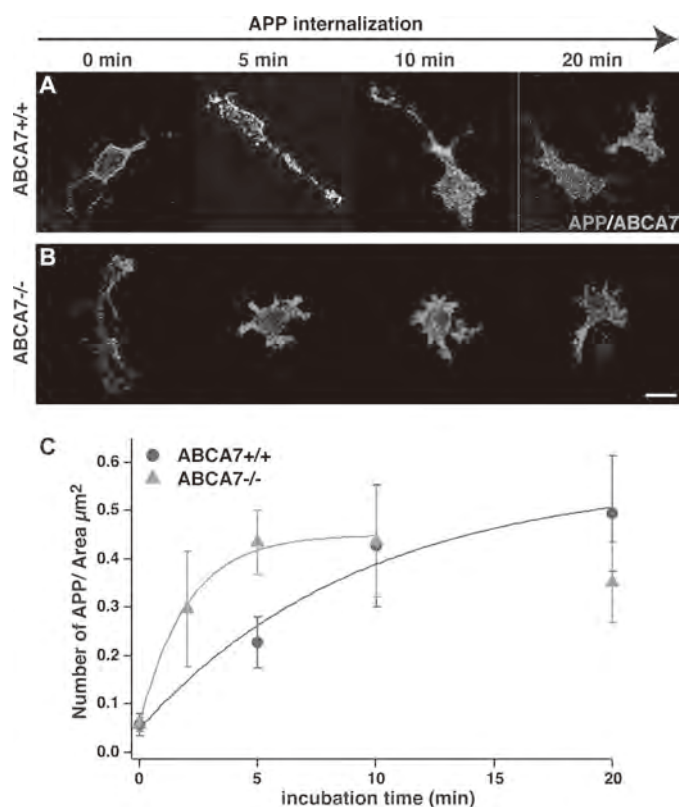


**FIGURE 8. Endocytosis of endogenous APP in ABCA7 knock-out cells.** Primary microglia cells from WT and ABCA7 knock-out mice were used to examine the rates of endocytosis for endogenous APP. Cell surface APP was labeled with 6E10 antibodies (red), and internalization was examined at 0, 5, 10, and 20 min. After fixation, cells were probed for endogenous ABCA7 (green). Cells expressing endogenous ABCA7 (ABCA7<sup>+/+</sup>) (A) displayed slower APP uptake of 15–20 min as compared with cells lacking ABCA7 (ABCA7<sup>-/-</sup>) (B), which exhibited APP endocytosis within the first 5 min of incubation. The scale bar represents 10 µm. C, quantitative analyses of APP internalization. The number of intracellular APPs was detected at each time point and divided by the area of the cells with Volocity. Data were fitted with exponential equation  $Y = y_0 + A \times \exp(-1/\text{Tau} \times X)$ .  $y_0$  of WT and knock-out (KO) are  $0.56891 \pm 0.13$  and  $0.44988 \pm 0.0207$ ,  $A$  of WT and KO are  $-0.52098 \pm 0.129$  and  $-0.39347 \pm 0.0287$ , and  $1/\text{Tau}$  of WT and KO are  $0.10604 \pm 0.0607$  and  $0.5003 \pm 0.0969$ , respectively (means  $\pm$  S.D.). The data represent means  $\pm$  S.D. (error bars).  $n = 13$ –24 in each group.

amyloid processing, the effects of loss of function on APP endocytosis were investigated. Primary microglia were isolated from wild-type and ABCA7 knock-out animals, and endogenous cell surface APP was labeled with monoclonal antibodies directed to the extracellular domain when cells were incubated at 4 °C (Fig. 8). Microglia were selected for this study as they express reasonable levels of both ABCA7 and APP (see Fig. 2) and have a morphology that makes them amenable to intracellular trafficking. Endocytosis was activated by bringing the cells to 37 °C, and internalization of the APP was monitored at different time points. After a 5-min incubation, the majority of the APP in wild-type cells was found at the surface and co-localized to some extent with plasma membrane ABCA7 (Fig. 8A). Some APP was internalized after 10 min, and progressively more cytoplasmic staining was observed at 20 min postincubation. In contrast, cells lacking ABCA7 exhibited a significant amount of intracellular APP after only 5 min of incubation (Fig. 8B). After 10 min, the majority of the endogenous APP was internalized, and similar staining was observed with longer incubations.

Quantitative analysis revealed that the velocity of APP internalization during the first 5 min for ABCA7<sup>-/-</sup> cells was significantly more rapid than the uptake observed in wild-type cells (Fig. 8C). It has been shown previously that APP is internalized over a short time frame of 15 min or less (34). To examine the internalized APP in more detail, cells were double labeled with the endosomal marker EEA1, which showed considerable overlap with APP as expected (Fig. 9A). In ABCA7 knock-out cells, a greater degree of co-localization of APP and endosomes was observed, which is consistent with the accelerated uptake upon loss of ABCA7 (Fig. 9B). Quantification of the immunofluorescence after 5 min of endocytosis revealed significant differences in the overlap of EEA1 and APP in ABCA7<sup>-/-</sup> cells as compared with wild type as a function of total endosomal staining or total APP (Fig. 9, C and D). These differences were not due to variations in the amounts of EEA1 or APP levels as these were observed to be the same in ABCA7<sup>-/-</sup> and wild-type cells (Fig. 9, E and F). Cumulatively, these findings indicate that the loss of ABCA7 results in a rapid uptake of APP to endosomal compartments, which would account for the increased A $\beta$  production seen both *in vitro* and *in vivo*.

### Discussion

The identification of ABCA7 as a susceptibility locus in recent genetic analyses has raised questions on how it may contribute to AD-related pathology and disease pathways. Our investigation examined the effects of ABCA7 on APP processing and A $\beta$  deposition as one of the early key events in AD. These *in vitro* and *in vivo* studies revealed that ABCA7 loss of function significantly increased APP proteolysis and A $\beta$  production. It is possible that changes in ABCA7 expression and/or activity may confer susceptibility through these aspects of the amyloid pathway. This would be consistent with recent studies that have demonstrated ABCA7 loss-of-function mutants and their association with increased risk for AD (35). In addition, changes in DNA methylation of several AD-related loci, including ABCA7, that correlated with amyloid load and neurofibrillary tangle density have been observed (36).

Knockdown of endogenous ABCA7 in HeLa cells resulted in an increase in sAPP $\beta$  processing of the endogenous protein indicative of increased amyloidogenic cleavage. This is in contrast to similar knockdown studies of various LOAD-related genes (e.g. BIN1, Clustrin, and CD33) where no effect on APP processing was observed, but ABCA7 was not examined in this particular investigation (37). In the current study, loss of ABCA7 in cells overexpressing APPS<sub>w</sub> resulted in increased  $\beta$ -cleavage products and A $\beta$  secretion. The A $\beta$ <sub>40</sub>:A $\beta$ <sub>42</sub> ratios for the TgCRND8-ABCA7<sup>-/-</sup> ( $0.439 \pm 0.173$ ) and TgCRND8-ABCA7<sup>+/+</sup> ( $0.533 \pm 0.286$ ) were comparable under these conditions, suggesting that there did not appear to be preferential  $\gamma$ -secretase cleavage at residue 42 versus 40. However, this was not the case for endogenous A $\beta$  in ABCA7 knock-out mice. In brain tissue of wild-type mice, ABCA7 was found to be slightly elevated during aging, and its deletion resulted in a gradual increase in A $\beta$ <sub>42</sub> over the 6-month period investigated. The difference in brain A $\beta$ <sub>42</sub> levels between wild-type and ABCA7 knock-outs was eliminated when animals were put on high fat diets, which have been shown previously to

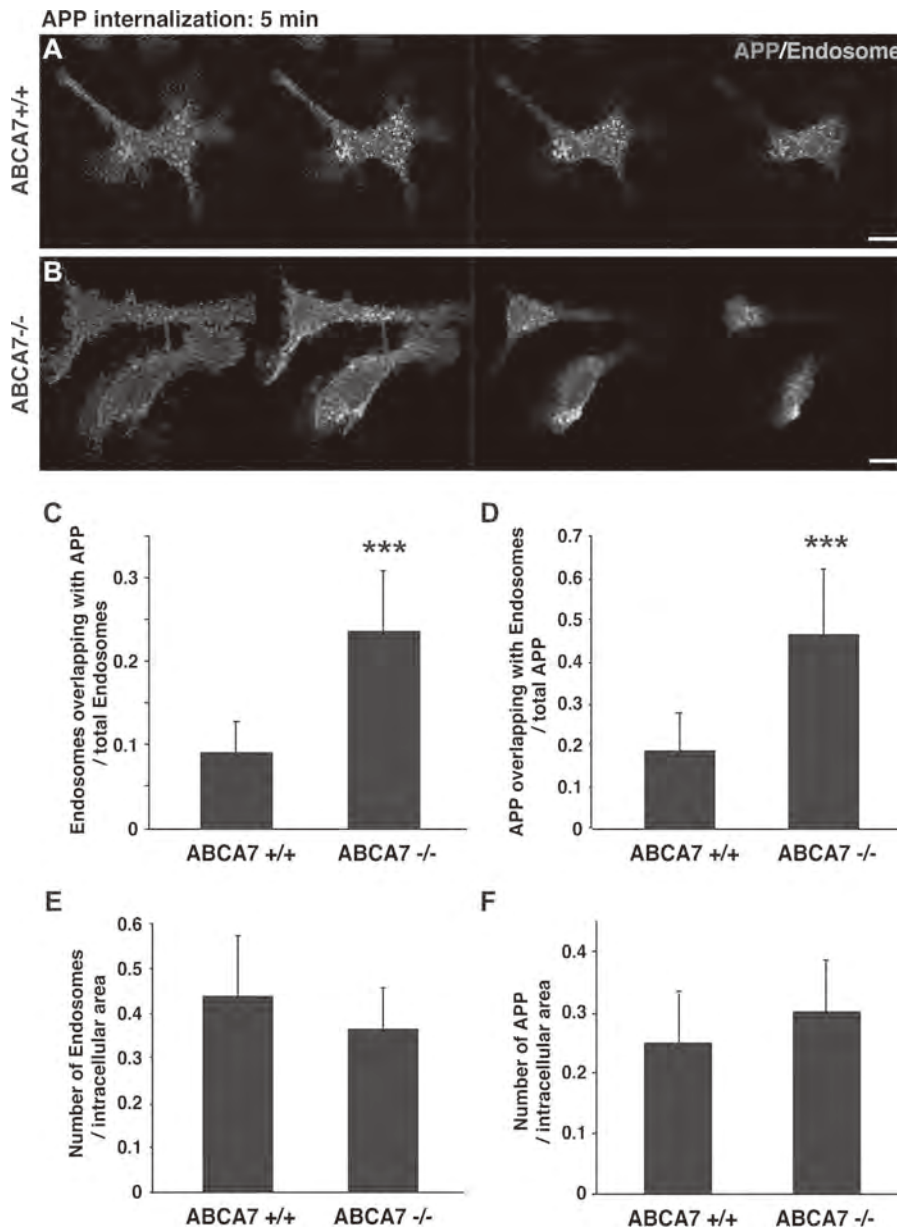


**FIGURE 9. Internalization of endogenous APP to endosomal compartments in ABCA7 knock-out cells.** Primary microglia cells from WT (A) and ABCA7 KO (B) mice were used to examine subcellular compartmentalization of APP and endosomes. After 5 min of APP endocytosis, more APP (red) overlapping with endosomes labeled with EEA1 antibodies (green) was observed in ABCA7 KO cells. The scale bars represent 10  $\mu$ m. C and D, quantitative analyses of subcellular compartmentalization for APP and endosomes. The number of subcellular endosomes overlapping with APP after 5 min of endocytosis was calculated and normalized with the total number of endosomes (C). The number of subcellular APPs overlapping with endosomes after 5 min of endocytosis was calculated and normalized with the total number of APPs (D). Endosomes overlapping with APPs and APPs overlapping with endosomes were significantly increased in ABCA7 KO cells as compared with wild-type cells. E and F, the numbers of subcellular endosomes and APPs in ABCA7 KO cells were comparable with those in WT cells. The data represent means  $\pm$  S.D. (error bars).  $n = 15$ . \*\*\*,  $p < 0.001$  by Student's  $t$  test.

up-regulate  $A\beta$  generation. Cumulatively, these findings indicate that ABCA7 has a direct impact on APP processing and  $\gamma$ -secretase. This may be mechanistically linked to the more rapid internalization and endosomal trafficking of APP that was observed for the ABCA7 knock-out cells.

It has been reported that mice lacking ABCA7 exhibit cognitive defects in the absence of any exogenous influences (38). A combination of behavioral tests was used to examine ABCA7 knock-out animals, and it was found that they had normal locomotion characteristics and fear conditioning-related memory and subtle differences in gender-specific impairments in some memory tasks. Only male knock-out mice exhibited impair-

ments in novel object recognition that was not observed in female knock-out mice (38). There are likely to be several pathways involved in the ABCA7 knock-out cognitive deficit, but it is of interest to note the increased  $A\beta_{42}$ , which may be a contributing factor as the animal ages. Additional studies, including the use of  $A\beta$  protease inhibitors, will be required to resolve these questions.

ABCA7 knock-out mice were crossed with an APP transgenic mouse, TgCRND8, to determine whether amyloid plaque levels and soluble  $A\beta$  were affected *in vivo*. We report here that examination of whole brain extracts revealed increases in soluble but not insoluble  $A\beta_{40}$  and  $A\beta_{42}$ . This observation is of

## ABCA7 and Amyloid Pathology

note because many prior studies have supported a role for soluble A $\beta$  oligomers in the synaptic and cognitive impairment during the early stages of AD (39–45). The conclusion that soluble A $\beta$  species are the relevant moiety in ABCA7 $^{-/-}$  mice is supported by plaque density quantification, which showed modest increases in the dense amyloid deposits (which are consistent with the observed increases in A $\beta$  production), but no statistical differences in overall number or size of diffuse plaques or total plaque counts were observed in the older transgenic mice (18 weeks of age).

In a recent study, ABCA7 knock-out mice were crossed to the J20 APP transgenic model of amyloid pathology (12). In contrast to our findings, J20-ABCA7 $^{-/-}$  mice had significantly increased insoluble A $\beta$  at the late stage of pathology development (17 months) but no obvious differences in the soluble peptides. The different observations may be due to the characteristics of the particular APP transgenic mice under investigation. The TgCRND8 transgenic mice are an aggressive model of AD amyloid pathology with plaque development at 3–4 months as compared with the 15–17-month time frame for the J20 model. The fact that we did not observe substantial changes in the insoluble A $\beta$  at 18 weeks in transgenic mouse models may be due to this rapid pace of pathology in the TgCRND8 mice that may potentially overwhelm clearance mechanisms.

Based on previous studies demonstrating significantly impaired phagocytosis in ABCA7 knock-out mice, it is quite feasible that ABCA7 does play a role in uptake and clearance of aggregated A $\beta$  plaques and aggregates (14, 18, 46, 47). This would be consistent with several other genome-wide association study candidates that have been shown to regulate microglial activity necessary for amyloid removal as opposed to APP processing and trafficking. For example, CD33 is elevated in AD tissue and was found to inhibit macrophage uptake of A $\beta$  in culture suggestive of impairments in phagocytosis (48). This was confirmed in CD33 knock-out mouse models crossed with APP transgenic mice that led to a substantial reduction in plaque density and levels of insoluble A $\beta$ . In addition, a recently identified risk factor, TREM2, is linked to neuroinflammation and complement-related pathways and has been suggested to be involved in A $\beta$  uptake (49, 50). However, our data indicate that ABCA7 also clearly has an impact on APP processing possibly through endocytosis-related pathways for which there are precedents with other AD at-risk genes.

SorLA (or Sorl1) for example is associated with LOAD, and changes in its expression have direct consequences for A $\beta$  production (51). SorLA regulates intracellular trafficking of APP and when expressed at high levels, similar to ABCA7, reduces A $\beta$  processing due to APP shuttling to endosomal and Golgi compartments (51, 52). SorLA-ablated mice when crossed to APP transgenic mice also have higher A $\beta$  levels (53). Another LOAD-related gene, PICALM, has been shown in some (54, 55) but not other studies (56) to regulate APP processing and amyloid deposition in the opposite direction. PICALM overexpression *in vitro* was found to increase A $\beta$ 40 and A $\beta$ 42 through a preferential endocytosis of APP and the active form of the  $\gamma$ -secretase complex. Similar effects were found *in vivo* using virally mediated expression that led to elevated soluble and insoluble A $\beta$ , whereas PICALM knockdown decreased both of these amyloid components (54).

A potential mechanism of action for ABCA7 can be envisioned along similar lines considering that ABCA7 co-localizes with LRP1 (18). It was observed that C1q-mediated enrichment of ABCA7 and LRP1 on the cell surface as well as membrane ruffles was markedly attenuated in hemizygous ABCA7 $^{+/-}$  macrophages, and this was associated with decreased phagocytic activity as compared with wild-type cells (18). LRP1 is also one of the principal regulators of APP endocytosis and subsequent A $\beta$  processing (for reviews, see Refs. 19 and 57). This is mediated by two phosphotyrosine binding domains in FE65 that interact with the NPXY motifs within LRP1 and APP to effectively link the two proteins (58). The resulting LRP1-APP binding results in a more rapid endocytosis of APP and A $\beta$  production (59, 60). It is therefore conceivable that disruptions in the ABCA7-LRP1 interaction lead to a dysregulation and enhancement of the LRP1-FE65-APP pathway to accelerate APP endocytosis that culminates in the observed increases in A $\beta$  production in the ABCA7 knock-out mice. This would be consistent with the observed increase in APP endocytosis in the primary mouse microglia cells lacking ABCA7. Comparable changes in APP processing for a related family member, ABCA2, that result from alterations in the trafficking of  $\gamma$ -secretase components, particularly nicastrin, have been observed (61).

Studies to date have presented two potential mechanisms by which ABCA7 may contribute to AD pathology that involve A $\beta$  production and/or clearance. Our current investigation supports an additional role for ABCA7 in APP processing leading to enhanced A $\beta$  secretion, which may be linked to endocytosis activity. Although we did not observe the same extent of plaque accumulation in our APP transgenic mouse model as was seen in other studies (12), our findings support a role for ABCA7-mediated amyloid processing that may be working in combination with amyloid removal as factors for ABCA7 at-risk allelic variants. Recent studies have led to the identification of multiple ABCA7 coding variants that may also result in loss of function (62, 63). It will be of considerable interest to determine the effects of these ABCA7 mutants on APP processing and A $\beta$  clearance. It is possible that ABCA7 may contribute to both pathways, and this study has focused on its impact on A $\beta$  production. The role of ABCA7, if any, in A $\beta$  removal is a key question and is the focus of separate future investigations.

*Author Contributions*—K. S. and P. E. F. coordinated the study and wrote the original version of the paper. K. S. acquired the data. K. S., S. A.-D., S. Y., P. S. G.-H., and P. E. F. made substantial contributions to the conception and design of the investigation as well as analysis and interpretation of the findings. All authors contributed to drafting the manuscript as well as revising it for clarity and intellectual contents.

*Acknowledgments*—We are very grateful for the supply of ABCA7 monoclonal antibody from Kyowa Hakko Kirin Co. Ltd. We also thank Rosemary Ahrens, Monika Duthie, Kathy Ha, and Kyung Han for invaluable technical assistance; Dr. Lili-Naz Hazrati for assistance with the amyloid immunohistochemistry; and Dr. Jennifer Griffin for assistance with primary cultures.

## References

- Hollingsworth, P., Harold, D., Sims, R., Gerrish, A., Lambert, J.-C., Carrasquillo, M. M., Abraham, R., Hamshe, M. L., Pahwa, J. S., Moskva, V., Dowzell, K., Jones, N., Stretton, A., Thomas, C., Richards, A., Ivanov, D., Widdowson, C., Chapman, J., Lovestone, S., Powell, J., Proitsi, P., Lupton, M. K., Brayne, C., Rubinsztein, D. C., Gill, M., Lawlor, B., Lynch, A., Brown, K. S., Passmore, P. A., Craig, D., McGuinness, B., Todd, S., Holmes, C., Mann, D., Smith, A. D., Beaumont, H., Warden, D., Wilcock, G., Love, S., Kehoe, P. G., Hooper, N. M., Vardy, E. R., Hardy, J., Mead, S., Fox, N. C., Rossor, M., Collinge, J., Maier, W., Jessen, F., Rüther, E., Schürmann, B., Heun, R., Kölsch, H., Van Den Bussche, H., Heuser, I., Kornhuber, J., Wiltfang, J., Dichgans, M., Frölich, L., Hampel, H., Gallacher, J., Hüll, M., Rujescu, D., Giegling, I., Goate, A. M., Kauwe, J. S., Cruchaga, C., Nowotny, P., Morris, J. C., Mayo, K., Sleegers, K., Bettens, K., Engelborghs, S., De Deyn, P. P., Van Broeckhoven, C., Livingston, G., Bass, N. J., Gurling, H., McQuillin, A., Gwilliam, R., Deloukas, P., Al-Chalabi, A., Shaw, C. E., Tsolaki, M., Singleton, A. B., Guerreiro, R., Mühleisen, T. W., Nöthen, M. M., Moebus, S., Jöckel, K.-H., Klopp, N., Wichmann, H.-E., Pankratz, V. S., Sando, S. B., Aasly, J. O., Barcikowska, M., Wszolek, Z. K., Dickson, D. W., Graff-Radford, N. R., Petersen, R. C., Van Duijn, C. M., Breteler, M. M., Ikram, M. A., Destefano, A. L., Fitzpatrick, A. L., Lopez, O., Launer, L. J., Seshadri, S., Berr, C., Campion, D., Epelbaum, J., Dartigues, J.-F., Tzourio, C., Alperovitch, A., Lathrop, M., Feulner, T. M., Friedrich, P., Riehle, C., Krawczak, M., Schreiber, S., Mayhaus, M., Nicolhaus, S., Wagenpfeil, S., Steinberg, S., Stefansson, H., Stefansson, K., Snædal, J., Björnsson, S., Jonsson, P. V., Chouraki, V., Genier-Boley, B., Hiltunen, M., Soininen, H., Combarros, O., Zelenika, D., Delepine, M., Bullido, M. J., Pasquier, F., Mateo, I., Frank-Garcia, A., Porcellini, E., Hanon, O., Coto, E., Alvarez, V., Bosco, P., Siciliano, G., Mancuso, M., Panza, F., Solfrizzi, V., Nacmias, B., Sorbi, S., Bossù, P., Piccardi, P., Arosio, B., Annoni, G., Seripa, D., Pilotto, A., Scarpini, E., Galimberti, D., Brice, A., Hannequin, D., Licastrò, F., Jones, L., Holmans, P. A., Jonsson, T., Riemenschneider, M., Morgan, K., Younkin, S. G., Owen, M. J., O'Donovan, M., Amouyel, P., and Williams, J. (2011) Common variants at *ABCA7*, *MS4A6A/MS4A4E*, *EPHA1*, *CD33* and *CD2AP* are associated with Alzheimer's disease. *Nat. Genet.* **43**, 429–435
- Naj, A. C., Jun, G., Beecham, G. W., Wang, L.-S., Vardarajan, B. N., Buross, J., Gallins, P. J., Buxbaum, J. D., Jarvik, G. P., Crane, P. K., Larson, E. B., Bird, T. D., Boeve, B. F., Graff-Radford, N. R., De Jager, P. L., Evans, D., Schneider, J. A., Carrasquillo, M. M., Ertekin-Taner, N., Younkin, S. G., Cruchaga, C., Kauwe, J. S., Nowotny, P., Kramer, P., Hardy, J., Huentelman, M. J., Myers, A. J., Barmada, M. M., Demirci, F. Y., Baldwin, C. T., Green, R. C., Rogava, E., St George-Hyslop, P., Arnold, S. E., Barber, R., Beach, T., Bigio, E. H., Bowen, J. D., Boxer, A., Burke, J. R., Cairns, N. J., Carlson, C. S., Carney, R. M., Carroll, S. L., Chui, H. C., Clark, D. G., Corneveaux, J., Cotman, C. W., Cummings, J. L., DeCarli, C., DeKosky, S. T., Diaz-Arrastia, R., Dick, M., Dickson, D. W., Ellis, W. G., Faber, K. M., Fallon, K. B., Farlow, M. R., Ferris, S., Frosch, M. P., Galasko, D. R., Ganguli, M., Gearing, M., Geschwind, D. H., Ghetti, B., Gilbert, J. R., Gilman, S., Giordani, B., Glass, J. D., Growdon, J. H., Hamilton, R. L., Harrell, L. E., Head, E., Honig, L. S., Hulette, C. M., Hyman, B. T., Jicha, G. A., Jin, L.-W., Johnson, N., Karlawish, J., Karydas, A., Kaye, J. A., Kim, R., Koo, E. H., Kowall, N. W., Lah, J. J., Levey, A. I., Lieberman, A. P., Lopez, O. L., MacK, W. J., Marson, D. C., Martiniuk, F., Mash, D. C., Masliah, E., McCormick, W. C., McCurry, S. M., McDavid, A. N., McKee, A. C., Mesulam, M., Miller, B. L., Miller, C. A., Miller, J. W., Parisi, J. E., Perl, D. P., Peskind, E., Petersen, R. C., Poon, W. W., Quinn, J. F., Rajbhandary, R. A., Raskind, M., Reisberg, B., Ringman, J. M., Roberson, E. D., Rosenberg, R. N., Sano, M., Schneider, L. S., Seeley, W., Shelanski, M. L., Slifer, M. A., Smith, C. D., Sonnen, J. A., Spina, S., Stern, R. A., Tanzi, R. E., Trojanowski, J. Q., Troncoso, J. C., Van Deerlin, V. M., Vinters, H. V., Vonsattel, J. P., Weintraub, S., Welsh-Bohmer, K. A., Williamson, J., Woltjer, R. L., Cantwell, L. B., Dombroski, B. A., Beekly, D., Lunetta, K. L., Martin, E. R., Kamboh, M. I., Saykin, A. J., Reiman, E. M., Bennett, D. A., Morris, J. C., Montine, T. J., Goate, A. M., Blacker, D., Tsuang, D. W., Hakonarson, H., Kukull, W. A., Foroud, T. M., Haines, J. L., Mayeux, R., Pericak-Vance, M. A., Farrer, L. A., and Schellenberg, G. D. (2011) Common variants at *MS4A4/MS4A6E*, *CD2AP*, *CD33* and *EPHA1* are associated with late-onset Alzheimer's disease. *Nat. Genet.* **43**, 436–441
- Reitz, C., Jun, G., Naj, A., Rajbhandary, R., Vardarajan, B. N., Wang, L.-S., Valladares, O., Lin, C.-F., Larson, E. B., Graff-Radford, N. R., Evans, D., De Jager, P. L., Crane, P. K., Buxbaum, J. D., Murrell, J. R., Raj, T., Ertekin-Taner, N., Logue, M., Baldwin, C. T., Green, R. C., Barnes, L. L., Cantwell, L. B., Fallin, M. D., Go, R. C., Griffith, P., Obisesan, T. O., Manly, J. J., Lunetta, K. L., Kamboh, M. I., Lopez, O. L., Bennett, D. A., Hendrie, H., Hall, K. S., Goate, A. M., Byrd, G. S., Kukull, W. A., Foroud, T. M., Haines, J. L., Farrer, L. A., Pericak-Vance, M. A., Schellenberg, G. D., Mayeux, R., and Alzheimer Disease Genetics Consortium (2013) Variants in the ATP-binding cassette transporter (*ABCA7*), apolipoprotein e  $\epsilon 4$ , and the risk of late-onset Alzheimer disease in African Americans. *JAMA* **309**, 1483–1492
- Pohl, A., Devaux, P. F., and Herrmann, A. (2005) Function of prokaryotic and eukaryotic ABC proteins in lipid transport. *Biochim. Biophys. Acta* **1733**, 29–52
- Wahrle, S. E., Jiang, H., Parsadanian, M., Hartman, R. E., Bales, K. R., Paul, S. M., and Holtzman, D. M. (2005) Deletion of *Abca1* increases  $A\beta$  deposition in the PDAPP transgenic mouse model of Alzheimer disease. *J. Biol. Chem.* **280**, 43236–43242
- Wahrle, S. E., Jiang, H., Parsadanian, M., Kim, J., Li, A., Knoten, A., Jain, S., Hirsch-Reinshagen, V., Wellington, C. L., Bales, K. R., Paul, S. M., and Holtzman, D. M. (2008) Overexpression of *ABCA1* reduces amyloid deposition in the PDAPP mouse model of Alzheimer disease. *J. Clin. Investig.* **118**, 671–682
- Koldamova, R., Staufienbiel, M., and Lefterov, I. (2005) Lack of *ABCA1* considerably decreases brain ApoE level and increases amyloid deposition in APP23 mice. *J. Biol. Chem.* **280**, 43224–43235
- Chan, S. L., Kim, W. S., Kwok, J. B., Hill, A. F., Cappai, R., Rye, K.-A., and Garner, B. (2008) ATP-binding cassette transporter A7 regulates processing of amyloid precursor protein in vitro. *J. Neurochem.* **106**, 793–804
- Abe-Dohmae, S., Ikeda, Y., Matsuo, M., Hayashi, M., Okuhira, K., Ueda, K., and Yokoyama, S. (2004) Human *ABCA7* supports apolipoprotein-mediated release of cellular cholesterol and phospholipid to generate high density lipoprotein. *J. Biol. Chem.* **279**, 604–611
- Hayashi, M., Abe-Dohmae, S., Okazaki, M., Ueda, K., and Yokoyama, S. (2005) Heterogeneity of high density lipoprotein generated by *ABCA1* and *ABCA7*. *J. Lipid Res.* **46**, 1703–1711
- Wang, N., Lan, D., Gerbod-Giannone, M., Linsel-Nitschke, P., Jehle, A. W., Chen, W., Martinez, L. O., and Tall, A. R. (2003) ATP-binding cassette transporter A7 (*ABCA7*) binds apolipoprotein A-I and mediates cellular phospholipid but not cholesterol efflux. *J. Biol. Chem.* **278**, 42906–42912
- Kim, W. S., Li, H., Ruberu, K., Chan, S., Elliott, D. A., Low, J. K., Cheng, D., Karl, T., and Garner, B. (2013) Deletion of *Abca7* increases cerebral amyloid- $\beta$  accumulation in the J20 mouse model of Alzheimer's disease. *J. Neurosci.* **33**, 4387–4394
- Linsel-Nitschke, P., Jehle, A. W., Shan, J., Cao, G., Bacic, D., Lan, D., Wang, N., and Tall, A. R. (2005) Potential role of *ABCA7* in cellular lipid efflux to apoA-I. *J. Lipid Res.* **46**, 86–92
- Iwamoto, N., Abe-Dohmae, S., Sato, R., and Yokoyama, S. (2006) *ABCA7* expression is regulated by cellular cholesterol through the SREBP2 pathway and associated with phagocytosis. *J. Lipid Res.* **47**, 1915–1927
- Tanaka, N., Abe-Dohmae, S., Iwamoto, N., and Yokoyama, S. (2011) Roles of ATP-binding cassette transporter A7 in cholesterol homeostasis and host defense system. *J. Atheroscler. Thromb.* **18**, 274–281
- Abe-Dohmae, S., and Yokoyama, S. (2012) *ABCA7*: a potential mediator between cholesterol homeostasis and the host defense system. *Clin. Lipidol.* **7**, 677–687
- Soscia, S. J., and Fitzgerald, M. L. (2013) The *ABCA7* transporter, brain lipids and Alzheimer's disease. *Clin. Lipidol.* **8**, 97–108
- Jehle, A. W., Gardai, S. J., Li, S., Linsel-Nitschke, P., Morimoto, K., Janssen, W. J., Vandivier, R. W., Wang, N., Greenberg, S., Dale, B. M., Qin, C., Henson, P. M., and Tall, A. R. (2006) ATP-binding cassette transporter A7 enhances phagocytosis of apoptotic cells and associated ERK signaling in macrophages. *J. Cell Biol.* **174**, 547–556
- Jaeger, S., and Pietrzik, C. U. (2008) Functional role of lipoprotein recep-

## ABCA7 and Amyloid Pathology

- tors in Alzheimer's disease. *Curr. Alzheimer Res.* **5**, 15–25
20. Bu, G., Cam, J., and Zerbinatti, C. (2006) LRP in amyloid- $\beta$  production and metabolism. *Ann. N.Y. Acad. Sci.* **1086**, 35–53
  21. Tanaka, A. R., Ikeda, Y., Abe-Dohmae, S., Arakawa, R., Sadanami, K., Kidera, A., Nakagawa, S., Nagase, T., Aoki, R., Kioka, N., Amachi, T., Yokoyama, S., and Ueda, K. (2001) Human ABCA1 contains a large amino-terminal extracellular domain homologous to an epitope of Sjögren's Syndrome. *Biochem. Biophys. Res. Commun.* **283**, 1019–1025
  22. Cole, R., and de Vellis, J. (2001) in *Protocols for Neural Cell Culture* (Fedoroff, S., and Richardson, A., eds) 3rd Ed., pp. 117–127, Humana Press, Totowa, NJ
  23. Hertz, L., Juurlink, B. H. J., Fosmark, H., and Schousboe, A. (1982) in *Neuroscience Approached Through Cell Culture* (Pfeiffer, S. E., ed) Vol. 1, pp. 175–186, CRC Press Boca Raton, FL
  24. Zhou, Y., Li, H. L., Zhao, R., Yang, L. T., Dong, Y., Yue, X., Ma, Y. Y., Wang, Z., Chen, J., Cui, C. L., and Yu, A. C. (2010) Astrocytes express N-methyl-D-aspartate receptor subunits in development, ischemia and post-ischemia. *Neurochem. Res.* **35**, 2124–2134
  25. Saura, J., Tusell, J. M., and Serratos, J. (2003) High-yield isolation of murine microglia by mild trypsinization. *GLIA* **44**, 183–189
  26. Jiang, Y., Mullaney, K. A., Peterhoff, C. M., Che, S., Schmidt, S. D., Boyer-Boiteau, A., Ginsberg, S. D., Cataldo, A. M., Mathews, P. M., and Nixon, R. A. (2010) Alzheimer's-related endosome dysfunction in Down syndrome is A $\beta$ -independent but requires APP and is reversed by BACE-1 inhibition. *Proc. Natl. Acad. Sci. U.S.A.* **107**, 1630–1635
  27. Chishti, M. A., Yang, D.-S., Janus, C., Phinney, A. L., Horne, P., Pearson, J., Strome, R., Zuker, N., Loukides, J., French, J., Turner, S., Lozza, G., Grilli, M., Kunicki, S., Morissette, C., Paquette, J., Gervais, F., Bergeron, C., Fraser, P. E., Carlson, G. A., St George-Hyslop, P., and Westaway, D. (2001) Early-onset amyloid deposition and cognitive deficits in transgenic mice expressing a double mutant form of amyloid precursor protein 695. *J. Biol. Chem.* **276**, 21562–21570
  28. Kim, W. S., Fitzgerald, M. L., Kang, K., Okuhira, K., Bell, S. A., Manning, J. J., Koehn, S. L., Lu, N., Moore, K. J., and Freeman, M. W. (2005) ABCA7 null mice retain normal macrophage phosphatidylcholine and cholesterol efflux activity despite alterations in adipose mass and serum cholesterol levels. *J. Biol. Chem.* **280**, 3989–3995
  29. Janus, C., Pearson, J., McLaurin, J., Mathews, P. M., Jiang, Y., Schmidt, S. D., Chishti, M. A., Horne, P., Heslin, D., French, J., Mount, H. T., Nixon, R. A., Mercken, M., Bergeron, C., Fraser, P. E., St George-Hyslop, P., and Westaway, D. (2000) A $\beta$  peptide immunization reduces behavioural impairment and plaques in a model of Alzheimer's disease. *Nature* **408**, 979–982
  30. Bachstetter, A. D., Norris, C. M., Sompol, P., Wilcock, D. M., Goulding, D., Neltner, J. H., St Clair, D., Watterson, D. M., and Van Eldik, L. J. (2012) Early stage drug treatment that normalizes proinflammatory cytokine production attenuates synaptic dysfunction in a mouse model that exhibits age-dependent progression of Alzheimer's disease-related pathology. *J. Neurosci.* **32**, 10201–10210
  31. Durk, M. R., Han, K., Chow, E. C., Ahrens, R., Henderson, J. T., Fraser, P. E., and Pang, K. S. (2014) 1 $\alpha$ ,25-Dihydroxyvitamin D3 reduces cerebral amyloid- $\beta$  accumulation and improves cognition in mouse models of Alzheimer's disease. *J. Neurosci.* **34**, 7091–7101
  32. Walter, J. (2012)  $\gamma$ -Secretase, apolipoprotein E and cellular cholesterol metabolism. *Curr. Alzheimer Res.* **9**, 189–199
  33. Tremblay, P., Bouzamondo-Bernstein, E., Heinrich, C., Prusiner, S. B., and DeArmond, S. J. (2007) Developmental expression of PrP in the post-implantation embryo. *Brain Res.* **1139**, 60–67
  34. Kinoshita, A., Fukumoto, H., Shah, T., Whelan, C. M., Irizarry, M. C., and Hyman, B. T. (2003) Demonstration by FRET of BACE interaction with the amyloid precursor protein at the cell surface and in early endosomes. *J. Cell Sci.* **116**, 3339–3346
  35. Steinberg, S., Stefansson, H., Jonsson, T., Johannsdottir, H., Ingason, A., Helgason, H., Sulem, P., Magnusson, O. T., Gudjonsson, S. A., Unnsteinsdottir, U., Kong, A., Helisalmi, S., Soininen, H., Lah, J. J., DemGene, Aarsland, D., Fladby, T., Ulstein, I. D., Djurovic, S., Sando, S. B., White, L. R., Knudsen, G.-P., Westlye, L. T., Selbaek, G., Giegling, I., Hampel, H., Hiltunen, M., Levey, A. I., Andreassen, O. A., Rujescu, D., Jonsson, P. V., Bjornsson, S., Snaedal, J., and Stefansson, K. (2015) Loss-of-function variants in ABCA7 confer risk of Alzheimer's disease. *Nat. Genet.* **47**, 445–447
  36. Yu, L., Chibnik, L. B., Srivastava, G. P., Pochet, N., Yang, J., Xu, J., Kozubek, J., Obholzer, N., Leurgans, S. E., Schneider, J. A., Meissner, A., De Jager, P. L., and Bennett, D. A. (2015) Association of brain DNA methylation in *SORL1*, *ABCA7*, *HLA-DRB5*, *SLC24A4*, and *BIN1* with pathological diagnosis of Alzheimer disease. *JAMA Neurol.* **72**, 15–24
  37. Bali, J., Gheini, A. H., Zurbruggen, S., and Rajendran, L. (2012) Role of genes linked to sporadic Alzheimer's disease risk in the production of  $\beta$ -amyloid peptides. *Proc. Natl. Acad. Sci. U.S.A.* **109**, 15307–15311
  38. Logge, W., Cheng, D., Chesworth, R., Bhatia, S., Garner, B., Kim, W. S., and Karl, T. (2012) Role of Abca7 in mouse behaviours relevant to neurodegenerative diseases. *PLoS One* **7**, e45959
  39. Lue, L. F., Kuo, Y. M., Roher, A. E., Brachova, L., Shen, Y., Sue, L., Beach, T., Kurth, J. H., Rydel, R. E., and Rogers, J. (1999) Soluble amyloid  $\beta$  peptide concentration as a predictor of synaptic change in Alzheimer's disease. *Am. J. Pathol.* **155**, 853–862
  40. Klein, W. L., Krafft, G. A., and Finch, C. E. (2001) Targeting small A $\beta$  oligomers: the solution to an Alzheimer's disease conundrum? *Trends Neurosci.* **24**, 219–224
  41. Selkoe, D. J. (2002) Alzheimer's disease is a synaptic failure. *Science* **298**, 789–791
  42. Gong, Y., Chang, L., Viola, K. L., Lacor, P. N., Lambert, M. P., Finch, C. E., Krafft, G. A., and Klein, W. L. (2003) Alzheimer's disease-affected brain: presence of oligomeric A $\beta$  ligands (ADDLs) suggests a molecular basis for reversible memory loss. *Proc. Natl. Acad. Sci. U.S.A.* **100**, 10417–10422
  43. Lesné, S., Koh, M. T., Kotilinek, L., Kaye, R., Glabe, C. G., Yang, A., Gallagher, M., and Ashe, K. H. (2006) A specific amyloid- $\beta$  protein assembly in the brain impairs memory. *Nature* **440**, 352–357
  44. Lacor, P. N., Buniel, M. C., Furlow, P. W., Clemente, A. S., Velasco, P. T., Wood, M., Viola, K. L., and Klein, W. L. (2007) A $\beta$  oligomer-induced aberrations in synapse composition, shape, and density provide a molecular basis for loss of connectivity in Alzheimer's disease. *J. Neurosci.* **27**, 796–807
  45. Tomiyama, T., Matsuyama, S., Iso, H., Umeda, T., Takuma, H., Ohnishi, K., Ishibashi, K., Teraoka, R., Sakama, N., Yamashita, T., Nishitsuji, K., Ito, K., Shimada, H., Lambert, M. P., Klein, W. L., and Mori, H. (2010) A mouse model of amyloid  $\beta$  oligomers: their contribution to synaptic alteration, abnormal tau phosphorylation, glial activation, and neuronal loss *in vivo*. *J. Neurosci.* **30**, 4845–4856
  46. Tanaka, N., Abe-Dohmae, S., Iwamoto, N., Fitzgerald, M. L., and Yokoyama, S. (2010) Helical apolipoproteins of high-density lipoprotein enhance phagocytosis by stabilizing ATP-binding cassette transporter A7. *J. Lipid Res.* **51**, 2591–2599
  47. Tanaka, N., Abe-Dohmae, S., Iwamoto, N., Fitzgerald, M. L., and Yokoyama, S. (2011) HMG-CoA reductase inhibitors enhance phagocytosis by upregulating ATP-binding cassette transporter A7. *Atherosclerosis* **217**, 407–414
  48. Griciuc, A., Serrano-Pozo, A., Parrado, A. R., Lesinski, A. N., Asselin, C. N., Mullin, K., Hooli, B., Choi, S. H., Hyman, B. T., and Tanzi, R. E. (2013) Alzheimer's disease risk gene CD33 inhibits microglial uptake of amyloid  $\beta$ . *Neuron* **78**, 631–643
  49. Guerreiro, R., Wojtas, A., Bras, J., Carrasquillo, M., Rogaeva, E., Majounie, E., Cruchaga, C., Sassi, C., Kauwe, J. S., Younkin, S., Hazrati, L., Collinge, J., Pocock, J., Lashley, T., Williams, J., Lambert, J. C., Amouyel, P., Goate, A., Rademakers, R., Morgan, K., Powell, J., St George-Hyslop, P., Singleton, A., Hardy, J., and Alzheimer Genetic Analysis Group (2013) TREM2 variants in Alzheimer's disease. *New Engl. J. Med.* **368**, 117–127
  50. Jonsson, T., Stefansson, H., Steinberg, S., Jonsdottir, I., Jonsson, P. V., Snaedal, J., Bjornsson, S., Huttenlocher, J., Levey, A. I., Lah, J. J., Rujescu, D., Hampel, H., Giegling, I., Andreassen, O. A., Engedal, K., Ulstein, I., Djurovic, S., Ibrahim-Verbaas, C., Hofman, A., Ikram, M. A., van Duijn, C. M., Thorsteinsdottir, U., Kong, A., and Stefansson, K. (2013) Variant of TREM2 associated with the risk of Alzheimer's disease. *New Eng. J. Med.* **368**, 107–116
  51. Rogaeva, E., Meng, Y., Lee, J. H., Gu, Y., Kawarai, T., Zou, F., Katayama, T., Baldwin, C. T., Cheng, R., Hasegawa, H., Chen, F., Shibata, N., Lunetta, K. L., Pardossi-Piquard, R., Bohm, C., Wakutani, Y., Cupples, L. A.,

- Cuenco, K. T., Green, R. C., Pinessi, L., Rainero, I., Sorbi, S., Bruni, A., Duara, R., Friedland, R. P., Inzelberg, R., Hampe, W., Bujo, H., Song, Y. Q., Andersen, O. M., Willnow, T. E., Graff-Radford, N., Petersen, R. C., Dickson, D., Der, S. D., Fraser, P. E., Schmitt-Ulms, G., Younkin, S., Mayeux, R., Farrer, L. A., and St George-Hyslop, P. (2007) The neuronal sortilin-related receptor SORL1 is genetically associated with Alzheimer disease. *Nat. Genet.* **39**, 168–177
52. Andersen, O. M., Reiche, J., Schmidt, V., Gotthardt, M., Spoelgen, R., Behlke, J., von Arnim, C. A., Breiderhoff, T., Jansen, P., Wu, X., Bales, K. R., Cappai, R., Masters, C. L., Gliemann, J., Mufson, E. J., Hyman, B. T., Paul, S. M., Nykjaer, A., and Willnow, T. E. (2005) Neuronal sorting protein-related receptor sorLA/LR11 regulates processing of the amyloid precursor protein. *Proc. Natl. Acad. Sci. U.S.A.* **102**, 13461–13466
  53. Dodson, S. E., Andersen, O. M., Karmali, V., Fritz, J. J., Cheng, D., Peng, J., Levey, A. I., Willnow, T. E., and Lah, J. J. (2008) Loss of LR11/SORLA enhances early pathology in a mouse model of amyloidosis: evidence for a proximal role in Alzheimer's disease. *J. Neurosci.* **28**, 12877–12886
  54. Xiao, Q., Gil, S.-C., Yan, P., Wang, Y., Han, S., Gonzales, E., Perez, R., Cirrito, J. R., and Lee, J.-M. (2012) Role of phosphatidylinositol clathrin assembly lymphoid-myeloid leukemia (PICALM) in intracellular amyloid precursor protein (APP) processing and amyloid plaque pathogenesis. *J. Biol. Chem.* **287**, 21279–21289
  55. Kanatsu, K., Morohashi, Y., Suzuki, M., Kuroda, H., Watanabe, T., Tomita, T., and Iwatsubo, T. (2014) Decreased CALM expression reduces A $\beta$ 42 to total A $\beta$  ratio through clathrin-mediated endocytosis of  $\gamma$ -secretase. *Nat. Commun.* **5**, 3386
  56. Wu, F., Matsuoaka, Y., Mattson, M. P., and Yao, P. J. (2009) The clathrin assembly protein AP180 regulates the generation of amyloid- $\beta$  peptide. *Biochem. Biophys. Res. Commun.* **385**, 247–250
  57. Bu, G. (2009) Apolipoprotein E and its receptors in Alzheimer's disease: pathways, pathogenesis and therapy. *Nat. Rev. Neurosci.* **10**, 333–344
  58. Pietrzik, C. U., Yoon, I.-S., Jaeger, S., Busse, T., Weggen, S., and Koo, E. H. (2004) FE65 constitutes the functional link between the low-density lipoprotein receptor related protein and the amyloid precursor protein. *J. Neurosci.* **24**, 4259–4265
  59. Ulery, P. G., Beers, J., Mikhailenko, I., Tanzi, R. E., Rebeck, G. W., Hyman, B. T., and Strickland, D. K. (2000) Modulation of  $\beta$ -amyloid precursor protein processing by the low density lipoprotein receptor-related protein (LRP) Evidence that LRP contributes to the pathogenesis of Alzheimer's disease. *J. Biol. Chem.* **275**, 7410–7415
  60. Cam, J. A., Zerbinatti, C. V., Li, Y., and Bu, G. (2005) Rapid endocytosis of the low density lipoprotein receptor related protein modulates cell surface distribution and processing of the  $\beta$ -amyloid precursor protein. *J. Biol. Chem.* **280**, 15464–15470
  61. Michaki, V., Guix, F. X., Vennekens, K., Munck, S., Dingwall, C., Davis, J. B., Townsend, D. M., Tew, K. D., Feiguin, F., De Strooper, B., Dotti, C. G., and Wahle, T. (2012) Down-regulation of the ATP-binding cassette transporter 2 (Abca2) reduces amyloid- $\beta$  production by altering nicastrin maturation and intracellular localization. *J. Biol. Chem.* **287**, 1100–1111
  62. Ghani, M., Lang, A. E., Zinman, L., Nacmias, B., Sorbi, S., Bessi, V., Tedde, A., Tartaglia, M. C., Surace, E. I., Sato, C., Moreno, D., Xi, Z., Hung, R., Nalls, M. A., Singleton, A., St George-Hyslop, P., and Rogava, E. (2015) Mutation analysis of patients with neurodegenerative disorders using NeuroX array. *Neurobiol. Aging* **36**, 545.e9–545.e14
  63. Cuyvers, E., De Roeck, A., Van den Bossche, T., Van Cauwenberghe, C., Bettens, K., Vermeulen, S., Mattheijssens, M., Peeters, K., Engelborghs, S., Vandenbulcke, M., Vandenbergh, R., De Deyn, P. P., Van Broeckhoven, C., and Sleegers, K. (2015) Mutations in ABCA7 in a Belgian cohort of Alzheimer's disease patients: a targeted resequencing study. *Lancet Neurol.* **14**, 814–822
  64. Bradford, M. M. (1976) A rapid and sensitive method for the quantitation of microgram quantities of protein utilizing the principle of protein-dye binding. *Anal. Biochem.* **72**, 248–254

Neurobiology:

**ATP-binding Cassette Transporter A7  
(ABCA7) Loss of Function Alters  
Alzheimer Amyloid Processing**

Kanayo Satoh, Sumiko Abe-Dohmae, Shinji  
Yokoyama, Peter St George-Hyslop and Paul  
E. Fraser

*J. Biol. Chem.* 2015, 290:24152-24165.

doi: 10.1074/jbc.M115.655076 originally published online August 10, 2015

NEUROBIOLOGY

CELL BIOLOGY

---

Access the most updated version of this article at doi: 10.1074/jbc.M115.655076

Find articles, minireviews, Reflections and Classics on similar topics on the JBC Affinity Sites.

Alerts:

- When this article is cited
- When a correction for this article is posted

Click here to choose from all of JBC's e-mail alerts

This article cites 63 references, 28 of which can be accessed free at  
<http://www.jbc.org/content/290/40/24152.full.html#ref-list-1>



Contents lists available at ScienceDirect

## Chemistry and Physics of Lipids

journal homepage: [www.elsevier.com/locate/chemphyslip](http://www.elsevier.com/locate/chemphyslip)

## Sequential change in physicochemical properties of LDL during oxidative modification

Toshimi Kido<sup>a</sup>, Kazuo Kondo<sup>b</sup>, Hiroshige Itakura<sup>c</sup>, Shinji Yokoyama<sup>d,\*</sup><sup>a</sup> Institute of Environmental Science of Human Life, Ochanomizu University, Bunkyo-ku, Tokyo 112-8610, Japan<sup>b</sup> Department of Food and Nutritional Science, Toyo University, Itakura-machi, Ora-gun, Gunma 374-0193, Japan<sup>c</sup> Shinagawa East One Medical Clinic, Minato-ku, Tokyo 108-0075, Japan<sup>d</sup> Nutritional Health Science Research Center, Chubu University, Kasugai 487-8501, Japan

## ARTICLE INFO

## Article history:

Received 15 August 2015

Received in revised form 26 October 2015

Accepted 27 October 2015

Available online 11 November 2015

## Keywords:

LDL

Cholesterol

Phospholipid

Oxidation

Copper ion

Apolipoprotein B

## ABSTRACT

Oxidized LDL is thought to be a highly atherogenic lipoprotein. Structural background of this pathogenesis, however, has not yet been well defined. Physicochemical characterization of this lipoprotein is still controversial, which therefore makes it difficult to take a mechanistic approach to its atherogenicity. We thus conducted investigation of time-dependent changes in chemical compositions and alternation of physical properties of LDL in detail during its oxidation induced by human embryonic endothelial cells and copper ions. The oxidation caused hydrolysis of glycerolipids being demonstrated as decrease of triglyceride and choline-phospholipid and increase of lysophosphatidylcholine. Fragmentation of apoB was also induced while over-all protein components stayed with the particles. The density of the particles continuously shifted to higher fractions for all the particles to reach  $d \geq 1.044$  after 10 h incubation. The average diameter of LDL, however, decreased from 28.1 nm to 25.6 nm by 5 h and increased to 27.1 nm towards 20 h incubation with the increase of discoid particles. These dynamic changes can be interpreted by losing fatty acyl group from the core lipid components perhaps due to oxidative degradation and by increase of surface lysophosphatidylcholine to cause remodeling of the particles.

© 2015 Elsevier Ireland Ltd. All rights reserved.

## 1. Introduction

One of the most rational hypotheses for the coronary risk of increased plasma low-density lipoprotein (LDL) involves chemical modification of LDL in plasma, due to its prolonged retention by decrease in the LDL receptor activity caused by genetic and/or environmental factors. In such circumstances, LDL has more chance to undergo degenerative changes such as oxidative modification (oxidized LDL, OxLDL). OxLDL is less sensitively recognized by the LDL receptor and rather processed by the “scavenger” receptor (SR) s of macrophages such as SR class A, SR class B (CD36), and SR class E (Lectin-like oxidized LDL receptor-1) (Ashraf and Gupta, 2011; Steinberg, 1997; Witztum and Steinberg, 1991; Yla-Herttuala et al., 1989). Uptake of modified lipoproteins by scavenger cells is not feedback-regulated by cellular sterol and results in accumulation of LDL lipids to the extent of generating “foam cells” as an initial stage of atherogenesis. Modes of intracellular lipid accumulation may differ by types of modification

of LDL (Lougheed et al., 1999). OxLDL may participate in other stages of the pathogenesis as well, such as endothelial dysfunction or the rupture of arterial plaque to cause acute coronary syndrome (Igarashi et al., 2004; Kugiyama et al., 1990; Kume, 2010; Kume and Gimbrone, 1994). Other types of modified LDL, perhaps enzymatically by metalloproteinase or cholesteryl ester hydrolase, may also contribute to these stages of pathogenesis (Torzewski et al., 2004). Pathophysiological relevance of this hypothesis is based on the findings that OxLDL is recovered from atherosclerotic vascular lesions (Morton et al., 1986). Since such modified LDL is found only a little in circulating blood plasma, oxidation of LDL is assumed to take place mainly in the vascular subendothelial site in vivo. The oxidative reaction is carried out non-enzymatically by reactive oxygen species (ROS) but perhaps more mediated with enzymes in vivo such as lipoxygenase and myeloperoxidase (Parthasarathy et al., 1989). Oxidative modification of LDL is therefore induced in vitro by copper ion (Zarev et al., 2002; Zarev et al., 2003) or by the treatment with human umbilical vein endothelial cells (HUVECs) (Steinbrecher et al., 1984) to mimic in vivo reactions. The former reaction has been frequently used as a simple and easy model reaction for LDL oxidation.

\* Corresponding author. Fax: +81 568 51 9698.

E-mail address: [syokoyam@isc.chubu.ac.jp](mailto:syokoyam@isc.chubu.ac.jp) (S. Yokoyama).

OxLDL has been studied extensively for its roles in atherogenesis and for its physical/chemical properties that may be related to such functions. During the oxidative process, LDL particles undergo various chemical and physical changes (Itabe, 2009; Zarev et al., 2003), including fragmentation of apolipoprotein B (apoB) (Fong et al., 1987), increase in lipid hydroperoxides (Spiteller, 2005), hydrolysis of phosphatidylcholine (PC) (Steinbrecher et al., 1984), generation of aldehydes by cleaving the peroxides, and carbonylation of apoB by direct oxidation or by reacting with aldehydes (Chen et al., 1992; Kato et al., 1999; Obama et al., 2007; Zarev et al., 2002). In any case, lipid molecules primarily undergo oxidative degradation and secondarily other changes take place such as chemical modification of apoB. Changes in physical properties of LDL, particularly decrease in size and increase of negative surface charge (Henriksen et al., 1983) may result in lower affinity for LDL receptor and increase of recognition and uptake by scavenger receptors.

However, there are some ambiguities on changes by oxidation in physical/chemical properties of LDL particles (Austin et al., 1988; Coresh et al., 1993). While the average density of human LDL was found increased from 1.036 to 1.070 g/ml by oxidative treatment with rabbit endothelial cell (Henriksen et al., 1981, 1983; Steinbrecher et al., 1987), the density of the LDL-size particles isolated from human atherosclerotic lesions was lower than that of plasma LDL (Morton et al., 1986). The findings on the size of LDL were also diverse, as decrease in the particle diameters (Hidaka et al., 2005) or its increase due to the particle aggregation or fusion (Meyer et al., 1996; Pentikainen et al., 1996) by oxidative modification of LDL. Therefore, systemic characterization is still required for properties of LDL during the course of its oxidative reaction in order to understand the basis of LDL oxidation.

Here, we investigated the effects of oxidative process of LDL on its physicochemical properties in detail in a systemic fashion focusing on changes in the buoyant density and the size of the particles. In this study, we used copper ion-mediated oxidation of LDL after verification of similarity of the products to HUVECs-induced OxLDL.

## 2. Materials and methods

### 2.1. Subjects

Fasting blood samples were collected in sodium EDTA-containing tubes from healthy female volunteers, and plasma samples were immediately separated by centrifugation at 3000 rpm, 4 °C for 15 min. Total cholesterol (TC), triglyceride (TG) and choline-phospholipid (PL) levels of plasma were determined enzymatically (DETERMINER L-TC II, DETERMINER L-TG II, DETERMINER L-PL, KYOWA MEDEX, TOKYO, Japan). LDL-cholesterol (LDL-C) and HDL cholesterol (HDL-C) of plasma were estimated using a Rapid Electrophoresis System (REP, Helena Laboratories, Saitama, Japan) (Kido et al., 2001). The experimental

protocol was approved by the Ethics Committee at Ochanomizu University granted for obtaining informed consents from the participants. Plasma lipid/lipoprotein profiles of the donors are listed in Table 1.

### 2.2. Isolation of LDL

Single-spin density gradient ultracentrifugation was employed for isolation of endotoxin-free LDL for HUVECs-mediated oxidation (Kamiyama et al., 2009), in order to avoid contamination of endotoxin in LDL isolated by a sequential ultracentrifuge method apparently from the silicone grease used to seal the slicing equipment identified in our preliminary evaluation. LDL was isolated from fasting plasma of three females (TC  $204.2 \pm 49.4$  mg/dl, LDL-C  $123.0 \pm 37.9$  mg/dl, HDL-C  $64.3 \pm 19.8$  mg/dl, TG  $95.0 \pm 29.5$  mg/dl, PL  $217.5 \pm 36.3$  mg/dl, age  $42 \pm 16$  years old). 2.2 ml of plasma was adjusted to 1.21 mg/dl by adding 0.715 g KBr. This mixture was transferred into a 5.1 ml centrifuge tube then being filled with saline-EDTA buffer ( $d = 1.006$  g/ml), and centrifuged at 100,000 rpm, 4 °C, for 40 min using a TLA 100.4 rotor (BECKMAN COULTER, Inc., CA, USA). The LDL fraction was collected by using a syringe, dialyzed against EDTA-free PBS for 48 h and filtered through a 0.45  $\mu$ m PVDF filter (Millex<sup>®</sup>-HV, Merck Millipore Ltd., Tullagreen, Carrigtwohill, Co., Cork, IRL.). LDL protein was determined using a Micro BCA<sup>™</sup> Protein Assay Kit (Thermo Scientific, Rockford, IL, U.S.A.). LDL for copper-oxidation was isolated as a density range 1.019–1.063 g/ml by sequential ultracentrifugation of fasting plasma of six females using the method of Havel et al. (Havel et al., 1955).

### 2.3. HUVECs-mediated LDL oxidation

LDL was prepared as described above (Section 2.2). HUVECs (Lonza Walkersville, Inc., Walkersville, USA) were cultured in EGM-2 (Lonza Walkersville, Inc., Walkersville, USA). The Cells were grown to confluence at 37 °C in 5% CO<sub>2</sub> and used for experiments at passage 4 (Saita et al., 2012). The medium was removed, and the cells were washed with Ham's F10 medium (Lonza Walkersville) and incubated with LDL (100  $\mu$ g protein/ml) for 20 h in Ham's F10 medium containing 3  $\mu$ M FeSO<sub>4</sub> and 10 nM CuSO<sub>4</sub>. LDL (100  $\mu$ g protein/ml) was also incubated without cells for 20 h in Ham's F10 medium or PBS as controls. Following incubation, the conditioned medium was collected and centrifuged at 1500 rpm, 4 °C for 5 min. The supernatant containing LDL was dialyzed for PBS, concentrated from 20 ml to 1.15 ml by using centrifugal filter Units (Amicon Ultra, Ultracel-100K, Merck Millipore Ltd., Tullagreen, Carrigtwohill, Co., Cork, IRL.), and centrifuged at 20,000  $\times$  g, 4 °C, for 1 min. The aliquot of the supernatant was subjected to agarose gel electrophoresis in a Rapid Electrophoresis System to evaluate the extent of oxidation. The supernatant, 800  $\mu$ l, was used to determine the changes in the buoyant density. The residue was used for electrophoretic analysis in nondenaturing gradient gel to examine particle size and measurements of lipids and protein.

### 2.4. Oxidation of LDL induced by copper

EDTA-free LDL solution, 1000  $\mu$ l of 2.0 mg protein/ml, and 250  $\mu$ M CuSO<sub>4</sub>, 100  $\mu$ l, both in PBS were added to 8900  $\mu$ l PBS in a 15 ml polypropylene tube, mixed gently and incubated at 37 °C for 0 to 20 h. The 10 ml EDTA-free LDL solution was incubated without CuSO<sub>4</sub> for 20 h as a control. To stop the incubation, EDTA was added to each sample to make the final concentration 0.25 mM followed by immediate cooling on ice (Esterbauer et al., 1992; Obama et al., 2007). The samples were concentrated from 10 ml to 1.15 ml by using centrifugal filter Units. After centrifugation at 20,000  $\times$  g, 4 °C, for 1 min, an aliquot of the supernatant

**Table 1**

Plasma lipid/lipoprotein profiles of donors used for LDL oxidation studies.

Subjects	Age	TC	LDL-C	HDL-C	TG	PL
	Years					
No.1	25	237.0	166.0	64.0	52.0	247.0
No.2	49	247.0	151.8	74.3	103.0	263.0
No.3	23	191.8	101.5	81.1	45.0	234.5
No.4	58	221.0	103.0	109.0	52.0	276.0
No.5	24	163.0	85.5	72.5	54.0	193.0
No.6	55	187.5	119.0	49.0	52.0	186.5

Total cholesterol (TC), triglyceride (TG) and choline-phospholipid (PL) were determined by enzymatic method. LDL-cholesterol (LDL-C) and HDL-cholesterol (HDL-C) were determined by electrophoresis method.

was further analyzed for electrophoretic mobility and density in ultracentrifugation.

### 2.5. Lipids assay of OxLDL

Lipid composition of the OxLDL induced by  $\text{Cu}^{2+}$  was analyzed in detail for the samples before concentration for electrophoresis or ultracentrifugation. TC, TG, PL and protein were measured as described above. TC was also chemically determined by the Abell–Kendall assay based on lipid saponification of serum samples, its extraction with hexane and color development using Liebermann–Burchard reagent (Abell et al., 1952). Lysophosphatidylcholine (lysoPC) was determined using AZWELL LPC Assay Kit (Alfresa Pharma Corporation, Osaka, Japan). ApoB was determined by immunoturbidimetric assay using ApoB Auto N “Diichi” (Sekisui Medical Co., Ltd., Japan).

### 2.6. Agarose gel electrophoresis of OxLDL

The concentrated sample was analyzed in agarose gel electrophoresis at 20 °C, 400V for 15 min using the Rapid Electrophoresis System. The lipoprotein bands were visualized by enzymatic staining of cholesterol as previously described (Kido et al., 2001). The condition of electrophoresis was chosen for the most efficient separation of LDL samples of 20-h oxidation from the pre $\beta$  to  $\alpha$ -positions in migration in order to distinguish the effect of various oxidative conditions on the LDL mobility.

### 2.7. Non-denaturing gradient gel electrophoresis of OxLDL

Non-denaturing gradient gel electrophoresis of oxidized LDL was carried out in 2–15% polyacrylamide gradient gels (Cosmo Bio Co., Ltd., Tokyo, Japan) at 4 °C, 120V for 18 h according to the method of Krauss and Burke (Krauss and Burke, 1982). Migration distance was calibrated with high molecular weight markers,

comprising thyroglobulin (669 kDa, stokes diameter 17 nm), ferritin (440 kDa, 12.2 nm) and catalase (232 kDa, 9.2 nm) (GE Healthcare UK Limited, Buckinghamshire, UK). The particle size of OxLDL was determined as previously described (Kondo et al., 2001).

### 2.8. SDS polyacrylamide gel electrophoresis of apo B

SDS polyacrylamide gel electrophoresis was performed to analyze degradation of apoB along with oxidation of LDL as follows: 20  $\mu\text{l}$  of the sample was mixed with 140  $\mu\text{l}$  of methyl alcohol, 200  $\mu\text{l}$  of chloroform and 600  $\mu\text{l}$  of diethyl ether sequentially under agitation and then immediately stored at  $-80\text{ }^\circ\text{C}$ , for 30 min. To follow centrifugation at 2000 rpm at 4 °C for 2 min, the upper phase was discarded. The residue was mixed with 140  $\mu\text{l}$  of methyl alcohol and 600  $\mu\text{l}$  of diethyl ether sequentially under agitation. To this residue 600  $\mu\text{l}$  of diethyl ether was added, mixed and the upper layer phase was discarded after centrifugation at 2400 rpm, 4 °C, for 2 min. Finally, the solvents were removed under a steam of  $\text{N}_2$  (Bligh and Dyer, 1959). ApoB was suspended in water and an aliquot (20  $\mu\text{l}$ ) was solubilized, by incubating in boiling water for 3 min after adding reducing buffer (5  $\mu\text{l}$ ) containing 4% SDS, 20% glycerol and 10% 2-mercaptoethanol. Samples were subjected to SDS polyacrylamide gel electrophoresis in 2–15% polyacrylamide gradient gel as described previously (Laemmli, 1970).

### 2.9. Classification of oxidized LDL by density

Oxidized LDL was classified as density ranges at cutoff densities of 1.019, 1.030, 1.044, 1.055, 1.063 and 1.125 g/ml. KBr-saline was prepared with specific densities of each above at 20 °C by adding solid KBr to 0.9% NaCl solution ( $d=1.006\text{ g/ml}$ ). Oxidized LDL, 800  $\mu\text{l}$  in PBS (solvent density = 1.006 g/ml), 2.0 ml of saline ( $d=1.006\text{ g/ml}$ ) and 110  $\mu\text{l}$  of KBr-saline ( $d=1.350$ ) were mixed

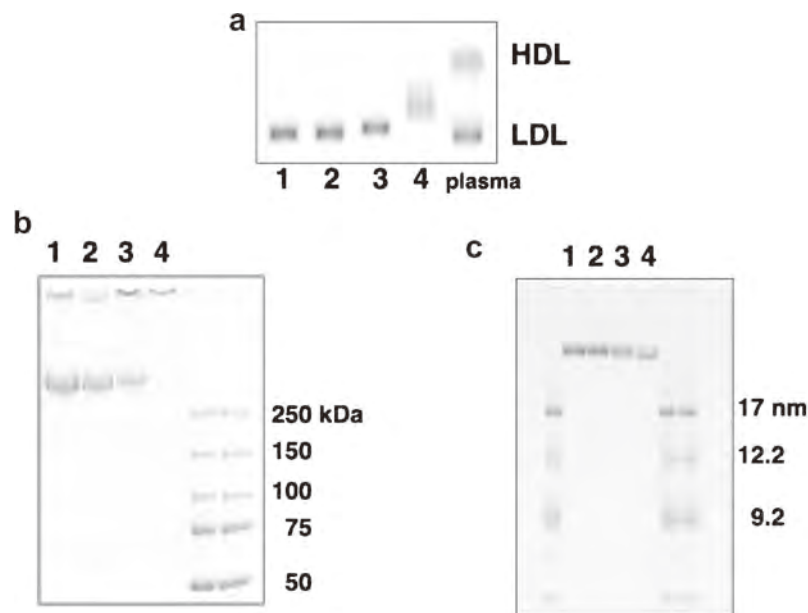


**Fig. 1.** Electrophoretic profiles of LDL oxidized with HUVECs. The oxidative conditions of LDL are as follows: (1) LDL/PBS (100  $\mu\text{g}$  protein/ml) was stored at 4 °C (native LDL). (2) LDL/PBS (100  $\mu\text{g}$  protein/ml) was incubated at 37 °C, for 20 h. (3) LDL / Ham's F10 (100  $\mu\text{g}$  protein/ml) was incubated at 37 °C, for 20 h. 4. LDL / Ham's F10 (100  $\mu\text{g}$  protein/ml) was incubated at 37 °C, for 20 h with HUVECs. Each panel demonstrate a typical profile of lipoproteins. (a) Agarose gel electrophoresis. The samples were electrophoresed using the Rapid Electrophoresis System (at 20 °C, 400 V for 15 min). After electrophoresis, the gel was dyed by cholesterol enzymatic staining. (b) SDS-polyacrylamide gel electrophoresis. The gel shows the degradation of apoB of OxLDL. The samples were electrophoresed on 2–15% polyacrylamide gradient gel at 30 mA/gel, room temperature, for 1 h after delipidation and stained with Coomassie Brilliant Blue. (c) Nondenaturing gradient gel electrophoresis to show the change in the particle size of OxLDL. The electrophoresis of oxidized samples was performed at 4 °C in 2–15% polyacrylamide gradient gels at 120 V for 18 h. Molecular size standards used are; thyroglobulin (17 nm), ferritin (12.2 nm) and catalase (9.2 nm).

**Table 2**  
Electrophoretic analysis of LDL oxidized with HUVECs.

Sample no.	Relative mobility	Apo B (%)	Diameter (nm)
1	1.0 ± 0.1	100.0 ± 27.4	27.2 ± 0.7
2	1.0 ± 0.1	93.2 ± 39.7	27.2 ± 0.7
3	1.2 ± 0.1	44.7 ± 12.1*	26.9 ± 0.9
4	1.7 ± 0.1***	4.4 ± 4.4**	26.2 ± 0.7

The table shows summary of electrophoretic analysis of LDL oxidized with HUVECs. The oxidative conditions of LDL are as follows:

1. LDL/PBS (100 µg protein/ml) was stored at 4 °C (native LDL)
2. LDL/PBS (100 µg protein/ml) was incubated at 37 °C, for 20 h
3. LDL/Ham's F10 (100 µg protein/ml) was incubated at 37 °C, for 20 h
4. LDL/Ham's F10 (100 µg protein/ml) was incubated at 37 °C, for 20 h with HUVECs

The relative contents of apoB (%) were obtained from the results of SDS-polyacrylamide gel electrophoresis and expressed as% against apoB content at oxidation for 0 h. The diameters were calculated from the results the nondenaturing gradient gel electrophoresis. The results are expressed in form, mean ± S.D.,  $n=3$ . Differences between groups were analyzed by One-Way Repeated measures ANOVA.

to adjust the density to 1.019 g/ml and the mixture was transferred to a 5.1 ml centrifuge tube and KBr-saline ( $d=1.019$  g/ml) was gently layered over the top, and centrifuged at 100,000 rpm, 4 °C, for 5 h using a TLA 100.4 rotor (Beckman Coulter, Inc., CA, USA). The top fraction (buoyant density 1.019 g/ml) was collected by slicing a tube at a position of 2.8 cm from the bottom and the bottom fraction was adjusted to density 1.030 g/ml by mixing with an appropriate amount of KBr-saline ( $d=1.350$  g/ml) for further centrifugation. This procedure was repeated to obtain the fractions with specific cutoff buoyant density of  $d=1.044$ , 1.055, 1.063 and 1.125 g/ml. TC, TG, PL and protein concentration of each fraction were determined by the same methods as described above.

### 2.10. Electron micrographic analysis of OxLDL

The OxLDL solutions were prepared as described above (Section 2.4.) and diluted 8-fold in PBS.

An aliquot of 5 µl of each sample was applied onto a copper grid supported by carbon vapor deposited formvar film (EM-fine grid F-300, Nisshin EM Corporation, Tokyo, Japan) for 30 s and the excess liquid was removed by blotting. 5 µl of 2% uranyl acetate solution was applied to the grid for 30 s for negative staining and then blotted. The grids were dried at room temperature and examined in a JEOL transmission electron microscope (JEM1400, JEOL Ltd., Tokyo, Japan). The micrographs were analyzed by Image J software from a public domain provided by United States National Institute

of Health (NIH). The diameter was calculated by measuring the area of particles assuming they are spherical. The ratio of deformed particles in approximately 500 particles was counted.

### 2.11. Statistical analysis

Results were expressed as mean ± SD. Differences between groups were analyzed by ANOVA using the Turkey test. The difference with a value of  $p < 0.05$  was considered significant.

## 3. Results

### 3.1. Endothelial cell-mediated LDL oxidation

LDL conditioned with HUVECs for 20 h was analyzed by electrophoresis. The results are shown in Fig. 1 and summarized in Table 2. Fig. 1a shows increase in relative mobility of LDL in agarose gel electrophoresis by the treatment reflecting the increase of negative surface electric charge of the LDL particles as an indicator for the LDL oxidation. The migration distance of LDL incubated with HUVECs in Ham's F10 was  $10.3 \pm 0.6$  mm in comparison to that of native LDL ( $6.2 \pm 0.6$  mm) ( $p < 0.001$ ). The migration distance of LDL incubated without HUVECs in Ham's F10 also increased slightly ( $7.4 \pm 0.6$  mm) not reaching significant difference from the native LDL. Fig. 1b shows the degradation of apoB during the oxidation process. The relative amount of apoB in LDL incubated with HUVECs in Ham's F10 and that in LDL incubated without HUVECs in Ham's F10 decreased to 4.4% and 44.7%, respectively, of the native LDL ( $p < 0.01$ ,  $p < 0.05$  respectively), being consistent with previous reports of apoB fragmentation as well as its denaturation (such as carbonylation) in amino groups of lysine, arginine, histidine and N-terminal amino groups that are functional for Coomassie staining. Some inaccuracy should be allowed in quantitative estimation of apoB since a part of the protein stays in the origin as aggregates due to the extremely insoluble nature of this protein. Fig. 1c shows changes in the diameter of OxLDL. The diameter of native LDL was  $27.2 \pm 0.7$  nm while it was  $26.2 \pm 0.7$  nm for the LDL incubated with HUVECs in Ham's F10 ( $p=0.0522$ ).

Changes in the density of LDL represented by cholesterol are shown in Fig. 2. As the oxidation proceeds, the density of LDL shifts heavier. The majority subclass  $d=1.030$ –1.044 represents decreased by the incubation and the subclass  $d > 1.044$  increased from 54.7% in LDL incubated without HUVECs in Ham's F10 to 77.7% in LDL incubated with HUVECs in Ham's F10, both significantly higher than that of the LDL stored at 4 °C ( $p < 0.05$ ,  $p < 0.001$  respectively).

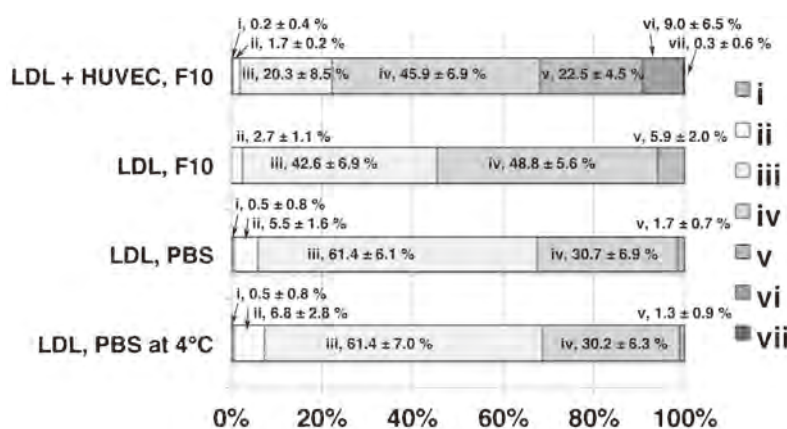


**Fig. 2.** Changes in the density subclass proportion of LDL during oxidation induced by incubation with HUVECs. Proportions are calculated on the basis of the cholesterol content in each subclass. LDL subclasses (i–vii) are defined as specific density ranges: (i)  $d < 1.019$ ; (ii)  $d = 1.019$ –1.030; (iii)  $d = 1.030$ –1.044; (iv)  $d = 1.044$ –1.055; (v)  $d = 1.055$ –1.063; (vi)  $d = 1.063$ –1.125; (vii)  $d > 1.125$ . The data are expressed as mean ± S.D.  $n=3$ .

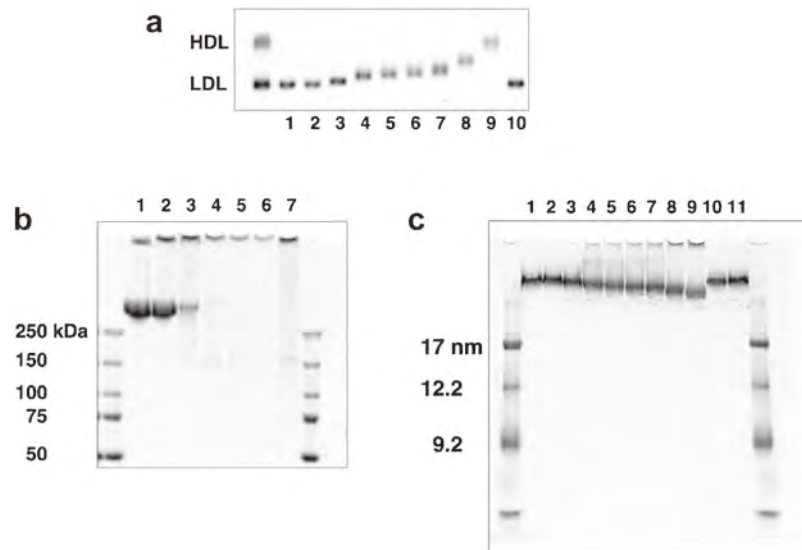


**Fig. 3.** Electrophoretic profiles of LDL oxidized by copper ion. The conditions for each electrophoresis are same as those for the experiments in Fig. 1. (a) Agarose gel electrophoresis. Lanes from left to right represent plasma as positional control, native LDL (1), LDL oxidized for 0 h (2), 1 h (3), 2 h (4), 3 h (5), 4 h (6), 5 h (7), 10 h (8), and 20 h (9), and LDL incubated for 20 h without copper (10). (b) SDS-polyacrylamide gel electrophoresis of apoB. Lanes 1–7 represent, native LDL (1), LDL oxidized for 0 h (2), 1 h (3), 2 h (4), 3 h (5), 4 h (6) and 5 h (7), respectively. The lanes in the both ends represent molecular weight markers. (c) Nondenaturing gradient gel electrophoresis. Lanes represent native LDL (1, 11), LDL oxidized for 0 h (2), 1 h (3), 2 h (4), 3 h (5), 4 h (6), 5 h (7), 10 h (8), and 20 h (9), and LDL incubated for 20 h without copper (10). The lanes at the both ends represent high molecular weight (HMW) markers.

### 3.2. Oxidation induced by Copper

LDL oxidized by copper ion was analyzed in electrophoresis. The results are shown in Fig. 3 and summarized in Table 3. Fig. 3a shows LDL migrates further in agarose gel in consistency with HUVECs-induced oxidation. The change by the 3-h incubation was equivalent to that caused by the HUVECs treatment for 20 h. After 20-h copper-induced oxidation, LDL sample migrated nearly to the  $\alpha$ -position, migration distance approximately 3.3-fold of intact LDL ( $p < 0.001$ ). This shift to the anode implied increased negative surface charge of LDL. Fig. 3b shows the degradation of apoB during the oxidation process. The amount of apoB decreased to 19.7% and 1.0% of unoxidized apoB by 1- and 2- h incubation, respectively ( $p < 0.001$ ), and it completely disappeared after 3-h oxidation. Fig. 3c shows changes in the diameter of OxLDL. Compared with native LDL ( $27.9 \pm 2.2$  nm), the diameters at 3-, 4-, 5-, 10-, and 20-h oxidation significantly decreased to  $26.7 \pm 1.6$  nm ( $p < 0.05$ ),  $26.6 \pm 1.5$  nm ( $p < 0.01$ ),  $26.3 \pm 1.2$  nm ( $p < 0.001$ ),  $25.7 \pm 1.0$  nm ( $p < 0.001$ ), and  $25.2 \pm 0.9$  nm ( $p < 0.001$ ), respectively. The results showed that similar changes in physical

properties were observed between HUVEC-mediated and copper-induced oxidation exhibited by diameter, surface charge and degradation of apoB, except that the latter condition seemed to provide more extreme oxidative condition. Accordingly, we examined changes in density, diameter, and lipid composition in more detail using copper-induced OxLDL.

Fig. 4 shows proportional change in density subclass of LDL as copper-induced oxidation proceeded, represented by cholesterol (a) or PL (b). Both profiles are almost identical. The proportion of the subclasses  $d > 1.044$  was  $63.8 \pm 8.1\%$  at 2-h oxidation exhibiting marked increase from that of native LDL ( $35.0 \pm 8.8\%$ ) ( $p < 0.001$ ). The proportion of heavier subclasses increased with progress of oxidation. All LDL was present in the density  $> 1.044$  subclass after 10-h oxidation, and most of LDL was shifted into the  $d = 1.063$ – $1.125$  subclass after 20-h oxidation. There was no significant change in the density distribution of LDL after incubated for 20 h with buffer alone. Density profile of LDL incubated with HUVECs in Ham's F10 was equivalent to that of 3-h copper-oxidation, being consistent with other parameters.

**Table 3**

Electrophoretic analysis of LDL oxidized by copper ion.

	Relative mobility	ApoB (%)	Diameter (nm)
1. Native LDL	$1.0 \pm 0.1$		$27.9 \pm 2.2$
2. Oxidation 0 h	$1.0 \pm 0.0$	$100.0 \pm 27.3$	$28.0 \pm 2.3$
3. Oxidation 1 h	$1.2 \pm 0.1$	$19.7 \pm 5.7^{***}$	$27.6 \pm 1.8$
4. Oxidation 2 h	$1.5 \pm 0.1^{***}$	$1.0 \pm 0.8^{***}$	$26.9 \pm 1.6$
5. Oxidation 3 h	$1.6 \pm 0.2^{***}$	–	$26.7 \pm 1.6^*$
6. Oxidation 4 h	$1.7 \pm 0.1^{***}$	–	$26.6 \pm 1.5^{**}$
7. Oxidation 5 h	$1.9 \pm 0.1^{***}$	–	$26.3 \pm 1.2^{***}$
8. Oxidation 10 h	$2.5 \pm 0.2^{***}$	–	$25.7 \pm 1.0^{***}$
9. Oxidation 20 h	$3.3 \pm 0.2^{***}$	–	$25.2 \pm 0.9^{***}$
10. Control 20 h	$1.1 \pm 0.1$	–	$27.7 \pm 2.0$

The table shows summary of electrophoretic analysis of LDL oxidized by copper ion. The relative contents of apoB (%) were obtained from the results of SDS-polyacrylamide gel electrophoresis and expressed as % against apoB content at oxidation for 0 h. The diameters were calculated from the results the nondenaturing gradient gel electrophoresis. The results are expressed in form, mean  $\pm$  S.D.,  $n = 6$ . Differences between groups were analyzed by one-way repeated measures ANOVA.

\*\*\* $p < 0.001$ , \*\* $p < 0.01$ , \* $p < 0.05$  vs. native LDL (relative mobility on agarose gel electrophoresis, diameter). \*\*\* $p < 0.001$  vs. LDL oxidized for 0 h (relative content of apoB).

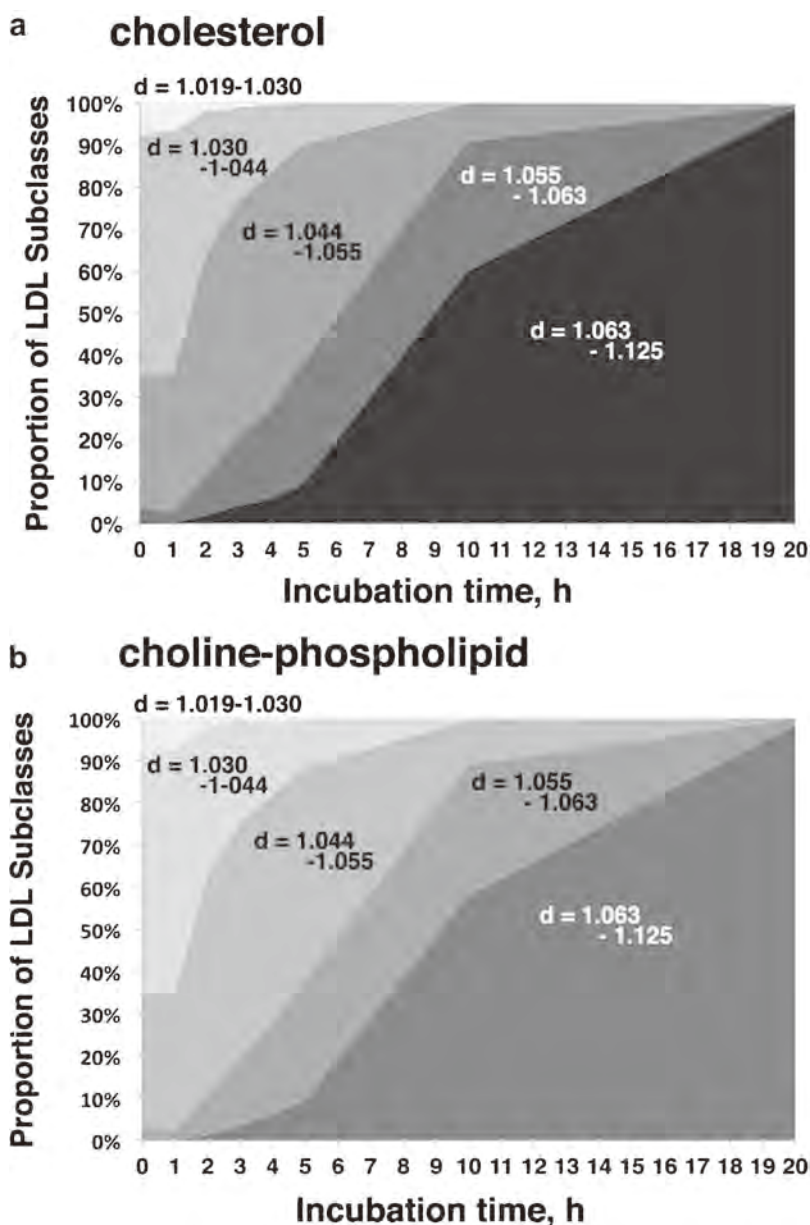


**Fig. 4.** Changes in the density subclass proportion of LDL during oxidation induced by incubation with copper. Changes in proportion are calculated on the basis of cholesterol (a) or PL (b). The data are expressed as averages of  $n=6$ .

**Table 4**  
Changes of composition of LDL by oxidation with copper ion.

	Protein, mg/ml	apoB, mg/dl	TC, mg/dl		TG, mg/dl	PL, $\mu\text{mol/L}$	LPC, $\mu\text{mol/L}$	LPC/PL, %
			Abell-Kendall	Enzymatic				
Native LDL	0.22 ± 0.01	28.5 ± 1.3	42.6 ± 1.4	43.0 ± 0.8	3.3 ± 1.7	317.8 ± 14.5	9.0 ± 3.9	2.8 ± 1.1
Oxidation 1 h	0.24 ± 0.02 <sup>†</sup>	27.8 ± 0.5	42.6 ± 2.2	42.4 ± 1.5	3.3 ± 1.4	317.8 ± 14.5	12.8 ± 4.3	4.0 ± 1.3
Oxidation 2 h	0.25 ± 0.02 <sup>***</sup>	27.0 ± 0.8	42.7 ± 1.5	40.9 ± 0.8	3.3 ± 1.7	319.4 ± 8.4	28.8 ± 8.4 <sup>***</sup>	9.0 ± 2.7 <sup>†</sup>
Oxidation 3 h	0.24 ± 0.02 <sup>**</sup>	26.3 ± 0.5 <sup>†</sup>	42.2 ± 1.5	39.8 ± 0.9 <sup>†</sup>	3.1 ± 1.7	313.0 ± 19.5	40.8 ± 4.7 <sup>***</sup>	13.0 ± 1.2 <sup>***</sup>
Oxidation 4 h	0.24 ± 0.01 <sup>†</sup>	26.0 ± 0.8 <sup>**</sup>	42.8 ± 1.2	38.9 ± 1.1 <sup>**</sup>	3.0 ± 1.4	313.0 ± 19.5	48.3 ± 4.2 <sup>***</sup>	15.5 ± 1.3 <sup>***</sup>
Oxidation 5 h	0.23 ± 0.01	24.8 ± 0.5 <sup>***</sup>	43.4 ± 0.8	37.4 ± 0.9 <sup>***</sup>	3.3 ± 1.0	309.7 ± 18.5	56.4 ± 3.1 <sup>***</sup>	18.2 ± 1.1 <sup>***</sup>
Oxidation 10 h	0.21 ± 0.01	23.0 ± 0.8 <sup>***</sup>	42.4 ± 1.0	32.1 ± 1.9 <sup>***</sup>	2.6 ± 1.1	300.1 ± 19.5 <sup>†</sup>	87.3 ± 2.3 <sup>***</sup>	29.2 ± 1.9 <sup>***</sup>
Oxidation 20 h	0.20 ± 0.01	19.5 ± 0.6 <sup>***</sup>	42.2 ± 0.5	25.9 ± 2.5 <sup>***</sup>	2.5 ± 1.0	289.4 ± 21.4 <sup>***</sup>	127.1 ± 10.2 <sup>***</sup>	44.1 ± 5.1 <sup>***</sup>
Incubation 20 h	0.22 ± 0.02	28.8 ± 1.0	43.1 ± 1.4	42.4 ± 0.5	3.1 ± 1.4	314.6 ± 23.4	10.2 ± 4.6	3.2 ± 1.3

Lipid /protein compositions of OxLDL induced by copper ion were analyzed in detail using donor plasma except for No.1 and 4 of Table 1. Total cholesterol (TC), triglyceride (TG), choline-phospholipid (PL) and Lysophosphatidylcholine (LPC) levels were determined by enzymatic method. TC was also chemically determined by the Abell-Kendall assay. The results are expressed in form, mean ± S.D.,  $n=4$ . Differences between groups were analyzed by one-way repeated measures ANOVA.

Table 4 shows the change in chemical composition of LDL by copper-induced oxidation before its concentration for further analysis. Total cholesterol measured by enzymatic method continuously decreased during the incubation by 40% from the original level. In contrast, chemical cholesterol assay by the method of Abell–Kendall showed the level of cholesterol completely stable throughout the incubation. The enzymatic assay is based on oxidation of its hydroxyl group by cholesterol oxidase after hydrolysis of esterified cholesterol that accounts for 60–70% of total cholesterol in LDL. Accordingly, unesterified (free) cholesterol that accounts for 30–40% of total cholesterol is exposed to copper-oxidation to exhaust the assay target and cause apparent decrease of the assay results value. On the other hand, TG assay is based on enzymatic oxidation of glycerol liberated from TG by lipase after free glycerol present in the sample is eliminated by pre-oxidation, so that the data represent a real amount of TG in the samples. PL assay pre-requires enzymatic hydrolysis of choline PL molecules to produce free choline molecules for specific oxidation and quantitation covering PC, sphingomyelin (SPM) and lysoPC. Thus, the copper-induced oxidative reaction should not influence the assay results. TG decreased by 24%, and non-lysoPL (total choline-PL-lysoPC)=PC+SPM decreased by 44% as lysoPC markedly increased and total choline PL remained constant. Increase of lysoPC reached approximately 14-fold of the intact LDL at 20-h oxidation ( $p < 0.001$ ). Total protein level of OxLDL measured by BCA method was more or less constant throughout the incubation. However, immunoreactive apoB level significantly decreased after 3-h incubation (native LDL vs 3-h oxidation  $p < 0.05$ , native LDL vs 4-h oxidation  $p < 0.01$ , native LDL vs 5-, 10-, and 20-h oxidation  $p < 0.001$ ). Changes in chemical composition in OxLDL were not influenced by concentration of the samples by using a membrane concentrator (data not shown) so that the results of the analyses reflected the changes described as above.

### 3.3. Electron micrographic analysis of oxidized LDL

The results of electron micrographic analysis of copper-oxidized LDL are shown in Figs. 5 and 6. Changes in the size during the incubation were demonstrated consistent with the analysis by gradient gel electrophoresis shown in Figs. 1 and 3. Intact LDL particles were mostly spherical with a mean diameter of  $28.1 \pm 1.9$  nm ( $n = 246$ ). The proportion of elliptic or discoidal particles increased with prolonged incubation and as 32.7% and 46.4% at 5-h and 10-h incubation, respectively. Some particles appeared in elliptic or rectangular shape after 5-h incubation, and substantial numbers of the particles were found in an amorphous appearance that has never been observed at earlier oxidation time. The average diameter of the particles at 3-, 5-, 10-, and 20-h oxidation were  $27.5 \pm 1.9$  nm ( $n = 246$ ),  $25.6 \pm 1.7$  nm ( $n = 196$ ),  $26.9 \pm 2.4$  nm ( $n = 167$ ),  $27.1 \pm 2.2$  nm ( $n = 246$ ), respectively. The mean longer and shorter axes of the elliptic particles ( $n = 41$ ) at 5-h oxidation were  $28.3 \pm 2.2$  nm and  $19.8 \pm 1.9$  nm, respectively, to give their mean volume calculated assuming as ellipsoid approximately 50% of that of the native LDL. The mean length and height of rectangular shapes ( $n = 15$ ) at 5-h oxidation were  $27.8 \pm 1.8$  nm and  $15.2 \pm 1.2$  nm to give their mean volume 79% of the native LDL assuming they are discoidal. The mean volume of the ellipsoid particles thus calculated at 10-h incubation was approximately 46% of the native LDL (longer axis:  $29.3 \pm 2.6$  nm, shorter axis:  $19.1 \pm 2.4$  nm,  $n = 21$ ) and that of the discoidal particles (length:  $26.7 \pm 2.8$  nm, height:  $16.6 \pm 3.3$  nm,  $n = 26$ ) was approximately 77% of native LDL. At 20-h incubation, discoidal particles got scarce and the mean volume of the ellipsoid (longer axis:  $28.0 \pm 2.6$  nm, shorter axis:  $20.4 \pm 2.3$  nm,  $n = 25$ ) was approximately 52.6% of the native LDL. LDL particles were almost exclusively spherical even after incubation for 20 h in PBS buffer as control. The mean particle

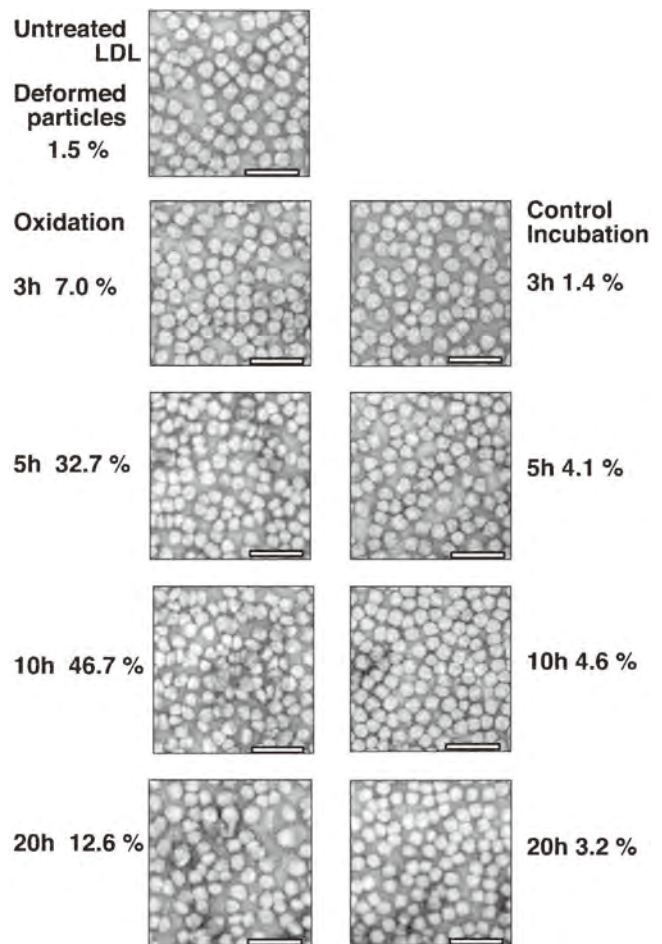


**Fig. 5.** Analysis of the copper-oxidized LDL particles in electron microgram. After OxLDL solutions were centrifuged at  $20,000 \times g$ ,  $4^\circ\text{C}$ , for 1 min, the supernatants were treated with 2% uranyl acetate solution for negative staining. All images were photographed at the same magnification, as a scale bar in each panel indicating 100 nm. The percentage indicates the relative appearance of deformed particles by scanning approximately 500 particles.

diameters ( $n = 246$ ) at the 3-, 5-, 10-, and 20-h control incubation were  $27.9 \pm 1.8$  nm,  $27.8 \pm 2.5$  nm,  $26.8 \pm 1.9$  nm, and  $27.0 \pm 2.0$  nm, respectively, showing very slight but significant decrease after 10-h incubation against the native LDL ( $p < 0.001$ ).

In this particular samples, the levels of LPC at 0-, 3-, 5-, 10-, 20-h oxidation and 20-h control incubation were 7, 33.5, 42.0, 65.5, 80.5 and  $7.5 \mu\text{mol/l}$ , respectively, to give the ratios of LPC/PL increase as 2.6%, 12.1%, 15.5%, 24.7%, 32.9% and 2.7% assuming total PL remained constant (Table 4) showing the increase by 11.5-fold compared by oxidation being consistent with the data in Table 4.

Fig. 6 summarizes size distribution of LDL at each incubation time as histogram profiles. The distribution peak shifts from 27 to 28 nm to 25–26 nm as the oxidation proceeds. However, the large size particles above 28 nm once almost disappear by the 5-h oxidation and increased after 10-h oxidation, in spite that the distribution peak remained same. The increase of the average LDL particle diameters after the apparent transient decrease by the 5-h oxidation was thus demonstrated to be due to the change in size distribution. It should be noted that the volume of the 30 nm particles is double of the 24 nm particles.

## 4. Discussion

It is a widely accepted concept that OxLDL is an “atherogenic” LDL and a potential marker for atherosclerosis risk, as being found

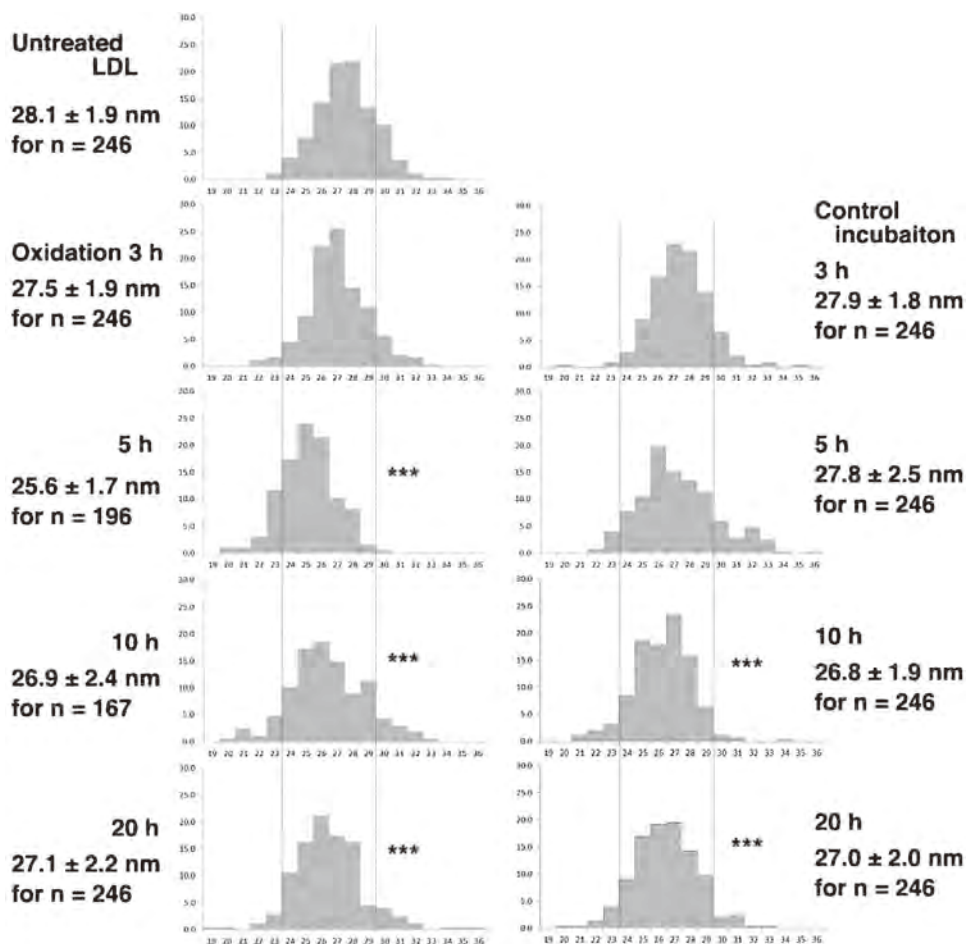


**Fig. 6.** Change in the size of LDL during copper-induced oxidation, based on the electron-micrographic analysis by using Image J software developed by United States National Institute of Health (NIH). The diameter of each particle was estimated by measuring the area of particles assuming they are spherical. Each graph represents histogram of diameters by scanning (nm on the abscissa) and the numbers of particles indicated (on the ordinate), and the data are expressed as mean  $\pm$  S.D. Differences from the untreated control were analyzed by one-way ANOVA. \*\*\* $p < 0.001$  vs. untreated LDL.

in circulation and vascular sub-endothelial layer. The mechanism for its pathogenic function however has not yet been very clear even after long history of investigation of OxLDL. One of the hypotheses is that abnormal size and density of OxLDL may interfere with normal LDL metabolism and lead to cholesterol accumulation in the scavenger cells. However, OxLDL consists of particles varying in size and density, and it is very uncertain if any of these particles are more atherogenic than others. Moreover, the results of the studies on physicochemical properties of OxLDL produced *in vitro* are controversial and conflicting. In an attempt to reconcile these problems, we investigated changes in the physicochemical properties of OxLDL in detail, focusing on their density and particle size.

Major changes in LDL by the oxidation are summarized as follows. (1) Particle size decreased and the density increased as the oxidation proceeds. (2) TG and PL seemed hydrolyzed to increase lysoPC. ApoB was degraded but its fragment products remain on the particles. (3) Advanced oxidation causes amorphous change of particles including forming ellipsoid and discoid and perhaps fusion of these particles. The findings are mainly on copper-oxidized LDL, which was confirmed equivalent to more “physiological” oxidation method by conditioning with HUVECs, as both methods showed similar changes in the density, size, electric charge and degradation of apoB. These changes were largely consistent with many other earlier findings including those of apparent contradictions (discussed in Section 1) as the present

study demonstrated the sequential changes in physical and chemical properties of LDL during oxidative modification were in time-dependent manners with respect to various parameters.

The density of copper-induced OxLDL increased with time of oxidation. The proportion of  $d > 1.044$  subclass represented  $63.8 \pm 8. \%$  after 2-h oxidation and denser LDL became more predominant as the oxidation proceeded, with most LDL shifting to the density 1.063–1.125 subclass (equivalent to HDL<sub>2</sub>) after 20-h oxidation. Similar results were obtained after HUVECs-induced oxidation, but to lesser extent. Changes in chemical composition are consistent with these findings. While protein components largely remain with the particles, lipid components must have decreased during the oxidation because the density of the particles increased. As substantial amount of glycerolipid is hydrolyzed, and lysophospholipid remained in the particles (Table 4), fatty acids cleaved from PC or TG might be removed from the particles. No data is available for the hydrolysis of cholesteryl ester in the present study but a previous report indicated such a reaction during the LDL oxidation (Esterbauer et al., 1992). As a result, surface components of the lipoprotein particles such as protein/peptides, PL including lysoPC may remain more-or less constant while the core lipid TG simply decreased. If cholesteryl ester is hydrolyzed, the core component decreased while the surface components of free cholesterol might increase.

After enzymatic hydrolysis of LDL-PL, lysoPC and fatty acids remained on the particles even in the presence of albumin

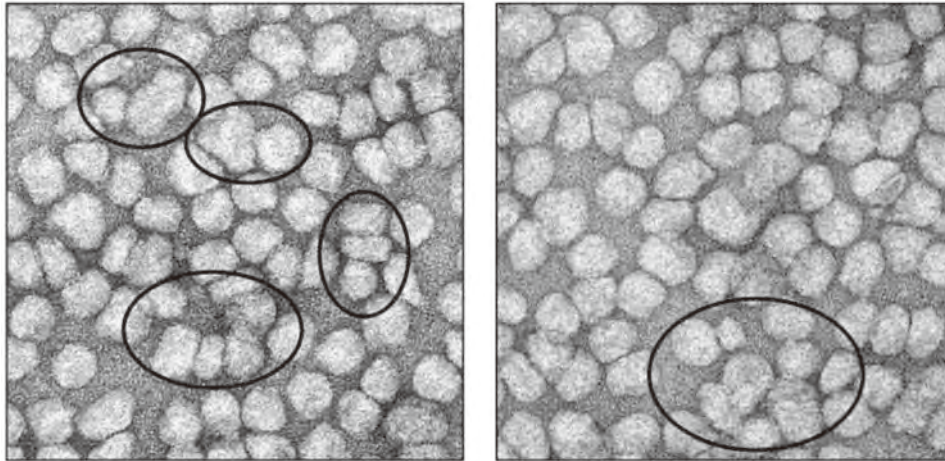


**Fig. 7.** Change in particle shape of LDL by copper-induced oxidation. The micrographs show the particles of LDL oxidized by copper ion for 10 h. Deformation of the particles in shape and size were observed, typically as indicated in circles.

(Aggerbeck et al., 1976). However, unsaturated fatty acids are degraded into lipid peroxides by oxidation, and decomposed into aldehydes including malondialdehyde, acrolein, and 4-hydroxy-2-nonenal in the oxidative reaction (Halliwell and Chirico, 1993). It is therefore conceived that these more water-soluble short chain aldehydes are readily shift to an aqueous phase from the LDL particle. Throughout repeated ultracentrifugation to isolate sub-fractions of OxLDL, only 1–2% of the protein was recovered in the bottom fraction, compared with 1% of native LDL. Therefore, it seems clear that the increased density of OxLDL is the result of the change in the lipid-protein ratio of OxLDL.

An apparent increase of the average diameter of LDL after the advanced/prolonged oxidative reaction was perhaps due to the presence of aggregation and/or fusion of the oxidized LDL that reduced in their size as being suggested in the analysis of size distribution profiles. In fact, the fusion process may be observed even in the view of electron-micrograms (Fig. 7). This may be supported by the findings in electrophoretic size analysis that the sizes of particles in the gel were reduced by the oxidation while we observed more material remained in the loading wells with the samples with prolonged time of oxidation. The particles varied in appearances as the oxidation proceeded. The average diameter of spherical OxLDL was smallest at 5-h oxidation and the proportion of deformed particle with smaller volume was highest at 10-h oxidation. This change may be recovered by further incubation for 20-h by aggregation or fusion of the LDL with reduced-size. This may not be reflected in non-denaturing gradient gel electrophoresis. The findings seem consistent with the report of deformation associated with the decrease of particle volume (Gomez et al., 2010). They showed that copper-induced OxLDL appeared predominantly in a discoid profile with a volume 50% smaller than native LDL.

LDL particles steadily become smaller by the oxidative incubation, but the particles with altered surface properties may aggregate and fuse. The fusion may be facilitated by the presence of lysoPC that accounts for 33–44% of PL at 20-h oxidation. PC and SPM with two carbon (acyl) chains compose a cylindrical shape while lysoPC with a single carbon chain is rather in a shape of cone. Therefore, lysoPC fits in the surface of smaller spheres or ellipsoids with higher curvature when the core lipids decrease. Non-lyso phospholipids with two carbon chains remain on the surface less curved that may be represented discoid as the core lipids reduced. When the core lipids decrease by hydrolysis, discoid particles are produced first, but small spherical or ellipsoids may be produced as lysoPC content increases on the surface. In addition, the changes in

elasticity and viscosity of the surface layer caused by an increase of lysoPC may also influence the shape. Some of these ideas are illustrated in Fig. 8.

The analyses here inevitably have limitations. Electrophoretic mobility may also be influenced by many other physical properties of the particles. The increased mobility observed in gradient gel electrophoresis might be exaggerated by a substantial increase of the negative charge on the particle surface. Density analysis is also

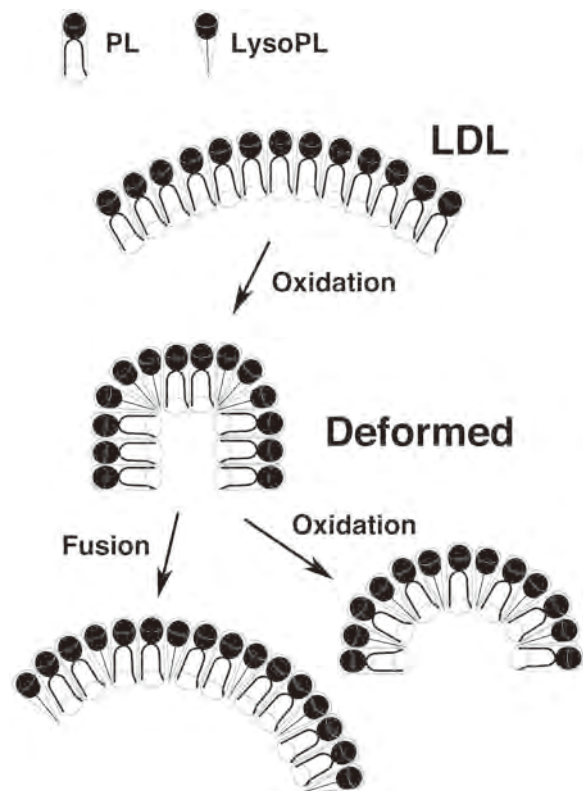


**Fig. 8.** Illustrated structural models for deformation of LDL particles. PC and sphingolipids with two hydrocarbon chains (PL) occupy a cylindrical space while lysoPC and lysosphingolipid (LysoPL) with a single hydrocarbon chain to fill rather a cone space. Ellipsoid particles may be structured with forming surface domain with high curvature by initial generation of lysoPL molecules. Further oxidation generates more lysoPL molecules and fatty acids that may leave lipoprotein particles, to form small spherical and perhaps to cause fusion of particles, making overall appearance rather amorphous.

affected by various factors of the nature of the particles and solvents. Negative staining in electron-microgram might include artifacts resulting from fixation and dehydration of particles on the grid. Changes such as apparent recovery of the LDL size after prolonged incubation might result from destabilization of particle surface, fixation or dehydration.

Further work is needed to address the cause of deformation and the apparent recovery in sphericity and particle size. Our results also showed that OxLDL resembles small dense LDL, a subfraction believed to strongly associate with arteriosclerosis (Austin et al., 1988; Galeano et al., 1998; McNamara et al., 1996). However the significance of this similarity (between OxLDL in vivo and small dense LDL) remains unclear. The advanced change in density may get close to that of HDL<sub>2</sub> that may interfere with assay of plasma HDL, but it also needs further clarification in their properties and physiological significance. Glycation is known to promote oxidation in conjunction with oxidation reactions (Kaneto et al., 1996), and the small dense LDL that often appears in diabetic patients might include OxLDL particles promoted by glycation. Our current methodology is ideally suited to examine the shape and size of glycated particles, which may shed further light on the changes we have observed with OxLDL.

### Conflict of interest

The authors declare that there is no conflict of interest.

### Acknowledgments

We wish to acknowledge Professor Noel Fidge (Monash University, Melbourne, Australia) for helpful discussions during the course of this work and during the preparation of the manuscript. Shinji Yokoyama was supported in part by MEXT-Supported Program for the Strategic Research Foundation at Private Universities (S1201007) and by Grant-in-aid from MEXT-Japan (15H02903).

### References

- Abell, L.L., Levy, B.B., Brodie, B.B., Kendall, F.E., 1952. A simplified method for the estimation of total cholesterol in serum and demonstration of its specificity. *J. Biol. Chem.* 195, 357–366.
- Aggerbeck, L.P., Kezdy, F.J., Scanu, A.M., 1976. Enzymatic probes of lipoprotein structure. Hydrolysis of human serum low density lipoprotein-2 by phospholipase A<sub>2</sub>. *J. Biol. Chem.* 251, 3823–3830.
- Ashraf, M.Z., Gupta, N., 2011. Scavenger receptors: implications in atherothrombotic disorders. *Int. J. Biochem. Cell Biol.* 43, 697–700.
- Austin, M.A., Breslow, J.L., Hennekens, C.H., Buring, J.E., Willett, W.C., Krauss, R.M., 1988. Low-density lipoprotein subclass patterns and risk of myocardial infarction. *JAMA* 260, 1917–1921.
- Bligh, E.G., Dyer, W.J., 1959. A rapid method of total lipid extraction and purification. *Can. J. Biochem. Physiol.* 37, 911–917.
- Chen, Q., Esterbauer, H., Jurgens, G., 1992. Studies on epitopes on low-density lipoprotein modified by 4-hydroxynonenal. Biochemical characterization and determination. *Biochem J.* 288 (Pt 1), 249–254.
- Coresh, J., Kwiterovich Jr., P.O., Smith, H.H., Bachorik, P.S., 1993. Association of plasma triglyceride concentration and LDL particle diameter, density, and chemical composition with premature coronary artery disease in men and women. *J. Lipid Res.* 34, 1687–1697.
- Esterbauer, H., Gebicki, J., Puhl, H., Jurgens, G., 1992. The role of lipid peroxidation and antioxidants in oxidative modification of LDL. *Free Radic. Biol. Med.* 13, 341–390.
- Fong, L.G., Parthasarathy, S., Witztum, J.L., Steinberg, D., 1987. Nonenzymatic oxidative cleavage of peptide bonds in apoprotein B-100. *J. Lipid Res.* 28, 1466–1477.
- Galeano, N.F., Al-Haideri, M., Keyserman, F., Rumsey, S.C., Deckelbaum, R.J., 1998. Small dense low density lipoprotein has increased affinity for LDL receptor-independent cell surface binding sites: a potential mechanism for increased atherogenicity. *J. Lipid Res.* 39, 1263–1273.
- Gomez, S.L., Monteiro, A.M., Rabbani, S.R., Bloise, A.C., Carneiro, S.M., Alves, S., Gidlund, M., Abdalla, D.S., Neto, A.M., 2010. Cu and Fe metallic ions-mediated oxidation of low-density lipoproteins studied by NMR, TEM and Z-scan technique. *Chem. Phys. Lipids* 163, 545–551.
- Halliwel, B., Chirico, S., 1993. Lipid peroxidation: its mechanism, measurement, and significance. *Am. J. Clin. Nutr.* 57, 715S–724S discussion 724S–725S.
- Havel, R.J., Eder, H.A., Bragdon, J.H., 1955. The distribution and chemical composition of ultracentrifugally separated lipoproteins in human serum. *J. Clin. Invest.* 34, 1345–1353.
- Henriksen, T., Mahoney, E.M., Steinberg, D., 1981. Enhanced macrophage degradation of low density lipoprotein previously incubated with cultured endothelial cells: recognition by receptors for acetylated low density lipoproteins. *Proc. Natl. Acad. Sci. U. S. A.* 78, 6499–6503.
- Henriksen, T., Mahoney, E.M., Steinberg, D., 1983. Enhanced macrophage degradation of biologically modified low density lipoprotein. *Arteriosclerosis* 3, 149–159.
- Hidaka, A., Inoue, K., Kutsukake, S., Adachi, M., Kakuta, Y., Kojo, S., 2005. Decrease in the particle size of low-density lipoprotein (LDL) by oxidation. *Bioorg. Med. Chem. Lett.* 15, 2781–2785.
- Igarashi, K., Tsuji, M., Nishimura, M., Horimoto, M., 2004. Improvement of endothelium-dependent coronary vasodilation after a single LDL apheresis in patients with hypercholesterolemia. *J. Clin. Apher.* 19, 11–16.
- Itabe, H., 2009. Oxidative modification of LDL: its pathological role in atherosclerosis. *Clin. Rev. Allergy Immunol.* 37, 4–11.
- Kamiyama, M., Kishimoto, Y., Tani, M., Utsunomiya, K., Kondo, K., 2009. Effects of equol on oxidized low-density lipoprotein-induced apoptosis in endothelial cells. *J. Atheroscler. Thromb.* 16, 239–249.
- Kaneto, H., Fujii, J., Myint, T., Miyazawa, N., Islam, K.N., Kawasaki, Y., Suzuki, K., Nakamura, M., Tatsumi, H., Yamasaki, Y., Taniguchi, N., 1996. Reducing sugars trigger oxidative modification and apoptosis in pancreatic beta-cells by provoking oxidative stress through the glycation reaction. *Biochem. J.* 320 (Pt 3), 855–863.
- Kato, Y., Mori, Y., Makino, Y., Morimitsu, Y., Hiroi, S., Ishikawa, T., Osawa, T., 1999. Formation of Nepsilon-(hexanonyl) lysine in protein exposed to lipid hydroperoxide. A plausible marker for lipid hydroperoxide-derived protein modification. *J. Biol. Chem.* 274, 20406–20414.
- Kido, T., Kurata, H., Matsumoto, A., Tobiyama, R., Musha, T., Hayashi, K., Tamai, S., Utsunomiya, K., Tajima, N., Fidge, N., Itakura, H., Kondo, K., 2001. Lipoprotein analysis using agarose gel electrophoresis and differential staining of lipids. *J. Atheroscler. Thromb.* 8, 7–13.
- Kondo, A., Muranaka, Y., Ohta, I., Notsu, K., Manabe, M., Kotani, K., Saito, K., Maekawa, M., Kanno, T., 2001. Relationship between triglyceride concentrations and LDL size evaluated by malondialdehyde-modified LDL. *Clin. Chem.* 47, 893–900.
- Krauss, R.M., Burke, D.J., 1982. Identification of multiple subclasses of plasma low density lipoproteins in normal humans. *J. Lipid Res.* 23, 97–104.
- Kugiyama, K., Kerns, S.A., Morrisett, J.D., Roberts, R., Henry, P.D., 1990. Impairment of endothelium-dependent arterial relaxation by lysolecithin in modified low-density lipoproteins. *Nature* 344, 160–162.
- Kume, N., 2010. Molecular mechanisms of coronary atherosclerotic plaque formation and rupture. *Nihon Rinsho* 68, 637–641.
- Kume, N., Gimbrone Jr., M.A., 1994. Lysophosphatidylcholine transcriptionally induces growth factor gene expression in cultured human endothelial cells. *J. Clin. Invest.* 93, 907–911.
- Laemmli, U.K., 1970. Cleavage of structural proteins during the assembly of the head of bacteriophage T4. *Nature* 227, 680–685.
- Lougheed, M., Moore, E.D., Scriven, D.R., Steinbrecher, U.P., 1999. Uptake of oxidized LDL by macrophages differs from that of acetyl LDL and leads to expansion of an acidic endolysosomal compartment. *Arterioscler. Thromb. Vasc. Biol.* 19, 1881–1890.
- McNamara, J.R., Small, D.M., Li, Z., Schaefer, E.J., 1996. Differences in LDL subspecies involve alterations in lipid composition and conformational changes in apolipoprotein B. *J. Lipid Res.* 37, 1924–1935.
- Meyer, D.F., Nealis, A.S., Macphee, C.H., Groot, P.H., Suckling, K.E., Bruckdorfer, K.R., Perkins, S.J., 1996. Time-course studies by synchrotron X-ray solution scattering of the structure of human low-density lipoprotein during Cu(2+)-induced oxidation in relation to changes in lipid composition. *Biochem. J.* 319 (Pt 1), 217–227.
- Morton, R.E., West, G.A., Hoff, H.F., 1986. A low density lipoprotein-sized particle isolated from human atherosclerotic lesions is internalized by macrophages via a non-scavenger-receptor mechanism. *J. Lipid Res.* 27, 1124–1134.
- Obama, T., Kato, R., Masuda, Y., Takahashi, K., Aiuchi, T., Itabe, H., 2007. Analysis of modified apolipoprotein B-100 structures formed in oxidized low-density lipoprotein using LC-MS/MS. *Proteomics* 7, 2132–2141.
- Parthasarathy, S., Wieland, E., Steinberg, D., 1989. A role for endothelial cell lipoxygenase in the oxidative modification of low density lipoprotein. *Proc. Natl. Acad. Sci. U. S. A.* 86, 1046–1050.
- Pentikainen, M.O., Lehtonen, E.M., Kovanen, P.T., 1996. Aggregation and fusion of modified low density lipoprotein. *J. Lipid Res.* 37, 2638–2649.
- Saita, E., Kishimoto, Y., Tani, M., Iizuka, M., Toyozaki, M., Sugihara, N., Kondo, K., 2012. Antioxidant activities of Perilla frutescens against low-density lipoprotein oxidation in vitro and in human subjects. *J. Oleo Sci.* 61, 113–120.
- Spiteller, G., 2005. The relation of lipid peroxidation processes with atherogenesis: a new theory on atherogenesis. *Mol. Nutr. Food Res.* 49, 999–1013.
- Steinberg, D., 1997. Lewis A. Conner Memorial Lecture. Oxidative modification of LDL and atherogenesis. *Circulation* 95, 1062–1071.
- Steinbrecher, U.P., Parthasarathy, S., Leake, D.S., Witztum, J.L., Steinberg, D., 1984. Modification of low density lipoprotein by endothelial cells involves lipid peroxidation and degradation of low density lipoprotein phospholipids. *Proc. Natl. Acad. Sci. U. S. A.* 81, 3883–3887.

- Steinbrecher, U.P., Witztum, J.L., Parthasarathy, S., Steinberg, D., 1987. Decrease in reactive amino groups during oxidation or endothelial cell modification of LDL. Correlation with changes in receptor-mediated catabolism. *Arteriosclerosis* 7, 135–143.
- Torzewski, M., Suriyaphol, P., Paprotka, K., Spath, L., Ochsenhirt, V., Schmitt, A., Han, S.R., Husmann, M., Gerl, V.B., Bhakdi, S., Lackner, K.J., 2004. Enzymatic modification of low-density lipoprotein in the arterial wall: a new role for plasmin and matrix metalloproteinases in atherogenesis. *Arterioscler. Thromb. Vasc. Biol.* 24, 2130–2136.
- Witztum, J.L., Steinberg, D., 1991. Role of oxidized low density lipoprotein in atherogenesis. *J. Clin. Invest.* 88, 1785–1792.
- Yla-Herttuala, S., Palinski, W., Rosenfeld, M.E., Parthasarathy, S., Carew, T.E., Butler, S., Witztum, J.L., Steinberg, D., 1989. Evidence for the presence of oxidatively modified low density lipoprotein in atherosclerotic lesions of rabbit and man. *J. Clin. Invest.* 84, 1086–1095.
- Zarev, S., Bonnefont-Rousselot, D., Cosson, C., Beaudoux, J.L., Delattre, J., Gardes-Albert, M., Legrand, A., Therond, P., 2002. In vitro low-density lipoprotein oxidation by copper or  $^{\bullet}\text{OH}/\text{O}^{\bullet}(2-)$ : new features on carbonylation and fragmentation of apolipoprotein B during the lag phase. *Arch. Biochem. Biophys.* 404, 10–17.
- Zarev, S., Bonnefont-Rousselot, D., Jedidi, I., Cosson, C., Couturier, M., Legrand, A., Beaudoux, J.L., Therond, P., 2003. Extent of copper LDL oxidation depends on oxidation time and copper/LDL ratio: chemical characterization. *Arch. Biochem. Biophys.* 420, 68–78.

# ABCA1-dependent sterol release: sterol molecule specificity and potential membrane domain for HDL biogenesis

Yoshio Yamauchi,<sup>1,\*†</sup> Shinji Yokoyama,<sup>§</sup> and Ta-Yuan Chang<sup>1,†</sup>

Department of Biochemistry II,\* Nagoya University Graduate School of Medicine, Nagoya 466-8550, Japan; Department of Biochemistry,<sup>†</sup> Geisel School of Medicine at Dartmouth, Hanover, NH 03755; and Nutritional Health Science Research Center and Department of Food and Nutritional Sciences,<sup>§</sup> Chubu University, Kasugai 487-8501, Japan

**Abstract** Mammalian cells synthesize various sterol molecules, including the C30 sterol, lanosterol, as cholesterol precursors in the endoplasmic reticulum. The build-up of precursor sterols, including lanosterol, displays cellular toxicity. Precursor sterols are found in plasma HDL. How these structurally different sterols are released from cells is poorly understood. Here, we show that newly synthesized precursor sterols arriving at the plasma membrane (PM) are removed by extracellular apoA-I in a manner dependent on ABCA1, a key macromolecule for HDL biogenesis. Analysis of sterol molecules by GC-MS and tracing the fate of radiolabeled acetate-derived sterols in normal and mutant Niemann-Pick type C cells reveal that ABCA1 prefers newly synthesized sterols, especially lanosterol, as the substrates before they are internalized from the PM. We also show that ABCA1 resides in a cholesterol-rich membrane domain resistant to the mild detergent, Brij 98. Blocking ACAT activity increases the cholesterol contents of this domain. Newly synthesized C29/C30 sterols are transiently enriched within this domain, but rapidly disappear from this domain with a half-life of less than 1 h. Our work shows that substantial amounts of precursor sterols are transported to a certain PM domain and are removed by the ABCA1-dependent pathway.—Yamauchi, Y., S. Yokoyama, and T.-Y. Chang. ABCA1-dependent sterol release: sterol molecule specificity and potential membrane domain for HDL biogenesis. *J. Lipid Res.* 2016. 57: 77–88.

**Supplementary key words** ATP binding cassette transporter A1 • acyl-CoA:cholesterol acyltransferase • cholesterol/efflux • cholesterol/trafficking • high density lipoprotein • lipid rafts • lanosterol • Niemann-Pick disease type C

*This work was supported by an American Heart Association Postdoctoral Fellowship (to Y.Y.), JSPS KAKENHI from the Japan Society for the Promotion of Sciences (to Y.Y. and S.Y., respectively), a MEXT-Supported Program for the Strategic Research Foundation at Private Universities from the Ministry of Education, Culture, Sports, Science and Technology of Japan (to S.Y.), and by a grant from the National Institutes of Health, HL060306 (to T.-Y.C.). Its contents are solely the responsibility of the authors and do not necessarily represent the official views of the National Institutes of Health. The authors declare no conflicts of interest.*

Manuscript received 18 September 2015 and in revised form 14 October 2015.

Published, JLR Papers in Press, October 24, 2015

DOI 10.1194/jlr.M063784

Copyright © 2016 by the American Society for Biochemistry and Molecular Biology, Inc.

This article is available online at <http://www.jlr.org>

Although cholesterol is an essential lipid, its accumulation in membranes is toxic to cells. Cholesterol homeostasis is tightly controlled in cells by elaborate systems (1, 2). Impairment of cholesterol homeostasis causes various congenital and acquired human diseases (3). In peripheral cells, two pathways play major roles to prevent the excess build-up of unesterified cholesterol: 1) its esterification by ACAT1 at the endoplasmic reticulum (ER); and 2) its release from cells by several ABC transporter proteins (2, 4, 5). Evidence suggests that ACAT1 and ABCA1 work in concert to eliminate excess cellular unesterified cholesterol (6, 7).

The cholesterol biosynthetic pathway involves the biosynthesis of a series of precursor sterols in addition to cholesterol. Lanosterol, a C30 sterol having three extra methyl groups, is the first sterol synthesized in the pathway and is structurally distinct from the C27 sterol, cholesterol. The dihydro-derivative of lanosterol (dihydrolanosterol), but not cholesterol, downregulates the protein stability of HMG-CoA reductase, the key enzyme in sterol biosynthesis (8, 9). Excess build-up of lanosterol in cells causes severe cytotoxicity (10, 11). In humans, abnormal accumulation of various precursor sterols, including lanosterol, due to deficiency in a distal cholesterol biosynthetic enzyme is associated with malformation syndromes (12, 13). It is therefore essential that cells are able to minimize the cellular build-up of precursor sterols. Others and we had previously shown that upon biosynthesis at the ER, substantial amounts of precursor sterols are transported to the plasma membrane (PM) (14–17). These precursor sterols are then rapidly transported back from the PM to the ER to undergo enzymatic demethylations and other reactions to be converted

Abbreviations: 9cRA, 9-*cis* retinoic acid; DRM, detergent-resistant membrane; ER, endoplasmic reticulum; HEK/hABCA1, HEK293 cells stably expressing human ABCA1; HSF, human skin fibroblast; LE, late endosome; LS, lysosome; MEF, mouse embryonic fibroblast; NPA, Niemann-Pick disease type A; NPC, Niemann-Pick disease type C; PM, plasma membrane; PNS, postnuclear supernatant; TX, Triton X.

<sup>†</sup>To whom correspondence should be addressed.

e-mail: [yyoshio@med.nagoya-u.ac.jp](mailto:yyoshio@med.nagoya-u.ac.jp) (Y.Y.); [Ta.Yuan.Chang@Dartmouth.edu](mailto:Ta.Yuan.Chang@Dartmouth.edu) (T.-Y.C.)

to cholesterol (17, 18). Circulating lipoproteins such as HDL contain small, but significant, amounts of various precursor sterols, including lanosterol and other methylated sterols (i.e., C28, C29, and C30 sterols) (19). Also, nonhepatic cells export various C27 precursor sterols, including desmosterol and lathosterol, to HDL and LDL (15, 16).

In extrahepatic cells, cellular cholesterol release is primarily carried out by HDL. The ABC transporter, ABCA1, plays an essential role in the generation of HDL. Defective mutation in the *ABCA1* gene causes Tangier disease, a familial HDL deficiency (20–22). ABCA1 mediates cellular cholesterol and phospholipid release to helical apolipoproteins, including apoA-I, which results in the formation of nascent HDL (23, 24). ABCA1 primarily resides in and mediates HDL biogenesis at the PM (25–27), while a small but significant amount of ABCA1 is also present in the endocytic compartments (28); internalized ABCA1 is degraded or recycled back to the PM (26). How ABCA1 acts to regulate lipid release has been the subject of much investigation [reviewed in (4, 29)], but the precise mechanism remains unsettled. Direct interaction between apoA-I and ABCA1 has been shown (30–32). It has also been reported that ABCA1 at the PM produces membrane deformation sites where apoA-I interacts and solubilizes lipids present in these domains to generate nascent HDL (33, 34). These results lead one to speculate that the lipid compositions of nascent HDL may reflect those of a membrane domain where nascent HDL is assembled. However, there has been controversy regarding the membrane domains where ABCA1 resides (35, 36).

In this work, we seek to determine the sterol specificity of ABCA1 as a lipid transporter. We also report the dynamic relationship between the potential membrane domain that contains ABCA1 and the newly synthesized lanosterol.

## MATERIALS AND METHODS

### Materials

apoA-I was prepared as previously described (37). Delipidation of FBS was performed as described (38). [ $^3\text{H}$ ]acetic acid and [ $^3\text{H}$ ]cholesterol were from American Radio Chemicals. TO901317, 9-*cis* retinoic acid (9cRA), and fatty acid-free BSA were from Sigma. An ACAT inhibitor, F12511, was a gift of Pierre Fabre Research (Castres Cedex, France). Other chemicals were from Fisher, Sigma, or Wako.

### Cell culture and media

Mouse embryonic fibroblasts (MEFs) from *Abca1*<sup>+/+</sup> (WT) and *Abca1*<sup>-/-</sup> mice were isolated and used for experiments, as previously described (18, 39). HEK293 cells stably expressing human ABCA1 (clone 293/2c, hereafter referred as to HEK/hABCA1) were established previously (40). WT CHO cells and 25RA CHO cells were employed as described (7, 17). 25RA cells contain a gain-of-function mutation in the cholesterol sensor, Scap (41, 42). Normal human skin fibroblast (HSF) lines were from Drs. Bzik and Brinckerhoff (Geisel School of Medicine at Dartmouth) (designated N-1, N-2, and N-3 in this work) and from Dr. Peter Pentchev, formerly at National Institutes of Health (designated

N-4). The normal HSF cell line, GM00038 (designated N-5), was obtained from Coriell Institute. Niemann-Pick disease type C (NPC) patient-derived HSF cell lines, NPC1 HSF GM03123 (designated C1-1) containing P237S/I1061T mutations in NPC1 protein and GM17912 (designated C1-2) containing P1007A/T1036M mutations in NPC1 protein, were from Coriell Institute. Another NPC1 HSF cell line, NIH 93.22 (designated C1-3) (mutations are not determined), was from Dr. Pentchev. The NPC2 HSF cell line, GM17910 (designated C2-1), which contains C93F/C93F mutations in NPC2 protein, was from Coriell Institute. Another NPC2 HSF cell line (designated C2-2) (mutations are not determined) was kindly provided from Dr. Yiannis A. Ioannou (Mount Sinai School of Medicine). Niemann-Pick disease type A (NPA) HSF cell line, GM00112, which contains L302P/L302P mutations in acid sphingomyelinase protein, was from Coriell Institute. Some of the HSF lines used here were employed in our previous study (17). HSFs and MEFs were grown in DMEM with penicillin and streptomycin supplemented with 10% FBS (17, 18). The human monocyte-like THP-1 cells were differentiated to macrophage-like cells by using the procedure described in (43). All cells were grown in humidified CO<sub>2</sub> incubators at 37°C. Media used are designated as follows: medium A contained 10 or 7.5% FBS, medium B contained 0.1% fatty acid-free BSA, medium D contained 5% delipidated FBS, and medium F contained no supplements.

### Sterol release assays

Cells (CHO, HEK293, HSFs, and MEFs) were seeded into 6-well plates, as described (7, 17, 18). HSFs and MEFs were pretreated or not pretreated with 9cRA (RXR ligand) and/or the synthetic LXR agonist, TO901317, as indicated in the figure legends, to induce ABCA1 expression. Afterwards, cells were incubated with or without apoA-I (5 or 10 µg/ml) in the presence or absence of 9cRA and/or TO901317 in medium B for various times, as indicated in the figure legends. The release of endogenously synthesized sterols was monitored after incubating cells with [ $^3\text{H}$ ]acetate (20 or 40 µCi/ml) for either a short or long period of time, as described in the figure legends. Alternatively, cells were labeled with [ $^3\text{H}$ ]cholesterol (0.1 µCi/ml). ABCA1-dependent sterol release was calculated by subtracting the values obtained without apoA-I from the values obtained with apoA-I. To identify each sterol species by GC-MS, HEK/hABCA1 cells were grown in 100 mm dishes. Lipid efflux was induced by incubating cells with apoA-I in medium B for 48 h. The medium from two 100 mm dishes was pooled for sterol analysis.

### Cell fractionation

Cells grown in 100 mm dishes at subconfluent stage were treated with 1.0 ml of TNE buffer [25 mM Tris-HCl (pH 7.5), 150 mM NaCl, 5 mM EDTA] that contained protease inhibitor cocktail (Sigma) and various detergents, according to procedures described (44), and 1.0% Triton X-100 (TX100), 1.0% Triton X-102 (TX102), 1.0% Brij 58, 1.0% Lubrol WX, 2.0% CHAPS, 1.0% CHAPSO, or 1.0% Tween 20 for 30 min at 4°C, or with 1.0% Brij 98 for 10 min at 37°C. After treatment with a detergent, cell lysates were harvested and homogenized with 10 strokes by using a Dura-Grind stainless steel dounce tissue grinder (Wheaton). Cell homogenate was spun twice at 1,000 *g* for 5 min; the resulting postnuclear supernatant (PNS) was subjected to Opti-Prep (Axis-Shield) or sucrose gradient ultracentrifugation, as described previously (45). Briefly, the PNS was mixed with Opti-Prep or with 80% sucrose (in TNE buffer) to be at 37.5 or 40% as a final concentration, respectively, and placed at the bottom of an ultracentrifuge tube. Optiprep (30%) or sucrose (30%) were layered and TNE buffer or 5% sucrose was then layered on the

top. After centrifugation at 200,000 *g* for 3 h at 4°C in a SW41 or SW60 rotor (Beckman), eight 0.5 ml fractions or eleven 1 ml fractions were collected from the top, respectively. Alternatively, PNS was centrifuged at 100,000 *g* for 60 min to isolate detergent-resistant membrane (DRM) as pellet and detergent-soluble fraction as supernatant (46).

### Lipid extraction and analysis

Cellular lipids were extracted by hexane/isopropanol (3:2, v/v). Lipids in medium or fractions from cell fractionation experiments were extracted by 4 vol of chloroform/methanol (2:1, v/v). Lipids extracted were dried under nitrogen gas at 40–45°C. Amounts of total cholesterol, free cholesterol, and choline-phospholipid were measured by colorimetric enzymatic assay systems, as described previously (7). Cholesteryl ester was determined by subtracting free cholesterol from total cholesterol. Cellular and medium lipids containing radio-labeled sterols were prepared by saponification, and nonsaponifiable fractions (containing labeled sterols) were separated by TLC in a solvent system of methylene chloride/ethyl acetate (97:3, v/v), as described (17). For GC-MS, extracted lipids were saponified and nonsaponifiable lipids (containing sterols) were isolated and dried under N<sub>2</sub> gas. Sterol derivatization and GC-MS analysis were performed essentially as described previously (17). Epicoprostanol served as an internal standard.

### Antibodies and immunoblot

Anti-human ABCA1 rabbit serum was produced previously (47). Other antibodies were obtained from commercial sources as follows; anti-caveolin-1 polyclonal antibodies (N-20) and anti-LAMP-2 monoclonal antibody (H4B4) from Santa Cruz Biotechnology, anti-flotillin-1 monoclonal antibody and anti-calnexin monoclonal antibody from BD Biosciences, and anti-β-actin monoclonal antibody from Sigma. Whole cell lysate was prepared by using lysis buffer [50 mM Tris-HCl (pH 7.5), 150 mM NaCl, 1% NP40, and protease inhibitor cocktail]. Protein concentration was determined by BCA protein assay (Pierce). Equal amounts of cell protein or equal amounts of fraction were subjected to SDS-PAGE and immunoblot analysis by using antibodies, as indicated in the figure legends.

### Statistical analysis

Data are presented as mean ± SD. Statistical analyses of results were performed using a two-tailed unpaired Student's *t*-test. The difference between two sets of values was considered significant when the *P* value was <0.05 (\**P* < 0.05, \*\**P* < 0.01, \*\*\**P* < 0.001).

## RESULTS

### Sterol specificity of ABCA1-mediated sterol release

To determine the specificity of sterol molecules in the ABCA1-dependent lipid release, we first employed the HEK293 cell system (40); these cells express neither ABCA1 nor any other ABC transporters involved in cholesterol release. HEK293 cells that ectopically express ABCA1 are therefore suitable to determine the ABCA1-specific sterol release. We incubated HEK/hABCA1 cells in medium without serum, but with apoA-I, collected the conditioned medium, and analyzed its sterol composition by GC-MS. The result showed that, in addition to a peak of the internal standard, epicoprostanol (retention time of

14.4 min), we found not only a major peak with a retention time of 15.3 min, but also other minor peaks, including one having a retention time of 17.1 min (Fig. 1A). Subsequent analysis (by molecular ion and fragmentation pattern analysis) identified the major peak as cholesterol and the second major peak as lanosterol (C30) (Table 1). The amount of lanosterol released was  $2.8 \pm 0.1\%$  (*n* = 3) of cholesterol. Other minor peaks were found to be desmosterol (C27), monomethylsterol (C28), and dimethylsterol (C29). The results indicate that, in addition to cholesterol, ABCA1 mediates the release of substantial amounts of lanosterol and other methylated sterols to apoA-I (Fig. 1A). Cellular sterol analyses showed that lanosterol content was  $0.6 \pm 0.2\%$  (*n* = 3) of cholesterol. The results described in Fig. 1A and Table 1 suggest that lanosterol is preferentially released from cells in an ABCA1-dependent manner. To test this interpretation, we compared apoA-I-mediated release of sterols synthesized de novo between parental HEK293 and HEK/hABCA1 cells (Fig. 1B, C) and between WT and *Abca1*<sup>-/-</sup> MEFs (Fig. 1D, E). We incubated these cells with apoA-I for 8 h in the presence of [<sup>3</sup>H]acetate (to label newly synthesized sterols) and analyzed [<sup>3</sup>H]-labeled sterols released from cells by TLC. This TLC system efficiently separates C29/C30 sterols (including lanosterol) from the C28 and the C27 sterols (17). The results showed that HEK/hABCA1 cells and WT MEFs released labeled C27 sterols and labeled C29/C30 sterols. These cells also released labeled C28 sterols, but in much smaller quantities (Fig. 1B, D). We calculated the labeled C29/C30 sterols or the labeled C27 sterols in the medium versus the same sterol species in cells. The result showed that, indeed, the C29/C30 sterols were released more efficiently than the C27 sterols (Fig. 1C, E). In HEK293 cells and *Abca1*<sup>-/-</sup> MEFs, none of the labeled sterols were released, demonstrating an essential role of ABCA1 in cholesterol and lanosterol release. In macrophages, ABCA1 plays a major role in cellular sterol efflux. We performed a similar [<sup>3</sup>H]acetate-labeling experiment in THP-1 human macrophage-like cells and analyzed radioactive sterols by TLC. The result showed that the same sterol specificity in apoA-I/ABCA1-mediated sterol release was also observed in the human macrophage-like cells (Fig. 1F, G). Together, these results show that lanosterol is a preferred sterol released from cells by the apoA-I/ABCA1 pathway.

### Newly synthesized sterols, but not recycling sterols, are the preferential source for ABCA1-dependent sterol release

The results presented in Fig. 1 suggest that ABCA1 preferentially releases newly synthesized sterols to apoA-I, shortly after these sterols arrive at the PM. To confirm this, we made use of HSFs isolated from NPC patients. In NPC1- or NPC2-deficient cells, cholesterol transport from the endosome to the PM is defective, but ER-to-PM sterol transport is normal (17, 48). We compared the release of endogenously synthesized sterols to apoA-I in HSFs isolated from normal and NPC subjects under various conditions (Fig. 2A). When cells were incubated with apoA-I for 8 h in the presence of [<sup>3</sup>H]acetate, the labeled C29/C30,

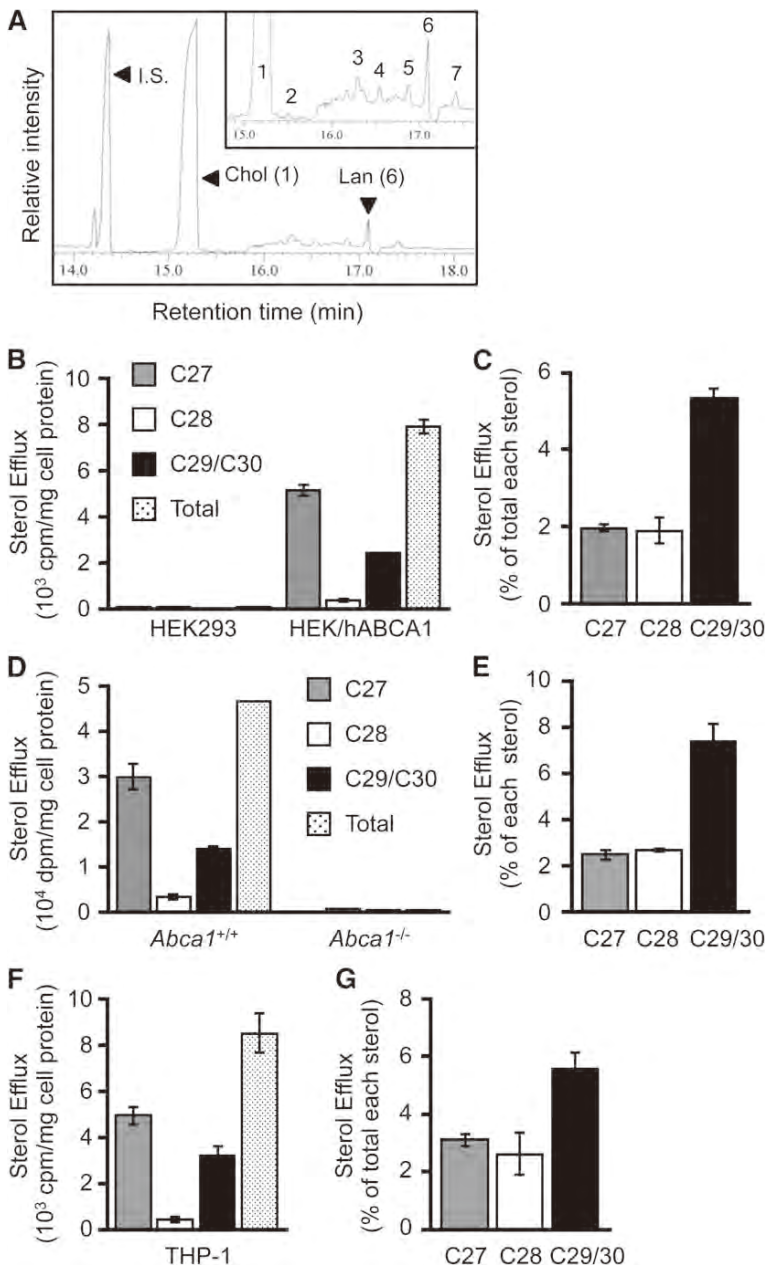


**Fig. 1.** Sterol specificity of ABCA1. A: GC-MS analysis of apoA-I-mediated sterol release. HEK/hABCA1 cells were incubated with apoA-I (10  $\mu$ g/ml). Lipids were extracted from medium, saponified, and analyzed by GC-MS, as described in Materials and Methods. The peaks of epicoprostanol [internal standard (I.S.)], cholesterol (Chol, peak 1), and lanosterol (Lan, peak 6) are indicated by arrowheads. Other minor peaks (2–5 and 7) are shown in the inset and described in Table 1. B–G: HEK293 and HEK/hABCA1 (B, C), and WT and *Abca1*<sup>-/-</sup> (D, E) MEFs were treated with 1  $\mu$ g/ml of TO901317 for 24 h, and differentiated THP-1 cells (F, G) were incubated with or without apoA-I in the presence of [<sup>3</sup>H]acetate for 8 h in 6-well plates. Lipids were extracted from medium and cells, and were saponified. Sterols were analyzed by TLC. Results are shown as cpm or dpm of [<sup>3</sup>H]sterol per milligram of cell protein (B, D, F) or as percent release relative to each [<sup>3</sup>H]sterol synthesized [medium/(medium + cell)  $\times$  100] (C, E, G). Error bars represent SD (n = 3).

C28, and C27 sterols were all available to apoA-I-mediated release in HSFs, and the release of C29/C30 sterol was more efficient than that of the C27 sterol (Fig. 2B). As expected, the release of all sterol species was not impaired in HSFs from NPC patients. When HSFs were pulse-labeled with [<sup>3</sup>H]acetate for only 2 h followed by chase with apoA-I, the lower radioactive counts in labeled sterols (due to rapid conversion of precursor sterols) only allowed us to monitor C27 sterols reliably, but the result again showed that the release of C27 sterols was not impaired in NPC HSFs (Fig. 2C). Instead, when cells were labeled with [<sup>3</sup>H]acetate for a prolonged period (16 h) followed by a long chase period without the labeled acetate (24 h), and were then incubated with apoA-I for 8 h, the result showed that the release of labeled C27 sterol was severely affected in

NPC HSFs (Fig. 2D). Under this condition, in normal HSFs, 99% of labeled sterols were C27 sterols; in NPC HSFs, only 84% of labeled sterols were C27 sterols, and C29/C30 and C28 sterols were approximately 7 and 9%, respectively. The build-up of labeled C29/C30 and C28 sterols in NPC mutant cells was previously reported (17). We then performed a third set of experiments by labeling HSFs with [<sup>3</sup>H]cholesterol for 16 h, chasing them without the label for 24 h, and then monitoring apoA-I-dependent cholesterol release. The result showed that when compared with the normal HSFs, the release of [<sup>3</sup>H]cholesterol was markedly reduced in NPC HSFs (Fig. 2E). Together, these results demonstrate that once arriving at the PM, a certain portion of all newly synthesized sterols are quickly releasable via the ABCA1/apoA-I system from

TABLE 1. Identification of sterols released to apoA-I in HEK/hABCA1 cells

Peak	Sterol (number of carbons)	Retention Time (min)	Protein (ng/mg)	Percent of Total
1	Cholesterol (C27)	15.3	4,392.6	93.6
2	Desmosterol (C27)	15.5	10.7	0.2
3	Monounsaturated monomethylsterol (C28)	16.3	41.6	0.9
4	Monounsaturated monomethylsterol (C28)	16.6	40.3	0.9
5	Monounsaturated dimethylsterol (C29)	16.9	48.9	1.0
6	Lanosterol (C30)	17.1	119.7	2.6
7	Diunsaturated dimethylsterol (C29)	17.4	40.4	0.9
	C27 sterols	—	4403.3	93.8
	C28 sterols	—	81.9	1.7
	C29/C30 sterols	—	208.9	4.5

HEK/hABCA1 cells were incubated with apoA-I. Sterols extracted from the conditioned medium were analyzed by GC-MS. The GC-MS profile is shown in Fig. 1A. The result shown is a typical result of three independent experiments.

the PM, with C29/C30 sterols as the preferred substrate. Later, the endogenously synthesized sterols traverse through other compartments, including the late endosome (LE)/lysosome (LS) compartment (49); their egression from the LE/LS for ABCA1/apoA-I-dependent release becomes dependent on NPC1 and NPC2 proteins.

This interpretation can also explain the previous reports showing that apoA-I/ABCA1-mediated release of radiolabeled cholesterol is impaired in NPC1-deficient macrophages and fibroblasts, when these cells are incubated with radiolabeled cholesterol for a long period of time (50, 51).

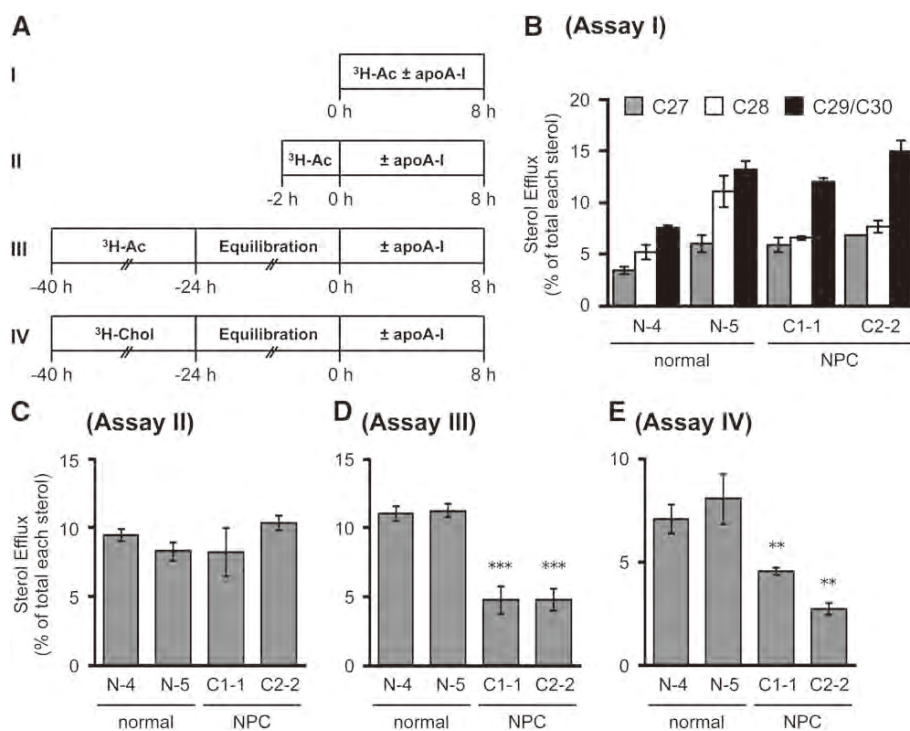


**Fig. 2.** Dependency of NPC1/NPC2 proteins of apoA-I-mediated release of sterols endogenously synthesized. A: Schematic procedures for pulse-chase experiments employed (assays I–IV). Cells were labeled with either [ $^3\text{H}$ ]acetate ( $^3\text{H-Ac}$ ) or [ $^3\text{H}$ ]cholesterol ( $^3\text{H-Chol}$ ). B–E: apoA-I-mediated release of labeled sterols in normal and NPC HSFs. HSFs from normal subjects (N-4 and N-5) or NPC patients (C1-1, NPC1 patient; C2-2, NPC2 patient) were seeded in 6-well plates and grown in medium A to subconfluent stage. Cells were then subjected to assay I, II, III, or IV by labeling cells with [ $^3\text{H}$ ]acetate or [ $^3\text{H}$ ]cholesterol as below. B: Cells pretreated with TO901317 (1  $\mu\text{g}/\text{ml}$ ) for 18 h were incubated with or without apoA-I (10  $\mu\text{g}/\text{ml}$ ) during the 8 h [ $^3\text{H}$ ]acetate (40  $\mu\text{Ci}/\text{ml}$ ) labeling period with TO901317. C: Cells were labeled with [ $^3\text{H}$ ]acetate (40  $\mu\text{Ci}/\text{ml}$ ) for 2 h followed by washing off the label and incubation with or without apoA-I (10  $\mu\text{g}/\text{ml}$ ) in the presence of TO901317 for 8 h. D, E: Cells were labeled with [ $^3\text{H}$ ]acetate (20  $\mu\text{Ci}/\text{ml}$ ) for 16 h in medium D (D) or with [ $^3\text{H}$ ]cholesterol (0.1  $\mu\text{Ci}/\text{ml}$ ) in medium A (E), followed by washing off the label and incubation with medium D with TO901317 for 24 h. The cells were then incubated with or without apoA-I (10  $\mu\text{g}/\text{ml}$ ) for 8 h in the presence of TO901317. Sterols were analyzed by TLC. Data shown are mean  $\pm$  SD ( $n = 3$ ). \*\* $P < 0.01$ , \*\*\* $P < 0.001$ .

Next, lipid release from normal and NPC HSFs exposed to apoA-I was examined in the absence (Fig. 3A) or presence (Fig. 3B) of LXR and RXR ligands. Genetic heterogeneity

exists among human cells of different origin. We thus used five normal and five mutant NPC (containing mutations in either NPC1 or NPC2) fibroblasts. The results showed that

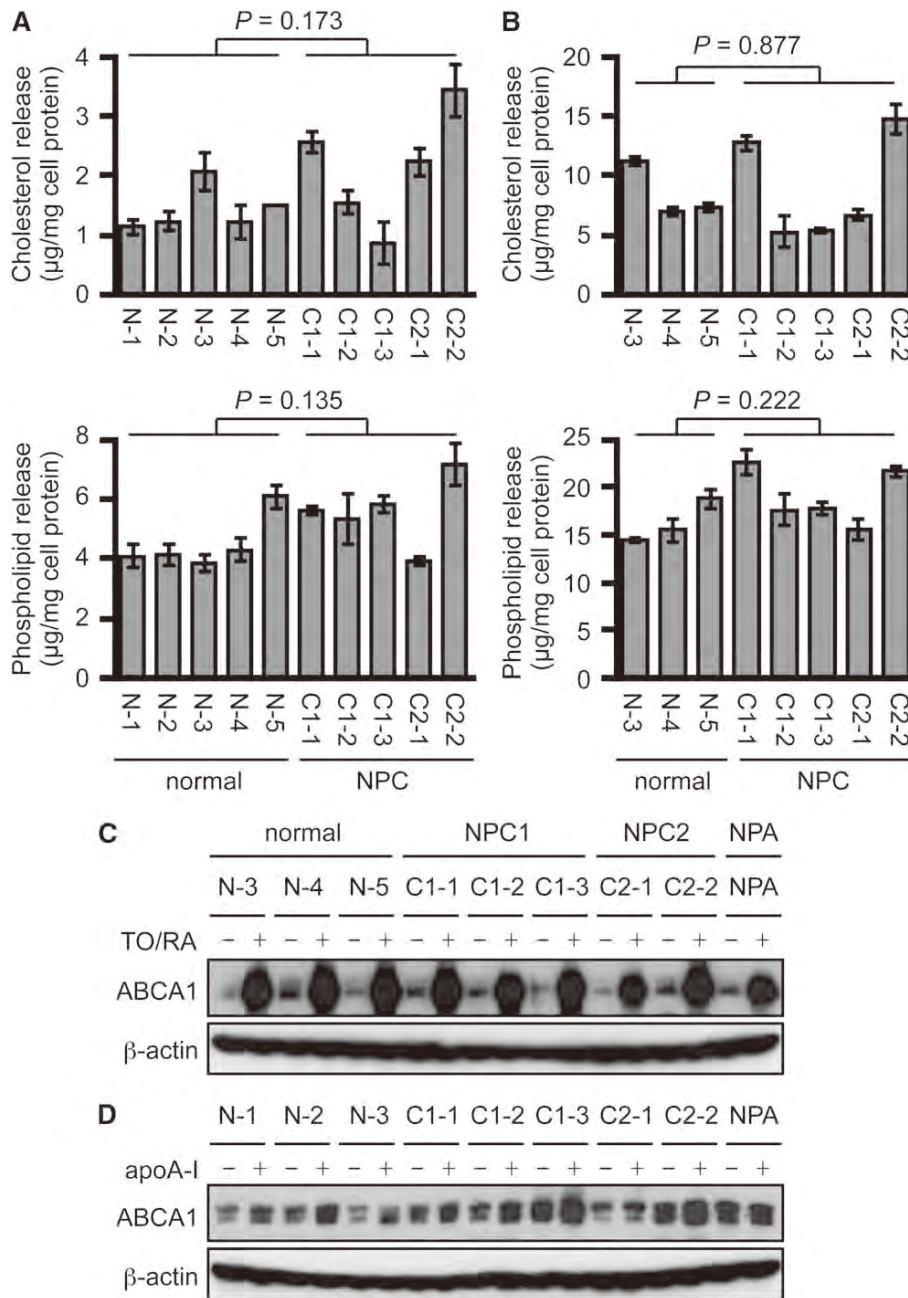


**Fig. 3.** ABCA1-dependent cholesterol release to apoA-I is not impaired in NPC human fibroblasts. A, B: apoA-I-mediated release of cholesterol and phospholipid in normal and NPC HSFs. HSFs were seeded in 6-well plates as in Fig. 2. Cells were then incubated with or without 10 µg/ml of apoA-I for 24 h. Before incubation with apoA-I, the cells were pretreated with TO901317 (1 µg/ml) and 9cRA (1 µg/ml) for 18 h to induce ABCA1 expression, and TO901317 and 9cRA were included during incubation with apoA-I (B). Cholesterol (upper panels) and phospholipids (lower panels) in medium were measured by the colorimetric enzymatic assays, and apoA-I-dependent release was calculated as described in the Materials and Methods. Amounts of cholesterol and phospholipid were normalized to amounts of cellular protein. Data shown are mean ± SD. Statistical significance was evaluated by Student's *t*-test between normal and NPC subjects and no significant changes were found. *P* values are indicated in each panel. C, D: ABCA1 protein expression. ABCA1 expression in normal and NPC HSFs was examined by immunoblot. Cells were either treated or not treated with TO901317 (TO) and 9cRA (RA) for 24 h (C) or with apoA-I (10 µg/ml) for 4 h (D).

apoA-I-mediated release of cholesterol and phospholipid was not impaired in NPC HSFs under both conditions (Fig. 3A, B). In both normal and NPC HSFs, the treatment with LXR and RXR ligands robustly increased cholesterol and phospholipid release. Cholesterol and phospholipid release was also not impaired in HSFs from a patient with NPA (data not shown). We also examined ABCA1 protein expression in normal and NPC HSFs treated or not treated with LXR and RXR ligands (Fig. 3C) or with apoA-I (Fig. 3D). LXR and RXR ligands transcriptionally increase ABCA1 expression, whereas apoA-I protects ABCA1 protein from degradation to increase its protein level (4, 6). Consistent with lipid release, the results showed that ABCA1 expression is not impaired in NPC and NPA HSFs (Fig. 3C, D). Because cholesterol transport from the LE/LS to the PM is impaired in NPC cells (52), these results indicate that ABCA1 preferentially utilizes de novo synthesized sterols before they are eventually endocytosed to the LE/LS. To confirm this interpretation, we calculated specific activity of de novo synthesized sterol released. Normal and NPC fibroblasts were incubated with or without apoA-I in the presence of [<sup>3</sup>H]acetate, and the mass and radioactivity of sterol released to medium and remaining in cells were determined. The results showed that, in normal HSFs, specific activity of newly synthesized sterol released was 1.34-fold higher than that of labeled sterols remaining in cells (Table 2), indicating that newly synthesized sterols are the preferential source available for ABCA1/apoA-I-dependent release. On the other hand, because the size of the preexisting cholesterol pool was much larger than that of the newly synthesized sterol pool, the preexisting PM cholesterol pool also contributed substantially to the mass of sterols released. In mutant NPC HSFs, the specific activity of newly synthesized sterols released was markedly increased over that of sterols remaining in the cells, because the labeled sterols not released to apoA-I began to recycle among various cellular compartments and, with time, a significant portion of them became partially immobilized and unavailable for release in these cells. Table 2 also shows that, in NPC cells, the rate of sterol synthesis is similar to normal cells despite the large accumulation of cholesterol. Together, these results demonstrate that ABCA1 preferentially releases newly synthesized sterols to apoA-I from the PM before they are internalized to the LE/LS and other cellular compartments.

### ABCA1 is present in the cholesterol-rich membrane domain

Our results suggest that newly synthesized sterols, including lanosterol, consist of a preferential sterol pool for the ABCA1/apoA-I system. Lanosterol and ABCA1 may thus colocalize at the same membrane domain; such a membrane domain has not been characterized. ABCA1 is a multi-span membrane protein and mainly acts at the PM to mediate HDL assembly (25–27, 33); however, the precise nature of the membrane domain where ABCA1 resides remains controversial. Depending on the detergents employed, ABCA1 has been reported to reside either in detergent-soluble membrane or partly in DRM; ABCA1 was recovered in detergent-soluble membrane when TX100 was used (35), while a fraction of this protein was recovered in DRM prepared using Lubrol WX (36). A recent work showed that lipid composition of nascent HDL particles generated by the ABCA1/apoA-I system is similar to that of lipid rafts (53). Heterogeneity of lipid raft domains has been reported; the protein and lipid contents/compositions of DRM vary greatly depending on the detergents used (44, 54). To further characterize membrane domain(s) where ABCA1 localizes, we employed eight different detergents (Table 3). The results showed that ABCA1 was largely soluble in most of the detergents tested, but was largely insoluble when Brij 98 or Tween 20 was used (Fig. 4A). Brij 98-DRM contained 67% of total cellular ABCA1 and the lipid raft marker caveolin-1, but the ER membrane marker, calnexin, or the LE/LS membrane marker, LAMP2, were excluded. In contrast, the Tween 20-DRM contained calnexin in addition to ABCA1 (Fig. 4A), indicating that, unlike Brij 98, Tween 20 could not completely solubilize the ER membrane. Cholesterol was highly enriched in Brij 98-DRM, with a free cholesterol/phospholipid ratio of 0.62; for TX100-DRM and for Tween 20-DRM, the values were 0.49 and 0.30, respectively (Table 3). To further confirm these results, after treating cells with Brij 98 or with TX100, cell lysate was subjected to density-gradient centrifugation. The results showed that buoyant Brij 98-DRM, but not TX100-DRM, contained ABCA1 in normal HSF (Fig. 4B). Additional results showed that, in THP-1 macrophage cell lysates, ABCA1 was also recovered in Brij 98-DRM, but not in TX100-DRM (Fig. 4C).

We previously reported that in CHO cells, pharmacological and genetic inactivation of ACAT1 increase ABCA1-dependent cholesterol and phospholipid release

TABLE 2. Specific activity for newly synthesized sterol release

Cell Line	Total [ <sup>3</sup> H]sterol (cpm)/mass cholesterol (μg)		Specific Activity for Newly Synthesized Sterol Release (medium/cell)
	Medium	Cell	
N-5	1,527/0.99 = 1,537.8	19,596/17.13 = 1144.1	1.34
C1-1	1,512/0.88 = 1,720.1	19,823/30.02 = 660.2	2.61
C2-2	1,432/1.58 = 931.1	19,296/92.75 = 208.1	4.47

Normal (N-5) and NPC (C1-1 and C2-2) HSFs pretreated with TO901317 (1 μg/ml) were incubated with or without apoA-I for 8 h in the presence or absence of [<sup>3</sup>H]acetate. Cholesterol and [<sup>3</sup>H]sterol in medium and cells were measured by an enzymatic assay or by a scintillation counter, as described in the Materials and Methods, and normalized to amounts of cellular protein. Counts per minute in [<sup>3</sup>H]sterols were divided by amounts of cholesterol in micrograms to determine specific activity for newly synthesized sterol release. Results shown are the average of triplicate assays.

TABLE 3. Characterization of DRM prepared by using different detergents in human fibroblasts

Detergent	Concentration (%)	Condition	ABCA1 in DRM <sup>a</sup>	FC in DRM <sup>a</sup>	PL in DRM <sup>a</sup>	FC/PL in DRM
Triton X-100	1.0	4°C, 30 min	4.8	36.2	22.4	0.49
Triton X-102	1.0	4°C, 30 min	5.4	75.0	30.2	0.59
Brij 58	1.0	4°C, 30 min	53.2	85.9	42.0	0.55
Brij 98	1.0	37°C, 10 min	67.0	79.8	32.3	0.62
Lubrol WX	1.0	4°C, 30 min	31.1	84.1	38.1	0.57
CHAPS	2.0	4°C, 30 min	36.0	13.2	11.3	0.35
CHAPSO	1.0	4°C, 30 min	8.7	16.2	10.4	0.41
Tween 20	1.0	4°C, 30 min	89.1	87.8	75.9	0.30

Normal HSF (N-5) was treated with various detergents, as indicated. Free cholesterol (FC) and phospholipid (PL) contents in DRM (pellet) and detergent-soluble fraction (supernatant) isolated in Fig. 4A were measured by colorimetric enzymatic assays. Amounts of ABCA1 were quantified by ImageJ software.

<sup>a</sup>Percent of total cellular ABCA1, free cholesterol, or phospholipid.

(7). The increase in cholesterol release was twice as much as the phospholipid release. Furthermore, the increase in phospholipid release was parallel to the increase in ABCA1 protein expression. These results suggested that ACAT inhibition expands a cholesterol pool in the PM that is preferentially utilized for ABCA1-dependent release. Here we sought to determine whether ACAT blockage increases cholesterol content in Brij 98-DRM. 25RA is a CHO mutant that accumulates large amounts of cholesteryl ester, as a consequence of increases in cholesterol synthesis and LDL uptake (41, 42). 25RA cells were treated or not treated with ACAT inhibitor for 6 h, and subjected to Brij 98-DRM preparation to examine changes in lipid composition in the membrane domain. The results showed that ACAT1 blockage caused a marked increase (approximately 2.5-fold) in cholesterol content in Brij 98-DRM (Fig. 5A). The treatment, however, had no effect on phospholipid content in this domain (Fig. 5B). Therefore, ACAT1 inhibition resulted in a robust increase in the cholesterol/phospholipid ratio of Brij 98-DRM. These results explain why ACAT1 blockage increases cholesterol release by 2-fold over ABCA1 protein expression and phospholipid release.

#### Newly synthesized C29/C30 sterols are transiently associated with the membrane domain rich in ABCA1

We next examined whether Brij 98-DRM is also enriched in newly synthesized lanosterol. We performed pulse/chase experiments in normal HSFs using [<sup>3</sup>H]acetate, and monitored the appearance and disappearance of newly synthesized C29/C30, C28, and C27 sterols in Brij 98-DRM. The results showed that, without the chase, the majority of the labeled C29/C30 sterols were found in Brij 98-DRM (Fig. 6A). As the chase time increased, the percentage of [<sup>3</sup>H] C29/C30 and C28 sterols rapidly decreased, while the percentage of [<sup>3</sup>H]C27 sterols increased in Brij 98-DRM and in cells (Fig. 6B). The half-life of C29/C30 sterols in the domain was much shorter than 1 h. The results thus suggest that newly synthesized sterols are rapidly transported to the PM microdomains where ABCA1 resides, and become available for ABCA1-dependent release.

## DISCUSSION

Our current work aims to determine the sterol molecule specificity of ABCA1 as the cellular lipid release

protein. The results reveal that ABCA1 prefers newly synthesized sterols, especially lanosterol, as the substrate. What determines the sterol specificity in this system is currently unknown, and we can only offer certain speculation at this point: At the PM, the ability of cholesterol to form stoichiometric complexes with phospholipids in part determines the “chemical reactivity” of cholesterol in membranes (55). Cholesterol molecules that exceed the binding capacity of phospholipids are considered more mobile, and can be depicted as “active cholesterol” (56). The structure of lanosterol is significantly different from that of cholesterol. It contains three extra methyl groups, the gem-dimethyl moieties at the C4 position, and another methyl group at the C14 position. It also contains a double bond at the C24 position. The C24 double bond in desmosterol causes weaker ability to form an ordered domain than cholesterol does (57). On the other hand, lanosterol was shown to have the ability to form liquid-ordered domains, and can induce membrane curvature formation in vitro (58). Therefore, lanosterol may not form as tight packing with phospholipids as cholesterol does (10), yet membrane domains containing this sterol may retain raft-like properties. The unique structural properties of lanosterol may thus allow it to be more mobile at the PM for ABCA1-dependent release. It was shown that ABCA1 creates a specific lipid-packing deformation site at the PM, and apoA-I recognizes and solubilizes such membrane domains to generate HDL (33, 34). HDL particles generated by ABCA1 are cholesterol-rich and have similar lipid composition to lipid rafts (53), suggesting that the ABCA1/apoA-I system generates HDL at a membrane domain containing significant amounts of cholesterol. Consistent with this notion, our detergent-based cell fractionation experiments showed that ABCA1 resides in a certain membrane domain resistant to Brij 98, a milder detergent than TX100, where cholesterol is highly enriched. This domain also contains newly synthesized lanosterol. This domain may retain a lipid raft-like nature, whereas it may be less ordered compared with TX100-DRM. Several additional lines of evidence produced in other laboratories also support the hypothesis that ABCA1 resides in a certain cholesterol-rich membrane domain. 1) A fraction of ABCA1 was recovered from DRM when Lubrol WX was used (36). 2) ABCA1 is palmitoylated, and this modification is crucial for its function (59). Palmitoylation of a transmembrane protein

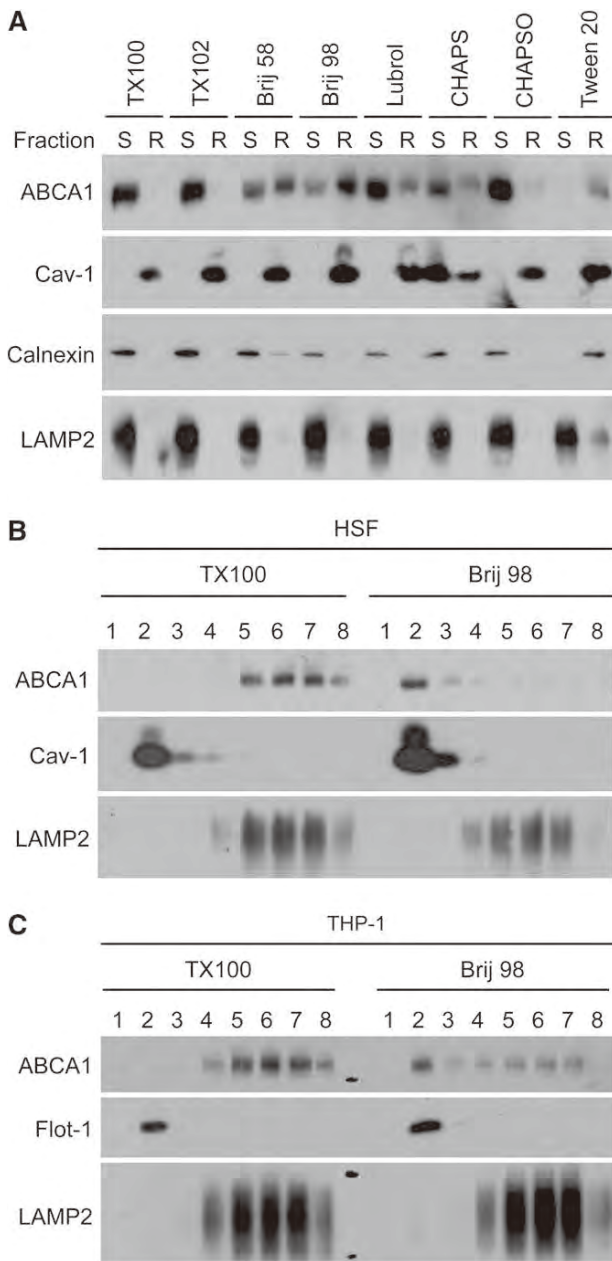


**Fig. 4.** ABCA1 resides in a distinct membrane domain. **A:** Normal HSFs (N-5) grown to subconfluent stage in 100 mm dishes (one dish per treatment) were treated with the indicated detergents, as described in the Materials and Methods. Cells were homogenized, and the PNS obtained was spun at 100,000 *g* for 1 h. The resultant DRM pellet (R) and detergent-soluble supernatant (S) were subjected to immunoblot analysis for ABCA1, caveolin-1 (Cav-1), calnexin, and LAMP-2. The detergents used are as follows: 1.0% Triton X-100 (TX100), 1.0% Triton X-102 (TX102), 1.0% Brij 58, 1.0% Brij 98, 1.0% Lubrol WX (Lubrol), 1.0% CHAPS, 2.0% CHAPSO, and 1.0% Tween 20. **B, C:** Normal HSFs (N-5) (**B**) or differentiated THP-1 cells (**C**) were treated with 1.0% TX100 or with 1.0% Brij 98 as above, and PNS was subjected to density gradient centrifugation by using OptiPrep, as described in the Materials and Methods. Eight 0.5 ml fractions collected from the top were subjected to immunoblotting with antibodies to ABCA1, Cav-1, flotillin-1 (Flot-1), or LAMP-2.

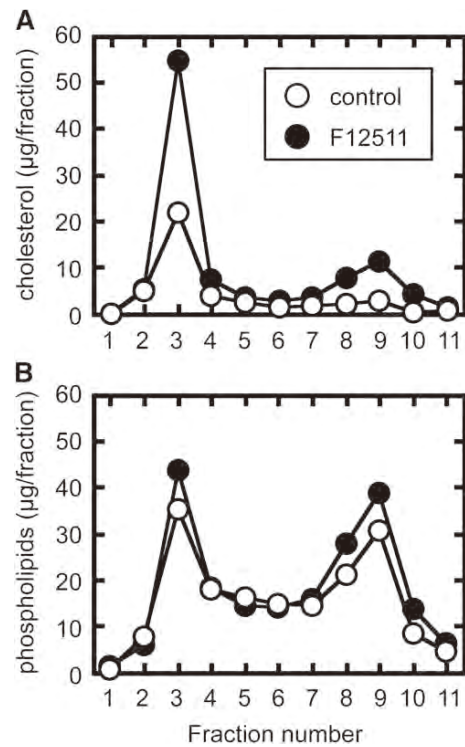


**Fig. 5.** Effect of an ACAT inhibitor on cholesterol contents in Brij 98-DRM. 25RA cells were treated or not treated with an ACAT inhibitor (1  $\mu$ M F12511) for 6 h. Cells were then treated with 1.0% Brij 98, and the PNS was subjected to sucrose density gradient centrifugation. Eleven 1 ml fractions were collected from the top. After extracting lipids from equal amounts of each fraction, amounts of free cholesterol (**A**) and phospholipid (**B**) were determined by enzymatic assays.

serves as a lipid raft-targeting signal (60). 3) Real-time tracking of single ABCA1 molecules showed that ABCA1 forms immobile homodimers in the absence of apoA-I. Upon apoA-I addition, ABCA1 rapidly became mobile (61). A GPI-anchored protein, a typical raft-associated molecule, also forms homodimers and becomes immobile, which results in the formation of homodimer rafts in a cholesterol-dependent manner (62). Based on these observations, we speculate that ABCA1 homodimers associate with lipid rafts, and cholesterol and sphingomyelin removal by apoA-I disrupts ABCA1-homodimer rafts.

Why should lanosterol be chosen as a preferred substrate for ABCA1? Because accumulation of lanosterol in the PM displays cytotoxicity (10, 11), cells need to “detoxify” lanosterol rapidly. Lanosterol is hardly a substrate of ACAT (63), because it contains the gem-dimethyl moieties at the C4 position, which produce severe steric hindrance to 3- $\beta$ -OH. This property incapacitates the ability of ACAT1 to detoxify lanosterol at the ER. Therefore, the preferential release of lanosterol by ABCA1-mediated HDL biogenesis may provide a means to limit the build-up of lanosterol. We recently reported that ABCA1 also facilitates PM-to-ER lanosterol movement for its conversion to cholesterol (18). At the ER, lanosterol is first converted to

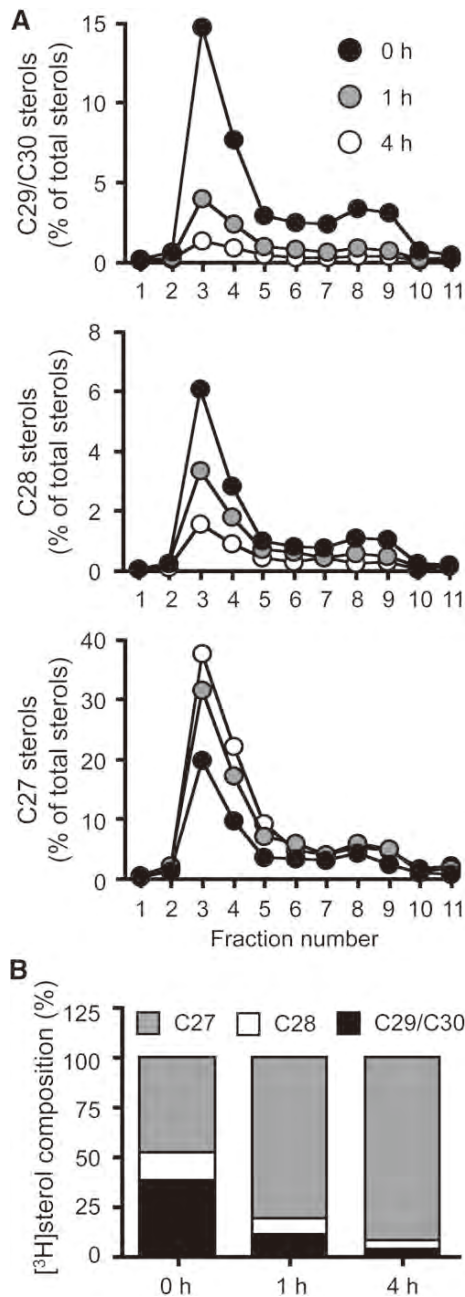


**Fig. 6.** Appearance and disappearance of newly synthesized lanosterol in Brij 98-DRM. A: Appearance and disappearance of precursor sterols in Brij 98-DRM. Normal HSFs (N-5) treated with TO901317 were pulse-labeled with [ $^3\text{H}$ ]acetate for 1 h in medium F. Afterwards, the cells were chased for 0, 1, or 4 h in medium F. PNS was subjected to sucrose density gradient analysis. Eleven 1 ml fractions were collected from the top. Lipids in each fraction were saponified, and C29/C30 (top), C28 (middle), and C27 (bottom) sterols were analyzed by TLC. Data shown are one of two representative experiments. B: Cellular compositions of newly synthesized sterols. Changes in labeled sterol compositions were plotted based on the above results.

dihydrolanosterol, which causes rapid degradation of HMG-CoA reductase protein to limit further biosynthesis of lanosterol (9). The potential toxicity of lanosterol at the PM can thus be minimized by the ABCA1-dependent

bidirectional lanosterol transport system. It is interesting to note that another ABC transporter, ABCG1, but not ABCA1, releases 7-ketocholesterol to HDL in addition to cholesterol (64). 7-Ketocholesterol is accumulated in atherosclerotic lesions, and induces macrophage apoptosis. Thus, ABCG1 protects macrophages from cytotoxicity of 7-ketocholesterol. In addition, ABCG1 and ABCG4 export desmosterol to HDL (65). HDL contains substantial amounts of precursor sterols, including lanosterol and desmosterol. Therefore, besides cholesterol as a common substrate, ABCA1, ABCG1, and ABCG4 may have different sterol specificity. These transporters may cooperatively act to protect cells from the build-up of cytotoxic sterols.

In conclusion, the current work identifies unique substrates for ABCA1: the de novo synthesized cholesterol and methylated precursor sterols arriving at a certain PM domain where ABCA1 is enriched can be rapidly removed by the ABCA1-dependent sterol release pathway before they are transported back to the ER. Our results also support a model where the ABCA1/apoA-I system generates HDL at the PM. **FIG**

The authors thank Dr. Sumiko Abe-Dohmae (Nagoya City University Medical School) for providing cells and Dr. Koichi Furukawa (Nagoya University Graduate School of Medicine) for his generous support.

## REFERENCES

- Brown, M. S., and J. L. Goldstein. 2009. Cholesterol feedback: from Schoenheimer's bottle to Scap's MELADL. *J. Lipid Res.* **50**(Suppl): S15–S27.
- Chang, T. Y., C. C. Chang, N. Ohgami, and Y. Yamauchi. 2006. Cholesterol sensing, trafficking, and esterification. *Annu. Rev. Cell Dev. Biol.* **22**: 129–157.
- Maxfield, F. R., and I. Tabas. 2005. Role of cholesterol and lipid organization in disease. *Nature.* **438**: 612–621.
- Yokoyama, S. 2006. Assembly of high-density lipoprotein. *Arterioscler. Thromb. Vasc. Biol.* **26**: 20–27.
- Tarling, E. J., T. Q. de Aguiar Vallim, and P. A. Edwards. 2013. Role of ABC transporters in lipid transport and human disease. *Trends Endocrinol. Metab.* **24**: 342–350.
- Oram, J. F., and J. W. Heinecke. 2005. ATP-binding cassette transporter A1: a cell cholesterol exporter that protects against cardiovascular disease. *Physiol. Rev.* **85**: 1343–1372.
- Yamauchi, Y., C. C. Y. Chang, M. Hayashi, S. Abe-Dohmae, P. C. Reid, T. Y. Chang, and S. Yokoyama. 2004. Intracellular cholesterol mobilization involved in the ABCA1/apolipoprotein-mediated assembly of high density lipoprotein in fibroblasts. *J. Lipid Res.* **45**: 1943–1951.
- Song, B. L., N. B. Javitt, and R. A. DeBose-Boyd. 2005. Insig-mediated degradation of HMG CoA reductase stimulated by lanosterol, an intermediate in the synthesis of cholesterol. *Cell Metab.* **1**: 179–189.
- Lange, Y., D. Ory, J. Ye, M. Lanier, F. Hsu, and T. Steck. 2008. Effectors of rapid homeostatic responses of endoplasmic reticulum cholesterol and 3-hydroxy-3-methylglutaryl-CoA reductase. *J. Biol. Chem.* **283**: 1445–1455.
- Bloch, K. E. 1983. Sterol structure and membrane function. *CRC Crit. Rev. Biochem.* **14**: 47–92.
- Xu, F., S. D. Rychnovsky, J. D. Belani, H. H. Hobbs, J. C. Cohen, and R. B. Rawson. 2005. Dual roles for cholesterol in mammalian cells. *Proc. Natl. Acad. Sci. USA.* **102**: 14551–14556.
- Kelley, R. I., and G. E. Herman. 2001. Inborn errors of sterol biosynthesis. *Annu. Rev. Genomics Hum. Genet.* **2**: 299–341.
- Porter, F. D. 2002. Malformation syndromes due to inborn errors of cholesterol synthesis. *J. Clin. Invest.* **110**: 715–724.

14. Echevarria, F., R. Norton, W. Nes, and Y. Lange. 1990. Zymosterol is located in the plasma membrane of cultured human fibroblasts. *J. Biol. Chem.* **265**: 8484–8489.
15. Johnson, W. J., R. T. Fischer, M. C. Phillips, and G. H. Rothblat. 1995. Efflux of newly synthesized cholesterol and biosynthetic sterol intermediates from cells. Dependence on acceptor type and on enrichment of cells with cholesterol. *J. Biol. Chem.* **270**: 25037–25046.
16. Lusa, S., S. Heino, and E. Ikonen. 2003. Differential mobilization of newly synthesized cholesterol and biosynthetic sterol precursors from cells. *J. Biol. Chem.* **278**: 19844–19851.
17. Yamauchi, Y., P. C. Reid, J. B. Sperry, K. Furukawa, M. Takeya, C. C. Chang, and T. Y. Chang. 2007. Plasma membrane rafts complete cholesterol synthesis by participating in retrograde movement of precursor sterols. *J. Biol. Chem.* **282**: 34994–35004.
18. Yamauchi, Y., N. Iwamoto, M. A. Rogers, S. Abe-Dohmae, T. Fujimoto, C. C. Chang, M. Ishigami, T. Kishimoto, T. Kobayashi, K. Ueda, et al. 2015. Deficiency in the lipid exporter ABCA1 impairs retrograde sterol movement and disrupts sterol sensing at the endoplasmic reticulum. *J. Biol. Chem.* **290**: 23464–23477.
19. Koivisto, P. V., and T. A. Miettinen. 1988. Increased amounts of cholesterol precursors in lipoproteins after ileal exclusion. *Lipids*. **23**: 993–996.
20. Brooks-Wilson, A., M. Marcil, S. M. Clee, L. H. Zhang, K. Roomp, M. van Dam, L. Yu, C. Brewer, J. A. Collins, H. O. Molhuizen, et al. 1999. Mutations in ABC1 in Tangier disease and familial high-density lipoprotein deficiency. *Nat. Genet.* **22**: 336–345.
21. Bodzioch, M., E. Orsó, J. Klucken, T. Langmann, A. Böttcher, W. Diederich, W. Drobnik, S. Barlage, C. Büchler, M. Porsch-Ozcurümez, et al. 1999. The gene encoding ATP-binding cassette transporter 1 is mutated in Tangier disease. *Nat. Genet.* **22**: 347–351.
22. Rust, S., M. Rosier, H. Funke, J. Real, Z. Amoura, J. C. Piette, J. F. Deleuze, H. B. Brewer, N. Duverger, P. Denèfle, et al. 1999. Tangier disease is caused by mutations in the gene encoding ATP-binding cassette transporter 1. *Nat. Genet.* **22**: 352–355.
23. Hara, H., and S. Yokoyama. 1991. Interaction of free apolipoproteins with macrophages. Formation of high density lipoprotein-like lipoproteins and reduction of cellular cholesterol. *J. Biol. Chem.* **266**: 3080–3086.
24. Francis, G. A., R. H. Knopp, and J. F. Oram. 1995. Defective removal of cellular cholesterol and phospholipids by apolipoprotein A-I in Tangier disease. *J. Clin. Invest.* **96**: 78–87.
25. Denis, M., Y. D. Landry, and X. Zha. 2008. ATP-binding cassette A1-mediated lipidation of apolipoprotein A-I occurs at the plasma membrane and not in the endocytic compartments. *J. Biol. Chem.* **283**: 16178–16186.
26. Lu, R., R. Arakawa, C. Ito-Osumi, N. Iwamoto, and S. Yokoyama. 2008. ApoA-I facilitates ABCA1 recycle/accumulation to cell surface by inhibiting its intracellular degradation and increases HDL generation. *Arterioscler. Thromb. Vasc. Biol.* **28**: 1820–1824.
27. Faulkner, L. E., S. E. Panagotopoulos, J. D. Johnson, L. A. Woollett, D. Y. Hui, S. R. Witting, J. N. Maiorano, and W. S. Davidson. 2008. An analysis of the role of a retroendocytosis pathway in ABCA1-mediated cholesterol efflux from macrophages. *J. Lipid Res.* **49**: 1322–1332.
28. Neufeld, E. B., A. T. Remaley, S. J. Demosky, J. A. Stonik, A. M. Cooney, M. Comly, N. K. Dwyer, M. Zhang, J. Blanchette-Mackie, S. Santamarina-Fojo, et al. 2001. Cellular localization and trafficking of the human ABCA1 transporter. *J. Biol. Chem.* **276**: 27584–27590.
29. Phillips, M. C. 2014. Molecular mechanisms of cellular cholesterol efflux. *J. Biol. Chem.* **289**: 24020–24029.
30. Oram, J. F., R. M. Lawn, M. R. Garvin, and D. P. Wade. 2000. ABCA1 is the cAMP-inducible apolipoprotein receptor that mediates cholesterol secretion from macrophages. *J. Biol. Chem.* **275**: 34508–34511.
31. Wang, N., D. Silver, P. Costet, and A. Tall. 2000. Specific binding of ApoA-I, enhanced cholesterol efflux, and altered plasma membrane morphology in cells expressing ABC1. *J. Biol. Chem.* **275**: 33053–33058.
32. Fitzgerald, M. L., A. L. Morris, A. Chroni, A. J. Mendez, V. I. Zannis, and M. W. Freeman. 2004. ABCA1 and amphipathic apolipoproteins form high-affinity molecular complexes required for cholesterol efflux. *J. Lipid Res.* **45**: 287–294.
33. Vedhachalam, C., P. T. Duong, M. Nickel, D. Nguyen, P. Dhanasekaran, H. Saito, G. H. Rothblat, S. Lund-Katz, and M. C. Phillips. 2007. Mechanism of ATP-binding cassette transporter A1-mediated cellular lipid efflux to apolipoprotein A-I and formation of high density lipoprotein particles. *J. Biol. Chem.* **282**: 25123–25130.
34. Segrest, J. P., M. K. Jones, A. Catte, M. Manchekar, G. Datta, L. Zhang, R. Zhang, L. Li, J. C. Patterson, M. N. Palgunachari, et al. 2015. Surface density-induced pleating of a lipid monolayer drives nascent high-density lipoprotein assembly. *Structure*. **23**: 1214–1226.
35. Mendez, A. J., G. Lin, D. P. Wade, R. M. Lawn, and J. F. Oram. 2001. Membrane lipid domains distinct from cholesterol/sphingomyelin-rich rafts are involved in the ABCA1-mediated lipid secretory pathway. *J. Biol. Chem.* **276**: 3158–3166.
36. Drobnik, W., H. Borsukova, A. Böttcher, A. Pfeiffer, G. Liebisch, G. J. Schütz, H. Schindler, and G. Schmitz. 2002. Apo A1/ABCA1-dependent and HDL3-mediated lipid efflux from compositionally distinct cholesterol-based microdomains. *Traffic*. **3**: 268–278.
37. Yokoyama, S., S. Tajima, and A. Yamamoto. 1982. The process of dissolving apolipoprotein A-I in an aqueous buffer. *J. Biochem.* **91**: 1267–1272.
38. Limanek, J. S., J. Chin, and T. Y. Chang. 1978. Mammalian cell mutant requiring cholesterol and unsaturated fatty acid for growth. *Proc. Natl. Acad. Sci. USA*. **75**: 5452–5456.
39. Hu, W., S. Abe-Dohmae, M. Tsujita, N. Iwamoto, O. Ogikubo, T. Otsuka, Y. Kumon, and S. Yokoyama. 2008. Biogenesis of HDL by SAA is dependent on ABCA1 in the liver in vivo. *J. Lipid Res.* **49**: 386–393.
40. Abe-Dohmae, S., Y. Ikeda, M. Matsuo, M. Hayashi, K. Okuhira, K. Ueda, and S. Yokoyama. 2004. Human ABCA7 supports apolipoprotein-mediated release of cellular cholesterol and phospholipid to generate high density lipoprotein. *J. Biol. Chem.* **279**: 604–611.
41. Chang, T. Y., and J. S. Limanek. 1980. Regulation of cytosolic acetoacetyl coenzyme A thiolase, 3-hydroxy-3-methylglutaryl coenzyme A synthase, 3-hydroxy-3-methylglutaryl coenzyme A reductase, and mevalonate kinase by low density lipoprotein and by 25-hydroxycholesterol in Chinese hamster ovary cells. *J. Biol. Chem.* **255**: 7787–7795.
42. Hua, X., A. Nohturfft, J. Goldstein, and M. Brown. 1996. Sterol resistance in CHO cells traced to point mutation in SREBP cleavage-activating protein. *Cell*. **87**: 415–426.
43. Sakashita, N., C. C. Chang, X. Lei, Y. Fujiwara, M. Takeya, and T. Y. Chang. 2010. Cholesterol loading in macrophages stimulates formation of ER-derived vesicles with elevated ACAT1 activity. *J. Lipid Res.* **51**: 1263–1272.
44. Schuck, S., M. Honsho, K. Ekroos, A. Shevchenko, and K. Simons. 2003. Resistance of cell membranes to different detergents. *Proc. Natl. Acad. Sci. USA*. **100**: 5795–5800.
45. Yamauchi, Y., K. Furukawa, K. Hamamura, and K. Furukawa. 2011. Positive feedback loop between PI3K-Akt-mTORC1 signaling and the lipogenic pathway boosts Akt signaling: induction of the lipogenic pathway by a melanoma antigen. *Cancer Res.* **71**: 4989–4997.
46. Röper, K., D. Corbeil, and W. B. Huttner. 2000. Retention of prominin in microvilli reveals distinct cholesterol-based lipid microdomains in the apical plasma membrane. *Nat. Cell Biol.* **2**: 582–592.
47. Arakawa, R., and S. Yokoyama. 2002. Helical apolipoproteins stabilize ATP-binding cassette transporter A1 by protecting it from thiol protease-mediated degradation. *J. Biol. Chem.* **277**: 22426–22429.
48. Abi-Mosleh, L., R. Infante, A. Radhakrishnan, J. Goldstein, and M. Brown. 2009. Cyclodextrin overcomes deficient lysosome-to-endoplasmic reticulum transport of cholesterol in Niemann-Pick type C cells. *Proc. Natl. Acad. Sci. USA*. **106**: 19316–19321.
49. Reid, P. C., S. Sugii, and T. Y. Chang. 2003. Trafficking defects in endogenously synthesized cholesterol in fibroblasts, macrophages, hepatocytes, and glial cells from Niemann-Pick type C1 mice. *J. Lipid Res.* **44**: 1010–1019.
50. Chen, W., Y. Sun, C. Welch, A. Gorelik, A. Leventhal, I. Tabas, and A. Tall. 2001. Preferential ATP-binding cassette transporter A1-mediated cholesterol efflux from late endosomes/lysosomes. *J. Biol. Chem.* **276**: 43564–43569.
51. Choi, H. Y., B. Karten, T. Chan, J. E. Vance, W. L. Greer, R. A. Heidenreich, W. S. Garver, and G. A. Francis. 2003. Impaired ABCA1-dependent lipid efflux and hypoalphalipoproteinemia in human Niemann-Pick type C disease. *J. Biol. Chem.* **278**: 32569–32577.
52. Karten, B., K. B. Peake, and J. E. Vance. 2009. Mechanisms and consequences of impaired lipid trafficking in Niemann-Pick type C1-deficient mammalian cells. *Biochim. Biophys. Acta*. **1791**: 659–670.
53. Sorci-Thomas, M. G., J. S. Owen, B. Fulp, S. Bhat, X. Zhu, J. S. Parks, D. Shah, W. G. Jerome, M. Gerelus, M. Zabalawi, et al. 2012. Nascent high density lipoproteins formed by ABCA1 resemble lipid

rafts and are structurally organized by three apoA-I monomers. *J. Lipid Res.* **53**: 1890–1909.

54. Pike, L. J. 2004. Lipid rafts: heterogeneity on the high seas. *Biochem. J.* **378**: 281–292.
55. Radhakrishnan, A., T. G. Anderson, and H. M. McConnell. 2000. Condensed complexes, rafts, and the chemical activity of cholesterol in membranes. *Proc. Natl. Acad. Sci. USA.* **97**: 12422–12427.
56. Steck, T. L., and Y. Lange. 2010. Cell cholesterol homeostasis: mediation by active cholesterol. *Trends Cell Biol.* **20**: 680–687.
57. Vainio, S., M. Jansen, M. Koivusalo, T. Róg, M. Karttunen, I. Vattulainen, and E. Ikonen. 2006. Significance of sterol structural specificity. Desmosterol cannot replace cholesterol in lipid rafts. *J. Biol. Chem.* **281**: 348–355.
58. Bacia, K., P. Schwille, and T. Kurzchalia. 2005. Sterol structure determines the separation of phases and the curvature of the liquid-ordered phase in model membranes. *Proc. Natl. Acad. Sci. USA.* **102**: 3272–3277.
59. Singaraja, R. R., M. H. Kang, K. Vaid, S. S. Sanders, G. L. Vilas, P. Arstikaitis, J. Coutinho, R. C. Drisdell, A. D. El-Husseini, W. N. Green, et al. 2009. Palmitoylation of ATP-binding cassette transporter A1 is essential for its trafficking and function. *Circ. Res.* **105**: 138–147.
60. Levental, I., D. Lingwood, M. Grzybek, U. Coskun, and K. Simons. 2010. Palmitoylation regulates raft affinity for the majority of integral raft proteins. *Proc. Natl. Acad. Sci. USA.* **107**: 22050–22054.
61. Nagata, K. O., C. Nakada, R. S. Kasai, A. Kusumi, and K. Ueda. 2013. ABCA1 dimer-monomer interconversion during HDL generation revealed by single-molecule imaging. *Proc. Natl. Acad. Sci. USA.* **110**: 5034–5039.
62. Suzuki, K. G., R. S. Kasai, K. M. Hirotsawa, Y. L. Nemoto, M. Ishibashi, Y. Miwa, T. K. Fujiwara, and A. Kusumi. 2012. Transient GPI-anchored protein homodimers are units for raft organization and function. *Nat. Chem. Biol.* **8**: 774–783.
63. Tavani, D. M., W. R. Nes, and J. T. Billheimer. 1982. The sterol substrate specificity of acyl CoA:cholesterol acyltransferase from rat liver. *J. Lipid Res.* **23**: 774–781.
64. Terasaka, N., N. Wang, L. Yvan-Charvet, and A. Tall. 2007. High-density lipoprotein protects macrophages from oxidized low-density lipoprotein-induced apoptosis by promoting efflux of 7-ketocholesterol via ABCG1. *Proc. Natl. Acad. Sci. USA.* **104**: 15093–15098.
65. Wang, N., L. Yvan-Charvet, D. Lütjohann, M. Mulder, T. Vanmierlo, T. Kim, and A. Tall. 2008. ATP-binding cassette transporters G1 and G4 mediate cholesterol and desmosterol efflux to HDL and regulate sterol accumulation in the brain. *FASEB J.* **22**: 1073–1082.

## ***INVITED COMMENTARY***

# **Gel Permeation HPLC Analysis Validates a Classical Spherical Space-filling Model for Lipoprotein Structure Opening Future Potential of the Technology**

Shinji Yokoyama

*Director of Nutritional Health Science Research Center and Professor of Food and Nutritional Sciences, Chubu University, Kasugai, Aichi 487-8501, JAPAN*

Plasma lipoproteins are complex particles of lipid and proteins primarily designated for extracellular transport of acyl glycerides and cholesterol. We conventionally measure lipid molecules included in these particles as empirical parameters for evaluation of lipoprotein concentration. However, such “concentration” of lipid represents neither the molecules of independent behaviour assumed from regular chemical reactions nor those of lipoprotein particles that in fact behave as “molecules” in solution. Early theoretical work by Shen and Kézdy proposed number of each component lipid molecule in various lipoprotein subclasses, based on the size of the particles, space occupying volume of lipid molecule, and a simple structural model that the particles are spherical composed of surface monomolecular layer of phospholipid and unesterified cholesterol, and spherical core of triglyceride and esterified cholesterol<sup>1, 2)</sup>. This model has become a prototype of various other models derived to interpret more complex experimental findings.

Lipoprotein subclasses are analyzed traditionally by ultracentrifugation and electrophoresis. However, the former is time-consuming, uneconomical and requires a large quantity of sample while the latter is only semi-quantitative. Hara and Okazaki have developed techniques to analyze lipoprotein subclasses by using molecular sieve high performance liquid chromatography for years<sup>3-8)</sup>, and this method has become one of the standard methods to analyze plasma lipoproteins. In principle, the GC-HPLC analysis gives particle size information along with the amounts of their lipid contents. On the other hand, a more-recently developed NMR analysis technique provides particle size and number at the same time<sup>9-12)</sup>. Since lipoprotein particle size is associated with some pathological conditions and their risk predicting power, these technologies

have gotten popular as competing each other. HPLC is more-time consuming but economical while NMR is more efficient but expensive.

In the article in this issue, Okazaki and her colleague reviewed the validity of their achievement that the GC-HPLC method is capable of providing pretty accurate particle size information of subclasses more than conventional classification by component analysis of elution profiles<sup>13, 14)</sup>. Based on these results, they attempted to fit the data accumulated to spherical model of lipoprotein structure above mentioned. There are two highlights in this bioinformatic analysis. For each subclass of lipoprotein particle, esterified and unesterified cholesterol was accurately estimated from the information of total cholesterol, triglyceride and particle size. They also derived an empirical equation for plotting the parameters of lipid composition to illustrate abnormal non-spherical lipoprotein particle. It was of course easy to show particle number of each lipoprotein subclass by this analysis.

The results clearly demonstrate advantage of the GC-HPLC method over other method in demonstrating complete profile of plasma lipoprotein. Clinical values of this analytical method should more be evaluated. And most of all, the results also demonstrated high validity of Shen and Kézdy model proposed 40 years ago.

## **References**

- 1) Shen, B. W.; Scanu, A. M.; Kezdy, F. J. Structure of human serum lipoproteins inferred from compositional analysis. *Proc. Natl. Acad. Sci. U S A.* **74**, 837-841 (1977).
- 2) Edelstein, C.; Kezdy, F. J.; Scanu, A. M.; Shen, B. W.

## S. Yokoyama

- Apolipoproteins and the structural organization of plasma lipoproteins: human plasma high density lipoprotein-3. *J. Lipid Res.* **20**, 143-153 (1979).
- 3) Hara, I.; Okazaki, M.; Ohno, Y. Rapid analysis of cholesterol of high density lipoprotein and low density lipoprotein in human serum by high performance liquid chromatography. *J. Biochem.* **87**, 1863-1865 (1980).
  - 4) Ohno, Y.; Okazaki, M.; Hara, I. Fractionation of human serum lipoproteins by high performance liquid chromatography. I. *J. Biochem.* **89**, 1675-1680 (1981).
  - 5) Okazaki, M.; Hara, I. Analysis of cholesterol in high density lipoprotein subfractions by high performance liquid chromatography. *J. Biochem.* **88**, 1215-1218 (1980).
  - 6) Okazaki, M.; Ohno, Y.; Hara, I. High-performance aqueous gel permeation chromatography of human serum lipoproteins. *J. Chromatogr.* **221**, 257-264 (1980).
  - 7) Okazaki, M.; Ohno, Y.; Hara, I. Rapid method for the quantitation of cholesterol in human serum lipoproteins by high performance liquid chromatography. *J. Biochem.* **89**, 879-887 (1981).
  - 8) Okazaki, M.; Shiraiishi, K.; Ohno, Y.; Hara, I. High-performance aqueous gel permeation chromatography of serum lipoproteins: selective detection of cholesterol by enzymatic reaction. *J. Chromatogr.* **223**, 285-293 (1981).
  - 9) Mallol, R.; Rodriguez, M. A.; Brezmes, J.; Masana, L.; Correig, X. Human serum/plasma lipoprotein analysis by NMR: Application to the study of diabetic dyslipidemia. *Progress NMR Spectrosc.* **70**, 1-24 (2013).
  - 10) Otvos, J. D.; Jeyarajah, E. J.; Bennett, D. W.; Krauss, R. M. Quantification of plasma lipoproteins by proton nuclear magnetic resonance spectroscopy. *Clin. Chem.* **37**, 377-386 (1991).
  - 11) Otvos, J. D.; Jeyarajah, E. J.; Bennett, D. W. *et al.* Development of a proton nuclear magnetic resonance spectroscopic method for determining plasma lipoprotein concentrations and subspecies distributions from a single, rapid measurement. *Clin. Chem.* **38**, 1632-1638 (1992).
  - 12) Ala-Korpela, M.; Korhonen, A.; Keisala, J.; Horkko, S.; Korpi, P.; Ingman, L. P.; Jokisaari, J.; Savolainen, M. J.; Kesaniemi, Y. A. <sup>1</sup>H NMR-based absolute quantitation of human lipoproteins and their lipid contents directly from plasma. *J. Lipid Res.* **35**, 2292-2304 (1994).
  - 13) Okazaki, M.; Usui, S.; Fukui, A.; Kubota, I.; Tomoike, H. Component analysis of HPLC profiles of unique lipoprotein subclass cholesterol for detection of coronary artery disease. *Clin. Chem.* **52**, 2049-2053 (2006).
  - 14) Okazaki, M.; Usui, S.; Ishigami, M.; Sakai, N.; Nakamura, T.; Matsuzawa, Y.; Yamashita, S. Identification of unique lipoprotein subclasses for visceral obesity by component analysis of cholesterol profile in high-performance liquid chromatography. *Arterioscler. Thromb. Vasc. Biol.* **25**, 578-584 (2005).

# SCIENTIFIC REPORTS

OPEN

## Bioinformatic Analysis of Plasma Apolipoproteins A-I and A-II Revealed Unique Features of A-I/A-II HDL Particles in Human Plasma

Received: 11 February 2016

Accepted: 21 July 2016

Published: 16 August 2016

Toshimi Kido<sup>1</sup>, Hideaki Kurata<sup>2</sup>, Kazuo Kondo<sup>3</sup>, Hiroshige Itakura<sup>4</sup>, Mitsuyo Okazaki<sup>5</sup>, Takeyoshi Urata<sup>6,7,\*</sup> & Shinji Yokoyama<sup>8</sup>

Plasma concentration of apoA-I, apoA-II and apoA-II-unassociated apoA-I was analyzed in 314 Japanese subjects (177 males and 137 females), including one (male) homozygote and 37 (20 males and 17 females) heterozygotes of genetic CETP deficiency. ApoA-I unassociated with apoA-II markedly and linearly increased with HDL-cholesterol, while apoA-II increased only very slightly and the ratio of apoA-II-associated apoA-I to apoA-II stayed constant at 2 in molar ratio throughout the increase of HDL-cholesterol, among the wild type and heterozygous CETP deficiency. Thus, overall HDL concentration almost exclusively depends on HDL with apoA-I without apoA-II (LpAI) while concentration of HDL containing apoA-I and apoA-II (LpAI:All) is constant having a fixed molar ratio of 2 : 1 regardless of total HDL and apoA-I concentration. Distribution of apoA-I between LpAI and LpAI:All is consistent with a model of statistical partitioning regardless of sex and CETP genotype. The analysis also indicated that LpAI accommodates on average 4 apoA-I molecules and has a clearance rate indistinguishable from LpAI:All. Independent evidence indicated LpAI:A-II has a diameter 20% smaller than LpAI, consistent with a model having two apoA-I and one apoA-II. The functional contribution of these particles is to be investigated.

High density lipoproteins (HDL) in human plasma are relatively small and mostly spherical lipid-protein complex particles, having diameters 10–15 nm being composed of several hundred lipid molecules and a few apolipoprotein (apo) molecules<sup>1</sup>, mainly apoA-I and apoA-II<sup>2</sup>. HDL plays a key role in transport of cholesterol from the tissues to the liver for excretion into the bile either as cholesterol itself or after conversion to bile acids. The basic structure of HDL is considered to be a microemulsion with core lipids of esterified cholesterol and a small amount of triglyceride surrounded with surface components of phospholipids, unesterified cholesterol and helical amphiphilic apolipoproteins<sup>1</sup>. HDL is however structurally heterogeneous in size, density and chemical composition<sup>3</sup>. HDLs are metabolically active and therefore unstable particles that undergo enzymatic reactions, transfer/exchange of component molecules and accordingly remodeling in plasma as they carry cholesterol<sup>4</sup>.

ApoA-I is a predominant protein component of HDL along with a secondary dominant apoA-II<sup>5–7</sup>. Because HDL is a small particle that will accommodate only a few protein molecules per particle, apoA-II cannot be present in all HDL particles so that some of the HDL particles inevitably contain only apoA-I<sup>2</sup>. Accordingly, HDL particles can largely be classified into two categories; those associated only with apoA-I (LpAI) and those with

<sup>1</sup>Institute of Environmental Science of Human Life, Ochanomizu University, Bunkyo-ku, Tokyo 112-8610, Japan.

<sup>2</sup>Division of Diabetes, Metabolism and Endocrinology, Department of Internal Medicine, The Jikei University School of Medicine, Nishi-Shimbashi, Minato-ku, Tokyo, 105-8461, Japan. <sup>3</sup>Department of Food and Nutritional Science, Toyo University, Itakura-machi, Ora-gun, Gunma 374-0193, Japan. <sup>4</sup>Shinagawa East One Medical Clinic, Minato-ku, Tokyo 108-0075, Japan. <sup>5</sup>Tokyo Medical and Dental University, Bunkyo-ku, Tokyo 113-8519, Japan. <sup>6</sup>International Mibyou (Pre Symptomatic Medicine) Medical Center, Sanuki-chou, Ryugasaki, Ibaraki 301-0033, Japan. <sup>7</sup>Department of Pharmacogenomics, Showa University, Hatanodai, Shinagawa-ku, Tokyo 142-8555, Japan. <sup>8</sup>Nutritional Health Science Research Center, Chubu University, Matsumoto-cho, Kasugai 487-8501, Japan. <sup>\*</sup>Present address: Department of Diabetes, Metabolism and Endocrinology, Showa University School of Medicine, Shinagawa-Ku Tokyo 142-8666, Japan. Correspondence and requests for materials should be addressed to S.Y. (email: syokoyam@isc.chubu.ac.jp)

<sup>2</sup>Division of Diabetes, Metabolism and Endocrinology, Department of Internal Medicine, The Jikei University School of Medicine, Nishi-Shimbashi, Minato-ku, Tokyo, 105-8461, Japan. <sup>3</sup>Department of Food and Nutritional Science, Toyo University, Itakura-machi, Ora-gun, Gunma 374-0193, Japan. <sup>4</sup>Shinagawa East One Medical Clinic, Minato-ku, Tokyo 108-0075, Japan. <sup>5</sup>Tokyo Medical and Dental University, Bunkyo-ku, Tokyo 113-8519, Japan. <sup>6</sup>International Mibyou (Pre Symptomatic Medicine) Medical Center, Sanuki-chou, Ryugasaki, Ibaraki 301-0033, Japan. <sup>7</sup>Department of Pharmacogenomics, Showa University, Hatanodai, Shinagawa-ku, Tokyo 142-8555, Japan. <sup>8</sup>Nutritional Health Science Research Center, Chubu University, Matsumoto-cho, Kasugai 487-8501, Japan. <sup>\*</sup>Present address: Department of Diabetes, Metabolism and Endocrinology, Showa University School of Medicine, Shinagawa-Ku Tokyo 142-8666, Japan. Correspondence and requests for materials should be addressed to S.Y. (email: syokoyam@isc.chubu.ac.jp)

both apoA-I and apoA-II (LpAI:AI) <sup>5,6,8</sup>. Human apoA-I is a single peptide of 243 amino acid residues <sup>9</sup> while apoA-II is a disulfide-linked homodimer of 77-residue peptides <sup>10</sup>. Both have several helical segments that are believed responsible for their reversible binding to lipoprotein surface, enhance cholesteryl ester transfer protein reaction <sup>11</sup> and generate HDL from cellular lipid in the presence of ABCA1 <sup>12</sup>. Granted that distribution of the two apolipoproteins are merely statistical, these two types of particles may substantially be different in their properties and functions. The major factors for this differentiation may be 1) very poor potency of apoA-II to “activate” lecithin: cholesterol acyltransferase (LCAT) in comparison to efficient activation by apoA-I <sup>13</sup>, resulting in poor generation of the core lipid of esterified cholesterol and poor capacity of inducing cell cholesterol release by its exchange pathway, and 2) stable binding of apoA-II to HDL particles compared to high exchangeability of apoA-I among HDL and other lipoproteins to make particles more “stable” <sup>14,15</sup>. These two types of HDL particles were demonstrated for differences in structure <sup>16–23</sup> and functions <sup>19,21,22,24</sup>. However, information of such HDL subpopulation is still limited, either quantitatively or qualitatively. Most of the observations are descriptive based on defined particles isolated from limited numbers of donors.

We therefore analyzed the data of apoA-I, apoA-II and physical association of apoA-I and apoA-II from more than 300 Japanese subjects previously collected and accumulated in 1994 <sup>25</sup>. The results revealed unique feature of HDL containing apoA-I and apoA-II, in comparison to that having apoA-I without apoA-II, and provide important insight on the function of HDL for cholesterol transport in human.

## Materials and Methods

**Study Subjects.** Blood samples were collected in 1994 from randomly selected subjects who visited Omiya City Clinic for regular health check-up, 177 males and 137 females, all upon informed consent in fasting state under unlinkable anonymity for individual identification <sup>25</sup>. After clotting, plasma and buffy coat were taken for determination of lipid and apolipoprotein levels, and CETP genotypes, respectively, at National Institute of Nutritional Sciences completed in 1994–1995. Protocol for the operation was retroactively in accordance with Ethical Guidelines for Epidemiological Research first installed in 2002 <<https://www.niph.go.jp/wadai/ekig-akurinri/guidelines.pdf>> and Ethical Guidelines for Medical and Health Research Involving Human Subjects in 2015 <<http://www.mhlw.go.jp/file/06-Seisakujouhou-10600000-Daijinkanboukouseikagakuka/0000080278.pdf>> by Ministry of Health, Labour and Welfare of Japan. A part of the data of this study was previously published elsewhere <sup>25</sup> and the current analysis of the data was approved by the Ethics Committee for Human Gene and Genome Research at Ochanomizu University.

**Measurements of lipids and apolipoproteins.** Fasting blood plasma was obtained by centrifugation of the blood at  $1200 \times g$  for 20 min at 4 °C. Total cholesterol (TC), triglyceride (TG), and HDL-cholesterol (HDL-C) levels in plasma were determined by enzymatic methods by using commercially available assay kits (SEIKEN T-CHO(S), SEIKEN FG-TG(II), SEIKEN HDL-CHO, respectively, DENKA SEIKEN, Ltd, Tokyo) in a biochemical analyzer TBA-60R (TOSHIBA MEDICAL SYSTEMS CORPORATION, Tochigi, Japan). ApoA-I and apoA-II were determined by using commercial immunoturbidimetry assay systems (apoA-I auto · 2, apoA-II auto · 2, Daiichi Pure Chemicals Co., Ltd., Tokyo). All procedures of measurement were done automatically with a biochemical analyzer COBAS MIRA (Roche Diagnostics Corporation, Indianapolis, USA).

**Measurement of apoA-I unassociated with apoA-II by rocket immunoelectrophoresis.** ApoA-I unassociated with apoA-II was determined with the HYDRAGEL LPAI PARTICLES Kit (Sebia, Issy-les-Moulineaux, France) by electroimmunodiffusion technique <sup>6,26</sup>. The standards and plasma samples (100-fold diluted in saline) were applied into the agarose gel containing anti-apoA-I antibody and excess amount of anti-apoA-II antibody and were electrophoresed at 20 °C, 150 V, for 3 h after diffusing for 20 min. We used our own migration condition as it had been verified to be accurate by intro-, inter-, and linearity-assay. After removing the remaining proteins, the gel was dried and stained with 0.2% acid violet in 10% acetic acid for 5 min. The gel was destained and dried, then the heights of the rockets of apoA-II-unassociated apoA-I were measured and its apoA-I concentration was determined with calibrated standard curve. This value was considered as apoA-I concentration on LpAI. ApoA-I concentration on LpAI:AI was calculated as [total apoA-I] – [apoA-I in LpAI]. The method was also validated with an independent technique by using combination of immunoprecipitation of LpAI:AI with anti-apoA-II antibody and turbidimetric immunoassay with anti apoA-I antibody <sup>27</sup> for 26 samples randomly chosen (Supplementary Figure).

**HPLC analysis.** Plasma sample was treated with anti-apoA-II antibody conjugated with Sepharose 4B gel to adsorb apoA-II-containing lipoprotein particles. The whole plasma and the supernatant after the treatment were analyzed by high performance liquid chromatography as described elsewhere <sup>3,28</sup>, by using four tandem TSKgel LipopropakXL columns (Tosoh, Japan) eluted with TSK eluent Lp-1 (Tosoh). Five-microliter plasma sample was analyzed by monitoring cholesterol concentration with an enzymatic assay system. The elution profile of LpAI:AI HDL was calculated as the HDL peak of total plasma minus that of the supernatant by using software for component analysis <sup>29,30</sup>.

**CETP genotype determination.** In order to differentiate the subjects of normal and modified HDL metabolism, CETP genotype was determined for intron 14 (1452G-A) and exon 15 (D442G) mutations, since the prevalence of these activity-deficient mutations are uniquely high among East Asians including Japanese <sup>31–33</sup>. Fasting blood was collected into a tube containing EDTA-2Na and centrifuged at  $1200 \times g$  for 20 min at 4 °C. Genomic DNA was extracted from buffy coat (leukocyte-enriched fraction) with IsoQuick nucleic acid extraction kit (MicroProbe Corp., Bothell, WA, USA). Purified DNA was dissolved in RNase-free water and stored at 4 °C. The DNA was amplified using primers designed for the domain including intron 14 and exon 15 of the CETP gene by polymerase chain reaction (PCR). After verifying amplification of the target DNA fragments of

approximately 1400 bp by agarose gel electrophoresis, 1  $\mu$ l of the DNA fragment solution was spotted onto a positively charged nylon membrane (Biohyne<sup>®</sup> B Nylon Membrane, NIPPON Genetics Co, Ltd., Japan) to detect four genotypes (intron 14 wild/variant and exon 15 wild/variant). The membranes were rinsed with 10 ml of 0.4 M NaOH-1 M NaCl solution for 2 min to denature DNA, dried, rinsed with 10 ml of 0.5 M Tris HCl-1 M NaCl for 2 min twice, dried, and baked in an UV linker to fix DNA. DNA was detected as follows by using a DIG Nucleic Acid Detection Kit (Boehringer Mannheim Biochemica, Germany). The membranes were pre-hybridized in 5  $\times$  SSC buffer (0.75 M NaCl, 0.075 M sodium citrate) containing 0.5% blocking reagent, 0.1% N-lauroylsarcosine Na-salt, and 0.02% SDS for an hour at 37°C. The DNA on the membranes were then hybridized overnight at 37°C applying digoxigenin labeled and non-labeled with a specific probe. Following hybridization, the membranes were washed twice in 5  $\times$  SSC containing 0.1% SDS for 10 min at 37°C. After washing membranes, Dig-labeled DNA was detected by enzyme-linked immunoassay using anti-digoxigenin alkaline phosphatase conjugate. A subsequent enzyme-catalyzed color reaction using 5-bromo-4-chloro-3-indolyl phosphate and nitroblue tetrazolium salt produced an insoluble blue precipitate that made hybrid molecules visible.

**Simplified Model Analysis for apoA-I Distribution Among HDL Particles.** In order to estimate contribution of any specific factor to distribution of apolipoproteins among HDL particles, the data was attempted to fit a simplified statistical probability model as defined below. The model was based on the assumptions; 1) All HDL particles have an equal number of independent “binding site” for helical apolipoproteins, 2) All the “binding sites” on HDL surface are occupied either with apoA-I or apoA-II. 3) Two disulfide-dimer apoA-II molecules displace one apoA-I with absolute priority with no reverse displacement due to high lipid-affinity of apoA-II<sup>14,15</sup>. The equations for fitting were derived using the same principle as those derived for apoE binding to microemulsions<sup>34</sup>. When the total number of HDL particle is N, the total number of apoA-II molecule is M and the number of binding site for apoA-II per single HDL particle is B (and therefore that for apoA-I is B/2), probability for a particular HDL particle to be unoccupied with apoA-II,  $P_e$ , is calculated as follows. Probability of the first binding site of the first HDL particle free from apoA-II is expressed as  $\left(1 - \frac{M}{NB}\right)$ , and likewise for the second binding site as  $\left(1 - \frac{M-1}{NB-1}\right)$ , the third as  $\left(1 - \frac{M-2}{NB-2}\right)$  and so on to the last binding site (number B) as  $\left(1 - \frac{M-B+1}{NB-B+1}\right)$ . Therefore,  $P_e = \prod_{i=0}^{B-1} \left(1 - \frac{M-i}{NB-i}\right)$  as for  $P_e = \left(1 - \frac{M}{NB}\right) \times \left(1 - \frac{M-1}{NB-1}\right) \times \left(1 - \frac{M-2}{NB-2}\right) \times \left(1 - \frac{M-3}{NB-3}\right) \times \dots \times \left(1 - \frac{M-B+2}{NB-B+2}\right) \times \left(1 - \frac{M-B+1}{NB-B+1}\right)$ . Since  $N \gg B$  and  $M \gg B$ , the equation can be simplified as  $P_e = \left(1 - \frac{M}{NB}\right)^B$  where  $\frac{M}{NB}$  can be considered as an average saturation of the binding site by apoA-II ( $r$ ). Thus,  $P_e = (1 - r)^B$ . Because it is assumed that all the binding sites unoccupied with apoA-II are occupied with apoA-I, the proportion of apoA-I in apoA-II-unassociated HDL (LpAI)(s) is  $s = \frac{NB \times P_e}{NB \times (1 - r)} = \frac{(1 - r)^B}{1 - r} = (1 - r)^{B-1}$ . However, if the clearance rate from plasma of LpAI and LpAI:AI is different, a constant factor,  $c$ , must be installed. Thus,  $s = c \times (1 - r)^{B-1}$ . This equation is converted into linearized format of  $\ln s = (B-1) \times \ln(1 - r) + \ln c$ . The value  $r$  is to be calculated from apoA-I/apoA-II molar ratio in plasma (R) as  $r = \frac{1}{2R+1}$  due to the assumption that all the apoA-I and apoA-II molecules are HDL-bound occupying all the “binding sites” and that two apoA-II molecules are equivalent to one apoA-I in the occupancy of the binding sites. Therefore, when the value of  $r$  and  $R$  are available, the data can be plotted according to this linearized form of the equation, yielding a slope as the number of apoA-II binding site and a Y-axis intercept as a parameter for the relative catabolic rate of two HDL species.

**Statistical analysis.** Difference between two groups was analyzed using Unpaired t-test, or Unpaired t-test with Welch's correction if the variance between the two groups cannot be assumed equal. Difference with  $p < 0.05$  was considered significant.

## Results and Discussion

Basic information of the study subjects is summarized in Table 1. Of the total 314 subjects, 177 were male and 137 were female. Mutations of the CETP gene were identified in 38 subjects; 6 (3 males and 3 females) as heterozygotes of 1452G-A in intron 14, 31 (17 males and 14 females) as heterozygotes of D442G and one male as a homozygote of D442G. HDL-C levels and the related parameters were higher in females than males and in heterozygous CETP deficiency than its wild type. The levels of HDL-C and apoA-I were consistent with other epidemiological data of Japanese<sup>35</sup>. Prevalence of D442G heterozygote was 9.9% and 1452G-A was 1.9%, being consistent with other survey among Japanese and East Asians<sup>31-33</sup>.

Figure 1 demonstrates relationship of apoA-I, apoA-II, and apoA-I in LpAI and LpAI:AI to HDL-C of the wild type subjects of CETP genotype. Plasma total ApoA-I increases linearly with HDL-C, and apoA-I in LpAI (apoA-II-free apoA-I) also increased along with HDL-C with a slope somewhat lower than total apoA-I (Panel A). On the other hand, apoA-II also linearly increased but only very slightly and apoA-I in LpAI:AI (apoA-II-associated apoA-I) increased but also only slightly along over the range of HDL-C increase (Panel B). Therefore, the increase of apoA-I along with the increase of HDL-C is largely accounted for by the increase of apoA-I in LpAI. Accordingly, the ratio of apoA-I in LpAI:AI to apoA-II remained constant at around 3 in weight, or 2 in molar ratio throughout the range of HDL-C increase (Panel C). This molar ratio is consistent with most of previous publications based on selected small numbers of samples<sup>17-19</sup>. Figure 2 shows the analyses of wild type samples for males and females separately (Panels A-D). In spite of substantial difference of these parameters between males and females, the relationships of the apolipoprotein parameters to HDL-C were all the same. ApoA-I/apoA-II ratio in LpAI:AI was also same at around 3 in weight and 2 in molar between males and females. The analysis for heterozygous CETP deficiency also yielded same results as the wild type subjects (Panel E, F). ApoA-I in LpAI thus increases by three times from 25 to 75 mg/dl over the increase HDL-C from 30 to 80 mg/dl,

	CETP Wild Type			CETP Variants	
	Total	Male	Female	heterozygote	homozygote
	n = 276	n = 156	n = 120	n = 37 (1452 G-A, 3 males, 3 females) (D442G, 17 males, 14 females)	n = 1 (D442G, 1 male)
Age (yrs)	47 ± 7	47 ± 7	47 ± 6	47 ± 6	54
TC (mg/dL)	192 ± 32	194 ± 35	189 ± 29	198 ± 32	227
TG (mg/dL)	125 ± 101	152 ± 124	91 ± 39	108 ± 56	210
HDL-C (mg/dL)	56 ± 14	51 ± 13	63 ± 13**	63 ± 16 <sup>§</sup>	48
apoA-I (mg/dL)	159 ± 28	154 ± 29	166 ± 25 <sup>††</sup>	168 ± 29	164
apoA-II (mg/dL)	37.0 ± 6.2	37.8 ± 6.6	36.0 ± 5.5 <sup>†</sup>	38.0 ± 5.0	37.1
apoA-I in LpAI (mg/dL)	52.3 ± 16.5	46.5 ± 14.5	59.7 ± 15.8**	56.7 ± 18.0	49.9
apoA-I in LpA-I:A-II (mg/dL)	107 ± 20	107 ± 22	106 ± 18	112 ± 17	114.1
apoA-I/apoA-II in LpA-I:A-II	2.90 ± 0.34	2.85 ± 0.32	2.97 ± 0.36*	2.94 ± 0.27	3.08

**Table 1. Characteristics of the study subjects.** The data are presented as Mean ± SD. \* and <sup>†</sup> indicate the results of Unpaired t test and Unpaired t test with Welch's correction, respectively, from wild type males as \*\*p < 0.001, \*p < 0.01, <sup>††</sup>p < 0.001, and <sup>†</sup>p < 0.05. <sup>§</sup>Indicates p < 0.01 from wild type total by the Unpaired t test.

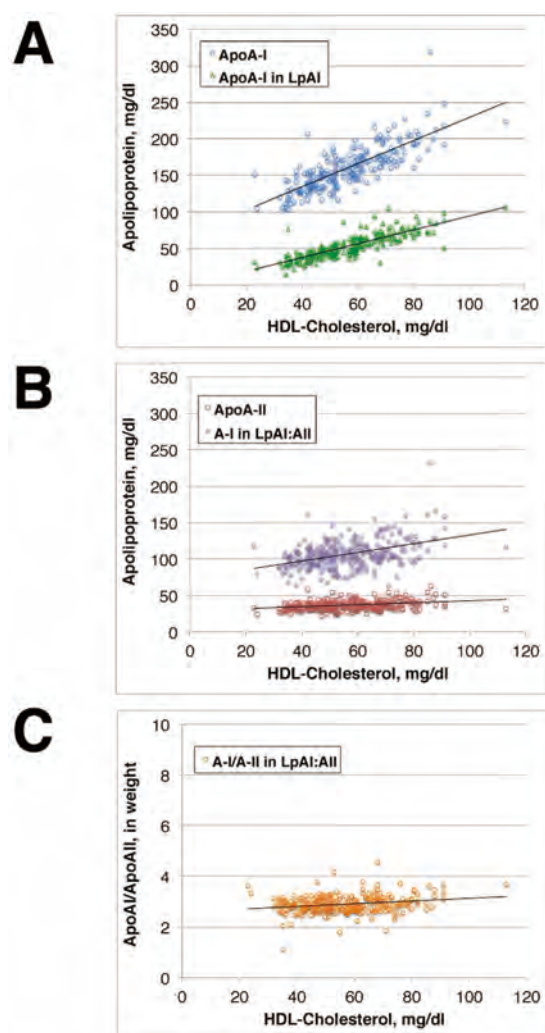


**Figure 1.** Plots against HDL-cholesterol, of total apoA-I and apoA-I in HDL without apoA-II (LpAI) (A), of apoA-II and apoA-I in HDL with apoA-II (LpAI:AII) (B), and weight ratio of apoA-I to apoA-II in LpAI:AII (C), of the subjects of wild type of CETP genotype.

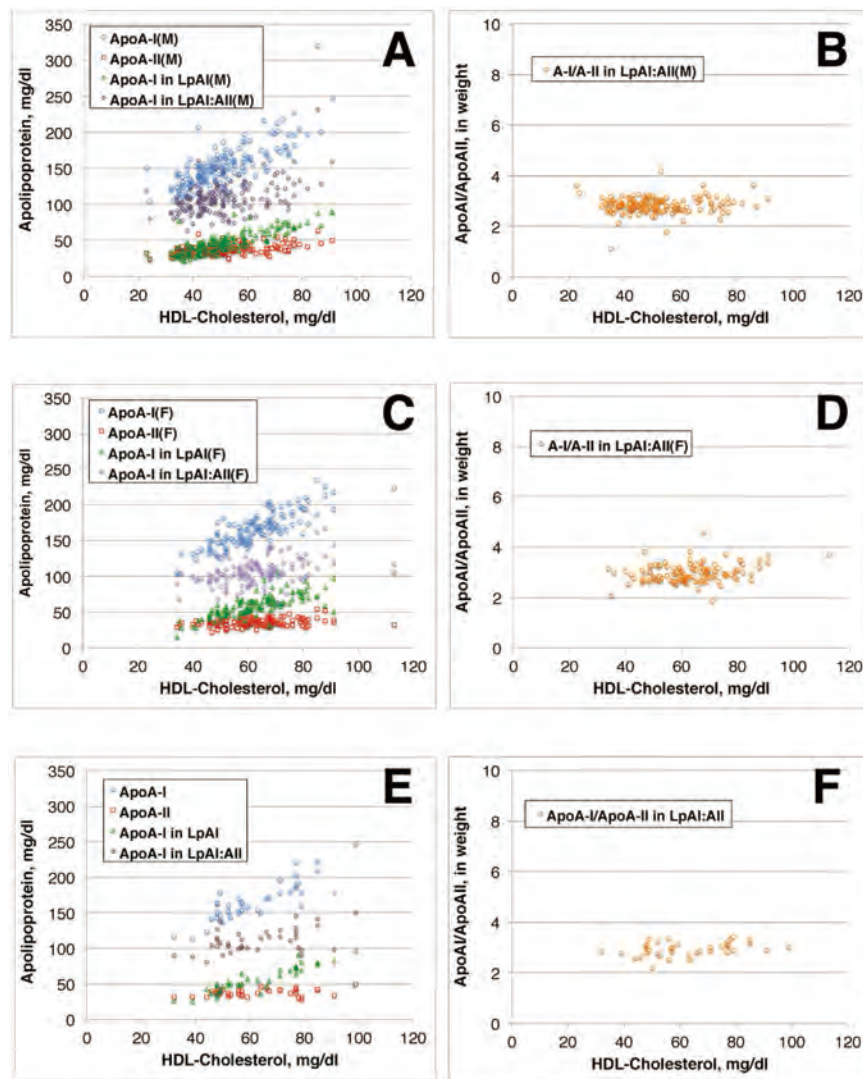


**Figure 2.** Plots against HDL-cholesterol, of total apoA-I and apoA-I in LpAI, apoA-II and apoA-I in LpAI:AII (A), and weight ratio of apoA-I to apoA-II in LpAI:AII (B) of the male subjects of wild type of CETP genotype. The same analyses for female subjects of the CETP wild type (C,D), and for the male and female subjects of heterozygous CETP mutants (E,F).

while apoA-I in LpAI:AII increased only less than 30%, from 90 to less than 120 mg/dl, over the same range of HDL-C, regardless of sex and CETP genotype.

From the results of the analysis above, it is concluded that human plasma contains constant amount of LpAI:AII particles containing a fixed molar ratio of apoA-I to apoA-II, 2 to 1, regardless of total HDL concentration. Increase of HDL thus predominantly depends on the concentration of LpAI.

It is wondered then whether distribution of apoA-I and apoA-II among HDL particles is regulated merely by statistical probability for occupying binding site as assumed earlier or involves any additional specific factor such as biochemical/biological reactions. The data were thus analyzed according to a model based on statistical distribution of apolipoproteins among “binding sites” of HDL surface<sup>34</sup>. An oversimplified statistical distribution model was applied as described in the method section. The data of the wild type subjects are plotted according to the linearized equation,  $\ln s = (B-1) \times \ln(1-r) + \ln c$ , as defined in the method section, in Fig. 3A. The results taken from a previous publication<sup>18</sup> were also plotted in the same graph. Both sets showed consistent profiles and gave similar linear fitting in this model. The least square linear regression best fit of the current data gave  $\ln s = 6.49 \times \ln(1-r) - 0.019$  while the previous sets gave a slope 10.3 and the intercept 0.56. Male and female data gave similar parameters when analyzed separately as  $\ln s = 5.96 \times \ln(1-r) - 0.14$  and  $\ln s = 5.82 \times \ln(1-r) - 0.102$ , respectively (Fig. 3B). Those of heterozygous CETP deficiency gave  $\ln s = 6.60 \times \ln(1-r) - 0.0014$  (Fig. 3C). Thus, from the set of the data analyzed here, number of apoA-II per particle (B) can be estimated 7–8 and c value is around 1. Therefore, on the assumption of homogeneous particle size of HDL, the average HDL particle

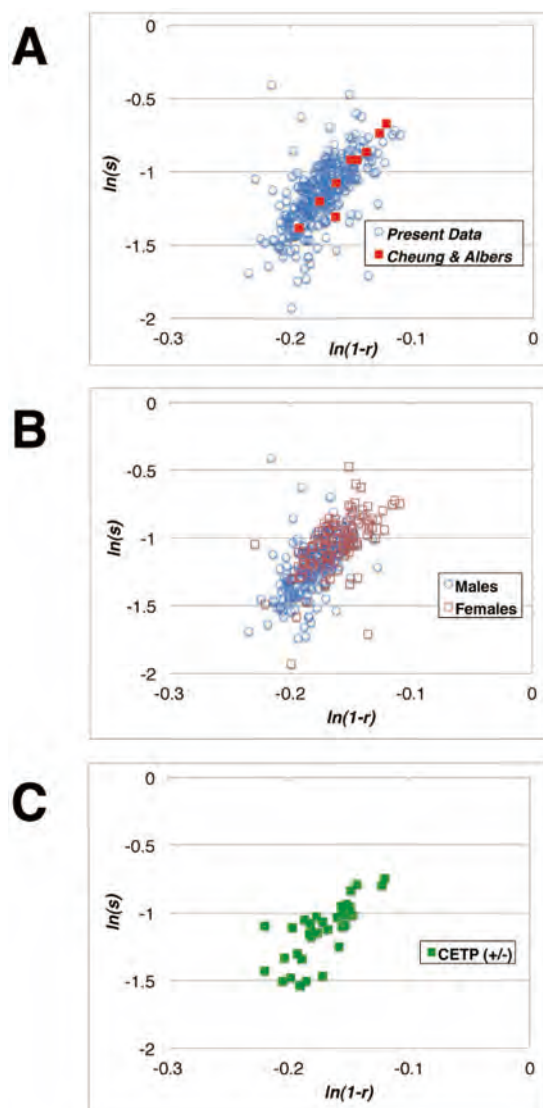


**Figure 3. Plots for consistency of LpAI / LpAI:AII distribution with statistical partitioning.** Panel A represents the plots for the wild type subjects with respect to CETP genotype of the current study, as well as those from the previous reports by Cheung and Albers<sup>18</sup>. Panel B shows the wild type subjects of the current study, male and female, shown separately. Panel C shows the same plot of the heterozygous CETP mutants. The equation used for the analysis is described in the method section of the text.

is capable of accommodating four apoA-I molecules or 6–9 of apoA-II. Distribution of apoA-II and apoA-I among the particles is thus not inconsistent with partitioning according to statistical probability.

Previous reports however indicated that HDL particles containing apoA-II (LpAI:AII) are smaller or heavier than those with apoA-I but without apoA-II (LpAI)<sup>16,17,19,22,28,36,37</sup>. We also confirmed this by HPLC analysis of human HDL, as demonstrated in Fig. 4. The peak of HDL containing apoA-II, LpAI:AII, was smaller than HDL containing apoA-I but not apoA-II, LpAI. The difference of the diameter was estimated as about 20%, consistent with the previous estimation<sup>16,19,22,36</sup>. LpAI:AII was shown to have apoA-I and apoA-II in a molar ratio of 2 (Figs 1 and 2). Assuming average LpAI accommodates four apoA-I molecules, LpAI:AII would fit to contain two apoA-I molecules and one apoA-II molecule because the alternative possibility of four apoA-I and two apoA-II molecules is unlikely. If the number of apolipoprotein binding site is proportional to the surface area of the particle, the diameter of LpAI:AII particles is smaller than average LpAI particles by about 20%, consistent with the measured values. Figure 5 illustrates the concept of this scheme. This model is consistent with volumetric simulation of apolipoprotein stoichiometry in HDL previously proposed by Kézdy and his colleagues<sup>36</sup> and more recently confirmed by HPLC analysis<sup>30</sup>. The scheme is somewhat inconsistent with the earlier assumption that apolipoprotein “binding site” number on HDL particles is same. The linearity of the plot in Fig. 3 may not be sensitive enough to detect this scale of the difference. This is also shown in Fig. 2 where the slope of apoA-I in LpAI plotted against HDL-C is more or less same between the wild type and the CETP mutants in which increase of HDL-C is generally considered due to the increase of the size of HDL.

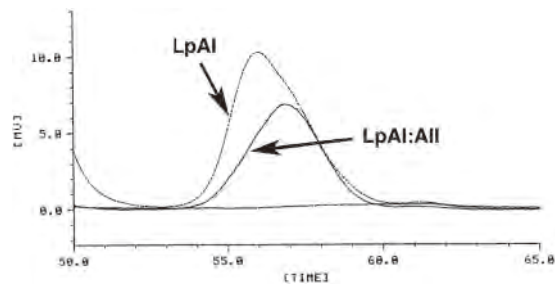


**Figure 4. Elution profile of cholesterol of LpAI and LpAI:AII with molecular sieve HPLC.** The method is described in detail in the text. The elution profile was monitored with total cholesterol before and after immunoremoval of apoA-II-containing HDL with immobilized anti-apoA-II antibody. The post-treatment profile represented LpAI and LpAI:AII was calculated by subtracting the LpAI profile from that of total HDL.

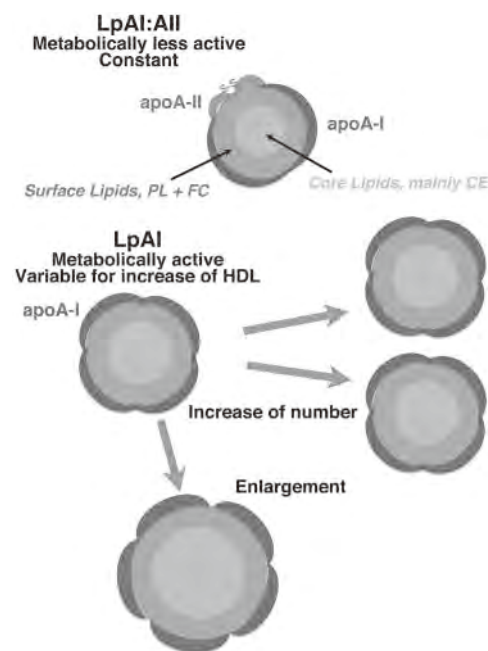


**Figure 5. Model for LpAI and LpAI:AII.** LpAI:AII particles contain one dimeric apoA-II and two apoA-I molecules, and are stable and perhaps metabolically less active with fixed constant amount. Average LpAI particles accommodate four apoA-I molecules, which are variable to determine total HDL concentration. The increase of HDL may be due to the increase of the number of LpAI or by the increase of HDL size to accommodate more apoA-I molecules. PL, phospholipid; FC, free cholesterol; CE, esterified cholesterol.

We here conclude that human plasma HDL is largely composed of two discrete types with respect to apoA-I/apoA-II composition, HDL having only apoA-I (LpAI) and that containing apoA-I and apoA-II (LpAI:AII). The concentration of the latter particle, containing two apoA-I and one apoA-II molecule(s) and smaller than LpAI, is relatively constant regardless of total plasma HDL concentration. On the other hand, LpAI particles having average number of four apoA-I molecules predominantly regulate plasma HDL concentration.

Distribution of apoA-I and apoA-II among HDL particles and thereby generation of LpAI and LpAI:AII seems thus in principle to be due to statistical probability based on common binding sites and higher affinity of apoA-II as defined in the model. However, once LpAI:AII particles are formed, they seem structurally more stable and unlikely change the size since this HDL maintains the fixed apoA-I/A-II molar ratio of 2. The concentration of this particle stays rather constant regardless of variation of total HDL concentration, so that it should be less active with respect to remodeling. However, significant difference in metabolic fate was not apparent in the analyses employed in this paper. More recent work on clearance or distribution of HDL apoproteins<sup>38,39</sup> also seem consistent with the current hypothesis. It is interesting that relative cholesteryl ester content to unesterified cholesterol is reportedly rather higher in LpAI:AII than LpAI<sup>20,22</sup> though apoA-I is known for more efficient “activation” of LCAT than apoA-II. The conclusions are largely consistent with previous discussion on these types of HDL.

Plasma HDL concentration predominantly depends on the concentration of LpAI, so this particle is a determinant of the risk for cardiovascular diseases. The increase in LpAI can be in their number or size, which could appear as a difference of surface/core ratio of the particles and may be represented by apoA-I/HDL-cholesterol ratio (Fig. 5). However, the slope of the apoA-I versus HDL-cholesterol plot for LpAI in Fig. 3 did not show significant difference among the wild type males and females and even heterozygotes of CETP deficiency. Thus, biochemical markers of HDL may not be sensitive enough to detect subtle change in the particle structure. It is of interest that heterozygotes of CETP deficiency exhibited the same profile as the wild type carriers with respect to structure and behavior of LpAI and LpAI:AII though they generally appear with increased size of HDL. More information is required for the size of the HDL subclasses in these subjects in order to understand roles of CETP in HDL interconversion.

The data here were based upon the rocket immunoelectrophoresis assay for differentiation of total apoA-I and apoA-II-associated apoA-I. The method potentially involves a number of problems as any other immuno-differential methods for the same purposes, such as specificity of the antibody, release of apoA-I from HDL, accuracy of quantitative staining, etc. The method was validated with an independent turbidimetric immunoassay<sup>27</sup>, which largely assured acceptable liability of the rocket immunoelectrophoresis method by showing linearity of the relationship between the two method (Supplementary Figure), except for apparently higher background in the reference method perhaps from the background turbidity. Thus, the conclusion here may be verified by using some other methods for differentiation of LpAI and LpAI:AII.

These two subclasses of HDL may largely represent HDL3 and HDL2, but their physiological significance such as functions in cholesterol transport or discriminating risks for any disease is not apparent<sup>6,19,20,22,40–43</sup>. Further analysis of the data accumulated here may reveal any pathophysiological significance and therefore rationale for measuring the subclasses.

## References

- Shen, B. W., Scanu, A. M. & Kézdy, E. J. Structure of human serum lipoproteins inferred from compositional analysis. *Proc Natl Acad Sci USA* **74**, 837–841 (1977).
- Edelstein, C., Kézdy, F. J., Scanu, A. M. & Shen, B. W. Apolipoproteins and the structural organization of plasma lipoproteins: human plasma high density lipoprotein-3. *J Lipid Res* **20**, 143–153 (1979).
- Okazaki, M., Hagiwara, N. & Hara, I. Heterogeneity of human serum high density lipoproteins on high performance liquid chromatography. *J Biochem* **92**, 517–524 (1982).
- Lewis, G. F. & Rader, D. J. New insights into the regulation of HDL metabolism and reverse cholesterol transport. *Circ Res* **96**, 1221–1232, doi: 10.1161/01.RES.0000170946.56981.5c (2005).
- Albers, J. J. & Aladjem, E. Precipitation of 125 I-labeled lipoproteins with specific polypeptide antisera. Evidence for two populations with differing polypeptide compositions in human high density lipoproteins. *Biochemistry* **10**, 3436–3442 (1971).
- Atmeh, R. F., Shepherd, J. & Packard, C. J. Subpopulations of apolipoprotein A-I in human high-density lipoproteins. Their metabolic properties and response to drug therapy. *Biochim Biophys Acta* **751**, 175–188 (1983).
- Barbaras, R., Puchois, P., Fruchart, J. C. & Ailhaud, G. Cholesterol efflux from cultured adipose cells is mediated by LpAI particles but not by LpAI:AII particles. *Biochem Biophys Res Commun* **142**, 63–69 (1987).
- Alaupovic, P. The concept of apolipoprotein-defined lipoprotein families and its clinical significance. *Curr Atheroscler Rep* **5**, 459–467 (2003).
- Brewer, H. B. Jr. *et al.* The amino acid sequence of human APOA-I, an apolipoprotein isolated from high density lipoproteins. *Biochem Biophys Res Commun* **80**, 623–630 (1978).
- Lux, S. E., John, K. M. & Brewer, H. B. Jr. Isolation and characterization of apoLp-Gln-II (apoA-II), a plasma high density lipoprotein containing two identical polypeptide chains. *J Biol Chem* **247**, 7510–7518 (1972).
- Ohnishi, T. & Yokoyama, S. Activation of human plasma lipid transfer protein by apolipoproteins. *Biochemistry* **32**, 5029–5035 (1993).
- Hara, H. & Yokoyama, S. Interaction of free apolipoproteins with macrophages. Formation of high density lipoprotein-like lipoproteins and reduction of cellular cholesterol. *J Biol Chem* **266**, 3080–3086 (1991).
- Chung, J., Abano, D. A., Fless, G. M. & Scanu, A. M. Isolation, properties, and mechanism of *in vitro* action of lecithin: cholesterol acyltransferase from human plasma. *J Biol Chem* **254**, 7456–7464 (1979).
- Lagocki, P. A. & Scanu, A. M. *In vitro* modulation of the apolipoprotein composition of high density lipoprotein. Displacement of apolipoprotein A-I from high density lipoprotein by apolipoprotein A-II. *J Biol Chem* **255**, 3701–3706 (1980).
- Edelstein, C., Halari, M. & Scanu, A. M. On the mechanism of the displacement of apolipoprotein A-I by apolipoprotein A-II from the high density lipoprotein surface. Effect of concentration and molecular forms of apolipoprotein A-II. *J Biol Chem* **257**, 7189–7195 (1982).
- Nestruck, A. C., Niedmann, P. D., Wieland, H. & Seidel, D. Chromatofocusing of human high density lipoproteins and isolation of lipoproteins A and A-I. *Biochim Biophys Acta* **753**, 65–73 (1983).
- Cheung, M. C. & Albers, J. J. Distribution of high density lipoprotein particles with different apoprotein composition: particles with A-I and A-II and particles with A-I but no A-II. *J Lipid Res* **23**, 747–753 (1982).
- Cheung, M. C. & Albers, J. J. Characterization of lipoprotein particles isolated by immunoaffinity chromatography. Particles containing A-I and A-II and particles containing A-I but no A-II. *J Biol Chem* **259**, 12201–12209 (1984).
- Ohta, T., Hattori, S., Nishiyama, S. & Matsuda, I. Studies on the lipid and apolipoprotein compositions of two species of apoA-I-containing lipoproteins in normolipidemic males and females. *J Lipid Res* **29**, 721–728 (1988).
- Ohta, T., Hattori, S., Murakami, M., Nishiyama, S. & Matsuda, I. Age- and sex-related differences in lipoproteins containing apoprotein A-I. *Arteriosclerosis* **9**, 90–95 (1989).
- Leroy, A., Toohill, K. L., Fruchart, J. C. & Jonas, A. Structural properties of high density lipoprotein subclasses homogeneous in protein composition and size. *J Biol Chem* **268**, 4798–4805 (1993).
- Ohta, T. *et al.* Structural and functional differences of subspecies of apoA-I-containing lipoprotein in patients with plasma cholesteryl ester transfer protein deficiency. *J Lipid Res* **36**, 696–704 (1995).
- Gordon, S. M., Deng, J., Lu, L. J. & Davidson, W. S. Proteomic characterization of human plasma high density lipoprotein fractionated by gel filtration chromatography. *J Proteome Res* **9**, 5239–5249, doi: 10.1021/pr100520x (2010).
- Boucher, J. *et al.* Apolipoprotein A-II regulates HDL stability and affects hepatic lipase association and activity. *J Lipid Res* **45**, 849–858, doi: 10.1194/jlr.M300431-JLR200 (2004).
- Kidou, T. *et al.* LpAI levels in Japan. *Atherosclerosis* **134**, 87 (1997).
- Coste-Burel, M., Mainard, F., Chivot, L., Auget, J. L. & Madec, Y. Study of lipoprotein particles LpAI and LpAI:AII in patients before coronary bypass surgery. *Clin Chem* **36**, 1889–1891 (1990).

27. Ishizuka, M. *et al.* The development of rapid method for LpA-I by turbidimetric immunoassay (in Japanese). *Japanese Journal of Medicine and Pharmaceutical Sciences* **39**, 1041–1046 (1998).
28. Okazaki, M. *et al.* Identification of unique lipoprotein subclasses for visceral obesity by component analysis of cholesterol profile in high-performance liquid chromatography. *Arterioscler Thromb Vasc Biol* **25**, 578–584, doi: 10.1161/01.atv.0000155017.60171.88 (2005).
29. Okazaki, M. Method for analyzing of lipoproteins. United States patent US 8,268,626 (2005, November 24).
30. Okazaki, M. & Yamashita, S. Recent Advances in Analytical Methods on Lipoprotein Subclasses: Calculation of Particle Numbers from Lipid Levels by Gel Permeation HPLC Using “Spherical Particle Model”. *J Oleo Sci* **65**, 265–282, doi: 10.5650/jos.ess16020 (2016).
31. Yokoyama, S. A potential screening factor for accumulation of cholesteryl ester transfer protein deficiency in East Asia: *Schistosoma japonicum*. *Biochim Biophys Acta* **1841**, 495–504, doi: 10.1016/j.bbali.2013.12.014 (2014).
32. Yokoyama, S. Unique features of high-density lipoproteins in the Japanese: in population and in genetic factors. *Nutrients* **7**, 2359–2381, doi: 10.3390/nu7042359 (2015).
33. Yokoyama, S., Okumura-Noji, K. & Lu, R. Prevention of fatal hepatic complication in schistosomiasis by inhibition of CETP. *J Biomed Res* **29**, 176–188, doi: 10.7555/jbr.29.20150005 (2015).
34. Yokoyama, S. Self-associated tetramer of human apolipoprotein E does not lead to its accumulation on a lipid particle. *Biochim Biophys Acta* **1047**, 99–101 (1990).
35. Yokoyama, S. *et al.* High-density lipoprotein levels have markedly increased over the past twenty years in Japan. *J Atheroscler Thromb* **21**, 151–160 (2014).
36. Segrest, J. P., Cheung, M. C. & Jones, M. K. Volumetric determination of apolipoprotein stoichiometry of circulating HDL subspecies. *J Lipid Res* **54**, 2733–2744, doi: 10.1194/jlr.M039172 (2013).
37. Gauthamadasa, K. *et al.* Speciated human high-density lipoprotein protein proximity profiles. *Biochemistry* **49**, 10656–10665, doi: 10.1021/bi1015452 (2010).
38. Singh, S. A. *et al.* Multiple apolipoprotein kinetics measured in human HDL by high-resolution/accurate mass parallel reaction monitoring. *J Lipid Res* **57**, 714–728, doi: 10.1194/jlr.D061432 (2016).
39. Reyes-Soffer, G. *et al.* Cholesteryl Ester Transfer Protein Inhibition With Anacetrapib Decreases Fractional Clearance Rates of High-Density Lipoprotein Apolipoprotein A-I and Plasma Cholesteryl Ester Transfer Protein. *Arterioscler Thromb Vasc Biol* **36**, 994–1002, doi: 10.1161/atvbaha.115.306680 (2016).
40. Puchois, P. *et al.* Effect of alcohol intake on human apolipoprotein A-I-containing lipoprotein subfractions. *Arch Intern Med* **150**, 1638–1641 (1990).
41. Bekaert, E. D. *et al.* Characterization of apoA- and apoB-containing lipoprotein particles in a variant of familial apoA-I deficiency with planar xanthoma: the metabolic significance of LP-A-II particles. *J Lipid Res* **32**, 1587–1599 (1991).
42. Asztalos, B. F. *et al.* Role of LCAT in HDL remodeling: investigation of LCAT deficiency states. *J Lipid Res* **48**, 592–599, doi: 10.1194/jlr.M600403-JLR200 (2007).
43. Asztalos, B. F., Tani, M. & Schaefer, E. J. Metabolic and functional relevance of HDL subspecies. *Curr Opin Lipidol* **22**, 176–185, doi: 10.1097/MOL.0b013e3283468061 (2011).

## Acknowledgements

The authors thank Dr. Takashi Nakagawa, Omiya City Clinic, for his helpful collaboration in collecting samples, and to Dr. Masahiko Hori, Home Healthcare Research, and Dr. Kazuyo Nakamura, Yokohama City University Medical Center, for their help in lipoprotein and apolipoprotein assays. They also thank Ms. Yuko Ueno, an undergraduate student at Toho University at that time, for her contribution to CETP genotyping. The work was supported in part by a grant from Japan Health Science Foundation and by MEXT-supported Program for the Strategic Research Foundation at Private Universities (S1201007) and by a Grant-in-Aid from MEXT-Japan (15H02903).

## Author Contributions

T.K. was responsible for collecting and analyzing the data and writing the manuscript, H.K. determined CETP genotypes, K.K. and H.I. planned, initiated and monitored the project, M.O. performed HPLC analysis of lipoproteins, T.U. was involved in validating the methods and S.Y. was responsible for data analysis and preparing the manuscript.

## Additional Information

**Supplementary information** accompanies this paper at <http://www.nature.com/srep>

**Competing financial interests:** The authors declare no competing financial interests.

**How to cite this article:** Kido, T. *et al.* Bioinformatic Analysis of Plasma Apolipoproteins A-I and A-II Revealed Unique Features of A-I/A-II HDL Particles in Human Plasma. *Sci. Rep.* **6**, 31532; doi: 10.1038/srep31532 (2016).



This work is licensed under a Creative Commons Attribution 4.0 International License. The images or other third party material in this article are included in the article's Creative Commons license, unless indicated otherwise in the credit line; if the material is not included under the Creative Commons license, users will need to obtain permission from the license holder to reproduce the material. To view a copy of this license, visit <http://creativecommons.org/licenses/by/4.0/>

© The Author(s) 2016

Supplementary materials for:

## Bioinformatic Analysis on Plasma Apolipoproteins A-I and A-II Revealed Unique Features of A-I/A-II HDL Particles in Human Plasma

Toshimi Kido<sup>a</sup>, Hideaki Kurata<sup>b</sup>, Kazuo Kondō<sup>c</sup>, Hiroshige Itakura<sup>d</sup>, Mitsuyo Okazaki<sup>e</sup>, Takeyoshi Urata<sup>f</sup> and Shinji Yokoyama<sup>g</sup>

<sup>a</sup>Institute of Environmental Science of Human Life, Ochanomizu University, Bunkyo-ku, Tokyo 112-8610, Japan

<sup>b</sup>Division of Diabetes, Metabolism and Endocrinology, Department of Internal Medicine, The Jikei University School of Medicine, Nishi-Shimbashi, Minato-ku, Tokyo, 105-8461, Japan

<sup>c</sup>Department of Food and Nutritional Science, Toyo University, Itakura-machi, Ora-gun, Gunma 374-0193, Japan

<sup>d</sup>Shinagawa East One Medical Clinic, Minato-ku, Tokyo 108-0075, Japan

<sup>e</sup>Tokyo Medical and Dental University, Bunkyo-ku, Tokyo 113-8519, Japan

<sup>f</sup>International Mibyou (Pre Symptomatic Medicine) Medical Center, Sanuki-chou, Ryugasaki, Ibaraki 301-0033, Japan and Department of Pharmacogenomics, Showa University, Hatanodai, Shinagawa-ku, Tokyo 142-8555, Japan

<sup>g</sup>Nutritional Health Science Research Center, Chubu University, Matsumoto-cho, Kasugai 487-8501, Japan

Correspondence should be addressed to: Shinji Yokoyama at Chubu University by [syokoyam@isc.chubu.ac.jp](mailto:syokoyam@isc.chubu.ac.jp).

The present address of Takeyoshi Urata: Department of Diabetes, Metabolism and Endocrinology, Showa University School of Medicine, Shinagawa-Ku Tokyo 142-8666, Japan

The work was supported in part by a grant from Japan Health Science Foundation and by MEXT-supported Program for the Strategic Research Foundation at Private Universities (S1201007) and by a Grant-in-Aid from MEXT-Japan (15H02903).

Legend for Supplementary Figure

Validation of the method to measure LpAI and LpAI:AI. Randomly chosen 26 samples from the wild type subjects were assayed for LpAI by immunoelectrophoresis and the reference method of turbidimetric immunoassay. The antibody was raised against human apoA-II and human apoA-I in goats plasma. Ten microliter sample serum was mixed with the antibody and detergent to make the solution 70  $\mu$ L to precipitate LpAI:AI and the supernatant 9  $\mu$ L was diluted with 300  $\mu$ L buffer and mixed with anti-human apoAI goat antibody to make the final incubation volume 409  $\mu$ L. Turbidity of the mixture was measured as absorbance at 600 nm as apoA-I unassociated with apoA-II as a parameter for LpAI. **A.** LpAI measured with turbidometric immunoassay (TIA) versus LpAI measured with immunoelectrophoresis (RKT). **B.** ApoA-I, apoA-II and LpAI:AI measured by TIA and RKT.

